PIERS 2013 Stockholm

Progress In Electromagnetics Research Symposium

Abstracts

August 12–15, 2013
Stockholm, SWEDEN

www.emacademy.org
www.piers.org

PIERS 2013 Stockholm Abstracts

Copyright © 2013 The Electromagnetics Academy. All rights reserved.

Published by

The Electromagnetics Academy
777 Concord Avenue, Suite 207
Cambridge, MA 02138

www.emacademy.org
www.piers.org

ISSN: 1559-9450
ISBN: 978-1-934142-25-7

Progress In Electromagnetics Research Symposium

August 12–15, 2013

Stockholm, SWEDEN

PIERS 2013 STOCKHOLM ORGANIZATION

PIERS 2013 Stockholm General Co-chairs

Sailing He, Royal Institute of Technology, SWEDEN

Kazuya Kobayashi, Chuo University, JAPAN

Raj Mittra, Pennsylvania State University, USA

Yury Shestopalov, Karlstad University, SWEDEN

Ke Wu, University of Montreal, CANADA

PIERS 2013 Stockholm Technical Program Committee Co-chairs

Yang Hao, University of London, UK

Iam-Choon Khoo, Pennsylvania State University, USA

Joshua Li, University of Electronic Science and Technology, CHINA

Ari Sihvola, Aalto University, FINLAND

Sune Svanberg, Lund University, SWEDEN

PIERS 2013 Stockholm Subcommittee 1
(CEM, EMC, Scattering and Electromagnetic Theory)

Weng Cho Chew, University of Illinois, USA, Lead Co-Chair
Jin-Fa Lee, Ohio State University, USA, Co-Chair
Er-Ping Li, A*STAR, Singapore, Co-Chair
Yoichi Okuno, Kumamoto University, Japan, Co-Chair

Dan Censor	Georgi N. Georgiev	Levent Gürel	Se-Yun Kim
Gerhard Kristensson	Karl J. Langenberg	Giuliano Manara	Frederic Molinet
Andrey V. Osipov	Burak Polat	Alexander B. Samokhin	Tapan K. Sarkar
Taner Sengör	Thomas Wriedt	Tsuneki Yamasaki	Nikolay Zernov

PIERS 2013 Stockholm Subcommittee 2
(Metamaterials, Plasmonics and Complex Media)

Che Ting Chan, Hong Kong University of Science and Technology, China, Co-Chair
Tie Jun Cui, Southeast University, China, Co-Chair
David R. Smith, Duke University, USA, Co-Chair
Sergei Tretyakov, Aalto University, Finland, Co-Chair

Hongsheng Chen	Shanhui Fan	Francisco J. García Vidal	Jensen T H Li
Yongmin Liu	Ross McPhedran	N. Asger Mortensen	Alexander Schuchinsky
Mário G. Silveirinha	Din Ping Tsai	Lei Zhou	

PIERS 2013 Stockholm Subcommittee 3
(Optics and Photonics)

El-Hang Lee, Fellow of Korean Academy of Science and Technology, South Korea, Lead Co-Chair
Lars Thylen, Royal Institute of Technology, Sweden, Co-Chair

Adibi Ali	Yasuhiko Arakawa	Giulio Cerullo	Hyuck Choo
Sonali Dasgupta	Shanhui Fan	Stefan W. Hell	Kazuo Hotate
Chia Chen Hsu	Masanori Koshiba	Liu Liu	Oliver Muecke
Ekmel Ozbay	Andrew Poon	John Sajeev	Ali Serpenguzel
Anand Srinivasan	Katarina Svanberg	Zheng Wang	Kiyotoshi Yasumoto

PIERS 2013 Stockholm Subcommittee 4
(Antennas and Microwave Technologies)

Maurizio Bozzi, University of Pavia, Italy, Co-Chair
Vincent Fusco, Queen's University Belfast, UK, Co-Chair
Xun Gong, University of Central Florida, USA, Co-Chair

Christophe Caloz	Dau-Chyrh Chang	Young Ki Cho	Chung-Kwang Chou
Takeshi Fukusako	Debatosh Guha	Koichi Ito	Eugene O. Kamenetskii
George A. Kyriacou	Kwai Man Luk	Ananda Mohan	Lotfollah Shafai
Reuven Shavit	Jan Vrba	Vadim V. Yakovlev	Jiang Zhu
Arcady Zhukov			

PIERS 2013 Stockholm Subcommittee 5
(Remote Sensing, Inverse Problems, Imaging, Radar and Sensing)

Kun-Shan Chen, National Central University, Taiwan, Co-Chair
Mats Gustafsson, Lund University, Sweden, Co-Chair
Jianchen Shi, University of California, Santa Barbara, USA, Co-Chair
Leung Tsang, University of Washington, USA, Lead Co-Chair

Wolfgang-Martin Boerner
Lorenzo Capineri
Valentin Freilikher
Martti Hallikainen
Akira Ishimaru
Ludmilla Kolokolova
Paolo Pampaloni
Motoyuki Sato
Takashi Takenaka
Rachid Talhi
Mitsuo Tateiba
Alexey A. Vertiy
Ganquan Xie
Alexander G. Yarovoy

PIERS 2013 Stockholm Local Organizing Committee

Sailing He (Chair)
Erik Forsberg (Co-chair)
Lech Wosinski (Co-chair)

Shuai Zhang
Clark Mei
Martin Norgren
Zhangwei Yu
Jiajia Chen

PIERS 2013 STOCKHOLM SESSION ORGANIZERS

J. Aizpurua
A. Alomainy
S. Anand
M. Antezza
H. Arai
Y. Arakawa
M. Backstrom
T. D. Bechtel
G. G. E. Bjork
T. Bolin
M. Bozzi
J. Bravo-Abad
F. Capasso
L. Capineri
A. Capozzoli
G. Cerullo
C. T. Chan
H. S. Chen
N.-K. Chen
X. D. Chen
W. C. Chew
H. Choo
W. C. H. Choy
A. Costanzo
T. J. Cui
D. X. Dai
S. Dasgupta
E. De Lera Acedo
J. V. De Luca
S. H. Fan
E. Forsberg
S. M. Gao
F. J. Garcia-Vidal
G. N. Georgiev
M. N. Georgieva-Grosse
E. Gescheidtova
A. A. Glazunov
B. Guizal
M. Gustafsson
M. T. Hallikainen
M. Hammar
Y. Hao
S. W. Hell
C. C. Hsu
P. G. Huggard
B. H. In't Veld
M. V. Ivashina
G. V. Jandieri
M. Jaroszewski
S. G. Jin
S. John
N. Y. Joly
E. O. Kamenetskii
E. M. Karchevskiy
I.-C. Khoo
K. Y. Kim
K. Kobayashi
Y. Kurylev
U. Leonhardt
E. P. Li
J. Li
A. Liseno
L. Liu
Y. M. Liu
Y. L. Lu
C. Luxey
Y. G. Ma
S. A. Maier
A. Massa
P. Millot
R. Mittra
F. Molinet
J. Mork
N. A. Mortensen
O. D. Muecke
I. Ndip
S. Nordebo
P. Nordlander
S. Ohnuki
Y. Okuno
C. K. Ong
C. Ozdemir
P. Pampaloni
S. L. Pan
A. Pellegrini
J. Perruisseau-Carrier
A. W. O. Poon
O. Quevedo-Teruel
K. Z. Rajab
C. J. Reddy
J. Reif
C. Ronda
T. Rylander
P. Saari
K. K. Samanta
A. B. Samokhin
T. Sengor
A. Serpenguzel
R. Shavit
Z. X. Shen
Y. V. Shestopalov
J. Shibayama
V. Shumeiko
A. B. Shvartsburg
A. S. Sigov
A. H. Sihvola
W. M. R. Simpson
Y. G. Smirnov
G. Somesfalean
C. M. Soukoulis
J. Stake
A. Stolin
K. Svanberg
S. Svanberg
T. Takenaka
R. Thottappillil
L. Thylen
L. Ukkonen
D. V. Valovik
J. Vrba
J. F. Wang
Z. Wang
K. Watanabe
W. Whittow
L. Wosinski
Y. Wu
G. Q. Xie
D.-X. Xu
T. Yamasaki
J. Yang
K. Yasumoto
C.-H. Yeh
Z. N. Ying
M. Zhadobov
J. X. Zhang
S. Zhang
L. Zhou
J. Zhu
A. P. Zhukov
J. Ziaja

PIERS 2013 STOCKHOLM SPONSORS

- ☐ Royal Institute of Technology, Sweden
- ☐ JORCEP (Sino-Swedish Joint Research Center of Photonics)
- ☐ Asian Office of Aerospace Research and Development
- ☐ City of Stockholm
- ☐ The Swedish Institute
- ☐ Swedish Research Council
- ☐ The Electromagnetic Academy at Zhejiang University, China
- ☐ The Electromagnetics Academy

PIERS 2013 STOCKHOLM EXHIBITORS

- ☐ CST — Computer Simulation Technology
- ☐ Simpleware Ltd.

THE ELECTROMAGNETICS ACADEMY

The Progress in Electromagnetics Research Symposium (PIERS) is sponsored by The Electromagnetics Academy.

The Electromagnetics Academy is devoted to academic excellence and the advancement of research and relevant applications of the electromagnetic theory and to promoting educational objectives of the electromagnetics profession. PIERS provides an international forum for reporting progress and advances in the modern development of electromagnetic theory and its new and exciting applications.

Founded by the late Professor Jin Au Kong (1942–2008) of MIT in 1989, The Electromagnetics Academy is a non-profit organization registered in USA.

PIERS Founding Chair:

Jin Au Kong, MIT, USA

President of The Electromagnetics Academy:

Professor Leung Tsang, University of Washington, Seattle, WA, USA

PIERS 2013 SESSIONS

1A1 2_FocusSession.SC2: Metamaterials and Plasmonics Based on Graphene . . . 13
1A2 2_FocusSession.SC3&2: New Developments in Non-reciprocal Electromagnetics and Optics . . . 27
1A3 3_FocusSession.SC3: Frontiers of Ultrafast Optics . . . 41
1A4 1_FocusSession.SC1: Foundations of Casimir Physics (with tutorials) . . . 53
1A5 SC3: Silicon Photonics . . . 63
1A6 SC1&4: Antenna Modeling and Simulation . . . 79
1A7 Advanced Photonic Materials and Nanophtonics . . . 91
1A8 SC5: Inverse Scattering Problems: Theory and Applications . . . 103
1A9 SC1: Novel Mathematical Methods in Electromagnetics . . . 115
1A10 SC1: Electromagnetics of Gradient Nanostructures and Heterogeneous Media . . . 129
1A11a Application of EM Field in Medicine and in Ecological Industrial Technologies . . . 139
1A11b SC1: Physics and Application of Nonlinear Materials and Devices . . . 147
1AK Poster Session 1 . . . 153
1P1 2_FocusSession.SC2: Plasmonics in the Quantum Regime 1 . . . 213
1P2 2_FocusSession.SC2: Metasurfaces for Wavefront Control . . . 229
1P3 1_FocusSession.SC1: Casimir Effect and Heat Transfer 1 . . . 243
1P4a SC4: Novel Frequency Selective Structures . . . 257
1P4b SC4: Innovative Materials/Metamaterials for Wireless Circuits and Miniaturized Antennas . . . 267
1P5 4_FocusSession.SC4: Advances in Millimeter-Wave and THz Circuit, Techniques and Applications 275
1P6 SC4: Multiband and Wideband Antenna and Array Techniques . . . 291
1P7a SC3: Optical Fiber Communications . . . 307
1P7b Industrial Forum on CEM (Computational Electromagnetics) Software . . . 317
1P8 SC3&4: Fano Resonances in Microwaves and Optics: Physics and Application . . . 323
1P9 SC1: Ultrawideband Nondiffracting and Accelerating Waves . . . 341
1P10a Remote Sensing of the Atmosphere, Ocean, Hydrology and Cryosphere . . . 355
1P10b SC1: Nonlinear and Inverse Problems in Electromagnetics . . . 363
1P11 SC1: Computational Electromagnetics . . . 369
1PK Poster Session 2 . . . 383
2A1 2_FocusSession.SC2: Transformation Optics 1 . . . 451
2A2 3_FocusSession.SC3: Recent Progress in Photonic Crystals 1 . . . 465
2A3 0_Focus Session: Education for Electromagnetics . . . 479
2A4 5_FocusSession.SC5: Microwave Remote Sensing of Snow Cover . . . 489
2A5 SC3: Lightwaves and Resonances in Confined Structures . . . 501
2A6 SC4: Small and Miniaturized Antenna Techniques . . . 513
2A7 3_FocusSession.SC3: Nonlinear Optics: Structured Materials, Functional Devices and Applications 1 . . . 527

2A8 SC1: Analytical and Numerical Techniques for Periodic Structures . . . 537
2A9a SC4: Paper-based Microwave Circuits and Antennas . . . 549
2A9b SC4: Circuit Modelling in Microwave Devices . . . 559
2A10 SC4: Antenna-channel Interactions and Multipath Wireless Channels . . . 567
2A11 SC1: Spectral Theory of Open Structures: Critical and Interaction Phenomena . . . 579
2AK Poster Session 3 . . . 589
2P1 3_FocusSession.SC3: Recent Progress in Photonic Crystals 2 . . . 649
2P2 4_FocusSession.SC4&3: Quantum Bits and Entanglement at Microwave Frequencies . . . 669
2P3 3_FocusSession.SC3: Optics for Bio-medical Diagnostics and Therapy Applications . . . 687
2P4 1_FocusSession.SC1: Casimir Effect and Heat Transfer 2 . . . 703
2P5a SC3: High Energy and High Power Applications in Photonic Crystal/Microstructured Fibres . . . 719
2P5b 3_FocusSession.SC3: Optical Angular Momentum and Its Applications . . . 727
2P6 SC4: Antenna and RF Measurements . . . 735
2P7a SC3: Integrated Nanophotonics for Optical Interconnects in Data Centers . . . 749
2P7b SC1: High Frequency/Asymptotic Methods . . . 761
2P8a SC5: Inverse Source Problems for Localization and Diagnostics . . . 769
2P8b SC5: Emerging Techniques and Applications in SAR/ISAR Imaging . . . 779
2P9 Extended/Unconventional Electromagnetic Theory, EHD(Electro-hydrodynamics)/EMHD(Electro-magneto-hydrodynamics), and Electro-biology . . . 791
2P10 SC1: Advanced Mathematical and Computational Methods in Electromagnetic Theory and Their Applications . . . 803
2P11b SC1: Computational Techniques in Electromagnetics and Applications . . . 819
2PK Poster Session 4 . . . 833
3A1 2_FocusSession.SC2: Microwave Metamaterials and Applications 1 . . . 901
3A2 2_FocusSession.SC2: Super Enhancement of Light with Plasmonic Nano-structures 1 . . . 913
3A3 3_FocusSession.SC3: Photonics of Quantum Dots and Its Applications . . . 925
3A4 1_FocusSession.SC1: EMC, Signal Integrity and Power Integrity for Semiconductor and High Speed Electronics . . . 939
3A5 SC3&4: Microwave Photonics . . . 951
3A6 4_FocusSession.SC4: Challenges for Small Antennas . . . 965
3A7a SC4: Ultra-wideband Antennas for Radio Astronomy . . . 981
3A7b SC4: Body-centric Wireless Communications . . . 987
3A8a GPU Computing in Electromagnetics . . . 997
3A8b SC1&3: Design and Simulation of Electromagnetic and Optical Devices . . . 1005
3A9a SC3: On-chip Optical Sensing Technologies and Devices . . . 1013
3A9b Action-at-a-distance Theories and Electrodynamics . . . 1023
3AK Poster Session 5 . . . 1029
3P1 2_FocusSession.SC2: Super Enhancement of Light with Plasmonic Nano-structures 2 . . . 1091
3P2 1_FocusSession.SC1: Multi-scale & Multi-physics Computational Electromagnetics . . . 1107
3P3a 3_FocusSession.SC3: Super-resolution in Bio-imaging and Sensing . . . 1121
3P3b 2_FocusSession.SC2: Plasmonics in the Quantum Regime 2 . . . 1131
3P4a 4_FocusSession.SC4&3: Radio over Fiber Systems and Components . . . 1143
3P4b SC2: Plasmonic Nanomaterials and Nanostrcutures for Photovoltaics and Optoelectronics in Energy 1 . . . 1153

3P5 SC2: Effective Medium Theories and Homogenization 1161
3P6 SC4: Active Antennas, MIMO and Beamforming Systems 1177
3P7a SC1: Intentional Electromagnetic Interference (IEMI) and EMC 1193
3P7b SC4: THz Technologies and Applications 1203
3P8a SC4: Advanced Magnetic Materials for Microwave Applications 1211
3P8b New Materials for EM Shielding — Materials and Technology 1219
3P9a SC4: Giant Magneto-impedance and EM Safety 1227
3P9b SC1: Advanced Techniques in Nanoelectromagnetics Applications 1235
3PK Poster Session 6 1241
4A1a 2_FocusSession.SC2: Transformation Optics 2 1313
4A1b 3_FocusSession.SC3: Photonics and Optoelectronics in Industry 1321
4A2 SC2: Non-linear Metamaterials and Plasmonics 1329
4A3 3_FocusSession.SC3: Progress in Optical Sensing and Environmental Monitoring 1341
4A4 SC4: Wireless Energy Transmission and Harvesting 1 1359
4A5 SC5: High Resolution Imaging with Penetrating Radar Scanners for Detection of Small or Low Contrast Objects 1375
4A6a SC3&2: Physics and Modeling of Laser-induced Periodic Surface Structures 1389
4A6b SC4: Millimeter-Wave and THz Components, Antennas and Arrays 1397
4A7 Integrated Optical Passive and Active Components for Communication and Sensing Applications 1405
4A8a Remote Sensing of the Earth, Ocean, and Atmosphere 1419
4A8b SC5: Advances in EM Imaging and Detection of Concealed Objects or People through Walls 1427
4AK Poster Session 7 1435
4P1 2_FocusSession.SC2: Microwave Metamaterials and Applications 2 1511
4P2 SC2: New and Novel Concepts on Metamaterials/Plasmonics 1525
4P3 SC2: Plasmonic Nanomaterials and Nanostrcutures for Photovoltaics and Optoelectronics in Energy 2 1543
4P4 SC2: Plasmonics beyond the Common Local-response Approximation 1555
4P5a SC4: Wireless Energy Transmission and Harvesting 2 1571
4P5b Antenna and Array 1579
4P6a Electromagnetic Modeling, Inversion and Applications 1591
4P6b SC4: MIMO Antennas 1597
4P7 Microwave and Millimeter Wave Circuits and Devices, CAD 1605
4P8a Medical Electromagnetics, Biological Effects 1619
4P8b SC3: Nonlinear Optics: Structured Materials, Functional Devices and Applications 2 1629
Author Index 1638

Session 1A1
2_FocusSession.SC2: Metamaterials and Plasmonics Based on Graphene

Nano-plasmonic Phenomena in Graphene: Toward Tunable Metamaterials
Dmitri N. Basov, ... 14

Charge Transport in Graphene and Light Propagation in Periodic Dielectric Structures with Metamaterials: A Comparative Study
Yury P. Bliokh, Valentin D. Freilikher, Franco Nori, ... 15

Uncovering Damping Mechanisms of Plasmons in Graphene
Hrvoje Buljan, Marinko Jablan, Marin Soljacic, ... 17

Graphene: Hybrid Optoelectronic and Voltage-gated Plasmonics
Naomi J. Halas, ... 18

Plasmonic Effects in Terahertz Photomixing in Double-graphene-layer Heterostructures
Maxim Ryzhii, Taiichi Otsuji, Akira Satou, Victor Ryzhii, Vladimir Mitin, Michael S. Shur, ... 19

Graphene Plasmonics: Guiding, Excitation and Strong SERS Enhancement
Sanshui Xiao, ... 20

A Comparison of Graphene and Metals as Conductors for Metamaterials and Plasmonics
Costas M. Soukoulis, ... 21

Active Graphene Metadevices at Terahertz Frequencies
Bumki Min, ... 22

Graphene-based Metamaterials and Plasmonics at Mid-infrared and Optical Frequencies
Philippe Tassin, ... 23

Inductive Tuning of Fano-resonant Metasurfaces Using Plasmonic Response of Graphene in the Mid-infrared
S. Hossein Mousavi, Kamil B. Alici, David Purtseladze, Nihal Arju, Kaya Tatar, David Y. Fozdar, Alexander B. Khanikaev, Gennady Shvets, Iskandar Kholmanov, Ji Won Suk, Yufeng Hao, Rodney S. Ruoff, ... 24

Studying the Optical Response of Graphene Using Electron Energy-loss Spectroscopy
Juan Carlos Idrobo, Wu Zhou, Florence J. Nelson, Zoran L. Miskovic, Alain C. Diebold, Stephen J. Pennycook, Sokrates T. Pantelides, ... 25

Graphene-based Hyperbolic Metamaterial and Its Applications
Tuo Chen, Sailing He, ... 26

Nano-plasmonic Phenomena in Graphene: Toward Tunable Metamaterials

D. N. Basov
University of California, San Diego, USA

Abstract— Infrared nano-spectroscopy and nano-imaging experiments have uncovered rich optical effects associated with the Dirac plasmons of graphene [1]. We were able to directly image Dirac plasmons propagating over sub-micron distances [2]. We have succeeded in altering both the amplitude and wavelength of these plasmons by gate voltage in common graphene/SiO_2/Si back-gated structures. Scanning plasmon interferometry has allowed us to visualize grain boundaries in CVD graphene. These experiments revealed that grain boundaries tend to form electronic barriers that impede both electrical transport and plasmon propagation. Our results attest to the feasibility of using electronic barriers to realize tunable plasmon reflectors: A precondition for implementation of various metamaterials concepts. Finally, we have carried out pump-probe experiments probing ultra-fast dynamics of plasmons in exfoliated graphene with the nano-scale spatial resolution.

REFERENCES

1. *Nano Lett.*, Vol. 11, 4701, 2011.
2. *Nature*, Vol. 487, 82, 2012.

Charge Transport in Graphene and Light Propagation in Periodic Dielectric Structures with Metamaterials: A Comparative Study

Yu. Bliokh[1,2], **V. Freilikher**[2,3], **and F. Nori**[2,4]

[1]Technion, Israel
[2]Advanced Science Institute RIKEN, Japan
[3]Bar-Ilan University, Israel
[4]University of Michigan, USA

Abstract— Highly unusual properties of graphene and of optical media with negative refractive indices had been indepen-dently predicted and studied theoretically long ago. At that time, however, these predictions were perceived as rather intriguing but unrealistic exotica, and remained unnoticed for about a half-century, until quite recently (and nearly simultaneously) they were embodied in real materials. This immediately triggered an explosion of interest and activ-ities, both in solid states physics and optics. Physicists also realized that the most unusual properties of the electron transport in graphene were peculiar to the propagation of light in dielectric systems with metamaterials. Inspired by the very unusual predictions and discoveries made in graphene, researches in optics started endeavors to reproduce the unique transport properties of graphene in specifically-designed dielectric structures. An additional incentive to these efforts came from the fact that while the elementary building blocks of graphene are fixed, the modern micro- and nanotechnologies enable manufacturing periodic dielectric samples with a variety of types and sizes of unit cells. Moreover, the electrodynamical parameters of photonic crystals can, in principle, be controlled by external fields providing unique opportunities to study condensed matter phenomena in optical ways. Furthermore, rather simple electrodynamical analogies furnish physical insights into such features of graphene as the Klein paradox, delocalization in one-dimensional disordered superlattices, etc..

In this presentation, we show that some of the exotic properties of charge transport in graphene can be repro-duced in the propagation of light through layered dielectric samples. Similarities and distinctions between Maxwell and Dirac equations, and between the corresponding boundary conditions are studied. Although the equations for the real electric and magnetic fields are essentially different from those for the Dirac electrons, under some con-ditions they can be reduced to the similar form. Therewith, the role of the refractive index in graphene is played by the difference between properly normalized values of the Fermi energy and the external electrostatic potential. The boundary conditions for a Dirac quasiparticle incident on a plane separating two areas with different potentials, and for an electromagnetic wave propagating through an interface between two layers of homogeneous dielectrics are, generally speaking, different. They coincide only when the impedances of the layers are equal, and the direction of the propagation is normal to the boundary.

The analytical and numerical analysis of the photonic band gap structures of infinite periodically-layered sys-tems reveals an infinite number of the so-called "diabolic points" (singular points of contact of two transparency zones) in the spectral diagrams. A distinction needs to be drawn between two types of these singularities: point-like transparency zones and point-like gaps in the spectrum because the transport properties of the corresponding finite periodic stacks of layers differ drastically in the vicinities of these points. Namely, waves with the frequencies with the frequencies lying on opposite sides of the singularities of the first type propagate through the samples in similar ways. In the same time, when two tangent spectral cones form a point-like gap, the electromagnetic radiation inte-racts with the same sample differently, depending to which cone its frequency belongs to. Studies of the propagation of beams of light show that only the diabolic points of this type posses the properties of genuine Dirac points. We demonstrate that in mono-type layered structures, just diabolic point of the first type can exist, while conical, Dirac-type singulariteis appear only in mixed (with alternating left- and right-handed layers) samples. Although the angular dependences of the transmission and reflection coefficients from a single interface in layered dielectrics and graphene superlatices are different, the spectral properties of these two structures are conceptually identical and entail similar features in the light and charge transport. Considering, as examples, the transmission of the Gaussian monochromatic beams of light and monoenergetic Dirac electrons through the corresponding (dielectric or graphene) samples we predict the following Dirac-point-induced effects: (i) two tangent Dirac cones influence the propagation of a beam in different ways: the beam is focused when the frequency (energy) belongs to the upper cone, and is defocused at frequencies (energies) lying in the lower one; (ii)

the transverse shift of the beam is anomalously small or even zero; (iii) the decay of the intensity at forbidden frequencies is diffusion-like; (iv) a spatial analog of the Zitterbewegung effect (i.e., trembling motion of the "center of gravity" of the energy flux) is observed in periodically-layered dielectric structures and in graphene super-lattices.

Uncovering Damping Mechanisms of Plasmons in Graphene

H. Buljan[1], **M. Jablan**[1], **and M. Soljačić**[2]

[1]Department of Physics, University of Zagreb, Bijenička c. 32, Zagreb 10000, Croatia
[2]Department of Physics, Massachusetts Institute of Technology
77 Massachusetts Avenue, Cambridge, MA 02139, USA

Abstract— The development of nanophotonics depends on our ability to confine and control light at scales much smaller than the wavelength of light. One, and perhaps the only viable path towards this goal, is to use surface plasmons — collective excitations of electrons and light at the interface of a conductor and a dielectric [1]. Plasmon wavelength can be much smaller than the wavelength of light in air at the same frequency of the wave, which enables smaller diffraction limit in the plane of propagation and exponentially strong confinement (at the scale of the plasmon wavelength) perpendicular to the plane of propagation. However there is a tradeoff: The strong subwavelength confinement of light is generally accompanied with large losses resulting in small propagation lengths of plasmonic excitations, imposing a large obstacle to development of nanophotonics. When graphene — a single sheet of carbon atoms organized in a honeycomb lattice with its extremely interesting electrical and optical properties — was isolated on a dielectric substrate [2], graphene plasmons became a very hot topic of research in the nanophotonic community due to their strong confinement of light, the possibility of control via gate voltage, and potentially smaller losses than in the previously used systems [3]. The understanding of plasmon losses in graphene is of key importance for their potential use in nanophotonics [3, 4]. There are a number of possible damping pathways for plasmons in graphene, which we discuss in light of the recent experiments [5–7] where plasmon graphene properties were studied. First we point out that Landau damping can be eliminated by doping (e.g., back-gate doping) of graphene. Second we discuss scattering from phonons and electron-electron scattering beyond random-phase approximation. Finally we address the role of impurities and attempt to provide the intrinsic limits on plasmon damping. Some other advantages of graphene plasmons as the possibility of operation in a broad frequency range (including THz) will be discussed.

REFERENCES

1. Barnes, W. L., A. Dereux, and T. W. Ebbesen, *Nature*, Vol. 424, 824–830, 2003.
2. Novoselov, K. S., et al., *Science*, Vol. 306, 666–669, 2004.
3. Jablan, M., H. Buljan, and M. Soljačić, *Phys. Rev. B*, Vol. 80, 245435, 2009.
4. Tassin, P., T. Koschny, M. Kafesaki, and C. M. Soukoulis, *Nat. Photonics*, Vol. 6, 259–264, 2011.
5. Yan, H., et al., *Nature Nanotechnology*, Vol. 7, 330–334, 2012.
6. Chen, J., et al., *Nature*, Vol. 487, 77–81, 2012.
7. Fei, Z., et al., *Nature*, Vol. 487, 82–85, 2012.

Graphene: Hybrid Optoelectronic and Voltage-gated Plasmonics

N. J. Halas
Rice University, Houston, TX, USA

Abstract— Graphene, with its unique electronic structure and its outstanding conductivity, is a material well suited for realizing new plasmonic functions and devices. Gold nanoantennas sandwiched between two graphene monolayers yield a photodetector that efficiently converts visible and near-infrared photons into electrons with an 800% enhancement of the photocurrent relative to the antennaless graphene device. This results in a graphene-based photodetector achieving up to 20% internal quantum efficiency in the visible and near infrared regions of the spectrum. This device can serve as a model for merging the light-harvesting characteristics of optical frequency antennas with the highly attractive transport properties of graphene in new optoelectronic devices [1]. By fabricating nanodisks and nanorings in a voltage-gated structure, we demonstrate the electrical and geometric tunability of graphene plasmon modes in the mid infrared region of the spectrum [2], a property well-suited for active plasmonics applications.

REFERENCES

1. Fang, Z., Z. Liu, Y. Wang, P. M. Ajayan, P. Nordlander, and N. J. Halas, "A graphene-antenna sandwich photodetector," *Nano Letters*, Vol. 12, 3808–3813, 2012.
2. Fang, Z., S. Thongrattanasiri, A. Schlather, Z. Liu, Y. Wang, P. Ajayan, P. Nordlander, N. J. Halas, and J. G. de Abajo, "Gated tunability and hybridization of localized plasmons in nanostructured graphene," *ACS Nano*, Vol. 7, 2388–2395, 2013.

Plasmonic Effects in Terahertz Photomixing in Double-graphene-layer Heterostructures

M. Ryzhii[1], **T. Otsuji**[2], **A. Satou**[2], **V. Ryzhii**[2], **V. Mitin**[3], **and M. S. Shur**[4]

[1]University of Aizu, Aizu-Wakamatsu 965-8580, Japan
[2]Tohoku University, Sendai 980-8577, Japan
[3]University at Buffalo, Buffalo, NY 14260, USA
[4]Rensselaer Polytechnic Institute, Troy, NY 12180, USA

Abstract— The energy spectrum of graphene layers (GLs) enables the interband photogeneration of electrons and holes by electromagnetic radiation from the terahertz to ultraviolet range.

Long momentum relaxation times in GLs promote the existence of weakly damped propagating and standing plasma waves in GL-heterostructures, in particular, in the gated GLs at terahertz (THz) frequencies. This opens up the prospects of creation of different THz plasma-wave GL-based devices, such as THz photomixers, surpassing those made of the standard heterostructures.

We propose the concept of voltage-controlled THz photomixing using the interband electron transitions due to the absorption of optical radiation from two lasers with close frequencies ($\Omega_1 \approx \Omega_2 \approx \Omega$) or ultrashort optical pulses in double-GL heterostructures [1].

The device operation is associated with the tunneling or thermionic inter-GL current and resonant excitation of plasma oscillations in GLs. One of GLs is occupied by electrons while another is occupied by holes due to the applied bias voltage. Each GL plays the role of the highly conducting gate for another GL.

Using the proposed double-GL photomixer (DG-PM) model, we analyze its operation and calculate the device characteristics. We demonstrate that the output power of the THz radiation exhibits sharp resonant peaks at the plasmonic resonant frequencies. Due to relatively high quantum efficiency of optical absorption in GLs and short inter-GL transit time, the proposed DG-PM operating in the regime of plasma oscillations can surpass the photomixers based on the standard heterostructures.

REFERENCES

1. Ryzhii, V., M. Ryzhii, V. Mitin, M. S. Shur, A. Satou, and T. Otsuji, *J. Appl. Phys.*, Submitted.

Graphene Plasmonics: Guiding, Excitation and Strong SERS Enhancement

Sanshui Xiao[1, 2]

[1]Department of Photonics Engineering, Technical University of Denmark
DK2800 Kongens Lyngby, Denmark
[2]Center for Nanostructured Graphene (CNG), Technical University of Denmark
DK2800 Kongens Lyngby, Denmark

Abstract— Propagation of graphene plasmons in nanoribbon waveguides is numerically investigated and excitation of the graphene plasmons in a continuous graphene monolayer is experimentally demonstrated. Interaction between a graphene monolayer with metallic nanostructures is further experimentally studied, and strong SERS enhancement for the graphene monolayer is observed with the aid of metallic nanostructures.

A Comparison of Graphene and Metals as Conductors for Metamaterials and Plasmonics

Costas M. Soukoulis[1, 2]

[1]Ames Lab, Iowa State University, USA
[2]IESL-FORTH, Crete, Greece

Abstract— Recent advances in metamaterials and plasmonics have promised a number of exciting applications, in particular at terahertz and optical frequencies. Unfortunately, the noble metals used in these photonic structures are not particularly good conductors at high frequencies, resulting in significant dissipative loss. Here, we address the question what is a good conductor for metamaterials and plasmonics. For resonant metamaterials, we develop a figure-of-merit for conductors that allows for a straightforward classification of conducting materials according to the resulting dissipative loss in the metamaterial. Application of our method predicts that graphene and high-Tc superconductors are not viable alternatives for metals in metamaterials. We also provide an overview of a number of transition metals, alkali metals and transparent conducting oxides. For plasmonic systems, we predict that graphene and high-Tc superconductors cannot outperform gold as a platform for surface plasmon polaritons (SPPs), as graphene has a smaller propagation length-to wavelength ratio. Graphene has a very strong confinement of SPPS and tunable devices at THz frequencies.

Active Graphene Metadevices at Terahertz Frequencies

Bumki Min
Department of Mechanical Engineering, KAIST
291 Daehak-ro, Yuseong-gu, Daejeon 305-751, Republic of Korea

Abstract— We show experimentally that various functionalities such as electrical/optical modulation of terahertz (THZ) waves and electrically-controlled memory operations in terahertz wave transmission can be achieved with active graphene metadevices. The active graphene metadevices are basically composed of four functional building blocks: Graphene, Meta-atoms, dielectric or ferroelectric spacers, and THz transparent electrodes. For the electrical modulation of terahertz waves, gate-controllable electronic properties of graphene are fully utilized. The gate-controlled change of graphene conductivity results in the modification of coupling between meta-atoms and graphene and this leads to the change in the terahertz transmission through the active graphene metadevices. Although the thickness of the embedded single-layer graphene is more than 'six' orders of magnitude smaller than the wavelength ($< \lambda/1,000,000$), the one-atom-thick layer, in conjunction with the meta-atoms, can modulate both the amplitude of the transmitted wave by up to 47% and its phase by more than 30° at room temperature. In addition, it is shown that, with nonresonant design of meta-atoms, broadband operation is possible with considerable modulation depth. For the demonstration of ultrafast modulation of terahertz waves, we performed ultrafast optical pump/terahertz probe measurements on the active graphene metadevices. The photo-generated nonequilibrium Dirac fermions and/or gate-induced equilibrium Dirac fermions of graphene effectively alter the polarization density in the meta-atoms, resulting in ultrafast index control with an extreme index contrast over $\Delta n \sim -3.4$, the value of which has never been observed in any natural photorefractive materials. Finally, the electrically-controlled memory operations in terahertz wave transmission are demonstrated in the active graphene metadevices. The memory operation is due to the hysteretic behaviour of charge density in graphene with a variation in gate voltage. However, this intrinsic hysteresis of CVD-grown graphene is not strong enough for the device to show non-volatile memory operation (retention time of ~ 20 minutes). Therefore, we replace the dielectric spacer with a ferroelectric layer of P(VDF-TrFE) in order to render the active graphene metadevices non-volatile. When being poled by electric gating, the ferroelectric layer provides long-lasting polarization states by which charge carriers in graphene layer can be controlled. Thus, two polarization states in the ferroelectric result in two distinct doping levels of graphene and lead to bistable states of terahertz wave transmission that last over 10^5 seconds.

Graphene-based Metamaterials and Plasmonics at Mid-infrared and Optical Frequencies

Philippe Tassin
Iowa State University, USA

Abstract— Graphene has recently been proposed as an alternative for metals as a platform for electromagnetic metamaterials and plasmonics in the mid-infrared and optical frequency bands. Both metamaterials and plasmonic systems rely on conducting materials, to generate large electric and magnetic dipole moments or to generate propagating charge oscillations, respectively. To investigate this possibility, we study the relation between the conductive properties of a material and the dissipative loss in a metamaterial made from that conducting material. We show that the optical resistivity multiplied by a geometrical term related to the thickness of the conductor is the appropriate figure of merit. The geometrical term is of particular importance when comparing graphene — a two-dimensional conductor — with metals. Finally, we investigate the propagation length of surface plasmon polaritons on graphene starting from experimental data of the mid-infrared conductivity of graphene.

REFERENCES

1. Tassin, P., T. Koschny, M. Kafesaki, and C. M. Soukoulis, "A comparison of graphene, superconductors and metals as conductors for metamaterials and plasmonics," *Nature Photonics*, Vol. 6, 259–264, 2012.
2. Zou, Y., P. Tassin, T. Koschny, and C. M. Soukoulis, "Interaction between graphene and metamaterials: Split rings vs. wire pairs," *Opt. Express*, Vol. 20, 12198–12204, 2012.

Inductive Tuning of Fano-resonant Metasurfaces Using Plasmonic Response of Graphene in the Mid-infrared

S. Hossein Mousavi[1], Kamil B. Alici[1], David Purtseladze[1], Nihal Arju[1], Kaya Tatar[1], David Y. Fozdar[1], Alexander B. Khanikaev[1], Gennady Shvets[1], Iskandar Kholmanov[2], Ji Won Suk[2], Yufeng Hao[2], and Rodney S. Ruoff[2]

[1]Department of Physics, The University of Texas at Austin, Austin, Texas 78712, USA
[2]Department of Mechanical Engineering and Materials Science Program
The University of Texas at Austin, Austin, Texas 78712, USA

Abstract— Graphene is widely known for its anomalously strong broadband optical absorptivity of 2.3% that enables seeing its single-atom layer with the naked eye. However, in the mid-infrared part of the spectrum graphene represents a quintessential lossless zero-volume plasmonic material. We experimentally demonstrate that, when integrated with Fano-resonant plasmonic metasurfaces, single-layer graphene (SLG) can be used to tune their mid-infrared optical response. SLG plasmonic response is shown to induce large blue shifts of the meta-surfaces resonance without reducing its spectral sharpness. This effect is explained by a generalized perturbation theory of SLG-metamaterial interaction that accounts for two unique properties of the SLG that set it apart from all other plasmonic materials: its anisotropic response and zero volume. These results pave the way to using gated SLG as a platform for dynamical spectral tuning of infrared metamaterials and meta-surfaces. We also demonstrate that meta-surfaces can be used for spectroscopic measurements of graphene's optical characteristics such as the complex-valued surface conductivity.

Metamaterials are typically comprised of highly resonant plasmonic elements which have a spectrally-narrow response. The ability to actively control the resonant constitutive elements of metamaterials enables dynamic tunability of their optical response and can potentially expand the range of their applications even further. A variety of approaches to achieving dynamic tunability have recently emerged. They rely on integrating metamaterials with various optically active materials such as semiconductors with electrically/optically controlled free carriers, liquid crystals, and nonlinear media.

Here we propose an approach to blue-shifting metamaterials resonances in the mid-infrared part of the spectrum by enveloping them in a "zero-volume" nearly-lossless plasmonic material: the single-layer grapheme (SLG). SLG, due to its vanishing out-of-plane polarizability, hence the name zero-volume, does not alter the capacitance, however, here we show both theoretically and experimentally, that it modifies the inductance, and accordingly induces blueshifting. We will present an analytic theory describing frequency-shifting of metamaterial resonances that takes into account both field expulsion (capacitance increase) and inductive response (inductance decrease) by anisotropic materials such as graphene will be presented. This theory clearly differentiates between the frequency tuning by common (isotropic) plasmonic materials and anisotropic materials such as graphene.

One interesting aspect of using Fano-resonant metamaterials functionalized by single-layer graphene is that reflectivity data can be used for characterizing graphene's optical properties such as graphene's complexvalued conductivity $\sigma(\omega)$. While graphene's response is strong in the visible/near-IR spectral ranges due to inter-band transitions, and in the THz due to high Drude-like conductivity, the mid-IR response of graphene is rather weak. Strong field enhancement in the immediate proximity of meta-surfaces can be used to enhance graphene's response and characterization in the mid-IR. Experimental results of such characterization and the supporting theory will be presented.

Studying the Optical Response of Graphene Using Electron Energy-loss Spectroscopy

Juan-Carlos Idrobo[1], Wu Zhou[1], Florence J. Nelson[2], Zoran L. Mišković[3], Alain C. Diebold[3], Stephen J. Pennycook[1,2], and Sokrates T. Pantelides[1,4]

[1]Materials Science & Technology Division, Oak Ridge National Laboratory
Oak Ridge, TN 37831, USA
[2]College of Nanoscale Science and Engineering, University at Albany
255 Fuller Rd., Albany, New York 12203, USA
[3]Department of Applied Mathematics, University of Waterloo
Waterloo, Ontario N2L 3G1, Canada
[4]Department of Physics & Astronomy, Vanderbilt University
Nashville, TN 37235, USA

Abstract— Graphene, due to its intrinsic two-dimensional and flexible structure, excellent electronic transport and unusual optical properties, is believed to be a very good candidate material for the next generation of plasmonic devices. All localized plasmon resonances observed so far in materials have been limited to the sub-10 nanometer scale, with a reported record of $\lambda/40$, where λ is the wavelength of the related plasmon excitation. In this talk, using aberration-corrected scanning transmission electron microscopy (STEM) and total energy first-principles calculations, we show that single point defects can enhance the optical response of, the so called, π and $\pi + \sigma$ plasmons of monolayer graphene at the atomic level. Our study shows that point defects in monolayer graphene represent a length scale smaller than $\lambda/200$, and suggest that the physical limit for the size of optoelectronic devices can be down to the single atom level. We will discuss in detail the methods to obtain the optical response of two-dimensional materials from electron energy-loss spectroscopy (EELS) experiments, and present further insights into whether the optical response of graphene is formed by plasmons or other electronic excitations.

ACKNOWLEDGMENT

This research was supported in part by NSF grant No. DMR-0938330 (WZ, J-CI), the Institute for Nanoelectronics Discovery and Exploration (INDEX)/Nanoelectronics Research Initiative (NRI) and the New York Center for National Competitiveness in Nanoscale Characterization (NC3), Oak Ridge National Laboratory's Shared Research Equipment (ShaRE) User Program (JCI), which is sponsored by the Office of Basic Energy Sciences, U.S. Department of Energy; the Materials Sciences and Engineering Division, Office of Basic Energy Sciences, U.S. Department of Energy (SJP, STP), and DOE Grant No. DE-FG02-09ER46554 (STP), the Natural Sciences and Engineering Research Council of Canada (ZLM). This research used resources of the National Energy Research Scientific Computing Center, which is supported by the Office of Science of the US DOE (contract No. DE-AC02-05CH11231).

Graphene-based Hyperbolic Metamaterial and Its Applications

Tuo Chen[1] **and Sailing He**[1,2]

[1]Centre for Optical and Electromagnetic Research, JORCEP
Zhejiang University, Hangzhou 310058, China
[2]Department of Electromagnetic Engineering, School of Electrical Engineering
Royal Institute of Technology, 100 44 Stockholm, Sweden

Abstract— The optical properties of graphene have been extensively studied. Recently the interest has shifted to the interaction between the graphene and THz electromagnetic wave. Graphene can exhibit some plasmonic response in THz, similar to a noble metal at optical frequency range. A hyperbolic metamaterial is a special medium described by a diagonal permittivity tensor with the principle components having opposite signs. A stack of graphene sheets, separated by dielectric layers, can be considered as a hyperbolic material with anisotropic electric properties. The dispersion for such a graphene-based metamaterial can be tuned from hyperbolic to elliptic by changing the applied voltage or the level of chemical doping. Graphene can be fabricated by CVD method and can be transferred by PMMA. Coupled with the dielectric layers, the graphene-based hyperbolic metamaterial could be made extremely thin compared to the operating wavelength. We demonstrate deep-subwavelength scale waveguides made of graphene-dielectric multilayered hyperbolic metamaterials that support ultra-high effective refractive indices. Numerical simulations based on both graphene-dielectric multilayers and the effective medium approach are performed to analyze the waveguide properties, including the propagation length and mode areas. We will also show that the unique hyperbolic dispersion of the graphene-based metamaterial can also be used as broadband THz light absorbers.

Session 1A2
2_FocusSession.SC3&2: New Developments in Non-reciprocal Electromagnetics and Optics

An Overview of Optical Isolation on Integrated Platforms
Richard M. Osgood, Jr., ... 28

Silicon-based Magneto-optical Isolator and Circulator Fabricated by Direct Bonding Technology
Yuya Shoji, K. Mitsuya, Tetsuya Mizumoto, ... 30

Optical Isolation and Mode Conversion Using Stimulated Brillouin Scattering in Multi-mode Waveguides
Christopher G. Poulton, Ravi Pant, I. Aryanfar, M. J. Steel, S. Fan, Benjamin J. Eggleton, ... 31

Magnetic Field Controlled Nonreciprocal Band-stop Filters for the W-band Using Magnetic Polariton Modes in Yttrium-iron Garnet
Maksym A. Popov, Igor V. Zavislyak, Gopalan Srinivasan, ... 32

Unidirectional Electromagnetic Edge Mode in Gyromagnetic Photonic Crystal Slab
Kexin Liu, Sailing He, ... 33

Faraday Rotation and Magneto-plasmonic Effects in Graphene
Alexey B. Kuzmenko, ... 34

Magnet-less Non-reciprocal Metamaterials
Toshiro Kodera, Dimitrios L. Sounas, Christophe Caloz, ... 35

Synthetic Faraday Rotation in Active Metamaterials
Zheng Wang, Zhiyu Wang, Jingyu Wang, Bin Zhang, Jiangtao Huangfu, John D. Joannopoulos, Marin Soljacic, Lixin Ran, ... 37

Photonic Transitions for Enabling Non Reciprocity in Silicon
Michal Lipson, ... 38

A Unidirectional Sub-wavelength Bend Waveguide with Arbitrary Angle Based on Magnetic Photonic Crystals
Yin Poo, Rui-Xin Wu, Renkai Li, Yan Yang, Chao Meng, ... 39

An Overview of Optical Isolation on Integrated Platforms

Richard Osgood, Jr.
Laboratory for Light-Surface Interactions, Columbia University, NY 10027, USA

Abstract— Optical isolation is a key technology for most integrated optical functions since it separates one optical system, say, forward travelling waves, from a second, backward travelling waves. Highly efficient isolation presents a difficult challenge since the most straightforward methods involve the integration of magnetic-garnet oxide materials with standard photonic integrated optical materials such as silicon, SiO_2 on Si, or InP-based III-V materials. Often these materials cannot be lattice matched or they may react with the magnetic materials. Our talk will review progress in integrated optical isolation devices and materials technology. The discussion will include review careful magnetic thin-film engineering to form micrometer-scale waveguide magnetic field [1, 2]. This approach eliminates the intrusive bulk magnets seen in many fiber-optics systems by using the magnetic near-field of thin-film magnetic materials. In addition, we will show that lift-off technology and other novel thin film processing methods, in many cases based on deep ion-implantation methods, enable hetero-integration of epitaxial garnet films without the use of complex heteroeptixial growth of oxides [3–5]. This approach enables us to highlight the recently demonstrated YIG/SOI isolators by our group [6, 7] and by others [8] and discuss their performance. Research in understanding the detailed science of the lift-off process has continued to advance in the last few years [9]. A final area of major improvement has been development of methods for the use of non-Faraday rotator designs, including the use of transverse magnetic fields for isolation [10, 11, 13]. Finally recently there have been attempts to surmount the materials challenges by using a series of novel optical phenomena for isolation, some for example, based on unidirectional lineshape effects in standard reciprocal materials and other approaches based on nanooptical-fabrication methods [14–16]. As will be brought out in the talk, this progress in our lab and others has been the result of major, key collaborations and independent work with/by other groups in the US, Europe, and Japan.

REFERENCES

1. Levy, M., I. Ilic, R. Scarmozzino, and R. M. Osgood, Jr., "Thin-film-magnet magneto-optic waveguide isolator," *Photon. Tech. Lett.*, Vol. 5, 198, 1993.
2. Levy, M., H. Hegde, F. J. Cadieu, R. Wolfe, V. J. Fratello, and R. M. Osgood, Jr., "Integrated optical isolators with sputter-deposited thin-film magnets," *Photon. Tech. Lett.*, Vol. 8, 903, 1996.
3. Levy, M., R. M. Osgood, Jr., A. Kumar, and H. Bakhru, "Epitaxial liftoff of thin oxide layers: Yttrium iron garnets onto GaAs," *Appl. Phys. Lett.*, Vol. 71, 2617–2619, 1997.
4. Levy, M., R. M. Osgood, Jr., A. Kumar, and H. Bakhru, "Crystal ion slicing of single-crystal magnetic garnet films," *J. Appl. Phys.*, Vol. 83, 6759–6761, 1998.
5. Izuhara, T., M. Levy, and R. M. Osgood, Jr., "Direct wafer bonding and transfer of 10 μm-thick magnetic garnet films onto semiconductor surfaces," *Appl. Phys. Lett.*, Vol. 76, 1261–1263, 2000.
6. Shoji, Y., I.-W. Hsieh, R. M. Osgood, Jr., and T. Mizumoto, "Polarization-independent magneto-optical waveguide isolator using TM-mode nonreciprocal phase shift," *J. Lightwave Technol.*, Vol. 25, No. 10, 3108–3113, 2007.
7. Shoji, Y., T. Mizumoto, H. Yokoi, I.-W. Hsieh, and R. M. Osgood, Jr., "Magneto-optical isolator with silicon waveguides fabricated by direct bonding," *Appl. Phys. Lett.*, Vol. 92, No. 7, 071117, 2008.
8. Pintus, P., F. Di Pasquale, and J. E. Bowers, "Integrated TE and TM optical circulators on ultra-low-loss silicon nitride platform," *Opt. Exp.*, Vol. 21, 5041, 2013.
9. Gaathon, O., J. D. Adam, S. V. Krishnaswamy, J. W. Kysar, S. Bakhru, H. Bakhru, D. O. Welch, and R. M. Osgood, Jr., "Planar single-crystal thin films of YAG obtained by ion implantation and thermal exfoliation," *Opt. Mater.*, Vol. 35, 25–28, 2012.
10. Fujita, J., M. Levy, R. U. Ahmad, R. M. Osgood, Jr., M. Randles, C. Gutierrez, and R. Villareal, "Observation of optical isolation based on nonreciprocal phase shift in a Mach-Zehnder interferometer," *Appl. Phys. Lett.*, Vol. 75, 998–1000, 1999.

11. Fujita, J., M. Levy, R. M. Osgood, Jr., L. Wilkens, and H. Dotsch, "Polarization-independent waveguide optical isolator based on nonreciprocal phase shift," *Photon. Tech. Lett.*, Vol. 12, 1510–1512, 2000.
12. Fujita, J., M. Levy, and R. M. Osgood, Jr., "Waveguide optical isolator based on mach-zehnder interferometer," *Appl. Phys. Lett.*, Vol. 76, 2158–2160, 2000.
13. Espinola, R. L., T. Izuhara, M.-C. Tsai, and R. M. Osgood, Jr., "Magneto-optical nonreciprocal phase shift in garnet/silicon-on insulator waveguides," *Opt. Lett.*, Vol. 29, 941, 2004.
14. Steel, M. J., M. Levy, and R. M. Osgood, Jr., "High transmission enhanced faraday rotation in one-dimensional photonic crystals with defects," *Photon. Tech. Lett.*, Vol. 12, 1171–1173, 2000.
15. Steel, M. J., M. Levy, and R. M. Osgood, Jr., "Photonic band gaps with defects and the enhancement of faraday rotation," *J. Lightwave Tech.*, Vol. 18, 1297–1308, 2000.
16. Steel, M. J., M. Levy, and R. M. Osgood, Jr., "Large magnetooptical Kerr rotation with high reflectivity from photonic band gap structures with defects," *J. Lightwave Tech.*, Vol. 18, 1289–1296, 2000.
17. Yu, Z. and S. Fan, "Optical isolation: A non-magnetic approach," *Nature Photonics*, Vol. 5, 517, 2011.
18. Shoji, Y., M. Ito, Y. Shirato, and T. Mizumoto, "MZI optical isolator with Si-wire waveguides by surface-activated direct bonding," *Opt Exp.*, Vol. 20, 18440, 2012.
19. Ghosh, S., S. Keyvavinia, W. Van Roy, T. Mizumoto, G. Roelkens, and R. Baets, "Ce:YIG/Silicon-on-insulator waveguide optical isolator realized by adhesive bonding," *Opt. Exp.*, Vol. 20, 1839, 2012.

Silicon-based Magneto-optical Isolator and Circulator Fabricated by Direct Bonding Technology

Y. Shoji, K. Mitsuya, and T. Mizumoto
Tokyo Institute of Technology, Japan

Abstract— We have investigated waveguide-type magneto-optical isolators and circulators. The devices are based on silicon photonic waveguides with an upper cladding layer of magneto-optic garnet. It is difficult to integrate a single-crystalline garnet having a large magneto-optical effect on silicon or any other waveguide platforms. Our approach is to use a direct bonding technology which realizes direct contact between two different materials without any adhesive.

Any interlayer between core and upper cladding reduces the nonreciprocal effect. Therefore, our approach enables more efficient nonreciprocal effect than any other approach using adhesive bonding or deposition with buffer layer.

Our direct bonding is carried out with plasma activation followed by pressing and annealing processes in a vacuum chamber.

The optical isolator is a Mach-Zehnder interferometer (MZI) with nonreciprocal and reciprocal phase shifters. The nonreciprocal phase difference is provided by a phase shift induced by the magneto-optical effect in a push-pull manner. The reciprocal one is induced by optical path difference. Therefore, constructive and destructive interference occur for forward and backward directions, respectively.

We demonstrated a silicon-based optical isolator for the first time. The first device was fabricated with shallow-etched rib waveguides, which had the advantage of low propagation loss at the sacrifice of large device size. The next device was fabricated with silicon-wire waveguides to minimize the size. In these devices, the operation bandwidth was narrow due to the immature fabrication for controlling the reciprocal phase shift. Recently, a silicon-based optical isolator was demonstrated with a high isolation ratio over 20 dB for a wavelength range of 8 nm. Also, silicon-based 4-port optical circulator was demonstrated by using a 2×2 MZI configuration. In this report, we describe the progress of magneto-optical isolators and circulators based on silicon waveguides.

Optical Isolation and Mode Conversion Using Stimulated Brillouin Scattering in Multi-mode Waveguides

C. G. Poulton[1,2,3], R. Pant[3], I. Aryanfar[3], M. J. Steel[1,4], S. Fan[1,3,5], and B. J. Eggleton[3]

[1]Centre for Ultrahigh Bandwidth Devices for Optical Systems (CUDOS), Australia
[2]School of Mathematical Sciences, University of Technology, Sydney, Australia
[3]School of Physics, University of Sydney, Australia
[4]School of Physics, Macquarie University, Australia
[5]Department of Electrical Engineering, Stanford University, USA

Abstract— We theoretically and numerically investigate Stimulated Brillouin Scattering as a mechanism for non-reciprocal mode conversion and isolation in multi-moded nanophotonic waveguides. We find that significant isolation ($> 20\,\mathrm{dB}$) can be achieved with realistic pump powers ($< 0.5\,\mathrm{W}$) and short waveguide lengths ($< 10\,\mathrm{cm}$).

Introduction: Stimulated Brillouin Scattering (SBS) is a coherent interaction in which two optical beams can excite acoustic vibrations; these acoustic waves then form a travelling index grating that can drive transitions between optical modes [1]. Because this transition is unidirectional it can be used as a source of non-reciprocity [1, 2]. Here we examine SBS-based non-reciprocal mode-conversion in integrated optical waveguides and present designs for compact nanophotonic isolators.

Isolator Configuration and Numerical Results: The configuration for SBS-based optical mode conversion is show in Figs. 1(a) and (b); the amount of mode conversion for a given pump power is shown in Fig. 1(c). We find that significant isolation ($> 20\,\mathrm{dB}$) can be achieved in chalcogenide waveguides: these glasses are not only highly nonlinear but also act as guides for both optical and acoustic waves [2]. We investigate non-reciprocal mode-conversion and isolation in a range of chalcogenide structures and show how the bandwidth depends critically on the waveguide geometry.

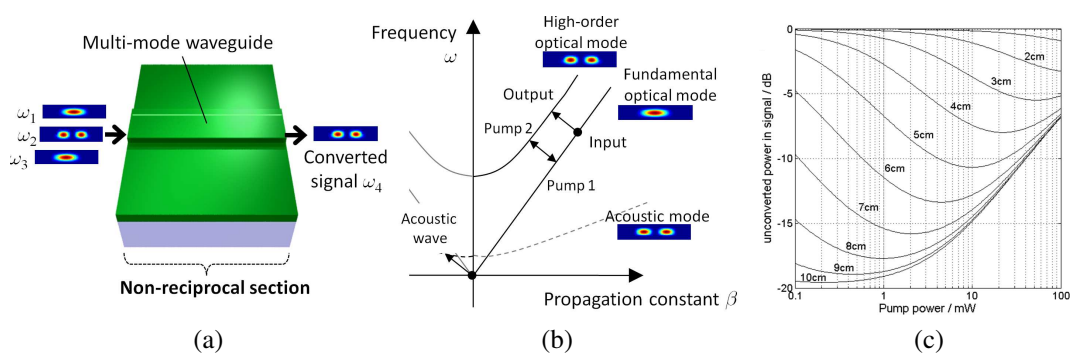

Figure 1: (a) One-way mode conversion in a multimode waveguide; (b) Dispersion diagram for SBS-driven inter-mode transitions; (c) Mode conversion as a function of pump power.

ACKNOWLEDGMENT

The authors aknowledge funding from ARC Discovery Projects DP130100832 and DP1096838, the Centre of Excellence CUDOS, and AFOSR/AOARD grant FA23861114030.

REFERENCES

1. Huang, X. and S. Fan, "Complete all-optical silica fiber isolator via stimulated brillouin scattering," *J. Lightwave Technol.*, Vol. 29, No. 15, 2267–2275, 2011.
2. Poulton, C. G., et al., "Design for broadband on-chip isolator using stimulated Brillouin scattering in dispersion-engineered chalcogenide waveguides," *Opt. Express*, Vol. 20, No. 19, 21235–21246, 2012.

Magnetic Field Controlled Nonreciprocal Band-stop Filters for the W-band Using Magnetic Polariton Modes in Yttrium-iron Garnet

M. A. Popov[1], **I. V. Zavislyak**[1], **and G. Srinivasan**[2]

[1]Radiophysics Department, Taras Shevchenko National University of Kyiv, Kyiv 01601, Ukraine
[2]Physics Department, Oakland University, Rochester, MI 48309, USA

Abstract— A new concept for magnetic field tunable nonreciprocal ferrite-based millimeter wave filter design has been suggested. Such filters can be built on the basis of standard W-band waveguide with flat rectangular ferromagnetic resonator (typical dimensions $2 \times 1 \times 0.4\,\mathrm{mm}^3$) situated on the middle of the wide metal wall and biased to saturation with perpendicular external DC magnetic field. The filter operating frequency is well above the ferromagnetic resonance (FMR).

The principle of operation of this filter is the excitation of magnetic polariton (MP) modes of the ferrite resonator by dominant H_{10} waveguide mode [1]. MPs propagate in the ferrite transversely to biased magnetic field direction and localize on the surface of wide waveguide wall. Impedance properties of metal contacted with surface of ferrite resonator play a vital part.

Polarization nature of nonreciprocity effect is based on the interaction of either co-polarized (elliptic of the same sign) or cross-polarized (elliptic of the different sign) electromagnetic oscillations in ferrite and electron plasma in the magnetized metal. Eigen modes of one polarization state does not excite and attenuation is less than 0.5 dB (see Figure), while other polarization, on the contrary, effectively excites and attenuation reaches 10–12 dB. It is shown that the observed effect is reversible with respect to both direction of external static magnetic field and direction of H_{10} wave propagation.

The theory that qualitatively explains the observed effect is presented. Theoretical evaluations give for maximum magnetic field filter frequency tuning expression $\Delta\omega = \omega_M(\omega_M + \omega_H)/2\omega_d$, where ω_d — dielectric resonance angular frequency, $\omega_H = \gamma H_0$, $\omega_M = \gamma 4\pi M$, M — saturation magnetization, γ — gyromagnetic ratio, H_0 — bias field.

Experiments have been performed on various ferrite resonators made from single-crystals, polycrystals and epitaxial films of yttrium-iron garnet (YIG) over the frequency range 75–110 GHz (W-band). Numerical modeling using HFSS finite element simulation has shown that the filter frequency is determined by excitation of EH_{131} dielectric resonance mode. Measured magnetic field frequency tuning of the filter was found to be 60–230 MHz. Isolation of almost 12 dB was obtained with very reasonable input and output standing wave ratio (SWR) values (less than 1.7), that makes the suggested filter design rather attractive.

Theoretical estimates show feasibility of such filters and isolators at frequencies over the entire sub-THz range.

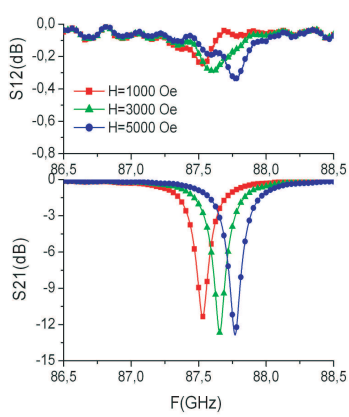

REFERENCES

1. Kaganov, M. I., N. B. Pustyl'nik, and T. I. Shalaeva, "Magnons, magnetic polaritons, magnetostatic waves," *Phys. Usp.*, Vol. 40, No. 2, 181–224, 1997.

Unidirectional Electromagnetic Edge Mode in Gyromagnetic Photonic Crystal Slab

Kexin Liu[1] **and Sailing He**[1, 2]

[1]Centre for Optical and Electromagnetic Research
State Key Laboratory of Modern Optical Instrumentation
Zhejiang University, Hangzhou, China
[2]Division of Electromagnetic Theory, School of Electrical Engineering
Royal Institute of Technology, Stockholm S-100 44, Sweden

Abstract— The unidirectional electromagnetic edge mode confined at the edge of two-dimensional (2D) gyromagnetic photonic crystals is an analogy of the chiral edge states, which characterizes the quantum Hall effect in 2D electron systems subject to a strong magnetic field. Here we theoretically and experimentally demonstrate that unidirectional electromagnetic edge mode could also be sustained by the edge of gyromagnetic photonic crystal slab (with finite height) under an external dc magnetic field. The gyromagnetic photonic crystal slab is formed by a triangular lattice of air holes in an yttrium-iron-garnet (YIG) slab or by a honeycomb lattice of YIG rods on a dielectric substrate. The applied magnetic field breaks the time-reversal symmetry of the three-dimensional (3D) system, and thus the original degeneracy point in k space, at which two dispersion surfaces intersect, is lifted, resulting in a photonic band gap below the light cone. At this band gap, the electromagnetic edge modes are localized horizontally to the slab edge, while confined by the index contrast in the vertical direction. To verify this, we calculate edge modes using the finite element methods together with the supercell technique. These edge modes are shown to possess group velocities pointing in only one direction, determined by the direction of the applied dc magnetic field. We also perform a simulation of unidirectional wave propagation in 3D geometry for a direct illustration using the finite integration technique. Moreover, the edge modes are shown to have good transmission under various types of defects and obstacles. Finally, we present an experimental demonstration of unidirectional electromagnetic edge modes on the zigzag edge of a honeycomb lattice of YIG rods on a dielectric substrate. The experiment shows that the edge modes are robust against defects and obstacles. The results of theoretical calculations are well consistent with the experimental data.

Faraday Rotation and Magneto-plasmonic Effects in Graphene

A. B. Kuzmenko
DPMC, University of Geneva, Quai ErnestAnsermet 24, 1211 Geneva 4, Switzerland

Abstract— Graphene attracts much attention as a novel optical and plasmonic material. Its electromagnetic response is exceptionally sensitive to a magnetic field due to the small cyclotron mass of the Dirac-like charge carriers. This does not only make infrared magneto-optics (infrared Hall effect) a valuable characterization tool, but also gives rise to giant magneto-optical effects potentially interesting for terahertz applications. I'll overview our magneto-transmission and Faraday rotation studies of large-scale single- and multilayer graphene grown epitaxially on the Si- and C-faces of silicon carbide respectively [1–3]. I'll consider peculiarities of the cyclotron resonance in quasiclassical and quantum regimes and touch upon the important effect of nanoscale inhomogeneites, such as terrace steps and thermal wrinkles that give rise to magneto.-plasmonic effects.

REFERENCES

1. Crassee, I., J. Levallois, A. L. Walter, M. Ostler, A. Bostwick, E. Rotenberg, T. Seyller, D. van der Mareland, and A. B. Kuzmenko, *Nature Physics*, Vol. 7, 48, 2011.
2. Crassee, I., J. Levallois, D. van der Marel, A. L. Walter, T. Seyller, and A. B. Kuzmenko, *Phys. Rev. B*, Vol. 84, 035103, 2011.
3. Crassee, I., M. Orlita, M. Potemski, A. L. Walter, M. Ostler, T. Seyller, I. Gaponenko, J. Chen, and A. B. Kuzmenko, *Nano Lett.*, Vol. 12, 2470, 2012.

Magnet-less Non-reciprocal Metamaterials

Toshiro Kodera[1], **Dimitrios L. Sounas**[2], **and Christophe Caloz**[3]

[1]Department of Electrical Engineering, Yamaguchi University, Ube 7558611, Japan
[2]Department of Electrical and Computer Engineering
The University of Texas at Austin, Austin, TX 78712, USA
[3]Department of Electrical Engineering, École Polytechnique de Montréal
Montréal, QC H3T 1J4, Canada

Abstract— *Gyrotropic* media are substances or materials that exhibit different responses to left-handed and right-handed circularly polarized waves, and hence rotate the polarization plane of linearly polarized waves. *Reciprocal* gyrotropic media are *biisotropic* (or chiral) media. They may exist in the form of natural substances, such as sugar, liquid crystals and quartz, or in the form of artificial materials made of twisted subwavelength scatterers dispersed in a host dielectric medium.

Non-reciprocal gyrotropic media are *anisotropic* media whose gyrotropic constitutive parameter (permittivity, permeability or conductivity) becomes a hermitian tensor under the application of a static magnetic field. They include magnetic materials ($\overleftrightarrow{\mu}$ for microwaves and $\overleftrightarrow{\epsilon}$ ideal isolator for optical waves), plasmas ($\overleftrightarrow{\epsilon}$ for both microwaves and optical waves) and graphene ($\overleftrightarrow{\sigma}$ for microwaves and $\overleftrightarrow{\epsilon}$ foroptical waves). They support Faraday rotation, where the polarization plane rotates in a fixed direction dictated by the biasing magnetic field irrespectively to the direction of wave propagation.

Among these non-reciprocal materials, the ferrimagnetic ones (ferrites) have been the enabling materials in the technology of electronic and photonic non-reciprocal components over the past

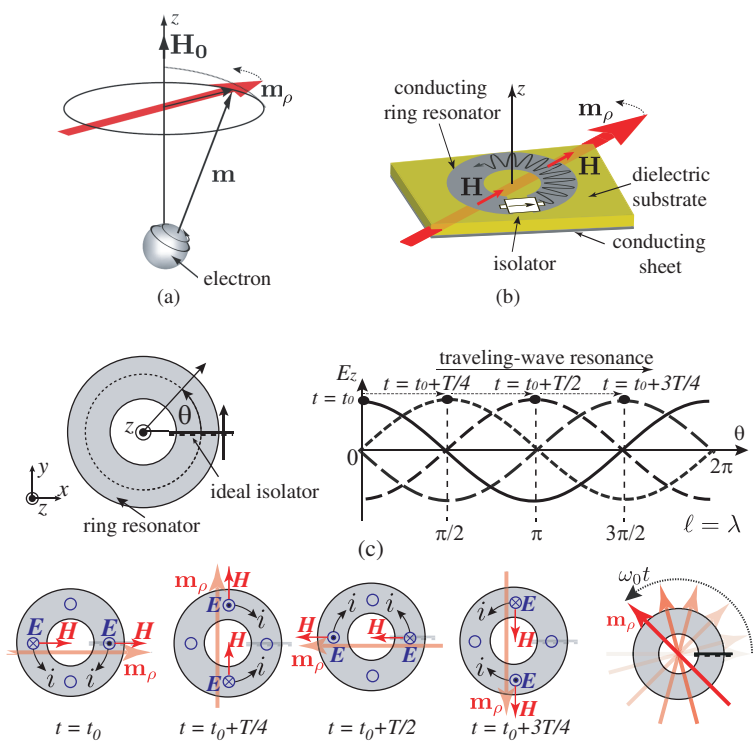

Figure 1: Principle of the MNM, mimicking a natural magnetic material. (a) Rotating magnetic moment in a natural magnetic material. (b) Rotating magnetic moment in the MNM, resulting from the presence of a unilateral semiconductor (transistor) load in a conducting ring. This structure is a reflection (Kerr) MNM, which may be turned into a transmission (Faraday) MNM by removing the conducting sheet and adding a second ring in the mirrorplaneof thefirstring. (c) Timeevolutionof theelectric field along the ring at four instants of the wave harmonic period. (d) Corresponding fields and effective magnetic dipole.

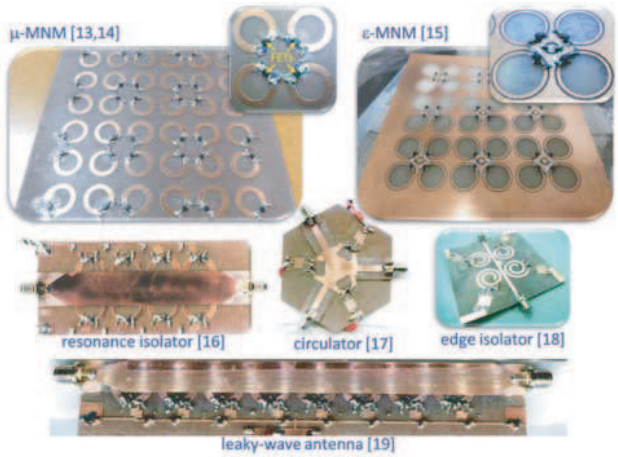

Figure 2: First MNM structures and applications.

60 years. However, this technology suffers of major drawbacks, associated with the nature of magnetic materials and the magnet required to bias them, including bulky size, heavy weight, circuit non-integrability, high cost and frequency restrictions.

To overcome these drawbacks, and to provide additional capabilities, such as multiple operation bands, broader bandwidth and higher design flexibility, we recently introduced a magnet-less non-reciprocal metamaterial (MNM) [1, 2], based on transistor-loaded conducting rings mimicking electron-spin precession in natural magnetic materials via rotating radial magnetic dipole moments. The operation principle of this MNM is depicted in Fig. 1. Several proof-of-concept MNM structures and devices have already been reported. Some of them are shown in Fig. 2.

REFERENCES

1. Kodera, T., D. L. Sounas, and C. Caloz, "Artificial faraday rotationusing a ring metamaterial structure without static magnetic field," *Appl. Phys. Lett.*, Vol. 99, 031114:1–3, July 2011.
2. D. L. Sounas, T. Kodera, and C. Caloz, "Electromagnetic modeling of a magnet-less non-reciprocal gyrotropic metasurface," *IEEE Trans. Antennas and Propagation*, Vol. 61, No. 1, 221231, Jan. 2013.

Synthetic Faraday Rotation in Active Metamaterials

Zheng Wang[1], **Zhiyu Wang**[2, 3], **Jingyu Wang**[2], **Bin Zhang**[2], **Jiangtao Huangfu**[2], **John D. Joannopoulos**[3], **Marin Soljačić**[3], **and Lixin Ran**[2]

[1]Department of Electrical and Computer Engineering
The University of Texas at Austin, Austin, Texas 78758, USA
[2]Department of Information and Electronic Engineering
Zhejiang University, Hangzhou 310027, China
[3]Department of Physics, MIT, Cambridge, MA 02139, USA

Abstract— Electromagnetic materials lacking local time-reversal symmetry, such as gyrotropic materials, are of keen interest and importance both scientifically and technologically. Scientifically, topologically-nontrivial phenomena, such as photonic chiral edge states, allow for reflection-free transport even in the presence of large disorder. Technologically, nonreciprocal photonic devices, such as optical isolators and circulators, play critical roles in optical communication and computing technologies due to their ability to eliminate cross-talk and feedback. Nevertheless, most known natural materials that lack local time-reversal symmetry require strong external fields and function only in a limited range of the electromagnetic spectrum. By taking advantage of metamaterials capable of translating the property of unidirectional active electronic circuits into effective dielectric response, we introduce a microwave gyrotropic metamaterial that does not require an external magnetic bias. Strong bulk Faraday-like effects, observed in both simulations and experiments, confirm non-reciprocity of the effective medium. This approach is scalable to many other wavelengths, and it also illustrates an opportunity to synthesize exotic electromagnetic materials.

Photonic Transitions for Enabling Non Reciprocity in Silicon

Michal Lipson
Cornell University, USA

Abstract— The key to enable non-reciprocity in silicon is the ability to perform photonics transitions: actively controlling the momentum and frequency of the photons (i.e., transitioning from one photonic state to another). This is enabled by the high performance of today's silicon photonic devices. Currently the speed of modulation can be faster than the time of flight of the light (at least in slow light devices). This enables one to modify the properties of the *light* by controlling the properties of the *structure* in which light is guided.

A Unidirectional Sub-wavelength Bend Waveguide with Arbitrary Angle Based on Magnetic Photonic Crystals

Yin Poo, Rui-Xin Wu, Renkai Li, Yan Yang, and Chao Meng
School of Electronic Science and Engineering, Nanjing University, Nanjing 210093, China

Abstract— The discovery of electromagnetic (EM) chiral edge state (CES) in nonreciprocal photonic crystals has attracted much attentions. With respect to its exotic property, the remarkable chiral edge states bring more flexible light manipulation and provide a new avenue for broom EM device fabrication. By constructing the degenerated point and using the condition of time reversal symmetry breaking of nonreciprocal PCs, the robust EM one-way characteristic of CES has been verified both theoretically and experimentally. However, such topological CES system has some limits for practical usage, since the degenerated point depends on lattice structure strictly inducing CES sensitive to the edge shape.

In this work, we focus on another mechanism of EM CES, the magnetic surface polaritons. By designing a magnetic photonic crystal (MPC) with honeycomb lattice, we report the experimental realizations of surface magneto plasmon (MP) induced CES modes at microwave frequencies. It is demonstrated that in the CES modes, EM wave can propagate in only one direction and be robust against the scatterings from disorders of various kinds. Quite different from topological CES, such MP induced CES can exist in both zigzag edge and armchair edge of PC ribbons. Meanwhile, CESs appearing in these two edges are both self-guided surface wave mode, which verifies MP induced CES is immune to the edge shapes. Later, a further band structure calculation demonstrates that the MP induced MPC is an instinct characteristic of MPC and insensitive to topological structures of PC. Based on the dramatic characteristic, a robust unidirectional subwavelength waveguides with various angles is designed. The bend subwavelength waveguide has a high transmission efficiency and can be tunable by bias magnetic field, which providing many potential applications in EM storage and optical communication.

Session 1A3
3_FocusSession.SC3: Frontiers of Ultrafast Optics

Attosecond Optical Synthesis: New Routes in Attosecond Science
Eleftherios Goulielmakis, ... 42

Multi-mJ Parametric Synthesizer Generating Two-octave-wide Optical Waveforms for Strong-field Experiments
Oliver D. Muecke, Shaobo Fang, Giovanni Cirmi, Shih-Hsuan Chia, Franz X. Kartner, Cristian Manzoni, Paolo Farinello, Giulio Cerullo, ... 43

Microjoule Isolated Attosecond Pulses by High-order Harmonic Generation
Eiji J. Takahashi, ... 44

Attosecond Dynamics of Electronic Wave Packets in Nitrogen
M. Reduzzi, C. Feng, W.-C. Chu, A. Dubrouil, F. Calegari, M. Nisoli, F. Frassetto, L. Poletto, C.-D. Lin, Giuseppe Sansone, ... 45

Attosecond Dynamics of Nano-localized Fields Probed by Photoelectron Spectroscopy
Frederik Süβmann, S. Zherebtsov, B. Förg, L. Seiffert, J. Schötz, V. Mondes, M. Förster, M. Krüger, J. Stierle, C. Peltz, J. Plenge, B. Ahn, D. Kim, S. Trushin, C. Graf, Peter Hommelhoff, E. Rühl, Ferenc Krausz, Thomas Fennel, Matthias F. Kling, ... 46

Applications of Ultrashort Pulses to Biomedical Imaging
Chris Xu, ... 47

Optical Parametric Oscillator Frequency Combs for High-resolution Metrology and Spectroscopy
Zhaowei Zhang, Teresa I. Ferreiro, Tom Gardiner, Derryck T. Reid, ... 48

High-field Multi-THz Technology and Its Applications for Nonlinear Spectroscopy
Alexej Pashkin, Bernhard Mayer, Christian Schmidt, Olaf Schubert, Marc Rebholz, Friederike Junginger, Sebastian Mährlein, Rupert Huber, Alfred Leitenstorfer, ... 49

Generation and Acceleration of Few-cycle Electron Pulses from Sharp Metal Tips
Christoph Lienau, ... 50

Ultrabright Femtosecond Electron Diffraction Breaks the Barrier to the Exploration of Coherent Molecular Motions in a Labile Organic Material
German Sciaini, R. J. Dwayne Miller, ... 51

Ultrafast Coherent X-ray Pulses from a Nanostructured Electron Beam
William S. Graves, ... 52

Attosecond Optical Synthesis: New Routes in Attosecond Science

E. Goulielmakis
Max-Planck-Institut für Quantenoptik, Hans-Kopfermann-Str. 1, Garching D-85748, Germany

Abstract— In the absence of attosecond laser pulses, which could directly drive bound electron motion with attosecond precision — just as femtosecond pulses induce and drive femtosecond polarization in atoms, molecules and solids-ultrafast science relied upon the extreme nonlinearity of strong field ionization of matter in order to attain attosecond temporal resolution [1] and to capture electrons in motion [2].

I will discuss how recent advances in attosecond photonics permit the synthesis the control and the measurement of attosecond pulses at optical frequencies. These, nearly unidirectional electromagnetic fields of visible radiation combine the extreme field strength of modern lasers, the dramatic resolution and temporal confinement of extreme ultraviolet attosecond pulses [3] and the tunability of light transients [4, 5] in a single light tool that we name the *attosecond light transient* (ALT).

I will show that, these precisely sculpted optical waves, can now offer new capabilities in controlling attosecond nonlinear dynamics of free and bound electrons in atoms and materials, beyond the strong field ionization regime, and thus enable the direct transfer of the techniques of nonlinear spectroscopy to the attosecond time domain, opening up the era of *attosecond nonlinear optics*.

REFERENCES

1. Corkum, P. B. and F. Krausz, *Nature Physics*, Vol. 3, 381, 2007.
2. Goulielmakis, E., *Nature*, Vol. 466, 793, 2010.
3. Goulielmakis, E., et al., *Science*, Vol. 320, 1614, 2008.
4. Wirth, A., et al., *Science*, Vol. 334, 195, 2011.
5. Hassan, M. Th., et al., *Rev. Sci. Instrum.*, Vol. 83, 111301, 2012.

Multi-mJ Parametric Synthesizer Generating Two-octave-wide Optical Waveforms for Strong-field Experiments

Oliver D. Mücke[1,3], Shaobo Fang[1,3], Giovanni Cirmi[1,3], Shih-Hsuan Chia[1,3], Franz X. Kärtner[1−4], Cristian Manzoni[5], Paolo Farinello[5], and Giulio Cerullo[5]

[1]Center for Free-Electron Laser Science, Deutsches Elektronen-Synchrotron DESY
Notkestraße 85, Hamburg 22607, Germany
[2]Physics Department, University of Hamburg, Luruper Chaussee 149, Hamburg 22761, Germany
[3]The Hamburg Center for Ultrafast Imaging, Luruper Chaussee 149, Hamburg 22761, Germany
[4]Department of Electrical Engineering and Computer Science and Research Laboratory of Electronics
Massachusetts Institute of Technology, Cambridge, Massachusetts 02139, USA
[5]IFN-CNR, Dipartimento di Fisica, Politecnico di Milano, Piazza Leonardo da Vinci 32, Milan 20133, Italy

Abstract— The coherent synthesis of custom-tailored, intense, few-cycle or even sub-cycle optical waveforms is currently one of the most intriguing and promising frontiers of attosecond science and strong-field physics, opening up unprecedented prospects, e.g., for precision control of strong-field interactions in atoms, molecules and solids, for the generation of intense isolated attosecond pulses, and for attosecond pump-probe spectroscopy employing ultrashort pulses in the VIS/IR and XUV/soft-X-ray regions. The key ingredients of coherent pulse synthesis are (i) the generation of an ultrabroad spectrum, (ii) extremely precise dispersion control over the whole bandwidth, (iii) sub-cycle timing synchronization as well as tight stabilization of the relative phases between the different pulses, and (iv) carrier-envelope phase (CEP) stability required for generating reproducible electric-field transients.

Recently, coherent pulse synthesis based on supercontinuum generation in a neon-filled hollow-core fiber compressor allowed the generation of sub-cycle $\sim$ 300-μJ optical pulses. However, the energy throughput of such hollow-core fiber compressors is limited by ionization losses in the gas medium, thus preventing further energy upscaling to the (multi-) mJ level, which is required for many interesting applications in attosecond science. In contrast, parametric synthesizers do not face an energy-scaling bottleneck, and spectral extension into the mid-IR region is particularly appealing for the realization of bright coherent tabletop high-harmonic sources in the water-window and keV X-ray region. In our earlier works, we already demonstrated coherent pulse synthesis between ultrabroadband 870-nm and 2.15-μm pulses based on optical parametric chirped-pulse amplification (OPCPA) resulting in a 15-μJ sub-cycle waveform and also between two optical parametric amplifiers (OPAs) with 1–2 μJ energy each. Here, we present our ongoing development of a novel multi-mJ 3-channel parametric synthesizer for generating a 2-octave-wide spectrum supporting a $\sim$ 1.9-fs pulse duration.

Our parametric synthesizer is driven by a cryogenically cooled Ti:sapphire chirped-pulse amplifier (150 fs, 18 mJ, 0.8 μm, 1 kHz). We first generate an ultrabroadband self-CEP-stabilized white-light continuum (0.5–2.5 μm) in a YAG crystal. This continuum is split using dichroic beam splitters and seeds three type-I BBO OPA channels, a VIS non-collinear OPA (NOPA), a NIR and an IR degenerate OPA (DOPA) channel, pumped by the pulses at 0.8 μm (IR DOPA) and by its second harmonic at 0.4 μm (VIS NOPA, NIR DOPA). After parametric amplification, the three OPA channel outputs are individually recompressed using double-chirped mirrors and recombined using dichroic beam splitters. To synthesize a coherent ultrashort waveform from these OPAs, the relative timing of the pulses will be tightly locked using feedback loops with balanced optical cross-correlators, that can achieve sub-cycle synchronization with $<$ 30-as RMS timing jitter.

After two amplification stages in each channel, the VIS NOPA and NIR DOPA, each yielding 40 μJ energy, continuously cover the region from 520 nm to 960 nm, the IR DOPA spectrum with 45 μJ extends from 1130 nm to 2290 nm. The combined spectrum supports the synthesis of 1.9-fs sub-cycle optical waveforms. In the third stages, the pulse energies are further scaled up to the multi-mJ level. So far we have obtained 1.7-mJ octave-spanning spectra from the IR DOPA and 200 μJ from the NIR DOPA, both corresponding to a 5.2-fs transform-limited pulse duration.

In this talk, we discuss the technological challenges of multi-mJ parametric waveform synthesis and our experimental results. We foresee that our multi-mJ 2-octave-wide 3-channel synthesizer will become a versatile tool for controlling strong-field interactions in atoms, molecules and solids and for attosecond pump-probe spectroscopy employing ultrashort pulses in the VIS/IR and XUV/soft-X-ray regions.

Microjoule Isolated Attosecond Pulses by High-order Harmonic Generation

Eiji J. Takahashi
Extreme Photonics Research Group, RIKEN Center for Advanced Photonics (RAP)
2-1 Hirosawa, Wako, Saitama 351-0198, Japan

Abstract— We successfully generated a microjoule isolated attosecond pulse for investigating attosecond nonlinear phenomena in atoms and molecules. Pulse duration of isolated attosecond pulse was directly evaluated to be 500 as by nonlinear autocorrelation method using the Coulomb explosion of N_2. Observed Coulomb explosion signal of N_2 guarantees that our isolated attosecond pulses are strong enough to induce the nonlinear phenomena in the XUV region.

To make a breakthrough for attosecond science, one of the most important issues is the development of high-power isolated attosecond pulses (IAPs) and/or attosecond pulse trains (APTs). At present high-power APTs have been successfully generated thanks to research on harmonic energy scaling using a loosely focusing geometry [1]. Although IAP were already obtained using a state-of-the-art Ti:sapphire laser system, output energy is still not sufficient for inducing nonlinear phenomena. Many researchers have been making a great effort to scale up the IAP energy thus far. Unfortunately, the highest IAP output energy was no more than a few tens nanojoule [2]. Since a phase-matching technique can't be utilized due to high ionization rate of target gas, a conversion efficiency is just 10^{-5} level [2] even if Xe gas was used. Thus, most of attosecond nonlinear optics experiments had been demonstrated by using APTs.

In this paper, we demonstrate the first generation and full characterization of microjoule-energy isolated attosecond pulses [3], which have sufficient power for inducing nonlinear phenomena in atoms and molecules as well as for attosecond-pump/attosecond-probe spectroscopy. Our generation scheme is based on the two-color (TC) infrared laser field synthesis [4] and the energy-scaling method [1] of HHG. As we previously reported [4], our optimized TC scheme for generating IAPs enables us not only to relax the requirements for the pump pulse duration (∼30 fs) but also to reduce ionization of the harmonic medium. This is a major advantage for efficiently generating intense IAPs, because neutral media allow us to use the phase-matching technique. Thus, we can realize the generation of intense IAPs with high conversing efficiency. In the experiment, an almost 100-fold energy-enhancement over previous results became possible by combining the energy-scaling method of Xe HHG with TC infrared waveform synthesis. The produced isolated pulses with a duration of 500 as (28–35 eV), as characterized by an nonlinear autocorrelation using the Coulomb explosion of N_2, and maximum energy up to 1.3 μJ open the door to the realm of nonlinear attosecond science. The peak power of our table-top light source reaches 2.6 GW, which even surpasses that of a compact free electron laser in the extreme-ultraviolet region, the peak brightness is estimated to be 10^{30} photons/(mm^{2}mrad^{2}s). The conversion efficiencies attained was 1.1×10^{-4} at the cutoff region. Furthermore, in our TC-HHG method, we created a mid-plateau region exhibiting a quasi-continuous spectrum with an energy of 10 μJ. By utilizing this quasi-continuous spectrum at the mid-plateau (14–27 eV), we also demonstrated the generation of a quasi-IAP. We evaluated the pulse duration of the main pulse of this quasi-IAP to be 375 as with ∼0.25 intensity satellite pulses at ±6.7 fs. We think that the presented method paves the way for the intense attosecond science frontier, which will certainly bring a great leap forward in research on ultrafast phenomena and nonlinear optics.

REFERENCES

1. Takahashi, E. J., et al., "Generation of highly coherent submicrojoule soft X rays by high-order harmonics," *Phys. Rev. A*, Vol. 66, 021802, 2002.
2. Sansone, G., et al., "High-energy attosecond light sources," *Nature Photonics*, Vol. 5, 655, 2011.
3. Takahashi, E. J., et al., "Generation of an isolated attosecond pulse with microjoule-level energy," *Quantum Electronics and Laser Science Conference*, QTh5B.10, 2012.
4. Takahashi, E. J., et al., "Infrared two-color multicycle laser field synthesis for generating an intense attosecond pulse," *Phys. Rev. Lett.*, Vol. 104, 233901, 2010.

Attosecond Dynamics of Electronic Wave Packets in Nitrogen

M. Reduzzi[1], C. Feng[1], W.-C. Chu[2], A. Dubrouil[1], F. Calegari[1], M. Nisoli[1], F. Frassetto[3], L. Poletto[3], C.-D. Lin[2], and G. Sansone[1]

[1]Dipartimento di Fisica, Politecnico Piazza Leonardo da Vinci, 32, Milano 20133, Italy
[2]Institute of Photonics and Nanotechnologies, National Research Council, Padova, Italy
[3]Physics Department, Kansas State University, Manhattan, USA

Abstract— Attosecond pulses can create broadband electronic wave packets whose time evolution depends on the bandwidth of the excitation pulse. In this work, we demonstrate the control of electronic wave packets created in nitrogen using a carrier-envelope-phase stabilized infrared pulse synchronized with the excitation pulse. The control is demonstrated by measuring the variations of the dipole radiation emitted by the electronic wave-packet as a function of the relative delay between the excitation and control pulse. We present results highlighting the presence of two different coupling mechanisms occurring in the manifold of excited states close to the ionization threshold of the molecule.

Introduction: The coherent superposition of several electronic states (i.e., an electronic wave-packet) evolves on a timescale that depends on the energy range covered by the levels. Different attosecond spectroscopic techniques have been used for the characterization of ultrafast dynamics such as attosecond streaking spectroscopy [1], ion chronoscopy [2], and attosecond transient absorption spectroscopy (ATAS) [3, 4]. Recently, this technique has been used for the investigation of absorption features associated to laser-dressed states in helium [5, 6].

Experimental Results: We performed an experiment aiming at investigating the ultrafast dynamics occurring in the manifold of states of nitrogen excited by tunable attosecond pulses. Around the ionization threshold ($I_p = 15.58\,\mathrm{eV}$), the absorption of nitrogen is characterized by two Rydberg series converging to the fundamental $X^2\Sigma_g^+$ and first excited $A^2\Pi_u$ ionic states. Above 17 eV, the absorption profile is characterized by two-series of Fano-Beutler resonances that converge to the excited ionic state $B^2\Sigma_u^+$. Using tunable attosecond pulses, it was possible to excite separately states below (or around) the first ionization threshold and states corresponding to the Fano-Beutler autoionizing series. A synchronized carrier-envelope-phase stable IR field was used to couple the two groups of states. The IR coupling modifies the time evolution of the electronic wave-packet, determining oscillations in the absorption lines.The oscillations presents a $T_0/2$ periodicity (T_0 is the optical cycle of the IR field) indicating a two-IR-photon mechanism. The experimental outcomes are in good agreement with theoretical simulations that describe the coupling between the bound excited states and the Fano-Beutler resonances.

REFERENCES

1. Kienberger, R., et al., "Atomic transient recorder," *Nature*, Vol. 427, No. 6977, 817–821, 2004.
2. Uiberacker, M., et al., "Attosecond real-time observation of electron tunnelling in atoms," *Nature*, Vol. 446, No. 7136, 627–632, 2007.
3. Wang, H., et al., "Attosecond time-resolved autoionization of argon," *Phys. Rev. Lett.*, Vol. 105, No. 14, 143002, 2010.
4. Goulielmakis, E., et al., "Real-time observation of valence electron motion," *Nature*, Vol. 466, No. 7307, 739, 2010.
5. Chen, S. H., et al., "Light-induced states in attosecond transient absorption spectra of laser-dressed helium," *Phys. Rev. A*, Vol. 86, No. 6, 063408, 2012.
6. Chini, M., et al., "Sub-cycle oscillations in virtual states brought to light," *Scient. Reports*, Vol. 3, 2045–2322, 2013.

Attosecond Dynamics of Nano-localized Fields Probed by Photoelectron Spectroscopy

F. Süßmann[1], S. Zherebtsov[1], B. Förg[1], L. Seiffert[2], J. Schötz[1], V. Mondes[3], M. Förster[1], M. Krüger[1], J. Stierle[1], C. Peltz[2], J. Plenge[3], B. Ahn[4], D. Kim[4], S. Trushin[1], C. Graf[3], P. Hommelhoff[1], E. Rühl[3], F. Krausz[1], T. Fennel[2], and M. F. Kling[1,4]

[1]Max Planck Institute of Quantum Optics, Hans-Kopfermann-Str. 1, Garching 85748, Germany
[2]Institute of Physics, University of Rostock, Universitätsplatz 3, Rostock 18051, Germany
[3]Physical Chemistry, FreieUniversitätBerlin, Takustr. 3, Berlin 14195, Germany
[4]Physics Department, POSTECH, San 31 Hyoja-Dong, Namku Pohang, Kyungbuk 790-784, Kore

Abstract— The application of nanosystems in the ultrafast regime requires control of nanoscopic fields on sub-cycle timescales. One of the most promising routes to the realization of electronics operating at light frequencies arises from applying waveform controlled fields to nanoscale systems, where the nanolocalized near-fields enable for ultimate temporal and spatial control of the relevant electron transport processes.

We have studied the momentum distribution of photoemission by few-cycle laser fields from dielectric nanospheres of different sizes. At low intensities ($< 3 * 10^{13}\,\mathrm{W/cm^2}$), a comparison of experimental data with numerical simulations identifies the additional Coulomb forces of the liberated electron cloud as an effective additional acceleration mechanism for distinct trajectories [1]. By varying the particle size, the imprint of propagation effects and a resulting asymmetric field enhancement distribution could be observed in the photoelectron momentum distributions and used for partial reconstruction of the local field amplitude. The mapping between position and momentum space is investigated by analyzing the correlation of the photoelectron's birth and detection angle. In the high intensity range ($> *10^{14}\,\mathrm{W/cm^2}$), the opto-electronic properties of the material are strongly affected by the driving laser field and a metallic character of the material is observed.

The efforts on the realization of nanoplasmonic attosecond streaking spectroscopy are presented. Such experiments would enable a real-time measurement of (plasmonic) near-field oscillations. Numerical simulations are used to identify the influence of the inhomogeneous near-field distributions on the streaking process [2]. First experimental results obtained from Au nanotipsshow clear streaking features of sub-micron localized near-fields.

REFERENCES

1. Zherebtsov, S., et al., "Carrier-envelope phase-tagged imaging of the controlled electron accelerationfrom SiO_2 nanospheres in intense few-cycle laser fields," *New Journal of Physics*, Vol. 14, No. 7, 075010, 2012.
2. Süßmann, F. and M. Kling, "Attosecond nanoplasmonic streaking of localized fields near metal nanospheres," *Physical Review B*, Vol. 84, No. 12, 121406(R), 2011.

Applications of Ultrashort Pulses to Biomedical Imaging

Chris Xu
School of Applied and Engineering Physics, Cornell University, Ithaca, NY 14853, USA

Abstract— Fiber optic communications have seen tremendous growth in the last 20 years, driven by the demand for bandwidth. In general, technologies deployed in telecom are robust, user friendly, low-cost, and compatible with volume production. On the other hand, biophotonic imaging technologies have also seen rapid development in the last 20 years. Optical coherence tomography, photo-acoustic microscopy, and multiphoton microscopy (MPM) are just a few examples that illustrate the emergence of optical imaging technologies for biomedical applications. In particular, the development of MPM, including multiphoton fluorescence (and/or harmonic generation) microscopy and coherent Raman scattering microscopy, was propelled in large part by the rapid technological advances in mode-locked lasers. Nevertheless, the complexity, cost, and sometimes availability of the excitation source pose significant challenges for MPM to become widely accessible in the research labs. Obviously, the requirement of a robust, fiber delivered, and low-cost ultrafast source is even more important for multiphoton imaging to become a diagnostic tool in the clinics. In this talk, we discuss the potential of applying ultrafast technologies to biomedical imaging. We will focus on novel light sources based on soliton self-frequency shift in optical fibers for multiphoton fluorescence imaging. Wavelength tunable, megawatt (MW) peak power solitons were generated in a photonic crystal rod at $\sim 1700\,\mathrm{nm}$. The MW solitons were applied in three-photon fluorescence microscopy for in vivo deep tissue imaging. Sub-cortical vasculatures and fluorescent protein labeled neurons were visualized for the first time in an intact mouse brain.

Optical Parametric Oscillator Frequency Combs for High-resolution Metrology and Spectroscopy

Zhaowei Zhang[1], **Teresa I. Ferreiro**[1], **Tom Gardiner**[2], **and Derryck T. Reid**[1]

[1]Scottish Universities Physics Alliance (SUPA), Institute of Photonics and Quantum Sciences
Heriot-Watt University, Riccarton, Edinburgh, EH14 4AS, UK
[2]National Physical Laboratory, Hampton Road, Teddington, London TW11 0LW, UK

Abstract— Laser frequency combs unite the spectroscopic precision of narrow-line CW lasers with the optical bandwidth of modelocked oscillators, while simultaneously providing a direct connection between optical and radio frequencies. Optical parametric oscillators (OPOs) can be used to extend the unique properties of laser frequency combs into the near- and mid-infrared, opening up new applications in sensing, metrology and spectroscopy. Here, we discuss recent progress in the development of Ti:sapphire- and Yb:fibre-pumped OPO frequency combs. In the context of precision metrology, results will be presented which show that OPO combs can be operated with reference-synthesizer-limited accuracies of the order of 10^{-12}, corresponding to an uncertainty in the absolute optical frequencies of only 100 Hz. The application of OPO combs to spectroscopy and gas sensing will also be described, in particular how a dual-OPO-comb source has been developed and employed for methane sensing at 3.3 μm. Finally, an outlook will be given defining the future challenges and opportunities for OPO-based femtosecond frequency combs.

High-field Multi-THz Technology and Its Applications for Nonlinear Spectroscopy

Alexej Pashkin[1], **Bernhard Mayer**[1], **Christian Schmidt**[1], **Olaf Schubert**[2], **Marc Rebholz**[1], **Friederike Junginger**[1], **Sebastian Mährlein**[3], **Rupert Huber**[2], **and Alfred Leitenstorfer**[1]

[1]Department of Physics and Center for Applied Photonics, University of Konstanz, Germany
[2]Department of Physics, University of Regensburg, Germany
[3]Fritz-Haber-Institut der Max-Planck-Gesellschaft, Berlin, Germany

Abstract— Two-dimensional spectroscopy is a powerful tool for study of ultrafast coherent dynamics and spectral correlations in condensed matter systems. Extension of this technique into THz spectral range provides access to fundamental low-energy excitations such as lattice vibrations in solids, inter-molecular motion in liquids or single-particle excitations of broken symmetry electronic states in superconductors and density wave systems.

Here, we employ our high-field multi-THz source [1] to perform two-dimensional spectroscopy using a intensive phase-stable transients with peak electric fields up to 5 MV/cm. The emerging coherent signals are detected by a field-resolved electro-optic sampling and can be discriminated using a Fourier filtering procedure. We present two recent examples of nonlinear THz experiments performed on bulk indium antimonide (InSb) and graphite samples.

We detect a clear four-wave mixing (FWM) response of InSb driven well below the interband resonance frequency. In spite of that, the time-domain FWM signals demonstrate a splitting which indicates a non-perturbative response to electric fields above 5 MV/cm [2]. Our simulations based on a simplified model of a two-level system demonstrate that the strong THz excitation can lead to a transient population inversion in spite of the strongly off-resonant character of the excitation.

In the thin graphite sample, exfoliated down to a thickness of 130 nm, we observe pronounced pump-probe signals. In contrast to this, the FWM signals are too weak and could not be detected. When the central frequency of the excitation pulses is set to 25 THz, the pump-probe spectra are dominated by absorption at frequencies above 24 THz. At lower frequencies we detect a moderate bleaching. Surprisingly, the same spectral signature shifted up by 5 THz is observed when the central frequency of the pump pulses is set to 30 THz. We suggest that the peculiar band structure of graphite should be responsible for the observed behavior.

REFERENCES

1. Junginger, F., A. Sell, O. Schubert, B. Mayer, D. Brida, M. Marangoni, G. Cerullo, A. Leitenstorfer, and R. Huber, *Optics Letters*, Vol. 35, 2645, 2010.
2. Junginger, F., B. Mayer, C. Schmidt, O. Schubert, S. Mährlein, A. Leitenstorfer, R. Huber, and A. Pashkin, *Phys. Rev. Lett.*, Vol. 109, 147403, 2012.

Generation and Acceleration of Few-cycle Electron Pulses from Sharp Metal Tips

C. Lienau[1, 2]

[1]Institut für Physik, Carl von Ossietzky Universität Oldenburg, Oldenburg, Germany
[2]Center of Interface Science, Oldenburg, Germany

Abstract— Sharp metallic nanotapers irradiated with few-cycle laser pulses are emerging as a source of highly confined coherent electron wavepackets with attosecond duration and strong directivity [1–6]. The possibility to steer, control or switch such electron wavepackets by light is expected to pave the way towards direct visualization of nanoplasmonic field dynamics and real-time probing of electron motion in solid state nanostructures. Such pulses can be generated by strong-field induced tunneling and acceleration of electrons in the near-field of sharp gold tapers within one half-cycle of the driving laser field. Here, we study for the first time the effect of the carrier envelope phase of few cycle laser pulses on the motion of electrons emitted from metallic nanostructures by strong-field tunneling.

We illuminate very sharp, single-crystalling gold tips with CEP-stable few-cycle near-infrared pulses at 1.5 µm and record angle-resolved kinetic energy spectra of the photoemitted electrons. Our experiments give first evidence for the effect of absolute phase of the laser pulses on the emission direction and kinetic energy distribution of the photoemitted electrons. We observe pronounced modifications of the photoelectron spectra when varying the CEP phase, paving the way towards a light-driven control of motion of electrons in the near field of metallic nanostructures on sub-femtosecond time scales and nanometer length scales. In my talk, I will give an introduction into this emerging field, discuss our own recent experimental observations and their interpretation within simple theoretical models and will give an outlook, illustrating possible applications of such electron sources.

REFERENCES

1. Hommelhoff, P., Y. Sortais, A. Aghajani-Talesh, and M. A. Kasevich, *Phys. Rev. Lett.*, Vol. 96, 077401, 2006.
2. Ropers, C., D. R. Solli, C. P. Schulz, C. Lienau, and T. Elsaesser, *Phys. Rev. Lett.*, Vol. 98, 043907, 2007.
3. Krüger, M., M. Schenk, and P. Hommelhoff, *Nature*, Vol. 475, 78, 2011.
4. Herink, G., D. R. Solli, M. Gulde, and C. Ropers, *Nature*, Vol. 483, 190, 2012.
5. Park, D. J., et al., *Phys. Rev. Lett.*, Vol. 109, 244803, 2012.
6. Piglosiewicz, B., et al., submitted, arXiv:1301.4074, 2013.

Ultrabright Femtosecond Electron Diffraction Breaks the Barrier to the Exploration of Coherent Molecular Motions in a Labile Organic Material

Germán Sciaini[1] and R. J. Dwayne Miller[1, 2]

[1]Max Planck Research Department for Structural Dynamics, Department of Physics
University of Hamburg, Center for Free Electron Laser Science
DESY, Hamburg D-22607, Germany
[2]Departments of Chemistry and Physics, University of Toronto
Toronto, Ontario M5S 3H6, Canada

Abstract— Over the last 20 years the development of ultrashort structural probes has been tremendous. Femtosecond laser-driven X-ray and electron sources, slicing techniques, and X-ray free electron lasers have been successfully applied for the study of ultrafast structural dynamics in a variety of samples. By combining the atomic spatial resolution of diffraction techniques with the temporal resolution of femtosecond spectroscopy, ultrafast diffraction has overcome the barrier to atomic exploration [1]. However, its application to labile organic crystals which can provide a molecular basis for the understanding of various attractive properties such as organic conductivity and optical switching remains unexplored. Composed by weak scattering centres, organic compounds often present low melting points and poor heat conduction. These facts impart tremendous constraints on source brightness to attain high-quality diffraction data before accumulative heating effects from the laser excitation degrade the sample or mask the structural dynamics. Here, we implemented a recently developed ultrabright, low repetition rate fs-electron source [2] to light up molecular motions in the organic salt $(\text{EDO-TTF})_2\text{PF}_6$ as it undergoes its photo-induced insulator-to-metal phase transition [3]. The structural evolution is monitored by recording time-delayed diffraction patterns following ultrafast laser excitation. High-quality images allowed us to identify hundreds of Bragg reflections showing time-dependent changes beyond the noise level. In the early stage of charge delocalization (0–5 ps), model refinement calculations indicate the formation of a transient intermediate structure (TIS) which is mostly driven by concerted "sliding" of flat EDO-TTF molecules and motion of PF_6 counter-ions. The flattening of bent EDO-TTF moieties seems, however, to be assisted by thermal relaxation that brings the system into a metallic-type state on the 100-ps timescale. The present work illustrates the potential of ultrabright fs-electron probes to provide an atomic perspective on complex structural dynamics relevant to chemistry and biology.

REFERENCES

1. Sciaini, G. and R. J. D. Miller, "Femtosecond electron diffraction: Heralding the era of atomically-resolved dynamics," (Invited Review) *Rep. Prog. Phys.*, Vol. 74, 096101, 2011.
2. Gao, M., H. Jean-Ruel, R. R. Cooney, J. Stampe, M. de Jong, M. Harb, G. Sciaini, G. Moriena, and R. J. D. Miller, "Full characterization of RF pulse compressed femtosecond electron pulses using ponderomotive scattering," *Opt. Express*, Vol. 20, 12048, 2012.
3. Gao, M., C. Lu, H. Jean-Ruel, L. C. Liu, A. Marx, K. Onda, S.-Y. Koshihara, Y. Nakano, X. Shao, T. Hiramatsu, G. Saito, H. Yamochi, R. R. Cooney, G. Moriena, G. Sciaini, and R. J. D. Miller, "Mapping molecular motions leading to charge delocalization with ultrabright electrons," *Nature*, Vol. 496, 343, 2013.

Ultrafast Coherent X-ray Pulses from a Nanostructured Electron Beam

William S. Graves
Massachusetts Institute of Technology, MA 02139, USA

Abstract— The advent of cathodes with nanoengineered features has enabled production of electron beams with density modulation at nanometer wavelength scale that are well suited to coherent x-ray production. The x-rays are produced in a form of inverse Compton scattering by resonant interaction of the electron nanobunches with a periodic electromagnetic field consisting of either a laser or terahertz pulse. The interaction of electrons with the laser or THz beam is similar to the interaction of an electron beam with a static magnetic undulator, except that the much shorter period of the laser or THz field allows x-rays to be produced at lower MeV electron energy instead of the GeV beams required for static undulators, decreasing the cost and size of the source.

The nanocathode produces electron beams that have a transverse spatial density modulation. Although the modulation is quickly smeared by the wide angular spread of electron trajectories, conventional linear optics can reimage the cathode with variable magnification after acceleration of the beam to final energy. Emittance exchange is an innovative method that is used to exchange the transverse periodic density modulation into a longitudinal (current) modulation. The period of this modulation is tunable over a wide range to match the desired output x-ray wavelength.

After emittance exchange the structured electron beam collides head on with the laser or THz pulse where it produces coherent x-rays. Simulation studies indicate that free electron laser gain occurs using electron beam parameters that are achievable at low charge and peak current with current technology. The predicted output is fully coherent, tunable, and highly stable, with properties similar to a seeded x-ray FEL although at lower peak power than large facilities. The required electron energy ranges from a few MeV to a few hundred MeV depending on the output wavelength and whether laser or THz is scattered. The radiation from such a compact device is directly useful and also can provide an x-ray seed pulse for a large XFEL.

Session 1A4
1_FocusSession.SC1: Foundations of Casimir Physics (with tutorials)

Casimir Forces — Forces from Nothing
Stefan Scheel, ... 54
Measurements of the Casimir Effect
Ricardo S. Decca, ... 55
Casimir Effect, Macroscopic QED, and the Nature of Thermal and Zero-point Self-forces
Thomas G. Philbin, ... 56
Quantum Electrodynamics in the Presence of Moving Bodies
Simon A. R. Horsley, ... 57
Computing Fluctuation-induced Interactions in Arbitrary Geometries
Alejandro W. Rodriguez, M. T. Homer Reid, Steven G. Johnson, ... 58
Casimir Force Calculations Using Domain Decomposition Methods
Phillip R. Atkins, Weng Cho Chew, M.-K. Li, ... 59
A Tutorial on Casimir Interactions between Nanostructured Materials
Diego A. R. Dalvit, ... 60
Casimir Torque: From Magnetoplasmons to Self-assembly of Nano Particles Arrays
Raul Esquivel-Sirvent, ... 61
Transmitting Signals from the Vacuum: Giant van der Waals and Casimir Interactions via Transmission Lines
Ephraim Shahmoon, Igor E. Mazets, Gershon Kurizki, ... 62

Casimir Forces — Forces from Nothing

Stefan Scheel
Institut of Physics, University of Rostock, Universitätsplatz 3, Rostock D-18055, Germany

Abstract— In the ground state of the quantized electromagnetic field, the expectation values of electric and magnetic fields vanish. However, as with all quantum mechanical quantities, such a statement refers only to an ensemble average over many realisations of identically prepared physical systems. At any given instance, however, a random field would be observed, thus leading to the notion of fluctuating electromagnetic fields. In 1948, H. B. G. Casimir was the first to predict that these ground-state fluctuations lead to an attractive force between two parallel metallic plates. Since the early experimental confirmation by M. J. Spaarnay in 1958, the number of experiments and related theoretical work has grown substantially.

The Casimir force and the closely related Casimir-Polder and van der Waals forces all belong to the class of dispersion interactions that are due to the zero-point fluctuations of the quantized electromagnetic field. In this talk, I will present the basic concepts of Casimir physics, its experimental consequences and applications of Casimir forces in nanoscience. I will show how all dispersion forces can be derived as ground-state expectiation values of the quantum Lorentz force, and how Casimir, Casimir-Polder and van der Waals forces are ultimately related to one another. Finally, I will give an overview over recent developments towards understanding thermal and motional effects.

Measurements of the Casimir Effect

Ricardo S. Decca
Department of Physics, Indiana University-Purdue University Indianapolis
Bldg. LD 154, 402 N. Blackford St., Indianapolis, IN 46202, USA

Abstract— In this presentation we review the results obtained with our technique towards the measurements of the Casimir interaction. Details of the experimental setup, effects of geometry, temperature and material properties are discussed and presented.

In our system a $R \sim 150\,\mu\text{m}$ sapphire sphere is Au coated and glued to a high quality mechanical oscillator. This oscillator is brought in closed proximity to a test sample. This sample can be made of different materials and/or have different geometries. The whole assembly is kept in high vacuum ($P \sim 10^{-7}$ Torr) and some electric and surface characterizations are performed over the surfaces.

The results obtained with our system will not only be used towards trying to get a deeper understanding of the Casimir interaction but to constraint the existence of hypothetical forces as well. Regarding this last topic our current efforts towards the improvement of "Casimir less" measurements will be presented. We will show that a judicious selection of the test sample and experimental setup allows improving current constraints in phase space for hypothetical forces in over two orders of magnitude at 100 nm.

Casimir Effect, Macroscopic QED, and the Nature of Thermal and Zero-point Self-forces

T. G. Philbin
University of Exeter, UK

Abstract— Casimir's original result on electromagnetic vacuum energy can be derived from the QED of light and particles, which was successfully formulated in the late 1940s. The Casimir effect in real materials, however, cannot be calculated using the QED of light and particles. Instead a theory of macroscopic QED is required, the quantized version of the macroscopic Maxwell equations. This theory of macroscopic QED was lacking for many decades, leading to a phenomenological approach to Casimir theory based on generalized thermodynamic relations (Lifshitz theory). We show how macroscopic QED can be constructed exactly like the QED of light and particles, and how the Casimir effect is the special case of macroscopic QED in thermal equilibrium (including zero temperature).

We also discuss thermal and zero-point electromagnetic fields on material boundaries, and the resulting self-forces. A proper treatment of material properties removes the divergence problems that have plagued the study of this interesting aspect of the zero-point and thermal Casimir effect.

Quantum Electrodynamics in the Presence of Moving Bodies

S. A. R. Horsley
University of Exeter, United Kingdom

Abstract— The vacuum state of the electromagnetic field close to a dielectric body is not the same in all reference frames. Here we show that this has some surprising consequences. For instance, if we attempt to quantize electromagnetism interacting with a uniformly moving medium (properly including effects of dispersion and dissipation), then the resulting Hamiltonian lacks a lower bound. Consequently, a detector placed close to a moving surface can be *excited* by the vacuum! It is shown that when the dielectric is allowed to change velocity then the Hamiltonian again becomes bounded from below, thus demonstrating that the source of the energy exciting the detector is the kinetic energy of the dielectric.

Computing Fluctuation-induced Interactions in Arbitrary Geometries

Alejandro W. Rodriguez[1, 2], **M. T. Homer Reid**[2], **and Steven G. Johnson**[2]

[1]School of Engineering and Applied Sciences, Harvard University, USA
[2]Department of Mathematics, Massachusetts Institute of Technology, USA

Abstract— We review recent numerical methods for calculating Casimir forces and fluctuation induced interactions between bodies of arbitrary shapes that exploit well-known techniques from classical electromagnetism. Our approach allows application of established and powerful computational techniques from nanophotonics, including the finite-difference and boundary-element methods, with little (if any) modifications. We demonstrate the efficiency and versatility of these techniques by computing the interaction of various complicated objects using a recently developed and free to use Casimir solver.

Casimir Force Calculations Using Domain Decomposition Methods

P. R. Atkins, W. C. Chew, and M.-K. Li
University of Illinois, Urbana, IL, USA

Abstract— The calculation of the Casimir force is a difficult multiphyics problem combining computational electromagnetics (CEM) and quantum physics over broadband frequencies. Traditional CEM methods can be used to calculate the Casimir force, but difficulties lie in the fact that the calculations must be performed over a broadband of frequencies using dense matrix methods. In an effort to expand the range of problems that can be simulated, we propose using a boundary element method and argument principle derivation of the Casimir force to derive a domain decomposition method to handle large, complex objects. The resulting calculation uses the Equivalence Principle Algorithm (EPA) to subdivide a complex problem to be into separate smaller subproblems that are recombined into a reduced matrix. This in turn allows for an effective reduction in the number of unknowns for a given structure making them feasible under dense matrix methods. To account for the low frequency demands of the Casimir calculation, a high-order point sampling scheme is required since close electrical proximity of the domain boundaries to the object's surface introduces high frequency noise. We demonstrate the advantages of the EPA by simulating large, finite, three-dimensional corrugated plates. Such geometries have previously only been modeled as infinite plates using two-dimensional techniques. The use of the EPA allows for the modeling of phenomenon like edge effects and for cases where the corrugations are unaligned.

A Tutorial on Casimir Interactions between Nanostructured Materials

Diego A. R. Dalvit
Theoretical Division, MS B213, Los Alamos National Laboratory, Los Alamos, NM 87545, USA

Abstract— In this tutorial I will review the state-of-the-art of theoretical, computational, and experimental techniques for studying Casimir interactions between nanostructured materials, including gratings and metamaterials. I will discuss different modeling and simulation approaches, such as the proximity force approximation, the effective medium approach, and exact techniques based on scattering theory. Some recent experiments on measuring Casimir forces in semiconducting and metallic gratings will be described, and the comparison between theory and experiment will be discussed.

Casimir Torque: From Magnetoplasmons to Self-assembly of Nano Particles Arrays

R. Esquivel-Sirvent
Instituto de Fisica, Universidad Nacional Autonoma de Mexico, Mexico

Abstract— Lifshitz theory predicts that, besides the usual Casimir force, two parallel optically anisotropic plates will experience a torque. This torque tends to align the principal optical axes of the plates [1, 2]. In this work, we present a theoretical calculation of the Casimir torque for two systems. First we consider two isotropic parallel plates where the anisotropy is induced using an external magnetic field. The anisotropy will in turn induce a torque. A case study we consider III-IV semiconductors such as *InSb* that can support magneto plasmons. The calculations of the torque are done in the Voigt configuration, that occurs when the magnetic field is parallel to the surface of the slabs [3]. The change in the dielectric function as the magnetic field increases has the effect of decreasing the Casimir force and increasing the torque. Thus, the external magnetic field is used to tune both the force and torque. The second example we present is the use of the Casimir torque in the non retarded regime to align arrays of nano particle slabs [4]. The torque is calculated within Barash and Ginzburg formalism in the nonretarded limit, and is quantified by the introduction of a Hamaker torque constant. Calculations are conducted between anisotropic slabs of materials including *BaTiO3* and arrays of Ag nano particles. Depending on the shape and arrangement of the Ag nano particles the effective dielectric function of the array can be tuned as to make it more or less anisotropic. We show how this torque can be used in self assembly of arrays of nano particles.

ACKNOWLEDGMENT

Partial support from Instituto de Fisica, UNAM and DGAPA-UNAM.

REFERENCES

1. Barash, Y. S., "Van der Waals interactions between anisotropic bodies," *Izv. VUZ. Radiofiz*, Vol. 16, No. 8, 1227–1234, 1973.
2. Munday, J. N., D. Iannuzzi, Y. Barash, and F. Capasso, "Torque on birefringent plates induced by quantum uctuations," *Phys. Rev. A*, Vol. 71, 042102–042102-9, 2005.
3. Esquivel-Sirvent, R., G. H. Cocoletzi, and M. Palomino Ovando, "Van der Waals torque induced by external magnetic fields," *J. App. Phys.*, Vol. 108, 114101–114101-5, 2010.
4. Esquivel-Sirvent, R. and G. C. Schatz, "Van der Waals torque coupling between slabs composed of planar arrays of nanoparticles," *J. Phys. Chem. C*, Vol. 117, 5492–5496, 2013.

Transmitting Signals from the Vacuum: Giant van der Waals and Casimir Interactions via Transmission Lines

Ephraim Shahmoon[1], **Igor Mazets**[2], **and Gershon Kurizki**[1]

[1]Department of Chemical Physics, Weizmann Institute of Science, Rehovot, Israel
[2]Vienna Center for Quantum Science and Technology, Atominstitut, TU Wien, Austria

Abstract— Quantum electromagnetic fluctuations induce forces between neutral particles, namely, the van der Waals (vdW) and Casimir interactions. Here we show that these fundamental interactions can be enhanced by **many orders of magnitude** upon changing the character of the mediating vacuum photon-modes. We consider two dipoles in the vicinity of any standard electric transmission line and find analytically that the interaction scales non-trivially with the inter-dipolar distance, resulting in a strong and long-range interaction. This may have profound implications on the non-additivity of vdW and Casimir interactions in many-particle systems, and opens the door for Casimir Physics in 1d. We discuss the possibilities of measuring this effect, e.g., in a coplanar waveguide line.

Session 1A5
SC3: Silicon Photonics

Ultra-high-speed Optical Signal Processing Using Silicon Photonics
Leif Katsuo Oxenlowe, Hua Ji, Asger Sellerup Jensen, Hao Hu, Hans Christian Hansen Mulvad, Michael Galili, Minhao Pu, Lars Hagedorn Frandsen, Kresten Yvind, ... 64

Using Silicon Nanophotonics for Digital and Analog Signal Processing with Reservoir Computing
Peter Bienstman, Kristof Vandoorne, Thomas Van Vaerenbergh, Martin Fiers, Bendix Schneider, Benjamin Schrauwen, Joni Dambre, ... 65

Maturing the CMOS-photonics-devices-library for the Development of Highly Integrated Circuits Dedicated to Optical Transmissions
Sylvie Menezo, B. Charbonnier, G.-H. Duan, L. Virot, J.-M. Fedeli, P. Grosse, B. Ben Bakir, ... 66

Tunable Self-coupled Optical Waveguide (SCOW) Resonator and Its Application in Optical Signal Processing
Linjie Zhou, Zhi Zou, Xiaomeng Sun, Jingya Xie, Liangjun Lu, Haike Zhu, Jianping Chen, ... 68

High Quality InP Localized Growth on (001) Silicon Substrate for Photonics Applications
Zhechao Wang, Marianna Pantouvaki, Mohan Paladugu, Bin Tian, Richard Olivier, Bender Hugo, Clement Merckling, Weiming Guo, Johan Dekoster, Matty Caymax, Joris Van Campenhout, Dries Van Thourhout, ... 69

40 Gbit/s Silicon Modulators and Detectors
Laurent Vivien, Delphine Marris-Morini, M. Ziebell, G. Rasigade, L. Virot, J. M. Hartmann, Eric Cassan, P. Crozat, D. Bouville, C. Baudot, F. Boeuf, J.-M. Fedeli, ... 70

Configurable Silicon Photonic Crystals
Stefan Prorok, Alexander Yu. Petrov, Manfred Eich, Jingdong Luo, Alex K. Y. Jen, ... 71

Direct Growth of Multi-quantum Wells on Micro and Nanostructures of Indium Phosphide on Silicon for Silicon Photonics
Sebastian Lourdudoss, Carl Junesand, Wondwosen Metaferia, Himanshu Kataria, Yanting Sun, ... 73

HONN Type and L-HONN Type Systems: Towards Digital Optical Cognitive Architectures of Robust Object Recognition
Ioannis Kypraios, ... 74

Optical Modulators and Routers for Photonic Networks-on-chip
Lin Yang, Jianfeng Ding, Ruiqiang Ji, Rui Min, ... 75

Silicon Based Optofluidics
Claude Renaut, Benoit Cluzel, Emmanuel Picard, Jean Dellinger, David Peyrade, Frederique de Fornel, Emmanuel Hadji, ... 76

Ultra-high-speed Optical Signal Processing Using Silicon Photonics

Leif Katsuo Oxenløwe, **Hua Ji**, **Asger Sellerup Jensen**,
Hao Hu, **Hans Christian Hansen Mulvad**, **Michael Galili**,
M. Pu, **Lars Hagedorn Frandsen**, **and K. Yvind**
DTU Fotonik, Department of Photonics Engineering, Technical University of Denmark
Ørsteds Plads, Building 343, Kgs. Lyngby 2800, Denmark

Abstract— In supercomputers, the optical inter-connects are getting closer and closer to the processing cores. Today, a single supercomputer system has as many optical links as the whole worldwide web together, and it is envisaged that future computing chips will contain multiple electronic processor cores with a photonic layer on top to interconnect them. For such systems, silicon is an attractive candidate enabling both electronic and photonic control. For some network scenarios, it may be beneficial to use optical on-chip packet switching, and for high data-density environments one may take advantage of the ultra-fast nonlinear response of silicon photonic waveguides. These chips offer ultra-broadband wavelength operation, ultra-high timing resolution and ultra-fast response, and when used appropriately offer energy-efficient switching.

In this presentation we review some all-optical functionalities based on silicon photonics. In particular we use nano-engineered silicon waveguides (*nanowires*) [1] enabling efficient phase-matched four-wave mixing (FWM), cross-phase modulation (XPM) or self-phase modulation (SPM) for ultra-high-speed optical signal processing of ultra-high bit rate serial data signals. We show that silicon can indeed be used to control Tbit/s serial data signals [2], perform 640 Gbit/s wavelength conversion [3] 640 Gbit/s serial-to-parallel conversion [4], 160 Gbit/s packet switching as well as all-optical regeneration [5]. We will also discuss the performance limitations of crystalline silicon and discuss emerging materials such as amorphous silicon [6].

ACKNOWLEDGMENT

European Research Council (ERC) project SOCRATES, Danish National Research Council (FTP) project NESTOR.

REFERENCES

1. Pu, M., et al., *Optics Communications*, Vol. 283, 3678, 2010.
2. Ji, H., et al., *OFC 2010*, postdeadline paper PDPC7, 2010.
3. Hu, H., et al., *OFC 2011*, postdeadline paper PDPA8, 2011.
4. Mulvad, H. C. H., et al., *ECOC'2011*, postdeadline paper, 2011.
5. Jensen, A. S., et al., *OECC'2013*, paper ThM1-2, 2013.
6. Kuyken, B., et al., *Opt. Lett.*, Vol. 36, No. 4, 552–554, 2011.

Using Silicon Nanophotonics for Digital and Analog Signal Processing with Reservoir Computing

Peter Bienstman[1], **Kristof Vandoorne**[1], **Thomas Van Vaerenbergh**[1], **Martin Fiers**[1], **Bendix Schneider**[1], **Benjamin Schrauwen**[2], **and Joni Dambre**[2]

[1]Photonics Research Group, NB-Photonics, Department of Information Technology
Ghent University, IMEC, Gent 9000, Belgium
[2]Department of Electronics and Information Systems, Ghent University
Sint-Pietersnieuwstraat 41, Gent 9000, Belgium

Abstract— Reservoir computing is a decade old framework from the field of machine learning to use and train recurrent neural networks and it splits the network in a reservoir that does the computation and a simple readout function. This technique has been among the state-of-the-art for a broad class of classification and recognition problems such as time series prediction, speech recognition and robot control. However, so far implementations have been mainly software-based, while a hardware implementation offers the promise of being low-power and fast. Despite essential differences between classical software implementation and a network of optical components, we will show that photonic reservoirs can offer a promising alternative for a hardware implementation.

We will show experimental and theoretical results on the use of a generic photonic reservoir on a silicon-on-insulator chip, which can be used to perform arbitrary digital calculations involving input from up to four bit periods in the past. Using simulations, we also show that such a network can handle more analog tasks like speech recognition.

We also show that phase is an important asset that can be exploited using an integrated photonics approach. By using complex-valued signals as opposed to traditional real-valued signals, the effective size of the reservoir doubles, which is beneficial for performance.

Maturing the CMOS-photonics-devices-library for the Development of Highly Integrated Circuits Dedicated to Optical Transmissions

S. Menezo[1], B. Charbonnier[2], G.-H. Duan[3], L. Virot[1], J. M. Fedeli[1], P. Grosse[1], and B. Ben Bakir[1]

[1]CEA LETI, Minatec, 17 rue des Martyrs, F-38054 Grenoble Cedex 9, France
[2]Orange Labs, 2 Avenue Pierre Marzin, Lannion 22307, France
[3]III-V lab, a Joint Lab of 'Alcatel-Lucent Bell Labs France'
'Thales Research and Technology' and 'CEA Leti', Campus Polytechnique
1, Avenue A. Fresnel, 91767 Palaiseau Cedex, France

Abstract— The complete CMOS-Photonics-devices library developed over the last 5 years in our 200 mm (8 inch) CMOS fab was previously reported. It includes monolithically integrated III-V-on-Silicon-lasers [1, 2], Silicon phase modulators arranged in Mach Zehnder (MZ) interferometers or Ring Resonators (RR) [3, 4], Germanium photo-detectors [5], and passive devices for colorless or Wavelength Division Multiplexing (WDM) circuitry [6]. When developing optoelectronic circuits built up from the integration of many elementary devices, one has to master the statistics of each device characteristics and performances, and their associated dispersions due to process variations. For that purpose, we have been developing highly automated 200 mm-wafer-level test procedures (optoelectronic tests from DC to 60 GHz). Statistical measurements of the main building blocks will be presented here, among which that of passive devices, hybrid III-V-on-Si lasers, Germanium-on-Si photodetectors, and Silicon modulators.

With an increased knowledge and maturity of the elementary devices, the circuit development is made more efficient. The trade-offs on devices performances are driven, on the one hand, by the search for a simpler and more robust integration process of the building blocks, and on the other hand, by the application requirements. Several photonic circuits are currently being developed, for applications ranging from telecom coherent-long-haul-transmissions down to a-few-cm-scale-communications. Some will be presented here, among which

- A coherent QPSK demodulator, integrating a hybrid III-V-on-Si laser [8] serving as the local oscillator (long haul).
- An optical IQ modulator.
- A reflective MZM providing with the Faraday Rotator Mirror effect for a polarization independent and self-coherent transmission (Optical Network Unit of Next Generation Passive Optical Networks) [9].
- Circuits for cm-scale-optical communications [10].

Trade-offs and updates will be discussed.

ACKNOWLEDGMENT

The research leading to these results has received funding from the French ANR under the projects 'IRT Photonique', FAON, MICROS, ULTIMATE and SILVER.

REFERENCES

1. Ben Bakir, B., et al., "Hybrid Si/III-V lasers with adiabatic coupling," *2011 8th IEEE International Conference on Group IV Photonics (GFP)*, 169–171, 2011.
2. Sciancalepore, C., et al., "III-V on Si photonic crystal VCSEL arrays for wavelength division multiplexing," *Photonic Tech. Letters*, 2013.
3. Ziebell, M., et al., "40 Gbit/s low-loss silicon optical modulator based on a pipin diode," *Optics Express*, Vol. 20, No. 10, 10591-6, 2012.
4. Thomson, D. J., et al., "An alignment tolerant high speed ring resonator based silicon optical modulator," *2012 IEEE 9th International Conference on Group IV Photonics (GFP)*, 198–200, 2012.
5. Vivien, L., et al., "Zero bias 40 Gb/s germanium waveguide photodetector on silicon," *Optics Express*, Vol. 20, No. 2, 1096, 2012.

6. Le Liepvre, A., et al., "Silicon integrated triplexer filters based on cascaded Mach-Zehnder interferometers for passive optical networks," *Photonic Tech. Letters*, 2012.
7. Charbonnier, B., et al., "Silicon photonics for next generation FDM/FDMA PON," *IEEE/OSA Journal of Optical Communications and Networking*, Vol. 4, No. 9, A29–A37, 2012.
8. Le Liepvre, A., et al., "Single-mode tunable hybrid III-V/Si laser with 45 nm wavelength range," *ECOC*, 2012.
9. Menezo, S., et al., "Reflective silicon Mach Zehnder modulator with faraday rotator mirror effect for self-coherent transmission," *Optical Fiber Communication Conference*, JTh2A.30, 2013.
10. Menezo, S., et al., "Evaluation of optical interconnects built up from a complete CMOS-photonics-devices-library," *OIC*, 2013.

Tunable Self-coupled Optical Waveguide (SCOW) Resonator and Its Application in Optical Signal Processing

Linjie Zhou, **Zhi Zou**, **Xiaomeng Sun**, **Jingya Xie**, **Liangjun Lu**, **Haike Zhu**, **and Jianping Chen**
State Key Laboratory of Advanced Optical Communication Systems and Networks
Department of Electronic Engineering, Shanghai Jiao Tong University, Shanghai 200240, China

Abstract— We present a novel type of resonators, the self-coupled optical waveguide (SCOW) resonators. SCOW resonators differ from the widely used microring resonators in that the light wave travelling inside the SCOW resonator is no longer simply clock-wise (CW) or counter-clockwise (CCW). Instead, both modes are excited and coupled through the central bridge waveguide. Unlike conventional coupled resonators in which resonance modes are mutually coupled resulting in symmetric and anti-symmetric super-modes, the CW and CCW modes in the SCOW resonators are sequentially coupled and the energy transfer is unidirectional from one mode to the other. Therefore, it exhibits quite distinct resonance behavior with respect to microring resonators. Due to the unidirectional coupling between the CW and CCW modes, the output transmission spectrum shows second-order resonance features. Looking into the propagation of light inside the SCOW resonator, we could find that the output is essentially resulted from the interference of two resonance paths with one side-coupling with and the other tunneling through the CW and CCW modes. By making use of silicon fabrication techniques, we demonstrate the SCOW resonators on silicon photonics platform. Our experimental results reveal that the output resonance spectrum can be either a single- or a dual-notch profile depending on the coupling coefficients of the two couplers and the cavity intrinsic loss.

SCOW resonators can also be coupled in series and in this case the transmission spectrum is more complicated because of the generation of Fabry-Perot (FP) resonances between two adjacent SCOW resonators. The output resonance profile is determined by both the SCOW and FP resonances. Upon controlling the frequency detuning between them, the resonance profile can be easily tailored. In our experiments, we design two-stage coupled SCOW resonators with various configurations of individual resonators. To realize active tuning, we embed p-i-n and p-i-p junctions into the waveguide connecting the two SCOW resonators. The former one is based on the free-carrier plasma dispersion effect, and the latter one is essentially a resistive micro-heater. In one SCOW configuration, the coupled-resonator induced transparency (CRIT) phenomenon is observed in the transmission spectrum with a sharp peak residing in a broad absorption valley. The sharp peak can be utilized for optical switching and optical delay. When the phase of the connection waveguide is tuned, The CRIT peak periodically moves inside the absorption valley. In another configuration, the transmission spectrum exhibits a deep notch, which can work as a notch filter. With the phase tuned, the bottom ripple of the notch filter is varied, which can be used to trim the stopband profile or correct the fabrication induced errors.

Given its versatility in resonance spectrum, the SCOW resonators can find rich applications in optical signal processing. The sharp and deep notch could be utilized for carrier suppression, differential operation on incoming optical signals, and so on. The dual notches could be used for dense wavelength conversion and signal multicasting by making good use of the closely-spaced two channels. The CRIT effect is an optical analog to electromagnetically induced transparency (EIT), which could be adopted for coherent manipulation of optical signals for delay, storage, and nonlinear and quantum information processing on the compact integrated platform with room temperature operation.

High Quality InP Localized Growth on (001) Silicon Substrate for Photonics Applications

Zhechao Wang[1], **Marianna Pantouvaki**[2], **Mohan Paladugu**[2], **Bin Tian**[1], **Richard Olivier**[2], **Bender Hugo**[2], **Clement Merckling**[2], **Weiming Guo**[2], **Johan Dekoster**[2], **Matty Caymax**[2], **Joris Van Campenhout**[2], **and Dries Van Thourhout**[1]

[1]INTEC Department, Ghent University-IMEC
Sint-Pietersnieuwstraat 41, Ghent 9000, Belgium
[2]IMEC, Kapeldreef 75, Heverlee 3001, Belgium

Abstract— Over the last decade, "silicon photonics" has evolved from a relatively new topic to one of the most competitive research field. It holds great promises to many applications, such as optical interconnects, sensing, and next generation commercial electronics. Great achievements have been made, although the indirect bandgap nature of silicon hinders the realization of active devices. Besides the efforts of bonding IIIVs materials on silicon for active applications, the possibility of integrating IIIVs on silicon in the epitaxy level reattracts enormous interests from the material science society. In this work, we present recent results of localized InP growth on exactly [001] oriented silicon substrate.

In order to accommodate the large lattice mismatch between InP and silicon, we start the epitaxial growth from a (001) silicon substrate covered by a patterned SiO_2 buffer. Modified shallow trench isolation (STI) process available in the IMEC 130 nm CMOS line is utilized to fabricate nano-scale holes and trenches in the SiO_2 layer. Thanks to the defect necking effect of a high aspect ratio trenches, most of the threading dislocations that propagates upwards in the trench will be annihilated by the trench sidewall, leaving the InP defect-free in the upper part of the trench. After the localized epitaxial growth that was carried out in a metalorganic vapour phase epitaxy (MOCVD) reactor, the material quality is analyzed by photoluminescence (PL) and transmission electron microcopy (TEM).

Figure 1(a) shows the schematics of the SiO_2 mask: trenches that are aligned along different orientations will be filled by InP during the growth. Figure 1(b) shows the PL image recorded by an ordinary silicon camera. Several images are joined together to give the full view of the PL emission from all the trenches. It is very interesting to find that the material quality is highly trench orientation dependent, and a rotation periodicity of 45° can be found. InP that is grown in [110] and [100] oriented trenches give the lowest PL intensity, while the InP grown in the [130] orientation family gives extremely high PL intensity. TEM analysis of the [130] oriented trench (see Figure 1(c)) shows that all the dislocations and anti-phase boundaries (APBs) are confined in the bottom trench, and the large lateral overgrown InP "cap" on top is ideal for IIIV active devices integrated on silicon.

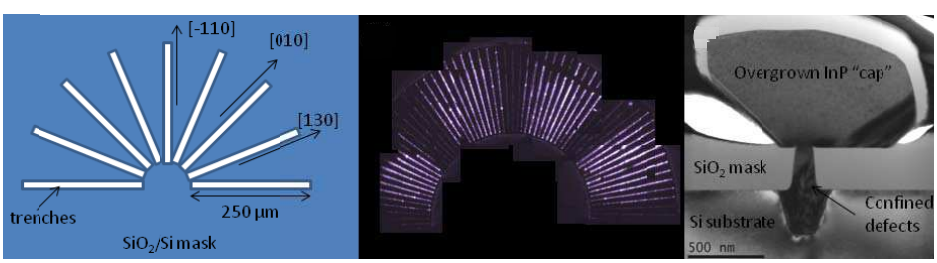

(a) (b) (c)

Figure 1: (a) Schematics of the SiO_2 mask that covers the silicon substrate. (b) Camera image of the PL emission from different trenches. (c) TEM image of the InP that is grown in the [130] oriented SiO_2 trench.

40 Gbit/s Silicon Modulators and Detectors

L. Vivien[1], D. Marris-Morini[1], M. Ziebell[1], G. Rasigade[1], L. Virot[1,2,3], J.-M. Hartmann[2], E. Cassan[1], P. Crozat[1], D. Bouville[1], C. Baudot[3], F. Boeuf[3], and J.-M. Fédéli[2]

[1]Institut d'Electronique Fondamentale, University Paris Sud
CNRS UMR 8622, Bât. 220, F-91405 Orsay Cedex, France
[2]CEA, LETI, Minatec Campus, 17 rue des Martyrs, F-38054 Grenoble Cedex 9, France
[3]STMicroelectronics, Silicon Technology Development, Crolles, France

Abstract— Silicon-based photonics has generated a strong interest in recent years, mainly for optical telecommunications and optical interconnects in microelectronic circuits. The main rationales of silicon photonics are the reduction of photonic system costs and the increase of the number of functionalities on the same integrated chip by combining photonics and electronics. Furthermore, the use of optical links for high speed on chip communications may dramatically reduce the power consumption of the global circuit. Numerous developments on photonic and optoelectronic building blocks have been then made including waveguides, modulators, lasers, and photodetectors. Recent results on ultrafast optical modulators based on carrier depletion effect and germanium photodetectors integrated in silicon on insulator (SOI) waveguides will be presented.

The modulator reported here is based on a 400 nm thick PIPIN diode allowing the achievement of a good trade-off between high bandwidth, high efficiency and low loss. The measured insertion loss was lower than 6 dB for a 4.7 mm long MZI modulator. Cut-off frequency up to 20 GHz and dynamic extinction ratio of about 7 dB at 40 Gbit/s has been achieved. In addition, insertion loss can be reduced down to 4.5 dB using 1 mm long active region, with an extinction ratio larger than 3 dB and cut-off frequency higher than 30 GHz.

Germanium (Ge) is a natural candidate for detection in silicon platform thanks to its strong absorption around $\lambda = 1.55\,\mu$m. In our approach, Ge is selectively grown at the end of a SOI waveguide in a silicon recess in order to achieve butt coupling integration. Such a configuration allows a very short absorption length (95% of the light intensity is absorbed over lengths of about 4 µm at 1.31 µm and less than 7 µm at 1.55 µm). 40 Gbit/s data transmission was obtained under zero-bias. The detector was a 10 µm long lateral pin diode. The responsivity was about 0.5 A/W at a wavelength of 1.55 µm.

These ultra-fast performances obtained with both optoelectronic devices constitute a new milestone towards the generations of several Tbs/s chips merging electronics and photonics.

Configurable Silicon Photonic Crystals

Stefan Prorok[1], **Alexander Yu. Petrov**[1], **Manfred Eich**[1], **Jingdong Luo**[2], **and Alex K. Jen**[2]

[1]Institute for Optical and Electronic Materials, Hamburg University of Technology
Eissendorfer Straße 38, Hamburg 21073, Germany
[2]Department of Materials Science and Engineering
University of Washington, Seattle, WA 98195-2120, USA

Abstract— Compact high Q resonators can dramatically enhance the light matter interaction. Examples for this are efficient four wave mixing and enhanced spontaneous emission due to Purcell effect [1, 2]. However the combination of high Q photonic crystal cavities and functional cladding materials such as nonlinear polymers and glasses has turned out to be challenging. The reported quality factors for polymer infiltrated silicon photonic crystal cavities are below 10 k [3].

We demonstrate that this challenge can be resolved by taking advantage of the bleaching effect in chromophore doped polymer claddings. As reported earlier bleaching either by UV light or by high energy electrons breaks the conjugated pi-bonds of the chromophore [4, 5]. This reduces the polarizability of the chromophore molecules and hence also the refractive index of the polymer blend. We showed that for a photonic crystal waveguide a reduction of the refractive index in the cladding material is equivalent to an effective reduction of the photonic crystal lattice constant. This means that the effective lattice constant can be trimmed by bleaching the cladding material. In order to proof this concept polymer coated photonic crystal waveguides are subjected to different electron doses. The transmission spectrum of the waveguides is measured before and after bleaching. A typical measurement after a dose of 200 μA/cm^2 is presented in Figure 1(a). A shift of 2.4 nm to shorter wavelengths is observed which corresponds to a reduction of the effective lattice constant of 630 pm. Doing this for several different doses it is possible to obtain the change of the effective lattice constant as a function of the electron dose. With the given system the effective lattice constant can be defined with a resolution of 7.8 pm which is a factor of 70 smaller than the lattice constant of crystal silicon.

As described by Takahashi et al. [6] photonic crystal heterostructure cavities can be created by adjoining two photonic crystal waveguides of lattice constant a separated by a waveguide section with a slightly larger lattice constant a'. Since the effective lattice constant can be reduced by bleaching it is possible to use the same approach in order to define a photonic crystal cavity. Figure 1(b) shows a light microscope image of a bleached cavity. Figure 1(c) shows the measured spectrum of the waveguide before and after bleaching. The cut-off of the waveguide is shifted to smaller wavelengths as before. Close to the cut-off a cavity with a quality factor of 99 k is observed.

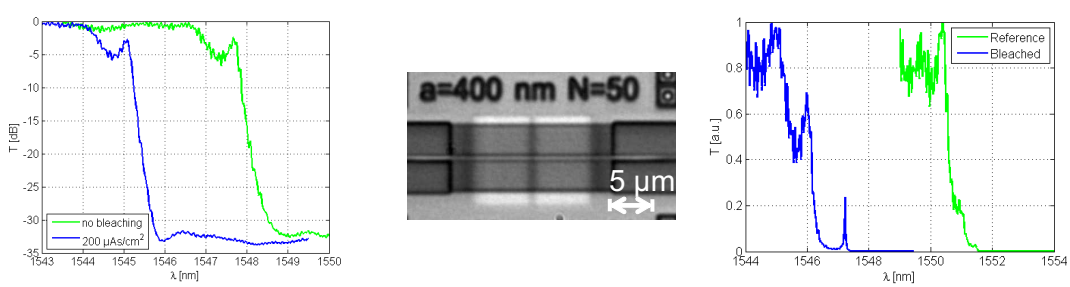

(a) (b) (c)

Figure 1: (a) Transmission spectrum of a waveguide before and after bleaching. (b) Light microscope image after cavity definition by bleaching. (c) Transmission spectrum of a waveguide before and after cavity definition by bleaching.

ACKNOWLEDGMENT

This work was supported by the German Research Foundation (DFG) under Grant DFG (EI 391/12-1). The authors acknowledge the support from CST, Darmstadt, Germany with their Microwave Studio software.

REFERENCES

1. Agha, I. H., Y. Okawachi, and A. L. Gaeta, *Opt. Express*, Vol. 17, 16209, 2009.
2. Hennessy, K., A. Badolato, M. Winger, D. Gerace, M. Atature, et al., *Nature*, Vol. 445, 896, 2007.
3. Wülbern, J. H., J. Hampe, A. Petrov, M. Eich, J. Luo, et al., *Appl. Phys. Lett.*, Vol. 94, 241107, 2009.
4. Vydra, J., H. Beisinghoff, T. Tschudi, and M. Eich, *Appl. Phys. Lett.*, Vol. 69, 1035, 1996.
5. Prorok, S., A. Y. Petrov, M. Eich, J. D. Luo, and A. K.-Y. Jen, *Opt. Lett.*, Vol. 37, 3114, 2012.
6. Takahashi, Y., H. Hagino, Y. Tanaka, B. S. Song, T. Asano, et al., *Opt. Express*, Vol. 15, 17206, 2007.

Direct Growth of Multi-quantum Wells on Micro and Nanostructures of Indium Phosphide on Silicon for Silicon Photonics

Sebastian Lourdudoss, **Carl Junesand**, **Wondwosen Metaferia**, **Himanshu Kataria**, **and Yanting Sun**
Laboratory of Semiconductor Materials
School of ICT, KTH, Electrum 229, Kista 16440, Sweden

Abstract— Integration of III-V's on silicon is a viable approach for silicon photonics and nanophotonics. There are several bonding and epitaxial approaches that have been reviewed recently in the literature [1–4]. Active hybrid silicon devices achieved through epitaxial growth of active III-V layers directly on SOI (silicon on insulator) wafers without the use of the intermediate step of growth on InP substrates is an important step to facilitate the integration of high density nano-scale photonic components and to reduce the cost. This would enable the transition of photonic devices to large area silicon substrates with several orders of magnitude reduction in cost, and a large increase in manufacturing capability to tap the potential of silicon photonics [3].

Towards reaching the goal of monolithic integration of lasers on Si, we demonstrate direct growth of multi-quantum wells (MQW) emitting at 1.55 µm on InP on Si. InP on silicon was achieved by epitaxial lateral overgrowth. The MQWs exhibit similar photoluminescence intensity as those grown on the reference InP substrate. This has been feasible with proper morphological optimisation to obtain InP on Si with low defect density $\sim 5 \times 10^6\,\mathrm{cm}^{-2}$ [5, 6]. In addition, we also explore the feasibility of achieving quantum dot (QD) structures on silicon as these are attractive for nanophotonic applications. QD lasers for example, are known to have remarkable reduction in threshold current, temperature-insensitive operation, and large modulation bandwidth [7–9]; in addition, luminescent QDs can be used to create single photon sources, entangled photon sources and quantum bits for quantum computation. In recent years various approaches for formation of QDs have been intensively studied to realize device-grade semiconductor QD structures. We demonstrate that templates with InP frusta on silicon for QD growth can be achieved by combining nanoimprinting and epitaxial growth. Morphological and optical studies of these templates are indicative of their potential for monolithic integration of QDs on silicon for silicon photonics and nanophotonics.

REFERENCES

1. Bolkhovityanov, Y. B. and O. P. Pchelyakov, "III-V compounds-on-Si: Heterostructure fabrication, application and prospects," *The Open Nanoscience Journal*, Vol. 3, 20–33, 2009.
2. Heck, M. J. R., H.-W. Chen, A. W. Fang, B. R. Koch, D. Liang, H. Park, M. N. Sysak, and J. E. Bowers, "Hybrid silicon photonics for optical interconnects," *IEEE J. Sel. Topics in Quant. Electron.*, Vol. 17, No. 2, 333–346, 2011.
3. Lourdudoss, S., "Heteroepitaxy and selective area heteroepitaxy for silicon photonics," *Current Opinion in Solid State and Materials Science*, Vol. 16, 91–99, 2012.
4. Lee, A., H. Liu, and A. Seeds, "Semiconductor III-V lasers monolithically grown on Si substrates," *Semicond. Sci. Technol.*, Vol. 28, 015027, 2013.
5. Metaferia, W., C. Junesand, M.-H. Gau, I. Lo, G. Pozina, L. Hultman, and S. Lourdudoss, "Morphological evolution during epitaxial lateral overgrowth of indium phosphide on silicon," *J. Crystal Growth*, Vol. 332, 27–33, 2011.
6. Junesand, C., C. Hu, Z. Wang, W. Metaferia, P. Dagur, G. Pozina, L. Hultman, and S. Lourdudoss, "Effect of the surface morphology of seed and mask layers on InP grown on Si by epitaxial lateral overgrowth," *J. Electron. Mater.*, Vol. 41, No. 9, 2345–2349, 2012.
7. Arakawa, Y. and H. Sasaki, "Multidimensional quantum well laser and temperature dependence of its threshold current," *Appl. Phys. Lett.*, Vol. 40, 939, 1982.
8. Asryan, L. V. and S. Luryi, "Temperature-insensitive semiconductor quantum dot laser," *Solid State Electron.*, Vol. 47, 205–212, 2003.
9. Bhattacharya, P., D. Klotzkin, O. Qasaimeh, W. Zhou, S. Krishna, and D. Zhu, "High-speed modulation and switching characteristics of In(Ga)As-Al(Ga)As self-organized quantum-dot lasers," *IEEE J. Sel. Top. Quantum. Electron.*, Vol. 6, 426–438, 2000.

HONN Type and L-HONN Type Systems: Towards Digital Optical Cognitive Architectures of Robust Object Recognition

Ioannis Kypraios
APEM R&D Computing Lab, Centre of Innovation & Enterprise, Begbroke Science Park
University of Oxford, Begbroke Hill, Woodstock Road, Begbroke, Oxfordshire OX5 1PF, UK

Abstract— We describe the biologically-inspired knowledge learning and knowledge representation architectures of both the hybrid optical neural network and logarithmic hybrid optical neural network family of object recognition systems. An object recognition system to be able to solve complex problems needs to combine a knowledge representation module with a knowledge learning module in its design. We focus on the non-linearity of the input information, the knowledge learning and adaptation to the input information, and the provision of an attentional mechanism by both families of systems' designs for selecting certain information in their knowledge learning process against other input. We present the effects of altering the knowledge representation can have on the problems' learned knowledge and the problem solving process. We study how the unconstrained- and logarithmic unconstrained-hybrid optical neural network object recognition systems apply an unconstrained representation of the problem's knowledge to maximize the search of solutions, how the constrained- and logarithmic constrained-hybrid optical neural network object recognition systems use effectively a guided search of problem solutions, and how the modified- and logarithmic modified-hybrid optical neural network object recognition systems implement memory-like architectures to recall certain solutions over others in the multidimensional search space. Further, we explore the effects that the grain size and the field width have in the knowledge representation and learning process. Though both the hybrid optical neural network and logarithmic hybrid optical neural network families of object recognition systems could be implemented in space domain as joint transform correlator architectures or be Fourier transformed and used as Fourier domain filters in 4-f Vander Lugt type optical correlators, we envision those biologically-inspired digital optical cognitive architectures to be ideally suited for integrated silicon photonics technologies on-chip.

Optical Modulators and Routers for Photonic Networks-on-chip

Lin Yang, **Jianfeng Ding**, **Ruiqiang Ji**, **and Rui Min**
State Key Laboratory on Integrated Optoelectronics, Institute of Semiconductors
Chinese Academy of Sciences, Beijing 100083, China

Abstract— The performance of chip multiprocessor (CMP) is determined not only by the number of the processor cores integrated on a die, but also by how efficiently they collaborate with each other. With more processor cores being integrated on a die, interconnects in CMP gradually move from traditional bus interconnects to more sophisticated networks-on-chip (NoC). With CMP continuously requiring more communication bandwidths, metallic-based electrical NoC gradually becomes the bottleneck for improving the performance of CMP due to its high power consumption, limited bandwidth and long latency. Recent studies have demonstrated that photonic NoC is a potential solution to overcome the limitations of its electrical counterpart.

Many architectures for photonic NoC have been widely studied, such as Mesh, Fat Tree and Clos. While, recent studies are gradually focused on Mesh NoC due to its symmetric architecture, good scalability, simple routing algorithm and easy implementation. A series of optical devices are required to construct the optical interconnect between two processor cores, such as lasers, modulators, multiplexers, waveguides, de-multiplexers and detectors. Such a point-to-point interconnect is the simplest communication mode. However, for network application environment, the processor core is required to communicate with other processor cores. This function is usually completed by optical router, which is located at each node of photonic NoC and connects the local processor core with other remote nodes.

In this paper, we will review the status of optical modulators and routers for photonic networks-on-chip and introduce our efforts on these topics. In the first section, we will introduce the 40 Gb/s carrier-depletion Mach-Zehnder silicon optical modulator with the extinction ratio of 15 dB. In the second section, we will introduce the 5-port optical router for Mesh photonic NoC and a universal method for constructing N-port non-blocking optical router for photonic NoC.

Silicon Based Optofluidics

Claude Renaut[1,2], Benoit Cluzel[2], Emmanuel Picard[1], Jean Dellinger[2], David Peyrade[3], Frederique de Fornel[3], and Emmanuel Hadji[1]

[1]Laboratoire SiNaPS, INAC/SP2M, UMR-E CEA/UJF-Grenoble 1
17 rue des Martyrs, 38054 Grenoble Cedex 9, France
[2]Laboratoire Interdisciplinaire Carnot de Bourgogne, UMR CNRS 6303
Université de Bourgogne, France
[3]Laboratoire Technologies Microélectroniques, CNRS/UJF-Grenoble 1/CEA
17 rue des Martyrs, 38054 Grenoble Cedex 9, France

Abstract— We report here on-chip optical trapping and handling of micrometer-sized dielectric particles in a microfluidic cell. We achieve single nanoparticle trapping as well as multiple particles assembly By wavelength induced field map tuning within a set of coupled nanobeam cavities, we also evidence particle motion control and handling between specific trapping sites. These results are proof-on-principles of a new range of optofluidics functionalities.

Nanobeam cavities appeared as one of the possible key players for silicon photonics. They provide very strong light confinement within an ultra-low volume [1] and allow achieving light localization down to sub-wavelength sized features [2].

If one set a couple of nanobeam twinned cavities (i.e., strictly identical) in the near-field of each others (i.e., for distances ranging from 50 to 200 nm), then the nanobeam cavities can evanescently couple. As a result of the coupling mechanism, new optical states arise. For instance, it has been observed [3] that for a set of two nanobeam cavities, the fundamental optical mode splits in two modes of different parities.

We suggest that this effect, formerly known while coupling harmonic oscillators, may open the road to a new range of silicon based optofluidics devices. The light localization within such a system of twinned cavities is indeed wavelength dependent and thus wavelength addressable. In odder words, the light can then be localized at different places on the chip depending on the wavelength. We recently demonstrated the operation of such an optical grid [4] by using an array of near-field optically-coupled twinned nanobeam cavities.

While tightly confined within the high optical index material, the evanescent part of the optical field can also translate into actual optical forces. As a result, we demonstrated the trapping and assembling of single micrometer or sub-micrometer sized nanocolloidal particles over a nanobeam cavity in a microfluidic cell [5].

We present here further developments of this concept towards silicon based on-chip optofluidics. We hence show that, once trapped, the near-field optical interaction between the particle and the nanobeam cavity allows recording its presence. This effect results from the interaction between the particle and the cavity, formerly observed between a nanometric NSOM tip and a cavity [6]. As a result, the actual number of trapped particles is detected.

We also evidence that the nanoparticles can be trapped and moved at nanometre scale. By designing specific nanobeam cavity networks, we demonstrate that different kinds of motions are achievable among which are the linear motion and the rotation.

This new architecture offers an unprecedented opportunity to mold on a chip the morphology of the optical field and opens therefore exciting new perspectives for the future development of nanoscale optofluidics with configurable optical traps, sensors or dynamic nano-tweezers.

REFERENCES

1. Velha, P., J. C. Rodier, P. Lalanne, J. P. Hugonin, D. Peyrade, E. Picard, T. Charvolin, and E. Hadji, "Ultracompact silicon-on-insulator ridge-waveguide mirrors with high reflectance," *Applied Physics Letters*, Vol. 89, 171121, 2006.
2. Lalouat, L., B. Cluzel, F. de Fornel, P. Velha, P. Lalanne, D. Peyrade, E. Picard, T. Charvolin, and E. Hadji, "Sub wavelength imaging of light confinement in high Q small V photonic crystal nanocavity," *Applied Physics Letters*, Vol. 92, 111111, 2008.
3. Foubert, K., L. Lalouat, B. Cluzel, E. Picard, D. Peyrade, F. de Fornel, and E. Hadji, "An air-slotted nanoresonator relying on coupled high-Q small-V Fabry Perot nanocavities," *Applied Physics Letters*, Vol. 94, 251111, 2009.

4. Cluzel, B., K. Foubert, L. Lalouat, J. Dellinger, D. Peyrade, E. Picard, E. Hadji, and F. de Fornel, "Addressable sub-wavelength grids of confined light in a multi-slotted nanoresonator," to appear in *Applied Physics Letters*, 2011.
5. Renaut, C., J. Dellinger, B. Cluzel, T. Honegger, D. Peyrade, E. Picard, F. de Fornel, and E. Hadji, "Assembly of microparticles by optical trapping with a photonic crystal nanocavity," *Applied Physics Letters*, Vol. 100, No. 10, 2012.
6. Cluzell, B., L. Lalouat, P. Velha, E. Picard, D. Peyrade, J.-C. Rodier, T. Charvolin, P. Lalanne, F. de Fornel, and E. Hadji, "A near-field actuated optical nanocavity," *Optics Express*, Vol. 16, No. 1, 279, 2008.

Session 1A6
SC1&4: Antenna Modeling and Simulation

Curve-fitting Formulas for Fast Determination of Frequency Band-notched Response of UWB Antennas
Ayman Ayd Ramadan Saad, Mohamed Mamdouh Mahmoud Ali, Elsayed Esam M. Khaled, ... 80

State of the Art Antenna Simulation Using the "System Assembly and Modeling" Approach
Wittig Tilmann, ... 81

MIMO Antenna Integration for LTE Operation
Peter Futter, Gopinath Gampala, C. J. Reddy, ... 82

A Novel Frequency-tunable Antenna with a Wide Tuning Range
Ningli Zhu, Wei Zhang, ... 83

Advanced Computational Tools for Antenna Design and Placement
C. J. Reddy, ... 84

An Improved Model for Estimating Radiated Emissions from a Printed Circuit Boards with Attached Cables
Boon Kuan Chung, Goh Jia Haw, ... 85

Design of Linear Biconical Antenna Array for the Generation of Trapezoidal Pattern
Alapati Sudhakar, C. Subba Rao, A. V. Yashwanth, ... 86

HFSS: Hybrid IE Solvers for Efficient Simulation of Complex Systems
Anders Edquist, Alain Michel, ... 87

HFSS with HPC for Large Finite Antenna Array Design Session
Anders Edquist, Alain Michel, ... 88

Patch and Ground Plane Design of Microstrip Antennas by Material Distribution Optimization
Emadeldeen Hassan, Eddie Wadbro, Martin Berggren, ... 89

Antenna Design for a Ground Penetrating Radar inside a Bottom Hole Assembly
Jan-Florian Höfinghoff, Ludger Overmeyer, ... 90

Curve-fitting Formulas for Fast Determination of Frequency Band-notched Response of UWB Antennas

Ayman Ayd R. Saad[1], **Mohamed Mamdouh M. Ali**[2], **and Elsayed Esam M. Khaled**[2]

[1]Kosseir Radio, Telecom Egypt, Kosseir 84712, Egypt
[2]Electrical Engineering Department, Assiut University, Assiut, Egypt

Abstract— Since the Federal Communication Commission (FCC) assigned 3.1–10.6 GHz frequency band of ultra-wideband (UWB) systems in February 2002 [1], UWB technology has been attracting considerable interests in both the academic and commercial domains due to the potentially high data rate (more than 110 Mbits/s) for short range, low power consumptions and easy connections to different devices such as wireless USB, PCs, high-definition TVs, etc.. Consequently, UWB antennas have received more and more attention, as the only non-digital part of UWB system. UWB antennas have more challenges to meet, namely, stable radiation pattern, gain, and group delay, all over the band. Covering this ultra wide bandwidth arouses a coexistence problem with narrowband technologies sharing with UWB some of the frequency bands such as WLAN operating in the band 5–6 GHz. To overcome this problem and avoiding interference, UWB antennas use filters to suppress dispensable bands. An alternative approach to notch-out specific frequencies is to design UWB antenna with frequency band-notch characteristic.

With the development of UWB antenna having frequency band-notched features, literature is congested with different designs in various topologies. However, the most popular method to obtain the notched band is to insert slots. The length of the slot may appear to be a nearly quarter-/half-wavelength at resonance [2].

The aim of this paper is to present approximated formulas that help researchers and UWB antennas designers to fast determine the frequency band-notched response of the nearly quarter-/half-wavelength resonators. The formulas are obtained using the curve-fitting technique. The process of finding the best fit equation with the available results is known as curve fitting. The obtained formulas describe a relationship between the total length of the resonator and the corresponding notched frequency. To verify the proposed methodology, the results obtained from the approximated formulas are compared with the results obtained from the EM simulator based on a prototype design of UWB antenna previously published in literature [3]. The validity of the proposed methodology is verified and high accuracy results are obtained.

REFERENCES

1. "Revision of part 15 of the communication's rules regarding ultra-wideband transmission systems," Federal Communications Commission, ET–Docket 98–153, FCC 02–48, 2002.
2. Kim, C., *Ultra-wideband Antenna, Microwave and Millimeter Wave Technologies: Modern UWB Antennas and Equipment*, I. Minin, Ed., In-Tech, Croatia, 2010.
3. Khaled, E. E. M., A. A. R. Saad, and D. A. Salem, "A proximity-fed annular slot antenna with different a band-notch manipulations for ultra-wide band applications," *Progress In Electromagnetics Research B*, Vol. 37, 289–306, 2012.

State of the Art Antenna Simulation Using the "System Assembly and Modeling" Approach

Wittig Tilmann
CST AG, Darmstadt, Germany

Abstract— Simulation is well established in modern antenna engineering as an essential part of the design process. However, antenna designs and concepts are numerous, and the number of applications gives rise to diverse design goals and requirements. When designing an antenna, it is important to remember that is not isolated in space — engineers must take into account matching and feeding networks, antenna placement, co-site interference, multiphysics effects and human exposure to fields, along with application-specific postprocessing analysis. Various simulation methods exist to address all these different tasks, and each has its own advantages and disadvantages.

During this presentation, we would like to show how these different approaches can be combined in one simulation environment to exploit their individual strengths, using hybrid solver methods and near- and far-field sources to link different simulation domains. With these "Complete Technology" and "System Assembly and Modeling" approaches, CST's state-of-the-art technology can simulate not just the electromagnetic properties of a device, but also the full circuit and system behavior, with incomparable speed and flexibility.

Several application examples will be used to demonstrate this approach to antenna simulation. All aspects of the antenna design workflow will be discussed, from choosing the right antenna type and dimensions, through selecting the optimal solver technology, to optimizing the antenna performance for a specific application, as well as designing feeding and matching circuits. The antennas demonstrated will range across small antennas as used in mobile communications (including MIMO configuration), reconfigurable and conformable body-wearable types, UWB, reflector antennas, and array antennas both large and small.

MIMO Antenna Integration for LTE Operation

Peter Futter[1], **Gopinath Gampala**[2], **and C. J. Reddy**[2]

[1]EM Software & Systems — S.A. (Pty) Ltd., Stellenbosch, South Africa
[2]EM Software & Systems (USA) Inc., Hampton, Virginia, USA

Abstract— 4G mobile broadband network technologies, like Long-Term Evolution (LTE), target increased bandwidth to deliver higher data speeds, improved network capacity and better spectrum utilisation [1]. Technologies like MIMO are exploited [1] to provide better channel performance. Despite the current trend towards larger tablet-like form factors, device geometry is typically thin and the antenna volume is still limited. The design requirements are multifaceted: antennas must offer good performance while occupying a small volume, in the proximity of multiple/multiband transmitters and densely integrated components, while delivering low mutual coupling needed for effective MIMO performance and still comply with specific absorption rate (SAR) limits. In [2], a novel electrically small antenna (ESA) design is derived for use in the 2.6 GHz LTE band and the MIMO performance is presented for the antenna and substrate. When the ESA is integrated into a device, the performance is influenced by components and the presence of the human body,which must be taken into account to ensure a robust and comprehensive design.

Method: This study focusses on the integration of the original ESA design into a mobile device and the interactions with its environment. Traditionally, this is approached by building and measuring prototypes at each design stage, which is costly and time consuming. Computational electromagnetic tools, like FEKO [3], offer numerical equivalents of these steps, which can reduce the number of prototype iterations that are needed. Rigorous optimisation and parametric analysis is performed to investigate the influence of components [4] (e.g., battery, display module, speaker, microphone, housing, etc.), all of which can be located in the reactive near-field of the antenna. Furthermore, the device is mostly used in close proximity to the human body, which degrades the total radiated power [4] (TRP) performance due to power absorption in the body.

Conclusions: The process of integrating the ESA into a modern mobile device form factor was presented and the interactions of the antenna and its environment were highlighted. The presented approach not only provides insight into a more robust design practice, but can facilitate early stage product development by identifying potentially problematic configurations.

REFERENCES

1. Ericsson, "LTE: An introduction," www.ericsson.com/res/docs/2011/lte_an_introduction.pdf.
2. Gampala, G., C. J. Reddy, O. Stäbler, and T. Hager, "Compact antenna for MIMO LTE mobile phone applications," *Micorwave Journal*, March 2012.
3. FEKO Suite6.2, www.feko.info, EM Software & Systems — S.A. (Pty) Ltd., P. O. Box 1354, Stellenbosch, 7599, South Africa.
4. Meshram, M. K., R. K. Animeh, A. T. Pimpale, and N. K. Nikolova, "A novel quad-band diversity antenna for LTE and Wi-Fi applications with high isolation," *IEEE Transactions on Antennas and Propagation*, Vol. 60, No. 9, September 2012.

A Novel Frequency-tunable Antenna with a Wide Tuning Range

Ningli Zhu and Wei Zhang
Institute of Microelectronics, Peking University, Beijing 100871, China

Abstract— In this paper a varactor-loaded antenna with a wide tuning range and good directivity is designed. The HFSS and ADS software simulates this antenna independently, and the results show that it realizes a 500 MHz tunable range, from 1.44 GHz to 2.06 GHz in HFSS, and 1.944 GHz to 2.568 GHz in ADS, moreover, there exists a perfect matching resistor. At the same time, the shape of the H radiation pattern is nearly omnidirectional at those chosen frequency points. Due to the limitation of processing technology, it's difficult to accurate to 0.3 mm. So it makes the effect of inductance larger than before, and the working frequency lower than before. The testing results of vector network analyzer show that this antenna realizes 370 MHz tunable range, from 1.52 GHz to 1.89 GHz. This proposed design has a simple structure and a compact dimension of 24.2 mm × 32 mm × 1.5 mm.

The proposed antenna is composed of two parts, one is the radiation part, and another is the coplanar waveguide feedline. The connection of the two parts is a J slot. As can be seen from surface electric field figure, the E-field across the CPW slots is asymmetric. This phenomenon indicates that the CPW odd mode as well as even mode is significantly influences the capability of this antenna. From this surface current picture, the horizontal line at the top of the antenna is not involved in the radiation, due to the odd symmetry of the distribution of the current. Accordingly, this narrow slit is equivalent to a loaded inductance. At the same time, the J-slot can be equivalent to the field current of the space radiation, which can be explained by the surface electric field.

The frequency tunable antenna, designed in this paper, has the advantage of small size, wide tunable range, good directivity, easy processing, which can be applied to near field wireless transmission system such as WLAN, Buletooth, UWB, ZigBee.

Advanced Computational Tools for Antenna Design and Placement

C. J. Reddy
EM Software & Systems (USA) Inc., Hampton, VA 23666, USA

Abstract— Recent advances in computational electromagnetic tools made antenna design possible along with integration of antennas on various ground, sea and air platforms. Full wave techniques such as Method of Moments (MoM), Multilevel Fast Multipole Method (MLFMM) along with asymptotic techniques such as Physical Optics (PO) and Uniform Theory of Diffraction (UTD) will be reviewed. Application of these and hybrid numerical techniques for antenna designs, antenna-platform interaction studies, EMI/EMC, bio-electromagentics and Radio Frequency Identification (RFID) system design. For many practical applications, sometimes it is necessary to study the electromagnetic behavior on a specific structure over a broad frequency band, and therefore it is important to have some benchmark data on computational resources needed for some commonly used numerical techniques. In this paper, a full-size air, ground and sea platforms are considered and the frequency limit is pushed at different bands using several numerical techniques. A benchmark study of computational resources required by available computational tools for electrically large platforms will be presented.

An Improved Model for Estimating Radiated Emissions from a Printed Circuit Boards with Attached Cables

Boon Kuan Chung and Goh Jia Haw
Universiti Tunku Abdul Rahman, Jalan Genting Kelang, Setapak, Kuala Lumpur 53300, Malaysia

Abstract— Common mode current induced on cable attached to a PCB has been a well known source of unintentional radiated emissions. The coupling mechanism of the common mode current to the cable can be divided into two types: voltage-driven and current-driven. In voltage-driven mechanism, the common mode current is induced by electric field that couples from traces on PCB to the cable. Previous work showed that these radiated emissions can be estimate based on the self-capacitance of the trace and the signal return plane but the method is only reasonably accurate at lower frequency. This paper develops a model which gives an extended frequency range up to 1 GHz. The formulation for the equivalent common-mode voltage source is improved by taking into account the driving point impedance of the cable which behaves as a wire antenna. The radiated emissions estimated by the improved model match well with the values from 3D electromagnetic simulation of the original PCB with attached cable. It represents an improvement compared to earlier model by 11 dB at 400 MHz to 18 dB at 800 MHz for board size of 10 cm×16 cm and cable length of 3 m. Similar improvements are obtained for other combinations of board size and cable length. The results show that the cable length is an important factor, in addition to the board area as suggested by earlier work, in determining the magnitude of the equivalent common-mode voltage source. Resonant of the wire antenna affects not only the radiated electromagnetic field but also the common-mode voltage source magnitude due to varying antenna impedance.

Design of Linear Biconical Antenna Array for the Generation of Trapezoidal Pattern

A. Sudhakar[1], **C. Subba Rao**[2], **and A. V. Yashwanth**[1]

[1]Department of ECE, RVR & JC College of Engineering
Chowdavaram, Guntur, Andhra Pradesh 522019, India
[2]Department of ECE, PVP Siddhartha Institute of Technology
Vijayawada, Andhra Pradesh 520007, India

Abstract— The radiation patterns of individual antennas are either omnidirectional or directional in shape. The patterns of linear arrays are either broad side or end fire in shape and the radiation patterns are omnidirectional in collinear arrays. These shapes are common and are widely used in many broad casting applications with a single element. Shape of the radiation pattern can be altered by using reflectors of various geometries. But these antennas with reflectors are heavy and are not suitable for present day applications where miniaturization is the prime requirement of any gadget. Array antennas are highly suitable for effectively controlling the radiation pattern properties such as position of nulls, number of side lobes and their amplitudes using parameters of the array such as input excitation of the elements and the separation between them. Geometrical shape of the array also plays an important role in determining the radiation properties but complex configurations are not preferred due to high cost. Complex shaped beams can be easily generated by using simple linear array antenna with excitation control. Excitation may be input amplitude or phase of the individual elements of the array. Amplitude control method is not usually preferred as the scanning of the beam is not possible and usually losses in the feed configuration are more. More over the amplitude taper between center element and edge elements becomes pronounced as the number of elements in the array increases. Control of excitation phase of individual elements to generate complex beam shapes is more optimum as the input amplitudes of the elements are maintained constant and is suitable for scanning the beam at high speeds. The radiation intensity from a linear array may be expressed as a Fourier Transform which consists of complex exponential term. Many times such transforms cannot be solved by standard methods. In such cases numerical or approximation methods are used to obtain desired result. In this paper a biconical linear array antenna is proposed to generate trapezoidal shaped radiation pattern using input phase control method. The stationary phase concept is used to evaluate required phase coefficients necessary for the elements of the proposed array to generate the Trapezoidal shaped radiation pattern which is highly useful in ground mapping and surveillance applications.

HFSS: Hybrid IE Solvers for Efficient Simulation of Complex Systems

Anders Edquist and Alain Michel
ANSYS, Sweden

Abstract— The 3D Electromagnetic field solver, HFSS, is widely used in the RF/Microwave industry for simulation of 3D microwave structures, including antenna and scattering problems. Recent trend in antenna design is towards system/platform simulation enabling installed performance to be evaluated. The challenge is to solve these electrically large models whilst maintaining accuracy and speed. To achieve this challenge HFSS combines hybridizations between different numerical schemes such as FEM and IE and domain decomposition method (DDM). This two methods and how they are used together will be describe in this paper.

HFSS is based on the Finite Element Method (FEM), which is very well suited to model arbitrary complex structures. The Integral Equation (IE) technique, introduced into HFSS as a new 3D solver in 2010, is better at simulating electrically large but simple, smooth structures. IE solver has been combined with the existing FEM solvers in a hybrid technique known as the Finite Element Boundary Integral (FE-BI) Method. The hybrid solver supports the hybridization of FEM and IE including perfect FEM absorber, rigorous two-way coupling, metallic IE region for large metallic structures and current flow across FEM and IE regions. The IE regions definition within the solve domain for metals and dielectric objects, allows the IE solver to be used directly on these objects, which helps to reduce overall mesh and solve time. A recent critical advancement allows metallic IE regions to touch FEM regions (see Fig. 1). This new ability marks HFSS as a true hybrid solver and opens up new simulation capabilities. Also, this is an essential feature for an automatic hybrid solver where decisions for which solver to use for a given region can be based on geometry and material without constraining how the various regions are connected.

Domain decomposition is a very powerful method that opens up vast computing resources due to its inherent capability for distributed computing.An important advantage for DDM is the ability to link different solution methods and physics. As stated before, HFSS hybrid solver can already combine FEM domains with IE domains. The coupling between disjoint domains is provided via a finite element-boundary integral (FE-BI) method which also works as a perfect truncation of FEM in the case of only one domain. The advantages of DDM-based FE-BI compared to traditional FE-BI include modularity of FEM and IE domains in terms of mesh and basis functions. This "non-conformal" ability better supports system architecture with "plug and play" of best solver for a given region.

This new state of the art technique enables engineers to tackle and new range of problems accurately and efficiently.

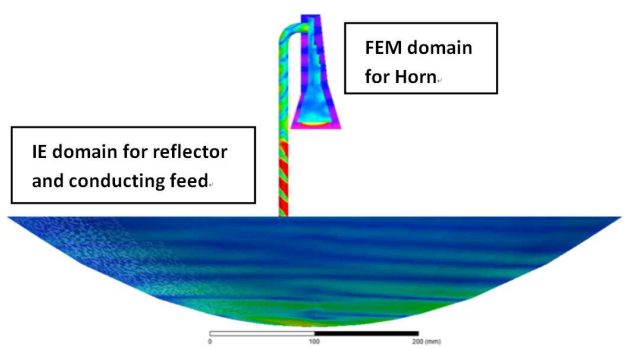

Figure 1.

HFSS with HPC for Large Finite Antenna Array Design Session

Anders Edquist and Alain Michel
ANSYS, Sweden

Abstract— The 3D Electromagnetic field solver, HFSS, is widely used in the RF/Microwave industry for simulation of a diverse range of microwave antenna structures, including smaller discrete structures such as patches, dipoles, horns etc. as well much larger scale antenna arrays. The Domain Decomposition Method (DDM) is a technique which enables a large 3D model's mesh and solution to be solved utilizing multiple cores/machines and shared memory resources (HPC). Whilst this technology can be applied to large arbitrary structures such as a reflectors or antenna in vehicle etc., large antenna arrays have unique properties related to their size and repetitive nature which are well suited to this technique. Traditionally, array designers have to rely on infinite array analysis using a unit cell approach to model large finite arrays. This approach neglects edge effects. The finite array DDM by operating on the antenna unit cell removes the need to handle repetitive detailed geometry, reduces model setup overhead and dramatically reduces time associated with meshing the structure and hence lowers overall solve time.The user specifies the unit cell by drawing it and the array mask thanks to a simple interface. This interface allows the user to define arbitrary arrangements and outlines for a repeating array (see Fig. 1). Once the unit cell is solved, the mesh from the unit cell will be imported for each cell of the array, no additional meshing is needed. Thanks to DDM, RAM is distributed across many computers/cores. All Mutual Coupling between elements are included as well as edge effect.

The finite array technology recently implemented within HFSS brings forward a robust, powerful capability for antenna array simulation, automating setup and post processing as well as offering dynamic control of elements in the array for investigating active array performance, whilst delivering an order of magnitude reduction in simulation time and resources required for the most challenging array models.

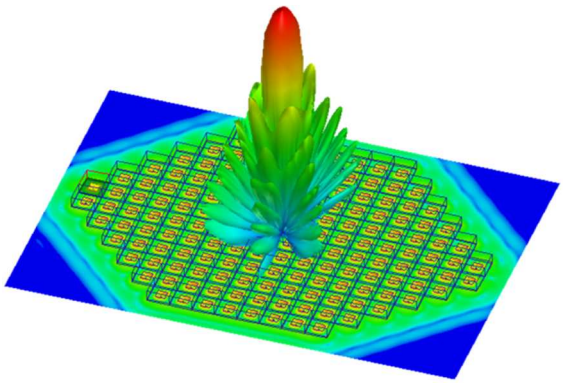

Figure 1.

Patch and Ground Plane Design of Microstrip Antennas by Material Distribution Optimization

Emadeldeen Hassan, **Eddie Wadbro**, **and Martin Berggren**
Department of Computing Science, Umeå University, Umeå SE-901 87, Sweden

Abstract— We propose a gradient-based material distribution approach to optimize the conductive parts of microstrip antennas. This kind of optimization was first developed for the design of load-carrying elastic structures [1]. The approach has been generalized to the design of various electromagnetic devices through optimization of the permittivity and permeability distributions. However, to the best of our knowledge, it is only in the article by Erentok and Sigmund [2] where the material distribution approach has been used to design conductive parts of antennas, and the design was there carried out for a single frequency only.

Our proposed approach is based on the solution of the 3D Maxwell's equation using the FDTD method. The design variables are the conductivity components on each Yee cell edge in the design domain. Given an incoming signal, the objective is to maximize the energy received by the microstrip antenna and transmitted to a coaxial cable. By the reciprocity theorem this is equivalent to minimizing the re ection coefficient of a transmitting microstrip antenna. The gradient of the objective function is based on a solution of an adjoint field problem, which is also a FDTD discretization of Maxwell's equations. The gradient is evaluated for an arbitrary number of design variables using only two FDTD simulations. The design variables are updated using the globally convergent method of moving asymptotes by Svanberg [3].

We design a microstrip antenna to operate at 1:5 GHz with 0.2 GHz bandwidth. The design process comprises two separate phases. In the first phase, the finite ground plane area is fixed to be a perfect electric conductor, and the antenna reflection coefficient is minimized by finding an optimal conductivity distribution over the patch area. In the second phase, we fix the radiating patch obtained from the first phase. Then we minimize the reflection coefficient of the antenna by optimizing the conductivity distribution over the ground plane area. After the first phase, the microstrip antenna has a reflection coefficient below -10 dB in the frequency band 1.48–1.55 GHz. After the design of the ground plane, the antenna bandwidth increase to 1.48–1.7 GHz; that is, the design of the ground plane increases the antenna bandwidth almost three times.

REFERENCES

1. Bendsøe, M. P. and O. Sigmund, *Topology Optimization: Theory, Methods and Applications,* Springer, 2003.
2. Erentok,A. and O. Sigmund, "Topology optimization of sub-wavelength antennas," *IEEE Transactions on Antennas and Propagation*, Vol. 59, No. 1, 58–69, 2011.
3. Svanberg,K., "A class of globally convergent optimization methods based on conservative convex separable approximations," *SIAM J. Optim*, Vol. 12, No. 2, 555–573, 2002.

Antenna Design for a Ground Penetrating Radar inside a Bottom Hole Assembly

Jan-Florian Höfinghoff and Ludger Overmeyer
Institute of Transport and Automation Technology, Germany

Abstract— Ground penetrating radar (GPR) is widely used as a sensing device for subsurface investigations in various applications as for example, archaeological studies, building inspection, open-cast mining and drilling. Common borehole GPR systems are integrated into a plastic housing used to investigate borehole surroundings after the drilling has taken place. However, there exists no operational GPR system implemented into the bottom hole assembly (BHA) for logging while drilling (LWD) or measurement while drilling (MWD) operations at UHF frequencies. This is mainly due to the negative influence of the metallic BHA on the antenna performance and the limited space for the integration of the necessary components.

This paper focuses on the implementation of a resistive loaded dipole antenna at 500 MHz into a BHA for GPR measurements during the drilling process. Resistive loaded antennas are widely used in ground penetrating radars, due to their good pulse radiation behavior and small size. Despite these facts their implementation into an antenna housing with absorber material and shielding leads to a quite cumbersome GPR device not suitable for integration into the limited free space of a metallic BHA. Furthermore, the metallic BHA itself influences the pulse radiation behavior of the antenna in a negative way. We therefore focused on developing an optimized antenna design that takes into account the limitations in pulse radiation due to the metallic influence. Moreover, we computed the mechanical stresses to illustrate that the antenna implementation does not inadmissibly compromise the mechanical stability of the BHA.

We firstly analyzed the anticipated antenna performance with an FEM simulation and afterwards built a prototype and compared the actual performance with the results deriving from the simulation. Moreover, we examined the developed antenna in field tests with the aid of a commercial GPR system, to prove that the antenna can operate efficiently in a practical application.

Session 1A7
Advanced Photonic Materials and Nanophtonics

X-ray Single-mode Diffraction from Si-nanowires on Silicon
Hsin-Yi Chen, Pei-Tze Chu, Shih-Lin Chang, ... 92

Exciton-polaritons in Organic-dye Nanofibers with Optical Anisotropies
Hiroyuki Takeda, Kazuaki Sakoda, ... 93

Large-area Metallic Photonic Crystals by Stacking and Rolling
Lindsey Anne Ibbotson, Jeremy J. Baumberg, ... 94

Optical Perception for Detection of Few-layer Graphenes
Yi-Sheng Wang, Jhe-Ming Yang, Ya-Ping Hsieh, Hsiang-Chen Wang, Raymond Chien-Chao Tsiang, 95

Layer Homogenization Method for Modeling Additive Color Effect in Natural Photonic Polycrystals — The Case of ***Entimus imperialis*** Weevil
Sébastien Mouchet, Jean-Pol Vigneron, Jean-François Colomer, Olivier Deparis, ... 96

Efficiency of Light Emission in Light Emitters Coupled to Surface Plasmons
Toufik Sadi, Jani Oksanen, J. Tulkki, ... 97

Optical and Plasmonic Properties of Metallic Nanostructure Arrays Grown on Optically Patterned Photochromic Thin Films
Duc Vu Anh, F. Fabbri, L. Martinelli, Y. Lassailly, K. Lahlil, J.-B. Boilot, T. Gacoin, J. Peretti, 98

Super-chiral Effects in Silicon Nano-sphere Clusters
Claudiu G. Biris, A. Al-Jarro, Nicolae C. Panoiu, ... 99

Monodisperse Silicon Colloids with Magnetic Response in the Optical Region: From Colloidal Suspensions to Photonic Crystals
Lei Shi, Justin T. Harris, Roberto Fenollosa, Isabelle Rodriguez, Xiaotang Lu, Brian A. Korgel, Francisco Meseguer, ... 100

Numerical Analysis of Grating and Prism Coupled Surface Plasmon Resonance
Sorin Miclos, Dan Savastru, Ion Lancranjan, Roxana Savastru, Constantin Opran, ... 101

X-ray Single-mode Diffraction from Si-nanowires on Silicon

Hsin-Yi Chen[1], **Pei-Tze Chu**[1], **and Shih-Lin Chang**[1,2]

[1]Department of Physics, National Tsing Hua University, Hsinchu, Taiwan
[2]National Synchrotron Radiation Research Center, Hsinchu, Taiwan

Abstract— Single-mode operation in x-ray diffraction from crystalline materials is very difficult to reach because many modes of wave propagation are simultaneously excited in crystals, thus hinders the application of single-mode x-ray diffraction in coherent x-ray optics and materials characterization. We report here a method of realizing single-mode diffraction by using singly-polarized x-rays wide angle incidence and grazing emergence diffraction from Si-nanowires and bare Si substrate. For a bare Si substrate, the surface diffracted and specular reflected beam of single-mode excitation are separated by different angular settings due to the extremely asymmetric diffraction at grazing emergence. For Si-wires on Si, single-mode diffraction is achieved by tuning the x-ray energy so as to have nearly grazing emergent reflection, or by decreasing the incident angle to both the Si-wires and Si substrate to satisfy the condition of total reflection. Dynamical theory of x-ray diffraction is employed to calculate the dispersion relation, linear absorption coefficient, excitation of mode of wave propagation, and intensity distribution. Single-mode operation can be understood from these dynamical calculations. An equation which determines the vertical component of the diffracted wavevector, Kz, as a function of photon energy and azimuth angle of rotation is derived from the diffraction geometry. It is proved that the diffraction from the Si-wires on Si is of single-mode, when the corresponding Kz is smaller or equal to zero. Synchrotron diffraction experiments also confirm this Kz relationship. This development opens up new opportunities of using crystal diffraction, in addition to optical reflection/refraction, for the design of coherent x-ray optics.

Exciton-polaritons in Organic-dye Nanofibers with Optical Anisotropies

Hiroyuki Takeda[1] **and Kazuaki Sakoda**[1,2]

[1]Photonic Materials Unit, National Institute for Materials Science (NIMS)
1-1 Namiki, Tsukuba, Ibaraki 305-0044, Japan
[2]Graduate School of Pure and Applied Science, University of Tsukuba
1-1-1 Tennodai, Tsukuba, Ibaraki 305-8571, Japan

Abstract— Recently, light propagation in organic-dye nanofibers has been experimentally observed at room temperature [1, 2]. However, this light propagation is very different from that in conventional dielectric waveguides. For example, leakage of light can be neglected even in sharply bent nanofibers with a radius of curvature less than 10 microns [3]. Moreover, group refractive indices exceed 10 [4], although in organic materials they are at most $n = 1.4 - 1.7$. The group refractive index is defined by $n_g = c/v_g$, where c is the speed of light in free space and v_g is the group velocity.

These properties result from exciton polaritons, which are the coupling of photons and excitons. In the interaction of photons and excitons, while two dispersion curves of lower and upper branches appear, a polariton gap appears between them. In the lower branch, a speed of light becomes slower near an exciton excitation energy. These properties are well known in isotropic bulk exciton polaritons.

Frenkel excitons in organic materials exist stably even at room temperature. However, since in organic-dye nanofibers transition dipole moments are uniformly oriented at a certain angle, exciton-polariton mediated light propagation strongly depends on optical anisotropies [5]. Assuming organic-dye films on glass substrates, we first calculate dispersion curves and light propagation by the plane wave expansion and finite-difference time-domain methods, respectively. We investigate the dependence of exciton polaritons on optical anisotropies. Group refractive indices can be estimated by both dispersion curves and Fabry-Perot peaks in light propagation. Results derived from these two methods coincide well. In organic-dye nanofibers on glass substrates, next, we calculate dispersion curves, and compare group refractive indices derived from the dispersion curves with those observed experimentally. We show that our theoretical model can successfully explain experimental results.

REFERENCES

1. Takazawa, K., "Waveguiding properties of fiber-shaped aggregates self-assembled from thiacyanine dye molecules," *J. Phys. Chem. C*, Vol. 111, No. 24, 8671–8676, 2007.
2. Takazawa, K., "Micron-sized rings self-assembled from thiacyanine dye molecules and their waveguiding properties," *Chem. Mat.*, Vol. 19, No. 22, 5293–5301, 2007.
3. Takazawa, K., "Flexibility and bending loss of waveguiding molecular fibers self-assembled from thiacyanine dye," *Chem. Phys. Lett.*, Vol. 452, Nos. 1–3, 168–172, 2008.
4. Takazawa, K., J. Inoue, K. Mitsuishi, and T. Takamasu, "Fraction of a millimeter propagation of exciton polaritons in photoexcited nanofibers of organic dye," *Phys. Rev. Lett.*, Vol. 105, No. 6, 067401, 2010.
5. Takeda, H. and K. Sakoda, "Exciton-polariton mediated light propagation in anisotropic waveguides," *Phys. Rev. B*, Vol. 86, No. 1, 205319, 2012.

Large-area Metallic Photonic Crystals by Stacking and Rolling

L. A. Ibbotson and J. J. Baumberg
NanoPhotonics Centre, Department of Physics, University of Cambridge, UK

Abstract— We present a promising new fabrication method capable of producing woodpile metallic photonic crystals over large areas. Nanopatterned metallo-polymeric thin films are stacked and rolled to produce flexible nanostructures with novel optical properties. This technique is cheap with a high-throughput, providing a scalable method for producing bulk three-dimensional (3D) photonic crystals.

The optical bandgaps of photonic crystals offer unique control over photon transport and energy selection, and rapid advances in nanofabrication have enabled the manufacture of 3D crystals with complete bandgaps at optical wavelengths [1, 2]. However the traditional lithographic methods of two-photon laser writing, ion beam milling and electron-beam lithography severely limit their overall volume due to high cost and low-throughput. Our technique for making metallic woodpile photonic crystals produces large-area polymer films spanned by gold nanowires with excellent uniformity that are stacked and rolled to produce a truly volumetric 3D photonic crystal (Figure 1(a)) [3].

Large-area polymer films are nanoimprinted with a grating profile upon which metallic wires are created by glancing angle deposition. These thin-film wire gratings are then captured onto a water surface where they can be stacked onto a substrate at customized orientations (Figure 1(b)) or rolled onto a rod. Rolling up a single film or series of stacked films is an efficient and easy way of building up a 3D structure with excellent layer uniformity. In addition these metallo-dielectric films can be induced to roll up spontaneously under selected conditions, demonstrating a promising new method of assembly (Figure 1(c)). The flexibility of the polymer films allows neighbouring layers to automatically align as the textures of the two films lock together, harnessing self-alignment for large scale nanoassembly. Preliminary optical measurements indicate that the structures are appropriate for use at optical wavelengths.

These metal-polymer photonic crystals are flexible and deformable, and so can be elastically tuned and used in arbitrarily curved geometries unlike conventional hard photonic crystals. This is the first demonstration of such a general and scalable approach towards producing truly bulk 3D optical metamaterials and will stimulate a wide range of work among broad scientific communities.

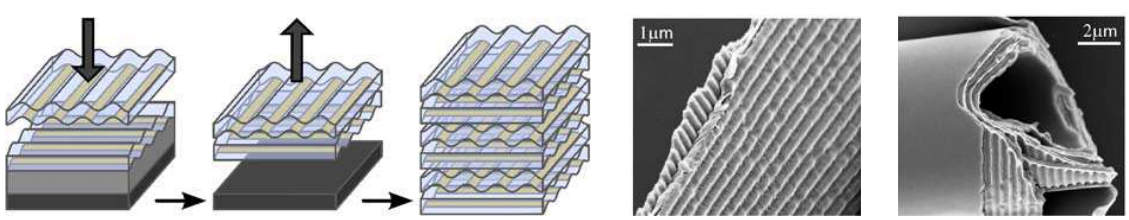

(a) (b) (c)

Figure 1: (a) Schematic of stacking films into a woodpile photonic crystal, (b) image from scanning electron microscopy of a bilayer with wires in perpendicular orientations and (c) a thin-film wire grating self-assembled into a 10 micron roll.

REFERENCES

1. Vasilantonakis, N., et al., *Adv. Mater.*, Vol. 24, No. 8, 1101–1105, 2012.
2. Tandaechanurat, A., et al., *Nature Photonics*, Vol. 5, 91–94, 2011.
3. Ibbotson, L. A. and J. J. Baumberg, *Nanotechnology*, 2013 (submitted).

Optical Perception for Detection of Few-layer Graphenes

Yi-Sheng Wang[1,2], **Jhe-Ming Yang**[1,2], **Ya-Ping Hsieh**[1,2], **Hsiang-Chen Wang**[1,2], **and Raymond Chien-Chao Tsiang**[3]

[1]Graduate Institute of Opto-Mechatronics, National Chung Cheng University
168, University Rd., Min-Hsiung, Chia-Yi 62102, Taiwan
[2]Advanced Institute for Manufacturing with High-tech Innovations (AIM-HI)
National Chung Cheng University, 168, University Rd., Min-Hsiung, Chia-Yi 62102, Taiwan
[3]Department of Chemical Engineering, National Chung Cheng University
168, University Rd., Min-Hsiung, Chia-Yi 62102, Taiwan

Abstract— Graphene has emerged to be an exciting material with potential applications. A remarkable feature of graphene is that it is a Dirac solid, with the electron energy being linearly dependent on the wave vector near the crossing points in the Brillouin zone. It also exhibits unusual fractional quantum Hall effect and conductivity behavior. The discovery of the fascinating properties of single-layer graphene has generated much interest in the physical and materials sciences. To distinguish graphene layers become a very important issue. Using the discriminant for each location of the RGB pixel, then calculate the colors of the graphene layers; it can distinguish the different layers of the image thought multi-spectral imaging technology. Therefore this method can save time for material characteristics measurements, such as Raman, TEM, and AFM. We quickly determine the layers of graphene samples from a microscope image.

Layer Homogenization Method for Modeling Additive Color Effect in Natural Photonic Polycrystals — The Case of *Entimus imperialis* Weevil

Sébastien Mouchet, Jean-Pol Vigneron, Jean-François Colomer, and Olivier Deparis
Department of Physics, University of Namur, 61 rue de Bruxelles, B-5000 Namur, Belgium

Abstract— Modeling the optical properties of photonic polycrystals is crucial for the investigation of photonic structures as well as for the design and fabrication of bioinspired devices [1, 2]. In this kind of approach, the calculation of the reflectance of photonic crystals having form anisotropic elements in the crystal unit cell, such as cylinders or parallelepipeds, often turns out to be problematic, especially when the reflectance spectrum has to be computed according to different crystal orientations as in polycrystals. The original method we propose here solves this problem in the specific case of a photonic crystal whose periodicity is such that it does not diffract the incident light [3]. A single crystal grain is first considered. For a given crystal orientation, the grain is sliced into layers and the periodic spatial variations of the dielectric function ε within each layer are homogenized. Thanks to that homogenization method, the calculation of the reflectance of a single grain in arbitrary orientation can be performed using standard thin film computation code, which considerably reduces the computation time. In a second step, the method takes into account the disorder in the crystal orientation of the photonic polycrystal by averaging reflectance spectra calculated for different crystal orientations and incidence angles.

We demonstrated the usefulness of our method by applying it to the study of a natural photonic polycrystal. Polycrystals found in living organisms are known to give rise to multiscale visual effect such as additive color effects. A nice example was found in cavities on the cuticle of the Brazilian weevil *Entimus imperialis* (Curculionidae). It is a remarkable example of additive color effect caused by photonic crystal grains [2, 4]. Although each photonic crystal grain produces a single bright iridescent color ranging from blue to orange, the orientation disorder gives rise to a non-iridescent green matt coloration perceived by the human eye (Fig. 1). This photonic structure is relevant for developing bioinspired applications. For instance, it has been recently replicated by Van Opdenbosch et al. in order to serve as biomimetic devices such as gas, temperature or pH sensors [5].

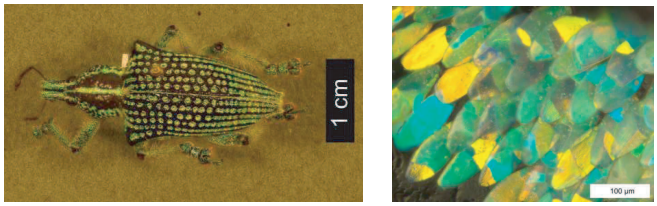

Figure 1: Additive color effect in the polycrystal grains of *Entimus imperialis* reflecting individual bright colors leads to a matt green coloration when observed in the far-field.

REFERENCES

1. Vigneron, J.-P. and V. Lousse, "Variation of a photonic crystal color with the Miller indices of the exposed surface," *Proc. SPIE*, Vol. 6128, 61281G, 2006.
2. Deparis, O. and J.-P. Vigneron, "Modeling the photonic response of biological nanostructures using the concept of stratified medium: The case of a natural three-dimensional photonic crystal," *Mater. Sci. Eng. B-Adv.*, Vol. 169, 12–15, 2010.
3. Mouchet, S., J.-F. Colomer, C. Vandenbem, O. Deparis, and J.-P. Vigneron, "Method for modeling additive color effect in photonic polycrystals with form anisotropic elements: The case of *Entimus imperialis* weevil," *Opt. Express*, submitted.
4. Mouchet, S., J.-P. Vigneron, J.-F. Colomer, C. Vandenbem, and O. Deparis, "Additive photonic colors in the Brazilian diamond weevil, *Entimus imperialis*," *Proc. SPIE*, Vol. 8480, 848003, 2012.
5. Van Opdenbosch, D., M. Johannes, X. Wu, H. Fabritius, and C. Zollfrank, "Fabrication of three-dimensional photonic crystals with tunable photonic properties by biotemplating," *Photonics Nanostruct.*, Vol. 10, 516–522, 2012.

Efficiency of Light Emission in Light Emitters Coupled to Surface Plasmons

T. Sadi, J. Oksanen, and J. Tulkki
Department of Biomedical Engineering and Computational Sciences
Aalto University, P. O. Box 12200, Aalto FI-00076, Finland

Abstract— Surface plasmons (SPs) have recently gained much attention due to their sub-wavelength localization and strong interactions in the near-field. These unique properties are expected to be essential in enhancing the light-matter interaction strength in next-generation photonic nanostructures such as new LEDs, solar cells, sub-wavelength microscopes and other miniaturized photonic devices. However, quantitative theoretical analysis, insight and optimization of the enhancement are challenging due to computational complexity and lack of simple analytical tools to evaluate the field profiles in structures incorporating a variety of lossy material layers and scattering elements.

We present a newly developed rigorous and transparent method suitable for modeling the fields and energy transfer in grated multi-layer structures. The method is based on a Green's function approach to solving Maxwell's equations and the fluctuational electrodynamics description of light emission [1]. The Green's function approach to fluctuational electrodynamics (GFED) has several benefits over other well-established numerical and coupled modes based analysis. For instance, it allows fairly accurate and relatively simple analytical approximations that inherently account for the plasmon and other optical losses. This feature makes the approach very appealing for estimating the effect of the plasmonic interactions on the overall efficiency of light emission in plasmonic-enhanced LEDs.

Two techniques are implemented within the Green's function framework to solve Maxwell's equations. The first technique uses analytical approximations involving the evaluation of the intensity of the optical modes present in the grated structure. The second technique involves a more accurate fully-numerical solution for the fields [1]. The properties of these techniques are compared to establish the validity limits of the analytical solutions. The solutions are used to evaluate the directional reflectivity and luminescence spectra of gallium nitride based LED structures incorporating metallic gratings [2], and to estimate the efficiency of light emission in these structures. The results enable substantial new quantitative insight into the properties of surface plasmons, luminescence enhancement and in particular the losses related to the plasmonic interactions in technologically interesting GaN structures.

REFERENCES

1. Sadi, T., J. Oksanen, P. Mattila, J. Bellessa, and J. Tulkki, "The Green's function description of emission enhancement in grated LED structures," *J. Selected Topics in Quantum Electronics*, 2013, Accepted.
2. Homeyer, E., P. Mattila, J. Oksanen, T. Sadi, H. Nykänen, S. Suihkonen, C. Symonds, J. Tulkki, F. Tuomisto, M. Sopanen, and J. Bellessa, "Enhanced light extraction from InGaN/GaN quantum wells with silver gratings," *Appl. Phys. Lett.*, Vol. 102, 081110, 2013.

Optical and Plasmonic Properties of Metallic Nanostructure Arrays Grown on Optically Patterned Photochromic Thin Films

D. Vu Anh, **F. Fabbri**, **L. Martinelli**, **Y. Lassailly**, **K. Lahlil**,
J.-P. Boilot, **T. Gacoin**, **and J. Peretti**
Laboratoire de Physique de la Matière Condensée, Ecole Polytechnique, CNRS, Palaiseau 91128, France

Abstract— Photochromic materials containing azobenzene derivatives exhibit spectacular photomechanical properties which allow to produce surface relieves upon illumination in the chromophore visible absorption band [1]. Size and shape of the photo-induced relief pattern can be tailored over a large scale ranging from a few tens of nanometers up to several microns by controlling the projected optical pattern [2]. These photochromic materials can be used as a photoactive substrate or as a template for the elaboration of metal/dielectric hybrid structures whose properties can be tuned and controlled by the geometrical characteristics of the subjacent patterned substrate.

We have used this approach to elaborate 2D arrays of noble metal nanostructures. As shown in Figs. 1(a)–1(c), combining holographic patterning of the photochromic film with directional metal deposition, various periodic patterns can be elaborated over large area. Such periodic noble metal patterns exhibit specific optical and plasmonic properties that we have investigated. In particular, we have directly obtained the dispersion relation of surface plasmons by measuring the optical reflection spectrum of the patterned thin film as a function of the incident angle under illumination through a total reflection prism. As the coupling of surface plasmons with light can be mediated by the 2D periodic pattern [3], different modes are observed which correspond to surface plasmons propagating in opposite directions and at both the metal/air and substrate/metal interfaces. At the intersection points of the different mode dispersion relations, plasmonic band gap opening is observed [4]. Some of these show intriguing features. The dispersion diagram of surface plasmons for plasmonic crystals of different geometrical parameters will be presented and discussed.

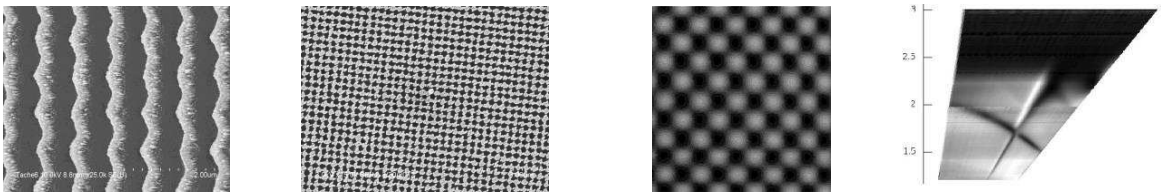

(a) (b) (c) (d)

Figure 1: (a) MEB image of single face gold coated azo-polymer arrays of 832 nm period. Gold is evaporated at grazing incidence. (b) MEB image of single face gold coated azo-polymer arrays of 250 nm period. Gold is evaporated at grazing incidence. (c) 2 µm × 2 µm shear force topography image of gold-coated surface relief grating of 250 nm period. Gold is evaporated at normal incidence. (d) Dispersion relation of surface plasmon modes measured on the patterned gold layers shown in (c).

Super-chiral Effects in Silicon Nano-sphere Clusters

C. G. Biris[1], **A. Al-Jarro**[2], **and N. C. Panoiu**[2]

[1]High Performance Computing Centre, West University of Timisoara, Romania
[2]Department of Electronic and Electrical Engineering
University College London, Torrington Place, London WC1E 7JE, United Kingdom

Abstract— We demonstrate that the scattered optical field of photonic nanostructures with intrinsic chirality, which are made of silicon spheres, exhibits strong optical chirality as well as enhanced circular differential scattering. In addition, our analysis shows that using such resonant chiral nanostructures allows one to easily achieve super-chiral optical fields whose optical chirality is more than two orders of magnitude larger than that of circularly polarized plane waves.

Plasmonic nano-scale structures that exhibit strong optical chirality have shown great potential in the design of ultra-compact optical devices due to their strong interaction with light [1]. We show in this work that one can use all-dielectric (silicon) nanostructures made of coupled resonators to achieve super-chiral optical fields, namely fields whose optical chirality is larger than that of circularly polarized plane waves. This enhanced optical chirality is achieved by arranging in a chiral pattern spheres made of silicon and tuning the frequency of the incident light to one of the optical resonances of the spheres. We use in our computational analysis a numerical approach based on a 3D implementation of the multiple scattering theory [2, 3].

The nano-cluster consists of Si spheres with radius $R = 230\,\text{nm}$, arranged in a chiral pattern. The cluster is excited by a circularly polarized plane wave with wavelength, $\lambda = 920\,\text{nm}$, which is chosen to coincide with one of the optical resonances (TE mode) of the spheres. The optical resonances are determined by computing the spectrum of the field enhancement at an arbitrary position near one of the spheres, as indicated in Figure 1. The chirality of the optical field, C, can be calculated once the field distribution is known [1]. For super-chiral fields, $|C| > 1$. Our analysis shows that the chirality of the optical field is strongly enhanced at the resonance wavelength when the cluster is perpendicularly illuminated by circularly polarized plane waves, the field being highly super-chiral in large domains. In particular, more than two orders of magnitude enhancement of the chirality is observed. Importantly, the chirality of the optical near-field also indicates a strong circular differential scattering of the chiral cluster we investigated.

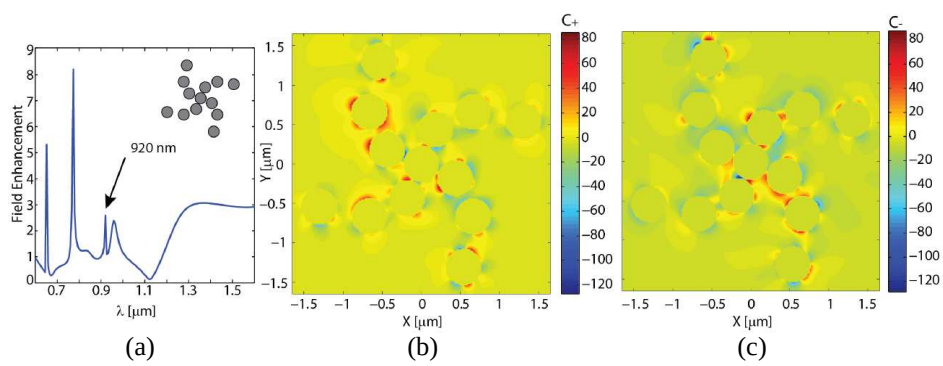

Figure 1: (a) Spectrum of the field enhancement and optical chirality of the scattered field of a chiral nano-sphere cluster for (b) C_+, and (c) C_-, circularly polarized light.

REFERENCES

1. Schaferling, M., D. Dregely, M. Hentschel, and H. Giessen, "Tailoring enhanced optical chirality: Design principles for chiral plasmonic nanostructures," *Phys. Rev. X*, Vol. 2, 031010, 2012.
2. Biris, C. G. and N. C. Panoiu, "Second harmonic generation in metamaterials based on homogeneous centrosymmetric nanowires," *Phys. Rev. B*, Vol. 81, 195102, 2010.
3. Mishchenko, M. I., L. D. Travis, and D. W. Mackowski, "T-matrix computations of light scattering by nonspherical particles: A review," *J. Quant. Spetrosc. Transfer*, Vol. 55, No. 5, 535–575, 1996.

Monodisperse Silicon Colloids with Magnetic Response in the Optical Region: From Colloidal Suspensions to Photonic Crystals

Lei Shi[1,3,4], **Justin T. Harris**[2], **Roberto Fenollosa**[1,3], **Isabelle Rodriguez**[1,3], **Xiaotang Lu**[2], **Brian A. Korgel**[2], **and Francisco Meseguer**[1,3]

[1]Centro de Tecnologias Fisicas, Unidad Asociada ICMM/CSIC-UPV
Universidad Politecnica de Valencia, Av. Los Naranjos s/n, Valencia 46022, Spain
[2]Department of Chemical Engineering, Texas Materials Institute
Center for Nano- and Molecular Science and Technolog
The University of Texas at Austin, Austin, Texas 78712, United States
[3]Instituto de Ciencia de Materiales de Madrid CSIC, Madrid 28049, Spain
[4]Department of Applied Physics, Aalto University, FI-00076, Finland

Abstract— Magnetic component, an indispensable part of electromagnetic wave, generally plays a negligible role in light matter interaction, because of the nonmagnatism nature of normal materials at optical frequency. The disclosure of metamaterials with strong magnetic response has broken this traditional concept. Fascinating new phenomena and applications, such as negative refraction, perfect lenses and even optical cloaking are realized. Although, from fundamental research point of view, metamaterials have already shown their distinctive ability of controlling light, two serious problems which prevent the usage of metamaterials in future applications still haven't been solved. One limitation comes from the intrinsic losses of metamaterials. The other limitation comes from the difficulties of the fabrication of large area two dimensional or three dimensional metamaterials which work in the near infrared and visible region.

In this presentation, we report that full dielectric silicon colloids could be used to solve these two limitations. Here, monodispersed high refractive index silicon colloids are firstly fabricated through 1) the decomposition of trisilane in organic solvent and 2) vacuum annealing processes. The experiment and the Mie theory results clearly show that not only the obtained single silicon colloid but also silicon colloids liquid suspension has strong magnetic response with low loss in the near infrared region. In addition, the first experimental results of a bottom up approach for developing a two dimensional silicon colloidal crystal with magnetic response will be reported. Furthermore, based on those "optical magnetism" silicon colloids, related applications concerning magnetic type optical forces are discussed. In conclusion, these results clearly indicate that the monodispersed silicon colloids could be a new building block for metamaterials applications and be easily applied to fabricate low loss two or three dimensional metamaterials.

REFERENCES

1. Shi, L., J. Harris, R. Fenollosa, I. Rodriguez, X. Lu, B. Korgel, and F. Meseguer, "Monodisperse silicon nanocavities and photonic crystals with magnetic response in the optical region," *Nat. Commun.*, accepted and to be published.
2. Shi, L., T. U. Tuzer, R. Fenollosa, and F. Meseguer, "A new dielectric metamaterial building block with a strong magnetic response below 1.5 micrometers region. Silicon colloids nanocavities," *Adv. Mater.*, Vol. 20, 5934–5938, 2012.
3. Shi, L., E. Xifre-Perez, F. J. Garcia de Abajo, and F. Meseguer, "Looking through the mirror: Optical microcavity-mirror image photonic interaction," *Opt. Express*, Vol. 20, 11247–11255, 2012.
4. Shi, L. and F. Meseguer, "Magnetic interaction in all silicon waveguide spherical coupler device," *Opt. Express*, Vol. 20, 22617–22626, 2012.

Numerical Analysis of Grating and Prism Coupled Surface Plasmon Resonance

Sorin Miclos[1], **Dan Savastru**[1], **Ion Lancranjan**[1], **Roxana Savastru**[1], **and Constantin Opran**[2]

[1]National Institute of R&D for Optoelectronics — INOE 2000
409 Atomistilor St., Magurele, Ilfov RO-077125, Romania
[2]Politehnica University of Bucharest, 313 Splaiul Independentei Ave., Bucharest, Romania

Abstract— The main purpose of the paper consists of presenting simulation results obtained in analyzing the surface plasmons excitation effect, presently commonly referred as surface plasmon resonance (SPR) and its main possible application as a highly accurate and sensitive sensor. Both electromagnetic wave coupling configurations to the medium, grating and Kretschmann prism configurations are investigated. In the grating coupling configuration, the performed numerical simulations are pointing mainly to nanowire and/or nanostructured gratings. The numerically simulation model developed in the case of the grating coupling configuration consider Cu, Au, Ag or other metal nanowire having a diameter of 40 nm to 800 nm, formed on dielectric substrates with a refractive index between 1.4 and 2.4, such as SF11, BK7 glasses, GaP and TiO2-o (rutile). The same range of dielectric materials is considered for the prism coupling configuration. The thin layers formed on the face of prism coupler is considered as being formed by up to 15 Cu, Au, Ag or other metal layers. Several shapes of the groves formed onto the high refractive index substrate are investigated, such as square/rectangular (including the rounded corner case), circular or elliptical. As the low-index background material air, water and sea-water were considered.

In order to get more insight into the plane electromagnetic wave propagation in such waveguides a simulation procedure is developed on the basis of the Finite Element and Finite Difference Time Domain methods and a finite element Helmholtz solver. For practical applications, it is of interest to evaluate how much electromagnetic radiation can be coupled into the medium. Therefore, the coupling coefficient of electromagnetic radiation from and into the medium using the grating and Kretschmann prism coupling configurations has been examined.

Session 1A8
SC5: Inverse Scattering Problems: Theory and Applications

Determination of the Optimal Value of the Radius of a Circular Cylindrical Post in a Rectangular Waveguide for Measurement of the Dielectric Permittivity
Roman Kushnin, Janis Semenjako, ... 104

Perturbation Approach to Boundary Reconstruction in a Multiple Waveguide Model
Martin Karl Norgren, ... 105

Successive Estimation Method for Microwave Tomography
Zhi Qi Meng, ... 106

Reconstruction of a Stratified Slab Using Time Reversal and Equivalent Fields
Takashi Takenaka, Toshifumi Moriyama, Toshiyuki Tanaka, ... 107

Explicit Regularization Method for Reconstructing Permittivity Distributions
Melike Erdogan, Mehmet Cayoren, Mehmet Abbak, Ibrahim Akduman, ... 108

Efficient Imaging of 3D Objects Located in a Layered Media with Rough Interfaces
Tolga Ulas Gurbuz, Birol Aslanyurek, Ibrahim Akduman, ... 109

Image Appraisal of Full Waveform Inverted GPR Data
Giovanni Meles, Stewart Greenhalgh, Hansruedi Maurer, Alan Green, ... 110

Microwave Detection of Specific Dielectric Targets behind Concrete Walls
Sinem Avci, O. Guren, Mehmet Cayoren, Ibrahim Akduman, ... 111

Permittivity Imaging by Addressable Defect of Surface-wave Structure on Two-dimensional Metamaterial in Millimeter-wave Range
Osamu Sakai, Go Itami, Tomohide Akiyama, Yoshinori Harada, ... 112

Guaranteed Estimates of Linear Continuous Functionals of Solutions and Right-hand Sides of the Helmholtz Equation in the Domains with Infinite Boundaries under Uncertainties
Yury Podlipenko, Yury V. Shestopalov, ... 113

Feasibility Study of Passive Bistatic Synthetic Aperture Radar for Imaging Small Objects
Motoyuki Sato, Takafumi Kitajyo, Kazunori Takahashi, ... 114

Determination of the Optimal Value of the Radius of a Circular Cylindrical Post in a Rectangular Waveguide for Measurement of the Dielectric Permittivity

Roman Kushnin and Janis Semenjako
Riga Technical University, Riga, Latvia

Abstract— This paper is inspired by a recently published paper, in which a very useful method for determination of the optimal radius of a dielectric post in a cylindrical metallic waveguide for measurement of the dielectric permittivity has been proposed. In this paper we propose an approach for determination of the optimal value of the radius of a circular cylindrical post in a rectangular waveguide, that is, such a value of the radius of the post at which measurement uncertainty takes minimum value. To accomplish this task, we employ the Monte Carlo method, as suggested in the GUM Supplement 1. This task requires a lot of computation time, since the Monte Carlo method requires a very large number of trials in order for estimation of the measurement uncertainty to be reliable and because each of these trials, in turn, requires solution of the inverse scattering problem, that in our case is being solved by iteratively minimizing the distance between simulated and measurement data. In order to accomplish this task in a reasonable amount of time, we need a very fast approach for solving the direct scattering problem, since the computation time required to solve the inverse scattering problem is proportional to that required by an algorithm for solving the corresponding direct scattering problem. Over the last several decades, there have been a number of approaches that have been proposed by various authors for solving the direct problem of scattering by a cylindrical post in a rectangular waveguide. All these approaches take the advantage of uniformity of both the magnetic and electric field components and the geometrical and electrical properties of the post in the direction that coincides with that of the electric field component of the dominant waveguide mode. This property allows one to carry out the analysis of the problem in two dimensions. Also, these approaches allow one to solve some part of the problem, where possible, analytically and the remaining part of the problem by numerical techniques that leads to significant reduction in the amount of computation time. From these approaches we have chosen one that provides reasonably accurate results and at the same time shows rapid convergence. For uncertainty estimation, we take into account measurement uncertainties contributed by imperfect measurements of the post radius, frequency and scattering data. Probability distributions for the mentioned quantities are assigned according to the principle of maximum entropy. In this paper two different measurement methods are considered. One of these methods is to measure scattering data at two different frequencies and the second method is to measure scattering data at two different positions of a movable short-circuit. Results obtained for both these methods and for both lossless and lossy posts are presented. Also, one of the aims of this paper is to ascertain whether the GUM framework is valid for the problem considered in this paper.

Perturbation Approach to Boundary Reconstruction in a Multiple Waveguide Model

M. Norgren
KTH Royal Institute of Technology, Sweden

Abstract— In electrical power transformers, local deformations of the windings increase the risk of failures, which may cause power outages. Hence, it is of interest to develop methods for detecting the onset of winding deformations, and in particular online methods that can be applied on transformers in operation. Recently, we have started to investigate a principle of positioning microwave antennas inside the transformer tank and use the microwave fields to reconstruct the shape of the windings.

With the purpose of detecting the onset of deformations, we are mainly interested in small deformations that can be analysed using methods for weak scattering. In an earlier work we have considered a simplistic parallel plate PEC waveguide model in which one of the plates approximates the surface of a transformer winding. The inverse problem of reconstructing deformations in the plate is solved by applying a first order perturbation method to the scattering problem.

In this work, we consider an extended model in which the two surfaces of a parallel plate waveguide approximate the iron core and the tank wall, respectively. In a section between these outer boundaries, we place parallelled thick PEC plates, modelling a layer winding with multiple layers. The frequencies are chosen such that in the spacings between the layers only TEM-modes propagate. On each side of the multilayered structure, we have empty regions in which the excitation and measurement antennas are supposed to be located. Hence, we have in these regions a more complicated situation with a multitude of propagating waveguide modes.

The forward scattering problem is solved in two steps. First, in each spacing between two winding layers (or between a layer and the wall/core), the TEM-mode scattering due to boundary deformations is solved by transmission line theory. Secondly, using the mode matching method, the fields in the spacings are connected to the fields in the surrounding regions, in which way the total scattering matrix is obtained.

For the inverse problem, the two-step procedure is applied in reversed order. We assume that in the measurement regions, we have a least as many propagating modes as the number of layer spacings. Hence, it is straight forward to invert the mode mode matching matrices, to de-embed the spacings from the measurement regions. In the final step, each spacing is handled separately as a parallel plate waveguide. The boundary deformations are reconstructed using a first order perturbation method applied to the reflection coefficients of the dominant TEM-mode. To handle the illposedness, we use the L-curve criterion to determine the appropriate regularization parameters. Reconstruction results are presented and influences from noisy data and model deficiencies are demonstrated.

Successive Estimation Method for Microwave Tomography

Zhiqi Meng
Department of Electrical Engineering, Fukuoka University, Fukuka, Fukuoka 814-0180, Japan

Abstract— Inverse scattering problem is one of the hot topics in fields of measuring, non-destructive inspection, biopsy, and so on. One of the common methods for solving inverse scattering problem is to formulate the problem as an optimization problem. In that case, usually there are many local minima in the search space because of the problem's complexity, and how to avoid the optimization algorithm to be trapped in local optima becomes a bottleneck to get true solution.

In this paper, we consider a microwave tomography for concrete diagnosis in 1D and 2D cases: radiating a pulse wave to a concrete body, measuring the scattered wave by a receiver antenna and estimating the distributions of permittivity $\varepsilon(x, y)$ and conductivity $\sigma(x, y)$ of the concrete body. A Finite-Difference Time Domain method (FDTD) is employed to analyze the scattered wave where $\varepsilon(x, y)$ and $\sigma(x, y)$ are known (direct problem). The inverse problem to estimate ε, σ of all Yee-cells in FDTD with information of the scattered wave is formulated as an optimization problem. Usually, the number of Yee-cells is very large, and optimizing a problem with a very large number of dimensions is difficult. Here we try to use the information more efficiently. Note that the timing of incident wave arrives at a cell may be different with that at another cell, and the scattered wave received by the receiver may be just from a part of cells in the early stages of measurement. We divided the time domain of measured signal of scattered wave into several time slots, one for estimating ε, σ of the cells in a sub-area the wave scattered from which is received by the receiver by that time. As a result, the number of dimensions of the "sub-optimization" can be reduced, and the optimization algorithm may avoid local minima. The objective variables are estimated step by step while the measurement time for scattered wave becomes longer and longer, and the solution in one step is used as an initial value in next step.

The numerical results of the "Successive Estimation Method" (SEM) mentioned above are compared with the traditional method by which all the objective variables in the diagnosis area are estimated with all measured information of scattered wave from begin to end at once. In either 1D or 2D case, the simulation experiments indicate the superiority of SEM.

Reconstruction of a Stratified Slab Using Time Reversal and Equivalent Fields

Takashi Takenaka, Toshifumi Moriyama, and Toshiyuki Tanaka
Graduate School of Engineering, Nagasaki University
1-14 Bunkyo-Machi, Nagasaki 852-8521, Japan

Abstract— There are a variety of applications for which it would be useful to know the distribution of material properties inside a given volume. As inverse scattering analysis provides techniques which visualize electrical property distribution of a domain of interest without destroying or damaging it, much research has been carried out in a lot of inverse scattering problems such as medical imaging, nondestructive testing and subsurface exploration. Electrical properties are reconstructed from measurements of the total fields on an observation surface enclosing the domain of interest after successively illuminating it by incident fields. Most inverse scattering methods, especially based on integral equations, assume knowledge of incident fields in the domain of interset. In [1], reconstruction was performed only from measured total field data. Using the field equivalence principle, we have proposed an alternative inversion method without knowledge of incident fields [2]. The method requires measurements of both electric and magnetic fields as in the reference [1]. Time reversal (TR) imaging has also been attracting much interest since it can achieve super-resolution and imaging a small scatterer in random media. Until recently, TR imaging techniques have mostly focused on detection and localization of point-like or small objects. We have presented a TR method which reconstruct image of inhomogeneous objects [3].

In this paper, a new inversion approach to reconstruction of the electrical parameter distributions of an object is introduced using time reversal and an equivalent problem. A key feature is that the proposed approach assumes no prior knowledge of the incident field illuminating the object and measurement of only the total electric field on an observation surface provides reconstruction of its electrical property distributions. For the sake of simplicity, we focus on a one-dimensional case, i.e., imaging of a stratified slab. The slab is irradiated by an electromagnetic short pulse. A part of the pulse is reflected and the other part is transmitted. The total electric field is measured at two points located in different sides of the slab. Only the collected data are used to reconstruct the electrical parameter distributions of the slab. We set up a problem equivalent to the original one in the interior region Ω bounded by two observation points. If the estimated slab is different from the original one, the electromagnetic field of the equivalent problem and the time reversed field are different from each other. A cost functional that expresses the misfit between the equivalent field and the time reversed field in the region Ω is introduced. Some numerical simulations were performed using a genetic algorithm for minimization of the functional and the results indicate the effectiveness of the proposed method.

REFERENCES

1. Gustafsson, M. and S. He, "An optimization approach to two-dimensional time domain electromagnetic inverse problems," *Radio Sci.*, Vol. 35, 525–536, Jan. 2000.
2. Takenaka, T. and T. Moriyama, "Inverse scatterimg approach based on the field equivalence principle: Inversion without a priori information on incident fields," *Optics Letters*, Vol. 37, 3432–3434, Aug. 2012.
3. Moriyama, T., T. Tanaka, and T. Takenaka, "Time reversal imaging without information of incident field," *Proc. of URSI-EMTS*, Hiroshima, Japan, May 2013, accepted.

Explicit Regularization Method for Reconstructing Permittivity Distributions

M. Erdoğan, M. Çayören, M. Abbak, and I. Akduman
Electrical and Electronics Faculty, Istanbul Technical University, Istanbul, Turkey

Abstract— Reconstructing the permittivity distribution of an object from the scattered electric field is a well-known inverse problem that is encountered in various domains such as measurement science, medical imaging or dielectric spectroscopy. Since the scattering of electromagnetic waves is a volumetric interaction, the dielectric reconstruction problem requires inverting two volumetric integral equations which are called the object and the data equations. Well known methods such as Distorted Born Iterative (DBIM) [1] and Contrast Source Inversion (CSI) [2] handle this inversion as an optimization problem where the dielectric distribution minimizes the difference between the measured and the calculated field values. This inversion is a highly non-linear, ill-posed problem thus some form of regularization procedure is needed. However, most methods handle regularization implicitly in an iterative manner.

We discuss the possibility of using explicit regularization in the inversion procedure. Instead of minimizing a cost functional that merges both integral equations as in CSI, we decompose the method into two parts: one is ill-posed and the other part is non-linear but well-posed. The main contribution of our works is on the ill-posed part where we presented a different regularization approach where a set of regularization parameters are used for inverting the data equation in Tikhonov sense. Instead of using a single regularization parameter which may not be enough for objects whose electrical dimensions are large, we modified the regularization parameters according to the distance between the source and observer positions. As the overall quality of the reconstruction is critically dependent on selected regularization parameters, we define a general guideline for choosing optimal regularization parameters through Morozov's discrepancy principle [3]. Preliminary results indicate the feasibility of the approach.

REFERENCES

1. Chew, W. and Y. Wang, "Reconstruction of two-dimensional permittivity distribution using the distorted born iterative method," *IEEE Trans. Med. Imag.*, Vol. 9, No. 2, 218–225, 1990.
2. Van den Berg, P. M. and R. E. Kleinman, "A contrast source inversion method," *Inverse Problems*, Vol. 13, No. 6, 1607, 1997.
3. Colton, D. and R. Kress, *Inverse Acoustic and Electromagnetic Scattering Theory*, Springer, 1998.

Efficient Imaging of 3D Objects Located in a Layered Media with Rough Interfaces

Tolga Ulaş Gürbüz[1], **Birol Aslanyürek**[2], **and Ibrahim Akduman**[1]

[1]Electrical-Electronics Engineering Faculty, Istanbul Technical University, Maslak 34469, Istanbul, Turkey
[2]Mathematical Engineering Department, Yildiz Technical University, Davutpasa 34210, Istanbul, Turkey

Abstract— During the last three decades enormous efforts have been devoted to the imaging problems whose aim is to recover the geometrical (location and shape) and physical (constitutive parameters) properties of inaccessible bodies. The imaging problems related to the buried bodies have an important place in this research area. This is due to the fact that these problems have direct applications in the areas such as medical imaging, geophysics, material tests etc. Although several methods have been developed for the solution of imaging problems related to the buried objects, these methods are valid under certain approximations and limitations that restrict their applications. So, the problem is open and needs to be developed by new methods with high resolution. On the other hand, one of the main classes of the inverse scattering problems for buried objects is the imaging of objects located in a layered media with rough interfaces. The complexity of the problem, which is due to the roughness of the surfaces, makes the problem more difficult compared to conventional inverse scattering problems with layered backgrounds having planar interfaces. In contrast with their practical importance, such problems have not been well investigated in the open literature. The main objective of this paper is to develop a fast and effective imaging method for 3D objects located in a layered media containing rough interfaces. The method is based on the Contrast Source Inversion algorithm [1] requiring the knowledge of the Greens function of the layered background that constitutes an interesting and difficult separate problem. In this work, the Buried Object Approach (BOA) is adapted to the present configuration to calculate the required Greens function [2]. The Greens function is represented in terms of infinite integrals in the spectral domain, which are computationally very costly. In order to overcome this difficulty, an approach based on the discrete complex images method (DCIM) [3] is applied and the calculation of the required components of the Greens function is significantly accelerated. Reconstruction is done via the Contrast Source Inversion algorithm. As an introduction to the full-vectorial 3D electromagnetic problem, the proposed approach is implemented in the 3D acoustic case and tested with several examples in order to see its efficiency and accuracy as well as applicability. It is shown that it yields accurate results both for geometrical and physical properties.

REFERENCES

1. Van Den Berg, P. M. and R. E. Kleinman, "A contrast source inversion method," *Inv. Prob.*, Vol. 13, 1607–1620, 1997.
2. Altuncu, Y., A. Yapar, and I. Akduman, "Buried object approach for solving scattering problems related to rough surfaces," *Canadian Journal of Physics*, Vol. 85, 39–55, 2007.
3. Aksun, M. I., "A robust approach for the derivation of closed-form Green's functions," *IEEE Trans. Microwave Theory and Tech.*, Vol. 44, No. 5, 651–658, 1996.

Image Appraisal of Full Waveform Inverted GPR Data

G. Meles[1], S. Greenhalgh[2], H. Maurer[2], and A. Green[2]

[1]School of Geosciences, University of Edinburgh
The Kings Buildings, West Mains Road, Edinburgh EH9 3JN, UK
[2]Institute of Geophysics, ETH Zurich, Sonneggstrasse 5, CH 8092 Zurich, Switzerland

Abstract— We have recently developed a novel method for explicitly computing the permittivity ε and conductivity σ sensitivity functions (Jacobian matrix $\mathbf{J}$) of ground penetrating radar (GPR) data, based on a time domain adjoint approach which uses a finite difference modeling method. This not only opens up the possibility for performing Gauss-Newton type inversions, which offer distinct advantages over standard gradient-based approaches, but also permits a methodology for assessing the reliability of inverted GPR images from full waveform data. Image appraisal is performed through a joint analysis of the eigenvalue spectrum of the pseudo Hessian matrix $\mathbf{H} = \mathbf{J}^T\mathbf{J}$ and the formal model resolution matrix $\mathbf{R} = (\mathbf{J}^T\mathbf{J} + \lambda\mathbf{I})^{-1}\mathbf{J}^T\mathbf{J}$, where λ is a damping value to stabilize the matrix inversion. In seismic and geoelectric inversion, the damping factor is often chosen as the median value of $\mathbf{H}$, but the justification for this is not clear. The diagonal values of $\mathbf{R}$ give the resolution of each cell in the model, with values varying from 0 (unresolved) to 1 (perfectly resolved). The off-diagonal elements convey the trade-offs (cross-coupling) between the different parameters, and the degree of image blurring. The eigenvalue distribution of the pseudo-Hessian matrix provides a measure of the information content of an experiment and shows the unresolved model space. The effect of model perturbation along a given eigenvector direction on the cost function is established in terms of the size of the corresponding eigenvalue. The relative eigenvalue range (RER), which is the width of the normalized spectrum (with entries assembled in descending eigenvalue order) at the level of the noise floor, is a measure of the resolved model space. Four and three-sided radar acquisition geometries (e.g., combination crosshole and borehole-to-surface) yield higher RER values than a one-sided (surface reflection) or two-sided (crosshole) experiment, indicating greater information content and smaller null spaces. Clearly, the better the angular and spatial coverage of the target, the more reliable the image. Resolution is not just a function of the recording geometry and the quantity measured but also the underlying model itself.

We show that cumulative sensitivity (i.e., the column sum of absolute values of the Jacobian) images can be used as a reasonable proxy for formal resolution. Cumulative sensitivity is far less expensive than obtaining the resolution matrix, which involves large matrix inversion and multiplication. We also show that only minor differences exist between the resolution images provided by normalized Jacobians for the full set of ε and σ parameters and the sub-Jacobians for the individual ε and σ values. Permittivity sensitivity values are typically 10^9 times larger than the conductivity values, because they involve a time derivative of the electric field ($i2\pi f$ term, where frequency f is $\sim 100\,\mathrm{MHz}$) as opposed the field itself. Without normalization of sensitivities or using sub-Jacobians, conductivity updating would be impossible.

To provide more insightful meaning to resolution, we have undertaken a singular value decomposition of the pseudo-Hessian matrix $\mathbf{W}\Omega\mathbf{D}^T = \mathbf{H}$ and then extract the eigenvectors of $\mathbf{D}$ corresponding to the 'a' largest singular values (because H is self adjoint, these are identical to the eigenvalues) of Ω: $\mathbf{A}_{ij} = \mathbf{D}_{ij}$, $i = (1, 2, \ldots, M)$; $j = (1, 2, \ldots, a < M)$. We then form an alternative expression for the resolution matrix $\mathbf{R}^a = \mathbf{A}\mathbf{A}^T$ and take the diagonal elements of R^a as representative of resolution in each cell. There is a close relationship between resolution provided by $\mathbf{R}$ and $\mathbf{R}^a$. The effect of the damping factor λ in the formal model resolution formula for $\mathbf{R}$ is basically equivalent to the role of a in the truncated SVD resolution $\mathbf{R}^a$. Small values of λ have a very similar effect as choosing small values of a. (i.e., just the most dominant eigenvalues). Since SVD resolution is clearly connected to the spectrum of the Hessian, and because the singular values of Ω and the eigenvalues of $\mathbf{H}$ are identical, it provides insight and guidance on the effect of damping in computing $\mathbf{R}$. However, SVD analysis is extremely expensive from a computational point of view and not intended for routine applications.

In this contribution we illustrate the sensitivity patterns, eigenvalue spectra and resolution plots for a variety of heterogeneous models and recording setups.

Microwave Detection of Specific Dielectric Targets behind Concrete Walls

S. Avcı, O. Güren, M. Çayören, and I. Akduman
Electrical and Electronics Faculty
Istanbul Technical University, Istanbul, Turkey

Abstract— Through-wall imaging where the aim is identify specific objects inside or behind the concrete walls, has gathered interest in parallel to increasing concerns for public security [1, 2]. While conducting targets can be effectively detected, dielectric targets still poses a great challenge. For the detection of specific dielectric targets by using microwaves, we extend the idea demonstrated in [3]. The method is based on surface impedance concept where the target's contribution to electric field is projected to the surface of the wall in terms of impedance boundary conditions. The surface impedance is reconstructed through analytical continuation of electrical field values which are measured in one side of the wall. As shown in [3], one can observe peak like behaviors in the reconstructed surface impedance which indicates the existence of targets at a specific position. However, detection rate deteriorates with the increase of various factors such as the distance between the target and the wall, the measurement noise and the thickness of the wall. To overcome such drawbacks and improve the overall efficiency of the method, here we presented additional steps. Instead of qualitative analysis of the reconstructed surface impedance to detect objects, we define a distance function which the reconstructed surface impedance is compared against and the numerical results higher than a predefined threshold indicates the existence of an object at a certain position. Interestingly, one can define different distance functions to accommodate the detection of different targets according to their electrical or geometrical properties. The preliminary results indicate improved noise tolerance and detection rate.

REFERENCES

1. Song, L.-P. and C. Yu, and Q. H. Liu, "Through-wall imaging (TWI) by radar: 2-D tomographic results and analyses," *IEEE Transactions on Geoscience and Remote Sensing*, Vol. 43, No. 12, 2793–2798, 2005.
2. Smith, G. E. and B. G. Mobasseri, "Robust through-the-wall radar image classification using a target-model alignment procedure," *IEEE Transactions on Image Processing*, Vol. 21, No. 2, 754–767, 2012.
3. Sahinturk, H., A. Yapar, and I. Akduman, "On the use of surface impedance in the detection and location of buried objects," *AEU Int. J. Electron. Commun.*, Vol. 58, No. 4, 249255, 2004.

Permittivity Imaging by Addressable Defect of Surface-wave Structure on Two-dimensional Metamaterial in Millimeter-wave Range

Osamu Sakai[1], **Go Itami**[1], **Tomohide Akiyama**[1], **and Yoshinori Harada**[2]

[1]Kyoto University, Japan
[2]Kyoto Prefectural University of Medicine, Japan

Abstract— Dielectric constant or permittivity of lesional tissues varies from normal ones due to difference of tissue structures, although the level of the variation depends on deceases. To monitor position(s) and size of such tissues noninvasively, several optical probes have been proposed, but limit of detection depth from the skin surface is certainly present since penetration depths of optical rays or lasers are in a millimeter range at most. Here, we propose to use millimeter waves for detection of mm-size lesional tissues for portable instruments available on sides of beds and/or during operation.

To obtain two-dimensional images, we used a metamaterial which supports spoof surface plasmons [1–3], which are surface waves propagating on the surface of the flat metallic structure. Assuring propagation of surface waves which penetrate into the material in a certain depth on one side, we installed a movable metal needle to disturb electromagnetic waves as a local defect. We calculated such a configuration by a numerical code based on the finite element method, and we confirmed that electric fields are spatially modified in a region just around the needle whose characteristic length is fairly smaller than the wavelength.

We performed experiments using a system composed of a millimeter-wave source, a detector, a metamaterial which is a simple perforated metal plate, and a movable metal needle which can scan every hole of the plate one by one. At 72.5 GHz, where spoof surface plasmons are present [3], we successfully reconfigured images of a metal pole and a metal triangle plate, and a rat lung taken from a whole body. Although the images did not perfectly match shapes of such real bodies, these experimental results verify that the concept of this imaging method is valid for detection of spatial variation of permittivity.

REFERENCES

1. Pendry, J. B., L. Martin-Moreno, and F. J. Garcia-Videl, *Science*, Vol. 305, 847, 2004.
2. Miyamaru, F. and M. Hangyo, *Phys. Rev. B*, Vol. 71, 165408, 2005.
3. Lee, D.-S., O. Sakai, and K. Tachibana, *Jpn. J. Appl. Phys.*, Vol. 48, 062004, 2009.

Guaranteed Estimates of Linear Continuous Functionals of Solutions and Right-hand Sides of the Helmholtz Equation in the Domains with Infinite Boundaries under Uncertainties

Yury Podlipenko[1] and Y. Shestopalov[2]

[1]Kiev National University, Ukraine
[2]Karlstad University, Sweden

Abstract— We consider the construction of guaranteed estimates [1, 2] of linear continuous functionals of the unknown solutions and right-hand sides of the Helmholtz equation [2, 3]; the boundary value problems under study are associated with the wave diffraction by a bounded body D situated in a domain K whose boundary stretches to infinity (e.g., a wedge or a layer) and Green's function is known [4]. We assume that right-hand sides of the equations entering the problem statement are not known; the only available information is that they belong to a bounded set of the space of square-integrable functions.

In order to solve these estimation problems we need additional data: observations in the form of certain linear transformations of the solution distorted by noise. The latter are realizations of the random fields with the unknown second moment functions belonging to a given bounded set in the appropriate functional space.

The approach set forth in [2, 3, 5] and developed in this study allows us to obtain optimal estimates of the unknown solution or right-hand sides of the equations and linear functionals, i.e., estimates sought in the class of functionals linear with respect to observations for which the maximal mean-square estimation error taken over all elements belonging to the aforementioned sets takes minimal value. Such estimates are called minimax or guaranteed estimates.

We obtain representations for these estimates and estimation errors in terms of solutions to certain integro-differential or integral equations in bounded subdomains of domain K.

REFERENCES

1. Nakonechnyi, O., Y. Podlipenko, and Y. Shestopalov, "Estimation of parameters of boundary value problems for linear ordinary differential equations with uncertain data," arXiv:0912.2872, 72.
2. Podlipenko, Y., Y. Shestopalov, and V. Prishlyak, "Estimation under uncertainties of acoustic and electromagnetic fields from noisy observations," arXiv:0910.2331, 93.
3. Podlipenko, Y., Y. Shestopalov, and V. Prishlyak, "Estimation of solutions of Helmholtz problems with uncertain data," *Proc. 2010 International Symposium on Electromagnetic Theory EMTS 2010*, 621–623, Berlin, Germany, August 15–19, 2010.
4. Podlipenko, Y. and Y. Shestopalov, "On the electromagnetic scattering problem for an infinite dielectric cylinder of an arbitrary cross section located in the wedge," *J. Math. Phys.*, Vol. 40, No. 10, 4888–4902, 1999.
5. Podlipenko, Y. and Y. Shestopalov, "Guaranteed estimates of functionals from solutions and data of interior Maxwell problems under uncertainties," *Springer Proceedings in Mathematics & Statistics*, Vol. 52, 2013.

Feasibility Study of Passive Bistatic Synthetic Aperture Radar for Imaging Small Objects

Motoyuki Sato, Takafumi Kitajyo, and Kazunori Takahashi
Center for Northeast Asian Studies, Tohoku University, Sendai 980-8576, Japan

Abstract— We have developed a passive bistatic radar system for fundamental understanding of such a system. Passive bistatic radar has been demonstrated for detecting isolated large objects such as flying airplanes, but not has been demonstrated for detection of relatively small objects. Ground Penetrating Radar (GPR) normally uses frequencies between 100 MHz and a few GHz, however, these frequencies are used by many communication and broadcasting purposes. Therefore, it is very difficult to obtain regal permission to use the wide frequency bandwidth in this frequency range. If we could use the electromagnetic waves transmitted from the exiting radio stations, we have a few advantages. Firstly, we do not have to get regal permission for frequency allocation, which enables the system operation easy, and secondly, the radar system has to have only receivers, which make the system simple, and power consumption can be reduced. On the contrary, we have to synchronize the receiver system to the transmitted waves to reconstruct the radar image.

We used a high speed digitizing Oscilloscope (Agilent E4407B, 20 GSa/s), which can acquire the real-time signal up to 7 GHz. Two Yagi-Uda array antennas were connected to the oscilloscope, and one antenna is directed to one of transmitting radio stations, and the other was directed to the target to be imaged. A metal trihedral corner reflector, which is composed from three 1 m by 1 m aluminum plates, was used as a target. One antenna is fixed for receiving the reference signal from a digital TV broadcasting station (536–542 MHz), which is about 2 km away from the receiving antenna, and the other antenna was moved on a rail, which receives the reflected wave from the target. The receiving antenna was moved along a 4-m straight rail, and data was acquired ever 2 cm. The cross correlation of each signal received at each position and the reference signal received at the fixed position is calculated, and the delay (lag) caused by the antenna position change was estimated. The cross correlation function is shown in Fig. 1.

The cross correlation function was used as a raw signal and synthetic aperture radar (SAR) processing was executed. Fig. 2 shows the reconstructed image. We can clearly identify the position of the coroner reflector.

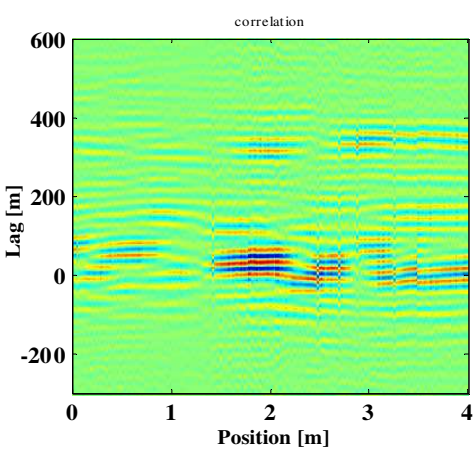

Figure 1: Cross correlation function.

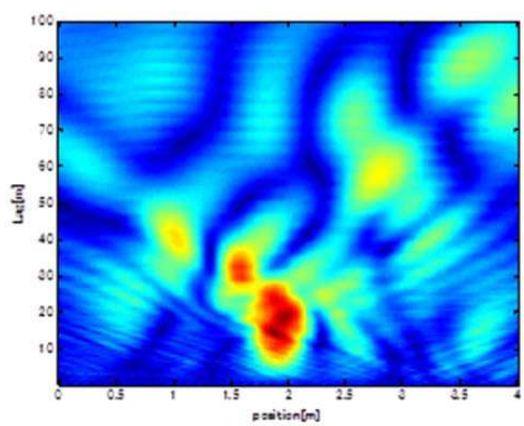

Figure 2: SAR image of a trihedral corner reflector.

Session 1A9
SC1: Novel Mathematical Methods in Electromagnetics

Mathematical Methods for the Doubly-fed Induction Generator
Giovanni Franco Crosta, Federica Bertini, Goong Chen, Nicholas Mai, ... 116

Wiener-Hopf Analysis of the High-frequency Diffraction by a Sinusoidal Strip
Toru Eizawa, Kazuya Kobayashi, ... 118

A Complete Set of Relativistic Time-domain Waveguide Modes in Hollow Waveguides
Ozlem Akgun, ... 119

Polyfunctional Properties of Resonant Scattering and Generation of Oscillations by Nonlinear Layered Media
Lutz Angermann, Vasyl V. Yatsyk, ... 120

Calculating the Scattering from Periodic Conducting Surfaces without Using Evanescent Modes, Part I: Existence of a Solution
Dayalan Prajith Kasilingam, Christopher Goonan, ... 121

Media Not Restricted by a Dispersion Equation
Ismo Veikko Lindell, Alberto Favaro, ... 122

Singular Modes in an Anisotropic Medium
Alexander B. Samokhin, Y. Fukumoto, ... 123

FDTD Simulation of Waveguide with Non-uniform Dielectric Slab
Aleksander P. Smirnov, A. N. Semenov, Yury V. Shestopalov, ... 124

Remarks on the Mathematical Solution of the Hollow Cavity Eigenvalue Problem
Gabriele Costanza, Andreas D. Ioannidis, ... 125

The Resolution of Identity: A Unifying Concept in Field Theory
Alireza R. Baghai-Wadji, ... 126

Asymptotic Analysis of the Whistler Waves Propagation in Space Plasma Thrusters
Davide Melazzi, Alessandro Cardinali, Marco Manente, Daniele Pavarin, ... 127

Electromagnetic and Gravitational Origin of Dark Energy in Kaluza-Klein $\boldsymbol{D = 5}$ Spacetime
Mohamed S. El Naschie, ... 128

Mathematical Methods for the Doubly-fed Induction Generator

Giovanni F. Crosta[1], **Federica Bertini**[1], **Goong Chen**[2], **and Nicholas Mai**[2]

[1]Inverse Problems & Mathematical Morphology Unit, Department of Earth and Environmental Sciences
University of Milan-Bicocca, 1, piazza della Scienza, MILAN, IT 20126, USA
[2]Department of Mathematics, Texas A&M University, College Station, TX 77843-3368, USA

Abstract—

Motivation: A wind turbine powertrain includes a three-phase generator and switching electronics. The two most frequently installed types of generators are the synchronous induction machine and the doubly-fed induction machine (DFIG for short) [1]. Since the wind field is substantially unpredictable, whereas power has to be delivered to the network at (possibly) constant frequency and voltage amplitude, control of the powertrain plays an essential role in the design and operation of a wind power plant. This work focuses on the model of the DFIG for control purposes.

Co-energy and the Legendre Transform: The general process of power conversion from mechanical to electrical and the operation of a DFIG can be modeled by applying the mathematical methods of analytical mechanics and group theory. For example, let an electric machine have P poles and let its rotor form a mechanical angle $\theta_{r,mech}$ in the stator frame; then the electrical angle of the rotor θ_r with respect to the stator is given by $\theta_r = \frac{P}{2}\theta_{r,mech}$ (multiplier effect of P) and the resulting (motor) torque T can be shown to read [2, 3]

$$T = \frac{\partial W'_{fld}[\vec{i}, \theta_r]}{\partial \theta_{r,mech}} = \frac{P}{2}\frac{\partial W'_{fld}[\vec{i}, \theta_r]}{\partial \theta_r}$$

where $\vec{i}$ is the vector of electric currents and $W'_{fld}[\vec{i}, \theta_r]$ is *co-energy*.

Standard textbooks do not generally introduce co-energy as the Legendre transform of the energy (stored in the magnetic field) with respect to magnetic flux linkage, $\vec{\lambda}$, nor point out the underlying differential geometric setting. Whereas $\vec{\lambda}$, as *energy* variables, are coordinates of the manifold $\mathcal{N}$, electric currents, $\vec{i}$, belong to the co-tangent bundle $T^*\mathcal{N}$ [4, 5]. The relation between co-energy and torque applies to any machine and can, in principle, deal with any functional dependence between $\vec{\lambda}$ and $\vec{i}$. Non-linear $\vec{\lambda}[\vec{i}]$ relations become of interest when saturation of the magnetic circuit has to be modeled.

Some examples and results in this direction will be provided.

The Blondel-Park Transformation and the Rotation Group: A linear DFIG is most effectively modeled in terms of stator and rotor flux linkages, $\vec{\lambda}_s$, $\vec{\lambda}_r$ (with obvious notation) and currents $\vec{i}_s$, $\vec{i}_r$, by means of inductance matrices. In the case of winding symmetry the equations read

$$\vec{\lambda}_s = \mathbf{L}_{ss} \cdot \vec{i}_s + L_x \mathbf{L}_{sr}[\theta_r] \cdot \vec{i}_r$$

and

$$\vec{\lambda}_r = L_x \mathbf{L}_{sr}^{\mathrm{Trs}}[\theta_r] \cdot \vec{i}_s + \mathbf{L}_{rr} \cdot \vec{i}_r.$$

The Blondel-Park transformation, which applies to electrical quantities of interest, is defined by the matrix

$$\mathbf{B}[\eta] := \sqrt{\frac{2}{3}} \begin{bmatrix} \cos[\eta] & \cos[\eta - \frac{2\pi}{3}] & \cos[\eta + \frac{2\pi}{3}] \\ -\sin[\eta] & -\sin[\eta - \frac{2\pi}{3}] & -\sin[\eta + \frac{2\pi}{3}] \\ \frac{1}{\sqrt{2}} & \frac{1}{\sqrt{2}} & \frac{1}{\sqrt{2}} \end{bmatrix}$$

where η stands for any of the electrical angles, usually denoted by θ, θ_r and $\beta(= \theta - \theta_r)$ respectively. As it is well known, the $\mathbf{B}[\eta]$'s form a one-parameter (η) group of unitary (power preserving) transformations.

The following properties can be shown to hold.

• Let $\mathbf{D}[\eta] := \mathbf{B}[0]^{-1} \cdot \mathbf{B}[\eta]$, then the exponential representation holds

$$\mathbf{D}[\eta] = e^{\eta \mathbf{F}},$$

where the matrix $\mathbf{F}$ is constant and is similar to the matrix $\mathbf{G}$, which row-wise reads $\mathbf{G} = [0\ 1\ 0| - 1\ 0\ 0|0\ 0\ 0]$

$$\mathbf{F} = \mathbf{B}[0]^{-1} \cdot \mathbf{G} \cdot \mathbf{B}[0].$$

• By letting $\frac{\partial \mathbf{L}_{sr}[\theta]}{\partial \theta} := \mathbf{M}[\theta]$, where $\mathbf{L}_{sr}$ is the mutual, stator-to-rotor, inductance matrix, application of the $\mathbf{D}[.]$ transformation turns the electric torque into a bilinear, antisymmetric form for $\mathbf{G}$.

The extent to which the use of $\mathbf{D}[.]$ in the non-linear case (e.g., [6]) still simplifies results, and the class of tractable non-linearities, [7, 8] are currently being investigated.

ACKNOWLEDGMENT

G. F. Crosta gratefully acknowledges the financial support of the home University's *Fondo di Ateneo per la ricerca*, from 2010 onwards and the research agreement between the home University and *Digicom* S.p.A., Gallarate, IT.

G. Chen, G. F. Crosta and N. Mai gratefully acknowledge the partial support by the *Texas* Norman Hackman Advanced Research Program Grant #010366-0149-2009 from the Texas Higher Education Coordinating Board.

REFERENCES

1. Hau, E., *Windkraftanlagen, 4. Auflage*, Springer, Berlin, D, 2008.
2. Fitzgerald, A. E. and C. Kingsley, Jr., *Electric Machinery*, 2nd Edition, McGraw-Hill, New York, NY, 1961.
3. Krause, P. C., *Analysis of Electric Machinery*, McGraw-Hill, New York, NY, 1986.
4. Maschke, B. M., A. J. Schaft van der, and P. C. Breedveld, "An intrinsic Hamiltonian formulation of the dynamics of LC-circuits," *IEEE Transactions on Circuits and Systems I: Fundamental Theory and Applications*, Vol. 42, No. 2, 73–82, 1995, ISSN 1057-7122.
5. Eberard, D., B. Maschke, and A. J. Schaft van der, "Conservative systems with ports on contact manifolds," *Proc. 16th IFAC World Congress*, Prague, CZ, IFAC, July 4–8, 2005.
6. Sullivan, C. R. and S. R. Sanders, "Models for induction machines with magnetic saturation of the main flux path," *IEEE Trans. Industry Appl.*, Vol. 31, No. 4, 907–917, 1995.
7. Youla, D. C. and J. J. Bongiorno, Jr., "A Floquet theory of the general linear rotating machine," *IEEE Trans. Circuits and Systems*, Vol. 27, No. 1, 15–19, 1980.
8. Liu, X. Z., G. C. Verghese, J. H. Lang, and M. K. Önder, "Generalizing the Blondel-Park transformation of electrical machines: Necessary and sufficient conditions," *IEEE Trans. Circuits and Systems*, Vol. 36, No. 8, 1058–1067, 1989.

Wiener-Hopf Analysis of the High-frequency Diffraction by a Sinusoidal Strip

T. Eizawa and K. Kobayashi
Chuo University, Japan

Abstract— The analysis of the scattering by gratings and periodic structures is an important subject in electromagnetic theory and optics. Various analytical and numerical methods have been developed thus far, and the diffraction phenomena have been investigated for a number of periodic structures [1]. However, the analysis in most of the past works is restricted to periodic structures of infinite extent and plane boundaries. Therefore, it is important to investigate scattering problems involving periodic structures without these restrictions. In [2], we have considered a strip with sinusoidal corrugation as an example of periodic structures of finite extent and non-plane boundaries, and analyzed the plane wave diffraction using the Wiener-Hopf technique together with the perturbation method. This paper is in continuation with our previous analysis [2], and we shall derive a uniform asymptotic expression of the scattered far field.

The geometry of the problem is shown in Figure 1, where ϕ^i is the incident field of E or H polarization. The surface of the strip is assumed to be infinitely thin, perfectly conducting, and uniform in the y-direction, and it is defined by $x = h \sin mz$ for $|z| \leq a$ where m and h are positive constants. Assuming that the corrugation amplitude of the strip is small compared with the wavelength, the original problem is replaced by the problem of diffraction by a flat strip with an impedance-type boundary condition. We also expand the scattered field using a perturbation series, and separate the diffraction problem into the zero- and the first-order boundary value problems. Introducing the Fourier transform for the scattered field and applying boundary conditions in the transform domain, the problem is formulated in terms of the zeroand first-order Wiener-Hopf equations. The Wiener-Hopf equations are solved via the factorization and decomposition procedure leading to the exact solution. However, the solution is formal in the sense that infinite branch-cut integrals with unknown integrands are contained. We shall further employ a rigorous asymptotics to derive an explicit high-frequency solution that is valid for the strip width large compared with the wavelength. Taking the Fourier inverse of the solution in the transform domain and applying the saddle point method, a uniform asymptotic expression of the scattered far field is derived explicitly in terms of the Fresnel integral. Representative numerical examples of the radar cross section are presented for various physical parameters, and far field scattering characteristics of the strip are discussed in detail.

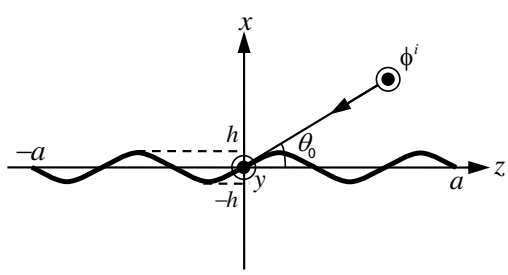

Figure 1: Geometry of the problem.

REFERENCES

1. Petit, R., Ed., *Electromagnetic Theory of Gratings*, Springer-Verlag, Berlin, 1980.
2. Eizawa, T., T. Matsuyama, and K. Kobayashi, "Plane wave diffraction by a strip with sinusoidal corrugation," *Progress In Electromagnetics Research Symposium Abstracts*, 248, Moscow, Russia, August 19–23, 2012.

A Complete Set of Relativistic Time-domain Waveguide Modes in Hollow Waveguides

Ö. Akgün
Department of Electrical and Electronics Engineering, Aksaray University, Aksaray, Turkey

Abstract— An initial-boundary value problem for the system of Maxwell's equations with time derivative is formulated and solved *rigorously* for transient modes in a hollow waveguide having a cross-section domain, S, invariable along the waveguide axis, Oz. We assume that the domain S is bounded by a closed singly-connected contour of arbitrary but smooth enough shape implying that none of its inner angles measured within S exceed π. We also assume that the waveguide surface has the physical properties of the perfect electric conductor. The cases of TE and TM waveguide modes are considered in parallel. Every modal field component is obtained as a product of a vector function of transverse coordinates, $(\mathbf{r})$, and a scalar amplitude dependent on axial coordinate, z, and time, t. The study can be reduced to solving two autonomous problems: *1) A modal basis problem.* Final result of this step is the definition of complete set in Hilbert space $\mathcal{L}_2(\mathcal{S})$ of eigensolutions dependent on $(\mathbf{r})$. The eigensolutions generate the basis elements and exhibit the field pattern configurations of the modal field components. *2) A modal amplitude problem.* It is proved that the amplitudes are generated by the solutions to the Klein-Gordon Equation (KGE) with z and t as independent variables. The KGE, which has been *directly* derived from Maxwell's equations, has remarkable properties of symmetry in the sense of the group theory. Solutions to the KGE are invariant under the relativistic Lorentz transformations and subjected to the causality principle. The main focus of this study is to give an insight to the function pairs leading to analytical solutions to the KGE resulting in non-sinusoidal modal amplitudes. Surely, the approach proposed here satisfies the correspondence principle which states that every new theory should reproduce the results of previously well-established theories as a limiting case in the domains of previous theories. Therefore, one of the aforementioned function pairs leads to sinusoidal modal amplitudes evaluated within the framework of well-studied time-harmonic field theory. The modal amplitudes presented here are found *explicitly* and expressed via products of the Bessel and the modified Bessel functions with arguments dependent on z and t.

Polyfunctional Properties of Resonant Scattering and Generation of Oscillations by Nonlinear Layered Media

Lutz Angermann[1] and Vasyl V. Yatsyk[2]

[1]Department of Mathematics, University of Technology at Clausthal
Erzstraße 1, Clausthal-Zellerfeld D-38678, Federal Republic of Germany
[2]O. Ya. Usikov Institute for Radiophysics and Electronics
National Academy of Sciences of Ukraine, 12 Ac. Proskura Str., Kharkiv 61085, Ukraine

Abstract— Nonlinear dielectrics with controllable permittivity begin to find broad applications in device technology and are subject of intense studies in the range of both radio and the optical frequencies. We focus on the development of a mathematical model, an effective algorithm and a self-consistent numerical analysis of the multifunctional properties of resonant scattering and generation of oscillations by nonlinear, cubically polarisable structures [1, 2]. The polyfunctionality of the nonlinear media will be caused by the interference mechanism between interacting oscillations — the incident oscillations as well as the scattered and generated oscillations at the frequencies of excitation/scattering and generation.

The study of the resonant properties of scattering and generation of oscillations by a nonlinear structure with a controllable permittivity in dependence on the variation of the intensities of the components of the exciting wave package is of particular interest. In the proposed paper we extend our former results and indicate the possibility of increasing the multifunctionality of electronic devices, of designing frequency multipliers and other electrodynamic devices containing nonlinear dielectrics with controllable permittivity.

ACKNOWLEDGMENT

This work was partially supported by the Visby Program of the Swedish Institute and by the joint Russian-Ukrainian RFBR-NASU Grant No. 12.02.90425-2012.

REFERENCES

1. Angermann, L. and V. V. Yatsyk, "The effect of weak fields at multiple frequencies on the scattering and generation of waves by nonlinear layered media," *Solutions and Applications of Scattering, Propagation, Radiation and Emission of Electromagnetic Waves*, 303–332, A. Kishk, Editor, InTech, Rijeka, Croatia, 2012.
2. Angermann, L. and V. V. Yatsyk, "The influence of weak fields at multiple frequencies on the process of resonant scattering and generation of oscillations by nonlinear layered structures," *Physical Bases of Instrumentation*, Vol. 2, No. 1, 48–71, 2013 (in Russian).

Calculating the Scattering from Periodic Conducting Surfaces without Using Evanescent Modes, Part I: Existence of a Solution

Dayalan Kasilingam and Christopher Goonan
Department of Electrical & Computer Engineering, University of Massachusetts Dartmouth
285 Old Westport Road, North Dartmouth, MA 02747-2300, USA

Abstract— In 1897, Lord Rayleigh published a classic paper in which he used periodic functions to describe the scattering from periodic surfaces. Known as the Rayleigh hypothesis, this method not only used periodic plane wave representations to describe the fields away from the periodic surfaces, but also inside the corrugated region of the surface. However, in the mid-sixties through the early eighties, many researchers challenged Rayleigh's approach of using plane wave representations for the fields inside the corrugated region of the periodic surface. Several of these papers used extensive complex analysis to show that the solutions were unstable when the periodic surface became quite rough. However in the past decade, other researchers have shown that despite these apparent limitations, the Rayleigh hypothesis gives valid results even for very rough surfaces. It has been argued by these researchers that the limitations were primarily a function of the computational accuracy and not implicit to the method itself. In this paper, we show that the Rayleigh hypothesis yields accurate results for scattering from periodic conducting surfaces even when the roughness is large. We also develop a new technique where the rough surface scattering problem is solved without the need to include the evanescent modes. In the new technique we have developed, we show the existence of a modal sub-space in which the boundary conditions are satisfied using only the incident propagating modes and the scattered propagating modes. This modal sub-space is chosen to be orthogonal to all the evanescent modes on the boundary. Thus by projecting the boundary conditions on to this sub-space, we derive a set of equations which only involve propagating modes. In a companion paper, we show how this model sub-space can be estimated without calculating the evanescent modes. In this paper, we calculate evanescent modes to show the existence of an appropriate modal sub-space which is orthogonal to all the evanescent modes. We show the existence of a solution and that the solution is unique. We show that the aforementioned limitations of the Rayleigh hypothesis do not prevent one from solving for scattering from periodic surfaces, even when the surface roughness is large. We derive a matrix form of a transfer function model, which describes the scattered fields in terms of the incident fields. The transfer function model describes the scattering for all possible combinations of incident waves. We show that this transfer function satisfies reciprocity and the conservation of power. The proposed method has several obvious advantages in not calculating the evanescent modes. In most scattering problems such as those in radar and remote sensing, one is only interested in the scattered signal or power in the far field. In these cases, one needs to find only the propagating fields and not the evanescent fields. Furthermore, computationally the evanescent modes are poorly conditioned because of their exponential dependence on depth and they also constitute an infinite set of modes. For periodic surfaces, the propagating modes represent a well-defined, finite set of modes. Thus purging the evanescent modes in the computation allows one to deal with well-conditioned matrices and eliminates the need for truncating an infinite series. This newly developed technique has the potential to be a powerful computational method for calculating scattering from rough surfaces.

Media Not Restricted by a Dispersion Equation

I. V. Lindell[1] and A. Favaro[2]

[1]Department of Radio Science and Engineering, Aalto University, Espoo, Finland
[2]Institute of Theoretical Physics, University of Cologne, Cologne, Germany

Abstract— Time-harmonic plane waves propagating in linear homogeneous and time-invariant electromagnetic media obey the space dependence $\exp(-j\mathbf{k}\cdot r)$, where the wave vector $\mathbf{k}$ is normally restricted by a dispersion equation $D(\mathbf{k}) = 0$, where the function $D(\mathbf{k})$ depends on the medium in question. For the general linear (bi-anisotropic) medium $D(\mathbf{k})$ is an algebraic function of the fourth order in $\mathbf{k}$. Special cases of the function can be used to define certain classes of media. For example, when the function can be decomposed as a product of two second-order functions, $D(\mathbf{k}) = D_1(\mathbf{k})D_2(\mathbf{k})$, a class of decomposable media can be defined in which all possible plane waves can be decomposed in two sets, one obeying the dispersion equation $D_1(\mathbf{k}) = 0$ and, the other one, $D_2(\mathbf{k}) = 0$. An example of a decomposable medium is the uniaxial anisotropic medium. As another special case, defining a more restricted class of media, the two functions may coincide, $D_1(\mathbf{k}) = D_2(\mathbf{k})$ which leaves just one second-order dispersion equation. In this case the medium appears nonbirefringent, whence this property defines the class of nonbirefringent media. An example of such a medium is the isotropic medium. Finally, it is possible to define media for which the dispersion function $D(\mathbf{k})$ vanishes identically for all $\mathbf{k}$, whence in such media there is no dispersion equation at all. Media in which plane waves are not restricted by a dispersion equation, like the one called skewon-axion medium, have recently emerged in various studies.

In this paper the problem of defining electromagnetic media which do not possess a dispersion equation is addressed in terms of four-dimensional formalism applying multivectors, multiforms and dyadics following the reference [1]. The outcome is that there are three classes of possible media, defined by the form of their medium bidyadics.

REFERENCES

1. Lindell, I. V., *Differential Forms in Electromagnetics*, Wiley and IEEE Press, New York, NY, 2004.

Singular Modes in an Anisotropic Medium

A. B. Samokhin and Y. Fukumoto
Moscow State Institute of Radio Engineering, Electronics and Automatics, Moscow, Russia

Abstract— We construct the singular mode corresponding to a spatial essential spectrum of the integral operator for the scattering of electromagnetic waves by a three-dimensional body of finite size with inhomogeneous and anisotropic dielectric permittivity tensor. The permittivity tensor field is assumed to be Holder continuous throughout the whole space. The singular volume integral equation transformed from Maxwell equations, makes is feasible to deduce explicit forms of both the continuous essential spectrum and the corresponding singular modes. The obtained singular mode is a natural extension of the previously obtained one for the iso-tropic case and is applicable to a much wider class of dielectric scattering bodies, for example for anisotropic plasma medium. A discussion is made of the possibility for realizability of electromagnetic waves, with finite energy, concentrated at a point in the medium.

FDTD Simulation of Waveguide with Non-uniform Dielectric Slab

A. P. Smirnov[1], **A. N. Semenov**[1], **and Y. V. Shestopalov**[2]

[1]Lomonosov Moscow State University, Moscow, Russia
[2]Karlstad University, Karlstad, Sweden

Abstract— Scattering in the time domain of electromagnetic waves in the elongated waveguide with non-uniform dielectric slab is considered. Electromagnetic field components are computed and investigation of energy transport in the guide is effected by using Finite Difference Time Domain (FDTD) method for different frequency ranges. Computation for the nonstationary Maxwell equation system is performed by efficient 3D FDTD solver EMWSolver3D created by authors of this paper. Simulation is performed for the H10-mode scattering from dielectric slab inclusions. Numerical computations for solving large-scale problems have been implemented on supercomputers of last generation. The model computations of empty waveguide without dielectric inclusions have shown that numerical dispersion arising during waves travelling in waveguide causes solution errors. Numerical phase velocity is shown to differ from the analytical phase velocity with the lapse of time that obstructs accurate finding of attenuation and propagation factors. In this respect method similar to Total Field/Scattered field has been proposed to specify waveguide mode with respect to numerical dispersion. The analytical solution of finite-difference equation for the H10-mode have been calculated for this purpose. Using the methods described above has allowed to compute the values of waveguide attenuation and propagation factors for different configurations of dielectric slab.

Remarks on the Mathematical Solution of the Hollow Cavity Eigenvalue Problem

G. Costanza[1] and A. D. Ioannidis[2]

[1]Lund University, Sweden
[2]Linnæus University, Sweden

Abstract— In this paper, we reconsider the classical eigenvalue problem for a perfectly conducting resonant cavity $\Omega \subset \mathbb{R}^3$, under a pure functional analytic point of view. This problem is obtained from the full Maxwell system with no currents by taking Fourier Transform (or applying a separation-of-variables technique) with respect to time and reads:

$$\mathcal{Q}e = \omega e. \tag{1}$$

Here we make use of the six-vector notation; $e := (\mathbf{E}, \mathbf{H})^T$ stands for the electromagnetic field, $\mathcal{Q}$ for the Maxwell operator

$$\mathcal{Q} := i \begin{bmatrix} 0 & -\mathrm{curl} \\ \mathrm{curl} & 0 \end{bmatrix}.$$

$\mathcal{Q}$ is realized in its weak sense as a maximally defined self-adjoint operator in the Hilbert space of square integrable fields over Ω; the perfect conductor boundary condition is absorbed in the domain of definition (corresponding Sobolev spaces for *curl* operator). A non-trivial solution of Eq. (1) is a pair (ω, e), where $\omega \in \mathbb{R}$ and e is a non-zero square integrable field. ω is then called an eigenfrequency of the cavity and e a corresponding resonant mode.

We pay special attention in the determination of the "correct space" for which the modes form an orthonormal basis, usually met as the problem of "completeness". This point is quite unclear in the existing literature and the main reasons of complication can be found in the problem of validity of Gauss equations and the big null space of $\mathcal{Q}$. In reality, one has to concern about Gauss equations only in the static case ($\omega = 0$).

It is worth noting here that usually Eq. (1) is solved by considering a set of four separate eigenvalue problems for the Laplacian, two vector (corresponding to solenoidal fields) and two scalar valued (from which irrotational fields are calculated). The decloupling of electric and magnetic fields is practically obtained by taking the square $\mathcal{Q}^2$. In our treatment, we insist on the original operator $\mathcal{Q}$ and we apply a variant of the Spectral Theorem for discrete operators, which seems to tackle the aforementioned difficulties.

Another close related complication arise when one tries to solve the inhomogeneous problem for an eigenfrequency ω

$$\mathcal{Q}e = \omega e + j, \tag{2}$$

where function j models the electromagnetic currents. We treat Eq. (2) in terms of Fredholm Alternative and we justify the common belief that the existence of currents "excite more modes" than one founds by just solving Eq. (1).

The Resolution of Identity: A Unifying Concept in Field Theory

A. R. Baghai-Wadji
University of Cape Town, South Africa

Abstract— The search for a unified regularization scheme of singularities arising in computational electromagnetics, along with the simultaneous quest for a systematic design of optimized analysis- and synthesis functions, have led to the insight that identity matrices and operators in finite and infinite dimensional Hilbert space play an all-important fundamental role. Consequently, the additive and multiplicative factorization of the identity matrix $\mathbf{I}$ and the identity operator $\hat{\mathbf{I}}$ in finite and infinite dimensional Hilbert space, has been identified, in this work, as a single unifying scheme in theoretical and computational electromagnetics. The discussion starts with the concept of the resolution of identity, and its manifestation as the completeness condition. Notions of generalized integral (series) transforms and inverse integral (series) transforms of field vectors, as well as co-variant and contra-variant field vector- and tensor components have been established in a unified manner. The discussion also embraces, in a natural way, the notion of spinors in three and higher dimensions. Apart from these rather physics-based considerations, the all-important computational aspects of basis, dual basis, wavelets, dual wavelets, frame and dual frames have also been covered in the paper. It is the author's conviction that various (traditionally conceived as disparate) areas of theoretical physics, mathematics, and mathematical physics, have been brought together here, thus proposing new venues for computational electromagnetics. The author is also convinced that the proposed method paves the way and invites powerful concepts and ideas from signal processing, theoretical physics and computer science into the arena of computational electromagnetics. The proposed methodology, inspired by physics, has its genesis in the modern functional analysis, in the form of multiresolution analysis. The proposed ideas are expected to find applications where classical electromagnetics, mesoscopic phenomena and quantum physics play a role, and thus physical phenomena in various scales must simultaneously be accounted for.

More specifically, operators in classical electrodynamics and the corresponding dual operators are reviewed, and factorized in their irreducible building blocks, utilizing factorization of differential identity operators. The Maxwells equations in general bi-anisotropic and inhomogeneous media are diagonalized in Cartesian coordinates. Maxwell equations in general curvilinear co-ordinates are transformed to local Cartesian coordinate systems. Problem-specific basis- and weighting (analysis- and synthesis) functions are constructed. Notions of non-orthogonality, and over-completeness have been discussed and explained in terms of the resolution of identity. A myriad of examples for the algebraic and operational resolution of identity have been presented, with the hope that experienced researchers and new comers to the field will both find the presented idea fresh and useful.

Asymptotic Analysis of the Whistler Waves Propagation in Space Plasma Thrusters

D. Melazzi[1], **A. Cardinali**[2], **M. Manente**[3], **and D. Pavarin**[1,4]

[1]CISAS "G. Colombo" Center of Studies and Activities for Space, University of Padua, Italy
[2]ENEA-EURATOM Association, Frascati, Rome, Italy
[3]Hit09, S.r.l., Padova, Italy
[4]Department of Industrial Engineering, University of Padua, Italy

Abstract— Recent advances in plasma-based propulsion systems have led to the development of electromagnetic Radio-Frequency (RF) plasma generation and acceleration systems, called Helicon Plasma Thruster (HPT) and derived from high density industrial helicon plasma sources.

HPT main components are: A gas feeding system, an RF antenna, and magnetic coils. The feeding system injects a neutral gas into a cylindrical vessel, wrapped by a RF antenna system working in the MHz range, ionizing the neutral gas and heating the plasma. The magnetic coils provide the axial magnetic field allowing for the propagation of helicon waves, and the confinement of plasma inside the cylindrical source. Additionally, the magnetic field lines at the exhaust section have to become divergent providing a "magnetic" nozzle effect on the magnetized plasma. The propulsive figures of merit (e.g., specific impulse and thrust efficiency) are strictly related to the power deposition inside the plasma source, requiring the optimization of the power coupled between the RF driven antenna and the plasma. Different models have been developed to study, design and optimize such a plasma propulsion system. All these models rely on the assumption that the confinement magnetic field is purely axial, constant and uniform as expected in helicon sources; however, experimental setups for HPTs can depart from this configuration due to dimension, mass and power budget limitations for space application purposes, generally leading to three-dimensional magnetic field configurations. We present a three-dimensional Ray-Tracing solver, called RAYWh (RAY-tracing Whistler), for the electromagnetic propagation and power deposition in plasma sources for space applications, where high density plasmas (ranging from 10^{17} to 10^{19} particles/m^3) are confined by general magnetic configurations with magnitude below $B < 0.15\,\mathrm{T}$. The 3D Maxwell-Vlasov equations have been solved by means of a WKB asymptotic expansion, to investigate the propagation and absorption of the whistler waves (excitation frequency is 13.56 MHz) under the influence of general confinement magnetic field, and axisymmetric realistic density profiles. The reduced set of the WKB equations for the wave phase and for the square amplitude of the electric field have been solved; additionally, the verification of WKB hypothesis has been monitored during the simulation. The Ray Tracing approach has been employed — for the first time — in the analysis of plasma sources for space applications. A direct comparison between common helicon sources with axial, constant and uniform confinement magnetic field, and plasma sources with actual confinement magnetic field lines revealed a propagative picture with mode conversions, cut-offs and resonances inside the source that affect the power deposition. Moreover, a comparison against a 1D (radial) full-wave solution showed that a strong variation of the axial wave number can lead to mode conversion to the slow branch of the propagation wave at the plasma edge, preventing the wave to reach the plasma bulk. The results are relevant for space thruster applications, but they can be fruitfully employed in industry plasma sources for the identification of the best source configuration (in terms of confinement magnetic field lines in addition to actual plasma density profiles), thus providing the maximum power transfer from the RF antenna to the plasma.

Electromagnetic and Gravitational Origin of Dark Energy in Kaluza-Klein $D = 5$ Spacetime

Mohamed S. El Naschie
Department of Physics, Faculty of Science, Alexandria University, Alexandria, Egypt

Abstract— Kaluza-Klein (K-K) theory is generally accepted as a partial unification of two of the fundamental interactions in Nature namely Electromagnetism and Gravity. In the present work we show against conventional expectation using transfinite quantization (i.e., Fractals) that K-K theory in conjunction with Penrose's Non-commutative (Fractal) space tiling leads to dual quantum relativity equations. The first is the ordinary energy equation of a quantum particle $E(O) = (\phi^5/2)mc^2$ where E is the Energy, m is the mass, c is the speed of light and $\phi = 2/(\sqrt{5}+1)$. On the other hand, the second dual equation corresponding to the dark energy of the quantum wave, i.e., of the Empty set is given by $E(D) = (5\phi^2/2)mc^2$.

Finally a third equation resulting from summing up the ordinary energy of the quantum particle and the dark energy of the quantum wave namely

$$\begin{aligned} E(O) + E(D) &= \left(\phi^5 + 5\phi^2\right) mc^2 \\ &= 2mc^2/2 \\ &= mc^2 \end{aligned}$$

is nothing else but Einstein's famous equation.

Recalling that $E(O) = (\phi^5/2)mc^2$; $mc^2/22$ is almost exactly equal to the value found from the WMAP and Supernova cosmological measurement which was awarded the 2011 Nobel Prize in Physics, we conclude that $E = mc^2$ is blind to any distinction between the ordinary energy which we can measure and the dark energy presumed so far to be "missing". It is further reasoned that ordinary energy is of opposite sign to dark energy, which could be traced mathematically to the negative sign of the empty set of the quantum wave or physically to the compactified dimension which is behind negative gravity and the recently measured acceleration of cosmic expansion.

Session 1A10
SC1: Electromagnetics of Gradient Nanostructures and Heterogeneous Media

Novel Technological Equipment for Gradient Optical Coatings Production
Nikolay F. Abramov, Oleg D. Volpian, Yuri A. Obod, ... 130

Reflectionless Tunneling of Light in Gradient Dielectric Nanostructures: Physical Fundamentals, Theoretical Basis and the First Experiments
Alexander Borisovich Shvartsburg, ... 131

Synthesis and Properties of the $LiNbO_3$ Thin Films Intended for Nanogradient Structures
Roman N. Zhukov, S. V. Ksenich, Alexandr S. Bykov, Dmitry A. Kiselev, Mikhail D. Malinkovich, Yuriy N. Parkomenko, ... 132

Magnetron Sputtering Deposition of Gradient Coatings for Photovoltaic Devices
Oleg D. Volpian, Anatoly I. Kuzmichev, Yuri A. Obod, ... 133

About Some Unusual Electrodynamic Properties of Negative Refraction Materials
Victor G. Veselago, ... 134

Multivariable Development of Gradient Optical Films Structures and Its Technological Applications
Oleg D. Volpian, Yuri A. Obod, Sergey V. Shkatula, ... 135

Application of X-ray Reflectometry for a Characterization of Graded Layers
Kirill D. Shcherbachev, Mikhail D. Malinkovich, Yuriy N. Parkhomenko, ... 136

Quantum Blooming: The Influence of the Detuning of the Antireflective Wells and the Phenomenon of Nonsymmetric Transmission
Alexander S. Kaklyugin, ... 137

Intermodal Coupling Induced Reflection in Tapered Slow Light Metamaterial Waveguide
Yingran He, Borui Li, Sailing He, ... 138

Novel Technological Equipment for Gradient Optical Coatings Production

N. F. Abramov[1], **O. D. Volpian**[1], **and Y. A. Obod**[2]

[1]JSC "M. F. Stelmakh R&D Institute "Polyus", Russia
[2]"Research and Production Company "Fotron-Auto" Ltd, Russia

Abstract— Optical coatings deposited on optical system parts greatly determine their energetic, spatial and spectrum characteristics. For example, in order to provide operating characteristics for modern laser systems, optical coatings must meet the following complex requirements: simultaneous multiple-wavelengths functioning, hard-driving modulation of optical characteristics, low optical losses, high resistance to high-power radiation and strong thermal and humid influences. The increasing requirements for operating characteristics of optical and laser systems have shown the need of novel optical coatings development, which will meet these requirements. Among these are nanogradient coatings, where the refractive index greatly changes along the layer thickness in a thin dielectric layers structure (for the thickness less than 100 nm) [1]. Gradient coatings, made of metamaterials and described in some sources are perspective for these applications [2].

Production of nanogradient coatings is a difficult technological problem. According to our research the best technique for high-quality optical dielectric thin-films production is the pulse magnetron sputtering technique in reactive gas medium [3]. The automated equipment for precision nanogradient optical coatings production using the dual-magnetron sputtering deposition technique has been created in JSC "M. F. Stelmakh R&D Institute "Polyus" and "RPC "Fotron-Auto" Ltd. The ion and photon assisted deposition technique has been applied. The technology of production of $1D_z$ gradient sub wave-thickness coatings has been developed using this equipment. As a result, the reproducible nanogradient optical structures with divers profile and modulation of refractive index were produced. Furthermore, developed control equipment and software let execute in situ reengineering of their structure when producing complex coatings.

Test results for the nanogradient coatings, which were produced using the developed equipment, have shown the conformity to radiation, climatic and mechanical requirements for onboard optical and laser systems. These optical and laser coatings have been successfully implemented and operated in avionic and space devices since some years.

REFERENCES

1. Kuzmichev, A. I., A. B. Shvartsburg, O. D. Volpian, Y. A. Obod, and P. P. Yakovlev, "Polarized light in nanogradient metamaterials," *Optical Complex Systems: OCS11*, Marseille, France, September 5–8, 2011.
2. Volpian, O. D. and A. I. Kuzmichev, "Negative waves refraction. Introduction in physics and technology of electromagnetic metamaterials," *Avers*, Kiev, 2012.
3. Volpian, O. D., A. I. Kuzmichev, Y. A. Obod, and P. P. Yakovlev, "Optical nanogradient metacoatings production using the reactive magnetron sputtering," *Mat. of 15th Intern. Conf.*, "High technologies in the industry of Russia — Materials and devices of functional electronics and microphotonics," *22th Intern. Symp.*, "Thin-films in electronics," 447–450, Moscow, 2009.

Reflectionless Tunneling of Light in Gradient Dielectric Nanostructures: Physical Fundamentals, Theoretical Basis and the First Experiments

A. B. Shvartsburg[1, 2]

[1]Joint Institute for High Temperatures Russian Academy of Sciences, Moscow, Russia
[2]JSC "M. F. Stelmakh R&D Institute" Polyus, Russia

Abstract— This research is devoted to the physical fundamentals and technological basis of a newly shaping branch of applied physics — dynamics of light waves in gradient dielectric nanofilms. These heterogeneous media can be viewed as planar dielectric photonic barriers, characterized by technologically controlled continuous spatial distributions of refractive index $n(z)$ across planes. To highlight the potential of these nanostructures in design of miniaturized subwavelength optical devices for visible and IR spectral ranges, the following corner–stone concepts of gradient nanophotonics are stressed out below:

Giant heterogeneity-induced dispersion of gradient structures, having nothing in common with the natural dispersion of materials, is determined by the geometrical parameters of profile $n(z)$ — it's shape, gradient and curvature; subject to these geometrical parameters the dispersion can be both normal and abnormal.

Flexible reflectance/transmittance spectra of gradient nanofilms in visible and IR spectral ranges are controlled by drastic influence of discontinuities of gradient and curvature of $n(z)$ profile on these spectra. Herein the classical Fresnel formulae, describing the reflectance and transmittance spectra of homogeneous films due to discontinuities of refractive indices, prove to be the limiting cases of more general results, visualizing the drastic influence of discontinuities of gradient and curvature of $n(z)$ profile on these spectra for gradient photonic barriers.

Resonant tunneling of light through the transparent gradient film with concave profile of dielectric susceptibility opens the new horizons for flexible amplitude-phase tuning of wave flows. Effective broadband reflectors, frequency-selective interfaces and miniaturized large angle polarizers, separating S- and P-polarized waves due to different tunneling regimes for these waves, are considered.

The perspective alternative to metal-based plasmonics, formed by nanogradient dielectric films with plasma — like characteristic frequencies, are shown to extend essentially the list of small losses and low cost materials, competing with golden and silver foils, used by optoelectronic devices.

New exactly solvable analytical models in electromagnetics of gradient media are developed. Owing to subwavelength thickness of photonic barriers the traditional suppositions about smallness or slowness of spatial variations of fields or media are invalid in these problems; new exact explicit solutions of Maxwell equations, following from suggested models, form the mathematical fundamentals of gradient nanophotonics.

Experimental basis of gradient nanophotonics is provided by magnetron sputtering of planar dielectric nanofilms with thickness less than 150 nm on the quartz substrates; simultaneous matched movement of two magnetrons, governed by special program, results in controlled formation of prescribed heterogeneous distributions of refractive index n across these films; the depth of spatial modulation of n inside the film is 25–30%.

Synthesis and Properties of the $LiNbO_3$ Thin Films Intended for Nanogradient Structures

R. N. Zhukov, S. V. Ksenich, A. S. Bykov, D. A. Kiselev, M. D. Malinkovich, and Yu. N. Parkhomenko
National University of Science and Technology "MISiS"
Leninskiy pr. 4, Moscow 119049, Russian Federation

Abstract— Lithium niobate ($LiNbO_3$) has been one of the promising ferroelectric materials for potential applications in the area of modulators, switches, actuators, surface acoustic wave devices, sensors, and wave guides because of its high piezoelectric, photorefractive, and nonlinear optical properties. However, thin films are advantageous over their bulk counterparts for various device applications. From a technological point of view, the prospect of $LiNbO_3$ thin films on Si substrates is particularly attractive in view to combine the ferro- and piezoelectric processing capabilities of with lithium niobate the obvious advantages of Si. Indeed, Si technology continues to dominate the microelectronics market, providing a rigid substrate ideal for lithographic techniques. This will make possible the development of integrated devices in which sources, detectors and electronics, as well as ferroelectric and waveguiding components may be produced on the same wafer.

The studied $LiNbO_3$ films were deposited by radio-frequencies magnetrom sputtering of the single-crystalline target in Ar/O = 1 atmosphere (0.6 Pa) on n-type Si (100) and Si (111) substrates ($\rho = 2\,\Omega \cdot \mathrm{cm}$) with SiO_2 buffer layer. The subsequent thermal annealing of the obtained structures has been done in air at 600°C. Atomic force microscopy measurements indicate that the surface roughness of the $LiNbO_3$ thin films was 4–10 nm, which meets the demands for practical waveguiding devices. The ferroelectric properties have been studied by visualization of the as-growth domain structure (vertical and lateral component polarization), recording induced ferroelectric states and the hysteresis loops by piezoresponse force microscopy using Scanning probe laboratory NTEGRA-Prima (NT-MDT, Russia).

Magnetron Sputtering Deposition of Gradient Coatings for Photovoltaic Devices

O. D. Volpian[1], **A. I. Kuzmichev**[2], **and Yu. A. Obod**[3]

[1]M. F. Stelmakh Research Institute — Polus, Vvedenskogo Str. 3, Moscow 117342, Russian Federation
[2]Electron Device Department, National Technical University "Kiev Polytechnical Institute"
Pobedy Prospect 37, KPI-2230, Kiev 03056, Ukraine
[3]Scientific-Manufacturing Enterprise "Fotron-Auto Ltd."
Novodanilovskaya Naberezhnaya 8, Moscow 117105, Russian Federation

Abstract— The development of photonics requests improved photovoltaic devices. An example is the solar energetics, the widespread introducing of which needs photovoltaic solar cells with maximum performance but minimal cost. This leads to a transition from usual thick single-crystal solar cells and batteries to thin-film (1–2 μm) structures. However, thin-film cells have their own shortcomings, mainly, small absorbency of light. In order to solve these problems, two approaches were proposed: the deposition of gradient subwavelength antireflection metacoatings onto the front surfaces and the use of metallic nanostructures and nanoparticles that support surface plasmons and plasmon polaritons. The gradient antireflective metacoatings with small thickness allow guiding practically full light flow into the thin-film cell regardless of wavelength and angle of incidence. The plasmon nanostructures, in turn, enable the higher efficiency of capture of light in thin layers, where it is converted into electricity. We discuss the potential of magnetron sputtering for fabrication of gradient antireflection metacoatings and plasmon nanostructures, designed to improve photovoltaic devices. Here, the gradient coating means a coating with 1D or 2D variable refraction index n.

For obtaining the variable n, dielectric compounds (oxides, nitrides, oxynitrides, fluorides, sulfides, etc.) may be deposited or co-deposited in PVD or CVD processes in reactive gas medium. We consider the best approach is use of the reactive pulse magnetron sputtering (RPMS) because this method, providing energy activation of the condensation process, ensures obtaining dense condensate with low surface roughness and low light scattering loss. Besides, this kind of magnetron sputtering meets the case of arc-free processes in reactive gas medium, deposition process stability, coating thickness uniformity, stability of deposited coatings against various factors. That is RPMS may ensure optical coatings of high quality.

A multicathode/target magnetron system with computer control and monitoring *in situ* has been developed, manufactured and employed for obtaining 1D and 2D gradient multi-wave antireflection coatings. 1D and 2D variation of n was received by parameter regulation of the combined deposition of different sputtered target materials (e.g., Si and Ti, or Nb, or Ta) in reactive gas mixture (e.g., Ar + O_2). Reflection spectra of the gradient metacoatings were measured and numerically calculated with use of specially adopted PC software. The practical reflection spectra of the manufactured gradient coatings were close to the calculated ones. The advantage of these coatings is that their physical thickness is less than the thickness of usual multilayer interference coatings with similar spectral characteristics. Testing the coatings showed they were stable against light laser radiation, environment and mechanics factors due to low optical loss, small thickness and high density of the deposited material. The RPMS system was also employed for deposition of metallic nanoparticles arrays over a substrate. Control of nanoparticle size was carried out by varying pulse parameters of sputtering magnetron power supply.

Obtained results demonstrate that the precisely controlled RPMS method of dielectric and metallic material deposition is a very perspective one for fabrication of high quality gradient and plasmon metacoatings for use in improved photovoltaic devices.

About Some Unusual Electrodynamic Properties of Negative Refraction Materials

V. G. Veselago
A. M. Prokhorov Institute of General Physics, Moscow 119991, Russia

Abstract— The process of mass transfer from the emitter to the receiver is considered for different connection between energy and momentum. Shown, in particular, that in the case when the energy is transferred by radiation, this relationship has the form $E = mv_{ph}v_{gr}$, where v_{ph}-phase velocity, and v_{gr}-group velocity.

From this equation immediately shows that in media with negative refraction radiation transfers the mass not from the transmitter to receiver, but rather from the receiver to the transmitter.

In addition, from the above conclusion follows, that the mass transferred from the transmitter to the receiver is determined not only by transferred energy, but also by transferred linear momentum, which may be associated with energy in different ways. Thus, the well-known relation $E = mc^2$ is a special case of relation $E = mv_{ph}v_{gr}$.

It is shown that the relation $E = mc^2$ corresponds to the transfer of energy from the transmitter to the receiver in the form of a moving material particle, and the relation $E = mv_{ph}v_{gr}$ corresponds to the transfer of energy in the form of electromagnetic waves. The first case can be described by the Abraham energy-momentum tensor, and the second case — with the help of the Minkowski tensor.

ACKNOWLEDGMENT

This work is partially supported by the Visby Program of the Swedish Institute in cooperation with Karlstad University.

Multivariable Development of Gradient Optical Films Structures and Its Technological Applications

Oleg D. Volpian[1], **Yuri A. Obod**[2], **and Sergey V. Shkatula**[2]

[1]Federal State Unitary Enterprise "M. F. Stelmakh Research Institute — Polus"
Moscow, Russian Federation
[2]Scientific-Manufacturing Enterprise "Fotron-Auto Ltd.", Moscow, Russian Federation

Abstract— Optical thin film coatings are the important element of photonic apparatus and need sophisticated approaches for their producing. Traditionally, an optical coating design is based on multilayer systems of alternating high n_h and low n_l refraction indexes and presents an interference system of a kind. Certain functional possibilities are given by another type of interference systems based on gradient coatings (e.g., rugate filters), where the refraction index $n(z)$ is gradually varied across the coating thickness [1, 2].

We have developed a set of programs allowing to calculate the spectral properties of planar thin-film interference structures with continuously varying refractive index across the film thickness and synthesize these structures for a given spectral properties. For the maximum approximation of the calculated structures to the real coating sscattering at the boundaries of layers caused by their roughness are included in their computer design, along with absorption and dispersion of the materials. The practice of making high-precision optical and laser coatings shows that even low roughness of the coating layer boundaries has a significant influence on their optical properties and its consideration in the design of coatings has become necessary.

A heuristic algorithm of global search for an extremum of the fitness function has been developed to design the optimal structure of the thin-film interference gradient [3].

We concentrated our effort on accuracy and stability of optical coatings.One of features used is subsequent layers re-design in situ during sputtering process by measuring deviations of spectral characteristics and calculating errors in initial design. This approach helps to create moresophisticated coatings with more simple optical control, which is equivalent to increase of optical control accuracy. Second approach is addition into coating fitness function information about its stability to minor errors in layer thickness and deviation of refractive index. Thus heuristic algorithm generates most stable designs for sputtering and structures are inherently less demanding for optical control.

REFERENCES

1. Volpian, O. D., A. I. Kuzmichev, Y. A. Obod, and P. P. Yakovlev, "The experience of optical coatings coverage by magnetron method. The problem the gradient coating obtaining," *III International Scientific-Technical Conference, "Vacuum Technology, Materials and Technology"*, Moscow, 2008.
2. Volpian, O. D., A. I. Kuzmichev, Y. A. Obod, and P. P. Yakovlev, "Optical nanogradient-metacoating production by reactive magnetron sputtering," *15th Int. Conf. "High Technology Industry in Russia — Materials and Devices of Functional Electronics and Microphotonics" and the 22th Int. Symp. "Thin Films in Electronics"*, 447–450, Moscow, 2009.
3. Shkatula, S. V., Y. A. Obod, and O. D. Volpian, "Engineering design methods of nanogradient optical coatings," in press.
4. Volpian, O. D. and A. I. Kuzmichev, "Magnetron deposition of optical coatings by magnetron power high frequency AC voltage," *Applied Physics*, Vol. 3, 34–51, 2008.
5. Volpian, O. D. and A. I. Kuzmichev, "Pulsed magnetron sputtering application for creation of optical metacoatings with the longitudinal refractive index nanogradient," *Electronics and Communication (Kiev)*, Vol. 2, No. 55, 28–33, 2010.

Application of X-ray Reflectometry for a Characterization of Graded Layers

K. D. Shcherbachev, **M. D. Malinkovich**, **and Yu. N. Parkhomenko**
National University of Science and Technology "MISiS"
Leninskiy pr. 4, Moscow 119049, Russian Federation

Abstract— Grazing incidence X-ray reflectometry (XRR) is a powerful tool for surface analysis of a density profile and a roughness of a sample surface and buried interfaces in the depth range of 0.2–500 nm. In the present report we demonstrate advantages of the method for characterization of Ta_2O_5-SiO_2 graded layers grown by radio-frequencies magnetron sputtering of the Ta and Si targets. XRR measurements were performed on D8 Discover (Bruker-AXS, Germany) multipurpose X-ray diffractometer equipped with a copper anode 2 kW sealed tube as an X-ray source. Due to large value of the graded layer thickness (about 200 nm) the high-resolution geometry was used. The high-resolution experimental setup was achieved by using a Göbel mirror coupled with a fourfold Ge(220) Bartels-type primary beam monochromator and a Ge(220) diffracted beam analyzer. With this configuration, a wavelength dispersion of the primary beam of $\Delta\lambda/\lambda \approx 7\times10^{-5}$ and a divergence of only 12 arcsec both for the primary and for the diffracted beams were achieved. In the experiment, we measured both specular and off-specular (diffuse) scattering to get a "pure" specular curve (difference between experimental specular and off-specular data). Analysis of the distribution of a specular and a off-specular scattering showed that the shape of the XRR curve depends on density distribution only. Thus, the simulation procedure which is based on Parratt's theory and assumed, that the density gradient can be treated as a multilayered structure composed of thin slices with different densities, can be used for fitting of the "pure" specular XRR curve.

Application of XRR allowed us to reveal a difference between technological design of the Ta_2O_5-SiO_2 graded layers and the measured density distribution profile. The method can be successfully used for the quality control of the layers with complex density profile on early stages of the growth technology development.

Quantum Blooming: The Influence of the Detuning of the Antireflective Wells and the Phenomenon of Nonsymmetric Transmission

A. Kaklyugin
Atmospheric Plasma Instant Technology Corp., Hangenbieten 67980, France

Abstract— The classical concept of tunneling with an exponential decrease of the amplitude of the penetrated wave and the appearance of the reflected wave adopted in quantum mechanics is to be completed by the possibility of quantum blooming, providing additional singular quantum wells. It is shown that such an addition to the classical inaccessible barrier allows dampingless traverse through the barrier [1].

This paper deals with the further development of the ideas of blooming barriers. It is shown that the "detuning" of one of the extra wells causes (so as it follows intuitively) a reflection of the incoming wave and weakening of the transmitted wave. Reflectance and transmission coefficients look out a resonance (Lorentz) profile those parameters are proportional to the detuning degree of the quantum well.

In the case of the detuning availability of both wells, the detuning influence of the opposite wells is to turn out nonsymmetrical. The symmetry breaking is to prove a consequence of the lack of bilateral symmetry of the problem: the incoming wave arrives on the blooming barrier from only one of the selected sides.

It is shown that under certain conditions the different sign detuning of the opposite antireflection wells may compensate for each other — The system of well-barrier-well is to happen navigable without attenuation. The barrier is by virtue of the nonsymmetrycal influence of detuning of the wells to prove transparent in one direction only.

REFERENCES

1. Kaklyugin, A. S., "Quantum blooming: The possibility of passing through the classically inaccessible area without attenuation," *PIERS Proceedings*, 513–519, Moscow, Russia, August 19–23, 2012.

Intermodal Coupling Induced Reflection in Tapered Slow Light Metamaterial Waveguide

Yingran He, Borui Li, and Sailing He
Centre for Optical and Electromagnetic Research
Zhejiang Provincial Key Laboratory for Sensing Technologies
Zhejiang University, Hangzhou 310058, China

Abstract— Metamaterial waveguide composed of left-handed material (LHM) and right-handed material (RHM) can considerably reduce the propagation velocity of guided light. For a specific slow light metamaterial waveguide, two guided modes, namely, a forward mode (where the net energy flow is parallel to the wave vector) and a backward mode (where the net energy flow is anti-parallel to the wave vector) coexist. These two modes degenerate at a critical thickness, leading to zero group velocity. For different operating light frequency, the corresponding critical thickness also varies. Subsequently a tapered waveguide is proposed to achieve completely standstill of incident light in a broad frequency, which is the so called "trapped rainbow storage of light". However, this conclusion is based on the applicability of "adiabatic approximation". Due to the degeneracy of the forward mode and backward mode, this approximation has already broken down in the critical thickness region. In the current work, the coupling between the forward mode and the backward mode in tapered metamaterial waveguide is thoroughly investigated. The mode matching technique is employed to calculate the energy reflection and transmission in a tapered waveguide. It is found that the energy carried by a forward mode will gradually be converted to backward mode as the result of the intermodal coupling when the light propagates inside the slow light waveguide. The conversion rate is especially large near the critical thickness region due to the similarity (both the wave vectors and the mode profiles) between the forward mode and backward mode. Eventually, all the incident energy will be transferred to backward mode and flow out of the waveguide, instead of completely trapping. The physical mechanism for energy reflection is further analyzed based on energy conservation and momentum conservation. A microwave experiment using spoof surface plasmon verifies our conclusion in an unambiguous way. Although the light cannot be trapped forever in the critical thickness region, our study shows that light pulse can indeed be trapped for a fairly long time in the slow light waveguide. By superposing a number of oscillating components with a central frequency, the finite trapping time can be obtained quantitatively. It is found that the trapping time is closely related to the tapering angle of the waveguide. If one would like to trap the light for a longer time, the tapering angle of the slow light waveguide should be made smaller.

Session 1A11a
Application of EM Field in Medicine and in Ecological Industrial Technologies

Magnetoelectric Current Sensor
Roman Valer'evich Petrov, Ivan N. Solovjev, Alexander Nikolaevich Soloviev, Mirza Imamovich Bichurin, ... 140

Microwave Power Absorption in Human Body for Non-invasive Glucose Monitoring
A. Elkady, Mohamed El-Hadidy, A. Medhat, A. Khorshid, A. Darwish, ... 141

Electrodynamic Model of Mitotic Spindle
Daniel Havelka, Michal Cifra, Jan Vrba, ... 142

Ultra Weak Photon Emission from *Saccharomyces Cerevisiae*
Katerina Cervinkova, Michaela Nerudova, Michal Cifra, Jiri Hasek, Jan Vrba, ... 143

Changes in DNA Methylation Wheat Seedlings in First and Second Generations under Influence of EHF EMI
Liya A. Minasbekyan, M. S. Abovyan, ... 144

Two Layers of Microwave Applicators: Comparing of SAR Distribution
Barbora Vrbova, Jan Vrba, ... 145

Magnetoelectric Current Sensor

R. V. Petrov, I. N. Solovyev, A. N. Soloviev, and M. I. Bichurin
Novgorod State University, Russian Federation

Abstract— For the safety, performance, and feedback control of the power supplies and electric circuits, it is often necessary for the circuit to better understand its load current. Protecting the supply circuits, for instance, against overloading and short-circuit conditions requires the system to self-monitor its current delivery. The tasks can be performed by the ME current sensors.

The ME current sensor uses the ME effect as a basis of its measurements. The ME effect is a polarization response to an applied magnetic field, or conversely a magnetization response to an applied electric field. ME behaviour exists as a composite effect in multiphase systems of piezoelectric and magnetostrictive materials. In a magnetostrictive-piezoelectric layered structure the interaction between the magnetic and electric subsystems occurs through mechanical deformation. It means that the ME effect is much stronger at frequencies corresponding to elastic oscillations called resonance frequencies.

The ME current sensors can be applied in many types of sensing devices and perform a function as a magnetic field sensor with some design changes. The sensors can detect currents and magnetic fields according to the purpose. If the quantity (parameter) to be sensed incorporates or can incorporate a magnetic field, the ME current sensor will perform the task.

The sensor consists of the ME composite, generator, rectifier and control systems.

The ME composite is a layered structure which includes a thin piezoceramic plate placed between two magnetostrictive layers of Metglas (FeBSiC) performing a function of electrodes. The PZT layer was poled in an electric field in the thickness direction. The ME laminate have been operated in a transverse mode, in which the applied magnetic fields ($H_{\sim}$, H_0) are in the plane direction of the laminate.

The frequency dependence for transverse ME voltage coefficients of the composite have obtained by solving electrostatic, magnetostatic and elasto-dynamic equations with the corresponding boundary conditions.

The ME current sensors have been designed and fabricated. The sensor works on the electromechanical resonance at the resonance frequency. The sensors sensitivity and ME voltage dependence has been researched by using the designed measurement setup.

The measurement setup includes two power supplies APS-7315 (Aktakom), multimeter HM 8112-3 (HAMEG instr.), oscilloscope ACIP-4226-3 (Aktakom) and an electromagnet.

The induced ME voltage across the PZT layer was measured as a function of the bias magnetic field (H_0) and the input conductor current (I) at a measurement frequency. The current flowed through the test conductor and had a range of 0 A to 1 A. The voltage of the power supply is 5 V.

An output ME voltage of the ME current sensor as a function of detecting input current under various DC magnetic bias has been obtained. The sensors sensitivity dependence has been obtained and analyzed. The sensors sensitivity depends on constructive and material parameters of ME composite and bias magnetic field. Then the operating point for the ME current sensor has been selected. The ME current sensor sensitivity is 2.2 V/A.

The sensor have been designed and fabricated for wireless detecting AC and DC leakage currents in electrical circuits.

ACKNOWLEDGMENT

The reported study was partially supported by the grant of the Federal Target Program "Scientific and pedagogical staff of innovative Russia" on 2009–2013 and by RFBR research project grant #13-02-98801.

Microwave Power Absorption in Human Body for Non-invasive Glucose Monitoring

A. Elkady[1], **M. El-Hadidy**[2], **A. Medhat**[2], **A. Khorshid**[1], **and A. Darwish**[1]

[1]American University in Cairo, Egypt
[2]CST-Middle East, Egypt

Abstract— The main objective of this contribution is to explore the penetration and absorption of electromagnetic millimeter waves in different human body regions for non-invasive glucose monitoring (NGM). Recently, the use of dielectric measurements for the purpose of NGM has been an area of much interest. However, currently no existing report can explore the power dissipation and penetration of electromagnetic waves for the NGM. This work is based on established empirical models of human tissue and standard human body models of the Electromagnetic (EM) simulation tools, such as CST Voxel Model. The Specific Absorption Rate (SAR) and the penetration depths are investigated for various frequencies and different regions of the human body to estimate the optimum real-world scenarios for non-invasive glucose monitoring (NGM). Recent empirical models of dielectric properties for estimating the blood glucose concentrations are applied at frequency range from 1 GHz to 10 GHz and blood glucose concentration from 10 mg/dl to 400 mg/dl. To further explore the effect for various NGM measurement scenarios, analysis of the radar cross section (RCS) is performed for major blood vessels of the neck, arm and thigh using the human body model. A comparative evaluation of RCS measurements for blood in free space and blood in blood vessels is presented in context of investigating the effect of power dissipation and penetration for dielectric NGM measurements.

Electrodynamic Model of Mitotic Spindle

Daniel Havelka[1,2], **Michal Cifra**[1,2], **and Jan Vrba**[1]

[1]Department of Electromagnetic Field/Department of Circuit Theory, Faculty of Electrical Engineering
Czech Technical University in Prague, Technická 2, Prague 166 27, Czech Republic
[2]Institute of Photonics and Electronics, Academy of Sciences of the Czech Republic
Chaberská 57, Prague 18251, Czech Republic

Abstract— Microtubules (MTs) are nano-micro protein filaments which are composed of hundreds or thousands of tubulin dimers and are one of three types of filament which create the cytoskeleton of eukaryotic cell. MTs which are composed of highly polar structures fulfil all conditions for generation of cellular electromagnetic field.

We approximate electric properties of the basic structure of a MT (tubulin heterodimer) as two elementary electric dipoles, which are situated into the centres of gravity of alpha and beta tubulin heterodimers. Also we approximate mechanical oscillations of tubulin heterodimers in one protofilament as mechanical oscillations of the chain of rigidparticles (acoustical brand of oscillations). In addition, we modelled microtubule networks during cell division (mitotic spindle). The models are composed of 200 microtubules (100-astral MTs and 100-kinetochore and polar MTs) and geometry of models resemble prolate spheroids with values of the major axis from 8 µm to 321 µm and of the minor axis from 6 µm to 117 µm. Frequencyband of oscillations of MTs which created model of mitotic spindle is in GHz region. The electric field around oscillating MTs was calculated as a vector sum of contributions from all elementary electric dipoles.

In this paper, we present results from calculations of electric intensity around models of microtubule networks. We also present time progress of electric field around models of mitotic spindles and the frequency spectra of oscillations of MTs.

Ultra Weak Photon Emission from *Saccharomyces Cerevisiae*

K. Červinková[1,2], M. Nerudová[1,2], M. Cifra[2], J. Hašek[3], and J. Vrba[1]

[1]Faculty of Electrical Engineering, Czech Technical University in Prague, Czech Republic
[2]Institute of Photonics and Electronics, Academy of Sciences of the Czech Republic, Czech Republic
[3]Institute of Microbiology, Academy of Sciences of the Czech Republic, Czech Republic

Abstract— This study deals with the topic of ultra weak photon emission (UPE) from yeasts *Saccharomyces cerevisiae*. UPE is a phenomenon resulting from reactions of reactive oxygen species (chemicals with an unpaired electron derived from molecular oxygen) and occures in all living organisms as a by-product of metabolic processes ongoing inter alia in mitochondria.

S. cerevisiae is a model organism applied in many fields of research and contributes significantly towards understanding of eukaryotic cell biology. Two types of *S. cerevisiae* mitochondrial mutations were used — *ptc5*Δ and *pkp1*Δ. Since *ptc5*Δ mutant has deleted *PTC5* gene encoding phosphatase enzyme which is significant in citric acid cycle its mitochondrial oxidative metabolism is reduced and it leads to decrease of reactive oxygen species production. Thus *ptc5*Δ mutant exhibits a lower photon emission compared to the *pkp1*Δ mutant.

Photomultiplier tube R4220P (Hamamatsu Photonics K.K.) with a measuring the range 185–710 nm with highest sensitivity at 410 nm was employed to detect photon emission. Cooling unit C9144 (Hamamatsu Photonics K.K.) was used to reduce termoemission of the photomultiplier to the lowest achievable value Average dark count of the system persisted around 0,07 counts per second. Measurement of the sample took place in a light-tight chamber specially designed for this purposes. Temperature inside the chamber was regulated by A2A (UWE Electronic) thermocontrol unit to the value 28° CPhoton emission was measured for 2 hours for each sample.

Changes in DNA Methylation Wheat Seedlings in First and Second Generations under Influence of EHF EMI

L. A. Minasbekyan and M. S. Abovyan
Department of Biophysics, Yerevan State University, 1 Alek Manukyan St, Yerevan 0025, Armenia

Abstract— In the cells *in vitro* can be occurred the changes in the gene expression on replay to the different stresses such as high temperature, hypoxia and other injurious factors. DNA methylation in critical regulatory regions is involved in regulating gene expression. There is an overall inverse correlation between DNA methylation in regulatory regions of genes and gene expression, and it was confirmed by whole-genome approaches. Nevertheless the role of modified 5-methylcytocine in controlling gene expression is unclear yet.

We study the level of DNA methylation of 4-day seedlings of hexaploid wheat in two generations. In our investigations we separate DNA from seedlings of control and treated by EHF EMI (Extremely High Frequencies Electromagnetic Irradiation) of soaked seeds on 3-rd day after treated. Part from each samples of treated seedlings growing in soil to get a harvest (obtained a second generation). The treatment of seeds we carried out in the range of 45–53 GHz frequencies of EMI. As we suggested EHF EMI can bring to some changes in aqua environment and DNA conformation, which can lead to changes in the level of DNA methylation. The data indicate that level of DNA 5 m-C changes in the first generation depend of EHF EMI frequencies and exposition. After that we have investigate the level of DNA methylation from 4-th day seedlings of seeds of new harvest (second generation), which was growing from the previously treated seedlings. Obtained in our study data shows that the changes in level of DNA methylation in first generation of seeds during the plant ontogeny partially conserved and pass to the seedlings of obtained seeds in second generation. So we have shown on the plant model that the changes in biological systems have epigenetic character and can conserve the whole life of plant and partially pass to the next generation.

Two Layers of Microwave Applicators: Comparing of SAR Distribution

Barbora Vrbova and Jan Vrba
Department of Electromagnetic Field, Faculty of Electrical Engineering
Czech Technical University in Prague, Technicka 2, 166 27 Prague 6, Czech Republic

Abstract— In this contribution we deal with simulations of SAR distribution obtained by ring (i.e., annular) array of microwave stripline type TEM mode applicators of the same type working at frequency 434 MHz. In this study we describe the SAR distribution created in the treated area by two layers of these applicators (in each of these two layer single applicators are configured in a ring situated around area to be treated). At first, we study the shape of SAR distribution created in homogeneous agar phantom, which represents only one type of tissue with defined dielectric parameters, in our case homogeneous phantom represents muscle tissue. The shape of this agar phantom is cylindrical with diameter 8 cm and represents human extremity. But human body is very inhomogeneous and 3D distribution of different tissues is very complicated. Because in real situation EM field diffuses through several types of tissue, then it is for hyperthermia treatment planning very important to use anatomically based models of human body. Therefore, we describe simulations of SAR distribution created in an anatomical model of calf of human body. The main aim of this study is to compare SAR distribution for changing distance between two layers of applicators. In each of both layers is the same number of applicators. We studied different cases of SAR distribution by using two, six and eight applicators positioned each from other by 90°. Distance between the layers is being increased in several steps. When distance between both layers of applicators is zero then the SAR distribution has maximum just in the centre of both layers. However, when the distance between the layers is being enlarged, local maxima of SAR distribution are created.

Session 1A11b
SC1: Physics and Application of Nonlinear Materials and Devices

A Possibility of Negative Differential Resistivity in Thin Ferroelectric Films
Alexander S. Sigov, ... 148
Leakage Currents in Sol-gel PZT Thin Films Doped by Lanthanum
Yu Podgorny, Alexander S. Sigov, A. Vishnevskiy, Konstantin Vorotilov, ... 149
Transformation of the Nanodomain State in the Frustrated Ferromagnet-antiferromagnet System
A. A. Berzin, Alexander I. Morosov, Alexander S. Sigov, ... 150
New Interpretation of Dielectric Spectrum of Water
Alexander A. Volkov, V. G. Artemov, A. V. Pronin, ... 151
Effect of Photodetector's Nonlinear Optical-to-electronic Conversion on the Specific Transmitting Characteristics of an Analog Fiber-wireless Link
Mikhail E. Belkin, ... 152

A Possibility of Negative Differential Resistivity in Thin Ferroelectric Films

A. Sigov
Moscow State Technical University of Radioengineering, Electronics and Automation (MIREA)
Vernadsky prosp. 78, Moscow 119454, Russia

Abstract— Leakage current is one of the key parameters that should be considered in operation of electronic devices with ferroelectric capacitors, such as FRAM and DRAM. The current-voltage $I(V)$ dependencies for some ferroelectric thin films demonstrate an apparent negative differential resistivity [1]. In this paper we show that in capacitor structures with a thin sol-gel PZT film this is an artifact, whose manifestation degree depends on the voltage ramp speed in $I(V)$ measurement process. PZT films ($Zr/Ti = 48/52$) are prepared by sol-gel techniques (annealing 650°C, 20 min, final film thickness of 220 nm) on 8″ silicon wafers with the Pt (150 nm)/TiO_2 (10 nm)/SiO_2 (300 nm)/Si structure. The films demonstrate dielectric hysteresis with remanent polarization of 23 μC/cm2 and coercive field of ∼52 kV/cm. $I(V)$ measurements are performed with the step voltage increase $\Delta U = 0.05$ V and 2, 5, 10 and 20 s delay time. As it can be seen from the figure, the leakage current decreases with the delay time in the whole range of applied voltage. There is the transition region with a negative or near-zero differential conductance (depending on the time delay) located between the low field (up to ∼40–50 kV/cm) and high field (> 115–120 kV/cm) regions. For the $I(V)$ dependence with the delay time of 2 s, the maximum value of negative differential conductivity occurs at a field strength of 103 kV/cm. In all cases the transition regions correspond well to the Dawber-Scott diffusion model [1]. This model considers ionization of oxygen vacancies in PZT layer located near to electrodes. A fitting model is developed, providing a good experimental data approximation in the transition region, and allowing one to obtain the potential barrier height, the oxygen vacancies concentration and estimation value of the charge mobility. In the low field region the data are well fitted whithin the model that considers the sum of ohmic and bias currents [2]. As to the high field region the Schottky-Simmons diffusion model gives adequate results.

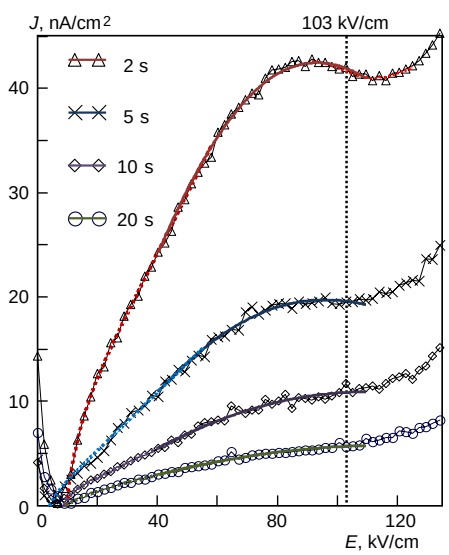

REFERENCES

1. Dawber, M. and J. F. Scott, "Negative differential resistivity and positive temperature coefficient of resistivity effect in the diffusion limited current of ferroelectric thin film capacitors," *J. Phys. Condens. Matter*, Vol. 16, 515–521, 2004.
2. Podgorny, Y. V., K. A. Vorotilov, and A. S. Sigov, "Leakage currents in thin ferroelectric films," *Physics of the Solid State*, Vol. 54, No. 5, 911–914, 2012.

Leakage Currents in Sol-gel PZT Thin Films Doped by Lanthanum

Yu Podgorny, **A. Sigov**, **A. Vishnevskiy**, **and K. Vorotilov**
Moscow State Technical University of Radioengineering, Electronics and Automation (MIREA), Russia

Abstract— PZT thin film is a promising material for nonvolatile memory and MEMS applications. Preparation of PZT thin films by sol-gel techniques suggests a high temperature annealing accompanied by lead oxide volatility. Sol-gel PZT films have a p-type conductivity mechanism as a result of lead vacancies formation. Doping by lanthanum is widely used to compensate hole conduction in PZT. In this report we have tried to establish main mechanisms of charge transport in sol-gel PZT films with different La concentrations in various regions of the electric field $Pb_{1-x}La_x(Zr_{0.48}Ti_{0.52})_{1-x/4}O_3$ films with $x = 0$, 0.02, 0.05, 0.08, and 0.1 are deposited by spin-on sol-gel techniques on platinum plated silicon substrates with intermediate pyrolysis of each layer at 400°C and final annealing at 650°C for 20 min. The final thickness of the PLZT films is about 240 nm. As expected doping by La effects on polarization behavior of PZT films, the values of remanent polarization P_r and coercive field E_c decrease with the increase of La content (23 μC/cm^2, 52 kV/cm respectively for undoped film; 7 μC/cm^2, 25 kV/cm for the film with $x = 0.02$ and so on). Current-voltage dependencies are studied at the voltage ramp speed of 0.005 and 0.0025 V/s. It was found that the I-V dependencies of all PLZT films have two characteristic regions: low- and high-voltage. In the low-voltage region (up to 80–90 kV/cm) the influence of La concentration is negligible and has no definite relationship, see the figure. The leakage current in this region is determined mainly by the high resistance of depletion region of the reverse-bias Schottky barrier at the electrode-ferroelectric interface, as a result the current is practically independent of La content. In the high-voltage region the Schottky barrier breakdown occurs above some threshold voltage and the current is mainly determined by the film bulk resistance. As a result the dependence of the leakage current on La concentration becomes particularly pronounced in this region. At the 2% La content, the leakage current in this region reduces by about two orders in contrast to an undoped PZT film. Further increase of La content leads to an increase of leakage current as a result of change in conductivity mechanism from p- to n-type. The conductivity mechanism in this case is a combination of a limited interface injection and bulk limited drift-diffusion.

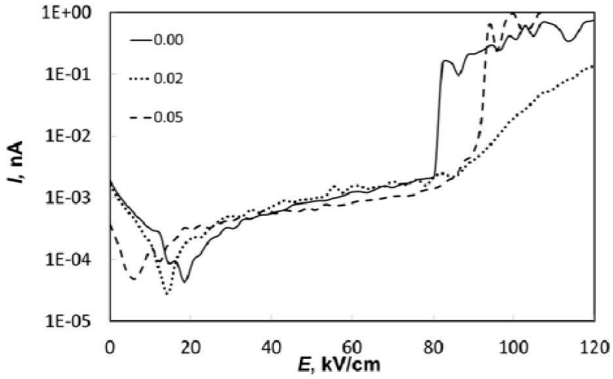

Transformation of the Nanodomain State in the Frustrated Ferromagnet-antiferromagnet System

A. A. Berzin, **A. I. Morosov**, **and A. S. Sigov**
Moscow State Technical University of Radioengineering, Electronics and Automation
Moscow 119454, Russia

Abstract— The existence of atomic steps at the interface of the nanolayer system "ferromagnet-antiferromagnet with uncompensated atomic planes parallel to the interface" brings about the frustration of the interlayer exchange interaction. When the exchange stiffness of the ferromagnet is lower than that of the antiferromagnet and the layer thicknesses are comparable, and when the characteristic distance between the edges of the neighboring atomic steps at the interface R exceeds a critical value, the ferromagnetic layer is divided into 180° domains due to frustrations. The new-type domain walls generated by the frustrations are nucleated at the edges of the atomic steps and penetrate the ferromagnetic layer, extending with the distance from the interface [1, 2]. If the external field applied collinearly to the domain magnetizations exceeds a critical value, it makes the single-domain state of the ferromagnetic layer more preferable. In this case, the domain walls perpendicular to the layer plane divide the antiferromagnetic layer into the 180° domains. The phenomenon of switching of the domain walls generated by frustrations in a two-layer ferromagnet-antiferromagnet nanostructure has been studied theoretically taking into account the energy of the uniaxial anisotropy beyond the exchange approximation. It was shown [3] that in the region of applicability of the exchange approximation, the switching occurs continuously in field, and, strictly speaking, it is not a phase transition. The thickness of the domain walls generated by the frustrations is dependent on the applied magnetic field and increases with decreasing field. The switching field corresponds to the field, at which the domain walls generated by the edges of the neighboring atomic steps at the interface between the layers occupy all the space between the atomic steps and begin to overlap. The thickness of the domain walls generated by the frustrations increases with varying layer thickness or with decreasing magnetic field, until it becomes equal to the thickness of the traditional domain wall in the material. Thereafter the thickness ceases to increase. When the distance R exceeds the thickness of the traditional domain wall in the antiferromagnet, the first-order phase transition takes place in a critical magnetic field, instead of the smooth transition. The domain wall energy in the antiferromagnetic layer is higher as compared to the ferromagnet. The critical magnetic field is found from the conditions of equality of the gain in the Zeeman energy and the loss of the domain wall energy. The phase diagram of the two-layer nanostructure has been constructed in the variables "the magnetic field — the characteristic distance between atomic step edges at the interface between the layers". We predict the existence of the critical point in the phase diagram. Unfortunately, we do not know experimental observations of the predicted switching phenomenon. The transition of a layer (ferromagnetic or antiferromagnetic) from the nanodomain to homogeneous state can be observed by studying its surface using spin-polarization scanning tunneling microscopy [4, 5].

REFERENCES

1. Morosov, A. I. and A. S. Sigov, *Phys. Solid State*, Vol. 46, 395, 2004.
2. Morosov, A. I. and A. S. Sigov, *Phys. Solid State*, Vol. 54, 219, 2012.
3. Berzin, A. A., A. I. Morosov, and A. S. Sigov, *Phys. Solid State*, Vol. 54, 2226, 2012.
4. Schlickum, U., N. Janke-Gilman, W. Wulfhekel, and J. Kirschner, *Phys. Rev. Lett.*, Vol. 92, 107203, 2004.
5. Wulfhekel, W., U. Schlickum, and J. Kirschner, *Microsc. Res. Tech.*, Vol. 66, 105, 2005.

New Interpretation of Dielectric Spectrum of Water

A. A. Volkov[1], **V. G. Artemov**[1], **and A. V. Pronin**[1,2]

[1]A. M. Prokhorov General Physics Institute, RAS, Moscow 119991, Russia
[2]Dresden High Magnetic Field Laboratory, HZ Dresden-Rossendorf, Dresden 01314, Germany

Abstract— New interpretation of the dielectric spectrum of water alternative to the Debye's approach is proposed. Instead of orientational motion of the molecular dipoles, as a basic factor in formation of the dielectric spectrum, we consider exclusively the diffusive motion of protons.

In accordance with the modern concept, protons, H^+, and hydroxyl ions, OH^-, are permanently generated and recombined in the volume of water due to the self-ionization of H_2O molecules [1–4]. Since free protons in water are not observed, they are considered to localize after their birth (on femtosecond time scale) on the neighboring neutral H_2O molecules. The excess proton converts the H_2O molecule into a charged complex H_3O^+ with a positive charge q^+, and leaves a "hole", OH^-, with a negative twin charge q^-. Subsequently, by a relay-race manner the q^+ and q^- charges wander diffusively over the H_2O molecules until they meet each other and recombine to produce a neutral H_2O. Due to mutual Coulomb attraction, a charge usually recombines with its own twin partner. Sometimes, however, the "twins" fail to meet each other and recombine with "foreign" partners (from the first configuration sphere of the ionized molecules). Thus, there are two recombination processes for the charges: fast and slow. Accordingly, there are short- and long-living charge carriers in water. The electrodynamic response of the carriers reveals itself in the panoramic spectrum of conductivity. By analogy with materials with high ionic conductivity (the superionics), we develop a model of hopping proton diffusion in water. This model comprehensively fits the experimental dielectric response of water in a broad frequency range, 10^4–10^{11} Hz [5]. The parameters of water, found by use of this model, bring us to the conclusion that the electrodynamics of water is mainly determined by the ability of H_2O molecules to dissociate rather than to form geometric structures.

REFERENCES

1. Geissler, P. L., C. Dellago, D. Chandler, J. Hutter, and M. Parrinello, "Autoionization in liquid water," *Science*, Vol. 291, 2121 2001.
2. Agmon, N., "Tetrahedral displacement: The molecular mechanism behind the debye relaxation in water," *J. Phys. Chem.*, Vol. 100, 1072, 1996.
3. Walbran, S. and A. A. Kornyshev, "Proton transport in polarizable water," *J. Chem. Phys.*, Vol. 114, 10039, 2001.
4. Bakker, H. J. and H.-K. Nienhuyst, "Delocalization of protons in liquid water," *Science*, Vol. 297, 587, 2002.
5. Volkov, A. A., G. Artemov, and A. V. Pronin, "Proton electrodynamics in liquid water," arXiv:1302.5048v1, 2013.

Effect of Photodetector's Nonlinear Optical-to-electronic Conversion on the Specific Transmitting Characteristics of an Analog Fiber-wireless Link

Mikhail E. Belk
Moscow State Technical University of Radio-Engineering, Electronics and Automation
Vernadskogo av., 78, Moscow, Russian Federation

Abstract— The contribution is focused upon a study of microwave-band pin-photodiode behavior under large-power large-signal modulated IR radiation. Typical realistic examples of this case are employments in short haul radio-over-fiber telecom systems [1] and microwave photonics phased-array antenna radar plants [2]. In a specific unit of their block schemes titled "active photonic antenna" [3], a photodetector usually is followed by transistor pre-amplifier and microstrip or patch antenna.

Generically, a photodiode as any electronic diode is a nonlinear device with a saturation effect and when it works in large-signal mode the fundamental signal is usually accompanied by a remarkable level of nonlinear distortions. Large-signal operation of photodetector in the above-mentioned systems called out an additional issue that a pre-amplifier must concurrently have low noise figure and enough high linearity. A good chance to circumvent this issue is in utilizing a special type high-linear photodetector and a scheme without pre-amplifier. But an employment of special type photodetectors that are structurally more complicate than standard ones might degrade the economical features. Thus, a direct linearity study of an active photonic antenna including a widespread top-illuminated photodiode, middle-power microwave transistor amplifier, and a patch microwave antenna is a subject of practical interest.

The presentation highlights the results of simulation experiments allowing testing by commercial ECAD tool AWR Microwave Office such specific parameters of multi-carrier analog transmission as output intercept points, power to phase conversion characteristics based on recently presented photodiode's large-signal electrical equivalent circuit model [4].

REFERENCES

1. Sauer, M., A. Kobyakov, and J. George, "Radio over fiber for picocellular network architectures," *IEEE J. of Lightwave Technol.*, Vol. 25, No. 11, 3301–3320 Nov. 2007.
2. Pappert, S. A. and B. Krantz, "RF photonics for radar front-ends," *IEEE Radar Conference*, 965–970, Apr. 2007.
3. Prakoso, T., N. Ngah, T. A. Rahman, and Z. Ghassemlooy, "A high gain active photonic antenna for high speed backhaul link: A system analysis," *17th International Conference on Telecommunications*, 455–461, 2010.
4. Belkin, M. E., "Multiscale computer aided design of microwave-band P-I-N photodetectors," *Photodetectors*, InTech, Croatia, 2012.

Session 1AK
Poster Session 1

A Novel Single Prism-based Setup for Simultaneous Shaping of Measuring Beams and Common-path Interferometry
Christoph Gerhard, Wolfgang Viöl, ... 156
Fractal Labyrinths and Planar Nanostructures
Vladimir I. Grachev, Alexander A. Potapov, Vitaly A. German, ... 157
Innovative Circuits to Detect Faults in Accelerator Pedal Sensor Wires to Reduce Unintended Acceleration in Modern Vehicles
Mohamad Rahal, Muhammad Usman, Ibrahim Rida, ... 158
Passive Super-Low Frequency Remote Sensing System
Nan Wang, Qiming Qin, ... 159
Multi-resolution Composite Linear DBF Array
Yue Tang, Yi-Long Lu, ... 160
Microstrip Antennas on a Cylindrical Surfaces
Rafal Lech, Wojciech Marynowski, Adam Kusiek, ... 161
UWB Coplanar Line Fed Antennas on the Conducting Planar and Cylindrical Surfaces
Rafal Lech, Wojciech Marynowski, Adam Kusiek, ... 162
Cheap UWB Coplanar Line Fed Antennas on Electrically Conductive Adhesive Tape
Wojciech Marynowski, Rafal Lech, Adam Kusiek, ... 163
Multi-band Circular Patch Antenna for Wideband Application
Ebrahim Sailan Alabidi, Muhammad Ramlee Kamarudin, Tharek Bin Abdul Rahman, Hashimu Uledi Iddi, ... 164
A Novel Compact Multiband H-shaped Patch Antenna Using CRLH Zeroth Order Resonator
Mohit Kumar Joshi, Ankit Kumar Ghosh, Akhilesh Mohan, ... 165
The Comparative Analysis of UWB Antennas with Complementary Characteristics: A Functionality in FS and Applicability for the Usage Close to Tissues
Tommi Tuovinen, Markus Berg, Erkki T. Salonen, ... 166
Optimized Reflector Position for Vlasov Antennas
Hilal El Misilmani, Mohammed Al-Husseini, Karim Y. Kabalan, Ali El-Hajj, ... 168
The Imbedding Method in the Internal Electrodynamics Problem of Parabolic Reflector Antennas
S. V. Boyarkin, Valery L. Kuznetsov, ... 170
Feasibility of Using an Absorptive Cover for Ice, Snow or Water Removal from Radome Surface
Aleksey Solovey, ... 171
Windowing of the Discrete Green's Function for Accurate FDTD Computations
Tomasz P. Stefanski, ... 172
Combined E and H Field Formulation of IPO (Iterative Physical Optics) for Metallic, Coated or Uncoated with Lossy or Non Lossy Dielectric Materials Cavities
A. Pajot, Nicolas Douchin, Henri-Jose Mametsa, ... 173
Global Base Approach to $\boldsymbol{H}$-polarized Wave Scattering by Conducting Circular Cylinders
Keníchiro Yashiro, ... 174
Simulations of Electromagnetic Pulses from Hypervelocity Impact Plasmas
Alexander Fletcher, Sigrid Close, ... 175
Advances in Surface Integral Equation for Nano-scale Optical Wireless Nanolink
Yang Shao, Zhen Peng, Jin-Fa Lee, Diego M. Solis, Jose Manuel Taboada, ... 176
Surface Integral Equation Methods for Multi-scale Composite Problems
Zhen Peng, Jin-Fa Lee, ... 177
The Coulomb Gauge Based Integral Equation
Xiaoyan Y. Z. Xiong, Y. H. Lo, Lijun Jiang, Wei E. I. Sha, ... 178
Radiative Transfer with Coherent Backscattering Compared to Exact Scattering Methods
Antti Penttila, K. Muinonen, E. Zubko, Michael I. Mishchenko, Janna M. Dlugach, D. W. Mackowski, G. Videen, ... 179

Optical Interaction of Two Closely Spaced Nanoholes in Au Film
M. Janipour, Tavakol Pakizeh, F. Hodjat-Kashani, ... 180
Novel All-optical Logic Gates Based on Microring Metal-insulator-metal Plasmonic Waveguides
Yaw-Dong Wu, Yung-Ta Hsueh, Tien-Tsorng Shih, ... 181
CRLH-TL Based Zeroth Order Resonance Antenna
Ankit Kumar Ghosh, Mohit Kumar Joshi, Akhilesh Mohan, ... 182
New Weakly-coupled Nearly Adapted Resonant Sensors for Microwave Range Measurements
Filippo Micheletti, Roberto Olmi, ... 183
Multi-layered Frequency Selective Surfaces for High Frequency Applications
Agâh Oktay Ertay, Can Suer, ... 184
A Novel Neural Network Model of a Microwave Transistor Using Particle Swarm Optimization
Ufuk Özkaya, Filiz Gunes, ... 185
Characteristic Planes of Microstrip and Unilateral Finline Tee-junctions
Alicia Casanueva Lopez, A. Leon, Angel Mediavilla Sanchez, Joe Helszajn, ... 187
Study of Longitudinally Magnetized Left-handed Cylindrical Ferrite Coupled Line Junction
Adam Kusiek, Wojciech Marynowski, Jerzy Mazur, ... 189
Nonreciprocal Devices Using Longitudinally Magnetized Left Handed Ferrite Coupled Line Junction
Wojciech Marynowski, Adam Kusiek, J. Mazur, ... 190
A K-band Direct Injection-locked Frequency Divider Using Harmonic LC Tanks
Chien-Pai Wu, Yen-Chung Chiang, ... 191
The Phase Noise Reduction of GaAs V-band Push-push VCO Using Slow-wave CPW Resonator Structures
Hsien-Chin Chiu, Min-Li Chou, Po-Yu Ke, Fan-Hsiu Huang, Hsuan-Ling Kao, ... 192
Novel Atmospheric Pressure Plasma-based Methods for Surface Modification and Hybrid Laser Ablation of Optical Glasses
Christoph Gerhard, Wolfgang Viöl, ... 193
A Versatile Atmospheric Pressure Plasma Source for Simultaneous Surface Treatment and Analysis
Christoph Gerhard, Stephan Bruckner, Wolfgang Viöl, ... 194
Shape Dependent Broadband Plasmonic Absorption in Metallic Nanoparticles for Efficient Organic Solar Cells
Xuanhua Li, Wallace C. H. Choy, Haifei Lu, Wei E. I. Sha, Ho-Pui Ho, ... 195
An Accurate and Robust Timing and Frequency Synchronization for Coherent Optical Systems
Lingchen Huang, Changjian Guo, Dawei Wangle, ... 196
Compressed Sensing for Velocity Estimation of CW Radar Using a Constrained Least Square Method
Jiwoong Yu, Tae Yun Lee, Seok Kim, Seeon Jeon, Min-Ho Ka, ... 197
Electromagnetic Signal Processing for Feature Extraction and Classification of Lossy Dielectric Targets
Gonul Turhan-Sayan, Basak Isik Barut, ... 198
Bivariate Statistical Analysis for Electromagnetic Reverberation Chamber
Suna Choi, Seungkeun Park, ... 199
Design of the Electric-fields Probe in the Personal Exposure Meter
Sang Il Kwak, Byung Chan Kim, Hyung-Do Choi, Young Joong Yoon, ... 201
GNSS-based Bistatic Synthetic Aperture Radar Image Formation via Compressive Sensing
Chunyang Dai, Liangjiang Zhou, Xingdong Liang, Yirong Wu, ... 203
Analysis and Design of Directional Couplers Based on Metal-insulator-metal (MIM) Plasmonic Waveguide
Fabrizio Frezza, Endri Stoja, ... 204
Capacitively-loaded Inductively-coupled Fed Loop Antenna with an Omnidirectional Radiation Pattern for UHF RFID Tags
Qi Liu, Yufeng Yu, Qiangsheng Huang, ... 205
Slot Embedded Microstrip Paper Based Substrate Antenna for Automotive Systems
Muhammad Yusof Ismail, W. N. Zaihasra, Norbahiah Misran, ... 206
Enhanced Fullwave-mode Technique for Multilayered Passive Circuits Including Ferrites with Arbitrary dc Magnetic Field Polarization
Mohamed Lamine Tounsi, Youcef Gaceb, Mustapha C. E. Yagoub, ... 207
Optimizing Photonic Crystal Filter in Defective 1D Periodic Media
Veysel Korkmaz, A. Cetin, ... 209

Design of Coplanar Sensor for the Permittivity Measurement of Thin Dielectric Samples
Manisha Shete, Mohammad Jaleel Akhtar, ... 210
Inverse Modeling of Pseudo-interdigital Bandpass Filters Using Artificial Neural Networks
Erdem Demircioglu, Murat H. Sazli, Orhan Sengul, S. Taha Imeci, Mesut Gokten, ... 211

A Novel Single Prism-based Setup for Simultaneous Shaping of Measuring Beams and Common-path Interferometry

C. Gerhard and W. Viöl
Laboratory of Laser and Plasma Technologies, University of Applied Sciences and Arts
Von-Ossietzky-Straße 99, Göttingen 37085, Germany

Abstract— In this contribution, we present a novel common-path interferometer setup with integrated beam shaping device. By the use of a single prism, unidirectional shaping of laser beams that are used for interferometry is made possible by compression or extension, respectively, of the initial beam profile. In this vein, elliptically-shaped diode laser beams are circularised by realising the required aspect ratio of both the fast and the slow axis [1]. Against this background, a mathematical description of single-prism beam shaping is provided. After shaping, both the measuring and reference beam propagate coaxially and pass a reference plane plate, comparable to a Fizeau interferometer setup. After reflection by the sample, a fraction of the interference signal is reflected towards a detector. As shown in Figure 1, this reflection is accomplished by the beam shaping prism which thus also acts as beam splitting device.

By this configuration, well-evaluable interferograms with a Michelson contrast of 0.42–0.45 were obtained [2]. The main advantage of the presented setup in terms of beam shaping is the fact that a wide range of different aspect ratios can be realised dynamically, where the resulting deflection of the optical axis is compensated by a foldable opto-mechanic setup. This allows the use of a number of different (diode) laser sources. It is thus an easy-to-use, cost-efficient and versatile alternative solution to conventional beam shaping devices such as fixed anamorphotic prism pairs in terms of experimental applications. Due to its common-path configuration, the presented interferometer features high immunity and stability, providing a comparatively high contrast without using any classically coated beam splitting device.

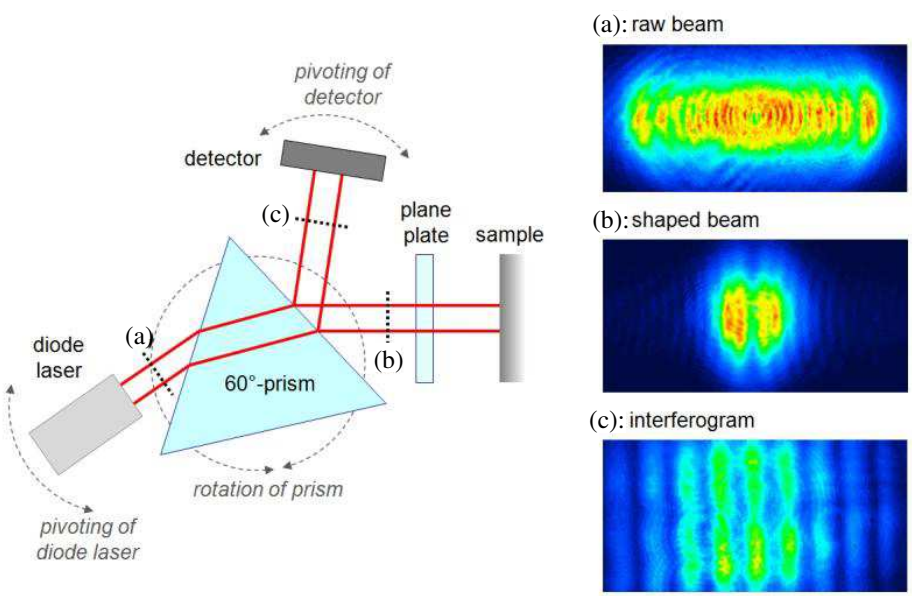

Figure 1: Interferometer setup including (a) integrated single-prism beam shaper, (b) resulting circularisation of the raw beam and (c) resulting interferogram.

REFERENCES

1. Gerhard, C., B. Bahr, S. Brückner, and W. Viöl, *J. Opt. Res.*, Vol. 14, 1–10, 2012.
2. Gerhard, C., J. Heine, B. Bahr, S. Brückner, and W. Viöl, *Measurement*, Vol. 46, 1291–1296, 2013.

Fractal Labyrinths and Planar Nanostructures

V. I. Grachev, **A. A. Potapov**, **and V. A. German**
Kotel'nikov Institute of Radio Engineering and Electronics, Russian Academy of Sciences, Russia

Abstract— Now are widely used fractal-topological methods of processing and analysis of nanostructures [1]. The paper deals with the application of fractal formalism to the tasks of reconstruction complicated images of microstructures of nano-modified materials based on fractal labyrinths [2], in particular, at equal fractal signatures of their parameters. Presents the elements of the fractal labyrinths theory and their use in computer image analysis of microstructures. Image of microstructures of nano-modified material obtained in a transmission electron microscope. Nanostructure — Pd labyrinth-like planar nanosystem on a copper grid formed on the Langmuir monolayer [3]. On image is especially pronounced the structure of the original fractal labyrinth. Its physical nature is the result of the dynamic nonequilibrium processes. Presents the results of fractal analysis of this TEM image: measured the fractal dimension D and fractal signatures (fractal kepstrums) of microsamples surface. Showed the mean value of the fractal dimension D and its root-mean-square value σ. In those cases, when the image is composed of fragments with different values of the estimates of the fractal dimension, it makes sense to produce clustering of images in order to highlight areas with approximately constant estimates of D. In the mode of clustering, specifying the desired range of local fractal dimensions ΔD, obtain a field D, for which all the values $D_i \in \Delta D$ are displayed in one color. The obtained data shows one of the main our conclusions reached earlier, namely, the point estimate of the fractal dimension leads to absurd results. For analysis of complex stochastic objects necessary and sufficient condition of unequivocal result is to obtain of fractal signatures and fractal cepstrum.

The problem of expanding entirely new class of fractal-scaling approaches under equal fractal signatures of the object and the background considered by the authors at an angle of mathematics of fractal structures and labyrinths. The concept of fractal labyrinths allows you to identify the parameters of complex stochastic nanostructures.

REFERENCES

1. Potapov, A. A., Yu. V. Gulyaev, S. A. Nikitov, A. A. Pakhomov, and V. A. German, "Noveyshie metody obrabotki izobrazheniy," *Newest Images Processing Methods*, 496, Moscow, Fizmatlit, 2008.
2. Potapov, A. A. and V. I. Grachev, "Fractal labyrinths: Physics and fractional operators," *PIERS Proceedings*, 1584–1587, Moscow, Russia, August 19–23, 2012.
3. Khomutov, G. B. and S. P. Gubin, *Mater. Sci. Eng. C*, Vol. 22, No. 2, 141–146, 2002.

Innovative Circuits to Detect Faults in Accelerator Pedal Sensor Wires to Reduce Unintended Acceleration in Modern Vehicles

Mohamad Rahal, Muhammad Usman, and Ibrahim Rida
Department of Electrical Engineering, University of Hail, P. O. Box 2440, Hail, Saudi Arabia

Abstract— All modern vehicles employ computerised management system to control the speed of the engine. *Electronic control unit* (ECU) is used to manage and control key functions in the vehicle such as opening the throttle angle. In addition, the ECU receives sensory inputs such as the accelerator pedal angle from the accelerator pedal position (APP) sensor. The advantages of employing computerised management system are: 1) increasing vehicle stability, 2) better fuel economy, and reduction of harmful emissions. However, the downside of using a computerised management system is that ECU must be able to cope with any abnormalities and faults. Recent studies have shown that they have been many cases of unintended acceleration incidents. Some of these cases were attributed to the inability of the ECU to detect short or open circuit faults in the APP sensor wires.

In this paper, a detection circuit is proposed that is able to detect, identify and localize both open and short circuit faults. Moreover, it has a simple realization and can be implemented in hardware or software form. The proposed circuit sends key commands to the ECU to place the engine in idle mode when specific faults occur on the APP sensor wires. Full simulation results and implementation architectures of the circuit will be presented in the conference.

Passive Super-Low Frequency Remote Sensing System

Nan Wang and Qiming Qin
Institute of Remote Sensing and Geographical Information System
Peking University, Beijing 100871, China

Abstract— Over the past decade, the Super-Low Frequency (SLF) remote sensing has undergone a revolution driven by its increasing use in geological applications and resource exploration. The SLF electromagnetic wave, originating from natural-source (passive) or controlledsource (active) within a general range of 3–3000 Hz, propagates through the surface of the earth a few kilometers deep, and then the correspondingly reflective or inductive wave carries abundant underground information. We have mainly focused on the passive remote sensing by developing a passive SLF remote sensing system, including the hardware and software system, to collect, process and analyze the SLF signal in order to extract the underground information.

The hardware system can be divided into three parts: the sufficient-sensitivity signal collector, the host computer and the power supply. The signal collector is used to sense SLF signal, and then a frequency sweep circuit under the host computers control can be utilized to digitally record high-quality SLF frequency spectrum data sets at every frequency point. By means of the Frequency-Depth model [1, 2], we can calculate the Amplitude-Depth curves of SLF signal in the real-time display on the computer screen. The characteristics of anomalies we are interested in can be interpreted by analyzing the SLF Amplitude-Depth curves.

The software system is in charge of data processing and final interpretation of SLF remote sensing. We have developed the pre-processing module, which includes data format transformation, stacking, filtering and normalization methods; the de-noising module aiming at filtering random noise and industrial electromagnetic interference; the interpretation module which builds the geological maps or profiles of underground anomalies; the typical geo-object database module. All the above modules help the SLF remote sensing to identify and extract representative underground anomalies by the enormous expansion of the earth observation.

Up until now, the passive Super-Low-Frequency (SLF) remote sensing system have successfully been applied to geothermal well surveys, petroleum and gas prospecting, fault identification and mining industry [2, 3].

REFERENCES

1. Burrell, G. A. and L. Peters, Jr., "Pulse propagation in lossy media using the low-frequency window for video pulse radar application," *Proceedings of the IEEE*, Vol. 67, 981–990, 1979.
2. Qin, Q. M., B. S. Li, R. B. Cui, H. B. Jiang, Q. P. Wang, Z. X. Zhang, and N. Zhang, "Analysis of factors affecting natural source SLF electromagnetic exploration at geothermal wells," *Chinese Journal of Geophysics-Chinese Edition*, Vol. 53, 685–694, 2010.
3. Hou, G., X. Qian, S. Wang, and J. Sun, "Possibility of the application of the ultra-long electromagnetic wave remote sensor to marine geological exploration," *Acta Geologica Sinica-English Edition*, Vol. 74, 391–394, 2000.

Multi-resolution Composite Linear DBF Array

Yue Tang and Yilong Lu
School of Electrical and Electronic Engineering
Nanyang Technological University, 50 Nanyang Avenue, 639798, Singapore

Abstract— This paper presents a multi-resolution composite linear Digital Beamforming (DBF) array based on the composite array concept. A composite array is a amalgamation of several uniform subarrays with different interelement spacings. Conventionally, a composite array is formed by several subarrays and each subarray has a half-wavelength spacing at a particular frequency; by doing so the composite array can get a constant mainlobe beamwidth in a wide frequency band. While in this paper, we propose a composite array with different spacing structure (from half a wavelength to several wavelengths) to achieve very narrow mainlobe beamwidth with much less array elements required by a uniform linear array.

The proposed composite array is based on multi-resolution concept. Each subarray could perform DBF with different resolution independently and super-resolution DBF could be obtained by combining multi-resolution DBF results of all the subarrays. Different with conventional DBF arrays that may perform continuous digital beam scanning with similar beamwidth over a relatively large look angle region, the proposed DBF array with multi-resolution subarrays could point the beams in the desired direction to achieve super-resolution beamwidth by a special digital processing. In the numerical experiments, the beamforming performance of proposed DBF array will be demonstrated in comparison to conventional DBF arrays with much more antenna elements.

Microstrip Antennas on a Cylindrical Surfaces

R. Lech, **W. Marynowski**, **and A. Kusiek**
Gdansk University of Technology, Gdansk, Poland

Abstract— Microstrip antennas localized on curved surfaces are becoming popular due to their advantages and possibilities of applications [1]. One advantage of using antennas with a curved surface is the possibility of integrating them with the object on which they are mounted. The other advantage is their wider, relatively to planar antennas, visible angular range. The arrays of radiators located on the surface of a cylinder may be the examples of such antenna that provide omni-directional radiation patterns in azimuth plane or provide, in this plane, the possibility of beam control. These arrangements can find their application in base stations for mobile communications systems.

In the analysis of conformal antennas one encounters the electromagnetic problem which consists in finding the electromagnetic field resulting from radiation sources placed on curved surfaces. It is a boundary problem, where the fields in the area outside antenna surface and the fields or current distribution on the radiating elements have to be matched.

The analysis of microstrip patch antennas mounted on a circular cylinder and fed by a probe is being conducted in the paper. The configuration contains an arbitrary number of substrate and superstrate layers (which can also be analyzed as air gaps). The full wave approach is being used to analyze the structure. Numerical results are obtained using a moment-method calculation. An efficient way of calculating a dyadic Green's function is presented here for arbitrary configuration of multilayered antena structure.

ACKNOWLEDGMENT

This work was supported from sources of National Science Center under grant decision No. DEC-2011/01/D/ST7/06639.

REFERENCES

1. Josefsson, L. and P. Persson, "Conformal array synthesis including mutual-coupling," *Electroinic Letters*, Vol. 35, No. 8, 625–627, April 1999.

UWB Coplanar Line Fed Antennas on the Conducting Planar and Cylindrical Surfaces

R. Lech, W. Marynowski, and A. Kusiek
Gdansk University of Technology, Poland

Abstract— The ultra-wideband (UWB) systems have become very attractive and drawn interests for their low operating power level, low complexity, high data rates and great capacity. They find application not only in wireless communication but are also used in see-through-wall radar-imaging [1] and ultra-wideband microwave imaging for the detection and localization of breast cancer [2]. One of the most essential parts of the UWB systems are antennas. They are required to operate in a wide frequency band, be compact and simple with small dimensions and light weight [3, 4]. When the antenna is designed on thin and flexible dielectric substrate it can be bent and placed on a curved surfaces. As authors have recently shown [5] the bending of coplanar fed UWB antennas does not significantly affect their performance.

Conformal antennas are becoming popular due to their many advantages and possibilities of applications [6, 7]. The advantages of using antennas with a curved surface arise not only from the possibility of integrating them with the object on which they are mounted on but also from the increase, relatively to planar antennas, of their visible angular range. The circular antenna arrays, or arrays of radiators located on the surface of a cylinder may be the examples of such antenna that provide omni-directional radiation patterns in azimuth plane or provide, in this plane, the possibility of beam control. Such antennas can be used, e.g., in base stations for mobile communications systems.

The analysis of UWB coplanar line fed antennas mounted on the planar or, when bend, on cylindrical surfaces is being investigated in the paper. The influence of curvature of the antennas as well as the proximity of metallic surface on their reflection coefficients and radiation patterns is investigated. A commercial softwares are used to design the UWB radiators and investigate the influence of the curvature. The obtained results are verified by own measurements of manufactured antenna prototypes.

ACKNOWLEDGMENT

This work was supported from sources of National Science Center under grant decision No. DEC-2011/01/D/ST7/06639.

REFERENCES

1. Yang, Y., Y. Wang, and A. E. Fathy, "Design of compact vivaldi antenna arrays for UWB see through wall applications," *Progress In Electromagnetics Research*, Vol. 82, 401–418, 2008.
2. Lazaro, A., D. Girbau, and R. Villarino, "Wavelet-based breast tumor localization technique using a UWB radar," *Progress In Electromagnetics Research*, Vol. 98, 75–95, 2009.
3. Chen, M. and J. Wang, "Compact CPW-fed circular slot antenna for ultra-wideband applications," *8th International Symposium Antennas, Propagation and EM Theory*, 7881, Nov. 25, 2008.
4. Marynowski, W. and J. Mazur, "Design of UWB coplanar antenna with reduced ground plane," *Journal of Electromagnetic Waves and Applications*, Vol. 23, No. 13, 1707–1713, 2009.
5. Lech, R., W. Marynowski, and A. Kusiek, "UWB microstrip antennas on a cylindrical surfaces," *Progress In Electromagnetics Research Symposium Abstracts*, Taipei, Mar. 25–28, 2013.
6. Josefsson, L. and P. Persson, "Conformal array synthesis including mutual-coupling," *Electroinic Letters*, Vol. 35, No. 8, 625–627, Apr. 1999.
7. Xu, Z., H. Li, Q.-Z. Liu, and J.-Y. Li, "Pattern synthesis of conformal antenna array by the hybrid genetic algorithm," *Progress In Electromagnetics Research*, Vol. 79, 75–90, 2008.

Cheap UWB Coplanar Line Fed Antennas on Electrically Conductive Adhesive Tape

W. Marynowski, R. Lech, and A. Kusiek
Gdansk University of Technology, Poland

Abstract— The ultra-wideband (UWB) systems have become very attractive for their many advantages and drawn interests of researchers and industry for over a decade now since the Federal Communications Commission (FCC) released the unlicensed frequency band of 3.1–10.6 GHz for commercial UWB applications. The UWB systems find application, e.g., in wireless communication, see-through-wall radar-imaging and imaging for the detection and localization of breast cancers. The UWB antennas should not only operate in a wide frequency band but also have compact and simple structure with small dimensions and light weight [1, 2]. Besides above requirements their production costs, especially for mass production, should also be as low as possible.

In this paper we investigate the modified version of UWB coplanar antenna proposed in [2] with reduced dimensions and absence of dielectric substrate. The antenna is designed to be fed by a coplanar line with reduced ground plane on a short brick of dielectric layer and the antenna resonator rings are placed in free space (the dielectric substrate is removed). In order to manufacture such antenna structure we utilize the electrically conductive adhesive tape. The designed antenna is produced with the use of laser structuring system, which cuts the antenna geometry on the tape. After this procedure the redundant tape can be easily removed resulting in the demanded antenna structure.

The investigation of antenna performance in terms of its reflection coefficient and radiation pattern is conducted in this paper. The influence of placing antenna on foil, paper, wood or glass is also tested experimentally.

ACKNOWLEDGMENT

This work was supported in part by Polish Ministry of Science and Higher Education from sources for science in the years 2012–2013 under Contract No. 0340/IP2/2011/71.

REFERENCES

1. Chen, M. and J. Wang, "Compact CPW-fed circular slot antenna for ultra-wideband applications," *8th International Symposium Antennas, Propagation and EM Theory*, 7881, Nov. 25, 2008.
2. Marynowski, W. and J. Mazur, "Design of UWB coplanar antenna with reduced ground plane," *Journal of Electromagnetic Waves and Applications*, Vol. 23, No. 13, 1707–1713, 2009.

Multi-band Circular Patch Antenna for Wideband Application

Ebrahim Sailan Aabidi, M. R. Kamarudin, T. A. Rahman, and Hashimu Uledi Iddi
Wireless Communication Centre (WCC), Universiti Teknologi Malaysia
UTM Skudai, Johor 81310, Malaysia

Abstract— This paper presents a multi-band circular patch antenna for wideband applications. The antenna operates at 1.5, 2.8, 4.0, 4.8, 7.5 and 8.8 GHz frequency bands. The antenna has been designed, simulated and fabricated on an FR4 substrate with dielectric constant (ε_r) of 4.4 and thickness of 1.6 mm. A dual feed approach has been used in the design of the proposed wideband antenna. The multi-band circular patch antenna is smaller than the conventional antenna for wideband application. The final optimized design is $50 \times 50\,\mathrm{mm}^2$. Figure 1 shows the prototype of a multi-band circular patch antenna. The measured and simulated return loss results and simulated radiation pattern results of proposed antenna has been presented.

Figure 2 shows the measured and simulated return loss result of the proposed multi-band circular patch antenna. The experimental results indicate wide impedance bandwidths (VSWR < 2) of 18% (1.27–1.51), 6.2% (2.66–2.83), 7.6% (3.8–4.1), 2.55% (4.74–4.86), 1.93% (7.5–7.65) and 1.35% (8.8–8.92) in the frequency bands. The dual feed improves the gain of the circular patch antenna which gives 4, 4.5, 3.2, 2.1, 6.8 and 1.5 at 1.5, 2.8, 4, 4.8, 7.5 and 8.8 GHz, respectively. The measured and simulated results show that the proposed antenna provides good performance in term of return loss and radiation pattern for wideband applications.

(a) (b)

Figure 1: Prototype of the proposed antenna. (a) Front view. (b) Back view.

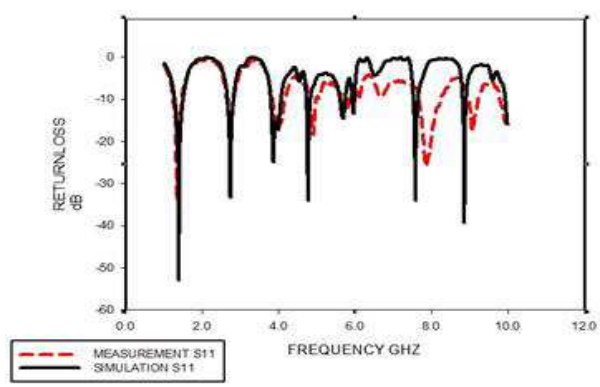

Figure 2: Return loss results.

A Novel Compact Multiband H-shaped Patch Antenna Using CRLH Zeroth Order Resonator

Mohit Kumar Joshi[1], **Ankit Kumar Ghosh**[1], **and Akhilesh Mohan**[2]

[1]The LNM-Institute of Information and Technology, Jaipur, India
[2]Indian Institute of Technology Rajasthan, Jodhpur, Rajasthan, India

Abstract— A novel design and simulation of multiband rectangular patch antenna loaded with Composite Right/Left Handed (CRLH) metamaterials is proposed. Its structure consists of two rectangular notched patches (H-shaped) on spiral slotted ground plane with mushroom like structure. The simulation is demonstrated using full wave EM simulator HFSS 13.0. The zeroth-order resonator (ZOR) properties are analysed. The proposed antenna has a total volume of $40.74 \times 15 \times 1.57\,\mathrm{mm}^3$ with substrate and size of single unit of patch is $6.5 \times 13\,\mathrm{mm}^2$ which makes it compact and suitable for portable devices. Maximum efficiency demonstrated here for different frequency bands are quite high in comparison with previously reported any kind of rectangular patch antenna. The antenna offers omnidirectional radiation patterns. Antenna gain and other antenna parameters are sufficient for wireless application such as GSM, Wi-Fi (5 GHz), WiBro, WiMAX and satellite communication.

Antenna Design and Results:

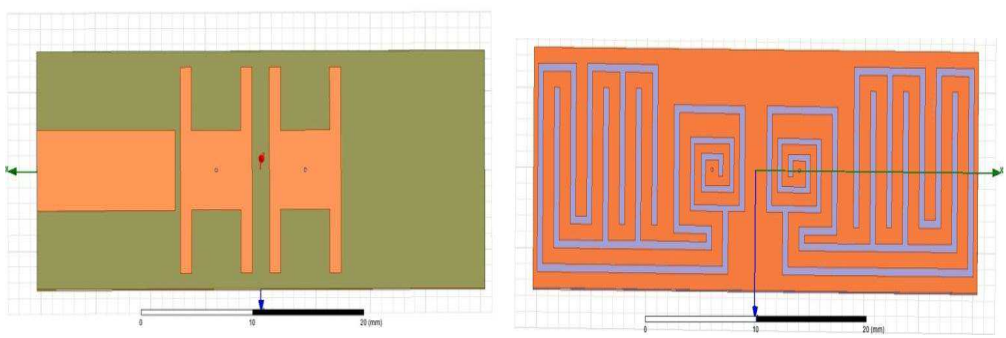

(a) (b)

Figure 1: (a) Geometry of proposed antenna (top view). (b) Geometry of proposed antenna (bottom view).

Six frequencies (a) 0.6500 GHz, (b) 3.0764 GHz, (c) 3.6434 GHz, (d) 4.1984 GHz, (e) 5.8412 GHz, (f) 6.0278 GHz are obtained by this proposed design of Antenna. At most of the operating bands, this antenna exhibits a monopole like radiation pattern. Highest gain 4.76 dBi is obtained with 90.39% efficiency at 5.8412 GHz band. The maximum return loss of 26.45 dB ($S_{11} = -26.45$ dB) is also obtained at 5.8412 GHz. This antenna covers GSM (650), WiBro, IEEE 802.11a Wi-Fi (5 GHz), WiMAX based applications and especially systems which operates in S-Band and C-Band. Maximum relative bandwidth 4.14% obtained at 3.6434 GHz with 86.4% efficiency and 2.29 dBi gain. H-shape and slotted ground plane leads to obtain desired results with miniature structure of antenna.

REFERENCES

1. Lai, A., K. M. K. H. Leong, and T. Itoh, "Infinite wavelength resonant antennas with monopolar radiation patterns based on periodic structures," *IEEE Trans. on Antennas Propagat.*, Vol. 55, No. 3, 868–876, Mar. 2007.
2. Zhu, J., M. A. Antoniades, and G. V. Eleftheriades, "A compact tri-band monopole antenna with single-cell metamaterial loading," *IEEE Trans. on Antennas Propagat.*, Vol. 58, No. 4, 1031–1038, Apr. 2010.
3. Baek, S. and S. Lim, "Miniaturized zeroth-order antenna on spiral slotted ground plane," *Proc. Electron Lett.*, Vol. 45, 1044–1047, Sep. 2009.

The Comparative Analysis of UWB Antennas with Complementary Characteristics: A Functionality in FS and Applicability for the Usage Close to Tissues

Tommi Tuovinen, **Markus Berg**, **and Erkki Salonen**
Centre for Wireless Communications, University of Oulu, Finland

Abstract— The properties of wearable antennas are proposed to investigate in the proximity of a body for wireless body area network (WBAN) usage. The present paper considers the operation of two complementary antennas based on Babinet's principle as $Z_{\text{slot}} = Z_0^2/4Z_{\text{dipole}}$ where Z_0 is a wave impedance and Z_{antenna} is input impedance. We examine the possibility to implement planar ultra wideband (UWB) complementary structures. Their applicability and discrepancies for UWB WBAN on-body usage are further evaluated. Such comparative study to investigate if these antennas may appear planar wearable UWB complementary structures, and how are they performed close to tissues is not carried out, according to the best knowledge of authors.

A complementarity for the dipole-slot pair is first studied by forming antennas that satisfy Babinet based on simulations and theoretical calculations. To achieve wearable capability, a 1.6 mm thick FR4 substrate is included to the same designs and validation reproduced. For the computation of Z_{slot}, the effective permittivity $\varepsilon_{eff} = (\varepsilon_r + 1)/2$ for the substrate is taken into account. Babinet's principle is concluded to match properly for the formulation of complementary antennas that are not using the substrate. However, although the structure complementarity occurs, they do not cover the same S_{11} BW. In case of a substrate is included, determination of the correct wave impedance is observed to be confusing: should one use ε_r or ε_{eff} for a substrate to define wave impedance for the medium. Apparently, complementary structures based on Babinet can be achieved with the inclusion of a substrate nevertheless they will not operate in the same S_{11} band. Based on the findings, the approach was changed to form planar UWB antenna structures that are the most equal each other satisfying the pattern duality. The results are shown in Figs. 1(b)–(c) with currents and E-fields (note: a substrate is not visible); presented structures are targeted to have equal -10 dB S_{11} BW and efficiency in FS. Good agreement based on

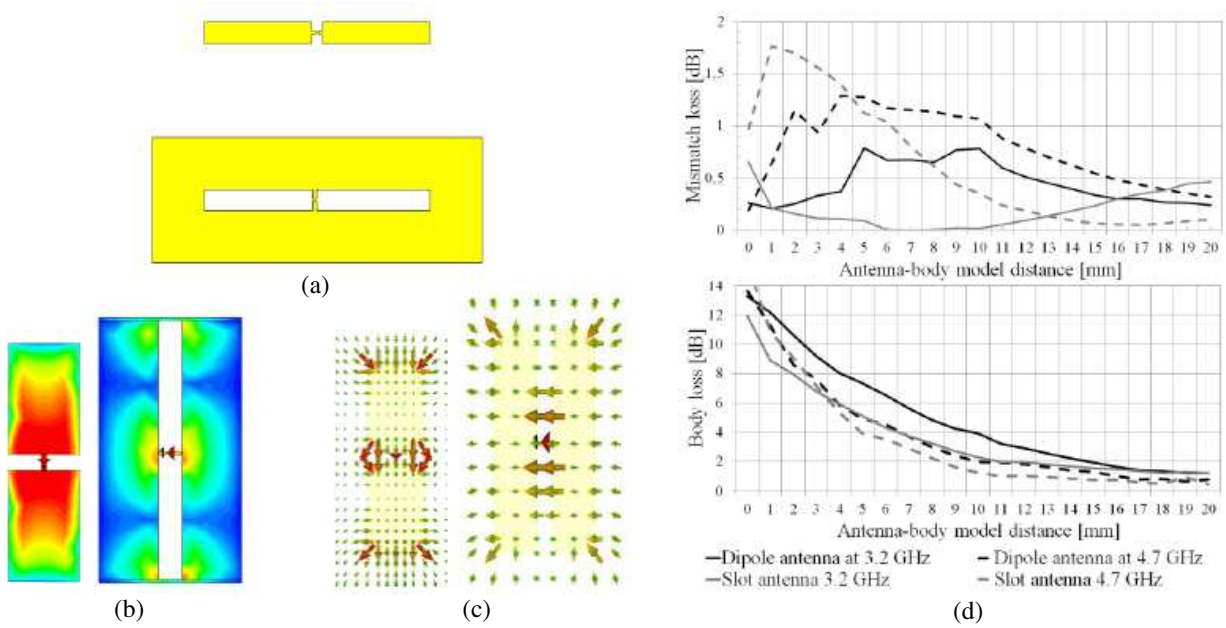

Figure 1: (a) Theoretical complementary antennas based on BP: a dipole (above) and slot (below), (b) instantenous currents [A/m], and (c) E-fields at 4 GHz at 0° phase. In (b) the color range is a logarithmic from 0 A/m (blue) to 5 A/m (red). (d) The proportion of an antenna mismatch (above) loss and a body loss (below). The behaviour is shown at 3.2 GHz and 4.7 GHz as a function of antenna-model distance through $0\,\text{mm} \leq D \leq 20\,\text{mm}$ in steps of 1 mm.

patterns is observed with respect to the duality, i.e., the interchange of fields. More details will be presented in the full paper.

To visualize the performance close to tissues, the operation above the rectangular tissue-equivalent model made of a skin (the dispersion for UWB is defined based on 2nd Debye model) is considered by Computer Simulation Technology (CST) simulations. Although equal antenna performance is noticed in free space, strong differences for the matching are observed both on contact the model and with the increased distance above the tissue model. This is visualized in Fig. 1(d). The behaviour of dipole is found to appear that of expected: corresponding properties are reported in the literature (i.e., the effect of tissues in reactive near-field of a dipole). The slot is observed to have the first rapid change in matching during the first millimetre with the increased distance. However, matching stays exceptional steady as the function of distance on the model. The differences of antennas on contact could be at least because of two reasons: 1) the pattern discrepancies because the power of slot propagates more strongly to $+/-z$ directions (the doughnut-shaped pattern for the dipole), hence the stronger effect of tissues for the slot could be rational explanation. 2) The E-fields of slot structure is over the slit area (see Fig. 1(c)), and if there appears tissues close to the slit, the stronger change for the Z_{slot} is understandable. Although the antennas start to show a performance close to free space after the 15 mm distance on tissues, the exact distance where an antenna is in safe is challenging to provide since of being a sum of many factors; the tissue combination (impossible to give the precise thicknesses for a body: only estimations), the effect of a substrate thickness, the size antennas near-fields, and so forth. Based on the observations, it seems that operating an antenna farther than the size of its reactive near-field above tissues, is proper indicator for attaining the satisfactory antenna performance and operation.

Optimized Reflector Position for Vlasov Antennas

H. M. El Misilmani[1,2], M. Al-Husseini[2], K. Y. Kabalan[1], and A. El-Hajj[1]

[1]American University of Beirut, Beirut 1107 2020, Lebanon
[2]Lebanese Center for Studies and Research, Beirut 2030 8303, Lebanon

Abstract— High Power Microwave (HPM) sources, such as the backward-wave Oscillator (BWO), the gyrotron, and the vircator (virtual cathode oscillator), generate power in cylindrically symmetric transverse electric TE_{0n} or transverse magnetic TM_{0n} modes. The side lobe generation, gain reduction, and inefficient power loading on the antenna aperture, make these modes unsuitable for driving conventional antennas. This gave the idea of using mode converters at the output of these sources to convert these modes into a plane-parallel linearly polarized beam. Vlasov antenna is one of the most known mode converters used. The well-known Vlasov types are the Step Cut and the Bevel Cut antennas. Step-cut, originally suggested by Vlasov, has sharp edges and therefore may suffer from electrical breakdown when radiating HPM. Bevel-cut, which was later suggested by Nakajima to avoid the sharp points of step cut, has a shape more suitable for HPM applications. However, Vlasov antenna with either cuts generates waves with the direction of maximum radiation shifted by some angle in the $\phi = 90°$ plane (assuming the antenna is placed along the Z-axis). Although several studies have been made to increase the gain of this antenna, which have mainly focused on adding a reflector to direct the radiated wave, none of these studies considered bringing back the maximum radiation along the axis of the waveguide.

In this paper, an optimized reflector position for Vlasov antennas is presented, which will help, with the proper rotation angle, to orient the radiated waves along the axis of the waveguide ($+Z$ direction in our case). In addition, with our proposed configuration, the reflector is directly attached to the waveguide structure, thus decreasing the size of the usual Vlasov antenna with reflectors, and eliminating the need for extra components to hold the waveguide and reflector together. The proposed reflector is applied to a bevel-cut and a step-cut Vlasov antenna to evaluate its performance.

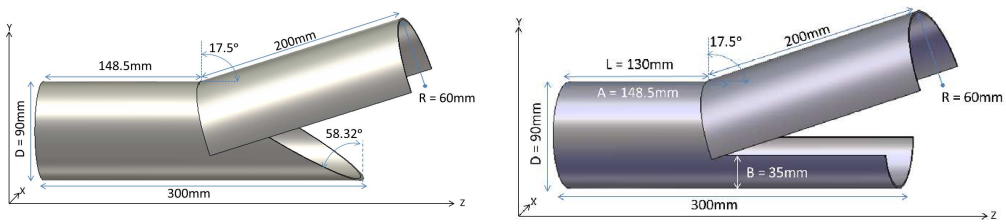

(a) Bevel-cut with optimized reflector (b) Step-cut with optimized reflector

Figure 1: Antenna configurations.

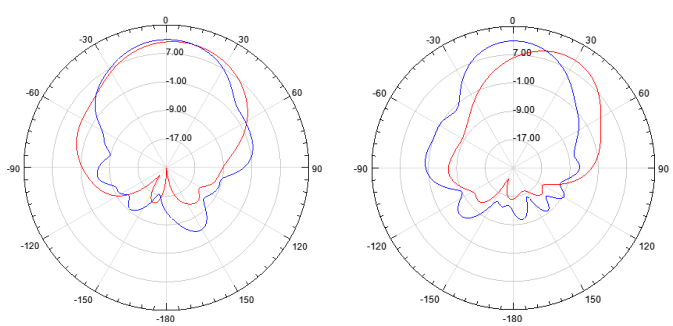

(a) (b)

Figure 2: Simulated radiation patterns, with initial bevel results shown in red and proposed design results in blue. (a) Red in the plane formed by the X-axis and the point of maximum radiation ($\theta = \theta_m, \phi = 90°$), blue in $\phi = 0°$ plane. (b) $\phi = 90°$ plane.

The presented Vlasov antenna consists of a circular waveguide of a radius of 45 mm and a length of 300 mm to operate at a frequency of 3 GHz. The presented bevel-cut Vlasov antenna has a cut angle of 58.32° chosen to give the maximum gain. The initial bevel cut antenna has a maximum gain of 10.3 dB, with a pattern rotated by an angle of $\theta = \theta_m = 28°$ in the $\phi = 90°$ plane. Adding a reflector, with an optimized radius of 60 mm, length of 200 mm, and an optimized rotation angle of 17.5° in the $\phi = 90°$ plane, has the effect of bringing back the direction of maximum radiation to the axis of the waveguide, i.e., $\theta = 0°$ and $\phi = 90°$. The proposed antenna with reflector, shown in Fig. 1(a), has a gain of 10.9 dB at 3 GHz and a reduced HPBW, as indicated in Figs. 2(a) and 2(b).

The same reflector is then attached to the step-cut Vlasov antenna, as shown in Fig. 1(b). By inspecting Fig. 3(b), the concept of adjusting the direction of maximum radiation along the waveguide axis is proven for a rotation angle of 17.5°, which is similar to the one used for the bevel-cut case.

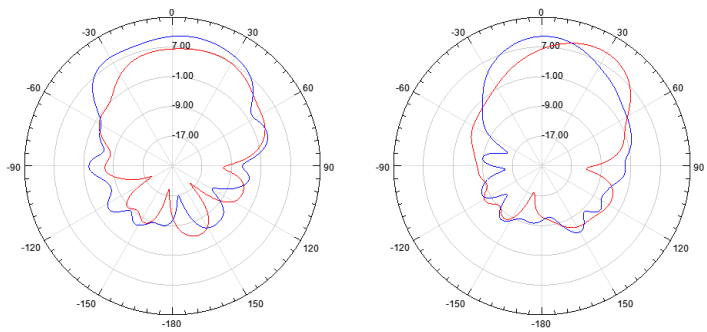

(a) (b)

Figure 3: Step cut simulated gain patterns, with initial step-cut results shown in red and proposed design results in blue. (a) Red in the plane formed by the X-axis and the point of maximum radiation ($\theta = \theta_m, \phi = 90°$), blue in $\phi = 0°$ plane. (b) $\phi = 90°$ plane.

The Imbedding Method in the Internal Electrodynamics Problem of Parabolic Reflector Antennas

S. V. Boyarkin and V. L. Kuznetsov
Moscow State Technical University of Civil Aviation, Russia

Abstract— Modern hybrid methods of computing parabolic reflector antennas include two steps. First step consists of evaluating surface currents on antenna reflector and a second one is computing far wavefields, generated by this currents. There is a natural question appears — is first step indeed necessary in reflector antennas theory.

In this paper we will demonstrate a different method that doesn't include computations of surface currents. Moreover, this new approach can be attributed to rigorous electromagnetic methods.

In proposed method the parabolic reflector considers as section of irregular waveguide or as a nonplanar end of shorted circular waveguide with diameter equals to reflector aperture diameter.

Field in any cross-section will be consider in eigenmodes basis of circular waveguide with corresponding section as it usually done in computations of irregular waveguides. The reflection coefficient in this way could be represented as 4-index matrix ${}_{\alpha,\beta}R_{n,m}$, where m — number and β — initial field mode type, n and α — corresponding parameters of reflected mode.

Value of this matrix coefficient is calculated by invariant imbedding method as a solution of equation

$$\frac{d\hat{R}^{+}_{nm}}{dz} = \sum_{k,l} \widehat{R}^{+}_{nk} \cdot \hat{\rho}^{-}_{kl} \cdot \widehat{R}^{+}_{lm} + \sum_{k} \widehat{R}^{+}_{nk} \cdot \hat{\tau}^{-}_{km} + \sum_{k} \hat{\tau}^{+}_{nk} \cdot \widehat{R}^{+}_{km} + \hat{\rho}^{+}_{nm} \tag{1}$$

For simplicity the α and β indexes doesn't shown in (1).

In this work we consider a case, then **f/D-**ration equals to 0.25, i.e., antenna feed is in the plane of the aperture and Equation (1) integrated in interval (0, **f**). Feed itself modeled by coaxial circular waveguide and computed by mode matching method.

The apparent advantage of proposed method is that it bears a geometrical transition from parabolic reflector to cylindrical waveguide, whose radiation in space could be described rigorous (L. A. Weinstein 1966). The combined solutions for reflector and infinitely short (virtual) section of cylindrical waveguide gives us the rigorous solution for radiation field of Parabolic Reflector Antennas.

Feasibility of Using an Absorptive Cover for Ice, Snow or Water Removal from Radome Surface

Aleksey Solovey
L-3 Communications ESSCO, 90 Nemco Way, Ayer, MA 01432, USA

Abstract— Radomes housing the antennas used for the microwave remote sensing of snow cover often are subjected by the snow and/or ice build-up on their surface. That build-up have extremely negative impact on all antenna transmit/receive characteristics. In this paper the feasibility of using a thin layer of absorptive and/or conductive dielectric cover for the ice, snow or water removal from the radome outer surface was investigated. Constrains on the design parameters and usability of such de-icing system were derived. The new de-icing approach that employs the effect of total internal reflection of radome outer skin is introduced.

To prevent or remove the ice, snow or water build-up from the radome surface (referred further as a de-icing) a chemical, mechanical, and thermal de-icing approaches were introduced at the early stage of radomes development. This paper investigates the feasibility of the particular type of thermal de-icing approach when the radome outer surface is covered by a heating layer of absorptive and/or conductive dielectric. The similar method that uses the heating wire mesh embedded into the radome outer skin was used for the reference. The infrared and hot air blowing de-icing approaches were not considered because those methods are suitable only for the metal space frame or thin solid laminate radomes whose wall has no thermo insulating core. For sandwich radomes with a low density core that works as a thermo insulator those approaches can be used only if the infrared radiators or hot air blowers are installed outside of the radome, which is impractical for most radome applications.

As a result of presented study the following were found. From the overall power consumption standpoint any thermal de-icing approaches required up to 1.3 kW/m^2 per 1 mm/hr precipitation and thus, are feasible for radomes with the de-icing area up to a few tens square meters. The well-known heating wire mesh de-icing approach can be used for the VP radiation at any frequencies and for the HP and CP radiations only at frequencies that are much higher than 10 GHz. The distance between heating wires should be about 3 cm with the wire length up to few meters, depending on voltage allowable and precipitation level. The de-icing approach that uses the polarization current induced by the quasi-stationary fields is uncompetitive with the heating wire mesh approach. The DC/50/60 Hz conductivity current de-icing approach can be used for linearly polarized radiation (VP, HP or slant) at any frequency. This gives it an edge over the heating wire mesh de-icing approach. With respect to the CP radiation, the DC/50/60 Hz conductivity current and the heating wire mesh de-icing approaches are the same. The new radome thermal de-icing approach is introduced. It uses the strip or wire type radiating antennas embedded into radome outer skin and employs the effect of total internal reflection. Although the most expensive, this approach can be used for linearly polarized radiation (VP, HP or slant) at any frequency and, depending on particular de-icing scenario, above 1 GHz for the CP radiation. That gives it an edge over both the heating wire mesh and the DC/50/60 Hz conductivity current de-icing approaches.

Windowing of the Discrete Green's Function for Accurate FDTD Computations

T. P. Stefański
Department of Microwave and Antenna Engineering, Gdansk University of Technology
Narutowicza 11/12, Gdansk 80-233, Poland

Abstract— Recently, the discrete Green's function (DGF) [1] has become a popular tool facilitating the finite-difference time-domain (FDTD) simulations. The DGF applications include electromagnetic computations on disjoint domains and implementation of nonlocal absorbing boundary conditions. In this way, free-space cells between scatterers and perfectly matched layers absorbing the electromagnetic wave at the mesh boundaries can be avoided in FDTD simulations. The above-mentioned advantages of the DGF implementation in FDTD simulators have resulted in several applications of this function in the design process of antennas. Savings in runtime and memory usage have been reported for computations of antenna characteristics using the convolution of current sources with DGF [2].

Unfortunately, numerical implementations of the DGF formulas are cumbersome. A three-dimensional dyadic DGF formula in [1, 2] was derived with the use of Jacobi orthogonal polynomials by applying operators to the impulse response of the scalar wave equation. On the other hand, Jeng's formula [3] has a very compact form but employs powers of Courant numbers and factorials that cause numerical problems for large time indices. In fact, feasibility of the DGF generation for a large time index is limited by current computing technology, i.e., size of available memory and computing power. Therefore, only short DGF waveforms can be generated with the use of existing computing resources. To overcome this limitation, the DGF waveform has to be truncated with the use of a windowing function for accuracy of computations. However, although windowing has been reported as an efficient method of the DGF truncation and a remedy for stability issues, the accuracy and usability of this technique have not been deeply investigated yet.

In this contribution, systematic evaluation of the applicability of parametric and nonparametric windowing functions for the DGF truncation is presented. The paper extends report [4], which evaluates the accuracy of the DGF truncation for the most frequently applied windowing functions, i.e., Hann, Hamming, Gaussian and exponential windows. In this contribution, the accuracy of the DGF windowing is demonstrated for other windowing functions useful in the digital signal processing, e.g., Barlet, Blackman and Kaiser windows.

The study concludes that abrupt truncation of the DGF waveforms results in an increase in the error of the electromagnetic field computations in comparison to the solution obtained for the DGF waveform truncated using a suitable windowing function. Truncation errors were compared for a wide range of parametric and nonparametric windowing functions and demonstrated the best performance for the Hann window.

REFERENCES

1. Vazquez, J. and C. G. Parini, "Discrete Green's function formulation of FDTD method for electromagnetic modelling," *Electron. Lett.*, Vol. 35, 554–555, Apr. 1999.
2. Ma, W., M. R. Rayner, and C. G. Parini, "Discrete Green's function formulation of the FDTD method and its application in antenna modeling," *IEEE Trans. Antennas Propag.*, Vol. 53, 339–346, Jan. 2005.
3. Jeng, S.-K., "An analytical expression for 3-D dyadic FDTD-compatible Green's function in infinite free space via z-transform and partial difference operators," *IEEE Trans. Antennas Propag.*, Vol. 59, 1347–1355, Apr. 2011.
4. Stefański, T. P., "Accuracy of the discrete Green's function formulation of the FDTD method," *IEEE Trans. Antennas Propag.*, Vol. 61, 829–835, Feb. 2013.

Combined *E* and *H* Field Formulation of IPO (Iterative Physical Optics) for Metallic, Coated or Uncoated with Lossy or Non Lossy Dielectric Materials Cavities

A. Pajot[1], **N. Douchin**[1], **and H. J. Mametsa**[2]

[1]OKTAL Synthetic Environment, 11, avenue du Lac, Vigoulet-Auzil 31 320, France
[2]ONERA DEMR, 2, Av. E. Belin, 31055 Toulouse Cedex 4, France

Abstract— A generalization of IPO (Iterative Physical Optics) is presented in this paper in order to solve the most general case of scattering concerning cavities whatever their cover: metallic, dielectric, metallic covered with dielectric layer .... Moreover, contrary to the majority of encountered papers relative to this problem, no restrictive hypothesis on the values of the dielectric permittivity and losses is assumed in our formulation.

Dielectric coating covers can have a significant effect on the scattering pattern of cavities. Most common technique used for analysis is the traditional dielectric PO (Physical Optics) formulation. Scattering for air-dielectric or air-multilayered dielectric interface is described in terms of electric and magnetic current on the interface. Exact solution of these currents could be achieved using integral equation resolution such as Moment Method. To save computation time, we use an asymptotic evaluation of the first order currents using GO (Geometrical Optics) by taking into account, the incident and reflected, electric and magnetic fields. The reflected fields are calculated from the matrix expression of Fresnel reflection coefficients obtain with a generalised multilayered medium. A combined field formulation using both electric and magnetic field has been developed.

This formulation is solved using an improved IPO approach. In standard IPO, currents are iteratively accumulated at sampling points, reradiating toward all other points at each iteration until convergence is reached to bring higher orders of physical optics bounces. With this method, convergence can require a large number of steps. To reduce this number of steps, we use an IPO formulation allowing us to use a general iterative linear system solver. It is shown that with this improved approach and a suitable linear system solver, currents converge very soon, especially for distant facets. For large cavity, this iterative method is really efficient and reaches enough precision for different scattering applications. Specific tasks have been focused on obtaining the number of iterations required in the IPO method when non-PEC cavities are considered. **First results are very satisfactory and an intensive validation phase is in progress.**

The primary incident field in the cavity is directly obtained through a SBR (Shooting and Bouncing Ray) technique modelling the incident plane wave. Understandably, on-going work on a complete hybridization of the formulation with our asymptotic software SE RAY-FERMAT dedicated to EM interactions calculations is under investigation.

Global Base Approach to H-polarized Wave Scattering by Conducting Circular Cylinders

K. Yashiro
Chiba University, Japan

Abstract— The scattering of a H-polarized plane wave by an arbitrary configuration of parallel circular cylinders with any radius is analysed by method of moments (MoM). The analysis objects is confined to circular cylinders. The scattered magnetic field is expressed as integral of the product of equivalent magnetic current and Green function, that is, the Hankel function of zero-th order.

The unknown current density on each cylinder is expanded with global base functions. Since the global base functions should be periodic along the periphery of the cross section of each circular cylinder in this case, they are chosen to be the exponential function with a pure imaginary argument. This choice of base is useful to reduce the number of the unknowns every cylinder without deteriorating the accuracy of solution. The integral of the product of Hankel function and the exponential function is calculated analytically by using Graf's addition theorem for Bessel functions.

The local polar coordinate system is introduced and the tangential component of the total electric field is derived by differentiating with respect to radial variable. Applying the boundary condition to the tangential component, it is set to be zero. The Galerkin's method is used to obtain the system of linear equations. In other words, the same exponential functions as base functions are chosen as weight functions. And the inner products of the resulting equations with the weight functions are calculated analytically. To do so, the addition theorem is applied to calculate the integral analytically, when the observation point and source point locates on different circle cylinders. The obtained matrix is symmetric and it is written as a matrix of which elements are matrices. The diagonal matrix are diagonalised ones.

To verify the method, the scattering from a circular cylinder with radius of one wavelength is considered. The solution is the same as the analytical one obtained by the separation of variables. The numerical data shows that the number of the unknowns can be reduced to one thirds for the conventional MoM. Furthermore, the comparison with previous work in case of five cylinders are presented. The numerical results obtained based on the above analysis are compared with those obtained by Elsherbeni by the conventional MoM [1]. A good agreement between them is observed. Some other numerical examples are given.

REFERENCES

1. Elsherbeni, A. Z., *Radio Science*, Vol. 29, 1023–1033, 1994.

Simulations of Electromagnetic Pulses from Hypervelocity Impact Plasmas

Alexander Fletcher and Sigrid Close
Department of Aeronautics and Astronautics, Stanford University, USA

Abstract— Hypervelocity micro-particles (mass $< 1\,\mathrm{ng}$), including meteoroids and orbital debris, routinely impact spacecraft. Meteoroids are interplanetary dust particles originating primarily from comets and asteroids with impact velocities up to $72\,\mathrm{km/s}$ if in solar orbit; and orbital debris are objects of human origin in orbit around Earth with impact velocities of $\sim 11\,\mathrm{km/s}$. Most meteoroids and some debris possess enough energy to ionize and vaporize themselves as well as a significant portion of the satellite material upon impact, forming a plasma in the impact crater that is initially dense ($\sim 10^{28}\,\mathrm{m}^{-3}$), but rapidly expands into the surrounding vacuum. The associated electrical effects and potential for damage to satellite electronics through these processes remains largely unknown. Numerous spacecraft have experienced electrical anomalies correlated with meteoroid activity and micro-particle scale momentum transfer events. This area of spacecraft engineering requires a deeper understanding of the underlying physics that occur upon formation and expansion of the plasma that results from an impact.

We present a series of computational multi-physics simulations of micro-particle impacts on spacecraft. These simulations incorporate elasticity and plasticity of the solid target, phase change and plasma formation, non-ideal plasma physics due to the high density and low temperature of the plasma, a fully kinetic description of the collisionless portion of plasma, and free space electromagnetic radiation. We use a particle-based method that is a variant of smoothed particle hydrodynamics in the high density limit (early stages of impact) and an electromagnetic particle-in-cell in the low density limit (collisionless plasma expansion into vacuum). A discontinuous Galerkin method is used for the coupled solution of Maxwell's equations.

In order to explain the impact induced RF radiation observed in both ground based Van de Graaff experiments and on spacecraft, we investigate a number of physical mechanisms including coherent oscillation of electrons and a current pulse due to the presence of a charged target. We find plasma temperatures of up to $60\,\mathrm{eV}$ in the crater, but these cool to $< 5\,\mathrm{eV}$ as the plasma expands. We also find that non-ideal plasma effects noticeably increase the amount of charge generated from a single impact. For a threshold micro-particle impact velocity, the plasma generates an electromagnetic pulse of sufficient strength to pose a threat to spacecraft electronics.

Advances in Surface Integral Equation for Nano-scale Optical Wireless Nanolink

Yang Shao[1], **Zhen Peng**[1], **Jin-Fa Lee**[1], **Diego M. Solís**[2], **and José M. Taboada**[3]

[1]The Ohio State University, Columbus, Ohio, USA
[2]University of Vigo, Vigo, Spain
[3]University of Extremadura, Caceres, Spain

Abstract— In the next generation of integrated circuits, one option to overcome the bandwidth limitations is wireless chip-to-chip and on-chip interconnects via integrated antennas. One of the main limitations of regular plasmonic waveguide links is the range of propagation due to the metal absorption losses. Hence, nano-optical wireless links using nanoantennas are considered in this work. To efficiently analyze the high-capability nano-scale wireless nanolink using matched directive nanoantennas in the visible range $\lambda_0 = 0.65\,\mu\text{m}$, we propose a surface integral equation domain decomposition method (SIE-DDM). The convergence of SIE-DDM depends heavily upon the transmission conditions (TCs). The use of the Robin TCs provides the needed convergence for many electromgnetic wave radiation and propagation problems. Nonetheless, the use of the Robin TC is proven to be not effective in addressing such applications. In the vicinity of large (negative) real part of the permittivity of conductors operating at THz frequency, electromagnetic field excitations propagate to the interface between a dielectric and a conductor, evanescently decay in the perpendicular direction to the interface, known as the surface plasmon polaritons (SPP). Subsequently, optimized TC is introduced in this work to provide fast and robust converging mechanism for wireless nanolink and allowing convergence when SPP effects take place. We demonstrate that the use of optimzed TC clearly enhances the convergence of the proposed SIE-DDM of the optical wireless nanolink.

Surface Integral Equation Methods for Multi-scale Composite Problems

Zhen Peng and Jin-Fa Lee
The Ohio State University, Columbus, Ohio, USA

Abstract— Full wave solution of electromagnetic wave scattering from a multi-scale and complex target with multiple materials has been a major research emphasis for computational electromagntetics. In this work, we shall present our efforts in combating a complex heterogeneous multi-scale electromagnetic scattering problem, viz. a plane wave scattering from a high-definition composite unmanned aerial vehicle (UAV) at X-band. Of particular concern is that this complex platform is partially coated with multi-layer electromagnetic absorbers, which include frequency selective surfaces, multi-layer impedance sheets and magnetic radar absorbing materials. Needless to say, such a multi-scale scattering problem is extremely challenging and taxes heavily on existing surface integral equation methods.

In this work, we shall present some recent advances in surface integral equation formulation to address this challenging large multi-scale composite system. There are three major technical ingredients in the proposed method:

a) A surface integral equation domain decomposition method (SIE-DDM) is proposed. The proposed SIE-DDM follows a hierarchical domain partitioning strategy. The entire computational domain is decomposed into a series of non-overlapping sub-regions. Each local sub-region is homogeneous with constant material properties and described by a closed surface. Through this decomposition, we have introduced at least two pairs of trace data as unknowns on interfaces between sub-regions (Multi-trace Formulation). This multi-trace feature admits two major benefits: the localized surface integral equation for the homogeneous sub-region problem is amenable to operator preconditioning; the resulting linear systems of equations readily lend themselves to optimized Schwarz methods.

b) We present a discontinuous Galerkin surface integral equation, herein referred to as IEDG, for the numerical solution of sub-domains. The proposed IEDG algorithm allows the implementation of the generalized combined field integral equation (G-CFIE) using square-integrable trial and test functions without any considerations of continuity requirements across element boundaries. It is possible to employ non-conformal surface discretizations of the targets.

c) In the method to be presented, we study a new optimized second order transmission condition to further improve the convergence in the SIE-DDM iterations. Numerical results are included to validate the accuracy and demonstrate the versatility of the proposed method.

The Coulomb Gauge Based Integral Equation

X. Y. Z. Xiong, Y. H. Lo, L. J. Jiang, and W. E. Sha
Department of EEE, The University of Hong Kong, Hong Kong, China

Abstract— The electric field integral equation (EFIE) method is one of modern simulation methods for scattering, radiation, and circuit problems. The popularity of the EFIE stems from the efficient surface triangulation, excellent numerical precision, and powerful capabilities to handle open and complex geometries. However, when the frequency tends to zero, the method-of-moment (MoM) solution of the EFIE using the Rao-Wilton-Glisson (RWG) basis functions suffers from the low-frequency breakdown, where the contribution from the vector potential is extremely imbalanced with that from the scalar potential. As a result, the matrix representation of the EFIE operator is highly ill conditioned and cannot be inverted reliably and efficiently.

Over the past few years, various approaches have been proposed to overcome the problem. As a quasi-Helmholtz decomposition and robust low-frequency solver, the looptree or loop-star decomposition separates the surface current into solenoidal and irrotational parts to capture the inductance and capacitance physics, respectively. But one pitfall associated with the loop-tree or loop-star method lies at the nontrivial loop-search process for complex geometries encountered in the circuit simulation. The recent developed augmented EFIE (A-EFIE) method, which employs current and charge as independent unknowns, can remedy the low-frequency breakdown and meanwhile avoid searching for loop bases. Furthermore, a similar AEFIE method in conjugation with the Calderon multiplicative preconditioner in nature removes the internal resonance corruption and preserves other merits of the EFIE.

All algorithms mentioned above formulate the EFIE using the Lorentz-gauge Green's function. In this paper, we investigate the EFIE represented by the Coulomb-gauge Green's function and explore its potential applications to solve the low-frequency problem. To solve the low-frequency breakdown inherent from the electric field integral equation (EFIE), the EFIE using the Coulomb-gauge Green's function of quasistatic approximation is proposed. Different from the commonly adopted Lorentz-gauge EFIE, the Coulomb-gauge EFIE separates the solenoidal and irrotational surface currents explicitly, which captures inductive and capacitive responses through electrodynamic and electrostatic Green's functions, respectively. By applying existing techniques such as the loop-tree decomposition, frequency normalization, and basis rearrangement, the Coulomb-gauge EFIE also can remedy the low-frequency breakdown problem. Through comparative studies between the Lorentz-gauge and Coulomb-gauge EFIE approaches from mathematical, physical and numerical aspects, the Coulomb-gauge EFIE approach shows the capability of solving low-frequency problems and achieves almost the same accuracy and computational costs compared to the Lorentz-gauge counterpart.

ACKNOWLEDGMENT

This work was supported in part by Hong Kong RGC (GRF 711511, 713011, and 712612), NSFC 61271158), and in part by the University Grants Council of Hong Kong (Contract No. AoE/P-04/08).

Radiative Transfer with Coherent Backscattering Compared to Exact Scattering Methods

A. Penttilä[1], K. Muinonen[1,2], E. Zubko[1], M. I. Mishchenko[3], J. M. Dlugach[4], D. W. Mackowski[5], and G. Videen[6]

[1]Department of Physics, University of Helsinki, P. O. Box 64, FI-00014, Finland
[2]Finnish Geodetic Institute, P. O. Box 15, Masala FI-02431, Finland
[3]NASA Goddard Institute for Space Studies, 2880 Broadway, New York, NY 10025, USA
[4]Main Astronomical Observatory, National Academy of Sciences of Ukraine
27 Zabolotny Street, Kyiv 03680, Ukraine
[5]Department of Mechanical Engineering, Auburn University, Auburn, AL 36849, USA
[6]Army Research Laboratory, Adelphi, MD 20783, USA

Abstract— Coherent backscattering (CB) has been recently quantitatively verified as an essential addition to the radiative transfer (RT) approach for correct backscattering enhancement [1]. We continue to develop the hybrid RT-CB code by comparing the results against exact simulations using superposition T-matrix method and its implementation MSTM [2]. We increase the number of spherical constituents in the simulations of a spherical cloud of particles to 2000 and consider the effect of increasing packing density (pD) of the material from 5% up to 30%. The results show good agreement with small pD (see Fig. 1) and slowly decreasing agreement with larger pD.

It is known that the RT approach is not valid for large pD. In Monte Carlo RT the direction of ray after scattering is computed for an independent scatterer. With high pD the particles will be in the near-fields of each other which will violate the assumption. The distance between consequent scattering events uses the concept of mean-free-path length but this assumes independent extinction efficiency and Poisson distributed locations. With comparisons against MSTM, we might be able to correct the RT-CB to better adapt to higher pD. Furthermore, non-spherical scatterers can be tested using, e.g., the discrete-dipole approximation to compute the scattering matrices.

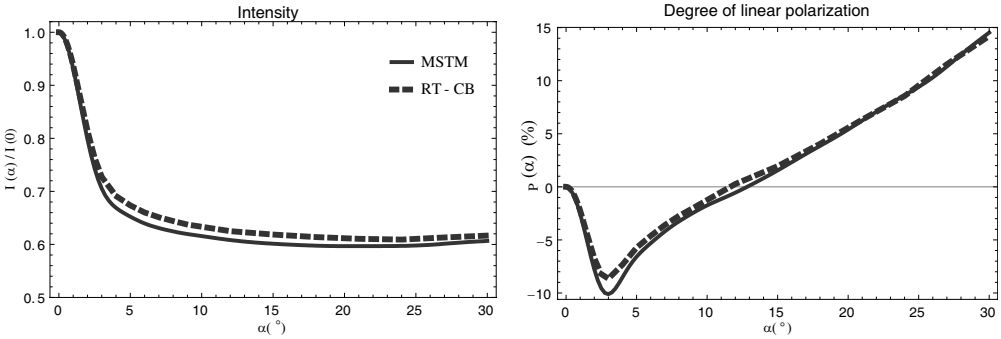

Figure 1: Normalized intensity and degree of linear polarization for phase angle range 0–30° using the MSTM (solid line) and RT-CB codes (dotted line). Computations are for spherical media with wavenumber times radius $kR = 68.4$ where 2000 spheres with radii $kr = 2$ and with refractive index $m = 1.31 + i0$ are randomly placed inside, resulting pD of 5%.

ACKNOWLEDGMENT

The computations presented have been made using CSC computing resources. CSC is the Finnish IT center for science and is owned by the Ministry of Education.

REFERENCES

1. Muinonen, K., M. I. Mishchenko, J. M. Dlugach, E. Zubko, A. Penttilä, and G. Videen, "Coherent backscattering verified numerically for a finite volume of spherical particles," *ApJ*, Vol. 760, No. 2, 118–128, 2012.
2. Mackowski, D. W. and M. I. Mishchenko, "A multiple sphere T-matrix Fortran code for use on parallel computer clusters," *JQSRT*, Vol. 112, No. 13, 2182–2192, 2011.

Optical Interaction of Two Closely Spaced Nanoholes in Au Film

M. Janipour[1], **T. Pakizeh**[2], **and F. Hodjat-Kashani**[1]

[1]Department of Electrical Engineering, Iran University of Science Technology, Tehran 1684613114, Iran
[2]Faculty of Electrical and Computer Engineering, K. N. Toosi University of Technology, Tehran 16314, Iran

Abstract— Two closely spaced nanoholes analyzed as two tiny interacting magnetic dipoles depending on the incident beam polarization [1–3]. It is demonstrated that the optical coupling mechanism between two nanoholes inherently has a magnetic property, unlike the electric dipoles which are mainly coupled through electric-fields [4]. It is obvious that, in comparison with a single hole, the transmission experiences two peaks for Fig. 1(b) where the long and short wavelength peaks are proportional to anti-phase and in-phase magnetic dipoles, respectively. The long wavelength peak considerably blue-shifts by increasing the distance, whereas the short wavelength peak partially red-shifts. It is obvious from Fig. 1(a) and Fig. 1(b) that the electric field is confined in the air region of nanoholes and thus unlike electric dipoles, coupling through electric fields for nanoholes is very weak, while coupling through magnetic fields is strong. The peak of Fig. 1(d) is due to the in-phase interaction of dipoles and experiences a little blue shift relative to single hole, which is caused by electric coupling of dipoles. The simulation is based on a three dimensional finite difference time domain (FDTD) method and it is considered that each nanohole dimension is $a = 100\,\text{nm}$, $b = 200\,\text{nm}$, and thickness $d = 100\,\text{nm}$. The separating distance between nanoholes (i.e., Δ) varies from 5 to 15 nm. Figs. 1(a) and 1(b) illustrate the electric fields for different polarizations and Figs. 1(c) and 1(d) show the normalized transmissions for two separated nanoholes with $\Delta = 10\,\text{nm}$.

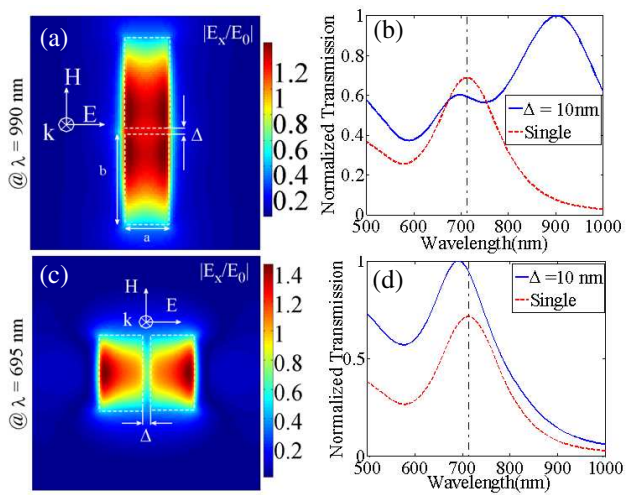

Figure 1: (a) and (b) The field profile of electric field component of two rectangular nanoholesin Au film at the proportional LSPR wavelengths. (b) and (d) The normalized transmission for (a) and (c), respectively.

REFERENCES

1. Pakizeh, T. and M. Käll, "Unidirectional ultracompact optical nanoantennas," *Nano Lett.*, Vol. 9, 2343–2349, 2009.
2. Maier, S. A., P. G. Kik, H. A. Atwater, S. Meltzer, E. Harel, B. E. Koel, and A. A. G. Requicha, "Local detection of electromagnetic energy transport below the diffraction limit in metal nanoparticle plasmon waveguides," *Nature Mater.*, Vol. 2, 229–232, 2003.
3. Bethe, H. A., "Theory of diffraction by small holes," *Phys. Rev. Lett.*, Vol. 66, 163–182, 1944.
4. Bohren, C. F. and D. R. Huffman, *Absorption and Scattering of Light by Small Particles*, Wiley, 1983.

Novel All-optical Logic Gates Based on Microring Metal-insulator-metal Plasmonic Waveguides

Yaw-Dong Wu, Yung-Ta Hsueh, and Tien-Tsorng Shih
Department of Electronic Engineering
National Kaohsiung University of Applied Sciences, Kaohsiung, Taiwan, R.O.C.

Abstract— In this paper, we proposed novel all-optical logic gates based on microring metal-insulator-metal (MIM) plasmonic waveguides. The proposed all-optical logic gates were numerically studied by the finite-difference time-domain method (FDTD). In recent years, surface plasmon has attracted much attention due to the potential of applications. Surface plasmons are existed at the interface of metals and dielectrics. It has highly localized to a metal surface that can have applications as sub-wavelength waveguides to guide light below the diffraction limit in conventional optics. The MIM structures consist of a dielectric waveguide and two metallic claddings, which strongly confine the incident light in the insulator region. MIM waveguides are prospective for the design of nanoscale all-optical devices shown strong localization, as well as relatively simple fabrication. Some devices based on the MIM waveguides have been studied numerically and experimentally, such as the filters based on ring resonators, tooth-shaped plasmonic waveguide filters, nanodisk resonator, Y-shaped combiners, and wavelength selective waveguides. We designed a MIM structure which consists of the symmetric ring resonators and straight waveguides. By utilizing the coupling property between straight waveguides and ring resonator waveguides and modulating the radii of the ring resonators, we can design an all-optical NOT logic gate. By changing the state of the control port, we can make outgoing field propagating in the output waveguide or not. According to the numerical results, the proposed device could really function as an all-optical NOT logic gate. It would be a potential key component in the application of the all-optical signal processing system.

CRLH-TL Based Zeroth Order Resonance Antenna

Ankit Kumar Ghosh[1], **Mohit Kumar Joshi**[1], **and Akhilesh Mohan**[2]

[1]The LNM-Institute of Information and Technology, Jaipur, India
[2]Indian Institute of Technology Rajasthan, Jodhpur, Rajasthan, India

Abstract— In this paper, a Zeroth order resonance antenna based on CRLH-TL technique is proposed. To achieve a compact size antenna utilizes the ZOR phenomenon and its reactive parameters determine the resonant frequency. It consists of a top patch and the meander lines are connected to the rectangular patch. Here the meander lines acts as an inductor and the rectangular patch as a virtual ground capacitor. The proposed antenna has the benefit of compact size and easy to fabricate. The efficiency of 70% and gain of 6.51 dB and operates at 2.934 GHz.

Antenna Design and Results: The antenna proposed in this paper exhibits higher gain and efficiency. The structure is implemented on a Rogers RT/Duroid 5880 substrate of size 26.5 mm × 28 mm and having a dielectric constant of 2.2 and thickness of 1.6 mm (62 mil). It consists of a top patch and the meander lines are connected to the virtual ground capacitor. Here the meander lines acts as an inductor and ground is provided by a rectangular patch (act as a virtual ground). The dimension of patch is 6 mm ∗ 6 mm. Each unit cell consists of a patch connected symmetrically to meanderlines. The width of the meander strip = 0.2 mm and gap between the strips = 0.2 mm. The gap between each unit cell = 0.2 mm. The virtual ground capacitor patch is of 3 mm ∗ 6 mm dimension. The spacing between the first patch with the feed line is 0.1 mm.

The radiation pattern and gain of 6.51 dB at $n = 0$ mode, frequency = 2.934 GHz. A return loss of 27.127 dB at 2.934 GHz is obtained. An efficiency of 70% is also obtained. This design has an increased gain and efficiency as compared with the previously reported metamaterial antennas.

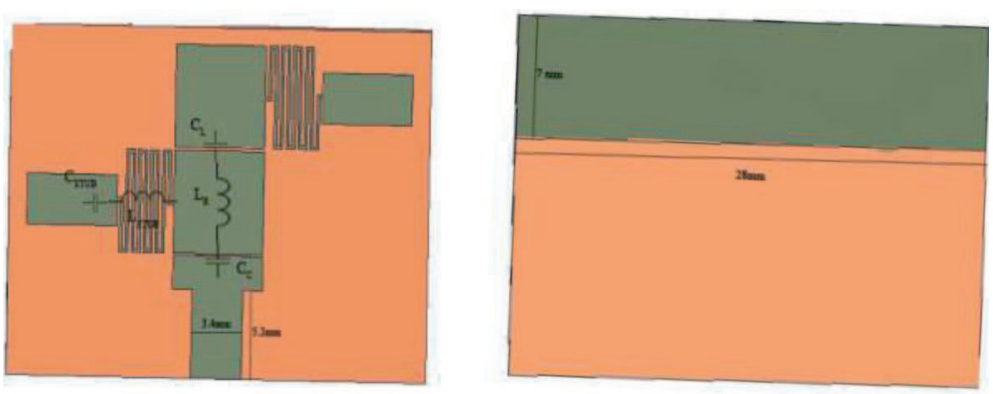

(a) (b)

Figure 1: (a) Top view of the CRLH-TL antenna, (b) bottom view of the CRLH-TL antenna.

REFERENCES

1. Lai, A., T. Itoh, and C. Caloz, "Composite right/left-handed transmission line metamaterials," *IEEE Microwave Mag.*, Vol. 5, Sep. 2004.
2. Sheeja, K. L, P. K Sahu, and S. K Behera, "Comparative study of CRLH TL based zeroth order resonance antenna," *2012 National Conference on Communications (NCC)*, 1–5, Feb. 3–5, 2012.

New Weakly-coupled Nearly Adapted Resonant Sensors for Microwave Range Measurements

F. Micheletti and R. Olmi
Institute for Applied Physics — National Research Council, IFAC-CNR
Via Madonna del Piano, 10, Sesto Fiorentino (Firenze) 50019, Italy

Abstract— This paper deals with issues related to the design of resonant probes for dielectric spectroscopy. One of the problems commonly faced with is the coupling of sensor ports with the impedance of the measurement system, in particular when this last is designed to operate in "matched" conditions.

This issue is particularly true at the feed port, where the reflected wave due to the port mismatch involves generator malfunctions like PLL lock failures or an increase of the phase noise.

In general the port matching is not achievable due to the resonant character of sensor, so that the problem can be solved by removing the reflected wave by using an isolator or an active buffer.

When a portable measurement system with small size and cost is desired, using one of the above solutions can represent a limit for energetic purpose and it can give rise to a sensible increase in size and in the overall cost of the system. Furthermore, these solutions can be not feasible when we need to deal with very large frequency bandwidths.

A possible solution is to design a weak coupling method for sensor ports, which involves a small perturbation of the feeding transmission line, resulting in a slight mismatch which does not imply issues with the synthesizer in every working situation of the sensor.

In this work methods are developed and discussed for effectively coupling the feeding lines of an actual system for dielectric spectroscopy to a resonant micro-strip sensor. Limitations of the original approach, based on a coplanar gap, are discussed and the solutions based on cross-over coupling are illustrated with their pros and cons relative to the above-mentioned issues.

Multi-layered Frequency Selective Surfaces for High Frequency Applications

Agâh Oktay Ertay and Can Suer
Electrical and Electronics Engineering Faculty
Istanbul Technical University, Maslak, Istanbul 34469, Turkey

Abstract— Structures involving Frequency Selective Surfaces (FSSs) are popular research topics in several fields such as Radar Cross Section (RCS), electromagnetic absorber and microwave filter design applications. Albeit basic properties of simple structures in the cm-wave region go back as far as 1946 [1], during the last four decades frequency selective surfaces became more and more important as several methods and approaches have been developed for different kind of materials and structures [2].

In the military aircraft industry, stealth technology takes a large place especially for surveillance and detection of threats without being detected itself. Although a large number of studies have been carried out for the structures involving Frequency Selective Surfaces, it is still required to develop multi-band methodologies to avoid multi-frequency scanners. The most difficult thing about Frequency Selective Surfaces is the design and the implementation of the structure that reduces the reflection coefficient — theoretically to zero —.

The aim of this paper is to compare the methodologies such as Jerusalem Cross, rectangular or circular slots and combine these specific structures if necessary to create a multiband Frequency Selective Surface that can be used for the applications mentioned above. C and X Bands will be investigated to satisfy the needs of the aircraft usage. The band coverage will be as wide as it can be along with the low thickness of the Frequency Selective Surface proportional to the wavelength λ. Full wave electromagnetics software tools are used to model the proposed structures. Reflection and transmission coefficient values are calculated through desired frequency bands. MATLAB is preferred for calculations of related to required values. Modifications of surfaces with different geometries are applied to the structures via EM design environments and simulation results are presented.

REFERENCES

1. Vardaxoglou, J. C., *Frequency Selective Surfaces Analysis and Design,* Research Studies Press Ltd., John Wiley & Sons Inc., 1997.
2. Munk, B. A., *Frequency Selective Surfaces: Theory and Design*, John Wiley, 2000.

A Novel Neural Network Model of a Microwave Transistor Using Particle Swarm Optimization

Ufuk Ozkaya[1] and Filiz Gunes[2]

[1]Department of Electronics and Communication Engineering
Suleyman Demirel University, Isparta 32260, Turkey
[2]Department of Electronics and Communication Engineering
Yıldız Technical University, Istanbul 34349, Turkey

Abstract— In microwave engineering, one of the most challenging tasks is modeling the nonlinear microwave devices with high accuracy. Adequate modeling the small-signal and/or noise behavior of a microwave transistor contributes significantly to the power gain, mismatching and noise performances of a microwave communication system. Commonly, equivalent circuit approach is used in small-signal and/or noise modeling tasks. This approach aims to represent the active device with a proper equivalent circuit and here equivalent circuit parameters are derived from the measured scattering and noise parameters. Since the intrinsic circuit elements of the equivalent circuit are bias- and frequency-dependent, extraction procedure involves time consuming recurrent processes. Also, the bias dependency gives rise to presence of several equivalent circuits with varied intrinsic parameters values. Especially in the last decade, soft computing methods have been implemented as alternative approaches in device modeling applications. Among these, ANN pioneered the modeling of microwave active devices and has provided significant progress. ANN models are constructed by generating a high-order analytical relation between input (bias conditions and frequency) and output (measured scattering parameters, noise parameters) data sets without requiring any additional physical information about the device. Recent works proves that ANN has the ability to model noise behavior of a microwave transistor based on bias condition and temperature and also small-signal behavior based on bias condition and neural networks models provide considerably good agreement between measured and simulated results.

In this work, a novel neural network modeling approach using particle swarm optimization (PSO) for the black-box modeling of a microwave transistor is presented and compared with the different ANN models. PSO algorithm is applied as an efficient learning algorithm to enhance the modeling accuracy of the neural network due to its inherent superior performance. Black-box model includes both small-signal and noise parameters. Since each model parameter has unequal analytical relation with bias conditions and frequency, neural network contains unique and parallel processing sub-networks for each model parameter as shown in Fig. 1(a). Each sub-network

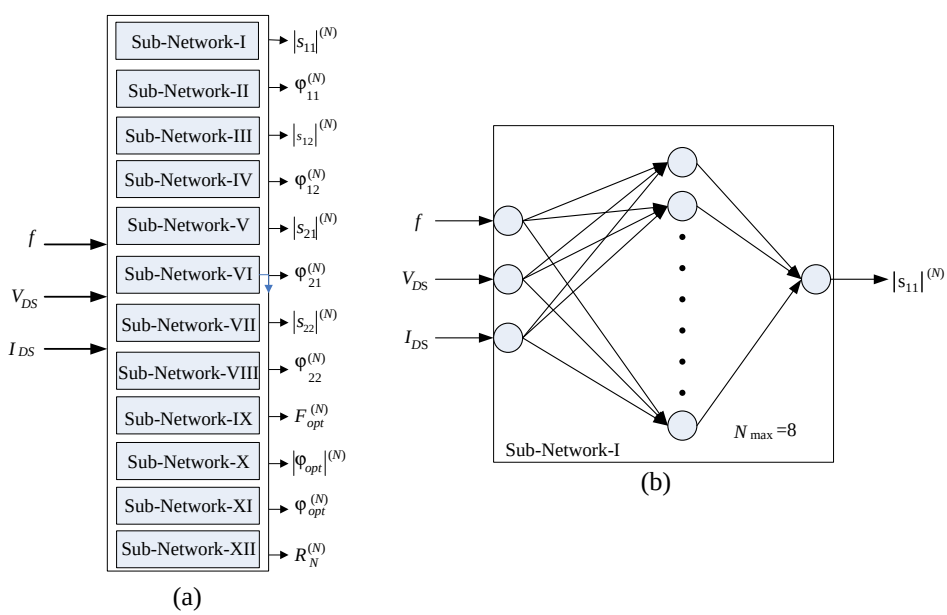

Figure 1.

topology is optimized so as to achieve the available best modeling accuracy as shown in Fig. 1(b). The proposed modeling approach is applied to pHEMT device and results are compared with conventional ANN models which are commonly used. This is verified that, among the models, the proposed modeling approach provides the best agreement between measured and simulated results. Results show that proposed approach has a high potential of accuracy and efficient device modeling.

Characteristic Planes of Microstrip and Unilateral Finline Tee-junctions

A. Casanueva[1], **A. Leon**[1], **A. Mediavilla**[1], **and J. Helszajn**[2]

[1]Universidad de Cantabria, Santander, Spain
[2]Heriot-Watt University, Edinburgh, UK

Abstract— The purpose of this paper is to establish the characteristic planes of microstrip and unilateral finline tee-junctions. A knowledge of these planes allow unique representations of these type of circuits. The former is an example of an H-plane or shunt network and the latter is one of an E-plane or series tee-junction. A unique set of reference planes which enters into the description of a three port E or H-plane tee-junctions are its characteristics planes. These planes correspond to the positions of a short circuit at one typical port that will decouple a second port from one input port. The purpose of this paper is to establish these planes in the cases of microstrip and unilateral finline circuits. This is done in each case for a number of different geometries. The spacing between the first two characteristic planes across the junction is 360 deg. in the case of the H-plane tee junction; it is 180 deg. in the case of the E-plane geometry. The parameters of E and H-plane tee-junctions are usually characterized at either the intersection between the symmetry planes of the main and side waveguides or at the physical opening of the junction. One other possibility is to adopt the characteristics planes for this purpose. Such planes provide a universal set of terminals in this class of network in both, microstrip line and waveguide. The concept of characteristics planes was first introduced in [1]. It has recently been applied in the descriptions of E and H-plane waveguide tee-junctions in WR-75 [2]. The purpose of this paper is to characterize microstrip in the H-plane and finline tee-junctions in the E-plane using this notation. This is done for both, parametric values of impedance levels and relative dielectric constants of the substrates. The scattering matrices of the circuits are separately calculated. This is done at an arbitrary frequency interval between 3 and 6 GHz. These sorts of junctions enter in the construction of filters circuits and also in the design of rat races and other microwave circuits. The eigenvalue problem of the H-plane circuit has been touched in [3]. The coordinate system adopted in [1]. is that at the intersection between the symmetry planes of the main waveguide and the side waveguide. Other authors, such as Mansour [4] have chosen the reference planes to coincide with the opening of the waveguides of the junction. The convention adopted here is to place the reference terminals at the characteristics planes of the junction. The convention adopted here is to place the reference terminals at the characteristics planes of the junction. It is indicated in Fig. 2(b) in the case of microstrip. The characteristics planes of the structure in Fig. 1(a) are summarized in Figs. 1(c) and 1(d). The corresponding standing wave patterns are illustrated in Figs. 1(e)–1(h). This is done for parametric values of impedance between 25 and 100 W over a frequency band between 3 and 6 GHz. The dielectric constant of the substrate is 3.12. The unilateral finline waveguide is an example of an E-plane geometry

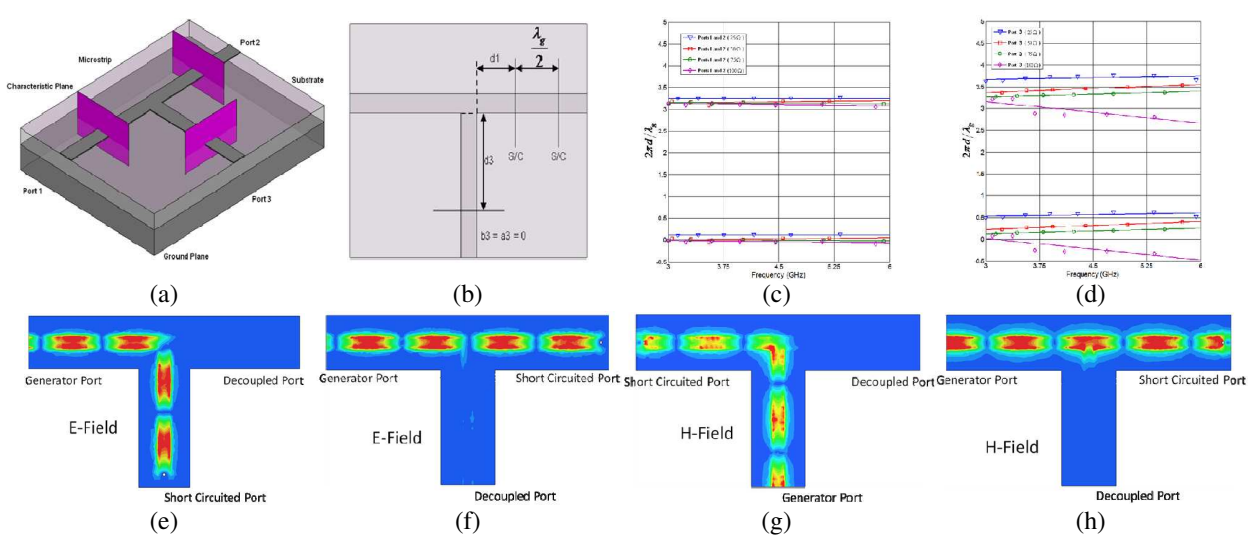

Figure 1.

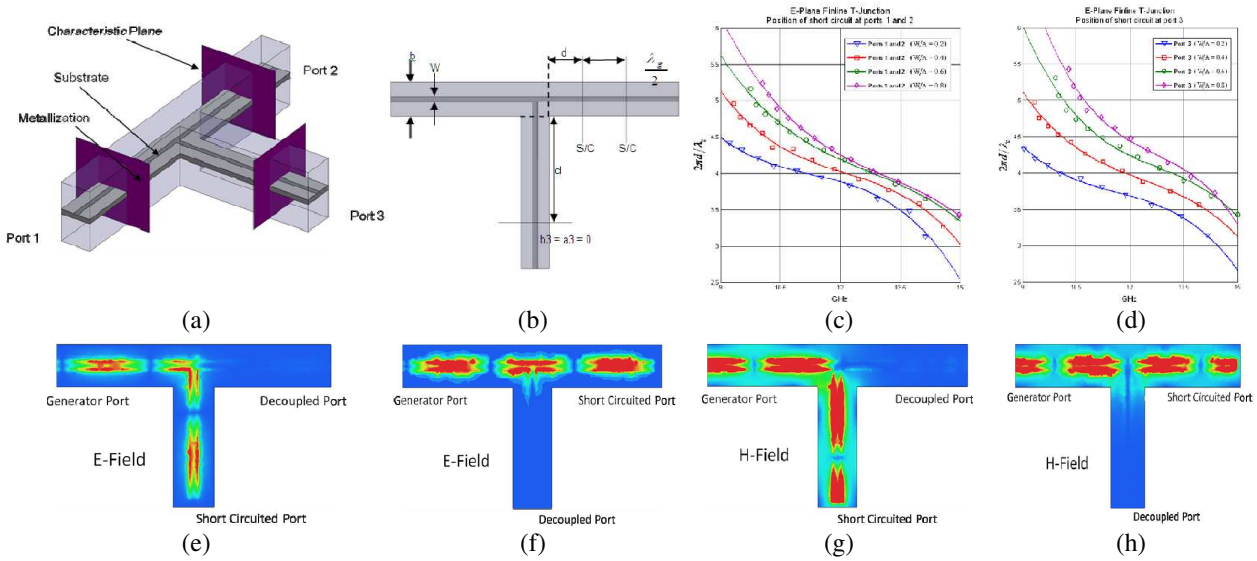

Figure 2.

it is described by the gap (w) and by the thickness (h) and by the dielectric constant of the substrate (ε_r). The relative dielectric constant employed in this work is 2.2 and the waveguide is WR-75. The schematic diagram under consideration is indicated in Fig. 2(a). The definitions of the reference planes are here arbitrarily taken at the openings of the waveguide of the rectangular waveguides of the junction rather than at those of the finline circuit. This is shown in Fig. 2(b). The analysis of the unilateral finline can be solved using the a spectral domain approach (SDA) together with a technique known as singular value decomposition (SVD) [5]. This type of planar transmission line differs from the microstrip case in that it is a dispersive structure. Figs. 2(c) and 2(d) define its characteristic planes. The standing wave patterns of the different possible experimental arrangements are shown in Figs. 2(e)–2(h).

ACKNOWLEDGMENT

The authors would like to thank the Spanish Ministry of Science and Innovation (MICINN-FEDER) by the financial support provided through project TEC2011-29126-C03-01 and CONSOLIDER-TERASENS CSD2008-00068.

REFERENCES

1. Allanson, J. T., R. Cooper, and T. G. Cowling, "The theory and experimental behaviour of right-angled junctions in rectangular-section wave guides," *IEE Proc.*, 1946.
2. Helszajn, J., M. Caplin, J. Frenna, and B. Tsounis, "Characteristics planes, scattering matrices and eigenvalues of E and H-plane waveguide Tee junctions," *IEEE MTT International Conference*, 2012.
3. Montgomery, C. G., R. H. Dicke, and E. M. Purcell, *Principles of Microwave Circuits*, McGraw-Hill Co., New-York, 1948.
4. Mansour, R. R. and J. Dude, "Analysis of microstrip T-junction and its application to the design of transfer switches," *IEEE Conference*, 1992.
5. Casanueva, A. and J. L. García, "An innovative fast powerful method for tackling electromagnetic eigenvalue problems for multistrip transmission lines," *IEEE Trans. Microwave Theory and Tech.*, Vol. 50, 36–40, Jan. 2002.

Study of Longitudinally Magnetized Left-handed Cylindrical Ferrite Coupled Line Junction

A. Kusiek, W. Marynowski, and J. Mazur
Gdansk University of Technology, Poland

Abstract— Nonreciprocal devices have been extensively used in modern microwave and millimeter system. Recently, the longitudinally magnetized ferrite coupled strip- or slotlines [1, 2] are being developed and employed to realize integrated nonreciprocal devices. Significant interest in these devices results from their advantages which are weak biasing magnetic field and wide operation bandwidth. So far, studies concerning FCL devices have been focused mainly on structures realized in planar line technology. Such structures allow one to obtain fully integrated FCL devices. However, due to the significant length of ferrite section, the main drawbacks are high insertion losses occurring in ferrite material [3] and large dimensions of the structure.

There were several attempts to improve performance and to reduce total dimensions of planar FCL devices. In order to reduce the dimensions of the planar FCL devices in [1] the circulator with appropriate matching networks at the ports ensuring multiple reflections was proposed. For presented device the FCL junction length reduction by a factor of two was obtained. The drawback of this structure was high value of insertion losses caused by multiple transmission of signal through the lossy ferrite junction. Also similar length reduction of FCL junction was achieved with the use of periodic left-handed/ferrite coupled line (LH-FCL) structures [4, 5]. However, for the simulated circulator utilizing LH-FCL section the insertion losses were not better than 4dB.

The promising results concerning losses were obtained for cylindrical ferrite junction [6]. In such configuration stronger gyromagnetic coupling occurs which is a result of high magnetic field concentration in the ferrite medium. These make possible to design shorter ferrite junctions ensuring lower insertion losses in comparison to planar ones. Since, the obtained insertion losses 1.5 dB in [6] are still at unacceptable level in this paper we focus on insertion losses reduction by miniaturization of CFCL section based on left handed (LH) periodic structures. The scattering parameters of CFCL/LH junction were obtained by cascading scattering parameters of N unit cells composed of short length CFCL connected with lumped reactance circuit. In the analysis of CFCL section the own hybrid technique combining metod-of-moments with mode-matching technique was applied. The obtained results have shown that it is possible to design $\pi/4$ Faraday rotation CFCL/LH junction with reduced length in comparison to conventional CFCL.

ACKNOWLEDGMENT

This work was supported by the Polish Ministry of Science and Higher Education from sources for science in the years 2012–2013 under Contract IP2011 028271 (decision No. 0282/IP3/2011/71).

REFERENCES

1. Meng, C. and R. Pietig, "Ferrite coupled-line circulator with reduced length," *IEEE Transactions on MTT*, Vol. 53, No. 8, 2572–2579, August 2005.
2. Yang, L.-Y. and K. Xie, "Design and measurement of nonuniform ferrite coupled line circulator," *Journal of Electromagnetic Waves and Applications*, Vol. 25, No. 1, 131–145, 2011.
3. Marynowski, W. and P. Kowalczyk, "Analysis of magnetic losses in ferrite coupled lines using SDA and hybrid root finding algorithm," *Progress In Electromagnetics Research Symposium Abstracts*, 635, Taipei, March 25–28, 2013.
4. Abdalla, M. A. and Z. Hu, "On the study of left-handed coplanar waveguide coupler on ferrite substrate," *Progress In Electromagnetics Research Letters*, Vol. 1, 69–75, 2008.
5. Abdalla, M. A. and Z. Hu, "Compact tuneable single and dual mode ferrite left-handed coplanar waveguide coupled line couplers," *IET Microwaves, Antennas Propagation*, Vol. 3, No. 4, 695–702, June 2009.
6. Kusiek, A., W. Marynowski, and J. Mazur, "Investigations of four-port circulator utilizing cylindrical ferrite coupled line junction," *Progress In Electromagnetics Research*, Vol. 134, 379–395, 2013.

Nonreciprocal Devices Using Longitudinally Magnetized Left Handed Ferrite Coupled Line Junction

W. Marynowski, **A. Kusiek**, **and J. Mazur**
Gdansk University of Technology, Poland

Abstract— The nonreciprocal devices utilizing longitudinally magnetized ferrite coupled lines (FCL) are important group of passive circuits. Recently, many research is carried on the miniaturization of FCL devices [1–4]. Generally they are focused on size reduction of whole circuit while the length of FCL section is unchanged.

Since, the losses of FCL devices are caused mainly by ferrite material [5, 6], the main attempt should be focused on FCL section size reduction. In [1] the length reduction of ferrite section is proposed using additional matching circuits at the input ports of FCL section. As a result the ferrite length is reduced to half of conventional FCL section, however the narrow-band operation is achieved.

In this paper the alternative technique for FCL section size reduction based on left handed (LH) periodic structures is described. Proposed ferrite LH structure is realized based on three strip FCL section and is named FCL-LH. The single section of such periodic structure is composed of short FCL in cascade with series capacitance and shunt inductance. In order to obtain the scattering parameters of FCL-LH junction of required length, this section is duplicated n times. Next the achieved junction is used in design of the circulator. The obtained results have shown that using FCL-LH junction, the nonreciprocal devices with reduced ferrite section length (in comparison to conventional FCL section) can be realized.

ACKNOWLEDGMENT

This work was supported in part by Polish Ministry of Science and Higher Education from sources for science in the years 2012-2013 under Contract No. 0340/IP2/2011/71.

REFERENCES

1. Cao, M. and R. Pietig, "Ferrite coupled-line circulator with reduced length," *IEEE Transactions on Microwave Theory and Techniques*, Vol. 53, No. 8, 2572–2579, August 2005.
2. Queck, C. K. and L. E. Davis, "Novel folding technique for planar ferrite-coupled-line circulators," *IEEE Transactions on Microwave Theory and Techniques*, Vol. 52, No. 5, 1369–1374, May 2004.
3. Marynowski, W., A. Kusiek, and J. Mazur, "Microstrip ferrite coupled line isolators," *International Conference MIKON*, Vol. 1, 342–345, Krakow, Poland, May 2006.
4. Queck, C. K. and L. E. Davis, "Butterfly-shape folding of a ferrite coupled line," *36th European Microwave Conference*, 1147–1150, September 2006.
5. Marynowski, W. and J. Mazur, "Study of nonreciprocal devices using three-strip ferrite coupled line," *Progress In Electromagnetics Research*, Vol. 118, 487–504, 2011.
6. Marynowski, W. and P. Kowalczyk, "Analysis of magnetic losses in ferrite coupled lines using sda and hybrid root finding algorithm," *Progress In Electromagnetics Research Symposium*, 635, Taipei, Taiwan, March 2013.

A K-band Direct Injection-locked Frequency Divider Using Harmonic LC Tanks

Chien-Pai Wu and Yen-Chung Chiang
National Chung Hsing University, Taiwan

Abstract— An injection-locked frequency divider implemented in the TSMC 0.18 μm CMOS process technology for K-band applications is proposed in this paper. The proposed frequency divider is based on the conventional complementary direct injection-locked frequency divider. By using the harmonic LC tank technique, the third order harmonic of the output signal from the frequency divider is enhanced and a balanced performance between the locking range and the output swing can be achieved. Compared with the conventional direct injection-locked frequency divider, the locking speed of the proposed frequency divider can also be improved. The chip size of the proposed frequency divider is $0.711 \times 0.776\,\mathrm{mm}^2$. The measured locking range is from 24.8 to 26.6 GHz under 0 dBm input power level and the core circuit draws a 5.4 mW dc-power from a 1.8-V supply.

The Phase Noise Reduction of GaAs V-band Push-push VCO Using Slow-wave CPW Resonator Structures

Hsien-Chin Chiu, **Min-Li Chou**, **Po-Yu Ke**, **Fan-Hsiu Huang**, **and Hsuan-Ling Kao**
Department of Electronics Engineering, Chang Gung University, Taoyuan, Taiwan, R.O.C.

Abstract— In the paper, the design of two fully integrated millimeter-wave (mmW) V-band push-push voltage controlled oscillators (VCOs) implemented in a 150-nm pHEMT process is presented. Both use slow-wave coplanar waveguide (CPW) structures transmission line resonators instead of a lumped LC tank to provide extended output frequency ranges and relatively low phase noise (PN). The LC tank with and without slow-wave features were employed in the two VCO circuits. The measured results of the manufacture chips were compared. The VCO with the slow wave feature showed a lower PN is -104.5 dBc/Hz at 1 MHz offset frequency. Compare with a without slow wave VCO, this with slow wave VCO design shows that the achieves lower phase noise average about 8 dBc at offset frequency 1 MHz. Varactor adjustment the oscillation frequencies for two VCOs, 53.2 to 57.1 GHz for without slow wave VCO and 53.8 to 55.4 GHz for with slow wave VCO. The two VCOs were developed for use in licensed V-band transceiver systems.

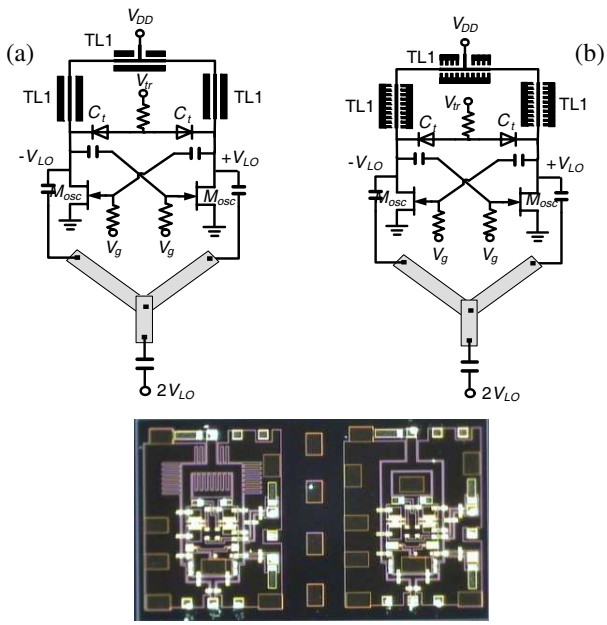

Figure 1: Circuit schematic of the designed V-band push-push VCOs. (a) LC-tank without slow-wave VCO. (b) LC-tank with slow-wave VCO.

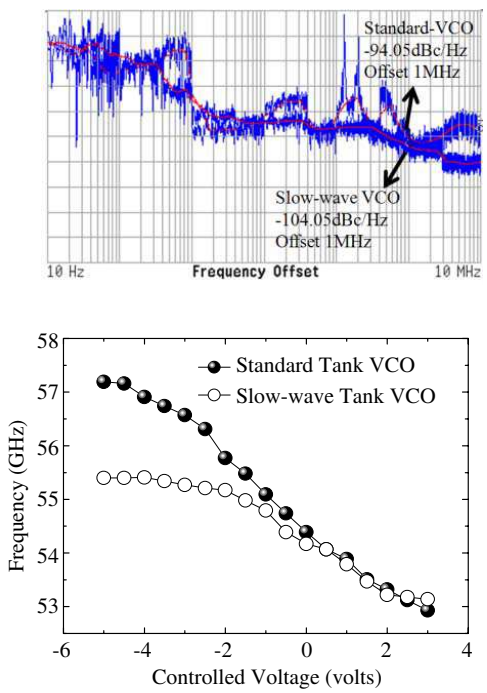

Figure 2: Measured VCO of tuning range.

Novel Atmospheric Pressure Plasma-based Methods for Surface Modification and Hybrid Laser Ablation of Optical Glasses

C. Gerhard and W. Viöl
Laboratory of Laser and Plasma Technologies, University of Applied Sciences and Arts
Von-Ossietzky-Straße 99, Göttingen 37085, Germany

Abstract— Cost- and energy-efficient modification and micro structuring of fused silica and other optical glasses is of great interest for a number of widely varying application areas such as optical telecommunication, medical engineering and metrology. In this contribution, we present an overview on recent research results and developments on atmospheric pressure plasma (APP)-based modification and ablation methods for such materials. Against this background, different approaches were developed, using different types of plasma discharge modes as well as both inert and chemically active process gases.

APP-induced modification of optical glasses is generally achieved by chemical reactions of both the glass surface and the reactive species provided by the applied plasma and the accompanying change in stoichiometry of the involved glass compounds. As an example, silicon dioxide is reduced to silicon suboxide near to the surface and hydrogen is implanted into deeper regions of the glass bulk material. These underlying effects can be used for modifying the index of refraction of fused silica [1]. As a consequence, the related dispersion and absorption characteristics are shifted significantly, resulting in an enhanced energy coupling during subsequent laser ablation. This allows improving laser ablation results (i.e., a higher ablation rate, higher contour accuracy and reduced surface roughness of the ablated area) and an optimised energy conversion [2–4]. In the case of APP-based ablation of fused silica, the ablation threshold was reduced by a factor of 4.6 with respect to pure laser ablation. Besides, surface smoothing of glassy materials as well as an enhanced laser ablation process can also be performed by applying inert process gases [5].

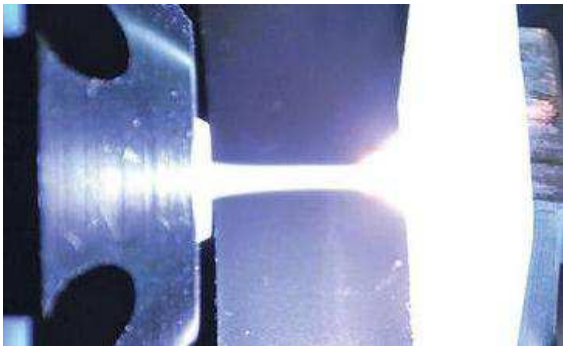

Figure 1: Example for hybrid atmospheric pressure plasma-based laser ablation of optical glass.

REFERENCES

1. Gerhard, C., D. Tasche, S. Brückner, S. Wieneke, and W. Viöl, *Opt. Lett.*, Vol. 37, 566–568, 2012.
2. Brückner, S., J. Hoffmeister, J. Ihlemann, C. Gerhard, S. Wieneke, and W. Viöl, *J. Laser Micro Nanoen.*, Vol. 7, 73–76, 2012.
3. Hoffmeister, J., C. Gerhard, S. Brückner, J. Ihlemann, S. Wieneke, and W. Viöl, *Physics Procedia*, Vol. 39, 613–620, 2012.
4. Gerhard, C., J. Heine, S. Brückner, S. Wieneke, and W. Viöl, *Laser Eng.*, Vol. 24, 391–403, 2013.
5. Gerhard, C., S. Roux, S. Brückner, S. Wieneke, and W. Viöl, *Appl. Opt.*, Vol. 51, 3847–3852, 2012.

A Versatile Atmospheric Pressure Plasma Source for Simultaneous Surface Treatment and Analysis

C. Gerhard[1], **S. Brückner**[2], **and W. Viöl**[1]

[1]Laboratory of Laser and Plasma Technologies, University of Applied Sciences and Arts
Von-Ossietzky-Straße 99, Göttingen 37085, Germany
[2]Institute of Energy Research and Physical Technologies, Clausthal University of Technology
Leibnizstraße 4, Clausthal-Zellerfeld 38678, Germany

Abstract— Atmospheric pressure plasma processes stand out due to a high degree of efficiency and a low maintenance effort and thus represent a reasonable alternative solution for a number of established energy-requiring methods. In this context, we present a novel versatile atmospheric pressure plasma source (APPS) as well as some of its already implemented and possible applications. The presented APPS allows realising two different discharge modes: an atmospheric pressure plasma jet and a fine and stable plasma beam, both based on a dielectric barrier discharge (DBD) and thus providing a "cold" plasma. As shown in Figure 1, this is achieved by a specific composition and circuitry of the involved internal and external electrodes.

As a further special feature, this patented APPS offers accessing the particular plasma coaxially. For instance, this characteristic can be used in order to implement a measuring fibre for plasma diagnostics applications or to guide a laser beam along the plasma jet or beam, respectively. It was shown that such a laser-plasma coupling allows enhancing the machining efficiency of laser ablation processes significantly by resulting energetic synergies [1, 2]. Due to the low temperature of the generated plasma (i.e., in the range of 20–50°C), temperature-sensitive materials can be treated without any damage of the surface. This effect was applied for the development of a novel spectroscopic measurement technique, where optical emission is excited by the plasma beam (see Figure 1) [3]. In comparison to laser-induced breakdown spectroscopy (LIBS), this plasma-induced ionisation spectroscopy allows measuring thin films such as contaminations without destroying the substrate material.

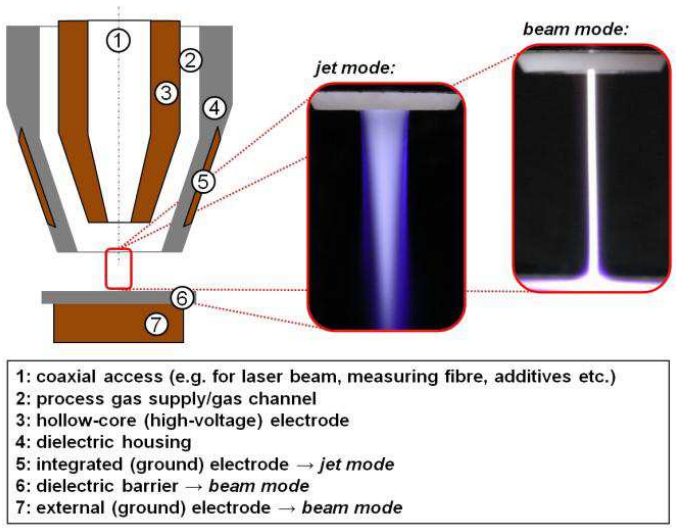

Figure 1: Scheme of the presented plasma source.

REFERENCES

1. Gerhard, C., S. Roux, S. Brückner, S. Wieneke, and W. Viöl, *Appl. Phys. A*, Vol. 108, 107–112, 2012.
2. Gerhard, C., S. Roux, S. Brückner, S. Wieneke, and W. Viöl, *Appl. Opt.*, Vol. 51, 3847–3852, 2012.
3. Brückner, S., S. Rösner, C. Gerhard, S. Wieneke, and W. Viöl, *Mater. Test.*, Vol. 53, Vol. 10, 639–642, 2011.

Shape Dependent Broadband Plasmonic Absorption in Metallic Nanoparticles for Efficient Organic Solar Cells

Xuanhua Li[1], Wallace C. H. Choy[1], Haifei Lu[2], Wei E. I. Sha[1], and H. P. Ho[2]

[1]Department of Electrical and Electronic Engineering, The University of Hong Kong
Pokfulam Road, Hong Kong, China
[2]Department of Electronic Engineering, Center for Advanced Research in Photonics
The Chinese University of Hong Kong, Shatin, NT, Hong Kong SAR 852, China

Abstract— Light trapping is an important topic for thin film organic solar cells (OSCs) to improve the light absorption and thus performances of OSCs. Recently, it is been widely reported that plasmonic effects in metallic nano-materials can enhance light trapping in OSCs. However, typical nanoparticles (NP) of high quality, i.e., mono-dispersive, only possess a single localized plasmonic resonant (LPRs) absorption peak, which inevitably limits the power conversion efficiency (PCE) enhancement to a narrow spectral range. Broadband plasmonic is obviously highly desirable. In this paper, we propose to combine Ag nanomaterials of different shapes including nanoparticles and nanoprisms for this purpose. The synthesized Ag nanoparticles and nanoprisms have maximum absorption peaks around 400 nm and 600 nm, respectively, which arise from LPRs of two different shapes of NPs. After mixing the two shaped Ag NPs, a broader absorption spectrum is obtained covering from 400 nm to 600 nm. By using the combined Ag nanomaterials in active layer of OSCs, we would like to achieve a broad wavelength range of absorption enhancement. Our theoretical and experimental studies show that the origin of the observed PCE enhancement comes from the simultaneous excitation of many plasmonic low-order and high-order resonances modes which are shape-, size- and polarization-dependent. Particularly for the Ag nanoprisms studied here, the high-order resonances result in higher contribution than low-order resonances to the absorption enhancement of OSCs through an improved overlap with the active material absorption spectrum. With the incorporation of the mixed nanomaterials into the active layer, wide band absorption improvement has been demonstrated and the short-circuit photocurrent density (Jsc) has improved by 17.91%. Finally, PCE enhances by 19.44% as compared to the pre-optimized control OSCs. Our results suggest a new approach to achieve higher overall enhancement through improving broadband absorption.

An Accurate and Robust Timing and Frequency Synchronization for Coherent Optical Systems

Lingchen Huang[1], **Changjian Guo**[2], **and Dawei Wangle**[1]

[1]Zhejiang University, Hangzhou 310058, China
[2]South China Normal University, Guangzhou 510006, China

Abstract— Owing to its high spectral efficiency and high receiver sensitivity, coherent optical (CO) polarization-division-multiplexing (PDM) technique has been actively investigated both in single carrier and multi-carrier optical systems for applications in the next-generation high-speed optical transport systems. At coherent receivers, timing and frequency synchronizations are critical procedures to ensure the proper functioning of following digital signal processing (DSP) algorithms. For CO-PDM-OFDM systems, several methods based on training symbols (TS) and auto-correlation have been proposed. However, these methods may suffer from narrow band interference, essentially the residual optical carrier in the optical fiber transmission, which may result from the insufficient modulation depth, or deliberate reservation for carrier phase estimation. Besides, due to the fiber chromatic dispersion (CD) and polarization mode dispersion (PMD), the correlation property of TS may be weakened after fiber transmission, which also results in the deterioration of synchronization performance.Here, a novel synchronization method is proposed to offer high interference, noise, and dispersion tolerance. A specially designed TS is used to generate a sharp timing metric compared to the S&C scheme3. And by compensating the link CD and applying a fine timing estimation, our proposed method can achieve nearly perfect timing estimation in both cases of back-to-back and long-haul transmission.The simulation results are shown below:

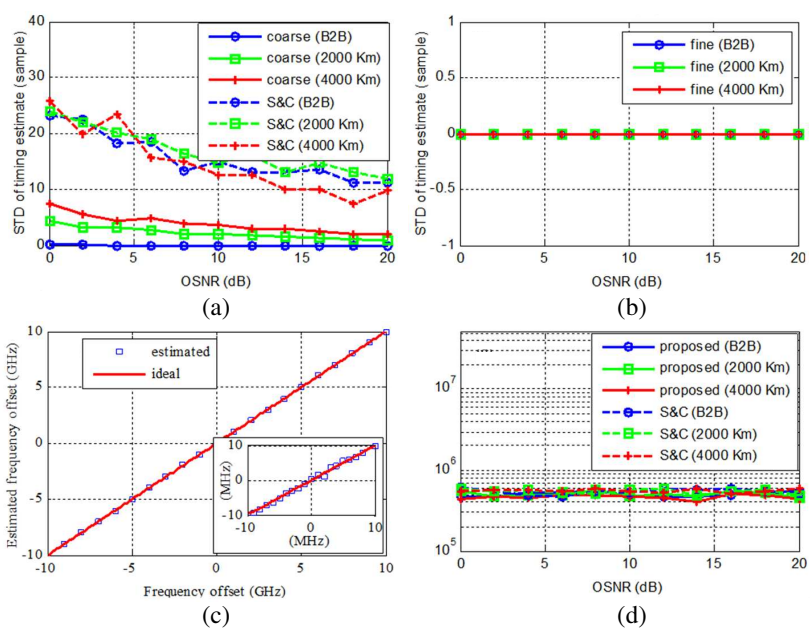

Figure 1: Simulation results of the proposed synchronization method.

Conclusion: A novel timing and frequency synchronization method is proposed to achieve accurate timing and frequency offset synchronization for coherent optical PDM systems. The proposed method provides robustness to interference, noise and dispersion. Simulation results show that its timing estimate STD approaches the ideal value of zero, while its frequency estimate accuracy achieves the order of magnitude of the laser line-width.

Compressed Sensing for Velocity Estimation of CW Radar Using a Constrained Least Square Method

Jiwoong Yu, **Tae-Yun Lee**, **Seok Kim**,
Se-Yeon Jeon, **and Min-Ho Ka**
School of Integrated Technology, Yonsei University, Incheon, Korea

Abstract— In spite of noise limitation, continuous-wave (CW) radar is widely used in near range. The CW radar is useful in velocity estimation by using the doppler frequency shift. Traditional doppler shift is calculated by FFT (Fast Fourier Transform) which is needed to enough number of received signal for high resolution. The maximum frequency resolution is proportional to the number of received signal. The accurate velocity estimation requires a long integration time. In this paper, we suggest new technique that estimates the velocity using compressed sensing. The received signal can be represented by a linear combination of sine and cosine function as frequency same. Dictionary consists of several frequencies of both sine and cosine function. Then, if received doppler frequency is closed to such a frequency of the dictionary, least square error is small between received signal and a linear combination of sine and cosine function. The frequency having a minimum least square error is represented by the best fit solution in time domain without FFT. This method improves the frequency resolution with the same integration time. As is well known, if the solution has a property of constrained sparse it can be solved with a L1 minimization. But proposed method is much faster and robust. Also, similar to compressed sensing, length of dictionary can be reduced by multiplying a normalized random matrix. This Study has demonstrated that the constrained least square method reduces a data sampling rate and improves the frequency accuracy.

ACKNOWLEDGMENT

This research was supported by the MKE (The Ministry of Knowledge Economy), Korea, under the "IT Consilience Creative Program" support program supervised by the NIPA (National IT Industry Promotion Agency) (NIPA-2013-H0203-13-1002).

REFERENCES

1. Skolinik, M. I., *Radar Handbook*, McGraw-Hill Professional, 2nd Edition, 1990.
2. Mahafza, B. R., *Radar Signal Analysis and Processing Using MATLAB*, Chapman & Hall/CRC, 2008.
3. Herman, M. A. and T. Strohmer, "High-resolution radar via compressed sensing," *IEEE Trans. Signal Process.*, Vol. 57, 2275–2284, 2009.
4. Smith, G. E., T. Diethe, Z. Hussain, J. Shawe-Taylor, and D. R. Hardoon, "Compressed sampling for pulse Doppler radar," *Radar Conference*, 887–892, Arlington, USA, May 2010.

Electromagnetic Signal Processing for Feature Extraction and Classification of Lossy Dielectric Targets

Gonul Turhan-Sayan and Basak I. Barut
Department of Electrical and Electronics Engineering
Middle East Technical University (METU), Ankara, Turkey

Abstract— Recognition of objects from their wideband radar signals is a challenging task due to the inherent problem of aspect and polarization dependency of electromagnetic scattered signals. Despite this fundamental complexity, electromagnetic target classifiers must be designed to satisfy high correct decision rates even under high-noise conditions. Several different methods have been demonstrated during the last decade for the extraction of target features with reduced aspect and polarization sensitivity from multi-aspect electromagnetic signal measurements in the resonance region. The common approach in all those feature extraction methods is to retrieve some information related to the target's complex natural resonance frequencies (i.e., target's system poles) which are known to be the aspect and polarization invariant characteristics of the given target. Methods for target feature extraction are almost always based on the use of signal processing techniques such as the Wigner distribution (WD) that is a time-frequency representation technique, principal component analysis (PCA), multiple signal classification (MUSIC) algorithm, the self-organizing map (SOM) that is a clustering type neural network as well as conventional or global optimization methods. Combinations of different signal processing techniques are used in recently proposed WD-PCA, MUSIC and WD-SOM methods which have been successfully demonstrated (by G. Turhan-Sayan et al.) for the classification of targets made of conductors and/or very low-loss (practically lossless) dielectric materials.

In literature, the WD-PCA technique has been successfully applied so far to recognize perfect conductor, perfect dielectric or dielectric coated conducting objects. In this paper, this technique will be demonstrated for the first time in literature for objects made of dispersive and lossy dielectric materials. Simulation results for target classifier design and testing will be demonstrated for canonical targets of spherical geometry having the same size but different material loss properties.

Bivariate Statistical Analysis for Electromagnetic Reverberation Chamber

Suna Choi and Seungkeun Park
Electronics and Telecommunications Research Institute (ETRI), Koera

Abstract—

Introduction: Reverberation chambers (RCs) have been widely attracting attention as electromagnetic (EM) testing facilities, performance evaluations of multiple-input-multiple-output handset antennas, etc.. Recently, to investigate the field properties in good-but-imperfect RCs, bivariate normal distributions (BNDs) with five parameters have been applied and categorized into eight types. We complete the mathematical expressions describing the magnitude and phase of electric fields. Moreover, we present the experimental results of electric fields in a real RC. Using the Goodness-of-fit (GoF) test, the magnitude and phase distributions of electric fields for the eight cases of BNDs are evaluated.

Bivariate Normal Distributions: For characterizing the electric fields, the BND of real and imaginary parts ξ and η is represented as $N(\mu_\xi, \mu_\eta;\, \sigma_\xi, \sigma_\eta;\, \rho)$, where μ_ξ and μ_η are the means for ξ and η, respectively, σ_ξ and σ_η are the standard deviations and ρ is the correlation coefficient between ξ and η. The BNDs are categorized into eight types according to the values of μ_ξ, μ_η, σ_ξ, σ_η, and ρ.

The magnitude or phase PDFs for two cases of $N(\mu_\xi, \mu_\eta;\, \sigma_\xi, \sigma_\eta;\, 0)$ and $N(0, 0;\, \sigma_\xi, \sigma_\eta;\, \rho)$ have not been reported as clearly explicit expressions. Thus, we present the two PDFs and complete the expressions for the magnitude and phase PDFs of BNDs.

1) For $N(\mu_\xi, \mu_\eta;\, \sigma_\xi, \sigma_\eta;\, 0)$ case: the phase PDF is

$$\begin{aligned} f_\phi(\phi) &= \frac{\sigma_\xi^3\sigma_\eta^3}{\pi A(\phi)} \exp\left[-\frac{\left(\mu_\xi^2\sigma_\eta^2 + \mu_\eta^2\sigma_\xi^2\right)}{2\sigma_\xi^2\sigma_\eta^2}\right] \\ &\quad \cdot \left\{\sqrt{\frac{\pi B_{\xi\eta}}{A(\phi)}}\cos(\phi-\alpha)\exp\left[\frac{B_{\xi\eta}}{A(\phi)}\cos^2(\phi-\alpha)\right]\operatorname{erfc}\left[-\frac{B_{\xi\eta}}{A(\phi)}\cos^2(\phi-\alpha)\right]+1\right\} \end{aligned}$$

where

$$\begin{aligned} A(\phi) &= \sigma_\xi^2\sigma_\eta^2\left[\sigma_\xi^2+\sigma_\eta^2-\left(\sigma_\xi^2-\sigma_\eta^2\right)\cos 2\phi\right], \\ B_{\xi\eta} &= \mu_\xi^2\sigma_\eta^4+\mu_\eta^2\sigma_\xi^4, \\ \cos\alpha &= \mu_\xi\sigma_\eta^2/\sqrt{B_{\xi\eta}}, \quad \sin\alpha = \mu_\eta\sigma_\xi^2/\sqrt{B_{\xi\eta}}, \end{aligned}$$

and $\operatorname{erfc}(\cdot)$ represents the complementary error function.

2) For $N(0, 0;\, \sigma_\xi, \sigma_\eta;\, \rho)$ case: the magnitude PDF is

$$f_r(r) = \frac{r}{\sigma_\xi\sigma_\eta\sqrt{1-\rho^2}}\exp\left[-\frac{\left(\sigma_\xi^2+\sigma_\eta^2\right)r^2}{4\sigma_\xi^2+\sigma_\eta^2\left(1-\rho^2\right)}\right] I_0\left[\frac{\sqrt{\left(\sigma_\xi^2+\sigma_\eta^2\right)^2+4\rho^2\sigma_\xi^2+\sigma_\eta^2}}{4\sigma_\xi^2+\sigma_\eta^2\left(1-\rho^2\right)}r^2\right]$$

where $I_0(z)$ is the zeroth order modified Bessel function of the first kind.

Measurement Results: To verify the bivariate normal distributions, complex electric field components were measured in the RC located at Ajou University, South Korea. In this experiment, three different frequencies of 1.8, 2.4, and 3.8 GHz were selected, and about 5,000 samples per each frequency were measured using a vector network analyzer and dipole antennas.

The T-test and F-test are applied to test the hypothesis of zero-mean, equal variance and zero correlation test for a 5% confidence level. Figure 1 shows that the rejection rates are 10–30%, which are non-negligible.

For the numerical comparison of the eight cases, the Kolmogorov-Smirnov (KS) and Anderson-Darling (AD) GoF tests are applied to the magnitude and phase PDFs. Figure 2 show the results

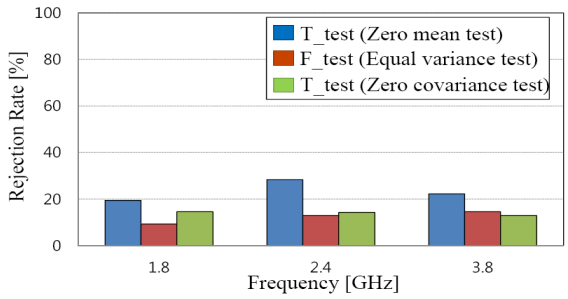

Figure 1: T and F test results for measurement data against the ideal assumption of parameters.

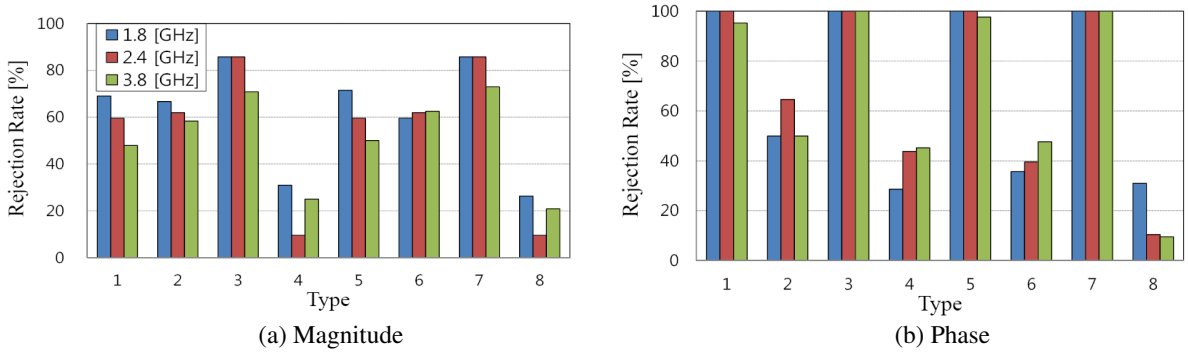

Figure 2: KS GoF results for measurement data against 8 types of PDFs.

from KS GoF test. The rejection rates of magnitude PDFs of the type 4 and type 8 are much less than that of type 1 (the ideal case). The phase PDFs of odd types are highly rejected than those of even types. The AD GoF test shows similar tendency with KS test.

Conclusion: We present the complete expressions for the magnitude and phase PDFs in RC using BNDs. Also, using the experiment and the goodness-of-fit test, the PDFs are compared and evaluatd. The results are helpful in better understanding the behavior of the fields in RCs.

Design of the Electric-fields Probe in the Personal Exposure Meter

Sang Il Kwak[1], **B. C. Kim**[1], **H. D. Choi**[1], **and Young Joong Yoon**[2]

[1]Radio Technology Research Department
Electronics and Telecommunications Research Institute (ETRI)
218 Gajeongno, Yuseong-gu, Daejeon, Korea
[2]Department of Electrical and Electronics Engineering, Yonsei University, Seoul, Korea

Abstract—

Introduction: This paper shows a development of the isotropic electric fields probe in the personal exposure meter. The personal exposure meter is a device for measurement of E-fields near the human body. To detect the exposed E-fields, a 3-axis E fields probe is used in the personal exposure meter. The probe is consists of three orthogonal infinitesimal dipole antennas with schottky diodes and lossy transmission lines using chip resistors. The proposed probe bandwidth is 10 MHz to 6 GHz and the isotropic deviation of the proposed probe radiation pattern is less than 0.5 dB in the simulation results. Finally, the fabricated probe will be shown and the properties of the probe such as a linearity and radiation pattern of the probe are presented.

Probe Design: Figure 1 shows the layout of the proposed E-fields probe. To measure the wideband services such as ISM devices (RFID, medical devices etc.), broadcasting and communications devices, the target frequency bandwidth is 10 MHz to 6 GHz. Using the Ref. [1], the size of the dipole antenna is calculated at target frequency. The size of the probe is 3 mm × 2 mm. A HSCH-5330 schottky diode is used and the spatial angle of the three dipoles is 54.74° for orthogonal property. To obtain highly resistive transmission line, chip resistors are used.

Results: To obtain the isotropic radiation characteristic of the probe, the parameter studies are performed [2]. The length of the transmission line is 65 mm and total height of the probe is 73.7 mm. Figure 2 shows the simulated radiation pattern of the probe. As shown in Figure 2 and Ref. [2], the isotropic deviation of the proposed probe is less than 0.5 dB.

Figure 3 shows the measured output voltage of the probe according to the input power. The measurement of the probe is using the GTEM cell (TESEQ GTEM 250). The GTEM cell can create uniform E-fields and the input power can be adjusted. As the input power is increased, the output voltage increases linearly. Also, the occupational exposure limits to protect human body at 2 GHz is 134 V/m. The proposed probe can measure the E-fields up to 267 V/m at 2 GHz. The measured radiation pattern of the probe is also using the GTEM cell. As the input power is fixed, the designed probe is rotated in the GTEM cell and measured output E-fields. The results will be shown at the conference.

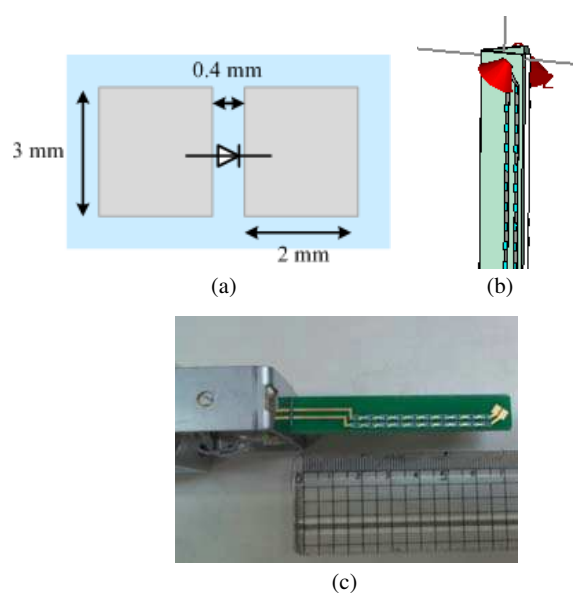

Figure 1: Layout of the proposed probe: (a) dipole, (b) probe, (c) probe with readout device.

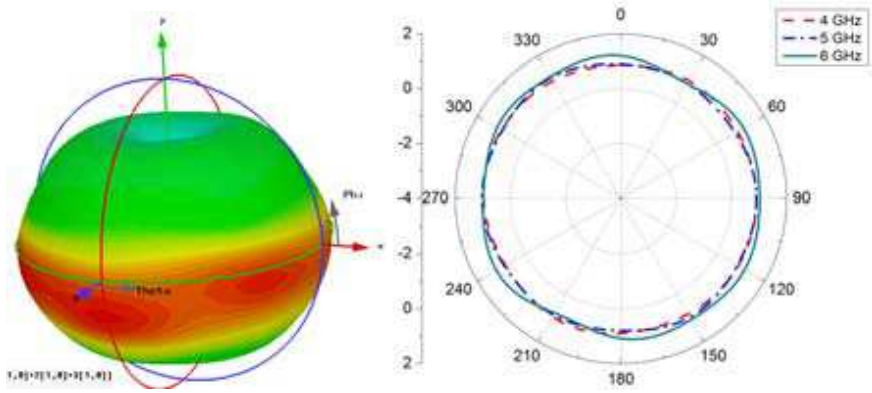

Figure 2: Simulated radiation pattern of the proposed probe.

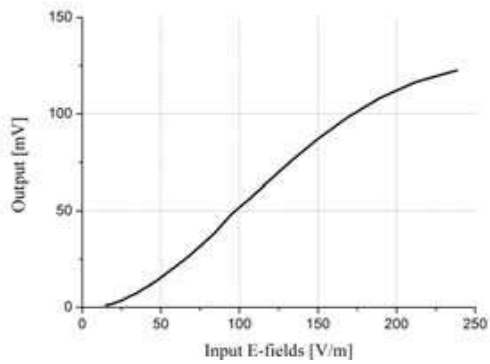

Figure 3: Measured output voltage according to the input E-fields at 2 GHz.

Conclusion: In this paper, the isotropic electric fields probe in the personal exposure meter is designed. To detect the exposed E fields, a 3-axis E-fields probe is used in the personal exposure meter. The probe is consists of three orthogonal infinitesimal dipole antennas with schottky diodes and lossy transmission lines using chip resistors. The bandwidth of the probe is 10 MHz to 6 GHz. The designed probe output voltage has a linear characteristic for the input power. Finally, the fabricated probe can be used in the personal exposure meter.

ACKNOWLEDGMENT

This work is supported by the KCC (Korea Communications Commission), under the R&D program supervised by the KCA.

REFERENCES

1. Bassen, H. I. and G. S. Smith, "Electric field porbes — A review," *IEEE Trans. Antennas and Propg.*, Vol. 31, 710–718, Sep. 1983.
2. Kwak, S. I., B. C. Kim, and H. D. Choi, "Analysis of isotropic deviation of the E-fields probe in the personal exposure measurement meter," *ICTC 2012*, 235–237, Oct. 2012.

GNSS-based Bistatic Synthetic Aperture Radar Image Formation via Compressive Sensing

Chunyang Dai, **Liangjiang Zhou**, **Xingdong Liang**, **and Yirong Wu**
Institute of Electronics, Chinese Academy of Sciences, Beijing, China

Abstract— Global Navigation Satellite System (GNSS) based bistatic synthetic aperture Radar (BiSAR) is a promising non-cooperative radar imaging system, and becomes to be a hot research topic in passive remote sensing area. This paper proposed a novel imaging configuration with multiple GNSS transmitters and one receiver, which can be equivalent to a large sparse two-dimensional antenna arrays. By this configuration, we can obtain focused sparse targets in the ground via compressive sensing (CS) even in zero coherent integration time. Simulations are also been conducted to validate the effectiveness of this newly imaging scheme. Corresponding results show that, our CS image formation algorithm can generate improved focused performance compared with traditional matching filtering method.

Analysis and Design of Directional Couplers Based on Metal-insulator-metal (MIM) Plasmonic Waveguide

Fabrizio Frezza and Endri Stoja
Department of Information Engineering, Electronics and Telecommunications
"La Sapienza" University of Rome, Via Eudossiana 18, Roma 00184, Italy

Abstract— In the last decade, a strong interest of the research community in the new field of plasmonics has been observed as a promising way to bridge the optics world with electronics [1]. By exploiting the negative permittivity of metals at optical frequencies, plasmonic waveguides offer a subwavelength confinement of the propagating modes allowing for highly integrated plasmonic circuits. In our view, the Metal-Insulator-Metal (MIM) [2] waveguide, similar to the parallel-plate waveguide, constitutes one of the most suitable in this context.

Efforts to apply well-consolidated techniques adopted in the microwaves are being made and different passive plasmonic components have been proposed by making use of transmission line theory [3].

In this study, we design and analyze a 3 dB branch coupler. Couplers are fundamental structures used in the microwaves for different purposes such as power division and phase shifting in antenna beam-forming networks [4]. The MIM waveguide employed to access the junction is made of a silica slab 50 nm thick emerged in silver and a recently developed analytical model for the characteristic impedance of the transmission line has been adopted [5]. The structure operates at the relevant telecommunications wavelength of 1.55 μm.

Finally, the solution provided by commercially available frequency domain full-wave simulator has been employed to compare the transmission line model results with and fine-tune the structure.

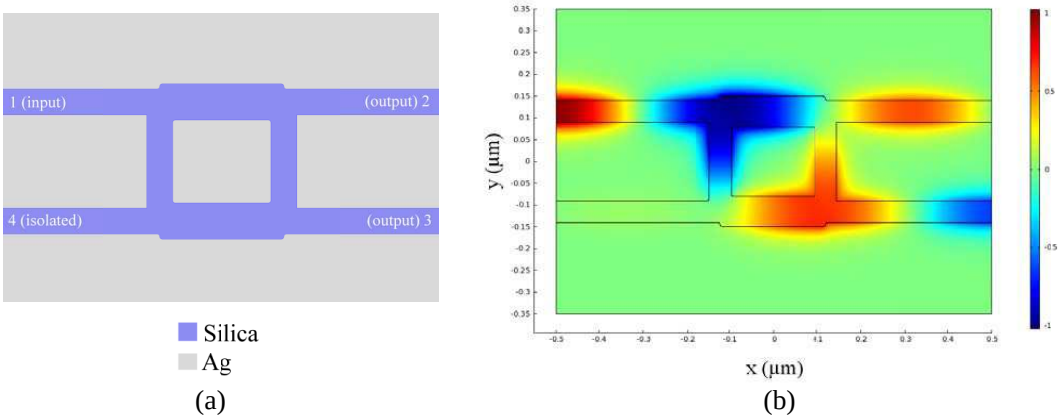

Figure 1: (a) Geometry of the structure and (b) normalized out-of-plane component of the magnetic field.

REFERENCES

1. Ozbay, E., "Plasmonics: Merging photonics and electronics at nanoscale dimensions," *Science*, Vol. 311, No. 5758, 189–193, January 2006.
2. Mayer, S., *Plasmonics: Fundamentals and Applications*, Springer, New York, 2007.
3. Veronis, G. and S. Fan, "Bends and splitters in metal-dielectric-metal subwavelength plasmonic waveguides," *Applied Physics Letters*, Vol. 87, No. 13, 131102(3), September 2005.
4. Pozar, D. M., *Microwave Engineering*, 2nd Edition, John Wiley & Sons Inc., New York, 1998.
5. Nejati, H. and A. Beirami, "Theoretical analysis of the characteristic impedance in metal-insulator-metal plasmonic transmission lines," *Optics Letters*, Vol. 37, No. 6, 1050–1052, March 2012.

Capacitively-loaded Inductively-coupled Fed Loop Antenna with an Omnidirectional Radiation Pattern for UHF RFID Tags

Qi Liu, **Yufeng Yu**, **and Qiangsheng Huang**
Center for Optical and Electromagnetic Research, Zhejiang University, Hangzhou 310027, China

Abstract— A capacitively-loaded inductively-coupled fed loop RFID tag antenna with an omnidirectional radiation pattern is proposed. With an inductively-coupled feed structure, it is convenient and accurate to achieve conjugate impedance matching condition. Concentration of surface current on the radiating loop is beneficial to improving the gain of antenna. The radiation pattern which is omnidirectional in antenna plane makes the proposed tag practicable mounted on top or bottom of target objects. The length of the antenna is only 43 mm, and the maximum simulated read range of the prototype is 14 m with 4 W of EIRP.

In this paper, a UHF RFID tag antenna with an omnidirectional radiating pattern is proposed. This antenna consists of a radiating loop and a concentric inductively-coupled feeding loop. The radiating loop loaded with four periodically spaced interdigital capacitors realizes uniform current distribution along the loop even when it is no longer electrically small. The feeding loop inserted with an interdigital capacitor which is inductively coupled to the radiating loop provides a convenient way for conjugate impedance matching. In this way, the proposed tag antenna can achieve an omnidirectional radiation pattern and good conjugate impedance matching with arbitrary size. With a size of $0.13\lambda_0 \times 0.13\lambda_0$ (λ_0 is the corresponding wavelength of the operating frequency), the antenna achieves a simulated reading range of above 10 meters with total transmitted power of 4 W. This maximum reading range is much further than the reading ranges of other tags of similar size. The obtained operating impedance bandwidth (< -3 dB) can cover the FCC band.

Slot Embedded Microstrip Paper Based Substrate Antenna for Automotive Systems

M. Y. Ismail[1], **W. N. Zaihasra**[1], **and N. Misran**[2]

[1]Wireless and Radio Science Centre (WARAS)
Universiti Tun Hussein Onn Malaysia (UTHM), Johor, Malaysia
[2]Institute of Space Science (ANGKASA), Universiti Kebangsaan Malaysia, Selangor, Malaysia

Abstract— The increased number of traffic congestion and collisions are the main problems in automotive field nowadays. In order to solve these problems, antennas with low cost and optimized performances are highly required. The conventional microstrip antennas for automotive systems are limited to short range communications due to its narrow bandwidth performance. In addition, the non-sustainable substrate materials used for conventional microstrip antennas are shown to be non-flexible to conform to the rigid surface of the vehicle structures. In this work, a new modified microstrip dipole antenna based on paper substrate is presented for the first time to be employed for automotive systems. A detailed analysis on the scattering parameters of the proposed microstrip dipole antenna embedded with slot configurations have been carried out using Ansoft HFSS^{V12} computer model. It has been shown that the proposed microstrip antenna based on paper substrate offers the lowest return loss of -25.82 dB and the widest bandwidth of 460 MHz as compared to Rogers RT/Duroid 5880 and FR-4 substrates. Furthermore, a mathematical formulation has been established for the estimation range on the detection of the targets of interest. The results show that the low loss and widest bandwidth performances allow the proposed microstrip dipole antenna to detect the targets of interest at an estimated range of 150 m from the main system. The introduction of slot configurations on the surface of the dipole element is shown to improve the bandwidth performance up to 520 MHz which can be applied for long range communications with an estimated range of 320 m from the main system. Moreover, a numerical algorithm based on the loss mechanism has been developed by using Finite Element Method (FEM) to verify the analysis performed using the scattering parameters of the proposed microstrip antenna.

Enhanced Fullwave-mode Technique for Multilayered Passive Circuits Including Ferrites with Arbitrary dc Magnetic Field Polarization

Mohamed Lamine Tounsi[1], **Youcef Gaceb**[1], **and Mustapha C. E. Yagoub**[2]

[1]Faculty of Electronics and Informatics, University U.S.T.H.B
BP 32, El Alia, Bab-Ezzouar, Algiers 16111, Algeria
[2]EECS, University of Ottawa, 800 King Edward, Ottawa, ON, K1N 6N5, Canada

Abstract— In recent years, the unique and interesting properties of ferrite materials have enabled them to be widely used in microwave circuits for various applications including non-reciprocal ones (circulators, isolators ...). However, to meet the ever-growing market demand on miniaturization and functionality, design and development of ferrite circuits have been facing a multitude of issues related to the complexity of their structures and the hybrid nature of the electromagnetic field.

This paper deals with the hybrid-mode analysis of the magnetic anisotropy in multilayered passive ferrites. Based on the spectral domain approach (SDA), the proposed technique takes into account the arbitrary polarization of the static magnetic field. To obtain the dyadic Green's functions for ferrite circuits with nondiagonal tensors depending on the arbitrary polarization of the static magnetic field (tangential or normal), the proposed method has been associated with the technical immittance approach [1] and generalized to biaxial anisotropic substrates [2].

Based on the polarization of the dc magnetic field responsible of the non-reciprocity, an original transition matrix was also introduced to simplify the evaluation of electromagnetic fields in all dielectric layers (i.e., three field components for LSE-LSM modes instead of five for TE-TM modes), leading to much faster computation rounds. All numerical results are in good agreement with those available in the literature.

Numerical Results: Figure 1 shows the dispersion effect on the phase shift $\Delta\beta$ for different values of the dielectric thickness 'h_d' for a suspended finline ferrite with four layers for an Ox polarization of the dc magnetic field. Note that the non-reciprocity is accentuated for high values of h_d. These results agree well with [3]. Figure 2 illustrates the dispersion chart for a suspended waveguide loaded with ferrite for an Oy polarization. The results show good agreement with those published [4–6]. Figure 3 shows the normalized propagation constant for the Oz polarization and the results agree well with [6].

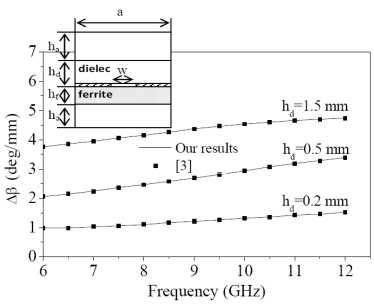

Figure 1: Phase shift variation $\Delta\beta$ versus frequency for an Ox polarization ($\varepsilon_f = 11.6$, $\varepsilon_d = 20$, $M_s = 1800\,\mathrm{A/cm}$, $H_0 = 300\,\mathrm{cm}$, $h_f = 0.635\,\mathrm{mm}$, $h_a = 10\,\mathrm{mm}$, $a = 20\,\mathrm{mm}$, $w = 1.27\,\mathrm{mm}$).

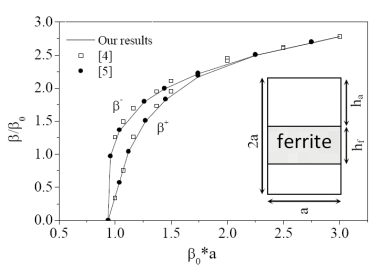

Figure 2: Dispersion chart of a suspended waveguide loaded with ferrite for an Oy polarization ($\varepsilon_f = 10$, $h_f = 0.5\,\mathrm{mm}$, $h_a = 1.25\,\mathrm{mm}$, $a = 1\,\mathrm{mm}$).

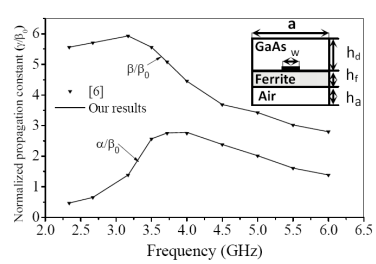

Figure 3: Normalized propagation constant for an Oz polarization ($\varepsilon_f = 17.7$, $\varepsilon_d = 10.2$, $M_s = 0.2267\,\mathrm{T}$, $h_f = 2.03\,\mathrm{mm}$, $h_d = 1.27\,\mathrm{mm}$, $h_a = 33\,\mathrm{mm}$, $w = 0.3\,\mathrm{mm}$, $a = 3\,\mathrm{mm}$).

REFERENCES

1. Itoh, T., "Spectral domain immitance approach for dispersion characteristics of generalized printed transmission lines," *IEEE Trans. on Microwave Theory and Tech.*, Vol. 39, 1021–1025, June 1991.

2. Tounsi, M. L., et al., "Generic spectral immittance approach for fast design of multilayered bilateral structures including anisotropic media," *IEEE Microwave and Wireless Components Letters*, Vol. 17, No. 6, 409–411, 2007.
3. Kitazawa, T., "Analysis of shielded striplines and finlines with finite metallization thickness containing magnetized ferrites," *IEEE Trans. Microwave Theory Tech.*, Vol. 39, No. 1, Jan. 1991.
4. Brankovic, V. J., D. V. Krupezevic, J. Ritter, and F. Arndt, "Efficient 2D FD-TD method for the rigorous analysis of arbitrarily shaped guided wave structures on general electrically and magnetically anisotropic substrates," *IEEE Trans. Microwave Theory Tech.*, Vol. 2, 1017–1020, 1994.
5. Angkaew, T., M. Matsuhara, and N. Kumagai, "Finite element analysis of waveguide modes: A novel approach that eliminates spurious modes," *IEEE Trans. Microwave Theory Tech.*, Vol. 35, 117–123, Feb. 1987.
6. Gaglione, S., private communication, Feb. 12, 2001.

Optimizing Photonic Crystal Filter in Defective 1D Periodic Media

V. Korkmaz[1] and A. Cetin[2]

[1]Information and Communication Technologies Authority (ICTA), Ankara, Turkey
[2]Department of Physics, Faculty of Arts and Sciences, Osmangazi University, Eskisehir, Turkey

Abstract— In this study, a narrow-band filter is designed in defective 1D photonic crystal structure using parameters and by selecting the appropriate material. Analyses are carried out in wavelength region of 1550 nm for Si/SiO_2 multilayer periodic structure by means of transfer matrix method (TMM). A defect was added to the periodic structure and photonic band properties of filter were investigated comparatively by changing some parameters such as layer thickness and parameters of material. Changing the angle of incidence of the light to system the behavior of transmission spectrum is observed. Multi-channel filter is optimized conveniently optical frequency region and to be used in applications such as wavelength division multiplexing (WDM).

Design of Coplanar Sensor for the Permittivity Measurement of Thin Dielectric Samples

Manisha Shete and M. Jaleel Akhtar
Department of Electrical Engineering, Indian Institute of Technology Kanpur, Kanpur 208016, India

Abstract— This work explores nondestructive permittivity measurement of thin dielectric samples using coplanar waveguide. A conductor backed coplanar is designed for 50 ohms and sample whose permittivity is to be measured is placed freely on top of this sensor. This structure of coplanar sensor with sample placed on it is referred as MCCPW (Multilayered conductor backed coplanar waveguide), scattering parameters of MCCPW structure are measured using VNA(Vector network analyzer) . To reduce effect of higher order modes the sample is placed at the center of coplanar sensor. From measured scattering parameters reflection and transmission coefficient is calculated, and using revised form of reflection theory, effective permittivity of the MCCPW structure is calculated. Fill factors are calculated from geometry of the MCCPW structure. In this paper, instead of using costly microwave probe stations for measurement of scattering parameters of coplanar, two SMA to coplanar end launchers are used. De-embedding technique is used to extract scattering parameters at the coplanar sample interface using transmission matrix method. Two coplanar sensors with length 25.4 mm and 50 mm are designed fabricated and tested to measure samples of practical lengths. The designed sensor is tested by extracting the permittivity of a number of reference samples from both the simulated and the experimental data.

Inverse Modeling of Pseudo-interdigital Bandpass Filters Using Artificial Neural Networks

Erdem Demircioglu[1], **Murat H. Sazli**[1], **Orhan Sengul**[2], **S. Taha Imeci**[3], **and Mesut Gokten**[4]

[1]Department of Electrics and Electronics Engineering, Ankara University, Tandoğan, Ankara, Turkey
[2]R & D Department, T. C. Başbakanlık, Ankara, Turkey
[3]Department of Electrics and Electronics Engineering, İstanbul Commerce University Küçükyalı, İstanbul, Turkey
[4]Department of R & D and Satellite Manufacturing, Turksat AS, Golbasi, Ankara, Turkey

Abstract— A neural network trained to model original EM problems can be called as the forward model where the model inputs are physical or geometrical parameters and outputs are electrical parameters. Conversely, neural network techniques are applicable to inverse modeling of microwave circuit design. In opposition to conventional statistical electromagnetic signal processing applications, inverse modeling techniques acquire electrical parameters as model input and geometrical properties as the output. Pseudo-interdigital bandpass microstrip filters offer compact and planar solutions to wide bandwidth filtering applications. They avoid the through vias required for short circuiting in conventional interdigital filters. Miniaturized microstrip bandpass filters are in demand for systems requiring small size and light weight. The coupling of the resonators in filter design must be adjusted using EM simulators. There are no analytical or numerical methods proposed for accurate determination of resonator spacing. The inverse modeling can be applied to accurately determine the resonators' locations consistent with desired filter specifications. The neural network training process of the inverse modeling has difficulties due to the nonuniqueness of the input-output relationship. The multivalued data must be divided into subgroups using derivative information and each individual group must be trained by itself. In the final modeling the subgroups are combined together to form the complete model. In this study, the applied inverse modeling technique includes segmentation, derivative division and subgroup combining of the pseudo-interdigital bandpass microstrip filter data. Efficient neural network modeling techniques have been presented and applied to microwave filter modeling and design. The inverse modeling technique has been formulated and the nonuniqueness of the input-output relationship has been addressed.

Session 1P1
2_FocusSession.SC2: Plasmonics in the Quantum Regime 1

Quantum Plasmonics: Plasmon Induced Electron Transfer Processes
Peter Nordlander, ... 214

Diamond Nanophotonics and Quantum Optics
Marko Loncar, ... 215

Atoms Coupled to Nanophotonic Waveguides: A Novel Platform for Quantum Optics
Darrick Chang, ... 216

Mediating between Light and Charge in Plasmonic Metamaterials
Naomi J. Halas, ... 217

Quantum Tunneling Seen Directly in the Plasmonic Resonance
Ventsislav K. Valev, Alan Sanders, Kevin J. Savage, Matthew M. Hawkeye, Ruben Esteban, Andrei G. Borisov, Javier Aizpurua, Jeremy J. Baumberg, ... 218

Quantum Effects in Tunneling Plasmonics
R. Esteban, A. G. Borisov, Peter Nordlander, Kevin J. Savage, Matthew M. Hawkeye, Jeremy J. Baumberg, Javier Aizpurua, ... 219

Signatures of Quantum Condensation in a Plasmonic Nanoparticle Array
S. R. K. Rodriguez, Johannes Feist, M. A. Verschuuren, F. J. Garcia Vidal, Jaime Gomez-Rivas, . 220

Quantum Statistics and Loss Compensation in Confined Surface Plasmon Polariton Waveguides
Stefan A. Maier, Yannick Sonnefraud, ... 221

Transformation-optics Insight into the Emergence of Quantum Effects in Plasmonic Dimers
Antonio I. Fernandez-Dominguez, ... 222

Room Temperature Plasmonic Nanowire Laser near the Surface Plasmon Frequency
Themistoklis P. H. Sidiropoulos, Sebastian Geburt, Robert Röder, Matthias Ogrisek, Stefan A. Maier, Carsten Ronning, Rupert F. Oulton, ... 223

Continuous Operation SPASER Based on Epitaxial Silver Films
Yu-Jung Lu, Jisun Kim, Hung-Ying Chen, Chun-Yuan Wang, Ming-Yen Lu, Bo-Hong Li, Xiang-gang Qiu, Wen-Hao Chang, Lih-Juann Chen, Shangjr Gwo, Chihhui Wu, Nima Dabidian, Charlotte E. Sanders, Chih-Kang Shih, Gennady Shvets, ... 225

A New Way to Excite Surface Plasmon Polaritons at Smooth Surfaces without Using Any Coupler — Quantum-interference-based Surface Plasmon Resonance Technique
Chunguang Du, ... 226

Emerging Plasmons Enhanced Ultrafast Light-matter Interactions
Min Ouyang, ... 227

Quantum Plasmonics: Plasmon Induced Electron Transfer Processes

Peter Nordlander
Laboratory for Nanophotonics, Department of Physics and Astronomy
Rice University, Houuston TX77251, USA

Abstract— Plasmon resonances can be tuned across the spectrum by simply changing the geometrical shape of a nanostructure. Plasmons can efficiently capture incident light and focus it to nanometer sized hotspots which can induce electronic and vibrational excitations in nearby structures [1]. For narrow plasmonic junctions, quantum mechanical tunneling can induce charge transfer across the gap leading to novel optical effects such as charge transfer plasmons [2–4]. The presence of molecules in the junction can further enhance such charge transfer and lead to yet new optical effects [5, 6]. Another important but still relatively unexplored effect is production of hot energetic electrons which can transfer into nearby structures and induce a variety of processes. This process is of quantum mechanical origin: the decay of plasmon quanta into electron-hole pairs. I will discuss how plasmon induced hot electrons can be used in various applications: such as to induce chemical reactions in molecules physisorbed on a nanoparticle surface [7, 8]; to inject electrons directly into the conduction band of a nearby substrate [9–11]; and to induce local doping of a nearby graphene sheet [12].

REFERENCES

1. Halas, N. J., et al., *Adv. Mat.*, Vol. 24, 4842, 2012.
2. Zuloaga, J., et al., *Nano Lett.*, Vol. 9, 2009.
3. Esteban, et al., *Nature Comm.*, Vol. 3, 825, 2012.
4. Thongrattanasiri, S., et al., *Laser Phot. & Rev.*, 2013, 10.1002/lpor.201200101.
5. Song, P., et al., *J. Chem. Phys.*, Vol. 134, 074701, 2011.
6. Song, P., et al., *Phys. Rev. B*, Vol. 86, 121410, 2012.
7. Huschka, R., et al., *JACS*, Vol. 133, 12247, 2011.
8. Mukherjee, S., et al., *Nano Lett.*, Vol. 13, 240, 2013.
9. Knight, M. W., et al., *Science*, Vol. 332, 702, 2011,
10. Fang, Z. Y., et al., *Nano Lett.*, Vol. 12, 3808, 2012.
11. Knight, M. W., et al., *Nano Lett.*, Vol. 13, 2013, 10.1021/nl400196z.
12. Fang, Z. Y., et al., *ACS Nano*, Vol. 6, 10222, 2012.

Diamond Nanophotonics and Quantum Optics

Marko Lončar
School of Engineering and Applied Science, Harvard University, Cambridge, MA 02138, USA

Abstract— Individual color centers in diamond have recently emerged as a promising solid-state platform for quantum communication and quantum information processing systems, as well as sensitive nanoscale magnetometry with optical read-out [1]. Performance of these systems can be significantly improved by engineering optical properties of color centers using nanophotonic approaches. I will describe a high-flux, room temperature, source of single photons based on an individual Nitrogen-Vacancy (NV) center embedded in a top-down nanofabricated, single crystal diamond nanowires [2], plasmonic nano-apertures [3], and all-diamond based optical cavities [4–6]. Using the nanowire geometry, for example, an order of magnitude brighter single photon source is realized, compared to an NV center in a bulk diamond [2]. By embedding diamond nanowires in metals 10-fold enhancement of NV's spontaneous emission, due to large Purcell effect provided by metallic nanocavity, was demonstrated [3]. Finally, single-photon emission of NVs inside ring [5] and photonic crystal resonator [6], fabricated directly in diamond, as well as single photon routing in an on-chip optical network has been achieved [5]. In addition to these applications I will discuss integrated all-diamond optical networks operating at telecom wavelengths [7] and their potential for on-chip frequency comb generation. Finally, single-crystal diamond nanomechanical resonators fabricated using our novel angle-etching approach [6] will be discussed.

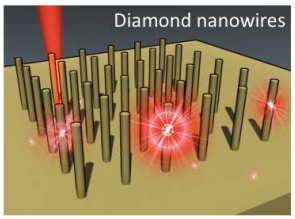

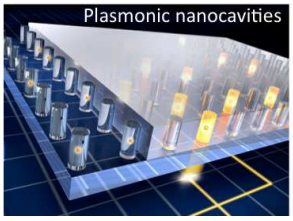

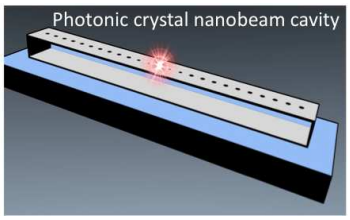

REFERENCES

1. For detailed review please see February 2013 issue of MRS Bulletin dedicated to physics and applications of NV centers.
2. Babinec, T. M., B. M. Hausmann, M. Khan, Y. Zhang, J. Maze, P. R. Hemmer, and M. Lončar, "A bright single photon source based on a diamond nanowire," *Nature Nanotechnology*, Vol. 5, 195, 2010.
3. Choy, J. T., B. M. Hausmann, T. M. Babinec, I. Bulu, and M. Lončar, "Enhanced single photon emission by diamond-plasmon nanostructures," *Nature Photonics*, Vol. 5, 738, 2011.
4. Babinec, T. M., J. T. Choy, K. J. M. Smith, M. Khan, and M. Lončar, "Design and focused ion beam fabrication of single crystal diamond nanobeam cavities," *J. Vac. Sci. Tech. B*, Vol. 29, 010601, 2011.
5. Hausmann, B. J. M., B. Shields, Q. Quan, P. Maletinsky, M. McCutcheon, J. T. Choy, T. M. Babinec, A. Kubanek, A. Yacoby, M. D. Lukin, and M. Lončar, "Integrated diamond networks for quantum nanophotonics," *Nano Letters*, Vol. 12, 1578, 2012.
6. Burek, M. J., N. P. de Leon, B. J. Shields, B. M. Hausmann, Y. Chu, Q. Quan, A. S. Zibrov, H. Park, M. D. Lukin, and M. Lončar, "Free-standing mechanical and photonic nanostructures in single-crystal diamond," *Nano Letters*, Vol. 12, 6084, 2012.
7. Hausmann, B. M., I. Bulu, P. B. Deotare, M. W. McCutcheon, V. Venkataraman, M. L. Markham, D. J. Twitchen, and M. Lončar, "Integrated high quality factor optical resonators in diamond," *Nano Letters*, 2013, DOI: 10.1021/nl3037454.

Atoms Coupled to Nanophotonic Waveguides: A Novel Platform for Quantum Optics

Darrick Chang
ICFO — The Institute of Photonic Sciences Mediterranean Technology Park
Castelldefels, Barcelona 08860, Spain

Abstract— Techniques to controllably interface atoms or other quantum emitters with optical fields form the basis for many applications in quantum information science. Thus far, the available techniques to efficiently couple single photons with atomic media fall into one of the following, mostly independent categories: 1) cavity QED, where atomic interactions with light are enhanced via a high-finesse cavity, 2) coherent coupling with atomic ensembles exhibiting large optical depths, and 3) the use of fields tightly focused to dimensions smaller than or approaching the single-atom scattering cross section, as can occur in plasmonic systems.

Here we describe a novel hybrid approach, which aims to overcome the technical challenges associated with the previous techniques and can lead to a scalable atom-photonic quantum interface. In particular, we consider an atomic ensemble coupled to a common waveguide, and show that a periodically arranged atomic lattice can function as a high-finesse cavity for the guided fields. Such a cavity can subsequently be used to strongly enhance the interactions between a specially designated "impurity" atom from within the ensemble and a single photon. Under realistic conditions, we show that it is possible to reach the "strong coupling" regime of cavity QED, where vacuum Rabi oscillations occur between the excited impurity atom and a single photon of the effective cavity. The strong coupling regime can be used as a resource to facilitate scalable quantum information networks.

Finally, we will discuss how such a system can give rise to large photon-mediated forces between atoms, which can be used for the investigation of novel condensed matter phenomena such as self-organization and lattice formation.

Mediating between Light and Charge in Plasmonic Metamaterials

N. J. Halas
Rice University, USA

Abstract— In addition to serving as nanoscale optical components, plasmonic nanoparticles and nanostructures participate in photon-to-electron and electron-to-photon conversion processes. When electrons are incident on a plasmonic cluster, they excite multiple modes of the system, some of which are radiative in nature. Examining the differences between optical and electron beam excitation of plasmonic clusters provides important insight into the coupled-oscillator nature of plasmonic systems [1]. Conversely, hot electrons generated by plasmon decay following optical excitation, can be utilized in photodetecting devices such as a "nanoantenna-diode", capable of distinguishing light of specific wavelengths and polarizations [2]. In this case, the plasmonic metamaterial controls the optical properties while the carrier-accepting media controls the electrical transport aspects of the device. Depending on geometry, quite narrowband spectral responses can be achieved, which lend themselves to new SPR-based sensing concepts [3]. An important variation of this type of device can be achieved with graphene, where the optoelectronic properties of graphene can be greatly enhanced by integrating this material with plasmonic nanoparticle antennas in a unique sandwich geometry [4]. Plasmon-generated hot electrons can also participate in chemical reactions at the nanoparticle surface, and are responsible for processes as diverse as light-induced melting of DNA [5] and the dissociation of diatomic molecules at nanoparticle surfaces [6].

REFERENCES

1. Lassiter, J. B., H. Sobhani, M. W. Knight, W. S. Mielczarek, P. Nordlander, and N. J. Halas, "Designing and deconstructing the fano lineshape in plasmonic nanoclusters," *Nano Letters*, Vol. 12, 1058–1062, 2012.
2. Knight, M. W., H. Sobhani, P. Nordlander, and N. J. Halas, "Photodetection with active optical antennas," *Science*, Vol. 332, 702–704, 2011.
3. Sobhani, A., M. W. Knight, Y. Wang, B. Zheng, N. S. King, P. Nordlander, and N. J. Halas, "Narrowband photodetection in the near-infrared with an EOT-plasmon-induced hot electron device," *Nature Communications*, online.
4. Fang, Z., Z. Liu, Y. Wang, P. M. Ajayan, P. Nordlander, and N. J Halas, "A graphene-antenna sandwich photodetector," *Nano Letters*, Vol. 12, 3808–3813, 2012.
5. Huschka, R., J. Zuloaga, M. W. Knight, L. Brown, P. Nordlander, and N. J. Halas, "Plasmon-assisted DNA release from nanoshells and nanorods," *Journal of the American Chemical Society*, Vol. 133, 12247–12255, 2011.
6. Mukherjee, S., F. Libisch, N. Large, O. Neumann, L. V. Brown, J. Cheng, B. Lassiter, E. A. Carter, P. Nordlander, and N. J. Halas, "Hot electrons do the impossible: Plasmon-induced dissocation of H_2 on Au," *Nano Letters*, Vol. 13, 240–247, 2012.

Quantum Tunneling Seen Directly in the Plasmonic Resonance

Ventsislav K. Valev[1], **Alan Sanders**[1], **Kevin J. Savage**[1], **Matthew M. Hawkeye**[1], **Rubén Esteban**[2], **Andrei G. Borisov**[2,3], **Javier Aizpurua**[2], **and Jeremy J. Baumberg**[1]

[1]NanoPhotonics Centre, Department of Physics, University of Cambridge, UK
[2]Material Physics Center CSIC-UPV/EHU and Donostia International Physics Center, DIPC
Paseo Manuelde Lardizabal 5, 20018 Donostia, San Sebastián, Spain
[3]Institut des Sciences Moléculaires d'Orsay
UMR 8214, CNRS, Université Paris Sud, Bâtiment 351, Orsay Cedex 91405, France

Abstract— The local field enhancement between two coupled plasmonic nanoparticles increases dramatically as the particles come closer together. According to classical theory, as the particles approach, the field between them increases infinitely, reaching a singularity, whereby it is impossible to predict electromagnetic properties beyond the "event horizon". In reality, as the nanoparticles approach, they eventually become close enough for electrons to be able to tunnel from one to the other. This tunneling enables the formation of a charge transfer plasmon, which dominates the electromagnetic behavior past the classical event horizon. It is precisely because quantum tunneling is not taken into account by the classical theory that an apparent singularity arises.

Through simultaneous measurement of both the electrical and optical properties of two gold nanostructures with controllable sub-nm separation, we reveal the quantum regime of tunnelling plasmonics and trace through it in unprecedented detail [1]. Furthermore, all observed phenomena show good agreement with recent quantum-based models of plasmonic systems [2].

Using two controllable 150 nm radius Au-coated, ball-type AFM tips, aligned tip-to-tip using a nonlinear electrostatic-force technique [3], we are able to observe the onset of the quantum tunnelling and subsequent entry into the quantum regime as tips are brought together. Plasmons in the cavity between tip surfaces are excited using a tightly focussed supercontinuum laser and studied via confocal, dark-field spectroscopy of back-scattered light from the cavity.

Findings indicate that the onset of quantum tunnelling establishes entry into a quantum regime in which the characteristic redshift of the gap plasmon modes reverses as modes transform into charge transfer plasmons. This implies the existence of a quantum limit for plasmonic field confinement and consequently the field enhancement of a plasmonic hot-spot. We therefore demonstrate that quantum mechanics is already important at the 0.3 nm scale at which tunnelling plasmonics begins to dominate. This understanding is fundamental for describing light-matter interactions down to the atomic scale. We predict the ultimate confinement volume for visible light, and show how zeptolitre photochemistry becomes possible.

REFERENCES

1. Savage, K. J., M. M. Hawkeye, R. Esteban, A. G. Borisov, J. Aizpurua, and J. J. Baumberg, *Nature*, Vol. 3, 2012.
2. Esteban, R., A. G. Borisov, P. Nordlander, and J. Aizpurua, *Nature Communications*, Vol. 3, 825, 2012.
3. Savage, K. J., M. M. Hawkeye, B. F. Soares, and J. J. Baumberg, *Applied Physics Letters*, Vol. 99, 053110, 2011.

Quantum Effects in Tunneling Plasmonics

R. Esteban[1], **A. G. Borisov**[2], **P. Nordlander**[3], **K. J. Savage**[4], **M. M. Hawkeye**[4], **J. J. Baumberg**[4], **and J. Aizpurua**[1]

[1]Material Physics Center CSIC-UPV/EHU and Donostia International Physics Center, DIPC
Donostia-San Sebastián, Spain
[2]Institut des Sciences Moléculaires d'Orsay
UMR 8214, CNRS — Université Paris Sud, Orsay Cedex, France
[3]Laboratory for Nanophotonics, Department of Physics, MS61
Rice University, Houston, Texas, USA
[4]Nanophotonics Centre, Cavendish Laboratory, University of Cambridge, Cambridge, UK

Abstract— Electron transfer due to quantum tunnelling between two metallic structures strongly modifies the plasmonic resonances of the system. For small particles, the resulting optical behaviour can be studied using Time-Dependent Density Functional Theory (TDDFT). The particles used in typical plasmonics applications, however, often have dimensions that are tens, hundreds of even thousands of nanometers long, and thus they are too large to be treated with state-of-the-art TDDFT.

Here, we present a Quantum Corrected Model (QCM) that includes the effect of quantum tunnelling in the calculation of the plasmonic response of large structures at subnanometer separation distances. The model requires to define an effective material in the region where tunnelling is happening, with the properties of the material given by exact quantum calculations from a simplified system. A standard solver of Maxwell equations can then be used to obtain the response of the entire system. QCM is straightforward to implement for arbitrary geometries, which can exhibit narrow gaps or particles in contact.

We first test the QCM results against small Na spheres that can be also simulated using TDDFT, and find very good agreement between both methods. Next, we consider the case of large Drude-like Au structures to illustrate the effect of tunnelling in realistic plasmonic systems formed by large nanometric structures. As expected from previous work in small particles, we observe a spectral redistribution of the modes for all the geometries and a collapse of the near-field enhancement at very short separation distances.

We also consider the experimental situation of two approaching gold tips, a system which we have recently tested to experimentally reveal quantum effects in plasmonic gaps at subnanometer separation distances. The modelled structures (longer than 1 micrometer), exceed by several orders of magnitude the sizes typically tackled with TDDFT. Notably, the measured and calculated far-field spectra are in good agreement, which further emphasizes the relevance of the proposed method to correctly address experimental situations. Moreover, our QCM simulations open the possibility to predict both the optimal near field enhancement and confinement expected, a task that has still not been yet reported experimentally.

Signatures of Quantum Condensation in a Plasmonic Nanoparticle Array

S. R. K. Rodriguez[1], **J. Feist**[2,*], **M. A. Verschuuren**[3], **F. J. García Vidal**[1], **and J. Gómez Rivas**[2,4]

[1]Center for Nanophotonics, FOM Institute AMOLF, c/o Philips Research Laboratories
Eindhoven, The Netherlands
[2]Departamento de Física Teórica de la Materia Condensada
Universidad Autónoma de Madrid, Madrid, Spain
[3]Philips Research Laboratories, Eindhoven, The Netherlands
[4]COBRA Research Institute, Eindhoven University of Technology, Eindhoven, The Netherlands

Abstract— Condensation of bosons, where a single quantum state is macroscopically populated, is a fascinating phenomenon spanning diverse areas of physics. It lies at the heart of superfluidity and superconductivity, as well as the Bose-Einstein condensation of ultracold atomic gases. A long-standing goal is to find systems in which condensation takes place at ever higher temperatures, even at or above room temperature. Bosonic quasi-particles in solids are excellent candidates due to their light effective masses, and signatures of condensation have been observed for semiconductor excitons and exciton-polaritons at temperatures of a few K, as well as for magnons and cavity photons at room temperature.

We present and discuss experimental signatures of quantum condensation of plexcitons at room temperature. The system under study consists of a periodic array of metallic nanorods covered by a polymer layer doped with an organic dye. The plexcitons in this system are bosonic quasiparticles formed by strong coupling between organic molecule excitons and surface lattice resonances (hybrid photonic-plasmonic states formed in nanoparticle arrays). The effective plexciton mass is seven orders of magnitude lower than the electron mass and two orders of magnitude below exciton-polaritons in semiconductor microcavities, enabling condensation at high temperatures. In addition, they can be easily pumped and observed due to their photonic component. By increasing the plexciton density through optical pumping, we observe signatures of thermalization and condensation, such as the emergence of Bogoliubov-Goldstone modes, despite the nonequilibrium character of this driven and dissipative system. In contrast to lasing, which requires inversion, condensation is a thermodynamic phase transition driven by the Bose statistics and can take place at lower pump powers. In addition to enabling studies of quantum phase transitions in new parameter regimes, plexciton condensation could thus potentially provide a path towards low-power coherent light sources.

*Presenting author: J. Feist (johannes.feist@uam.es).

Quantum Statistics and Loss Compensation in Confined Surface Plasmon Polariton Waveguides

Stefan A. Maier and Yannick Sonnefraud
Imperial College London, UK

Abstract— Surface plasmon polariton waveguides based on thin metal slabs are a powerful means for propagation of electromagnetic energy in highly confined modes. Here we examine the quantum statistics of single surface plasmon polaritons propagating on such waveguides after excitation via grating-coupling of single photons [1]. We demonstrate that the quantum statistics and quality of the field remain unaffected by the considerable loss in these sustems, and assess the potential of this system for quantum interference experiments.

We further demonstrate, in the classical regime, complete loss compensation and indeed surface plasmon amplification in this waveguide system when coupled to a thin-film system showing strong optical gain, for pump fluences as low as $200\,\mu\mathrm{J/cm}^2$ [2].

REFERENCES

1. Di Martino, G., Y. Sonnefraud, S. Kéna-Cohen, M. Tame, S. K. Özdemir, M. S. Kim, and S. A. Maier, "Quantum statistics of surface plasmon polaritons in metallic stripe waveguides," *Nano Letters*, Vol. 12, 2504, 2012.
2. Kéna-Cohen, S., P. N. Stavrinou, D. D. C. Bradley, and S. A. Maier, "Confined surface plasmon-polariton amplifiers," *Nano Letters*, Vol. 13, 1323, 2013.

Transformation-optics Insight into the Emergence of Quantum Effects in Plasmonic Dimers

A. I. Fernández-Domínguez
The Blackett Laboratory, Department of Physics, Imperial College London, London SW7 2AZ, UK

Abstract— Recently, an elegant transformation-optics approach has been used to describe the optical properties of nanoparticle dimers within the local approximation [1, 2]. In this talk, we further develop this quasi-analytical methodology to investigate the emergence of nonlocal and quantum tunnelling effects in this geometry. Specifically, the impact of these quantum phenomena in the light harvesting and focusing capabilities of dimers of touching and separated nanowires [3, 4] will be discussed in detail.

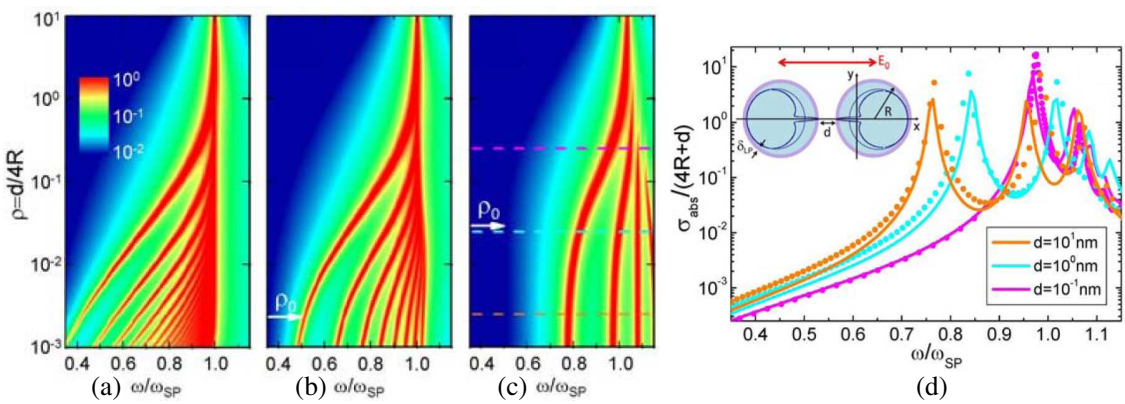

Figure 1: Upper panels show absorption spectra as a function of the relative gap size for three different degrees of nonlocality: local (a), $\beta = 10^5$ m/s (b) and $\beta = 10^6$ m/s (c). Panel (d) plots the theoretical (lines) and numerical (dots) cross section for three gaps sizes ($R = 10$ nm).

REFERENCES

1. Aubry, A., et al., *Nano Lett.*, Vol. 10, 2574, 2010.
2. Fernández-Domínguez, A. I., et al., *Phys. Rev. Lett.*, Vol. 105, 266807, 2010.
3. Fernández-Domínguez, A. I., et al., *Phys. Rev. Lett.*, Vol. 108, 106802, 2012.
4. Fernández-Domínguez, A. I., et al., *Phys. Rev. B*, Vol. 86, 241110R, 2012.

Room Temperature Plasmonic Nanowire Laser near the Surface Plasmon Frequency

Themistoklis P. H. Sidiropoulos[1], **Sebastian Geburt**[2], **Robert Röder**[2], **Matthias Ogrisek**[2], **Stefan A. Maier**[1], **Carsten Ronning**[2], **and Rupert F. Oulton**[1]

[1]Imperial College London
Prince Consort Road, London UK-SW7 2BZ, United Kingdom
[2]University of Jena, Max-Wien-Platz 1, Jena D-07743, Germany

Abstract— The reduction in the size of semiconductor lasers has opened a path for future on-chip light sources for communications and sensing applications [1]. However, their minimum size is limited by the classical diffraction limit of light. Research has focused on surface plasmon based lasers to circumvent this limit, due to their nature of mixing light and electrons at the metal surface and thus generating intense optical localization [2]. Hybrid plasmonic nanowire lasers are of great interest as they allow mode sizes as small as $\lambda^2/400$, are simple to fabricate, and allow a strong field confinement [3]. Until now, lasing from sub wavelength semiconductor nanowires has only been achieved at cryogenic temperatures. In this work, we present the first room temperature hybrid-plasmonic semiconductor nanowire laser operating at UV frequencies. We show that ZnO nanowires sitting on a Silver substrate, emitting at 385 nm at room temperature, generate lasing surface plasmons very close the surface plasmon frequency.

Experiments are conducted on ZnO nanowires separated from a Silver substrate by a thin LiF gap layer of about 10 nm thickness. The nanowires were optically pumped (100 fs pulses @ 800 kHz) at 355 nm and the band edge luminescence was monitored spectrally at room temperature. We have observed plasmonic laser emission occurring for pump powers moderately larger than non-metal samples in the $\mathrm{GWcm^{-2}}$ range (Fig. 1(b)). Evidence for the lasing of plasmonic modes arises from a range of tests. Firstly, the optical modes of ZnO nanowires on glass substrates do not lase for diameters smaller than around 170 nm [4], whereas their plasmonic counterparts operated for diameters as small ∼100 nm. We also verify surface plasmons lasing by polarization measurements of the emitted light. We have also observed a blue shift in laser emission at threshold with decreasing nanowire diameter, which we associate with both higher loss and slower group velocity, which we believe could be evidence for operation near the surface plasmon frequency, where the group velocity is expected to tend zero or even can become negative (Fig. 1(a)).

These preliminary studies highlight the feasibility of surface plasmon lasers operating near the surface plasmon frequency, despite the extremely high losses associated with fast electron scattering of electrons in metals [5].

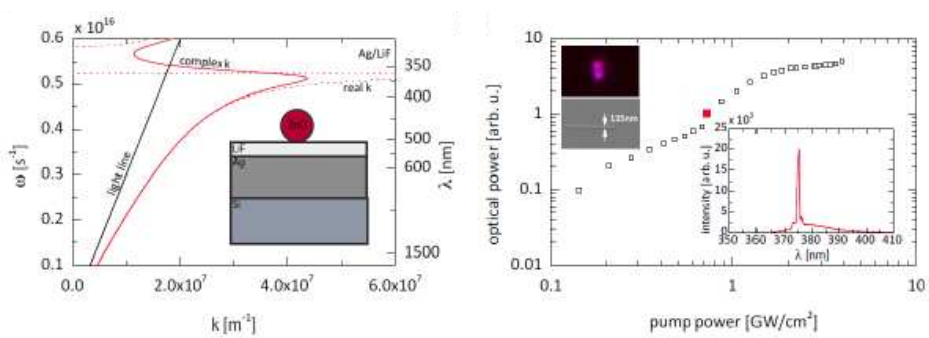

(a) (b)

Figure 1: (a) Surface plasmon polariton dispersion relation for Ag/LiF interface. (b) Pump vs. output power of a 135 nm wide lasing nanowire. (Inset) Lasing spectrum of the nanowire close to threshold (marked by the filled square).

REFERENCES

1. Oulton, R. F., "Surface plasmon lasers: Sources of nanoscopic light," *Materials Today*, Vol. 15, 592–600, 2012.

2. Hill, M. T., M. Marell, E. S. P. Leong, B. Smalbrugge, Y. Zhu, M. Sun, P. J. Veldhoven, E. J. Geluk, F. Karouta, Y.-S. Oei, R. Nötzel, C.-Z. Ning, and M. K. Smit, "Lasing in metal-insulator-metal sub-wavelength plasmonic waveguides," *Opt. Express*, Vol. 17, 11107, 2009.
3. Oulton, R. F., V. J. Sorger, T. Zentgraf, R.-M. Ma, C. Gladden, L. Dai, G. Bartal, and X. Zhang, "Plasmon lasers at deep subwavelength scale," *Nature*, Vol. 461, 629–632, 2009.
4. Zimmler, M. A., F. Capasso, S. Müller, and C. Ronning, "Optically pumped nanowire lasers: Invited review," *Semicond. Sci. Technol.*, Vol. 25, 024001, 2010.
5. Khurgin, J. B. and G. Sun, "Practicality of compensating the loss in the plasmonic waveguides using semiconductor gain medium," *Appl. Phys. Lett.*, Vol. 100, 011105, 2012.

Continuous Operation SPASER Based on Epitaxial Silver Films

Yu-Jung Lu[1], **Jisun Kim**[1], **Hung-Ying Chen**[1], **Chun-Yuan Wang**[1], **Ming-Yen Lu**[1], **Bo-Hong Li**[1], **Xianggang Qiu**[1], **Wen-Hao Chang**[1], **Lih-Juann Chen**[1], **Shangjr Gwo**[1], **Chihhui Wu**[2], **Nima Dabidian**[2], **Charlotte E. Sanders**[2], **Chih-Kang Shih**[2], **and Gennady Shvets**[2]

[1]Department of Physics, National Tsing-Hua University, Hsinchu 30013, Taiwan
[2]Department of Physics, The University of Texas at Austin, Austin, Texas 78712, USA

Abstract— A nanolaser is a key component for on-chip optical communications and computing systems. I will describe a low-threshold, continuous-wave nanolaser based on surface plasmon amplification by stimulated emission of radiation. The plasmonic nanocavity is formed between an atomically smooth epitaxial silver film and a single optically pumped semiconductor nanorod acting as gain medium. The atomic smoothness of the metallic film is crucial for reducing the modal volume and plasmonic losses. Bimodal lasing with similar pumping thresholds was experimentally observed, and polarization properties of the two modes were used to unambiguously identify them with theoretically predicted modes. This nanolaser is a true SPASER: It surves as the source of surface plasmons and relies on plasmonic confinement.

I will discuss the physics behind the recent demonstration [1] of a nanolaser based on an optically-pumped semiconductor nanorod (sub-wavelength in all three dimensions) placed on an epitaxially-grown atomically-smooth silver film. The 480 nm long and 60 nm wide nanorod consists of a gain InGaN core embedded inside a GaN shell. By choosing the appropriate composition of InGaN, nano-lasing across the entire visible range is enabled. Our computational modeling reveals that this nanolaser is a "true" SPASER. To prove that point, the energy loss balance was numerically calculated and used to show that the emission of surface plasmon polaritons (SPPs) from the two tips of the laser is the largest loss mechanism: larger than Ohmic losses and far-field emission. It is demonstrated that the continuous Ag film plays two roles: (a) as the enabler of sub-wavelength mode confinement (lasing modes volumes as small as $V = 0.03\lambda^3$), and (b) as the supporting medium for the SPPs emitted by the SPASER. Numerical simulations reveal that the resulting plasmonic/semiconductor cavity support two modes with high quality factors and Purcell factors exceeding unity. The two modes are shown to have different spatial symmetries resulting in very distinct polarization signatures that are confirmed by the experiment. The two modes are shown to be plexitons, i.e., hybridized states comprised of semiconductor excitons and plasmonic modes.

The role of the atomically-smooth Ag film will be explained in this talk. First-principles simulations of the single-crystalline (no grain boundaries) and poly-crystalline (grainy) silver films reveals that SPP scattering by grain boundaries plays the decisive role in lasing suppression for the latter case. Specifically, it is shown that the plasmonic mode's volume explodes due to this scattering. Revealingly, smaller Ohmic losses in single-crystalline silver is shown to be a relatively minor advantage. These conclusions will be backed up by additional experiments comparing extraordinary optical transmission in single-crystalline and poly-crystalline films. Finally, the relatively broad bandwidth of the lasing lines will be theoretically explained.

REFERENCES

1. Lu, Y., et al., "Plasmonic nanolaser using epitaxially grown silver film," *Science*, Vol. 337, 450, 2012.

A New Way to Excite Surface Plasmon Polaritons at Smooth Surfaces without Using Any Coupler — Quantum-interference-based Surface Plasmon Resonance Technique

Chunguang Du
State Key Laboratory of Low-Dimensional Quantum Physics
Department of Physics, Tsinghua University, Beijing, China

Abstract— In this talk, I propose a new way to excite surface plasmon polaritons (SPPs) on a smooth metal surface by laser fields without using prism and any other coupler. The SPR system is simply made up of a non-structured metal film, and a substrate made of an atomic medium. It is found that when the laser beams are incident on the air-metal interface with a proper angle, the SPP at the metal-substrate interface can be resonantly excited due to atomic quantum effects, such as Electromagnetically induced transparency (EIT) [1] or other related effects.

The surface plasmon polaritons (SPPs) are highly confined, non-radiative surface waves associated with collective electron charge oscillations propagating along a dielectric-metal interface. The SPPs can be excited with, e.g., the Kretschmann geometry of the attenuated total reflection method [2]. A remarkable feature of the surface plasmon resonance (SPR) system is their highly sensitive response to changes in the refractive index near the metal surface, which has already been exploited in, for example, biosensors [3]. For ordinary SPR systems, a prism, a waveguide, or other couplers are necessary for matching light and SPPs wave-vectors. However, the SPR system proposed in this talk has no coupler, and the SPPs are resonantly excited due to atomic quantum effects. To my knowledge, there is no report on this excitation way of SPPs. Although recently I have investigated the EIT-based modulation of SPR systems for prism-coupling cases [4], the SPR system proposed in this talk is different from that cases in principle. It is also found that, the loss of the surface plasmon polaritons can not be eliminated by the EIT medium. However, if another optical pump (e.g., an incoherent field) is applied, the loss can be eliminated completely, and the SPR resonance will be very sharp.

Other quantum interference effects such as quantum beats are also investigated, and found to be also applicable for excitation and modulation SPPs without coupler. The inherent quantum-feature of such kind effects can lead to a lot of new phenomena which are absent in ordinary SPR systems, and the excition way without couplers provides a new idea of realization of more compact nanophotonic devices.

ACKNOWLEDGMENT

This work is supported by the National Natural Science Foundation of China (Grant No. 11274197) and partially supported by the '973' program (Grant No. 2010CB922904) of the Ministry of Science and Technology (MOST), China.

REFERENCES

1. Fleischhauer, M., A. Imamoglu, and J. P. Marangos, *Rev. Mod. Phys.*, Vol. 77, 633, 2005.
2. Raether, H., *Surface Plasmons on Smooth and Rough Surfaces and on Gratings*, 10–18, 118–123, Springer-Verlag, Berlin, Heidelberg, 1988.
3. Abdulhalim, I., M. Zourob, and A. Lakhtakia, *Electromagnetics*, Vol. 28, 214, a Mini-Review, 2008.
4. Du, C. G., *Applied Physics A*, Vol. 109, 797, 2012.

Emerging Plasmons Enhanced Ultrafast Light-matter Interactions

Min Ouyang
College Park, University of Maryland, USA

Abstract— In this talk I will present a few recent advances from my research group, centering on emerging plasmons enhanced nanoscale light-matter interactions. Through the bottom-up nanoscale materials engineering, fundamental physics properties and coupling interactions, such as plasmon, exciton, and phonon, can be finely tailored within nanostructures. This allows opportunity to explore novel physics, including nanoscale resonant plasmon-exciton coupling, in a precisely engineered artificial hybrid metalsemiconductor nanostructure, and thus to achieve significant enhancement of the lightmatter interactions with manifestation of such as optical Stark effect. Such enhanced nanoscale light-matter interactions can be further applied for ultrafast coherent manipulation of quantum process.

Session 1P2
2_FocusSession.SC2: Metasurfaces for Wavefront Control

Holographic Metasurfaces
Federico Capasso, ... 230
Flat Optics: Controlling Wavefronts with Optical Antenna Metasurfaces
Nanfang Yu, Federico Capasso, ... 231
Ultrathin Optical Plasmonic Metadevices Based on Phase Discontinuity
Xianzhong Chen, Lingling Huang, Holger Muhlenbernd, Guixin Li, Benfeng Bai, Qiaofeng Tan, Guofan Jin, Cheng-Wei Qiu, Thomas Zentgraf, Shuang Zhang, ... 232
Beam Transformation Using Spin-optical Metasurfaces with Pancharatnam-Berry Phase Elements
Jensen Li, Ming Kang, Guixin Li, Shumei Chen, Edwin Yue-Bun Pun, Kok Wai Cheah, ... 233
Spectrally Selective Flat Reflective Lenses for Photovoltaic Applications
Sergiy Valyukh, ... 234
Fixed and Reconfigurable THz Reflectarrays Using Graphene
Eduardo Carrasco, Julien Perruisseau-Carrier, ... 235
Controlled Reflection from a Reflectarray of Optical Dielectric Resonator Nano-antennas
Longfang Zou, Withawat Withayachumnankul, Charan Manish Shah, Arnan Mitchell, Madhu Bhaskaran, Sharath Sriram, Christophe Fumeaux, ... 236
Gradient-index Meta-surfaces as a Bridge Linking Propagating Waves and Surface Waves
Qiong He, Shulin Sun, Shiyi Xiao, Xin Li, Che Qu, Lei Zhou, ... 238
High-efficiency Anomalous Light Reflections by Gradient Meta-surfaces
Shulin Sun, Kuang Yu Yang, Chih-Ming Wang, Ta-Ko Juan, Wei Ting Chen, Chun Yen Liao, Qiong He, Shiyi Xiao, Wen-Ting Kung, Guang-Yu Guo, Lei Zhou, Din Ping Tsai, ... 239
Gap Plasmon Based Gradient Metasurfaces for Control of Reflected Light
Sergey I. Bozhevolnyi, ... 240
Spoof Surface Plasmons on Ultrathin Corrugated Metal Structures
Tie Jun Cui, Xiaopeng Shen, ... 241
Metasurfing Substrate Integrated Waveguides to Mold the Radiation from Leaky Waves
Jose Luis Gomez Tornero, George Goussetis, Yingjie Jay Guo, ... 242

Holographic Metasurfaces

Federico Capasso
School of Engineering and Applied Sciences, Harvard University, Cambridge, MA 02138, USA

Abstract— Flat photonics based on metasurfaces is an active area of research as means to manipulate the wavefront of scattered light in arbitrary ways [1]. Nanostructured surfaces can also be used to convert arbitrary incident light beams into surface waves such as surface plasmons and viceversa. For example plasmonic gratings and lenses are routinely used to convert free-space beams into propagating surface waves and vice versa. So far, this approach has been limited to simple light beams, such as plane waves or Gaussian beams. We will present a powerful generalization of plasmonic structures to couple more complex wavefronts. This approach is based on the principle of holography: the coupler is designed as the interference pattern of the incident vortex beam and focused surface plasmon polaritons (SPPs). We have integrated these holographic plasmonic interfaces into commercial silicon photodiodes, and demonstrated that such devices can selectively detect the orbital angular momentum of light [2]. We have also demonstrated new plasmonic couplers that generate upon illumination, new diffractionless SSPs, which unlike surface plasmon Airy beams propagate in a straight line: the cosine-Gauss beam (CGB) [3] and the plasmonic bottle beam (PBB) [4]. The CGB is generated by a launcher consisting of intersecting metallic gratings that produce different degrees of confinement; diffractionless propagation distances approaching 100 microns have been demonstrated by NSOM imaging. By analogy to the three dimensional optical bottle beams, the PBB features a lattice of plasmonic bottles, i.e., closed regions of dark focii alternated with high intensity regions. Such bottle beam is created using three gratings by the interference of a two-dimensional nondiffracting cosine-Gauss beam with a quasi-plane wave. By controlling the propagation constant of the cosine-Gauss beam, we can change the numbers and the size of the plasmonic bottles. Such beams could become important for particle trapping.

Finally we report a new type of holographic interface, which after being designed for a given wavelength, is able to manipulate the three fundamental properties of light (phase, amplitude and polarization) over a broad wavelength range. The design strategy relies on replacing the large openings of conventional holograms by arrays of sub-wavelength apertures, oriented to locally select a particular state of polarization. The resulting optical element can therefore be viewed as the superposition of two independent structures with very different length scales, i.e., a hologram with each of its apertures filled with nanoscale openings to transmit only a desired state of polarization. As an implementation we have fabricated a nano-structured holographic plate that can generate radially polarized optical beams from circularly polarized incident light and we have demonstrated that it can operate over a broad range of wavelengths. The ability of a single holographic interface to shape simultaneously amplitude, phase and polarization of light can find widespread applications in photonics.

ACKNOWLEDGMENT

The author gratefully acknowledges collaborations with: P. Genevet, J. Lin, M. A. Kats, R. Blanchard, A. She, M. Petit, B. Cluzel and F. de Fornel.

REFERENCES

1. Yu, N., P. Genevet, F. Aieta, M. A. Kats, R. Blanchard, G. Aoust, J. P. Tetienne, Z. Gaburro, and F. Capasso, *IEEE J. of Selected Topics in Quantum Electronics*, Vol. 19, 4700423, 2013.
2. Genevet, P., J. Lin, M. A. Kats, and F. Capasso, *Nature Communications*, Vol. 3, 1278, 2012.
3. Lin, J., J. Dellinger, P. Genevet, B. Cluzel, F. de Fornel, and F. Capasso, *Physical Review Letters*, Vol. 109, 93904, 2012.
4. Genevet, P., J. Dellinger, R. Blanchard, A. She, M. Petit, B. Cluzel, M. A. Kats, F. de Fornel, and F. Capasso, *Optics Express*, Vol. 21, 10295, 2013.

Flat Optics: Controlling Wavefronts with Optical Antenna Metasurfaces

Nanfang Yu[1] and Federico Capasso[2]

[1]Department of Applied Physics and Applied Mathematics
Columbia University, New York, NY 10027, USA
[2]School of Engineering and Applied Sciences
Harvard University, Cambridge, MA 02138, USA

Abstract— Conventional optical components rely on the propagation effect to control the phase and polarization of light beams. One can instead exploit abrupt phase and polarization changes associated with scattered light from optical resonators to control light propagation. In this talk, we discuss the optical responses of anisotropic plasmonic antennas and a new class of planar optical components ("metasurfaces") based on arrays of these antennas. The essence of these designs is using the array to create a phase gradient $d\Phi/dr$, which is equivalent to an effective wavevector along the interface, to bend the propagation of light. To demonstrate the versatility of metasurfaces, we show the design and experimental realization of a number of flat optical components: (a) metasurfaces with a constant interfacial phase gradient that deflect light into arbitrary directions; (b) metasurfaces with spiral phase distributions that create optical vortex beams of well-defined orbital angular momentum; (c) planar lenses and axicons that generate spherical wavefronts and non-diffracting Bessel beams, respectively; and (d) metasurfaces with anisotropic optical responses that create light beams of arbitrary polarization over a wide wavelength range.

By using phased antennas to create a circular interfacial phase distribution $\Phi = L\varphi$, where L is an integer and φ is the azimuthal angle, we imparted orbital angular momentum of $L\hbar$ to an incident beam, creating a vortex beam in transmission [1, 2]. The power flow or Poynting vector of this peculiar beam follows a spiral trajectory, which has been visualized by interferometry. By imposing a hyperboloidal phase profile or other appropriate radial phase distributions on an interface, we have demonstrated flat lenses with a number of desirable properties, including large numerical aperture, absence of spherical aberration and reduced comatic aberration [3]. By tailoring the spatial distribution of polarization response, we have demonstrated optically thin quarter-wave plate that generate high-quality circularly-polarized light over a broad wavelength range [4].

REFERENCES

1. Yu, N., P. Genevet, M. A. Kats, F. Aieta, J. P. Tetienne, F. Capasso, and Z. Gaburro, *Science*, Vol. 334, 333–337, 2011.
2. Genevet, P., N. Yu, F. Aieta, J. Lin, M. A. Kats, R. Blanchard, M. O. Scully, Z. Gaburro, and F. Capasso, *Appl. Phys. Lett.*, Vol. 100, 13101, 2012.
3. Aieta, F., P. Genevet, M. A. Kats, N. Yu, R. Blanchard, Z. Gaburro, and F. Capasso, *Nano Lett.*, Vol. 12, 4932–4936, 2012.
4. Yu, N., F. Aieta, P. Genevet, M. A. Kats, Z. Gaburro, and F. Capasso, *Nano Lett.*, Vol. 12, 6328–6333, 2012.

Ultrathin Optical Plasmonic Metadevices Based on Phase Discontinuity

Xianzhong Chen[1], **Lingling Huang**[1, 2], **Holger Mühlenbernd**[3], **Guixin Li**[4], **Benfeng Bai**[2], **Qiaofeng Tan**[2], **Guofan Jin**[2], **Cheng-Wei Qiu**[5], **Thomas Zentgraf**[3], **and Shuang Zhang**[1]

[1]School of Physics & Astronomy, University of Birmingham, Birmingham, B15 2TT, UK
[2]State Key Laboratory of Precision Measurement Technology and Instruments
Department of Precision Instruments, Tsinghua University, Beijing 100084, China
[3]Department of Physics, University of Paderborn, WarburgerStraβe 100, Paderborn D-33098, Germany
[4]Department of Physics, Hong Kong Baptist University, Hongkong, China
[5]Department of Electrical and Computer Engineering, National University of Singapore
4 Engineering Drive 3, Singapore 117576, Singapore

Abstract— Recently, the concept of interfacial phase discontinuities has been proposed and the devices based on this new concept have been demonstrated experimentally at infrared wavelength. Such ultrathin metasurfaces consisting of a monolayer of subwavelength plasmonic resonators are capable of generating local abrupt phase changes and can be used for controlling the wavefront of electromagnetic waves. Based on this principle, a linear gradient of the phase discontinuity at the interface was previously realized, leading to anomalous reflection and refraction described by a generalized Snell's Law. In practice, the parameters of the antennas need to be carefully engineered to cover the whole [0, 2π] phase range while maintaining uniform scattering amplitude. However, as the phase discontinuities rely on a delicate design of two plasmonic resonances along orthogonal directions, both the phase shift and the scattering amplitude are intrinsically wavelength dependent.

We consider the abrupt phase change that occurs for a circularly polarized light converted to its opposite helicity. The metamorphosing phase shift, ranging from 0 to 2π, is realized by a metasurface consisting of an array of metallic nanorods with the same geometry but spatially varying orientations. The phase discontinuity depends on the orientation of dipole antennas, and can be reversed by flipping the circular polarization of incident light. We experimentally demonstrated dispersionless phase discontinuity devices for controlling light propagation, a dual-polarity plasmonic metalens in the visible range and helicity dependent directional surface plasmon polariton excitation using a metasurface with interfacial phased is continuity. The purely planar geometry of such metadevices enables promising integration into other nanodevices by using the conventional micro- and nanofabrication processes.

Beam Transformation Using Spin-optical Metasurfaces with Pancharatnam-Berry Phase Elements

Jensen Li[1], **Ming Kang**[2], **Guixin Li**[3], **Shumei Chen**[3], **Edwin Yue-Bun Pun**[4], **and K. W. Cheah**[3]

[1]School of Physics and Astronomy, University of Birmingham, Birmingham B15 2TT, UK
[2]Department of Physics and Materials Science, City University of Hong Kong, Kowloon, Hong Kong, China
[3]Department of Electronic Engineering, City University of Hong Kong, Hong Kong, China
[4]Department of Physics, Baptist University, Kowloon Tong, Kowloon, Hong Kong, China

Abstract— Metasurfaces, a varying profile of specially designed nanostructures on an optically thin surface, are able to introduce abrupt phase change across or reflected from an interface [1, 2]. The spatial phase profile can be used for beam steering through the manipulation of the linear momentum. It can also be used for generating optical vortex beam through the manipulation of orbital angular momentum. One would therefore expect metasurface can also provide a flexible platform to control the spin angular momentum of a light beam through spin-orbit coupling. In fact, metasurfaces have been recently used to realize a much stronger optical spin hall effect, a manefest of spin angular momentum flowing into the linear momentum, than previous approaches [3]. Here, we study how metasurfaces can transform optical beams with spin angular momentum flowing into orbital angular momentum. In particular, we construct metasurfaces using circular rings of Pancharatnam-Berry phase elements to control the spin-orbit coupling. We experimentally demonstrate transverse angular splitting between the two spins in light trajectory, also associated to the optical spin Hall effect, using the geometric-phase route. The spin-orbit coupling is further controlled to generate orbital rotation with an observation of a rotated profile of Stokes ($S3$) parameter. The investigations may give rise to a class of ultra-thin spin-optical metasurfaces in maniulating optical vortex beams with spin-orbit transformations as an extra degree of freedom.

REFERENCES

1. Yu, N., P. Genevet, M. A. Kats, F. Aieta, J. P. Tetienne, F. Capasso, and Z. Gaburro, *Science*, Vol. 334, 333, 2011.
2. Ni, X., N. K. Emani, A. V. Kildishev, A. Boltasseva, and V. M. Shalaev, *Science*, Vol. 335, 427, 2012.
3. Yin, X. B., Z. Ye, J. Rho, Y. Wang, and X. Zhang, *Science*, Vol. 339, 1405, 2013.

Spectrally Selective Flat Reflective Lenses for Photovoltaic Applications

Sergiy Valyukh
Laboratory of Applied Optics, Department of Physics, Chemistry and Biology
Linköping University, Linköping SE-581 83, Sweden

Abstract— Many techniques for light trapping in photovoltaic cells and for concentration of sunlight onto the active layers are applied to increase efficiency of photovoltaic systems and to decrease their costs. However, this leads often to temperature increase of the photovoltaic material that, in turn, has a detrimental effect on the energy conversion efficiency and life time of the photovoltaic cell [1]. The main reason of the temperature increase is the absorption of the incoming sunlight within spectral range that is not converted into electrical energy. The situation can be improved dramatically by the use of reflectors and lenses with selective spectral properties. For practical applications, these reflectors and lenses are desired to be flat and thin. The goal of the present work is to present such reflective lenses.

The proposed spectrally selective reflective lenses are based on volume Bragg gratings (Figure 1). In contrast to numerous selective reflectors utilizing coatings, these reflectors do not absorb the light. The light of the "needed" spectral range is reflected to the active material, whereas the rest light passes through the grating without absorption. In opposite to the volume Bragg gratings utilised in many applications (usually lasers), the spectrum of the reflected light from the lenses proposed by us is relatively broad. One way of realization of such reflecive lenses is to use a cholesteric liquid crystal (ChLC) polymer. The broad spectral band is achieved due to the high birefringence and the pitch deviations. The high reflectance (close to 100%) can be obtained owing to two layers of ChLC polymers with opposite handedness. The lens effect is accomplished because the orientations of the helical axes of the ChLC vary in space and these axes are not strictly linear. The desired distribution of the helical axes is achieved due to non-uniform alignment conditions in the ChLC cell before polymerisation.

Figure 2 shows the distribution of the calculated electromagnetic field reflected from the structure presented in Figure 1. The incident light has a plane wavefront, whereas the wavefront of the reflected light is spherical that is inherent to a lens.

As one of the examples of practical implementation, we are going to demonstrate how the proposed reflective lenses can increase efficiency of the folded PV cells [2].

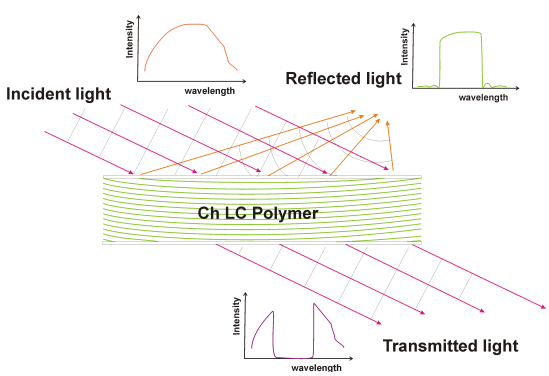

Figure 1: Reflective ChLC lens.

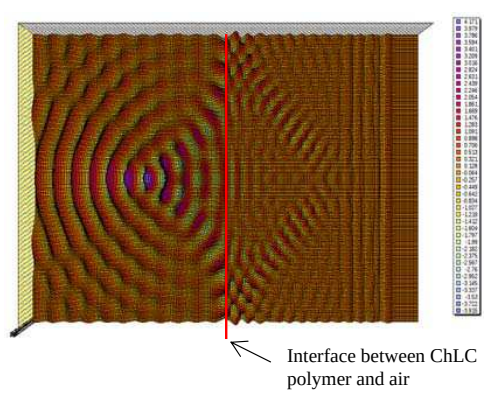

Figure 2: Distribution of the electric field reflected from ChLC lens (air is left from the interface ChLC-air).

REFERENCES

1. Royne, A., C. J. Dey, and D. R. Mills, "Cooling of photovoltaic cells under concentrated illumination: A critical review," *Sol. Energy Mater. Solar Cells*, Vol. 86, No. 4, 451–483, 2005.
2. Andersson, V., K. Tvingstedt, and O. Inganäs, "Optical modeling of a folded organic solar cell," *J. App. Phys.*, Vol. 103, 094520, 2008.

Fixed and Reconfigurable THz Reflectarrays Using Graphene

Eduardo Carrasco and Julien Perruisseau-Carrier
Adaptive MicroNano Wave Systems
Ecole Polytechnique Fédérale de Lausanne (EPFL), Switzerland

Abstract— The use of graphene for implementing the reflectarray concept at THz or above is proposed. The reflector in a reflectarray system, as symbolized in Fig. 1, produce a nonuniform reflection phase profile, to locally control the deflection of an incoming wave (here produced by a 'feed' antenna). Therefore 'arbitrary' far field can be created via complex phase profile on the reflector, similar to the phased array principle. Reflectarray are especially interesting due to their low loss and quasi-planar structure and are envisioned for different applications including satellite antennas. As a result advanced analysis and design techniques have been developed (create complex beams, reduce loss, increase bandwidth, etc.) as well as new capabilities (transformation or twisting of polarization on the reflector, multi-frequency operation, dynamic reconfiguration, etc.).

Here, we first show the detailed design of a fixed reflectarray antenna using graphene, where the reflection phase is controlled by locally changing the size of graphene patches operating around their plasmonic resonance at THz. The proposed reflectarray has been designed at 1.3 THz and comprises more than 25000 elements of size about $\lambda/16$. The array reflective unit cell is analyzed using a full vectorial approach, taking into account the variation of the angle of incidence and assuming local periodicity. Good performance is obtained in terms of bandwidth, cross-polar and grating lobes suppression, proving the feasibility of graphene-based reflectarrays and other similar spatially-fed structures at Terahertz frequencies.

Second, a dynamically-reconfigurable implementation is proposed. In this case, instead of controlling the phase by different patch dimensions, we use the change in the complex conductivity of graphene when biased by an electric field to *independently and dynamically* control the phase of the reflected field at each element of the array. An elementary cell is optimized and its scattering parameters computed, demonstrating a dynamic phase range of 300° and good loss figure for realistic chemical potential variations. Finally, a circuit model is proposed and shown to very accurately predict the element response.

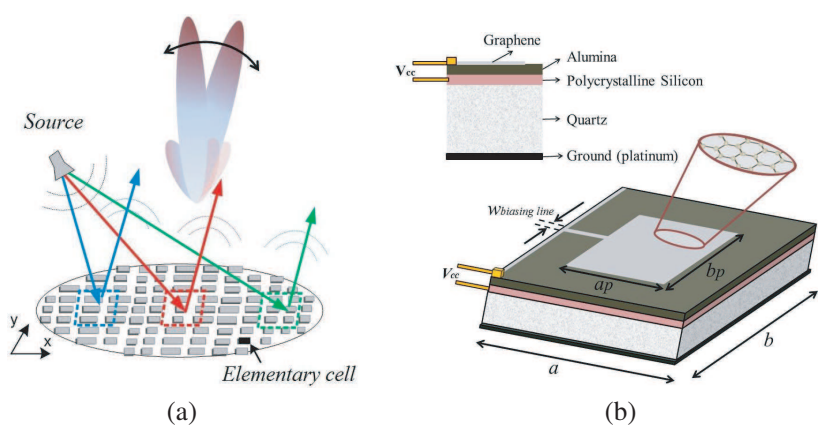

Figure 1: (a) General reflectarray concept. (b) Reconfigurable graphene reflective cell.

Controlled Reflection from a Reflectarray of Optical Dielectric Resonator Nano-antennas

L. Zou[1], W. Withayachumnankul[1], C. M. Shah[2], A. Mitchell[2], M. Bhaskaran[2], S. Sriram[2], and C. Fumeaux[1]

[1]School of Electrical & Electronic Engineering, The University of Adelaide, Adelaide, SA 5005, Australia
[2]School of Electrical and Computer Engineering, RMIT University, Melbourne, VIC 3001, Australia

Abstract— Previous studies on dielectric resonator antennas (DRAs) have demonstrated their high radiation efficiency (> 90%) with negligible loss in the millimeter wave range, whilst the performance of conventional metallic antennas rapidly degrades with increasing frequency. This motivates the use of DRAs as optical antennas. In that perspective, Yang et al. [1] suggested to use resonant dielectric elements to reduce conductive loss in infrared reflectarrays and a concept of dielectric Yagi-Uda geometry was proposed in [2] for possible scaling to optical frequencies.

To extend the concept of DRA from radio-frequencies towards the visible spectrum, we have designed an optical DRA reflectarray for operation at 633 nm visible red light. The optical reflectarray provides a platform for evaluating the function of optical cylindrical DRs operating in their fundamental HEM_{11} mode through observation of a predefined far-field beam angular deflection off the angle of specular reflection. A similar principle of gradient meta-surface has been successfully employed for metallic resonators [3].

The proposed reflectarray is composed of 6-element sub-arrays forming a 60° progressive phase shift along the X direction, as shown in Fig. 1 [4]. The selected material for the DRs is TiO_2 (titanium dioxide) due to its optical properties, manufacturability and functionality. The TiO_2 resonators with variable radii and a fixed height of 50 nm were deposited on a silicon wafer coated with a 200 nm silver layer (see scanning electron micrograph (SEM) of Fig. 2(a)). With each DR separated by 310 nm from centre to centre, the reflectarray deflects an incident beam by 20° off the specular reflection direction, as shown in Fig. 2(b). Although the zeroth-order spatial harmonic (specular reflection) is observed in the measurement because of the fabrication imperfection, the expected beam shaping capacity of the reflectarray is proved by the power ratio of 4.42 between the deflected beam and the specular reflection. This concept provides a new building block for planar optical components and opens a new research area alternative to purely metallic optical antennas.

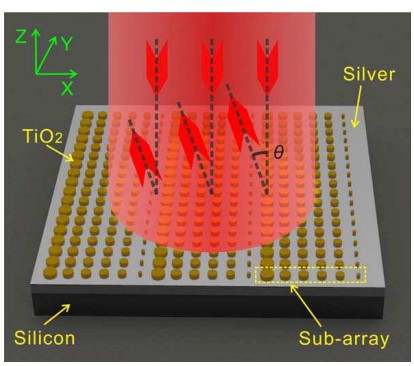

Figure 1: Schematic showing a partial view of 6-element DRA reflectarray with DR height of 50 nm and diameters of 66, 154, 170, 180, 193 and 242 nm.

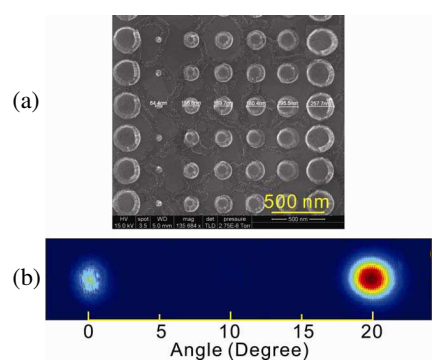

Figure 2: (a) SEM revealing an area on the fabricated 6-element reflectarray. (b) Beam reflection patterns obtained from a CCD camera. Angle of 0° denotes the direction of the specular reflection.

REFERENCES

1. Yang, F., P. Nayeri, A. Elsherbeni, J. Ginn, D. Shelton, G. Boreman, and Y. Rahmat-Samii, "Reflectarray design at infrared frequencies: Effects and models of material loss," *IEEE Trans. Antennas Propag.*, Vol. 60, No. 9, 4202–4209, Sep. 2012.

2. Filonov, D. S., A. E. Krasnok, A. P. Slobozhanyuk, P. V. Kapitanova, E. A. Nenasheva, Y. S. Kivshar, and P. A. Belov, "Experimental verification of the concept of all-dielectric nanoantennas," *Appl. Phys. Lett.*, Vol. 100, No. 20, 201113, 2012.
3. Sun, S., K. Yang, C. Wang, T. Juan, W. Chen, C. Liao, Q. He, S. Xiao, W. Kung, G. Guo, L. Zhou, and D. Tsai, "High-efficiency broadband anomalous reflection by gradient metasurfaces" *Nano Letters*, Vol. 12, 6223–6229, 2012.
4. Zou, L., W. Withayachumnankul, C. Shah, A. Mitchell, M. Bhaskaran, S. Sriram, and C. Fumeaux, "Dielectric resonator nanoantennas at visible frequencies," *Opt. Express*, Vol. 21, No. 1, 1344–1352, Jan. 2013.

Gradient-index Meta-surfaces as a Bridge Linking Propagating Waves and Surface Waves

Qiong He, Shulin Sun, Shiyi Xiao, Xin Li, Che Qu, and Lei Zhou
Department of Physics, Fudan University, Shanghai 200433, China

Abstract— Controlling electromagnetic (EM) waves freely is a dream for researchers. While manipulating propagating waves (PWs) or surface waves (SWs) has separately become possible using transformation optics, a bridge that can link PWs with SWs at will has not yet been found and is highly desired to make the full control over EM waves possible. Here, we demonstrate that a specific gradient-index meta-surface can convert a PW to an SW with theoretically 100% efficiency. Distinct from conventional devices such as prism or grating couplers, here the momentum mismatch between PW and SW is compensated by the reflection-phase gradient of the meta-surface, and perfect PW-SW conversion can happen for any incidence angle larger than a critical value. Experiments, including both far-field and near-field characterizations, are performed to verify this idea in the microwave regime, which are in excellent agreement with full-wave simulations. In addition, we demonstrated that such SWs bounded on the meta-surfaces, which are driven by incident PWs, can be guided out to flow as surface plasmons on another system supporting eigen surface EM modes [1]. Our findings may pave the road for many applications, including flat lens [2], high-efficiency surface plasmon couplers [3], anti-reflection surfaces, light absorbers.

REFERENCES

1. Sun, S. L., et al., *Nature Materials*, Vol. 11, 426, 2012.
2. Li, X., et al., *Opt. Lett.*, Vol. 37, 4940, 2012.
3. Qu, C., et al., *Europhys. Lett.*, Vol. 101, 54002, 2013.

High-efficiency Anomalous Light Reflections by Gradient Meta-surfaces

Shulin Sun[1,2,3], **Kuang-Yu Yang**[4], **Chih-Ming Wang**[5], **Ta-Ko Juan**[5], **Wei Ting Chen**[4], **Chun Yen Liao**[2], **Qiong He**[1], **Shiyi Xiao**[1], **Wen-Ting Kung**[5], **Guang-Yu Guo**[2,7], **Lei Zhou**[1], **and Din Ping Tsai**[2,3,7]

[1]Physics Department, Fudan University, Shanghai 200433, China
[2]Department of Physics, National Taiwan University, Taipei 10617, Taiwan
[3]National Center for Theoretical Sciences, National Taiwan University, Taipei 10617, Taiwan
[4]Graduate Institute of Applied Physics, National Taiwan University, Taipei 10617, Taiwan
[5]Institute of Opto-Electronic Engineering, National Dong Hwa University, Hualien 97401, Taiwan
[6]Physics Department, Fudan University, Shanghai 200433, China
[7]Graduate Institute of Applied Physics, National Chengchi University, Taipei 11605, Taiwan
[8]Research Center for Applied Sciences, Academia Sinica, Taipei 115, Taiwan

Abstract— Manipulating light in a controllable manner is highly desired in photonics research. Recently, we showed that a new type of gradient meta-surface can convert a propagating wave to a surface wave with 100% efficiency provided that the phase gradient is large enough, and experimentally verified the idea in the microwave regime [1]. Now we further pushed this idea to higher frequency region. Combining both theory and experiment, we demonstrated that a carefully designed gradient meta-surface supports high-efficiency anomalous reflections for near-infrared light following the generalized Snell's law, and the reflected wave becomes a bounded surface wave as the incident angle exceeds a critical value [2]. Compared to previously studied meta-string of V-shaped antennas, the gradient meta-surfaces work around ~ 850 nm with broad-band functionality (750–900 nm), exhibit much higher conversion efficiency ($\sim 80\%$) to the anomalous reflection mode at normal incidence, and keep light polarization unchanged after the anomalous reflection. Our results can lead to many practical applications, such as polarization and spectral beam splitters, anti-reflection coating, light absorber, etc..

REFERENCES

1. Sun, S., Q. He, S. Xiao, Q. Xu, X. Li, and L. Zhou, *Nature Materials*, Vol. 11, 426, 2012.
2. Sun, S., K.-Y. Yang, C.-M. Wang, T.-K. Juan, W. T. Chen, C. Y. Liao, Q. He, S. Xiao, W.-T. Kung, G.-Y. Guo, L. Zhou, and D. P. Tsai, *Nano Letters*, Vol. 12, 6223, 2012.

Gap Plasmon Based Gradient Metasurfaces for Control of Reflected Light

Sergey I. Bozhevolnyi
Department of Technology and Innovation, University of Southern Denmark
Odense DK-5230, Denmark

Abstract— Plasmonic metasurfaces, i.e., nm-thin surface metal nanostructures with subwavelength-sized lattice units, have recently attracted considerable attention due to their abilities to efficiently control both phase and amplitude of transmitted and reflected radiation. We have recently shown that metal nanostructures, in which the top layer consists of a periodic array of nanobricks, thus supporting gap surface plasmon (GSP) resonances, offer improved control of the phase of the reflected light. At the same time, by choosing a subwavelength periodicity and weak coupling between the nanobricks and the metal underlay one can strongly suppress the strong absorption typically related to GSP resonances (that can also be advantageously used for efficient and broadband suppression of light reflection), thereby allowing one to design efficient, compact (i.e., subwavelength thick) and background-free (i.e., no diffraction and no scattering into other polarizations) wave plates in reflection. The understanding of light reflection by arrays of GSP resonators led us to further developments, including the design of highly efficient and background-free (i.e., no diffraction and no scattering into other polarizations) plasmonic metasurfaces providing strong phase gradients in the reflected optical fields at the same polarization as that of the incident one. This work, which is currently in progress, opens exciting avenues for very efficient (up to 90%) and broadband manipulation of reflected optical fields in a manner similar to what has recently been shown with V-shaped optical antennas that however influence only the orthogonal polarization with a limited efficiency. We envision many interesting applications for these structures in nanophotonics, including the possibility of realization of efficient and broadband flat mirrors strongly focusing incident radiation in reflection. Further results obtained in this direction will be presented at the conference.

Spoof Surface Plasmons on Ultrathin Corrugated Metal Structures

Tie Jun Cui and Xiaopeng Shen
State Key Laboratory of Millimeter Waves, Southeast University, Nanjing 210096, China

Abstract— Surface plasmons (SPs) are highly localized electromagnetic (EM) waves with exponential field decay from the interface of metal and dielectric. Based on the geometry of metal, SPs are generally classified into two types: surface plasmon polaritons (SPPs) as the propagating modes which exist on the extended interface of metal and air, and localized surface plasmons (LSPs) which exist on small metal particles. Due to the advantages to confine EM waves in a subwavelength scale, both SPPs and LSPs have found wide applications. However, SPs only exist in the optical frequency. In the microwave and terahertz frequencies, artificial structures have to be used to produce spoof SPPs and LSPs. Spoof SPPs have been intensively investigated in recent years using metal surfaces decorated with one-dimensional arrays of subwavelength grooves, two-dimensional arrays of subwavelength holes or dimples, and three-dimensional metal wires with periodic array of radial grooves. However, such structures have two shortcomings. First, they are non-planar structures with a vertical dimension of decorations, yielding the inconvenience for fabrications. Second, they cannot control the bending of surface waves freely. In fact, the natural SPPs can neither be controlled to propagate along an arbitrarily-designed path freely on metal surfaces in the optical frequency.

In this presentation, we introduce a planar plasmonic metamaterial on thin metal films with nearly zero thickness. From the theoretical simulations and experiments, we show that spoof SPPs can propagate along a thin metal film by corrugating its edge with periodic array of grooves [1]. Such a planar plasmonic metamaterial can sustain highly localized SPPs along two orthogonal directions in the terahertz and microwave regions in broadband by keeping good modal shape and propagating long distance with low bending loss. The ability to bend spoof SPPs freely on thin film makes the planar plasmonic metamaterial more practical to produce plasmonic devices in the terahertz frequency, such as the 90° bend, splitter and ring resonator. Experiments in the microwave frequency validate the feasibility of planar plasmonic metamaterial. Based on the above idea, we also present the concept of conformal surface plasmons (CSPs) [2], i.e., the surface plasmon waves that can propagate on ultrathin and flexible films to long distances. The flexible ultrathin films can be bent, folded, and even twisted to mould the flow of CSPs.

In the second part of the presentation, we propose and experimentally demonstrate the spoof localized surface plasmons (LSPs) on a planar textured metallic disk at the microwave frequencies [3]. We design and realize the plasmonic metamaterial using ultrathin metal film printed on a thin dielectric substrate and observe the multipolar plasmonic resonances in both numerical simulations and experiments, including the dipole, quadrupole, hexapole, octopole, decapole, dodeca-pole, and quattuordec-pole modes. The simulation and experiment results have very good agreements. We show that the spoof LSP resonances are sensitive to the disk's geometry and local dielectric environments, and hence the ultrathin textured metallic disk has potential applications as plasmonic sensor in the microwave and terahertz frequencies.

REFERENCES

1. Shen, X. and T. J. Cui, "Planar plasmonic metamaterial on a thin film with nearly zero thickness," *Appl. Phys. Lett.*, 2013 (accepetd for publication).
2. Shen, X., T. J. Cui, D. Martin-Canob, and F. J. Garcia-Vidal, "Conformal surface plasmons propagating on ultrathin and flexible films," *Proceedings of the National Academy of Science*, Vol. 110, No. 1, 40–45, 2013.
3. Shen, X. and T. J. Cui, "Ultrathin plasmonic metamaterial for spoof localized surface plasmons," Scientific Report, 2013 (submitted for publication).

Metasurfing Substrate Integrated Waveguides to Mold the Radiation from Leaky Waves

Jose Luis Gomez-Tornero[1], **George Goussetis**[2], **and Jay Guo**[3]

[1]Technical University of Cartagena, Spain
[2]Heriot-Watt University, UK
[3]CSIRO ICT Centre, Australia

Abstract— We show our latest developments in the application of the metasurfing concept to Substrate Integrated Waveguide (SIW) technology. It is described how this simple and versatile guiding medium can be conveniently modified and modulated to control the conversion from propagating waves to surface/leaky waves, and to mold their propagation and radiation features with the general application to wavefront control (amplitude and phase).

Theoretical aspects and practical designs are described, covering frequencies from Ku band (12–18 GHz) to W-band (75–111 GHz), and showing fabricated prototypes and experimental results. The synthesis of different and exotic propagating wavefront shapes will be theoretical described and validated with full-wave simulations and experiments. Also, this theory will be linked with holography.

Different exciting applications are described, such as static near- and far-field pattern shaping, and also dynamic-electronically reconfigurable beam shaping. 1D and 2D SIW configurations, rectilinear and conformal shapes, and passive/active (tunable) devices will be described. Free-space operation (leaky wave control) and host-substrate operation (surface wave control) will be also distinguished.

The frequency-spatial decomposition is also described, with interesting applications such as electrical prisms for analog signal processing, frequency steerable near-field lenses for microwave/mm-wave sensing/imaging and heating, novel quasi-optical spatial bandpass filters/multiplexers, or novel and simple radiative (propagative) Bessel beam launchers and tailored surface wave launchers which present arbitrary amplitude distributions.

In the field of wireless telecommunications and chip-to-chip wireless interconnects, the beam-squint reduction will be also discussed, showing how this simple SIW technology allows flexible design and shaping of the spatial and spectral response in both near and far-field radiation regimes.

In this 20 minute talk, the presenting author will show comprehensive illustrations and animations of the simulated electromagnetic fields, fabricated prototypes and experimental results, covering a wide range of physical phenomena and potential applications.

Session 1P3
1_FocusSession.SC1: Casimir Effect and Heat Transfer 1

Anomalous Heat Transport Regimes in Complex Plasmonic Networks
Philippe Ben-Abdallah, ... 244
Evanescent-wave Heat Transfer at Cryogenic Temperatures in a Parallel Plane Geometry
Richard S. Ottens, V. Quetschke, G. Mueller, D. H. Reitze, David B. Tanner, ... 245
Near-field Thermal Emission near Non-local Dielectrics
Karl Joulain, Y. Ezzahri, F. Singer, ... 246
Revisiting Thermal Emission in the Near-field with a Thermal Radiation Scanning Tunnelling Microscope
Arthur Babuty, Karl Joulain, Pierre-Olivier Chapuis, Jean-Jacques Greffet, Yannick De Wilde, ... 247
Measuring Radiative Heat Transfer Enhancement at the Nanoscale
Emmanuel Rousseau, Alessandro Siria, Guillaume Jourdan, Sebastian Volz, Fabio Comin, Joel Chevrier, Jean-Jacques Greffet, ... 248
Control of Near-field Heat Transfer in Nanostructures
Michal Lipson, ... 249
On Experiments of Near-field Heat Flow between a SPM-tip and a Monolayer Dielectric Island
Achim Kittel, D. Hellmann, L. Worbes, ... 250
Measurements of the Heat Transfer in Near Field Regime and the Influence of Graphene Layer
Joel Chevrier, P. J. Van Zwol, ... 251
Continuous Transition of Heat Transport across a Closing Vacuum Gap from Thermal Radiation to Thermal Conduction
Bair V. Budaev, David D. Bogy, ... 252
Theory of the Dynamical Casimir Effect in Superconducting Circuits
Goran Johansson, ... 253
Experiments on the Dynamical Casimir Effect in Superconducting Circuits
Per Delsing, ... 254
On the Foundations of Electromagnetic Fluctuation Forces
Carsten Henkel, V. E. Mkrtchian, ... 255

Anomalous Heat Transport Regimes in Complex Plasmonic Networks

P. Ben-Abdallah
Laboratoire Charles Fabry, UMR 8501, Institut d'Optique, CNRS, Université Paris-Sud 11
2, Avenue Augustin Fresnel, 91127 Palaiseau Cedex, France

Abstract— Resonant plasmonic structures networks have been widely used to modify the optical properties of composite materials thanks to multiple scattering interactions. During the last decade these collective interactions mechanims have been largely exploited to design the optical properties of materials. In this work we show that these interactions can also be used to tailor the heat transport properties.

When two media out of thermal equilibrium are separated by a subwavelength separation gap it is well known that a huge heat flux is transferred by photon tunneling [1] from the hot medium toward the cold one. In presence of resonant surface modes [2] such as surface plasmons or surface polaritons, collective electrons or partial charges oscillations coupled to the light waves at the surface, the radiative heat flux exchanged between these media can even surpass by several orders of magnitude the heat flux exchanged between two blackbodies.

During the last five years [3–6], the near-field heat transfers in nanostructures networks have been investigated. A detailed study of three body systems has allowed in particular to identify different many body exaltation mechanisms due to the presence of configurational resonance. However, to date, numerous questions of fundamental importance remain unsolved in complex plasmonic networks and the physics of heat transport is mainly unknown. In this work we focus our attention on the study of heat transport regimes driven by the near-field interactions in these networks. We demonstrate the existence of anomalous heat transport regimes due to near-field interactions and we propose a new generation of composite materials able to transport heat faster than the classical diffusion.

REFERENCES

1. Polder, D. and M. Van Hove, *Phys. Rev. B*, Vol. 4, 3303, 1971.
2. Volokitin A. I. and B. N. J. Persson, *Rev. Mod. Phys.*, Vol. 79, 1291, 2007.
3. Ben-Abdallah, P., K. Joulain, J. Drevillon, and C. Le Goff, *Phys. Rev. B*, Vol. 77, 075417, 2008.
4. Ben-Abdallah, P., S. A. Biehs, and K. Joulain, *Phys. Rev. Lett.*, Vol. 107, No. 11, 114301, 2011.
5. Yannopapas, V. and N. V. Vitanov, *Phys. Rev. Lett.*, Vol. 110, 044302, 2013.
6. Messina, R., M. Antezza, and P. Ben-Abdallah, *Phys. Rev. Lett.*, Vol. 109, 244302, 2012.

Evanescent-wave Heat Transfer at Cryogenic Temperatures in a Parallel Plane Geometry

Richard S. Ottens[1], **V. Quetschke**[2], **G. Mueller**[1], **D. H. Reitze**[3], **and D. B. Tanner**[1]

[1]Department of Physics, University of Florida, USA
[2]Department of Physics and Astronomy, University of Texas at Brownsville, USA
[3]LIGO Laboratory, California Institute of Technology, USA

Abstract— Evanescent-wave heat transfer is the process by which near-field radiation effects are used to transfer heat from one body to another. These evanescent waves allow a thermal transmission across vacuum gaps on the scale of microns. With decreasing gap size, the heat transfer rises rapidly, substantially exceeding the far-field blackbody radiation limit. We experimentally demonstrate evanescent-wave heat transfer in a macroscopic geometry between two parallel plates of sapphire around 300 K between 2.5 µm and 100 µm. Our experimental results are in good agreement with theoretical predictions made by Polder and Van Hove. A recent upgrade to make our experiment more precise in measuring distance and in temperature stabilization will be described. Experiments where we cool our experiment to cryogenic temperatures will also be discussed. The goal is to insure that the theory can still accurately predict the evanescent-wave heat transfer effect. By understanding and controlling this process, especially at cryogenic temperatures, it will be possible to cool large substances when other methods of heat transfer are limited due to experimental constraints. Such constraints are found in potential cryogenic operations of Laser Interferometer Gravitational-wave Observatories (LIGO). Future versions of LIGO will use cryogenic operation of the optics in conjunction with increased laser power to increase sensitivity. A problem arises in that the laser will heat up the optics. The optics will be in vacuum and are seismically isolated by complicated pendulum systems. These conditions prevent normal methods of heat transfer of convection and conduction to be used; moreover far-field radiative heat transfer would not provide sufficient cooling power. Methods for using evanescent-wave heat transfer to solve cryo-LIGO's cooling difficulties will be discussed.

ACKNOWLEDGMENT

Supported by NSF Grant PHY-1205512 LIGO DCC# LIGO-G1300400.

Near-field Thermal Emission near Non-local Dielectrics

K. Joulain, Y. Ezzahri, and F. Singer
Institut Pprime, CNRS, Université de Poiters, ENSMA, Poitiers, France

Abstract— The work presented here focuses on the way to calculate near-field radiative thermal emission above a dielectric which optical properties are described with a non-local dielectric constant. The dielectric non locality has been described by two models. In the first one, dielectric properties are local as long as the wave vector is smaller than $2\pi/a$ where a is the lattice parameter. For higher wave vectors, the material can be considered as transparent. We show with this modeling that heat transfer between two semi-infinite planar non-local dielectrics modeled as described above do not diverge as the distance is reduced but saturates at separation distances smaller than a. Similar results are predicted for the density of energy. In a second part of the work, thermal emission of a non-local material is simulated from first principles. The material is here constituted by elementary dipoles situated at the nodes of a 3D square lattice with a period equal to a. Each dipoles is thermalized at a certain temperature T and exhibit a polarizability α. By application of the fluctuation-dissipation theorem to the elementary dipoles, we obtain the electromagnetic field anywhere above and in the materials. We deduce from the fluctuating fields quadratic electromagnetic quantities such as the density of energy or the Poynting vector. When the medium is diluted, we show that the emitted field can be seen as the sum of individual dipoles. When the medium is dense like in a solid, multiple interactions between dipoles have to taken into account. The polarizability is modified and an expression of a dressed polarizability can be established calculating the dipoles Green functions. We show here again that in both cases the density of energy above a such semi-infinite planar non-local material do not diverge as the distance to the interface is reduced. The energy density saturates as the distance is reduced below the lattice parameter a.

Revisiting Thermal Emission in the Near-field with a Thermal Radiation Scanning Tunnelling Microscope

Arthur Babuty[1], **Karl Joulain**[2], **Pierre-Olivier Chapuis**[3,4], **Jean-Jacques Greffet**[5], **and Yannick De Wilde**[1]

[1]Institut Langevin, ESPCI ParisTech, CNRS, 75238 Paris Cedex 05, France
[2]Institut P', CNRS, Université de Poitiers, 86022 Poitiers, France
[3]Catalan Institute of Nanotechnology (ICN), Campus UAB, 08193 Bellaterra, Spain
[4]Centre de Thermique de Lyon (CETHIL), CNRS, INSA Lyon, UCBL, 69621 Villeurbanne, France
[5]Laboratoire Charles Fabry, Institut d'Optique, CNRS, Université Paris-Sud, 91127 Palaiseau, France

Abstract— The thermal radiation scanning tunnelling microscope is a near-field probe based on the scattering of the thermal emission in the near-field by the metal tip of an atomic force microscope. Spatial maps of the TRSTM signal allows one recording the spatial variations of the local electromagnetic density of states (EM-LDOS) at a frequency (typically in the mid-infrared) set by a filter [1]. We report local spectra of the near-field thermal emission recorded by a Fourier transform infrared spectrometer, using a tungsten tip as a local scatterer coupling the near-field thermal emission to the far field [2]. Spectra recorded on silicon carbide and silicon dioxide exhibit temporal coherence due to thermally excited surface waves. Finally, we evaluate the ability of this spectroscopy to probe the frequency dependence of the electromagnetic local density of states.

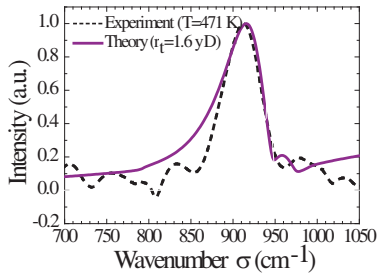

Figure 1: (Dashed curve) Spectrum of the near-field thermal emission measured on silicon carbide (SiC) showing the partial temporal coherence due to thermally excited surface phonon polaritons, and (full curve) theoretical fit based on a model in which the tungsten tip is approximated by a spherical dipole which interacts with the surface of the sample, and including retardation [2].

REFERENCES

1. De Wilde, Y., F. Formanek, R. Carminati, B. Gralak, P.-A. Lemoine, J.-P. Mulet, K. Joulain, Y. Chen, and J.-J. Greffet, "Thermal radiation scanning tunnelling microscopy," *Nature*, Vol. 444, 740–743, 2006.
2. Babuty, A., K. Joulain, P.-O. Chapuis, J.-J. Greffet, and Y. De Wilde, "Blackbody spectrum revisited in the near field," *Physical Review Letters*, 2013, in press.

Measuring Radiative Heat Transfer Enhancement at the Nanoscale

Emmanuel Rousseau[1,2,3], **Alessandro Siria**[4,5], **Guillaume Jourdan**[5], **Sebastian Volz**[6], **Fabio Comin**[7], **Joël Chevrier**[4], **and Jean-Jacques Greffet**[1]

[1]Laboratoire Charles Fabry de l'Intitut d'Optique
CNRS UMR 850, Campus Polytechnique, Palaiseau Cedex 91127, France
[2]Université Montpellier 2, Laboratoire Charles Coulomb UMR 5221, Montpellier F-34095, France
[3]CNRS, Laboratoire Charles Coulomb UMR 5221, Montpellier F-34095, France
[4]Institut Néel, CNRS, Université Joseph Fourier, Grenoble 38042, France
[5]CEA/LETI MINATEC, Grenoble 38042, France
[6]Laboratoire EM2C, CNRS UPR 288, École Centrale Paris
Grande Voie des Vignes, Châtenay, Malabry 92295, France
[7]ESRF, 6 Rue Horowitz, Grenoble Cedex 38042, France

Abstract— It has been predicted theoretically that for distances smaller than the peak wavelength of the blackbody spectrum, radiative heat transfer can be increased by the contribution of evanescent waves [1]. This enhancement can reach several orders of magnitude for materials supporting resonances in the IR such as surface phonon-polariton or surface plasmon-polariton [2–4].

These effects have already been observed but a quantitative comparison is still missing. We have measured the heat flux between a sphere and a plate as a function of the sphere-plate distance [5]. We show that experimental and theoretical results are consistent in the range 50 nm–2 µm. Particularly, the distance dependence is well reproduced by the theory.

For a sphere with a radius of 20 µm, the heat flux exchanged with a plate is in the order of tens of nanoWatts. To measure the radiative heat tranfer, a very sensitive device is needed. The fluxmeter used in our experiment is a bimorph based on an AFM cantilever. Such fluxmeters can measure fluxes variations as small as 10 pW [6]. The bimorph bending is proportional to the flux and is measured using an optical interferometric technique based on the device used in [7] to measure the Casimir force. The experimental results are compared with theoretical calculations based on the Derjaguin approximation [8] commonly used to compute the Casimir force between a sphere and a plane. The transition regime between far field and near field is well reproduced. These results strongly support previous theoretical works and pave the way to engineering radiative heat transfer in the mesoscopic regime. Possible applications are heat assisted magnetic recording or heat assisted lithography.

REFERENCES

1. Volokitin, A. I. and B. N. J. Persson, *Rev. Mod. Phys.*, Vol. 79, 1291–1329, 2007.
2. Joulain, K., J.-P. Mulet, F. Marquier, R. Carminati, and J.-J. Greffet, *Surf. Sci. Rep.*, Vol. 57, 59–112, 2005.
3. Rousseau, E., M. Laroche, and J. J. Greffet, *Appl. Phys. Lett.*, Vol. 95, 231913, 2009.
4. Rousseau, E., M. Laroche, and J. J. Greffet, *JQSRT*, Vol. 111, 1005, 2010.
5. Rousseau, E., A. Siria, G. Jourdan, S. Volz, F. Comin, J. Chevrier, and J.-J. Greffet, *Nature Photonics*, Vol. 3, 514, 2009.
6. Lai, J., T. Perazzo, Z. Shi, and A. Majumdar, *Sensors & Actuators A: Physical*, Vol. 58, 113–119, 1997.
7. Jourdan, G., A. Lambrecht, F. Comin, and J. Chevrier, *J. Eur. Phys. Lett.*, Vol. 85, 31001, 2009.
8. Derjaguin, B. V., I. I. Abrikosova, and E. M. Lifshitz, *Quaterly. Rev. Chem. Soc.*, Vol. 10, 295–329, 1956.

Control of Near-field Heat Transfer in Nanostructures

Michal Lipson
School of Electrical and Computer Engineering, Kavli Institute at Cornell
Cornell University, Ithaca, NY, USA

Abstract— We show the ability to tailor the photonic density of states in the IR and manipulate near field thermal radiation in nanostructures. This is achieved by inducing strong interaction between Photons in the IR and optical phonons. Using this principle we have recently demonstrated the ability to coon down localized hotspots by tens of degrees at submicrometer gaps near-field radiative cooling of a nano membrane. These results pave the way for realizing other new effects based on resonant heat transfer, like thermal rectification and negative thermal conductance.

On Experiments of Near-field Heat Flow between a SPM-tip and a Monolayer Dielectric Island

A. Kittel, **D. Hellmann**, **and L. Worbes**
University of Oldenburg, Germany

Abstract— We have investigated the influence of thin films of a dielectric material on the near-field mediated heat transfer at the fundamental limit of single monolayer islands on a metallic substrate. We present spatially resolved measurements by near-field scanning thermal microscopy showing a distinct enhancement in heat transfer above NaCl islands compared to the bare Au(111) film. The experimental results show a pronounced increase of the heat transfer by means of evanescent electromagnetic fields above a monolayer NaCl film. The method facilitates the possibility of developing designs of nanostructured surfaces with respect to specific requirements in heat transfer down to a single atomic layer.

Measurements of the Heat Transfer in Near Field Regime and the Influence of Graphene Layer

J. Chevrier and P. J. Van Zwol
Institut Néel, CNRS, Universite Joseph Fourier Grenoble, BP 166, 38042 Grenoble Cedex 9, France

Abstract— Heat can be exchanged between two surfaces through emission and absorption of thermal radiation. For distances smaller than the peak wavelength of the blackbody spectrum, radiative heat transfer can be increased by the contribution of evanescent waves. This contribution can be viewed as energy tunnelling through the gap between the surfaces. On the basis of results published in [1], we shall here present a detailed quantitative comparison between theory and experiments in the nanometre range. We shall describe an experimental setup that allows measurement of conductance for gaps varying between 30 nm and 2.5 µm. We shall then show how the systematic use of this machine has enabled us to measure the heat transfer in near field regime for different materials including VO2 which presents a prototypical metal insulator transition. Further we have investigated the change of the near field contribution to heat transfer when one surface is covered with graphene. Indeed owing to its two dimensional electronic structure, graphene exhibits many unique properties. One of them is a wave vector and temperature dependent plasmon in the infrared range. Theory predicts that due to these plasmons, graphene can be used as a universal material to enhance nanoscale radiative heat exchange for any dielectric substrate. Based on [2], we shall report on radiative heat transfer experiments between SiC and a SiO_2 sphere which have non matching phonon polariton frequencies, and thus only weakly exchange heat in near field. Heat flux contribution of graphene epitaxially grown on SiC wil be shown to dominate at short distances. The influence of plasmons on radiative heat transfer is further supported with measurements for doped silicon. These results highlight graphene's strong potential in photonic nearfield and energy conversion devices.

REFERENCES

1. Rousseau, E., A. Siria, G. Jourdan, S. Volz, F. Comin, J. Chevrier, and J.-J. Greffet, *Nat. Photonics*, Vol. 3, 514, 2009.
2. Van Zwol, P. J., S. Thiele, C. Berger, W. A. De Heer, and J. Chevrier, *Phys. Rev. Lett.*, Vol. 109, 264301, 2012.

Continuous Transition of Heat Transport across a Closing Vacuum Gap from Thermal Radiation to Thermal Conduction

B. V. Budaev and D. B. Bogy
University of California, Berkeley, USA

Abstract— For a long time conductance and radiation have been viewed as different mechanisms of heat transport based on different physical phenomena. Conduction dominates heat transport in solids, it is governed by the Fourier law and is described by the heat/diffusion equation. Radiation appears as the only means for heat exchange across a vacuum gap, it is governed by the laws of electromagnetism and, therefore, is described in terms of Maxwell's equations.

However, in the beginning of active exploration of heat transport at micro and nano scales it was noticed that the conventional theory of radiative heat transport provides calculations that differ from experiment. Thus, while the classical theory predicts the heat transport coefficient between two half-spaces separated by a vacuum gap should be independent of the gap's width H, it is observed [1] that the heat transfer coefficient starts increasing when H decreases below a few microns, and more recent experiments [2] suggest that the increase is proportional to $1/H^2$ as the gap vanishes.

Although these observations contradict classical theories of radiative heat transport, they agree with common sense which suggests that when H becomes comparable with interatomic distances then the radiation heat transport across it should evolve to heat conductance over the interface. In particular, the thermal resistance of a vacuum gap should gradually evolve to the interface thermal resistance, known as Kapitsa resistance.

Our study of nanoscale heat transport explores the observation that heat conduction is also (as radiation) due to electromagnetic forces. Indeed, it is well known that a material body, even an electrically neutral one, is surrounded by an electromagnetic field that rapidly decays with distance. Therefore, when the distance H between bodies becomes close to the interatomic distance, the molecules of two separated bodies start interacting directly via the short-range electric forces, as if they belong to a single body. And as the distance of separating bodies increases, at some point, this short-range interaction becomes equal to the long-range interactions responsible for radiation, and this provides a gradual transition between the radiative heat transport and heat conductance.

In particular, our analysis estimates that the heat flux related with the Casimir (or van der Walls) effect for approaching bodies behaves as $H \to 0$ like $\sim 1/H^8$ and starts exceeding the flux due to heat radiation at the distances of the order $\sim 5\,\mathrm{nm}$ and below [3, 5]. We expect that this phenomenon may find application in the design of Heat Assistance Magnetic Recording (HAMR) systems where the spacing between the head and disk is less than 5 nm.

We also demonstrate that our concepts imply that for intremediate range separations, between $H \sim 10\,\mathrm{nm}$ and $H \sim 3000\,\mathrm{nm}$, the heat transport coefficient follows the rate $1/H^2$ observed in [2], and these concepts also provide, for the first time, reasonably accurate order of magnitude estimates of interface Kapitsa resistance, which has remained illusive since the 1940s.

REFERENCES

1. Cravalho, E. G., C. L. Tien, and R. P. Caren, "Effect of small spacing on radiative transfer between two dielectrics," *J. Heat Transport*, Vol. 89, No. 3, 351–358, 1967.
2. Narayanaswamy, A., S. Shen, L. Hu, X. Chen, and G. Chen, "Breakdown of the planck blackbody radiation law at nanoscale gaps," *Appl. Phys. A*, Vol. 96, 357–362, 2009.
3. Budaev, B. V. and D. B. Bogy, "On the role of acoustic waves (phonons) in equilibrium heat exchange across a vacuum gap," *APL*, Vol. 99, No. 5, 053109-1–053109-3, 2011.
4. Budaev, B. V. and D. B. Bogy, "Mechanisms of heat flux across a nano-scale gap: HAMR without optics," *Digest of the 22nd Magnetic Recording Conference TMRC-2011*, 57–58, Minneapolis, MN, USA, Jul. 2011.
5. Budaev, B. V. and D. B. Bogy, "An extension of Khalatnikov's theory of Kapitsa thermal resistance," *Ann. der Physik*, Vol. 523, No. 3, 208–225, 2011.

Theory of the Dynamical Casimir Effect in Superconducting Circuits

G. Johansson
Department of Microtechnology and Nanoscience, MC2
Chalmers University of Technology, S-41296 Göteborg, Sweden

Abstract— The dynamical Casimir effect was recently demonstrated in a superconducting circuit [1]. In this presentation, I will discuss the theory behind this experimental demonstration [2, 3]. In particular, I will discuss the boundary condition for a 1D electromagnetic field confined to a microwave transmission line terminated by a superconducting quantum interference device (SQUID) (see Fig. 1). By modulating the external magnetic flux through the SQUID, the boundary condition can be modulated rapidly. The boundary condition is equivalent to an oscillating mirror, and the effective velocities of this mirror can approach the speed of light. I will also discuss the non-classical correlations in the output field [4] as well as the possibility to use this system to investigate relativistic effects on the quantum teleportation protocol [5].

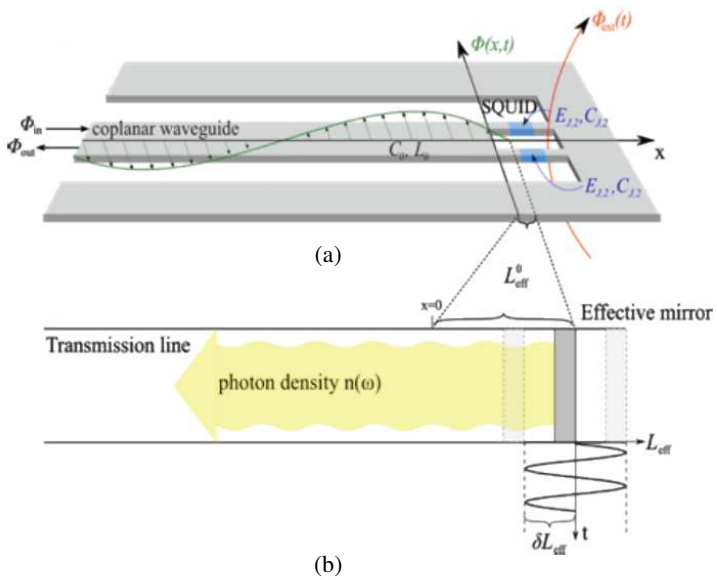

Figure 1: (a) Schematic of a microwave transmission line (a coplanar waveguide — CPW) terminated by a superconducting quantum interference device (SQUID). The SQUID imposes a boundary condition in the CPW that can be parametrically tuned by changing the externally applied magnetic flux through the SQUID. (b) The setup in (a) is equivalent to a waveguide with tunable length or to a mirror with tunable position.

REFERENCES

1. Wilson, C. M., G. Johansson, A. Pourkabirian, M. Simoen, J. R. Johansson, T. Duty, F. Nori, and P. Delsing, "Observation of the dynamical Casimir effect in a superconducting circuit," *Nature*, Vol. 479, 376–379, 2011.
2. Johansson, J. R., G. Johansson, C. M. Wilson, and F. Nori, "Dynamical Casimir effect in a superconducting coplanar waveguide," *Physical Review Letters*, Vol. 103, 147003, 2009.
3. Johansson, J. R., G. Johansson, C. M. Wilson, and F. Nori, "Dynamical Casimir effect in superconducting microwave circuits," *Physical Review A*, Vol. 82, 052509, 2010.
4. Johansson, J. R., G. Johansson, C. M. Wilson, P. Delsing, and F. Nori, "Nonclassical microwave radiation from the dynamical Casimir effect," to appear in *Physical Review A*, 2013.
5. Friis, N., A. R. Lee, K. Truong, C. Sabín, E. Solano, G. Johansson, and I. Fuentes, "Relativistic quantum teleportation with superconducting circuits," *Physical Review Letters*, Vol. 110, 113602, 2013.

Experiments on the Dynamical Casimir Effect in Superconducting Circuits

P. Delsing
Chalmers University of Technology, S-41296 Göteborg, Sweden

Abstract— The Dynamical Casimir Effect (DCE) was recently observed in a superconducting circuit consisting of a coplanar transmission line with a tunable electrical length [1]. The rate of change of the electrical length can be made very fast (a substantial fraction of the speed of light) by modulating the inductance of a superconducting quantum interference device at high frequencies ($\sim 10\,\mathrm{GHz}$). Broadband generation of photons is observed and in addition, we detect two-mode squeezing in the emitted radiation, which is a signature of the quantum character of the generation process. A new related experiment, with a doubly tunable cavity is also discussed. The cavity is terminated by one SQUID in each end, so that the cavity can be parametrically pumped in different ways. In particular the difference between the breathing mode and the translational mode of the cavity is discussed [2].

REFERENCES

1. Wilson, C. M., et al., "Observation of the dynamical casimir effect in a superconducting circuit," *Nature*, Vol. 479, 376, 2011.
2. Svensson, I. M., "Photon generation in a doubly tunable resonator," Masters Thesis, Chalmers University of Technology, 2012.

On the Foundations of Electromagnetic Fluctuation Forces

C. Henkel[1] and V. E. Mkrtchian[2]

[1]Institute of Physics and Astronomy, Universität Potsdam, Germany
[2]Institute for Physical Research, Armenian Academy of Sciences
Ashtarak-1, 0203, Republic of Armenia

Abstract— Quite early in their development, theories for mechanical forces arising from electromagnetic fluctuations (dispersion interactions of the van der Waals, Casimir-Polder, and Casimir type) allowed for situations out of global mechanical or thermodynamic equilibrium [1–4]. A Casimir pressure calculation, for example, based on the stress tensor, implicitly uses external force applied to objects or boundaries to maintain mechanical equilibrium against the electromagnetic interaction. Discussions and recent measurements of Casimir and Casimir-Polder forces in a distance range between 100 nm and a few μm actually call for descriptions with at least two different temperatures, and this has amplified theoretical work from different directions. Examples are fluctuation-dissipation relations combined with the assumption of local thermodynamic equilibrium, applied to the Casimir interaction between bodies at different temperatures [5–8], and the semiclassical Rytov theory applied to Casimir-Polder forces on ultracold atomic gases near solid substrates at room temperature [9–11]. Another setting are friction forces arising from the relative motion between two objects [12–16]. We discuss recent results for non-equilibrium Casimir-Polder interactions and for radiative friction forces [17, 18]. A particularly interesting example is provided by relativistic motion above a graphene sheet where radiative friction is revealing quite some detail on the quasi-particle response around the Dirac point (graphene plasmon dispersion and loss) [19, 20].

An alternative approach is based on non-equilibrium field theory, as formulated by Keldysh and Schwinger. For the problem of electromagnetic heat transfer between dielectric surfaces, it has been shown to yield the same answer as the semiclassical Rytov theory [21]. We construct and discuss the correlation functions (Keldysh Green functions) for the archetypal two-plate geometry based on a path integral formulation of the non-equilibrium quantum field theory. One of our aims is to evaluate the impact of generalized boundary conditions, including relative motion and near-surface scattering and loss, on electromagnetic dispersion interactions [22].

ACKNOWLEDGMENT

We acknowledge funding from the *Deutsche Forschungsgemeinschaft*.

REFERENCES

1. Rytov, S. M., Y. A. Kravtsov, and V. I. Tatarskii, *Elements of Random Fields*, *Principles of Statistical Radiophysics*, Vol. 3, Springer, Berlin, 1989.
2. Lifshitz, E. M. and L. P. Pitaevskii, *Statistical Physics (Part 2)*, Ch. VIII, *Course of Theoretical Physics*, Landau and Lifshitz, 2nd Edition, Vol. 9, Pergamon, Oxford, 1980.
3. Dorofeyev, I. A. and E. A. Vinogradov, *Phys. Rep.*, Vol. 504, 75, 2011.
4. Buhmann, S. Y., *Dispersion Forces I, Springer Tracts in Modern Physics*, Vol. 247, Springer, Heidelberg, 2012.
5. Dorofeyev, I. A., *J. Phys. A*, Vol. 31, 4369, 1998.
6. Bimonte, G. and E. Santamato, *Phys. Rev. A*, Vol. 76, 013810, 2007.
7. Krüger, M., T. Emig, and M. Kardar, *Phys. Rev. Lett.*, Vol. 106, 210404, 2011.
8. Messina, R. and M. Antezza, *Europhys. Lett.*, Vol. 95, 61002, 2011.
9. Henkel, C., K. Joulain, J. P. Mulet, and J. J. Greffet, *J. Opt. A*, Vol. 4, S109, 2002.
10. Obrecht, J. M., R. J. Wild, M. Antezza, L. P. Pitaevskii, S. Stringari, and E. A. Cornell, *Phys. Rev. Lett.*, Vol. 98, 063201, 2007.
11. Dedkov, G. and A. Kyasov, *Tech. Phys. Lett.*, Vol. 34, 950, 2008.
12. Kardar, M. and R. Golestanian, *Rev. Mod. Phys.*, Vol. 71, 1233, 1999.
13. Volokitin, A. I. and B. N. J. Persson, *Rev. Mod. Phys.*, Vol. 79, 1291, 2007.
14. Dedkov, G. V. and A. A. Kyasov, *J. Phys.: Cond. Matt.*, Vol. 20, 354006, 2008.
15. Philbin, T. G. and U. Leonhardt, *New J. Phys.*, Vol. 11, 033035, 2009.
16. Pendry, J. B., *New J. Phys.*, Vol. 12, 033028, 2010.

17. Haakh, H., F. Intravaia, C. Henkel, S. Spagnolo, R. Passante, B. Power, and F. Sols, *Phys. Rev. A*, Vol. 80, 062905, 2009.
18. Pieplow, G. and C. Henkel, *New J. Phys.*, Vol. 15, 023027, 2013.
19. Wunsch, B., T. Stauber, F. Sols, and F. Guinea, *New J. Phys.*, Vol. 8, 318, 2006.
20. Koppens, F. H. L., D. E. Chang, and F. J. García de Abajo, *Nano Lett.*, Vol. 11, 3370, 2011.
21. Janowicz, M., D. Reddig, and M. Holthaus, *Phys. Rev. A*, Vol. 68, 043823, 2003.
22. Dorofeyev, I. A., preprint arxiv:1302.6740.

Session 1P4a
SC4: Novel Frequency Selective Structures

Three-dimensional Dual-band Frequency Selective Structure Using Microstrip Lines
Bo Li, Zhongxiang Shen, ... 258

A Triple-mode Passband Filter with Improved Upper-stopband Performance
Huan Yang, Shaobin Liu, Xiang-Kun Kong, Hui-Chao Zhao, Bo-Rui Bian, ... 260

Embedding Grating Mirror in Resonant Cavity-enhanced Absorber Structures for Mid-infrared Detectors Applications
Moshe Zohar, Mark Auslender, Shlomo Hava, ... 261

Three-dimensional Loaded Dipoles for Applications in Frequency Selective Structures
Amir Khurrum Rashid, Shan Ullah, S. A. Nauroze, ... 262

Automated Design of Frequency Selective Surfaces with the Application to Wi-Fi Band-stop Filter
Pavel Tomasek, Stanislav Gona, ... 264

Ultra-low Density Microwave Absorber Based on Frequency Selective Surface of Ferromagnetic Nano-films
Meng Zhang, Tian Jiang, Jinglong Fan, Yijun Feng, ... 265

Angular Stable Three-dimensional Convoluted-dipole for the Applications in Band-stop Frequency Selective Surfaces
Shan Ullah, Farooq Ahmad Tahir, M. A. Tarar, Amir Khurrum Rashid, ... 266

Three-dimensional Dual-band Frequency Selective Structure Using Microstrip Lines

Bo Li and Zhongxiang Shen
School of Electrical and Electronic Engineering, Nanyang Technological University
50 Nanyang Avenue, Singapore 639798, Singapore

Abstract— Recently, three-dimensional (3-D) frequency selective structures (FSS) with multi-mode cavities/resonators were demonstrated to exhibits superior filtering response by introducing multiple transmission zeros/poles at finite frequencies [1–4]. In this paper, we present a new design of a 3-D dual-band FSS with closed band spacing and high selectivity at each band. The proposed FSS, as shown in Fig. 1(a), consists of a two-dimensional periodic array of two vertically placed microstrip-line structures and two inserted "T-type" metallic pieces. Figs. 1(b) and 1(c) illustrate the front and side views of a unit cell. There are two shielded parallel microstrip lines, named as strips 1 and 2, are printed on two different substrates 1 and 2. The two microstrip lines are shorted to ground (PEC) by two centered via holes, respectively. In addition, two "T-type" metallic pieces are inserted between two substrates, which are in contact with two microstrip lines, respectively. This FSS shows dual-passband behavior due to multiple resonances constructed. The first passband is formed by two microstrip-line resonators along strip 1, and the second passband is realized by another two microstrip-line resonators along strip 2. Moreover, transmission zeros closed to the two passbands are obtained by couplings between the air and substrate modes, which greatly increase the selectively of the presented FSS.

An example of the proposed FSS is designed to operate at the two center frequencies of 5.2 GHz and 8.0 GHz. Fig. 2 illustrates the simulated transmission and reflection coefficients of the designed FSS for TE polarization under incidence angles of 0° and 40° It is seen that two passbands can be successfully achieved with stable filtering response even when the incident angle increases from 0° to 40°.

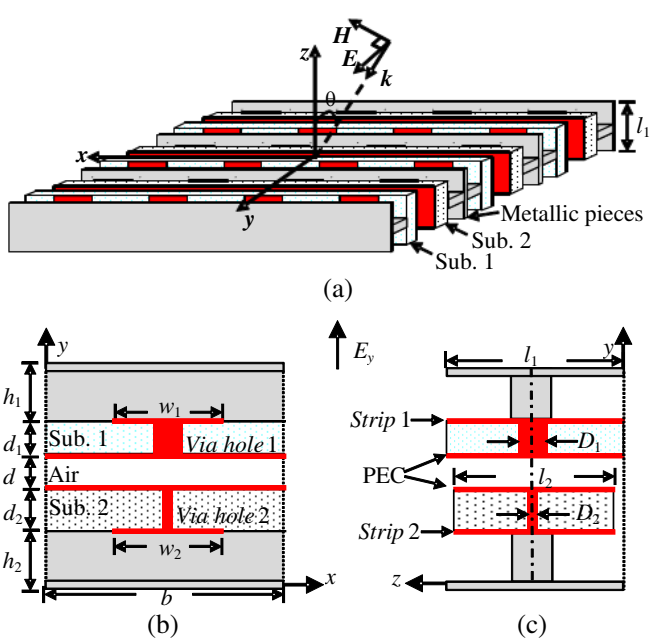

Figure 1: Structure of the miniaturized band-stop FSS. (a) Perspective view. (b) Front view of a unit cell (xy plane). (c) Side view of a unit cell (yz plane).

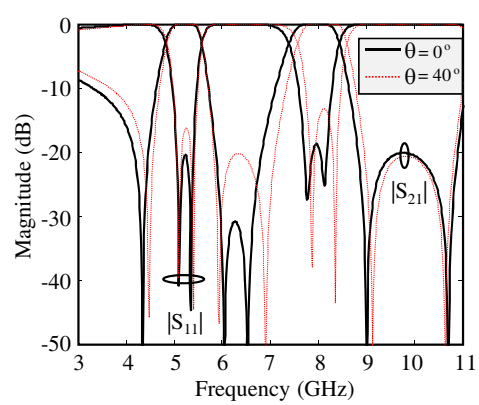

Figure 2: Simulated S parameters of the dual-band FSS (b = 6.0 mm, h_1 = 1 mm, h_2 = 1.2 mm, d_1 = 0.8 mm, d_2 = 1.3 mm, d = 0.7 mm, w_1 = 5 mm, w_2 = 2.5 mm, l_1 = 10.4 mm, l_2 = 10 mm, D_1 = 1.8 mm, D_2 = 1.4 mm, $\varepsilon_{r1} = 3.55$, $\varepsilon_{r2} = 10.2$).

REFERENCES

1. Rashid, A. K. and Z. Shen, "A novel band-reject frequency selective surface with pseudo-elliptic response," *IEEE Trans. on Antennas and Propag.*, Vol. 58, No. 4, 1220–1226, 2010.
2. Rashid, A. K. and Z. Shen, "Scattering by a two-dimensional periodic array of vertically placed microstrip lines," *IEEE Trans. on Antennas and Propag.*, Vol. 59, No. 7, 2599–2606, 2011.
3. Rashid, A. K., Z. Shen, and B. Li, "An elliptical bandpass frequency selective structure based on microstrip lines," *IEEE Trans. on Antennas and Propag.*, Vol. 60, No. 10, 4661–4669, Oct. 2012.
4. Li, B. and Z. Shen, "Miniaturized bandstop frequency-selective structure using stepped-impedance resonators," *IEEE Antennas and Wireless Propag. Lett.*, Vol. 11, 1112–1115, Nov. 2012.

A Triple-mode Passband Filter with Improved Upper-stopband Performance

Huan Yang[1], **Shao-Bin Liu**[1], **Xiang-Kun Kong**[1,2], **Hui-Chao Zhao**[1], **and Bo-Rui Bian**[1]

[1]College of Electronic and Information Engineering
Nanjing University of Aeronautics and Astronautics, Nanjing 210016, China
[2]Jiangsu Key Laboratory of Meteorological Observation and Information Processing
Nanjing University of Information Science and Technology, Nanjing 210044, China

Abstract— In this letter, a high selectivity triple-mode microstrip bandpass filter (BPF) with loaded stubs is proposed. This filter consists of a half-wavelength transmission line with two different open-ended stubs at the line center. Compared with conventional uniform stub, the circular impedance-stepped stub can improve the performance of the upper-stopband. This filter can generate three operation modes, which can be easily adjusted individually. Owing to the symmetrical structure, we can apply the odd-even-mode method to analysis. When the coupling is weak, the even-modes frequency can be flexibly controlled by the open-ended stubs. By use of the two unsymmetrical stubs, two transmission zeros are brought out at low and high rejection bands, which leads to high selectivity. Simulated results show that the central frequency is 6.3 GHz with 3-dB fractional bandwidth of 49%. Its upper-stopband from 8.4 to 16.7 GHz with a rejection level of about −25 dB is extended. As a result, the measured performance agrees well with the simulation.

Embedding Grating Mirror in Resonant Cavity-enhanced Absorber Structures for Mid-infrared Detectors Applications

Moshe Zohar, Mark Auslender, and Shlomo Hava
Department of Electrical and Computer Engineering
Ben-Gurion University of the Negev, P. O. B. 653, Beer-Sheva 84105, Israel

Abstract— Incorporating a photosensitive (optically active) layer into Fabry-Perot (FP) cavity enhances the layer's sensitivity (emissivity) due to reflections of light between the cavity mirrors. Strongest enhancement occurs when the phase difference between each succeeding reflection (round-trip phase), satisfies the resonance condition (which is in fact that of highest resonant transmission through empty FP cavity)

$$\delta_0 = 4\pi n_c(\lambda_0)\, t_c/\lambda_0 + \varphi_f(\lambda_0) + \varphi_b(\lambda_0) = 2\pi m,$$

where λ_0 is a resonance wavelength, m is an integer; n_c and t_c is refractive index (RI) and length of the cavity; φ_f and φ_b is the reflection phase of front and back FP cavity mirror, respectively.

High performance photodetectors (PDs) and imagers in MWIR range (3–10 μm) are attracting increasing interest due to the wide applications in security surveillance, chemical sensing, and industrial processes monitoring [1, 2]. Promising technology is using the resonant cavity enhanced (RCE) absorption [3]. So far, the RCE PDs designs commonly employed [3] distributed Bragg reflectors (DBRs), i.e., stacks of quarter-wave pairs of high/low (H/L) RI layers, both for the front mirror (one that is further away from the illuminated side) and back mirror.

In this presentation, we propose RCE PDs in which the front mirror is a grating structure, designed to act as perfect retroreflector, and the back mirror is a DBR. Optical absorbance of a thin semiconductor embedded in the resonant cavity of this novel type (assuming that the absorption is efficiently converted into photoconductive or photovoltaic response) is further maximized. We apply this idea to $Hg_{0.7}Cd_{0.3}Te$ (MCT) in a CdTe cavity [4]. In our design the irradiation and back mirror ($Hg_{0.6}Cd_{0.4}Te$/CdTe DBR grown on a CdZnTe substrate) scheme is the same as in the conventional design [4] while the front mirror instead of Ge/SiO DBR [4] is a Ge-grating/layer structure.

For a fair comparison, we optimized the conventional and grating-based RCE MCT-absorber structure in parallel using a smart round-trip and mirrors' phases engineering. The optimized grating-mirror based RCE MCT-absorber attains $\sim 97\%$ efficiency with the mirrors twice thinner than in the conventional DBR-based structure optimized to attain only $\sim 83\%$ efficiency in the best case.

The obtained results indicate that the novel grating-mirror based type of RCE PDs meets the combined challenges of significantly increasing the efficiency and reducing the overall complexity and size of the entire device, in comparison with the conventional RCE PDs.

REFERENCES

1. Wang, J., J. Hu, P. Becla, A. M. Agarwal, and L. C. Kimerling, *Opt. Express*, Vol. 18, 12890, 2010.
2. Rogalski, A., J. Antoszewski, and L. Faraone, *J. Appl. Phys.*, Vol. 105, 091101, 2009.
3. Unlu, M. S. and S. Strite, *J. Appl. Phys.*, Vol. 78, 607, 1995.
4. Wehner, J. G. A., R. H. Sewell, J. Antoszewski, C. A. Musca, J. M. Dell, and L. Faraone, *J. Electron. Mater.*, Vol. 34, 710, 2005.

Three-dimensional Loaded Dipoles for Applications in Frequency Selective Structures

A. K. Rashid[1], **S. Ullah**[2], **and S. A. Nauroze**[1]
[1]National University of Computer and Emerging Sciences, Pakistan
[2]National University of Science and Technology, Pakistan

Abstract— Conventional frequency selective surfaces consist of simple two-dimensional (2-D) unit-cell shapes like dipoles, loops, etc. [1, 2]. A number of variations to earlier simple shapes have been proposed over the last three decades, which lead to an advantage in certain applications [3–5]. This quest for finding the best shape continues till date, and more recently, a few three-dimensional unit-cell shapes have also been considered [6, 7]. Freedom of variation in third dimension actually offers more flexibility in designing innovative unit-cell geometries. It appears prudent to efficiently use the third dimension (thickness) of a frequency selective structure (FSS) in order to obtain improved performance of certain parameters. Based on that, it may be useful to reconsider the conventional FSS shapes, and modify them to utilize the freedom of third dimension. This may lead to better and interesting FSS designs, which may also be easy to analyze and fabricate with the present computational and manufacturing technology.

Dipole constitutes one of the earliest shapes used in FSS designs [1]. It has been a preferred choice for application in linearly polarized FSSs. A number of other FSS shapes have actually been derived from a dipole unit-cell, and they include loaded-dipoles [3], meander-lines [4], crossed-dipoles [8], Jerusalem cross [9], tri-poles [10], etc.. These modified forms basically lead to more compact shapes, which can also be applied in dual-polarized FSS.

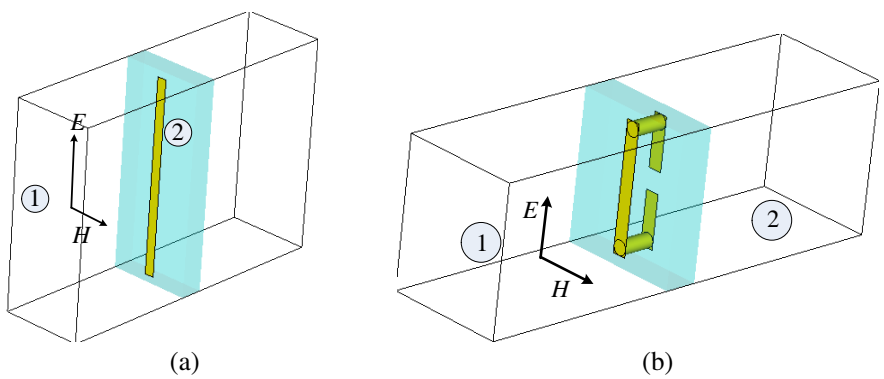

Figure 1: Unit-cell of (a) a conventional FSS consisting of unloaded strip dipoles. (b) The proposed FSS based on three-dimensionally loaded strip dipoles.

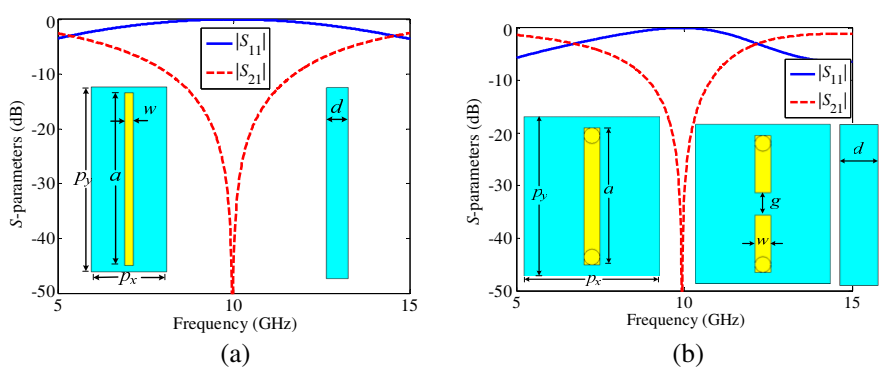

Figure 2: S-parameters of a conventional FSS compared with those of the proposed FSS, when two structures are printed on the same substrate ($\varepsilon_r = 2.2$) and designed for the same resonant frequency. $p_x = 6\,\text{mm}$, $w = 0.7\,\text{mm}$, $d = 1.6\,\text{mm}$. (a) Unloaded case: $p_y = 15\,\text{mm}$, $a = 14\,\text{mm}$. (b) Loaded case: $p_y = 7.1\,\text{mm}$, $a = 6.1\,\text{mm}$, $g = 1\,\text{mm}$.

We study an FSS consisting of a 2-D periodic array of strip dipoles, which have been loaded with two cylinders and strips, along the thickness of the FSS. The two cylinders represent the two via-holes, which connect the opposite sides of a printed circuit board (PCB). Figure 1 compares the unit-cell shape of a conventional FSS with that of our proposed structure. We print strips on the opposite sides of a PCB, and then join them through via-holes. Unlike the 2-D loading of dipoles [3], our proposed loading along the thickness of an FSS, does not affect the horizontal period of the original unloaded dipoles. With the proposed loading, it appears possible to realize a desirably small vertical period A quick example is shown in Figure 2, whereby the unit-cell dimensions of a conventional FSS (unloaded dipoles) can be compared with that of our proposed FSS when both are designed for the same resonant frequency. It is seen that the vertical period p_y of the loaded dipole is less than half of the vertical period of an unloaded dipole. Horizontal period p_x, spacing between the elements p_y–a, substrate height d, dielectric constant ε_r, and width of the strips w has been kept identical for the two cases. More results and comparisons are part of the full paper.

REFERENCES

1. Munk, B. A., *Frequency Selective Surfaces: Theory and Design*, John Wiley & Sons Inc., 2000.
2. Wu, T. K., *Frequency Selective Surface and Grid Array*, John Wiley & Sons Inc., 1995.
3. Munk, B. A., R. G. Kouyoumjian, and L. Peters, "Reflection properties of periodic surfaces of loaded dipoles," *IEEE Trans. on Antennas and Propag.*, Vol. 19, No. 5, 612–617, Sep. 1971.
4. Parker, E. A. and A. N. A. El-Sheikh, "Convoluted array elements and reduced size unit cells for frequency selective surfaces," *IEE Proc. Microwaves, Antennas and Propag.*, Vol. 138, No. 1, 19–22, Feb. 1991.
5. Zheng, S. F., Y. Z. Yin, H. L. Zheng, Z. Y. Liu, and A. F. Sun, "Convoluted and interdigitated hexagon loop unit cells for frequency selective surfaces," *Electron. Lett.*, Vol. 47, No. 4, 233–235, Feb. 2011.
6. Luo, G. Q., W. Hong, Q. H. Lai, K. Wu, and L. L. Sun, "Design and experimental verification of compact frequency-selective surface with quasi-elliptic bandpass response," *IEEE Trans. on Microwave Theory and Tech.*, Vol. 55, No. 12, 2481–2487, Dec. 2007.
7. Rashid, A. K., Z. Shen, and B. Li, "An elliptical bandpass frequency selective structure based on microstrip lines," *IEEE Trans. on Antennas and Propag.*, Vol. 60, No. 10, 4661–4669, Oct. 2012.
8. Hamdy, S. M. A. and E. A. Parker, "Influence of lattice geometry on transmission of electromagnetic waves through arrays of crossed dipoles," *IEE Proc. Microwaves, Antennas and Propag.*, Vol. 129, No. 1, 7–10, Feb. 1982.
9. Anderson, I., "On the theory of self-resonant grids," *The Bell System Technical Journal*, Vol. 54, No. 10, 1725–1731, 1975.
10. Pelton, E. L. and B. A. Munk, "Periodic antenna surface of triple slot elements," United States Patent 3,975,738, Aug. 17, 1976.

Automated Design of Frequency Selective Surfaces with the Application to Wi-Fi Band-stop Filter

P. Tomasek and S. Gona
Tomas Bata University in Zlin, The Czech Republic

Abstract— This article presents a technique for analysis and automated design of frequency selective surfaces. In this work the method of moments is used to analyse a planar periodic structure. Then, the method of moments is combined with a local optimization technique for automated design of filters reflecting given goals. Before performing the design by the local techniques, the necessary system parameters of the filter are derived from the given tolerance channel of the filter. These parameters include the order of the filter and the shape of the periodic element of the filter. The approach allows to automate the whole process of the filter design and frees the user from the detailed knowledge of the filter design theory.

For the practical part of the paper, the algorithm of Levenberg-Marquardt is chosen as a local optimization method. Whole process of automation is implemented in Matlab. An optimization of a band-stop filter for Wi-Fi signals serves as a practical example. A Wi-Fi device communicating under standard 802.11b or 802.11g uses a specific channel which has frequency between 2.412 and 2.484 GHz. Therefore the goal is to design a band-stop filter which ideally does not transmit mentioned band of frequencies. The geometry of Jerusalem-cross serves as a structure to be optimized. Four design variables are defined for optimization: The width and the height of a periodic cell (a square), the width of an arm and two other variables which influence the length of an outer arm and the length of the whole structure of the Jerusalem-cross. This filter consists of two dielectrically separated conductive layers which make the filter more narrow-band. S-parameters of the final optimized geometry of the Wi-Fi filter are presented in the paper.

Ultra-low Density Microwave Absorber Based on Frequency Selective Surface of Ferromagnetic Nano-films

Meng Zhang, Tian Jiang, Jinlong Fan, and Yijun Feng
School of Electronic Science and Engineering, Nanjing University, Nanjing 210093, China

Abstract— Frequency selective surfaces (FSSs) have been successfully used in constructing microwave absorbers which demonstrate the ability of modifying and improving its absorbing performances. In this paper, microwave absorber based on ferromagnetic nano-films have been proposed and investigated with structure similar to that of the Salisbury screen except that the resistive sheet is replaced by FSS of square arrays of the nano-films. We have explored the FSS absorber from three aspects: electromagnetic full-wave simulation, equivalent circuit model and the actual sample measurement. By carefully tuning the patch size, the thickness of the dielectric spacers and the specifications of the ferromagnetic nano-films, we obtain the optimized performance of broadband microwave absorbing. Due to the light weight of the nano-films, the proposed absorbers can achieve an ultra-low surface density less than $0.25\,\mathrm{kg/m^2}$.

The designed microwave absorber consists of a FSS layer of ferromagnetic nano-films and a conducting back-plane, separated by a low-loss, foam dielectric spacer. The FSS layer is a sheet of ferromagnetic nano-films consisting of alternating Fe/SiO_2 nano-films prepared with E-beam evaporation. The unit cell of the FSS pattern is a square patch as shown in Fig. 1(a). The free-space reflectivity characteristics of the FSS absorber were measured for linearly polarized illumination over the frequency range of 2 to 18 GHz in a calibrated NRL arch. Fig. 1(b) shows the measured reflectivity responses of an optimized sample. The designed absorber can achieve -10 dB absorbing bandwidth up to 12 GHz in the 2–18 GHz frequency band. By adjusting the geometric parameters of the FSS layer we can fine-tune the work frequency of the composite structure. The FSS absorber with advantages of controllable parameters, extremely light weight, large area, and flexible texture promises applications in electromagnetic wave protection, electromagnetic compatibility, as well as radar stealth technology.

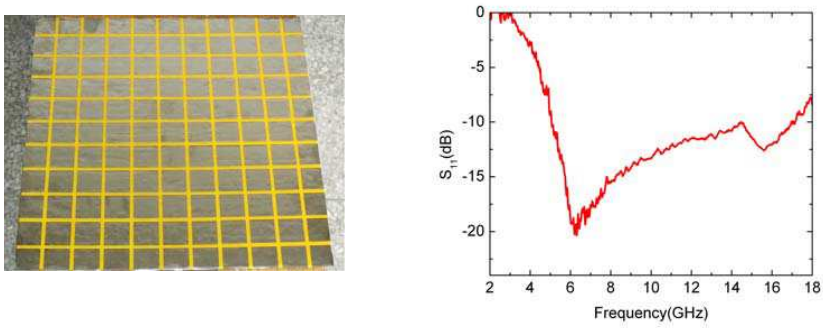

(a) (b)

Figure 1: (a) A sheet of ferromagnetic nano-films with square patches. (b) Measured reflectivity spectra for the FSS absorber sample.

ACKNOWLEDGMENT

Supported by the National Nature Science Foundation of China (60990322, 60990320, 60801001, 61101011), the Key Grant Project (313029) and the Ph.D. Programs Foundation (20100091110036, 20120091110032) of Ministry of Education of China.

Angular Stable Three-dimensional Convoluted-dipole for the Applications in Band-stop Frequency Selective Surfaces

Shan Ullah[1], **F. A. Tahir**[1], **M. A. Tarar**[1], **and A. K. Rashid**[2]

[1]School of Electrical Engineering and Computer Science (SEECS)
National University of Sciences and Technology (NUST), Pakistan
[2]National University of Computer and Emerging Sciences (NUCES-FAST), Pakistan

Abstract— A band-stop frequency selective structure using three-dimensional (3-D) convoluted dipole with improved angular stability (stable resonance with respect to angle of incidence) has been proposed in this research. Frequency selective surface (FSS) using three cycles two-dimensional (2-D) convoluted dipoles are studied for both TE- and TM-polarized incidence wave and found to be less angular stable in case of TM-polarization. However, the proposed 3-D convoluted dipole has utilized the third-dimension (thickness) of the traditional 2-D design efficiently to reduce the vertical period which in turn has improved the angular stability for both TE- and TM-polarized incidence. A comparative analysis of 2-D and 3-D three cycle convoluted dipoles with different geometric shapes and dimensions with respect to angular stability has been presented in this research paper.

Session 1P4b
SC4: Innovative Materials/Metamaterials for Wireless Circuits and Miniaturized Antennas

Miniaturised Antennas over High Impedance Surfaces
Kenneth Lee Ford, Daniel Graham Holtby, Alan Tennant, Richard J. Langley, ... 268

Steering Electromagnetic and Acoustic Waves at Scales Independent of the Wavelength with Metamaterials
Nadege Kaina, Mathias Fink, Geoffroy Lerosey, ... 269

On-chip Integrated Millimeter-wave Antennas on a Local Porous Si Substrate
Panagiotis Sarafis, Chuan-Lun Hsu, Gustavo Ardila, Philippe Benech, Androula G. Nassiopoulou, . 271

Reflectance Spectroscopy of $Ba_{3+x}Zn_{1+y}Nb_2O_9$ Perovskites
W. De La Cruz, S. Moodie, J. Manson, David A. Crandles, Dymitro Grebennikov, P. Mascher, ... 272

Stability and Noise in Active Metamaterials
Khalid Z. Rajab, Yifeng Fan, Deepak Singh Nagarkoti, Yang Hao, ... 273

Design of Advanced Microwave Filters Using the Metamaterial Approach
Dmitry V. Kholodnyak, V. M. Turgaliev, J. Ni, S. Qian, A. S. Rusakov, Irina B. Vendik, J.-S. Hong, 274

Miniaturised Antennas over High Impedance Surfaces

K. L. Ford, **D. G. Holtby**, **A. Tennant**, **and R. J. Langley**
Department of Electronic & Electrical Engineering, The University of Sheffield
Mappin Street, Sheffield S1 3JD, United Kingdom

Abstract— The design of Electrically Small Antennas (ESA), High Impedance Surfaces (HIS) and meta-materials has been a topic of much interest for many years. Particularly of interest is the use of such structures for low frequency applications ($< 1\,\mathrm{GHz}$), where classic antenna/HIS designs become physically large. For such applications miniaturisation techniques are important, however, raise design challenges, such as maintaining radiation efficiency, bandwidth, input match etc. The work carried out at Sheffield has also had a focus of providing platform tolerance using antennas over high impedance surfaces, so that the structure can be placed close to any surface without the performance deteriorating significantly.

This invited paper will present the challenges and proposed solutions for designing ESA and miniaturised HIS for low frequencies ($\sim 400\,\mathrm{MHz}$) as well as the performance of ESA over HIS, in order to achieve platform tolerance. The proposed ESA solutions are based on the use of split ring resonator antennas, which can be designed to have a largest dimension of $\sim \lambda/10$, whilst still achieving good input match and efficiency. To achieve the dimensional requirements the use of lumped reactive elements is employed. A similar miniaturisation technique is chosen in designing low frequency HIS, i.e., use of lumped reactive elements, where unit cell sizes of $< \lambda/70$ have been achieved. Combining the ESA and HIS to provide a compact platform tolerant device is not trivial due to the complex field interactions.

Full field simulations and design approaches will be presented investigating issues, such as the limitation in the dimensions of ESA over HIS structures to provide platform tolerance, accurate modelling of the structures (including lumped component parasitic effects) and measurements of realised designs.

Steering Electromagnetic and Acoustic Waves at Scales Independent of the Wavelength with Metamaterials

N. Kaina, M. Fink, and G. Lerosey
Institut Langevin, ESPCI ParisTech, France

Abstract— We study metamaterials that are arranged on a spatial scale much smaller than the free space wavelength and we show, using a microscopic approach that they present a hybridization band that only results from the local resonance. We show that we can tailor the unit cells locally to shape the flow of waves at deep subwavelength scales. We experimentally validate our approach demonstrating cavities, waveguides, corners and splitters with $\lambda/40$ dimension in electromagnetism and $\lambda/14$ dimension in acoustics. Finally, we prove that those results do not depend on the spatial order of the medium.

It is known that photonic crystals exhibit band gaps due to their translationnal symmetries. This property can be used to create defect cavities or waveguides for example in ordrer to control the flow of wave at a scale of the wavelength. Conversely, metamaterials, that are man made materials organized at a scale much smaller than the wavelength, are consequently usually studied under an effective medium approach and are often considered to be governed by near field interactions.

Here we prove using a macroscopic model based on the transfer matrix formalism, that this assertion is generally incorrect and that the properties of such medium can be only driven by the far field coupling between the local resonance at f_0 and the incoming plane wave. We interprete the dispersion relation of metamaterials at the light of this hybridation: indeed, the wave reradiated by the resonant unit cell of the medium can be either in phase for frequencies below f_0 (in that case, the wave propagates in the medium, which corresponds to the knowned high index band) or in anti-phase above f_0, thus leading to a band gap (the negative effective property band).

Thus, understanding that the band gap in some metamaterials arise from interference effects only, we show that it allows us to induce local modifications of the medium to create cavities and waveguides to steer the wave at dimensions of the order of the period of the medium, which can be very small compared to the wavelength. We present experimental results that illustrate this concept using both electromagnetism (array of copper wires) and acoustic (array of soda cans) metamaterials such as cavities, straight, corner and T-shaped waveguides in which the confinement reaches $\lambda/40$ in electromagnetic and $\lambda/14$ in acoustics. The experimental results show that it is possible to steer the waves even through 90° bend with unity efficiency.

In addition, we stress out that the medium can be spatially disordered since the band gap do not originate from the spatial structure but from the local resonance. We present the case of cavities

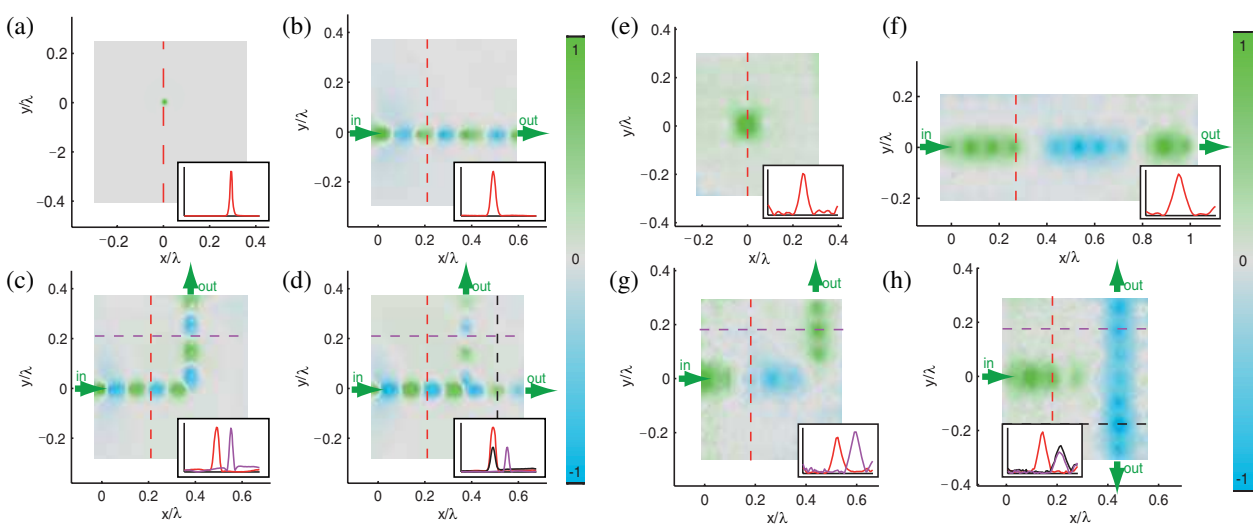

Figure 1: Deep subwavelength cavities and waveguides in (a)–(d) electromagnetic metamaterial, (e)–(h) and acoustic metamaterial.

in two samples, one periodic and one spatially random in the electromagnetic domain. In both samples, the band gap is observed and a cavity is successfully created, with a Q factor of 500 and a modal volume of $\lambda/10000$, leading to very high Purcell factors.

In conclusion, this work proves that it is possible to merge the properties of photonic crystals and metamaterials, leading the way to the possibilities of molding the flow of waves at wish and at scales independent of the wavelength.

REFERENCES

1. Lemoult, F., N. Kaina, M. Fink, and G. Lerosey, *Nature Physics*, Vol. 9, 5560, 2013.
2. Kaina, N., F. Lemoult, M. Fink, and G. Lerosey, *App. Phys. Lett.*, accepted 2013.

On-chip Integrated Millimeter-wave Antennas on a Local Porous Si Substrate

Panagiotis Sarafis[1], **Chuan-Lun Hsu**[2], **Gustavo Ardila**[2], **Philippe Benech**[2], **and Androula Nassiopoulou**[1]

[1]NCSR Demokritos, IMEL, Terma Patriarchou Grigoriou, Aghia Paraskevi, Athens 153 10, Greece
[2]IMEP-LAHC, Grenoble Université, 3 Parvis Louis Néel, CS 50257, Grenoble Cedex 38016, France

Abstract— Antennas in the mm-wave frequencies have a small size since the associated wavelength is in the mm range. This enables their on-chip integration for use either as free-space antennas or in intra-chip interconnects. However, the leaky standard CMOS substrate (1–10 Ω·cm) introduces a lot of losses in RF [1] that significantly affect their performance. In order to overcome this problem, we have used a local porous Si (PSi) substrate, on which the antennas were integrated. This local porous Si substrate technology has been demonstrated as an effective technology for high performance RF passive devices [2–4]. The main advantages of porous Si regarding on-chip antenna integration, can be summarized in its low RF losses, its tunable relative permittivity between 1.5 and 11.9, the ability to be locally formed and its compatibility with batch Si processing. The achieved low values of dielectric permittivity with this materials, give the possibility of higher frequency antennas on them, than on bulk Si.

In this work we explore the advantages of local PSi substrate technology for the on-chip integration of small antennas. In this respect, we have fabricated transmitter-receiver pairs of identical conductor-backed dipole antennas both on PSi and on standard CMOS Si wafers and we compared their performance. The metal thickness of the antennas was 250 nm, the metal width was between 2–5 μm and their length between 800–2000 μm. The slim antenna configuration has been chosen in order to reduce occupied surface. Moreover, the antennas can be shortened in order to reach higher operating frequencies and get connected directly to nanolines and nano-interconnects without transition structure. The antennas were designed for the operating frequencies 50, 90 and 105 GHz.

The antennas were fabricated using Al metallization and were measured from 0.5 GHz up to 110 GHz using a vector network analyzer. As expected, the same antennas on PSi operate at higher frequencies compared to those on bulk crystalline Si. Moreover, through the transmitter-receiver pairs we could extract the in-plane antenna gain, which was found at −12 dBi for antennas on PSi and at −18 dBi for antennas on Si. Both results are attributed to the low losses and the low relative permittivity of PSi that limits the insertion loss and prohibits the emergence of larger modes of surface waves into the substrate. This allows, in a given frequency, increased power efficiency for antennas on PSi as compared to antennas on Si.

The above results demonstrate the superiority of the local porous Si substrate technology in RF and mm-wave antennas, in addition to the obtained excellent performance of other RF passive devices on PSi (e.g., coplanar waveguide transmission lines, inductors).

ACKNOWLEDGMENT

This work was supported by the EU Network of Excellence Nanofunction through the EU Seventh Framework Programme for Research under Contract 257375).

REFERENCES

1. Triantafyllou, A., A. Farcy, P. Benech, F. Ndagijimana, O. Exshaw, C. Tinella, O. Richard, C. Raynaud, and J. Torres, "Intra-chip wireless interconnections based on high performances integrated antennas," *Solid-State Electronics*, Vol. 49, No. 9, 1477–1483, Sep. 2005.
2. Issa, H., P. Ferrari, E. Hourdakis, and A. G. Nassiopoulou, "On-chip high-performance millimeter-wave transmission lines on locally grown porous silicon areas," *IEEE Transactions on Electron Devices*, Vol. 58, No. 11, 3720–3724, Nov. 2011.
3. Sarafis, P., E. Hourdakis, and A. G. Nassiopoulou, "Dielectric permittivity of porous Si for use as substrate material in Si-integrated RF devices," *IEEE Transactions on Electron Devices*, Vol. 60, No. 4, 1436–1443, Apr. 2013.
4. Sarafis, P., E. Hourdakis, and A. G. Nassiopoulou, "Advanced Si-based substrates for RF passive integration: Comparison between local porous Si layer technology and trap-rich high resistivity Si," *Solid-State Electronics*, to appear in 2013.

Reflectance Spectroscopy of $Ba_{3+x}Zn_{1+y}Nb_2O_9$ Perovskites

W. De La Cruz[1], **S. Moodie**[1], **J. Manson**[1],
D. A. Crandles[1], **D. Grebennikov**[2,3], **and P. Mascher**[2]

[1]Brock University, St. Catharines, ON, Canada
[2]McMaster University, Hamilton, ON, Canada
[3]Western University, London, ON, Canada

Abstract— Complex perovskites $Ba_{2.7}ZnNb_2O_9$, $Ba_{2.97}ZnNb_2O_9$, $Ba_{3.015}ZnNb_2O_9$, $BaZn_{0.93}Nb_2O_9$ and $BaZn_{1.005}Nb_2O_9$ which are all near stoichiometric composition ($Ba_3ZnNb_2O_9$) were studied via reflectance spectroscopy for photon energies between 0.006 eV and 1 eV. These materials are of interest as potential dielectric resonator materials which require large ϵ_1 (to enable device miniaturization), large $Q \approx \epsilon_1/\epsilon_2$ (for selectivity) and small temperature dependence of optical functions (for device stability). The dielectric functions were modeled by fitting the reflectance spectra to both Lorentz oscillator and factorized dielectric functions in order to get a sense of the uncertainty in extrapolating the measured far-infrared dielectric function to the microwave (MW) region (300 GHz). Both models suggest that for the stoichiometric composition $\epsilon_1 \approx 40$ while the extrapolated value of ϵ_2 has more uncertainty. The extrapolated value of $Q = 2000$ at room temperature at MW frequency for $Ba_3ZnNb_2O_9$ and Q is largest near stoichiometric composition. ϵ_1 is only weakly composition dependent, except for the sample furthest from stoichiometric composition ($Ba_{2.7}ZnNb_2O_9$). Comparison of the present data for $Ba_3ZnNb_2O_9$ with previous work reveals that the phonon scattering rates and low frequency ϵ_2 are much higher in the present samples yielding lower Q values, which were prepared at somewhat higher temperature than previous workers. It is possible that microstructure — which depends strongly on sample preparation temperature — is influencing ϵ_2 in the microwave region more strongly than deviation from ideal stoichiometry $Ba_3ZnNb_2O_9$.

Stability and Noise in Active Metamaterials

Khalid Z. Rajab, Yifeng Fan, Deepak Singh Nagarkoti, and Yang Hao
School of Electronic Engineering & Computer Science
Queen Mary University of London, United Kingdom

Abstract— Passive metamaterials suffer from inherent limitations, including losses and narrow bandwidths that can limit the performance of a number of interesting applications, including free-space invisibility cloaks and superlenses, among others. These limitations are imposed by causality, and lead to the high levels of dispersion of near-zero or negative properties (ε, μ or n for example). In order to circumvent these limitations, active metamaterials have been proposed that can reduce the levels of dispersion, and possibly add gain to the effective media. A significant drawback of active inclusions is the possibility for instability in the material; an issue that does not plague their passive counterparts. In this presentation, we will discuss aspects of stability in active metamaterials. Furthermore, we will provide the foundations for the analysis of noise; an important, and potentially limiting factor which has largely been ignored.

Our discussion will begin with the analysis of stability in active media. By developing equivalent circuit models of the structures, one may analyse the feedback relationships of both finite and infinite systems, including effects such as mutual coupling. These feedback relationships will allow us to investigate stability using the Nyquist criterion, and will allow us to develop simple stability bounds that can be verified through full-wave simulations. We will then present a matrix-approach to noise analysis which, again, will allow us to investigate the performance of both finite and infinite structures. We will examine the noise figures of active metamaterials with enhanced bandwidths, and compare their performance to their narrowbanded passive counterparts. This work is particularly important to future investigations into active or nonlinear metamaterials, at any frequency range.

Design of Advanced Microwave Filters Using the Metamaterial Approach

D. V. Kholodnyak[1], V. M. Turgaliev[1], J. Ni[2], S. Qian[2], A. S. Rusakov[1], I. B. Vendik[1], and J.-S. Hong[2]

[1]St. Petersburg Electrotechnical University "LETI", St. Petersburg, Russia
[2]Heriot-Watt University, Edinburgh, UK

Abstract— Metamaterial transmission lines (TLs) have been widely used to design microwave devices with an enhanced performance, e.g., with extended operational bandwidth, reduced size or those operating over multiple frequency bands. The metamaterial TLs are artificial structures consisting of a host TL (microstrip, coplanar waveguide etc.) loaded with reactive elements (inductances, capacitances) or resonators such as split-ring resonators (SRRs) and complementary split-ring resonators (CSRRs).

Most of practical designs of the metamaterial TLs use the composite right/left-handed (CRLH) TL approach as it allows taking into account the parasitic right-handed (RH) effects which are always present in practice. Besides, the CRLH TLs give some additional degrees of freedom to a design of broadband or multiple-band microwave devices. On the other hand, the parasitic RH effects can be often neglected or compensated. The use of the pure left-handed (LH) TL model simplifies the design procedure. Feasibility of the LH TL approach was confirmed by many practical designs reported in literature.

The paper presents the design of advanced microwave filters based on the both CRLH TL and LH TL approaches. Different bandpass filter examples including those designed for dual-band and ultra-wideband (UWB) applications are presented. The filters were fabricated as multilayer integrated circuits using the low temperature co-fired ceramics (LTCC) technology and the liquid crystal polymer (LCP) lamination technology which both suit well for the implementation of the metamaterial TLs.

The use of a transversal signal-interference structure in combination with the artificial RH and LH TLs made it possible to design a compact two-pole bandpass filter with an improved out-of-band rejection. A high performance was experimentally achieved for the LCP filter with the centre frequency of 2.06 GHz and the 3-dB passband of 24%. The measured in-band insertion loss is as low as 1.5 dB. The effective filter size (excluding the microstrip feed lines) is only 5.8 mm × 4.8 mm corresponding to 0.06×0.05 of the guided wavelength λ_g.

Due to its bandpass nature, a balanced CRLH TL is very suitable for UWB filter design. A UWB filter was designed based on the symmetrical CRLH TL unit cell. A capacitive cross-coupling providing a transmission zero above the passband was introduced between the input and output of the filter structure to increase the characteristic slope. The filter implemented on a multilayer LCP substrate has the entire size of 13 mm × 9.5 mm. Experimentally obtained frequency response of the filter is in a good agreement with the results of circuit and EM simulations.

Since the conventional immittance inverters operate properly in a very limited frequency band, they can be hardly used to design multi-band filters. Immittance inverters that are able to operate over all the frequency bands of interest are required instead. The so-called dual composite right/left-handed (D-CRLH) TL is very attractive to design immittance inverters for dual-band applications. We introduced the D-CRLH TL-based dual-band immittance inverter operating at two different frequencies which can be chosen almost arbitrary. Another advantage of such an immittance inverter is a transmission zero between the two operational frequencies that improves the out-of-band rejection.

The SRRs and CSRRs have been recently used to design dual-band filters in the substrate integrated waveguide (SIW) technology. A novel dual-mode SIW-based resonator consists of a miniaturized capacitively loaded cavity and a CSRR etched on the cavity top cover. The capacitively loaded cavity operates at the lower resonant frequency while the higher resonance of the dual-mode resonator is provided by the CSRR. A three-pole dual-bandpass filter for WLAN application at 2.3–2.5 GHz and 5.1–5.8 GHz was designed using the developed dual-mode resonators. According to the EM simulation results, the filter insertion loss in two passbands is as low as 1.1 dB and 1.3 dB. The filter implemented on a multilayer printed circuit board occupies the area of 30 mm × 10 mm.

Session 1P5
4_FocusSession.SC4: Advances in Millimeter-Wave and THz Circuit, Techniques and Applications

InP and GaN mm-wave Transistor Electronics at ETH-Zurich
Colombo R. Bolognesi, ... 276

Millimeter-wave Signal Generation by Nonlinear Optical Effect in Rectangular Waveguides
Hiroshi Murata, ... 277

Millimeter Wave Biomedical Applications for Microfluidic Platforms
Bart K. J. C. Nauwelaers, Ilja Ocket, ... 278

Photoimageable Substrate Integrated Waveguide (SIW) and Components for Advanced Millimetre-wave and Sub-mmW Systems (SoP)
Kamal K. Samanta, ... 279

Modular Antenna Array Concept for Millimeter-wave Beam-steering Applications
U. Johannsen, M. Imran Kazim, A. Bart Smolders, Matti H. A. J. Herben, ... 280

LTCC-based Millimeter-wave System-on-package
Langis Roy, ... 281

Substrate Integrated Waveguide (SIW) Technology for the Next Generation of Microwave and mm-Wave Systems
Maurizio Bozzi, ... 282

Integrated Terahertz Electronics for Imaging and Sensing Applications
Jan Stake, Huan Zhao, Vladimir Drakinskiy, Aleksandra Malko, Johanna Hanning, Robin Dahlback, Aik-Yean Tang, Peter J. Sobis, Tomas Bryllert, ... 283

Monocrystalline Silicon Microwave MEMS
Joachim Oberhammer, Umer Shah, Zargham Baghchehsaraei, Fritzi Topfer, Nikolai Chekurov, Mikael Sterner, Nutapong Somjit, ... 284

Novel Passive Devices for Sub-millimeter Wave Applications
Khaled Elgaid, ... 285

Low-cost Miniaturized 122 GHz SiP Radar Sensor
Yaoming Sun, ... 286

High-peak-power and Tunable Terahertz-wave Generation by Using Nonlinear Parametric Conversion
Shinichiro Hayashi, Kouji Nawata, Kodo Kawase, Hiroaki Minamide, ... 287

Terahertz Spectroscopic Imaging for Graphene Conductance Metrology
Jonas Due Buron, Dirch Hjort Petersen, Filippo Pizzocchero, Bjarke Sorensen Jessen, Tim Booth, Peter Boggild, Peter Uhd Jepsen, ... 289

Analysis and Design of Multi-mode Dielectric Waveguide Interconnect with Planar Excitation
Nemat Dolatsha, Amin Arbabian, ... 290

InP and GaN mm-wave Transistor Electronics at ETH-Zurich

C. R. Bolognesi
Millimeter-Wave Electronics Group (MWE), ETH-Zürich, Zürich 8092, Switzerland

Abstract— The MWE Group of the ETH-Zurich was established in 2006 and is active in several domains of mm-wave transistor research, spanning technologies such InP low-noise pHEMTs to GaN-based mm-wave transistors on Silicon and SiC substrates. The presentation will discuss InP/GaAsSb — based double heterostructure bipolar transistors (DHBTs) as well as GaN-based HEMTs in terms of small- and large-signal properties.

InP/GaAsSb DHBTs provide the best reported cutoff-frequency vs. breakdown voltage trade-off thanks to an advantageous type-II band alignment enabling the growth of grading-free base/collector heterojunctions merging the excellent high-field transport properties of InP with the low turn-on voltages associated with the GaAsSb base bandgap of $\sim 0.72\,\mathrm{eV}$. The devices have demonstrated current gain cutoff frequencies as high as 600 GHz at 300 K, as well as maximum oscillation frequencies exceeding 675 GHz. The prospects for all-electronic THz local oscillator sources will be considered.

AlInN/GaN and AlGaN/AlN/GaN high electron mobility transistors (HEMTs) are excellent candidates for the generation of significant power output at microwave and millimeter-wave frequencies. In the present work, we will among others characterize the performance of AlInN/GaN HEMTs grown on SiC substrates. The epitaxial layers consist, from the substrate up, of a 2 µm GaN buffer, a 1 nm AlN spacer, 3 nm $Al_{0.83}In_{0.17}N$, and a 2 nm GaN cap. Hall measurements revealed a mobility of $1470\,\mathrm{cm}^2/\mathrm{V}\cdot\mathrm{s}$. A post-process sheet resistance of $260\,\Omega/\square$ was measured on Van der Pauw test structures. Transistors with gate lengths of $L_G = 200\,\mathrm{nm}$ in source to drain gaps of 1, 2, and 4 m were defined by electron beam lithography and lift-off.

Load-pull measurements were performed at 40 GHz in class A/B at a bias corresponding to about 15% $I_{\mathrm{DS,MAX}}$, and the load was optimized for the best P_{OUT}. Fig. 1 below shows a power sweep performed on a 200 nm gate device with a distance of 0.75 µm to the source, for a source-drain distance of 4 µm, biased at VGS = −2.6 V and VDS = 35 V. At 2 dB compression, a maximum power density of 5.85 W/mm was achieved with a peak power-added-efficiency of 15%. Other devices displayed higher PAE, up to 30%, but with lower $P_{\mathrm{OUT,MAX}}$. To our knowledge, this is the highest power density ever achieved in AlInN HEMTs at 40 GHz.

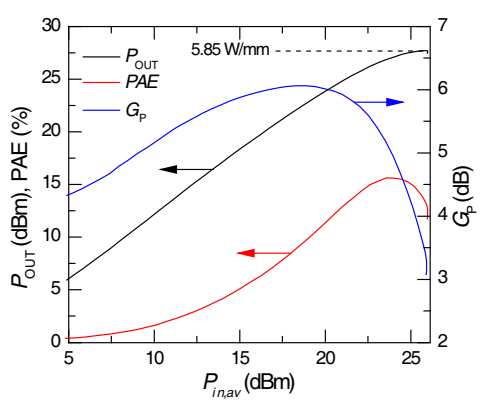

Millimeter-wave Signal Generation by Nonlinear Optical Effect in Rectangular Waveguides

Hiroshi Murata
Graduate School of Engineering Science, Osaka University, Japan

Abstract— Recently, electromagnetic-waves in millimeter-wave (MMW) and THz frequency bands have been attracting attention for many application fields: over 10 Gb/s wireless communications, high-resolution imaging, sensing, radar, and astronomical physics. Difference frequency generation (DFG) based on the second order nonlinear optical effect is a potential candidate for the MMW/THz-wave signal generation. By using DFG, it is possible to generate a MMW/THz signal at a desired frequency by simply tuning the frequency difference between the two coherent lightwaves. In addition, the generated signal power increases as frequency increases owing to the Manley-Rowe relationship. Therefore, the DFG-based signal generation is rather attractive at higher-frequency ranges up to THz. Advanced photonic technologies developed for optical fiber communication systems (optical amplifiers, high-speed vector modulators, frequency shifters, comb generators, and sharp-cut filters) are also applicable to control/improve DFG responses.

We have proposed new MMW/THz-wave signal generation devices by use of a rectangular waveguide embedded with a nonlinear optical crystal. Utilizing DFG of two coherent lightwaves, MMW signals can be injected into MMW circuits with negligible distortion of circuit characteristics since a light wavelength is below 1% of MMW/THz-wave wavelengths. Adopting this technique to a MMW rectangular waveguide resonator, adiabatic coupling of a DFG MMW signal into a resonator mode can be obtained. For the phase matching between lightwaves and MMW waveguide mode, quasi-phase-matching (QPM) technique by polarization reversal structures is applicable. In the experiment, 15 GHz-/30 GHz-/60 GHz-band microwave/MMW signals were obtained successfully from fabricated devices using a straight single-mode rectangular waveguide embedded with z-cut LiTaO3 crystal. The measured frequency responses were in good agreement with the theoretical frequency responses. New functional devices for modulation of a MMW/THz-wave and for optical signal temporal/spatial correlation are also obtainable by use of DFG in MMW circuits.

In presentation, the operation principles, analysis, fabrication, and experimental results of the several DFG devices will be discussed in detail.

Millimeter Wave Biomedical Applications for Microfluidic Platforms

Bart K. J. C. Nauwelaers and Ilja Ocket
ESAT-TELEMIC, KU Leuven, Kasteelpark Arenberg 10, Leuven, Heverlee 3001, Belgium

Abstract— In recent years, the use of millimeter waves and microwaves in biomedical microfluidic platforms has seen increased interest. Especially sensing approaches for measuring concentrations in minute volumes of liquid have been reported by a number of authors. These methods essentially rely on the available contrast in dielectric response between different compounds or between living cells and their buffer solution. These sensors assume a uniform solution and use simple mixing formulas. Also at the KU Leuven, these types of structures are under investigation and will be briefly discussed as an introduction to this talk.

However, when cell solutions are investigated with a very low concentration of cells, the solution can no longer be considered as uniform, especially when the cell is close to e.g., the CPW structure used for sensing. In these cases the effect of non-uniformity will have to be taken into account and the sensor will respond differently when the same cell is in a different position. To account for this, we can either find ways to correct for the position of the cell or we can find sensor topologies where the position of the cell does not impact the sensor response that much. The second approach is followed at the KU Leuven and some ideas will be discussed in this talk.

The aforementioned sensors are mostly targeted at automated high throughput screening where the cells pass by in a microfluidic channel. Another application that can be envisaged is the extension of cell membrane impedance spectroscopy towards higher frequencies with the aim of developing models for the cell *interior* as opposed to only monitoring the cell membrane. This kind of application is challenging for many reasons, most notably because of the small sizes involved, the uncertain inherent dielectric contrast available within a cell, and the dynamic nature of cells.

The topic of electromagnetic modeling of living cells is in its very early stages at our lab, but we will present our perspective on what we feel is possible and which issues need to be tackled to achieve useful data for biologists, pharmacologists, toxicologists, etc..

Photoimageable Substrate Integrated Waveguide (SIW) and Components for Advanced Millimetre-wave and Sub-mmW Systems (SoP)

Kamal K. Samanta[1, 2]

[1]Institute of Microwaves and Photonics, University of Leeds, Leeds, LS2 9JT, UK
[2]Milmega/Teseq Ltd, Ryde, Hampshire, PO33 2DD, UK

Abstract— Due to the unique advantages of short wavelength, there is ever-growing extensive applications of millimetre wave (mmW) and sub-millimetre wave (Sub-mmW) bands, ranging from high speed wireless and space/satellite communication to radar and imaging. These advanced applications require development of high performance and compact components and systems with ever growing product functionality at a reasonable cost. The Multichip module (MCM) or System-on/in-package (SoP/SiP) technologies with high quality off-chip passive components and interconnects have been widely respected as an excellent stand for addressing these requirements.

For millimeter-wave and sub-mmW modules, due to an increase of loss in planar microstrip (MS) and coplanar waveguide (CPW) lines, there has been huge interest in low loss alternatives. These include MEMS waveguides, NRD waveguide and Substrate Integrated Waveguide (SIW). Out of these, the SIW comes out as an extremely capable due to the simple fabrication process and ease of integration with MMICs and other components. The SIW is being realized using LTCC, MMIC, standard MIC/PCB, laminate, post wall, and multilayer photoimageable thick-film (P-TF). Unfortunately, most of these circuit technologies (except thin and high loss MMIC and P-TF) employ rows of via holes (fence-post), which starts to become too close together for high frequency operation. At the same time, using conventional thick-film, it is very difficult to achieve fine conductor geometry, requires for compact passive/lumped components at a high frequency. To address the lack of dimensional precision as well as via resolution, recently developed advanced multilayer photoimageable thick-film technology is found to be very promising, straightforward and ease to fabricate, and meets the high frequency requirements at a low cost [1]. The technology is highly suitable to produce multilayer SIWs with photoimaged filled trench via, giving operation beyond 180 GHz, and also a wide range of precisely defined lumped elements, passive components and modules are realized with remarkably high performance and miniaturization [1, 2].

This paper describes the realization of compact and high performance millimeter-wave and sub-millimeter wave SIW lines and passive components, including antenna and filters using novel multialyer/3D photoimageable thick film technology for advanced MCM/SoP applications. The multilayer SIW, supported on a multilayer MCM substrate are studied in terms of S-parameters and impedance for different modes and with various cavity dimensions to optimize performance as well as miniaturization. The multilayer photoimageable SIW components demonstrates high performance, superior to the reported results from most of the MCM technologies, and is expected to bring a novel solution to the realization of challenging SIW based cost-effective millimeter-wave and sub-mmW systems.

REFERENCES

1. Samanta, K. K., D. Stephens, and I. D. Robertson, "Design and performance of a 60 GHz multi-chip-module receiver employing substrate integrated waveguides," *IEE Proc. of MAP*, Vol. 1, 961–967, Oct. 2007.
2. Samanta, K. K. and I. D. Robertson, "Advanced multilayer thick-film system-on-package technology for miniaturized and high performance CPW microwave passive components," *IEEE Trans. on CPMT*, Vol. 1, No. 11, 1695–1705, Nov. 2011.

Modular Antenna Array Concept for Millimeter-wave Beam-steering Applications

U. Johannsen, **M. I. Kazim**, **A. B. Smolders**, **and M. H. A. J. Herben**
Eindhoven University of Technology, the Netherlands

Abstract— Steerable antenna arrays are of particular importance for consumer electronics applications in the millimeter-wave band. However, the exact array size depends on the specific application scenario. Therefore, a modular array concept is proposed in this paper that meets the cost requirements of the consumer electronics market. Moreover, since circular polarization is desired due to the line-of-sight nature of the communication channel at those frequencies, special attention is placed on the construction of circularly-polarized antenna arrays. Finally, a deflector design is proposed that allows to extend the scan-range of the proposed modular antenna array.

LTCC-based Millimeter-wave System-on-package

Langis Roy
Department of Electronics, Carleton University, Ottawa, Canada

Abstract— Recent advances in LTTC System on Package (SoP) design show that miniaturization, component count reduction and cost effectiveness can be compatible with increased functionality, agility and efficiency of mm-wave wireless components. This presentation will consist of three parts.

First, a brief overview will be provided of the 3D co-design of active chips and passives in the realization of highly functional wireless front-ends. It will be shown that good System on Chip (SoC) design can lead to good SoP design.

Next, the use of 3D geometries in LTCC will be presented as an effective technique for achieving enhanced integrated antenna performance in a 60 GHz balanced antipodal Vivaldi antenna design.

Finally, the recent introduction of ferrite tapes into the LTCC ceramic material system will be discussed, highlighting several new tunable microwave and millimeter-wave components (antennas, phase shifters, circulators) that have been realized this way.

Substrate Integrated Waveguide (SIW) Technology for the Next Generation of Microwave and mm-Wave Systems

Maurizio Bozzi
Department of Electrical, Computer and Biomedical Engineering
University of Pavia, Pavia 27100, Italy

Abstract— Substrate integrated waveguide (SIW) technology represents an emerging approach for the implementation of compact, low-loss and cost effective components, circuits, antennas and complete systems at microwave and millimeter-wave frequency. The interest in SIW technology is booming in the last few years, as shown by the exponentially increasing number of scientific publications, special sessions and workshops at international conferences, and by the number of industries interested in SIW applications. It appears that SIW technology is bound to become the paradigm for the implementation of cost-effective millimeter-wave systems in the next decade.

SIW structures permit to realize traditional rectangular waveguides in planar form: they are implemented in dielectric substrates by using two rows of metalized holes that connect the two ground planes of the substrate. SIW structures can be implemented by adopting standard PCB fabrication process, as well as advanced LTCC technology. Different fabrication technologies and materials, including silicon, have been recently proposed. SIW technology combines the advantages of classical microstrip circuits (low cost, easy fabrication, compact size, low weight) and metallic waveguides (low losses, complete shielding, high power handling capability). The major advantage of SIW technology is the possibility to integrate entire wireless systems, according to the system-on-substrate (SoS) approach: this approach allows integrating passive structures, active components, and antennas in a single substrate, thus avoiding transitions and reducing losses and parasitic effects.

This paper present state-of-the-art results of SIW components and antennas, advanced modeling techniques, current research trends of SIW systems at microwaves and mm-waves, and the use of novel materials and fabrication technologies (including paper, plastic and textile).

Integrated Terahertz Electronics for Imaging and Sensing Applications

Jan Stake[1,2,4], **Huan Zhao**[1,2], **Vladimir Drakinskiy**[1,2], **Aleksandra Malko**[2], **Johanna Hanning**[1,2], **Robin Dahlbäck**[2], **Aik-Yean Tang**[1,2], **Peter Sobis**[1,2,3], **and Tomas Bryllert**[1,2,4]

[1]GigaHertz Centre, Sweden
[2]Terahertz and Millimetre Wave Laboratory
Department of Microtechnology and Nanoscience
Chalmers University of Technology, SE-41296 Göteborg, Sweden
[3]Omnisys Instruments AB, SE-4313, V. Frölunda, Sweden
[4]Wasa Millimeter Wave AB, Göteborg, Sweden

Abstract— Compact heterodyne receivers operating in the sub-millimeter wave band above 300 GHz are needed for earth observation instruments, space science missions and ground-based applications such as security scanners. Existing terahertz heterodyne receivers are usually bulky due to complex hybrid integration and there is a strong need for an terahertz monolithic integration circuit (TMIC) technology that allows for higher circuit functionality, ease of assembly, and low loss at terahertz frequencies. This talk provides an overview of research on terahertz integrated diodes and circuits carried out in the GHz centre at Chalmers. For instance, we will present progress on integration techniques for HBV multipliers and Schottky diode mixers. Moreover, we will present results from full S-parameter characterization of on-chip components at terahertz frequencies. Finally, the use of terahertz waves in biology, environmental monitoring and security will be presented.

Monocrystalline Silicon Microwave MEMS

Joachim Oberhammer, Umer Shah, Zargham Baghchehsaraei, Fritzi Töpfer, Nikolai Chekurov, Mikael Sterner, and Nutapong Somjit
School of Electrical Engineering, KTH Royal Institute of Technology, Stockholm, Sweden

Abstract— This paper gives an over view of recent achievements in microwave micro-electromechanical systems (microwave MEMS) at KTH Royal Institute of Technology, Stockholm, Sweden.

The first topic is MEMS-tuneable microwave high-impedance metamaterial surfaces which were conceptualized for local tuning of the electromagnetic resonance frequency of a surface wave on a high-impedance surface. The fabrication and characterization of such surfaces in the W-band is presented. Applications for which prototype devices were implemented include beam-steering for car radar, leaky-wave antennas, waveguide-integrated tuneable backs hort phase-shifters. RF characterization and realiability data is presented.

The second topic is a micromachined phase shifter which in the 75–110 GHz band. The phase shifter is based on a micromachined dielectric block which is vertically moved by integrated MEMS actuators to achieve a tuning of the propagation constant of a micromachined transmission line. A 4.25-bit 75–110 GHz phase shifter was implemented with a best phase-shift per dB loss (98.3°/dB at 110 GHz), best insertion loss per bit (0.82 dB/bit at 110 GHz), and best return loss (better than 12 dB for the whole W-band) ever reported in literature. Reliability data of 1 billion cycles, power handling of > 40 dBm, and high linearity of IIP3 > 48 dB mare presented.

The third topic covers 3-dimensional micromachined coplanar transmission lines with integrated MEMS actuators which move the sidewalls of these transmission lines. With this concept, multistables witches, tuneable capacitors, tuneable couplers, and tuneable filters have been implemented and characterized for 1–40 GHz frequencies. The tuneable capacitors achieve a tuning in upto 7 discrete steps from 44 to 106 fF, a Q of upto 90 at 40 GHz (highest Q for a tuneable capacitor in that frequency band), high self-actuation robustness (> 42 dBm), high linearity (> 65 dBm), and high reliability (> 1 billion cycles without degradation of pull-in/pull-out voltage).

Finally, silicon-micromachined near-field and far-field sensor and antenna interfaces are presented, including a micromachined planar lens antenna and a tapered dielectric rod measurement probe for medical applications (skin cancer diagnosis).

Novel Passive Devices for Sub-millimeter Wave Applications

Khaled Elgaid
Engineering Electronics & Nano Engineering
University of Glasgow, Glasgow G12 8LT, United Kingdom

Abstract— Passives of reconfigurable millimeter wave applications using elevated structures and MEMS have become more attractive as the demand for multiband high Q components such as integrated antennas has increased. Reconfigurable passives provide greater levels of functionality to a system by eliminating the need for complicated wideband solutions. Reconfiguring antennas can enhance their performance by providing the ability to adapt to new operating scenarios. MEMS switches have been introduced as a prime candidate to replace the conventional solid state switches and in reconfigurable antennas utilisations. This work covers the rapid development of vertical integration and MEMS switch technology and their limitations and advantages at millimetre-wave regimes and focuses on cantilever beam metal-contact MEMS switches. We propose a new design of a low-actuation voltage cantilever beam MEMS switches for high-frequency applications, which can overcome the limitations associated with cantilever MEMS switches. The antenna design demonstrates the feasibility of reconfigurable printed antennas on high dielectric substrates at G-band. Several examples of high performance millimeterwave passive structures and including a new concept for feeding a proximity-coupled elevated patch antenna will be introduced. The antennas are fabricated on SI-GaAs substrate based on surface micromachining technology without need of etching the substrate.The results show that the bandwidth is 15 GHz, determined from 10 dB return loss and the gain is about 7.18 dB at G-band frequencies (140–220 GHz) with nearly constant broadside radiation pattern over its bandwidth. The authors believe this to be the best reported performance of a micro-machined antenna operating in the G-band frequency range to date. Other examples of such applications will be presented.

Low-cost Miniaturized 122 GHz SiP Radar Sensor

Yaoming Sun
IHP, Im Technologiepark 25, 15236 Frankfurt (Oder), Germany

Abstract— A complete 122 GHz radar chipset is presented including its major mmW building blocks. The radar features a sub-harmonic transmitter and receiver frontend. A design-for-test (DFT) has been used in the transmitter to detect the absolute output power as well as the antenna matching. Digital designs are introduced to perform the on-chip linear frequency modulation. Furthermore, all the analog building blocks can be controlled by a Serial-to-Peripheral Interface (SPI) reducing the number of bond pads and increasing programmability. This chipset is tested in a surface mountable package including antenna. The packaged radar has 0 dBm output power in the TX path and up to 36 dB gain in the receiver path. Its total power dissipation is 350 mW. The VCO phase noise is around −96 dBc/Hz at 1 MHz offset.

Introduction: State-of-the-art BiCMOS and CMOS technologies nowadays provide sufficient performance for mm-wave applications at more than 100 GHz and offer low cost. ISM bands are preferable for low-cost commercial applications, too, because they are license-free and product certification is comparably simple. The ISM band at 122 GHz (1 GHz bandwidth) is suitable for the implementation of low-cost radar sensors.

At higher frequencies on- and off-chip antennas require less area which is very attractive for ultra-compact radar systems. A further important aspect of low-cost radar systems is high-volume chip testing. At frequencies beyond 100 GHz this would be extremely expensive — if not impossible at all. Hence on-chip mm-wave test will be mandatory if volume applications are targeted.

This talk covers the topics from the design of the critical building blocks to the final packaged radar testing. Low-cost and low-power are the major design targets. SiP package concept and antenna design will also be briefly discussed.

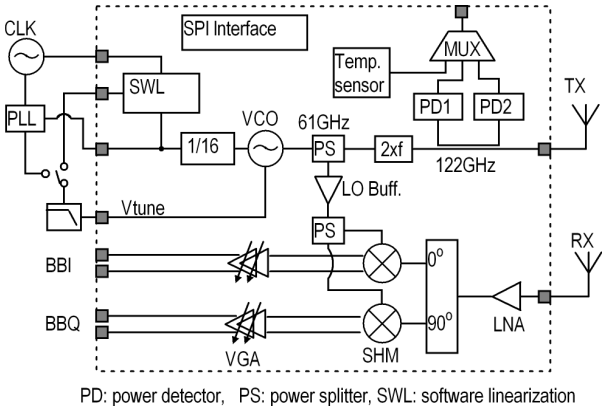

Figure 1: Radar system architecture.

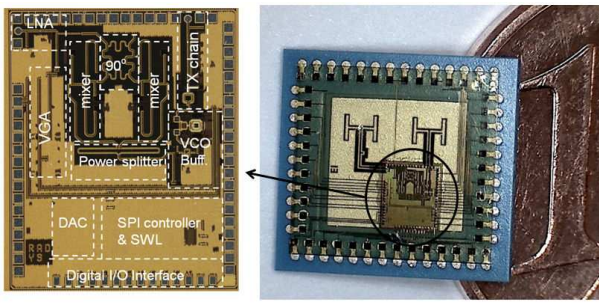

Figure 2: Chipset and package photo.

Figure 1 shows the radar system block. A push-push 60 GHz Colpitts VCO is used to drive the transmitter and receiver front-end. The 30 GHz VCO fundamental is coupled to the divider input, resulting in a robust dividing operation. The receiver chain includes an LNA, a 90-degree coupler, two passive sub-harmonic mixers (SHM) and two VGAs forming a quadrature receiver. The software linearization (SWL) block is a mixed signal design. It can measure the VCO frequency tuning curve and perform the FMCW linear frequency ramps. In transmit path, an edge coupler and two power detectors are used as DFT. It can detect both the forward and reflected power to/from the antenna. Based on the detector outputs, the antenna matching can be calculated. When the digital functionality is disabled, the chipset works as an analog radar. Its frequency can be stabilized by an external PLL.

The chipset has been packaged into a surface mountable package, where antennas are also realized as shown in Fig. 2. The final package has a dimension of only $8 \times 8\,\mathrm{mm}^2$. All the high frequency interfaces are contained in the package. Therefore, FR4 board can be used to demonstrate the radar functionality. When working as Doppler radar, the radar can detect hand movement as well as a single piece of paper.

High-peak-power and Tunable Terahertz-wave Generation by Using Nonlinear Parametric Conversion

Shin'ichiro Hayashi[1], **Kouji Nawata**[1], **Kodo Kawase**[1,2], **and Hiroaki Minamide**[1]

[1]RIKEN, Japan
[2]Nagoya University, Japan

Abstract— We developed a high peak power, narrowband and tunable injection-seeded terahertz-wave parametric generator using frequency conversion in a nonlinear MgO:$LiNbO_3$ crystal, which operates at room temperature. The powerful emission, peak power of > 1 kW, linewidth of < 5 GHz, and tuning range of 1–2.8 THz, was obtained and the output was measured by a calibrated pyroelectric detector.

Introduction: Recently, the technologies available in the terahertz frequency range have made great progress with the development of new methods for generating and detecting the terahertz radiation. Improved sources and detectors allow terahertz radiation to be applied in solving real-world problems. In particular, high power output of terahertz waves has attracted much interest into terahertz applications such as terahertz nonlinear spectroscopy, large-area terahertz wave imaging, and sensitive analysis using terahertz waves.

In our laboratory, we have been studying terahertz-wave parametric sources using noncollinear phase matching in MgO:$LiNbO_3$ as widely tunable terahertz-wave sources based on stimulated polariton scattering [1]. The terahertz-wave parametric generator/oscillator (TPG/TPO) allow building systems that are not only compact, but also operate at room temperature, making them suitable as practical sources. In principle, both a narrow linewidth and a wide tunability are possible in injection-seeded TPG/TPO (is-TPG/is-TPO) systems with single-longitudinal-mode near-infrared pumping and seeding beams [2].

In this paper, we developed a high-peak-power, single-longitudinal-mode, widely-tunable is-TPG. The output over 1 kW peak-power measured with a calibrated detector is reported.

Experimental Setup and Results: The is-TPG consists of a pumping source, amplifiers, a seeding source and the nonlinear crystal. The pumping source is a microchip Nd^{3+}:YAG laser [3]. The pumping beam is amplified in two amplifiers in double pass configurations. The seeding beam from external cavity diode laser is also amplified by an Yb-doped fiber amplifier. We used a 50-mm-long nonlinear MgO:$LiNbO_3$ crystal. A Si-prism placed on the surface of the crystal acts as an efficient output coupler. The terahertz-wave output was measured using a calibrated pyroelectric detector (Spectrum Detector Inc.: SPI-A-65 THz).

Figure 1 shows power spectrum of our is-TPG. When the pumping energy was about 14 mJ/pulse and seeding power of 500 mW (CW), it was possible to tune the wavelength of terahertz wave from 1.0–2.8 THz. The observed maximum peak power of terahertz-wave was more than 1 kW, then, by blocking seeding beam, the output power decreased less than 1 W. The tuning curve has a broad bandwidth, with a flat region around 1.4–2.2 THz. The tuning range is limited by

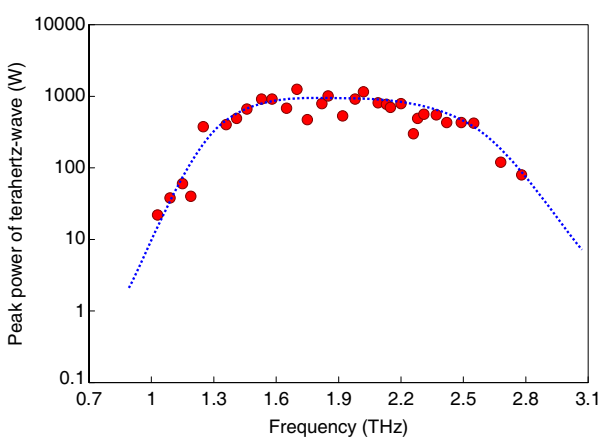

Figure 1: Power spectrum of the is-TPG.

the TPG gain and absorption by $LiNbO_3$. In low or high frequency region, less than 1.4 THz or above 2.6 THz, the output terahertz-wave decreased, because of low gain or high absorption coefficient in each region. We expect this source offer advantages for many applications.

ACKNOWLEDGMENT

The authors would like to thank Prof. T. Taira of IMS and Prof. H. ITO of RIKEN for useful discussions.

REFERENCES

1. Piestrup, M. A., R. N. Fleming, and R. H. Pantell, "Continuously tunable submillimeter wave source," *APL*, Vol. 26, 418–421, 1975.
2. Kawase, K., J. Shikata, and H. Ito, "Terahertz wave parametric source," *J. Phys. D: Appl. Phys.*, Vol. 34, R1–R14, 2001.
3. Sakai, H., H. Kan, and T. Taira, "> 1 MW peak power single-mode high-brightness passively Q-switched Nd^{3+}:YAG microchip laser," *Opt. Express*, Vol. 16, 19891–19899, 2008.

Terahertz Spectroscopic Imaging for Graphene Conductance Metrology

Jonas Due Buron[1], **Dirch Hjort Petersen**[2], **Filippo Pizzocchero**[2], **Bjarke Sørensen Jessen**[2], **Tim Booth**[2], **Peter Bøggild**[2], **and Peter Uhd Jepsen**[1]

[1]Department of Photonics Engineering, Technical University of Denmark, Denmark
[2]Department of Micro- and Nanotechnology, Technical University of Denmark, Denmark

Abstract— Photonics-based generation and detection of electromagnetic radiation at terahertz (THz) frequencies has advanced significantly in the past decades. In particular, time-domain methods based on femtosecond laser technology has enabled generation and detection of broadband THz transients at the fundamental single-cycle limit. Such transients are highly versatile in spectroscopic sensing applications relying on some of the unique contrast mechanisms found in the THz range, as will be discussed with relevant cases of THz imaging and spectroscopy.

The characterization of the electrical conductivity of thin films is immensely important in a range of modern technologies, including transparent top electrodes in solar cells and touch screens. The conductivity of such surfaces is characterized by contact methods such as four-point probing which is inherently slow due to the delicate mechanical contact required. Here we will discuss a novel characterization method of the conductivity of thin films based on contactless THz spectroscopic imaging. In particular, the potential for wafer-scale mapping of the conductivity of single-layer graphene [1] will be discussed.

Applying spectroscopy with the highest possible bandwidth and the highest possible time resolution has recently enabled new insight into the THz-frequency physics of a range of solid-state materials. We will discuss ultrafast conductivity dynamics in polymer solar cells [2] and vibrational dynamics in soft glasses [3].

REFERENCES

1. Buron, J. D., D. H. Petersen, P. Bøggild, D. G. Cooke, M. Hilke, J. Sun, E. Whiteway, P. F. Nielsen, O. Hansen, A. Yurgens, and P. U. Jepsen, "Graphene conductance uniformity mapping," *Nano Lett.*, Vol. 12, 5074–5081, 2012.
2. Cooke, D. G., F. C. Krebs, and P. U. Jepsen, "Direct observation of sub-100 fs mobile charge generation in a polymer-fullerene film," *Phys. Rev. Lett.*, Vol. 108, 056603, 2012.
3. Zalkovskij, M., C. Z. Bisgaard, A. Novitsky, R. Malureanu, D. Savastru, A. Popescu, P. U. Jepsen, and A. V. Lavrinenko, "Ultrabroadband terahertz spectroscopy of chalcogenide glasses," *Appl. Phys. Lett.*, Vol. 100, 031901, 2012.

Analysis and Design of Multi-mode Dielectric Waveguide Interconnect with Planar Excitation

Nemat Dolatsha[1,2] and Amin Arbabian[3]

[1]EE Department, ETHZ University, Zurich, Switzerland
[2]EE Department, Stanford University, Stanford, CA, USA
[3]Center of Integrated Systems (CIS), EE Department, Stanford University, Stanford, CA, USA

Abstract— There is a large demand to substantially increase overall system bandwidth as well as connectivity at all levels- from individual ICs to backplanes. As aggregate link data rate requirements are approaching Tbps levels, current physical channels are nearing their limits. To this end, a power and data-rate "wall" is emerging on the horizon. This is in terms of maximum "data flux density" (bandwidth per unit width) and link efficiency (in terms of energy per bit) when the bandwidth of conventional planar onboard transmission lines is pushed to tens of GHz. In improving data bandwidth, main culprits are the high-loss, dispersion, cross-talk and reflections in the conventional planar TEM electrical channel. Optical fiber links have been extensively used in longhaul communication and are now also slowly making their way into the short-range arena. However, the associated power and cost overhead (due to precision packaging and the addition of electro-optical modules) pose limitations on adaptability for ubiquitous board-level interconnects.

In this paper, we propose a structure that addresses these concerns. An all-electrical, low-cost and easy to package wideband chip-to-chip serial link on a multi-mode dielectric waveguide is proposed. Dielectric waveguides made of simple dielectric strips are known for very low transmission loss at mm-wave and sub-THz frequencies. Here, the signal is coupled from the silicon chip, simultaneously, to the fundamental and polarization-orthogonal E_x^{11} and E_y^{11} waveguide modes using planar electric and slot dipole antennas, respectively. Excitation with planar feed antennas simplifies the assembly and enables the use of conventional packaging with CMOS transceivers. Fig. 1 shows a conceptual schematic of the proposed structure. This multi-mode excitation approach doubles the capacity of a single line without sacrificing robustness or adding implementation cost and complexity. As a result, two independent (isolation of better than 55 dB between excitation sections) ultra-wideband 30 GHz channels, each from 90 GHz to 120 GHz, are demonstrated. The large available bandwidth will be channelized in frequency for optimal overall efficiency and throughput with a mmwave CMOS transceiver. Various design aspects of the structure (excitation sections and the waveguide design) are examined and discussed. In addition, the general trend for bandwidth-per-pitch (for a single mode) and maximum length of the link in terms of operating frequency are approximated and shown in Fig. 1(b). When combined with appropriate frequency channelization and interleaving, these links can achieve aggregate data rates approaching several Tbps over distances as long as one meter.

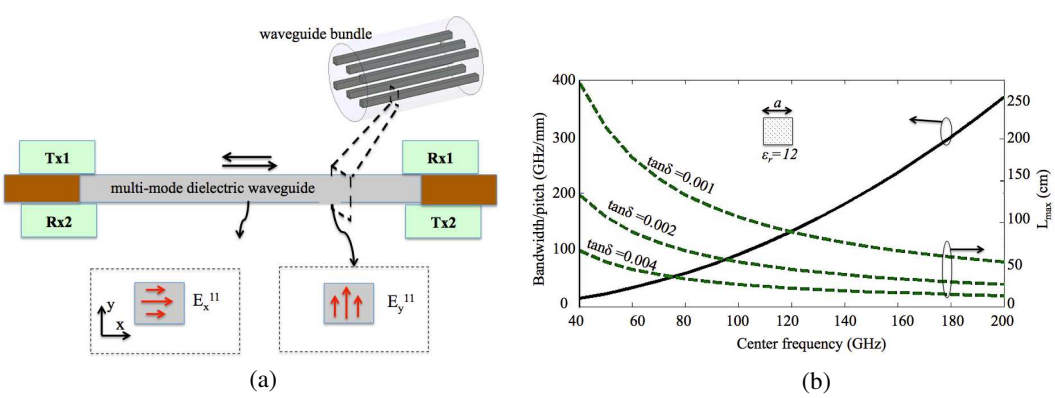

Figure 1: (a) Conceptual schematic of the proposed multi-mode dielectric waveguide for chip-to-chip interconnects or active cables. (b) The general trend for bandwidth-per-pitch (for a dual mode excitation) and maximum length of the link in terms of operating frequency.

Session 1P6
SC4: Multiband and Wideband Antenna and Array Techniques

A Review of Broadband Array Antenna Technologies
Anthony Keith Brown, Yongwei Zhang, ... 292

Design Considerations for a Low-frequency Vivaldi Array Element
Alberto Tibaldi, Giuseppe Virone, Federico Perini, Jader Monari, Muhammad Zunnoorain Farooqui, Mauro Lumia, Oscar Antonio Peverini, Giuseppe Addamo, Riccardo Tascone, Renato Orta, ... 293

Optimization and Performance Tradeoffs of Phased Array Antenna Configurations for Radio Astronomy
Nima Razavi-Ghods, T. Clavier, F. Glineur, David Gonzalez-Ovejero, Eloy de Lera Acedo, Christophe Craeye, ... 295

Ultra-Wideband Tightly Coupled Phased Array Antenna for Low-Frequency Radio Telescope
Eman O. Farhat, Kristian Z. Adami, Yongwei Zhang, Anthony Keith Brown, Charles V. Sammut, . 296

EM Simulations, Beam Modeling and Calibration of Ultra-wideband Array Antennas for Radio Astronomy
Eloy De Lera Acedo, David Gonzalez-Ovejero, C. Raucy, J. Harris, Nima Razavi-Ghods, Christophe Craeye, ... 297

A Wideband Circularly-polarized Antenna — Self-grounded Monopole Array with Low Axial Ratio over Large Coverage
Jian Yang, ... 298

Recent Developments of Multiband and Wideband Reflectarrays
José Antonio Encinar Garcinuño, Manuel Arrebola, Carolina Tienda, Mariano Barba, Eduardo Carrasco, ... 299

Quasi Conformal Transformation Optics for the Design of Ultra Wide Band Lenses
Oscar Quevedo-Teruel, R. C. Mitchell-Thomas, Y. Hao, ... 300

A Compact Triple-band Filtering Microstrip Patch Antenna with the Same Polarization Planes
Yun-Jui Lee, Shyh-Jong Chung, ... 301

A Study of Partial Resonance Control for Edge Elements in a Finite Array
Christos I. Kolitsidas, B. Lars G. Jonsson, ... 302

Broadband, High Gain, See-through Antenna for WiFi, WiMax and LTE 2600 Radio Networks
Pierre-Antoine Garcia, Tchanguiz Razban-Haghighi, Anne Chousseaud, E. Motta Cruz, ... 303

A Fractal Microstrip Array Antenna with Slots Feeding Network for DTV Reception
Jianhua Zhou, Bingyang Liang, Baiqiang You, Qing Liu, Xingjing Yan, ... 304

Recent Developments in Analysis and Design of a Low Noise Connected Array Feed for the Australian SKA Pathfinder
Stuart G. Hay, ... 305

A Review of Broadband Array Antenna Technologies

A. K. Brown and Yongwei Zhang
School of Electrical and Electronic Engineering, University of Manchester, UK

Abstract— This paper presents a overview of broadband phased array technologies being used by, or under consideration for, radio astronomy. The emphasis is on phased arrays up to a few GHz frequency and covering several octaves of bandwidth, although the principles are equally applicable to other frequency ranges.

In designing these arrays it is important to consider the whole structure as a complete radiating system — the elements themselves, how they are disposed (that is the array geometry) and how each element interacts with its neighbours (the mutual coupling effect) over the range of frequencies and scan angles required.

Following a brief review of the fundamentals of broadband antennas, and in particular arrays, this paper will present some candidate element types for different performance requirements. Next, the overall array geometry, in particular different types of sparse or thinned arrays, is considered and design trade offs presented. Finally the mutual coupling phenomena and its computation is introduced.

For maximal pattern control a fully filled array is normally assumed. It is shown how in certain types of arrays the mutual coupling can be used to good advantage to produce wide band structures. Using a particular example of such a structure, the Octagonal Rings Array (ORA), the impact of introducing a level of array thinning to an otherwise fully filled highly coupled array will be presented.

Design Considerations for a Low-frequency Vivaldi Array Element

A. Tibaldi[1], **G. Virone**[2], **F. Perini**[3], **J. Monari**[3], **M. Z. Farooqui**[1], **M. Lumia**[2], **O. A. Peverini**[2], **G. Addamo**[2], **R. Tascone**[2], **and R. Orta**[1]

[1]Dipartimento di Elettronica e Telecomunicazioni (DET), Politecnico di Torino
Corso Duca degli Abruzzi 24, Torino 10129, Italy
[2]Istituto di Elettronica e di Ingegneria dell'Informazione e delle Telecomunicazioni (IEIIT), Consiglio National Research Council of Italy (CNR) c/o Politecnico di Torino
Corso Duca degli Abruzzi 24, Turin 10129, Italy
[3]Istituto di Radioastronomia (IRA), Istituto Nazionale di Astrofisica (INAF)
Via Fiorentina 3513, Medicina (BO) 40059, Italy

Abstract— The Square Kilometer Array (SKA) represents one of the most interesting instruments of the new-generation radio astronomy [1]. One of the SKA main subsystems is the low-frequency Aperture Array (AA-low), which has to operate in the [70, 450] MHz band. In the recent years, a dual-polarization Vivaldi array element has been proposed as a potential candidate for AA-low [2]. The main advantages of this configuration are a good single ended $50\,\Omega$ matching with low cross-polarization in the principal planes owing to the symmetry of the antenna. Furthermore, the antenna is self-standing, does not require bulky dielectric parts and can be manufactured in a gridded version [3].

A cavity-backed Vivaldi antenna has been adopted in order to reduce the ground noise contribution and to obtain a more symmetrical radiation pattern, compared to [2]. The new geometry is sketched in Figure 1. This work deals with a design strategy to maximize the sensitivity, i.e., $A_{eff}(\hat{r}) = T_{sys}$ for such an array element in the overall operative bandwidth, where $A_{eff}(\hat{r})$ is the effective area in a given observation direction $\hat{r}$ and T_{sys} is the system noise temperature. It should be noted that $T_{sys} = T_{ant} + T_{rec}$; T_{ant} and T_{rec} are the antenna and receiver noise temperatures, respectively.

The antenna radiation patterns, and hence the respective effective areas, are computed with full-wave simulations. Starting from these data, the evaluation of the antenna noise temperature T_{ant} is carried out by means of a simplified Cortes model [4] which returns two noise contributions: $T_{ant,\,sky}$ (related to the noise coming from the sky) and $T_{ant,\,gnd}$ (related to the noise coming from the ground). For this study, the receiver temperature contribution T_{rec} is instead considered antenna-independent owing to the suitable matching properties of the antenna.

A significant set of parametric analyses has been performed in order to find the finest solution according to the sensitivity goal function described above. Such data have been arranged in order to obtain a synthetic representation of the effect of the various geometrical parameters. An example of the design-oriented representation of the sensitivity is reported in Figure 1, which shows a contour plot of the minimum A_{eff}/T_{sys} (within the required 45° sky coverage and the

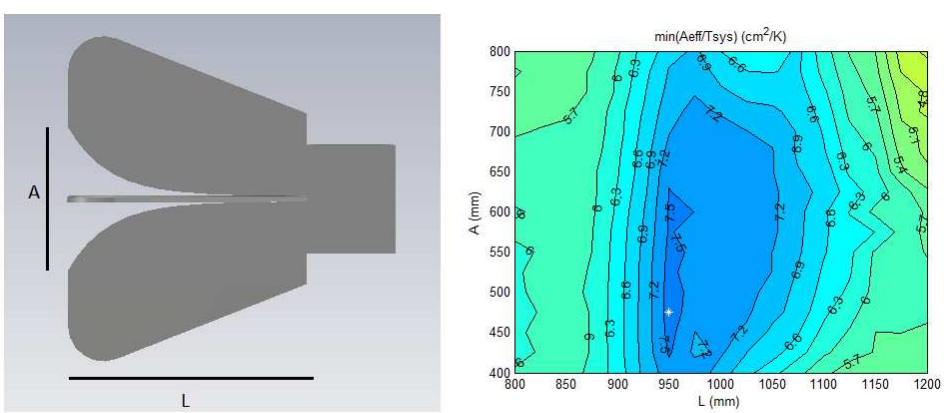

(a) (b)

Figure 1: (a) The geometry of the structure; (b) an example of $\min_{\vartheta,f}\{A_{eff}/T_{sys}\}$ contour plot.

operative frequency band) as a function of the geometry of the structure. The highest value of A_{eff}/T_{sys} in Figure 1 corresponds to the best parameters set.

Both the design considerations and the obtained results will be discussed in more detail at the conference.

REFERENCES

1. http://www.skatelescope.org/.
2. Virone, G., G. Addamo, O. A. Peverini, and R. Tascone, "Broadband array element for the SKA low-frequency aperture array," *ICEAA*, Sep. 12–16, 2011.
3. Virone, G., R. Sarkis, C. Craeye, G. Addamo, and O. A. Peverini, "Gridded vivaldi antenna feed system for the northern cross radio telescope," *IEEE-AP*, Vol. 59, No. 6, Part 1, 2011.
4. Bolli, P., F. Perini, S. Montebugnoli, G. Pelosi, and S. Poppi, "Basic element for square kilometer array training (BEST): Evaluation of the antenna noise temperature," *IEEE-AP*, Vol. 50, No. 2, 58–65, Apr. 2008.

Optimization and Performance Tradeoffs of Phased Array Antenna Configurations for Radio Astronomy

N. Razavi-Ghods[1], **T. Clavier**[2], **F. Glineur**[2], **D. Gonzalez-Ovejero**[3], **E. de Lera Acedo**[1], **and C. Craeye**[2]

[1]Cavendish Astrophysics, University of Cambridge, Cambridge, CB3 0HE, UK
[2]ICTEAM, Universite Catholique de Louvain, 1348 Louvain-la-Neuve, Belgium
[3]Information Engineering Department, University of Siena, Siena 53100, Italy

Abstract— Wideband phased array antenna technologies are widely used for radar systems and satellite communications.In the last decade, phased arrays have also become one of the most important technologies used for radio astronomy applications due to their high flexibility as well as low cost implementation. Several low-frequency wideband radio astronomy telescopes such as LOFAR, PAPER and MWA currently use phased arrays and in the next few years the largest of these telescopes, aptly named the Square Kilometre Array (SKA) will be developed comprising of a quarter million antennas in the first phase of operation [1].

Whilst regular lattice configurations have been implemented widely for various applications, there are limitations to using these for wideband radio astronomy where the average spacing is chosen at the low end of the band resulting in non-ideal grating responses on the sky at the high end of the band [2]. This has led to studies of non-regular arrays which can be optimized to give the desired performance. There are many important aspects to the design of a non-regular phased array,not least of which is the location of the antennas in the array. This has a major impact on the side lobe distribution and beam size as well as overall cost. The design of such arrays will thus aim at optimizing the distribution of a fixed number of antennas within a given perimeter in order to achieve the performance requirements.

As this problem involves a large number of variables (two for each element), solving it is computationally challenging and simple heuristics to adapt positions of the antennas are unlikely to provide satisfactory results. Here, we purpose a method for the optimization of the positions of elements in large non-regular arrays with constant weights. The method is based on complementary contributions of global and local changes of the array configuration and relies on three main steps. The following design constraints are considered: minimal separation of antennas, maximum size of the array and fixed main beam width. The level of the side lobes is reduced via the minimization of a new type of flexible averaging cost function based on an L_p-norm. Furthermore, we place these optimizations in the context of a large radio astronomy telescope such as the SKA and analyse the performance trade-offs.

REFERENCES

1. De Vaate, J., E. De LeraAcedo, G. Virone, A. Jiwani, N. Razavi, F. Perini, K. Zarb-Adami, J. Monari, S. Padhi, G. Addamo, O. Peverini, S. Montebugnoli, A. Gunst, P. Hall, A. Faulkner, and A. Van Ardenne, "Low frequency aperture array developments for phase 1 SKA," *XXXth URSI General Assembly and Scientific Symp.*, 1–4, Aug. 13–20, 2011.
2. Razavi-Ghods, N., E. De LeraAcedo, A. El-Makadema, P. Alexander, and A. Brown, "Analysis of sky contributions to system temperature for low frequency SKA aperture array geometries," *Experimental Astronomy*, Vol. 33, No. 1, 141–155, 2012.

Ultra-Wideband Tightly Coupled Phased Array Antenna for Low-Frequency Radio Telescope

E. O. Farhat[1], **K. Z. Adami**[1, 2], **Y. Zhang**[3], **A. K. Brown**[3], **and C. V. Sammut**[1]

[1]University of Malta, Malta
[2]University of Oxford, United Kingdom
[3]The University of Manchester, United Kingdom

Abstract— This paper introduces a different approach to a broadband array design for a low frequency radio telescope, presenting a low profile ultra-wideband tightly coupled phased array antenna with integrated feedlines. The approach consists of applying broadband techneques to an array of capacitively coupled, planar element pairs with an octagonal fractal geometry. Designed as a low cost, low loss, dual-polarised wideband array, this antenna is optimised for operation between 50 and 250 MHz. Simulations have shown that the antenna has a wide-scanning ability with a low cross-polarisation level, over the operational frequency range.

EM Simulations, Beam Modeling and Calibration of Ultra-wideband Array Antennas for Radio Astronomy

E. de Lera Acedo[1], **D. Gonzalez-Ovejero**[2], **C. Raucy**[3], **J. Harris**[1], **N. Razavi-Ghods**[1], **and C. Craeye**[3]

[1]Cavendish Astrophysics, University of Cambridge, Cambridge, CB3 0HE, UK
[2]Information Engineering Department, University of Siena, Siena 53100, Italy
[3]ICTEAM, Universite catholique de Louvain, Louvain-la-Neuve 1348, Belgium

Abstract— The Square Kilometre Array (SKA) [1] represents the next big step in Radio Astronomy. With a collecting area larger than 1 square kilometre, the SKA-AAlow will be one of the 3 instruments forming the SKA. The main science goals of the SKA include probing the Epoch of Re-ionization and the detection of pulsars in our Galaxy [2].

The frequency range of the SKA-AAlow instrument spans from 50 MHz up to at least 350 MHz. The SKA will be an interferometer. For the AAlow instrument, each of the hundreds of stations will be formed with hundreds and up to thousands of disconnected elements arranged in an irregular lattice [3]. Electromagnetic (EM) simulations accounting for the effects of mutual coupling are essential in the design process of the array antennas. Smooth, predictable patterns are desired for the SKA in order to facilitate the calibration process. The authors present here a powerful EM simulation code based on the Method of Moments [4] capable of simulating large irregular arrays such as SKA stations [5]. At present, this code is capable of simulating one of the candidate elements proposed to be used for the AAlow instrument, an ultra-wideband log-periodic antenna, SKALA [3]. Several experiments have been conducted to validate the accuracy of the code [6, 7]. In line with these developments, the authors have been working on a calibration scheme for the SKA, based on very accurate EM simulations of the arrays. In this calibration scheme, the antenna weights in the array can be represented and corrected by a few tens of coefficients by using a projection of the measured main beam onto the reference main beam, which has been simulated using the fast code. Details of this scheme and an update on the code will be given during the presentation.

REFERENCES

1. www.skatelescope.org.
2. "Science with the square kilometre array," *New Astronomy Reviews*, Vol. 48, C. Carilli, S. Rawlings, Eds., Elsevier, December 2004.
3. De Lera Acedo, E., "SKALA: A log-periodic antenna for the SKA," *Proceedings of the International Conference on Electromagnetics in Advanced Applications (ICEAA)*, Cape Town, September 2012.
4. González-Ovejero, D. and C. Craeye, "Interpolatory macro basis functions analysis of non-periodic arrays," *IEEE Transactions on Antennas and Propagation*, Vol. 59, No. 8, 2011.
5. Gonzalez-Ovejero, D., E. de Lera Acedo, N. Razavi-Ghods, and C. Craeye, "Fast MBF based method for large random array characterization," *Proc. IEEE Ant. Propag. Soc. Int. Symp. (APS-URSI)*, 1–4., 2009
6. Raucy, C., E. de Lera Acedo, N. Razavi-Ghods, and C. Craeye, "Characterization of SKA-AAlow antenna elements in the array environment," *Proceedings of the International Conference on Electromagnetics in Advanced Applications (ICEAA)*, Cape Town, September 2012.
7. Raucy, C., E. de Lera Acedo, N. Razavi-Ghods, D. González-Ovejero, and C. Craeye, "Low-cost near field pattern measurement technique for aperture array characterization," *European Conference on Antennas and Propagation, EuCAP*, Goteborg, April 2013, to be presented.

A Wideband Circularly-polarized Antenna — Self-grounded Monopole Array with Low Axial Ratio over Large Coverage

Jian Yang
Department of Signals and Systems, Chalmers University of Technology, Goteborg S41296, Sweden

Abstract— A new wideband circularly-polarized antenna — self-grounded monopole array is presented in the paper. This antenna has low axial ratio over a large coverage with a compact size. This characteristic is important in many applications. The design is done via an optimization process with a nature inspired algorithm — social civilization algorithm. The results will be presented in the conference.

Recent Developments of Multiband and Wideband Reflectarrays

J. A. Encinar[1], **M. Arrebola**[2], **C. Tienda**[3], **M. Barba**[4], **and E. Carrasco**[4]

[1]Ciudad Universitaria, Spain
[2]Universidad de Oviedo, Spain
[3]ESA ESTEC, Netherlands
[4]Universidad Politécnica de Madrid, Spain

Abstract— Printed reflectarrays combine certain advantages of reflector antennas and phased arrays to produce focused and contoured beams. They are manufactured on a planar substrate using printed circuit technology and can offer the possibility of beam steering as phased arrays when controllable phase shifters are used; on the other hand, the feeding mechanism (as in a reflector antenna) eliminates the complexity and losses of the feeding network used in planar arrays. However, the major limitation of reflectarrays is the narrow-band behaviour, but recent developments based on stacked patches of varying size, patches aperture-coupled to delay lines and dual-reflector configurations have significantly overcome this limitation [1–3].

The talk will show recent developments of reflectarray antennas carried out by Universidad Politécnica de Madrid and Universidad de Oviedo that demonstrate the wide-band performance or dual frequency operation for some specific applications. The first example is a reflectarray at X-band, which has been designed to operate in 20% bandwidth using delay lines aperture-coupled to the printed patches [2]. Dualfrequency operation is demonstrated in a second example [4], in which a Ka-band terminal antenna has been designed to provide an uplink in V polarization at 30 GHz and a downlink in H polarization at 20 GHz using separate feed-horns. Some reflectarray demonstrators covering the transmit (12 GHz) and receive (14 GHz) frequencies for satellite antennas in Ku-band are presented in the following examples. A single-offset reflectarray antenna made of three stacked arrays of varying-sized patches conveniently optimized has demonstrated a satisfactory compliance with very stringent requirements in both frequency bands for South-America coverage [5]. Finally, a wide-band performance (12 GHz–15 GHz) is demonstrated by a dual-reflectarray antenna [3], which also provides very low levels of cross-polarisation in dual linear polarization.

ACKNOWLEDGMENT

The work presented here has been supported by the European Space Agency (ESA) and by the Spanish Commission for Science and Technology (CICYT, TEC2010-17567).

REFERENCES

1. Huang, J. and J. A. Encinar, *Reflectarray Antennas*, John Wiley, 2008.
2. Carrasco, E., J. A. Encinar, and M. Barba, "Bandwidth improvement in large reflectarrays by using true-time delay," *IEEE Trans. on Antennas and Propagat.*, Vol. 56, 2496–2503, 2008, doi:10.1109/TAP.2008.927559.
3. Tienda, C., J. A. Encinar, M. Arrebola, M. Barba, and E. Carrasco, "Design, manufacturing and test of a dual-reflectarray antenna with improved bandwidth and reduced cross-polarization," *IEEE Trans. on Antennas and Propagat.*, Vol. 61, No. 3, 1180–1190, 2013, doi:10.1109/TAP.2012.2228620.
4. Encinar, J. A. and M. Barba, "Design manufacture and test of Ka-band reflectarray antenna for transmitting and receiving in orthogonal polarization," *ANTEM-AMEREM 2010*, Ottawa, Canada, Jul. 5–9, 2010, doi:10.1109/ANTEM.2010.5552500.
5. Encinar, J. A., M. Arrebola, L. F. de la Fuente, and G. Toso, "A transmit-receive reflectarray antenna for direct broadcast satellite applications," *IEEE Trans. on Antennas and Propagat.*, Vol. 59, No. 9, 3255–3264, Sep. 2011, doi:10.1109/TAP.2011.2161449.

Quasi Conformal Transformation Optics for the Design of Ultra Wide Band Lenses

O. Quevedo-Teruel, R. C. Mitchell-Thomas, and Y. Hao
Queen Mary, University of London, E1 4NS, UK

Abstract— Optical transformation can be used to link one coordinate system of one space to any other, while retaining the same electromagnetic propagation behaviour of the original [1, 2]. The outcome of such a transformation is the necessity to fill the space with a material with both magnetic and dielectric properties. There are several routes to take when employing transformation optics, and three of these are: non-Euclidean [3], analytical [4] and quasi-conformal transformation [5]. The analytical transformation results in the necessity of anisotropic materials in the implementation of designs. Furthermore, non-Euclidean transformations can be difficult to match to practical applications [6]. On the other hand, the quasi-conformal technique allows the design of full dielectric and isotropic configurations at the price of assuming an approximation of the conformal anisotropy [7].

Lenses were not commonly used at microwave frequencies due to their large size compared with the wavelength and their bulky shapes. However, the transformation optics tool can be used to reduce the size of conventional high quality lenses, such as the Luneburg lens [8, 9] which has desirable properties such as the ability to produce highly directive steerable beams, but has the disadvantage of being spherical in shape. In this talk, we will show how quasi-conformal transformation can be used to manipulate the shape of conventional lenses maintaining their frequency independency.

ACKNOWLEDGMENT

This work was funded by the Engineering and Physical Sciences Research Council, UK, under a Program Grant (No. EP/I034548/1) entitled The Quest for Ultimate Electromagnetics Using Spatial Transformations (QUEST).

REFERENCES

1. Leonhardt, U., "Optical conformal mapping," *Science*, Vol. 312, No. 5781, 1777–1780, 2006.
2. Pendry, J. B., D. Schurig, and D. R. Smith, "Controlling electromagnetic fields," *Science*, Vol. 312, No. 5781, 1780–1782, 2006.
3. Leonhardt, U. and T. G. Philbin, *Geometry and Light: The Science of Invisibility*, Dover, Mineola, 2010.
4. Roberts, D. A., N. Kundtz, and D. R. Smith, "Optical lens compression via transformation optics," *Opt. Express*, Vol. 17, No. 19, 16535–16542, Sep. 2009.
5. Kundtz, N. and D. R. Smith, "Extreme-angle broadband metamaterial lens," *Nat. Mater.*, Vol. 9, No. 129, 2010.
6. Quevedo-Teruel, O., R. C. Mitchell-Thomas, and Y. Hao, "Frequency dependence and passive drains in fish-eye lenses," *Phys. Rev. A*, Vol. 86, No. 5, Nov. 2012.
7. Tang, W., Y. Hao, and F. Medina, "Broadband extraordinary transmission in a single subwavelength aperture," *Opt. Express*, Vol. 18, No. 16, 16946–16954, Aug. 2010.
8. Quevedo-Teruel, O., W. Tang, and Y. Hao, "Isotropic and nondispersive planar fed Luneburg lens from Hamiltonian transformation optics," *Opt. Lett.*, Vol. 37, 4850–4852, 2012.
9. Quevedo-Teruel, O. and Y. Hao, "Directive radiation from a diffuse Luneburg lens," *Opt. Lett.*, Vol. 38, 392–394, 2013.

A Compact Triple-band Filtering Microstrip Patch Antenna with the Same Polarization Planes

Y.-J. Lee and S.-J. Chung
Institute of Communications Engineering, National Chaio Tung University, Hsinchu 30010, Taiwan

Abstract— A novel compact filtering microstrip patch antenna with triple-band operation is presented for WLAN/TD-LTE wireless applications. The proposed design is composed of a patch with slot-loaded parasitic elements and a stepped-impedance resonator which shares the same apertured ground. The slot-loaded parasitic elements are incorporated into the non-radiating edges of a microstrip patch which is operated in the second band. The parasitic elements are worked for the first and third bands. The coupling between the main patch and slot-loaded parasitic elements is realized by controlling the vertical and horizontal gaps. Using full-wave simulator HFSS, the broadside coupling coefficient can be extracted to determine the dimension of the aperture. The proposed triple-band antenna is fabricated on two FR4 substrates. It has similar broadside radiation patterns in both E- and H-planes in the three frequency bands. Meanwhile, the antenna provides good selectivity as well as the same polarization planes.

REFERENCES

1. Chuang, C.-T. and S.-J. Chung, "A compact printed filtering antenna using a ground-intruded coupled line resonator," *IEEE Trans. Antennas Propag.*, Vol. 59, No. 10, 3630–3637, Oct. 2011.
2. Lin, C.-K. and S.-J. Chung, "A compact filtering microstrip antenna with quasi-elliptic broadside antenna gain response," *IEEE Antennas Wireless Propag. Lett.*, Vol. 10, 381–384, 2011.
3. Lee, Y.-J. and S.-J. Chung, "A compact dual-band filtering microstrip antenna with the same polarization planes," *Proc. Asia-Pacific Microwave Conference (APMC)*, 1178–1180, Kaohsiung, Taiwan, Dec. 2012.
4. Maci, S., G. B. Gentili, P. Piazzesi, and C. Salvador, "Dual-band slot-loaded patch antenna," *IEE Proc. Microw. Antennas Propag.*, Vol. 142, No. 3, 225–232, Jun. 1995.
5. Wi, S.-H., Y.-S. Lee, and J.-G. Yook, "Wideband microstrip patch antenna with U-shaped parasitic elements," *IEEE Trans. Microw. Antennas Propag.*, Vol. 55, No. 4, 1196–1199, Apr. 2007.
6. Hong, J. S. and M. J. Lancaster, *Microstrip Filter for RF/Microwave Application*, J. Wiley & Sons, New York, 2001.

A Study of Partial Resonance Control for Edge Elements in a Finite Array

C. I. Kolitsidas and B. L. G. Jonsson
Division of Electromagnetic Engineering, School of Electrical Engineering
KTH Royal Institute of Technology, Stockholm SE-100 44, Sweden

Abstract— Future wireless base station are expected to have the ability to support all existing commercial frequency bands as well as new emerging wireless technologies. This implies that the corresponding RF-air interface should be able to cover all these frequency bands simultaneously. Furthermore on top of the classic multiplexing techniques spatial division (SDMA-Spatial Division Multiple Access) needs to be employed in order to achieve maximum network capacity, low interference and power efficiency at a low visual impact device. The latter two are very important since the majority of base stations are used in urban environments.

An implementation possibility for the RF-air interface is a mid-sized, wideband, wide scan angle antenna array. The classic array design procedure starts with the unit cell analysis where the element is considered in an infinitely periodic structure. This design procedure has been proven efficient for large array antenna systems where most elements are approximately in an infinite periodic environment. The outermost elements in a finite array suffer from "edge effects" which are caused by the finiteness of the array. Applying the same design procedure in the mid-sized arrays is a challenge as most of the elements of the array can be considered to be influenced by the array's edge effects. The edge effects are mainly caused by the multiple reflections from the edges of the array. The reflections cause variations at the element currents which, in turn, can be translated as a resonance shift at the antenna impedance. The severity of this shift depends on the scanning angle and bandwidth of the array.

This work is focused on studying the element resonant shifting on a mid-sized array of strongly coupled dipoles over a ground plane. First we model the shifting in the resonance behavior for a finite $\times$ infinite array of these strongly coupled dipoles for different scanning angles. This initial study provides an insight in each element shifted resonance behavior as a function of scan angle and the element surrounding. At this point we introduce as design parameters a partially controllable second order resonance at the edge elements of the structure. Also the interelement coupling is considered as tunable design parameter. Tuning these design parameters we can partially control the direction of the second order shift, resulting in non-uniform elements. Changing the resonance shift of the edge elements in the finite sized structure according to the study creates a possibility to partially control how edge effects influence the array performance. Combining these features the ultimate goal of this study is to compensate and utilize the edge effects in the mid-sized arrays by introducing this form of non-uniform elements architecture in the finite array.

Broadband, High Gain, See-through Antenna for WiFi, WiMax and LTE 2600 Radio Networks

P.-A. Garcia[1,2], **T. Razban**[1], **A. Chousseaud**[1], **and E. Motta Cruz**[2]

[1]LUNAM, Université de Nantes, IETR UMR 6164, rue Christian Pauc, Nantes 44306, France
[2]Bouygues Telecom, 76 rue des Français Libres, Nantes 44263, France

Abstract— This paper demonstrates the feasibility of broadband, high gain, see-through antennas for radio networks where low visual impact is needed. A single linear polarization, proximity-coupled stacked patch antenna is proposed. Borosilicate glass is used for substrates, but its high permittivity ($\epsilon_r = 4.7$), leads to inefficient unilayer patch antennas, with isotropic gains lower than 5 dBi. However, adding two stacked superstrates of this material allows a substantial increase of the gain, up to 7.3 dBi. The latter configuration offers the opportunity to add resonant patches, so the bandwidth can be broadened. A 2.1–2.8 GHz bandwidth (30% relative bandwidth) is proposed, with VSWR < 1.5, covering WiMax (around 2.3 GHz and 2.5 GHz), WiFi (2.4–2.483 GHz) and LTE2600 (2.5–2.69 GHz) frequency bands.

Antenna is manufactured with a proprietary process, which is neither based on ultrathin metallic film deposition, nor Transparent Conductive Oxides (TCO) deposition, nor any thin or thick film complex deposition process, such as Sputtering or Chemical Vapor Deposition (CVD). We use a simple, low cost process, based on Printed Circuit Board (PCB) technology, to create thick (17 µm) meshed conductors on glass substrate. The gridded mesh is made of 50 µm wide horizontal and vertical strips, with a 450 µm interspacing. This resolution is high enough to make the conductive patterns quite discreet with respect to human eye acuity, with an estimated optical transparency greater than 80%. This high resolution also ensures meshed conductors to have a radioelectric behavior comparable to plain conductors at this frequency spectrum, since the interspacing is very low compared to the minimum operating wavelength ($\lambda_0 = 100$ mm at 3 GHz).

Substrates thicknesses are 3.3 mm, to ensure glass mechanical resistance, and to limit the impact of thickness tolerance (±0.2 mm) on impedance variation. In our case, thickness tolerance relative to nominal thickness is ±6%, which is comparable to classic substrate technology. Substrates sizes ($91 \times 91\,\text{mm}^2$) have been chosen to allow the use of antenna in arrays, and to maximize transparency by avoiding large (7 mm wide) 50 Ω microstrip lines.

The impedance matching strategy relies on the idea of combining impedance *loops*, that can be seen on Smith chart. These loops are created by patches resonances. However, this initial combination can occur for any complex impedance, not necessarily 50 Ω. Therefore, we first look for loops combination, and then we match the resulting impedance to a 50 Ω coaxial cable, using single or multisection transformers.

Further antenna design considerations, antenna prototyping, impedance measurement and radiation measurement will be discussed in the full paper.

A Fractal Microstrip Array Antenna with Slots Feeding Network for DTV Reception

Jianhua Zhou, Bingyang Liang, Baiqiang You, Qing Liu, and Xingjing Yan
Department of Electronic Engineering, Xiamen University, Xiamen, Fujian 361005, China

Abstract— A Cantor fractal microstrip array antenna of multi-ports with equal amplitude and phase with slots feeding network is designed for DTV reception. The performances of the antenna array are optimized with different feeding networks and array matrices. The simulation shows that applying Cantor fractal elements, the mutual coupling strength between the array elements is decreased effectively and the antenna is miniaturized. The samples of designed $4 \times 4/8 \times 8$ planar arrays and 4×4 slot coupling array were fabricated. The measurement results agreed very well with the simulation, which indicate a relatively high efficiency and relative bandwidth of 3.08% and 3.81% respectively.

Based on a FR4 board with the relative permittivity of 2.2 and the dimensions of $W = 60\,\text{mm}$, $L = 58\,\text{mm}$, $h = 0.8\,\text{mm}$, we designed a 4×4 uniform planar array with Cantor elements, as shown in Fig. 1.

By feeding network supplied with slot coupling technology, the radiation energy of proposed antenna system could be controlled well, which has been proved with 4×4 and 8×8 feeding system. In our design, fractal antenna elements can reduce the outlet of antenna with little radiation loss, and the coupling energy can be modulated by slots with separated feeding network providing more reliable multi-ports for the feeding system. We also found that combining all these techniques, the gain, bandwidths and phase center could be improved further significantly.

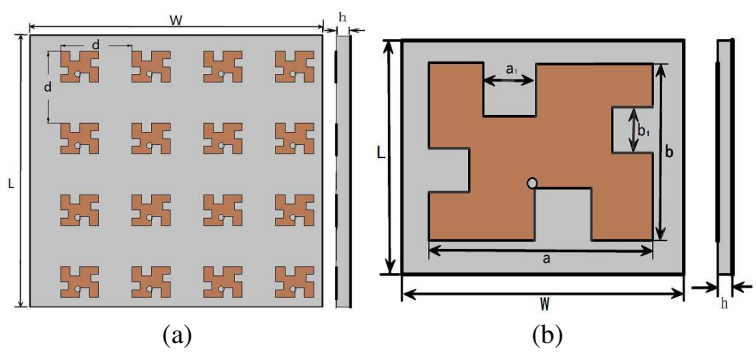

Figure 1: Configuration of the proposed 44 Cantor array antenna. (a) Planar array. (b) Cantor element.

Recent Developments in Analysis and Design of a Low Noise Connected Array Feed for the Australian SKA Pathfinder

Stuart G. Hay
CSIRO ICT Centre, P. O. Box 76, Epping, NSW 1710, Australia

Abstract— A key requirement for next-generation radiotelescopes such as the Australian SKA Pathfinder (ASKAP) is for large areas of sky to be surveyed quickly and deeply. This can only be done if it is possible to image a large area of the sky with multiple individual beams simultaneously, with sensitivity not significantly less than traditional single-pixel receivers.

Multiple-beam receiver systems are not new. A number of telescopes use multiple feed horns at the focus of a dish. The spacing between the feed horns is such that it is only possible to capture part of the energy at the focus. Also, the off-axis feed horns cannot compensate for aberration. An alternative approach with a number of advantages is to place a phased array feed (PAF) at the focus. The PAF captures most of the incident energy and by weighting and summing the signals of the individual PAF elements, multiple beams with high sensitivity can be produced. Such beamforming is performed in the digital domain in real time, allowing calibration of the element responses and the flexibility to tailor beam properties such as spacing, sidelobes and cross polarization to best suit a range of astronomy requirements.

CSIRO has developed a novel PAF based on a planar connected array. In this structure, neighbouring elements of a chequerboard array of conducting patches are connected by two-wire transmission lines that divert the array signals through low-noise amplifiers (LNAs) situated behind a groundplane. Connecting the array elements in this way allows operation over a wide frequency range with the array element spacing less than half the minimum wavelength. The approach requires accurate analysis and design of the array in concert with LNAs that have differential impedances in the order of 300 ohm. Recent developments are described in the analysis and design in order to achieve good low-noise and high-sensitivity performance over the 0.7–1.8 GHz frequency range required for the ASKAP telescope.

REFERENCES

1. Schinckel, A. and J. Bunton, T. Cornwell, I. Feain, and S. Hay, "The australian SKA pathfinder," *SPIE Astronomical Telescopes and Instrumentation*, Amsterdam, Netherlands, July 2012.
2. Hay, S. G., J. D. O'Sullivan, and R. Mittra, "Connected patch array analysis using the characteristic basis function method," *IEEE Trans. Ant. Prop.*, Vol. 59, No. 3, 2011.
3. Shaw, R. D., S. G. Hay, and Y. Ranga, "Development of a low-noise active balun for a dual-polarized planar connected-array antenna for ASKAP," *International Conference on Electromagnetics in Advanced Applications*, Cape Town, South Africa, 2012.

Session 1P7a
SC3: Optical Fiber Communications

Performance Analysis of the Injection of a Transparent Assist Light in a SOA Amplifying a CO-OFDM Transmission System
Hamidreza Khaleghi, Ammar Sharaiha, Pascal Morel, Thierry Rampone, ... 308
Wavelength-dependent Switching of a Nonlinear Optical Loop Mirror
Olivier Pottiez, Baldemar Ibarra-Escamilla, E. A. Kuzin, ... 310
XGM Wavelength Conversion of an Optical OFDM Signal in a RSOA over a 90 nm Range
Mohamad Hamze, Ammar Sharaiha, Ali Hamié, Mikael Guegan, ... 312
Channel Estimation Using Superimposed Training for Coherent Optical OFDM Systems
Changjian Guo, Han Zhang, Lingchen Huang, Sailing He, ... 313
Sub-frame Carrier Phase Estimation for Coherent Optical Orthogonal Frequency Division Multiplexing System
Xuezhi Hong, Sailing He, ... 314

Performance Analysis of the Injection of a Transparent Assist Light in a SOA Amplifying a CO-OFDM Transmission System

Hamidreza Khaleghi, **Ammar Sharaiha**, **Pascal Morel**, **and Thierry Rampone**
UEB, ENIB, Lab-STICC UMR CNRS (6285), CS 73862, 29238 Brest Cedex 3, France

Abstract— Using large optical bandwidth Semiconductor Optical Amplifiers (SOA) is extensively studied as a solution for amplifying the future broadband high data rate optical transmission networks. Specific research is focused on the non-linear impacts of SOAs on the data pattern of amplified signals.

A solution to improve performances of a SOA used as an inline amplifier is to increase its linear operating regime by increasing its output saturation power. A method to enhance the output saturation power, without changing the amplifier operating point in terms of gain level and NF, is to inject into the SOA an optical continuous wave (CW) pump signal at the gain transparency wavelength (transparent assist light) using a counter-propagation configuration, as shown in Figure 1(a). The improvement of its performances on conventional On-Off Keying (OOK) signals has been previously proved [1]. In this paper, it is numerically investigated for a 10.94 Gb/s QPSK (Quadrature Phase-Shift Keying) CO-OFDM (Coherent Optical-Orthogonal Frequency Division Multiplexing) signal including 128 subcarriers by using an experimentally validated simulation platform [2].

An enhancement of about 4.2 dB is obtained for the output saturation power. In addition, the coupling factor amplitude-phase (Alpha Factor) remains constant over a wide range of powers. By evaluating the Error Vector Magnitude (EVM) of a received QPSK CO-OFDM signal with this configuration and by comparing with results where no assist light is used, an improvement in the EVM is observed for high input powers (Figure 1(b)) leading to a larger input power range (about 2.5 dB more) for a given EVM. It can be shown that this improvement is due to a reduction of non-linear effects, especially the Four-Wave Mixing (FWM) effect which is the principal cause of the performance degradation for an OFDM signal, while the other parameters of the SOA remain unchanged.

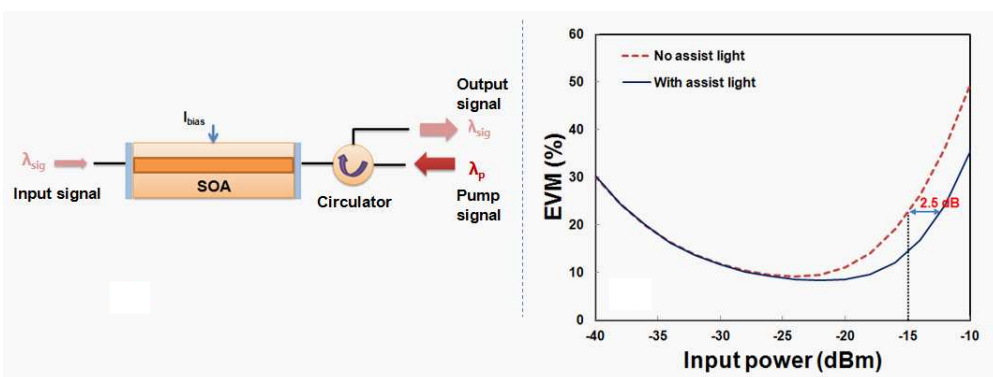

(a) (b)

Figure 1: (a) Optical pumping at the SOA gain transparency with a counter-propagating configuration. (b) Simulated EVM of a QPSK CO OFDM signal as a function of the input power without (dotted line) and with (continuous line) pump at the gain transparency wavelength (1416 nm). The signal wavelength is 1540 nm and the bias current is 200 mA.

ACKNOWLEDGMENT

This work is supported by European Funds for regional development (FEDER) and by the French National Research Agency (ANR) in the frame of UltraWIDE project (ANR 2010 VERS 011 06) and the Images & Réseaux cluster (http://www.images-et-reseaux.com/en).

REFERENCES

1. Amaya, M., et al., "Comparison between co- and counter-propagative optical injection near the transparency wavelength on SOA static and dynamic performances," *Opt. Commun.*, Vol. 246, No. 1–3, 67–71, 2005.

2. Khaleghi, H., et al., "Experimental validation of numerical simulations and performance analysis of a coherent optical-OFDM transmission system employing a semiconductor optical amplifier," *IEEE J. Lightwave Technol.*, Vol. 31, No. 1, 161–170, January 2013.

Wavelength-dependent Switching of a Nonlinear Optical Loop Mirror

O. Pottiez[1], **B. Ibarra-Escamilla**[2], **and E. A. Kuzin**[2]

[1]Centro de Investigaciones en Óptica, Loma del Bosque 115
Col. Lomas del Campestre, Leon, Gto. 37150, Mexico
[2]Departamento de Optica, Instituto Nacional de Astrofísica Óptica y Electrónica
L. E. Erro 1, Puebla, Pue. 72000, Mexico

Abstract— The Nonlinear Optical Loop Mirror (NOLM) [1] is a versatile and low-cost device whose potential has long been recognized for applications like ultra fast optical switching and signal processing (regeneration, wavelength conversion, demultiplexing, etc.). Switching is obtained through the optical Kerr effect, when the symmetry in the Sagnac interferometer structure of the device is broken in some way. Although conventional schemes are power-asymmetric (by the use of an asymmetric coupler, or by inserting asymmetrically a gain or loss element in the loop), a birefringence asymmetry (e.g., a wave retarder (WR) inserted assymetrically in the loop) is also effective, taking advantage of the polarization dependence of the Kerr nonlinearity (nonlinear polarization rotation). Such a polarization-imbalanced NOLM, including a 50/50 coupler and a quarter-WR, was proposed and studied previously [2], and the enhanced flexibility of its switching characteristic, which can be controlled though the WR angle and inpult polarization, makes it very promising for applications like high-quality data regeneration, for example [3].

With most NOLM schemes, the nonlinear response does not depend on the signal wavelength. For some applications however, in particular in WDM systems, wavelength-dependent operation is highly desirable. Unfortunately, very few wavelength-sensitive NOLM designs can be found in the literature. In [4], wavelength dependence was introduced in a NOLM though the insertion of a chirped grating. Wavelength confined switching (switching at the grating wavelength only) was demonstrated experimentally.

Because the polarization-imbalanced NOLM relies on a birefringent element, a WR, to provide switching, and as birefringence is wavelength-dependent by nature, this setup is intrinsically able to support wavelength dependent switching, without the need for any additional wavelength-selecting element. In this work, we study a NOLM including a 50/50 coupler, a piece of fiber of length L and a WR taking the form of a few cm of polarization-maintaining (PM) fiber [Figure 1(a)]. Input polarization to the NOLM is linear, forming a 45° angle with the WR axes. For two wavelengths λ_1 and λ_2 separated by $\Delta\lambda$, the phase shift $\Delta\phi$ of the WR differs by $\delta(\Delta\lambda) = 2\pi L_{\mathrm{WR}}\Delta\lambda/(L_B\lambda_c)$, where L_{WR} and L_B are the PM fiber length and beat length, and λ_c is the central wavelength. We show that the switching characteristic is a sinusoidal function of input power, whose switching power P_π depends on the signal wavelength, as a consequence of the WR delay variation [Figure 1(b)]. Through slight adjustments of the WR birefringence, which can be performed mechanically or thermally, the ratio between switching powers at λ_1 and λ_2 can be set to any value. A potential application is simultaneous regeneration of different WDM channels presenting different power levels. WR adjustment also allows making one switching power infinite for one wavelength (no switching) and finite for the other (switching), allowing WDM demultiplexing. Hence we believe that this work paves the way for the design of a range of novel wavelength-sensitive devices for WDM applications.

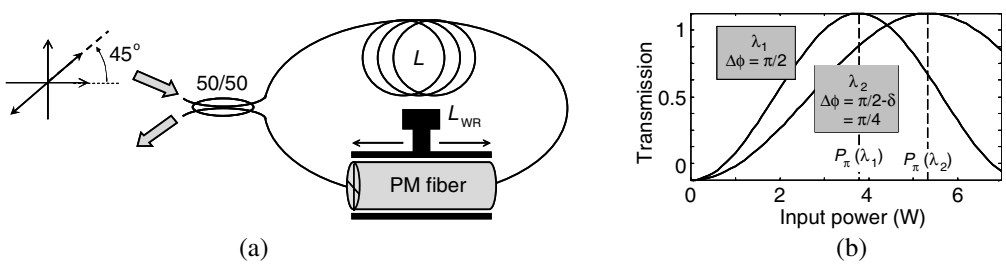

Figure 1: (a) NOLM scheme; (b) examples of switching characteristics for 2 wavelengths separated by 1.9 nm in the 1550 nm region ($L_{\mathrm{WR}} = 10$ cm, $L_B = 1$ mm, $\sigma = \pi/4$). Switching power is given by $P_\pi = 6\pi/(\lambda L \sin\Delta\phi)$, $L = 500$ m is fiber length and $\gamma = 10$/W/km the nonlinearity.

ACKNOWLEDGMENT

This work is funded by CONACYT grant #130681.

REFERENCES

1. Doran, N. J. and D. Wood, *Opt. Lett.*, Vol. 13, 56, 1988.
2. Kuzin, E. A., N. Korneev, J. W. Haus, and B. Ibarra-Escamilla, *J. Opt. Soc. Am. B*, Vol. 18, 919, 2001.
3. Pottiez, O., E. A. Kuzin, B. Ibarra-Escamilla, F. Gutierrez-Zainos, U. Ruiz-Corona, and J. T. Camas-Anzueto, *IEEE Photon. Technol. Lett.*, Vol. 17, 154, 2005.
4. Pattison, D. A., P. N. Kean, W. Forysiak, I. Bennion, and N. J. Doran, *Opt. Lett.*, Vol. 20, 362, 1995.

XGM Wavelength Conversion of an Optical OFDM Signal in a RSOA over a 90 nm Range

Mohamad Hamzé[1,2], Ammar Sharaiha[1], Ali Hamié[1,2], and Mikael Guégan[1]

[1]UEB, ENIB, Lab-STICC UMR CNRS (6285), CS 73862, 29238 Brest Cedex 3, France
[2]Arts, Sciences, and Technology University in Lebanon (AUL), Lebanon

Abstract— Today, the use of new advanced transmission modulation formats such as OOFDM (Optical Orthogonal Frequency Division Multiplexing) has become a hot research topic in the field of high-speed optical communications [1, 2]. In this paper, we present for the first time as far as we know an experimental work on wavelength conversion of an optical OFDM signal using the RSOA as a wavelength converter by using the cross gain modulation (XGM), We experimentally (Figure 1) perform the conversion of the OOFDM signal for 16 QAM-OOFDM modulation formats over 90 nm for an electrical bandwidth of 500 MHz, 1 GHz, and 2 GHz. with an effective transmitted data of 1.875 Gb/s, 3.75 Gb/s, and 7.5 Gb/s respectively. At the RSOA input, we inject a pump OOFDM signal at 1556 nm which corresponds to the RSOA peak gain and a CW optical probe signal from a tunable laser source varying from 1520 nm to 1610 nm. At the RSOA output, we obtain at the probe wavelength an up and down wavelength conversion. After direct photo-detection, we calculate the error vector magnitude (EVM) of the converted signal response. For 16-QAM-OOFDM format, we show that we can transmit the 500 MHz signal for a 90 nm range, the 1 GHz signal for an 80 nm range, and the 2 GHz signal for a 30 nm range (Figure 2).

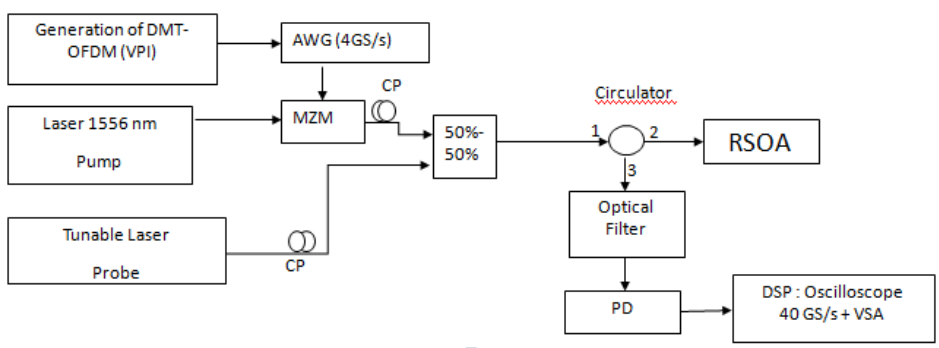

Figure 1: Experimental setup (C.P: polarization controller, MZM: mach Zehnder modulator, AWG: arbitrary wave generator, VSA: vector signal analyzer, PD: photodetector).

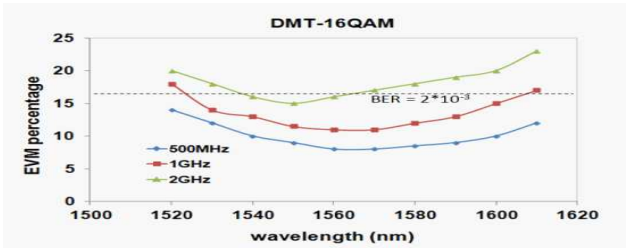

Figure 2: EVM of the converted signal versus wavelength for 16 QAM-OOFDM format.

REFERENCES

1. Qian, D., N. Cvijetic, J. Hu, and T. Wang, "Optical OFDM transmission in metro/access networks," *Optical Fiber Communication. Conf.*, Paper OMV1, San Diego, CA, USA, 2009.
2. Chow, C. W., C. H. Yeh, Y. F. Wu, H. Y. Chen, Y. H. Lin, J. Y. Sung, Y. Liu, and C.-L. Pan, "13 Gbit/s WDM-OFDM PON using RSOA-based colourless ONU with seeding light source in local exchange," *Electronics Letters*, Vol. 47, No. 22, 1235–1236, October 2011.

Channel Estimation Using Superimposed Training for Coherent Optical OFDM Systems

Changjian Guo[1], **Han Zhang**[1], **Lingchen Huang**[2], **and Sailing He**[3]

[1]South China Normal University, Guangzhou 510006, China
[2]Zhejiang University, Hangzhou 310058, China
[3]Royal Intstitute of Technology, Kista SE-164 40, Sweden

Abstract— Coherent optical orthogonal frequency division multiplexing (CO-OFDM) is considered to be one of the promising modulation formats for 100-Gb/s and beyond optical transmission systems due to its high spectral efficiency, high flexibility and its natural combination with digital signal processing (DSP). In recent DSP based CO-OFDM systems, pilot symbols (preambles) and pilot subcarriers are used for channel estimation, which consumes valuable bandwidth, resulting in significant bandwidth loss. Here, we propose an overhead free channel estimation method for CO-OFDM systems based on superimposed training, and show that, channel estimation can be robustly accomplished without sacrificing any bandwidth. Superimposed training (ST) are well studied in wireless literatures. In ST based channel estimation schemes, periodic training sequences are arithmetically added to the information data streams in either time-domain or frequency domain. The channel state information (CSI) is then extracted by exploiting the first-order statistics of the received signal at receiver. In this way, no extra bandwidth is lost. We show through simulation that by symbol-by-symbol averaging and iterative feed-back, the estimation accuracy can be significantly improved. We consider single polarization CO-OFDM systems for simplicity. The simulation results are shown in Figure 1.

Conclusion: We have presented a robust/bandwidth-efficient CE method for CO-OFDM systems, and have shown through simulation that 1) increasing the number of symbols transmitted per block helps to increase the estimation performance; 2) iterative feed-back is useful for large SPR and small averaging number, while optimal SPR values exist; 3) the ST based CE performance is comparative to that of preamble-based schemes when an appropriate SPR value is used.

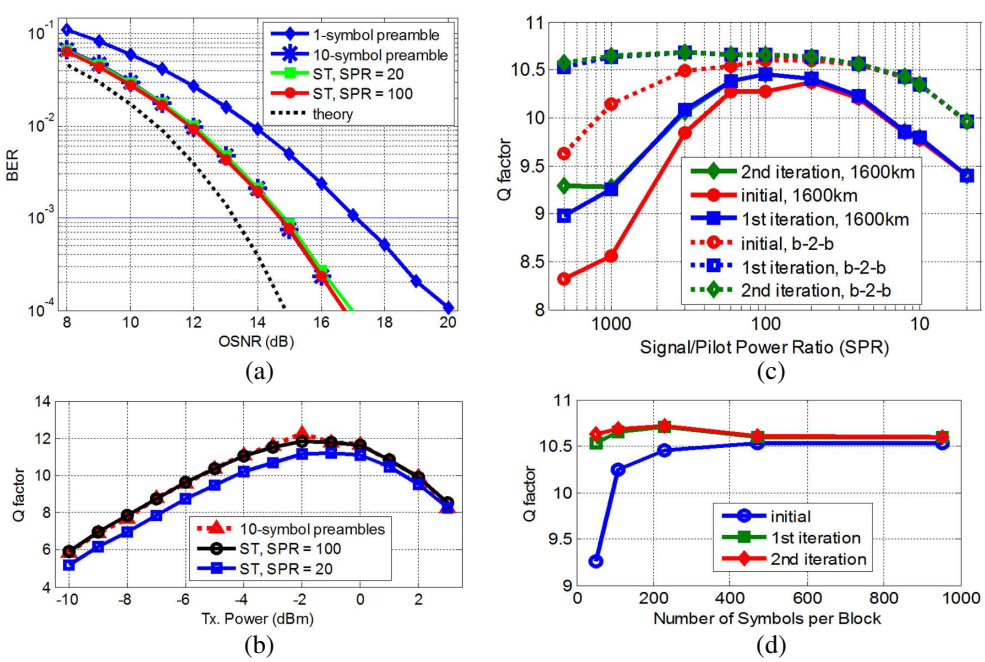

Figure 1: Simulation results of an ST based 56-Gb/s CO-OFDM systems. (a) Back-to-back performance. (b) Q factors vs. Tx. power after 1600 km SSMF transmission. (c) Performance under different SPR values. (d) Q factor vs. number of symbols used for averaging.

Sub-frame Carrier Phase Estimation for Coherent Optical Orthogonal Frequency Division Multiplexing System

Xuezhi Hong[1] **and Sailing He**[1, 2]

[1]ZJU-SCNU Joint Research Center of Photonics, South China Normal University
Guangzhou 510006, China
[2]Joint Research Center of Photonics of the Royal Institute of Technology (Sweden)
Lund University (Sweden) and Zhejiang University
Zhejiang University, Hangzhou 310058, China

Abstract— Coherent optical orthogonal frequency division multiplexing (CO-OFDM) has been intensively studied for its high spectral efficiency (SE) and high tolerance to chromatic dispersion (CD) [1]. However, compared to the single-carrier counterpart, the CO-OFDM system is more sensitive [2] to the phase noise contributed by the free-running lasers at the transmitter and the receiver. In order to compensate for the inter-carrier-interference (ICI) and common phase error caused by the phase noise, carrier phase estimation (CPE) [2–4] is carried out by digital signal processing (DSP) after coherent detection.

In [2–4], CPE is done frame by frame. In this paper, we propose to use sub-frame carrier phase estimation to improve the phase noise tolerance of CO-OFDM system. The basic idea of sub-frame CPE is to divide a single CO-OFDM frame to several sub-frames during the phase estimation stage. Details of sub-frame CPE algorithm are depicted in Fig. 1. The coarse carrier phase is first estimated with pilot subcarriers using conventional single-frame CPE. After channel equalizer (BCJR here), we make tentative hard decision on received data. The IFFT of tentative

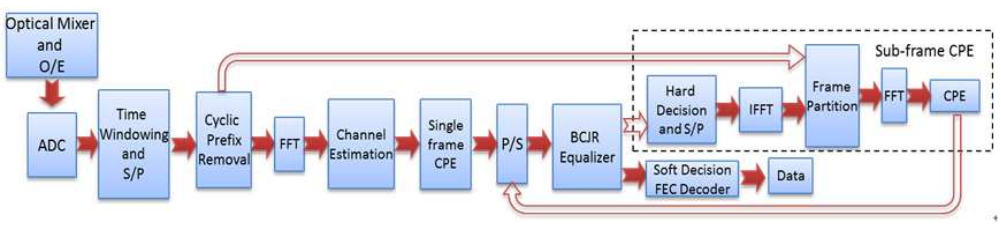

Figure 1: DSP diagrams for CO-OFDM with sub-frame CPE.

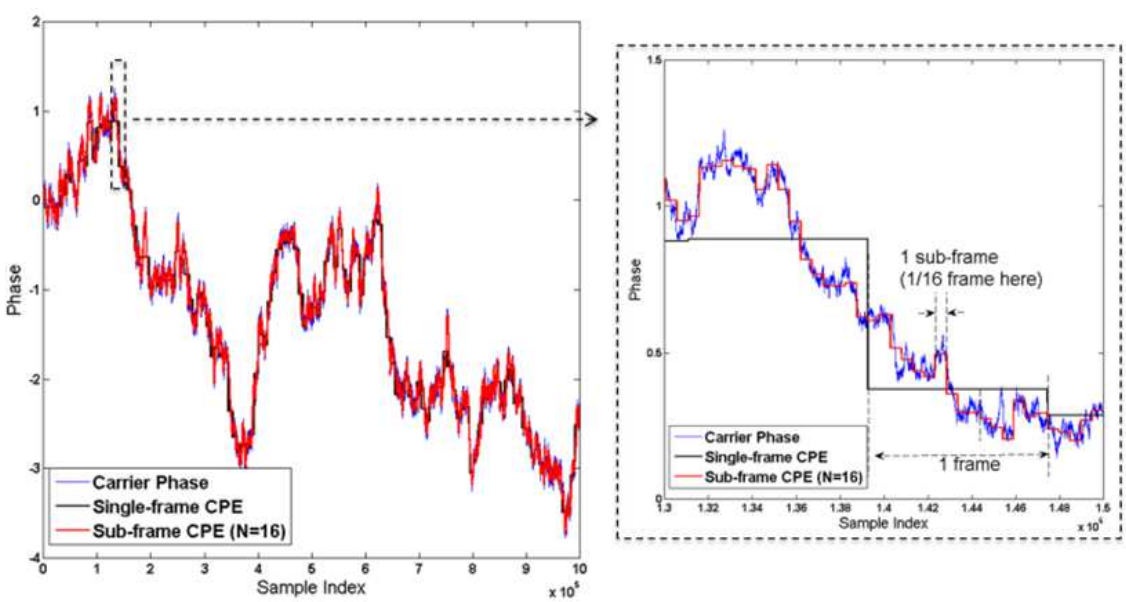

Figure 2: Estimated phase by sub-frame CPE (red) and single-frame CPE (black) and truecarrier phase (blue). Sub-frame CPE provides more accurate phase estimation compared with single-frame CPE.

decisions and received data (with cyclic prefix removed) are then partitioned to several sub-frames to get CPE for each sub-frame.

As shown in Fig. 2, compared with single-frame CPE (black), sub-frame CPE (red) can provide a better estimation of the time varying carrier phase (blue). Therefore, more accurate phase noise compensation can be done with sub-frame CPE. The effectiveness of proposal in long distance fiber transmission system will be presented in the conference.

REFERENCES

1. Shieh, W., et al., *OFDM for Optical Communications*, 2009.
2. Yi, X., et al., *IEEE JLT*, Vol. 26, No. 10, 1309–1316, 2008.
3. Yang, C., et al., *IEEE PTL*, Vol. 22, No. 1, 51–53, 2012.
4. Cao, S., et al., *IEEE PTL*, Vol. 24, No. 22, 2067–2069, 2012.

Session 1P7b
Industrial Forum on CEM (Computational Electromagnetics) Software

Advances in Commercial Field Solver FEKO
Ulrich Jakobus, Peter Futter, C. J. Reddy, ... 318

Workflow to Create 3D Image-based, Simulation Ready Electromagnetic Models
Kerim Genc, Paul Segars, Dane Thompson, Marc Horner, Rebecca Bryan, Simon Richards, Philippe Young, ... 319

New Fast Modeling Algorithms in Commercial Software Tools for High-gain Antennas
Erik Jorgensen, O. Borries, M. Zhou, P. Meincke, N. Vesterdal, ... 320

CEM in the Multiphysics Context
Magnus Olsson, ... 321

Recent Advances in the Computational Electromagnetics Code Efield
Bo Strand, E. Abenius, ... 322

Advances in Commercial Field Solver FEKO

Ulrich Jakobus[1], **Peter Futter**[1], **and C. J. Reddy**[2]

[1]EM Software & Systems — S.A. (Pty) Ltd, Stellenbosch, South Africa
[2]EM Software & Systems (USA) Inc., Hampton, Virginia, USA

Abstract— FEKO is a general purpose 3D computational electromagnetics code incorporating many different solver technologies (e.g., MoM, FEM, UTD, PO, MLFMM, various hybrid combinations of these, MTL cable harness modelling) and also offers advanced support for modern computer hardware (e.g., GPU computing, clusters, multicore etc.). Applications of FEKO covers areas such as antenna design, antenna placement, bio-electromagnetics, electromagnetic compatibility, radar analysis or microwave components.

In this paper, we present some of the recent advances made to the solver of FEKO:

- The characteristic mode analysis (CMA) feature was added which based on the MoM solver will extract data like modal significance or characteristic angle for modes. Visualization of these provide a tool in understanding the fundamental current distributions on antennas and their environment, which is a very useful tool for antenna design engineers.
- The MoM/SEP (Method of Moments/Surface Equivalence Principle) was combined with the planar multilayer Green's function allowing to model finite size 3D objects buried in multilayer substrates/earth, but also at the same time allowing to truncate such multilayer substrates to finite sizes without actually meshing them (i.e., then modelling finite sized substrates of planar patch antennas in a very efficient manner).
- A special array solver was added to FEKO which allows to model large finite size array antennas in a very efficient and memory economical manner. This is achieved by using a kind of perturbation technique which still models edge effects accurately.
- FEKO's GPU (graphical processing unit) computing ability was extended to support multiple GPUs and is compatible with the latest graphics hardware (e.g., NVIDIA Kepler K20) with excellent compute performance.
- For MoM codes the traditional linear rooftop RWG (Rao-Wilton-Glisson) type basis functions on triangular patches are very popular and have also been used in FEKO. These have been extended to also support higher order basis functions (up to order 3.5) which allow mesh sizes of up to about one wavelength (instead of lambda/10 for RWG) resulting in a significant reduction in the overall number of unknowns required to model a given structure, while maintaining (or even increasing) the solution accuracy.

Workflow to Create 3D Image-based, Simulation Ready Electromagnetic Models

Kerim Genc[1], **Paul Segars**[2], **Dane Thompson**[3], **Marc Horner**[3], **Rebecca Bryan**[1], **Simon Richards**[1], **and Philippe Young**[1]

[1]Simpleware Ltd., Exeter, UK
[2]Carl E. Ravin Advanced Imaging Laboratories, Department of Radiology
Duke University Medical Center, Durham, NC, USA
[3]ANSYS, Inc., Canonsburg, PA, USA

Abstract— Creating 3D meshes of multi-part structures from medical scan data (PET, SPECT, CT, MRI, ultrasound etc.) continues to open up exciting new possibilities for the application of electromagnetic (EM) methods to a wide range of biomedical problems including RF ablation, nerve stimulation, hyperthermia and MRI safety [1]. However, such modeling requires a population of accurate simulation compatible human body models and significant challenges to creating such models have prevented them from becoming readily available for industry. These challenges include:

1) **Dataset Availability** — Due to health care industry privacy rules and the expense of creating a virtual population of MRI and/or CT scan data, there are very few readily available dataset repositories of human phantoms for industry to use [2–4].
2) **Segmentation Difficulty** — Segmentation of scan datasets (intelligent labeling of voxel groups on a per object basis) is an extremely man-hour intensive process. Depending on the quality of images and segmentation, this is often measured in terms of man-months or man-years for properly labeling objects within a single body model. The time required for this step has precluded patient specific modeling or hopes for a timely creation of an FE compatible virtual population.
3) **Clean CAD Model Extraction** — Once the data is segmented, extracting usable CAD surface models of the various tissues/layers/objects in the human body is not straight forward. If the CAD model contains coincident spline (NURBS) surface interfaces between tissues, the ability to create a mesh may be slowed significantly or prevented completely. Likewise, faceted volumetric meshes and CAD geometry must contain conformal face mapping between touching objects. This mapping can be very challenging since traditional part-by-part meshing and geometry extraction approaches risk gaps between, or node penetration into adjacent parts, requiring manual and time consuming repair.

We established a potential solution to these challenges through a fast and efficient workflow. The process begins with newly available anatomical geometries and culminates in a solved multi-object computational simulation. Taking advantage of the new series of 4D extended cardiac-torso (XCAT) phantoms created by Segars and colleagues [5], we use a semi-automated smart segmentation routine in ScanIP (Simpleware Ltd., Exeter, UK) to convert these datasets into multi-object simulation ready geometry files that are imported into HFSS (ANSYS Inc., Canonsburg, PA) for electromagnetic simulation. We were able to leverage these technologies to create a proof of concept that may be expanded upon to enable timely patient specific EM biomedical simulation across a population of models generated in the XCAT phantom data set.

REFERENCES

1. Young, P., T. Beresford-West, S. Coward, B. Notarberardino, B. Walker, and A. Abdul-Aziz, "An efficient approach to converting three-dimensional image data into highly accurate computational models," *Phil. Trans. R. Soc.*, Vol. 366, 3155–3173, 2008.
2. Ackerman, M., "The visible human project: A resource for education," *Acad. Med.*, Vol. 74, 667–670, 1999.
3. Park, J., M. Chung, S. Hwang, Y. Lee, D. Har, and H. Park, "Visible Korean human: Improved serially sectioned images of the entire body," *IEEE Trans. Med. Imaging*, 352–360, 2005.
4. http://www.itis.ethz.ch/itis-for-health/virtual-population/human-models/.
5. Segars, W. P., S. Mendonca, J. Grimes, G. Sturgeon, and B. M. W. Tsui, "4D XCAT phantom for multimodality imaging research," *Med. Phys.*, Vol. 37, 4902–4915, 2010.

New Fast Modeling Algorithms in Commercial Software Tools for High-gain Antennas

E. Jørgensen, O. Borries, M. Zhou, P. Meincke, and N. Vesterdal
TICRA, Denmark

Abstract—

CEM in the Multiphysics Context

M. Olsson
COMSOL AB, Sweden

Abstract—

Recent Advances in the Computational Electromagnetics Code Efield

B. Strand and E. Abenius
Efield AB/ESI, Sweden

Abstract—

Session 1P8
SC3&4: Fano Resonances in Microwaves and Optics: Physics and Application

A Tunable Fano Resonance between LSPR and SPP Modes for Improved Refractive Index Sensing
Kristof Lodewijks, Jef Ryken, Wim Van Roy, Gustaaf Borghs, Liesbet Lagae, Pol Van Dorpe, ... 324

Interference of Whispering Gallery Modes in Photonic and Plasmonic Microcavities
Keiji Sasaki, ... 325

Plasmonic Fano Resonances in 3D: Applications to Biosensing, Graphene Spectroscopy, and Super-resolution Imaging
Chihhui Wu, Alexander Khanikaev, Hossein Mousavi, Nihal Arju, Nima Dabidian, Farbod Shafiei, Elaine Li, Gennady Shvets, Ronen Adato, Ahmet Ali Yanik, Hatice Altug, ... 326

Asymptotic Fano-type Formula for Anomalous Transmission in Photonic Crystal Films
Aaron D. Jackson, Stephen P. Shipman, Stephanos Venakides, ... 327

Fano Resonances in Disordered Systems
Alexander N. Poddubny, Mikhail V. Rybin, Mikhail F. Limonov, Yuri S. Kivshar, ... 328

Probing Decoherence through Fano Resonances
Stefan Gehler, U. Kuhl, Hans-Jurgen Stockmann, A. Barnthaler, Stefan Rotter, Florian Libisch, J. Burgdorfer, ... 329

Fano-resonance Spectra in Microwave Structures with Magnetostatic-magnon Particles
Eugene O. Kamenetskii, G. Vaisman, Reuven Shavit, ... 330

Time-domain Differentiation of Optical Pulses in Reflection and in Transmission Using the Same Resonant Grating
Dmitry Alexandrovich Bykov, L. L. Doskolovich, N. V. Golovastikov, ... 331

Fano Resonances via the Characterisation of Individual Hybridized Plasmonic Nanocavities
Yannick Sonnefraud, ... 332

Nanosensors with Dark Plasmonic Modes
Benjamin Gallinet, ... 333

Plasmonic Fano Resonances: Light Harvesting Applications
Peter Nordlander, ... 334

Field Enhancement and Spectrum Shaping in Self-assembled (Opto) Plasmonic Molecules: From Fano Resonances to Optical Vortices
Bjorn M. Reinhard, ... 335

Engineered Absorption Enhancement and Induced Transparency in Fano-resonant Plasmonic and Molecular Systems
Hatice Altug, Ronen Adato, Alp Artar, Shyamsunder Erramilli, ... 336

Classical Analogues of Electromagnetically Induced Transparency and Absorption in Effective Metamaterials
Philippe Tassin, ... 337

Fano Effect in the Optical Micro-cavity Coupling
Fang-Wen Sun, Fang-Jie Shu, Chang-Ling Zou, Chun-Hua Dong, Guangcan Guo, ... 338

Studies of Fano Resonances in Microwave Structures with Magnetostatic-magnon Particles and Dielectric Loadings
M. Berezin, Eugene O. Kamenetskii, Reuven Shavit, ... 339

A Tunable Fano Resonance between LSPR and SPP Modes for Improved Refractive Index Sensing

Kristof Lodewijks[1,2], **Jef Ryken**[1,3], **Wim Van Roy**[1], **Gustaaf Borghs**[1,4], **Liesbet Lagae**[1,4], **and Pol Van Dorpe**[1,4]

[1]IMEC, Kapeldreef 75, B-3001 Leuven, Belgium
[2]Department of Electrical Engineering (ESAT), KU Leuven, Leuven, Belgium
[3]Department of Biosystems (MeBioS), KU Leuven, Leuven, Belgium
[4]Department of Physics and Astronomy, KU Leuven, Leuven, Belgium

Abstract— It is well established that by measuring the phase next to the amplitude of localized and propagating surface plasmon modes, the line width of the resonances can be significantly reduced [1, 2], resulting in an increased Figure-Of-Merit (FOM) for refractive index sensing, and potentially lower detection limits. Here we show how spectroscopic ellipsometry can be utilized to study the interaction between localized (LSPR) and propagating (SPP) surface plasmon modes in periodic arrays of gold nanoparticles on top of a thin dielectric spacer and a continuous gold film. We observe pronounced anti-crossing behavior between the LSPR and SPP modes, which can be exploited to increase the refractive index sensitivity of the LSPR mode. When the modes show strong interaction, the line shape of both resonances becomes highly asymmetric, indicative of strong Fano interference. The measured phase difference between the modes shows a large increase when the interaction is strong, which allows for a more fundamental understanding of the interaction between the different plasmon modes. In phase-sensitive refractive index sensing experiments on randomly distributed and periodic arrays of the same nanoparticles, we show that the FOM is enhanced up to 4 and 25 times respectively, compared to the intensity based measurements. In the former case this effect can be attributed to the phase-based measurements only, while in the latter the FOM is additionally enhanced by the reduction of inhomogeneous broadening and the enhanced refractive index sensitivity due to the Fano interference with the propagating SPP mode.

REFERENCES

1. Huang, Y. H., et al., *Ann. Der Fys.*, Vol. 524, 637–662, 2012.
2. Lodewijks, K., et al., *Nano Lett.*, Vol. 12, 1655–1659, 2012.

Interference of Whispering Gallery Modes in Photonic and Plasmonic Microcavities

Keiji Sasaki
Research Institute for Electronic Science, Hokkaido University, Sapporo 001-0020, Japan

Abstract— We present Fano resonances and Fano-like effects occurring in photonic and plasmonic microcavity systems. The first topic concerns a high-Q microspherical cavity coupled with a tapered optical fiber. Multimode waves propagating in the taper are coupled with a single whispering gallery mode (WGM) of the glass sphere, and their coherent interference results in Fano resonance. The asymmetric line shapes of the transmission spectra change periodically with scanning of the coupling position along the taper. The observed period is due to modal dispersion in the tapered fiber [1]. The second topic is related to localized surface plasmon (LSP) cavity systems. When an incident electric field couples with electron oscillations in a metal nanodisk, surface charge density waves propagate circularly around the disk's edge. The resonance condition for the round-trip propagation determines the angular modes, which correspond to the WGMs. When multiple WGMs are simultaneously excited, they interfere with each other, which results in Fano-like resonances appearing in the far-field scattering spectra. We investigated the nanoscale spatial shapes of the LSP fields within hot spots of a gold nanodisk dimer system, which exhibit complicated fine structures, rather than single peaks. The nanopatterns are created by constructive and destructive interferences of dipolar, quadrupolar, and higher-order multipolar plasmonic modes, which can be drastically altered by controlling parameters of the excitation optical system [2]. We also introduce Fano-like resonance in an optically driven atomic force microscope cantilever and its application to nonvibrating tapping-mode near-field optical microscope [3].

REFERENCES

1. Chiba, A., H. Fujiwara, J. Hotta, S. Takeuchi, and K. Sasaki, "Fano resonance in a multimode tapered fiber coupled with a microspherical cavities," *Appl. Phys. Lett.*, Vol. 86, 261106, 2005.
2. Tanaka, Y., A. Sanada, and K. Sasaki, "Nanoscale interference patterns of gap-mode multipolar plasmonic fields," *Sci. Rep.*, Vol. 2, 764, 2012.
3. Kadri, S., H. Fujiwara, and K. Sasaki, "Fano-like resonance in an optically driven atomic force microscope cantilever," *Opt. Express*, Vol. 19, 2317, 2011.

Plasmonic Fano Resonances in 3D: Applications to Biosensing, Graphene Spectroscopy, and Super-resolution Imaging

Chihhui Wu[1], **Alexander Khanikaev**[1], **Hossein Mousavi**[1], **Nihal Arju**[1], **Nima Dabidian**[1], **Farbod Shafiei**[1], **Elaine Li**[1], **Gennady Shvets**[1], **Ronen Adato**[2], **Ahmet Ali Yanik**[2], **and Hatice Altug**[2]

[1]Department of Physics, The University of Texas at Austin, Austin, Texas 78712, USA
[2]Department of Electrical Engineering and Computer Science, Boston University, Boston, MA 02215, USA

Abstract— It will be demonstrated how precise information about the structure of protein and graphene monolayers (thickness, bond orientation, dipole strength) can be obtained using Fanoresonant metamaterials. Three-dimensional orientation of proteins on the surface of a plasmonic sensor is shown to reveal itself through the strength of the Fano feature. A novel diffractionbeating technique, Polarization Spectro-Tomography, will be introduced.

Plasmonic metamaterials are engineered artificial media with tailored electromagnetic response over a broad range of frequencies: from visible to THz. Their optical properties go beyond those achievable using naturally-occurring optical materials, exhibiting a number of exotic phenomena which include negative refractive index, strong chirality, and indefinite electric permittivity. Metamaterials manifesting these unusual optical properties are typically comprised of highly-resonant plasmonic elements (e.g., split-ring resonators) which have a spectrally-narrow response and high local field concentration. Owing to these properties, plasmonic metamaterials and single meta-molecules have recently emerged as a powerful photonic platform for sensing applications and have been used for linear and nonlinear surface-enhanced spectroscopies. Especially important for biosensing applications are infrared metamaterials, because bio-molecules possess mid-infrared vibrational fingerprints that can be used for their identification, thereby improving specificity of bio-detection.

I will demonstrate how high-Q Fano-resonant modes of a infrared plasmonic metamaterials matched to vibrational molecular fingerprints can be used for sensing of molecular monolayers [1], which is accomplished by calculating the difference reflectivity. I will demonstrate: (i) vibrational fingerprinting and measurement of the thickness of the binding protein; (ii) detection and determination of the thickness of the antibody monolayer using as a molecular yardstick; (iii) determination of spatial orientation of the proteins with respect to the metal surface normal. The latter measurement is a remarkable application of Fano resonances to three-dimensional structure retrieval of bio-molecules.

I will also demonstrate blue-shifting of metamaterial resonances by strongly anisotropic materials such as single-layer graphene [2]. In addition, infrared spectroscopy of graphene and extraction of its complex-valued frequency-dependent conductivity is enabled. An experimental demonstration of a novel three-dimensional spectroscopic ruler, called "plasmonic protractor", will be presented [3]. Using a new far-field technique, Polarization Spectro-Tomography (PST), we use the plasmonic protractor to localize "dark" quantum dots on the surface of a "bright" nanosphere with super-resolution accuracy. Potentially this could lead to a new labeling technique for biomolecules. The experimental data validating the PST concept will be presented for a "dark" nanorod brought in contact with a nanosphere using an AFM.

REFERENCES

1. Wu, C., A. B. Khanikaev, R. Adato, N. Arju, A. A. Yanik, H. Altug, and G. Shvets, "Fano-resonant asymmetric metamaterials for ultrasensitive spectroscopy and identification of molecular monolayers," *Nature Materials*, Vol. 11, 69, 2012.
2. Mousavi, S. H., I. Kholmanov, K. B. Alici, D. Purtseladze, N. Arju, K. Tatar, D. Y. Fozdar, J. W. Suk, Y. Hao, A. B. Khanikaev, R. S. Ruoff, and G. Shvets, "Inductive tuning of fano-resonant metasurfaces using plasmonic response of graphene in the mid-infrared," *Nano Letters*, Vol. 13, 1111, 2013.
3. Shafiei, F., C. Wu, Y. Wu, A. B. Khanikaev, P. Putzke, A. Singh, X. Li, and G. Shvets, "Plasmonic nano-protractor based on polarization spectro-tomography," *Nature Photonics*, 2013 (in press).

Asymptotic Fano-type Formula for Anomalous Transmission in Photonic Crystal Films

Aaron Jackson[1], **Stephen P. Shipman**[2], **and Stephanos Venakides**[3]

[1]Bloomberg, New York, USA
[2]Department of Mathematics, Louisiana State University, USA
[3]Department of Mathematics, Duke University, USA

Abstract— We obtain a Fano-type asymptotic formula for the *anomalous transmission* of electromagnetic plane waves through a film of finite thickness and non-metallic dielectric permittivity distribution that is 2D periodic in space. Our calculation assumes lossless materials and surrounding medium and applies to the range of incident frequencies for which there is only one propagating mode. Periodicity is the only restriction on the geometry of the film. The anomalous transmission occurs near values of the frequency and of the Bloch wavevector at which there is a *bound state*, that is a field, localized in the vicinity of the film. The bound states that we examine are *nonrobust*; occurring at normal incidence (zero Bloch wavevector), they disappear upon perturbation of the angle of incidence or, equivalently, of the Bloch wavevector. It is this dissolution of the bound state that produces the transmission anomaly.

We follow a radically different path from the original calculation of Ugo Fano. His approximation of neglecting the mutual interaction of the states of the continuous spectrum is not relevant in our approach. The present work extends the result of Shipman and Venakides (films with one-dimensional periodicity such as an infinite array of parallel rods, and a specific polarization) to films with two dimensional periodicity and any polarization.

To explain our derivation, let us assume for simplicity that the film, immersed into a surrounding medium of infinite extent, consists of a single dielectric material with doubly periodic structure. The *boundary-integral* formulation of the Maxwell equations involves the tangential components of the EM fields along the interface of the two media. The tangential source field is expressed as the result of a linear integral operator acting on the tangential total field, that is then calculated by solving this equation. The bound state, being sourceless, occurs at wave parameters (frequency and Bloch wavevector) at which the linear operator has a zero eigenvalue.

Assuming that perturbing these wave parameters in a small vicinity produces a unique, nonzero, necessarily small eigenvalue, we use this eigenvalue to scale the amplitude of the incident wave. We obtain two other amplitudes, the one of the reflected and the one of the transmitted waves. We utilize the following properties of the three amplitudes: (1) All three are analytic functions of the frequency and of the two wavenumbers that constitute the wavevector. (2) All three equal zero at the bound state. (3) They participate in the classic equation of the conservation of energy. (4) The zeroes of the eigenvalue have nonpositive imaginary part. The first and second properties allow us to invoke the *Weierstrass preparation* theorem for each of the three amplitudes. This theorem expresses the zero set of an analytic function of several variables (frequency and the two components of the wavevector in our case) as the zero set of a polynomial in one of the variables (frequency) with coefficients that are analytic in the other variables (components of the wavevector) near a zero of the function (frequency and wavevector of a bound state). It writes the function as the product of two factors. (a) One factor is the polynomial, just described, that vanishes at the zero set of the function. This is a monic polynomial in the detuning (frequency deviation from bound state). The coefficients, which depend on the wavevector, are also zero at the bound state. (b) The second factor is just an analytic function which is nonzero at the bound state. We have assumed that the eigenvalue at the bound state is simple (perturbations produce only one branch of zeros). The polynomial factor is then of first degree. We now factor each of the three amplitudes in this way, retaining only terms up to a certain order. We then determine some of the expansion constants by forcing conservation of energy. The undetermined parameters in the leading behavior of the formula for transmission profile depend on the geometrical and dielectric structure of the film as well as on the polarization of the incident wave.

Fano Resonances in Disordered Systems

A. N. Poddubny[1,2], **M. V. Rybin**[1,2], **M. F. Limonov**[1,2], **and Yu. S. Kivshar**[1,3]

[1]National Research University for Information Technology, Mechanics and Optics, Russia
[2]Ioffe Physical-Technical Institute, Russia
[3]Australian National University, Australia

Abstract— Fano resonance is a well-known phenomenon, [1] generally manifested as an asymmetric profile of a narrow band in the spectrum due to the interference between the interaction with the continuum and with discrete state. Here we focus on the novel type of Fano resonances arising in the optical transmission spectra of the disordered and lossy photonic crystals.

Light localization in disordered systems and Bragg scattering in regular periodic structures are considered traditionally as two entirely opposite phenomena: disorder leads to degradation of coherent Bragg scattering whereas Anderson localization is suppressed by periodicity. Here we demonstrate the Fano-like interference between resonant Bragg scattering on one hand and light localization and absorption on the other hand. We show, that contrary to a common belief and even physical intuition, the interference between various multiple scattering pathways, prerequisite to Fano resonances, does survive the disorder and the losses.

We focus one-dimensional photonic crystal consisting of alternating layers A and B. The structure is subjected to a specific type of disorder: the dielectric constants of the layers are complex and fluctuating from layer to layer, different layers are statistically independent (see Figure 1). Depending on the strength of losses, disorder and the ration between layer thicknesses the structure transmission can be either suppressed or enhanced at the Bragg condition. This results in the Fano-like resonances in the transmission spectra.

Our results are supported by direct transfer matrix calculations, analytical solution of Fokker-Planck equation and two-wave approximation of the diffraction theory generalized for disordered system. Proposed theory explains experimental observations of Fano resonance in opals [2]. This type of Fano resonance has a general nature and can be manifested in a variety of the lossy and disordered [3] systems allowing for Bragg diffraction.

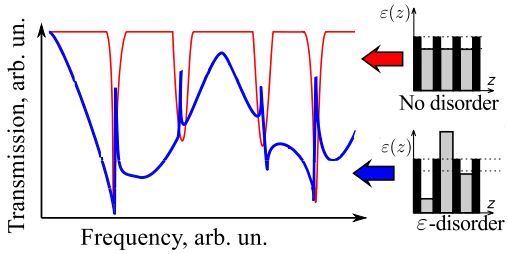

Figure 1: Light transmission spectra through periodic (thin lines) and disordered (thick lines) structures.

REFERENCES

1. Fano, U., "Effects of configuration interaction on intensities and phase shifts," *Phys. Rev. B*, Vol. 124, 1866, 1961.
2. Rybin, M. V., et al., "Fano resonance between Mie and Bragg scattering in photonic crystals", *Phys. Rev. Lett.*, Vol. 103, 023901, 2009.
3. Poddubny, A. N., M. V. Rybin, M. F. Limonov, and Y. S. Kivshar, "Fano interference governs wave transport in disordered systems," *Nature Commun.*, Vol. 3, 914, 2012.

Probing Decoherence through Fano Resonances

S. Gehler[1], **U. Kuhl**[1,2], **H.-J. Stöckmann**[1], **A. Bärnthaler**[3], **S. Rotter**[3], **F. Libisch**[3], **and J. Burgdörfer**[3]

[1]Fachbereich Physik, Philipps-Universität Marburg, Renthof 5, D-35032 Marburg, Germany
[2]LPMC, CNRS UMR 7336, Université de Nice Sophia-Antipolis, F-06108 Nice, France
[3]Institute for Theoretical Physics, Vienna University of Technology, A-1040 Vienna, Austria

Abstract— We investigate the effect of decoherence on Fano resonances in wave transmission through resonant scattering structures [1, 2]. We show that the Fano asymmetry parameter q follows, as a function of the strength of decoherence, trajectories in the complex plane that reveal detailed information on the underlying decoherence process [3]. In particular, we study dephasing and dissipation as the two prototypical decoherence mechanisms.

We find that dephasing leads to a circular dependence of the complex Fano q-parameter on the dephasing strength. Dissipation, in contrast, evolves on a straight line in the complex plane when increasing the dissipation strength. This difference allows us to distinguish between these two different decoherence mechanisms by analyzing the evolution of the Fano q-parameter. To demonstrate this explicitly, we test our predictions in microwave experiments using metallic cavities with different absorption coefficients and at different temperatures. To contrast these results for dissipative transport with those for dephasing, we numerically simulate transport through a dephasing cavity and reanalyze previously published data on temperature dependent transport through quantum dots [4]. The results are in good agreement with our theoretical predictions, thereby demonstrating that the Fano q-parameter contains valuable information, not only on the degree, but also on the specific type of decoherence present in an experiment.

Thus the Fano q-parameter is a good candidate to investigate and determine the decoherence processes in resonant quantum transport.

REFERENCES

1. Rotter, S., F. Libisch, J. Burgdörfer, U. Kuhl, and H.-J. Stöckmann, "Tunable Fano resonances in transport through microwave billiards," *Phys. Rev. E*, Vol. 69, 046208, 2004.
2. Clerk, A. A., X. Waintal, and P. W. Brouwer, "Fano resonances as a probe of phase coherence in quantum dots," *Phys. Rev. Lett.*, Vol. 86, 4636, 2001.
3. Bärnthaler, A., S. Rotter, F. Libisch, J. Burgdörfer, S. Gehler, U. Kuhl, and H.-J. Stöckmann, "Probing decoherence through fano resonances," *Phys. Rev. Lett.*, Vol. 105, 056801, 2010.
4. Zacharia, I. G., D. Goldhaber-Gordon, G. Granger, M. A. Kastner, Yu. B. Khavin, H. Shtrikman, D. Mahalu, and U. Meirav, "Temperature dependence of Fano line shapes in a weakly coupled single-electron transistor," *Phys. Rev. B*, Vol. 64, 155311, 2001.

Fano-resonance Spectra in Microwave Structures with Magnetostatic-magnon Particles

E. O. Kamenetskii, G. Vaisman, and R. Shavit
Microwave Magnetic Laboratory, Department of Electrical and Computer Engineering
Ben Gurion University of the Negev, Beer Sheva, Israel

Abstract— Microwave ferrite structures with a reduced dimensionality brings into play new effects, which should be described based on the quantized picture and demonstrate the properties of artificial atomic structures. Magnetostatic-magnon (MS-magnon) [or magnetic-dipolar-mode (MDM)] oscillations in a mesoscopic ferrite-disk particle are quantized microwave oscillations, which are characterized by energy eigenstates, power-flow vortices and non-zero helicity [1–4]. These oscillations are observed or as the frequency-domain spectrum at a constant bias magnetic fields, or as the magnetic-field-domain spectrum at a constant frequency. For electromagnetic waves irradiating a quasi-2D MS-magnon disk, this small ferrite sample appears as a vortex topological defect with time symmetry breaking. Long radiative lifetimes of MS-magnon modes combine strong subwavelength confinement of electromagnetic energy with a narrow spectral line width carrying the signature of Fano resonances. Due to existence of two coalescent resonances with different chirality one has behaviors of very narrow transparency and reflectivity in the MS-magnon spectrum (Fig. 1). First experimental evidence of the Fano-resonance spectra in microwave structures with MS-magnon ferrite-disk particles have been given in Ref. [5]. Perhaps the most straightforward application of Fano resonances in MS-magnon structures is in the development of microwave sensors for chemical and biological objects with chiral properties [6, 7].

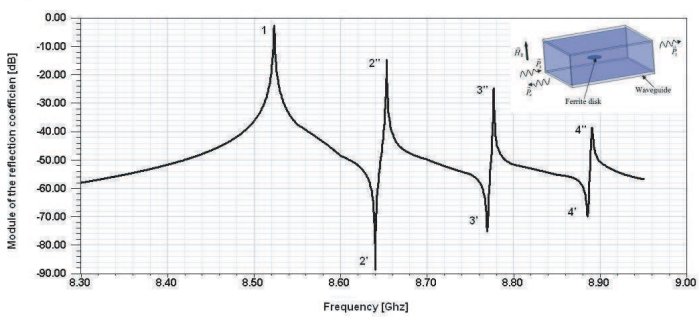

Figure 1: Fano-resonance spectrum in a microwave waveguide with a MS-magnon ferrite disk [4].

REFERENCES

1. Kamenetskii, E. O., "Vortices and chirality of magnetostatic modes in quasi-2D ferrite disc particles," *J. Phys. A: Math. Theor.*, Vol. 40, 6539, 2007.
2. Kamenetskii, E. O., M. Sigalov, and R. Shavit, "Manipulating microwaves with magnetic-dipolar-mode vortices," *Phys. Rev. A*, Vol. 81, 053823, 2010.
3. Kamenetskii, E. O., "Helical-mode magnetostatic resonances in small ferrite particles and singular metamaterials," *J. Phys.: Condens. Matter*, Vol. 22, 486005, 2010.
4. Kamenetskii, E. O., R. Joffe, and R. Shavit, "Coupled states of electromagnetic fields with magnetic-dipolar-mode vortices: MDM-vortex polaritons," *Phys. Rev. A*, Vol. 84, 023836, 2011.
5. Kamenetskii, E. O., A. K. Saha, and I. Awai, "Interaction of magnetic-dipolar modes with microwave-cavity electromagnetic fields," *Phys. Lett. A*, Vol. 332, 303, 2004.
6. Kamenetskii, E. O., R. Joffe, and R. Shavit, "Microwave magnetoelectric fields and their role in the matter-field interaction," *Phys. Rev. E*, Vol. 87, 023201, 2013.
7. Joffe, R., E. O. Kamenetskii, and R. Shavit, "Novel microwave near-field sensors for material characterization, biology, and nanotechnology," *J. Appl. Phys.*, Vol. 113, 063912, 2013.

Time-domain Differentiation of Optical Pulses in Reflection and in Transmission Using the Same Resonant Grating

D. A. Bykov, **L. L. Doskolovich**, **and N. V. Golovastikov**
Image Processing Systems Institute of the Russian Academy of Sciences, Samara 443001, Russia

Abstract— The interaction of light with resonant diffraction gratings (DGs) is in the focus of active research. The resonant DGs exhibit a wide variety of extraordinary (resonant) optical effects, including extraordinary optical transmission, total absorption of incident light, generation of high-intensity evanescent fields with nanoscale features. The diffraction of an optical pulse by a resonant DG can result in substantial changes in the pulse envelope shape [1]. This makes resonant DGs a highly efficient instrument for the implementation of the required pulse transformations (pulse shaping). The transformation of incident pulse envelope implemented by resonant diffraction grating can be described in terms of the passing of an optical signal through a linear time-invariant (LTI) system with the transfer function proportional to the grating transmission (reflection) coefficient. In the vicinity of the resonances associated with the excitation of quasi-guided eigenmodes the resonant features in the grating transmission (reflection) spectrum are represented by Fano profiles. Under certain conditions the Fano profiles can efficiently approximate the transfer function of differentiating (integrating) LTI system [2, 3]. In particular, in our previous work [2] we have demonstrated that the resonant DG can efficiently perform the first-order differentiation of an optical pulse. However, in [2], the possibility of differentiation was considered only in transmission.

In the present work, we consider the general form of the optical pulse transformation implemented by a resonant DG. Special attention is paid to resonant DGs performing the differentiation in reflection. We demonstrate that the same resonant DG can efficiently differentiate both in transmission and in reflection. In this case, the differentiation operations are performed for different central frequencies of the incident pulse corresponding to zeros of reflection and transmission coefficients. The relations between the amplitude of the transformed pulse and the differentiation quality are studied and compared for both operation regimes (in reflection and in transmission). Numerical simulations based on the rigorous coupled-wave analysis demonstrate high-quality differentiation of picosecond pulses in reflection and transmission using the same DG.

ACKNOWLEDGMENT

This work was financially supported by RFBR grants Nos. 12-07-13113, 12-07-00495, 13-07-00464, and 11-07-00153 and RF Presidential grant No. NSh-4128.2012.9.

REFERENCES

1. Vabishchevich, P., V. Bessonov, F. Sychev, M. Shcherbakov, T. Dolgova, and A. Fedyanin, "Femtosecond relaxation dynamics of surface plasmon-polaritons in the vicinity of Fano-type resonance," *JETP Lett.*, Vol. 92, 575–579, 2011.
2. Bykov, D. A., L. L. Doskolovich, and V. A. Soifer, "Temporal differentiation of optical signals using resonant gratings," *Opt. Lett.*, Vol. 36, 3509 (3pp), 2011.
3. Bykov, D. A., L. L. Doskolovich, and V. A. Soifer, "Integration of optical pulses by resonant difraction gratings," *JETP Lett.*, Vol. 95, 6–9, 2012.

Fano Resonances via the Characterisation of Individual Hybridized Plasmonic Nanocavities

Yannick Sonnefraud
Experimental Solid State Group, Physics Department
Imperial College London, London SW7 2AZ, UK

Abstract— Fano resonances can be found in many physical systems presenting a coherent interaction of a broad mode with a sharp dark mode. Plasmonic nanostructures can serve as model systems for a variety of fascinating classical oscillator physics, and one effect they allow to study well is those Fano resonances. The coherent coupling of plasmonic cavities brought to close proximity can lead to the hybridisation [1] of their modes, and to Fano type of lineshape. This has first been predicted by simulations in dolmen [2] and ring-disk system [3], and the first experimental demonstrations soon followed [4, 5]. In this presentation we will point out the key features necessary for the excitation of Fano resonances and the methods used to characterize single plasmonic nanocavities. Confocal extinction measurements give access to the far-field radiation properties of the cavities; whereas the local field enhancement and the charge distribution of the modes at play can be accessed using scattering near-field optical microscopy (s-SNOM). We will show that combining a s-SNOM with a tunable laser source can allow to observe the interactions locally around the Fano dip.

REFERENCES

1. Prodan, E., C. Radloff, N. J. Halas, and P. Nordlander, *Science*, Vol. 302, 419, 2003.
2. Zhang, S., D. A. Genov, Y. Wang, M. Liu, and X. Zhang, *Phys. Rev. Lett.*, Vol. 101, 047401, 2008.
3. Hao, F.,Y. Sonnefraud, P. Van Dorpe, S. A. Maier, N. J. Halas, and P. Nordlander, *Nano Letters*, Vol. 8, 3983, 2008.
4. Verellen, N., Y. Sonnefraud, H. Sobhani, F. Hao, V. V. Moshchalkov, P. Van Dorpe, P. Nordlander, and S. A. Maier, *Nano Letters*, Vol. 9, 1663, 2009.
5. Sonnefraud, Y., N. Verellen, H. Sobhani, G. A. Vandenbosch, V. V. Moshchalkov, P. Van Dorpe, P. Nordlander, and S. A. Maier, *ACS Nano*, Vol. 4, 1664, 2010.

Nanosensors with Dark Plasmonic Modes

B. Gallinet
CSEM SA, CSEM Muttenz, Switzerland

Abstract— Plasmonic modes with long radiative lifetimes, dark modes, combine strong nanoscale light confinement with a narrow spectral line width carrying the signature of Fano resonances, making them very promising for nanophotonic applications such as sensing, lasing, and switching. Their coupling to incident radiation, also known as radiance, determines their optical properties. The use of dark plasmonic modes as sensing platforms is discussed with a general approach. It is theoretically and experimentally demonstrated that the radiance of a plasmonic mode can be classified into three distinct regimes. In the weak coupling regime, it is shown that geometrical displacements of the order of a few ångstroms can be detected optically by measuring the radiance. The development of ultrasensitive sensors based on radiance sensing has potential in a wide range of applications such as molecular rulers, nanoscale temperature, hydrogen or pH sensors. In the intermediate regime, the electromagnetic energy stored in the mode is maximal, with large electric field enhancements that can be exploited in surface enhanced spectroscopy applications. Fano-resonant systems also possess a steep spectral dispersion which makes them promising for refractive index sensors, in particular biochemical sensors and immunoassays. It is analytically and numerically shown that the intrinsic spectral width determines the strength of this dispersion, and depends on the penetration of the electric field in the metallic nanostructure. A figure of merit, given by the ratio of the dark mode sensitivity to its intrinsic width is introduced. Finally, the large-scale fabrication of Fano-resonant nanostructures using nanoimprint lithography is shown, which paves the road towards their practical implementation in low-cost sensing devices.

REFERENCES

1. Gallinet, B. and O. J. F. Martin, "Influence of electromagnetic interactions on the line shape of plasmonic Fano resonances," *ACS Nano*, Vol. 5, 8999, 2011.
2. Gallinet, B., T. Siegfried, H. Sigg, P. Nordlander, and O. J. F. Martin, "Plasmonic radiance: Probing structure at the angstrom scale with visible light," *Nano Letters*, Vol. 13, 497, 2013.

Plasmonic Fano Resonances: Light Harvesting Applications

Peter Nordlander
Laboratory for Nanophotonics, Department of Physics and Astronomy
Rice University, Houston TX77251, USA

Abstract— Metallic nanostructures with their ability of confining and enhancing incident light offer unique possibilities for manipulating light at the nanoscale [1]. Plasmonic nanostructures can also exhibit coherence effects such as Fano resonances where the interference between superradiant and subradiant modes produces extinction features with characteristic narrow and asymmetric line shapes [2]. Due to their narrower spectral width compared to standard plasmon resonances, Fano resonances can provide very large LSPR refractive index sensitivity [3] and provide large electric field enhancements for surface enhanced spectroscopies [4]. Depending on the coupling between the subradiant and superradiant mode, Fano interference can be classified into specific regimes: a weak coupling regime suitable for LSPR sensing; and a critical coupling regime providing large field enhancements suitable for plasmon enhanced spectroscopies [5]. Finally Iwill discuss several recent applications where the unique light capturing capability provided by plasmonic Fano resonances have been exploited to enhance the coupling of light to nearby structures [6, 7].

REFERENCES

1. Halas, N. J., et al., *Adv. Mat.*, Vol. 24, 4842, 2012.
2. Lassiter, J. B., et al., *Nano Lett.*, Vol. 12, 1058, 2012.
3. Lassiter, J. B., et al., *Nano Lett.*, Vol. 10, 3184, 2010.
4. Ye, J., et al., *Nano Lett.*, Vol. 12, 1660, 2012.
5. Gallinet, B., et al., *Nano Lett.*, Vol. 13, 497, 2013.
6. Fang, Z. Y., et al., *Nano Lett.*, Vol. 12, 3808, 2012.
7. Fang, Z. Y., et al., *ACS Nano*, Vol. 6, 10222, 2012.

Field Enhancement and Spectrum Shaping in Self-assembled (Opto) Plasmonic Molecules: From Fano Resonances to Optical Vortices

Björn M. Reinhard
Department of Chemistry and The Photonics Center
Boston University, Boston, MA 02215, USA

Abstract— Conventional approaches for achieving giant E-field enhancements in gap antennas of noble metal nanoparticles (NPs) suffer from the short dephasing times of localized surface plasmons (LSPs) caused by high dissipative and radiative losses in NPs. There is, consequently, a need for alternative design approaches that can create slowly dephasing resonances in the spectra of plasmonic structures. Fano resonances that occur through interference of broad superradiant and sharp subradiant plasmon modes have recently attracted significant interest for engineering plasmonic nanostructures with sharp spectral responses. In this presentation I will briefly review the physical nature underlying the electromagnetic coupling mechanisms that give rise to Fano resonances in plasmonic nanostructures and then expand this concept to hybrid optoplasmonic structures that contain both plasmonic nanoantennas and dielectric whispering gallery mode (WGM) resonators. Versatile nanofabrication approaches are absolute key for the practical realization of these materials. I will review different template guided self-assembly approaches developed in the Reinhard Laboratory that allow for an efficient fabrication of plasmonic and optoplasmonic molecules with even intricate morphologies. In the last part of the seminar I will introduce an alternative strategy for increasing the dephasing times of plasmonic modes in plasmonic and optoplasmonic molecules based on "storing" the electromagnetic energy in optical vortices. (Opto) plasmonic molecules generate a defined phase landscape that can be shaped to create phase singularities that generate optical vortices at defined locations in space. One experimental implementation of this concept, which provides spectral resonances at multiple frequencies, is achieved by integration of a gold nanoparticle dimer chain into a periodic NP array. The experimental characterization of this structure and its working principle will be discussed in detail.

Engineered Absorption Enhancement and Induced Transparency in Fano-resonant Plasmonic and Molecular Systems

Hatice Altug[1,2], Ronen Adato[2], Alp Artar[1], and Shyam Erramilli[1]

[1]Electrical and Computer Engineering, Boston University, Boston, MA 02215, USA
[2]Biomedical Engineering, Ecole Polytechnique Federale de Lausanne, 1024, Switzerland

Abstract— Coupled plasmonic resonators have become the subject of significant research interest in recent years as they provide a route to dramatically enhanced light-matter interactions. This is important for applications involving slow light, sensor and general metamaterial design. Often, the design of these coupled mode systems draws intuition and inspiration from analogies to atomic and molecular physics systems. In particular, they have been shown to mimic quantum interference effects, such as electromagnetically induced transparency (EIT) and Fano resonances. Interaction between the coupled modes in Fano-resonant systems is described using standard coupled harmonic oscillator model. In this work we demonstrate that this standard treatment neglects a fundamental and important relationship between the driving force applied to the system and its damping rate. We then develop an intuitive and powerful picture of the interaction that addresses this issue and therefore satisfies fundamental time-reversal symmetry and reciprocity considerations. We apply our model and demonstrate its consequences through a series of analytical and numerical calculations and experimental measurements.

Broadly, this treatment is required to correctly describe the fundamental behavior of coupled plasmonic modes, which can be thought of the building blocks for a wide range of important physical systems. Significantly, the coupling between a plasmonic resonance and a weak molecular absorber forms the basis for the surface enhanced absorption effect. We first demonstrate, through analytical scattering calculations of such a system, that the absorption spectra may alternatively resemble the commonly observed EIT like sharp spectral dip at the absorption line or the converse effect, a superimposed peak, usually referred to as analogous to electromagnetically induced absorption (EIA). We additionally show that, not only is our approach necessary for the accurate prediction of surface enhanced absorption spectra, but it additionally implies that the standard intuition of increased field enhancement leading to increased signal is not necessarily the case. We show, for example, that structures, which support high field enhancement, may yet yield negligible surface enhanced absorption signal as a result of effects predicted by our model. We verify these seemingly unexpected effects through analytical and numerical calculations, as well as a surface enhanced infrared absorption (SEIRA) spectroscopy experiment using a metamaterial perfect absorber. Finally, we conclude by noting that our model is completely general, and applies equally well to fully plasmonic systems, such as the 'dolmen metamaterial' originally used to generate the plasmonic analogue to EIT. In a unifying manner, not only can the behavior of the meta-molecule be treated identically to a natural molecular absorption line, but we show that a transition between behaviors typically described as EIT and its converse, EIA, can occur as a straightforward consequence of the effects described in this work.

Classical Analogues of Electromagnetically Induced Transparency and Absorption in Effective Metamaterials

Philippe Tassin
Iowa State University, USA

Abstract— We review our work on the classical analogue of electromagnetically induced transparency (EIT) and absorption (EIA) in metamaterials where a radiating oscillator interacts through the near fields with a dark oscillator. We have demonstrated the EIT effect in microwave metamaterials involving meta-atoms made from metallic and from superconducting constituent elements, reaching group delays of 300 ns or slowdown factors of approximately 250,000. Subsequently, we discuss a simple two-oscillator model that accounts for the coupling between the radiative oscillator and we show that this model can be used to accurately model the scattering parameters of EIT metamaterials, including the transmission and group delay spectra. The model further suggests that a peak instead of a minimum in the absorption spectrum can be obtained when the radiation damping in the bright oscillator is sufficiently small. This classical analogue of EIA was subsequently verified experimentally.

REFERENCES

1. Tassin, P., L. Zhang, T. Koschny, E. N. Economou, and C. M. Soukoulis, "Low loss metamaterials based on classical electromagnetically induced transparency," *Phys. Rev. Lett.*, Vol. 102, 053901, 2009.
2. Zhang, L., P. Tassin, T. Koschny, C. Kurter, S. M. Anlage, and C. M. Soukoulis, "Large group delay in a microwave metamaterial analogue of electromagnetically induced transparency," *Appl. Phys. Lett.*, Vol. 97, 241904, 2010.
3. Kurter, C., P. Tassin, L. Zhang, T. Koschny, S. M. Anlage, and C. M. Soukoulis, "Classical analogue of electromagnetically induced transparency with a metal-superconductor hybrid metamaterial," *Phys. Rev. Lett.*, Vol. 107, 043901, 2011.
4. Tassin, P., L. Zhang, R. Zhao, A. Jain, T. Koschny, and C. M. Soukoulis, "Electromagnetically induced transparency and absorption in metamaterials: The radiating two-oscillator model and its experimental confirmation," *Phys. Rev. Lett.*, Vol. 109, 187401, 2012.

Fano Effect in the Optical Micro-cavity Coupling

Fang-Wen Sun[1], **Fang-Jie Shu**[2], **Chang-Ling Zou**[1], **Chun-Hua Dong**[1], **and Guang-Can Guo**[1]

[1]Key Laboratory of Quantum Information
University of Science and Technology of China, Hefei, Anhui 230026, China
[2]Department of Physics, Shangqiu Normal University, Shangqiu 476000, China

Abstract— Fano effect is usually found in the spectroscopy and has been well studied in various physical systems, since it has been discovered to discuss different interference phenomena. It comes from the competition and interference between two possible paths with different spectral properties. For example, in the optical micro-cavity, there are different optical resonant modes with different quality factors. The coupling between those modes will show Fano effect and electromagnetically induced transparency like effect. Here, we will demonstrate the Fano effect in the optical coupling to a Whispering Gallery Mode (WGM) micro-cavity. Theoretical studies have shown the Fano effect will be found in the optical spectrum. In the perpendicular coupling to WGM cavity with a waveguide or fiber taper, all spectrum lineshapes are asymmetric Fano-like lineshapes instead of expected symmetric Lorentz-shape dip for the parallel coupler. The incident light will undergo a tunnel coupling to the WGMs and be reflected at both the waveguide end and the cavity boundary. Thus, the detected reflective light is composed of the light tunneling from the WGMs and the reflected light on the interfaces. The interference between different components results in the Fano spectrum. In the free space coupling through barrier tunneling, similar Fano effect can also be observed as a result of multiple cylinder wave interference. In experiment, we demonstrated the Fano effect in the normal parallel coupling. Due to the coupling between WGMs with different quality factors and the fiber taper, both the symmetric electromagnetically induced transparency like and asymmetric Fano-like line was observed by changing the coupling strength.

Studies of Fano Resonances in Microwave Structures with Magnetostatic-magnon Particles and Dielectric Loadings

M. Berezin, E. O. Kamenetskii, and R. Shavit
Microwave Magnetic Laboratory
Department of Electrical and Computer Engineering
Ben Gurion University of the Negev, Beer Sheva, Israel

Abstract— In Ref. [1], we gave a general description of Fano-resonance spectra in microwave structures with magnetostatic-magnon (MS-magnon) ferrite-disk particles. These Fano resonances were previously experimentally observed in [2, 3]. In the present work, we analyze the effects of different dielectric loadings in such microwave structures on the behavior of Fano resonances. Based on numerical and experimental studies, we show that Fano-resonance spectra of MS-magnon particles are very sensitive to material parameters and geometry of dielectric loadings.

The nature of interaction of MS-magnon ferrite-disk particles with microwave irradiation is well described by topological properties of the fields. These properties are characterized by topological factors of the fields: power-flow vortices and the helicity parameters [4–7]. Study of these topological structures of the fields is the basis of the present work on MS-magnon Fano resonances in microwave systems.

REFERENCES

1. Kamenetskii, E. O., G. Vaisman, and R. Shavit, "Fano-resonance spectra in microwave structures with magnetostatic-magnon particles," Submitted to *Progress In Electromagnetics Research Symposium*, Stockholm, Sweden, August 12–15, 2013.
2. Kamenetskii, E. O., A. K. Saha, and I. Awai, "Interaction of magnetic-dipolar modes with microwave-cavity electromagnetic fields," *Physics Letters A*, Vol. 332, 303, 2004.
3. Sigalov, M., E. O. Kamenetskii, and R. Shavit, "Electric self inductance of quasi-2D magnetic-dipolar-mode ferrite disks," *J. Appl. Phys.*, Vol. 104, 053901, 2008.
4. Kamenetskii, E. O., M. Sigalov, and R. Shavit, "Manipulating microwaves with magnetic-dipolar-mode vortices," *Phys. Rev. A*, Vol. 81, 053823, 2010.
5. Kamenetskii, E. O., R. Joffe, and R. Shavit, "Coupled states of electromagnetic fields with magnetic-dipolar-mode vortices: MDM-vortex polaritons," *Phys. Rev. A*, Vol. 84, 023836, 2011.
6. Berezin, M., E. O. Kamenetskii, and R. Shavit, "Topological-phase effects and path-dependent interference in microwave structures with magnetic-dipolar-mode ferrite particles," *J. Opt.*, Vol. 14, 125602, 2012.
7. Kamenetskii, E. O., R. Joffe, and R. Shavit, "Microwave magnetoelectric fields and their role in the matter-field interaction," *Phys. Rev. E*, Vol. 87, 023201, 2013.

Session 1P9
SC1: Ultrawideband Nondiffracting and Accelerating Waves

New Applications for Non-diffracting Light Fields
Kishan Dholakia, ... 342

Focus Wave Modes Based on Moving Sources and Angular Spectrum Representation
Colin J. R. Sheppard, ... 343

Complexified Spherical Waves and Their Sources in the Physical Space
Azat M. Tagirdzhanov, Aleksei P. Kiselev, ... 344

High-field Bessel Pulses and Shock-front Assisted Resonant Radiation
Thomas W. Roger, Chunyong Li, Mohammed F. Saleh, Samudra Roy, Fabio Biancalana, Daniele Faccio, ... 345

Localized Pulsed Waves in Hyperbolic Media
Ioannis M. Besieris, Amr M. Shaarawi, ... 346

Spatiotemporal Properties of Broadband Axicon Fields
Rahul Dutta, Kimmo Saastamoinen, Jari Turunen, Ari T. Friberg, ... 347

Energy Transport Velocity for Various Localized and Accelerating Pulsed Waves
Peter Saari, O. Rebane, Ioannis M. Besieris, ... 348

Non-diffractive Light Beams and Bullets in Nonlinear Media with Dissipation
Miguel A. Porras, ... 349

Spherical Light, Arbitrary Nonparaxial Accelerating Beams and Femtosecond Laser Micromachining of Curved Profiles
Francois Courvoisier, A. Mathis, L. Froehly, M. Jacquot, R. Giust, L. Furfaro, John M. Dudley, . 350

Generation and Characterization of Ultrawideband Airy Pulses
Peeter Piksarv, A. Valdmann, Heli Valtna-Lukner, R. Matt, Peter Saari, ... 351

Three-dimensional Nonparaxial Accelerated Waves and Pulses That Follow Circular Paths
Miguel A. Alonso, Miguel A. Bandres, Ido Kaminer, Mordechai Segev, ... 352

Sub-3-cycle Linear Light Bullets
Martin Bock, Ruediger Grunwald, ... 353

Temporal Focusing and Focus Wave Modes
Colin J. R. Sheppard, Elijah Y. S. Yew, Peter T. C. So, ... 354

New Applications for Non-diffracting Light Fields

Kishan Dholakia
School of Physics and Astronomy, University of St Andrews, UK

Abstract— The last decade has seen immense advances in photonics based methods for imaging and manipulation. However in many photonics fields there is a recognition that using the direct form a laser output — the Gaussian beam — is insufficient for a number of applications in manipulation and beyond [1].

I will describe the use of propagation invariant ('non-diffracting') light fields for applications such as particle manipulation, cell transfection and imaging. These light fields, as the name suggests retain their transverse intensity profile upon propagation. Bessel light fields and Airy light fields are prime examples of such beams.

In terms of light assisted targeted drug delivery through photoporation, we can use a Bessel light mode to relax the constraint of accurately locating the cell membrane with a tightly focused light beam. As the most prominent method of such cell transfection is a multiphoton process with a femtosecond laser this turns out to be a very advantageous method to improve usefulness of the method [2, 3]. Shaping the output of a microscopic optical fibre with conical or other lens types leads to endoscopic variants of photoporation that may be useful.

In terms of imaging, Single plane illumination (light sheet) microscopy (SPIM) offers a myriad of unique advantages. Orthogonal detection allows rapid imaging of large, three-dimensional, samples of living tissue. Illumination with a thin sheet of light ensures high contrast by minimizing the fluorescent background. Moreover, by restricting the sample exposure to a single plane, photobleaching and damage are minimized, crucial when imaging photo-sensitive samples over a larger period of time. Recent enhancements to the original technique attempt to overcome the inherent trade off between axial resolution and field-of-view of conventional light sheet microscopy. To date, this was only achieved by compromising on one or more of its key advantages: high contrast, time-resolution, or minimal sample exposure. I will discuss the use of appropriate light fields for wavefront correction [4] and enhancement within this imaging modality.

REFERENCES

1. Dholakia, K. and T. Čižmár, "Shaping the future of manipulation," *Nature Photonics*, Vol. 5, 335–342, 2011.
2. Tsampoula, X., et al., "Femtosecond cellular transfection using a nondiffracting light beam," *Appl. Phys. Lett.*, Vol. 91, 053902, 2007.
3. Rudhall, A., et al., "Exploring the ultrashort pulse laser parameter space for membrane permeabilisation in mammalian cells," *Sci. Reports*, Vol. 2, 858, 2012.
4. Dalgarno, H. I. C., et al., "Wavefront corrected light sheet microscopy in turbid media," *Appl. Phys. Lett.*, Vol. 100, 191108, 2012.

Focus Wave Modes Based on Moving Sources and Angular Spectrum Representation

Colin J. R. Sheppard
Istituto Italiano di Tecnologia, via Morego 30, Genova IT 16163, Italy

Abstract— Saari presented a model for the focus wave mode (FWM) based on the field of a moving source and sink combination [1]. An alternative representation is based on appropriate summation of a polychromatic angular spectrum of plane waves, equivalent to a polychromatic summation of Bessel beams, which are each solutions of the Helmholtz equation. The group velocity then gives the velocity of the moving source. Solutions can be found that are consistent with sources traveling with velocities less than, or greater than, the speed of light, in addition to the usual focus wave mode solution that travels at the speed of light [2]. We call these the generalized FWMs. The X-wave is a special case of the superluminal solution. In contrast, pulsed Gaussian beams can be considered as the field of a stationary, pulsating, source/sink pair [3, 4]. A different solution that has been investigated is made up of identical spectral components, which we have called a Type 1 pulse [4].

Using a causal, (time-) spectral distribution given by a shifted gamma distribution, we find that an integration over Bessel beams gives a Laguerre-Gaussian variation, exhibiting weak sidelobes [5]. So we see there is a fundamental connection between Bessel and Gaussian beams. Comparison of the source and angular spectrum models requires a consistent form of the (space-) spectral representation of a source and sink: the usual representation of a source in theoretical physics is non-causal [6, Page 612] (for the 4D case), so we use a causal form, which is similar to that well-known in signal processing [7]. This leads to a straightforward spectral representation of a complex source/sink beam [8]. As any integration over Bessel beams is still a solution of the Helmholtz equation, a further extension of the pulsed solutions can be developed, which includes the generalized focus wave modes (including FWM and X-waves) and the Type 1 pulses as special cases.

REFERENCES

1. Saari, P. and K. Reivelt, "Generation and classification of localized waves by Lorentz transformations in Fourier space," *Phys. Rev. E*, Vol. 69, 036612, 2004.
2. Sheppard, C. J. R., "Generalized Bessel pulse beams," *Journal of the Optical Society of America A*, Vol. 19, 2218–2222, 2002.
3. Saari, P., "Evolution of subcycle pulses in nonparaxial Gaussian beams," *Optics Express*, Vol. 8, 590–598, 2001.
4. Sheppard, C. J. R. and X. Gan, "Free-space propagation of femto-second light pulses," *Optics Comm.*, Vol. 133, 1–6, 1997.
5. Sheppard, C. J. R., "Bessel pulse beams and focus wave modes," *Journal of the Optical Society of America A*, Vol. 18, 2594–2600, 2001.
6. Jackson, J. D., *Classical Electrodynamics,* John Wiley & Sons, New York, 1962.
7. Bracewell, R. N., "The Fourier transform and its applications," *McGraw-Hill Electrical and Electronic Engineering Series,* McGraw Hill, New York, 1978.
8. Sheppard, C. J. R. and M. D. Sharma, "Spatial frequency content of ultrashort pulsed beams," *Journal of Optics A: Pure and Applied Optics*, Vol. 4, 549–552, 2002.

Complexified Spherical Waves and Their Sources in the Physical Space

A. M. Tagirdzhanov[1] **and A. P. Kiselev**[1, 2, 3]

[1]St. Petersburg State University, Russia
[2]Steklov Mathematical Institute St. Petersburg Department, Russia
[3]Institute of Problems of Mechanical Engineering, Russia

Abstract— We address spherical waves complexified by a complex shift in a coordinate of the point source. They have been studied since early 1970th in both time-harmonic and non-time-harmonic cases as exact localized solutions of the wave equation. We deal with the fundamental mode described by $u = \frac{f(\theta_*)}{R_*}$, where $R_* = \sqrt{x^2 + y^2 + (z - ia)^2}$, $a > 0$ is a free positive constant, $\theta_* = R_* - ct$ is a complex phase and $f(\theta_*)$ is an arbitrary function describing the wave form. Such a function satisfies the inhomogeneous wave equation $u_{xx} + u_{yy} + u_{zz} - c^{-2}u_{tt} = F$ with a certain source function $F = F(x, y, z, t)$, which is a generalized function supported by a 2D surface in the real 3D physical space. Here, $c > 0$ is the constant wave speed. The function F is dependent on the wave form f as well as on the definition of branch of the square root in the "complex distance" R_*. Unlike several earlier research, where sources in complex space were discussed, we focuss on explicit finding the source function F in the real physical space for a rather arbitrary wave form f. The procedure of finding the source function F for non-time-harmonic case is based on that presented earlier by the authors for the time-harmonic case. For different definitions of the branch of the square root, we consider several particular examples of the wave forms allowing localized wave fields.

High-field Bessel Pulses and Shock-front Assisted Resonant Radiation

T. W. Roger[1], **C. Li**[1], **M. F. Saleh**[2], **S. Roy**[2], **F. Biancalana**[1,2], **and D. Faccio**[1]

[1]School of Engineering and Physical Sciences, SUPA, Heriot-Watt University, UK
[2]Max Planck Institute for the Science of Light, Gunther-Scharowsky Str. 1, Erlangen 91058, Germany

Abstract— Resonant radiation (RR), commonly known as dispersive-wave or Cerenkov emission is a well studied effect caused by the propagation of a soliton in an optical fibre. The presence of higher-order dispersion causes light to scatter through a resonant-like process to a blue-shifted frequency. Here we use a class of optical pulses known as Bessel pulses to reach extremely high peak intensities, while simultaneously suppressing transverse beam reshaping and self focusing induced collapse. This combination of properties allows us, for the first time, to access a new kind of resonant radiation that appears even with normal group velocity dispersion (GVD). Theoretical modelling shows that these modes are a direct consequence of high laser pulse intensities. The relation, $k_z(\omega) = k_z(\omega_{\rm IN}) + (\omega - \omega_{\rm IN})/v$, is the fundamental momentum conservation relation that determines the wavelength of the RR. In normal GVD and considering the phase matching condition between pump pulse and RR then Taylor expanding we generalise this relation such that

$$k_z(\omega) - k_z(\omega_{\rm IN}) - (\omega - \omega_{\rm IN})/v = \sum_{m=2}^{\infty} \frac{\beta_m}{m!} \Delta\omega^m = \gamma P(1 + \tau_{\rm shock}\Delta\omega) \tag{1}$$

We have introduced the additional term, $\gamma P \tau_{\rm shock} \Delta\omega$, where $\tau_{\rm shock} \sim 1/\omega_{\rm IN}$ and accounts for dispersion that arises in the presence of intense shock fronts. We have verified both numerically and experimentally that this relation indeed correctly predicts the formation of new RR modes. As an example, in Fig. 1 we show the experimental evolution of the spectral broadening created in bulk fused silica as the pump energy is increased. At a certain pump energy threshold (5.5 µJ) the light is scattered to a new resonant mode. The dashed line in the figure at $E = 5.5\,\mu$J shows the fit obtained from Eq. (1) — the shock induced RR appears as a conical emission at a wavelength that is blue-shifted by nearly one octave. At very high pump energies the pulse eventually collapses and forms a filament characterised by temporal pulse splitting and complex spatio-temporal dynamics that cover the structure of the shock-induced RR.

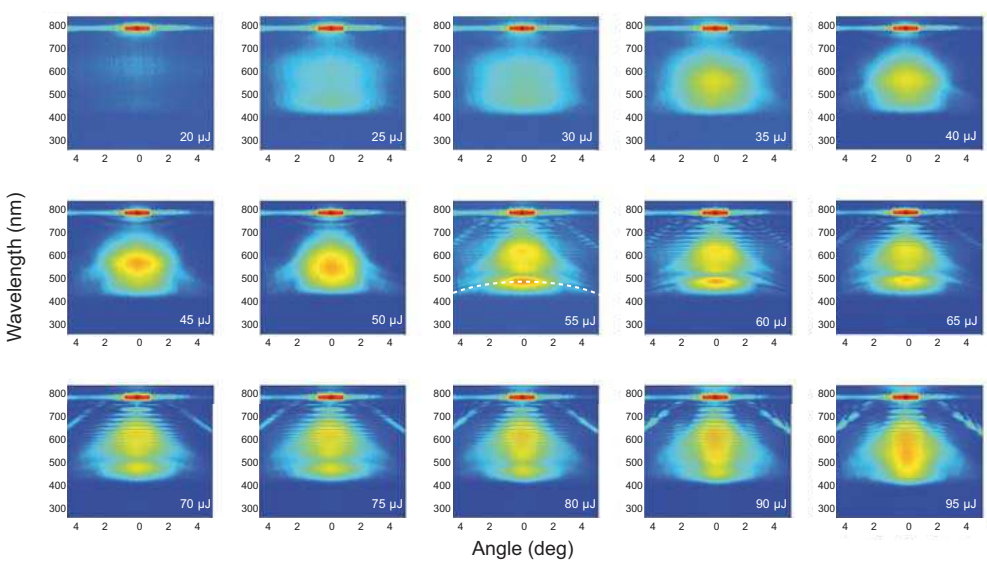

Figure 1: The evolution of supercontinuum and later (55 µJ) the resonant radiative peak as the pumping energy is increased. The super continuum is created in bulk fused silica via an intense Bessel pulse. A fit has been made using Eq. (1) to find the RR wavelength, which follows the expected shape of the conical emission.

Localized Pulsed Waves in Hyperbolic Media

I. M. Besieris[1] and A. M. Shaarawi[2]

[1]The Bradley Department of Electrical and Computer Engineering, VPI&SU
Blacksburg, Virginia 24061, USA
[2]The Physics Department, The American University in Cairo
P. O. Box 74, New Cairo 11835, Egypt

Abstract— Consider a nonmagnetic uniaxially anisotropic material with diagonal electric permittivity matrix elements $\varepsilon_{xx}, \varepsilon_{yy} = \varepsilon_{xx}, \varepsilon_{zz}$. If both elements are positive, the dispersion relation is described by an ellipsoid. Within a certain frequency band, however, it may turn out that one diagonal element is positive and the other negative. Then, the dispersion relation is described by a hyperboloid. Under these conditions, the material is referred to as a *hyperbolic medium*. Such a medium can be realized with metal-dielectric nanolayers or nanowire composites in the optical regime. Source-free, transverse magnetic electromagnetic fields in the frequency domain are expressed in terms of an appropriately defined Hertz vector potential $\vec{\Pi}(\vec{r},\omega) = \tilde{\Pi}_e(\vec{r},\omega)\hat{z}$ governed by the equation

$$\left(\nabla_t^2 + \frac{\varepsilon_{zz}}{\varepsilon_{xx}}\frac{\partial^2}{\partial z^2} + \frac{\varepsilon_{zz}}{\varepsilon_0}k^2\right)\tilde{\Pi}_e(\vec{r},\omega) = 0; \quad k \equiv \omega/c.$$

This expression is a de Broglie-like equation for $\varepsilon_{xx} < 0$ and $\varepsilon_{zz} > 0$, and a Klein-Gordon-like equation for $\varepsilon_{xx} > 0$ and $\varepsilon_{zz} < 0$, with a *timelike* z coordinate. For both cases, large classes of spatially localized solutions $\tilde{\Pi}_e(\vec{r},\omega)$ are available. A parabolic approximation of the de Broglie-like equation along the y direction yields an equation analogous to that arising in the study of bidispersion. Using hyperbolic rotations, a broad class of skewed, nonspreading, "accelerating" Airy solutions can be obtained.

The study of propagation of pulsed signals in hyperbolic media is complicated, in general, due to the frequency dependence of the permittivity matrix elements. Consider, however, a *canonical* situation whereby the permittivity matrix elements are constant within a certain frequency regime. Then, approximately, one has

$$\left(\nabla_t^2 - \frac{|\varepsilon_{zz}|}{\varepsilon_{xx}}\frac{\partial^2}{\partial z^2} + \frac{|\varepsilon_{zz}|}{\varepsilon_0}\frac{1}{c^2}\frac{\partial^2}{\partial t^2}\right)\Pi_e(\vec{r},t) = 0$$

in the time domain for $\varepsilon_{xx} > 0$ and $\varepsilon_{zz} < 0$. A large class of spatiotemporally localized luminal, subluminal and superluminal pulsed solutions to this equation can be derived. These solutions differ substantially from the analogous ones in isotropic free space.

Spatiotemporal Properties of Broadband Axicon Fields

R. Dutta, K. Saastamoinen, J. Turunen, and A. T. Friberg
Department of Physics and Mathematics, University of Eastern Finland, Joensuu FI-80101, Finland

Abstract— We examine the space-time properties of approximately propagation-invariant fields [1] generated by achromatic and diffractive axicons, illuminated with collimated isodiffracting Gaussian beams with different spectral coherence properties. The spectral field distribution in front of the axicon (the plane $z = 0$) is assumed to be of the rotationally symmetric form

$$U(\rho';\omega) = \left(\frac{2}{\pi\omega^2}\right)^{1/2} \left(\frac{\omega}{\bar{\omega}}\right)^{1/2} \sqrt{S(\omega)} \exp\left(-\frac{\omega}{\bar{\omega}}\frac{\rho'^2}{\omega^2}\right), \tag{1}$$

where

$$S(\omega) = \frac{S_0}{\Gamma(2n)\bar{\omega}} \left(2n\frac{\omega}{\bar{\omega}}\right)^{2n} \exp\left(-2n\frac{\omega}{\bar{\omega}}\right). \tag{2}$$

In these expressions ρ' is the transverse radial coordinate, n is a real number, $\bar{\omega}$ is the peak angular frequency of $S(\omega)$, w is the $1/e$ width of the field at $\omega = \bar{\omega}$, and Γ denotes the Gamma function. An achromatic axicon is described by a complex-amplitude transmission function

$$t(\rho';\omega) = \exp[-i(\omega/c)\sin\theta\rho'], \tag{3}$$

and for a diffractive axicon $\sin\theta = 2\pi c/d\omega$, where d is the radial period of the circular grating. By applying Fresnel diffraction theory and the method of stationary phase for single integrals, we find that the field at a distance z behind the axicon takes the form

$$U(\rho, z;\omega) = C\omega\sqrt{S(\omega)} \exp\left(-\frac{\omega}{\bar{\omega}}\frac{z^2}{\omega^2}\sin^2\theta\right) J_0\left(\frac{\omega}{c}\sin\theta\rho\right) \exp\left[i\omega\left(\frac{z}{v} + \frac{\rho^2}{2cz}\right)\right], \tag{4}$$

where C is a constant and $v = c/(1 - \sin^2\theta/2)$. Assuming a fully spectrally coherent field and applying the usual Fourier-transform relationship, the temporal intensity profile of the incident field is found to have a sharply peaked shape with half-width at half-maximum (HWHM) at $t = T$,

$$\bar{\omega}T = \sqrt{2^{1/(n+3/2)} - 1}\left(n + \rho'^2/\omega^2\right). \tag{5}$$

On the optical axis ($\rho = 0$) of an achromatic axicon, the intensity is also of symmetric sharply peaked form with HWHM value at $t_r = T_r$,

$$\bar{\omega}T_r = \sqrt{2^{1/(n+2)} - 1}(n + z^2/L^2). \tag{6}$$

where $t_r = t - z/v$ and $L = w/\sin\theta$ is the effective propagation-invariant range of the axicon field (the axial position at $z = L$ receives a stationary-point contribution from a ring of radius $\rho' = w$). In view of Eq. (6), the axial intensity profile broadens with z, which is consistent with the corresponding broadening of the incident pulse duration in the radial direction as given by Eq. (5). In the case of refractive axicons, also the Bessel field exhibits off-axis modulation of the temporal intensity profile. For diffractive axicons, however, the temporal intensity at any transverse plane is position-independent, but it depends on the longitudinal position. Compared to achromatic axicons, the temporal profiles are time-delayed, broader, and nonsymmetric with long trailing tails.

In addition to fully spectrally coherent pulses, we consider spectrally incoherent (stationary) light with the same spectrum, given by Eq. (2), as in the case of spectrally coherent pulses. Now the temporal coherence properties are is of main concern and, by applying the Wiener-Khintchine theorem, we obtain for achromatic axicons symmetric distributions of the complex degree of temporal coherence both for the incident field and the axial field behind achromatic axicons. The spatial coherence becomes partial as for ideal polychromatic propagation-invariant fields [2].

REFERENCES

1. Turunen, J. and A. T. Friberg, "Propagation-invariant optical fields," *Progr. Opt.*, Vol. 54, 1–88, 2009.
2. Turunen, J., "Space-time coherence of polychromatic propagation-invariant fields," *Opt. Express*, Vol. 16, 20283–20294, 2008.

Energy Transport Velocity for Various Localized and Accelerating Pulsed Waves

P. Saari[1], **O. Rebane**[2], **and I. M. Besieris**[3]

[1]Institute of Physics, University of Tartu, Riia 142, Tartu 51014, Estonia
[2]Laser Diagnostic Instruments AS, Valukoja 7, Tallinn 11415, Estonia
[3]The Bradley Department of Electrical and Computer Engineering
Virginia Polytechnic Institute and State University, Blacksburg, VA 24060, USA

Abstract— Despite the fact that the energy energy velocity of localized waves has been considered by several authors, still the literature lacks a sufficiently rigorous and comprehensive treatment of this issue.

We undertook a theoretical study of local and plane-integrated energy transport in various X-type waves, both scalar and vectorial ones of different polarization properties. Some of main results of the study are the following:

(i) as it follows from a general theoretical derivation, no EM field can transport energy faster than c even in the case of superluminal pulses;
(ii) the spatial distribution of the Poynting vector, the energy density and its transport velocity, calculated by means of scalar approximation formulas practically coincide with the results of exact vectorial approach, except for some subtleties;
(iii) the energy flux density for all double-conical (X-type) localized waves is converging before the central intensity maximum (apex) and diverging after it; in other words, these waves have a negative lateral energy velocity component in the leading (backward-directed) cone and a positive one in the rear (forward-directed) cone.

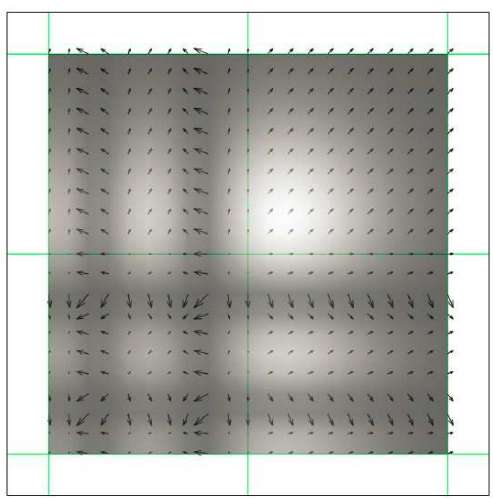

Figure 1: Vector field plot of the transverse component of the energy transport velocity in a cross section of a 2D Airy beam. On the background, the energy density in the region of the main Airy maximum (in upper right quadrant) has been indicated by grey scale.

Non-diffractive Light Beams and Bullets in Nonlinear Media with Dissipation

M. A. Porras
Departamento de Física Aplicada y Grupo de Sistemas Complejos
Universidad Politécnica de Madrid, Rios Rosas 21, Madrid 28013, Spain

Abstract— We review the properties of nonlinear lossy light bullets (LLBs), a family of non-diffractive and non-dispersive light wave packets in homogeneous, isotropic, nonlinear media sustained by a dynamic balance between nonlinear energy dissipation and self-focusing. The properties of LLBs differ substantially from those of other well-known families of non-diffractive, nonlinear light bullets, as solitary, conical, or dissipative light bullets. LLBs are substantially nonlinear and multidimensional (two or three dimensional) waves, and feature a rather complex structure in space and time. They survive to nonlinear losses and rebuild after obstacles, but these properties do not result from a peculiar geometry, as in conical light bullets, or from a gain that balances the losses, as in dissipative light bullets. The stationary propagation of LLBs in media with nonlinear losses results from the refilling effect of self-focusing, which creates a continuous energy flux from a widespread energy reservoir in the periphery of the light bullet towards the intense, central core of the bullet, where energy is continuously absorbed. The stability properties of LLBs against perturbations are studied in detail. Nonlinear losses not only do not prevent from the existence of stationary propagation, but also provide stability. In fact, the LLB with maximum intensity supported by a nonlinear medium shows maximum stability properties, and acts as an attractor of the two-dimensional or three-dimensional self-focusing dynamics in media with nonlinear losses. The existence of this attractor can explain many facts of the observed self-focusing and filamentation dynamics of standard (Gaussian-like) light wave packets when collapse is halted by nonlinear losses.

Spherical Light, Arbitrary Nonparaxial Accelerating Beams and Femtosecond Laser Micromachining of Curved Profiles

F. Courvoisier, A. Mathis, L. Froehly, M. Jacquot, R. Giust, L. Furfaro, and J. M. Dudley
Département d'Optique P.M. Duffieux, Institut FEMTO-ST
UMR 6174 CNRS, Université de Franche-Comté, Besançon Cedex 25030, France

Abstract— We review our recent results applying caustics wave theory to the generation of arbitrary curved accelerating beams and their use in the field of femtosecond laser materials processing. We report experimental realization of highly nonparaxial accelerating beams with circular, parabolic and quartic trajectories that extend over more than 95° of arc as well as spherical optical fields. We also report femtosecond laser curved edge profiling.

Accelerating optical beams are a novel class of electromagnetic wave associated with a localized intensity maximum that propagates along a curved trajectory. In the nonparaxial regime, beams accelerating along circular, parabolic (Weber beams) and elliptic (Mathieu beams) trajectories were predicted from Maxwell's equations and experimentally demonstrated [1–3]. Here, we review our recent results on generating arbitrary nonparaxial accelerating beams with another approach, i.e., from optical caustics, and report an important novel application, i.e., curved laser processing.

Caustics accurately describe non-paraxial wave propagation using an appropriate wave-diffraction integral. In our case, Debye-Wolf integral is used to determine the phase mask to be applied at the entrance plane of a high numerical aperture aplanatic microscope objective [4]. Analytical integra- tion provides results identical to those obtained from Maxwell's equations and numerical integration also allows other arbitrary profiles. Figure 1(a) shows the experimental intensity distribution of a 632.8 nm beam accelerating on a circular trajectory. The high agreement with the target trajectory (dashed white line) is shown in the magnified views A and B. This approach also allowed us to generate spherical fields, as predicted by [2]. Figures 1(b)–(c) show experimentally generated field that takes the form of a spherical cap extended down to the equator.

The same approach was applied to the spatial shaping of amplified femtosecond pulses at 800 nm and we used it for a novel technique of femtosecond laser micromachining [5]. Figure 1(d) presents a 3D view of a silicon sample where the initial square-cut edge was processed into a circle. We anticipate a broad range of applications in different technological fields such as the processing of flat panels and photonic components.

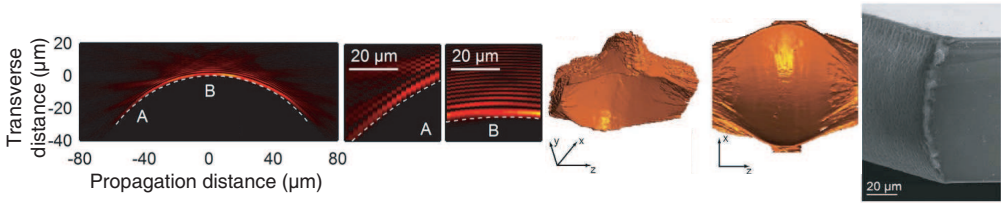

(a) (b) (c) (d)

Figure 1: (a) Intensity distribution of a highly nonparaxial beam accelerating along a circle. (b)–(c) 3D isointensity surface of experimental spherical field (radius 50 μm). (d) SEM view of a 100 μm thick silicon sample with the edge processed as a circular profile.

REFERENCES

1. Kaminer, I., et al., *Phys. Rev. Lett.*, Vol. 108, No. 163901, 2012.
2. Alonso, M. A., et al., *Opt. Lett.*, Vol. 37, No. 5175, 2012.
3. Aleahmad, P., et al., *Phys. Rev. Lett.*, Vol. 109, No. 203902, 2012.
4. Courvoisier, F., et al., arXiv:1304.3469, 2013.
5. Mathis, A., et al., *Appl. Phys. Lett.*, Vol. 101, No. 071110, 2012.

Generation and Characterization of Ultrawideband Airy Pulses

P. Piksarv, A. Valdmann, H. Valtna-Lukner, R. Matt, and P. Saari
Institute of Physics, University of Tartu, Riia 142, Tartu 51014, Estonia

Abstract— The laterally accelerating Airy beams have gained widespread attention ever since their introduction to the field of optics by Siviloglou and Christodoulides in 2007 [1]. In addition to the propagation along the parabolic trajectory in nondiffractive manner maintaining the transverse confinement over propagation distances much greater than the Rayleigh range of a Gaussian beams, the Airy beams have found to exhibit self-healing properties allowing bending the trajectory of light around obstacles. These features have made the Airy beams attractive for applications like optical micromanipulation, micro-machining and laser-induced plasma channel formation, etc.

The Airy profile and the lateral acceleration of the beam arises from the cubic spatial phase. Most commonly, the Airy beams are generated using spatial light modulators (SLM). Pulses with a temporal Airy profile have been introduced as well and have been particularly found to be resistant to material dispersion [2]. Theoretically, the pulsed Airy beams have many variants as their monochromatic constituents can be freely shifted in time and space. However, experimentally the generation mechanisms impose strong restrictions on the type of broadband Airy pulses. Therefore a thorough characterization of Airy pulse formation by an SLM is needed in order to fully understand these limitations.

In this paper, we present full spatiotemporal characterization of ultrabroadband Airy pulse and Airy-Bessel wave packet generators. The measurements with a few micrometer spatial and almost one-wave-cycle temporal resolution have been performed using a white light spatial spectral interferometry setup based on the SEA TADPOLE ultrashort pulse characterization technique [3, 4]. Our results are important for generating real near-single-cycle laterally accelerating Airy pulses and show how Airy-Bessel wave packets can be used to suppress the material induced temporal spread of ultrashort pulses.

ACKNOWLEDGMENT

This work has been supported by the Estonian Science Foundation and by the European Regional Development Fund. P. P. has been partially supported by the European Social Fund.

REFERENCES

1. Siviloglou, G. A. and D. N. Christodoulides, "Accelerating finite energy Airy beams," *Opt. Lett.*, Vol. 32, No. 8, 979–981, 2007.
2. Chong, A., W. H. Renniger, D. N. Christodoulides, N. Demetrios, and F. W. Wise, "Airy-Bessel wave packets as versatile linear light bullets," *Nat. Photon.*, Vol. 4, No. 2, 103–106, 2010.
3. Piksarv, P., H. Valtna-Lukner, A. Valdmann, M. Lõhmus, R. Matt, and P. Saari, "Temporal focusing of ultrashort pulsed Bessel beams into Airy-Bessel light bullets," *Opt. Express*, Vol. 20, No. 15, 17220–17229, 2012.
4. Piksarv, P., A. Valdmann, H. Valtna-Lukner, R. Matt, and P. Saari, "Spatiotemporal characterization of ultrabroadband Airy pulses," *Opt. Lett.*, Vol. 38, No. 7, 1143–1145, 2013.

Three-dimensional Nonparaxial Accelerated Waves and Pulses That Follow Circular Paths

Miguel A. Alonso[1], **Miguel A. Bandres**[2], **Ido Kaminer**[3], **and Mordechai Segev**[3]

[1]The Institute of Optics, University of Rochester, Rochester, NY 14627, USA
[2]Instituto Nacional de Astronomía, Óptica y Electónica, Calle Luis Enrique Herro No. 1 Sra. Ma. Tonantzintla, Pue, CP 72840, Mexico
[3]Physics Department, Solid State Institute, Technion, Haifa 32000, Israel

Abstract— We present nonparaxial generalizations of accelerating beams whose intensity features describe circular paths, both for scalar and electromagnetic fields. Several cases are discussed, corresponding to different shapes of the caustic sheets. We pay special attention to fields associated with coordinate frames displaying rotational symmetry around a given axis and that allow the analytic solution of the Helmholtz equation through separation of variables. For these fields, the maxima describe full circular paths. For many practical purposes (e.g., in particle manipulation applications), one must use fields whose angular spectrum is limited to a "forward-propagating" hemisphere. We therefore discuss the effect that limiting the angular spectrum has on the bending properties of these fields. In particular, if the field's directionality is enforced through a directional apodization factor resulting from an imaginary spatial displacement, the resulting directional accelerated fields are still expressible in closed form. In the case of fields resulting from separation in spherical coordinates, closed-form pulsed solutions are also accessible.

For many of the nonparaxial accelerated fields presented here, the main intensity maximum (or maxima) corresponds to the intersection of two caustic sheets, as in the case of paraxial two-dimensional Airy beams. However, unlike in the paraxial case where the transverse cross-sections of these caustic sheets can be straight, the cross-sections of the nonparaxial fields unavoidably bend outwards. This behavior is explained through a ray-optical treatment. This treatment allows the calculation of the expression for the second caustic sheet given the first, and permits the design of other circular accelerated beams beyond those associated with separation of variables. Finally, we discuss the design of optical reflectors that would generate the desired nonparaxial caustic profiles.

Sub-3-cycle Linear Light Bullets

Martin Bock and Ruediger Grunwald
Max-Born-Institute for Nonlinear Optics and Short-pulse Spectroscopy, Germany

Abstract— Ultrashort-pulsed Bessel and Airy beam are often presented as examples of linear light bullets. A basic difficulty for the temporal invariance of such beams, however, is related to spatially variable path differences of the constituting waves. In the case of Bessel beams, only the central lobes ("needle beams") result from the interference of waves of equal phase and transfer ultrashort pulses nearly without distortions. Airy beams are asymmetric caustics formed by waves with continuously changing tilt angle of the wavefront. In both cases, the corresponding geometrical dispersion alters the pulse duration if no sophisticated pre-compensation is introduced. A different behavior is found for a particular class of undistorted progressive wave phenomena we refer to as "highly localized wavepackets (HLWs)". HLWs are a generalization of needle beams and can flexibly be generated by programming high-resolution phase axicons with low-dispersion spatial light modulators (SLMs). They combine (a) a spatially and temporally invariant propagation over extended depth ranges, and (b) an intensity profile containing a minimum of radial oscillations. Therefore it is better justified to interprete free-space HLWs as "linear light bullets" compared to the case of the radially oscillating and temporally unstable Bessel and Airy beams. We show how reconfigurable HLWs can easily be generated and adaptively be corrected by appropriate transformations of the phase maps and how they can serve as building blocks for complex nondiffracting patterns. Experimental results are reported for flexibly shaping sub-3-cycle pulses of a Ti:sapphire laser with a liquid-crystal-on-silicon (LCoS)-SLM. Applications for highly sensitive techniques of pulse diagnostics combining the properties of wavefront sensing and nonlinear autocorrelation are presented. The detection of few-cycle vortex beams with a nondiffracting wavefront sensor is demonstrated. Because of the unprecedented temporal transfer properties, HLWs are predicted to play a key role in the spatio-temporal diagnostics of sub-femtosecond pulses. Currently, the capability of MEMS axicons to shape HLWs for nonlinear plasmon excitation and nanostructuring is studied.

Temporal Focusing and Focus Wave Modes

Colin J. R. Sheppard[1], **Elijah Y. S. Yew**[2], **and Peter T. C. So**[2, 3]

[1]Istituto Italiano di Tecnologia, Genova, Italy
[2]Singapore-MIT Alliance for Research and Technology (SMART), Singapore
[3]Department of Biological Engineering, Massachusetts Institute of Technology, USA

Abstract— There is great current interest in the technique of temporal focusing, where an ultrashort pulsed beam is split into spectral components, which are then combined to give rise to ultrashort pulses only in the focal region of a lens. This effect is similar to the method used for pulse dispersion compensation using prism or grating pairs [1]. As nonlinear effects are enhanced by ultrashort pulse excitation, these nonlinear effects, such as two-photon fluorescence, are comparatively confined to this focal plane [2–4].

The technique of temporal focusing bears some similarity to the method of producing localized pulses termed the focus wave mode (FWM) [5]. The focus wave mode has also been generalized to the case of pulses that propagate at arbitrary speeds [6]. The connections between work in the fields of temporal focusing and FWMs is investigated, which could lead to improved understanding and designs for temporal focusing.

Effectively, in temporal focusing a train of localized pulses is used to illuminate a region of a sample. This train of pulses can be scanned to illuminate different parts of the sample. The conventional focus wave mode geometry is rotationally symmetric, producing a train of pulses that propagate along the optical axis. In off-axis positions the pulse shape is degraded. We consider different FWM geometries such as two-dimensional geometries. In two dimensions, the analog of the Bessel beam is the cosine beam, which should not really be considered a beam as all the lobes are of equal strength. But in the same way that the strength of the Bessel beam side lobes is reduced in a focus wave mode [7], so too this occurs for the cosine beam case.

REFERENCES

1. Fork, R. L., O. E. Martinez, and J. P. Gordon, "Negative dispersion using pairs of prisms," *Opt. Lett.*, Vol. 9, 150–152, 1984.
2. Oron, D., E. Tal, and Y. Silberberg, "Scanningless depth resolved microscopy," *Optics Express*, Vol. 13, 1468–1476, 2005.
3. Tal, E., D. Oron, and Y. Silberberg, "Improved depth resolution in video-rate line-scanning multiphoton microscopy using temporal focusing," *Opt. Lett.*, Vol. 30, 1686–1688, 2005.
4. Zhu, G., J. van Howe, M. Durst, W. Zipfel, and C. Xu, "Simultaneous spatial and temporal focusing of ultrashort pulses," *Optics Express*, Vol. 13, 2153–2159, 2005.
5. Brittingham, J. N., "Focus wave modes in homogeneous Maxwell's equations: Transverse electric mode," *J. Appl. Phys.*, Vol. 54, 1179–1189, 1983.
6. Sheppard, C. J. R., "Generalized Bessel pulse beams," *Journal of the Optical Society of America A*, Vol. 19, 2218–2222, 2002.
7. Sheppard, C. J. R., "Bessel pulse beams and focus wave modes," *Journal of the Optical Society of America A*, Vol. 18, 2594–2600, 2001.

Session 1P10a
Remote Sensing of the Atmosphere, Ocean, Hydrology and Cryosphere

Towards a Comprehensive Model of Ice Sheet Scattering Properties at VHF and P-band for Design and Optimization of Multichannel Ice Sounding Techniques
Ulrik Dam Nielsen, Theresa M. Stumpf, Peng Seng Tan, Prasad Gogineni, Jorgen Dall, ... 356

Electromagnetic Monitoring of Sea Ice Processes
Kenneth Morgan Golden, ... 358

Analysis of GRACE-derived Terrestrial Water Storage in Boreal and Subarctic Environments in Canada
Kalifa Goita, ... 359

Applying Particle Swarm Optimization to Polarimetric Decomposition Technique with Phase Rotation of Covariance Matrix
Toshifumi Moriyama, ... 360

Using DInSAR Phase to Carry out Sub-surface SAR Imaging from Space
Keith Morrison, John Bennett, ... 361

Semi-automatic Polarimetric SAR Image Classification by MD PSO Based Dynamic Clustering
Turker Ince, Serkan Kiranyaz, Moncef Gabbouj, ... 362

Towards a Comprehensive Model of Ice Sheet Scattering Properties at VHF and P-band for Design and Optimization of Multichannel Ice Sounding Techniques

U. Nielsen[1], **T. M. Stumpf**[2], **P. S. Tan**[2], **P. Gogineni**[2], **and J. Dall**[1]

[1]Technical University of Denmark, Denmark
[2]Center for Remote Sensing of Ice Sheets, University of Kansas, USA

Abstract— There is an urgent need to improve ice-sheet models to predict the contribution of large ice sheets to level rise in a warming climate. Knowledge of bed topography and basal conditions is essential for improving these models but observations of these features are missing for many key areas of the polar ice sheets. Multichannel ice-sounders can measure ice sheets in great detail and are capable of profiling their geological features from the surface to the bedrock. Today, airborne sounders, like the Multichannel Coherent Radar Depth Sounder/Imager (MCoRDS/I) developed by the University of Kansas's Center for Remote Sensing of Ice Sheets (CReSIS), are collecting large volumes of ice-sheet measurements. Although a spaceborne sounder does not currently exist, the feasibility of such a sensor is being studied using the POLarimetric Airborne Radar Ice Sounder (POLARIS), developed by the Technical University of Denmark. Both space-based and airborne sounders are needed to provide complete data sets to the scientific community. A space-based sounder would be capable of the broad coverage over the interior of the ice sheets that cannot be realized from an aircraft at low altitude, while airborne sensors are needed for detailed measurements of the fast-flowing outlet glaciers that cannot be sounded from high altitudes due to their heavily crevassed surfaces and lossy ice.

Detecting weak echoes from deep within the ice sheet in the presence of both volume clutter from inclusions in the ice and surface clutter from the air-ice interface is a major technical challenge for both space-based and airborne sounders. Advanced array-processing techniques are needed to mitigate the effects of undesirable clutter contributions. In order to improve and optimize those techniques, we must be able to simulate their performance in realistic clutter environments. Currently there are no comprehensive scattering models for polar ice sheets that account for both surface scattering at the air-ice and ice-bed interfaces as well as volume scattering from within the ice. To address this gap in the literature, we are using real data to characterize the ice sheet and develop a first-order approximation of its scattering properties at VHF and P-Band. These models will be integrated into a simulator that will be used to optimize and validate our array processing approaches.

The Integral Equation Surface Backscattering Model (IEM) [1] can be used to model backscatter at both the air-ice and ice-bed interfaces. The IEM requires specification of roughness, correlation length, and shape of the roughness spectrum at each interface. We are using surface elevation data from NASA's Airborne Topographic Mapper (ATM) that were collected in a very dense grid over Russell Glacier in Greenland and using a geostatistical approach to estimate the roughness parameters. To characterize roughness at the bed in the absence of fine resolution bed topography, we are considering an approach based on radar data. Ice sounder data can be used to estimate roughness and backscatter from the leading and trailing edges of the bed echo respectively [2–4]. This analysis can be performed with data collected over the exposed bedrock of a retreated glacier as well as with data collected from ice-covered bed. We are using documented observations of different types of ice inclusions [5–8] to model the volume clutter as an inhomogeneous medium consisting of a dominant ice background with inclusions.

This study presents our methods for estimating surface and subsurface ice sheet scattering characteristics along with preliminary backscatter results.

REFERENCES

1. Fung, A. K. and K. S. Chen, *Microwave Scattering and Emission Models for Users*, Artech House, Norwood, 2009.
2. Brown, G. S., "The average impulse response of a rough surface and its application," *IEEE Trans. Antennas Propagat.*, Vol. 25, 67–74, 1977.
3. Niamsuwan, N., "Electromagnetic scattering models for the global ice sheet mapping orbiter demonstrator," Ph.D. Thesis, The Ohio State University, 2009.

4. Niamsuwan, N., J. T. Johnsona, and K. C. Jezek, "Modeling the nadiral low-frequency pulse return of one-dimensionally rough surfaces," *Waves in Random and Complex Media*, Vol. 21, No. 1, 184–197, 2011.
5. Smith, B. M. E. and S. Evans, "Radio echo sounding: Absorption and scattering by water inclusion and ice lenses," *Journal of Glaciology*, Vol. 11, No. 61, 133–146, 1972.
6. Watts, R. D. and A. W. England, "Radio-echo sounding of temperate glaciers: Ice properties and sounder design criteria," *Journal of Glaciology*, Vol. 17, No. 73, 39–48, 1976.
7. Bamber, J. L., "Enhanced radar scattering from water inclusions in ice," *Journal of Glaciology*, Vol. 34, No. 118, 293–296, 1988.
8. Ueltzhöffer, K. J., et al., "Distribution of air bubbles in the EDML and EDC (Antarctica) ice cores, using a new method of automatic image analysis," *Journal of Glaciology*, Vol. 56, No. 196, 339–348, 2010.

Electromagnetic Monitoring of Sea Ice Processes

Kenneth M. Golden
Department of Mathematics, University of Utah, USA

Abstract— Polar sea ice is a key component of Earth's climate system, and a leading indicator of climate change. As a material sea ice is a composite of pure ice with brine and air inclusions. The brine microstructure hosts extensive algal and bacterial communities which sustain life in the polar oceans. While global climate models predict declines in sea ice, they have significantly underestimated the recent dramatic losses observed in the summer Arctic sea ice pack. We focus here on sea ice transport processes which are critical to the role that sea ice plays in climate, and which must be understood better to more realistically represent sea ice in climate models.

Fluid flow through sea ice mediates a broad range of geophysical and biological processes in the polar marine environment. For example, the evolution of melts ponds and sea ice albedo, which is critical to climate modeling, is constrained by drainage through the porous brine microstructure. Fluid flow also governs snow-ice formation, the evolution of the salt budget, and biomass build-up sustained by nutrient fluxes. However, for brine volume fractions below about 5%, columnar sea ice is effectively impermeable to fluid flow. In two different experiments conducted in the Arctic and Antarctic, we have found that this critical transition in fluid flow exhibits a strong electrical signature, with sea ice resistivity sharply rising over three orders of magnitude near the brine connectivity threshold. The data are accurately explained by percolation theory for the effective resistivity of sea ice, treated as a composite of ice and brine, with the same universal critical exponent of 2 which captures the behavior of the effective fluid permeability. The data were obtained using cross-borehole tomography and a novel direct measurement technique on extracted sea ice cores.

Our results demonstrate that classical lattice models of phase transitions in statistical physics and theories of homogenization can help unravel the complexity of transport in this multiscale random medium. The theory enables electrical classification of sea ice layers in terms of their fluid flow properties, thus connecting specific electrical signatures to important transport processes such as melt pond drainage, CO_2 pumping, and nutrient fluxes. The findings also have implications for measuring ice thickness, an important gauge of the impact of global warming. Promising techniques for advanced airborne or surface-based measurements of ice thickness depend on the interaction of electromagnetic fields with sea ice. These techniques, and the interpretation of the data to obtain thickness information, rely on knowledge of the electrical properties of sea ice, and how they vary with depth, temperature, salinity, and ice type. The results presented here shed significant light on such issues. Finally, our findings lay the foundation for electromagnetic monitoring of transport phenomena in sea ice, which can help track key transitions in the state of polar sea ice and improve projections of its fate and impact on ecosystems.

Analysis of GRACE-derived Terrestrial Water Storage in Boreal and Subarctic Environments in Canada

Kalifa Goïta
Centre d'applications et de recherches en télédétection, Département de Géomatique Appliquée
Université de Sherbrooke, Sherbrooke, Québec J1K 2R1, Canada

Abstract— The Gravity Recovery and Climate Experiment (GRACE) satellite mission measure variations in Earth's gravity field which are linked to mass distribution. Over land surface, the temporal variations in the gravity field are mainly due to terrestrial water storage change (TWS). The gravimetric data provided by GRACE can be converted to TWS, which corresponds to the vertically integrated measure of all water features, namely snow, ice, surface water, soil moisture and groundwater. Therefore additional independent information is required to isolate the different components. In this study, GRACE-derived TWS are analysed over different regions in Canada, especially the Canadian Prairies (Western Canada) and Quebec (located in Eastern Canada). The Canadian Prairies are mainly dominated by agriculture lands in the south and boreal forests in the north. Quebec is covered by a gradient of ecosystems from mixed boreal forest in the south to tundra in the north. During the winter period, all the areas are covered by snow, with more important quantities in Quebec. Ten years of GRACE data are analysed (2002–2012). The equivalent water thickness anomalies show interesting seasonal and interannual variations, with a sharp contrast between the winter (positive anomalies) and the summer periods (negative anomalies) in both the Prairies and Quebec. The influence of snow water equivalent (SWE) on TWS variations is examined, in addition to land cover characteristics such as the forest cover distribution. SWE was extracted from GlobSnow products derived from spaceborne passive microwave measurements using semi-empirical radiative transfer model and data assimilation. During the summer period, GRACE TWS were analysed in relation with soil moisture information derived from the Advanced Microwave Scanning Radiometer-Earth Observing System (AMSR-E) and the Advanced Scatterometer (ASCAT) soil moisture products. Overall snow cover appears as an important parameter driving TWS variations.

Applying Particle Swarm Optimization to Polarimetric Decomposition Technique with Phase Rotation of Covariance Matrix

Toshifumi Moriyama
Department of Electrical and Electronic Engineering
Graduate School of Engineering, Nagasaki University, Nagasaki 852-8521, Japan

Abstract— In recent years, polarimetric decomposition technique is attracted to get the valuable information from the covariance and coherency matrices which are made by the data of polarimetric synthetic aperture radar (POLSAR). The information obtained by the polarimetric decomposition can be expected to retrieve the physical parameters of natural targets and to do the classification of SAR image. Adaptive-Non-Negative-Eigenvalue Decomposition (ANNED) method, which was proposed in [1], is one of useful decomposition techniques [2]. This method is a model based decomposition technique and has a capability to estimate the mean orientation angle and a degree of randomness for the volume scattering for each pixel in an image. However, it takes long time to get the decomposition parameters because all combinations are estimated to search a most fitted candidate of decomposition parameters. In order to reduce the calculation time, the generalized eigenvalue problem has been used in ANNED [3]. In this paper, particle swarm optimization (PSO) is applied to ANNED with the generalized eigenvalue problem. Thus, more fast calculation of ANNED is achieved and it is possible that POLSAR image with many pixels can be analyzed by ANNED. Moreover, it is considered that a phase rotation of measured covariance matrix is applied to ANNED. The phase rotation is expected to reduce an effect of polarimetric orientation angle shift and to improve the POLSAR analysis such as classification. Numerical results based on the proposed technique will be shown in the presentation.

REFERENCES

1. Arii, M., J. J. van Zyl, and Y. Kim, "Adaptive model-based decomposition of polarimetric SAR covariance matrices," *IEEE Transactions on Geoscience and Remote Sensing*, Vol. 49, No. 3, 1104–1113, Mar. 2011.
2. Freeman, A. and S. L. Durden, "A three-component scattering model for polarimetric SAR data," *IEEE Trans. Geosci. Remote Sens.*, Vol. 36, No. 3, 964–973, May 1998.
3. Takizawa, R., H. Yamada, and Y. Yamaguchi, "Consideration of scattering component decomposition of POLSAR image using general volume scattering model," IEICE Technical Report, Vol. SANE2010-150, 71–76, Jan. 2011.
4. Singh, G., Y. Yamaguchi, and S.-E. Park, "4-component scattering power decomposition with phase rotation of coherency matrix," *Porc. of IEEE Geosci. and Remote Sens. Symp.*, 4103–4106, Jul. 2011.

Using DInSAR Phase to Carry out Sub-surface SAR Imaging from Space

Keith Morrison[1] **and John Bennett**[2]

[1]Department of Informatics & Systems Engineering
Cranfield University, Shrivenham, Swindon SN6 8LA, UK
[2]Department of Electronic & Electrical Engineering
University of Sheffield, Mappin Street, Sheffield S1 3JD, UK

Abstract— The goal of carrying out sub-surface imaging from space or aircraft has so far remained elusive. SAR is the main imaging tool for airborne and spaceborne radar platforms, and allows rapid, repeat imaging of large parts of the earth's surface. However, whilst it can provide high-resolution discrimination in azimuth and range, it is ambiguous in the vertical direction, providing little or no height information in a scene. As a consequence, schemes for overcoming scene layover to allow discrimination between surface and buried features have relied on high-resolution, nadir-looking, ground-based systems or very low-flying aerial platforms. However, the use of these systems places severe restrictions on the size of the area that can be investigated or accessed, making large-scale surveys costly in time and money. Ground-penetrating radars seek to spatially isolate features in backscatter, and hence are limited to a vertical resolution prescribed by the platform's formal spatial resolution. To address this problem, here we propose a novel scheme for subsurface imaging which exploits the effect a varying volumetric soil moisture, mv, has on the sub-surface phase signal (mv is a dimensionless ratio representing the fraction of the total volume of soil that is occupied by the water contained in the soil). Whereas the return from a sub-surface feature experiences phase changes in sympathy to variations in soil moisture, these are absent from the phase history of surface features. A theoretical framework will be presented describing the temporal differential interferometric SAR (DInSAR) phase history of a scene. The model describes the observed phase changes in terms of retardation of the signal by the soil dielectric properties, which are dependent upon the moisture content. The ability to exploit the scheme relies on two central tenets in the model; 1) that the DInSAR phase is linear with change in mv and 2) that the phase is independent of the incidence angle the scene is observed at. The linearity of the differential phase across the mv range means the starting value of mv is not needed. That the DInSAR phase is independent of viewing angle can be understood by the competition of two equal phase terms which act upon the wave, but opposite in sign. An increased dielectric constant slows the propagation of the wave, increasing the phase path. However, increased dielectric constant acts so as to refract the wave towards the normal, reducing the path length. This allows us to ignore refraction, which similarly negates the need to have knowledge of absolute values of mv. Because we are using a phase signal, the scheme is applicable at large stand-off distances from airborne and spaceborne platforms.

Semi-automatic Polarimetric SAR Image Classification by MD PSO Based Dynamic Clustering

Turker Ince[1], **Serkan Kıranyaz**[2], **and Moncef Gabbouj**[2]

[1]Department of Electrical and Electronics Engineering, Izmir University of Economics, Izmir, Turkey
[2]Department of Signal Processing, Tampere University of Technology, Finland

Abstract— In this study, a new systematic approach for semi-automatic classification of polarimetric synthetic aperture radar (PolSAR) image is proposed. The feature extraction block utilizes traditionally used SAR features including the complete coherency (or covariance) matrix information, features derived from various target decomposition theorems, the backscattering power and the selected texture features from gray-level cooccurrence matrix (GLCM). Classification of the information in multi-dimensional PolSAR data space by dynamic clustering is addressed as an optimization problem and recently proposed multi-dimensional particle swarm optimization (MD-PSO) technique is applied to find optimal clusters in a given input data space, distance metric and a proper validity index function. An experimental study is performed using the fully polarimetric San Francisco Bay AIRSAR dataset to analyze and compare the results of classification with the state of the art techniques.

Session 1P10b
SC1: Nonlinear and Inverse Problems in Electromagnetics

New Propagation Regime for Nonlinear Guided Waves: Coupled Electromagnetic TE-TM Wave Propagation
Dmitry V. Valovik, ... 364
Reconstruction of Permittivity and Permeability Tensors of Anisotropic Materials in a Rectangular Waveguide from the Reflection and Transmission Coefficients at Different Frequencies
Yury G. Smirnov, Yury V. Shestopalov, Ekaterina D. Derevyanchuk, ... 365
Parameter Optimization of Waveguide Filters Employing Analysis of Closed-form Solution
Pavel Tomasek, Yury V. Shestopalov, ... 366
Modelling of Resonant Scattering and Generation of Oscillations for Nonlinear Media
Lutz Angermann, Vasyl V. Yatsyk, ... 367
The Formation Process of Nanoclusters in the Metal Surface Layer, Initiated by Nonlinear Tunneling Dynamics in the Electrostatic Field
Igor I. Artemov, Vladimir D. Krevchik, Mikhail B. Semenov, Alexey V. Sokolov, Sverlana B. Menshova, ... 368

New Propagation Regime for Nonlinear Guided Waves: Coupled Electromagnetic TE-TM Wave Propagation

D. V. Valovik
Penza State University, 40 Krasnaya Street, Penza 440026, Russia

Abstract— It is well known that purely nonlinear guided TE and TM waves exist in a plane waveguide with Kerr nonlinearity. It turns out that there is more general regime, so called regime of nonlinear coupled TE-TM wave propagation in a nonlinear layer.

In this regime we have sum of two independent waves (TE and TM) that create new (nonlinear) polarization (so called coupled TE-TM wave). TE and TM waves that form this nonlinear TE-TM wave we call pseudopolarizations (pseudo-TE and pseudo-TM, respectively). It is proved that in this case each pseudopolarization can propagate at its own frequency (ω_E and ω_M, respectively) and has its own propagation constant (γ_E and γ_M for pseudo-TE and pseudo-TM waves, respectively).

In this report coupled electromagnetic TE-TM wave propagation in a nonlinear dielectric layer filled with lossless, nonmagnetic, and isotropic medium is considered. The layer is located between two half-spaces with constant permittivities. The permittivity in the layer is described by Kerr law. The physical problem is reduced to a two-parameter eigenvalue problem for Maxwell's equations. We look for coupled eigenvalues of the problem and reduce the question to the analysis of the corresponding system of two dispersion equations. It is shown that the new waveguide regime for coupled TE and TM wave exists in a layer with Kerr nonlinearity. Existence of coupled eigenvalues is proved and localization of coupled eigenvalues is given.

The problem when $\omega_E \neq \omega_M$, as it is known to the author, have not been considered in literature. This regime is seemed to be interesting for, at least, two reasons: we obtain exact results about existence of coupled TE-TM waves; this model can be applied to study nonlinear interaction of two types of waves (pseudo-TE and pseudo-TM) at different frequencies. We should note that frequencies ω_E and ω_M do not depend on each other.

Reconstruction of Permittivity and Permeability Tensors of Anisotropic Materials in a Rectangular Waveguide from the Reflection and Transmission Coefficients at Different Frequencies

Yu. G. Smirnov[1], **Yu. V. Shestopalov**[2], **and E. D. Derevyanchuk**[1]

[1]Penza State University, Russia
[2]Karlstad University, Sweden

Abstract— Determination of electromagnetic parameters of anisotropic dielectric bodies of complicated structure is an urgent problem. However, as a rule, these parameters cannot be directly measured (because of composite character of the material and small size of samples), so that numerical solution to the corresponding forward and inverse electromagnetic problems must be applied. We develop a method of solution [1] to the inverse problem of reconstructing permittivity and permeability tensors of anisotropic materials in the form of diaphragms (sections) in a single-mode waveguide of rectangular cross section from the transmission and reflection coefficients measured at different frequencies. Components of the permittivity and permeability tensors of composite materials can be considered as effective parameters. The method enables in particular obtaining solutions in a closed form in the case of one-sectional diaphragm. For multi-sectional diaphragms, we solve the inverse problem by means of numerical solution to a nonlinear equation system. Solvability and uniqueness of the system are studied and convergence of the method is proved.

In the case of thin diaphragms we obtain approximate formulas for the permittivity and permeability tensors and compare analytical and calculated permittivity and permeability tensors of anisotropic materials. Results of numerical modeling are presented for different types of anisotropic materials; the metamaterials are also considered. The developed solution techniques for the inverse problem under study can be applied in nanotechnology, optics, and design of microwave devices.

REFERENCES

1. Shestopalov, Y. and Y. Smirnov, "Determination of permittivity of an inhomogeneous dielectric body in a waveguide," *Inverse Problems*, Vol. 27, 095010–095022, 2011.

Parameter Optimization of Waveguide Filters Employing Analysis of Closed-form Solution

P. Tomasek[1] and Y. V. Shestopalov[2]

[1]Tomas Bata University in Zlin, The Czech Republic
[2]Karlstad University, Sweden

Abstract— Recent findings [1, 2] have demonstrated that the transmission coefficients for a waveguide of rectangular cross-section loaded with multi-layered parallel-plane dielectrics can be determined in a closed form and analysed as a function of several real or complex variables. Consequently, the analysis of the transmitted and reflected fields in terms of the scattering matrix formalism can be performed explicitly. These results can be efficiently applied for modelling of waveguide filters. This article presents a technique based on the method set forth in [1, 2] for the computation and optimization of the transmission coefficients of waveguide filters formed by multi-sectional diaphragms in a waveguide of rectangular cross-section. An approach for designing band-stop and band-pass filters is proposed employing analysis of closed-form solutions and numerical multi-parameter optimization [3, 4] which allows to automate the process of the filter design. The users only have to set the parameters of the waveguide and define the required goal of optimization: which band of frequencies should be transmitted or reflected and what design variables should be used for the optimization (e.g., thickness of the diaphragm, permittivity of its material, number of sections, or the thickness of the separation between the sections).

As examples, numerical optimization of several band-stop filters with multi-layered diaphragms using two design variables are performed and the transmission coefficients of the final optimized structure of the waveguide filters are calculated.

REFERENCES

1. Shestopalov, Y. and Y. Smirnov, "Inverse scattering in guides," *J. Phys.: Conf. Ser.*, Vol. 346, 012019, 2012.
2. Shestopalov, Y., Y. Smirnov, and E. Derevyanchuk, "Permittivity determination of multi-sectional diaphragm with metamaterial layers in rectangular waveguide," *PIERS Proceedings*, Taipei, March 25–28, 2013.
3. Chan, R., R. Mittra, and T. Cwik, "Techniques for analyzing frequency selective surfaces — A review," *IEEE*, Vol. 76/12, 1593–1615, 1988.
4. Antoniou, A. and W. S. Lu, *Practical Optimization: Algorithms and Engineering Applications*, Pvt. Limited, Springer, India, 2009.

Modelling of Resonant Scattering and Generation of Oscillations for Nonlinear Media

Lutz Angermann[1] and Vasyl V. Yatsyk[2]

[1]Department of Mathematics, University of Technology at Clausthal
Erzstraße 1, Clausthal-Zellerfeld D-38678, Federal Republic of Germany
[2]O. Ya. Usikov Institute for Radiophysics and Electronics
National Academy of Sciences of Ukraine, 12 Ac. Proskura Str., Kharkiv 61085, Ukraine

Abstract— Based on a model of resonant scattering and generation of waves on an isotropic nonmagnetic nonlinear layered dielectric structure, which is excited by a packet of plane waves, we compare two numerical algorithms — the preset field approximation and the self-consistent method for simulating various effects of the fields at multiple frequencies. The mathematical model consists of a system of boundary-value problems of Sturm-Liouville type and of an equivalent system of one-dimensional nonlinear Fredholm integral equations of the second kind. Various effects caused by the nonlinearity of the structure were investigated using analytical and numerical techniques [1–3]. It could be observed that only the self-consistent approach ensures the physically important law of the balance of energy. The results principally indicate how to control the generated field by means of the intensity of the exciting field. In particular, they offer the possibility of designing a frequency multiplier and other electrodynamic devices containing nonlinear dielectrics with controllable permittivity.

ACKNOWLEDGMENT

This work was partially supported by the Visby Program of the Swedish Institute and by the joint Russian-Ukrainian RFBR-NASU Grant No. 12.02.90425-2012.

REFERENCES

1. Angermann, L., Y. V. Shestopalov, and V. V. Yatsyk, "Modeling and analysis of wave packet scattering and generation for a nonlinear layered structure," *Multiphysics Modeling in Microwave Power Engineering*, 21–26, E. M. Kiley and V. V. Yakovlev, Editors, University of Bayreuth, Germany, 2012; *14th Seminar Computer Modeling in Microwave Engineering and Applications*, Bayreuth, Mar. 5–6, 2012.
2. Angermann, L. and V. V. Yatsyk, "The effect of weak fields at multiple frequencies on the scattering and generation of waves by nonlinear layered media," *Solutions and Applications of Scattering, Propagation, Radiation and Emission of Electromagnetic Waves*, 303–332, A. Kishk, Editor, InTech, Rijeka, Croatia, 2012.
3. Angermann, L. and V. V. Yatsyk. "The influence of weak fields at multiple frequencies on the process of resonant scattering and generation of oscillations by nonlinear layered structures," *Physical Bases of Instrumentation*, Vol. 2, No. 1, 48–71, 2013 (in Russian).

The Formation Process of Nanoclusters in the Metal Surface Layer, Initiated by Nonlinear Tunneling Dynamics in the Electrostatic Field

I. I. Artemov, **V. D. Krevchik**, **M. B. Semenov**, **A. V. Sokolov**, **and S. B. Menshova**
Penza State University of Russia, Russia

Abstract— One of the possible mechanisms for the nanoclusters formation in the metal surface layer under the cavitation regime for sound capillary effect, has been considered. Physical basis of this mechanism is electron exchange between nanoparticles by dissipative tunneling with subsequent formation of dipoles. As a result, the mechanism of the dipole-dipole interaction can turn on between the nanoparticles themselves, and with the interior of the broken bonds in microcracks due to the electrostatic image forces, which leads to the formation of nanoclusters. It is shown, that the effective Young's modulus of the nanostructured surface layer is defined by the relation between the rate of tunneling transfer in an electric field and the frequency of the ultrasonic wave. It is found that in the case of the dense regular chain of microcracks the effective Young's modulus of the surface layer is mainly determined by Young's modulus of the nanoparticles material. The obtained theoretical results can form the basis of technology to improve the efficiency of grinding, including and for rather brittle materials. For example, the results of the experiment on the processing of ferrite materials using the process fluid, modified by the copper nanoparticles are showed a reduction of roughness by 12%. By electron microscopy data, the surface of the treated material becomes more homogeneous due to overgrowth of microcracks net by the copper nanoparticles.

Session 1P11
SC1: Computational Electromagnetics

Computing Ground-Wave Electric Field at MF Band via FDTD Method
Fernando Tomas Pachon Garcia, Jesus Manuel Paniagua-Sanchez, Maria Montana Rufo-Perez, Antonio Jimenez-Barco, ... 370

Longitudinal Voltages, Induced by Parallel Overhead Transmission Lines Magnetic Field
Nina B. Rubtsova, M. Sh. Misrikhanov, S. G. Murzin, A. Yu. Tokarskij, ... 371

Finite Volume Frequency Domain Method for Nonlinear Media
Harish Bhat, Garnet J. Vaz, ... 372

Effective HF Modeling of Passive Devices Based on Frequency Dependent Hodge Operators and Model Order Reduction
Gabriela Ciuprina, Daniel Ioan, Mihail-Iulian Andrei, ... 373

Image Restoration of Two-dimensional Signal Sources with Superresolution
Boris A. Lagovsky, Alexander B. Samokhin, ... 374

Femtosecond Laser Pulse Breakdown of a Single Water Microdroplet
E. S. Efimenko, A. A. Murzanev, Yu. A. Malkov, A. N. Stepanov, ... 375

Stability Analysis of Predictor-corrector Based Quasi-explicit MOT-TDIE Solvers
Huseyin Arda Ulku, Hakan Bagci, ... 376

A PMCHWT Surface Integral Equation Solver for Analyzing Transient Plasmonic Interactions
Ismail Enes Uysal, Huseyin Arda Ulku, Hakan Bagci, ... 377

A Stable and Explicit MOT Solver for the Time Domain Volume Electric Field Integral Equation
Sadeed Bin Sayed, Huseyin Arda Ulku, Hakan Bagci, ... 378

A Direct Spectral Domain Method for Near-ground Microwave Radiation by a Vertical Dipole above Earth in the Presence of Atmospheric Refractivity
Rajib Bhattacharjea, Christopher R. Anderson, Gregory David Durgin, ... 379

A Variational Approach to Compute Singular Axisymmetric Electromagnetic Fields
Franck Assous, I. Raichik, ... 380

Electromagnetic Sources and Observers in Motion X — Unification of Electromagnetism and Gravity
Selwyn Edgar Wright, ... 381

Computing Ground-Wave Electric Field at MF Band via FDTD Method

F. T. Pachón-García, J. M. Paniagua-Sánchez, M. Rufo-Pérez, and A. Jiménez-Barco
Polytechnic School, University of Extremadura, Av. de la Universidad s/n, Cáceres 10003, Spain

Abstract— This paper presents a study about calculations of electric field at medium frequency (MF: 300 kHz–3 MHz), based on 2D finite-difference time-domain (FDTD) method. Variations of electric field with land conductivity and with typified mountains are evaluated, and the results are validated with Millington expressions and parabolic-equation finite-element method (PE-FEM) method, agreeing well. The interest of introducing this technique for calculating levels of electric field is that it includes reflection, diffraction, surface wave, and takes into account backscattering. Therefore it provides a more robust solution in non-ideal environments with difficult terrain, being this a first step to analyze how suitable its use is, in terms of time consuming and accuracy of results for this frequency band.

Entering into details, firstly a 2D FDTD method in Cartesian coordinates was implemented, being possible to select the spatial and temporal resolution according to the working frequency and a reasonable compromise between the grid resolution and the time required for execution. In the space, a section of land is included in the low part, allocating the transmitter and the receiver 1 cell above the earth, being surrounded all the space by perfect matched layer (PML). Regarding the selected source, it was a Gaussian pulse at the frequency of study. Concerning the characteristics of the terrain, different sections of land were used with conductivities between 2–30 mS/m depending on the transitions to analyze; and when mountains wanted to be included, Gaussian shaped hills were incorporated to the space. Secondly, the results were contrasted on the one hand with the Millington curve approaches for flat earth, applying GRWAVE software from ITU, and on the other hand, FEM for hilly terrain, using FEMIX software from IEEE members.

Longitudinal Voltages, Induced by Parallel Overhead Transmission Lines Magnetic Field

N. B. Rubtsova[2], **M. Sh. Misrikhanov**[1], **S. G. Murzin**[1], **and A. Yu. Tokarskij**[3]

[1]JSC Federal Network Company, Moscow, Russian Federation
[2]Federal State Budgetary Institution 'Research Institute of Occupational Health' under the Russian Academy of Medical Sciences, Moscow, Russian Federation
[3]JSC Federal Network Company Branch "Main Power Networks of the Center" Moscow, Russian Federation

Abstract— Under parallel overhead transmission line (TL) maintenance linemen safety requires to know the voltage equal voltage induced by return current in the ground in circuit of parallel line magnetic field (MF). The equations received on Carson' integral $J(r,\theta) = P + jQ$, where r, θ — integral parameters, with use of electromagnetic wave penetration into ground, are applied to definition of induced voltage value. Applicability of these equations is limited by "dead zone" on "r" parameter (under r change from 0.25 up to 5). In recalculation to a distance between parallel TL, for example for $\rho = 50\,\text{Ohm}\cdot\text{m}$ ground resisitivity, these equations application lead to very high error in case of $100\,\text{m} < a < 1800\,\text{m}$.

The mathematical model of voltage induced by parallel lines MF calculation with use of equivalent depth of return induced current is offered.

Induced in repaired TL voltage $\dot{E}$ is combined from created by parallel line wire current MF, voltage created currents induced in the ground by parallel line wire current MF, and voltage induced by return current in the ground in circuit of parallel line. Before and after "dead zone" voltage modules $\dot{E}_K$ and $\dot{E}$ have good concurrence, and inside of this zone $\dot{E}$ module curve unlike $\dot{E}_K$ does not leave to zone of big error.

Finite Volume Frequency Domain Method for Nonlinear Media

Harish S. Bhat and Garnet J. Vaz
Applied Mathematics Unit, University of California, Merced, USA

Abstract— A typical approach to compute the steady-state response for nonlinear electromagnetic media is to step the system forward in time until all transients have decayed. We present a finite volume frequency domain (FVFD) method that computes steady-state solutions of Maxwell's equations for two-dimensional nonlinear media without recourse to time-stepping. The method naturally handles general nonlinearities including the Kerr nonlinearity, spatial discontinuities in the permittivity and permeability, and different types of meshes.

In this work, we discretize the domain using a conforming triangulation. By averaging Maxwell's equations in each cell, we obtain a coupled system of nonlinear ordinary differential equations, with the coupling governed by the connectivity (i.e., the dual graph) of the mesh. This coupled system may be interpreted as Kirchhoff's laws for a network of voltage-dependent capacitors and inductors, together with boundary resistors and sources. We apply a fixed point iterative method to determine the steady-state solution of the coupled system. Numerical experiments show that, under a wide variety of conditions, the fixed point method converges. The FVFD method we develop here is a generalization to nonlinear media of a method devised previously for linear media [2].

In order to study the properties of the FVFD method, we develop a novel distributed memory implementation using the Portable, Extensible Toolkit for Scientific Computation (PETSc) [1]. The implementation leverages the fact that each iteration of the fixed point method naturally decouples into two steps. The first step requires only local computation of spectral data, and thus does not require interprocessor communication. The second step requires the solution of a linear system, which we handle using parallel numerical linear algebra solvers that are part of PETSc. Using this implementation, we study the accuracy, stability, speed, and scalability of the FVFD method in comparison with other leading techniques.

ACKNOWLEDGMENT

We gratefully acknowledge support from UC Merced's Graduate Research Council together with support from the U.S. Department of Energy (Contract No. DE-AC02-05CH11231, Subaward 7041635).

REFERENCES

1. Balay, S., W. D. Gropp, L. C. McInnes, and B. F. Smith, "Efficient management of parallelism in object-oriented numerical software libraries," *Modern Software Tools in Scientific Computing*, 163–202, Birkhäuser Press, Boston, USA, 1997.
2. Bhat, H. S. and B. Osting, "Kirchhoff's laws as a finite volume method for a planar Maxwell system," *IEEE Transactions on Antennas and Propagation*, Vol. 59, No. 10, 3772–3779, 2011.

Effective HF Modeling of Passive Devices Based on Frequency Dependent Hodge Operators and Model Order Reduction

Gabriela Ciuprina, **Daniel Ioan**, **and Mihail-Iulian Andrei**
Politehnica University of Bucharest
Spl. Independentei 313, Bucharest 060042, Romania

Abstract— Designers of integrated circuits require models for passive components which describe all relevant electromagnetic field effects at high frequency. These effects are quantified by the Maxwell equations of the full wave (FW) electromagnetic field. In the Finite Integration Technique (FIT), by applying the global form of electromagnetic field equations on the mesh elements (elementary faces and their borders), a system of differential algebraic equations, called Maxwell Grid Equations (MGE) is obtained [1]. However, due to high conductivity ($\sigma \gg \omega\varepsilon$), the electromagnetic field inside metallic conductors can be considered a magneto-quasi-static (MQS) one. In our approach, MGE for MQS regime are combined with the Hodges operators, which describe the material behavior. In the classical FIT approach, the discrete Hodge operators $\vec{M}_\nu$ and $\vec{M}_\sigma$ and are constant diagonal matrices, which can be built by independent averaging of material constants $\nu = 1/\mu$ and σ over each cell. In order to describe field effects at high frequency such as skin and proximity effects, the cell dimensions have to be much less than the skin depth. In order to keep the number of cells at a reasonable level, non-uniform grids could be used, with peripheral cells smaller than internal ones. Even so, the number of cells required by a reasonable accuracy can be relatively high. To avoid this drawback, it was proposed to replace the Hodge operators used in classical FIT with others appropriate for the description of high field effects in conductors. This paper continues the research in [2, 3].

The final validation was carried out for a more complex problem consisting of two coupled inductors (Fig. 1), for which measurements are available. It is important to emphasize that, the finally a reduced compact netlist consists of lumped circuit elements with constant parameter values is obtained, whose behaviour is able to catch the frequency dependence of the original field problem.

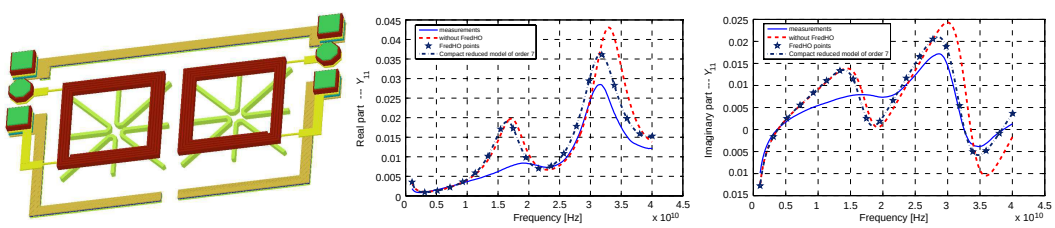

Figure 1: Frequency characteristic — with or without FredHO for two coupled spiral inductors.

ACKNOWLEDGMENT

The work is funded by the Joint Research Project PN-II-PT-PCCA-2011-3 (ANCS, CNDI-UEFISCDI), contract No. 5/2012.

REFERENCES

1. Weiland, T., "A discretization method for the solution of Maxwell's equations for 6 component fields," *AE, Electronics and Communication*, Vol. 31, 116–120, 1977.
2. Ioan, D. and M. Piper, "FIT models with frequency fependent hodge operators for HF effects in metallic conductors," *Progress In Electromagnetics Research Symposium Abstracts*, Pisa, Italy, Mar. 28–31, 2004.
3. Ciuprina, G., D. Ioan, C. B. Dita, and M. I. Andrei, "Frequency parameterized models for planar on-chip inductors," *Scientific Computing in Electrical Engineering*, 2012.
4. Gustavsen, B. and A. Semlyen, "Rational approximation of frequency responses by vector fitting," *IEEE Trans. Power Delivery*, Vol. 14, 1052–1061, 1999.
5. Palenius, T. and J. Roos, "Comparison of reduced-order interconnect macromodels for time-domain simulation," *IEEE Trans. Microwave Theory and Techniques*, Vol. 52, No. 9, 2240–2250, 2004.

Image Restoration of Two-dimensional Signal Sources with Superresolution

B. A. Lagovsky and A. B. Samokhin
Moscow State Institute of Radio Engineering and Automation (Technical University), Russia

Abstract— Generalization of the known methods for two-dimensional image restoration problem is essentially complicates the algorithms greatly increases the processing time of signals. The use of parallel processors to obtain satisfactory results sometimes requires.

Considered promising for two-dimensional problems of image restoration with superresolution radiation sources are algebraic methods for solving one-dimensional problems.

They were to present the approximate solutions in the form of finite expansions given by a sequence of functions with unknown coefficients. A generalization of algebraic methods to two-dimensional problem does not lead to a serious complication of algorithms. The numerical solution time varies slightly.

The dependence of the envelope of the received signal $U(x, y)$ is a linear Fredholm integral equation of the first kind type of two-dimensional convolution

$$U(x, y) = \int\limits_{\Omega} f(x - x', y - y') I(x', y') dx' dy' \tag{1}$$

where $I(x, y)$ — two-dimensional angular distribution of emitted (or reflected) signal, $f(x, y)$ — the radiation pattern. The problem is to restore the $I(x, y)$ based on the analysis of the signal $U(x, y)$ and the known $f(x, y)$ with the best possible angular resolution exceeding the Rayleigh criterion.

This problem belongs to a class of inverse. It is It is ill-posed, because not satisfy the second and third requirements correctness of Hadamard.

To search sustainable solution initially sought distribution $I(x, y)$ is represented as an expansion in a finite system of orthogonal two-dimensional functions with unknown coefficients. The expansion coefficients are found from the system of linear algebraic equations obtained on the basis of (1).

Algebraic methods allow consistently approach to the maximum for each problem angular resolution.

The resolution and its limits were studied in the mathematical model. Archived resolution is 4 times higher than the Rayleigh criterion. In addition, it has been a good source localization signals. Intensities were used with a small error, which amounted to 5.2%.

Femtosecond Laser Pulse Breakdown of a Single Water Microdroplet

E. S. Efimenko, **A. A. Murzanev**, **Yu. A. Malkov**, **and A. N. Stepanov**
Institute of Applied Physics, Russian Academy of Sciences
46 Ulyanov st., Nizhny Novgorod, Russia

Abstract— The recent significant progress in the development of femtosecond laser has resulted in a considerable number of available sources and their application in various fields of science and technology. The use of such systems for atmospheric research, in particular in the framework of the Teramobile project, increases the importance of accounting for various nonlinear impact on laser radiation propagation through the atmosphere. The presence of water in air vapor or aerosols may substantially change the conditions of laser radiation propagation, so the effects associated with the interaction of intense radiation with aerosols require careful study. Tight focusing conditions realized inside water droplets lead to substantial intensity gain in focal spots and, hence, to rapid ionization. The scattered laser radiation experiences strong spectra modification, which can be used for remote atmosphere probing. In turn, the overdense plasma produced inside a water droplet absorbs a significant part of the pulse energy leading to high energy deposition, the medium rapidly becomes a mixture of overheated water, vapor and overdense plasma — so this object may be of interest for studying matter under extreme conditions.

In the present work we study the interaction of a 30 μm water microdroplet with a 70 fs laser pulse by direct modeling the Maxwell equation via a three-dimensional FDTD code, including Kerr nonlinearity, multiphoton, tunnel and avalanche ionization of the medium, electron-ion recombination and nonlinear energy absorption. This approach, in contrast to the traditional analysis based on the Mie theory, allows describing complex self-consistent dynamics of microdroplet breakdown accounting for plasma backreaction on laser pulse and therefore studying breakdown characteristics, including energy deposition, scattering and spectra modification. The numerical modeling in a wide range of input intensities from 10^{11} to 10^{14} W/cm^2 showed that, for intensities below 10^{13} W/cm^2, plasma is formed mainly near focus, reaching densities up to 3 10^{22} cm^{-3} and absorbs 75–80% of incident energy, which leads to maximum local energy deposition comparable with 20–30 kJ/cm^3. The backscattered radiation experiences a strong blueshift, but is considerably influenced by absorption. For intensities exceeding 10^{13} W/cm^2 corresponding to water breakdown threshold, rapid ionization occurs already at the input boundary, so the main part of the pulse is backreflected. Finally, we compared the numerical results and the experimental work done by our group.

Stability Analysis of Predictor-corrector Based Quasi-explicit MOT-TDIE Solvers

H. Arda Ülkü and Hakan Bağcı
Division of Computer, Electrical, and Mathematical Sciences and Engineering (CEMSE)
King Abdullah University of Science and Technology (KAUST)
Thuwal 23955-6900, Saudi Arabia

Abstract— Implicit marching on-in-time (MOT) time domain integral equation (TDIE) solvers require at every time step inversion of a matrix system of equations, termed implicit MOT system here. Implicit MOT matrix is sparse when spatial discretization size is around $c\Delta t$, where c is the speed of light and Δt is time step. Under high-frequency excitation Δt is small and this condition is usually met and the implicit MOT system can be solved efficiently using an iterative solver. On the other hand, under low-frequency excitation, $c\Delta t$ is significantly larger than the spatial discretization size and the implicit MOT matrix becomes denser. Consequently, its iterative solution cannot be carried out efficiently. To remedy this problem, recently a quasi-explicit MOT scheme that uses a predictor-corrector scheme to solve the time domain magnetic field integral equation (MFIE) has been developed [1]. This new scheme requires at every time step inversion of a matrix system of equations, termed explicit MOT system here. Explicit MOT matrix is the Gram matrix that is obtained from discretization of the self-term contribution of the MFIE and is always sparse and well-conditioned regardless of Δt. It has been shown that the quasi-explicit MOT solver produces accurate results and Δt can be as large as that of the implicit MOT solver without sacrificing from accuracy. The stability of the MOT solvers is usually investigated by observing the late time response of the time dependent solution. Additionally, the stability properties of the solution can be shown by an algebraic analysis of the MOT system [2].

In this work, an algebraic stability analysis for the quasi-explicit MOT-MFIE solver, which uses $PE(CE)^m$ type predictor-corrector schemes will be presented. The analysis is an extension of the one described in [2]; the extension takes into account the predictor and corrector coefficients as well the number of corrector step repetitions while constructing the companion matrix of the quasi-explicit MOT system. Then, the locations of the companion matrix's eigenvalues are used to investigate the stability of the solver. Indeed, this algebraic analysis, which is executed on several examples, demonstrates that the explicit MOT solution is stable.

REFERENCES

1. Ulku, H. A., et al., *IEEE Trans. Antennas Propagat.*, submitted.
2. Walker, S. P., et al., *Int. J. Numer. Model.: Electron. Networks, Device Fields*, Vol. 474, No. 15, 459–474, 2002.

A PMCHWT Surface Integral Equation Solver for Analyzing Transient Plasmonic Interactions

I. Enes Uysal, H. Arda Ülkü, and Hakan Bağcı
Division of Computer, Electrical, and Mathematical Sciences and Engineering (CEMSE)
King Abdullah University of Science and Technology (KAUST)
Thuwal 23955-6900, Saudi Arabia

Abstract— Device design based on manipulation of plasmonic wave interactions at nanoscale often requires characterization of scattering and absorption response of the prototype to the changes in various parameters such the local refractive index, geometric dimensions and aspect ratios, and the direction and polarization of the incident fields. Due to the high geometric complexity and intricacy of the proposed designs, fully- and even semi-analytical methods cannot be used for the task of characterization and analysis of plasmonic wave interactions. To undertake this task, numerical full-wave time domain solvers have been developed. These solvers mostly rely on finite difference time domain (FDTD) method or its extensions.

Time domain surface integral equation (TDSIE) solvers are a promising alternative to FDTD schemes in terms of computational efficiency and accuracy; this is attributed to two features: (i) they only discretize interface surfaces and (ii) implicitly enforce the radiation condition. These properties render the TDSIE solvers especially useful in simulating plasmonic wave interactions, where if FDTD techniques were employed, volume discretizations would have to be dense due fast decaying fields in the vicinity of metal-dielectric interfaces (resulting in long simulation times) and approximate absorbing boundary conditions would have to be applied to truncate the computation domain (resulting in inaccuracies in the scattered field response). Despite these advantages, use of TDSIE solvers in simulating plasmonic wave interactions has not been widely reported.

In this work, a TDSIE solver is proposed for analyzing transient plasmonic interactions. The proposed solver utilizes the well-known Poggio-Miller-Chan-Harrington-Wu-Tsai (PMCHWT) SIE formalism [1] to describe the scattered fields in terms of equivalent surface electric and magnetic currents introduced at material interfaces and the time domain Green function of the plasmonic medium [2]. Equivalent currents are expanded in terms of Rao-Wilton-Glisson (RWG) [3] functions in space and polynomial interpolants [4] in time. Inserting these expansions into the TDSIE and Galerkin testing the resulting equation at time samples results in a matrix system of equations. This matrix system is solved for current expansion coefficients using the marching-on-in-time (MOT) technique.

At the presentation, accuracy, stability, and real-life applicability of the MOT-TD-PMCHWT solver for plasmonic scatterers will be demonstrated via numerical examples.

REFERENCES

1. Medgyesi-Mitschang, L. N., et al., *J. Opt. Soc. Am. A*, Vol. 11, No. 4, 1383–1398, 1994.
2. Wilhelmsson, H., et al., *Physica Scripta.*, Vol. 52, 102–107, 1995.
3. Rao, S. M., *IEEE Trans. Antennas Propagat.*, Vol. 30, No. 3, 409–418, 1982.
4. Manara, D. G., et al., *IEEE Trans. Antennas Propagat.*, Vol. 45, No. 3, 527–532, 1997.

A Stable and Explicit MOT Solver for the Time Domain Volume Electric Field Integral Equation

Sadeed Bin Sayed, **H. Arda Ülkü**, **and Hakan Bağcı**
Division of Computer, Electrical, and Mathematical Sciences and Engineering (CEMSE)
King Abdullah University of Science and Technology (KAUST)
Thuwal 23955-6900, Saudi Arabia

Abstract— Time domain volume integral equation (TDVIE) solvers are becoming attractive alternatives to finite difference time domain and time domain finite element methods for analyzing transient electromagnetic wave interactions on inhomogeneous dielectric objects. Classical volume electric field integral equation (VEFIE) solversdiscretize the unknown flux density induced inside the object using Schaubert-Wilton-Glisson (SWG) [1] and polynomial interpolants [2] in time. Testing the discretized VEFIE using Galerkin procedure at sampling points in time results in a matrix system, which is solved by marching on-in-time (MOT) algorithm.

The MOT scheme can be either explicitor implicit. Implicit MOT solvers usually provide a stable solution, but require at every time step inversion of a matrix system that becomes dense when the time step size is large. On the other hand classical explicit MOT solvers do not require matrix inversion but are more likely to be unstable [3]. Typically, explicit solvers can be made stable using finer time steps at the cost of significant increase in computation time.

In this work, a stable and explicit MOT solver that employs a predictor-corrector scheme to efficiently solvethe time domain VEFIE is described. Spatial discretization of VEFIE is carried out in the same way as the implicit MOT-VFIE solver but the time marching is constructed in the form of a traditional $PE(CE)^m$ scheme. The stability and accuracy of the time marching are controlled using successive over relaxation (SOR) applied at each repetition of the corrector step. As opposed to its implicit counterpart, the explicit solver requires at every time step inversion of a matrix system with a Gram matrix that is sparse and well-conditioned regardless of time step size. It should be noted here that the $PE(CE)^m$ scheme can be constructed using classical polynomial based methods (e.g., Adam-Moulton, Adam-Bashforth, backward difference formula) or novel numerical methods based on exponential fitting [4]. Unlike the classical explicit MOT solvers, the proposed solver can work with large time steps as in its implicit counterpart. Numerical results demonstrate thatit provides faster solution especially for small permittivity values — compared to implicit MOT solver,and is capable of providing stable solution even when the implicit solver fails.

REFERENCES

1. Schaubert, D. H., et al., *IEEE Trans. Antennas Propag.*, Vol. 32, No. 1, 77–85, 1984.
2. Manara, G., et al., *IEEE Trans. Antennas Propag.*, Vol. 45, No. 3, 527–532, 1997.
3. Al-Jarro, A., et al., *IEEE Trans. Antennas Propag.*, Vol. 60, No. 11, 5203–5214, 2012.
4. Glaser, A. and V. Rokhlin, *J. Sci. Comput.*, Vol. 38, No. 3, 368–399, 2009.

A Direct Spectral Domain Method for Near-ground Microwave Radiation by a Vertical Dipole above Earth in the Presence of Atmospheric Refractivity

R. Bhattacharjea[1, 2], C. R. Anderson[2], and G. D. Durgin[1]

[1]Georgia Institute of Technology, USA
[2]United States Naval Academy, USA

Abstract— We present an analytically rigorous computational model for long-range radiation by a vertical dipole above a realistic Earth in the presence of atmospheric refractivity gradients. Weak refractive gradients are observed across the EM spectrum above the earth, where solar irradiance drives temperature and humidity gradients in height; these, in turn, affect the index-of-refraction of air. Although methods exist for calculating EM fields in this context, this work represents a significant improvement in fidelity, rigor, and generality over previous models, which use empirical rules, ad hoc collections of simple closed-form approximations, or asymptotic approximations including the paraxial approximation or ray-based approximations. These other methods are limited in their range of validity with respect to some or all of the following parameters: 1) minimum and maximum propagation range, 2) maximum propagation angle, 3) allowable ground permittivity, and 4) allowable atmospheric gradients. Also, ray-based and paraxial approximation formulations inherently represent solutions to the eikonal equation and the paraxial (or parabolic) one-way wave equation, respectively, and NOT the wave equation embedded in Maxwell's equations. What's more, these methods generally must use approximate boundary conditions to model surfaces, and approximate radiation boundary conditions to make simulation in finite domains possible. As such, these techniques are valid methods for EM modeling insofar as the eikonal or paraxial equations with approximate boundary conditions are valid approximations of Maxwell's equations with true boundary conditions, which of course is not the case in general. While approximate methods are currently used for long range propagation modeling, they naturally lead to questions about non-approximate methods. We conceive of the present model then as a kind of reference solution for very general, long range EM problems. The environmental model is a multilayered uniaxial "stackup", representing lossy (not perfectly conducting) ground and a refractivity profile of the atmosphere. Beginning with Maxwell's equations for the potential of a dipole embedded in this multilayered medium, we use analytical full-wave, planewave spectrum (Fourier transform) techniques to reduce the original 3D problem to a 1D transmission-line-like problem in the spatial-wavenumber domain of planewaves. We do not develop the transmission line analogy in terms of circuit quantities as other have done in the analysis of multilayered printed circuit boards, and instead directly work with EM field quantities. As such, the 1D problem is efficiently solved by enforcing tangential field continuity conditions at layer interfaces, resulting in a sparse matrix operator that can be solved in $O(n)$ operations, where n is the number of layers in the environmental model. This matrix solution corresponds to the height dependence of the fields in all layers for a given planewave in the spectral expansion of the fields. To arrive at a 3D field solution, the height dependence of the fields is integrated over a suitable subset of all the planewaves in an inverse Fourier transform integral, commonly known as a Sommerfeld integral in this context. The integrals are evaluated partially in closed form and partially using efficient numerical quadratures. The integration kernels are smoothed by a singularity extraction procedure, and the extracted terms are analytically integrated. The remainder of the integrals can be evaluated using two different types of quadratures that are selected based upon the range at which the fields should be evaluated. For short ranges to intermediate ranges, adaptive Clenshaw-Curtis quadratures can be used to very accurately calculate the Sommerfeld integrals, while in the long range regime, Filon quadrature leads to solutions that are accurate. The end result is always the values of the fields at a grid of points in height and range. Examples of propagation in various refractive environments and ground conditions are compared against analytical results and those of other models in the literature. We qualitatively identify the conditions under which guided propagation modes of the atmospheric profile are the dominant mode of propagation. While we note that the methodology of the calculations is analogous to methods used in the EM modeling of multilayer printed circuit boards, multi-segment transmission lines, or the theory of multilayered optical coatings, we have observed that this is the first work to apply such rigorous techniques to long range propagation in realistic atmospheres and realistic ground conditions.

A Variational Approach to Compute Singular Axisymmetric Electromagnetic Fields

F. Assous[1] **and I. Raichik**[2]

[1]Ariel University, Israel
[2]Bar-Ilan University, Israel

Abstract— We propose a new variational approach to compute the axisymmetric Maxwell equations in singular domains, as for example non convex polygonal domains. We show that the key point to solve this problem is related to the solution of Laplace-like operators in the singular domain. For instance to compute the singular magnetic field $B = (B_r, B_z)$, one needs to solve the static problem

$$\text{curl B: } = \frac{\partial B_r}{\partial z} - \frac{\partial B_z}{\partial r} = f.$$

This problem is singular in the sense that for a non-convex axisymmetric domain ω, the space of solutions (says W) is *not a subspace* of the Sobolev space H^1. Nevertheless, W can be decomposed into two subspaces, i.e., $W = W_R \oplus W_S$, where W_R is a regular subspace, that is a subspace of H^1 in which one can easily compute a numerical solution. The difficulty comes from the singular subspace W_S, that has been proved to be a finite-dimensional subspace, the dimension being the number of reentrant corners is the domain ω. Moreover, a basis function w_S of W_S can be characterized as the solution to

$$\begin{aligned} &\text{curl } w_S = P_S \quad \text{in } \omega, \\ &\text{div } w_S = 0 \quad \text{in } \omega, \\ &w_S \cdot \nu = 0 \quad \text{on } \partial\omega. \end{aligned}$$

Here, the right-hand side P_S is singular, that it belongs to L^2 but not to H^1, and solves the following Laplace-like equation

$$\Delta' P_S := \frac{\partial^2 P_S}{\partial r^2} + \frac{\partial^2 P_S}{\partial z^2} + \frac{1}{r}\frac{\partial P_S}{\partial r} - \frac{P_S}{r^2} = 0 \quad in\ \omega, \quad P_S = 0 \quad \text{on } \partial\omega.$$

Similar problem can be established for the electric field $E = (E_r, E_z)$. Hence, the key point is to compute P_S, which can not be solved by a standard finite element method, which would give $P_S = 0$. In this talk, we propose a new method to efficiently compute P_S, and then the electromagnetic field. It consists in decomposing the domain ω into 2 subdomains, and to derive an *ad hoc* variational formulation, in which the interface conditions are imposed through a method deduced from a Nitsche approach. Numerical examples to illustrate our method will be shown in the talk.

Electromagnetic Sources and Observers in Motion X — Unification of Electromagnetism and Gravity

Selwyn E. Wright
Moor Lane Laboratory, ECASS Technologies Ltd, HD8 0QS, UK

Abstract— This tenth paper in the series of EM Sources and Observers in Motion is complimentary to paper IX dealing with the Nature of Gravity. Motional Electromagnetic (EM) and gravitational theories appear to have two inherent deficiencies that have prevented them from becoming a unified theory. (α) Not recognising that the propagation medium (ether) is the essential thread that runs through these developments. (β) Not realising that EM waves and gravity are two forms of the same field — unsteady electric and steady difference electric fields. A New Relativity theory (NR) re-establishes a preferred frame of reference, re-uniting classical and modern physics. It appears that all observed actions at a distance are based on a propagation medium, and that EM, gravitational and inertial fields use the same electrical medium. The only difference from classical theories, is that time and structure of EM systems shrink with motion through the medium, gravity compresses the medium, and residual gravity within the universe provides the inertial field. All predictions involving observations have to satisfy the wave equation through its propagation medium. All causal observations, which currently support Einstein's Special Relativity (SR) (1905) and General Relativity (GR) (1915), are predicted using the medium based theory. The ether-less aspects of SR and GR are non causal (not predictable). NR predicts SR and GR properties in a straight forward physical manner with a medium, without ambiguity or paradox.

Measurements, based on Einstein's SR and GR, such as Kramer et al. (2006) on binary pulsars, are causal, (predictable). They are not ether-less as Einstein claimed. Einstein used Lorentz's (1899) medium based Transform (LT) and field equations based on a propagation medium, Einstein did not appear to realise the equations he used were medium based, not believing in an ether. Einstein's ether-less concept of relativity is not supported by the medium based LT, where interaction with the EM medium is essential. Ether-less claims and predictions, such as simultaneity, time travel and no absolute time and space, are non causal, they cannot be measured. Einstein not accepting the medium's presence, believed that the general wave equation could not distinguish between source and observer motion, nor distinguish between stationary and moving medium reference frames. The new theory accommodates these additional features, predicts the medium based measured aspects of SR and GR and identifies the ether-less, non causal aspects of relativity.

Wright (2010)[1]–(2012)[8], has shown that Einstein's ether-less relativity, based on his inertial frame, is non causal, it cannot predict measured observations. Without a medium relativity cannot explain how the simple Doppler effect occurs, how a moving more dense medium than a vacuum can convect light, how an impulsive wave is formed in Cerenkov (1934) radiation, how two systems can move apart physically, greater than the speed of light, but not relative to each other. Nor distinguish between light propagation on Earth, around the Earth or through the Solar System and beyond. Einstein's invariant ether-less inertial frame cannot predict propagation time asymmetry or explain the inconsistency of predicting ether-less and medium based motional properties, both at the same time. To account for these measured observations, the medium's presence has to be accepted, Einstein's concept of relative motion rejected, and the medium based LT extended for both source and observer motion. None of the observations can be observed without a medium.

Those who believe there is nothing wrong with Einstein's relativity ignore fundamental unanswered questions such as; how does light propagate, or how can one solve the wave equation for propagating waves, without a propagation medium? Removing the medium is against basic wave theory, creating a discontinuity between classical and modern physics. There is no evidence, or causal model that can support Einstein's ether-less universe. Further, after a century of SR and GR, there have been no significant developments to explain what gravity is, how it is propagated and how it is related to EM waves. This theory identifies and establishes the existence of a well defined measured propagation medium and unifies it with gravity. There is now sufficient evidence to re-think our basic EM model by reinstating the EM medium for the propagation of EM waves and gravity, and recognising that gravity is the attraction between dissimilar charges.

Session 1PK
Poster Session 2

Numerical Modeling of Perfect Lens Using FDTD Method
Aleksander P. Smirnov, A. N. Semenov, V. V. Shevchenko, ... 386
Power Network Vulnerability Analysis via Compressed Sensing
Harish S. Bhat, Garnet J. Vaz, Juan C. Meza, ... 387
CFmaxwell — The Program Code for FDTD Modelling of Very Large Size Problems
Andrey V. Zakirov, Vadim D. Levchenko, ... 388
Performance Analysis of Blind Calibration in Five-port Receivers Based on Blind Source Separation
Francisco Vidal, Adriao Duarte Doria Neto, Allan Medeiros, Bernard Huyart, ... 389
Propagation Measurement of a Partially Open Drain: An Examination of the LOS and NLOS Sections
Anwuna Kingsley Awelemdy, Soo Yong Lim, Kah Phooi Seng, ... 390
A Comparison between 2-D and 3-D Models for Outdoor Radiowave Propagation
Zeina El Ahdab, Funda Akleman, ... 391
Analysis of the Benefits of Diversity Polarization in Wireless Networks
Inigo Cuinas, Manuel Garcia Sanchez, ... 392
Conception of Radio Frequency Link in the Radio of 3.5 GHz in Consonance with the National Brazilian Rules and International Legislation
Theoma M. Sanchez Otobo, Horacio Tertuliano Filho, C. A. Dartora, Eduil Nascimento Junior, E. Cherubini Rolin, ... 393
Some Insights on the Amount of Fading in Radio Channels
Hassan El-Sallabi, Khalid A. Qaraqe, Erchin Serpedin, ... 394
RF Identification (RFID) Reader with Long Read Range in the UHF Band
Jae-Young Jung, Kyu-Won Han, Chan-Won Park, ... 395
Simulation and Implementation of TDOA Monitoring System for Broadcasting Interferences
Yao-Tang Chang, ... 396
Design Guidelines of a Microwave Active Front-end Receptor: A LNA Approach
J. C. Bonoto, C. E. Capovilla, Humberto Xavier De Araújo, ... 397
Statistical Analysis of On-body Radio Propagation Channel for Body-centric Wireless Communications
Hasliza A. Rahim, Fareq Malek, Nurbaizatul Badrul Hisham, Mohd Fariz Abd Malek, ... 398
Path Loss Characterization of Body-to-body Radio Propagation Channel on the Angular Variations
Hasliza A. Rahim, Fareq Malek, A. Izwan Ahmad, Mohd Fariz bin Haji Abd Malek, ... 399
The Influence of Textile Dielectric Properties in On-body Radio Communication Channel Performance at 2.45 GHz
Hasliza A. Rahim, Fareq Malek, Mohd Fariz Abd Malek, ... 400
Mathematical and Numerical Analysis of Dielectric Waveguides by the Integral Equation Method
Evgeny M. Karchevskiy, Yury V. Shestopalov, ... 401
Linear-operator Theory for Inhomogeneous Omega Planar Waveguides
Antonio L. Topa, ... 402
Coupled Electromagnetic Wave Propagation in Space and around Surfaces and Interfaces
Michael James Underhill, ... 403
Two Types of Electromagnetic Induction Existing in Nature
Vladimir A. Leus, Ray T. Smith, Simon Maher, ... 404
The Stability of EM Particles and Predicted Mass Ratios
Michael James Underhill, ... 405
A Novel Approach for the Construction of Dirac's Delta Functions
Alireza R. Baghai-Wadji, ... 407
Electromagnetic Sources and Observers in Motion IX — Nature of Gravity
Selwyn Edgar Wright, ... 408
Energy Continuity Equation for Electromagnetic Waves in Dispersive Lossy Medium
Oleg B. Vorobyev, ... 409

Electromagnetic Force on Neutral Particles
Boon Kuan Chung, ... 411
The Uniqueness Theorems in the Electromagnetic Wave Theory and Quasi-periodical Solutions of the Periodical Diffraction Problems
Nikolai B. Pleshchinskii, ... 412
The Over-determined Boundary Value Problems for the Maxwell Equations Set in the Orthogonal Coordinates and Some Applications for the Electromagnetic Wave Diffraction Problems
Nikolai B. Pleshchinskii, ... 413
Plasma Treatment as a Versatile Technique for Preparation of Plasmonic Nanoantenna Arrays
Lucie Štolcová, Mária Domonkos, Tibor Ižák, Jan Proška, Marek Procházka, Alexander Kromka, . 414
The Dispersive Properties of the Three-dimensional Photonic Crystals with Diamond Lattices Containing the Epsilon-negative Materials
Hai Feng Zhang, Wenping He, Shaobin Liu, Yu-Qing Chen, ... 415
A New Triple-band Polarization-insensitive Wide-angle Microwave Metamaterial Absorber
Bo-Rui Bian, Shaobin Liu, Hai Feng Zhang, Bin-Xiang Li, Ben Ma, ... 416
Studies on Fano Resonances in Subwavelength Plasmonic Nanostructures
J. Fiala, P. Kwiecien, Ivan Richter, ... 417
Spectral Density Analysis of Thin Gold Films: Thickness and Structure Dependence of the Optical Properties
Pia C. Lansaker, E. Tuncer, I. Valyukh, H. Arwin, C. G. Granqvist, Gunnar A. Niklasson, ... 418
Variable Forbidden Regions in Metamaterial Planar Waveguide with Nonlinear Cladding
Yaw-Dong Wu, Ming-Hsiung Cheng, Tien-Tsorng Shih, ... 419
New All-optical Switch Based on the Local Nonlinear Plasmonic Mach-Zehnder Interferometer Waveguides
Yaw-Dong Wu, Sheng-Rong Hong, Tien-Tsorng Shih, ... 420
Broadband High Efficiency Amplifier for a Cognitive Radio System
Ahmed Eissa Fathy Khorshid, Ali M. Darwish, Islam A. Eshrah, Hossam A. H. Fahmy, Mohamed El-Hadidy, ... 421
Magnetoelectric Microwave Module for Phased Array
Roman Valer'evich Petrov, Mirza Imamovich Bichurin, Alexander Sergeevich Tatarenko, ... 423
Failure Analysis of Ferrite Sheet Used in NFC Antenna
Soon-Mi Hwang, Kwan-Hun Lee, ... 424
High Tunable and Low Loss Capacitor Using a BZN/BST/BZN Multi-layer Thin Film Dielectric for Reconfigurable RF Circuit Applications
Young Chul Lee, ... 425
Large-signal Properties of 3C-SiC/Si Heterojunction DDR IMPATT Devices at Terahertz Frequencies
Suranjana Banerjee, Aritra Acharyya, Monojit Mitra, Joyoti Prasad Banerjee, ... 426
A High Efficiency Broadband Supply Modulator Based on Switch-mode Operations for Polar Transmitters
Fei You, Bohai Zhang, Zhebin Hu, Songbai He, ... 427
Separation of Overlapped Compressed Cyclostationary Signals Using Adaptive FRESH Filtering
Said Esmail El-Khamy, Amr El Helw, Azza Mahdy, ... 429
Development of Non-contacting System for Detection of Driver's Sleepiness Using UWB Radar
Tae Yun Lee, Se-Yeoun Jeon, Jiwoong Yu, Seok Kim, Min-Ho Ka, ... 430
Depth-image Coding Using Neural Networks for 3D Video Transmission
Yih-Chuan Lin, Pu-Jian Hsu, ... 431
Research on Possibilities of Abnormal Tissues Diagnostic by THz Reflection Spectra
Anna A. Ezerskaya, E. A. Strepitov, I. V. Prozheev, O. A. Smolyanskaya, ... 433
Characterization of Dissipation Due to Quasiparticles and Dielectric Loss in a Josephson Metamaterial
J. Hassel, Pasi Lahteenmaki, A. Timofeev, Gheorghe Sorin Paraoanu, Pertti J. Hakonen, ... 435
Ultrafast Rotational Dynamics of Illuminated Particles and Stimulated Emission
Ana Asenjo-Garcia, Alejandro Manjavacas, F. Javier Garcia De Abajo, ... 436
A Dual-band Antenna with a Choke-circuit on the Ground Plane
The-Nan Chang, Jyun-Ming Lin, ... 437
RFID Tag on PCB in UHF Band
Won-Kyu Choi, Seung-Hwan Jeong, Chan-Won Park, Haewon Son, ... 438

Deep Defect Detection Using Eddy Current Testing with AMR Sensor
Dong Feng He, Mitsuharu Shiwa, ... 439
Comparative Study on Graphene-based Artificial Magnetic Conductor (AMC)
Xuchen Wang, Wen-Yuan Li, Wen-Sheng Zhao, Jun Hu, Ying-Ying Xu, Qiangsheng Huang, ... 440
Risk Assessment for University Students Occupationally Exposed to Electromagnetic Fields in Turkey
Fulya Callialp Kunter, Yagmur Kirkagac, ... 441
Single Layer Meta-material Lens with Graded Refractive Index
Mohamad-Ali Bitar, Y. Nasser, Mohammed Al-Husseini, Karim Y. Kabalan, ... 442
Problem of Coupled Electromagnetic TE-TE Wave Propagation in Nonlinear Anisotropic Layer
Yury G. Smirnov, ... 443
Stability of Nonlinear 2D-tunnel Bifurcations in Systems of Interacting Quantum Molecules in the Metamaterial Matrix
Vladimir D. Krevchik, Vladimir I. Volchikhin, Igor I. Artemov, Mikhail B. Semenov, Roman V. Zaitsev, Alexey V. Razumov, Ascar K. Aringazin, Kenji Yamamoto, Tikhon A. Gubin, ... 444
Slotted Patch Antenna Loaded with Metamaterial
Surabhi Dwivedi, Vivekanand Mishra, Yogesh P. Kosta, ... 445
Metamaterial Included Slotted Patch Antenna versus Metamaterial Cover over Patch
Surabhi Dwivedi, Vivekanand Mishra, Yogesh P. Kosta, ... 446
Effect of the Simultaneous Impact of Opioid Drug (Tramadol) and Electromagnetic Field (EMF) on Lipid Peroxidation
Pawel Bodera, Wanda Stankiewicz, Malgorzata Paluch, Malgorzata Krzyzowska, Bozena Antkowiak, 447
Snow Cover Effect on Brightness Temperature of Arctic Ice Fields Based on SSM/I Data
Vasiliy V. Tikhonov, D. A. Boyarskii, I. A. Repina, M. D. Raev, E. A. Sharkov, T. A. Alexeeva, . 448
Wavelets and Morphological Filter (Alternating Sequential Filters) for Robust Multiscale Image Segmentation
Med Ali Hamdi, Karim Saheb Ettabaa, ... 449

Numerical Modeling of Perfect Lens Using FDTD Method

A. P. Smirnov[1], **A. N. Semenov**[1], **and V. V. Shevchenko**[2]

[1]Lomonosov Moscow State University, Russia
[2]Kotel'nikov Institute of Radio-Engineering and Electronics of RAS, Russia

Abstract— We introduce numerical implementation of perfect lens based on dispersive metamaterials described by Drude model. There are several approaches to dealing with the metamaterials in case of Maxwell equations. This implementation is based on Maxwell equations approximation in integral form on Yee lattice, performed by 3-dimensional FDTD solver EMW Solver 3D created by authors of this paper. Numerical solution of 3-dimensional perfect lens problem described by left-handed material finite dielectric slab with cylindrical source is provided. The behaviour of numerically obtained solutions matches theoretical proposals of geometric optics about perfect lens. The numerical permittivity in 3-dimensional case has been computed and, according to the mismatch between the numerical and analytical values of permittivity introduced by the discretization in FDTD, the way to correct such a mismatch has been applied. Finite-sized left-handed materials slabs excited by a line source have been investigated by using the proposed technique for various transverse dimensions of the slab, and their subwavelength imaging capability has been confirmed. Solutions obtained with numerical simulation of perfect lens for various transverse dimensions of the slab are congruent to theoretically predicted results. It is shown that surface plasmons appears on boundary of the structure and it does not introduce distortion in the image.

Power Network Vulnerability Analysis via Compressed Sensing

Harish S. Bhat, Garnet J. Vaz, and Juan C. Meza
Applied Mathematics Unit, University of California, Merced, USA

Abstract— Combinatorial/discrete optimization arises naturally in several electromagnetic problems of recent interest: synthesis of linear arrays [1, 2] and design of media with prescribed scattering properties [3, 4], for instance. Here we focus on a vulnerability analysis problem for electric power networks [5], another example featuring combinatorial optimization. For a given network of buses and lines, the problem is to find the smallest set of lines such that failure of these lines leads to failure of the network. Here we show how a compressed sensing approach applied to a continuous relaxation yields solutions of the vulnerability analysis problem. The methodology we develop is general and can be applied to other discrete electromagnetic problems [1–4].

We first discuss how failure of the network is modeled using the power flow equations. When all lines are in operation, the power flow equations are satisfied by a particular configuration of bus phases, loads, and generators. When one or more lines fail, nonlinear programming can be used to find the smallest adjustment to the phases, loads, and generators such that the power flow equations can once again be satisfied. We refer to this nonlinear programming problem as the load-shedding subproblem.

The overall problem can be framed as a bilevel optimization problem [6]. The problem is to find the smallest set of lines such that, when these lines removed from the network, the solution of the load-shedding subproblem is greater than a prespecified severity level. Here the outer optimization problem is discrete, while the inner load-shedding subproblem is continuous.

Such nested optimization problems are difficult, and hence we pursue a continuous relaxation: instead of treating the operability of a line as a binary variable, we take the operability to be a real number in $[0, 1]$. Then we replace the outer optimization problem by a continuous problem in which we minimize the L^1 norm of the line operability vector. We show numerical evidence that this approach yields sparse solutions in which the number of non-zero elements of the line operability vector is very small. By comparison with the brute force solution of the original bilevel problem, we establish that our compressed sensing approach yields optimal solutions for a very large fraction of randomly generated networks. Finally, we discuss the scalability of our approach to large-scale problems.

ACKNOWLEDGMENT

This work was supported by the U.S. Department of Energy (Contract No. DE-AC02-05CH11231, Subaward 7041635).

REFERENCES

1. Liu, D., Q.-Y. Feng, and W.-B. Wang, "Discrete optimization problems of linear array synthesis by using real number particle swarm optimization," *Progress In Electromagnetics Research*, Vol. 133, 407–424, 2013.
2. Morabito, A. F., A. Massa, P. Rocca, and T. Isernia, "An effective approach to the synthesis of phase-only reconfigurable linear arrays," *IEEE Trans. Ant. Prop.*, Vol. 60, No. 8, 3622–3631, 2012.
3. Ye, X. Z., X. D. Chen, Y. Zhong, and K. Agarwal, "Subspace-based optimization method for reconstructing perfectly electric conductors," *Progress In Electromagnetics Research*, Vol. 100, 119–128, 2010.
4. Chen, Y.-S., Y.-C. Chan, H.-J. Li, E. J. Rothwell, R. O. Ouedraogo, and S.-Y. Chen, "A self-structuring electromagnetic scatterer," *IEEE Trans. Ant. Prop.*, Vol. 60, No. 4, 1931–1941, 2012.
5. Donde, V., V. López, B. Lesieutre, A. Pinar, C. Yang, and J. Meza, "Severe multiple contingency screening in electric power systems," *IEEE Trans. Power Sys.*, Vol. 23, No. 2, 406–417, 2008.
6. Pinar, A., J. Meza, V. Donde, and B. Lesieutre, "Optimization strategies for the vulnerability analysis of the electric power grid," *SIAM J. Optimization*, Vol. 20, No. 4, 1786–1810, 2010.

CFmaxwell — The Program Code for FDTD Modelling of Very Large Size Problems

A. V. Zakirov[1] and V. D. Levchenko[2]

[1]Moscow Institute of Physics and Technology, Russia
[2]Keldysh Institute of Applied Mathematics, Russia

Abstract— We offer `CFmaxwell` — the program code for 3D Finite-Difference Time-Domain (FDTD) modelling of up-to-date artificial optical and electromagnetic devices and materials such as photonic crystals, metamaterials, antennas etc.. There are many other FDTD libraries and solvers, but in general they aimed on relatively small problems (up to billion Yee cells in computational grid). So it is impossible to use them for the full significant exploring of electromagnetic processes in structures with the scale of characteristic sizes by an order of magnitude.

The code is based on the Local-Recursive nonLocal-Asynchronous Algorithms (LRnLA), which makes possible to reach peak rate of program's effectiveness in problems with very large computational grid size ($\gtrsim 10^{12}$ Yee cells). "Effective" algorithm means such one, that has real rate coming up to theoretical. In the work the implementation of such algorithm is offered for Maxwell's equations' modeling. `CFmaxwell` is primarily designed realistic fully 3D modelling and for problems in which the characteristic dimensions should vary by many times (for example, the size of one cell of photonic crystal's lattice and the linear physical size of the sample).

One may set different boundary conditions, including PML. Also following models for material equations have been realized: simple linear undispersion materials, Drude dispersion model with several terms, anisotropic media. In report it will be shown the effectiveness of `CFmaxwell` in comparison with other FDTD codes at different parameters and grid sizes.

Performance Analysis of Blind Calibration in Five-port Receivers Based on Blind Source Separation

F. Vidal[1], **A. Duarte**[2], **A. Medeiros**[3], **and B. Huyart**[4]

[1]Department of Environmental and Technological Sciences, UFERSA, Brazil
[2]Department of Computer Engineering and Automation, UFRN, Brazil
[3]Department of Electrical Engineering, UFRN, Brazil
[4]Department of Communications and Electronics, Telecom ParisTech, France

Abstract— The diversity of currently available wireless services (GSM, UMTS, WiMax, LTE and IEEE 802.15) requires that multi-mode transceivers are able to support many wireless communication standards that operate in several frequency bands with low cost, low power dissipation and high integration. The conventional superheterodyne receiver makes it difficult to achieve these goals, mainly due to the need for expensive external analog filters to eliminate image response. The direct conversion receiver, also called zero-IF or homodyne receiver, is one of the candidates to meet these needs.

In order to solve these problems and satisfy the requirements for small size, low cost and wideband, designers have been directing their efforts to design other receivers architecture. A new direct conversion receivers architecture based on the six-port reflectometer have been proposed as multimode and multiband or software receiver operating with digital signal processors (DSPs). Advantages such as phase and amplitude demodulations, compatibility with DSP and broadband specification, have made of five-port architecture a great choice for software defined radio application.

Five-port direct conversion receiver has been demonstrated as an interesting alternative for application in software-defined radio since its design is simple and it can operate in a wide range of frequencies. However, in order to carry out in-phase and quadrature demodulation, the five-port receiver must be calibrated for each frequency and modulation type. In this paper, we evaluate the performance of a blind calibration procedure based on blind source separation (BSS) for three algorithms JADE, FastICA as well as an iterative clustering approach called k-means algorithm, taking advantage of the fact that no prior knowledge about the signal is necessary.

An experimental prototype has been fabricated using microstrip components for 2.4 GHz frequency band. Simulation and measurement results are presented to validate the proposed approach.

Propagation Measurement of a Partially Open Drain: An Examination of the LOS and NLOS Sections

Anwuna Kingsley Awelemdy, Soo Yong Lim, and Kah Phooi Seng
Sunway University, Malaysia

Abstract— This paper presents field measurement results collected from inside a partially open drain at 2.4 GHz, a frequency band that is commonly deployed for wireless local area networks. The motivation of this paper stems from the need to better understand the behaviour of radio waves in partially open drains environment, in terms of signal coverage and attenuation characteristics. Partially open drains are a common sight in several Asian countries. Their design and shapes are similar to a certain degree to that of tunnels, except that they have one less reflecting wall on top. This is one major difference compared to the drainage systems in the US and Europe because the drainage systems in those regions are primarily below ground and covered. Previous research in this area has shown that the existence of the partially open drains makes up an additional channel in which the radio signal can travel. In this work, we are interested to further scrutinize the partially open drain environment in two sections, namely the line-of-sight (LOS) and non-line-of-sight (NLOS) sections using an empirical approach. Towards this end, one Data Acquisition Unit (DAU) has been assembled and tested to be used for data collection. Field measurements are taken at intervals of 30 cm using two dipole antennas that are oriented for vertical-vertical polarization. The repeatability of the measurement results is verified by consecutive measurements. In the full paper, details of the DAU will be reported together with the repeatability of the field measurement results. In addition, discussion and insights will be offered to analyze the measurement results collected from inside a partially open drain at LOS and NLOS sections. The direct research output of this work is highly relevant to the wireless communications systems design in many Asian cities, where partially open drains dominate.

A Comparison between 2-D and 3-D Models for Outdoor Radiowave Propagation

Zeina El-Ahdab and F. Akleman
Electronics & Communication Engineering Department
Istanbul Technical University, Istanbul 34469, Turkey

Abstract— The prediction of the electromagnetic wave propagation characteristics of an outdoor environment, such as the propagation loss and the propagation factor, is of wide interest because it allows us to model and thus to improve the communication systems implemented in a given environment whether in the near field or far field of the emitting source. Different methods have been considered in the past such as empirical methods [1] and site-specific deterministic methods [2]; these methods either ignore details of the terrain topology or solve an approximate model. More recent work is based on a parabolic approximation to the Helmholtz equation that assumes forward scattering. However, most of the formulations are two-dimensional (2-D) in nature and assume a propagation in a 2-D plane [3, 4]. As has been shown that a 3-D formulation better models the propagation environment would reduce the errors resulting from the 2-D modeling. In this paper we analyze and compare the results obtained by 2-D and 3-D formulation of the parabolic equation based solution of radiowave propagation problem in rural and urban environments. In this study both flat earth and irregular terrains are considered. In urban environment the buildings are allowed to be lossy or perfectly conducting, while in rural environment the refractivity variations of troposphere, which effects the long range radiowave propagation characteristics, are also included. Although using a 3-D model does improve in most cases the average error with respect to measurements or other techniques than that of a 2-D model, the trade-off between the error reduction/accuracy and the complexity of the 3-D formulation as well as the length of the implementation can be considered in some cases to be inefficient depending on the requirements of the communication system in consideration. In this study the validity region of 2D approximations for radiowave propagation will be presented by comparing the results with the data obtained using more realistic solutions based on 3D algorithms.

ACKNOWLEDGMENT

We thank The Scientific and Technological Research Council of Turkey for the support it is offering to the research we are pursuing.

REFERENCES

1. Janaswamy, R., *Radiowave Propagation and Smart Antennas for Wireless Communications*, Kluwer, Boston, MA, 2000.
2. Bertoni, H. L., *Radio Propagation for Modern Wireless Systems*, Prentice Hall PTR, Saddle River, NJ, 2000.
3. Janaswamy, R. and J. B. Andersen, "Path loss predictions in urban areas with irregular terrain topography," *Wireless Personal Commun.*, Vol. 12, No. 3, 255–268, Mar. 2000; Also see the addendum in *Wireless Personal Commun.*, Vol. 14, No. 3, 303–304, Sep. 2000.
4. Sevgi, L., C. Uluisik, and F. Akleman, "A MATLAB-based two-dimensional parabolic equation radiowave propagation package," *IEEE Antennas and Propagation Magazine*, Vol. 47, No. 4, 164–175, 2005 (SCI (B)).

Analysis of the Benefits of Diversity Polarization in Wireless Networks

I. Cuiñas and M. García Sánchez
Department of Teoría do Sinal e Comunicacións, Universidade de Vigo, Spain

Abstract— Fading effects acquire vital importance in the process of designing and planning a radio link in systems operating at frequencies below 10 GHz. Particularly, an due to multipath phenomenon, fast fading appear as a key factor. This kind of fading is frequency selective, and can represent the propagation dominant factor in the digital radio link systems that operate in the spectral range quoted.

All the present work is based on measurement conducted within different indoor scenarios, both furnished and empty, with various dimensions The outcomes of such campaigns have been analyzed, and they present several fading events. These results, combined with the electromagnetic behavior of the materials at walls, floor and ceiling, have been processed in order to reduce these impairments.

This study addresses one of the mechanisms designed to minimize these adverse effects, which are diversity techniques; and among them, the polarization diversity at reception, by assessing the suitability of their use. The improvements in propagation conditions obtained as a result of the use of polarization diversity (i.e., reduction of percentage of fading event duration) will be quantified in indoor environments in a frequency range centered on 5.8 GHz, which has direct application in the planning of wireless local area network (WLAN).

Other advantages of diversity techniques, in addition to reducing the percentage of time a given fading influence, are the increased reliability (the existing redundancy), or, depending on the combination of signal processing and subsequent reception, to achieve improvements in quality parameters as signal to noise relation or the error rate. Therefore, the mechanisms of diversity constitute a fundamental contribution to combat the effects of multipath propagation.

ACKNOWLEDGMENT

This work was partially funded by Spanish Ministry of Economy and Competitiveness, State Secretary for Research under project TEC2011-28789-C02-02, that was co-funded using European Regional Development Funds (ERDF), as well as the Galician Regional Government under project CN 2012/260 "Consolidation of Research Units: AtlantTIC".

Conception of Radio Frequency Link in the Radio of 3.5 GHz in Consonance with the National Brazilian Rules and International Legislation

T. M. Sanchez Otobo[1,2], H. Tertuliano Filho[1,2], C. A. Dartora[1,2], E. Nascimento Júnior[1,2], and E. Cherubini Rolin[1,2]

[1]Department of Electrical Engineering, Federal University of Parana
C.P: 19011, Centro Politécnico, Jardim das Américas, Curitiba, PR 81531-990, Brazil
[2]Department of Electrical Engineering, Federal Institute of Education
C.P: 19011, Centro Politécnico, Jardim das Américas, Palmas, PR 81531-990, Brazil

Abstract— In Brazil, most of the research works in radio propagation found in the literature are based on unlicensed bands of 900 MHz, 2.4 GHz, 5.4 GHz and 5.8 GHz, because they offers a wide range of applications of interest with the advantage of being free of charge to any user, as far as they do not interfere with other licensed services and if their operation level do not exceed 1 Watt of power transmission. However, for those who use a licensed band (e.g., 2.5 GHz, 3.5 GHz, 7.5 GHz and 8.5 GHz), despite the priority of band use, the Brazilian law for frequency range and service, controlled by the Agency of the Brazilian Telecommunications Services — ANATEL (in accord with international organizations) provides a strong impositions of rules, precedents, decrees and laws that cause, in some cases, projects that are carried out by transposition of frequency or even a complete non-observance. Research centers develop their projects based on theoretical logic but the Brazilian companies do it in complete dissonance with the academic world. Under this scene, the regulatory agency uses successive and constant decrees, to regulate these licensed bands because of the growing number of new applications and services. Due to the huge number of legislative parameters, the radio link designer often neglects important standards or lanes modification, because of lack of knowledge. Within this universe, this article relates how a licensed frequency band specifies a project conducted in strict observance of these standards, where only technical design constraints are considered. After a careful analysis of these projects, a comparative analysis is made with the aim of investigating the impact of the legislation in the design of radio link. Thus, the designer who is subject to these varying norms will be aware of the principal aspects to be considered.

Some Insights on the Amount of Fading in Radio Channels

Hassan El-Sallabi[1], **Khalid Qaraqe**[1], **and Erchin Serpedin**[2]

[1]Wireless Communications Laboratory, Electrical Engineering Department
Texas A&M University at Qatar, Qatar
[2]Electrical and Computer Engineering Department, Texas A&M University
College Station, TX, USA

Abstract— Wireless radio channels are known of their fading phenomena, where received signal fluctuates randomly due to multipath arrival of radio signal to the receiver point. Fading phenomena are known of fast fading and slow fading. Slow fading (aka shadow fading) describes the signal variation slowly over tenths of wavelength distance. It is usually modeled as lognormal. The fast fading which results due to phase difference of multipath components is defined by locations of scatterers and their electrical parameters as well as the location and height of the transmitter and receiver and their antenna patterns. The geometry of the propagation scenarios defines the angular and delay domain properties of the channel. These properties are directly related to fast fading. The fast fading has been modeled in literature with many models based on existence or non-existence of line of sight (LOS) component. The widely known models are the Rayleigh model for non-line of sight (NLOS) component and Rice model when LOS component exist.

Radio channel characterization is usually done for stationary or mobile devices with fixed antenna orientation; assuming talking scenario where handheld is hold to head or a laptop of fixed position. The recent advance in smartphone technology, the mobile device not only can move but can also rotate. This rotation can make faster direction changes than mobility. The rotation of the device changes the antenna pattern relative to vertical and horizontal polarization for different inclination angles. This polarization change in antenna pattern due to device rotation will have an impact on fading profile, which is measured with amount of fading measure.

The investigation of this work is simulation based using multi-ray RF multi-dimensional propagation model. The number of rays is determined by number of reflections and existence or not LOS components. For indoor scenario, multiple reflections from side and opposite walls as well as ceiling and floors are considered. The model ray parameters are derived from geometry using electromagnetic image theory and vector operations to extract needed angles for every ray in terms of angle of arrivals and departures as well as surface reflection angles.

This work will present a measure of severity of fading in terms of amount of fading (AF). The AF is defined in [1] as

$$\mathrm{AF} = \frac{var\{\alpha^2\}}{E\{\alpha\}^2} \tag{1}$$

where α is the instantaneous fading amplitude of a complex fading channel, $E\{\cdot\}$ and $ar\{\cdot\}$ are the statistical mean and variance, respectively.

In this work, we present an experimental investigation on the amount of fading as a measure of fading severity in radio channels. The presented results are for indoor environments and assume a multi-dimensional ray based model. The amount of fading of Rayleigh channel, which is equal to one, is used as a reference to know if the channel is less or more severely affected than Rayleigh radio channel. For the tested environment, it has been found that placing the antenna of indoor cell at a height close to the pedestrian height leads to less fading than placing it on the ceiling and at this preferred height. The amount of fading for line of sight propagation conditions exhibits higher correlation with coherence time than that corresponding to non-line of sight propagation.

REFERENCES

1. Charash, U., "Reception through Nakagami multipath channels with random delays," *IEEE Trans. Commun.*, Vol. 27, No. 4, 657–670, Apr. 1979.

RF Identification (RFID) Reader with Long Read Range in the UHF Band

Jae-Young Jung, Kyu-Won Han, and Chan-Won Park
Electronics and Telecommunications Research Institute (ETRI), Republic of Korea

Abstract— In this paper, the design of a long read range UHF RFID reader using a novel carrier leakage suppression method is presented. The read range is one of the key parameters in RFID systems and is frequently evaluated for RFID system assessment. A read range of about 20 m may be appropriate for the emerging application of long read range RFID systems, such as vehicle toll systems and the management of airline cargo containers and shipbuilding yard equipment. Most Class-1 commercial readers show a receiving sensitivity of −60 to −70 dBm and it is very difficult to find a reader with a sensitivity of below −80 dBm due to a leakage power from the transmitter in a reader. We developed and demonstrated through experiment in the laboratory environment in the carrier-to-tag data ratio by more than 36 dBc in the UHF RFID band, which is consistent with our simulation results. When inserted between the reader antenna and a Class-1 RFID reader, measurements show that the reader can successfully demodulate the generated tag signal for a power level of −80 dBm, which corresponds to the backscattered power at 20 m distance. The read range of the reader with the proposed carrier leakage suppression front-end is verified again in a completely real environment. The measured read range is found to be greater than 20 m for a commercial battery-assisted passive (BAP) tag, which is more than twice the read range of conventional reader. We showed that a Class-3 RFID system for a long read range of 20 m can be successfully established with BAP tags and the Class-1 reader with the proposed carrier leakage suppression front-end.

Simulation and Implementation of TDOA Monitoring System for Broadcasting Interferences

Yao-Tang Chang
Department of Information Technology, Kao Yuan University, Kaohsiung 82151, Taiwan

Abstract— Since the rapid developing of economy in Taiwan in recently years, a large numbers of constructions have made the changes of the terrain surrounding the radio monitoring stations rapidly. Hence, the accuracy performance of the radio monitoring station configured by signal angle of arrival (AOA) location technology has been seriously degraded. In this paper, the simulated result of 20 km $\sim$ 30 km coverage area is evaluated. Furthermore, the implementation and experiments supported by the radio frequency interference have been governed by authority of national communication commissions (NCC) in Taiwan. The results show that the locating accuracy at circle error probability (CEP) 50% is less than 950 m distance under multi-path effect in metropolitan area. Hence, the solution of integrated the AOA/TDOA technologies can be applied and the interference transmitter characterized with low transmitted power, burst and weak signal and metropolitan interference is easy identified, analyzed (located) and prevented.

Design Guidelines of a Microwave Active Front-end Receptor: A LNA Approach

J. C. Bonoto[1], **C. E. Capovilla**[2], **and H. X. Araujo**[1]

[1]Universidade Federal de São João Del Rei — UFSJ, Ouro Branco, Brazil
[2]Universidade Federal do ABC — UFABC, Santo André, Brazil

Abstract— In this work, the design guidelines of a BiCMOS 0.35 µm front-end receptor, including a LNA — Low Noise Amplifier, Mixer and Oscillator to attend the Brazilian 4G technology, will be shown. In this context, this paper aims the improvement and development of new technologies to meet the growing demands on the communication and mobile field.

The current economic scenario, coupled with the lifestyle that people have in their homes, always seeking comfort and connectivity, makes increase the need for faster electronic devices with high efficiency and low cost. These devices have features to make life easier and give comfort to people. Among these features, can be cited the use of the internet as a vehicle of communication through mobiles, something unimaginable in the early twenty-first century.

In order for such expectations becomes fulfilled, it took many technological advances in the electronic field, including in the stage of RF (radio frequency) devices for communications, which is considered the basis for many advances, due to the growing demand for data traffic, voice and image, increasing the need of high speeds transfers that support these services, making it essential that there be a monitoring of its technological development.

The progress related to the RF microelectronic happened in a faster way, thus requiring constant updating and training of researchers and technicians involved in this area. This search for knowledge is due to the fact that the market always needs new devices. Therefore, in this work it will be shown the design guidelines of a 0.35 µm BiCMOS Front-end for the Brazilian 4G Technology. It will be shown since the hand calculation to the final layout which will be manufactured by the AMS — Austria Micro System Foundry.

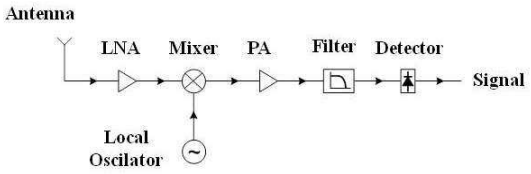

Figure 1: A generic front-end receptor.

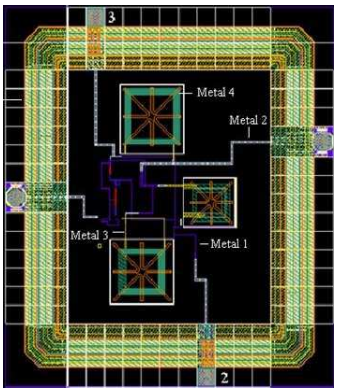

Figure 2: Preliminary LNA layout.

Statistical Analysis of On-body Radio Propagation Channel for Body-centric Wireless Communications

H. A. Rahim[1], **F. Malek**[1], **N. Hisham**[1], **and M. F. A. Malek**[2]

[1]Embedded, Networks and Advanced Computing Research Cluster (ENAC)
School of Computer and Communication Engineering
Universiti Malaysia Perlis, P. O. Box 77, d/a Pejabat Pos Besar, Kangar 01000, Malaysia
[2]MISC LNG Japan MISC Berhad, Yokohama, Japan

Abstract— This paper presents the statistical analysis of on-body radio propagation channel utilizing textile monopole antenna at 2.45 GHz. The measurement campaign was carried out in the anechoic chamber, considering stationary movement of the human body. The position of the transmitted antenna was fixed on the right of the upper arm of the human body and the received antenna was varied on several different potential on-body locations for body-centric wireless communication (BCWC) applications. The investigation was aimed to characterize the reflection coefficient and path loss of on-body radio channel when the antenna was placed in the vicinity of human body. The lognormal and normal distributions were considered in characterizing the on-body radio propagation channel. The measured reflection coefficient values were then compared to the simulated environment using CST HUGO body model software. The HUGO model was defined at $8 \times 8 \times 8 \times 8\,\mathrm{mm}^3$ voxel resolution.

The results showed that the measured reflection coefficient of four on-body positions experienced an upward frequency shift at a maximum of 22.3% compared to the simulated reflection coefficient values due to the body coupling effect. In the anechoic chamber, the highest path loss was found for upper arm-left ankle link while the lowest path loss was observed on the upper arm-right chest link, proving that the closer a received antenna to the transmitted antenna, the better signal reception will be obtained. Based on the measurement results, it could be seen that the lognormal distribution fits very well to the on-body radio channel for narrowband frequency.

Path Loss Characterization of Body-to-body Radio Propagation Channel on the Angular Variations

H. A. Rahim[1], **F. Malek**[1], **A. I. Ahmad**[1], **and M. F. A. Malek**[2]

[1]Embedded, Networks and Advanced Computing Research Cluster (ENAC)
School of Computer and Communication Engineering
Universiti Malaysia Perlis, P. O. Box 77 d/a Pejabat Pos Besar, Kangar 01000, Malaysia
[2]MISC LNG Japan MISC Berhad, Yokohama, Japan

Abstract— This paper investigated the path loss characteristics of body-to-body radio propagation channel in a controlled lab environment using a pair of simple structure textile path antennas operating at 2.45 GHz. A line-of-sight (LOS) case was considered in this measurement campaign. The transmitted antenna was mounted parallel to a right upper arm of the first human body, separated by 2 mm air gap and the received antenna was placed on a left upper arm of second human body. The orientation between transmitted antenna on the first body and received antenna on the second body was carried out for 0, 90 and 180 degrees. The distance between transmitted antenna on the first body and received antenna on the second body was varied from 40 to 180 cm for each orientation angle. Both of the subjects were in a static movement throughout the measurement campaign. This investigation was carried out to observe the path loss variation in LOS scenario in terms of orientation angle and distance variation between two human bodies.

The results showed that the path loss varied differently when the received antenna was oriented in different angles. It was noticed that the path loss increased by a maximum of 10–12 dB when the antennas separation between the first body and the second body increased for all orientation angles. The results also showed that the path loss varied up to 4.1 dB from 0° to 90° orientation angle and increased by 3 dB when the angle was oriented from 0° to 180°.

The Influence of Textile Dielectric Properties in On-body Radio Communication Channel Performance at 2.45 GHz

H. A. Rahim[1], **F. Malek**[1], **and M. F. A. Malek**[2]

[1]Embedded, Networks and Advanced Computing Research Cluster (ENAC)
School of Computer and Communication Engineering, Universiti Malaysia Perlis
P. O. Box 77, d/a Pejabat Pos Besar, Kangar 01000, Malaysia
[2]MISC LNG Japan MISC Berhad, Yokohama, Japan

Abstract— This paper presents the characterization of on-body radio communication channel considering the effect of textile dielectric properties at 2.45 GHz. The experiment was performed in the anechoic chamber, involving six subjects that utilized a pair of omni-directional antenna, textile monopole. Four types of textiles with different dielectric properties were considered in this investigation; cotton, nylon, satin and polyester. The transmitted antenna was positioned on a fixed location, right upper arm of the human body and the received antenna position was varied on seven realistic on-body locations for both line-of-sight (LOS) and non-line-of-sight (NLOS) scenarios. This investigation was carried out to determine whether the dielectric properties of textile clothing give significant effect on the characterization of on-body radio communication channel. The path loss model was derived for on-body radio communication channel for LOS and NLOS scenarios. The comparison of path loss values between with and without textile cases was also presented in this work. The result showed that the path loss exponent for both LOS and NLOS scenarios was affected by the dielectric properties of textile. Besides, the thickness of textile also played a significant role in path loss variation of on-body radio channel.

Mathematical and Numerical Analysis of Dielectric Waveguides by the Integral Equation Method

E. Karchevskiy[1] and Y. Shestopalov[2]

[1]Kazan Federal University, Russia
[2]Karlstad University, Sweden

Abstract— Many different numerical techniques are applied for computing eigenmodes of dielectric waveguides [1, 2]; namely, finite-element, finite-difference, beam propagation, and spline collocation methods and multidomain spectral approach. Often the authors concentrate on the algorithm's aspects and physical interpretation of the numerical results rather than on fundamental mathematical aspects including the existence, properties, and distribution of the spectra on the complex plane of the spectral parameter. In this study, we propose a new approach to mathematical and numerical analysis of the dielectric waveguides based on the methods of spectral theory of operator-valued functions [3, 4] and integral equations (IEs) [4–6]. The eigenvalue problems for the determination of natural modes (surface, leaky, and complex eigenmodes) of inhomogeneous optical waveguides and step-index optical waveguides with the smooth cross-sectional boundary are formulated [3–5] for the time-harmonic Maxwell equations with partial radiation conditions at infinity in the cross-sectional plane. The initial problems are reduced with the aid of the IE method (using appropriate Green functions) to nonlinear spectral problems with Fredholm integral operators. Theorems on the spectrum localization are proved. It is shown that the sets of all eigenvalues of the initial problems may consist of isolated points on the Reimann surface of the spectral parameter (longitudinal wavenumber) and each eigenvalue depends continuously on the frequency and permittivity and can appear or disappear only at the boundary of the Reimann surface.

The initial problems for surface waves are reduced to linear eigenvalue problems for integral operators with real-valued symmetric weakly singular kernels. The existence, localization, and dependence of the spectrum on parameters are investigated. The collocation and Galerkin methods for the calculation of natural modes are proposed, the convergence of the methods is proved, and some results of numerical experiments are discussed.

REFERENCES

1. Horikis, T. P., "Dielectric waveguides of arbitrary cross sectional shape," *Applied Mathematical Modeling*, Vol. 37, No. 7, 5080–5091, 2013.
2. Xiao, J. and X. Sun, "Full-vectorial mode solver for anisotropic optical waveguides using multidomain spectral collocation method," *Optics Communications*, Vol. 283, No. 14, 2835–2840, 2010.
3. Shestopalov, V. P. and Yu. V. Shestopalov, *Spectral Theory and Excitation of Open Structures*, Peter Peregrinus Ltd., 1996.
4. Chernokozhin, E., Y. Smirnov, and Y. Shestopalov, *Logarithmic Integral Equations in Electromagnetics*, VSP Int. Science Publishers, Utrecht, Boston, Köln, Tokyo, 2000.
5. Kartchevski, E. M., A. I. Nosich, and G. W. Hanson, "Mathematical analysis of the generalized natural modes of an inhomogeneous optical fiber," *SIAM J. Appl. Math.*, Vol. 65, No. 6, 2033–2048, 2005.
6. Dautov, R. Z. and E. M. Karchevskiy, *Integral Equations Method and Exact Nonlocal Boundary Conditions in the Theory of Dielectric Waveguides*, Kazan State University, Kazan, 2009.

Linear-operator Theory for Inhomogeneous Omega Planar Waveguides

António L. Topa
Instituto de Telecomunicações and Instituto Superior Ténico
Technical University of Lisbon, Lisbon, Portugal

Abstract— The omega medium has been first proposed in [1], as a new type of artificial bianisotropic media. An omega medium consists of small omega-shaped microstructures printed onto a dielectric substrate and then stacked. An incident electric field induces both electric and magnetic polarization on such printed elements. Omega media are nonchiral, since these polarization vectors are perpendicular to each other. This distinctive feature of omega media implies that the orientation of the doping elements in the host isotropic medium cannot be random but must be parallel to a unique preferred direction.

In this paper, a linear-operator formalism for the analysis of inhomogeneous omega planar waveguides is presented. Using the theory of linear operators, the problem of guided electromagnetic wave propagation is reduced to an eigenvalue equation related to a 2×2 matrix differential operator [2]. Based on the transverse electromagnetic field equations an eigenvalue problem is then obtained. For each eigenvalue the corresponding eigenfunction represents a transverse mode function of the waveguide. Hence, the orthogonality properties of these eigenfunctions can be used to represent the electromagnetic field as a superposition of mode functions, as long as completeness is guaranteed.

A complete spectral representation for the electromagnetic field of planar multilayered waveguides inhomogeneously filled with omega media is obtained. Using the concept of adjoint waveguide [3], general bi-orthogonality relations for the hybrid modes (either from the discrete or from the continuous spectrum) are derived.

In order to have a complete field representation in open omega waveguides, these relations are of utmost importance when choosing an appropriate set of mutually orthogonal radiation modes. One should note that this linear-operator formalism is applicable to multilayered planar waveguides with inhomogeneous layers. However, in the case of homogeneous layers the general formalism reduces to an algebraic 2×2 coupling matrix eigenvalue problem [4].

REFERENCES

1. Engheta, N. and M. M. I. Sadaoun, "Novel pseudochiral or Ω-medium and its applications," *Proceedings of PIERS'91*, 339, Cambridge, MA, Jul. 1991.
2. Topa, A. L., C. R. Paiva, and A. M. Barbosa, "New biorthogonality relations for inhomogeneous biisotropic planar waveguides," *IEEE Trans. Microwave Theory Tech.*, Vol. 42, 629–634, Apr. 1994.
3. Friedman, B., *Principles and Techniques of Applied Mathematics,* Wiley, New York, 1956.
4. Topa, A. L., "Linear operator formalism in the analysis of omega planar layered waveguides," *Proc. ICECECE 2012 — International Conference on Electrical, Computer, Electronics and Communication Engineering*, Paris, France, Aug. 2012.

Coupled Electromagnetic Wave Propagation in Space and around Surfaces and Interfaces

Michael J. Underhill
Underhill Research Ltd, Lingfield, UK

Abstract— The discovery of Electromagnetic (EM) Coupling [1–7] has an impact on the understanding of propagation of waves in free space, in homogeneous and inhomogeneous solids, and at the interfaces between these.

In free space or in uniform homogenous solids, as a consequence of EM coupling, we find that different types of plain wave travelling in the same direction can co-exist. They can be defined as having substantially different wave impedances $Z_w = E/H$. Based on the assumption that the asymptotic value of EM coupling for free space is $\kappa_0 = 1/2\pi$ we find values for stable linearly polarised wave impedances that are not $Z_0 = 120\pi$ (377 Ohms). Additionally it follows that pairs of orthogonally linear or circularly polarised waves in the same volume may exist. Even if these waves are very lightly coupled, there will be preferred asymptotically stable wave impedances, reached at some distance from the source. This opens up the possibility that there are many types of free-space EM waves that have not yet been investigated. Note that any mathematical analysis has to include the EM coupling factor for the wave components under consideration.

Surface waves have been shown to extend with a distance profile above and below the surface between two materials or between a material and free space. The mean evanescent wave distance is found to be inversely proportional to the square root of frequency [1–4]. At higher frequencies ($\ll$ 20 MHz) the surface waves can have interlaced layers of alternating high and low wave impedance. It is possible to select one of these layers for stable propagation of the major part of the supplied surface wave energy. However the layers are partially coupled and some energy is also conveyed in adjacent layers. It is possible for two adjacent or nearby layers to be excited simultaneously initially with equal power in each layer. Whether there is a phase relationship that keeps the powers equal in both layers and with low radiation loss as the waves propagate, is under investigation.

Also under investigation is whether it is possible to have a stable 'tube' of radiation where one field component is radially directed and the complementary field is solenoidal [1, 2, 8]. Such a (self-focussed) wave could have much less spreading and expansion with distance. The source antenna for such a wave would then effectively be a high gain small antenna. However one possible difficulty is that there is likely to be an addition self focussing or defocusing action that is wave power dependent.

REFERENCES

1. Underhill, M. J., "The phase noise spectrum and structure of photons?," *Proc. 16th EFTF-2010*, 8 pages, Noordwijk, Netherlands, Apr. 13–16, 2010.
2. Underhill, M. J., "A physical model of electro-magnetism for a theory of everything," *PIERS Online*, Vol. 7, No. 2, 196–200, 2011.
3. Underhill, M. J., "Maxwell's transfer functions," *PIERS Proceedings*, 1766–1770, Kuala Lumpur, Malaysia, Mar. 27–30, 2012.
4. Underhill, M. J., "A local ether lens path integral model of electromagnetic wave reception by wires," *PIERS Proceedings*, 1005–1008, Moscow, Russia, Aug. 19–23, 2012.
5. Underhill, M. J., "Antenna pattern formation in the near field local ether," *PIERS Proceedings*, 1009–1012, Moscow, Russia, Aug. 19–23, 2012.
6. Underhill, M. J., "Anomalous ground wave tilt measured over wet ground," *IET Conf. on Ionospheric Radio Systems and Techniques 2012*, Royal York Hotel, York, UK, May 15–17, 2012.
7. Underhill, M. J., "Wideband small loop-monopole HF transmitting antenna with implications for Maxwell's equations and the Chu criterion," *PIERS Proceedings*, Taipei, Mar. 25–28, 2013.
8. Underhill, M. J., "Electromagnetic structures and inertias of particles including the higgs boson," *PIERS Proceedings*, Taipei, Mar. 25–28, 2013.

Two Types of Electromagnetic Induction Existing in Nature

Vladimir A. Leus[1], **Ray T. Smith**[2], **and Simon Maher**[3]

[1]Sobolev Institute of Mathematics, Novosibirsk 630090, Russia
[2]Wirral Metropolitan College, Wirral L62 0AY, UK
[3]Department of Electrical Engineering and Electronics, University of Liverpool, Liverpool L69 3GJ, UK

Abstract— "Transformer EMF" and "Motional EMF" — these are two well known terms to denote two different sources of electromagnetic induction. However, the physical characteristics of both forms of induction always remain unclear; moreover they tend to be subsumed under the same comprehensive "flux rule" where they inevitably tend to lose their individual traits. The situation reminds one of a movie shown on a screen by a cine-projector with a defocussed lens: the light flux is the same, but details of the scene vanish from sight. In this paper we present both the results of our investigation and an examination of the mechanism of induction in order to provide a clearer insight into the phenomenon. The experimental arrangement comprises a large scale transformer consisting of movable single turn coils wound onto rectangular frames. The primary coil is powered by a signal generator providing alternating current over a variable frequency range while the secondary output is connected to an oscilloscope. Some specific type transformers were also used. Measurements of transformer EMF were carried out at several frequencies and with variable conditions of shielding of the inductor and receiver. In comparison, the motional EMF was examined due to the free fall of a permanent magnet — a uniformly magnetized sphere. In this case the changing magnetic influence was detected by measuring the EMF in a stationary conducting loop also with different shielding conditions. All results provide evidence for the existence in nature of two quite distinct types of electromagnetic (we might add "and magnetoelectric") induction. A suggested theoretical analysis, based on examination of the wave equation, corroborates this significant conclusion.

The Stability of EM Particles and Predicted Mass Ratios

Michael J. Underhill
Underhill Research Ltd., Lingfield, UK

Abstract— Feasible electromagnetic structures for all particles have been proposed [1–3]. These support the proposition that 'Everything is Electromagnetic' and therefore there is 'An Electromagnetic Theory of Everything'. The prime basis for the 'Electromagnetic Model' is the discovery of Electromagnetic (EM) Coupling [1–8].

One mechanism that needs to be explained in electromagnetic terms is the physical process that gives rise to the measured stable masses of all the sub-atomic particles in the Standard Model [9]. This paper is an examination of the factors that may contribute to the stability of the EM models of particles.

It is proposed that any form of energy has a *gravitational* mass in accordance with $E = mc^2$. This includes the energy in fields or low density particles such as photons and neutrinos [3]. Also in [3] an EM coupling mechanism was given for the *inertial* mass of particles having a dense central core. In this case inertial mass is defined to be equal to gravitational mass. Low density forms of energy such as heat light and EM and gravitational fields are considered to be 'dark matter' having a low inertia.

The 'core-atmosphere' particle model in [10] is assumed as the basis for finding particle stability conditions. The core consista of concentrated 'substance' ψ_1 and it creates a surrounding potential ϕ_2 by electromagnetic coupling. The potential in turn creates diffuse substance ψ_2, which is the main constituent of the atmosphere, the other constituent being the potential itself. Matter or energy is the product of substance with the potential $E = \psi \times \phi$. (Current times potential is energy.) The core substance ψ_2 in its local potential ϕ_1 is ordinary matter, and the atmosphere is dark matter $E_d = \psi_2 \times \phi_2$. The substance can be considered to be 'current' in one form or another. The substance of the atmosphere in turn creates a third potential ϕ_3. At any point the potentials and the currents have to be in equilibrium for the particle to have a stable shape profile and stable energy.

The electromagnetic model of a particle requires it to have a dominant line frequency, if it is stable, or a wider frequency spectrum if is not stable (as for the Higgs particle [10]. In general the dominant frequency f of a particle is given by the empirical relationship $E = hf$ where $E = mc^2$ is the energy of the particle, and m is its mass. The conditions for stability are more stringent as a result of the particle frequency and mass being inter-related. The phases of the potentials and any time delays in the creation processes have to be taken into account. The paper will define the factors that have to be taken into account for the derivation of particle stability equations and what further research may be necessary.

REFERENCES

1. Underhill, M. J., "The phase noise spectrum and structure of photons?," *Proc. 16th EFTF*, 8, Noordwijk, Netherlands, April 13–16, 2010.
2. Underhill, M. J., "A physical model of electro-magnetism for a theory of everything," *PIERS Online*, Vol. 7, No. 2, 196–200, 2011.
3. Underhill, M. J., "Electromagnetic structures and inertias of particles including the higgs boson," *PIERS Proceedings*, Taipei, March 25–28, 2013.
4. Underhill, M. J., "Maxwell's transfer functions," *PIERS Proceedings*, 1766–1770, Kuala Lumpur, Malaysia, March 27–30, 2012.
5. Underhill, M. J., "A local ether lens path integral model of electromagnetic wave reception by wires," *PIERS Proceedings*, 1005–1008, Moscow, Russia, August 19–23, 2012.
6. Underhill, M. J., "Antenna pattern formation in the near field local ether," *PIERS Proceedings*, 1009–1012, Moscow, Russia, August 19–23, 2012.
7. Underhill, M. J., "Wideband small loop-monopole hf transmitting antenna with implications for Maxwell's equations and the Chu criterion," *PIERS Proceedings*, Taipei, March 25–28, 2013.
8. Underhill, M. J., "Coupled electromagnetic wave propagation in space and around surfaces and interfaces," *PIERS Proceedings*, Stockholm, Sweden, August 12–15, 2013 (Not yet accepted for publication).

9. http://en.wikipedia.org/wiki/Standard_Model.
10. Underhill, M. J., "Electromagnetic structures and inertias of particles including the higgs boson," *PIERS Proceedings*, Taipei, March 25–28, 2013.

A Novel Approach for the Construction of Dirac's Delta Functions

A. R. Baghai-Wadji
University of Cape Town, South Africa

Abstract— In recent works a series of Dirac delta functions were constructed from Poisson's equations in isotropic or an-isotropic dielectric media subject to simple boundary conditions. The construction of delta functions was also briefly touched upon in connection with Maxwell's equations in unbounded free space. The present paper generalizes the previously introduced ideas and applies them to more general cases; provides physical interpretation of the results; and offers a recipe on how to employ the constructed Dirac delta functions in regularizing singular surface integrals arising in computational electromagnetics in isotropic, anisotropic, or bi-anisotropic media. To sketch the underlying ideas for constructing physics-based problem-tailored Dirac delta functions, consider the following general problem. Let the system of partial differential equations (PDEs) $\mathcal{L}\mathbf{\Psi}(\mathbf{x}) = \mathbf{s}(\mathbf{x})$ be given. Solve this system of PDEs subject to given boundary conditions. Here, $\mathcal{L}$ is a differential matrix operator; $\mathbf{\Psi}(\mathbf{x})$ is the solution to be determined; $\mathbf{s}(\mathbf{x})$ is a given source function (direct problem); and $(\mathbf{x}) = (x_1, x_2, x_3)$. In applications we are mostly faced with indirect problems. This distinction is, however, not relevant in our present discussion. To solve this problem consider $\mathcal{L}\mathbf{G}(\mathbf{x}) = \mathbf{u}\delta(\mathbf{x} - \mathbf{x}')$, subject to the boundary conditions of the original problem, or simplified boundary conditions, as it is the case in the majority of practical problems. Here, $\mathbf{G}$ refers to the dyadic Green's functions; $\mathbf{u}$ is a unit vector in space; and $\delta(\mathbf{x} - \mathbf{x}')$ is the Dirac delta function in symbolic form. In our discussion the latter specification; i.e., "symbolic" form or "symbolic" representation plays a significant role. The construction Green's functions usually requires the transformation of the equations into spectral domain. Utilizing the sifting property of the symbolic delta function, the simple exponentially harmonic Fourier transform of the delta function is immediate. The major point is here that no integral representations are required for the delta function in order to construct the Green's functions associated with the problem.

Assume the dyadic Green's functions have been determined. As a rule, and by way of construction, Green's functions $\mathbf{G}(\mathbf{x})$ are obtained in terms of Fourier-type integrals. Substitute the expression for the obtained Green's function into the equation $\mathcal{L}\mathbf{G}(\mathbf{x}) = \mathbf{u}\delta(\mathbf{x} - \mathbf{x}')$. Thus, the left-hand side gives integral representations for the symbolic delta function $\delta(\mathbf{x} - \mathbf{x}')$ appearing at the right-hand side, following a few careful manipulatory steps. It can be shown that not only integral representations for the Dirac delta functions, but also for Cauchy Principle Values, associated with the problems at hand, can be constructed.

The present paper details the underlying ideas along with the implications for the regularization of the associate singularities of the Green's functions. The aforementioned discussion should justify the claim that the pro-posed method is a problem-tailored regularization technique.

Electromagnetic Sources and Observers in Motion IX — Nature of Gravity

Selwyn E. Wright
Moor Lane Laboratory, ECASS Technologies Ltd, HD8 0QS, UK

Abstract— This is the ninth paper in the series of EM sources and observers in Motion. Two given in Xian China, two in Cambridge USA, two in Marrakech Morocco and two in Moscow Russia. This Paper IX is a companion paper to Paper X, the Unification of Electromagnetism and Gravity also presented at this symposium. Gravity has similar properties to the electric field. Both are attractive, their intensity is dependent on the inverse square law with distance, they use the same medium and have a propagation (retarded) time delay. Generally, a distribution of positive and negative charges will produce internally an attractive force and externally a residual difference attractive electric field. This residual field will tend to zero as the distribution size goes to zero.

But for a finite distribution this field remains finite, capable of attracting similar multipole charge distributions contained in matter. This appears to be the basis of gravity explaining how dissimilar charges from gravitational matter always attract. Thus unsteady electric (electromagnetic), steady difference electric (gravitational), and residual gravity fields throughout the universe (inertial) are all electrical and use the same propagation medium. This allows the Lorentz transform, gravity and accelerating frames to be compared directly. Einstein's invariant inertial frame, which Einstein based his ether-less predictions, is shown to be non causal. A medium based variant propagation frame supports a Propagation Time Asymmetric model predicting all wave behaviour both classical and EM.

Most of the matter in the universe is thought to be comprised of just negatively charged electrons and two types of charged quarks, having fractional values of charge q, an up quark 'u' ($q = 2/3$) and a down quark 'd' ($q = -1/3$). The main field contributors are therefore the proton $q = u + u + d = 2/3 + 2/3 - 1/3 = 1$ and the electron $q = -1$. Even possibly the neutron $q = d + d + u = -1/3 - 1/3 + 2/3 = 0$, if its quarks, under high pressure, can be reconstructed into positive and negative charges. Using a point atomic model an equal number of negative electrons and positive protons, with their corresponding electric fields cancel, creating a neutral atom. However, a finite distribution of dissimilar charges will always produce an attractive steady residual difference field. This can be easily demonstrated with dissimilar magnetic or charged poles. These basic fields appears to play an important part in the attraction of atoms and molecules and therefore gravity.

According to van der Waals (1873) induced dipoles from molecules with permanent bipolar fields and induced dipoles, causes an attraction between individual atoms and molecules. These attractive dipole fields, in the near field, determine their liquid and gaseous phases and the pulling together of mercury beads and soap films. They are local, having a very rapidly reducing field strength with distance. Also London (1937), predicted that electrons orbiting at large distances around atomic nuclei repel (displace) electron orbits of neighbouring atoms and molecules. These unbalanced orbits then create a mass/spring induced dipole field, oscillating at imaginary non propagating frequencies, resulting in a rapidly decaying reactive field with distance. However, low atomic number molecules can have high and low energy levels. These result in strong and weak attractive near fields creating both solids and gases with similar atomic numbers, i.e., their attraction is not proportional to the atomic number.

Although these van der Waals type attractive fields are electrostatic, they do not appear to be gravitational, they are local fields holding the molecules together. For gravity we are looking for attractive electrical dipole fields that propagate into the radiation far field, i.e., decaying according to the inverse square law and whose strength (weight) tends to be proportional to the atomic number. The model that best fits this description is the Atomic Residual Difference Field (ARDF) whose attractive field is proportional to the atomic number (number of pairs of dissimilar charges in the atom). From quantum mechanical grounds, the difference residual field should form in the reactive near field, at the atomic level. The field summation from all atoms and molecules in the vicinity would then be attractive and decay into the propagation far field according to the inverse square law, the same as gravity.

Energy Continuity Equation for Electromagnetic Waves in Dispersive Lossy Medium

O. B. Vorobyev
Stavropol Institute of Radio Communications, Russia

Abstract— The Poynting theorem for the electromagnetic waves in a causally dispersive medium with inherent losses is clarified on the base of examination of the notion of the energy density of the electromagnetic field. In contrast with the static and quasi-static fields, the average energy density of the electromagnetic field is not reduced to the energy densities of the macroscopic electric and magnetic fields.

The energy densities of the electro- and magnitostatic fields correspond to the energy densities of the non-propagating fields in free space and the energy of the static polarization and magnetization of a medium. The energy density of the macroscopic electromagnetic field in a dispersive medium with negligible losses in the frequency regions of normal dispersion is described by the Brillouin formula. The Brillouin energy density of the macroscopic fields corresponds to the energy density of the fields in free space and the energy of the electromagnetic oscillations in structural elements of the dispersive medium.

Similar to the case with the static fields, the Brillouin formula was derived as a sum of the energy densities of the electric and magnetic fields described by the corresponding constitutive parameters. The Brillouin formula, presented as an expression for the energy density of the electromagnetic field using the refractive index and the Poynting vector, was employed in the calculation of the group velocity. Both interpretations of the Brillouin formula are correct for a lossless medium. However, the model of the dispersive medium with negligible losses is applicable in the frequency regions of transparency while the Brillouin formula leads to the unphysical negative energy densities of the fields in the frequency regions of anomalous dispersion.

The energy densities of the macroscopic electric and magnetic fields in a dispersive medium with losses were expressed by functions of magnitudes of the constitutive parameters. In contrast, the Brillouin formula depends on the real parts of the constitutive parameters. The dispersive and dissipative components of the electric (magnetic) energy density corresponding to the electromagnetic oscillations in the structural elements of the medium were taken into account using the real and imaginary parts of the electric (magnetic) susceptibility. The energy densities of the macroscopic electric and magnetic fields in a dispersive medium with losses were also expressed by functions of the Lorentz constitutive and microscopic parameters. In accordance with the latter model, the energy of the electromagnetic oscillations was linked with the energy of mechanical oscillations of the electrons in the Lorentz model. The results of the latter approaches demonstrate that some aspects of the description of the energy parameters of the microscopic fields are not essential on the macroscopic level. The generalization of the Brillouin formula is not restricted by the Lorentz model and does not depend upon microscopic parameters.

Nevertheless, the generalized energy densities of the quasi-static macroscopic electric and magnetic fields in a medium with losses do not fully correspond to the energy density of the electromagnetic waves. The power density of the energy dissipation of the electric and magnetic fields depends on the imaginary parts of the permittivity and permeability. That leads to different dissipation rates of the energy densities of the electric and magnetic fields. In comparison, the propagation of the electromagnetic field in the case of a lossless medium is equivalent to the concurrent propagation of the energy densities of the electric and magnetic fields in accordance with the Brillouin formula. Description of the propagation of the electromagnetic wave as a whole becomes a primary task.

The definition of the energy density of the electromagnetic field using the Poynting vector and refractive index has fundamental importance for the accurate calculation of the energy density and velocity. The constitutive parameters describe the electric and magnetic properties of a quasi-continuous medium, whereas the refractive index is necessary to take into account reciprocation of those parameters for a correct description of the electromagnetic field in accordance with Maxwell's theory. Dependence of the energy density of the electromagnetic field on the Poynting vector yields a straightforward generalization of the group velocity for the frequency ranges, where the group velocity ceases to have meaning of the energy velocity. The energy velocity depends on the refractive index and characteristic impedance of a lossy medium. The Poynting theorem is identified as the energy continuity equation for the time averaged Poynting vector and energy

velocity in agreement with the concept of the energy density of the macroscopic electromagnetic field in a dispersive medium with losses.

Electromagnetic Force on Neutral Particles

Chung Boon Kuan
Universiti Tunku Abdul Rahman, Malaysia

Abstract— The theory of charged particles acceleration is well understood and widely used in many applications. In some cases, collections of particles that are neutral may be accelerated by charge separation effects. Two examples are magnetic acceleration of a plasma and deflection of atoms by a magnetic gradient (Stern-Gerlach experiment). According to the Lorentz force law, the electromagnetic force is proportional to the net charge and velocity of a particles ($F = qv \times B$). So, it seems impossible to accelerate a fundamentally neutral particle. However, another form of Lorentz force law states that the electromagnetic force is proportional to the current ($F = I \times B$). The current can be an induced current as in the case of induction motor. This gives the idea that it may be possible to yield a Lorentz force by applying a time-varying electric field and magnetic field at perpendicular direction through a neutral particle. The time-varying electric field will polarize the particles and induce an alternating current. Interaction between the induced current and the time-varying magnetic field at a suitable phase relationship will produce a Lorentz force that is always in a certain direction perpendicular to both the electric field and the magnetic field. The existence of the force would mean the neutral particle can be accelerated and the motion can be controlled. This would give rise to many practical applications. Simulation using CST EM Studio has shown some promising results. An experiment has be set up to investigate the relationship between the Lorentz force and the field strength, optimum phase difference between electric and magnetic fields, frequency of the time-varying sources, and material property (dielectric constant, permeability, and conductivity) of the particles. A Helmholtz coil is used to generate a uniform ac magnetic field, while a parallel-plates system provides a uniform ac electric field. The ac voltage connected to the Helmholtz coil is phase shifted by a phase-shifter network. Its voltage is then stepped up by a high-voltage transformer and applied to the parallel-plates. Smoke or steam is released through the electromagnetic field region and the deflection of it is recorded using a high-speed digital video camera. The force on the particles can then be calculated.

The Uniqueness Theorems in the Electromagnetic Wave Theory and Quasi-periodical Solutions of the Periodical Diffraction Problems

N. B. Pleshchinskii
Kazan Federal University, Russia

Abstract— The simple method to prove the uniqueness of the solution of the electromagnetic wave diffraction problems is proposed in the case of loss-free media. The set of the diffraction problems on the thin conducting screens in the wave-guided structures are considered. The over-determined boundary value problem method is used. It is shown that the limited absorption principle is correct for the considered problems.

The uniqueness conditions of the solution of the integral equations with difference kernel are obtained as an auxiliary result. These conditions are used to prove the Floquet theorem: the solution of the quasi-periodical wave diffraction on the periodical set of the heterogeneities can be the quasi-periodical wave (Floquet wave) only.

The case of diffraction problem on the bi-periodical set of thin conducting screens in the opened space is considered in detail as an example. The boundary value problem is equivalent to the dual summatorial functional equation for the Floquet coefficients. It is proved that this problem is equivalent to the regular infinite set of the linear algebraic equations for the coefficients of decomposition of the electromagnetic field by Floquet harmonics. By this set of equations the algorithms are constructed for numerical solving the diffraction problem.

The Over-determined Boundary Value Problems for the Maxwell Equations Set in the Orthogonal Coordinates and Some Applications for the Electromagnetic Wave Diffraction Problems

N. B. Pleshchinskii
Kazan State University, Russia

Abstract— The necessary and sufficient conditions of solvability of the over-determined problems for the Maxwell equations set are obtained in the cases of Cartesian, cylindrical and spherical coordinates. These conditions are used by reduction of the electromagnetic wave diffraction problems on the thin conducting screen placed on the coordinate surfaces to integral or summatorial equations. Moreover, these conditions can be used for regularization of the integral equations of the first kind obtained by solving the diffraction problems.

In the case on three-dimensional problems of electrodynamics the over-determined problems appear when both the tangential components of the electric vector and of the magnetic vector are given on the boundary of the partial domains.

It is shown that the conditions of solvability of the over-determined problems can be obtained in the different form. The common form is the dependence of the Fourier transforms or Fourier coefficients of the boundary functions. But the mixed form is possible when both expressions participate.

The set of the three-dimensional diffraction problems on the thin conducting screens in the waveguided structures is considered as examples.

Plasma Treatment as a Versatile Technique for Preparation of Plasmonic Nanoantenna Arrays

L. Štolcová[1], M. Domonkos[1], T. Ižák[2], J. Proška[1], M. Procházka[3], and A. Kromka[2]

[1]Department of Physical Electronics, Faculty of Nuclear Sciences and Physical Engineering
Czech Technical University in Prague, Břehová 7, 115 19 Prague 1, Czech Republic
[2]Institute of Physics, Academy of Sciences of the Czech Republic
Cukrovarnická 10, 162 00 Prague 6, Czech Republic
[3]Faculty of Mathematics and Physics, Institute of Physics
Charles University, Ke Karlovu 5, 121 16 Prague 2, Czech Republic

Abstract— Metal nanostructures supporting localized surface-plasmon resonance (LSPR) have attracted growing research interest in the last decades due to their ability to confine light and produce high enhancement of the local electromagnetic field in their vicinity. These effects gave rise to novel scientific methods, such as surface-enhanced spectroscopies [1].

In this contribution, we report on the preparation of diverse plasmonic nanoantennas prepared by the self-assembly of polystyrene (PS) spheres, followed by plasma treatment, and gold sputter coating. These simple, relatively low-cost, and high-throughput techniques enable to produce meso-scale structures with certain features as small as a few nanometres, thus to control comfortably the optical response of the metal nanostructures (determined primarily by their size, shape, and mutual distances), and create large periodic arrays of rationally designed plasmonic substrates. By adjusting the plasma etching conditions and character (i.e., reactive ion etching or pulsed linear-antenna microwave plasma [2]), self-assembled monodisperse polystyrene beads either decrease their size to form non-close packed spheres, create long necks toward adjacent spheres (Fig. 1(a)), or transform to corrugated anisotropic structures known as nanocorals (Fig. 1(b)). The possibility of utilizing the prepared nanostructure arrays both as a template and/or a mask for metal deposition and producing 2D plasmonic nanoantennas further enhances the versatility of the described technique.

Selected types of nanoantenna arrays, i.e., nanocorals and hollow semishells (Fig. 1(c)) obtained from spheres 471 nm and 253 nm in diameter, were successfully tested as substrates for surface-enhanced Raman scattering (SERS) by measuring SERS spectra of 4-aminothiophenol, a prototypical SERS probe, at submicromolar concentrations.

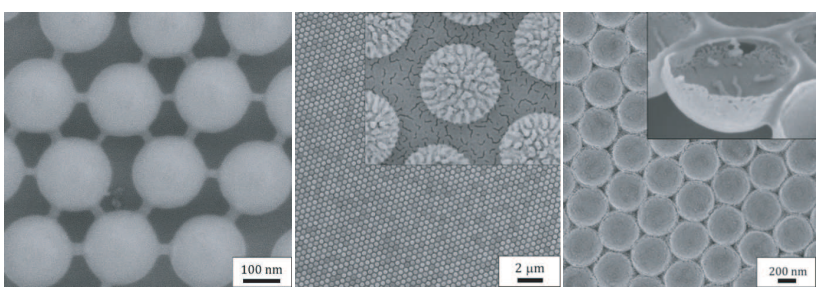

(a) (b) (c)

Figure 1: Plasmonic nanoantennas produced by self-assembly of PS spheres (471 nm or 253 nm in diameter), plasma etching, and gold sputter coating: (a) PS "ball-and-stick" structure, (b) gold nanocorals, (c) 20 nm thick gold semishells.

ACKNOWLEDGMENT

This work was supported by the Czech Science Foundation grants No. P205/13/20110S and P108/12 /G108 (AK, TI).

REFERENCES

1. Willets, K. A. and R. P. Van Duyne, *Annu. Rev. Phys. Chem.*, Vol. 58, 267–297, 2007.
2. Kromka, A., et al., *Proc. of 3rd NANOCON Int. Conference*, 271–279, Brno, Czech Republic, 2011.

The Dispersive Properties of the Three-dimensional Photonic Crystals with Diamond Lattices Containing the Epsilon-negative Materials

Hai-Feng Zhang[1, 2], **Wen-Ping He**[2], **Shao-Bin Liu**[1], **and Yu-Qing Chen**[2]

[1]College of Electronic and Information Engineering
Nanjing University of Aeronautics and Astronautics, Nanjing 210016, China
[2]Nanjing Artillery Academy, Nanjing 211132, China

Abstract— In this paper, dispersive properties of three-dimensional (3D) photonic crystals (PCs) with diamond lattices composed of the isotropic positive-index materials and epsilon-negative materials are theoretically investigated based on a modified plane wave expansion (PWE) method. The eigenvalue equations of such structure (spheres with epsilon-negative materials inserted in the dielectric background) are deduced. It can be obviously seen that a photonic band gap (PBG), a flatbands region, and two stop band gaps (SBGs) in the Γ-X and Γ-L directions appear, respectively. The results show that the upper edges of flatbands region can not be tuned by any parameters except for the electronic plasma frequency. The first PBG and the first SBGs above the flatbands region in the Γ-X and Γ-L directions for the 3D PCs can be modulated by the filling factor, relative dielectric constant and electronic plasma frequency, respectively. However, the damping factor has no effect on the locations of the first PBG and the first SBGs above the flatbands region in the Γ-X and Γ-L directions.

A New Triple-band Polarization-insensitive Wide-angle Microwave Metamaterial Absorber

Bo-Rui Bian[1], **Shao-Bin Liu**[1, 2], **Hai-Feng Zhang**[1], **Bin-Xiang Li**[1], **and Ben Ma**[1]

[1]College of Electronic and Information Engineering
Nanjing University of Aeronautics and Astronautics, Nanjing 210016, China
[2]State Key Laboratory of Millimeter Waves, Southeast University, Nanjing 210000, China

Abstract— We propose a new triple-band absorber in microwave frequencies in which the design, analysis, fabrication and measurement of the absorber is presented. The absorber is constructed of a periodic array of tetra-lashing triangle resonators printed on a dielectric material backed by metal ground. By adjusting the geometry parameters of the structure, we can realize a triple-band polarization-insensitive wide-angle absorber in three different resonator modes. Experiment results demonstrate excellent absorption rates in the designed frequency bands over wide angles of incident waves for both transverse electric and magnetic polarizations and have good correspondence with the required results.

Studies on Fano Resonances in Subwavelength Plasmonic Nanostructures

J. Fiala, **P. Kwiecien**, **and I. Richter**
Department of Physical Electronics, Faculty of Nuclear Sciences and Physical Engineering
Czech Technical University in Prague, Brehova, 11519 Prague 1, Czech Republic

Abstract— Recently, by utilizing our experience with the analysis of interactions at the nanoscale of the periodical subwavelength hole array structures and fishnet metamaterials [1], our interest has been turned into characterization of resonances for the case of 'inversed' structures, being thus, e.g., periodical arrays of metallic nanoparticles. Such subwavelength-scaled plasmonic nanostructures have newly gained much interest for their applications in surface plasmon resonance (SPR) biosensing as well as surface-enhanced Raman scattering (SERS) spectroscopy activities primarily because their response to light can be effectively reshaped, based on the application needs.

With our aim being the understanding and revelation of an interplay between resonances localized in individual particles and lattice resonances originating in the array, a simple model that characterizes an isolated building blocks in terms of equivalent induced dipoles of both magnetic and electric character, and a lattice resonances originating in coupling of such dipoles is being developed based on the previous work of Garcia de Abajo [2]. Indeed, it has been observed that metallic nanoparticles can sustain localized plasmon excitations which travel across neighbors. This phenomenon can be utilized to transmit light energy along chains of subwavelength particles, thus providing some basic constituents for plasmonic sensors, for example.

The interaction among particles in the periodic arrays appears to be governed by the lattice sums and is dominated by their singularities, which originate in accumulation of in-phase scattered fields. Also in the context of plasmonic resonances, Fano interferences are a powerful tool to exhibit very sharp and strong features due to what is known as lattice resonances, where the interaction between a discrete state and a continuum gives rise to resonant suppression and enhancement of scattering, resulting in a typical asymmetric resonance shape, as was also observed in case of extraordinary optical transmission. These are given by the interference of the LSPR (broad state) with the in-plane scattered light at the Rayleigh anomaly position (discrete state). It has been found that Fano resonances exhibit a very strong sensitivity to changes of the local environment as well as a sharp spectral dispersion [3, 4], thus providing a perspective application to SPR sensing potential.

The results of our studies on Fano resonant responses on several selected subwavelength-structured nanoplasmonic systems will be shown and discussed in a detail. As an example, one of the representative structures within our study is formed by identical spherical/cylindrical gold nanoparticles which form a periodical lattice with a periodicity L, height of a cylinder h, and radius r, with the aim of utilizing such a structure as an efficient platform for SPR sensing.

ACKNOWLEDGMENT

This work was financially supported by the Czech Science Foundation (projects P205/10/0046 and P205/12/G118).

REFERENCES

1. Fiala, J., P. Kwiecien, and I. Richter, "The physics and design possibilities of plasmonic-based fishnet metamaterial structures," *Proceedings SPIE 8697 of the 18th Czech-Polish-Slovak Optical Conference on Wave and Quantum Aspects of Contemporary Optics*, Ostravice, Czech Republic, September 2012.
2. Garcia de Abajo, F. J., "Site and lattice resonances in metallic hole arrays," *Opt. Exp.*, Vol. 14, No. 1, 7–18, 2006.
3. Miroshnichenko, A., S. Flach, and Y. Kivshar, "Fano resonances in nanoscale structures," *Rev. Mod. Phys.*, Vol. 82, 2257–2289, 2010.
4. Luk'yanchuk, B., N. I. Zheludev, S. A. Maier, N. J. Halas, P. Nordlander, H. Giessen, and C. T. Chong, "The Fano resonance in plasmonic nanostructures and metamaterials," *Nat. Mater.*, Vol. 9, 707–715, 2010.

Spectral Density Analysis of Thin Gold Films: Thickness and Structure Dependence of the Optical Properties

P. C. Lansåker[1], E. Tuncer[2], I. Valyukh[3], H. Arwin[3], C. G. Granqvist[1], and G. A. Niklasson[1]

[1]The Ångström Laboratory, Department of Engineering Sciences
Uppsala University, P. O. Box 534, SE-751 21 Uppsala, Sweden
[2]3M Austin Center, EEBG/CRML, Austin, TX 78726, USA
[3]Laboratory of Applied Optics, Department of Physics, Chemistry and Biology
Linköping University, SE-58183 Linköping, Sweden

Abstract— The purpose of this paper is to study the feasibility and the limitations of representing the optical properties of ultrathin gold films by effective medium theories. We perform an analysis of the spectral density function (SDF) [1–3], which was obtained by inverting experimental optical measurements. The SDF describes the effect of nanostructure on the effective optical properties of the films. Gold films with mass thicknesses in the range of 1.4 to 9.2 nm were deposited by DC magnetron sputtering onto glass substrates. The film structure evolved from gold island films to a percolating gold network and finally we obtained a homogenous film. The area fractions of gold on the substrates were estimated from image analysis of scanning electron micrographs and the geometric thicknesses of the films were found to be between 4.0 nm and 9.2 nm. Optical measurements in the range 0.25 to 2 µm were carried out by spectroscopic ellipsometry, and the effective complex dielectric function of the films was determined. The gold films were modeled as mixtures of gold and air, and a general effective medium description using the spectral density function was used to describe their optical properties. The experimental effective dielectric function was inverted by a numerical Monte-Carlo technique [3, 4] in order to obtain the SDF. The results showed a broad and rather featureless SDF with a few superimposed peak structures, both for island structures and percolating films. The broad featureless SDF background is qualitatively similar to the result from Bruggeman effective medium theory, but it must be realized that we cannot experimentally explore the region of large spectral parameters ($x > 0.5$). It seems that the Bruggeman theory can be considered as a first approximation to the optical properties of nanostructured gold films. Our results illustrate the usefulness of the SDF in describing the effective optical properties of nanostructured thin metal films.

REFERENCES

1. Bergman, D. J., *Phys. Rep.*, Vol. 43, 377–407, 1978.
2. Bergman, D. J., *Annals Phys.*, Vol. 138, 78–114, 1982.
3. Tuncer, E., *Materials*, Vol. 3, 585–613, 2010.
4. Tuncer, E., *Phys. Rev. B*, Vol. 71, 012101, 2005.
5. Bruggeman, D. A. G., *Ann. Phys.*, Leipzig, 5 Folge, Vol. 24, 636–679, 1935.

Variable Forbidden Regions in Metamaterial Planar Waveguide with Nonlinear Cladding

Yaw-Dong Wu, Ming-Hsiung Cheng, and Tien-Tsorng Shih
Department of Electronic Engineering, National Kaohsiung University of Applied Sciences
Kaohsiung, Taiwan, R.O.C.

Abstract— In this paper, we used the modal theory to analyze TE waves in the three-layer planar waveguide with the metamaterial guiding film and the nonlinear cladding layer, and derive a formula for the guiding power density. The power density is very helpful to analyze the forbidden regions of the proposed waveguide structure. In recent years, the metamaterial in the planar waveguide has been widely studied in many researches. The feature of the metamaterial includes the permittivity ε and the permeability μ less than zero. The forbidden regions always exist in the three-layer planar waveguide with the metamaterial guiding film and the nonlinear cladding layer. In this study, the guiding power density can help to provide a clear picture of forbidden regions in the metamaterial film with different permeability values. The numerical results show that the forbidden regions are different in metamaterial film with the same width but the permeability values are different. The greater permeability value is, the narrower the forbidden region is. The study shows that the value of guiding power density is less than zero at metamaterial and is greater than zero at right-handed medium. Therefore, the guiding power density is at the opposite direction because the values of permeability are positive and negative. It agrees with the phenomenon of negative refraction in metamaterial. The simulation result is helpful to find out the propagation situation of the TE polarized waves.

New All-optical Switch Based on the Local Nonlinear Plasmonic Mach-Zehnder Interferometer Waveguides

Yaw-Dong Wu, Sheng-Rong Hong, and Tien-Tsorng Shih
Department of Electronic Engineering
National Kaohsiung University of Applied Sciences, Kaohsiung, Taiwan, R.O.C.

Abstract— In this paper, we proposed a new all-optical switch based on the local nonlinear metal-insulator-metal (MIM) plasmonic Mach-Zehnder (MZ) interferometer waveguides. The proposed structure is composed of the local Kerr-type nonlinear MIM plasmonic MZ interferometer waveguide and the straight MIM plasmonic control waveguide. In recent year, the surface plasmon has attracted much attention due to the potential of application. Surface plasmon polariton (SPP) is an electromagnetic excitation at the interface of dielectrics and metals, which can be used to control light in subwavelength. The the local Kerr-type nonlinear MIM plasmonic MZ interferometer waveguide is used in this switching structure for its large third-order nonlinear susceptibility and ultrafast response properties. Some important optical properties of the switching structure have been studied numerically by the finite-difference time-domain method (FDTD), including the transmission characteristics and the switching effect. The proposed new all-optical switching structure shows great advantages of the ultracompact device size and the ultrafast switching effect. By properly fixing the input signal power and changing the control power, the output signal beam will show the switching effect. In this structure, we can found that the proposed all-optical switch exhibits an excellent switching effect. It would be a potential key component in the application of the ultra-high-speed data processing system.

Broadband High Efficiency Amplifier for a Cognitive Radio System

Ahmed E. Khorshid[1], **Ali M. Darwish**[2], **Islam A. Eshrah**[1], **Hossam A. H. Fahmy**[1], **and Mohamed El-Hadidy**[2]

[1]Department of Electronics and Communications Engineering, Cairo University, Egypt
[2]Department of Electronics Engineering, American University in Cairo, Egypt

Abstract— In this paper we describe the design and the implementation of aclass-J power amplifier, intended to be used in a cognitive radio system operating in the TV band, achieving a percentage bandwidth of 60%, covering the band from 0.5–0.95 GHz. Class J mode was selected in order to achieve high PAE (power added efficiency) over a broadband. The suggested design was first simulated, after precisely selecting the multi-harmonic impedance terminations, showing promising performance. Then circuit implementation was carried out, where the measured results showed good match with the simulated ones. This is the first class-J implementation in the TV band. To our knowledge, this is the highest efficiency for such a wide bandwidth PA reported in this band.

Introduction: Cognitive radio is an emerging area of tremendous opportunity for providing affordable broadband wireless access to more people. Our challenge was in building the front end of a TV Band Device (TVBD). The proposed TVBD is supposed to cover a very wide frequency range (500–950 MHz) covering an octave. Developing an inexpensive, efficient, and broadband power amplifier is proposed in this research.

Previous Class-J designs were investigated [2–4], yet none of them was operating in our band of interest. To our knowledge, this is the first design for a Class-J operating in the TV band. Compared to other generally designed Class-J amplifier, this design achieves the largest percentage bandwidth (60%), with the highest efficiency (60–80%) achieved over such bandwidth and at such high gain and high output power. In [2] for example, only 50% bandwidth was achieved with efficiency between (60–70%). Cree's CGH40010 — 10 W GaN (Gallium Nitride) high electron mobility transistor device was used in this research. Excessive load-Pull measurements were carried out on Microwave office software in order to select the proper impedance termination for the fundamental and 2nd harmonics tones. Simulation (both circuit and EM simulations) results showed excellent PAE over that wide band of frequencies, ranging between (60%–80%), with 20 dB gain and 40 dBm output power. Stability of the circuit was then checked using both the μ-test and the K-Δ test. The circuit is then fabricated with both the input and output matching circuits, where measurements confirmed the results previously obtained from the simulation.

Theory: Class-J mode is defined [1] as a mode in which the voltage has harmonic components which make it tend asymptotically towards a half-wave rectified sine-wave through the selection of a reactive component at the fundamental load and a suitably phased second harmonic component. The starting point in class-J design is deep class-AB mode, that's why it can be expected to have the same linear performance as a class-AB amplifier operating at the same conduction angle.

Simulation: Simulation was carried out using the model of Cree's CGH40010 GaN HEMT on the AWR design environment. Load-Pull measurements were used to get the value for the optimum load, where we had to compromise between maximizing the efficiency and maximizing

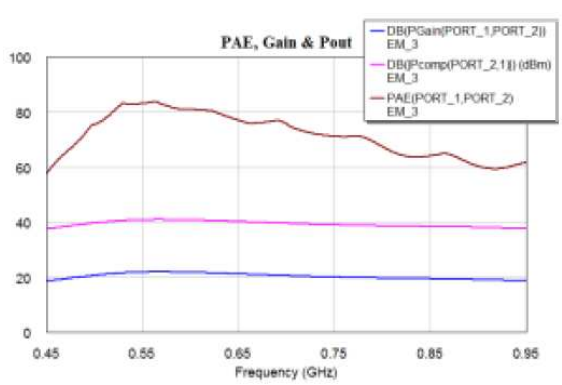

Figure 1: Simulation results (PAE, gain and pout).

Figure 2: Circuit implementation.

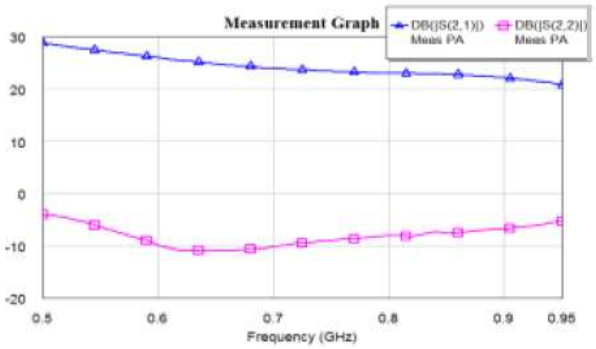

Figure 3: Measured results (S_{21}, S_{22}).

the gain over such a broadband. After the proper selection of such terminations, circuit and EM simulations were carried out showing the performance in Fig. 1.

Practical Implementation: The design was then fabricated as shown in Fig. 2. Results were then measured, showing very good match with the simulation results. Part of the results is shown in Fig. 3. The rest will be presented in the full paper.

Conclusion: In this paper a broadband class-J PA was designed and implemented to operate in the TV band. Excellent PAE was achieved (above 60%) over the band from 500–950 MHz, with 20 dB gain and 40 dBm output power. Both simulation and measured results were obtained, confirming the design methodology and the expected results.

REFERENCES

1. Cripps, S. C., *RF Power Amplifiers for Wireless Communications*, 2nd Edition, Artech House, Norwood, MA, 2006.
2. Wright, P., J. Lees, J. Benedikt, P. J. Tasker, and S. C. Cripps, "A methodology for realizing high efficiency class-J in a linear and broadband PA," *IEEE Transactions on Microwave Theory and Techniques*, Vol. 57, No. 12, 3196–3204, Dec. 2009.
3. Moon, J., et al., "Investigation of a class-J power amplifier with a nonlinear Cds for optimized operation," *IEEE Transactions on Microwave Theory and Techniques*, Vol. 58, No. 11, 2800–2811, Nov. 2010.
4. Wright, P., J. Lees, P. J. Tasker, J. Benedikt, and S. C. Cripps, "An efficient, linear, broadband class-J-mode PA realised using waveform engineering," *IEEE MTT-S Int. Microw. Symp. Dig.*, 653–656, 2009.

Magnetoelectric Microwave Module for Phased Array

R. V. Petrov, **M. I. Bichurin**, **and A. S. Tatarenko**
Novgorod State University, Russia

Abstract— The central problem of microwave technology is the design of receiver, transmitter and receiver-transmitter modules of phased array system (PAS) with specified characteristics. They must address diverse requirements of PAS in sensitivity, power, frequency range, etc.. Layered ferrite-piezoelectric structure is an ideal target for a microwave devices and PAS. Electromechanical, ferromagnetic and magnetoacoustic resonances, magnetic dipole and electric dipole transitions in these structures allow to design the new magnetoelectric (ME) microwave devices for PAS module. Development and application of new layered ferrite-piezoelectric structures with advanced properties will significantly improve the performance of PAS modules as a whole. In this work, the design of ME microwave devices for PAS modules are proposed.

The base elements of the ME receiver module of PAS are receiving microstrip antenna, preselector filter, attenuator, phase shifter, amplifier and the detector.

For example, it is known a module designed by company CJSC "Micran, Research & Production Company" (Russian) which have the next characteristics: dynamic range of gain control is 23 dB, the adjustment range of phase is 360-degree with increments 5.6 degrees, receiver noise figure is no more than 5 dB. We propose the module with the comparable characteristics and following parameters: the adjustment range of the phase is 360 degrees (continuously regulated), receiver noise figure is not more than 0.9 dB that exceeds the characteristics of the "Micran" module in the several times. The offered decision based on ME devices improves the sensitivity of the system and provides advantages for the module as a whole.

The implementation of transceiver modules is possible on a single substrate technology, and separately for the devices. Hybrid technologies allow to combine separately fabricated devices into a single module. The advantage of the technology can provide integrated, combining production of all ME devices in a single technological cycle. Ferrite-piezoelectric heterostructures are ideal for studies on wide-band magnetoelectric interactions between the magnetic and electric subsystems that are mediated by mechanical forces. Such structures show a variety of magnetoelectric phenomena including microwave ME effects. The phenomenon can be used for design of electrical tuning microwave ME resonators and devices on their basis. The specific focus is on ME effects when electromagnetic modes close to ferromagnetic resonance are excited in the ferrite. In the presence of an electric field, the piezoelectric deformation in the bilayer structures will manifest as an internal magnetic field in the ferrite. Tunability of the ME devices characteristics in the chosen working range can be executed by application of an electric field. This electric tuning is relatively fast and is not power-consuming. According to our estimates the receiver ME microwave module at a frequency of 10.525 GHz can provide a dynamic range of 30 to 50 dB with noise figure less than 0.9 dB.

ACKNOWLEDGMENT

The reported study was partially supported by the grant of the Federal Target Program "Scientific and pedagogical staff of innovative Russia" on 2009–2013 and by RFBR research project #13-02-98801.

Failure Analysis of Ferrite Sheet Used in NFC Antenna

Soon-Mi Hwang and Kwan-Hun Lee
Korea Electronics Technology Institute (KETI), Republic of Korea

Abstract— The Near Field Communication (NFC) is a technology which reads the information built in products and objects by using radio frequency in definite distance. NFC is a contactless communication, operates in 13.56 MHz frequency band, with low cost and easy to use features [1]. In the NFC communication process, information transfers through the electromagnetic induction as the high frequency RFID. And the field distribution in the same near zone becomes more complex and may also include an electrostatic or magnetostatic component. So the antenna performance is one of the core problems [2].

Ferrites are found to be effective in diminishing electromagnetic influence [3]. And the ferrite absorbers such as ferrite sheet are widely used to optimize the antenna performance in near-field communications [4].

Ferrite sheet for NFC antenna is used in a variety of environments, and 'product reliability' is important as much as the function of each part. If products are developed and used without an enough environment conformance test as NFC antenna is applied in various applied environment and overall society, social chaos and economical damage will be expected from the disorder and malfunction of NFC working system. Therefore, research and analysis of reliability in various NFC application fields, study of the test criteria and methods according to the applied environment, and planning for reliable environmental evaluation standard should be carried out so that the final users can feel relieved and introduce NFC stable system. This thesis studies the main failure modes and the failure mechanisms of Ferrite sheet for designing the life-time.

To verify aforementioned reasons for the failure of Ferrite sheet, a environment test was carried out according to RS C0043; (Electromagnetic wave absorption sheet, Reliability standards). Five kinds of test; (High temperature test, Low temperature test, Thermal Shock test, High temperature and humidity test, Vibration test) were carried out. The test item for performance verification is permeability. And as a result, We knew that the major failure stress of the ferrite sheet are thermal shock and high temperature.

Thermal Shock test was carried out in high temperature ($125\pm2^\circ$C), low temperature ($-55\pm2^\circ$C) and run for 30 minutes. And the Ferrite sheet failed sporadically after 500 cycles. If a device made of metal soild like ferrite sheet has long-term exposure to sudden temperature changes, it can result in cracks in body. This crack is caused the circuit open and changes the characteristic of the device.

High temperature test was carried out in ($125 \pm 2^\circ$C). And the Ferrite sheet failed sporadically after 600 h. If a ferrite sheet has long-term exposure to high temperature, deformation occurs. This deformation changes the characteristic of the device.

After the environment test, the failed samples were carefully examined with Environmental Scanning Electron Microscope (ESEM) and 2D X-ray. Analysis result, product cracks and deformation was found.

REFERENCES

1. Li, L., Z. Gao, and Y. Wang, "NFC antenna research and a simple impedance matching method," *International Conference on Electronic and Mechanical Engineering and Information Technology (EMEIT)*, 3968–3972, Aug. 12–14, 2011.
2. Augustine, R., T. Alves, M. Zhadobov, B. Poussot, T. Sarrebourse, R. Sauleau, M. K. Thomas, and J.-M. Laheurte, "SAR reduction of wearable antennas using polymeric ferrite sheets," *European Conference on Antennas and Propagation (EuCAP)*, 1–3, Apr. 12–16, 2010.
3. Jung, Y.-B., S.-H. Lee, H.-J. Oh, and T.-J. Jeon, "Research on the influence of absorbing sheet for electrical performance of NFC antenna," *Journal of Institude of Korean Electrical and Electronics Engineers*, Vol. 16, No. 3, 167–172, 2012.
4. Jung, Y.-B., S.-H. Lee, H.-J. Oh, and T.-J. Jeon, "Research on the influence of absorbing sheet for electrical performance of NFC antenna," *Journal of Institude of Korean Electrical and Electronics Engineers*, Vol. 16, No. 3, 167–172, 2012.

High Tunable and Low Loss Capacitor Using a BZN/BST/BZN Multi-layer Thin Film Dielectric for Reconfigurable RF Circuit Applications

Young Chul Lee
Department of Electronics Engineering, Mokpo National Maritime University (MMU), Korea

Abstract— In this paper, a high tunable and low loss capacitor using a multi-layer dielectric of BZN/BST/BZN is designed and fabricated for reconfigurable RF applications. By utilizing a high tunable BST ferroelectric and low-loss BZN paraelectric thin film dielectric, a multi-layer dielectric of BZN/BST/BZN obtained a tunability of 47% and $\tan\delta$ of 0.005. The fabricated tunable capacitor on a quartz wafer using this multi-layer dielectric achieved a Q factor of 10 and a tunability of 60% at 800 MHz and 15 V. Its size is $327 \times 642\,\mu m^2$.

Large-signal Properties of 3C-SiC/Si Heterojunction DDR IMPATT Devices at Terahertz Frequencies

Suranjana Banerjee[1], **Aritra Acharyya**[2], **Monojit Mitra**[3], **and J. P. Banerjee**[2]

[1]Academy of Technology, West Bengal University of Technology
Adisaptagram, Hooghly, West Bengal 712121, India
[2]Institute of Radio Physics and Electronics, University of Calcutta
92, APC Road, Kolkata, West Bengal 700009, India
[3]Bengal Engineering and Science University, India

Abstract— The authors have made an attempt to study the large-signal properties of 3C-SiC/Si anisotype heterojunction Double-Drift Region (DDR) Impact Avalanche Transit Time (IMPATT) devices designed to operate at 0.3 and 0.5 THz. A large-signal simulation technique developed by the authors which is based on non-sinusoidal voltage excitation model [1–3] is used for the present study. Two different heterojunction structures: N-3C-SiC/p-Si and n-Si/P-3C-SiC have been considered for comparison with Si homojunction DDR IMPATTs. The results show that n-Si/P-3C-SiC heterojunction DDR structure of IMPATTs excel all other structures with respect to DC to RF conversion efficiency and RF power output at 0.3 and 0.5 THz frequencies. The design considerations and large-signal results presented in this paper will be worthwhile for the future experimentalists and encourage them to fabricate DDR n-Si/P-3C-SiC heterojunction IMPATTs operating at THz regime for several possible THz applications such as THz imaging [4], spectroscopy [5], bio-sensing [6], quality inspection in various industrial branches [7–9], medical and pharmaceutical applications [10, 11], THz astronomy [12] etc.

REFERENCES

1. Acharyya, A., S. Banerjee, and J. P. Banerjee, "Large-signal simulation of 94 GHz pulsed DDR silicon IMPATTs including the temperature transient effect," *Radioengineering*, Vol. 21, No. 4, 1218–1225, 2012.
2. Acharyya, A., S. Banerjee, and J. P. Banerjee, "Effect of junction temperature on the large-signal properties of a 94 GHz silicon based double-drift region impact avalanche transit time device," *Journal of Semiconductors*, Vol. 34, No. 2, 024001–12, 2013.
3. Acharyya, A., S. Banerjee, and J. P. Banerjee, "A proposed simulation technique to study the series resistance and related millimeter-wave properties of Ka-band Si IMPATTs from the electric field snap-shots," *International Journal of Microwave and Wireless Technologies*, Vol. 5, No. 1, 91–100, 2013.
4. Chan, W. L., J. Deibel, and D. M. Mittleman, "Imaging with terahertz radiation," *Rep. Prog. Phys.*, Vol. 70, 1325–1379, 2007.
5. Grischkowsky, D., S. Keiding, M. Exter, and C. Fattinger, "Far-infrared time-domain spectroscopy with terahertz beams of dielectrics and semiconductors," *J. Opt. Soc. Am. B*, Vol. 7, 2006–2015, 1990.
6. Debus, C., and P. H. Bolivar, "Frequency selective surfaces for high sensitivity terahertz sensing," *Appl. Phys. Lett.*, Vol. 91, 184102–3, 2007.
7. Yasui, T., T. Yasuda, K. Sawanaka, and T. Araki, "Terahertz paintmeter for noncontact monitoring of thickness and drying progress in paint film," *Appl. Opt.*, Vol. 44, 6849–6856, 2005.
8. Stoik, C. D., M. J. Bohn, and J. L. Blackshire, "Nondestructive evaluation of aircraft composites using transmissive terahertz time domain spectroscopy," *Opt. Express*, Vol. 16, 17039–17051, 2008.
9. Jördens, C., and M. Koch, "Detection of foreign bodies in chocolate with pulsed terahertz spectroscopy," *Opt. Eng.*, Vol. 47, 037003, 2008.
10. Fitzgerald, A. J., B. E. Cole, and P. F. Taday, "Nondestructive analysis of tablet coating thicknesses using terahertz pulsed imaging," *J. Pharm. Sci.*, Vol. 94, 177–183, 2005.
11. Siegel, P. H., "Terahertz technology in biology and medicine," *IEEE Trans. Microwave Theory & Tech.*, Vol. 52, 2438–2447, 2004.
12. Siegel, P. H., "THz instruments for space," *IEEE Trans. Antenn. Propag.*, Vol. 55, 2957–2965, 2007.

A High Efficiency Broadband Supply Modulator Based on Switch-mode Operations for Polar Transmitters

Fei You, Bohai Zhang, Zhebin Hu, and Songbai He
School of Electronic Engineering, University of Electronic Science and Technology
Chengdu 611731, China

Abstract— In this paper, a high efficiency broadband supply modulator is proposed. This modulator is built based on class-E amplifiers and class-E inverters. The envelope reconstruction is realized by $\Delta\Sigma$ modulations. The feasibility of high efficiency operations is verified by numerical simulations and experiments. The simulation of theoretical WCDMA signals' envelope amplification shows over 70% average eciency. The simulations of the modulator operating at 1.28 GHz built by TSMC 130 nm CMOS devices shows 43.3% average efficiency for 40 MHz baseband signals' envelopes. The experimental board for 3.84 MHz WCDMA signals' envelope modulator built by discrete transistors shows 45.6% average efficiency.

The proposed supply modulator is shown in Figure 1. The output envelope modulation is realized by the on-offstates of transistor T2 controlled by the $\Delta\Sigma$ modulator's outputs from the baseband digital circuits. The envelopes can be recovered by a low-pass filter.

In simulations of WCDMA baseband signals' envelopes modulation, the average efficiency of this modulator, operating at 122.88 MHz, is 76% for $L_{dc} = 0.5\,\mu$H. The normalized mean square error (NMSE) is about -15.8 dB. Another simulation is built based on TSMC 130 nm CMOS device designed at 1.28 GHz. The bandwidth of the envelopes is wider than 80 MHz. The average eciency and NMSE is measured to be 43.3% and -20.66 dB respectively for this modulator example.

The experimental modulator is designed for $V_{dd} = 10$ V and $P_o = 2$ W at 122.88 MHz. LDMOS transistors MRF21010 are used to build the supply modulator. Diodes BAT54 are adopted for Da and Dr in Figure 1. The photo of the FPGA board and the supply modulator is shown in Figure 2.

The measured effiiency of the supply modulator, when connected transistor T2 is turned off is 57.8%. The average efficiency is measured to be 45.6% for WCDMA signal's envelope of 5.8 dB PAPR. The NMSE is about -9.5 dB.

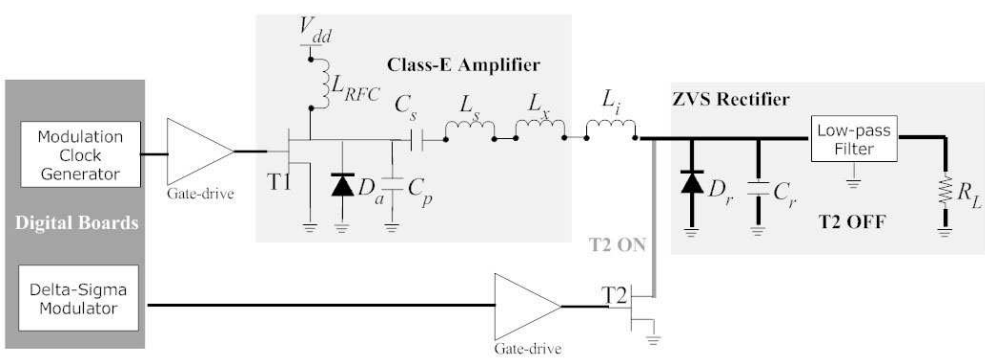

Figure 1: The basic configurations of the proposed supply modulator.

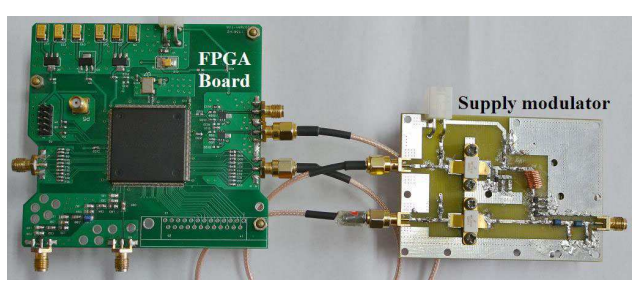

Figure 2: The picture of the experimental supply modulator operating at 122.88 MHz.

ACKNOWLEDGMENT

This work was supported by the National Natural Science Foundation of China under Grant 61001032 /F010501.

Separation of Overlapped Compressed Cyclostationary Signals Using Adaptive FRESH Filtering

Said E. El Khamy[1], **Amr El-Helw**[2], **and Azza Mahdy**[2]

[1]Department of Electrical Engineering, Faculty of Engineering
Alexandria University, Alexandria, Egypt
[2]Department of Electronics and Communication Engineering
Arab Academy for Science & Technology & Maritime Transport, Cairo, Egypt

Abstract— One important property of cyclostationary signals is interference removal. This is accomplished by implementing Frequency Shifting filter. FRESH filters are adaptive filters upon which their operation depends on a correlative property of cyclic signals, that is, for a cyclic signal, the two spectral components of a cyclostationary signal shifted at $f+\alpha/2$ and $f-\alpha/2$ are correlated. As a consequence, there exists spectrum redundancy between the two components. By knowing the required set of cycle frequencies of the signal of interest, these filters can remove an interfering signal. The optimum adaptive FRESH filter is implemented for the SOI being a raised-cosine bandpass BPSK signal and the interference signal being a square-root raised-cosine bandpass BPSK signal. Their carrier frequencies are defined to be overlapped by a certain offset frequency Δf. Further, the same filter is implemented in the wavelet domain and it is shown that it is able to separate spectrally overlapped signals after first level wavelet decomposition of the input signal. The purpose of reducing the sequence length is to reduce the processing time taken to separate spectrally overlapped signals. The idea is illustrated by applying multilevel wavelet decomposition to the input signal. Moreover, the processing time taken to separate the signals after first-level wavelet decomposition is shorter than that in case of implementing the FRESH filter without compressing the input signal. A reduction percentage of the processing time applying first-level wavelet decomposition is achieved. Accordingly, the average value of error increases. Also the more we compress the input signal, the worse the average error.

Development of Non-contacting System for Detection of Driver's Sleepiness Using UWB Radar

Tae-Yun Lee, **Se-Yeon Jeon**, **Jiwoong Yu**, **Seok Kim**, **and Min-Ho Ka**
School of Integrated Technology, Yonsei University, Incheon, Korea

Abstract— Drowsy driving is a major cause of automobile crash. To reduce it, many researches were and still are being. Parameters for detecting sleepiness are investigated by previous studies. So the majority of research has progressed to estimate these parameters. And developed systems are mostly image processing using optical/infrared camera or estimating vital sign using contacting system. Some systems combine these but that must have two or more sensors. In this paper, we suggest novel technique that detects the driver's sleepiness using UWB radar. When human fall into the sleep, breathing and heartbeat rate reduce than normal state. So if we can measure this change, we can detect driver's sleepiness. UWB radar can measure human vital sign, especially breathing and heartbeat rate. Its accuracy is very high enough to be used medical equipment. So that is sufficient to use for sleepiness detection. Although breathing and heartbeat rate are good parameter for sleep state, that are not enough for driver's sleepiness detection system because that don't estimate sleep attack (micro-sleep). When human falls into sleep attack, eyes are closed and head loses power. So we add another parameter that is head movement for detecting sleep attack. UWB radar can estimate these parameters at the same time using just one. It is advantage for driver's sleepiness detection system because the system is much cheaper and lighter than other systems. Another advantage of suggested method is non-contacting. And UWB radar can be used all-day-and-night and all-weather. For this study we make similar to driving environment. The result shows the possibility of UWB radar for Detection of driver's sleepiness.

ACKNOWLEDGMENT

This research was supported by the MKE (The Ministry of Knowledge Economy), Korea, under the "IT Consilience Creative Program" support program supervised by the NIPA (National IT Industry Promotion Agency)" (NIPA-2013-H0203-13-1002).

REFERENCES

1. Giusti, A., C. Zocchi, and A. Rovetta, "A noninvasive system for evaluating driver vigilance level examining both physiological and mechanical data," *IEEE Trans. Intelligent Transportation System*, Vol. 10, No. 1, 127–134, March 2009.
2. Ueno, H., M. Kaneda, and M. Tsukino, "Development of drowsiness detection system," *Proceedings of Vehicle Navigation and Information Systems Conference*, 15–20, Yokohama, Japan, August 1994.
3. Lazaro, A., D. Girbau, and R. Villarino, "Analysis of vital signs monitoring using an IR-UWB radar," *Progress In Electromagnetics Research*, Vol. 100, 265–284, 2010.
4. Yarovoy, A. G., L. P. Ligthart, J. Matuzas, and B. Levitas, "UWB radar for human being detection," *Aerospace and Electronic Systems Magazine*, Vol. 21, No. 3, 10–14, 2006.

Depth-image Coding Using Neural Networks for 3D Video Transmission

Yih-Chuan Lin and Pu-Jian Hsu
Department of Computer Science and Information Engineering
National Formosa University, Yunlin 63201, Taiwan

Abstract— With the advances of multimedia technology, a variety of 3D video applications have been growingly penetrated in our daily live. Owning to its high transmission bit-rate, delivering the 3D video sequences across wired or wireless networks is a challenging task for 3D video communication. As for the data-rate reduction of transmitting the 3D videos, the texture and the associated depth information are encoded separately, in which H.264/AVC standard is used for encoding the texture part of 3D video, and a special designed coder is applied to the encoding of depth-image sequence. In this paper, a neural-network depth image compression scheme is proposed to take the advantage of higher correlation between the texture and depth information for increasing the compression ratio. Considering machine learning approach in depth images, video compression [1–4], and 3D shape applications [5–7], a new neural network approach is studied to effectively compress the depth-image sequence in 3D videos.

The incoming 3D video, which includes one video-texture sequence and the associated depth-image sequence, is separated into a series of group-of-picture (GOP), each consisting of one I-frame and several P-frames. Based on the structure, NNs are employed to identify the foreground objects in the depth image associated to the I-frame of each GOP, and to model the depth values over the foreground object, respectively. Beside the bitstream of H.264/AVC for the video texture information, all of the weight values of NNs for depth information of each GOP are transmitted to the receiver for rending stereoscopic-views of 3D video.

With preliminary experiments on five 3D test videos, called "Interview", "Cg", "Orbi", "Puppy", and "Soccer", the proposed 3D video transmission approach is found to be promising in terms of rate-distortion performance when comparing to the H.264/AVC codec. Figure 1 depicts the rate-distortion performance of the preliminary experiments. In the figure, x-axis represents the PSNR (dB), y-axis is the total bits of coded depth-image, the blue lines denote the rate distortion curve of H.264, and red lines indicate the performance of our proposed method.

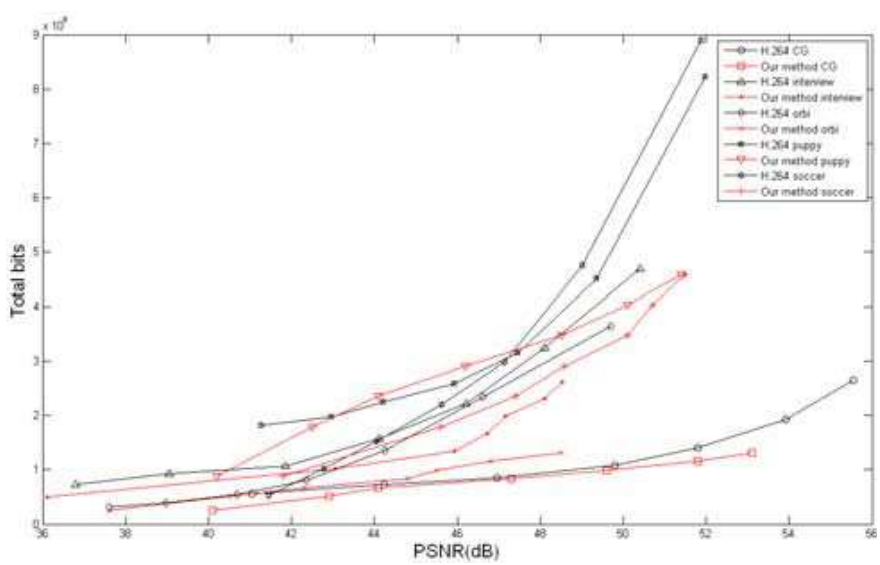

Figure 1: Rate-distortion performance of the proposed approach and comparison with H.264/AVC.

REFERENCES

1. Harman, P., J. Flack, S. Fox, and M. Dowley, "Rapid 2D to 3D conversion," *Proceedings of SPIE*, 78, 2002.

2. Zhang, Y. and M. M. Zhang, "Application of artificial neural network in video compression coding," *2008 IEEE ICIII*, 207–210, 2008.
3. Anna Durai, S. and E. Anna Saro, "Image compression with back-propagation neural network using cumulative distribution function," *IJES*, Vol. 3, 185–189, 2007.
4. Varekamp, C. and B. Barenbrug, "Improved depth propagation for 2D to 3D video conversion using key-frames," *Proc. of 4th IET Conf. on Visual Media Production*, 1–7, 2007.
5. Grossberg, S., L. Kuhlmann, and E. Mingolla, "A neural model of 3D shape-from-texture: Multiple-scale filtering, boundary grouping, and surface filling-in," *Vision Research*, Vol. 47, No. 5, 634–672, 2007.
6. Fanany, M. I. and I. Kumazawa, "A neural network for recovering 3D shape from erroneous and few depth maps of shaded images," *Pattern Recognition Letters*, Vol. 25, No. 4, 377–389, 2004.
7. Malika, A. S., H. Nisarb, and T. Choib, "A Fuzzy-Neural approach for estimation of depth map using focus," *Applied Soft Computing*, Vol. 11, No. 2, 1837–1850, 2011.

Research on Possibilities of Abnormal Tissues Diagnostic by THz Reflection Spectra

A. A. Ezerskaya, **E. A. Strepitov**, **I. V. Prozheev**, **and O. A. Smolyanskaya**
St.-Petersburg National Research University Information Technologies, Mechanic & Optic, Russia

Abstract— It was investigated THz reflection spectra of human tissues (skin with various pathologies, vessels with atherosclerotic plaques). It was ascertained of characteristic absorption lines. Was shown the possibility of non-invasive diagnosis of in-vivo.

One of the most interesting applications of THz radiation is a medicine [1], and in particular the direction of the optical methods of diagnostics of diseases in dermatology, in particular monitoring the healing of dermatitis, without disturbing the integrity of the dressing.

Note that this line of 1.87 THz reflection characteristic of the skin, but its amplitude will vary depending on the type and stage of dermatitis. The result is also influenced by the reflection from the structure of vessels and capillaries (especially hematoma), whose dimensions are comparable with the wavelength of the THz radiation. The distance between the capillaries in an average of about 700 microns (250–1500 microns), the size of blood vessels ranging from 25 mm (diameter of the aorta) to 8 microns (diameter of capillaries) at the wavelength of the radiation used 150–3000 microns.

Special interest is non-invasive monitoring of the healing of dermatitis, without destroying the dressing. It was investigated the healing of thermal burns of the skin of the 2nd degree, covered with plaster bactericidal.

The skin is not unhealed thermal burn has expressed a reflection of high frequencies in the range of 1.6–2 THz, very clearly points out such a line of reflection as 1.67, 1.74, 1.87, 1.89 THz. The

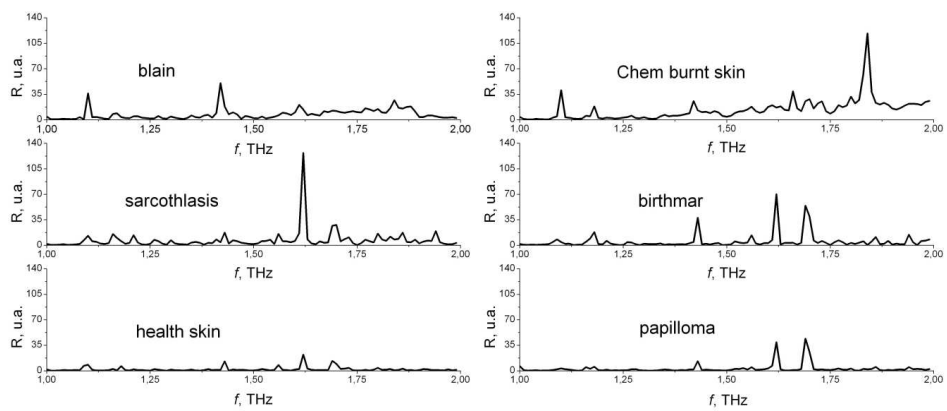

Figure 1: The reflection spectra of THz pulse from different parts of the skin.

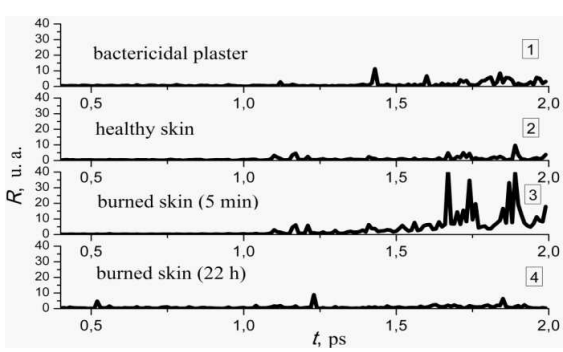

Figure 2: The spectra of the reflected terahertz radiation from a bactericidal plaster (1), the healthy skin area (2), thermal burns of human skin (5 minutes after the burn) (3), thermal burns of the skin (22 hours after burn) (4).

lines of reflection at these frequencies are present in the spectrum of healthy skin, but less evident. Modulus of the spectral components of healthy skin is 4–5 times less than for the skin to unhealed thermal burn. The plot with the healing thermal burn has singularities in the reflection spectrum of THz radiation at a frequency band of 0.52 and 1.23 THz, which are absent in samples of healthy skin and skin with fresh thermal burns.

Healthy skin, thermal burns, healed and unhealed, have a clear spectral differences in the terahertz range. This allows real-time monitoring of the process of healing of dermatitis, in this case, thermal burn, without removing the dressing.

Therefore, using the technique of terahertz diagnostics can monitor the healing process dermatitis, burns, and in particular, in-vivo.

REFERENCES

1. Tuchin, V. V., *Handbook of Photonics for Biomedical Science*, editor, Taylor & Francis Group, LLC, 809, 2010.

Characterization of Dissipation Due to Quasiparticles and Dielectric Loss in a Josephson Metamaterial

J. Hassel[1], **P. Lähteenmäki**[2], **A. Timofeev**[1], **G. S. Paraoanu**[2], **and P. J. Hakonen**[2]

[1]VTT Technical Research Centre, Finland
[2]O. V. Lounasmaa Laboratory, Aalto University, Finland

Abstract— The dynamical Casimir effect is a process by which the vacuum fluctuations of a field are transformed into real particles (typically photons) by the action of an external modulation. This modulation changes a parameter entering the Euler-Lagrange equations of the system. If this change is realized over a length much smaller than the wavelength of the field, the process can be assimilated to a change in a boundary condition [1]. If the change is realized over a length of the same order as the wavelength, the process can be regarded as a modulation of the index of refraction [2]. In both cases, photons are generated at two frequencies that sum up to the pump (modulation) frequency.

In this talk I will present our experiments [2] on the dynamical Casimir effect, observed by the modulation of the kinetic inductance per unit length of an array of SQUIDs. To measure the outgoing radiation, we couple the array into a transmission line, by using a low-dissipation (no-dielectric) capacitor realized with FIB (focused ion beam). This forms a cavity with quality factor $Q = 50$–100 and a resonant frequency tunable by magnetic field. We pump the device at 10.8 GHz and measure the photons created by the dynamical Casimir effect at a frequency around 5.4 GHz.

We give a treatment of correlations and entanglement in our system that includes dissipation. Standard criteria of non-separability are then used to show that the photons generated by this process in a non-classical state, as expected from general theoretical considerations. By examining the covariance matrix extracted from the experimental data, we prove that the photons created by the dynamical Casimir effect are in an entangled state. Additionally, we provide a direct experimental demonstration of squeezing below the vacuum level.

REFERENCES

1. Wilson, C. M., G. Johansson, A. Pourkabirian, M. Simoen, J. R. Johansson, T. Duty, F. Nori, and P. Delsing, "Observation of the dynamical Casimir effect in a superconducting circuit," *Nature*, Vol. 479, 376–379, 2011.
2. Lähteenmäki, P., G. S. Paraoanu, J. Hassel, and P. J. Hakonen, "Dynamical casimir effect in a josephson metamaterial," *Proc. Natl. Acad. Sci.*, Vol. 110, No. 11, 4234–4238, USA, 2013.

Ultrafast Rotational Dynamics of Illuminated Particles and Stimulated Emission

A. Asenjo-Garcia, **A. Manjavacas**, **and F. J. García de Abajo**
IQFR, CSIC, Serrano 119, Madrid 28006, Spain

Abstract— We study the electromagnetic torque and scattering properties of a rotating particle in vacuum subject to external illumination. A complex interplay between the light frequency and the particle rotation frequency is observed. Under resonance conditions, the particle produces inelastic scattering at frequencies separated from the incoming light frequency by twice the rotation frequency, depending on the polarization of the external light. Inelastic scattering dominates over the elastic component over wide ranges of light and rotation frequencies. The predicted frequency shifts and resonant torque are shown to be observable under feasible experimental conditions. If the particle is illuminated with circularly polarized light, it will be accelerated and the acceleration time can be calculated. Performing a calculation of the equilibrium temperature between the particle and the environment, we observe that the particle achieves very high rotational frequencies in very short times without being heated, thus supporting the viability of experiments exploring inelastic light scattering and centrifugal explosion of spinning particles under extreme rotation conditions. Furthermore, within certain limits, it is possible to achieve a negative extinction cross-section, which implies that there is stimulated emission, which allow us to speculate with the idea of making a laser consisting on rotating particles.

A Dual-band Antenna with a Choke-circuit on the Ground Plane

The-Nan Chang[1] and Jyun-Ming Lin[2]

[1]Tatung University, Taipei, Taiwan
[2]Simula Technology Inc., Tayuan, Taiwan

Abstract— Dual-band printed antenna has extensively been investigated in the literature. The bandwidth of each band is better wide enough to comply with various applications. Though there are many methods to enhance the bandwidth of a single-band antenna, methods to increase both bandwidths of the lower and higher band of a dual-band antenna are seldom addressed.

The bandwidth of a single-band PIFA antenna could be maximized by varying the length of the ground plane [1]. It does not notice the possibililty of applying the length-adjusting method to increase both bandwidths of a dual-band antenna. In this symposium, we extend the length-adjusting method to enhance both bandwidths of a dual-band PIFA antenna by adding a choke circuit in the ground plane. The dual-band PIFA is obtained by introducing a meandered slot on a planar plate to create two frequency bands. The physical length of the printed circuit board is determined by the central frequency of the lower-band part of the dual-band antenna. Then, a properly located choke circuit is added with an aim to equivalently reducing the length of the printed circuit board when the antenna is operated in the higher-band part of the antenna. One feature of the choke circuit is that it can block the current flow at a desired frequency. This property is employed here to block current flow toward the end of the printed circuit board at the higher-band part of the dual-band antenna. Since the bandwidth of a PIFA antenna depends largely on the length of the printed circuit board, the bandwidth enhancement for both bands can be realized.

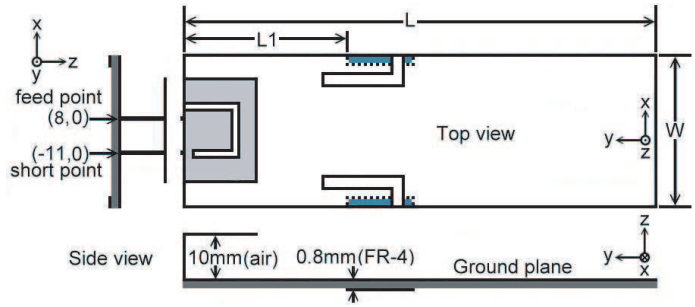

REFERENCES

1. Wu, T.-Y. and K. L. Wong, *Microwave and Optical Technology Letters*, Vol. 32, No. 4, 249–251, Feb. 2002.

RFID Tag on PCB in UHF Band

Won-Kyu Choi[1], **Seung-Hwan Jeong**[1], **Chan-Won Park**[1], **and Hae-Won Son**[2]

[1]Electronics and Telecommunications Research Institute (ETRI), Republic of Korea
[2]Chonbuk National University, Republic of Korea

Abstract— This paper presents a tiny RFID tag which can be directly mounted on a PCB in electronic products as a solution to tracking PCBs within the electronics industry. The designed RFID tag consists of the tag chip, two capacitors and the 3-turn rectangular loop antenna. The RFID tag with the loop antenna utilizes a ground plane of a PCB as an additional radiator by an inductive coupling. So the tag do not necessarily require direct connection to a PCB ground plane and can simply be mounted on a ground plane of a PCB using normal adhesive or sticky tape. The designed tiny RFID tag is made up of a thin dielectric substrate, FR-4, which a part of the 3-turn rectangular loop is patterned on the top side of and the ground plane of the tag on the bottom side of. The structure of the 3-turn loop antenna is completely realized by the metallic patterns etched on the top side of the dielectric body and formed inside the body and 6 via-holes. The RFID tag chip and two capacitors are assembled on the top side of the dielectric body. The tag is $10 \times 1.8 \times 1$ mm in size and the fractional bandwidth for a reflection coefficient of less than -3 dB is about 4.2% at 920 MHz. The reading distance of the tag ranges from 0.3 to 0.7 m depending on a size of a PCB ground plane. Two capacitors of 3.6 and 3.9 pF are used in series for matching between the 3-turn loop antenna and tag chip.

Deep Defect Detection Using Eddy Current Testing with AMR Sensor

D. F. He and M. Shiwa
National Institute for Material Science, Sengen 1-2-1, Tsukuba 305-0047, Japan

Abstract— Eddy current testing (ECT) is an efficient surface and near surface inspection method. To detect deep defect in conductive materials, like aluminum, copper and steel, high sensitive magnetic field sensors at low frequency are needed. We developed high sensitive anisotropic magneto resistive sensor and used it for ECT. Compared with other sensors, AMR sensor has the advantages of good sensitivity at low frequency, easy operation, big dynamic range, and flat frequency response in a big bandwidth. Due the high magnetic field sensitivity of AMR sensor at low frequency, the ECT system can be used to detect deep defect. The excitation coil was 50 turns with the diameter of about 30 mm. The amplitude of the excitation current was about 20 mA, and the excitation frequency was 32 Hz. The AMR sensor was put at the center of the excitation coil, and the sensing direction of the AMR sensor is not perpendicular but parallel with the plane of the excitation coil. By this arrangement, the background field produced the excitation coil can be compensated. Using this ECT system, we successfully detect the deep crack defect in an aluminum plate with the depth of 15 mm, and the signal-to-noise ratio was good.

Comparative Study on Graphene-based Artificial Magnetic Conductor (AMC)

X.-C. Wang, **W.-Y. Li**, **W.-S. Zhao**, **J. Hu**,
Y.-Y. Xu, **and Q.-S. Huang**
Centre for Opt. & EM Research, Zhejiang Provincial Key Lab for Sensing Technologies
State Key Lab of MOI, Zhejiang University, Hangzhou 310058, China

Abstract— In this work, the graphene is employed to form artificial magnetic conductor (AMC). The main drawback of conventional AMC ground plane is its relatively narrow bandwidth compared to the ultra-wide bandwidth (UWB) antenna. Typically, there are two ways to broaden the bandwidth of the AMC: 1) Modify the AMC structure such as using via holes or adopting multilayer FSS over a grounded substrate; and 2) insert varactor diodes between the AMC units. However, these methods become tough at very high frequencies (for example THz) due to the complex manufacturing process. In our work, it is demonstrated that both the resonance frequency and bandwidth of graphene-based AMC can be tuned by varying the external electric field (changing the chemical potential of graphene). The resonance frequency can be tuned from 1.88 THz to 2.67 THz. The operation bandwidth, which is defined in the frequency range corresponding to the reflection phases between $+90°$ and $-90°$ can reach as wide as 50% while μ_c is changed from 0.4 eV to 1 eV. It is also found that the graphene-based AMC will be more reflective as μ_c increases. Parametric study is also conducted to investigate the impacts of patch period D, patch gap g, substrate thickness t, and substrate permittivity ε_r on the reflection phase of graphene-based AMC. Additionally, the graphene-based AMC with different geometries are examined and compared. The tunability of AMC ground plane is mainly determined by the equivalent capacitance contributed by the structure. It is found that a larger structural capacitance means that the reactance contributed by graphene dominates thus a better tunability can be attained.

Risk Assessment for University Students Occupationally Exposed to Electromagnetic Fields in Turkey

Fulya Callialp Kunter and Yagmur Kirkagac
Department of Electrical & Electronics Engineering
Engineering Faculty, Marmara University, Istanbul 34722, Turkey

Abstract— With the development of wireless communication technology, the evaluation and estimation of the effective amount of electromagnetic field (EMF) distribution in areas connected with human activities has grown in importance, in order to satisfy public and governmental safety regulations. Following these efforts, the environment and personnel protection aspects become a very important task. In this light, for the first time in Turkey, an assessment of exposure to radio frequency (RF) EMF for students of Marmara University located in Anatolian Region, Istanbul have been performed in order to check the fulfillment of safety regulations.

The objective of this survey is to characterize electric and magnetic field exposure of university students in Turkey. In the first step of the survey, spot measurements are recorded to determine the locations in the university campus, where the electric and magnetic field levels are maximum. Secondly, at given points, electric and magnetic fields are measured and recorded every 10 seconds during daily activities of subjects with a Power Frequency Field Strength Meter. Measurements are taken in a sufficient number of points, in order to construct surface plots of the fields. By analyzing data obtained, cumulative probability distributions of magnetic fields on some specific locations are evaluated. The results indicate that the recorded levels in all the cases are below the limits. The authors consider that the results of EMF measurements presented in this paper are very useful also for people who are exposed to RF in their daily lives.

ACKNOWLEDGMENT

This work is supported by Marmara University Research Foundation Project Code: FEN-D-080212-0029.

Single Layer Meta-material Lens with Graded Refractive Index

M. A. Bitar, Y. Nasser, M. Al-Husseini, and K. Y. Kabalan
ECE Department, American University of Beirut, Beirut 1107 2020, Lebanon

Abstract— Meta-material lenses are of great importance in radiometry process, which allows the measurement of the temperature profiles in magnetic confinement fusion devices [1]. In practice, optical systems are optimized for a single frequency scenario leading to losses in the transverse resolution at other frequencies. Thus, the increase and optimization of the transverse resolution require different focal points for different frequencies.

In the literature, meta-material lenses with frequency dependent focal points have been proposed [2] to replace the conventional optical systems, where the surface of the lens is divided into several zones. Each zone would provide a certain phase-shift for a certain frequency, and hence having a specific focal point for a specific frequency. This was achieved earlier using layered structure. The layered structure consisted of periodic arrangements of capacitive patches and inductive wire grids, separated by a dielectric material, where, in each zone the capacitive patches and inductive wire grids act as band pass filters allowing certain frequencies and providing a specific phase-shift [3]. However, this appeared to be complex to design and manufacture due to the layered structure [2].

In this paper a meta-material lens with frequency dependent focal points using a single dielectric layer is investigated. In the proposed lens design, the surface of the single layer dielectric material is also divided into zones, however the different phase-shift for each frequency is achieved through having a different permittivity in each zone. As shown in Figure 1, different permittivity in each zone is achieved by means of perforations of a specific radius in each zone [4], which is less complex in design and in fabrication. The perforations are distributed according to squared cell elements where each cell element has four perforations [5]. This would allow the lens to have a graded index of refraction, and hence it would be able to simultaneously focus at several objects located at different distances, emitting at different frequencies. The design in this paper is based on a lens with two zones, where each zone is optimized for a specific frequency. Hence the lens would allow two different focal points each for a given frequency.

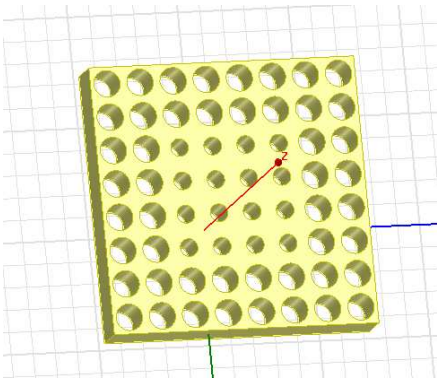

Figure 1: Two zones with perforations of specific radius in each zone.

REFERENCES

1. Hutchinson, I. H., *Principles of Plasma Diagnostics*, Cambridge Univ. Press, 2002.
2. Capecchi, W. J., N. Behdad, and F. A. Volpe, "Numerical optimization of reverse chromatic abberation in planar metamaterial lenses," 2011.
3. Al-Joumayly, M. and N. Behdad, "A generalized method for synthesizing low-profile, band-pass frequency selective surfaces with non resonant constituting elements," *IEEE Trans. Antennas and Prop.*, Vol. 58, No. 12, 4033–4041, Dec. 2010.
4. Muldavin, J. B. and G. M. Rebeiz, "Millimeter-wave tapered-slot antennas on synthesized low permittivity substrates," *IEEE Trans. Antennas and Prop.*, Vol. 47, No. 8, Aug. 1999.
5. Zainud-Deen, S. H., S. M. Gaber, and K. H. Awadalla, "Transmitarray using perforated dielectric material for wideband applications," *Progress In Electromagnetics Research M*, Vol. 24, 1–13, 2012.

Problem of Coupled Electromagnetic TE-TE Wave Propagation in Nonlinear Anisotropic Layer

Yury G. Smirnov
Penza State University, Penza 440600, Russia

Abstract— Propagation of two TE coupled electromagnetic waves in a nonlinear plane layer is considered. Nonlinearity in the anisotropic layer is described by Kerr law. It is shown that new nonlinear propagation regime exists for a pair of TE waves. Physical problem is reduced to a nonlinear two-parameter eigenvalue problem for a system of (nonlinear) ordinary differential equations. It is proved that TE and TE waves that form (nonlinear) coupled TE-TE wave can propagate at two different frequencies with different propagation constants, respectively. These frequencies can be chosen independently. Existence of surface coupled TE-TE waves is proved. Intervals of localization of coupled eigenvalues are found.

We study nonlinear interaction between two polarized TE electromagnetic waves propagating in different orthogonal directions. The waves propagate in a nonlinear dielectric anisotropic layer placed between two linear isotropic half-spaces. The nonlinearity in the layer is described by Kerr law. This geometrical structure represents a nonlinear waveguide. It is shown that these two TE waves form new polarization that exists in nonlinear media. This new polarization we call coupled TE-TE wave. On the basis of the results obtained in we prove here that coupled TE-TE wave propagates at its own two frequencies and has its own two propagation constants.

We reduce the problem to the nonlinear twoparameter transmission eigenvalue problem for Maxwell's equations. This approach was proposed in [1].

REFERENCES

1. Smirnov, Y. G. and D. V. Valovik, "Coupled electromagnetic TE-TM wave propagation in a layer with Kerr nonlinearity," *Journal of Mathematical Physics*, Vol. 53, No. 12, 123530-1-24, 2012.

Stability of Nonlinear 2D-tunnel Bifurcations in Systems of Interacting Quantum Molecules in the Metamaterial Matrix

V. D. Krevchik[1], V. I. Volchikhin[1], I. I. Artemov[1], M. B. Semenov[1], R. V. Zaitsev[1], A. V. Razumov[1], A. K. Aringazin[2], K. Yamamoto[3], and T. A. Gubin[1]

[1]Penza State University of Russia, Russia
[2]Eurasian National University, Kazakhstan
[3]International Medical Center, Japan

Abstract— The problem of controllability for 2D-tunnel bifurcations in systems with quantum molecules in a dielectric matrix of a metamaterial in the external electric field at finite temperature has been investigated. Usage of the quantum tunneling with dissipation theory to study the interaction of quantum molecules with contact environment is productive, because, despite of the instanton approach usage, it is possible to obtain the main results in the analytical form with account of the environment influence on the process of tunneling, whereas other commonly used approaches give not such possibility. A theoretical study of the electric field influence on the 2D-quantum tunneling for quantum molecules in the matrix of a metamaterial (with negative effective permittivity) at finite temperature has been fulfilled in the instanton approximation. It is shown that a stable regime of 2D-bifurcations in such matrix can take place in a more narrower range of parameters than in case of usual dielectric matrix. An important problem in this case is to identify the range of experimentally realizable values of the relative dielectric permittivity (including negative values) for the matrix environment, which allow to realize the 2D-bifurcations regime. A range of the control parameters (electric field, temperature, and the relative permittivity of the metamaterial matrix), in which the regime of stable 2D-bifurcations in the system of quantum molecules, as well as in the system "AFM/STM cantilever-quantum dot or quantum molecule" can take place, has been theoretically investigated. The "phase diagram" for the stable 2D-bifurcations regime for tunnel current in the matrix of a metamaterial in dependence on controllable parameters (the inverse temperature, electric field intensity and values of the (negative) relative permittivity for the heat-bath environmental matrix), has been represented. It is shown that in contrast to usual dielectric matrices in case of the metamaterial matrix the region of stable 2D-bifurcation is significantly narrowed, which is probably due to inversion of the sign of the tunneling particles interaction.

Slotted Patch Antenna Loaded with Metamaterial

Surabhi Dwivedi[1], **Vivekanand Mishra**[1], **and Yogesh P. Kosta**[2]

[1]ECED, S.V.N.I.T., Surat, India
[2]Marwadi Education Foundation's Group of Institutions, Rajkot, India

Abstract— Two ways to simulate a patch antenna has been demonstrated. The return loss is obtained for simple and slotted patch and compared with the metamaterial included slotted patch response. The deviation in solution time and the results are the important factors that are considered. Miniaturization of the patch antenna is to the core of our effort and the enhancement of bandwidth is obtained by slotting of the patch. Microstrip antennas are a relatively new generation of antennas and are preferable for many applications over the broad frequency range from 500 MHz to 50 GHz also called "patch antennas" or "printed antennas" or "planar antennas".

Metamaterial Included Slotted Patch Antenna versus Metamaterial Cover over Patch

Surabhi Dwivedi[1], **Vivekanand Mishra**[1], **and Yogesh P. Kosta**[2]

[1]ECED, S.V.N.I.T., Surat, India
[2]Marwadi Education Foundation's Group of Institutions, Rajkot, India

Abstract— A metamaterial is introduced into the cover of a patch antenna and its band structure is analyzed. The metamaterial cover with correct selection of the working frequency increases the patch antenna's directivity. Based on the methodology, optimization of structure is proposed for the application of metamaterials as antenna substrate to primarily enhance directivity by minimizing its refractive index. The experimental results are presented thoroughly and compared with the analytic calculations. This paper aims to review and critically discuss the comparison of a metamaterial included patch and metamaterial cover over the patch. An analytical method is used to predict the features of the simulation results, implying that within a certain frequency range, comparison can be made between these two models. The S-parameters as a performance matrix are obtained from antenna simulations carried on CADFEKO Silverlite version 5.5. Simulations have been carried out for different shapes of microstrip patch antenna in the microwave regime in HFSS 13.0.

Effect of the Simultaneous Impact of Opioid Drug (Tramadol) and Electromagnetic Field (EMF) on Lipid Peroxidation

P. Bodera[1], **W. Stankiewicz**[1], **M. Paluch**[2], **M. Krzyzowska**[3], **and B. Antkowiak**[2]

[1]Department of Microwave Safety, Military Institute of Hygiene and Epidemiology
Kozielska 4, Warsaw 01-163, Poland
[2]Department of Pharmacology and Toxicology, Military Institute of Hygiene and Epidemiology
Kozielska 4, Warsaw 01-163, Poland
[3]Department of Regenerative Medicine, Military Institute of Hygiene and Epidemiology, Poland

Abstract— Regulation of signal transduction in the brain depends on the transportation of lipids, where plasma low density lipoproteins (LDL) and high density lipoproteins (HDL) are involved.

HDL-like lipoproteins, found in cerebrospinal fluid, play a role in lipid transportation in the central nervous system.

Lipoproteins are susceptible to lipid peroxidation, which is triggered by reactive oxygen species (ROS), produced and found in the brain and peripheral tissue.

The presence of oxidized LDL (ox-LDL) in demyelinating plaques in the brain during the course of multiple sclerosis (MS), and the increase of antibodies against ox-LDL in plasma suggests this disease is associated with oxidative damage of lipoproteins.

An increase in the production of ROS and RNS as a result of the impairment of the antioxidant system may contribute to lipoprotein peroxidation in MS.

The electromagnetic field (EMF), which is widely encountered in the environment, is produced both for technological applications (e.g., power lines, mobile phones), as well as in medicine for diagnostic, e.g., magnetic resonance imaging (MRI), and therapeutic purposes as radiofrequency and microwave ablation and hyperthermia in e.g. aesthetic dermatology. EMF, as one environmental factor, may be involved in a number of metabolic processes which generate oxidants and antioxidants.

Currently, several reports have been published which present deleterious effects of EMF exposure. Special attention is addressed to assessing the potentially harmful effects of EMF on the brain and other important organs for existence.

Our xperiments were performed on healthy rats, and on rats with persistent inflammatory state, induced by Complete Freund's Adjuvant (CFA) injection.

Animals were placed 1 meter from the EMF source, and exposed to the far-field range of an antenna at 1800 MHz with the additional modulation identical to that generated by mobile phone GSM 1800, and the value of effective electric field 20 V/m and effective magnetic field value 0.05 A/m. Rats were given one or five (once a day) 15 minutes exposures or were sham-exposed with no voltage applied to the field generator in control groups. Immediately before EMF exposure (the last one in the case of five exposures), particular groups of rats were intraperitoneally injected with tramadol in the 20 mg/kg dose or vehicle (*aqua pro injectione*) in the 1 ml/kg volume.

Lipid peroxidation (LPO) was estimated by measuring the concentration of the colored complex formed by malondialdehyde (MDA), end product of LPO during reaction with externally added thiobarbituric acid (TBA).

We observed statistically important differences in lipid peroxidation between control group (CON) and both groups CFA/EMF and tramadol (TRAM)/(EMF).

The differences of the lipid peroxidation level in rats' blood were particularly visible after 5 times of EMF radiation, particularly higher in the groups under exposure: control (CON/EMF) and TRAM/EMF, versus control group (CON), without EMF exposure.

The received data may suggest that longer EMF exposure may affect some biological structures, which are responsible for free radical scavenging mechanisms.

Our study may suggest the impact of EMF radiation on the development of brain tumors, because ROS are thought to take part in oncogenesis and cellular differentiation.

Snow Cover Effect on Brightness Temperature of Arctic Ice Fields Based on SSM/I Data

V. V. Tikhonov[1], **D. A. Boyarskii**[1], **I. A. Repina**[1, 2], **M. D. Raev**[1], **E. A. Sharkov**[1], **and T. A. Alexeeva**[3]

[1]Remote Sensing of the Earth Department, Space Research Institute, Russian Academy of Sciences, Russia
[2]A. M. Obukhov Institute of Atmospheric Physics, Russian Academy of Sciences, Russia
[3]Arctic and Antarctic Research Institute, Russia

Abstract— The presence of snow on the surface of ice considerably influences the radiation characteristics of the "water surface — ice cover — snow cover — atmosphere" system. This work discusses the effect of snow cover on brightness temperature of Arctic ice fields.

Wavelets and Morphological Filter (Alternating Sequential Filters) for Robust Multiscale Image Segmentation

Med Ali Hamdi[1] **and Karim Saheb Ettabaa**[2,3]

[1]Laboratoires Des Matériaux, Molécules, Université de Carthage
Institut National des Sciences Appliquées et de Technologies, Tunisia
[2]Laboratoire de Recherche en Informatique Arabisée, et Documentique Intégrée (R.I.AD.I)
Ecole Nationale des Sciences de l'Informatique
Campus Universitaire de Manouba, Manouba, Tunis 3020, Tunisie
[3]Télécom Bretagne, Laboratoire ITI, Technopôle Brest Iroise CS 81828, Brest Cedex 39318, France

Abstract— Image segmentation is a fundamental problem in image analysis. It provides a partitioning of the image, where each region should represent a different object. With this information, it is possible to accomplish quantitative object measurements, such as size, shape and position, with many practical applications (for example, measurement of the size and shape of tumors in medical images). A powerful tool for image processing based on mathematical morphology is the ASF. However, small fluctuations in the image gray values (usually due to noise) produce spurious morphological gradients, which cause oversegmentation. To overcome this problem, many techniques based on watersheds have been proposed, as the *levelings* approach and theedge-preserving statistical noise reduction approach.

In this paper, we propose, a new multiscale segmentation technique based on wavelets and ASF. The first step of this approach describes the considered image in multiple resolutions using an orthogonal wavelet decomposition based on resolution 3^J and gradient magnitudes by applying the Prewitt edge detector. In the second step, to apply the ASF, an adaptive threshold is used to remove small magnitudes. This initial segmentation is projected to higher resolutions using the inverse wavelet transform, until the full resolution segmented image is obtained. The proposed approch relies on region merging to further reduce oversegmentation produced by watersheds which allows the selection of the initial resolution for applying the Wavelet transform, and projects the segmentation result back into the original full resolution, without significant loss of edge definition. The initial resolution was chosen in accordance with the resolution of the image, the size of the desired objects and the amount of noise contamination. Therefore, smaller objects are segmented when finer initial resolutions are selected, while less and larger objects are obtained for coarser resolutions. A region merging process was also suggested to further reduce oversegmentation. Experimental results indicates that the proposed approach performs well for both inherent and artificial noise contamination. In particular, it is robust in the presence of intense noise. The proposed method is completely adaptive: after the selection of the initial resolution 2^J, it does not require any user defined parameter. Future work will concentrate on combining the segmentation result obtained with different starting resolutions, extending the method to color image segmentation, and combining this approach with energy-based segmentation techniques.

Session 2A1
2_FocusSession.SC2: Transformation Optics 1

Transformation Optics Shapes Metamaterials
John B. Pendry, ... 452
Transformation Optics Based Cloaking
Gunther Uhlmann, Allan Greenleaf, Yaroslav Kurylev, Matti Lassas, ... 453
Manipulating Surface Plasmon Waves: Several Design Examples through Transformation Plasmon Optics
Yijun Feng, Zhengzhong Yu, Bo Zhu, Junming Zhao, Tian Jiang, ... 454
Trapping Light by Mimicking Gravitational Lensing
C. Sheng, Hui Liu, Y. Wang, S. N. Zhu, Dentcho A. Genov, ... 455
Phase Preservation in Transformation Optics
Baile Zhang, George Barbastathis, Cheng-Wei Qiu, Yuan Luo, ... 457
Cloaked Sensors via Transformation Optics
Allan Greenleaf, Yaroslav Kurylev, Matti Lassas, Gunther Uhlmann, ... 458
Schrödinger's Hat: A Cloaked Electromagnetic, Acoustic and Quantum Amplifier
Matti Lassas, Allan Greenleaf, Yaroslav Kurylev, Ulf Leonhardt, Gunther Uhlmann, ... 459
Bianisotropic Transformation Media with Additional Polarization and Impedance Control
Jensen Li, Fu Liu, ... 460
Anomalous Propagation, Flux Control and Percolation of EM Waves in Inhomogeneous Zero-index Materials
J. Luo, Yun Lai, ... 461
Broadband Isotropic Cloak Designed by Conformal Mapping
Yungui Ma, ... 462
Visualization of Pulse Propagation and Optical Forces in Graded-index Optical Devices
Alireza Akbarzadeh, Cheng-Wei Qiu, Tomas Tyc, Aaron J. Danner, ... 463

Transformation Optics Shapes Metamaterials

John Pendry
Imperial College London, London SW7 2AZ, UK

Abstract— Metamaterials offer a huge range of new electromagnetic properties: negative refraction, spatial inhomogeneity to name only two. To exploit the possibilities offered in this new world we need a new design tool. Maxwell's equations are exact at the classical level but lack transparency; Snell's law is elegantly visual, an aid to the imagination, but fails to account for many vital aspects of electromagnetism. Transformation optics retains an intuitive appeal, replacing the rays of Snell's law with the field lines of Maxwell whose equations is represents exactly.

Transformation Optics Based Cloaking

Gunther Uhlmann[1,5], **Allan Greenleaf**[2], **Yaroslav Kurylev**[3], **and Matti Lassas**[1]

[1]Department of Mathematics and Statistics, University of Helsinki, 00014, Finland
[2]Department of Mathematics, University of Rochester, Rochester, NY 14627, USA
[3]Department of Mathematical Sciences, University College London, London WC1E 6BT, UK
[4]School of Physics and Astronomy, University of St. Andrews, St Andrews, Scotland KY16 9SS, UK
[5]Department of Mathematics, University of Washington, Seattle, WA 98195, USA

Abstract— In this talk, I will give a general overview of the joint work with A. Greenleaf, Y. Kurylev and Matti Lassas on using transformation optics to achieve invisibility or approximate invisibility. This work started in the case of electrostatics in [1, 2] and the same principle has been applied to achieve invisibility for acoustic waves (Helmholtz equations) and electromagnetic waves (Maxwell's equations). I will also discuss invisibility for matter waves (Schroedinger equation). A survey of some of the results can be found in [3].

REFERENCES

1. Greenleaf, A., M. Lassas, and G. Uhlmann, "Anisotropic conductivities that cannot be detected by EIT," *Physiol. Meas.*, Vol. 24, 413, 2003.
2. Greenleaf, A., M. Lassas, and G. Uhlmann, "On nonuniqueness for Calderon's inverse problem," *Math. Res. Lett.*, Vol. 10, 685, 2003.
3. Greenleaf, A., Y. Kurylev, M. Lassas, and G. Uhlmann, "Cloaking devices, electromagnetic wormholes and transformation optics," *SIAM Review*, Vol. 51, 3–33, 2009.

Manipulating Surface Plasmon Waves: Several Design Examples through Transformation Plasmon Optics

Yijun Feng, **Zhengzhong Yu**, **Bo Zhu**, **Junming Zhao**, **and Tian Jiang**
School of Electronic Science and Engineering
Nanjing University, Nanjing 210093, China

Abstract— Surface plasmon polaritons (SPPs) are surface electromagnetic waves propagating along the dielectric-metal interface, which are well confined along the interface and limited to sub-wavelength scales, therefore could lead to miniaturized optical integrated circuits and devices with scales smaller than the light wavelength [1, 2]. As transformation optics (TO) is based on the form-invariant of Maxwell's equations, it applies to all EM waves including SPPs. Recently, some efforts have been made in successful application of TO to the efficient manipulation of the SPP waves, which give birth to the so-called transformation plasmon optics [3, 4]. With the help of metamaterials, different plasmonic structures have been theoretically proposed to manipulate the SPP waves, such as the invisibility cylinder or carpet cloak, SPP wave propagation on curved surface, or SPP beam shifter. Besides the theoretical studies, experimental explorations have been carried out on constructing and verifying the performance of a plasmonic Luneburg lens and a plasmonic Eaton lens by spatially varying the thickness of a thin dielectric film on the metal [5].

In this presentation, we continue the theoretical studies on designing plasmonic structures and devices for manipulating the SPPs through transformation plasmon optics. We will present several design examples including SPP beam squeezer, bend, omni-directional absorber, as well as SPP couplers across different gaps in a dielectric/metal interface. The couplers for SPP waves across discontinuities or gaps in a dielectric/metal interface have been designed through complementary medium and folded-geometry TO. Detailed design procedures and three-dimensional full-wave simulations will be demonstrated to verify their functionality. Aiming at practical applications, we will also focus on the design of SPP wave bend and omni-directional absorber constructed by conventional dielectric cladding with varying thickness on silver surface, which could facilitate the practical realization.

ACKNOWLEDGMENT

Supported by the National Nature Science Foundation of China (60990322, 60990320, 60801001, 61101011), the Key Grant Project (313029) and the Ph.D. Programs Foundation (20100091110036, 20120091110032) of Ministry of Education of China.

REFERENCES

1. Gramotnev, D. K. and S. I. Bozhevolnyi, "Plasmonics beyond the diffraction limit," *Nat. Photonics*, Vol. 4, 83, 2010.
2. Barnes, W. L., A. Dereux, and T. W. Ebbesen, "Surface plasmon subwavelength optics," *Nature*, Vol. 424, 824, 2003.
3. Huidobro, P. A., M. L. Nesterov, L. Martín-Moreno, and F. J. García-Vidal, "Transformation optics for plasmonics," *Nano Lett.*, Vol. 10, 1985–1990, 2010.
4. Liu, Y., T. Zentgraf, G. Bartal, and X. Zhang, "Transformational plasmon optics," *Nano Lett.*, Vol. 10, 1991–1997, 2010.
5. Zentgraf, T., Y. M. Liu, H. Mikkelsen, J. Valentine, and X. Zhang, "Plasmonic Luneburg and Eaton lenses," *Nat. Nanotech.*, Vol. 6, 151, 2011.

Trapping Light by Mimicking Gravitational Lensing

C. Sheng[1], H. Liu[1], Y. Wang[1], S. N. Zhu[1], and D. A. Genov[2]

[1]National Laboratory of Solid State Microstructures, Department of Physics
Nanjing University, Nanjing 210093, China
[2]College of Engineering and Science, Louisiana Tech University, Ruston, Louisiana 71270, USA

Abstract— We propose a distorted optical waveguide around a microsphere to mimic curved spacetimes caused by the "gravitational fields". Gravitational lensing effects analogues are experimentally demonstrated and this can be used to prospective light harvesting.

One of the most fascinating predictions of the general theory by Einstein is gravitational lensing, the bending of light in close proximity to massive stellar objects, which wrap space and time due to their powerful gravitational pull. Recently, artificial optical materials were proposed to study the various aspects of curved spacetimes such as light trapping and Hawking's radiation [1–5]. However, the development of experimental "toy" models that simulate gravitational lensing in curved spacetimes remains a challenging problem, especially for a visible light. Here, we propose utilizing a distorted optical waveguide around a microsphere to mimic curved spacetimes caused by the "gravitational fields" with high precision. Both far-field gravitational lensing effects and the critical phenomenon in close proximity to the photon sphere of degenerated stars or "black hole" analogues are experimentally demonstrated. Furthermore, the proposed curved waveguide can be used as an omnidirectional absorber with prospective light harvesting and microcavity applications.

A curved waveguide is fabricated in the experiment during the fabrication process, a PMMA resist is mixed with oil-soluble CdSe/ZnS quantum dots and a powder consisting of microspheres 32 μm in diameter is then added to the mixture. The solution is deposited on the silver film through a spin-coating process. In the region near the microsphere, the waveguide thickness gradually increases due to surface tension effects before and during the baking process. The curved waveguide consists of an air/PMMA/silver/SiO_2 multilayer stack and can be considered as step-index planar waveguides. To study the ray propagation in close proximity to the microsphere, a 405 nm light from a CW laser is coupled into the waveguide through a grating. It excites the quantum dots that then reemit at 605 nm. The obtained fluorescence image is then used to analyze the ray trajectory. The incident light is deflected as it passes in the vicinity of the microsphere. The excitation point is gradually moved along the grating and toward the microsphere. The change in the fluorescence pattern, which captures the interaction of the incident beam with the inhomogeneous effective refractive index of the waveguide, is presented in Fig. 3. We observe a gradual increase in the light deflection as the distance to the microsphere decreases. These results are reminiscent to the gravitational lensing as well as the existence of a photon sphere in stellar objects such as ultracompact neutron stars and black holes[33]. Hence, our system may provide a useful "toy" model to study the electromagnetic scattering and light capture due to such unique celestial objects.

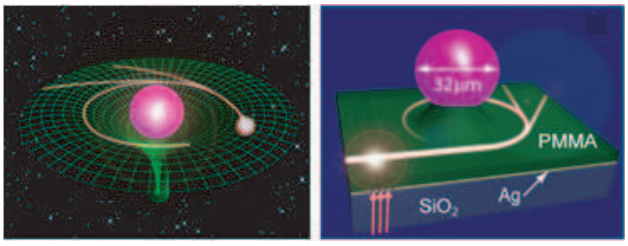

(a) (b)

Figure 1: (a) Depiction of light deflection by the gravitational field of a massive stellar object. (b) The schematic view of the distorted optical waveguide formed around a microsphere and used to emulate the deflection of light by a gravitational field.

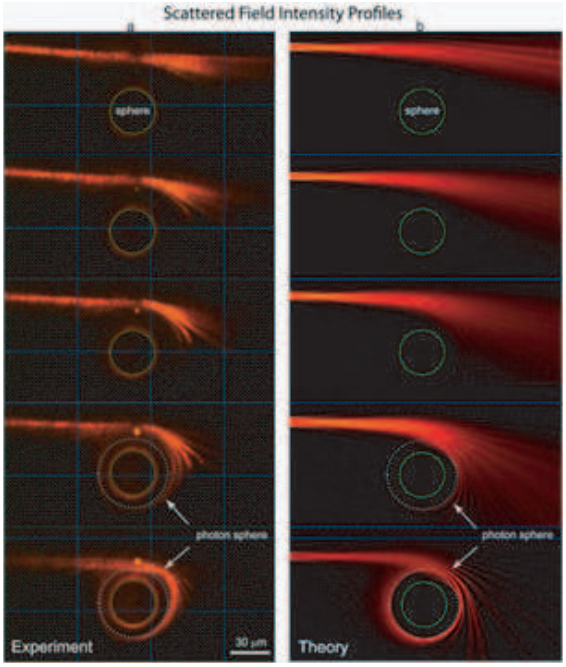

REFERENCES

1. Pendry, J. B., D. Schurig, and D. R. Smith, "Controlling electromagnetic fields," *Science*, Vol. 312, 1780–1782, 2006.
2. Leonhardt, U., "Optical conformal mapping," *Science*, Vol. 312, 1777–1780, 2006.
3. Shalaev, V. M., "Transforming light," *Science*, Vol. 322, 384–386, 2008.
4. Smolyaninov, I. I., V. N. Smolyaninova, A. V. Kildishev, and V. M. Shalaev, "Anisotropic metamaterials emulated by tapered waveguides: Application to optical cloaking," *Phys. Rev. Lett.,* Vol. 102, 213901, 2009.
5. Genov, D. A., S. Zhang, and X. Zhang, "Mimicking celestial mechanics in metamaterials," *Nature Phys.*, Vol. 5, 687–692, 2009.

Phase Preservation in Transformation Optics

Baile Zhang[1], **George Barbastathis**[2,3], **Chengwei Qiu**[4], **and Yuan Luo**[5]

[1]School of Physical and Mathematical Sciences, Nanyang Technological University, Singapore
[2]Singapore-MIT Alliance for Research and Technology Centre, Singapore
[3]Department of Mechanical Engineering, Massachusetts Institute of Technology, United States
[4]Department of Electrical and Computer Engineering, National University of Singapore, Singapore
[5]Center for Optoelectronic Biomedicine, National Taiwan University, Taiwan

Abstract— The outstanding wave manipulation capability of transformation optics comes from its unique property in recovering both ray trajectory and optical path length. However, very few experiments have been done so far to verify this dual-recovery property from viewpoints of both ray trajectory and optical path length simultaneously. The experimental diculties arise from the fact that most previous optical transformation optics devices only work at the nano-scale; the lack of inter- comparison between data from both optical path length and ray trajectory measurement in these experiments obscured the fact that the ray path was subject to a subwavelength lateral shift that was otherwise not easily perceivable and, instead, was pointed out theoretically [1]. Here, we use a simple macroscopic transformation optics device of phase-preserved optical elevator, which is a typical birefringent optical phenomenon that can virtually lift an optical image by a macroscopic distance, to demonstrate decisively the unique optical path length preservation property of transformation optics. The recovery of ray trajectory is first determined with no lateral shift in the reflected ray. The phase preservation is then verified with incoherent white-light interferometry without ambiguity and phase unwrapping.

REFERENCES

1. Zhang, B., et al., *Phys. Rev. Lett.*, Vol. 104, 233903, 2010.

Cloaked Sensors via Transformation Optics

Allan Greenleaf[1], **Yaroslav Kurylev**[2], **Matti Lassas**[3], **and Gunther Uhlmann**[4]

[1]University of Rochester, Rochester, NY 14627, USA
[2]University College London, London WC1E 6BT, UK
[3]University of Helsinki, Helsinki FIN-00014, Finland
[4]University of Washington, Seattle, WA 98195, USA

Abstract— It has been widely stated in the literature that transformation optics based cloaking, besides rendering the cloaked region invisible to detection by scattering of incident waves, also shields the region from those same waves. We show that this is not the case, demonstrating a coupling between the cloaked and uncloaked regions. Careful choice of parameters allow this coupling to be strengthened, leading to effective cloaks with decreased shielding. The sensor modes we describe are close to but distinct from interior resonances, which destroy cloaking, particularly in the near field. These resonances can be exploited via the insertion of a layer within the cloaked region whose surface impedance induces an appropriate Robin boundary condition. There are three regimes: (1) At a fixed frequency ω and an approximate cloak parameter ρ, both cloaking and shielding are effective for generic values of the impedance. (2) At and very near a resonant value $\alpha_{res}(\rho)$ of the impedance, both shielding and cloaking are severely degraded. (3) At a distinct but nearby sensing value of the impedance, $\alpha_{sen}(\rho)$, with $|\alpha_{sen}(\rho) - \alpha_{res}(\rho)| \sim c\rho$, a balance is formed between the penetration of the incident wave and the outflow from the resonance, so that approximate cloaking is still highly effective but the wave inside the cloaked region contains zeroth mode information about the incident wave. As one application, we describe how to use transformation optics to hide sensors in the cloaked region and yet enable the sensors to efficiently measure waves incident on the exterior of the cloak, an effect similar to the plasmon based approach of Alu and Engheta [1].

REFERENCES

1. Alu, A. and N. Engheta, *Phys. Rev. Lett.*, Vol. 102, 233901, 2009.

Schrödinger's Hat: A Cloaked Electromagnetic, Acoustic and Quantum Amplifier

Matti Lassas[1], **Allan Greenleaf**[2], **Yaroslav Kurylev**[3], **Ulf Leonhardt**[4], **and Gunther Uhlmann**[1,5]

[1]Department of Mathematics and Statistics, University of Helsinki, 00014, Finland
[2]Department of Mathematics, University of Rochester, Rochester, NY 14627, USA
[3]Department of Mathematical Sciences, University College London, London WC1E 6BT, UK
[4]School of Physics and Astronomy, University of St. Andrews, St Andrews, Scotland KY16 9SS, UK
[5]Department of Mathematics, University of Washington, Seattle, WA 98195, USA

Abstract— Transformation optics and metamaterials have made possible designs and devices producing effects on wave propagation not seen in nature, including invisibility cloaks for electrostatics [1, 2], electromagnetism (EM) [3–5], acoustics and quantum mechanics (QM). Here we describe a class of invisible reservoirs and amplifiers for waves, which we refer to as *Schrödinger hats*. The unifying mathematical principle on which these are based admits such devices for any time harmonic waves modeled by either the Helmholtz or Schrödinger equation, e.g., polarized waves in electromagnetism, acoustical waves and matter waves in quantum mechanics. Schrödinger hats occupy one part of a parameter-space continuum of wave-manipulating structures which also contains standard transformation optics based cloaks, resonant cloaks and cloaked sensors.

At nonzero frequencies, ideal (i.e., perfect) cloaking produces a decoupling between the parts of the wave in the cloaked region and its exterior, and one has both cloaking (the undetectability of the object within the cloak) and shielding (the inability of the wave to penetrate into the cloaked region) [6]. In more realistic approximate cloaking, there is generically only a weak coupling between the regions; however, if the frequency (for acoustic or EM cloaks) or energy (for QM cloaks) is an eigenvalue for the interior region, then there exist resonant (or trapped) states which simultaneously destroy both cloaking and shielding [7]. Near such a resonance, it is possible to design the cloak parameters so that the flow of the wave from the exterior into the cloak and vice versa are precisely balanced. This restores and even improves cloaking, while allowing a moderate penetration of the cloaked region by the incident wave, leading to the possibility of transformation optics-based cloaked sensors. A different approach previously led to sensors in plasmonic cloaking [8]. We show here that it is possible to go beyond the limited coupling allowed by cloaked sensors and give designs, based on an overarching mathematical principle, for devices which we call *Schrödinger hats*, acting as invisible reservoirs and amplifiers for waves and particles. Schrödinger hats (SH) exist for any wave phenomenon modeled by either the Helmholtz or Schrödinger equation. Some of the presented results have been published in [9].

REFERENCES

1. Greenleaf, A., M. Lassas, and G. Uhlmann, "Anisotropic conductivities that cannot be detected by EIT," *Physiol. Meas.*, Vol. 24, 413, 2003.
2. Greenleaf, A., M. Lassas, and G. Uhlmann, "On nonuniqueness for Calderon's inverse problem," *Math. Res. Lett.*, Vol. 10, 685, 2003.
3. Leonhardt, U., "Optical conformal mapping," *Science*, Vol. 312, 1777, 2006.
4. Pendry, J., D. Schurig, and D. Smith, "Controlling electromagnetic fields," *Science*, Vol. 312, 1780, 2006.
5. Schurig, D., et al., "Metamaterial electromagnetic cloak at microwave frequencies," *Science*, Vol. 314, 977, 2006.
6. Greenleaf, A., Y. Kurylev, M. Lassas, and G. Uhlmann, "Full-wave invisibility of active devices at all frequencies," *Comm. Math. Phys.*, Vol. 275, 749, 2007.
7. Greenleaf, A., Y. Kurylev, M. Lassas, and G. Uhlmann, "Approximate quantum cloaking and almost-trapped states," *Phys. Rev. Lett.*, Vol. 101, 220404, 2008.
8. Alù, A. and N. Engheta, "Cloaking a sensor," *Phys. Rev. Lett.*, Vol. 102, 233901, 2009.
9. Greenleaf, A., Y. Kurylev, M. Lassas, U. Leonhardt, and G. Uhlmann, "Schrodinger's hat: Electromagnetic, acoustic and quantum amplifiers via transformation optics," *PNAS*, Vol. 109, No. 26, 10169–10174, 2012.

Bianisotropic Transformation Media with Additional Polarization and Impedance Control

Jensen Li[1] and Fu Liu[2]

[1]School of Physics and Astronomy, University of Birmingham, Birmingham B15 2TT, UK
[2]Department of Physics and Materials Science, City University of Hong Kong, Kowloon, Hong Kong, China

Abstract— The conventional approach of transformation optics is mainly enabled by metamaterials with varying indices and anisotropies in both the dielectric permittivity and magnetic permeability tensors. Being inspired by the parallel development for homogeneous metamaterials that the artificial atoms with lower symmetries or with magneto-electric coupling can provide exotic optical properties such as huge optical activity, electromagnetic-induced transparency and asymmetric transmission, etc., the ability of transformation optics is far from being fully utilized by only covering a limited palette of optical responses. Some of the recent theoretical approaches are already going into this direction [1–6]. Here, we further investigate two dimensional transformation optical devices enabled by generally bianisotropic metamaterials. In particular, we explore the additional degrees of freedom in controlling polarization and impedance, comparing to the conventional approach. We will discuss illustrative examples in designing transformation optical devices with the generally bianisotropic metamaterials. For example, we can design a device to achieve complete cross-polarization conversion. We can also obtain additional impedance control when a transformation optical device is matched to an object.

REFERENCES

1. Cheng, X., H. Chen, B.-I. Wu, and J. A. Kong, "Cloak for bianisotropic and moving media," *Progress In Electromagnetics Research*, Vol. 89, 199–212, 2009.
2. Thompson, R. T., S. A. Cummer, and J. Frauendiener, *J. Opt.*, Vol. 13, 024008, 2011.
3. Horsely, S. A. R., *New J. Phys.*, Vol. 13, 053053, 2011.
4. Popa, B.-I. and S. A. Cummer, *Phys. Rev. A*, Vol. 84, 063837, 2011.
5. Castaldi, G., S. Savoia, V. Galdi, A. Alù, and N. Engheta, arxiv:1210.7629.
6. Zhang, Y.-L., L.-N. Shi, X.-Z. Dong, Z.-S. Zhao, and X.-M. Duan, arxiv:1301.6954.

Anomalous Propagation, Flux Control and Percolation of EM Waves in Inhomogeneous Zero-index Materials

J. Luo and Y. Lai
Wave Functional Materials Lab, School of Physical Science and Technology
Soochow University, Suzhou, China

Abstract— Zero-index materials possess many unique transmission properties [1–6], such as tunneling waveguide, wave front engineering, etc. In this work, we present two peculiar transmission phenomena of zero-index materials that are unseen in any other systems before.

Firstly, in *inhomogeneous* zero-index materials with one principle component of the permittivity tensor near zero and the impedance matched in that propagation direction, we observe a unique anomalous propagation behavior of electromagnetic waves, which makes the transmission rate extraordinarily high, even for random systems [7]. Moreover, unprecedented arbitrary control of energy flux can be easily achieved in such systems, which implies potential important applications such as sub-wavelength energy focusing, 1D cloaking, and free routing of waves [7].

Secondly, in random media embedded in a background of 3D homogeneous zero-index materials with both permittivity and permeability near zero, a unique phenomenon of electromagnetic wave percolation is observed [8]. Similar to usual percolation of fluids through porous materials, there exists a percolation threshold at which the transmission is suddenly changed. However, the condition of the electromagnetic wave percolation threshold is distinctly different from the usual percolation threshold due to the nature of EM waves.

Both of the above peculiar transmission behaviors of zero-index materials are understood by theoretical analyses, and verified by numerical simulations with finite element method.

REFERENCES

1. Silveirinha, M. and N. Engheta, *Phys. Rev. Lett.*, Vol. 97, 157403, 2006.
2. Edwards, B., A. Alù, M. E. Young, M. Silveirinha, and N. Engheta, *Phys. Rev. Lett.*, Vol. 100, 033903, 2008.
3. Liu, R., Q. Cheng, T. Hand, J. J. Mock, T. J. Cui, S. A. Cummer, and D. R. Smith, *Phys. Rev. Lett.*, Vol. 100, 023903, 2008.
4. Huang, X., Y. Lai, Z. H. Hang, H. Zheng, and C. T. Chan, *Nat. Mater.*, Vol. 10, 582, 2011.
5. Hao, J., W. Yan, and M. Qiu, *Appl. Phys. Lett.*, Vol. 96, 101109, 2010.
6. Nguyen, V. C., L. Chen, and K. Halterman, *Phys. Rev. Lett.*, Vol. 105, 233908, 2010.
7. Luo, J., et al., to be published.
8. Luo, J., et al., to be published.

Broadband Isotropic Cloak Designed by Conformal Mapping

Yungui Ma
Center for Optical and Electromagnetic Research, State Key Lab of Modern Optical Instrumentation
Zhejiang University, Hangzhou 310058, China

Abstract— Since Pendry's first cloaking theory and their successive experiment [1, 2], electromagnetic cloak has experienced important advancement both in frequency bands from microwave to optics [3, 4] and in geometries evolving from two to three dimensions [5, 6] excited by the modification of the original theory using quasi-conformal mapping [7]. However, as we know now this technique involves with unequal coordinate-axis compression/extension in transformation and only produces weak anisotropic cloaking media [8]. One of the negative outcomes is that it inherently makes device actually detectable parallel the lateral direction and the other problem is in implementation, which is very hard to configure a device hiding large objects under the isotropic material approximation. In this talk we will present our new results on pure conformal mapping to design a complete isotropic invisible cloak and demonstrated such a device. Near-field measurement shows our device has very good cloaking performance and broad frequency response. This pure dielectric approach could be technically extent to higher frequencies and other potential device applications.

REFERENCES

1. Pendry, J., D. Schurig, and D. R. Smith, "Controlling electromagnetic fields," *Science*, Vol. 312, 1780–1782, 2006.
2. Schurig, D., J. J. Mock, B. J. Justice, S. A. Cummer, J. B. Pendry, A. F. Starr, and D. R. Smith, "Metamaterial electromagnetic cloak at microwave frequencies," *Science*, Vol. 324, 977–980, 2006.
3. Liu, R., C. Ji, J. J. Mock, J. Y. Chin, T. J. Cui, and D. R. Smith, "Broadband ground-plane cloak," *Science*, Vol. 323, 366–369, 2009.
4. Valentine, J., J. S. Li, T. Zentgraf, G. Bartal, and X. Zhang, "An optical cloak made of dielectrics," *Nat. Mater.*, Vol. 8, 568–571, 2009.
5. Ma, H. F. and T. J. Cui, "Three-dimensional broadband ground-plane cloak made of metamaterials," *Nat. Comm.*, Vol. 1, 124, 2011, DOI: 10.1038/ncomms1126.
6. Xu, S., X. Cheng, S. Xi, R. Zhang, H. O. Moser, Z. Shen, Y. Xu, Z. Huang, X. Zhang, F. Yu, B. Zhang, and H. Chen, "Experimental demonstration of a free-space cylindrical cloak without superluminal propagation," *Phys. Rev. Lett.*, Vol. 109, 223903, 2012.
7. Li, J. S. and J. B. Pendry, "Hiding under the carpet: A new strategy for cloaking," *Phys. Rev. Lett.*, Vol. 101, 203901, 2008.
8. Zhang, B. and B.-I. Wu, "Electromagnetic detection of a perfect invisibility cloak," *Phys. Rev. Lett.*, Vol. 103, 243901, 2009.

Visualization of Pulse Propagation and Optical Forces in Graded-index Optical Devices

Alireza Akbarzadeh, **Cheng-Wei Qiu**, **Tomáš Tyc**, **and Aaron J. Danner**
Department of Electrical and Computer Engineering
National University of Singapore, Singapore 117576, Singapore

Abstract— Light-matter interaction has been of great significance over the past century and huge efforts have been put forth to understand the physics of optical force and photon momentum within media. The Abraham-Minkowski dilemma is the most famous topic of concern in this field which has created controversy among both theoretical and experimental researchers. Besides rich literature of the controversial Abraham-Minkowski dilemma, researchers have also explored light-matter interaction in practical applications. Optical tweezers, particle trapping by light, tractor beams and optical lift are bold examples of recent research into exciting applications. In most of the designs and analyses related to radiation pressure and optical torque, however, it is common to solve the electrodynamic problem from a full-wave perspective and then use this as a starting point to determine the interaction between light and media. Solving a full-wave scattering problem for complex media can be computationally intensive. We know that geometrical optics as a strong tool can be used in many different situations to study the behavior of light to a very good approximation, provided the problem under consideration meets the necessary criteria of the geometrical optics domain. In this presentation, we are going to show a general method to calculate the distribution of the bulk and surface force density within a medium on the basis of the ray-tracing technique and also the limitations of such a method. We will also examine deep connections between geometrical optics (ray tracing) and wave optics through the geometry of optical cavities by presenting several illustrative wave and ray-based animations.

ACKNOWLEDGMENT

This work is supported by the Singapore National Research Foundation (NRF) under CRP Award No. NRF-CRP 4-2008-06.

Session 2A2
3_FocusSession.SC3: Recent Progress in Photonic Crystals 1

Materials, Morphologies and Fabrication Approaches for Photonic Applications
Cefe Lopez, ... 466

Observation and Use of Internal Water in Silica Photonic Structures
Alvaro Blanco, ... 467

Opto-mechanical Interaction in Flexible Photonic Crystals
Marko Loncar, ... 469

Optical Trapping and Back-actions Effects in Hollow Photonic Crystal Cavities
Nicolas Descharmes, Ulagalandha Perumal Dharanipathy, Zhaolu Diao, Mario Tonin, Romuald Houdre, ... 470

Towards PhoXonic Crystals: Optomechanics in Corrugated Beams
D. Navarro-Urrios, J. Gomis-Bresco, M. Oudich, F. Alzina, Alejandro Martinez, A. Griol, D. Puerto, Y. Pennec, S. El-Jallal, Bahram Djafari-Rouhani, C. M. Sotomayor-Torres, ... 471

Mode-symmetry Requirement for Creating Photonic Dirac Cones in the Brillouin-zone Center
Kazuaki Sakoda, ... 472

Photonic Crystals-based Functional Devices for Silicon Photonics
Lech Wosinski, ... 473

InP-based Photonic Crystal Waveguide Technology: Material Properties and Applications
Srinivasan Anand, ... 474

Purely Nonlinear Photonic Crystals in Quadratic Media
Katia Gallo, ... 475

Photonic Crystal L3 Cavities in Lithium Niobate Self-suspended Membranes
Severine Diziain, Reinhard Geiss, Matthias Zilk, Frank Schrempel, Ernst-Bernhard Kley, Andreas Tünnermann, Thomas Pertsch, ... 477

Combining Ag Nanostructure Plamonics with SiO_2 Nanosphere Opal Photonic Crystal for Biosensing
Yue-Heng Li, Ti Yi Kao, Pei-Chang Tsai, Jian-Hung Lin, Chia Chen Hsu, Hung-Chih Kan, ... 478

Materials, Morphologies and Fabrication Approaches for Photonic Applications

Cefe López
Instituto de Ciencia de Materiales de Madrid (CSIC)
3, Sor Juana Inés de la Cruz, Madrid 28049, Spain

Abstract— Advanced photonic materials are essentially based on structures sculpted to feature sizes comparable to or shorter than the wavelength of light. Even single-material structures may present interesting features like light diffraction and photonic band-gaps; diffusion and localization etc. [1].

When more components come into play the properties expand and offer new possibilities. This is the case, for example, when passive dielectrics are mixed with chromophoric compounds or metals are coupled with dielectrics [2]. Beside the choice of materials the interplay between order and disorder occupies a central position in designing functions [3].

I will examine how in this context self-assembly and templating lend themselves very useful to create structures to serve as thermal switches, humidity sensors, ordinary or random lasers, etc..

In particular the synthesis of opals -and often the infiltration of guest materials inside them- involves water. This is present in relatively large amounts and imparts interesting properties whose nanoscale study links optics with mechanical properties. Materials aspects presented by opals at micrometer scale can serve to understand wet granular materials [4].

Lasers created upon these photonic structures can be based on single [5] or FRET-coupled DNA-supported dyes. This strategy improves the performance of single dyes and expands their potential through tuneable coupling.

Addressing selected modes [6] among the immense number composing the spectrum of a random laser constitutes the ultimate challenge in trying to control the seemingly uncontrollable properties of photonic structures built by self-assembly. In certain cases this can be done with engineered pumping enabling remarkable new levels of control over their emission properties such as mode locking [7], mode extension [8] etc..

REFERENCES

1. Galisteo-López, J. F., et al., "Self-assembled photonic structures," *Advanced Materials*, Vol. 23, 30–69, 2011.
2. López-García, M., et al., "Enhancement and directionality of spontaneous emission in hybrid self-assembled photonicplasmonic crystals," *Small*, Vol. 6, 1757–61, 2010.
3. García, P. D., R. Sapienza, and C. López, "Photonic glasses: A step beyond white paint," *Advanced Materials*, Vol. 22, 12–19, 2010.
4. Gallego-Gómez, F., V. Morales-Flórez, A. Blanco, N. De la Rosa-Fox, and C. López, "Water-dependent micromechanical and rheological properties of silica colloidal crystals studied by nanoindentation," *Nano Letters*, Vol. 12, 4920–4, 2012.
5. Gottardo, S., et al., "Resonance-driven random lasing," *Nature Photonics*, Vol. 2, 429–432, 2008.
6. Leonetti, M. and C. López, "Active subnanometer spectral control of a random laser," *Applied Physics Letters*, Vol. 102, 071105, 2013.
7. Leonetti, M., C. Conti, and C. López, "The mode-locking transition of random lasers," *Nature Photonics*, Vol. 5, 615–617, 2011.
8. Leonetti, M., C. Conti, and C. López, "Tunable degree of localization in random lasers with controlled interaction," *Applied Physics Letters*, Vol. 101, 051104, 2012.

Observation and Use of Internal Water in Silica Photonic Structures

A. Blanco
Instituto de Ciencia de Ciencia de Materiales de Madrid ICMM-CSIC
C/Sor Juana Inés de la Cruz 3, Madrid 28049, Spain

Abstract— Recently, it has been shown that silica artificial opals possess a PBG controlable by simple heating on a hot plate [1]. Submicrometer silica spheres easily form high-quality face-centered-cubic (fcc) structures displaying a Bragg peak (the lowest energy PBG) in the visible range. Given the hydrophilic character of silica, these opals inherently contain a substantial amount of molecular water (as much as 8 wt.% in as-grown samples) physisorbed on the silanol groups at the spheres surface. This water is partially placed between the spheres forming necks, leading to a nonclose-packed arrangement, so that the opal lattice parameter directly depends on the amount of water. Thus, controlled desorption of this water upon moderate opal heating induced large effects in the opal photonic properties, mostly due to shrinking of the lattice parameter in up to ~ 12 nm. Complete water removal (achieved at $\sim 120°$C) leads to a pronounced blueshift of the Bragg peak of 25 nm. PBG changes are reversible upon cooling down to room temperature (RT) by virtue of spontaneous water re-adsorption. By *in situ* measuring PBG behavior with temperature one can extract relevant fundamental knowledge regarding water morphology and adsorption in silica colloidal systems [2, 3]. Further, this internal water plays an important role in Azo-Molecules photo-alignment [4] or in the mechanical properties of these systems [5]. Furthermore, we have recently succeeded in observing this water by standard electronic microscopy as shown in Figure 1 [6].

Once the presence of water is characterized we are able to use it for different means. The amount of adsorbed water and its distribution can be controlled by modifying the chemistry of the silica surface, from hydrophilic to hydrophobic through thermal annealing. By doing this we can acquire deep knowledge on silica chemistry and use it to tune the structure photonic response. Further, although thermal effects regarding the whole structure (sample size around some square centimeters) are usually rather slow (seconds) we can bring this response to the millisecond range by inducing local heating [7]. The opal was photoirradiated with a focused 488-nm Ar^+-laser while measuring the opal reflectance spectrum in order to monitor *in situ* the PBG changes. Photoirradiation significantly affected the spectrum of the infiltrated opal in a reversible fashion (Figure 2(a)). Under light exposure the Bragg peak shifted to shorter wavelengths (up to 13 nm) within a few milliseconds and rapidly shifted back to the original position after turning the light off. Simultaneously, the bandgap width decreased (up to 5%) during irradiation, also reversibly. Thus, the photoinduced PBG changes were fast and, without external stimulus, fully reversible, and the shift distance directly depended on the irradiation intensity I. Additionally, the overall performance was reproducible over millions of cycles. All these issues are greatly relevant for switching applications demanding not only spontaneous reverse effect but also accurate response and fidelity in a fast fashion.

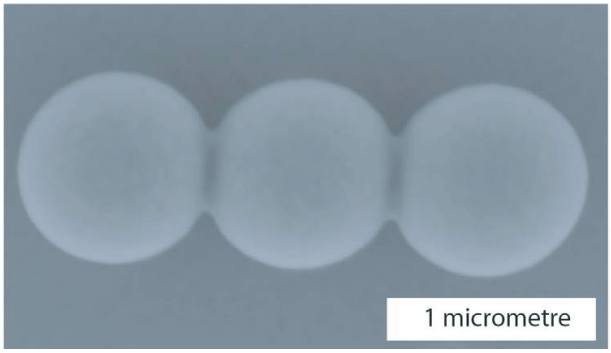

Figure 1: Field emission electron microscope image of water bridges connecting three silica spheres.

REFERENCES

1. Gallego-Gómez, F., A. Blanco, V. Canalejas-Tejero, and C. López, *Small*, Vol. 7, 1838, 2011.
2. Gallego-Gómez, F., A. Blanco, and C. López, *Langmuir*, Vol. 37, 13992, 2012.

3. Gallego-Gómez, F., A. Blanco, and C. López, *J. of Phys. Chem. C*, Vol. 116, 18222, 2012.
4. Gallego-Gómez, F., A. Blanco, D. Gomayo, and C. López, *Adv. Funct. Mater.*, Vol. 21, 4109, 2011.
5. Gallego-Gómez, F., V. Morales-Flórez, A. Blanco, N. De la Rosa-Fox, and C. López, *Nano Letters*, Vol. 12, 4920, 2012.
6. Blanco, A., F. Gallego-Gómez, and C. López, *J. Phys. Chem. Lett.*, Vol. 4, 1136, 2013.
7. Gallego-Gómez, F., A. Blanco, and C. López, *Adv. Mater.*, Vol. 24, 6204, 2012.

Opto-mechanical Interaction in Flexible Photonic Crystals

Marko Lončar
School of Engineering and Applied Science, Harvard University, Cambridge, MA 02138, USA

Abstract— Much of the work in the field of integrated nanophotonics has been done in silicon-on-insulator (SOI) platform, motivated by a need for efficient on-chip optical interconnects. At the same time, owing to mature fabrication techniques, SOI is an ideal playground for the development of novel photonic devices and exploration of interesting physical phenomena. In my talk I will discuss interaction between optical and mechanical degrees of freedom of free-standing photonic crystal nanobeam cavities, and realization of dynamically tunable/programmable optical filters based on this phenomena. I will also introduce an optomechanical system based on silicon photonic-crystal membrane suspended above a SOI substrate that gives rise to strong repulsive optical forces. The interplay between the optomechanical and photo-thermal-mechanical dynamics will be discussed, and cooling and amplification of the mechanical motion demonstrated. Finally, I will present our work on integrated on-chip optical networks, based on silicon-on-sapphire (SOS) platform, operating at mid-infrared wavelength range (wavelength of 4.5 microns).

Optical Trapping and Back-actions Effects in Hollow Photonic Crystal Cavities

Nicolas Descharmes, Ulagalandha Perumal Dharanipathy,
Zhaolu Diao, Mario Tonin, and Romuald Houdré
Institut de Physique de la Matière Condensée, École Polytechnique Fédérale de Lausanne (EPFL)
Station 3, CH-1015 Lausanne, Switzerland

Abstract— Since the first demonstration of optical trapping in the 1980s, progresses in nanofabrication have enabled the emergence of a variety of on-chip trapping techniques aimed at lower trapping powers, smaller system footprints, and manipulation of nanometer-sized particles. The ability to confine large electromagnetic fields in volumes beyond the diffraction limit is at the core of all these advances. Subwavelength confinement gives rise to large field gradients capable of generating unprecedented optomechanical forces on small dielectric particles. Appropriately designed photonic crystal defects, which we refer to as hollow cavities in analogy to the hollow core fibre terminology, can feature optical modes with a large fraction of the field being located in air. Such a highly localized and resonant field can be exploited to realize optical traps exhibiting specific features linked to their resonant nature.

In this talk, we will report on the experimental demonstration of optomechanical coupling between a resonant optical field and a nanoparticle through trapping forces. Resonant optical trapping, when achieved in a hollow photonic crystal cavity is accompanied by cavity back-action effects that result from two mechanisms, which are characterized and discussed. Firstly the effect of the particle on the resonant field is measured as a shift in the cavity eigenfrequency. Secondly, the effect of the resonant field on the particle is shown as a wavelength-dependent trapping strength. The existence of two distinct trapping regimes, intrinsically particle specific, is also revealed. Long optical trapping ($> 10\,\mathrm{min}$) of $500\,\mathrm{nm}$ dielectric particles is achieved with very low intracavity powers ($< 120\,\mu\mathrm{W}$).

Towards PhoXonic Crystals: Optomechanics in Corrugated Beams

D. Navarro-Urrios[1], **J. Gomis-Bresco**[1], **M. Oudich**[3], **F. Alzina**[1], **A. Martínez**[2], **A. Griol**[2], **D. Puerto**[2], **Y. Pennec**[3], **S. El-Jallal**[3], **B. Djafari Rouhani**[3], **and C. M. Sotomayor-Torres**[1, 4, 5]

[1]Catalan Institute of Nanotechnology, Campus UAB, Edifici ICN2, Bellaterra 08193, Spain
[2]Nanophotonics Technology Center, Universitat Politècnica de València
Building 8F, 2nd Floor Camino de Vera, s/n, Valencia 46022, Spain
[3]Institut d'Electronique, Microélectronique et Nanotechnologie, UMR CNRS 8520, Université Lille 1
59655 Villeneuve d'Ascq, France
[4]Department of Physics, Universitat Autònoma de Barcelona, Bellaterra (Barcelona) 08193, Spain
[5]Catalan Institution for Research and Advanced Studies (ICREA), Barcelona 08010, Spain

Abstract— Optomechanical (OM) crystals are quasiperiodic structures in which it is possible to achieve simultaneous control of light and sound enhancing optomechanical interactions. These interaction can be engineered on a chip-scale platform [1] which makes them attractive for science and possible information processing and transduction. Here we report on the optical, mechanical and optomechanical properties of a Silicon based 1D corrugated beam with dual phononicand photonic band gaps [2], excited by means of a microlooped tapered optical fiber.

As we show in Figure 1(a), the unit-cell contains a hole in the middle and two symmetric stubs on the sides. Figure 1(b) shows a scanning electron microscope micrograph of one of the OM crystals. The defect region consists of 12 central cells in which the pitch (a), the radius of the hole (r) and the stubs length (d) aredecreased in a quadratic way towards the center. total number of cells is 32 and the whole device length is about 15 µm. The particular resonator design localises simultaneously high quality factor photonic and phononic modes, presenting photo-elastic and moving-boundary coupling rates of about 1 MHz.

Once in resonance with one of those modes, the thermally activated mechanical motion causes the transmitted field to be phase modulated around its steady-state value, which is directly measured in the RF spectrum. Q_{opt} of up to 35000 were measured. Evidence of the whispering gallery modes within the microlooped tapered fibre has been fond. The OM devices present strong transduced resonances in different spectral regions. A maximum $Q_{mec} = 4700$ has been measured in the highest energy regionat 7.25 GHz.

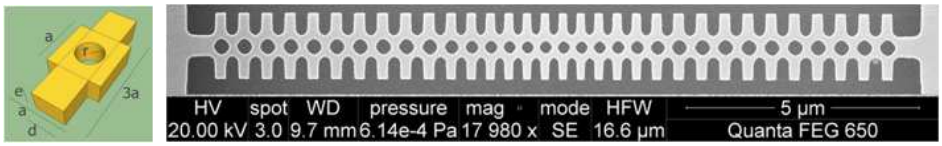

(a) (b)

Figure 1: (a) Representation of the unit cell. (b) A SEM micrograph of a device.

REFERENCES

1. Eichenfield, M., J. Chan, R. Camacho, K. J. Vahala, and O. Painter, *Nature*, Vol. 462, 78–82, 2009.
2. Pennec, Y., B. Djafari Rouhani, C. Li, J. M. Escalante, A. Martinez, S. Benchabane, V. Laude, and N. Papanikolaou, *AIP Advances*, Vol. 1, 041901, 2011.

Mode-symmetry Requirement for Creating Photonic Dirac Cones in the Brillouin-zone Center

Kazuaki Sakoda[1,2]

[1]National Institute for Materials Science, 1-1 Namiki, Tsukuba 305-0044, Japan
[2]University of Tsukuba, 1-1-1 Tennodai, Tsukuba 305-8571, Japan

Abstract— The linear dispersion relation in the Brillouin-zone center of periodic optical structures, which is often called (photonic) Dirac cone, has been attracting considerable interest [1], since it realizes interesting phenomena like scatter-free waveguides and lenses of arbitrary shapes. Huang et al. [2] clarified that isotropic Dirac cones can be created by accidental degeneracy of two modes for square and triangular dielectric photonic crystals. On the other hand, we showed for metamaterials characterized by well-defined electromagnetic resonant states that the combination of A_1 and E modes of the square lattice and the combination of A_{1g} and T_{1u} modes of the simple cubic lattice create isotropic Dirac cones, while the combination of E_1 and E_2 modes of the triangular lattice leads to isotropic double Dirac cones [3, 4]. We also extended the $\mathbf{k} \cdot \mathbf{P}$ theory to the vector electromagnetic field and derived a necessary condition by which we could easily select candidates for mode combinations that enabled the creation of the Dirac cone [5]. From the structure of a matrix that determines the first-order correction (linear in k) to eigen frequencies, we can obtain the analytical solution of dispersion curves and judge the presence of the Dirac cone. The results of the analytical calculation agreed with the numerical photonic-band calculation. Two such examples are shown in Fig. 1, where isotropic double Dirac cones with two quadratic dispersion surfaces are found.

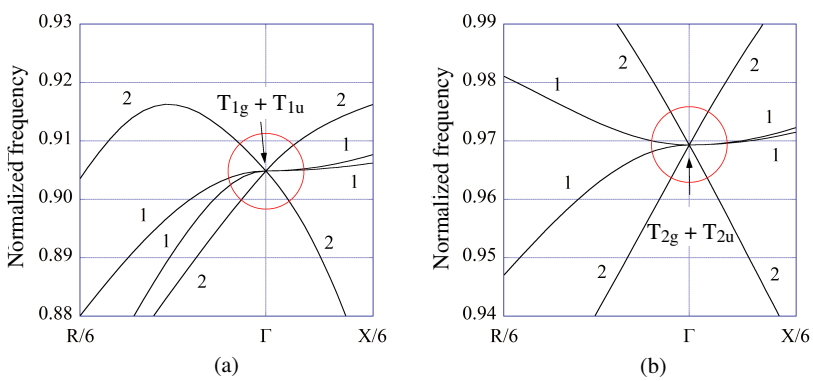

Figure 1: Dispersion curves of photonic crystals composed of the simple-cubic lattice of dielectric spheres with a dielectric constant of 12.6 (GaAs). The vertical axis is the normalized frequency ($\omega a/2\pi c$), and the horizontal axis is the wave vector in the $R(= (\pi/a, \pi/a, \pi/a))$, and $X(= (\pi/a, 0, 0))$ directions, where a is the lattice constant, c is the speed of light, and $R/6$, for example, means that the horizontal axis is magnified by six times. The radius of the spheres was tuned to 0.160 a for (a) and 0.210 a for (b) to realize accidental degeneracy. The number associated with each dispersion curve is the multiplicity of the mode. Both cases give isotropic double Dirac cones and two auxiliary quadratic dispersion surfaces.

REFERENCES

1. Chan, C. T., Z. H. Hang, and X. Huang, "Dirac dispersion in two-dimensional photonic crystals," *Adv. Opto. Electronics*, Vol. 2012, 313984, 2012 and references therein.
2. Huang, X., Y. Lai, Z. H. Hang, H. Zheng, and C. T. Chan, "Dirac cones induced by accidental degeneracy in photonic crystals and zero-refractive-index materials," *Nature Mater.*, Vol. 10, No. 8, 582–586, 2011.
3. Sakoda, K., "Dirac cone in two- and three-dimensional metamaterials," *Opt. Express*, Vol. 20, No. 4, 3898–3917, 2012.
4. Sakoda, K., "Double Dirac cones in triangular-lattice metamaterials," *Opt. Express*, Vol. 20, No. 9, 9925–9939, 2012.
5. Sakoda, K., "Proof of the universality of mode symmetries in creating photonic Dirac cones," *Opt. Express*, Vol. 20, No. 22, 25181–25194, 2012.

Photonic Crystals-based Functional Devices for Silicon Photonics

Lech Wosinski[1, 2]

[1]School of Information and Communication Technology, Royal Institute of Technology, Kista 16440, Sweden
[2]Joint Research Center of Photonics of the Royal Institute of Technology (Sweden) and Zhejiang University (JORCEP)
Zhejiang University, Hangzhou 310058, China

Abstract— In this paper we present some specific applications of silicon-based photonic crystals for realization of functional devices for telecom and sensing.

Silicon platform is a technology of choice for microelectronics and recently became also a preferable platform for photonics due to great advantage of CMOS fabrication compatibility allowing for advanced standards for high accuracy fabrication, high yield and possibility for mass production. Silicon is also a preferable material for MEMS applications due to its excellent mechanical properties and well established processing technology. Here we discuss some nanophotonic solutions using photonic crystal-based components including filters, polarization splitters and sensors.

A variety of passive and active devices based on photonic crystals have been demonstrated in recent years. Here we restrict us to passive 1D and 2D structures.

PhC-based waveguides and devices are in active research period. For waveguiding they introduce usually more loss than nanowire-based guiding elements, but PhCs are preferably used, where their peculiar properties, especially unique dispersion relations can be exploit for applications, which are difficult to realize otherwise, such as negative dispersion, slow light or super-high wavelength selectivity. Nano-structured elements can also be sensitive for environmental changes that open new applications of such devices for optical sensing, solar cells and biomedicine. Practical components based on photonic crystals are under development, short behind the nanowire-based photonic integrated circuits.

Small-band filters based on 2D Photonic crystals can be realized with help of a photonic nanowire and a suspended silicon photonic crystal membrane with a missing hole, which acts as a high quality factor cavity, vertically coupled with a nanowire waveguide situated 250 nm below the membrane. From the light that is transmitted through the nanowire, the wavelength that is in resonance with the cavity is reflected back whereas the rest of light is not affected. In an alternative design a PhC and a photonic nanowire are combined using a surface-mode cavity for on-side coupling between silicon nanowire waveguide and photonic crystal surface cavity formed on the interface between the PhC slab and the air gap.

Polarization beam splitter with positive and negative refracted beams is a good example of using negative refraction for practical photonic application. Designing a band structure of the PhC in a proper way it is possible to achieve negative refraction (for a specific frequency range) in an essentially positive index medium.

Pillar array-based optical sensor is a good example of using a 2D photonic crystal of pillar tpe. Compared to hole array based PhCs, pillar arrays have several advantages for sensing applications, although they are more difficult to fabricate, especially, when large aspect ratio is needed. The advantages include the fact that a pillar array has a much larger percentage of void space. Here the cavity with more than 80% of air space was fabricated and tested. The big connected open space inside the cavity makes it much easier for the infiltration of the analytes. We have experimentally realized a pillar array-based 2D photonic crystal microcavity suitable for biosensing. For refractive index change of 0.01, a resonance peak wavelength shift is 3.5 nm.

ACKNOWLEDGMENT

This work was supported by "the Swedish Research Council (VR) through its Linn?us Center of Excellence ADOPT", as well as project VR-621-2010-4379.

InP-based Photonic Crystal Waveguide Technology: Material Properties and Applications

S. Anand
School of Information and Communication Technology, KTH Royal Institute of Technology
Electrum 229, Kista S164 40, Sweden

Abstract— Photonic crystal (PhC) components in InP-based materials are of practical importance not only for their unique properties but also for integration with conventional optoelectronic components on InP or Si substrate. Control over PhC fabrication methods and material properies — electrical, composition, electronic defect states and optical — is central to realize high device performances. Here, specific to InP-based PhCs we address nanofabrication methods, electrical conduction and material modification to tailor carrier lifetimes.

We present the state-of-the-art high aspect ratio etching of InP-PhCs illustrating how to go beyond the fundamental fabrication limits to reduce optical losses to intrinsic levels. Thermally driven mass-transport is shown to be an effective post-fabrication technique to obtain nearly cylindrical holes, with excellent depth and shape uniformity [1]. The efficacy of this procedure is validated by the high yield and reliability of PhC waveguides [2]. By mode-gap engineering in photonic crystal waveguides we demonstrate coarse wavelength filtering, including structural and temperature tuning. Transmission mini-stop bands with $> 35\,\mathrm{dB}$ attenuation, $12\,\mathrm{nm}$ bandwidth and ultra-sharp edges, dropping over $30\,\mathrm{dB}$ in intensity in a $\sim 4\,\mathrm{nm}$ wavelength change are obtained [1–5]. By appropriate design of heterojunction photonic crystal waveguides, both drop and pass filter functions are possible [4, 5]. In contrast to cavity-resonance based filters where the peak transmission is limited by loss of the optical cavity, these filters show high peak transmission intensity [4]. The performance of these waveguides can be tuned by cascading PhC waveguides.

Carrier (lateral) transport in etched PhCs is analysed, highlighting the consequences of surface Fermi-level pinning on conductivity [6] and ways to reduce resistance. Material modifications to obtain ultra-short carrier lifetimes [7, 8] and chemical surface passivation [9] for improving carrier lifetimes are discussed.

REFERENCES

1. Shahid, N., S. Naureen, M.-Y. Li, M. Swillo, and S. Anand, *J. Vac. Sci. Technol. B*, Vol. 29, 031202, 2011.
2. Shahid, N., S. Naureen, and S. Anand, *Phys. Status Solidi C*, Vol. 9, No. 7, 1670, 2012.
3. Shahid, N., N. Speijcken, S. Naureen, M.-Y. Li, M. Swillo, and S. Anand, *Appl. Phys. Lett.*, Vol. 98, 081112, 2011.
4. Shahid, N., M. Amin, S. Naureen, M. Swillo, and S. Anand, *Optics Express*, Vol. 19, 21074, 2011.
5. Shahid, N., M. Amin, S. Naureen, and S. Anand, *AIP Advances*, Vol. 3, 032136, 2013.
6. Berrier, A., M. Mulot, G. Malm, M. Östling, and S. Anand, *J. Appl. Phys.*, Vol. 101, 123101, 2007.
7. Berrier, A., Y. Shi, J. Siegert, S. Marcinkevicius, S. He, and S. Anand, *J. Vac. Sci. Technol. B*, Vol. 27, 1969, 2009.
8. Berrier, A., Y. Shi, J. Siegert, S. Marcinkevicius, S. He, and S. Anand, *Proc. SPIE*, 6989, 2008, doi:10.1117/12.781231.
9. Naureen, S., N. Shahid, R. Sanatinia, and S. Anand, *Adv. Funct. Mater.*, 2012, doi: 10.1002/adfm.20120220.

Purely Nonlinear Photonic Crystals in Quadratic Media

Katia Gallo
Department of Applied Physics, KTH — Royal Institute of Technology
Roslagstullsbacken 21, SE-106 91 Stockholm, Sweden

Abstract— Ferroelectric materials such as $LiNbO_3$ provide the unique possibility to structure the optical nonlinearity by means of electric field poling techniques [1]. This has led to the development of a wide variety of novel devices, ranging from integrated optical chips for advanced signal processing to efficient parametric sources of entangled photon pairs [2, 3].

The extension of poling techniques to two dimensions has enabled a new class of *purely nonlinear* photonic crystals [4, 5], and quasi-crystals [6], in which the optical response is tailored by mechanisms intrinsically associated to the quadratic nonlinearity, as opposed to conventional photonic crystals, based on refractive index structuring. This entails new degrees of freedom in the design and implementation of multi-port optical frequency conversion devices, and gives rise to novel nonlinear effects stemming from the coherent interplay of multiple resonances in the 2D lattice.

Quadratic [$\chi^{(2)}$] photonic crystals were first demonstrated in bulk hexagonally poled $LiNbO_3$ and subsequently implemented in integrated formats [5, 7]. Several experimental and theoretical studies have addressed the novel functionalities affordable in this structures with particular reference to optical frequency upconversion, with demonstrations of multi-beam second and higher harmonic generation [5–7], tunable spatial solitons [8], and multistep cascading [9].

More recent investigations concerning frequency down-conversion in hexagonally poled $LiTaO_3$ crystals have also highlighted the possibility to achieve a coherent locking of distinct three-wave-mixing processes during optical parametric generation via a shared signal or idler [10, 11]. This results in novel parametric schemes whereby the simultaneous excitation of multiple resonances by a single pump gives rise to twin beams sharing the same spectral properties as a consequence of a coherent exchange mediated by the 2D nonlinear lattice.

The talk will briefly introduce the technology and design principles for quadratic photonic crystals in $LiNbO_3$ and $LiTaO_3$ materials and provide a few examples of optical functionalities affordable on this platform, ranging from optically tunable spatial solitons to multi-beam parametric generators, with a particular focus on recent developments concerning frequency down-conversion, and their implications for the engineering of novel parametric light sources for classical and quantum optics applications.

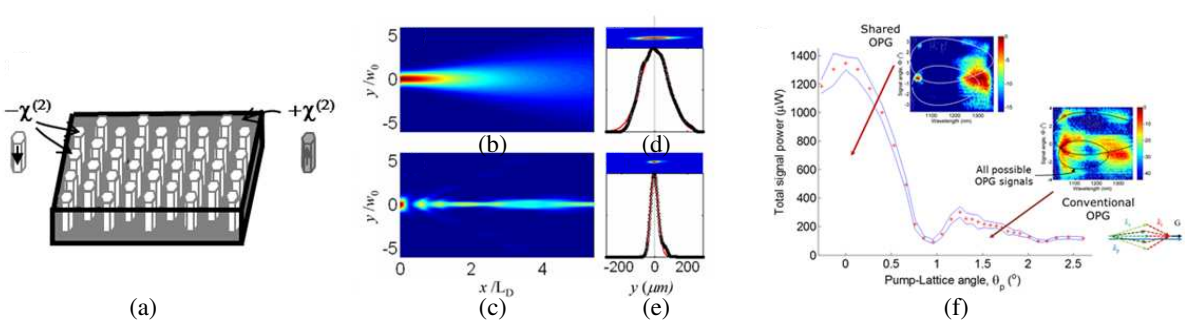

Figure 1: (a) Schematic illustration of a $\chi^{(2)}$ purely nonlinear photonic crystal. (b)–(e) Spatial soliton formation in 2D nonlinear photonic crystals: simulated nonlinear beam propagation in the lattice at: (b) low powers and (c) above the soliton formation threshold; (d)–(e) corresponding experimental results (transverse beam profiles recorded at the output of a photonic crystal waveguide in $LiNbO_3$) for the two cases. (f) Optical parametric generation in hexagonally poled LiTaO3. Signal output power as a function of the pump incidence angle (θ_p), highlighting the efficiency enhancement associated to the onset of twin-beam optical parametric generation (i.e., the coherent locking of two distinct lattice resonances, (here occurring for $\theta_p \sim 0$).

REFERENCES

1. Yamada, M., N. Nada, M. Saitoh, and K. Watanabe, *Appl. Phys. Lett.*, Vol. 62, 435, 1993.

2. Liu, S., K. J. Lee, F. Parmigiani, J. Kakande, K. Gallo, P. Petropoulos, and D. J. Richardson, *Opt. Expr.*, Vol. 19, 11705, 2011.
3. Tanzilli, S., W. Tittel, M. Halder, O. Alibart, P. Baldi, N. Gisin, and H. Zbinden, *Nature*, Vol. 437, 116, 2005.
4. Berger, V., *Phys. Rev. Lett.*, Vol. 81, 4136, 1998.
5. Broderick, N. G. R., G. W. Ross, H. L. Offerhaus, D. J. Richardson, and D. C. Hanna, *Phys. Rev. Lett.*, Vol. 84, 4345, 2000.
6. Bratfalean, R., A. C. Peacock, N. G. R. Broderick, K. Gallo, and R. Lewen, *Opt. Lett.*, Vol. 30, 424, 2005.
7. Gallo, K., C. Codemard, C. B. E. Gawith, J. Nilsson, P. G. R. Smith, N. G. R. Broderick, and D. J. Richardson, *Opt. Lett.*, Vol. 31, 1232, 2006.
8. Gallo, K., A. Pasquazi, S. Stivala, and G. Assanto, *Phys. Rev. Lett.*, Vol. 100, 053901, 2008.
9. Saltiel, S. and Y. Kivshar, *Opt. Lett.*, Vol. 31, 3321, 2006.
10. Gallo, K., M. Levenius, F. Laurell, and V. Pasiskevicius, *Appl. Phys. Lett.*, Vol. 98, 161113, 2011.
11. Levenius, M., V. Pasiskevicius, and K. Gallo, *Appl. Phys. Lett.*, Vol. 101, 121114, 2012.

Photonic Crystal L3 Cavities in Lithium Niobate Self-suspended Membranes

Séverine Diziain, **Reinhard Geiss**, **Matthias Zilk**, **Frank Schrempel**, **Ernst-Bernhard Kley**, **Andreas Tünnermann**, **and Thomas Pertsch**
Institute of Applied Physics, Abbe Center of Photonics, Friedrich-Schiller-Universität Jena
Max-Wien-Platz 1, Jena 07743, Germany

Abstract— Photonic crystal cavities have been proposed to confine the light into small volumes and thus to enhance nonlinear optical phenomena. Most of the work devoted to this topic has been focused on semiconductors, with either third or second order nonlinearities. III-V semiconductors have high quadratic susceptibilities but can suffer from absorption phenomena due to their electronic bandgap which can limit the nonlinear process efficiency in the visible and near-infrared wavelength range.

Lithium niobate, a ferroelectric crystal which is transparent in this wavelength range, is an alternative as host material with quadratic nonlinear properties for photonic crystal based devices. Moreover, this material, characterized by electrooptic, piezoelectric and photoelastic properties allows the realization of active photonic devices. In this work we report on photonic crystal L3 cavities fabricated by ion-beam enhanced etching and focused ion beam milling in a X-cut lithium niobate wafer. The resulting samples, consisting of a photonic crystal cavity drilled in a thin free standing lithium niobate layer benefit from the highest possible light confinement in the vertical direction based on a refractive index contrast mechanism. The light confinement in the plane originates from a photonic band gap effect. The cavities, designed to be multiresonant at telecom wavelengths, exhibit quality factors of several hundred. Their linear optical properties are theoretically and experimentally investigated as a function of their geometries. Second harmonic generation is also demonstrated with a continuous wave incident beam. Since second harmonic intensity scales as the square of the quality factor, an enhancement of the quadratic effect of several 10^4 has been reached in freestanding lithium niobate photonic crystal cavities compared to the bulk material.

Combining Ag Nanostructure Plamonics with SiO_2 Nanosphere Opal Photonic Crystal for Biosensing

Yue-Heng Li, **Ti Yi Kao**, **Pei-Chang Tsai**, **Jian-Hung Lin**, **Chia-Chen Hsu**, **and Hung-Chih Kan**
Department of Physics, National Chung Cheng University
Min Hsiung, Chia-Yi 621, Taiwan, R.O.C.

Abstract— We combine the localized surface plasmonic resonance (LSPR) effect of Ag nanostructures with the photonic bangap property of SiO_2 nanosphere opal photonic crystal to produce surface enhanced fluorescence (SEF) substrate suitable for biosensing applications with ultra-high sensitivity Using the self-assembly approach we decorated the top layer SiO_2 nanosphere in the opal with nanometer size Ag caps as shown in Figures 1(a) and 1(b). Plasmonic properties of the Ag nanocaps strongly interact with that of the opal photonic crystal, leading to dramatic change in its reflection spectrum. As shown in Figure 1(c), the reflection peak that signatures the presence of photonic bandgap is converted into a dip in the reflection spectrum. Transmission spectrum measurement shows a nearly uniform reduction of 50% in the transmission for the Ag-cap decorated opal. This suggests that the dip results from absorption, most likely due to excitation of LSPR on the Ag caps, which is supported by our preliminary results of numerical simulation. More interestingly, the spectral position of the dip follows that of the reflection peak when the incident angle of incident light changes. To test for the biosensing application, we first coated a layer of BSA-bt molecules on the sample and then allowed Cy3-tagged streptavidin bio-molecules to covalently bonded to BSA-bt layer. We excited the fluorophores with a 532 nm laser beam and measured the fluorescent emission intensity from the sample. In comparison with a glass slide, the fluorescent intensity was enhanced by a factor of 70.

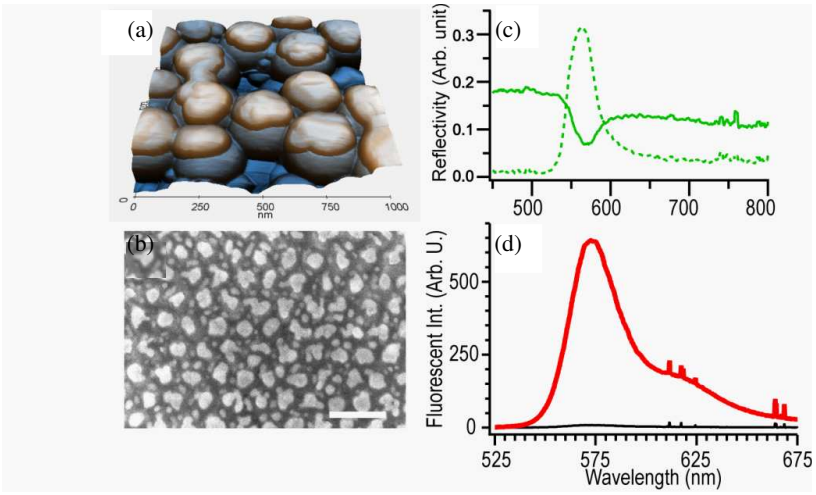

Figure 1: (a) AFM image of Ag cap decorated opal. (b) The SEM images of the same sample. The size of the scale bar is 500 nm. (c) The reflection spectrum of a bare opal (dashed curve) and Ag-cap decorated opal (solid) curve measured at normal incidence. (d) Fluorescent spectra of Cy3 molecules coated on Ag-decorated opal (red thick solid curve) and those coated on the glass slide (black thin solid curve).

Session 2A3
0_Focus Session: Education for Electromagnetics

Comparing Electromagnetics Education in China, Hong Kong, and USA
Weng Cho Chew, Lijun Jiang, Wen Xun Zhang, Xin-Qing Sheng, Jin Pan, ... 480
Just in Time: Teaching Electromagnetics in the 21st Century
Rajeev Bansal, ... 481
Electromagnetics Basic Courses: A Student-activating Approach
Jari J. Hanninen, ... 482
Computer-aided Teaching of Electromagnetics: Is It for Real?
Raj Mittra, ... 483
Using Web Quizzes to Assess Concept Understanding and Pacing the Students
Daniel Sjoberg, ... 484
Impact of Counselling Programs on the Academic Results at Telecommunication Engineering Degree
M. Edita De Lorenzo Rodriguez, Artemio Mojón, Generosa F. Manín, Cristina L. Bravo, Inigo Cuinas, 485
Challenges in Electromagnetics Education Design as a Part of Curriculum Reform Process
Kirsti Keltikangas, Keijo Nikoskinen, ... 486
Understanding Matching Circuits; Plastic Made Quasioptical Multilayer Matching Unit Design at X-band
Tugrul Aydogmus, İnan Kopcal, Gizem Kahya, Yalçin Albayrak, Selcuk Helhel, Sukru Ozen, ... 487
Virtual Laboratory for Microwave Devices
D. S. Gubsky, I. V. Mamay, Viacheslav V. Zemlyakov, ... 488

Comparing Electromagnetics Education in China, Hong Kong, and USA

W. C. Chew[1], **L. J. Jiang**[2], **W. X. Zhang**[3], **X. Q. Sheng**[4], **and J. Pan**[5]

[1]University of Illinois, Urbana, Champaign, USA
[2]University of of Hong Kong, Hong Kong, China
[3]South-East University, Nanjing, China
[4]4Beijing Institute of Technology, Beijing, China
[5]University of Electronic Science and Technology, Chengdu, China

Abstract— We compare electromagnetics (EM) education in three regions of the world: China, Hong Kong, and USA. All three regions have varied history and hence their educational institutions are affected by their historical background.

Education in China is strongly influenced by the Soviet model due to the initial infusion of technology knowledge from Russia during the early years of modern Chinese history. Electromagnetics was under radio physics, and an entire university was devoted to an area such as the University of Electronic Science and Technology in Chengdu, China. Electrical engineering (EE) is divided into heavy current EE or weak current EE. Power engineering is under heavy current while information engineering is under weak current. The electromagnetics curricula are also influenced by such classification. Chinese team teaching is very well organized, with the use of modern technologies such as the Internet, audiovisual equipment and slides, laboratory, and software. Knowledge is often imbibed from overseas. It reflects the rapid technology advancements in China.

The education system in Hong Kong started with the UK tradition. The UK system is more laissez faire than others. Some of these traditions are apparent in Hong Kong universities. There were no course requirements for PhD students, and no weekly home-works for undergraduates, but it is changing. The lack of good technology jobs in Hong Kong has diverted good local students from engineering. Nevertheless, being the gateway to the West, Hong Kong still attracts many outstanding mainland Chinese students who excel in their classes. An old three-year bachelor degree program is now replaced with a four-year curriculum, aligning it with the world's norm. It was hard to fit in undergraduate EM education in the old UK system, but the four-year bachelor offers more flexibility.

EM Education in US has gone on a different path. The Yankee ingenuity and the American penchant for self-criticism, openness, and soul searching has produced some of the best universities in the world: American universities lead in innovation. The curricula in US also change rapidly with time. In the postwar period, EM was very important, and many American text books were written to underscore its importance. It also correlated well with the vast resource the government had invested in research. Many universities require two undergraduate courses in EM. However, as technology evolves, with other emerging technologies, classical EM is not central to electrical engineering. Nano-electronics, photonics, computer science and computer engineering become increasingly important. Hence, it is still hotly debated as to how to teach students a difficult subject, EM, with the modern constraints.

Just in Time: Teaching Electromagnetics in the 21st Century

Rajeev Bansal
University of Connecticut, Storrs, USA

Abstract— Once upon a time, a standard four-year undergraduate curriculum in electrical engineering (EE) in the US required a full year devoted to electromagnetics (EM), with often a semester devoted to static fields and another to electromagnetic waves, transmission lines, radiation, etc.. However, as new engineering topics related to electronic/photonic/digital/computer-technologies have seeped into the modern EE curriculum (which remains stuck at four years), university faculty members (and their industrial advisory boards) have often engaged in spirited debates on which subjects constitute *core* knowledge. As a consequence, current EE curricula are all over the map, ranging from a *required* full-year of EM to an *optional* one-semester course. It is not that people do not realize the important role of EM in their lives (from microwave ovens to cellular wireless networks), there simply are too many important engineering subjects that are deemed just as worthy of inclusion in the modern EE curriculum.

I would like to propose a *restructuring* of the first (often the *only*) course in engineering electromagnetics so that it will excite the imaginations of not only electrical engineers but also other science/engineering students (with standard calculus and physics as prerequisites). The course will not be encyclopedic but will still draw material from both static and dynamic fields. Furthermore, each lecture will start with a question related to everyday life (e.g., are cell phones safe to use?), then proceed with an investigation of the issue, initially non-mathematically (the "short answer") and then lead to a more detailed theoretical exposition (the "long answer"). Students will learn how to *formulate* good engineering problems. Mathematical concepts will be introduced as needed ("just in time") and the treatment will *not* be general but rather as simple as possible in the context of the problem. Additional mathematical material may be covered in homework assignments or small projects. Such an approach to teaching network theory has been tried successfully by Mung Tiang at Princeton University and is presented in his recent book [1].

It may be noted in passing that the current ABET accreditation criteria for electrical engineering programs emphasize that students, in addition to mastering the technical content, become conversant with the *societal* and *ethical* implications of technologies and learn to place the engineering subject matter in the broader *global* context. The restructured EM course also goes some distance in filling that niche in a student's technical education. Another goal is to entice the reader into pursuing the sources for a lecture topic to delve more deeply into the subject ["*life-long learning*"].

REFERENCES

1. Chiang, M., *Networked Life: 20 Questions and Answers*, Cambridge University Press, 2012.

Electromagnetics Basic Courses: A Student-activating Approach

J. J. Hänninen
Department of Radio Science and Engineering, Aalto University School of Electrical Engineering, Finland

Abstract— Many electrical engineering students consider the electromagnetics basic courses difficult and even repelling. A poor motivation level combined with weak mathematical skills makes it difficult for the students to solve complex exercise problems; and even worse, the conceptual understanding of the subject matter may remain thin. To tackle these problems an activation-based approach has been tested on two electromagnetics basic courses in the Aalto University School of Electrical Engineering. The courses are five ECTS credit points each, and they cover the fundamentals of static and dynamic field theory. "Traditional" lectures have not been abandoned altogether, but they have been enlivened with activating verbal questions (direct teacher-student interaction) and with clicker questions probing the conceptual understanding of the subject matter (indirect teacher-student interaction). Assisted sessions for solving exercise problems are provided, too. Participation in the lectures and exercise sessions is voluntary. The course grades are based on homework (60% of total points) and on an exam (40% of total points). Five of the ten homework answers are submitted individually, and the other five are submitted as group work. Belonging to a group of two or three students is a compulsory prerequisite for submitting group work answers; this policy has been strictly enforced with success. Writing a short comment about the learning experience of a problem grants the student one bonus point in the individual problems; in group work the assessment of learning is a required part of the answer — it serves as a certificate of participation of the student. The exam tests both the conceptual understanding of the matter and mathematical problem-solving skills.

The activity-based approach has been positively received by the students. However, the approach is on its first round, so it is not yet possible to assess the effectiveness of the method compared to earlier lectures-exercises-exam approaches. So far the major insight gained by the teachers has been how difficult it is for the students to express their ideas in writing and how total the lack of conceptual understanding may be. Based on the lessons learned, the next course realizations may see differences, for example, in the execution and structure of the lectures and exercise sessions. It may be necessary to encourage or even require a more regular class attendance of the students.

The presentation of the paper will consist of a slide presentation but also of hands-on clicker use by the audience to demonstrate the activation principle.

Computer-aided Teaching of Electromagnetics: Is It for Real?

Raj Mittra
Electromagnetic Communication Lab, The Pennsylvania State University, University Park, PA 16802, USA

Abstract— We all know that the computers, though they are good tools for number-crunching, don't inspire students to do the type of thinking that is needed to learn Electromagnetic Theory and practice. Thus, it is not uncommon to find that knowledgeable people in our field believing that pairing Electromagnetics with computers in the context of teaching EM, and saying those two words in the same breath, is almost an "oxymoron," which we should shy away from as best as we can. And yet, there is no denying of the fact that today's students, who are weaned on Facebook, Twitter and other vehicles for social media, naturally gravitate towards the plethora of readily accessible commercial computer codes to solve their problems. One consequence of this is that the students have the tendency, once they have completed a formal course in EM,to rapidly wipe out from their minds what little theory they might have learnt in an EM class — and rely primarily, and heavily, on the computer instead — to tackle real-world problems involving antennas, propagation and the like that they are asked to solve. We all know, from the student feedback we get, that learning EM theory from the usual textbooks is challenging, and the student can easily get lost in the quagmire of vector algebra, differential and integral equations, Green's functions, and so on — the necessary evils that they have to be willing to contend with and digest, in order to survive in an EM course. It is also a fact that only a select few brave souls emerge from their undergraduate experience in EM courses to take up the challenge to go on to postgraduate school and to specialize in Electromagnetics, as the dwindling population of students in M.S. and Ph.D. programs in EM clearly seems to indicate.

Unequivocally, the $64K question before us, of course, is: "Can we fix this problem in EM Education that appears to rear its ugly head in almost all developed counties and, if so, how?" One approach that has been used with considerable success is setting up Lab demos that intrigues the students, at least in undergraduate courses, and convinces them that EM need not be dull — it is not just a pile of boring equations — but that itcan indeed be interesting if taught via the use of these demos and experiments,which expose them to the hands-on learningexperience. In this talk, we would propose that the above approach be complemented by what might be labeled as "computer-aided EM teaching," where the students are encouraged, by using computers, to learn their EM theory,to interpret them in a way that helps them better understand the physical meaning of those abstruse equations, and to apply them to successfully solve real-world problems. Some examples that illustrate such computer-sided EM instruction will be presented in the paper, and the experience of teaching graduate level students using this approach will be shared with the audience.

Using Web Quizzes to Assess Concept Understanding and Pacing the Students

Daniel Sjöberg
Electrical and Information Technology, Lund University
Box 118, 221 00 Lund, Sweden

Abstract— We have used the free web application moodle (http://moodle.org) to publish short questionnaires after each week of teaching. The students' understanding of the concepts discussed during the week are tested by different types of questions, typically multiple choice, short calculations, matching of alternatives etc. The students' answers are graded by the system, and some automatic feedback can be given. This provides the students with a tool they can use to check their understanding, and also helps keeping them in phase with the intended pace of the course. We have found it most useful to test only the basic concepts; the students' ability to synthesize different concepts is tested with other means like traditional exercises, since this is seldom suited for automatic grading.

The system has been used and evaluated in different types of courses: large compulsory courses (around 100 students, compulsory in year 1 or 2), and in small advanced courses (around 20–40 students, elective in year 4). It is observed that the talented students do not need to spend much more than a few minutes with the tests, whereas the struggling students may spend up to hours with the questions. From our evaluations, we conclude that 1) the students appreciate modern course elements that are well aligned with the rest of the course, 2) the system has encouraged them to spend time with the subject matter, and 3) the teacher has to do relatively little work once the questions have been formulated. The latter point means this system can provide a large group of students with feedback, without necessarily increasing the workload of the teacher.

Impact of Counselling Programs on the Academic Results at Telecommunication Engineering Degree

E. de Lorenzo, A. Mojón, G. F. Manín, C. L. Bravo, and I. Cuiñas
School of Telecommunication Engineering, Universidade de Vigo, Spain

Abstract— Traditionally, academic results of undergraduates at Engineering degrees, in general, and particularly at Telecommunication Engineering degrees seem to be far from the aptitudes and competences of such selected students. And this occurs mainly during the first year at the University degree. This common trend could be observed in statistics from Universities along the World. However, our schools and faculties are receiving, year by year, most of the best secondary school students.

A first analysis would highlight a common behavior of such students: their academic results are better once they have adapted their study skills to that required in the University, and when they feel themselves as residents at the campus. So, different strategies could be applied to help the students to land on the campus and to adapt their habits to the life at the University.

The objective of this contribution is to share our experience in the School of Telecommunication Engineering, at the University of Vigo. Usually, the students arrived first time the School without any help, and they began attending lessons. Some years ago, an incipient tutoring program was implemented, and few results were obtained as the joining was optional and the professors in charge had no materials to understand the student's situation. Recently, a full tutoring program has been implemented, with mandatory registration for students and an organized timetable for the activities.

Statistics of last years support an increment in the students that attend the different tests along the season and the final exams, but also an improvement in the qualifications our students obtain, related to their participation in the tutoring program.

The explanation of our personal and group tutoring plan, the analysis of its effects in terms of students and tutors satisfaction, and the evaluation of the improvement in academic results would be the contents of the contribution and the corresponding full paper in case of being accepted for presentation in PIERS 2013.

ACKNOWLEDGMENT

This work was partially funded by Galician Regional Government under project CN 2012/260 "Consolidation of Research Units: AtlantTIC".

Challenges in Electromagnetics Education Design as a Part of Curriculum Reform Process

Kirsti Keltikangas and Keijo Nikoskinen
School of Electrical Engineering, Aalto University, Finland

Abstract— Aalto University was established in 2010 as a merger of three different universities; Helsinki University of Technology (TKK), Helsinki School of Economics, and University of Arts and Design.Currently, it consists of six Schools; the School of Arts, Design and Architecture, the School of Business, the School of Chemical Technology, the School of Electrical Engineering, the School of Engineering, and the School of Science Already in 2010, it was decided that teaching evaluation process (TEE) was designed for the whole university focusing on the practices and issues of planning, management, implementation, and development of the undergraduate and graduate degree programmes. The TEE process took place in 2010–2011, and its results, suggestions and ideas for the degree programmes are used in the curriculum design at Aalto Schools [1]. Later on, the university management launched a curriculum renewal process at the Schools. As a first result, new Bachelor programmes in engineering fields will be instigated in September 2013.

Accordingly, the curriculum design is also in progress at the Aalto School of Electrical Engineering (ELEC). Aims in the design have been, for instance, fluency and flexibility of the study path. Furthermore, links between different courses and substances have been significant as well. Courses in electromagnetics form the basis of the Degree Programme of Electronics and Electrical Engineering at Aalto ELEC. Together with courses in circuit analysis theory, they give theoretical foundation for the further studies at Aalto ELEC. However, learning electromagnetics is very challenging [2]. Teachers and professors seek new pedagogical methods how to teach the very theoretical substance in a way that students form conceptual understanding, and are able to apply the theoretical knowledge into practical problem-solving tasks. One of the essential methods in teaching electromagnetics is to integrate possible practical solutions and examples to the theoretical substance.

In the curriculum design process at Aalto ELEC, the importance of pedagogical approach and collective planning between different levels (School, departments, and teachers) has been emphasised. Additionally, when the new programmes for Aalto ELEC were designed, the starting point was the substance. Physics and electromagnetic field theory teachers and professors examined the existing courses as a unity, and designed new courses to respond the larger area of knowledge that students learn in their Degree. During the following years of study, feedback and other data will be collected on the adoption of the new, designed courses. Moreover, even more interesting it will be to analyse whether the entire comprehension of the students in this very difficult and theoretical field will increase.

REFERENCES

1. Levander, L. and R. Koivisto Aalto, eds., "Learning together — Towards enhancing the co-creation of education," Project Report, University Teaching and Education Evaluation, 2010–2011, Unigrafia, Helsinki, 2011.
2. Leppävirta, J., H. Kettunen, and A. Sihvola, "Complex problem exercises in developing engineering students' conceptual and procedural knowledge of electromagnetics," *IEEE Transactions on Education*, Vol. 54, No. 1, 63-66, 2010.

Understanding Matching Circuits; Plastic Made Quasioptical Multilayer Matching Unit Design at X-band

Tugrul Aydogmus, Inan Kopcal, Gizem Kahya,Yalcın Albayrak, Selcuk Helhel, and Sukru Ozen
Electrical and Electronics Engineering Department
Akdeniz University, Campus, Antalya 07058, Turkey

Abstract— 800 mm × 500 mm certain number of plastic cards having 1 mm thickness have been used as quasioptical matching unit at X-band frequencies. Varying number of plastics cards were placed varying positions between transmitting and receiving antennas, and complex S_{21} and S_{11} parameters were measured for each position in order to calculate transmission and reflection coefficient of designed setup. Obtained results showed that increased number of plastic cards from 1 to 6 resulted in decreasing transmission as expected, but certain number of plastics (5 plastics) at a certaing frequency (7 GHz–9 GHz) behaves as resonanting circuit. Manually adjusted multilayered plastic slots can be automised as continues microwave adaptation, and proposed setup is quite understandable by students.

Virtual Laboratory for Microwave Devices

D. S. Gubsky, **I. V. Mamay**, **and V. V. Zemlyakov**
Physics Department, Southern Federal University, Russia

Abstract— Computer simulation of the behavior of the measuring equipment and microwave devices is essential for engineer's educational process. It allows creating virtual laboratory workshops which are equal to their "real" analogs. Created virtual labs can describe the behavior of measuring devices, studied microwave devices and their interaction at a sufficient educational level. The creation of virtual labs that can be used for remote and online education is also available.

In this paper the method of computer simulation of microwave devices and special laboratory workshops is described.

Simulated laboratory has a module structure. The basis for constructing a model of the specific workshop is a concept of the abstract "device" with layout is identical to the installation of a real one. The device behavior is described by the terms "signal" and "function". Devices have a set of input and output signals and are capable to establish connection between each other in a certain way. Each device module is a separate software component realized by Visual C++ code. Therefore the general functional package is easily extensible and depends on a set of modules.

As an example the laboratory work which includes sweep frequency generator, VSWR/Attenuation Scope and a narrowband waveguide filter was simulated. The software interface allows changing the frequency tags and filter configuration to carry out all necessary measuring characteristics.

Created virtual laboratory based on independent modules allowing expanding and modifying the set of devices that are investigated in the workshop without affecting the core of the package. A main feature of this implementation is to represent the studied devices in the form of "black boxes", which behavior can be determined not only by a mathematical model, but also by an output of the external simulation tools for example CST Microwave Studio and by measured data of real experiments.

REFERENCES

1. Gupta, T., A. S. M. Prachi, M. J. Akhtar, and K. V. Srivastava, "Development of the virtual lab module for understanding the concepts of electric and magnetic field patterns in rectangular waveguides and cavities," *International Journal of Online Engineering*, Vol. 8, No. 3, 12–21, 2012.
2. Gómez-Tornero, J. L., D. Cañete-Rebenaque, F. D. Quesada-Pereira, and A. Álvarez-Melcón, "Interactive lab to learn radio astronomy, microwave & antenna engineering at the Technical University of Cartagena (Spain)," *International Journal of Online Engineering*, Vol. 7, No. 1, 10–18, 2011.
3. Kara, A., E. Aydin, M. E. Ozbek, and N. Cagiltay, "Design and development of a remote and virtual environment for experimental training in electrical and electronics engineering," *9th International Conference on Information Technology Based Higher Education and Training, ITHET 2010*, 194–200, 2010.

Session 2A4
5_FocusSession.SC5: Microwave Remote Sensing of Snow Cover

Electromagnetic Models in Active and Passive Microwave Remote Sensing of Terrestrial Snow
Leung Tsang, Kung-Hau Ding, Xiaolan Xu, Simon H. Yueh, ... 490

Development of the Snowcover and Its Observable Parameters
Christian Matzler, Marin Schneebeli, ... 491

Passive Microwave Observations of Snow Using AMSR2 Measurements: Progress in Satellite-based Observation Retrievals and Uncertainty Estimation
Richard Kelly, Nastaran Saberi, ... 492

Airborne Microwave Radiometer Measurements of Snow on Lake Ice in Winter 2013
Martti Tapani Hallikainen, Matti Vaaja, Jaakko Seppänen, Anssi Hakkarainen, ... 493

Advancing the Characterisation of Snow Parameters Sharpens Our Understanding of Active and Passive Microwave Signatures — And Vice Versa
Christian Matzler, Mike Schwank, A. Wiesmann, M. Proksch, Martin Schneebeli, Juha Lemmetyinen, J. Pulliainen, K. Rautiainen, Anna Kontu, ... 494

Multilayer Dense Medium Radiative Transfer Combined with NMM3D Boundary Conditions with Application to Terrestrial Snow Scattering at X Band and Ku Band
Shurun Tan, Wenmo Chang, Xiaolan Xu, Leung Tsang, Juha Lemmetyinen, Simon H. Yueh, ... 496

Monitoring of Dynamic Changes in Alpine Snow with Terrestrial Radar Imagery
Andreas Wiesmann, Tazio Strozzi, Rafael Caduff, Jessica Papke, Christian Matzler, ... 497

The Sensitivity of Radar Backscattering to Snow Characteristics
X. Xiong, Marco Brogioni, A. Crepaz, Simonetta Paloscia, Paolo Pampaloni, Emanuele Santi, J. C. Shi, ... 498

Characterization of Snow Cover Areas by Change Detection Applied to COSMO-SkyMed Images
Simone Pettinato, E. Santi, S. Paloscia, Bruno Aiazzi, Andrea Garzelli, ... 499

Electromagnetic Models in Active and Passive Microwave Remote Sensing of Terrestrial Snow

Leung Tsang[1], **Kung Hau Ding**[2], **Xiaolan Xu**[3], **and Simon Yueh**[3]

[1]Department of Electrical Engineering, University of Washington, Seattle, WA 98195, USA
[2]Wright Patterson AirForce Laboratory, OH 45433, USA
[3]Jet Propulsion Laboratory, M/S 300-233, Pasadena, CA 91109, USA

Abstract— We describe the electromagnetic models that have been applied to active and passive microwave remote sensing of terrestrial snow. For snow water equivalent, there are two satellite missions, the CoREH2O (Cold Regions Hydrology High-Resolution Observatory) and the SCLP (Snow Cold Land Process), that are being considered respectively by the European Space Agency and NASA.

In microwave scattering by terrestrial snow, snow is considered a dense medium with densely packed inhomogenieties. We describe the work of dense media radiative transfer (DMRT) theory that incorporate coherent effects of scattering by densely packed particles. Three approaches have been used to obtain the effective permittivity, phase matrix and scattering coefficients of DMRT equations. They are (i) the analytical theory of the quasicrystalline approximation (QCA) and correlated ladder approximation, (ii) the Foldy Lax multiple scattering equations, and (iii) the bicontinuous media model with discrete dipole approximation. Results of frequency, polarization and grain size dependences of dense media scattering are illustrated and compared with experimental data of measurements on terrestrial snow.

Development of the Snowcover and Its Observable Parameters

Christian Mätzler[1] and Marin Schneebeli[2]

[1]Gamma Remote Sensing, Gümligen, Switzerland
[2]WSL Institute for Snow and Avalanche Research, SLF, Davos, Switzerland

Abstract— The snowcover consists of ice particles that are precipitated after formation in the atmosphere. Any landscape changes dramatically between snow-free and snow-covered conditions. Associated with the visible changes are significant impacts on interactions and exchange processes at the surface. The details of these effects strongly depend on the snowcover properties, such as snow height, density, temperature, liquid-water content (if $T = 0°\mathrm{C}$), snow structure (often characterised by a grain size, but including also stratification, surface roughness and other variables), and impurities. Due to the fact that the snow temperature is not far below the melting temperature of ice, the snowpack undergoes continuous modifications that are called snow metamorphism, a term used in geology to describe structural changes. In order to understand the development of the snowcover we need objective methods to measure all relevant parameters. The development of useful and accurate methods has not been an easy task. An overview of methods and their improvements over time will be presented.

Passive Microwave Observations of Snow Using AMSR2 Measurements: Progress in Satellite-based Observation Retrievals and Uncertainty Estimation

Richard Kelly and Nastaran Saberi
Interdisciplinary Centre on Climate Change
Department of Geography and Environmental Management
University of Waterloo, Waterloo, Ontario N2L 3G1, Canada

Abstract— Passive microwave observations of snow from space-based instruments have been available for nearly 35 years to estimate snow accumulation. With our improved understanding of both snowpack physical state evolution processes and the controls on the spatial variability of snow accumulation, retrieval science has improved through the incorporation of new knowledge of snowpack physical characteristics and the microwave properties of snow and non-snow surfaces. An independent snow accumulation product that is primarily based on satellite-derived observations and static ancillary data that was developed for the Advanced Microwave Scanning Radiometer — EOS (AMSR-E) has been extended for the Advanced Microwave Scanning Radiometer — 2 (AMSR2) instrument aboard the Global Change Observation Mission — Water. The product is designed for measuring snow accumulation globally using a parsimonious retrieval approach.

The development of the AMSR2 retrieval approach is described. A surface air temperature estimator is implemented from previous work and is used to estimate bulk snow grain size and a simple time-dependent densification model provides daily bulk snow density. In turn these variables are used along with AMSR2 brightness temperature observations to constrain the inversion of snow water equivalent from a dense media radiative transfer model. Efforts are made to ensure that changes in snow water equivalent (SWE) from one day to the next are conservative, mostly through ensuring that grain size growth and densification follow conservative change trajectories during the below-freezing part of the winter time. Results are compared with *in situ* observations from the 2012–2013 winter in North America and with the Canadian Meteorological Centre's snow analysis system that estimates SWE and snow depth from WMO snow depth observations and a temperature index model.

Airborne Microwave Radiometer Measurements of Snow on Lake Ice in Winter 2013

Martti Hallikainen, **Matti Vaaja**, **Jaakko Seppänen**, **and Anssi Hakkarainen**
Department Radio Science and Engineering, Aalto University
P. O. Box 13000, Aalto 00076, Finland

Abstract— Spaceborne microwave radiometry provides information on terrestrial snow characteristics including the water equivalent of dry snow. In northern regions the effect of land-cover categories, especially boreal forests and lakes, to the brightness temperature must be eliminated in order to obtain reasonable accuracy. We have investigated the brightness temperature behavior of snow on lake ice compared to that of snow on ground by conducting airborne radiometer measurements over two lakes in southern Finland over a period of several winters, covering various snow conditions encountered during early winter, mid-winter and late winter (melting period). The flight path includes, in addition to the two lakes, a forested area and an open, mostly agricultural area.

The main instrument has been our HUTRAD system, which operates at 6.8, 10.7, 18.7, 23.8, and 36.5 GHz, providing data for both vertical and horizontal polarization at an incidence angle of 50 degrees off nadir. Some data have been collected, additionally, using our HUT-2D interferometric imaging radiometer, which operates at 1.4 GHz. In-situ measurements have been made simultaneously with airborne data collection.

This paper presents results from our most recent flights conducted on 5 April 2013 (HUTRAD data set) and 11 April 2013 (HUTRAD data set in the morning and HUTRAD and HUT-2D data sets in the afternoon). On 5 April we had dry snow conditions with 10–15 cm of snow on top of lake ice and 40–50 cm of snow on ground. On 11 April we had 5–10 cm of snow on lake ice and 40–50 cm of snow on ground. In the morning the snow cover was dry (except the bottom layers on ground), whereas in the afternoon the topmost snow layers were wet due to air temperature rising above 0°C. The radiometer data indicate that (a) under dry snow conditions the results depend substantially on frequency, and (b) wet snow on top practically removes frequency dependence, except for the lowest frequencies. The results for snow on lake ice are different from those for snow on ground and, additionally, there is a difference between the results for the larger and smaller lake.

Advancing the Characterisation of Snow Parameters Sharpens Our Understanding of Active and Passive Microwave Signatures — And Vice Versa

C. Mätzler[1], M. Schwank[1,4], A. Wiesmann[1], M. Proksch[2], M. Schneebeli[2], J. Lemmetyinen[3], J. Pulliainen[3], K. Rautiainen[3], and A. Kontu[3]

[1]Gamma Remote Sensing, Gümligen, Switzerland
[2]WSL Institute for Snow and Avalanche Research SLF, Davos, Switzerland
[3]Finnish Meteorological Institute (FMI), Helsinki, Finland
[4]Swiss Federal Institute of Forest, Snow and Landscape, WSL, Mountain Hydrology and Torrents Birmensdorf, Switzerland

Abstract— The requirements for information on the cryosphere from regional to global scale initiated theoretical and experimental studies to explore the interaction between microwaves and the snowcover, including the relevant influences of the environment. A new collaboration between interested partners was initiated by studies in support of two ESA missions: (1) the SMOS Mission observing the earth surface with an imaging radiometer at 1.4 GHz, and (2) the proposed Earth Explorer Mission, COREH2O, for retrieving snow properties from Synthetic Aperture Radars at 9 and 17 GHz. Both studies made use of the test site of the Finnish Meteorological Institute (FMI) at Sodankylä in Northern Finland, instrumented with local radiometers and scatterometers covering the frequency range of interest and with several in-situ sensors. Several aspects of the studies have already been presented at conferences, ESA reports and journal publications. Here we will show what we learned from the in-situ and ground based microwave observations, and their comparisons with model expectations

As an example, during early winter the backscattering coefficient decreased with time while the snowpack was growing. This was against the expectation that volume scattering increases with increasing snow volume. First the variation was believed to be a signature of soil freezing. However, it turned out that melt metamorphism and its slow relaxation to winter snow was responsible for the changes. The available scheme was unable to quantify the variation of the snow structure with sufficient accuracy. On the other hand, the signal variation reveals the capability of microwave sensors to observe structural changes in snow and thus to feed back to the advancement of physical snow models.

Another example is related to radiometer observations at 1.4 GHz. Since snowpacks are highly transparent at this frequency, it was expected that dry snow does not influence the microwave emission. It will be shown that this way of arguing is misleading, since effects of refraction and impedance matching by snow can be significant.

The examples emphasise the need for realistic models and the objective characterisation of the relevant parameters. Recent improvements in measurement methods have led to the hope that the development of adequate snow-physical models will soon be possible. They will provide us with the temporal evolution of snow and soil parameters. These parameters are required as input to the forward models and their output will be used for comparison with remote sensing observations in data-assimilation schemes. Ill-conditioned inversion methods can be avoided in this way.

An important advancement realised over the last years is the improved characterisation of snow structure by at least three different methods to replace the subjective estimation of grain size:

1) Snow-Micro-Penetrometer (SMP) for one-dimensional (vertical) profiles of snow hardness and spatial correlation length. This is a rapid sampling method, suitable for fieldwork.
2) Near-infrared imaging of two-dimensional views of the specific surface area is also suitable for fieldwork, but requiring snow pits, and thus is not suitable for repeated observations at the identical place.
3) X-ray tomography for (small) 3-dimensional snow samples to determine the ice matrix with high resolution. Snow samples are collected in the field. The analysis takes place in a cold room.

The main structure parameter, the correlation length, can be determined from all three methods. The full 3-dimensional correlation function can be obtained from Method 3, only. All methods have been applied in Sodankylä by the SLF group. The introduction of at least one of these methods as a standard observation still has to wait for its realisation.

Apart from snow structure, we also need snow density, temperature and liquid-water content in microwave forward models, including the temporal and spatial variation of all parameters. Advancing the characterisation of these properties will improve the simulation capability of microwave observables, like brightness temperatures and backscattering coefficients. Furthermore, the comparison of modelled and measured values will feed back to the modelling of snow parameters and to the delicate processes of snow metamorphism.

Multilayer Dense Medium Radiative Transfer Combined with NMM3D Boundary Conditions with Application to Terrestrial Snow Scattering at X Band and Ku Band

Shurun Tan[1], **Wenmo Chang**[1], **Xiaolan Xu**[2], **Leung Tsang**[1], **Juha Lemmetyinen**[3], **and Simon Yueh**[2]

[1]Department of Electrical Engineering, University of Washington, Seattle, WA 98195, USA
[2]Jet Propulsion Laboratory, M/S 300-233, Pasadena, CA 91109, USA
[3]Arctic Research Unit, Finnish Meteorological Institute, Finland

Abstract— In two proposed satellite missions, CoReH2O of ESA, and SCLP of NASA, the radar remote sensing of terrestrial snow at X and Ku band are used. In this paper, we apply the Dense Medium Radiative Transfer (DMRT) theorywith multilayer snow structures and rough snow-ground interface. Both QCA and the bicontinuous medium model are used to calculate the bi-static scattering property of each snow layer. The NMM3D is used to derive the rough surface boundary condition. Interpolation is used to obtain the full-directional bi-scattering coefficient for the rough surface The model is applied to the SnowSAR data from ESA snow field measurement campaign carried out in Finland in March 2011.

We first applied the first order theory. An explicit expression is derived that accounts for transmission and attenuation and expresses the backscattering as the sum from each layer and the rough surface. Next we applied the multiple scattering theory. The diffuse intensity is decomposed into Fourier series in the azimuth direction. The phase matrix and the rough surface boundary conditions are also decomposed into harmonics. Each harmonic is solved numerically with Eigen-quadrature approach by matching boundary conditions. The quadrature solution takes into account the full multiple scattering effects. The bi-scattering of the rough surface is also systematically coupled into the snow volume multiple scattering effects.

The effect of stickiness parameter τ in QCA is studied. Variations of stickiness parameters give a variety of frequency dependences, size dependences and angular dependences of scattering coefficients and phase matrices at X band and Ku band. We also studied such frequency, size and angular dependences of the bicontinuous model as well as the ratio of cross polarization to co-polarization.

The rough surface scattering effect is also studied. The backscattering of rough surface plays a significant part in terrestrial snow scattering at X band. The dependence of rough surface scattering on rms height, correlation length and ground permittivity is used to determine the rough surface parameters.

Monitoring of Dynamic Changes in Alpine Snow with Terrestrial Radar Imagery

Andreas Wiesmann, Tazio Strozzi, Rafael Caduff, Jessica Papke, and Christian Matzler
GAMMA Remote Sensing AG, Gumligen, Switzerland

Abstract— Remote sensing of snow with active and passive microwaves has a long tradition. Terrestrial instruments are used to investigate the interaction of snow with microwaves at selected locations, air- and space-borne sensors are used to image larger areas. While the terrestrial instruments are mobile and can be brought to selected test areas they are usually doing point measurements. Satellite based instruments on the other hand, have a given observation geometry and observation schedule. These constraints limit the potential to investigate dynamic processes in the snowpack spatially, especially of slopes. Terrestrial imaging radars such as the GPRI (GAMMA Portable Radar Interferometer), overcome some of these constraints due to their portability, operating range of several kilometers, image acquisition time of about 30 seconds and the possibility to do repeat acquisitions within minutes.

In our presentation we discuss results of campaigns conducted with a GPRI in the Swiss Alps covering dry and wet snow conditions as well as measurements before and after an artificial avalanche release. The investigation covers the analysis of backscatter information spatially and in time as well as the interferometric analysis of the corresponding time series. The interferometric processing allows to gather information on the temporal decorrelation within the snowpack and to retrieve spatial displacement information.

The interferometric decorrelation is linked with changes in the snowpack structure. Consequently a drop in coherence is mainly an indicator for changes of the snowpack. They can be induced by short term effects like an avalanche release, or by slow restructuring such as snow metamorphism. If the correlation between two image acquisitions is high the interferometric phase can be interpreted. The phase reveals information about changes in the wave propagation to and from the target. Main contributions come from the displacement of the target area (e.g., speed and extent of creeping snow) along the line of sight, as well as changes in the atmospheric conditions.

The Sensitivity of Radar Backscattering to Snow Characteristics

C. Xiong[1], M. Brogioni[2], A. Crepaz[3], S. Paloscia[2], P. Pampaloni[2], E. Santi[2], and J. C. Shi[1]

[1]Institute of Remote Sensing Applications, Chinese Academy of Sciences, Beijing, China
[2]Institute of Applied Physics-National Research Council, Florence, Italy
[3]Avalanche Center, Arabba, Italy

Abstract— The importance of snow cover monitoring in the study of global changes, in the management of water resources, and in risk prevention is well known. Research carried out to investigate the potential of Synthetic Aperture Radars (SAR) in monitoring snow characteristics has shown that, at the frequencies of currently in orbit Synthetic Aperture Radars (C- and X-bands) wave penetration is very high in dry snow and very low in wet snow. Experiments conducted at 9 GHz on artificially packed dry snow showed a good sensitivity of σ° to snow depth. Following studies pointed out no significant difference between radar observations of bare soils and regions covered by natural dry snow at 10.4 GHz. However, recent investigations showed a noticeable relationship between X-band backscattering and snow water equivalent (SWE) when snow depth (SD) is higher than about 60 cm. The same investigations pointed out the effects of layering structure on microwave emission and backscattering.

In this paper, the effects of multilayer structure of snowpack and its temporal evolution on backscattering have been investigated by using a multilayer version of the Dense Medium Radiative Transfer model implemented for the active remote sensing.

In order to make this study as general as possible a few "synthetic" snow profiles, representative of typical cases of dry snow cover in the Alps were realized. The parameters taken into consideration were: grain size, snow density and layer thickness. These "synthetic" profiles were obtained by analyzing 26 snow profiles obtained in winter 2010–2011, when the snow depth was frequently greater than 60 cm, and by extracting simplified profiles that summarize the main characteristics for each period of the season. The analysis was limited to dry snow by considering only the measurements taken obtained from late fall to early springtime. During the first period the snow cover was dry, although in some cases it showed some evidence of temporary melting, testified by the presence of layers made by melt forms, in particular by melt-freeze crusts. First of all we took into consideration the layering of snow cover, with the indication of the present grains, which is a fundamental element in charactering the snow cover. Successively, for each layer, we have extracted the values of density and size of prevalent grains. It should be noted that, often, in the survey two types of grains are indicated, but, in this analysis, only the dominant sizes have been taken into consideration.

The model used for this analysis simulates the natural snowpack by means of a stratified medium composed by spherical ice scatterers embedded in air, overlying a rough homogeneous half-infinite medium. The snow layers interfaces, these are assumed to be flat. Backscattering from soil was simulated by using the Advanced Integral Equation Method (AIEM) for the co-polar components and the semi-empirical approach by Oh et al. 1992 for the cross-polar terms. Volume scattering from dry and wet snow was computed by using a multi-layer version of the Dense Medium Radiative Transfer Theory in the Quasi Crystalline Approximation (DMRT-QCA) with sticky particles. In this volume scattering model the position of the ice spheres is described by the Percus-Yevik distribution. For each layer the radiative transfer equation was solved by using the Discrete-order Eigenvalues Method, using the phase matrix described in Tsang et al. 2007, which account for the multiple scattering effects. The boundary conditions for solving the RT equations where finally determined by using a cubic spline interpolation to interpolate from the Snell's angles to the quadrature ones.

Characterization of Snow Cover Areas by Change Detection Applied to COSMO-SkyMed Images

S. Pettinato[1], **E. Santi**[1], **S. Paloscia**[1], **B. Aiazzi**[1], **and A. Garzelli**[2]

[1]Institute of Applied Physics, National Research Council, Firenze, Italy
[2]Department of Information Engineering and Mathematical Sciences
University of Siena, Siena, Italy

Abstract— The use of satellite data for a timely monitoring of the Earth's surface has become ever more appealing and effective in the last decades. Quantitative snow cover investigation can provide important information on global changes and water resource management, as well as food and avalanche risk prevention. Optical sensors have been proven capable of monitoring snow cover in cloud-free conditions, and several systems have been developed for operational monitoring of snow parameters from remote sensing data. However, only microwave sensors are able to acquire data independently of daylight and in adverse weather conditions. In particular, spaceborne X-band SAR systems (COSMO-SkyMed and TerraSAR-X) can provide accurate localization of snow-covered areas, exploit high/low penetration in dry/wet snow and estimate of the snow water equivalent (SWE) in the case of dry snow. In general, backscattering coefficients higher than the snow-free case can be detected, by assuming that the backscattering enhancement is due to snow characterized by a SWE greater than 100 mm and therefore able to contribute to the radar response at the X-band. In this paper, an experimental study on the characterization of snow cover areas on COSMO-SkyMed images is presented. Different data processing approaches are tested and experimentally compared:

1. Process multi-temporal SAR images to detect a backscattering change due to wet snow which typically ranges from -3 to -2 dB with respect to snow-free soil.
2. Apply a classical change detection algorithm based on semi-automatic thresholding of the logarithm of the ratio image between two SAR images acquired at different dates.
3. Apply a non-parametric change detection algorithm on two-date SAR images based on mean-shift clustering.

It should be noted that the first approach requires geo-coded and radiometrically calibrated multi-temporal SAR images, the second approach needs accurate de-speckling and suffers from the trade-off between noise reduction and preservation of spatial resolution, while the third approach has been proven to be effective also on 1-look SAR image data at very high spatial resolution. Preliminary results on Single-Look-Complex CSK images (Himage data in Stripmap acquisition mode) acquired in September 2011, December 2011 and January 2012 on an alpine region in Northern Italy show that the results obtained by applying the third approach are very promising since they provide accurate localization of the snow covered areas and reduced false alarm rate with respect to the first two classical approaches. Experimental results on PingPong Stripmap images will be also presented in the final paper and objectively assessed by using ground truth data.

Session 2A5
SC3: Lightwaves and Resonances in Confined Structures

Microring Resonators: The Road toward Practical Implementations
Joyce K. S. Poon, ... 502

Planar WGM Resonators: Vertical Evanescent Coupling for Complete On-chip Integration
Mher Ghulinyan, ... 503

Mode Selection for Subwavelength Aluminum/Silica Coated Semiconductor Circular Nanoresonators
Yong-Zhen Huang, Chu-Cai Guo, Jin-Long Xiao, Yue-De Yang, ... 504

Broad Band Second Harmonic Generation in Crystalline Whispering Gallery Mode Resonators
Florian Sedlmeir, Martin Hauer, Josef U. Furst, Harald G. L. Schwefel, ... 505

Modelling Kerr Comb Generation in Whispering Gallery Mode Resonators with a Periodic 1D Lugiato-Lefever Equation
Yanne Kouomou Chembo, Curtis R. Menyuk, ... 506

Multilayer Slab Waveguide Distributed Feedback Dye Laser Sensors
Christoph Vannahme, Cameron L. C. Smith, Michael Leung, Frank Richter, Mads B. Christiansen, Petur G. Hermannsson, Anders Kristensen, ... 507

Ab Initio Model of Lasing in Nanowires
Vladimir G. Bordo, ... 508

Characterization of Fringing Far-infrared Reflectance Spectra of Indium Phosphide
Jheng-Hong Yang, Pei-Kang Chung, Hong-Wen Hsieh, Shun-Tung Yen, ... 509

Improvement of Infrared Single-photon Detectors Absorptance via Grating-anomalies on Integrated Plasmonic Structures
Gábor Szekeres, Áron Sipos, András Szenes, Mária Csete, ... 510

Coupled Microcavity Lasers and Sensing Applications
Lei Xu, ... 512

Microring Resonators: The Road toward Practical Implementations

Joyce K. S. Poon
Department of Electrical and Computer Engineering
University of Toronto, Canada

Abstract— Despite decades of research, micro-resonator devices have not found widespread commercial adoption and have not replaced workhorse interferometric based photonic devices, such as Mach-Zehnder interferometers or arrayed waveguide gratings. The main roadblocks are the notoriously high sensitivity of the optical characteristics of microcavity devices to dimensional variations, environmental fluctuations, and nonlinearities.

In recent years, the availability of silicon photonic foundries coupled with the need for energy-efficient and compact photonic components for short reach networks (e.g., datacenters, board-to-board) have renewed interest in micro-resonators, especially microring resonators for integrated photonic circuits. The longstanding implementation challenges of micro-resonators motivate a fundamental re-consideration of the design and implementation of microring devices with a focus on fabrication tolerance, tunability, and functionality.

In this talk, I will describe my group's efforts on this front. I will present silicon microrings with improved tolerance to dimensional variations, tunable microring modulators with high extinction ratios, and modulators that break the linewidth limitations of resonant modulation. I will describe how these concepts can be extended to other types of high index contrast waveguide devices, resonant modulators, and lasers, including those in hybrid integration platforms. Innovative architectures and design approaches are needed for microrings to realize their potential as essential elements in large-scale integrated photonic circuits.

Planar WGM Resonators: Vertical Evanescent Coupling for Complete On-chip Integration

Mher Ghulinyan
Advanced Photonics and Photovoltaics Unit, Fondazione Bruno Kessler, Povo I-38123, Italy

Abstract— We will report on the realization and characterization of a silicon-based integrated optical platform which implements a vertical coupling scheme between a Whispering-gallery mode (WGM) resonator and a buried dielectric waveguide. The vertical coupling allows for the separation of the resonator and the waveguide into different planes, permitting one to realize the optical components in different materials and of thicknesses. This geometry has important implications on both the new and unexpected physics of the vertical evanescent coupling, but as well on the various possibilities to integrate in a monolithic way several resonator systems which currently can be probed by using only fiber-taper techniques.

Physics of the Vertical Evanescent Coupling: In contrast to the usual in-plane resonator-waveguide coupling geometry, the vertical one is characterized by an oscillatory behavior of the effective coupling as a function of the vertical gap [1]. This behavior manifests itself as oscillations in both the resonant waveguide transmission and the mode quality factor (Q). In particular, in contrast to the existence of a unique critical coupling gap for the in-plane geometry, the multiple critical coupling can occur at distinctly different vertical gaps in the vertical geometry. We will present an analytical description based on coupled-mode theory and a two-port beam-splitter model of the waveguide-resonator vertical coupling, developed for arbitrary phase-matching conditions. The model is validated by successful interpretation of experimental observations.

Freestanding Resonators: The vertical coupling approach enables the realization of freestanding WGM resonators suspended in air over the dielectric bus waveguides [2]. This is achieved by a partial removal of the sacrificial layer between the resonator and the waveguide using a selective dry or wet etch. We demonstrate the feasibility of our approach for wafer-scale mass fabrication of freestanding planar resonators suspended in air and coupled to integrated bus waveguides. This opens the door for the realization of stable all-integrated resonator systems for optomechanical and metrological applications and has the potential to substitute today's complicated fiber-taper coupling schemes.

Wedge Resonators: Engineering of ultra-high Q's (UHQ) in planar resonators by using conventional semiconductor processing can be achieved by realizing a shallow-angle wedge at the rim of microdisk resonators. In a wedge geometry the cavity modes are pushed away from the device edge, boosting thus the scattering loss-related Q. Even though, the integration of UHQ wedge resonators with side-coupled dielectric waveguides cannot be realized because of fundamental technological limitations. We will show here that a fully integrated wedge resonator with bus waveguides on a silicon chip is achieved by using a vertical coupling scheme [3]. In this approach, the cavity and the waveguide lay in different planes. This permits to realize the shallow-angle wedge while the waveguide remains intact. Therefore, the precise size-control and the robustness against post-processing operation due to its monolithic integration makes this system a prominent platform for industrial-scale integration of ultra-high-Q devices into planar lightwave chips.

REFERENCES

1. Ghulinyan, M., F. Ramiro-Manzano, N. Prtljaga, R. Guider, I. Carusotto, A. Pitanti, G. Pucker, and L. Pavesi, "Oscillatory vertical coupling between a whispering-gallery resonator and a bus waveguide," *Phys. Rev. Lett.*, Vol. 110, 163901, 2013.
2. Ghulinyan, M., R. Guider, G. Pucker, and L. Pavesi, "Monolithic whispering-gallery mode resonators with vertically coupled integrated bus waveguides," *IEEE Photonics Technol. Lett.*, Vol. 23, 1166, 2011.
3. Ramiro-Manzano, F., N. Prtljaga, L. Pavesi, G. Pucker, and M. Ghulinyan, "A fully integrated high-Q whispering-gallery wedge resonator," *Opt. Express*, Vol. 20, 22934, 2012.

Mode Selection for Subwavelength Aluminum/Silica Coated Semiconductor Circular Nanoresonators

Yong-Zhen Huang, Chu-Cai Guo, Jin-Long Xiao, and Yue-De Yang
State Key Laboratory on Integrated Optoelectronics
Institute of Semiconductors, Chinese Academy of Sciences, Beijing 100083, China

Abstract— Nanocavity semiconductor lasers have attracted great attention for the potential applications in photonic integrated circuits and on-chip optical interconnect. However, the spatial spreads of the confined mode field distributions beyond the physical boundaries of dielectric cavities will limit the reduction of the cavity sizes and the integrated density of photonic integrated circuits. Metallic coated nanocavities can use the surface-plasmon polaritons for plasmon nanolasers with device size down to less than 100 nm, and confine optical modes in subwavelength size cavities. In this report, we investigate the mode characteristics for circular semiconductor nanolasers coated by silica/aluminum on the bottom and sidewalls. The mode characteristics of the metallic-confined nanoresonators are simulated by 3D FDTD technique and the Padé approximation. Mode spectra over wide frequency range from 1350 to 1750 nm are obtained from the FDTD simulation for resonators with semiconductor core height of 800 nm and radii of 250, 450, and 750 nm. The simulated mode field patterns show that the high-Q resonant modes can be the first, the second, and the third order longitudinal (vertical) modes. The mode interval of high-Q modes can be larger than the wavelength range of the gain spectrum and the mode selection can determine the lasing temperature range of a nanolaser with the reduction of the cavity size. The position of the active region is important for the high order longitudinal mode to have a large optical confinement factor. Finally, the simulated mode spectra are compared with the lasing spectra of the fabricated aluminum coated InAlGaAs/InP circular nanolasers. The mode selection related to the cavity size and location of the active region are critical for nanocavity lasers to work over a wide temperature range.

Broad Band Second Harmonic Generation in Crystalline Whispering Gallery Mode Resonators

F. Sedlmeir[1,2], **M. Hauer**[1], **J. U. Fürst**[1,2], **and Harald G. L. Schwefel**[1,2]

[1]Max Planck Institute for the Science of Light, Erlangen 91058, Germany
[2]Institute for Optics, Information and Photonics
University of Erlangen-Nuremberg, Erlangen 91058, Germany

Abstract— Crystalline whispering gallery mode (WGM) resonators confine the light by total internal reflection along the equator of a convex dielectric. We report on a new class of birefringent crystalline WGM resonators, which are birefringent with their optic axis tilted with respect to the rotational symmetry axis. In such a system, the eigen polarizations of the extra ordinary beam changes continuously around the equator, and thus its refractive index. Nevertheless, when coupling light into the resonator, clear resonance spectra are visible and support high quality factors ($Q > 10^7$). Furthermore, the oscillating refractive index allows for a new type of broad band phase-matching in non-linear processes. First, we will briefly discuss the polarization of such resonances in a prism coupled magnesium fluoride WGM resonator. Contrary to the standard z-cut resonators, we find resonances that are ideally coupled with left hand circular polarized light. Furthermore we characterize the polarizations of light coupled out at different positions along the rim of the resonator. Even with linearly polarized incoupled light, the out-coupled light displays a complex polarization behavior in the far-field. Following the short introduction, we will focus on the novel type of phase-matching. In the second experiment we utilize the oscillating refractive index for phase-matching of a non-linear $\chi^{(2)}$ process. Therefore we fabricated a x-cut lithium niobate WGM resonator. In a x-cut resonator, only the refractive index seen by the quasi transverse magnetic resonance oscillates and the ordinary refractive index stays constant. Thus, such a resonator features always four regions where perfect phase-matching can be achieved. The usual z-cut resonator, requires the dispersion curves to be carefully matched by temperature tuning and then provides rather narrow band phase-matching. Here we can report on successful broad band second harmonic generation, in a x-cut lithium niobate WGM resonator from 1550 nm to 775 nm. We will show the range in which phase-matching is possible and discuss the efficiencies.

Modelling Kerr Comb Generation in Whispering Gallery Mode Resonators with a Periodic 1D Lugiato-Lefever Equation

Yanne K. Chembo[1] and Curtis R. Menyuk[2]

[1]Optics Department, FEMTO-ST Institute, CNRS UMR6174
Route de Gray, Besançon cedex 25030, France
[2]Department of Computer Science and Electrical Engineering, University of Maryland
Baltimore County, 1000 Hilltop Circle, Baltimore, Maryland 21250, USA

Abstract— Kerr combs are a set of equidistant spectral components generated through the optical pumping of an ultra-high Q whispering gallery mode resonator with Kerr nonlinearity. Kerr comb generators are characterized by their conceptual simplicity, structural robustness, small size, and low power consumption. Thus, Kerr combs are promising candidates to replace femtosecond mode-locked lasers in applications where these features are of particular relevance. The theoretical understanding of Kerr comb generation in whispering gallery mode resonators is currently the focus of worldwide activity that is motivated by the wide range of potential applications and by the necessity of understanding the complex light-matter interactions that are due to the strong confinement of long-lifetime photons in nonlinear media. A modal expansion has recently been proposed to describe Kerr comb formation. This expansion uses a large set of coupled nonlinear ordinary differential equations, each of which governs the evolution of one of the whispering gallery modes. Each equation describes the evolution of one of the modes. This modal expansion is in excellent agreement with the experimental measurements. In this communication, we show that the total intra-cavity field that is obtained by summing up all the modal contributions obeys a variant of the Lugiato-Lefever equation. This equation leads to an alternative paradigm for Kerr comb generation. We also explain how the spatiotemporal model can also be extended to include higher-order nonlinear effects that are difficult to account for in the modal formalism. We finally show that observed Kerr comb spectra are generally the signature of cavity solitons or Turing patterns.

Multilayer Slab Waveguide Distributed Feedback Dye Laser Sensors

C. Vannahme, C. L. C. Smith, M. Leung, F. Richter, M. B. Christiansen, P. G. Hermannsson, and A. Kristensen
Department of Micro- and Nanotechnology, Technical University of Denmark, DTU Nanotech
Østeds Plads, Building 344, Kgs. Lyngby 2800, Denmark

Abstract— Organic dye-based distributed feedback (DFB) lasers are widely tunable laser light sources in the visible wavelength range and exhibit low-cost, simple fabrication, low threshold and single-mode emission [1]. Precise emission wavelength modeling is essential for understanding and optimization of DFB lasers. Here, we present a simple yet precise model for calculating the emission wavelength of multilayer DFB lasers. We find that experimental and calculated wavelength values are in compelling agreement for hybrid nanoimprinted Ormocomp-TiO_2 (doped with Pyrromethene 597) first order DFB lasers [2]. Applying the model, we explain the occurrence of different laser light polarization, i.e., transvers electric (TE) or transvers magnetic (TM) emission. We further explore hybrid Ormocomp-TiO_2 second order DFB lasers as highly sensitive refractive index sensors featuring narrow linewidth and thus high quality spectral resolution. Design guidelines for high performance sensing are given and the influences of layer thicknesses and grating period on wavelength and wavelength shifts are discussed in this context [3]. This is used for optimizing the laser sensors towards highest sensitivity and thus lowest detection limits. We show that the additional TiO_2 layer can increase the sensitivity by a factor of 5 making the laser sensors competitive with state-of-the-art photonic crystal sensors. In addition, single-mode biological second order distributed feedback dye lasers are presented [4]. The active core of these lasers consists of vitamin B_2 doped gelatin which is spin-coated onto a nanoimprinted grating structure in low-index polymer. These single-mode biological lasers represent a next step towards all-biological lasers where the resonator is formed from structured biological material. Such devices could be biocompatible and eventually biodegradable laser light sources and laser sensors.

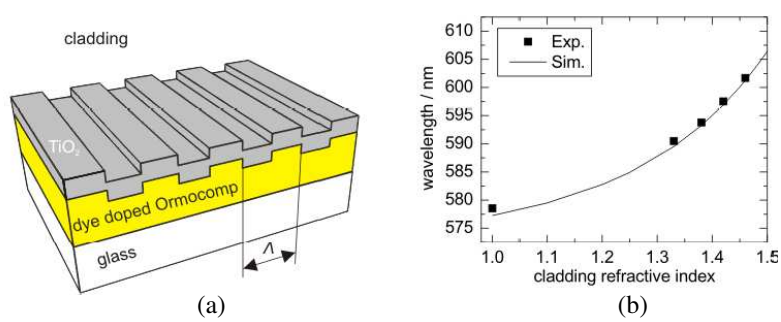

Figure 1: (a) Schematic of hybrid Ormocomp-TiO_2 distributed feedback laser with grating period Λ. (b) Example of experimental and simulated emission wavelength values.

REFERENCES

1. Grivas, C. and M. Pollnau, "Organic solid-state integrated amplifiers and lasers," *Laser Photonics Rev.*, Vol. 6, 419–462, 2012.
2. Vannahme, C., C. L. C. Smith, M. B. Christiansen, and A. Kristensen, "Emission wavelength of multilayer distributed feedback dye lasers," *Appl. Phys. Lett.*, Vol. 101, 151123, 2012.
3. Vannahme, C., F. Maier-Flaig, U. Lemmer, and A. Kristensen, "Single-mode biological distributed feedback laser," *Lab Chip*, 2013, DOI: 10.1039/C3LC50140J.
4. Vannahme, C., M. Leung, F. Richter, C. L. C. Smith, P. G. Hermannsson, and A. Kristensen, "Nanoimprinted distributed feedback lasers comprising TiO_2 thin films: Design guidelines for high performance sensing," in preparation.

Ab Initio Model of Lasing in Nanowires

V. G. Bordo
NanoSYD, Mads Clausen Institute, University of Southern Denmark, Denmark

Abstract— Recent advances in nanotechnology have led to the possibility to fabricate nanowires which can lase under pumping conditions. They can be currently grown from both inorganic and organic materials and demonstrate lasing at both optical and electrical pumping. This progress paves a way to diverse applications of nanowire lasers in nanoscale optical and optoelectronic devices.

To be able to design nanolasers and optimize their operation one needs to have deep understanding of elementary optical processes which lead to lasing. So far, to describe nanolaser action one utilizes the conventional laser equations which have been obtained for laser cavities of dimensions much larger than the laser field wavelength. One of the key approximations which has been used to derive such equations implies that both the field and polarization in the laser cavity are described by plane waves which are slowly modulated in both time and space. The latter assumption is obviously not fulfilled in nanocavities where the field changes essentially on the scale of the wavelength. Moreover, such equations involve some semi-phenomenological parameters, in particular the photon decay rate and the modal gain, which cannot be well defined for a nanocavity. Another aspect related to small sizes of a nanocavity is the fact that the atoms or molecules of the active medium are in the close proximity of the cavity walls that implies a significant role of the cavity-quantum-electrodynamical effects. One takes partly such effects into account by means of introducing the population decay rate modified by the Purcell factor in the rate equations. The rate equations do not contain, however, information about the phase of the light field and thus are incomplete. All these arguments reveal that the laser equations should be revisited from the beginning in order to provide a basis for a proper nanolaser design.

Recently we have developed an *ab initio* analytical model which is capable to describe rigorously electromagnetic field in a cylindrical nanocavity of arbitrary diameter and length. This model allows one to calculate Fabry-Pérot modes of a cylindrical nanowire and the Purcell factor in a cylindrical nanocavity. In this talk, that approach is applied to derive the laser equations for a nanowire from first principles and thus to fill this gap in the nanolaser theory. We use the developed theory to design a nanowire laser which can operate without a population inversion.

Characterization of Fringing Far-infrared Reflectance Spectra of Indium Phosphide

Jheng-Hong Yang, Pei-Kang Chung, Hong-Wen Hsieh, and Shun-Tung Yen
Department of Electronics Engineering and Institute of Electronics
National Chiao Tung University, Hsinchu 30010, Taiwan

Abstract— We use fringing patterns in a high-resolution reflectance spectrum of a thin semi-transparent indium phosphide layer to identify the spectral features. The patterns result from interference between reflected waves from the parallel surfaces of the layer. Since the intensity of the reflected waves having traveled within the layer varies with absorption of the material, variation of fringe amplitude is observed. By observing local minima of fringe amplitude, we identify nine obvious features. Spectral positions of these features agree well with those obtained by transmission, absorption, or Raman experiments. The absorption mechanism in the measured spectral range has been known to be dominated by two-phonon sum and two-phonon difference processes. Both processes involve absorption of a photon that virtually excites a transverse optical phonon. In the sum process, the excited phonon decays an harmonically into two phonons with their energy sum equal to the energy of the absorbed photon. In the difference process, mediated by the excited phonon, a phonon is annihilated and a higher-energy phonon is emitted with their energy difference equal to the energy of the photon. The processes are characterized by joint two-phonon density of states. Since absorption associated with the processes varies with the joint density of states, the fringe amplitude is expected to vary accordingly. The local minima of fringe amplitude can therefore be related to singularities in the joint density-of-states spectrum around which the density of states vary rapidly with frequency. We then find critical points in the Brillouin zone by which the singularities are caused.We find that the critical points are all on the boundary of the irreducible wedge of the Brillouin zone, including the faces, lines, and vertices. The result is different from that of a previous work. Our analysis is applicable to other semi-transparent materials.

Improvement of Infrared Single-photon Detectors Absorptance via Grating-anomalies on Integrated Plasmonic Structures

Gábor Szekeres, Áron Sipos, András Szenes, and Mária Csete
Department of Optics and Quantum Electronics, University of Szeged, Hungary

Abstract— The optimal illumination directions are determined by numerical method (via COMSOL software package) for superconducting nanowire single-photon detectors (SNSPDs) comprising (i) optical-cavity covered by a gold reflector (OC-SNSPD), (ii) nano-cavity-array closed by horizontal and vertical gold segments (NCAI-SNSPD), and (iii) three types of nano-cavity-deflector-array consisting of longer vertical gold segments neighboring each nano-cavity (NCDAI-SNSPD_1), additional trench at the anterior side of each deflector (NCDAI-SNSPD_2), and two deflectors neighboring each nano-cavity at both sides (NCDAI-SNSPD_3), which are integrated into the absorbing meandered niobium-nitride (NbN) pattern. The wavelength dependent NbN absorptance as well as the near-field distribution are inspected to uncover the origin of the observed nanophotonical phenomena.

In OC-SNSPDs the highest 27% NbN absorptance is attained at perpendicular incidence onto the NbN pattern in P-orientation ($\gamma = 0°$) due to the **E**-field antinode at the silica substrate interface. In NCAI- and NCDAI-SNSPDs the S-orientation ($\gamma = 90°$) is more advantageous, which result in coupled resonances on the nano-cavity-array. In NCAI-SNSPD enhanced 34% NbN absorptance is attained at perpendicular incidence, a local maximum of 29% appears at 20.8° polar angle (V point) due to grating-coupled backward propagating Brewster-Zenneck waves, and the global maximum of 70.3% is attained at the 80° plasmonic Brewster angle (PBA). The Fano-shaped wavelength dependent NbN absorptance exhibits plasmonic-band-gap (PBG) at the local maximum, while large absorptance is observable in a broad wavelength interval at the PBA. In NCDAI-SNSPDs strongly enhanced 74.8/75.1/83.3% NbN absorptance is attainable at $\sim$ 19°–20° tilting (M* points) at the center of the inverted PBG. At these global maxima in NCDAI-SNSPDs the integrated grating couples to partially bounded backward propagating surface waves with wavelength equal to that of SPPs, however, these waves are synchronized with the cavities. Additional trenches in NCDAI-SNSPD_2 result in FWHM increase, while two

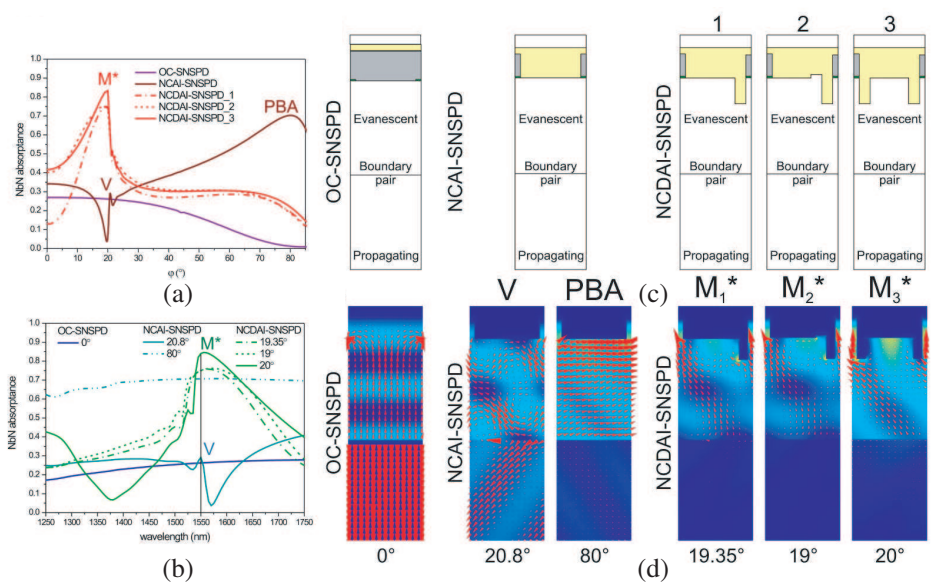

Figure 1: Comparison of the NbN absorptance (a) as a function of polar angle and (b) wavelength at the extrema on angle-dependent curves in different designs. (c) Schematic drawings of OC-, NCAI- and NCDAI-SNSPDs, above the "Boundary pair" the incoming, evanescent and scattered fields are superimposed, while below the "Boundary pair" the scattered fields are presented separately. (d) The normalized **E**-field and power-flow in one unit cell of different designs at the extrema on the polar-angle dependent NbN absorptance at 1550 nm.

neighbouring deflectors in NCDAI-SNSPD_3 ensure higher absorptance, however cause parallel band-width narrowing.

The 792.5 nm integrated pattern periodicity matches the condition of optimal nano-cavity illumination in NCAIand NCDAI-SNSPDs as well as ensures resonant transmission, moreover the deflectors make possible efficient coupling between localized and propagating modes. The length of the meandered NbN pattern enables parallel electric optimization, the experimental feasibility is ensured via silica substrate that can be etched easily.

Coupled Microcavity Lasers and Sensing Applications

Lei Xu
Key Lab for Micro and Nano Photonic Structures, Department of Optical Science and Engineering
Ministry of Education, Fudan University, Shanghai 200433, China

Abstract— Whispering gallery mode (WGM) resonators are high cavity quality factor (Q) resonators. In recent years, ultra-high Q whispering gallery resonators with various structures have been reported, such as glass spheres, micro-toroids, capillary tubes, crystal disks, to mention a few. The ultra-Q nature of WGM leads to many new optical properties to appear in a small cavity size, such as ultra-low threshold lasing, weak light optical nonlinearity, mechanic resonant mode cooling and single particle sensing.

Up to now, most reported high Q WGM resonators are single cavity structure. In the past years, we delevoped coupled cavity structure that composed of two size mismatched ring cavities. When these two cavities are coupled to each other, we realized new optical properties such as single frequency lasing, unidirectional lasing and ultrahigh sensitive sensing.

The coupled microcavity lasers compses two cavities that have a little different sizes. Both of the cavities can generate WGM resonance, but their free spectral range (i.e., mode spacing) is slightly different. The WGM Light generated from one microdisk can enter partly to the other cavity through coupling. By using coupled cavity structure, we were able to suppress the multi-mode nature of WGM and generate single frequency lasing.

WGM resonators are good candidates for high sensitive bio and chemical sensors. The sensitivity of WG mode sensors is mostly in a range of 10–100 nm/RIU. In 2009, we demonstrated that coupled ring laser is an excellent sensor structure. Lasing intensity, rather than WGM resonance shift, gives the sensing signal and a detection limit as high as 80 pg/ml was achieved, this is equivalent to a $Q = 107$ passive resonator sensor. More recently, We demonstrated the ultrahigh sensitivity mechanism by using a coupled optofluidic ring laser. The new sensor consists of one ring laser and one optofluidic tube. The optofluidic tube also serves as sensing element. Majority portion of the WG mode distributes in the tube, very high sensitivity is expected. Experimentally, a sensitivity of 5930 nm/RIU was achieved, which is two orders of magnitude higher than conventional ring resonator sensors, and one order of magnitude higher than evanescent field engineered ring resonator sensors.

Session 2A6
SC4: Small and Miniaturized Antenna Techniques

Small Antenna Analysis Using Convex Optimization
Mats Gustafsson, ... 514

An Alternative Derivation of the Equivalent Networks for Spherical Modes Using the Extended Kuroda Transform
James S. McLean, Robert Sutton, Heinrich D. Foltz, ... 515

Ultra Thin and Transfer Tattoo UHF RFID Tags
J. C. Batchelor, D. O. Oyeka, B. M. Turki, Edward A. Parker, S. G. Yeates, V. Sanchez-Romaguera, 517

Radiation Efficiency of Low-profile and Electrically Small Printed Antennas with Capacitive Feeding Structure
Takeshi Fukusako, Hiroyuki Maema, ... 518

Analysis, Design and Experimental Verification of a Miniature Printed, Coupled-loops Antenna
Hubregt J. Visser, Stefan Lem, ... 519

A Miniaturized Archimedean Spiral Antenna with Polarization Diversity
Jonathan M. Rigelsford, ... 520

Multi-Mode Reconfiguration of a Compact Ultra-wideband Antenna
Akram Alomainy, Tamer Aboufoul, Clive Parini, ... 521

Design of Compact Antenna Deigns for WLAN/WiMAX Bands and for Dual Band-notched UWB Applications
Yingsong Li, Wenxing Li, Raj Mittra, William Whittow, ... 522

Design of Miniature Multiband Fractal CPW-fed Antenna for Telecommunication Applications
Ines Rouissi, Imen Ben Trad, Jean-Marie Floc'h, Muntasir Sheikh, Hatem Rmili, ... 523

A Stacked Microstrip Antenna with CSRR Arrays for Beidou Navigation System
Baiqiang You, Lizhi Li, Yang Zhao, Jianhua Zhou, Jie Li, ... 525

Small Antenna Analysis Using Convex Optimization

Mats Gustafsson
Department Electrical and Information Technology, Lund University, Box 118, SE-221 00 Lund, Sweden

Abstract— The performance of antennas is constrained by the size (measured in wavelengths) of the antenna structure [1, 2]. The trade-off between performance and size are expressed by physical limitations that provide bounds solely based on the shape and size of the design volume. Chu [3] analyzed the stored and radiated energies in the exterior of a sphere circumscribing the antenna to determine a lower bound on the Q-factor, Q. The bound was generalized to arbitrary sized and shaped antennas in [4] under the assumption of $Q \gg 1$.

In [5], optimal currents and physical bounds are formulated as convex optimization problems [6] using the expressions for the stored energies presented by Vandenbosch [7], see also [8]. The convex optimization problems are used to determine optimal current distributions on arbitrary shaped antennas for minimum Q, maximal $G = Q$, superdirective antennas, antennas with prescribed radiated fields [5, 9], and losses. This generalizes the physical bounds in [1, 3, 4, 9] in many ways. We also show how losses and antennas embedded in structures can be included in the bounds. The presented results are for arbitrary shaped structures but restricted to antenna structures composed of metallic or dielectric materials. We also restrict the size of the antenna structure to less than approximately half a wavelength to obtain positive semidefinite energy expressions, see [8, 9]. The theoretical results are illustrated with numerical simulations for antennas confined to planar rectangles.

REFERENCES

1. Volakis, J., C. C. Chen, and K. Fujimoto, *Small Antennas: Miniaturization Techniques & Applications*, McGraw-Hill, New York, 2010.
2. Hansen, R. C. and R. E. Collin, *Small Antenna Handbook*, Wiley, 2011.
3. Chu, L. J., "Physical limitations of omni-directional antennas," *J. Appl. Phys.*, Vol. 19, 1163–1175, 1948.
4. Gustafsson, M., C. Sohl, and G. Kristensson, "Physical limitations on antennas of arbitrary shape," *Proc. R. Soc. A*, Vol. 463, 2589–2607, 2007.
5. Gustafsson, M. and S. Nordebo, "Optimal antenna currents for Q, superdirectivity, and radiation patterns using convex optimization," *IEEE Trans. Antennas Propagat.*, Vol. 61, No. 3, 1109–1118, 2013 (in press).
6. Boyd, S. P. and L. Vandenberghe, *Convex Optimization*, Cambridge University Press, 2004.
7. Vandenbosch, G. A. E., "Reactive energies, impedance, and Q factor of radiating structures," *IEEE Trans. Antennas Propagat.*, Vol. 58, No. 4, 1112–1127, 2010.
8. Gustafsson, M. and B. L. G Jonsson, "Stored electromagnetic energy and antenna Q," Technical Report LUTEDX/(TEAT-7222)/1–25/(2012), Lund University, Department of Electrical and Information Technology, P. O. Box 118, S-221 00 Lund, Sweden, 2012, http://www.eit.lth.se.
9. Gustafsson, M., M. Cismasu, and B. L. G. Jonsson, "Physical bounds and optimal currents on antennas," *IEEE Trans. Antennas Propagat.*, Vol. 60, No. 6, 2672–2681, 2012.

An Alternative Derivation of the Equivalent Networks for Spherical Modes Using the Extended Kuroda Transform

J. S. McLean[1], **R. Sutton**[1], **and H. D. Foltz**[2]

[1]TDK R. & D. Corp., Cedar Park, TX, USA
[2]Department of Electrical Engineering, University of Texas Pan-American, Edinburg, TX, USA

Abstract— The equivalent lumped-element ladder networks originally derived by Chu [1–3] which represent electromagnetic spherical modes are invaluable for the understanding of numerous phenomena including radiation from electrically-small antennas. One strong impetus for this approach is that it enables the application of the the rigorous Fano-Bode limitation on impedance matching, which applies strictly to lumped-element networks [5, 6]. The equivalent networks in Refs. [1–3] were derived entirely using the recursion relations for the spherical Bessel functions. The equivalent network for TM-to-R modes is shown in Fig. 1. Thal [3] also gave a two-port network describing the propagation of the spherical modes in a spherical shell or region. The network simplified for the TM_{01} mode is shown in Fig. 2. Whereas Chu and Harrington gave one-port lumped-element networks which would predict wave impedances, Thal presented a two-port network from which the field quantities at two (or more) values of R could be obtained. Thal's equivalent network consisted of lumped elements and a length of uniform transmission line. Thus, the network could be described in microwave terminology as a mixed lumped and distributed network. The model is remarkable because it is a combination of lumped elements and *uniform* transmission line. Thal's analysis also facilitates the understanding of so-called "spherical wire antennas" [4]. We note that Thal's two-port model of a spherical shell contains positive lumped elements (positive inductances and capacitances) on one end of the uniform transmission line and negative lumped elements (negative inductors and capacitors) on the other. In the highly refined area of microwave circuit analysis, Kobayashi [7] derived a set of what he termed "extended Kuroda transforms" that apply very generally to mixed lumped and distributed networks. Here, using Kobayashi's extended Kuroda transforms [8], we derive Thal's equivalent circuit directly from the a nonuniform transmission line model [9] for the spherical modes. Such a nonuniform transmission line model for spherical modes has been presented in Ref. [10].

Finally, we consider the analogous acoustic problem and show that a two-port mixed lumped and distributed equivalent network for the acoustic monopole identical to that obtainable from Thal's model was given by Benade [11], but derived using an entirely different approach. Like Thal's model, Benades model includes a uniform transmission line with a positive "conicity inertance" on one end and a negative one on the other. A two-port representation for acoustic monopole radiation equivalent to Benade's model, Thal's model, and Kobayashi's model is shown in Fig. 3. Such a model would be most beneficial in the understanding of energy storage and impedance matching in the area of electrically-small antennas and, as noted earlier, enables the application of the Fano-Bode theory to the problem of electrically-small antennas. Finally, the model also provides insight into time-domain behavior as the rational function representation provides details of the complex plane behavior of the system such as the location of poles and zeroes.

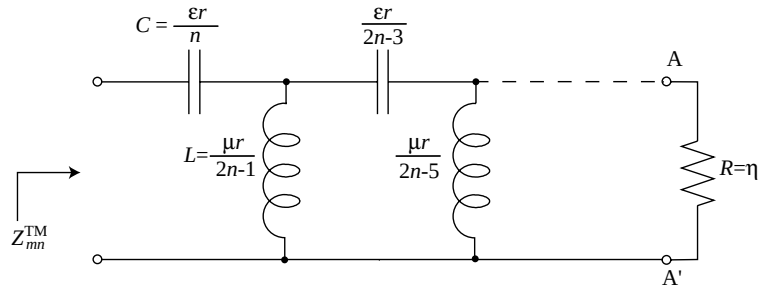

Figure 1: Equivalent circuit for spherical for spherical TM-to-R modes as shown in Figures 5–6 of Ref. [1] and Ref. [2]. On the right hand end of the network is a load which does represent far field radiation of power. However, the port comprised by the two terminals A-A′ shown on the right is fictitious.

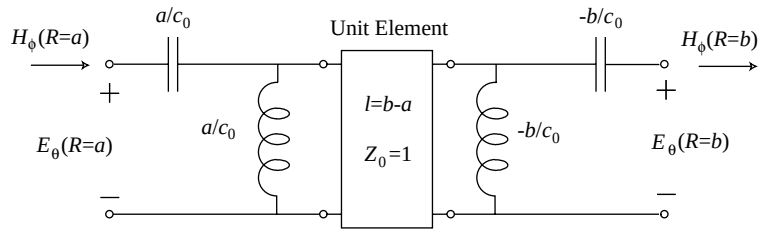

Figure 2: Equivalent circuit for spherical shell supporting TM_{01} modes with inner radius a and outer radius b as given in Ref. [3]. Note that the lumped elements on the right side of the unit element are negative. Also note the directions of the currents. Finally note that the network in Ref. [3] is flipped right to left in relation to this one. As noted in Ref. [3], if two spherical shells were cascaded, these elements would cancel with the positive counterparts on the next shell. If $b \to \infty$, the negative series capacitance would become a short while the negative shunt inductance would become an open circuit.

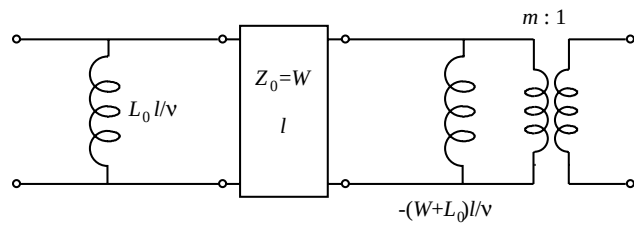

Figure 3: Representation of acoustic monopole mode or rigid-walled acoustic conical horn using the nomenclature in Ref. [7]. The ideal transformer on the right accounts for the transformation of area. Note that the conicity inertance on the right is negative.

REFERENCES

1. Chu, L. J., "Physical limitations on omnidirectional antennas," *Journal Applied Physics*, Vol. 19, 1163–1175, 1948.
2. Harrington, R. F., *Time Harmonic Electromagnetic Fields,* McGraw-Hill, New York, 1961.
3. Thal, Jr., H. L., "Exact analysis of spherical waves," *IEEE Trans. Antennas Propagat.*, Vol. 26, No. 2, 282–287, 1978.
4. Thal, Jr., H. L., "New radiation Q limits for spherical wire antennas," *IEEE Trans. Antennas Propagat.*, Vol. 54, No. 2, 2757–2763, Oct. 2006.
5. Fano, R. M., "Theoretical limitations on the broadband matching of arbitrary impedances," *J. Franklin Institute*, Vol. 249, 57–83, Jan. 1950; 139–155, Feb. 1960.
6. Villalobos, M. C., H. D. Foltz, J. S. McLean, and I. Sen Gupta, "Broadband tuning limits on UWB antennas based on fanos formulation," *Proc. 2006 IEEE Antennas and Propagation International Symposium*, 171–174, Albuquerque, NM, Jul. 9–14, 2006.
7. Kobayashi, K., Y. Nemoto, and R. Sato, "Kurodas identity for mixed lumped and distributed circuits and their application to nonuniform transmission lines," *IEEE Trans. Microwave Theory Tech.*, Vol. 29, No. 2, 81–86, 1981.
8. Kuroda, K., "Derivation methods of distributed constant filters from lumped constant filters," Text for Lectures at *Joint Meeting of Kansai Branch of IECE*, 32, Japan, Oct. 1952.
9. Ghose, R. N., *Microwave Circuit Theory and Analysis,* McGraw-Hill, New York, 1963.
10. Marcuvitz, N., *Waveguide Handbook,* IET, 1951.
11. Benade, A. H., "Equivalent circuits for conical waveguides," *J. Acoust. Soc. Am.*, Vol. 83, 1764–1769, May 1988.

Ultra Thin and Transfer Tattoo UHF RFID Tags

J. C. Batchelor[1], **D. O. Oyeka**[1], **B. M. Turki**[1], **E. A. Parker**[1], **S. G. Yeates**[2], **and V. Sanchez-Romaguera**[2]

[1]School of Engineering, University of Kent, UK
[2]School of Chemistry, University of Manchester, UK

Abstract— This paper describes inkjet printing as a digital fabrication tool for the manufacture of RFID tags on flexible and porous substrates (i.e., paper). The RFID tag presented is a single layer, ultrathin UHF tag in the form of a transfer tattoo [1] which evolved from ultra-thin, substrate insensitive tag designs [2]. Operation has been demonstrated when mounted direct on the skin with initial read ranges in the region of 1m and subsequent improvements have enabled read range increases. The implications of ink sintering processes for paper based transfer tattoos will be discussed as specifically applied to this work [3], and resulting patch conductivities and read ranges highlighted for tags printed on tattoo transfer paper [4]. Recent developments in selective ink layering will be outlined to illustrate the benefits to cost effective fabrication and efficient tattoo patch operation. Finally, work integrating additional components to improve transponder efficiency will be presented and leading to the concept of an ultra-thin battery for power assisted tagging where on-skin read ranges of 6m are possible. The issues for fabrication will be discussed for deposition and fabrication of such ultra-low profile sensitive tattoo tags.

REFERENCES

1. Ziai, M. and J. Batchelor, "Temporary on-skin passive UHF RFID transfer tag," *IEEE Transactions on Antennas and Propag.*, Vol. 59, No. 10, 3565, 2011.
2. Ziai, M. and J. Batchelor, "Thin ultra high-frequency platform insensitive radio frequency identification tags," *IET Microw. Antennas Propag.*, Vol. 4, 390–398, 2010.
3. Sanchez-Romaguera, V., M. B. Madec, and S. G. Yeates, "Ink-jet printing of conductive polymers for smart textiles and flexible electronics," *Materials Research Society Symposium Proceedings, 1192E (Materials and Devices for Flexible and Stretchable Electronics)*, Paper #: 1192-PP14-04, 2009.
4. http://www.craftycomputerpaper.co.uk/.-Inkjet-Tattoo-Paper_CPJ316I.htm.

Radiation Efficiency of Low-profile and Electrically Small Printed Antennas with Capacitive Feeding Structure

Takeshi Fukusako and Hiroyuki Maema
Department of Computer Science & Electrical Engineering
Kumamoto University, 2-39-1, Kurokami, Chuo-ku, Kumamoto 860-8555, Japan

Abstract— Some effects of a capacitive feeding structure with printed low-profile and electrically small antennas are discussed. In this structure, a feeding plate is installed in between a ground plane and a radiating element so that the radiator can be coupled capacitive; therefore, this feeding structure has a duality to the inverted-F antenna. At the same time, variations in impedance characteristics with respect to the structural parameters are discussed.

This structure feeds the antenna by voltage. Considering the effect of the ohmic loss, this talk is also devoted to the difference in radiation efficiency between the capacitive structure and the inverted-F structure for an example of electrically small meandered line antennas with a low-profile structure. Moreover, the authors show that the radiation efficiency can be improved by reducing the equivalent permittivity of the substrate by making a small air-gap in the substrate. As a result, a radiation efficiency of 67% has been achieved for thickness of $0.01\lambda_0$ and $k_0a < 0.5$. (k_0: wavenumber at the resonant frequency, a: radius of a sphere surrounding the antenna.) Some ways to construct the gap are discussed considering practical fabrications.

Finally, for some variations in feeding structure and element shapes, the variations in radiation efficiency are also discussed.

Analysis, Design and Experimental Verification of a Miniature Printed, Coupled-loops Antenna

Hubregt J. Visser[1, 2] **and Stefan Lem**[2]

[1]Holst Centre/IMEC, Eindhoven, The Netherlands
[2]Eindhoven University of Technology, Eindhoven, The Netherlands

Abstract— Recently, an electrically small, self-resonant, inherently 50 Ω-matched antenna has been introduced [1]. The antenna consist of a small loop antenna integrated into a larger loop antenna that is capacitively loaded, see Figure 1. The dimensions of the larger loop determine the resonance frequency while the dimensions of the smaller loop determine the input impedance. Since designing such an antenna by iteratively employing a full-wave analysis program will be very time consuming, the development of an all-analytical approximate model has been undertaken. To facilitate the model development, the antenna configuration of Figure 1 has been slightly modified, see Figure 2. To start with, the two loops have been separated and positioned on both sides of the dielectric slab. Then the capacitive loading has been given the shape of a coplanar strip in line with the large loop strip conductor. Approximate models have been developed for the small and large strip loops, the feed gap of the small loop, the coupling between the loops [1], the coplanar strip capacitor and the effects of the dielectric slab. The separate models as well as the combined model will be discussed and it will be shown how this approximate model can generate a predesign in a very short time. The predesign is used as input for the full-wave analysis program and is fine-tuned in typically two iterations. Measurements performed on realized prototypes will be shown.

In addition to this balanced antenna model and design, the first full-wave simulation and measurement results for an unbalanced design, excited with a coplanar waveguide, will be presented. The size of the antenna will be discussed with respect to radiation efficiency.

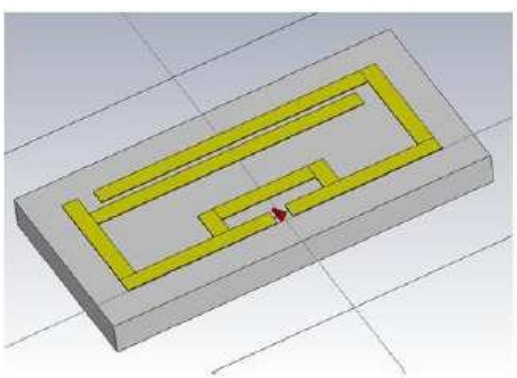

Figure 1: Small loop antenna according to [1].

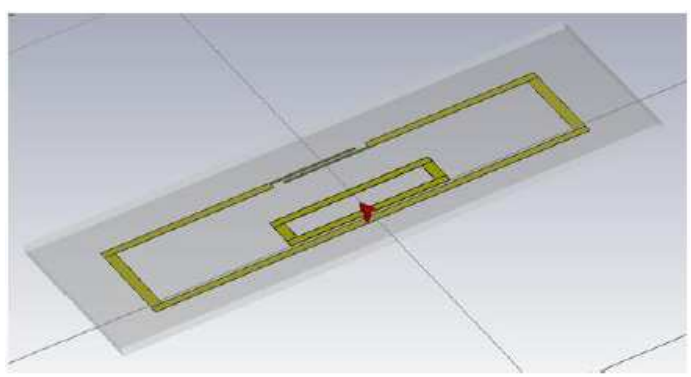

Figure 2: Modified antenna to aid in analytic modeling.

REFERENCES

1. Zhang, J. and O. Breinbjerg, "Self-resonant electrically small loop antennas for hering-aids applications," *Proceedings LAPC*, 1–5, 2010.

A Miniaturized Archimedean Spiral Antenna with Polarization Diversity

Jonathan M. Rigelsford
Department of Electronic & Electrical Engineering, The University of Sheffield
Mappin Street, Sheffield S1 3JD, United Kingdom

Abstract— This paper presents a miniaturized linearly polarized quad-arm Archimedean spiral antenna with polarisation diversity. The antenna comprises two spiral driven elements positioned above a circular reflector and operates at 1.7 GHz. The design has a simulated gain of 8 dBi and having a diameter of 44.5 mm, the driven element has an aperture reduction of 49% when compared to a standard half-wavelength dipole operating at the same frequency. The simulated axial ratio of the antenna is found to be greater than 38 dB at the resonant frequency and therefore linear polarisation has been maintained despite the spiral geometry. Measured results are in good agreement with those predicted by theory and the antenna is shown to have a good 50 Ω input impedance. The paper continues to present different techniques for dielectrically loading the antenna to further reduce its size while maintaining its operational performance. These miniaturized designs provide an aperture reduction of greater than 55% when compared to a standard half-wavelength dipole operating at the same frequency and without degrading the antennas performance. An example is presented whereby the antenna has been directly printed onto a glass substrate with a conductive silver ink.

Suitably scaled versions of the designs could be used for applications such as MIMO systems which require a reduced antenna aperture size necessary for small inter-element spacing and for HF/VHF applications where the very large aperture of a linearly polarized antenna may be prohibitive.

Multi-Mode Reconfiguration of a Compact Ultra-wideband Antenna

Akram Alomainy, **Tamer Aboufoul**, **and Clive Parini**
School of Electronic Engineering and Computer Science
Queen Mary University of London, Mile End Road, London E1 4NS, United Kingdom

Abstract— A novel and simple reconfigurable single element ultra-wideband monopole antenna realised in a compact design is presented. The antenna occupies overall dimensions of $34 \times 31 \times 0.88\,\text{mm}^3$, which makes it suitable for handheld devices. The ultra-wideband antenna can be frequency reconfigured to work in specific frequency bands and limit the impact of out-of -band interferers; this is very useful for cognitive devices front ends. Moreover, the antenna exhibits notched band operation to limit the interference of HIPERLAN/2 (5.15–5.35 GHz).

Another interesting feature of the proposed multimode antenna is that its polarisation can be reconfigured at specific frequencies to generate circular polarised (CP) radiation; this can improve the signal reception in multipath fading environments regardless of the orientation of the portable cognitive radio devices. The CP radiation can also be switched to either right hand circular polarisation (RHCP) or left hand circular polarisation (LHCP). The simulated reflection coefficient, radiation patterns, gain and total efficiency of the ultra-wideband mode and the multi-reconfiguration modes are presented. The compactness, simplicity and flexibility of the proposed multimode antenna make it a good candidate for future cognitive radio consumer-level devices.

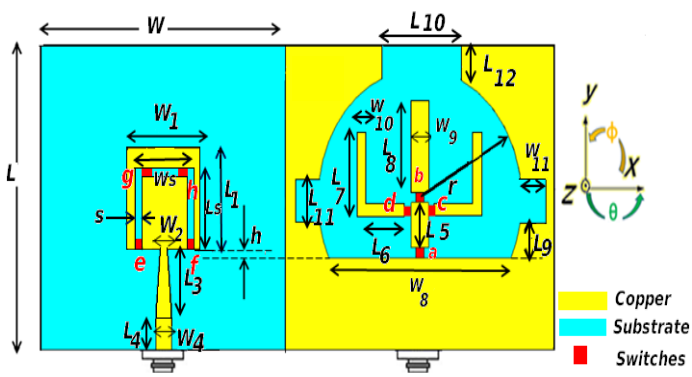

$34 \times 31 \times 0.88\ \text{mm}^3$

Design of Compact Antenna Deigns for WLAN/WiMAX Bands and for Dual Band-notched UWB Applications

Yingsong Li[1], **Wenxing Li**[1], **Raj Mittra**[2], **and William Whittow**[3]

[1]College of Information and Communications Engineering
Harbin Engineering University, Heilongjiang, Harbin 150001, China
[2]Electromagnetic Communication Laboratory, The Pennsylvania State University
University Park, PA 16802, USA
[3]School of Electrical, Electronic and Systems Engineering
Loughborough University, Loughborough LE11 3TU, UK

Abstract— Recently, rapid evolution of wireless communication systems has fueled the need to design antennas for portable terminals suitable for Wireless Local Area Networks (WLANs), as well as for Worldwide Interoperability for microwave access (WiMAX). There is ever growing commercial pressure to reduce the antenna size to keep pace with the decreasing size of the electronics.

In this talk, we first present the design of a dual-band (3.5 GHz and 5.8 GHz), meandered monopole antenna for WLAN/WiMAX applications, which is fed by an asymmetric coplanar strip (ACS). The proposed antenna is comprised of an asymmetric ground plane, an ACS-fed structure, and coupled meandered monopole-type of radiating elements that are designed to provide the two desired operation bands, namely 3.5 GHz and 5.8 GHz. The two resonance frequencies of the antenna can be controlled by adjusting the dimensions of the radiating elements, namely the two meandered monopoles, and the gap between them which controls the coupling. The designed antenna has a small size, which is only 20 mm $\times$ 12 mm including the ground plane. Simulated and measured results will be presented to demonstrate that the proposed dual-band antenna is well suited for WLAN and WiMAX applications.

The talk will then go on to discuss the extension of some of the above concepts to the design a reconfigurable Ultrawideband (UWB) antenna with one or more notches for interference suppression, and will include illustrative experimental results for this type of antenna as well.

Design of Miniature Multiband Fractal CPW-fed Antenna for Telecommunication Applications

I. Rouissi[1], **I. Ben Trad**[2,3], **J. M. Floc'h**[3], **M. Sheikh**[4], **and H. Rmili**[4]

[1]SYSCOM, ENIT, Université de Tunis-El Manar, Tunis 1002, Tunisia
[2]INNOV'COM, Sup'Com, City of Communication Technologies, Ariana 2083, Tunisia
[3]IETR, INSA Rennes, 20 Avenue Buttes des Coësmes, Rennes 35043, France
[4]Faculty of Engineering, Electrical and Computer Engineering Department
King Abdulaziz University, P. O. Box 80204, Jeddah 21589, Saudi Arabia

Abstract— A miniature planar fractal antenna has been introduced in this paper for multi-standard wireless communication systems. The multifrequency structure was based on Hilbert curve at the second iteration and fed using the CPW technology. The performed monopole was designed using the EM Simulator HFSS v11 from Ansoft. Simulation results show that it resonates at several frequencies used in applications such as GSM900, WLAN, ISM, WiFi, and WiMAX. A prototype was manufactured and characterized and measurements show that this compact monopole antenna can be used for a wide variety of telecommunication applications.

Antenna Design: The compact fractal second-iteration antenna of size $27 \times 28\,\text{mm}^2$ based on Hilbert curve is shown in Fig. 1. It is printed on FR4 substrate with relative permittivity $\varepsilon_r = 4.4$ and thickness $h = 1.6\,\text{mm}$. The CPW monopole antenna has been fed by a $50\,\Omega$ SMA connector. The optimized design parameters are as following: $a = 5\,\text{mm}$, $Wp = 1\,\text{mm}$, $Lp = 17\,\text{mm}$, $Lf = 6\,\text{mm}$, $Wf = 1\,\text{mm}$, $s = 0.11\,\text{mm}$, $Wg = 5\,\text{mm}$, $Lg = 12.89\,\text{mm}$, $S_1 = 1\,\text{mm}$.

Results: The Hilbert curve fractal antenna was realized and measured results agree well with simulation. In fact, the compact structure has a multiband behavior as it can be seen in Fig. 3.

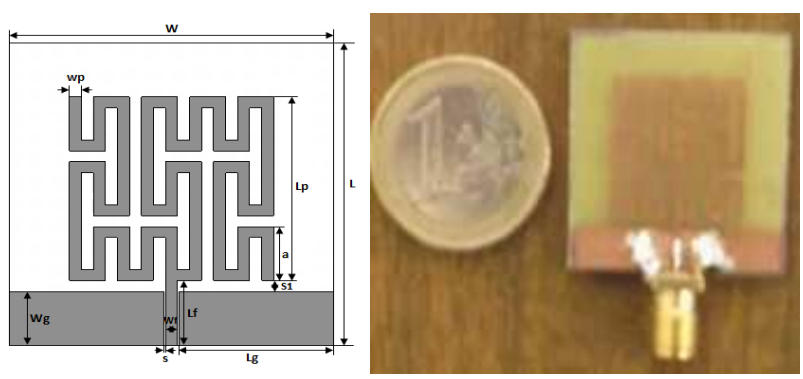

(a) (b)

Figure 1: The fractal antenna: (a) geometry and (b) prototype.

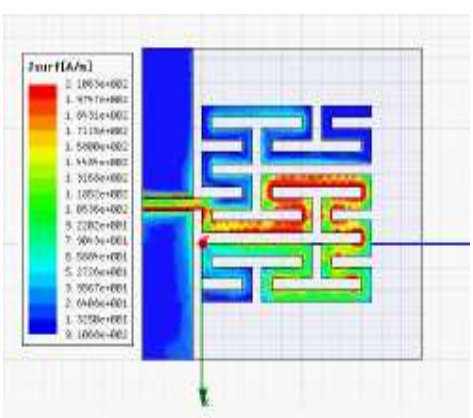

Figure 2: Surface current distribution for $F = 0.96\,\text{GHz}$.

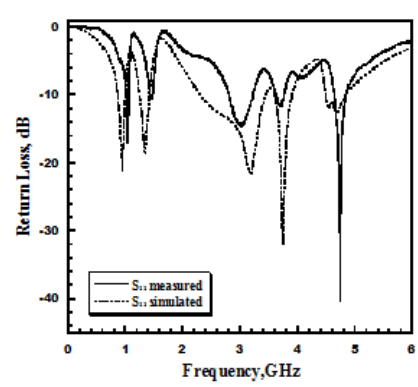

Figure 3: Measured and simulated return loss.

The desired bands are achieved to a large extent. The 2D measured radiation patterns on E-plane and H-plane at 1.024 GHz and 4.73 GHz frequencies are presented in Fig. 4. It can be concluded that the antenna behaves as a monopole and its radiation performance is maintained over the 0.1–6 GHz range.

The surface current distribution changes depending on the operating frequency. Fig. 2 depicts the surface current distribution at the 0.96 GHz frequency which is localized along the micro strip line due to the existing EM coupling with the ground plane and chiefly at the center of the Hilbert curve and the right edges.

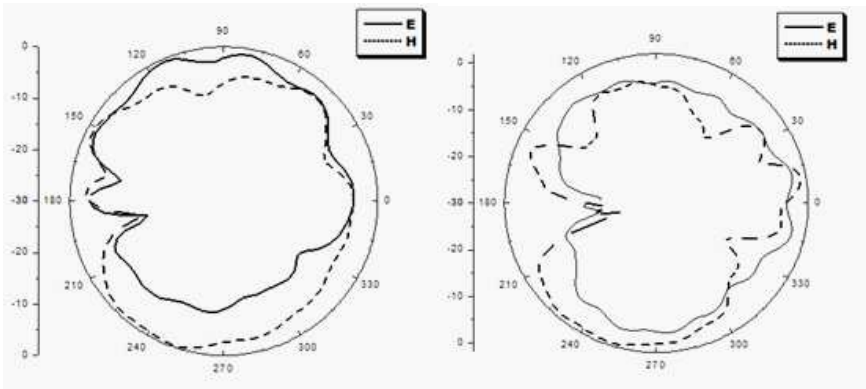

(a) (b)

Figure 4: Measured radiation patterns at frequencies: (a) 1.024 GHz; (b) 4.73 GHz.

A Stacked Microstrip Antenna with CSRR Arrays for Beidou Navigation System

Baiqiang You, **Lizhi Li**, **Yang Zhao**, **Jianhua Zhou**, **and Jie Li**
Department of Electronic Engineering, Xiamen University, Xiamen, Fujian 361005, China

Abstract— A double-feeding and dual-band circularly polarized stacked microstrip antenna is presented for Beidou Navigation System. CSRR arrays are used for the miniaturization of the proposed antenna, together with slotting and corner cutting for circular polarization. Simulation results show that the proposed antenna covers 1.61 GHz and 2.5 GHz. The 10 dB impedance bandwidth and 3 dB axial-ratio bandwidth for lower band are 11.8 MHz and 2.8 MHz respectively, and that for higher band are 165 MHz and 65.7 MHz respectively. The obvious widened bandwidths of the latter are caused by the stacked structure.

The configuration of the proposed double-feed dual-band circularly polarized stacked microstrip patch antenna is shown in Figure 1.

The parameters of the proposed antenna are relatively independent and easy to be regulated in the stimulation design. Its mechanism is discussed by the antenna input impedance and a conceptual circuit model. The proposed antenna, with size of only 36 mm × 33 mm × 6 mm, has been fabricated and measured. There has been good agreement between stimulation and measurement results, confirming the suitability for Beidou navigation application.

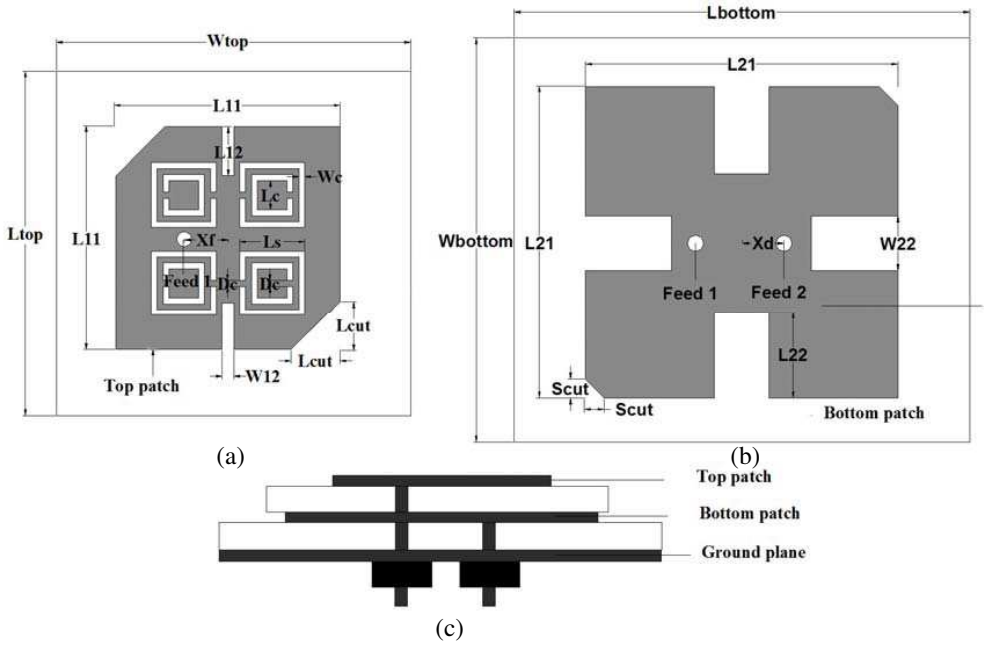

Figure 1: Configuration of the proposed antenna with (a) top patch, (b) bottom patch and (c) lateral view.

Session 2A7
3_FocusSession.SC3: Nonlinear Optics: Structured Materials, Functional Devices and Applications 1

Nonlinear Optics at the Few-photon Level in Rb-filled Photonics Crystal Fibers
Alexander L. Gaeta, ... 528

Nonlinear Processes in Planar Photonic Crystal Structures and Circuits
Jeff F. Young, ... 529

Second Harmonic Nanoparticles in Biological Imaging
Ye Pu, Demetri Psaltis, ... 530

Liquid Crystals for Broadband (Optical-terahertz-microwave) Tunable Nano-photonic Structures and All-optical Switching
Iam-Choon Khoo, ... 531

Nanodomain Engineered Ferroelectrics for Nonlinear Optical Applications
Fredrik Laurell, C. Canalias, A. Zukauskas, C. Liljestrand, Valdas Pasiskevicius, ... 532

Generation of a Harmonic Frequency Comb for the Synthesis of Arbitrary Optical Waveforms
Andy Kung, ... 533

Two-photon Absorption in Graphene
Wei Ji, ... 534

Ultrafast Nonlinearities of Metallic 3D Metamaterials
Ventsislav K. Valev, Petros Farah, Stefano Salvatore, Silvia Vignolini, Ullrich Steiner, Jeremy J. Baumberg, ... 535

Large Area Enhancement of Optical Nonlinearities of Ultrathin Gold Films
Stefano De Zuani, Tobias Knoblauch, Audrey Berrier, Bruno Gompf, Martin Dressel, ... 536

Nonlinear Optics at the Few-photon Level in Rb-filled Photonics Crystal Fibers

Alexander L. Gaeta
Cornell University, USA

Abstract— Rubidium-filled photonics band-gap fibers offer the prospect of performing nonlinear optics at ultralow light levels. Producing a significant vapor density within such fibers is non-trivial, and I will describe recent experiments that are able to produce optical densities exceeding 1000 at room temperature. Through use of this platform, nonlinear optics at the few-photon level is possible either through cross-phase or cross-absorption modulation. This indicates that our system can be employed to realize the recently proposed weak-nonlinearity based quantum computation paradigm and also quantum non-demolition measurement of photon number.

Nonlinear Processes in Planar Photonic Crystal Structures and Circuits

Jeff F. Young
Advanced Materials and Process Engineering Laboratory
Department of Physics and Astronomy, University of British Columbia
6224 Agricultural Rd. Vancouver, BC, V6T 1Z1, Canada

Abstract— Planar photonic crystals offer a versatile platform for fabricating optical micro/nanostructures in which the photonic density of states can be engineered over a wide range. There are several demonstrations of how this flexibility can be used in isolated microcavities, waveguides, resonators etc., to reduce the optical power requirements for nonlinear studies, in a variety of high refractive index host materials. Advances in processing techniques, especially in the silicon-on-insulator (SOI) material system, are now being used to fabricate fully-integrated nonlinear optical *circuits*.

This talk will first review some examples of early work on isolated structures, both in III-V and silicon planar slab hosts. Recent advances in CMOS-foundry based, large scale optical circuit fabrication, and their impact on nonlinear optical studies will be described, using as an example, recent progress on the development of single-photon sources in SOI circuits. These examples not only illustrate the ways in which the photonic density of states can effectively enhance the second and third order nonlinear response of the host materials, but also reveal nonlinear aspects of how resonant excitonic transitions in semiconductor quantum dots couple to circuit-bound photons in silicon.

Second Harmonic Nanoparticles in Biological Imaging

Ye Pu and Demetri Psaltis
Laboratory of Optics, School of Engineering, EPFL, BM 4.107, Station 17, Lausanne 1015, Switzerland

Abstract— Second harmonic generation (SHG) is a nonlinear optical process where two incident photons are combined into one photon with doubled frequency. Only efficient in crystalline materials that lack a symmetry center, SHG forms excellent optical contrast in most biological cells and tissues. As such, nanocrystals capable of SHG, generally of non-centrosymmetric materials, are an emerging new type of nonlinear optical nanoprobes. By up-converting the excitation light into frequency-doubled photons, they provide a contrast forming capability similar to fluorescence agents. Dramatically different from fluorescence, however, the process of SHG is ultrafast, lossless, and coherent. As a result, second harmonic nanoprobes emit a steady signal that is neither fading (bleaching) nor blinking, which are ubiquitous issues with fluorescent probes. The absence of photobleaching and emission intermittency is therefore a particularly important feature that is likely to complement the widely used fluorescent agents in many biomedical imaging applications. Recently, biomolecule conjugations and a significant emission enhancement have been achieved in these nanoprobes, paving the way for their deployment in the field of molecular imaging. Furthermore, the coherent emission from the SHG process provides unique opportunities for the application of coherence domain techniques that are not available with fluorescent agents. Through harmonic holography, which records holograms with second harmonic signals emitted from the SHG nanoprobes, three-dimensional (3D) images can be captured with only one frame of two-dimensional (2D) hologram. The technique was later extended to restore a focus behind a turbid medium through digital phase conjugation. More recently, scanning imaging in 2D and 3D domain were achieved by scanning the restored focus through the memory effect in the scattering medium.

Liquid Crystals for Broadband (Optical-terahertz-microwave) Tunable Nano-photonic Structures and All-optical Switching

I. C. Khoo
Electrical Engineering Department, Pennsylvania State University, University Park, PA 16802, USA

Abstract— Liquid crystals possess extraordinarily large optical nonlinearities that are suitable for all-optical switching over a very broad spectral regime from the visible to infrared and beyond [1, 2]. Most of the underlying mechanisms such as field induced collective molecular and crystalline reorientation, coupled flows-reorientation, thermal and electrostrictive effects are non-resonant in nature. In conjunction with their extraordinarily large birefringence in the visible-terahertz-microwave regime [3], liquid crystals are extremely attractive as the active ingredients in the development of metamaterials and plasmonic nano-structures, (liquid crystals on silicon) LCOS-waveguides and -resonator [4–8] for applications throughout this electromagnetic spectrum. We present the results of recent theoretical studies/simulations of the dynamical aspects of these mechanisms and experimental feasibility demonstrations of all-optical switching operations. With Blue-Phase liquid crystals (BPLC), their 3-D photonic crystal structure and optical anisotropy allow polarization-free nonlinear optical switching and wave mixing processes. The freedom from surface alignment requirements also enable easy integration of BPLC in complex nano-structures and geometries that are difficult to implement with other phases such as nematicsor ferroleectrics.

REFERENCES

1. Khoo, I. C., "Extreme nonlinear optics of nematic liquid crystals," *J. Opt. Soc. Am. B*, Vol. 28, A45–A55, 2011 (Invited paper in Focus Issue dedicated to *50th Anniversary of Nonlinear Optics*).
2. Khoo, I. C. and A. Diaz, "Multiple-time-scales dynamical studies of nonlinear transmission of pulsed lasers in a multi-photon absorbing organic material," *J. Opt. Soc. Am. B*, Vol. 28, No. 7, 1702–1710, 2011.
3. Xu, H., O. Trushkevych, N. Ollings, and W. A. Crossland, "Measurement of dielectric anisotropy of some liquid crystals for microwave applications," *Mol. Cryst. Liq. Cryst.*, Vol. 502, 235–244, 2009.
4. Khoo, I. C., A. Diaz, J. Liou, M. V. Stinger, J. Huang, and Y. Ma, "Liquid crystals tunable optical metamaterials," *IEEE J. Selected Topics in Quantum Electronics, Special Issue*, Vol. 16, 410–417, 2010.
5. Bossard, J. A., et al., "Tunable frequency selective surfaces and negative-zero-positive index metamaterials based on liquid crystals," *IEEE Transactions on Antennas and Propagation*, Vol. 56, 1308–1320, 2008.
6. Zhao, Y., et al., "Light-driven tunable dual band absorber with liquid-crystal-plasmonic asymmetric nanodisk array," *Appl. Phys. Letts.*, Article # 053119, 2012 and references therein.
7. Khoo, I. C., et al., "Blue-phase liquid crystal cored optical fiber array with photonic bandgaps and nonlinear transmission properties," *Optics Express*, Vol. 21, 4319–4327, 2013.
8. Ptasinski, J., S. W. Kim, L. Pang, I. C. Khoo, and Y. Fainman, "Optical tuning of silicon photonic structures with nematic liquid crystal claddings," *Optics Letts.*, 2013, submitted.

Nanodomain Engineered Ferroelectrics for Nonlinear Optical Applications

F. Laurell, C. Canalias, A. Zukauskas, C. Liljestrand, and V. Pasiskevicius
Applied Physics Department, KTH, Roslagstullsbacken 21, Stockholm 10691, Sweden

Abstract— We review the recent advances in fabrication of nanodomain engineered ferroelectrics and discuss the use of these materials in second-order nonlinear optical interactions.

Quasi-phase matching (QPM) devices with sub-μm periodicity enable the realization of unique nonlinear interactions that are impossible to obtain in ordinary birefringent phase matched nonlinear media [1–4]. One example is the mirrorless optical parametric oscillator (MOPO) which exploits counter-propagating nonlinear interaction to achieve the distributed feedback necessary for the oscillation to start. Implementation of these devices demands a reliable technology for structuring the nonlinearity of the material on the nanometer scale. Sub-μm domain engineering is not a straightforward task since not only new lithographic techniques are needed but also methods to control the lateral domain-growth have to be established. $KTiOPO_4$ (KTP) is considered to be the most suitable material for sub-μm domain engineering due to its large ferroelectric domain propagation velocity anisotropy. In this contribution we report on the progress in fabrication techniques for sub-μm domain gratings in KTP and RKTP. Their performance as QPM devices will be discussed. Focus will be on the mirrorless parametric oscillator where its unique optical properties will be reviewed. Other devices like the backward second harmonic generator and the elcectro-optic Bragg filter will also be discussed.

REFERENCES

1. Canalias, C. and V. Pasiskevicius, "Mirrorless optical parametric oscillator," *Nature Phot.*, Vol. 1, 459–462, 2007.
2. Canalias, C., V. Pasiskevicius, M. Fokine, and F. Laurell, "Backward quasi-phase-matched second-harmonic generation in submicrometer periodically poled flux-grown $KTiOPO_4$," *Appl. Phys. Lett.*, Vol. 86, 181105-1–3, 2005.
3. Zukauskas, A., V. Pasiskevicius, and C. Canalias, "Second-harmonic generation in periodically poled bulk Rb-doped $KTiOPO_4$ below 400 nm at high peak-intensities," *Opt. Express*, Vol. 21, 1395, 2013.

Generation of a Harmonic Frequency Comb for the Synthesis of Arbitrary Optical Waveforms

Andy Kung[1, 2]

[1]Institute of Atomic and Molecular Sciences, Academia Sinica, Taipei, Taiwan
[2]Institute of Photonics Technologies, National Tsing Hua University, Hsinchu, Taiwan

Abstract— An optical field waveform synthesizer in the femtosecond to attosecond regime is the analog to a radio-frequency or microwave function generator that provides microwave fields to control mesoscopic electronic behavior in the nanosecond and longer time scales but extends it to the attosecond regime [1]. It is a significant emerging technology because such waveforms afford a capability to attain microscopic control of electronic motion in the attosecond time scale. Periodic waveforms can be synthesized by the Fourier technique that is the coherent superposition of a comb of harmonic frequencies [2, 3]. Thus efficient generation of a harmonic frequency comb is of current interest in this field.

Among various approaches to the generation of the harmonic frequency comb, nonlinear optical frequency mixing in a photonic crystal designed to satisfy quasi-phase-matching condition is deemed to be the most effective because of its high conversion efficiency. Using cascaded nonlinear mixing in a monolithic PPLN crystal we generated up to 7 harmonics of a fundamental infrared laser pulse [4] and successfully demonstrated the synthesis of ultrafast optical field waveforms of various shapes using five of the harmonic components [5]. Greater waveform fidelity and stability are obtained using CW harmonics. We have proposed a scheme to produce watt-level multiple harmonics using a combination of nonlinear optical devices comprising of QPM photonic crystals. The progress of this work will be described in this conference.

REFERENCES

1. Goulielmakis, E., V. S. Yakovlev, A. L. Cavalieri, M. Uiberacker, V. Pervak, A. Apolonski, R. Kienberger, U. Kleineberg, and F. Krausz, *Science*, Vol. 317, 769, 2007.
2. Hänsch, T. W., *Opt. Commun.*, Vol. 80, 71, 1990.
3. Chan, H.-S., Z.-M. Hsieh, W.-H. Liang, A. H. Kung, C.-K. Lee, C.-J. Lai, R.-P. Pan, and L.-H. Peng, *Science*, Vol. 331, 1165, 2011.
4. Hsu, W.-C., Y.-Y. Lai, C.-J. Lai, L.-H. Peng, C.-L. Pan, and A. H. Kung, *Opt. Lett.*, Vol. 34, 3496, 2009.
5. Chan, H.-S., Z.-M. Hsieh, L.-H. Peng, and A. H. Kung, *Opt. Lett.*, Vol. 37, 2805, 2012.

Two-photon Absorption in Graphene

Wei Ji
National University of Singapore, Singapore

Abstract— It has been widely demonstrated that graphene is an excellent saturable absorber and has great potential in mode-locking technique. Recently, we observed, from both quantum perturbation theory and experiment, that two-photon absorption (TPA) also plays an important role in the nonlinear response of graphene [1]. The observation was carried out on bilayer epitaxial graphene in the spectral range from 780 to 1100 nm. Here we present our latest experimental results on CVD-grown, multilayer ($\sim$ 10) graphene on quartz with a spectral range extended from the near infrared (NIR) region of 780–1100 nm to a visible region of 535–780 nm.

By assuming the linear dispersion of the energy structure near the Dirac point, our theory [1] predicts the TPA coefficient of monolayer graphene to be

$$\beta^{monolayer} = \frac{4\pi^2}{\varepsilon_\omega \omega^4 \hbar^3} \left(\frac{\upsilon_F e^2}{c} \right)^2 \tag{1}$$

which gives a TPA coefficient of $\sim 0.3\,\mathrm{cm/MW}$ at 800 nm, too insignificant to be detected under our experimental conditions. In order to achieve a detectable TPA signal, we have stacked N layers of CVD-grown graphene on quartz substrate. For such stacked graphene samples, the TPA signal should be enhanced by a factor of $N^2/(1+N\pi\alpha/2)^8$, where N is the number of layers and $\pi\alpha \approx 0.023$ [2].

We have conducted both pump-probe and Z-scan measurements with $120 \sim 200$ fs laser pulses on the 10-layer sample. To simulate the measured Z-scans, we have found that the total absorption coefficient must be expressed as $\alpha_0/(1+I/I_s)+\beta I$, where α_0 is the linear absorption coefficient of the graphene sample, I_s is the saturation intensity, and I is the light intensity. The Z-scans cannot be fit if we switch off TPA (by setting $\beta = 0\,\mathrm{cm/MW}$). Values of the saturation intensity are measured to be in the range from 2 to $10\,\mathrm{GW/cm^2}$, depending on the photon energy. Our results reveal a quadratic dependence of the I_s-values on the photon energy. Interestingly, the measured TPA spectrum deviates from Eq. (1) in the visible region. This is anticipated as our theory is invalid in the spectrum far away from the Dirac point. As the photon energy moves away from the Dirac point and approaches the saddle point (M) in the band structure of graphene, a so-called excitonic Fano resonance [3] becomes important. In fact, our linear (or one-photon) absorption spectrum clearly demonstrates that this resonance dominates in the visible and UV region with a peak near ~ 4.6 eV and a broad-band feature covering the entire visible region. If we shift this resonance band to the corresponding two-photon transition region, it shows that the measured TPA is in agreement with the spectral dependence of the excitonic Fano resonance.

REFERENCES

1. Yang, H., X. Feng, Q. Wang, H. Huang, W. Chen, A. T. S. Wee, and W. Ji, "Giant two-photon absorption in bilayer graphene," *Nano Lett.*, Vol. 11, 2622, 2011.
2. Hendry, E., P. J. Hale, J. Moger, A. K. Savchenko, and S. A. Mikhailov, "Coherent nonlinear optical response of graphene," *Phys. Rev. Lett.*, Vol. 105, 097401, 2010.
3. Chae, D.-H., T. Utikal, S. Weisenburger, H. Giessen, K. V. Klitzing, M. Lippitz, and J. Smet, "Excitonic fano resonance in free-standing graphene," *Nano Lett.*, Vol. 11, 1379, 2011.

Ultrafast Nonlinearities of Metallic 3D Metamaterials

Ventsislav K. Valev, **Petros Farah**, **Stefano Salvatore**,
Silvia Vignolini, **Ulli Steiner**, **and Jeremy J. Baumberg**
NanoPhotonics Centre, Department of Physics, University of Cambridge, UK

Abstract— The optical properties of metals have become of extreme interest recently due to the rise of the fields of plasmonics and metamaterials. Engineering metallic nanostructures at sub-wavelength scales has been shown to lead to metamaterials with novel optical properties [1]. Realizing three-dimensional (3D) metallic architectures for visible wavelengths has proven experimentally challenging, as it requires unit cells and features on the 10 nm scale. Our recent breakthrough in fabricating reliable 3D metamaterials on large-scales with unit cells of 50 nm and below allows investigation of their modified optical nonlinearities.

Through a block-copolymerbased self-assembly technique we produce 3D metamaterials with spectral features in the visible region, built on a gyroidal architecture [2, 5]. These materials exhibit a number of novel optical properties including anisotropic linear and circular dichroism.

Using a phenomenological model, derived from metamaterial theory, an effective dielectric function for the gold gyroid films is produced which successfully reproduces their linear optical response. By applying this model to samples with tuned structural parameters we have shown that nanostructuring the gold inhibits the free motion of the metallic electrons. As a result, the electrons in these nanostructures appear twice as heavy to a driving electromagnetic field (doubling their effective mass). Furthermore the nanostructured gold leads to a large increase in the damping of the electrons.

The nonlinear response of these nanostructured metamaterials is investigated and found to be over an order of magnitude stronger than bulk gold. Using a novel broadband lock-in technique [3], we spectrally resolve the transient changes in the optical properties of the metamaterial. The spectra are evaluated simultaneously across the entire optical range. From these spectra, the changes to the parameters of the dielectric function producing the nonlinear response have been identified. Through this we see how small optically-induced perturbations of the intrinsic dielectric function of gold lead to large changes in the effective parameters of the metamaterial, transiently increasing the electron effective mass by 50% over a few picoseconds.

Nanostructured metallic metamaterials, such as the ones presented here, offer a new route for exploiting the strong nonlinearities of metals in a new class of nonlinear materials. Founded on our understanding of the intrinsic nonlinear response of gold [4], we are able to investigate the response of such 3D gyroid metamaterials. Their optical response based on the transient perturbation of the gold dielectric functions gives a range of new tuning mechanisms and elicits insight into the mechanisms governing the metamaterial novel optical properties.

REFERENCES

1. Pendry, J. B., et al., "Extremely low frequency plasmons in metallic mesostructures," *Phys. Rev. Lett.*, Vol. 76, 4773, 1996.
2. Vignolini, S., et al., "A 3D optical metamaterial made by self-assembly," *Adv. Mater.*, Vol. 24, OP23, 2012.
3. Smith, R. J., et al., "Parallel detection in laser ultrasonics," *J. Phys. Conf. Ser.*, Vol. 214, 012006, 2010.
4. Farah, P., et al., "Ultrafast nonlinearities of minibands in metallodielectric Bragg resonators," *Phys. Rev. B*, Vol. 84, 125442, 2011.
5. Salvatore, S., et al., "Tunable 3D extended, self-assembled gold metamaterials with enhanced light transmission," *Adv. Mater.*, 2013, in Press.

Large Area Enhancement of Optical Nonlinearities of Ultrathin Gold Films

Stefano De Zuani, Tobias Knoblauch, Audrey Berrier, Bruno Gompf, and Martin Dressel
Physikalisches Institut, Universtät Stuttgart, Pfaffenwaldring 57, Germany

Abstract— Controlling the nonlinear properties of a material is very attractive for novel photonic applications. In particular, modifying the material at the nanoscale influences both its linear and non-linear optical properties. Plasmonic nanostructures attract nowadays lots of interest as they show good prospects for enhancement of nonlinearities. However, most of the fabricated nanostructures are confined to small active areas and cannot yield large area field enhancements. Here we propose to use evaporated thin films of noble metals around the percolation threshold, where the sample geometry can be controlled in order to maximize the field enhancements. Such samples can be fabricated over large areas at wafer scale. The nonlinear properties of the sample are monitored by the collection of second harmonic generated signal under Nd:YAG laser illumination.

When a metal is evaporated onto an insulating substrate, the atoms are migrating on the surface and start to form isolated clusters. Close to percolation the metallic particles form a network of almost touching nanoparticles where the area of large field enhancement can be maximized. Crossing the percolation, the insulator to metal transition occurs and the conductivity of the film increases [1]. The optical conductivity of such ultrathin metal films is dominated by a Drude component starting at the percolation threshold in the low frequency range and by the localized surface plasmon resonances of the isolated particles. The interplay of both components leads to a predicted dielectric anomaly in the infrared region with a divergence of the real part of the dielectric constant at the insulator to metal transition [2, 3]. We control the approach to percolation using metallic seeds as templates, by pre-heating the substrate, or by modifying its surface properties. The evolution of the optical properties of the sample is controlled by in-situ monitoring during evaporation. Scanning electron and atomic force microscopy provide information about the topography of the samples. We present a systematic study of the linear and nonlinear properties of ultrathin gold layers around the percolation threshold in order to correlate the dielectric anomaly in the real dielectric constant, the maximum of the local field enhancements and the nonlinear signal of the films. The role of the capacitive coupling of the almost touching gold clusters on the nonlinear properties of the metallic film is also discussed as well as further methods to control the enhancement. This work brings fundamental understanding of the nonlinear properties of ultrathin metallic films and it opens the way to an active tailoring of the nonlinear signals.

REFERENCES

1. Clerc, J. P., G. Giraud, J. M. Laugier, and J. M. Luck, *Adv. Phys.*, Vol. 39, 191, 1990.
2. Efros, A. L. and B. I. Shklovskii, *Phys. Stat. Sol. B*, Vol. 76, 475, 1976.
3. Hövel, M., B. Gompf, and M. Dressel, *Phys. Rev. B*, Vol. 81, 035402, 2010.

Session 2A8
SC1: Analytical and Numerical Techniques for Periodic Structures

Two-dimensional Band Solitons in Defected Optical Lattices
Jianhua Zeng, Boris A. Malomed, ... 538
Modal Analysis of Lamellar Gratings: A New Formulation Based on B-splines Expansion
Gérard Granet, ... 539
Differential Method for Imperfectly Periodic Gratings
Koki Watanabe, ... 540
Coupled Mode Formulation of Two Contra-directional Photonic Crystal Waveguide Couplers
Vakhtang Jandieri, Kiyotoshi Yasumoto, ... 541
Single Layer Cylindrical Frequency Selective Structures for Radome Applications
Elia Di Salvo, Fabrizio Frezza, Endri Stoja, Nicola Tedeschi, ... 542
Analysis of Scattering from Doubly Periodic Layers with Non Parallel Interfaces by Means of the Curvilinear Coordinate Method
Gérard Granet, ... 543
Analytic Dispersion Relation of Periodic Array of Magnetodielectric Circular Cylinders
Woo-Jin Byun, Yong Heui Cho, Do-Hoon Kwon, ... 544
Surface Plasmon Resonance Structure with Ferromagnetic Grating
Jaromir Pistora, Jaroslav Vlcek, Michal Lesnak, ... 545
Comparison between Two Methods for Directivity Enhancement of Antennas through 2-D EBGs
Silvio Ceccuzzi, Lara Pajewski, Cristina Ponti, Giuseppe Schettini, ... 546
Leakage Loss of Post-wall Waveguides Based on a Model of Two-dimensional Photonic Crystal Waveguides
Kiyotoshi Yasumoto, Hiroshi Maeda, Vakhtang Jandieri, ... 547

Two-dimensional Band Solitons in Defected Optical Lattices

Jianhua Zeng[1] and Boris A. Malomed[2]

[1]State Key Laboratory of Low Dimensional Quantum Physics
Department of Physics, Tsinghua University, Beijing 100084, China
[2]Department of Physical Electronics, School of Electrical Engineering
Faculty of Engineering, Tel Aviv University, Tel Aviv 69978, Israel

Abstract— Periodic (lattice) potentials have played an increasingly important role in the control of optical and matter waves. The potentials can be induced, severally, by optical lattice (OL) in Bose-Einstein condensates (BECs) [1], and by photonic crystals (periodic dielectric) in optics [2]. In much the same way as a semiconductor crystal affects the electron motion, the periodic potentials allow the possibilities of creating different kinds of solitons, both ordinary ones (exist within semi-infinite gap of the relevant band spectrum) and gap solitons, supported by a balance between the lattice potentials and self-attractive or repulsive nonlinearity, respectively, see a recent review [3]. More recently, the soliton dynamics in nonlinear lattices [3–5] and parity-time OL [6], have also drawn a lot of attention. Recently, a new type of localized state, the so-called truncated nonlinear Bloch waves (or gap waves as they only appear in finite bandgaps), has been observed [7–9]. However, it is still an open question to find stable localized modes in Bloch bands.

Here, by means of numerical methods, we demonstrate that, under the action of the self-focusing nonlinearity, a new type of two-dimensional (2D) band solitons (reside in the Bloch bands of the eigenvalue spectrum) could also be stabilized in an OL with a single defect. The band solitons are completely stable in the first band, and partly stable in the second. Together with the regular solitons populating the semi-infinite bandgap, and gap solitons nested in the first finite bandgap (between the first and second Bloch bands), the band solitons form a continuous family covering the entire band structure. Besides, stable 2D gap solitons pinned to the defect can also be generated in the same model. The present system for OL with multiple defects can support stable dipole-mode solitons and vortices too, in the first band and bandgap alike. Our results suggest new opportunities for using defected OL to create and stabilize 2D band and gap solitons in self-focusing media. The predicted solitons can be created in Bose-Einstein condensates and photonic crystals.

REFERENCES

1. Pethick, C. J. and H. Smith, *Bose-Einstein Condensate in Dilute Gas*, Cambridge University Press, Cambridge, 2008.
2. Joannopoulos, J. D., S. G. Johnson, J. N. Winn, and R. D. Meade, *Photonic Crystals: Molding the Flow of Light*, Princeton University Press, Princeton, 2008.
3. Kartashov, Y. V., B. A. Malomed, and L. Torner, "Solitons in nonlinear lattices," *Rev. Mod. Phys.*, Vol. 83, 247–305, 2011.
4. Zeng, J. and B. A. Malomed, "Stabilization of one-dimensional solitons against the critical collapse by quintic nonlinear lattices," *Phys. Rev. A*, Vol. 85, 023824, 2012.
5. Zeng, J. and B. A. Malomed, "Two-dimensional solitons and vortices in media with incommensurate linear and nonlinear lattice potentials," *Phys. Scr.*, Vol. T149, 014035, 2012.
6. Zeng, J. and Y. Lan, "Two-dimensional solitons in PT linear lattice potentials," *Phys. Rev. E*, Vol. 85, 047601, 2012.
7. Anker, T., M. Albiez, R. Gati, S. Hunsmann, B. Eier-mann, A. Trombettoni, and M. K. Oberthaler, "Nonlinear self-trapping of matter waves in periodic potentials," *Phys. Rev. Lett.*, Vol. 94, 020403, 2005.
8. Alexander, T. J., E. A. Ostrovskaya, and Yu. S. Kivshar, "Self-trapped nonlinear matter waves in periodic potentials," *Phys. Rev. Lett.*, Vol. 96, 040401, 2006.
9. Bennet, F. H., T. J. Alexander, F. Haslinger, A. Mitchell, D. N. Neshev, and Y. S. Kivshar, "Observation of nonlinear self-trapping of broad beams in defocusing waveguide arrays," *Phys. Rev. Lett.*, Vol. 106, 093901, 2011.

Modal Analysis of Lamellar Gratings: A New Formulation Based on B-splines Expansion

Gérard Granet[1, 2]

[1]Clermont Universite, Universite Blaise Pascal, LASMEA, BP 10448, Clermont-Ferrand F-63000, France
[2]CNRS, UMR 6602, LASMEA, Aubiere F-63177, France

Abstract— Among the many existing rigorous methods for analyzing diffraction by periodic or aperiodic structures, Fourier based methods like the differential method, the Fourier Modal method, and the C method, are certainly the most popular. For that reason, they have been intensively researched and they can now handle most problems in optics and photonics. The above three methods share a common feature: they are based on an expansion of the field in terms of periodic functions. The intrinsic drawback of such a representation is that it requires a large number of terms to describe efficiently electromagnetic fields with sharp variations as is the case with highly conducting gratings. We are thus lead to seek alternative expansions. Within the framework of numerical modal methods, polynomial expansions have already been used. Similarly, the method of lines [1] and the finite difference method in the frequency domain [2] may be considered as modal methods in which the field is expanded on pulse basis. The above formulations of the modal method compared favorably with the Fourier modal method for metallic gratings. Following the pioneering work of Edee et al. [3], this presentation is devoted to the modal method in which adaptive spatial resolution and a piecewise linear representation of the field are introduced.

The presentation is organized as follows: first, we present the grating problem and its solution in terms of eigenmodes; then, the matrix from which eigenmodes are obtained is derived by using the method of moments [4] in copnjontion with B-spline expansion. Various numerical variants of the method are implemented. Lastly, we compare the convergence rate of the present methods with that of the finite difference modal method and of the Fourier Modal Method.

REFERENCES

1. Pregla, R. and W. Pasher, *The Method of Lines Techniques for Microwaves and Millimeter-wave Passive Structures*, Wiley Interscience, 1989.
2. Lalanne, P. and J. P. Hugonin, "Numerical performance of finite-difference modal method for the electromagnetic analysis of one-dimensional grating," *J. Opt. Soc. Am.*, Vol. 17, No. 6, June 2000.
3. Edee, K., P. Schiavone, and G. Granet, "Analysis of defect in extreme UV lithography mask using a modal method based on nodal B-spline expansion," *J. J. A. P.*, Vol. 44, 6458–6462, 2005.
4. Harrington, R., *Field Computation by Moment Methods*, The Macmillan, New York, 1968.

Differential Method for Imperfectly Periodic Gratings

Koki Watanabe
Fukuoka Institute of Technology, Japan

Abstract— This paper considers the two-dimensional electromagnetic scattering problem of diffraction gratings in which structural periodicity is locally collapsed, and presents a spectral-domain formulation based on the differential method [1] and the pseudo-periodic Fourier transform (PPFT) [2]. The differential method is a widely used approach in the analyses of diffraction gratings for the plane-wave incidence. The Floquet theorem asserts that the fields in periodic structures are expressed in a superposition of the Floquet-modes, which are the eigenmodes with pseudo-periodic property. The plane-wave excites only one Floquet-mode in a perfectly periodic structure, and the excited fields have a pseudo-periodic property. This implies that the analysis region can be reduced to only one periodicity cell and the fields have equidistant discrete spectra in the wavenumber space. Therefore, the field components can be expressed in the generalized Fourier series expansions, and many numerical approaches to periodic structures are based on the Floquet theorem. However, the structure under consideration is an imperfectly periodic structure and approaches based on the Floquet theorem cannot be applied directly. To solve the difficulty, the PPFT is introduced. The PPFT converts an arbitrary function into pseudo-periodic one and the scattering problem from imperfectly periodic structure becomes possible to be formulated by the conventional grating theory. The PPFT uses a transform parameter that relates to the wavenumber and the transformed function has a periodic property in terms of the parameter. The discretization scheme required in the spectral-domain approach can be considered only inside the Brillouin zone owing to this periodicity.

REFERENCES

1. Vincent, P., "Differential methods," *Electromagnetic Theory of Gratings*, 101–121, R. Petit, Editor, Springer-Verlag, Berlin, 1980.
2. Watanabe, K. and K. Yasumoto, "Two-dimensional electromagnetic scattering of non-plane incident waves by periodic structures," *Progress In Electromagnetics Research*, Vol. 74, 241–271, 2007.

Coupled Mode Formulation of Two Contra-directional Photonic Crystal Waveguide Couplers

Vakhtang Jandieri[1] and Kiyotoshi Yasumoto[2]

[1]School of Electronics Engineering and Computer Science
Kyungpook National University, Republic of Korea
[2]College of Information Science and Technology, Nanjing Forestry University, China

Abstract— Photonic crystals are periodic structures that prohibit the propagation of electromagnetic waves at some frequencies. Photonic crystals have inspired a lot of interest due to their wide application for controlling the propagation of light. A photonic crystal waveguide (PCW) is made by removing a row of either air columns or dielectric rods that result in multimode guiding. If the PCWs are placed in close proximity, a coupled PCW is formed and the optical power is efficiently transferred from one PCW to another [1]. It allows us to realize high performance ultra-compact power dividers, filters and couplers in integrated optics.

Recently, K. Yasumoto and V. Jandieri have proposed the coupled-mode formulation for two coupled PCWs [2]. Using a perturbation theory, the first-order coupled-mode equations have been systematically derived, which govern the evolution of the modal amplitudes in each individual PCW. The proposed coupled-mode formulation has been successfully applied to analyze the propagation constants of the supermodes of the coupled symmetric pillar and air-hole type directional PCWs [2].

In this paper the proposed coupled-mode formulation [2] is applied to study the contra-directional coupling between two asymmetric PCWs, consisting of the hexagonal lattice of the air-hole circular rods situated in a dielectric medium. The geometry of the problem is illustrated in Fig. 1. The dielectric permittivity of the background medium is $\varepsilon_s = 11.56\varepsilon_0$ and the radius of the air-holes is $r = 0.38h$, where h is a period of the photonic crystals. The width of the upper PCW is $0.8\sqrt{3h}$ and the width of the lower photonic crystal, which is displaced by a distance $0.5h$ with respect to the upper PCW, is $(\sqrt{3}/2 + 0.2)h$. The dispersion diagrams of the isolated PCWs as well as the coupled PCWs are numerically studied. When the modes of two isolated PCWs interact at the phase matching point, the repulsion effect between the modes appears and the contra-directional phenomenon between the forward and backward waves occurs. Based on the proposed coupled-mode formulation, the optical power exchange between the PCWs is investigated and the transmission spectra at different output ports of the PCWs are analyzed. The effect of the barrier layers between the PCWs on the transmission spectra and the coupling length of the PCWs device are studied in a very detail.

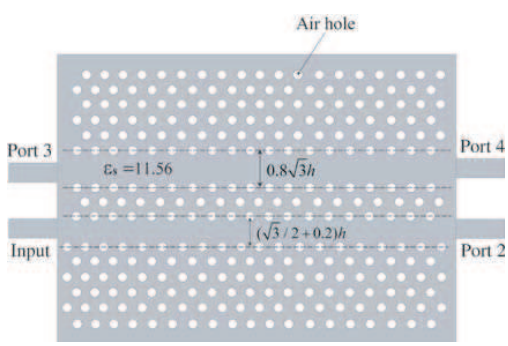

Figure 1: Cross-sectional view of two contra-directional photonic crystals waveguide couplers.

REFERENCES

1. Qiu, M. and M. Swillo, "Contra-directional coupling between two-dimensional photonic crystal waveguides," *Photonics & Nanostructures — Fundamentals & Applications*, Vol. 1, 23–30, 2003.
2. Yasumoto, K., V. Jandieri, and Y. Liu, "Coupled-mode formulation of two-parallel photonic crystal waveguides," *Journal of the Optical Society of America A*, Vol. 30, 96–101, 2013.

Single Layer Cylindrical Frequency Selective Structures for Radome Applications

E. Di Salvo, **F. Frezza**, **E. Stoja**, **and N. Tedeschi**
Department of Information Engineering, Electronics and Telecommunications
Sapienza University of Rome, Via Eudossiana 18, Rome 00184, Italy

Abstract— An analysis technique is proposed for Cylindrical Frequency Selective Surfaces (CFSS), at microwave wavelength, particularly useful for antenna radome applications.

Frequency Selective Surfaces (FSS) have been an extensive research topic since a long time, but the case of CFSS, which are of interest for antenna radome applications, has been less studied in the literature [1, 2].

Figure 1 shows the infinitely long cylindrical structure we have considered. It may consist of free-standing conducting rectangular patches, or of a perfectly conducting circular cylinder perforated with axial slots. Patches or slots are located periodically along the circumferential direction φ (T_φ periodicity) and along the axial direction z (T_Z periodicity).

For the case of free-standing conducting patches, a cylindrical wave with TM polarization ($E_\varphi = 0$; $H_Z = 0$), generated by an electric line current located on the cylinder axis, is considered. For the case of free-standing slots, a cylindrical wave with TE polarization ($E_Z = 0$; $H_\varphi = 0$) generated by a magnetic line current located on the cylinder axis is considered. It is assumed $w < l/10$ and $w < \lambda/20$ where λ is the wavelength of the incident field. Scattered fields are calculated with a Matlab code implemented by ourselves, according to the procedure described in [2]: however, we have extended this formulation for structures with a larger number of circumferential patches/slots (e.g., more than 64). Using approximated expressions [3, 4] and Miller's algorithm, numerical problems of overflow and underflow of Matlab variables due to large-order and large-argument Bessel functions have been avoided.

The opacity, or transparency, of the surfaces for a suitable frequency range in terms of transmission/reflection coefficients is computed. Comparison with previous results given in the literature and with data obtained through Electromagnetic Simulators have been performed.

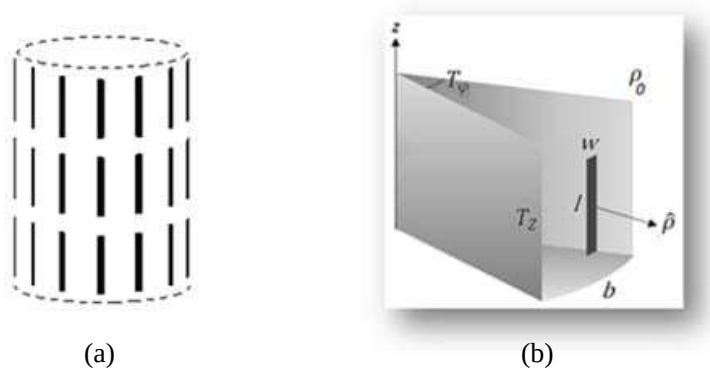

Figure 1: (a) Cylindrical frequency selective surface, made by conducting patches or slots. (b) Relevant unit cell parameters.

REFERENCES

1. Cwik, T., "Coupling into and scattering from cylindrical structures covered periodically with metallic patches," *IEEE Transactions on Antennas and Propagation*, Vol. 38, 220–226, February 1990.
2. Uzer, A. and T. Ege, "Radiation from a current filament located inside a cylindrical frequency selective surface," *ETRI Journal*, Vol. 26, No. 5, 481–485, October 2004.
3. Abramowitz, M. and I. A. Stegun, Editors, *Handbook Of Mathematical Functions: With Formulas, Graphs, and Mathematical Tables*, Dover, New York, 1972.
4. Watson, G. N., *A Treatise on the Theory of Bessel Functions*, Cambridge University Press, London, 1962.

Analysis of Scattering from Doubly Periodic Layers with Non Parallel Interfaces by Means of the Curvilinear Coordinate Method

Gérard Granet[1, 2]

[1]Clermont Universite, Universite Blaise Pascal, LASMEA, BP 10448, Clermont-Ferrand F-63000, France
[2]CNRS, UMR 6602, LASMEA, Aubiere F-63177, France

Abstract— We consider the problem of scattering from doubly periodic layers with non parallel interfaces. In fact, this problem is reduced to the canonical case of a layer with two periodic faces separated by a mean distance h. Functions $a_1(x, y)$ and $a_2(x, y)$ describe the upper and lower interfaces respectively. The only restriction is that all faces of the structure should have the same periodicity.

The solution to the electromagnetic problem is obtained by using the Curvilinear Coordinate Method which is an exact modal method based on Maxwell's equations under covariant form written in a non-orthogonal coordinate system [1]. In our previous work [2, 3], we have presented the implementation of this covariant formalism for analyzing 1D and 2-D multilayer structures. The present work deals with a new development of the Curvilinear Coordinate Method as applied to scattering from layers with non identical faces. Indeed, since each face is associated to a coordinate system, it is necessary to match eigensolutions obtained in one coordinate system to those obtained in the other one. The above approach has already been used in the case of singly periodic structures. For the first time, it is implemented for doubly periodic layers. The key point of the method is the derivation of the whole solution from a single potential as is done in classical wave-gude theory. This potential is obtained as a solution of the scalar Helmholtz equation written in curvilinear coordinates. Lastly, boundary conditions are written with the S-matrix algorithm in which we separate carefully interface S-matrix and layer S-matrix.

REFERENCES

1. Chandezon, J., D. Maystre, and G. Raoult, "A new theoretical method for diffraction gratings and its numerical application," *J. Opt.*, Vol. 11, 235–241, Paris, 1980.
2. Granet, G., J. P. Plumey, and J. Chandezon, "Scattering by a dielectric layer with non identical faces," *Pure and Applied Optics*, Vol. 4, 1–5, 1995.
3. Granet, G., "Analysis of diffraction by surface-relief crossed gratings with use of the Chandezon method: Application to multilayer crossed gratings," *J. Opt. Soc. Am. A*, Vol. 15, 1121–1131, 1998.

Analytic Dispersion Relation of Periodic Array of Magnetodielectric Circular Cylinders

W. J. Byun[1], **Y. H. Cho**[2], **and D.-H. Kwon**[3]

[1]Electronics and Telecommunications Research Institute (ETRI), Korea
[2]Mokwon University, Korea
[3]University of Massachusetts Amherst, USA

Abstract— A periodic array of two-dimensional (2D) magnetodielectric circular cylinders is analyzed with a standard mode-matching technique (MMT) and common-area concept in order to get the dispersion relation of a periodic waveguide. Although the elements of an array is not connected each other with respect to the propagation direction, it can be used for a reliable transmission line. A great example of this type is a substrate integrated waveguide (SIW) or a terahertz transmission line composed of nanowires. The field representations of a unit cell are given in the Cartesian and circular cylindrical coordinate systems. Since the array has a finite periodicity, we need the Cartesian coordinate system in the unit cell to consider a periodic array. The mixed coordinate characteristics in the geometry make it difficult for us to apply a standard MMT. To this end, we introduce a MMT based on the Floquet theorem and common-area concept which was proposed for the mixed coordinate systems. By matching the boundary conditions around a magnetodielectric circular cylinder in the unit cell, we obtain analytic simultaneous equations for the dispersion relation. An elementary root searching algorithm is enough to find a propagation constant with which the determinant of simultaneous equations is zero. The dispersion results showed the wave guiding condition for a robust transmission and will be compared with the scattering behaviors of the same geometry. The scattering equations for a periodic array of 2D magnetodielectric circular cylinders have been already proposed in the previous work. Our approach for the dispersion relation can be easily extended to the structures composed of PEC (Perfect Electric Conductor) and PMC (Perfect Magnetic Conductor) instead of magnetodielectric materials.

Surface Plasmon Resonance Structure with Ferromagnetic Grating

Jaromír Pištora[1], **Jaroslav Vlček**[2], **and Michal Lesňák**[1]

[1]Nanotechnology Centre, VSB — Technical University of Ostrava
17. Listopadu 15, Ostrava-Poruba 708 33, Czech Republic
[2]Department of Mathematics, VSB — Technical University of Ostrava
17. Listopadu 15, Ostrava-Poruba 708 33, Czech Republic

Abstract— Theoretical model of magneto optical binary grating with cylindrical micro dots, where the permittivity anisotropy is induced by external magnetic field has been presented [1]. As showed obtained results, the ratio r/Λ (the dot radius r and period Λ) influences magneto-optical (MO) response more expressively than small changes of a single parameter. The non-reciprocity of MO reflection response by surface plasmon excitation in a planar glass/Fe/Au/air system with prism coupling was analyzed with aim to find the optimal thicknesses of metallic layers with regard to the reflectance sensitivity to an external magnetic field [2].

In our recent contribution we combine plasmon wave structure with periodic magneto-optical system (Fig. 1).

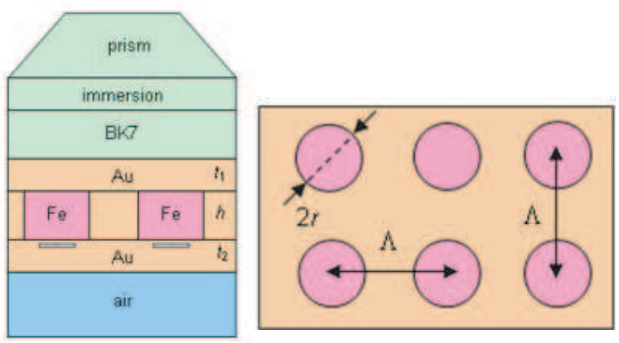

Figure 1: MO-SPR geometry.

We analyzed for different periodicity Λ ($\Lambda = 4000\,\text{nm}$, $400\,\text{nm}$, fill factor $F = \pi r^2/\Lambda^2 = 0.24$) and golden films thicknesses t_1 (from 0 to 15 nm) and t_2 (from 20 to 5 nm) the reflectance and Kerr magneto-optical parameters of applied structure. The dot thickness has been fixed to 20 nm, the incidence 632.8 nm laser beam was p-polarized. The results show the sharp reflectance extreme (up to $R_p = 0.85$) as function of incidence angle. This dependance is importantly modified by t_1 Au film thickness. The influence of magneto-optical activity of Fe grating has been studied by Kerr effect in longitudinal configuration. The maximum of rotation achieves to 4 mdeg, the extreme ellipticity value is about 3 mdeg. The influence of t_1 thickness on Kerr parameters is observed too. The achieved results offer new approaches for MO surface plasmon resonance sensing elements.

REFERENCES

1. Vlček, J., J. Pištora, D. Ciprian, T. Yamaguchi, and K. Postava, "Modelling of two-dimensional magneto optical gratings," *Trans. Mag. Soc. Jap.*, Vol. 2, 179–182, 2002.
2. Vlček, J., M. Lesňák, J. Pištora, and O. Životský, "Magneto-optical sensing of magnetic field," *Opt. Comm.*, Vol. 286, 372–377, 2013.

Comparison between Two Methods for Directivity Enhancement of Antennas through 2-D EBGs

S. Ceccuzzi, L. Pajewski, C. Ponti, and G. Schettini
Department of Engineering, "Roma Tre" University, Roma, Italy

Abstract— Electromagnetic Band-Gap (EBG) materials have been repeatedly proven to be a passive, effective means of enhancing the directivity of single radiators, thus allowing to avoid the use of complex arrays relying on troublesome feeding networks. Two methods mainly received attention in this sense: the one realizes a resonator antenna by sandwiching the radiator in between a ground plane and an EBG material working in the bandgap, while the other embeds it inside an EBG structure working at the edge of the bandgap. In the former case a cavity is created and the periodically spaced elements act as a partially reflecting surface, while in the latter configuration, the EBG structure behaves like an epsilon near zero material and can generate equiphase wavefronts at its boundaries.

Both mechanisms have been theoretically explained and experimentally demonstrated, however archived literature misses an exhaustive benchmark between them; this is indeed the aim pursued by this paper. The comparison is presented for a set of two-dimensional EBG structures, consisting of either triangular or square arrangements of dielectric cylinders, excited by a 8 GHz, TM-polarized, line source. After a preliminary lattice design based on the dispersion diagrams and transmission curves, different finite-size configurations, obtained by changing the number of layers as well as the amount of cylinders per layer, have been locally optimized with a full-wave solver. The two approaches of directivity enhancement are compared in terms of radiative and geometrical parameters also with reference to the performance of a single line source radiating in presence of a ground plane. In addition the radiation patterns of the most attractive configurations are shown.

The resonator antenna generally gives the highest directivities, but there are operative conditions in which it is outperformed by the method with embedded source. In details, the former approach results more suitable in case of low-profile arrangements, i.e., very few layers with many rods, while the latter one better fits compact configuration, having more layers with few cylinders. In general, depending on specific requirements, each method features strengths and weaknesses, which are fully discussed in the paper together with sketching further relevant analyses such as dual-band antennas or three-dimensional structures.

Leakage Loss of Post-wall Waveguides Based on a Model of Two-dimensional Photonic Crystal Waveguides

Kiyotoshi Yasumoto[1], **Hiroshi Maeda**[1], **and Vakhtang Jandieri**[2]

[1]Faculty of Information Engineering, Fukuoka Institute of Technology, Fukuoka 811-0295, Japan
[2]School of Electrical Engineering and Computer Science
Kyungpook National University, Daegu 702-701, Republic of Korea

Abstract— Post-wall waveguides, also called laminated waveguides or substrate integrated waveguides [1], have received a growing attention because of their promising applications to planar circuit components operating in the microwave and millimeter wave frequency range. A post-wall waveguide, as illustrated in Fig. 1, is composed of periodic arrays of conducting circular posts embedded in a dielectric substrate that connect two parallel conducting plates. Although the post arrays in both sides may be N-layered, Fig. 1 shows a simple structure formed by a single array. This sort of periodic waveguide is quite similar to a two-dimensional photonic crystal waveguide [2] formed by parallel circular conducting rods which are infinitely long in the y direction. Recently we have proposed a novel semi-analytical approach [3] for post-wall waveguides based on the model of two-dimensional photonic crystal waveguide (PCW). The modal properties of the post-wall waveguide can be analyzed using the generalized reflection and transmission matrices [2] of N-layered post arrays viewed from the guiding region, which is expressed in term of the T-matrix of the isolated circular rod and the lattice sums for the periodic arrangement of the rods.

The post-wall waveguide is inherently a laterally open structure so long as the number N of the post array layers is finite. A part of the electromagnetic energy may leak out through the periodic gaps between adjacent posts, thus resulting in a leakage loss. If the gap length $h - 2r$ in Fig. 1 is sufficiently smaller than the half of wavelength and the post walls are stacked with enough number, the leakage effect and hence the attenuation in propagation may be treated as a small perturbation. In this paper, we incorporate the perturbation theory based on the energy conservation principle in the model of photonic crystal waveguides and analyze the leakage loss of the post-wall waveguide.

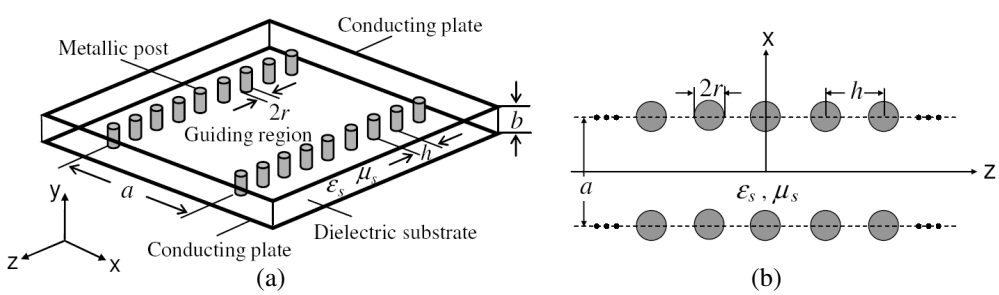

Figure 1: Schematic of a post-wall waveguide. (a) 3-D view and (b) transversal view in the x-z plane.

ACKNOWLEDGMENT

This work was supported in part by Grant-in-Aid for Scientific Research (C) 24560430.

REFERENCES

1. Deslandes, D. and K. Wu, "Accurate modeling, wave mechanisms, and design considerations of a substrate integrated waveguide," *IEEE Trans. Microwave Theory Tech.*, Vol. 54, No. 6, 2516–2526, 2006.
2. Yasumoto, K., H. Jia, and K. Sun, "Rigorous modal analysis of two-dimensional photonic crystal waveguides," *Radio Sci.*, Vol. 40, No. 6, RS6S02, 2005.
3. Yasumoto, K., H. Maeda, and V. Jandieri, "Modal analysis of post-wall waveguides based on a model of two-dimensional photonic crystal waveguides," *PIERS Proceedings*, Taipei, March 25–28, 2013.

Session 2A9a
SC4: Paper-based Microwave Circuits and Antennas

Manufacturing and Applications of Screen-printed RFID Tags on Paper Substrate
Johanna Virkki, Toni Björninen, Sari Merilampi, Lauri Sydanheimo, Leena Ukkonen, ... 550

Printable RFID Antenna with Embedded Sensor and Calibration Functions
Yasar Amin, Rajeev Kumar Kanth, Pasi Liljeberg, Adeel Akram, Qiang Chen, Li-Rong Zheng, Hannu Tenhunen, ... 552

Implementation of Substrate Integrated Waveguide (SIW) by Inkjet-printing on Paper Substrate
Riccardo Moro, Sangkil Kim, Maurizio Bozzi, Manos M. Tentzeris, ... 553

On the Influence of Edge Roughness in High-speed RFID Antenna Manufacturing Processes
Jinlan Gao, Johan Siden, Hans-Erik Nilsson, ... 554

Design of Sierpinski Grid Patch Antenna for Multiband Application
Rajeev Kumar Kanth, Pasi Liljeberg, Hannu Tenhunen, Yasar Amin, Qiang Chen, Axel Janstch, Li-Rong Zheng, Harish Kumar, ... 556

A Battery Free RFID Sensor for Quality Detection of Food Products
Dat-Son Nguyen, Gia-Tam Phan, Tien-Thong Pham, Nguyen-Ngan Le, Mau-Chien Dang, Smail Tedjni, ... 557

Manufacturing and Applications of Screen-printed RFID Tags on Paper Substrate

Johanna Virkki[1], **Toni Björninen**[1], **Sari Merilampi**[2], **Lauri Sydänheimo**[1], **and Leena Ukkonen**[1]

[1]Department of Electronics and Communications Engineering
Tampere University of Technology, P. O. Box 692, Tampere 33101, Finland
[2]Faculty of Technology and Maritime Management
Satakunta University of Applied Sciences, Tekniikantie 2, Pori 28600, Finland

Abstract— Paper is ubiquitous in everyday life and a truly environmental-friendly, low-cost, and high potential substrate for electronics. However, applying electronics on paper is challenging [1]. The paper surface is not only very rough compared to plastics, but is also porous. While this is detrimental for most electronic devices manufactured directly onto paper substrates, there are also approaches that are compatible with the rough and absorptive paper surface [1–3]. Our approach is to use screen printing to fabricate an RFID (radiofrequency identification) tag antenna pattern directly on paper. The reason for this is the future goal of all-printed [4] RFID tag on paper, in which also the semiconductor chip would be printed and no additional process steps would then be required. This kind of product would offer cost savings and countless applications.

RFID is an effective automatic identification technology. In passive RFID systems, the RFID tag has no on-board power source and it uses the power emitted from the reader to energize itself and backscatter its data. Passive RFID tags are simple in structure, light in weight, inexpensive, and offer virtually unlimited operational lifetime and long read ranges. With passive RFID systems, the product information is restored throughout the lifecycle, especially if the tag is solid part of the product [5].

In this study, passive ultra high frequency (UHF) RFID tag antennas were manufactured by screen printing polymer thick film silver ink, mainly consisting of silver particles mixed in polyester resin (particle sizes from 3 to 15 µm), on a paper substrate. Plain copy paper (80 g/m^2) was used as the substrate material. After printing, the tags were cured for 20 minutes in 120°C. This manufacturing process is described more detailed in the full paper. After printing and curing, NXP UCODE G2iL ICs were attached to the samples using a conductive silver epoxy resin. The characteristics of the manufactured RFID tags were measured in different end applications (See Figure 1). The measurements were conducted with an RFID tester containing an RFID reader unit with a capability to a power-frequency sweeps. We performed two different measurements: path loss and threshold power measurement.

Screen printed passive UHF RFID tags on a paper substrate offer a great potential, e.g., for packaging industry, libraries, and postal services. According to our measurements, their performance is without a doubt sufficient for many such applications. The measurement results are presented in the full paper.

(a) (b)

Figure 1: An antenna printed on (a) a paper substrate and an RFID tag used in a paper package and (b) in an envelope.

REFERENCES

1. Tobjörk, D. and R. Österbacka, "Paper electronics," *Advanced Materials*, Vol. 23, No. 17, 1935–1961, 2011.
2. Blayo, A. and B. Pineaux, "Printing processes and their potential for RFID printing," *Conference on Smart Objects and Ambient Intelligence: Innovative Context-aware Services: Usages and Technologies*, 2005.
3. Shaker, G., S. Safavi-Naeini, N. Sangary, and M. M. Tentzeris, "Inkjet printing of ultrawideband (UWB) antennas on paper-based substrates," *IEEE Antennas and Wireless Propagation Letters*, Vol. 10, 111–114, 2011.
4. Subramanian, V., J. M. J. Frechet, P. C. Chang, D. C. Huang, J. B. Lee, S. E. Molesa, A. R. Murphy, D. R. Redinger, and S. K. Volkman, "Progress toward development of all-printed RFID tags: Materials, processes, and devices," *Proceedings of the IEEE*, Vol. 93, No. 7, 1330–1338, 2005.
5. Dobkin, M., *The RF in RFID*, Wiley, New York, 2010.

Printable RFID Antenna with Embedded Sensor and Calibration Functions

Y. Amin[1,2], R. K. Kanth[3], P. Liljeberg[3], A. Akram[2], Q. Chen[1], L.-R. Zheng[1], and H. Tenhunen[1,3]

[1]iPack VINN Excellence Center, Royal Institute of Technology (KTH), Stockholm, Sweden
[2]Telecommunication Engineering Department, University of Engineering and Technology Taxila, Pakistan
[3]Turku Centre for Computer Science, University of Turku, Finland

Abstract— In this paper, an RFID tag antenna which has incorporated humidity sensor functionality along with calibration mechanism due to distinctiveness of its structural behavior, is proposed. The sensor-enabled antenna is directly printed on paper substrate using state-of the-art inkjet printing technology for realizing the eco-friendly and ultra-low cost wireless sensor network (WSN) module. The antenna has reduced profile that paves the way for small item level tagging and monitoring. The effect of humidity on paper-based antenna characteristics along with other electromagnetic parameters is investigated to evaluate the antenna performance under realistic operating conditions. The proposed antenna exhibits wider operational bandwidth and extended read range while at the same time provides an additional degree of freedom for sensor calibration. In addition, sustainability and environmental impact analysis is performed which validates the tag's eco-friendliness.

The antenna has to counter the dielectric variations of the substrate in a precise, controlled mode while demonstrating linear parametric change for realizing humidity sensor and its calibration relative to specified humidity levels without being undetected. Consequently, the antenna is composed of four classifiable elements which provide stability as well as variability in order to exhibit sensory and radiating physiognomies. The substrate adopted is Kodak photopaper of 250 µm thickness (280 gm/m^2) with dielectric permittivity of $\varepsilon_r = 3.2$, and loss tangent $\tan\delta = 0.077$, characterized at 1 GHz@25°C, and NXP UCODE G2XM RFID Al strap is selected, for instance the goal IC impedance at 915 MHz is 13.3–j122Ω is preferred. However, the principle of operation for the proposed antenna is not IC dependent.

The novel progressive ladder contours play the important role for customizing the sensor calibration by varying the length of segments. It is observed that the coupling between electromagnetic characteristics of the paper substrate and radiating elements is significantly aided by these contours. The coupling features and stabilized performance in the far-field region are likewise alleviated by quadrangular end-tip loading by adjusting the length and spacing of segments. The computer-aided design of the antenna is performed by using the commercial full-wave simulator ANSYS HFSSTM. The prototype antenna is directly printed on paper by employing Dimatix DMP-2800 printer. The dimensions of the proposed antenna are optimized and calibrated for measuring every 20% RH change.

An RFID tag antenna which has instinct characteristics of a humidity sensor and potentiality of customizable calibration, is designed, fabricated and validated. It is observed that the explicit incorporation of ink and paper substrate is crucial for igniting the destabilisation effect, which is exploited in a regulated mechanism by the structural alignment of the proposed antenna. The design flexibility of the antenna resourcefully provides the effective calibration of the humidity sensor in accordance with defined requirements. In addition, this structure is eco-friendly, flexible and ultra-low cost, thus making this antenna well suited for realizing ubiquitous wireless sensor networks.

Implementation of Substrate Integrated Waveguide (SIW) by Inkjet-printing on Paper Substrate

Riccardo Moro[1], **Sangkil Kim**[2], **Maurizio Bozzi**[1], **and Manos Tentzeris**[2]

[1]Department of Electrical, Computer and Biomedical Engineering
University of Pavia, Pavia 27100, Italy
[2]Georgia Institute of Technology, Atlanta, GA 30309, USA

Abstract— Significant efforts have been spent in the last years for the development of novel wireless systems to be adopted for the implementation of the future wireless sensor networks (WSN) and the Internet of Things (IoT). The implementation of these wireless networks will require thousands or millions of wireless sensor nodes, which should be small and cost-effective and, at the same time, with low or zero environmental impact. Among available choices, planar technologies appear an effective solution for the implementation of this class of wireless systems.

The realization of microwave circuits in planar technologies, such as microstrip or coplanar waveguide, is traditionally based on the chemical etching of the metalized layers of the substrate. This fabrication technique produces a significant effect on the environment, both during the production of the circuit and at the end of its life time. In order to reduce this negative aspect, new substrates have been proposed, based on innovative materials never used before for electronics applications. The use of paper and recyclable plastic have been considered for the fabrication of microwave components. In particular, paper exhibits promising characteristics for the implementation of RF and microwave circuits, such as the complete eco-compatibility, the large availability, and the extremely low cost. Moreover, the implementation of electronic devices on paper can be performed by ink-jet printing, with no need of chemical etching or use of acids.

In this paper, the implementation of substrate integrated waveguide (SIW) components on paper substrates is presented. SIW structure, which is similar to a classical rectangular waveguide realized in planar form, consists of a dielectric substrate with top and bottom metallization and two rows of metal cylinders that define the side walls of the waveguide. The main advantage of SIW technology is the possibility to monolithically integrate a complete system in a single substrate, with no need of interconnects or transitions between elements fabricated with different technologies. This feature dramatically reduces losses and parasitics, according to the "System on Substrate" (SoS) concept. Moreover the implementation of SIW structures on paper permits to exploit the mechanical flexibility of the substrate by realizing conformal and multilayered configurations.

SIW interconnects, components, and antennas were implemented by ink-jet printing on paper substrate, demonstrating the applicability of paper-based technology to SIW structures. The design and the steps of the fabrication process will be described and the achieved results will be presented.

On the Influence of Edge Roughness in High-speed RFID Antenna Manufacturing Processes

J. Gao, J. Sidén, and H.-E. Nilsson
Mid Sweden University, Sundsvall, Sweden

Abstract— Antenna robustness is becoming an ever more important issue. An originally great antenna design can for example suffer from physical damages when used in a harsh environment or being unintentionally detuned due to unforeseen nearby materials or environmental factors. High-speed and low-cost manufacturing processes can introduce high mechanical manufacturing tolerances, which provide uncertainties in an antenna's outer dimensions as well as in the surface- and line-roughness of the its geometry.

Previous work on antenna robustness with regards to mechanical tolerances and random damages has primarily been directed toward arrays and reflector antennas. Other presented work includes characterization of mechanical robustness performance for embedded annular ring type antennas for GPS applications by using drop weight impact tests. Work also exists where studies have been performed upon the effect of environmental stress by exposing antennas to physical bending, high humidity levels and temperature cycling, and how different stresses may accelerate the effects of another stress. Performance degradation due to elongation of electrical structures has been investigated where antennas are printed with silver ink on stretchable PVC. Statistical methodologies for evaluation of antenna susceptibility to various types of random physical damages for "buck shots" and "scratches" has similarly been studied.

The last decade's rapid expansion of RFID-technology has constituted a driving force for low-cost antenna manufacturing methods. Printed RFID tag antennas have received high attention in the literature while etched and milled antennas so far represent the largest amount of manufactured tag antennas. While surface roughness for screen printed RFID antennas has been described before, this work characterizes performance degradation for antennas with a smooth surface but whose edges has received a rough pattern. Such rough patterns can for example occur in the subtractive production process in which high-speed milling is used on metallic foils.

As compared to the statistical approaches presented in earlier publications, this work follows a deterministic approach when applying distortions to antenna structures. Deviations are introduced to an antenna structure by applying a triangle wave pattern that is uniformly distributed around the original lines' edges. The triangular pattern causing the roughness is quantified by the wave-patterns period length and its peak amplitude. The wave-pattern's amplitude is swept from a relatively small value that hardly affects the original antenna properties up to the extreme case where the roughness' subtractive parts meet each other. That is, up the point where the conductive traces cease to be connected. Antennas with wide lines can thus be evaluated for a higher maximum edge roughness than antennas with thin lines.

Results show that, as expected, the performance degradation for an RFID tag antenna increases with increased edge roughness. It is observed that the input return loss for the investigated antennas shows a relatively good impedance match for a low level of edge roughness. The input return loss then increases in an almost linear fashion up to about $-10\,\mathrm{dB}$ for the highest possible roughness with the triangle wave pattern defined. The results also show that the impedance changes due to edge roughness is almost identical for the investigated antennas' line widths when the roughness level is normalized to its specific antenna line width. For the specific antenna structure that is used in this work it is thereby concluded that the level of performance degradation due to edge roughness, in terms of input return loss, is related to the structure's line width and not only related to the total level of roughness.

It is also observed that applying rough edge patterns decreases the bandwidth for the specific antennas under test from about 60 MHz to about 40 MHz for each investigated antenna line width.

Much of the previous work on RFID tag antennas has focused on printing the antennas with electrically conductive ink, with a conductivity that is significantly lower than antennas that are etched or milled from solid metal. The effect that a hypothetical printing process, which creates traces with finite conductivity and rough edges, would have on an RFID tag antenna was therefore also investigated. The results show that ohmic losses increases significantly for rough-edged antennas with a sheet resistance of $50\,\mathrm{m}\Omega/\square$ as compared to corresponding $50\,\mathrm{m}\Omega/\square$ smooth lined antennas.

It is concluded that antennas that are at risk for receiving a high degree of edge roughness are also at risk of receiving a significant degree of performance degradation. Such antennas should be designed to be electromagnetically robust against this kind of manufacturing issues. Future work should evaluate whether different types of RFID tag antennas are more and less sensitive to edge roughness. The results of such evaluation could advantageously constitute the base for creating design guidelines for antennas that are robust against edge roughness.

Design of Sierpinski Grid Patch Antenna for Multiband Application

R. K. Kanth[1], **P. Liljeberg**[1], **H. Tenhuen**[1], **Y. Amin**[2],
Q. Chen[2], **A. Janstch**[2], **L. R. Zheng**[2], **and H. Kumar**[3]

[1]Turku Centre for Computer Science, University of Turku, Joukahaisenkatu 3-5 B, Turku 20520, Finland
[2]School of Information and Communication Technology
Royal Institute of Technology, KTH Forum, Isafjordsgatan 39, Kista, Stockholm 164 40, Sweden
[3]Department of Electronics and Communication Engineering, Bhagwant Institute of Technology
Muzaffarnagar, UP, India

Abstract— In this paper, we have attempted to design a planar Sierpinski fractal antenna in stacked configuration for multiband application. The stacked configuration of Sierpinski fractal patch and Sierpinski grid are employed to improve the multiband characteristics. The operating frequencies obtained are at 3.3 GHz, 5 GHz, 5.74 GHz and 5.9 GHz which covers the bands useful for HIPERLAN2 frequencies and for implementation in futuristic WiFi enabled devices and PCI Cards for mobile internet. The simulated results show that the operating frequencies obtained are spread over a wide range of frequency band compared to the simple Sierpinski fractal patch antenna.

In the first step, only up to the second stage of the Sierpinski gasket is considered. For the first stage, a simple triangular patch with the length of each side 32 mm is placed on a substrate of thickness 1.6 mm and permittivity 4.4 is considered. Location of the coax feed placed on the patch is -3, 20.5 (x_f, y_f) from the centre of the patch's base (offset). Resonant frequencies obtained were 5.07 and 5.72 GHz. The second stage of the Sierpinski gasket (1st iteration) is then obtained using the Sierpinski gasket design method described above. With this configuration the resonant frequencies obtained were at 5.51 and 5.62 GHz. But in this case too the operating frequencies were only two with the slight frequency shift.

In the next step a grid with the width of 1.0 mm is formed, whose dimensions are same as that of the second stage of the Sierpinski gasket. This Grid is constructed on a foam substrate of thickness 1.6 mm and permittivity 1.06 and is placed over the previous structure. This way a stacked configuration is obtained in which the lower structure is Sierpinski gasket on FR4 where as the upper structure is grid on a foam of thickness 1.6 mm. The lower patch is coaxially fed. With this configuration the operating frequency obtained are 3.3 GHz, 5 GHz, 5.75 GHz and 5.9 GHz, which are widely spreaded over the frequency band.

It is evident from the return loss characteristics of three structures, which within the range of 6 GHz. only two operating frequencies were obtained with the simple triangular patch and the Sierpinski fractal patch (1st iteration). With the Sierpinski fractal patch (1st iteration) resonant frequencies were at 5.51 and 5.62 GHz and give rise to a wide band antenna whose return loss is less than -10 dB from 5.49 Hz to 5.67 GHz.

The third configuration in which Sierpinski fractal patch and Sierpinski grid were considered in the stack configuration, with Sierpinski fractal patch as probe fed and Sierpinski grid as parasitic patch, the resonant frequency obtained are four, which are at 3.3 GHz, 5 GHz, 5.75 GHz and 5.9 GHz.

The gain of this novel antenna is within the desired frequency is always more than 5.5 dBi. The radiation pattern characteristics at all the frequencies are almost same. At frequency 5.9 GHz the gain is slightly reduced but is still greater than 5 dBi.

The proposed antennas are potential candidates for implementation on paper substrate for greater degree of eco-friendliness, and usability in future flexible electronic circuits.

A Battery Free RFID Sensor for Quality Detection of Food Products

Dat-Son Nguyen[1, 2], Gia-Tam Phan[1], Tien-Thong Pham[1], Nguyen-Ngan Le[1], Mau-Chien Dang[1], and Smail Tedjni[2]

[1]Laboratory for Nanotechnology, Vietnam National University — Ho Chi Minh City
Community 6, Linh Trung Ward, Thu Duc District, Ho Chi Minh City, Vietnam
[2]Laboratoire de Conception et d'Intégration des Systèmes, Université de Grenoble
50 rue Barthélémy de Laffemas, BP 54, 26902 Valence Cedex 9, France

Abstract— In this paper, we propose the use of passive UHF RFID tags as a wireless sensor in order to detect the quality of food products. K. G. Ong [1] proposed an analytical formula to calculate the permittivity of food products during the increasing of bacteria concentration through the impedance of embedded structure in food products. On the other hand, Ghatass [2] estimated the freshness of beef by calculating the permittivity and conductivity from measured capacitance and inductance. Based on these data, the RFID tag sensor includes plural pairs of antenna/chip where each pair of antenna/chip is designed to operate over a range of permittivity value of the food. Knowing the variation of the permittivity of food over time (due to aging), we can detect when the food becomes contaminated with the measurement of each pair's read-range. The experimental and simulation results have shown the potential of this technique for real-world applications of food traceability. In addition, the results of this work allow considering the use of this approach for medical applications in real-world. As we known, the permittivity of human muscle and tissue is very close to the permittivity of meat such as pork or beef. Sensitivity study should be conducted in order to better optimize the sensor and predict its performance.

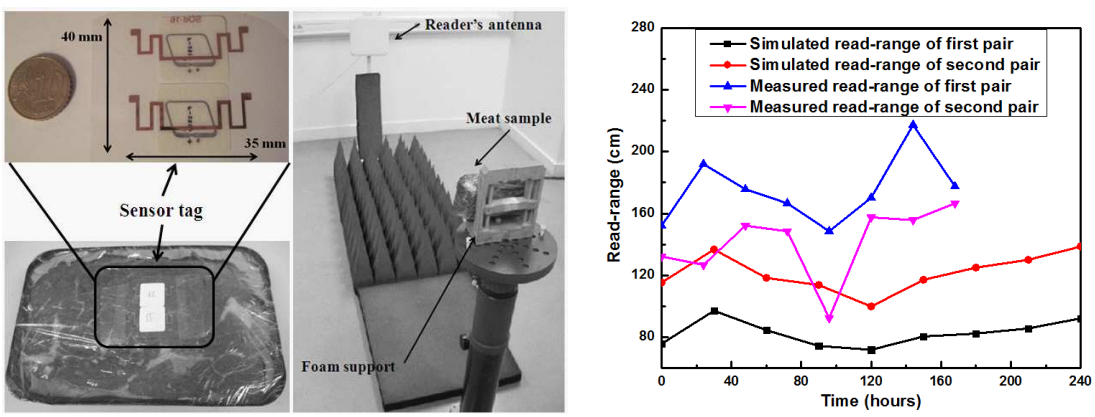

Figure 1: The measurement configuration and characterized results of designed RFID sensor tag.

REFERENCES

1. Ong, K. G., J. S. Bitler, C. A. Grimes, et al., "Remote query resonant-circuit sensors for monitoring of bacteria growth: Application to food quality control," *Sensor MDPI*, 219–232, Feb. 2002.
2. Ghatass, Z. F., M. M. Soliman, and M. M. Mohamed, "Dielectric technique for quality control of beef meat in the range 10 kHz–1 MHz," *American-Eurasian Journal of Scientific Research*, Vol. 3, 62–69, 2008, ISSN 1818-6785.

Session 2A9b
SC4: Circuit Modelling in Microwave Devices

A Microstrip-fed Printed Slot Antenna for 3G/Bluetooth/WiMAX and UWB Applications with 3.6 GHz Band Rejection
Mohamed Mamdouh Mahmoud Ali, Ayman Ayd Ramadan Saad, Elsayed Esam M. Khaled, ... 560

Symmetrical T-stubs Coupled Miniature Square Open-loop Dual-band Bandpass Filter for C- and X-band Applications
Ram Krishna Maharjan, Nam-Young Kim, ... 561

2.4-GHz CMOS Direct Conversion Receiver Using Standard-cell Deep N-well BJT
Wei-Ling Chang, Chinchun Meng, Jin-Siang Syu, Chia-Ling Wang, Guo-Wei Huang, ... 562

Theoretical Study of the Coupling Factor of Open-ended Coupled Transmission Lines at First Resonant Frequencies under Quasi-TEM Propagation
Enrique Bronchalo, Miguel Ángel Sanchez-Soriano, German Torregrosa-Penalva, Angela Coves Soler, 564

A V-band Low Noise Amplifier with 18.1 dB Gain and 6.3 dB NF in 90-nm CMOS Process Technology
Chiu-Hsiang Hsu, Yen-Chung Chiang, ... 565

The Band-pass SIW-filter Based on L-ridged Rectangular Waveguide
Viacheslav V. Zemlyakov, ... 566

A Microstrip-fed Printed Slot Antenna for 3G/Bluetooth/WiMAX and UWB Applications with 3.6 GHz Band Rejection

Mohamed Mamdouh M. Ali[1], **Ayman Ayd R. Saad**[2], **and Elsayed Esam M. Khaled**[1]

[1]Electrical Engineering Department, Assiut University, Assiut, Egypt
[2]Kosseir Radio, Telecom Egypt, Kosseir 84712, Egypt

Abstract— This paper presents a design and a circuit modeling of a compact and simple wide-slot antenna for 3G/Bluetooth/WiMAX and UWB applications, with 3.6 GHz band-notched characteristics. A rectangular wide– slot controls the low frequency band and impedance matching of the proposed antenna. A modified rectangular tuning stub is used to enhance and control the operating bandwidth at high frequency band. The proposed antenna is successfully simulated, designed, and measured showing an impedance bandwidth about 7.75 GHz, from 1.9 to 9.65 GHz, for UMTS (1.920 $\sim$ 2.170 GHz)/Bluetooth (2.4 $\sim$ 2.484 GHz)/WiMAX (2.5 $\sim$ 2.96 GHz) and UWB (3.1 $\sim$ 9.65 GHz) applications with good radiation characteristics. To reduce unwanted interference with UWB communication system, the antenna employed a U-shaped slot in the microstrip feeding line provided a band-rejection performance (3.2 $\sim$ 4.0 GHz) for WiMAX technology.

In order to consider the effect of integrating the proposed antenna with a whole communication system simulation, the equivalent circuit of proposed antenna is obtained based on Vector Fitting (VF) technique. The frequency domain input impedance/admittance of the antenna can be simulated by an electromagnetic (EM) simulator or measured using a vector network analyzer is fitted by VF technique and a rational function is obtained. The rational function is converted into SPICE-compatible lumped-element equivalent circuit. It is noted that, approximating rational functions through VF is a great tool that can be used to create equivalent circuits based on scattering parameter data. A major limitation in the creation of these equivalent circuits is the presence of negative resistors which makes the circuit non-physical, although the stability and enforcing of passivity. One of the key advantages of the proposed modeling methodology in this paper is avoiding the non-physical circuit elements. Calculation results show that this methodology is effective over the ultra-wide bandwidth.

The results elucidate the validity of the proposed antenna usage in the multi-band operation and also present a good strategy for physical circuit modeling of the ultra-wide bandwidth antenna. The measured data show very good agreement with the simulated results along with the equivalent circuit results.

Symmetrical T-stubs Coupled Miniature Square Open-loop Dual-band Bandpass Filter for C- and X-band Applications

Ram Krishna Maharjan and Nam-Young Kim
RFIC Center, Kwangwoon University
447-1 Wolgye-dong, Nowon-ku, Seoul 139-701, Korea

Abstract— A compact microstrip symmetrical T-stubs coupled dual-band square open-loop bandpass filter with asymmetrical feed lines is proposed. English letter T-shaped stub is inserted inside-wall of each square loop resonator. The maximum coupling can be possible by optimizing the open-loop gap, the spacing of the two open-loop resonators, the orientation of the loaded T-stubs, and controlling parameters of T-stubs inside the square loop resonators. The asymmetrical port terminals also enhance to couple electromagnetic (EM) energy by maintaining $50\,\Omega$ impedance matching with input/output devices. The open gap between the two loops of the filter structure strongly inhibits the flow of DC current and out-of-band signals. The face-to-face open sides of the loops orientation build up strong electric fields and inserted T-stubs are subjected to generate the magnetic coupling through the open gaps; as a result, the combined coupling gives an effective EM coupling in the proposed filter with adequate transmission and reflection coefficients for dual-band frequencies. The first and second band resonant frequencies were measured at 5.85 GHz and 9.35 GHz, respectively. The measured return losses (S_{11}) of the fabricated filter are of -14.6 dB and -14.8 dB; and insertion losses (S_{21}) are of 1.5 dB and -1.7 dB, at the first and the second resonant frequencies of the dual-band bandpass filter, respectively. The spurious suppression was measured to be more than -35 dB at out-band frequencies in all of four transmission zeros. The design analysis for this research primarily focuses on applying the highly compatible size and planarity of a type reliable bandpass filter utilized for the combined C- and X-band frequencies in a single communication system, and therefore this proposed bandpass filter can be used for fusion application in modern remote sensing satellite systems.

2.4-GHz CMOS Direct Conversion Receiver Using Standard-cell Deep N-well BJT

Wei-Ling Chang[1], **Chinchun Meng**[1], **Jin-Siang Syu**[1], **Chia-Ling Wang**[1], **and Guo-Wei Huang**[2]

[1]Department of Electrical and Computer Engineering
National Chiao Tung University, Hsinchu 300, Taiwan
[2]National Nano Device Laboratories, Hsinchu 300, Taiwan

Abstract— In 0.18 µm CMOS foundry process, npn2, npn5 and npn10 deep n-well vertical npn BJTs as shown in Figure 1(a) are provided with emitter size of 2×2, 5×5 and $10 \times 10\,\mu m^2$, respectively. A BJT is known to have a low flicker noise corner and thus can be employed in the mixer core of a Gilbert mixer and the subsequent IF amplifier for a low-flicker-noise direct conversion receiver. Standard BJT cells are routinely fabricated and thus preferred in the circuit design. However, there is a lack of rf model and performance for the standard BJT cells. The measured S parameters reveal that the peak ft as shown in Figure 1(b) reaches 2.6 GHz, 2.3 GHz

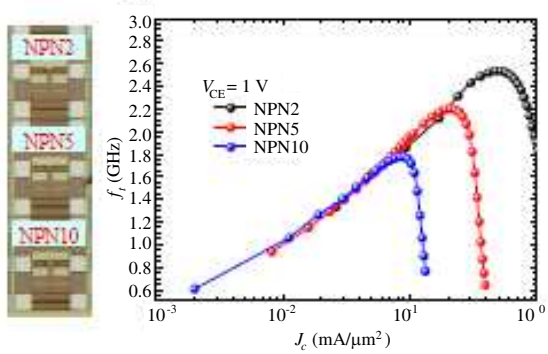

(a) (b)

Figure 1: (a) Die photo of npn2, npn5 and npn10 deep n-well vertical npn BJTs. (b) f_t of BJTs, respectively.

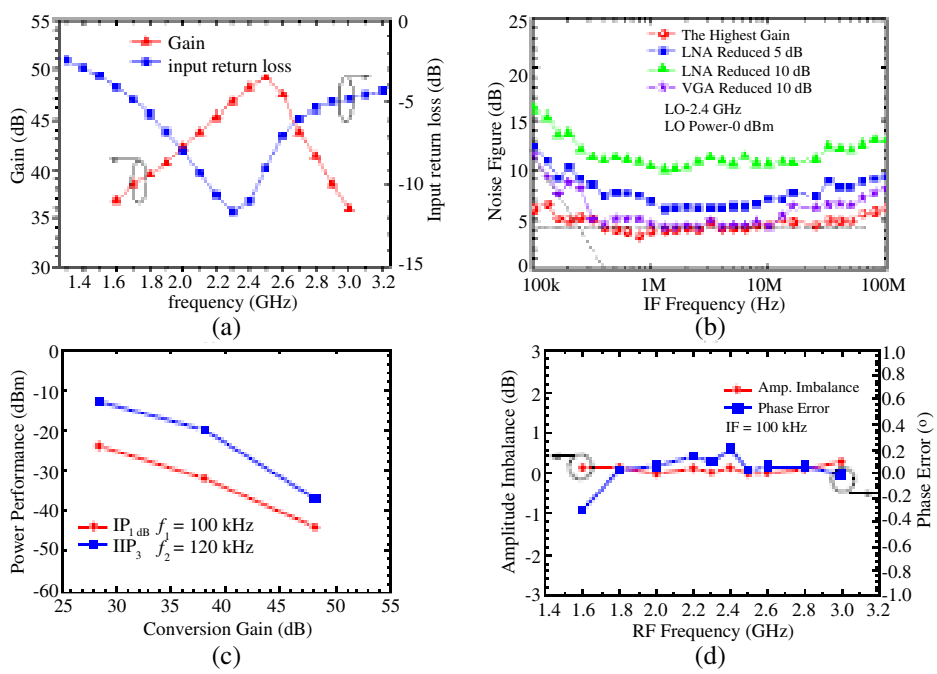

Figure 2: (a) CG and return loss with respect to RF frequency. (b) Noise figure. (c) Power performance. (d) I/Q imbalance.

and 1.8 GHz for npn2, npn5 and npn10, respectively. Emitter Current crowding effect which makes the current flowing at the emitter edge can account for the results. Thus, npn2 BJT has less emitter current crowding and is chosen to design the 2.4 GHz direct conversion receivers in 0.18 µm CMOS technology. The circuit topology of the receiver is identical to the circuit in reference 1 except the $2 \times 2\,\mu m^2$ standard BJT cell is exclusively used for all the BJT devices [1]. Two area-saved 3D inductors are employed to optimize the LO power performance by inductive peaking technique. The receiver has 48 dB gain and 11 dB input return loss at 2.4 GHz as shown in Figure 2(a). Figure 2(b) indicates the flicker noise of 6 dB at IF = 100 kHz, and of 4 dB for IF > 300 kHz. The conversion gain ranges from 50 to 30 dB by LNA gain tuning. The $IP_{1\,dB}$ and IIP_3 is −24 and −13 dBm at CG = 30 dB as shown in Figure 2(c). The I/Q channel gain and phase imbalance is shown in Figure 2(d). The supply voltage is 1.8 V, and the current consumption is only 4.8 mA.

REFERENCES

1. Syu, J.-S., C. C. Meng, and C.-L. Wang, "2.4-GHz low-noise direct-conversion receiver with deep N-well vertical-NPN BJT operating near cutoff frequency," *IEEE Trans. Microw. Theory Tech.*, Vol. 59, No. 12, 3195–3205, Dec. 2011.

Theoretical Study of the Coupling Factor of Open-ended Coupled Transmission Lines at First Resonant Frequencies under Quasi-TEM Propagation

E. Bronchalo[1], **M. A. Sánchez-Soriano**[2], **G. Torregrosa**[1], **and A. Coves**[1]

[1]Departamento de Ingeniería de Comunicaciones, Universidad Miguel Hernández de Elche
Elche, Alicante 03202, Spain
[2]Lab-STICC, Université Bretagne Occidentale, Brest, France

Abstract— In this work we present the results of a theoretical study on identical, open-ended transmission lines coupled with arbitrary coupling strength under the assumption of quasi-TEM propagation. The study focuses on the coupling factor between resonant lines, as this parameter has a great practical interest in the design of RF and microwave filters [1].

The coupling factor of a pair of identical resonators is usually calculated from the two resonant frequencies into which the fundamental frequency of the non-coupled resonators is split [2]. This method leads a unique coupling factor for the two resonant frequencies. In our work, we have used the definitions of electric, magnetic and total coupling factors based on the ratio of coupled and uncoupled energies at a given resonance [3]. Exact expressions for the resonant frequencies, voltage and current distributions have been used to calculate the different energies and the coupling factors at the two first resonant frequencies split from the fundamental one as a consequence of the coupling. The theoretical expressions obtained are valid for arbitrary coupling strength and for TEM or quasi-TEM propagation, as different phase velocities of the two propagation modes in the coupled region can be considered.

These theoretical expressions have been used to carry out several comparative studies: a) The electric, magnetic and total coupling factors as functions of the coupling length are compared for the two first resonant frequencies. b) The total coupling factors based on the energetic definition are compared with the one based on the resonant frequencies. c) The dependence of the coupling factors with the coupling length is compared for TEM and quasi-TEM propagation. Finally, the bandwidth between resonant frequencies as a function of the coupling factor is also compared for TEM and quasi-TEM propagation.

ACKNOWLEDGMENT

This work has been supported by the Spanish Ministry of Science and Innovation under the coordinated project TEC2010-21520-C04-02.

REFERENCES

1. Sánchez-Soriano, M. A., E. Bronchalo, and G. Torregrosa-Penalva, "Parallel-coupled line filter design from an energetic coupling approach," *IET Microw. Antennas Propag.*, Vol. 5, No. 5, 568–575, 2011.
2. Hong, J.-S. and M. J. Lancaster, *Microstrip Filters for RF/Microwave Applications*, John Wiley & Sons, New York, 2001.
3. Tyurnev, V. V., "Coupling coefficients of resonators in microwave filter theory," *Progress In Electromagnetics Research B*, Vol. 21, 47–67, 2010.

A V-band Low Noise Amplifier with 18.1 dB Gain and 6.3 dB NF in 90-nm CMOS Process Technology

Chiu-Hsiang Hsu and Yen-Chung Chiang
National Chung Hsing University, Taiwan

Abstract— In this paper, a three-stage low noise amplifier (LNA) implemented in the TSMC 90-nm CMOS process technology for V-band applications is proposed. The proposed low noise amplifier consists of three common-source stages with inductive degeneration. We use microstrip lines for input/output matching and as loads for all stages. The chip size of the proposed low noise amplifier is $0.608 \times 0.636\,\mathrm{mm}^2$. The measured peak gain is 18.1 dB at 59.9 GHz with 3 dB bandwidth from 58 to 62.4 GHz. The lowest measured noise figure (NF) is 6.3 dB at 61 and 63.5 GHz, respectively, and NF is from 6.3 dB to 8 dB for the 57–64 GHz frequency range. The measured input 1 dB compression point ($P_{1\,\mathrm{dB}}$) is −19 dBm and input third intercept point (IIP3) is −10 dBm. The proposed circuit draws a 32.6 mW dc-power from a 1.2-V supply.

The Band-pass SIW-filter Based on L-ridged Rectangular Waveguide

V. V. Zemlyakov
Faculty of Physics, Southern Federal University, Russia

Abstract— The modern technologies of design and production of integrated circuits open up possibilities of integration in the structure of 3-D elements, in particular rectangular waveguides and cavity resonators on their basis. Such technology has the name — SIW (Substrate Integrated Waveguide). The main feature of SIW structures is that they keep the advantages of classical waveguides — big transmission capacity, low losses, completely shielded structure, high good quality of resonators; gaining features of planar structures — the small sizes and weight, low cost of production [1]. The SIW technology can be successfully used for development of compact band-pass filters. There are some approaches on creation of the waveguide filters on inductive diaphragms and transverse junctions with direct, and with quarter-wave links are known. In this work the structure of the waveguide filter on evanescent waveguides is offered. As a basic element of the filter the new type of a waveguide of complex cross-section — L-ridged rectangular waveguide is proposed. The investigation of electrodynamic properties of such waveguide shows the possibility of its effective application at development of band-pass filters due to the small wave impedance, low cut-off frequency and high good quality of the resonators created on its basis [2].

The filter synthesis was carried out on the basis of the author's electrodynamic methods developed for classical waveguides, and the subsequent transfer of geometry on SIW structure. The calculation of parameters of the final device was carried out by CST Microwave Studio. The total length of the filter is 28 mm and the band-width 4%. The in-band return loss is below −20 dB.

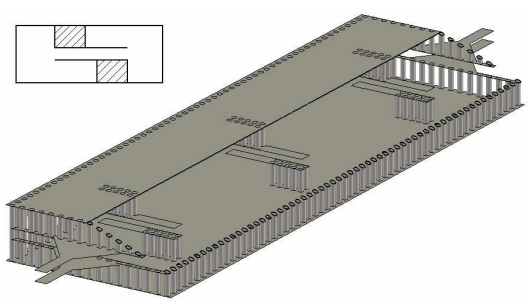

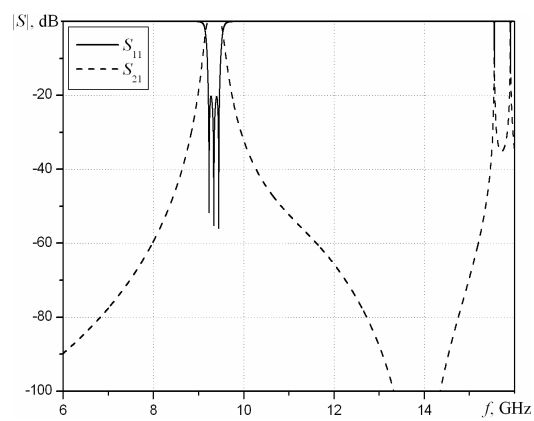

REFERENCES

1. Bozzi, M., L. Perregrini, and K. Wu, "Modeling of conductor, dielectric, and radiation losses in substrate integrated waveguide by the boundary integral-resonant mode expansion method," *IEEE Trans. on Microwave Theory and Technique*, Vol. 56, No. 12, 3153–3161, 2008.
2. Zargano, G. F., V. V. Zemlyakov, and V. V. Krivopustenko, "Electrodynamic analysis of eigenmodes in a rectangular waveguide with two L-shaped septa," *Journal of Communications Technology and Electronics*, Vol. 56, No. 3, 259–268, 2011.

Session 2A10
SC4: Antenna-channel Interactions and Multipath Wireless Channels

Cooperative Communications Based on Smart Antenna Systems Using PSO Algorithm
Ahmed Magdy Mohamed, Korany Ragab Mahmoud, Samir Sayed, ... 568

Reader Antenna Beam Width Optimization under Multiple Channel Effects in a UWB-RFID System
Alain Sibille, ... 569

Evaluation of UWB Chipless RFID System Performance Considering Indoor Multipath Propagation Channel and Real World Aspects
Mohamed El-Hadidy, A. Fawky, B. Nagy, Maher Mohamed Ahmed Khaliel, Esmat Abdel-Fattah Abdallah, H. Elhennawy, Thomas Kaiser, ... 571

Lognormal Shadow Fading Arising from Inhomogeneous Radio Wave Diffusion
Dmitry Chizhik, Jonathan Ling, Reinaldo A. Valenzuela, ... 572

On the Use of Huygens' Sources for Synthetic Propagation Environments with the Application in MIMO Over-the-air Testing
Afroza Khatun, Keijo Nikoskinen, ... 573

Characterization of the Field Distribution in a Reverberation Chamber for MIMO Channel Emulation
Andres Alayon Glazunov, ... 574

Variability of Radio Channel Characteristics in Different Indoor Environments
Hassan El-Sallabi, Khalid A. Qaraqe, Erchin Serpedin, ... 575

Novel Methodology for Increasing the Reading Range of the UWB Passive RFID Chipless Tags Considering Power Regulations
Mohamed El-Hadidy, B. Nagy, Maher Mohamed Ahmed Khaliel, A. Fawky, E. Abdallah, H. Elhennawy, Thomas Kaiser, ... 576

Stochastic Modeling of Ultra Wideband Propagation Channels within a Small Spacecraft
Miyuki Hirose, T. Kobayashi, ... 577

Cooperative Communications Based on Smart Antenna Systems Using PSO Algorithm

Ahmed Magdy[1], **K. R. Mahmoud**[1], **and S. Sayed**[1, 2]

[1]Department of Electronics, Communications, and Computers Engineering
Helwan University, Cairo, Egypt
[2]Department of Electronic and Electrical Engineering University College London, London, UK

Abstract— The concept of cooperative communication has been proposed to improve link capacity, transmission reliability and network coverage in multiuser wireless communication networks. Different from conventional point-to-point and point-to-multipoint communications, cooperative communication allows multiple users or stations in a wireless network to coordinate their packet transmissions and share each other's resources, thus achieving cooperative diversity or user cooperative diversity. As a promising application of cooperative communication in multirate wireless networks, a low data-rate station can use a neighboring station as a relay to forward its information to destination station.

In this paper, an adaptive cooperative protocol based on smart antenna system is proposed using UCA geometry of 12 elements. The array feeding elements are optimized using the PSO algorithm to synthesize the beampattern. The results are compared with those obtained in previous work using Uniform Linear Array (ULA). In addition, the best strategy for transmission to give the lowest BER is considered.

Simulation results prove enhancement in performance when using the proposed adaptive strategy based UCA smart antenna. Simulation results show beam patterns comparison of smart antenna for different geometries (UCA and ULA) from relay to destination and from the source to destination. It is found that, both arrays have the capability to direct the main beam toward incoming signal from source and from relay to destination. From results, it is clear that the directed power toward the intended direction using UCA is better than that obtained by ULA by approximately 17%. Also, it can be noticed that an extra undesired main beam in the broadside direction is obtained in the ULA geometry. In general, the results obtained by UCA are better than those obtained from ULA for both directions. It is found that, the performance of the proposed adaptive UCA outperforms the all other protocols for low and high SNR. The proposed switching technique using adaptive UCA is better than the adaptive ULA by at least 3 dB for the same BER at 10^{-2}.

Reader Antenna Beam Width Optimization under Multiple Channel Effects in a UWB-RFID System

Alain Sibille[1,2]

[1]Telecom ParisTech/LTCI, Paris, France
[2]ENSTA ParisTech, Palaiseau, France

Abstract— This work addresses the performance of a system of four Ultra Wide Band (UWB) readers for the detection and localization of RFID tags operating in modulated backscattering. Several effects involving the radio channel between the tags and the readers compete in the system performance, which are very much depending on the major parameters of the reader antennas. Based on a model of these effects, it is possible to optimize this performance, in terms of detection and localization coverage.

RFID devices will progressively penetrate our private and professional lives and will be part of the "Internet of Things" in the coming years. However, in addition to a simple identification of objects through the tags attached to them, the localization capability will very much enhance the services available from such devices. Ultra Wide Band (UWB) radio communications offer an excellent (sub-meter) location accuracy and are very attractive for this purpose. In order to combine this capability with extremely low on-tag power consumption, a modulated backscattering approach is currently investigated [1, 2]. The system consists of 4 readers at the corners of a rectangular area, which first wake-up the tags through a UHF signal, then send a coded UWB interrogation signal that is backscattered (BS) by them. In order to detect and identify the tags by the system of readers, the BS signal is modulated through a coded sequence of open circuit and short circuit loads connected at the tag antenna terminals. From the measurement of the BS delay, it is also possible to triangulate and determine the tag location.

Although this operation principle is simple, it incurs in practice a number of detrimental effects, which must be mitigated in order to achieve an optimal performance. The main problem is the extremely strong attenuation of the BS signal, which suffers a power loss given by the 4th power of the distance. A 2nd problem is the masking effect by objects, which often further increases the attenuation for some of the readers. A 3rd one is the interference between readers, which is much higher than the BS signal, owing to a decrease by only the 2nd power of the distance. Finally, a 4th effect is the clutter, which can also dominate by several orders of magnitude the tag modulated signal.

All of these effects depend, to some extent, on the characteristics of the reader antennas. In other words, an appropriate optimization of the latter may significantly improve the overall system performance. However, since the tag locations can vary over the prescribed area and since many characteristics are of statistical nature, it is necessary to base the optimization on coverage maps taking into account this statistical character and the various effects mentioned above. This is what has been done in the present work, by adjusting the beam widths in both planes of the antenna pattern, as well as the tilt angle. The computation of the coverage is based on a simplified model of the multidimensional propagation channel [3], developed from several channel measurement campaigns. The results show a strong impact of the beam widths on the

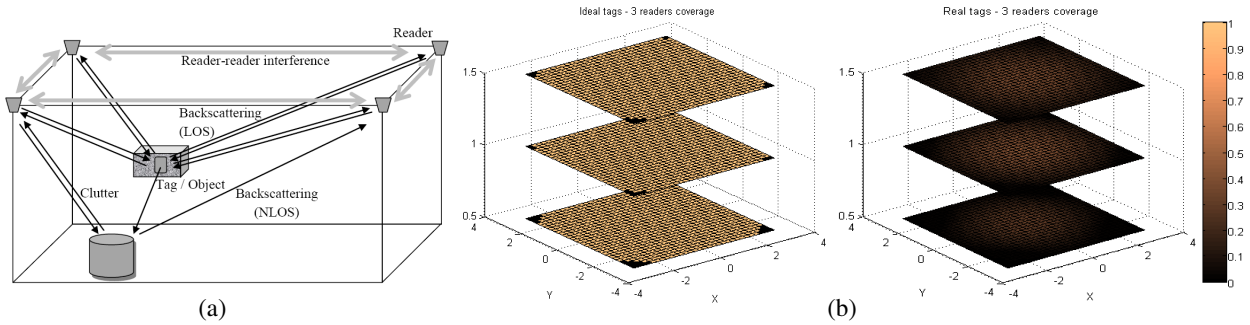

Figure 1: (a) SELECT scenario [2], (b) example of coverage maps for ideal tags and for a statistical model of tags on objects.

coverage maps, either in the case of ideal tags or in that of more realistic situations where the tags are placed on objects. The presentation will give an overview of these results.

ACKNOWLEDGMENT

This work took place thanks to the European Commission 7th framework program FP7/2007-2013 under grant No. 257544 [2].

REFERENCES

1. D'Errico, R., M. Bottazzi, F. Natali, E. Savioli, S. Bartoletti, A. Conti, D. Dardari, N. Decarli, F. Guidi, F. Dehmas, L. Ouvry, U. Alvarado, N. Hadaschik, C. Frankek, Z. Mhanna, M. Sacko, Y. Wei, and A. Sibille, "An UWB-UHF semi-passive RFID system for localization and tracking applications," *IEEE RFID TA*, Nice, France, Nov. 5–7, 2012.
2. "Smart and efficient location, identification and cooperation techniques (SELECT)," http://www.selectwireless.eu/.
3. Sibille, A., Z. Mhanna, M. Sacko, R. Contreras, V. Casadei, and R. D'Errico, "Channel modeling for backscattering based UWB tags in a RTLS system with multiple readers," *European Conference on Antennas and Propagation*, Gothenburg, Apr. 8–12, 2013.

Evaluation of UWB Chipless RFID System Performance Considering Indoor Multipath Propagation Channel and Real World Aspects

M. El-Hadidy[1], **A. Fawky**[1], **B. Nagy**[1], **M. Khaliel**[1], **E. Abdallah**[2], **H. Elhennawy**[3], **and T. Kaiser**[1]

[1]Institute of Digital Signal Processing, Duisburg-Essen University, Germany
[2]Ain-Shams University, Cairo, Egypt
[3]Electronic Research Institute, Cairo, Egypt

Abstract— Main objective of this contribution is to evaluate the overall performance of the Ultra Wide Band (UWB) Radio Frequency Identification (RFID) system based on chipless RFID tags, within the UWB range from 3.1 to 10.6 GHz. In this work, a ray-tracing tool "*Wireless Insite*" is used to consider the channel multipath components and the real environmental effects as fading, frequency dependence, transmission, reflections, diffractions and polarization dependence. Furthermore, an Electromagnetic (EM) simulation tool "*CST Microwave Studio*" is used to compute the Frequency Coding Response (FCR) and the Radar Cross Section (RCS) of the UWB-chipless-RFID tag. The system is based on an 8-bit FCR concept of a compact printable orientation independent chipless RFID tag. The tag consists of a circular patch loaded with N multiple slot ring resonators, where each resonator is relevant to a frequency component in the FCR. Simulation results show constructive guidelines for designing multiuser UWB RFID communications and enhancing the channel estimation process of the chipless RFID tag systems. System evaluation would consider several parameters as Bit Error Rate (BER), FCR word length, and the maximum reader-tag range. This enables the insertion of the advanced communication techniques as Interference Alignment (IA), Cognitive Radio (CR) and Massive Multiple Input Multiple Output (MIMO) for passive RFID systems.

Lognormal Shadow Fading Arising from Inhomogeneous Radio Wave Diffusion

Dmitry Chizhik, **Jonathan Ling**, **and Reinaldo A. Valenzuela**
Alcatel Lucent, USA

Abstract— Indoor radio propagation is receiving an increasing amount of attention from telecommunications industry due to deployment of indoor radio nodes whose coverage and mutual interference are at the heart of defining achievable communication rates. Effective propagation modeling is often needed in locations where only limited environmental information is available. In this work, diffusion theory has been found to provide a simple yet accurate expression for the average received radio power loss indoors in non-line-of-sight propagation. Effective specific absorption is the sole parameter. In this work the diffusion model is extended to account for shadow fading. It is found that variation in scatterer density provides a stochastic mechanism explaining the log-normal nature of observed average power variations, usually termed "shadow fading". The standard deviation of power variation is found to increase with range (as $r^{1/2}$ at short ranges), in agreement with measurements and unlike accepted models.

The average specific intensity is taken to obeys the diffusion equation with spatially varying scattering cross-section. This variation is attributed to variation in wall and furniture density and composition. It is assumed to be known only statistically with a specified spatial covariance. The resulting variation in received power is found to be a lognormal process, with a range-dependent standard deviation. At short ranges the standard deviation scales with range as $\sqrt{x}$, which is the same dependence as would arise when modeling the absorption as a random walk in one dimension. For longer ranges, the standard deviation scales with x as a slower function $\sqrt{\ln x}$. This may be attributed to path diversity in 3D: variations are somewhat less dramatic with range if the diffusion allows the photons to arrive at the receiver while going around obstacles rather than trying to penetrate the obstacles. The significance of diffusion as a propagation mechanism is its ability to introduce a natural "curtain" beyond which distant interferers are much attenuated.

On the Use of Huygens' Sources for Synthetic Propagation Environments with the Application in MIMO Over-the-air Testing

Afroza Khatun and Keijo Nikoskinen
SMARAD, Department of Radio Science and Engineering, School of Electrical Engineering
Aalto University, P. O. Box 13000, AALTO, Espoo 00076, Finland

Abstract— To support the increased demand for higher data rate transmission, new multi-antenna terminals are being emerged exploiting the advances in multiple-input multiple-output (MIMO) technique. However, MIMO technique not only opens up new opportunities, but also needs a realistic test methodology to evaluate the MIMO terminal performances. Since the MIMO terminal performance is a combination of antenna characteristics, multi-path radio propagation conditions, radio frequency, baseband hardware, and software, it need to be tested in a controlled environment. Over-the-air (OTA) testing, that has been used for single-input single-output (SISO) performance evaluation, is an obvious choice also for MIMO performance evaluation, additionally radio-propagation channel must be taken into account. Several possible MIMO-OTA test methodologies have been proposed in research and standardization forums with the purpose to be capable of creating such an electromagnetic field environment which represents the true environment where the device is exposed during its normal operation.

One possible way to achieve the conditions representing the actual radio-channel environment is through exploitation of multi-probe technology where probes are placed on a circle in 2-D case or on a sphere in 3-D case around the device under test (DUT) in an anechoic chamber. With the help of the channel models developed for different radio-propagation environments, these probes are used to synthesize such radio-channel conditions inside the test volume that emulate the actual conditions where the device would be used in practice.

One of the key issues addressed in anechoic chamber based method is the optimum distance between the DUT and the probe circle (sphere) which directly points the required size of the chamber. The cost will be increased for large chamber. The purpose of this paper is to investigate the Huygens' principle in this context. With the proper electronics, it is possible to map the existing field environment into such excitation currents at the Huygens' sources on the test surface enclosed the DUT. And with this Huygens' principle the field outside of the test volume would be zero. In this way, the actual radio-channel environment may be created inside a test volume in laboratory conditions. Hence the required chamber will be small enough in size as the Huygens' sources are placed on the surface of the test volume which reduces the cost significantly. In Fig. 1, an illustration of a 2-D MIMO-OTA test system using Huygens' sources located on a circle around the test zone is presented. In the final manuscript the synthesis technique using the Huygens' sources will be presented in details.

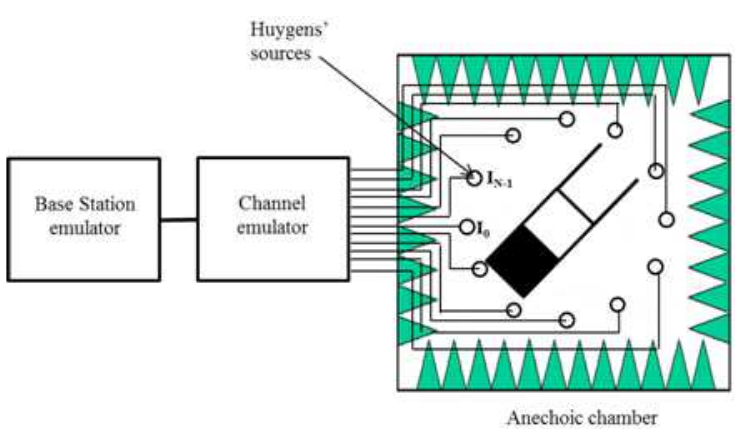

Figure 1: An illustration of a possible MIMO-OTA test system with N equally spaced Huygens' sources placed on a circle around the test zone where the DUT is located.

Characterization of the Field Distribution in a Reverberation Chamber for MIMO Channel Emulation

A. Alayon Glazunov
Electromagnetic Engineering, KTH-Royal Institute of Technology, Sweden

Abstract— Over The Air (OTA) testing of wireless devices such as mobile phones has become crucial to ensure their adequate performance in wireless cellular networks. OTA measurements involve the emulation of realistic propagation environments in controlled laboratory conditions, which can be roughly divided into two main categories depending on the type of measurement chamber used [1]. To the first category belong techniques involving an anechoic chamber where the walls of the chambers absorb the radiated energy allowing generating a propagation channel with the desired directional distribution of waves impinging at the wireless device. The second category of techniques employs a reverberation chamber (RC) which relies on a minimum of absorption of electromagnetic energy resulting in a more isotropically distributed field. In this contribution we focus our attention on the latter technique.

The produced field variation inside a mode-stirred RC is ideally homogeneous. Each of the in-phase and quadrature field components are independent identically distributed zero-mean complex Gaussian variables resulting in a Rayleigh distributed magnitude of the field component and uniformly distributed phase. An ideal RC provides a reference wireless channel which, in addition to the mentioned properties, has the following characteristics: isotropic AoA or AoD (Angle of Departure) distributions at the receive and the transmit antenna, respectively; exponential decay of the power delay profile and balanced powers in the vertical and orthogonal polarizations. However, as well-known, realistic environments do not always behave in that particular way. Therefore, the aim of our contribution is to experimentally investigate means of changing the propagation characteristics in a RC for OTA testing of Multiple Input Multiple Output (MIMO) antenna systems.

The focus has been on the multidimensional characterization of the channel transfer function and the channel impulse response along the positions of a virtual array. We investigate the impact of different arrangements in the reverberation chamber on the average power, the Ricean K-factor and array antenna correlation. The arrangements include combining radio frequency absorbers with different orientations of a directive antenna to achieve changes of the channel behavior along the array. A number of 40 positions separated 0.233λ from each other are considered at the center frequency of 1 GHz and over a 120 MHz bandwidth. The analysis shows that the channel behavior is, as expected, rather homogeneous along the array when averaging over frequency and time. However, if we look at a specific frequency we can observe non-negligible variations of, e.g., the received signal power and the Ricean K-factor indicating that a careful arrangement of the physical environment inside the RC can result in a variety of channel behaviors. This opens up for further studies of the use of RC that are large in size to produce different field distributions at different areas inside a RC chamber. This can, in principle, be used to emulate various MIMO channels such as single-user MIMO, but also multi-user MIMO systems as well as the so called very large MIMO antennas.

REFERENCES

1. Alayón Glazunov, A., V. M. Kolmonen, and T. A. Laitinen, "MIMO over-the-air testing," *LTE-advanced and Next Generation Wireless Networks — Channel Modelling and Propagation*, Chapter 15, John Wiley & Sons, October 2012.

Variability of Radio Channel Characteristics in Different Indoor Environments

Hassan El-Sallabi[1], **Khalid Qaraqe**[1], **and Erchin Serpedin**[2]

[1]Wireless Communications Laboratory, Electrical Engineering Department
Texas A&M University at Qatar, Qatar
[2]Electrical and Computer Engineering Department, Texas A&M University, College Station, TX, USA

Abstract— Radio channel characteristics in different domains are determined by scatterers distribution, locations of transmitter and receiver, their antenna patterns, frequency, bandwidth and mobility in the channel either one end of the radio communication link, or both and/or scatterers in the environment. The distribution of scatterers varies for indoor and outdoor, which would be reflected on radio channel characteristics (RCC). The impact of antenna patterns at transmitter and receiver on RCC of single input, single output channel is determined by pattern 1) horizontal and vertical beamwidth, which reflect directionality property of the antenna, 2) pointing direction, 3) antenna tilt, 4) antenna rotation. The movement of the mobile device introduces different temporal and directional variations of the RCC. The amount of variation depends on aforementioned parameters in addition to amount of randomness and distributions of scatterers in the communications channel. The personnel movements in indoor channel are also a main source of temporal and spatial variability of the radio channel.

The investigation of this work is simulation based using multi-ray RF multi-dimensional propagation model. The number of rays is determined by number of reflections and existence of LOS components or not. For indoor scenario, multiple reflections from side and opposite walls as well as ceiling and floors are considered. The model ray parameters are derived from geometry using electromagnetic image theory and vector operations to extract needed angles and path length for every ray in terms of angle of arrivals and departures as well as surface reflection angles.

In this work, we will focus our studies on three different indoor environments representing lecture hall, corridors and convention center. The lecture hall environment represents scenario where delay and directional properties are comparably affected by close by walls, ceiling and floor. The corridor represents scenario where two reflecting surfaces are at larger distance from each other relative to other corresponding walls. So, their effect will represent a couple of far indoor scatterers that would result in isolated cluster in large delays and opposite angle or arrivals relative to the tested geometry. The third tested indoor environment is the convention center. This represents scenario where every two opposite surfaces are far from each other in terms of indoor dimensions. These far distances between opposite surfaces will be reflected in terms of delay and directional properties of the channel as well as transmitter and receiver.

This work presents a characterization of the radio channel of the next evolution of Wi-Fi standard IEEE802.11ac with a bandwidth of 80 MHz around the frequency range of 5 GHz for three different indoor environments: a lecture hall, corridor and banquet hall. These environments are selected to represent three different levels of dispersion in the delay and direction domains. The very wide bandwidth results in high resolution in the delay domain and leads to splitting delay clusters as the distance between transmitter and receiver increases. The radio channel of this system is expected to have a variable number of delay clusters with different excess delays per cluster. The spread and geometric distance distribution of scatterers are the main factors that determine the cluster characteristics of this radio channel.

Novel Methodology for Increasing the Reading Range of the UWB Passive RFID Chipless Tags Considering Power Regulations

M. El-Hadidy[1], **B. Nagy**[1], **M. Khaliel**[1], **A. Fawky**[1], **E. Abdallah**[2], **H. Elhennawy**[3], **and T. Kaiser**[1]

[1]Institute of Digital Signal Processing
Duisburg-Essen University, Germany
[2]Ain-Shams University, Cairo, Egypt
[3]Electronic Research Institute, Cairo, Egypt

Abstract— This paper presents a reading methodology for RFID readers to overcome the problem of the limited reading range and enhance the reading efficiency of the UWB chipless tags in a noisy environment. We apply this methodology on passive UWB chipless tag consists of a circular patch loaded with multiple rings resonators. The main problem of these passive chipless tags is that the reflected UWB power is hardly detected, because the transmitted UWB power is dramatically low by the FCC regulations. In this work is a new methodology has been developed to make the best use of the restricted UWB regulations to increase the effective radiated power by the RFID reader. This leads to a significant improvement of the reader range and the overall system performance. The FCC regulation states that the maximum allowed limit for the Effective Isotropic Radiated Power (EIRP) for an UWB device operating in the 3.1–10.6 GHz must not exceed than −41.3 dBm/MHz. However, the FCC regulations allows a peak level of emission with a maximum of 0 dBm, contained within a bandwidth of 50 MHz centered at the frequency at which the highest emission occurs. Therefore, the methodology depends on detecting the presence of a tag in a carrier sense manner using frequency sweeping and hoping techniques, instead of sending an UWB signal. The link budget analysis shows a considerable enhancement in the RFID system range and improving the signal to noise ratio at the reader. Simulation results show the expected improvement of the overall system performance.

Stochastic Modeling of Ultra Wideband Propagation Channels within a Small Spacecraft

M. Hirose and T. Kobayashi
Wireless Systems Laboratory, Tokyo Denki University, Japan

Abstract— A use of ultra wideband (UWB) technology within spacecrafts has been proposed with a view to (partly) replacing conventional wired onboard data buses with wireless connections [1]. Adaptation of wireless technologies in spacecrafts could contribute to: reduction of cable weight (and launching cost as a result), more flexibility in layout of spacecraft subsystems, and reliable connections at rotary, moving, and sliding joints. However, multipath propagation in semi-closed metal enclosures, such as spacecrafts, restricts the transmission performance. To realize the above benefits, multipath propagation affecting the transmission performance must be scrutinized. In this present paper, UWB channels within a small scientific satellite was measured and statistically analyzed, based on a modified Saleh-Valenzuela (SV) model [2], which modeled indoor UWB propagation channels. The modified SV model is based on a cluster concept of rays. The clusters, as well as the multipath components within a cluster, arrive according to Poisson processes with different rates. The received power of both the cluster and the rays within a cluster decays exponentially.

A mechanical test model (MTM) of a small scientific satellite was used for the measurements. The MTM was a rectangular parallelepiped, approximately 0.4 m × 0.5 m × 0.4 m. Frequency- (from 3.1 to 10.6 GHz) and time-domain propagation gains were measured with a microwave vector network analyzer. The transmitting and receiving antennas were omnidirectional, vertically-polarized, low-VSWR UWB monopole antennas. The transmitting antenna was fixed in an open space within the MTM, and the receiving antenna was scanned within a limited region, as shown in Fig. 1.

Delay profile measured in the MTM indicated that rays arrived in clusters, as shown in Fig. 2, where clustering was carried out heuristically. The arrival time intervals of the clusters and the rays within each cluster were observed to follow exponential distribution. This means that their arrivals can be modeled as Poisson processes. Arrival rates of the clusters and the rays within a cluster were found to be 0.15 ± 0.05 and 2.09 ± 0.25 [1/ns], respectively. The power decay factors of the clusters and the rays within a cluster respectively ranged from 0.08 to 0.19 ns and from 0.63 to 0.94 ns. These values found almost independent of the position of the receiving antenna. This was because the conductive enclosure caused abundant multipaths. The multipath gain coefficients were found to follow a lognormal distribution, which was also used in the modified SV model.

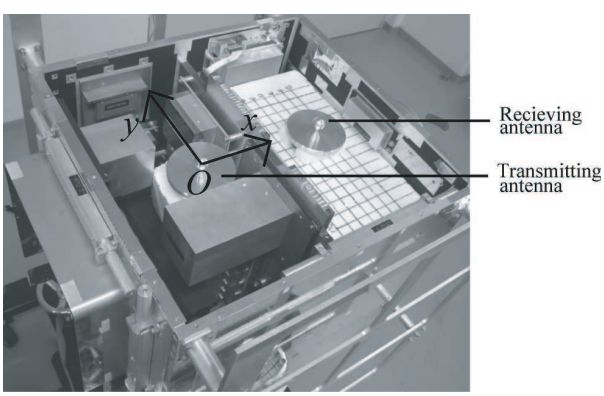

Figure 1: The measurement setup in a mechanical test model of a small scientific satellite. The top lid was closed during the measurements.

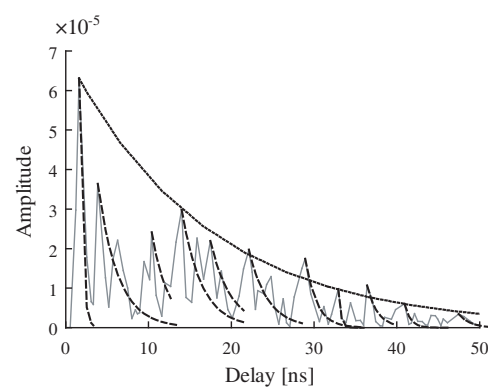

Figure 2: An example of the measured delay profile. The dotted and dashed lines represent exponential decay of the clusters and rays within each cluster, respectively.

REFERENCES

1. Matsubara, A., A. Tomiki, T. Toda, and T. Kobayashi, "Measurements and characterization of ultra wideband propagation within spacecrafts — Proposal of wireless transmission for replacing wired interface buses," *Advances in Spacecraft Technologies*, 61–74, IN-TECH, Vienna, Austria, Feb. 2011, ISBN978-953-307-551-8.
2. Molisch, A. F., et al, "IEEE 802.15.4a channel model — Final report," Submitted to *IEEE 802.15 WPAN Low Rate Alternative PHY Task Group 4a (TG4a)*, Nov. 2004, doc: IEEE 802.15.04-0662-01-004a.

Session 2A11
SC1: Spectral Theory of Open Structures: Critical and Interaction Phenomena

Reduced Volume Integral Formulations for an Open Waveguide Based on the Cylindrical Vector Wave Expansion
Sven Nordebo, Andreas Ioannidis, Borje Nilsson, ... 580

Eigenmodes in Problems of Scattering and Generation of Oscillations on a Nonlinear Layer
Lutz Angermann, Vasyl V. Yatsyk, ... 581

Spectral Theory of Wave Propagation: Survey of Recent Results
Yury V. Shestopalov, ... 582

Plasmonic Cavity Modes: Black-hole Phenomena Captured by Perfectly Matched Layers
Anne-Sophie Bonnet-Ben Dhia, Camille Carvalho, Lucas Chesnel, Patrick Ciarlet, Jr., ... 583

Resonant Frequency Doubling of Electromagnetic Waves in a Magnetoplasma: Analogy of the Non-linear Laser Crystal
Nikolay Sergeevich Erokhin, Alexander Borisovich Shvartsburg, ... 584

The Reconstruction of Dielectric Profile of a Layer for the Harmonic Wave Case
Nikolai B. Pleshchinskii, D. N. Tumakov, ... 585

Cylindrically Shaped Apertures and Guidance of Waves by Using Hankel Transformation and the Exact Approach Technique
Taner Sengor, ... 586

Adaptive Artificial Boundary Conditions for Schrödinger Equation with Un-instantaneous Nonlinearity
Vyacheslav A. Trofimov, Anton D. Denisov, Mikhail V. Fedotov, Alexander S. Prokopenko, ... 587

Reduced Volume Integral Formulations for an Open Waveguide Based on the Cylindrical Vector Wave Expansion

S. Nordebo, A. D. Ioannidis, and B. Nilsson
Linnaeus University, Sweden

Abstract—

Introduction: The analysis of the dispersive behavior of open waveguides is a research field that raises many interesting questions regarding the qualitative properties of the spectrum [7, 11], and which has important applications in fiber optic communications [1], as well as with the modeling of propagating waves on a power cable [8]. As an example is given in [7] a spectral characterization of the generalized natural modes of an inhomogeneous optical fiber with arbitrary cross-section without a sharp boundary.

The volume equivalence principle in connection with the strongly singular free space Greens dyadic for Maxwell's equations is a generic technique to derive integral equations in scattering theory, see, e.g., [2–4, 6, 10]. A discussion on several different derivations is given in [10] regarding general composite volume media. A rigorous mathematical derivation of the volume integral under the hypothesis of a discontinuity of the electric permittivity across the dielectric boundary and no electric conductivity is given in [6]. Numerical aspects involving Galerkin formulations for general inhomogeneous scatterers are treated in [2] including comparative numerical results for higher-order basis functions.

In this paper, we give reduced volume integral formulations for an open and cylindrically symmetrical waveguide based on the cylindrical vector wave expansion. The waveguide material is assumed to be non-magnetic and with an arbitrary radial variation in the real valued relative permittivity. Based on the expansion of the free space Green's dyadic in terms of the cylindrical vector waves [5], it is shown that the volume integral equation [6, 10] reduces to a system of one-dimensional integral equations, one system for each azimuthal index and each with a discontinuous kernel which is singular at the origin. The Fourier variable of the cylindrical vector wave expansion plays the role of a spectral parameter. Furthermore, it is demonstrated how the Floquet condition [5, 9] for waveguides periodic in the longitudinal direction leads to a corresponding system of two-dimensional integral equations defined over a unit cell of the waveguide. Spectral issues, asymptotic properties and numerical issues are discussed.

REFERENCES

1. Agrawal, G. P., *Fiber-optic Communication Systems*, John Wiley & Sons, Inc., Hoboken, New Jersey, 2010.
2. Botha, M. M., "Solving the volume integral equations of electromagnetic scattering," *Comput. Phys.*, Vol. 218, 141–158, 2006.
3. Budko, N. V. and A. B. Samokhin, "On the eigenvalues of the volume integral operator of electromagnetic scattering," *SIAM J. Sci. Comput.*, Vol. 28, No. 2, 682–700, 2006.
4. Chew, W. C., *Waves and Fields in Inhomogeneous Media*, IEEE Press, Piscataway, NJ, 1995.
5. Collin, R. E., *Field Theory of Guided Waves*, 2nd Edition, IEEE Press, New York, 1991.
6. Costabel, M., E. Darrigrand, and E. H. Koné, "Volume and surface integral equations for electromagnetic scattering by a dielectric body," *Comput. Appl. Math.*, Vol. 234, 1817–1825, 2010.
7. Kartchevski, E. M., A. I. Nosich, and G. W. Hanson, "Mathematical analysis of the generalized natural modes of an inhomogeneous optical fiber," *SIAM J. Appl. Math.*, Vol. 65, No. 6, 2033–2048, 2005.
8. Nordebo, S., B. Nilsson, T. Biro, G. Cinar, M. Gustafsson, S. Gustafsson, A. Karlsson, and M. Sjöberg, "Wave modeling and fault localization for underwater power cables," *International Conference on Electromagnetics in Advanced Applications (ICEAA11)*, 698–701, 2011.
9. Peterson, A. F., S. L. Ray, and R. Mittra, *Computational Methods for Electromagnetics*, IEEE Press, New York, 1998.
10. Sancer, M. I., K. Sertel, J. L. Volakis, and P. V. Alstine, "On volume integral equations," *IEEE Trans. Antennas Propagat.*, Vol. 54, No. 5, 1488–1495, 2006.
11. Shestopalov, V. and Y. Shestopalov, *Spectral Theory and Excitation of Open Structures*, Peter Peregrinus, Ltd., London, 1996.

Eigenmodes in Problems of Scattering and Generation of Oscillations on a Nonlinear Layer

Lutz Angermann[1] and Vasyl V. Yatsyk[2]

[1]Department of Mathematics, University of Technology at Clausthal
Erzstraße 1, D-38678 Clausthal-Zellerfeld, Federal Republic of Germany
[2]O. Ya. Usikov Institute for Radiophysics and Electronics of the National Academy of Sciences of Ukraine
12 Ac. Proskura Str., Kharkiv 61085, Ukraine

Abstract— We have obtained a variety of numerical results that describe important properties of the nonlinear permittivities of the layers as well as their scattering and generation characteristics. In the frequency domain, the resonant scattering and generation properties of nonlinear structures are determined by the proximity of the excitation frequencies of the nonlinear structures to the complex eigenfrequencies of the corresponding homogeneous linear spectral problems with the induced nonlinear dielectric permeability of the medium. The approximate solution of the self-consistent nonlinear problems was obtained by solving linear problems with an induced nonlinear dielectric permeability. The analytical continuation of these linear problems into the region of complex values of the frequency parameter allowed us to switch to the analysis of spectral problems [1–3]. By introducing a variable which describes the ratio of the Q-factor of eigenoscillations at the excitation and generation frequencies, we were able to show the following. For an increasing amplitude of the exciting field, an increase of the generated energy in the higher harmonics is accompanied by a monotonic decrease of the relative Q-factor of the eigenoscillations, and this is the case for canalising as well as decanalising nonlinear layers. The paper presents results of the effect of a weak field at the doubled excitation frequency on the scattering and generation of oscillations. It is shown that inclusion of a weak field at a multiple frequency increases the portion of the generated energy.

ACKNOWLEDGMENT

This work was partially supported by the Visby Program of the Swedish Institute and by the joint Russian-Ukrainian RFBR-NASU grant No. 12.02.90425-2012.

REFERENCES

1. Angermann, L., Y. V. Shestopalov, and V. V. Yatsyk, "Modeling and analysis of wave packet scattering and generation for a nonlinear layered structure," *Multiphysics Modeling in Microwave Power Engineering*, 21–26, E. M. Kiley and V. V. Yakovlev, Editors, University of Bayreuth, Germany, 2012; *14th Seminar Computer Modeling in Microwave Engineering and Applications*, Bayreuth, March 5–6, 2012.
2. Angermann, L. and V. V. Yatsyk, "The effect of weak fields at multiple frequencies on the scattering and generation of waves by nonlinear layered media," *Solutions and Applications of Scattering, Propagation, Radiation and Emission of Electromagnetic Waves*, 303–332, A. Kishk, Editor, InTech, Rijeka, Croatia, 2012.
3. Angermann, L. and V. V. Yatsyk, "The influence of weak fields at multiple frequencies on the process of resonant scattering and generation of oscillations by nonlinear layered structures," *Physical Bases of Instrumentation*, Vol. 2, No. 48–71, 2013 (in Russian).

Spectral Theory of Wave Propagation: Survey of Recent Results

Yury Shestopalov
Karlstad University, Sweden

Abstract— The spectral theory of open structures [1, 2] that employs advanced methods of the theory of nonselfadjoint operators and operator-valued functions (OVFs) offers a universal approach to the solution of boundary value problems for linear and nonlinear partial differential equations arising in electromagnetic and acoustics. The theory includes mathematical techniques for modeling the interaction of oscillations and waves in terms of the analysis of the spectral and various critical points (CPs) of multi-parameter OVFs, in particular, integral and infinite-matrix (summation) OVFs when some of the operator parameters are varied. Interaction of oscillations in a cylindrical slotted resonator whose cross section is formed by two rectangular domains [3] may be taken as an example. The initial boundary eigenvalue problem for the Helmholtz equation or Maxwell equations is reduced to a Fredholm integral equation with logarithmic singularity or to infinite systems with respect to the unknown Fourier coefficients of the solution. It turns out that some CPs of the OVF are associated with the points where one or several eigenvalues merge and interaction of oscillations may occur in this case; namely, the electromagnetic field distributions become unstable with respect to small variations of certain parameters of the structure (geometric, permittivity etc.) in the vicinities of critical values. A recent fundamental result establishing global existence of the discrete eigenwave spectra has brought the spectral theory of wave propagation in guides to a qualitatively new level: for a wide class of metal-dielectric guides it was shown [4] that (1) there exists a countable set of the points of complex spectrum of eigenwaves located in a strip of known width on the complex plane and (2) the corresponding system of eigenvectors and associated vectors is doubly complete with finite defect. Thus, there is no continuous spectrum of eigenwaves and the location of the spectra can be efficiently determined using the operator pencil methods developed in [4]. The latter can be applied as alternative technique to the analysis of the wave propagation in waveguides of arbitrary cross section with various dielectric inclusions.

REFERENCES

1. Shestopalov, V. P. and Yu. V. Shestopalov, "Spectral theory and excitation of open structures," Peter Peregrinus Ltd., 1996.
2. Chernokozhin, E., Y. Smirnov, and Y. Shestopalov, *Logarithmic Integral Equations in Electromagnetics*, VSP Int. Science Publishers, Utrecht, Boston, Köln, Tokyo, 2000.
3. Yu. Shestopalov, Y. Okuno, and N. Kotik, "Oscillations in slotted resonators with several slots: Application of approximate semi-inversion," *Progress In Electromagnetics Research*, Vol. 39, 193–247, 2003.
4. Yu. Shestopalov, Y. Okuno, and N. Kotik, "Oscillations in slotted resonators with several slots: Application of approximate semi-inversion," *Journal of Electromagnetic Waves and Applications*, Vol. 17, No. 5, 755–757, 2003.
5. Yu. Shestopalov and Y. Smirnov, "Eigenwaves in waveguides with dielectric inclusions: Spectrum," *Appl. Analysis*, 2013, to appear.

Plasmonic Cavity Modes: Black-hole Phenomena Captured by Perfectly Matched Layers

A.-S. Bonnet-Ben Dhia[1], **C. Carvalho**[1], **L. Chesnel**[2], **and P. Ciarlet, Jr.**[1]

[1]POEMS, UMR 7231 CNRS-INRIA-ENSTA, France
[2]Department of Mathematics and Systems Analysis, Aalto University, Finland

Abstract— Consider a cavity made of a dielectric material with a metal inclusion, which are separated by an interface. We assume that, in a given frequency range, the metal's permittivity $\epsilon = \epsilon(\omega)$ is a negative real number. We consider the time-harmonic Maxwell equations for the Transverse Magnetic polarization. We look for the cavity resonances by studying the linearized eigenvalue problem (dependence in ω of ϵ frozen): $Au = \omega^2 u$. When ϵ changes sign at the interface, the operator A is self-adjoint with a discrete spectrum if and only if [1]: the ratio κ_ϵ of permittivities between the dielectric and the metal is such that $\kappa_\epsilon \neq -1$ (for a smooth interface); or κ_ϵ doesn't belong to a *critical interval* strictly larger than $\{-1\}$ (when the interface has corners). The eigenvalues $(\omega_i^2)_i$ consist in two sequences of real numbers with finite multiplicity tending respectively to $\pm\infty$. Inside the critical interval (excluding $\kappa_\epsilon = -1$), due to singular phenomena occuring at the corners, a new functional framework is required. In [2, 3] an extension of the operator A is given which recovers the resolvent's compactness property. It takes into account singular functions whose gradient is not square integrable at the corners. These singularities, selected by a limiting absorption principle [2], can be interpreted as waves propagating along the interface towards the corners: they are called black-hole plasmonic waves.

To be able to compute these black-hole waves with Finite Elements, we propose an original use of PMLs. By the Euler change of variables $(r, \theta) \longrightarrow (\log(r), \theta)$ we transform a disk centered at each corner into an open waveguide [2] which we can troncate with PMLs. Numerical results confirm that the PMLs' method is efficient to ensure the stability of the Finite Element approximation. Outside the critival interval, the eigenvalue's approximation is stable under some conditions on the mesh [4]. Inside the critical interval, the extended operator's spectrum includes complex eigenvalues which clearly proves its non self-adjointness. Moreover, we can prove that all eigenvalues are such that $\mathrm{Im}(\omega^2) \leq 0$, which is numerically verified.

Once the linearized eigenproblem is fully understood, we can solve in principle the exact *nonlinear* eigenproblem. For instance, the resonances could be obtained with the help of a fixed point algorithm.

ACKNOWLEDGMENT

We thank the DGA for its financial support.

REFERENCES

1. Bonnet-Ben Dhia, A.-S., L. Chesnel, and P. Ciarlet, Jr., "T-coercivity for scalar interface problems between dielectrics and metamaterials," *Math. Mod. Num. Anal.*, Vol. 46, 1363–1387, 2012.
2. Bonnet-Ben Dhia, A.-S., L. Chesnel, and X. Claeys, "Radiation condition for a non-smooth interface between a dielectric and a metamaterial," *Math. Mod. Meth. App. Sci.*, 2012.
3. Bonnet-Ben Dhia, A.-S., M. Dauge, and K. Ramdani, "Analyse spectrale et singularités dún problème de transmission non coercif," *C. R. Acad. Sci. Paris, Ser. I*, Vol. 328, 717–720, 1999.
4. Chesnel, L. and P. Ciarlet Jr., "T-coercivity and continuous Galerkin methods: Application to transmission problems with sign changing coefficients," *Numer. Math.*, 2012.

Resonant Frequency Doubling of Electromagnetic Waves in a Magnetoplasma: Analogy of the Non-linear Laser Crystal

N. S. Erokhin[1] **and A. B. Shvartsburg**[1, 2]

[1]Institute of Space Researches, RAS, Moscow, Russia
[2]Laser Center "Pole", Moscow, Russia

Abstract— This research is devoted to a new non-linear effect — resonant doubling of the frequencies of EM waves in the gaseous magnetoplasma. The physical fundamentals of this effect are:

1. The EM wave field in the magnetoplasma is characterized by vector polarization structure;

owing to magnetoplasma anisotropy this structure depends upon the direction of wave propagation [1]. The component of wave's electric field, parallel to the wave vector, provides the perturbation of plasma electron density, oscillating with the wave frequency ω; the travelling wave is scattering on this oscillating perturbation. This self-action results in the generation of wave with frequency 2ω.

2. This non-linear effect is shown to possess the resonant strengthening, when the refractive index of the travelling wave and its second harmonic obey to the resonant condition of phase synchronism: $n(\omega) = n(2\omega)$. This condition, well known in laser physics [2], can be fulfilled in the wide spectral ranges, determined by plasma density, magnetic field and the direction of propagation.

3. It is remarkable, that this resonant condition is fulfilled, in particular, in the magnetoplasma of the upper Ionosphere. Due to spatial variations of electron density in these regions the resonant conditions arise in the restricted altitudinal areas with scales about tens of kilometers [3] for the waves with frequencies about several MHz; hereat the transformation coefficient of this resonant SHG process with respect to energy at the distance about tens of wavelengths can exceed 10%.

This effect opens the perspectives for non-linear remote sensing of plasma density both in the laboratory and Space plasmas. Comparison of travelling times of two nanosecond pulses with frequencies ω and 2ω provides the location of the place, where the resonant conditions are fulfilled, meanwhile the efficiency of SHG opens the way to the estimation of parameters of this region.

REFERENCES

1. Mikhailovskii, A. B., *Electromagnetic Instabilities in an Inhomogeneous Plasma*, Hilger, 1992.
2. Mendoza, B. S. and W. L. Mochan, *Phys. Rev. B*, Vol. 53, 4999, 1996.
3. Shvartsburg, A., V. Kuzmiak, and G. Petite, *Physics Reports*, Vol. 452, 34, 2007.

The Reconstruction of Dielectric Profile of a Layer for the Harmonic Wave Case

N. B. Pleshchinskii and D. N. Tumakov
Kazan Federal University, Russia

Abstract— Let the plane electromagnetic harmonic wave fall on a layer of thickness L with unknown refractive index from a homogenous isotropic medium. It is necessary to reconstruct the refractive index $n(x)$ measuring the reflected and the transited waves of several frequencies. We suppose that profile of the refractive index is varied continuously.

The direct diffraction problem with the known refractive index is reduced to an ordinary differential equation with necessary boundary conditions. These conditions are formed by elimination of two semi-infinite domains from the wave guide structure. The direct diffraction problem on the layer for arbitrary continuous profiles is solved numerically.

Let us assume that M measurements are executed and values of fields on the layer's borders are obtained as a result. We will solve iteratively the direct problem in order to solve the inverse problem. The direct problem is solved with the refractive index which was received at a previous iteration. We will minimize the functional

$$\begin{aligned} F(n(x)) \;=\; & \sum_{j=1}^{M} \left\| u^j(0) - \hat{u}_0^j \right\| + \sum_{j=1}^{M} \left\| u^j(L) - \hat{u}_L^j \right\| \\ & + \alpha \left\| n(x) \right\| + \beta_1 \left\| n(0) - n_0 \right\| + \beta_2 \left\| n(0) - n_L \right\|, \end{aligned} \tag{1}$$

where $\hat{u}_0^j$ and $\hat{u}_L^j$ are known values of the field for experiment with number j, $u^j(0)$ and $u^j(L)$ are calculated values of the field on the current iterative step on both sides $x = 0$ and $x = L$ of the layer. The values α, β_1 and β_2 are regularization parameters; values n_0 and n_L are known values of refractive index on the layer's borders. The extremal problem is solved by the gradient method.

The algorithm for reconstruction of the refractive index is tested. The profile of approximate refractive index is in accord with the accurate profile by correct choice of frequencies. The algorithm of selection of "measurement" frequencies is presented. Dependences of the accuracy of the approximate solution on various parameters are shown.

Cylindrically Shaped Apertures and Guidance of Waves by Using Hankel Transformation and the Exact Approach Technique

T. Sengor
Yildiz Technical University, Turkey

Abstract— The main goal of this paper is to present an effective semi-analytical and computational method for studying on apertures and guidance of electromagnetic waves involving cylindrical discontinuities. The approach is based on the application of the Exact Approach Technique by Integral Representations, EATIR [1]. Some pre-applications were given with the aid of Hankel's integral transformation for planarly and/or cylindrically symmetrical cases with both of the perfectly and imperfectly electrical conducting waveguides [2–7]. Some cases involving dielectric apertures were studied [8, 9]. First, a review of previously studied configurations is given. Second, cylindrical apertures on cylindrical waveguides and cylindrical strip coatings on dielectric waveguides and cylindrical openings are presented.

REFERENCES

1. Sengor, T., "The exact approach technique by integral representations," *The XXVIII Moscow International Conference on Antenna Theory and Technology*, Moscow, Russia, September 22–24, 1998.
2. Sengor, T. and H. P. Partal, "The exact computational solution approach by integral representation with an application to radiation characteristics of aperture antennas," *1996 IEEE AP-S International Symposium and Radio Science Meeting, AP-S Digest*, Vol. 3, 1832–1835, Baltimore, Maryland, USA, July 21–26, 1996.
3. Sengor, T. and H. P. Partal, "Simulating the radiation characteristics of circular impedance discs," *Proceedings of the International Conference on Electromagnetics in Advanced Applications, ICEAA 97*, 211–214, Torino, Italy, September 15–18, 1997.
4. Kalaycioglu, K., "Exact numerical solution approximation in scattering problems with cylindrical geometries by integral representations," MSEE Thesis supervised by Sengor, December 1997.
5. Saglam, A., "Exact numerical solution approximation in scattering problems of cylindrical geometries with impedance by integral representations," MSEE Thesis supervised by Sengor, January 1999.
6. "Decrease of side lobe effects by circular aperture antenna configurations," Turkey Science and Technical Research Organization, TUBITAK-BAYG 313(93)-5482, Starting Date: October 1993.
7. Erkut, C. and T. Sengor, "Imaging of dielectric apertures on curved patches," *PIERS Proceedings*, 1112, Washington, USA, July 24–28, 1995.
8. Sengor, T., "The electromagnetic radiation mechanism in faults: Aperture antenna array in fractal structure," *European Geosciences Union General Assembly 2006*, Nisan 02-07, Vienna, Austria, 2006.

Adaptive Artificial Boundary Conditions for Schrödinger Equation with Un-instantaneous Nonlinearity

V. A. Trofimov, **A. D. Denisov**, **M. V. Fedotov**, **and A. S. Prokopenko**
Lomonosov Moscow State University, Moscow 119992, Russia

Abstract— Enhancement of a computer simulation performance is one of the urgent problems. A possible way to do this consists in implementing artificial boundary conditions applied for the numerical solution of equation under consideration. As it well-known [1–6], such approach is widely applies for computer simulation of wave propagation in linear and nonlinear medium. In particular, various types of artificial boundary conditions were proposed for Schrödinger equation [5, 6]. Mainly, such conditions were developed for such equation with instantaneous nonlinear response of medium or in the linear case. In present report [7], we proposed the adaptive artificial boundary conditions for Schrödinger equation describing a nonlinear propagation of terawatt laser pulse in glass taking into account the multi-photon absorption and non-stationary generation of free carriers of charges and Kerr nonlinear response of medium. This process is described by the nonlinear Schrödinger equation together with time-dependent equation with respect to concentration of free electrons.

For considering set of the equations in 1D case, we constructed two-layer non-explicit scheme, which is conservative one in the case of transparent medium. To realize the adaptive artificial boundary conditions, the analysis of instantaneous frequency of optical pulse near the boundaries of time interval under consideration is provided. This value of frequency is used in the boundary conditions. Obviously, the instantaneous frequency depends on propagation coordinate and time. Therefore, using the constant value of frequency in the boundary conditions is ineffective way for developing of the artificial boundary conditions.

On the base of computer simulation, we show high efficiency of an approach, developed by us.

ACKNOWLEDGMENT

This work is partly supported by the Russian Foundation for Basic Research.

REFERENCES

1. Schürmann, H. W., Y. Smirnov, and Y. Shestopalov, "Integral equation approach for the propagation of TE-waves in a nonlinear dielectric cylindrical waveguide," *J. Nonlinear Math. Phys.,* Vol. 11, 256–268. 2004.
2. Xu Z. and H. Han, "Absorbing boundary conditions for nonlinear schrödinger equations," *Phys. Rev.*, Vol. 74, 037704, 2006.
3. Xu, Z., H. Han, and X. Wu, "Adaptive absorbing boundary conditions for Schrödinger-type equations: Application to nonlinear and multi-dimensional problems," *J. Comput. Phys.*, Vol. 225, 1577–1589, 2007.
4. Fibich, G. and S. Tsynkov, "High order two-way artificial boundary conditions to nonlinear wave propagation with back-scattering," *J. Comput. Phys.*, Vol. 171, No. 2, 632–677, 2001.
5. Antoine, X., A. Arnold, C. Besse, M. Ehrhardt, and A. Schadle, "A review on transparent and artificial boundary conditions technique for linear and nonlinear Schrödinger equations," *Commun. Comput. Phys.*, Vol. 4, 729–796, 2008.
6. Tereshin, E. B., V. A. Trofimov, and M. V. Fedotov, "Conservative finite-difference scheme for the problem of propagation of a femtosecond pulse in a nonlinear photonic crystal with nonreflecting boundary conditions," *Computational Mathematics and Mathematical Physics*, Vol. 46, No. 1, 152–164, 2006.
7. Trofimov, V. A. and A. D. Denisov, "Adaptive artificial boundary conditions for 2D schrodinger equation," *Abstracts of Reports on "Fifth Conference on Numerical Analysis and Applications"*, 50–51, Lozenetz, Bulgaria, 2012.

Session 2AK
Poster Session 3

Benefits of Using Wireless Sensor Networks to Predict Plagues in Vineyards
Inigo Cuinas, Sergio Cervera, Jose Antonio Gay-Fernandez, ... 592
Electro-responsive and Dielectric Characteristics of Graphene Oxide Based Composites
Wen Ling Zhang, Hyoung Jin Choi, ... 593
Heterogeneous Oscillator Model of Cardiac Conduction System
Elena Ryzhii, Maxim Ryzhii, ... 594
GP GPU Acceleration of a PO Based RF Simulation Software Dedicated to Radar Simulation in Large Scale and Complex Environments
A. Boudet, Nicolas Douchin, P. Pitot, ... 595
Phase Delay of Alternating Multi-layers of Meta-materials and Dielectrics
Jonghun Lee, Cherl-Hee Lee, ... 596
Hybrid Metal-dielectric Ring Resonators for Optical Magnetism and Magnetic Metamaterials Down to Ultraviolet Wavelengths
Jianwei Tang, Sailing He, ... 597
Atomistic Approach for the Field Enhancement in Quantum Plasmonic Nanostructures
Tuomas Rossi, Arto Sakko, R. M. Nieminen, ... 598
Graphene Waveguides of Ultra-small Mode Areas and Ultra-large Effective Refractive Indices
Sailing He, Xizhou Zhang, Yingran He, ... 599
Fe:BN Nanoceramic — Negative Refraction Material in the Wide Frequency Range
Karen Oganisian, A. Vogt, P. Gluchowski, K. Orzechowski, W. Strek, ... 600
Fano Resonance in Simple and Single Plasmonic Particle
Yuan Zhang, Sailing He, ... 601
Design and Application of Multi-slots AMC Structure Having Metamaterial Characteristic for 2.45 GHz Band
Seung Woo Lee, Nam Kim, Seung-Yeup Rhee, ... 602
Bundle Block Adjustment with Optical and SAR Images
Shuai Xing, Qing Xu, Wei Sun, Jiansheng Li, Yu He, ... 603
Airborne Interferometric SAR Experiment with Multi-carrier Frequencies Using both Chirp and Noise Signals
Yunhua Zhang, Wenshuai Zhai, Xueyan Kang, Xiaojin Shi, Xiang Gu, Yueying Tang, ... 604
Micro-doppler Analysis of Rotating Targets in Dual-channel Bistatic SAR
Meng Lv, ... 605
Snow Wetness Estimation from Polarimetric SAR Image
Manickam Surendar, G. Singh, Avik Bhattacharya, G. Venkataraman, P. A. Bharathi, ... 606
Optical Data Storage Using Diffractive Optical Elements
Shuhei Yoshida, Kai Yamada, Noriyuki Unno, Jun Taniguchi, Manabu Yamamoto, ... 607
Multi-dimensional Shift Multiplexing for Holographic Data Storages
Shuhei Yoshida, Keiko Yamamoto, Hiroyuki Kurata, Manabu Yamamoto, ... 608
Characterization of Zinc-tin-oxide Films Deposited by Radio Frequency Magnetron Sputtering at Various Substrate Temperatures
Ik-Jae Lee, Nark-Eon Sung, Keun Hwa Chae, Ray Conley, ... 609
Design of New ITO Electrodes for High Sensitive Capacitive Touch Panel
Huai-Yi Chen, Hsi-Ting Huang, ... 610
On the Modeling of an External Cavity Tunable Laser ECTL Source with Finite Mirror Dimensions
Ahmed Mohamed Fawzy, Salwa El-Sabban, Ibrahim I. Ibrahim, Diaa Khalil, ... 612
Polarization-insensitive and Broadband Plasmonic Silicon Schottky Diode for Detection of Sub-bandgap Photons
Liu Yang, Pengfei Kou, El Hang Lee, Sailing He, ... 613
The Fabrication of AlGaN Ultraviolet-B Metal-semiconductor-metal Photodetectors with a MgZnO Thin Film Filter

Ming-Jer Jeng, Jun-Yan Chang, Liann-Be Chang, Ray-Ming Lin, Li-Zen Hsieh, ... 614
Omnidirectional Absorber Based on Collision Plasma Heterostructures
Xiang-Kun Kong, Shaobin Liu, Hai Feng Zhang, Bo-Rui Bian, Hui-Chao Zhao, Huan Yang, ... 615
Size Reduction of Narrowband Hairpin Bandpass Filter Using Fractal Koch Geometry
Achmad Munir, Teguh Praludi, Mohammad Ridwan Effendi, ... 616
Design of a Compact Dual-mode Dual-band Microstrip Bandpass Filter Based on Semi-fractal CSRR
Mushtaq A. Alqaisy, Jawad K. Ali, Chandan Kumar Chakrabarty, Goh Chin Hock, ... 617
Odd-order Bandstop Filter (BSF) Topology with Inter-resonator Coupling Structures
Tae-Hak Lee, Kangho Lee, Chang-Soo Ahn, Young Sik Kim, Juseop Lee, ... 618
Dual-band Impedance Matching Network with Transmission Zeros Using Resonators
Phirun Kim, Girdhari Chaudhary, Yongchae Jeong, Jongsik Lim, ... 619
Highly Miniaturized Forced-mode Ring Resonator
Jose Roberto Reyes Ayona, ... 620
A Novel Approach to Increase the Multipactor Level in Microwave Transformer
Tiancun Hu, Wanzhao Cui, ... 621
Design and Realization of a C-band Impedance Transformer
Tiancun Hu, Wanzhao Cui, ... 622
Synthesis of Non-uniform Planar Lines and Coupled Line Filters Using Inverse Scattering Approach
Harishankar Prasad, Mohammad Jaleel Akhtar, ... 623
Calculating the Scattering from Periodic Conducting Surfaces without Using Evanescent Modes, Part II: Formulation of the Solution
Dayalan Prajith Kasilingam, Christopher Goonan, ... 624
Changes in the Degree of Polarization of a Stochastic Electromagnetic Plane-wave Pulse Scattered by a Spherical Medium
Liuzhan Pan, Chaoliang Ding, ... 625
Some Ideas Yet Unattempted in Georadar Full Waveform Inversion
Giovanni Meles, Stewart Greenhalgh, Hansruedi Maurer, Alan Green, ... 626
Compton Effect in the Medium with Non-unity Refractive Index
S. G. Chefanov, A. G. Chefranov, Vinay Venugopal, ... 627
An Acoustic Inverse Scattering Problem for Spherical Coating Materials with Radially Inhomogeneous Profile
Egemen Bilgin, Ali Yapar, ... 628
Reflection of TEM Waves from a Finite Gap on the Inner Wall of a Coaxial Waveguide
Ozge Yanaz Cinar, Sinan Aksimsek, ... 629
Properties of One-way Magnetooptic Nanostructures in THz Range
P. Kwiecien, Vladimir Kuzmiak, Ivan Richter, Jiri Ctyroky, ... 630
Broadband Characterization Using Stripline Structure
Ellen Yoshie Sudo Lutif, Alberto Jose de Faro Orlando, Antonio Carlos da Cunha Migliano, ... 632
Few-quantum-dot Lasing in Photonic Crystal Nanocavities
Jin Liu, S. Ates, S. Stobbe, M. Lorke, Peter Lodahl, ... 633
Investigations on Two-wavelength Holographic Recording in Thick Phenanthrenequinone-doped Poly(Methyl Methacrylate) Photopolymer
June Hua Lin, Shiuan Huei Lin, Ken-Yuh Hsu, ... 635
Optical Control of Guided-mode-resonance in the Waveguide Grating Structures with Azo-dye Polymers
Jian-Hung Lin, Yu Chung Huang, Jian Hao Huang, Hung-Chih Kan, Chia Chen Hsu, ... 636
Design and Simulation of Optimized Ultra-wideband Saddle Antenna
Alapati Sudhakar, Devabhaktuni Madhavi, ... 637
Printed Yagi-Uda Antenna for WLAN Applications
Amira El-Tokhy Ali, Deena A. Salem, ... 638
Digital Public Safety Radio Communication
Eduil Nascimento Junior, Horacio Tertuliano Filho, Jose-Ricardo Descardeci, C. A. Dartora, Theoma M. Sanchez Otobo, E. Cherubini Rolin, ... 639
A Compact UWB Antenna with Wide Band-notch at 5 GHz for WLAN Band
Qurratulain, Neela Chattoraj, ... 640
Effect of Stationary Magnetic Fields on Different Bacterial Strains
Pavel Krepelka, Eliska Hutová, Karel Bartušek, ... 642

Enhanced Spectrum Planning in Cognitive System Based on Reinforcement Learning
Robert Urban, Eliska Hutová, Dusan Nespor, ... 643
2D Simulations of Bioelectrical Properties of Thorax by EIT
Ksenia Ostanina, Jarmila Dedkova, Tomas Kriz, ... 644
Estimation of the Air Ion Mobility Spectrum by Means of a Gerdien Tube with a Segmented Inner Electrod
Zdeněk Roubal, Pavel Krepelka, ... 645
Study about Effects Induced by Temporal-variability of Ionosphere on Medium-Earth-Orbit SAR Azimuth Imaging
Liang Li, Jun Hong, Feng Ming, ... 646
Technique Problems in Designing the on-chip EMI Sensor Array
Tao Su, Yehua Yang, Zixin Wang, ... 647
Design and Synthesis of Multi Resonant Planar Antenna Using Particle Swarm Optimization Method
B. Rama Sanjeeva Reddy, Damera Vakula, N. V. S. N. Sarma, ... 648

Benefits of Using Wireless Sensor Networks to Predict Plagues in Vineyards

I. Cuiñas, S. Cervera, and J. A. Gay-Fernández
Department Teoría do Sinal e Comunicacións, Universidade de Vigo, Spain

Abstract— Wireless sensor networks (WSNs) have been proposed as a key tool in improvement of agriculture goods quality, as a mean to control different parameters related to the biological activity and growing rhythm of the plants. Wine sector is especially interested in such technology: the final product (the wine) has important added value, but its quality is strongly dependent to the vines health and development during several months a year.

This abstract, and the subsequent related paper, is intended to describe the experience in installing and operating a WSN with different meteorological sensors in a vineyard at a Spanish denomination of origin area, as well as the processing of collecting data to analyze the most troublesome plague in the region, the mildew.

The system consists of six motes, each provided by four sensors (temperature, humidity, leaf wetness, and so on), a coordinator, and a gateway to link the data to the world (i.e., the Internet) via a GPRS connection. This set of sensors is collecting data since more than two years, each 5 minutes, constructing what could be seen as time varying signals that could be processed and analyzed.

The application of methods as EPI, POM, Goidanich, RAI, Milvit, or Plasmo allows us to provide the biologists taking care of the vineyards with a mildew alert system, in order they to decide the actions or products to apply the plants each time. This scientific alert procedure could reduce the number of applied treatments, as it breaks the traditional period-based treatment and supports the decision of cure when it is need. Then, a reduction in costs could be obtained: both economics (products and work-time to apply them) and ecological (less chemical products incorporated to the soil and plants).

An analysis of the processing procedures and the estimation of cost reduction after using such method will be presented along the final paper and at the conference.

ACKNOWLEDGMENT

This work was partially funded by Spanish Ministry of Economy and Competitiveness, State Secretary for Research under project TEC2011-28789-C02-02, that was co-funded using European Regional Development Funds (ERDF), as well as the Galician Regional Government under project CN 2012/260 "Consolidation of Research Units: AtlantTIC".

Electro-responsive and Dielectric Characteristics of Graphene Oxide Based Composites

Wen Ling Zhang and Hyoung Jin Choi
Department of Polymer Science and Engineering, Inha University, Incheon 402-751, Korea

Abstract— Due to its excellent physical and chemical properties, graphene a two-dimensional sheet of sp^2-bonded carbon has become an exciting material with many potential applications, such as sensors, batteries, catalyst supports, field-effect transistor, conducting ink and capacitors [1]. The oxidized and exfoliated graphite (graphene oxide, GO) was reported as the precursor to prepare graphene using the reduction process. GO is an interesting material because of its excellent dispersion stability and various functional groups In addition, the low electrical conductivity of the GO is also favorable in our study for GO-based composite as an electrorheological (ER) smart material. Here, the ER fluids are in general the suspensions composed of polarizable particles dispersed in insulating medium oils [2]. The dispersed particles get polarized and form chain/column like structures under the applied electric field. Therefore, their rheological properties such as shear stress, apparent shear viscosity and dynamic modulus can be controlled by the external electric field stimulus The ER characteristics can be improved by combining materials with suitable electrical conductivity and high dielectric constant. The achievable polarizability is related to the parameters of the permittivity and the dielectric relaxation time and these parameters can be analyzed by fitting the well known Cole-Cole equation [3]. In this work, fabrication of GO-based composites with inorganic (silica) [4] and organic (poly(glycidyl methacrylate) particles in addition to GO itself [5] is reported, along with their ER properties and dielectric constants measured using a rotational rheometer and a LCR meter, respectively.

REFERENCES

1. Shi, W., J. Zhu, D. H. Sim, Y. Y. Tay, Z. Y. Lu, X. J. Zhang, H. Zhang, H. H. Hng, and Q. Yan, *J. Mater. Chem.*, Vol. 21, 3422–3427, 2011.
2. Choi, H. J. and M. S. Jhon, *Soft Matter*, Vol. 5, 1562–1567, 2009.
3. Cole, K. S. and R. H. Cole, *J. Chem. Phys.*, Vol. 9, 341, 1941.
4. Zhang, W. L. and H. J. Choi, *Langmuir*, Vol. 28, 7055, 2012.
5. Zhang, W. L., Y. D. Liu, H. J. Choi, and S. K. Kim, *ACS Appl. Mater. Interf.*, Vol. 4, 2267, 2012.

Heterogeneous Oscillator Model of Cardiac Conduction System

E. Ryzhii and M. Ryzhii
Complex Systems Modeling Laboratory, University of Aizu, Japan

Abstract— The study of heart electrical behavior utilizing mathematical and computer models with different approaches and levels of details is very popular research subject today. It is very important for deeper understanding of origins of life-treating cardiac arrhythmias and improvement of their prevention and treatment.

We propose a mathematical model of human heart consisting of modified Van der Pol equations for self-sustained oscillating and quiescent excitable systems with time-delay coupling. Accordingly, the heart electrical activity is described by a system of delayed differential equations.

The model allows generating physiologically correct electrical signals of action potentials of all three major natural pacemakers (sinoatrial node (SAN), atrioventricular node (AVN), and Purkinje fiber (PKJ)) as well as atrial (ATR) and ventricular (VTR) muscle response.

Resulting dynamic response of the oscillator system is obtained in the form of the electrocardiogram (ECG) which is one of the most important clinically comparable characteristic of human heart electrical activity.

The performed numerical simulations demonstrated good qualitative agreement with normal cardiac electrical rhythm. We also tested the proposed model to reproduce some well-known arrhythmias.

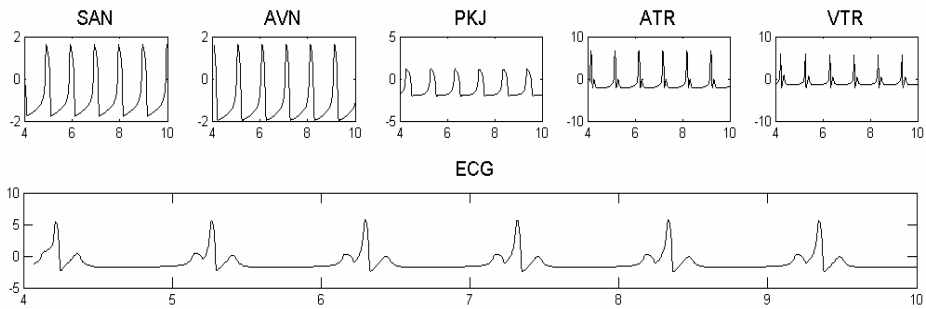

GP GPU Acceleration of a PO Based RF Simulation Software Dedicated to Radar Simulation in Large Scale and Complex Environments

A. Boudet, **N. Douchin**, **and P. Pitot**
OKTAL Synthetic Environment, 11, avenue du Lac, Vigoulet-Auzil 31 320, France

Abstract— SE-RAY-EM software is based on a combination of Shooting and Bouncing Rays (SBR) technique, that has been optimized to calculate efficiently the intersections between rays from a transmitter towards a 3D database and back to a receiving point, and EM models for computing propagation, reflection and diffraction. These models are the formulations of Geometrical Optics (GO), Physical Optics (PO) and Equivalent Current Method (ECM). An operating strategy enables unified calculation for the near or far EM scattered fields from the scenes. The "forward scattering" approach based on the equivalence principle is also used to compute EM fields in the shadow region. Since it relies on asymptotic methods SE RAY-EM is well suited for computing the EM interactions of an incident wave with complex 3D models of large scale environments and objects at high frequencies typically in the 1–100 GHz range.

Existing works have shown that GP GPU acceleration is well suited for ray tracing applications. EM asymptotic simulations based on ray tracing simulation can benefit from that technology, with the following difficulties.

Computation of phases requires double precision: though GPU double precision capabilities are improved at each GPU generation, double precision numbers cost also twice as much registers than float numbers and twice as much memory bandwidth. So avoiding double computations while preserving phase precision is necessary.

For physical optics simulations, high frequency computation needs very precise surface sampling. To be efficient, it is necessary to reduce the number of samples to compute. As on existing SE-RAY-EM CPU renderer, we choose to implement an adaptive antialiasing process that reduces the samples number while achieving the precision requirements. Adaptive antialiasing process on a highly parallel architecture is not obvious as the number of rays to trace can actually explode. It must be controlled without consuming too much memory and keeping a high level of parallelism.

In this paper, we discuss on the way to solve such problems. We also present the SE-RAY-EM computation scheme on its existing CPU version and compare it to the new GP GPU version. Results and comparison with the CPU version of SE-RAY-EM are presented.

Phase Delay of Alternating Multi-layers of Meta-materials and Dielectrics

Jonghun Lee and Cherl-Hee Lee
Robotics Research Division, Daegu Gyeonbuk Institute of Science & Technology, Korea

Abstract— An artificial metamaterials (MTM) having simultaneously negative permittivity (ε) and permeability (μ), which is referred to as left-handed materials (LHM), was first proposed by Veselage in 1968. The MTM have received considerable attentions after the experimental realizations, such as a prism-shaped sample, flat lens, filter and antennas, photonic crystals at the infrared region, surface plasmon waveguides at visible frequencies, and cloaking. One of some extraordinary properties of the MTM is that the Poynting vector of a plane wave is in the opposite direction of the phase velocity at certain frequencies. According to this property, because the MTM has a phase difference with conventional dielectrics, an alternating multilayer formed by the MTM and dielectrics can decrease and even compensate the phase difference. In this paper, the phase delay of an alternating multilayered slab with an arbitrary thickness is studied to decrease the phase difference between MTM slabs and dielectric slabs. We study the propagation characteristics of electromagnetic waves in one-dimensional periodic structures composed of alternating layers, especially, the dispersion equation, dispersion curves, and transmission and reflection ratio by transfer matrix method. For simplicity, our investigation was confined to only TE guided modes, $E_y(x)\exp[-j(\beta z - \omega t)]$, where ω is the angular frequency of the field and β is the propagation constant in z-direction. Using the boundary conditions, the tangential components E_y, and H_z are continuous at all the boundaries, and the new dispersion equation of guided modes can be obtained. In periodic structures with negative index MTM, we can achieve some of most interesting features of the phase delay that can be used as a phase compensator.

Hybrid Metal-dielectric Ring Resonators for Optical Magnetism and Magnetic Metamaterials Down to Ultraviolet Wavelengths

Jianwei Tang[1] **and Sailing He**[1, 2]

[1]Centre for Optical and Electromagnetic Research
JORCEP [Sino-Sweden Joint Research Center of Photonics]
Zhejiang Provincial Key Laboratory for Sensing Technologies, Zhejiang University
East Building No. 5, Zijingang Campus, Zhejiang University, Hangzhou 310058, China
[2]Department of Electromagnetic Engineering, Royal Institute of Technology, Stockholm 100 44, Sweden

Abstract— In order to engineer the magnetic permeability, people developed magnetic metamaterials composed of subwavelength artificial magnetic resonators, which can be treated as effectively homogeneous media by homogenization. Optical magnetic resonators can be realized through metallic structures supporting magnetic plasmonic modes, such as split-ring resonators (SRRs) and cut-wire pairs. However, the operation of metallic structures at optical frequencies is limited by the kinetic energy of the electrons in the metal, leading to saturation of the magnetic response when we push the operating frequency deeper into the optical frequency by size scaling. All-dielectric magnetic resonators have no saturation effect and have a much lower loss than metallic structures. However, if the refractive index of the constituent dielectric material is not large enough, the homogenization of all-dielectric resonators will be unreasonable. This limits the use of all-dielectric magnetic resonators as homogenizable magnetic metamaterials at short optical wavelengths due to the lack of dielectric materials of very high indices at short optical wavelength. Therefore, it is still necessary to develop elegant designs for realization of homogenizable magnetic metamaterials at short optical wavelengths, such as the blue, violet and ultraviolet regions. We proposed a hybrid metal-dielectric ring resonator mainly composed of a high index dielectric material TiO_2 with some gaps filled with metal (e.g., Ag). The hybrid metal-dielectric ring resonator can overcome both the saturation problem of SRRs and the homogenization problem of all-dielectric magnetic resonators, and therefore can form homogenizable magnetic metamaterials at short wavelengths down to the ultraviolet wavelength range. An analytical LC model was developed to describe the magnetic resonances of ring resonators, including the proposed hybrid ring resonator, the split-ring resonator and the all-dielectric ring resonator. In the framework of the LC model, we compared the hybrid ring resonator with the split-ring resonator to interpret how hybrid ring resonators can overcome the saturation problem to exhibit strong magnetic resonance down to ultraviolet wavelengths, and we compared the hybrid ring resonator with the all-dielectric ring resonator to interpret how hybrid ring resonators can overcome the homogenization problem to form homogenizable magnetic metamaterials.

Atomistic Approach for the Field Enhancement in Quantum Plasmonic Nanostructures

T. Rossi, A. Sakko, and R. M. Nieminen
COMP Centre of Excellence, Department of Applied Physics, Aalto University, Finland

Abstract— Collective oscillation of valence electron plasma in a metallic nanostructure, i.e., localized surface plasmon resonance, induces strong local electric field around the structure. This field enhancement phenomenon is utilized in many practical applications, e.g., in surface-enhanced Raman spectroscopy and chemical sensing. Plasmon resonances are described successfully with classical electrodynamics down to structure sizes of tens of nanometers, but the quantum effects become increasingly significant as the feature size further decreases. Previously, the field enhancement phenomenon has been studied with quantum mechanical methods mainly by utilizing the jellium approximation, where the atom nuclei are replaced with a uniform positive background charge density [1]. This approach simplifies computations, but may fail to predict correctly, e.g., screening of the d-electrons and close-contact behaviour between surfaces with atomic features.

In the present work, we study plasmonic excitations and associated field enhancements in nanostructures with the full atomistic structure. We apply quantum mechanical time-dependent density functional theory, which is a standard first principles tool for calculating photoabsorption spectrum of molecules and nanostructures. We have implemented a general field enhancement calculation method to a local version of GPAW code [2]. In this work, we describe our implementation and present results for nearly-touching metallic nanostructures. The results are compared with classical electrodynamical calculations as well as with previously published results involving jellium approximation [3].

REFERENCES

1. Morton, S. M., D. W. Silverstein, and L. Jensen, "Theoretical studies of plasmonics using electronic structure methods," *Chem. Rev.*, Vol. 111, No. 6, 3962–3994, 2011.
2. Enkovaara J., et al., "Electronic structure calculations with GPAW: A real-space implementation of the projector augmented-wave method," *J. Phys.: Condens. Matter*, Vol. 22, No. 25, 253202, 2010.
3. Zuloaga, J., E. Prodan, and P. Nordlander, "Quantum description of the plasmon resonances of a nanoparticle dimer," *Nano Lett.*, Vol. 9, No. 2, 887–891, 2009.

Graphene Waveguides of Ultra-small Mode Areas and Ultra-large Effective Refractive Indices

Sailing He[1,2], **Xizhou Zhang**[1,2], **and Yingran He**[1,2]

[1] Centre for Optical and Electromagnetic Research
JORCEP (Sino-Swedish Joint Research Center of Photonics)
Zhejiang Provincial Key Laboratory for Sensing Technologies
Zhejiang University, Hangzhou 310058, China
[2]Department of Electromagnetic Engineering
Royal Institute of Technology, Stockholm 10044, Sweden

Abstract— The plasmonic property of graphene in THz frequency has attracted much attention recently. The complex conductivity of a graphene layer can be tuned flexibly by controlling the chemical potential via the electric field, magnetic field or chemical doping. In THz range, the graphene layer can exhibit plasmonic response similar to a noble metal at optical frequencies. Here we use this unique plasmonic property to design ultra-small waveguides. The waveguide modes supported by various graphene structures of finite width are investigated extensively.

The waveguide mode of a single graphene nanoribbon placed in free space is first studied. The effective index is obtained using FEM simulation. The dependence of the effective index on the width of graphene nanoribbon is derived. It is found that the graphene nanoribbon can operate at a single-mode region if its width is small enough. An extremely small mode area of $1.3 \times 10^{-7}\lambda_0^2$ is obtained, which is the smallest mode area that has ever been reported (to the best of our knowledge). Then a slot waveguide structure composed of graphene, silica and silicon is proposed. The large refractive index contrast between the silica and silicon leads to greatly enhanced electric field in the silica layer. It is found that there is an optimized thickness for silica to achieve the largest figure of merit [which is defined as the ratio of $\mathrm{Re}(n_{eff})$ to $\mathrm{Im}(n_{eff})$].

The waveguide constructed by two identical graphene nanoribbons with nanometer gap size is also investigated. Two kinds of coupling configurations, namely, the side-side coupling and top-bottom coupling are studied. There are symmetric mode and anti-symmetric mode for both configurations due to the presence of mode coupling. For the side-side coupling, it is found that the symmetric mode can squeeze the optical energy effectively into the gap between the two nanoribbons. The waveguide mode area depends critically on the gap size. A smaller gap size will lead to a smaller mode area. For the top-bottom coupling, it is found that the effective refractive index over 150 can be readily achieved by changing the gap size between the two ribbons. The effective refractive index can be nearly triple as large as that for the single ribbon. The ultra-large effective refractive index can be utilized to design ultra-compact optical components, such as an ultra-small ring cavity.

Fe:BN Nanoceramic — Negative Refraction Material in the Wide Frequency Range

K. Oganisian[1], **A. Vogt**[2], **P. Gluchowski**[1], **K. Orzechowski**[2], **and W. Strek**[1]

[1]Institute of Low Temperature and Structure Research, PAS, Okolna 2, Wroclaw 50-422, Poland
[2]Faculty of Chemistry, Wroclaw University, F. Joliot-Curie 14, Wroclaw 50-383, Poland

Abstract— We report the Fe:BN composite that revealed the metamaterial-like behavior in the wide frequency range. The structural investigation showed the core-shell structure where BN layers coat Fe cores. It was found that the values of permittivity and magnetic permeability are negative simultaneously at frequencies above 10 MHz that suggests to the negative refractive index for this compound in the range up to 1 GHz as minimum. We assume that within the simple model of isolated nanoparticle at applied electromagnetic field the obtained results can be described. We suppose that this material can be very promising for radiofrequency application.

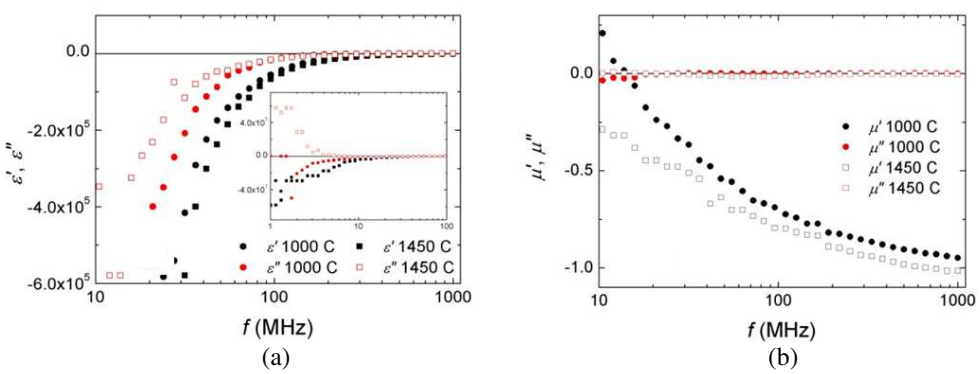

Figure 1: (a) Permittivity and (b) permeability as a function of frequency of Fe:BN compound obtained at 1000°C and 1450°C.

Fano Resonance in Simple and Single Plasmonic Particle

Yuan Zhang[1] **and Sailing He**[1, 2, 3]

[1]ZJU-SCNU Joint Research Center of Photonics, South China Normal University
Guangzhou 510006, China
[2]Centre for Optical and Electromagnetic Research
Zhejiang Provincial Key Laboratory for Sensing Technologies
JORCEP [Sino-Sweden Joint Research Center of Photonics]
Zhejiang University, Hangzhou, China
[3]Department of Electromagnetic Engineering, Royal Institute of Technology
Stockholm 100 44, Sweden

Abstract— In the last decades, great expectation has been placed on the plasmonic structures because of their remarkable ability of electromagnetic (EM) field confinement and enhancement, which, therefore, could be very useful to areas of optical communication, optical sensing, bio-engineering, nano-science, nanotechnology and so on. Researchers have done many theoretical and experimental works to understand the EM behaviors about various kinds of plasmonic structures. A kind of interesting work in these studies is the Fano resonance in plasmonic system, which comes from the interaction between different plasmonic resonant modes. Excellent works have been done on this topic both theoretically and experimentally. Several structures have been proposed to produce evident Fano resonance, such as Dolmen structure, Ring-disk system, or asymmetric Split-ring resonator etc.. The typical characteristic of these proposed structures is they always contain several (two or more) metallic components with different size or shape in one unit cell. Such a composed plasmonic system will lead to multi-resonance because of the mode hybridization. Some broad and narrow ones of these modes may overlap with each other, which makes the opportunity for Fano resonance. However, these plasmonic structures are somehow complex as they always have different parts demanding accuracy of position. This will increase the fabrication difficulty or the size of unite cell (note that one of the advantage of the plasmonic devices is their ultra-compact size in dimension). In this proposal, we make our effort to design a simple and single metallic particle show evident Fano resonance. The proposed plasmonic system just contains one metallic particle with asymmetric profile. The asymmetric feature will make the narrow (dark) mode of the particle excitable and give it chance to interfere with the broad (bright) dipolar mode. By numerical simulation tools, we will investigate the Fano resonance in such an asymmetric metal particle and try to explain its original reason. Finally, we show how to tune the Fano resonance position in the spectrum by changing the geometry parameters of the particle profile.

Design and Application of Multi-slots AMC Structure Having Metamaterial Characteristic for 2.45 GHz Band

Seungwoo Lee[1], **Nam Kim**[1], **and Seung-Yeop Rhee**[2]

[1]Chungbuk National University, Korea
[2]Chonnam National University, South Korea

Abstract— New concept metamaterial which is designed on normal FR-4 substrate is suggested. The designed structure is composed by transformed symmetrical slots (artificial magnetic conductors), and is focused on the WLAN application for 2.45 GHz band. The AMC unit cell has a high impedance surface characteristic, wider frequency range than conventional cells, and no via-holes. The designed cell is applied to a reflector which is consisted of periodically arrayed cells, for verifying the performance. When a 2.45 GHz dipole or monopole antennas is placed at one-tenth distance on the suggested reflector, the AMC reflector is perfectly working and shows 3 dB increased of the radiation efficiency. To verify the reduction of human effects, the reflector is inserted in the mobile phone case (fake version designed by our lab.). The calculated peak SAR (specific absorption rate) of the human head model is only 0.006 averaged over 1 g. In conclusion, the designed reflector could be shielded the EMF generated by the 2.45 GHz antennas.

Bundle Block Adjustment with Optical and SAR Images

Shuai Xing, Qing Xu, Wei Sun, Jiansheng Li, and Yu He
Zhengzhou Institute of Surveying and Mapping, Zhengzhou, China

Abstract— Block adjustment is one of key techniques in photogrammetry, which can achieve orientation parameters of images and coordinates of pass points in a large area efficiently and simultaneously. Up to now, what researched by block adjustment has not changed, it has been always the images photographed by one sensor at variant time and position. Since different photogrammetry and remote sensing sensors have been produced, the technique processing different images achieved by different sensors has been proposed. Most works have been concentrated in radiative and physical processing, but there was few people noticed multi-sensor images could be used to realize combined position. In this paper the combined bundle block adjustment model with optical and SAR remote sensing images has been constructed, and its some key problems have been studied.

First, the geometric equations and block adjustment models for linear array push-broom optical image and SAR image are briefly reviewed. Since the linear array push-broom image is acquired with linear sensors by scanning the earth surface, different exterior orientation elements of each image line can be calculated by the collinearity equation with ground control points (gcps). The relation between ground and image coordinates for a SAR image is established by the Doppler and Range equations proposed by F. Leberl.

Secondly, the combined bundle block adjustment model with optical and SAR images has been constructed. It includes three problems, construction of observation equations, computation of the weight matrix and space intersection with multi-image.

Observation equations of the combined bundle block adjustment model include observation equations of each pass point and gcp in each image and *fake observed value* observation equations of each optical image. Observation equations of each pass point and gcp have been constructed according to which image their corresponding image points were in. If one pass point were both in optical and SAR images, a group of observation equations of this point have been constructed in every image based on which was optical or SAR image. The *fake observed value* observation equation of one optical image has been introduced for solving correlation of exterior orientation parameters of linear array push-broom image.

After normalizing observation equations of the combined bundle block adjustment model, the normal equations have been achieved. But there is a key problem of solving the normal equations, which is the computation of the weight matrix. As usual, weights of observation equations of each pass point and gcp in optical image are decided with experience and always constants. But weights of observation equations of each pass point and gcp in SAR image are different since the F. Leberl model. So we deduced the equations to calculate weights of observation equations in SAR image according to covariance promulgation law.

Ground coordinates of pass point were computed with space intersection. When one pass point appeared in different images, multi-image space intersection has been used to compute its ground coordinates.

Then the frame of block adjustment process has been proposed, which included two steps. The first step was preliminary block computation, which calculated preliminary values of unknowns. The second step was block adjustment.

Thirdly, four space-borne imageries in Beijing achieved at variant time, including two optical (SPOT5, SPOT4) and two SAR (ERS-2, Radarsat-1) images, are used in the experiment. The covering area of four images is mainly city and partly mountain, and the maximum altitude difference is 600 m. We designed two schemes to prove the feasibility and performance of the proposed model. First scheme, we randomly chose two, three or four out of the four images to construct 11 adjustment combinations. Block adjustments of all adjustment combinations were finished successfully, which proved the proposed model was feasible. Second scheme, we chose four out of 11 adjustment combinations, and using 6 distributions of gcps to test accuracy of block adjustment. Experiment results proved that the accuracy of combined block adjustment was consistent with traditional block adjustment, and the elements and laws of affecting the accuracy of combined block adjustment are similar with traditional block adjustment.

Finally, the characteristics and application of the combined block adjustment have been summarized. It is feasible to carry on the combined block adjustment experiment using our model with a great deal of images in large area.

Airborne Interferometric SAR Experiment with Multi-carrier Frequencies Using both Chirp and Noise Signals

Yunhua Zhang, Wenshuai Zhai, Xueyan Kang, Xiaojin Shi, Xiang Gu, and Yueying Tang
Center for Space Science and Applied Research, CAS, China

Abstract— Airborne interferometric SAR experiment with Ku-band mult-carrier frequencies using both chirp and noise signals was conducted over small mountain area and topographies were obtained for each frequency. Three carrier frequencies, i.e., 13.78 GHz, 13.98 GHz, and 14.18 GHz have been used. Results show that the results of different frequencies are very well agreed with each other and by combining them together, much better results can be obtained. The performance of noise signal also meets our expectation although the SNR is reduced about 3 dB as the transmitted power reduced. Besides the cross-track interferometric experiment, along-track interferometric experiment was also conducted over a city. In this experiment, moving targets in a lake were detected.

Results show that by using chaotic noise signal, three measurements are used to estimate the baseline.

Micro-doppler Analysis of Rotating Targets in Dual-channel Bistatic SAR

Meng Lv
Department of Information Science and Electronic Engineering
Zhejiang University, Hangzhou 310027, China

Abstract— The micro-motions of structures in a target, such as the rotor of a helicopter, the scanning antenna of a ship, the vibrations of vehicle engines, may induce additional frequency modulations on the returned radar signals and generate sidebands about the center Doppler frequency of the target's body, which is known as the micro-Doppler effect. Extraction of micro-Doppler signature is very useful for target classification and recognition. In recent years, the researches of micro-Doppler extraction methods are widely discussed. However, few of them are based on bistatic SAR which has many advantages. Bistatic SAR may have a counter-stealth capability and the receivers are passive which are undetectable. Rotation is a typical micro-motion form. Most of the published researches on analysis of the rotation target did not pay enough attention to the interference of ground clutter. However, ground clutter caused by the presence of stationary targets makes the extraction of the micro-Doppler signature difficulty, which may submerge the signals of rotating targets. In this paper, based on the configuration of bistatic SAR with a dual-channel fixed receiver, a new micro-Doppler signature extraction method is used to extract the micro-Doppler features and estimate parameters of rotating targets. The received signals' expressions of rotating targets are established in the case of dual-channel fixed-receiver bistatic SAR. With displaced phase center antenna technique, the ground clutter is suppressed and the signals of rotating targets are reserved in the range-compressed data domain. Then the mathematical expressions of micro-Doppler are derived. The fractional Fourier transform is adopted to compensate for the radar Doppler shift and the Gabor transform method is utilized for extraction of micro-Doppler information caused by rotating targets and parameter estimation. Finally, the effectiveness of the proposed method is confirmed through simulations.

Snow Wetness Estimation from Polarimetric SAR Image

M. Surendar[1], **G. Singh**[2], **A. Bhattacharya**[1], **G. Venkataraman**[1], **and P. A. Bharathi**[1]

[1]Indian Institute of Technology, Bombay, Mumbai, India
[2]Niigata University, Niigata, Japan

Abstract— Avalanche modeling, snow melt runoff and hydrological investigation requires timely information about spatial variability of snow properties, among them the snow wetness of a snowpack is very important. Over the past few years, several attempts have been made using active microwave remote sensing systems for the detection of snowpack parameters. The scope of this study is to develop a methodology to retrieve snowpack parameters using decomposition scheme of fully polarimetric SAR data. In this study the Radarsat-2 fine quad polarization data was acquired on 7th February 2012 over Manali and Dhundi (center Lat/Long: N32°22′05″/E77°15′00″, Himachal Pradesh, India).

Here a new approach has been attempted to estimate the snow surface wetness. General four component scattering power decomposition with unitary transformation (G4U) is used in this study. In this decomposition unitary transformation is applied to the coherency matrix twice. The T_{23} (helix component) element of the coherency matrix becomes zero after the application of the double rotation. The double bounce scattering is assumed to be absent in the wet snow condition and the surface and volume scatterings are only considered for snow pack wetness estimation. The surface snow dielectric constant is derived using the generalized Freeman surface parameter and the volume snow dielectric constant is derived using the Cloude's volume parameter. The volume scattering component of the snow is derived under a uniform distribution condition. The Cloude's volume parameter and the generalized Freeman surface parameter can be expressed with the rotated coherency matrix elements. These parameters are then related to Fresnels transmission coefficients which then lead to derive dielectric constant map through an iterative process. The snow dielectric constant is then used for estimating snow wetness directly by using an empirical relation.

The estimated snow wetness is validated with the field measurement. This algorithm has shown that the mean absolute error of 1.395% of volume which is better than the previous algorithms used for dual-pol SAR images.

Optical Data Storage Using Diffractive Optical Elements

S. Yoshida, K. Yamada, N. Unno, J. Taniguchi, and M. Yamamoto
Tokyo University of Science, 6-3-1 Niijuku, Katsushika-ku, Tokyo 125-8585, Japan

Abstract— The diffractive optical element (DOE) can transform wavefront, and generate arbitrary intensity distribution. DOE is used for forming or homogenization of the beam, and aberration correction, and others. In this study, we focus on these functions of DOE, and examined the possibility as read-only memory (ROM) type storage usage of the DOE.

The DOE based optical data storage is thought of as a kind of holographic data storage (HDS) using thin holograms. In the HDS, digital data is recorded and read out as modulated two-dimensional page data, instead of bit-by-bit recording in conventional optical disks. Therefore, HDS actualize high data transfer rate. Additionally, the feature of the hologram makes multiplexing recording.

In order to examine the possibility as storage usage of the DOE, we design and optimize phase distribution of the DOE using the iterative method with regularization. In the optimization process, we use iterative Fourier transform algorithm (IFTA) that is known as Gerchberg-Saxton (GS) algorithm. Optimized phase distribution is implemented as multistep surface concavo-convex structure. Multistep surface concavo-convex structure actualizes high diffraction efficiency.

Designed and optimized DOE is fabricated by ultraviolet (UV) nanoimprinting technology. By adopting nanoimprinting technology, high productivity can be expected. Molds for nanoimprinting is made by electron beam (EB) cutting, and mask patterns for EB cutting is generated based on optimized phase distribution. DOEs are duplicated on the silicon (Si) substrate as reflection-type elements. Fabricated DOE is evaluated in the experiment. We verify that DOE for optical data storage can be actualized through the approach.

Multi-dimensional Shift Multiplexing for Holographic Data Storages

S. Yoshida, K. Yamamoto, H. Kurata, and M. Yamamoto
Tokyo University of Science, 6-3-1 Niijuku, Katsushika-ku, Tokyo 125-8585, Japan

Abstract— Holographic data storage (HDS) is a next-generation optical storage that uses the principles of holography. Assuming a read/write laser wavelength of λ and considering that the recording density is proportional to squared λ in a conventional optical disk while being proportional to cubic λ in HDS, the HDS recording density is potentially greater than that of a conventional optical disk.

The multiplex holographic recording method is an important factor that affects the recording capacity of this storage. Various multiplex recording methods have been proposed so far. In this study, we focus on shift multiplexing with spherical waves and examined the possibility of high-density recording using this method. Since a spherical wave can be regarded in some locations as overlapping plane waves advancing in different directions, the shape of the diffraction grating recorded as a hologram is a function of the location in the recording medium. Therefore, multiplex recording is enabled in this system by simply displacing the recording medium. We propose a method of shift multiplex recording that combines the in-plane direction and depth direction of the recording medium.

In conventional shift multiplexing with spherical waves, shift multiplexing is usually carried out with respect to the direction parallel to the plane of the recording medium. By focusing on the fact that shift selectivity is also in the depth direction, we examined the possibility of a multiplex recording method that combines multiple shift directions. We report on numerical and experimental evaluation results of our high-density recording and reproduction system based on this principle.

Characterization of Zinc-tin-oxide Films Deposited by Radio Frequency Magnetron Sputtering at Various Substrate Temperatures

Ik-Jae Lee[1], **Nark-Eon Sung**[1], **Keun Hwa Chae**[2], **and Ray Conley**[3]

[1]Pohang Accelerator Laboratory (PAL), South Korea
[2]Korea Institute of Science and Technology (KIST), South Korea
[3]Brookhaven National Laboratory (BNL), USA

Abstract— Zinc-tin-oxide (ZTO) thin films were grown by radio frequency magnetron sputtering on glass substrates at various substrate temperatures. The effects of substrate temperature on the crystalline behavior and electrical and optical properties of the films were studied. The ZTO films were amorphous and maintained their stable amorphous state up to a substrate temperature of 350°C. With increasing substrate temperature, the ZTO films crystallized through a solid-state reaction, normally transforming from $ZnSnO_3$ at temperatures in the range of 450–550°C into stable zinc stannate, Zn_2SnO_4, at temperatures above 650°C. The XRD and EDS results indicate that the ZTO films deposited at temperatures of above 650°C are Zn_2SnO_4 films with a face-centered cubic spinel structure. The Hall mobility of the films was in the range of 22.7–23.5 cm^2/V s in the amorphous phase and 15.4–19.6 cm^2/V s in the crystalline phase. The carrier concentration reached 8.287×10^{19} cm^{-3}, resulting in a minimum resistivity of $8.75 \times 10^{-3}\Omega\cdot$cm in the film deposited at 750°C. The average transmittance in the visible region was $\geq 85\%$, and the band gap showed a red-shift in the amorphous phase and a blue-shift in the crystalline phase.

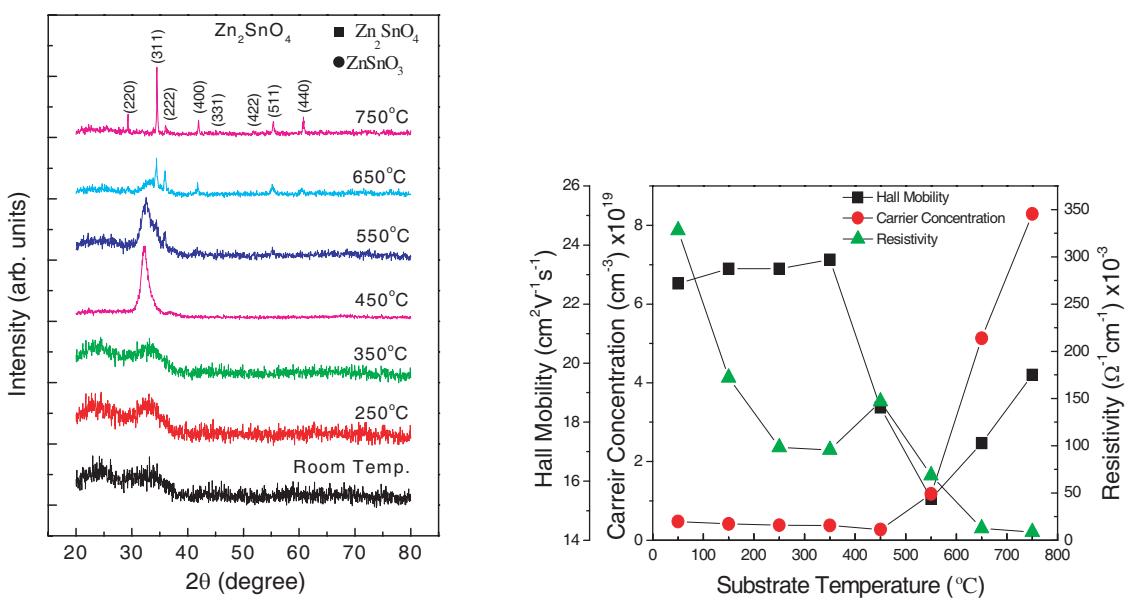

(a) (b)

Figure 1: (a) XRD diffraction patterns of ZTO thin films deposited on glass substrates by RF magnetron sputtering atvarious substrate temperatures. (b) Variation in Hall mobility, carrier concentration and resistivity of the ZTO films as a function of substrate temperature.

Design of New ITO Electrodes for High Sensitive Capacitive Touch Panel

Huai-Yi Chen and Hsi-Ting Huang
Department of Electronic Engineering, Huafan University, Taiwan, R.O.C

Abstract— Touch panel technology has been more and more widely applied in electronic products. The structure of general touch panels can be divided mainly into resistive and capacitive types. The latter's performance is better as compared with the former. Typically, the electrode of capacitive touch panel is rectangular or diamond like in shape. However, we designed in this paper new chain-shaped and mountain-shaped touch panel electrodes. Their simulated capacitive sensing gains were about 30%, higher than those of traditional ones. In addition, we also found that with the decrease of the ratio of glass thickness (H) to electrode thickness (h), the capacitive sensing gain is higher.

The COMSOL multi-physics engineering simulation software was used to design the indium tin oxide (ITO) electrode of capacitive touch panel in this study. Fig. 1 shows the cross-sectional structure of the touch panel we attempted to design. Fig. 2 shows the structure and size of the touch panel with rectangular, diamond-shaped, chain-shaped, and mountain-shaped touch electrode, respectively. The placement of the ITO electrodes is parallel. The dielectric constant of human fingers was set to 5 in the simulation. The touch panel capacitance without the touch of human fingers was C, the amount of increase in the capacitance of touch panel after the touch of human fingers was ΔC, and the capacitive sensing gain was defined as $\Delta C/C$. The simulation results of C, ΔC, and $\Delta C/C$ for touch panels with four different electrodes are shown in Table 1. Table 2 lists the variations of C, ΔC, and $\Delta C/C$ for the capacitive touch panel with chain and mountain-shaped electrodes at different ratio of H/h. Under the same size of environment parameters, we demonstrated from simulation that capacitive sensing gains of touch panels with

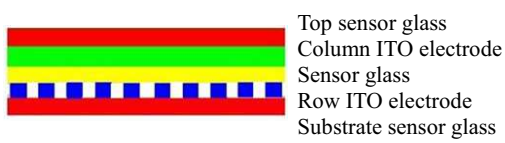

Figure 1: Cross-sectional view of a touch panel.

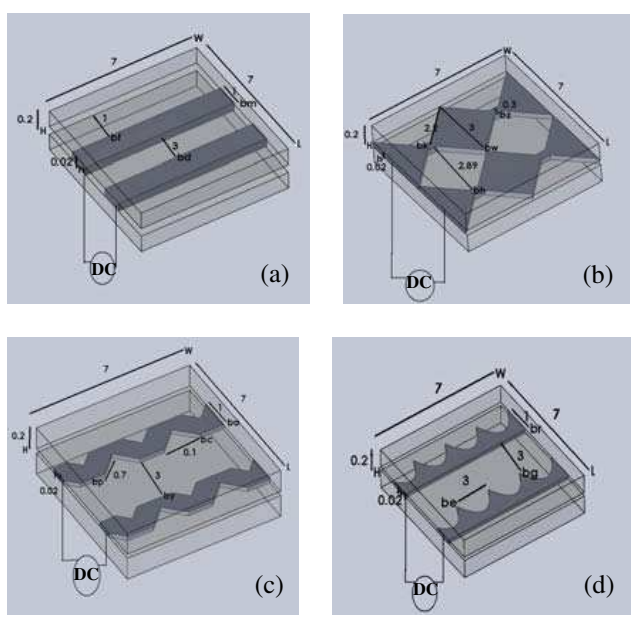

Figure 2: Structure and size of a touch panel with (a) rectangular, (b) diamond-shaped, (c) chain-shaped, and (d) mountain-shaped electrode (unit: 10 μm).

Table 1: Simulated capacitance changes (ΔC) and gains ($\Delta C/C$) for touch panels with different electrodes.

	C (fF)	ΔC (fF)	$\Delta C/C$
Rectangular electrode	0.447	0.126	28%
Diamond-shaped electrode	0.798	0.177	22%
Chain-shaped electrode	0.293	0.087	30%
Mountain-shaped electrode	0.274	0.081	29%

Table 2: Comparison of capacitance changes and gains as a function of the ratio of glass thickness (H) to ITO electrode thickness (h) for touch panels with chained-shaped and mountain-shaped electrodes.

	Chain-shaped electrode			Mountain-shaped electrode		
(H/h)	C (0.1 fF)	ΔC (0.1 fF)	$\Delta C/C$	C (0.1 fF)	ΔC (0.1 fF)	$\Delta C/C$
10	2.93	0.87	30%	2.74	0.81	29%
20	5.43	0.77	14%	5.08	0.72	14%
30	7.67	0.69	8%	7.16	0.64	8%

chain and mountain-shaped electrodes were higher than those of touch panels with traditional common rectangular and diamond-shaped electrodes.

On the Modeling of an External Cavity Tunable Laser ECTL Source with Finite Mirror Dimensions

Ahmed Fawzy[1], **Salwa El-Sabban**[1], **Ibrahim Ismail**[1], **and Diaa Khalil**[2]

[1]Electronic and Communication Engineering Department, Faculty of Engineering
Helwan University, Helwan, Cairo, Egypt
[2]Electronic and Communication Engineering Department, Faculty of Engineering
Ain-Shams University, Abbassia, Cairo, Egypt

Abstract— MEMS mirrors are very promising candidates for External Cavity Tunable Laser ECTL sources. When using the Deep Reactive Ion Etching DRIE technology, these mirrors can be monolithically integrated with their actuators on a single Si die while the laser chip is assembled on the same die. Such configuration has great potential in integrated optoelectronics on a silicon platform and for these reasons it has been previously investigated both theoretically and experimentally in the discrete and continuous tuning regimes. However, its continuous tuning model in the literature, is based on weak (or moderate) reflections from an infinite external mirror, while in the practical realizations this mirror is usually metallized and has a finite aperture limited by the height of the device layer in the SOI wafer used in the DRIE technology. To account for these differences and allow for more precise engineering of the MEMS based ECTL we developed a model that describes the behavior of the ECTL taking into account both the diffraction of the optical beam in the external cavity and the high reflection coefficient of the external mirror. The model is based on the use of the Plane wave Expansion Method PEM to describe the propagation outside the laser cavity. We first develop an expression for the laser frequency shift due to optical feedback signal that is not limited to weak reflections. The propagation in the external cavity is then modeled in the spectral domain while the reflection from a mirror of finite dimensions is modeled in the spatial domain and the FFT technique is used to move between the two domains. The results show that both the tuning range ($\lambda_{\max}$–$\lambda_{\min}$) and the tuning sensitivity $d\lambda/dx$ depend on the length of the external cavity as it would be expected. Based on our calculations, the external cavity dimensions can be engineered for a required tuning range. The model opens the door also for the optimization of the external mirror shape for a specific laser performance.

Polarization-insensitive and Broadband Plasmonic Silicon Schottky Diode for Detection of Sub-bandgap Photons

Liu Yang, **Pengfei Kou**, **El Hang Lee**, **and Sailing He**
Centre for Optical and Electromagnetic Research
Zhejiang Provincial Key Laboratory for Sensing Technologies
State Key Laboratory of Modern Optical Instrumentations
Zhejiang University, Hangzhou 310058, China

Abstract— We proposed a novel polarization-insensitive and broadband Au-Si Schottky diode. Based on internal photoemission (IPE), sub-bandgap photons in the optical communication wavelength range can be detected. It consists of a lossless Si ridge waveguide with its top and sidewalls covered by an Au thin film, which also works as a Schottky contact. After absorbing photons, carriers in the Au film become hot, which are also called hot carriers. If they gain sufficient energy which is higher than the Schottky barrier, they can jump over the barrier, be swept in Si and collected by the Al Ohmic electrode, becoming photocurrent. Assuming that elastic reflections occur for the hot carriers if they are not emitted, IPE probability and thus internal quantum efficiency (IQE) are calculated analytically and are found to be greatly enhanced by a thin Au film. Then, finite-difference time domain method is employed to simulate the light propagation and absorption in Au. According to both IQE and absorption, responsivity spectra of our photodetector are calculated. The simulation results show that our photodetector has polarization-insensitive and broadband (at least 400 nm considered here) opto-electric responses because both polarized plasmonic modes can be excited with comparable imaginary parts of the effective refractive indices. Moreover, the responsivity is strongly enhanced by the tightly confined optical fields around the Au-Si interfaces together with the high IPE-induced IQE enhanced by the thin Au film. Due to the small size of the Schottky diode, our photodtector has very small dark current.

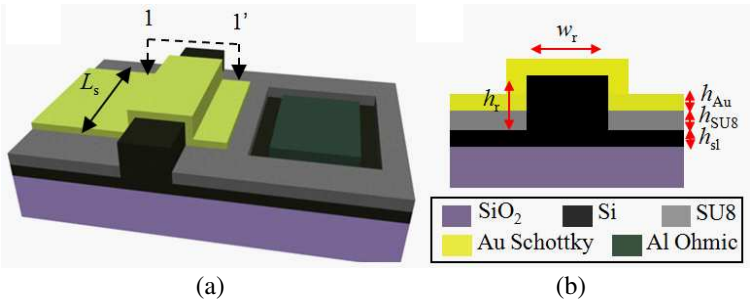

Figure 1: (a) 3D, (b) 2D (along plane 1-1') schematic diagrams of our Si photodetector.

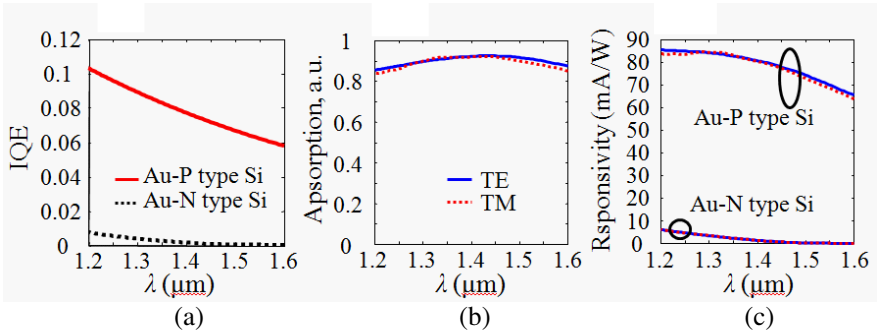

Figure 2: (a) IQE, (b) absorption and (c) responsivity spectra of the Au-Si based Schottky diode.

The Fabrication of AlGaN Ultraviolet-B Metal-semiconductor-metal Photodetectors with a MgZnO Thin Film Filter

Ming-Jer Jeng[1], **Jun-Yan Chang**[2], **Liann-Be Chang**[1], **Ray-Ming Lin**[1], **and Li-Zen Hsieh**[3]

[1]Department of Electronic Engineering and Green Technology Research Center
Chang Gung University, Taiwan
[2]Department of Electrical Engineering, Chung-Cheng Institute of Technology
National Defense University, Taiwan
[3]Department of Electrical Engineering, Hwa Hsia Institute of Technology, Taiwan

Abstract— The UV-B light is most harmful to human skin. It can cause the skin cancer. How to detect UV-B light is very worthy of study. Comparing with the conventional UV photodetector, such as Si-based photodectors, the UV detectors based on wide band gap semiconductors such as SiC, GaN and ZnO have the advantage of higher efficiency, lower noise and dark current, etc.. Therefore, high performance UV-B photodetector is fabricated by AlGaN materials with an MgZnO thin film filter. Good quality of an epitaxial layer means it has a good photoresponse due to suppressing dark current effectively. The SiC substrate is used to deposit a good quality of AlGaN epi-layer due to good lattice match with AlN materials. An AlN nucleation layer was deposited on SiC substrate as a buffer layer. An undoped $Al_{0.26}Ga_{0.74}N$ layer was subsequently grown and followed by an AlN capping layer. An AlN capping can form two degree electron gas at the interface of AlN/AlGaN. It can increase photocurrent significantly to enhance photoresponsivity. We choose a high resistance and good filter performance material of $Mg_{0.44}Zn_{0.56}O$ as UV-B filter. The $Mg_{0.44}Zn_{0.56}O$ layer will be deposited by a sputter. The Mg0.44Zn0.56O layer with a thickness of 280 nm can effectively filtered out the wavelength below 280 nm. The light with a wavelength below 315 nm will be absorbed at the undoped $Al_{0.26}Ga_{0.74}N$ layer. A high light-to-dark current ratio can be achieved as high as $\sim 10^4$.

Omnidirectional Absorber Based on Collision Plasma Heterostructures

Xiang-Kun Kong[1,2], **Shao-Bin Liu**[1], **Hai-Feng Zhang**[1,3], **Bo-Rui Bian**[1], **Hui-Chao Zhao**[1], **and Huan Yang**[1]

[1]College of Electronic and Information Engineering
Nanjing University of Aeronautics and Astronautics, Nanjing 210016, China
[2]Jiangsu Key Laboratory of Meteorological Observation and Information Processing
Nanjing University of Information Science and Technology, Nanjing 210044, China
[3]Nanjing Branch, Artillery Academy of the PLA, Nanjing 211132, China

Abstract— A broadband omnidirectional absorber which is realized by hererostructures containing a collision plasma layer and a ternary plasma Bragg mirror is theoretically investigated. A collision plasma layer and an appropriate dielectric layer are put on the top of the ternary plasma photonic crystals to obtain a broadband omnidirectional absorption. It is shown to absorb roughly 70% of all available electromagnetic wave in a relative omnidirectional absorption band width 0.58 GHz with plasma width 3 mm in PCs. The band edges are impacted by the range of reflection band gap and the decrease of absorption range for TM wave at large incidence. This kind of hererostructures offer additional opportunities to design novel optoelectronic devices.

Size Reduction of Narrowband Hairpin Bandpass Filter Using Fractal Koch Geometry

Achmad Munir[1], **Teguh Praludi**[2], **and Mohammad Ridwan Effendi**[1]

[1]Radio Telecommunication and Microwave Laboratory
School of Electrical Engineering and Informatics
Institut Teknologi Bandung, Indonesia
[2]Research Center for Electronics and Telecommunication
Indonesian Institute of Sciences, Indonesia

Abstract— In this paper, an implementation of fractal Koch geometry concept for reducing size of conventional narrowband Hairpin bandpass filter (BPF) is investigated numerically and experimentally. The proposed BPF which is utilized the 1st iteration of fractal Koch geometry referred as fractal Hairpin BPF is constructed of 5 elements on Rogers RO4350 dielectric substrates with the thickness of 1.524 mm. Prior to hardware realization, the filter is numerically designed to have center frequency of 3 GHz with the minimum bandwidth of 200 MHz and its characteristics are compared to the conventional Hairpin BPF. From the characterization results, it is shown that the physical size of fractal Hairpin BPF can be reduced up to approximately 20% from the conventional one with the similarity on other parameters such as return loss, insertion loss and 3 dB working bandwidth.

Design of a Compact Dual-mode Dual-band Microstrip Bandpass Filter Based on Semi-fractal CSRR

Mushtaq A. Alqaisy[1], **Jawad K. Ali**[2], **Chandan K. Chakrabarty**[1], **and Goh C. Hock**[1]

[1]Department of Electronics and Communication Engineering
College of Engineering, Universiti Tenaga Nasional, Malaysia
[2]Microwave Research Group, Department of Electrical Engineering
University of Technology, Iraq

Abstract— Various complementary split ring resonators (CSRRs) are used as defected ground structures (DGSs) in the bandpass filter (BPF) design for different communication applications. In this paper, a hybrid CSRR has been introduced as a DGS in the ground plane of a dual-mode microstrip BPF to produce a new compact filter with dual band response. The proposed CSRR structure is essentially based on the conventional square double ring one, but with the inner ring made in the form Minkowski-like pre-fractal curve. Simulation and performance evaluation of the proposed filter have been carried out using a method of moment based EM simulator; the IE3D. Simulation results show that the resulting filter offers a dual passband response. The higher passband is attributed to the dual mode microstrip ring structure, while the lower passband is as a result of the embedded CSRR DGS structure, which implies an extra filter miniaturization. Results also show that the position of the lower passband could be varied, to certain extent, without affecting the position of the higher passband. This can be performed by the application of higher fractal iteration level to the inner split ring and/or dimension scaling of the whole CSRR structure. This feature makes the proposed filter suitable as a candidate for use in a wide variety of communication systems incorporating dual band operation.

Odd-order Bandstop Filter (BSF) Topology with Inter-resonator Coupling Structures

T.-H. Lee[1], K. Lee[1], C.-S. Ahn[2], Y.-S. Kim[1], and J. Lee[1]

[1]Department of Computer and Radio Communications Engineering
Korea University, Seoul 136-713, Republic of Korea
[2]The 3rd. R&D Institute-2, Agency for Defense Development, Republic of Korea

Abstract— In this presentation, we show the odd-order bandstop filter (BSF) topologies with inter-resonator coupling structures. Resonators which construct the conventional BSFs are coupled to a transmission line separated by 1/4 or 3/4 wavelength along the transmission line, but they are not coupled to each other. Since the conventional BSF topology does not have inter-resonator couplings, it is not suitable for designing bandstop-to-bandpass or bandstop-to-all-pass switchable filters. Recently, BSFs which include the inter-resonator coupling structures are utilized to achieve the reconfigurability of its functions from bandstop to bandpass or all-pass [1–3]. However, only even-order BSF topologies have been discussed up to date. We present a synthesis method for odd-order BSF topologies containing inter-resonator couplings. It is shown that the presented BSF topologies can be synthesized in such a way that it exhibits the same frequency response that the conventional BSF topologies can generate by exploring the relationship between the presented topologies and the conventional topologies. For example, a coupling matrix for 3rd-order BSF which possesses two inter-resonator coupling structures is extracted from a coupling matrix related to the conventional BSF using the relationship, and the higher odd-order filters with inter-resonator couplings are synthesized. Two different frequency responses, Butterworth and Equi-ripple, can also be generated by the proposed BSF topology.

ACKNOWLEDGMENT

This work was supported by Agency for Defense Development (Contract number: UD120046FD).

REFERENCES

1. Lee, J. E. N., H. H. Sigmarsson, D. Peroulis, and W. J. Chappell, "New bandstop filter circuit filter topology and its application to design of a bandstop-to-bandpass switchable filter," *IEEE Trans. Microw. Theory Tech.*, Vol. 61, No. 3, 1114–1123, Mar. 2013.
2. Naglich, E., J. Lee, D. Peroulis, and W. J. Chappell, "A tunable bandpass-to-bandstop reconfigurable filter with independent bandwidths and tunable response shape," *IEEE Trans. Microw. Theory Tech.*, Vol. 58, No. 12, 3370–3379, Dec. 2010.
3. Naglich, E., J. Lee, D. Peroulis, and W. J. Chappell, "Switchless tunable bandstop-to-all-pass reconfigurable filter," *IEEE Trans. Microw. Theory Tech.*, Vol. 60, No. 5, 1258–1265, May 2012.

Dual-band Impedance Matching Network with Transmission Zeros Using Resonators

Phirun Kim[1], **Girdhari Chaudhary**[1], **Yongchae Jeong**[1], **and Jongsik Lim**[2]

[1]Chonbuk National University, Republic of Korea
[2]Soonchunhyang University, Republic of Korea

Abstract— Various wireless communication standards such as wireless local area networks (WLAN), wideband code division multiple access (WCDMA), Long term evolution (LTE) etc. have been developed throughout the world and apparently more standards are to emerge in the near future. The integration of separate standards into one unit increases the size, cost and complexity of systems. For this purpose, the design of matching networks for the multi-band components such as power amplifiers is essential. The multi-band impedance matching networks are the basic design issues in the multi-band RF circuits and systems. The conventional dual-band matching network mainly pays attention to match between two consecutive circuits at just two operating frequencies and rarely consider the out-of-band suppression characteristics. In this paper, the dual-band impedance matching network with the out-of-band suppression with transmission zeros is proposed (Figs. 1 and 2). The proposed network can match two frequencies simultaneously and suppress the out-of-band unwanted signals which can also ease the filtering burden of the RF front-end. Two steps are required to realize the proposed dual-band matching network. First, two T-type single band matching networks are designed at each operating frequency. Secondly, two single band matching networks are converted into the dual-band matching network by the compliance of reactance and susceptance at the single band matching network (Fig. 1). For experimental validation of proposed structure, the dual-band matching network for extracted the source and load impedances (Table 1) of the power amplifier operating at two center frequencies of 881 MHz and 2.14 GHz is designed and measured. From experiment, it found that, the measured results have good agreement with the extracted impedance matching points (Figs. 3 and 4).

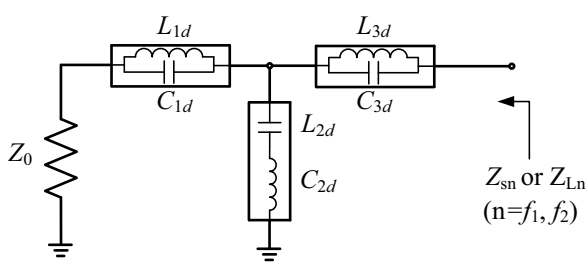

Figure 1.

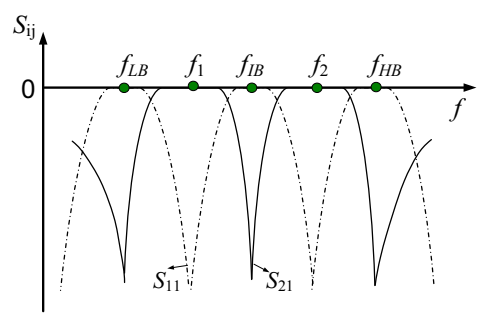

Figure 2.

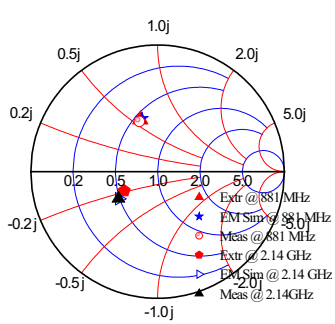

Figure 3.

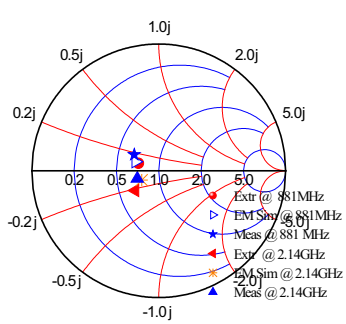

Figure 4.

	Items	f_1= 881 MHz	f_2= 2.14 GHz
Source impedance	Extracted impedance	27.829+j28.168	23.391-j9.4287
	Dual-Band M/N EM simulation	28.2+j29.125	24.69-j12.305
	Measurement	28.052+j27.081	24.515-j12.174
Load impedance	Extracted impedance	36.08+j4.41	39.859-j6.783
	Dual-Band M/N EM simulation	34.13+j5.12	37.88-j5.62
	Measurement	32.9+j8.88	35.344-j4.61

Table 1.

Highly Miniaturized Forced-mode Ring Resonator

Jose Roberto Reyes Ayona
Instituto Nacional de Astrofisica Óptica y Electrónica
Luis Enrique Erro # 1, Sta. María Tonantzintla, Puebla 72840, Mexico

Abstract— The resonance frequency of a close-square ring resonator (f_c) mainly depends on its dimensions and they are related as $l = n\lambda_g$, where l is the total length of the square ring resonator, λ_g is the guided-wavelength and n is the mode number [1]. When a gap is placed on the ring, the resonance frequency is reduced to half its previous value ($f_o = f_c/2$). Figure 1 shows the current distribution at the resonance frequency for (a) the close ring and open ring (b). Close ring current distribution shows two maxima and two minima, open ring shows just one maximum and one minimum at opposing locations.

When a via to ground is added at one side of the gap, the current distribution has the maximum right next to the minimum (c) and the resonance frequency is reduced to half ($f_{ov} = f_o/2 = f_c/4$). The use of interdigital capacitors will reduce the resonance frequency even more. For example, a 1.2 cm × 1.2 cm resonator on a material with $\varepsilon_r = 4.4$, shown on Figure 1(d), resonates at 560 MHz. To resonate at the same frequency, the dimensions of a conventional open ring would have to be of 3.26 cm × 3.26 cm (86% area size reduction). The miniaturized novel resonator presented here has an external coupling that goes from ≈ 2 to 100 s (with tapped line). Internal coupling can be: electric, magnetic or mixed. Mixed coupling is needed to design filters having transmission zeros [2]. Four conventional resonators are required to have a two transmission zeros filter, transmission zeros can be obtained using the miniaturized forced-mode ring resonators.

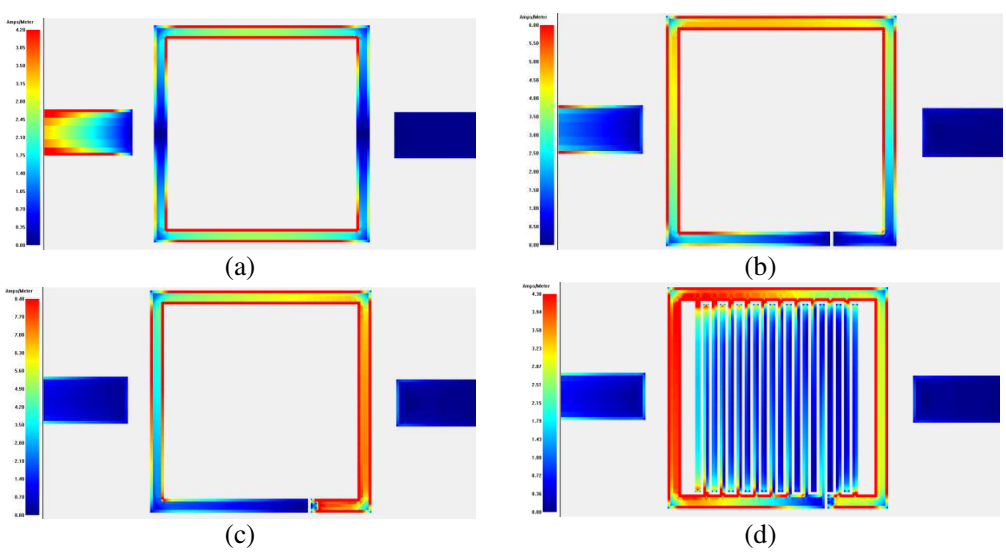

Figure 1: Current distribution at resonance frequency for (a) close ring resonator, (b) open ring resonator, (c) via and gap ring resonator, and (d) highly miniaturized forced-mode ring resonator.

REFERENCES

1. Chang, K. and L. H. Hsieh, "Microwave ring circuit and related structures," 2nd Edition, Wiley, New Jersey, 2004.
2. Hong, J. S. and M. J. Lancaster, *Trans. on Microwave Theory and Techniques*, Vol. 48, No. 7, 1098, 2000.

A Novel Approach to Increase the Multipactor Level in Microwave Transformer

Tiancun Hu and Wanzhao Cui
Science and Technology on Space Microwave Laboratory
Xi'an Institute of Space Radio Technology, P. O. Box 710100, Xi'an, Shannxi, China

Abstract— Multipactor breakdown is a serious risk in all type of high power microwave antenna working in satellite payload, new generation telecommunication satellites are designed to cater for constantly increasing number of users, asking for higher and higher bit rate, in the same frequency multiplex. The conjunction of both tendencies implies increasing power level of RF equipment downstream from the power amplifiers. In this situation, multipactor breakdown can occur in satellite antenna system, such as waveguide transformers, the effect is especially important for the satellites antenna system, since multipactor breakdown can lead to a failure in the whole satellite transponder.

We have presented a novel approach to improve the multipactor threshold using dielectric materials, which is placed in the critical areas, where the multipactor threshold is lowest. The electric filed is disturbed that the secondary electrons are emitted against the electric filed, and they are not able to accelerate back across the gap. Hence, an improvement in the multipactor threshold should be expected. In order to verify the approach, a waveguide transformer is designed, the minimum gap of which is filled with the dielectric materials whose permittivity is 3.15. For the calculation of the threshold input power with the multipactor calculator, the Voltage Magnification Factor (VMF) has to be calculated in these critical areas at the frequencies of 3.95 GHz, the VMF is defined as the ratio between the voltage along the critical distance and the input voltage. The VMF of the waveguide transformer without dielectric filling is 3.12, The VMF of the waveguide transformer with dielectric filling is 0.36, representing an improvement in the multipactor threshold with respect to the original waveguide transformer.

Design and Realization of a C-band Impedance Transformer

Tiancun Hu and Wanzhao Cui
Science and Technology on Space Microwave Laboratory
China Academy of Space Technology (CAST), Xi'an, China

Abstract— Impedance Transformer is an important component in the design of microwave and millimeter System, which can be used to match the impedances of microwave components with different impedances. Since impedance mismatches may severely deteriorate the overall performance of electronic systems. In high-power applications, the standing electromagnetic wave resulting from mismatch in a transmission line is highly undesirable as it leads to amplitudes of voltage and current which might be several times higher than those in a matched line. This can lead to disruption or even damage of the dielectric in the transmission line. A reflected electromagnetic wave can also result in frequency pulling of signal generators connected to the mismatched transmission line, thereby shifting the oscillation frequency from the desired.

The most widely used class of impedance transformers is that of cascaded quarter-wave transformers, for which the maximum flatness (binomial) and equi-ripple (Chebyshev) synthesis procedures are well known. In this paper, we designed a C-band impedance transformer using a synthesis tool named FEST3D (Full-wave Electromagnetic Simulation Tool), which analyses complex passive microwave components by means of advanced modal techniques. It provides a quick synthesis tool to design an impedance transformer. Many parameters such as waveguide type, height, lower frequency, upper frequency, order and return loss can be selected for deciding the characteristic of the impedance transformer. In order to validate the design and simulation, the C-band impedance transformer has been manufactured. The fabricated impedance transformer with silver plated aluminium body with dimension of $210 \times 80 \times 50$ mm, the performance is measured using the Agilent network analyzer E8363C, the measured results of S parameters are agree well with the simulation results.

Synthesis of Non-uniform Planar Lines and Coupled Line Filters Using Inverse Scattering Approach

Harishankar Prasad and M. Jaleel Akhtar
Department of Electrical Engineering, Indian Institute of Technology, Kanpur 208016, India

Abstract— A novel analytical concept for the reconstruction of physical structures of a non uniform transmission line is presented here. The method is based on the solution of an inverse scattering problem, and involves the reconstruction of the impedance profile corresponding to the dimensions of the coplanar waveguide line in terms of its specified frequency response. The overall procedure requires the re-formulation of the famous Riccati differential equation in terms of the spectral domain reflection coefficient data and the impedance profile. The formulated Riccati equation is then solved using the proposed renormalization technique, which helps in obtaining a closed form solution of the unknown impedance profile in terms of the inverse Fourier transform of the reflection coefficient data in the specified frequency band. The impedance profile is finally transformed into the geometry of the coplanar waveguide line using the standard relationships. The validation of the overall procedure is checked by designing a number of coplanar waveguide (CPW) lines. The design is independently verified using CST microwave studio, a 3-D field simulator, and are fabricated based on the numerical simulation. This concept is used to design coupled line filters. Coupled line filters are used extensively in front end of communication and microwave systems. In this paper, a novel approach is used to design coupled line filters using microwave inverse scattering. This method involves synthesis of parallel line coupled filters for specified scattering parameter response over wide frequency band. The over all procedure requires the reformulation of Riccati equation in term of spectral domain reflection data and the impedance. An algorithm proposed above, to determine impedance profile of planar lines as a function of length. After getting impedance profile, this impedance is going to be converted into even and odd mode impedances for type of filter response, bandwidth, center frequency and number of coupled section of desired filters. The proposed approach may be used for continuously varying transmission structures also. The design is independently verified using CST microwave studio, a 3-D field simulator, and fabricated on the basis of numerical simulation. Here, we have discussed a novel technique using inverse scattering approach to design microwave filters. This technique is better than the conventional methods used which were inaccurate when a transmission line consists of multiple discontinuities or continuously varying transmission lines. This reconstruction technique is applicable to many other physical structures as long as those structures can be represented by equivalent transmission-line representations. Filters designed by inverse scattering offers several advantages over other methods, i.e., faithful frequency response over a wide frequency band and no sharp impedance discontinuities. An electromagnetic inverse scattering approach has been employed to design, fabricate and test a number of coplanar waveguide filters. The proposed technique is shown to be applicable to continuously varying planar geometry taking into account the multiple reflection. The measured data are compared with the specified frequency response of the filter. The result of the developed filters are found to be within 2–3% of the specified frequency response.

Calculating the Scattering from Periodic Conducting Surfaces without Using Evanescent Modes, Part II: Formulation of the Solution

Dayalan Kasilingam and Christopher Goonan
Department of Electrical & Computer Engineering, University of Massachusetts Dartmouth, USA

Abstract— The Rayleigh hypothesis for calculating the fields due to scattering from periodic surfaces was first formulated by Lord Rayleigh and applied to periodic gratings in the 1900's. In the Rayleigh method, the fields are represented in terms of plane waves both above the periodic surface and inside the corrugated region of the periodic surface. Due to its compactness, the Rayleigh method is computationally more efficient than other semi-analytical methods such as the integral equation method. However, in later years, the Rayleigh method was shown to be invalid for periodic surfaces with large steepness. Many researchers challenged Rayleigh's approach of using plane wave representations for the fields inside the corrugated region of the periodic surface. Several of these papers used extensive complex analysis to show that the solutions were unstable when the periodic surface became quite steep. However in the past decade, other researchers have shown that despite these apparent limitations, the Rayleigh hypothesis gives valid results even for very steep surfaces. It has been argued by these researchers that the limitations were primarily a function of the computational accuracy and not implicit to the method itself. In part I of this paper, we showed that the Rayleigh method can be used for calculating the fields from periodic conducting surfaces, even when the steepness was large. We also showed the existence of a modal sub-space which was orthogonal to all the evanescent modes at the boundary. By projecting the boundary conditions on to this sub-space, we showed that the propagating scattered fields can be found in terms of the incident fields. This was accomplished by calculating the evanescent modes and using their functional form to derive the modal sub-space orthogonal to the evanescent modes. We derive a matrix form of a transfer function model, which describes the scattered fields in terms of the incident fields. The transfer function model describes the scattering for all possible combinations of incident waves. For each mode, we generate a matrix whose one-dimensional, null-space represents the functional form of that mode. This matrix is generated using the modal propagation constants and the surface slopes. Since the method depends on the surface slopes, this technique works for surfaces with continuous slopes. By combining these matrices, one is able to define the modal sub-space which is orthogonal to the evanescent modes. For this technique to be of practical value, it is critical that the method of finding the modal sub-space not involve calculating the evanescent modes themselves. This technique accomplishes this by estimating the sub-space in terms of the propagation constants and surface slopes. The technique is shown to work for a variety of different surfaces with varying surface steepness. The new technique has many computational advantages. In most applications, such as those in radar and remote sensing, one is only interested in the scattered power in the far field. In these cases, one needs to find only the propagating fields and not the evanescent fields. Furthermore, computationally the evanescent modes are poorly conditioned because of their exponential dependence on depth and they also constitute an infinite set of modes. For periodic surfaces, the propagating modes represent a well-defined, finite set of modes. Thus purging the evanescent modes in the computation allows one to deal with well-conditioned matrices and eliminates the need for truncating an infinite series. This newly developed technique has the potential to be a powerful computational method for calculating scattering from rough surfaces. This new technique can be applied to modeling the behavior of gratings in applied optics, the scattering of RF and microwave signals in radar and remote sensing, the propagation properties of metamaterials and the scattering of acoustical signals in sonar and ultrasound systems.

Changes in the Degree of Polarization of a Stochastic Electromagnetic Plane-wave Pulse Scattered by a Spherical Medium

Liuzhan Pan and Chaoliang Ding
Department of Physics, Luoyang Normal University, Luoyang 471022, China

Abstract— In recent years the statistical properties of the light generated by scattering have been studied extensively due to their considerable interest in medical diagnostics and imaging, remote sensing of the atmosphere and ocean, and so on. However, in most cases, the treatment of scattering of the field was confined to the case that the incident field is statistically stationary. In this paper, the scattering of a stochastic electromagnetic plane-wave pulse on a deterministic spherical medium is investigated. Analytical formula for the degree of polarization (DOP) of the scattered field in the far zone is derived. Let pulse duration $T_0 \to \infty$, our formula can be applied to study the scattering of a stationary stochastic electromagnetic light wave. Numerical results show that the DOP of the far zone field is closely determined by the size of the spherical medium when the incident field is a stochastic electromagnetic plane-wave pulse, which is much different from the case when the incident field is a stationary stochastic electromagnetic light wave, where the degree of polarization of the far zone field is independent of the size of medium. One may obtain the information of the spherical medium by measuring the scattering-induced changes in the DOP of a stochastic electromagnetic plane-wave pulse.

Some Ideas Yet Unattempted in Georadar Full Waveform Inversion

G. Meles[1], S. Greenhalgh[2], H. Maurer[2], and A. Green[2]

[1]School of Geosciences, University of Edinburgh
The Kings Buildings, West Mains Road, Edinburgh EH93JN, United Kingdom
[2]Institute of Geophysics, ETH Zurich, Sonneggstrasse 5, Zurich CH 8092, Switzerland

Abstract— Georadar full wave form inversion for elucidating the shallow subsurface is now commonplace. It yields significantly higher resolution images than conventional tomographic techniques based on first arrival times and pulse amplitudes, or reflection imaging techniques. Despite the successes, there are still a number of areas in need of extension or improvement. For a start, all approaches are generally based on a 2D model assumption. This assumption is often questionable but of equal concern is the infinite line source in the medium invariant (y) direction, which is implicit in 2D modeling. Actual antennae are better approximated as point sources, which give rise to quite different wave propagation characteristics. The 3D to 2D transformation filter which is normally applied to convert the point source field data to match the line source modeled data is strictly only valid in the far field for a homogeneous full space and does not account for interference effects in heterogeneous media. Nor are intrinsic 3D effects, like out of plane events (sideswipe) accommodated in the analysis. 3D and 2.5D inversion schemes are strictly needed but they are computationally demanding in terms of memory and run time. The 2.5D approach is a compromise approach when the assumption of a 2D model is valid, but it is still two orders of magnitude more demanding than 2D modeling.

In crosshole surveys, using vertical borehole dipole antennae, only TM modes involving both the vertical (z) and horizontal (x) components of the electric field in the medium, are taken into account, whereas in surface surveys in which the transmitter antenna can be oriented horizontally, TE modes with the electric field in the transverse y direction are exploited. Ideally, combined TE and TM mode inversions should be carried out, especially for borehole-to-surface experiments.

Nearly all GPR full waveform inversions are implemented in the time domain and assume constant (time invariant) values for the permittivity ε and conductivity σ at each cell. In the presence of material dispersion (frequency dependence of ε and σ) it is preferable to perform the inversion in the frequency domain where such frequency dependence can be readily accommodated. In the time-domain, it involves difficult and computer intensive convolutions. Other attractions of working in the frequency domain are that successful inversions can be achieved with just a few frequencies rather than the entire data as in a time domain approach, and the local minimum trapping problem is reduced by starting at low frequency.

An obvious future direction is to move away from gradient-based inversion schemes to more advanced Gauss-Newton of full Newton approaches. We have recently developed the necessary methodology for explicit computation of the Jacobian and pseudo-Hessian matrices but as yet have not implemented this approach because of the computational challenges associated with the large dimensions of the pseudo Hessian matrix to be inverted and multiplied. Emphasizing the later portions of the radargrams and compensation for radiation/reception pattern effects on sensitivity are also promising areas for further work. Without such time-variant boosting and gradient conditioning/normalization, the inversion is captured by the stronger direct arrivals and the more diagnostic later arriving reflected and diffracted signals are down-played.

Source signal estimation is a critical area in need of further research. Most finite difference time domain modeling schemes use what are called hard sources (impressing a specified electric field (or voltage) as a function of time at the source position in the grid), but the theory really requires that a soft source (impressing a given current density function) be used. To a first approximation, to generate the same electric field in the medium, the hard source has to be the time integral of the soft source waveform, but this is often overlooked. Transmitter and receiver coupling variations along the boreholes or at the surface of the Earth will cause different waveforms at each recording point and ideally these should be solved for in the inversion. A frequency-domain scheme to do this for seismic waveform inversion was recently developed by us and could be adapted to the GPR case.

Compton Effect in the Medium with Non-unity Refractive Index

S. G. Chefranov[1], **A. G. Chefranov**[2], **and Vinay Venugopal**[3]

[1]A. M. Obukhov Institute of Atmospheric Physics, RAS, Moscow, Russia
[2]Eastern Mediterranean University, Famagusta, North Cyprus
[3]Division of Physics, VIT University, Chennai Campus, Chennai, India

Abstract— The foundations of the modern quantum theory of electro-magnetic radiation and its interaction with medium is constituted by the Einstein's theory of photo-effect and the theory of Compton effect. However, in the theory proposed by Compton and subsequent refinements, the medium features in explicit form are not generally accounted at all. This theory is based on the relationship between the photon momentum and its energy that may takes place only in vacuum, but not in a medium with non-unity refractive index n. Here we use Abraham's representation for the momentum of a photon in medium for the creation of a new consistent Compton effect theory accounting for media features. A condition, different to that obtained in [1], under which anomalous Compton effect is possible, is defined. In this case, due to the photon scattering on a moving electron, the photon's energy can increase when the electron velocity is above a threshold value in analogy with the Vavilov-Cherenkov radiation effect [2, 3]. In our theory we also give a new description of the parameters for scattered electrons [4], which is important for the experimental determination of the dependence of the Compton effect in medium on refractive index n.

REFERENCES

1. Pardy, M., "Compton effect in dielectric medium," v1 1, Jun. 2004, arXiv: hep-ph/0406008.
2. Chefranov, S. G., *Phys. Rev. Lett.*, Vol. 93, 254801, 2004.
3. Chefranov, S. G., *JETP*, Vol. 126, 333, 2004, arXiv: 1205.3774.
4. Venugopal, V. and P. S. Bhagdikar, *Physics Education*, Vol. 29, No. 1, Article No. 3, India, 2013, arXiv: 1202.4572.

An Acoustic Inverse Scattering Problem for Spherical Coating Materials with Radially Inhomogeneous Profile

E. Bilgin and A. Yapar
Electrical and Electronics Engineering Faculty, Istanbul Technical University, Istanbul, Turkey

Abstract— The objective of this study is to reconstruct the acoustical parameters of the coating material surrounding a sound-soft spherical object. Electromagnetic inverse scattering problems related to coated objects have a significant importance for practical applications such as design of special lenses or radar cross section reduction. The scalar acoustic inverse problem also has theoretical significance and can be considered as an introductory study for the vectorial electromagnetic case.

In this work, the compressibility of the coating material is assumed to have one-dimensional variation along the radial direction. Although the problem is a three-dimensional one, it can be reduced to a one-dimensional form using the spherical symmetry. To this end, the angular dependency of the acoustic field is expressed in terms of tesseral harmonics. The one-dimensional formulation is then obtained using the orthogonality of these functions over a spherical surface. The resulting formulation consists of two classical integral equations, known as the *object* and *data* equations. The aim of the inverse problem is to determine the unknown acoustical profile of the coating material via measurement of the scattered field over a spherical surface outside the spherical object, in the case of a point source excitation. This inversion is achieved using the Newton method. In this method the system of one-dimensional integral equations is solved iteratively starting with an initial estimation of the unknown acoustical profile. Since the inverse problem is ill-posed by nature, a regularization technique must be used in order to obtain a solution. In this work the classical Tikhonov regularization is applied for this purpose. The method applied in this work is first used in [1] to reconstruct the one-dimensional variation of the acoustical profile of a simple spherical object. In the present work, the approach applied in [1] is extended to the case of spherical coatings surrounding a sound-soft sphere. Numerical simulations demonstrate that the method is quite effective in determining smoothly varying continuous profiles and provides a useful approximation for layered profiles. However as expected for a Newton based iterative approach, the success of the method is strongly dependent on the choice of the initial guess and regularization parameter.

REFERENCES

1. Bilgin, A. Y. and T. Yelkenci, "An acoustic inverse scattering problem for spheres with radially inhomogeneous compressibility," *J. Acoust. Soc. Am.*, (will appear in April 2013).

Reflection of TEM Waves from a Finite Gap on the Inner Wall of a Coaxial Waveguide

Ö. Yanaz Çınar[1] and S. Akşimşek[1, 2]

[1]Gebze Institute of Technology, Turkey
[2]Istanbul Kültür University, Turkey

Abstract— Electromagnetic wave propagation in waveguides has been an interesting topic and subject to various engineering problems, such as microwave filters [1] and microwave measurement techniques [2]. In this study, reflection of a TEM wave from a finite gap on the inner wall of a coaxial waveguide with perfectly conducting walls (see Figure 1), which can function as a microwave filter, is analyzed rigorously by applying direct Fourier transform and reducing the problem into the solution of a modified Wiener-Hopf equation of the third type in a similar fashion to that of [3]. Applying the classical Wiener-Hopf procedure, Fredholm integral equations of the second type are determined, which are solved via the law of residues as described in [3]. The solution for the field terms are determined in terms of infinite number of unknown coefficients which satisfy an infinite set of linear algebraic equations. These equations are solved numerically and the effect of area ratio and the gap length on the reflection coefficient is presented graphically at the end of the analysis. The same problem is then analyzed by applying the mode matching technique [4], which is widely used in previous works related to waveguides. Following the classical mode-matching procedure, the reflection coefficient is determined and it is compared to the one obtained via the Wiener-Hopf technique.

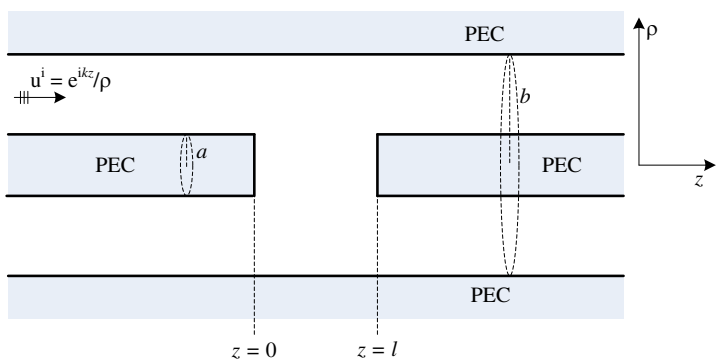

Figure 1: The geometry of the problem.

REFERENCES

1. Hwang, K. C. and H.-J. Eom, "Tunable notch filter of ferrite-filled grooves in parallel plates," *IEEE Microwave and Wireless Components Letters*, Vol. 15, No. 5, 363–365, 2005.
2. Huang, R. and D. Zhang, "Application of mode matching method to analysis of axisymmetric coaxial discontinuity structures used in permeability and/or permittivity measurement," *Progress In Electromagnetics Research*, Vol. 67, 205–230, 2007.
3. Çınar, G., H. Öztürk, and Ö. Yanaz Çınar, "Reflection and transmission of plane acoustic waves in an infinite annular duct with a finite gap on the inner wall," *Mathematical Methods in Applied Sciences*, Vol. 34, No. 2, 220–230, 2011.
4. Mittra, R. and S. W. Lee, *Analytical Techniques in the Theory of Guided Waves*, McMillan and Company, New York, 1971.

Properties of One-way Magnetooptic Nanostructures in THz Range

P. Kwiecien[1], V. Kuzmiak[2], I. Richter[1], and J. Čtyroký[2]

[1]Department of Physical Electronics, Faculty of Nuclear Sciences and Physical Engineering
Czech Technical University in Prague, Břehová, 11519 Prague 1, Czech Republic
[2]Department of Guided-Wave Photonics, Institute of Photonics and Electronics AS CR, v.v.i.
Chaberská 57, 182 51 Prague 8, Czech Republic

Abstract— For photonics to become a realistic alternative to electronics compact integrated optical analogs of one-way electronic devices such as diodes and transistors, are needed. Most of the nonreciprocal devices and one-way devices are based on nonlinear optics and magneto-optical effects. Unidirectional propagation can arise not only from a strong electromagnetic spectral asymmetry in the presence of an external magnetic field based on the simultaneous breaking of space and time-reversal symmetry [1] but it may also occur due solely due to the geometry of the structure [2–4]. Many conventional metal surfaces support localized surface plasmon polariton modes that can be excited using prism-coupling methods which, however cannot be applied in THz frequency range. After Pendry et al. [5] proposed the concept of spoof plasmons which is based on the introduction of a periodic texture to a conducting surface, an extensive experimental and theoretical work has been reported on the excitation and confinement of surface waves using surface corrugations. However, fabrication of the grating in a metallic substrate has proved to be challenging. Unlike metals, the dielectric properties of semiconductors can be adjusted by controlling the dopant concentration which in turn determines the degree of confinement and the loss for the plasmonic wave. Surface plasmon polaritons in the THz range are technologically important because they provide a possibility to develop subwavelength-scale device and offer the only possibility to investigate nanoscale systems in THz frequencies. By extending our previous work [6, 7], we developed an efficient D numerical technique based on the MO aperiodic rigorous coupled wave analysis (MOaRCWA). In our in-house tool, an artificial periodicity is imposed within a periodic 1D RCWA method, in the form of the complex transformation and/or uniaxial perfectly matched layers. Our approach, in which several key improvements have been implemented, namely allows to deal with anisotropic medium described by a general form of permittivity/permeability tensor and thus allows to describe SPP propagation in nanostructures in the presence of the external magnetic field in all three MO configurations. To study unidirectional properties in terahertz frequency range we applied both analytical methods [8] and numerical simulations by using MOaRCWA technique [9]. Specifically, based on our previous investigation of one-way waveguides consisiting of metal/MOPhC interface [10], we focused on the structures containing interface InSb/dielectric interface. The dispersion relation of such structures are known to exhibit a number of interesting features associated with both surface and bulk polaritonic modes [11, 12] which are shown to be reflected in their transport properties. Our work has been partially motivated by recent investigation of Au/dielectric/InSb sandwiched guiding structures [13]. The results obtained demonstrate variety of interesting features for both planar and structured interfaces and are discussed in the context of recent experiments.

ACKNOWLEDGMENT

This work was financially supported by the Czech Science Foundation project P205/10/0046.

REFERENCES

1. Figotin, A. and I. Vitebsky, *Phys. Rev. E*, Vol. 63, 066609, 2001.
2. Serebryannikov, A. E., *Phys. Rev. B*, Vol. 80, 155117, 2009.
3. Kuzmiak, V. and A. A. Maradudin, *Phys. Rev. A*, Vol. 86, 043805, 2012.
4. Stolarek, M., et al., *Opt. Lett.*, Vol. 38, 839, 2013.
5. Pendry, J. B., L. Martın-Moreno, and F. J. Garcia-Vidal, *Science*, Vol. 305, 847–848, 2004.
6. Čyroký, J., P. Kwiecien, and I. Richter, *J. of Lightwave Technology*, Vol. 28, 2969, 2010.
7. Kwiecien, P., I. Richter, and J. Čyroký, *OWTNM*, Cambridge, April 2010.
8. Dmitriev, V. and A. O. Silva, "Nonreciprocal properties of surface plasmon-polaritons at the interface between two magnetized media: Exact analytical solutions," *Progress In Electromagnetics Research Letters*, Vol. 21, 177–186, 2011.
9. Kwiecien, P., V. Kuzmiak, I. Richter, and J. Čyroký, *SPIE Optics and Optoelectronics*, Prague, April 2013.

10. Kuzmiak, V., S. Eyderman, and M. Vanwolleghem, *Phys. Rev. B*, Vol. 86, 045403, 2012.
11. Wallis, R. F., J. J. Brion, E. Burstein, and A. Harstein, *Phys. Rev. B*, Vol. 9, 3424, 1974.
12. Kong, F., K. Li, H. Huang, B.-I. Wu, and J. A. Kong, "Analysis of the surface magnetoplasmon modes in the semiconductor slit waveguide at terahertz frequencies," *Progress In Electromagnetics Research*, Vol. 82, 257–270, 2008.
13. Hu, B., Q. J. Wang, and Y. Zhang, *Opt. Lett.*, Vol. 37, 1895, 2012.

Broadband Characterization Using Stripline Structure

Ellen Yoshie Sudo Lutif[1, 2], **Alberto José de Faro Orlando**[1], **and Antonio Carlos da Cunha Migliano**[2]

[1]Aerospace Technological Institute (ITA), CTA, Brazil
[2]Institute of Advanced Studies (IEAv), CTA, Brazil

Abstract— The finite difference time domain method has been used to design, simulate, and validate the measurement results for the stripline structure. An analysis of the resonant characteristics for a broadband waveguide by using the finite difference time domain method for the description of the electromagnetic behavior of the cell discontinuities in the analysis of the transmission and reflection coefficients, permits in the 500 MHz–10 GHz frequency band the achievement of a good precision for the results. We will analyses the relation $w/h = 1.1$. The sample shows a good transmission in the PCB stripline structure. An electromagnetic wave is formatted of the type TEM. The results show that Stripline EM field distribution is more symmetrical offering better control over even/odd mode impedance. Characteristic impedance is very sensitivity to the ratio of center conductor width to dielectric thickness and relativity insensitive to the ratio of center-conductor thickness to dielectric thickness. The stripline structure is then implemented on Alumina substrate and measured in the laboratory. The measurement and simulation results are found to be close in the frequency range.

Few-quantum-dot Lasing in Photonic Crystal Nanocavities

J. Liu[1,2], S. Ates[1], S. Stobbe[1], M. Lorke[1], and P. Lodahl[1]

[1]DTU Fotonik, Department of Photonics Engineering, Technical University of Denmark
Ørsteds Plads 343, Kgs. Lyngby DK-2800, Denmark
[2]South China Academy of Advanced Opto-Electronics, South China Normal University
Guangzhou 510006, China

Abstract— Photonic crystal nanolasers have attracted great interest both for fundamental research and applications in the past decade. In photonic crystal cavities, the leakage to optical modes is strongly reduced, which increases the spontaneous emission coupling factor, β. This is a crucial parameter for the threshold characteristics of lasers. With increasing β, the well-known step-like threshold behavior becomes smoother. Although the smooth lasing transitions of photonic crystal nanolasers were observed and fitted by traditional rate equation models [1], a systematic comparison between experiments and more advanced semiconductor models of photonic crystal nanolasers is still missing [2]. The goal of this work is to get a deep understanding of the quantum dots based nanocavity lasers by comparing experiments to theory.

Excitation power dependent cavity mode intensity and linewidth are shown in Fig. 1(a). In regimes I and III, the output intensity increases linearly with the input power. A smooth nonlinear increase of output power can be clearly traced in regime II, which is the signature of onset of lasing. The theory predicts a similar behaviour as observed experimentally by assuming realistic parameters of cavity quality factor $Q = 7800$, the number of quantum dots $N = 4$, spontaneous emission coupling factor $\beta = 0.15$ and the mode volume $V = 0.52\,\mu\text{m}^3$. The linewidth decreases in regime I, is stable in regime II, and slowly decreases in regime III [3]. Saturation is observed in regime IV.

The emission spectra with low pumping power and the decay rates of quantum dots are shown in Fig. 1(b). Below saturation, many exciton peaks in the spectra can be indentified as well as the fundamental cavity mode around 950 nm. Only three quantum dots have comparable decay rates to that of the emission at the wavelength of the cavity mode and most of the decay rates from quantum dots are strongly inhibited by the photonic band gap. This indicates that only a few quantum dots are feeding the cavity mode in the lasing transition process.

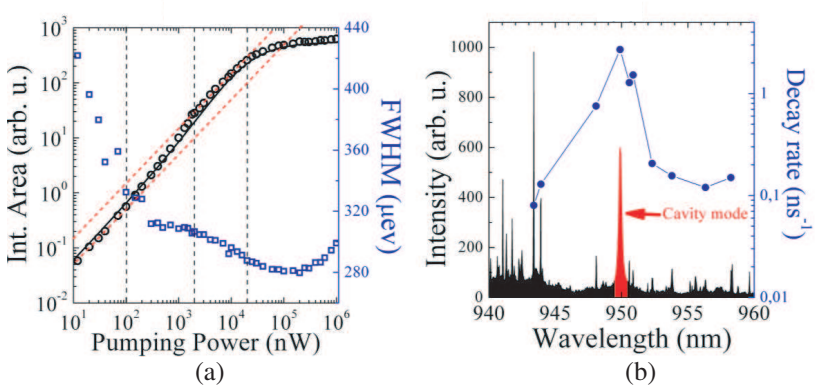

Figure 1: (a) The output power (black circles) and the linewidth (blue squares) of the cavity mode as a function of excitation power. The solid line shows the theoretical curve as explained in the text. Red lines are guides to the eye for a linear increase of output power with a slope of one. (b) The emission spectra (black) of quantum dot-cavity system for 100 nW pumping power and decay rates (blue circles) for different wavelength. The cavity mode is highlighted in red.

REFERENCES

1. Strauf, S., K. Hennessy, M. T. Rakher, Y.-S. Choi, A. Badolato, L. C. Andreani, E. L. Hu, P. M. Petroff, and D. Bouwmeester, "Self-tuned quantum dot gain in photonic crystal lasers," *Phys. Rev. Lett.*, Vol. 96, 127404, 2006.

2. Gies, C., J. Wiersig, M. Lorke, and F. Jahnke, "Semiconductor model for quantum-dot-based microcavity lasers," *Phys. Rev. A*, Vol. 75, 013803, 2007.
3. Björk, G. A. Karlsson, and Y. Yamamoto, "On the linewidth of microcavity lasers," *Appl. Phys. Lett.*, Vol. 60, 304, 1992.

Investigations on Two-wavelength Holographic Recording in Thick Phenanthrenequinone-doped Poly(Methyl Methacrylate) Photopolymer

June Hua Lin[1], **Shiuan Huei Lin**[2], **and Ken Y. Hsu**[1]

[1]Department of Photonics, National Chiao Tung University, Hsinchu 30010, Taiwan, R.O.C.
[2]Department of Electrophysics, National Chiao Tung University, Hsinchu 30010, Taiwan, R.O.C.

Abstract— Holographic recording using two-wavelength processes, in which the red (even near-infrared) laser is used for recording and the blue (even UV) light was used for optically gating provides several important features over conventional single-wavelength recording [1–5]. The features include the ability to record holograms with longer-wavelength lasers, nondestructive readout before material become saturated and the ability to selective recording by gating the sensitivity of the recording medium optically. If these features were combined with volume holography, one could have more freedoms for designing optical system and/or creating innovative ideas of applications. Thus, materials and techniques for two-wavelength holographic recording have been of great scientific interest.

In this presentation we report our investigation on two-wavelength holography in thick Phenanthrenequinone-doped Poly(methyl methacrylate) Photopolymer, PQ/PMMA. We first describe the absorption spectrum and light-induced absorption change measurements in samples, so as to select the appreciate wavelengths of gating and recording laser beams. The two-wavelength holographic recording in 2-mm thick PQ/PMMA sample at 647 nm under gating of an additional laser at 325 nm is then demonstrated. We then present a theoretical model and experimental verification of the model for two-wavelength holographic recording in PQ/PMMA. With optimum recording conditions, the diffraction efficiency can reach 40%. To the best of our knowledge it is the first demonstration to perform the two-wavelength holographic recording in a millimeter thick PQ/PMMA photopolymer. Bragg selectivity curve of a 2-mm thick volume hologram and image hologram reconstruction are also tested, suggesting our PQ/PMMA to be attractive candidate for two-wavelength volume holographic application.

ACKNOWLEDGMENT

Financial support by NSC, Taiwan under contracts NSC 101-2221-E-009-111-MY3, NSC 101-2221-E-009-112-MY3 and by Ministry of Education, Taiwan under AUT program is gratefully acknowledged.

REFERENCES

1. Kippelen, B., S. R. Marder, E. Hendrickx, J. L. Maldonado, G. Guillemet, B. L. Volodin, D. D. Steele, Y. Enami, Sandalphon, Y. J. Yao, J. F. Wang, H. Röckel, L. Erskine, and N. Peyghambarian, "Infrared photorefractive polymers and their applications for imaging," *Science*, Vol. 279, 54–57, 1998.
2. Shimizu, M., M. Schelper, K. Mochida, T. Hiyama, M. Adachi, Y. Sasaki, S. Akiyama, S. Maeda, H. Kanbara, and Y. Mori, "A novel strategy for two-photon holographic recording: Stepwise two-photon absorption of α-quinquethiophene followed by energy transfer to an aryl azide," *Adv. Mater.*, Vol. 19, 1826–1829, 2007.
3. Nguyen, L. H., M. Straub, and M. Gu, "Acrylate-based photopolymer for two-photon microfabrication and photonic applications," *Adv. Funct. Mater.*, Vol. 15, 209–216, 2005.
4. Buse, K., A. Adibi, and D. Psaltis, "Non-volatile holographic storage in doubly doped lithium niobate crystals," *Nature*, Vol. 393, 665–668, 1998.
5. Chen, P. L., S. L. Cho, J. H. Lin, S. H. Lin, K. Y. Hsu, and C. Sien, "Two-wavelength holographic recording in thick phenanthrenequinone-doped poly(methyl methacrylate) photopolymer," *Opt. Eng.*, Vol. 51, 030503, 2012.

Optical Control of Guided-mode-resonance in the Waveguide Grating Structures with Azo-dye Polymers

Jian Hung Lin[1], **Yu Chung Huang**[1], **Jian Hao Huang**[2], **Hung-Chih Kan**[1], **and Chia Chen Hsu**[1, 2]

[1]Department of Physics, National Chung Cheng University, Ming Hsiung, Chia Yi 621, Taiwan
[2]Graduate Institute of Optomechatronics, National Chung Cheng University
Ming Hsiung, Chia Yi 621, Taiwan

Abstract— A simple and promising method is presented for optical control of guided-mode-resonance (GMR) in a waveguide grating structure (WGS). The GMR mode shows high sensitivity to the change of the refractive index in the cladding or waveguide layer resulted from the photo-isomerization of disperse-red-one (DR1) molecules induced by the pump beam. By setting up a detector to monitor the light intensity reflected or transmitted from the WGS at the wavelength of the GMR peak positions, we demonstrate optical modulation capability with our GMR filter.

REFERENCES

1. Lin, J. H., Y. C. Huang, N. D. Lai, H. C. Kan, and C. C. Hsu, *Optics Express*, Vol. 20, 377, 2012.

Design and Simulation of Optimized Ultra-wideband Saddle Antenna

A. Sudhakar[1] and D. Madhavi[2]

[1]Department of ECE, RVR & JC College of Engineering
Chowdavaram, GUNTUR-522019, Andhra Pradesh, India
[2]Department of Physics, RVR & JC College of Engineering
Chowdavaram, GUNTUR-522019, Andhra Pradesh, India

Abstract— Ultra-Wideband (UWB) is an emerging technology for short range wireless communications with high data rates as well as radar applications. In this paper an optimized saddle flared type structure of ultra wideband antenna is modeled and simulations are performed using CST microwave studio package. This ultra wideband antenna is based on using of two smoothly shaped flares of a simple geometric structure- the saddle. The first flare, larger in size, serves as an antenna base, reflector and one of the radiator arms. The second flare, smaller in size, operates as other arm of the radiator. An apparent idea is exploited in this design that an ideal UWB antenna would operate as a broadband well matched transformer for the current at its driving ports to the radiated fields that leave the antenna aperture. Besides terminal matching, the antenna would provide a necessary spatial distribution of the radiated energy. A novel design of a simple saddle antenna is presented and discussed. The antenna geometrical models are created. The antenna design is numerically optimized by profound analysis of the effects of parameters on antenna radiation characteristics. This antenna presents a relatively compact physical structure to operate in ultra wideband applications. The terminal characteristics and radiation patterns of the optimized saddle antenna in the ultra wideband range are presented. In particular, this antenna demonstrates a frequency independent behavior holding small variations for the input impedance and constant beam width. The proposed antenna exhibits an efficient use of occupied physical space, beam stability and approximately 5 dB gain with more than front to back ratio. The consistent directivity of the antenna ensures it a prominent place in the field of wireless communication.

Printed Yagi-Uda Antenna for WLAN Applications

Amira El-Tokhy Ali[1] and Deena A. Salem[2]

[1]Electrical and Communication Department, Modern Science and Arts University (MSA)
6th October City, Egypt
[2]Microstrip Department, Electronic Research Institute (ERI), Dokki, Cairo, Egypt

Abstract— Printed Yagi-Uda antennas have lately, gained popularity for its end fire radiation pattern, low profile, small size, light weight, and low cost, along with ease of fabrication and installation All these characteristics made it highly demanded for diverse applications in various communication systems. Ref. [1] utilized optimization techniques to obtain the optimum dimensions of Yagi-Uda antenna. The size of the presented antenna was about $91.56 \times 21.8\,\mathrm{mm}^2$ with resonance frequency of 5.8 GHz with FBW of 11% and gain that exceeded 11 dB. The length may be attributed to the use of five directors.

Later Ref. [2] implemented a MIMO system using the design presented in [1] but with resonant frequency of 5.2 GHz to obtain omni-directional radiation pattern. The size of the single element was reduced by 20% to reach $3.4 \times 60\,\mathrm{mm}^2$ without significant degradation in the single element's gain which reduced to 9.6 dB.

In this paper, a printed Yagi-Uda antenna was designed where total size is reduced to $2.4 \times 60\,\mathrm{mm}^2$ to be used for WLAN (5.2–5.28 GHz) applications. In this antenna, a horizontal extension of the feed line and three directors are printed on the top of a FR4 substrate with dielectric constant = 4.5, $\tan\delta = 0.02$ and thickness 1.5 mm. On the other side of the substrate a partial ground plane with a mirror image of the feed line and the horizontal extension are printed. The two horizontal sections formed the driver dipole. Parametric analysis was carried out to minimize the dimensions to be used for USB applications for devices that are not equipped with WLAN access point. To ensure that the performance of the designed antenna does not vary with the presence of the casing, the design was re-simulated including casing with materials of 2.5 and 4.5 dielectric constants with thickness 0.8 mm. The substrate was extended by two cm for the circuitry of the dongle.

The designed antenna has a small size of $W \times L = 24 \times 60\,\mathrm{mm}^2$, substrate thickness $h = 1.5$ mm, with a driver of width 9.9 mm, and three directors of widths 16.5, 15.5 mm, and 15.5 mm, with separations of 9 mm, 8 mm, and 13 mm. The operational bandwidth extended from 5.09–5.36 GHz to include WLAN applications. Furthermore, the design was re-simulated extending the ground plane by 2 cm to consider the circuitry required for USB applications, and with a dielectric casing for two different dielectric constants, 2.5 and 4.5, for the casing with 2.5 dielectric constant the design was adjusted to maintain the same bandwidth and same resonant frequency by changing the driver width to 11.2 mm.

As for the casing of dielectric constant 4.5, and to maintain the same bandwidth and resonant frequency a wider casing was required which violates the advantage of small size of the designed antenna. The antenna was fabricated using photolithographic technique and measured using VNA HP8719ES and very good agreement was achieved.

REFERENCES

1. Sedighy, S. H., A. R. Mallahzadeh, M. Soleimani, and J. Rashed-Mohassel, "Optimization of printed Yagi antenna using invasive weed optimization (IWO)," *IEEE Antennas and Propag. Letters*, Vol. 9, 1275–1279, 2010.
2. Khaleel, H. R., H. M. Al Rizzo, and D. G. Rucker, "Printed Yagi-Uda antenna array for MIMO systems," *IEEE AP-S*, 2012.

Digital Public Safety Radio Communication

E. Nascimento Junior[1], **H. Tertuliano Filho**[1], **J. R. Descardeci**[2], **C. A. Dartora**[1], **T. M. Sanchez Otobo**[1], **and E. C. Rolin**[1]

[1]Department of Electrical Engineering, Federal University of Paraná, Brazil
[2]Department of Electrical Engineering, Federal University of Tocantins, Brazil

Abstract— The present work aims to show a comparison between the various radio systems digital standards as APCO-25 TETRA and TETRAPOL. The realization of operational tests of the same on the pitch under severe conditions, adjustments for use by federal law, stare and local enforcement agencies, in all Brazil, especially in the border regions of the country. After discussion about each standard of interest and comparative way, the first contribution was in the presentation of the results between the standards and comparison between the systems. Once compared the data, was made a compilation of the characteristics of the equipment used and tested links to finally guide the Brazilian Government by SENASP, ENAFRON group, in the definition of the best system, its applicability and functionality in police institutions, as well as their strategic integration with defense sectors, that by understand that region of international borders. A predictive modeling system software professional coverage was used and an algorithm developed in Matlab®, which made it possible to checking signal coverage. Were taken into consideration for altimetry data algorithm development and morphological settings. A part of the preliminary result obtained can be observed in Figure 1.

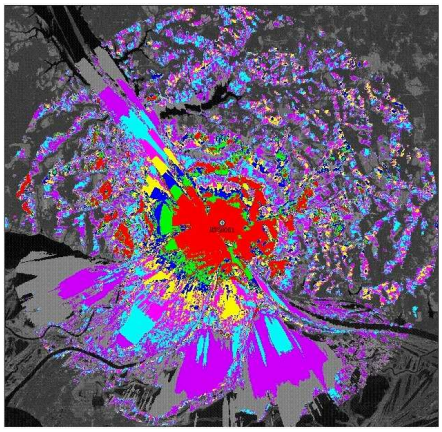

Figure 1: Data obtained of prediction of coverage in Oriximiná, Pará, Brazil with the CelPlan wireless global technologies.

A Compact UWB Antenna with Wide Band-notch at 5 GHz for WLAN Band

Qurratulain and Neela Chattoraj
ECE Department, Birla Institute of Technology, Mesra, Ranchi-835215, India

Abstract— Ultra-wideband (UWB) has come up as a revolutionary and contemporary wireless technology in the last decade. It has generated a great deal of interest for use in the industry and academia.

In this paper the design of a small and compact ultra-wideband (UWB) printed monopole antenna having whole size of $24 \times 32\,\text{mm}^2$ with band notch characteristic is proposed. This antenna is designed to cover the FCC bandwidth for UWB applications (3.1–10.6 GHz) and has a band-notch to filter the 5.15–5.825 GHz band. First the planar tapered square printed monopole microstrip antenna is realized, simulated and fabricated on Glass epoxy substrate having a relative permittivity of 4.36 and a substrate height of 1.567 mm. By using beveling technique in the patch and strip-line feed, the compact size and wide impedance bandwidth of this antenna is obtained. The geometry of the proposed antennas is shown in Figures 1(a) & 1(b). To obtain the frequency rejection characteristic a U slot is inserted in the patch as shown in Figure 1(b). The rejected frequency is calculated from the following formula to be

$$f_{notch} = \frac{c}{2L_{slot}\sqrt{\varepsilon_{eff}}} \tag{1}$$

where L_{slot} is the total length of the slot, ε_{eff} is the effective dielectric constant, and c is the speed of light. We take the total slot length calculated from (1) into account initially and then adjust the geometry of the design. The snapshots of fabricated antennas are shown in Figures 2(a)

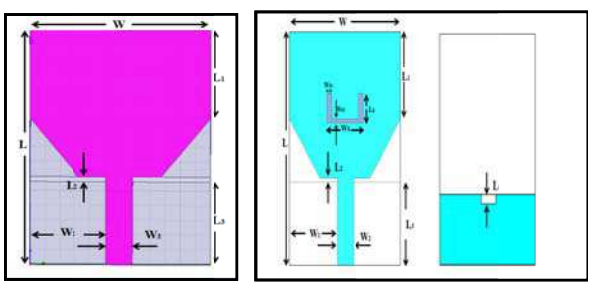

(a) (b)

Figure 1: Geometry for the proposed antenna, (a) without notch, (b) with notch.

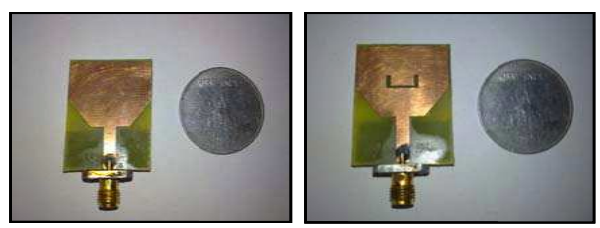

(a) (b)

Figure 2: Snapshot of the fabricated antennas, (a) without notch, (b) with notch.

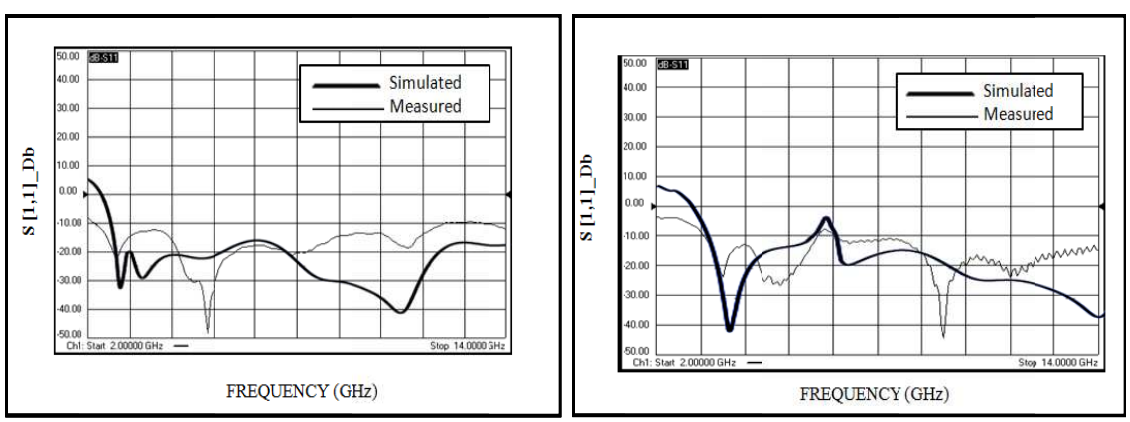

(a) (b)

Figure 3: Comparison of return loss curves for proposed antenna, (a) without notch, (b) with notch.

& 2(b). The simulated and measured results show that the proposed antenna achieves a wide bandwidth from 3 to 14 GHz with successful band-notching. The comparison of simulated and measured return loss curves for proposed antenna without and with the U slot for filtering are as shown in Figures 3(a) & 3(b) respectively. UWB performance parameters of return loss, radiation pattern, group delay and current distribution are studied. The simulated results are well supported by measured results of the prototype of the antenna fabricated. More results will be presented in the full paper.

Effect of Stationary Magnetic Fields on Different Bacterial Strains

P. Krepelka[1], **E. Hutova**[1], **and K. Bartusek**[2]

[1]Department of Theoretical and Experimental Electrical Engineering
Brno University of Technology, Technicka 12, Brno 612 00, Czech Republic
[2]Institute of Scientific Instruments, Academy of Sciences of the Czech Republic
Kralovopolska 147, Brno 612 64, Czech Republic

Abstract— The authors discuss the effects of stationary magnetic fields on the growth, morphology, and chemical composition of colonies of bacteria. The bacterial strains applied in the experiment were Lactobacillus acidophillus, Staphylococcus epidermidis, Enterococcus durans and Escherichia coli, all in the form of colonies cultivated on the growth medium and in an isotonic diluent. Homogeneous or gradient stationary magnetic field modified these bacterial cells by a exhibiting the magnetic flux density value of 1 T. The modified bacterium was compared with a control sample placed in the same conditions outside the magnetic field.

Using neodymium magnets, we generated ten different magnetic field types of diverse densities and defined configurations. The model of the magnetic field structure was computed by a finite element method (ANSYS) and experimentally verified via measurement with a Hall effect sensor. The experiment was carried out under stable ambient conditions to eliminate possible effects of the environment. We used standard image processing methods to observe the structure and size of the bacterial colonies on Petri dishes; subsequently, the extracted image descriptors were statistically evaluated.

Within follow-up stages of the research, changes in the chemical composition of bacterial cells will be monitored. If the magnetic field influences the metabolism of the bacteria, then their membrane structure and ratio of lipids, proteins and polysaccharides will change. These variations will bring an effect on the number and strength of the molecular bonds. An appropriate technique for the determination of these changes appears to consist in the vibration spectrum; the observation of the variations is performed by means of the NIR spectrum. Although interpretation of the NIR spectra is a difficult task, this method is suitable for the measurement of water-based samples. The changes are to be evaluated via analysis of the principal components and application of the artificial neural net.

Enhanced Spectrum Planning in Cognitive System Based on Reinforcement Learning

R. Urban, E. Hutova, and D. Nespor
Department of Theoretical and Experimental Electrical Engineering
Brno University of Technology, Technicka 12, Brno 612 00, Czech Republic

Abstract— Generally acceptable approach of spectrum allocation is inefficient. Frequency spectrum is allocated according to the global frequency plans for large geographical areas. This method leads to massive underutilization of some parts of the frequency spectrum. Other parts are massively used at selected places. Regarding to these facts, deploying of the new worldwide wireless service is now nearly impossible due to the totally overfilled frequency spectrum plans around. One possible solution of this problem in frequency spectrum is offered by using dynamic spectrum sharing or resource management, which could be operated by cognitive system [1]. To apply cognitive feature, data about spectrum situation are essential. There are several research projects focusing on spectrum survey measurements, such as [2, 3]. Cognitive radio is distinguishing following two types of the users. Primary users have privilege to use their frequency band according to the paid license. On the other hand, secondary users are searching for unused parts of spectrum in current time at current location and they are using it to optimize wireless traffic. This paper introduces novel approach of finding the best available channel for secondary users based on reinforcement learning from spectrum survey data introduced in [3]. We are able to study several completely different environments in this spectrum survey. The main focus is on cellular network bands such as UMTS and GSM. The reinforcement learning algorithm returns the vector of the best channels, which could be used for spectrum sharing by secondary users with minimal impact to primary user's communication parameters. Based on this information we are able to plan secondary user's frequency allocation and minimize chance of interference between both primary and secondary users. Nonetheless to say, that better spectrum planning brings decreasing of the radiation power and decreasing of the microwaves smog to biological tissues as well. The effects of the enormous electromagnetic radiation are widely discussed [4].

ACKNOWLEDGMENT

This work was supported by the project CZ.1.07/2.3.00/30.0005 of Brno University of Technology and GACR 13-09086S.

REFERENCES

1. Mitola, J., *Cognitive Radio Architecture: The Engineering Foundations of Radio XML*, N. J. Hoboken, Wiley-Interscience, 2006.
2. Shared Spectrum Company (SSC), 2011, http://www.sharedspectrum.com/papers/spectrum-reports/.
3. Urban, R., T. Korinek, and P. Pechac, "Broadband spectrum survey measurements for cognitive radio applications," *Radioengineering*, Vol. 21, No. 4, 2012.
4. Adair, E. R., K. S. Mylacraine, and B. L. Cobb, "Partial-body exposure of human volunteers to 2450 MHz pulsed or CW fields provokes similar thermoregulatory responses," *Bioelectromagnetics*, Vol. 22, 246–259, 2001.

2D Simulations of Bioelectrical Properties of Thorax by EIT

K. Ostanina, J. Dedkova, and T. Kriz
Department of Theoretical and Experimental Electrical Engineering
Brno University of Technology, Technicka 3082/12, Brno 616 00, Czech Republic

Abstract— The conventional Electrical Impedance Tomography (EIT) is a non-invasive imaging method of internal structure of the investigated object using spatial conductivity and relative permittivity distributions obtained from measurements of surface voltages and the known injected current.

The EIT image reconstruction is an ill-posed inverse problem of finding such internal impedivity distribution, which minimizes certain optimization criteria. The impedivity is defined

$$\mathbf{z} = \sigma + j \cdot 2\pi f \varepsilon_0 \varepsilon_r,$$

where σ is the conductivity, ε_r is the relative permittivity, ε_0 is the permittivity of free space and f is the frequency.

In the article, the improved EIT algorithm for reconstruction images of an internal impedivity distribution of the human thorax tissue is described. This approach of imaging was applied to the several computer simulations, which demonstrate the real rang of application of the proposed algorithm. Obtained reconstruction results will be presented. All reconstruction process properties will be also discussed.

ACKNOWLEDGMENT

The research described in the paper was financially supported by the project of the BUT Grant Agency FEKT-S-11-5.

REFERENCES

1. Holder, D. C., Ed., *Electrical Impedance Tomography: Methods, History and Applications,* Institute of Physics Publishing, London, 2005.
2. Miklavčič, D., N. Pavšelj, and F. X. Hart, "Electric properties of tissues," *Wiley Encyclopaedia of Biomedical Engineering*, M. Akay, Ed., John Wiley & Sons, Inc., 2006.

Estimation of the Air Ion Mobility Spectrum by Means of a Gerdien Tube with a Segmented Inner Electrod

Z. Roubal and P. Křepelka
Department of Theoretical and Experimental Electrical Engineering
Brno University of Technology, Kolejní 2906/4, Brno 612 00, Czech Republic

Abstract— Light negative air ions demonstrably exhibit positive influence on the human organism. The concentration of these ions can be effectively used as the integral criterion for the evaluation of air purity, and there also exists a multitude of other applications. The presented aspiration method enables us to establish the concentration of air ions in the atmosphere. In a gerdien tube fitted with a one-piece inner electrode, measurement of the saturation characteristics must be performed to facilitate the determination of the air ion mobility spectrum. The characteristics represent the relation of the measured current through the inner electrode to the polarization voltage. The measurement is time-intensive and sensitive to temporal fluctuations of the air ion concentration during the measurement. For this reason, a gerdien tube of the first type is used; the device comprises a segmented inner electrode, and the air ion mobility spectrum can be estimated (for two polarization voltages) from individual currents of the inner electrode segments. However, due to the overlapping between the functions G that characterize the transmission functions of the individual electrodes, estimation of the air ion spectrum is not an explicit task. The paper describes the application of the method of least squares, which performs iterative estimation of the air ion spectrum from the measured currents. A suitable regularization method will facilitate an increase of the solution stability; the estimated and the original air ion spectra will be compared to enable the evaluation of applicability for the method.

ACKNOWLEDGMENT

The research described in the paper was financially supported by project of the BUT Grant Agency, FEKT-S-11-5/2012 project from Education for Competitiveness Operative Programme CZ.1.07.2.3.00.20.0175, (Electro-researcher).

REFERENCES

1. Roubal, Z., M. Steinbauer, and Z. Szabó, "Modeling of saturation characteristic of an aspiration condenser," *PIERS Online*, Vol. 6, No. 1, 26–30, 2010.
2. Kondrashova, M. N., E. V. Grigigorreko, A. N. Tikhonov, T. V. Sirota, A. V. Temnov, I. G. Stavrovskaya, N. I. Kosyakova, N. V. Lange, and V. P. Tikonov, "The primary physicochemical mechanism for the beneficia biological/medical effects of negative air ions," *IEEE Trans. Plasma Scien.*, Vol. 28, No. 1, 230–237, 2000.
3. Tammet, H. F., "The aspiration method for determination of atmosphericion spectra," *IPST*, Jerusalem, 1970.
4. Bartušek, K., P. Fiala, T. Bachorec, and E. Kadlecova, "Accuracy of air ion field measurement," *PIERS Online*, Vol. 2, No. 6, 640–643, 2006.
5. Bartušek, K., "Meření spektrálních charakteristik iontových polí," *Elektrorevue* [online], 2001, http://www.elektrorevue.cz/clanky/01038/index.html.
6. Roubal, Z. and M. Steinbauer, "Design of electrometric amplifier for aspiration condenser measurement," *PIERS Proceedings*, 1430–1434, Xi'an, China, March 22-26, 2010.
7. Steinbauer, M., P. Fiala, K. Bartušek, and Z. Szabó, "Experiments with accuracy of air ion field measurement," *PIERS Proceedings*, 1062–1066, Hangzhou, China, March 24–28, 2008.

Study about Effects Induced by Temporal-variability of Ionosphere on Medium-Earth-Orbit SAR Azimuth Imaging

Liang Li[1,2,3], **Jun Hong**[1,2], **and Feng Ming**[1,2]

[1]Institute of Electronics, Chinese Academy of Sciences, Beijing 100190, China
[2]Sciences and Technology on Microwave Imaging Laboratory, Beijing 100190, China
[3]University of Chinese Academy of Sciences, Beijing 100049, China

Abstract— An analysis model for ionospheric effects on azimuth imaging of Medium-Earth-Orbit SAR (MEOSAR) is established based on the system characteristics of MEOSAR and the temporal-variability of ionosphere. The effects caused by the quadratic and cubic phased errors induced by ionosphere gradients on azimuth imaging are analyzed. The results of the analysis show that both the quadratic phase error and the cubic phase error being neglected for Low-Earth-orbit SAR (LEOSAR) will deteriorate the azimuth imaging for MEOSAR. Moreover, the ionospheric effects become more and more serious with the increasing of SAR altitude.

Technique Problems in Designing the on-chip EMI Sensor Array

Tao Su, **Yehua Yang**, **and Zixin Wang**
School of Physics and Engineering, Sun Yat-sen University, Guangzhou, China

Abstract— The methods for modeling and optimizing the electromagnetic immunity of integrated circuits (ICs) are demanded by the electronic industry. When electromagnetic interference (EMI) is applied on an IC, the EMI signal is spread in the on-chip power distribution network (OCPDN). Efforts on modeling have started to simulate two-dimension (2D) voltage distribution in the OCPDN. Moreover, the EMI optimization is intent to manage the voltage of the whole chip instead of a single node. To check the validation of the model and to see the effect of the optimization, it is very interesting to measure the 2D EMI voltage distribution in the OCPDN.

Current on-chip measurement techniques are not suitable for measuring the 2D on-chip EMI distribution in real time. Some techniques measure on-chip voltages of only a few locations while the others need to store the voltages and output them after the EMI injection.

The motivation of this work is to establish a method which can qualitatively measure the 2D profile of the EMI voltage in OCPDN. The approach proposed in this paper is an on-chip EMI sensor array (OCEMISA). The array contains sensor cells being distributed uniformly on the chip. The cells can send feedback signals indicating the cells' status. The cell status is a function of the local EMI voltage. EMI above certain threshold cause the cell to fail. There are three critical properties in the OCEMISA:

- The cell response to its local supply voltage only.
- The feedback signals of cells of the whole array are accessible.
- The location of the failed cell can be identified from the feedback pattern.

What this paper detailed are two designs of OCEMISA and their technique problems. The first design uses a pulse generator as the sensor cell. Each cell generates repeated pulses as the feedback. The pulses of a row or column of cells within one cycle form a pulse train at the monitoring port. By measuring and examining the feedback signals on the monitoring port, locations of the failed cells are identified. The design face three key problems: first, some failure modes share the same feedback signals; second, the IC process variation prevents the feedback signal forming a stable pattern; a considerable number of monitoring ports are required.

The second design uses ring oscillator as the sensor cell. Different cell use the rings of different length so that each cell has its own unique oscillation frequency. A ring oscillator generates a switching noise on the supply of the chip. The switching noise has a fundament frequency component at oscillator frequency of the oscillator. By measuring the switching noise on the supply pin, the status of the cells can be monitored. The design face three key problems: first, frequency of the switching noise may overlay with the frequency of the EMI; second, the IC process variation cause the oscillation frequency to be deviated from the expected value and to be unstable; to measure the switching noise is not easy.

The paper illustrates the two designs in details. Theoretical analyses with formulas are performed to show the origins, behaviors and solutions of the technique problems. Measurement results on FPGA prototypes are given to show the implementation problems. The paper points out one direction of the next effort to make OCEMISA real.

Design and Synthesis of Multi Resonant Planar Antenna Using Particle Swarm Optimization Method

B. Rama Sanjeeva Reddy, D. Vakula, and N. V. S. N. Sarma
National Institute of Technology, Warangal, India

Abstract— This paper presents a novel evolutionary optimization methodology for multi resonant planar antenna design for mobile communication applications. The design criterion was to obtain satisfactory antenna return loss and bandwidth for three frequency bands. Based on a pre-determined planar antenna structure, the geometrical parameters are extracted and optimized by PSO. The synthesized structure has been analyzed numerically by considering an antenna prototype. The synthesis procedure is automatically performed by means of an iterative PSO-based optimization strategy. The fitness function of the optimization is calculated by the PSO program. The feasibility of PSO algorithm allows improved optimization efficiency and less computational time assessed through simulations.

Session 2P1
3_FocusSession.SC3: Recent Progress in Photonic Crystals 2

Recent Progress in Photonic Crystals and Their Applications
Susumu Noda, ... 650

Cavity Quantum Electrodynamics with Three-dimensional (3D) Photonic Bandgap Crystals
Willem L. Vos, Léon A. Woldering, ... 651

3D Photonic Crystals for Photon Management in Solar Cells
Ralf B. Wehrspohn, Alexander Sprafke, ... 653

3D Photonic Crystals with Controlled Deterministic Aperiodic Disorder
Michael Renner, Erik Waller, Georg Von Freymann, ... 655

Quantum Optical Devices Based on Photonic Crystal Nanocavities
Hisashi Sumikura, Muhammad Danang Birowosuto, Masaya Notomi, ... 656

Solid-state Cavity-QED in Quantum Dot-photonic Crystal Nanocavity Coupled Systems
Yasuhiko Arakawa, S. Iwamoto, Yasutomo Ota, Aniwat Tandaechanurat, ... 657

Photonic Crystals for Integrated Quantum Circuits
Thang Ba Hoang, Sartoon Fattahpoor, Leonardo Midolo, Dondu Sahin, Andrea Fiore, Alessandro Gaggero, Francesco Mattioli, Roberto Leoni, Johannes Beetz, Matthias Lermer, Sven Hoefling, Martin Kamp, ... 658

Hybrid III-V Semiconductors/Silicon on Insulator Photonics Crystals Cavities for Ultrafast Switching and Memories
Fabrice Raineri, Alexandre Bazin, Paul Monnier, Isabelle Sagnes, Rama Raj, ... 659

Photonic Crystal Cavities for Optical Switching
Jesper Mork, Y. Yu, Mikkel Heuck, Philip T. Kristensen, K. Yvind, ... 660

Optical Delay in Silicon Photonic Crystals: Accelerating Slow Light
Daryl M. Beggs, Isabella H. Rey, Tobias Kampfrath, Nir Rotenberg, Laurens Kuipers, Thomas F. Krauss, ... 661

Optical Amplification Resulting from Two-level Population Inversion Using Photonic Crystals
Hiroyuki Takeda, ... 663

Tunnelling of Vacuum Fluctuations in a 3D Photonic Band Gap; Strongly Inhibited Spontaneous Emission
Elahe Yeganegi, Ad Lagendijk, Allard P. Mosk, Willem L. Vos, ... 664

Advanced Photonic Crystal Structures for Nano-scale Photonic Integrated Circuity
Imanol Andonegui, Isidro Calvo, Angel J. Garcia-Adeva, ... 666

Investigation of High- and Low-refractive-index-based Defect Cavities Formed in Three-dimensional Photonic Crystals
Mike P. C. Taverne, Ying-Lung Daniel Ho, X. Zheng, L. Chen, Martin Lopez Garcia, John G. Rarity, 667

Recent Progress in Photonic Crystals and Their Applications

Susumu Noda
Department of Electronic Science and Engineering, Kyoto University, Kyoto 615-8510, Japan

Abstract— I will report on the recent progresses in 2D and 3D photonic crystals, including 2D high-Q nanocavities-based new phenomena, novel lasers including ultra-compact Si Raman lasers, thermal emission control, and on-demand 3D optical guiding, etc.. In 2D photonic crystals, (1) high-Q nanocavity-based new phenomena, including strong coupling between distant nanocavities and its dynamic control [1], (2) ultra-compact Si Raman lasers [2], (3) new materials (SiC) [3–5] and their applications to nonlinear optical phenomena, (4) broad-area photonic crystal lasers with an ability of 1D and 2D beam scanning [6, 7] and (5) thermal emission control via simultaneous control of photonic and electronic states [8, 9] will be described.

In 3D photonic crystals, I will show that on-demand 3D optical guiding has now become possible [10], where horizontal and (slightly oblique) vertical waveguides including sophisticated bends have been successfully integrated, through which a clear 3D optical guiding has been observed.

Such progresses in 2D and 3D photonic crystals indicate that photonic crystal research has now entered much more advanced phases towards realization of ultimate control of photons.

REFERENCES

1. Sato, Y., Y. Tanaka, J. Upham, Y. Takahashi, T. Asano, and S. Noda, *Nature Photonics*, Vol. 6, 56, 2012.
2. Takahashi, Y., Y. Inue, M. Chihara, T. Asano, M. Terawaki, and S. Noda, unpublished.
3. Song, B. S., S. Yamada, T. Asano, and S. Noda, *Optics Exp.*, Vol. 19, 11084, 2011.
4. Yamada, S., B. S. Song, T. Asano, and S. Noda, *Optics Lett.*, Vol. 36, 3981, 2011.
5. Yamada, S., B. S. Song, T. Asano, and S. Noda, *Appl. Phys. Lett.*, Vol. 99, 201102, 2011.
6. Kurosaka, Y., S. Iwahashi, Y. Liang, K. Sakai, E. Miyai, W. Kunishi, D. Ohnishi, and S. Noda, *Nature Photonics*, Vol. 4, 447, 2011.
7. Iwahashi, S., T. Nobuoka, T. Okino, and S. Noda, unpublished.
8. Zoysa, M., T. Asano, K. Mochizuki, A. Oskooi, T. Inoue, and S. Noda, *Nature Photonics*, Vol. 6, 535, 2012.
9. Inoue, T., M. Zoysa, T. Asano, and S. Noda, *Appl. Phys. Lett.*, Vol. 102, 191110, 2013.
10. Ishizaki, K., M. Koumura, K. Gondaira, and S. Noda, *Nature Photonics*, Vol. 7, 133, 2013.

Cavity Quantum Electrodynamics with Three-dimensional (3D) Photonic Bandgap Crystals

Willem L. Vos[1] and Léon A. Woldering[2]

[1]Complex Photonic Systems (COPS), MESA+ Institute for Nanotechnology
University of Twente, AE Enschede 7500, The Netherlands
[2]Transducer Science and Technology (TST), MESA+ Institute for Nanotechnology
University of Twente, AE Enschede 7500, The Netherlands

Abstract— Three-dimensional (3D) photonic crystals with a 3D photonic bandgap play a fundamental role in cavity quantum electrodynamics (cQED). In the bandgap, the local density of optical states — equal to the density of vacuum fluctuations — is inhibited [1]. A photonic bandgap offers many prospects for new physics. First, an eagerly pursued phenomenon is the complete inhibition of spontaneous emission [2, 3]: an excited quantum emitter — atom, molecule, or quantum dot — with its transition frequency tuned to the 3D bandgap remains excited for a very long time [4], since it cannot emit a photon [5]. Any interaction mediated by vacuum fluctuations is affected by the 3D bandgap. Hence the gap will modify blackbody radiation, and affect dipole-dipole interactions including Förster resonant energy transfer that is prominent in biology and chemistry [6]. The radical suppression of optical modes in the bandgap is unique to photonic crystals, and is only limited by the crystal's extent.

Second, bandgap cQED physics becomes even richer by introducing point defects. Isolated resonances appear in the bandgap. Here the light is spatially localized within a tiny volume that is less than a cubic micron [7]. Such a photonic bandgap cavity is a true "nanobox for light". Since the density of states in a nanobox is enhanced, an embedded emitter experiences an enhanced emission rate: the Purcell effect.

Third when a gain medium is introduced in a nanobox, such a system promises a thresholdless laser [2, 3]. Only one resonance exists in a photonic bandgap cavity, and the vacuum is shielded, thus no competing spontaneous emission occurs into modes other than the lasing mode [8], and the laser quickly switches on [9].

Fourth, a main theme in cQED is the breaking of the weak coupling approximation. There are two main ways to break this limit: a well-known approach is to embed a two-level quantum emitter in a high-finesse cavity. When a quantum of energy is reversibly exchanged, the emitter and the cavity are in a coherent superposition, called QED strong coupling [10]. This limit has been realized with pillars, ring cavities, and 2D photonic crystal cavities, but not yet with nanoboxes. Other ways to break the weak-coupling limit are to operate close to a van Hove singularity, or to rapidly modulate the vacuum around the quantum emitter [11], using ultrafast all-optical switching [12].

Fifth, in quantum physics there is an active interest in decoherence, i.e., loss of coherence of a system that is in a quantum superposition. A consequence of decoherence is that a quantum system irreversibly becomes classical, which is undesired for quantum information processing [13]. An important component of decoherence in cQED corresponds to the escape or emission of photons [14]. Hence shielding of vacuum fluctuations by a 3D photonic bandgap offers opportunities to make optical quantum systems robust to decoherence. We will also give an overview of the current status regarding the fabrication of 3D photonic bandgap crystals [15–17], and discuss applications.

REFERENCES

1. John, S. and J. Wang, *Phys. Rev. Lett.*, Vol. 64, 2418–2421, 1990.
2. Bykov, V. P., *Sov. Phys. JETP*, Vol. 35, 269–273, 1972.
3. Yablonovitch, E., *Phys Rev. Lett.*, Vol. 58, 2059, 1987.
4. Leistikow, M. D., A. P. Mosk, E. Yeganegi, S. R. Huisman, A. Lagendijk, and W. L. Vos, *Phys. Rev. Lett.*, Vol. 107, 193903, 2011.
5. Ogawa, S., M. Imada, S. Yoshimoto, M. Okano, and S. Noda, *Science*, Vol. 305, 227–229, 2004.
6. Blum, C., N. Zijlstra, A. Lagendijk, M. Wubs, A. P. Mosk, V. Subramaniam, and W. L. Vos, *Phys. Rev. Lett.*, Vol. 109, 203601, 2012.
7. Joannopoulos, J. D., S. G. Johnson, J. N. Winn, and R. D. Meade, *Photonic Crystals: Modeling the Flow of Light*, Princeton University Press, Princeton, 2008.

8. Björk, G., A. Karlsson, and Y. Yamamoto, *Phys. Rev. A*, Vol. 50, 1675–1680, 1994.
9. Tandaechanurat, A., S. Ishida, D. Guimard, M. Nomura, S. Iwamoto, and Y. Arakawa, *Nature Photon.*, Vol. 5, 91–94, 2010.
10. Haroche, S., "Cavity quantum electrodynamics," *Fundamental Systems in Quantum Optics*, 767–940, North Holland, Amsterdam, 1992.
11. Lagendijk, A., "Vibrational relaxation studied with light," *Ultrashort Processes in Condensed Matter*, 197–238, Plenum, New York, 1993.
12. Euser, T. G., A. J. Molenaar, J. G. Fleming, B. Gralak, A. Polman, and W. L. Vos, *Phys. Rev. B*, Vol. 77, 115214:1–6, 2008.
13. Nielsen, M. A. and I. L. Chuang, *Quantum Computation and Quantum Information*, Cambridge University Press, 2000.
14. Mabuchi, H. and A. C. Doherty, *Science*, Vol. 298, 1372–1377, 2002.
15. Takahashi, S., K. Suzuki, M. Okano, M. Imada, T. Nakamori, Y. Ota, K. Ishizaki, and S. Noda, *Nature Mater.*, Vol. 8, 721–725, 2009.
16. Staude, I., M. Thiel, S. Essig, C. Wolff, K. Busch, G. von Freymann, and M. Wegener, *Opt. Lett.*, Vol. 35, 1094–1096, 2010.
17. Van den Broek, J. M., L. A. Woldering, R. W. Tjerkstra, F. B. Segerink, I. D. Setija, and W. L. Vos, *Adv. Func. Mater.*, Vol. 22, 25, 2012.

3D Photonic Crystals for Photon Management in Solar Cells

Ralf B. Wehrspohn[1, 2] and Alexander Sprafke[1]

[1]Institute of Physics, Martin-Luther-University Halle-Wittenberg, Halle 06120, Germany
[2]Institute for Mechanics of Materials, Fraunhofer IWM, Halle 06120, Germany

Abstract— Photon management is a key element to optimize the optical and electro-optical performance of solar cells. The potential of 3D photonic crystals for photon management in solar cells and the corresponding concepts are discussed.

Introduction: Photovoltaics comprise the most promising technologies for renewable and sustainable energy sources, especially in the context of protecting our environment, climate, and resources. Reducing the costs of photovoltaic systems is essential to accelerate the market launch and the distribution of this innovative technology. To notably reduce costs a significant increase of the conversion efficiency from solar to electrical energy is necessary.

A promising route to increase the conversion efficiency of a solar cell is to increase the absorption probability for the incoming photons and thus increasing the photocurrent density by an optical light path enhancement. Strategies to increase the optical light path by utilizing optical effects such as interference, light trapping, diffraction, and concentration are subsumed under the term photon management. Photon management can be implemented by the use of optical nanostructures, e.g., structured surfaces and photonic crystals. Here, we present optical concepts for light management, focusing on purely dielectric structures. After a short review of light trapping concepts, the potential of 3D photonic crystals [1, 2] for improved light trapping applications are presented.

Photonic Concepts for Photon Management in Solar Cells: The main goal of light trapping is to increase the optical light path inside the solar cell. Conventional light trapping designs are ususally non-resonant and range from simple back-side mirrors to light-randomizing surfaces, e.g., inverted pyramids or randomly textured interfaces.

Resonant structures, such as gratings, directionally change the incoming light due to their diffraction properties. Ideally, i.e., maximized light path enhancement, the diffracted light travels parallel to the solar cell surface.

Angular-selective structures for light-trapping use direction-selective filters which decrease the angle of acceptance of and the re-emission from the solar cell without any concentrating optics [4]. Combined with a two-axis tracking system this concept is also called ultra-light trapping.

Energy-selective structures for light trapping are applicable to serial-connected tandem solar cells. Intermediate reflective layers (IRL) have been suggested to modify the photon distribution to reduce the current mismatch between the cells [5]. Therefore, the IRLs have to be spectrally selective and matched to the optical properties of the adjacent top and bottom cell. Additionally, the IRLs need to be conductive to avoid ohmic losses.

3D Photonic Crystals for Photovoltaics: The combination of spectral and angular selectivity and diffractive effects lead to optical properties which make 3D photonic crystals attractive for photon management applications [6].

Placed on top of a solar cell, a 3D photonic crystal structure can act as a ultra-light trapping device. The structure should exhibit high transmission in the direction pointing to the sun so that the photons can reach the solar cell. In all other directions the structure should be opaque to prevent the escaping of light that was not absorbed. We present numerical calculations for model systems and give design rules for improved 3D photonic crystal ultra-light trapping.

3D photonic crystals, such as inverted opals, integrated between the top and the bottom cell of a tandem solar cell form a new category of IRLs since they combine reflective and diffractive properties simultaneously in one single functional layer. We show numerically and experimentally, that an increased efficiency is expected for 3D inverted opals compared to simple thin films or Bragg stacks [7, 8].

Placed on the backside of a solar cell, 3D photonic crystals allow to combine the effects of a back-side mirror and a grating with much higher flexibility than the linear combination of both. Promising concepts utilizing 3D photonic crystals as back reflectors have been suggested, but no experiments have been carried out for crystalline silicon solar cells yet.

Conclusion: Possible applications of 3D photonic crystals implementing photonic concepts for photon management have been discussed and numerical and experimental results have been

presented. In summary, 3D photonic crystals offer exciting opportunities to increase the efficiency of solar cells.

REFERENCES

1. Yablanovitch, E., "Inhibited spontaneous emission in solid-state physics and electronics," *Phys. Rev. Lett.*, Vol. 58, 2059, 1987.
2. John, S., "Strong localization of photons in certain disordered dielectric superlattices," *Phys. Rev. Lett.*, Vol. 58, 2486, 1987.
3. Yablanovitch, E. and G. D. Cody, "Intensity enhancement in textured optical sheets for solar cells," *IEEE Trans. Electron. Devices*, Vol. 29, 300, 1982.
4. Ulbrich, C., S. Fahr, J. Upping, M. Peters, T. Kirchartz, C. Rockstuhl, R. B. Wehrspohn, A. Gombart, F. lederer, and U. Rau, "Directional selectivity and ultra-light-trapping in solar cells," *Phys. Status Solidi A*, Vol. 205, 2831, 2008.
5. Yamamoto, K., et al., "Large area thin film Si module," *Sol. Energy Mater. Sol. Cells*, Vol. 74, 449, 2002.
6. Wehrspohn, R. B. and J. Upping, "3D photonic crystals for photon management in solar cells," *J. Opt.*, Vol. 14, 024003, 2012.
7. Bielawny, A., C. Rockstuhl, and R. B. Wehrspohn, "Intermediate reflectors for enhanced top cell performance in photovoltaic thin-film tandem cells," *Opt. Express*, Vol. 17, 8439, 2009.
8. Upping, J., et al., "Three-dimensional photonic crystal intermediate reflectors for enhanced light-trapping in tandem solar cells," *Adv. Mater.*, Vol. 23, 3896, 2011.

3D Photonic Crystals with Controlled Deterministic Aperiodic Disorder

Michael Renner, **Erik Waller**, **and Georg von Freymann**
Department of Physics and Research Center OPTIMAS
University of Kaiserslautern, 67663 Kaiserslautern, Germany

Abstract— Introducing disorder in a controlled way into photonic crystals allows studying the disorder-related change of the underlying transport mechanisms. Recently, controlled disorder has been introduced by mixing different ratios of spheres of different materials and assembling them into fcc opaline photonic crystals [1]. This leads to a random distribution of the defective sites.

Here, we introduce deterministic aperiodic disorder in woodpile photonic crystals. Deterministic aperiodic structures offer the possibility to reproducibly create specific potential landscapes whose Fourier components are determined by the underlying aperiodic sequence. In accordance with Lebesgues spectral theorem the Fibonacci, Thue-Morse and Rudin-Shapiro sequences are examples of the three basic spectral measures, namely pure-point, singularly-continuous and absolutely-continuous, respectively. Especially, the Rudin-Shapiro series is said to be indiscernible from randomly disordered samples concerning their diffraction patterns/properties [2]. Varying the structural parameters, i.e., filling fraction and lattice spacing, according to the aperiodic sequences allows us to introduce deterministic aperiodic disorder into the photonic crystals.

Samples are fabricated via direct laser writing in negative-tone photoresist. Using a dip-in lithography approach, samples of considerable height (> 70 unit cells) are prepared with constant high quality throughout the volume. Employing additionally a galvanometric scanning unit, large volumes can be filled, reducing writing times by about two orders of magnitude. After development the samples are characterized with reflectance and time-resolved transport measurements as well as with Laue diffraction. The different types of aperiodic disorder can clearly be discerned in the Laue diagrams. Results from the samples with deterministic aperiodic disorder are compared to such from randomly disordered samples.

REFERENCES

1. Garcia, P. D., et al., *Phys. Rev. A*, Vol. 84, 023813, 2011.
2. Baake, M. and U. Grimm, *J. Phys. Conf. Ser.*, Vol. 226, 012023, 2010.

Quantum Optical Devices Based on Photonic Crystal Nanocavities

Hisashi Sumikura[1,2], **Muhammad D. Birowosuto**[2], **and Masaya Notomi**[1,2]

[1]NTT Nanophotonics Center, Nippon Telegraph and Telephone Corporation, Japan
[2]NTT Basic Research Laboratories, Nippon Telegraph and Telephone Corporation, Japan

Abstract— We have demonstrated cavity-enhanced spontaneous emissions from a quantum dot and impurities in semiconductors. Photonic crystal nanocavities enable us to obtain a fast and efficient single photon emitter and a large emission enhancement of the impurities working as quantum bits. These devices are able to be the key of the optical devices in future quantum telecommunication networks.

The cavity-enhanced spontaneous emission, which is known as the Purcell effect, has long been studied on semiconductors because it is attractive in relation to the development of fast and efficient light emitting devices. Since the enhanced emission rate is proportional to the Q/V of the cavity (V is a mode volume), photonic crystal (PhC) nanocavities with a high Q and a small V are suitable to obtain a large emission enhancement. Here we have demonstrated the PhC-cavity-enhanced spontaneous emissions from an InAs quantum dot (QD) and radiative copper impurities in Si in terms of developing quantum optical devices.

For quantum key distribution on quantum telecommunication, single photon emitters are needed in telecom band wavelength around 1550 nm. Although few studies reported single photon emission in the telecom band, however their emission efficiency and operation speed are limited. In this study, we successfully fabricated InP PhC cavities embedding an InAs QD and observed cavity-enhanced single photon emission around 1550 nm for the first time [1]. This device shows fast (> 1 GHz) and bright single photon emission due to the Purcell effect and the high emission extraction efficiency of the PhC cavities. This result contributes to the realization of the high-speed and energy-efficient quantum telecommunication.

In addition, impurities doped in Si are promising candidates for quantum bits (qubits) because their long-lived spin can store bit information for a long time. However, the optical interaction is inefficient because the nonradiative Auger process is stronger than the radiative process of Si. Our study focused on the bright copper isoelectronic centers (Cu-IECs) as qubits, which are free from the Auger process. We developed a novel method for doping the Cu-IECs to Si PhC cavities and demonstrated the intense Cu-IEC emission enhanced by the PhC cavity [2]. The enhanced emission rate is $0.91\,\mathrm{ns}^{-1}$, which is 30 times larger than that in flat Si. This enhancement factor is largest in solid state systems. Our Si-based device suggests a quantum optical device compatible with Si photonics platforms.

ACKNOWLEDGMENT

We thank R. Nötzel, S. Matsuo and E. Kuramochi for their help in fabrication, and H. Taniyama for numerical simulation. This work is partially supported by the National Institute of Information and Communications Technology (NICT) in Japan.

REFERENCES

1. Birowosuto, M. D., H. Sumikura, S. Matsuo, H. Taniyama, P. J. van Veldhoven, R. Nötzel, and M. Notomi, "Fast Purcell-enhanced single photon source in 1550-nm telecom band from a resonant quantum dot-cavity coupling," *Sci. Rep.*, Vol. 2, 321, 2012.
2. Sumikura, H., E. Kuramochi, H. Taniyama, and M. Notomi, "Ultrafast spontaneous emission of copper-doped silicon enhanced by an optical nanocavity," in preparation.

Solid-state Cavity-QED in Quantum Dot-photonic Crystal Nanocavity Coupled Systems

Y. Arakawa[1,2], **S. Iwamoto**[1,2], **Y. Ota**[1,2], **and A. Tandaechanurat**[1,2]

[1]Institute for Nano Quantum Information Electronics, The University of Tokyo
4-6-1 Komaba, Meguro-ku, Tokyo 153-85-5, Japan
[2]Institute of Industrial Science, The University of Tokyo
4-6-1 Komaba, Meguro-ku, Tokyo 153-85-5, Japan

Abstract— Cavity quantum electrodynamics (cavity-QED) addresses the interaction of atom-like emitters with photons in cavities under the weak or the strong coupling regime, providing a platform for developing new concepts in light sources and quantum information processing devices. The strong coupling has been observed between single quantum dots [1] and high-quality semiconductor nanocavities. Recently, much effort has been devoted to development of high Q two-dimensional and three-dimensional photonic crystal nanocavities embedded with active quantum dots for investing the light-matter interaction in semiconductors [2–4]. In this presentation, we discuss our recent advances in the quantum dots-photonic crystal nanocavity coupled systems. These include the fabrication of high quality two-dimensional photonic crystal nanocavities ($Q > 50,000$), the generation of spontaneous two photon emission from a single quantum dot [2], and the realization of lasing oscillation with single quantum dot gain [5, 6]. We also report on an efficient intra-cavity frequency doubling to generate coherent visible light [7].

REFERENCES

1. Arakawa, Y. and H. Sakaki, *Appl. Phys. Lett.*, Vol. 40, 939, 1982.
2. Arakawa, Y., S. Iwamoto, M. Nomura, A. Tandaechanurat, and Y. Ota, *IEEE J. of Sel. Top. Quant. Electron.*, Vol. 18, 1818, 2012.
3. Ota, Y., S. Iwamoto, N. Kumagai, and Y. Arakawa, *Phys. Rev. Lett.*, Vol. 107, 233602, 2011.
4. Tandaechanurat, A., S. Ishida, D. Guimard, M. Nomura, S. Iwamoto, and Y. Arakawa, *Nature Photonics*, Vol. 5, 91, 2010.
5. Nomura, M., N. Kumagai, S. Iwamoto, Y. Ota, and Y. Arakawa, *Opt. Express*, Vol. 17, 15975, 2009.
6. Nomura, M., N. Kumagai, S. Iwamoto, Y. Ota, and Y. Arakawa, *Nature Physics*, Vol. 6, 279, 2010.
7. Ota, Y., S. Iwamoto, N. Kumagai, and Y. Arakawa, unpublished.

Photonic Crystals for Integrated Quantum Circuits

T. B. Hoang[1], **S. Fattahpoor**[1], **L. Midolo**[1], **D. Sahin**[1], **A. Fiore**[1], **A. Gaggero**[2], **F. Mattioli**[2], **R. Leoni**[2], **J. Beetz**[3], **M. Lermer**[3], **S. Höfling**[3], **and M. Kamp**[3]

[1]COBRA Research Institute, Eindhoven University of Technology
P. O. Box 513, 5600 MB Eindhoven, The Netherlands
[2]Istituto di Fotonica e Nanotecnologie (IFN), CNR, Via Cineto Romano 42, Rome 00156, Italy
[3]Technische Physik, Universität Würzburg, Würzburg 97074, Germany

Abstract— Quantum information processing (QIP) has become a major field of research since switching from classical to quantum bits will open up completely new possibilities in communication and computing. Research in QIP is going into different directions, e.g., quantum simulation, quantu computing or quantum cryptography. The latter allows a secure exchange of cryptographic keys and can be regarded as the first commercial application of QIP. Quantum cryptography makes use of single or entangled photons as quantum bits since they have a low decoherence and can be transmitted over wide distances. Up to now, most of the experiments that make use of single photons have been realized by bulky setups based on discrete components, either coupled via free-space transmission or by optical fibers. The realization of complex quantum circuits based on these approaches becomes increasingly difficult. Therefore, the integration of basic building blocks for the generation, manipulation and detection of single photons on a chip is required in order to advance the state-of-the-art of photonic QIP in both science and applications. While passive quantum circuits based on integrated optics have already been demonstrated, the integration of sources and detectors is far more challenging due to the very different requirements concerning materials and fabrication technology. The talk will present recent results on the use of photonic crystals (PhCs) in integrated quantum circuits.

On-chip single photon sources were realized using self-assembled quantum dots (QDs) in photonic crystal waveguides. Due to the size variation of the QDs, a tuning mechanism is required to match the emission wavelength of the dots with resonances of the PhC or that of other quantum dots. One possibility is to use the quantum confined Stark effect, which has allowed us to demonstrate widely tuneable waveguide single-photon sources. Further components required for on-chip quantum circuits are beam splitters, couplers and filters, which can also be realized with a small footprint using photonic crystals. For the sake of completeness, I'll also briefly discuss the integration of single-photon detectors based on NbN nanowires patterned onto GaAs/AlGaAs waveguides. This detector technology is fully compatible with single-photon sources described above.

ACKNOWLEDGMENT

This work was supported by the European Commission within the FP7 project QUANTIP, the state of Bavaria, the Dutch Technology Foundation STW, applied science division of NWO and the Technology Program of the Ministry of Economic Affairs.

Hybrid III-V Semiconductors/Silicon on Insulator Photonics Crystals Cavities for Ultrafast Switching and Memories

F. Raineri[1,2], A. Bazin[1], P. Monnier[1], I. Sagnes[1], and R. Raj[1]

[1]Laboratoire de Photonique et de Nanostructures, CNRS, Marcoussis 91460, France
[2]Université Paris Diderot, Paris Cedex 13, France

Abstract— Hybrid platforms combining semiconductor compounds with Silicon on Insulator (SOI), have a huge potential for photonic integration as they draw benefit from Si for CMOS compatibility and for fabricating ultra compact low loss optical circuitry and from III-V semiconductors for active devices. Within this context, the use of photonic crystals (PhC) should represent a disruptive solution in the drive towards low-power consuming nano circuitry. Indeed, these structures have shown for the last 10 years their great capacity to enhance light-matter interaction and have allowed impressive demonstration of low threshold and ultrafast laser emission [1], ultrafast switching [2] and memories [3]. This approach was recently implemented to obtain low threshold laser emission efficiently coupled into SOI waveguides [4].

In this presentation, we will show that InP-based PhC cavities heterogeneously integrated onto a SOI waveguide circuitry can be used to obtain optical memories and ultrafast all optical gates. The demonstrated optical memories rely on the bistability obtained in the regime of injection locking of a PhC quantum well (QW) nanolaser. These memories were demonstrated to exhibit memory time longer than 2 seconds with fast switching times (below 100 ps) and weak switching energies (1 fJ).

To obtain the ultrafast all optical gates, we optimised the nonlinear response of the III-V semiconductor through the manipulation of the carrier lifetime in InP-based materials by growing InGaAs QWs at the very surface of the heterostructure. Moreover the processing of these λ-scale structures induces irremediably the creation of defects at the etched interfaces which results in further reduction of the carrier lifetime. Ultrafast swtiching activated with low energy as low as 40 fJ, is demonstrated in InGaAs surface QW Photonic crystals on SOI. The recovery time of the switch is shown to be faster than 15 ps. These result allowed the demonstration of 20 GHz wavelength conversion using sub milliwatt peak powers.

REFERENCES

1. Matsuo, S., A. Shinya, T. Kakitsuka, K. Nozaki, T. Segawa, T. Sato, Y. Kawaguchi, and M. Notomi, "High-speed ultracompact buried heterostructure photonic-crystal laser with 13 fJ of energy consumed per bit transmitted," *Nature Photon.*, Vol. 4, 648–654, 2010.
2. Husko, C., A. De Rossi, S. Combrié, Q. Vy Tran, F. Raineri, and C. W. Wong, "Ultrafast all-optical modulation in GaAs photonic crystal cavities," *Appl. Phys. Lett.*, Vol. 94, 021111, 2009.
3. Nozaki, K., A. Shinya, S. Matsuo, Y. Suzaki, T. Segawa, T. Sato, Y. Kawaguchi, R. Takahashi, and M. Notomi, "Ultralow-power alloptical RAM based on nanocavities," *Nature Photon.*, Vol. 6, 248–252, 2012.
4. Halioua, Y., A. Bazin, P. Monnier, T. J. Karle, G. Roelkens, I. Sagnes, R. Raj, and F. Raineri, "Hybrid III-V semiconductor/silicon nanolasers," *Opt. Express*, Vol. 19, 9221–9231, 2011.

Photonic Crystal Cavities for Optical Switching

J. Mork, Y. Yu, M. Heuck, P. T. Kristensen, and K. Yvind
Technical University of Denmark, Kgs. Lyngby, Denmark

Abstract— A high-quality optical cavity can be realized by embedding a defect in a photonic crystal lattice, typically a membrane structure. The cavity can be excited via coupling to a (defect) waveguide and be used as the basis for all-optical switches and memories, as demonstrated in the literature. In this paper, we present theoretical and experimental results for different photonic crystal structures. We consider an InP membrane embedded in air and mainly focus on interactions due to Kerr effects and the dispersion of carriers excited by two-photon absorption. For modelling and design we use FDTD simulations in combination with coupled mode theory, exploiting perturbation results for the quasi-normal modes excited in the cavity.

In the presentation, four topics will be emphasized: (1) Energy-bandwidth trade-off and limitations to the switching speed due to patterning effects. (2) Use of Fano resonances for reducing the switching energy. A simple design enabling the realization of different Fano factors is suggested and demonstrated experimentally. The bandwidth-energy product is shown to be favourable for Fano structures as compared to standard Lorentzian filters. (3) Demonstration of a 4-port structure. A design for a 4-port structure is suggested and realized experimentally. This configuration allows to separate control and data signal for systems applications. (4) Proposal and analysis of a switch exploiting coherent control. It is shown that the switch can be operated in a regime where the switching speed is much faster than the cavity lifetime and the optimum excitation scheme minimizing the switching energy is identified.

Optical Delay in Silicon Photonic Crystals: Accelerating Slow Light

Daryl M. Beggs[1,3], **Isabella H. Rey**[2], **Tobias Kampfrath**[1], **Nir Rotenberg**[1], **L. Kuipers**[1], **and Thomas F. Krauss**[2]

[1]FOM Institute AMOLF, Science Park 104
Amsterdam 1098XG, The Netherlands
[2]School of Physics & Astronomy, University of St. Andrews
North Haugh, St. Andrews KY16 9SS, UK
[3]Centre for Quantum Photonics
University of Bristol, Bristol BS8 1TL, UK

Abstract— We demonstrate an ultrafast, continuously tuneable integrated delay line in silicon made-up entirely of a photonic crystal waveguide [1]. Whereas previous quasi-static examples have used the slow thermo-optic effect to tune the *waveguide* from the fast-light to the slow-light regime, we use an indirect photonic transition of the *pulse*, converting it from slow-light to fast-light, and offering the possibility of true bit-by-bit dynamic control of individual pulses. In analogy with indirect electronic transitions in semiconductors (where the simultaneous absorption of a photon and a phonon is needed to change both energy and momentum), an indirect photonic transition requires changes in both frequency and wavevector, which can be provided by a stimulus that involves temporal and spatial perturbations.

The indirect photonic transition is illustrated in Fig. 1. The delay line is a single 300 m long photonic crystal waveguide (Fig. 1(c)), with the red dispersion curve in Figs. 1(a) and (b). A signal pulse is loaded into the first 80 µm tuning section of the waveguide, where it undergoes adiabatic frequency conversion [2, 3]. This process is triggered by a pump pulse that decreases the refractive index of the waveguide material by $\Delta n = -7 \times 10^3$, providing the required dn/dt and shifting the dispersion of the tuning section to the blue line. The remaining 220 µm of the waveguide then acts as a dispersive medium, in that the speed of the pulse in this section depends on its final frequency after the adiabatic frequency conversion. The transition from pumped to unpumped regions provides the spatial modulation (dn/dx) needed for the horizontal transition (Fig. 1(a)) on the dispersion diagram.

Our delay line exploits the group velocity difference between initial and final states of this indirect transition, and we have demonstrated tuneable delays of up to 20 ps in a waveguide just 300 µm in length [1]. The delay of the light pulse can be continuously tuned by controlling the magnitude of the frequency shift via the pump power. Also, by controlling the delay of one pulse in a chain of two, we have shown bit-by-bit control of individual pulses is possible by exploiting our ultrafast approach. The scheme is fully compatible with silicon optoelectronics, as the required wavelength shift could also be produced by carrier injection/depletion, removing the need for an external pump laser. Hence, our integrated tuneable delay line provides an important missing piece of the

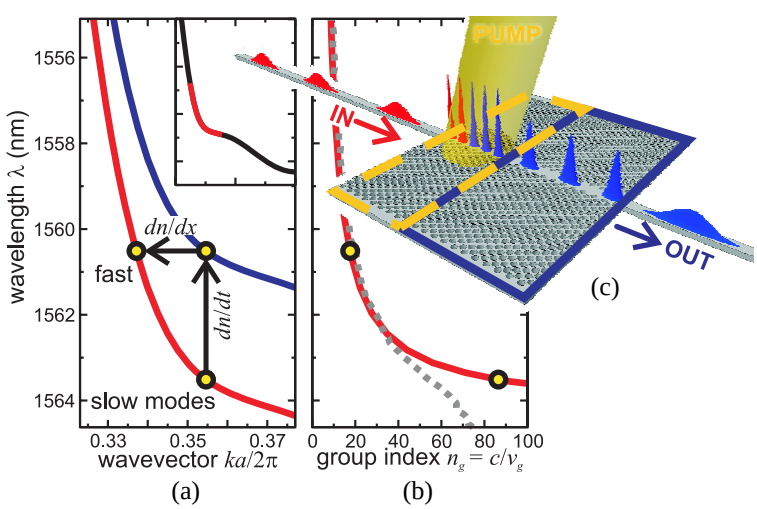

Figure 1.

silicon photonics puzzle, bringing the full implementation of all-optical networks on silicon chips a step closer towards reality.

REFERENCES

1. Beggs, D. M., et al., "Ultrafast tunable optical delay line based on indirect photonic transitions," *Phys. Rev. Lett.*, Vol. 108, 213901, 2012.
2. Kampfrath, T., et al., "Ultrafast adiabatic manipulation of slow light in a photonic crystal," *Phys. Rev. A*, Vol. 81, 043837, 2010.
3. Beggs, D. M., et al., "Ultrafast tilting of the dispersion of a photonic crystal and adiabatic spectral compression of light pulses," *Phys. Rev. Lett.*, Vol. 108, 033902, 2012.

Optical Amplification Resulting from Two-level Population Inversion Using Photonic Crystals

Hiroyuki Takeda
Photonic Materials Unit, National Institute for Materials Science (NIMS)
1-1 Namiki, Tsukuba, Ibaraki 305-0044, Japan

Abstract— Steady-state population inversion is generally considered impossible in two-level atoms. Therefore, three-level or four-level atoms are necessary. However, if two-level population inversion were possible to achieve, it might provide new applications for optical materials. From this scientific interest, a possibility of two-level population inversion has been discussed for a long time [1–4]. Photonic crystals composed of periodic dielectric materials are considered as powerful candidates to achieve two-level population inversion [1, 5].

In photonic crystals, electromagnetic local densities of states abruptly change near photonic band edges. Especially in photonic band gaps, they become very small, which enables the inhibition of spontaneous emission. When an external laser with the frequency ω_L is input to two-level atoms, there appear three frequency components ω_L and $\omega_L \pm 2\Omega$ (Mollow triplet) in radiative electromagnetic waves. It is assumed that two-level atoms are incorporated into photonic crystals, and that they are coherently excited by an external laser. When the contrast of electromagnetic local densities of states at $\omega = \omega_L \pm 2\Omega$ is very large, population inversion can be achieved by an external laser even in two-level atoms [2, 5].

After two-level population inversion is achieved by an external laser, another signal light is assumed to be input to photonic crystals with two-level atoms. Then, it is expected that the signal light is amplified. However, properties of optical amplification in two-level population inversion are very different from those in three-level or four-level one [6]. Although in three-level or four-level population inversion a pumping frequency has to be larger than an atomic transition frequency, in two-level population inversion this condition is not always necessary. Moreover, although in three-level or four-level population inversion optical amplification is obtained at the atomic transition frequency, in two-level population inversion it is obtained at two specific frequencies ($\omega = \omega_L \pm 2\Omega$). I show these properties in concrete geometries of optical materials by using the semiclassical Maxwell-Bloch theory [6].

REFERENCES

1. Lindberg, M. and C. M. Savage, "Steady-state two-level atomic population inversion via a quantized cavity field," *Phys. Rev. A*, Vol. 38, No. 10, 5182–5192, 1988.
2. John, S. and T. Quang, "Collective switching and inversion without fluctuation of two-level atoms in confined photonic systems," *Phys. Rev. Lett.*, Vol. 78, No. 10, 1888–1891, 1997.
3. Stace, T. M., A. C. Doherty, and S. D. Barrett, "Population inversion of a driven two-level system in a structureless bath," *Phys. Rev. Lett.*, Vol. 95, No. 10, 106801, 2005.
4. Hughes, S. and H. J. Carmichael, "Stationary inversion of a two level system coupled to an off-resonant cavity with strong dissipation," *Phys. Rev. Lett.*, Vol. 107, No. 19, 193601, 2011.
5. Florescu, M. and S. John, "Single-atom switching in photonic crystals," *Phys. Rev. A*, Vol. 64, No. 3, 033801, 2001.
6. Takeda, H., "All-optical modulation and amplification resulting from population inversion in two-level systems using a photonic-crystal cavity," *Phys. Rev. A*, Vol. 86, No. 1, 013803, 2012.

Tunnelling of Vacuum Fluctuations in a 3D Photonic Band Gap; Strongly Inhibited Spontaneous Emission

Elahe Yeganegi, Ad Lagendijk, Allard Mosk, and Willem Vos
Complex Photonic Systems (COPS), MESA + Institute for Nanotechnology
University of Twente, The Netherlands

Abstract— An infinite photonic band gap crystal provides an environment for a light source that is even quieter than vacuum [1, 2]. The complete absence of vacuum fluctuations can be interpreted as zero density of states and vice versa. It is well known that the characteristics of spontaneous emission of light depend strongly on the environment of the light source. According to quantum electrodynamics, the emission rate of a two-level quantum emitter as described by Fermi's "golden rule", is factorized into one part describing the emitter's properties and a second part describing the effect of the environment on the light field via the local density of optical state (LDOS). The radiative decay rate of the emitters is proportional to the local density of optical states (LDOS) [3]. In certain three-dimensional crystals, a frequency range exist for all polarizations for which light is not allowed to propagate in any direction, called the 3D photonic band gap [4, 5]: A frequency range where the density of vacuum fluctuations vanishes in an ideal infinitely large and perfect system. The absence of vacuum fluctuations leads to complete inhibition of the spontaneous emission.

While many great advances towards a band gap have been made, no complete inhibition has ever been observed to date. Recently, the very first study of spontaneous emission inside real 3D photonic band gap crystal has been done by our group [2, 6]. In our new experiments we have observed an inhibited emission of $18x$ at the frequency near the center of the band gap. The time-resolved decay curves show evidence for intriguing finite-size effects whereby vacuum fluctuations tunnel into the band gap.

Unfortunately, most theories assume crystals of infinite extent, where the inhibition in the band gap is also infinite, as vacuum fluctuations don't exist inside the crystal. Here we propose a model to calculate the local density of states (LDOS) in the band gap of a finite photonic crystal based on tunneling of the vacuum fluctuations into the crystal. We test our model for one-dimensional situations where direct analytic calculations exist for direct model verifications. This model helps to interpret spontaneous emission rates measured in a finite photonic band gap crystal based on tunneling of vacuum fluctuation in a 3D photonic band gap.

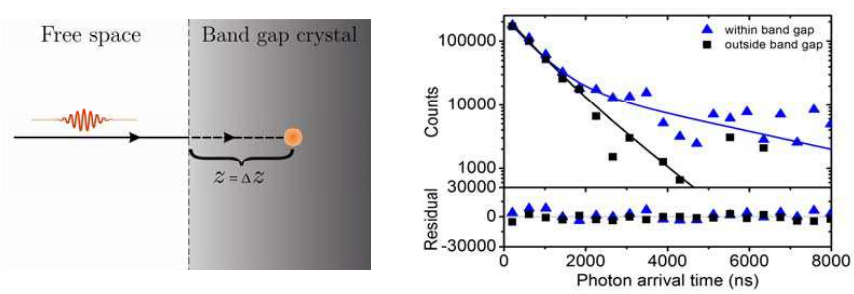

(a) (b)

Figure 1: (a) Schematic drawing of a light source (orange sphere) embedded in a semi-infinite 1D photonic band gap crystal. The source is located at a depth $z = \Delta z$. The interface between the crystal and free space is indicated by the vertical dashed line. The red pulse represents vacuum fluctuations in free space. (b) Time resolved emission measured on PbS quantum dots in the photonic crystal outside the band gap (black squares), and inside the band gap (blue triangles) showing an inhibited emission rate.

REFERENCES

1. Yablonovitch, E., "Inhibited spontaneous emission in solid-state physics and electronics," *Phys. Rev. Lett.*, Vol. 58, 2059, 1987.

2. Leistikow, M. L., A. P. Mosk, E. Yeganegi, S. R. Huisman, A. Lagendijk, and W. L. Vos, "Inhibited spontaneous emission of quantum dots observed in a 3D photonic band gap," *Phys. Rev. Lett.*, Vol. 107, 193903, 2011.
3. Vats, N., S. John, and K. Butch, "Theory of fluorescence in photonic crystals," *Phys. Rev. A*, Vol. 65, 043808, 2002.
4. Busch, K. and S. John, "Photonic band gap formation in certain self-organizing systems," *Phys. Rev. E*, Vol. 58, 3896, 1998.
5. Joannopoulos, J. D., S. G. Johnson, J. N. Winn, and R. D. Meade, *Photonic Crystals: Modeling the Flow of Light*, 2nd Edition, Princeton University Press, Princeton, 2008.
6. Van den Broek, J. M., L. A. Woldering, R. W. Tjerkstra, F. B. Segerink, I. D. Setija, and W. L. Vos, "Inverse-woodpile photonic band gap crystals with a cubic diamond-like structure made from single-crystalline silicon," *Adv. Func. Mater.*, Vol. 22, 25–31, 2012.

Advanced Photonic Crystal Structures for Nano-scale Photonic Integrated Circuity

Imanol Andonegui[1], **Isidro Calvo**[2], **and Angel J. Garcia-Adeva**[1]

[1]Departamento de Fisica Aplicada I, E.T.S. Ingenieria de Bilbao
Universidad del Pais Vasco (UPV/EHU), Alda. Urquijo s/n, Bilbao 48013, Spain
[2]Departamento de Ingenieria de Sistemas y Automatica, E.U. Ingenieria Tecnica de Vitoria
Universidad del Pais Vasco (UPV/EHU), C/Nieves Cano 12, Vitoria 01006, Spain

Abstract— Photonic crystals (PC) have generated a surge of interest in the last decades as they offer the possibility to control the propagation of light to an unprecedented level. The prospect of attaining a fully functional photonic device that tackles light propagation in subwavelength scale requires breaking the spatial symmetry of PCs. However, novel designs on aperiodic PC clusters entails dealing with several correlated parameters. Moreover, investigating all feasible combinations of structural parameters for a particular application demands a lot of computational effort, which scales exponentially with the number of parameters. Currently, the process of designing a PC structure that complies with one or many conflicting objectives is strongly based on intuition, rather than on a rigorous mathematical technique, which usually yields to non-optimum scenarios. We found that global optimization heuristic and evolutionary algorithms are very well suited to deal with this problem. They provide a global optimum for one or various functional objectives at a reasonable computational cost. The results obtained by these methods clearly outperform intuitive design procedures and trial-and-error based models. We illustrate this by using a series of inverse-designed practical photonic devices, such as, an abrupt and short stage of broadband PC waveguide tapers, sharp PC waveguide bends, broadband PC beam splitters and Y-junctions, hih-Q PC resonant cavities, and reduced modal volume and compact PC multiplexers, among others.

Investigation of High- and Low-refractive-index-based Defect Cavities Formed in Three-dimensional Photonic Crystals

M. P. C. Taverne, Y.-L. D. Ho, X. Zheng, L. Chen, M. L. Garcia, and J. G. Rarity
Centre for Communications Research, Department of Electrical and Electronics Engineering
University of Bristol, UK

Abstract— The confinement of light in one-dimensional (1D) and two-dimensional (2D) systems is always partly reliant on total internal reflection at a low refractive index boundary, hence a key loss component is out-of-waveguide scattering. Fabricated structures often show much lower Q-factors than predicted in theory because of surface scattering and the difficulties of trapping of light in low refractive index defects. Hence, we are investigating a system where these losses are almost fully suppressed because the cavity is fabricated in a structure with a full three-dimensional (3D) bandgap at the resonant frequency. Furthermore, recent results on the implementation of slot-waveguides and air hole photonic-crystal fiber have inspired us to take a new approach for low refractive index guiding and trapping of light in 3D nanostructures.

The design and simulation of these 3D structures uses off the shelf software [MIT Photonic-Bands (MPB)] and our in house finite-difference time-domain (FDTD) software. We report results obtained from models of nanocavities in woodpile structures showing full photonic bandgaps. As these structures are inside full bandgap materials we expect to be able to trap light in both high- and low-refractive-index-based defect cavities. For high-index based defect cavities in three-dimensional (3D) woodpile photonic crystal lattices, we show a high-Q factor of $7 * 10^5$ and a modal volume V of $1.29 * (\lambda/(2n))^3$ for a cubic defect of size $(0.5, 0.5, 0.25) * a$ where "a" is the vertical period. In present simulations we are looking at results from low-index based cavities, i.e., where the defect and woodpile have a lower index than the backfill material. We will also present the fabrication of woodpile photonic crystals containing defects using a direct laser writing (DLW) system and preliminary optical characterization using Fourier Image Spectroscopy technique, which is based on the observation of the spatial optical Fourier transform response of the structures.

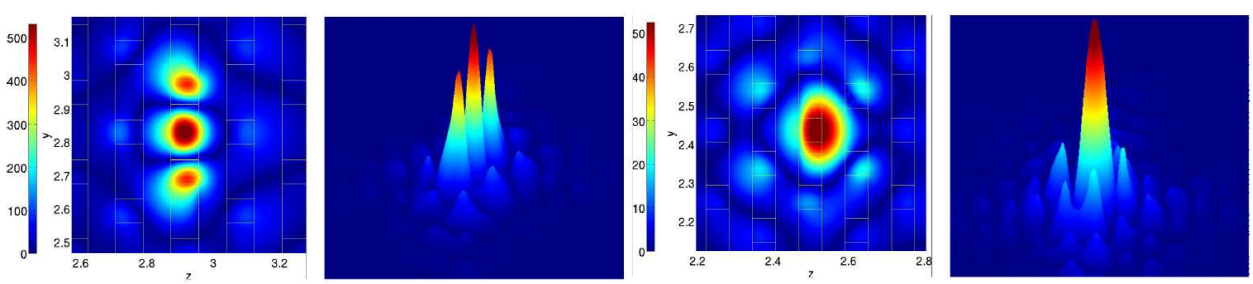

Figure 1: Frequency snapshots of $|Ex|$ in the central X plane for (a), (b) a high-index defect-based cavity and (c), (d) a low-index defect-based cavity. Both correspond to a defect of size $(0.5, 0.5, 0.25) * a$.

The ultimate goal is the simulation and eventual fabrication of a high-Q nanocavity containing a two-level 'atom' showing strong coupling with the electromagnetic field. This can be used to implement efficient single photon sources, ultra-low power optical switches and quantum memory based on spin [3].

REFERENCES

1. Ho, Y.-L. D., et al., "FDTD simulation of inverse three-dimensional face-centered cubic photonic crystal cavities," *IEEE J. Quantum Electron.*, Vol. 47, 1480–1492, 2011.
2. Ho, Y.-L. D., et al., "Modelling, fabrication and measurement of 3-D photonic crystal defect layer in woodpile structures," *Photonics Photon*, Vol. 12, Durham, UK, September 3–6, 2012.
3. Hu, C. Y., et al., "Loss-resistant state teleportation and entanglement swapping using a quantumdot spin in an optical microcavity," *Phys. Rev. B*, Vol. 47, 115303, 2011.

Session 2P2
4_FocusSession.SC4&3: Quantum Bits and Entanglement at Microwave Frequencies

Exploring Quantum Properties of Propagating Microwave Photons
Andreas Wallraff, ... 670

The Josephson Mixer, a Swiss Army Knife for Microwave Quantum Optics
E. Flurin, N. Roch, Francois Mallet, Michel H. Devoret, Benjamin Huard, ... 671

Controlling the Trajectory of a Superconducting Qubit by Measurement Based Feedback
P. Campagne-Ibarcq, E. Flurin, N. Roch, D. Darson, P. Morfin, M. Mirrahimi, Michel H. Devoret, Francois Mallet, Benjamin Huard, ... 672

Scattering of Photons and Limits of Ultrastrong Light-matter Coupling in Open Transmission Lines
B. Peropadre, D. Zueco, Juan Jose Garcia-Ripoll, ... 673

Quantum Optics with Microwave Photons in Superconducting Circuits
Per Delsing, ... 674

Nonclassical Photon Pair Production in a Voltage-biased Josephson Junction
Olivier Parlavecchio, Max Hofheinz, Carles Altimiras, Patrice Roche, Patrice Bertet, Denis Vion, Philippe Joyez, Daniel Esteve, Fabien Portier, ... 675

Simulation of Motional Averaging with a Superconducting Circuit
Jian Li, Matti P. Silveri, K. S. Kumar, J.-M. Pirkkalainen, Antti Vepsalainen, W. C. Chien, Jani Tuorila, Mika A. Sillanpaa, Pertti J. Hakonen, Erkki V. Thuneberg, Gheorghe Sorin Paraoanu, 676

Microwave Photon Detection Based on the Cross-Kerr Effect
Goran Johansson, ... 677

Giant Cross-Kerr Effect for Propagating Microwaves Induced by an Artificial Atom
Io-Chun Hoi, Anton F. Kockum, Tauno Palomaki, Thomas M. Stace, Bixuan Fan, Lars Tornberg, Sankar R. Sathyamoorthy, Goran Johansson, Per Delsing, C. M. Wilson, ... 678

Quantum Deformed Richardson-Gaudin Model
Petr Kulish, Alexander Stolin, H. Johanesson, ... 679

Entanglement Sudden Death for a Two-particle Gaussian State
Tony C. Dorlas, A. Guesquiere, ... 680

Ultrafast Quantum Nondemolition Measurement Based on two Inductively Coupled Transmons
Etienne Dumur, Igor Diniz, Alexey Feofanov, Thomas Weissl, Bruno Kung, Cecile Naud, Olivier Buisson, Wiebke Guichard, Alexia Auffeves, ... 681

Generation of Non-classical Electromagnetic Fields by Magnetic-dipolar-mode Ferrite Particles
Eugene O. Kamenetskii, ... 683

Proton Beam Induction of Quantum Correlations in Silicon Nanocrystal
Vesna I. Berec, ... 684

Parametric Resonance in Tunable Superconducting Cavities
Waltraut Wustmann, Vitaly Shumeiko, ... 685

Exploring Quantum Properties of Propagating Microwave Photons

Andreas Wallraff
ETH Zurich, Zurich, Switzerland

Abstract— Using modern micro and nano-fabrication techniques combined with superconducting materials we realize quantum electronic circuits in which we create, store, and manipulate individual microwave photons. The strong interaction of photons with superconducting quantum two-level systems allows us to probe fundamental quantum effects of microwave radiation and also to develop components for applications in quantum technology. Previously we have realized on-demand single photon sources which we have characterized using correlation function measurements [1] and full quantum state tomography [2]. For this purpose we have developed efficient methods to separate the quantum signals of interest from the noise added by the linear amplifiers used for quadrature amplitude detection [3]. We now regularly employ superconducting parametric amplifiers [4] to perform nearly quantum limited detection of propagating electromagnetic fields. These enable us to probe the entanglement which we generate on demand between stationary qubits and microwave photons freely propagating down a transmission line [5]. Using two independent microwave single photon sources, we have recently performed Hong-Ou-Mandel experiments at microwave frequencies [6] and have probed the coherence of two-mode multi-photon states at the out-put of the beam-splitter. The non-local nature of such states may prove to be useful for distributing entanglement in future small-scale quantum networks.

REFERENCES

1. Bozyigit, D., et al., *Nat. Phys.*, Vol. 7, 154, 2011.
2. Eichler, C., et al., *Phys. Rev. Lett.*, Vol. 106, 220503, 2011.
3. Eichler, C., et al., *Phys. Rev. A*, Vol. 86, 032106, 2012.
4. Eichler, C., et al., *Phys. Rev. Lett.*, Vol. 107, 113601, 2011.
5. Eichler, C., et al., *Phys. Rev. Lett.*, Vol. 109, 240501, 2012.

The Josephson Mixer, a Swiss Army Knife for Microwave Quantum Optics

E. Flurin[1], **N. Roch**[1], **F. Mallet**[1], **M. H. Devoret**[2,3], **and B. Huard**[1]

[1]Laboratoire Pierre Aigrain, Ecole Normale Supérieure, CNRS (UMR 8551), Université P. et M. Curie
Université D. Diderot, 24, Rue Lhomond, 75231, Paris Cedex 05, France
[2]Collège de France, 11 Place Marcelin Berthelot, F-75231, Paris Cedex 05, France
[3]Department of Applied Physics, Yale University
P. O. Box 208284, New Haven, Connecticut 06520-8284, USA

Abstract— The possibility to couple various mesoscopic systems to microwave signals and the availability of high performance microwave instruments make microwave quantum optics a very promising component for future quantum machines. In this talk, I will present how the Josephson mixer can fill several roles in the toolbox of microwave quantum optics. When the pump tone is the sum of the two other mode frequencies, it acts as a phase-preserving quantum limited amplifier. When only vacuum fluctuations feed its two ports, it produces Einstein-Podolsky-Rosen (EPR) states of microwave light shared over two transmission lines at arbitrarily separated mode frequencies. Using a noise-interferometric experiment, we were able to demonstrate a production rate of more than 6 millions entangled bits per second, comparable to current achievements in optics. When the pump tone is the difference of the two other mode frequencies, it acts as a dissipationless up or down-converter for microwave signals. Coupling the mixer to an isolated resonator on one port, we were able to make a quantum memory for microwaves. The memory can hold a quantum signal as long as the internal losses of the resonator permit and can be written and read on-demand at a rate given by half that of the other port's coupling.

Controlling the Trajectory of a Superconducting Qubit by Measurement Based Feedback

P. Campagne-Ibarcq[1], E. Flurin[1], N. Roch[1], D. Darson[1], P. Morfin[1], M. Mirrahimi[2], M. H. Devoret[3], F. Mallet[1], and B. Huard[1]

[1]Laboratoire Pierre Aigrain, Ecole Normale Superieure, CNRS (UMR 8551)
24, rue Lhomond, 75231, Paris Cedex 05, France
[2]INRIA Rocquencourt, France
[3]College de France and Yale University, New Haven, Connecticut, USA

Abstract— The mere observation of the state of a quantum object in time modifies its trajectory. The control of the state of a qubit hence abides by different rules than for its classical counterpart. In measurement based feedback, an observer acquires information about the state of the qubit in a non-destructive manner, and optimally corrects for its deviations from a targeted trajectory. In the case of a projective measurement using appropriate pointer states, the measurement itself helps correcting the trajectory. The remaining randomness in the measurement outcome leads non-deterministically to quantum jumps into undesired states. A conditional manipulation of the qubit allows to switch it back to the desired state.

In this talk, I will present an experiment on a superconducting qubit in cavity, the 3-dimensional transmon, in which we were able to measure and manipulate conditionally the qubit in much less than its relaxation and coherence times. Three feedback schemes are demonstrated. One is based on a strong readout of the qubit, followed by a quick reset conditioned by the measurement result. It allowed us to cool down the qubit by lowering the first excited state occupation down to a fraction of a percent. Symmetrically, this scheme can be used to stabilize the excited state. A second scheme consists in driving Rabi oscillations using a coherent field tuned at the qubit transition frequency, and read out its state strongly every half a period. Quantum Zeno effect then locks the Rabi oscillations on the readout periodicity. In case a measurement reveals an undesired quantum jump (mostly due to relaxation), the setup reacts by applying a fast π-pulse to the qubit, putting it back to the targeted position on the Bloch sphere. Thus, we can stabilize permanently Rabi oscillations with contrast greater than 70%. Finally, we were able to stabilize Ramsey fringes using a similar scheme including $\pi/2$-pulses in order to effectively measure the qubit along σ_X instead of σ_Z in the Bloch sphere. This set of trajectory stabilizations using digital processing offers great promise for more elaborate quantum control procedures.

Scattering of Photons and Limits of Ultrastrong Light-matter Coupling in Open Transmission Lines

B. Peropadre[1], **D. Zueco**[2], **and J. J. García-Ripoll**[1]

[1]Instituto de Física Fundamental, CSIC, Spain
[2]ICMA-Unizar, Spain

Abstract— We discuss, using new and non-perturbative models, the limits of interaction strength between propagating photons and flux qubits. We show that the deep ultrastrong light-matter coupling can be achieved using *ordinary* transmission lines using *ordinary* flux qubits. We also show that it is possible to model the qubit-photon interaction using the tools of Matrix Product States, and present results on the scattering of photons by ultrastrongly coupled qubits.

The most interesting advantage of superconducting circuits is the possibility of achieving the strongest qubit-photon couplings in the field of quantum information processing. This fact was suggested theoretically [1], with initial experimental demonstrations using flux qubits [2, 3].

We have developed a different way to quantize a flux qubit which is galvanically coupled to an open transmission line. Without any perturbative approximation, we derive the qubit-photon coupling numerically, demonstrating that the ultrastrong and deep ultrastrong couplings are within reach already for three-junction qubits.

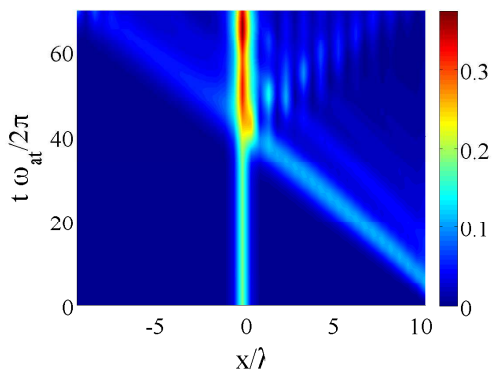

Figure 1: A single photon of wavelength λ is emitted from a qubit with frequency $\omega := 1$ at $x = 10/\lambda$ and scattered ultrastrongly by a similar qubit at $x = 0$.

Using the numbers from these simulations we have studied the dynamics of two ultrastrongly coupled qubit with propagating photons in an open transmission line. We can study the entanglement properties and scattering properties of the qubits using the tools of Matrix Product States [4].

ACKNOWLEDGMENT

B.P. and J.J.G.R. acknowledge support from the Spanish MINECO Project FIS2012-33022, from the European project PROMISCE and from the CAM research consortium QUITEMAD S2009-ESP-1594.

REFERENCES

1. Bourassa, J., et al., "Ultrastrong coupling regime of cavity QED with phase-biased flux qubits," *Phys. Rev. A*, Vol. 80, No. 3, 032109, 2009.
2. Niemczyk, T., et al., "Circuit quantum electrodynamics in the ultrastrong-coupling regime," *Nat. Phys.*, Vol. 6, No. 10, 772–776, 2010.
3. Forn-Díaz, P., et al., "Observation of the Bloch-Siegert shift in a qubit-oscillator system in the ultrastrong coupling regime," *Phys. Rev. Lett.*, Vol. 105, No. 23, 237001, 2010.
4. Garcia-Ripoll, J. J., "Time evolution algorithms for matrix product states and DMRG," *New J. Phys.*, Vol. 8, 305, 2006.

Quantum Optics with Microwave Photons in Superconducting Circuits

P. Delsing
Chalmers University of Technology, S-41296 Göteborg, Sweden

Abstract— We study an artificial 3 level atom in the form of a transmon qubit coupled to superconducting 1D transmission line [1]. Strong interaction between the artificial atom and photons is revealed in the reflection of propagating microwaves and substantial extinction (99.6%) of the transmission has been observed. A strong control pulse, at the frequency corresponding to the transition between the two upper states, is used to route a weak probe tone at lower transition frequency. The maximum on-off ratio is 99% with a rise and fall time on the order of 10 ns. This fast controllable router provides a fundamental building block for quantum optics on chip. The radiation reflected from the artificial atom can be shown to be non-classical, we observe clear antibunching of the reflected signal and superbunching in the transmitted signal [2]. The artificial atom also displays a very strong cross Kerr effect. With a probe signal tuned to the 0–1 transition and a control signal tuned to the 1–2 transition (both signals at the signal photon level) we observe a cross Kerr effect of up to 25 degrees/photon.

REFERENCES

1. Hoi, I.-C., et al., *Physical Review Letters*, Vol. 107, 073601, 2011.
2. Hoi, I.-C., et al., *Physical Review Letters*, Vol. 108, 263601, 2012.
3. Hoi, I.-C., et al., Arxiv 1207.1203, 2012.

Nonclassical Photon Pair Production in a Voltage-biased Josephson Junction

Olivier Parlavecchio[1], **Max Hofheinz**[2], **Carles Altimiras**[1,3], **Patrice Roche**[1], **Patrice Bertet**[1], **Denis Vion**[1], **Philippe Joyez**[1], **Daniel Esteve**[1], **and Fabien Portier**[1]

[1]SPEC-IRAMIS-DSM-CEA Saclay, CNRS/MPPU/URA 2464, 91191 Gif sur Yvette Cedex, France
[2]SPSMS-INAC-DSM-CEA, 17 rue des Martyrs, 38054 Grenoble Cedex 9, France
[3]Laboratorio NEST, Istituto Nanoscienze CNR & Scuola Normale Superiore di Pisa, Italy

Abstract— The dynamical Coulomb blockade (DCB) of tunnelling is a quantum phenomenon in which tunneling of charge through a small tunnel junction is modified by its electromagnetic environment [1]. The sudden charge transfer associated with tunneling generates photons in the electromagnetic modes of the environment. In a normal metal tunnel junction, biased at voltage V, the energy eV of a tunnelling electron can be dissipated both into quasiparticle excitations in the electrodes and into photons. At low temperature energy conservation forbids tunneling processes emitting photons with total energy higher than eV, which reduces the conductance at low bias voltage [1]. In a Josephson junction, DCB effects are more prominent since at bias voltages smaller than the gap voltage $2\Delta/e$ quasiparticle excitations cannot take away energy and the entire energy of tunneling Cooper pairs has to be transformed into photons in the impedance for a dc current to flow through the junction [1]. We have recently observed and characterized the radiation associated to the flow of Cooper pair connected to a microwave resonator [2]. Our new experiment can be schematically represented by Fig. 1: A Josephson junction is placed between two microwave resonators and voltage biased at voltage V, such that $2eV = hv_1 + hv_2$. The tunnelling of a Cooper pair is then associated to the emission of one photon into each of the resonators. Our setup routes the photons leaking out of each resonators into a separate microwave amplifier, allowing to detect and analyse the emitted radiation at room temperature. It has recently been shown by Leppagänkas [3] and co-workers that the radiation emitted by these two photon-processes is non classical, and that it violates a classical Cauchy-Schwarz inequality for two mode power cross-correlated fluctuations. The basic idea is that the probability of emitting a photon in each of the resonators during the observation time τ is higher that the geometric mean of the probability of emitting two photons in either one of them. Preliminary measurements suggest that this is the case, and we will report on our experimental investigations of this effect.

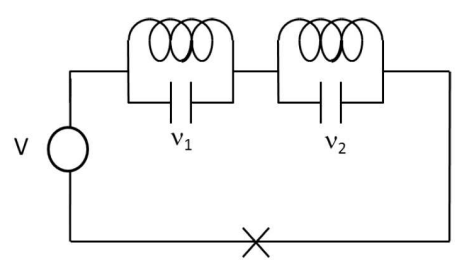

Figure 1: Principle of the experiment: A Josephson junction is embedded within two microwave resonators of frequency v_1, v_2. If the junction is voltage biased at voltage $2eV = hv_1 + hv_2$, Cooper pairs can flow through the junctions, emitting photons in the two resonators via a non classical process.

REFERENCES

1. Ingold, G.-L. and Y. V. Nazarov, *Single Charge Tunneling*, edited by H. Grabert and M. H. Devoret, Plenum, New York, 1992.
2. Hofheinz, M., F. Portier, Q. Baudouin, P. Joyez, D. Vion, P. Bertet, P. Roche, and D. Esteve, *Phys. Rev. Lett.*, Vol. 106, 217005, 2011.
3. Leppäkangas, J., G. Johansson, M. Marthaler, and M. Fogelström, arXiv:1210.6276, 2012.

Simulation of Motional Averaging with a Superconducting Circuit

J. Li[1], **M. P. Silveri**[2], **K. S. Kumar**[1], **J.-M. Pirkkalainen**[1], **A. Vepsäläinen**[1], **W. C. Chien**[3], **J. Tuorila**[2], **M. A. Sillanpää**[4], **P. J. Hakonen**[1], **E. V. Thuneberg**[2], **and G. S. Paraoanu**[1]

[1]O. V. Lounasmaa Laboratory, Aalto University, P. O. Box 15100, Aalto FI-00076, Finland
[2]Department of Physics, University of Oulu, P. O. Box 3000, FI-90014, Finland
[3]Department of Physics, National Chung Hsing University
250 Kuo Kuang Road, Taichung 40227, Taiwan
[4]Department of Applied Physics, Aalto University, Aalto FI-00076, Finland

Abstract— We consider a superconducting circuit consisting of a capacitively-shunted charge qubit (a transmon) embedded in a superconducting waveguide resonator. Two microwave fields are applied to the system: one, at the frequency of the resonator, is used for measurement, while the other, around the Larmor frequency of the qubit, is used to drive the qubit. In addition, the qubit frequency is modulated by a random telegraph noise with externally-controlled amplitude and characteristic jumping frequency. Surprisingly, by adding noise in this way a new, "motional averaged" spectral line is formed with a linewidth smaller than the amplitude of the random modulation [1]. We have also succeeded in driving Rabi oscillations on the motional averaged line, demonstrating the formation of hybrid states of the transmon and modulation field, with transitions that can be coherently driven.

When modulating the system sinusoidally, we observe a rich spectral structure, resembling a Landau-Zener interference pattern. However, direct Landau-Zener transitions are prohibited in our system by the fact that the frequency of the modulation is much smaller than the energy level separation. We show that in this case the transitions occur through the absorption of photons from the driving field; we call this process "photon-assisted Landau-Zener effect".

For the values of the fields used in our experiment we show that, in a rotating frame, the system reaches the ultrastrong coupling regime. Our setup can also be seen as the simulation of the effect of coupling an externally-controlled fluctuation to a qubit. We anticipate that the experimental demonstration of motional averaging presented in this work will provide a novel route to improving the dephasing times of existing superconducting qubits.

REFERENCES

1. Li, J., M. P. Silveri, K. S. Kumar, J.-M. Pirkkalainen, A. Vepsäläinen, W. C. Chien, J. Tuorila, M. A. Sillanpää, P. J. Hakonen, E. V. Thuneberg, and G. S. Paraoanu, "Motional averaging in a superconducting qubit," *Nat. Commun.*, Vol. 4, 1420, 2013.

Microwave Photon Detection Based on the Cross-Kerr Effect

G. Johansson
Department of Microtechnology and Nanoscience — MC2, Chalmers University of Technology
S-41296 Göteborg, Sweden

Abstract— In recent years, the field of circuit quantum electrodynamics (circuit QED) has become one of the most promising platforms in the study of light-matter interaction. Within circuit QED, there is now growing interest in studying propagating fields interacting with artificial atoms. Theoretically, coherent coupling between an atom or superconducting qubit and a one-dimensional continuum of modes has been discussed for some time [1], and there exist now a growing number of experiments investigating this system in a circuit QED setup [1].

The cross-Kerr effect, whereby the phase of one field is changed proportional to the intensity of another, arises from the nonlinear response of an atomic medium to applied fields. It is usually described phenomenologically in terms of a third order term in the nonlinear polarizability, a description that is valid when the applied fields are strong and absorption is weak. In particular, the cross-Kerr has been suggested as a mechanism for nondemolition photon measurements.

The very strong nonlinearities achievable in circuit QED leads to a giant cross-Kerr effect also for a single artificial atom, which was recently demonstrated experimentally [2]. This system is thus a promising candidate for the realization of a microwave photon detector. However, a careful analysis leads to the conclusion that single-photon sensitivity cannot be reached straightforwardly in this setup [3]. I will discuss this limitation, which holds under quite general conditions. I will also discuss the possibility to find alternative routes, to still approach the quantum limit [4].

REFERENCES

1. Peropadre, B., J. Lindkvist, I.-C. Hoi, C. M. Wilson, J. J. Garcia-Ripoll, P. Delsing, and G. Johansson, "Scattering of coherent states on a single artificial atom," *New Journal of Physics*, Vol. 15, 035009, 2013.
2. Hoi, I.-C., C. M. Wilson, G. Johansson, T. Palomaki, T. M. Stace, B. Fan, and P. Delsing, "Giant cross Kerr effect for propagating microwaves induced by an artificial atom," e-print arXiv:1207.1203
3. Fan, B., A. F. Kockum, J. Combes, G. Johansson, I.-C. Hoi, C. Wilson, P. Delsing, G. J. Milburn, and T. M. Stace, "Breakdown of the cross-Kerr scheme for photon counting," *Physical Review Letters*, Vol. 110, 053601, 2013.
4. Sathyamoorthy, S. R., "Quantum non-demolition detection of propagating microwave photons," MSc thesis, Chalmers University of Technology, Gothenburg, Sweden, 2012.

Giant Cross-Kerr Effect for Propagating Microwaves Induced by an Artificial Atom

Io-Chun Hoi[1], **Anton F. Kockum**[1], **Tauno Palomaki**[1], **Thomas M. Stace**[2], **Bixuan Fan**[2], **Lars Tornberg**[1], **Sankar R. Sathyamoorthy**[1], **Göran Johansson**[1], **Per Delsing**[1], **and C. M. Wilson**[1,3]

[1]Department of Microtechnology and Nanoscience (MC2)
Chalmers University of Technology, Göteborg SE-412 96, Sweden
[2]Centre for Engineered Quantum Systems, School of Physical Sciences
University of Queensland, Saint Lucia, Queensland 4072, Australia
[3]Electrical and Computer Engineering Department, Institute for Quantum Computing
University of Waterloo, Waterloo, Canada

Abstract— We investigate the effective interaction between two microwave fields, mediated by a transmon-type superconducting artificial atom which is strongly coupled to a coplanar transmission line. The interaction between the fields and atom produces an effective cross-Kerr coupling. We demonstrate average cross-Kerr phase shifts of up to 20 degrees per photon when both coherent microwave fields at the single-photon level. Our results provide an important step towards quantum applications with propagating microwave photons.

Quantum Deformed Richardson-Gaudin Model

P. Kulish[1], **A. Stolin**[2], **and H. Johanesson**[2]

[1]Steklov Mathematical Institute, St. Petersburg, Russia
[2]University of Gothenburg, Sweden

Abstract— The Richardson model is an integrable spin 1/2 finite chain with a special Hamiltonian, which eigenstates can be constructed algebraically. Quantum group theory provides a possibility to deform the Hamiltonian preserving integrability.

More exactly, we use the so-called Jordanian r-matrix to deform the Hamiltonian of the Richardson model. In order to preserve integrability of the model, we need to insert a special nilpotent term into the auxiliary L-operator, which generates integrals of motion of the system. Moreover, the quantum inverse scattering method enables us to construct eigenstates of the deformed Hamiltonian. These states have a complicated entanglement structure and they require a further invesigation.

Entanglement Sudden Death for a Two-particle Gaussian State

T. C. Dorlas[1] and A. Guesquière[2]

[1]School of Theoretical Physics, Dublin Institute for Advanced Studies
10 Burlington Road, Dublin 4, Ireland
[2]Department of Mathematical Physics, NUI Maynooth, Maynooth Co. Kildare, Ireland

Abstract— We investigate the evolution of an initially entangled Gaussian state of two particles interacting with heat baths. Using a master equation for their evolution we show that when the particles do not interact, there is entanglement sudden death, i.e., the entanglement vanishes at a finite time. Introducing an interaction between the particles the evolution of the entanglement is more complicated. Depending on the strength of the interaction the entanglement can either disappear or fluctuate and approach a non-zero constant value for large times.

Ultrafast Quantum Nondemolition Measurement Based on two Inductively Coupled Transmons

Étienne Dumur, **Igor Diniz**, **Alexey Feofanov**, **Thomas Weissl**, **Bruno Küng**, **Cecile Naud**, **Olivier Buisson**, **Wiebke Guichard**, **and Alexia Auffèves**
Institut Néel, CNRS, Universié Joseph Fourier, Boîte Postale, 166, 38042 Grenoble Cedex 9, France

Abstract— We present a theoretical study of a quantum nondemolition (QND) readout scheme based on a diamondshaped artificial atom coupled to a microwave resonator in a circuit quantum electrodynamics (CQED) architecture [1].

The device consists of two transmons coupled by a large inductance. A transmon, composed of a small Josephson junction shunted by an interdigitated capacitor, behaves as a nonlinear LC parallel oscillator. The circuit leads to an in-phase and an out-of-phase anharmonic oscillator coupled via a cross-Kerr-like term. The in-phase oscillating mode corresponds to the logical qubit which exhibits a relatively low resonance frequency. The out-of-phase oscillating mode is used as an ancilla qubit with a relatively high resonance frequency [2]. The ancilla qubit is strongly coupled to a resonator. Depending on the state of the logical qubit, $|g\rangle$ or $|e\rangle$, the ancilla will be resonantly or dispersively coupled to the resonator leading to a large contrast of the transmitted microwave signal (Figure 2). In our proposed measurement scheme, the large detuning between the logical qubit and the resonator and their very weak mutual coupling prevent qubit relaxation due to the Purcell effect.

To estimate precisely the contrast of the transmitted microwave, we take into account nonlinear effects between the ancilla and the resonator. It leads to a drastic reduction of the contrast at large microwave power.

In addition we introduce the noise through an effective temperature T_N and a bandwidth B of our measurement circuit. We have performed a statistical study of the photon distribution obtained at the end of the amplification chain. The fidelity of this novel QND measurement can be extracted as function of the experimental parameters such as T_N, B, lifetime τ of the photon inside the resonator, acquisition time and microwave power.

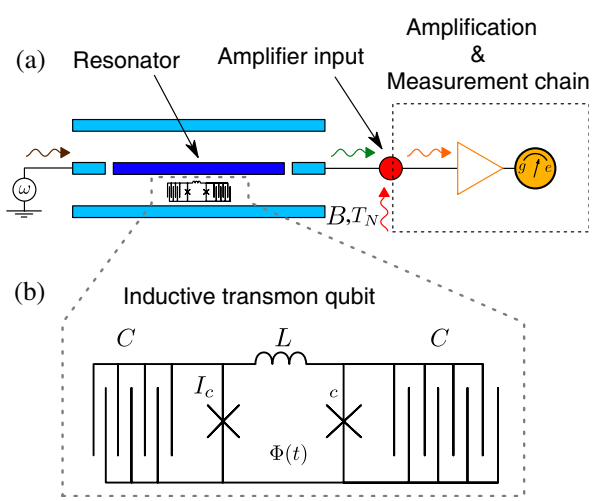

Figure 1: (a) Schematic circuit for a fast QND readout. The incident microwave signal of frequency ω is transmitted through the resonator coupled to the superconducting device. The microwave signal is amplified and detected. The noise amplifier is illustrated by an additional microwave source at the amplifier input. (b) The superconducting device realized by two transmons coupled by a large inductance.

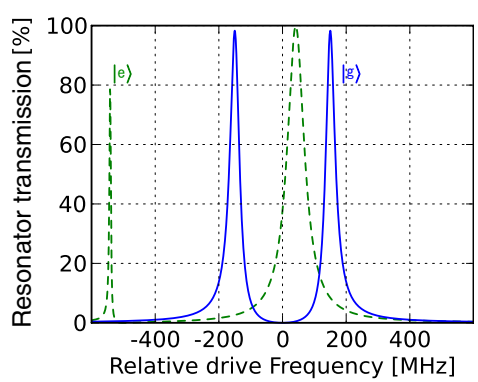

Figure 2: Resonator transmission for the two logical qubit states as a function of microwave signal frequency with the photon lifetime $\tau = 4\,\mathrm{ns}$ and a very weak microwave power signal $p = 0.001\,\mathrm{photon}\cdot\mathrm{ns}^{-1}$. Blue solid curve: logical qubit state $|g\rangle$. Green dashed curve: logical qubit state $|e\rangle$. The frequency is centered on the bare resonator frequency.

We will discuss the trade-off between all these parameters. This original scheme can be implemented with a state-of-the-art Josephson parametric amplifier,leading to a predicted QND measurement with very high fidelity, up to 99.9%, in a very short measurement time, down to 60 ns.

We will present the experimental circuit that we are realizing for the implementation of this idea and the preliminary experimental results.

REFERENCES

1. Diniz, I., E. Dumur, O. Buisson, and A. Auffèves, "Ultrafast quantum nondemolition measurements based on a diamond-shaped artificial atom," *Phy. Rev. A*, to be published.
2. Lecocq, F., I. M. Pop, I. Matei, E. Dumur, A. K. Feofanov, C. Naud, W. Guichard, and O. Buisson, "Coherent frequency conversion in a superconducting artificial atom with two internal degrees of freedom," *Physical Review Letters*, Vol. 108, 2012.

Generation of Non-classical Electromagnetic Fields by Magnetic-dipolar-mode Ferrite Particles

E. O. Kamenetskii
Microwave Magnetic Laboratory, Department of Electrical and Computer Engineering
Ben Gurion University of the Negev, Beer Sheva, Israel

Abstract— In a subwavelength region of microwave electromagnetic (EM) fields, one can observe fields with the "electric-magnetic democracy" very different from the "electric-magnetic democracy" in free-space Maxwellian fields. To distinguish such unusual field structures we term them as magnetoelectric (ME) fields. We show that there exist point sources of microwave ME fields — the ME particles. These particles are represented by small quasi-2D ferrite disks with the magnetic-dipolar-mode (MDM) [or magnetostatic-magnon] spectra [1, 2]. ME fields are characterized by unique symmetry properties. There are the fields with helicity effects and power-flow-density vortices [3–5]. There is a very peculiar mechanism of scattering of microwave EM fields by ME particles. In contrast to small metal particles with electrostatic (plasmon) resonances, where there is strong localization of electric fields [6], in small ferrite particles with magnetostatic-magnon resonances one has strong localization of both magnetic and electric fields. One of the main features of the ME-field spectra is discrete energy eigenstates. We give a theoretical background of properties of the microwave ME fields. We show new results of numerical studies of microwave ME fields [5, 7–9].

REFERENCES

1. Kamenetskii, E. O., *Phys. Rev. E*, Vol. 63, 066612, 2001.
2. Kamenetskii, E. O., M. Sigalov, and R. Shavit, *J. Phys.: Condens. Matter*, Vol. 17, 2211, 2005.
3. Kamenetskii, E. O., *J. Phys. A: Mathematical and Theoretical*, Vol. 40, 6539, 2007.
4. Kamenetskii, E. O., *J. Phys.: Condens. Matter*, Vol. 22, 486005, 2010.
5. Kamenetskii, E. O., R. Joffe, and R. Shavit, *Phys. Rev. E*, Vol. 87, 023201, 2013.
6. Tribelsky, M. I. and B. S. Luk'ynchuk, *Phys. Rev. Lett.*, Vol. 97, 263902, 2006.
7. Kamenetskii, E. O., M. Sigalov, and R. Shavit, *Phys. Rev. A*, Vol. 81, 053823, 2010.
8. Kamenetskii, E. O., R. Joffe, and R. Shavit, *Phys. Rev. A*, Vol. 84, 023836, 2011.
9. Berezin, E., O. Kamenetskii, and R. Shavit, *J. Opt.*, Vol. 14, 125602, 2012.

Proton Beam Induction of Quantum Correlations in Silicon Nanocrystal

Vesna I. Berec[1, 2]

[1]Department of Physics, University of Belgrade, Serbia
[2]Institute of Nuclear Sciences, Vinča, P. O. Box 522, Belgrade 11001, Serbia

Abstract— Permanent system size decreasing trend of communication systems defined by Moore's Law, by 2015 will imply the implementation of elements as memory units comparable to individual atoms and charge. Accordingly, the quantum effects at the subatomic level will have a decisive influence on the development of information technology. We investigate induction-generation of mutual quantum correlations — entanglement, which implies accurate control, manipulation and transfer of quantum information — qubits addressable for modeling and implementation in quantum channels and network systems. The proposed investigation employs the quantum communication protocol based on the transmission model of hyperchanneled protons and the Monte Carlo simulations of spin systems in silicon nanocrystals.

The quantum electrodynamical nature of entanglement as an essential quantum property that establishes mutual predictable correlation of particles of energy/matter is investigated using the precisely guided proton beam through a ^{29}Si nanocrystal axial channel on a basis of screened Moliere's interaction potential. Numerical solutions of equations of motion of protons correspond to hyperchanneled proton spatial and angular distributions in the phase space.

REFERENCES

1. Kimble, H. J., "The quantum internet," *Nature*, Vol. 453, 1023–1030, 2008.
2. Morton, J. J. and B. W. Lovett, "Hybrid solid-state qubits: The powerful role of electron spins," *Annu. Rev. Condens. Matter Phys.*, Vol. 2, 189–212, 2011.
3. Guidi, V., A. Mazzolari, D. De Salvador, and L. Bacci, "Deflection of MeV protons by an unbent half-wavelength silicon crystal," *Phys. Rev. Lett.*, Vol. 108, 014801, 2012.
4. Berec, V., "Quantum entanglement and spin control in silicon nanocrystal," *PLoS ONE*, Vol. 7, No. 9, e45254, 2012, doi:10.1371/journal.pone.0045254.

Parametric Resonance in Tunable Superconducting Cavities

Waltraut Wustmann and Vitaly Shumeiko
Chalmers University of Technology, S-41296 Goteborg, Sweden

Abstract— We present a theory of parametric resonance in tunable superconducting cavities. We take into consideration the nonlinearity introduced by the SQUID attached to the cavity, and damping due to connection of the cavity to a transmission line. In the particular case of degenerate parametric resonance, with a pump frequency close to twice the fundamental cavity resonance, we study in detail the nonlinear classical dynamics of the cavity field below and above the parametric threshold, featuring regimes of multistability and parametric radiation.

We investigate the phase-sensitive amplification of external signals on resonance, as well as amplification of detuned signals, and relate the amplifier performance to that of linear parametric amplifiers. We also discuss applications of the device for dispersive qubit readout.

Beyond the classical response of the cavity, we investigate small quantum fluctuations around the amplified classical signals. We evaluate the noise power spectrum both for intrinsic field in the cavity and in the output. Other quantum statistical properties, are addressed as well, such as squeezing spectra, second order coherence and two-mode entanglement.

Session 2P3
3_FocusSession.SC3: Optics for Bio-medical Diagnostics and Therapy Applications

Nanoscopy with Focused Light and Its Relevance to the Biomedical Sciences
Stefan W. Hell, ... 688

Laser-activated Nanocomposite Biomaterials for Photothermal Therapies and Drug Release
Roberto Pini, Paolo Matteini, Fulvio Ratto, Francesca Rossi, Sonia Centi, Francesca Tatini, ... 689

Optimization of Optical Excitation of Upconversion Nanoparticles for Quicker Microscopy and Deeper Tissue Imaging with Higher Quantum Yield
Qiu Qiang Zhan, Sailing He, ... 691

Shaping Light for Biophotonics
Kishan Dholakia, ... 692

Active Rotational Microrheology Using an Optically Trapped Sphere and Its Applications to Biology and Medicine
Lachlan J. Gibson, Daryl Preece, Timo A. Nieminen, Halina Rubinsztein-Dunlop, ... 693

Laser-made 3D Scaffolds for Tissue Engineering Applications
Maria Farsari, ... 694

Optical Sensor Based on LSPR Phenomenon to Reveal Cholesterol Concentrations for Biomedical Applications
Richard Tarparelli, Renato Iovine, Lucio Vegni, ... 695

Non-intrusive Gas Sensing of Human Body Cavities Using Diode Laser Absorption Spectroscopy
Märta Lewander, Patrik Lundin, Emilie Krite Svanberg, Sven Lindberg, Vineta Fellman, Gabriel Somesfalean, Stefan Andersson-Engels, Sune Svanberg, Katarina Svanberg, ... 696

Multiphoton Multispectral Fluorescence Lifetime Tomography for the Evaluation of Basal Cell Carcinomas
Rakesh Patalay, Clifford B. Talbot, Yuriy Alexandrov, Martin O. Lenz, Sunil Kumar, Sean Warren, Ian Munro, Mark A. A. Neil, Karsten Konig, Paul M. W. French, Anthony Chu, Gordon W. H. Stamp, Chris Dunsby, ... 697

Non-contact Optical Skin Assessment for Dermatology and Anaesthesiology
Janis Spigulis, Ilze Lihacova, Dainis Jakovels, Ilona Kuzmina, A. Lihachev, Uldis Rubins, ... 698

Novel Optical Waveguide Theory and Novel Electrical Circuit Theory of Photoreceptors in the Human Retina
Anhui Liang, Leiting Hu, ... 699

Laser Detection of Tissue Disease
Francesco S. Pavone, ... 700

Microcirculation Imaging with Light
Martin J. Leahy, Joey Enfield, S. Daly, Hrebesh Molly Subhash, ... 701

Nanoscopy with Focused Light and Its Relevance to the Biomedical Sciences

Stefan W. Hell
Max Planck Institute for Biophysical Chemistry, Göttingen, Germany

Abstract— For a long time the resolution of any light microscope relying on focused light has been considered incapable of resolving details that are finer than about half of the light's wavelength (> 250 nm). The diffraction resolution barrier has been a serious impediment for the life sciences because focused light is the only means by which one can access the interior of living cells noninvasively. However, in the last two decades novel fluorescence microscopy approaches have been developed that allowed overcoming the diffraction barrier. Today, fluorescence microscopy investigations with resolution 20–30 nm have become routine and are being applied to various areas in the life sciences, from living cell cultures to tissues, such as the brain of living rodents. Developments improving the imaging speed as well as the resolution to the sub-10 nm scale are underway. We will discuss how the resolution-limiting role of diffraction can be neutralized and highlight the potential of emerging 'far-field fluorescence nanoscopy' for the biomedical sciences.

REFERENCES

1. Hell, S. W., "Far-field optical nanoscopy," *Science*, Vol. 316, 1153–1158, 2007.
2. Hell, S. W., "Far-field optical nanoscopy," *Single Molecule Spectroscopy in Chemistry*, ed., A. Gräslund, R. Rigler, and J. Widengren, 365–398, Springer, Berlin, 2009.

Laser-activated Nanocomposite Biomaterials for Photothermal Therapies and Drug Release

Roberto Pini[1], **Paolo Matteini**[1], **Fulvio Ratto**[1], **Francesca Rossi**[1], **Sonia Centi**[2], **and Francesca Tatini**[1]

[1]Institute of Applied Physics, National Research Council of Italy, Florence, Italy
[2]Clinical Physiopathology Department, University of Florence, Florence, Italy

Abstract— Stimuli-responsive polymeric biomaterials have attracted much attention for their prospective application in several fields including biomedicine, biotechnology and biosensing. Here we discuss the exploitation of a light stimulation produced by a laser source to "activate" biomaterials hybridized with suitable photothermal enhancers. We will present into more details two exemplary laser-activated biomaterials, which we have recently developed and characterized as viable solutions to critical issues in tissue repair and drug delivery applications.

Laser-assisted tissue repair or laser welding has been proposed to close chronic accidental and surgical wounds. Typically, laser light is delivered 1) to a wound site to be repaired which has been stained with an exogenous optical absorber or 2) to a photoresponsive medical dressing (e.g., patches, stents, etc) placed in intimate contact with the tissue to be repaired, in order to produce a photothermal effect. The endogenous tissue or the externally applied dressing respond to the thermal stimulus producing different chemostructural modifications such as denaturation and fusion, which can mediate the repair of the wound. An exemplary application is corneal laser welding, which is obtained by staining the cut edges of a stromal tissue with the photosensitizer Indocyanine green and by irradiating them with a near-infrared laser light to produce collagen denaturation and reorganization of the noncollagenous components, which can ultimately sustain wound closure and tissue fusion. We have recently engineered an hybrid bioadhesive consisting in a chitosan film doped with gold nanorods (GNRs) that can be activated by NIR laser light. These films (0.8 cm diameter, 40 µm thickness) are insoluble, flexible, resistant and stable in a physiological environment. The use of GNRs provides amplified optical absorbance of the laser light due to efficient plasmon bands in the NIR window, where tissue components and chitosan are mostly transparent. Upon laser irradiation a well-localized photothermal effect can thus be produced in the film, which is in turn stimulated to produce adhesion with a proximal tissue surface (e.g., arterial wall, tendon, lens capsule). The excellent biocompatibility and biodegradability of chitosan make it a preferred choice for such biomedical applications as wound dressing, tissue engineering and drug delivery.

Capitalizing on this previous experience, we have succeeded in fabricating an implantable device for on demand chemical release in the form of a light-activated sponge-like nanocomposite scaffold. The sponge consists of a porous chitosan scaffold containing a dispersion of GNRs, which acts as an absorber of the incoming laser light, and of thermosensitive polymeric micelles, which serve as a reservoir for the drug molecules to be released. The photothermal response of the nanoparticles contained inside the sponge triggers a contraction in proximal micelles, thus promoting the expulsion of the drug that in turn is released from the sponge to the external environment. We proved the possibility of regulating the temperature generated in the sponge by laser illumination with a continuous wave diode laser light through a variation in the laser intensity (in the 0.3–0.5 W cm^{-2} range) and with a linear relationship within the temperature range of interest for the activation of the release (40–45°C). The peculiar physiochemical and structural properties of the nanocomposite sponges impart a number of interesting features to this drug release system, including the possibility of spatially confining the therapeutic treatment as well as of precise control of the amount of released drug as a function of duration and power of the excitation light.

REFERENCES

1. Pini, R., F. Rossi, P. Matteini, and F. Ratto, "Laser tissue welding in minimally invasive surgery and microsurgery," *Biophotonics. Series: Biological and Medical Physics, Biomedical Engineering*, Chapter 15, 275–299, L. Pavesi, P. M. Fauchet (Eds.), Springer-Verlag, Berlin, 2008.
2. Rossi, F., P. Matteini, F. Ratto, L. Menabuoni, I. Lenzetti, and R. Pini, "Laser tissue welding in ophthalmic surgery," *J Biophotonics*, Vol. 1, 331–342, 2008.

3. Matteini, P., F. Rossi, L. Menabuoni, and R. Pini, "Microscopic characterization of collagen modifications induced by low-temperature diode laser welding of corneal tissue," *Lasers Surg. Med.*, Vol. 39, 597–604, 2007.
4. Matteini, P., F. Ratto, F. Rossi, S. Centi, L. Dei, and R. Pini, "Chitosan films doped with gold nanorods as laser-activatable hybrid bioadhesives," *Adv. Mater.*, Vol. 22, 4313–4316, 2010.
5. Matteini, P., M. R. Martina, G. Giambastiani, F. Tatini, R. Cascella, F. Ratto, C. Cecchi, G. Caminati, L. Dei, and R. Pini, "Light-responsive nanocomposite sponges for on demand chemical release with high spatial and dosage control," *J. Mater. Chem. B*, 2013, DOI: 10.1039/C2TB00310D.

Optimization of Optical Excitation of Upconversion Nanoparticles for Quicker Microscopy and Deeper Tissue Imaging with Higher Quantum Yield

Qiuqiang Zhan[1] and Sailing He[1, 2, 3]

[1]ZJU-SCNU Joint Research Center of Photonics, Centre for Optical and Electromagnetic Research
South China Academy of Advanced Optoelectronics
South China Normal University (SCNU), Guangzhou 510006, China
[2]Centre for Optical and Electromagnetic Research, JORCEP
Zhejiang Provincial Key Laboratory for Sensing Technologies
Zijingang Campus, Zhejiang University (ZJU), Hangzhou 310058, China
[3]Department of Electromagnetic Engineering, Royal Institute of Technology, Stockholm 10044, Sweden

Abstract— Relatively low quantum yield (QY), time-consuming scanning and strong absorption of light in tissue are some of the issues present in the development of upconversion nanoparticles (UCNPs) for biomedical applications. In this work we systematically optimized several aspects of optical excitation of UCNPs to improve their applicability in bioimaging and biotherapy. A novel multi-photon evanescent wave (EW) excitation modality is proposed for UCNP-based microscopy. The scanning-free, ultrahigh contrast and high spatiotemporal resolution method could simultaneously track a few particles in a large area with a speed of up to 350 frames per second. The HeLa cancer cell membrane imaging was successfully performed using $NaYF_4$: 20% Yb^{3+}/2% Er^{3+} targeting nanoparticles. Studies with different tissues were made to illustrate the impact of optical property parameters on the deep imaging ability of 920-nm band excitation. In the experiments a semiconductor laser with a 920 nm wavelength was used to excite UCNPs in tissue phantom at five depths. Our experimental and computational results have shown that in UCNP-based diffusion optical imaging with 920-nm laser excitation could lead to larger imaging depth range compared to traditional 974-nm excitation in a wide dynamic range of tissue species. As the QY is power density dependent, a pulsed laser is proposed to improve the QY of UCNPs. This proposal is promising in drastically increasing the imaging depth and efficiency of photodynamic therapy. These three methods/aspects about UCNP performance are related to each other. For example, pulsed excitation could be used in a TIRF method to further improve the speed of imaging, and appropriate excitation wavelength shift together with pulsed excitation could further improve the deep imaging ability. These proposed optical optimizations will improve the applicability of UCNPs and further catalyze their development in the field of biomedical optics.

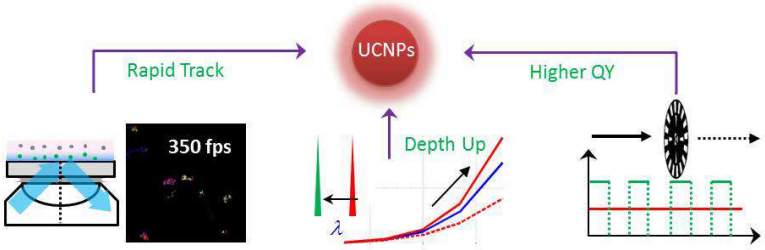

Shaping Light for Biophotonics

Kishan Dholakia
SUPA, School of Physics and Astronomy, University of St Andrews
Fife KY16 9SS, Scotland

Abstract— A review of shaped light fields will be presented with an emphasis on optical manipulation, imaging and biophotonics.

Laser light typically emanates in what is termed a standard Gaussian beam. As we solve the basic equations for light propagation, we recognize this mode as a "fundamental" solution used by most lasers. However, it is becoming critically apparent, to a wide range of cutting-edge science, that the basic form of light propagation is insufficient for numerous applications and indeed that our very understanding of the propagation of light needs to be re-addressed. Light fields possessing on axis phase singularities (Laguerre-Gaussian modes) [1] have come to the fore over the last two decades. The concept of light diffraction is also pertinent: by considering light fields composed of plane waves that undergo equivalent phase shifts upon axial propagation one can define propagation invariant ("non-diffracting") beams. This includes the family of Bessel, Airy and Mathieu light modes [2]. Ultimately, if we group all of these topics under the framework of optimal far-field propagation or optical beam shaping, we see that a very wide range of fields within the science community is seeking to engineer and exploit the characteristics of light.

A key example is optical manipulation. This is a powerful non-contact technique where micrometre sized particles can be grabbed, moved and generally manipulated solely with light. Optical tweezers is the most popular way to implement these forces using a single tightly focused light beam. The use of "shaped light fields" such as vortex, Bessel and Airy modes have continued to play a key role in the field as well as the ability to propagate light through turbid media (disordered materials) [3]. This can be extended to explore new forms of endoscopy using a multimode fibre.

In this talk, I will review some of the key advances in shaped optical fields over the last decade with an emphasis on studies in biophotonics. I will particularly discuss new directions in imaging in this talk.

REFERENCES

1. Allen, L., et al., *Phys. Rev. A*, Vol. 45, 8185, 1992.
2. Mazilu, M., D. J. Stevenson, F. J. Gunn-Moore, and K. Dholakia, *Laser & Photonics Reviews*, Vol. 4, No. 4, 529–547, 2010.
3. Čižmár, T., M. Mazilu, and K. Dholakia, *Nature Photonics*, Vol. 4, 388–394, 2010.
4. Cizmar, T. and K. Dholakia, *Nature Comm.*, Vol. 3, 1027, 2012.

Active Rotational Microrheology Using an Optically Trapped Sphere and Its Applications to Biology and Medicine

Lachlan J. Gibson, Daryl Preece, Timo Nieminen, and Halina Rubinsztein-Dunlop
School of Mathematics and Physics, The University of Queensland, Brisbane, QLD 4072, Australia

Abstract— Traditional rheology studies the flow and deformation of macroscopic materials ($\sim$ mL) in response to applied stresses. In contrast, microrheology explores microfluidic responses. Typically this information is inferred by observing the dynamics of micron-sized probe particles embedded in the material. Through these methods colloids, polymer networks and fluids with mesoscopic inhomogeneities have been studied. Such systems are jointly denoted as complex fluids because they exhibit both viscous and elastic behaviours. In biomedicine these so called viscoelastic fluids arise frequently and changes in their rheological behaviour have been linked to the development of some diseases, including arthritis and dry eye. For studies of onset of these conditions only extremely small volumes of the liquid are available and therefore the use of microrheologically based methods is advantageous and in many cases the only type method that can be uses.

Viscoelastic fluids are prevalent in many biological systems, from the synovial fluid between bone joints to the cytoplasm inside a cell. Many of these fluids are highly inhomogeneous or preferably available in ultra-small volumes so their precise mechanical properties, rheology, are largely unknown and difficult to test. To unable studies of such systems, we have developed an optical tweezers microrheometer capable of conducting viscoelastic measurements in picoliter volumes with the highest spatial resolution available to particle tracking microrheometers. Using a highly focused linearly polarised laser beam we can trap micron size birefringent vaterite crystalline spherical particles both angularly and in 3D. The sphere's birefringence causes polarisation changes on an incident laser beam which we measure. This polarisation tracking allows the angle to be monitored over time with high precision permitting the observation precise data over a broad frequency range ($\sim$ 0.1–1000 Hz). In comaparison, conventional large scale rheometers are inferior since they are limited by inertial effects and therefore, only produce lower frequency data ($\sim$ 1–100 Hz). Our microrheological measurements have excellent quantitative agreement with measurements conducted by a large scale bulk rheometer for ethanol, water and Celluvisc eye drops. By observing the rotation of the probe driven by alternating angularly offset traps our method finds rheological information about the local region in which the probe is positioned unhindered by close boundaries. Such information is typically inaccessible to other translational or multi-probed microrheometers yet vital to future research in highly inhomogeneous, intracellular, rare or difficult to obtain fluids.

Laser-made 3D Scaffolds for Tissue Engineering Applications

Maria Farsari
IESL-FORTH, N. Plastira 100, Heraklion, Crete 70013, Greece

Abstract— A critical component for successfully engineering complex 3D tissue from a cell source is the production and utilisation of the appropriate 3D scaffold. Indeed, cells seeded on a flat surface grow typically in a monolayer fashion, while 3D cell cultures can only be achieved via their growth in a 3D micro-environment. The success of these scaffolds in their use for tissue engineering is critically dependent on their mechanical and surface properties, and microstructure.

Here, we present our recent results into the fabrication of 3D scaffolds of a series of novel materials using Direct fs Laser Writing (DLW) by multiphoton polymerization. These are:

(a) Biodegradable polylactide-based scaffolds for neural and bone tissue engineering applications. We study neuronal cell growth on them, to specifically assess neurocompatibility [1]. In addition, we grow pre-osteoblasts and investigate the effect of porosity on their adhesion and proliferation.

(b) Organic-inorganic hybrid scaffolds for bone tissue engineering. These are functionalized with self-assembling peptides which are designed for promoting either a) nucleation of calcium phosphates or b) adhesion, proliferation and differentiation of preosteoblasts.

This study indicates that DLW is a feasible fabrication route for making 3D tissue engineering scaffolds with reproducible feature shape and sizes.

REFERENCES

1. Melissinaki, V., et al., "Direct laser writing of 3D scaffolds for neural tissue engineering applications," *Biofabrication*, Vol. 3, 045005, 2011.

Optical Sensor Based on LSPR Phenomenon to Reveal Cholesterol Concentrations for Biomedical Applications

R. Tarparelli, **R. Iovine**, **and L. Vegni**
Department of Engineering, University of Roma Tre, Via Vito Volterra 62, Rome 00146, Italy

Abstract— In this contribution a nanodevice based on Localized Surface Plasmon Resonance (LSPR) phenomenon for biological characterization operating in the Visible and Near Infrared frequency Regime is proposed. We analyze the possibility to use plasmonic nanoparticles arranged in array configuration to detect in a ultra-sensitive way different cholesterol concentrations of the lipid membrane. Recently, it was shown that elevate levels of cholesterol of the lipid membrane can be associated to a tumor initial stage. For example, it is referred that the breast cancer and the prostate cancer cell contained lipid with high values of cholesterol. The main reasons, referred in literature, are:

- cancer cells tends to accumulates cholesterol in their cell membrane which facilitates pro-carcinogenic cell signaling;
- high cholesterol level is vital for carcinogenesis because it activates several proteins signals such as Sonic Hedgehog (SH) and Akt.

Therefore, these results indicate the importance of the evaluation of cholesterol concentrations of the lipid membrane.

The proposed device allows to evaluate different cholesterol concentration by permittivity measurements. Nowadays, it is well known that the optical properties of nanoparticles depend on the dielectric properties of the background environment. This behavior is already exploits in several sensing application based on LSPR phenomenon. In this work an electromagnetic enhancement of this mechanism is necessary because the permittivity of the lipid membrane shows small changes when different values of cholesterol are considered. This enhancement is obtained arranging the nanoparticles in array structure. Full-wave simulations confirm that in this configuration the device is able to reveal small change of cholesterol concentration.

Non-intrusive Gas Sensing of Human Body Cavities Using Diode Laser Absorption Spectroscopy

Märta Lewander[1], **Patrik Lundin**[1,2], **Emilie Krite Svanberg**[3], **Sven Lindberg**[4], **Vineta Fellman**[5], **Gabriel Somesfalean**[2], **Stefan Andersson-Engels**[2], **Sune Svanberg**[2,7], **and Katarina Svanberg**[6,7]

[1]GASPOROX AB, Lund, Sweden
[2]Department of Physics, Lund University, Lund, Sweden
[3]Department of Anesthesiology and Intensive Care Medicine
Lund University, Lund, Sweden
[4]Department of Oto-Rhino-Laryngology, Lund University, Lund, Sweden
[5]Department of Pediatrics, Lund University, Lund, Sweden
[6]Department of Oncology, Lund University, Lund, Sweden
[7]Centre for Optical and Electromagnetic Research
South China Normal University, Guangzhou, China

Abstract— This paper addresses a new optical approach of assessing information about the gas inside human cavities non-intrusively, utilizing diode laser absorption spectroscopy. The technology has shown feasible to the paranasal sinuses; maxillary and frontal sinuses, the mastoid bone, the intestine, and the lungs. The gas information can provide clinically important information in the diagnosis of sinusitis and otitis and in the infant case may give valuable information about the lung function of prematurely born babies.

Today no easy reliable method for diagnosis of the paranasal sinuses exists which results in a large over-prescription of antibiotics. The diode laser absorption spectroscopy method described here, provides an alternative where the physician at a primary care clinic can obtain support in his/her diagnosis of sinusitis. The laser-based method is referred to as GASMAS, GAs in Scattering Media Absorption Spectroscopy, and was invented by the Lund University group. The method enables gas sensing of free gas located inside a scattering medium, such as human tissue. In the case of gas monitoring of the maxillary sinuses, located behind the cheekbone, the light can either be injected from the inside of the mouth or from the outside on the cheek. The light emerging out through the cheekbone is detected and provides information about the gas inside the sinus. Information on both the gas amount and the respiration of the sinus can be achieved by measuring the gases oxygen and water vapour. In a clinical study of 40 patients the GASMAS method was compared to CT findings of the maxillary and frontal sinus with very good correlation [1] suggesting it to be a feasible diagnostic tool. The mastoid bone, a porous bone located behind the ear, was similarly investigated. The light was then injected below the ear and detected behind the ear. Good correlation was found with CT and also with the gas volume of the mastoid bone [2].

Utilizing GASMAS to monitor oxygen inside the lungs of prematurely born babies provides an attractive alternative to today's methods where ionizing radiation is used as well as to indirect measurements of, e.g., the oxygenation of the blood or of the oxygen in the exhaled air. The lungs are one of the last organs to be developed during the pregnancy and need to be carefully monitored for prematurely born babies. Simulations and measurements of models to scale with the premature case indicate that lung monitoring of prematurely born infants should be possible [3]. The feasibility of GASMAS monitoring has also been demonstrated on full-term born infants. The next step in the development of this alternative diagnosis method would be a clinical trial of prematurely born babies.

REFERENCES

1. Lewander, M., S. Lindberg, T. Svensson, R. Siemund, K. Svanberg, and S. Svanberg, "Non-invasive diagnostics of the maxillary and frontal sinuses based on diode laser gas spectroscopy," *Rhinology*, Vol. 50, 26, 2011.
2. Lindberg, S., M. Lewander, T. Svensson, R. Siemund, K. Svanberg, and S. Svanberg, "Method for studying gas composition in the human mastoid cavity by use of laser spectroscopy," *Annals of Otology, Rhinology & Laryngology*, Vol. 121, 217, 2012.
3. Lewander, M., A. Bruzelius, S. Svanberg, K. Svanberg, and V. Fellman, "Nonintrusive gas monitoring in neonatal lungs using diode laser spectroscopy: Feasibility study," *Journal of Biomedical Optics*, Vol. 16, 127002, 2011.

Multiphoton Multispectral Fluorescence Lifetime Tomography for the Evaluation of Basal Cell Carcinomas

Rakesh Patalay[1,2], Clifford Talbot[1], Yuriy Alexandrov[1], Martin O. Lenz[1], Sunil Kumar[1], Sean Warren[1], Ian Munro[1], Mark A. A. Neil[1], Karsten König[4], P. M. W. French[1], Anthony Chu[2], Gordon W. H. Stamp[5], and Chris Dunsby[1,3]

[1]Photonics Group, Department of Physics, Imperial College London
South Kensington Campus, London, UK
[2]Department of Dermatology, Imperial College Healthcare NHS Trust, London, UK
[3]Department of Medicine, Imperial College Healthcare NHS Trust, London, UK
[4]JenLab GmbH, Jena, Germany
[5]CRUK London Research Institute, London, UK

Abstract— Two photon microscopy of tissue autofluorescence enables label free, non-invasive imaging of the skin. Autofluorescence arises from endogenous fluorophores such as collagen, elastin, melanin, NAD(P)H and flavins. The ability to image intracellular proteins associated with metabolism and extracellular proteins allows for a degree of both functional and structural imaging.

We have adapted a commercial CE marked two photon tomograph (DermaInspect, JenLab GmbH) for multispectral fluorescence lifetime detection and spectral imaging. It allows the collection of depth resolved fluorescence intensity, fluorescence lifetime and fluorescence emission spectral images with submicron resolution laterally and $< 2\,\mu\text{m}$ vertically, to a depth of $200\,\mu\text{m}$. A femtosecond pulsed laser was used to excite the tissue at a wavelength of 760 nm. The autofluorescence from the skin was then collected into four spectral channels in the range 360–655 nm using time correlated single photon counting for the intensity and lifetimes images and a CCD based spectrometer for the emission spectra.

We present a detailed study using multispectral multiphoton fluorescence lifetime imaging to differentiate basal cell carcinoma cells (BCCs) from normal keratinocytes. Images were acquired from 19 freshly excised BCCs and 27 samples of normal skin (*in* & *ex vivo*). Features from fluorescence lifetime images were used to discriminate BCCs with a sensitivity/specificity of 79%/93% respectively. A mosaic of BCC fluorescence lifetime images covering $1\,\text{mm}^2$ is also presented, demonstrating the potential for tumour margin delineation. Using 10,462 manually segmented cells from the image data, we quantify the cellular morphology and spectroscopic differences between BCCs and normal skin.

Statistically significant increases were found in the fluorescence lifetimes of cells from BCCs in all spectral channels, ranging from 19.9% (425–515 nm spectral emission) to 39.8% (620–655 nm emission). A discriminant analysis based diagnostic algorithm allowed the fraction of cells classified as malignant to be calculated for each patient. This yielded a receiver operator characteristic area under the curve for the detection of BCC of 0.83. We also rank a range of morphological and spectroscopic parameters by their ability to discriminate BCC from normal skin, which provides useful information for the future development of imaging instrumentation and image analysis algorithms.

Non-contact Optical Skin Assessment for Dermatology and Anaesthesiology

J. Spigulis, I. Lihacova, D. Jakovels, I. Kuzmina, A. Lihachev, and U. Rubins
Biophotonics Laboratory, Institute of Atomic Physics and Spectroscopy, University of Latvia, Latvia

Abstract— Several techniques for real time assessment of in-vivo skin have been developed, implemented in prototype devices and tested in clinical environment. Evaluation of skin pathologies and their healing after photo-therapy was performed by means of multispectral imaging analysis using the CRI camera *Nuance* [1–4]. Later original designs of devices for spectral imaging of skin under multi-colour LED illumination have been proposed and clinically tested [5–7]. Currently a prototype device for non-contact multimodal skin imaging is under development [8]. It combines RGB colour imaging at polarized white LED illumination with spectral imaging at four selected wavelength bands, photoplethysmography imaging (PPGI) of skin blood perfusion [9] and imaging of skin autofluorescence photo-bleaching rates [10].

Photoplethysmography video-imaging technique for remote control of regional anaesthesia (RA) efficiency before and during surgeries [11] deserves a special attention. This technology has been successfully tested at Riga Traumatology and Orthopaedic Hospital during wrist surgeries. Physiological response to RA is a notable increase of peripheral microcirculation that can be detected by the PPGI device as increased amplitude of skin blood pulsations; it serves as the START signal for surgery.

REFERENCES

1. Jakovels, D. and J. Spigulis, "2-D mapping of skin chromophores in the spectral range 500–700 nm," *J. Biophoton.*, Vol. 3, No. 3, 125–129, 2010.
2. Kuzmina, I., I. Diebele, J. Spigulis, L. Valeine, A. Kempele, and A. Abelite, "Contact and contactless diffuse reflectance spectroscopy: Potential for recovery monitoring of vascular lesions after intense pulsed light treatment," *J. Biomed. Opt.*, Vol. 16, No. 4, 040505, 2011.
3. Kuzmina, I., I. Diebele, D. Jakovels, J. Spigulis, L. Valeine, and J. Kapostinsh, "Towards non-contact skin melanoma selection by multispectral imaging analysis," *J. Biomed. Opt.*, Vol. 16, No. 6, 060502, 2011.
4. Diebele, I., I. Kuzmina, A. Lihachev, J. Spigulis, J. Kapostinsh, A. Derjabo, and L. Valaine, "Clinical evaluation of melanomas and common nevi by spectral imaging," *Biomed. Opt. Express*, Vol. 3, No. 3, 467–472, 2012.
5. Spigulis, J., "Biophotonic technologies for noninvasive assessment of skin condition and blood microcirculation," *Latv. J. Phys. Techn. Sci.*, Vol. 49, No. 5, 63–80, 2012.
6. Bekina, A., I. Diebele, U. Rubins, J. Zaharans, A. Derjabo, and J. Spigulis, "Multispectral assessment of skin malformations by modified video-microscope," *Latv. J. Phys. Techn. Sci.*, Vol. 49, No. 5, 4–8, 2012.
7. Jakovels, D. and J. Spigulis, "RGB imaging device for mapping and monitoring of hemoglobin distribution in skin," *Lith. J. Phys.*, Vol. 52, No. 1, 50–54, 2012.
8. Spigulis, J., V. Garancis, U. Rubins, E. Zaharans, J. Zaharans, and L. Elste, "A device for multimodal imaging of skin," *Proc. SPIE*, Vol. 8574, 2013 (in press).
9. Rubins, U., V. Upmalis, O. Rubenis, D. Jakovels, and J. Spigulis, "Real-time photoplethysmography imaging system," *Proc. IFMBE*, Vol. 34, 183–186, 2011.
10. Spigulis, J., A. Lihachev, and R. Erts, "Imaging of laser-excited tissue autofluorescence bleaching rates," *Appl. Opt.*, Vol. 48, No. 10, D163–D168, 2009.
11. Miščuks, A., R. Erts, U. Rubīns, J. Spīgulis, and M. Mihelsons, "Method and device for determination of regional anaesthesia," Latvian patent LV14444, 2012.

Novel Optical Waveguide Theory and Novel Electrical Circuit Theory of Photoreceptors in the Human Retina

Anhui Liang and Leiting Hu
Nanjing University of Posts and Telecommunications, China

Abstract— Anhui Liang first proposed and reported the photoreceptors of eyes of vertebrates (including human) are active optical waveguides and quantum-well semiconductor photodetectors in 1998 (see [1]), some important vision phenomena can be explained by the quantum-well detector theory. We first reported the outer segments of human cones are single-mode waveguides in 1998. We first discovered that the mode field diameters of cones' outer segments are equal to or close to their geometrical diameters, and this phenomena may play important roles for human to recognize distances and shapes precisely. In this talk, we first discover (to our knowledge) that the three points, which are the highest resolution wavelength 495 nm, Golden Ratio value 496 nm of the wavelength separation between the blue and green cones' absorption peaks, the rod's absorption peak 498 nm, are coincide or very close, we shall discuss the significance and potential mechanics behind this phenomena. We shall discuss several other new phenomena (in human eyes and bodies,) which are related to Golden Ratio. For the well known Golden Ratio phenomena (e.g., If an object's position relative to the width of a picture's width is Golden Ratio, the picture will be felt most comfortable.) and new Golden Ratio phenomena, we find that the deeper reasons for those phenomena are energy saving, fast and less steps to find objects. We first propose that the retina's circuits are quite close to those of photodetector receiver circuits which are widely used in optical communication systems. Thorough the comparison between the the retina's circuits and photodetector receiver circuits in optical communication systems, we gain a lot of deeper understanding on the human retina's circuits.

Because human's photoreceptors are with optimum structures and very energy saving, we first proposed to design photodetectors and detector arrays of optical communication by emulating human's photoreceptors (i.e., optical communication bionics). By mimicking human eyes, we proposed the mixed detector arrays with tapered and straight waveguides, and these kind of detectors array will have high sensitivity and wide dynamic range. To study on this major (i.e., optical communication bionics) further will lead very significant discoveries.

REFERENCES

1. Liang, A., *The Japan Society of Applied Physics*, No. 3, paper 17p-ZA-1, 1998.

Laser Detection of Tissue Disease

Francesco S. Pavone
European Laboratory for Non Linear Spectroscopy, University of Florence, Via N. Carrara 1, Italy

Abstract— In the first part of this talk a brief review on the non linear laser imaging techniques will be displayed. In particular, two photon fluorescence microscopy, lifetime imaging, multispectral imaging, second harmonic generation microscopy principles will be described.

In the second part of the talk there will be an overview on the applications of these techniques in the field of biomedical imaging. In particular, tumor detection in tissue imaging applications will be shown in different fields, from urology to gastrointestinal surgery, dermatology and brain surgery.

Morpho-functional characterization of tissue pathologies will be displayed as an interesting tool for tumor early diagnosis. Other type of non tumor disease applications will be also shown together with the demonstration on using laser imaging for follow up of laser therapies.

In the last part of the talk, a fiber based endoscope based on multidimensional spectral detection (one photon fluorescence, lifetime and Raman detection) will be described with particular applications of tumor detection.

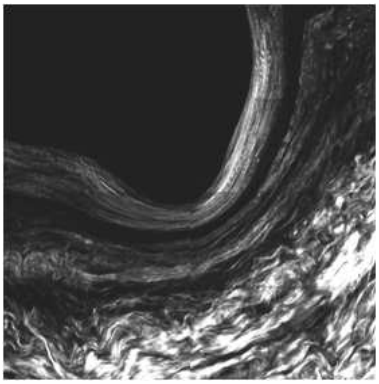

Figure 1: Collagen fibers (second harmonic signal) and elastine fibers (two photon) in the stroma area of a tumor in a basal cell carcinoma.

Microcirculation Imaging with Light

M. J. Leahy[1], **J. Enfield**[2], **S. Daly**[2], **and H. Subhash**[1]

[1]Tissue Optics & Microcirculation Imaging Group, School of Physics
National University of Ireland, Galway, Ireland
[2]TOMI, Department of Physics, University of Limerick, Ireland

Abstract— As more evidence emerges that 2D biology does not adequately represent the 3D in vivo target, the need for improved structural and functional imaging in three dimensions is more pressing. Light has significant advantages in that they can be safe, low cost, with sufficient resolution and molecule specific. The objective is to put (patho-) physiological function in its structural context in the living organism. This should be achieved with spatial and temporal resolution which are sufficient to observe the phenomenon of interest. We have developed several innovations in in vivo imaging in an effort to further this goal. Correlation mapping Optical Coherence Tomography (cmOCT) provides the functional information relating to the microcirculation, full-range OCT permits doubling the range while providing the highest sensitivity at the centre of the image and through the zero delay line. Finally, we have developed a scheme which permits miniaturizing OCT for deployment in primary care and other low cost applications.

Blood flow provides oxygen and removes waste while maintaining shape, temperature and blood pressure. This can be determined in high resolution using Doppler optical coherence tomography (OCT) methods, but this requires great phase stability and is difficult for horizontal vessels. Alternative methods were developed based on speckle variance of the structural image intensity have been used in tumour microvascular imaging with high-frequency ultrasound [1] and more recently with OCT [2]. Typically eight or more frames are required. This method reduces the sensitivity to the angle of red cell movement with respect to the laser beam. The calculated variance is in the range of $\pm\infty$ and is dependent on the chosen window size. There is therefore some difficulty with its interpretation and a dependence on *a priori* structural knowledge. In a more complex approach, velocities moving into the tissue away from the surface are mapped into one image and velocities moving out of the tissue toward the surface into a second image by means of the Hilbert transform and subsequent fast Fourier transform, giving good separation of flow and structure [3].

Methods: To overcome these difficulties we developed correlation mapping OCT (cmOCT) [4], which is an elegant solution requiring only to adjacent frames. The frames must be well within the lateral resolution of the system or better still they should be repeat B-scans in the same location before moving to take another pair of B-Scans. Areas which have a high correlation are therefore non-moving structures and the areas with low correlation are moving. Then the correlation between these two OCT B-frames is determined by cross-correlating a grid from adjacent frames. Such simple analysis can give rise to exquisite images detailing all the smallest capillaries in the human body as per the examples in Figure 1.

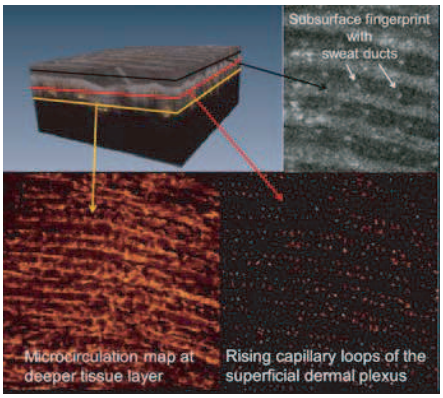

Figure 1: Capillary loops following the pattern of the fingerprint.

Conclusion: Imaging the microcirculation in its native structural context is more feasible using cmOCT and this will aid discovery and diagnosis in a safe and fit for purpose method.

ACKNOWLEDGMENT

This study was supported by NBIP Ireland funded under the Higher Education Authority PRTLI Cycle 4, co-funded by the Irish Government and the EU — Investing in your future and IRCSET.

REFERENCES

1. Needles, A., et al., "Interframe clutter filtering for high frequency flow imaging," *Ultrasound in Medicine and Biology*, Vol. 33, 591–600, 2007.
2. Liu, X., et al., "Spectroscopic-speckle variance OCT for microvasculature detection and analysis," *Biomedical Optics Express*, Vol. 2, 2995–3009, 2011.
3. Wang, R. K., et al., "Three dimensional optical angiography," *Optics Express*, Vol. 15, 4083–4097, 2007.
4. Jonathan, E., J. Enfield, and M. Leahy, "Correlation mapping method for generating microcirculation morphology from optical coherence tomography (OCT) intensity images," *J. Biophotonics*, 2010.

Session 2P4
1_FocusSession.SC1: Casimir Effect and Heat Transfer 2

Transition from Near-field Thermal Radiation to Phonon Interfacial Conduction
Gang Chen, ... 704
Casimir-Polder Forces in Thermal Nonequilibrium
Stefan Scheel, ... 705
Single Mode Thermal Field with a Microwave Cavity Parametric Amplifier
C. Braggio, G. Carugno, F. Della Valle, G. Galeazzi, A. Lombardi, Giuseppe Ruoso, D. Zanello, . 706
Casimir Energies in a One-dimensional Cavity with a Fluctuating Boundary
Salvatore Butera, Roberto Passante, ... 707
Aspects of Metamaterials in the Casimir Effect
Didier Felbacq, R. Messina, B. Bellomo, Mauro Antezza, ... 708
Casimir Forces on a Silicon Micromechanical Chip
Ho Bun Chan, J. Zou, Z. Marcet, Alejandro W. Rodriguez, M. T. Homer Reid, Alexander P. McCauley, I. I. Kravchenko, T. Lu, Y. Bao, S. G. Johnson, ... 709
Casimir Friction for Media of Finite Density
Johan S. Hoye, Iver Brevik, ... 710
Current Measurements of Casimir Interactions: Are Electrostatic Patches Important?
Ricardo S. Decca, ... 711
Non-equilibrium Critical Casimir Forces
Andrea Gambassi, ... 712
Casimir-polder Forces: From Quantum Friction to Chiral and Non-Onsager Media
Stefan Yoshi Buhmann, ... 713
Quantum Friction from Shearing the Vacuum
Rongkuo Zhao, John B. Pendry, ... 714
Casimir Momentum of a Chiral Molecule in a Magnetic Field
Manuel Donaire, Bart A. Van Tiggelen, G. L. J. A. Rikken, ... 715
Near Field Radiative Heat Transfer in Microstructured Geometries
Alejandro W. Rodriguez, ... 716
Quantum Friction: A Case Study of the Fluctuation-dissipation and Quantum Regression Theorems
Diego A. R. Dalvit, Ryan Behunin, Francesco Intravaia, ... 717

Transition from Near-field Thermal Radiation to Phonon Interfacial Conduction

Gang Chen
Mechanical Engineering Department, Massachusetts Institute of Technology
Cambridge, MA 02139, USA

Abstract— When the spacing between two surfaces is less than the dominant wavelength of thermal radiation, heat transfer between the two surfaces can significantly exceed the blackbody limit. Radiative heat transfer at small spacing is usually described by Rytov's fluctuating electrodynamics formulation which is based on the macroscopic Maxwell equations and continuum descriptions such as dielectric functions. In the past, we have demonstrated experimentally that near-field thermal radiation can far-exceed the far-field blackbody limit and the experimental results are in agreement with the Rytov's fluctuating electrodynamics description. However, in the limit when two surfaces are in contact, heat transfer is described in terms of heat conduction and phonon transport. Today there is no unified theory that can describe the power transferred between two bodies as a function of their separation down to the zero gap contact limit. We develop an approach using lattice dynamics and the microscopic Maxwell equations to bridge the theories of conduction and radiation. Experimentally, we investigate near-field thermal radiation between two objects at extremely small separations using a sphere-plate geometry. To measure near field thermal radiation from tens of nanometers down to direct contact, we fabricate and characterize a new type of cantilever which can decouple thermal and force signals to eliminate the parasitic deflection of the cantilever due to the force effect. Surface phonon-polariton and surface-plasmon contributions to near-field radiation heat transfer will be discussed.

ACKNOWLEDGMENT

This work is supported by DOE BES (DE-FG02-02ER45977) and UIUC MURI.

Casimir-Polder Forces in Thermal Nonequilibrium

Stefan Scheel
Institut of Physics, University of Rostock, Universitätsplatz 3, D-18055 Rostock, Germany

Abstract— Dispersion forces such as Casimir and Casimir-Polder forces arise due to fluctuations of the quantised electromagnetic field. In thermal equilibrium, these forces can be computed by envoking the linear fluctuation-dissipation theorem which leads to the well-known Lifshitz formalism. If, however, an atom or molecule is prepared in some energy eigenstate, this constitutes an out-of-equilibrium nonstationary state. In almost all experimental realisations involving cold atoms or molecules and room temperature surfaces, this is typically the case.

I will first briefly review the dynamical approach to dispersion forces based on the formalism of macroscopic quantum electrodynamics. The latter is based on a source-quantity expansion of the electromagnetic field in terms of dynamical variables that describes collective excitations of the field and the absorbing matter. I will show how absorption and emission of thermal photons by the atom or molecule can lead to repulsive transient forces until thermalisation is completed and thermal equilibrium has been reached. As an example of how these new repulsive forces can be used, I will describe their effect on chiral molecules in chiral Fabry-Perot cavities and the resulting possibility to separate enantiomers in the gas phase.

In the case of large thermal photon numbers, I will show that the Casimir–Polder force can become independent of temperature. This statement holds strictly only for potentials that are due to low-energy atomic or molecular transitions interacting with metallic bodies whose plasma frequency is larger than any atomic resonance frequency. I will present criteria for the validity of this statement and give expressions for the leading-order corrections to this result. As an illustrative example, I will consider the Casimir-Polder interaction of highly excited Rydberg atoms with metallic surfaces.

Single Mode Thermal Field with a Microwave Cavity Parametric Amplifier

C. Braggio[1, 2], G. Carugno[2], F. Della Valle[3], G. Galeazzi[4], A. Lombardi[4], G. Ruoso[4], and D. Zanello[5]

[1]Dipartimento di Fisica e Astronomia, Via F. Marzolo 8, Padova I-35131, Italy
[2]INFN, Sezione di Padova, Via F. Marzolo 8, Padova I-35131, Italy
[3]Dipartimento di Fisica and INFN, Sezione di Trieste, Via A. Valerio 2, Trieste I-34127, Italy
[4]INFN, Laboratori Nazionali di Legnaro, Viale dell'Università 2, Legnaro I-35020, Italy
[5]INFN, Sezione di Roma, Piazzale A. Moro 1, Roma I-00185, Italy

Abstract— In our effort to study the Dynamical Casimir Effect [1, 2] we have built a parametric amplifier based on a microwave resonant cavity whose proper frequency can be modulated by means of a variable capacitance diode (varicap). By proper tuning of the varicap, extremely large gain can be obtained, thus allowing to measure the very small amounts of thermal energy contained in an extremely narrow frequency band.

The properties of thermal radiation are generally described by applying the laws of statistical mechanics to the radiation in equilibrium at temperature T. The radiation consists of a continuum spectrum of modes whose energy density is described by Planck's formula. When analyzing radiation inside a high Q resonator, we have to consider that only a single mode of the field is possible, i.e., only photons with energy E around $h\nu_r$, with ν_r the resonance frequency of the cavity, are present. When the mode is populated by n photons, the energy of the mode is $E_n = (n + 1/2)h\nu_r$. The probability $P_\nu(n)$ of finding n photons in the cavity is then:

$$P_\nu(n) = \frac{1}{\bar{n}+1}\left(\frac{\bar{n}}{\bar{n}+1}\right)^n \tag{1}$$

where $\bar{n}$ is the mean photon number $\bar{n} = [\exp(h\nu_r/k_BT) - 1]^{-1}$. Equation (1) is the Bose-Einstein distribution, having the peculiar characteristic to be super Poissonian, with variance $(\Delta n)^2 = \bar{n}(1 + \bar{n})$. The Planck spectrum has been measured several times with extremely high accuracy, the most remarkable measurement being the cosmic microwave background. This is not the case of the single mode photon distribution, described by (1), since when selecting a very narrow frequency band the number of photons is reduced below detectability. On the other hand, enlarging the measurement band will soon spoil the single mode reducing its variance as: $(\Delta n)^2 = \bar{n}(1 + \bar{n}/\mu)$, with μ the number of modes.

We have recently studied a super Poissonian single mode thermal field inside a high Q resonator kept at room temperature, i.e., with $\bar{n} \sim 10^3$ [3]. The measured distribution of the thermal photons inside the resonator follows the distribution probability (1). This measurement has been possible due to a novel type of parametric amplifier having extremely large amplitude gain and frequency selectivity. We will present the characteristic features of this parametric amplifier, based on a 1.5 GHz microwave resonator and a varicap. The system has now been tested at liquid nitrogen and liquid helium temperatures. The corresponding spectra of thermal radiation, with $\bar{n} \sim 10^2$, has been obtained.

The system we have built proves to be a powerful and versatile tool for the measurement of very small signals. In principle, being the thermal radiation in the cavity the limiting noise, this amplifier can reach quantum limited performance when operating at a temperature where the average thermal photon number is smaller than one.

Our result could pave the way for the measurement of the Dynamical Casimir effect [1, 2, 4], finding also possible applications in the development of low energy detectors.

REFERENCES

1. Braggio, C., et al., *Europhys. Lett.*, Vol. 70, 754, 2005.
2. Dodonov, V. V., *Phys. Scripta*, Vol. 82, 038105, 2010.
3. Braggio, C., et al., *New J. Phys.*, Vol. 15, 013044, 2013.
4. Wilson, C. M., et al., *Nature*, Vol. 479, 376, 2011.

Casimir Energies in a One-dimensional Cavity with a Fluctuating Boundary

Salvatore Butera and Roberto Passante
Dipartimento di Fisica e Chimica, Università degli Studi di Palermo, CNISM
Via Archirafi 36, I-90123 Palermo, Italy

Abstract— We consider a massless scalar field in a one-dimensional cavity with one fixed and one mobile wall. We assume that the mobile wall is also subjected to a harmonic potential, and its mechanical degrees of freedom are treated quantum-mechanically. The wall's position has thus quantum fluctuations around the equilibrium position.

The possible motion of the wall makes the cavity length variable, and this gives rise to a wall-field interaction and an effective interaction between the modes of the cavity. We use an effective Hamiltonian, originally introduced by C. K. Law, to describe our system in terms of field modes relative to the equilibrium position of the mobile wall. We obtain by perturbation theory the *dressed* ground state of the wall-field coupled system, which contains pairs of virtual quanta of the field and excitations of the wall's mechanical degrees of freedom.

We evaluate the average number of virtual excitations in each mode of the cavity, induced by the effective wall-field interaction, as well as the renormalized field energy density inside the cavity. We show that the quantum fluctuations of the wall's position significantly affect the field energy density in the cavity, in particular in the proximity of the mobile wall. We also consider a statistical average of the energy density on the position of the fluctuating boundary, in order to discuss the known problem of the divergence of field energy densities at the boundaries. All these quantities are then compared with analogous quantities for a cavity with fixed walls. We find a correction to the Casimir potential energy and to the field energy density in the cavity, due to the position fluctuations of the cavity wall, and discuss how these corrections depend on relevant parameters of the mobile wall, in particular its plasma frequency, mass and frequency of the harmonic potential. Observability of these new effects is also discussed, as well as the relation to the dynamical Casimir effect.

Aspects of Metamaterials in the Casimir Effect

D. Felbacq, **R. Messina**, **B. Bellomo**, **and M. Antezza**
Laboratory Charles Coulomb, University of Montpellier 2, France

Abstract— A lot of work has been devoted to the calculation of Casimir forces between objects of simple geometry such as planes, cylinders or spheres. More recently, more complicated geometries such as gratings or rough surfaces were considered. There is now a raising interest in the Casimir effect in much more complicated systems, namely metamaterials, that can exhibit very specific, and tailorable, electromagnetic behavior. In this talk, I will give a brief introduction to the physics of metamaterials, with a specific view on their interest for the community fo researchers interested in the Casimir effect.

Casimir Forces on a Silicon Micromechanical Chip

H. B. Chan[1], **J. Zou**[1,2], **Z. Marcet**[1,2], **A. W. Rodriguez**[3,4], **M. T. H. Reid**[5], **A. P. McCauley**[6], **I. I. Kravchenko**[7], **T. Lu**[1], **Y. Bao**[2], **and S. G. Johnson**[4]

[1]Department of Physics, The Hong Kong University of Science and Technology
Clear Water Bay, Kowloon, Hong Kong, China
[2]Department of Physics, University of Florida, Gainesville, Florida 32611, USA
[3]School of Engineering and Applied Sciences, Harvard University
Cambridge, Massachusetts 02138, USA
[4]Department of Mathematics, Massachusetts Institute of Technology
Cambridge, Massachusetts 02139, USA
[5]Research Laboratory of Electronics, Massachusetts Institute of Technology
Cambridge, Massachusetts 02139, USA
[6]Department of Physics, Massachusetts Institute of Technology
Cambridge, Massachusetts 02139, USA
[7]Center for Nanophase Materials Sciences, Oak Ridge National Laboratory
Oak Ridge, Tennessee 37830, USA

Abstract— The Casimir force originates from the quantum fluctuations of the electromagnetic field. It leads to an attraction between electrically neutral plates with a vacuum gap that becomes measureable at nanoscale separations. Under the trend of miniaturization, such quantum electrodynamical effects are expected to play an important role in nanomechanical devices. With recent advances, repulsive Casimir forces have been demonstrated in experiments involving fluids and predicted for vacuum gaps under specific conditions. Such repulsive Casimir forces can potentially prevent stiction in nanomechanical systems. Nevertheless, utilization of the Casimir force on the chip level remains a major challenge because all experimental observations of the Casimir force so far require an external object to be manually positioned close to the mechanical element.

We demonstrate that the Casimir force can be the dominant interaction between single-crystalline silicon components on a semiconductor chip, in the absence of external objects. The geometry involves two microfabricated beams with near-square cross sections, the distance between which can be decreased from 1.8 µm to ~ 260 nm. One of the beams acts as the force-sensing element. The force gradient exerted on this beam is measured using magnetomotive transduction. For controlling the distance between the two beams, we use a comb actuator integrated on the same substrate, in which electrostatic forces push the second beam towards the force-sensing beam. No external alignment of the interacting bodies is necessary because they are defined in a single lithographic step. Another advantage is that the distance of the interacting elements to their common support is reduced to ~ 70 µm, about a factor of 1000 smaller than conventional experiments. The improved mechanical stability minimizes long-term drifts in the gap between the interacting objects. In addition to providing a compact platform for Casimir force measurements, this scheme also opens the possibility of tailoring the Casimir force using lithographically defined nanostructures of non-conventional shapes on a single chip.

Casimir Friction for Media of Finite Density

Johan S. Høye[1] **and Iver Brevik**[2]

[1]Department of Physics, Norwegian University of Science and Technology, Trondheim, Norway
[2]Department of Energy and Process Engineering, Norwegian University of Science and Technology
Trondheim, Norway

Abstract— This work is a continuation of our earlier papers on Casimir friction for a pair of particles at low relative velocity [1–4] and also earlier papers. As usual, we consider the situation where two thick plates are separated by a small gap, one plate moving longitudinally with respect to the other. The new element in the present analysis is to allow the media to be dense. The situation becomes then more complex due to induced dipolar correlations, both within the two planes, and between the planes. We show that the structure of the problem can be simplified by regarding the two plates to be a generalized version of a pair of particles. It turns out that macroscopic parameters such as the permittivity suffice to describe the friction in the finite density case also. Somewhat remarkably, the particle density does not occur explicitly in the Casimir friction force expression. The force is predicted to be very small, far beyond what is practically measurable. Finally, we point out how the statistical methods that we are using, correspond to field theoretical methods more commonly in use.

REFERENCES

1. Høye, J. S. and I. Brevik, *Eur. Phys. J. D*, Vol. 61, 335, 2011.
2. Høye, J. S. and I. Brevik, *Eur. Phys. J. D*, Vol. 64, 1, 2011.
3. Høye, J. S. and I. Brevik, *Eur. Phys. J. D*, Vol. 66, 149, 2012.
4. Høye, J. S. and I. Brevik, *Int. J. Mod. Phys. A*, Vol. 27, 126001, 2012.

Current Measurements of Casimir Interactions: Are Electrostatic Patches Important?

Ricardo S. Decca
Department of Physics, Indiana University-Purdue University Indianapolis
Bldg. LD 154, 402 N. Blackford St., Indianapolis, IN 46202, USA

Abstract— Precise measurements of the Casimir force at separations under a micrometer between the Au-coated surfaces have shown that the magnitude of the force can be better understood if a plasma model is used for the low frequency extrapolation of the dielectric constant for Au. Using a Drude model (or any model that takes into account dissipation) yields a difference of over three standard deviations between the measurements and the theoretical calculations.

Among the plausible explanations for this unexpected discrepancy, the existence of electrostatic patches has gained momentum in the last couple of years. In an attempt to quantify the effect of patches we have performed measurements between a sapphire sphere (radius $\sim 150\,\mu\text{m}$) coated with thermally evaporated Au and a single crystal of Au. The measurements are performed at 10^{-7} Torr, not low enough to prevent contamination on the sample. We characterize the single crystal Au surface by performing in-situ Kelvin probe microscopy. Our results show a remarkable agreement with the plasma model.

Non-equilibrium Critical Casimir Forces

Andrea Gambassi
SISSA — International School for Advanced Studies and INFN, via Bonomea 265, Trieste 34136, Italy

Abstract— In 1948, Hendrik Casimir predicted that two uncharged conducting surfaces in vacuum attract each other due to the quantum fluctuations of the electromagnetic field which are spatially confined by these surfaces. The classical analogue of this effect originates from the confinement of thermal fluctuations in fluids near continuous phase transitions, such as the demixing of a mixture of two liquids. Early indirect experimental evidence of the equilibrium force of these fluctuations — the so-called critical Casimir force — were provided by detailed studies of complete wetting films. Its first direct measurement, instead, has been possible only thirty years after its first theoretical investigation by Michael Fisher and Pierre-Gilles de Gennes in 1978, by monitoring the Brownian motion of a micrometer-sized colloidal particle close to a surface.

I will present recent advances in the theoretical and experimental study of the universal properties of this novel fluctuation-induced force, discussing in particular its nonequilibrium behavior and possible relevant applications to soft matter systems.

Casimir-polder Forces: From Quantum Friction to Chiral and Non-Onsager Media

S. Y. Buhmann
Imperial College London, UK

Abstract— Quantum friction describes the predicted drag force on two perfectly smooth parallel dielectric plates which are in relative motion to each other. Mediated by zero-point fluctuations of the electromagnetic field, the existence of this vacuum shear force has been contested. A simple model case to discuss this question is the Casimir-Polder force on a single ground-state atom moving parallel to a stationary dielectric or metal plate. On the basis of macroscopic quantum electrodynamics, one finds that for a dissipative plate, there is indeed a friction force which converts the atom's kinetic energy into heat. Generalising the problem to an excited atom, we find that resonantly enhanced quantum friction or acceleration is possible as mediated by the coupling of internal atomic excitations to surface plasmons. Here, the difference between the energy emitted by the atom and the energy absorbed by the plasmon is balanced by the change in the atom's kinetic energy.

To describe the same process from the perspective of a moving plate rather than an atom, one requires macroscopic quantum electrodynamics in moving, absorbing dielectrics. To an observer at rest, such moving media appear to exhibit electromagnetic cross-susceptibilities. We outline a quantisation scheme for the electromagnetic field in for a general class of linear, cross-polarisable media. It contains both chiral materials and media that violate the Onsager reciprocity theorem. As an application, we show that chiral media give rise to discriminatory Casimir-Polder forces on the enantiomers of chiral molecules and that non-reciprocal media could be used to detect CP-violating effects in molecules.

REFERENCES

1. Scheel, S. and S. Y. Buhmann, "Casimir-Polder forces on moving atoms," *Phys. Rev. A*, Vol. 80, No. 4, 042902, 2009.
2. Buhmann, S. Y., D. T. Butcher, and S. Scheel, "Macroscopic quantum electrodynamics in nonlocal and nonreciprocal media," *New J. Phys.*, Vol. 14, 083034, 2012.
3. Butcher, D. T., S. Y. Buhmann, and S. Scheel, "Casimir-Polder forces between chiral objects," *New J. Phys.*, Vol. 14, 113013, 2012.
4. Buhmann, S. Y., *Dispersion Forces II — Many-body Effects, Excited Atoms, Finite Temperature and Quantum Friction*, Springer, Heidelberg, 2012.

Quantum Friction from Shearing the Vacuum

Rongkuo Zhao and J. B. Pendry
The Blackett Laboratory, Department of Physics, Imperial College London
London SW7 2AZ, United Kingdom

Abstract— Van der Waals force, generally called Casimir force in the long-rang retarded limit, is a fluctuation-induced electromagnetic interaction between the instantaneous correlated charge pairs arising from quantum fluctuations on one surface and the induced opposite image charges on the other. This force dominates the interactions in nanodevices and causes stictions. Geckos inherit the ability to control this quantum force and manage to scamper on a smooth ceiling. What happens if a gecko slides along the wall? As indicated in Fig. 1(a), because of the dispersion (i.e., loss or electric resistance) of the materials, the induced image charges will not be able to follow up instaneously, showing a slightly delay. The lateral component of electromagnetic interaction will pull the quantum fluctuated charge back and equivalently produce a friction acting on the flat surface via the shearing vacuum. This quantum phenomenon, named 'quantum friction', was firstly correctly described in 1997 [1].

The quantum frictional force acting on a small sphere rotating near a surface as shown in Fig. 1(b) was theoretically investigated [2]. The existence of this noncontact quantum friction at zero temperature was confirmed. The surface can enhance the frictional force by several orders of magnitude, compared to that for the sphere rotating in the vacuum as studied in [3]. Quantum friction can be maximized by choosing materials with poor conductivity like graphite or semiconductors. For some semiconductor materials which support surface wave excitations, quantum friction can be further enhanced by several orders of magnitude. The prominent enhancement and the realistic geometry open up the possibility of experimental verification. In this talk, we will present our recent progresses on this topic.

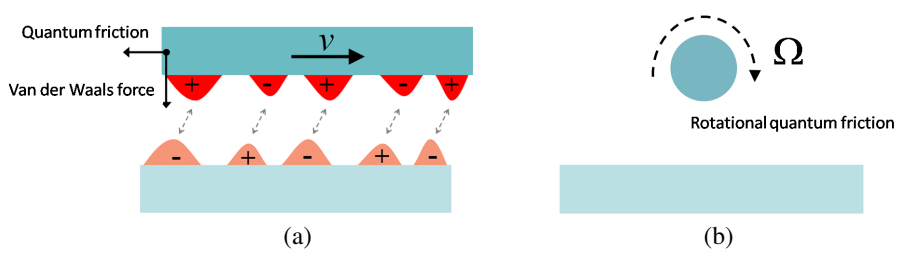

Figure 1: (a) Neutral perfect smooth surfaces shearing against each other with velocity v encounter a noncontact friction because of the correlated quantum fluctuation of the charges on the surfaces [1]. (b) A spherical particle rotates near a surface also encounters a rotational quantum frictional force.

REFERENCES

1. Pendry, J. B., *J. Phys. Condens. Matter*, Vol. 9, No. 10, 301, 1997.
2. Zhao, R., A. Manjavacas, F. J. García de Abajo, and J. B. Pendry, *Phys. Rev. Lett.*, Vol. 109, 123604, 2012.
3. Manjavacas, A. and F. J. García de Abajo, *Phys. Rev. Lett.*, Vol. 105, 113601, 2010.

Casimir Momentum of a Chiral Molecule in a Magnetic Field

M. Donaire[1,2], B. A. van Tiggelen[1], and G. L. J. A. Rikken[2]

[1]Université Grenoble 1/CNRS, LPMMC UMR 5493, B. P. 166, Grenoble 38042, France
[2]LNCMI, UPR 3228 CNRS/INSA/UJF Grenoble 1/UPS, Toulouse & Grenoble, France

Abstract— We present a full QED calculation which shows that the quantum vacuum coupled to a chiral molecule in a magnetic field provides a kinetic 'Casimir' momentum on the molecule directed along the magnetic field, proportional to its rotatory power and the fine structure constant and inversely proportional to its electrical polarizability [1].

Our molecular model is that of Condon [2]. In it an only oscillator, fully anisotropic, determines the optical activity of the molecule. Its harmonic potential is perturbed by its Coulomb interaction with the neighboring atomic groups within the molecule. This interaction breaks the mirror symmetry. In addition, a strong external magnetic field is applied which brakes time reversal symmetry. Under these conditions, it is symmetry-allowed for the oscillator to acquire a kinetic momentum [3]. We prove that this effect is entirely due to the interaction of the molecule with the electromagnetic (EM) vacuum field.

Our calculation is perturbative and free of divergences. It involves processes in which an only virtual photon is created and annihilated. The transfer of momentum from the EM vacuum to the oscillator can be understood as a result of the conservation of a total pseudo-momentum made of the addition of the kinetic momentum of the oscillator and the momentum of the EM field. We find that the kinetic momentum acquired by the molecule due to its interaction with the vacuum field is equal in magnitude and opposite sign to the momentum of the vacuum field. We refer to the latter as Casimir momentum, which is further decomposed into a longitudinal momentum, proportional to the gauge field, and the usual transverse momentum [4]. Interestingly, we find that the dominant contribution comes the longitudinal momentum. In addition, we find that the Doppler effect due to the internal motion of the oscillator is essential in the contribution of the transverse momentum.

We estimate the orders of magnitude of this effect in actual chiral compounds. Using the experimental data of their rotatory power and index of refraction, for a magnetic field of 10 T, we obtain molecular velocities of the order of nm/s.

REFERENCES

1. Donaire, M., B. A. van Tiggelen, and G. L. J. A. Rikken, arXiv:1304.6767.
2. Condon, E. U., *Rev. Mod. Phys.*, Vol. 9, 432, 1937.
3. Feigel, A., *Phys. Rev. Lett.*, Vol. 92, 020404, 2004.
4. Cohen-Tannoudji, C., J. Dupont-Roc, and G. Grynberg, *Atom-photon Interactions. Basic Processes and Applications*, Wiley, New York, 1998.

Near Field Radiative Heat Transfer in Microstructured Geometries

Alejandro W. Rodriguez
Massachusetts Institute of Technology, USA

Abstract— When two bodies of unequal temperatures are brought close to one another, heat, in the form of stochastic EM waves, is transferred from the hotter to the colder body. Although radiative heat transfer between far-away bodies (in the far field) has been well understood for decades, this phenomenon is just beginning to be explored in the near field (bodies separated by distances smaller than the thermal wavelength, i.e., seven microns near room temperature), where the contributions of evanescent waves lead to orders of magnitude larger heat transfers than in the far field. In this talk, we describe recent progress in the development of numerical methods that exploit the generality and efficiency of standard numerical techniques from classical computational EM to enable the design of nanostructured surfaces whose heat transport deviate significantly from the transport between planar geometries. Specifically, we describe a surface-integral-equation formulation of the problem that allows direct application of the boundary-element method of classical EM, which we exploit to compute heat transfers in various complex geometries.

Quantum Friction: A Case Study of the Fluctuation-dissipation and Quantum Regression Theorems

Diego A. R. Dalvit[1], **Ryan Behunin**[2], **and Francesco Intravaia**[3]

[1]Los Alamos National Laboratory, USA
[2]Yale University, USA
[3]University of Nottingham, UK

Abstract— Quantum friction, a drag force on scatterers (atoms, solids, etc.) in relative motion due to quantum and thermal fluctuations of the electromagnetic field, has attracted much attention recently. However, several authors have obtained quite different results for this force, making different predictions as to its dependence on the velocity of the atom and the atom-surface separation. The aim of this talk is to shed light on the apparent contradictory predictions by using general concepts of quantum statistical mechanics and comparing predictions arising from the exact flluctuation-dissipation theorem with the approximate quantum regression hypothesis.

Session 2P5a
SC3: High Energy and High Power Applications in Photonic Crystal/Microstructured Fibres

Challenges and Opportunities for Next-generation Fibers for High-power Laser Sources
Johan Nilsson, ... 720

High Average Power, Widely Tunable Femtosecond Laser Source from Red to Mid-infrared Based on an Yb-fiber-laser-pumped OPO
Ming-Lie Hu, Chengling Gu, Jingtao Fan, Limeng Zhang, Ching-Yue Wang, ... 721

Development and Perspectives of High Repetition Rate Attosecond Sources
Cord L. Arnold, M. Miranda, P. Rudawski, J. Guo, C. M. Heyl, E. Witting-Larsen, E. Lorek, J. Mauritsson, T. Binhammer, O. Prochnow, A. L'Huillier, ... 722

Self-focusing in Optical Fibers
Alexander L. Gaeta, ... 723

High-power Laser Pulse Compression for Optimized High-harmonic Generation in Short Hollow Fibers
Peter Horak, P. N. Anderson, T. J. Butcher, J. G. Frey, W. S. Brocklesby, ... 724

Generation of Tunable Ultraviolet Light in Kagomé-lattice Hollow-core Photonic Crystal Fibre
Nicolas Y. Joly, John C. Travers, K. F. Mak, F. Tani, Philipp Hölzer, Wonkeun Chang, P. St. J. Russell, ... 725

Challenges and Opportunities for Next-generation Fibers for High-power Laser Sources

Johan Nilsson
Optoelectronics Research Centre, University of Southampton, Southampton SO17 1BJ, England

Abstract— Advances in fiber design and manufacturing underpin the impressive progress of fiber lasers in output power and other performance parameters that we have seen in the last 15 years. Despite this progress, many of the challenges that were encountered early on still remain, but at a different level, where tolerances, etc., are becoming increasingly stringent. In addition, new requirements are added by the increasing importance of thermal effects as the power gets higher, the fiber get shorter, and the cores get larger. Furthermore, new device approaches also add requirements, on phase fidelity in case of coherent beam combination in phased-array geometries to give just one example.

Microstructured fibers has played and will continue to play an important part of this in several different ways. At one level, the stack-and draw fabrication approach of microstructured fibers allows for unsurpassed control of refractive index and dopant distribution. Fabricated rods of different composition can be precisely characterized before they are stacked in a preform and drawn into fiber. The resulting features can be so small that they are not resolved by the light field, so that refractive index profiles that are effectively perfectly flat can be realized.

The large index step provided by air:glass surfaces in microstructured fibers also providesmany advantages. This is true even when the waveguiding relies on average-index effects in large waveguides, with the definition of the inner cladding in jacketed air-clad fibers being one important example.

The ability to create large index steps for high-NA waveguides and to reduce unwanted index variationsis extremely important. However arguably more interesting in terms of waveguide physics is the ability to manipulate the dispersion and to create waveguide filters that guide some wavelengths but not others.

I will discuss the roles these different features of microstructured can play in emerging applications and devices.

High Average Power, Widely Tunable Femtosecond Laser Source from Red to Mid-infrared Based on an Yb-fiber-laser-pumped OPO

Minglie Hu, **Chengling Gu**, **Jingtao Fan**, **Limeng Zhang**, **and Ching-Yue Wang**
Ultrafast Laser Laboratory
Key Laboratory of Opto-Electronic Information Science and Technology of Ministry of Education
College of Precision Instruments and Opto-Electronics Engineering
Tianjin University, Tianjin 300072, China

Abstract— Femtosecond laser sources in visible, infrared and mid-infrared ranges are of great importance in many applications including biophotonics, optical microscopy and time resolved spectroscopy. Optical parametric oscillators (OPO) or amplifiers (OPA) pumped by femtosecond Ti:sapphire lasers have been the source of choice in the past for this range. Nowadays, the rapid progress in ultrafast fiber lasers leads to the development of a new generation of compact and robust femtosecond laser sources and inspires the development of fiber-based OPO. We demonstrate highly efficient generation of widely tunable femtosecond pulses based on intracavity second harmonic generation (SHG) and sum frequency generation (SFG) in a MgO-doped periodically poled $LiNbO_3$ optical parametric oscillator (OPO), which is pumped by a Yb-doped large-mode-area photonics crystal fiber femtosecond laser Red and near infrared from intracavity SHG and SFG and infrared signal directly obtained from OPO. A 2 mm β-BaB_2O_4 is applied for Type I ($oo \rightarrow e$) intracavity SHG and SFG, and then femtosecond laser pulses over $610 \sim 668$ nm from SFG and $716 \sim 970$ nm from SHG are obtained with high efficiency In addition, the oscillator simultaneously generates signal and idler femtosecond pulses over 1450 nm $\sim$ 2200 nm and 2250 nm $\sim$ 4000 nm, respectively.

Development and Perspectives of High Repetition Rate Attosecond Sources

C. L. Arnold[1], M. Miranda[1], P. Rudawski[1], J. Guo[1], C. M. Heyl[1], E. Witting-Larsen[1], E. Lorek[1], J. Mauritsson[1], T. Binhammer[2], O. Prochnow[2], and A. L'Huillier[1]

[1]Department of Physics, Lund University, P. O. 118, Lund 22100, Sweden
[2]VENTEON Laser Technologies GmbH, Hertzstr. 1b, Garbsen 30827, Germany

Abstract— After the initial realization of attosecond pulses in 2001 [1, 2], the first decade of attosecond science was mainly conditioned by establishing the field and exploring ultrafast dynamics of rather simple electronic systems. The second decade is dominated by physical questions of much greater complexity [3], for which today's tools are not adequate. To appropriately address these questions, a new generation of attosecond pulse sources is indispensable.

In particular, the development of high repetition rate attosecond sources is of great interest for a number of applications. To, e.g., unravel electron correlations often involves coincidence detection schemes [4], which by definition can only record single events per attosecond laser pulse. Such an experiment strongly benefits from an increase in repetition rate, but not necessarily from an increase in pulse energy. The same accounts for time-resolved electron microscopy, combining nanometer spatial with attosecond temporal resolution, which at low repetition rate is strongly compromised by space charge effects [5].

We currently develop a high repetition rate attosecond source based on optical parametric chirped pulse amplification (OPCPA) laser technology. OPCPA overcomes two main limitations of traditional chirped pulse amplification (CPA), i.e., it directly allows for few-cycle pulse duration without post compression schemes and it easily scales to high repetition rates. In practice, this results in more control on the generation of attosecond pulses and faster repetition of attosecond experiments.

Consequently, together with VENTEON laser technologies a high repetition rate OPCPA laser system, based on a Titanium:Sapphire front end and a Ytterbium-doped fiber CPA laser chain as pump source, was developed and recently installed in Lund. It emits pulses at 200 kHz to 2 MHz repetition rate, with pulse duration < 7 fs (2.5 optical cycles), and up to 10 μJ pulse energy. Due to its compactness the system features excellent carrier envelope phase (CEP) stability, a prerequisite for the reproducible generation of single attosecond pulses (SAPs).

Efficient generation of attosecond pulses via high-order harmonic generation (HHG) in gaseous targets however remains a challenge at high repetition rate. Because of the low energy of the driving pulse, tight focusing into the generation gas is required, what greatly reduces the generation volume and complicates phase-matching. An interesting approach could be the use of hollow core photonic crystal fibers. So-called Kagomé fibers recently have attracted much attention in the ultrafast community due to their unique possibility for pulse self-compression at ionizing intensities [6, 7]. This might allow for a unique high repetition rate source of single attosecond pulses.

The talk will summarize our current development of a high repetition rate attosecond source and applications will be highlighted.

REFERENCES

1. Paul, P. M., et al., *Science*, Vol. 292, 1689, 2001.
2. Hentschel, M., et al., *Nature*, Vol. 414, 509, 2001.
3. Krausz, F. and M. Ivanov, *Rev. Mod. Phys.,* Vol. 81, 163, 2009.
4. Månsson, E., et al., in revision.
5. Mårsell, E., et al., *Ann. Phys*, Vol. 525, 162, 2013.
6. Travers, J., et al., *J. Opt. Soc. Am. B,* Vol. 28, 12, 2011.
7. Hölzer, P., et al., *Phys. Rev. Lett.*, Vol. 107, 203901, 2011.

Self-focusing in Optical Fibers

Alexander Gaeta
Cornell University, USA

Abstract— Recent developments of high-power fiber lasers and amplifiers demonstrate operation at power levels within fibers that approach or exceed the critical power for self-focusing. I will discuss the dynamics of self-focusing in optical waveguides and the potential for raising the threshold power for self-focusing above that in bulk media.

High-power Laser Pulse Compression for Optimized High-harmonic Generation in Short Hollow Fibers

P. Horak[1], **P. N. Anderson**[1], **T. J. Butcher**[1], **J. G. Frey**[2], **and W. S. Brocklesby**[1]

[1]Optoelectronics Research Centre, University of Southampton, Southampton SO17 1BJ, UK
[2]Chemistry, Faculty of Natural and Environmental Sciences, University of Southampton
Southampton SO17 1BJ, UK

Abstract— High-harmonic generation (HHG) driven by high-power femtosecond lasers is a promising route towards tabletop sources of coherent radiation at extreme ultraviolet (XUV) and soft X-ray wavelengths. In order to maximize conversion efficiency and to obtain attosecond pulse lengths of the harmonics, pump pulse lengths down to the few-cycle regime are required. Traditionally, this has been achieved by nonlinear spectral broadening in gases and subsequent dispersion compression or by self-compression in laser-induced filaments. Here we investigate an alternative method that is simpler to implement experimentally, based on multimode nonlinear propagation effects in short, centimeter-length, gas-filled hollow fibers operating in the high-ionization regime.

We use an advanced multimode generalized nonlinear Schrödinger equation that includes ionization and plasma effects to simulate pulse propagation in such a system [1]. We show how plasma defocusing and modal interference effects lead to spatio-temporal compression of 50-fs input pulses to the few-cycle regime. The simulations predict that highly compressed pulses are generated and maintained for significant propagation distances over a wide range of parameters such as input pulse energy, gas pressure, and capillary diameter. We also extend the scheme to novel wavelengths and driving pulse lengths. As an example, we demonstrate how few-hundred femtosecond pulses from a state-of-the-art high repetition rate fiber laser can be compressed in hollow-core fibers by reducing the core diameter. Microstructured hollow core fibers provide significant advantages in this situation compared to capillaries by allowing us to reduce the propagation losses by orders of magnitude.

Based on our simulations we have recently implemented an improved design of our experimental setup for investigating HHG in short capillaries. This has resulted in a 40-fold increase of the observed flux of generated high-harmonic radiation around 29 nm wavelength reaching up to 1.5×10^9 photons per pulse [2].

In a next step, we are now combining our model of pump pulse propagation with simulations of the time-dependent Schrödinger equation of the electron wavefunction of single gas atoms [3]. While this is an extremely demanding problem computationally, it will provide a full $3+1$ dimensional ab-initio model of HHG in hollow fibers. Preliminary results predict that isolated attosecond XUV pulses can be generated on-axis using the pulse compression technique described above where both pump compression and HHG occur within the same short (4 cm long) hollow fiber.

REFERENCES

1. Chapman, R. T., T. J. Butcher, P. Horak, F. Poletti, J. G. Frey, and W. S. Brocklesby, *Opt. Express*, Vol. 18, 13279, 2010.
2. Butcher, T. J., P. N. Anderson, P. Horak, W. S. Brocklesby, R. T. Chapman, and J. G. Frey, *Phys. Rev. A*, Vol. 87, 043822, 2013.
3. Anderson, P. N., P. Horak, J. G. Frey, and W. S. Brocklesby, *CLEO-Europe/IQEC 2013*, paper CG-P.10, Munich, Germany, May 12–16, 2013.

Generation of Tunable Ultraviolet Light in Kagomé-lattice Hollow-core Photonic Crystal Fibre

N. Y. Joly, J. C. Travers, K. Mak, F. Tani, P. Hölzer, W. Chang, and P. St. J. Russell
Max-Plank Institute for the Science of Light, Guenther-Scharowsky Str. 1, Erlangen 91058, Germany

Abstract— We review recent work on the generation of tunable ultraviolet-to-visible light in gas-filled hollow-core photonic crystal fiber. The generated wavelengths range from 180 nm to 550 nm.

Kagomé-lattice hollow-core photonic crystal fiber (kagomé-PCF) is a special type of fiber which exhibits weak anomalous dispersion that varies slowly with wavelength from the UV to the IR. When filled with gas, it is possible to adjust the whole landscape of the dispersion [1] and to shift the zero dispersion wavelength from the ultraviolet (UV) to the infrared (IR) [2]. Combined with a broad transmission window and a high-damage threshold, gas-filled kagomé-PCF is a perfect system for studying the propagation of high peak power pulses in gases, soliton-related effects and spectral-broadening, especially in the UV region. Such systems have been used to demonstrate soliton self-compression followed by the emission of UV dispersive waves in the normal dispersion region [3]. They have also been used to demonstrate plasma-driven soliton blue shifting [4].

Here we present recent results on UV dispersive wave emission tunable from below 180 nm to 550 nm (Fig. 1), the tunability being made possible largely by the choice of noble gas, the pressure, the pulse energy and duration and of course the fibre design. For a weakly polarizable gas such as Ne, the contribution of normal dispersion at pressures of a few bar is very weak, so that the zero dispersion wavelength of the combined gas + fibre system is in the deep UV far from the pump wavelength (800 nm. This results in dispersive wave emission in the vacuum UV. In contrast, for a more polarisable gas such as Xe, the zero-dispersion wavelength lies closer to the pump-wavelength a fewbar pressure, leading to the emission of dispersive waves at longer wavelengths.

This unique tunable source of bright vacuum-UV-to visible radiation, based simply on a short length of gas-filled hollow core PCF, is likely to have many applications in, e.g., spectroscopy and lithography and has also been suggested as a source for seeding free-electron lasers [5].

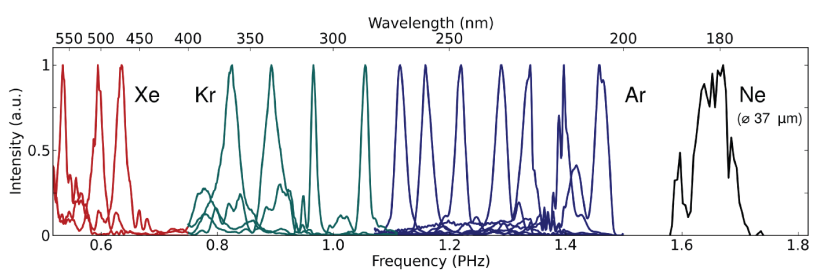

Figure 1: Tunability of the dispersive wave emission for gas-filled kagomé-PCF, optimized so as to produce a well-localised spectral peak in each case. Note that for the Ne result the core diameter was 37 μm, whereas it was 27 μm in all other cases. Pulse energies of more than 75 nJ in the deep- UV, with relative bandwidths of $\sim 3\%$, are generated from pump pulses of a few μJ (after [4]).

REFERENCES

1. Nold, J., et al., "Pressure-controlled phase matching to third harmonic in Ar-filled hollow-core photonic crystal fiber," *Opt. Lett.*, Vol. 35, 2922–2924, 2010.
2. Travers, J. C., et al., "Ultrafast nonlinear optics in gas-filled hollow-core photonic crystal fibers," *J. Opt. Soc. Am. B*, Vol. 28, A11–A26, 2011.
3. Joly, N. Y., et al., "Bright spatially coherent wavelength-tunable deep-UV laser source using an Ar-filled photonic crystal fiber," *Phys. Rev. Lett.*, Vol. 106, 203901, 2011.
4. Mak, K., et al., "Tunable vacuum-UV to visible ultrafast pulse source based on gas-filled kagome-PCF," *Opt. Express*, Vol. 21, 10942–10953, 2013.
5. Joly, N. Y., et al., "Seeding of SPARC-FEL with a tunable fibre-based source," *34th International Free-Electron Laser Conference*, Nara, Japan, 2012.

Session 2P5b
3_FocusSession.SC3: Optical Angular Momentum and Its Applications

Light's Orbital Angular Momentum and Its Application to the Remote Detection of a Spinning Object
Miles J. Padgett, Martin P. J. Lavery, ... 728
Ultrafast Optical Rotation of Gold Nanoparticles in Water
Anni Lehmuskero, Robin Ogier, Tina Gschneidtner, Peter Johansson, Mikael Kall, ... 729
Optical Angular Momentum Modes for Optical Communication
L. Mauritz Andersson, Gunnar G. E. Björk, ... 730
Generation of Classical and Quantum Sources of Light with Well Defied Orbital Angular Momentum
Nidia Escamilla Bojorges, Z. Gress Mendoza, Sara Cruz y Cruz, Víctor Velázquez Aguila, ... 731
Applying Humblet's Decomposition of the Electro-magnetic Angular Moment in Metallic Waveguides
Eilert Berglind, G. Bjork, ... 732
Spin-orbit Interaction and Uncertainty-type Inequalities for Strongly Focused Fields
Miguel A. Alonso, ... 733
Photon's Angular Momentum and Center-of-mass Reference Frame
Chun-Fang Li, Zi-Hua Xin, ... 734

Light's Orbital Angular Momentum and Its Application to the Remote Detection of a Spinning Object

M. Padgett and M. Lavery
School of Physics and Astronomy, University of Glasgow, Scotland, UK

Abstract— The linear momentum of light is encompassed in Maxwell's equations [1] and was shown in 1901 by Lebedew to cause the the recoil of a mechanical object [2]. The angular momentum of a light beam is also implicit within Maxwells equations and was explicitly considered by Poynting who drew analogies between optical and mechanical systems to deduce that, for circularly polarised light, the ratio between its angular momentum and its energy was $1/\omega$ [3], (where ω is the angular frequency).

Nowadays accepting the concept of a photon with an energy $\hbar\omega$ leads directly to the familiar descriptions of the linear and spin angular momentum of the photon being $\hbar k$ and $\hbar$ respectively, where $k = 2\pi/\lambda$. The $\hbar$ quantisation of this spin angular momentum is consistent with the interaction of light and dipole transitions within atomic systems. In 1932 Darwin (grandson of the originator of evolution) recognised that higher-order transitions required an optical angular momentum of integer multiples of $\hbar$ [4]. He postulated that this extra momentum could be produced as a recoil torque when the centre of mass of the atomic system was slightly displaced from the optical axis.

Sixty years after Darwin, Allen, Woerdman and co-workers proposed that beams with helical phasefronts described by a phase cross-section $\exp(i\ell\phi)$, had an angular momentum of $\ell\hbar$ per photon [5]. This orbital angular momentum (OAM) is distinct from, and additional to, the spin angular momentum associated with the polarisation state of the light.

Over the course of the last 20 years studies of OAM have attracted significant interest in applications ranging from optical manipulation to imaging [6]. Beyond applications, the analysis of problems in this angular basis has provided new insight to phenomena ranging from rotational frequency shifts to angular uncertainty relationships. In quantum science, OAM emphasised spatial modes as one parameter within a large state space thereby giving basis sets for new tests and demonstrations of high-dimensional entanglement.

In our latest work we show that by analysing the orbital angular momentum of the light scattered from a spinning object we can observe a frequency shift many times greater than the rotation rate of the object itself. This rotational frequency shift is still present when the angular momentum vector is parallel to the observation direction, i.e., when the linear Doppler shift is zero. Our findings, including the multiplicative enhancement of the frequency shift, have potential applications in both terrestrial and astronomical settings for the remote detection of rotating bodies.

REFERENCES

1. Maxwell, J. C., "A dynamical theory of the electromagnetic field," *Philosophical Transactions for the Royal Society of London*, 1865.
2. Lebedew, P., "Untersuchungen ber die Druckkrfte des Lichtes," *Annalen der Physik*, Vol. 311, 433, Wiley Online Library, 1901.
3. Poynting, J. H., "The wave motion of a revolving shaft, and a suggestion as to the angular momentum in a beam of circularly polarised light," *Proc. R. Soc. Lon.*, Ser. A, Vol. 82, 560, 1909.
4. Darwin, C. G., "Notes on the theory of radiation," *Proc. R. Soc. Lon.*, Ser. A, Vol. 136, 36, 1932.
5. Allen, L., M. W. Beijersbergen, R. J. C. Spreeuw, and J. P. Woerdman, "Orbital angular-momentum of light and the transformation of Laguerre-Gaussian laser modes," *Phys. Rev. A*, Vol. 45, 8185, 1992.
6. Yao, A. M. and M. J. Padgett, "Orbital angular momentum: Origins, behavior and applications," *Adv. Opt. Photon.*, Vol. 3, 161, 2011.

Ultrafast Optical Rotation of Gold Nanoparticles in Water

Anni Lehmuskero[1], **Robin Ogier**[1], **Tina Gschneidtner**[2], **Peter Johansson**[1,3], **and Mikael Kall**[1]

[1]Department of Applied Physics, Chalmers University of Technology, S-412 96 Göteborg, Sweden
[2]Department of Chemical and Biological Engineering, Chalmers University of Technology S-412 96 Göteborg, Sweden
[3]School of Science and Technology, Örebro University, S-701 82 Örebro, Sweden

Abstract— Controlling the position and movement of small objects with light is an appealing way to manipulate delicate samples, such as living cells or nanoparticles. It is well-known that optical gradient and radiation pressure forces caused by a focused laser beam enables trapping and manipulation of objects with strength that is dependent on the particle's optical properties. Objects can even be set into rotational motion simply by targeting them with a beam of circularly polarized light. Here we show that this effect, which is caused by transfer of photon spin angular momentum, can make gold nanoparticles with $\sim 200\,\mathrm{nm}$ radii rotate at frequencies that reach several kilohertz in water [1]. We show that the high rotation frequency is the combined result of favorable optical particle properties and a low local viscosity due to substantial heating of the particles surface layer. The results suggest possible applications in nanofluidics, optical sensing and micro-tooling of soft matter.

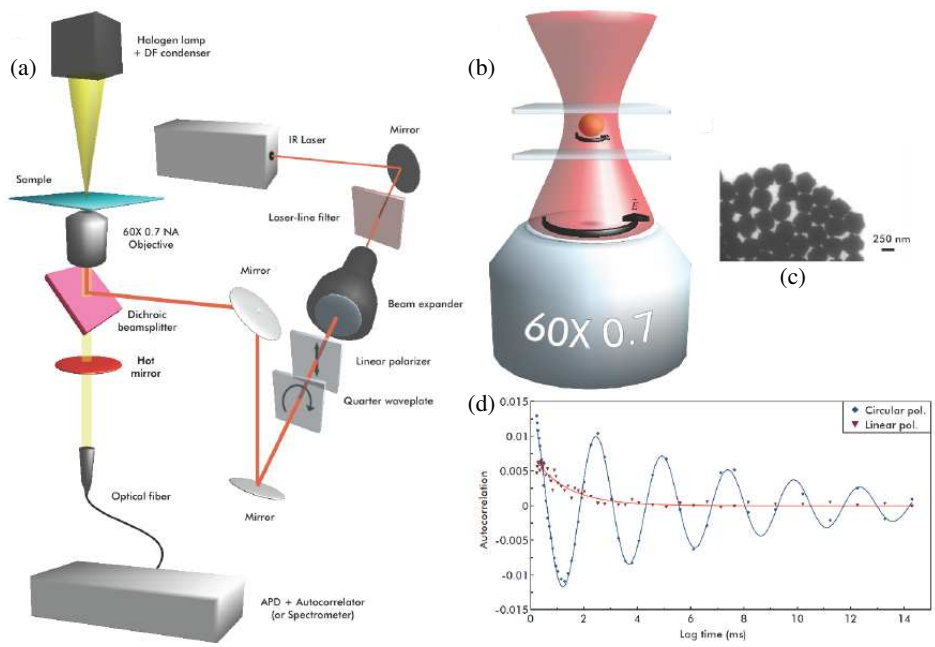

Figure 1: Spinning gold nanoparticles by light. (a) Schematic of the setup. The near-infrared trapping laser beam ($\lambda_L = 830\,\mathrm{nm}$) is expanded to fill the back aperture of the objective and circularly polarized using appropriate optics components. The sample is also illuminated with white light through a dark field (DF) condenser. The light scattered from the trapped particle is recorded by an avalanche photo diode (APD) and analyzed by an autocorrelator. (b) A gold particle is optically trapped between two cover glass slides and pushed against the upper cover glass by the radiation pressure. The particle starts to rotate by absorbing spin angular momentum from the circularly polarized laser beam. (c) Transmission electron microscope image of the gold particles. The particles have a round shape with an average radius of 200 nm. The irregular deviations from perfect sphericity results in a light scattering intensity that fluctuate with the periodicity of the optical rotation. (d) Intensity autocorrelation functions for a particle subject to circular (blue squares) and linearly polarized laser light (red triangles). The solid lines represent fits to the data using an analytical model of the intensity correlation functions.

REFERENCES

1. Lehmuskero, A., et al., submitted.

Optical Angular Momentum Modes for Optical Communication

L. Mauritz Andersson and Gunnar Björk
Royal Institute of Technology (KTH), AlbaNova University Center, Stockholm SE-106 91, Sweden

Abstract— Communication through the use of optical angular momentum modes is analyzed.

Optical angular momentum modes [1] can be used to encode information. Here we study to what extent they can provide additional communication capacity for small detectors below the spatial resolution of traditional modes.

A possible orthogonal set of modes with well defined optical angular momentum about the optical axis is the Laguerre-Gauss modes. Consider an optical intensity detector of radius r and area $A = \pi r^2$ capable of distinguishing orthogonal optical angular momentum modes into different channels. Assume the L-G modes k to be centered on the detector and have a mode radius of $w \gg r$. Further assume that the total photon flux transmitted in each mode is N_k.

The photon flux received for the $l = 0$ and $l = \pm 1$ angular momentum detectors become

$$n_0 \approx N_0 \frac{2r^2}{w^2}, \quad n_1 \approx N_0 \frac{2r^4}{w^4}. \tag{1}$$

Now if we want to have reliable communication we need to get a signal to noise ration (SNR) above a certain threshold. Assuming only quantum shot noise contribution, the SNR becomes

$$\mathrm{SNR} = \sqrt{nt} = \sqrt{n/\mathrm{BW}}, \tag{2}$$

where t is the integration time for a bit. The communication bandwidth is $\mathrm{BW} = 1/t$. Thus, in order for the different channels to have the same SNR the transmitter photon flux have to be

$$N_0 \approx \frac{\mathrm{SNR}^2\ \mathrm{BW}}{2(r/w)^2}, \quad N_1 \approx \frac{\mathrm{SNR}^2\ \mathrm{BW}}{2(r/w)^4}. \tag{3}$$

Therefore the relative power in the two transmitter modes need to be

$$P_1/P_0 = N_1/N_2 = (w/r)^2, \tag{4}$$

showing that the power penalty for the first vortex mode scales as the inverse of the detector area, when the detector is small compared to the transmitted mode radius. For higher modes the power penalty scales even worse, proportional to $(w/r)^{2|l|}$.

The conclusion is therefore that far field multichannel communication using vortex modes comes at a great power cost.

For the case of detector size bigger than the transmitted mode size the power penalty is essentially unity. However in this case any set of spatially orthogonal modes are equally useful for communication. However, this case is equivalent to "near field" communication, where the transmitting antenna size is comparable to the detector distance.

In broadcasting, when the detector is offset from the optical axis, the detected vortex modes are no longer orthogonal and detrimental cross-talk will increase rapidly with increasing offest. This is a manifestation of the fact that the angular momentum of an optical mode has an optical axis [2] in contrast to polarization.

REFERENCES

1. Allen, L. and M. Padgett, *Twisted Photons*, Wiley-VCH, 2011.
2. Allen, L., "The poynting vector in Laguerre-Gaussian beams and the interpretation of their angular momentum density," *Opt. Comm.*, Vol. 184, No. 1–4, 67–71, 2000.

Generation of Classical and Quantum Sources of Light with Well Defied Orbital Angular Momentum

Nidia E. Bojorges[1], **Z. Gress Mendoza**[1], **Sara Cruz y Cruz**[1], **and Víctor Velázquez Aguilar**[2]

[1]Unidad Profesional Interdisciplinaria en Ingeniería y Tecnologías Avanzadas (UPIITA)
Instituto Politécnico Nacional (IPN), Av. Instituto Politécnico Nacional 2580
Barrio la Laguna Ticomán, Gustavo A. Madero, México D.F. 07340, Mexico
[2]Facultad de Ciencias, Universidad Nacional Autónoma México (UNAM)
Av. Universidad 3000, Circuito Exterior S/N Delegación Coyoacán
C.P. 04510 Ciudad Universitaria, México D.F., Mexico

Abstract— Information and quantum engineering are branches of science that have increasingly gained interest in recent years. One of their most promising goals is to understand how quantum physics can be used to improve the transmission, processing and manipulation of information, as well as how to generate new technologies. Of the great number of processes occurring at the quantum level, the interaction of radiation with matter is of fundamental importance since it may give us a deep insight of how the properties of radiation can be used to manipulate quantum systems. In particular, the ability of light to transmit energy, linear and angular momentum offers high perspectives in this sense.

The energy, linear momentum and polarization of radiation are concepts which are well studied. However, the description of light orbital angular momentum is still under development. The study of this phenomenon intends to give a better understanding of the transference of orbital angular momentum between matter and light at the microscopic level. Additionally, a detailed study of the spatial correlation of light with well defined orbital angular momentum offers a number of exciting novel applications as, for example, optical atomic and molecular manipulation, optical trapping, communications and quantum entanglement just to mention few ones. In this context, the generation of sources of light with well defined orbital angular momentum is of crucial importance.

In this work we present a theoretical and experimental study of the optical orbital angular momentum. In the first place, the solutions of wave equation with well defined orbital angular momentum (the Laguerre-Gauss modes) are presented. Next, the generation of sources of Laguerre-Gauss modes in the classical regime is addressed and the corresponding spatial correlation is observed. Similar experiments in the quantum regime are carried out with Spontaneous Parametric Down Converted photons. These experiments allow us to conclude that converted photons also acquire well defined orbital angular momentum.

Applying Humblet's Decomposition of the Electro-magnetic Angular Moment in Metallic Waveguides

E. Berglind and G. Björk
Department of Applied Physics, Royal Institute of Technology (KTH), Stockholm 10691, Sweden

Abstract— In a seminal paper, Humblet [1] decomposed the electro-magnetic angular moment of a classical field as a sum of three parts: the orbital angular moment, the spin, and the more unfamiliar surface angular moment [2]. In this contribution we present the result of such decomposition for various waveguides.

We investigate two hollow, metal waveguides with rectangular and circular cross sections, respectively. The waveguides are excited with two TE_{nm} eigen-modes [3] driven in phase quadrature. We also investigate two TEM-waveguides with four metallic boundaries, pair-wise driven in phase quadrature. Two better known modes are used as references: A plane, circularly polarized wave and a "twisted" TE-Bessel beam [4, 5], both of infinite extent and with no metallic boundaries.

When the results are normalized to the energy density, the decomposition yields reasonable results. For example, the spin per photon is never larger than $\hbar$ (or smaller than $-\hbar$) and for some mode combinations it vanishes. However, the normalized orbital angular moment is not bounded in general, but can also be zero for certain mode combinations. It is worth emphasizing that the surface angular moment is not always zero, which often assumed. Even in some simple modes (e.g., plane, circularly polarized waves) without boundary or confinement this term cannot be neglected.

The angular moment of superpositions of TM_{nm} modes follow the same general pattern as the TE_{nm} modes since the Maxwell equations are dual with respect to the **E**- and **H**-fields.

Although not often discussed in the literature, we hence show that angular moment is built into the eigen-mode description of the fields in the waveguide. Therefore, electromagnetic angular moment and orbital angular moment do not provide any degrees of freedom that are not already covered by the eigen-mode description.

REFERENCES

1. Humblet, J., "Sur le moment d'impulsion d'une onde electromagnetique," *Physica (Utrecht)*, Vol. 10, 585, 1943.
2. Crichton, J. H. and P. L. Marston, "The measurable distinction between the spin and orbital angular momenta of electromagnetic radiation," *Electron. J. Differential Equations*, Vol. 4, 37, 2000.
3. Collin, R. E., *Foundations for Microwave Engineering*, Chapter 3, McGraw-Hill, New York, 1992.
4. Durnin, J., "Exact solutions for nondiffracting beams. I. The scalar theory," *J. Opt. Soc. Am. A*, Vol. 4, 651–654, 1987.
5. Durnin, J., J. J. Miceli, Jr., and J. H. Eberly, "Diffraction-free beams," *Phys. Rev. Lett.*, Vol. 58, 1499, 1987.

Spin-orbit Interaction and Uncertainty-type Inequalities for Strongly Focused Fields

Miguel A. Alonso
The Institute of Optics, University of Rochester, Rochester, NY 14627, USA

Abstract— The study of the angular momentum of light has been the focus of a large body of work in recent years, motivated in part by the discovery that this momentum can be partially transferred from the optical field to a particle or particles that the field illuminates. Particular emphasis has been placed on the longitudinal component of the orbital angular momentum, which relates to the phase structure of a field around a given axis, and the spin angular momentum, related to the fields polarization. While for paraxial beams these two contributions to the total angular momentum are independent, beyond the paraxial regime they have been shown to be interconnected.

Uncertainty-type relations provide fundamental lower or upper bounds for quantities that give a local or global characterization of a field. For example, a direct analogue of the Heisenberg uncertainty relation states that the product of the spatial and directional spreads of a beam (measured in terms of second moments of the intensity) must be equal to or greater than a given constant proportional to the wavelength, the lower bound of such a relation being achieved only for Gaussian beams. This inequality is the basis for the definition of the so-called beam quality factor, M^2. Generalizations of this type of inequality to the nonparaxial regime have been studied by several authors. Here, the influence of the orbital and spin (if applicable) angular momenta on the relation between the spatial and directional spreads of free nonparaxial fields (both scalar and electromagnetic) are studied, leading to new uncertainty-type inequalities. These inequalities describe how these two types of angular momentum affect the minimum spatial spread of a focused field of given angular spread.

REFERENCES

1. Alonso, M. A., "The effect of orbital angular momentum and helicity on the uncertainty-type relations between focal spot size and angular spread," *J. Opt.*, Vol. 13, 064016, 2011.
2. Bliokh, K. Y., M. A. Alonso, E. A. Ovstrovskaya, and A. Aiello, "Angular momenta and spin-orbit interaction of nonparaxial light in free space," *Phys. Rev. A*, Vol. 82, 063825, 2010.

Photon's Angular Momentum and Center-of-mass Reference Frame

Chun-Fang Li and Zi-Hua Xin
Department of Physics, Shanghai University, China

Abstract— A new representation, called Jones representation, is introduced to canonically quantize the radiation field. Being different from the Maxwell wavefunction that is defined in the laboratory reference frame and is constrained by the transversality condition, the Jones wavefunction is defined in the so-called inner reference frame. It is the position vector with respect to the inner reference frame that is canonically conjugate to the momentum. Nevertheless, the inner reference frame is not associated with the laboratory reference frame simply by a spatial translation. Instead, the origin of the inner reference frame with respect to the laboratory reference frame is described by an operator in the Jones representation. A new degree of freedom is also identified to determine this operator. The notion of inner reference frame can be regarded as a natural generalization of the classical concept of center of mass in the quantum theory. As a matter of fact, for the eigen excitations such as the plane-wave modes and the diffraction-free modes, the origins of their inner reference frames become their centers of mass with respect to the laboratory reference frame. Based on these observations, the angular momentum of photon is shown to satisfy the commutation relations that were obtained by [1] from a consideration of the second quantization.

REFERENCES

1. Van Enk, S. J. and G. Nienhuis, "Commutation rules and eigenvalues of spin and orbital angular momentum of radiation fields," *J. Mod. Opt.*, Vol. 41, 963–977, 1994.

Session 2P6
SC4: Antenna and RF Measurements

VHF EMF Portable Radio Assessment
Nina B. Rubtsova, Sergey Yu. Perov, Elena Bogacheva, Quirino Balzano, Niels Kuster, ... 736

Conductivity and Permittivity Measurements of Children and Adult's Hands Covering Mobile Communications Frequency Bands
Chinthana J. Panagamuwa, Ian Howells, William Whittow, ... 737

Optimal Size of Waterproofed Shielded Loop Antenna in a Tissue-equivalent Liquid to Calibrate SAR Probe in HF Band
Nozomu Ishii, Ryosuke Takezawa, Hidenori Toyoshima, Lira Hamada, Soichi Watanabe, ... 738

Characterization of HF RFID Tags Exposed to Moisture Based on Threshold Power Measurement
Toni Bjorninen, Jukka Voutilainen, Lauri Sydanheimo, Leena Ukkonen, ... 739

Non-invasive Antenna Pattern Characterization Using Time-domain and Frequency-domain Measurement Techniques
Tian Hong Loh, David Humphreys, Philip Miller, ... 741

Far Field Gain Estimation Method for Japanese Broadband Antenna Standard Using Time-frequency Analysis
Satoru Kurokawa, Michitaka Ameya, Masanobu Hirose, ... 742

RCS Measurement of a Patch Antenna with Resistive Load in a Compact Anechoic Chamber
Naobumi Michishita, Tadashi Chisaka, Yoshihide Yamada, ... 743

Complex Antenna Pattern Measurement by Spherical Scanning and Phase Retrieval Method
Hiroyuki Arai, Eriko Ohashi, ... 744

Extended $\boldsymbol{S}$-parameter Method for Radiation Characteristics and Mutual Coupling of Multiport Antennas
Takashi Yanagi, Toru Fukasawa, Hiroaki Miyashita, ... 745

Path Loss Characteristics in a Civil Laboratory Building at a Frequency of 2.4 GHz
Supachai Phaiboon, Adchara Kampan, ... 746

New Applications and Measurement Results by MIMO Transmission
Kentaro Nishimori, ... 747

Detection Reliability Analysis of Passive DAS RFID System
Abdelmoula Bekkali, Abdullah Kadri, Michael J. Crisp, Richard V. Penty, ... 748

VHF EMF Portable Radio Assessment

Nina Rubtsova[1], **Sergey Perov**[1], **Elena Bogacheva**[1], **Quirino Balzano**[2], **and Niels Kuster**[3]

[1]Federal State Budgetary Institution 'Research Institute of Occupational Health' under the Russian Academy of Medical Sciences, Moscow, Russian Federation
[2]Department of Electrical and Computer Engineering, University of Maryland, Maryland, USA
[3]Foundation for Research on Information Technologies in Society, Zurich, Switzerland

Abstract— The safety of human users of portable transmitters in occupational conditions is an issue of interest, because these radiofrequency (RF) devices are often placed in vicinity of the human body. Portable transmitters are the essential personal communication devices for many different professions. These devices can be operated hand held in front of the face or strapped to the body of the user. In this operational condition the RF currents on the antenna and the radio case are in the immediate vicinity of the human body and, thus, can cause the highest possible exposure level to some part of the body of the user. For this reason, it is necessary to evaluate the exposure of the human body close to portable radio transmitters at VHF, the band of operation of many such devices.

According to the Russian measurement recommendations, the electromagnetic fields exposure from portable transmitters Radiy 301 (Izevsky radiozavod, Russia), the devices under test (DUT), was evaluated at 4.5 meter from source. This distance is recommended as the control point at 170 MHz for portable communication devices. The electric field strength measurements were carried out using the NARDA NBM-550 (Narda Safety Test Solutions, USA) which is included in the Russian state register of measuring equipment.

Also Specific Absorption Rate (SAR) measurements were performed for the exposure from the electromagnetic fields of the DUT. SAR measurements were carried out using the dosimetric system DASY 52 NEO (SPEAG AG, Switzerland). The DUT was located in a special holder under the standard flat phantom ELI4 in touch position and at distances of 5, 10 and 50 mm from the phantom. The dielectric properties of the tissue simulating liquid were $\varepsilon = 52.58$; $\sigma = 0.80\,\mathrm{Sm/m}$.

The area scan covered all the parts of the device including the antenna. The portable radio transmitter operated at maximum output power (5 W) and the operating frequency was 171 MHz. Several radios were tested to evaluate the spread of SAR level caused by manufacturing tolerance. The SAR patterns and the depth of penetration of the RF energy in the simulated human body will be presented in detailed. A summary of the results is given in the paragraph below.

The SAR data show that the levels of human body exposure under normal DUT usage are from 0.5 to 0.2 W/kg which are not be above the EU limits (Directive 2004/40/EC, CR 1999/519/EC). But the measured electric field strength is higher than reference level at the control point. The measured values are from 2.08 to 2.25 V/m. The maximum permissible electric field strength at the control point is 1.5 V/m (SanPiN 2.1.8/2.2.4.1190-03), which is the minimum health and safety requirement for exposure of workers to the risks arising from exposure to electromagnetic fields. Hence excessive use of these portable transmitter models may be potentially harmful to human health. Therefore the operational transmit time of this type of equipment per work shift must be limited by the Russian occupational health compliance rules. For this reason, the power of exposure parameter must be time restricted and, to enforce the Russian occupational hygienic/safety standards, timers are necessary to limit the RF transmission intervals over a person's working day.

Conductivity and Permittivity Measurements of Children and Adult's Hands Covering Mobile Communications Frequency Bands

Chinthana Panagamuwa, Ian Howells, and William Whittow
Centre for Mobile Communications Research, School of Electronic, Electrical and Systems Engineering
Loughborough University, Loughborough, LE11 3TU, United Kingdom

Abstract— Smart phones have become more than simple communication devices; for many they are indispensable (fashion) accessories capable of running sophisticated applications. The use of these mobile phones by children is becoming more widespread. In this changing climate, the health effects of radiation from mobile phones on children in particular, takes on added importance. In order to assess the Specific Absorption Rate (SAR) in human tissue, the conductivity and permittivity of the tissue must be studied. Measuring permittivity and conductivity of biological tissue at microwave frequencies has been investigated over a number of decades. Researchers have used live and dead animals as well as adult volunteers to measure the electrical properties of tissue. Numerous full-body human phantom models are now available for EM simulations of SAR. Although a number of studies have developed mathematical functions to extrapolate child data from adult, actual measured conductivity and permittivity data for children is much harder to source.

As part of a larger project looking at how the hand holding a mobile phone affects the power absorbed in the head, this study investigates the use the open-ended coaxial probe technique for measuring skin permittivity and conductivity. The paper then presents data collected from the palms of child and adult volunteers. We present permittivity and conductivity data coving the frequency range from GSM 900 to 1800.

First we investigate how the force with which the probe is pushed on to the volunteer's hand affects the measured data. As the probe pushes into the palm, the blood is forced away from the contact point which then changes the dielectric properties of the skin. We investigate this effect in an attempt to find the optimum force necessary to produce an accurate measurement of the palm permittivity and conductivity.

The study shows that for a realistic force, the s-parameter measurements taken from the probe can take up to 20 seconds to settle to their final value. The final value and the time taken to settle to the final value are clearly dependent on the force applied to the probe. There are considerable differences in the results obtained with minimal force on the palm compared to the measurements using maximum realistic force. This is mainly due to the changein blood circulation at the point of contact. The study highlights the importance and difficulty of choosing the correct force to apply and the correct time at which to take the measurement. This problem is exacerbated for children's hands where the skin is more supple, thinner and has a higher moisture content.Results from a preliminary volunteer based study of 26 people (half of which were children) showed that the skin conductivity at 1710 MHz ranged from 1 S/m for an 8 year old to 0.4 S/m for a 50 year old. This is indicative of the general trend over the 26 volunteers.

Optimal Size of Waterproofed Shielded Loop Antenna in a Tissue-equivalent Liquid to Calibrate SAR Probe in HF Band

Nozomu Ishii[1], **Ryosuke Takezawa**[1], **Hidenori Toyoshima**[1], **Lira Hamada**[2], **and Soichi Watanabe**[2]

[1]Graduate School of Science and Technology, Niigata University, Japan
[2]National Institute of Information and Communications Technology, Japan

Abstract— Recently, the wireless power transmission (WPT) technology in the HF band has been getting a lot of attention. One issue should be considered to realize the WPT technology is to ensure its safety in view of electromagnetic exposure. There are some exposure guidelines for the electromagnetic fields in the HF band, for example, setting exposure limits for electric field, magnetic field and specific absorption rate (SAR). We focus on the SAR to evaluate the exposure of the electromagnetic fields to the human body. SAR has been employed for the compliance test to the radio radiation protection guidelines of mobile communication devices from 30 MHz to 6 GHz. In our study, the probe calibration for standard SAR measurement based on extended Friis transmission formula in the GHz band can be expanded to the HF band. For the mobile communication devices, the electric-field type probes are used to detect the electric field intensity in the tissue-equivalent liquid of the standard SAR measurement system to obtain SAR, because the electric field intensity is superior to the magnetic field intensity. However, in the HF band, the electric field intensity is inferior to the magnetic field intensity so that the magnetic-field type reference antenna or loop antenna can be a strong candidate. In this paper, a waterproofed shielded loop antenna operated in the liquid will be examined. Our developed probe calibration or gain estimation in the liquid in the GHz band is to face the two identical antennas in the liquid and to estimate the far-field gain as the distance between them is changed. The wavelength in the HF band is much larger than the GHz band. For the physical limitation, it is impossible to assign the distance enough to satisfy the far-field criterion in the practical system so that the gain of the antenna in the HF band should be determined in the extremely near-field region. However, we present one solution to shorten the required minimum distance (about 0.1 wavelength in the liquid) by selecting the appropriate diameter of the loop antenna (0.638 wavelength in the liquid). This fact is ensured by the method of moments and experiment. It leads to the possibility that the gain of the waterproofed shielded loop antenna and SAR probe can be calibrated at a considerable short distance.

Characterization of HF RFID Tags Exposed to Moisture Based on Threshold Power Measurement

Toni Björninen[1], **Jukka Voutilainen**[2], **Lauri Sydänheimo**[1], **and Leena Ukkonen**[1]

[1]Department of Electronics and Communications Engineering, Tampere University of Technology
P. O. Box 692, FI-33101, Tampere, Finland
[2]Voyantic Ltd., Kutojantie 11, FI-02630, Espoo, Finland

Abstract— We investigated the impact of moisture on the operation of fully assembled high-frequency (HF) ISO 15693 compliant radio-frequency identification (RFID) tags operating at the frequency of 13.56 MHz. In the tag performance characterization, we use an active measurement technique based on the ramping of the output power of the reader during wireless communication with the tag under test.

From the measurement of a wetted tag (Smartrac Block^{TM}) we obtained the results shown in Fig. 1. The figure shows the minimum reader output power (threshold power; Pth), which enabled a response from the tag at a given frequency. In the full paper, we will also discuss how this parameter relates to the magnetic field intensity at the tag's location given the reader hardware. We will also compare the results from the active measurement with results from the more conventional HF tag characterization based on the measurement of the reader antenna impedance variations when it is loaded with the coupled tag.

As seen from the results in Fig. 1, the moisture caused a significant down-shift in the frequency of the best antenna-IC power transfer (frequency of the lowest threshold power) and additional reduction of the tag sensitivity. The physical mechanisms behind this phenomenon are discussed in more detail in the full paper. As seen from the results in Fig. 1, a way to alleviate these undesired effects is to purposefully tune the tag in air at a higher frequency. This way, smaller performance variation at the actual operation frequency (13.56 MHz) is attained; Pth varied 6.5 dB instead of 15 dB at the optimum operation frequency of 13.86 MHz. In the full paper we will show how this variability affects the maximum interrogation distance of the tag.

Alternatively, the observed frequency-shift in the tag's response can be exploited in the development of inductively powered low-cost wireless humidity sensor tags. The threshold power based sensing may provide a simpler mechanism for sensor readout compared with the reader antenna input impedance based method utilized in vapour and pressure sensors based on 13.56 MHz tags [1, 2]. Compared with ISO 18000-6 compliant the UHF RFID humidity sensor tags [3, 4], the implementation at 13.56 MHz could provide a more reliable readout since the near field wireless channel is localized and thus free from multipath.

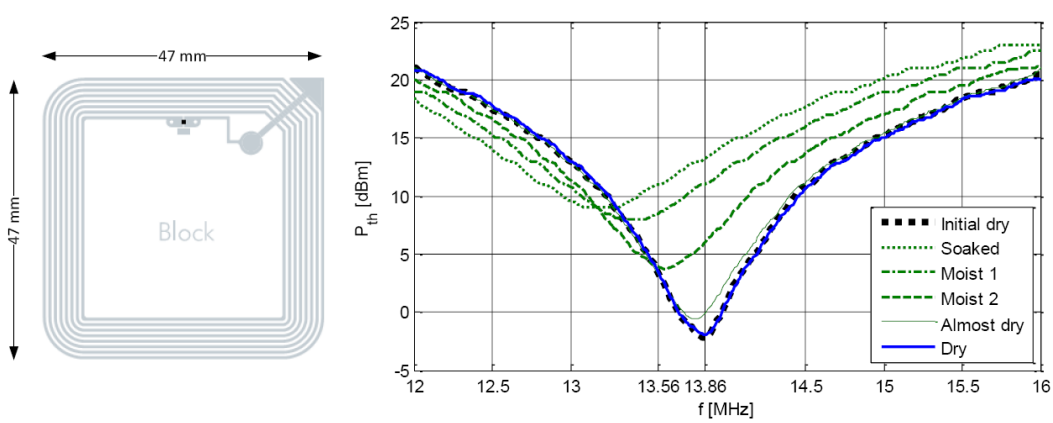

Figure 1: Tested tag and its threshold power during the wetting test.

REFERENCES

1. Potyrailo, R. A., C. Syrman, W. G. Morris, S. Go, Y. Lee, J. Cella, and K. S. Chichak, "Selective quantitation of vapors and their mixtures using individual passive multivariable RFID sensors," *IEEE RFID Conf. Digest*, 22–28, Orland, FL, USA, Apr. 14–16, 2010.

2. Surman, C., R. A. Potyrailo, W. G. Morris, T. Wortley, M. Vincent, R. Diana, V. Pizzi, J. Carter, and G. Gach, "Temperature-independent passive RFID pressure sensors for single-use bioprocess components," *IEEE RFID Conf. Digest*, 78–84, Orland, FL, USA, Apr. 12–14, 2011.
3. Virtanen, J., L. Ukkonen, T. Björninen, A. Z. Elsherbeni, and L. Sydänheimo, "Inkjet printed humidity sensor for passive UHF RFID systems," *IEEE Trans. Instrum. Meas.*, Vol. 60, No. 8, 2768–2777, Aug. 2011.
4. Gao, J., J. Sidén, H.-E. Nilsson, and M. Gulliksson, "Printed humidity sensor with memory functionality for passive RFID tags," *IEEE Sensors*, Early Access Article in IEEE Xplore, 2013.

Non-invasive Antenna Pattern Characterization Using Time-domain and Frequency-domain Measurement Techniques

T. H. Loh, D. A. Humphreys, and P. Miller
National Physical Laboratory, Teddington, Middlesex, United Kingdom

Abstract— At the UK national physical laboratory we have replaced the standard metal coaxial feed by an optical fibre system that does not support common-mode currents and has minimal effect on the antenna radiation-pattern. This system is particularly useful for measuring antenna systems where the impact of the RF feed is significant [1].

Traditional frequency-domain (FD) antenna pattern characterisation is based on measurement of the vector RF voltages as a function of angle (θ and φ) using a vector network analyser (VNA) at a number of pre-set frequencies. The dwell-time at each frequency is sufficiently long that the process can be treated as static. In time-domain (TD) antenna characterisations [2] the frequency content is embedded in the source and received waveforms, typically an impulse. Provided the TD measurement system is linear, equivalent results are expected for either TD or FD stimulus.

This paper presents an investigation on the performance limitations due to time-domain multi-sine stimuli [3] with different Peak-to-Average-Power Ratios (PAPRs) on non-invasive radiation pattern measurements of a broadband antenna over 500 MHz to 4500 MHz and compare these results with frequency domain quasi-CW measurements using a VNA. The TD waveforms were chosen to provide an evenly-spaced grid of frequencies within the antenna passband. These were a train of short pulses with a high peak-to-average power ratio (PAPR) and a Schroeder multi-sine with a low PAPR.

The measurement setup within the FAC remains unchanged while interchanging the TD and FD equipment. The results show that the Schroeder multi-sine results were superior to the high-PAPR stimulus because of the higher average power and suggest that the PAPR of the time domain stimulus waveform directly affects the system dynamic range and the uncertainty of the results. The TD approach can be used to measure modulated waveforms and provide results equivalent to a VNA but have the disadvantage of additional complexity and the choice of TD stimuli will affect measurement accuracy.

REFERENCES

1. Loh, T. H., M. Alexander, P. Miller, and A. Betancort, "Interference minimisation of antenna-to-range interface for pattern testing of electrically small antennas," *4th European Conference on Antennas and Propagation (EuCAP)*, 1–5, Apr. 2010.
2. Allen, O. E., D. A. Hill, and A. R. Ondrejka, "Time-domain antenna characterizations," *IEEE Trans. on EMC*, Vol. 35, No. 3, 339–346, Aug. 1993.
3. Schroeder, M. R., "Synthesis of low-peak-factor signals and binary sequences with low auto-correlation," *IEEE Trans. on Information Theory*, Vol. 16, 85–89, Jan. 1970.

Far Field Gain Estimation Method for Japanese Broadband Antenna Standard Using Time-frequency Analysis

S. Kurokawa, M. Ameya, and M. Hirose
National Institute of Advanced Industrial Science and Technology, Tsukuba, Ibaraki, Japan

Abstract— We propose a new estimation method for far-field antenna factor and gain of broadband antenna at near distance. Our proposed method is based on the techniques of a time domain analysis and a time-frequency analysis using a short time Fourier transform. Our proposed method can be determined the estimated antenna distance at each frequency to estimate the far field gain. In the case of Bi-conical antenna, the difference between far-field gain and the estimated gain using our proposed method is less than 0.2 dB at 5 m antenna distance in the frequency range from 30 MHz to 240 MHz. In the case of Log-periodic dipole array antenna for EMI measurement, the difference between far-field gain and the estimated gain using our proposed method is less than 0.25 dB at 5 m antenna distance in the frequency range from 300 MHz to 1200 MHz.

RCS Measurement of a Patch Antenna with Resistive Load in a Compact Anechoic Chamber

Naobumi Michishita, **Tadashi Chisaka**, **and Yoshihide Yamada**
National Defense Academy, Japan

Abstract— To reduce the radar cross section (RCS) of various structures, the radio absorber material is employed. In the antenna structures, the RCS reduction is required without using typical wave absorber. Recently, the monostatic RCS of a patch antenna with different terminal loads has been investigated. An appreciable RCS reduction were ensured by varying the terminal conditions of open, short, and dummy. We have also achieved an additional reduction by applying high resistive load. When the patch antenna is terminated with 500 Ω, the RCS reduction of 15 dB is verified through both simulation and measurement. To measure a lower RCS value, the setup condition of measurement environment needs to be examined in detail. In this paper, the RCS measurement method of the patch antenna with resistive load in a compact anechoic chamber is investigated. For measuring monostatic RCS, transmitting and receiving antennas are placed in proximity to each other. Therefore, the reduction of mutual coupling between antennas is important to ensure the dynamic range of the measurement. The effect of several setup conditions in the compact anechoic chamber are estimated quantitatively by simulation and measurement. The mutual coupling characteristics between transmitting and receiving horn antennas are shown when their separation increases. The effects of inserting the sheet type wave absorber and the measurement setup at target side are also discussed.

Complex Antenna Pattern Measurement by Spherical Scanning and Phase Retrieval Method

Hiroyuki Arai and Eriko Ohashi
Graduate School of Engineering, Yokohama National University, Japan

Abstract— This paper presents complex antenna pattern measurement by spherically scanned probe and phase retrieval method. Built-in antennas are widely used for handheld devices such as smart phones and tablet PCs. Complex radiation pattern given by measurement of amplitude and phase distributions are necessary to estimate MIMO channel capacity for arbitral incoming wave distributions and arbitral cross polarization ratio. Phase-less measurements are often used in millimeter frequency band for electrically large sized aperture antenna using phase retrieval method. This technique has been applied for planar scanning probe for reflector antennas. To introduce this method for wireless devices of mobile communication in UHF band, a spherical scanning probe is necessary due to low gain characteristics of test antennas. For small sized measurement facilities, near field to far filed transformation is attractive for the above applications, then this paper presents field transformation procedure assuming magnetic field probe for amplitude measurements. Electrically small magnetic field probes reduce the mutual coupling with test devices and minimize the size of scanning space. We derive near field to far field transformation for magnetic near field distributions measurement firstly, and clarify the condition to apply phase retrieval method. A key parameter in this method is to select the position of two amplitude measurement planes. This paper discusses this parameter by the simulation with a half-wavelength ($\lambda/2$) dipole, a $3\lambda/2$ dipole and a folded F-shaped antenna on rectangular ground plane and shows optimal position of two measurement planes. We also verify the results by measurements.

Extended S-parameter Method for Radiation Characteristics and Mutual Coupling of Multiport Antennas

T. Yanagi, T. Fukasawa, and H. Miyashita
Mitsubishi Electric Corporation, Japan

Abstract— When a coaxial cable is connected an antenna, unbalanced current may be induced on the outside of the cable and causes a measurement error. This error becomes large in the case that an antenna and a ground plane are small. Therefore, it is important for antenna measurement to eliminate influence of coaxial cables connected to antennas. The S-parameter method is known as one of the method to reduce influence of coaxial cables for measurement of a balanced antenna inpedance. This method is useful and widely used to measure the impedance characteristics of many kinds of antennas because it does not require any special equipment for measurement except two cables. However, it has been applied for measurements of impedance and radiation pattern of only one antenna element. In this paper, an extended S-parameter method (ESPM) for accurate measurements of reflection, mutual coupling and radiation characterisitics of multiport antennas that can reduce the influence of the coaxial cables is proposed. First, the ESPM for multiport antennas is formulated. Two coaxial cables are connected to each antenna in this method. Impedance and mutual coupling characteristics with reducing influence of the coaxial cables are obtained by synthesizing measured S-parameters under the condition that unbalanced currents on the outside of the coaxial cables are canceled. Radiation pattern with reduced unbalanced currents can be calculated from array patterns with excitation coefficients derived by the measured S-parameters. Next, we apply the proposed method to two closepositioned monopole antennas mounted on a small ground plane and demonstrate the validity and effectiveness of the proposed method by measurement. It is shown that accurate measurement results can be obtained using the proposed method.

Path Loss Characteristics in a Civil Laboratory Building at a Frequency of 2.4 GHz

Supachai Phaiboon[1] **and Adchara Kampan**[2]

[1]Electrical Engineering Department, Faculty of Engineering
Mahidol University, Salaya, Nakhorn Pathom 73170, Thailand
[2]Technology of Information System Management, Faculty of Engineering
Mahidol University, Salaya, Nakhorn Pathom 73170, Thailand

Abstract— This paper presents indoor radio wave propagation characteristics of a civil laboratory building at a frequency of 2.4 GHz. We performed path loss measurements and modeled measured data with fuzzy regression. This model provides both large scale fading and boundary limitation in which almost measured data is contained. There are five path loss categories namely LOS, NLOS same room, LOS with NLOS same room, NLOS different rooms, and LOS with NLOS all rooms. These categories provide different path loss characteristics in each environment. Comparing between conventional models and purposed models show that the purposed models provide a better prediction within boundaries for all categories, especially for LOS model and partition attenuation factor (PAF) model. It is also found that machine arrangements do not affect significantly the path loss prediction.

New Applications and Measurement Results by MIMO Transmission

Kentaro Nishimori
Faculty of Engineering, Niigata University
8050 2-no-cho, Ikarashi, Nishi-ku, Niigata 950-2181, Japan

Abstract— The growing popularity of smart phones and wireless LANs has set the demand for achieving broadband wireless transmission within a limited frequency band. Multiple input multiple output-orthogonal frequency division multiplexing (MIMO-OFDM) systems have been developed because they promise to increase the channel capacity compared to single input single output (SISO) systems. Moreover, multi-user MIMO (MU-MIMO) systems have recently attracted much attention as a technology that enhances the total system capacity by generating a large virtual MIMO channel between a base station and multiple user terminals (UTs).

In this paper, we propose new applications by using MIMO transmission. First, we focus on the application of security systems. An intruder detection using array signal processing is proposed using single input multiple output (SIMO) channel. In this paper, an intruder detection method, which utilizes channel matrix in MIMO channels, is proposed in order to enhance detection performance using SIMO channel. We call this method *MIMO Sensor*. Although the channel capacity on the MIMO transmission is severely degraded in time variant channels, we can take advantage of this feature in MIMO Sensor applications. Since not only receiving but also transmitting diversity effects are obtained by using MIMO transmission, higher reliability for the intruder detection is expected by using the MIMO Sensor compared to the SIMO sensor. We propose an use of time correlation function for channel matrix in the MIMO channel.

We evaluate the effectiveness of proposed method by using the measured propagation channel data when considering an actual intruder by a person in an actual indoor environment. We compare the detection performance of SIMO/MIMO sensors which have same number of channel responses: 4×1 SIMO and 2×2 MIMO.

As the second topic, the collision detection method by using MIMO transmission is proposed. This paper proposes an interference detection method in MIMO transmission, which utilizes periodical preamble signals in a frequency domain. The signals are mapped in only several subcarriers in short preamble signals of IEEE802.11a/g/n based OFDM signals and the signal in a time domain is transformed by IFFT at the transmitter. At the receiver site, the subcarriers at which only interference arrive can be found by employing FFT. Propose method utilize this feature and efficiently detects the interference. By measurements throughout MIMO-OFDM signals using dual polarization antenna, it is shown that the proposed method can receive the interference at the null carrier in OFDM signal.

Detection Reliability Analysis of Passive DAS RFID System

Abdelmoula Bekkali[1,*], Abdullah Kadri[1], Michael Crisp[2], and Richard V. Penty[2]

[1]Qatar Mobility Innovations Center (QMIC), Doha, Qatar
[2]Electrical Division, Department of Engineering, University of Cambridge, UK
*abdelmoulab@qmic.com

Abstract— Radio frequency identification (RFID) is a rapidly developing technology which uses wireless communication for automatic identification of objects. The passive RFID tag successful detection and reader reliable reading range remain the most critical issues for successful deployment of passive ultra high frequency (UHF) RFID systems in diverse applications such as asset management, access control, and industrial automation. The main factors influencing the reliability of a tag response include tag location and orientation, multipath fading and communication blind spot. Recently it has been shown that an improved communication coverage can be achieved by employing distributed antenna system (DAS). By applying concepts of DAS system to RFID system, it is possible to overcome the limitation of the existing passive UHF RFID systems, enabling a few reader antennas to provide reliable coverage over a wide area. The DAS RFID system is based on a novel technique whereby two or more spatially separated transmit and receive antennas are used to enable greatly enhanced tag detection performance over longer distances using antenna diversity combined with frequency and phase hopping. In this paper, we present a performance evaluation of the DAS RFID to achieve 100% detection rate of passive tags in a laboratory harsh environment. Performance metrics like received signal strength indication (RSSI) and the probability that an RFID reader successfully detects RFID tags in its interrogation zone, are measured and analyzed. The obtained results will be used for designing the multi-cell DAS RFID system for wider passive RFID coverage.

Session 2P7a
SC3: Integrated Nanophotonics for Optical Interconnects in Data Centers

Photonics Communications: From Global Reach to Photonic Interconnect Networks on Multicore Architecture Chips: The Role of Low Power Nanophotonics in Data Centers
Lars Thylen, ... 750

Active Plasmonics for Datacom Applications
Sergey I. Bozhevolnyi, ... 751

Multiplexing Technologies and Devices Enabling Tera-bit Photonic Network-on-chip
Daoxin Dai, ... 752

Plasmonic Nanophotonic Devices for Optical Interconnects
Qiang Li, Weichun Zhang, Jing Wang, Yi Song, Jie Tian, Min Yan, Min Qiu, ... 753

Chip-level Assembly of Silicon Photonics in Optical Interconnects
Antonio La Porta, Ibrahim Murat Soganci, Jens Hofrichter, Folkert Horst, Bert Jan Offrein, ... 754

Surface Plasmonics and Metallic Cavity Nanolasers
Cun Zheng Ning, K. Ding, D. B. Li, L. J. Yin, Z. C. Liu, ... 755

Integration of III-V Device Structures on Silicon for Optical Interconnects
Sebastian Lourdudoss, Carl Junesand, Wondwosen Metaferia, Himanshu Kataria, Yanting Sun, ... 757

Silicon Platform-based Nanophotonics for Interconnect Applications
Lech Wosinski, Fei Lou, Lars Thylen, ... 758

Active Plasmonic Circuitry
Alexey V. Krasavin, Anatoly V. Zayats, ... 759

Photonics Communications: From Global Reach to Photonic Interconnect Networks on Multicore Architecture Chips: The Role of Low Power Nanophotonics in Data Centers

Lars Thylen
Royal Institute of Technology, Kista, Sweden

Abstract— Photonics communications is evolving from the global network to encompass ever shorter distances, not only in smaller cellular phone cells but in much shorter connections. The current impending introduction of photonics interconnects in cabinet backplanes will be followed by intra board and eventually on chip connections, though at a slower pace than predicted in an optimistic article in IEEE Spectrum in 2002. For the emerging multi- and many-core architectures, core counts are expected to double every 18 months and the bandwidth required to support concurrent computation on all cores will increase by orders of magnitude. Architecture studies and analysis of power dissipation and bandwidth requirements point to integrated nanophotonics as a solution , partly because its length independent power dissipation.

Thus, photonics interconnection based on nano-scale photonic integrated circuit technology and optical waveguides of different types are of prime importance and the rapid development of the photonic integration technology is showing great promises for the deployment in the next generation data centers, including reduced power consumption, small footprint and increased functionalities. Such nanophotonics technology would include diverse materials and devices using compound semiconductors, group four semiconductors, dielectric wires, micro-rings, photonic crystals, nanowires, plasmonics, metamaterials, polymers and of course nanostructures. But continued progress is required not least in the practical implementation.

This contribution will elaborate on systems and architectures issues as well as the hurdles and possibilities of further decreasing device footprint.

Active Plasmonics for Datacom Applications

Sergey I. Bozhevolnyi
Department of Technology and Innovation, University of Southern Denmark
Odense DK-5230, Denmark

Abstract— The massive growth of telecom and data communication traffic in the last decade has spurred the interest in a new nanophotonics platform, which is based on guiding surface plasmon polaritons by metal stripes, which serve as waveguiding cores in plasmonic waveguides With metal stripes being intrinsic components of plasmonic waveguides, plasmonics provides a "naturally" energy-efficient platform for merging broadband optical links with intelligent electronic processing, instigating a great promise for low-power and small-footprint active functional circuitry. The first active Dielectric-Loaded Surface Plasmon Polariton (DLSPP) thermo-optic (TO) switches with successful performance in single-channel 10 Gb/s data traffic environments have led the inroad towards bringing low-power active plasmonics in practical traffic applications. In this talk, active plasmonics for Wavelength Division Multiplexed (WDM) switching applications is considered, using the smallest TO DLSPP-based Mach-Zehnder interferometric switch reported so far and showing its successful performance in 4×10 Gb/s low-power and fast switching operation. The demonstration of the WDM-enabling characteristics of active plasmonic circuits with an ultra-low power $\times$ response time product represents a crucial milestone in the development of active plasmonics towards real telecom and datacom applications, where low-energy and fast TO operation with small-size circuitry is targeted. Power monitoring in plasmonic DLSPP-based circuits using internal Wheatstone bridges for measuring the resistance of gold stripes that support the propagation of DLSPP modes is also discussed.

Multiplexing Technologies and Devices Enabling Tera-bit Photonic Network-on-chip

Daoxin Dai
Centre for Optical and Electromagnetic Research
State Key Laboratory for Modern Optical Instrumentation
Zhejiang Provincial Key Laboratory for Sensing Technologies
Zhejiang University, Zijingang Campus, Hangzhou 310058, China

Abstract— Optical interconnect has been regarded as a very promising solution for satisfying the increasing demands of high bandwidth for future massively-parallel chip multiprocessors. In order to enhance the optical transmission capacity, multiplexing technologies are still needed.

A straightforward way is introducing the wavelength-division-multiplexing (WDM) technology, which has been developed very successfully for long-haul optical communication networks. DWDM might be a good option regarding the potential for ultra-high capacity. However, many (even tens of) laser sources with different wavelengths are needed, which is quite expensive due to the high package cost and the low yield. The management for wavelength tuning, routing and switching in a DWDM system is also pretty complicated, expensive, and power-consumed. Besides, one has to precisely align and stabilize the emission wavelengths of all the laser sources as desired by e.g., controlling the temperature of the chip carefully. This will introduce lots of complexity for the chip driver as well significant excess power consumption. This is not desired because low power consumption is required in photonic networks-on-chip. Therefore, coarse WDM (CWDM) is a potentially better way to be low-cost option for photonic network-on-chip.

In order to improve the capacity further, one could use the so-called "spatial-division multiplexing (SDM)", i.e., with multi-core or multimode optical waveguides/fibers, which have attracted intensive attention for long-haul optical fiber communications in the past decades. In this way, the independent signals are carried by different cores or modes in parallel. Recently multimode SDM technology has been developed with few-mode fibers which only support a few modes and some complicated free-space optical setups are introduced for mode (de)multiplexing. However, it is still very difficult to extend for having more modes included. In contrast, for on-chip optical networks, the situation is much better because the optical signal propagates along planar optical waveguides within the chip and the eigen-modes could be converted, transferred, as well as coupled conveniently between planar optical waveguides. It is not difficult to design and fabricate some complex photonic integrated circuits to handle (e.g., multiplex/demultiplex) the eigen-modes. Thus, it becomes very attractive and convenient to develop multimode SDM technology for on-chip optical networks. The capacity of the multimode SDM link can be improved more by combining the multimode SDM and polarization-division-multiplexing (PDM) with the assistance of polarization handling devices, e.g., polarization rotators (PR) and polarization-beam splitters (PBSs).

In this paper, we will give a review for our recent work on on-chip multiplexing technologies and devices to enable Tera-bit optical interconnects, including CWDM, SDM, PDM, and the hybrid technology of them.

Plasmonic Nanophotonic Devices for Optical Interconnects

Qiang Li[1], **Weichun Zhang**[1], **Jing Wang**[2], **Yi Song**[2], **Jie Tian**[2], **Min Yan**[2], **and Min Qiu**[1,2]

[1]State Key Laboratory of Modern Optical Instrumentation
Department of Optical Engineering, Zhejiang University, Hangzhou 310027, China
[2]School of Information and Communication Technology
Royal Institute of Technology, Electrum 229, Kista 164 40, Sweden

Abstract— Plasmonic nanophotonic devices have shown tremendous potentials in photonic integration due to their capability of subwavelength confinement. However, the main obstacle for plasmonic devices is the high loss. Thus proper design and optimization of plasmonic modules are of great significance.Here we will review our recent results concerning plasmonic waveguides (PWs) and plasmonic couplers [1–5]. Guiding modes, propagation losses, couplers, and photothermal heating due to light absorption, are presented for applications in photonic integrated circuits.

Silver nanowires could function as low loss waveguides for SPP modes at optical communication wavelength [1]. It is found that when the metal nanowires are located on a SiO_2 substrate, the long-range SPP (LRSPP)-like modes cannot be supported owing to asymmetry. While for the short-range SPP (SRSPP)-like guiding mode, it has a cutoff radius for wavelength longer than 682 nm [5]. When the metal nanowires are immersed in a SiO_2 matrix, both SRSPP-like modes and LRSPP-like modes can be guided. However, only the LRSPP modes have cutoff radii.

While for plasmonic couplers, two kinds of hybrid plasmonic couplers utilizing directional coupling and taper coupling are exploited to achieve high coupling efficiency [2, 3]. The broadband, high-efficiency direct coupling between wire waveguide and metal-dielectric-metal plasmonic gap waveguide is also realized with a planar plasmonic coupler [4]. These optical interconnect modules have the potential for high-quality signal routing components in photonic integrated circuits.

REFERENCES

1. Li, Q., S. Wang, Y. Chen, M. Yan, L. Tong, and M. Qiu, "Experimental demonstration of plasmon propagation, coupling and splitting in silver nanowire at 1550 nm wavelength," *IEEE J. Sel. Top. Quantum Electron.*, Vol. 17, 1107, 2011.
2. Li, Q., Y. Song, G. Zhou, Y. Su, and M. Qiu, "Asymmetric plasmonic-dielectric coupler with short coupling length, high extinction ratio, and low insertion loss," *Opt. Lett.*, Vol. 35, 3153, 2010.
3. Song, Y., J. Wang, Q. Li, M. Yan, and M. Qiu, "Broadband coupler between silicon waveguide and hybrid plasmonic waveguide," *Opt. Express*, Vol. 18, 13173, 2010.
4. Tian, J., S. Yu, W. Yan, and M. Qiu, "Broadband high-efficiency surface-plasmon-polariton coupler with silicon metal interface," *Appl. Phys. Lett.*, Vol. 95, 013504, 2009.
5. Li, Q. and M. Qiu, "Plasmonic wave propagation in silver nanowires: Guiding modes or not?," *Opt. Express*, Vol. 21, 8587, 2013.

Chip-level Assembly of Silicon Photonics in Optical Interconnects

A. La Porta, I. M. Soganci, J. Hofrichter, F. Horst, and B. J. Offrein
IBM Research — Zurich, Saeumerstrasse 4, Rueschlikon 8803, Switzerland

Abstract— Integrated silicon nanophotonics combines optical functionalities with CMOS electronics on a single silicon die. It represents a key technology to provide low-power, high-bandwidth and high-density transceiver chips for numerous applications, such as optical interconnects for computing systems. However, the system-level assembly effort remains present and the overall density advantages are limited by the packaging and optical connector cost. As a consequence, novel packaging schemes are required. We propose to assemble the silicon photonic chip using standard chip-attachment techniques such as flip-chip bonding technology with single-mode polymer waveguides on the chip carrier substrate. This packaging scheme allows to scale up the optical fan-in/out of the chip and to minimize the assembly overhead. When necessary, fiber connectors can be placed off-chip at the edge of the carrier. A single-mode polymer optical waveguide technology compatible with flip-chip soldering was established. We demonstrate propagation losses of 0.3 dB/cm at 1310 nm and 0.8 dB/cm at 1550 nm.

Three assembly schemes were identified for the optical connection of the silicon photonic chip to the polymer waveguides on the carrier substrate: vertical coupling using grating elements and mirrors, lateral coupling with microlenses and adiabatic/proximity coupling. The last two approaches are the most promising in terms of assembly considerations, optical coupling losses, optical alignment tolerances and scalability.

The lateral coupling scheme is implemented using a dual lens coupling scheme with silicon microlens arrays. The silicon microlens arrays are realized using wafer-level processing. Passive alignment was employed to attach the lens array to the silicon photonic chip using a set of mechanical features defined in the lens array and in the silicon photonic chip. Similarly, silicon lens arrays are attached to the carrier and aligned to the polymer waveguide. The dual-lens scheme was designed to provide expansion of collimated optical beams with 20 µm of alignment tolerance for an additional coupling loss of 1 dB.

For the adiabatic coupling, the optical connection is realized by providing a direct contact or proximity between silicon tapered waveguides and the core of the single-mode polymer waveguide on the carrier. 5 µm of horizontal alignment tolerance is achievable using adiabatic coupling.

In conclusion, chip-level assembly of silicon photonic devices soldered onto a carrier with single-mode polymer waveguides offer high interconnection density with low assembly overhead. Two optical coupling approaches to execute on this concept were presented.

Surface Plasmonics and Metallic Cavity Nanolasers

C. Z. Ning, K. Ding, D. B. Li, L. J. Yin, and Z. C. Liu
School of Electrical, Computer and Energy Engineering
Arizona State University, Tempe, AZ 85287, USA

Abstract— Miniaturization has been an eternal theme for electronics and photonics since the dawn of the semiconductor era. Size reduction of photonic devices has been driven both by the rich physics and by promising applications in future nanophotonic systems. In the last decades, several new concepts of smaller lasers have been demonstrated such as photonics crystal lasers, microdisk lasers, photonic wire lasers, and nanowire lasers. However, further size reduction of such dielectric-cavity laser becomes exceedingly challenging when the wavelength becomes the eventual roadblock [1]. To significantly reduce the sizes of semiconductor lasers in all three dimensions beyond the limit of dielectric-cavity lasers, a semiconductor-metal core-shell structure was proposed and systematically analyzed with plasmonic resonant behavior included [2]. It was demonstrated by a detailed study taking into account the full plasmonic dispersion that the net modal gain of a semiconductor core can overcome the metal loss in the shell. The first experimental demonstration of lasing in such a core-shell structure in near infrared was soon reported by Hill et al. [3]. Since then, experimental and theoretical studies of plasmonic or metallic cavity nanolasers have flourished and rapid progress has been made over the last several years.

In this talk, we will present a summary overview of our efforts since 2006 in developing the metallic cavity nanolasers. We will start with a brief overview of short history and a background introduction to the plasmon-photon interactions, showing how such interactions might lead to a nanolaser of ever shrinking size. Recent progress in theoretical [2, 4, 5] and experimental studies [7–9] will then be presented, including the demonstration of the first nanolaser with a below-diffraction limit size [6], our recent efforts in raising the operating temperature of such nanolasers [7, 8], and the eventual realization of the first room temperature subwavelength size nanolasers [9].

Through the presentation, special emphasis will be placed on the unique features of such nanolasers that distinguish them from the conventional semiconductor lasers of pure dielectric cavities. We will also discuss some of attracting features that are yet to be realized experimentally, including the possibility of giant modal gain [4] and interesting features of confinement factor [5]. Finally, we will discuss new designs towards further miniaturization [10].

REFERENCES

1. Ning, C. Z., "Semiconductor nanolasers," *Phys. Stat. Sol. B*, Vol. 247, 774, 2010.
2. Maslov, A. V. and C. Z. Ning, "Size reduction of a semiconductor nanowire laser using metal coating," *SPIE Proceed.*, Vol. 6468, 64680I, 2007.
3. Hill, M. T., Y.-S. Oei, B. Smalbrugge, Y. Zhu, T. de Vries, P. J. van Veldhoven, F. W. M. van Otten, T. J. Eijkemans, J. P. Turkiewicz, H. de Waardt, E. J. Geluk, S.-H. Kwon, Y.-H. Lee, R. Nötzel, and M. K. Smit, "Lasing in metallic-coated nanocavities," *Nat. Photonics*, Vol. 1, No. 10, 589–594, 2007.
4. Li, D. B. and C. Z. Ning, "Giant modal gain, amplified surface plasmon-polariton propagation, and slowing down of energy velocity in a metal-semiconductor-metal structure," *Phys. Rev. B*, Vol. 80, 153304, 2009.
5. Li, D. B. and C. Z. Ning, "Peculiar features of confinement factors in a metal-semiconductor waveguide," *Appl. Phys. Lett.*, Vol. 96, 181109, 2010.
6. Hill, M. T., M. Marell, E. S. P. Leong, B. Smalbrugge, Y. Zhu, M. Sun, P. J. van Veldhoven, E. J. Geluk, F. Karouta, Y. S. Oei, R. Nötzel, C. Z. Ning, and M. K. Smit, "Lasing in metal-insulator-metal sub-wavelength plasmonic waveguides," *Opt. Express*, Vol. 17, 11107, 2009.
7. Ding, K., Z. Liu, L. Yin, H. Wang, R. Liu, M. T. Hill, M. J. H. Marell, P. J. van Veldhoven, R. Nötzel, and C. Z. Ning, "Electrical injection, continuous wave operation of subwavelength-metallic-cavity lasers at 260 K," *Appl. Phys. Lett.*, Vol. 98, 231108, 2011.
8. Ding, K., Z. C. Liu, L. J. Yin, M. T. Hill, M. J. H. Marell, P. J. van Veldhoven, R. Nötzel, and C. Z. Ning, "Room-temperature continuous wave lasing in deep-subwavelength metallic cavities under electrical injection," *Phys. Rev. B*, Vol. 85, 041301(R), 2012.

9. Ding, K., M. T. Hill, Z. C. Liu, L. J. Yin, P. J. van Veldhoven, and C. Z. Ning, "Record performance of electrical injection sub-wavelength metallic-cavity semiconductor lasers at room temperature," *Opt. Express*, Vol. 21, 4728–4733, 2013.
10. Li, D. and C. Z. Ning, "Interplay of various loss mechanisms and ultimate size limit of a surface plasmon polariton semiconductor nanolaser," *Opt. Exp.*, Vol. 20, 16348–16357, 2012.

Integration of III-V Device Structures on Silicon for Optical Interconnects

Sebastian Lourdudoss, **Carl Junesand**, **Wondwosen Metaferia**, **Himanshu Kataria**, **and Yanting Sun**
Laboratory of Semiconductor Materials, School of ICT, KTH, Electrum 229, Kista 16440, Sweden

Abstract— Integration of III-V's on silicon is a viable approach for silicon photonics and nanophotonics. These technologies are also promising for optical interconnects [1]. Optical interconnects represent perhaps the strongest contender in replacing copper interconnects in integrated circuits [2], and Si/SiO_2-based waveguides are the obvious choice since they can be fabricated in a CMOS-compatible process [3]. Urino et al. demonstrated for the first time high density optical interconnects integrated with lasers, modulators and photodetectors on single silicon substrate [4]. In their integration scheme, lasers were hybridly bonded on to the SOI platform. In many of the transceiver modules proposed by several companies there is no satisfactory solution for integrating laser monolithically is so far available.

Integration of III-V devices on silicon can be done also by epitaxial methods but it hitherto remains not that well explored especially for optical interconnects. There are several bonding and epitaxial approaches that have been reviewed recently in the literature [5–8]. Active hybrid silicon devices achieved through epitaxial growth of active III-V layers directly on SOI (silicon on insulator) wafers without the use of the intermediate step of growth on InP substrates is an important step to facilitate the integration of high density nano-scale photonic components and to reduce the cost. This would enable the transition of photonic devices to large area silicon substrates with several orders of magnitude reduction in cost, and a large increase in manufacturing capability to tap the potential of silicon photonics [7]. In this presentation we explore certain feasible methods of integrating III-V devices on silicon for optical interconnects. We indicate that multi-quantum wells and quantum dots can indeed be grown on silicon platform with the feasibility of coupling it to the silicon waveguide.

REFERENCES

1. Miller, D. A. B., "Optical interconnects to electronic chips," *Appl. Opt.*, Vol. 49, F59–F70, 2010.
2. Beausoleil, R. G., P. J. Kuekes, G. S. Snider, S.-Y. Wang, and R. S. Williams, "Nanoelectronic and nanophotonic interconnect," *Proc. IEEE*, Vol. 96, No. 2, 2008.
3. Jalali, B., "Can silicon change photonics?," *Phys. Stat. Sol. (A)*, Vol. 205, No. 2, 213–224, 2008.
4. Urino, Y., et al., "First demonstration of high density optical interconnects integrated with lasers, optical modulators, and photodetectors on single silicon substrate," *Optics Express*, Vol. 19, B159–B165, 2011.
5. Bolkhovityanov, Yu. B. and O. P. Pchelyakov, "III-V compounds-on-Si: Heterostructure fabrication, application and prospects," *The Open Nanoscience Journal*, Vol. 3, 20–33, 2009.
6. Heck, M. J. R., H.-W. Chen, A. W. Fang, B. R. Koch, D. Liang, H. Park, M. N. Sysak, and J. E. Bowers, "Hybrid silicon photonics for optical interconnects," *IEEE J. Sel. Topics in Quant. Electron.*, Vol. 17, No. 2, 333–346, 2011.
7. Lourdudoss, S., "Heteroepitaxy and selective area heteroepitaxy for silicon photonics," *Current Opinion in Solid State and Materials Science*, Vol. 16, 91–99, 2012.
8. Lee, A., H. Liu, and A. Seeds, "Semiconductor III-V lasers monolithically grown on Si substrates," *Semicond. Sci. Technol.*, Vol. 28, 015027, 2013.

Silicon Platform-based Nanophotonics for Interconnect Applications

Lech Wosinski[1,2], **Fei Lou**[1,2], **and Lars Thylen**[1,2]

[1]School of Information and Communication Technology, Royal Institute of Technology, Kista 16440, Sweden
[2]Joint Research Center of Photonics of the Royal Institute of Technology (Sweden) and Zhejiang University (JORCEP)
Zhejiang University, Hangzhou 310058, China

Abstract— In this paper we present our technology based on silicon platform used for fabrication of nanophotonic devices as well as novel components with hybrid plasmonic nanowire waveguides.

Over past decade silicon photonics established its position as an important photonic platform, mainly due to compatibility to microelectronic fabrication and great advantage of CMOS process compatibility allowing for high accuracy, high yield and possibility for mass production. This technology is intended to drive optical interconnect applications that demand high-volume and low-cost production of a wide scale of interconnect components and structures for data communication from data centers to intra-core architectures.

We have designed and fabricated a variety of passive devices based on Si nanowire waveguides allowing to build highly integrated structures. For the inter- and intra-core communication the size of these structures is constrained by the diffraction limit of light. To go below this limit, plasmonic structures based on metal-dielectric interfaces have been proposed although their intrinsic high losses make their use with the available metal films impractical. Recently a new type of "hybrid plasmonic waveguides" was developed that allows for similar light confinement as in a metal-insulator-metal structure, but with much longer propagation lengths. Here a very thin low-index dielectric layer (slot layer) is sandwiched between a metal from one side and a high-index dielectric from the other side. Using this structure a number of different components based on hybrid plasmonic waveguides have been simulated and/or fabricated including waveguide couplers and splitters, different ring and disk resonators, polarisation beam splitters etc. This provides the way to realize subwavelength functional components for future ultra-compact integrated structures for optical interconnects and other applications.

ACKNOWLEDGMENT

This work was supported by "the Swedish Research Council (VR) through its Linnæus Center of Excellence ADOPT", as well as project VR-621-2010-4379.

Active Plasmonic Circuitry

A. V. Krasavin and A. V. Zayats
Department of Physics, King's College London, Strand, London WC2R 2LS, United Kingdom

Abstract— A variety of plasmonic and Si-photonic waveguiding geometries has recently been proposed to act as possible optical interconnects. In this context, plasmonics which is dealing with surface electromagnetic excitations in metallic structures, provides a great deal of flexibility in photonic integration since with surface plasmons the problem of light manipulation can be reduced from three to two dimensions. The electromagnetic field enhancement effects associated with surface plasmons and specific to them field confinement near metal interfaces result in the strong sensitivity of plasmonic mode to dielectric surroundings, thus facilitating all-optical and electronic control of their propagation. Moreover, utilizing more complex arrangements of plasmonic nanostructures such as plasmonic crystals and metamaterials complete control over surface plasmon dispersion can be achieved. In this talk we will overview plasmonic approaches for achieving subwavelength guiding and manipulation of optical signals [1–9]. Generation, detection, amplification and modulation of plasmonic signals in the integrated circuitry will also be discussed.

REFERENCES

1. Krasavin, A. V. and A. V. Zayats, "Silicon-based plasmonic waveguides," *Opt. Exp.*, Vol. 18, 11791–11799, 2010.
2. Krasavin, A. V. and A. V. Zayats, "Guiding light at the nanoscale: Numerical optimization of ultrasubwavelength metallic wire plasmonic waveguides," *Opt. Lett.*, Vol. 36, 3127–3129, 2011.
3. Wurtz, G. A., W. Dickson, D. O'Connor, R. Atkinson, W. Hendren, P. Evans, R. Pollard, and A. V. Zayats, "Guided plasmonic modes in nanorod assemblies: Strong electromagnetic coupling regime," *Opt. Exp.*, Vol. 16, 7460–7470, 2008.
4. Wurtz, G. A., R. Pollard, W. Hendren, G. P. Wiederrecht, D. J. Gosztola, V. A. Podolskiy, and A. V. Zayats, "Designed ultrafast optical nonlinearity in a plasmonic nanorod metamaterial enhanced by nonlocality," *Nature Nanotech.*, Vol. 6, 107–111, 2011.
5. Krasavin, A. V. and A. V. Zayats, "Electro-optic switching element for dielectric-loaded SPP waveguides," *Appl. Phys. Lett.*, Vol. 97, 041107, 2010.
6. Bolger, P. M., W. Dickson, A. V. Krasavin, L. Liebscher, S. G. Hickey, D. V. Skryabin, and A. V. Zayats, "Amplified spontaneous emission of surface plasmon polaritons and limitations on the increase of their propagation length," *Opt. Lett.*, Vol. 35, 1197–1199, 2010.
7. Krasavin, A. V., T. P. Vo, W. Dickson, P. M. Bolger, and A. V. Zayats, "All-plasmonic modulation via stimulated emission of co-propagating surface plasmon polaritons on a substrate with gain," *Nano Lett.*, Vol. 11, 2231–2235, 2011.
8. Fedyanin, D. Y., A. V. Krasavin, A. V. Arsenin, and A. V. Zayats, "Surface plasmon polariton amplification upon electric injection in highly-integrated plasmonic circuits," *Nano Lett.*, Vol. 12, 2459–2463, 2012.
9. Krasavin, A. V., S. Randhawa, J.-S. Bouillard, J. Renger, R. Quidant, and A. V. Zayats, "Optically-programmable nonlinear photonic component for dielectric-loaded plasmonic circuitry," *Opt. Exp.*, Vol. 19, 25222–25229, 2011.

Session 2P7b
SC1: High Frequency/Asymptotic Methods

High-frequency Scattering by Strongly Elongated Spheroids
Ivan Viktorovitch Andronov, Frederic Molinet, ... 762

Diffraction by an Acute-angled Dielectric Wedge: The $\boldsymbol{H}$-polarization Case
Marcello Frongillo, Gianluca Gennarelli, Giovanni Riccio, ... 763

An Alternative Treatment of the Problem in "A New Fast Physical Optics for Smooth Surfaces by Means of a Numerical Theory of Diffraction" about Saddle Stationary Phase Point
Jun Zhang, Tie Jun Cui, ... 764

Improved Asymptotic Expansion of the Dyadic Potential in the Line Integral Representation of the Physical Optics Integral
Frederic Molinet, ... 765

Numerical Evaluation of Creeping Waves for EM Scattering by Arbitrary Convex Conducting Bodies of Revolution
Jun Zhang, Tie Jun Cui, ... 766

Time-domain SBR Method for Fast Transient Analysis of Scattering from Large PEC Objects
Xiao Zhou, Tie Jun Cui, ... 767

High-frequency Scattering by Strongly Elongated Spheroids

I. V. Andronov[1] **and F. Molinet**[2]

[1]University of St. Petersburg, Russia
[2]Société MOTHESIM, France

Abstract— Many advances in the theory of diffraction were due to the high-frequency asymptotic methods, which provide relatively simple formulae for the fields in the form of series by inverse fractional powers of the large parameter $k\rho$, where k is the wave number and ρ is the characteristic radius of surface curvature in the plane of incidence. However for strongly elongated bodies the usual asymptotic approach fails. This happens because besides $k\rho$ another large parameter ρ/ρ_t, where ρ_t is the radius of transverse curvature, which characterizes the rate of elongation, is present in the problem formulation. Bodies with $\rho/\rho_t = O((k\rho)^\delta)$, $\delta < 1/3$ do not present difficulties and usual asymptotics are valid for such problems. When $1/3 \leq \delta < 2/3$ we deal with moderately elongated bodies in the terminology of [1]. In this case the structure of asymptotic expansions does not change and the influence of the large transverse curvature can be taken into account by introducing effective impedance in the boundary conditions [2]. Bodies with $\delta \geq 1$ have transverse dimensions of the order of the wavelength or smaller.

The most interesting case is the case of strongly elongated body when $2/3 \leq \delta < 1$. The asymptotic technique for the description of diffraction by bodies of revolution characterized by the relation

$$\chi \equiv k\rho \left(\frac{\rho_t}{\rho}\right)^{3/2} = O(1),$$

which corresponds to $\delta = 2/3$, was developed in [3, 4], where induced currents on a perfectly conducting surface were studied.

In this paper we extend the approach to describe far fields. For that we apply Stratton-Chu formula to the currents derived in the cited above papers. This allows asymptotics of the total scattering cross-section of a perfectly conducting strongly elongated spheroid to be derived for axial incidence. The leading order approximation is

$$\Sigma = -\frac{8}{\chi}\mathrm{Im}\left(\int_{-\infty}^{+\infty} \frac{\dot{F}_{-\frac{1}{2}}\left(t,\frac{\chi}{2}\right) H^+_{\frac{1}{2}}\left(t,\frac{\chi}{2}\right) + F_{-\frac{1}{2}}\left(t,\frac{\chi}{2}\right) \dot{H}^+_{\frac{1}{2}}\left(t,\frac{\chi}{2}\right)}{\dot{H}^+_{-\frac{1}{2}}\left(t,\frac{\chi}{2}\right) H^+_{\frac{1}{2}}\left(t,\frac{\chi}{2}\right) + H^+_{-\frac{1}{2}}\left(t,\frac{\chi}{2}\right) \dot{H}^+_{\frac{1}{2}}\left(t,\frac{\chi}{2}\right)} \frac{dt}{1+e^{-2\pi t}}\right),$$

where F and H^+ are Coulomb wave functions [5] and dot denotes derivative.

Numerical analysis of this formula shows that when $\chi \to \infty$, that is the body becomes not elongated, the total scattering cross-section Σ tends to the well known classical limit of 2. For finite values of the elongation parameter $\Sigma > 2$ if $\chi > \chi_0$ and $\Sigma < 2$ if $\chi < \chi_0$, where $\chi_0 \approx 1.95$.

REFERENCES

1. Andronov, I. V. and D. Bouche, "Asymptotic of creeping waves on a strongly prolate body," *Ann. Télécommun.*, Vol. 49, No. 3–4, 205–210, 1994.
2. Molinet, F., I. Andronov, and D. Bouche, *Asymptotic and Hybrid Methods in Electromagnetics*, The IEE, London, 2005.
3. Andronov, I. V., "High frequency asymptotics of electromagnetic field on a strongly elongated spheroid," *PIERS Online*, Vol. 5, No. 6, 536–540, 2009.
4. Andronov, I. V., D. P. Bouche, and M. Duruflé, "High-frequency diffraction of plane electromagnetic wave by an elongated spheroid," *IEEE Transactions on Antennas and Propag.*, Vol. 60, No. 11, 5286–5295, 2012.
5. Abramowitz, M. and I. A. Stegun, Editors, *Handbook of Mathematical Functions with Formulas, Graphs, and Mathematical Tables*, Dover Publications, New York, 1972.

Diffraction by an Acute-angled Dielectric Wedge: The H-polarization Case

M. Frongillo[1], **G. Gennarelli**[2], **and G. Riccio**[1]

[1]D.I.E.M., University of Salerno, Via Ponte Don Melillo, Fisciano (SA) 84084, Italy
[2]Institute for Electromagnetic Sensing of the Environment
National Research Council, Via Diocleziano 328, Naples 80124, Italy

Abstract— Diffraction by penetrable wedges is a canonical problem having an important role in many applications, and constitutes a very challenging problem from the analytical point of view.

The existing approaches provide approximate analytical or heuristic solutions, or attempt to solve the problem in an exact sense by using function theoretic techniques or by combining analytical and numerical techniques to compute integral equations. Uniform Asymptotic Physical Optics (UAPO) solutions were proposed by the authors in [1] and [2] for evaluating the field diffracted by right- and obtuse-angled lossless dielectric wedges when a plane wave impacts on them at normal incidence. They were expressed in closed form and given in terms of the Geometrical Optics (GO) response of the structure and the transition function of the Uniform Geometrical Theory of Diffraction (UTD) [3]. As a consequence, they resulted to be manageable and easy to implement in a computer code. Numerical tests and comparisons with Finite Difference Time Domain (FDTD) data assessed their accuracy. The time domain UAPO diffraction coefficients associated to the right-angled geometry were derived in [4] by taking advantage of the knowledge of their frequency domain counterparts [1].

The goal of this work is to propose a useful formulation for the field diffracted by an acute-angled lossless dielectric wedge illuminated by a TE_z (H-polarized) plane wave. Two separate diffraction problems relevant to the dielectric region and the surrounding space are tackled and solved by formulating the corresponding radiation integrals in terms of electric and magnetic equivalent PO surface currents lying on the internal and external faces of the wedge. For each observation domain, the UAPO solution for the diffracted field is derived in the UTD framework by means of a useful approximation, analytical manipulations and uniform asymptotic evaluations of the resulting integrals. This leads to closed form expressions containing the Fresnel reflection and transmission coefficients of the structure and the UTD transition function [3]. As expected, the here proposed UAPO solutions for the diffracted field allow one to compensate the GO discontinuities in the internal and external regions.

REFERENCES

1. Gennarelli, G. and G. Riccio, "A uniform asymptotic solution for diffraction by a right-angled dielectric wedge," *IEEE Trans. Antennas Propag.*, Vol. 59, 898–903, 2011.
2. Gennarelli, G. and G. Riccio, "Plane-wave diffraction by an obtuse-angled dielectric wedge," *J. Opt. Soc. Am. A*, Vol. 28, 627–632, 2011.
3. Kouyoumjian, R. G. and P.H. Pathak, "A uniform geometrical theory of diffraction for an edge in a perfectly conducting surface," *Proc. of IEEE*, Vol. 62, 1448–1461, 1974.
4. Gennarelli, G. and G. Riccio, "Time domain diffraction by a right-angled penetrable wedge," *IEEE Trans. Antennas Propag.*, Vol. 60, 2829–2833, 2012.

An Alternative Treatment of the Problem in "A New Fast Physical Optics for Smooth Surfaces by Means of a Numerical Theory of Diffraction" about Saddle Stationary Phase Point

Jun Zhang and Tie Jun Cui
State Key Lab of Millimeter Waves, Department of Radio Engineering
Southeast University, Nanjing 210096, China

Abstract— In one interesting literature about computing the physical optics (PO) integral by numerical steepest descend method, when considering the case that the integration domain had a saddle stationary phase point, the authors obtained a one dimensional integral along x axis, on which there existed higher order up to third poles at the origin after performing the integral about the variable of y. In order to avoid tackling this singular integral, they used a technique called Abel's summation technique to solve the problem ingeniously. In fact some classical electromagnetic textbooks use the similar technique abundantly to derive some integrals on the path of which there are *simple poles*. In particular the physical meaning of the technique in spectral domain can be summarized as studying the medium with tiny loss firstly and then taking the limit to obtain the result for the lossless medium.

However, some literatures have stated that if there are even-order poles on the path of integral, the integral will be divergent. In appearance the integral the authors obtain satisfies the condition, but why is the integral convergent? The aim of this paper is to clear this doubt. In the end of our investigation, we have found that actually higher order poles have no contribution to the final result. For the motivation of academic interest to acquire a general law, we go further to consider arbitrary polynomials of higher degree for the amplitude term in the PO integral. In such a case, the orders of the poles can be arbitrary numbers and make our analysis much more complicated. Fortunately, we also find the phenomenon that all higher order poles have no contribution successfully.

Comparing with the authors' technique, we can conclude that out method can reveal the influence of the higher order poles more clearly. It seems that we should pay the cost that the coefficients before all orders of poles must be evaluated accurately while the authors need only compute the residue. However from our analysis one can easily find that the derivations of coefficients for all orders of poles are the same and therefore, we believe the tasks we fulfill should also be accomplished by them.

Improved Asymptotic Expansion of the Dyadic Potential in the Line Integral Representation of the Physical Optics Integral

Frédéric Molinet
MOTHESIM, 9, Villa Pierre Loti, L'Hay-les-Roses 94240, France

Abstract— A way to reduce the complexity of evaluating the Physical Optics (PO) integral consists in making use of the possibilities related in the literature, to transform radiation integrals which are surface integrals, to line integrals. Following the work of Maggi, Miyamoto, Rubinowicz and Asvestas, an exact line integral representation of the PO scattered field from a perfectly conducting flat plate, illuminated by an Hertzian dipole, has been obtained by Johansen and Breinbjerg [1]. The monostatic case which has been excluded by these authors has been treated recently by Gordon [2]. However the integrand of the line integral along the rim of the radiating surface exhibits a pole singularity at geometrical optics shadow boundaries. Despite being analytically integrable it renders the numerical integration inaccurate or time consuming. An approach which overcomes this difficulty has been developed by Albani [3].

The case of double interactions of the PO field generated by a dipole in front of two non-coplanar plates has been considered in [4]. We have shown that the double surface integral can be transformed exactly in a double line integral along the contours of two plates with the addition of an integral along the generatrixes of a cone having the observation point as the tip and the contour of the second plate as the basis. In [4] we have shown that this last integral also called the dyadic potential function can be decomposed into a set of elementary integrals which have no stationary point in the domain of integration and which can be evaluated asymptotically by integration by parts. This approach however breaks down at the Geometrical Optics boundaries.

In the present paper, we consider the singularities of the integrand of the double line integral at the Geometrical Optics boundaries and construct an improved asymptotic expansion of the dyadic potential function.

The same technique can also be applied to the dyadic potential function of the transformed PO integral corresponding to a single diffraction, which for an arbitrary incident field is not exactly integrable, but can be evaluated asymptotically in a large domain of observation.

Numerical results showing the efficiency of the method are shown.

REFERENCES

1. Johansen, P. M. and O. Breinbjerg, *IEEE ANP*, Vol. 43, 689–696, Jul. 1995.
2. Gordon, W., *IEEE ANP*, Vol. 60, 2587–2589, May 2012.
3. Albani, M., *IEEE ANP*, Vol. 59, 586–594, Feb. 2011.
4. Molinet, F., *Progress In Electromagnetics Research Symposium Abstracts*, 698, Moscow, Russia, Aug. 19–23, 2012.

Numerical Evaluation of Creeping Waves for EM Scattering by Arbitrary Convex Conducting Bodies of Revolution

Jun Zhang and Tie Jun Cui
State Key Lab of Millimeter Waves, Department of Radio Engineering
Southeast University, Nanjing 210096, China

Abstract— We present numerical implementations on creeping waves for the electromagnetic (EM) scattering by arbitrarily shaped convex bodies of revolution (BOR) that are modeled by the nonuniform rational B-spline (NURBS) surfaces. Since the trajectory of creeping ray is geodesic, the first task of the paper isto make geodesic tracing on BOR surfaces. For BOR, the geodesic equation can be simplified from the original second-order differential equation to the first-order. Simulation results show that either the second-order or the first-order format can obtain good results if the step of discretization is chosen small enough. After geodesic tracing, we perform the scattering integrations with the expression of equivalent creeping current on each single strip bounded by two adjacent geodesic rays. Since the integrand is oscillatory, a fast method for evaluating the integral is suggested. By meshing the strip to small triangle cells, we approximate the phase of the creeping current by a linear function in each cell. If the amplitude of the creeping current is approximated by a constant in the integration cell, the integral can be expressed by a closed-form formula. This method has been shown much more efficient than the ordinary integration method.

Time-domain SBR Method for Fast Transient Analysis of Scattering from Large PEC Objects

Xiao Zhou and Tie Jun Cui
Department of Radio Engineering, Southeast University, Nanjing 210096, China

Abstract— The interest in the analysis of transient wave phenomena has been growing primarily due to the many recent advances which are taking place in the development of ultra-wide band (or short pulse) radar and their associated antennas for remote sensing and target identification applications; in additional, there has always been a significant interest in the effects of natural and man-made electromagnetic pulse (EMP) on complex radiating systems such as aircraft and spacecraft. It is natural to analyze transient electromagnetic (EM) wave phenomena directly in the time domain (TD). Even though conventional frequency-domain (FD) solution, in conjunction with fast Fourier transform (FFT) can be employed to obtain TD solutions, that is very time consuming since a wide frequency range needs to be considered. There are various numerical TD method such as finite-difference time-domain (FDTD) or TD integral equation approaches, but these numerical solutions for analyzing transient phenomena become intractable when the pulse width of transient incident field is very narrow compared with the geometrical dimensions of scattering object. Recently, direct use of physical optics (PO), physical theory of diffraction (PTD), equivalent edge current (EEC), geometric theory of diffraction (GTD), uniform theory of diffraction (UTD) in the time domain has been has been of interest. The advantages are several. These quasi-analytical solutions can provide closed form solutions which contain physical interpretation of transient wave behavior. Efficient and faster computation, more suitable solutions when pulse width is narrow compared with the geometrical dimensions of scattering object, feasibility to implement a hybrid solution by combination with various time domain methods such as FDTD and TLM.

In this paper, a time-domain version of shooting and bouncing rays (TD-SBR) method is developed to analyze the transient scattering from large perfectly conducting objects excited by a general time impulsive astigmatic wavefront. It is a method combining the method of time-domain geometrical-optics (TDGO) and time-domain physical-optics (TDPO). In TDGO, transient electromagnetic propagation is first represented with reflection and the divergence of optical rays. The electromagnetic properties of magnitude, direction and time decay are then added on top of the ray traces to mimic the properties of waves. In addition, this paper employs an analytic signal representation for the transient fields when formulating a ray based TD solution where the actual time response is the simply the real part of the analytic function. The use of the analytic time functions allows one to circumvent in a simple manner some complexities that arise when inverting into the TDGO ray fields which pass through caustics. In TDPO, a time-domain PO integral is formulated under the incidence of plane waves and observation in the far-field region. Then the surface integral over S is reduced to a line integral around the boundary of S. When S is a polygon, the line integral is further reduced to a closed-form expression, which is very similar to the well-known Gordon formula in the evaluation of PO integral in the frequency domain. When S is arbitrarily shaped, the integral evaluation is also efficient once the polygon mesh is given. Combining TDGO and TDPO methods, TD-SBR begins the computation by launching numerous rays from the sources, usually antennas or regions of plane waves. The magnitude of the rays is dependent upon the pattern of the source. Each ray then propagates through the computational domain and bounces between the target surfaces under study using the TDGO method. Next, the transient electromagnetic fields at each hit point are converted into surface currents using the TDPO methods and re-radiated towards all observation points. Finally, the transient fields at each observation point are summed up to represent the final transient electromagnetic field computed at the corresponding location of the computational domain.

Session 2P8a
SC5: Inverse Source Problems for Localization and Diagnostics

Explicit Reconstruction of Power Line Conductors Using a Two-dimensional Model
Martin Karl Norgren, ... 770
Reflection of TEM Waves by a Step Discontinuity on the Inner Wall of a Coaxial Waveguide
Gokhan Cinar, Sinan Aksimsek, Borje Nilsson, Sven Nordebo, Ozge Yanaz Cinar, ... 771
Reconstruction Strategies for Clinical Microwave Imaging
Andreas Fhager, Hoi-Shun Lui, Mikael Persson, ... 772
Conductor Locations Reconstruction in a Cylindrical Winding Model
Mariana Dalarsson, Martin Karl Norgren, ... 773
The Eigenvalue Problem for a Bianisotropic Cavity
Eftychia Argyropoulou, Andreas D. Ioannidis, ... 774
Power Cables and Basis Properties for Lossy Closed Waveguide Modes
Borje Nilsson, Anders Andersson, Gokhan Cinar, Andreas D. Ioannidis, Sven Nordebo, ... 775
Source Reconstruction for Radome Diagnostics
Kristin Persson, Mats Gustafsson, Gerhard Kristensson, Björn Widenberg, ... 776
An Inverse Scattering Technique Based on Finite Element — Boundary Integral Method
Emre Kilic, Thomas F. Eibert, ... 777
Characterization of Antenna Current Distributions Using Angular Momentum of the Farfield Amplitude
Jonas Friden, ... 778

Explicit Reconstruction of Power Line Conductors Using a Two-dimensional Model

M. Norgren
KTH Royal Institute of Technology, Sweden

Abstract— We consider a two-dimensional approximation of the magnetic inverse source problem of reconstructing the positions and currents of very long parallel conductor structures. In electric power engineering, such inverse source problems appear in contact-free measurements of currents in e.g., power lines, bus bars and cables. The magnetic field is measured by a set of sensors located in the vicinity of the conductors, and the currents and/or positions are determined by inversion of the direct map from the currents to the magnetic field, using a suitable model of the problem.

Here, the inverse source problem is solved using a technique that have been considered previously in magnetoencephalography for locating dipolar sources. In our case, the input data is the magnetic field on a contour surrounding the conductors to be reconstructed. Using the magnetic field and a harmonic function in a scalar-vector Green identity, we obtain a Green reciprocation formula, from which an explicit reconstruction algorithm is derived that provides both the positions and currents of the conductors. Mathematically, the Green identity approach removes influences of external disturbances, but practically a finite number of measurements must be used, which introduces modelling errors.

The numerical implementation of the algorithm is described and the sensitivity versus the number of measurement points is investigated. Also, we test the sensitivity of the algorithm against random noise in the measurement data. We find that the algorithm is highly sensitive to both numerical errors and uncertainties in the measured data, and these problems accelerate when increasing the number of conductors. Hence, if positions and currents are to be reconstructed simultaneously, a very large number of measurement points will be needed and the magnetic field sensors must have a very high precision.

Clearly, there are practical difficulties with the full reconstruction problem, but the algorithm is also an interesting alternative for the reduced problem of reconstructing the currents only. Since the Green formalism cancels external disturbances it can be used as guideline for determining optimal sensors positions and for the processing of measurement data.

Reflection of TEM Waves by a Step Discontinuity on the Inner Wall of a Coaxial Waveguide

G. Çınar[1], S. Akşimşek[1,2], B. Nilsson[3], S. Nordebo[3,4], and Ö. Yanaz Çınar[1]

[1]Gebze Institute of Technology, Turkey
[2]Istanbul Kültür University, Turkey
[3]Linnaeus University, Sweden
[4]Lund University, Sweden

Abstract— Electromagnetic wave propagation in waveguides has been an interesting topic and subject to various engineering problems, such as microwave filters and microwave measurement techniques, one of which is the measurement setup described in [1], where experiments utilizing electromagnetic pulses have been performed on a 80 km long High Voltage Direct Current (HVDC) power cable in a factory [2] and on the 250 km long Baltic HVDC power cable [3]. Low frequency electromagnetic modeling of this measurement setup is very interesting as there exist many scattering mechanisms such as different inner and outer radii of two connected coaxial cables (step discontinuity on the outer and inner walls), different dielectric media, etc.. Among these, scattering by a step discontinuity on the outer wall of a coaxial waveguide has been analyzed by the authors, recently [4]. In this study, reflection of a TEM wave from a step discontinuity on the inner wall of a coaxial cable (see Figure 1) is analyzed rigorously by applying direct Fourier transform and reducing the problem into the solution of a modified Wiener-Hopf equation of the second type. The solution for the field terms are determined in terms of infinite number of unknown coefficients which satisfy an infinite set of linear algebraic equations. These equations are solved numerically and the effect of area ratio on the reflection coefficient is presented graphically at the end of the analysis. The same problem is then analyzed by applying the mode matching technique, which is widely used in previous works related to waveguides. Following the classical mode-matching procedure, the reflection coefficient is determined and it is compared to the one obtained via the Wiener-Hopf technique.

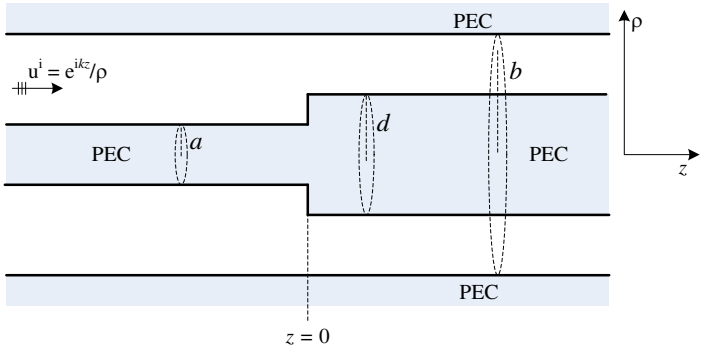

Figure 1: The geometry of the problem.

REFERENCES

1. Nilsson, B., G. Çınar, S. Nordebo, and Ö. Yanaz Çınar, "Asymptotic methods for long distance monitoring of power cables," *The Sixth International Conference "Inverse Problems: Modeling and Simulation"*, Antalya, Turkey, May 2012.
2. Nordebo, S., B. Nilsson, T. Biro, G. Çınar, M. Gustafsson, S. Gustafsson, A. Karlsson, and M. Sjöberg, "Electromagnetic dispersion modeling and measurements for HVDC power cables," Technical Report LUTEDX/(TEAT-7211)/132/(2011), Department of Electrical and Information Technology, Lund University, P. O. Box 118, S-221 00 Lund, Sweden, 2011.
3. Nordebo, S., B. Nilsson, T. Biro, G. Çınar, M. Gustafsson, S. Gustafsson, A. Karlsson, and M. Sjöberg, "Wave modeling and fault localization for underwater power cables," *Proceedings of 13th International Conference on Electromagnetics in Advanced Applications (ICEAA11)*, Torino, Italy, September 2011.
4. Akşimşek, S., G. Çınar, B. Nilsson, and S. Nordebo, "TEM wave scattering by a step discontinuity on the outer wall of a coaxial waveguide," *IEEE Trans. Microwave Theory and Techniques*, submitted.

Reconstruction Strategies for Clinical Microwave Imaging

Andreas Fhager[1], **Hoi-Shun Lui**[2], **and Mikael Persson**[1]

[1]Department of Signals and Systems, Chalmers University of Technology, Sweden
[2]The University of Queensland, Australia

Abstract— Microwave imaging is an interesting alternative being extensively researched. It has the potential to solve problems in several important clinical areas, for example stroke diagnostics, breast cancer imaging. However the technique is general and may have applications in a great variety of other application areas. The strategy in microwave imaging is that the object under investigation, e.g., the breast or the head, is surrounded by a number of transmitting and receiving antennas. In the measurements each antenna is operated as a transmitter as well as a receiver for every possible combination of antennas. Based on these measurements a dielectric image of the internal parts of the body is reconstructed. We are using an iterative time domain algorithm to reconstruct the dielectric parameters of the target object. It is based on electromagnetic simulations of the antenna system and the image is reconstructed based on a comparison with the scattering measurements of pulses for the different transmitter/receiver combinations. The difference between the measured and the simulated signals is used to update the dielectric properties in the target region. As the reconstruction of the target object is iteratively refined, the simulated and measured signals converge. The assumption is that when the difference is sufficiently small the reconstruction is completed.

In our current work we investigate how different measurement schemes using cross- and co-polarization measurements and the matching medium affect the ability to perform accurate reconstructions. We also investigate how the skin, a high contrast tissue surrounding the outer parts of the body affect the final reconstructiom.

Conductor Locations Reconstruction in a Cylindrical Winding Model

M. Dalarsson and M. Norgren
Division of Electromagnetic Engineering, School of Electrical Engineering
Royal Institute of Technology, Stockholm SE-100 44, Sweden

Abstract— Power transformers are critical components of an electric power grid and their occasional failures reduce the power supply ability of the grid severely. In operation, power transformers are subject to several degradation mechanisms, e.g., thermal degradation at hot spots, partial discharges due to local over-stress, deformations of the windings caused by mechanical forces from short circuit currents, and increased levels of moisture in the cellulose insulation due to decomposition. In this paper we continue the study of a new proposed principle for on-line diagnostics of power transformers in operation. The existing diagnostic tools are either based on relatively coarse methods or off-line methods that require disconnection from the grid and imply a non-service stress of the transformer.

We insert antennas inside the transformer tank above and below the winding to radiate and measure microwave fields that interact with the metallic structure and the insulation. The responses from the different modes of the radiated waves are shown to be sensitive to mechanical deformations that could be caused by electromagnetic forces due to short-circuit currents and possible manufacturing weaknesses. The goal is to be able to identify and quantify deformations of the individual winding segments or individual turns from measurements of the scattered fields at both ends.

As a simplified model for the present study, we model the transformer as a coaxial waveguide where the overall outer cylinder represents the transformer tank wall while the overall inner cylinder represents the iron core that conducts the magnetic flux. In between there is a set of cylindrical conductor structures representing the winding segments or turns. The actual inner and outer cylindrical waveguide boundaries are then determined depending on the region under consideration. The propagation problem is solved accurately and efficiently by conventional waveguide theory, using the exact Bessel functions as well as modematching and cascading techniques.

Assuming that waves may be launched at both ends of the waveguide, the inverse problem is to determine the locations of the individual conductors, from measurements of the scattered fields at both ends. Using a waveguide environment, the cut-off frequencies of the modes imply restrictions on how much information that can be obtained from measurements at various frequencies. The dominant TEM-mode yields information at all frequencies, while the higher order modes enter as the frequency increases. The multiplemodes can therefore be required to improve the reconstructions which implies that many antennas may be needed in the measurement system. We envisage optimization as a suitable method for solving the inverse problem and we obtain a qualitative agreement between the reconstructed and actual cylindrical winding positions.

ACKNOWLEDGMENT

This work was funded by the Swedish Energy Agency, Project Nr 34146-1.

The Eigenvalue Problem for a Bianisotropic Cavity

E. Argyropoulou[1] and A. D. Ioannidis[2]

[1]National and Kapodistrian University of Athens, Greece
[2]Linnaeus University, Sweden

Abstract— This research discusses the propagation problem of a time harmonic electromagnetic field (time convention is taken to be $e^{-i\omega t}$) inside a perfectly conducting bounded domain $\Omega \subset \mathbb{R}^3$ (cavity). We assume that the cavity is filled with a bianisotropic medium. This problem is formally formulated as an eigenvalue problem for a linear operator pencil

$$\mathcal{Q}e = \omega M(\omega)e. \qquad \text{(EP)}$$

Here we employ the six-vector notation and $e := (\mathbf{E}; \mathbf{H})^T$ stands for the electromagnetic field, $\mathcal{Q}$ for the self-adjoint Maxwell operator

$$\mathcal{Q} := i \begin{bmatrix} 0 & -\text{curl} \\ \text{curl} & 0 \end{bmatrix},$$

and $M = M(\omega)$ for the material matrix

$$M := \begin{bmatrix} \varepsilon & \xi \\ \zeta & \mu \end{bmatrix}.$$

Our approach is functional analytic and we pose the problem in an appropriate Hilbert space. We do not make any special assumption on M apart that its entries are essentially bounded with respect to the spatial variable $r \in \Omega$ and analytic with respect to $\omega \in D$, where D is a domain in the complex plane.

A non-trivial solution for (EP) is a pair $(\omega; e)$, where ω is a complex number and e is a non-zero square integrable function. ω is then referred as an eigenfrequency of the cavity and e as a corresponding mode. By using the "analytic Fredholm alternative", we show that (EP) admits countably many eigenvalues with no accumulation point; in addition, corresponding eigenspaces are finite dimensional. We also provide a characterization of eigenelements of bianisotropic cavity by using the eigenelements of hollow cavity (when $M = I$) and the material matrix.

Finally, we discuss some ideas about the inverse problem, that is, how to reconstruct the material matrix M if eigenelements $(\omega_n; e_n)$ of problem (EP) are known. This discussion involves the generally difficult problem of the completeness of eigenvectors and, more precisely, the question whether they provide a Riesz basis.

Power Cables and Basis Properties for Lossy Closed Waveguide Modes

Börje Nilsson[1], **Anders Andersson**[2], **Gökhan Cinar**[3], **Andreas Ioannidis**[1], **and Sven Nordebo**[1]

[1]Linnæus University, Sweden
[2]Jönköping University, Sweden
[3]Gebze Institute of Technology, Turkey

Abstract— Closed waveguide modes without losses are relatively simple to analyze. They are eigenfunctions to a self-adjoint operator and results on basis and orthogonality properties follow from wellknown results in functional analysis. With losses, the situation is more complicated and the lossless theory is not directly applicable. In general there are both discrete and non-discrete modes but only the former are present in closed waveguides. The modelling of a junction between a measurement coaxial cable and a power cable motivates a detailed study of the discrete modes, their basis, orthogonality and biorthogonality properties in particular. After a brief introduction to power cable modelling, a state of the art of basis properties of eigenfunctions are given based on functional analysis. It is concluded that the most efficient results are based on perturbations of well-known systems. The perturbations can be described in various ways in terms of operator, eigenvector or eigenvalue. It is the actual problem formulation that determines how the perturbation should be formulated.

Source Reconstruction for Radome Diagnostics

Kristin Persson[1], **Mats Gustafsson**[1],
Gerhard Kristensson[1], **and Björn Widenberg**[2]

[1]Department of Electrical and Information Technology
Lund University, Box 118, Lund SE-221 00, Sweden
[2]Radomes & Antennas, GKN Aerospace Applied Composites
Box 118, Linkping SE-580 13, Sweden

Abstract— Visualization of electromagnetic field and currents facilitates our understanding of the interaction between fields and devices. This is easily accomplished in numerical simulations where the electromagnetic fields can be computed directly. It is much harder in most measurement situations where the fields cannot be measured directly and must instead be reconstructed from measurements of the fields outside the object or volume of interest. This reconstruction requires the solution of an inverse source problem. Source reconstruction is useful in applications such as non-destructive diagnostic of antennas and radomes [1–7].

In this presentation, we use source reconstruction for radome diagnostics. Defects caused by metallic and dielectric patches as well as dislocations in frequency selective surfaces (FSS) are imaged from far-field data.

REFERENCES

1. Persson, K. and M. Gustafsson, "Reconstruction of equivalent currents using a near-field data transformation — With radome applications," *Progress In Electromagnetics Research*, Vol. 54, 179–198, 2005.
2. Alvarez, Y., F. Las-Heras, and M. R. Pino, "Reconstruction of equivalent currents distribution over arbitrary three-dimensional surfaces based on integral equation algorithms," *IEEE Trans. Antennas Propagat.*, Vol. 55, No. 12, 3460–3468, 2007.
3. Cappellin, C., A. Frandsen, and O. Breinbjerg, "Application of the SWE-to-PWE antenna diagnostics technique to an oset reector antenna," *IEEE Antennas and Propagation Magazine*, Vol. 50, No. 5, 204–213, 2008.
4. Eibert, T. F. and C. H. Schmidt, "Multilevel fast multipole accelerated inverse equivalent current method employing Rao-Wilton-Glisson discretization of electric and magnetic surface currents," *IEEE Trans. Antennas Propagat.*, Vol. 57, No. 4, 1178–1185, 2009.
5. Persson, K., M. Gustafsson, and G. Kristensson, "Reconstruction and visualization of equivalent currents on a radome using an integral representation formulation," *Progress In Electromagnetics Research*, Vol. 20, 65–90, 2010.
6. Jorgensen, E., D. W. Hess, P. Meincke, O. Borries, C. Cappellin, and J. Fordham, "Antenna diagnostics on planar arrays using a 3D source reconstruction technique and spherical near-field measurements," *2012 6th European Conference on Antennas and Propagation (EUCAP)*, 2547–2550, 2012.
7. Persson, K., M. Gustafsson, G. Kristensson, and B. Widenberg, "Radome diagnostics — Source reconstruction of phase objects with an equivalent currents approach," Technical Report LUTEDX/(TEAT-7223)/1–22/(2012), Department of Electrical and Information Technology, Lund University, P. O. Box 118, S-221 00 Lund, Sweden, 2012, http://www.eit.lth.se.

An Inverse Scattering Technique Based on Finite Element — Boundary Integral Method

Emre Kılıç and Thomas F. Eibert
Institute for High-Frequency Engineering
Technische Universität München, Munich 80290, Germany

Abstract— A novel decomposition technique is addressed for the inverse scattering of three dimensional objects in free-space. It is assumed that the unknown object is illuminated by a number of sources producing incident fields at different frequencies. Scattered electric fields, due to the contribution of the unknown object to the total electric fields are assumed to be measured either in far field region or near field region. Exploiting equivalence principle, a closed surface including the unknown object and excluding sources is defined in order to decompose the inverse scattering problem, which is ill-posed and nonlinear, into two parts. While the first one is linear but ill-posed, the second one is non-linear. In the first step of the proposed technique, unknown surface electric and magnetic currents on the closed surface are introduced in order to model the scattered electric field in a boundary integral representation. The resulting integral equation is linear and ill-posed. Rao-Wilton-Glisson basis functions on triangles are employed to discretize the boundary integral equation with appropriate testing functions. The multilevel fast multilevel method is adapted in order to reduce the computational burden. In the equivalence principle, surface currents due to incident fields produce null fields outside the closed surface and negative incident fields inside the closed surface. In order to eliminate this null-space of integral equation, the fields inside the closed surface produced by surface currents are forced to be zero. A regularized solution of the integral equation is obtained by the GMRES algorithm. Once surface currents are obtained, the inverse scattering problem is reduced to a cavity problem with inhomogeneous boundary condition which forms the second part of the problem. Tetrahedral elements are used to discretize the solution domain surrounded by the closed surface. The unknown electric field is expanded by using curl-conforming basis functions. Material properties are assumed to be constant within each tetrahedron. After employing finite element method, a nonlinear system of equations is obtained and solved iteratively in the sense of Newton's method in order to reconstruct properties of the object. As primary results, promising reconstructions are obtained.

Characterization of Antenna Current Distributions Using Angular Momentum of the Farfield Amplitude

Jonas Friden
Ericsson Research, Ericsson AB, Sweden

Abstract— Angular momentum, as known in Quantum Mechanics, is applied to the Spherical Wave Expansion (SWE) of the farfield amplitude of an antenna. The angular momentum and its projection on a given axis are defined as weighted sums of the mode amplitudes. Fundamental symmetry operations, translations and rotations, of the angular momentum operator are used to minimize the magnitude of angular momentum and to characterize its directional properties. Especially, a unique translation, minimizing the magnitude of the angular momentum, is guaranteed and defines the radiation center. This provides a well-defined definition and method to calculate a reference point corresponding to minimal phase variations of the farfield amplitude. The method can be applied to any farfield pattern corresponding to positive definite radiated power. Results using measured and simulated farfield patterns for a range of antenna types are shown.

Session 2P8b
SC5: Emerging Techniques and Applications in SAR/ISAR Imaging

Improved Classification of Targets Using a Fusion of the Range Profile and the Inverse Synthetic Aperture Radar Image
In-O. Choi, Sang-Hong Park, ... 780

Wide-field Circular SAR Imaging Studies Based on Ground-based Experiments
Sevket Demirci, Enes Yigit, Betul Yilmaz, Caner Ozdemir, ... 781

An Accurate High Resolution ISAR Image Reconstruction Method Based on 2-D Nonuniform Fast Fourier Transform
Xin-Yi He, K. Cai, ... 783

Short-range Ground-based SAR Imaging Experiments: Application of Back-projection Algorithm
Enes Yigit, Sevket Demirci, Betul Yilmaz, Caner Ozdemir, ... 784

Compressed Sensing Based Near-field Inverse Synthetic Aperture Radar Imaging
Caner Ozdemir, Sevket Demirci, Enes Yigit, Betul Yilmaz, ... 786

Huynen Dichotomy-based Radar Target Adaptive Extraction
Dong Li, Yunhua Zhang, ... 788

Huynen Dichotomy-based Unsupervised Terrain Classification
Dong Li, Yunhua Zhang, ... 789

Improved Classification of Targets Using a Fusion of the Range Profile and the Inverse Synthetic Aperture Radar Image

I. O. Choi and S. H. Park
Department of Electronic Engineering, Pukyong National University, Busan, Korea

Abstract— The range profile (RP) and the inverse synthetic aperture radar (ISAR) image are the useful radar signature used to classify unknown targets because they can be used regardless of day-night and weather conditions. RP is derived by compressing the wideband radar signal into the high-resolution one and ISAR is derived by coherently processing RPs and conducting the translational motion compensation. However, the classification using the two methods is heavily dependent on flight condition [1]. When the target is flying in the direction of the radar line of sight (LOS), the classification ratio (P_c) derived using ISAR is degraded significantly because the image plane formed by the vertical angular variation causes scatters to be distributed in a narrow region on the image. On the other hand, when the target is flying in the vertical direction of LOS, P_c by RP is degraded due to the dominant peak that makes each target look similar. Therefore, it is necessary to develop an efficient method that can provide high P_cs regardless of the flight direction. This paper proposes an efficient method to classify targets using a classifier-level fusion of RP and ISAR and a scenario-based construction method of the training database. Simulation results using the five targets composed of point scatterers prove that the proposed method yields P_cs $\geq 98\%$ when the targets are flying in a variety of directions at both short and long ranges.

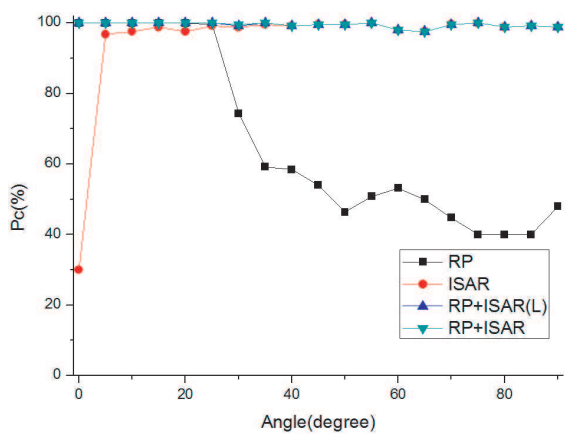

Figure 1: Classification result versus flight direction.

ACKNOWLEDGMENT

This research was supported by Basic Science Research Program through the National Research Foundation of Korea (NRF) funded by the Ministry of Education, Science and Technology (2012R1-A1A1002047).

REFERENCES

1. Park, S.-H., J.-H. Lee, and K.-T. Kim, "Performance analysis of the scenario-based construction method for real target ISAR recognition," *Progress In Electromagnetics Research*, Vol. 128, 137–151, 2012.

Wide-field Circular SAR Imaging Studies Based on Ground-based Experiments

S. Demirci[1], **E. Yigit**[2], **B. Yilmaz**[1], **and C. Ozdemir**[1]

[1]Department of Electrical-Electronics Engineering, Mersin University, Mersin, Turkey
[2]Vocational School of Technical Sciences, Mersin University, Mersin, Turkey

Abstract— Circular synthetic aperture radar (CSAR) is a term generally used to refer to synthetic aperture radar (SAR) systems wherein the radar-carrying platform at a fixed height moves along a circular path while the radar beam illuminates the ground region that falls inside the scanning circle [1]. Since this type of a spotlight scenario provides observation of the target over acomplete azimuthal coverage of 360 degrees, it can achieve highly sharpresolved imageswhen compared to linear SAR scenarios. Additionally, the resolution in vertical direction and hence the height information of the scene can be obtained by the help of the single pass of the radar only. Despite these unique features, a major challenge forCSARis the imaging of large-sized scenes. More clearly, if the scene's radius is a significant fraction of the SAR path radius (i.e., wide-field scenario), various contributions from the scatterers superpose in the same range-azimuth cell, resulting in a layover phenomenon [2]. Layover effects actually arise from the two-dimensional (2D) representation of a three-dimensional (3D) objectand can significantly degrade the SAR imaging quality. In this scope, this attribute of the wide-field CSAR imaging was investigated through ground-based (i.e., low attitude and smallscanning radius) CSAR imaging studies of point targets and as well as complex target vehicles such as cars and backhoes. A modified back-projection algorithm was used in all image reconstruction tasks.

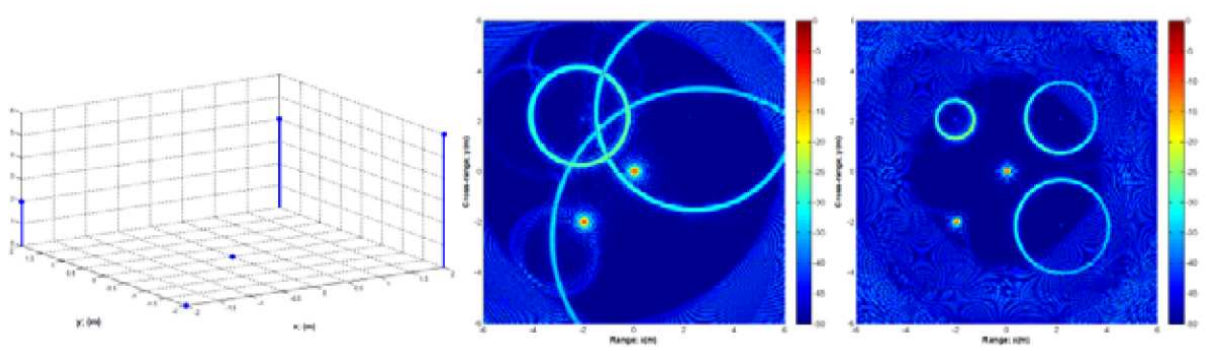

(a) (b) (c)

Figure 1: (a) Multiple point targets in 3D space. Ground plane imaging results for (a) $\theta = 45°$, (b) $\theta = 23.5°$, depression angles.

In the first simulation, it was aimed to obtain the images of various isotropic point targets located at different heights. The targets were placed in 3D space as shown in Fig. 1(a) and then the backscattering data were acquired for the two different cases of depression angle, i.e., $\theta = 45°$ and $\theta = 23.5°$. For the first case of $\theta = 45°$, both the height h of the radar from the ground and the radius of the circular path R_g was set to 21.54 m. In the latter case, the depression angle value of 23.5° was obtained by setting these values to $h = 9.54$ m and $R_g = 21.9$ m. In both situations, the frequency data were collected within the bandwidth of 4.5 to 6 GHz sampled at 501 points and the azimuth data were collected within the full aperture of 360° sampled with 0.25° steps. The results of the ground plane imaging are shown in Figs. 1(b) and 1(c). Some observations from these results are as follows: (i) The response is focused when the height of the target z_t, is equal to the height of the imaging plane z_f, otherwise it is shown up a defocused ring. (ii) As the difference between the z_f and z_t increases, the radius of the defocusing ring increases and its width decreases. (iii) The radius of the defocusing ring is also shown to be larger as the depression angle gets closer to the 45°. In the second simulation, the point spread function (PSF) analysis of a radially displaced point target on the ground plane was performed. The results shown in Fig. 2 demonstrate that, as the distance of the scatterer to the imaging center increases, the original ring-shaped characteristic become elliptical-shaped and asymmetric about the z-axis. Finally,

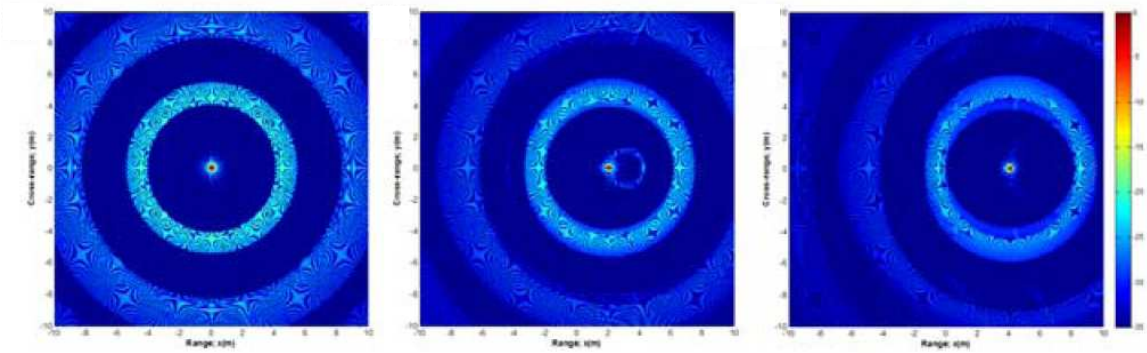

(a) (b) (c)

Figure 2: PSF images of a point target: (a) at the imaging center, (b) displaced 2 m along the x-axis and (c) displaced 4 m along the x-axis.

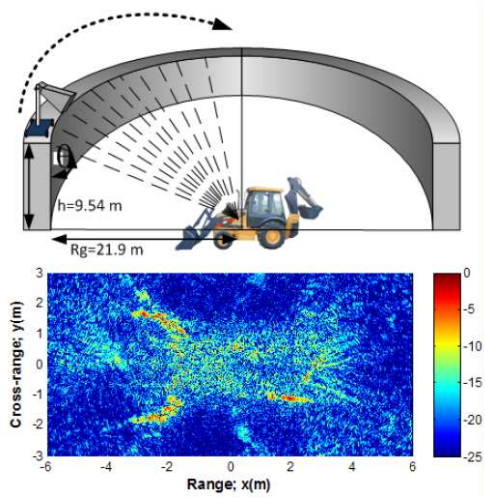

Figure 3: Ground-based CSAR imaging of a backhoe. Top: geometry, Bottom: 270° aperture CSAR image.

the wide-field CSAR imaging challenges were investigated through real, ground-based imaging experiments. With the geometry shown in Fig. 3, the near-field CSAR images of various vehicles were acquired.An example imaging result of a backhoe is shown in Fig. 3, for a total scanning aperture of 270° and a depression angle of $\theta = 23.5°$.

REFERENCES

1. Soumekh, M., *Synthetic Aperture Radar Signal Processing with MATLAB Algorithms*, Wiley, New York, 1999.
2. Dungan, K. E. and L. C. Potter, "Classifying civilian vehicles using a wide-field circular SAR," *Algorithms for Synthetic Aperture Radar Imagery XVI, Proc. SPIE*, E. G. Zelnio and F. D. Garber, Eds., Vol. 7337, 2009.

An Accurate High Resolution ISAR Image Reconstruction Method Based on 2-D Nonuniform Fast Fourier Transform

X. Y. He and K. Cai
Science and Technology on Electromagnetic Scattering Laboratory, China

Abstract— We present a new method to reconstruct high resolution inverse synthetic aperture radar (ISAR) images. When the far-field data arranged in the polar format, the two-dimensional (2-D) image can be reconstructed by a 2-D Fourier transform directly. But the fast Fourier transform (FFT) is failed for the data do not falling on a Cartesian grid. We introduce the 2-D nonuniform fast Fourier transform (NUFFT) to reconstruct the ISAR image. It is the first time to use NUFFT technology to achieve ISAR imaging. Instead of interpolating the input data, NUFFT interpolate the exponential function for each sampling point. The technology could easily extend to high dimensional by tensor product. The 2-D NUFFT is very suitable to reconstruct SAR image. Two examples will be shown to demonstrate that the reconstructed images have higher resolution than the general method when using the same data.

Short-range Ground-based SAR Imaging Experiments: Application of Back-projection Algorithm

Enes Yigit[1], **Sevket Demirci**[2], **Betul Yilmaz**[2], **and Caner Ozdemir**[2]

[1]Vocational School of Technical Sciences, Mersin University, Mersin, Turkey
[2]Department of Electrical-Electronics Engineering, Mersin University, Mersin, Turkey

Abstract— Synthetic aperture radar (SAR) is an important remote sensing and imaging technique capable of generating high resolution images of stationary target on the ground, and it becomes an important tool in military intelligence, surveillance, and reconnaissance [1, 2]. Since conventional SAR systems has an implementation difficulty, high cost and long data collection time; ground based SAR (GB-SAR) systems; however, are easier to implement, cheaper in hardware and faster in data collection and therefore they become more preferable recently [3, 4]. Also; maintenance and improvement of the system are clearly versatile providing arbitrary choices in frequency, interferometry, polarimetry and incidence angle so, it can be used as a test-bed for an advanced concept design of airborne or space borne SAR system. Unlike conventional SAR systems that observe large regions of earth, GB-SAR systems can acquire high resolution images of interested earth portions of limited sizes. Therefore; it may be used in many specialized applications such as unstable slopes monitoring, environment monitoring, investigation of artificial structures, observation of mature grain and etc. [5, 6].

In this study, an experimental study on ground based-synthetic aperture (GB-SAR) radar imagery was accomplished to image terrestrial regions by the help of a GB-SAR data collection setup. It consists of Vector Network Analyzer (VNA-Anritsu MS2026C), antennas (C-band), manual controlled rail-scanner, and the control computer as seen in Fig. 1(a). VNA is used as the stepped frequency continuous wave radar system operating between 5 kHz and 6 kHz. The antennas that were used in the quasi-monostatic mode are of pyramidal horn types that have half-power beam widths of approximately 23° at 5 GHz. The system was installed on a balcony of a 9 m-high building and look angle of the antennas were arranged 23° as shown in Fig. 1(b). The length of synthetic aperture was 10 m for total of 200 discrete measurement points. The frequency of VNA was altered with 5 MHz discrete steps ranging from 4.5 GHz to 6 GHz for a total of 301 frequencies. The final SAR image of the road, reconstructed by back-projection algorithm (BPA), is shown in Fig. 1(c). Some observations from this result are as follows: The responses from ground targets like rubbish bin, sidewalk and safety zone are focused when the heights of the targets are approximately equal to the height of the imaging plane; otherwise it is shown up a defocused reflection. As seen from the Fig. 1(b), the position of the pole is approximately $x = 4.25$ m and $y = 16.5$ m. However; the reflection from the pole is seen approximately at $x = 4.25$ m and $y = 14$ m as seen in Fig. 1(c). This is because of the length of the pole and depression angle of the antenna. When the depression angle gets closer to the 0° the defocusing distance is also shown to be smaller. Hence, when the short range GB-SAR image is interpreted, this depression angle effect must be taken in to account. Consequently the short-range GB-SAR

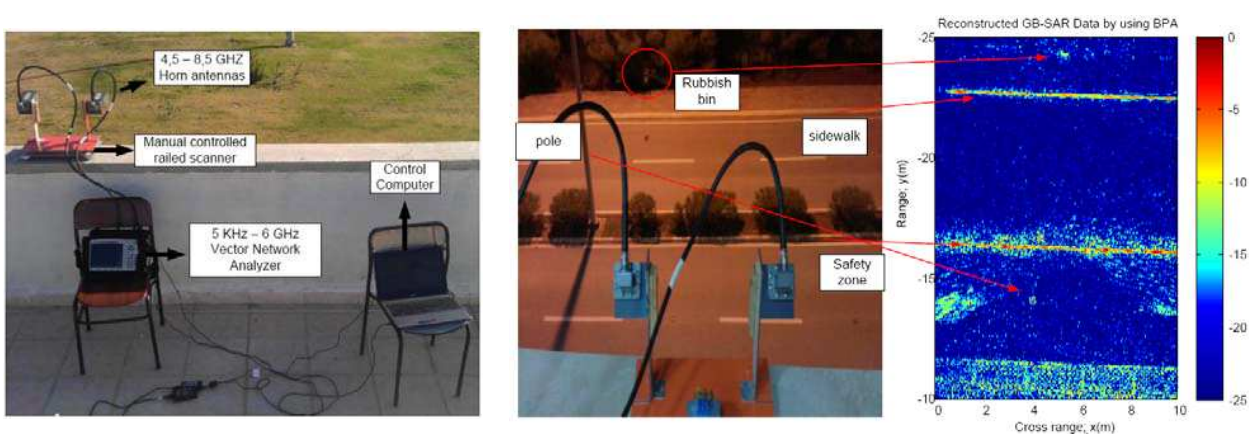

(a) (b) (c)

Figure 1: (a) Ground based SAR imaging setup, (b) the road to be imaged, (c) GB-SAR image of the road.

imaging techniques were investigated through real, ground-based imaging experiments and some imaging difficulties are exhibited.

REFERENCES

1. Mao, X. H., D. Y. Zhu, and Z. D. Zhu, "Signatures of moving target in polar format spotlight SAR image," *Progress In Electromagnetics Research*, Vol. 92, 47–64, 2009.
2. Chan, Y. K. and S. Y. Lim, "An introduction to synthetic aperture radar (SAR)," *Progress In Electromagnetics Research B*, Vol. 2, 27–60, 2008.
3. Cazzani, L., C. Colesanti, D. Leva, G. Nesti, C. Prati, F. Rocca, and D. Tarchi, "A ground-based parasitic SAR experiment," *IEEE Trans. Geosci. Remote Sensing*, Vol. 38, No. 5, 2132–2141, 2000.
4. Cho, B. L., Y. K. Kong, H. G. Park, and Y. S. Kim, "Automobile-based SAR/InSAR system for ground experiments," *IEEE Trans. Geosci. Remote Sensing*, Vol. 3, No. 3, 401–405, 2006.
5. Pieraccini, M., G. Luzi, D. Mecatti, L. Noferini, and C. Atzeni, "Ground-based SAR for short and long term monitoring of unstable slopes," *Proceedings of the 3rd European Radar Conference*, 92–95, 2006.
6. Zhou, Z. S., V. Boerner, and M. Sato, "Development of a ground-based polarimetric broadband SAR system for non-invasive ground-truth validation in vegetation monitoring," *IEEE Trans. Geoscience and Remote Sensing*, Vol. 42, No. 9, 1803–1810, 2004.

Compressed Sensing Based Near-field Inverse Synthetic Aperture Radar Imaging

C. Ozdemir[1], S. Demirci[1], E. Yigit[2], and B. Yilmaz[1]

[1]Department of Electrical-Electronics Engineering, Mersin University, Mersin, Turkey
[2]Vocational School of Technical Sciences, Mersin University, Mersin, Turkey

Abstract— The newly developed theory of compressed sensing (CS) states that it is possible to reconstruct sparse or compressible signals from a small set of linear measurements. Besides, if properly selected (i.e. random, noisy-like), the number of these measurements can be much smaller than the Nyquist rate, which in turn may provide clear advantages over conventional systems. In the context of synthetic aperture radar (SAR), this high under-sampling capability may give rise to a reduction in transmission/reception of radar signals, a reduction in on-board storage constraints, etc. Consequently, the feasibility of using CSin SAR imaging has become a trending topicandan increasing research has begun to benefit from this new framework [1, 2]. Most of the existing studies [1], however, deal with simulation data. Yet, there are few realistic examples [2], which have shown the application of CS to SAR imaging to be challenging in practice. In this contribution, these challenges are investigated through both simulation and real, near-field inverse synthetic aperture radar (ISAR) imaging studies.

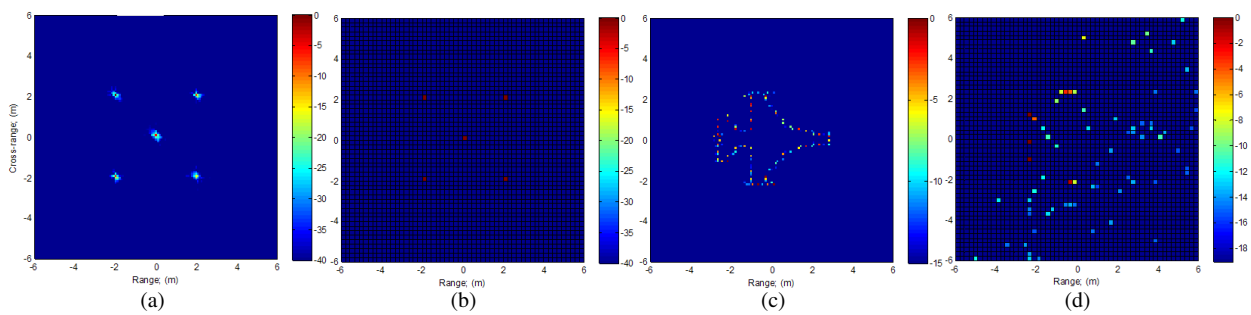

Figure 1: Simulation results: (a), (c): back-projection based, (b), (d): CS-based imaging of point targets.

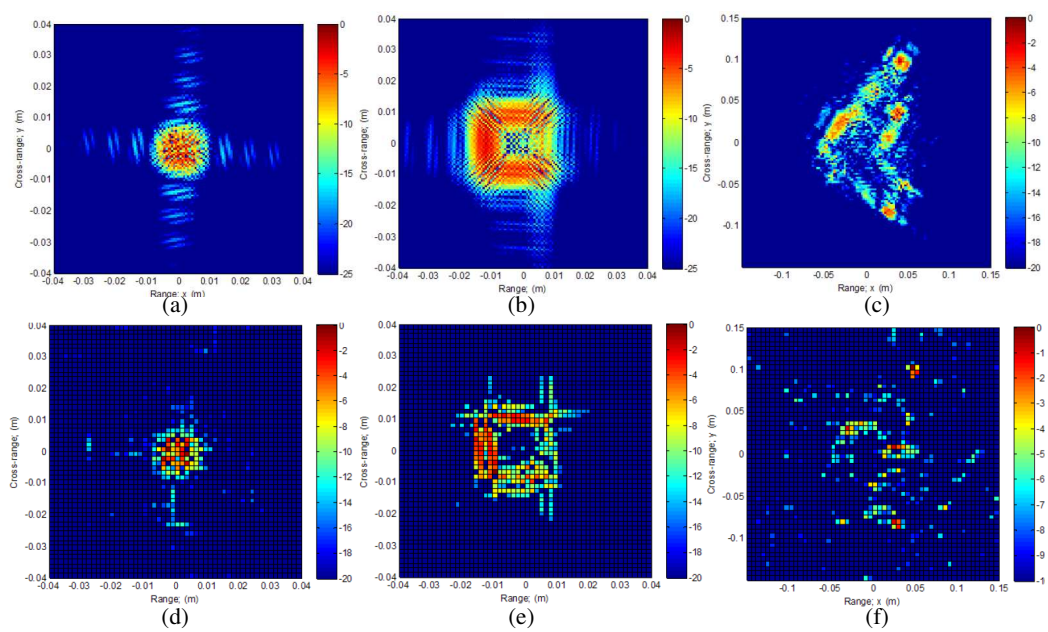

Figure 2: Experimental results: (a), (b), (c): back-projection based, (d), (e), (f): CS-based imaging of cube and a gun targets.

First, some simulation examples were carried out under the isotropic point scattering assumption. The frequency data was gathered within the bandwidth of 4 to 6 GHz sampled at 501 points and the azimuth data were collected within the full aperture of 360° sampled with 0.25° steps. The back-projection based imaging results are shown in Figs. 1(a) and (c) for referencing purposes. The results of the application of an orthogonal matching pursuit based decompression scheme are shown in Figs. 1(b) and (d). Second, CS based imaging of real data was studied. The experiments were performed in an anechoic chamber room and the W-band data of small cube targets and a metallic gun were acquired for an 1.3 m antenna-to-target distance and a full aperture angular scanning. Figs. 2 (a) and (b) shows the reference images wherein the targets were 1 cm^3 and 2 cm^3 metallic cubes. The corresponding CS-based imaging results are shown in Figs. 2(d) and (e) which were reconstructed by using the 4200 samples out of the total 92160 measurement data. Finally, a metallic gun whose reference image is shown in Fig. 2(c) was tried as a more complex imaging target. In this case, the angular step was set to 0.25° thereby giving a total of $256 \times 1441 = 368896$ frequency-angle sampling points. The CS result that exploits only 5200 random samples of this data is shown in Fig. 2(f) which clearly demonstrates the success of CS at the expense of an increased computational complexity.

REFERENCES

1. Baraniuk, R. and P. Steeghs, "Compressive radar imaging," *2007 IEEE Radar Conference*, 128–133, 2007.
2. Rilling, G., M. Davies, and B. Mulgrew, "Compressed sensing based compression of SAR raw data," *Proc. of SPARS'09 (Signal Processing with Adaptive Sparse Structured Representations)*, Saint-Malo (F), April 2009.

Huynen Dichotomy-based Radar Target Adaptive Extraction

Dong Li and Yunhua Zhang
Key Laboratory of Microwave Remote Sensing
Chinese Academy of Sciences, Beijing 100190, China

Abstract— Huynen dichotomy is the first formalized target polarimetric decomposition, but it has not been widely used because it may not obtain stable and unique target dichotomy for some special cases. There exist other Huynen-like target dichotomies, such as the Holm-Barnes decomposition and Yang decomposition, which improve Huynen dichotomy with different considerations, but may also aggravate the potential application of Huynen-like target dichotomies because for a given target coherence matrix we probably have different target dichotomies. There is no unified criterion to direct us to adaptively select the appropriate target dichotomy algorithm. We consider the main reason restricting the application of Huynen dichotomy is its preference for target symmetry and regularity. We find that from the physical realizablility conditions on Kennaugh matrix for both the single and distributed targets, there exist two other target dichotomies which prefer scattering non-symmetry and irregularity, respectively. They along with the Huynen dichotomy adaptively compose a Huynen canonical dichotomy, which can achieve an integrated description of target symmetry, regularity, non-symmetry, and irregularity. Based on the invariance of N-target, the algorithm is further extended for a generalized Huynen dichotomy, which includes nine dichotomy sub-algorithms and the existing Huynen-like dichotomies are all unified in it. The generalized Huynen dichotomy enables us an adaptive target extraction and classification because each sub-algorithm prefers different scatterings. By adaptively filtering the noisy scattering, the generalized dichotomy can well strengthen the target scattering. From Huynen dichotomy and Holm-Barnes decomposition to the Huynen canonical dichotomy, and further to the generalized Huynen dichotomy, a convergence to Cloude decomposition is achieved in retrieving the dominant scattering mechanism. The relative residue on the single target Pauli vector extractions between generalized dichotomy and Cloude decomposition is the least, especially on the Frobenius norm of the extracted Pauli vector, the average relative residue is just 0.99% on the AIRSAR San Francisco data. Therefore, a consistency between Huynen dichotomy and Cloude decomposition is achieved in a sense.

Huynen Dichotomy-based Unsupervised Terrain Classification

Dong Li and Yunhua Zhang
Key Laboratory of Microwave Remote Sensing
Chinese Academy of Sciences, Beijing 100190, China

Abstract— Since Dr. S. R. Cloude proposed using the coherence matrix to analyze the target polarimetric phenomena, decomposition of the target Kennaugh matrix developed by Huynen can be then equivalently transformed to the decomposition of target coherence matrix. Cloude and Pottier probabilistically interpret the random target scattering as three orthogonal single target scatterings represented by the eigenvectors of coherence matrix appearing with the probabilities proportional to the eigenvalues. A scattering α angle and an entropy H are then developed from the model to index the scattering mechanism and randomness, respectively. The two parameters compose an unsupervised H/α target classification scheme which has been widely used in SAR polarimetry. Nevertheless, the Cloude-Pottier random scattering model has an inherent drawback that the three obtained target scatterings are mutually orthogonal, which may impact the average estimation of the scattering parameters such as α angle. Although some alternatives to H/α have been developed recently, they are still based on the Cloude-Pottier decomposition. In this paper, we revisit H/α algorithm from the viewpoint of target dichotomy. Huynen dichotomy is the first formalized target polarimetric decomposition algorithm, but it has not been widely used because it only prefers target symmetry and regularity. By generalizing it to the scattering scenarios of non-symmetry, irregularity, and their hybrids, we can achieve an integrated characterization of the radar targets [1]. Based on the generalized dichotomy, a nine-symbol Bernoulli scheme is used to statistically model the random media scattering. The model is more reasonable than the Cloude-Pottier three-symbol Bernoulli scheme because the single target scatterings from it are not mutually orthogonal. Two Huynen characteristic parameters, i.e., the Huynen α angle and the scattering fraction of polarization (FoP) are then developed from the model to describe target scattering mechanism and randomness, respectively, and a Huynen FoP/α unsupervised terrain classification scheme is finally obtained which is demonstrated to be well consistent with the H/α classifier.

REFERENCES

1. Li, D. and Y. Zhang, "Huynen dichotomy-based radar target adaptive extraction," Submitted to PIERS 2013 in Stockholm.

Session 2P9
Extended/Unconventional Electromagnetic Theory, EHD(Electro-hydrodynamics)/EMHD(Electro-magneto-hydrodynamics), and Electro-biology

Scattered Intensity Distribution at near the Glass Transition of Charged Fibrous Virus (fd) Suspensions
Kyongok Kang, ... 792

Deep Field Penetration in Cylindrical Conductors
Francisco Eugenio Mendonca Da Silveira, ... 793

NMR Lens — Mapping of the Magnetic Field
Dusan Nespor, Tomas Kriz, Radek Kubasek, Pavel Fiala, ... 794

A Measurement System for Electrical Impedance Tomography
Tomas Kriz, Zdeněk Roubal, Jiří Rez, ... 795

Identification of Bacteria Strains via Advanced Methods for the Statistical Processing of Near-infrared Spectra
Pavel Krepelka, ... 796

The Effect of a Magnetic Field on the Speed of Temperature Change
Eliska Hutová, Karel Bartušek, Pavel Fiala, ... 797

Response of a Layered Medium to an Obliquely Incident Wave
Radim Kadlec, Pavel Fiala, I. Běhunek, ... 798

Low-level Measurement of the Electric Field Intensity around a Heterogeneous Structure
Pavel Fiala, Martin Friedl, Jan Mikulka, I. Behunek, Z. Szabo, ... 799

Consequences of the Extended Field Theory
Konstantin Meyl, ... 800

Automated Segmentation of Brain Tumor Edema in FLAIR MRI Using Symmetry and Thresholding
Pavel Dvorak, Karel Bartušek, W. G. Kropatsch, ... 801

Scattered Intensity Distribution at near the Glass Transition of Charged Fibrous Virus (fd) Suspensions

Kyongok Kang
Forschungszentrum Juuelich, Institute of Complex Systems (ICS-3)
Soft Condensed Matter, ICS-3 52425 Juuelich, Germany

Abstract— We recently reported on the structural particle arrest, found to occur at a low ionic strength due to the caging of charged rods in the potential set up by their neighbors through long-ranged electrostatic interactions [1, 2]. The glass transition exists far above the isotropic-nematic coexistence concentration, and during the equilibration, the texture dynamics of poly nematic domains undergo severe slowing down behaviors with various orientations in the equilibrium time. Also the relaxation time of density fluctuations as probed by dynamic light scattering, which has shown the unusual scattered intensity distribution during the equilibration.

REFERENCES

1. Kang, K. and J. K. G. Dhont, *Phys. Rev. Lett.*, Vol. 110, 015901, 2013.
2. Kang, K. and J. K. G. Dhont, *Soft Matter*, Vol. 6, 273, 2010.

Deep Field Penetration in Cylindrical Conductors

F. E. M. Silveira
Centro de Ciências Naturais e Humanas, Universidade Federal do ABC, Santo André, Brazil

Abstract— Recent investigations in the phenomenon of deep field penetration in cylindrical conductors have been motivated by the possibility of optically manipulating power flows in photonic nanowires. The basic aspects of the subject are rediscussed by taking into account inertial effects due to charge carriers. Inertial effects are described by introducing a finite relaxation time for the current density. The resulting generalized Ohm's law can be rigorously justified in the framework of extended irreversible thermodynamics [1–5]. A generalization of the diffusion equation is derived and its solution is parametrized in terms of the surface current and impedance. The real and imaginary parts of the latter are related, as usual, to the surface resistance and inductance, respectively. It is found that the surface inductance attains a minimum if the radius of the conductor acquires a critical value. It is also shown that such a situation should occur at low frequencies, for which the relaxation time is of the order of the diffusion time of the electric field. The proposed formulation is then applied to aluminum at room temperature, and it is found that the minimum inductance scales as 22.1 fH for a critical radius of the order of 35.1 nm. This shows that inertial effects should be important at the nanoscale. The results presented here may be of interest for investigations in the subject of nanophotonics. More generally, the experimental validation of the proposed theory would suggest that extended irreversible thermodynamics is the basic theory that determines the constitutive relations, which describe dissipative processes.

REFERENCES

1. Silveira, F. E. M. and J. A. S. Lima, *J. Phys. A: Math. Theor.*, Vol. 42, 095402, 2009.
2. Silveira, F. E. M. and J. A. S. Lima, "Skin effect from extended irreversible thermodynamics perspective," *Journal of Electromagnetic Waves and Applications*, Vol. 24, Nos. 2–3, 151–160, 2010.
3. Silveira, F. E. M. and S. M. Kurcbart, *Europhys. Lett.*, Vol. 90, 44004, 2010.
4. Silveira, F. E. M. and S. M. Kurcbart, *Int. J. Eng. Sci.*, Vol. 52, 22, 2012.
5. Silveira, F. E. M., *Physica A*, Vol. 392, 1818, 2013.

NMR Lens — Mapping of the Magnetic Field

D. Nespor, **T. Kriz**, **R. Kubasek**, **and P. Fiala**
Department of Theoretical and Experimental Electrical Engineering
Brno University of Technology, Technická 3082/12, Brno 616 00, Czech Republic

Abstract— Electromagnetic field is possible to manipulate by means of dielectric materials. Electromagnetic field will be affected due to values of dielectric constant ε_r and permeability μ_r. The lens was constructed as periodic structure of single split ring resonators (SSR). A negative effective permeability μ_r can be imposed on this structure. The main problem is to set up the resonance frequencies of the resonators. The resonance frequency is very sensitive and it is possible to very easily change it by the interaction with others resonators or by the interactions with objects in the surrounding area (parts of the NMR system, measured object, probe sensors etc. ...). This is the reason, why is so complicated to set resonant frequency exactly. NMR system has one disadvantage and that it is no possible to change frequency of the RF electromagnetic field. So it is impossible to find out resonant frequency of the resonators interaction with NMR system and eventually with measured object. This paper contains measurement methodology for mapping of the magnetic flux density in the reactive field of the resonators. Measuring workplace simulates RF electromagnetic field in NMR system with frequency sweeping possibility. This makes it possible to monitor manipulation of the magnetic field and dependence of the resonant frequency of the resonators interacting with surrounding objects.

A Measurement System for Electrical Impedance Tomography

T. Kříž, Z. Roubal, and J. Rez
Department of Theoretical and Experimental Electrical Engineering
Brno University of Technology, Kolejní 2906/4, Brno 612 00, Czech Republic

Abstract— The authors present a measurement system designed to facilitate tests within electrical impedance tomography (EIT). More concretely, this system provides the input data for EIT-based conductivity image reconstruction. The realized setup includes a generator, a voltage-to-current converter, a switching unit, an accurate AC multimeter, and a measuring device. This device contains 16 stainless steel electrodes; a pair of the directly opposed electrodes is connected to the converter, and voltage is easured on the other electrodes. The current electrodes are periodically excited. For each instance of current excitation, a set of voltages is measured; thus, we obtain $n(n-1)$ of measured voltage values, where n expresses the number of the electrodes. The measurement system is fully automated. To control the measurement, we created a program in the HP VEE environment. The measured sample consists in a saline solution, in which agar-based objects exhibiting different conductivity are placed; these objects then form inhomogenities. The intermittent excitation applied prevents the occurrence of electrolysis. The measurement is realized with several conductivity values as well as with various locations and number of inhomogenities in the saline solution.

As the EIT method considerably depends upon the noise level and the accuracy of the measured values, it was necessary to use the principles of low-level measurement. The paper describes the application of these principles to the switching unit. Within the follow-up stages of the research, the measured voltage values will be compared to the numerical model of the measured task, and we will evaluate the measurement accuracy and errors as well as their influence on the instability of conductivity reconstruction.

Identification of Bacteria Strains via Advanced Methods for the Statistical Processing of Near-infrared Spectra

Pavel Krepelka
Department of Theoretical and Experimental Electrical Engineering
Brno University of Technology, Technicka 12, Brno 616 00, Czech Republic

Abstract— The NIR absorption spectrum contains information related to molecular bonds of the examined sample. When the energy quantum from a source of light equals the energy necessary for the transition of a bond to a higher vibration level, the light is absorbed; in the measured spectrum, this effect can be observed in the form of an absorption band. Based on interpretation of these bands, chemical compounds can be determined or quantified. However, the processes become more complicated in the NIR part of the spectrum. Because the value of delivered energy is higher, most absorption bands are caused by overtones rather than by the fundamental transition of vibration conditions. Due to these effects, the absorption bands overlap, gain in width, and are difficult to interpret. The classification is usually carried out by means of traditional chemometric methods such as principal component analysis and partial least squares regression; these techniques were used for the identification of bacterial strains in a fluid medium during transmission measurement. The authors also introduce other processing methods, for example the artificial neural net and fuzzy logic techniques. The main advantage of the neural net approach consists in its simplicity and ability to provide high-speed evaluation; however, it is computationally demanding to learn the method. Fuzzy modeling then respects the shape and position of absorption peaks, which enables us to easily interpret the acquired spectrum. All the above-described methods are employed (and subsequently compared) in the process of identifying some bacterial strains.

The Effect of a Magnetic Field on the Speed of Temperature Change

E. Hutova, **K. Bartusek**, **and P. Fiala**
Department of Theoretical and Experimental Electrical Engineering
Brno University of Technology, Technická 3084/12, Brno 616 00, Czech Republic

Abstract— When the temperature drops below 0°C, in the animal cells and organisms containing water, the water will freeze and occurs the death of the living structures. Experiments performed on living organisms show that the magnetic field reduces the effects of hypothermia affecting the cells of the living organisms and reduce the mortality of the cells.

This paper deals with the influence of magnetic field on the inanimate nature. It was created a mathematical model using the physical parameters, which describes the rate of temperature change of the defined sample of material. It was performed the experimental measurement of the temperature change of the cooper sensor in a stationary homogeneous and gradient magnetic field. The sample was to 10 times cooled to the point of the boiling nitrogen (−195.80°C to 77.35 K), at the selected time was removed and placed in an area where was heated to a temperature of −20°C. Using the measuring centre and 4 temperature sensors (2 temperature measuring sample and 2 for measuring the ambient temperature) were recorded the temperature change of the sample and the time, which was required to heating a defined temperature difference. This experiment was repeated in the presence of two magnetic fields. The results of the experiment were consistent with the mathematical model and contribute to the description of physical processes during cooling of the biological tissues.

Response of a Layered Medium to an Obliquely Incident Wave

R. Kadlec, **P. Fiala**, **and I. Běhunek**
Department of Theoretical and Experimental Electrical Engineering
Brno University of Technology, Technická 3082/12, Brno 616 00, Czech Republic

Abstract— The authors report on an analytical solution of the propagation, reflection and refraction of broadband electromagnetic signals within multilayer optical materials. The presented solution is processed in the Matlab program, which is suitable for a specifically oriented detailed analysis of a general problem.

The paper includes a theoretical analysis and references to the generated algorithms. Comparison of the parameter changes is supported by graphical outputs of the algorithms. Algorithms created in the Matlab environment are verified by means of programs based on the finite element method, namely the ANSYS program.

Response of layered material is dependent on the thickness of each layer. A result of algorithm shows the response of layers of different thickness. The wave is sent from a source in the form of a single pulse. The response is shown for the electric field strength **E** and magnetic field strength **H**, ie the amplitude and the phase.

The methods described in this paper are well-suited for the analysis of beam refraction to the other side from the perpendicular line during the passage through the boundary. This phenomenon occurs in metamaterials.

ACKNOWLEDGMENT

The research described in the paper was financially supported by the Czech Science Foundation (13-09086S), project of the BUT Grant Agency FEKT-S-11-5/1012 and project from Education for Competitiveness Operative Programme CZ.1.07.2.3.00.20.0175 (Electro-researcher).

REFERENCES

1. Dedek, L. and J. Dedková, *Elektromagnetismus*, 232, Brno, VITIUM, 2000, ISBN 80-214-1548-7.
2. Steinbauer, M., R. Kubásek, and K. Bartušek, "Numerical method of simulation of material influences in MR tomography," *Progress In Electromagnetics Research Letters*, Vol. 1, 205–210, 2008.
3. Fiala, P., E. Kroutilová, M. Steinbauer, P. Dohnal, M. Hadinec, and K. Bartušek, "The effect of non-homogeneous parts into materials," *PIERS Online*, Vol. 3, No. 8, 1245–1249, 2007.
4. Hadinec, M., P. Fiala, E. Kroutilová, M. Steinbauer, and K. Bartušek, "Method for magnetic field approximation in MR tomography," *PIERS Online*, Vol. 3, No. 8, 1250–1253, 2007.

Low-level Measurement of the Electric Field Intensity around a Heterogeneous Structure

P. Fiala, M. Friedl, J. Mikulka, I. Behunek, and Z. Szabo
Department of Theoretical and Experimental Electrical Engineering
Brno University of Technology, Technická 3082/12, Brno 616 00, Czech Republic

Abstract— The paper presents the measurement of the electric field intensity in the area of a biological structure. The measured quantity can be evaluated remotely, without touching the plant, and this is a factor of exceptional importance for field applications. But the decisive aspect consists in the possibility of deciphering the information (about a living object) that may be carried by the electric field. Therefore, the most vital problem is to find out whether the electric field will be utilizable for contactless diagnostics. The principle of the method will consist in electric charge measurement on the electrodes of a capacitive sensor, exhibiting the elimination of interferences and leakage currents. Theoretical analysis will be performed to enable the setting of the measurement method sensitivity with respect to anticipated diurnal magnitudes of the electric field in different instantaneous weather conditions. The measurement method using one test tree within the stand will be analyzed; the group of other related steps comprises modification proposals for the sensor and the measurement methodology, comparison with the theoretical model, and direct comparison with the data evaluated by other laboratory or experimental techniques.

ACKNOWLEDGMENT

The research described in the paper was financially supported by the GACR 13-09086S grant, a project of the BUT Grant Agency, No. FEKT-S-11-5/1012 and project from Education for Competitiveness Operative Programme CZ.1.07.2.3.00.20.0175 and CZ.1.07/2.3.00/30.0005.

REFERENCES

1. Meleschenko, S. N., "Nature of changes in electrical properties of plant tissue with change in the external conditions," *Biofyzika*, Vol. 10, No. 3, 507–513, 1965.
2. Aubrecht, L., Z. Stanek, and J. Koller, "Systematic study of the characteristics of the point to-plane corona on natural objects," *Proceedings of the International Congress on Plasma Physics 25th EPS Conference on Controlled Fusion and Plasma Physics*, 2431–2433, ECA 22C, Prague, 1998.
3. Aubrecht, L., J. Koller, and Z. Staněk, "Onset voltages of atmospheric corona discharges on coniferous trees," *Journal of Atmospheric and Solar Terrestrial Physics*, Vol. 83, 1901–1906, 2001.
4. Steinbauer, M., P. Fiala, K. Bartušek, and Z. Szabó, "Experiments with accuracy of air ion field measurement," *PIERS Proceedings*, 1062–1066, Hangzhou, China, March 24–28, 2008.
5. Vojtek, T., M. Steinbauer, P. Fiala, and K. Bartušek, "Gerdien condenser measuring and numerical modeling of air ion fields," *Applied Electronics*, 225, 2006, ISBN: 978-80-7043-442-0.

Consequences of the Extended Field Theory

Konstantin Meyl
Faculty of Computer and Electrical Engineering, Furtwangen University, Germany

Abstract— We all learned from our textbooks, that the field equations according to Maxwell do not describe potential vortices in the dielectric such as vortex losses in capacitors. But this was yesterday. Since Science and Nature have reported in 2009 about the development of magnetic monopoles by the German Helmholtz Society [9] the 3rd Maxwell equation (div $B = 0$) is describing only a special case and we have to consider about the consequences and the impact to what we learned about electrodynamics.

In the contribution in PIERS 2012 in Moscow [1] from the new and extended field equations the pointing vector was derived with one loss term in addition, based on the new development but avoiding any postulates. The present contribution at PIERS 2013 is continuing the published ide-as from 2012, with the aim, to prove the losses of capacities.

It will be shown, that still visible proves are published, like vortex spots in high voltage capacities. The frequency dependence of the loss factor, calculated by the Lorentz model, compared with calculations as vortex losses, according to the new and extended field theory show very clear the importance and power of this new theory.

Thus the calculated potential-vortex and its effect on the dielectric medium can be measured and its existence made evident through observable natural phenomena.

Automated Segmentation of Brain Tumor Edema in FLAIR MRI Using Symmetry and Thresholding

P. Dvorak[1, 2], K. Bartusek[2], and W. G. Kropatsch[3]

[1]Department of Telecommunications, Faculty of Electrical Engineering and Communication
Brno University of Technology, Technická 12, Brno 612 00, Czech Republic
[2]Institute of Scientific Instruments of the ASCR, v.v.i., Královopolská 147, Brno 612 64, Czech Republic
[3]Pattern Recognition and Image Processing Group, Institute of Computer Graphics and Algorithms,
Faculty of Informatics, Vienna University of Technology, Favoritenstr. 9/186-3, Vienna A-1040, Austria

Abstract— Nowadays, the brain tumor detection and segmentation in MR images is a developing issue. There are many research teams producing different and interesting methods and algorithms for this particular task of medical image processing. Many of them are semi-automatic, but the aim of current research, and of this work, is to find a fully automatic method.

This paper focuses on the automatic brain tumor segmentation in FLAIR images. This type of contrast images was selected because of the visibility and manifestation of tumors in this image type. Since in axial plane of healthy brain, the approximate left-right symmetry exist, it is used as the prior knowledge for searching of the approximate tumor location. It assumes that the tumor is not located symmetricaly in both hemispheres, which is met in most cases. For the detection, the multiresolution approach is used. Since the tumor mostly manifests as a hyperintense area in FLAIR images, it is extracted using thresholding. For the automatic determination of the threshold, the Otsu's algorithm is used. This work does not deal with the tumor presence detection. One of our previous work is concentrated on this topic. The main reason for the brain tumor segmentation is for its classification. This will be done by applying the resulting mask of the proposed method to perfusion MR images. Since perfusion images are of very low contrast, the pathological area, it means the tumor and a potential edema around it, has to be detected and segmented in another type of MR images.

Session 2P10
SC1: Advanced Mathematical and Computational Methods in Electromagnetic Theory and Their Applications

Wiener-Hopf Analysis of the Diffraction by a Thin Material Strip
Takashi Nagasaka, Kazuya Kobayashi, ... 804

Hypothesis for the Identity of the $\boldsymbol{L_2(c,\rho,n)}$ and $\boldsymbol{\hat{L}_2(\hat{c},\hat{\rho},\hat{n})}$ Numbers and Its Application in the Theory of Waveguides
Georgi Nikolov Georgiev, Mariana Nikolova Georgieva-Grosse, ... 805

On the Reflection and Shadow Regions Related to a Half-plane Illuminated by a Uniformly Moving Line Source
Serkan Barak, Kadir Durgut, Ali Alkumru, ... 807

Propagation and Compression of Plane-wave Pulses in a Lossy Plasma
Natalie A. Cartwright, ... 808

An Analysis of a Strip Antenna Located at an Interface between Free Space and a Magnetoplasma
Alexander V. Kudrin, T. M. Zaboronkova, Anna S. Zaitseva, ... 809

Optical Solitons in Birefringent Fibers with Kerr and Log Law Nonlinearities
Anjan Biswas, Luminita Moraru, ... 810

Scattering of a Plane Wave by the End-face of a Two-dimensional Waveguide System
Akira Komiyama, ... 811

Symmetries in Scalar Potential Scattering
Giovanni Franco Crosta, ... 812

Exactly Solvable High Frequency Model of a Coil of Finite Length
Dierk Bormann, ... 814

Complex Permittivity Determination of Homogeneous Objects Loaded in Circular Waveguide via Integral Equation Method
Ahmet Aydogan, Funda Akleman, ... 815

Electromagnetic Response of Self-complementary Metasurfaces
Yosuke Nakata, Yoshiro Urade, Toshihiro Nakanishi, Masao Kitano, ... 816

Numerical Study of a Discontinuous Galerkin Time Domain Method for the Propagation of Electromagnetic Waves in Dispersive Media
Maciej Klemm, Stephane Lanteri, Claire Scheid, J. Viquerat, ... 817

Comparison of Uni- and Bi-directional Approaches to the Simulation of Intense Few-cycle Laser Pulses Propagating in an Optical Waveguide
Leonid S. Konev, Yuri A. Shpolyanskiy, ... 818

Wiener-Hopf Analysis of the Diffraction by a Thin Material Strip

T. Nagasaka and K. Kobayashi
Chuo University, Japan

Abstract— The analysis of the scattering by material strips is an important subject in electromagnetic theory and radar cross section (RCS) studies. Volakis [1] has analyzed the plane wave diffraction by a thin material strip using the dual integral equation approach and the extended spectral ray method together with approximate boundary conditions. In [1], Volakis first solved rigorously the diffraction by a single material half-plane, and subsequently obtained a high-frequency solution to the original strip problem by superposing the singly diffracted fields from the two independent half-planes and the doubly/triply diffracted fields from the edges of the two half-planes. Therefore his analysis is mathematically not rigorous from the viewpoint of boundary value problems, and may not be applicable unless the strip width is relatively large compared with the wavelength. In this paper, we shall consider the same strip geometry as in Volakis [1], and analyze the plane wave diffraction using the Wiener-Hopf technique.

The geometry of the strip is shown in Figure 1, where μ_r and ε_r denote the relative permeability and the relative permittivity of the material, respectively, and ϕ^i is the incident field of E or H polarization. Introducing the Fourier transform of the scattered field and applying approximate boundary conditions [2] in the transform domain, the problem is formulated in terms of the simultaneous Wiener-Hopf equations, which are solved exactly via the factorization and decomposition procedure. However, the solution is formal since branch-cut integrals with unknown integrands are involved. We shall further employ a rigorous asymptotic method to derive a high-frequency solution to the Wiener-Hopf equations, which accounts for all the higher order multiple diffraction effects. The scattered field is evaluated asymptotically by taking the inverse Fourier transform and applying the saddle point method. It is to be noted that our final solution is uniformly valid in incidence and observation angles. Numerical examples of the RCS for various physical parameters are presented and far field scattering characteristics of the strip are discussed in detail. Some comparisons with Volakis [1] are also provided.

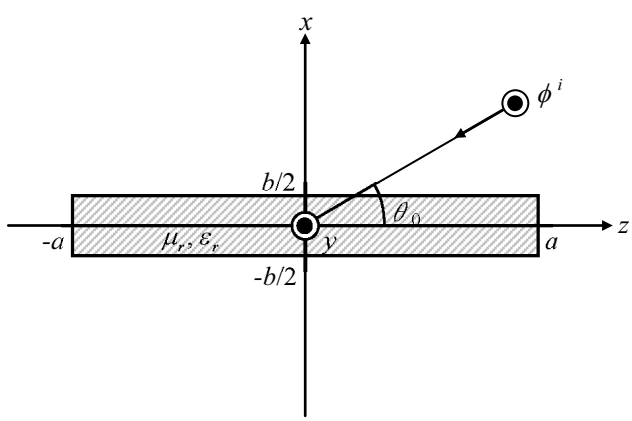

Figure 1: Geometry of the problem.

REFERENCES

1. Volakis, J. L., "High-frequency scattering by a thin material half plane and strip," *Radio Sci.*, Vol. 23, No. 3, 450–462, 1988.
2. Senior, T. B. A. and J. L. Volakis, *Approximate Boundary Conditions in Electromagnetics*, IEE, London, 1995.

Hypothesis for the Identity of the $L_2(c,\rho,n)$ and $\hat{L}_2(\hat{c},\hat{\rho},\hat{n})$ Numbers and Its Application in the Theory of Waveguides

Georgi Nikolov Georgiev[1] **and Mariana Nikolova Georgieva-Grosse**[2]

[1]Faculty of Mathematics and Informatics
University of Veliko Tirnovo "St. St. Cyril and Methodius"
Veliko Tirnovo BG-5000, Bulgaria
[2]Consulting and Researcher in Physics and Computer Sciences
Gerlingen D-70839, Germany

Abstract— $L_2(c,\rho,n)$ numbers in which c is an arbitrary real, ρ is real, positive, less than unity and n is a natural number, are called finite positive real ones, determined through the relations [1]. i) In case $c \neq l$, $l = 0,-1,-2,\ldots$: $L_2(c,\rho,n) = \lim\limits_{k_-\to-\infty} K_{2-}(c,\rho,n,k_-) = \lim\limits_{k_-\to-\infty} M_{2-}(c,\rho,n,k_-)$ where $K_{2-}(c,\rho,n,k_-) = |k_-|\chi^{(c)}_{k_-,n}(\rho), M_{2-}(c,\rho,n,k_-) = |a_-|\chi^{(c)}_{k_-,n}(\rho)$ and $\chi^{(c)}_{k_-,n}(\rho)$ is the nth positive purely imaginary zero in x of the function $F_2(a,c;x,\rho) = \Phi(a,c;x)\Psi(a,c;\rho x) - \Phi(a,c;\rho x)\Psi(a,c;x)$ in that $\Phi(a,c;x)$ and $\Psi(a,c;x)$ are the Kummer and Tricomi confluent hypergeometric functions [2] ($n = 1,2,3,\ldots$) with $a \equiv a_-$, $a_- = c/2 - jk_-$ — complex, $x = jz$, z — real, positive, k_- — real, negative and ρ — real, positive, $0 < \rho < 1$, (c, n — fixed). ii) Stipulating that $c = l$ and ε is an infinitesimal positive real number: $L_2(c,\rho,n) = \lim\limits_{\varepsilon\to0} L_2(l-\varepsilon,\rho,n) = \lim\limits_{\varepsilon\to0} L_2(l+\varepsilon,\rho,n)$. It holds: $L_2(c,\rho,n) = L_2(2-c,\rho,n)$, $c \neq l$, $L_2(l,\rho,n) = L_2(2-l,\rho,n)$, $L_2(1+h,\rho,n) = L_2(1-h,\rho,n)$, $h \neq l$, $L_2(1+l,\rho,n) = L_2(1-l,\rho,n)$, h — real number, $h \neq l$. The notion $\hat{L}_2(\hat{c},\hat{\rho},\hat{n})$ number is advanced in a similar manner [3]. To distinguish both cases, however, it is accepted in the second one to introduce hats " ˆ" above all the symbols involved. Besides, unlike previously, now the quantities $\hat{a}$, $\hat{c}$, $\hat{\rho}$, $\hat{x}$ are real, $\hat{\chi}^{(\hat{c})}_{\hat{k}_-,\hat{n}}(\hat{\rho})$ stands for the $\hat{n}$th positive real zero of the function $F_2(\hat{a},\hat{c};\hat{x},\hat{\rho}) = \Phi(\hat{a},\hat{c};\hat{x})\Psi(\hat{a},\hat{c};\hat{\rho}\hat{x}) - \Phi(\hat{a},\hat{c};\hat{\rho}\hat{x})\Psi(\hat{a},\hat{c};\hat{x})$ in $\hat{x}$, $\hat{x} > 0$ $\hat{a} = \hat{c}/2 + \hat{k}_-$ — real, negative, ($\hat{a} \neq -\hat{m}$, $\hat{m} = 1,2,3,\ldots$), $\hat{c}$ — restricted positive or negative real number, different from zero or a negative integer ($\hat{c} \neq \hat{l}$, $\hat{l} = 0,-1,-2,\ldots$), (in both cases $\hat{a} < \hat{c}$), $\hat{x}$ — real, positive, $\hat{k}_- = \hat{a} - \hat{c}/2$ — real, negative, $\hat{\rho}$ — real, positive, $0 < \hat{\rho} < 1$, $\hat{n} = 1,2,\ldots,\hat{t}$, $\hat{t}$ — finite positive integer, whose numerical equivalent is determined by the parameters of F_2 [3].

In this study a hypothesis is advanced that if $c \neq l$ and $\hat{c} \neq \hat{l}$ ($l = \hat{l}$), on condition that $c = \hat{c}$, $n = \hat{n}$ and $k_- = \hat{k}_-$ — large, negative, it is fulfilled: i) $\chi^{(c)}_{k_-,n}(\rho) \approx \hat{\chi}^{(\hat{c})}_{\hat{k}_-,\hat{n}}(\hat{\rho})$; ii) $K_{2-}(c,\rho,n,k_-) \approx M_{2-}(c,\rho,n,k_-) \approx \hat{K}_{2-}(\hat{c},\hat{\rho},\hat{n},\hat{k}_-) \approx \hat{M}_{2-}(\hat{c},\hat{\rho},\hat{n},\hat{k}_-)$; iii) $L_2(c,\rho,n) \approx \hat{L}_2(\hat{c},\hat{\rho},\hat{n})$. Moreover, in the vicinity of the points $l = \hat{l}$, assuming that $\varepsilon = \hat{\varepsilon} \to 0$ it is true: $L_2(l-\varepsilon,\rho,n) \approx \hat{L}_2(\hat{l}-\hat{\varepsilon},\hat{\rho},\hat{n})$, $L_2(l+\varepsilon,\rho,n) \approx \hat{L}_2(\hat{l}+\hat{\varepsilon},\hat{\rho},\hat{n})$, $L_2(l,\rho,n) \approx \hat{L}_2(\hat{l},\hat{\rho},\hat{n})$.

The identity $c = \hat{c} = 3$ finds application in the theory of coaxial waveguide, entirely filled with azimuthally magnetized remanent ferrite, propagating rotationally symmetric *TE* modes [1, 3, 4]. The physical interpretation of the truthfulness of the identity of numbers reflects the coincidence of specific envelope curves in the phase diagrams of the waves in case of negative magnetization which restrict the phase characteristics from higher (lower) frequencies provided normal (slow) waves are supported in the structure.

REFERENCES

1. Georgiev, G. N. and M. N. Georgieva-Grosse, "Theory of the L numbers: Definition, computational modeling, properties and application," *Proc. Thirteenth Int. Conf. Electromagn. Adv. Applicat. ICEAA'11*, 544–547, in CDROM, Turin, Italy, September 12–16, 2011, (Invited Paper in the Special Session "Future challenges in mathematical and computational electromagnetics and its applications," organized by G. N. Georgiev and M. N. Georgieva-Grosse).
2. Tricomi, F. G., *Funzioni Ipergeometriche Confluenti*, Edizioni Cremonese, Rome, Italy, 1954.
3. Georgiev, G. N. and M. N. Georgieva-Grosse, "Theory of the $\hat{L}_2(\hat{c},\hat{\rho},\hat{n})$ numbers and its application to the slow wave propagation in the coaxial ferrite waveguide," *Progress In Electromagnetics Research Symposium Abstracts*, 249–250, Moscow, Russia, August 19–23, 2012; *PIERS Proceedings*, 450–455, Moscow, Russia, August 19–23, 2012.

4. Georgiev, G. N. and M. N. Georgieva-Grosse, "A property of the $L(c, \rho, n)$ numbers and its application to waveguide propagation," *Proc. XXIX URSI General Assembly*, BK.6(120), in CDROM, Chicago, IL, USA, August 7–16, 2008.

On the Reflection and Shadow Regions Related to a Half-plane Illuminated by a Uniformly Moving Line Source

Serkan Barak, **Kadir Durgut**, **and Ali Alkumru**
Department of Electronics Engineering, Gebze Institute of Technology
41400, Gebze, Kocaeli, Turkey

Abstract— As it is well known, the investigation of the scattering of electromagnetic waves by moving scatterers such as communication satellites, guided missiles, and modern swift vehicles are of importance from both pure scientific and engineering point of view. The same occurs also when the source is in motion with respect to the scatterer, for example moving line antennas. The motion of the scatterer or source modulates the scattered wave and causes complicated issues which can be enumerated as the well-known Doppler shift in frequency, aberration in propagation direction, edge or wedge diffracted waves and the deformation of the reflection and shadow boundaries or regions.

The works devoted to *rigorous* analysis of the phenomena cited above are rather few because in the case of *accelerated* motion it needs the application of the General Theory of Relativity, which causes very tough mathematical difficulties. When the motion is *uniform*, however, a rigorous and elegant analysis can sometimes be done rather easily by considering the concepts of the Special Theory of Relativity [1]. So, in the open literature, there are many interesting works devoted to the case of uniformly moving scatterers or sources [2–8].

The aim of this work is to reveal the effect of motion of a source on the determination of the reflection and shadow zones or boundaries which have a crucial importance on the diffraction phenomenon. To this end, one considers the canonical structure formed by a perfectly conducting half-plane illuminated by a time-harmonic and uniformly moving infinitely long line source which is parallel to the edge of the corresponding half-plane (see Figure 1.). The phenomena of aberration, Doppler shift and edge-diffraction for this problem are already investigated in [8]. Therefore this study can be considered as the complementary for [8] on the part of obtaining the shadow and reflection regions. The method to determine these regions or the shapes of the corresponding boundaries is presented rigorously. In order to show some illustrative examples for different values of the velocity of the line source, the numerical evaluations are still continuing.

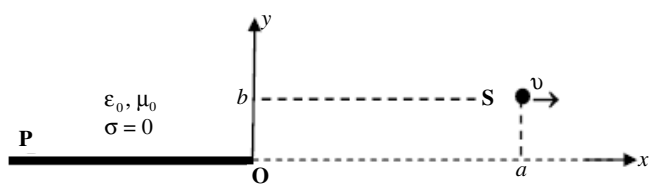

Figure 1: A source **S** moving with velocity $\upsilon = \upsilon \mathbf{e}_x$ with respect to perfectly conducting half-plane **P**.

REFERENCES

1. Pauli, W., *Theory of Relativity*, Pergamon Press, N.Y., 1958.
2. Censor, D., "Scattering of electromagnetic waves by a cylinder moving along its axis," *Microwave Theory and Techn.*, Vol. 17, 154–158, 1969.
3. Idemen, M. and A. Alkumru, "Influence of the velocity on the energy patterns of moving scatterers," *Journal of Electromagnetic Waves and Applications*, Vol. 18, No. 1, 3–22, 2004.
4. Idemen, M. and A. Alkumru, "Relativistic scattering of a plane-wave by a uniformly moving half-plane," *IEEE Trans. Antennas and Propagat.*, Vol. 54, 3429–3440, 2006.
5. Tsandoulas, G. N., "Low-frequency diffraction by moving conducting strips," *J. Opt. Soc. Amer.*, Vol. 59, 1357–1360, 1969.
6. Lang, K. C., "Diffraction of electromagnetic waves by a moving impedance wedge," *Radio Sci.*, Vol. 6, 655–663, 1971.
7. Shimura, T., H. Ochi, and Y. Watanabe, "Time-reversal communication with moving source-receiver in shallow water," *Jap. J. Appl. Phys.*, Vol. 45, 4847–4852, 2006.
8. Idemen, M. and A. Alkumru, "Influence of motion on the edge-diffraction," *Progress In Electromagnetics Research B*, Vol. 6, 153–168, 2008.

Propagation and Compression of Plane-wave Pulses in a Lossy Plasma

N. A. Cartwright
State University of New York at New Paltz, USA

Abstract— Asymptotic methods are used to provide an asymptotic approximation, valid for large propagation distances, of rectangular-modulated pulses through a lossy plasma. A study of matched signals and their effect on pulse compression is then given. Although the theory of pulse compression in dispersive media has been discussed for more than forty years, this is the first application of this theory to a material that exhibits loss and does not employ the group velocity approximation.

Introduction: Communication and imaging systems require pulses with a large intensity and short duration for the purposes of signal detection and signal resolution. However, the dispersive material through which a pulse propagates causes pulse broadening and attenuation. Compression methods based on group delay, space-time rays, and matched signals were the topic of a many papers [1–6] during the 1970's. A later treatment is found in [7]. Although matched filtering for dispersive and attenuative material using asymptotic methods was discussed in [4–6], previous applications of matched-filtering have been restricted to lossless material, or lossy material whose dispersive properties are approximated by a Taylor series.

Study: Here, we consider a causal dielectric permittivity that exhibits both dispersion and attenuation appropriate for a lossy plasma. Uniform asymptotic methods are used to obtain the propagated field of a rectangular-modulated signal with either a fixed carrier frequency or linearly-chirped frequency. This propagated signal is seen to be the sum of three components: the high, low, and carrier frequency responses of the material to the applied field. We consider matched filters, with amplitude and phase distortion, based on these three components, and their effect on pulse compression. The results are then given.

ACKNOWLEDGMENT

This work has been supported, in part, by the United States Air Force Office of Scientific Research under AFOSR Grant # FA9550-13-1-0013.

REFERENCES

1. McIntosh, R. E. and S. E. El-Khamy, "Compression of transmitted pulses in plasmas," *IEEE Trans. Antennas and Propagation*, Vol. 18, No. 2, 236–241, 1970.
2. McIntosh, R. E. and S. E. El-Khamy, "Optimum pulse transmission through a plasma medium," *IEEE Trans. Antennas and Propagation*, Vol. 18, No. 5, 666–671, 1970.
3. McIntosh, R. E. and S. E. El-Khamy, "Optimum transionospheric pulse transmission," *IEEE Trans. Antennas and Propagation*, Vol. 21, No. 2, 269–273, 1973.
4. Felsen, L. B., "Asymptotic theory of pulse compression in dispersive media," *IEEE Trans. Antennas and Propagation*, Vol. 19, No. 3, 424–432, 1971.
5. Connor, K. A. and L. B. Felsen, "Complex space-time rays and their application to pulse propagation in lossy dispersive media," *Proc. of IEEE*, Vol. 62, No. 11, 1586–1598, 1974.
6. El-Khamy, S. E., "On pulse compression in dispersive media," *IEEE Trans. Antennas and Propagation*, Vol. 27, No. 3, 420–422, 1979.
7. Albright, B. J. and S. C. Cowley, "Behavior of wave packets and pulse compression," *J. Geophys. Res.*, Vol. 101, 17259–17271, 1996.

An Analysis of a Strip Antenna Located at an Interface between Free Space and a Magnetoplasma

A. V. Kudrin[1], **T. M. Zaboronkova**[2], **and A. S. Zaitseva**[1]

[1]University of Nizhny Novgorod, Russia
[2]Technical University of Nizhny Novgorod, Russia

Abstract— We consider the problem of finding the current distribution of a linear antenna in the form of an infinitesimally thin, perfectly conducting, narrow strip located at an interface between free space and a magnetoplasma. The strip is infinitely long and perpendicular to an external dc magnetic field superimposed on the plasma medium. The current on the strip surface is excited by a time-harmonic voltage creating a given electric field which is aligned with the strip and differs from zero in a narrow gap of it. The semi-infinite magnetoplasma occupying one half-space is assumed resonant. By resonant magnetoplasma, we mean a cold, collisionless magnetized plasma in which the refractive index of one of the characteristic waves tends to infinity when an angle between the wave normal direction and the external dc magnetic field approaches a certain value determined by the plasma parameters. In this case, the classical thin-antenna theory cannot be employed readily since no matter how small the cross section of the antenna conductor might be physically, it is always possible to find some wave normal direction for which one wavelength in the plasma medium will become less than the conductor cross-sectional extent and the antenna conductor will appear to be "thick".

At first, we write the total field excited by the unknown antenna current and satisfy the boundary conditions for the tangential electric- and magnetic-field components at the interface of the two half-spaces. Then, using the boundary conditions for the tangential electric-field components on the strip surface, we derive integral equations for the surface current density. We analyze the properties of the kernels of the integral equations and represent the kernels as sums of singular and nonsingular parts. It is shown that in the considered case, the properties of the integral equations admit their analytical solution for the antenna current if the strip is sufficiently narrow. The obtained closed-form solution describes the current distribution both along and across the strip and makes it possible to find the antenna input impedance. The derived expressions allow a reasonably precise check of the results of approximate theories such as that of the transmission line theory for a strip antenna located at the interface between a magnetoplasma and free space. We also compare the results of the performed analysis with those previously obtained by various methods for similar linear antennas immersed an unbounded homogeneous resonant magnetoplasma [1, 2].

ACKNOWLEDGMENT

This work was supported by the Russian Foundation for Basic Research (project No. 12–02–00747-a), the Government of the Russian Federation (contract No. 11.G34.31.0048), the Russian Ministry of Science and Education (contract No. 14.B37.21.1292), and the Greek Ministry of Education through the project THALIS (RF-EIGEN-SDR).

REFERENCES

1. Adachi, S., T. Ishizone, and Y. Mushiake, "Transmission line theory of antenna impedance in magnetoplasma," *Radio Sci.*, Vol. 12, No. 1, 23–31, 1977.
2. Zaboronkova, T. M., A. V. Kudrin, and E. Yu. Petrov, "Electrodynamic characteristics of a strip antenna in a magnetoplasma," *J. Commun. Technol. Electron.*, Vol. 57, No. 3, 296–300, 2012.

Optical Solitons in Birefringent Fibers with Kerr and Log Law Nonlinearities

Anjan Biswas[1] and Luminita Moraru[2]

[1]Department of Mathematical Sciences, Delaware State University
1200 N DuPont Hwy, Dover, DE 19901-2277, USA
[2]Department of Chemistry, Physics and Environment, Faculty of Sciences
University "Dunarea de Jos", Str. Domneasca, nr. 111, Galati 800201, Romania

Abstract— The dynamics of optical solitons in birefringent fibers, with the presence of perturbation terms, will be addressed. The perturbation terms are due to inter-modal dispersion, third order dispersion, nonlinear dispersion and self-steepening. There are two types of nonlinerarity that will be taken into consideration. They are the Kerr law and the logarithmic law. Both bright and dark soliton solutions will be obtained. Several constraint conditions fall out, as a required condition, for the existence of the soliton solutions. The DWDM system will also be considered for log law nonlinearity.

Scattering of a Plane Wave by the End-face of a Two-dimensional Waveguide System

Akira Komiyama
Osaka Electro-Communication University, Hatsu-cho, Neyagawa-shi 572-8530, Japan

Abstract— An image fiber is composed of a large number of cores embedded in a single cladding, which is used to transmit directly an optical image. By illuminating the end-face of an image fiber with a laser beam a diffraction pattern reflecting the arrangement of cores can be simply observed. We can see experimentally that the diffraction pattern does not almost depend on the polarization of the laser beam. In this paper we deal with the problem from a theoretical point of view.

The reflection and transmission of a guided mode by the cut-end of a dielectric slab waveguide and the coupling of a beam wave to a dielectric slab waveguide have been treated by the boundary integral equation [1, 2]. In their papers the approximated form of the Green's function in a waveguide region has been used and the integral equation has been solved numerically. The analytical treatment of the boundary integral equation is very difficult.

The scattering of an electromagnetic wave from a dielectric body has been treated by the volume integral equation for the electric field [3]. The scattered field is the field radiated from the electric polarization induced in a dielectric body by the incident field and the physical image is very clear. The solution of the volume integral equation can be easily expanded into a perturbation series and each term of the series can be derived analytically. The analytical representation gives a deep understanding of the scattering properties of a dielectric body.

The scattering of a plane wave by the end-face of a waveguide system composed of a large number of cores and a single cladding has been treated by the volume integral equation for the electric field and it has been shown that the far scattered field does not almost depend on the polarization of an incident wave [4]. However, only the first order term of the perturbation solution has been derived there and the contributions of the higher order terms have not been clarified.

In this paper, the scattering of a plane wave by the end-face of a two-dimensional waveguide system is treated by solving straightforwardly a wave equation for the electric field. The unknown scattered field is expanded into a perturbation series with respect to the difference of refractive indices of core and cladding. The first and second order terms of the series are analytically derived and it is shown that the second order term is sufficiently small and can be ignored.

REFERENCES

1. Nishimura, E., N. Morita, and N. Kumagai, "Theoretical treatment of arbitrary shaped cut-ends of dielectric optical waveguide," *IECE Trans. Electron.*, Japanese Edition, Vol. J65-C, No. 7, 537–544, 1982.
2. Nishimura, E., N. Morita, and N. Kumagai, "Theoretical study on the coupling of two-dimensional Gaussian beam to a dielectric slab waveguide," *IECE Trans. Electron.*, Japanese Edition, Vol. J67-C, No. 5, 474–481, 1984.
3. Richmond, J. H., "Scattering by a dielectric cylinder of arbitrary cross section shape," *IEEE Trans. Antennas and Propagation*, Vol. 13, No. 3, 334–341, 1965.
4. Taki, A. and A. Komiyama, "Scattering of plane wave from the end-face of a threedimensional waveguide system," *IECE Trans. Electron.*, Vol. E94-C, No. 1, 63–67, 2011.

Symmetries in Scalar Potential Scattering

Giovanni F. Crosta
Inverse Problems & Mathematical Morphology Unit, Department of Earth and Environment
University of Milan-Bicocca, 1, piazza della Scienza, Milan, IT 20126, Italy

Abstract—

Motivation: The elastic scattering of the mass-less ($\omega^2 = c^2k^2$) complex scalar field by a potential, $q[\cdot]$, of bounded support is a prototype model which finds applications to acoustics and electromagnetics in a classical (i.e., non quantum mechanical) setting. Also, it provides the framework for direct and inverse obstacle scattering problems [1] from far-zone data, represented either by the complex-valued scattering amplitude, $A[\cdot]$, or by the modulus thereof (a.k.a the *scattering magnitude*). Of particular interest are the symmetries of the scattered wave, $u[\cdot]$ and of the quantities derived therefrom ($A[\cdot]$, $|A[\cdot]|^2$) caused by symmetry operations on $q[\cdot]$, such as translation, rotation, reflection, and scaling. An equally important problem is the separation of true from false symmetries, as it will be clarified below. This investigation is motivated by the analysis of scattering patterns of environmental interest, where the pattern "degree of symmetry" has been introduced on a heuristic basis [2].

Scattering by a Translated or Rotated Potential: Let k (> 0) and $\vec{\alpha} \in S^2$ respectively denote the wavenumber and incidence direction of a unit amplitude plane wave $u_{\rm inc}[\vec{x}; k, \vec{\alpha}] := \mathrm{e}^{\mathrm{i}k\vec{\alpha}\cdot\vec{x}}$. Let the potential, $q[\cdot]$, be a real-valued, bounded function, supported in the sphere of radius a (> 0) centered at the origin

$$q \in Q_a^\infty := \{q : q[\vec{x}] = q[\vec{x}]^*; \quad q[\vec{x}] = 0 \text{ for } |\vec{x}| > a; \quad q[\cdot] \in L^\infty(B_a[\mathbf{O}])\}. \tag{1}$$

Then the following operators can be defined.

Def. (*translation, rotation and reflection operators*)

Let $\vec{b} \in I\!R^3$, $\vec{\gamma} \in S^2$, $\mathbf{D}_\gamma \in \mathrm{SO}(3)$ and q_0 stand for the reference potential. Then $\mathcal{T}_b$, $\mathcal{D}_\gamma$ and $\mathcal{R}$ respectively are the operators of translation by $\vec{b}$, rotation by $\vec{\gamma}$ and reflection, which act on $q_0[\cdot]$ according to [3]

$$q_b[\vec{y}] = (q_0 \circ \mathcal{T}_b)[\vec{y}] = q_0[\vec{y} - \vec{b}]; \;\; q_\gamma[\vec{y}] = (q_0 \circ \mathcal{D}_\gamma)[\vec{y}] = q_0[\mathbf{D}_\gamma^{-1} \cdot \vec{y}]; \;\; q_r[\vec{y}] = (q_0 \circ \mathcal{R})[\vec{y}] = q_0[-\vec{y}]. \tag{2}$$

One further requires $q_b[\cdot],\ q_\gamma[\cdot] \in Q_a^\infty$.

If $\Phi[\vec{x} - \vec{y}]$, with $\vec{x}, \vec{y} \in I\!R^3$, stands for the fundamental solution to the Helmholtz equation $(\nabla^2 + k^2)\Phi[\vec{x} - \vec{y}] = \delta[\vec{y}]$, subject to the Sommerfeld radiation condition, then the scattered wave, $u_{\rm sc}[\vec{x}; \vec{\alpha}, k, q]$, is the solution to the integral equation

$$u_{\rm sc}[\vec{x}; \vec{\alpha}, k, q] = \int_{B_a[\mathbf{O}]} \Phi[\vec{x} - \vec{y}] \left(\mathrm{e}^{\mathrm{i}k\vec{\alpha}\cdot\vec{y}} + u_{\rm sc}[\vec{y}; \vec{\alpha}, k, q]\right) q[\vec{y}] \mathrm{d}^3 y. \tag{3}$$

Since the solution to Eq. (3) is the limit of the (iterative) Born sequence, the following two results can be proved.

Thm. 1 (Born *sequence for the translated potential*).

Let $\vec{x} \in I\!R^3 \backslash \overline{B_a[\mathbf{O}]}$ be fixed, $\vec{\eta} := \vec{y} - \vec{b}$, $u_{\rm sc}^{(0)} := 0$ and $n \geq 1$ (integer), then

$$u_{\rm sc}^{(n+1)}[\vec{x}; \vec{\alpha}, k, q_b] = \mathrm{e}^{\mathrm{i}k\vec{\alpha}\cdot\vec{b}} \int_{B_a[\mathbf{O}]} \Phi\left[\vec{x} - \vec{\eta} - \vec{b}\right] \left(\mathrm{e}^{\mathrm{i}k\vec{\alpha}\cdot\vec{\eta}} + u_{\rm sc}^{(n)}[\vec{\eta}; \vec{\alpha}, k, q_0]\right) q_0[\vec{\eta}] \mathrm{d}^3\eta. \tag{4}$$

Thm. 2 (Born *sequence for the rotated potential*).

Let $\vec{x}$, $u_{\rm sc}^{(0)}$ and n as above. Also, let $\vec{\eta} := \mathbf{D}_\gamma^{-1} \cdot \vec{y}$ and $\vec{\beta} := \mathbf{D}_\gamma^{-1} \cdot \vec{\alpha}$, then

$$u_{\rm sc}^{(n+1)}[\vec{x}; \vec{\alpha}, k, q_\gamma] = \int_{B_a[\mathbf{O}]} \Phi\left[\vec{x} - \mathbf{D} \cdot \vec{\eta}\right] \left(\mathrm{e}^{\mathrm{i}k\vec{\beta}\cdot\vec{\eta}} + u_{\rm sc}^{(n)}\left[\vec{\eta}; \vec{\beta}, k, q_0\right]\right) q_0[\vec{\eta}] \mathrm{d}^3\eta. \tag{5}$$

Rem. The recursion formulas of Eqs. (4) and (5) are of non-local type, because $\Phi[\vec{x} - .]$ is NOT evaluated at the integration variable, $\vec{\eta}$. The reason for keeping $\vec{x}$ fixed is dictated by the analysis of experimental data [2].

Invariance Results for the Squared Scattering Magnitude:

Def. (*the scattering amplitude from the first* Born *approximation*)

Let $\vec{\alpha}' := \vec{x}/|\vec{x}|$, then the scattering amplitude derived from the first Born approximation and due to the reference potential, q_0, is defined by

$$A_{1B}[\vec{\alpha}'; \vec{\alpha}, k, q_0] := -(1/4\pi) \int_{B_a[\mathbf{O}]} \mathrm{e}^{-\mathrm{i}k(\vec{\alpha}'-\vec{\alpha})\cdot\vec{y}} q_0[\vec{y}] \mathrm{d}^3 y. \tag{6}$$

With by now obvious notation, Eq. (2) in particular, the following properties can be easily shown to hold.

Thm. 3 (*invariance properties*).

$$|A_{1B}[\vec{\alpha}'; \vec{\alpha}, k, q_b]|^2 := |A_{1B}[\vec{\alpha}'; \vec{\alpha}, k, q_0]|^2; \tag{7}$$

$$|A_{1B}[\vec{\alpha}'; \vec{\alpha}, k, q_r]|^2 := |A_{1B}[\vec{\alpha}'; \vec{\alpha}, k, q_0]|^2; \tag{8}$$

Discussion: Thms. 1 and 2 characterize the symmetries of the scattered wave exactly. Some symmetry properties of the scattering amplitude have been investigated before [4]. As it could be easily shown, the first Born approximation, from which Eq. (6) follows, brings in an uncountably infinite set of false symmetries with respect to translation and rotation. False symmetries will be presented in detail.

ACKNOWLEDGMENT

The financial support by the following sources is gratefully acknowledged: *a*) Contract W911NF 11-1-0277 R&D 1449-BC-01 granted to Università Milan-Bicocca by the US Army RDECOM ACQ CTR, *b*) the home University's *Fondo di Ateneo per la ricerca*, from 2010 onwards, and *c*) the research agreement between the home University and *Digicom* S.p.A., Gallarate, IT.

REFERENCES

1. Ramm, A. G., *Scattering by Obstacles*, Reidel, Dordrecht, 1986.
2. Aptowicz, K. B., R. G. Pinnick, S. H. Hill, Y.-L. Pan, and R. K. Chang, "Optical scattering patterns from single aerosol particles at Adelphi, Maryland, USA: A classification relating to particle morphologies," *J. Geophys. Res.*, Vol. 111, D12212, 2006.
3. Altmann, S., *Rotations, Quaternions, and Double Groups*, Dover, Mineola, NY, 2005.
4. Ramm, A. G., "Symmetry properties of scattering amplitudes and applications to inverse problems," *J. Math. Anal. Appl.*, Vol. 156, No. 2, 333–340, 1991.

Exactly Solvable High Frequency Model of a Coil of Finite Length

Dierk Bormann[1,2]

[1]ABB Corporate Research, Power Technologies, Västerås S-721 78, Sweden
[2]Royal Institute of Technology, School of Electrical Engineering, Stockholm S-100 44, Sweden

Abstract— In the present paper a simple, analytical high-frequency model of a long, homogeneous coil, with or without iron core, is formulated and analyzed. A practical realization of this model is the high-voltage winding of a voltage measurement transformer. Typical high-voltage windings of power transformers are similar but present additional complications due to the disk structure of windings and to interleaving.

Our model is essentially a transmission line model, extended by adding homogeneously distributed stray capacitances which connect different sections of the line ("series capacitances") as well as mutual inductances between different sections. Deviations from homogeneity as well as coil-end effects can be handled at a later stage by perturbation theory, which is also briefly addressed.

It has been pointed out repeatedly in the literature (see for instance Ref. [1]) that adding series capacitance to a transmission line model (as a means to describe a transformer winding) leads to an upper limit frequency for propagating modes. At frequencies above that limit, the winding essentially behaves as a capacitance network. Surprisingly, as we show here using our model, this effect is reversed (i.e., the limit frequency is moved back to infinity) by the presence of mutual inductance.

We also report measurements on a real voltage transformer and show that they are in excellent agreement with the predictions of our model. The measurements display a characteristic deviation from the simple transmission line behavior, affecting the location of poles and zeros of the winding admittance function relative to each other, which is explained by our model in a natural way.

In conclusion, we believe that our simple analytical model will be a powerful tool for further assessing the transient and high-frequency response of real voltage transformers and other simple coils in electrical machines. Moreover, it may be a useful starting point for modeling and understanding more complex types of coils.

REFERENCES

1. Greenwood, A., *Electrical Transients in Power Systems*, 2nd Ed., 344, John Wiley, New York, 1991.

Complex Permittivity Determination of Homogeneous Objects Loaded in Circular Waveguide via Integral Equation Method

A. Aydogan[1, 2] and F. Akleman[2]

[1]Electrical and Electronics Engineering Department, Marmara University, Istanbul, Turkey
[2]Electronics and Communication Engineering Faculty, Istanbul Technical University, Istanbul, Turkey

Abstract— In this paper, an integral equation approach is presented for the complex permittivity determination of arbitrarily shaped homogenous objects loaded in circular waveguide. The integral equation based reconstruction algorithm has been introduced for similar inverse problems in rectangular waveguides [1, 2] and it can easily be shown that the proposed method is applicable to waveguides with arbitrary cross sections if the related dyadic Green's function of the empty waveguide is known. In order to formulate the integral equation based inverse algorithm,first the well-known data and object equations, containing electric type dyadic Green's function of empty waveguide are obtained. It should be noted that the data and object equations can be solved with different techniques to determine the permittivity of the objects partially/fully loaded in a waveguide. In this paper, a Newton based iterative algorithm is applied as in [2], where the nonlinear data equation is linearized by first order Taylor expansion using Frechet derivative of the integral operator. During the solution, the integral equations are converted to matrix equations through a Moment Method based approach, where integration of dyadic Green's function at each discrete cell is required. In order to validate and verify the integral equation formulation, first the direct problem related to circular waveguide loaded with inhomogeneous and arbitrarily shaped lossy dielectric is solved and the scattered parameters are compared with the results obtained via Mode Matching and HFSS [3]. The main problem encountered in the solution of direct scattering problem by means of Method of Momentsis the integration of dyadic Green's function of empty circular waveguide in the source region, which is handled using a pie-type meshing to obtain an analytical integration [3]. In this study, complex permittivity determination of non-magnetic, arbitrarily shaped and homogeneous material using the scattered electric fields in the circular waveguide is considered. The inverse algorithm for partially filled circular waveguide is applied for objects with different geometries and electrical parameters, and satisfactory results are obtained also in the presence of random noise.

REFERENCES

1. Akleman, F., "Reconstruction of complex permittivity of a longitudinally inhomogeneous material loaded in a rectangular waveguide," *IEEE Microwave and Wireless Components Letters*, Vol. 18, No. 3, 158–160, March 2008.
2. Kilic, E., F. Akleman, B. Esen, D. M. Ozaltin, O. Ozdemir, and A. Yapar, "3-D imaging of inhomogeneous materials loaded in a rectangular waveguide," *IEEE Transactions on Microwave Theory and Techniques*, Vol. 58, No. 5, 1290–1296, May 2010.
3. Aydogan, A. and F. Akleman, "Validation of mom-based direct scattering analysis in circular waveguide for appropriate mesh-type decision," *2012 International Conference on Mathematical Methods in Electromagnetic Theory (MMET)*, 275–278, August 28–30, 2012.

Electromagnetic Response of Self-complementary Metasurfaces

Y. Nakata, Y. Urade, T. Nakanishi, and M. Kitano
Department of Electronic Science and Engineering, Kyoto University
Nishikyo-ku, Kyoto 615-8510, Japan

Abstract— Artificial structured metallic thin screens (metasurfaces) have attracted considerable interest for unusual electromagnetic properties. Given a metasurface, we can construct the complementary one by using inversion operation which interchanges holes and metals. The Babinet principle relates scattering fields of the complementary metasurface to those of original one. It is valid not only for metasurfaces made of perfect electric conductors, but also for those with resistive elements. In order to treat the latter case, we must use the extended inversion operation instead of the above one [1]. By applying the extended operation, the metasurface with the surface impedance Z_s is transformed to complementary one with $Z'_s = Z_0^2/(4Z_s)$, where Z_0 is the impedance of free space.

The Babinet principle is based on invariant property of the Maxwell equations in free space under the duality transformation between electric and magnetic fields. It is expected that metasurfaces with structural symmetry matching to the dual symmetry of electromagnetic fields have specific scattering properties. In this paper, we study electromagnetic response of self-complementary metasurfaces which are congruent to their complementary ones obtained by the extended inversion operation. First of all, we show the general property of self-complementary metasurfaces: the complex reflectance r and transmittance t of the metasurfaces for circularly-polarized plane waves should satisfy $r = -1/2$, $t = 1/2$ independent of frequency. This is proved by the following facts: (i) the Babinet principle extended to metasurfaces with resistive elements, (ii) the transmittance of self-complimentary metasurface is the same as original one. Secondly, we show that the half power of an incident plane wave is absorbed by the self-complementary metasurface with rotational symmetry in the wide frequency range. Finally, these theoretical prediction are confirmed by the three-dimensional numerical simulation for a checker-board metasurface with resistive elements. For double-side excitation by two plane waves, such the metasurface can acts as a perfect absorber.

REFERENCES

1. Baum, C. E. and H. N. Kritikos, *Electromagnetic Symmetry*, (Eds.), Taylor & Francis, Washington, 1995.

Numerical Study of a Discontinuous Galerkin Time Domain Method for the Propagation of Electromagnetic Waves in Dispersive Media

M. Klemm[1], **S. Lanteri**[2], **C. Scheid**[2,3], **and J. Viquerat**[2]

[1]University of Bristol, UK
[2]INRIA Sophia Antipolis, France
[3]J. A. Dieudonné Laboratory
University of Nice-Sophia Antipolis, France

Abstract— The use of nano metallic structures in optics allows to benefit from new features or improved properties of the considered device. One may in particular think to light enhancement and the capabilities to exploit the properties of surface plasmons to manipulate the propagation of electromagnetic waves. In this context, there is a need of an accurate numerical modeling. In term of modeling, since one would consider the interaction of electromagnetic waves with metals at the nano scales and optical frequencies, electric dispersion of the media can not be neglected. In other words, one has to take into account the polarization of the electrons in the metal that reflects the delay of their response to the electric field. Thus the constitutive relation linking the electric displacement to the electric field is given in terms of a time convolution between an effective timedependent permittivity and the time dependent electric field. Modelization then relies on the set of Maxwell's equations linearly coupled to an ordinary differential equation describing the evolution of the polarization of the electrons. Several models exist to describe dispersion and, for the most classical (Drude, Drude-Lorentz) they have been widely used in the literature. Concerning discretization aspects, the majority of studies relies on Finite Difference Time Domain (FDTD) methods due to their nice features as, in particular, straightforward implementation. However, for nanophotonics applications, the space and time scales, in addition to the geometrical characteristics of the considered nanostructures can be particularly challenging for an accurate and efficient application of the FDTD method. In this regard, numerical discretization could benefit from a Discontinuous Galerkin approach. Indeed, as unstructured mesh-based and potentially high order methods, Discontinuous Galerkin methods are exible and could be able to deal with these stakes. They have already demonstrated their potentialities for being considered as viable alternatives to the FDTD method (see, e.g., [1]).

In this work, we propose a complete study of a Discontinuous Galerkin numerical scheme for the approximation of the propagation of electromagnetic waves in dispersive media. The particularity of this scheme is that it relies on a centered approximation for the uxes and a leap frog scheme for the approximation in time as in [2]. Furthermore, it leads to a non dissipative scheme. We first go through the description of some dispersion models (from a Drude model to a generalized version inspired from [3]). Then we develop the numerical analysis by proving a result of stability and convergence for the different models. Finally, we validate our tridimensional implementation on numerical test cases, from academic ones to more realistic ones, to confirm the pertinence of our approach.

REFERENCES

1. Busch, K., M. König, and J. Niegemann, "Discontinuous Galerkin methods in nanophotonics," *Laser Photonics Review*, Vol. 34, No. 10, 1–37, 2011.
2. Fezoui, L., S. Lanteri, S. Lohrengel, and S. Piperno, "Convergence and stability of a discontinuous Galerkin time-domain method for the 3D heterogeneous Maxwell equation on unstructured meshes," *ESAIM: M2AN*, Vol. 39, 1149–1176, 2005.
3. Vial, A., T. Laroche, M. Dridi, and L. Le Cunff, "A new model of dispersion for metals leading to a more accurate modeling of plasmonic structures using the FDTD method," *Applied Physics A*, Vol. 103, 849–853, 2011.

Comparison of Uni- and Bi-directional Approaches to the Simulation of Intense Few-cycle Laser Pulses Propagating in an Optical Waveguide

Leonid S. Konev and Yuri A. Shpolyanskiy
National Research University of Information Technologies, Mechanics and Optics
Kronverkskiy pr. 49, Saint-Petersburg 197101, Russia

Abstract— Evolution of intense few-cycle femtosecond optical pulses in silica-core telecommunication-type single-mode optical fiber is under consideration. Mathematical model of the process can be represented by the set of bidirectional equations for counter-propagating forward and backward waves [1, 2]. The set is analogous to the full second-order scalar wave equation for the total field. In the spectral domain it can be written in the form:

$$\partial_z G_\pm = \pm ik(\omega)G_\pm \pm \frac{1}{2}ik(\omega)N_\omega(E_+ + E_-), \tag{1}$$

$$N_\omega(E) = 4\pi F[P_{NL}(E)]/n^2(\omega), \tag{2}$$

where z is coordinate along the propagation axis, $E_\pm$ are fields with energy transfers in forward and backward directions, respectively, and $G_\pm$ are their spectral densities, ω is frequency, $k(\omega) = \omega n(\omega)/c$ is wavenumber, n is refractive index, c is velocity of light, N_ω is nonlinear operator in frequency domain, P_{NL} is nonlinear response of the medium, F is Fourier transform.

Commonly used approximation of unidirectional propagation [3, 4] implies absence of the backward wave, hence leads to an error that should be estimated. With initial conditions corresponding to the unidirectional approach (zero initial backward field) we solve set (1) numerically. Our simulations show that in case of instantaneous cubic nonlinearity backward wave occurs during evolution of the forward-propagating pulse. It consists of two parts propagating in opposite directions, which agrees with [1]. First one travels backward and can be explained as reflection of intense initial pulse from jump of refractive index induced via nonlinearity. The other travels forward along with the forward pulse, and appears due to nonlinear coupling of forward and backward waves. Inhomogeneity of the refractive index propagates along with the forward pulse due to instant nonlinearity in the model, so self-reflection does not occur during further pulse propagation.

To analyze the observed behavior of the backward wave we derive and solve a simplified set of equations, which can be applied over distances of a few central wavelengths. The solution of this set provides an analytical estimate of the error of unidirectional approximation and helps us to obtain consistent initial conditions eliminating the initial reflected field. Our numerical simulations show that the estimate and initial conditions are adequate even for the full set of equations.

Raman nonlinearity of fused silica will be added to the model. We expect continuous generation of self-reflected fields due to the inertial nature of Raman response.

REFERENCES

1. Kinsler, P., S. B. P. Radnor, and G. H. C. New, "Theory of directional pulse propagation," *Physical Review A*, Vol. 72, 063807, 2005.
2. Kolesik, M., P. T. Whalen, and J. V. Moloney, "Theory and simulation of ultrafast intense pulse propagation in extended media," *M. IEEE Journ. of Selected Topics in QE*, Vol. 18, No. 1, 494–506, 2012.
3. Agrawal, G. P., *Nonlinear Fiber Optics*, 466, Academic Press, San Diego, 2001.
4. Bespalov, V. G., S. A. Kozlov, Y. A. Shpolyanskiy, and I. A. Walmsley, "Simplified field wave equations for the nonlinear propagation of extremely short light pulses," *Physical Review A*, Vol. 66, 013811, 2002.

Session 2P11b
SC1: Computational Techniques in Electromagnetics and Applications

Effect of a Metal Dispersion on Characterizing Terahertz Devices in the FDTD Analysis
Jun Shibayama, Shingo Ozaki, Yosuke Uchizono, Junji Yamauchi, Hisamatsu Nakano, ... 820

Current Density Estimation and Visualization for Exposed Live Transmission Line Workers
Chokri Ahmed Belhadj, Nabil M. Maalej, ... 821

Computational Investigations on Plasmonic Waveguides of THz Waves
Qing Cao, ... 822

Distribution of Energy Flow by Dielectric Waveguides Composed of Dielectric Circular Cylinders and Air-hole Type Circular Cylinders Array
Ryosuke Ozaki, Tsuneki Yamasaki, ... 823

An Efficient Implementation of Yasuura's Method of Modal Expansion by Sequential Accumulation
M. Kawano, T. Matsuda, Yoichi Okuno, ... 824

Three Dimensional Electromagnetic Simulations of VLF/LF Antennas in Natural Environments with FDTD Method
Julien Vincent, Pierre Borderies, Jean-Rene Poirier, Vincent Gobin, ... 825

Novel Edge-based Smoothed Finite Element Time Domain Method
Khaled Sami R. Atia, Salah Sabry Ahmed Obayya, ... 826

A Grating-based Plasmon Biosensor via Phase Detection with Wide Measurement Range
Ziqian Luo, Taikei Suyama, Xun Xu, Yoichi Okuno, Sailing He, ... 828

Parallel Performance of the Multi-threaded ICCG Solver in Electromagnetic Finite Element Analyses on the Latest Processors
Kazuki Semba, Koji Tani, Takashi Yamada, Takeshi Iwashita, Yasuhito Takahashi, Hiroshi Nakashima, ... 830

Detection of Electromagnetic Radiation during the Earthquake Preparation Process
Fedir Dudkin, Valeriy Korepanov, ... 831

Effect of a Metal Dispersion on Characterizing Terahertz Devices in the FDTD Analysis

J. Shibayama, **S. Ozaki**, **Y. Uchizono**, **J. Yamauchi**, **and H. Nakano**
Faculty of Science and Engineering, Hosei University, Tokyo, 184-8584, Japan

Abstract— For guiding terahertz (THz) waves, two parallel metal plates have often been employed [1]. In the THz regime, metal is often regarded as a perfect electric conductor (PEC) due to a very shallow skin depth of electromagnetic fields. Note, at higher THz frequencies, that the effect of a metal dispersion begins to exist [2]. However, little attention has been directed towards the frequency ranges not only for which the PEC approximation is valid, but also for which a metal dispersion should be considered.

In this study, we analyze a terahertz stop band filter and a resonator consisting of metal gratings [3] using the finite-difference time-domain (FDTD) method [4], with special attention to the treatment of metal. Numerical results based on the PEC approximation are compared to those with a metal dispersion being taken into account by the Drude model. It is shown that the results of the resonator for the PEC model are favorably compared with those for the Drude model at frequencies of less than 1 THz. However, care must be taken at higher frequencies, since not only the transmittance at the resonance remarkably reduces for the Drude model, but also its resonance frequency deviates, in comparison with those for the PEC model. Metal mesh structures are also investigated using the periodic FDTD. The differences are found to be relatively small, due to less metal absorption from thin metal structures.

REFERENCES

1. Harsha, S. S., N. Laman, and D. Grischkowsky, "High-Q terahertz Bragg resonances within a metal parallel plate waveguide," *Appl. Phys. Lett.*, Vol. 94, No. 9, 091118-1–3, 2009.
2. Leal-Sevillano, C. A., J. A. Ruiz-Cruz, J. R. Montejo-Garai, and J. M. Rebollar, "Field propagation in circular hollow waveguides with non-ideal metallic conductors from microwaves to terahertz frequencies," *IEEE Trans. Microwave Theory Tech.*, Vol. 59, No. 12, 3013–3022, 2011.
3. Shibayama, J., Y. Uchizono, J. Yamauchi, and H. Nakano, "Wideband analysis of a stop band filter and a resonator at THz frequencies," *IEEE Topical Conf. Antennas Propag. Wireless Comm.*, 888–890, 2012.
4. Shibayama, J., R. Ando, A. Nomura, J. Yamauchi, and H. Nakano, "Simple trapezoidal recursive convolution technique for the frequency-dependent FDTD analysis of a Drude-Lorentz model," *IEEE Photon. Technol. Lett.*, Vol. 21, No. 2, 100–102, 2009.

Current Density Estimation and Visualization for Exposed Live Transmission Line Workers

C. A. Belhadj[1] and N. Maalej[2]

[1]Electrical Engineering Department
King Fahd University of Petroleum and Minerals, Dhahran 31261, Saudi Arabia
[2]Physics Department, King Fahd University of Petroleum and Minerals, Dhahran 31261, Saudi Arabia

Abstract— This paper is about estimation and visualization of the current densities for live transmission line workers body tissues. The purpose of this investigation work was to evaluate the safety level of an exposed high voltage transmission line worker externally and internally. A typical utility 132-kV, 60 Hz transmission line was considered. The charge simulation method was used to compute the external electric field and Biot-Savart law was used for the magnetic field estimation. The live-line worker exposure simulation was conducted using EPRI's WorkStation. Three exposure scenarios were selected for the simulation studies. The first one was for a worker standing in the bucket close to conductor phase A and about 2 m away from the conductor. The second was for a worker standing in the bucket close to conductor of phase B and about 2 m away from the conductor. The third was for a worker standing in the bucket close to conductor phase C and about 2 m away from the conductor. To estimate the organs internal induced electric field and current densities, Finite Difference Time Difference computational algorithm method was implemented using EMPIRE commercial software. Visible Human model was used to investigate several tissues. Tissues such as Cerebellum, Gray Matter, White Matter, Heart, Nerve (Spine), Cerebral Spinal Fluid, Eye (Aqueous Humor), Kidneys, Liver, Lung (Inner), Lung (Outer), Pancreas, Spleen, Feet and Ankles, Hands and Wrist were considered for investigation and for visualization. Such visualization gives the relative intensity value of the current density as well as its location in the tissue section. As a matter of fact the maximum value is represented by the dark red color.

The highest computed values of 6.485 KV/m and of 663.51 mG respectively for the external electric and magnetic fields were found and compared with their respective Maximum Permissible Level according to the IEEE, ICNIRP, ACGIH, NRPB guidelines for occupational exposure for power frequency. The highest induced maximum current density in all the tissues was found to be below the ICNIRP and the NRPB limit of 10 mA/m^2. The visualization of the anatomical structure of the tissue has revealed the location of the maximum current density value as well the relative intensity value of the current density in the layer. In general the highest values for each organ are obtained at the border between different tissues.

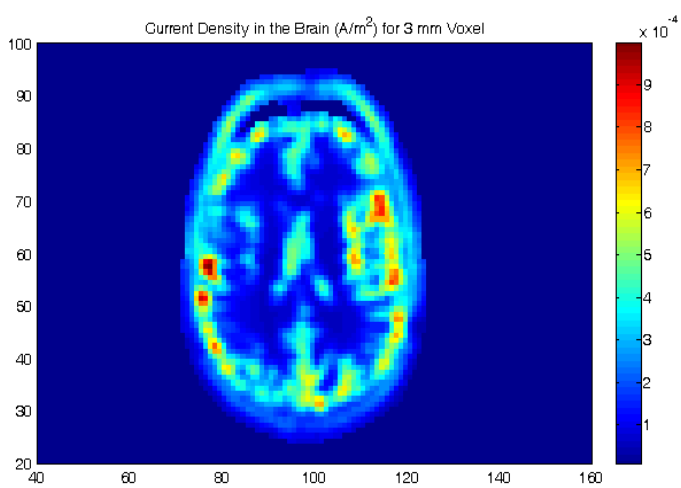

Figure 1: Current density in the brain (A/m^2).

Computational Investigations on Plasmonic Waveguides of THz Waves

Qing Cao
Department of Physics, Shanghai University
99 Shangda Road, Baoshan District, Shanghai 200444, China

Abstract— Recent years, terahertz technology has attracted a lot of research interests. In particular, people have paid much attention on the important component of terahertz waveguides. In 2004, metal wire waveguides [1] were rediscovered as effective THz waveguides. This simple waveguide has the advantages of low loss and negligible dispersion. It was then quickly explained that the waveguide effect of a single metal wire comes from the azimuthally polarized surface plasmons (APSP) [2]. Several recurrence formulas had been derived to calculate the effective index n_{eff} of the metal wire APSP in both large scale and nanoscale [3–5]. They are in good agreement with the numerical calculations for 11 nonmagnetic metals in the whole spectral region of terahertz waves. For sub-skin-depth diameter, the recurrence formula is very simple, and the mode field size is simply proportional to the radius of the metal wire [4].

In 2007, a two-wire waveguide was proposed [6]. It has low bending loss. Here, a high efficient plasmonic connector called tapered dual elliptical plasmon waveguide is suggested for the coupling of terahertz wave from an approximate plate waveguide to a two-wire waveguide. As shown in Fig. 1, through putting the long axis b decreases slowly (enough for coupling process to meet the WKB approximation), the two-ellipse structure gradually degenerates into two metal wires and couples terahertz waves into a two-wire waveguide.

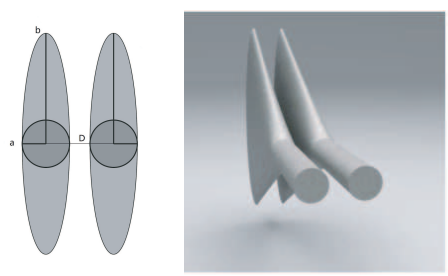

Figure 1: Tapered dual elliptical plasmon waveguides.

By using a finite element method (FEM) software (COMSOL Multiphysics), we get the effective index n_{eff} of each 2-D cross-section of the tapered dual elliptical plasmon waveguide. And then by use of the integral of equation below, we numerically calculate the coupling efficiency, which can be as high as about 94%.

$$\eta = \exp\left[-2k_0 \int_0^l \mathrm{Im}(n_{eff})dz\right]$$

REFERENCES

1. Wang, K. and D. M. Mittleman, "Metal wires for terahertz waveguiding," *Nature*, Vol. 432, 376–379, 2004.
2. Cao, Q. and J. Jahns, "Azimuthally polarized surface plasmons as effective terahertz waveguides," *Opt. Express*, Vol. 13, 511–518, 2005.
3. Yang, J., Q. Cao, and C. Zhou, "An explicit formula for metal wire plasmon of terahertz wave," *Opt. Express*, Vol. 17, 20806–20815, 2009.
4. Yang, J., Q. Cao, and C. Zhou, "Theory for terahertz plasmons of metallic nanowires with sub-skin-depth diameters," *Opt. Express*, Vol. 18, 18550–18557, 2010.
5. Yang, J., Q. Cao, and C. Zhou, "An analytical recurrence formula for the zero-order metal wire plasmon of terahertz wave," *J. Opt. Soc. Am. A*, Vol. 27, 1608–1612, 2010.
6. Mbonye, M., R. Mendis, and D. M. Mittleman, "A terahertz two-wire waveguide with low bending loss," *Appl. Phys. Lett.*, Vol. 95, 233506, 2009.

Distribution of Energy Flow by Dielectric Waveguides Composed of Dielectric Circular Cylinders and Air-hole Type Circular Cylinders Array

Ryosuke Ozaki and Tsuneki Yamasaki
Department of Electrical Engineering, College of Science and Technology, Nihon University, Japan

Abstract— Optical wave propagation in periodic structures waveguide such as photonic crystals waveguides has been both theoretical and practical interest in many areas of physics and engineering. In periodic structures such as photonic crystals structure, it is known that a frequency stop band occurs. Also, in general, photonic crystals such as optical nanostructures with periodically permittivity distribution are known as technology which can be controlled the light in the periodic structure by interaction of both the wave nature of light and periodicity. They have expected the development in integrated optics circuit device. Therefore, in the design of photonic crystals structure with periodic constants same as optical wavelength, it is very important to investigate the stop band region or photonic band gaps. As these applications, for example, there are optical devices such as an optical branching filter, optical resonator, and optical coupler. But, it is not analyzed the stop band area in Bragg region in detailed, many numerical analysis are shown only the distribution of electromagnetic fields by utilizing the FDTD method, TD-BPM method, and another numerical techniques.

In previous paper, we have analyzed the propagation characteristics of dielectric waveguide composed of air-hole type circular cylinders array, investigated the complex propagation constants in the first stop band regions and distribution of energy flow by using the combination of an improved Fourier series expansion method and multilayer method. As numerical results, it is shown that we can be obtained the confinement efficiency compared with dielectric circular cylinders array for case of various permittivities for TE_0 mode.

In this paper, we have analyzed the distribution of energy flow for dielectric waveguide with defects consists of air-hole type circular cylinders and dielectric circular cylinders array as shown in Fig. 1(a) and investigated the influence of confinement efficiency for defects area compared with air-hole circular cylinders array in all region.

Numerical results are given for the complex propagation constants in the first stop band region and the distribution of energy flow by using the propagation constants at the guided area of dominant mode for the case of various permittivity and structures in the middle layer for TE_0 mode.

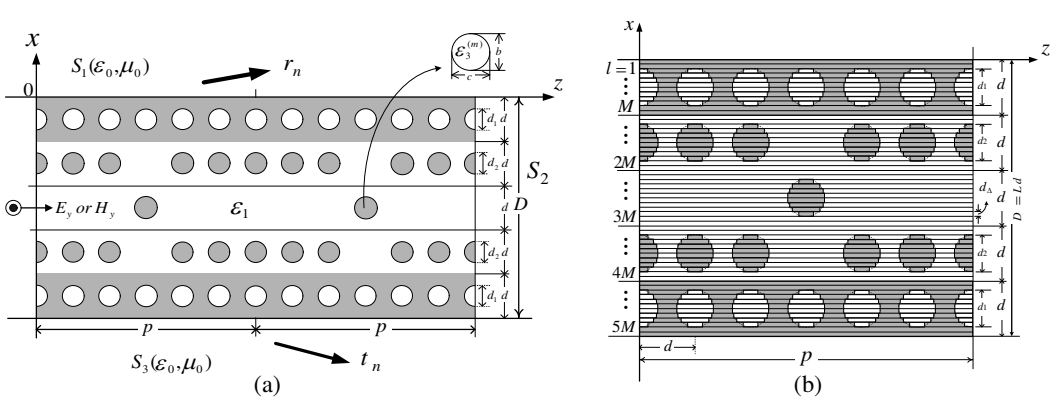

Figure 1: Structures of dielectric waveguides composed of dielectric circular cylinders and air-hole type circular cylinders array. (a) Coordinate system. (b) Approximated multilayer method.

An Efficient Implementation of Yasuura's Method of Modal Expansion by Sequential Accumulation

M. Kawano[1], **T. Matsuda**[2], **and Y. Okuno**[3]

[1]Lumerical Solutions Inc., Canada
[2]Kumamoto National College of Technology, Japan
[3]Graduate School of Science and Technology, Kumamoto University, Japan

Abstract— Yasuura's method [1] is a standard technique for numerical solution to the boundary value problems of the Helmholtz equation. In that method, the approximate solution is formed as a linear combination of modal functions and the expansion coefficients are determined so that the approximate solution satisfies the boundary conditions in a least squares sense. The numerical algorithm of the method is, therefore, formulated as the least squares problem: Find the solution vector $\mathbf{A}$ minimizing the Euclidean norm

$$I = ||\Phi\mathbf{A} - \mathbf{b}||^2. \tag{1}$$

In Eq. (1), Φ is Jacobian of a $J \times M$ matrix, $\mathbf{A}$ and $\mathbf{b}$, respectively, are an M- and J-dimensional column vector. Φ can be classified into two types of a matrix, a dense matrix and a banded one:

$$\Phi = \begin{bmatrix} \Phi_1 \\ \Phi_2 \\ \cdots \\ \Phi_L \end{bmatrix} \quad \text{and} \tag{2}$$

$$\Phi = \begin{bmatrix} \Phi_{11} & \Phi_{12} & 0 & \cdots & 0 \\ 0 & \Phi_{22} & \Phi_{23} & \ddots & \vdots \\ \vdots & \ddots & \ddots & \ddots & 0 \\ 0 & \cdots & 0 & \Phi_{LL} & \Phi_{LL+1} \end{bmatrix}. \tag{3}$$

For example, when we eapply Yasuura's method to a light scattering problem from a cluster of nanoparticles, Φ consists of L block matrices $\Phi_\ell(\ell = 1,, 2, \ldots, L)$ with L being the number of particles as shown in Eq. (2). In the case of a diffraction problem by multilayered periodic structures which hare stacked thin-films periodically corrugated, Φ becomes to be a block bi-diagonal matrix of Eq. (3) where L is the number of layers. Least squares problems can be solved by the orthogonal transformation of Jacobian such as a QR decomposition [2]. The application of a QR decomposition method to the entire matrix Φ of Eqs. (2) or (3), however, requires a huge amount of memory at one time and takes a long computation time as L increases. Sequential processing and parallel computation save computational complexity of the least-squares problem having Φ with structure of Eqs. (2) or (3). In this presentation, we show that the sequential accumaltion processing [2] is significantly effective for a numerical implementation of the least-squares problem that arises in the application of Yasuura's method to light scattering by a cluster of nanoparticles or diffraction from multilayered periodic structures. In the numerical computation using sequential accumaltion, the QR decomposition of the submatrix consisting of the block matrices Φ_ℓ (or $\Phi_{\ell,\ell}$ and $\Phi_{\ell,\ell+1}$) is sequentially executed L times. As a result, computer storage is significantly saved in comparison with that of a QR decomposition without sequential accumulation and a computation time is reduced.

ACKNOWLEDGMENT

This work is supported in part by a grant-in-aid 22560045 from JSPS in Japan.

REFERENCES

1. Yasuura, K., "A view of numerical methods in diffraction problems," *Progress in Radio Science 1966–1969*, 257–270, W. V. Tilson and M. Sauzade, eds., 1986.
2. Lawson, C. L. and R. J. Hanson, *Solving Least Squares Problems*, Prentice-Hall, Englewood Cliffs, 1974.

Three Dimensional Electromagnetic Simulations of VLF/LF Antennas in Natural Environments with FDTD Method

J. Vincent[1,2], **P. Borderies**[1], **J.-R. Poirier**[2], **and V. Gobin**[1]

[1]Electromagnetism and Radar Department, ONERA, Toulouse, France
[2]Research Group in Electromagnetism, LAPLACE, Toulouse, France

Abstract— In this paper, we investigate the effects of multiple environments on antenna matching and electric field propagation in complex environments at low frequencies. The system is computed in time domain with FDTD method.

Introduction: VLF and LF antennas have been mainly used for long distance broadcasting and submarine communications, since last century. Recent studies [1] show the behaviour of low frequency antennas. These investigations are extended by introducing several types of antennas in natural environments. FDTD Method is used in order to simulate wire antennas on a ground plane. The Earth's soil interaction is taken into account for various frequencies. The main aim of this paper is to show the effects of the environment on antenna properties and to favour surface wave propagation.

Antenna Design: FDTD Method is used in order to simulate an inverted-L antenna and a quarter-wavelength monopole antenna. Wires are designed with Holland model [2], which include the possibility of adding voltage sources and impedances. The inverted-L antenna is intrinsically matched.

Natural Environments: The natural environment creates various scattering and diffraction mechanisms that must be accounted for. Two principal situations are proposed: the effect of a forest and the existence of a hill near the antennas.

It has been shown that a forest can be represented by a dielectric slab for a frequency up to 100 MHz [3]. The value of the relative permitty ε_r is 1.065 and the conductivity σ is $10^{-3}\,\mathrm{S{\cdot}m^{-1}}$. It is very interesting to analyse the propagation of the electric field when the forest is in the nearfield of the antenna, in particular if the long wire of the inverted-L antenna is upon the dielectric slab. Then several layers of dielectric are used and the antennas are placed in different positions: on the hillside or on the hilltop.

Conclusion: Our study shows the effects of multiple environments on the propagation of electric field and on antenna matching with FDTD simulations. The effects of a lossy earth, including obstacles such as hills and forested areas are observed.

REFERENCES

1. Larbi, B., "Modélisation de structures antennaires VLF," Ph.D. Thesis, Université Nice-Sophia Antipolis, 2006.
2. Holland, R. and L. Simpson, "Finite-difference of EMP coupling to thin struts and wires," *IEEE Transactions on Electromagnetic Compatibility*, Vol. 23, No. 2, 88–97, May 1981.
3. Tewari, R. K., S. Swarup, and M. N. Roy, "Evaluation of relative permittivity and conductivity of forest slab from experimentally measured data on lateral wave attenuation constant," *International Journal of Electronics*, Vol. 61, 597–605, Nov. 1996.

Novel Edge-based Smoothed Finite Element Time Domain Method

Khaled S. R. Atia and S. S. A. Obayya
Centre For Photonics and Smart Materials, Zewail City of Science and Technology
Sheikh Zayed District, 6th of October City, Giza, Egypt

Abstract— In this paper, new formulation for edge-based smoothed finite element time domain method (ES-FETDM) is proposed for studying forward wave propagation in longitudinally varying optical waveguides. The derivative of the shape function in the ES-FETDM formulation is based on the line integral over "smoothed domain" around each edge in the mesh. Therefore, the suggested method using the Pade approximation is more accurate and more computationally efficient than the conventional finite element time domain method with linear triangular element mesh or quadrilateral elements. In addition, the investigated ES-FETDM has no spurious non-zero-energy modes. Therefore the proposed method is stable and works well for time domain problems. The numerical results show the effectiveness of the proposed ES-FETDM in the analysis of reflections of both transverse electric and transverse magnetic polarized pulses in waveguiding structures containing arbitrarily shaped discontinuities. In order to avoid non-physical reflections from the computational window edges, the perfectly matched layer boundary condition is introduced.

The suggested ES-FETDM is introduced for solving Maxwell's equations in time domain. In this formulation, a mesh of elements is required. In addition, the problem domain Ω is then divided into a set of Ns "non-overlap" and "no-gap" smoothing domains Ω_s^k such that $\Omega = \bigcup_{k=1}^{N_s} \Omega_s^k$ and $\Omega_s^i \cap \Omega_s^j = \phi$, $i \neq j$ as shown in Fig. 1. In the ES-FETDM, smoothed Galerkin weak form is used instead of Galerkin weak form as follows;

$$\frac{-1}{c^2}[M]\frac{d^2\{\phi\}}{dt^2} - 2j\frac{w_o}{c^2}[M]\frac{d\{\phi\}}{dt} + \left([K] + \frac{w_o^2}{c^2}[M]\right)\{\phi\} = \{0\} \tag{1}$$

where $\{\phi\}$ is the global electric or magnetic field vector, $\{0\}$ null vector

$$[K] = \sum_{k=1}^{N_s} B^T p B \tag{2}$$

$$[M] = \sum\nolimits_e \iint_e q[N_e][N_e]^T dxdy \tag{3}$$

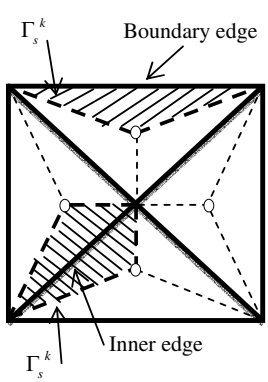

Figure 1: Triangular elements (solid lines) and the edge-based smoothing domains (shaded areas).

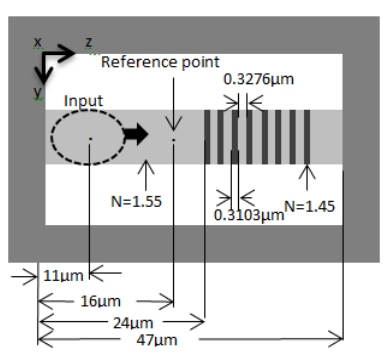

Figure 2: Optical grating with modulated refractive indces.

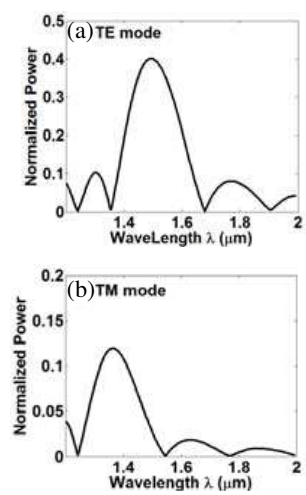

Figure 3: Reflection characteristics of an optical grating for: (a) TE and (b) TM modes.

where $p = 1$, $q = n^2$ for TE Mode while $p = \frac{1}{n^2}$, $q = 1$ for TM Mode. In addition B can be expressed as

$$B = \begin{bmatrix} b_{Ix} \\ b_{Iy} \end{bmatrix}, \quad b_{Ih} = \frac{1}{A_s^k} \int_{\Gamma_s^k} n_h N_I d\Gamma \tag{4}$$

where $h = x$ or y, n_h is the outward normal component in h direction, N_I is the shape function of node I associated with the smoothed domain, and A_s^k is the area of smoothed domain. The suggested method is used for studying the waveguiding structures containing arbitrarily shaped discontinuities as shown in Fig. 2. Fig. 3 shows the reflection characteristics of an optical grating for TE and TM modes.

A Grating-based Plasmon Biosensor via Phase Detection with Wide Measurement Range

Ziqian Luo[1], **Taikei Suyama**[2], **Xun Xu**[3], **Yoichi Okuno**[4], **and Sailing He**[1, 5]

[1]Academy of Advanced Optoelectronics, South China Normal University, Guangzhou, China
[2]Akashi National College of Technology, Akashi, Japan
[3]Faculty of Engineering, Kyushu Sangyo University, Fukuoka, Japan
[4]Graduate School of Science and Technology, Kumamoto University, Kumamoto, Japan
[5]Centre for Optical and Electromagnetic Research, Zhejiang University, Hangzhou, China

Abstract— Surface plasmon excitation on a metal grating causes an obvious change in the reflected phase as the material index changed [1]. Thus, grating based plasmon biosensors via phase detection were reported to have great potential on medical and physiological applications [2–5]. However, the magnitude of a phase shift cannot be more than 180°, high resolution means a narrow measurement range in refractive index. In this work, we scan the surface plasmonic resonance phenomenon around the environment index range as $1.27 < n < 1.35$, and find very similar patterns of phase shift (Fig. 1). We summerize rules of phase shift patterns between different index range, and recommend an optical set-upmethod that can determine a wide measurement range of refractive index by combining all small workspaces.

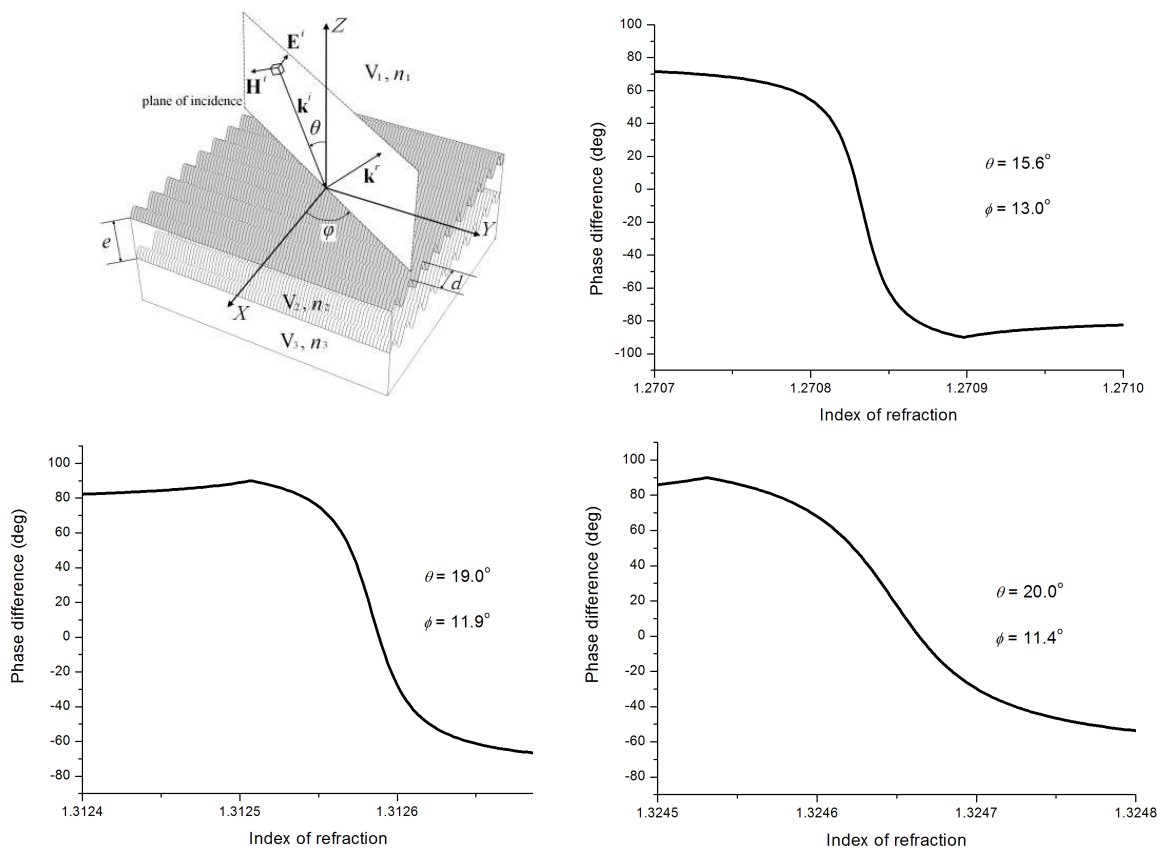

Figure 1: Similar phase shift patterns in different refractive index environment.

REFERENCES

1. Nelson, S. G., K. S. Johnston, and S. S. Yee, "High sensitivity surface plasmon resonance sensor based on phase detection," *Sensors and Actuators B*, 35–36, 187–191, 1996.
2. Homola, J., "On the sensitivity of surface plasmon resonance sensors with spectral interrogation," *Sensors and Actuators B*, Vol. 41, 207–211, 1997.

3. Homola, J., I. Koudela, and S. Yee, "Surface plasmon resonance sensor based on diffraction gratings and prism couplers: sensitivity comparison," *Sensors and Actuators B: Chemical*, Vol. 54, Nos. 1–2, 1624, 1999.
4. Kuo, W.-K. and C.-H. Chang, "Phase detection properties of grating-coupled surface plasmon resonance sensors," *Optics Express*, Vol. 18, No. 19, 19656–19664, 2010.
5. Luo, Z., T. Suyama, X. Xu, and Y. Okuno, "A grating-based plasmon biosensor with high resolution," *Progress In Electromagnetics Research*, Vol. 118, 527–539, 2011.

Parallel Performance of the Multi-threaded ICCG Solver in Electromagnetic Finite Element Analyses on the Latest Processors

K. Semba[1,2], K. Tani[1], T. Yamada[1], T. Iwashita[3], Y. Takahashi[4], and H. Nakashima[3]

[1]Engineering Division, JSOL Corporation, Tokyo, Japan
[2]Graduate School of Informatics, Kyoto University, Kyoto, Japan
[3]Academic Center for Computing and Media Studies, Kyoto University, Kyoto, Japan
[4]Department of Electrical Engineering, Doshisha University, Kyoto, Japan

Abstract— We introduce results of a performance analysis for a multi-threaded incomplete Cholesky conjugate gradient (ICCG) solver applied to a linear system derived from a finite-element electromagnetic-field analysis (FEA). In the FEA, a linear sparse iterative solver typified by an ICCG accounts for most of the computational time, and thus a speedup of the solver is always wanted. Accordingly, we have investigated the use of multi-threaded parallel processing in the FEA. While the multi-threaded iterative solver is used in a shared memory parallel computational node such as a PC comprised of multi-core processors, it can also work as an internal solver in a distributed memory parallel solver based on a domain decomposition technique for a cluster of computational nodes.

Earlier in our research, we developed a multi-threaded ICCG solver using algebraic block multi-color (ABMC) ordering [1]. The ABMC ordering is one of the parallel ordering techniques, and it shows better solver performance than conventional multi-color ordering in an FEA of practical systems such as IPM motors. However, it was found that the convergence of the solver is significantly degraded when an effect of the external circuit is taken into account. Consequently, we proposed a new parallelization technique in which the unknowns related to the external circuit are dealt with separately from the unknowns for the field variables during the reordering process [2]. The new parallel solver exhibits good convergence for the model with the external circuit.

In the present research, we examine the parallel multi-threaded solver in FEA conducted on the latest processors. Numerical tests for the performance evaluation were conducted on a latest multi-core processor (Intel® Xeon® E5) and an Intel® Xeon Phi™ Coprocessor based on Intel® MIC architecture. Because the program for the parallel solver is written using OpenMP, its modification for the Xeon Phi™ only requires the insertion of several directives. The numerical result from the IPM motor model analysis shows a 6.4-fold speedup compared with the sequential solver using eight cores of Intel® Xeon® E5 processor (Table 1), although the older Intel® Xeon® X5560 processor gave us a poor eight-core speedup of 2.6-fold [2]. This is mainly due to the improvements in memory bandwidth for the latest processor. The numerical result on 60 cores of the Intel® Xeon Phi™ Coprocessor will be reported at the conference and in the full paper.

Table 1: Parallel performance of ICCG solver with ABMC reordering.

Number of threads	1	2	4	8
Number of iterations	4044	3972	3955	3949
Time sec	199.31	106.53	56.22	31.19
Speedup	1.00	1.87	3.54	6.39

REFERENCES

1. Iwashita, T., H. Nakashima, and Y. Takahashi, "Algebraic block multi-color ordering method for parallel multi-threaded sparse triangular solver in ICCG method," *IEEE 26th International Parallel Distributed Processing Symposium*, 2012.
2. Semba, K., K. Tani, T. Yamada, T. Iwashita, Y. Takahashi, and H. Nakashima, "Parallel performance of multi-threaded ICCG Solver based on algebraic block multi-color ordering in finite element electromagnetic field analyses," *15th Biennial IEEE Conference on Electromagnetic Field Computation*, 2012.

Detection of Electromagnetic Radiation during the Earthquake Preparation Process

Fedir Dudkin and Valery Korepanov
Lviv Centre of Institute for Space Research, 5-A Naukova Str., Lviv 79060, Ukraine

Abstract— The generation of electromagnetic (EM) fieled accompanies practically all natural physical processes and often is used for their characterization. The EM methods were also analyzed for the efficiency of the solution of one of the greatest modern problems — detection of the precursors of the future earthquakes (EQ). It was believed that first of all seismic variations have to carry information about EQ preparation process, but multiple experiments showed that this method can not be used for the precursors selection. Many other phenomena preceding EQ were studied and as for today, in many publications it was stated that the variations of the magnetic field are often detected before EQ.

The greatest problems which impede the reliable detection of the magnetic precursors are following: (i) very low intensity of anticipated seismo-EM signals, (ii) difficulty at separation of weak seismo-EM signals from the background natural EM fields of ionospheric and magnetospheric origin, (iii) and finally the poor precision of the localization of precursor source position. The combination of these difficulties leads to the reduction in confidence and criticism of seismo-EM signals detection possibility, but a great amount of experimental data allowed though coming to general agreement that the most promising frequency band to detect such signals is ULF — from ~ 0.0001 to 0.1 Hz.

The present report describes a new approach to solve these problems.

First a dedicated high-sensitive 3-component magnetometer system for ULF range was created and successfully tested in seismoactive regions. For the separation and localization of EQ magnetic precursors the polarization ellipse technique has been developed to process the measurements data acquired from 3-component magnetometers. It was shown that the calculations based on polarization ellipse parameters obtained from at least two distant points allow successful discrimination of seismo-EM signals from the natural background, as well as rather good localization the source of these signals.

The theoretical background of the proposed method is presented. The method was successfully tested in three seismoactive regions with greatly different conditions of EM precursor generation: Koyna-Warna region in the southern part of Deccan Volcanic Province, Western India; Panzhihua region, Sichuan province, China and Kanto region, Japan. The lithospheric magnetic precursors were found in frequency range 0.07–0.0005 Hz in dependence of local geomorphological conditions and an EQ focal depth. The results of these experimental verifications are given which confirm the proposed method efficiency and give hope, with its further improvement, to the progress in the EQ precursors reliable detection.

ACKNOWLEDGMENT

These works are partly supported by SSAU contract 1-05/08.

Session 2PK
Poster Session 4

Maxwell Equations of Electromagnetic and Gravitational Fields in the Curved Spaces
Zi-Hua Weng, ... 836
Adjoint Fields of Electromagnetic and Gravitational Fields in the Curved Spaces
Zi-Hua Weng, ... 837
Dense Waves in Electromagnetic and Gravitational Fields
Zi-Hua Weng, ... 838
Numerical Modelling of Heat Flow Distribution Based on the Nodal Heating Method
Eva Kroutilová, Pavel Fiala, Premysl Dohnal, Radim Kadlec, ... 839
Approaches to the Modelling of Multilayer Materials
Eva Kroutilová, Pavel Fiala, Premysl Dohnal, Radim Kadlec, ... 840
How Strict is the Validity Range of the Dipole Approximation for a Dielectric Mixture?
Changhe Yang, Liang Li, Jian Wan, Zhanli Chen, ... 841
Inhomogeneous Spatially Dispersive Electromagnetic Media
Jonathan Gratus, Matthew Jack McCormack, ... 842
The Influence of the Aspect-ratio on the Effective Optical Response of Metallic Nanowire Media
Anderson Oliveira Silva, Ivo T. Leite, J. M. Teixeira, J. P. Araujo, J. W. C. A. Costa, Maria T. R. Giraldi, Pedro A. S. Jorge, A. Guerreiro, ... 843
An Electromagnetic Meta-lens Based on a New SRR Type for Antenna Gain Enhancement
Akram Boubakri, Fethi Choubeni, ... 845
Multifunctionalized Self-supported (Nano) Membranes as Integrated Platform for Plasmonic Metamaterials
Zoran Jaksic, Filip Radovanovic, Aleksandra Nastasovic, Jovan Matovic, ... 846
Automatic Tracking of Bandpass Sampling OFDM Signal in Mobile Environment
Xin Wang, Heung-Gyoon Ryu, ... 848
A Reconfigurable Miniaturized Spiral Monopole Antenna for TV White Spaces
Mohamad Y. Abou Shahine, Mohammed Al-Husseini, Youssef Nasser, Karim Y. Kabalan, Ali El-Hajj, 849
Dual Polarized High Front-to-back Ratio Microstrip Slot Antenna
Mohamed S. El-Gendy, Haythem Hussein Abdullah, Esmat Abdel-Fattah Abdallah, ... 850
A Proximity-fed Elliptical-shaped Aperture UWB Antenna with Triple Band-rejection Property
Mohamed Mamdouh Mahmoud, Ayman Ayd Ramadan Saad, Elsayed Esam M. Khaled, ... 851
Design and Development of Reconfigurable Microstrip Patch Antenna Using MEMS Switch for Ku-band Application
Prafulla Chandra Prasad, Neela Chattoraj, ... 852
Wideband Patch Antenna for X-band Applications
Amal Harrabi, Tchanguiz Razban-Haghighi, Yann Mahe, Lotfi Osman, Ali Gharsallah, ... 854
A Fractal-based Printed Slot Antenna for Multi-band Wireless Applications
Seevan F. Abdulkareem, Ali J. Salim, Ali I. Hammoodi, Jawad K. Ali, ... 855
Picosecond Erbium-doped Fiber Laser Using Carbon Nanotube Coated Abrupt Tapers
Kuan-Hao Lin, Hsiang-Ting Peng, Tsung-Hsun Yang, Feng-Zhou Liu, Nan-Kuang Chen, Der-Yi Hsu, 856
Measurement of Evanescent Optical Force Based on Dual Fiber Sagnac Loop Interferometers
Gia-Ling Cheng, Hsiang-Ting Peng, Zhao-Ying Chen, Nan-Kuang Chen, ... 858
Birefringence in Dispersion-engineered Short-pass Edge Fiber
Yi-Kun Lee, Nan-Kuang Chen, ... 860
Orbital Angular Momentum of Light Generated at the Fiber End
Bin Zhou, ... 861
Effects of the Length Variations of LYSO and Plastic Optical Fiber on the Energy Spectrum Responses of a Fiber-optic Radiation Sensor
Wook Jae Yoo, Kyoung Won Jang, Sang Hun Shin, Dayeong Jeon, Byung Gi Park, Sin Kim, Joo-Hyun Moon, Seunghyun Cho, Bongsoo Lee, ... 862

A Novel Multipath Limiting Quadrifilar Helix Antenna for Local Area Augmentation System
James A. Quinlan, Daniel N. Aloi, ... 863
A Transfinite Set Theory for Particle-wave Duality, Wave Collapse and Quantum Entanglement
Ji-Huan He, M. S. Elnaschie, ... 864
Adapting the New IRI-Plas Model to Satellite Data in the High-latitude Ionosphere
Olga A. Maltseva, N. S. Mozhaeva, ... 865
Short-temporal Magnetosphere-ionosphere Predictors of Catastrophic Earthquakes
Nadezda P. Sergeenko, Andrey L. Kharitonov, ... 866
Exploring and Exploiting Polarization Properties of Angle Cut Whispering Gallery Resonators
Florian Sedlmeir, Martin Hauer, Josef U. Furst, Harald G. L. Schwefel, ... 867
Compact Low Phase Noise Oscillator Using Symmetrical Square Open-loop with Loaded T-stubs Resonator
Sung-Jin Cho, Nam-Young Kim, ... 868
Miniaturized Dual-band Artificial Magnetic Conductor with Easy Control of Second/First Resonant Frequency Ratio
Son Xuat Ta, Ikmo Park, ... 869
A Wide-stopband EMI Filter for Power-line
Jin-Sup Kim, Se-Hwan Choi, Sang-Kuk Kim, Dong-Joon Lim, Jong-Kyu Kim, ... 870
A Computational Model of Slim Speaker Using Transmission Line Enclosure Modeling
Jin-Sup Kim, Heung-Euy Kim, Se-Hwan Choi, Yoon-Seok Heo, ... 871
A Lumped-element Absorptive Bandstop Filter Topology with Perfect Impedance Matching
Kangho Lee, Tae-Hak Lee, Young Sik Kim, Juseop Lee, ... 872
Open Stub Band-pass Filter Using Stepped Impedance Resonator for Size Reduction
Ki-Cheol Yoon, Hyunwook Lee, Joung-Geun Park, Jaegook Lee, Tae-Young Kim, Tae-Sung Jung, Jong-Chul Lee, ... 873
Compact Reconfigurable Dual Mode Resonator with Switchable Band Using RF PIN Diodes
Hesham Abd Elhady Mohamed, Heba B. El-Shaarawy, Esmat Abdel-Fattah Abdallah, Hadia M. El-Henawy, ... 874
Lightweight Polypropylene-metal Based Nanocomposites and Their Electromagnetic Shielding Response
Javier Arranz-Andres, Pilar Marín, Ana M. Aragon, Maria L. Cerrada, ... 875
Optical Control Charge State of Nitrogen Vacancy Defects in Diamond
Xiangdong Chen, Changling Zou, Fangwen Sun, ... 876
Electromagnetic Field as Human Health Risk Factor: EMF Safety Ensuring by Hygienic Standardization
I. V. Bukhtiyarov, Nina B. Rubtsova, Yu. P. Paltsev, L. V. Pokhodzey, Sergey Yu. Perov, ... 877
Design of an Optimal Multi-layered Electromagnetic Absorber through the Central Force Optimization Algorithm
Jorge González, Iván Amaya, Rodrigo Correa, ... 878
Peculiarities of Relativistic TWT Operation near the Cyclotron Resonance
Mikhail I. Fuks, Edl Schamiloglu, Yongdong Li, ... 879
Narrow Bipolar Pulses and Associated Microwave Radiation
Mohd Riduan Ahmad, Mona Riza Mohd Esa, Vernon Cooray, ... 880
Coaxial Reflection Probe for Measurements of Temperature and Frequency Dependent Dielectric-properties of Low-loss Liquids
Jan Vrba, Jr., ... 881
Design of Stripline Kicker for Tune Measurements in the MAX IV 3 GeV Ring
David Olsson, ... 883
Compact Microstrip Patch Antenna for Ultra-wideband Applications
Waqas Mazhar, M. A. Tarar, Farooq Ahmad Tahir, Shan Ullah, Farooq Ahmad Bhatti, ... 884
Self-similarity in pSi Multilayer Structures
Dan Sidney Diaz-Guerrero, Luis Manuel Gaggero-Sager, A. David Ariza-Flores, ... 885
A Theoretical Investigation of the Influence of Underground Power Cable Parameters on Magnetic Field Levels
Ivan Rostovskiy, Oleksandr Okun, Sergey Shevchenko, Leena Korpinen, ... 886
On Double Scattering in Lidar Sounding of the Atmosphere with Simple Non-spherical Particles
Piero Bruscaglioni, ... 887

Analysis of Metallic Terahertz Structures Using FDTD Method
Jorge R. Sosa-Pedroza, Méndez Rodíguez, M. Galaz-Larios, Mauro Alberto Enciso-Aguilar, Manuel Benavides-Cruz, ... 888
Possible Methods for Limiting Magnetic Fields outside a High Voltage Power Substation by Changing the Phase Sequence of Busbar Wires
Oleksandr Okun, Sergey Shevchenko, Leena Korpinen, ... 889
FOSLL* Dual Potential Method for Time Harmonic Maxwell's Equations in 3D
Juhani Kataja, ... 890
An Improvement Method of Diversity Effect for the Linear Polarization Diversity by Decreasing the XPD Value
Deock-Ho Ha, ... 891
A Two-dimension Generalized Electro-magneto-thermo Elastic Diffusion with Thermal Relaxation
Shaaban EL-Shahat Mohamed Khader, Mona El-Shahat Mohamed Khedr, ... 893
Numerical Study of Dual-frequency Stacked Annular-ring Microstrip Antenna
Abderraouf Messai, A. Bourayou, Skander Aris, Tarek Fortaki, ... 894
Analysis of Electromagnetic Shielding Effectiveness by the Change in the Distance of the Antenna
Jeong-Ju Bang, Ho-Je Kang, Chang-Su Huh, Woo-Chul Park, Sun-Mook Hwang, ... 895
SVM Approach for Hyperspectral Images Classification
Karim Saheb Ettabaa, Med Ali Hamdi, Imed Riadh Farah, Bassel Souleiman, ... 896
Analysis of Multisection Rectangular Waveguide Impedance Transformers
Debendra Kumar Panda, Sanjay Chouhan, Ajay Chakraborty, ... 897
A Compact Elliptic Bandpass Filter Using Cross-coupled Miniaturised Hairpin Resonators Packaged by COB Method
C. Wang, Y. Li, Nam-Young Kim, ... 898
A Compact Dual-band Bandpass Filter with High-selectivity and Tunable Passband for WiMax and WLAN Applications
C. Wang, Y. Li, Nam-Young Kim, ... 899

Maxwell Equations of Electromagnetic and Gravitational Fields in the Curved Spaces

Zi-Hua Weng
School of Physics and Mechanical & Electrical Engineering
Xiamen University, Xiamen 361005, China

Abstract— J. C. Maxwell was first to adopt simultaneously the quaternion and the vectorial terminology to describe the electromagnetic theory. The algebra of quaternions was invented by W. R. Hamilton in 1843, meanwhile the octonion, as the ordered pair of quaternions, was invented independently by J. T. Graves in 1843 and A. Cayley in 1845. The paper introduces the octonion space into the field theory, to describe simultaneously the physical features of electromagnetic and gravitational fields. The result reveals that the connection coefficient and the curvature of the curved octonion space can impact directly the field equations of electromagnetic and gravitational fields.

The viewpoint of R. Descartes, M. Faraday, and A. Einstein etc claims that, the field is an irreducible element of physical description, while the space-time is only the extension of the field and does not claim existence on its own. It means that the space-time extended from the electromagnetic field is different from the one extended from the gravitational field. They are quite similar but independent to each other.

According to the viewpoint of W. R. Hamilton and J. C. Maxwell etc., the space-time in the physics can be considered as the quaternion space. Therefore two space-times, which extended respectively from the electromagnetic and gravitational fields, both can be considered as the quaternion space, and they may be flat or curved quaternion space. These two quaternion spaces are perpendicular to each other so that they can combine together to become an octonion space, and they may be flat or curved octonion space correspondingly.

In the curved quaternion space for the gravitational field, the quaternion orthogonality defines the quaternion parallel transport, covariant derivative, metric coefficient, connection coefficient, and curvature etc. The decomposition of the definition formula of gravitational source deduces the field equations of gravitation in the curved quaternion space. Two components of gravitational strength can induce to each other. The experimental measurement about the gravitational field equations in the curved quaternion space for the gravitational field, will find the offset of the curved quaternion space departure from the flat quaternion space.

In the curved quaternion space for the electromagnetic field, the quaternion orthogonality defines the quaternion parallel transport, covariant derivative, metric coefficient, connection coefficient, and curvature etc. The decompounding of the definition formula of electromagnetic source infers the field equations of electromagnetics in the curved quaternion space. Two components of electromagnetic strength will induced to each other. The experimental measurement about the electromagnetic field equations in the curved quaternion space for the electromagnetic field, may discover the offset of the curved quaternion space departure from the flat quaternion space.

ACKNOWLEDGMENT

The authors are grateful for the financial support from the National Natural Science Foundation of China under grant number 60677039.

Adjoint Fields of Electromagnetic and Gravitational Fields in the Curved Spaces

Zi-Hua Weng
School of Physics and Mechanical & Electrical Engineering
Xiamen University, Xiamen 361005, China

Abstract— The algebra of quaternions was adopted firstly by J. C. Maxwell to describe the physics feature of electromagnetic fields, presently the quaternion is used to depict the gravitational field also. However the quaternion space for electromagnetic field is independent to that for gravitational field. These two quaternion spaces can be combined together to become the octonion space. The quaternion space may be either flat or curved, accordingly the octonion space, which consisted of these two quaternion spaces, is either flat or curved.

In the curved quaternion space for gravitational field, there are the field potential and the operator $\diamondsuit_g$ of gravitational field. The operation of the operator $\diamondsuit_g$ on the gravitational potential will yield the field strength and field source of gravitational field. The definition formula of gravitational source will deduce the gravitational field equations, including Newton's law for gravitation. The operation of the operator $\diamondsuit_g$ on the electromagnetic potential will yield the field strength and field source of electromagnetic field. The definition formula of electromagnetic source will infer the electromagnetic field equations, including Maxwell's equations.

In the curved quaternion space for electromagnetic field, there are the field potential and the operator $\diamondsuit_e$ of electromagnetic field. The operation of the operator e on the gravitational potential will yield the adjoint field of gravitational field with the adjoint field strength and adjoint field source etc.. The adjoint field of gravitational field possesses some features of electromagnetic fields. The operation of the operator $\diamondsuit_e$ on the electromagnetic potential will yield the adjoint field of electromagnetic field with the adjoint field strength and adjoint field source etc.. The adjoint field of electromagnetic field possesses some features of gravitational fields.

The results reveal that the connection coefficient and curvature of curved octonion space will impact directly on the physics features of electromagnetic field, gravitational field, adjoint field of gravitational field, and adjoint field of electromagnetic field etc..

ACKNOWLEDGMENT

The authors are grateful for the financial support from the National Natural Science Foundation of China under grant number 60677039.

Dense Waves in Electromagnetic and Gravitational Fields

Zi-Hua Weng
School of Physics and Mechanical & Electrical Engineering
Xiamen University, Xiamen 361005, China

Abstract— At present the quaternion space can be used to describe the feature of gravitational fields. In the quaternion space, the vectorial radius can be combined with the integral of gravitational potential to become the compounding vectorial radius. The latter can be considered as the vectorial radius of quaternion compounding space (function space). Correspondingly the quaternion velocity and the gravitational potential can be combined together to become the compounding potential.

The operation of the quaternion operator on the compounding potential can deduce the compounding strength and compounding source of gravitational field. The decomposition of definition formula of compounding source yields the field equations and wave equation of gravitational field in the quaternion compounding space. According to the wave equation in the quaternion compounding space, the transmission direction of compounding strength (wave) originated from one point is perpendicular to the acceleration of gravity and velocity curl simultaneously, and it is generally along the tangent direction of star trajectory, in the orbit motion model of stars around the galaxy center. When the compounding strength transmits to other points, the differentiation of compounding strength appears in the tangent and radial directions. These two components will impact the other stars' orbit motions, to result in the corresponding dense wave.

The quaternion space was adopted to depict the electromagnetic field by J. C. Maxwell. However the quaternion space for electromagnetic field is independent to that for gravitational field. In the quaternion space for electromagnetic field, the vectorial radius can be combined with the integral of electromagnetic potential to become the compounding vectorial radius. The latter can be considered as the vectorial radius of quaternion compounding space (function space) for electromagnetic field. Correspondingly the quaternion velocity and the electromagnetic potential can be combined together to become the compounding potential.

The operation of the quaternion operator on the electromagnetic compounding potential can infer the compounding strength and compounding source of electromagnetic field. The decompounding of definition formula of compounding source produces the field equations and wave equation in the quaternion compounding space for electromagnetic fields. According to the wave equation of electromagnetic fields in the quaternion compounding space, the propagation direction of compounding strength (wave) originated from one point is perpendicular to the electric intensity and magnetic flux density simultaneously, and it is generally along the tangent direction of trajectory of negative trial charge, in the orbit motion model of negative trial charges around the positive electric charge. When the compounding strength of electromagnetic field transmits to other points, the discrimination of compounding strength appears in the tangent and radial directions. These two components will impact the orbit motions of other negative trial charges, to result in the corresponding dense wave.

ACKNOWLEDGMENT

The authors are grateful for the financial support from the National Natural Science Foundation of China under grant number 60677039.

Numerical Modelling of Heat Flow Distribution Based on the Nodal Heating Method

Eva Kroutilova, **Pavel Fiala**, **Premysl Dohnal**, **and Radim Kadlec**
Department of Theoretical and Experimental Electrical Engineering
Brno University of Technology, Technicka 12, Brno 616 00, Czech Republic

Abstract— The paper presents a solution of the thermal problem based on the modified nodal heating method. This technique exploits the classic nodal voltage method, and thus the vector of unknown quantities contains mainly nodal heating oriented from the individual independent nodes to the reference node. The vector of unknown quantities is nevertheless extended to include certain nodal thermal fluxes, the heating of ideal sources in particular. Test examples of a switchgear are shown as an instance of the solution.

ACKNOWLEDGMENT

This work was supported by the Czech Science Foundation (13-09086S), project of the BUT Grant Agency FEKT-S-11-5/1012 and project from Education for Competitiveness Operative Programme CZ.1.07.2.3.00.20.0175, (Electro-researcher).

REFERENCES

1. Cap, M., P. Marcon, K. Bartušek, et al., "Measuring of temperature fields using MR tomography," *PIERS Proceedings*, 1040–1042, Cambridge, USA, July 5–8, 2010.
2. Kadlecová, E., "Automated system of calculation of reflecting surface of light sources," Disertation thesis, VUT v Brně, FEKT, Brno, 2004.
3. Kroutilová, E. and T. Bachorec, "Modelovani teplotnich pomeru v rozvadeci," Vyzkumna zprava, VUT v Brne, FEKT, UTEE, Brno, 2007.
4. Kadlec, R., E. Kroutilova, and P. Fiala, "Multiple reflection from layered heterogeneous medium," *PIERS Online*, Vol. 7, No. 7, 633–636, 2011.
5. Mikulka, J., T. Kriz, E. Kroutilová, and P. Fiala, "Numerical modeling of light sources with R-FEM method in CFX environment," *PIERS Proceedings*, 424–427, Xi'an, China, March 22–26, 2010
6. Kadlecová, E. and P. Fiala, "New directions in modeling the lighting systems," *Radioengineering*, roč, Vol. 13, č, No. 4, 75–80, 2004, ISSN: 1210-2512.
7. Kadlec, R., P. Fiala, and E. Kroutilová, "Numerical modeling by raytracing," *Proceedings of the International Workshop on Teleinformatics and Electromagnetic Field*, 14, UTEE, FEKT VUT v Brně, Paris, 2008, ISBN: 9788021437180.
8. Kadlec, R., E. Kroutilová, and P. Fiala, "Multiple reflection from layered heterogeneous medium," *PIERS Online*, Vol. 7, No. 7, 633–636, 2011.
9. Kroutilová, E., "Hybridní numerické metody," Habilitation thesies, VUT v Brně, FEKT, UTEE, May 2013.
10. Kadlec, R., P. Fiala, and D. Nespor, "Electromagnetic wave propagation in heterogeneous structures," *PIERS Online*, Vol. 6, No. 7, 613–616, 2010.

Approaches to the Modelling of Multilayer Materials

Eva Kroutilova, **Pavel Fiala**, **Premysl Dohnal**, **and Radim Kadlec**
Department of Theoretical and Experimental Electrical Engineering
Brno University of Technology, Technicka 12, Brno 616 00, Czech Republic

Abstract— The authors evaluate the applicability of different numerical methods in the solution of practical problems related to material engineering. In this context, the paper presents various approaches to solving the transmission of electromagnetic waves through a multilayer material that consists of environments with different material properties. The proposed solutions can be used, for example, in the modelling of the propagation of electromagnetic waves in metamaterials and nanostructures.

ACKNOWLEDGMENT

This work was supported by the Czech Science Foundation (13-09086S), project of the BUT Grant Agency FEKT-S-11-5/1012 and project from Education for Competitiveness Operative Programme CZ.1.07.2.3.00.20.0175, (Electro-researcher).

REFERENCES

1. Kadlecová, E., "Automated system of calculation of reflecting surface of light sources," Disertation thesis, VUT v Brně, FEKT, Brno, 2004.
2. Kadlecová, E. and P. Fiala, "New directions in modeling the lighting systems," *Radioengineering*, roč, Vol. 13, č, No. 4, 75–80, 2004, ISSN: 1210-2512
3. Kadlec, R., P. Fiala, and E. Kroutilová, "Numerical modeling by raytracing," *Proceedings of the International Workshop on Teleinformatics and Electromagnetic Field*, 14, UTEE, FEKT VUT v Brně, Paris, 2008, ISBN: 9788021437180.
4. Kadlec, R., E. Kroutilová, and P. Fiala, "Multiple reflection from layered heterogeneous medium," *PIERS Online*, Vol. 7, No. 7, 633-636, 2011.
5. Kroutilová, E., "Hybridní numerické metody," Habilitation thesies, VUT v Brně, FEKT, UTEE, May 2013.
6. Kadlec, R., P. Fiala, and D. Nespor, "Electromagnetic wave propagation in heterogeneous structures," *PIERS Online*, Vol. 6, No. 7, 613–616, 2010.

How Strict is the Validity Range of the Dipole Approximation for a Dielectric Mixture?

Changhe Yang, Liang Li, Jian Wan, and Zhanli Chen
School of Civil Engineering and Architecture, Nanchang University, China

Abstract— Various physical models or numerical simulations have been made to provide exact solutions for a dielectric mixture with an arbitrary concentration of inclusions. The evaluation on the interactions among inclusions directly determines the accuracy of various mixing models for a given mixture. The interactions among inclusions mainly depend on two parameters: the dielectric mismatch $\varepsilon_i/\varepsilon_e$ between the inclusions ε_i and the environmental media ε_e, and the volume fraction f of the inclusions. A simple approach is the dipole approximation without considering the interactions for small dielectric mismatch or small volume fraction, but it is not fit for large dielectric mismatch and large volume fraction for which the contributions of higher-multipole may be significant.

This paper investigates the validity range of the dipole approximation for a dielectric mixture with spherical inclusions through electric field analyses according to a new criterion: if the maximum perturbation on an arbitrarily selected sphere surface caused by the interactions among spheres is less than a given allowable error, the dipole approximation is considered acceptable. For an arbitrarily selected sphere, the difference (the relative error) between the FEM result and the dipole approximation is actually caused by the interactions among spheres. We define it as the perturbation on the central sphere due to all the other spheres. A theoretical formula for calculating the validity range of the dipole approximation is derived. It shows that the validity range depend on three parameters, the dielectric mismatch, the volume fraction of inclusions, and the allowable error. The calculated results by this formula are compared with those numerically obtained by the FEM (Finite Element Method). The good agreement between them indicates the credibleness of this formula.

Inhomogeneous Spatially Dispersive Electromagnetic Media

Jonathan Gratus[1,2] **and Matthew McCormack**[1,2]

[1]Physics Department, Lancaster University, LA1 4YB, UK
[2]The Cockcroft Institute, Sci-Tech Daresbury, Keckwick Lane
Daresbury, Warrington, WA4 4AD, UK

Abstract— The constitutive properties of a medium which is temporally and spatially dispersive and inhomogeneous are dependent on the temporal frequency ω, the wavenumber $\mathbf{k}$ and the position $\mathbf{x}$. Warm plasmas are naturally inhomogeneous and spatially dispersive [1, 2]. In accelerator science small balls of plasma, created from the cavity walls, may disturb the cavity's RF fields. A detailed knowledge of the behaviour of electromagnetic fields in a laser-plasma interactions is crucial for the design of laser-plasma-wakefield accelerators. How the radiation generated by the accelerated elections modified by the plasma, for example as it leaves the bubble regime, could be modelled using a spatially dispersive and inhomogeneous constitutive relations.

Spatially dispersive and inhomogeneous media may also be constructed as a metamaterial leading to direct experimental testing of the responses.

Since $\mathbf{x}$ and $\mathbf{k}$ are conjugate variables one can ask what is meant when one writes the permittivity as $\varepsilon(\omega, \mathbf{k}, \mathbf{x})$. I shall present two complementary approaches, using integral and differential representation. For media which are spatially dispersive no single mode solution to Maxwell's equations exist. Instead one must look for packet solutions which combine several spatial frequencies for each temporal frequencies ω. This becomes especially relevant when investigating wavelike solutions with wavelengths comparable in size to the inhomogeneities.

I will present two types of inhomogeneities for which solutions can be found. One is a medium where the constitutive relations are discontinuous. These media were first considered by Pekar as additional boundary conditions in 1957, but have been researched since. I will also consider a medium where the constitutive relations vary periodically.

REFERENCES

1. Gratus, J. and R. W. Tucker, "Covariant constitutive relations, Landau damping and non-stationary inhomogeneous plasmas," *Progress In Electromagnetics Research M*, Vol. 13, 145–156, 2010.
2. Gratus, J. and R. W. Tucker, "Covariant constitutive relations and relativistic inhomogeneous plasmas," *Journal of Mathematical Physics*, Vol. 52, No. 26, 2011.

The Influence of the Aspect-ratio on the Effective Optical Response of Metallic Nanowire Media

Anderson O. Silva[1,2,3], **Ivo T. Leite**[1], **J. M. Teixeira**[4], **J. P. Araujo**[4,5], **J. W. C. A. Costa**[2,3], **M T. R. Giraldi**[5], **P. Jorge**[1], **and A. Guerreiro**[1,6]

[1]INESC TEC, UOSE (National Institute of Engineering Systems and Computers)
R. Campo Alegre, Porto 4169-007, Portugal
[2]LEA (Applied Electromagnetic Laboratory)
C. U. José da Silveira Neto, Belém, Brazil
[3]Federal University of Para, C. U. José da Silveira Neto, Belém, Brazil
[4]IFIMUP/IN (Material Physics Institute/University of Porto)
R. Campo Alegre, Porto 4169-007, Portugal
[5]IME (Military Engineering Institute)
Instituto Militar de Engenharia, Rio de Janeiro, Brazil
[6]Faculty of Sciences/University of Porto
R. Campo Alegre, Porto 4169-007, Portugal

Abstract— The field of Plasmonics has played a central role in manipulating lightwaves bellow the diffraction limit. Surface plasmon-polariton (SPP) excitations are waves that propagate along the metal-dielectric interface due to the resonant interaction between photons and collective electronic oscillations at the metallic surface. The effective wavelength of SPP waves is much smaller than the wavelength of the incident light and can reach high degree of energy confinement at nanoscale [1]. Several classes of artificially nanostructured materials have attained SPP waves as the core of extraordinary optical phenomena, such as: negative refraction [2], subwavelength imaging [3] and surface enhanced Raman spectroscopy (SERS) [4]. The developments in nanofabrication techniques together with the rapid evolution in computational modeling has allowed handling SPP waves for a large variety of applications, giving rise to a new generation of photonic devices fully compacted in subwavelength dimensions, as superlenses, scanning near-field optical microscopes, perfect absorbers, nano-optical sensors, to name a few [5]. In the macroscopic framework, the properties of SPP waves are tailored according to relations that can be obtained from the effective permeability μ and permittivity □ parameters in the material design. Within this context, nanowire media has proven to be a versatile building block to sustain SPP resonances. Such media allows spanning SPP wave propagation from elliptic to hyperbolic dispersion relations, opening the possibility to reach a broad range of refraction regimes by adjusting its geometric parameters or the spectrum of the incident light [6].

This work investigates the influence of the aspect ratio (the relation between nanowire height h and radius r) on the effective optical response of periodic arrays of metallic nanowires. To perform this, we applied 3D Finite Element Method to theoretically estimate the corresponding SPP behavior as the ratio h/r varies along a periodic structure composed by Ag nanowires embedded in alumina background. Calculation of reflectance and transmittance coefficients computed at the visible and near infrared ranges and several angles of incidence demonstrates that a multiband-channel profile can be obtained and modulated owing to changes in the aspect-ratio for TM-polarization. With this study, we aim to map the impact of varying the aspect-ratio on the overall optical properties of the nanowire medium and provide a reliable insight in how it affects usefulness in practical applications, as environmental and biochemical nano-optical sensors.

REFERENCES

1. Bozhevolnyi, S. I., *Plasmonic Nanoguides and Circuits*, Pan Stanford Publishing, Singapore, 2009.
2. Pendry, J. B., "Negative refraction makes a perfect lens," *Physical Review Letters*, Vol. 85, No. 18, 3966–3969, 2000.
3. Lu, W. T. and S. Sridhar, "Superlens imaging theory for anisotropic nanostructured metamaterials with broadband all-angle negative refraction," *Physical Review B*, Vol. 77, No. 23, 1–4, 2008.
4. Kneipp, K., H. Kneipp, I. Itzkan, R. Dasari, and M. Feld, "Surface-enhanced Raman scaterring and biophysics," *Journal of Physics: Condensed Matter*, Vol. 14, N. 18, 597–624, 2002.
5. Maier, S. A., *Plasmonics – Fundamentals and Applications*, Springer, United Kingdom, 2007.

6. Custodio, L. M., C. T. Sousa, J. Ventura, J. M. Teixeira, P. V. S. Marques, and J. P. Araujo, "Birefringence swap at the transition to hyperbolic dispersion in metamaterials, *Physical Review B*, Vol. 85, No. 16, 1–6, 2012.

An Electromagnetic Meta-lens Based on a New SRR Type for Antenna Gain Enhancement

Akram Boubakri and Fethi Choubeni
INNOV'COM Lab, Higher School of Communications, Carthage University, Ariana, Tunisia

Abstract— Meta-lens introduced by J. Pendry on 2000 are lenses based on metamaterials in order to go beyond the diffraction limit and ameliorate the resolution of the structure. Those metamaterials are known to promise subwavelength focusing through negative refraction index and consist an alternative of the ordinary lens and even has the power to focus the evanescent mode waves. Electromagnetic super lens or meta-lens can be realized in the microwave band with a negative index slab made with SRR and wire.

Here, this work is based on the use of meta-lens made with a new SRR type called Diamond SRR which is characterized by a relative bandwidth of about 88.37% which is to the present day the best value in the literature compared to other SRR types. Associated with a rectangular patch antenna working in the X band this meta-lens improve the antenna gain of about 2 dB and the −3 dB aperture of about 20 degree and decrease the backward radiation.

Multifunctionalized Self-supported (Nano) Membranes as Integrated Platform for Plasmonic Metamaterials

Zoran Jakšić[1], **Filip Radovanović**[1], **Aleksandra Nastasović**[2], **and Jovan Matovic**[3]

[1]Centre of Microelectronic Technologies and Single Crystals
Institute of Chemistry, Technology and Metallyrgy, University of Belgrade
Njegoševa 12, Belgrade 11000, Serbia
[2]Centre for Chemistry, Institute of Chemistry, Technology and Metallyrgy
University of Belgrade, Njegoševa 12, Belgrade 11000, Serbia
[3]Institute for Sensor and Actuator Systems, Technical University Vienna
Gusshausstrasse 27-29/366-MST, Vienna A-1040, Austria

Abstract— Plasmonics is a burgeoning field of electromagnetics that ensures electromagnetic fields confinement and manipulation at nanoscale through the use of metal-dielectric nanostructures [1]. Some of its application areas include, e.g., enhanced light trapping in photodetectors or solar cells, photo-assisted catalysis and ultra-sensitive chemical and/or biological sensors. One of the important platforms for plasmonics are freestanding nanomembranes, structures with a thickness below 100 nm and extremely large aspect ratios, often in excess of 1,000,000 [2, 3]. Nanomembranes are electromagnetically symmetrical, support propagation of long-range surface plasmons polaritons and can be used to enhance the design freedom in all of the above quoted application fields. In their basic form nanomembranes are simple and with relatively limited applicability, but their field of use and tailorability can be vastly expanded through nanocompositing [4].

We considered the possibility to fabricate nanomembranes that behave as quasi-2D plasmonic crystals and simultaneously incorporate nanopores with built-in active nanoparticles. To this purpose we combined lamination and inclusion of nanofillers into the membrane host. For the basic material we chose macroporous crosslinked copolymers based on glycidyl methacrylate (GMA). The epoxy group present in GMA molecule is readily transformed into a plethora of various functional groups (e.g., amine, thiol, pyridine, dithiocarbamate) that further serve as affinity enhancers and thus ensure the usability of the plasmonic membranes as pre-concentrators of selected agents. GMA has already been successfully used for enzyme immobilization and heavy and precious metals adsorption [5]. To form GMA-based membranes we used a recently proposed method combining the traditional immersion precipitation with photopolymerization and crosslinking of functional monomers [6] Further functionalization is obtained by in-situ formation of noble metal nanoparticles directly within the GMA host. In this way ultrathin structures with simultaneous plasmonic, adsorbent and catalytic functionality are obtained.

We considered the use of the our structures for plasmonic metamaterial-based chemical sensors [7] where separator, pre-concentrator and ligand are integrated into a single structure with the plasmonic crystal. We also considered the possibility to use our structures for plasmonic enhancement of photocatalytic reactions in microreactors. Our approach gives a highly tailorable element compatible with microelectromechanical systems (MEMS) and readily transferable across platforms.

REFERENCES

1. Barnes, W. L., A. Dereux, and T. W. Ebbesen, "Surface plasmon subwavelength optics," *Nature*, Vol. 424, No. 6950, 824–830, 2003.
2. Jiang, C., S. Markutsya, Y. Pikus, and V. V. Tsukruk, "Freely suspended nanocomposite membranes as highly sensitive sensors," *Nature Mater.*, Vol. 3, No. 10, 721–728, 2004.
3. Jakšić, Z., S. M. Vuković, J. Buha, and J. Matovic, "Nanomembrane-based plasmonics," *J. Nanophotonics*, Vol. 5, 051818.1-20, 2011.
4. Jakšić, Z. and J. Matovic, "Functionalization of artificial freestanding composite nanomembranes," *Materials*, Vol. 3, No. 1, 165–200, 2010.
5. Nastasović, A., Z. Sandić, L. Suručić, D. Maksin, D. Jakovljević, and A. Onjia, "Equilibrium and kinetics study on hexavalent chromium adsorption onto diethylene triamine grafted glycidyl methacrylate based copolymers," *J. Hazard. Mater.*, Vol. 171, 153–159, 2009.

6. Radovanovic, P., M. Kellner, J. Matovic, R. Liska, and T. Koch, "Asymmetric membranes with interpenetrating proton-conducting morphology made by a combination of immersion precipitation and photopolymerization," *J. Memb. Sci.*, Vol. 401, 254–261, 2012.
7. Jakšić, Z., O. Jakšić, Z. Djurić, and C. Kment, "A consideration of the use of metamaterials for sensing applications: Field fluctuations and ultimate performance," *J. Optics A — Pure Appl. Opt.*, Vol. 9, No. 9, S377–S384, 2007.

Automatic Tracking of Bandpass Sampling OFDM Signal in Mobile Environment

Xin Wang and Heung-Gyoon Ryu
Department of Electronic Engineering, Chungbuk National University, Cheongju 361-763, Korea

Abstract— In this paper, a combined OFDM system and bandpass sampling method using Multiple Signal Classification (MUSIC) algorithm for automatic (angle of arrival) AOA tracking is discussed. And we propose a new method that adding (time division multiplexing) TDM with bandpass sampling in the same time to avoid interference due to RF filter characteristics. Also, we consider Doppler effect for the targets' movement in mobile environment and after compensating the Doppler effect with a valid range, the system performances well. Computer simulation results show that the performances of MUSIC spectrum for AOA due to various conditions and demonstrates the accuracy of AOA estimations.

A Reconfigurable Miniaturized Spiral Monopole Antenna for TV White Spaces

M. Y. Abou Shahine[1], **M. Al-Husseini**[2], **Y. Nasser**[1], **K. Y. Kabalan**[1], **and A. El-Hajj**[1]

[1]American University of Beirut, Beirut 1107 2020, Lebanon
[2]Lebanese Center for Studies and Research, Beirut 2030 8303, Lebanon

Abstract— TV white space (TVWS) refers to the unused portions of the spectrum in the TV band, which can be used for new services and applications. TVWS has interesting benefits where radio signals in this part of the spectrum have a very long range and are excellent in building penetration, in addition to that the spectrum is huge, free, unlicensed and globally harmonized.

A reconfigurable miniaturized planar spiral monopole antenna suitable for TVWS applications is presented in this paper. A square spiral monopole antenna is designed on a 105 mm × 40 mm FR4 epoxy substrate of thickness $h = 0.8$ mm and fed by a 2 mm width microstrip line over a partial ground plane. The size of the spiral structure is 50 mm × 30 mm with a width of 1 mm and a gap of 5 mm between the spirals as shown in Fig. 1. The designed antenna operates in the higher part of the UHF band (600–800 MHz) with a gain of 1 dB, which is good given the small size of this antenna. Frequency reconfigurability is obtained by inserting a tunable inductor (Chip Inductor — 0603CT) on the spiral monople as shown in Fig. 1 (red color) and modifying its inductance. The size of the tunable inductor is compatible with the size of the spiral and its inductance ranges between 1 and 56 nH.

Figure 2 shows the reflection coefficient plots for different inductance values. As shown, frequency reconfigurability is achieved and the antenna can operate on different bands in the 600–800 MHz band. These bands range between 15 to 20 MHz which is suitable for TVWS applications. The radiation patterns of this antenna are omni-directional over its bands of operation, as shown in Fig. 3, with almost equal radiation in the H-plane, and radiation with the shape of digit 8 in the E-plane. Detailed and verified results will be included in the full paper.

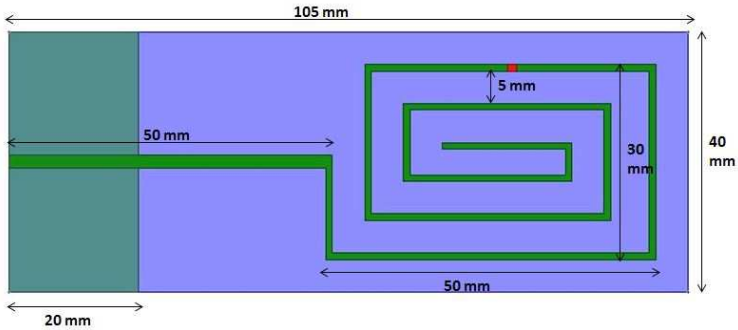

Figure 1: Antenna configuration.

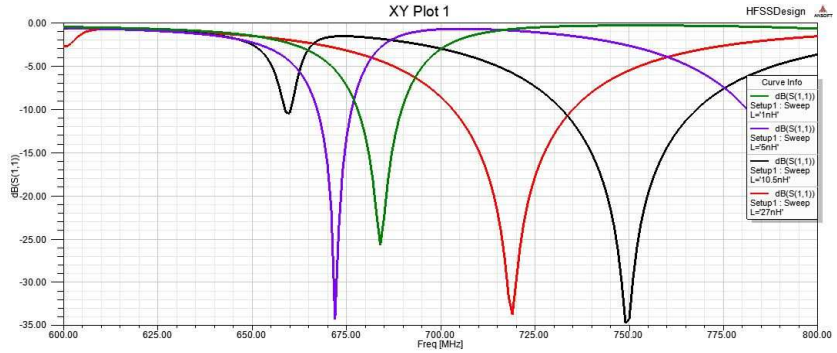

Figure 2: Simulated reflection coefficients for different inductance values.

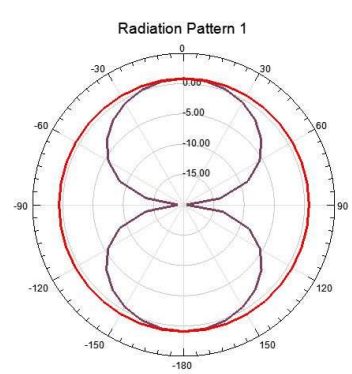

Figure 3: Simulated radiation patterns.

Dual Polarized High Front-to-back Ratio Microstrip Slot Antenna

Mohamed S. El-Gendy, **Haythem H. Abdullah**, **and Esmat A. Abdallah**
Electronics Research Institute, Dokki, Giza, Egypt

Abstract— Due to capacity problems in the conventional GSM 900 band used in mobile phone communication systems and narrow spectral bandwidth, operators had to use additional licenses for multi-bands operating frequency such as DCS 1800 (Digital Cellular system), PCS 1900 (Personal Communications Service), UMTS 2100 (Universal mobile Telecommunication system) in order to overcome these problems. Also, dual feed transceiver systems are facing the problem of poor isolation between the transmitting and the receiving ports. One of the most important parameter is the front-to-back ratio (FBR) which is almost achieved on one band and deteriorates on the other.

A novel dual-band dual-polarized microstrip slot antenna used in mobile base stations is proposed. The antenna supports the operating bands of GSM900 (0.88–0.96) GHz, DCS1800 (1.71–1.88) GHz, PCS1900 (1.85–1.99) GHz, and UMTS2100 (1.92–2.17) GHz in mobile phone base stations. The simulation port isolation between the two ports less than 45 dB overall operating bands. The average front-to-back ratio is 17.15 dB at GSM900, 29.12 dB at DCS1800, 18.47 dB at PCS1900 and 16.03 dB at UMTS2100.

Five layers of FR4 and foam are used to design the antenna. Three layers of FR4 dielectric material with dielectric constant $\varepsilon_r = 4.5$ and height 1.5 mm and two air/foam layers ($\varepsilon_r = 1$). The use of FR4 material is to reduce the cost of the antenna in addition to its rigidity in construction. The two foam layers are placed one between the transmitting feed layer and the FR4 dielectric substrate layer of the first reflector and the second foam layer is placed between the first reflector and the second reflector. Four Teflon (PTFE) spacers at the edges are used in order to fix the five layers of the antenna. The overall antenna dimension is about $300 \times 300 \times 73.175\,\text{mm}^3$.

The dual polarization can be achieved using two orthogonal microstrip feed layers look like the U-shape are placed underneath the FR4 substrate material on the opposite side of the ground plane in order to excite a two orthogonal radiating slots. The ordinary rectangular slot etched on the ground plane doesn't give the performance of the dual band operation used in mobile communication. A novel configuration of step rectangular cross slot etched on the ground plane which acts as a radiating layer is utilized to achieve the dual band operation used in mobile communication bands than rectangular slot.

High front-to-back ratio is obtained at both operating bands utilizing two reflectors underneath the radiating slot. The length of the first square reflector is 0.3 of the wavelength at the lower frequency band 915 MHz, and is placed at quarter waveleng that the upper frequency band apart from the radiating slot at 1940 MHz,which acts as a radiator at the lower band (915 MHz) and as a reflector at the upper frequency band (1940 MHz). The second square reflector is placed at quarter wavelength at the frequency band apart from the radiating slot at 915 MHz.

A prototype of the antenna element with optimized dimensions has been simulated using CST STUDIO SUITE 2012 and fabricated using photolithographic process. Finally, the measured and the simulated results of the proposed antenna are compared. Consistency, between the simulated and measured scattering parameters is observed.

A Proximity-fed Elliptical-shaped Aperture UWB Antenna with Triple Band-rejection Property

Mohamed Mamdouh M. Ali[1], **Ayman Ayd R. Saad**[2], **and Elsayed Esam M. Khaled**[1]

[1]Electrical Engineering Department, Assiut University, Assiut, Egypt
[2]Kosseir Radio, Telecom Egypt, Kosseir 84712, Egypt

Abstract— The ultra-wideband (UWB) communications have drawn much attention since the U.S. Federal Communication Commission authorized, in 2002, the unlicensed use of the UWB with a frequency range of 3.1–10.6 GHz for commercial purposes [1]. As one of the essential components in UWB communication systems, the UWB antenna has been rapidly developed. However, the existence of other wireless narrowband standards that already occupy frequencies in the UWB band, such as wireless local area network, WLAN (5.15–5.35 GHz and 5.725–5.825 GHz) and worldwide interoperability for microwave access, WiMAX (3.3–3.9 GHz), require rejection of certain frequencies within the UWB band. Various solutions have been studied in literature to generate single, dual or even triple frequency band notches, based on embedding resonators into the main body of UWB antenna [2–4].

In this paper, a novel elliptical-shaped aperture UWB antenna with triple band-notched property is proposed. The antenna is compact with size of $22.5 \times 24\,\text{mm}^2$. Matching between a sector-disk patch and the 50 Ohm microstrip line is manipulated through a proximity-feed technique. Double shunt stubs are used to enhance the impedance bandwidth of the antenna. The band notches of WiMAX at 3.6 GHz, lower WLAN of 5.25 GHz and upper WLAN at 5.775 GHz are realized by embedding a reversed F-shaped slot in the patch, a reversed U-shaped slot in the feed line, and adding a parasitic flipped C-shaped strip around the patch, respectively. The antenna is fabricated and the experimental results show that the designed antenna has an impedance bandwidth of 3.2–11.6 GHz for VSWR less than 2, except three frequency stop-bands of 3.20–4.19, 5.02–5.32, and 5.51–6.10 GHz. Moreover, a SPICE-compatible equivalent circuit model of the proposed antenna is obtained using a rational function modeling based Vector Fitting (VF) technique. The validity of the proposed methodology is achieved. The proposed antenna provides almost omnidirectional patterns, relatively flat gain and high radiation efficiency over the entire UWB frequency excluding the rejected bands.

REFERENCES

1. Revision of Part 15 of the *Communication's Rules Regarding Ultra-Wideband Transmission Systems*, ET-Docket 98–153, FCC 02–48, Federal Communications Commission, 2002.
2. Khaled, E. M., A. R. Saad, and D. A. Salem, "A proximity-fed annular slot antenna with different a band-notch manipulations for UWB applications," *Progress In Electromagnetics Research B*, Vol. 37, 289–306, 2012.
3. Li, C. M. and L. H. Ye, "Improved dual band-notched UWB slot antenna with controllable notched band-widths," *Progress In Electromagnetics Research*, Vol. 115, 477–493, 2011.
4. Liao, X. J., H.-C. C. Yang, N. Han, and Yang Li, "Aperture UWB antenna with triple band-notched characteristics," *Electronics Letters*, Vol. 47, No. 2, 77–79, January 2011.

Design and Development of Reconfigurable Microstrip Patch Antenna Using MEMS Switch for Ku-band Application

Prafulla Chandra Prasad and Neela Chattoraj
Department of Electronics and Communication Engineering
Birla Institute of Technology, Mesra, Ranchi, Jharkhand, India

Abstract— Reconfigurable multi-band antennas are attractive for many military and commercial applications where it is required to have a single common antenna that can be dynamically reconfigured to transmit (or receive) on multiple frequency bands. The patch antennas lead to considerable savings in size, weight and cost. They find applications in space based radar, communication satellites, electronic intelligence, and aircraft navigations besides many other communications and sensing applications. The proposed frequency of 15 GHz and 15.65 GHz belong to 14.4 to 15.35 GHz and 15.63 to 15.7 GHz band respectively with application in Fixed Satellite Service (FSS), Mobile Satellite Communication (Up-Link), Space research and Aeronautical Navigation.

The design of printed microstrip antenna is reported in Ku-Band for wireless applications in this paper. The planar, very small, thin antenna with coaxial probe feed of 50 Ω is first realized at 15 GHz on a PTFE substrate having a dielectric constant of 2.5 and a substrate thickness of 1.6 mm to achieve impedance bandwidth of more than 2 GHz as shown in Fig. 2. Simulations have been carried out with the Ansoft HFSS 13 to determine antenna's performance like Return Loss, Impedance matching, Bandwidth (VSWR < 2), Gain (6 dB) and Radiation patterns.

On moving towards reconfigurability, the structure under investigation is shown in Fig. 1. The schematic structure consist of two patches, one is driving patch of dimension $5 * 5.7\,\mathrm{mm}^2$ and another defined as wing patch of dimension $5 * 1\,\mathrm{mm}^2$ separated by 1 mm. MEMS (Micro electro Mechanical System) switch as contact is applied between the gap and it changes the antenna topology structure with RF switch. When the switch closes, the wing patch is coupled with main patch by an inductance. When the switch opens, the wing patch is coupled with main patch by a

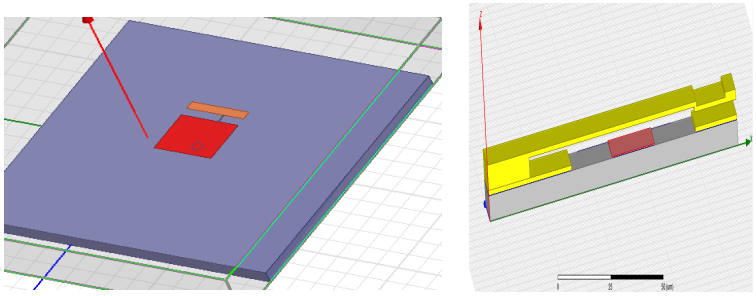

Figure 1: Proposed antenna & MEMS switch.

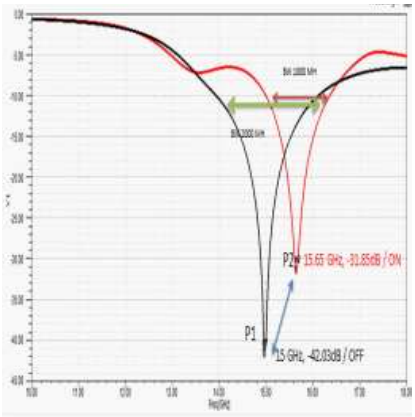

Figure 2: Return loss.

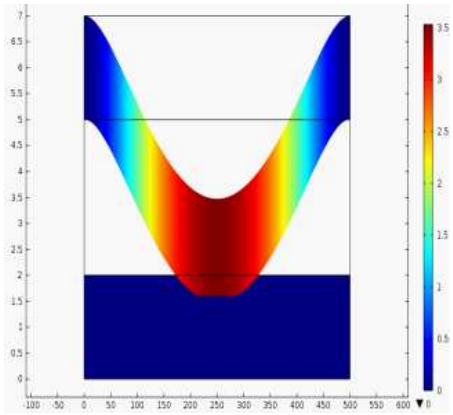

Figure 3: Beam deflection.

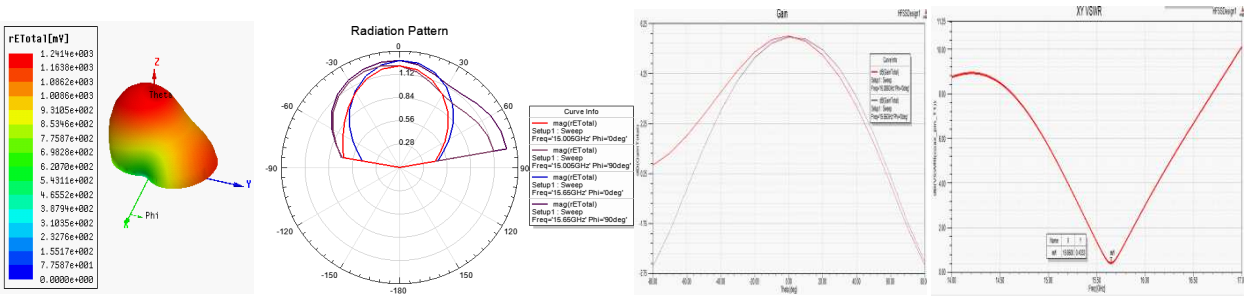

Figure 4: 3D radiation pattern, 2D pattern, gain (6.3) and VSWR (0.4) at two frequencies.

capacitance. The simulation results show that the antenna can change the work frequency from 15 GHz to 15.65 GHz in Ku band with the switch. Mechanical deflection of beam is realized by Comsol multiphysics in Fig. 3.

Wideband Patch Antenna for X-band Applications

A. Harrabi[1], **T. Razban**[2], **Y. Mahe**[3], **L. Osman**[4], **and A. Gharsallah**[1]

[1]Faculty of Sciences of Tunis, Tunisia
[2]LUNAM, IETR UMR 6164, France
[3]Polytech'Nantes, Nantes, France
[4]Higher School of Communication of Tunis, Tunisia

Abstract— Many systems impose strong constraints in terms of bandwidth. The most common techniques used to achieve a typical bandwidth of 20% are based on the alignment or the superposition of several different levels of dielectric and resonators. The first solution leads to a relatively large size of the element. The second solution is limited by the resonant frequency. In fact, the increasing frequency implies that the technological constraints on the alignment of the different layers become drastic. In this article, the design of a broadband planar antenna operating in X-band is presented.

In a given technology, the bandwidth is generally determined by the thickness, the dielectric substrate as well as the geometry of the antenna. Aiming a bandwidth greater than 20% is not yet possible with a simple rectangular patch antenna. It is then necessary to change the geometry to remove this lock.

The suggested antenna has a polygonal shape with a circular slot and it shows that a bandwidth of 2 GHz has been obtained for a central frequency of 9.75 GHz. In spite of the changing in the antenna geometry its size still small about $0.7\lambda_0 \times 0.7\lambda_0$. The radiation pattern has the same characteristics of the rectangular patch antenna. The article details step by step the design procedure, discusses the results and compares the proposed antenna to a simple rectangular antenna.

A Fractal-based Printed Slot Antenna for Multi-band Wireless Applications

Seevan F. Abdulkareem, **Ali J. Salim**, **Ali I. Hammoodi**, **and Jawad K. Ali**
Microwave Research Group, Department of Electrical Engineering
University of Technology, Iraq

Abstract— Fractal geometries have shown to be attractive for antenna designers because of the unique features they offer. In this paper, a printed fractal based slot antenna has been introduced to be used in multi-band wireless applications. The slot structure of the proposed antenna is of an octagonal shape with a Koch fractal curve of the second iteration is applied on each of its sides. The slot structure has been etched on the ground plane of a substrate with relative permittivity of 4.4 and 1.6 mm thickness. On the reverse side of the substrate, a 50 ohm microstrip line feed has been etched. To enhance the coupling with the slot, the feed line has been loaded with a circular stub with embedded complementary circular split ring resonator. Based on the lowest resonant frequency, it has been found that the largest dimension of the proposed antenna slot structure is less than half the guided wavelength. Parametric study shows that the resulting antenna offers a multi-band behavior with enhanced gain and fractional bandwidths, besides the reasonable radiation characteristics throughout the resonating bands. With appropriate dimension scaling, the proposed antenna could be a suitable candidate for use in a wide variety of multi functions wireless applications.

Picosecond Erbium-doped Fiber Laser Using Carbon Nanotube Coated Abrupt Tapers

Kuan-Hao Lin[1], **Hsiang-Ting Peng**[1], **Tsung-Hsun Yang**[1], **Feng-Zhou Liu**[1], **Nan-Kuang Chen**[1,2], **and Der-Yi Hsu**[3]

[1]Department of Electro-Optical Engineering, National United University, Miaoli 360, Taiwan, R.O.C.
[2]Optoelectronics Research Center, National United University, Miaoli 360, Taiwan, R.O.C.
[3]Hortek Crystal Co., LTD., Hsinchu 300, Taiwan, R.O.C.

Abstract—

Introduction: In the past few years, Single-wall carbon nanotube (SW-CNT) materials have attracted much attention, especially for their applications in fiber lasers [1, 2] and communication [3, 4] and so far. Which is the known as based on saturable absorbers (SAs), several techniques have been proposed to fabricate the optical fiber based CNT-SAs, such as inserting the SW-CNT between two optical fiber connectors [1, 2], depositing the SW-CNTs onto the tapered fibers [5] or D-shaped fibers [6, 7]. For the CNT-SAs mechanism and interaction length has been proposed, CNT are sprayed randomly on either a D-shaped fiber or a tapered fiber that can broaden the propagating mode, and therefore the mode will contact the outside of the optical fiber to interact with the deposited materials by evanescent field. Compare with immediate on the fiber end surface that not easily damaged when light launched into fiber end-faces, still maintain the optical properties. In this work, we introduce a new method that CNT-SAs sprayed on interaction length fiber optic component shorter than before published research, CNT-SAs success sprayed coating on Single mode fiber-28 (SMF-28) with abrupt taper that with CNT-SAs insert into ring cavity erbium-doped fiber lasers (EDFLs).

Experimental Set-up and Measurements: Figure 1(a) shows the experimental setup of our EDFLs, in order to achieve SAs effect was success by inserting an AT-CNT-SAs in the laser cavity. The abrupt tapering technique and employed in laser ring cavity to achieve pulse EDFLs was been demonstrated [8–10]. To fabrication, the unjacketed SMF-28 was heated and stretched using a point hydrogen flame fiber-tapering workstation, the tip portion flame can provide a higher heating temperature and smaller tip flame range to heating fiber, then bi-directionally pulled away to achieve single abrupt taper has uniform tapered length and diameter of 2.59 mm and 57.9 µm are shown in Fig. 1(b). When light signal is split into two parts by the abrupt taper to propagate in the core and the cladding along the same fiber, and abrupt taper region diameter with a suddenly changed profile to break the adiabaticity of power so that evanescent field are quickly leaks out form the core to the cladding. According the physical phenomena, the CNT sprayed on abrupt taper region by sprinkler head, it was fabricated by mixing about 0.05 g CNT in 20 ml 99.5% alcohol and then ultrasonic cleaner for 30 minutes. The superluminescent diodes (SLDs) is launched into the abrupt taper-CNT and the spectral responses recorded by an optical spectrum analyzer (OSA) under the resolution (RES) of 1 nm, as shown in Fig. 1(c). The

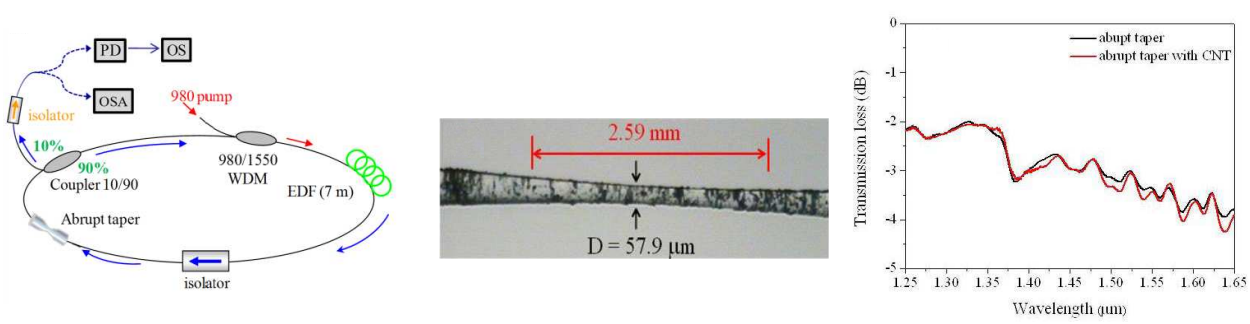

Figure 1: (a) The experimental setup of erbium-doped fiber lasers. WDM: wavelength division multiplexer, OSA: optical spectrum analyzer, EDF: erbium-doped fiber, PD: photo diode, OS: oscilloscope. (b) The device structure of abrupt taper with coating CNT under 200x microscope. (c) The Spectral responses of an abrupt tapered with CNT.

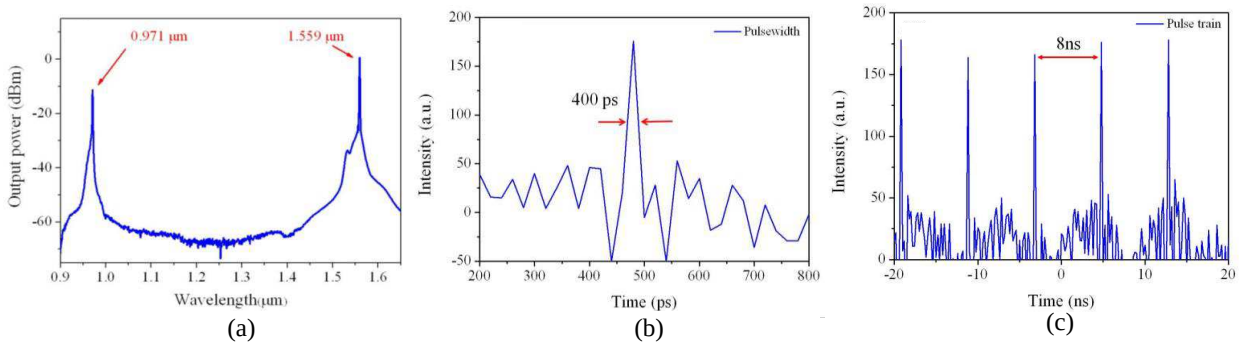

Figure 2: (a) Output laser spectrum of EDFLs. (b) The laser pulsewidth is 400 ps. (c) The pulsed output with pulse train. The repetition rate is 8 ns.

tapering process causing slightly interference when SMF-28 was heated by used hydrogen flame forming core-offset between core and cladding.

The EDFLs composed of 7 m long EDF (POFC EDFH 1090), the laser through coupler, total 10% energy is retrieved for the laser output, other 90% of the energy still propagate into the laser cavity. The laser output has connected OSA and oscilloscope, the photo diode was used to convert laser signals to electrical signals launched into oscilloscope, result shown as Figs. 2(a) and Fig. 2(b). Optical isolator is added to the cavity to ensure feedback laser The output pulse train verifies the pulse formation by our EDFLs with abrupt taper-CNT, the repetition rate is 8 ns, shown as Fig. 2(c).

Conclusion: In conclusion, we have demonstrated picoseconds EDFLs by incorporating an abrupt taper-CNT into the laser ring cavity. This all-fiber scheme is simple, cost-effective.

REFERENCES

1. Nicholson, J. W., R. S. Windeler, and D. J. DiGiovanni, "Optically driven deposition of single-walled carbon-nanotube saturable absorbers on optical fiber end-faces," *Opt. Express*, Vol. 15, 9176–9183, 2007.
2. Zhou, D. P., L. Wei, B. Dong, and W. K. Liu, "Tunable passively Q-switched erbium-doped fiber laser with carbon nanotubes as a saturable absorber," *IEEE Photon. Technol. Lett.*, Vol. 22, 9–11, 2010.
3. Chow, K. K., M. Tsuji, and S. Yamashita, "Single-walled carbon-nanotube-deposited tapered fiber for four-wave mixing based wavelength conversion," *Appl. Phys. Lett.*, Vol. 96, 061104, 2010.
4. Chow, K. K. and S. Yamashita, "Four-wave mixing in a singlewalled carbon-nanotube-deposited D-shaped fiber and its application in tunable wavelength conversion," *Opt. Express*, Vol. 17, 15608–15613, 2009.
5. Kieu, K. and M. Mansuripur, "Femtosecond laser pulse generation with a fiber taper embedded in carbon nanotube/polymer composite," *Opt. Lett.*, Vol. 32, 2242–2244, 2007.
6. Song, Y. W., S. Yamashita, and S. Maruyama, "Single-walled carbon nanotubes for high-energy optical pulse formation," *Appl. Phys. Lett.*, Vol. 92, 021115, 2008.
7. Song, Y. W., S. Yamashita, E. Einarsson, and S. Maruyama, "All-fiber pulsed lasers passively mode locked by transferable vertically aligned carbon nanotube film," *Opt. Lett.*, Vol. 32, 1399–1401, 2007.
8. Chen, N. K. and Z. Z. Feng, "Effect of gain-dependent phase shift for tunable abrupt-tapered Mach-Zehnder interferometers," *Opt. Lett.*, Vol. 35, 2109–2011, 2010.
9. Tian, Z. and S. S.-H. Yam, "In-Line Abrupt Taper Optical Fiber Mach-Zehnder Interferometric Strain Sensor," *IEEE Photon. Technol. Lett.*, Vol. 21, 161–163, 2009.
10. Chen, N. K., Z. Z. Feng, and S. K. Liaw, "All-fiber pulsewidth tunable actively Q-switched erbium fiber laser using abrupt-tapered Mach-Zehnder block filter," *Laser Phys. Lett.*, Vol. 7, 363–366, 2010.

Measurement of Evanescent Optical Force Based on Dual Fiber Sagnac Loop Interferometers

Gia-Ling Cheng[1], **Hsiang-Ting Peng**[1], **Zhao-Ying Chen**[1], **and Nan-Kuang Chen**[1,2]

[1]Department of Electro-Optical Engineering, National United University
Miaoli 360, Taiwan, R.O.C.
[2]Optoelectronics Research Center, National United University, Miaoli 360, Taiwan, R.O.C.

Abstract— We investigate the method of measurement of optical attractive force based on two conjugated fiber micro Sagnac loop interferometers. Each micro Sagnac loop interferometers (SLI) was prepared by using an tightly twist tapered fiber with a tapered diameter of around 2.4 µm. The micro SLI has a total device length of 2.02 mm and a radius of curvature of 35.7 µm when it is made. In general, the fiber evanescent field is strongly exposed to the outside when the fiber is tapered down to a diameter of approaching a wavelength scale. The intensity of the evanescent field drops quickly outward along the radial direction to generate the optical attractive force. The optical attractive force can be strong enough to attractive microparticles surrounding the tapered fiber [1, 2]. Moreover, the Van der Walls force can also be available in the microfiber with a very smooth fiber surface. It would be very interesting if the optical attraction force can be measured. According to the strong exposure of the evanescent field at the bent tapered [3], dual micro Sagnac loop interferometers are employed to detect the optical attractive force. In this work, the singlemode fiber (SMF-28) was heated using micro hydrogen flame and then stretched outward bilaterally until a diameter of 2.36 µm is reached. The tapered fiber was then tightly twisted by two rotators with a distance of about 20 cm in between. Subsequently, the rotators were moved a little bit close to each other, the SLI can thus be achieved. Because the interaction length is long enough so that the power over-coupling can occur for many times. Because of the optical path length difference (OPLD) produced from the two counter-propagating signal passing through the micro loop, it can generate the interferences. Figure 1 shows the experimental set-up of the two micro SLI that are close to each other. The white-light source comprising multiple superluminescent diodes (SLD, 1250–1650 nm) is launched into the SLI B. In measurement, when a 975 nm laser is launched into a the SLI A, the evanescent field will be enhanced at the loop of the SLI. Due to the varying pump power at 975 nm and the small displacement between the two SLI, the spectral responses are changed and recorded by an optical spectrum analyzer (OSA) to investigate the optical attractive force.

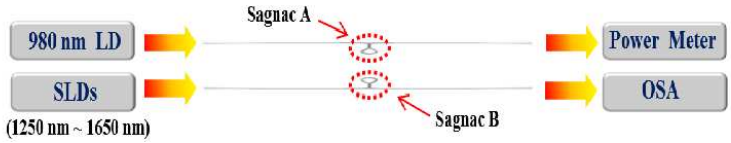

Figure 1: Schematic diagram of the dual Sagnac loop interferometers and experimental set-up for measuring optical attractive force.

(a) (b) (c)

Figure 2: Optical microphotographs of micro Sagnac loop interferometer constructed by tightly twisted tapered fiber under the (a) 50X and (b) 1000X and (c) 1000X CCD microscope.

REFERENCES

1. Brambilla, G., G. Senthil Murugan, J. S. Wilkinson, and D. J. Richardson, *Opt. Lett.*, Vol. 32, 3041–3043, 2007.

2. Lian, Z., P. Horak, X. Feng, L. Xiao, K. Frampton, N. White, J. A. Tucknott, H. Rutt, D. N. Payne, W. Stewart, and W. H. Loh, *Opt. Express*, Vol. 20, 29386, 2012.
3. Carmon, T., S. Y. T. Wang, E. P. Ostby, and K. J. Vahala, *Opt. Express*, Vol. 15, 7677, 2007.

Birefringence in Dispersion-engineered Short-pass Edge Fiber

Yi-Kun Lee[1] and Nan-Kuang Chen[1, 2]

[1]Department of Electro-Optical Engineering, National United University, Miaoli 360, Taiwan, R.O.C.
[2]Optoelectronics Research Center, National United University, Miaoli 360, Taiwan, R.O.C.

Abstract— Dispersion engineering by employing optical liquid surrounding silica tapered fiber has been proposed and used for S-band fiber amplifiers and wavelength/pulsewidth stretchable mode-locked femtosecond fiber lasers [1–3] and supercontinuum generation [4]. However, polarization maintaining is also important and helpful for improving the conversion efficiency for nonlinearity and has not yet discussed. To achieve this goal, a highly birefringence in dispersion-engineered micro-tapered fiber must be substantially introduced. In this work, we demonstrate a polarization dependent single mode fiber (PD-SMF) made by tapering single mode flat clad (SM-FC) fiber. The SM-FC fiber has different cladding diameter in horizontal and vertical axis and they are 125 µm and 80 µm, respectively. A hydrogen flame is used to heat and stretch the SM-FC fiber. When the tapered fiber's diameter along the short axis is down to be about 10 µm, the evanescent field will significantly extend outside the cladding. Under this situation, the effective index along the long and short axis will be different which give rise to birefringence and produce the dispersive evanescent tunneling losses along long and short axes. Fig. 1 shows the experimental set-up for birefringent dispersion engineering in tapered flat-clad fiber. A polarization controller is used to control the state of polarization of input lights. Fig. 2 shows the cross-sectional view of the SM-FC fiber in which the core diameter is 8.5 µm and the diameters of long axis and short axis cladding are 125 µm and 80 µm, respectively. Fig. 3 is the PD-SMF's cross-sectional microphotograph with the long and short axis diameter of 7 µm and 4.5 µm, respectively. The birefringent dispersion engineering is highly promising for applications in nonlinear optics.

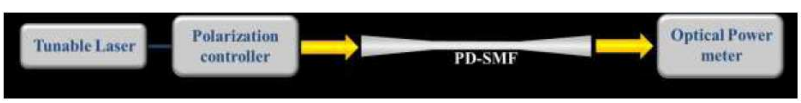

Figure 1: Experimental set-up of the birefringent fiber short-pass filters.

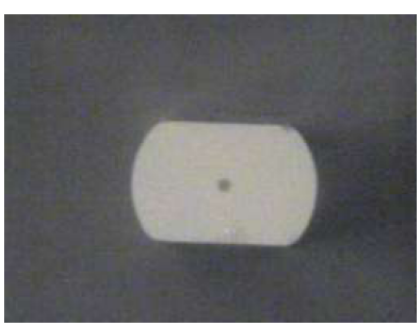

Figure 2: The cross-sectional view of the SM-FC.

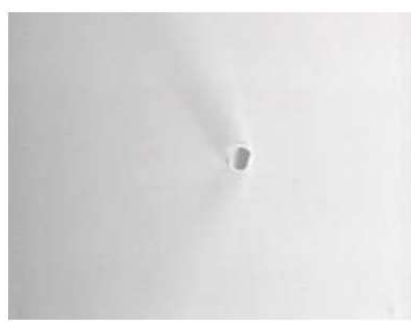

Figure 3: The cross-sectional view of the PD-SMF.

REFERENCES

1. Chen, N. K., K. C. Hsu, S. Chi, and Y. Lai, "Tunable Er^{3+}-doped fiber amplifiers covering S and C + L bands over 1490–1610 nm based on discrete fundamental-mode cutoff filters," *Opt. Lett.*, Vol. 31, 2842–2844, 2006.
2. Chen, N. K., J. W. Lin, F. Z. Liu, and S. K. Liaw, "Wavelength-tunable Er^{3+}-doped fs mode-locked fiber laser using short-pass edge filters," *IEEE Photon. Technol. Lett.*, Vol. 22, 700–702, 2010.
3. Chen, N. K., F. Z. Liu, H. P. Chuang, Y. Lai, S. D. Yang, J. W. Lin, S. K. Liaw, Y. C. Chang, C. B. Huang, and S. Chi, "Highly efficient femtosecond pulse stretching by tailoring cavity dispersion in erbium fiber lasers with an intracavity short-pass edge filter," *Opt. Express*, Vol. 19, 15879–15884, 2011.

Orbital Angular Momentum of Light Generated at the Fiber End

Bin Zhou
Centre for Optical and Electromagnetic Research, South China Academy of Advanced Optoelectronic
South China Normal University, Guangzhou 510006, China

Abstract— The orbital angular momentum of light (OAM) was first realized by Allen et al. in 1992 [1] and has already given rise to many developments in optical manipulation, quantum information processing etc. [2, 3]. In the past two years, the possibility of using the OAM light in optical communication has been demonstrated, as OAM light beams with different order are orthogonal [4]. The research activities nowadays are mainly focused on the free space communication nowadays [4, 5], however it is the fiber communication dominates the market actually. Fiber devices for all fiber OAM communication are needed.

In this paper, an all fiber OAM generator is proposed. We use a serial of ring structures whose width increase with linearly angle (see Fig. 1(a)). Then the effective medium index n_{eff} would be $n_{eff} = 1 + (n-1)\varphi/2\pi$, where n is the reflective index of silica. After an incident light with foundation mode goes through this structure, a vortex beam appears in case the phase delay difference at the angle 0 and 2π is $2\pi l$, where l is the quantum number. A ring fiber which can support the OAM light beams [6] was used to couple the generated OAM beam (see Fig. 2(b)).

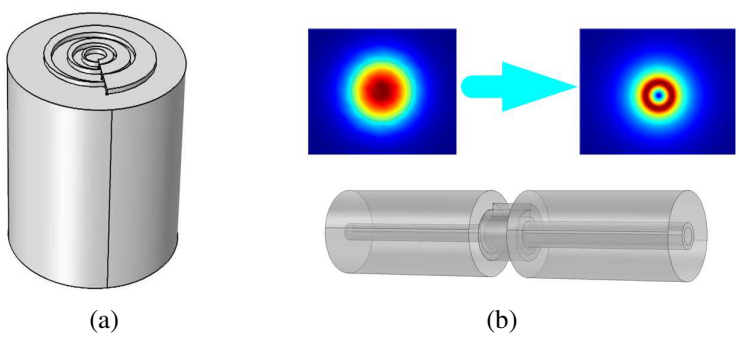

Figure 1: (a) The profile of the OAM generator at the end of a fiber. (b) In fiber OAM mode generating and coupling structure.

REFERENCES

1. Allen, L., et al., *Phys. Rev. A*, Vol. 45, 8185–8189, 1992.
2. Franke-Arnold, S., et al., *Laser Photon. Rev.*, Vol. 2, 299–313, 2008.
3. Yao, A. M., et al., *Adv. Opt. Photon.*, Vol. 3, 161204, 2011.
4. Wang, J., et al., *Nature Photonics*, Vol. 6, 488–496, 2012.
5. Cai, X., et al., *Science*, Vol. 338, No. 6105, 363–36619, 2012.
6. Yue, Y., et al., *IEEE Photonics Journal*, Vol. 4, No. 2, 2012.

Effects of the Length Variations of LYSO and Plastic Optical Fiber on the Energy Spectrum Responses of a Fiber-optic Radiation Sensor

W. J. Yoo[1], K. W. Jang[1], S. H. Shin[1], D. Jeon[1], B. G. Park[2], S. Kim[3], J. H. Moon[4], S. Cho[5], and B. Lee[1]

[1]School of Biomedical Engineering, Research Institute of Biomedical Engineering
Konkuk University, Chungju 380-701, Korea
[2]Department of Energy & Environmental Engineering, College of Engineering
Soonchunhyang University, Asan 336-745, Korea
[3]Department of Nuclear & Energy Engineering, Institute for Nuclear Science & Technology
Jeju National University, Jeju 690-756, Korea
[4]Department of Nuclear & Energy Engineering, College of Energy & Environment
Dongguk University, Gyeongju 780-714, Korea
[5]Department Organic Materials & Fiber Engineering
College of Engineering, Soongsil University, Seoul 156-743, Korea

Abstract— The scintillating fiber-optic radiation sensors (SFORSs) for gamma spectroscopy have thus far not been deployed on a commercial scale due to both their small sensing volume and light attenuation in the optical fiber. The physical properties of sensing element are very important in the scintillation detector and it should be specially considered for SFORS because its sensing size is in a few mm and thus it cannot completely absorb the energy of charged particles. In general, the energy spectroscopy outcome corresponding to various interactions between the gamma-ray and the scintillation material depends on the physical and optical properties of the scintillator including size, density, effective atomic number, peak emission, scintillating light conversion efficiency, and transparency. In order to transmit scintillating light having energy spectrum information, the length of an optical fiber should be also considered.

In this study, we developed a small-sized SFORS having the flexible and insertable characteristics for remote gamma-ray energy spectroscopy in narrow places such as pipes and holes. As a small sensing element of the SFORS, a cerium-doped lutetium yttrium orthosilicate (LYSO) crystal was used considering the many advantages of the LYSO as compared with the other scintillators which were used in the past. Using the fabricated SFORS, we measured the inherent gamma energy spectrum of a Co-60 and then analyzed the effects of the length variations of an LYSO crystal and a plastic optical fiber (POF) on the energy spectrum responses of the SFORS. Based on the results of this study, it is expected that a novel SFORS which has capabilities in real-time and remote measurements can be developed to obtain gamma-ray energy spectra.

A Novel Multipath Limiting Quadrifilar Helix Antenna for Local Area Augmentation System

James A. Quinlan and Daniel N. Aloi
Department of Electrical and Computer Engineering, Oakland University, Rochester, MI, USA

Abstract— This paper describes the design of a Multipath Limiting Antenna (MLA) for use on Global Positioning Systems (GPS) Local Area Augmentation System (LAAS). GPS is a Global Navigation Satellite System (GNSS) operated by the United States Government. GPS satellites broadcast their time and position on Bands L1 and L2; receivers use this information to calculate their position. Well designed receivers can achieve horizontal and vertical accuracy of 3 meters and 5 meters, respectively, 95% of the time. LAAS is an aircraft landing system using Differential GPS (DGPS), in which a reference station broadcasts the difference between the measured satellite pseudoranges and the known fixed position of the receiver antenna. LAAS receivers have accuracy and reliability increases that allow for automated landing of aircraft, if the LAAS reference station meets stringent requirements. A critical requirement is that the LAAS reference antenna is an MLA with a gain pattern that varies little above the horizon and is deeply attenuated below, to reduce the detrimental effects of ground-based multipath.

Several other antennas have been designed for LAAS, usually achieving good performance on the L1 or L2 bands. This new antenna performs well on both L1 and L2, with independent feeds and element arrays that share the same phase center. This independence allows accurate independent tuning of the GPS bands.

Some LAAS antennas are Integrated MLA, integrating separate high azimuth and low azimuth antenna arrays to achieve the necessary gain pattern for MLA definition. This new antenna uses single arrays to achieve its pattern, eliminating extra tuning and bifurcation of the phase center. Also, several LAAS antennas use dipoles or slanted dipoles in a quadrature pattern as some or all of their radiating elements. Dipoles require distance from ground plane object for good performance, forcing their feed systems to be compacted along the support frame for an array. This increases the complexity of their construction. This antenna uses a Quadrifilar Helix Antenna (QHA) as its radiating element. QHA is frequently used for narrow-beam satellite communication and is known for being highly circularly polarized with excellent cross-polarization rejection. The QHA designed in this paper has been modified for wide-beam operation, and for close proximity to ground plane objects. This allows the design and placement of a feed disk underneath each QHA element, simplifying the overall feed system. The feed disks use stripline RF rat-race structures, achieving excellent phase performance, minimal losses, and predictable performance variability.

Accurate, multiband MLAs with simplified construction will allows for proliferation of LAASs and an increase to automated navigation, and the antenna described uniquely meets these qualifications.

A Transfinite Set Theory for Particle-wave Duality, Wave Collapse and Quantum Entanglement

Ji-Huan He[1] **and M. S. Elnaschie**[2]

[1]National Engineering Laboratory for Modern Silk, College of Textile and Clothing Engineering Soochow University, P. O. Box 52, 199 Ren-Ai Road, Suzhou Industrial Park, Suzhou 215123, China
[2]Department of Physics, Alexandria University Alexandria, Egypt

Abstract— We start from K-theory and E-Theory and reason that the Zero set is given by its bi-dimensions $D_o = (o, \phi)$ where $\phi = 2/(\sqrt{5}+1)$ and represents physically the inside of a quantum-like state namely the quantum particle while the Empty set is given by $D_{-1} = (-1, \phi^2)$ and represents the outside of the quantum-like state namely, the quantum wave. It is then evident that any attempt to take measurements will penetrate the outside i.e., the Empty "quantum wave" and cause it to be non-empty. Such change converts the Empty set to a Zero set as manifested in the "processes" of a wave collapse. From these basic principles and based on the Zero measure, Cantorian space time in which D_o and D_{-1} are defined, we reach the conclusion that the maximal generic quantum probability of entanglement between n quantum particles is given by $P = (\phi^n)(\frac{1-\phi}{1+\phi}) = \phi^n\phi^3 = \phi^{n+3}$. For $n = 2$ one finds the celebrated Hardy quantum entanglement of two quantum particles while for $n = o$ we find the intrinsic probability of quantum spacetime which is equal to the dimensionless Unruh temperature. On the other hand when $n = 3$ we have $P = \phi^6$ which is the Imirzi parameter that connects loop quantum gravity and superstring theory. Finally we utilize all the preceding results within the framework of particle-wave duality to derive two energy expressions; one for the quantum particle (the Zero set) and one for the quantum wave (the Empty set) and find that the sum is equal to Einstein's expression where $E = mc^2$ E (Particle) $= (5\phi^2/2)mc^2$ and E (Wave) $= \left|-(5\phi^2/2mc^2\right| = (5\phi^2/2)mc^2$. Thus E (Wave) $= E$ (Dark Energy). In addition the negative sign is the indication of the connection between Dark Energy and Anti-Gravity.

Adapting the New IRI-Plas Model to Satellite Data in the High-latitude Ionosphere

O. A. Maltseva and N. S. Mozhaeva
Institute for Physics Southern Federal University, Stachki, 194, Rostov-on-Don 90, 344090, Russia

Abstract— Empirical models of the ionosphere play an important role in determining the propagation conditions in the near space. The most dynamic is the International Reference Ionosphere (IRI) model because it is constantly modified. A number of studies have shown that the IRI model is a good description of average conditions, not only in the middle-, but also in high-latitude regions. The new IRI-Plas version of it has several advantages: It introduces a new parameter Hsc for the basic topside height, includes plasmaspheric part of the N(h)-profile, and, most importantly, allows the adaptation of the model to experimental values of the total electron content TEC, in addition to experimental values of the critical frequency foF2 and the maximum height hmF2. This allows us to determine model N(h)-profiles for instantaneous conditions. In this paper, the testing of these profiles according to the incoherent scatter radars shows some peculiarities of the correspondence between these profiles. One of them is determined by the fact that the range of the experimental values of the TEC (the values of the global maps JPL, CODE, UPC, ESA are used) is large. This leads to a whole set of N(h)-profiles. To choose a profile that is closest to the experimental one, the IRI-Plas model is adapted to the plasma frequency at the height of CHAMP and DMSP satellites (separately for each satellite and together). This adaptation allows, first, to get the new value of the TEC(fne), in-second, to analyze the behavior of N(h)-profiles during the disturbances. In the first problem, it is obtained, that the values of the TEC(fne) adapted for N(h)-profiles fall in the range of global maps. They are close to the TEC(CODE) for conditions of high solar activity. The second problem includes typical distributions of N(h)-profiles for individual stations and for the latitudinal dependence on the chain of stations Kiruna, Lycksele, Uppsala. For comparison, the chain was added by mid-latitude stations Juliusruh, Rome. Since the feature of high-latitude ionosphere is a higher degree of disturbance than in the middle latitudes, there is no data of foF2 quite often. In these cases, the values of foF2, used for adaptation, were obtained by calculation from the experimental values of the TEC using medians of the ionospheric equivalent thickness τ(med). For three or four flights of satellites in the day over stations, it can be seen what stage of perturbations cover the entire area from high to low latitudes, where the state of the ionosphere is already close to the quite one, where the redistribution of ionization occurs.

Short-temporal Magnetosphere-ionosphere Predictors of Catastrophic Earthquakes

N. P. Sergeenko and A. L. Kharitonov
Pushkov Institute of Terrestrial Magnetizm, Ionosphere and Radiowave Propagation of the Russian Academy of Sciences, Moscow, Russia

Abstract— The analysis of ionosphere-geomagnetic predictors of catastrophic earthquakes is carried out. Files of values of critical frequencies of $F2$ ionosphere layer of a world network of ionosphere stations of vertical sounding f_0F2 were the main source of the information about ionosphere irregularities. It was calculated the relative variation δf_0F2, that excluded regular seasonal and daily variations. For the description of geomagnetic disturbances *Dst,* and AE-indexes were used. *Dst* — the index characterizes occurrence and development of a large-scale planetary geomagnetic storm. For identification of effects of substorms in an ionosphere AE-indexes were used, the indignant periods were considered when $AE > 100\,\mathrm{nT}$. The analysis of data has illustrated formation traveling large-scale irregularities of electronic concentration of the positive sign in the peak of the ionosphere near the epicenter of earthquake and increase of the intensity of anomaly of a local magnetic field. For the first time splashes AE-index characterizing amplitude of the auroral electrojet 15–17 hours prior to the moment of the main push are found out. Existence of this effect on examples of nuclear explosions on various latitudes zones is confirmed.

The analysis spent in this paper has shown that the geophysical chain of the connected short-term semidiurnal harbingers of catastrophic earthquakes in magnetosphere, geomagnetic field and an ionosphere is visible. Tectonic preparation of earthquake can lead to generation magnetosphere substorms (AE-splashes) and to formation in the peak of an ionosphere traveling large-scale irregularities of electronic concentration.

Data of the spent researches concern area of studying short-term magnetosphere-ionosphere harbingers of earthquakes with advance time approximately 10–15 hours. In a combination to other already studied harbingers results of the this paper can be used in algorithms of the geophysical forecast of time and a place of the future earthquake.

Exploring and Exploiting Polarization Properties of Angle Cut Whispering Gallery Resonators

F. Sedlmeir[1,2,3], **M. Hauer**[1],
J. U. Fürst[1,2], **and Harald G. L. Schwefel**[1,2]

[1]Max Planck Institute for the Science of Light, Erlangen 91058, Germany
[2]Institute for Optics, Information and Photonics
University of Erlangen-Nürnberg, Erlangen 91058, Germany
[3]Erlangen Graduate School in Advanced Optical Technologies (SAOT)
Friedrich-Alexander Université Erlangen-Nürnberg, Germany

Abstract— Long photon confinement and high fields densities, both desirable for nonlinear processes, require good optical resonators. Some of the best optical resonators with a small footprint are whispering gallery mode (WGM) resonators. Their principle is based on continuous total internal reflection at the interface of a round dielectric. Currently birefringent WGM resonators are fabricated fully symmetric to their rotational axis. In WGM resonators fabricated from uniaxial crystals this symmetry axis coincides with the optic axis, such that the modes are either parallel (TM) or perpendicular (TE) polarized. Thus nonlinear conversion processes between these polarizations can be phasematched with the help of dispersion. However this type of phasematching is extremly narrowband and needs to be tuned very carefully via temperature.

In a non z-cut resonator, where the optic axis is tilted with respect to the symmetry axis, we expect the extraordinary part of the light to experience a position dependend phase velocity as the angle between the k-vector and the optic axis changes continuously. This enables local phasematching between the two eigenpolarization states for a very broad wavelength regime.

In order to understand the modal structures of such resonators we investigated a slightly birefringent MgF_2 WGM resonator, cut at an angle of 20° with respect to the optic axis. We report on the farfield polarization properties of several modes with different input polarizations depending on the outcoupling position on the resonators rim. We show that this polarization can depend strongly on position and is in general elliptical.

Additionally we investigate an x-cut lithium niobate resonator showing that there is still a strict separation between classical TE and TM modes. The index of refraction of the TM mode (extraordinary polarization) is expected to change during the light travels along the rim as it changes the angle between k-vector and optic axis continuously. This index variation enables a broadbanded phasematching for nonlinear conversion. We show this by pumping the resonator at 1550 nm and measuring a second harmonic output signal. Conversion efficiencies are reported and a qualitative theoretical description will be given.

Compact Low Phase Noise Oscillator Using Symmetrical Square Open-loop with Loaded T-stubs Resonator

S. J. Cho and N. Y. Kim
RFIC Center, Kwangwoon University, 447-1 Wolgye-dong, Nowon-ku, Seoul 139-701, Korea

Abstract— The design of a miniaturized microstrip stubs-loaded square open-loop with asymmetrical feeder lines resonator and its implementation to a microwave oscillator is studied in this paper. The adopted resonator is based on a combination of electric and magnetic couplings in the central open-gaps of the square loop resonators. Moreover, the combined couplings generation electromagnetic (EM) flux between the two square open-loop resonators. The maximum coupling can be obtained by adjusting the open-loop gap, mounting the two open-loop resonators spacing, and the orientation of loaded-stubs inside the loop resonators. The asymmetrical port terminals also help to couple EM energy by maintaining 50 Ω impedance matching with input/output devices. The improved high Q factor characteristics and the higher transmission zero can be obtained high oscillator power and low phase noise characteristics.The resonator performance shows a return loss of −24.8 dB and an insertion loss of −1.6 dB at 6 GHz. In addition, according to design and performance of the resonator, this structure resulted in an optimized oscillator. The oscillator with this proposed resonator shows a good phase noise performance of −104.03 dBc/Hz at a 100 kHz offset from the carrier frequency of 6.2 GHz with an output power of 14.21 dBm.

Miniaturized Dual-band Artificial Magnetic Conductor with Easy Control of Second/First Resonant Frequency Ratio

Son Xuat Ta and Ikmo Park
Department of Electrical and Computer Engineering, Ajou University, Suwon, Korea

Abstract— The artificial magnetic conductor (AMC) surface has been widely used as an artificial ground plane or reflector in many different antenna types to enhance antenna performance while achieving profile miniaturization. An AMC works as a perfect magnetic conductor at resonant frequencies with the 0° phase of the reflected wave when illuminated by a normally incident plane wave. Its bandwidth is defined as the frequency range over which the phase of the reflection coefficient is between ±90° [1].

In many applications, an antenna works at different frequencies simultaneously; consequently, the AMC requires multi-band operation that can match with the antennas working frequencies. Several different AMC structures have been developed for multiband operation. The AMCs implemented with various shapes of patches [2, 3] on a unit cell have been used to achieve dual-band characteristics. However, owing to the lack of miniaturization, most of these AMCs have a large unit-cell size compared with the effective wavelength. Dual-frequency operation can also be achieved using two layers of a square patch with varactor diodes [4] or double patches incorporated with lumped capacitors [5]. However, both techniques increase the complexity and cost of the AMC.

In this paper, a novel miniaturized AMC is proposed for dual-band operation. An AMC unit cell that employs four slots in the metallic patch is used for achieving not only miniaturization but also easy control of the second/first resonant frequency ratio. The second/first resonant frequency ratio can be varied from 1.5 to 3.3 by simply changing the slot shape for a given metallic patch size. A dual-band antenna composed of a wideband monopole suspended over the proposed AMC surface is designed and tested to validate this approach. The measurements result in a satisfactory and good matching condition for the dual-band antenna. Considering its controllable frequency ratio, ease of fabrication, and miniaturized size, the proposed AMC structure has potential for use in dual-band wireless communication.

REFERENCES

1. Clavijo, S., R. E. Diaz, and W. E. McKinzie, "Design methodology for Sievenpiper high-impedance surfaces: An artificial magnetic conductor for positive gain electrically small antennas," *IEEE Transactions on Antennas and Propagations*, Vol. 51, No. 10, 2678–2690, Oct. 2003.
2. Zhu, S. and R. Langley, "Dual-band wearable textile antenna on an EBG substrate," *IEEE Transactions on Antennas and Propagations*, Vol. 57, No. 4, 926–935, Apr. 2009.
3. Mantash, M., M. E. de Cos, A. Tarot, S. Collardey, K. Mahdjoubi, and F. Las-Heras, "Dualband textile hexagonal artificial magnetic conductor for WiFi wearable applications," *Eur. Conf. Antennas Propag. (EUCAP)*, 1395–1398, 2012.
4. Lee, H. J., K. L. Ford, and R. J. Langley, "Dual band tunable EBG," *Electron. Lett.*, Vol. 44, No. 6, 392–393, Mar. 2008.
5. Saad, R. and K. L. Ford, "Miniaturised dual-band artificial magnetic conductor with reduced mutual coupling," *Electron. Lett.*, Vol. 48, No. 8, 425–426, Apr. 2012.

A Wide-stopband EMI Filter for Power-line

Jin-Sup Kim[1], **Se-Hwan Choi**[1], **Sang-Kuk Kim**[2], **Dong-Joon Lim**[2], **and Jong-Kyu Kim**[1]

[1]Wireless Communication Research Center, Korea Electronics Technology Institute, R. O. Korea
[2]Dongil Technology LTD., R. O. Korea

Abstract— EMI (Electromagnetic Interference) filter using feed through capacitors exhibits wide stopband characteristics. This type of EMI filters are used to provide RF isolation between power distribution services and noise sensitive local power distribution systems. This type of EMI filters generally needs a high current capacity and a high insertion loss of 80 dB from 10 MHz to 40 GHz is required. In this paper, the characteristics of the inductor and capacitor at high frequencies are investigated. The prototype filter is implemented and its performance is verified from the measured results. This paper describes the design process and validation of the design by testing using the MIL-STD-220C.

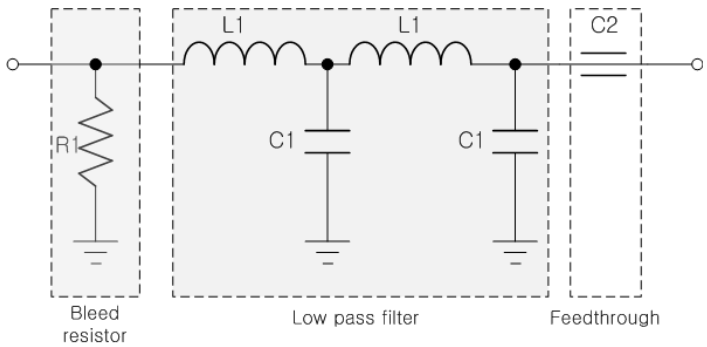

Figure 1: Equivalent circuit of the proposed wide-stopband EMI filter.

A Computational Model of Slim Speaker Using Transmission Line Enclosure Modeling

Jin-Sup Kim[1], **Heung-Euy Kim**[2], **Se-Hwan Choi**[1], **and Yoon-Seok Heo**[3]

[1]Wireless Communication Research Center, Korea Electronics Technology Institute, R. O. Korea
[2]Hanbit T&I., R. O. Korea
[3]Chung Cheong University, R. O. Korea

Abstract— In this paper, we have developed a thin, slim speaker using transmission line model. In order to predict low frequency performance of loudspeakers, the lumped parameter model is useful. However, it doesn't consider enclosure model. This paper discusses a computational model of the vented band-pass enclosure using Backman's low-frequency method for slim speaker enclosure model. Simulation results were compared with experimental results.

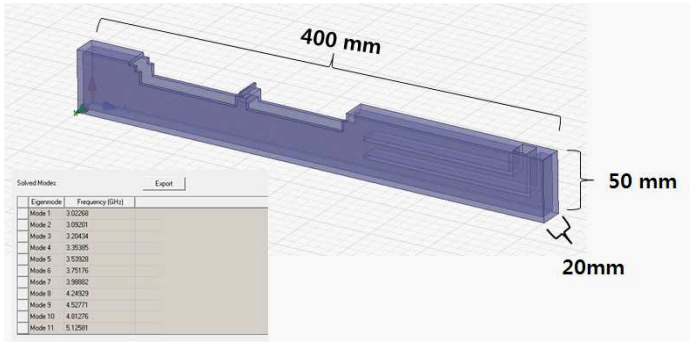

Figure 1: Slim speaker enclosure model for 3-D EM simulation.

A Lumped-element Absorptive Bandstop Filter Topology with Perfect Impedance Matching

K. Lee, T.-H. Lee, Y.-S. Kim, and J. Lee
Department of Computer and Radio Communications Engineering
Korea University, Seoul 136-713, Republic of Korea

Abstract— In these days, bandstop filters have been considered essential parts in microwave engineering because of eliminating jamming, unwanted signals and harmonics of microwave circuits. They also play an important role in concurrent transmission and receiving system. Since recent microwave systems require small-sized components, enormous amount of researches have been devoted to developing small-size bandstop filters. It has been reported that absorptive bandstop filters using low-Q lumped elements are suitable for small-size bandstop filter structures since they can be realized without quarter-wavelength transmission line between resonators. In addition to this, absorptive bandstop filters exhibit good performance with low-Q resonators since they can theoretically have infinite attenuation at the center frequency. Therefore, most of recent studies have focused on absorptive bandstop filters with lumped-elements. However, the conventional lumped-element absorptive bandstop filter does not work with extremely low-Q resonators since it lose the unique characteristic of the absorptive response at the center frequency if the Q-factor is close to 1.

In this paper, a new lumped-element absorptive bandstop filter topology is proposed. The new topology exhibits the absorptive characteristic even though the resonator Q-factor is close to 1. This topology uses one parallel resonator and two series resonators. It can realize good attenuation in spite of using extremely low-Q resonators. In addition, this topology theoretically exhibits the perfect matching over the entire frequency range whereas the conventional absorptive bandstop filter shows perfect matching only at the center frequency. Therefore, it also has superiority in the sense that it can be conveniently cascaded with other 50 Ohm components without any restriction since this topology has perfect matching regardless of Q-factor of each resonator and frequency.

ACKNOWLEDGMENT

This work was supported by the Basic Science Research Program through the National Research Foundation of Korea (NRF) funded by the Ministry of Education, Science, and Technology (2012R1-A1A1004665).

Open Stub Band-pass Filter Using Stepped Impedance Resonator for Size Reduction

K. C. Yoon[1], H. Lee[2], J. G. Lee[2], J. G. Park[2], T. Y. Kim[2], T. S. Jung[2], and J. C. Lee[2]

[1]RFIC Research Center, Kwangwoon University, 447-1 Wolgye-Dong, Nowon-ku, Seoul 139-701, Korea
[2]Department of Radio Science & Engineering, Kwangwoon University
447-1 Wolgye-Dong, Nowon-ku, Seoul 139-701, Korea

Abstract— This paper shows an open-stub narrow band-pass filter using a stepped-impedance-resonator (SIR). A SIR is adopted instead of transmission line to reduce the size of the BPF on the low dielectric substrate. The size of the conventional narrow BPF is reduced by more than 50% of its length of the transmission line within the inverter. The experimental results show that the insertion loss is 0.85 dB, return loss is 20.8 dB, and the fractional bandwidth is 10% at the center frequency of 5.8 GHz. The size of the filter is $12.7 \times 18.56\,\mathrm{mm}^2$.

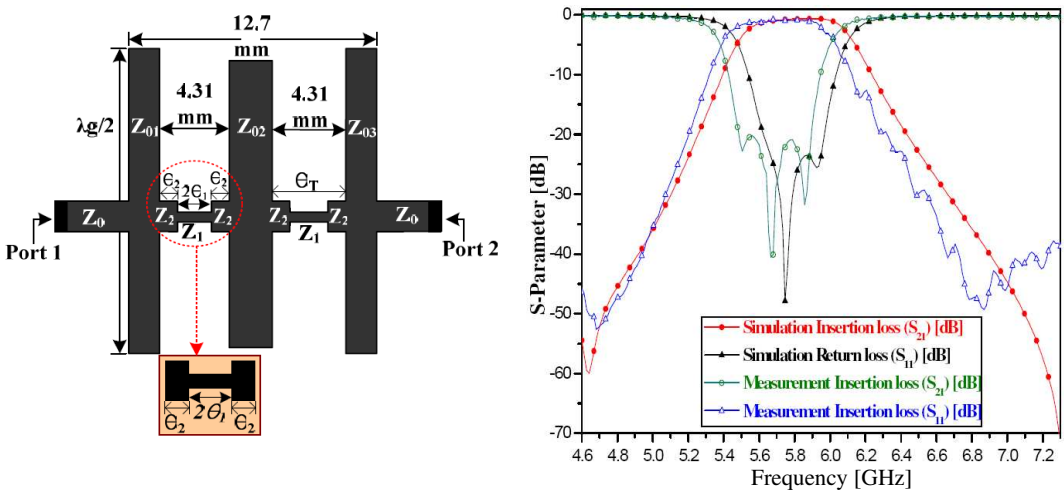

(a) (b)

Figure 1: (a) A proposed open stub BPF using SIR, and (b) simulation and measurement results of a proposed BPF with SIR.

ACKNOWLEDGMENT

This work was supported by the National Research Foundation of Korea (NRF) grant funded by Korea government (MEST) (No. 2011-0029625).

REFERENCES

1. Yoon, K. C. and J. C. Lee, "Design of a 5.8 GHz narrow band-pass filter with second harmonic suppression using the open stubs," *Microwave Optical Technology Lett.*, Vol. 50, No. 7, 1763–1766, Jul. 2008.
2. Zhang, H. and K. J. Chen, "Miniaturized coplanar waveguide bandpass filters using multi-section stepped-impedance resonator," *IEEE Trans. Microwave Theory Tech.*, Vol. 54, No. 3, 1090–1095, Mar. 2006.

Compact Reconfigurable Dual Mode Resonator with Switchable Band Using RF PIN Diodes

Hesham A. Mohamed[1], **Heba B. El-Shaarawy**[2], **Esmat A. Abdallah**[1], **and Hadia El-Hennawy**[3]

[1]Electronics Research Institute, Giza, Egypt
[2]Electronics and Communications Engineering Department, Faculty of Engineering
Cairo University, Giza, Egypt
[3]Electronics and Communications Engineering Department, Faculty of Engineering
Ain Shams University, Cairo, Egypt

Abstract— In modern communication systems, a single filter cannot perform the requisites for all operating bands. The use of multiple filters occupy a large surface area, therefore reconfigurable filter constitute an interesting solution to this problem [1]. Microstrip filters are one of the most important parts of many passive and active microwave and millimeter wave devices employed to suppress the harmonics. Recently, a bandpass filter is reported with good rejection performance [2].

In this paper, a new miniaturized reconfigurable dual-mode stub-loaded resonator, which consists of a microstrip resonator with internal coupled lines and an open-circuited stub is presented. Based on the odd and even-mode equivalent circuits, the resonant characteristics of the proposed microstrip resonator are investigated. RF PIN diode is used to switch the passband between GSM (1.83 GHz) and LTE-7 (2.6 GHz), and when changing the location of diode filter could switch its passband from GSM (1.83 GHz) to UMTS (2.1 GHz) with asymmetric responses. The measured results for asymmetric frequency response has attenuation slope of 46.84 dB/GHz in the lower and 97.14 dB/GHz in the upper transition bands. Measured results on the filter show a very good agreement with the simulations where a 1.83 GHz center frequency with a 280 MHz bandwidth was obtained for the GSM state, and a 2.72 GHz, center frequency with a 144 MHz bandwidth was obtained for the LTE-7 filter state. The above bandpass filter that has one transmission zero and its bandwidth is limited to 18%, is only suitable for narrow-band applications. To overcome this limitation, a defected ground structure (DGS) has been proposed and implemented in the fabrication. The parameters like sharpness factor, bandwidth and two transmission zeros are obtained. The DGS patterned enhanced the performance such as a 3 dB bandwidth reached 63%, insertion loss of −0.5 dB and great sharpness (the transition band between stop-band and pass-band is only 0.048 GHz from 1.7982 GHz to 1.8466 GHz, the transition band between pass-band and stop-band is only 0.0666 GHz from 3.4329 GHz to 3.4995 GHz), and the sharpness is 351 dB/GHz in low frequency edge and 255 dB/GHz in high frequency edge.

This filter has the merit of compact size, wideband and low insertion loss. Switchable filters can reduce the complexity of a system by allowing filter reconfigurability instead of having switched filter banks. The designed and fabricated filter is done on Rogers substrate (RO3010) with thickness of 0.635 mm, relative dielectric constant of 10.2 loss tangent = 0.0023 and the metallization thickness of 0.017 mm and simulated using CST 2011. The overall filter dimension is 26 mm × 15 mm with 75% reduction in size compared to other filters published in literature.

REFERENCES

1. Xiang, Q.-Y., Q.-Y. Feng, and X.-G. Huang, "A novel microstrip bandstop filter and its application to reconfigurable filter," *Journal of Electromagnetic Waves and Applications*, Vol. 26, Nos. 8–9, 1039–1047, 2012.
2. Hua, C., C. Chen, C. Miao, and W. Wu, "Microstrip bandpass filters using dual-mode resonators with internal coupled lines," *Progress In Electromagnetics Research*, Vol. 21, 99–111, 2011.

Lightweight Polypropylene-metal Based Nanocomposites and Their Electromagnetic Shielding Response

Javier Arranz-Andrés[1], **Pilar Marín**[2], **Ana M. Aragón**[2], **and María L. Cerrada**[1]

[1]Instituto de Ciencia y Tecnología de Polímeros (ICTP-CSIC)
Juan de la Cierva 3, Madrid 28006, Spain
[2]Instituto de Magnetismo Aplicado (UCM-ADIF-CSIC)
Departamento de Física de Materiales, UCM, P. O. Box 155, Las Rozas, Madrid 28230, Spain

Abstract— Electromagnetic interference (EMI), is considered a modern environmental pollution that can produces very important adverse effects on electronic equipments, like false operation because of unwanted electromagnetic waves and leakage of information in wireless telecommunications [1] as well as potential biological and health hazards (e.g., cancer) associated with exposure to electromagnetic fields [2].

Dependence of the electromagnetic shielding effectiveness on filler volume fraction has been investigated from attenuation upon reflection measurements over a broad frequency range in hybrids based on Polymer-Metal nanoparticles. The polymer chosen was polypropylene, a commodity polyolefin produced at industrial level due to its applicability in many diverse fields as a result of its attractive physical and mechanical properties, low price, lightweight and easy processability. The metallic components incorporated to infer the basic requirements to promote shielding were different contents of spherical nanoparticles of copper and aluminum with an average diameter of 25 and 18 nm respectively. In spite of the high amount in weight reached of metallic nanoparticles, these are in the final materials homogenously distributed and dispersed in aggregates of small size involving, as average, 3–6 nanoparticles. The main macroscopic properties are maintained or improved in the nanocomposites compared with those exhibited by the pristine polypropylene and significant shielding characteristics are boosted in the hybrids with the highest nanoparticle contents. The results show that these composites can be used as radar attenuating materials to decrease the reflectivity of a metal sheet. An attenuation of 20 dB has been observed in the case of incorporating Cu nanoparticles at 15 Vol.%. This effect is less important in the case of Al nanoparticles addition.

ACKNOWLEDGMENT

Financial support of Ministerio de Ciencia e Innovación, MICINN (project MAT2010-19883) is acknowledged. J. Arranz-Andrés is grateful to the CSIC JAE-Doc Program for the financial support.

REFERENCES

1. Chung, D. D. L., "Materials for electromagnetic interference shielding," *J. Mater. Eng. Perform.*, Vol. 9, 350–354, 2000.
2. Bausch, J., "Study reveals health risks of mobile phones and wireless networks," *Electronic Products*, Vol. 54, 2012.

Optical Control Charge State of Nitrogen Vacancy Defects in Diamond

Xiangdong Chen, **Changling Zou**, **and Fangwen Sun**
Key Lab of Quantum Information, University of Science and Technology of China
Hefei 230026, China

Abstract— The nitrogen vacancy (NV) in diamond is a potential candidate for nanoscale magnetometry, quantum computation and biological label, because of its stable fluorescence and long coherence time of the electronic spin state. Studies showed that the charge state of this defect will be changed by optical excitation. The movement of an electron changes the NV center between negative NV^- and neutral NV^0. This feature can be used for high resolution microscopy, but it also affects the stability of fluorescence and prevents the high fidelity quantum control of NV center. Therefore it is essential to further understand and control the charge state switch of NV center, and improve the proportion of NV^- for broad applications.

In this work, we measured the charge state with different excitation laser wavelengths and powers, and studied the impact of magnetic field. The charge state of NV center is detected through the intensity of fluorescence. As the spectra of NV^- and NV^0 are different, we can selectively detect the fluorescence of NV^-. Then high photon counts come from the negative charge state NV^-. In our results, we found remarkable wavelength and power dependence of the charge state of NV center. The dependence can be explained by the diamond energy band structure and NV energy level. The charge state conversion process was demonstrated to be single-photon process with short wavelength, in contrast to two-photon process with long wavelength. Further more, it found that the charge state conversion rates of two-photon process is affected by the magnetic field. This effect is resulted from the electron spin mixing with perpendicular magnetic. The population of negative NV^- is increase with the magnetic field. As the negative NV^- is the one with interest features, the results would help to improve the fidelity of quantum computation and magnetometry.

REFERENCES

1. Wildanger, D., J. R. Maze, and S. W. Hell, "Diffraction unlimited all-optical recording of electron spin resonances," *Phys. Rev. Lett.*, Vol. 107, 017601, 2011.
2. Aslam, N., G. Waldherr, P. Neumann, F. Jelezko, and J. Wrachtrup, "Photo induced ionization dynamics of the nitrogen vacancy defect in diamond investigated by single shot charge state detection," *New J. Phys.*, Vol. 15, 013064, 2013.
3. Beha, K., A. Batalov, N. B. Manson, R. Bratschitsch, and A. Leitenstorfer, "Optimum photoluminescence excitation and recharging cycle of single nitrogen-vacancy centers in ultrapure diamond," *Phys. Rev. Lett.*, Vol. 109, 097404, 2012.

Electromagnetic Field as Human Health Risk Factor: EMF Safety Ensuring by Hygienic Standardization

I. V. Bukhtiyarov, **N. B. Rubtsova**, **Yu. P. Paltsev**, **L. V. Pokhodzey**, **and S. Yu. Perov**
Federal State Budgetary Institution 'Research Institute of Occupational Health' under the Russian Academy of Medical Sciences, Moscow, Russian Federation

Abstract— Human health electromagnetic safety is the problem of compartability.

Electromagnetic fields (EMF) occupational exposure is risk factor of possible long-term effects: early atherosclerosis; coronary heart disease; essential hypertention; cancer (leukemia, brain tumors); congenital malformations; neurodegenerative diseses (Alzheimer's dementia, Parkinson's disease, ALS).

WHO/International Agency for Research on Cancer (IARC) has classified as possibly carcinogenic to humans (Group 2B): extremely low frequency magnetic field as childhood leukemia risk factor; radiofrequency EMF from wireless phone as glioma (a malignant type of brain cancer) risk factor.

Hygienic standards play the leading role in solving EMF safety problem. EMF hygienic standardization in Russia is based on the results of hygienic, clinical-physiological, epidemiological and experimental studies. Hygienic norms are developed for discrete frequency ranges. In Russia there are hygienic standards of occupational exposure of hypo-geomagnetic conditions, static electric and magnetic fields, 50 Hz EMF and radiofrequency EMF (from 10 kHz up to 300 GHz).

The main discrepancy of Russian and international EMF hydienic standardization approaches are in concepts of "cumulative" or "acute" factor effects, correspondingly. Hence EMF hygienic norms in RF are time dependent, comprising a principle "protection by time". The progress in EMF hygienic safety problem solving is time dependent norms for frequencies from 3 Hz up to 10 kHz development, as well as attempt of near zone EMF adequate evaluation (for > 300 MHz frequency range) principles.

Design of an Optimal Multi-layered Electromagnetic Absorber through the Central Force Optimization Algorithm

J. E. González, I. Amaya, and R. Correa
Escuela de Ingenierías Eléctrica, Electrónica y de Telecomunicaciones
Universidad Industrial de Santander, Bucaramanga, Santander, Colombia

Abstract— Electromagnetic absorbers are elements designed to avoid (or at least reduce) reflection of electromagnetic energy in a given frequency band, which could otherwise be harmful to living beings, or simply cause interference with other electronic equipment. Thus, this article presents the results achieved by using a metaheuristic for optimizing their design in the frequency range of wireless communications, i.e., between 0.8 and 1.9 GHz. In this case, the algorithm proposed by Formato in 2007, i.e., Central Force Optimization (CFO), was used. Moreover, the approach laid out by Qubati and Dib in 2010, i.e., acceleration clipping, was also implemented. Results are compared between these two variants, and using different initial distributions (i.e., uniform, mixed, and random). Furthermore, a two-stage process was executed, striving to reduce the number of dimensions of the problem, thus allowing for further optimization. In the first stage of this procedure, all unknowns were considered (i.e., two variables for each layer, each one representing a given material and its thickness), and the algorithm was run 10 times. During the second stage, the materials of the best run were fixed, and the algorithm was also executed 10 times, just that in this case it only had to operate on half of the dimensions (i.e., one for each layer, which represents the fixed material thickness). It was found that, for a three layered electromagnetic absorber, better results than previously reported ones for Particle Swarm Optimization (PSO) and for interval analysis, were possible, though only for the modified CFO algorithm.

Peculiarities of Relativistic TWT Operation near the Cyclotron Resonance

Mikhail I. Fuks[1], **Edl Schamiloglu**[1], **and Yong-Dong Li**[2]

[1]Department of Electrical & Computer Engineering
University of New Mexico, Albuquerque, NM 87131-0001, USA
[2]Xi'an Jiaotong University, Xi'an 710049, China

Abstract— The main obstacle to achieving high amplification in a relativistic traveling wave tube (TWT) is inevitable parasitic feedback attributed to reflections of the operating wave at mismatches in the interaction space. Practically all attempts to weaken this feedback are associated with sectioning the interaction space in order to minimize the electrodynamic coupling between them. For this, reflections from the ends of the slow wave structure (SWS) are reduced, thereby providing the best match to the load. In addition, absorbers or drift channels in which the electromagnetic signal at the operating frequency cannot pass are used. Above all, sections with different azimuthal symmetry are employed. Typically in the last section of the interaction space the input signal is the microwave current of the bunched electron beam that was produced earlier.

An additional means to weaken parasitic feedback is proper choice of the guide magnetic field H where the interaction of a fast cyclotron wave of the undisturbed electron beam with the wave, which is responsible for feedback, results in suppression of this wave. The region of magnetic field where the feedback is suppressed (the so called "region of cyclotron absorption" (RCA)) can be used for amplification of an external signal [1].

This paper describes this phenomenon in detail and is based on particle-in-cell (PIC) simulations using the code MAGIC. For example, for a relativistic X-band TWT with intentionally strong reflections we show that the RCA is significantly reduced and even disappears when the length of the SWS increases, which limits gain. Nevertheless, inside the stationary RCA we demonstrate the possibility of wide band amplification controlled by the value of the magnetic field H.

When we approach the field H from values outside the RCA to its stationary boundaries that represent distinctive thresholds of generation — the increment of increasing oscillations becomes so small that it appears as generation with a delay with respect to the saturation level of oscillations. The closer one is to the RCA, the longer is the delay. In an attempt to identify the stationary RCA boundaries we discontinued PIC simulations when the delays become several μs, much longer than typical pulse durations of applied voltages for relativistic microwave sources. Thus, the experimentally found RCA are significantly wider than the stationary RCA, which motivated its use for amplification. Most often an experimentalist does not know whether or not the feedback is suppressed. Because of this, if during the voltage pulse it appears that there is no generation, the temptation is to use the found RCA in order to amplify an external signal. However, such attempts outside the stationary RCA lead to immediate locked generation. We found that generation can be locked not only using a variable external signal, but also using a video signal when the spectral component of the leading edge at the frequency of free oscillations (Fourier integral from the leading edge over its pulse duration) significantly exceeds the noise level.

In our PIC simulations an external signal was injected by use of a driver with given current density J in the first SWS period at its minimal radius. We measure the input power by integrating $J * E$ over the volume of the driver (here E is the electric field excited by current density J).

REFERENCES

1. Fuks, M. I., M. B. Goykhman, N. F. Kovalev, A. V. Palitsin, and E. Schamiloglu, "Controlled amplification in a TWT using the guide magnetic field," *IEEE Trans. Plasma Sci.*, Vol. 36, 647–654, 2008.

Narrow Bipolar Pulses and Associated Microwave Radiation

M. R. Ahmad[1,3], **M. R. Mohd Esa**[2,3], **and V. Cooray**[3]

[1]FKEKK, Universiti Teknikal Malaysia Melaka, Malaysia
[2]FKE, Universiti Teknologi Malaysia, Malaysia
[3]Department of Engineering Science, Uppsala University, Sweden

Abstract— Narrow Bipolar Pulses (NBPs) is a special type of intra-cloud lightning discharge activities. It is known with other names also such as Narrow Bipolar Events (NBEs), energetic intracloud events, and Compact Intracloud Discharges (CIDs). NBP signatures have been measured by using various methods such as broadband antenna systems, HF-VHF direct measurement systems (filter-detector receiver), and satellitebased systems. To the best of our knowledge, there are no attempts have been made to measure NBP signatures at microwave region so far. In this paper, observations of microwave radiation from thunderstorms have been made during the northeast monsoon season of 2012 in Malaysia. Fast electric field change recording and broadband microwave receiver systems have captured simultaneous records of NBPs electric field change and microwave radiation, respectively. Strong noise-like burst of microwave radiation pulses associated with NBP events were detected. The total duration of the microwave bursts of the pulses is in the range between 2 and 8 µs for both NNBPs and NPBPs. More than 70% of the recorded radiation bursts arrived a few microseconds before the onset of the corresponding NBPs. The analyzed temporal characteristics of the microwave radiation bursts for both NNBPs and NPBPs are similar and indistinctive. In contrast, the analyzed NNBPs and NPBPs temporal characteristics are distinctive to some extent.

Coaxial Reflection Probe for Measurements of Temperature and Frequency Dependent Dielectric-properties of Low-loss Liquids

J. Vrba
Faculty of Biomedical Engineering, Czech Technical University in Prague, Czech Republic

Abstract— Results of laboratory and field tests have shown that the high-power MW-field-induced separation of Oil and Water (O-W) emulsions has a potential to become [1] a chemical-free alternative to conventional separation processes. The separation mechanism of this process has not been fully understood yet and there is a need for further research. In the separation mechanism temperature and frequency dependent dielectric properties of the two main emulsion components, of water and oil, play an important role. While the temperature and frequency dependent model of dielectric properties of water already exists [2], a lack of in professional literature published dielectric properties of oils was found out.

An existing measurement coaxial reflection probe [3] suitable for measurements of frequency dependent dielectric properties of low-loss liquids was adapted here. Both probes consist mainly of a coaxial transmission-line section filled with the measured liquid and short circuited at one end. Instead of the evaluation of dielectric properties of the Liquid Under Test (LUT) for every frequency point, the general model of dielectric properties of liquids, the Cole-Cole model [4] consisting of four real parameters, was used and these parameters were extracted directly.

A number of modifications made here led to an improved measurement performance in terms of significantly easier evaluation of LUT dielectric properties as well as easier probe handling. The probe was manufactured and the type A evaluations of the uncertainties were performed. Measurements of different liquids with known dielectric properties, so called standard liquids were performed as well. A comparison of the here evaluated values of dielectric properties of the standard liquids with data published in professional literature verified here presented probe geometry and measurement procedure.

Furthermore, the probe was equipped here with a heat exchanger. Therefore, it is possible to measure dielectric properties of LUT at different temperatures. This new feature of the probe was tested and verified for temperatures in the temperature range from 10 to 70°C. Dielectric properties of sunflower and olive oil were measured in temperature and frequency range from 10 to 70°C and from 1 to 3000 MHz, respectively and corresponding empirical temperature and frequency models were created.

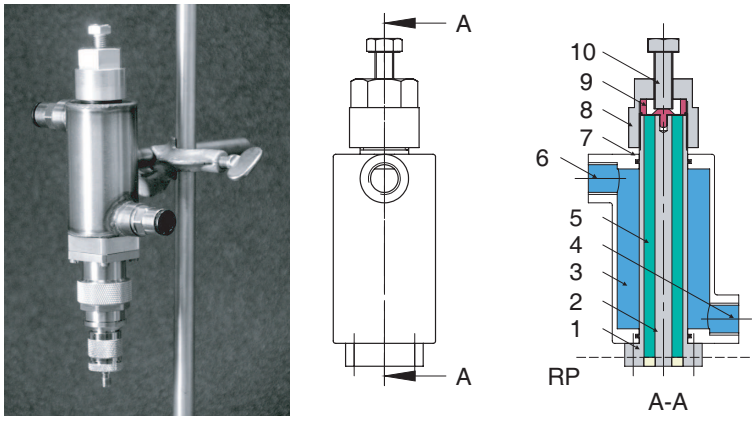

(a) (b)

Figure 1: (a) Picture of the probe with the heat exchanger. During the measurement, the probe was equipped with a thermal insulation, which is omitted here in order to show the probe's geometry. (b) A simplified technical drawing and a section of the measurement probe with the heat exchanger. (1) and (2) are the outer and the inner conductor of the coaxial probe, respectively, (3) water, (4) water inlet, (5) LUT, (6) water outlet, (7) heat exchanger, (8) nut, (9) short-circuit, (10) bolt. Thermal insulation is omitted here in order to simplify the picture.

REFERENCES

1. Hubrich, M., B. Schmidt, M. Kozariszczuk, A. John, R. H. Jansen, J. Vrba, and J. Wellenbuescher, "Ecologically friendly microwave treatment of oil emulsions as contribution to conserving resources by effluent free manufacture in industry," Project No. 01RI0616B, Tech. Rep. No. 4.61.163, VDEh-Betriebsforschungsinstitut GmbH (BFI), VDEh-Betriebsforschungsinstitut, Sohnstr. 65, Duesseldorf 40237, June 2010.
2. Ellison, W. J., "Permittivity of pure water, at standard atmospheric pressure, over the frequency range 0–25 THz and the temperature range 0–100°C," *Journal of Physical and Chemical Reference Data*, Vol. 36, No. 1, 1–18, 2007.
3. Cataldo, A., E. Piuzzi, G. Cannazza, and E. De Benedetto, "Dielectric spectroscopy of liquids through a combined approach: Evaluation of the metrological performance and feasibility study on vegetable oils," *IEEE Sensors Journal*, Vol. 9, No. 10, 1226–1233, 2009.
4. Cole, K. S. and R. H. Cole, "Dispersion and absorption in dielectrics i. Alternating current characteristics," *The Journal of Chemical Physics*, Vol. 9, No. 4, 341, 1941.

Design of Stripline Kicker for Tune Measurements in the MAX IV 3 GeV Ring

D. Olsson
MAX IV Laboratory, Lund University, Sweden

Abstract— The MAX IV laboratory will be a national synchrotron light source with two electron storage rings. The larger 3 GeV ring will have a circumference of 528 m, and the smaller 1.5 GeV ring a circumference of 96 m. The *betatron tune*, Q in a ring is defined as the number of betatron oscillations during one revolution. If Q is an integer or a simple fraction, there is a risk of resonant growth in the beam. Therefore, the ring lattice is tuned to avoid that. During commissioning and routine operation of the rings, the ability to measure Q is important. In both rings, the electron beam is excited by one traveling wave stripline kicker fed by RF. The beam oscillations are then monitored by a close by located button *beam position monitor*, BPM. However, the possibility of using the stripline kickers as BPMs in normal operation is also considered. The two rings will have different vacuum chambers, so different stripline designs have to be developed. Stripline kickers with four electrodes are considered since they allow beam excitation both in vertical and horizontal direction independently of each other. Parameters such as wake impedance and heat loading must be kept at an acceptable level, while the striplines have to be matched to the line impedance. The effective kick and field homogeneity should also be maximized.

In this paper, the design of the kicker for tune measurements in the 3 GeV ring is reported. Numerical tools such as COMSOL Multiphysics and CST Particle Studio have been used to verify the design.

Compact Microstrip Patch Antenna for Ultra-wideband Applications

W. Mazhar[1, 2], M. A. Tarar[2], F. A. Tahir[2], Shan Ullah[2], and F. A. Bhatti[1]

[1]Military College of Signals (MCS)-Rawalpindi
National University of Sciences and Technology (NUST), Islamabad, Pakistan
[2]School of Electrical Engineering and Computer Science (SEECS)
National University of Sciences and Technology (NUST), Islamabad, Pakistan

Abstract— In this paper a novel design of compact microstrip UWB antenna with step impedance microstrip line is proposed. The antenna consists of a rectangular patch with slits on the top face and a partial ground with slots at the rear end. The antenna with dimension of 34 mm × 36 mm ($L \times W$) is fabricated on FR-4 epoxy dielectric with relative permittivity of 4.4. The designed antenna has the capability of operating between 3 GHz to 10.26 GHz with a 7.26 GHz bandwidth ($f_h - f_l$). The proposed antenna has Omni-directional radiation pattern on most of the operating band. Radiation pattern is measured in antenna anechoic chamber. Feed line used has characteristic impedance of 50 Ω. The proposed antenna is anaylzed in both frequency and time domain to check its appropriateness for UWB applications. SMA female connector is used for feeding. Antenna parameters such as return loss and radiation pattern show reasonable agreement with the simulated results.

Self-similarity in pSi Multilayer Structures

D. S. Díaz-Guerrero, L. M. Gaggero-Sager, and A. D. Ariza-Flores
Universidad Autonoma del Estado de Morelos, Mexico

Abstract— Porous silicon is a promising material due to its versatility in the variation of refractive index. It also has the advantages that it is not to expensive to produce in the laboratory. The usual systems considered using pSi are of the periodic type, e.g., supelattices, Bragg, etc..

Other kind of systems, such as the Cantor-like multilayer structures, has been studied in the past. In those systems it has been found traces of scaling properties, in the reflectance curves, between different generations of the system. Nevertheless, a true self-similarity has not been achieved yet. Hence it worth to explore another type of multilayer systems.

In this work, we calculate the reflectance curves for a multilayer system based on a previous one, which we called the Gaggero-Pujals system. This is a variant of the usual Cantor-like construction as in it one uses the Cantor set complement and also scales the refractive index of the new layers. The reflectance curves obtained shows a complex structure, part of which is repeated in a self-similar fashion for higher frequencies.

This self-similar structure is analyzed in order to find the scaling factor and other possible symmetry transformations. It is found that the transformation is indeed a translation mixed with a scaling in frequency. It is also found that the these properties appears in different generations of the system, giving the possibility of a more reach scaling transformation. This is compared with previous findings for related systems with the purpose of stress the differences between Cantor-like and the Gaggero-Pujals systems.

A Theoretical Investigation of the Influence of Underground Power Cable Parameters on Magnetic Field Levels

Ivan Rostovskiy[1], **Oleksandr Okun**[1], **Sergii Shevchenko**[1], **and Leena Korpinen**[2]

[1]Department of Electrical Energy, National Technical University "Kharkiv Polytechnic Institute"
Kharkiv, Ukraine
[2]Department of Electronics and Communications Engineering, Tampere University of Technology
Tampere, Finland

Abstract— High voltage power objects, such as substations, cables, and overhead transmission lines, are sources of low frequency magnetic fields. They cover major populated areas. In recent years, revised regulations limiting magnetic field levels in Ukraine have been introduced. Therefore, our group has previously considered magnetic field levels generated by high voltage power substations and power lines. The aim of this study is to investigate the influence of construction-based and grounding system parameters of underground three-phase power cables on magnetic flux density levels at 0.5 m above the surface of the ground. In Ukraine, several types of grounding methods are used: grounding at the start and the end point of cables, grounding at the start or the end point, and without grounding at the ends. It is calculated that the last two grounding systems are the worst in terms of the magnetic field levels due to the absence of induced current in a shield. Values of induced currents in a shield of a cable could reach values that are close to values in a core. Therefore, it is possible to decrease magnetic field levels above cables by increasing the currents in the shield. It will be presented in an example of computation of 6–10 kV cables that current increase could be performed by varying the cable parameters, such as the distance between phases and a cross-section of the shield. It is noted that the currents in the shield lead to losses of energy and reduce cable lifetime. Thus, it is finally recommended to augment currents in a shield only at places where magnetic fields of power cables reach the regulation limits and are located in proximity to populated objects and areas.

On Double Scattering in Lidar Sounding of the Atmosphere with Simple Non-spherical Particles

Piero Bruscaglioni
University of Florence, Italy

Abstract— In the lidar sounding of clouds and fogs multiple scattering is widely dealt with. The cases of non-spherical particles, e.g., ice crystals, have also dealt with, in the cases of random orientation of the particle axes. For Monte Carlo procedures the Mueller matrices can be developed, with their dependence on the angle incidence-scattering directions. In these cases the extinction coefficient of the medium can be independent of radiation polarization. In case of non-spherical particles with non-random axes orientation the extinction cross section of a particle depends on the orientation and the polarization of the incident radiation. However, it is well known that even in this case one can define a couple of **polarization modes** for which the medium extinction coefficient maintains during the radiation propagation in a certain direction. These modes can be derived from the characteristics of the particles and their orientation. If one wants to follow the trajectories, as in Monte Carlo codes, one should divide each of them into two modes of polarization, and follow each trajectory until a further scattering point is found via the opportune probability law for distance, different for each mode. Then Monte Carlo procedures can become cumbersome. However, the case of double scattering can be dealt with correctly by geometrical considerations in simple cases of a homogeneous medium with uniform density. This was made for spherical particles and results positively compared with Monte Carlo results (Refs. [1–3]) . The overall geometry of the broken trajectories can be maintained for non-spherical particles by, however, doubling the trajectories at each partial tract, according to the relevant polarization modes. As for spherical particles (Ref. [3]) each trajectory from the starting point, the first scattering, the second scattering and the receiver is determined by geometrical considerations and the chosen time length. The attenuation of the path is determined by the extinction coefficients of the medium for each considered mode at each path step. In the procedure of Ref. [3], dealing with spherical particles, a double integration was needed with respect to angles of scattering and positions of first scattering point. For non-spherical particles the actual contribution to the received power depends on the direction of the starting direction. In the non-spherical case a further angular variable is needed, together with an angular integration with respect to the symmetry axis of the considered beam. The paper would present the relevant mathematics, and possibly a series of numerical results for very simple small particles.

REFERENCES

1. Bruscaglioni, P., "Simple way of introducing the optical theorem for non-spherical particles," *Il. Nuovo. Cimento.*, Vol. 30C, 647–651, 2007.
2. Bruscaglioni, P., A. Ismaelli, and G. Zaccanti, "Testing of a Monte Carlo procedure for evaluating multiple-scattering effects on lidar returns from clouds," *Il. Nuovo. Cimento.*, Vol. 21, 393–402, 1998.
3. Bruscaglioni, P., "On the contribution of double scattering to lidar rerturns from clouds," *Opt. Commun.*, Vol. 27, 9–12, 1978.

Analysis of Metallic Terahertz Structures Using FDTD Method

J. Sosa-Pedroza[1], **M. Rodríguez**[1], **M. Galaz**[1], **M. Enciso-Aguilar**[1], **and M. Benavides-Cruz**[2]

[1]Instituto Politécnico Nacional, Escuela Superior de Ingeniería Mecánica y Eléctrica
Unidad Profesional Adolfo López Mateos, Edificio Z-4 3er Piso, D.F. 07738, México
[2]Campus Poza Rica, Universidad Veracruzana, Veracruz, México

Abstract— We present in this paper application of the full three dimensional (3D) Finite Difference Time Domain Method to characterize the Electromagnetic propagation on a metallic nanostructure at THz frequencies. Using a frequency dependent dielectric function based on the Lorentz-Drude Model, Maxwell Equations are modified to include for this frequency range. Then, equations are discretized to apply the technique of 3D Finite Difference Time Domain Method to some samples of metallic structures. To consider effects between field and matter we use two concepts to modify Maxwell Equations, Lorentz Force and Drude plasma concept.

Drude model effects, considers free electrons on matter, supposing it as free electron plasma; it is used to predict optical properties of good conductors. If we consider W_p as intra-band transitions plasma frequency, model represents dielectric properties given by:

$$\varepsilon_r(\omega) = 1 - \frac{\Omega_p^2}{\omega^2 - j\omega\gamma} \tag{1}$$

Furthermore, as electrons have an intra-band oscillation, they produce a polarization density current $\mathbf{J}_{p,k}$, leading to equation:

$$\frac{d}{dt}\mathbf{J}_{p,k} = \varepsilon_0 f_k \omega_p^2 \mathbf{E} - \omega_{0k}^2 \mathbf{P}_k - \gamma_k \mathbf{J}_{p,k} \tag{2}$$

Equation (7) modifies Maxwell equations as:

$$\nabla \times \mathbf{E} = \mu \frac{\partial \mathbf{H}}{\partial t} \tag{3}$$

$$\nabla \times \mathbf{H} = \varepsilon \frac{\partial \mathbf{E}}{\partial t} + \sum_{k=0}^{K} \mathbf{J}_{p,k} \tag{4}$$

Results: Using (8) and (9) is possible to transform differential into incremental equations, as the FDTD model defines. Figure 1 shows analysis of a gold strip of $12 \times 30\,\mathrm{nm}$, we can see the effect of plane wave impinging on it, producing a charge accumulation in the vector polarization direction, resembling charge and field distribution of a dipole antenna.

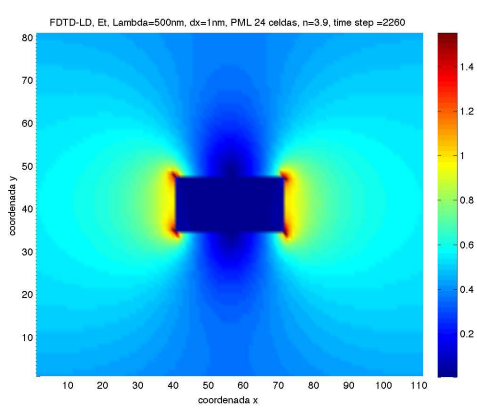

Figure 1.

Possible Methods for Limiting Magnetic Fields outside a High Voltage Power Substation by Changing the Phase Sequence of Busbar Wires

Oleksandr Okun[1], **Sergii Shevchenko**[1], **and Leena Korpinen**[2]

[1]Department of Electrical Energy, National Technical University "Kharkiv Polytechnic Institute"
Kharkiv, Ukraine
[2]Department of Electronics and Communications Engineering, Tampere University of Technology
Tampere, Finland

Abstract— In recent years in Ukraine, active work has been carried out on the revision of the existing magnetic field limits, as specified by Ukrainian regulations. The newly proposed limit will be 0.5 μT, and as such, some power objects may not comply with this limit value. It is known that magnetic field limiting methods related to constructive changes are usually quite expensive. Therefore, of special importance for this purpose, in our opinion, is the changing phase sequence method. The aim of our study is to examine the method for limiting magnetic fields outside high voltage power substation. In general, high voltage power substations are characterized by horizontal multilevel performance of busbar wires with the same phasing in the cells. It is the worst variant in terms of the level of magnetic fields generated outside a power substation. But at the same time, this configuration makes it possible to change the phase sequence of the busbars of neighboring layers and neighboring cells (low and high voltage side of power transformer), which finally facilitates a reduction in magnetic field levels. It is suggested to consider, in the first stage, the given phase-sequence methods on a typical examples of a Ukrainian 110 kV power substation made according to the 'two blocks of line-transformer' scheme in two-dimensional form, taking into account busbar design and mode characteristics. Then, in the final stage, consider the three-dimensional form based on a simulation model with finite element methodology previously used in studying magnetic field distribution at two typical power substations in Ukraine. It is finally shown (and will be presented in the paper) that implementation of the proposed strategies significantly reduces magnetic flux density values outside of the territory of power substations located in populated areas.

FOSLL* Dual Potential Method for Time Harmonic Maxwell's Equations in 3D

J. Kataja
Department of Radio Science and Engineering, Aalto University, Finland

Abstract— The paper studies the first order system LL* (FOSLL*) finite element method for time harmonic Maxwell's equations in three dimensional cavities. Using the FOSLL* approach, a FE (finite element) method to compute the mapping $\hat{\mathbf{n}} \times \mathbf{H} \mapsto \hat{\mathbf{n}} \times \mathbf{E}$ and its inverse is derived. This leads to a finite element method posed in

$$D_E(\Omega) = H^1(\Omega)/\mathbb{C} \times H_{\overset{\circ}{DC}}(\Omega) \times H_{\overset{\circ}{DC}}(\Omega) \times H_0^1(\Omega), \quad \text{or} \tag{1}$$

$$D_M(\Omega) = H_0^1(\Omega) \times H_{\overset{\circ}{DC}}(\Omega) \times H_{\overset{\circ}{DC}}(\Omega) \times H^1(\Omega)/\mathbb{C} \tag{2}$$

where $H_{\overset{\circ}{DC}}$ is the set of L_2 integrable vector fields whose normal component vanishes on the boundary and which have L_2 integrable divergence and curl. Likewise, $H_{\overset{\circ}{DC}}$ consists of L_2 vector fields which have square integrable divergence and curl and whose tangential component vanishes on the boundary.

The method is based on Picard's extended Maxwell system which makes the system automatically stable at static limit. At static limit the usual scalar and vector potentials coincide with the FE solutions but at non-zero frequency the FE solutions cannot be identified with the usual potentials.

The FOSLL* is a least-squares finite element method and thus the derived FE system will always have a positive definite hermitian stiffness matrix allowing one to use conjugate gradient Krylov subspace iteration in a natural manner. More specifically, given an operator equation $LU = f$ in a Hilbert space, the stiffness matrix corresponds with the bilinear form $(u, v) \mapsto \langle L^*u, L^*v\rangle$ in the discrete subspace, where $\langle\cdot,\cdot\rangle$ is the inner product and L^* is the adjoint of the operator L. The boundary data is given as a natural boundary condition on the right hand side of the variational formulation.

If the domain Ω is convex, nodal vector elements lead to an optimal convergence rates in terms of the mesh parameter h.

REFERENCES

1. Cai, Z., T. A. Manteuffel, S. F. McCormick, and J. Ruge, "First-order system LL* (FOSLL*): Scalar elliptic partial differential equations," *SIAM J. Numer. Anal.*, Vol. 39, No. 4, 1418–1445, 2001.
2. Lee, E. and T. A Manteuffel, "FOSLL* method for the eddy current problem with three-dimensional edge singularities," *SIAM J. Numer. Anal.*, Vol. 45, No. 2, 787–809, 2007.
3. Picard, R., "On the low frequency asymptotics in electromagnetic theory," *J. Reine Angew. Math.*, Vol. 1984, 50–74, 1984.

An Improvement Method of Diversity Effect for the Linear Polarization Diversity by Decreasing the XPD Value

Deock-Ho Ha
Department of Information and Communications Engineering
Pukyong National University, Busan, Korea

Abstract— Generally, it is well known that circular polarization diversity is more effective than that of linear polarization diversity in short range wireless environment. This is because the cross correlation coefficient of circular polarized waves shows extremely small value in short range wireless environment. In this paper, in order to evaluate the diversity effect more accurately, we calculated correlation coefficient considering the XPD value obtained from the measurement data of linear polarized waves. From the measurement analysis using the theoretical formula, it can be also seen that the linear polarization diversity reception scheme to create extremely less XPD value improve the diversity effect as well as circular polarization diversity.

Introduction and Analysis Results: To investigate the diversity effect, the cross correlation coefficient between the two received branch signals has usually been employed. In this paper, in order to predict the diversity effect, we analyzed the correlation coefficient characteristic due to the XPD (Cross Polarization Discrimination) value between the two polarized waves received by polarization diversity model. Especially, in order to evaluate the diversity effect more accurately, we calculated correlation coefficient considering the XPD value obtained from the measurement data of 5.9 GHz frequency band based on WAVE (Wireless Access in Vehicular Environments).

In this paper, in order to evaluate the diversity effect more accurately, we calculated correlation coefficients considering the XPD value obtained from the measurement data. From the analysis results, the diversity effect of circular polarization diversity is better than that of the linear polarization diversity. Otherwise, in the case of conventional linear polarization diversity, it was also seen that an optimum reception scheme to create extremely low XPD value can improve the diversity effect as well as circular polarization diversity.

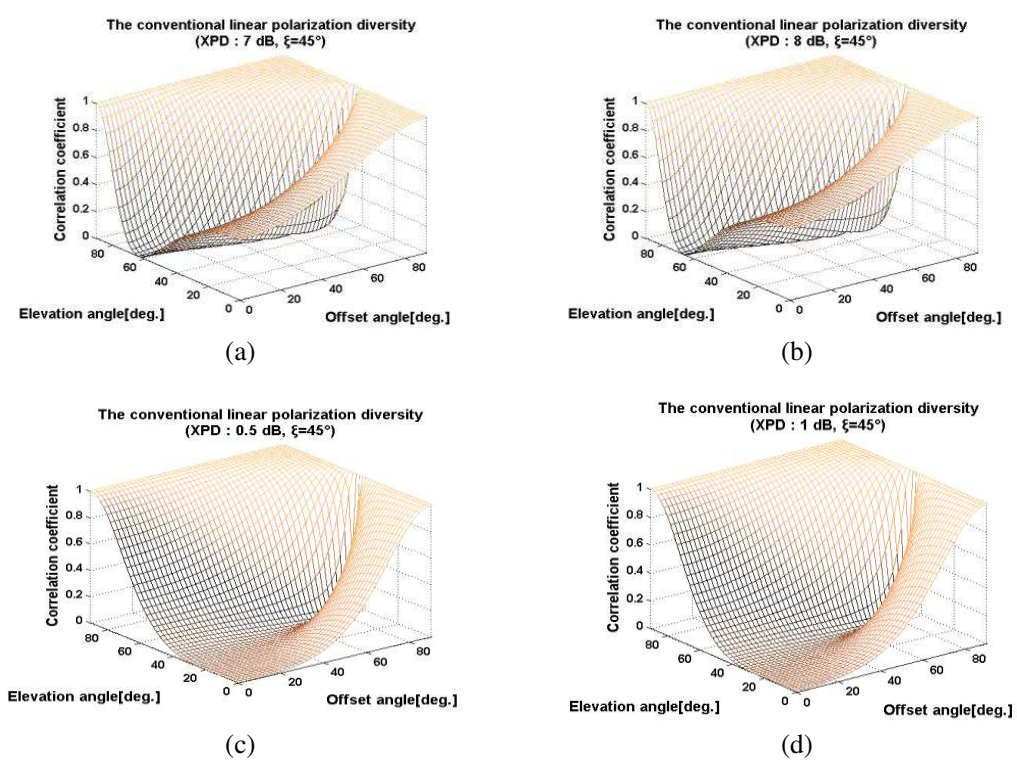

Figure 1: Correlation coefficients for the linear polarization diversity. (a) Real measured XPD value (7.0 dB), (b) real measured XPD value (8.0 dB), (c) supposed XPD value (0.5 dB), (d) supposed XPD value (1.0 dB).

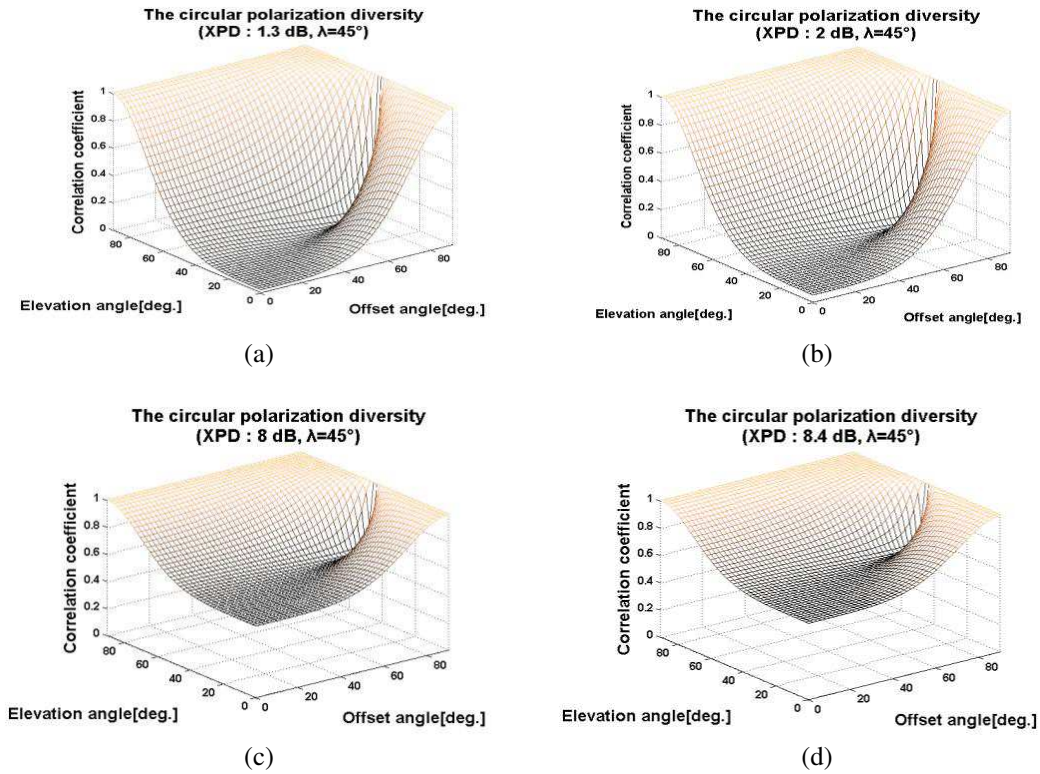

Figure 2: Correlation coefficients for the circular polarization diversity. (a) Real measured XPD valure (1.3 dB), (b) real measured value (2.0 dB), (c) supposed XPD value (8.0 dB), (d) supposed XPD value (8.4 dB).

Figure 1 and Figure 2 show the comparisons of two polarization diversity schemes. the correlation coefficient values of the circular polarization diversity as shown in the Figures 1(a), (b), is much lower than that of linear polarization diversity of the Figures 2(a), (b). This is because the XPD value of the circularly polarized wave was also much lower than that of the linearly polarized wave. So it can be inferred that the circular polarization diversity is more effective diversity scheme to reduce multi-path fading in short range wireless propagation environments. It was also seen that the XPD factor should be considered to estimate the diversity effect more accurately.

Meanwhile, we can see another conditions in the Figures 1(c), (d) and Figures 2(c), (d). In these cases, we considered a supposed XPD value which could not be expected the actual XPD value in each real measurement conditions. Namely, it could not be expected a low XPD value of 0.5 and 1.0 dB for the case of the linear polarization diversity reception of the Figures 2(c), (d) as well as high XPD value of 8.0 and 8.4 dB in circular polarization diversity reception of the Figures 1(c), (d). As shown Figures 2(c), (d) for the case of linear polarization diversity, it was also foreseen that an optimum reception scheme to create extremely low XPD value can improve the diversity effect. Because the XPD value could be varied by the reflection characteristic of polarization wave, the linear polarization diversity reception scheme to create extremely low XPD value could improve the diversity effect remarkably as well as circular polarization diversity. This will be the further research subject which will be composed diversity branches.

Consequently, the XPD factor should be considered to estimate the diversity effect more accurately.

A Two-dimension Generalized Electro-magneto-thermo Elastic Diffusion with Thermal Relaxation

Sh. EL. Khader[1] and M. Khedr[2]

[1]Department of Mathematical, Theoretical Physics Atomic Energy Authority, Egypt
[2]Department of Physics, Faculty of Science, Alexandria University, Egypt

Abstract— The present paper is aimed at study the effects of diffusion on thermoelastic interaction in an isotropic, thermally and electrically conducting half-space whose surface is taken to be traction free and subjected to a time dependent thermal shock where there is an initial magnetic field parallel to the bounding plane. The chemical potential is also assumed to be a known function of time on the bounding plane. Laplace and exponential Fourier transform techniques are used to obtain the solution by a direct approach. The solution of the problem in the physical domain is obtained by using a numerical method for the inversion of the Laplace transforms based on Fourier series expansions. The distributions of the temperature, the displacement, the stress and the induced magnetic and electric fields are obtained. The numerical values of these functions are represented graphically.

Numerical Study of Dual-frequency Stacked Annular-ring Microstrip Antenna

A. R. Messai[1], **A. Bourayou**[2], **S. Aris**[1], **and T. Fortaki**[2]

[1]Department of Electronics, Faculty of Sciences Technology
Constantine 1 University, Constantine 25000, Algeria
[2]Electronics Department, Faculty of Technology, Batna University, Batna 05000, Algeria

Abstract— Conventional microstrip antennas, consisting of a single conducting patch on a grounded dielectric substrate, have received much attention in recent years due to their many advantages, including low profile, light weight and easy integration with printed circuits [1]. However, due to their resonant behavior, they radiate efficiently only over a narrow band of frequencies, with bandwidths typically only a few percent. Dualfrequency structures are useful in situations where the antenna is required to operate efficiently at two distinct frequencies. Conventional microstrip antennas do not guarantee this type of operation. A more complex configuration, consisting of two microstrip patches in a stacked configuration, offers performance features that are not usually obtainable from the single-patch single-dielectric configuration. These features include higher gain, wider bandwidth and dual-frequency characteristics [2].

While the rectangular and the circular microstrip patches are probably the most extensively studied patch shapes, the annular ring microstrip patch also deserved special attention, because it can yield a larger bandwidth compared to other conventional microstrip patches by a proper choice of the dimensions of the annular ring patch and the mode of operation.

Owing to the inherent narrow bandwidth of microstrip patch antennas around their operating resonant frequencies, it is important to develop accurate algorithms for the computation of those resonant frequencies [1].

In the current paper, we investigate the dual-frequency behavior of stacked annular-ring microstrip patches fabricated on a two-layered substrate. As in [2] and [3], we consider both the case where the size of the top annular-ring patch is larger than the one of the bottom annular-ring patch and the opposite case. A rigorous analysis is performed using a dyadic Green's function formulation where the mixed boundary value problem is reduced to a set of coupled vector integral equations using the vector Hankel transform. Galerkin's method is employed in the spectral domain to solve the integral equations. The space-domain basis functions are chosen to be the TM current modes of the two magnetic-wall annular ring cavities. The calculated results are compared with experimental data and shown to be in excellent agreement. Finally, it is important to note that from the different executions of the developed program, it is found that the two constitutive resonators of the stacked structure, which determine the dual-frequency behavior of the microstrip antenna, depend on the relative sizes of the annular-ring patches. This result is in accordance with that discovered theoretically for stacked rectangular patches [2].

REFERENCES

1. Fortaki, T., L. Djouane, F. Chebbara, and A. Benghalia, "Radiation of rectangular microstrip patch antenna covered with a dielectric layer," *International Journal of Electronics*, Vol. 95, No. 9, 989–998, 2008.
2. Fortaki, T., L. Djouane, F. Chebbara, and A. Benghalia, "On the dual-frequency behavior of stacked microstrip patches," *IEEE Antennas and Wireless Propagation Letters*, Vol. 7, 310–313, 2008.
3. Benkouda, S., M. Amir, T. Fortaki, and A. Benghalia, "Dual-frequency behaviour of stacked high Tc superconducting microstrip patches," *Journal of Infrared, Millimeter, and Terahertz Waves*, Vol. 32, 1350–1366, 2011.

Analysis of Electromagnetic Shielding Effectiveness by the Change in the Distance of the Antenna

Jeong-Ju Bang[1], **Ho-Je Kang**[1], **Chang-Su Huh**[1], **Woo-Chul Park**[2], **and Sun-Mook Hwang**[3]

[1]INHA University, Korea
[2]Korea Testing & Research Institute, Korea
[3]Hanwha Corporation, Korea

Abstract— Electromagnetic shielding effectiveness of HEMP protection facility is very important. Some standard for the HEMP facilities were established to test them correct method. There are MIL-STD-188-125-1 and IEEE-STD-299 of the method for measuring the shielding effectiveness of facilities. Transmit antenna is placed outside the facility in se test. However, standard SE test is impossible if space for installing the transmission antenna is small. In this study, we suggested improved SE measurement method based on the actual experimental results.

SVM Approach for Hyperspectral Images Classification

Karim Saheb Ettabaa[1,2], **Med Ali Hamdi**[3], **Imed Riadh Farah**[1,2], **and Basel Solaiman**[2]

[1]Laboratoire de Recherche en Informatique Arabisée, et Documentique Intégrée (R.I.AD.I)
Ecole Nationale des Sciences de l'Informatique, Campus Universitaire de Manouba
Manouba, Tunis 2010, Tunisie
[2]Télécom Bretagne, Laboratoire ITI, Technopôle Brest Iroise CS 83818, Brest Cedex 29238, France
[3]Laboratoires Des Systèmes et Traitement du Signal, Ecole Nationale d'lngenieurs de Tunis, Tunisia

Abstract— Analyzing rapidly and automatically multi-temporal hyperspectral remotely sensed imagery is widespread interest in several applications as land cover mapping, flood monitoring and surface deformation. Hyperspectral images are rich in information. Indeed, hyperspectral imaging sensors measure the energy of the received light in hundreds of narrow spectral bands in each spatial position in the image. Thus, every pixel can be represented as a high-dimensional vector of reflectance of the material in this pixel across the wavelength dimension, this spectral information is called the spectral signature of the material. The high number of spectral bands acquired by hyperspectral sensors increases the capability to identify the different objects represented in the image.

In this research, we tried to classify a series of multi-temporal hyperspectral images of "hyperion". In this case,the problem of spectral variation over the time occurs, in fact, many researches proved that the spectral information is unstable over the time, it is affected by several phenomenon such as weather and climatic effects. So two images taken on the same area but at different times and under different conditions can lead to different spectral signatures for the same objects which leads to a false interpretation, analysis or classification.

Most classification methods process each pixel alone without taking into account the spatial and temporal correlation between images acquired at different dates. So the use of standard classifiers, such as neural networks and "Maximum likelihood" algorithm, can't improve their performance in terms of accuracy and precision.

To solve the problem of the spectral variation over the time in multi-temporal hyperspectral images classification, we propose a classification system based on the use of Support Vector Machines (SVM). It is a multi-class classification system each class present a material and each material is submitted by m spectral signatures registered in m different times. So we tried to train the classifier by the use of many spectral signatures registered in different times for each class. Therefore, the classifier can take into consideration the variation of spectral information over the time.

To implement this system, we are in front of a multiclass SVM problem. Indeed, SVMs were originally designed for binary classification, after, it has been extended for multiclass classification. In fact, there are two types of approaches for multiclass SVM, "one against all" strategy and "one against one". To select the adequate strategy, we tried to apply this two methods and to choose the most efficient. We tried also to use different SVM kernel functions (Linear kernel, Polynomial kernel, Radial Basis Function kernel).

The experimental results proves that the classification system ensures the best overall accuracy when we used "one against all" multiclass SVM approach with RBF kernel.

Despite the presence of spectral variation over the time problem, the proposed system allows to have significant classification accuracies for each class (varied between 90% and 100%). So we can note that this system can solve this problem in the multi-temporal hyperspectral images classification.

Analysis of Multisection Rectangular Waveguide Impedance Transformers

Debendra Kumar Panda[1], **Sanjay Chouhan**[1], **and Ajay Chakraborty**[2]

[1]Jawaharlal Institute of Technology
Borawan, Kasrawad, Khargone, Madhya Pradesh 451228, India
[2]BIT Mesra, India

Abstract— A method of moment based analysis of multisection waveguide impedance transformer has been presented using multiple cavity modeling technique (MCMT). Every discontinuity is modeled with a cavity. Several cavities are formed to describe the whole structure. The analyzed waveguide structure has good agreement with the MCMT and CST microwave studio simulated data. Previously MCMT has been applied to analyze the single and double section impedance transformers. The author try to describe, the methodology applied to analyze these structures are well suited to analyze other structures also, which can minimize time and manpower by adopting the cumbersome hit and trial methods.

In this paper, MCMT is used to analyze multisection waveguide impedance transformer. The technique involves in replacing all the apertures and discontinuities of the waveguide structures, with equivalent magnetic current densities so that the given structures can be analyzed using only magnetic field integral equation. This methodology has been used to examine the result of three and four section impedance transformers which increases the no of junctions from 3 to 4 and 5.

Arndt, Tucholke and Wriedthave given data for multi-section double plane step transformers between X, Ku, K and Ka band waveguides. All the same dimensions are considered in this paper. Matlab codes has been written to analyze these structures. MCMT data obtained for the magnitude of reflection coefficient from the present theory have been compared with CST Microwave Studio simulated data for three and four section waveguide impedance transformer from Ku to X, K to Ku and Ka to K band.

The magnitude of reflection coefficient of a three section waveguide impedance transformer from Ku to X band ($15.8 \times 7.9\,\mathrm{mm}^2$ to $22.86 \times 10.16\,\mathrm{mm}^2$) obtained which shows that it is less than 0.04 in frequency span of 10–14 GHz. The magnitude of reflection coefficient of a three section waveguide impedance transformer from K to Ku band shows that it is less than 0.03 in the frequency span of 15–19 GHz. The same for Ka to K band, it is less than 0.08 over a frequency range of 26–36 GHz. The reflection co-efficient for four sections waveguide impedance transformers are also obtained and compared with CST microwave studio data.

REFERENCES

1. Arndt, F., U. Tucholke, and T. Wriedt, "Computer-optimized multi-section transformers between rectangular waveguides of adjacent frequency bands," *IEEE Transactions on Microwave Theory and Techniques*, Vol. 32, No. 11, 1479–1484, November 1984.
2. Panda, D. K. and A. Chakraborty, "Analysis of single section impedance transformer using multiple cavity modeling technique," *2010 International Conference on Communication, Computers and Devices*, Kharagpur, India, December 10–12, 2010.
3. Panda, D. K. and A. Chakraborty, "Analysis of two section impedance transformer using multiple cavity modeling technique," *International Journal of Engineering and Innovative Technology (IJEIT)*, Vol. 2, No. 5, 107–112, November 2012.

A Compact Elliptic Bandpass Filter Using Cross-coupled Miniaturised Hairpin Resonators Packaged by COB Method

C. Wang, Y. Li, and N. Y. Kim
RFIC Center, Kwangwoon University
447-1 Wolgye-dong, Nowon-ku, Seoul 139-701, Korea

Abstract— A compact bandpass filter (BPF) using miniaturized hairpin resonator is presented for X-band radar applications. The proposed BPF is fabricated on a conventional 6-inch GaAs substrate using integrated passive device (IPD) semiconductor fabrication process. A miniaturized hairpin resonator and a COB packaging method are used to reduce the dimensions and improve the performance of the X-band BPF. Good agreement between the simulated and measured responses has been observed, indicating the validity of the circuit and packaging design strategies. The bare-chip measurements reveal an insertion loss of less than 1.4 dB in the 10.7 to 11.7 GHz passband; the passband return loss is better than −20 dB. The measured insertion loss for the COB-packaged BPF is better than 2.3 dB; the passband return loss is better than −14.8 dB. The area covered by the fabricated BPF is only $3.86 \times 2.5\,\mathrm{mm}^2$. The measured responses show that this BPF successfully covers the X-band frequency with a good insertion loss and return loss across the passband. A comparison of X-band BPFs by using different technologies is summarized and demonstrated. To the best of our knowledge, the presented BPF has the best RF performances with the smallest dimension size, compared to the other X-band BPFs in terms of insertion loss, return loss, and dimension as well as transmission zeros. The proposed BPF may be used very efficiently in X-band radio engineering applications.

A Compact Dual-band Bandpass Filter with High-selectivity and Tunable Passband for WiMax and WLAN Applications

C. Wang, Y. Li, and N. Y. Kim
RFIC Lab, Department of Electronic Engineering, College of Electronics and Information Engineering
Kwangwoon University, Nowon-Gu, Seoul 139-701, Republic of Korea

Abstract— A dual-band bandpass filter with compact size and high selective performance is presented using the combination of an embedded double E-type stepped-impedance resonator and open-loop resonators. The proposed dual-band filter has the capability to achieve different passband frequencies, both resonance frequencies can be conveniently and independently controlled without enlarging outline circuit size, and four transmission zeros near the edges of the passband are achieved to obtain a high-level selectivity. A comparison of simulated and measured results verifies the design and shows that two central frequencies of the fabricated filter are located at the desired 2.5 GHz (WiMax application) and 5.4 GHz (WLAN application) with 3 dB fractional bandwidths of 14.0% and 10.3%, respectively. The measured return losses are higher than 20 dB while insertion losses are less than 0.9 dB in each of the two passbands. In this design, the proposed scheme provides sufficient isolation between the two specific passbands, thus each passband can be individually tuned. The embedded structure can further miniaturize the dimensions of the overall structure, furthermore, four transmission zeros are realized near the passband edges which result in a high selectivity level. Good agreement between the simulated and measured results validates the correctness of the proposed design approach. The simple planar structure, compact size, passbands controllability and high selectivity make the proposed BPF attractive for modern wireless communication systems.

Session 3A1
2_FocusSession.SC2: Microwave Metamaterials and Applications 1

Microwave Metamaterial Antennas
Tie Jun Cui, Huifeng Ma, ... 902
Super/Zero Scattering Characteristics of Circular SRR Arrays
Yuan Zhang, Erik Forsberg, Sailing He, ... 903
New Strategies for Designing Broadband Absorber Cloaks in the Microwave Regime Using Transformation Electromagnetics
Raj Mittra, ... 904
Broadband Magnetic Carpet Cloak without Lateral Shift of Scattering Wave
Hongsheng Chen, Su Xu, Runren Zhang, Baile Zhang, Fa-Xin Yu, ... 905
Surface Wave Reflection, Transmission and Scattering from an Impedance Discontinuity
Simon James Berry, S. Horsley, Alastair P. Hibbins, J. Roy Sambles, ... 906
Transparent Metal Film Based on Metamaterials and Slow-light Meta-surface
Qiong He, Shiyi Xiao, Zhengyong Song, Xin Li, Lei Zhou, ... 907
Stability Characterization of Active Artificial Magnetic Conductors
Yifeng Fan, Khalid Z. Rajab, Yang Hao, ... 908
Directivity Enhancement of an X-band Horn Antenna Loaded by a Wire Medium
Antonio Tomaz, Joaquim J. Barroso, Ugur Cem Hasar, Alberto Jose De Faro Orlando, ... 909
Enabling Asymmetric Electromagnetic Wave Propagation with Polarization Dependent Chiral Metamaterials
Yijun Feng, Junming Zhao, Linxiao Wu, Bo Zhu, Ci Huang, Tian Jiang, ... 910
Electric Field Tunable Domain Ferromagnetic Resonances in (111) Yttrium-iron Garnet Films
Maksym A. Popov, Igor V. Zavislyak, Gopalan Srinivasan, ... 911

Microwave Metamaterial Antennas

Tie Jun Cui and Hui Feng Ma
State Key Laboratory of Millimeter Waves, Southeast University, Nanjing 210096, China

Abstract— Metamaterials have attracted great attentions due to their ability to control electromagnetic waves and the unusual properties. This presentation will be focused on the application of metamaterials in microwave antennas, exploring better performance and/or new features of antennas. Three types of metamaterial antennas are presented: zero-index material antennas, small patch antennas for wireless communications, and metamaterial lens antennas.

We propose and experimentally demonstrate two kinds of anisotropic zero-index materials (AZIMs) in the Cartesian and cylindrical coordinates, respectively. The Cartesian AZIMs (such as z component of permittivity or permeability tensor equals zero) are shown to generate perfectly plane waves in the z direction, resulting in high-directivity antennas. We make two-dimensional (2D) and three-dimensional (3D) experiments to verify such new features. On the contrary, the radially AZIMs (radial component of permittivity or permeability tensor in the cylindrical coordinate equals zero) will always produce omnidirectional radiations regardless the numbers and positions of sources inside AZIM. We also show experimentally the powerful ability of AZIM to reach high-efficiency spatial power combination for the omnidirectional radiations. We experimentally demonstrate efficient methods to improve the bandwidth and radiation efficiency of patch antennas and reduce the coupling among patch antenna array using metamaterials, which are important to the wireless communications (e.g., MIMO systems).

We present two kinds of metamaterial lens antennas. First, we demonstrate a series of 3D broadband, low loss, dual polarization, and high-directivity planar lens antennas which are realized using gradient-index metamaterials, which have excellent features and superior performance than traditional antennas (horns or Rotman lenses). Second, we propose and realize a 3D Luneburg lens with flattened focal surface using the transformation optics. The novel 3D lens has great advantages to the conventional uniform-material lens and spherical Luneburg lens with no aberration, zero focal distance, a flattened focal surface, and the ability to form images at extremely large angles. It can be directly used as a high-gain antenna to radiate or receive narrow beams in large scanning angles for dual polarizations.

Super/Zero Scattering Characteristics of Circular SRR Arrays

Yuan Zhang[1], **Erik Forsberg**[2], **and Sailing He**[1, 2, 3]

[1]ZJU-SCNU Joint Research Center of Photonics
South China Normal University, Guangzhou 510006, China
[2]Centre for Optical and Electromagnetic Research
Zhejiang Provincial Key Laboratory for Sensing Technologies
JORCEP [Sino-Sweden Joint Research Center of Photonics]
Zhejiang University, Hangzhou, China
[3]Department of Electromagnetic Engineering, Royal Institute of Technology
Stockholm 100 44, Sweden

Abstract— The past decades have seen a significant development of the fields of metamaterials and plasmonics. The strong interest is motivated by the possibility to control the electromagnetic response that metamaterial patterns or plasmonic structures allow, which promises to have a significant impact in physics, optics and material science. The scattering characteristic of an object is of big importance in many applications and hence the ability to be able to manipulate it is of strong interest. In military applications the desire is often to achieve as small as possible a scattering cross section, e.g., to hide an aircraft from enemy radar, which is the original motivation for metamaterial cloaking. In contrast, other applications benefit from an increased scattering cross section as in the case of some passive RFID tags or metallic nanoparticles in surface-enhanced Raman scattering (SERS) applications. In this paper, we propose and study the scattering characteristic of a circular array of split-ring resonators (SRRs). In this work we propose a circular SRR arrays and study their scattering characteristics. By studying the scattering spectrum, we will show the localized surface plasmons (LSPs) like modes of the proposed structure, which scatters a much larger amount of energy of the incident wave than a dielectric or a PEC structure of same dimensions does. At the same time, at a certain frequency the proposed structure will not scatter any electromagnetic wave at all, acting as a zero scattering object. In addition, we also study the scattering characteristic of a PEC cylinder with spoofed surface which also show the LSPs like resonance at microwave band. We believe that the controllable scattering characteristics that the proposed structure displays may have important applications such as, e.g., a passive RFID tag which needs large scattered field response to an incident wave or for cloaking applications as the structure is able to hide a dielectric target with high refractive index.

New Strategies for Designing Broadband Absorber Cloaks in the Microwave Regime Using Transformation Electromagnetics

Raj Mittra
Penn State University, USA

Abstract— In this presentation we take a fresh look at the problem of designing *thin* cloaks or blankets, which reduce scattering from arbitrary objects over a broad frequency band in the microwave regime, say 2–18 GHz, for arbitrary polarization and incident angles. We present a strategy for addressing this problem which is somewhat different from the traditional approach of "Geometry Modification" via coordinate transformation that forms the basis for the Transformation Optics (TO) paradigm for such designs.

We mention at the outset that we restrict our attention in this presentation to designing blankets using the TO that reduce the scattering cross-section of radar targets, primarily in the reflection region, when the target is interrogated either by a monostatic or bistatic radar. Our objective is to work with realistic materials to design the blanket, those that can be fabricated in the Lab, have small thicknesses, and exhibit very wideband characteristics despite their small thicknesses, in the range of a few millimeters. This is in contrast to the TO-designed "invisible" cloaks that must rely on Metamaterials, since the TO paradigm typically calls for material parameters (relative ε and μ) that are either less than unity, or tend to infinity in certain regions in a manner dictated by the TO paradigm, which make thistype of cloak inherently narrowband as well as extremely polarization-sensitive. We also ensure in our design process that we choose the characteristics of the cloak material such that it can handle incident fields impinging upon the target at an arbitrary angle, and with an arbitrary polarization, as is the case in a real-world scenario. We mention here that such blankets (or cloaks) are not only useful in the context of radar applications, but also in a scenario where a reflector and a monopole (or dipole) antenna share the same platform, and the obstruction caused by the monopole causes the far-end sidelobes of a reflector to rise.

The paper will present a number of examples to illustrate the application of the new strategy for absorber design, alluded to above, and will compare the performances of these absorbers with those of the legacy TO-based designs for cloaks in the microwave regime. The interested reader may find further details in [4].

REFERENCES

1. Leonhardt, U. and T. Tyc, "Broadband invisibility by non-euclidean cloaking," *Science*, Vol. 323, 110–112, 2009.
2. Pendry, J. B., D. Schurig, and D. R. Smith, "Controlling electromagnetic fields," *Science*, Vol. 312, 1780–1782, 2006.
3. Schurig, D., J. J. Mock, B. J. Justice, S. A. Cummer, J. B. Pendry, A. F. Starr, and D. R. Smith, "Metamaterial electromagnetic cloak at microwave frequencies," *Science*, Vol. 314, 977–980, 2006.
4. Mittra, R. and Y. D. Zhou, "Designing cloaks and absorbing blanketsfor scattering reduction using field andimpedance transformation techniques," *Computational Electromagnetics — Recent Advances and Engineering Applications*, R. Mittra, Ed., Springer Verlag, NY, in press.

Broadband Magnetic Carpet Cloak without Lateral Shift of Scattering Wave

Hongsheng Chen[1,2], **Su Xu**[1,2], **Runren Zhang**[1,2], **Baile Zhang**[3,4], **and Faxin Yu**[5]

[1]The Electromagnetics Academy at Zhejiang University
Zhejiang University, Hangzhou 310027, China
[2]Department of Information Science & Electronic Engineering
Zhejiang University, Hangzhou 310027, China
[3]Division of Physics and Applied Physics, School of Physical and Mathematical Sciences
Nanyang Technological University, Singapore 637371, Singapore
[4]Centre for Disruptive Photonic Technologies
Nanyang Technological University, Singapore 637371, Singapore
[5]School of Aeronautics and Astronautics, Zhejiang University, Hangzhou 310027, China

Abstract— Carpet cloaks, or ground-plane cloaks, have attracted wide interests since 2008. Quasi-Conformal Mapping is widely used to design broad band carpet cloak [1]. However, theoretical work showed that Quasi-Conformal Mapping may raise lateral shift of scattering wave, which makes the carpet cloak detectable [2]. Here, we report a broadband magnetic carpet cloak without lateral shift for TE-polarized microwaves. The cloaking behavior is confirmed over a broad bandwidth from 2–7 GHz both in simulation and experiment.

REFERENCES

1. Li, J. and J. B. Pendry, *Phys. Rev. Lett.*, Vol. 101, 2008.
2. Zhang, B., T. Chan, and B.-I. Wu, *Phys. Rev. Lett.*, Vol. 104, 2010.

Surface Wave Reflection, Transmission and Scattering from an Impedance Discontinuity

S. J. Berry, S. Horsley, A. P. Hibbins, J. R. Sambles
University of Exeter, UK

Abstract— The propagation and scattering of electromagnetic surface waves is of significance in a range of applications including radar cross section reduction and low profile antenna design. Any discontinuity on a surface that supports a surface wave will either cause a reflection or scattering into the adjacent medium or it will do both to the incident wave. The strengths of these effects are important to quantify to allow one to establish the correct functionality of surface wave devices. Here we investigate the reflection, transmission and scattering coefficients from the impedance discontinuity from a metallic patch array to the Sievenpiper mushroom array. These two metamaterial surfaces have very different dispersions for the fundamental transverse magnetic (TM) mode. Hence, as a function of frequency, a range of impedance discontinuities between the two surfaces are achievable, providing transmission across the boundary from near 100%, at low frequencies, to 0% above the cutoff frequency of the fundamental TM mode of the Sievenpiper array. The reflection coefficients are determined by measuring the interference between the incident wave and the wave reflected at the discontinuity using a scanning electric field probe and a plane surface wave source. This same system is used to map the electric fields of the scattered wave above the surface and the fields on the transmission side of the discontinuity, to determine both the scattering and transmission coefficients. These results are compared to finite element method modelling. In addition, an analytical expression for these coefficients is presented by using an impedance approximation for each metamaterial.

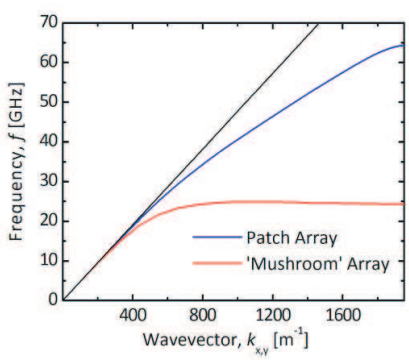

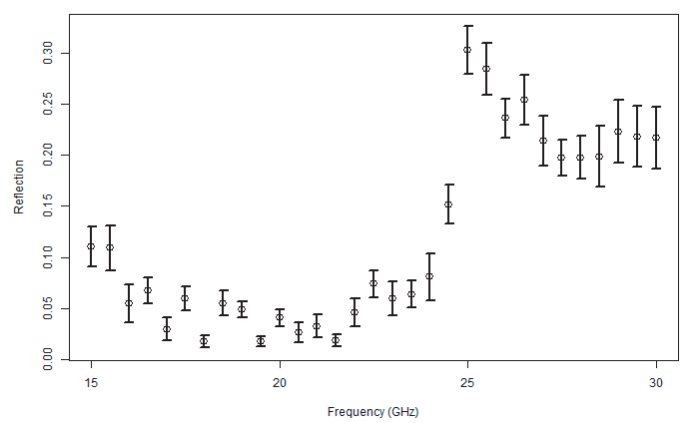

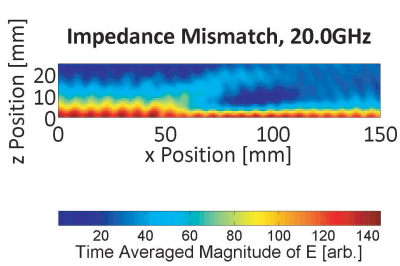

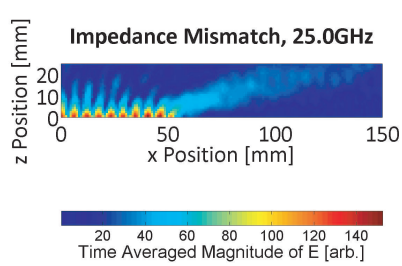

Transparent Metal Film Based on Metamaterials and Slow-light Meta-surface

Qiong He, **Shiyi Xiao**, **Zhengyong Song**, **Xin Li**, **and Lei Zhou**
State Key Laboratory of Surface Physics
and Key Laboratory of Micro and Nano Photonic Structures (Ministry of Education)
Fudan University, Shanghai 200433, China

Abstract— In this presentation, we firstly proposed a scheme to make a continuous metal film transparent in optical regime, with light scattered from the metal film cancelled by those from two composite layers consisting of metallic and dielectric stripes. we found that the entire system have two perfect transmission bands when the geometrical and material parameters satisfy certain conditions (see Fig. 1(b)): the upper high-T band at $P \approx \lambda$. is very narrow, and is easily identified as the SPP-aided EOT; the lower and broader high-T band is governed by the scattering cancellation mechanism (SCM) which can be explained by the mode-expansion theory. The SCM transparency fully retains the conductance of the targeted metal and is robust against incidence angle as well as structural disorders. As a proof of concept, we performed microwave and terahertz experiments [1, 2] to verify all theoretical predictions.

In the second part, we show a photo trapping effect of a designed meta-surface [3], with measured longest trapping time of near 5 ns for a microwave pulse with a center frequency of 5.5 GHz. Such a slow-light effect is governed by the anormalous dispersion and surface plasmon-exciatations, which is more significant in thinner samples owing to stronger hybridizations. The light-matter interactions are remarkably enhanced in such devices, leading to perfect light absorption and enhanced nonlinear harmonic generations, which are demonstrated by microwave experiments and full-wave simulations.

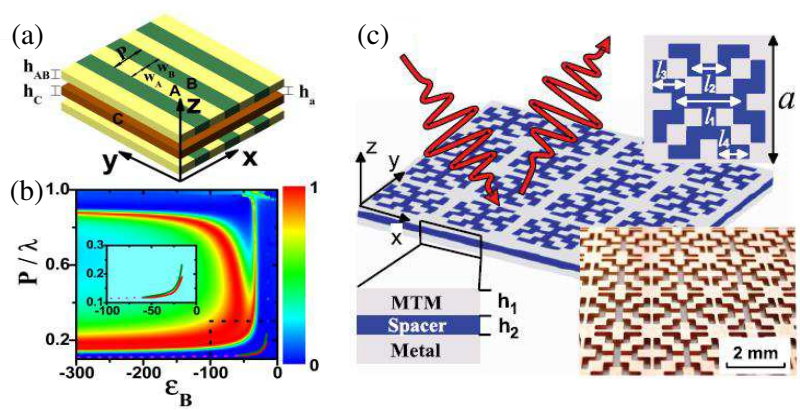

Figure 1: (a) Geometry of the structure studied in this work. (b) FEM calculated transmittance through the structure as functions of ε_B and P/λ. (c) Geometry of the designed slow-light meta-surface.

REFERENCES

1. Song, Z. Y., et al., "Making a continuous metal film transparent via scattering cancellations," *Appl. Phys. Lett.*, Vol. 101, 181110, 2012.
2. Maluream, R., et al., "A new method for obtaining transparent electrodes," *Opt. Express*, Vol. 20, 22770, 2012.
3. Xiao, S. Y., et al., "Enhancement of light-matter interactions in slow-wave metasurfaces," *Phys. Rev. B*, Vol. 85, 085125, 2012.

Stability Characterization of Active Artificial Magnetic Conductors

Yifeng Fan, Khalid Z. Rajab, and Yang Hao
School of Electronic Engineering and Computer Science
Queen Mary University of London, London E1 4NS, United Kingdom

Abstract— Active artificial magnetic conductors (AMCs) loaded with non-Foster elements has been proposed as an effective method to overcome the physical limitations of passive AMC and greatly increase the bandwidth. However, like any other active systems, active AMCs also have disadvantages, one of which is the possibility of instability due to the active incorporations. In this paper, the stability of non-Foster loaded AMCs will be investigated based on the circuit model and the detailed analytical solution will be given as well as the simulations.

Introduction: Artificial magnetic conductor (AMC) is a type of metamaterial that exhibits the performance of perfect magnetic conductors (PMCs) over a limited bandwidth [1, 2]. Possible applications for AMCs include antenna radiation pattern enhancement [3], antenna gain increase [4], and other microwave devices [5, 6].

It is desirable for the AMC bandwidth to be as wide as possible while passive AMCs are physically limited as the upper limit of their bandwidth was derived in Ref. [7]. Although there has been an extensive amount of research to increase the bandwidth of AMCs, active AMCs loaded with non-Foster circuits have been proposed as an effective means to achieve the bandwidth enhancement [8, 9]. However, the stability analysis of active AMCs which is necessary for any active devices has not been given enough attention yet. In this article, the detailed requirements of non-Foster loads for active AMCs with respect to stability are investigated with analytical solutions. Furthermore, a sample active AMC based on the stability design criterion will be provided and verified by full-wave simulations.

REFERENCES

1. Sievenpiper, D., L. Zhang, R. Broas, N. Alexopolous, and E. Yablonovitch, "High-impedance electromagnetic surfaces with a forbidden frequency band," *IEEE Trans. Microw. Theory Tech.*, Vol. 47, No. 11, 2059–2074, 1999.
2. Costa, F., S. Genovesi, and A. Monorchio, "On the bandwidth of high-impedance frequency selective surfaces," *IEEE Antennas Wireless Propag. Lett.*, Vol. 8, 1341–1344, 2009.
3. Huang, Y., A. De, Y. Zhang, T. Sarkar, and J. Carlo, "Enhancement of radiation along the ground plane from a horizontal dipole located close to it," *IEEE Antennas Wireless Propag. Lett.*, Vol. 7, 209–215, 2008.
4. Feresidis, A. P., G. Goussetis, S. Wang, and J. C. Vardaxoglou, "Artificial magnetic conductor surfaces and their application to low-profile high-gain planar antennas," *IEEE Trans. Antennas Propag.*, Vol. 7, 294–297, 2005.
5. Yang, F.-R., K.-P. Ma, Y. Qian, and T. Itoh, "A novel TEM waveguide using uniplanar compact photonic-bandgap (UC-PBG) structure," *IEEE Trans. Microw. Theory Tech.*, Vol. 47, 2092–2098, 1999.
6. Sievenpiper, D. F., J. H. Schaffner, H. Jae Song, R. Y. Loo, and G. Tangonan, "Two-dimensional beam steering using an electrically tunable impedance surface," *IEEE Trans. Antennas Propag.*, Vol. 51, 2713–2722, 2003.
7. Samani, M. F. and R. Safian, "On bandwidth limitation and operating frequency in artificial magnetic conductors," *IEEE Antennas Wireless Propag. Lett.*, Vol. 9, 228–231, 2010.
8. Ding, Y. and V. Fusco, "Loading artificial magnetic conductor and artificial magnetic conductor absorber with negative impedance convertor elements," *Microw. Opt. Tech. Lett.*, Vol. 54, 2111–2114, 2012.
9. Gregoire, D. J., C. R. White, and J. S. Colburn, "Wideband artificial magnetic conductors loaded with non-foster negative inductors," *IEEE Antennas Wireless Propag. Lett.*, Vol. 10, 1586–1589, 2011.

Directivity Enhancement of an X-band Horn Antenna Loaded by a Wire Medium

A. Tomaz[1], **Joaquim J. Barroso**[2], **Ugur C. Hasar**[3], **and Alberto J. Faro Orlando**[1]

[1]Technological Institute of Aeronautics (ITA), São José dos Campos, SP, Brazil
[2]National Institute for Space Research (INPE), São José dos Campos, SP, Brazil
[3]University of Gaziantep, Gaziantep, Turkey

Abstract— With the advent of metamaterials in the 2000s [1], ultra-refractive phenomena provided by wire media have increasingly been used in a variety of applications, including for instance transport of near-field images and directive emission [2]. On the basis of full-wave electromagnetic simulation, the present work reports on a comparative study of the enhanced radiation properties of a commercial X-band horn antenna loaded by a wire medium. Acting as an artificial dielectric the wire medium consists of an array of parallel metallic wires installed into the antenna with the wires oriented in the direction of the electric field. Performance of the original empty horn antenna is then compared with the same antenna when loaded by the artificial structure. A performance comparison of both antennas at 8.87 GHz is presented in Fig. 1(a), where it is clearly apparent that the E-plane radiation pattern for the loaded antenna yields significantly reduced side lobes. In addition, we can see in Fig. 1(b) that the intensity of the radiated electric field is far more concentrated along the antenna axis.

Moreover, the present paper discusses how a periodic array of parallel metallic wires is properly designed so as to enable specific device operation over a usable bandwidth. Construction and implementation details of the periodic array of metallic parallel wires, in addition of functional results of the antennas such as return loss and gain are also given.

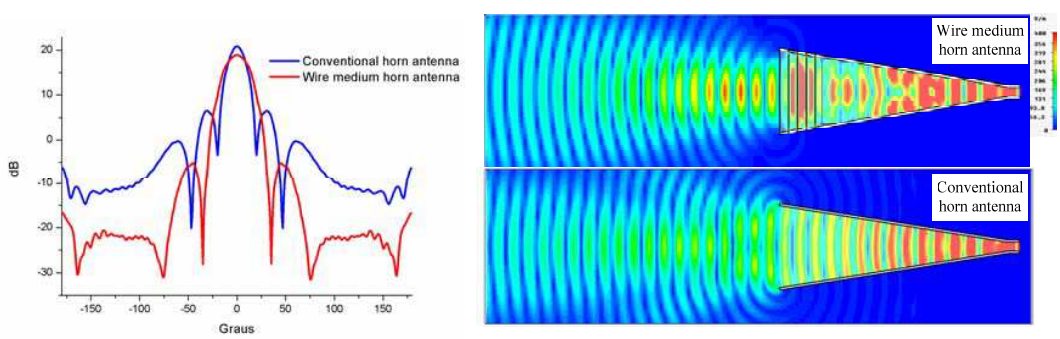

(a) (b)

Figure 1: (a) Radiation patterns and (b) electric field intensities radiated by the conventional and wire-medium loaded antennas at 8.87 GHz.

REFERENCES

1. Chen, H., B.-I. Wu, and J. A. Kong, "Review of electromagnetic theory in left-handed materials," *Journal of Electromagnetic Waves and Applications*, Vol. 20, No. 15, 2137–2151, 2006.
2. Simovski, C. R., P. A. Belov, A. V. Atrashchenko, and Y. S. Kivshar, "Wire metamaterials: Physics and applications," *Adv. Mater.*, Vol. 24, 4229–4248, Aug. 2012.

Enabling Asymmetric Electromagnetic Wave Propagation with Polarization Dependent Chiral Metamaterials

Yijun Feng, Junming Zhao, Linxiao Wu, Bo Zhu, Ci Huang, and Tian Jiang
School of Electronic Science and Engineering, Nanjing University, Nanjing 210093, China

Abstract— Recently, chiral metamaterials, as a kind of artificial structured materials, have been proposed with intriguing property that could be used to achieve many customized functionalities such as the negative refraction and the manipulation of electromagnetic (EM) polarizations. By breaking the mirror symmetry of the chiral structures either in the propagation direction or in the perpendicular plane, these chiral structures could be utilized to manipulate the polarization states of EM waves and have shown novel features, such as giant optic activity, nonlinearity and circular dichroism. Moreover, asymmetric EM wave transmission of circular polarizations has been reported in planar chiral metamaterials, where the partial conversion of the incident EM wave into one of the opposite handedness is asymmetric for the opposite directions of propagation [1–3]. This asymmetric transmission phenomenon is irrelevant to the non-reciprocity of the Faraday Effect in magneto-optical media, while originates from the interaction of EM radiation with sophisticated chiral metamaterial structures.

In this presentation, we will discuss on how to utilize polarization dependent chiral metamaterials to enable the EM wave asymmetric propagation, as well as one-way absorption of linearly polarized EM waves. We will first give a theoretical analysis on a kind of bi-layered chiral metamaterials with specific structure asymmetry that enables the asymmetric EM wave transmission only for linear polarization. Then by constructing a proof-of-concept metamaterial sample with twisted split ring resonator patterns on both sides of a dielectric slab, we will demonstrate experimentally substantial asymmetric transmission for linear polarizations, while none for circular polarizations at microwave frequency. Finally, we will report a one-way EM energy absorber based on a composite chiral metamaterial structure, which allow EM energy of linear polarized wave propagating along one direction, but being fully absorbed along the opposite direction. By scaling down the structures, we believe these proposed concepts could be utilized in other frequency band, such as terahertz and optical range, and extend the significant ability of metamaterial for EM wave manipulation.

ACKNOWLEDGMENT

Supported by the National Nature Science Foundation of China (60990322, 60990320, 60801001, 61101011), the Key Grant Project (313029) and the Ph.D. Programs Foundation (20100091110036, 20120091110032) of Ministry of Education of China.

REFERENCES

1. Zhukovsky, S. V., A. V. Novitsky, and V. M. Galynsky, *Opt. Lett.*, Vol. 34, 1988–1990, 2009.
2. Fedotov, V. A., P. L. Mladyonov, S. L. Prosvirnin, A. V. Rogacheva, Y. Chen, and N. I. Zheludev, *Phys. Rev. Lett.*, Vol. 97, 167401, 2006.
3. Singh, R., E. Plum, C. Menzel, C. Rockstuhl, A. K. Azad, R. A. Cheville, F. Lederer, W. Zhang, and N. I. Zheludev, *Phys. Rev. B*, Vol. 80, 153104, 2009.

Electric Field Tunable Domain Ferromagnetic Resonances in (111) Yttrium-iron Garnet Films

M. A. Popov[1], **I. V. Zavislyak**[1], **and G. Srinivasan**[2]

[1]Radiophysics Department, Taras Shevchenko National University of Kyiv, Kyiv 01033, Ukraine
[2]Physics Department, Oakland University, Rochester, MI 48309, USA

Abstract— The results of experimental investigation of electric field tuning of magnetic resonances in composite ferrite/piezoelectric YIG/PZT structure with YIG epitaxial film being in multiple-domain or saturated states are presented. Electric field tuning of resonance frequency being attributed to the appearance of stress induced first-order uniaxial magnetocrystalline anisotropy [1]. Electric field (instead of magnetic field) control of microwave properties enables construction of simpler, more compact, planar ferrite devices. Noteworthy, that domain resonances always exist in lower magnetic field (and in some cases even without it), than classical ferromagnetic resonance, reducing the challenge for permanent magnetic bias.

The 10 µm thick liquid phase epitaxy (111) YIG film was investigated. YIG film was glued to thick disk-shaped lead titanate-zirconite (PZT) slab. Resonator was situated on shorted section of microstrip line, with external magnetic field created using solenoid coil and applied in-plane $\langle 110 \rangle$ crystal axis. Domains observations via magnetooptical Faraday effect confirmed, that in moderate magnetic field the periodic stripe domain structure with period approximately 10 µm was formed, aligned along external magnetic field direction.

During the RF measurements, the reflection coefficient S_{11} of ferrite-piezoelectric structure for different static magnetic and/or electric fields in 0.01–1.5 GHz frequency range was recorded using vector network analyzer and the frequency vs. H field dependence for main magnetic resonance for different values of applied to piezoelectric static voltage were extracted (See figure). Measurements have shown that main domain mode exists in 800–1000 MHz range and demonstrates noticeable tuning of 120 MHz (14% of central frequency). This value is close to the best obtained results for magnetostatic mode in perpendicularly biased saturated ferrite film, despite that here magnetic field is actually laying in-plane and is much lower, that in former case. E-field tuning of magnetic resonance frequency in YIG film in saturated state was found to be considerably (5–6 times) smaller.

These results open up possibilities for practical applications of E-field tunable domain resonances. Indeed, we get 14% central frequency E-field tuning, which takes place in extremely low bias magnetic field (few tens of Oe), making this type of structure promising candidate for compact, lightweight, planar, UHF-band voltage-tunable microwave devices.

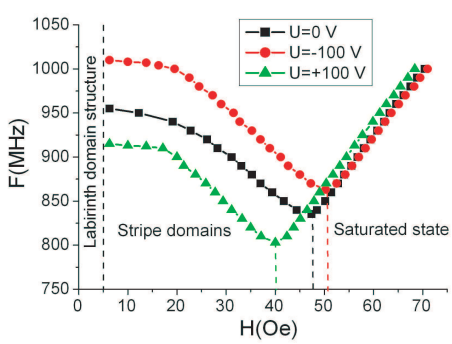

REFERENCES

1. Popov M. A. and I. V. Zavislyak, "Mechanism of electric frequency tuning in composite resonators based on epitaxial ferrite films," *Technical Physics Letters*, Vol. 38, No. 9, 865–868, 2012.

Session 3A2
2_FocusSession.SC2: Super Enhancement of Light with Plasmonic Nano-structures 1

Surface-enhanced Infrared Absorption (SEIRA) Spectroscopy Using Nanoantennas Tuned to Chemical Moieties
Lisa V. Brown, K. Zhao, Peter Nordlander, Naomi J. Halas, ... 914

Fano Lines and Signal Enhancement in IR Vibrational Spectroscopy
Annemarie Pucci, ... 915

Enhancement of Directionality, Emission Decay Rate and Gain for Emitters in Plasmonic and Hybrid Plasmonic-dielectric Systems
A. Femius Koenderink, ... 916

Designing Plasmonic Nanoparticles for Broadband Collection and Concentration of Light
Yu Luo, John B. Pendry, ... 917

Elucidating the Signatures of Electromagnetic Hot Spots and Fano Interferences in Electron Energy-loss and Cathodoluminescence Spectroscopies via Multiscale Electrodynamics Simulations
David J. Masiello, ... 918

Super Enhancement of Light in Self-assembled Multiscale Nanoparticle Cluster Arrays and Discrete Optoplasmonic Molecules
Bjoern M. Reinhard, ... 919

Activated Vibrational Modes and Fermi Resonance in Tip-enhanced Raman Spectroscopy
Hongxing Xu, ... 920

Real-time and Ultra-sensitive Infrared Absorption Biospectroscopy of Molecular Interactions with Plasmonic Nano-antennas
Hatice Altug, Ronen Adato, ... 921

Dependence of SERS Intensity on Geometrical Structures of Metals Formed Using Anodic Porous Alumina
Hideki Masuda, Toshiaki Kondo, Takashi Yanagishita, Kazuyuki Nishio, ... 922

Optical Nanoantennas: Directionality, Super Enhancement, and Single Molecule Raman Spectroscopy
Kenneth B. Crozier, ... 923

Surface-enhanced Infrared Absorption (SEIRA) Spectroscopy Using Nanoantennas Tuned to Chemical Moieties

L. V. Brown, K. Zhao, P. Nordlander, and N. Halas
Rice University, Houston, TX, USA

Abstract— The development of antenna structures for surface-enhanced infrared absorption spectroscopy (SEIRA) is a topic of intense and growing interest for extending IR spectroscopy to zeptomolar quantities and ultimately to the single molecule level. We have shown that strong infrared spectroscopic enhancements can be obtained from individual gold nanoantennas using conventional infrared spectrometric sources, where the antenna structure dimensions can be tuned to enhance the IR modes of specific chemical moieties [1]. Simulations of the electric field intensity in the antenna junction region reveal a maximum SEIRA enhancement factor of more than 12,000. These findings open new opportunities for analyzing infrared vibrations of exceptionally small quantities of molecules through widely accessible means. This general approach can be refined by modifications in antenna geometry and substrate material for further enhancements in sensitivity, and to selectively probe vibronic states of molecules and nanosystems of interest.

REFERENCES

1. Brown, L. V., et al., *Journal of the American Chemical Society*, Vol. 135, 3688–3695, 2013.

Fano Lines and Signal Enhancement in IR Vibrational Spectroscopy

Annemarie Pucci
Kirchhoff Institute for Physics, Heidelberg University
Im Neuenheimer Feld 227, Heidelberg 69120, Germany

Abstract— Plasmon-polariton excitations of metal particles can couple to other excitations of similar energy, which in the IR gives rise to vibrational signal enhancement. Fano lines from vibrational excitation can appear several orders of magnitude stronger than the signals in purely vibrational systems. Signal-enhancement factors depend on the resonance behaviour of the metal particles but also on parameters of the vibrating system. The talk will present examples with molecular vibrations and phonons.

Enhancement of Directionality, Emission Decay Rate and Gain for Emitters in Plasmonic and Hybrid Plasmonic-dielectric Systems

A. F. Koenderink
Center for Nanophotonics, FOM Institute AMOLF, Science Park 104, 1098 XG Amsterdam, Netherlands

Abstract— In recent years, plasmonic antennas have emerged as the optical nano-structures of choice to control single molecule fluorescence, absorption, spectroscopy and emission directivity. I will present recent work along two distinct lines of reasoning. Firstly, we pursue 'hybrid' antennas, where antennas are placed in dielectric environments that modify LDOS, such as moderate-Q cavities, interfaces or waveguides. On basis of nanomechanical manipulation we can controllably manipulate the coupling in such hybrid systems, including fluorophores. I will show how figures of merit, such as the joint Purcell factor, in hybrid systems arise from that of the constituent antenna and environment, and how the environment allows to create, e.g., efficient waveguide-interfacing to antennas. Ultimately, we aim to realize 'practical Q' hybrid systems, i.e., antenna-cavity hybrids with a quality factor of around 100, yet the mode volume of a plasmon antenna. Secondly, I will show how collective effects in lattices allow to control radiation directivity. In particular, in fluorescence correlation spectroscopy we have found that finite clusters of holes in metal film can be used to create directional antennas with strongly enhanced collection efficiency pre molecule. In the inverse structure, i.e., metal particle arrays, we find that similar lattice resonances allow to realize plasmonic distributed feedback lasers that we study using single-shot nanosecond pulsed spectroscopy and Fourier imaging.

Designing Plasmonic Nanoparticles for Broadband Collection and Concentration of Light

Yu Luo and J. B. Pendry
Department of Physics, Imperial College London, London, UK

Abstract— The ability of harvesting light and efficiently concentrating its energy into a nanoscale active center is highly desired for many applications, such as fluorescence, Raman scattering, single-molecule detection, and nonlinear effect. Surface plasmons have made these applications possible through a strong interaction between the incident light and free electrons in the metal. Critical to these goals is an ability to fully characterize and model the plasmonic properties of metallic nanostructures. In this contribution, a systematic strategy is proposed, based on transformation optics, to investigate a broad variety of plasmonic nanostructures. We exploit the fact that a finite nanoparticle with sharp geometrical features (such as edges or corners) can behave like an infinite plasmonic system and can exhibit a continuous absorption cross-section over a broad frequency band [1]. Comprehensive discussions are also provided on how the edge rounding at the sharp boundary affects the local field enhancement as well as the energy and bandwidth of each plasmonic resonance [2]. In particular, we will generalize this theory to design three-dimensional blunt structures (such as the one shown in Fig. 1) and show how to control their plasmonic resonances by tuning the geometry of the nanoparticle [3].

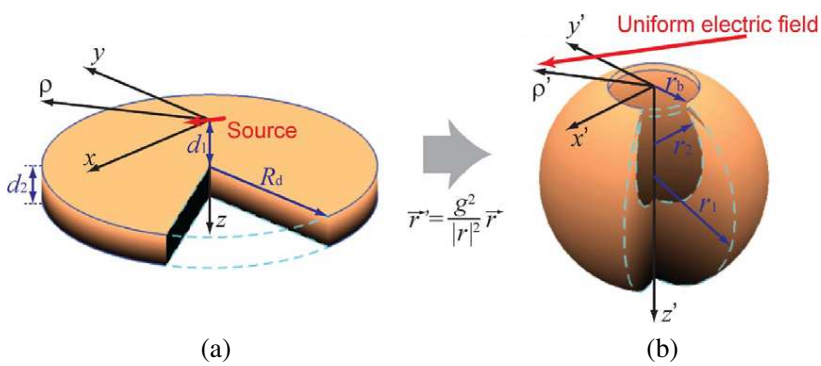

Figure 1: A 3D transformation maps (a) a metal disk excited by a point source to (b) a nano-bowl with a blunt edge illuminated by a uniform electric field.

REFERENCES

1. Pendry, J. B., A. Aubry, D. R. Smith, and S. A. Maier, *Science*, Vol. 337, 549, 2012.
2. Luo, Y., D. Lei, S. A. Maier, and J. B. Pendry, *Phys. Rev. Lett.*, Vol. 108, 023901, 2012.
3. Fernández-Domínguez*, A. I., Y. Luo*, A. Wiener*, J. B. Pendry, and S. A. Maier, *Nano Lett.*, Vol. 12, 5946, 2012 (*Equal contribution).

Elucidating the Signatures of Electromagnetic Hot Spots and Fano Interferences in Electron Energy-loss and Cathodoluminescence Spectroscopies via Multiscale Electrodynamics Simulations

David J. Masiello
Department of Chemistry, University of Washington, Seattle, WA 98195-1700, USA

Abstract— Electron energy-loss spectroscopy (EELS) performed in the scanning transmission electron microscope (STEM) offers a powerful means by which to study nanoscale light-matter inter- actions with sub-angstrom-scale spatial resolution. This technique is now being applied to probe surface-plasmon-supporting metal nanostructures, where a wealth of new information is being revealed that was previously unobtainable with standard optical techniques. These experiments provide an impetus for the implementation of theoretical methodologies capable of elucidating the differences between optically- and electronically-driven plasmons and their associated nanophotonic properties. In this talk, I will discuss our recent work in this area aimed at determining the signatures of electromagnetic hot spots, such as those responsible for single molecule surface-enhanced Raman scattering (SMSERS), in STEM/EELS based upon multiscale numerical simulations. I will also introduce a class of exotic interference features known as Fano resonances and predict, via simulations, their appearance in EELS and cathodoluminescence.

Super Enhancement of Light in Self-assembled Multiscale Nanoparticle Cluster Arrays and Discrete Optoplasmonic Molecules

Björn M. Reinhard
Department of Chemistry and The Photonics Center, Boston University, Boston, MA 02215, United States

Abstract— Traditional gap antenna approaches require a minimization of the interparticle separation to achieve giant electromagnetic E-field enhancements. Since chemical self-assembly approaches enable the fabrication of gap structures below the resolution limit of state-of-the-art top-down fabrication approaches, such as electron beam lithography, they are of high interest for realizing strongly coupled plasmonic nanostructures as well as for accessing the non-local/quantum plasmonic coupling regime. This presentation will give an overview of molecularly programmed and template guided self-assembly approaches developed for realizing clusters with narrow gap and size distributions at pre-defined locations. The dependence of the near- and far-field response on gap and cluster size, as well as on cluster configuration is analyzed through optical spectroscopy and supporting electromagnetic simulations. While near-field coupling in individual nanoparticle clusters achieves efficient electromagnetic hot-spot formation, the integration of clusters into extended arrays that support delocalized photonic-plasmonic supermodes achieves an additional boost through a cascaded electromagnetic field enhancement in the array. Design strategies for simultaneously maximizing short- and long-range electromagnetic coupling in multiscale nanoparticle cluster arrays (NCAs) with optimized cascaded eletromagnetic field enhancement will be elaborated. An alternative approach for boosting the field enhancement of individual NP antennas is based on their integration into the evanescent field of a whispering gallery mode (WGM) resonator. The plasmon antenna further localizes the evanescent field associated with the individual WGMs. A rational fabrication approach for discrete optoplasmonic molecules that contain plasmonic anntennas at pre-defined locations in the equatorial plane of a microcavity resonator will be introduced, and experimental and theoretical indications of efficient photonic-plasmonic model coupling in the fabricated hybrid structures will be presented.

Activated Vibrational Modes and Fermi Resonance in Tip-enhanced Raman Spectroscopy

Hongxing Xu
Beijing National Laboratory for Condensed Matter Physics
Institute of Physics, Chinese Academy of Sciences
No. 8, 3 South Street, ZhongGuanCun, Beijing 100190, China

Abstract— Tip-Enhanced Raman spectroscopy (TERS) is a high-sensitivity and high spatial-resolution optical analytical technique with nanoscale resolution beyond the diffraction limit of light, which was discovered more than one decade ago by Stöckle et al. [1]. In TERS a sharp metal tip is used to create a "hot site" to excite the localized surface plasmons and consequently enhance the electromagnetic field and Raman signals in the vicinity of the tip apex [1–5]. Since the tip can be moved three dimensionally to control the position of "hot site" and the corresponding enhancement factor by changing the gap distance between the tip and the substrate, TERS thus overcomes one of the most severe restrictions in the application of surface enhanced Raman scattering (SERS), which usually requires roughness of metal surfaces or aggregations of metal nanoparticles to create "hot sites", but hardly to be controlled. TERS may solve a wide variety of problems in high vacuum (HV) single crystal surface science, electrochemistry, heterogeneous catalysis, microelectronics, and tribology. In order to conduct spectroscopy sensitive to ambient conditions on a variety of specimens, the use of an HV environment is mandatory [5].

In this talk, by exploring the advantages of TERS, we investigate this long-standing issue, the appearance of normally unseen Raman modes of PATP, in SERS. Using p-aminothiophenol (PATP) molecules adsorbed on a gold substrate as prototypical examples, we observed the Raman spectra in high vacuum tip-enhanced Raman spectroscopy (HV-TERS), which are very different from normal Raman spectra of this compound. Raman-active symmetric modes and IR-active asymmetric modes of DMAB are simultaneously observed in the HV-TERS Raman spectra. Much narrower and much more activated (from IR-active) Raman modes in our TERS study than previously reported SERS spectra of DMAB gives more complete vibrational spectroscopic information and confirm strongly the putative production of DMAB. The activation of IR active modes to be Raman active is primarily attributed to enhanced electromagnetic field gradient effects within the gap region of the tip-surface geometry. The enhanced dynamical responses further result in the splitting of some vibrational modes caused by Fermi resonances in the vibrational spectra involving the coupling of a fundamental mode and the overtone or a combinational mode. These findings help to establish the power of TERS and substantially broaden the versatility of TERS as a promising technique for single-molecule spectroscopy. We also investigate plasmon-assisted chemical reactions for other molecules, where the electrons needed in the chemical reaction contributed from "hot" electrons decayed by plasmons [6, 7].

REFERENCES

1. Stöckle, R. M., Y. D. Suh, V. Deckert, and R. Zenobi, *Chem. Phys. Lett.*, Vol. 318, 131, 2000.
2. Pettinger, B., B. Ren, G. Picardi, R. Schuster, and G. Ertl, *Phys. Rev. Lett.*, Vol. 92, 096101, 2004.
3. Zhang, W., X. Cui, B. S. Yeo, T. Schmid, C. Hafner, and R. Zenobi, *Nano Lett.*, Vol. 7, 1401, 2007.
4. Bailo, E. and V. Deckert, *Chem. Soc. Rev.*, Vol. 37, 921, 2008.
5. Steidtner, J. and B. Pettinger, *Phys. Rev. Lett.*, Vol. 100, 236101, 2008.
6. Sun, M. T., Z. L. Zhang, H. R. Zheng, and H. X. Xu, *Scientific Reports*, Vol. 2, 647, 2012.
7. Sun, M. T., Y. R. Fang, Z. Y. Zhang, and H. X. Xu, *Phys. Rev. E*, Vol. 87, 020401(R), 2013.

Real-time and Ultra-sensitive Infrared Absorption Biospectroscopy of Molecular Interactions with Plasmonic Nano-antennas

Hatice Altug[1, 2] **and Ronen Adato**[1]

[1]Biomedical Engineering Department, Ecole Polytechnique Federale de Lausanne, Switzerland
[2]Electrical and Computer Engineering and Biomedical Engineering Departments
Boston University, Boston, USA

Abstract— IR absorption spectroscopy is a powerful biochemical analysis technique as it extracts detailed molecular structures of samples in a label-free fashion [1, 2]. Such information is highly desirable in many fields including biology. In this talk, we will demonstrate a plasmonic chip based technology for performing ultra-sensitive infrared (IR) absorption spectroscopy in aqueous solutions, capable of monitoring biomolecule interactions at the sub-monolayer level in real-time [3]. In leveraging engineered plasmonic antennas for IR absorption enhancement, our results represent a dramatic advance over previous studies, being the first demonstration of their use for biologically significant measurements in solution. Notably, such kinetic measurements are fundamentally challenging in traditional IR spectroscopy due to sensitivity limitations and the extremely strong absorption bands of liquid water, which routinely prohibit analysis in aqueous solutions. Our plasmonic system overcomes these challenges, enabling us to monitor in real-time protein and nano-particle binding events at high sensitivity. Compared to traditional label-free approaches our technology is based on molecular bond-specific IR absorption signatures, therefore it even enables observation of minute volumes of water displacement during molecular interactions.

In comparison with the current state of the art in IR spectroscopy, which require sampling volumes several thousand times larger and cumbersome, bulky macroscopic optics, our results offer overall sensitivity improvements of over an order of magnitude in an ultra-compact chip based technology. As such, our technology represents a dramatic and transformative advancement in the compatibility of IR absorption spectroscopy with modern and next generation sample preparation and handling techniques including microfluidics, optical trapping, high-throughput scanning. Significantly, our results open the door for both next generation IR sensors and spectroscopy tools and have the potential to enable a new class of measurements critical for understanding basic biological function as well as important aspects of e.g., disease progression and treatment.

REFERENCES

1. Neubrech, et al., *Physical Review Letters*, 2008.
2. Adato, et al., *Proceedings of National Academy of Sciences*, 2009.
3. Adato and Altug, under review, February 2013.

Dependence of SERS Intensity on Geometrical Structures of Metals Formed Using Anodic Porous Alumina

Hideki Masuda, **Toshiaki Kondo**, **Takashi Yanagishita**, **and Kazuyuki Nishio**
Department of Applied Chemistry, Tokyo Metropolitan University
1-1 Minamiosawa, Hachioji, Tokyo 192-0397, Japan

Abstract— The fabrication processes for nanostructures of noble metals are attracting attention due to its capability for enhancement of the electric field of incident light originated from localized surface plasmon resonance (LSPR). The various types of applications based on the enhanced electric field have been proposed such as sensing or energy conversion [1]. Precise control of the sizes and shapes of the metal nanostructures is important because the degree of the enhancement of electric field is substantially dependent on the shape and arrangement of the nanostructure of the metals. Anodic porous alumina, which is formed by anodization of Al in acidic electrolyte, is a typical self-ordered material and is promising candidate for the starting structure of geometrically controlled nanostructured metals [2–4]. Advantage of the use of anodic porous alumina for the preparation of the metal nanostructures is its controllability of the dimension of the metal nanostructures besides its easiness of the preparation. In the present report, the precise control of the geometrical structure of arrays of ordered metal nanodots using anodic porous alumina and their application to substrates for surface-enhanced Raman scattering (SERS) measurements are described. Ordered array of shape controlled Au nanodots were prepared using anodic porous alumina as an evaporation mask. The shape (circular, square etc.) and arrangement of nanodots were controlled by adjusting the geometrical structure of pores in anodic porous alumina. The aspect ratios of the Au dots were also controlled. Dependence of the SERS intensity on the geometrical structures of metals was investigated. The enhancement factors of the incident light intensity around the metal nanostructures were analyzed by numerical calculations based on the FDTD (finite-difference time-domain) method. The fabrication processes described in the present report make it possible to prepare an ordered array of geometrically controlled nanostructures of metals, which allow the effective enhancement of the electric field of incident light.

REFERENCES

1. Kondo, T., K. Nishio, and H. Masuda, *Appl. Phys. Express*, Vol. 2, 032001, 2009.
2. Masuda, H. and K. Fukuda, *Science*, Vol. 268, 1466, 1995.
3. Kondo, T., F. Matsumoto, K. Nishio, and H. Masuda, *Chem. Lett.*, Vol. 37, 466, 2008.
4. Kondo, T., H. Miyazaki, K. Nishio, and H. Masuda, *J. Photochem. Photobiol. A*, Vol. 221, 119, 2011.

Optical Nanoantennas: Directionality, Super Enhancement, and Single Molecule Raman Spectroscopy

Kenneth B. Crozier
School of Engineering and Applied Sciences, Harvard University
MD147, 33 Oxford Street, Cambridge, MA 02138, USA

Abstract— Optical nanonantennas present a means for overcoming the mismatch between the wavelength of light and dimensions of nanostructures. Here, I present recent work from my group [1, 2] on the use of optical nanoantennas for surface-enhanced Raman scattering (SERS). SERS employs plasmonic nanostructures to enhance the Raman cross section of molecules by orders of magnitude. Much emphasis in SERS substrate design has been on finding nanostructures with larger electric field enhancement. Recently, the importance of directionality in SERS has been recognized. I will discuss recent work [1] in which we use a technique termed "energy momentum spectroscopy" to directly observe directional Raman scattering molecules on optical nanoantennas. I will furthermore discuss recent work [2] in which we experimentally demonstrate an optical antenna chip that achieves directional SMSERS. More than a thousand single molecule events are observed, revealing that an unprecedented near-unity fraction of optical antennas have single molecule sensitivity. SMSERS is one of the few methods of obtaining the vibrational spectrum of a single molecule and presents opportunities for understanding chemical and biological systems at a fundamental level. Indeed, it is speculated that it may one day enable the observation of a single molecule undergoing a chemical reaction. We anticipate that this work will be very beneficial for such fundamental scientific studies but also in technological applications. In addition, we foresee wider applications of antenna approaches to other types of single emitters used in quantum optics and sensing.

REFERENCES

1. Zhu, W., D. Wang, and K. B. Crozier, "Direct observation of beamed raman scattering," *Nano Letters*, Vol. 12, 6235–6243, 2012.
2. Wang, D., W. Zhu, M. D. Best, J. P. Camden, and K. B. Crozier, "Directional raman scattering from single molecules in the feed gaps of optical antennas," *Nano Letters*, DOI: 10.1021/nl400698w.

Session 3A3
3_FocusSession.SC3: Photonics of Quantum Dots and Its Applications

Advances in Quantum Dot Lasers for Photonic and Electronic Convergent Systems
Yasuhiko Arakawa, K. Tababe, ... 926

1.5 m InP Based QD Lasers for High-speed Optical Communication Systems
Johann Peter Reithmaier, V. Ivanov, V. Sichkovskyi, D. Gready, G. Eisenstein, ... 927

MBE Growth of III-V Droplet Quantum Dots for the Application to Nano Photonics
Jin Dong Song, E. H. Lee, J. S. Kim, ... 929

Light-matter Interaction of Quantum Dots and Nanowires in Novel High-Q Photonic Crystal Cavities at Telecom Wavelength
Muhammad Danang Birowosuto, Hisashi Sumikura, A. Yokoo, M. Takiguchi, Masaya Notomi, ... 930

Wavelength Tunability of Two-wavelength Emission Laser with Semiconductor Quantum Dots
Kouichi Akahane, Naokatsu Yamamoto, Atsushi Kanno, Keizo Inagaki, Toshimasa Umezawa, Tetsuya Kawanishi, Takashi Endo, Yasunori Tomomatsu, Toshio Yamanoi, ... 931

Teleportation Using Electrically Generated Entangled Photons from a Quantum Dot
Jonas Nilsson, R. M. Stevenson, K. H. A. Chan, J. Skiba-Szymanska, M. Lucamarini, M. B. Ward, Anthony J. Bennett, C. L. Salter, I. Farrer, D. A. Ritchie, A. J. Shields, ... 932

Quantum Optics with Photonic Nanowires and Photonic Trumpets: Basics and Applications
Jean-Michel Gérard, Julien Claudon, M. Munsch, J. Bleuse, A. Delga, Niels Gregersen, J. Mork, 933

On-chip Quantum Optics Using Electrically Driven Quantum Dot — Micropillar Cavities
C. Hopfmann, F. Albert, E. Stock, Matthias Lermer, C. Schneider, S. Höfling, A. Forchel, Martin Kamp, Stephan Reitzenstein, ... 934

Highly-efficient Light-matter Interaction with Quantum Dots in Photonic Crystals
Peter Lodahl, ... 935

Controlling the Spontaneous Emission from Single Quantum Dots with Electromechanical Photonic Crystal Cavities
Leonardo Midolo, F. Pagliano, Thang Ba Hoang, T. Xia, F. W. M. Van Otten, L. H. Li, E. H. Linfield, Matthias Lermer, S. Hofling, Andrea Fiore, ... 936

Classical to Quantum Transition for Heat Transfer between Two Clusters
Shiyun Xiong, Kaike Yang, Roberto D'Agosta, Pietro Cortona, Sebastian Volz, ... 937

Advances in Quantum Dot Lasers for Photonic and Electronic Convergent Systems

Y. Arakawa[1,2] **and K. Tababe**[1,2]

[1]Institute for Nano Quantum Information Electronics, The University of Tokyo
4-6-1 Komaba, Meguro-ku, Tokyo 153-85-5, Japan
[2]Institute of Industrial Science, The University of Tokyo
4-6-1 Komaba, Meguro-ku, Tokyo 153-85-5, Japan

Abstract— Quantum dot lasers [1] are promising as light sources for application to both telecommunication and Si photonic integrated circuits, owing to its high temperature-stability and low power consumption [2]. In this presentation, we discuss recent progress in the III–V quantum dot lasers, including high-temperature operation of 1.3 μm InAs/GaAs quantum dot lasers on silicon substrates [3, 4]. Moreover, development of silicon optical interposer systems realizing a high bandwidth-density over 10 Tbps/cm^2 is also mentioned.

ACKNOWLEDGMENT

This work was in part supported by the JSPS through the FIRST Program, METI through the Future Pioneering Projects, and MEXT through the Project for Developing Innovation Systems, and Intel Corporation.

REFERENCES

1. Arakawa, Y. and H. Sakaki, *Appl. Phys. Lett.*, Vol. 40, 939, 1982.
2. Otsubo, K., N. Hatori, M. Ishida, S. Okumura, T. Akiyama, Y. Nakata, H. Ebe, M. Sugawara, and Y. Arakawa, *Jpn. J. of Appl. Phy.*, Vol. 43, L1124, Express Letter, 2004.
3. Tanabe, K., K. Watanabe, and Y. Arakawa, *Optics Express*, Vol. 20, B315–B321, 2012.
4. Tanabe, K., K. Watanabe, and Y. Arakawa, *Sci. Rep.*, 349, 2012.

1.5 m InP Based QD Lasers for High-speed Optical Communication Systems

J. P. Reithmaier[1], V. Ivanov[1], V. Sichkovskyi[1], D. Gready[2], and G. Eisenstein[2]

[1]Institute of Nanostructure Technologies and Analytics (INA), CINSaT, University of Kassel
Heinrich-Plett-Str. 40, Kassel 34132, Germany
[2]Department of Electrical Engineering, Technion, Haifa 32000, Israel

Abstract— A review will be given on the latest development of high-speed directly modulated 1.55 µm lasers based on high model gain quantum dot material [1–3]. Static and dynamic properties of short cavity lasers will be presented exhibiting data rates well beyond 20 GBit/s [4]. The impact of structural and operational parameters will be discussed and compared with a simulation model, which includes the complex carrier dynamics in quantum dot laser materials [5, 6].

Figure 1 shows low-temperature photoluminescence (PL) of a laser structure consisting of 6 stacked high-density InAs/InAlGaAs quantum dot layers grown on (001) InP substrates. Due to the reduced height variation a PL linewidth of 31 meV is observed. The inset show an $1 \times 1\,\mu m^2$ AFM image of a test sample grown by the same growth conditions.

In Figure 2, the small and large signal modulation response of a 275 µm long ridge waveguide laser are shown exhibiting a record value in digital modulation of 22 GBit/s with a clear open eye (3 dB extinction ration).

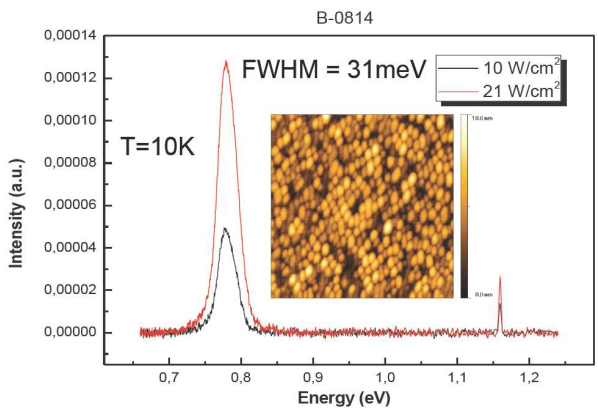

Figure 1: Narrow linewidth low-temperature photoluminescence of InAs QDs embedded in a laser with 6 QD layers at two different excitation densities. The weak higher energy peak is related to the QD embedding quaternary material. The inset shows an AFM image of surface QDs grown by similar conditions.

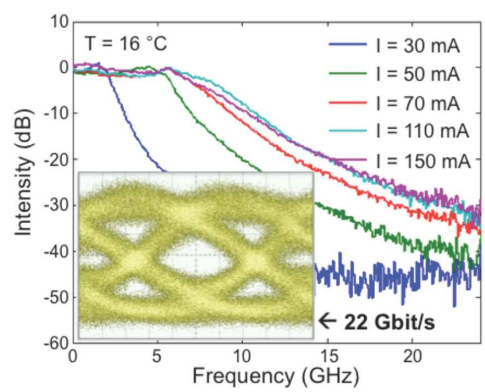

Figure 2: Small signal response of 275-µm long RWG QD laser for different bias current. The inset shows the eye diagram for 22 GBit/s digital modulation.

REFERENCES

1. Gilfert, C., E. M. Pavelescu, and J. P. Reithmaier, "Influence of the As2/As4 growth modes on the formation of quantum dot like InAs islands grown on InAlGaAs/InP (100)," *Appl. Phys. Lett.*, Vol. 96, 191903, 2010.
2. Gilfert, C., V. Ivanov, N. Oehl, M. Yacob, and J. P. Reithmaier, "High gain 1.55 µm diode lasers based on InAs quantum dot like active regions," *Appl. Phys. Lett.*, Vol. 98, 201102, 2011.
3. Gready, D., G. Eisenstein, C. Gilfert, V. Ivanov, J. P. Reithmaier, *IEEE Photon. Technol. Lett.*, Vol. 24, 809, 2012.
4. Reithmaier, J. P., V. Ivanov, V. Sichkovskyi, C. Gilfert, K. Kozhuharov, A. Rippien, F. Schnabel, N. Felgen, K. Fuchs, D. Gready, and G. Eisenstein, "Static and dynamic characteristics of InAs/AlGaInAs/InP quantum dot lasers operating at 1550 nm," *IPRM Conf.*, Kobe, Japan, May 2013.

5. Gready, D. and G. Eisenstein, "Carrier dynamics and modulation capabilities of 1.55 μm quantum dot lasers," accepted for publication in special issue of *IEEE Sel. Top. Quant. Electron.*, 2013.
6. Gready, D., G. Eisenstein, M. Gioannini, I. Montrosset, D. Arsenijevic, H. Schmeckebier, M. Stenbrauch, and D. Bimberg, "On the relationship between small and large signal modulation capabilities in highly non-linear quantum dot lasers," accepted for publication in *Appl. Phys. Lett.*, 2013.

MBE Growth of III-V Droplet Quantum Dots for the Application to Nano Photonics

Jin Dong Song[1], **E. H. Lee**[1], **and J. S. Kim**[2]

[1]Center for Opto-Electronic Convergence Systems, Korea Institute of Science and Technology
Seoul 136-791, South Korea
[2]Department of Physics, Yeungnam University, Gyeongsangbuk-Do 712-749, South Korea

Abstract— The droplet epitaxy (DE) method has the merit of the growth of various quantum structures, such as quantum rings, disks, coupled QDs and concentric quantum double rings, as well as low density QDs, due to a perfect separation of group 3 and 5 [1, 2]. In addition, larger GaAs DE QDs can be grown on AlGaAs without strain effect, for larger oscillation strength, compared with InAs QDs on GaAs.

For low density GaAs DE QDs, easier handling of them has huge merit in a Silicon-based industry, since GaAs DE QDs as a single photon source with an emission of $\sim 700\,\mathrm{nm}$ could be applied to low-cost and more sensitive silicon array detectors. Consequently, an efficient fabrication and measurement of quantum structures, based on DE growth, would be helpful for mass production of various devices.

The DE method has nolimitation on the choice of substrate material for nanostructure growth. As a result, (i) the growth of homo-epitiaxial nanostructures, such as GaAs QDs on GaAs substrates, and (ii) the formation of ultra large-sized QDs applicable to antireflective nanostructures are possible. That is, the formation of antireflection layers can be achieved on GaAs-based solar cells, without additional process or vacuum-breaking.

In this presentation, 1) the authors will present the mass-producible uniform growth and position retrieval of low density GaAs DE QDs of $\sim 4\,\mathrm{QDs}/\mu\mathrm{m}^2$ over 2 inch substrate. 2) the feasibility of DE-based nano-structure as an antireflection layer will be discussed. Finally, 3) various applications of DE such as a template for coupled InAs QDs, quantum ring structure and P-based DE will be covered.

REFERENCES

1. Mano, T., T. Kuroda, S. Sanguinetti, T. Ochiai, T. Tateno, J. S. Kim, T. Noda, M. Kawabe, K. Sakoda, G. Kido, and N. Koguchi, *Nano Lett.*, Vol. 5, 425, 2005.
2. Lee, E. H., J. D. Song, J. J. Yoon, M. H. Bae, I. K. Han, W. J. Choi, S. K. Chang, Y. D. Kim, and J. S. Kim, *J. of Appl. Phys.*, Vol. 113, 154308, 2013.

Light-matter Interaction of Quantum Dots and Nanowires in Novel High-Q Photonic Crystal Cavities at Telecom Wavelength

M. D. Birowosuto[1,2], H. Sumikura[1,2], A. Yokoo[1,2], M. Takiguchi[1,2], and M. Notomi[1,2]

[1]NTT Basic Research Laboratories, NTT Corporation
3-1 Morinosato Wakamiya, Atsugi, Kanagawa 243-0198, Japan
[2]NTT Nanophotonics Center, NTT Corporation
3-1 Morinosato Wakamiya, Atsugi, Kanagawa 243-0198, Japan

Abstract— Single photon source at telecom wavelength is an important feature for the quantum communication networks, quantum repeaters, and all optical quantum information processing via optical fibers. Single InAs/InP or InAsP/InP quantum-dots (QDs) are attractive emitters while coupling this single QD with a cavity yields a faster and brighter single photon source [1]. Here we demonstrate fast single photon source at 1.55-μm telecom band from the coupling of the single InAs/InP QD with the cavity of the photonic crystals (PhC) [2]. We observe a very fast lifetime of 0.2 ns from XX at 22 K (zero detuning). This fast lifetime is due to Purcell effect with five-time emission rate enhancement. Also at zero detuning, the photon correlation measurement shows an antibunching with $g^2(0)$ of 0.1. This fast single photon source at telecom band has a potential to improve the modulation rate of the long-distance quantum networks.

The PhC cavity in this experiment was incorporated in the PhC design prior the fabrication process. For this conventional cavity with embedded quantum dots, we do not have full control with the cavity creation and the location while we can not move the emitter relative to the maximum field of the cavity. Therefore, we envisage a novel high-Q position-controlled cavity using a single III-V nanowire (NW) and silicon PhC [3]. This cavity is created simply by putting single NW into the groove in the waveguide of photonic crystals. In such cavity, we can tune the cavity position using atomic force microscopy tip while we can define the position of the emitter through the NW growth. For the realization of this position-controlled cavity, we used $\sim$ 90-nm-diameter InP NW embedded with 10 InAsP QDs [4]. From photoluminescence (PL) spectra, a strong narrow peak around 1.3 μm is attributed to the cavity peak with Q of 7,100. We did not observe this peak before the NW was placed in the groove (bare silicon on insulator (SOI) substrate) and we found that this InAsP QD emission peak possesses the cavity polarization. This is the first demonstration of subwavelength high-Q position-controlled cavity. Such cavity will be useful for the movable devices, which is integrated with silicon. For fundamental research, our works will be useful in the advent of the research of the light matter interaction between the emitter and the cavity at telecom wavelength.

ACKNOWLEDGMENT

This work was supported by Core Research for Evolutional Science and Technology — Japan Science and Technology Agency (CREST-JST). The authors would like to acknowledge R. Nötzel, S. Matsuo, G. Zhang, K. Tateno, and E. Kuramochi for providing samples.

REFERENCES

1. Shields, A. J. , "Semiconductor quantum light sources," *Nature Photon.*, Vol. 1, No. 4, 215, 2007.
2. Birowosuto, M. D., H. Sumikura, S. Matsuo, H. Taniyama, P. J. van Veldhoven, R. Noetzel, and M. Notomi, "Fast purcell-enhanced single photon source in 1,550-nm telecom band from a resonant quantum dot-cavity coupling," *Sci. Rep.*, Vol. 2, 321, 2012.
3. Birowosuto, M. D., A. Yokoo, H. Taniyama, E. Kuramochi, M. Takiguchi, and M. Notomi, "Design for ultrahigh-Q position-controlled nanocavities of single semiconductor nanowires in two-dimensional photonic crystals," *J. of Appl. Phys.*, Vol. 112, 113106, 2012.
4. Birowosuto, M. D., A. Yokoo, G. Zhang, K. Tateno, E. Kuramochi, H. Taniyama, M. Takiguchi, and M. Notomi, in preparation.

Wavelength Tunability of Two-wavelength Emission Laser with Semiconductor Quantum Dots

Kouichi Akahane[1], **Naokatsu Yamamoto**[1], **Atsushi Kanno**[1], **Keizo Inagaki**[1], **Toshimasa Umezawa**[1], **Tetsuya Kawanishi**[1], **Takashi Endo**[2], **Yasunori Tomomatsu**[2], **and Toshio Yamanoi**[2]

[1]National Institute of Information and Communications Technology
4-2-1, Nukui-Kitamachi, Koganei, Tokyo 184-8795, Japan
[2]Koshin Kogaku Co., Ltd., 69-3, Bodai Hadano, Kanagawa 259-1302, Japan

Abstract— A two-wavelength emission laser can be used to generate millimeter and terahertz waves by irradiating high-speed photodiodes or nonlinear crystals. Electromagnetic waves at such frequencies have recently become important for high-speed wireless communication and accurate sensing. We have developed a quantum dot (QD) wavelength-tunable two-wavelength emission laser with a narrow linewidth and stable emission wavelength. In this study, we investigate the characteristics of the wavelength tunability for a two-wavelength emission laser consisting of a GaAs-based laser diode chip with InAs QDs as the gain medium and external cavity. The laser structure with InAs QDs was grown on GaAs (001) substrates by solid-source molecular-beam epitaxy. After the growth of the QD laser wafer, the ridge waveguide was fabricated. An external cavity laser system was constructed using the QD gain chip, an optical band-pass filter, and an etalon filter. The single-emission tunable laser is a conventional configuration in which the peak position of transmission by the band-pass filter is set to that of the etalon filter. The emission wavelength ranges from 1223.0 nm to 1265.8 nm. On the other hand, the configuration for a two-wavelength emission laser was modified from the conventional one. We observed two-mode lasing with a frequency separation of about 100 GHz, which is in good agreement with the free spectral range of the etalon filter. Because a clear beat signal was observed in the interference measurement, laser emission at the two wavelengths can be considered to have occurred simultaneously. Mode hopping and competition were largely suppressed by using QDs as the gain medium because the QDs have a delta-function-like density of states, so each of them contributed to the laser emission individually, stabilizing the laser emission wavelength. This two-mode lasing was obtained from 1228.5 nm to 1256.8 nm. This tunability is slightly narrower than that of single-mode emission, which can be attributed to the gain curve of the InAs QDs. However, two-mode emission also has a wide wavelength tunability, so it can be used for high-performance sensing.

Teleportation Using Electrically Generated Entangled Photons from a Quantum Dot

J. Nilsson[1], **R. M. Stevenson**[1], **K. H. A. Chan**[1,2], **J. Skiba-Szymanska**[1], **M. Lucamarini**[1], **M. B. Ward**[1], **A. J. Bennett**[1], **C. L. Salter**[1,2], **I. Farrer**[2], **D. A. Ritchie**[2], **and A. J. Shields**[1]

[1]Cambridge Research Laboratory, Toshiba Research Europe Limited
208 Science Park, Milton Road, Cambridge, CB4 0GZ, United Kingdom
[2]Cavendish Laboratory, University of Cambridge
JJ Thomson Avenue, Cambridge, CB3 0HE, United Kingdom

Abstract— We present results of quantum teleportation mediated by electrically generated entangled photon pairs emitted by a quantum dot based entangled-light-emitting-diode (ELED) [1]. Quantum teleportation, in which the quantum state of a particle is transferred onto a remote particle, underpins several quantum information applications, such as the realization of near-deterministic quantum logic [2] and the extension of quantum communication over longer distances [3].

Our device is based on InAs quantum dots embedded in a p-i-n diode structure [4]. We implement our teleportation circuit in single mode fibre and using single photon detectors. An entangled photon pair produced in the radiative cascade from the biexciton state of the quantum dot is shared between two parties Alice and Bob. For the purpose of the experiment the device also supplies the input photon carrying the polarisation state to be teleported.

Experimentally we measure time-resolved three-photon correlations between cross-polarised photon detections (H-V) by Alice and some polarisation P by Bob. Teleportation is performed for in total six input states over the Poincaré sphere with an average fidelity of 0.704 ± 0.016, beating the classically achievable limit of 2/3 (see Figure 1).

By creating electrically faster, pulsed devices and with optical cavity engineering, quantum teleportation with higher fidelity and without post-selection will be possible. The performance of photonic quantum information implementations is already today limited by accidental generation of multiple photons in Poissonian sources. The unique single-photon nature of our device and its electrical operation offers a path to alleviate this problem.

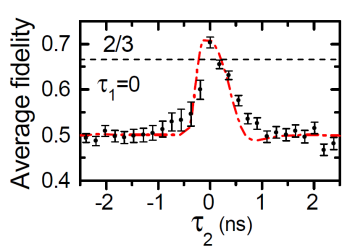

Figure 1: Average teleportation fidelity for six polarisation input states, plotted as a function of Bob's detection time τ_2 when Alice registers a coincidence ($\tau_1 = 0$).

REFERENCES

1. Nilsson, J., et al., "Quantum teleportation using a light emitting diode," *Nature Photon.*, advance online publication, February 24, 2013 (DOI 10.1038/nphoton.2013.10).
2. Knill, E., R. Laflamme, and G. J. Milburn, *Nature*, Vol. 409, 46–52, 2001.
3. Briegel, H.-J., et al., *Phys. Rev. Lett.*, 81, 5932–5935, 1998.
4. Salter, C. L., et al., *Nature*, Vol. 465, 594, 2010.

Quantum Optics with Photonic Nanowires and Photonic Trumpets: Basics and Applications

J. M. Gérard[1], J. Claudon[1], M. Munsch[1], J. Bleuse[1], A. Delga[1], N. Gregersen[2], and J. Mørk[2]

[1]CEA-CNRS-UJF Joint Group 'NanoPhysique et SemiConducteurs'
CEA, INAC, SP2M, Grenoble 38054, France
[2]DTU Fotonik, Technical University of Denmark, Kongens Lyngby DK-2800, Denmark

Abstract— Optimizing the coupling between a localized quantum emitter and a single-mode optical channel represents a powerful route to realise bright sources of non-classical light states. Reversibly, the efficient absorption of a photon impinging on the emitter is key to realise a spin-photon interface, the node of future quantum networks.

Besides optical microcavities [1], photonic wires have recently demonstrated in this context an appealing potential [2, 3]. For instance, single photon sources (SPS) based on a single quantum dot in a vertical photonic wire with integrated bottom mirror and tapered tip have enabled for the first time to achieve simultaneously a very high efficiency (0.72 photon per pulse) and a very pure single photon emission ($g^{(2)}(0) < 0.01$). Furthermore, photonic wires with an elongated cross-section provide polarization control of the spontaneous emission of embedded emitters [4].

However, the performance of photonic wire SPS with tapered tips is sensitive to minute geometrical details and optimum behaviour is only obtained for ultra-sharp tips. Photonic trumpets [5], which exploit the opposite tapering strategy, overcome this important limitation. Moreover, they feature a Gaussian far-field emission, a strong asset for most applications. We report on the first implementation of this strategy and demonstrate an ultra-bright SPS (first-lens external efficiency: 0.75 ± 0.1) [5]. More generally, photonic trumpets appear as a very promising template to explore and exploit in a solid-state system the unique optical properties of "one-dimensional atoms".

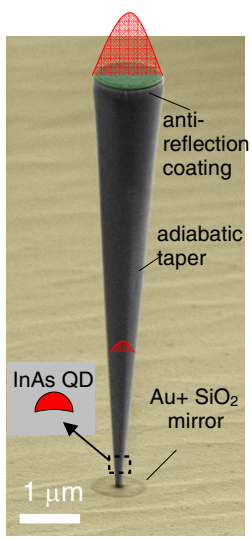

Figure 1: Colorized scanning electron micrograph of a GaAs photonic trumpet (from [5]).

REFERENCES

1. Gérard, J. M., et al., *Phys. Rev. Lett.*, Vol. 81, 1110, 1998.
2. Friedler, I., et al., *Opt. Exp.*, Vol. 17, 2095–2110, 2009.
3. Claudon, J., et al., *Nature Photon.*, Vol. 4, 174, 2010.
4. Munsch, M., et al., *Phys. Rev. Lett.*, Vol. 108, 077405, 2012.
5. Munsch, M., et al., *Phys. Rev. Lett.*, Vol. 110, 177402, 2013.

On-chip Quantum Optics Using Electrically Driven Quantum Dot — Micropillar Cavities

C. Hopfmann[1], F. Albert[2], E. Stock[1], M. Lermer[2], C. Schneider[2], S. Höfling[2], A. Forchel[2], M. Kamp[2], and S. Reitzenstein[1]

[1]Institut für Festkörperphysik, Technische Universität Berlin, Berlin, Germany
[2]Technische Physik, Universität Würzburg, Würzburg, Germany

Abstract— The prospect of studying quantum optics in the solid state and the quest for quantum light sources in the field of quantum communication has triggered enormous efforts in the development of micro- and nanocavity systems with embedded quantum dots (QDs). These structures exploit cavity quantum electrodynamics (cQED) effects and can act as efficient non-classical light sources and as high-β microlasers. Initially, QD-microcavities were exclusively excited optically by external lasers, while significant technological progress has enabled electrical pumping in advanced structures.

Here we report for the first time on an on-chip quantum optics experiment where an integrated microlaser excites a QD-micropillar cavity operating in the weak coupling regime of cQED. Our approach combines two very active but so far independent routes of cQED, namely high-β lasing and light-matter interaction at the quantum in a novel, integrated device concept. This concept is illustrated in Fig. 1(a) and relies on the fact that micropillar cavities allow for the localization of vertically emitting modes and laterally emitting whispering gallery modes (WGMs). We take advantage of these unique opportunity provided by the micropillar geometry to utilize an electrically pumped WGM micropillar as in-plane laser source. The integrated WGM microlaser resonantly excites radially displaced QD-micropillars. This specific configuration allows us to perform for the first time on-chip quantum optics in the cQED regime using an integrated coherent light source.

The high quality electrically pumped WGM lasers were studied by means of micro-electroluminescence spectroscopy and show single mode emission, threshold currents below 10 µA and β-factors of about 0.1 at low temperature. Emission from such a WGM laser was used to resonantly excite a target quantum dot in an adjacent micropillar with a diameter of 2.5 µm via p-shell excitation. It is interesting to note, that resonant excitation schemes are crucial for generation of indistinguishable photons and are not feasible in conventional approaches for electrically driven quantum light sources based on simple pin-diodes.

Resonant p-shell pumping was then applied to excite a QD-micropillar system where a single QD exciton (X) was shifted through resonance with the fundamental cavity mode (C) by means temperature tuning (cf. Fig. 1(b)). In this experiment, weak coupling associated with a Purcell factor of 4.1 was observed for the first time in a quantum device with an integrated coherent light source [1].

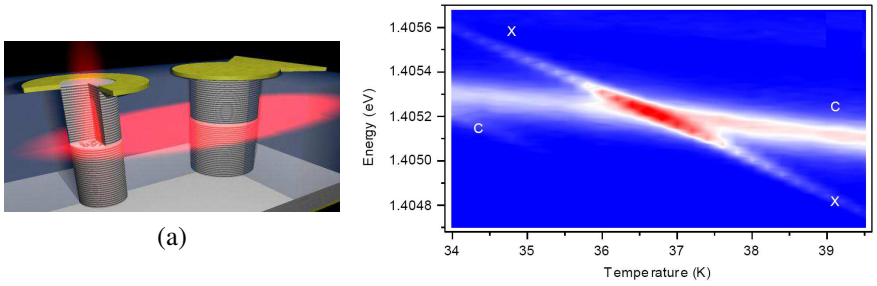

Figure 1: (a) Schematic view of device design for on-chip quantum optics (left panel). (b) Demonstration of Purcell enhancement of a QD-micropillar under resonant pumping via an electrically driven internal WGM microlaser.

REFERENCES

1. Stock, E., et al., *Adv. Mat.*, 2012, DOI: 10.1002/adma.201202778.

Highly-efficient Light-matter Interaction with Quantum Dots in Photonic Crystals

Peter Lodahl
Quantum Photonics Group, Niels Bohr Institute, University of Copehagen
Blegdamsvej 17, Copenhagen 2100, Denmark

Abstract— 2D photonic-crystal membranes fabricated in GaAs containing InGaAs quantum dots provide a very successful platform for all-solid-state quantum optics experiments. In a photonic crystal, the light-matter interaction strength can be tailored, i.e., either enhanced or suppressed by controlling the lattice constant of the structure. We present the experimental demonstration that the spontaneous emission rate of a single quantum dot can be suppressed by up to a factor of 70 in the 2D photonic-crystal membranes [1]. This ability to suppress coupling to radiation modes efficiently enables single-photon coupling efficiencies (the β-factor) approaching unity in photonic-crystal waveguides [2, 3] thereby outperforming competing methods based on plasmonic nanostructures or dielectric nanowires. The role of disorder in the form of fabrication imperfections is explored and found to lead to Anderson localization of light enabling cavity quantum electrodynamics by exploiting disorder as a way to enhance light-matter interactions that is remarkably efficient [4–6]. Furthermore, a surprisingly far reaching Purcell effect is explained as being due to the non-Markovian interaction of the quantum dot with phonons [7].

REFERENCES

1. Wang, Q., S. Stobbe, and P. Lodahl, *Phys. Rev. Lett.*, Vol. 107, 167404, 2011.
2. Lund-Hansen, T., S. Stobbe, B. Julsgaard, H. Thyrrestrup, T. Sunner, M. Kamp, A. Forchel, and P. Lodahl, *Phys. Rev. Lett.*, Vol. 101, 113903, 2008.
3. Thyrrestrup, H., L. Sapienza, and P. Lodahl, *Appl. Phys. Lett.*, Vol. 96, 231106, 2010.
4. Sapienza, L., H. Thyrrestrup, S. Stobbe, P. D. Garcia, S. Smolka, and P. Lodahl, *Science*, Vol. 327, 1352, 2010.
5. Thyrrestrup, H., S. Smolka, L. Sapienza, and P. Lodahl, *Phys. Rev. Lett.*, Vol. 108, 113901, 2012.
6. Garcia, P. D., S. Stobbe, I. Sollner, and P. Lodahl, *Phys. Rev. Lett.*, Vol. 109, 253902, 2012.
7. Madsen, Kaer, Kreiner-Møller, Stobbe, Nysteen, Mørk, and Lodahl, submitted: arxiv:1205.5623v1.

Controlling the Spontaneous Emission from Single Quantum Dots with Electromechanical Photonic Crystal Cavities

L. Midolo[1], F. Pagliano[1], T. B. Hoang[1], T. Xia[1], F. W. M. van Otten[1], L. H. Li[2], E. H. Linfield[2], M. Lermer[3], S. Höfling[3], and A. Fiore[1]

[1]Eindhoven University of Technology, P. O. Box 513, Eindhoven NL-5600MB, The Netherlands
[2]School of Electronic and Electrical Engineering, University of Leeds, Leeds LS2 9JT, United Kingdom
[3]Technische Physik and Wilhelm Conrad Röntgen Research Center for Complex Material System Universität Würzburg, Am Hubland, Würzburg D-97074, Germany

Abstract— Recent progress in the fabrication of micro-opto-electromechanical systems (MOEMS) on III/V semiconductors has opened novel perspectives in controlling the spectral properties of nano-photonic devices by coupling them to mechanical degrees of freedom. This possibility turns out to be quite attractive especially for quantum dots (QDs)-based devices, such as single photon sources, in which the spontaneous emission of the emitter can be significantly enhanced or suppressed by the surrounding electromagnetic environment (Purcell effect). We present a device based on single self-assembled InAs QDs coupled to an electromechanically tunable GaAs photonic crystal cavity (PCC). The tunable cavity allows us to modify the excitonic decay rate in real-time by adjusting the wavelength detuning between the resonant mode and the emitter. The PCCs have been etched on two closely spaced parallel membranes whose distance can be modified via electrostatic actuation. This novel structure provides several advantages compared to other electromechanical approaches discussed so far in the literature, such as the complete isolation of the actuation from the optically active areas and the absence of quality factor deterioration. Moreover it can be operated at cryogenic temperatures ($\sim 10\,\mathrm{K}$) without significantly affecting the energy emission of single QDs. We modified the spontaneous emission rate by over a factor of ten and observed a reversible tuning range of 13 nm with less than 5 V applied bias. These results will open the way to fully tunable and Purcell-enhanced single photon sources for applications in quantum photonic integrated circuits and networks.

Classical to Quantum Transition for Heat Transfer between Two Clusters

Shiyun Xiong[1], **Kaike Yang**[2], **Roberto D'Agosta**[2], **Pietro Cortona**[3], **and Sebastian Volz**[1]

[1]Laboratoire d'Énergétique Moléculaire et Macroscopique
Combustion, UPR CNRS 288, École Centrale Paris, 92295, Châtenay-Malabry, France
[2]Nano-Bio Spectroscopy Group and ETSF Scientific Development Centre
Departamento Fisica de Materiales, Universidad del Pais Vasco UPV/EHU, E-20018 San Sebastian, Spain
[3]Laboratoire Structures, Propriétés et Modélisation des Solides
UMR CNRS 8580, École Centrale Paris, 92295, Châtenay-Malabry, France

Abstract— Near Field Radiation between two objects separated by distances where the dipole/multipole approximation applies has been extensively investigated in the past while it is still unclear which mechanism takes place when the gap reduces to shorter lengths. In this paper, heat transfer through a chain composed by identical non-contacting silica clusters is calculated with the Nonequilibrium Green's Functions method. When the gap distance d between two clusters remains larger than 3 to 4 Angstroms, the thermal conductance decreases according to the power law $d^{-5.4}$, which can be explained by a dipole-dipole interaction or long-range Coulomb interactions. The power law however changes to d^{-21} when the distance becomes smaller than 3 to 4 Angstroms, which corresponds to the quantum region of interaction when electrons are shared by both clusters. This critical gap distance d_c is confirmed by *ab-initio* calculations showing that the electronic wave functions indeed merge when the gap becomes smaller than 3 to 4 Angstroms. This quantum interaction leads to the dramatic increase of the coupling between neighbour clusters. The critical gap distance d_c also corresponds to the transition from continuous ($d < d_c$) to discrete ($d > d_c$) phonon transmission spectra and density of states. The current study may provide a better understanding of the mechanisms at play in the near field radiation between two clusters at short distances.

Session 3A4
1_FocusSession.SC1: EMC, Signal Integrity and Power Integrity for Semiconductor and High Speed Electronics

Advances of EMC in TSV Based 3D Integrated Circuits
Er Ping Li, ... 940

Electromagnetic Interactions between Interconnected Patch-ring (IPR) Structures and Planes in Electronic Packages and PCBs
Ivan Ndip, Micha Bierwirth, Stephan Guttowski, Herbert Reichl, Klaus-Dieter Lang, ... 941

Stored Energies of Emission Sources
Geyi Wen, ... 942

Efficient Equivalent-circuit Representation of High-speed Interconnects for Broadband Simulation with Arbitrary Terminations
Marco Leone, Andreas Mantzke, ... 943

Isolation Capability of a Circulator under High Amplitude Surge Pulse Attacking
Chien-Fu Shih, Liann-Bie Chang, Ching-Chi Lin, Tung-Wuu Huang, Ping-Yu Kuei, ... 945

Low Electrical Crosstalk Design Results of Monolithic Integraed Bi-directional Optoelectronic Transceiver and Its Package
Sungil Kim, ... 946

The Rigorous Helmholtz Decomposition for Signal Integrity
Xiaoyan Y. Z. Xiong, Lijun Jiang, Wei E. I. Sha, ... 947

Electrical Modeling of Through-Silicon Vias (TSV) with Ohmic Contact in Silicon Interposer
De-Cao Yang, Madhavan Swaminathan, Er Ping Li, ... 948

Fast Macromodel-based Transient Simulation of High-speed Channels with Nonlinear Terminations
S. B. Olivadese, Stefano Grivet-Talocia, ... 949

Recent Advances in 3D-IC EMC Measurement Methods
Jianfei Wu, Etienne Sicard, J. Li, ... 950

Advances of EMC in TSV Based 3D Integrated Circuits

Erping Li
National University of Singapore, Singapore

Abstract— Rapid growth and convergence of digital computing and wireless communication have been driving the semiconductor technology in today's nanometer regime to continue its evolution following the scaling law, i.e., Moore's law at the semiconductor transistor device and on-chip level, and "More than Moore" at the intra-chip interconnect and packaging level. The through-silicon via (TSV) technology, which is explored by many researchers for three-dimensional (3D) integration, represents such a latest example of scaling. It has the potential benefits of improving the electrical performance including speed, bandwidth and functionality, and reducing power consumption by shortening the interconnection path in the 3D ICs. However, the development of nano-scaled integrated circuits and 3D integration faces several challenges in terms of electrical performance, such as the electromagnetic compatibility (EMC) between circuits, signal integrity (SI) and power integrity (PI) in electronic integration are of vital importance. In addition, the material property on electromagnetic performance, aging effects, thermal-electrical coupling. This presentation will cover the advances and challenges of EMC modeling, measurement, design in semiconductor integrated circuits and the system package integration.

Electromagnetic Interactions between Interconnected Patch-ring (IPR) Structures and Planes in Electronic Packages and PCBs

Ivan Ndip[1,2], **Micha Bierwirth**[2], **Stephan Guttowski**[1], **Herbert Reichl**[1,2], **and Klaus-Dieter Lang**[1,2]

[1]Fraunhofer IZM, Gustav-Meyer-Allee 25, Berlin 13355, Germany
[2]Technische Universität Berlin, Straße des 17, Juni 135, Berlin 10623, Germany

Abstract— The continuous demand for portable and multifunctional wireless electronic products has fueled the need for the integration of RF/analogue, digital, MEMS and a myriad of other mixed-signal components/subsystems on a single chip or electronic package. For further miniaturization of wireless products, these components must be integrated in very close proximity to each other. However, compact integration of mixed-signal components can only be achieved if efficient noise suppression/isolation methods are used, especially when the components share the same power distribution network (PDN). This is because noise, e.g., simultaneous switching noise (SSN), generated from digital components may propagate through the cavity of power-ground planes and couple to sensitive components, thereby causing either detuning of RF/analogue circuits, false switching of digital circuits or even malfunctioning of the entire system.

Amongst the numerous noise suppression/isolation methods studied so far, electromagnetic band gap (EBG) structures, based on Svienpipper's work on high impedance surfaces, have received the greatest attention because of their efficiency in suppressing noise propagation in a wide range of frequencies. Consequently, many EBG configurations have been developed within the last decade. Examples include planar EBGs, mushroom-type EBGs and hybrid EBGs. However, EBGs have many disadvantages which limit their application in system design. For example, since they are periodic structures, at least one of their metal layers is always segmented into many periodic unit cells. Each cell consists of a patch and inductive metal strips/branches. In some cases, surface mount capacitors and inductors are used to increase the design freedom. These surface-mount components and the periodic patches as well as the metal branches take-up much of the package/board space and leave little space for placement and routing of the "actual" components needed for system functionality. Furthermore, the branch inductances of EBG cells greatly obstruct charge delivery from bypass capacitors to switching devices. Lastly, due to the periodicity of the patches, transmission lines routed above the patterned layers of EBGs suffer from return-path discontinuity (RPD) problems, which severely degrade their electrical performance.

To overcome these limitations, a new noise suppression/isolation structure, the interconnected patch-ring (IPR) structure, was proposed in [1]. The IPR is just as effective as EBGs in suppressing noise propagation but has many advantages over EBGs. For example, only a small portion of one of its metal layer is patterned along its periphery and no surface mount components are needed. Hence, when IPRs are used, a higher integration density in electronic packages and boards is achieved, no obstruction of charge delivery occurs and transmission lines have less RPD problems than when routed over EBGs.

However, when IPRs are integrated/embedded in electronic packages and printed circuit boards (PCBs) they may suffer from de-tuning effects and lose their stopband characteristics, because of the electromagnetic interactions between the IPRs and metal layers routed above them. To prevent this, the impact of these metal layers must be extensively investigated at the beginning of the design cycle. In [1], this impact was not studied.

Therefore, in this paper, the electromagnetic interactions between interconnected-patch ring (IPR) structures and planes in electronic packages and PCBs are extensively discussed. The IPRs are first designed, fabricated and measured. An excellent correlation is obtained measurement and simulation. The effects of integrating the IPRs in multilayered substrates are then studied. Our results show that EM interactions between an IPR and a plane that is placed above the IPR causes the excitation of parallel-plate modes which leads to the disappearance of the stopband of the IPR. We then investigate and implement design measures to prevent this disappearance.

REFERENCES

1. Ndip, I., S. Guttowski, and H. Reichl, "A novel interconnected patch-ring (IPR) structure for noise isolation," *Proc. IEEE International Symposium on Electromagnetic Compatibility*, 328–333, Austin, TX, USA, August 17–21, 2009.

Stored Energies of Emission Sources

Geyi Wen
College of Electronic and Information Engineering
Nanjing University of Information Science and Technology, Nanjing 210044, China

Abstract— In order to understand electromagnetic interference in an electronic system, we need to know the emission source as well as its influence on other parts of the system. In many situations the interference (emissions) comes from the current distributions (emission sources) whose extensions are comparable to the wavelength. To identify how the electromagnetic field energy is transferred to a nearby component (receptor), the properties of the electromagnetic stored energies around the emission sources must first be elucidated. In this article, the methods for evaluating the stored electromagnetic energies generated by an arbitrary current distribution are investigated. Expressions for the stored electromagnetic energies have been derived and have been validated by numerical examples. These expressions provide physical insight into the coupling mechanisms of the emission source. For example, when the stored magnetic (or electric) field energy is dominant, the coupling is mainly inductive (or capacitive). One of the methods of reducing the coupling is to properly design the emission sources (structures) to make the intensity of the stored energies as small as possible. For this reason, the minimization of stored energies is also investigated in this article. It has been demonstrated that an optimal current distribution that minimizes the stored energies exists for a specified emission structure. The optimal current distribution may be determined by solving a generalized eigenvalue equation deduced from the minimization of stored energies. Numerical results are also presented in this article.

Efficient Equivalent-circuit Representation of High-speed Interconnects for Broadband Simulation with Arbitrary Terminations

Marco Leone and Andreas Mantzke
Otto-von-Guericke-University of Magdeburg, Germany

Abstract— In the recent years various macromodeling approaches have been developed for signal interconnections, relying on different mathematical effort and application range. In this paper we present a passive and intrinsically stable Foster equivalent-circuit model with accelerated convergence. Given an arbitrary homogenous transmission line, fully specified by the physical length l and the frequency dependent p.u.l. parameters R', L', G', C' (Fig. 1).

Based on the Greens function of the 1D-wave equation, the following accelerated solution for the frequency dependent mutual-impedance Z_{ij} can be obtained:

$$Z_{ij} = \frac{1}{j\omega C_0 + G_0} + j\omega \tilde{L}_{ij} + \sum_{n=1}^{N} \frac{v_n^i v_n^j}{\frac{1}{j\omega L_n} + j\omega C_n + G_n} \tag{1}$$

relating the voltage V_i at the port position x_i to the current I_j at x_i. The first term includes the static capacitance C_0 and the conductance G_0, as given by the p.u.l line parameters. The second term in (1)

$$\tilde{L}_{ij} = L_{ij} - \sum_{n=1}^{N} v_n^i v_n^j L_n \tag{2}$$

includes the static mutual inductance L_{ij}, for which a closedform expression has been developed. It provides convergence acceleration for the sum in the third term of (1). The truncation order

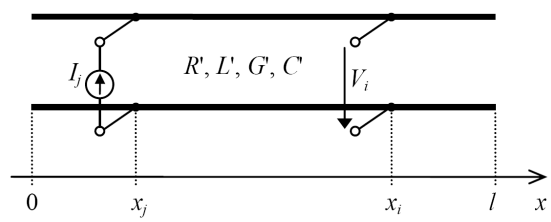

Figure 1: Transmission line with source and observation port.

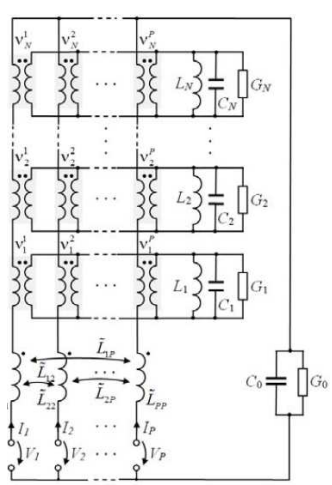

Figure 2: Accelerated equivalent-circuit for a multiport transmission-line.

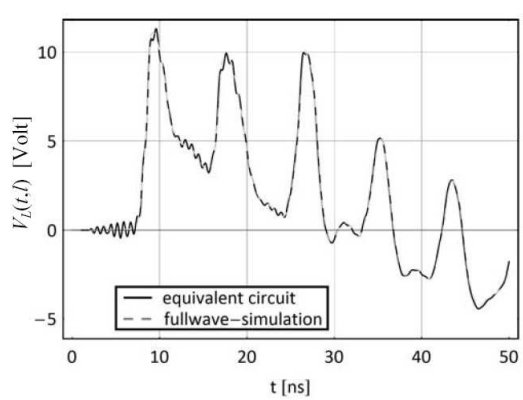

Figure 3: Voltage response at line end ($l = 1\,\mathrm{m}$), excited by a triangular voltage pulse at $x = 0$, with zener-diode protection at $x = l/8$ ($N = 11$).

N can be safely estimated by

$$N \gtrsim 2l\sqrt{L'C'}\,f_{\max} \tag{3}$$

with respect to the required frequency bandwidth $f_{\max}$. The impedance solution (1) can be cast into a Foster-type multiport equivalent circuit (Fig. 2) with the modal circuit parameters L_n, C_n and G_n which are available in closed form, and the position dependent factors

$$v_n^i = \sqrt{2}\cos(n\pi x/l) \tag{4}$$

represented by the turn ratios of ideal transformers.

As validation example we consider a lossy transmission line of $l = 1\,\mathrm{m}$ length and characteristic impedance $Z_C \approx 24\,\Omega$. The line is excited at $x = 0$ by a triangular voltage impulse with $50\,\mathrm{V}$ amplitude and rise/fall time $\tau = 2\,\mathrm{ns}$. A simple overvoltage protection consisting of two counter-directed zener diodes (SMF5.0A) is connected at $x = 0.8\,\mathrm{m}$.

Figure 3 shows the simulated voltage response across the load impedance $R_L = 50\,\Omega$ at the line end ($x = l$). The visible reflections are due to the impedance mismatches by the diodes and by R_L. Referring to (3), the minimum mode order for our equivalent circuit is roughly estimated by $f_{\max} \approx 1/\tau = 500\,\mathrm{MHz}$, resulting in $N > 5$. Using $N = 11$ we obtain a very good agreement with the reference 3D fullwave simulation of a commercial solver (CST MWS). The latter took about 15 min based on an S-parameter frequency sweep (62 frq. steps) with subsequent IFFT, while our equivalent network model required only 30 s with a customary SPICE solver.

Isolation Capability of a Circulator under High Amplitude Surge Pulse Attacking

Chien-Fu Shih[1], **Liann-Be Chang**[1], **Ching-Chi Lin**[1], **Tung-Wuu Huang**[1], **and Ping-Yu Kuei**[2]

[1]Department of Electronic Engineering & Green Technology Research Center
Chang Gung University, 259 Wenhwa 1st Road, Kweishan
Taoyuan 333, Taiwan, R.O.C.
[2]Department of Electrical and Electronic Engineering
Chung Cheng Institute of Technology
National Defense University, Taoyuan 335, Taiwan, R.O.C.

Abstract— A three port 4 GHz microwave circulator is adopted here for surge isolation testing. The circulator is terminated with high power 50 ohm on the third port. It has a 0.8 dB forward inserting loss and 15 dB return loss around 4 GHz with 50 ohm load. An electromagnetic pulse simulator with a waveform of double exponential is adopted in this study. Its short circuit peak current is 160 A, rise time 20 ns and FWHM (full width at half maximum) of 500 ns.

First, the pulse source simulator is connected directly to a 50 ohm load, and after reverse surge stressing, a peak current of 85 A is observed. Second, the source is connected to the isolator and then to 50 ohm load. The residual peak current is measured down to 15 Amperes. Third, the source is series connected to the isolator, a small high voltage capacitor, and then to 50 ohm load. The residual peak current is measure dropped to 3 Amperes. Thus, the total energy of residual transient voltage still remains safe even with a quarter watt load.

As a whole, the behavior of circulator under a high and fast surge pulse attacking has not been explored before. Most of the related discussion was made on low power or continuous wave only. In this research, the proposed simple configuration can reduce the high inject pulse current from 160 A down to 3 A. The device is also tested using a Network Analyzer with the correspondent configurations at 4 GHz. The insertion loss rises only from 0.8 to 1.8 dB for the extra capacitor and connectors. The return loss is still 15 dB without any change.

Low Electrical Crosstalk Design Results of Monolithic Integraed Bi-directional Optoelectronic Transceiver and Its Package

Sungil Kim
Future Technology Research Department, Creative Future Research Laboratory
Electronics and Telecommunications Research Institute
138 Gajeong-ro, Yuseong-gu, Daejeon 305700, Korea

Abstract— In this paper, we have proposed electrical crosstalk reduction scheme for a monolithic integrated bi-directional optoelectronic transceriver (M-BiDi) using an ion implantation technique. We have also presented a package design results for the M-BiDi based on a conventional transistor outline (TO)-CAN style. Implant isolation characteristics for a 1.25 Gbps M-BiDi, which is a key component to constitute gigabit passive optical networks (PONs) for a fiber-to-the-home (FTTH) were analyzed and measured. Also, we derived an equivalent circuit of the implant structure under various DC bias conditions. The 1.25 Gbps M-BiDi consists of a laser diode with a monitor photodiode as a transmitter and a photodiode as a digital data receiver on the same InP wafer. According to IEEE 802.3ah and ITU-T G.983.3 standards, a receiver sensitivity of the digital receiver has to satisfy under -24 dBm @ BER $= 10^{-12}$. Therefore, the electrical crosstalk levels have to maintain less than -86 dB from DC to 3 GHz. From analysed and measured results of an implant structure, the 1.25 Gbps M-BiDi with the implant area of 20 µm and 200 µm distance between the laser diode and monitor photodiode, and between the monitor photodiode and digital photodiode, satisfies the electrical crosstalk level. These implant characteristics can be used for a design and a fabrication of an optoelectronic systyem-on-a chip (SoC) design, and expended to a mixed-mode SoC field.

The Rigorous Helmholtz Decomposition for Signal Integrity

X. Y. Z. Xiong, L. J. Jiang, and W. E. Sha
Department of EEE, The University of Hong Kong, Hong Kong, China

Abstract— The vector field analysis is fundamentally important in fields of mathematics, physics and engineering. It is also one important stage for signal integrity and power integrity analysis for todays complex integrated circuits and printed circuit boards.

The Helmholtz's theorem states that any sufficiently smooth, decaying vector field in three dimensions can be decomposed into the sum of a curl-free (CF)/irrotational and a divergence-free (DF)/solenoidal vector components. The Helmholtz decomposition (HD) could capture field features, such as sources, sinks and vortices. Thus it is a powerful visual tool in several applications involving aerodynamic design, detection of flow features, computer graphics, etc.. This theorem is also of great importance in electromagnetic (EM) and microwave engineering applicable from low to high frequency ranges. Compared to the loop-tree decomposition that is a quasi-HD and breaks down at high frequencies, the HD can capture both circuit physics and the wave physics properly, which will be presented in numerical results.

Moreover, in contrast to the visual form of the total surface current obtained, the decomposed CF and DF parts respectively reproduce the capacitive and inductive coupling of a complex EM system. Hence, the HD can be employed as a postprocessing tool to understand and analyze EM responses.

In this talk, we will introduce a new development of the surface integral equation (SIE) method for realizing the HD for the arbitrary current (vector field) defined on a simply connected planar surface. The HD is applied to analyze the high-frequency coupled transmission line and low-frequency structure that demonstrate its rigorous properties and efficiency for EM field analysis. The work provides theoretical foundation, numerical method and physical understanding for the HD, which are not only important in electromagnetics and microwave engineering but also in fluid, elastic wave, and other areas. From our results, compared with the low-frequency loop-tree methods, we could get much cleaner vision of the capacitive and inductive coupling relationship in the parasitic circuit system which is critical to signal integrity and power integrity.

ACKNOWLEDGMENT

This work was supported in part by Hong Kong RGC (GRF 711511, 713011, and 712612), NSFC 61271158), and in part by the University Grants Council of Hong Kong (Contract No. AoE/P-04/08).

Electrical Modeling of Through-Silicon Vias (TSV) with Ohmic Contact in Silicon Interposer

De-Cao Yang[1, 2], **Madhavan Swaminathan**[2], **and Er-Ping Li**[2]

[1]Zhejiang University, China
[2]Georgia Institute of Technology, USA

Abstract— Through-silicon via (TSV) interconnects is used for vertical stacking of integrated circuit (IC) chips on silicon interposer. Because of the short pitch between TSV interconnects, crosstalk modeling for TSV arrays becomes important. Many approaches have been proposed for modeling TSVs [1]. In [2], the electrical design and physics-based modeling of a new signal-ground-signal (SGS) TSV signaling scheme that uses grounded TSVs has been proposed for 3D stacking of ICs. However, the proposed model in assumes a perfect ohmic contact for the metal-silicon interface of the ground TSV. As a result, the contact resistance and capacitance for metalsilicon interface and the effect of doping concentration on crosstalk has not been taken into account. In addition, since silicon substrates for IC dies are usually grounded and have zero potential, the ohmic contact for ground TSVs may not be necessary for ICs but can be useful for silicon interposer.

In this presentation, high-density through-silicon via (TSV) interconnects in silicon interposer require effective crosstalk-reduction signaling schemes and rigorous crosstalk modeling techniques. In this paper, we propose a rigorous model for grounded TSVs with ohmic contact. The proposed model takes into account contact resistance, doping density, and doping-region capacitance for the metal-silicon interface of grounded TSVs. The comparison between modeling results and full-wave simulations validates the accuracy of the proposed model for signal-ground-signal vias.

REFERENCES

1. Li, E. P., *Electrical Modeling and Design of 3D Integrated System*, Wiley-IEEE Press, New York, 2012.
2. Ndip, I., et al., "High-frequency modeling of TSVs for 3-D chip integration and silicon interposers considering skin-effect, dielectric quasi-TEM and slow-wave modes," *IEEE Transactions on CPMT*, Vol. 1, No. 10, 1627–1641, 2011.

Fast Macromodel-based Transient Simulation of High-speed Channels with Nonlinear Terminations

S. B. Olivadese and S. Grivet-Talocia
Politecnico di Torino, Italy

Abstract— This paper presents a systematic approach for the fast simulation of high-speed channels terminated by nonlinear drivers and receivers. This problem is relevant for the assessment of analog signal quality in high-speed data transmission, for which the correct communication between system parts may be seriously compromised if the relevant parasitic effects due to electromagnetic interactions are not properly taken into account.

There are several difficulties in the verification ow of terminated high-speed channels. The electrical connection between drivers and receivers is usually provided by a multiconductor system of nets placed in close proximity and undergoing an irregular routing through chip, package, cards, boards and connectors. Due to the high frequency spectral content of the transmitted signals, such structures have to be treated as distributed models, that are usually characterized in the frequency domain through their multiport Scattering matrices. The latter are computed by assembling different models of the channel parts computed at a discrete set of frequencies over the band of interest. On the other hand, drivers and receivers are complex nonlinear circuits, requiring system simulation in the time domain.

This work addresses the transient simulation problem by casting all system parts as reduced-order macromodels that approximate with good accuracy their electrical behavior. The channels are represented as linear time-invatiant systems having a transfer matrix with elements expressed by delay-rational functions of frequency. The delay terms represent signal propagation, whereas the corresponding rational coefficients represent attenuation, dispersion and all other nonideal effects. The time-domain representation of these macromodels is equivalent to a recursive convolution operator that is very efficient to compute. The driver and receiver macromodels are constructed as a combination of various submodels, including a nonlinear static part representing the DC characteristic, connected to a linear part representing dynamic effects in fixed logic states. Also these macromodels are cast as a time-domain operators represented by a combination of recursive convolutions and nonlinear function evaluations.

All macromodels are assembled into a global system that is solved through a dedicated iterative scheme based on a Waveform Relaxation formulation. As a result, complete transient system simulations are achieved in very fast runtime, outperforming traditional approaches. The proposed technique is demonstrated on a set of high-speed channels found in real hardware products.

Recent Advances in 3D-IC EMC Measurement Methods

J. Wu[1], **E. Sicard**[2], **and J. Li**[1]

[1]College of Electronic Science and Engineering
National University of Defense Technology, Changsha, Hunan 410073, China
[2]National Institute of Applied Sciences, Toulouse 31077, France

Abstract— For 3D-ICs, the multiple active dies are stacked on top of each other which bring more EMC problems like vertical die to die EMI coupling, crosstalk in bonding or TSVs, increasing amount of radiation, worse thermal ageing effects and so on. To characterize the 3D-IC EMC issues, the EMC test is a big challenge as some 2D-IC measurement methods may no longer suitable for 3D-ICs.

Due to the 3D-IC defects and the defects-induced circuit failures, people are concerning a lot on TSV defects test. There are external and internal accesses for 3D-IC EMC test. The external access can use probes, nano contactor or non-contact testing. The internal access is design-for-test (DfT) whose architecture is based on IEEE Std 1500 or IEEE Std 1149.1.

The International Electro-technical Commission (IEC) has released two major standards for IC EMC measurements. One for IC radiated and conducted emissions (IEC 61967) and another for IC susceptibility (IEC 62132). One new project concerning measurement methods to characterize IC transient susceptibility (IEC 62215) is also conducted. While applying in 3D-IC EMC tests, the existing or publishing methods for IC tests have some challenge. So some non-standard methods should be proposed for 3D-IC EMC testing. The proposed methods are on-chip sampling test, contactless probing test, skate probe, combined IC EMC standard methods and so on.

Session 3A5
SC3&4: Microwave Photonics

Electro-optic Engineering for Microwave Photonics Applications
Davide Janner, V. Pruneri, ... 952

Microwave Photonics Signal Processing with on-chip Stimulated Brillouin Scattering
David Marpaung, ... 953

Microwave Photonic Filter and Photonic Differentiator Employing Integrated Silicon Waveguide
Jianji Dong, ... 954

All Optical Frequency Conversion Utilizing Nonlinear Dynamics of Semiconductor Lasers Subject to Optical Square Wave Injection
Shao-Wei Peng, Yu-Shan Juan, ... 955

New Approach to Electronic Band Gap Filtering Structures Combining Microstrip and Dielectric Resonators
Bahareh Moradi, Ursula Martinez-Iranzo, Oriol Ymbern, Cynthia Martinez, Julian Alonso, Joan Garcia-Garcia, ... 956

Dispersive Fourier Transformation for Microwave Photonics Applications
Chao Wang, ... 957

Challenging Aspects of Terahertz Terabit Wireless Communications
Xianbin Yu, Michael Galili, Peter Uhd Jepsen, Leif K. Oxenlwe, ... 959

Polarization-modulated Photonic Analog Links
Shilong Pan, ... 960

Multiband-OFDM Ultra Wideband Wireless Signals over Fiber Transmission
John Xiupu Zhang, Bouchaib Hraimel, Dongya Shen, Taijun Liu, ... 961

An Efficient and Flexible Satellite Repeater Based on Optical Frequency Combs Technology
Xinwu Yang, Kun Xu, Jie Yin, Yitang Dai, Feifei Yin, Jianqiang Li, Hua Lu, Tao Liu, Yuefeng Ji, 962

Microwave Frequency Multiplication Based on Double-pass Modulation and Fiber Ring Microwave Photonic Filters
Zuowei Xu, Hongyan Fu, Zhiping Cai, Zhangwei Yu, ... 963

Electro-optic Engineering for Microwave Photonics Applications

D. Janner[1] **and V. Pruneri**[1, 2]

[1]ICFO-Institut de Ciencies Fotoniques, Mediterranean Technology Park
Castelldefels, Barcelona 08860, Spain
[2]ICREA-Institució Catalana de Recerca i Estudis Avançats, Barcelona E-08010, Spain

Abstract— Optical-to-electrical and electrical-to-optical conversion of microwave signals play a central role in microwave photonics links. High speed processing at microwave frequencies is difficult and expensive to realize in the electrical domain, while in the optical domain it can be more easily realized using photonic circuits and fiber based processing. However these latter solutions are not always inexpensive and easy to integrate. Another approach is represented by directly introducing microwave filtering in the electrical-to-optical conversion step, for example by using domain engineered electro-optic modulators. Domain engineering is a well known technique used to invert locally the spontaneous polarization of $LiNbO_3$ single crystals, that correspondingly produces a sign reversal of the electro-optic coefficient. Its application to Mach-Zehnder or even simpler waveguide circuits has strong potentials in microwave photonics, ranging from optical signal processing to enhanced bandwidth modulation and detection of microwave fields. In the talk, we will give few examples of domain micro-structuring and its applications in microwave photonics links.

Microwave Photonics Signal Processing with on-chip Stimulated Brillouin Scattering

David Marpaung
Centre for Ultrahigh Bandwidth Devices for Optical Systems (CUDOS)
School of Physics, University of Sydney, Australia

Abstract— Integrated microwave photonics (IMWP) is an emerging field in which microwave signals are processed in an optical chip scale. Key advantages of IMWP include footprint reduction, energy efficiency, and potential cost reduction. On the other hand, stimulated Brillouin scattering has been widely used for a number of microwave photonics signal processing tasks, such as wideband phase shifting, true time delay, and microwave filtering. But until very recently, SBS is largely limited to optical fibers. Here, we harness SBS effect in a chip scale to enable various IMWP signal processing tasks. We focus on the generation of an SBS-based microwave notch filter with a record performance in terms of 3-dB bandwidth, stop-band attenuation, frequency tunability, and energy efficiency operation.

Microwave Photonic Filter and Photonic Differentiator Employing Integrated Silicon Waveguide

Jianji Dong
Wuhan National Laboratory for Optoelectronics
Huazhong University of Science and Technology, Wuhan 430074, China

Abstract— Silicon integrated devices have been a hot topic in the area of integrated microwave photonics for ultrafast analog signal processing due to their maturity, compatibility with CMOS technology, immunity to electromagnetic interference, and compactness for it has high index contrast between Si and SiO_2 etc.. Microwave photonic filter (MPF) and photonic differentiator (DIFF) are very useful tools in ultrafast analog signal processing. In this talk, we demonstrate several schemes to implement MPF and photonic DIFF using silicon cascaded Mach-Zehnder interferometers and cascaded microring resonators. Especially high order DIFF and reconfigurable MPF are addressed.

All Optical Frequency Conversion Utilizing Nonlinear Dynamics of Semiconductor Lasers Subject to Optical Square Wave Injection

Shao-Wei Peng and Yu-Shan Juan
Department and Institute of Photonics Engineering
Yuan Ze University, 135 Yuan-Tung Road, Taoyuan County 32003, Taiwan

Abstract— Recently, nonlinear dynamics of the optically dynamical injection systems are of interested. Potential applications in microwave photonics such as broadband microwave frequency comb generation are demonstrated through an optically pulse-injected semiconductor laser. To the best of our knowledge, most studies focused on the nonlinear dynamics of the traditional continuous wave injection and dynamical pulse and sine wave injection. Nonlinear characteristics of the semiconductor laser subject to optical square wave injection are investigated the first time. In this work, nonlinear dynamics and characteristics of a semiconductor laser subject to optical square wave injection are investigated numerically. The periodic optical square waveforms for injection are generated from a laser (master laser) by using an external EO modulator on a laser (master laser). Under proper operational conditions, namely the repetition frequency and injection strength of the injected light, harmonic and sub-harmonic frequency-locked states with different locking ratios are observed at the output of the injected laser (slave laser). By examination of the electrical power spetra and time series generated from both the injection waveform and injected laser ouput, all optical frequency conversion are observed. The peaks of the injected laser output are induced by the injected square wave with repetition frequency of 1 GHz. The existence and enhancement of high-order harmonics lays on the foundation of frequency conversion. When applying a stronger injection level to the semiconductor laser, the conversion ratio can be continuously tuned to a higher value. As the result, the conversion ratio of 23 times is achieved due to the effect of bandwidth broadening in optical injection system. The proposed scheme possesses the advantages of low cost, compact, less system complexity, and more flexibility in frequency tuning which also shows the potential of high frequency microwave signal generation.

New Approach to Electronic Band Gap Filtering Structures Combining Microstrip and Dielectric Resonators

Bahareh Moradi[1], **Ursula Martinez-Iranzo**[1], **Oriol Ymbern**[2], **Cynthia Martinez**[2,3], **Julian Alonso**[2], **and Joan Garcia-Garcia**[1]

[1]Grupo de Aplicaciones Electromagnéticas Industriales-GAEMI
Departament d'Enginyeria Electrònica de la Universitat Autònoma de Barcelona
Campus de Bellaterra, 08208 Cerdanyola del Vallés, Barcelona, Spain
[2]Grupo de Sensores y Biosensores
Departamento de Química Analítica de la Universitat Autònoma de Barcelona
Campus de Bellaterra, 08208 Cerdanyola del Vallés, Barcelona, Spain
[3]Institute for Integrative Nanosciences, IFW Dresden, Helmholtzstrasse 20, 01069 Dresden, Germany

Abstract— A novel design combining standard microstrip resonators with high dielectric constant resonators, for design of low-pass and band-pass filtering electromagnetic band gaps (EBG) structures, operating in the range from 1 to 20 GHz is presented in this paper.

The basic cell of the EBG is compoused by a standard microstrip ring and a Dielectric Resonator (DR) embedded in the PCB, in such a way that the microstrip ring act as a feed structure for some of the dielectric resonator resonant modes. The DR is generated depositing commercial high dielectric constant Epoxy paste (CREATIVE 122-06 pad-printable high dielectric constant epoxy paste, with a value of $\varepsilon_r = 45$). The technological process is compatible with Low Temperature Cofired Ceramics (LTCC) technology. As an illustrative example a low band pass filter at 2.6 GHz has been designed and fabricated obtaining a good agreement between full 3D electromagnetic simulation and measurement. The simulations have been performed using the Agilent Empro 2012.9 software. The geometry of the proposed structure, consist in a 3 cells EBG each one formed by a cylindrical DR with 2 mm diameter and 1.27 mm height, and 1.3 mm width microstrip ring resonator with an inner radius of 2.3 mm. In order to obtain the best performance in the range of interest, the 50 mil Roger substrate RO3010 (characterized by a loss tangent $\delta = 0.0022$ and $\varepsilon_r = 10.2$), has been used to design the prototype.

Work is in progress to obtain design rules to control the filtering characteristics (impedance matching, operating frequencies, bandwidth, etc.) through geometrical parameter and to combine the response to improve standard filters.

Dispersive Fourier Transformation for Microwave Photonics Applications

Chao Wang
School of Engineering and Digital Arts, University of Kent
Canterbury, CT2 7NT, United Kingdom

Abstract— Dispersive Fourier transformation (DFT) maps the broadband spectrum of an optical pulse into a time stretched waveform using chromatic dispersion [1]. Owing to its capability of real-time pulse-by-pulse spectroscopic measurement and manipulation, DFT has become an emerging technique for ultrafast signal generation and continuous single-shot measurements in optical communications, optical sensing, spectroscopy and imaging, where the speed of traditional instruments falls short [2].

In this paper, the principle and implementation methods of DFT are introduced and its widespread applications in microwave photonics systems are presented. The most obvious and straightforward application of DFT is real-time spectroscopy, where the instantaneous spectral characteristics of an ultrashort optical pulse are encoded onto its temporal intensity variation. Fast dynamic phenomena that are encoded onto the optical spectrum can be now acquired and slowed down in the time domain so that they can be digitized and analyzed in real-time. Compared to traditional optical spectroscopy instruments, DFT-based real-time spectroscopy offers a few orders of magnitude higher measurement speed. As two examples of ultrafast real-time spectroscopy, ultrafast gas absorption spectroscopy [3] and fiber Bragg grating interrogation [4] are introduced. DFT technique can also be applied in photonic-assisted microwave arbitrary waveform generation [5], where the spectrum of the optical pulse is manipulated on purpose using an optical spectral shaper. By properly designing the response of the spectral shaper, a microwave waveform with its shape identical to that of the shaped optical spectrum can be produced [6–9]. In another application of DFT, due to the one-to-one mapping relation between spectrum and time, the spectrum shape of the pulse can be changed in a fast and reconfigurable manner using temporal modulation — a technique called time-domain spectral shaping. One example of this technique is instantaneous microwave frequency identification based on temporal channelization [10]. The final microwave photonics application of DFT technique is ultrafast real-time imaging [11], which is made possible by employing additional spatial dispersion to encode the spatial information (image) onto the pulse spectrum. The images can then be reconstructed from the temporally stretched optical pulses. With its capability of fast continuous capturing, DFT-based imaging technique is expected to be useful for high-throughput screening of rare objects or events.

REFERENCES

1. Muriel, M. A., J. Azana, and A. Carballar, "Real-time Fourier transformer based on fiber gratings," *Opt. Lett.*, Vol. 24, 1, 1999.
2. Goda, K. and B. Jalali, "Dispersive Fourier transformation for fast continuous single-shot measurements," *Nat. Photon.*, Vol. 7, 102, 2013.
3. Goda, K., C. Wang, and B. Jalali, "Broadband dispersive Fourier-transform spectroscopy in the 800 nm range," submitted.
4. Wang, C. and J. P. Yao, "Ultrafast and ultrahigh-resolution interrogation of a fiber Bragg grating sensor based on interferometric temporal spectroscopy," *J. Lightwave Technol.*, Vol. 29, 2927, 2011.
5. Wang, C. and J. P. Yao, "Advanced fiber Bragg gratings for photonic generation and processing of arbitrary microwave waveforms," *2010 IEEE International Topical Meeting on Microwave Photonics*, 414–417, 2010.
6. Wang, C., F. Zeng, and J. P. Yao, "All-fiber ultrawideband pulse generation based on spectral-shaping and dispersion-induced frequency-totime conversion," *IEEE Photon. Technol. Lett.*, Vol. 19, 137, 2007.
7. Wang, C. and J. P. Yao, "Simultaneous optical spectral shaping and wavelength-to-time mapping for photonic microwave arbitrary waveform generation," *IEEE Photon. Technol. Lett.*, Vol. 21, 793, 2009.
8. Wang, C. and J. P. Yao, "Photonic generation of chirped millimeter-wave pulses based on nonlinear frequency-to-time mapping in a nonlinearly chirped fiber Bragg grating," *IEEE Trans. Microw. Theory Tech.*, Vol. 56, 542, 2008.

9. Wang, C., M. Li, and J. P. Yao, "Continuously tunable photonic microwave frequency multiplication by use of an unbalanced temporal pulse shaping system," *IEEE Photon. Technol. Lett.*, Vol. 22, 1285, 2010.
10. Wang, C. and J. Yao, "High-resolution microwave frequency measurement based on temporal channelization using a mode-locked laser," *2012 IEEE MTT-S InternationalMicrowave Symposium Digest (MTT)*, 2012.
11. Goda, K., A. Mahjoubfar, C. Wang, A. Fard, J. Adam, D. R. Gossett, A. Ayazi, E. Sollier, O. Malik, E. Chen, Y. Liu, R. Brown, N. Sarkhosh, D. Di Carlo, and B. Jalali, "Hybrid dispersion laser scanner," *Sci. Rep.*, Vol. 2, 445, 2012.

Challenging Aspects of Terahertz Terabit Wireless Communications

Xianbin Yu, Michael Galili, Peter Uhd Jepsen, Leif K. Oxenlwe
DTU Fotonik, Department of Photonics Engineering
Technical University of Denmark, DK-2800, Kgs. Lyngby, Denmark

Abstract— The increasing demand on fast wireless communications, e.g., huge data file transferring and mobile broadband access, has driven wireless communication systems into a path towards Terabit era. Terahertz (THz) technology is promising due to its unique features, such as unlimited bandwidth available and minimum human health threat. However, a number of technical challenges need to be overcome to achieve such an ultrafast data rate of Terabit in the THz frequency band. This presentation overview the key technologies and challenging aspects of a THz Terabit communication system, from a system point of view, in terms of THz generation and link power budget. The THz atmospheric absorption is another critical issue to limit wireless communication range.

Polarization-modulated Photonic Analog Links

Shilong Pan
Microwave Photonics Research Laboratory, College of Electronic and Information Engineering
Nanjing University of Aeronautics and Astronautics, Nanjing 210016, China

Abstract— Power-efficient analog photonic links (APLs) for radio over fiber systems based on polarization modulators (PolMs) are presented. The PolM together with a polarizer can perform amplitude modulation and phase modulation with adjustable ratio, so the peak of the frequency response of a dispersive link can be shifted to a desired frequency, which can compensate the dispersion-induced power fading. In addition, with two of the PolMs placed in parallel, the third-order nonlinear distortion can be fully suppressed. The PolM-based APLs are simple, compact and power efficient.

Multiband-OFDM Ultra Wideband Wireless Signals over Fiber Transmission

Xiupu Zhang[1, 2], **Bouchaib Hraimel**[2], **Dongya Shen**[1], **and Taijun Liu**[3]

[1]School of Information Science & Engineering, Yunnan University, Kunming, China
[2]Advanced Photonic Systems Lab, Concordia University, Montreal, Canada
[3]College of Information Science & Engineering, Ningbo University, Ningbo, Zhejiang, China

Abstract— Multiband-OFDM ultra wideband signals-over-fiber transmission is reviewed considering the impact of modulator nonlinearity, fiber dispersion, optical receiver response, wireless interference and optical crosstalk. Enabling techniques to improve modulation efficiency are discussed. Photonic techniques for simultaneous millimeter-wave up/down conversion and optical subcarrier modulation are also reported.

Summary: Orthogonal frequency division multiplexing (OFDM) ultra-wideband (UWB) signal has attracted many applications. Due to UWB characteristics, UWB over fiber has been considered as a promising technique for distribution of UWB wireless signals. OFDM does not require complicated chromatic dispersion management for transmission and also makes spectrum resources utilized efficiently. Despite its advantages, OFDM is very susceptible to nonlinearities from optical transmission, such as nonlinearities from optical transmitter/receiver and semiconductor optical amplifier (SOA) etc.. In short-distance of radio over fiber (RoF), direct-detection is better applied to optical OFDM due to its simplicity. We will review the impact of the combined effect of fiber dispersion and nonlinearities of optical transmitter and receiver's response on the OFDM subcarriers for multiband (MB)-OFDM UWB over fiber with Mach-Zehnder modulator (MZM) or electro-absorption modulator (EAM). It was found that there are optimum RF modulation indexes for optical transmitter with MZM or EAM, and the best optical receiver is with Chebyshev-II response. MB-OFDM transmission over fiber is mainly limited by laser phase noise converted relative intensity noise and phase distortion induced by fiber dispersion. Higher modulation index is limited by amplitude and phase distortion to OFDM signal induced by optical transmitter and receiver response nonlinearities and fiber dispersion.

In subcarrier multiplexing UWB over Fiber (SCM-UoF), the antenna at the base station may receive in-band narrowband jammers falling within the bandwidth of the MB-OFDM UWB signals. It was found that the interferer-to-UWB peak power ratio of the in-band interferers must be maintained below certain level to ensure acceptable performance of the received MB-OFDM UWB signal.

Crosstalk due to out of band interferers in SCM-UoF can occur through second order nonlinearity of the electro-optic modulator and the use of direct detection. It was found that out of band interference can be mitigated using mixed polarization technique or biasing the modulator at quadrature bias for second order nonlinearity suppression.

When WDM technique is introduced to MB-OFDM UWB over fiber, adjacent channel crosstalk may destroy OFDM signal's orthogonality and thus limit transmission. Our investigation showed that MB-OFDM UWB over fiber WDM system is robust to linear crosstalk, as high as $-5\,\mathrm{dB}$, from adjacent channels.

Since the UWB over fiber is operated at a low RF modulation index and MB-OFDM UWB has a low power spectral density, it was found that required optical power at optical receiver in UWB over fiber is reasonably higher than that in radio over fiber with non-OFDM modulation schemes. To improve the modulation efficiency, new modulation techniques were reviewed: Optical double-sideband subcarrier modulation immune to fiber chromatic-dispersion-induced RF power fading, and optical single sideband (OSSB) with tunable optical carrier to sideband ratio modulation.

Simultaneous photonic frequency up/down-conversion and optical subcarrier modulation of millimeter-wave MB-OFDM UWB are also reviewed.

An Efficient and Flexible Satellite Repeater Based on Optical Frequency Combs Technology

Xinwu Yang[1], **Kun Xu**[1], **Jie Yin**[2], **Yitang Dai**[1], **Feifei Yin**[1], **Jianqiang Li**[1], **Hua Lu**[2], **Tao Liu**[2], **and Yuefeng Ji**[1]

[1]State Key Laboratory of Information Photonics and Optical Communications
Beijing University of Posts and Telecommunications, Beijing 100876, China
[2]Beijing Institute of Satellite Information Engineering, Beijing 100086, China

Abstract— As the problems of frequency spectrum congestion and orbital resource depletion driving today's telecom satellite to operate at C, Ku, Ka, V and even higher bands, multi-band and multi-channel signals handlings, such as multiple local oscillators distribution, band to band conversion, beam to beam cross connection, have become extremely inefficiency, inflexible, costly and complex.

Recently, microwave photonics, with its unique characteristics of parallel signal processing over an extremely wide bandwidth, has been implemented to handle multi-band RF signals in several practical applications such as the European Space Agency's SAT'N LIGHT project [1] and the Atacama Large Millimeter Array (ALMA) [2], where the corresponding functions can hardly be realized by their electrical counterparts.

In this work, we propose a high efficient and flexible satellite repeater with parallel processing ability based on optical frequency combs technology. The proposed scheme consists of three sections, a multi-band local oscillator generation section, an inter- & intra-band frequency conversion section and a channel switching section. It is worth noting that only three frequency-fixed microwave sources are needed for the whole system and theoretically more than 7 bands (L to Ka) of microwave generation and frequency conversion can be supported. In the first section, dual coherent optical frequency combs with different center wavelength and frequency spacing are generated through electro-optic modulation technique. By heterodyning the generated dual-combs, multiple photonic microwave local oscillators within different frequency bands (e.g., C, Ku, K, etc.) are achieved. Then, simultaneous inter- and intra-band microwave frequency conversion are implemented by adding a signal replication module to the first section. Input signal are optically mixed with one of the combs and replicated over each comb lines. After heterodyne with the other comb and optical periodical filtering process, the converted frequencies within different frequency bands are obtained in separated channels. In the channel switching section, an optical 4×4 MEMS switch routes the channelized signal within different bands to different output ports.

In a word, the first section provides multi-band local oscillators, the second and third section complete band to band conversion and beam to beam cross-connection respectively. We carry out a proof of concept experiment, in which an input C band frequency of 6.1 GHz is successfully converted to 4.1 GHz, 3.9 GHz, 11.9 GHz, 19.9 GHz, etc. in each channel. System impairments are assessed by modulating the input frequency with a 10 Mbps QPSK signal and about 9.3% EVM degradation compared with back to back condition is observed at 0 dBm input power. However, all the measured results are far below the maximum EVM limit of 31.6% for QPSK signal in a very wide power range.

REFERENCES

1. Sotom, M., B. Benazet, A. Le Kernec, and M. Maignan, "Microwave photonic technologies for flexible satellite telecom payloads," *35th European Conference on Optical Communication (ECOC)*, Vienna, Austria, Sept. 20–24, 2009.
2. Cliché, J.-F. and B. Shillue. "Precision timing control for radioastronomy. Maintaining femtosecond synchronization in the atacama large millimeter array," *IEEE Control Systems Magazine*, Vol. 26, No. 1, 19–26, 2006.

Microwave Frequency Multiplication Based on Double-pass Modulation and Fiber Ring Microwave Photonic Filters

Zuowei Xu[1], **Hongyan Fu**[1,*], **Zhiping Cai**[1], **and Zhangwei Yu**[2]

[1]Department of Electronic Engineering, School of Information Science and Engineering
Xiamen University, Xiamen 361005, China
[2]Department of Applied Physics, Royal Institute of Technology (KTH)
Roslagstullsbacken 21, Stockholm 10691, Sweden

Abstract— Photonic generation of high frequency microwave signal has been intensively studied in the last few years, due to its advantages such as the capability of generating high quality microwave signal with high frequency and wideband tunability, etc.. There are many techniques to generate microwave signal in optical domain, and the external modulation method is one of the important techniques that enjoys the advantages such as, high signal stability, good tunability and system simplicity. To generate high order harmonics, normally two or several modulators are used, and also a well-designed and fabricated optical filter is needed to select the desirable harmonics, which will both increase the complexity and cost of the generation system.

In this article, a novel approach to generate high frequency microwave signal with double-pass modulation and a fiber ring based microwave photonic filter is proposed and experimentally demonstrated. The light is modulated by a commercial Mach-Zehnder modulator (MZM), and after that the doublepass modulation is realized by connecting the output of the MZM with a fiber loop which is formed by connecting an EDFA between two output ports of a 50 : 50 fiber coupler, thus the modulated optical light from the MZM can be amplified and reflected back to the MZM again and re-modulated by the microwave signal via the same MZM High order harmonic signals are generated and enhanced based on the nonlinear characteristics of the large signal modulation and the dual-pass modulation process. By beating these harmonics on the photodiode (PD), high frequency microwave harmonic signals which are integral multiple of the low frequency drive signal can be generated. A fiber ring based tunable incoherent microwave photonic filter (MPF) is used to select the desirable harmonics to beat on the PD. The length of fiber ring can be designed, so that the frequency of odd harmonics and even harmonics are located in the notch points $((n + 0.5)FSR,\ n = 0,\ 1,\ 2,\ \ldots)$ and the maximum points $((2n + 1)FSR,\ n = 0,\ 1,\ 2,\ \ldots)$ of the fiber ring based MPF respectively, where FSR is the free spectra range of the MPF. In this way, the odd harmonics can be suppressed and even harmonics remains. By using a cascaded fiber ring based microwave photonic filter with another ring length, the even harmonics of the remained signal after the first filter can be selected. In our experiment, by modulating the drive signal of 3 GHz, the 2nd harmonic of 6 GHz has been generated with the signal-to-noise ration of more than 20 dB by using one fiber ring based MPF. The odd harmonics are well suppressed and the 4th harmonic of 12 GHz can also be generated by using two cascaded fiber ring based MPFs. Our experimental results are limited by the bandwidth of the MZM, and higher frequency microwave signal can be generated by increasing the frequency of driving signal, as well as the bandwidth of the devices, such as MZM and PD.

The proposed approach of photonic generation of microwave signal can generated high quality microwave signal with high frequency, good tunability, and it is very easy to implement, which shows good application potential in the fiber wireless communication systems.

*Corresponding author: Hongyan Fu (fuhongyan@xmu.edu.cn).

Session 3A6
4_FocusSession.SC4: Challenges for Small Antennas

A Look at the Small Challenges in the Small Antenna Design
Zhinong Ying, Raj Mittra, ... 966
Optimization of Resonant and Antiresonant Properties of Electrically Small Antennas with Single, Coupled, and Multiple Resonances
Oleg B. Vorobyev, ... 967
Antenna Bandwidth Optimization by Global Optimization Algorithms with Single Frequency Simulation
Marius Cismasu, Mats Gustafsson, ... 969
Optimum Geometry for an Electrically-small, Layered Magnetic Dipole Antenna
James S. McLean, Heinrich D. Foltz, Robert Sutton, ... 971
Gain Enhancement of a Fractal Antenna Using Partial Substrate Removal
Neeraj Rao, Dinesh Kumar Vishwakarma, ... 973
An Overview of Physical Bounds on Small Antennas
Mats Gustafsson, ... 975
Compact Dual Printed MIMO Antennas for Mobile Handsets Covering GSM/UMTS/WLAN and LTE
Sultan Shoaib, Imran Shoaib, Nosherwan Shoaib, Xiaodong Chen, Clive G. Parini, ... 976
Stored Energies and Antenna Q, Electric and Magnetic Case
B. Lars G. Jonsson, Mats Gustafsson, ... 977
Challenge of Small Multi-port Antenna for Compact MIMO Mobile Terminal
Zhinong Ying, ... 978
Compact Quad-band PIFA Antenna for LTE Handsets with MIMO and Low Mutual Coupling
Khaled A. Abdelwahab, Esmat Abdel-Fattah Abdallah, Mohamed Aboul El-Dahab, ... 979

A Look at the Small Challenges in the Small Antenna Design

Zhinong Ying[1] and Raj Mittra[2]

[1]Sony Mobile Corporation, Lund, Sweden
[2]EMC Laboratory, The Pennsylvania State University, University Park, PA-16802, USA

Abstract— Designing small antennas is a very challenging problem, especially when they operate in a complex environment such as the one found in a mobile phone, are surrounded by various paraphernalia, e.g., an acoustic component, a battery and a camera, and are limited to a small piece of real estate because of relentless trend toward miniaturization being followed by the manufacturers. In addition, the requirements to meet the coverage at multiple frequencies, multi-standard and the SAR criterion exacerbate the problem even further and continue to present continuous challenges to the designer.

In this paper, we first examine ways by which we can cope with some of the fundamental limits imposed by the physics of the problem at human body effect, and then look at creative ways by which we can attempt to meet these challenges. We describe some strategies for systematic antenna designs to cover multiple frequencies and MIMO type of approaches for increasing the throughput, even within the constraints of limited space that present formidable challenges to the development of MIMO-type designs. We examine the viability of non-Foster designs to enhance the bandwidth and how we can deal with the instability problems that inherently plague these designs. We also identify some potential application of Metamaterials that might help solve some of the problems identified above, and attempt to separate facts from fiction, insofar as the promises of these materials that are often touted as being the "cure-alls" for all of our problems.

Optimization of Resonant and Antiresonant Properties of Electrically Small Antennas with Single, Coupled, and Multiple Resonances

O. B. Vorobyev
Stavropol Institute of Radio Communications, Russia

Abstract— The small antennas relative to the radiated (scattered) wavelengths ($ka < 0.5 \ldots 1$) have a significant practical and fundamental importance. The concept of the lower bound on the quality factor facilitated the design of several outstanding antennas, including wire antennas with single and double resonances. The performance properties of the antennas are defined by the distribution of inductance in the wire structures. The properties of the macroscopic electromagnetic field in a medium comprised of electrically small elements, such as an ordered wire structure, are described by the effective negative permittivity. The wire antennas can be associated with the axially symmetric electrically small dipole antennas in the shells with the negative permittivity. Analysis of the symmetric antennas (scatteres) in the shells revealed that the optimal performance of the electrically small antennas is achieved for the antennas, which are tuned on resonance in antiresonant ranges.

Comparison of electrically small dipoles of different shapes with an equal electrical size displays that the radiation resistance is maximal for the spherical mode TM_{01}. Since the capacitive reactance of a fringe capacitance is minimal in this mode too, the radiation quality factor of the spherical antenna with the electrical current along its surface represents the lower bound on the quality factor of the electrically small antenna Q_{lb}. Generally, the electrical size and shape of an electrically small antenna determine the lower bound on the radiation quality factor, which is valid for scattering too. According to Mie's theory for a sphere and the approximate Rayleigh model for the spheroids, the shape and electrical size of a sub-wavelength particle designate negative permittivity for resonant scattering of a quasi-static electric field.

The power of antenna radiation of the antenna tuned on antiresonance is maximal in the case of the constant amplitude of the input current. Because of antiresonance, the magnitude of the current at the interface of the antenna with free space exceeds the input current of the antenna. Even though the power of the antenna radiation is comparatively low at an antiresonant frequency for the constant amplitude of the input voltage, a lower bound on the radiation quality factor of a specific antenna corresponds to the antiresonant frequency. A similar kind of antiresonance is involved in resonant scattering of an electromagnetic field on sub-wavelength particles with the power of the scattered (radiated) electromagnetic field proportional to $(ka)^4$. The shape of an electrically small antenna controls the antiresonant properties and a lower bound on the radiation quality factor of a specific antenna. The internal structure of an electrically small antenna is tuning the central frequency of the bandwidth in relation to the antiresonant frequency, and owing to that, the radiation quality factor.

Few practice antennas with a single impedance resonance provide the radiation quality factor $Q \leq 1.5Q_{lb}$. In accordance with the model of an electrically small antenna in the shell, the quality factor of the antenna with a single resonance is $Q = \frac{|\varepsilon|+1}{|\varepsilon|}Q_{lb}$, where $|\varepsilon| = 2 + 2.4(ka)^2$ is the antiresonant negative permittivity. The lower bound on the radiation quality factor is unreachable for the electrically small antennas with a single resonance. That, however, is possible for the antennas with closely spaced resonances around an antiresonant frequency. An electrically small antenna is tuned on a single resonant frequency higher (lower) than the closest antiresonant frequency by means of the inductance (capacitance). The antenna is tuned on the coupled resonances around the antiresonant frequency by a resonant sub-circuit comprised of series inductance and capacitance. The quality factor of the antenna with sufficiently coupled resonances is close to the lower bound on the quality factor.

Dispersion of the effective negative permittivity imposes fundamental constraints on optimization of electrically small antennas in accord with the concept of the lower bound on the quality factor. The wider is the bandwidth of an electrically small antenna with coupled resonances, the wider is the corresponding range of the effective negative permittivity, defined in the case of a non-resonant wire structure by the Drude model. Bandwidths of the antennas with single and coupled resonances are limited by the dispersion, which detunes the surface plasmon resonance at the interface of the antenna and fringing medium. A multi resonant electrically small antenna, which satisfies the condition of causality, corresponds to the antenna shell with the effective

permittivity described by the multi resonant Lorentz model. Functional parameters of multi resonant electrically small antennas, such as fractal antennas, are limited by a comparatively strong frequency dependence of the Lorentz permittivity.

Antenna Bandwidth Optimization by Global Optimization Algorithms with Single Frequency Simulation

M. Cismasu and M. Gustafsson
Department of Electrical and Information Technology, Lund University
Box 118, Lund 221 00, Sweden

Abstract— This work describes a method to compute antenna Q from the electromagnetic solution at a single frequency. The electric and magnetic energies stored in the fields excited by an antenna and the radiated power are computed using the results by Vandenbosch [1] and Geyi [2], see also [3]. This computation follows the procedure described in [4, 5]. The Q factor can be used as a direct measure of antenna bandwidth based on a input impedance resonance model [6].

The approach described above is implemented by slightly modifying a standard Method of Moments solver (MoM) [4, 5]. These modifications do not increase the computation time significantly due to the fact that such solvers compute most of the necessary quantities.

The method can be integrated in global optimization algorithms [7]. Here, a genetic algorithm (GA) [8], is used to optimize rectangular radiating structures and structures with a fixed rectangular ground plane. The GA/MoM procedure is followed [9]. Block matrix decomposition is used to reduce the optimization time for structures with fixed ground planes [9]. Antenna Q and resonance are the optimization criteria chosen for illustration purposes. In addition resonance is considered as equality of stored electric and magnetic energies in order to verify the validity of the expressions in [1, 4].

The quality of the optimization solutions is evaluated using physical bounds. These bounds can be used as a stop criterion for an optimization process. The comparison with physical bounds for rectangular structures [4, 10], and structures with a rectangular ground plane [5], shows that the optimized structures perform close to their physical limitations. It also sustains the theory presented in [5] for antennas with a rectangular ground plane. The commercial solver E field has provided simulation data that agree very well with the theoretical results.

The single frequency antenna Q computation method may reduce the optimization time for some radiating structures. Little computational overhead is necessary to implement this method in standard MoM solvers. Physical bounds can be used to compare the performance of optimized structures. "Genetic" characteristics yielded by an optimization process may prove useful for the manual design of other radiating structures.

ACKNOWLEDGMENT

The support of the Swedish Research Council is gratefully acknowledged.

REFERENCES

1. Vandenbosch, G. A. E., "Reactive energies, impedance, and Q factor of radiating structures," *IEEE Trans. Antennas Propagat.*, Vol. 58, No. 4, 1112–1127, 2010.
2. Geyi, W., "A method for the evaluation of small antenna Q," *IEEE Trans. Antennas Propagat.*, Vol. 51, No. 8, 2124–2129, 2003.
3. Gustafsson, M. and B. L. G. Jonsson,, "Stored electromagnetic energy and antenna Q," Tech. Rep. LUTEDX/(TEAT-7222)/1-25/(2012), Lund University, 2012, http://lup.lub.lu.se/record/3241376/file/3241431.pdf.
4. Gustafsson, M., M. Cismasu, and B. L. G. Jonsson, "Physical bounds and optimal currents on antennas," *IEEE Trans. Antennas Propagat.*, Vol. 60, No. 6, 2672–2681, 2012.
5. Gustafsson, M. and S. Nordebo, "Optimal antenna currents for Q, superdirectivity, and radiation patterns using convex optimization," *IEEE Trans. Antennas Propagat.*, Vol. 61, No. 3, 1109–1118, 2013.
6. Yaghjian, A. D. and S. R. Best, "Impedance, bandwidth, and Q of antennas," *IEEE Trans. Antennas Propagat.*, Vol. 53, No. 4, 1298–1324, 2005.
7. Fletcher, R., *Practical Methods of Optimization*, John Wiley & Sons, Ltd., Chichester, 1987.
8. Thors, B., H. Steyskal, and H. Holter, "Broad-band fragmented aperture phased array element design using genetic algorithms," *IEEE Trans. Antennas Propagat.*, Vol. 53, No. 10, 3280–3287, 2005.

9. Rahmat-Samii, Y. and E. Michielssen, *Electromagnetic Optimization by Genetic Algorithms*, ser. Wiley Series in Microwave and Optical Engineering, J. Wiley, 1999.
10. Gustafsson, M., C. Sohl, and G. Kristensson, "Illustrations of new physical bounds on linearly polarized antennas," *IEEE Trans. Antennas Propagat.*, Vol. 57, No. 5, 1319–1327, 2009.

Optimum Geometry for an Electrically-small, Layered Magnetic Dipole Antenna

J. S. McLean[1], **H. D. Foltz**[2], **and R. Sutton**[1]

[1]TDK R. & D. Corp., 1101 Cypress Creek Road, Cedar Park, TX 78613, USA
[2]University of Texas Pan-American, USA

Abstract— Several features differentiate the magnetic dipole from its electric counterpart making it more appropriate for some applications. The most obvious one is that such an antenna is well suited for radiating horizontal polarization near ground. However, another important characteristic of the magnetic dipole is that the presence of a magnetic core tends to exclude magnetic energy from the interior of the antenna [1–3, 9–12]. This exclusion of energy takes place even when the material is intrinsically lossy [4, 5] and an antenna will still operate efficiently provided the product of the frequency and the magnitude of the complex relative permeability is significantly greater than unity. As all known magnetic materials exhibit significant loss in the upper HF and VHF frequency ranges as well as above, this mechanism is very important. Materialloaded spherical-wire magnetic dipoles make more effective use of a spherical volume than do the simple loop and the solenoid or loop-stick designs. Hence, they provide performance more closely approaching the physical limitation on radiation Q for a spherical volume [6–8]. It has been found that the spherical wire magnetic dipole antenna can be realized using a shell or mantle of magnetic material, optimally placed over a conducting core as shown in Fig. 1 [?, 13, 14]. The magnetic mantle concept is to some degree appropriate for magnetic thin film materials. Magnetic thin film materials have an advantage over bulk magnetic materials in that their dispersion characteristics are superior. More specifically, bulk ferrite materials have been shown to exhibit dispersion characteristics which are predicted by Snoek's law which states that the product of the low frequency or static initial permeability and the resonance frequency (the loss tangent peak) is essentially constant; that is, increasing the resonance frequency requires reducing the static permeability. However, magnetic thin films and other heterogenous magnetic structures can circumvent this limitation to an extent [16, 17].

Thus, the paradigm of an optimum, low-profile, magnetic dipole antenna could possibly take the form of a generalized convex deformation in a conducting ground plane covered by one or more magnetic thin film layers and a top layer of metallization. Although optimum core parameters for spherical wire magnetic dipole antennas (such as mantle thickness and permeability) have been published, to the author's knowledge no argument has been put forth to show that the spherical or hemispherical shape itself is optimum. Therefore, we explore the effect of the deformation of a layered hemispherical wire antenna employing a magnetic mantle over a conducting core. More specifically, we quantitatively examine the effect on the radiation Q and radiation efficiency of increasing the height along the magnetic dipole axis and increasing the cross section transverse to the dipole axis.

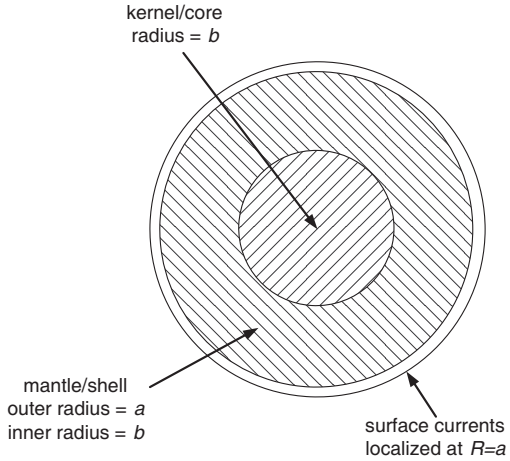

Figure 1: Spherical wire magnetic dipole employing an inhomogeneous core consisting of a magnetic mantle covering a conducting kernel.

REFERENCES

1. Wheeler, H. A., "Small antennas," *IEEE Trans. Antennas Propagat.*, Vol. 23, No. 4, 462–469, Jul. 1975.
2. Wheeler, H. A., "Fundamental limitations in small antennas," *Proc. IRE*, Vol. 35, No. 12, 1479–1484, Dec. 1947.
3. Bellett, P. T. and C. J. Leat, "An investigation of magnetic antennas for ground penetrating radar," *Progress In Electromagnetics Research*, Vol. 43, 257–271, 2003.
4. McLean, J. S., H. Foltz, and R. Sutton, "Electrically-small TE01 mode spherical wire antennas employing lossy magneto-dielectric materials," *Proc. International Workshop on Antenna Technology*, Lisbon Portugal, Mar. 2010.
5. McLean, J. S. and R. Sutton, "An efficient, low-profile antenna employing lossy magnetodielectric materials," *Proc. International Workshop on Antenna Technology*, 261–264, Tuscon, Arizona, Mar. 2012.
6. Thal, Jr., H. L., "New radiation Q limits for spherical wire antennas," *IEEE Trans. Antennas and Propagat.*, Vol. 54, 2757–2763, Oct. 2006.
7. Best, S. R., "A low Q electrically small magnetic (TE Mode) dipole," *IEEE Antennas and Wireless Propagat. Lett.*, Vol. 8, 572–575, Jun. 2009.
8. Best, S. R., "A new electrically small TE mode dipole," *Proc. Int. Workshop on Antenna Technol.*, Mar. 2009.
9. Breinbjerg, O. and O. S. Kim, "Minimum Q electrically small spherical magnetic dipole antenna — Theory," *Proc. International Symposium on Antennas and Propagation — ISAP2009*, Bangkok, Thailand, Oct. 2009.
10. Breinbjerg, O. and O. S. Kim, "Minimum Q electrically small spherical magnetic dipole antenna — Practice," *Proc. International Symposium on Antennas and Propagation — ISAP2009*, Bangkok, Thailand, Oct. 2009.
11. Kim, O. S., "Low-Q electrically small spherical magnetic dipole antennas," *IEEE Trans. Antennas and Propagat.*, Jul. 2010.
12. Kim, O. S., O. Breinbjerg, and A. D. Yaghjian, "Electrically small magnetic dipole antennas with quality factors approaching the Chu lower bound," *IEEE Trans. Antennas and Propagat.*, Vol. 58, No. 6, 1898–1906, 2010.
13. Kim, O. S. and O. Breinbjerg, "Lower bound for the radiation q of electrically small dipole antenna with solid magnetodielectric core," *IEEE Trans. Antennas and Propagat.*, Vol. 59, No. 2, 679–681, Feb. 2011.
14. Kim, O. S. and O. Breinbjerg, "Decreasing the radiation quality factor of magnetic dipole antennas by a magnetic-coated metal core," *20th International Conference on Applied Electromagnetics and Communications (ICECOM 2010) Proceedings*, Dubrovnik Croatia, Sept. 20–23, 2010
15. McLean, J. S., R. Sutton, and H. Foltz, "Broadband, electrically-small spherical-wire and generalized loop antennas exploiting inhomogeneous magnetic cores," *20th International Conference on Applied Electromagnetics and Communications (ICECOM 2010) Proceedings*, Dubrovnik Croatia, Sept. 20–23, 2010.
16. Acher, O. and S. Dubourg, "A generalization of Snoeks law to ferromagnetic films and composites," *Physical Review B*, Vol. 77, No. 10, Art. No. 104440, Mar. 2008.
17. Rozanov, K. N., "Achers constraint on the high-frequency magnetic performance of composites," *Proc. General Assembly and Scientific Symposium, 2011 XXXth URSI*, Aug. 13–20, 2011.

Gain Enhancement of a Fractal Antenna Using Partial Substrate Removal

Neeraj Rao and Dinesh Kumar Vishwakarma
PDPM Indian Institute of Information Technology, Design & Manufacturing, Jabalpur, India

Abstract— Many ways of enhancing gain and bandwidth of a microstrip patch antenna have been suggested in literature. The microstrip patch antenna resonates at a single frequency. In this paper, a novel antenna design for enhancing the resonant frequencies and the gain of a multiband antenna has been proposed. The frequencies are increased by the use of fractal designs and the gain is enhanced by using partial substrate removal on a dielectric (Fig. 1) [1].

A microstrip patch antenna is widely used in compact and portable communication devices due to its small size, thin profile configurations, conformity and low cost. In spite of these remarkable advantages, the patch suffers some serious drawbacks like single resonant frequency. Bandwidth can be increased but at the cost of size of the patch, making it large and bulky. To overcome this problem, a fractal design has been used, in this paper to make it multiband. There are different types of losses in antenna, one of which is surface wave loss due to of the permittivity of the material and thickness of the substrate. Due to excitation of surface waves, patch antenna also suffers from reduced gain and efficiency as well as unacceptably high levels of cross-polarization and mutual coupling within an array environment at high frequencies. In this paper, part of the substrate surrounding the patch have been strategically removed to suppress surface wave losses, and thereby increasing the gain.

It is known that microstrip patch antenna resonates for a particular frequency, the antenna has a set of radiating edges for this frequency. The number of frequencies can be increased by increasing the number of edges and also by increasing the inductance and capacitance generated within the patch. This is done by the use of fractal geometry so as to increase the number of radiating edges and also to increase the set of inductance and capacitances which combine to generate the resonant frequency of the antenna.

But the number of frequencies is added at the cost of the gain of the antenna, the gain of the fractal patch antenna is low as compared to the gain of the patch antenna without fractal design. Therefore methods must be implemented to enhance the gain of the fractal patch. To enhance the gain of the multiband antenna, techniques like Electromagnetic Band Gap structures are not appropriate because they enhance the gain of the antenna only for a particular frequency not for all the frequency [2]. Therefore the method to enhance the gain must be such that it enhances the gain of antenna for all the frequencies. The method proposed in this paper is partial substrate removal. In this technique the removed layer stops the propagation of surface waves and also reduces the dielectric loss. It forms a cavity below the removed portion because of it the gain for all frequency is not enhanced by the same amount. But the gain is enhanced for all the frequencies by this technique. The presence of the dielectric enhances the amount of radiation coupled to the substrate by a factor of $e^{(\text{function of } \varepsilon)}r$. Therefore presence of the substrate enhances the backward radiation and can be overcome by the proposed technique. Removing the substrate partially stops the propagation of surface wave in the substrate, which reduces the power coupled in backward direction and enhances the forward coupled power [3]. As a result the gain increases.

The proposed antenna has been implemented using CST Studio Suite^{TM} 2011 and tested for removal of substrate in various configurations like — along radiating and non-radiating edges, making trenches of different widths all-around the patch, below the patch and on all its sides. These configurations have been analyzed for removal of substrate on half of the layer from top. Analysis of resulting reflection loss, gain and bandwidth shows that using the proposed antenna design, best gain-bandwidth trade-off is achieved by removal of substrate surrounding the fractal patch. The single frequency of microstrip patch for the substrate of height 4 mm and with the dielectric constant of ($\varepsilon_r = 4$) is 5.74 GHz. The resonant frequencies increases for iteration 2 with 3 resonant frequencies and 2 well defined resonant frequencies (4.78 GHz and 7.5 GHz) for iteration 4. And the gain has been increased from 7.345 dB and 6.692 dB to 7.909 dB and 8.248 dB. Hence, the proposed antenna design based on partial substrate removal on half of the dielectric layer surrounding the fractal patch enhances the gain of the fractal antenna.

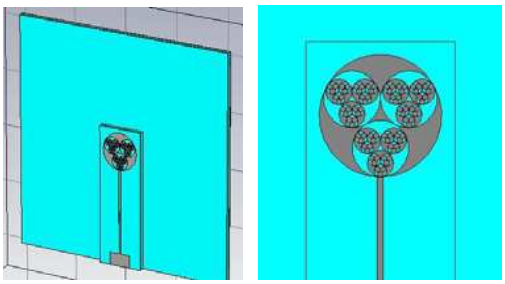

Figure 1: Proposed antenna design using partial substrate removal around the fractal patch.

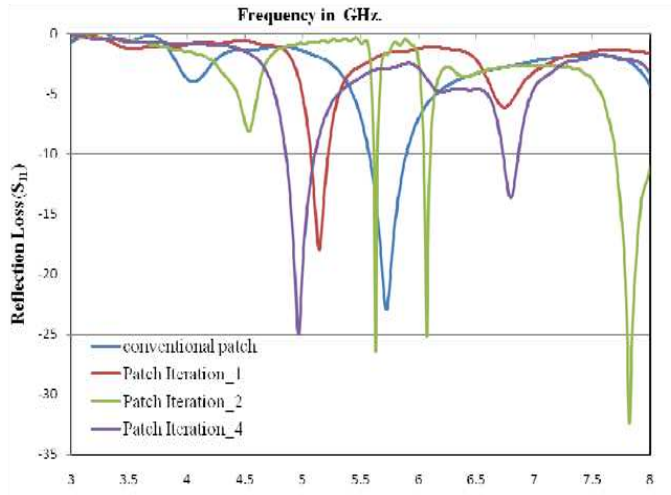

Figure 2: Reflection loss (in dB) for different iterations of fractal patch showing the multiband behaviour.

REFERENCES

1. Li, D. and J.-F. Mao, "A Koch-like sided fractal bow-tie dipole antenna," *IEEE Transactions on Antennas and Propagation*, Vol. 60, No. 5, May 2012.
2. Yablonovitch, E. and D. Siecenpiper, "High-impedance electromagnetic surfaces with a forbidden frequency band," *IEEE Transactions on Microwave Theory and Techniques*, Vol. 47, No. 11, Nov. 1999.
3. Rao, N. and D. K. Vishwakarma, "Gain and bandwidth enhancement of a microstrip antenna using partial substrate removal in multiple-layer dielectric substrate," *PIERS Proceedings*, 1285–1289, Suzhou, China, Sept. 12–16, 2011.

An Overview of Physical Bounds on Small Antennas

Mats Gustafsson
Department of Electrical and Information Technology, Lund University
Box 118, SE-221 00 Lund, Sweden

Abstract— It is well known that antenna performance deteriorates with the physical size (measured in wavelengths) of the antenna. The tradeoff between the performance and the size is expressed by physical bounds or limitations. Physical limitations are very useful because they provide a bound on the performance based on the shape and size of the design volume. The concept of physical bounds for electrically small antennas was first introduced more than half a century ago by Chu and Wheeler [1, 2]. Chu used spherical waves to express the stored and radiated energies outside the smallest circumscribing sphere of the antenna structure [1]. This approach has dominated the research on small antennas and offers many results on the Q-factor, Q, see [3] for an overview. The physical bounds were generalized to arbitrary shapes using the forward scattering sum rule in [4, 5]. These bounds have also been verified for several antennas with electrical size up to $k_0a \approx 1:5$. Arbitrary shapes are also analyzed in [6–9]. In [10], optimal currents and physical bounds for minimum Q, maximal $G = Q$, superdirective antennas, and antennas with prescribed radiated fields are presented. This generalizes the physical previous bounds in many ways.

In this presentation, an overview of the development from the work of Chu to today is presented.

REFERENCES

1. Chu, L. J., "Physical limitations of omni-directional antennas," *J. Appl. Phys.*, Vol. 19, 1163–1175, 1948.
2. Wheeler, H. A., "Fundamental limitations of small antennas," *Proc. IRE*, Vol. 35, No. 12, 1479–1484, 1947.
3. Volakis, J., C. C. Chen, and K. Fujimoto, *Small Antennas: Miniaturization Techniques & Applications*, McGraw-Hill, New York, 2010.
4. Gustafsson, M., C. Sohl, and G. Kristensson, "Physical limitations on antennas of arbitrary shape," *Proc. R. Soc. A*, Vol. 463, 2589–2607, 2007.
5. Gustafsson, M., C. Sohl, and G. Kristensson, "Illustrations of new physical bounds on linearly polarized antennas," *IEEE Trans. Antennas Propagat.*, Vol. 57, No. 5, 1319–1327, May 2009.
6. Yaghjian, A. D. and H. R. Stuart, "Lower bounds on the Q of electrically small dipole antennas," *IEEE Trans. Antennas Propagat.*, Vol. 58, No. 10, 3114–3121, 2010.
7. Vandenbosch, G. A. E., "Simple procedure to derive lower bounds for radiation Q of electrically small devices of arbitrary topology," *IEEE Trans. Antennas Propagat.*, Vol. 59, No. 6, 2217–2225, 2011.
8. Thal, H. L., "Q bounds for arbitrary small antennas: A circuit approach," *IEEE Trans. Antennas Propagat.*, Vol. 60, No. 7, 3120–3128, 2012.
9. Gustafsson, M., M. Cismasu, and B. L. G. Jonsson, "Physical bounds and optimal currents on antennas," *IEEE Trans. Antennas Propagat.*, Vol. 60, No. 6, 2672–2681, 2012.
10. Gustafsson, M. and S. Nordebo, "Optimal antenna currents for Q, superdirectivity, and radiation patterns using convex optimization," *IEEE Trans. Antennas Propagat.*, Vol. 61, No. 3, 1109–1118, 2013 (in press).

Compact Dual Printed MIMO Antennas for Mobile Handsets Covering GSM/UMTS/WLAN and LTE

Sultan Shoaib[1], **Imran Shoaib**[1], **Nosherwan Shoaib**[2], **Xiaodong Chen**[1], **and C. G. Parini**[1]

[1]Queen Mary, University of London, Mile End Road, E1 4NS, London, United Kingdom
[2]Politecnico Di Torino, Corso Duca degli Abruzzi, Turin 24 10129, Italy

Abstract— A dual printed multiple-input multiple-output (MIMO) antenna system for mobile handsets is presented. The proposed antenna is capable of covering GSM 1800 (1710–1880 MHz), GSM 1900 (1850–1990 MHz), UMTS (1920–2170 MHz), WLAN (2400–2480 MHz) and LTE (2500–2690 MHz) frequency bands. The proposed MIMO system is composed of two coupled-fed monopole antennas that are diagonally printed in mirrored configuration on the non-grounded portion of the system circuit board. The circuit board used is FR-4 substrate of relative permittivity of 4.4, loss tangent 0.02 and an overall volume of $110 \times 65 \times 0.8\,\text{mm}^3$ with each antenna occupying a small area of $24 \times 14.5\,\text{mm}^2$. A dual printed decoupling structure is etched into the ground plane to improve isolation between the two antennas. Each decoupling structure consists of a slot cut into the ground plane. Additionally two inverted-L-shaped ground branches have been extended into non-grounded portion to improve the isolation between the two antennas. The isolation of the proposed MIMO antenna is better than 15 dB over all the frequency bands covered by the antenna. The envelop correlation coefficient is also calculated to evaluate the diversity performance of the MIMO antenna.

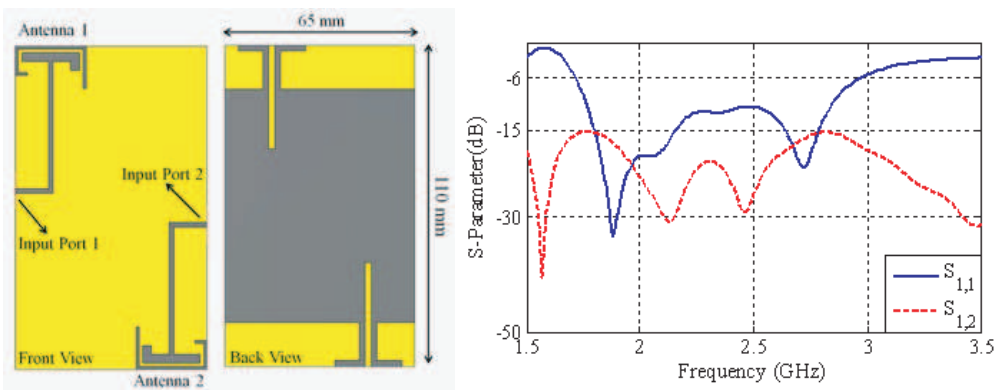

(a) (b)

Figure 1: (a) Front view and back view of the proposed dual printed MIMO antennas for mobile handsets. (b) S-parameter of the proposed antennas.

REFERENCES

1. Li, W.-Y. and W.-J. Chen, "Concurrent 2-port/3-port MIMO antenna system for UMTS/LTE2500 operation in the mobile phone," *2011 IEEE International Symposium on Antennas and Propagation (APSURSI)*, 1918–1921, July 3–8, 2011.
2. Chu, Q.-X. and J.-F. Li, "A compact wider dual-band MIMO antenna array for mobile phone," *2010 IEEE International Conference on Wireless Information Technology and Systems (ICWITS)*, 1–4, August 28–September 3, 2010.
3. Yang, C., Y. Yao, J. Yu, and X. Chen, "Novel compact multiband MIMO antenna for mobile terminal," *International Journal of Antennas and Propagation*, Vol. 2012, Article ID 691681, 9 pages, 2012.
4. Zeng, Q., Y. Yao, S. Liu, J. Yu, P. Xie, and X. Chen, "Tetraband small-size printed strip MIMO antenna for mobile handset application," *International Journal of Antennas and Propagation*, Vol. 2012, Article ID 320582, 8 pages, 2012.

Stored Energies and Antenna Q, Electric and Magnetic Case

B. L. G. Jonsson[1] and M. Gustafsson[2]

[1]KTH — Royal Institute of Technology, Sweden
[2]Lund University, Sweden

Abstract— First principle limitations on bandwidth have recently been derived for small arbitrarily shaped antennas as well as for unidirectional array antennas. These bounds provide physical limitations on the available bandwidth performance, given electrical size.

There are currently two different methods to derive these first principle bounds, energy-based limitations and sum-rule based limitations. In this letter we investigate how generalized stored energies yield such first-principle bandwidth limitations for small antennas of arbitrary shape. The stored energies presented here are an extension of the Vandenbosch integral representation energies. They were recently shown to be equivalent to the electric(magnetic) energy with the far-field energy subtracted. The energies are applied to different geometrical shapes of small antennas.

Given an arbitrarily shaped small antenna, we also present the optimization problem that determines the antenna Q and hence the antennas bandwidth. This optimization problem is investigated in detail for electric and magnetic sources and their combinations for differently shaped antennas.

For certain cases, we show that the optimization problem can be reduced to a constrained optimization problem with a well-defined Euler-Lagrange equation. The corresponding critical points of the optimization problem are shown to correspond to a certain eigenvalue problem where the dipole-moments become the eigenvectors. Explicit examples of both analytic and numerical examples are shown and discussed. We also show that a key challenging integral vector equation can be reformulated into an equivalent scalar problem, which is faster and easier to solve.

These results generalize earlier published results on bandwidth limitations. For the electric source cases it agrees with the existing results.

Challenge of Small Multi-port Antenna for Compact MIMO Mobile Terminal

Zhinong Ying
Network Research Laboratory, Research and Technology
Sony Mobile Communication AB, Sweden

Abstract— For MIMO and diversity application in Wi-Fi such as 11n, ac, 3.5G and 4G such as HSPA and LTE systems, the multi-antenna system require low mutual coupling loss and low pattern correlation between antennas in order to realize good diversity or MIMO performance. The main challenges to the mobile terminal antenna are small size, built in, multi-band and carrier aggregation for different MIMO system. For example, a smart phone needs to support more than ten 4G and 3.5G networks and all 2G and 3G networks for global coverage and roaming, which means up to dozens of cellular RF bands. Another important issue to be considered in designing antennas for mobile phone is reduction and control of SAR values (Specific Absorption Rates) which could be caused by RF radiation from multiple radio and antenna in the mobile phone. The SAR should be as low as possible, especially against the human brain. The handset with multiple transmitters and antennas in MIMO system will increase the complexity of the near field problem. In addition, Hearing aid compatibility (HAC) is required for mobile phone in some countries, which will also increase the complexity of the antenna designs.

In this paper, author will describe the fundamental issues of compact MIMO antenna system such as antenna efficiency, bandwidth, and correlation; and introduce the new parameter to character the MIMO performance by study of some fundamental antennas like orthogonal dipole; parallel dipole and co-ground monopole. Secondly, some MIMO performance improvement technique by using decoupling and de-correlation and orthogonal mode techniques will be described, some design example of multi-band, MIMO antenna design in mobile terminal will be presented. Finally, author will give some example to address the challenge of SAR issue of multi-transmitter and multi antenna mobile handset.

Compact Quad-band PIFA Antenna for LTE Handsets with MIMO and Low Mutual Coupling

Khaled A. Abdelwahab[1], **Esmat A. Abdallah**[2], **and Mohamed Aboul-Dahab**[1]

[1]The Arab Academy for Science and Technology, Cairo, Egypt
[2]Electronics Research Institute, Dokki, Giza, Egypt

Abstract— The digital era we live in has sparked numerous innovations in the smart phone market especially during the past decade. Market requirements for more compact and high capacity handsets are becoming more challenging by the day. Compact diversity antennas in the handset are needed more than ever now, at a time where Long Term Evolution (LTE) networks are being deployed in several countries. Multiple Input Multiple Output (MIMO) antennas have been shown to increase the overall capacity by being able to deliver simultaneous speed by utilizing multi-path signals. Closely spaced antennas in the mobile handset have become an ever increasing challenge due to mutual coupling between antenna elements.

Planar Inverted F-Shaped Antennas (PIFA) have been widely recognized in mobile handsets due to their compact size and multi-band capabilities. They are also known to have simple designs, thus enabling them to be commercially available. By using shorting mechanisms, PIFA antennas can resonate at quarter-wavelengths thus reducing the conventional half-wave patch antenna length by 50%. Having low SAR values due to their reduced backward radiation, makes PIFA antennas of considerable value. Narrow bandwidth has been known to be one of the limitations of PIFA antennas. The shorting via is one of the reasons for this limitation. To achieve wide bandwidth we may vary the ground size, include defected ground structures (DGS) and/or electromagnetic band-gap (EBG) structures.

The proposed structure consists of two PIFA antennas with meandered lines as well as a parasitic patch, all of which are shorted to the ground by using a shorting strip at an appropriate location. Multi-band operation in the LTE frequency bands (Band 13 "US 700 Upper C" 746–787 MHz, Band 2 "PCS 1900" 1850–1990 MHz, Band-1 "IMT 2100" 1920–2170 MHz) and the Wi-Fi (IEEE 802.11y.2008) frequency band (3600–3700 MHz) is achieved by cutting three slots into the PIFA antenna and including interdigitated capacitive strips. A folded patch at the back side of the dielectric substrate has been connected to the meandered line to increase the electrical length of the antenna thus achieving a low first resonant frequency.

It has been found that etching different DGS structures such as the Star-shape and the I-shape into the ground plane decreases the mutual coupling between the two antenna elements by more than 65 dB. Envelope correlation coefficient (ECC) and mean effective gain (MEG) have been studied in order to evaluate the operation of the MIMO antenna which was found to be satisfactory. The proposed antenna is optimal for the latest smart phone packaging dimensions. At the same time capacity is increased by incorporating two antenna elements to function as 2×2 MIMO with minimum mutual coupling between them.

Session 3A7a
SC4: Ultra-wideband Antennas for Radio Astronomy

Ultra-wideband Feeds for the Advanced Instrumentation Program of the Square Kilometer Array
Miroslav Pantaleev, ... 982

Wideband Receivers for VLBI2010 Applications
Anders Emrich, T. Ekebrand, S. Andersson, J. Jonsson, J. Yang, Miroslav Pantaleev, Per-Simon Kildal, ... 983

Initial Comparison Study of Two Alternative Feeds for the SKA Band 1: Eleven Feed and Quad-ridge Horn
Marianna V. Ivashina, Oleg Iupikov, Jian Yang, ... 984

Sensitivity and Performance Analysis of Large Antenna Arrays for Radio Astronomy
Arnold Van Ardenne, ... 985

The Antenna Performance of Chinese Spectral Radio Heliograph
Sha Li, Yihua Yan, Zhijun Chen, ... 986

Ultra-wideband Feeds for the Advanced Instrumentation Program of the Square Kilometer Array

Miroslav Pantaleev
Onsala Space Observatory, Chalmers University of Technology, Sweden

Abstract— The Square Kilometer Array Project (SKA) enters design phase aiming construction readiness in about 2–3 years. The initial configuration of SKA will consist of 260 Offset Gregorian 15 m dishes located in South Africa and equipped with 2 : 1 and 3 : 1 feeds and receivers. The final configuration of SKA, one kilometer collecting area will have dishes equipped with Wide Band Single Pixel Feeds (WBSPF). Onsala Observatory is leading the effort on the design and prototyping of WBSPF for the final configuration of SKA. In the talk, I will introduce the SKA project and discuss the WBSPF we consider as the best candidates.

Wideband Receivers for VLBI2010 Applications

A. Emrich[1], **T. Ekebrand**[1], **S. Andersson**[1], **J. Jönsson**[1],
J. Yang[2], **M. Pantaleev**[2], **and P.-S. Kildal**[2]

[1]Omnisys Instruments AB, Sweden
[2]Chalmers University of Technology, Sweden

Abstract— Omnisys is currently developing and delivering VLBI2010 receivers for the geodetic VLBI network users. The receiver is cryogenic and very wideband covering 2–14 GHz. It consists of a cryogenic dewar with a rather large window, a broadband feed, low noise amplifiers as well as different types of support electronics.

The current design is based on the well known 11-feed, INP low noise amplifiers from Low Noise Factory while the rest of the receiver system electronics comes from Omnisys.

The detailed design and performance verification results will be presented. Planned future development activities will also be described.

Initial Comparison Study of Two Alternative Feeds for the SKA Band 1: Eleven Feed and Quad-ridge Horn

Marianna Ivashina, **Oleg Iupikov**, **and Jian Yang**
Department of Signals and Systems, Chalmers University of Technology, Goteborg, Sweden

Abstract— We present an initial comparison study of the performance of two alternative feeds — Circular Eleven antenna and quad-ridge horn (QRH) — for the Off-set Gregorian reflector antenna system, such as considered for the Square Kilometer Array (SKA) radio telescope baseline design, for Band 1 of 0.3–1.05 GHz. The geometry of the reflector system is selected based on the US DVA-1 design (see Fig. 1(a)) for which the diameters of the main reflector and sub-reflector are equal to 15 m and 3.99 m, respectively, and the half subtended angle of the latter is 55° (both reflectors are shaped). To perform this study, we have used the simulated far-field pattern data of the Eleven antenna and QRH feeds that have been modeled at 2–14 GHz (for the VLBI2010 application); hence assuming that these feed designs can be scaled to the low frequencies of the SKA Band 1. The frequency scaling of the original designs has been realized such to meet the 3 : 1 bandwidth requirement for Band 1, under the constraint that the feed aperture that should not exceed the area of 90 cm × 90 cm. This constraint implies that the diameter of the feed aperture should be within the range of 1.05–3.15λ over 0.3–1.05 GHz. Comparison between the antenna efficiencies obtained when the Off-set Gregorian antenna is fed either with the Eleven feed or the Quad-ridge horn has been carried out by using the GRASP software (PO/PTD), and the results are shown on Fig. 1(b). These initial results indicate that Eleven antenna feed satisfies the efficiency requirements over the entire frequency band, while the QRH has about 12% reduced efficiency at higher frequencies; and rapid efficiency drop below 480 MHz due to the low-frequency cut-off occurring around this frequency. Hence, the dimensional constraints have more stringent implication on the performance of the QRH feed, as compared to the Eleven antenna. On the other hand, the Eleven antenna feed suffers from higher spillover noise temperature contribution due to its relatively broad pattern for the given sub-reflector; this noise contribution varies between 14 and 18 K from 600 to 1050 MHz in contrast to 8–10 K for the QRH feed. Our future work will include improvement of the considered feed designs for Band 1; and optimization of their performance in combination with the reflector optics. The latter is a part of the large collaborative effort within the SKA Dish consortium involving several partners from South Africa, Australia, Canada, China and others.

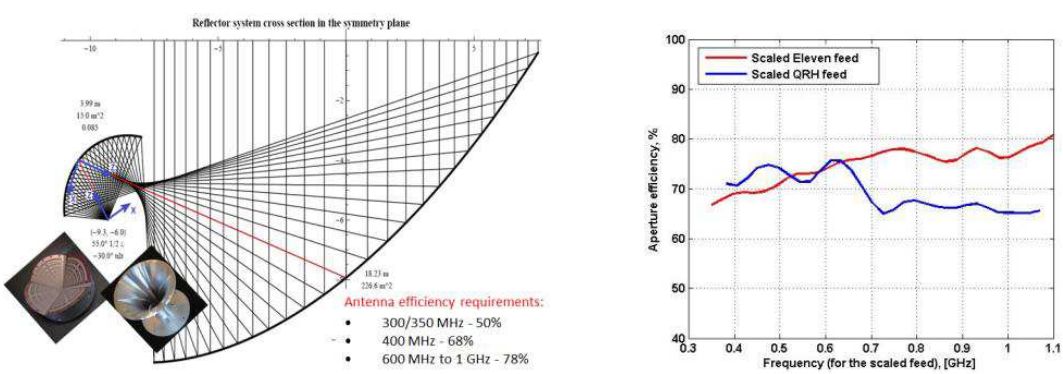

(a) (b)

Figure 1: (a) Geometry of the DVA-1 reflector system. (b) Aperture efficiency.

Sensitivity and Performance Analysis of Large Antenna Arrays for Radio Astronomy

A. Van Ardenne[1, 2]

[1]Netherlands Institute for Radio Astronomy (A-STRON)
P. O. Box 2, 7990 AA Dwingeloo, The Netherlands
[2]Chalmers Technical University, Gothenbörg, Sweden

Abstract— Since the inception around 1990 of the need that radio astronomy requires a much bigger collecting area then any existing telescope for sensitivity reasons to observe the early red-shifted neutral hydrogen universe toward cosmological distances, relatively incoherent efforts became organized over the last decades on a global scale. Now known as the Square Kilometre Array ("SKA") referring to its effective collecting aperture, under the auspices of the SKA Organization (see: www.skatelescope.org) it is in the first design phase to ultimately operate from 50 MHz up to 20 GHz. This frequency range is required to answer key astrophysical science questions complimenting observing instrument developments in other frequency domains ranging from (sub)mm to IR into the optical and beyond. This contribution will focus on the development of large so-called Aperture (Phased arrays) distributed in stations and operating in concert in so-called aperture array synthesis mode. The developments for these started from 1995 initially as a dedicated early R&D program at ASTRON, then toward a European effort with global participation for an array to operate from 400–1400 MHz ("EMBRACE") and presently as element of a development program for the SKA. Parallel to these efforts, a new window on the universe was opened at lower frequencies from 30 MHz–250 MHz for the development in what is now the LOFAR telescope (see: www.lofar.org) operating in Europe as the International LOFAR Telescope ("ILT").

This antenna systems are capable to operate over multi-octave frequency bandwidth with large operating field of views ("sky-coverage"). Being electronically controlled, flexible simultaneous multi beaming capability is only limited by the computing resources and could therefore be expanded over time. Figure 1 illustrates this capability in principle. A key attribute is to make these systems much more (say: 50–>100 times) capable for radio astronomy on most if not all performance scales compared with existing instruments at an "affordable" level for the size of the planned SKA.

We will briefly address the steps toward their present performance and analyze their capabilities and the upcoming developments.

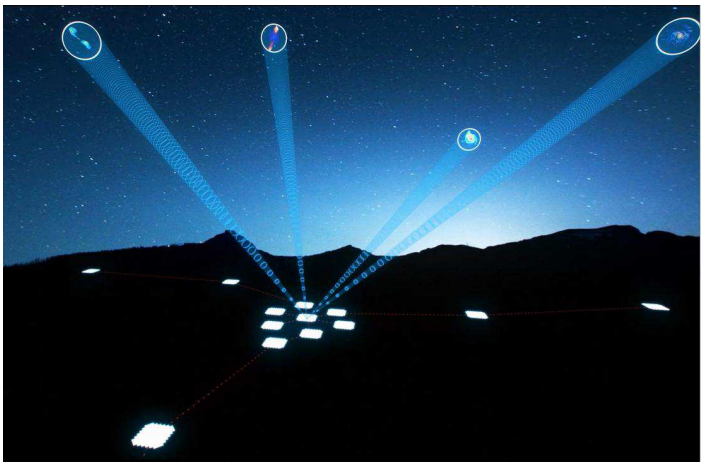

Figure 1: Artist impression of Aperture Array simultaneous multi-beam observation (courtesy Swinburne Univ. Australia). The status and performance of Arrays like this in the meter-decimeter wavelength range are topic of this contribution.

The Antenna Performance of Chinese Spectral Radio Heliograph

Sha Li, **Yihua Yan**, **and Zhijun Chen**
Chinese Academy of Sciences, Beijing, China

Abstract— Recently, there is an increasing interest in antennas with ultra-wide band feed in connection with proposed scientific systems, such as Square Kilometre Array (SKA), Atacama Large millimetre/submillimeter Array (ALMA), Chinese Spectral Radio Heliograph (CSRH) et al. CSRH is a solar Radio heliograph which will produce solar images over a frequency range of 0.4 GHz to 15 GHz. It is consisted of two arrays. CSRH-I contains 40 4.5 m antennas covering 0.4 GHz to 2 GHz, CSRH-II includes 60 2 m antennas covering frequencies from 2 to 15 GHz. To achieve this, feed with dual polarized wide impedance bandwidth, low profile, symmetrical radiation patterns are considered. In this work, efforts are made to achieve VSWR ≤ 2 over the 2.32 octave band in CSRH-I array. The feed has almost constant beam width and the measured axis ratio is nearly below 2.5 dB in the whole frequency band. The basic configuration of this feed is two parallel dipoles, which is half wavelength apart and with 11 dBi directivity. The feed and the radiation pattern is also measured in Mingantu Observatory.

Session 3A7b
SC4: Body-centric Wireless Communications

Reliable and Energy Efficient Communications for Wireless Biomedical Implant Systems
Georgia D. Ntouni, A. S. Lioumpas, Konstantina S. Nikita, ... 988

Numerical Investigation of Body-worn Ultra Wideband Antenna Localisation Techniques for Motion Capture Applications
Richa Bharadwaj, Akram Alomainy, Clive G. Parini, ... 989

Characterization of Electro-textiles Using Wireless Reflectometry for Optimization of Wearable UHF RFID Tags
Karoliina Koski, Elham Moradi, Arnaud Vena, Toni Björninen, Lauri Sydanheimo, Leena Ukkonen, Yahya Rahmat-Samii, ... 990

On the Stochastic Characterization of Wearable Antennas
Paolo Nepa, Giuliano Manara, ... 991

Active Textile Multi-antenna Systems for Energy-efficient Body-centric Communication
Hendrik Rogier, Sam Agneessens, Arnaut Dierck, Frederick Declercq, Patrick Van Torre, Luigi Vallozzi, Emmeric Tanghe, Guenter Vermeeren, Wout Joseph, ... 992

Analysis of On-body Propagation at 60 GHz Using Skin-equivalent Phantoms and Common Textiles
Anda Raluca Guraliuc, Maxim Zhadobov, Ronan Sauleau, ... 993

Evaluation of Antenna/Human Body Interactions in BAN Scenarios at Millimeter Waves
Maxim Zhadobov, Nacer Chahat, Stanislav I. Alekseev, Carole Leduc, Anda Raluca Guraliuc, Ronan Sauleau, ... 994

Broadband Vivaldi Array Antenna for On-body Communication
Xiao Li, Xianyue Wu, Constantinos Constantinou, Peter S. Hall, Yuriy I. Nechayev, Alice Pellegrini, Yang Hao, ... 995

Reliable and Energy Efficient Communications for Wireless Biomedical Implant Systems

G. D. Ntouni, A. S. Lioumpas, and K. S. Nikita
School of Electrical and Computer Engineering, National Technical University of Athens, Greece

Abstract— Wireless Body Area Networks (WBAN)s are attracting much research interest for biomedical applications, especially for patient monitoring, offering significant advantages in comparison with conventional systems, such as portability and ubiquity, as well as reduced risk of infection and failure. During the last years, the implant devices tend to comprise a complete wireless transceiver, enabling the remote control of the monitoring [1]. In contrast to conventional wireless communication systems (e.g., wireless sensor networks — WSNs), medical implants are characterized by much stricter limitations on size, reliability and power consumption, with the latter being of critical importance, since the replacement of the implants usually requires an invasive procedure. Towards this goal, the concept of cooperative communications [2] have been applied to WBANs [3], providing important advantages.

In this paper, taking into account a realistic wireless propagation environment based on the IEEE P802.15 channel model [4] (which considers devices that could be placed inside or on the surface of human body), we aim to minimize the power consumption of the implant device, by utilizing on-body relay devices, while providing the necessary link reliability in terms of the Average Bit Error Rate (ABER). In this way, the complexity and power consumption are transferred from the in-body device to the on-body relay, which is an efficient approach since they can be easily replaced, in contrast to the in-body implants. The results of this work indicate that the placement of the wearable relays on the human body (e.g., chest,wrist) plays an important role for both the total power consumption and the wireless link quality in terms of the ABER. Several different scenarios are investigated, which give insight into the system requirements and its behavior under realistic wireless environments and power considerations. Some preliminary results are illustrated in Fig. 1.

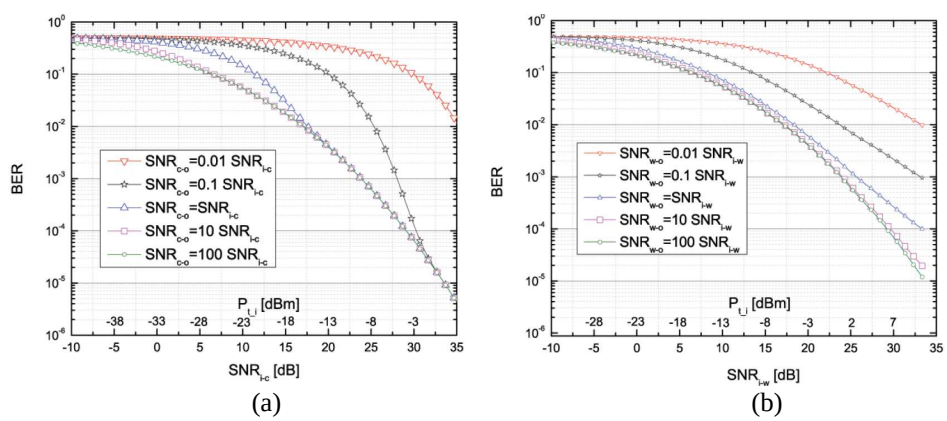

Figure 1: ABER against implant transmission power using a relay on (a) chest and (b) wrist (Distances: head implant to chest relay: 30 cm, head implant to wrist relay: 50 cm, relay to access point: 2 m).

REFERENCES

1. Ullah, S., H. Higgins, B. Braem, B. Latre, C. Blondia, I. Moerman, S. Saleem, Z. Rahman, and K. S. Kwak, "A comprehensive survey of wireless body area networks," *Journal of Medical Systems*, Vol. 36, No. 3, 1065–1094, 2010.
2. Michalopoulos, D. S., A. S. Lioumpas, G. K. Karagiannidis, and R. Schober, "Selective cooperative relaying over time-varying channels," *IEEE Transactions on Communications*, Vol. 58, No. 8, 2402–2412, 2010.
3. Arrobo, G. E. and R. D. Gitlin, "Improving the reliability of wireless body area networks," *Proceedings of the Annual International Conference of the IEEE Engineering in Medicine and Biology Society, EMBC*, 2192–2195, Boston, U.S.A, August 2011.
4. Yazdandoost, K. Y. and K. Sayrafian-Pour, "Channel model for body area network (BAN)," *IEEE802.15.6 Technical Contribution*, document ID: 15-08-0780-09-0006, 41–56, 2009.

Numerical Investigation of Body-worn Ultra Wideband Antenna Localisation Techniques for Motion Capture Applications

Richa Bharadwaj, **Akram Alomainy**, **and Clive Parini**
School of Electronic Engineering and Computer Science, Queen Mary University of London
Mile End Road, London E1 4NS, United Kingdom

Abstract— Localisation and motion tracking using body-worn sensors is emerging as an important research area for based on Ultra Wideband technology. Motion tracking itself is motivated by a variety of applications such as training of athletes, patient monitoring in medicine, localisation of people in home or office environment. The choice of sensors, such as compact, efficient and low cost UWB antenna makes human localisation and activity monitoring a promising new application made possible by advances in UWB technology. Impulse Radio UBW technology offers various advantages such as high accuracy, robustness, low cost, high data rate, capability of signals to penetrate through many obstacles, easy implementation and low energy consumption making it suitable for short range human localisation.

An accuracy of 10 to 15 cm is achieved in commercial localisation systems with operating range of 50 cm and also sub-millimetre range accuracy is possible using carrier based UWB systems as proposed in literature. In this paper UWB 3D human body localisation is studied using 14 different sensors on the body using CST simulations in presence of different obstacles and the accuracy is compared with situation when no obstacle is present. The objective of the work is to achieve accurate localisation of the human body using data fusion time of arrival and peak detection techniques.

The frequency range used in the simulation is from 3 to 4 GHz and sine modulated Gaussian pulse is used for signal transmission. Single layer human body model consisting of muscle tissue having dielectric permittivity at 3.5 GHz (centre frequency) with 14 sensors is simulated using CST Microwave Studio. The height of the human body is 1.72 m and has average built. The Tapered Slot UWB antennas are used as sensors and base stations (BS), which are positioned near the vertices of a cube which has dimensions of $2 \times 2 \times 1.8\,\mathrm{m}^3$. The position of the BS antennas is chosen in such a way that localisation information can be obtained accurately in 3 dimensional (3D) with respect to BS1.

Block of glass $(150 \times 150 \times 5)\,\mathrm{cm}^3$ and wood $(100 \times 100 \times 20)\,\mathrm{cm}^3$ have been considered as objects that act like obstacles during the localisation simulation. It is observed that there is distortion in received pulse leading to variation in range value between BS and sensor on body. More variation, delay and distortion of received signal is observed for glass object as it has higher permittivity of 4.28 in comparison to wood which has a permittivity of 1.4. It is observed that different base stations give different received signal output depending on line of sight (LOS) or non line of situation (NLOS). As expected there is more error obtained in estimation of sensor positions located on the human model due to presence of obstacles. The overall average accuracy in 3D localisation is around 2.5 to 4.5 cm using time of arrival data fusion method. Presence of obstacle leads to reduction in accuracy of results (2 to 3 cm reduction) with glass showing higher decrease (4 to 6 cm) of average error in comparison to wood (3 to 4.5 cm).

Characterization of Electro-textiles Using Wireless Reflectometry for Optimization of Wearable UHF RFID Tags

K. Koski[1], E. Moradi[1], A. Vena[1], T. Björninen[1], L. Sydänheimo[1], L. Ukkonen[1], and Y. Rahmat-Samii[2]

[1]Tampere University of Technology, Tampere, Finland
[2]University of California, Los Angeles, CA, USA

Abstract— The need of wearable radio frequency identification (RFID) tags in wireless body-centric communication applications is increasing rapidly. Flexible and maintenance-free wearable tags are desired in wireless sensor systems in security, healthcare, and biomedical applications. Tags made of conductive threads and fabrics are good candidates for on-body communication applications thanks to their flexibility, light-weight and integrability in normal clothing.

Optimization of antennas for wearable RFID tags demands comprehensive knowledge of the electrical properties of the conductive material used in the antenna structure. Embroidered patterns and conductive fabrics do not have uniform conductive structures and it is difficult to define an exact thickness for them. Hence, it is not convenient to use the conductivity or the resistivity to characterize their performance. Instead, a better candidate is the sheet resistance, which is independent on the thickness of the conductive structure.

First we propose a novel technique to wirelessly determine the sheet resistance of various wearable antenna materials using wireless reflectometry measurements. For this purpose, a high-quality-factor scatterer is designed and fabricated of each studied material (Fig. 1). A copper scatterer is included as a reference scatterer. We show that the sheet resistance can accurately be extracted by comparing the height and width of the resonant peak in the measured and simulated radar cross section (RCS) values of the scatterer.

Previously, an embroidered dipole tag has been modelled as a uniform homogeneous pattern with a designated thickness and conductivity. However, to be more accurate, the inhomogeneous pattern (Fig. 2) has to be divided into several distinct regions where each region can be regarded as homogeneous. For each region we are able to determine the sheet resistance using the proposed wireless reflectometry measurement technique. This enables the modelling of the embroidered dipole as an infinitely thin inhomogeneous conductor with distinct sheet resistance values. We then compare wearable ultra-high frequency (UHF) dipole RFID tags fabricated using conductive sewing thread and various conductive fabrics.

The sheet resistance can be used as a key parameter to characterize the wearable antenna performance. In the future, we will use the sheet resistance as a design parameter to optimize wearable tag antennas that could be used in smart multifunctional daily garments or in protective clothing for harsh environments.

Figure 1: Scatterers of various conductive fabrics used in the wireless reflectometry measurements.

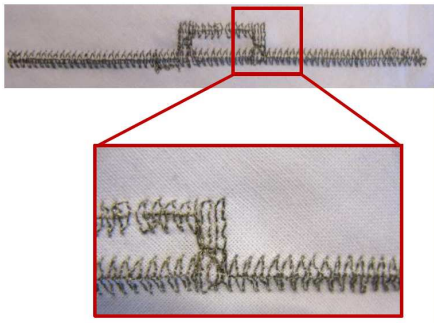

Figure 2: An embroidered dipole tag showing the inhomogeneous pattern created from conductive thread.

On the Stochastic Characterization of Wearable Antennas

P. Nepa and G. Manara
Department of Information Engineering, University of Pisa, Via G. Caruso 16, Pisa 56122, Italy

Abstract— Wearable antennas for body centric communications, which can operate in the frequency range from VHF to UHF and UWB bands, are reviewed. Their distinctive requirements are highlighted, which are quite different from those required to more conventional antennas for mobile terminals, access points and base stations. Also, specific attention is devoted to those parameters that can be used to characterize such class of antennas, since their characterization needs for a stochastic approach that can account for performance variations associated to the natural movements of the person wearing the wireless device.

Introduction: Body centric communications are attracting a considerable attention in several scenarios, going from the Ambient Assisted Living to the entertainment and military devices, just to mention a few of them. As a consequence, several studies have been reported on wearable antenna design, as well as on on-body propagation analysis and modelling [1–5]. An updated overview on wearable antennas is here presented, for both off-body and on-body communication systems.

When designing antennas, typical antenna parameters, as gain and return loss, are usually considered as deterministic quantities. Actually, wearable antenna parameters are random quantities since the natural movements of the person carrying the antenna introduce severe multipath phenomena and attenuation variability. Therefore, wearable antenna performances should be evaluated as random processes, whose parameters will depend on the antenna location on the body and on the degree of mobility of the person. Therefore, starting from some results already presented for mobile phone antennas [6] or antennas integrated in a life jacket [7], a systematic stochastic approach to the characterization of wearable antennas is here presented.

REFERENCES

1. Hall, P. S., Y. Hao, V. I. Nechayev, A. Alomain, C. C. Constantinou, C. Parini, M. R. Kamarudin, T. Z. Salim, D. T. M. Heel, R. Dubrovka, A. S. Owadall, W. Song, A. A. Serra, P. Nepa, M. Gallo, and M. Bozzetti, "Antennas and propagation for on-body communication systems," *IEEE Antennas and Propagation Magazine*, Vol. 49, No. 3, 41–58, 2007.
2. Hall, P. S. and Y. Hao, *Antennas and Propagation for Body-centric Wireless Communications*, Artech House, Norwood, MA, 2006.
3. Declercq, F. and H. Rogier, "Active integrated wearable textile antenna with optimized noise characteristics," *IEEE Trans. Antennas and Propagation*, Vol. 58, No. 9, 3050–3054, 2010.
4. Serra, A. A., A. R. Guraliuc, P. Nepa, G. Manara, I. Khan, and P. S. Hall, "Dual-polarisation and dual-pattern planar antenna for diversity in body-centric communications," *IET Microwaves, Antennas & Propagation*, Vol. 4, No. 1, 106–112, 2010.
5. Kamarudin, M. R., Y. I. Nechayev, and P. S. Hall, "Antennas for on-body communication systems," *IEEE International Workshop on Antenna Technology: Small Antennas and Novel Metamaterials*, 17–20, Mar. 7–9, 2005.
6. Carro, P. L., J. de Mingo, and P. G. Ducar, "Analysis of the antennastochastic effective gain in mobile environments," *69th IEEE Vehicular Technology Conference, VTC*, 1–5, Spring, 2009.
7. Serra, A., P. Nepa, and G. Manara, "A wearable two-antenna system on a life jacket for Cospas-Sarsat Personal Locator Beacons," *IEEE Trans. Antennas and Propagation*, Vol. 60, No. 2, Part 2, 1035–1042, 2012.

Active Textile Multi-antenna Systems for Energy-efficient Body-centric Communication

Hendrik Rogier, **Sam Agneessens**, **Arnaut Dierck**, **Frederick Declercq**, **Patrick Van Torre**, **Luigi Vallozzi**, **Emmeric Tanghe**, **Günter Vermeeren**, **and Wout Joseph**
Department of Information Technology, Ghent University, Belgium

Abstract— The last decade, we have witnessed a tremendous evolution in sensor networks deployed on the human body. Nodes in such a body area network monitor different life signs of the wearer, as well as environmental conditions. In addition, they exchange information and communicate wirelessly to a remote monitoring station or command post, which, in turn, feeds back commands, warnings or alarms. A well-known issue is the power consumption of these body-centric smart systems, requiring heavy batteries that may cause discomfort to the wearer and that require frequent recharging. In particular, the wireless communication module is one of the main consumers of energy in each sensor node.

In this contribution, we review active textile multi-antenna systems as a means to reduce the power-consumption while maintaining reliable communication in wireless off-body links. The key idea is that a garment offers a large platform, in which one can easily deploy multiple antennas of sufficient size to provide high gain and large radiation efficiency in the presence of a human body. Yet, it is important that this multi-antenna system does not disturb the movements or the comfort of the wearer. Hence, the antennas should be low-weight, flexible and breathable. Therefore, we fabricate the antennas using the same materials as found in the garments, allowing seamless integration. The active electronics circuits, such as the transceiver, sensors and battery, are then placed on a small flexible polyimide carrier, such that they may be integrated directly underneath the textile antenna's ground plane, resulting in a compact flexible module. Each active antenna module is optimized to yield maximum performance and minimal energy consumption by adopting a dedicated full-wave/circuit co-design strategy. Next, we apply multiple-input multiple-output (MIMO) techniques to create highly reliable wireless off-body links at reduced transmit power. It will be shown that, both for Line-of-Sight as for non-Line-of-Sight propagation, in most cases beamforming at the transmit side yields lower bit error rates than space-time coding, provided some diversity gain is implemented at the receive side. In addition, it will be demonstrated that high diversity orders can only be obtained by means of space-time coding provided that highly reliable channel estimates are available at the receiver side. Data-driven channel tracking may be applied by the receiver to obtain such channel estimates without excessive overhead in terms of pilot symbols. Finally, we consider cooperative communication techniques to set up reliable connections between an implanted antenna and a remote monitoring station. A wearable on-body antenna system will be presented that serves as a repeater, reliably relaying the data from the implanted antenna to a remote access point, while allowing the implanted system to operate at low power.

Analysis of On-body Propagation at 60 GHz Using Skin-equivalent Phantoms and Common Textiles

Anda R. Guraliuc, **Maxim Zhadobov**, **and Ronan Sauleau**
Institute of Electronics and Telecommunications of Rennes (IETR)
University of Rennes 1, Rennes 35042, France

Abstract— Medical applications including health monitoring and ambient assisted living, military applications, entertainment and sport applications, all envision the use of wearable wireless sensors. 60-GHz band becomes more and more attractive for body area network (BAN) applications offering several key advantages including compact size of components and devices, high data rates (typically up to several Gb/s), high level of security and reduced interference with neighboring BANs.

The propagation at 60 GHz is characterized by high atmospheric attenuation related to the free-space losses and resonant oxygen-induced absorption. At these frequencies, the human body is electrically large and the interaction with millimeter waves is characterized by a significant reflection due to the dielectric contrast between the complex dielectric permittivity of the skin and free space, which depends on the polarization and angle of incidence (typically 40% for the normal incidence), as well as by the superficial absorption of the transmitted power to the body [M. Zhadobov et al., "Millimeter-wave interactions with the human body: state of knowledge and recent advances," *Int. J. Microw. Wirel. Technol.*, Vol. 3, No. 2, 237–247, Apr. 2011]. For future BANs operating in the proximity of the human body, it is important to investigate the on-body propagation at 60 GHz including the effect of clothing on the propagation channel.

In this analysis, we studied numerically and experimentally the propagation at 60 GHz along a skin-equivalent phantom with and without clothing. A skin-equivalent phantom is prepared as described in [N. Chahat et al., "Broadband tissue-equivalent phantom for BAN applications at millimeter waves," *IEEE Trans. Microw. Theory Tech.*, Vol. 60, No. 7, 2259–2266, Jul. 2012], and its dielectric properties are determined using an open-ended coaxial slim probe. The dielectric properties of the textiles are determined using a free space technique with reflection/transmission quasi-optical setup. The path gain between two linearly-polarized standard V-band open-ended waveguides is measured in the presence of the textiles with different dielectric properties and thicknesses placed over a skin-equivalent phantom with or without an air gap. It is well known that in an on-body scenario the field polarization affects differently the path gain behavior [N. Chahat et al., "On-body propagation at 60 GHz," *IEEE Trans. Antennas Propag.*, Vol. 61, No. 4, 1876–1888, Apr. 2013]. As a consequence, the analysis is performed for both V polarization (E-field normal to the body surface) and H polarization (E-field tangential to the body surface). Results show that the presence of a textile on the skin-equivalent phantom can improve the path gain. For instance, a layer of the 0.2 mm-thick cotton ($\varepsilon_r = 2$ and $\tan\delta = 0.02$) produces a typical increase of 5–10% of the path gain. Numerical results indicate that an air gap between the cotton textile and the skin-equivalent phantom can reduce the path gain by 10%–12%. Complete results will be presented at the conference.

ACKNOWLEDGMENT

This study was supported by Labex CominLabs and Brittany Region under ResCor/BoWi project and by "Centre National de la Recherche Scientifique (CNRS)", France.

Evaluation of Antenna/Human Body Interactions in BAN Scenarios at Millimeter Waves

Maxim Zhadobov[1], **Nacer Chahat**[1, 2], **Stanislav I. Alekseev**[3], **Carole Leduc**[1], **Anda Guraliuc**[1], **and Ronan Sauleau**[1]

[1]Institute of Electronics and Telecommunications of Rennes (IETR), UMR CNRS 6164
University of Rennes 1, Rennes, France
[2]NASA Jet Propulsion Laboratory, California Institute of Technology, Pasadena, CA, USA
[3]Institute of Cell Biophysics, Puschino, Russia

Abstract— The millimeter-wave band, mainly 57–66 GHz range, has been identified as highly promising for future BAN technologies. One of the main features differentiating 60-GHz band from lower frequency BAN is confidentiality and low interference with neighboring networks, which has been demonstrated to be crucial for body-centric and inter-BAN communications. In addition, it provides other advantages including high data rates [typically beyond 5 Gb/s], reduced size of antennas and sensors, high accuracy for localization, that can be exploited for new applications (e.g., immersive video games).

At these frequencies, the power absorption in the body is superficial and essentially limited to the skin and cornea [1]. Because of this particularity, dosimetric techniques available at lower microwave frequencies used for the quantification of the power absorption in the body cannot be applied at millimeter waves. The purpose of this study is to implement a dosimetric approach at millimeter-wave frequencies allowing investigating the specific absorption rate (SAR), incident power density (IPD) and power density (PD) in the skin or tissue-equivalent phantoms. These characteristics are retrieved from the superficial temperature dynamics recorded using a high-resolution infrared camera.

As an application example, the SAR and IPD distributions are simulated and determined experimentally for a microstrip patch antenna array placed 5.6 mm above from a skin-equivalent phantom [2]. The array is characterized in free space and on a homogeneous skin-equivalent phantom in terms of reflection coefficient, radiation pattern, and antenna efficiency. Experimentally the SAR and IPD are found by fitting the analytical solution of the bio-heat transfer equation to the measured heating dynamics. The experimental and numerical results are in a very good agreement. They demonstrate that for the considered scenario the impact of the body on the antenna characteristics is almost negligible, and even relatively high radiated powers (up to 550 mW) result in exposure levels that are below international exposure limits.

ACKNOWLEDGMENT

This work was supported by "Agence Nationale de la Recherche" (ANR), France under Grants ANR-09-RPDOC-003-01 (Bio-CEM project) and by a joint grant of French National Center for Scientific Research (CNRS) and Russian Academy of Sciences (grant No. EDC25185).

REFERENCES

1. Zhadobov, M., N. Chahat, R. Sauleau, C. Le Quement, and Y. Le Dréan, "Millimeter-wave interactions with the human body: State of knowledge and recent advances," *International Journal of Microwave and Wireless Technologies*, Vol. 3, No. 2, 237–247, 2011.
2. Chahat, N., M. Zhadobov, L. Le Coq, S. I. Alekseev, and R. Sauleau, "Characterization of the interactions between a 60-GHz antenna and the human body in an off-body scenario," *IEEE Transactions on Antennas and Propagation*, Vol. 60, No. 12, 5958–5965, 2012.

Broadband Vivaldi Array Antenna for On-body Communication

Xiao Li[1], **Xianyue Wu**[1], **Constantinos Constantinou**[1], **Peter S. Hall**[1], **Yuriy Nechayev**[1], **Alice Pellegrini**[2], **and Yang Hao**[2]

[1]University of Birmingham, UK
[2]Queen Mary, University of London, UK

Abstract— On-body communications in the millimetre wave frequency band promise higher data rates and highly improved security and resistance to interference. However, propagation at these frequencies also suffers from high propagation losses and, therefore, the use of high gain antennas, on one hand, and multi-hop communication links, on the other, can be required. A broadband, low profile, low cost Vivaldi antenna array is proposed in this work for use in wireless body-area networking (WBAN) applications in the 60 GHz unlicensed frequency band. The array is fed by a substrate integrated waveguide (SIW) structure and incorporates an isolation via wall which improves the impedance matching effectively and makes the return loss more than 10 dB over the whole band from 57 GHz to 64 GHz (see Figure 1). Two arrangements of two-element Vivaldi antenna arrays (shown in Figure 2) are proposed for use in on-body multi-hop communications. The antennas were fabricated on a single-layer substrate Rogers RT5880 and measured. The measurement results are in good agreement with the simulation results. The measured peak gain of the proposed array is 10.7 dBi and the 3-dB beamwidths in the E- and H-planes are 36° and 52°, respectively, at 60 GHz. The effect of the human body proximity was investigated through electromagnetic simulations and it was found that, at a separation of 5 mm from the skin, the return loss and the H-plane pattern of the Vivaldi antenna remain unaffected while the main beam in the E-plane (perpendicular to the skin) is raised approximately 10° relative to the skin surface.

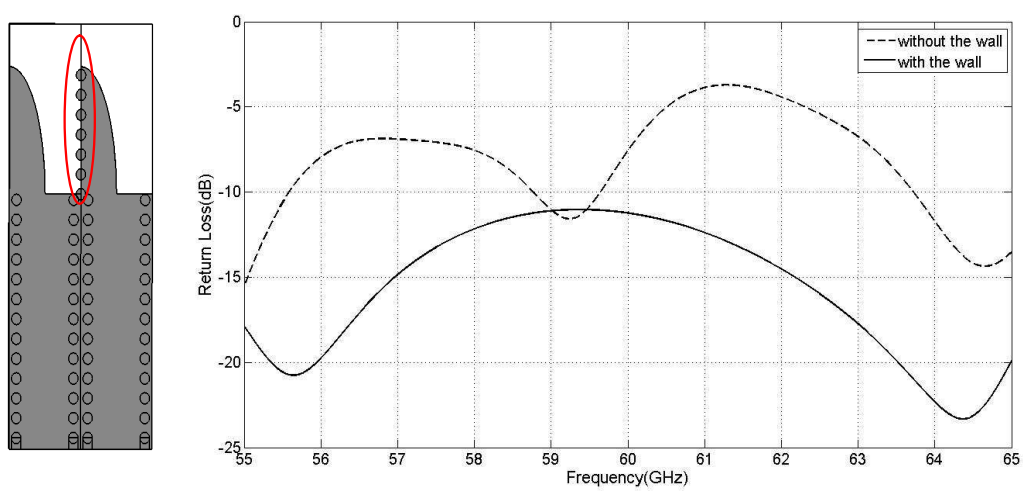

(a) (b)

Figure 1: Two-element Vivaldi array with the isolation via wall, (a) antenna top view, (b) return loss.

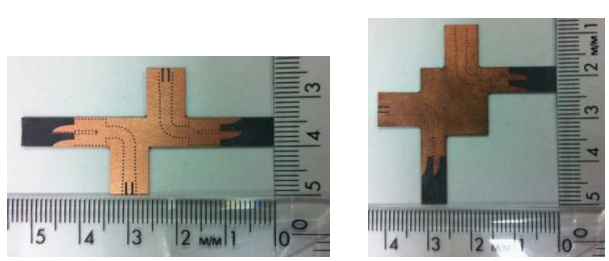

(a) (b)

Figure 2: Multi-hop on-body antennas, (a) back-to-back version, and (b) right-angle version.

Session 3A8a
GPU Computing in Electromagnetics

Large-scale Three-dimensional FDTD Calculation on GPU Clusters for Estimating the Specific Absorption Rate in a Human Body
Tomoaki Nagaoka, Soichi Watanabe, ... 998

B-CALM: An Open-source multi-GPU-based 3D-FDTD with Multi-pole Dispersion for Plasmonics
Pierre Wahl, Dany Sebastien Ly Gagnon, Christof Debaes, David A. B. Miller, Hugo Thienpont, .. 999

GPU-optimized Parallel Preconditioners for Finite-element Models Using Element-by-element Strategies
Imre Kiss, Zsolt Badics, Szabolcs Gyimothy, Jozsef Pavo, ... 1000

GPU-based Particle-in-Cell Plasma Simulation in PICADOR: Optimization Techniques
Sergey Bastrakov, Evgeny S. Efimenko, Arkady Gonoskov, Iosif Meyerov, Igor Surmin, ... 1001

Interactive FDTD Simulation Using LRnLA Algorithms
Vadim D. Levchenko, Ivan A. Goryachev, A. Yu. Perepelkina, ... 1002

Dynamic Parallelism in Reflectarray Antenna Analysis and Synthesis on GPU
Amedeo Capozzoli, Claudio Curcio, Angelo Liseno, Giovanni Toso, ... 1003

Large-scale Three-dimensional FDTD Calculation on GPU Clusters for Estimating the Specific Absorption Rate in a Human Body

Tomoaki Nagaoka and Soichi Watanabe
National Institute of Information and Communications Technology, Japan

Abstract— The increasing use of radio-frequency (RF) applications has led to the growing presence of electromagnetic waves in various locations. On the other hand, there is a growing concern regarding the effects of electromagnetic (EM) waves emanating from wireless communication devices on the health of humans. The safety of the RF-EMF is evaluated on the basis of the specific absorption rate (SAR), which is the amount of RF energy absorbed per unit weight of the body and is used as a measure of the thermal effects on the body caused by the absorption of EM energy.

Researchers have carried out a detailed SAR estimation with a numerical simulation using the fine-resolution and anatomically realistic human models. Three-dimensional finite-difference time-domain (FDTD) method has been the method used most often in these studies with the human models having complex shapes and internal structure.

High-performance computer systems, such as supercomputers, were until a few years ago generally needed to perform the FDTD calculation with computational human models, because the calculation runs very slowly and requires a large amount of computational memory. To accelerate the computational speed of the FDTD method and realize large-scale computing with the human model, we created multi-node GPU clusters and implemented the FDTD code on the GPU clusters with Compute Unified Device Architecture. Our GPU clusters consist of the nine nodes. The seven GPU boards (NVIDIA C2070 or C0275) are mounted on each node.

In this presentation, we present the CUDA implementation of the three-dimensional FDTD method and performance of the GPU-based FDTD method on GPU clusters. We also demonstrate the large-scale SAR calculations with the high-resolution human model.

B-CALM: An Open-source multi-GPU-based 3D-FDTD with Multi-pole Dispersion for Plasmonics

Pierre Wahl[1], **Dany-Sebastien Ly-Gagnon**[2], **Christof Debaes**[1], **David A. B. Miller**[2], **and Hugo Thienpont**[1]

[1]Brussels Photonics Team B-PHOT, Department of Applied Physics and Photonics
Vrije Universiteit Brussel, Belgium
[2]Department of Electrical Engineering, Stanford University, CA 940305, USA

Abstract— Finite-Difference Time-Domain (FDTD) simulations play a prominent role in numerical electromagnetic calculations in nanophotonics, where three dimensional full-field simulations are required. Also, FDTD simulations for metallic nanostructures in a broad optical spectrum require an accurate modeling of the permittivity of dispersive materials. Here, we present the algorithms behind B-CALM (Belgium-CAlifornia Light Machine), an open-source 3D-FDTD solver simultaneously operating on multiple Graphical Processing Units (GPUs) and efficiently utilizing multi-pole dispersion models while hiding latency in inter-GPU memory transfers by overlapping communication and computation. This overlap is done by utilizing a 1D decomposition of the computational domain and by computing the bordering halos first and by transferring the results to an adjacent GPU while the inner cells are being computed. As long as the time required for this communication is longer than the time required for the computing of the inner cells in each GPU, the communication overhead can almost be completely hidden. While overlapping computation and communication for GPU FDTD has been reported before [1], multi-GPU multi-pole dispersion has, to our knowledge, only been shown on single a GPU through the split kernel approach [2–4]. In addition, the transfers implemented in [1] are performed with staging transfers through a host memory buffer decreasing the bandwidth. In this work, we ease this by using new CUDA-aware Message Passing Interface (MPI) libraries that always use the fastest transfer possible. As computation and communication overlap, this increased bandwith only marginally affects performance when using a small amount of GPUs. However, the higher bandwidth reduces the number of inner cells that are required to hide the communication. This allows the use of more GPUs while still maintaining a simple 1D domain decomposition, whereas a more complicated and less efficient 2D decomposition would have been required otherwise. In FDTD, the parts of the simulation space that need to be processed as output need to be dumped to the host memory at regular intervals. For large simulations, these outputs can be very large and need to be stored on disk. Also for these transfers, we hide the communication overhead by overlapping them with computation. Our architecture shows a reduction in computing times for multi-pole dispersion models and 95% of the maximum linear speed-up with respect to the amount of used GPUs. We benchmark B-CALM by computing the absorption efficiency of a metallic nanosphere in a broad spectral range with a six-pole Lorentz model and compare it with Mie theory and with MEEP, a widely used Central Processing Unit (CPU)-based FDTD simulator.

REFERENCES

1. Hwan, K., Q. Kim, and H. Park, "Overlapping computation and communication of three-dimensional FDTD on a GPU cluster," *Computer Physics Communications*, Vol. 183, No. 11, 2012.
2. Wahl, P., D. S. Ly-Gagnon, C. Debaes, D. A. B. Miller, and H. Thienpont, "B-CALM: An open-source GPU-based 3D-FDTD with multi-pole dispersion for plasmonics," *2011 11th International Conference on Numerical Simulation of Optoelectronic Devices (NUSOD)*, 11–12, 2011.
3. Shahmansouri, A. and B. Rashidian, "GPU implementation of split-field finite-difference time-domain method for Drude-Lorentz dispersive media," *Progress In Electromagnetics Research*, Vol. 125, 55–77, 2012.
4. Lee, K. H., I. Ahmed, R. S. Goh, E. H. Khoo, E. P. Li, and T. G. Hung, "Implementation of the FDTD method based on Lorentz-Drude dispersive model on GPU for plasmonics applications," *Progress In Electromagnetics Research*, Vol. 116, 441–456, 2011.

GPU-optimized Parallel Preconditioners for Finite-element Models Using Element-by-element Strategies

I. Kiss[1], **Z. Badics**[2], **Sz. Gyimóthy**[1], **and J. Pávó**[1]

[1]Budapest University of Technology and Economics, Budapest, Hungary
[2]Tensor Research LLC, Andover, MA, USA

Abstract— In this contribution we present some efficient GPU-optimized preconditioners for the solution of FE (finite element) models in computational electromagnetics. Although several techniques accelerating the FE method have already been implemented on GPUs [1, 2], they usually suffer from the strict limitation of the available GPU memories. Since large scale FE problems need large storage capacity, the few GBs of available memory on GPUs must be continuously cached to the global system memory through the relatively slow bus system.

In contrast, we propose an acceleration technique based on the EbE (element-by-element) FE framework [3] that exhibits highly improved locality and minimization of data movement compared to other FE implementations on GPUs. The EbE technique has long since been known to be able to perform operations in Krylov-subspace iterative solvers without actually assembling the global system matrix. Therefore, the method has originally been constructed for low memory computers [4]. The foundation of the method is based on the recognition that the assembling operation of the element matrices to form the global system matrix is a linear operation. Therefore certain calculations with the system matrix — like for example a matrix-vector product — can be traced back to the level of finite elements, thus, converted to calculations with the individual element matrices.

Since all the computations are performed on the element level, traditional preconditioning techniques that rely on the assembled matrix are not usable. Therefore efficient preconditioning methods that can be constructed and applied without the presence of the assembled matrix are developed. Among these, the Hughes-Winget and the Gauss-Seidel EbE preconditioners are investigated in this work. The main challenge using these preconditioners arises from our EbE implementation of the iterative solver. Namely, instead of storing the local element matrices, we recompute them in each iteration. In this way the memory consumption of the method is kept on the minimum, that is, a memory bounded problem is transformed into a computation bounded one. NVIDIA's parallel computing solution, the Compute Unified Device Architecture (CUDA), is utilized to perform the required element-wise computations in parallel.

Summing up, the aim of this paper is to extend the scope of problems GPUs can effectively handle by utilizing several different preconditioners that are suitable to the EbE implementation of Krylov-subspace iterative solvers. Relying on the fact that it is cheaper to recompute element matrices and form the preconditioner than continuously cache the global system matrix between the GPU and the system memory, we do not need to store the element matrices or the preconditioners but rather recompute them in each iteration.

REFERENCES

1. Bolz, J., I. Farmer, E. Grinspun, and P. Schröder, "Sparse matrix solvers on the GPU: Conjugate gradients and multigrid," *ACM Trans. Graph.*, Vol. 22, 917–924, July 2003.
2. Cevahir, A., A. Nukada, and S. Matsuoka, "Fast conjugate gradients with multiple GPUs," *ICCS 2009*, G. G. van Albada, J. Dongarra, and P. Sloot, Eds., Vol. 5544, 893–903, 2009.
3. Kiss, I., S. Gyimóthy, Z. Badics, and J. Pávó, "Parallel realization of the element-by-element FEM technique by CUDA," *IEEE Trans. on Magnetics*, Vol. 48, No. 2, 507–510, 2012.
4. Carey, G. F., E. Barragy, R. McLay, and M. Sharma, "Element-by-element vector and parallel computations," *Commun. Appl. Numer. Methods*, Vol. 4, No. 3, 299–307, 1988.

GPU-based Particle-in-Cell Plasma Simulation in PICADOR: Optimization Techniques

Sergey Bastrakov[1], **Evgeny Efimenko**[2], **Arkady Gonoskov**[2], **Iosif Meyerov**[1], **and Igor Surmin**[1]

[1]N. I. Lobachevsky State University of Nizhny Novgorod, Russia
[2]Institute of Applied Physics, RAS, Nizhny Novgorod, Russia

Abstract— Simulation of plasma dynamics with the Particle-in-Cell method is one of the currently high-demand areas of computational physics. Solving up-to-date physical problems often requires large-scale plasma simulation. Therefore there is a need for high-performance implementation of the method for both traditional and heterogeneous systems.

In the recent years there has been a growing interest in efficient implementation of the Particle-in-Cell algorithm for GPUs. The main challenge is to obtain both highly parallel particle processing and efficient global and shared memory access pattern. A promising approach, popularized by the PIConGPU code, is tile-based particle processing.

PICADOR [1, 2] is a tool for three-dimensional plasma simulation based on the Particle-in-Cell method capable of using CPUs and GPUs of a heterogeneous cluster system. We utilize the widely used technique of storing and processing particles by tiles (supercells). During the particle push and current deposition stages the particles of a tile are processed by the threads of a thread block using shared memory for field interpolation and current accumulation. The need for performing reduction of thread results for current accumulation implies either usage of atomic operations or storing the thread results in the global or shared memory. PICADOR has originally chosen the latter alternative resulting in the efficient current deposition kernel. The tradeoff is a severe constraint on the block size and, consequently, low device occupancy. For example, for the $2 \times 2 \times 2$ tiles the maximum block size is only 128 threads in double precision. On Fermi GPUs this approach allows achieving $3\times$ speedup over 8 CPU cores with double precision and $5\times$ — with single precision. However, this approach becomes rather inefficient for Kepler GPUs having much more cores per multiprocessor with the same amount of shared memory. Therefore there is a need for different optimization approaches.

We analyze the widely used optimization techniques for GPUs and study how Fermi-specific optimizations behave on Kepler GPUs. We present the recent developments in PICADOR concerning Kepler-specific optimizations.

REFERENCES

1. Bastrakov, S., R. Donchenko, A. Gonoskov, E. Efimenko, A. Malyshev, I. Meyerov, and I. Surmin, "Particle-in-cell plasma simulation on heterogeneous cluster systems," *Journal of Computational Science*, Vol. 3, 474–479, 2012.
2. Bastrakov, S., I. Meyerov, V. Gergel, A. Gonoskov, A. Gorshkov, E. Efimenko, M. Ivanchenko, M. Kirillin, A. Malova, G. Osipov, V. Petrov, I. Surmin, and A. Vildemanov, "High performance computing in biomedical applications," *Procedia Computer Science*, 2013, accepted.

Interactive FDTD Simulation Using LRnLA Algorithms

V. D. Levchenko, **I. A. Goryachev**, **A. Yu. Perepelkina**
Keldysh Institute of Applied Mathematics, Russia

Abstract— The approach, based on Finite-Difference Time-Domain (FDTD) method, has been useful tool for numerical electrodynamics simulation recently. It permits to reconstruct full electromagnetic fields' dynamics and treat complex as well as nonlinear material properties in a natural way. Alternately, essential limitations of the approach operations had been defined by high computational complexity as compare to spectral and integral methods.

Things are improving due to the advance of computational power of novel general-purpose graphics processing unit (GPGPU). The last generation of GPGPU namely Nvidia Kepler and AMD GCN with the TeraFlops performance level potentially make it possible to interactive solving of numerical electrodynamics problem with moderate data size (up to 10^9 of Yee cell's). The graphics possibilities of GPU card allow to visualize calculated electromagnetic fields distribution in space without overhead for saving big volume data in slow disk memory.

The key point in the approach implementation are the effective algorithms of calculations which take into account the sophisticated hierarchy of memory and parallel levels of heterogeneous compute node. The original Local Recursive non-Local Asynchronous (LRnLA) algorithms allow come up to tens percents of peak performance in actual numerical electrodynamics problems.

The paper describes the algorithms for 2D and 3D simulations, their cuda implementation for Nvidia Titan GTX and examples of applications.

Dynamic Parallelism in Reflectarray Antenna Analysis and Synthesis on GPU

A. Capozzoli[1], **C. Curcio**[1], **A. Liseno**[1], **and G. Toso**[2]

[1]Dipartimento di Ingegneria, Elettrica e delle Tecnologie dell'Informazione
Università di Napoli Federico II, via Claudio 21, Napoli 80125, Italy
[2]Antenna and Sub-Millimeter Wave Section, Electromagnetics Division
TEC-EEA, European Space Agency, ESA
ESTEC, Keplerlaan 1, PB 299, 2200 AG Noordwijk, The Netherlands

Abstract— Microstrip reflectarrays combine some of the appealing features of microstrip patch arrays and reflectors and have recently raised interest in many applications, as direct broadcast satellite (DBS) services, Earth remote sensing and micro-spacecraft missions, to mention just a few. Indeed, they are flexible like arrays, and they do not require the use of cumbersome beamforming networks as reflectors. They are low cost, can be faceted or conformed and can be aesthetically pleasing for commercial applications.

To achieve high performance reflectarrays, as needed for example in satellite telecommunications, radiative models accounting for all the antenna degrees of freedom and exploiting the minimum number of approximations are required. To deal with them, accurate, efficient and effective design strategies, possibly based on sophisticated multistep strategies to guarantee a satisfactory degree of reliability are requested [1, 2]. Electrically large, high performance reflectarrays having hundreds or thousands of control parameters entail high computational burden, so implementations on massively parallel architectures are mandatory to perform large-scale, accurate computations.

We discuss the computationally critical steps of the synthesis procedure [1, 2] and present their implementation and optimization on Graphic Processing Units (GPUs) in Compute Unified Device Architecture (CUDA) language. The attention is focused on two points: the fast evaluations of the radiation operator and of the functional gradient as well as the fast implementation of the optimization algorithms.

Concerning the former, different tools are described, depending on the features of the considered reflectarray and on the involved model simplifications, as the 'p-series' representation and the 2D Non-Uniform FFT (NUFFT) of both NER (Non-Equispaced Results) and NED (Non-Equispaced Data) types. A deep optimization of the respective CUDA codes has been carried out in terms of memory management and transfers, latency hiding, branch path analysis, instruction selection, use of atomic instructions, paying particular attention to the improvements achieved by one of the ultimate features of NVIDIA Kepler cards, namely, *dynamic parallelism*. Dynamic parallelism is the capability of a GPU of assigning tasks to itself and aims at simultaneously simplifying programming and improving the performance.

As Matlab has become a common platform for technical computing, interfacing of these procedures to standard Matlab scripts is also detailed.

Results are presented by using cards from the latest NVIDIA GPU family architecture, namely, Kepler K20c.

REFERENCES

1. Capozzoli, A., C. Curcio, G. D'Elia, A. Liseno, and P. Vinetti, "Fast CPU/GPU pattern evaluation of irregular arrays," *Applied Comput. Electromagn. Soc. J.*, Vol. 25, No. 4, 355–372, Apr. 2010.
2. Capozzoli, A., C. Curcio, G. D'Elia, A. Liseno, G. Toso, and P. Vinetti, "Aperiodic and non-planar array of electromagnetic scatterers, and reflectarray antenna comprising the same," World Patent Nr. WO/2011/033388, published on Mar. 24, 2011, Priority Data Nr. 09425356.4 Filed on Sep. 16, 2010.
3. Capozzoli, A., C. Curcio, A. Liseno, and G. Toso, "Phase-only synthesis of flat aperiodic reflectarrays," *Progress In Electromagnetics Research*, Vol. 133, 53–89, 2013.

Session 3A8b
SC1&3: Design and Simulation of Electromagnetic and Optical Devices

Resonantly Confined Modes in Si/SiO_2 Micro-structured Optical Fibers
Yasuo Ohtera, Haruka Hirose, Hirohito Yamada, ... 1006

Efficient Time-domain Technique for the analysis of Circularly Symmetric Plasmonic Waveguides
Jun Shibayama, Takuto Oikawa, Junji Yamauchi, Hisamatsu Nakano, ... 1008

Design of a Novel Miniaturized Composite Right/Left-handed Leaky Wave Antenna
Cheng-Lung Kao, Fu-Chiarng Chen, ... 1009

Eigenmode Analysis for Designing Plasmonic Devices by an Integral Solver
Seiya Kishimoto, Shinichiro Ohnuki, Yoshito Ashizawa, Katsuji Nakagawa, ... 1010

All-dielectric Planar Chiral Nanogratings with Large Optical Activity
Yuu Wakabayashi, Yukinori Shigenaga, Junji Yamauchi, Hisamatsu Nakano, ... 1011

Design of All-optical Magnetic Recording System Using Plasmonic Antennas and Particulate Media
Shinichiro Ohnuki, Y. Takano, T. Kato, Yoshito Ashizawa, Katsuji Nakagawa, ... 1012

Resonantly Confined Modes in Si/SiO_2 Micro-structured Optical Fibers

Yasuo Ohtera, **Haruka Hirose**, **and Hirohito Yamada**
Graduate School of Engineering, Tohoku University
Aramaki-Aza-Aoba 6-6-04, Aoba-ku, Sendai 980-8579, Japan

Abstract— Due to the recent advance in fiber fabrication technologies, a variety of micro-structured fibers (MSFs) consisting of various materials has been enabled. In addition to conventional all-silica photonic crystal fibers, all-solid MSFs such as chalcogenide glass fibers and Si/SiO_2 fibers [1] have also been developed. Their have been gathering interest for potential applications to wideband light sources, filters, and sensors. For the above applications, one of the straightforward ways to enhance the interaction between light fields and the materials or to improve the device sensitivity is, to include some kind of resonance mechanism to the guidance principle of the fiber itself. In the previous PIERS we have demonstrated that a class of MSFs consisting of circularly-arranged solid rods had an ability to confine light in the continuum regime [2]. The key principle is the guided-mode resonance (GMR) that the rod array exhibit. Highly wavelength sensitive property of GMR made the guiding condition also wavelength selective. However, estimated propagation loss was large ($\sim 10\,\mathrm{dB/mm}$) due to the limited index contrast assumed ($n = 1.8/1.45$).

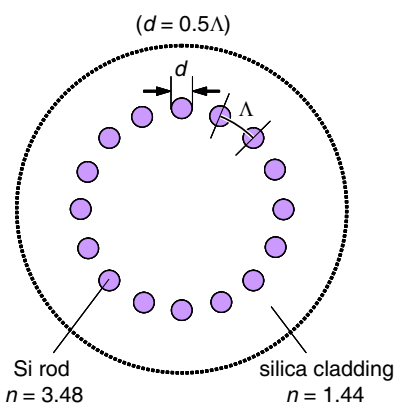

Figure 1: Schematic view of the fiber. 36 Si rods are circularly arranged with a pitch Λ.

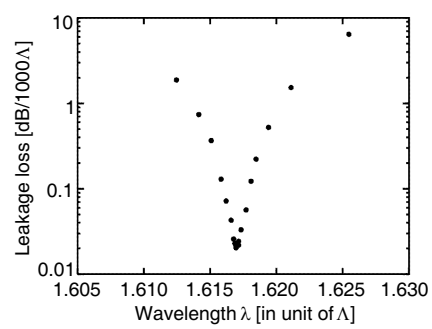

Figure 2: Leakage loss of the resonantly guided mode (RGM).

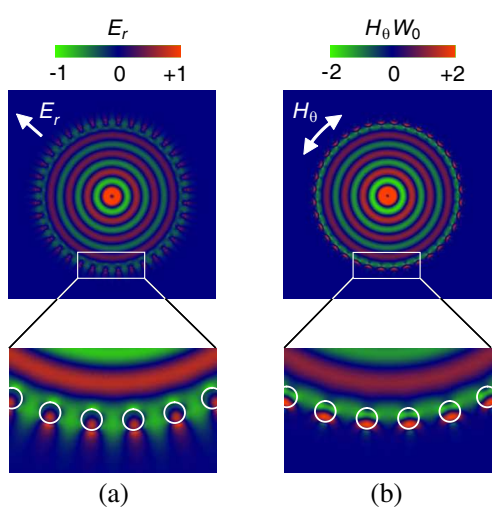

Figure 3: Mode field profiles at the minimum loss wavelength. (a) Radial component of the E-field. (b) Angular component of the H-field. ($W_0 = 120\pi$ is the impedance in vacuum.).

In this paper, we demonstrate a low-loss propagation capability of the resonantly guided modes (RGMs) in simple high-index contrast MSFs. Figure 1 shows a schematic view of the fiber. An array of Si rods ($n = 3.48$) is circularly arranged in a silica ($n = 1.44$) background. Cylindrical waves with concentric wavefronts are efficiently reflected by the array, and confined in the center region of the fiber. Figure 2 shows a calculated leakage loss of an RGM. At $\lambda = 1.617\Lambda$ (Λ is the distance between the rods), the minimum loss was found to be $\sim 0.021\,\mathrm{dB}/1000\Lambda$, which becomes $\sim 21\,\mathrm{dB/m}$ if $\Lambda = 1\,\mu\mathrm{m}$. The main leakage path was the radiation loss of the whispering gallery modes that travels along the array. The loss increases as $120\,\mathrm{dB/m}$ for a detuning of $\Delta\lambda = 1\,\mathrm{nm}$. Figure 3 shows mode field profiles of the RGM at the minimum loss point. The field was also localized in the vicinity of the Si rods, which is a typical feature of GMR. In the conference we will discuss the detail of the propagation characteristics, polarization of the modes, and the degree of field enhancement.

ACKNOWLEDGMENT

This work has been supported by JSPS KAKENHI 24656041.

REFERENCES

1. Sazio, P. J. A., et al., *Science*, Vol. 311, 1583–1586, 2006.
2. Ohtera, Y., H. Hirose, and H. Yamada, "Resonantly confined modes in optical fibers with circularly aligned high-index rods," *Progress In Electromagnetics Research Symposium Abstracts*, 146, Taipei, March 25–28, 2013.

Efficient Time-domain Technique for the analysis of Circularly Symmetric Plasmonic Waveguides

J. Shibayama, T. Oikawa, J. Yamauchi, and H. Nakano
Faculty of Science and Engineering, Hosei University, Japan

Abstract— For guiding surface plasmon polaritons, several circularly symmetric waveguides consisting of negative dielectrics have been proposed, which are known as one-dimensional optical waveguides [1]. Because of the circular symmetry, these waveguides can be successfully treated in body-of-revolution (BOR) coordinates. Recently, implicit BOR finite-difference time-domain (FDTD) methods have been developed on the basis of the locally one-dimensional (LOD) scheme for the efficient analysis of circularly symmetric structures [2–4]. The LOD-based methods offer the unconditional stability with respect to a time step size. Note, however, that these methods have not been extended to a frequency-dependent version that is mandatory for the analysis of surface plasmon polaritons in time domain.

The purpose of this work is to develop a frequency-dependent LOD-BOR-FDTD for the efficient analysis of circularly symmetric plasmonic waveguides. The Drude-Lorentz model, often used to express a metal dispersion, is taken into account using the trapezoidal recursive convolution technique. To absorb outgoing waves, we introduce the convolutional perfectly matched layer [4, 5] into the BOR coordinates. The method is finally simplified using the fundamental scheme providing a matrix-operator-free formulation in the right-hand sides [3, 6]. It is shown that the number of arithmetic operations is significantly reduced in the right-hand sides of the resultant equations, compared to that without the fundamental scheme. To assess the developed method, we analyze pulse propagation of the surface plasmon polariton along a metal rod waveguide. A reduction of the computation time is discussed in comparison with the explicit BOR-FDTD, with attention to the accuracy with a large time step size beyond the stability limit. As an application, we investigate the reflection characteristics of a metal rod waveguide with gratings.

REFERENCES

1. Takahara, J., et al., "Guiding of a one-dimensional optical beam with nanometer diameter," *Opt. Lett.*, Vol. 22, No. 7, 475–477, 1997.
2. Shibayama, J., et al., "LOD-BOR-FDTD algorithm for efficient analysis of circularly symmetric structures," *IEEE Microw. Wireless Compon. Lett.*, Vol. 19, No. 2, 56–58, 2009.
3. Shibayama, J., et al., "Efficient LOD-BOR-FDTD implementation based on a fundamental scheme," *IEEE Photon. Technol. Lett.*, Vol. 24, No. 11, 957–959, 2012.
4. Rana, M. M. and A. S. Mohan, "Rotationally symmetric (RS)-LOD-FDTD with CPML for analysing resonant structures," *Int. Sym. Antennas Propag. (ISAP)*, 930–933, 2012.
5. Ahmed, I., et al., "Convolutional perfectly matched layer for an unconditionally stable LODFDTD method," *IEEE Microw. Wireless Compon. Lett.*, Vol. 17, No. 12, 816–818, 2007.
6. Tan, E. L., "Fundamental schemes for efficient unconditionally stable implicit finite-difference time-domain methods," *IEEE Trans. Antennas Propag.*, Vol. 56, No. 1, 170–177, 2008.

Design of a Novel Miniaturized Composite Right/Left-handed Leaky Wave Antenna

Cheng-Lung Kao and Fu-Chiarng Chen
Department of Electrical Engineering, Institute of Communications Engineering
National Chiao Tung University, 1001 Tahsueh Rd., Hsinchu 300, Taiwan

Abstract— This paper presents the design of a novel miniaturized composite right/left-handed (CRLH) leaky wave antenna. This miniaturized CRLH leaky wave antenna utilizes coplanar waveguide (CPW) structure and metal-insulator-metal (MIM) capacitor in order to reach a high leakage constant and provide bi-direction frequency-scanning capability. The equivalent circuit model of the proposed CRLH structure unit cell will be presented and discussed. The extraction of the equivalent circuits component values will be also presented. The dispersion diagrams of the CRLH antenna unit cell from the results of full wave HFSS simulation, measurement and the equivalent circuit will be presented and compared. Furthermore, we use this miniaturized CRLH leaky wave antenna to implement a three-dimensional steering beam antenna. The proposed beam steering antenna includes two miniaturized CRLH leaky wave antennas, two switching circuits made by PIN-diodes to control phase shifter, and a 2-port power divider. By controlling the PIN diodes and the phases of the antenna array, the steering beam antenna can be switched in three dimensions. The CRLH leaky wave antenna is implemented on Rogers RT/Duroid 5880 with thickness = 1.57 mm, relative permittivity = 2.2, and loss tangent = 0.0009. In addition, the proposed antenna is compact and low-profile. The simulation and measurement results will be presented and discussed.

Eigenmode Analysis for Designing Plasmonic Devices by an Integral Solver

S. Kishimoto, **S. Ohnuki**, **Y. Ashizawa**, **and K. Nakagawa**
College of Science and Technology, Nihon University, Japan

Abstract— Analysis of electromagnetic problems for metallic nano objects plays an important role for developing plasmonic devices such as nanoscale antennas for ultra-high density magnetic recording [1]. In this research area, the finite difference time domain (FDTD) method is commonly used [2]. Recently, the integral solver has been attracted attention [3, 4]. In this talk, electric fields near nano objects are investigated by integral solvers for designing nanoscale devices. Especially, specific plasmon resonance modes can be computed by solving an eigenmode problem. To verify the computational accuracy, we investigate resonance modes for a metallic nano sphere and compare computational results to the exact Mie series solution.

Using our proposed method, nanoscale antennas for ultra-fast and high-density magnetic recording are designed. We will show that the designed antenna can produce high intensity electric fields and can be localized to achieve more than 2 Tbits/inch^2 recording density.

REFERENCES

1. Stanciu, C. D., F. Hansteen, A. V. Kimel, A. Kirilyuk, A. Tsukamoto, A. Itoh, and T. Rasing, "All-optical magnetic recording with circularly polarized light," *Phys. Rev. Lett.*, Vol. 99, No. 4, 047601-1–047601-4, 2007.
2. Nakagawa, K., Y. Ashizawa, S. Ohnuki, A. Itoh, and A. Tsukamato, "Confined circularly polarized light generated by nano-size aperture for high density all-optical magnetic recording," *J. Appl. Phys.*, Vol. 109, No. 7, 07B735-1–07B735-3, 2011.
3. Mayergoyz, I. D., Z. Zhang, and G. Miano, "Analysis of dynamics of excitation and dephasing of plasmon resonance modes in nanoparticles," *Phys. Rev. Lett.*, Vol. 98, No. 14, 147401-1–147401-4, 2007.
4. Kishimoto, S., S. Ohnuki, Y. Ashizawa, K. Nakagawa, and W. C. Chew, "Time domain analysis of nanoscale electromagnetic problems by a boundary integral equation method with fast inverse laplace transform," *Journal of Electromagnetic Waves and Applications*, Vol. 26, Nos. 8–9, 997–1006, 2012.

All-dielectric Planar Chiral Nanogratings with Large Optical Activity

Y. Wakabayashi, **Y. Shigenaga**, **J. Yamauchi**, **and H. Nakano**
Faculty of Science and Engineering, Hosei University, Tokyo 184-8584, Japan

Abstract— Considerable interest has been directed towards the optical activity caused by the chiral planar nanostructures [1–5], often referred to as planar chiral nanogratings (PCNGs). A typical PCNG consists of a silica substrate and high-index C_4 (fourfold rotational) symmetry elements such as gammadion-shaped nanoparticles, which are periodically arrayed on a homogeneous layer. We have analyzed all-dielectric PCNGs [4], using the finite-difference time-domain (FDTD) method with the periodic boundary condition (PBC) [6]. In addition to the gammadion-shaped PCNG, we have investigated a windmill-shaped PCNG, which shows that the polarization rotation behavior becomes somewhat insensitive to a wavelength change compared with that for the gammadion-shaped one.

In this study, as an alternative to the PCNGs with the C_4 symmetry nanoparticles (ridge-type), we analyze the PCNG with gammadion-shaped grooves (groove-type). The similarity and difference between the ridge- and groove-type PCNGs are revealed, using the periodic FDTD method. The wavelength responses for both types are divided into two regions with respect to wavelength $\lambda = 0.75\,\mu\text{m}$. In the shorter wavelength region ($\lambda < 0.75\,\mu\text{m}$), both the polarization rotation and elliptization take place, whereas, in the longer wavelength region ($\lambda > 0.75\,\mu\text{m}$), the ellipticity is zero regardless of the polarization rotation. It is worth mentioning that, for the groove-type, the polarization rotation is achieved around $\lambda = 0.76\,\mu\text{m}$ with a rotation angle of 6 degrees, maintaining a high transmissivity of more than 83%. This constant polarization rotation alleviates the fabrication accuracy. Further consideration is directed towards the eigenmode fields of the PCNGs. For this purpose we employ the beam-propagation method based on Yee's mesh (YMBPM) [7]. To effectively evaluate the eigenmodes of periodic structures, we apply the PBC to the YM-BPM. It is found for the fundamental mode that the field localizes in the high-index region. On the other hand, for the higher-order modes, the fields are mainly confined to the slit (air region) between the high-index regions.

REFERENCES

1. Papakostas, A., A. Potts, D. M. Bagnall, S. L. Prosvirnin, H. J. Coles, and N. I. Zheludev, "Optical manifestations of planar chirality," *Phys. Rev. Lett.*, Vol. 90, No. 10, 107404, 2003.
2. Bai, B., Y. Svirko, J. Turunen, and T. Vallius, "Optical activity in planar chiral metamaterial: Theoretical study," *Phys. Rev. A*, Vol. 76, No. 2, 023811, 2007.
3. Kuwata-Gonokami, M., N. Saito, Y. Ino, M. Kauranen, K. Jefimovs, T. Vallius, J. Turunen, and Y. Svirko, "Giant optical activity in quasi-two-dimensional planar nanostructures," *Phys. Rev. Lett.*, Vol. 95, No. 22, 227401, 2005.
4. Wakabayashi, Y., J. Yamauchi, and H. Nakano, "FDTD analysis of all-dielectric planar chiral metamaterials with large optical activity," *ISAP 2009*, Bangkok, Thailand, WF1, 2009.
5. Ohtera, Y., "Analysis of polarization characteristics of sub-wavelength chiral periodic structure," *IEICE Tech. Rep.*, Vol. 112, No. 401, EST2012-96, 211–216, 2013.
6. Taflove, A. and S. Hagness, *Computational Electrodynamics: The Finite-difference Time-domain Method*, Artech House, Norwood, MA, 2000.
7. Lee, S. M., "Finite-difference vectorial-beam-propagation method using Yee's discretization scheme for modal fields," *J. Opt. Soc. Am. A*, Vol. 13, No. 7, 1369–1377, 1996.

Design of All-optical Magnetic Recording System Using Plasmonic Antennas and Particulate Media

S. Ohnuki, **Y. Takano**, **T. Kato**, **Y. Ashizawa**, **and K. Nakagawa**
College of Science and Technology, Nihon University
1-8-14 Surugadai, Kanda, Chiyoda-ku, Tokyo 101-8308, Japan

Abstract— Recently, ultrafast magnetization reversal has been discovered and the experimental results show that it occurs by illuminating a 40 fs circularly polarized laser pulse [1]. Compared with conventional magnetic recording, the speed can be accelerated about 100,000 times faster. To realize high-density recording using the ultrafast magnetization reversal, we propose a novel system using plasmonic antennas and particulate media [2]. Plasmonic antennas can generate the localized circularly polarized light in nanoscale spots and one-bit information can be stored into each particulate medium.

In this talk, we will discuss stability of our recording system. To change the shape of plasmonic antennas and the distance between antennas and particulate media, we evaluate the total intensity enhancement, the degree of circular polarization, and the figure of merit in terms of the Stokes parameters. To simulate electromagnetic fields in dispersive media, the finite-difference time-domain method with the auxiliary differential equation is applied.

REFERENCES

1. Stanciu, C. D., F. Hansteen, A. V. Kimel, A. Kirilyuk, A. Tsukamoto, A. Itoh, and T. Rasing, "All-optical magnetic recording with circularly polarized light," *Phys. Rev. Lett.*, Vol. 99, 047601-1–047601-4, Jul. 2007.
2. Nakagawa, K., Y. Ashizawa, S. Ohnuki, A. Itoh, and A. Tsukamoto, "Confined circularly polarized light generated by nano-size aperture for high density all-optical magnetic recording," *J. Appl. Phys.*, Vol. 109, 07B735-1–07B735-3, Apr. 2011.

Session 3A9a
SC3: On-chip Optical Sensing Technologies and Devices

Silicon Nanophotonics On-chip Sensing
Peter Bienstman, Sam Werquin, Cristina Lerma Arce, Elewout Hallynck, Tom Claes, Jan-Willem Hoste, Daan Martens, ... 1014

SiC Based pH Sensor with Gd_2O_3/Si_3N_4 Gate Dielectrics
D. H. Ko, C. S. Huang, Liann-Bie Chang, Jer-Ming Jeng, C. S. Lai, Y. T. Lin, Chow Lee, ... 1015

Optical Sensing and Particle Manipulation Using Silicon-based Microresonators in Optofluidic Chips
Andrew Wing On Poon, Ting Lei, Jiawei Wang, ... 1016

Directional Plasmonic Nanoantennas for Spectroscopy and Sensing
Timur Shegai, Vladimir D. Miljkovic, P. Johansson, Mikael Kall, ... 1017

Group IV Photonics Platforms for Sensing Applications
Goran Z. Mashanovich, M. Nedeljkovic, X. Chen, J. Soler Penades, G. Madalinski, M. Muneeb, Gunther Roelkens, H. M. H. Chong, G. T. Reed, ... 1019

New Fabrication and Instrumentation Techniques for Nanoplasmonic Biosensors
Sang-Hyun Oh, ... 1020

Detection of Environmental Contaminants Using an Optical Refractometer and Silicon-on-Insulator (SOI) Devices
John E. Saunders, Weijian Chen, Chris Brauer, Jack A. Barnes, Scott S.-H. Yam, Dan-Xia Xu, Hans-Peter Loock, ... 1021

Silicon Nanophotonics On-chip Sensing

Peter Bienstman, Sam Werquin, Cristina Lerma Arce, Elewout Hallynck, Tom Claes, Jan-Willem Hoste, and Daan Martens
Photonics Research Group, NB-Photonics, Department of Information Technology
Ghent University-IMEC, Gent 9000, Belgium

Abstract— Silicon nanophotonics is a very promising platform for integrated biosensing due to its high index contrast and mass fabrication potential. Ring resonators are particularly attractive because they allow very accurate determination of refractive index.

In this paper, several advances in silicon ring resonator biosensors are presented. First, we address the problem that due to the high index contrast, small deviations from perfect symmetry lift the degeneracy of the normal resonator mode. This severely deteriorates the quality of the output signal. To address this, we discuss an integrated interferometric approach to give access to the unsplit, high-quality normal modes of the microring resonator.

Second, we also demonstrate how we can integrate ring-resonator based sensing chips in a plastic reaction tube while at the same time still allowing for sample flow. This is achieved by using laser ablation to create holes through the chip.

We also show a different scheme with through-chip fluidics which can lead to improved analyte delivery and show an improvement of at least a factor of 3 in delivery time.

In addition, we present a multimodal sensing technique which simultaneously allows us to measure thicknees and refractive index of biolayers. This opens the door towards high-throughput study of conformational changes in biomolecules, which is very promising for drug discovery research.

SiC Based pH Sensor with Gd_2O_3/Si_3N_4 Gate Dielectrics

D. H. Ko[1,2], C. S. Huang[2], L. B. Chang[2], J. M. Jeng[2], C. S. Lai[3], Y. T. Lin[3], and C. Lee[4]

[1]Department of Chemical Sciences
University of Auckland, Auckland 1010, New Zealand
[2]Department of Optoelectronic Engineering
Chang Gung University, Kweishan, Taoyuan 333, Taiwan
[3]Department of Electronic Engineering
Chang Gung University, Kweishan, Taoyuan 333, Taiwan
[4]Department of Physics, University of Central Florida, Orlando, FL 32816, USA

Abstract— Wide band gap Silicon Carbon material has more robust mechanical and chemical properties than the narrow band gap silicon material. For the first time, single layer Gd_2O_3 and Si_3N_4 dielectrics have been deposited onto SiC semiconductor substrates to perform pH sensing capability and have been compared to Si based device in this research. We have also investigated the pH sensing properties of Gd_2O_3 and Si_3N_4 composite dielectric in terms of pH hysteresis and time drift effects when deposited on both Si and SiC substrates.

From the data gathered, the optimum values for sensitivity and linearly is 42.75 mV/pH and 99.6% respectively. Due to the nature of silicon carbide substrate in having a wider band gap, we have demonstrated and verified that it may be incorporated in the application of biosensor materials. Not only does the substrate exhibit properties of high sensitivity and low noise to ratio, but also as a direct bandgap light emitting material itself that is able to be made into blue-ray diodes on the backside. Also, prior studies have shown that SiC have more practical advantages than conventional silicon substrate such as: higher hardness, wear-resistance, low chemical activity, good oxidation resistance, low thermal expansion coefficient, high thermal conductivity, high electric field break down and high maximum current density. In order to obtain an accurate measurement for pH-ISFET by using SiC substrate, in this paper, we have investigated hysteresis effect, time drift semiconductor interface and pH sensor characteristics. Overall, it is evident that the use of SiC substrate promotes several prospective developments in the field of biomedical sensors.

Optical Sensing and Particle Manipulation Using Silicon-based Microresonators in Optofluidic Chips

Andrew W. Poon, Ting Lei, and Jiawei Wang
Photonic Device Laboratory, Department of Electronic and Computer Engineering
The Hong Kong University of Science and Technology, Clear Water Bay, Hong Kong, China

Abstract— In this talk, we will review our latest breakthroughs in optical sensing and particle manipulation using silicon-based microresonators in optofluidic chips.

For optical sensing using microresonators, we are interested in using the spatial domain instead of the conventional spectral domain. We employ coupled-resonator optical waveguides (CROWs) comprising silicon or silicon nitride (SiN) cascaded microring resonators. The multiple cascaded microring resonators give us a number of eigenstates within an in homogeneously broadened passpand. Each eigenstate displays a unique spatial mode-field intensity distribution that is sensitive to the cladding refractive index. Thus it is conceivable that by imaging the elastic light scattering in the far field from the mode-field intensity distributionat a fixed wavelength, we can detect from the pattern variations the change in the cladding refractive index. Our preliminary experiments in 1550 nm wavelengths using a silicon CROW of eight cascaded microrings cladded with various concentrations of sodium chloride salt solutions suggest a detection-limit of 10^{-5} RIU.

The principle for on-chip optical manipulation of particles concerns using optical gradient forces in the vertical and lateral directions to trap multiple micrometer- or submicrometer-sized particles to the integrated waveguide top surface, and using optical scattering force in the longitudinal direction to propel the particles along the waveguide. As the particles interact with the evanescent field on the waveguide surface, the particles experience a large field gradient toward the waveguide surface without any focusing optics, which are commonly required in conventional laser-based optical tweezers. Over the past 5 years, our research group, along with other research groups in this young and bourgeoning field, has successfully demonstrated on the SiN photonics platform in 1550 nm wavelengths particle-manipulation devices including microring resonator-based particle add-drop filters, microdisk resonator-based particle buffers and waveguide junction-based planar optical tweezers that trap only one or two particles. Our on-going experiments reveal that multiple particles can be accumulated on a microring resonator and a whispering-gallery-mode microdisk resonator, and sensed in real time by measuring the resonance shifts using a broadband excitation source and an optical spectrum analyzer. We thus envision that the nascent interdisciplinary field of silicon-based optofluidics for sensing and particle manipulation has a lot of unchartered avenues to offer to electromagnetic theorists and experimentalists.

Directional Plasmonic Nanoantennas for Spectroscopy and Sensing

T. Shegai[1], **V. D. Miljković**[1], **P. Johansson**[1,2], **and M. Käll**[1]

[1]Bionanophotonics, Chalmers University of Technology, Göteborg, Sweden
[2]School of Science and Technology, Örebro University, Örebro, Sweden

Abstract— Plasmonic nanoantennas are well known for their ability to amplify signals from sub-wavelength sources. However, until recently, the directionality of the emission received comparatively little attention. Here we describe recent experimental and theoretical investigations of the directional emission from various types of plasmonic antennas composed of Au or Ag nanostructures [1–5]. As illustrated below, examples include nanowire antennas and different types of subwavelength nanoparticle dimers of relevance for surfaceenhanced spectroscopy and plasmonic sensing.

Single crystal silver nanowires act as broadband unidirectional antennae for visible light [4]. The degree of directionality can be controlled through the nanowire radius and its dielectric environment and the effect can be interpreted in terms of socalled leakage radiation from surface plasmons propagating in a single direction along the wire. We measure a forward-to-backward emission ratio exceeding 15 dB and an angular spread of 4 deg. for wires with radii of the order 150 nm on glass in air.

The angular distribution of surface enhanced Raman scattering (SERS) emitted by individual aggregates of gold nanoparticles is illustrated through the results in Fig. 2 [5]. The emission closely agrees with what can be calculated for a single point dipole oriented parallel to the dimer axis. In particular, we find that most of the radiation appears at angles exceeding the critical angle of the air-glass interface supporting the dimer. The results demonstrate that angle-resolved imaging can be used as a fast and facile method for determination of the three-dimensional orientation and symmetry of the SERS "transition dipole" and emphasize the importance of using optics with sufficiently high NA for collecting the "forbidden light" cone.

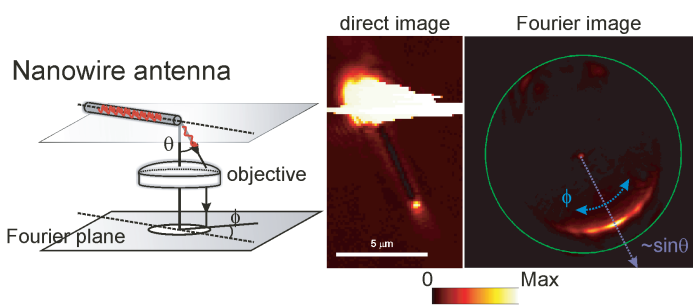

Figure 1: Unidirectional nanowire emission [4]. The upper left tip of the wire is excited with focused white light and the elastic emission remaining part is recorded in the Fourier and direct image planes.

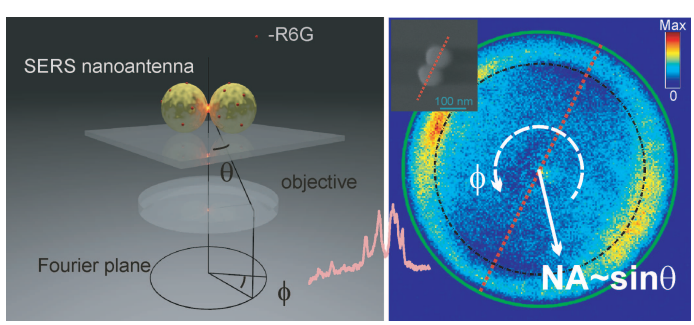

Figure 2: Fourier imaging of SERS emission dominated by a "hot spot" in the gap between two Au nanoparticles [5].

REFERENCES

1. Alaverdyan, Y., B. Sepúlveda, L. Eurenius, E. Olsson, and M. Käll, "Optical nanoantennas based on nanoholes in thin metal films," *Nature Phys.*, Vol. 3, 884, 2007.
2. Pakizeh, T. and M. Käll, "Unidirectional ultracompact optical nanoantennas," *Nano Lett.*, Vol. 9, 2343, 2009.
3. Shegai, T., Y. Huang, H. Xu, and M. Käll, "Coloring fluorescence emission with silver nanowires," *Appl. Phys. Lett.*, Vol. 96, 103114, 2010.
4. Shegai, T., V. Miljkoviç, K. Bao, H. X. Xu, P. Nordlander, P. Johansson, and M. Käll, "Unidirectional broadband light emission from metal nanowire antennae," *Nano. Lett.*, 2011, in press.
5. Shegai, T., B. Brian, V. Miljkoviç, and M. Käll, "Angular distribution of light from individual Raman nanoantennae," *ACS Nano*, in press.

Group IV Photonics Platforms for Sensing Applications

G. Z. Mashanovich[1], M. Nedeljkovic[1], X. Chen[1], J. Soler Penades[1], G. Madalinski[2], M. Muneeb[3], G. Roelkens[3], H. M. H. Chong[2], and G. T. Reed[1]

[1]Optoelectronics Research Centre, University of Southampton, Southampton SO17 1BJ, UK
[2]Electronics and Computer Science, University of Southampton, Southampton SO17 1BJ, UK
[3]Photonics Research Group — NB-Photonics, Ghent University-IMEC, Ghent B-9000, Belgium

Abstract— The mid-infrared (MIR) wavelength region has attracted interest due to a host of important application areas, such as sensing, medical diagnostics, industrial control, communications, defence and security [1, 2]. Of particular importance is the so-called 'fingerprint' region where high selectivity sensing can be achieved. Integrated, compact, low cost and low energy solutions in group IV materials will have significant advantages over expensive and bulky spectrometers currently used.

Due to absorption properties of photonic materials [3], variety of potential applications and several fabrication issues in the MIR, different material platforms need to be considered for this wavelength range. In the last 3 years, MIR devices in SOI [4, 5], SOS [6], Si on porous Si (SiPSi) [7], and Geon-Si [8] have been reported. SOI platform is probably the most desirable, as it has been extensively used for telecommunication wavelengths and fabrication recipes and designed rules are mature and can be readily transferred to the MIR. We have investigated this platform up to 4 µm and showed that the propagation loss can as low as 3 dB/cm for 400 nm thick SOI waveguides and at the wavelength of 3.8 µm. We have also demonstrated passive components based on this structure, including multimode interference (MMI) splitters, ring resonators, Mach-Zehnder interferometers (MZIs) [4], and spectrometers [9].

In order to extend the operational wavelength range even further, we have examined suspended structures in which the buried oxide layer has been removed [5]. Our simulations show that this structure can be used up to 6.5 µm for the Si overlayer thickness of 500 nm [10]. For the fingerprint region, the most promising candidate is Ge, and different Ge-based platforms can be considered.

ACKNOWLEDGMENT

This work has been supported by the Royal Society (Goran Mashanovich's URF "Mid-infrared Silicon Photonics") and by EPSRC through "UK Silicon Photonics" programme.

REFERENCES

1. Soref, R. A., "Group IV photonics for the mid infrared," *SPIE Photonics West*, 2013.
2. Soref, R. A., *Nature Photonics*, Vol. 4, 495, 2010.
3. Palik, E. D., *Handbook of Optical Constants of Solids*, Vol. 1, Academic, London, 1985.
4. Milosevic, M. M., et al., *Appl. Phys. Lett.*, Vol. 101, 121105, 2012.
5. Reimer, C., et al., *Opt. Express*, Vol. 20, 29361, 2012.
6. Shankar, R., et al., *Appl. Phys. Lett.*, Vol. 102, 051108, 2013.
7. Milošević, M. M., et al., *8th IEEE Group IV Photonics conference*, London, UK, 2011.
8. Chang, Y.-C., et al., *Opt. Letters*, Vol. 37 2883, 2012.
9. Muneeb, M., et al., *Optics Express*, 2013.
10. Chen, X., et al., *EOS Annual Meeting 2012*, Aberdeen, UK, September 25–28, 2012.

New Fabrication and Instrumentation Techniques for Nanoplasmonic Biosensors

Sang-Hyun Oh
Department of Electrical and Computer Engineering, University of Minnesota
Minneapolis, MN 55455, USA

Abstract— The research field of nanoplasmonics has emerged in synergy with advances in nanofabrication. Among various applications of nanoplasmonic devices, biosensing in particular has shown great promise to extend the sensitivity and functionality of commercially successful instruments based on surface plasmon resonance. This presentation will first focus on high-throughput fabrication technologies for nanoplasmonics, including template-stripping nanofabrication for making ultrasmooth patterned metals, large-area patterning of periodic structures via nano-imprint lithography and interference lithography, and surface modification using atomic layer deposition. The second part of the presentation will discuss how to combine nanoplasmonic sensor chips with free-space optics and microfluidics to construct high-performance biosensing instruments. Techniques for surface modification, microfluidic sample injection, parallel optical detection, and data analysis will be described. In addition to refractometric biosensing, we will discuss applications of ultra-thin metallic nanogap structures and sharp metallic tips for surface-enhanced Raman spectroscopy of biological analytes.

Detection of Environmental Contaminants Using an Optical Refractometer and Silicon-on-Insulator (SOI) Devices

John E. Saunders[1], **Weijian Chen**[2], **Chris Brauer**[1], **Jack A. Barnes**[1], **Scott S.-H. Yam**[2], **Dan-Xia Xu**[3], **and Hans-Peter Loock**[1]

[1]Department of Chemistry, Queen's University, 90 Bader Lane, Kingston, Ontario K7L 3N6, Canada
[2]Department of Electrical and Computer Engineering, Queen's University
19 Union Street, Kingston, Ontario K7L 3N6, Canada
[3]National Research Council of Canada, 1200 Montreal Road, Ottawa, Ontario K1A 0R6, Canada

Abstract— Detection of environmental contaminants in the field requires compact, sensitive and specific sensors. Many types of refractive index sensors are sensitive, but often not chemically specific. Functionalizing the devices with coatings that interact with an analyte of interest can provide the needed specificity. Here, we assess functionalized polymers and other materials as extraction matrices for volatile organic compounds and aqueous heavy metals using a lab-built Abbe-type refractometer and Silicon-on-Insulator (SOI) ring resonators. The lab-built refractometer focuses the output of a near-infrared diode laser (1550 nm) onto the interface between a prism and a slide coated with our extraction matrix. For thick films, only light reaching the interface at an incident angle greater than the critical angle is reflected producing a light-dark interface on a CCD camera. In thin films, on the other hand, light is reflected from both the bottom and top surface of a film causing an interferogram at the CCD camera. Using Fourier analysis of the interferograms we simultaneously extract the thickness and refractive index changes of materials while exposed to a variety of solvent vapours. This allows us to quantify the uptake in solid-phase microextraction materials such as modified polydimethylsiloxane films. The versatility of this technique stems from the ability to measure both solid and liquid films from below, while still leaving the top surface accessible for analyte introduction.

We apply similar extraction materials to micro-ring resonators made on SOI wafers by the National Research Council of Canada using e-beam lithography and deep-reactive ion etching. Silicon waveguides 260 nm high by 450 nm wide are coated with a protective cladding layer of 2 µm of silicon dioxide with windows opened for chemical sensing. On the chip, the waveguides are structured as double coiled ring resonators and Mach-Zehnder Interferometers in both individual devices and in array formats. Due to the high refractive index contrast and dimensions of the waveguides, a strong evanescent field is present and refractive index changes as low as 1×10^{-4} over the exposed devices can be detected. The SOI devices have been functionalised with the same modified polydimethylsiloxane polymer and exposed to numerous volatile organic compounds. Uptake was compared to refractometer results to understand the role that film swelling plays in refractive index changes.

On a different chip, tetrasulfide functionalized mesoporous silicates were condensed around Pluronic F-127 surfactant to form a highly periodic nanometer pore-sized material that binds heavy metals irreversibly and strongly. Once spin-coated onto SOI ring resonators, and surfactant extracted, the chips were exposed to aqueous heavy metal solutions. Initial experiments have shown detection of Pb^{2+} and Hg^{2+} ions, in the low ppm to high ppb range. Partial recovery has been observed after acid treatment of the exposed films. Experiments are underway to better quantify the uptake and determine the detection limits of this setup.

Session 3A9b
Action-at-a-distance Theories and Electrodynamics

Magnetic Field Expulsion in Perfect Conductors — The Magnetic Equivalent of Thomson's Theorem
Miguel C. N. Fiolhais, Hanno Essen, ... 1024
The Darwin-Breit Magnetic Interaction and Superconductivity
Hanno Essen, Miguel C. N. Fiolhais, ... 1025
On a Method of Solving Mixed-type FDEs
C. K. Raju, ... 1026
Variational Electrodynamics
Jayme Vicente De Luca, ... 1027
The Magnetic Force as a Kinematical Consequence of the Thomas Precession
David C. Lush, ... 1028

Magnetic Field Expulsion in Perfect Conductors — The Magnetic Equivalent of Thomson's Theorem

Miguel C. N. Fiolhais[1] and Hanno Essén[2]

[1]LIP, Department of Physics, University of Coimbra, Coimbra 3004-516, Portugal
[2]Department of Mechanics, KTH, Stockholm 10044, Sweden

Abstract— Thomson's theorem states that electric charge density on metal conductors, at static equilibrium, is distributed on the surface of the conductors in such a way that the interior electric field is zero, and the electric field on the surface must be perpendicular to the surface. In this paper, we present a theorem for static magnetic fields, analogous of the Thomson theorem of electrostatics. We prove, by making use of a variational principle, that the minimization of the magnetic field energy corresponds to the magnetic field expulsion of perfect conductive systems through surface currents. As a result, the current density distributes itself on the surface of the ideal conductor so that the interior magnetic field becomes zero, while the surface magnetic field is perpendicular to both the current density and the surface normal.

This result is put into the context of superconductivity, and leads us to conclude the Meissner effect is not a pure quantum effect, restricted to superconductors, but rather a magnetostatic equilibrium state as a consequence of zero resistivity. In addition, the London equations are derived following an approach by Pierre-Gilles de Gennes where *"the superconductor finds an equilibrium state where the sum of the kinetic and magnetic energies is minimum, and this state, for macroscopic samples, corresponds to the expulsion of magnetic flux"*. For further confirmation, the same result is also derived in the classical limit of the Coleman-Weinberg model, the most successful quantum macroscopic theory of superconductivity.

Several examples are presented to corroborate the result of our theorem. In particular, explicit solutions for minimal energy magnetic field configurations are analyzed, and found to be in agreement with our statement.

The Darwin-Breit Magnetic Interaction and Superconductivity

H. Essén[1] **and M. C. N. Fiolhais**[2]

[1]KTH, Sweden
[2]University of Coimbra, Portugal

Abstract— A number of facts indicating the relevance of the Darwin magnetic interaction energy in the superconducting phase are pointed out. The magnetic interaction term derived by Darwin is the same as the, so called, Breit term in relativistic quantum mechanics. While this term always is a small perturbation in few body systems it can be shown to be potentially dominating in systems of large numbers of electrons. It is therefore a natural candidate in the explanation of emergent phenomena — phenomena that only occur in sufficiently large systems. The dimensionless parameter that indicates the importance of the magnetic energy is the number of electrons times the classical electron radius divided by the size of the system. The number of electrons involved are only the electrons at the Fermi surface; electrons with lower energy cannot contribute to current density and thus not to the magnetic field.

The conventional understanding of superconductivity has always been problematic and no really reductionistic derivation exists. The idea that the inductive inertia, due to magnetism, is important in the explanation of superconductivity was first advanced by Frenkel and later brought up by Welker before it was prematurely discarded. So were theories involving Wigner crystallization. We speculate that the answer requires the combination of a Wigner lattice and the Darwin interaction. We point out that the Darwin interaction can be shown to have the right order of magnitude to explain the energy scales involved in normal superconductors. The London magnetic moment of rotating superconductors and the Meissner effect and their connection are discussed next. The London moment is shown indicate that the number of electrons involved in the superconducting condensate is such that the Darwin interaction cannot be neglected.

On a Method of Solving Mixed-type FDEs

C. K. Raju
Albukhary International University, Alor Setar 05200, Malaysia

Abstract— The absorber theories of Wheeler-Feynman [1, 2] and others [3] have logical defects, pointed out long ago [4] but never addressed by proponents of the theory. Also, a key motivation of the Wheeler-Feynman theory no longer applies: the problem of runaways with radiation damping has been resolved differently. Runaways arise due to the mathematically incorrect conversion of functional differential equations (FDEs) of electrodynamics to ordinary differential equations, [5] and, conversely, runaways may be controlled by reverting to FDEs [6]. Nonetheless, absorber theories brought to light the important possibility that small amounts of advanced radiation may exist, as my absorber theory explicitly predicted [4]. If advanced radiation does exist, the equations of (classical) electrodynamics would be mixed-type FDEs. A method of solving such mixed-type FDEs is required to design proper experiments to detect advanced radiation [7, 8].

Subsequently, mixed-type FDEs were proposed [9] as a general model for physics, independently of any absorber theory (including mine). This new, direct-action model corresponds to starting (in field-theoretic terms) with a mixture of the form $(1-c_a)F_{ret}+c_aF_{adv}$, with $c_a \approx 0$ (estimated to be 10^{-12}). This "tilt in the arrow of time" is not a hypothesis, since mixed-type FDEs are the most general form compatible with known physics. Instead of putting $c_a = 0$ on some metaphysical "principle of causality", one should decide it through physics. This requires the non-causal theory ($c_a \neq 0$) to be compared with the causal theory, against observations. Mundane observation, however, repeatedly shows that future is not entirely determined by the past. From the qualitative theory of mixed-type FDEs, this favours the case $c_a \neq 0$ [9, 10]. Further, for small c_a, the same qualitative theory allows one to infer a microphysical structure of time, corresponding to a quantum logic [11]. That is, (classical) mixed-type electrodynamics provides a simple model to explain the most puzzling aspect of quantum mechanics, namely the interference of probabilities (or the non-existence of a joint probability distribution for canonically conjugate variables).

For quantitative experimental tests (and to observationally fix the value of c_a), we need a general technique to solve mixed-type FDEs. This paper explains such a technique for the 1 and 2 body problems of mixed-type electrodynamics (as distinct from the 2-body problem of retarded electrodynamics for which a technique is already available [12]).

REFERENCES

1. Wheeler, J. A. and R. P. Feynman, *Rev. Mod. Phys.*, Vol. 17, 157–181, 1945.
2. Wheeler, J. A. and R. P. Feynman, *Rev. Mod. Phys.*, Vol. 21, 425–433, 1949.
3. Hoyle, F. and J. V. Narlikar, *Proc. R. Soc. A*, Vol. 277, 1–23, 1964.
4. Raju, C. K., "Classical time-symmetric electrodynamics," *Journal of Physics A: Math. Gen.*, Vol. 13, 3303–3317, 1980.
5. Raju, C. K., "Electromagnetic time," *Time: Towards a Consistent Theory*, Chapter 5b, 116–135, Kluwer Academic, Dordrecht, 1994, http://arxiv.org/pdf/0808.0767v1.
6. Raju, S. and C. K. Raju, "Radiative damping and functional differential equations," *Modern Physics Letters A*, Vol. 26, No. 35, 2627–2638, 2011.
7. Partridge, R. B., *Nature*, Vol. 244, 263–265, 1973.
8. Heron, M. L. and D. T. Pegg, *J. Phys. A: Math. Gen.*, Vol. 7, 1965–1969, 1974.
9. Raju, C. K., *Time: Towards a Consistent Theory*, Vol. 65 of *Fundamental Theories of Physics*, Kluwer Academic, Dordrecht, 1994.
10. Raju, C. K., "Time travel and the reality of spontaneity," *Foundations of Physics*, Vol. 36, 1099–1113, 2006.
11. Raju, C. K., "Quantum-mechanical time," *Time: Towards a Consistent Theory*, Chapter 6b, Kluwer Academic, 1994, http://arxiv.org/pdf/0808.1344v1.
12. Raju, C. K., "The electrodynamic 2-body problem and the origin of quantum mechanics," *Foundations of Physics*, Vol. 34, No. 6, 937–962, 2004.

Variational Electrodynamics

Jayme Vicente De Luca
Departamento de Física, Universidade Federal de São Carlos
Via Washington Luis, km 235, São Carlos 13565-905, Brazil

Abstract— We generalize Wheeler-Feynman electrodynamics of point charges. The generalized electrodynamics postulates the minimization of a finite action functional defined by the *integral* of a product of velocities evaluated at (different) times along continuous trajectories satisfying boundary conditions in past and future. For two-body boundary segments sufficiently close to circular orbits of large radii, we prove that the boundary-value problem has a unique solution depending continuously on the boundary segments positions, velocities and accelerations. The unique solution in general has velocity discontinuities, henceforth broken extremum. Electromagnetic fields of these finite segments of trajectories with velocity discontinuities are derived quantities that can be extended to a bounded region $\mathcal{B}$ of space-time. For boundary segments with a finite number of velocity discontinuities, extended fields are defined in all point of $\mathcal{B}$ with the exception of a finite number of spherical wave fronts. The extended fields satisfy the integral laws of classical electrodynamics for most surfaces and curves inside $\mathcal{B}$.

The extremum conditions along regular segments (Euler-Lagrange equations) are *neutral differential delay* equations with state-dependent deviating arguments. At corner points, broken extrema satisfy the Weierstrass-Erdmann corner conditions that *partial energies* and *momenta* are *continuous*. Such generalization is surprisingly necessary to include bounded two-body orbits with vanishing far-fields. As an application, we discuss some details of the hydrogenoid atomic model and its *variational boundary-value* problem with past and future boundary conditions. Our simple model predicts a finitely measured neighbourhood of periodic broken extrema with vanishing far-fields right at the atomic magnitude.

Last, it time allows, we shall give further details on the hydrogenoid model. We have varied the mass ratio by three orders of magnitude and the model predicts spectra in agreement with experiment for hydrogen, muonium and positronium.

The Magnetic Force as a Kinematical Consequence of the Thomas Precession

David C. Lush
2462 63rd Ave SE, Mercer Island, Washington 98040, United States

Abstract— This talk will describe how an examination of the interaction of two classical charged particles from the point of view of relativistic kinematics provides insight into the nature of the magnetic force, as well as possibly revealing the necessity of other forces that may correspond to the strong and weak fundamental forces. The magnetic force is viewed as arising as a consequence of the Thomas precession, as seen by an observer co-moving with a charged test particle accelerating under the influence of the Coulomb field of another, non-accelerating, charge. The accelerated observer with a component of motion non-radial to the field-source particle sees the rest frame of the field-source particle as Thomas precessing, but the absence of Coriolis force in the source particle rest frame, which is an inertial reference frame, appears to the accelerated observer as a tangible force that is termed an anti-Coriolis force. The part of this anti-Coriolis force that remains after the accelerated observer performs a sequence of Lorentz transformations, as needed to describe the motion in a laboratory frame where the field-source particle is uniformly translating, is identified with the magnetic force on the test particle. However, the accelerated observer also sees a similar lack of centrifugal and Euler forces in the field-source particle rest frame as requiring other tangible forces. In particular, he predicts an anticentrifugal force that is always attractive and may plausibly overcome Coulomb repulsion in the highly relativistic limit and at nucleonic scale, similarly to the strong fundamental force. The magnetic interaction between two highly-accelerating relativistic charges is then examined and shown to be equivalent to the expected anticentrifugal force in the case of circular motion.

Session 3AK
Poster Session 5

Comparison of Cylindrical FDTD with Cartesian Subcell Modeling for Circularly Shaped Objects
Stefan Kirsch, Rolf Schuhmann, ... 1032
Nonreciprocal Properties of Cylindrical Junction Loaded with Axially-symmetrical Ferrite Post
Adam Kusiek, Wojciech Marynowski, J. Mazur, ... 1033
Development of Graphical User Interface for Modern FDTD Simulation Tool
Sławomir Orłowski, Tomasz P. Stefanski, ... 1034
Examination of Discrete Green's Function Approach to Absorbing Boundary Condition in FDTD Method
Michal Wiktor, Tomasz P. Stefanski, ... 1035
Driven Eigenproblem Computation for 2D Periodic Structures
Huanlei Chen, Thomas F. Eibert, W. Che, ... 1036
Hight Order FD Computation of TE and TM Modes in Single Grid
Alessandro Fanti, M. Simone, Giuseppe Mazzarella, ... 1037
Application of Magnetic Moment Method to an Hall Effect Thrusters
Rania Oubaid, Y. Lefevre, Jean-Rene Poirier, C. Henaux, R. Vilamot, ... 1038
3D Conductivity Image Reconstruction Based on Electrical Impedance Tomography
Tomas Kriz, Jarmila Dedkova, ... 1039
An Electrical Explanation of the Electrical Behavior of Metals
Sara Liyuba Vesely, Alessandro Alberto Vesely, ... 1040
Widely Tunable Mid-IR Difference-frequency Generation Based on a Cylindrical Periodically Poled $LiNbO_3$ Crystal
Xuefei Qin, Weidong Zhou, ... 1042
Flower-shaped Dipole Based Nano-antenna for Energy Harvesting
Mohamed Hussein, Nihal F. F. Areed, Mohamed Farhat O. Hameed, Salah Sabry Ahmed Obayya, ... 1043
Prototype of Semi-transparent Photovoltaic Module for Greenhouse Roof Applications
Akira Yano, Josuke Nakata, ... 1045
Organic Solar Cells Using Transparent Graphene Cathode with Al-TiO_2 Interfacial Layer
Di Zhang, Fengxian Xie, Peng Lin, Wallace C. H. Choy, ... 1046
Light Trapping Enhancement of Inverted Polymer Solar Cells with a Nanostructured Scattering Rear Electrode
Pan-Pan Cheng, Lei Zhou, Jie-Ai Li, Yanqing Li, Jianxin Tang, ... 1047
Design of the Planar Antenna for Flexible Tablet
Se-Hwan Choi, Jae-Young Lee, Kyu-Bok Lee, ... 1048
Dual Polarization Array Antenna for WLAN
Ho-Jun Lee, Min-Ki Woo, Nae-In Lee, Gene Yoo, ... 1049
Near Field Antenna Measurement System for Radar Antenna Investigation
Mateusz Mazur, Wlodzimierz Zieniutycz, Adam Kusiek, Wojciech Marynowski, ... 1050
Design of Beam-steering Antenna Based on Stacked Structure
Wen-Chung Liu, Yu-Fan Lin, Chao-Ming Wu, ... 1051
A Methodology for Short Basis Velocity Measurement in Moving Objects
Pavel Fiala, Martin Friedl, Michal Kovac, Vladimir Benes, R. Koci, I. Behunek, ... 1052
Coherent Detected Secure Point-to-Point Optical Fiber Transmission Using Ultra-dense Optical Spectral Phase Coding (UD-SPC)
Xuezhi Hong, Yang Lu, Sailing He, ... 1053
Scaling Features in Graphene Multilayer Structures
Dan Sidney Diaz-Guerrero, Luis Manuel Gaggero-Sager, ... 1055
Potential Like Profile in Reflection Coefficient for a Graphene Multilayer System
Dan Sidney Diaz-Guerrero, Luis Manuel Gaggero-Sager, ... 1056
Harmonic and Intermodulation Performance of Contact-type MEM Microswitches

Muhammad Taher Abuelma'atti, ... 1057
Dependence of Ferromagnetic Resonance Measurements with Temperature in Permalloy Nanostructured Arrays
Ana García Flores, Víctor Javier Raposo Funcia, José Ignacio Iñiguez de la Torre, Marcelino Zazo Rodríguez, Carolina Redondo Esteban, David Navas Otero, ... 1058
Airborne Interferometric Altimetry Experiment over Lake with Multi-carrier Frequencies
Yunhua Zhang, Wenshuai Zhai, Xueyan Kang, Xiaojin Shi, Xiang Gu, Yueying Tang, ... 1059
A Method for Simultaneous Gas and Light Path Retrievals from Space-based Spectroscopic Observations of Greenhouse Gases
Sergey Oshchepkov, Andrey Bril, Tatsuya Yokota, Yukio Yoshida, Thomas Blumenstock, Nicholas M. Deutscher, Susanne Dohe, Ronald Macatangay, Isamu Morino, Justus Notholt, Markus Rettinger, Christof Petri, Matthias Schneider, Ralf Sussman, Osamu Uchino, Voltaire Velazco, Debra Wunch, ... 1060
Giant Magnetoimpedance Effect in Nanocrystalline Microwires
A. Talaat, Valentina Zhukova, Mihail Ipatov, J. M. Blanco, M. Churyukanova, S. Kaloshkin, E. Kostitcyna, E. Shuvaeva, V. Sudarchikova, L. González-Legarreta, B. Hernando, Arkady P. Zhukov, 1061
Monitoring System for Solar Activity in the Very Low Frequency Band
Edwin Andres Quintero Salazar, Ivan Dario Arellano Ramirez, ... 1062
Long-term Observation of GPS Phase Fluctuations near the Geomagnetic Equator in the Peruvian Sector
Chien-Chih Lee, Wei-Sheng Chen, Fang-Dar Chu, ... 1063
Transmission of Electromagnetic Signals of Measurement-While-Drilling System in the Rock
Zoya A. Pyatakova, A. I. Arkhipov, ... 1064
Characteristic Change of Particulate Matter in Osaka of Japan by Transboundary Pollution
Makiko Nakata, Itaru Sano, Sonoyo Mukai, ... 1065
Radiation Simulation Code for Aerosol Remote Sensing in the Aerosol Events
Sonoyo Mukai, Masayoshi Yasumoto, Itaru Sano, Makiko Nakata, ... 1066
Comparison of Satellite Altimetric Waveform Retracking Algorithms in the Niger River Delta
Kalifa Goita, Adama Diepkilé, ... 1067
Astronaut Monitoring for Bow Shock Front of Petergius Nebular
Shigehisa Nakamura, ... 1068
Spacecraft Monitoring for Magnetic Field of Planet Mercury
Shigehisa Nakamura, ... 1069
Monitoring for Sea Caldera Formed at Tsunami Earthquake
Shigehisa Nakamura, ... 1070
Micromachined Band Stop Resonator for Millimeter-wave Applications
Alina Cristina Bunea, Dan Neculoiu, ... 1071
Design of a Coplanar Waveguide to Substrate Integrated Waveguide Transition for LTCC Technology
Dan Neculoiu, Alina Cristina Bunea, ... 1072
Design of Two-stage Low Noise Amplifier Based on Non Simultaneous-conjugate-matching Technique
Yana Taryana, Achmad Munir, ... 1073
Theoretical Analysis of Frequency Characteristic and Resonance Mode of Anisotropic Artificial Dielectric Resonator Encapsulated in Circular Waveguide
Hepi Ludiyati, Andriyan Bayu Suksmono, Achmad Munir, ... 1074
A Two Order Bandpass Filter Designed with Lowpass Filter Sections
Xing Jian Zhong, Jundong Ye, De-Xin Qu, Rong Huang, ... 1075
Development of an Embedded Wafer Level Package Technology and Evaluation of Its Electrical Performance Using RF Switch IC
Se-Hoon Park, Jong-In Ryu, Jong Min Yook, Young-Ho Kim, Duck-Kyun Choi, ... 1076
70 GHz Tx and Rx LCP SoP Module for Point-to-point Millimetre Wave Applications
Young Chul Lee, ... 1078
Study of the Electromagnetic Compatibility in Hospitals in Argentina and Spain
Claudio Muñoz, Roxana Saint-Nom, Miguel Ángel Navarro, Oscar Gutiérrez Blanco, Francisco Saez De Adana, ... 1079
Photonic-assisted Measurement of Electromagnetic Coupling into a Generic Object
Dong-Joon Lee, Chi-Hyun Cho, Jeong-Il Park, No-Weon Kang, ... 1080
The Design and Implementation of an EMC Pre-compliance Board

F. R. L. Silva, L. R. Ribeiro, L. P. Dias, W. J. Santos, C. E. Capovilla, Humberto Xavier De Araújo, 1081
Magnetoelectric Transducers
Roman Valer'evich Petrov, Alexander Nikolaevich Soloviev, Ksenia Valerievna Lavrentieva, Ivan N. Solovjev, Vladimir M. Petrov, Mirza Imamovich Bichurin, ... 1083
Shielding Effectiveness of Plasma Coated Multi-layered Shields
Pinar Deniz Tosun, Sukru Ozen, Selcuk Helhel, ... 1084
Surge Test of High Power Radar Module Used in Military
Soon-Mi Hwang, Chul-Hee Kim, Kwan-Hun Lee, ... 1085
A Novel Approach to Impulsive Noise Analysis in PLC In-door Systems
Monica V. Avalos, Jose Hector Caltenco-Franca, Roberto Linares-Miranda, Jose Alfredo Tirado-Mendez, ... 1086
Multifunctional Reconfigurable Antenna Systems and Technologies
Bedri A. Cetiner, Hema Swaroop Mopidevi, Zhouyuan Li, Yasin Damgaci, ... 1087
Metamaterial Inspired Microstrip Patch
Surabhi Dwivedi, Vivekanand Mishra, Y. P. Kosta, ... 1088
Experimental Graduate Projects on Electromagnetism in Physics Courses
J. Iñiguez, V. Raposo, A. G. Flores, M. Zazo, Pablo Hernandez-Gomez, ... 1089
RF Heating of Conducting Film/Silicon Substrate Structure: The Heat Explosion Theory Approach
Misha Sinder, Joshua Pelleg, Victor Meerovich, Vladimir Sokolovsky, ... 1090

Comparison of Cylindrical FDTD with Cartesian Subcell Modeling for Circularly Shaped Objects

S. Kirsch and R. Schuhmann
Theoretische Elektrotechnik, Technische Universität Berlin, Germany

Abstract— Nowadays, numerical simulation of electromagnetic fields and waves has become an integral part of the design process in a variety of applications. Due to its simplicity and extensibility, the most common simulation method is the Finite Difference Time Domain (FDTD) algorithm, whose origins can be traced back to a publication from 1966 [1]. While the basic principle of this method now prevails for about half a century, other aspects of the initial proposal since have been modified, generalized or extended in manifold directions.

What remains common to most of them is the way material parameters (e.g., permittivity) are mapped to the computational mesh. Each (primary) mesh cell usually contains only one distinct material, which requires the mesh generator to align mesh faces with material discontinuities in order to avoid discretization errors. However, for the sake of a reasonably coarse mesh this error often is accepted or even can't be prevented at all, if, for example, a circularly shaped boundary is supposed to be mapped to a Cartesian mesh.

This particular case of disagreement between Cartesian meshes and circular material distributions usually leads to the loss of second order convergence and has given rise to two particular modifications of FDTD in its pristine formulation:

Cylindrical FDTD [2]: The mesh edges are no longer aligned to coordinate lines of a Cartesian coordinate system, but instead to those of a cylindrical one. Therefore, circular objects can often be discretized with much smaller discretization error. However, the FDTD algorithm's numerical stability depends on a sufficiently small time step, which, in turn, depends on the smallest mesh edge. This circumstance turns out to be very disadvantageous for cylindrical meshes due to their inherently small mesh edges in the vicinity of the origin. An attempt to solve this problem has been proposed recently [3]. It is based on dividing the computational domain and treating the part close to the origin (semi-)implicitly.

Subcell Modeling: This class of extension to FDTD does not depend on material conforming meshes. Instead, grid cells being cut by different materials (so-called cutcells) are subject to a special treatment in order to restore the algorithm's second order convergence. Two different cases have to be considered. If one part of the cutcell is filled with Perfect Electric Conductor (PEC), restricting the cell's edge lengths and facet areas to the non-PEC part yields a very accurate representation of the fields' behavior [4]. On the other hand, if a cutcell contains two different dielectric materials, an effective medium with anisotropic properties has been proposed [5].

The objective of this contribution is to determine which method yields more accurate results under the constraint of comparable computational effort. For this purpose, a numerical example is simulated with a cylindrical FDTD method and a Cartesian FDTD algorithm with Subcell Modeling. Both methods' accuracy is determined numerically and compared against each other.

REFERENCES

1. Yee, K., "Numerical solution of initial boundary value problems involving Maxwell's equations in isotropic media," *IEEE Trans. Antennas Propag.*, Vol. 14, No. 3, 302–307, 1966.
2. Weiland, T., "Time domain electromagnetic field computation with finite difference methods," *Intl. J. of Num. Mod.: El. Networks, Devices and Fields*, Vol. 9, No. 4, 295–319, 1996.
3. Kirsch, S. and R. Schuhmann, "Cylindrical FDTD with improved time step size based on hybrid newmark-beta discretization," *Proc. of Intl. Symposium on Electromagnetic Theory*, Hiroshima, Japan, May 2013, in press.
4. Krietenstein, B., et al., "The perfect boundary approximation technique facing the big challenge of high precision field computation," *Proc. of the XIX Intl. Linear Accelerator Conference*, 860–862, August 1998.
5. Farjadpour, A., et al., "Improving accuracy by subpixel smoothing in the finite-difference time domain," *OSA Optics Letters*, Vol. 31, No. 20, 2972–2974, 2006.

Nonreciprocal Properties of Cylindrical Junction Loaded with Axially-symmetrical Ferrite Post

A. Kusiek, **W. Marynowski**, **and J. Mazur**
Gdansk University of Technology, Poland

Abstract— The waveguide nonreciprocal devices [1–4] are essential components of recent civil and military wireless communication systems. These devices are constructed by inserting properly magnetized ferrite post into multi-port waveguide junction. The nonreciprocal properties of the ferrite loaded junction allow to design isolators, circulators [1, 3] or phase-shifters [4]. Recent research on nonreciprocal devices are focused on structures offering wide operation bandwidth and low insertion losses. Moreover, since the analysis of the waveguide nonreciprocal devices with the use of commercial software is time-consuming, there is also a demand for highly efficient and accurate analysis techniques of these devices.

In this paper the nonreciprocal properties of cylindrical waveguide junction loaded with axially-symmetrical posts are studied. The accurate and numerically efficient hybrid approach is proposed for the analysis of investigated structure. This approach is based on the representation of ferrite post by an effective sphere with the known boundary conditions defined by impedance matrix Z [5]. In order to determine Z-matrix of the ferrite post with irregular shape we utilize the finite-difference frequency-domain (FDFD) technique. Then by enforcing continuity of the waveguide transverse electric and magnetic fields on the surface of effective sphere the scattering parameters of investigated junction are calculated. In our analysis we focus on axially-symmetrical posts. This allows us to reduce the three dimensional formulation of FDFD to two-and-a half one and as a result to speed up the analysis. The presented numerical results are verified with the ones obtained from commercial software. Based on the obtained results the applications of investigated cylindrical ferrite loaded junction to nonreciprocal devices are pointed out.

ACKNOWLEDGMENT

This work was supported by the Polish Ministry of Science and Higher Education from sources for science in the years 2012–2013 under Contract IP2011 028271 (decision No. 0282/IP3/2011/71).

REFERENCES

1. Li, X., E. Li, and G. Guo, "Design of X-band H-plane waveguide Y-junction circulator," *2012 International Workshop on Microwave and Millimeter Wave Circuits and System Technology (MMWCST)*, 1–4, 2012.
2. Razavipour, H., G. Askari, F. Fesharaki, and H. Mirmohammad-Sadeghi, "A new high-power, dual-band, E-plane, ferrite circulator," *IEEE EUROCON 2009, EUROCON'09*, 20–25, 2009.
3. Wu, H. C. and W. B. Dou, "Field structures of waveguide junction circulators with irregular shaped ferrite simulated based on exact treatment," *Progress In Electromagnetics Research*, Vol. 57, 33–54, 2006.
4. Mazur, M., E. Sedek, and J. Mazur, "Propagation in a ferrite circular waveguide magnetized through a rotary four-pole magnetic field," *Progress In Electromagnetics Research*, Vol. 68, 1–13, 2007.
5. Kusiek, A. and J. Mazur, "Hybrid finite-difference/mode-matching method for analysis of scattering from arbitrary configuration of rotationally-symmetrical posts," *Progress In Electromagnetics Research*, Vol. 110, 23–24, 2010.

Development of Graphical User Interface for Modern FDTD Simulation Tool

S. Orłowski and T. P. Stefański
Department of Microwave and Antenna Engineering
Gdansk University of Technology, Narutowicza 11/12, Gdansk 80-233, Poland

Abstract— The finite-difference time-domain (FDTD) method has been applied to a variety of problems in microwave and antenna engineering, electromagnetic compatibility and photonics [1]. Although the FDTD algorithm is relatively easy to implement in software, simulations with the use of this method also require execution of pre- and post-processing tasks. Moreover, a fully functional and easy to use graphical user interface (GUI) is highly desired. Currently, several simulation tools based on the FDTD method are available on the market. Unfortunately, software techniques and technologies used for the development of these tools have not been identified and described in the literature. Moreover, GUIs of commercial tools have been under development for several years hence their development processes are not flexible and open for introduction of novel software technologies.

From the software engineering point of view, development of the stand alone software package for the FDTD method is a challenge due to its complexity. This process requires the development of the engine for FDTD computations, GUI, as well as pre- and post-processing modules. C and/or C++ are languages of choice in the case of computational engine and some pre-processing modules while other modern and high-level languages are natural choice for GUI and post-processing modules. To accelerate computations, parallel processing on central processing unit and graphics processing unit is widely employed. Graphics libraries are necessary to visualize the computational domain and simulation output consisting of 1-D, 2-D and 3-D data. To sum up, the development of any electromagnetic simulation tool involves various computer architectures, languages, technologies and supporting libraries.

In this contribution, we describe the development of GUI for the in-house written FDTD solver. It facilitates drawing of 3-D objects, generates material matrices, supports human body CAD models and displays simulation results. The OpenGL library is employed to visualize the FDTD computational domain, place 3-D objects and assign material parameters to each object. Moreover, the GPU-accelerated method for the material matrix generation was implemented inside the developed GUI [2]. Due to unmanaged nature of OpenGL, we have introduced managed wrapper over native OpenGL functionalities.

We have chosen C# as a language for the GUI development within Microsoft .NET Framework [3]. C# is a managed language and its compilation produces managed code that is executed by the Common Language Runtime virtual machine. On the other hand, the FDTD computational engine is an unmanaged code that directly runs under the control of operating system. To deal with both managed and unmanaged environments, C++/CLI has been introduced [4]. Using this language, we can utilize the FDTD engine with pre-processed data and we can expose this functionality to GUI. We have introduced layered software architecture with the following layers: (i) unmanaged FDTD engine, (ii) wrapper for unmanaged code (C++/CLI), (iii) managed GUI (C#). Main advantage of this layered architecture stems from isolation of components of the FDTD solver which simplifies design, development and testing processes. For the GUI development, the model-view-presenter (MVP) design pattern has been used. It produces streamlined and reusable code that is easy to test.

REFERENCES

1. Taflove, A. and S. C. Hangess, *Computational Electrodynamics: The Finite-Difference Time-Domain Method*, 3rd Edition, Artech House, Boston, MA, 2005.
2. Orlowski, S. and T. P. Stefanski, "Material matrix generation for FDTD simulations using open GL," *The 7th European Conference on Antennas and Propagation*, 2584–2588, Gothenburg, Apr. 8–12, 2013.
3. The C# Language Specification, Ver. 4.0 ECMA Library, 2006, http http://www.ecma-international.org/publications/files/ECMA-ST/Ecma-334.pdf.
4. The C++/CLI Language Specification, Ver. 1.0, ECMA Library, 2005, http://www.ecma-international.org/publications/files/ECMA-ST/ECMA-372.pdf.

Examination of Discrete Green's Function Approach to Absorbing Boundary Condition in FDTD Method

M. Wiktor[1] and T. P. Stefanski[2]

[1]Gdansk Medical University, M. Skodowskiej-Curie 3a, Gdansk 80-210, Poland
[2]Gdansk University of Technology, Narutowicza 11/12, Gdansk 80-233, Poland

Abstract— Consistent coupling of integral operators with the finite-difference time-domain (FDTD) method requires discrete formulation of the fundamental electromagnetic theorems and a discrete equivalent of the Green's function, known as the FDTD-compatible Green's function or the discrete Green's function (DGF) [1–3]. Computing a convolution of current sources with the dyadic DGF allows one to obtain the FDTD solution without execution of the time-marching procedure. Implementation of the absorbing boundary condition (ABC) in the FDTD method is one of the key DGF applications. Consistency with the electromagnetic theory on a grid guarantees the highest accuracy of such an ABC.

Since the impulse response of the grid can be calculated in advance for each time step and any cell position, boundary values can be found yielding absorption of outgoing waves. Several attempts to utilize DGF as ABC have been presented in the literature [2, 3]. In [2], the electric field at the domain boundary is calculated as the convolution of DGF with the magnetic field measured next to the boundary. Although the reported reflection error is better than $-50\,\mathrm{dB}$, such calculations employing the field measured over a single Huygens surface causes numerical problems. In the case of imperfect ABC implementation, a reflected wave propagates in the opposite direction to the domain boundary. In this way, the field at the domain boundary is calculated as the convolution of DGF with the reflected wave which, according to our observations, can cause numerical instability.

In this paper, we propose another strategy for the calculation of the field at ABC. The value of interest is calculated using the convolution of DGF with equivalent current sources measured over two displaced Huygens surfaces next to the boundary. Sampling both components of the electromagnetic field suppresses the instability of the algorithm when the residual wave is reflected from the boundary.

In this contribution, we examine DGF-based ABC on a simple 1-D example. Despite the simplicity of the investigated problem, almost all numerical issues can be demonstrated in this way. We show that the convolution of DGF with equivalent current sources measured over two displaced Huygens surfaces provides almost exact ABC, yielding reflection error comparable to the numerical noise level (approximately $-300\,\mathrm{dB}$). However, the computational overhead of this ABC implementation increases at each iteration because the convolution computations involve all previous next-to-boundary field samples. Truncation of DGF or, equivalently, truncation of field buffers is a natural way to improve the efficiency of the discussed technique. We examine the effects of such a truncation that are visible as spurious echo pulses propagating just after the DGF truncation. This pulses are delayed, and the reflection error caused by this phenomena has different origin compared to other ABC schemes. In this paper, we examine strategies for truncation of the DGF waveform, including windowing technique. We show that at a reasonable computational cost, the error level can be kept below $-100\,\mathrm{dB}$.

REFERENCES

1. Stefański, T. P., "Accuracy of the discrete Green's function formulation of the FDTD method," *IEEE Trans. Antennas Propag.*, Vol. 61, No. 2, 829–835, 2013.
2. Ma, W., "Discrete Green's function formulation of the FDTD method and its application," Ph.D. Thesis, Queen Mary University of London, 2004, available online at: www.elec.qmul.ac.uk/antennas/documents/weili-ma-thesis.pdf.
3. Holtzman, R. and R. Kastner, "The time-domain discrete Green's function method (GFM) characterizing the FDTD grid boundary," *IEEE Trans. Antennas Propag.*, Vol. 49, No. 7, 1079–1093, 2001.

Driven Eigenproblem Computation for 2D Periodic Structures

Huanlei Chen[1], **Thomas F. Eibert**[1], **and Wenquan Che**[2]

[1]Lehrstuhl für Hochfrequenztechnik, Technische Universität München, Germany
[2]Department of Communication Engineering, Nanjing University of Science and Technology, China

Abstract— Periodic structures like metamaterials and substrate integrated waveguides (SIWs), are becoming the research focus in resent years. The study about dispersion and attenuation behaviors helps to better understand and design periodic structures. However, the large model size, the fine details and the often open geometry, make the model of periodic structures a complicated complex eigenproblem. The driven eigenproblem computation analyzes the dispersion and attenuation behavior of periodic structures by solving the corresponding excitation problem in the eigenvalue domain. Different from the purely mathematical approaches of common eigenproblem solvers in [1, 2], the driven method analogizes the unit cell of periodic structures to a resonator model and simplifies the eigenvalue determination for large numerical systems by monitoring the resonance behavior. Comparing with time-domain excitation techniques, the driven method works directly in the eigenvalue domain and be able to concentrate the entire excitation energy in one isolated eigenmode [3]. With appropriately arranged excitation, e.g., port excitation or distribution current densities excitation, one or more particular modes can be stimulated in the unit cell of periodic structures. By searching the extremum for the field quantities, the corresponding pairs of (resonance frequency, wavevector) as eigenvalues can be obtained. This converts the eigenvalue searching to a maximization approach. The driven method was implemented in hybrid finite element boundary integral (FEBI) [4], where complex wavevectors for propagating modes with attenuations or leaky and evanescence modes are supported. Along with the start vector estimation methods based on previous solutions, some effective optimization techniques, e.g., Brent's method and Powell's quadratically convergent method, were employed to achieve fast convergence in the repeated solution of excitation problems with slightly varying parameters [5]. The driven method was proved to be efficient and accurate in one dimensional periodic structures, like corrugated dielectric slab [5] and composite right-/left-handed (CRLH) leaky wave antenna based on SIW [6]. Further, the driven method was employed to two dimensional metamaterials in this work. A mushroom structure [7] was analyzed to demonstrate the versatility of the driven method.

REFERENCES

1. Xu, F., K. Wu, and W. Hong, "Finite-difference time-domain modeling of periodic guided-wave structures and its application to the analysis of substrate integrated nonradiative dielectric waveguide," *IEEE Trans. Microw. Theory Tech.*, Vol. 55, No. 12, 2502–2511, 2007.
2. Deslandes, D. and K. Wu, "Accurate modeling, wave mechanisms, and design considerations of a substrate integrated waveguide," *IEEE Trans. Microw. Theory Tech.*, Vol. 54, No. 6, 2516–2526, 2006.
3. Eibert, T. F., Y. Weitsch, H. Chen, and M. E. Gruber, "Solving periodic eigenproblems by solving corresponding excitation problems in the domain of the eigenvalue," *Progress In Electromagnetics Research*, Vol. 126, 65–84, 2012.
4. Eibert, T. F. and J. L. Volakis, D. R. Wilton, and D. R. Jackson, "Hybrid FE/BI modeling of 3D doubly periodic structures utilizing triangular prismatic elements and a MPIE formulation accelerated by the Ewald transformation," *IEEE Trans. Antennas and Propagation*, Vol. 47, No. 5, 843–850, May 1999.
5. Chen, H., T. F. Eibert, and W. Che, "The eigenproblem computation with the brent's method acceleration," *European Conference on Antennas and Propagation (EuCAP)*, Prague, Czech, March 2012.
6. Chen, H., C. H. Schmidt, W. Che, and T. F. Eibert, "Dispersion and attenuation analysis of substrate integrated waveguide by driven eigenproblem computation," *European Conference on Antennas and Propagation (EuCAP)*, 643–646, Rome, Italy, April 2011.
7. Sanada, A., C. Caloz, and T. Itoh, "Planar distributed structures with negative refractive index," *IEEE Trans. Microw. Theory Tech.*, Vol. 52, No. 4, 1252–1263, 2004.

Hight Order FD Computation of TE and TM Modes in Single Grid

A. Fanti, **M. Simone**, **and G. Mazzarella**
University of Cagliari, Italy

Abstract— An accurate knowledge of the cut-off frequency and field distribution of waveguide modes is important in many waveguide problems. We can quote, among others, the analysis of waveguide junction using mode matching and the solution of waveguide problems with sources. Apart from same simple geometries, mode computation cannot be done in closed form, so that suitable numerical techniques must be used. Among them, finite difference techniques (FD), despite of their long history, are still very popular for their simplicity and computational effectiveness. One of their main drawback, however, is the requirement of two different grids, namely one for TE modes and the other for TM modes, due to the different boundary condition required by the Hertz potentials. Aim of the communication is to explore, and assess, the feasibility of use of a single grid for both TE and TM modes. Apart from the computational issues involved, this would simplify significantly the use of mode matching in function analysis. Numerical solution of this eigenvalue problem using the FD approach requires that both the Helmholtz equation and the boundary condition (for either TE or TM modes) must be replaced by a discretizead version, e.g., replacing derivatives with finite approximations. This transform the Helmholtz equation into a matrix eigenvalue problem, whose eigenvectors contains the samples of the Hertz potential at the discretization nodes. The discretized version is obtained using the same Hight-order Taylor approximation of the Hertz potential, both for the internal points and for the boundary conditions. The requirement of different grids stems out from this choice. It is therefore possible to use a single grid (either the old TE or the old TM) if different Taylor expansions are used for the points closer to the boundary. The eigenvalue problem can then be solved by linear algebra tecniques. The resulting matrix is highly sparse, since, for each row of it, no more than 5 elements can be different from zero. Therefore, very effective routines can be used to compute the smallest eigenvalues (the only ones of interest) and the corresponding eigenvectors, i.e., the field distribution of the modes inside the waveguide. To verify the validity of approach to FD computation of waveguide modes, we have analyzed square rectangular and circular waveguides, and compared the eigenvalues and the eigenvectors of the first few TE and TM modes with their exact values. The typical sparse matrix obtained by the FD allows an effective computation of the eigenvalues and eigenvectors, with a very good accuracy. Actually, compared with analytical results, the relative error is less 0.3%.

Application of Magnetic Moment Method to an Hall Effect Thrusters

R. Oubaid, **Y. Lefevre**, **J. R. Poirier**, **C. Henaux**, **and R. Vilamot**
INPT, LAPLACE, ENSEEIHT, CNRS, University of Toulouse, Toulouse, France

Abstract— The 3D magnetostatic moments method (MoM) is applied to a Hall effect thrusters (HETs) to take into account its geometrical and physical symmetries. To make MoM more practical, a mesh with irregular hexahedral elements is used. The results are compared with the 3D finite element method (FEM).

Hall effect thrusters (HETs) shown in (Fig. 1(a)) has been defined and realized in [1] The computation of magnetic field present within the channel of the thruster is realized using a 3D finite element model. The 3D FEM model requires a large number of elements for the discretization of the ferromagnetic materials and surrounding air volume Unfortunately, this it leads to a high CPU time and memory consumption Because of its drawbacks, we studied another method, which is the 3D magnetostatic moment method MoM A major advantage of this method is that there is no need to mesh the space and a few elements will be used to mesh the ferromagnetic materials This method has already been developed in [2] and has been applied to a low frequency antenna [3] where simplified geometry is used. Here, the ferromagnetic materials of HET are meshed with irregular trilinear (eight-node) hexahedral elements. Thus, the code MoM in [3] which is based on the integral volume equations is developed to compute an integral over a complex geometry and, also to take into account geometrical and physical symmetries of the HET. Therefore using this method, one eighth of the structure has been studied, unlike the problems treated by the method of moments in [2, 3] that studied the whole structure.

On (Fig. 1(b)), the radial component of the flux density within the channel of HET is calculated by both (MoM) method and the 3D finite element method (FEM).

In the final paper, the measured results will be compared with results of the FEM and MoM.

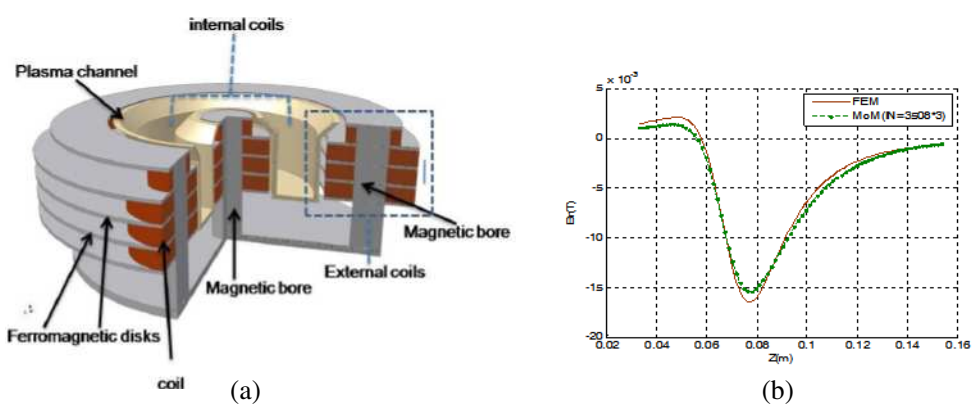

Figure 1: (a) Principal of the parametric magnetic circuit (HET). (b) Distributions of the radial component Br of the flux density: computed by MoM and FEM

REFERENCES

1. Henaux, C., R. Vilamot, L. Garrigues, and D. Harrib, "A new flexible magnetic circuit for a hall effect thruster," *Proceedings of the 32nd International Electric Propulsion Conference*, IEPC-2011-291, 2011.
2. Chadebec, O., J. L. Coulomb, and F. Janet, "A review of magnetostatic moment method," *IEEE Trans. Magn.*, Vol. 42, 515–520, Apr. 2006.
3. Rania, O., Y. Lefevre, and J.-R. Poirier, "Efficient computation of the magnetic field of low-frequency antenna," *AES 2012: Advanced Electromagnetics Symposium*, Apr. 16–19, 2012.

3D Conductivity Image Reconstruction Based on Electrical Impedance Tomography

T. Kříž and J. Dědková
Department of Theoretical and Experimental Electrical Engineering
Brno University of Technology, Kolejní 4, Brno 612 00, Czech Republic

Abstract— The authors present the application of deterministic methods for the calculation of conductivity images in electrical impedance tomography (EIT). Reconstruction based on EIT is predominantly characterized as the solution of a 2D problem; however, this paper contains a description of the conductivity reconstruction procedure utilizing three-dimensional models. Within electrical impedance tomography, the calculation of conductivity is realized using measured voltages on the electrodes placed at the edge of the examined object. In the course of the calculation process, an electric current source is connected to the sample. A direct current source enables us to obtain electrical conductivity distribution in the investigated object; with an alternating current source, we acquire the values of both the amplitude and the phase of the measured voltage and are thus able to obtain impedivity distribution. As a nonlinear inverse problem, the calculation of conductivity based on the measured voltage values is highly ill-posed. The reconstruction process is described as the minimization of a suitably selected function. In order to ensure stability of the solution, the Tikhonov regularization method is used; here, the regularization term complements the objective function. Then, the objective function is expressed as

$$\Psi(\sigma) = \frac{1}{2}\sum \left\|\mathbf{U}_M - \mathbf{U}_{\mathrm{FEM}}(\sigma)\right\|^2 + \alpha \left\|\mathbf{R}\sigma\right\|^2.$$

The paper describes a mathematical model of the solved 3D conductivity reconstruction problem. The time intensity and general accuracy of the solution are monitored, and the authors indicate the acquired numerical results.

An Electrical Explanation of the Electrical Behavior of Metals

S. L. Vesely[1] **and A. A. Vesely**[2]

[1]I.T.B. — C.N.R., Italy
[2]Via L. Anelli 13, Milano, Italy

Abstract— Electronic measurement and control devices find more and more applications in technology and basic sciences, and call for *innovative designs and materials* specifically studied for them. The branch of science committed to expound the performance of materials is condensed matter physics, which is rooted in quantum mechanics. The latter inherited a number of measurable properties from classical mechanics, thermology, electrology, etc.. However, some contextual assumptions that were essential for defining their original meanings might have been left out of it[1]. Besides, the study of the *electromagnetic performance* of those materials (and designs) lays entirely within electromagnetic phenomenology. Thus, in some way, such study resembles that of received signals in the transmission of intelligence. That is, the *logical basis* underlying the applications of information theory to communications engineering could be amended so as to apply to electromagnetic phenomena in general (unencoded). This approach is different from quantum theoretical approaches, even those following the same information-oriented trend, which can take a stochastic approach [1], or consider quantum information as the basic category from which all else flows [2].

For this paper, we restrict to metallic matter, and revisit the link among three different effects of its; that is, electrical conduction, thermal conduction, and metallic reflection[2]. That's interesting not only for the relationships between raw and encoded received signals, but also because condensed matter physics is an offspring of Sommerfeld's update of Drude's model.

Wiedemann and Franz explored the relationship between thermal and electrical conductivity, about 1850. They measured temperature differences along homogeneous metal rods, using a thermopile, and interpreted them as a heat flow, according to Fourier[3]. They examined several metals and obtained an average value of thermal conductivity k for each one. Comparing that value with the direct electrical conductivity σ_{DC} of the same metal, as found in the literature, they concluded $k/\sigma_{DC} = const$. Later on, Drude produced a model of metals, which called for a comparison between the electrical behavior and the kinetic theory of gases. It was suggested that that model can be extended to higher frequency electrical vibrations, which result in thermal agitation ascribable to the metal's free electrons. Rubens and Hagen had the idea to verify Drude's model by considering a different feature of metals than thermal conductivity, such as the reflective power of metallic mirrors. As it was already known that Drude's model fails in the optical range, they devised a technique for measuring the reflective power in the far infrared (8–51 µm). That technique brought the discovery of residual rays, the fitting of Planck's black body radiation curve[4], and paved the way to quantum mechanical modeling of metals. As a first step, though, it was found that there is an absorbed fraction A of the impinging radiation — the complement of the reflected fraction R — which satisfies the relationship: $1 - R \equiv A \propto 1/\sqrt{\sigma_{DC}}$. The infrared behavior of metals can also be derived directly from the Ampère-Maxwell equation by formulating boundary conditions at the air-metal interface, as Emil Cohn did for poor conductors.

None of those experiments worked out how heating upon contact is related to the Joule effect[5]. Thus, it is not clear whether the formula $R \approx 1$, that qualifies good mirrors in that same optical range where $R + T = 1$ qualifies transparent dielectrics, is still valid in the Rubens-Hagen range, where dielectrics strongly reflect residual rays. Nowadays it is possible to consider metal behavior over the whole frequency range, and thus it is possible to investigate in which cases metals can be used to amplify (enhance) rather than magnify (enlarge) a signal.

[1]The unified point of view, related to the concept of an absolute system of units introduced by Gaußand W. Weber, uses universal constants as conversion factors between quantities of different kind. However, for example, a thermopile works differently from a gas thermometer, due to the thermal gradients across its junctions.

[2]The authors presented a preliminary account of this subject at AES 2012 in Paris.

[3]Metal rods fed at one end function as monopole antennas; usually they are employed to convert alternate electric current into radiation. However, they can radiate input heat too.

[4]In the far infrared the curve can be fitted by the Rayleigh-Jeans law. However, in Rubens' lab the Wien distribution law for a (photon) gas was prevailing.

[5]Those experiments were devised to validate thermodynamical models of electrical phenomena, rather than investigating whether there are connections between the Joule effect and the transducer properties shown by antennas.

REFERENCES

1. Jaynes, E. T., "Electrodynamics today," *Proceedings of the Fourth Rochester Conference on Coherence and Quantum Optics*, 495–509, Rochester, USA, Jun. 1977.
2. Timpson, C. G., "Information, immaterialism, instrumentalism: Old and new in quantum information," *Philosophy of Quantum Information and Entanglement*, A. Bokulich and G. Jaeger, eds., Cambridge University Press, Cambridge, 2010.

Widely Tunable Mid-IR Difference-frequency Generation Based on a Cylindrical Periodically Poled $LiNbO_3$ Crystal

Xuefei Qin and Weidong Zhou
Institute of Information Optics, Zhejiang Normal University, Jinhua 321004, China

Abstract— Based on the dispersion property of the periodically poled $LiNbO_3$ (PPLN), the quasi-phase matching (QPM) band for the pump can evolve to two separate bands, and the spacing between them can be increased with the decrease of the crystal temperature. Two such separate QPM bands can be used for increasing the idler tuning range when the crystal temperature is set to adapt the pump tuning. With the technique, tunable mid-infrared radiation $2.8 \sim 3.56\,\mu m$ with a power level of $\sim 100\,\mu W$ is generated by quasi-phasematched difference-frequency mixing of a Nd:YAG laser and a tunable-diode laser in multigrating PPLN. The generated mid-infrared radiation is suitable for sensitive high-resolution spectroscopy of molecules.

Flower-shaped Dipole Based Nano-antenna for Energy Harvesting

Mohamed Hussein[1], **Nihal F. F. Areed**[2], **Mohamed Farhat O. Hameed**[1], **and S. S. A. Obayya**[1]

[1]Centre for Photonics and Smart Materials, Zewail City of Science and Technology
Sheikh Zayed District, 6th of October City, Giza, Egypt
[2]Electronics and Communications, Faculty of Engineering, Mansoura University, Egypt

Abstract— In this paper, a novel design of nano-antenna for energy harvesting is proposed and analyzed using finite difference time domain method. The new design consists of three elements nano-antenna with elliptical shape and with air gap. The numerical simulations are investigated for improving the harvesting efficiency of the nano-antennas within the wavelength range from 400 nm to 1450 nm. The suggested design has maximum efficiency at 500 nm where the irradiance of the sun is maximum. The proposed nano-antenna can enhance the efficiency of harvesting the solar energy and total harvesting efficiency over the conventional dipole antenna by 15% and 32.7%, respectively.

The worldwide energy demand, during the last years, is strongly increased and as a consequence the deleterious effects due to the combustion of fossil are apparent. Recently, renewable energies give strong contributions to power generation without increasing environmental pollutions. In particular, solar energy is largely used because it is a freely available source and the technology utilized to get electricity is relatively low cost. There are several approaches that have been pursued to harvest energy from the sun including the photovoltaic (PV) [1] and nano-antenna techniques [2]. In this paper, three different configurations for nano elements for energy harvesting are introduced and analyzed by using 3D finite difference time domain (FDTD) method [3]. Figure 1(a) shows the conventional dipole antenna which consists of two rectangular elements of equal length L, and height H separated by a distance G. However, each element of the first suggested structure has elliptical shape with air gap as shown in Figure 1(b) separated by a distance G. Each element of height H has minor and major radii a_1, and b_1, respectively. However, the elliptical shape air gap has major and minor radii a_2, and b_2, respectively. Next, the second configuration of the nano-antenna revealed in Figure 2(a) is considered. In this configuration, each element consists of two ellipses with the same size and with rotation angle θ between their major axes as shown in Figure 2(a). Finally, to increase the capability of energy harvesting, a flower shaped nano-antenna, shown in Figure 2(b), is suggested. The proposed flower

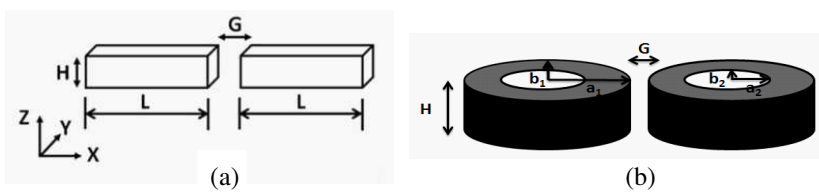

Figure 1: (a) Conventional dipole antenna. (b) The proposed one element elliptical dipole nano-antenna.

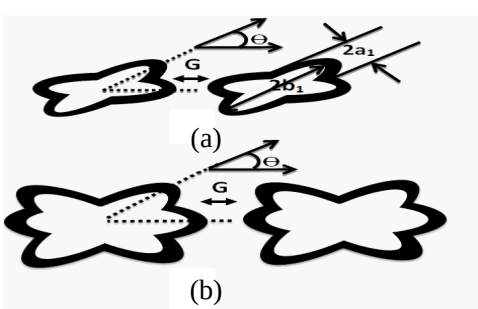

Figure 2: (a) Top view for elliptical two elements nano-antenna. (b) The proposed flower dipole antenna.

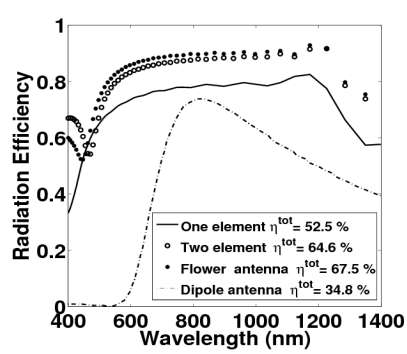

Figure 3: Variation of wavelength dependent radiation of the dipole presented by [9] and the proposed dipole with different number of elements.

nano-antenna dipole is composed of multiple ellipses, with rotation angle $\theta = 10°$, to harvest energy within the wavelength range from 400 nm to 1450 nm. Figure 3 shows the calculated radiation efficiency of the conventional dipole nano-antenna [2], and the three suggested configurations nano-antennas. In this investigation, the traditional dipole nano antennas has width of $W = 40$ nm, height $H = 40$ nm and $L = 250$ nm. However, the dimension of the proposed nano-antennas are $H = 40$ nm, $G = 10$ nm, $a_1 = 125$ nm, $b_1 = 40$ nm, $a_2 = 110$ nm, and $b_2 = 20$ nm. It is evident from Figure 3 that the flower shaped dipole shows an increase in the radiation efficiency and the total harvesting efficiency by 15% and 32.7%, respectively over the conventional dipole antenna. In addition, the radiation efficiency of the flower nano-antenna is greater than that of the one ellipse and two ellipses based nano-antenna shown in Figure 1(b) and Figure 2(a).

REFERENCES

1. Sabaawi, A. M. A., C. C. Tsimenidis, and B. S. Sharif, "Infra-red spiral nano-antennas," *Loughborough Antennas and Propagation Conference (LAPC)*, 1–4, Nov. 12–13, 2012.
2. Vandenbosch, G. A. E. and Z. Ma, "Upper bounds for the solar energy harvesting efficiency of nano-antennas," *Nano Energy*, Vol. 1, No. 3, 494–502, May 2012.
3. Sulivan, D. M., "Electromagntic simulation using the FDTD method," *IEEE Press Series on RF and Microwave Technology*, 1–9, 2000.

Prototype of Semi-transparent Photovoltaic Module for Greenhouse Roof Applications

Akira Yano[1] **and Josuke Nakata**[2]

[1]Faculty of Life and Environmental Science, Shimane University, Matsue, Shimane 690-8504, Japan
[2]Sphelar Power Corporation, Fushimi, Kyoto 612-8201, Japan

Abstract— Electricity consumption has been increasing in modern greenhouse cultivation for operations such as heating, cooling, ventilation, irrigation, and lighting appliances for plant growth environment control. Therefore, efficient use of sustainable energy is one of the most important objectives for greenhouse crop productions. In this paper, we prototyped a micro-spherical cell semi-transparent photovoltaic (PV) module for greenhouse roof applications.

The micro-spherical cell is measuring a mere 1.8 mm across and the p-n junction covers its almost entire outer surface, which enables the cell to capture sunlight from all directions. The module was built with 1500 individual spherical cells, embedded in 107 mm × 95 mm laminated glass plates. The module transparency is almost 60%, which allows the most sunlight entering in the greenhouse for promising plant photosynthesis. The micro-spherical cell module is less dependent on the angle of incidence of light compared with conventional flat PV modules. In addition, the cells generate electricity from sunlight impinging from both sides of the module because the cells are embedded in the transparent glass plates. For this reason, the module is suitable for use on the roof of greenhouses, where the major component of the sunlight irradiates from the top, but the minor component scattered by plants, the ground, and the greenhouse structure from the bottom is also available.

The performance of the module was studied. The module was mounted 2 m above the ground and fixed with the elevation angle of 25 degree facing north. The output power of 417 mW was obtained in the situation where the irradiation from the top and the bottom were 819 W/m^2 and 124 W/m^2, respectively. The conversion efficiency calculated from the amount of bifacial solar radiation was 4.3%, which is considerably high if we take into account the level of the module transparency. The design of the module makes it very attractive, but the module needs to be enlarged to the size compatible with conventional greenhouse roof glass for testing possible negative effects of shading on plant growth.

ACKNOWLEDGMENT

This study was partly supported by JSPS KAKENHI Grant Number 24580370.

Organic Solar Cells Using Transparent Graphene Cathode with Al-TiO_2 Interfacial Layer

Di Zhang, Fengxian Xie, Peng Lin, and Wallace C. H. Choy
Department of Electrical and Electronic Engineering
The University of Hong Kong, Pokfulam Road, Hong Kong, China

Abstract— While there are challenges in tuning the properties of graphene (surface wettability, work function alignment and carrier transport) for realizing efficient graphene cathode in organic solar cells (OSCs), a two-step Al-TiO_2 composite is proposed and demonstrated to modify single-layer graphene as efficient cathode for OSCs. We find that the evaporated aluminum (Al) nanoclusters benefit the graphene cathode by simultaneously achieving two goals, namely improving the surface wettability for subsequent TiO_2 deposition and reducing its work function to offer favorable energy alignment. To address challenges related to charge extraction in OSCs, solution-processed TiO_2 with excellent electron transport can offer charge extraction enhancement to the graphene cathode, which is essential to realizing efficient device performance. However, it is a well-known issue for methods such as spin coating to produce uniform films on the initially hydrophobic graphene, even with the improved wettability from Al nanoclusters. The undesired morphology of TiO_2 by such methods considerably inhibits its effectiveness in enhancing charge extraction for the graphene cathode. We propose and demonstrate a self-assembly method to deposit the solution-processed TiO_2 on the Al-covered graphene for forming the Al-TiO_2 composite layer. Compared with spin-coating, the self-assembly method is found to achieve more uniform coating on the graphene surface, with highly controllable thickness. Consequently, the graphene cathode modified with Al-TiO_2 composite in inverted OSCs gives rise to an enhanced power conversion efficiency of 2.58%, which is two-fold of the previously best reported efficiency (1.27%) for graphene cathode OSCs. Meanwhile, the efficiency of OSCs using graphene cathode reaches $\sim 75\%$ performance of control devices using indium tin oxide cathode.

Light Trapping Enhancement of Inverted Polymer Solar Cells with a Nanostructured Scattering Rear Electrode

Pan-Pan Cheng, **Lei Zhou**, **Jie-Ai Li**, **Yan-Qing Li**, **and Jian-Xin Tang**
Jiangsu Key Laboratory for Carbon-Based Functional Materials & Devices
Institute of Functional Nano & Soft Materials (FUNSOM)
Soochow University, Suzhou 215123, China

Abstract— High performance inverted polymer solar cell is demonstrated by introducing a nanostructured backscattering rear electrode, which is fabricated by embedding silver nanoparticle (NP) arrays into the MoO_3 hole extraction layer. As verified by characterizing and simulating the electrical and optical properties, such a nanostructured rear electrode can achieve an improved cell performance by maintaining simultaneously high open-circuit voltage and fill factor values, while providing excellent short-circuit current enhancement through efficient backscattering-induced light trapping. A careful optimization of the nanostructured rear electrode can result in polymer solar cells with an enhanced power conversion efficiency of 7.21%, as compared to 6.26% of the reference cell with a flat electrode. It is noteworthy that the method described here offers a convenient and scalable way for inexpensive and high-performance polymer solar cell designs.

Design of the Planar Antenna for Flexible Tablet

Sehwan Choi, Jaeyoung Lee, and Kyubok Lee
Korea Electronics Technology Institute, Republic of Korea

Abstract— Recently, the interest of flexible electronics is increased as development of flexible e-papers and e-books. Several companies announced concept models of flexible mobile phones and flexible e-books. But flexible electronics is not completed even if the display is bent, because many parts in flexible electronics are still rigid. The technology of flexible display is mature, but research about the other parts of flexible electronics except the display has not been studied.

Various researches about flexible materials, components and electronics are under development in order to implement flexible electronics. The most important characteristic of flexible electronics is that the performance of each components and modules must be unchanged or little changed when their shape is deformed. Generally, the frequency response of RF electronic components is changed when physical shape of them is modified. This causes a decline of data-rate and out-of-service in wireless communication. Recently, in commercial wireless communication, because most RF modules are miniaturized by integrated circuits, flexible circuits can be implemented by that rigid ICs are mounted on flexible substrates. But the performance of general antennas are sensitive to the ground size, bending or stretching.

In this paper, planar antenna is designed for flexible tablet. Flexible tablet patterns are fabricated on the fabricated on the LCP (Liquid Crystal Polymer) substrate with the thickness of 100 μm. The proposed antenna is also fabricated on the same substrate. This antenna operates at 2.4 GHz for Zigbee communication. Antenna is simulated by Ansys HFSS and measured by Agilent E5071c network analyzer. As results of the measurement, when the antenna is flat, this antenna has the bandwidth of about 160 MHz and the radiation efficiency of 79%. When the antenna is bent 45 degrees, this antenna has the bandwidth of about 150 MHz and the radiation efficiency of 71%. The center frequency is also changed from 2.42 GHz to 2.38 GHz.

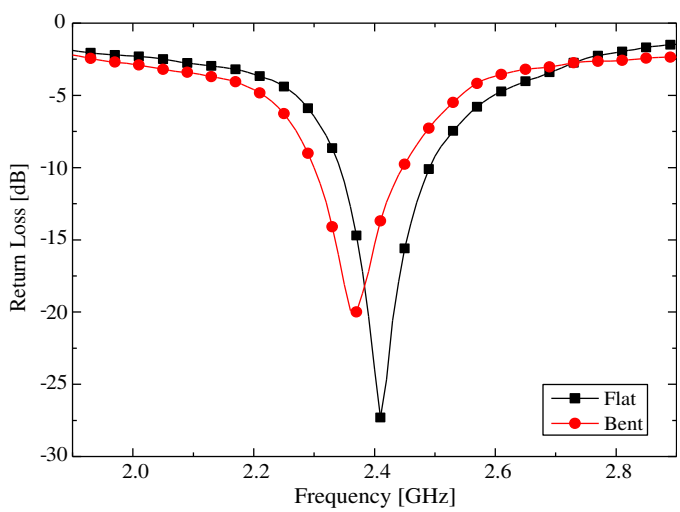

Figure 1: Return loss variation of the proposed antenna.

Dual Polarization Array Antenna for WLAN

Ho-Jun Lee[1], **Min-Ki Woo**[2], **Nae-In Lee**[2], **and Gene Yoo**[2]

[1]Convergence Communication Components Research Center
Korea Electronics Technology Institute, South Korea
[2]Innonet Co., Ltd., South Korea

Abstract— This paper present analysis, design, and simulation of dual feed dual polarization microstrip patch antenna for WLAN applications. The proposed antenna configuration is shown in Figure 1. Antennas in this paper are simulated by using the Ansoft simulation software high-frequency structure simulator(HFSS). A prototype of this antenna was fabricated on FR4 substrate with thickness $h = 1\,\text{mm}$ and dielectric constant $\varepsilon_r = 4.4$. The dimensions of the fabricated antenna, which is etched on $100\times260\times5\,\text{mm}$ substrate. The measurements of electrical characteristics such as radiation patterns, VSWR, and return loss of the implemented antenna were conducted in an anechoic chamber equipped with a HP 8510C network analyzer and far field measurement system. The measured gain of the antenna is from 6.98 to 8.09 dBi. Figure 2 shows a photograph of the fabricated antenna. We manufactured the antenna based on the results of optimized simulation results and measured characteristics of the suggested antenna in the anechoic chamber. Details of the proposed antenna designs are described, and typical experimental results are presented and discussed.

Table 1: Antenna electrical specification.

Frequency Range		2400 ∼ 2500 MHz
Polarization		±45°
Band Width		100 MHz
Array		1 ∗ 4 Array
Gain		≤ 6dBi
Beam width	Horizontal	≥ Nominal 60°
	Vertical	≥ Nominal 50°
F-B ration		≥ 10 dB
VSWR		≤ 1 : 20
Impedance		50 Ω
Maximum input power		≤ 10 W

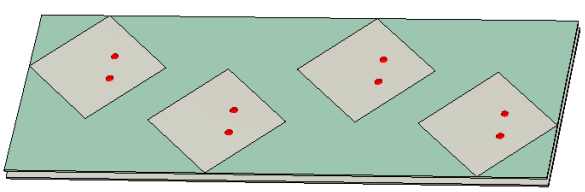

Figure 1: Proposed antenna.

Figure 2: Photograph of the fabricated antenna.

REFERENCES

1. Stutzman, W. L. and G. A. Thiele, *Antenna Theory and Design*, 2nd Edition, Hohn Wiley & Sons, New York, 1998.
2. Balanis, C. A., *Antenna Theory Analysis and Design*, 2nd Edition, Wiley & Sons, 1997.

Near Field Antenna Measurement System for Radar Antenna Investigation

Mateusz Mazur, Włodzimierz Zieniutycz, Adam Kusiek, and Wojciech Marynowski
Gdansk University of Technology, Poland

Abstract— The purpose of this work was to investigate capabilities of developed near field (NF) antenna pattern measurement system in investigation of radar antennas. The novel radars require advanced antenna technologies to fulfill requirements like fast electronic beam scanning or multi-beam pattern. It effects in increased requirements for antenna measurements systems capabilities, especially speed of measurements, ability to test separated radiating elements.

For relatively huge radar antennas far field (FF) measurement method requires long range to fulfill far field condition defined as $R_{\min} = 2D^2/\lambda$ (where D — maximum dimension of aperture, λ — wavelength in free space). But to minimize deviations in side lobe level measurements extended range is recommended. For not electronically controlled antennas when all radiating elements are in phase and direction of main beam is normal to the antenna aperture only azimuth and elevation patterns are measured. In that case all side lobes appears in azimuth and elevation pattern cuts. When direction of main beam is changed (beam is scanned) the side lobes appear out of two main pattern cuts. To measure them in FF 3D rotable antenna table is required. Pointed above features cause relatively high costs of FF range and carried out measurements.

The alternative solution is NF measurement. Reduced occupied area, reduced costs of equipment especially when anechoic chamber is not required are main advantages. NF scanning allows to detect all near and far side lobes during one measurement (for developed planar scanner in range $\pm 75^\circ$ for θ and ϕ directions). The tests speed depends on chosen VNA/Spectrum analyzer and its setting. In a table below the two measurement methods are compared for radar antenna with $D \approx 2.2\,\mathrm{m}$ ($2.1\,\mathrm{m} \times 0.5\,\mathrm{m}$) working in 5 GHz band ($\lambda = 6\,\mathrm{cm}$).

Recently carried out tests with radar antenna sub arrays at FF range and at developed NF scanner confirm good agreement between both methods. Test measurements indicated that the absence anechoic chamber has minor influence on measured patterns due to scanner construction where metal elements are almost fully removed from tested antenna aperture area and reflections are suppressed with absorbing materials. NF equipment allows also to make measurements significantly faster in limited angle range, sufficient for detection of over average side lobes related to different main beam directions.

A significant advantage of NF measurements is ability to detect faults in antenna aperture because testing probe is scanning signals over all radiating elements. As construction of scanner is flexible, after easy mechanical adaptation it may be implemented directly on radar antenna at its installation site allowing to extend radar diagnostic tests.

	FF measurement	**NF measurement**
Size of measurement systems	Range: $160\,\mathrm{m}/\approx 450\,\mathrm{m}$	Minimum $3\,\mathrm{m} \times 4\,\mathrm{m}$ room Scanners dimensions: $2.4\,\mathrm{m} \times 1.4\,\mathrm{m}$
Angle range	Full	Limited: $\pm 75^\circ$ for θ and ϕ
Number of measured points to obtain 1° resolution for range of θ and ϕ from -75° up to $+75^\circ$	22800 points	≈ 1200 points — (minimum resolution $\lambda/2$ between measured points). ≈ 4800 points for resolution $\lambda/4$
Energetic effort	The whole antenna is rotated	Only probe and scanner elements are in movement
Processing	Results obtained directly	Post processing required

ACKNOWLEDGMENT

This work was supported by the Polish Ministry of Science and Higher Education and carried out within the framework of The National Center for Research and Development under agreement LIDER/21/94/L-2/10/NCBiR/2011.

Design of Beam-steering Antenna Based on Stacked Structure

Wen-Chung Liu[1], **Yu-Fan Lin**[2], **and Chao-Ming Wu**[1]

[1]Department of Aeronautical Engineering, National Formosa University, Yunlin 632, Taiwan, R.O.C.
[2]Institute of Electro-Optical and Materials Science, National Formosa University
Yunlin 632, Taiwan, R.O.C.

Abstract— Recently, antennas with beam-steering property for adaptive application are becoming important for use in modern functional radar/sensor communication systems. Conventional beam-steering pattern is achieved by means of mechanical physic like turning the antenna by using a servo-motor. However, an alternative way of the electrically scanned phase array for realizing such function has been investigated. In this study, we present a stacked patch antenna capable of frequency scannability over a wild frequency range for beam steering. As shown in Fig. 1(a), the proposed design consists of a circular parasitic patch, a meandered strip feeder, and a defected ground plane. Two substrate layers were used for supported these conductors. By optimally selecting the geometry parameters of the antenna, a wide impedance-matching bandwidth and a scannable beam based on frequency dependence can be achieved. Constructed prototypes of the obtained design were experimentally studied and explore good wideband operation with −10 dB impedance bandwidths of 2.3 GHz, ranging from 3.8 to 6.1 GHz (Fig. 1(b)). The beam-steering property of an elevation angle, from the z-axis, of −70°, 40°, and −180° at 3.81, 4.37, and 5.19 GHz, respectively, has also been obtained (Fig. 1(c)). Agreement between the measurement and simulation is good. Additionally, details of effects of the geometry dimensions of this design on the beam-steering performance and the physical implementation for the optimized configuration are all presented and discussed.

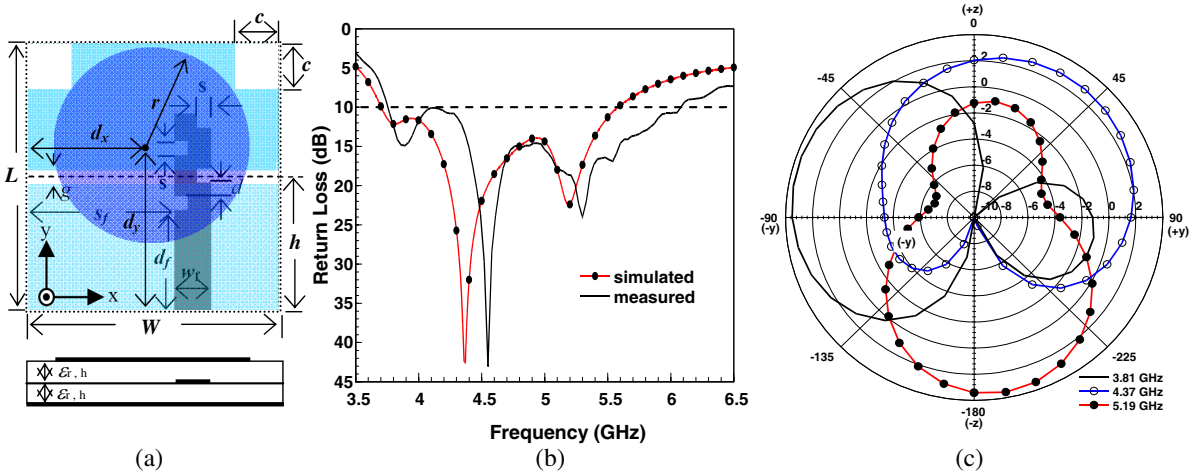

(a) (b) (c)

Figure 1: (a) Configuration of the proposed stacked beam-steering antenna. (b) Measured and simulated return loss versus frequency of the proposed design. (c) Frequency scannability of analytical H-plane radiation patterns at 3.81, 4.37, and 5.19 GHz, respectively.

ACKNOWLEDGMENT

This work was supported by the National Science Council of the Republic of China under Grant NSC 101-2221-E-150-016.

A Methodology for Short Basis Velocity Measurement in Moving Objects

P. Fiala, M. Friedl, M. Kovac, V. Benes, R. Koci, and I. Behunek
Department of Theoretical and Experimental Electrical Engineering
Brno University of Technology, Technická 3082/12, Brno 616 00, Czech Republic

Abstract— The velocity of various objects is currently measured within a large number of disciplines and activities. This paper presents velocity measurement in single-shot nonlinear processes, which occur only once and are thus characterized by zero repeatability. The measurement methods must therefore enable the recording, saving, and retroactive evaluation of the processes at a pre-defined accuracy; all these operations are performed to facilitate comparison of the recorded event and other similar processes. The methods commonly applied in the measurement of object velocity are based on optical and electromagnetic effects. In this context, the main disadvantage of optoelectronic methods consists in that the detector cannot be placed immediately behind the plasma source (or, generally, objects other than the projectile). Further problematic aspects can be identified in the emitted raw powder particles, muzzle flash, and shock wave, namely spurious effects leaving a track where the information from the launched projectile could be lost. However, the electromagnetic method described in the paper does not possess the disadvantages of the optical methods. We therefore present a design of an induction sensor fitted with an electronic signal processing system; this design is based on numerical evaluation of the relativistic effect occurring in the application of the electromagnetic principle of position sensing/object velocity [1]. The final part of the paper contains a discussion of the measured results.

ACKNOWLEDGMENT

The research described in the paper was financially supported by a grant of the Czech Ministry of Industry and Trade, No. FR-TI1/001, Czech Science Foundation (13-09086S), a project of the BUT Grant Agency, No. FEKT-S-11-5/1012 and project from Education for Competitiveness Operative Programme CZ.1.07.2.3.00.20.0175 (Electro-researcher).

REFERENCES

1. Szabó, Z. and P. Fiala, "EMHD effects come through at linear moving objects analysis," *PIERS Online*, Vol. 7, No. 1, 1173–1177, 2011.

Coherent Detected Secure Point-to-Point Optical Fiber Transmission Using Ultra-dense Optical Spectral Phase Coding (UD-SPC)

Xuezhi Hong[1], **Yang Lu**[2, 3, 4], **and Sailing He**[1, 2, 3, 4]

[1]ZJU-SCNU Joint Research Center of Photonics
South China Normal University (SCNU), Guangzhou 510006, China
[2]Joint Research Center of Photonics of the Royal Institute of Technology, Sweden
[3]Lund University, Sweden
[4]Zhejiang University (ZJU), Zhejiang University, Hangzhou 310058, China

Abstract— With the prevalent of cloud-based applications, e.g., cloud computing/storage, huge amount of data need to be synchronized timely among data centers at different locations. High speed optical fiber communication is considered as a prominent candidate for the point-to-point (P2P) communication between two nodes of the same cloud. The security of such P2P communication system is becoming increasingly important. Recently, some schemes have been proposed to enhance the security of the direct-detected optical fiber communication system [1, 2]. Time domain multi-code parallel coding is employed in [1] to generate an emulated multi-user CDMA signal which is of high security against eavesdropping in P2P communication system.

In this paper, we propose and study a long distance coherent detected P2P secure transmission scheme with multi-code spectral phase coding (SPC)-orthogonal frequency division multiplexing (OFDM) [3] based ultra-dense optical spectral phase coding (UD-SPC). The maximal spectral efficiency of our system can be two times of thetraditional one [4]. In the context of SE, our system is called ultra-dense optical spectral phase coding (UD-SPC) system.

Figure 1 depicts our scheme for long distance P2P secure optical fiber transmission. The electrical encoded signals are imprinted on optical carrier with an optical I/Q modulator. In the CDM encoding step, each data symbol in the same block is spread with a pre-allocated code of length N, respectively. The spread data of the M symbols are then added up. After CDM encoding, the data is converted to time domain samples by IFFT. At the receiver side, coherent detection is employed. The decoding process is done after FFT. Figs. 2(a)–(c) show the decoding output in different number of codes. To increase the number of simultaneously transmitted codes, the multilevel BCJR equalization is employed to suppress the cross-talk among non-orthogonal codes. Fig. 2(d) shows the decoding output with wrong code decoder. The eavesdropper with wrong decoder cannot get access to the transmitter information. The simulation results of 400 km fiber transmission will be presented at the conference.

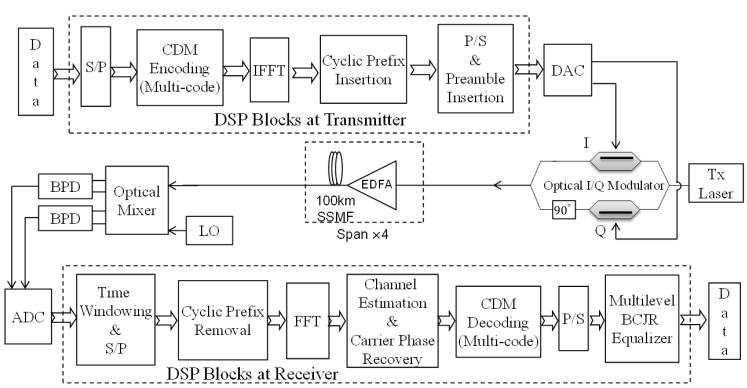

Figure 1: Long distance P2P UD-SPC secure optical fiber transmission scheme.

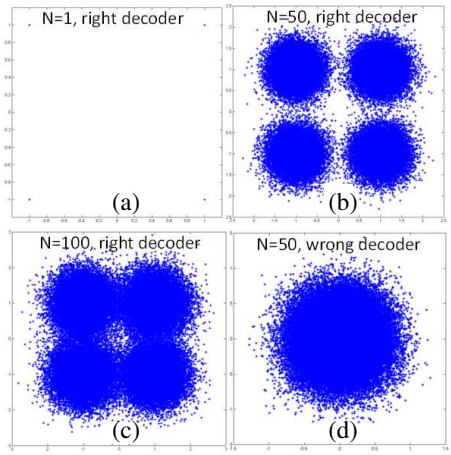

Figure 2: Decoding outputs in different scenarios.

REFERENCES

1. Wang, Z., et al., *IEEE PTL*, Vol. 22, No. 19, 1410–1412, 2010.
2. Zhang, L. J., et al., *IEEE PLT*, Vol. 23, No. 14, 998–1000, 2011.
3. Shieh, W., et al., *OFDM for Optical Communications*, 2009.
4. Toliver, P., et al., *OFC/NFOEC*, PDP 7, 2007.

Scaling Features in Graphene Multilayer Structures

D. S. Diaz-Guerrero and L. M. Gaggero-Sager
Facultad de Ciencias, Universidad Autónoma del Estado de Morelos, Morelos, Mexico

Abstract— Graphene based systems are important for its relativistic like transport properties. It is clear that the research of its properties has accumulated a considerable amount to this date. But one subarea that has no received much attention is the self-similar graphene based multibarrier systems. In this context, self-similar refers to the so called prefractals. The practical importance of this kind of systems is that they would enable us to build structures with specific physical scaling properties, such as transmission coefficient wich is directly related to current density.

In this work we consider a new type of self-similar potentials, generated as usual based on the Cantor construction. The main difference from other self-similar structures is that, from generation to generation, every barrier is scaled in the x-axis. Also, every new barrier added is scaled in the energy axis. Finally, as the barriers are scaled in the x-axis there is the chance of placed the scaled barrier at will. In this case we placed them in the right hand side of his predecessor place.

We called this potential, the evanescent potential. With a few generations of this potential we calculate the transmission coefficient as function of the energy. In the resultant curves, we found evidence of scaling laws between different generations. This evidence indicates that this type of structures propagates in some sense the scaling properties of the potentials to the transmission coefficient, and hence presumably to other related physical properties. Scaling properties like those described here are difficult to find in this type of systems, as they are very sensitive to the particular form of the multilayer system. Hence, we believe that this new potential have the key features in its construction, that make it possible.

Potential Like Profile in Reflection Coefficient for a Graphene Multilayer System

D. S. Diaz-Guerrero and L. M. Gaggero-Sager
Universidad Autónoma del Estado de Morelos, Mexico

Abstract— Using a graphene setup, in this work we study, theoretically, the reflection coefficient for a multilayer system which is cuasi self-similar and has mirror symmetry with respect to the center of the structure. The main result is that the reflection coefficient resembles the form of the potential, even more the discrete Fourier transform also resembles the form of the potential.

This system is not strictly self-similar, as it can not be obtain as a scaled copy of some subset of it. Nevertheless, it is approximately self-similar and as such it is possible to speculate, with our results, about the behavior of more complicate features as electron mobility or even the eigenfunctions. Thus, the proposed potential and it's reflection coefficient having nontrivial geometrical features give the possibility of find self-similarity in relativistic systems.

Harmonic and Intermodulation Performance of Contact-type MEM Microswitches

Muhammad Taher Abuelma'atti
King Fahd University of Petroleum and Minerals, Box 203, Dhahran 31261, Saudi Arabi

Abstract— This paper presents a new technique for predicting the harmonic and intermodulation performance of the contact-type MEMS microswitch under multi-sinusoidal excitation. The special cases of the contact-type MEMS microswitch excited by two and sixteen equally-spaced equal-amplitude sinusoids are considered in detail and the feasibility of obtaining closed-form mathematical expressions for the even- and odd-order harmonics and intermodulation products, of any order, is studied. The results show that the relative third-order intermodulation rapidly deteriorates when the number of sinusoids applied to the contact-type MEMS microswitch is increased. The results obtained are in excellent agreement with the previously reported measurements and simulation results.

Dependence of Ferromagnetic Resonance Measurements with Temperature in Permalloy Nanostructured Arrays

A. G. Flores[1], V. Raposo[1], J. Iñiguez[1], M. Zazo[1], C. Redondo[2], and D. Navas[2]

[1]Departamento de Física Aplicada, Universidad de Salamanca, E-37071, Salamanca, Spain
[2]Departamento de Química Física, Universidad del País Vasco
Barrio Sarriena s/n, 48940 Lejona (Vizcaya), Spain

Abstract— Dynamic properties of magnetic nanostructures have recently been intensively studied due to their potential application in high density perpendicular recording media, magnetic sensors or microwave devices. To understand magnetization processes in these materials it should be considered the intergrain exchange coupling, magnetic dipolar interactions and the anisotropy fields. The anisotropies fields can be investigated by various techniques. One of these techniques is the ferromagnetic resonance spectroscopy due to the fact that the resonance field depends directly on the anisotropy field strength and its angular spread. In order to understand the dynamic fenomena in these samples line arrays of Permalloy have been prepared using interference lithography. The film thickness is of 50 nm for different lattice period.

Ferromagnetic resonance measurements have been carried out at a frequency of 9.54 GHz as a function of H at different temperatures from 85 K to room temperature. The dependence of the absorption lines with temperature is shown in the following Figure:

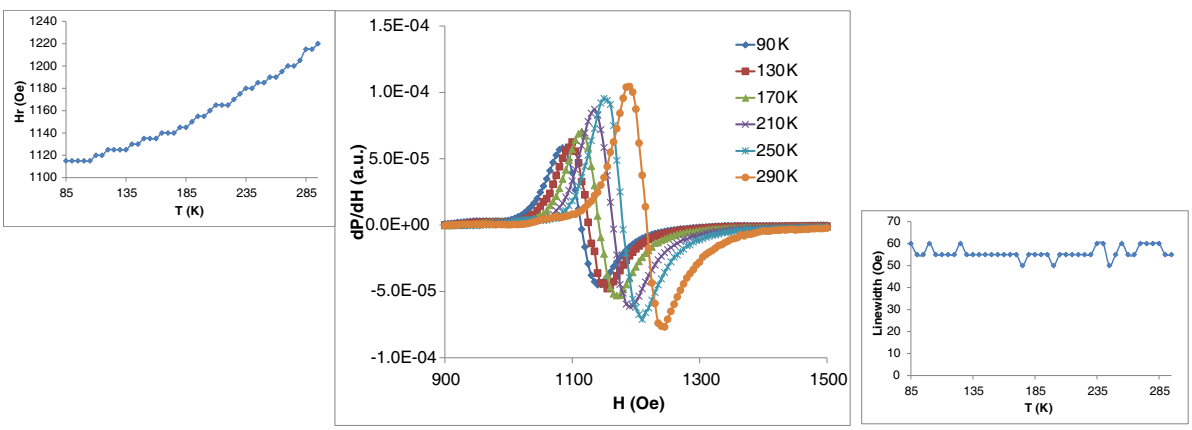

From these measurements it can be obtained the variation with temperatures of the resonance field and the linewidth. An increase of the resonance field with increasing temperature has been obtained. This behaviour can be explained by the relation between resonance field, frequency and the anisotropy field. The linewidth is kept constant throughout the temperature range. This fact make these sample suitable for microwave devices.

Airborne Interferometric Altimetry Experiment over Lake with Multi-carrier Frequencies

Yunhua Zhang, Wenshuai Zhai, Xueyan Kang, Xiaojin Shi, Xiang Gu, and Yueying Tang
Center for Space Science and Applied Research, CAS, China

Abstract— As we know the big challenge for realizing wide-swath observation over ocean for radar altimeter using interferometry is to accurately estimate the roll angle of the baseline because the retrieved height is greatly influenced by this angle. For example, the required accuracy can be as high as 0.1 arcsecond for SWOA or SWOT. However it is very difficult to achieve this accuracy based on the current satellite hardware techniques. We have to find another approach. In this paper we will show that by using the nadir interferometric two beams, the obtained interferometric phase (InPha) can help us to estimate the baseline status. The basic idea is that the InPha is related to actual observation geometry, i.e., the baseline status, height of platform, incidence angles as well as the topography of the target. If we can rule out the possibility of height variation of platform or the target, then we can relate the phase variation to the baseline status (rolling angle and baseline length). An airborne interferometric altimetry experiment over lake with multi-carrier frequencies was carried out to test this idea and promosing results were obtained. The results show that the obtained interferometric phases can very well reflect the variations of attitude and baseline status.

A Method for Simultaneous Gas and Light Path Retrievals from Space-based Spectroscopic Observations of Greenhouse Gases

Sergey Oshchepkov[1], **Andrey Bril**[1], **Tatsuya Yokota**[1], **Yukio Yoshida**[1], **Thomas Blumenstock**[2], **Nicholas M. Deutscher**[3,4], **Susanne Dohe**[2], **Ronald Macatangay**[4], **Isamu Morino**[1], **Justus Notholt**[3], **Markus Rettinger**[5], **Christof Petri**[3], **Matthias Schneider**[2], **Ralf Sussman**[5], **Osamu Uchino**[1], **Voltaire Velazco**[4], **and Debra Wunch**[6]

[1]National Institute for Environmental Studies, Tsukuba, Japan
[2]Karlsruhe Institute of Technology, IMK ASF, Karlsruhe, Germany
[3]Institute of Environmental Physics, University of Bremen, Germany
[4]Centre for Atmospheric Chemistry, School of Chemistry, University of Wollongong, Australia
[5]Karlsruhe Institute of Technology, IMK-IFU, Garmisch-Partenkirchen, Germany
[6]California Institute of Technology, Pasadena, California, USA

Abstract— We have developed an improved Path length Probability Density Function (PPDF) method to retrieve concentrations of greenhouse gases and light path modifications simultaneously from space-based spectroscopic observations of light reflected and scattered from the Earth's surface and the atmosphere. The target quantity to retrieve is the column-average greenhouse gas mole fraction. The light path modification is involved in the retrieval process to account for high variability in the optical properties of aerosols and clouds through the atmosphere. This method has been applied to process radiance spectra measured by the Greenhouse gases Observing SATellite (GOSAT), which is in orbit since 23 January 2009. The measurements of radiance spectra were provided by the Thermal And Near-infrared Sensor for carbon Observation — Fourier Transform Spectrometer (TANSO-FTS) in the short wave infrared bands at 0.76, 1.6, and 2.0 µm as the center with a high spectral resolution (interval) of about 0.2 cm^{-1}. To test the improved method we have compared PPDF-based CO_2 retrievals with those derived from FTS ground-based measurements for Total Carbon Column Observing Network (TCCON) at 12 TCCON validation sites (http://www.tccon.caltech.edu/). We analyzed GOSAT observations during 26 months from June 2009 collecting GOSAT single scans within a circle of 5° radius centered at each TCCON site. The analyzed ground-based FTS data were mean values measured within 1 hour of the GOSAT overpass time. This comparison showed a good agreement of the satellite PPDF-based CO_2 retrievals as compared with ground-based FTS measurements of CO_2 over TCCON sites.

Giant Magnetoimpedance Effect in Nanocrystalline Microwires

A. Talaat[1], **V. Zhukova**[1], **M. Ipatov**[1], **J. M. Blanco**[2], **M. Churyukanova**[3], **S. Kaloshkin**[3], **E. Kostitcyna**[3], **E. Shuvaeva**[3], **V. Sudarchikova**[3], **L. Gonzalez-Legarreta**[4], **B. Hernando**[4], **and A. Zhukov**[1, 5]

[1]Dpto. Fisica de Materiales, UPV/EHU, San Sebastian 20018, Spain
[2]Dpto. de Física Aplicada, EUPDS, UPV/EHU, San Sebastian 20018, Spain
[3]National University of Science and Technology "MISIS", Moscow 119049, Russia
[4]Dpto. de Física, Universidad de Oviedo, Calvo Sotelo s/n, Oviedo 33007, Spain
[5]IKERBASQUE, Basque Foundation for Science, Bilbao 48011, Spain

Abstract— We studied GMI effect and magnetic properties of Finemet-type FeCuNbSiB microwires. We observed that GMI magnetic field and frequency dependences and magnetic softness of composite microwires produced by the Taylor-Ulitovski technique can be tailored either controlling magnetoelastic anisotropy of as-prepared FeCuNbSiB microwires or controlling their structure by heat treatment or changing the fabrication conditions. GMI effect has been observed in as-prepared Fe-rich microwires with nanocrystalline structure.

Monitoring System for Solar Activity in the Very Low Frequency Band

Edwin A. Quintero and Iván D. Arellano
Department of Physics, Technological University of Pereira, Vereda La Julita, Pereira, Colombia

Abstract— The characteristic phenomena of solar activity, among which stand out solar flares, protuberances, sunspots, and coronal mass ejection (CME), release large amounts of radiation composed of ions, which upon reaching the outer layers of the earth interact with the particles present there, modifying their electrical characteristics. Among the possible consequences caused by this series of events, interferences are presented in the geolocation, telecommunications, satellite operations, space monitoring, radio navigation, electrical networks and fuel transportation networks. In order to begin monitoring solar activity, the Alfa Orion astronomy research group planned and executed a project for the design and construction of a signal detection system to operate in the very low frequency band of the electromagnetic spectrum (17–25 kHz VLF band). This system is formed by a detection stage composed of an array of loop antennas, a filtering and signal conditioning stage, and a processing and visualization stage based on a computer graphic interface. The system enables quantitative measurement of variable frequency, signal strength, signal to noise ratio, and power spectral density (PSD) of the received signals.

Long-term Observation of GPS Phase Fluctuations near the Geomagnetic Equator in the Peruvian Sector

Chien-Chih Lee[1], **Wei-Sheng Chen**[1], **and Fang-Dar Chu**[2]

[1]General Education Center, Chien Hsin University of Science and Technology
No. 229, Jianxing Rd., Zhongli, Taoyuan 32097, Taiwan
[2]National Standard Time and Frequency Lab of Telecommunication Laboratories
Chunghwa Telecom Co. Ltd., No. 99, Dianyan Rd., Yangmei, Taoyuan 32601, Taiwan

Abstract— This study investigates a long-term climatology of the nighttime F-region irregularities in the equatorial ionosphere, using GPS phase fluctuations. The GPS phase fluctuations are obtained from the observed data of AREQ station (16.47°S, 71.49°W), which is located in the Peruvian sector. The data period is 1996–2006, which is in the 23rd solar cycle. The results show that the GPS phase fluctuations occur frequently in the equinoctial and summer months, but rarely in the winter months. Moreover, the occurrences of GPS phase fluctuations are high in pre-midnight, but low in post-midnight. For the strength of GPS phase fluctuations, the strength is stronger during high solar activity; while the strength is weaker during low solar activity.

Transmission of Electromagnetic Signals of Measurement-While-Drilling System in the Rock

Z. A. Pyatakova and A. I. Arkhipov
Gubkin Russian State University of Oil and Gas, Russia

Abstract— Measurement While Drilling (MWD) systems are widely used to provide the information about trajectory of the well. The information signal from the source located in bottomhole assembly propagates through the ground.

The information from the bottom is transmitted by means of one of the channels of communication: electromagnetic or hydraulic. The first study of electromagnetic communication channel was carried out in 1959–1962 by S. Y. Litvinov, I. K. Sarkisov, E. A. Polyakov, O. P. Shishkin. Electromagnetic communication channel is widely used in the Soviet Union, because it does not impose specific requirements to the drilling mix and mud pumps.

Despite of the wide commercial application of this channel, physics of electromagnetic wave propagation from the MWD-system is still poorly understood. This is due to many factors that may be included in the model (diffuse system), as well as the high cost of field experiments.

The authors attempted to theoretically justify the physical phenomena occurring during the propagation of low-frequency signals transmitted by MWD-systems. The characteristic frequency of the radiation source is about several Hertz. That is why oil wells and rocks can be represented as a system with lumped parameters and one can build an equivalent electrical circuit consisting of linear elements: resistors and capacitors.

We considered semi-infinite heterogeneous medium and calculated its resistance and capacity on the basis of electrostatic approximation. The nonuniform structure of electric field radiated by the source is taken into account. So, we obtained effective parameters of the rock that match the concrete MWD system that is, in fact, self consistent model of low-frequency signal damping.

Impedance of the environment increases with decreasing of the distance between the wells and the increase can be seen on the output voltage of the receiver. We calculated output voltage for the cluster of two close wells approaching to each other and showed that output voltage on the receiver device can be an indicator of the distance between wells. Thus, the MWD-system with electromagnetic communication channel gets additional function of controlling the distance between the wells, which may be useful for killing well drilling, or to prevent the intersection with cluster drilling.

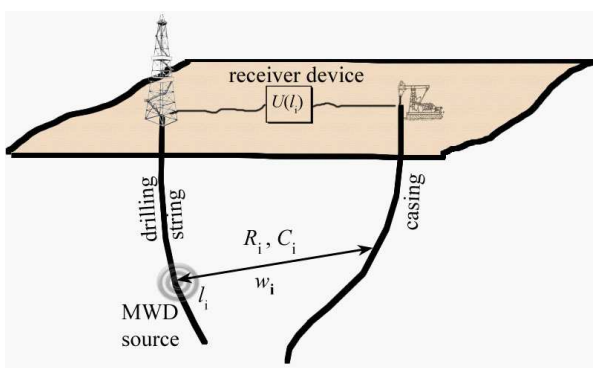

Figure 1: Geometry of the problem, R_i, C_i are effective resistance and effective capacity of the medium, w_i is distance between wells, l_i is the position of the source.

Characteristic Change of Particulate Matter in Osaka of Japan by Transboundary Pollution

Makiko Nakata, Itaru Sano, and Sonoyo Mukai
Kinki University, 3-4-1 Kowakae, Higashi-Osaka 577-8502, Japan

Abstract— Air pollution has become a serious issue in China. Especially problematic are fine particle called PM2.5, whose diameter is 2.5 micrometers or less. Automobiles, factories, coal-burning power plants and heaters at home using coal are the sources of PM2.5 in China. Japan's standard is a daily average of 35 micrograms in one cubic meter of air. The corresponding Chinese standard is 75 micrograms. The Chinese environment protection ministry said that up to a quarter of China was covered with thick fog in February 2013. The problem has become particularly acute, raising health concerns in neighboring parts of Asia including Japan as winds carry the pollution. A noticeable change in characteristics of particulate matter was observed in Japan when pollutant air was transported from China. In this work, we focus on the temporal change of particulate matter around Higashi-Osaka located on the east side of Osaka, the second-largest city in Japan. We take advantage of simultaneous observations on the campus of Kinki University in Higashi-Osaka. Radiometric data supplied by a Cimel instrument were analysed using a standard AERONET (Aerosol Robotics Network) processing system. An SPM (suspended particulate matter) sampler set up at the same AERONET site on the roof of a building at Kinki University about 50 m above sea level. We also set up a standard LIDAR (Light Detection and Ranging) network governed with NIES (National Institute for Environmental Studies) at the same site. The SPM sampler provides particle information about the concentrations of $PM_{2.5}$, PM_{10} and OBC separately. To investigate the change of size and composition of particulate matter, we analyse the particulate matter with a scanning electron microscope (SEM) coupled with an energy-dispersive X-ray analyser (EDX). We used sampling data from the SPM sampler. The component analysis shows that the rate of sulphur increases when pollution suffered from China. In spring, not only pollutants from automobiles and factories but also Asian dust are carried by the wind. Individual particle analysis using SEM/EDX showed the temporal variation of particles properties such as size, shape and components during dust events. The results of the analyses indicate that non-spherical particles with large particle sizes were dominant. LIDAR observations also indicates high depolarisation ratio in the middle of the dust event. The component analysis shows that the rate of silicon, which is possibly from soil particles, became dominant at the peak of the dust event and remained high following the dust event.

Radiation Simulation Code for Aerosol Remote Sensing in the Aerosol Events

Sonoyo Mukai, Masayoshi Yasumoto, Itaru Sano, and Makiko Nakata
Kinki University, Japan

Abstract— It is known that the extreme concentrations of aerosols in the atmosphere prevent aerosol monitoring with surface-level sun/sky photometers, whereas satellites can still be used to observe the Earth's atmosphere from the space. This is why aerosol remote sensing with satellites is well known to be useful and effective. Therefore this work is aimed at developing the practical and efficient algorithms for retrieving aerosol characteristics from space in the aerosol events, which represent the excessive loading of aerosols in the atmosphere

Our aerosol retrieval flow is simple. The optimized aerosol properties are estimated by comparing satellite measurements with the numerical values of radiation simulations, i.e., radiative transfer problem, in the Earth-atmosphere-surface model. Finally retrieved aerosol characteristics are validated by the ground measurements This work is restricted into radiative transfer problem for aerosol remote sensing and ground measurements for validation

The standard radiative transfer problems in a case of finite optical thickness have been treated. It is found that numerical calculations of radiation simulation take lots of time in aerosol events such as dust storms or biomass burning plumes The idea of successive order of scattering is fundamentally related to the probabilistic approach to the theory of radiative transfer in a case of semi-infinite medium. Then our new computation code for implementing the method of successive order of scattering (MSOS) is practically applied for space-based measurements by MODIS The retrieved results on the characteristics of dust particles in the yellow sand storm or biomass burning aerosols are validated with the aerosol properties given at near AERONET sites and/or model simulations.

Comparison of Satellite Altimetric Waveform Retracking Algorithms in the Niger River Delta

Kalifa Goïta and Adama Diepkilé
Centre d'applications et de Recherches en Télédétection
Département de Géomatique Appliquée, Université de Sherbrooke
Sherbrooke (Québec), J1K 2R1, Canada

Abstract— The satellite altimetric waveform is the basic altimetric data, and is represented as the energy backscattered by the ground surface as a function of the time. Retracking algorithms are required to reprocess the data in order to determine effective satellite-ground range information. In this study we compared different retracking algorithm using data from Topex-Poseidon, Envisat and Jason 2 over the Niger River Delta located in Mali (West-Africa). During the flooding period the Delta resembles to an interior sea of about 20 000 km^2, with water level of up to 11 m in some areas of the river bed. Several areas of the flooded basin are covered with herbaceous vegetation (*echinocloa stagnina*, locally named bourgou), which always stands above the water level. Ice-1, ICE-2, Ocean and Sea-Ice algorithms were analysed and compared to a new algorithm we developed based on the water-cloud model. This latter was used to integrate the volume diffusion. Bourgou herbs and rice cultures in the Delta were assimilated to wheat fields, which characteristics have already been tested in water-cloud model. For surface backscattering computation, we used the small fluctuations model. The new algorithm simulates a theoretical waveform which is compared to the measured one in order to extract the relevant parameters. For the study purposes, a field work was conducted in the Delta in 2009, before and during the flooding period, to measure the evolution of the water level at different locations.

The comparison of Ice-1, ICE-2, Ocean and Sea-Ice algorithms shows that their results are quite similar, except for Ocean algorithm, which has weak correlations with the others, and appears not suitable for the Delta. Overall the Ice-1 algorithm seems more appropriate. The results obtained with the water-cloud algorithm are closer to those obtained with Ice-1, ICE-2 and Sea-Ice. They show a highest correlation with Ice-1 ($R^2 = 0.84$). The comparison of the water level estimated using each retracking algorithm with Envisat data to the measured water levels, shows errors in the range of 40 to 56 cm, with the smallest error for the water-cloud algorithm. However, we observed some information loss with the model.

Astronaut Monitoring for Bow Shock Front of Petergius Nebular

Shigehisa Nakamura
Kyoto University, Japan

Abstract— This work concerns to an astronaut monitoring for a bow shock front of the Petergius Nebular. This is a case of the applications of the electromagnetic waves in the infrared band which is introduced for this purpose of monitoring. The author had worked ever in the field of satellite monitoring of the earth surface, though in this work, a passive sensor of infrared signals is reversed to the space outside of the planet earth. A brief note is given on what found at a monitoring under a mission operated as ASTRO-F conducted by JAXA after launched in 2006.

Spacecraft Monitoring for Magnetic Field of Planet Mercury

Shigehisa Nakamura
Kyoto University, Japan

Abstract— A brief note is introduced about spacecraft monitoring for magnetic field of the planet Mercury. A review of the related researches is introduced first for a convenience to clarify what is the main purpose of this work. Recent spacecraft monitoring of the magnetic fields around the planet Mercury is interesting at comparing to what have been studied about the magnetic field around the planet earth. What is the observed result in the MESSENGER project for a spacecraft monitoring of Mercury's environment, is introduced for demonstrating that what have been observed on and around the earth. This could be taken to be similar to the cases of the pattern found around Mercury in a linealized theoretical model. The findings at spacecraft monitoring cover the instability in Mercury's magnetic field. This finding could be a trigger of the advanced research for magnetic disturbance evolution as a physical process around the planet earth. Some part of this work might be looked as if it was quite similar to what found during satellite thermal monitoring of an ocean front evolution on the earth.

Monitoring for Sea Caldera Formed at Tsunami Earthquake

Shigehisa Nakamura
Kyoto University, Japan

Abstract— The author introduces a key to forming process of sea caldera at tsunami earthquake. Special reference after satellite monitoring shows a specific pattern of the earth surface displacements around the seismic, epicenter of the tsunami earthquake. The available satellite data is in the area on land around 500 km square. The other geological survey in the coastal zone seems to support the process of the sea caldera formation. The author notes a brief note to the sea caldera especially in relation to the 2011 tsunami earthquake in the northwestern Pacific.

Micromachined Band Stop Resonator for Millimeter-wave Applications

Alina-Cristina Bunea and Dan Neculoiu
National Institute for Research and Development in Microtechnologies, IMT Bucharest
Str. Erou Iancu Nicolae 126A, Bucharest 077190, Romania

Abstract— Band stop resonators (BSR) with deep rejections can be used in a variety of applications such as notch filters and sensors. A planar topology consisting of a capacitive interdigital structure with a shorted digit, which acts as an inductor was described in [1] for a microstrip approach. The structure demonstrated a deep rejection at several GHz. We propose a similar layout, in a coplanar waveguide (CPW) topology, suspended on a thin dielectric membrane, processed through silicon micromachining. This technology is well suited for the fabrication of high-performance circuits and devices working in the millimeter-wave range up to 110 GHz [2]. Removing the silicon under the structure leads to better RF performance by reducing the dielectric losses and increasing the self-resonance frequency of the interdigital capacitor. Several test structures are shown in Fig. 1(a), where the transparency of the dielectric membrane can be noticed.

The design and optimization of these devices is not a trivial task. A flexible 3D electromagnetic (EM) model was developed in the full-wave simulation tool CST Microwave Studio. The design offers full control over every layout parameter, including the number of digits and the position of the shorted digit. The sloped transitions which result from the wet micromachining of the ⟨100⟩ silicon are also included in the model (Fig. 1(b)). The simulations were validated through experimental results. Fig. 1(c) shows a very good agreement between simulations and measurements for a 11 digits structure, which demonstrated a rejection of −30 dB at 30 GHz. The measurements were performed using standard on wafer characterization techniques.

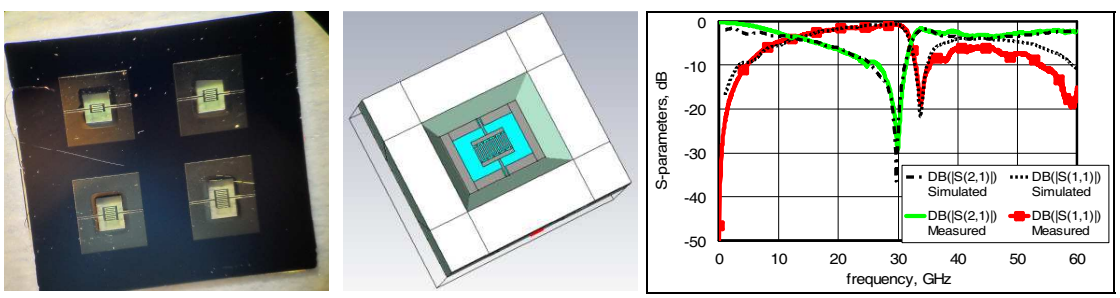

(a) (b) (c)

Figure 1: (a) Photo of fabricated test structures; (b) 3D EM model of the membrane supported BSR developed in CST MWS; (c) Comparison between simulation and measurement results for a 11 digits structure.

REFERENCES

1. Lancaster, M. J., F. Huang, A. Porch, B. Avenhaus, J.-S. Hong, and D. Hung, "Miniature superconducting filters," *IEEE Trans. Microwave Theory Tech.*, Vol. 44, No. 7, 1339–1346, 1996.
2. Bunea, A. C., D. Neculoiu, and A. Müller, "Analytic and electromagnetic investigation of millimeter wave membrane supported CPWs processed on high resistivity silicon," *Romanian Journal of Information Science and Technology*, Vol. 14, No. 3, 269–283, 2011.

Design of a Coplanar Waveguide to Substrate Integrated Waveguide Transition for LTCC Technology

Dan Neculoiu and Alina-Cristina Bunea
National Institute for Research and Development in Microtechnologies, IMT Bucharest
Str. Erou Iancu Nicolae 126A, Bucharest 077190, Romania

Abstract— Usually rectangular waveguides are difficult to integrate in complex millimeter wave systems. One alternative is to try and integrate them in the substrate, building a substrate integrated waveguide (SIW). This can easily be achieved by using the Low-Temperature Co-fired Ceramics (LTCC) technology, where rows of metallic vias and metal plates embedded in dielectric are used to define the SIW geometry. This type of waveguide offers the benefits of the classical rectangular waveguide, at low cost, small size and with easy integration using the system-inpackage (SiP) approach. Many new circuits and devices based on the SIW technology have been developed in the past few years [1]. One common issue is related to the feeding/extraction of the signal through transitions to microstrip or coplanar waveguide (CPW).

In this work a Ka band (26.5–40 GHz) grounded coplanar waveguide (GCPW) to SIW transition was designed and characterized. The transition starts from a 50 Ohm CPW transmission line, continues with a quarter-wavelength impedance transformer section and feeds the SIW using a double 90° bend on each of the CPW slots (Fig. 1(a)). The SIW has a width of 2.4 mm, the diameter of the vias is 0.1 mm and the vias pitch 0.25 mm, with a height of 0.288 mm. The dielectric tape considered is Ferro A6-M with a dielectric permittivity of 5.9. The calculated cut-off frequency of the SIW is $\sim$ 26.15 GHz.

The electromagnetic model for the GCPW-to-SIW transition was developed in CST Microwave Studio and was parameterized for optimization. For characterization purposes, two transitions were connected back-to-back, resulting in a test structure that was measured on-wafer. A comparison between the simulated and measured reflection and insertion losses is shown in Figs. 1(b) and 1(c). There is a very good agreement and the structure shows good behavior in the whole Ka band.

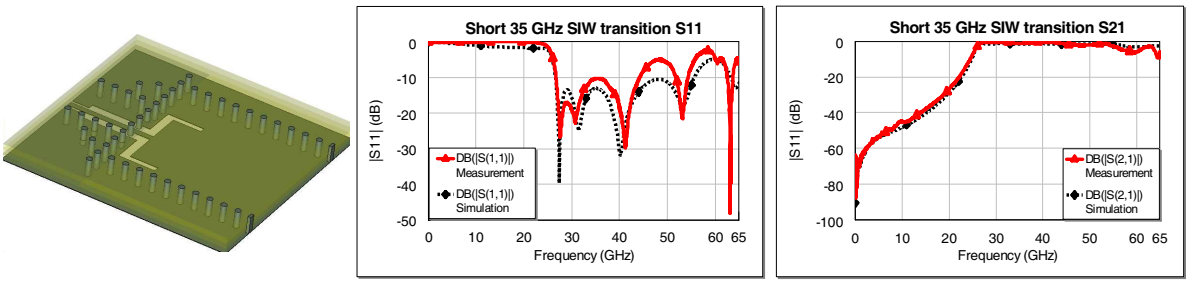

(a) (b) (c)

Figure 1: (a) 3D EM model in CST MWS; (b) Reflection losses of two back-to-back CPW-to-SIW transitions; (c) Insertion losses of two back-to-back CPW-to-SIW transitions.

REFERENCES

1. Bozzi, M., A. Georgiadis, and K. Wu, "Review of substrate-integrated waveguide circuits and antennas," *IET Microwaves, Antennas & Propagation*, Vol. 5, No. 8, 909, 920, June 6, 2011.

Design of Two-stage Low Noise Amplifier Based on Non Simultaneous-conjugate-matching Technique

Yana Taryana[1] **and Achmad Munir**[2]

[1]Research Center for Electronics and Telecommunication
Indonesian Institute of Sciences, Indonesia
[2]Radio Telecommunication and Microwave Laboratory
School of Electrical Engineering and Informatics
Institut Teknologi Bandung, Indonesia

Abstract— Usually a low noise amplifier (LNA) is designed based on a method of simultaneous-conjugate-matching technique to obtain a desired maximum gain. Unfortunately, the maximum gain which is obtained from the above method is almost followed by arise of values in noise figure (NF) and voltage standing wave ratio (VSWR). Therefore to minimize NF and VSWR, in this paper a non simultaneous-conjugate-matching technique is proposed to design 2-stage LNA working at S-band frequency. In the design process, the ADS software is applied to determine the value of desired trade-off between the amplifier parameters such as gain, NF and VSWR. The 2-stage LNA which is deployed on an Arlon DiClad527 uses BJT transistors of BFP420 and microstrip lines for matching the impedances at the input and output ports. From the characterization results, it shows that the proposed LNA produces the gain of 28 dB at 3 GHz with NF and VSWR less than 2.8 and 1.5, respectively.

Theoretical Analysis of Frequency Characteristic and Resonance Mode of Anisotropic Artificial Dielectric Resonator Encapsulated in Circular Waveguide

Hepi Ludiyati, **Andriyan Bayu Suksmono**, **and Achmad Munir**
Radio Telecommunication and Microwave Laboratory
School of Electrical Engineering and Informatics
Institut Teknologi Bandung, Indonesia

Abstract— The property of artificial dielectric resonator with anisotropic permittivity encapsulated in a circular waveguide is analyzed theoretically with the focus on its frequency characteristic and resonance mode. The theoretical analysis is required to investigate the specific property of resonator prior the implementation for some applications in microwave region. By applying Maxwell's equations with proper boundary conditions for circular waveguide, the related equations for calculating the resonant frequency of resonator for some resonance modes is determined. In the analysis, to obtain the anisotropic property of resonator, the permittivity is assumed to be different in each axis, i.e., ρ, φ, z axes of coordinate cylinder. The analysis result shows that the anisotropic permittivity can be used to improve the spurious property of resonator, or in other word it is implementable for resonance mode selection which depends on the value of permittivity.

A Two Order Bandpass Filter Designed with Lowpass Filter Sections

Xing J. Zhong, Jun D. Ye, De X. Qu, and Rong Huang
College of Communication Engineering, PLA University of Science & Technology, Nanjing 210007, China

Abstract— Signal suppression in stopband is an important issue in a bandpass filter design. A direct method of enhancing the stopband performance of the bandpass filter is adding a lowpass filter with wide stopband before or after the bandpass filter. This method may make the whole structure larger. Is it possible to imbed a lowpass filter in the bandpass filter? This paper does a initial study about imbedding a lowpass filter section in the design of a two order bandpass filter. The lowpass filter sections in this paper were derived from stepped impedance lowpass filter of order three with a slot inserted in the middle of the low impedance transmission line. This slot provide the needed coupling between the two resonators of the bandpass filter. And because of the slot, though the lowpass filter section has a wide stopband, it is different from traditional lowpass filter that it may have large insertion loss in the passband of it. But the larger insertion loss does not affect the performance of the bandpass filter. The passband of the lowpass filter section is below 2.5 GHz, and the stopband is extended from 2.5 GHz to 8 GHz. The constructed resonator from these lowpass filter sections is resonating about 1.92 GHz in the passband of the lowpass filter, thus lets the bandpass filter composed of them have a passband with center frequency about 1.92 GHz. And like the lowpass filter section suppressed the signals in a wide band, the bandpass filter also have a wide stopband from 2.5 GHz to about 8 GHz with minimum insertion loss larger than 20 dB. Measured results accord well with the simulated results, showing good performance of the filter.

Development of an Embedded Wafer Level Package Technology and Evaluation of Its Electrical Performance Using RF Switch IC

Se-Hoon Park[1,2], **Jong-In Ryu**[2], **Jong-Min Yook**[2], **Young-Ho Kim**[1], **and Duck-Kyun Choi**[1]

[1]Division of Materials Science & Engineering, Hanyang University, Seoul 133-791, Korea
[2]System Packaging Research Center, Korea Electronics Technology Institute
#68 Yatap-Dong, Bundang-Gu, Seongnam-Si, Gyeonggi-Do 463-816, Korea

Abstract— Recently, there has been strong demand for EWLP (Embedded wafer level package) technology as SiP (system in package) platform due to its low cost, small foot print and good electrical performance, so it has been considered as one of promising package solutions for the high frequency application [1–3]. Moreover, good electrical performance caused by short interconnection length and a high metal pattern resolution enables low-loss transmission lines [3, 4]. In this paper, EWLP technology was developed and its interconnection performance was evaluated using RF switch IC. EWLP was realized by epoxy molding, epoxy film lamination, laser via drilling and Cu plating for integration. For EWLP module fabrication, ABF (Ajinomoto bonding film) was laminated on re-arrayed switch ICs in molding wafer and then in order to reduce interconnection length, their I/O pads were interconnected by micro Cu vias and redistributed Cu patterns instead of wire bonding method (see Fig. 1). As a result, almost 50% size reduction was realized by EWLP technology, compared to wire bonding method. RF switch IC was also interconnected with PCB using normal gold wire bonding method for the comparative study on RF performance. SP3T (single pole triple through) IC was selected as RF switch IC and RF performance of both modules were compared by measuring IL (insertion loss) and RL (return loss) using test board. 2.4 GHz, one of ISM (Industry-Science-Medical) band, was selected as test frequency. IL of EWLP and of wire-bonding module was revealed as almost 0.6 dB as depicted in Fig. 2 and PCB loss of test board is almost 0.4 dB. RL of EWLLP and wire-bonding module are better than 20 dB and 16 dB, respectively. RL of EWLP module was relatively improved at 2.4 GHz, compared to that of wire bonded IC module, whereas IL of both modules did not show big difference. In this study, it is obtained that EWLP technology is one of good solutions to improve RF performance and reduce package size at competitive process cost.

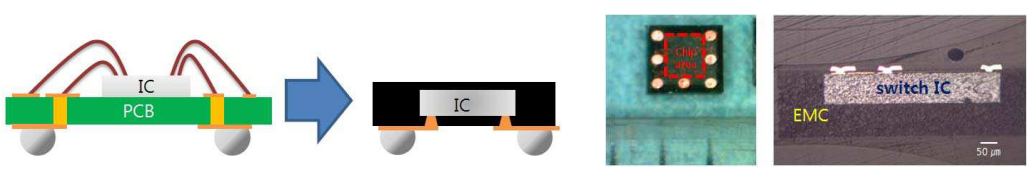

(a) (b)

Figure 1: (a) The schematics of EWLP structure. (b) Embedded switch IC package module.

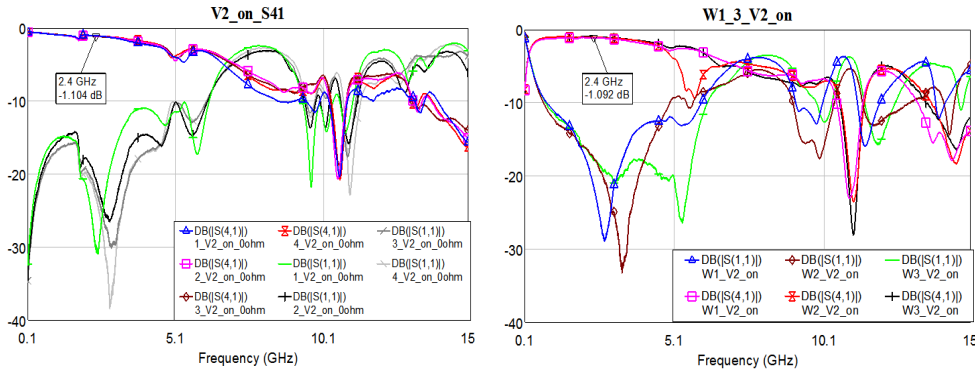

(a) (b)

Figure 2: (a) The results of EWLP structure. (b) Results of wire bonding structure.

REFERENCES

1. Carson, F., K. Ishibashi, S. W. Yoon, P. C. Marimuthu, and D. Shariff, "Development of super thin TSV PoP," *2010 IEEE CPMT Symposium Japan*, 1–4, 2010.
2. Jin, Y., X. Baraton, S. W. Yoon, Y. Lin, P. C. Marimuthu, V. P. Ganesh, T. Meyer, and A. Bahr, "Next generation eWLB (embedded wafer level BGA) packaging," *12th EPTC*, 520–526, 2010.
3. Issakov, V., G. Knoblinger, K. Pressel, G. Sommer, and R. Weigel, "High-Q inductors embedded in the fan-out area of an eWLB," *IEEE Transaction on Components, Packaging and Manufacturing Technology*, Vol. 2, No. 8, 1280–1292, 2012.
4. Wojnowski, M., R. Lachner, J. Böck, C. Wagner, F. Starzer, G. Sommer, K. Pressel, and R. Weigel, "Embedded wafer level ball grid array (eWLB) technology for millimeter-wave applications," *13th EPCT*, 423–429, 2011.

70 GHz Tx and Rx LCP SoP Module for Point-to-point Millimetre Wave Applications

Young Chul Lee
Department of Electronics Engineering, Mokpo National Maritime University (MMU), Korea

Abstract— In this paper, a 70 GHz Amplitude-Shift-Keying (ASK) transmitter and receiver system-on-package (SoP) module based on a liquid-crystal polymer (LCP) substrate has been presented for point-to-point wireless communication applications. Two frequency multipliers (MTLs), a driver amplifier (DA), high-gain LNA block, ASK modulator and de-modulator are integrated in the metal-backed LCP substrate. The size of the fabricated Tx and Rx SoP module are $30.11 \times 22.54 \times 2.15\,\mathrm{mm}^3$ and $22.95 \times 22.54 \times 2.15\,\mathrm{mm}^3$, respectively.

Study of the Electromagnetic Compatibility in Hospitals in Argentina and Spain

C. Muñoz[1], R. Saint-Nom[1], M. A. Navarro[2], O. Gutiérrez[2], and F. Saez de Adana[2]

[1]Centro Argentino de Estudios en Radiocomunicaciones y Compatibilidad Electromagnética (CAERCEM), Instituto Tecnológico de Buenos Aires (ITBA)
Buenos Aires, Argentina
[2]Dpto. de Ciencias de la Computación, Universidad de Alcalá, Alcalá de Henares, Spain

Abstract— This paper presents a study of the effect of the radiation of electronic equipments in hospital. A comparative study between Argentinean and Spanish hospitals has been performed. The work consists in two parts: a campaign of orientation to be aware of the knowledge of the personal of the hospitals about the problem, and the technical part consisting on a measurements campaign in different hospitals to study the failure produced in different equipments due to the presence of electromagnetic interferences such as the use of mobile phones. The study of this problem has been of special interest lately in countries as USA and Canada and this paper tries to obtain some regulations that can be applied to the Argentinean and Spanish cases. More than fifty hospitals have been studied in both countries, considering the following aspects: the awareness about the problem of the personal in the hospitals, if the hospitals have made previous studies of this type, the appearance of problems in medical equipment due to this interference, the origin of the interference, and the failures appeared in computers due to the electromagnetic interference. The results show the lack of prevision of most hospitals regarding this issue and the appearance of several problems, especially in medical equipment, due to the interference. Therefore, the conclusion is the necessity of providing a regulation to avoid the problem, which is the final objective of this paper.

Photonic-assisted Measurement of Electromagnetic Coupling into a Generic Object

Dong-Joon Lee, **Chi-Hyun Cho**, **Jeong-Il Park**, **and No-Weon Kang**
Center for Electromagnetic Wave, Korea Research Institute of Standards and Science
267 Gajeong-Ro, Yuseong-Gu, Daejeon 305-340, Korea

Abstract— Analyses of internal fields inside generic objects have been performed to enhance the immunity of such objects against external electromagnetic influences [1–3]. In this paper, we present a minimally invasive electric field measurement system utilizing mature photonic technology to evaluate the electromagnetic influences of a generic missile object. The internal electric fields — coupled into a generic missile cavity — are investigated using a fiber-coupled electro-optic field sensor with its associated photonic system. The operation principle and design scheme of the sensor are discussed first. Then, the sensitivity of the electro-optic sensor is characterized by calibrating the sensor with a commercial field probe. The minimum detectable field level is less than 1 V/m and the sensor's dynamic sensing range is over 100 dB [4]. We used a standard gain horn antenna at the R band to generate a calculable incident field toward the generic missile. The field level arriving at the object is typically about 60 V/m but can be built up to be 28 dB larger at multiple resonant frequencies as the fields couple into and accumulate inside the missile cavity (as shown in Figure 1, incident fields are normalized to 0 dB). The measured resonance characteristic of the generic cavity shows good agreement with the computational data. This indicates that the electromagnetic susceptibility of an electronic sub-system with an enclosed metallic cavity can be readily exploited with the photonic-assisted system presented here. The strength and spectra of the resonant fields passed through the aperture of the hollow generic cavity with various cylindrical structures are presented. This measurement system is quite effective at measuring actual fields without the need for a probe compensation procedure; thus it can be utilized for shielding a generic system against intentional electromagnetic threats as the interiors of the generic objects become highly sophisticated.

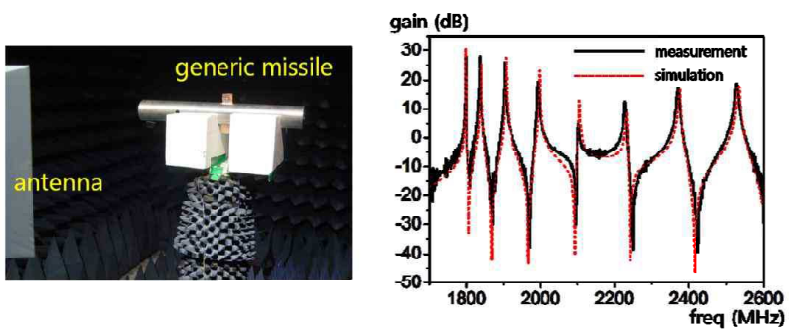

(a) (b)

Figure 1: (a) A system for electromagnetic coupling measurement and (b) fields in the missile sample.

REFERENCES

1. Bäckström, M., J. Lorén, G. Eriksson, and H. J. Åsander, "Microwave coupling into a generic object. Properties of measured angular receiving pattern and its significance for testing," *Proc. 2001 IEEE Int. Symp. on Electromagnetic Compatibility*, 13–17, Montreal, 2001.
2. Junqua, I., L. Guibert, and J. P. Parmantier, "Assessment of high frequency coupling in a generic object by the power balance method," *Proc. 18th Int. Zurich Symp. on Electromagnetic Compatibility*, 397–400, Munich, 2007.
3. Fisahn, S., H. Garbe, and F. Sabath, "Protective properties of a generic missile enclosure to different electromagnetic influences," *Proc. 2007 IEEE Int. Symp. on Electromagnetic Compatibility*, 1–6, Honolulu, 2007.
4. Lee, D. J., J. Y. Kwon, N. W. Kang, and J. F. Whitaker, "Calibrated 100 dB dynamic range electro-optic sensor for high power applications," *Optics Express*, Vol. 18, 14437–14450, 2011.

The Design and Implementation of an EMC Pre-compliance Board

F. R. L. Silva[1], L. R. Ribeiro[1], L. P. Dias[1], W. J. Santos[1], C. E. Capovilla[2], and H. X. Araujo[1]

[1]Universidade Federal de São João Del Rei — UFSJ, Ouro Branco, Brazil
[2]Universidade Federal do ABC — UFABC, Santo André, Brazil

Abstract— In this work, the EMC — Electromagnetic Compatibility of Integrated Circuits, electronic boards and home appliances is deal with the use of a conducted emission technique. In general, as the IC the major responsible of unintentional emissions and coupling, some specific pre-compliance setup tests were employed to analyze these detrimental effects to the system as a whole. Therefore, EMC Pre-Compliance Board — EPCB was designed and built. Additional techniques were used to improve the EPCB in terms of frequency range and performance. It is also shown others pre-compliance setup tests to evaluate the disturbance caused by an IC. Simulated and experimental results are compared to validate the EPCB test setup.

Nowadays, the necessity to control the electromagnetic emissions and interference between circuits and electronic devices becomes a crucial point to assure its correct operation inside an electromagnetic environment. Some approaches were designed to support the pre-compliance tests (EMC/EMI/EMS) setups, which are not designed to replace the well-known compliance equipments (anechoic chamber, stirring chamber, blue test chamber, etc.) but, it gives a previously information about the device behavior. All of them have consolidated standards and regulations.

The electrical circuit of any electronic device produces some kind of noise, which can reach levels of power that interfere in undesired ways on the operation of the equipment around and the environment as a whole. Each device generates a characteristic noise, due to its electrical circuit. Depending on the electromagnetic emission of these noises, other electronic devices can then receive the interference by a path of radiation or, much less frequently a direct electrical connection.

The analysis of conducted emission aims to measure how much electromagnetic radiation (noise) is conducted in an electronic equipment to the grid by the power cord. Such issuance may not exceed the established standards, so that the overcoming of the imposed limit causes interference in the operation of other devices that are connected on the same network.

In this context, the EPCB test setup will be used between the power cord of the device under test and the power outlet, to verify if the DUT meets the standards of conducted emission. Simulated and experimental results are compared to validate the EPCB test setup.

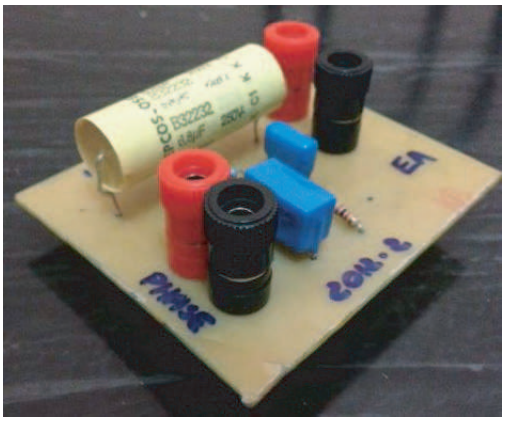

Figure 1: EPCB setup test.

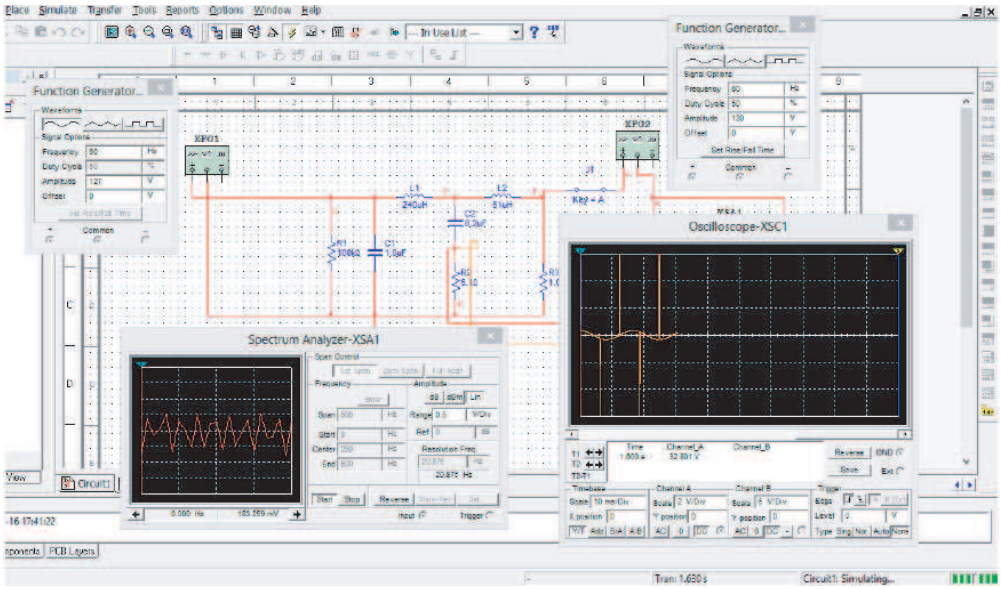

Figure 2: EPCB preliminary simulations.

REFERENCES

1. Montrose, M. I. and E. M. Nakauchi, *Testing for EMC Compliance*, Wiley Interscience, New York, 2004.
2. Araujo, H. X. and L. C. Kretly, "An EM simulation and design a GTEM chamber for EMC pre-compliance tests on electronic board and ICs in 500 MHz–18 GHz range," *Momag 2010*, Vila Velha, Brazil, August 2010.
3. Konigstein, D. and D. Hansen, "A new family of TEM-cells with enlarged bandwidth and optimized working volume," *Proceedings of the 7th International Zurich Symposium on Electromagnetic Compatibility*, 127–130, Zurich, March 1987.
4. Dhia, S. B., M. Ramdani, and E. Sicard, *Electromagnetic Compatibility of Integrated Circuits: Techniques for Low Emission and Susceptibility*, Springer, New York, 2006.
5. De Araujo, H. X. and L. C. Kretly, "EMC pre-compliance test of RFIC and RF systems using a laboratory GTEM chamber," *PIERS Proceedings*, 896–900, Moscow, Russia, August 19–23, 2012.

Magnetoelectric Transducers

R. V. Petrov, A. N. Soloviev, K. V. Lavrentyeva, I. N. Solovyev, V. M. Petrov, and M. I. Bichurin
Novgorod State University, Russia Federation

Abstract— Magnetoelectric (ME) effects have deserved careful study during the last decade due to energy transfer from magnetic (electric) field to electric (magnetic) one. ME materials have a wide range of potential applications. In this work, two types of the ME transducers are considered. The first one is the piezoelectric transformer with magnetic phase (PTM). PTM relates to the field of electronics, its new direction called magnetoelectric electronics. PTM is a main part of a secondary power source. The main objectives of this work are the modeling of processes in the structure, method of equivalent circuits, and analysis of amplitude-frequency characteristics.

PTM is a combination of magnetostrictive and piezoelectric components. The input section consists of two parts. The first one is designed to have even number piezoelectric layers. The second one is designed as a multilayer structure of magnetic material (Metglas). The input section is responsible for converting the electrical signal into the mechanical vibrations. The magnetostrictive component converts the variable constituent of the magnetic field into the elastic vibrations. The magnetostrictive component should have high magnetostriction to give an effective increase of the mechanical vibrations magnitude in the output section. It leads to increase the amplitude of mechanical vibrations created by piezoelectric and magnetostrictive effects.

The output section is performed in the form of the piezoelectric element with thickness polarization. The output one converts the mechanical vibrations into an electrical signal at the same frequency.

The piezoelectric transformer without magnetic phase (PT) and PTM have been compared. The PTM parameters, e.g., an output voltage, a transformation coefficient, are two times more than the PT parameters. The PTM output voltage and the transformation coefficient are 5 V and 5, respectively. The voltage of the power supply is 1 V.

The second type of the transducers is ME variable inductor. Inductors are known to be basis electronic elements and widely used in variety of applications, such as voltage regulation, power harmonic filters, voltage-controlled oscillators, filters, and matching networks in wireless systems. Developments in power electronics and wireless communication systems have given rise to an increased demand for tunable inductors with large tunability, high quality factors, and low energy consumption. For instance, magnetic films based tunable inductors have large tunability range but a large constant current is required for producing a large magnetization change in magnetic films.

In this research, a variable inductor with magnetoelectric composite core is discussed. The core consists of magnetostrictive-piezoelectric layered structure which is known to exhibit ME coupling. In a case of converse ME effect, applied electric field induces a strain mediated magnetization of magnetic phase. ME coupling leads to a change in magnetic induction and thus in inductance.

As an example, we considered the Metglas — lead zirconate titanate (PZT) — Metglas trilayer. Layers are bonded together with epoxy and are used as the core. Variation of dc voltage across the piezoelectric layer gives rise to a change in inductance. The maximum change of inductance is 70% for operation frequency of 100 kHz. Theoretical estimates are in good agreement with data.

ACKNOWLEDGMENT

The reported study was partially supported by the grant of the Federal Target Program "Scientific and pedagogical staff of innovative Russia" on 2009–2013 and by RFBR research project #13-02-98801.

Shielding Effectiveness of Plasma Coated Multi-layered Shields

P. D. Tosun[1], **S. Ozen**[2, 3], **and S. Helhel**[2, 3]

[1]Faculty of Engineering and Physical Sciences, University of Surrey, UK
[2]Electrical and Electronics Engineering, Akdeniz University, Turkey
[3]Industrial and Medical Applications of Microwaves Research and Application Centre
Akdeniz University, Turkey

Abstract— Shielding and shielding effectiveness (SE) are two important concepts concerning preventation of electromagnetic interference. Multi-layered shielding structures are used for electromagnetic interference (EMI) shielding for the last few decades. Combined shielding materials or coated shields form this kind of structures. Combined shielding materials have electromagnetic incompatibility problems due to their apertures existing in the structures. This is a problem which is caused by the process when combining the materials to form these structures. Plasma polymerization technique is simply coating of desired material on a surface, under high energy vacuum conditions. This technique can be applied to various surfaces by different types of high energy sources. In general, plasma coating systems are proved to be very effective in terms of coating stability and performance. Therefore, computer modelling of such structures were carried out to investigate the shielding effectiveness of these multi-layered shields. Two and three layered shielding models were generated. For two layered models; metal on metal structures, for three layered models; two layers of metal coatings on glass surface were investigated. 2.5 dB decrement at the 0.25 Hz resonance frequency was observed at two layered models. High frequency analyses were conducted for three layered structures with coating thicknesses 100 µm and 0.1 cm. Shielding effectiveness values were recorded similarly but overall values of shielding effectiveness declined due to the drop of reflection loss value of the shield. Surface thickness' effect on the EMI shielding was tested as well. SE value of 30–40 dB was noted for 10 cm thick structures. This value proved that the thickness of the surface material of the multi-layered structure increases the overall SE because of high absorption loss value of the shield.

Surge Test of High Power Radar Module Used in Military

Soon-Mi Hwang, Chul-Hee Kim, and Kwan-Hun Lee
Korea Electronics Technology Institute (KETI), Republic of Korea

Abstract— The radar module is used for communication in a civilian or military. In general, radar module is exposed to the outside, on the means of moving or fixed in a certain place. It should be guaranteed sufficient immunity for a variety of environmental stresses that can occur in the Outdoor. GaN Power Amplifier Module is the most critical part of the high-power communication systems is used in aviation, military radar transmitter [1, 2].

Surge means a higher transient voltage than normal voltage. And surge is one of the major causes of failure in radar module. It refers to the movement of high electricity caused by electrical or mechanical switching. When such high electricity power moves to other device for an instant, it damages the device's low power circuit. Surges impinging on electronic equipment may cause damage, or in lesser cases, operational upset [3]. Below some level dependent on equipment design, no effect is observed. Above this level, a surge may cause the operation of the equipment to change state, without any long-term effect on the circuit components. But, at a higher level, there may be enough energy to cause breakdown in critical components.

In this paper, we evaluate the surge immunity of high-power radar modules used in the military.

Surge test was done on GaN Power Amplifier radar Module, according to the international standard, IEC61000-4-5 standard [4]. The standard waveform for the IEC 61000-4-5 surge test is a single impulse specified by two waveforms at the same time, as a 1.2/50 µs voltage impulse into an open circuit and an 8/20 µs impulse into a short circuit. The effective output impedance of the surge generator, defined as ratio of the peak open-circuit voltage to the peak short-circuit current, is 2 ohm ±10%.

It was tested from 1 kV until failure occurs by adding 200 V. Check for changes in the output of GaN Power Amplifier Module to determine the presence of faults. As a result, current increase and power unstable occurred in the level of 4 kV.

Examining the failed sample from Surge test, we found there was a change in power input pin's resistance and capacitance of the sample. Looking closely at the internal circuit with an optical microscope showed us trace of burning in the circuit's capacitor and chip-type inductor. Surge caused sudden rush of high electricity, which led to failure of the power part circuit's insulation.

REFERENCES

1. Singhal, S., "GaN-ON-Si failure mechanisms and reliability improvements," *44th Annual IEEE International Reliability Physics Symposium Proceedings*, 95–98, March 26–30, 2006.
2. Ohki, T., "Reliability of GaN HEMTs: Current status and future technology," *IEEE International Reliability Physics Symposium*, 61–70, April 26–30, 2009.
3. Smith, S. B and R. B. Standler, "The effects of surges on electronic appliances," *IEEE Transactions on Power Delivery*, Vol. 7, No. 3, 1275–1282, July 1992.
4. IEC 61000-4-5, Electromagnetic Compatibility (EMC) Test, Surge Test, 2001.

A Novel Approach to Impulsive Noise Analysis in PLC In-door Systems

Mónica V. Avalos, J. H. Caltenco, R. Linares-Miranda, and J. A. Tirado-Méndez
Laboratorio de Compatibilidad Electromagnética, Instituto Politécnico Nacional
SEPI-ESIME-Zacatenco, Programa de Posgrado en Ing. Electrónica, México, D.F., Mexico

Abstract— In this paper a novel approach to statistical modeling using the Gamma function applied to Impulsive Noise generated by inductive loads is illustrated and its application to In-Home Power Line Communication in the bandwidth 1–30 MHz.

Nowadays, although the systems of communications PLC is an alternative to high-speed data transmission they are still affected for several problems that are investigation topics, just as the one impulsive noise generated by inductive loads. In this work an analysis of this noise is presented in the systems PLC of wide band, starting from measurement of the noise generated for motors of AC. The result is presented as the Amplitude Probability Distribution of the impulsive noise and their relationship with the probability of Bit Error Rate.

In the experimental work, the noise was measured using Electromagnetic Interference Test Receiver, a Current Probe and a Load Impedance Stabilization Network.

Multifunctional Reconfigurable Antenna Systems and Technologies

Bedri A. Cetiner, **Hema Swaroop Mopidevi**,
Zhouyuan Li, **and Yasin Damgaci**
Department of Electrical and Computer Engineering, Utah State University, USA

Abstract— This paper presents a review of the design methodologies and reconfiguration mechanisms for Multifunctional Reconfigurable Antenna (MRA) systems developed at Utah State University. It is well known that switches are the main building blocks of an MRA which is capable of dynamically reconfiguring its properties (frequency, radiation pattern, and polarization) based on the change in propagating medium. The switching technologies used can be classified into i) Micro Electro Mechanical Systems (MEMS) [1, 2] ii) solid state switches and iii) liquid metal switch [3]. Switch performance, ease of integration, reliability, and ease of fabrication are the important metrics for switch selection. The design methodologies of an MRA are broadly classified into three categories based on integrating switches: i) within the geometry of the driven antenna [1, 2] ii) into a parasitic pixel layer [4, 5] and iii) a hybrid approach, where switches are integrated both in the driven antenna and parasitic layer. The selection of a design methodology is based on the following factors: Radio Frequency (RF) power handling capability of switch, number of switches used, compactness of structure, bias circuitry design, ease of fabrication of antenna, and switch integration. For example, while methodology (i) can be advantageous in creating a compact design, the RF power handling capability of MRA is limited. Parasitic layer based approach can alleviate this difficulty at the cost of increase in antenna volume. Finally, a hybrid approach might combine the advantages of both methodologies. Also, different feeding mechanisms namely: i) coaxial fed ii) microstrip fed iii) aperture coupled and iv) Coplanar Waveguide (CPW) fed; have their own pros and cons when coupled with a particular design methodology. The simulations and measurements of important prototypes are presented and compared.

REFERENCES

1. Zohur, A., H. Mopidevi, D. Rodrigo, M. Unlu, L. Jofre, and B. A. Cetiner, "RF MEMS reconfigurable two-band antenna," *IEEE Antennas and Wireless Propagation Letters*, Vol. 12, 72–75, 2013.
2. Unlu, M., H. Mopidevi, A. Zohur, and B. A. Cetiner, "Frequency reconfigurable, 220–5000 MHz, five-band RF MEMS PIFA," *2012 IEEE 55th International Midwest Symposium on Circuits and Systems (MWSCAS)*, 65–68, Aug. 5–8, 2012.
3. Rodrigo, D., L. Jofre, B. A. Cetiner, "Circular beam-steering reconfigurable antenna with liquid metal parasitics," *IEEE Transactions on Antennas and Propagation*, Vol. 60, No. 4, 1796–1802, Apr. 2012.
4. Yuan, X., Z. Li, D. Rodrigo, H. S. Mopidevi, O. Kaynar, L. Jofre, and B. A. Cetiner, "A parasitic layer-based reconfigurable antenna design by multi-objective optimization," *IEEE Transactions on Antennas and Propagation*, Vol. 60, No. 6, 2690–2701, Jun. 2012.
5. Cetiner, B., Li, Z., D. Rodrigo, and L. Jofre, "A new class of antenna array with a reconfigurable element factor," *IEEE Transactions on Antennas and Propagation*, Voi. PP, No. 99, 2013.

Metamaterial Inspired Microstrip Patch

Surabhi Dwivedi[1], **Vivekanand Mishra**[1], **and Yogesh P. Kosta**[2]

[1]ECED, S.V.N.I.T., Surat, India
[2]Marwadi Education Foundation's Group of Institutions, Rajkot, India

Abstract— An introduction is presented on radome structure. And radome structure (patch cover) modeling and design concepts are studied and comparisons are made with the MTM included patch. Various advantages are evaluated over the existing technology.

Over the past decade, the need for small, compact and low cost antennas has increased tremendously for applications such as wireless communications and radar. Microstrip patch antennas, though popular for these applications, are difficult to miniaturize, since their resonant frequency is determined by the dominant (TMZ110) mode of the patch cavity (the region immediately beneath the patch). Nevertheless, numerous miniaturization techniques using shorting posts, active loading or high permittivity dielectrics have been conceived to lower the resonant frequency of patch antennas without increasing their size. Unfortunately, as the demand for ever smaller patch antennas increases, these techniques fail to produce the required size reductions.

Experimental Graduate Projects on Electromagnetism in Physics Courses

J. Íñiguez[1], V. Raposo[1], A. G. Flores[1], M. Zazo[1], and P. Hernández-Gómez[2]

[1]Departamento de Física Aplicada, Universidad de Salamanca, Salamanca E-37071, Spain
[2]Departamento de Electricidad y Electrónica, Universidad de Valladolid, Valladolid E-47071, Spain

Abstract— In recent years an increasing relevance of the graduate works in physics at our universities is being recognized. Unfortunately it is not easy to provide enough interesting ideas on experimental assignments to our students in order to satisfactorily develop these projects and often we resort to theoretical, bibliographic or computational works. Efforts should be made to increase the experimental project ratio including subjects that can be completed with an additional theoretical task or some numerical simulation.

Here we propose a set of selected ideas that we have developed or are currently in progress in our laboratory of electromagnetism. There are basically studies on electromagnetic induction in conductive materials and electrodynamic systems in which the presence of magnetic forces are relevant. A few examples are discussed here:

i. The first one corresponds to the study of the damped fall of a magnet through a hollow conducting tube, in which, after a simple calculation of the induced current, we can calculate the conductivity of the tube according to its radius and wall thickness.
ii. The second is a proposal concerning with the measurement of electrical conductivity in metallic tubes based on the screening of the magnetic field inside it at low frequencies.
iii. Another is related to a study on magnetic levitation by induced ac currents in non-magnetic conductors at low frequencies allowing us to distinguish the two components of the current responsible for levitation and heating respectively.
iv. One more is related to a simple and precise method to measure the electrical conductivity in nonferromagnetic tubes rods and slabs without electric contacts. The results are readily obtained by analyzing the eddy currents in the sample when it is subjected to an harmonic magnetic field and can be obtained from a measurement of the phase of the induced voltage in a short probe coil located inside the tube or around the rod or slab when the sample is axially excited by a long primary coil.
v. Another interesting idea corresponds to the analysis of the behavior of a small-scale model of a magnetic levitation system based on the Induct rack concept. Drag and lift forces acting on our prototype moving above a continuous copper track are studied analytically following a simple low-speed approach.
vi. And finally we present a study on magnetic actuators based on rare-earth permanent magnets concerning the correct choice of the aspect ratio and volume.

RF Heating of Conducting Film/Silicon Substrate Structure: The Heat Explosion Theory Approach

M. Sinder[1], J. Pelleg[1], V. Meerovich[2], and V. Sokolovsky[2]

[1]Department of Materials Engineering, Ben Gurion University, Beer Sheva 84105, Israel
[2]Physics Department, Ben Gurion University, Beer Sheva 84105, Israel

Abstract— To achieve the required properties of conducting film/silicon substrate structures for their application in microelectronics, these structures have to be heated up to $\sim 1000°$C. Quality of the obtained structures substantially depends on the heating rate. It was recently shown that the procedure of heating by RF magnetic field can be successfully applied in technological processes of fabrication of films and layers of metals, silicides, borides or nitrides on silicon substrates. Analysis of the heating kinetics is based on the solution of Maxwell's equations coupled with nonlinear and non-stationary thermal equation taking into account the dependence of resistivity and heat capacity on the temperature.

In the present work the heating kinetics is analyzed as a function of film thicknesses, sheet resistances of the conducting layers, specimen dimensions, their thermal parameters, as well as the amplitude and frequency of applied RF magnetic field. The approximate analytical expressions for the temporal dependence of temperature were obtained. It was shown that, depending on the relation between the structure parameters and applied field, two regimes of the heating can be realized. The first one is characterized by the heating of the structure up to a finite temperature determined by equilibrium between dissipated power loss due to eddy-currents and heat transfer to environment. The second regime corresponds to fast unlimited temperature increase (heat explosion). The conditions for the heat explosion were obtained. It was shown that the explosion includes two stages: a slow increase in temperature in the first stage which can be prolonged tens of seconds and even minutes, and by high increase rate (of the order of 10^{3}°C/s) in the second stage. Just during this second stage, new phase formation in the conducting film/silicon structures is analyzed.

Session 3P1
2_FocusSession.SC2: Super Enhancement of Light with Plasmonic Nano-structures 2

Control of Field Confinement and Quality Factor in Plasmonic Nanocavities
Stefan A. Maier, Yannick Sonnefraud, ... 1092
Plasmonics for Single-molecule Photochemistry and Structure-specific Nanoscopy
Zee Hwan Kim, ... 1093
Plasmon Waveguiding in Nanowires and Nanoparticle Chains
Stephan Link, ... 1094
Active Control of THz Field Enhancements in Semiconductor Plasmonic Resonators
Jaime Gomez-Rivas, ... 1095
Quantum Emitter Coupled to a Plasmonic Nanoantenna
Dana-Codruta Marinica, Javier Aizpurua, Andrey G. Borisov, ... 1096
Super-resolution Imaging of Plasmonic Nanostructures
Katherine A. (Kallie) Willets, ... 1097
Approaching the Strong Coupling Limit in Single Plasmonic Nanoparticles Interacting with J-aggregates
G. Zengin, Goran Johansson, P. Johansson, Mikael Kall, Timur Shegai, ... 1098
Kerr Effect Enhancement in Ni Antidot Hexagonal Nanostructures
Emil Melander, Erik Ostman, Evangelos Th. Papaioannou, Vassilios Kapaklis, Bjorgvin Hjorvarsson, 1100
An Analytical Model for Rod-type Nano-sized Optical Antennas
Liang Peng, Niels Asger Mortensen, ... 1101
Electron-beam Interaction with Plasmon Fields: A New Enhanced Electron Spectral Microscopy
Ana Asenjo-Garcia, F. Javier Garcia de Abajo, ... 1102
Size-effects on Optical Properties of Asymmetric Plasmonic Nanodisk Trimer
M. Ahmadsimab, Tavakol Pakizeh, ... 1103
Plasmonic Nano-structures Enhance the Intensity of Femtosecond Light Pulses Causing Highly Localized Nano-deformations
Ventsislav K. Valev, Victor V. Moshchalkov, Thierry Verbiest, Jeremy J. Baumberg, ... 1104
Optical Raman Mapping of a Single Molecule with Sub-nm Resolution
Zhenchao Dong, ... 1106

Control of Field Confinement and Quality Factor in Plasmonic Nanocavities

Stefan A. Maier and Yannick Sonnefraud
Imperial College London, UK

Abstract— A hybrid plasmonic-photonic nanocavity combining high spatial field localization with sharp spectral linewidth is presented, based on the coupling of plasmonic resonances in metallic nanospheres with higher-order Fabry Perot modes in dielectric thin films [1]. The basic physics of this hybrid system will be discussed, together with applications in LSPR sensing and thin film metrology.

We furthermore present a technique for the assessment of plasmonic hot spots based on the observation of strain in graphene layers deposited on top of metallic nanocavities [2].

REFERENCES

1. Schmidt, M. A., D. Y. Lei, L. Wondraczek, V. Nazaal, and S. A. Maier, "Hybrid nanoparticle-microcavity-based plasmonics nanosensors with improved detection resolution and extended remote-sensing ability," *Nature Communications*, Vol. 3, 1108, 2012.
2. Heeg, S., R. Fernandez-Garcia, A. Oikonomou, F. Schedin, R. Narula, S. A. Maier, A. Vijayaraghavan, and R. Reich, "Polarized plasmonic enhancement by Au nanostructures probed through Raman scattering of suspended graphene," *Nano Letters*, Vol. 13, 301, 2013.

Plasmonics for Single-molecule Photochemistry and Structure-specific Nanoscopy

Zee Hwan Kim
Department of Chemistry, Korea University, Seoul 136-701, Korea

Abstract— I will present my research group's recent investigation on how the localized plasmons of a nanoparticle interacts with another plasmon, and with nearby molecules. The talk will cover two different yet related topics. First, I will talk about the use of gap-plasmons to locally induce photochemical reactions, and to follow chemical kinetics of individual organic molecules using the surface-enhanced Raman scattering (SERS). As a second topic, I will talk about the use of near-field coupling between a scanning probe and graphenes to visualize/identify the stacking domains (e.g., ABA versus ABC-type stacking in triple layer) hidden in multilayer graphenes.

Plasmon Waveguiding in Nanowires and Nanoparticle Chains

Stephan Link
Laboratory for Nanophotonics, Department of Chemistry
Department of Electrical and Computer Engineering, Rice University, Houston, Texas 77005, USA

Abstract— Using light to exchange information offers large bandwidths and high speeds, but the miniaturization of optical components is limited by diffraction. Converting light into electron waves in metals, i.e., surface plasmons, allows one to overcome this problem. Using a novel imaging method based on far-field fluorescence microscopy, Bleach Imaged Plasmon Propagation (BlIPP), we determined plasmon propagation distances in chemically prepared gold and silver nanowires and straight and bent chains of assembled gold and silver nanoparticles. BlIPP is based on the plasmonic near-field induced photobleaching of a dye coated over the nanostructure to report the surface plasmon propagation. For gold nanowires, we identified higher order plasmon modes as the lowest order mode is quenched by the dye molecules. For nanoparticle chains with 90 degrees turns, we found that plasmon propagation occurs around the corners with minimal losses compared to straight chains. Finally, we realized gain of surface plasmons in silver nanowires by optically pumping a dye doped polymer matrix. Electrodynamic calculations complement our experimental studies and aid in the assignment of the measured plasmon modes.

Active Control of THz Field Enhancements in Semiconductor Plasmonic Resonators

Jaime Gómez Rivas
FOM Institute for Atomic and Molecular Physics AMOLF
c/o Philips Research Eindhoven, The Netherlands

Abstract— The large field enhancement in subwavelength volumes associated to surface plasmon polaritons (SPPs) has made of plasmonic resonances an important instrument for the sensitive detection of functionalized surfaces. Most of the work on SPP sensing has focused on surface polaritons at the interface between noble metals and dielectrics at optical and near-infrared frequencies. This focus is motivated by the efficient coupling of the electromagnetic field to the surface charges at these frequencies and the enhanced confinement of the polariton field. In this presentation we will discuss how to extend the field of plasmonic sensing to lower frequencies. In particular, we show that semiconductors offer an excellent platform for far-infrared and THz plasmonics. The lower permittivity of semiconductors at these frequencies compared to metals, which is due to the much lower carrier density, leads to a pronounced plasmonic behavior that can be exploited for the development of THz semiconductor plasmonic devices. Near-field enhancements in deep subwavelength volumes associated to plasmonic resonances in semiconductors can be actively controlled in ultra-short time scales with an optical pump of carriers. "Super" fast and large THz enhancement in semiconductor plasmonic structures have the potential to improve significantly the detection limits of plasmon-based biological and chemical THz sensors.

Quantum Emitter Coupled to a Plasmonic Nanoantenna

Dana C. Marinica[1], **Javier Aizpurua**[2,3], **and Andrey G. Borisov**[1]

[1]Institut des Sciences Moléculaires d'Orsay, UMR 8214, Université Paris-Sud
Bâtiment 351, Orsay Cedex 91405, France
[2]Material Physics Center, CSIC-UPV/EHU
Paseo Manuel de Lardizabal 5 20018, Donostia-San Sebastían, Spain
[3]Donostia International Physics Center, DIPC
Paseo Manuel de Lardizabal 5 20018, Donostia-San Sebastían, Spain

Abstract— We address here the optical properties of a quantum dipole emitter coupled to a metal nanoparticle dimer. Within the linear regime, and for separation distances between the particles for which no charge transfer occurs, the optical response of the system is calculated using a quantum approach based on TDDFT. Comparison with the results obtained through a classical treatment shows a very good agreement, including in the case of the strong coupling regime. Thus established classical model is then used to see how the spectral signatures change in the case where charge transfer is possible between the dipolar emitter and the metalic nanoparticles.

Super-resolution Imaging of Plasmonic Nanostructures

Katherine A. (Kallie) Willets
Department of Chemistry, University of Texas at Austin, USA

Abstract— Noble metal nanoparticles can support localized surface plasmons, which lead to enhanced electromagnetic fields at the nanoparticle surface and allow for a host of surface-enhanced spectroscopies, such as surface-enhanced Raman scattering (SERS). While extensive theoretical calculations have predicted how these enhanced electromagnetic fields are distributed on the nanoparticle surface, experiments that reveal how the enhanced electromagnetic fields interact with molecules on the surface of nanoparticles are extremely difficult due to the diffraction limit of light. Because the metal nanoparticles are smaller than the wavelength of light, they appear as diffraction limited spots in optical images, obscuring the local electromagnetic field enhancements and the molecule-metal interactions. This talk will describe how super-resolution imaging can be used to probe enhanced electromagnetic fields in SERS as well as map the size and shape of plasmonic nanostructures.

Approaching the Strong Coupling Limit in Single Plasmonic Nanoparticles Interacting with J-aggregates

G. Zengin[1], G. Johansson[2], P. Johansson[1,3], M. Käll[1], and T. Shegai[1]

[1]Department of Applied Physics, Chalmers University of Technology, Göteborg 412 96, Sweden
[2]Department of Microtechnology and Nanoscience
Chalmers University of Technology, Göteborg 412 96, Sweden
[3]School of Science and Technology, Orebro University, Orebro 701 82, Sweden

Abstract— In this paper we present recent experimental observations of strong plasmon-exciton coupling on a single plasmonic nanoparticle level. We report Rayleigh scattering from individual silver nanorods coupled to the J-aggregate form of the cyanine dye TDBC as a function of plasmon-exciton detuning. The measured single particle spectra exhibited a strongly suppressed scattering rate at wavelength corresponding to the J-aggregate absorption band, signaling strong interaction between the localized surface plasmon of the metal core and the exciton of the surrounding molecular shell. In the context of strong coupling theory, the observed "transparency dips" correspond to an average vacuum Rabi splitting of the order of 100 meV, which approaches the plasmon dephasing rate and, thereby, the strong coupling limit for the smallest investigated particles. These findings could pave the way towards ultra-strong light-matter interaction on the nanoscale and active plasmonic devices operating at room temperature.

Introduction: Plasmonic cavities and optical antennas possess a number of superior properties, such as strong local electromagnetic field amplification and broadband room-temperature operation. On the other hand, they exhibit relatively low quality factors ($Q < 100$) and typically possess only weak nonlinearities, thereby essentially prohibiting active control. One way to overcome this limitation could be to combine plasmonic structures with quantum light sources (dyes, quantum dots, etc.) that would allow active manipulation by, for example, all-optical means.

Results: In this paper, we give one promising example of a hybrid system consisting of a silver nanorod surrounded by a thin J-aggregate shell [1]. Plasmons in the metal core are shown to strongly interact with the excitons in the organic shell of our structures. We report dark-field microscopy measurements on a single nanoparticle level, which allowed us to accurately extract plasmon decoherence rates, not broadened by inhomogeneous ensemble. We have observed more than 20 individual nanoparticles of slightly different size and plasmon resonance position. Structural characterization by SEM confirms that in every case the particles were single isolated silver nanorods. Based on a coupled dissipative oscillator model we deduce vacuum Rabi splitting of the order of 100 meV, a value that approaches the plasmon decoherence rates for the smallest

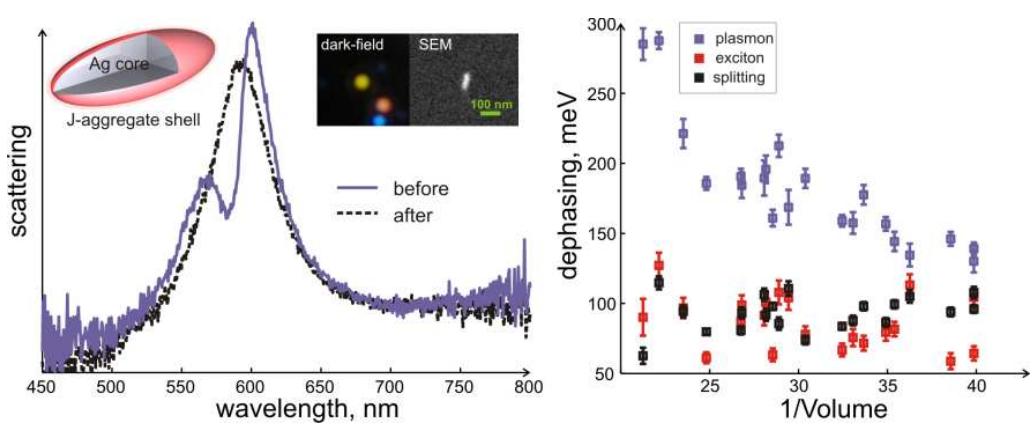

Figure 1: (a) Scattering of individual Ag nanorod surrounded with a thin shell of J-aggregate before and after illumination with a 532 nm laser. Inset shows a schematic drawing of the plasmon-exciton hybrid and experimental dark-field and SEM image of a single rod. (b) Plasmon and exciton dephasing rates as well as vacuum Rabi splitting extracted from about 20 individual rods of various sizes. The strong coupling limit, i.e., $2g > (\gamma_{pl}, \gamma_0)$, is approached for the smallest rods.

studied particles. Based on a quasi-static model we estimate the number of molecules to be of the order of 1000 per nanoparticle in our experiments, which allows us to deduce the Jaynes-Cummings coupling energy of the order of 1–1.5 meV for silver nanorods.

Conclusion: In conclusion, we have shown that a single silver nanorod covered by a thin shell of organic dye in J-aggregate form approaches the strong coupling regime at room temperature.

ACKNOWLEDGMENT

We acknowledge financial support: Swedish Research Council, Swedish Foundation for Strategic Research & GöranGustafsson Foundation.

REFERENCES

1. Zengin, G., et al., "Approaching the strong coupling limit in single plasmonic nanoparticles interacting with J-aggregates," submitted.

Kerr Effect Enhancement in Ni Antidot Hexagonal Nanostructures

Emil Melander[1], **Erik Östman**[1], **Evangelos Th. Papaioannou**[2], **Vassilios Kapaklis**[1], **and Björgvin Hjörvarsson**[1]

[1]Department of Physics and Astronomy, Division of Materials Physics, Uppsala University
Box 516, Uppsala 75120, Sweden
[2]Department of Physics, TU Kaiserslautern, Germany

Abstract— Angular resolved transverse magneto-optical Kerr effect (TMOKE) measurements provide a versatile tool for optical characterization of plasmonic nanostructures and show how plasmons couple to the applied magnetic field. These measurements show TMOKE enhancements that are closely connected to the plasmonic resonances of the nanostructures. This is seen even without noble metal layers that are traditionally used as the most important enhancing parameter.

Measurements with these methods on hexagonal arrays of circular holes in thin Ni films (Ni covered with Au [1] as well as pure Ni [2]) are presented and compared with reference Ni films. The hole sizes of the two samples are 250 nm for the Au covered Ni and 220 nm for the pure Ni, the periodicities are 470 nm for the Au covered and 450 nm for the pure Ni.

Drops in reflectivity,enhanced magneto-optical activity and transmission are reported which are closely connected with the formation of surface plasmons. One signature feature of plasmons, the drop in reflectivity followed by the Fano resonance, is shown to yield an increased magneto-optical asymmetry and therefore an increased sensitivity in the measurement even though the signal-to-noise ratio from the light source is significantly decreased. See Fig. 1 for the case of Au covered Ni and Fig. 2 for pure Ni. By comparing the two cases one can see that even though the plasmonic signal (in reflectivity) is much smaller for the pure Ni (less than 10% change in reflectivity compared to that of the Au covered Ni) the magneto-plasmonic signal is only about 20% smaller (0.048% compared to 0.06% for the Au covered Ni) which shows that magneto-optical methods have a higher sensitivity to the plasmonic states and can also be used to characterize the magneto-plasmonic properties.

With this type of patterned nanostructures, we have shown that is possible to enhance the magneto-optical activity due to the coupling to the plasmonic resonance in pure magnetic Ni (self-passivation thickness ~ 1 nm). This enables purely magnetic plasmonic structures (no noble metal required) and paves the way for circuits where the applied magnetization can be a great tool for controlling, enhancing and sensing the plasmonic effects.

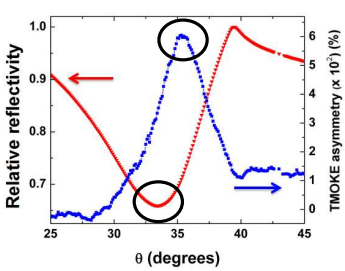

Figure 1: The normalized relative reflectivity (divided by a reference Ni thin film) as a function of incidence angle for the Au covered Ni antidot nanostructure [1]. The TMOKE asymmetry coincides well with the plasmonic resonance showing a large increase of the signal.

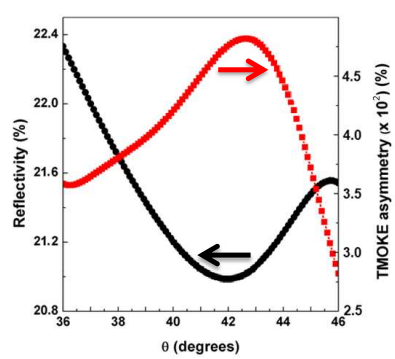

Figure 2: By using pure Ni antidot nanostructures one can obtain almost the same magneto-plasmonic enhancement as with nobl metal caps even though the optical contrast (dip in reflectivity) is very low [2].

REFERENCES

1. Papaioannou, E. Th., et al., *Opt. Express*, Vol. 19, 23867, 2011.
2. Melander, E., et al., *Appl. Phys. Lett.*, Vol. 101, 063107, 2012.

An Analytical Model for Rod-type Nano-sized Optical Antennas

Liang Peng[1] **and Niels Asger Mortensen**[2]

[1]Department of Electronic Engineering and Information Science
Hangdian University, Hangzhou, China
[2]Department of Photonics Engineering, Technical University of Denmark
Kongens Lyngby, Denmark

Abstract— We model and analysis both the resonance and radiation characteristics of rod-type nano-sized optical antennas. With a waveguide cavity model, we analytically solve the radiation problem of the rod-type nanoantennas with closed formulas for the internal and the radiated fields. We show that the radiation efficiency may be drastically improved by increasing the radius of the nanoantennas. Our theoretical work is quite general and is potentially applied to optimize the nano-sized antennas.

The schematic of the rod-type nanoantenna is shown in Figure 1. The imaginary part of the inner impedance of the nanoantenna is zero when resonance occurs, see Figure 2(a) and Figure 2(c). The near field (H-field) distributions in the lowest two resonance modes are shown in Figure 2(b) and Figure 2(d). In deriving the closed form expressions of the internal fields, the reflection at the waveguide end is reasonably considered. Combing the reflection at the waveguide end, we further show in detail that the radiation efficiency of the nanoantenna is mainly dominated by the resonance, see Figure 3. The consistence between the theoretical estimation and the simulated results directly reflects the validity of our theory, which may stimulate the optimal design of the nanoantenna system, such as to improve the emission efficiency of a single photon quantum dot.

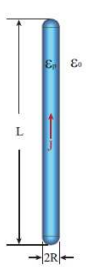

Figure 1: The schematic of nano antenna.

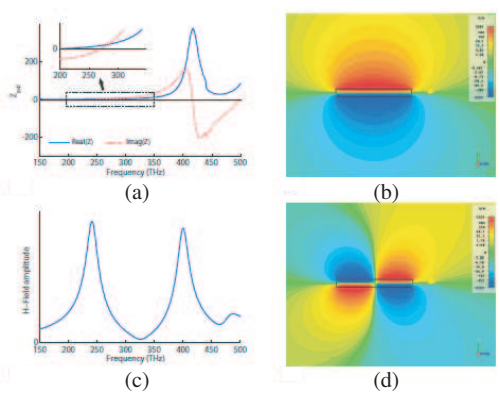

Figure 2: Resonance characteristics of nano rod antenna.

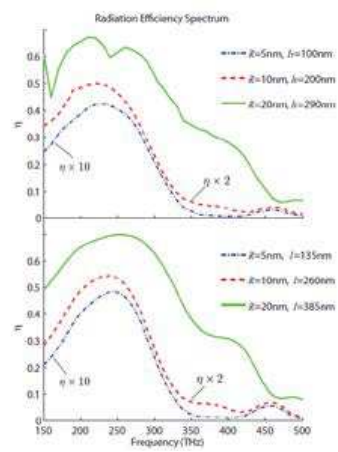

Figure 3: The radiation efficiency of nano rod antenna.

ACKNOWLEDGMENT

This work was financially supported by the Starting Program of Hangdian University (No. KYS045612004).

Electron-beam Interaction with Plasmon Fields: A New Enhanced Electron Spectral Microscopy

A. Asenjo-Garcia and F. J. García de Abajo
IQFR, CSIC, Serrano 119, Madrid 28006, Spain

Abstract— The interaction of swift electrons with strong evanescent light fields scattered by a nanostructure (e.g., by excitation of a plasmon by an external laser beam) can produce energy gains in the electrons and stimulated photon emission, which have been recently elucidated by direct solution of Schrödinger equation for the electron-light interaction in the presence of the nanostructure. In particular, it is possible to observe a complex evolution of the electron states in the sub-femtosecond regime while the electron is subject to the induced evanescent field produced by light scattering at the nanostructure. Non-Poissonian distributions of energy gains and losses can be observed in the spectra of the transmitted electron. This electron-light interaction can provide detailed information on the optical properties of the sampled nanostructures in the time and frequency domains. We study space-resolved spectroscopy in plasmon-supporting metallic structures. Taking advantage of plasmonic resonances, spectroscopy can be performed by varying the illumination frequency at low light intensities that are affordable under continuous wave illumination conditions. We predict energy, space, and time resolutions that go several others of magnitude beyond those of existing techniques.

Size-effects on Optical Properties of Asymmetric Plasmonic Nanodisk Trimer

Masoud Ahmadsimab and Tavakol Pakizeh
Faculty of Electrical and Computer Engineering, K. N. Toosi University of Technology, Tehran 16314, Iran

Abstract— We present the size and configuration effects on optical properties of an asymmetric silver (Ag) nanodisk trimer based on the dipole interaction model and numerical analysis. The nanostructure is made of three Ag nanodisks with the diameter D and thickness T, and the edge-to-edge distance of 10 nm. In the considered asymmetric trimer, the angle $\theta = 70°$ such that the distances between the two nanodisks $r_1 = r_2 = D + 10$ nm. Opposite to the symmetric Ag trimers [1, 2], the asymmetric plasmonic nanostructure exhibits three peaks in its optical extinction spectrum, seen in Fig. 1(a). Interestingly, for the trimer with $D = 100$ nm and $T = 25$ nm, this new mode occurs at about 600 nm wavelength between the two modes described for the symmetric trimer [1, 2]. Since this property is due to the plasmonic interactions of the plasmonic nanoparticles [4, 5], the configuration and the size of the nanodisks remarkably affects on this mode [3] as shown in Fig. 1(b). There, the diameter increases from $D = 60$ nm to 120 nm while the aspect ratio of the disks is kept constant ($D/T = 4$). A red shift in the resonance wavelengths because of the stronger optical interactions of the plasmonic resonances in the introduced hybridized asymmetric system is observed. Additionally, for the asymmetric trimer with smaller nanodisks ($D = 60$ nm) the lower energy modes are merged, and consequently only two distinct peaks can be seen in the optical response. This is similar to the results obtained for the symmetric Ag trimers [1, 2]. Moreover, the complex effects of symmetry breaking could no longer be described by the group theory [2]. Thus, we apply the coupled dipole approximation (CDA) method in order to describe the effects of symmetry breaking on the plasmon resonances in such asymmetric nanostructures.

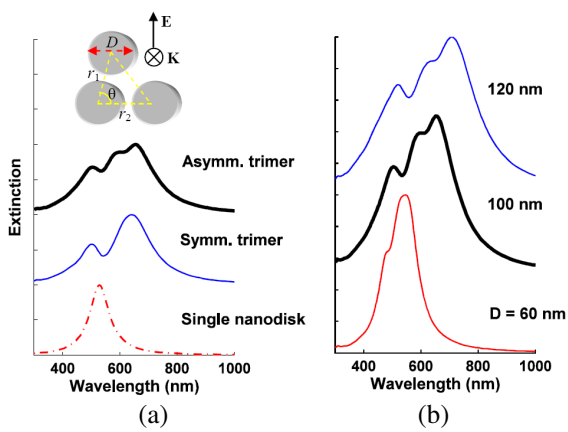

Figure 1: (a) A comparison of optical extinction spectra of the single Ag nanodisk and symmetric trimer with an asymmetric Ag trimers. (b) Optical property of an asymmetric trimer for different diameters, D.

REFERENCES

1. Alegret, J., et al., *J. Phys. Chem. C*, Vol. 112, 14313–14317, 2008.
2. Brandel, D. W., et al., *J. Phys. Chem. B*, Vol. 110, 12302–12310, 2006.
3. Kelly, K. L., et al., *J. Phys. Chem. B*, Vol. 107, 668–677, 2003.
4. Novotny, L. and B. Hecht, *Principles of Nano-optics*, Cambridge University Press, UK, 2006.
5. Fan, D. W., et al., *Nano Letters*, Vol. 10, 4680, 2010.

Plasmonic Nano-structures Enhance the Intensity of Femtosecond Light Pulses Causing Highly Localized Nano-deformations

V. K. Valev[1], V. V. Moshchalkov[2], T. Verbiest[2], and J. J. Baumberg[1]

[1]NanoPhotonics Centre, Department of Physics, University of Cambridge, UK
[2]Superconductivity and Magnetism & Pulsed Fields Group
INPAC, K.U. Leuven, Belgium

Abstract— Recently, metallic nanostructures were demonstrated to exhibit properties that could significantly impact a variety of scientific disciplines, such as medicine [1], chemistry [2] physics [3], material science and engineering [4]. In all of these examples, one of the chief properties driving potential applications is the surface plasmon resonance. Here we show that surface plasmons can be controlled to drive nanostructure buckling in highly-localised regions, enabling optical control of nanomanipulation, as well as direct mapping of the localized plasmonic states.

Surface plasmons are coherent electron oscillations that can occur in metallic nanostructures, for visible light excitation. Because in such cases surface plasmons govern the optical properties of the nanostructures at the visible wavelengths, imaging the plasmons, i.e., mapping their field enhancements in nanostructured materials is highly desirable. For instance, cathodoluminescence [5] and electron energy loss spectroscopy [6] both offer the high resolution of a scanning electron microscope, though they can only be used in vacuum. An alternative can be found in apertureless, scanning near-field scattering-type optical microscopy (s-SNOM) [7], although the interaction between the tip of the microscope in this case could constitute a significant complication.

The imaging of surface plasmons is of great importance because it provides a direct way to map and understand the local electric fields that are responsible for the unusual electromagnetic properties of metamaterials. Based on the use of ultrafast laser pulses, which allow high peak and low average laser intensities, we demonstrate a method for mapping the plasmonic nanopatterns.

We show that upon illuminating nanostructures made of gold, nickel or palladium above a certain laser fluence threshold, local melting can occur in the plasmonic hotspots but not in the rest of the nanostructures [8–10]. Consequently, the surface plasmon patterns can be imprinted on the structures themselves. More specifically, this imprinting is done through nanobump and nanojet formations, which are due to local melting and hydrodynamic processes in the regions where the plasmonic local field enhancements are the largest. In highly absorbing materials, such as nickel, the plasmonic currents bounce from the edges and can result in reinforced hotspots, whereas hotspots towards the middle of the nanostructure can be attenuated due to absorption of the plasmonic currents. These nanobumps and nanojets allow for subsequent imaging with scanning electron microscopy (SEM) or atomic force microscopy (AFM. The imprinting constitutes a fast, robust and user-friendly visualization method that can be applied to large sample area.

REFERENCES

1. Huang, X., W. Qian, I. H. El-Sayed, and M. A. El-Sayed, "The potential use of the enhanced nonlinear properties of gold nanospheres in photothermal cancer therapy," *Lasers Surg. Med.*, Vol. 39, 747, 2007.
2. Dostert, K.-H., M. Alvarez, K. Koynov, A. del Campo, H.-J. Butt, and M. Kreiter, "Near field guided chemical nanopatterning," *Langmuir*, Vol. 28, 3699–3703, 2012.
3. Pendry, J. B., "Negative Refraction," *Contemp. Phys.*, Vol. 45, 191, 2004.
4. Engheta, N., "Circuits with light at nanoscales: Optical nanocircuits inspired by metamaterials," *Science*, Vol. 317, 1698, 2007.
5. Vesseur, E. J. R., R. de Waele, M. Kuttge, and A. Polman, "Direct observation of plasmonic modes in Au nanowires using high-resolution cathodoluminescence spectroscopy," *Nano Lett.*, Vol. 7, 2843, 2007.
6. Nelayah, J., et al., "Mapping surface plasmons on a single metallic nanoparticle," *Nat. Phys.*, Vol. 3, 348–353, 2007.
7. Hillenbrand, R., F. Keilmann, P. Hanarp, D. S. Sutherland, and J. Aizpurua, "Coherent imaging of nanoscale plasmon patterns with a carbon nanotube optical probe," *Appl. Phys. Lett.*, Vol. 83, 368, 2003.

8. Valev, V. K., A. V. Silhanek, Y. Jeyaram, D. Denkova, B. De Clercq, V. Petkov, X. Zheng, V. Volskiy, W. Gillijns, G. A. E. Vandenbosch, O. A. Aktsipetrov, M. Ameloot, V. V. Moshchalkov, and T. Verbiest, "Hotspot decorations map plasmonic patterns with the resolution of scanning probe techniques," *Phys. Rev. Lett.*, Vol. 106, 226803, 2011.
9. Valev, V. K., D. Denkova, X. Zheng, A. I. Kuznetsov, C. Reinhardt, B. N. Chichkov, G. Tsutsumanova, E. J. Osley, V. Petkov, B. De Clercq, A. V. Silhanek, Y. Jeyaram, V. Volskiy, P. A. Warburton, G. A. E. Vandenbosch, S. Russev, O. A. Aktsipetrov, M. Ameloot, V. V. Moshchalkov, and T. Verbiest, "Plasmon-enhanced sub-wavelength laser ablation: Plasmonic nanojets," *Adv. Mater.*, Vol. 24, No. 10, OP29–OP35, 2012.
10. Valev, V. K., W. Libaers, U. Zywietz, X. Zheng, M. Centini, N. Pfullmann, L. O. Herrmann, C. Reinhardt, V. Volskiy, A. V. Silhanek, B. N. Chichkov, C. Sibilia, G. A. E. Vandenbosch, V. V. Moshchalkov, J. J. Baumberg, and T. Verbiest, "Nanostripe length-dependence of plasmon-induced material deformations," 2013, submitted.

Optical Raman Mapping of a Single Molecule with Sub-nm Resolution

Zhenchao Dong
Hefei National Laboratory for Physical Sciences at the Microscale
University of Science and Technology of China, Hefei 230026, China

Abstract— Visualizing individual molecules with chemical recognition is a longstanding target in catalysis, bio-science, and molecular nanotechnology. Molecular vibrations provide a valuable "fingerprint" for this identification. The vibrational spectroscopy based on tip-enhanced Raman scattering (TERS) has opened a path to obtain enhanced spectral signals thanks to the strong localized plasmonic field produced at the tip apex. The use of TERS has been pioneered by several groups in an effort to drive down the spatial resolution with chemical identification through vibrational fingerprints. However, the best spatial resolution of the TERS imaging reported to date is still limited to a few nm, obviously not adequate for resolving a single molecule chemically. Here we demonstrate unprecedented sub-molecular Raman spectral imaging with spatial resolution below 1 nm, resolving even the inner structure of a single molecule and its configuration on the surface. This is achieved via a double-resonance process by spectrally matching the resonance of the nanocavity plasmon to the molecular vibronic transitions, thanks to exquisite tuning capability provided by low-temperature ultrahigh-vacuum scanning tunneling microscopy. Our spectral-matching technique not only allows for chemical imaging at the single-molecule level, but also offers a new avenue to study nonlinear optical processes and photochemistry of a single molecule.

Session 3P2
1_FocusSession.SC1: Multi-scale & Multi-physics Computational Electromagnetics

Negative Optical Pressure in Plasmonic Cavities
Hui Liu, Che Ting Chan, Shi-Ning Zhu, ... 1108

Realization of Multidirectional Microwave Cloaks Based on Thin Dielectric Coatings
Yaroslav Urzhumov, Nathan Landy, Tom Driscoll, David R. Smith, ... 1109

The Multiple Scale Expansion Method for Nanophotonics
Didier Felbacq, Brahim Guizal, ... 1111

Surface Integral Equation Solvers in Nanophotonics
Jose Manuel Taboada, Fernando Obelleiro, D. M. Solis, Jose Luis Rodriguez, Luis Landesa, ... 1112

High Accurate Simulations to the Interaction between Electromagnetic Waves and Particles in Complicated Environment
Jianwei You, Tie Jun Cui, ... 1113

hieLPS: A Hierarchical Loop Basis Poisson Solver for Electrostatic Problems
Zu-Hui Ma, Weng Cho Chew, Lijun Jiang, ... 1114

Multiphysics and Electromagnetics
Weng Cho Chew, L. J. Jiang, Wallace C. H. Choy, Jun Z. Huang, Wei E. I. Sha, Phillip R. Atkins, Yumao Wu, Yongpin Chen, ... 1115

Model Order Reduction Methods for Efficient Quantum Transport Simulation of Nanoelectronic Devices
Jun Z. Huang, Weng Cho Chew, Jie Peng, Chi-Yung Yam, Lijun Jiang, Guan-Hua Chen, ... 1116

Nonlinear and Quantum Optics with the Spectral Element Method
Ma Luo, Qing Huo Liu, ... 1117

High Efficiency Polymer Solar Cells Achieved by Using Plasmonic Electrically Functionalized Electron Transport Layer
Wallace C. H. Choy, ... 1118

Grounding Grid Safety Evaluation under Lightning Current
Farhan Hanaffi, Wah Hoon Siew, Igor Timoshkin, ... 1119

Negative Optical Pressure in Plasmonic Cavities

H. Liu[1], **C. T. Chan**[2], **and S. N. Zhu**[1]

[1]National Laboratory of Solid State Microstructures, Department of Physics
Nanjing University, Nanjing 210093, China
[2]Department of Physics, Nano Science and Technology Program
Hong Kong University of Science and Technology, Clearwater Bay, Hong Kong, China

Abstract— It is well known that metamaterials are composed from many artificial plasmonic cavities, and such plasmonic resonance can be realized in the visible or infrared frequency range. In this work [1], we designed a plasmonic cavity comprising a patch and a slab (see Fig. 1). A strong plasmon resonance mode could be excited in this structure (see Fig. 2). At the resonance, the kinetic energy of conduction electrons is found to induce a strong negative optical pressure (see Fig. 3). A Lagrangian model is proposed to describe the salient features. The mechanism and theoretical model reported in this paper could have potential applications in many other subwavelength optomechanical plasmonic structures, such as selective optical trapping [2], parallel-plate metallic cavity [3], and metallic FP cavities [4].

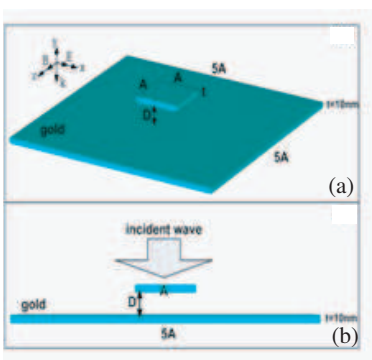

Figure 1: Schematic of nanocavity with two gold patches.

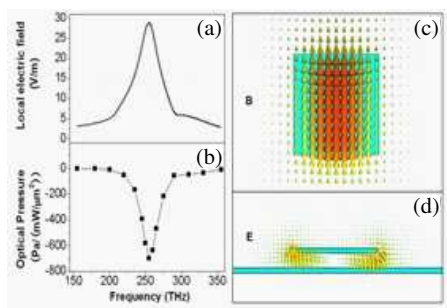

Figure 2: The frequency dependence of (a) local electric field between two patches and (b) optical pressure between two patches (with $A = 200\,\mathrm{mm}$, $D = 30\,\mathrm{nm}$); (c) Magnetic field (on y-cut middle layer) and electric field (on z-cut middle layer) at the resonance frequency.

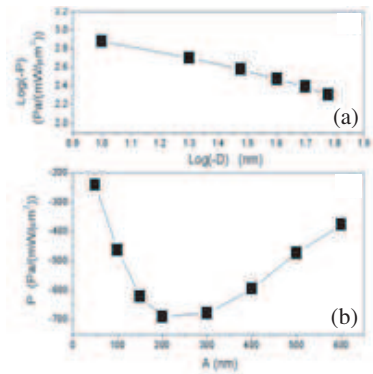

Figure 3: (a) The log-log relationship between optical pressure P and distance D (with $A = 600\,\mathrm{nm}$); (b) the dependence of optical pressure P on the size parameter A (with $D = 30\,\mathrm{nm}$).

REFERENCES

1. Liu, H., N. G. Jack, S. B. Wang, Z. F. Lin, Z. H. Hang, C. T. Chan, and S. N. Zhu, "Strong light-induced negative optical pressure arising from the kinetic energy of conduction electrons in plasmonic cavities," *Phys. Rev. Lett.*, 2011, accepted.
2. Zheng, J., H. Liu, S. M. Wang, T. Li, J. X. Cao, L. Li, C. Zhu, Y. Wang, S. N. Zhu, and X. Zhang, "Selective optical trapping based on strong plasmonic coupling between gold nanorods and slab," *Appl. Phys. Lett.*, Vol. 98, 083117, 2011.
3. Wang, S. B., N. G. Jack, H. Liu, H. Zheng, Z. H. Hang, and C. T. Chan, "Sizable electromagnetic forces in parallel-plate metallic cavity," *Phys. Rev. B*, Vol. 84, 075114, 2011.
4. Huang, C. P., S. B. Wang, X. G. Yin, Y. Zhang, H. Liu, Y. Y. Zhu, and C. T. Chan, "Enhanced electromagnetic pressure in a sandwiched reflection grating," *Phys. Rev. B*, Vol. 86, 085446, 2012.

Realization of Multidirectional Microwave Cloaks Based on Thin Dielectric Coatings

Yaroslav A. Urzhumov, **Nathan Landy**, **Tom Driscoll**, **and David R. Smith**
Center for Metamaterials and Integrated Plasmonics, Duke University
130 Hudson Hall, Box 90271 Durham, North Carolina 27708, USA

Abstract— In this presentation, we report theoretical development, stereolithographic fabrication and experimental testing of a multidirectional invisibility device operating in a sub-band (9.7–10.1 GHz) of the microwave X-band, for in-plane propagating TE-polarized waves. The device consists of a relatively thin (approximately one free-space wavelength) annulus filled with a binary dielectric composite (ABS/air). The dielectric component has negligible loss in the X-band and the dielectric constant of $\varepsilon = 2.45 \pm 0.01$.

Design methodology The binary composites are designed using topology optimization — a method that allows exploration of arbitrary topologies of the voids in a matrix of another material. The resulting shapes can be rather complicated, and structural integrity of the solid matrix is not guaranteed. We have experimented with a variety of initial guesses for the iterative optimization algorithm based on SNOPT and adjoint sensitivity method, as implemented in COMSOL, and determined that initial guesses with a sufficiently low concentration of voids typically lead to optimized solutions with a single, contiguous dielectric matrix. This topological class of shapes is easily amenable to fabrication without additional steps. The optimization goal is to minimize the scattered field norm averaged over a closed surface surrounding the structure consisting of a PEC cylinder and the "cloaking" dielectric shell. We have obtained a number of solutions in which the total scattering is reduced to less than 10^{-3} of the scattering from a bare PEC cylinder.

Fabrication To fabricate shape-and-topology optimized dielectric composites, we use a polymer-based stereo-lithographic technique known as Fused Deposition Modeling (FDM). This technique is used in commercially available 3D Printer Pack of Stratasys Inc. The dielectric component is the ABS, a hard plastic with negligible dielectric loss in the microwave X-band. FDM is a layer-by-layer method, with a minimum feature size of about 0.9 mm.

Material characterization To ensure accurate design of the cloak, we performed in-house characterization of ABSplus material supplied by Stratasys. This was accomplished by loading a rectangular waveguide (WR-90 standard) with a 120 mm length of plastic and measuring the phase delay in transmission in the entire X-band (8–12 GHz). The best fit is obtained with a lossless dielectric constant, $\varepsilon = 2.45 \pm 0.01$.

Testing While the invisibility device is designed to conceal an infinitely long PEC cylinder, our test is conducted in a 2D mapping chamber — a parallel-plate waveguide surrounded by microwave absorbers, which supports a free-space-like TEM mode propagation in the 8–12 GHz band, where it mimics free space. The cloaking de-vice was reduced to a slice that nearly fits the vertical space of the 2D mapper. The PEC cylinder was mimicked by a sufficiently thick copper foil annulus filled with an absorber. The remaining gap between the cloak slice and the moving plate of the 2D mapper was accounted for at the design stage by using an effective dielectric constant given by $\epsilon_{eff} = ((1-f)\epsilon_{\mathrm{ABS}}^{-1} + f)^{-1}$, where f is the filling fraction of air. The maps of electric field obtained in this fashion are in good agreement with full-wave simulations.

Conclusions Theoretically, we found that shape-and-topology optimization produces unidirectional and multi-directional invisibility devices based on binary dielectric composites (ABS + air) for a variety of shapes and thicknesses of the composite shell. The cloaking shell can be as thin as one free-space wavelength, regardless of the size of the concealed object. The concealed object can be 10–20 wavelengths in diameter, in which case the cloaking payload can be in the range of 80–90%. It seems likely that for larger objects, even higher payload ratios can be obtained. For the experimentally tested sample, the bandwidth of "transparency window" was about 4% (0.4 GHz at 10 GHz). This type of device is inexpensive to fabricate, easily to deploy, and it should find its applications in wireless communications, where it could assist communications in obstruction-crowded environments.

REFERENCES

1. Urzhumov, Y. A. and D. R. Smith, "Low-loss directional cloaks without superluminal velocity or magnetic response," *Opt. Lett.*, Vol. 37, 4471, 2012.

2. Landy, N. and D. R. Smith, "A full-parameter unidirectional metamaterial cloak for microwaves," *Nature Mat.*, Vol. 12, 25, 2013.

The Multiple Scale Expansion Method for Nanophotonics

D. Felbacq[1,2] and B. Guizal[1]

[1]Laboratory Charles Coulomb, University of Montpellier 2, France
[2]Institut Universitaire de France, France

Abstract— The multiple scale expansion is a powerful theoretical tool for analyzing the behavior of periodic structures possessing several different scales. It can be used for quantum and classical waves, whether acoustic or electromagnetic. Basically, the method requires to identify a small parameter describing the rapid oscillations of the system considered. Then an expansion of the field (electromagnetic, thermal, acoustical, quantal) in power of this small parameter is assumed. It furnishes a very convenient way of deriving the effective equation at the different orders of the expansion. It can be used for scalar equations such as the Helmholtz equation or the heat equation, or for vectorial equations such as the Maxwell system. In this work, we will deal with both scalar equations (for polarized light) as well as the full Maxwell system. The multiple scale expansion works in its basic form for parameters (e.g., permittivity or permeability) that do not take extreme values. We will develop an extension of the theory which is able to deal with strongly resonant structures such as that arising in the field of metamaterials. We shall demonstrate the usefulness of this tool by deriving the effective behavior of resonant photonic structures made of collections of rods or spheres. These basic objects can store light under the guise of open cavity modes and this induces very specific effective constitutive relations when they are organise into a periodic lattice. It will be also shown that these objects admit homogenization above the first band, i.e., above the so-called quasi-static regime.

Surface Integral Equation Solvers in Nanophotonics

J. M. Taboada[1], **F. Obelleiro**[2], **D. M. Solís**[2], **J. L. Rodríguez**[2], **and L. Landesa**[1]

[1]Departamento Tecnología de los Computadores y Comunicaciones
University of Extremadura, Spain
[2]Departamento Teoría do Sinal e Comunicacións, University of Vigo, Spain

Abstract— Surface-integral-equation (SIE) techniques based on the method of moments (MoM) [1–3] help us to obtain accurate solutions in different problems in computational electromagnetics. Especially, rigorous Maxwell integral equation solvers are extended to new demanded areas in the context of nanoscience and nanotechnology [4–6]. The research in the optical plasmonic properties of metallic nanoparticles and artificial materials (metamaterials) has generated an growing interest, due to their ability to route and manipulate light at nanometer length scale surpassing the classical diffraction limit. The optical response of metals is quite different from the metallic conductivity observed at low frequencies. In optics, the penetration of fields cannot be neglected, and the plasmonic response of metals makes it impossible to directly downscale the radio-frequency and microwave solutions to the optical regime. Otherwise, by properly engineering the underlying subunits, metamaterials can exhibit exotic optical properties that are not attainable in naturally occurring materials, such as prominent magnetic response or negative index of refraction. The range of applications of plasmonics and metamaterials is wide, covering many different disciplines such as biomedical sensing, information and communications technologies, enhanced solar cells and lighting, compact inter/intra-chip optical interconnects, disease diagnosis and treatment, among many other applications.

Otherwise, SIE-MoM approach yield very efficient and highly accurate representations of these new electromagnetic problems, taking into account all the physical constraints as determined by the shape and the complex dielectric constants of the particles. It only needs to model the material boundary surfaces and interfaces, thus greatly reducing the number of unknowns. Besides, the latest breakthroughs in integral-equation algorithmic like MLFMA-FFT [3, 7] can be applied to enable the solution of large-scale problems with high numbers of unknowns. To assess the validity of the proposed formulation in optics, several results will be shown, including the complete design of an optical wireless nanolink for inter/intra-chip communications using specifically designed directive nanoantennas and impedance matching elements [8].

REFERENCES

1. Song, J., C. Lu, and W. C. Chew, "Multilevel fast multipole algorithm for electromagnetic scattering by large complex objects," *IEEE Trans. Antennas Propagat.*, Vol. 45, 1488–1493, Oct. 1997.
2. Taboada, J. M., M. G. Araujo, J. M. Bertolo, L. Landesa, F. Obelleiro, and J. L. Rodriguez, "MLFMA-FFT parallel algorithm for the solution of large-scale problems in electromagnetic," *Progress In Electromagnetics Research*, Vol. 105, 15–30, 2010.
3. Taboada, J. M., M. G. Araújo, F. Obelleiro, J. L. Rodríguez, and L. Landesa, "MLFMA-FFT parallel algorithm for the solution of extremely large problems in electromagnetics," *Proceedings of the IEEE*, Vol. 101, No. 2, 350–363, Feb. 2013.
4. Rivero, J., J. M. Taboada, L. Landesa, F. Obelleiro, and I. García-Tunon, "Surface integral equation formulation for the analysis of left-handed metamaterials," *Opt. Express*, Vol. 18, 15876–15886, 2010.
5. Taboada, J. M., J. Rivero, F. Obelleiro, M. G. Araujo, and L. Landesa, "Method of moments formulation for the analysis of plasmonic nanooptical antennas," *J. Opt. Soc. Am. A*, Vol. 28, No. 7, Jul. 2011.
6. Araújo, M. G., J. M. Taboada, D. M. Solís, J. Rivero, L. Landesa, and F. Obelleiro, "Comparison of surface integral equation formulations for electromagnetic analysis of plasmonic nanoscatterers," *Opt. Express*, Vol. 20, No. 8, 9161–9171, 2012.
7. Araújo, M. G., D. M. Solís, J. Rivero, J. M. Taboada, and F. Obelleiro, "Solution of large-scale plasmonic problems with the multilevel fast multipole algorithm," *Optics Letters*, Vol. 37, No. 3, 416–418, 2012.
8. Solis, D. M., J. M. Taboada, F. Obelleiro, and L. Landesa, "Optimization of an optical wireless nanolink using directive nanoantennas," *Opt. Express*, Vol. 21, No. 2, 2369–2377, 2013.

High Accurate Simulations to the Interaction between Electromagnetic Waves and Particles in Complicated Environment

Jianwei You and Tiejun Cui
School of Information Science and Engineering, Southeast University, Nanjing 210096, China

Abstract— The interactions between the plasma particles and the electromagnetic field can be described by Maxwell's equations and the Newton-Lorentz's equations. However, it is almost impossible to solve such complicated interactions using traditionally analytical methods. With the development of the high performance computer, some numerical approaches have been investigated in the plasma simulations. In such approaches, the hybrid method of Finite Difference Time Domain (FDTD) with Particle-In-Cell (PIC) method has been widely used. In the past decades, some perfect works have been reported to develop the FDTD-PIC method. The parallel techniques have been applied to increase the simulation scale and accelerate its computational efficiency. Some electron emission theories and better collision models have been proposed to broaden its applications in discharge vacuum tubes, high-power microwave sources, plasma accelerators, and plasma stealth, etc..

However, there has been a little work to eliminate the staircase error of the traditional FDTD-PIC method. Actually, the staircase error is a big challenge not only in the FDTD method but also in the PIC simulation. And it is particularly serious when the geometric models are curved objects. In order to overcome the staircase errors in the traditional plasma simulation methods, we have first proposed a conformal hybrid algorithm of Time-Domain Finite-Integration Theorem with Particle-in-Cell method (TDFIT-PIC). In order to implement the conformal TDFIT-PIC hybrid method, we have given a fast and efficient extraction technique for TDFIT's conformal information, and proposed a new extraction technique of the conformal sections for PIC method. These extraction techniques are named as the extraction of conformal information (ECI) technique by us. Based on our fast and efficient ECI technique, the naturally conformal superiority of the TDFIT method can be utilized to successfully overcome the staircase error in electromagnetic simulation. On the other hand, due to the implementation of the conformal PIC method, the geometric information of the curved boundary can be more accurately approximated. Thus, the collision error of the traditional PIC simulation can be great restrained. In many complicated real-world applications, the accuracy and robust of our conformal method have been validated.

hieLPS: A Hierarchical Loop Basis Poisson Solver for Electrostatic Problems

Zu-Hui Ma[1, 2], **Weng Cho Chew**[2], **and Li Jun Jiang**[1]

[1]Department of Electrical and Electronic Engineering
The University of Hong Kong, Hong Kong, China
[2]Department of Electrical and Computer Engineering
University of Illinois at Urbana-Champaign, Urbana, IL 61801, USA

Abstract— Numerical solutions of Poisson's equation are of great importance in various scientific and engineering problems, especially for electrostatic problems. Recently, a novel Poisson solver, which based on quasi-Helmholtz decomposition of field and loop-tree bases technique, has been proposed to solve 2D electrostatic problems. This method provides a new alternative to solve Poisson's equation faster than traditional Finite Element Method (FEM). However, the solution time would increase dramatically when higher accuracy is required.

In this paper, we will present a new multilevel method for solving Poisson's equation by using hierarchical loop bases. We term this new method as hierarchical Loop basis Poisson Solver (hieLPS). It extends previous Poisson solver through loop-tree basis to a multilevel mesh. The basic idea of this new method is to solve Poisson's equation by a two-step procedure: At the first stage, the electric flux is expressed as a summation of tree-space part and loop-space part; We find the tree-space part by a fast tree solver and then solve the loop-space part through a iterative process. Second, the potential distribution is solved rapidly with a fast solution of $O(N)$ complexity. Since finding the loop part of electric flux is the most critical part and dominates the computational time, we use hierarchical loop bases to construct a multilevel system. It speeds up the iteration procedure and then reduces the whole solution time remarkably. Numerical experiments show that a linear computational complexity has been achieved. Because this method is independent of any uniformity restriction on the applied meshes, it is simpler and is an alternative of multilevel multigrid method.

Multiphysics and Electromagnetics

W. C. Chew[1], **L. J. Jiang**[2], **W. C. H. Choy**[2], **J. Z. Huang**[2], **W. E. I. Sha**[2], **P. R. Atkins**[1], **Y. M. Wu**[1], **and Y. P. Chen**[3]

[1]University of Illinois, Urbana, Champaign, USA
[2]University of of Hong Kong, China
[3]University of Electronic Science and Technology, China

Abstract— We will discuss possibilities for multiphysics research related to electromagnetics (EM). Inherently, classically EM entails the tale of three physics: when the frequency is low, circuit physics rules. At mid frequency, wave physics prevails, while at high frequency, ray physics reigns.

At low frequency, Kirchhoff current law (KCL) and Kirchhoff voltage law (KVL) can be used to study many complicated topologies for circuits. Many devices are described by lumped elements and their V-I relations. Even though the full bounty of Maxwell's theory is not apparent, it is actually embedded in circuit physics.

At mid frequency, E and H field couple with each other through space yielding wave phenomena allowing the communication of signals through vast distances such as the galaxy. It is also at this frequency that information can be encoded in the wave and be teleported through vast distances. Interferometric physics becomes important and are used in imaging and beam-forming and many other devices.

At high frequency, EM wave behaves like particles: The wave travels in straight rays, reflects, and refracts like particles. Ray physics or ray optics can be used for many technology developments.

The advances in fabrication technologies enable the making of sub-optical wavelength structures giving rise to the field of nano-optics. Due to the difference in material properties at optical frequencies, many interesting phenomena, previously not occurring in microwave, emerge in nano-optics. In particular, nano-plasmonics, nano-antenna, nano-array are hotly studied areas.

The advent of modern physics brings in quantum physics opening the realm of quantum optics and quantum information. For instance, the study of photon traps, spontaneous emission, Purcell effect, Casimir force all involve quantum optics concepts. The former three can be used to enhance the performance of solar cells, LED, photo detectors, while the latter is important for N/MEMS technology.

In nano-electronic transport, Poisson-Boltmann equation or its likes are indispensable. Hence, expeditious methods to perform the co-simulation of Schrodinger equation and Poisson's equation are important in device simulation. This can be done via the effective mass Schrodinger model, the k.p method, tight-binding method, or the DFT method via the use of the non-equilibrium Green's function method.

We will review these connections in this presentation.

Model Order Reduction Methods for Efficient Quantum Transport Simulation of Nanoelectronic Devices

Jun Z. Huang[1,2], **Weng Cho Chew**[1,2], **Jie Peng**[3], **Chi-Yung Yam**[3], **Li Jun Jiang**[1], **and Guan-Hua Chen**[3]

[1]Department of Electrical and Electronic Engineering
The University of Hong Kong, Hong Kong, China
[2]Department of Electrical and Computer Engineering
University of Illinois at Urbana-Champaign, Urbana, IL 61801, USA
[3]Department of Chemistry, The University of Hong Kong, Hong Kong, China

Abstract— With the advances of nano-technologies, the feature size of nanoelectric devices has been shrunk to electron wavelength size, a regime where wave physics becomes increasingly important. In addition, there are many emerging devices that are purely built upon quantum mechanical effects, such as the band-to-band tunneling field-effect transistors (FETs). To understand and predict the electrical behaviors of these small devices therefore require full quantum models. However, these models usually require solving the wave function or the Green's function of the whole device region with open boundary conditions, which are computationally very challenging. To accelerate the simulation, we have applied several model order reduction (MOR) techniques that are widely used in computational electromagnetics (CEM).

First, asymptotic waveform evaluation (AWE) combined with complex frequency hopping (CFH) algorithm is successfully adopted to characterize electron conduction over a wide energy range. This technique is particularly useful to analyze the transmission spectrum and the local density of states. N-type silicon nanowire FETs with ionized impurity and surface roughness scattering are shown as examples. Second, to simulate hole conduction in nanowire structures, we project the multi-band k.p Hamiltonian into a much smaller subspace constructed by sampling the Bloch modes of each cross-section layer. Together with fast algorithms for solving the eigenmodes, we can simulate large cross-section p-type silicon nanowire FETs as well as III-V ones. A novel device, junctionless transistor, is then studied and compared to the classical inversion-mode transistor. Third, by making use of the crystal structures and the short-range interactions of tight binding schemes, we can condense the Hamiltonian matrix of the periodic leads and thus speed up the open boundary treatment in atomistic simulations.

Nonlinear and Quantum Optics with the Spectral Element Method

Ma Luo and Qing Huo Liu
Department of Electrical and Computer Engineering
Duke University, Durham, North Carolina 27708, USA

Abstract— Nonlinear optics and quantum optics have many emerging applications, for example, in second harmonic generation (SHG) and nano-lasers. However, rigorous numerical computation for nonlinear and quantum optics is challenging with the traditional finite difference and finite element methods because of their large numerical dispersion errors. In this work, we propose to apply the spectral element method, a highly accurate high-order method, to simulate nonlinear and quantum optics in both frequency and time domains.

In the frequency domain, we use the SEM for the simulation of nonlinear optical effects and the associated second harmonic generation (SHG). Because nonlinear optical coefficients are usually small for most materials, the SHG effect is weak in general. Moreover, as optical materials are usually dispersive, there is a phase mismatch between the fundamental frequency and second harmonic fields, further weakening the SHG effect. Various design methods have been proposed to enhance the SHG effect, including the use of anisotropic crystal optical materials, some semiconductor materials with relatively large nonlinear optical coefficients, periodic structures to modify the dispersion relation, and microcavity resonant modes to increase the density of states. Here by using the SEM we design an air-bridge multiple layer photonic crystal slab based on the structure of GaAs/AlAs distributed Bragg reflector. We show that the SHG can be enhanced by ten orders of magnitude.

In the time domain, we model a nano-laser by directly solving the coupled Maxwell-Bloch equations using the spectral element time domain (SETD) method. Currently, many investigations on nano-laser divide the simulation of electromagnetic field and gain medium into two steps: (a) A linear optics electromagnetic field simulation tool (such as finite difference time domain method) is used to simulate the nano-cavity, which gives the Q factor, mode volume and mode pattern of the nano-cavity. (b) These parameters are input into the rate equations of the laser modeling to study the properties of the laser; the coupling between the gain medium and the optical mode (for example the frequency pulling effect) is modeled by a perturbation method. This scheme gives reasonable results for a large-size laser; however, when the size of the laser is smaller and the coupling becomes stronger, such a perturbation method is inadequate, and a simulation tool based on the first principle of the lasing is necessary. Here we apply the SETD method as the first principle to solve the coupled Maxwell-Bloch equations. Numerical results show the efficacy of the SETD method and its applications.

High Efficiency Polymer Solar Cells Achieved by Using Plasmonic Electrically Functionalized Electron Transport Layer

Wallace C. H. Choy
Department of Electrical and Electronic Engineering
The University of Hong Kong, Pokfulam Road, Hong Kong, China

Abstract— Optical effects of the plasmonic structures and the materials effects of the metal nanomaterials have recently been individually studied for enhancing performance of polymer solar cells (PSCs). In this work, differently, the effects of plasmonically induced carrier generation and enhanced carrier extraction of the carrier transport layer (i.e., plasmonic-electrical effects) in PSCs are investigated. We propose and demonstrate enhanced charge extraction in TiO_2 as a highly efficient electron transport layer by the incorporation of metal nanoparticles (NPs). While PSCs using pristine TiO_2 can only operate by UV activation (< 400 nm, otherwise poor S-shape J-V characteristics are exhibited), efficient device performance is demonstrated by using Au NPs incorporated TiO_2, at a plasmonic wavelength (560–600 nm) far longer than the originally necessary UV light. By optimizing the concentration ratio of the Au NPs in the NP-TiO_2 composite, the performances of PSCs with various polymer active layers are enhanced and efficiency of 8.74% is reached. In order to understand the fundamental physics, an integrated optical and electrical model (i.e., a multiphysics model), which takes into account plasmonic-induced hot carrier tunneling probability and extraction barrier between TiO_2 and the active layer, is introduced here. From experimental and theoretical studies, we attribute the enhanced charge extraction under plasmonic illumination to the strong charge injection of plasmonically excited electrons from NPs into TiO_2. The mechanism favors trap filling in TiO_2 which can lower the effective energy barrier and facilitate carrier transport in PSCs. The work can contribute to new approaches and knowledge to utilize plasmonically electrical nanostructures in organic optoelectronic devices for enhancing device performance.

Grounding Grid Safety Evaluation under Lightning Current

Farhan Hanaffi[1,2], **Wah Hoon Siew**[1], **and Igor Timoshkin**[1]

[1]University of Strathclyde, UK
[2]Universiti Teknikal Malaysia Melaka, Malaysia

Abstract— Every day, demand to electrical supply keep increase make more challenging to provide high efficiency system to ensure constant power can be delivered to customers. Consequently, a lot of new substation technology and design are developed which required more safety grounding design. Lightning is one of the natural phenomena that can inject huge current through the system by direct strike or indirect strike. In lightning protection system, grounding is a main element to provide low impedance path for unwanted current through the soil. In substation grounding design, touch voltage and step voltage are two main parameters to consider, there are very important to keep the parameters as low as possible to increase level of safety. Although the grounding response and safety limit are quite different under lightning condition, most of standards still base on power frequency safety hazard. There are no guidelines that consider fast transient response in grounding design. It challenges to get best protection for human and equipment under lightning condition. In this paper finite element method (FEM) is used to solved full Maxwell equation in order to model and analysis grounding grid behaviour under lightning current. The simulations are done in 3D using Comsol Multiphysic package. Results of this paper are compared with previous experiment data for validity. The purpose of this paper to analysis ground potential rise due to lightning current and evaluate safety limit on human base on energy limit of 50J as proposed by Dalziel [1].

REFERENCES

1. Dalziel, C. F., "A study of the hazards of impulse currents," *Power Apparatus and Systems, Part III. Transactions of the American Institute of Electrical Engineers*, Vol. 72, 1032–1043, 1953.

Session 3P3a
3_FocusSession.SC3: Super-resolution in Bio-imaging and Sensing

Template-stripped Metallic Pyramids for Reproducible Near-field Optical Microscopy
Sang-Hyun Oh, ... 1122
STED Nanoscopy Combined with Optical Tweezers Reveals Protein Dynamics on Densely Covered DNA
Iddo Heller, Gerrit Sitters, Onno D. Broekmans, Stefan W. Hell, Erwin J. G. Peterman, Gijs J. L. Wuite, ... 1123
Nanoscopy with Focused Light
Stefan W. Hell, ... 1124
Imaging Biological Processes with Quantitative High Spatiotemporal Resolution Microscopy
Melike Lakadamyali, ... 1125
Dissecting Plasma Membrane Organization with STED(-FCS) Fluorescence Microscopy
Christian Eggeling, ... 1126
Diffraction-unlimited Optical Lithography in Three Dimensions
Joachim Fischer, Martin Wegener, ... 1127
Characterization of Spatial Organization of Proteins in Metastasizing Cells and in Platelets — Openings for Future Diagnostic Applications
Jerker Widengren, ... 1128
Single Cell Analysis by Super-resolution Barcoding
Eric Lubeck, Long Cai, ... 1129

Template-stripped Metallic Pyramids for Reproducible Near-field Optical Microscopy

Sang-Hyun Oh
Department of Electrical and Computer Engineering, University of Minnesota
Minneapolis, MN 55455, USA

Abstract— Nanofabricated metallic tips are at the core of important research in single-molecule spectroscopy, near-field scanning optical microscopy (NSOM), tip-enhanced Raman spectroscopy (TERS), as well as potential applications such as heat-assisted magnetic recording (HAMR). While challenging to fabricate, much progress has been made towards the reliable production of sharp metallic probes. We will discuss the various factors that go into the design of metallic tips, high-throughput fabrication, and packaging issues. In particular, we will focus on template-stripping nanofabrication techniques that enable mass-production of ultrasmooth and sharp (10 nm) Au and Ag pyramids for reproducible near-field optical microscopy.

STED Nanoscopy Combined with Optical Tweezers Reveals Protein Dynamics on Densely Covered DNA

Iddo Heller[1,2], **Gerrit Sitters**[1,2], **Onno D. Broekmans**[1,2], **Stefan W. Hell**[3], **Erwin J. G. Peterman**[1,2], **and Gijs J. L. Wuite**[1,2]

[1]Department of Physics and Astronomy
VU University Amsterdam, Amsterdam, The Netherlands
[2]LaserLaB Amsterdam, VU University Amsterdam, Amsterdam, The Netherlands
[3]Department of NanoBiophotonics
Max Planck Institute for Biophysical Chemistry, Göttingen, Germany

Abstract— Dense coverage of DNA by proteins is a ubiquitous feature of cellular processes such as DNA organization, replication, and repair. We present a single-molecule approach capable of visualizing individual DNA-binding proteins on densely covered DNA and in presence of high protein concentrations. Our approach combines optical tweezers with multicolor confocal and STED fluorescence microscopy. Proteins on DNA are visualized at a resolution of 50 nm, a 6-fold resolution improvement over confocal microscopy. High temporal resolution (< 50 ms) is ensured by fast one-dimensional beam scanning. Individual trajectories of proteins translocating on DNA can thus be distinguished and tracked with enhanced precision. We demonstrate our multimodal approach by visualizing the assembly of dense nucleoprotein filaments with unprecedented spatial resolution in real time. Experimental access to the force-dependent kinetics and motility of DNA-associating proteins at biologically relevant protein densities is essential for linking idealized *in vitro* experiments with the *in vivo* situation.

Nanoscopy with Focused Light

Stefan W. Hell
Max Planck Institute for Biophysical Chemistry, Göttingen, Germany

Abstract— Throughout the 20th century it has been widely accepted that, at the end of the day, a light microscope relying on conventional lenses (far-field optics) cannot discern details that are finer than about half the wavelength of light ($> 200\,\mathrm{nm}$). However, in the 1990s, it was discovered that overcoming the diffraction barrier is viable and that fluorescent samples can be resolved virtually down to molecular dimensions. Here we discuss the simple yet powerful principles that allow us to neutralize the resolution-limiting role of diffraction. In a nutshell, features residing closer than the diffraction barrier are prepared in different molecular (quantum) states so that they are distinguishable for a brief detection period. As a result, the resolution-limiting role of diffraction is overcome, and the interior of transparent samples, such as living cells and tissues can now be imaged non-invasively at the nanoscale using focused visible light. Finally, we demonstrate the relevance of emerging 'far-field optical nanoscopy' to various areas, especially to the life and the material sciences.

REFERENCES

1. Hell, S. W., "Far-field optical nanoscopy," *Science*, Vol. 316, 1153–1158, 2007.
2. Hell, S. W., "Far-field optical nanoscopy," *Single Molecule Spectroscopy in Chemistry*, A. Grälund, R. Rigler, J. Widengren, Eds., 365–398, Springer, Berlin, 2009.

Imaging Biological Processes with Quantitative High Spatiotemporal Resolution Microscopy

Melike Lakadamyali
ICFO — Institut de Ciències Fotòniques
Av. Carl Friedrich Gauss, 3, Castelldefels, Barcelona 08860, Spain

Abstract— In the past decade the diffraction limit of resolution in far field fluorescence microcopy has been surpassed. Revolutionary techniques have been developed that provide nanoscale resolution in fluorescence images of biological samples. In this talk, I will review the "localization based" super-resolution microscopy techniques, such as Stochastic Optical Reconstruction Microscopy (STORM), in terms of the technical advances since their first development. I will specifically emphasize the biological applications of these techniques and highlight the wealth of novel information that can now be obtained at an unprecedented level of detail.

Dissecting Plasma Membrane Organization with STED(-FCS) Fluorescence Microscopy

Christian Eggeling[1, 2]

[1]MRC Human Immunology Unit, Weatherall Institute of Molecular Medicine, University of Oxford, UK
[2]Department of NanoBiophotonics, Max Planck Institute for Biophysical Chemistry, Göttingen, Germany

Abstract— Stimulated Emission Depletion (STED) far-field microscopy allows the study of living cells with nanoscale resolution, otherwise impeded by the limited spatial resolution of conventional microscopes [1]. Besides the recording of images, the combination of STED with single-molecule sensitive spectroscopic tools such as Fluorescence Correlation Spectroscopy (FCS) discloses complex dynamical processes hidden to the conventional observations [2–4]. For example, STED-FCS offers novel insights into important cellular processes, such as lipid-lipid and lipid-protein interactions in the plasma membrane of living cells, and their role in cellular functionality [4–9]. Improved insights into heterogeneities are realized by recent technological developments of the STED-FCS approach [10–12]

REFERENCES

1. Hell, S. W., "Far-field optical nanoscopy," *Science*, Vol. 316, 1153, 2007.
2. Kastrup, L., et al., "Fluorescence fluctuation spectroscopy in subdiffraction focal volumes," *Phys. Rev. Lett.*, Vol. 94, 178104, 2005.
3. Blom, H., et al., "Fluorescence fluctuation spectroscopy in reduced detection volumes," *Curr. Pharm. Biotechnol.*, Vol. 7, 51, 2006.
4. Ringemann, C., et al., "Exploring single-molecule dynamics with fluorescence nanoscopy," *New J. Physics*, Vol. 11, 103054, 2009.
5. Eggeling, C., et al., "Direct observation of the nanoscale dynamics of membrane lipids in a living cell," *Nature*, Vol. 457, 1159, 2009.
6. Polyakova, S. M., et al., "New GM1 ganglioside derivatives for selective single and double labelling of the natural glycosphingolipid skeleton," *Eur. J. Org. Chem.*, 5162, 2009.
7. Kolmakov, K., et al., "Red-emitting rhodamine dyes for fluorescence microscopy and nanoscopy," *Chem. Eur. J.*, Vol. 16, 158, 2010.
8. Mueller, V., et al., "STED nanoscopy reveals molecular details of cholesterol- and cytoskeleton-modulated lipid interactions in living cells," *Biophys. J.*, Vol. 101, 1651, 2011.
9. Honigmann, A., et al., "STED microscopy detects and quantifies liquid phase separation in lipid membranes using a new far-red emitting fluorescent phosphoglycerolipid analogue," *Faraday Discussion*, 2012, doi:10.1039/C2FD20107K.
10. Vicidomini, G., et al., "Sharper low power STED nanoscopy by time gating," *Nat. Meth.*, Vol. 8, 571, 2011.
11. Honigmann, A., et al., "Super-resolution STED microscopy advances with yellow CW OPSL," *Laser Focus World*, Vol. 48, 75, 2012.
12. Mueller, V., et al., "CW DPSS lasers make STED microscopy more practical," *Biophotonics*, Vol. 19, 30, 2012.

Diffraction-unlimited Optical Lithography in Three Dimensions

J. Fischer[1] **and M. Wegener**[1, 2]

[1]Institut für Nanotechnologie, Karlsruhe Institute of Technology (KIT)
Karlsruhe D-76021, Germany
[2]Institut für Angewandte Physik and DFG-Center for Functional Nanostructures (CFN)
KIT, Karlsruhe D-76128, Germany

Abstract— In some regards, optical lithography is just the opposite process of optical lithography. While microscopy aims at getting information about a three-dimensional object non-invasively, lithography aims at forming a three-dimensional object according to existing information. Nevertheless, lithography and microscopy share common limitations like the resolution limit imposed by diffraction.

For example, three-dimensional (3D) multi-photon direct laser writing (DLW) allows for the fabrication of nearly arbitrary 3D polymer structures inside a photoresist volume. Yet the resolution of 3D DLW is limited by diffraction. We have recently shown that a combination of 3D DLW and stimulated emission depletion (STED) or a STED-like mechanism yields an improved resolution in optical lithography. For this purpose, a specially designed photoresist containing 7-diethylamino-3-thenoylcoumarin is used in combination with a femtosecond Ti:Sa oscillator and a 532 nm continuous wave laser.

The smallest distances between adjacent features demonstrated in the lateral and in the axial direction fall below the diffraction limit for the first time. Moreover, these values surpass all previously published ones — even when compared to setups using shorter excitation wavelengths or chemically modified photoresists. This improved resolution has already enabled novel photonic devices that would have not been possible with regular DLW: A so-called carpet cloak operating at visible light frequencies as well as a 3D photonic crystal possessing a complete photonic bandgap in the visible.

A more detailed investigation of the analysis of the underlying depletion mechanism is performed using a pump-probe-like lithography setup with a pulsed tunable depletion laser. We identify stimulated emission by the temporal and spectral signature, as well as a slower depletion mechanism that is subject to current investigations.

Characterization of Spatial Organization of Proteins in Metastasizing Cells and in Platelets — Openings for Future Diagnostic Applications

Jerker Widengren
Exp. Biomol. Physics, Department of Applied Physics
Royal Institute of Technology (KTH)
Albanova University Center, Stockholm 106 91, Sweden

Abstract— Characterization of up- and/or down-regulation in the expression of specific disease-related proteins in cells is widely used in clinical diagnostics, not the least in cancer diagnostics. The remarkable progress in optical far-field nanoscopy now makes it possible to further consider also possible disease-specific features in the spatial distribution patterns of certain proteins within the cells. We have used ultrahigh resolution stimulated emission depletion (STED) microscopy to characterize protein distribution patterns within cultured cells, representing normal fibroblast cells, and cells from a corresponding matched metastasizing cell line [1], and distribution patterns in platelets, of proteins involved in the regulation of blood vessel formation [2]. In these studies, we can resolve features in the protein distribution patterns which are clearly different between normal and metastasizing fibroblast cells, and upon various forms of activation of the platelets. This opens interesting possibilities for subcellular diagnostics, on a small number of cells, and possibly at a quite early stage of a disease process.

REFERENCES

1. Rönnlund, D., A. K. B. Gad, H. Blom, P. Aspenström, and J. Widengren, "Spatial organization of proteins in metastasizing cells," *Cytometry A*, Accepted.
2. Rönnlund, D., Y. Yang, H. Blom, G. Auer, and J. Widengren, "Fluorescence nanoscopy of platelets resolves platelet-state specific storage, release and uptake of proteins, opening for future diagnostic applications," *Advanced Healthcare Materials*, Vol. 1, No. 6, 707–713, 2012.

Single Cell Analysis by Super-resolution Barcoding

Eric Lubeck[1] **and Long Cai**[1, 2]

[1]Program in Biochemistry and Molecular Biophysics, USA
[2]Division of Chemistry and Chemical Engineering, California Institute of Technology
Pasadena, CA 91125, USA

Abstract— Fluorescence microscopy is a powerful quantitative tool for exploring regulatory networks in single cells. However, the number of molecular species that can be measured simultaneously is limited by the spectral separability of fluorophores. Here we demonstrate a simple but general strategy to drastically increase the capacity for multiplex detection of molecules in single cells by using optical super-resolution microscopy (SRM) and combinatorial labeling. The basis for this new approach are the following: given the 10 nanometers resolution of a super-resolution microscope and a typical cell a size of $(10\,\mu\text{m})^3$, individual cells contains effectively 10^9 super-resolution pixels or bits of information. Most eukaryotic cells have 10^4 genes and cellular abundances of 10–100 copies per transcript. Thus, under a super-resolution microscope, an individual cell has 1000 times more pixel volume or information capacities than is needed to encode all transcripts within that cell. As a proof of principle, we labeled mRNAs with unique combinations of fluorophores using Fluorescence in situ Hybridization (FISH), and resolved the sequences and combinations of fluorophores with SRM. We measured the mRNA levels of 32 genes simultaneously in single yeast cells. These experiments demonstrate that combinatorial labeling and super-resolution imaging of single cells provides a natural approach to bring systems level analysis into single cells.

Session 3P3b
2_FocusSession.SC2: Plasmonics in the Quantum Regime 2

Efficient Coupling of Semiconductor Quantum Dots to Plasmon Nanostructures: Light-matter Interaction Beyond the Dipole Approximation
Peter Lodahl, ... 1132

Spontaneous Emission Enhancement at Finite-length Metal Nanowires
Konstantin Filonenko, Morten Willatzen, Vladimir G. Bordo, ... 1133

Theoretical Modelling and Experimental Study of Quantum Interactions between Molecules and Plasmonic Meta-molecules
Nicolae C. Panoiu, Edward J. Osley, Paul A. Warburton, ... 1134

Electron Energy-loss Spectroscopy of Ag Nanoparticles: Evidence of Nonlocal Blueshift
N. Asger Mortensen, ... 1135

Real-time Observation of Ultrafast Rabi Oscillations between Excitons and Plasmons in J-aggregate/Metal Hybrid Nanostructures
Christoph Lienau, ... 1136

Engineering Vacuum and Thermal Fluctuations Using Hyperbolic Metamaterials
Zubin Jacob, ... 1138

Quantized Optical Transparency of Plasmonic Nanoarrays due to Resistive Coupling of Localised Plasmons
Alexander N. Grigorenko, ... 1140

Coherent Interaction of Plasmonic Structures with Single Emitters: From Super Absorption to Cloaking
Xuewen Chen, ... 1141

Efficient Coupling of Semiconductor Quantum Dots to Plasmon Nanostructures: Light-matter Interaction Beyond the Dipole Approximation

Peter Lodahl
Quantum Photonics Group, Niels Bohr Institute, University of Copenhagen, Denmark

Abstract— The potential of using surface-plasmons polaritons for enhancing light-matter interaction has been realized recently [1], which has motivated a new research frontier in quantum plasmonics. Coupling a single quantum emitter, e.g., a quantum dot, to a highly confined plasmon excitation enables spontaneous emission control or efficient channeling of single photons into preferred directions. Self-assembled quantum dots are mesoscopic emitters with typical dimension on the order of 5–10 nm. The spatial extension and the asymmetry of exciton wavefunctions imply that the point-dipole description of light-matter interaction is not necessarily sufficient in particular not in the case of coupling to plasmon nanostructure, where a very rapidly varying electromagnetic is present. We will discuss recent experimental findings of the breakdown of the dipole approximation observed for InAs quantum dots coupled to plasmons at a dielectric-metal interface [2]. The potential of exploiting such mesoscopic light-matter enhancement will be discuss within the scope of a general theory for light-matter interaction beyond the dipole approximation [3]. Finally, we will discuss the prospects of efficient single-photon sources obtained by coupling single InAs quantum dots to plasmon nanowires [4].

REFERENCES

1. Chang, D. E., A. S. Sørensen, P. R. Hemmer, and M. D. Lukin, *Phys. Rev. Lett.*, Vol. 97, 053002, 2006.
2. Lykke Andersen, M., S. Stobbe, A. S. Sørensen, and P. Lodahl, *Nature Physics*, Vol. 7, 215, 2011.
3. Stobbe, S., P. T. Kristensen, J. E. Mortensen, J. M. Hvam, J. Mørk, and P. Lodahl, *Phys. Rev. B*, Vol. 86, 085304, 2012.
4. Chen, Y., N. Gregersen, T. R. Nielsen, J. Mørk, and P. Lodahl, *Opt. Express*, Vol. 18, 12489, 2010.

Spontaneous Emission Enhancement at Finite-length Metal Nanowires

K. Filonenko[1], **M. Willatzen**[2], **and V. Bordo**[1]

[1]NanoSyd, Mads Clausen Institute, Syddansk Universitet, Alsion 2, DK-6400 Sønderborg, Denmark
[2]Department of Photonics Engineering, Technical University of Denmark
DTU Fotonik, Building 345 West, DK-2800 Kongens Lyngby, Denmark

Abstract— We study spontaneous emission enhancement of a two-level atomic system placed near a finite-length metal nanowire. It is shown that spontaneous emission characteristics exhibit significant changes as compared to the case of an infinite wire. The differences arise essentially due to the boundary conditions for tangential field components at the end facets of a finite wire. The semi-analytical method developed by one of us enables both quantitative and qualitative analysis of spontaneous emission in finite-length cavities. We investigate the modes of a metal nanowire using interpolation of experimental data for different metals and calculate the Purcell and β factors. In particular, the attention is paid to the first two surface plasmonic modes TM0 and HE1, which exist below cutoff for the other modes. We calculate the dependence of the Purcell factor on the two-level system distance from the nanowire for several emitter transition frequencies and different orientations of the transition dipole moment. The results are compared to those obtained in the case of an infinite structure and to the radiative and nonradiative contributions to the total spontaneous emission rate. We also calculate the dependence of the Purcell and β factors on the nanowire radius. The resulting Purcell factor for the TM0 plasmonic mode exceeds all other contributions in a broad range of nanowire radii and separation distance values. It is obtained that the β-factor has sufficiently large values for some range of these parameters. The modes with high Purcell and β factors can potentially be used as lasing modes in plasmonic nanolasers.

Theoretical Modelling and Experimental Study of Quantum Interactions between Molecules and Plasmonic Meta-molecules

Nicolae C. Panoiu[1,2], **Edward J. Osley**[1,3], **and Paul A. Warburton**[1,3]

[1]Department of Electronic and Electrical Engineering, University College London
Torrington Place, London WC1E 7JE, United Kingdom
[2]Thomas Young Centre, London Centre for Nanotechnology, University College London
17-19 Gordon Street, London, WC1H 0AH, United Kingdom
[3]London Centre for Nanotechnology, University College London
17-19 Gordon Street, London WC1H 0AH, United Kingdom

Abstract— Recently there has been an increasing interest in the basic science and technological applications of light matter interaction at the nanoscale. In this context, quantum plasmonics is emerging as a research area that provides an ideal test bed where new ideas and phenomena pertaining to the classical and quantum aspects of the interaction between electromagnetic waves and sub-micrometre sized particles can be studied at deep sub-wavelength scale, primarily because plasmonic nano-structures facilitate and enhance the optical coupling between light and matter. As part of these new exciting developments, we have recently developed a quantum mechanical theoretical model [1], which fully describes the interaction between molecules and plasmonic meta-molecules (plasmonic nano-structures that have a series of optical resonances). More specifically, we have demonstrated experimentally that the coupling between tuneable broadband modes of an array of asymmetric plasmonic meta-molecules [2] and a vibrational mode of carbonyl bond of poly(methyl methacrylate) produces a Fano-like resonance, which can be tuned *in situ* by simply varying the polarization of incident light. The interaction between the localized plasmon modes of the plasmonic meta-molecule and the molecular resonance was also investigated using both rigorous electromagnetic calculations and a quantum mechanical model describing the quantum interference between a discrete state (the vibrational mode of the molecule) and two continua (the broad plasmon resonances). The predictions of our quantum mechanical model were in very good agreement with the experimental data and provided an intuitive interpretation, at the quantum level, of the plasmon molecule optical coupling. In addition to a review of all these recent developments, we will outline several ideas for future work.

REFERENCES

1. Osley, E. J., C. G. Biris, P. G. Thompson, R. R. F. Jahromi, P. A. Warburton, and N. C. Panoiu, "Fano resonance resulting from a tunable interaction between molecular vibrational modes and a double-continuum of a plasmonic metamolecule," *Phys. Rev. Lett.*, Vol. 110, 087402, 2013.
2. Thompson, P. G., C. G. Biris, E. J. Osley, O. Gaathon, R. M. Osgood, N. C. Panoiu, and P. A. Warburton, "Polarization-induced tunability of localized surface plasmon resonances in arrays of sub-wavelength cruciform apertures," *Opt. Express*, Vol. 19, 25035, 2011.

Electron Energy-loss Spectroscopy of Ag Nanoparticles: Evidence of Nonlocal Blueshift

N. Asger Mortensen[1, 2]

[1]Department of Photonics Engineering, Technical University of Denmark, DK-2800 Kgs. Lyngby, Denmark
[2]Center for Nanostructured Graphene, Technical University of Denmark, DK-2800 Kgs. Lyngby, Denmark

Abstract— The recent developments in analytical scanning transmission electron microscopes (STEM) equipped with a monochromator and electron energy-loss spectroscopy (EELS) gives the possibility of accessing the near-field energy distribution of the plasmon resonance of individual nanoparticles on a subnanometer scale with an energy resolution better than 0.2 eV. With STEM EELS it is possible to correlate the structural and chemical information on the nanometer scale, with the spectral information of the surface plasmon (SP) resonance of single isolated nanoparticles. STEM EELS is thus perfectly suited to probe and access plasmonic nanostructures and SP resonances at length scales where quantum mechanics is anticipated to become important.

In this paper we study experimentally the SP resonance energy of chemically grown isolated spherical Ag nanoparticles with STEM EELS. A significant blueshift of the SP resonance energy of 0.5 eV is measured when the particle diameter decreases from 26 down to 3.5 nm. This dependence of the SP resonance with the size of noble metal nanostructures is believed to be a signature of quantum properties of the free-electron gas. We therefore interpret the observed blueshift using three models for a metallic sphere embedded in a homogeneous background material: a classical Drude model with a homogeneous electron density profile in the metal, a semiclassical model corrected for an inhomogeneous electron density associated with quantum confinement, and a semiclassical nonlocal hydrodynamic description of the electron density. All of the three approaches are based on calculating the optical response and thereby also the resonance energies of the nanoparticle through the quasistatic polarizability. Effects due to spill-out and quantum tunneling are neglected.

Figure 1 displays the resonance energy of the SP as a function of the diameter of the nanoparticles. Along with the EELS measurements, we show the local-response Drude model (red line) and the semiclassical local-response model (blue line). Furthermore, the hydrodynamic nonlocal-response model is also depicted (green solid line). We see that the latter two models provide a qualitative explanation for the observed blueshift, but the theoretical predictions show smaller blueshifts than observed experimentally. The quantitative agreement between the two different theoretical models and the discrepancy with the larger observed blueshift suggest that the assumption of a homogeneous background is inadequate to describe the presence of the substrate. The symmetry breaking induced by the presence of the substrate leads to a higher degree of electron density inhomogeneity in the nanoparticle, producing a stronger blueshift than for a particle in a homogeneous background. We thus attribute the larger measured blueshift to effects due to the presence of the substrate.

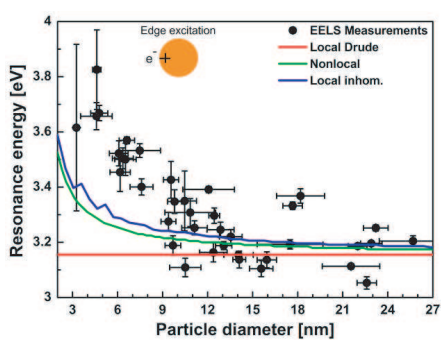

Figure 1: Nanoparticle SP resonance energy as a function of the particle diameter. The dots are EELS measurements taken at the surface of the particle, and the lines are theoretical predictions.

REFERENCES

1. Raza, S., N. Stenger, S. Kadkodazadeh, S. V. Fischer, N. Kostesha, A.-P. Jauho, A. Burrows, M. Wubs, and N. A. Mortensen, *Nanophotonics*, Vol. 2, 2013, in press.

Real-time Observation of Ultrafast Rabi Oscillations between Excitons and Plasmons in J-aggregate/Metal Hybrid Nanostructures

Christoph Lienau
Institut für Physik, Carl von Ossietzky Universität, Oldenburg 26111, Germany

Abstract— Surface plasmon polaritons (SPPs), optical excitations at the interface between a metal and a dielectric, carry significant potential for guiding and manipulating light on the nanoscale. Their weak optical nonlinearities, however, hinder active device fabrication, e.g., for all-optical switching or information processing. Recently, strong optical dipole coupling between SPPs and nonlinear quantum emitters with normal mode splittings of up to 700 meV has been demonstrated [1, 2]. The predicted ultrafast energy transfer between quantum emitters and SPP fields could be a crucial microscopic mechanism for switching light by light on the nanoscale. Here, we present the first real-time observation of ultrafast Rabi oscillations in a J-aggregate/metal nanostructure, evidencing coherent energy transfer between excitonic quantum emitters and SPP fields. We demonstrate coherent manipulation of the coupling energy by controlling the exciton density on a 10-fs timescale, a step forward towards coherent, all-optical ultrafast plasmonic circuits and devices.

We investigate a metal-molecular aggregate hybrid nanostructure consisting of a 50-nm-thick J-aggregated cyanine dye-polymer film spin-coated on a gold grating. Such a sample is a prototype system for exploring strong coupling between excitons and SPPs and shows the formation of upper (UP) and lower (LP) exciton-SPP polaritons with a normal mode splitting of 110 meV [2]. The physical cause for the clear anti-crossing, a periodic energy exchange between excitons and SPPs and the resulting Rabi oscillations are investigated in real-time by resonant ultrafast pump-probe spectroscopy (Fig. 1(a)). The LP response shows distinct oscillations in differential reflectivity with a Rabi period of ~ 25 fs (Fig. 1(b)).

These oscillations are caused by an interesting and new physical mechanism. The ultrashort pump laser impulsively launches a SPP wavepacket and thus induces coherent population oscillations between excitons and SPPs. We find that the exciton population reduces the normal mode splitting due to state filling. Therefore, transient oscillations in exciton density induced by coherent X-SPP population transfer give rise to a periodic modulation of the normal mode splitting and thus the optical nonlinearity on a 10-fs timescale. This may be seen as a new approach to control the SPP response of metallic nanostructures by coupling SPPs to active quantum systems and providing an ultrafast switching functionality to their otherwise linear response. We believe that this is a promising route towards active all-optical nano-photonic circuits and devices.

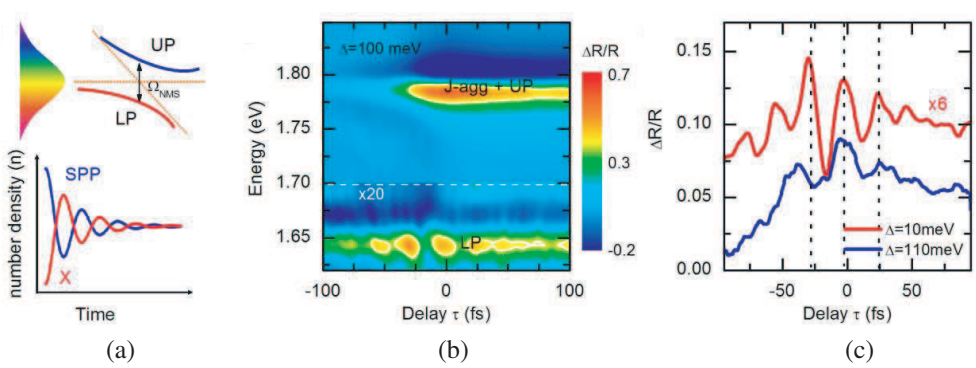

Figure 1: (a) An ultrafast resonant excitation of the hybrid nanostructure overlapping with UP and LP captures the population oscillation between Xs and SPPs. (b) Differential reflectivity spectra showing the distinct Rabi oscillations on the LP. The UP nonlinearity is masked by the bare dye nonlinearity. (c) Time traces for two X-SPP detuning, Δ, showing Rabi oscillations with a period of ~ 25 fs, slightly increasing with decreasing detuning.

REFERENCES

1. Schwartz, T., J. A. Hutchison, C. Genet, and T. W. Ebbesen, "Reversible switching of ultrastrong light-molecule coupling," *Phys. Rev. Lett.*, Vol. 106, 196405, 2011.
2. Vasa, P., R. Pomraenke, G. Cirmi, E. De Re, W. Wang, S. Schwieger, D. Leipold, E. Runge, G. Cerullo, and C. Lienau, "Ultrafast manipulation of strong coupling in metal-molecular aggregate hybrid nanostructures," *ACS Nano*, Vol. 4, 7559, 2010.
3. Vasa, P., W. Wang, R. Pomraenke, M. Lammers, M. Maiuri, C. Manzoni, G. Cerullo, and C. Lienau, "Real-time observation of ultrafast Rabi oscillations between excitons and plasmons in J-aggregate/metal hybrid nanostructures," *Nat. Photon.*, 128–132, 2013.

Engineering Vacuum and Thermal Fluctuations Using Hyperbolic Metamaterials

Zubin Jacob
Department of Electrical and Computer Engineering, University of Alberta
Edmonton, Alberta T6G 2V4, Canada

Abstract— We show that the broadband enhancement in the photonic density of states of hyperbolic metamaterials leads to a platform for enhancing vacuum and thermal fluctuations. We consider various applications in near-field thermal engineering and quantum nanophotonics.

The electrical engineer is often concerned with controlling the coherent state of light (as in a laser), a mechanical engineer might be more interested in controlling radiation from thermal fluctuations while a physicist looks for ways to manipulate the non-classical properties of light. In this talk, we will argue that metamaterials present a unified platform to engineer all three states of light. We will consider different classes of metamaterials (epsilon-near-zero, magnetic, hyperbolic and others) each with its unique potential for controlling light-matter interaction. We also develop the fluctuational electrodynamics of HMMs to analyze the role of the broadband enhancement in the density of states [1, 2] on the thermal and vacuum fluctuations. Our work paves the way for engineering the thermal emission using metamaterials for applications such as near-field thermophotovoltaics and near-field thermal sources. We will also show that metamaterials can enhance and direct spontaneous emission in a broad bandwidth for applications such as single photon sources.

We show that the characteristic dispersion of the high-k states (topological transitions in the isofrequency surface [3]) manifests itself in the thermal emission beyond the black body limit. We also show that the proposed effect can be experimentally verified in a practical implementation of the HMM. Following the seminal work of Rytov [4], which considers electromagnetic fields generated by equilibrium thermal fluctuations, we use the fluctuation-dissipation theorem and the green's tensor [5] of the HMM to calculate the emitted energy density in the near field of an HMM in equilibrium at temperature T. The final expression of thermal emission depends on the scattering matrix of the structure and can be directly applied to HMMs and multilayered structures. In the extreme near field, the thermal emission can be approximated by $u(z, \omega, T) \approx U_{BB}(\omega, T)\mathrm{Im}(r^p)/(2k_0 z)^3$ for a medium with no magnetic response.

One approach [6] to achieving the extreme anisotropy characteristic of HMMs is by using a metal-dielectric super-lattice structure where the thickness of each layer is far below the operating wavelength. We consider here a phonon-polaritonic metal (silicon carbide SiC) where the coupling between the optical phonons and light causes the real part of the permittivity to become negative in the Reststrahlen band. In Fig. 1, we show the topology of the isofrequency surfaces and near field thermal radiation as predicted by effective medium theory. A remarkable agreement is seen between the optical phases and the near field thermal emission with the hyperbolic phase showing super-planckian thermal emission. We have also confirmed these analytical results with a practical structure taking into account, absorption, dispersion and finite patterning scale. In Fig. 2, the fill fraction of the metal is chosen to be 0.25, so that a type I HMM response is achieved from 178 THz to 182 THz and a type II HMM response is achieved in between 149 THz and 162 THz. For the multilayer structure, the thickness of the SiC layers are 50 nm and the thickness of the SiO_2 layers are 150 nm. The total number of layers are $N = 10$ achieving a net thickness of 1 micron. On comparing the effective medium predictions with the wave-vector resolved local density of states in practical structure we see an excellent agreement of the optical phases as well as presence of the high-k modes. The multilayer structure behaves as an effective dielectric in the dark band where there are no high-k modes. Thus the topological transitions predicted in the optical phase diagram are achieved in the practical structure. Our predicted effect should be experimentally discernible from other routes of super-Planckian thermal emission using the topological transitions [2, 3] manifested in thermal emission.

In conclusion, we have established near field thermal emission in a broad bandwidth exceeding the black body limit as well as thermal topological transitions in hyperbolic metamaterials. This work paves the way for near-field thermal and quantum engineering using metamaterials for applications as thermophotovoltaics [7], near-field thermal stamping [8] and broadband single photon sources.

REFERENCES

1. Shchegrov, A. V., et al., "Near-field spectral effects due to electromagnetic surface excitations," *Phys. Rev. Lett.*, Vol. 85, 1548–1551, 2000.
2. Narimanov, E., I. Smolyaninov, Z. Jacob, et al., *Appl. Phys. Lett.*, Vol. 100, 181105, 2012.
3. Krishnamurthy, H. N. S., Z. Jacob, et al., "Topological transistions in metamaterials," *Science*, Vol. 336, 205, 2012.
4. Rytov, S. M., Y. A. Kravtsov, and V. I. Tatarskii, *Principles of Statistical Radiophysics 3*, Springer-Verlag, Berlin, 1989.
5. Tsang, L., et al., "Microwave thermal emission from a stratified medium with nonuniform temperature distribution," *J. Appl. Phys.*, Vol. 46, 5127–5133, 1975.
6. Guo, Y., et al., "Broadband super-Planckian thermal emission from hyperbolic metamaterials," *Appl. Phys. Lett.*, Vol. 101, 131106, 2012.
7. Narayanaswamy, A. and G. Chen, "Surface modes for near field thermophotovoltaics," *Appl. Phys. Lett.*, Vol. 82, 3544, 2003.
8. Pendry, J. B., "Radiative exchange of heat between nanostructures," *J. Phys.: Condens. Matter*, Vol. 11, 6621, 1999.

Quantized Optical Transparency of Plasmonic Nanoarrays due to Resistive Coupling of Localised Plasmons

A. N. Grigorenko
School of Physics and Astronomy, University of Manchester, Manchester, M13 9PL, UK

Abstract— We describe a plasmonic system in which relative optical transparency is determined solely by the fine structure constant. The system consists of a regular array of gold nanoparticles fabricated on a thin metallic sublayer. We show that its relative transparency can be quantized in the near-infrared, which we attribute to resistive coupling of localized plasmons through the quantized contact resistance between the nanoparticles and the metallic sublayer. Our results open new possibilities in the exploration of universal dynamic conductance in plasmonic nanooptics.

Coherent Interaction of Plasmonic Structures with Single Emitters: From Super Absorption to Cloaking

Xuewen Chen
Max Planck Institute for the Science of Light
Friedrich-Alexander University Erlangen-Nürnberg
Erlangen 91058, Germany

Abstract— The past decade witnessed a great interest in the effect of plasmonic structures on the optical properties of atoms and molecules. In the studied cases, the metallic structure usually acts as an optical antenna to modify the spontaneous emission, opens new nonradiative channels or enhances the Raman cross section [1].

We have asked the question how a single quantum emitter could affect the optics of a metallic structure. In particular, we have examined two extreme regimes of very small particles, where their optical properties are dominated by absorption and of "large" nanoparticles dominated by scattering. To treat the coherent interaction of an incident light with a composite of a metallic particle and a quantum emitter, we have developed a general theoretical platform based on quantized radiation in absorptive and inhomogeneous media and have examined the response of the composite in various configurations [2].

In this talk, I will present the results of the coherent interaction in extreme regimes. In the case of a small metallic structure, we demonstrate that a quantum emitter either compensates for the losses or enhances the absorption by up to 1000 times. While in the case of larger structures, we show that a single atom or molecule can eliminate both scattering and absorption so that the metallic structure is cloaked. This is particularly impressive because the plasmonic structure alone would nearly fully block the incident light! Since the emitter transition can be manipulated in various ways (Stark effect, photoswitching, optical pumping, etc.) the composite system or a macroscopic array of such structures act as active metamaterials and allow active switching of the beam.

REFERENCES

1. *Optical Antennas*, edited by M. Agio and A. Alù, Cambridge University Press, 2013.
2. Chen, X. W., V. Sandoghdar, and M. Agio, *Phys. Rev. Lett.*, 2013, in press.

Session 3P4a
4_FocusSession.SC4&3: Radio over Fiber Systems and Components

Intelligent Radio-over-fiber System Based on MWP for the Broadband Access and Ubiquitous Sensing
Kun Xu, ... 1144

Fiber-wireless Links Supporting High-capacity W-band Channels
J. J. Vegas Olmos, Idelfonso Tafur Monroy, ... 1145

Wired and Wireless Seamless MIMO Transmissions in Millimeter-wave Radio-over-Fiber Systems
Yuki Yoshida, ... 1146

Carrier Phase and Amplitude Manipulation for Linearization and Dispersion Compensation in Radio-over-fiber Systems Using Mach-Zehnder Modulator
Shangyuan Li, Xiaoping Zheng, Fan Wei, Hanyi Zhang, Bingkun Zhou, ... 1147

Digitized RF Transport for Fiber-wireless in a World of Digital Optical Networks
Christina Lim, Yizhuo Yang, Ampalavanapillai Nirmalathas, ... 1148

Linearization Techniques for Broadband Radio over Fiber Transmission
John Xiupu Zhang, Bouchaib Hraimel, Ran Zhu, Dongya Shen, Taijun Liu, ... 1150

A Study on OFDM Millimeter-wave Radio over Fiber System
Tam Hoang Thi, Mitsuji Matsumoto, ... 1151

Intelligent Radio-over-fiber System Based on MWP for the Broadband Access and Ubiquitous Sensing

Kun Xu
State Key Laboratory of Information Photonics and Optical Communications
Beijing University of Posts and Telecommunications, China

Abstract— Broadband, ubiquitous and convergent transmission and access of information has become the most important engine to push forward the development of the modern information society. Thus, broadband access and ubiquitous sensing of information has been rapidly developed as the important and necessary performance demand of the future high-performance information system. However, the current microwave and digital technologies have become less and less competent for the requirement of the future information network and high-performance digital receiving system. As a result, some brand-new solutions are strongly desired to be explored to keep the pace of the fast development of the modern information society.

Microwave photonics with combination of microwave and lightwave is found to be an effective solution to broadband access and ubiquitous sensing, of which the fundamental theory is to use photonic technologies to generate, transmit, process, and control microwave signals. Microwave photonic takes full advantages of the respective merits of microwave technology and lightwave technology to compensate the drawbacks of each other and eventually bridges the gap between microwave and lightwave effectively. Specifically speaking, microwave photonics makes use of the wideband, high-speed and low SWaP of photonics technology to achieve the high-quality generation of broadband microwave signal, high dynamic range transmission of analog microwave information, high-resolution processing of high-frequency microwave signal, flexible signal controlling, reconfigurable dynamic networking and the coordination between microwave and lightwave in the distributed networks. Taking advantage of the microwave photonics technology, we proposed intelligent radio-over-fiber (I-RoF) distributed antenna system (DAS) for the green, broadband access and ubiquitous sensing applications. The I-RoF DAS provide a promising solution for the future multi-service broadband green access and ubiquitous sensing applications. In the physical layer, the analog-optic links with high spur-free dynamic range (SFDR) are mathematical modeled and experimentally established. Furthermore, the different topologies (star, tree, etc.) of ROF network are proposed for the complex application environment. In the media access control (MAC) layer, an optimized MAC model for dynamic reconfigurable ROF network is proposed to overcome the impact of additional delay induced by the optical fibers. Moreover, by applying the intelligent DAS, the efficient utilization and dynamic management of the optical and microwave resources is realized. Consequently, an intelligent radio-over-fiber (I-RoF) distributed antenna system is implemented with the function modules of intelligent sensing and photonic RF switching, which provides a promising solution to the converged broadband access and sensor networks.

As the development of microwave photonics, it will be widely deployed in the national strategy industries such as broadband wireless communications, defense, aerospace and medical industry. Based on a national 973 project that Beijing University of Posts and Telecommunications leads, the intelligent radio-over-fiber based on microwave photonics' researches and applications in broadband access and ubiquitous sensing will be given in this talk.

Fiber-wireless Links Supporting High-capacity W-band Channels

J. J. Vegas Olmos and I. Tafur Monroy
Department of Photonics Engineering, Technical University of Denmark, Kgs. Lyngby 2800, Denmark

Abstract— Seamless convergence of fiber-optic and the wireless networks is of great interest for enabling transparent delivery of broadband services to users in different locations, including both metropolitan and rural areas. Current demand of bandwidth by end-users, especially using mobile devices, is seeding the need to use bands located at the millimeter-wave region (30–300 GHz), mainly because of its inherent broadband nature. In our lab, we have conducted extensive research on high-speed photonic-wireless links in the V-band (50–75 GHz) and the W-band (75–110 GHz). In this paper, we will present our latest findings and experimental results on the W-band, specifically on its 81–86 GHz sub-band. These include photonic generation of millimeter-wave carriers and transmission performance of broadband signals on different types of fibers and span lengths.

Wired and Wireless Seamless MIMO Transmissions in Millimeter-wave Radio-over-Fiber Systems

Yuki Yoshida
Graduate School of Engineering, Osaka University
2-1 Yamada-oka, Suita, Osaka 565-0871, Japan

Abstract— Seamless connection between wired (optic fiber) and wireless (radio) networks is an attractive technology not only for the "last-mile problem" in access networks including mobile backhauls, but also for the enhancement of network resilience against a disaster. In particular, on March 11, 2011, the Great East Japan Earthquake cut off a large number of optical fiber cables, and the most of broadband services were disconnected. The temporal deployment of broadband connections using wired and wireless converged systems immediately after a disaster has been strongly desired for rescue and surveillance, since the re-establishment of the optical back-haul network takes 1–2 years long. Millimeter-wave (MMW) radio with radio-over-fiber (RoF) technology is a prominent solution for providing wired/wireless seamless connection with a capacity greater than 10 Gbps, which is capable for a fast protection link for recovery. The capacity also meets the demand for backhauling the high-speed wireless systems such as IMT-advanced or for relaying the upcoming optical access systems such as 10 G-PON.

In this talk, the recent development of the "Agile deployment capability of highly resilient optical and radio seamless communication systems" program (the commissioned research of the National Institute of Information and Communications Technology, Japan) is introduced. Key technologies are 1) efficient W-band radio (75–110 GHz), whose available bandwidth is > 30 GHz with low atmospheric attenuation of < 1 dB/km, signal generations using photonic direct up-conversion, 2) DSP (digital signal processing)-aided optical coherent receiving techniques which offers the > 30 GHz ultra-wideband signal reception, as well as 3) wireless/wired seamless multiple-input-multiple-output (MIMO) transmissions providing further capacity and robustness to the RoF link. We also present some experimental demonstrations including the 74.4 Gbps wired and wireless seamless MIMO transmission utilize W-band radio (75–110 GHz) and fiber's polarization channels.

Carrier Phase and Amplitude Manipulation for Linearization and Dispersion Compensation in Radio-over-fiber Systems Using Mach-Zehnder Modulator

Shangyuan Li, Xiaoping Zheng, Fan Wei, Hanyi Zhang, and Bingkun Zhou
Tsinghua National Laboratory for Information Science and Technology
Department of Electronic Engineering, Tsinghua University, Beijing 100084, China

Abstract— In radio-over-fiber (ROF) systems, electrical signal modulates the optical carrier, converting the electrical signal to optical domain and generating the up-converted signal bands. Comparing to the ideal modulation process, an actual modulation process would deteriorate the modulated signal and generate distorted sidebands, leading to a reduction of the dynamic range. Meanwhile, the chromatic dispersion, originated from the transmission fiber or other devices, can also change the phase relationship between the carrier and the modulated sidebands, introducing power fading to the modulated signal and causing significant signal degradation. Most traditional compensation methods have only focused on one of these two issues. However, for such an ROF system, they should better be treated simultaneously.

Mach-Zehnder modulators (MZM) is generally treated as an electrical to optical (EO) converter. However, recent progresses show that the MZM (or an MZM with complex structures) can play far more than an EO converter. Special utilizations of the MZM can achieve linearization or dispersion compensation, and even resolve both the issues simultaneously. In this paper, we reviewed the fundamental principles, techniques, systems and applications that using MZMs to control the phase and amplitude of the optical carrier, to achieve multi-functions, including EO conversion, linearization and dispersion Compensation, simultaneously.

By controlling the phase and amplitude of the optical carrier, the phase and amplitude relationship between the carrier and the sidebands can be altered accordingly. Analysis shows that the nonlinear distortion and fiber dispersion can be suppressed and compensated simultaneously, if a specific phase and amplitude condition between the carrier and the sidebands is settled. Such a condition can be achieved using a dual-parallel MZM (DPMZM), which has two sub-modulators that lie on a parent modulator. By tuning the three biases of the DPMZM, dispersion and nonlinear distortion can be treated at the same time. Further studies show that such a technique can help establishing a frequency doubled opto-electronic oscillator (OEO), or a low-interference dual-direction RoF links.

Digitized RF Transport for Fiber-wireless in a World of Digital Optical Networks

Christina Lim, Yizhuo Yang, and Ampalavanapillai Nirmalathas
Department of Electrical and Electronic Engineering, The University of Melbourne, VIC 3010, Australia

Abstract— Fiber-wireless technology is able to unify the future telecommunication infrastructure by using a common backhaul network to support both wired and wireless services. Despite the elegance of the fiber-wireless architecture, previous study has shown that the performance is severely limited by the nonlinearity in the optoelectronic frontend [1]. Previously we have introduced and demonstrated the use of digitized wireless signal transport to overcome the inherent nonlinearity issue [2]. In this paper, we review how this transport strategy is able to improve the performance of fiber-wireless links while being compatible with a predominantly digital world.

Digitized RF-over-Fiber (DRoF) Transport of OFDM Wireless Signals: Figure 1 shows the digitized radio-over-fiber (DRoF) concept using bandpass sampling technique that undersamples the wireless signals with sampling rate proportional to the wireless message bandwidth that relaxes the ADC/DAC requirements within the remote base stations [3]. Since the wireless signal is transported digitally, the optical link can maintain its dynamic range independent of the fiber transmission distance until when the received signal goes below the link sensitivity. Fig. 2 shows the experimental setup for the DRoF transport of wideband OFDM signal (128 carriers, 80 modulated with 4-QAM, data rate of 1.25 Gb/s) generated using arbitrary waveform generator (AWG) [4]. The upconverted OFDM signal was bandpass sampled, digitally processed and externally modulated onto a DFB laser. The optical signal was transported over 20 km of fiber, detected and digitally processed off-line. Shown in Fig. 3 is the error vector magnitude (EVM) performance of the OFDM signals at 6–10 GH RF frequency as a function of ADC bit resolutions and the corresponding optical bit rates. The dashed line indicates error-free reception for 4-QAM signal. The performance improves with increasing ADC resolution before leveling off at an ADC bit-resolution of 6 bits. Also shown in Fig. 3 are the 4-QAM constellations of the original and the recovered signal after transmission with 4, 6 and 8 bit resolution. It can be seen that error-free transmission is achieved for wideband OFDM transmission using DRoF with ADC bit resolution as low as 4 bits with a total optical bit rate of 4 Gb/s.

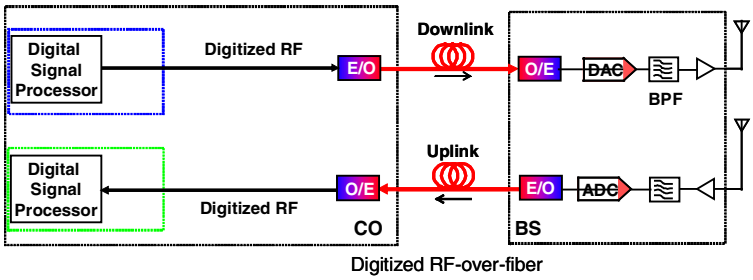

Figure 1: Digitized RF-over-fiber transport.

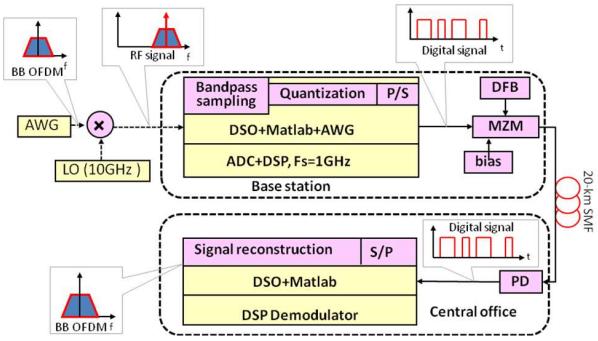

Figure 2: Experimental setup.

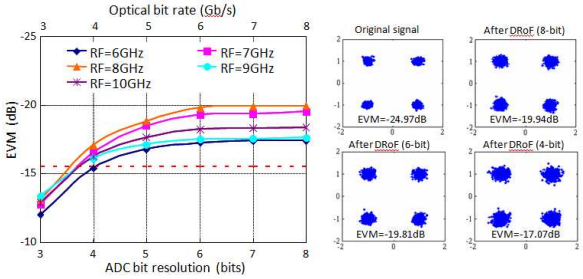

Figure 3: EVM performance and constellation diagram.

Conclusions: We have experimentally demonstrated the DRoF scheme for the transport of wideband OFDM wireless signals to increase the fiber-wireless capacity.

REFERENCES

1. Kurniawan, T., et al., *IEEE MTT*, Vol. 54, 921–928, 2006.
2. Gamage, P. A., et al., *Proc. MWP2008/APMP2008*, 15–18, 2008.
3. Akos, D. M., et al., *IEEE Trans. Comm.*, Vol. 47, 993–988, 1999.
4. Yang, Y., et al., *Proc. OFC*, OTu2H.6, 2012.

Linearization Techniques for Broadband Radio over Fiber Transmission

Xiupu Zhang[1, 2], **Bouchaib Hraimel**[2], **Ran Zhu**[2], **Dongya Shen**[1], **and Taijun Liu**[3]

[1]School of Information Science & Engineering, Yunnan University, Kunming, China
[2]Department of Electrical & Computer Engineering, Concordia University, Montreal, Canada
[3]College of Information Science & Engineering, Ningbo University, Ningbo, Zhejiang, China

Abstract— Linearization techniques are reviewed for broadband radio over fiber transmission. Three linearization techniques based on optical mixed polarization, analog predistortion and digital predistortion are summarized.

Summary The current wireless signal distribution based on optical digital transmission or microwave point to point transmission is not appropriate for next generation broadband wireless access networks (BWAN) that can support data rate of up to 10–20 Gb/s. Analog radio over fiber (ARoF) is considered a key enabling technology for BWAN because of its optical broadband and cost effective seamless integration to wireless technologies and transparent to radio frequency carriers and data protocols. Because of its analog modulation nature, ARoF transmission is very susceptible to intrinsic nonlinearities from the electro-optical modulation (EOM) and any other optical and electronic components that are used for transmission. Therefore, the deployment of ARoF in BWAN requires cost effective broadband linearization. Linearization is not a new research topic and two types of linearization had been proposed: analog and digital predistortion. Unfortunately, the proposed techniques were narrow band, typically limited to 20 MHz.

Due to the above, broadband linearization techniques have been intensively developed. In this presentation, we will review linearization techniques using optical mixed polarization (OMP), analog predistortion circuit (APDC) and digital predistortion. The OMP, making use of the two polarization states of light and the polarization dependence of the optical modulator to compensate for its nonlinearity, is used to linearize optical modulators, such as Mach-Zehnder modulator (MZM) and electro-absorption modulator (EAM). Using OMP for MZM and EAM, spurious free dynamic range (SFDR) is improved by more than 10 dB. By combining OMP and semiconductor optical amplifier (OSA) for an MZM, a record SFDR of 130 dB/Hz$^{4/5}$ and more than 10 dB of improvement in error vector magnitude (EVM) have been achieved for multiband-OFDM ultra-wideband signal. Broadband APDCs (in 2∼6 GHz and 7∼18 GHz bands) have been designed using broadband reflective Schottky diodes. An improvement of more than 10 dB in SFDR has been achieved over 10 GHz. Using digital predistortion (DPD) to linearize sparse multi-band RF signals in subcarrier multiplexed (SCM) ARoF, a 15 dB suppression of adjacent power ratio (ACPR) is achieved in two 64 QAM modulated OFDM signals on 2.4 and 3.6 GHz bands.

A Study on OFDM Millimeter-wave Radio over Fiber System

Tam Hoang Thi and Mitsuji Matsumoto
Graduate School of Global Information and Telecommunication Studies, Waseda University, Tokyo, Japan

Abstract— In this paper, we investigate and theoretically analyze the performance of OFDM based signal transmission over Millimeter-Wave Radio-over-Fiber systems in term of SDR (signal to distortion ratio) and BER (bit error rate). A novel configuration which has ability to transmit very high bit-rate data at a rather low cost is proposed. Moreover, the factors that affect the performance of this system are shown.

Introduction: At the present, the development of new services that require higher bit-rate such as video conference, HD video etc drives the network provider to upgrade the network to higher speed. On the other hand, the services price should be reduced due to competitive pressure. Therefore, we need a new technology that can provide huge bandwidth at a rather lower cost. Radio over fiber technology at millimeter wave can be a good candidate. The reason is that the license-free spectrum at 60 GHz is free and such high frequency can provide very broad bandwidth. However, signal transmission at extremely high frequencies faces many challenges such as high attenuation. In addition, the size of radio cell is very small so the number of base station will rise sharply. Radio over fiber technology is used because in this technology, the structure of base station is simple and as the result, the cost is low. Besides, the importance of OFDM based signal has increased in relation to the definition of standards, like LTE and WiMAX. It is necessary to analysis performance of the new system that transmit OFDM based signal over millimeter wave over Radio over Fiber. The combination of those advanced technologies is supposed to bring good results and this can be good candidate for next generation network.

The system model is shown at the figure below. Mach Zehnder Modulator is used as the external modulator.

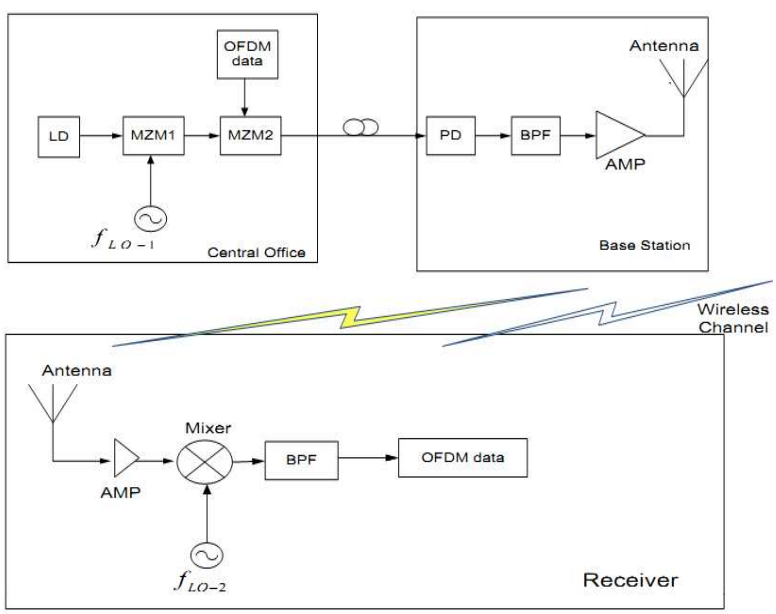

Session 3P4b
SC2: Plasmonic Nanomaterials and Nanostrcutures for Photovoltaics and Optoelectronics in Energy 1

Plasmonic Scattering Studies of Photo-chemically Generated Metallic Nanoparticles on Optical Fiber Double-tapers through Evanescent Field Interference
Aaron Ho-Pui Ho, Jiajie Chen, Zhiwen Kang, Haixi Zhang, Haifei Lu, Wallace C. H. Choy, Nan-Kuang Chen, ... 1154

Organic Solar Cells with Efficiency of ∼9% Achieved by Using Multiple Plasmonic Nanostructures
Wallace C. H. Choy, ... 1155

Modeling Coherent and Incoherent Light-trapping Elements in Solar Cells
Aimi Abass, Bjorn Maes, ... 1156

Plasmon-enhanced Light Harvesting of Dye Molecules in Gratzel Solar Cells
Tao Chen, ... 1157

A Comprehensive Simulation on Plasmonic and Nanostructured Solar Cells
Xiaofeng Li, Nicholas P. Hylton, Vincenzo Giannini, Yaohui Zhan, Kan-Hua Lee, Ned J. Ekins-Daukes, Stefan A. Maier, ... 1158

Surface Texturing of High-power Flip-chip LEDs by Femtosecond Pulsed Laser-induced Periodic Structures
Yi-Hong Lin, Yi-Hao Wang, Ping-Han Wu, Chung-Wei Cheng, Hsiang-Chen Wang, Raymond Chien-Chao Tsiang, ... 1159

Conjugated Polymers in Nanopatterned Photovoltaic Cells for Efficient Light Harvesting
Eunkyoung Kim, ... 1160

Plasmonic Scattering Studies of Photo-chemically Generated Metallic Nanoparticles on Optical Fiber Double-tapers through Evanescent Field Interference

Aaron H. P. Ho[1], **Jiajie Chen**[1], **Zhiwen Kang**[1], **Haixi Zhang**[1], **Haifei Lu**[2], **Wallace C. H. Choy**[2], **and Nan-Kuang Chen**[3]

[1]Department of Electronic Engineering
Chinese University of Hong Kong, Shatin, Hong Kong, China
[2]Department of Electrical and Electronic Engineering
University of Hong Kong, Pokfulam, Hong Kong, China
[3]National United University, Miaoli, Taiwan, R.O.C.

Abstract— We report a novel metallic nanoparticle (NP) synthesis scheme involving near-field optical interference fringes generated on the surface of fiber double-taper. The periodic distribution of the NPs has distinctive plasmonic scattering spectral characteristics caused by both the fringes as well as the localized plasmonic modes of the NPs. Interplay between various resonance modes may offer the possibility of high efficiency light scattering, thus leading to potential optoelectronic applications including non-linear optical conversion, photo-induced catalysis and photonic sensors. Nano-optical trapping and energy localization using the NP fringes is also discussed.

Organic Solar Cells with Efficiency of ∼9% Achieved by Using Multiple Plasmonic Nanostructures

Wallace C. H. Choy
Department of Electrical and Electronic Engineering, The University of Hong Kong
Pokfulam Road, Hong Kong, China

Abstract— Polymer-fullerene-based bulk heterojunction (BHJ) solar cells have many advantages including low-cost, low-temperature fabrication, semi-transparency, and mechanical flexibility [1, 2]. However, there is a mismatch between optical absorption length and charge transport scale [3, 4]. These factors lead to recombination losses, higher series resistances and lower fill factors. Attempts to optimize both the optical and electrical properties of the photoactive layer in organic solar cells (OSCs) inevitably result in a demand to develop a device architecture that can enable efficient optical absorption in films thinner than optical absorption length [5, 6]. Here, we report the use of multiple metallic nanostructures to achieve the broad light absorption enhancement, increased short-circuit circuit (J_{sc}) and improved fill factor (FF) simultaneously based on a new small-bandgap polymer donor of poly {[4,8-bis-(2-ethyl-hexyl-thiophene-5-yl)-benzo[1,2-b:4,5-b']dithiophene-2,6-diyl]-alt-[2-(2-ethyl-hexanoyl)-thieno[3,4-b]thiophen-4,6-diyl]} (PBDTT-T-C-T) in BHJ cells [7]. The multiple metallic nanostructure consists of 2D arrays of metallic nanograting electrode as a back reflector and metallic nanoparticles (NPs) with different geometries embedded into the active layer. Apart from the waveguide modes and diffractions, we simultaneously introduce hybridized surface plasmonic resonances (from Ag nanograting) and localized plasmonic resonances (from Au and Ag NPs [8]) to successfully achieve a broadband absorption enhancement. The detail understanding has been described with our theoretically studies. Consequently, we improve PCE to ∼9% [9] by improving both optical and electrical properties of single-junction OSCs through introducing dual plasmonic nanostructures which contribute to the practical application of OSCs for photovoltaics.

REFERENCES

1. Park, S. H., A. Roy, S. Beaupré, S. Cho, N. Coates, J. S. Moon, D. Moses, M. Leclerc, K. Lee, and A. J. Heeger, *Nat. Photon.*, Vol. 3, 297, 2009.
2. Chen, H. Y., J. H. Hou, S. Q. Zhang, Y. Y. Liang, G. W. Yang, Y. Yang, L. P. Yu, Y. Wu, and G. Li, *Nat. Photon.*, Vol. 3, 649, 2009.
3. Wöhrle, D. and D. Meissner, *Adv. Mater.*, Vol. 3, 129, 1991.
4. Blom, P. W. M., V. D. Mihailetchi, L. J. A. Koster, and D. E. Markov, *Adv. Mater.*, Vol. 19, 1551, 2007.
5. Atwater, H. A. and A. Polman, *Nat. Mater.*, Vol. 9, 205, 2010.
6. Nalwa, K. S., J. M. Park, K. M. Ho, and S. Chaudhary, *Adv. Mater.*, Vol. 23, 112, 2011.
7. Huo, L., S. Zhang, X. Guo, F. Xu, Y. Li, and J. Hou, *Angew. Chem. Int. Ed.*, Vol. 50, 9697, 2011.
8. Li, X. H., W. C. H. Choy, H. F. Lu, W. E. I. Sha, and H. P. Ho, "Efficiency enhancement of organic solar cells by using shape dependent broadband plasmonic absorption in metallic nanoparticles," *Adv. Funct. Mat.*, DOI: 10.1002/adfm.201202476.
9. Li, X., W. C. H. Choy, L. Huo, F. Xie, W. E. I. Sha, B. Ding, X. Guo, Y. Li, and J. Hou, *Adv. Mater.*, Vol. 24, 3046, 2012.

Modeling Coherent and Incoherent Light-trapping Elements in Solar Cells

A. Abass[1] and B. Maes[2]

[1]Electronics and Information Systems (ELIS), Ghent University
Sint-Pietersnieuwstraat 41, B-9000 Gent, Belgium
[2]Micro and Nanophotonic Materials Group, Faculty of Science
University of Mons, B-7000 Mons, Belgium

Abstract— Advanced thin-film photovoltaic or light emission devices incorporate multiple types of light management features. For light-trapping purposes one often employs wavelength-scale gratings on the front, and disordered, diffusive reflectors on the bottom side. We present a modeling method able to deal with these mixed elements together in a 2D or 3D device. The calculations handle the front grating effects in a fully coherent way, whereas for the bottom diffuser a plane-wave reflection spectrum is used.

With this method we can explore the complex interplay between the various scattering elements, and we present results for a thin-film silicon device. We show that a judicious combination of a front grating with a Lambertian back diffuser provides for the best absorption performance, better than any single element separately. In addition, we can optimize the global device with respect to various parameters: period, active layer thickness, specular component of the back diffuser etc. Finally, we can compare the same device with a coherent or incoherent reflector, offering the insight that a diffusive reflector has important advantages for certain silicon thicknesses.

The simulation algorithm works in two phases. First, we calculate rigorously the response of the front structure (active layer included) to incoming plane waves from the air side, and from the bottom side. This is manageable because we need only one incidence direction from air (the direction of the sun), and we calculate only one period of the grating structure. In the second phase, the power flows of the incoming and reflected plane waves are added and iteratively adjusted until we obtain a correct balance of absorption, reflection and transmission. It is only in the second phase that we include the plane-wave scattering properties of the back reflector, potentially with a specular part. This has the advantages that we do not need to rigorously simulate a large cell for the disordered reflector, and that we can re-use the calculated plane wave responses (of the first phase) for all kinds of back reflectors.

Combined coherent light-trapping features have been proposed as a step towards the ultimate absorption enhancement. Here, however we broaden the set of possible enhancement mechanisms by exploring coherent and incoherent structures together. The calculation method is versatile as it can handle dielectric and metallic features, in 2D or 3D settings, with arbitrary properties for the diffusive back-reflector.

ACKNOWLEDGMENT

This work is part of the Flemish IWT-SBO project SiLaSol (Number 3E100243).

Plasmon-enhanced Light Harvesting of Dye Molecules in Gratzel Solar Cells

Tao Chen
Department of Physics, The Chinese University of Hong Kong, Shatin, N. T. Hong Kong, China

Abstract— In dye-sensitized solar cell, dye molecules possessing strong absorption ranging from full visible to near infrared region is preferable for high photovoltaic conversion efficiency. However, to date, nearly all of the dye molecules only have strong absorption at specific regions. On the other hand, light trapping by plasmonic metal nanoparticles has been proven as an efficient way to improve light harvesting through: (1) scattering light to increase the effective optical path length, (2) focusing light to enhance optical density and (3) propagating surface plasmon polaritons. The plasmon band of the metal nanoparticle is dependent on the size and morphology of the metal nanoparticle. This tunable surface plasmon resonance allows the selective enhancement of light absorption of dye molecules in specific wavelength regions to span the strong spectral response.

In this talk, I will present our recent research in the enhancement of light harvesting of dye molecules by plasmonic metal nanoparticles. I will pay special attention on the use of one-dimensional Au nanorods to enhance low-photon energy light harvesting of Ru-based dye molecule (N719). In specific, the light absorption of N719 in the visible range (500–600 nm) is strong, while the absorption coefficient significantly decreases over longer wavelengths. By using Au nanorod with longitudinal absorption band at 600–700 nm, the light harvesting of N719 is considerably enhanced. This use of plasmonic metal nanoparticles to enhance the light harvesting offers an alternative a way to the development of dye molecules.

A Comprehensive Simulation on Plasmonic and Nanostructured Solar Cells

Xiaofeng Li[1,2], **Nicholas P. Hylton**[3], **Vincenzo Giannini**[3], **Yaohui Zhan**[1,2], **Kan-Hua Lee**[3], **Ned J. Ekins-Daukes**[3], **and Stefan A. Maier**[3]

[1]Institute of Modern Optical Technologies
Key Lab of Advanced Optical Manufacturing Technologies of Jiangsu Province
Soochow University, Suzhou, Jiangsu 215006, China
[2]Key Lab of Modern Optical Technologies of Education Ministry of China
Soochow University, Suzhou, Jiangsu 215006, China
[3]Blackett Laboratory, Department of Physics, Imperial College London, London SW7 2AZ, UK

Abstract— The pursuit of high light-conversion efficiency in thin-film solar cells (SCs) demands the incorporation of advanced nanostructures. Due to the large number of "degrees of freedom" for optimally designing these types of SCs, an accurate performance prediction is crucial. In addition, the numerical analysis for plasmonic nanostructured solar cells presents strong difficulties due to the highly localized and intense field around the metal nanoparticles. This brings a challenge in simulation since it requires high-dimensional, detailed modelling of the behaviour of photons in the optical domain and carriers in the electrical domain. In this talk, we present a comprehensive multi-dimensional simulation that links the photonic response and the carrier dynamic processes (generation, diffusion, drift, recombination, etc.) in the same numerical platform. The modelling technique allows us to extensively evaluate the light-trapping and electronic collection performance of different types of solar cells so that optimization strategies can be obtained. We will show in detail how the model is established in the Comsol environment, including the electromagnetic calculation, the link between the optical and electrical domains, the simulation of nonlinear dynamic behaviours of carriers, and the boundary/interface treatment. Finally, two application examples will be shown, including plasmonic and single-nanowire SCs based on various photovoltaic materials, with our experimental results provided for comparison.

Surface Texturing of High-power Flip-chip LEDs by Femtosecond Pulsed Laser-induced Periodic Structures

Yi-Hong Lin[1,2], **Yi-Hao Wang**[1,2], **Ping-Han Wu**[3], **Chung-Wei Cheng**[3], **Hsiang-Chen Wang**[1,2], **and Raymond Chien-Chao Tsiang**[4]

[1]Graduate Institute of Opto-Mechatronics, National Chung Cheng University
168, University Rd., Min-Hsiung, Chia-Yi 62102, Taiwan
[2]Advanced Institute for Manufacturing with High-Tech Innovations (AIM-HI)
National Chung Cheng University, 168, University Rd., Min-Hsiung, Chia-Yi 62102, Taiwan
[3]ITRI South, Industrial Technology Research Institute
No. 8, Gongyan Rd., Liujia District, Tainan 73445, Taiwan
[4]Department of Chemical Engineering, National Chung Cheng University
168, University Rd., Min-Hsiung, Chia-Yi 62102, Taiwan

Abstract— We report on the femtosecond laser direct structuring of the sapphire flip side surfaces of high-power flip-chip LEDs by laser-induced-periodic-surface-structures (LIPSS). It was found that the period of the laser-induced ripples was much dependent on the incident laser fluence. Through finely adjusting laser fluence and pulse number, uniform ripples could be formed on the sapphire surface. This method enables the control of the structure sizes with high precision. Our study shows that the light extraction from such LEDs increases strongly with increasing line sizes.

Conjugated Polymers in Nanopatterned Photovoltaic Cells for Efficient Light Harvesting

Eunkyoung Kim
Department of Chemical and Biomolecular Engineering, Yonsei University
50 Yonsei-ro, Seodaemun-gu, Seoul 120-749, South Korea

Abstract— A simple, fast, and universal nanopatterning methodology was explored for boosting the light harvesting efficiency of photovoltaic cells containing conjugated polymers (CPs), by a light-trapping technique. By using readily available pastes and elastomeric nanostamps, well-arrayed mesoporous inorganic oxide films were prepared. The nanopatterned film was applied in dye-sensitized solar cells (DSSCs) as a potoelectrode that contained CP as a hole conductor. In this structure CPs were grown in situ via solid state polymerization, inside nanopores of mesoporous inorganic oxide to give conductive channels as polymerization proceeds. The iodine-free solid-state DSSCs with N719 dye showed a 40% increase in the current density and high efficiency, reaching 7.03%, which is one of the highest values reported for I_2-free solid-state DSSCs with N719 dye to date. Our approach with direct nanopatterning of mesoporous inorganic oxide films was scalable to large areas and universally applicable to a variety of solar cells utilizing inorganic oxides, quantum dots, or organic materials. Further application of the light-trapping nanostructure using different oxides and polymers will be discussed.

REFERENCES

1. Kim, J., J. Koh, B. Kim, J. Kim, and E. Kim, "Nanopatterning of mesoporous inorganic oxide films for efficient light harvesting of dye-sensitized solar cells," *Angew. Chem. Int. Ed.*, Vol. 51, No. 28, 6864, 2012.
2. Bhuvana, T., B. Kim, X. Yang, H. Shin, and E. Kim, "Reversible full color generation with yellow electrochromic polymer patterns," *Angew. Chem. Int. Ed.*, Vol. 52, No. 4, 1180, 2013.
3. Kim, J., J. Koh, B. Kim, S. Ahn, H. Ahn, D. Ryu, J. Kim, and E. Kim, "Enhanced performance of I_2-free solid-state dye-sensitized solar cells with conductive polymer up to 6.8%," *Adv. Funct. Mater.*, Vol. 23, No. 36, 4168, 2011.

Session 3P5
SC2: Effective Medium Theories and Homogenization

Frequency-dependent Corrections in the Theory of Homogenization of Hyperbolic Metamaterials
Lyudmila Gumen, Edgar Reyes Ayona, Jesus Arriaga, Arkadii A. Krokhin, ... 1162

Effective Material Parameters of Hyperbolic Metamaterials with Hydrodynamic Nonlocal Response
Wei Yan, Martijn Wubs, N. Asger Mortensen, ... 1163

Retrieving Electromagnetic Properties of Anisotropic Magnetic Metamaterials: An Effective-medium Theory
Shiyang Liu, Zhifang Lin, Siu-Tat Chui, ... 1164

Effective-medium Properties of Meta-materials Studied by a Quasi-mode Method
Shulin Sun, Lei Zhou, ... 1165

Photonic Band Engineering of Zero-refractive-index Materials
Zhi Hong Hang, ... 1166

Dispersion Engineering through Mixing Formulas
Ari Henrik Sihvola, Henrik Wallen, ... 1167

Equal-potential Approach to Realize the Homogenization of Metamaterials
Liang Peng, Niels Asger Mortensen, ... 1168

Effective Medium Obtained by Eigenmode Boundary Field Analysis
Yun Lai, Y. Wu, P. Sheng, Z. Q. Zhang, ... 1169

Theory of the Photoelastic Effect and Effective Photoelastic Constants of 2-D Photonic Crystals
Zoya A. Pyatakova, ... 1170

Theoretical Design of a Two-dimensional Acoustic Metafluid with Anisotropic Effective Mass Density
Jesus Arriaga, Lyudmila Gumen, Arkadii A. Krokhin, ... 1171

Bubbly Water as a Dispersive Acoustic Metamaterial
Pi-Gang Luan, Kao-Der Chang, ... 1172

Dark Acoustic Metamaterials
Jun Mei, Guancong Ma, Min Yang, Zhiyu Yang, Weijia Wen, Ping Sheng, ... 1173

3D Numerical Simulations and Measurements of Effective Dielectric Properties of Oil-in-Water Emulsions
Jan Vrba, Jr., ... 1174

Frequency-dependent Corrections in the Theory of Homogenization of Hyperbolic Metamaterials

Lyudmila Gumen[1], **Edgar Reyes Ayona**[2], **Jesús Arriaga**[2], **and Arkadii Krokhin**[3]

[1]Universidad Popular Autónoma del Estado de Puebla, Mexico
[2]Universidad Autónoma de Puebla, Mexico
[3]University of North Texas, USA

Abstract— Modeling and design of layered hyperbolic metamaterials is based on the well-known results for the components of dielectric tensor of binary superlattice

$$\varepsilon_{\parallel} = f\varepsilon_m + (1-f)\varepsilon_d, \quad \frac{1}{\varepsilon_{\perp}} = \frac{f}{\varepsilon_m} + \frac{1-f}{\varepsilon_d}. \tag{1}$$

Here ε_m and ε_d are the dielectric constants of the constituents and f is the filling fraction of the material m. While these equations are obtained in the static limit ($\omega \to 0$) they are frequently used for metallo-dielectric structures where $\varepsilon_m(\omega \to 0) \to -\infty$. This singular behavior of the dielectric function of metal leads to formation of gap at low frequencies and plasma-like dispersion relation for the Bloch modes of 1D photonic crystal. Relations (1) are valid for frequencies above the gap but below the first photonic band gap, i.e., in the long-wavelength limit, where the wavelength exceeds the period of the structure, $\lambda \gg d$. Metal, however, exhibits strong frequency dispersion even in the long-wavelength limit giving rise to considerable disagreement between the results of the effective-medium theory Eq. (1) and exact values of the dielectric tensor [1].

Here we propose a method of calculation of frequency-dependent corrections to the electrostatic formulas (1). We consider propagation along the axis of a periodic structure with period $d = a+b$ where $\varepsilon_m = \varepsilon_m(\omega) < 0$. The dispersion relation in this case is given by the following Rytov equation:

$$\cos kd = \cosh\left(\frac{\omega a}{c}\sqrt{|\varepsilon_m|}\right)\cos\left(\frac{\omega b}{c}\sqrt{\varepsilon_b}\right) - \frac{1}{2}\left(\sqrt{\frac{\varepsilon_b}{|\varepsilon_m|}} - \sqrt{\frac{|\varepsilon_m|}{\varepsilon_b}}\right)\sinh\left(\frac{\omega a}{c}\sqrt{|\varepsilon_m|}\right)\sin\left(\frac{\omega b}{c}\sqrt{\varepsilon_b}\right). \tag{2}$$

In the long-wavelength limit, $kd \ll 1$, the effects of frequency dispersion becomes essential when the phase accumulated in the metallic layer is much greater than that in the dielectric layer, i.e.

$$\frac{\omega b}{c}\sqrt{\varepsilon_b} \ll 1, \quad \frac{\omega a}{c}\sqrt{|\varepsilon_m|} \sim 1. \tag{3}$$

Expansion of the trigonometric functions in Eq. (2) leads to a simplified dispersion relation $k = k(\omega)$. This relation can be used for calculation of the phase and group velocities,

$$V_{ph} = \frac{\omega}{k} = \frac{c}{n_{\parallel}(\omega)}, \quad V_g = \frac{d\omega}{dk} = \frac{c}{n_{\parallel} + \omega\frac{dn_{\parallel}}{d\omega}}. \tag{4}$$

Here $n_{\parallel}(\omega)$ is the effective index of refraction for propagation along the direction of periodicity. Forming a product $c^2/(V_{ph}V_g)$ we come to the following differential equation for $n_{\parallel}^2(\omega)$:

$$n_{\parallel}^2(\omega) + \frac{1}{2}\omega\frac{dn_{\parallel}^2}{d\omega} = f\varepsilon_m(\omega) + (1-f)\varepsilon_d + \phi(\omega). \tag{5}$$

Here function $\phi(\omega)$ contains frequency-dependent corrections obtained from the long-wavelength expansion of Eq. (2). Solution of differential Eq. (5) leads to the effective dielectric function $\varepsilon_{\parallel}(\omega) = n_{\parallel}^2(\omega)$ which gives better approximation than the static value Eq. (1). Similar procedure is also applicable for calculation of frequency-dependent corrections to the static result for $\varepsilon_{\perp}$. Analytical and numerical results for these dielectric function will be presented.

REFERENCES

1. Orlov, A. A, P. M. Voroshilov, P. A. Belov, and Y. S. Kivshar, "Engineered optical nonlocality in nanostructured metamaterials," *Phys. Rev. B*, Vol. 84, 045424, 2011.

Effective Material Parameters of Hyperbolic Metamaterials with Hydrodynamic Nonlocal Response

Wei Yan, Martijn Wubs, and N. Asger Mortensen
DTU Fotonik, Department of Photonics Engineering
Technical University of Denmark, DK-2800 Kongens Lyngby, Denmark

Abstract— Hyperbolic metamaterials (HMMs), owing an indefinite permittivity or permeability tensor, have a novel hyperbolic dispersion curve without cut-off, which leads to a lot of interesting phenomena and applications, e.g., evanescent wave transport for perfect imaging, and enhanced light matter interaction. Usually, HMMs are composed of periodic metal-dielectric structure, and are described by macroscopical effective material parameters in the local response approximation (LRA). Here, beyond the LRA, we take the nonlocal response of free electron gas in the metal into account based on a linearized semi-classical hydrodynamics model, and derive the nonlocal corrected effective material parameters. It is demonstrated that, in both weak and strong nonlocal response regime, i.e., the nonlocal longitudinal wavelength is much larger than the unit-cell (weak regime) or comparable with the unit-cell (strong regime), the nonlocal response shows an important role in modifying effective material parameters, and accordingly distorts the hyperbolic dispersion curve. Further, based on the corrected material parameters, we investigate how the nonlocal response affects the imaging performance of a HMM lens, and setting up a ceiling for the density of states.

Retrieving Electromagnetic Properties of Anisotropic Magnetic Metamaterials: An Effective-medium Theory

Shiyang Liu[1, 2], **Zhifang Lin**[2], **and S. T. Chui**[3]

[1]Institute of Information Optics, Zhejiang Normal University, Jinhua, Zhejiang 321004, China
[2]State Key Laboratory of Surface Physics (SKLSP), Key Laboratory of Micro and Nano Photonic Structures (Ministry of Education), Department of Physics, Fudan University, Shanghai 200433, China
[3]Bartol Research Institute, University of Delaware, Newark, DE 19716, USA

Abstract— By arranging an array of single-crystal yttrium-iron-garnet (YIG) ferrite rods periodically in the air, we construct a kind of metamaterials with intrinsic magnetic response. It is accordingly called magnetic metamaterials (MMs). To investigate the electromagnetic (EM) properties of MMs, we develop an effective-medium theory (EMT) based on coherent potential approximation. It is demonstrated that a negative index metamaterial (NIM) is realized by use of MM, which can be magnetically tuned by an external magnetic field (EMF) from a negative index to positive index. This can be corroborated by the calculation of the photonic band diagrams and the effective constitutive parameters. In addition, a nonreciprocal magnetic surface plasmon (MSP) resonance can be excited at the surface of an MM slab.

Effective-medium Properties of Meta-materials Studied by a Quasi-mode Method

Shulin Sun[1, 2] **and Lei Zhou**[1]

[1]Surface Physics Laboratory (State Key Laboratory), Physics Department
Fudan University, Shanghai 200433, China
[2]National Center for Theoretical Sciences at Taipei (Physics Division), Department of Physics
National Taiwan University, Taipei 10617, Taiwan

Abstract— In the spirit of the generalized coherent potential approximation, we established a "quasi-mode" method [1] to study the effective medium properties of electromagnetic (EM) meta-materials. Embedding the meta-material under study into a background medium with tunable permittivity and permeability, we calculate the Green's functions of EM waves traveling inside the medium by considering the scatterings caused by the meta-material. The density of states (DOS), the self-energy, and the mean free path of a mode can be calculated with the knowledge of the Green's function given. The effective permittivity and permeability of the meta-materials can then be determined by maximizing the DOS, which is a function of the permittivity and permeability of the background medium. Compared with the standard S-parameter retrieval method [2], the present approach overcomes the multiple solution problems that exist in previous methods. Moreover, the "mean free path" obtained in present method is helpful to judge qualitatively how good are the effective medium parameters that we obtained for the meta-materials. As the illustrations of our theory, we performed numerical calculations based on the finite element method to study the effective-medium properties of both split ring and metallic wire resonators. Recently, we introduced a new three-dimensional negative refraction index meta-material in near-infrared region with a broad band. The optical response is quite robust against the position deviation of the structure. Based on the numerical simulations, the effective medium parameters and negative refraction effect are systematically studied.

Photonic Band Engineering of Zero-refractive-index Materials

Zhi Hong Hang
Department of Physics, Soochow University, 1, Shizi Street, Suzhou 215006, China

Abstract— Using two-dimensional photonic crystals, we successfully constructed a zero-index material, with both permittivity and permeability equal to zero [1]. By carefully tuning the properties of photonic crystal cylinders, a triply-degenerate state at the Brillion zone center can be formed and with the help of effective medium theory, the effective parameter of this photonic crystal can be described.

Though our major previous works concentrated on the interesting wave propagation properties inside this zero-refractive-index photonic crystal, the accidental degeneracy induced triply-degenerate states have very fruitful physics to be discussed. The band diagram will strongly affect the electromagnetic pulse propagation inside the photonic crystal. The linear dispersions form Dirac-like cones and induce Zitterbewegung-like phenomenon to incident electromagnetic pulse while the coupling to the extra magnetic longitudinal band sheet will cause multi-component oscillations of the transmitted pulse. Anomalous Doppler effect is also one of the charming characteristics of photonic crystals. We will show, with the complex band diagram, the Doppler effect inside this zero-refractive-index photonic crystal is also interesting. By breaking the symmetry of the zero-index photonic crystal, we can engineer the photonic band diagram and tune the electromagnetic wave propagation properties. The photonic band engineering method discussed can also be applied to other two- and three-dimensional photonic crystals with different lattice symmetries.

REFERENCES

1. Huang, X., Y. Lai, Z. H. Hang, H. Zheng, and C. T. Chan, "Dirac cones induced by accidental degeneracy in photonic crystals and zero-refractive-index materials," *Nature Materials*, Vol. 10, 582, 2011.

Dispersion Engineering through Mixing Formulas

A. Sihvola and H. Wallén
Department of Radio Science and Engineering
Aalto University School of Electrical Engineering, Espoo, Finland

Abstract— Matter and geometry are intimately connected in electromagnetics. On one hand, material objects can be defined by their boundaries and internal geometrical structures, and on the other, the microgeometry determines the macroscopic electromagnetic response of the material sample. Hence it is also to be expected that geometrical parameters of the microstructure of a piece of material affect its dispersive characteristics (dispersion meaning here the frequency dependence of electromagnetic material parameters). Insulating boundaries stop current flow in media that contain conducting inclusions, polarization concentration across inclusions produce dipole moments that vibrate following the incident radiation, and geometry-dictated resonances shape the response function of the composite medium. Dispersion of a composite is hence a function of all the components' dispersions, and this function is moulded by the structural geometric parameters. This observation gives possibilities to engineer desired dispersion characteristics by tailoring the internal material structure in a clever way.

As has been shown [1], using mixing formulas, certain basic principles can be derived which tell how the dispersive function of the component materials are transformed to another type of dispersion in the homogenized composite. As examples we may list the mixing-forced change of the relaxation frequency in mixtures containing polar inclusions (Debye dispersion) and the transformation of a Drude-type dispersion typical of noble metals into a resonating Lorentz-dispersion when the metal inclusions are non-touching in the composite. Dispersion metamorphoses of this type and more general ones will be analyzed in the talk.

REFERENCES

1. Sihvola, A. and H. Wallén, "Homogenization of amorphous media," *Amorphous Nanophotonics*, Rockstuhl and Scharf, Ed., Springer, 2013.

Equal-potential Approach to Realize the Homogenization of Metamaterials

Liang Peng[1] **and Niels Asger Mortensen**[2]

[1]Department of Electronic Engineering and Information Science
Hangdian University, Hangzhou, China
[2]Department of Photonics Engineering, Technical University of Denmark
Kongens Lyngby, Denmark

Abstract— We propose a general description of electrically induced resonances (EIR) in metamaterials (MMs) comprising subwavelength unit cells. Based on classical electrodynamics, we found that EIR is governed by an equal-potential effect. Our theory accounts for the EIR phenomena and can give a renewed definition of the effective electric field and hence effective permittivity for MMs made of either dielectrics or metals as well as combinations thereof. The EIR, inherent to the periodic structures, may be the unifying origin of recently observed anomalous electromagnetic phenomena, e.g., the enhanced transmission, the suppressed transmission and the enhanced absorption by a variety of metal film structures in the terahertz range.

In the design and fabrication of MMs, metallic structures are successfully being applied in the microwave range. At the same time, rod-type structures made of dielectrics with a large permittivity have also been suggested as another route potentially applied in the terahertz and optical range. Although these two classes of MMs can realize similar macroscopic EM responses such as anomalous effective permittivity, they do not seem connected due to the apparent different theory bases and design methodologies, which indicates that the common physics behind the MMs still needs to be revealed. In order to clearly advance our fundamental understanding of those EM phenomena in MMs, a unifying theoretical description is essential. The scalar potential offers an attractive solution to this challenge.

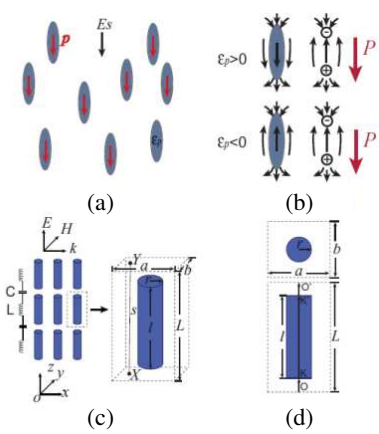

Figure 1: Polarization of MMs.

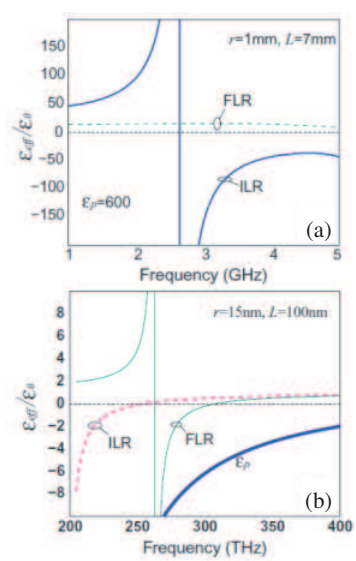

Figure 2: Dispersive permittivity.

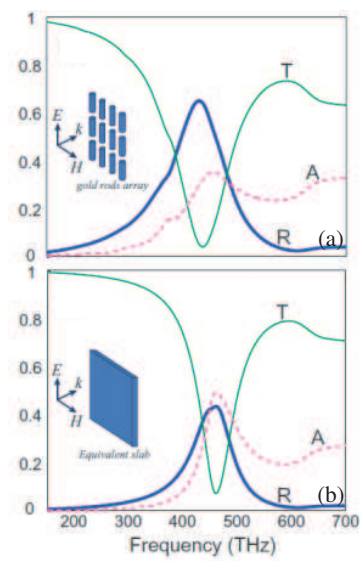

Figure 3: EM response of MMs.

ACKNOWLEDGMENT

This work was financially supported by the Starting Program of Hangdian University (No. KYS045612004).

REFERENCES

1. Peng, L. and N. A. Mortensen, "Equal-potential interpretation of electrically induced resonances in metamaterials," *New Journal of Physics*, Vol. 13, 053012, 2011.

Effective Medium Obtained by Eigenmode Boundary Field Analysis

Y. Lai[1], **Y. Wu**[2], **P. Sheng**[3], **and Z. Q. Zhang**[3]

[1]Wave Functional Materials Lab, School of Physical Science and Technology
Soochow University, Suzhou, China
[2]Division of Mathematical and Computer Sciences and Engineering
King Abdullah University of Science and Technology
Thuwal 23955-6900, Kingdom of Saudi Arabia
[3]Department of Physics, Hong Kong University of Science and Technology
Clear Water Bay, Kowloon, Hong Kong, China

Abstract— A large variety of metamaterials may be regarded as effective medium described by several effective parameters. Due to the local resonances within metamaterial building blocks, the effective parameters cannot be simply obtained by previous effective medium theories which are obtained in the quasi-static limit. This makes effective medium description of metamaterials an extremely interesting topic.

In this work [1, 2], we try to obtain the effective medium parameters from analysis on the eigenmode boundary fields. It is shown that these boundary fields carries the enough information to describe the physical properties of metamaterials and therefore, may be used to retrieve effective medium parameters.

We demonstrate two examples: one is an elastic metamaterial comprised of complicated structures [2]. By analyzing the eigen-mode boundary fields, we successfully described the metamaterial with a set of parameters and predicted unusual acoustic propagation in this metamaterial. Another example is an electromagnetic metamaterial which exhibits zero parameters [1]. Again, we successfully retrieved zero indexes as well as the finite group velocity when permittivity and permeability are near zero.

REFERENCES

1. Lai, Y., et al., to be published.
2. Lai, Y., Y. Wu, P. Sheng, and Z. Q. Zhang, "Hybrid elastic solids," *Nature Materials*, Vol. 10, 620, 2011.

Theory of the Photoelastic Effect and Effective Photoelastic Constants of 2-D Photonic Crystals

Z. A. Pyatakova
Gubkin Russian State University of Oil and Gas, Russia

Abstract— Photonic crystals (PC) are prospective media for acousto-optic devices because their photoelastic parameters are not limited to material constants and can be controlled by means of structuring [1, 2]. Photoelastic effect in photonic crystals cannot be reduced to photoelastic effects in its components, and its consequent theory is now developing. There are at least three mechanisms of the influence of elastic wave on optical parameters of photonic crystals:

1) modulation of material dielectric constants ε_1 and ε_2,

2) modulation of the shape of inclusions,

3) modulation of the lattice period.

The aim of the present work is to estimate the relative contribution of each from these mechanisms that can help engineers to construct effective photoelastic media based on photonic crystals. We consider an infinite 2-D photonic crystal (Fig. 1) from two materials — matrix and cylindrical inclusions which form square lattice. Acoustic and electromagnetic waves are incident in-plane, acoustic wave can be longitudinal or shear, electromagnetic has TE or TM polarization.

We analyzed the relative influence of these mechanisms on the optical properties of photonic crystals with different refractive index contrasts. The results of calculation show that mechanism 3 — modulation of the lattice period — gives very weak influence comparable to others. Mechanism 2 is sufficient for photonic crystals with high refractive index contrast, so such structures can be used as effective photoelastic media. We also found that different mechanisms can destructively interfere with each other in a certain range of filling factors, and good photoelastic parameters of matrix and inclusions not guarantee that photonic crystal would have good photoelastic properties.

On the basis of analytical model for acousto-optical figure of merit of photonic crystals [3] we developed analytical formulae for effective photoelastic constants of photonic crystals for different polarizations of light and sound. It is shown that effective photoelastic constant strongly depend on filling factor and angle between wavevectors of light and sound, and it is maximum than light and sound are collinear. So, developed theory allows optimization of photonic crystals for applications in acousto-optics.

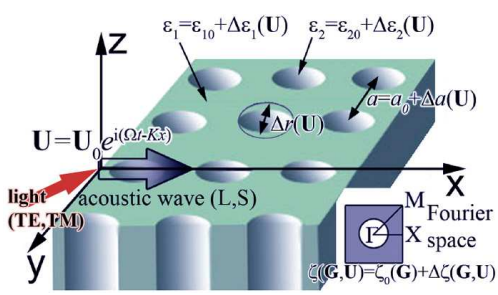

Figure 1: Geometry of the problem: 2D PC with square lattice.

REFERENCES

1. Krishnamurthy, S. and P. V. Santos, "Optical modulation in photonic band gap structures by surface acoustic waves," *J. Appl. Phys.*, Vol. 96, 1803, 2004.
2. Ma, H., S. Qu. and Z. Xu, "Photonic crystals based on acousto-optic effects," *J. Appl. Phys.*, Vol. 103, 104904, 2008.
3. Pyatakova, Z. A. and G. V. Belokopytov, "Acousto-optic efficiency of 2-dimensional photonic crystals," *Technical Physics Letters*, Vol. 37, No. 1, 1–4, 2011.

Theoretical Design of a Two-dimensional Acoustic Metafluid with Anisotropic Effective Mass Density

J. Arriaga[1], **L. Gumen**[2], **and A. A. Krokhin**[3]

[1]Instituto de Física, Benemérita Universidad Autónoma de Puebla
18 Sur y San Claudio, Edif. 110 B, Ciudad Universitaria, Puebla 72570, México
[2]Universidad Popular Autónoma del Estado de Puebla, 21 Sur 11, Puebla 72160, México
[3]Department of Physics, University of North Texas
1155 Union Circle 311427, Denton, TX 76203, USA

Abstract— The effective mass density is one of the most basic and important parameters in the study of elastic wave interactions with materials. In this work, we report an effective dynamic mass density for a two-component, two-dimensional (2D) periodic fluidCsolid composite in which the fluid constitutes the host medium. Fluids and glasses are naturally isotropic in the absence of external fields, and anisotropy is a property which is usually associated with crystal solids. Anisotropy may, however, be artificially stimulated by embedding periodic structures in naturally isotropic fluids. Then these artificial structures — so called phononic crystals — may have very unusual properties. Within a narrow band of frequencies of sound the effective mass or the effective elastic modulus of specially designed phononic crystals may become anisotropic, take negative values, or acquire abnormally large imaginary part. Due to such "strange" properties that do not exist for natural materials these artificial structures are usually called *metamaterials* or *metafluids*. Using the plane-waves expansion method proposed in Ref. [1] we derive (in the long wavelength limit) a formula for the effective mass tensor of the metafluid. The proposed formula is very general and it is valid for arbitrary Bravais lattices and arbitrary filling fractions of the cylinders. In particular, we calculate the effective mass tensor for sound waves in air with embedded lattice of aluminum cylinders having different cross sections. We consider cylinders with circular and triangular cross sections arranged in both rectangular and hexagonal lattice. The proposed method of calculation may find numerous applications for tailoring of metafluids with prescribed anisotropy which is necessary for design of acoustic cloaks [2].

REFERENCES

1. Krokhin, A. A., J. Arriaga, and L. Gumen, *Phys. Rev. Lett.*, Vol. 91, 264302, 2003.
2. Cummer, S. A. and D. Schurig, *New J. Phys.*, Vol. 9, 45, 2007.

Bubbly Water as a Dispersive Acoustic Metamaterial

Pi-Gang Luan[1] and Kao-Der Chang[2]

[1]Department of Optics and Photonics, National Central University, Jhongli 320, Taiwan
[2]Mechanical and Systems Research Laboratories, Industrial Technology Research Institute
Hsin-Chu City 31040, Taiwan

Abstract— A metamaterial usually refers to an artificial structure consisting of periodically arranged resonators having unusual properties such as negative index of refraction or strong anisotropy in a frequency range low enough so that the structure can be thought of as an effective medium [1]. In this paper, using a well known model in acoustic oceanography for describing the pulsating behavior of a single air bubble in water [2] under the influence of external sound field, we show that the composite system consisting of periodically arranged small bubbles in water is an acoustic metamaterial having negative dynamical modulus in a low frequency range [3]. According to this simple model, a bubble gluing with a layer of water pulsates back and forth like an isotropic oscillator, and the radial oscillating motion of this oscillator is coupled with the external sound field. When the frequency of the sound field is close to the resonance frequency of these oscillators, a band gap is created, just like a polariton band gap appears when electromagnetic waves are strongly coupled with the optical-branch phonons in an ionic crystal. For a low filling fraction of bubbles in water (0.1% or 1%), we estimate the upper and lower boundaries of the 'polariton gap', and find that the prediction agrees very well with the exact result obtained from the band gap calculation of this bubbly-water phononic crystal. Based on this model we further show that the acoustic energy density and the 'Poynting vector' (energy current density) of the sound field can be derived from the coupled dynamical equations of this acoustical-mechanical system. We also discuss how to construct the Lagrangian and Hamiltonian densities for this system so that we can study the dynamical behaviors of the polariton-like excitations in this medium using the language of field theory.

REFERENCES

1. Solymar, L. and E. Shamonina, *Waves in Metamaterials*, Oxford University, 2009.
2. Medwin, H. and C. S. Clay, *Fundamentals of Acoustical Oceanography*, Academic Press, 1997.
3. Fang, N., D. J. Xi, J. Xu, M. Ambati, W. Srituravanich, C. Sun, and X. Zhang, "Ultrasonic metamaterials with negative modulus," *Nature Materials*, Vol. 5, 452–456, 2006.

Dark Acoustic Metamaterials

Jun Mei[1], **Guancong Ma**[2], **Min Yang**[2], **Zhiyu Yang**[2], **Weijia Wen**[2], **and Ping Sheng**[2]

[1]Department of Physics, South China University of Science and Technology, Guangzhou 510641, China
[2]Department of Physics, Hong Kong University of Science and Technology, Hong Kong, China

Abstract— The attenuation of low-frequency sound has always been a challenging task because the intrinsic dissipation of materials is inherently weak in this regime. In this work, we show that by using thin elastic membranes decorated with designed patterns of rigid platelets, the resulting acoustic metamaterials can absorb 86% of the acoustic waves at $\sim$ 170 Hz, with two layers absorbing 99% at the lowest frequency resonant mode as well as at higher frequency modes. The sample is thus acoustically 'dark' at those frequencies. Finite element simulations of the resonant mode patterns and frequencies are in excellent agreement with the experiments. In particular, the measured displacement profiles of the resonant modes show discontinuities in the slope around the platelet perimeters, implying significantly enhanced curvature energy is concentrated in these small volumes, which are minimally coupled to the radiation modes. This thereby gives rise to strong absorption similar to a cavity system, even though the system is geometrically open. This is characterized by the fact that at resonances, the overall energy density in the system can be two to three orders of magnitude larger than the incident wave's energy density.

3D Numerical Simulations and Measurements of Effective Dielectric Properties of Oil-in-Water Emulsions

J. Vrba
Faculty of Biomedical Engineering, Czech Technical University in Prague, Czech Republic

Abstract— Results of laboratory and field tests have shown that the high-power MW-field-induced separation of Oil and Water (O-W) emulsions has a potential to become [1] a chemical-free alternative to conventional separation processes. The separation mechanism of this process has not been fully understood yet and there is a need for further research. An important area of this research is development of an accurate method for estimation of the effective dielectric properties of treated emulsions.

An existing 2D concept for the numerical estimation of effective dielectric properties of mixtures with random droplets' distribution [2–6] was adapted here and expanded into 3D.

As in the original concept [2–6], the electric field distribution is computed here with the commercial and well-proven FEM simulation tool COMSOL Multiphysics®. A MATLAB® script was written which automatically generates a random mixture (impenetrable spherical inclusions randomly placed in the cubic computation domain) and assigns a proper boundary condition to every face located on the outer walls of the computation domain as well as the corresponding dielectric parameters to each subdomain. The script also controls other simulation parameters, e.g., temperature and frequency, and it also starts the COMSOL simulation and performs evaluation of volume integrals in order to obtain the effective dielectric properties. The duration of one simulation is several minutes (approx. 2–4 min. depending on the complexity of the problem — oil/water volume fraction), therefore for each frequency and temperature even tens of simulations are manageable and statistical quantities, e.g., mean values and standard deviations, can be computed.

The expansion of the concept to 3D introduces a new possibility for direct comparison of simulation results with measured values. Here Water-in-Oil (W/O) as well as Oil-in-Water (O/W) emulsions were considered. First simulated effective permittivity of the both emulsion kinds were compared to data estimated using two mixing formulas: Maxwell Garnett and Bruggeman [7]. The Maxwell Garnett mixing formula fits better than the Bruggeman mixing formula. Especially for the O/W emulsion, the Maxwell Garnett mixing formula fits very well.

Furthermore, dielectric properties of O/W emulsions were measured using a commercial system Dielectric Probe Kit from Agilent Technologies®. The measured data were compared with the dielectric properties estimated using the Maxwell Garnett mixing formula and with the numerical concept. All three compared data fit well each other.

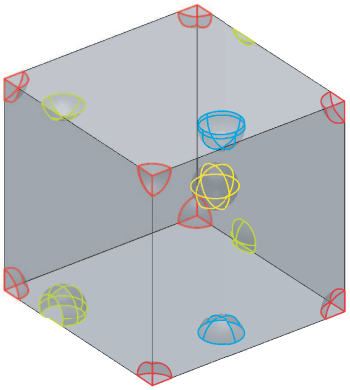

Figure 1: 3D view of a unit cell with 4 droplets in total. To make the geometry periodical with a spatial period in all three dimensions equal to the unit cell edge length a, the droplets exceeding unit cell side wall(s) have to have their counterpart on the opposite wall(s). Yellow, blue, green and red marked droplets exceed none, one, two and three unit cell walls, respectively.

REFERENCES

1. Hubrich, M., B. Schmidt, M. Kozariszczuk, A. John, R. H. Jansen, J. Vrba, and J. Wellenbuescher, "Ecologically friendly microwave treatment of oil emulsions as contribution to conserving resources by effluent free manufacture in industry," Project No. 01RI0616B, Tech. Rep. No. 4.61.163, VDEh-Betriebsforschungsinstitut GmbH (BFI), VDEh-Betriebsforschungsinstitut, Sohnstr. 65, Duesseldorf 40237, June 2010.
2. Krakovsky, I. and V. Myroshnychenko, "Modeling dielectric properties of composites by finite-element method," *Journal of Applied Physics*, Vol. 92, No. 11, 6743, 2002.
3. Brosseau, C., "A finite-element simulation study of the complex effective permittivity of two-phase random composite materials," *COMSOL Multiphysics Users Conference 2005*, November 2005.
4. Myroshnychenko, V. and C. Brosseau, "Finite-element method for calculation of the effective permittivity of random inhomogeneous media," *Physical Review E*, Vol. 71, 016701, January 2005.
5. Myroshnychenko, V. and C. Brosseau, "Finite-element modeling method for the prediction of the complex effective permittivity of two-phase random statistically isotropic heterostructures," *Journal of Applied Physics*, Vol. 97, No. 4, 044101, 2005.
6. Myroshnychenko, V. and C. Brosseau, "Effective complex permittivity of twophase random composite media: A test of the two exponent phenomenological percolation equation," *Journal of Applied Physics*, Vol. 103, No. 8, 084112, 2008.
7. Sihvola, A., *Electromagnetic Mixing Formulae and Applications*, The Institution of Engineering and Technology, May 2000.

Session 3P6
SC4: Active Antennas, MIMO and Beamforming Systems

Design of a Frequency and Null Switchable Microstrip Antenna
Ajit Yadav, Chinthana J. Panagamuwa, Robert D. Seager, ... 1178
Robust Antenna Array Beamforming under Some Uncertain Environment
Ju-Hong Lee, Wen-Chen Lo, ... 1179
Flexible 3-D Printed Substrates for Antenna Applications
S. S. Bukhari, William Whittow, ... 1181
Estimation of Direction of Arrival Algorithms
Tuna Orul, Erkan Afacan, ... 1182
Using Subwavelength Diffraction Gratings to Design Open Microwave Cavities
Matthieu Dupre, M. Fink, Geoffroy Lerosey, ... 1184
A Study of SNR Degradation due to Impedance Mismatch in ESPAR Antennas
V. Daskalaki, K. Maliatsos, Athanasios G. Kanatas, ... 1186
A Tunable Multiband Handset Antenna Operating at VHF and UHF Bands
Luyi Liu, Jonathan M. Rigelsford, Richard Langley, ... 1187
Antenna Array with Meshed Elements for Beamforming Applications
Eric R. Escobar, Nicholas J. Kirsch, R. Brough Turner, ... 1188
Compound Reconfiguration in Reflectarrays for Cognitive Radio Applications
Julien Perruisseau-Carrier, Eduardo Carrasco, ... 1189
Performance of Capacity Optimized Line-of-sight MIMO HAP-to-train Architectures
Emmanouel T. Michailidis, Paraskevi N. Daskalaki, Athanasios G. Kanatas, ... 1190
Actively-matched Antennas for UHF Applications
Khalid Z. Rajab, Deepak Singh Nagarkoti, Yifeng Fan, Yang Hao, ... 1192

Design of a Frequency and Null Switchable Microstrip Antenna

Ajit Yadav, **Chinthana Panagamuwa**, **and Robert Seager**
Centre for Mobile Communications Research
School of Electronic, Electrical and Systems Engineering
Loughborough University, Loughborough LE11 3TU, United Kingdom

Abstract— A compact microstrip patch antenna that is both frequency and beam switchable using RF PIN diodes is proposed in this paper. The antenna is able to switch between three distinct resonant frequencies and at each frequency, it switches its radiation pattern in five different directions. A major benefit of this antenna is that at each operational frequency, the impedance bandwidth remains unchanged as the radiation pattern nulls are switched between the five different directions. No additional phase shifters or impedance matching circuits are required to obtain the proposed reconfigurablity. The antenna is printed on low-cost FR4 substrate and measures only 40×40 mm in size. Simulated and measured scatter parameters, radiation patterns, and efficiency results are presented and discussed. The antenna is best suited for null steering applications in emerging wireless networks.

Robust Antenna Array Beamforming under Some Uncertain Environment

Ju-Hong Lee[1] and Wen-Chen Lo[2]

[1]Department of Electrical Engineering, Graduate Institute of Communication Engineering
Graduate Institute of Biomedical Electronics and Bioinformatics, National Taiwan University
No. 1, Sec. 4, Roosevelt Rd., Taipei 10617, Taiwan
[2]Graduate Institute of Communication Engineering, National Taiwan University
No. 1, Sec. 4, Roosevelt Rd., Taipei 10617, Taiwan

Abstract— This paper presents an adaptive antenna array beamformer with robust capabilities against an uncertain environment including steering angle mismatch and finite array data samples. To cope with the uncertainties, we develop an estimation method in conjunction with a support vector machine (SVM) to obtain an appropriate estimate of the actual array response vector for the desired signal and a SVM-based beamformer's weight vector. By using only the a *posteriori* information of the received antenna array data, the estimation method invokes an appropriate objective function and a gradient-based algorithm for the estimation of the desired signal's array response vector. Using the estimate of the desired signal's array response vector, we utilize a SVM-based iterative reweighted least-square (IRWLS) algorithm to find a weight vector for robust antenna array beamforming against the uncertain environment. The convergence property of the proposed method is guaranteed. The novelty of the proposed method is that using the estimation method provides a more appropriate guess for the actual array response vector to alleviate the difficulty of determining the angular mainlobe beamwidth (the uncertainty region) and the number of the constraint angles when using SVM-based beamforming techniques [1]. Moreover, using the SVM-based IRWLS algorithm enhances the capability of the estimation-based method [2] in dealing with strict restrictions on the number of available array data snapshots. We present a computer simulation example to show that the proposed method outperforms the existing techniques [1, 2] under the considered uncertainty.

Example: We use a uniform linear array with 8 array sensors and inter-element spacing equal to half of the desired signal wavelength. The background noise is white Gaussian with zero mean and variance equal to one. The desired signal with signal-to-noise ratio (SNR) 10 dB has 0° direction angle and two interferers with interference-to-noise ratio (INR) 20 dB have direction angles equal to 60 and 80 degrees, respectively. The simulation results of using the techniques of [1] and [2] are obtained by adjusting the required parameters to the optimal values for comparison. Figure 1 shows the array output signal-to-interference plus noise ratio (SINR) versus the number of array data snapshots for steering angle error = 2° after 50 Monte-Carlo runs. We note that the proposed method outperforms the techniques of [1] and [2] under finite data snapshot effect.

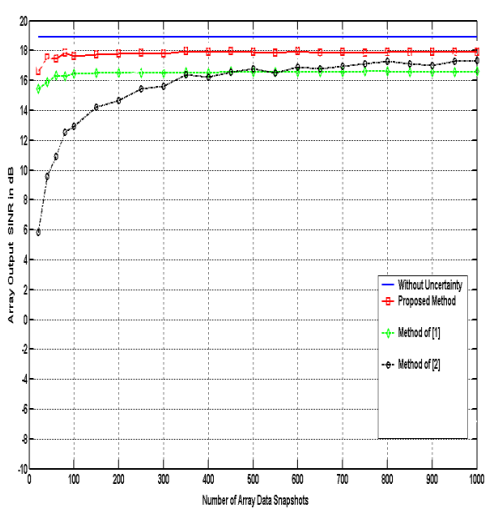

Figure 1.

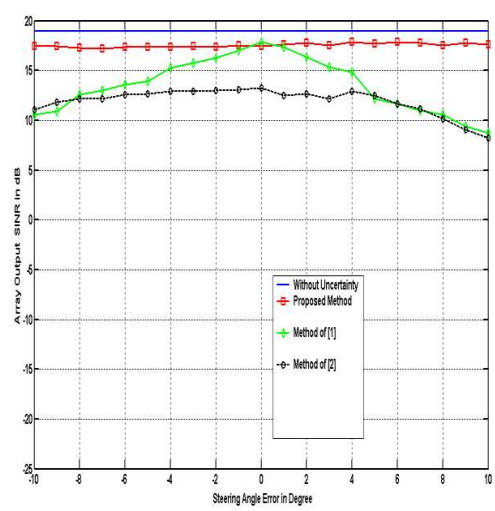

Figure 2.

Figure 2 depicts the array output SINR versus the steering angle error by using 100 array data snapshots after 50 Monte-Carlo runs. Again, we note that the proposed method outperforms the techniques of [1] and [2] for the considered uncertain environment.

REFERENCES

1. Gaudes, C. C., I. Santamaría, J. Vía, E. M. Gómez, and T. S. Paules, "Robust array beamforming with sidelobe control using support vector machines," *IEEE Trans. on Signal Processing*, Vol. 55, No. 2, 574–584, Feb. 2007.
2. Lee, J.-H., K.-P. Cheng, and C.-C. Wang, "Robust adaptive array beamforming under steering angle mismatch," *Signal Processing*, Vol. 86, No. 2, 296–309, Feb. 2006.

Flexible 3-D Printed Substrates for Antenna Applications

S. S. Bukhari and W. G. Whittow
School of Electronic, Electrical and Systems Engineering
Loughborough University, Loughborough, LE11 3TU, UK

Abstract— Consumer demand for small devices with wireless connectivity has put increasing pressure on antenna engineers to improve electromagnetic performance. These design constraints are exacerbated by increasing demand for improved bandwidth, efficiency and frequency coverage. It is often a challenging exercise to optimize the size-bandwidth-efficiency ratio [1].

This paper will investigate the effect of altering the dielectric substrate section of the antenna as opposed to the conducting elements. Previously, it has been established that creating textured dielectrics where the permittivity of the substrate is not uniform can lead to improved bandwidth [2], however, the geometries were difficult to fabricate using conventional methodologies. The advent of additive manufacturing (AM) techniques such as 3-D printing now enables any shape with intricate internal geometry to be created directly from a CAD file. These processes can potentially reduce costs by additively only using material where it is required. Currently, there are a wide range of polymers suitable for 3-D printing and these have a range of physical properties and flexible substrates can be easily created. This has direct relevance for wearable antenna systems. Furthermore, holes can be included to allow the antenna to be breathable. By leaving *gaps* in the CAD model — heterogeneous structures with air as the 2nd material can be considered. Emerging AM techniques allow multiple materials to be printed together and in the near future dielectrics and metals will be printable in one process. The author has previously shown that the heterogeneous substrates can be used to control multi-band performance [3] and 3D substrates can be used to improve EM performance [4].

REFERENCES

1. Wheeler, H. A., "Fundamental limitations of small antennas," *Proceedings of the IRE*, Vol. 35, No. 12, 1479–1484, 1947.
2. Psychoudakis, D., Y. H. Koh, J. L. Volakis, and J. H. Halloran, "Design method for aperture-coupled microstrip patch antennas on textured dielectric substrates," *IEEE Transactions on Antennas and Propagation*, Vol. 52, No. 10, 2763–2766, 2004.
3. Whittow, W. G., C. C. Njoku, Y. C. Vardaxoglou, and J. Joubert, "Designing multi-band and high bandwidth antennas with heterogeneous substrates," *IEEE Tropical Conference on Antennas and Propagation in Wireless Communications (APWC)*, 2012.
4. Whittow, W. G., "Microstrip patch antennas with 3-dimensional substrates," *Loughborough Antennas & Propagation Conference (LAPC)*, 2012.

Estimation of Direction of Arrival Algorithms

T. Orul[1] and E. Afacan[2]

[1]Ministry of Labour and Social Security, Turkey
[2]Electrical and Electronics Engineering Department, Gazi University, Turkey

Abstract— Determination of signal sources has been used for both military applications such as radar systems, location finding systems, electronic warfare systems and daily life applications such as mobile communication systems, the determination of mine reservations, the detection of illegal radio broadcasting and finding the lost mountaineers.

MUSIC and ESPRIT algorithms are two of the most widely known and used signal source estimation techniques. This study aims the comparison of the estimation performances of these two techniques.

In this study, the signals coming toward uniform linear antenna arrays are estimated using MUSIC and ESPRIT algorithm. Estimation performances of them related to signal arrival angle are compared with each other. Beside this comparison, effects of number of array elements, change in singal to noise ratio, number of signals and direction of arrival on estimation performance for MUSIC Algorithm are observed. On the other hand, effects of sampling frequency are observed for ESPRIT Algorithm in addition to the effects, which are observed for MUSIC Algorithm.

The obtained results show that MUSIC algorithm gives more accurate and definite results for moderately low SNR, whereas ESPRIT algorithm gives accurate results for moderately high SNR. (see Figure 1 and Table 1).

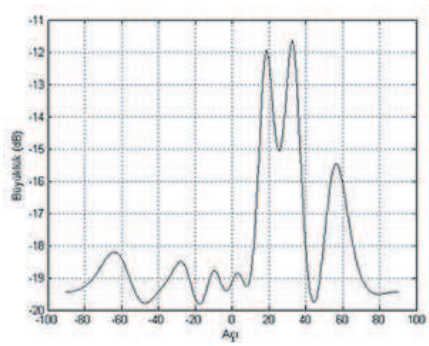

Figure 1: Estimation of direction of arrival for SNR = 0, $M = 10$, $D = 2$, Direction of arrival (θ) = 20, 30.

Table 1: Effects of SNR on estimation performances of ESPRIT algorithm ($M = 15$).

	Angle of arrival and Error Rate						Avg. Error Ratio (%)
SNR	°20	Error (%)	°50	Error (%)	°70	Error (%)	
0	6.71	66.40	18.05	63.89	62.63	10.51	46.93
10	19.69	1.54	30.86	38.27	60.48	13.59	17.80
20	5.45	72.70	22.23	55.52	64.09	8.42	45.55
30	20.70	3.53	55.99	11.99	62.79	10.28	8.604
40	19.95	0.24	49.34	1.30	69.35	0.91	0.821
60	20.01	0.07	50.45	0.90	69.95	0.06	0.346
80	19.99	0.00	50.01	0.03	70.02	0.03	0.024
100	20.00	0.00	50.00	0.00	69.99	0.00	0.00

On the other hand, when we looked at the effects of the number of array elements, the performances of both MUSIC and ESPRIT Algorithms are directly proportionate to this parameters. But, this increases computational complexity for MUSIC. Because of the fact that ESPRIT does not required scanning all space, it provides ease of calculation and decrease in capacity and cost.

REFERENCES

1. Schmidt, R. O., "Multiple emitter location and signal parameter estimation," *Proc. of RADC Spectrum Estimation Workshop*, 243–258, Griffiss AFB, NY, 1979.
2. Roy, R. and T. Kailath, "ESPRIT — Estimation of signal parameters via rotational invariance techniques," *IEEE Transactions on Acoustics, Speech and Signal Processing*, Vol. 37, No. 7, 1989.
3. Orul, T., "Direction of arrival estimation methods for smart antenna systems," M.Sc. Thesis, Institute of Science and Technology, Gazi University, Ankara, Turkey, June 2012.

Using Subwavelength Diffraction Gratings to Design Open Microwave Cavities

M. Dupré, M. Fink, and G. Lerosey
Institut Langevin, ESPCI ParisTech & CNRS, France

Abstract— Wave propagation in microwave cavities is a major topic of interest in various fields of research ranging from fundamental physics with the notions of quantum fidelity or level repulsion of states, to electrical engineering which embraces electromagnetic compatibility and antenna measurements. The behavior of waves in such complex media can be analytically calculated for the case of regular cavities and many statistical approaches have been proposed to predict it in chaotic ones [1, 2]. Up to date, most works devoted to these propagation media concentrated on the study of the wave fields inside the cavities, since the latter are usually 2D or 3D shapes enclosed by metallic walls which conceal the electromagnetic fields perfectly. The usual way to couple such cavities to the exterior consists in carving a hole which supports propagating modes in one of its metallic walls, hence realizing so called open microwave cavities in fundamental physics, or cavity backed slot antennas in electrical engineering [3]. In the optical domain, however, open cavities have been studied for a long time. Indeed, at those frequencies metals are no longer good conductors, and a silver film a hundred nanometer thick constitutes a semi-transparent mirror. Such mirrors have been used intensively to devise lasers for instance. Similarly high contrast subwavelength gratings have been used recently in so called vertical-cavity surface-emitting laser [4].

Here we propose to use binary subwavelength gratings, which are periodic patterns of metal and dielectric organized at the subwavelength scale, as semi-transparent mirrors for cavities at any frequency. We show that tuning the geometrical parameters of such gratings permits to obtain a mirror with any desired transparency. Replacing one of the walls of a cavity by a subwavelength grating, we achieve a quasi 2 dimensional microwave open cavity. We show that it gives rise to a specific radiation pattern in the far field with only discrete frequencies and angles of emission. Hence we make an antenna which directivity is dependent on the frequency. We prove that going from a regular to a chaotic cavity, the radiation pattern tends to become isotropic.

It is well known that in a microwave cavity, only quantized frequencies are allowed, due to boundary conditions that impose to the tangential electric field and normal magnetic field to be zero on a perfectly conducting wall. A sub-wavelength grating placed on one wall of the cavity introduces radiative losses. Sub-wavelength holes and gratings have a very poor transmittance, but this is an advantage in our case: the sub-wavelength grating behaves as a mirror with a reflection coefficient which can be very high. The transmission coefficient is tunable through the fill factor of the grating, directly impacting the Q factor and the bandwidth of the resonances.

Sub-wavelength gratings are known to only transmit the zero order to the far field. This means that wave vectors are conserved: a stationary wave of a given wave vector in the cavity radiates a propagating wave of the same wave vector. Hence, in the case of a 2D cavity and for a given mode (n_x, n_y) of frequency f_{n_x,n_y}, only a propagating wave of wave vector $\mathbf{k_{n_x,n_y}}$ radiates to the far-field. This corresponds to an angle $\theta_{n_x,n_y} = \pm\arctan(\frac{n_x}{n_y}\frac{L_y}{L_x})$ as shown on the Fig. 1. We can see that the cavity only emits in a given direction for a given frequency. Then we discuss what is expected if we introduce disorder in the cavity, by considering a chaotic cavity or a random

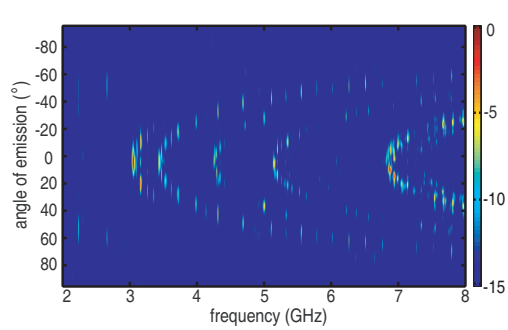

Figure 1: Measure of the emission pattern (dB).

grating. We show that the emission pattern tends to become isotropic. Indeed, randomizing the grating broadens the angular pattern at a given frequency, while a chaotic cavity gives rise to distribution of wave vectors that is no longer discrete. We believe that this type of open microwave cavity will have many applications, for instance to design highly directive antennas, MIMO antennas, radars or detectors, or to study the physics of open cavities.

REFERENCES

1. Stein, J. and H.-J. Stöckmann, "Experimental determination of billiard wave functions," *Phys. Rev. Lett.*, Vol. 68, 2867, 1992.
2. Gutzwiller, M. C., "Periodic orbits and classical quantization conditions," *Journ. of Math. Phys.*, Vol. 12, 343, 1971.
3. Stevenson, A. F., "Theory of slots in rectangular wave-guides," *Journ. of Appl. Phys.*, Vol. 19, 24, 1948.
4. Huang, M. C. Y., et al., "A surface-emitting laser incorporating a high-index-contrast subwavelength grating," *Nat. Photon.*, Vol. 1, 119, 2007.

A Study of SNR Degradation due to Impedance Mismatch in ESPAR Antennas

P. Daskalaki, K. Maliatsos, and A. G. Kanatas
Department of Digital Systems, University of Piraeus, Greece

Abstract— The deployment of conventional MIMO systems at mobile terminals has been delayed due to implementation difficulties regarding the required array size and the need for multiple RF chains. The recently introduced Beamspace MIMO (BS-MIMO) can offer high multiplexing and beamforming capabilities using a single active element and a number of parasitic elements. Moreover, BS-MIMO benefits from the use of compact array geometries. Electrically-Steerable Parasitic Array Radiator (ESPAR) antennas are a perfect fit for the beamspace concept and it was shown that they can provide the needed aerial degrees of freedom for beamspace transmission outperforming conventional systems for small inter-element distances. Beamspace processing using ESPAR antennas is performed with the application of appropriate values to the time-varying reactance loads at the parasitic elements. The use of ESPAR arrays in BS-MIMO induces several research challenges. Due to strong mutual coupling, the feeding of the active element is responsible for the currents induced to the parasitic elements. The reconfigurable antenna pattern produced from the BS-MIMO system can be determined with proper selection of the mutual impedance matrix and the load matrix that are used to mathematically calculate the currents at the antenna elements. However, the dynamic variation of the reactance values at the parasitic elements will also change the impedance value at the active element, an effect that is not yet taken into account to the mathematical model that describes the array. This paper presents results for the SNR degradation due to the impedance mismatch of the active element for ESPAR antennas. Simulation results are provided, while the non-linear relationship between the loading matrix and the radiation patterns is examined thoroughly. Moreover, a comparison of the radiation patterns and the SNR degradation for various ESPAR antennas is conducted, as well as the impact of the mismatch to the achieved degrees of freedom by each array is determined. Finally, the effect of the mismatch at the performance of a BS-MIMO system is evaluated.

A Tunable Multiband Handset Antenna Operating at VHF and UHF Bands

Luyi Liu[1], **Jonathan M. Rigelsford**[2], **and Richard Langley**[2]

[1]Antenova Ltd., Stow-cum-Quy, Cambridge, CB25 9AR, UK
[2]Department of Electronic & Electrical Engineering, The University of Sheffield
Mappin Street, Sheffield S1 3JD, United Kingdom

Abstract— Cognitive radio requirements demand reconfigurability from mobile devices ranging from base stations to telephone handsets. Changing the resonant frequency of an antenna can be achieved in many ways, for example by using pin diodes, varactor diodes and MEMs switches and by varying substrate permittivity using nematic liquid crystals (LC), ferrites or ferroelectrics.

Broadcast channel reception is becoming more desirable for modern mobile phone handsets. FM radio (88–108 MHz) and DVB-H (digital video broadcasting — handheld, 470–702 MHz) antennas present some of the most challenging requirements due to the low frequency of the broadcasts. DVB-H features a large fractional bandwidth ($\sim 40\%$) and low operating frequency (470–702 MHz). This is reflected in the implementation guidelines, currently indicating a realized gain of -10 dBi (at 470 MHz) to -7 dBi (at 702 MHz) as acceptable, where the realized gain G is gain reduced by the matching losses. In comparison, FM radio with 20.8% fractional bandwidth at around 100 MHz is even more difficult to realize due to its very low operating frequency, although there are currently no specified requirements for gain or radiation efficiency. Therefore, producing an antenna with acceptable antenna characteristics which operates over a wide frequency band from 88MHz to 2175 MHz, is a huge challenge for low frequency mobile terminal antenna designs where the physical size of the terminal is so small particularly near 100 MHz.

This paper presents a compact multiband tunable PIFA system which is operational from 88 to 2175 MHz whereby a varactor diode is used as an active tuning component. The antenna was designed to cover the mobile telephone bands (GSM850, 900, 1800, 1900, UMTS) by controlling the value of the capacitance across the gap in the slotted PIFA. FM radio (76–108 MHz) and mobile television DVB-H (470–702 MHz) broadcast bands were added by designing an appropriate matching circuit into the system. The antenna measured $\lambda/15 \times \lambda/43 \times \lambda/91$ at 470 MHz and was easily integrated into a small mobile phone handset. Simulations have been verified by measurements.

Antenna Array with Meshed Elements for Beamforming Applications

E. R. Escobar[1], **N. J. Kirsch**[1], **and R. B. Turner**[2]

[1]University of New Hampshire, USA
[2]NetBlazr, Inc., USA

Abstract— As demand for wireless networking increases, there is a growing need for reconfigurable systems that accommodate network change and varying demand. Mesh and heterogeneous networks potentially address these needs, but easily deployed systems use omni-directional antennas that limit performance and indoor units that restrict most such networks to a single building. High performance is possible using directional antennas to minimize interference and outdoor mounting allows inter-building links to form neighborhood networks. But such systems can be difficult or expensive to deploy. Easily installed high performance networks are possible with antennas installed indoors in windows, but the appearance and size of such traditional antennas are unacceptable. The solution is an optically transparent multi-element antenna with electronic beamforming and beamsteering that eliminates aiming and supports automatic reconfiguration.

There is a significant amount of prior work on optically transparent antennas made from materials such as Indium Tin Oxide (ITO), AgGL, and silver nanowires. This work shows that the there is a trade-off in conductivity and transparency, yet reasonable efficiency can be achieved. While suitable for some applications, these materials can also be difficult to fabricate. Therefore, we consider microstrip antennas made with thin conductive wires in an open mesh (or grid) configuration that provides 85%–90% optical transmittance.

In our work, we present a eight-element array of dual polarized mesh antennas suitable for inter-building connectivity. Our contribution includes details of the design of the patch antennas elements taking into consideration the transparency of the wire thickness and grid density. This design includes details regarding patch modifications and inter-element spacing to address mutual coupling, fit overall physical design goals, and achieve high enough spatial diversity for beamforming applications. The performance of the antenna array is modeled in HFSS and compared to similarly designed arrays made from non-transparent materials (FR-4 and copper). Additionally we include an analysis of the resulting beamwidth and scan angles of the array using beamforming techniques.

Compound Reconfiguration in Reflectarrays for Cognitive Radio Applications

Julien Perruisseau-Carrier and Eduardo Carrasco
Adaptive MicroNano Wave Systems, Ecole Polytechnique Fédérale de Lausanne (EPFL), Switzerland

Abstract— We discuss the application of the reconfigurable reflectarray structure to cognitive radio, or in general to applications requiring a high degree of dynamic flexibility in the radiated fields (frequency, power pattern, polarization).

Reflectarrays are known to be excellent directive antenna solutions for low-loss and lowcost electronic beamscanning in quasi-planar structures. However, the reflectarray approach is also particularly prone to reconfiguration in terms of operation frequency, or polarization, for reasons that will be explained at the conference. Of particular interest is the ability to design reflectarrays with advanced compound reconfigurability, namely the simultaneous but independent control of more than one antenna parameters. As an example, [1] presented a reflectarray cell capable of independently scanning two beams corresponding to orthogonal linear polarization, or to dynamically control the polarization of the field independently of beamscanning. Other recent designs of our team demonstrate the continuous tuning of the operation frequency, or dual-band operation, while again preserving the independent scanning capabilities.

An overview of our recent results on compound reconfigurable reflectarrays will be presented and discussed in the context of cognitive radio applications.

REFERENCES

1. Perruisseau-Carrier, J., "Dual-polarized and polarization-flexible reflective cells with dynamic phase control," *IEEE Trans. Antennas Propag.*, 2010.

Performance of Capacity Optimized Line-of-sight MIMO HAP-to-train Architectures

Emmanouel T. Michailidis,
Paraskevi N. Daskalaki, **and Athanasios G. Kanatas**
Department of Digital Systems, University of Piraeus
80 Karaoli & Dimitriou St., Piraeus 18534, Greece

Abstract— The growing exigencies for efficient high-speed Internet access and video and file transfer services in railways [1] have prompted the development of satellite and wireless terrestrial networks. Geostationary earth orbit (GEO) satellites intend to exploit line-of-sight (LoS) connections, whereas the terrestrial cellular infrastructure preserves link availability in propagation environments, where the direct communication to the satellite might not be feasible, i.e., tunnels and train stations. In recent years, the high-altitude platforms (HAPs) have also emerged [2]. HAPs are quasi-stationary aerial platforms flying at a height approximately 20 km above the ground, in the stratosphere [3]. To meet the long-term evolution for railway (LTE-R) requirements and enhance the achievable data throughput, the application of the multiple-input multiple-output (MIMO) technology seems inevitable [4]. This paper assesses the capacity performance of HAP-to-train MIMO channels at mm-wave frequencies, under clear sky conditions. Although signal transmissions at these frequencies are usually associated with fixed wireless access (FWA) services, currently there is a clear trend to extend the applicability of these services to mobile scenarios [5]. Then, mobility effects, such as multipath, shadowing, and blockage, which are also encountered at lower frequency bands, may exist due to the local environment in the vicinity of the trains. Nevertheless, the sparse multipath in the railway environment [6] and the high elevation angles of the HAP with respect to the trains lead to nearly LoS propagation. Conceptually, this correspond to a rank-deficient MIMO channel matrix and low spectral efficiency due to the increased spatial correlation introduced by the linear relationship of the phases of the received signals [7]. However, using specifically designed antenna arrays at optimal positions, a full-rank MIMO channel may be achieved [8]. In this paper, the validity of the geometrical design recommendations and the maximum capacity criterion introduced in [8] are investigated for HAP-to-train LoS-MIMO scenarios. The parameters of interest are the height and the elevation angle of the platform, the carrier frequency, and the array configuration. The sensitivity to non-optimal design in terms of the positioning and orientation of the arrays is also studied. The numerical results underline the potential capacity gain of the optimized HAP-to-train MIMO architecture.

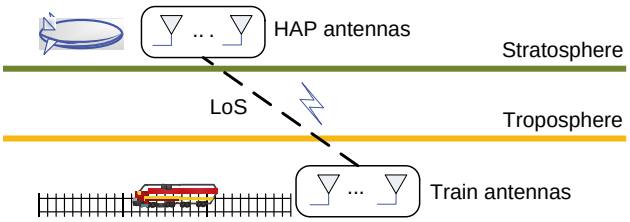

Figure 1: A simple representation of a HAP-to-train LoS-MIMO communication system.

REFERENCES

1. Karimi, O. B., J. Liu, and C. Wang, "Seamless wireless connectivity for multimedia services in high speed trains," *IEEE J. on Selec. Areas in Commun.*, Vol. 30, No. 4, 729–739, May 2012.
2. White, G. P. and Y. V. Zakharov, "Data communications to trains from high-altitude platforms," *IEEE Trans. on Vehic. Technol.*, Vol. 56, No. 4, 2253–2266, Jul. 2007.
3. Mohammed, A., A. Mehmood, F. Pavlidou, and M. Mohorcic, "The role of high-altitude platforms (HAPs) in the global wireless connectivity," *Proc. IEEE*, Vol. 99, No. 11, 1939–1953, Nov. 2011.
4. Paulraj, A. J., D. A. Gore, R. U. Nabar, and H. Bolcskei, "An overview of MIMO communications — A key to gigabit wireless," *Proc. IEEE*, Vol. 92, No. 2, 198–218, 2004.

5. Morlet, C., A. B. Alamañac, G. Gallinaro, L. Erup, P. Takats, and A. Ginesi, "Introduction of mobility aspects for DVB-S2/RCS broadband systems," *Int. Journal on Space Communications*, Vol. 21, Nos. 1–2, 5–17, 2007.
6. Gao, L., Z. Zhong, B. Ai, and L. Xiong, "Estimation of the Ricean K factor in the high speed railway scenarios," *Proc. of the IEEE Wireless Communications and Networking Confenrence (WCNC'08)*, 775–779, 2008.
7. Jin, S., X. Gao, and X. You, "On the ergodic capacity of rank-1 Ricean-fading MIMO channels," *IEEE Trans. on Inform. Theory*, Vol. 53, No. 2, 502–517, 2007.
8. Michailidis, E. T. and A. G. Kanatas, "Capacity optimized line-of-sight HAP-MIMO channels for fixed wireless access," *Proc. International Workshop on Satellite and Space Communications (IWSSC 2009)*, 73–77, Siena, Tuscany, Italy, Sep. 10–11, 2009.

Actively-matched Antennas for UHF Applications

Khalid Z. Rajab, Deepak Singh Nagarkoti, Yifeng Fan, and Yang Hao
School of Electronic Engineering & Computer Science, Queen Mary University of London, UK

Abstract— In this paper, we discuss the broadband impedance matching of electrically-small antennas. Negative impedance converter (NIC) circuits can demonstrably improve the performance of electrically-small antennas by cancelling their reactive components over a large range of frequencies. However, this is at the expense of both stability and noise. The inclusion of active components may lead to instability if not carefully designed, while Johnson-Nyquist noise may be amplified through the system. We will discuss methods for the analysis and design of both of these issues.

Specifically, we present a methodology based on the Nyquist criterion, applied for the thorough design of stable negative NIC-loaded antennas. This technique can be used to analyse the performance of combinations of either simulated or measured circuits, consisting of either NIC matching components and/or antennas. It is suitable for application to active/passive and linear/nonlinear systems. We also analyse noise by subjugating every resistor to a noise source, in order to determine the noise figures for the matched antennas. By determining the signal-to-noise ratios over the frequency band, we can show that these actively-matched antennas outperform their passively-matched counterparts.

Finally, we present stable fabricated NIC circuits. We use these fabricated NICs to confirm the stability analysis methods that we have developed, as well as to demonstrate through measurement that they may be used for the broadband impedance matching of various classes of electrically-small antennas. This form of active matching is envisioned to be particularly useful from the low MHz to UHF bands, where the wavelength is large, but parasitics and transistor performance may be controlled to the extent required to maintain stability.

Session 3P7a
SC1: Intentional Electromagnetic Interference (IEMI) and EMC

IEMI — A General Background and Military Experience
Mats Backstrom, ... 1194
A Survey of Low Cost UWB Sources for Conducted IEMI
Lars Ole Fichte, ... 1195
On the Feasibility of Low-power IEMI Attacks on Communication and Control Lines
Akiyoshi Tatematsu, Marcos Rubinstein, Farhad Rachidi, Nicolas Mora, Sana Sliman, ... 1196
IEMI and EMC Considerations for Large Systems — Smart Grid Aspects
Daniel Mȧnsson, ... 1197
Threat and Detection of High Power Microwaves
Michael Suhrke, ... 1198
An Experimental Characterization of Substation Impulsive Noise for a RF Channel Model
Minh Au, F. Gagnon, Basile L. Agba, ... 1199
On the Spectral Domain Approach to Long-range Propagation along a Strip Conductor above a Finite Conducting Ground of High-frequency Disturbances Induced by an Arbitrary Dipole Source
Ben Oakes, ... 1200
Wavelet Analysis of the First Pulse of Initial Breakdown Process in Lightning Discharges
Mona Riza Mohd Esa, Mohd Riduan Ahmad, Vernon Cooray, ... 1201

IEMI — A General Background and Military Experience

Mats Bäckström
Saab Aeronautics, KTH Royal Institute of Technology, Sweden

Abstract— Our society is rapidly becoming more and more dependent on electrical and electronic systems for its function. This dependence comprise almost all aspect of modern life, from entertainment, sports and leisure activities to structures of critical importance for the basic functions of the society, such as transmission of electrical power, medical care, telecommunications, transportation, banking and finance, food and water supply, emergency services, radio/television and decision making. The widespread reliance on electronics, also in mission- and safety-critical applications of fundamental importance, brings the question of its robustness against electromagnetic interference (EMI) into focus. Of special interest is the rapidly spreading use of new types of wireless systems since these by their nature are open systems and thus easy to interfere with and difficult to protect.

Interference may be caused by natural sources such as lightning and electrostatic discharges, or by the immense number of man-made emitters of electromagnetic energy. In the latter case the interference may be unintentional due to lack of compatibility between the electromagnetic emission (conducted or radiated) from one electronic apparatus and the susceptibility of nearby equipment. It may also be intentional, where the sole purpose is to disturb or destroy the function of the system under attack. The notion Intentional EMI (IEMI) refers to intentional attacks on electronics-based system by use of electromagnetic energy. The attack can be executed by electromagnetic radiation or by injecting electromagnetic energy onto e.g., power or signals cables. Irradiation is often carried out at higher frequencies, injection often at lower frequencies. An attack can lead to a disturbance of a system or even cause permanent damage to parts of it. The latter usually requires relatively high energy or high power.

While IEMI threats have been recognized for decades by the military, in the latest decade or so also the threat against civil systems has got an increased attention. The military heritage means that there is a wealth of knowledge regarding system effects as well as methods for protection and verification which can be of great use in protecting the civil society. However, vital parts of the society's technical infrastructure consists, in contrast to most military systems, of large complex and distributed system, i.e., system of systems. These are also often easily accessible for a perpetrator. This means that IEMI research has to widen its focus from vulnerability and protection at the level of components and subsystems to also include analyses of consequences for the society at large as well as strategies for implementation of well-balanced and cost efficient protection measures. Furthermore, a wide range of measures such as access restriction, surveillance, radiation detection, emergency planning etc. have to be considered and implemented.

A Survey of Low Cost UWB Sources for Conducted IEMI

Lars Ole Fichte
Helmut Schmidt University, Hamburg, Germany

Abstract— Most research activity in the field of Intentional Electromagnetic Interference is focussed on threats by signal propagating in free space, and which couple into the critical device via aperture or cable. Yet, if a harmful signal can be injected directly into cable, the range of propagation is much longer. In this paper we discuss the suitability of commercial available (COTS-commercial of the shelf) high voltage sources for the generation of cheap and simple ultra wide band pulse (UWB) devices, which can be used to inject fast transients directly into power or data grids. The used sources must be handy to be mobile and to be fit in small unremarkable casings. Therefore, some mobile voltage sources, like TASER, stun-gun and fence energizers (EFE) were analysed. The ideal source should fullfill the following requirements: power line independent power supply, high output voltage and small housing Their potential to disturb or damage electronic equipment directly is discussed, as well as the effort which is needed to modify them for optimised injection by adding additional self-made components. Additionally, the propagation of the generated signals on common power lines is discussed. In order to get some information of the conducting properties of a power supply network for frequencies up to 1GHz we measured the scattering parameter S_{21} (transmission) for some key elements of a network: power supply cable and a multi-socket connector using a network analyser. The results show a strong damping at frequencies above 500 MHz.

On the Feasibility of Low-power IEMI Attacks on Communication and Control Lines

Akiyoshi Tatematsu[1,2], **Marcos Rubinstein**[3], **Farhad Rachidi**[1], **Nicolas Mora**[1], **and Sana Sliman**[3]

[1]Swiss Federal Institute of Technology, Switzerland
[2]Central Research Institute of Electric Power Industry (CRIEPI), Kanagawa, Japan
[3]University of Applied Sciences Western Switzerland, HEIG-VD, Yverdon, Switzerland

Abstract— The risk of IEMI on critical infrastructure has gained much attention in the past few years due, on the one hand, to the development of high power electromagnetic sources and, on the other hand, to the proliferation of information on the Internet that could allow individuals or organizations with only moderate or even no technical skills to build or simply to acquire such sources. In addition, there is a growing awareness that society is heavily and increasingly dependent on the permanent availability and accessibility of services based on sensitive electronics and communication networks.

A large number of IEMI scenarios published in the literature deal with the use of high power sources for the disturbance or destruction of components and subsystems. These studies are based on the energy in the fields and it is assumed, implicitly or explicitly, that the higher the power, the higher the deleterious effect.

In this work, we study the feasibility of another type of attack in which it is not the power level but the "semantics" of the electromagnetic interference that is used as a vector and to measure its effectiveness. The principle of this type of attack is the injection, through radiated or conducted means, of low intensity signals that are indistinguishable from actual physical layer waveforms that transport higher layer protocols in digital communication networks.

To show the feasibility of such an attack, we use a specific case in which a wave impinges on a line with a propagation direction parallel to the line axis and we show that the required field levels are achievable with available sources.

IEMI and EMC Considerations for Large Systems — Smart Grid Aspects

D. Månsson
Division of Electromagnetic Engineering, Royal Institute of Technology (KTH)
Teknikringen 33, Stockholm 100 44, Sweden

Abstract— The smart grid concept is a grid design philosophy that diversifies power grids and the electricity markets. A "smart grid" is herein defined as:

"An interconnected and interdependent non-linear system, wherein money, information and energy are flowing multidirectionally over domain boundaries wherein different limitations and demands may exist."

The implementation of the smart grid concept is a viable solution for diminishing global environmental impact of the modern society. However a deep penetration of "prosumers" (i.e., a combined producer/consumer) and distributed generation in urban environments could lead to significant problems from an electromagnetic compatibility (EMC) viewpoint. Traditional classification methods, used for small isolated systems, are inadequate tools to investigate, improve and evaluate mitigation measures for large distributed infrastructures such as a smart grid.

Therefore, herein is a classification method originally developed to investigate the vulnerability of large distributed systems from intentional electromagnetic interference (IEMI) used. It employs three main variables:

- Accessibility, the ability of gaining access to the different parts of the facility or critical components belonging to it.
- Consequence of a disturbance.
- Susceptibility of the system, which is further subdivided into.
  - Receptivity, the degree of the facility's ability to mitigate disturbances between and within electromagnetic topological zones.
  - Sensitivity, the different upset threshold levels of the equipment and subsystems inside the facility.
  - Redundancy, the availability of backup systems and ability to "degrade gracefully".

The results are thereafter used to form an estimate of the vulnerability of the system.

In this paper the method is used to analyze the smart grid concept to investigate if the smart grid is, from an EMC and IEMI viewpoint for a large distributed system, an improvement or deterioration compared to traditional power grids (and the aspects that is attached to them).

Threat and Detection of High Power Microwaves

Michael Suhrke
Fraunhofer INT, Appelsgarten 2, Euskirchen 53879, Germany

Abstract— The paper starts with an overview on the threat of High Power Microwaves (HPM) with special emphasis on the vulnerability of critical infrastructures. Fraunhofer INT conducts HPM susceptibility tests of electronic devices and systems already for 20 years. The paper will give some examples of those tests with special relevance to the HPM threat to critical infrastructures. The investigation of susceptibility thresholds at Fraunhofer INT is done in its TEM waveguide which allows the generation of field strengths up to some kV/m, depending on location of test objects. Another testing environment is a reverberation chamber permitting field strengths of more than 10 kV/m.

As HPM attacks can be done covertly and failures and malfunctions of electronic systems cannot be traced back immediately to an electromagnetic attack, HPM detection is an important part of protection against these attacks. Therefore, the last part of the paper begins with an overview on available detectors and continues with the description of detector development done at Fraunhofer INT for surveillance of critical or premium facilities and for search and forensics after an HPM attack in addition to the basic warning function. Extended features include display of threat field strength in a wide frequency range, large amplitude dynamics (i.e., detection range), display of pulse number or repetition rate and pulse width together with directional and polarisation independence of the receiving antenna. The detectors are able to detect electromagnetic signals with field strengths up to 10 kV/m, are immune to field strengths of more than 10 kV/m and are able to detect sources at medium distance (i.e., field strengths down to at least 100 V/m). This is complemented by the ability of detection of the direction of an HPM attack.

An Experimental Characterization of Substation Impulsive Noise for a RF Channel Model

M. Au[1], F. Gagnon[1], and B. L. Agba[2]

[1]Electrical Engineering Department, École de Technologie Supérieure, Montréal, Canada
[2]IREQ (Hydro-Québec), Varennes, Canada

Abstract— Although, wireless communications for smart grid applications reduced costs and complexity in substations, the required performances depend on transmitted signals quality. Deploying wireless communication system, wireless sensors networks, for example, in a substation is problematic due to electromagnetic (EM) noise. The latter is partial discharges from high voltage (HV) equipments, electrical arcs from circuit breakers, etc..

This paper deals with EM noise emitted by partial discharges (PD). PD pulses are highly impulsive and occur when the apply voltage is sufficient high. In this condition, an ionization process takes place in HV equipments containing imperfections such as cavities, asperities, etc.. Our research work is to define metrics and methodology for electromagnetic noise characterization. This approach gives substantial information about RF channel in substations environments in which impulsive noise are omnipresent. This information will be useful for accurate channel modelling to ensure high quality in the transmitted signal.

In this contribution, measurement setup and methodology are developed. The measurement setup includes:

- A Rhode and Schwarz log periodic antenna. Wideband from 0.8–26 GHz.
- A High pass filter from 780–3200 MHz.
- A RF amplifier from 30–3000 MHz with output power up to 12.8 dBm.
- A limiter broadband from 30–6000 MHz. It protects against unwanted signals up to 2.5 W.
- A Lecroy oscilloscope with 256 M samples max with 40 Gs/s max sample rate.

We record PD pulse sequences for a large observation time at RF range. The measurement methodology is based on the knowledge of some substation physical parameters such as the voltage applied to HV equipments. The recorded waveform is a combination of PD sources randomly located and the ambient noise of the substation.

For impulsive noise characterization in substation, we present some main metrics:

- Energy or amplitude distribution.
- PD occurrence distribution.
- Inter-arrival time distribution.
- The phase resolved partial discharge (PRPD).

Although many measurements campaigns are carried out in various substations, this paper is only focused on the results from 735 kV substation. The results show the erratic behaviour of PD pulse sequences. We also observe that PD pulse occurrences are strongly correlated to AC voltage of the substation. Thus, impulsive noise in substation can be seen as a random process where PD evens are dependent to the AC voltage.

Our research work characterize the electromagnetic environment in a substation. This work allows us to model accurately RF channel in substation. Our future work will extend the analysis by taken into account PD sources location.

On the Spectral Domain Approach to Long-range Propagation along a Strip Conductor above a Finite Conducting Ground of High-frequency Disturbances Induced by an Arbitrary Dipole Source

Ben Oakes
Royal Institute of Technology, Stockholm

Abstract— Electric arcing may occur between the pantograph and contact line above electric locomotives while in motion. The sparks emit electromagnetic disturbances with a wide frequency spectrum. Some of the wave energy follows the metallic structure of the railways and overhead wires. Energy from high frequency radiation does not only propagate along the wire structures, but also radiates from the structures. From EMC point of view, it is of interest to study the attenuation of the currents along these wire structures above a finite conducting ground, to predict the radiation from them and determine how far from the rails sensitive electrical devices may be placed.

In a layered structure, computing the surface currents along a strip conductor is simpler than a circular wire since the strip conforms with the geometry. A wire of arbitrary cross section can be replaced by a strip if the thin wire approximation holds and neglecting proximity effects. An infinitely thin and infinitely long PEC strip is considered, placed in half-space 1, parallel with the planar interface between two half-spaces (1 and 2) with arbitrary material properties: ε_1, μ_1 and ε_2, μ_2. At an arbitrary point in half-space 1, an elemental electric dipole is placed representing the arcing above the train. The problem is very generic hence the dipole may represent intentional as well as unintentional arcing. The task is to compute the current in the direction of the strip along a long but finite length of strip. The fields resulting from the currents can later be calculated.

The method used is the mode matching technique in the spectral domain. This type of method has frequently been used for studying propagation along thin planar strip conductors on substrates, though it has now shown useful also for power line problems. As we are considering a planar structure, we may decompose the fields into TM and TE components. Requiring only conditions on horizontal field components on the strip and planar interface between the halfspaces (continuity of the horizontal wave vector) and the orthogonality of TM and TE modes, the scattered fields from the strip and planar interface can be calculated. With knowledge of all fields and the boundary conditions on the PEC strip and expanding the spectral current density into an infinite series of Bessel functions, the integral equation for the spectral current is derived for strips of arbitrary width. Further, the "full wave equation"is simplified for narrow strips, i.e., only considering currents in the direction of the strip and neglecting proximity effects, assuming the dipole is not too close to the strip or planar surface, the strip current is expanded only to the zeroth order Bessel function.

A semi-infinite integral over the derived expression for the spectral current density is evaluated with Matlab's `quadl`, over the horizontal wave vector component perpendicular to the direction of the strip. Of course, the integral can only be evaluated within a finite range so leading behaviors are extracted off the integrands and their explicit integrals are added, resulting in a faster convergence. Several numerical problems occur however, due to the presence of poles in the integrand: excitation of the TEM mode, i.e., propagation in the direction of the strip. This is treated by adding small losses to the wave vector and having smaller a step size near the poles. The trapezoidal rule with a complex argument is thus used for the inverse transformation of the spectral current.

Numerical results using high ε_2 have been compared with those for a PEC ground and are very similar, which is expected. Especially good results occur with the dipole directed in the same direction as the strip. This is due to the reduced presence of the TEM mode. For dipoles in other directions, the numerical solutions require finer tuning, although even they have been shown to be reasonable, especially for lossy half-spaces.

Wavelet Analysis of the First Pulse of Initial Breakdown Process in Lightning Discharges

Mona Riza Mohd Esa[1,3], **Mohd Riduan Ahmad**[2,3], **and Vernon Cooray**[3]

[1]Universiti Teknologi Malaysia, UTM Skudai, Johor, Malaysia
[2]Universiti Teknikal Malaysia Melaka, Malaysia
[3]Division of Electricity, Department of Engineering Sciences
Uppsala University, Uppsala, Sweden

Abstract— Wavelet transformation is used in order to seek for differences in the initial breakdown process between negative cloud-to-ground flash (CG−), positive CG (CG+), cloud flash (IC), and isolated breakdown (IB) processes. 72 waveforms were selected from 885 waveforms recorded between May and August 2010 at the premise of Uppsala University, Uppsala, Sweden. The analysis was conducted only on the first electric field pulse for each lightning process and the output from the wavelet transformation is plotted as normalized power spectrum. The first pulses in CG− are found to radiate intensely in average frequency between 195 and 1694 kHz. The energy radiated by the first pulses of CG+ mainly concentrated in the average frequency between 57 and 599 kHz. As for the IC, the first pulses found to be spread out in the average frequency between 461 and 3570 kHz and for IB, the energy spread out between 44 and 279 kHz. The CG+ and IB flashes tend to radiate at lower frequency region within smaller range compared to CG− and IC. IB has the smallest frequency range around 235 kHz while the frequency range of IC and CG− are more than 10 times and 6 times larger than IB, respectively. Furthermore, IC and CG− have comparable initial-to-overshoot peak ratio with 1.70 and 1.61, respectively, which higher than CG+ and IB at least with a factor of 1.4. It can be speculated that the initial breakdown processes of IC and CG− flashes are most likely initiated from the same discharge process in the thundercloud and differ from the discharge process of CG+ and IB.

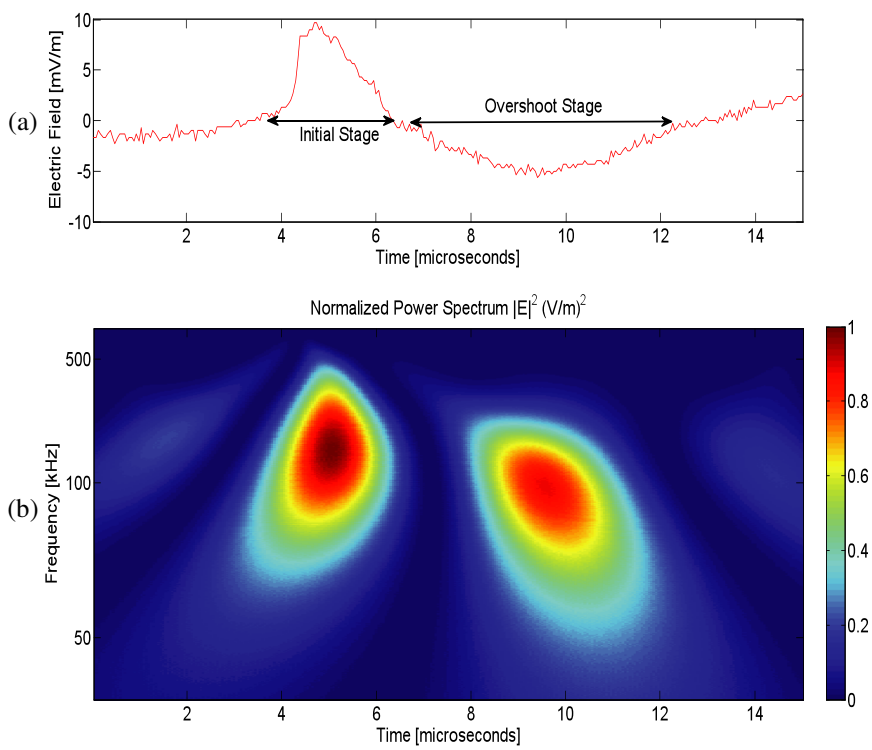

Figure 1: The upper plot is the first pulse of negative cloud-to-ground flash recorded on 15th of August 2010 and the lower plot is the normalized wavelet power spectrum of pulse in the upper plot.

Session 3P7b
SC4: THz Technologies and Applications

Si-based Devices Technologies toward THz
Albert Chin, Hsuan-Ling Kao, ... 1204

Towards Developing a Dielectric Metrology for the Life Sciences
Robert S. Donnan, Alex McIntosh, Bin Yang, Oleksandr Sushko, Junyi Qui, ... 1205

Tri-reflector Compact Antenna Test Range for Millimetre/Sub-millimetre Wave and THz Antenna Measurement
Junsheng Yu, Xiaoming Liu, Xiaodong Chen, Yuan Yao, Cheng Yang, Zejiang Lu, ... 1206

Steerable THz Emission by Optical Coherent Control
Heiko Fueser, Mark Bieler, ... 1207

Characterization of THz Pulse Pumped by High Power Pulse Amplified by Double-clad Yb-doped Fiber Amplifier
Junichi Hamazaki, Norihiko Sekine, Shingo Saito, Iwao Hosako, ... 1209

Si-based Devices Technologies toward THz

Albert Chin[1] **and Hsuan-Ling Kao**[2]

[1]Department of Electronic Engineering, National Chiao Tung University, Hsinchu 300, Taiwan
[2]Department of Electronic Engineering, Chang Gung University, Tao-Yuan 333, Taiwan

Abstract— The microwave performance of both cut-off-frequency (f_t) and maximum-oscillation-frequency ($f_{\max}$) improves as continuously scaling down the MOSFET. Nevertheless, the fundamental challenge of Si-based technology is the much poorer performance of microwave passive devices than those on GaAs. The measured loss of Si-based CPW transmission line is as high as 5 dB/mm at 110 GHz, which prevents any high performance Si circuit at sub-THz regime. This is due to the high-frequency loss, noise, and cross-talk generated from the low resistivity (10 Ω-cm) Si substrate compared with the insulating (10 MΩ-cm) GaAs substrate.

To improve the high-frequency loss of passive devices on Si, we invented a simple ion-implantation process that can translate the 10 Ω-cm resistivity into semi-insulating (1 MΩ-cm). Very low 0.5 dB/mm loss was measured in Si-based transmission line at 110 GHz that is close to EM simulation. Such semi-insulating Si can be maintained up to 1.1 THz from femto-second time-resolved photo-reflectance measurement.

The microwave loss can also couple into CPW-connected MOSFET during noise measurement and cause wrong noise modeling. To address this issue, an equivalent circuit de-embedding method and microstrip line shielding layout were reported by us. Very low minimum noise figure ($NF_{\min}$) of 0.3 $\sim$ 0.4 dB at 10 GHz was obtained in 40-nm MOSFET, with $\sim$ 200 GHz ft and 425 GHz $f_{\max}$. Both the f_t and $f_{\max}$ are expected into THz at 10-nm node MOSFET around year 2015.

Both the ion-implantation translated semi-insulating Si and microstrip line noise shielding method were adopted by IC foundry.

Towards Developing a Dielectric Metrology for the Life Sciences

Robert S. Donnan, Alex McIntosh, Bin Yang, Oleksandr Sushko, and Junyi Qui
School of Electronic Engineering and Computer Science, Queen Mary University of London, UK

Abstract— There is a growing interest and challenge in performing time-resolved dielectric spectrometry of soft condensed-matter systems. Group molecular motions are thought to play a fundamental role in governing the functional character of a 'system' — e.g., in proteins. Vector Network Analysers driving quasi-optical networks and, THz Time-Domain Spectrometry are now uniquely coming into their own alongside established methodologies of XRD and NMR to throw further light on microscopic processes in bio-chemistry. This talk outlines early adventure in adapting and developing antenna and microwave metrologies to study dynamic systems.

Tri-reflector Compact Antenna Test Range for Millimetre/Sub-millimetre Wave and THz Antenna Measurement

Junsheng Yu[1], **Xiaoming Liu**[1], **Xiaodong Chen**[2], **Yuan Yao**[1], **Cheng Yang**[1], **and Zejian Lu**[1]

[1]School of Electronic Engineering, Beijing University of Posts and Telecommunications
Box 279, No. 10 Xi-Tu-Cheng Road, Haidian District, Beijing 100876, China
[2]School of Electronic Engineering and Computer Science, Queen Mary University of London
Mile End Road, London, E1 4NS, UK

Abstract— The Compact Antenna Test Range (CATR), which generates a pseudo-plane wave in a very short distance, is commonly employed to measure electrically large aperture antennas for the applications in space remote sensing and radio astronomy. With the increasing operating frequencies, the design of a CATR becomes a technical challenge. For instance, in 2009, the European Space Agency (ESA) launched two space telescopes, the Planck and the Herschel, with their antennas being 3.5 m and 1.5 m in diameter, covering frequency ranges of 30–857 GHz and 448 GHz to 5 THz, respectively [1]. The conventional far field method requires a long distance to achieve useable quiet zone, make it impractical for millimetre antenna measurement. The near field measurements at high frequency suffer a number of difficulties, including scanning inaccuracy, phase errors, long scanning time and so forth. Therefore, a CATR is a feasible approach to measure large aperture antennas in the millimetre and sub-millimetre wave ranges. The most common reflector type CATR is using a single parabolic reflector in an offset arrangement. The drawback of a single reflector CATR is often referred to as its low quiet zone usage, typically 30%. There also exists shaped dual-reflector CATR, which means both the sub-reflector and main reflector are shaped, can provide 60% quiet zone usage. As in general, the main reflector is the most expensive item in the construction of a CATR, the cost of a shaped dual-reflector CATR may increase sharply in comparison with single reflector one. On the other hand, it is well known that most optical telescopes have spherical main reflectors and considerable knowledge exists in how to produce accurate spherical surfaces. In order to use a spherical main reflector in a CATR, a tri-reflector configuration has to be employed. This paper presents the design of a Cassegrain-Gregorian (CG) tri-reflector CATR, as shown in Fig. 1, operating from 40–500 GHz, through a dynamic ray-tracing approach [2, 3]. The design utilises two shaped sub-reflectors and a spherical main reflector and is verified by using a commercial Physical Optics (PO) package, GRASP version 9. It is found that a high quiet zone usage up to 70% is achieved.

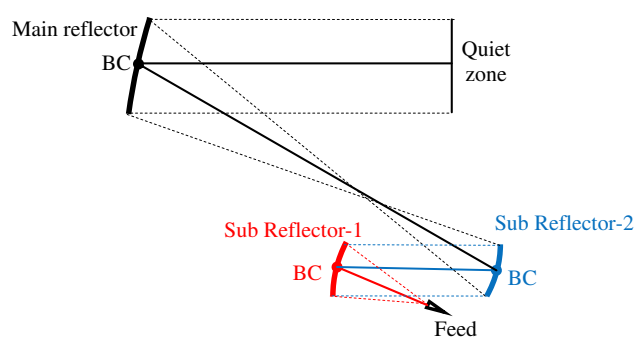

Figure 1: The configuration of a Cassegrain-Gregorian tri-reflector compact antenna test range. BC: Beam Centre.

REFERENCES

1. Döyle, D., G. Pilbratt, and J. Tauber, "The Herschel and Planck space telescopes," *Proceedings of the IEEE*, Vol. 97, No. 8, 1–9, Aug. 2009.
2. Kildal, P.-S., "Synthesis of multireflector antennas by Kinematic and dynamic ray tracing," *IEEE Trans. on Antennas and Propagations*, Vol. 38, No. 10, 1587–1599, Oct. 1990.
3. Deschamps, G. A., "Ray techniques in electromagnetics," *Proceedings of the IEEE*, Vol. 60, No. 9, 1022–1035, Sept. 1972.

Steerable THz Emission by Optical Coherent Control

Heiko Füser and Mark Bieler
Physikalisch-Technische Bundesanstalt, Bundesallee 100, Braunschweig D-38116, Germany

Abstract— We demonstrate fast and reliable steering of THz radiation based on coherent control of all-optically excited ultrafast currents in bulk GaAs. Changing the phase of the optical excitation, steering angles of ~ 8 degrees are realized. The approach demonstrated here overcomes the limitations of previous THz beam steering techniques that are based on mechanical movement of either the excitation source or of beam-shaping apertures [1, 2].

The experiments are performed on a semi-insulating GaAs sample with (110) crystal orientation, being excited by normally incident optical pulses (100 fs, 820 nm). The photoexcitation of the semiconductor leads to complex temporal and spatial dynamics of the generated charge carriers, being dependent on different physical effects. Using linearly polarized light with a photon energy above the GaAs bandgap for excitation, two main current components occur:

(i) Shift currents due to the nonlinear susceptibility $\chi^{(2)}$ [3]. This current flow can be chosen to be directed parallel to one of the crystallographic axis along the surface of the GaAs crystal. In the following, we consider currents along the $[1\bar{1}0]$ direction. This current direction can be reversed by changing the polarization of the optical excitation by 90°. Accordingly, the radiated THz field will reverse its sign.

(ii) Surface field currents resulting from carrier acceleration due to the bending of the band structure near the surface of the crystal [4]. Here, the current flow is directed perpendicular to the GaAs surface. This current contribution does not depend on the polarization of the excitation pulse. Hence, no change in the radiation field occurs when changing the polarization properties of the laser pulse.

Looking at the superposition of the THz fields emitted by those two currents, interference effects result in a tilt of the overall emission pattern, refer to Fig. 1(a). The tilting angle β is inversed when switching the sign of the shift current direction. To demonstrate this effect, a standard electro-optic sampling setup is used. The generated THz radiation is collected and focused onto a ZnTe detection crystal using two off-axis parabolic mirrors (OPM). The experimental geometry is chosen such that only THz fields polarized along the $[1\bar{1}0]$ direction of the GaAs sample are detected. To measure the spatial distribution of the electrical field, a slit (7 mm width) is positioned in between the OPMs. Moving the slit parallel to the $[1\bar{1}0]$ direction and measuring the THz peak-to-peak signal, the emission patterns as shown in Fig. 1(b) result. As can be seen, a steering of about 8 degrees is obtained when switching the excitation polarization.

In the scope of this work, we introduce a simple model based on dipole emitters representing both current contributions. Using this model, the superposition of the electromagnetic field distributions is evaluated, including refraction and diffraction effects as well as the numerical aperture of the experimental setup. As depicted in Fig. 1(b), the model fits the measured data

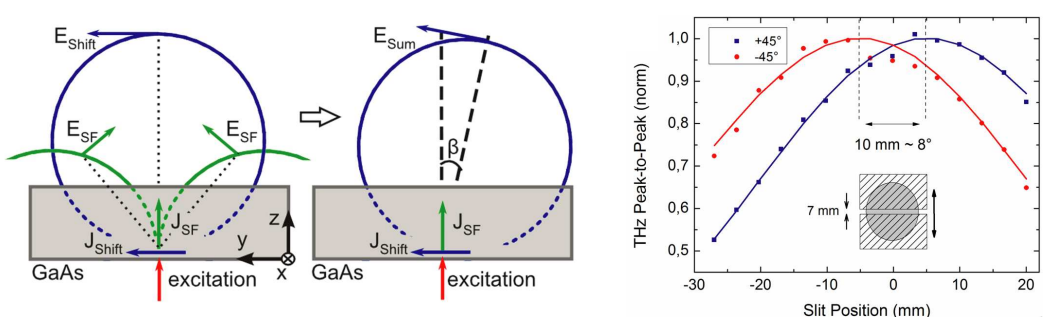

Figure 1: (a) Electrical fields resulting from shift and surface-field currents, E_{Shift} and E_{SF}, respectively. Due to interference effects, the propagation direction of the net electrical field is tilted by β with respect to the z-direction. (b) Spatially resolved peak-to-peak THz signal (dots) and simulations (lines) for $+/-45°$ excitation polarization with respect to the $[1\bar{1}0]$ direction.

very well. Additionally, we can use the model to explain the measured dependence of the steering angle on the pump intensity and the size of the excitation spot (not shown).

REFERENCES

1. Maki, K., et al., *Opt. Express*, Vol. 16, 10158, 2008.
2. Drysdale, T. D., et al, *Appl. Opt.*, Vol. 47, 2382, 2008.
3. Sipe, J. E., et al., *Phys. Rev. B*, Vol. 61, 5337, 2000.
4. Zhang, X. C., et al., *J. Appl. Phys.*, Vol. 71, 326, 1992.

Characterization of THz Pulse Pumped by High Power Pulse Amplified by Double-clad Yb-doped Fiber Amplifier

J. Hamazaki, N. Sekine, S. Saito, and I. Hosako
National Institute of Information and Communications Technology, Japan

Abstract— High-power broadband terahertz (THz) generation has attracted much attention for various THz applications, such as THz spectroscopy. In THz frequency region, various samples show characteristic finger-print absorption spectra. However, terahertz pulse with high-power broadband spectrum at high repetition rate ($\sim 100\,\mathrm{MHz}$) is not well developed. Therefore, it is difficult to evaluate absorbance with strong absorbance or thick samples, owing to low-power of THz pulse. Thus, high-power broadband THz generation is desired.

To generate high-power broadband THz pulse, optical rectification effect is generally used, by using an ultra-short high-power pump pulse and a nonlinear crystal. In the case of pump pulse with a wavelength of $\sim 1\,\mu\mathrm{m}$, typically GaP is used as a nonlinear crystal. In this technique, higher-power and broader-band THz pulse is obtained by using higher-power pulse with shorter pulse width. Therefore, higher-power ultra-short pump pulse is required.

In these days, double-clad Yb-doped fiber (DC-YDF) has attracted much attention for realizing high-power highly-efficient amplifier. It is known that Yb-doped fiber (YDF) has large gain and broad gain spectrum (1.0–1.1 μm). Furthermore, DC-YDF has extremely larger gain than usual YDF. Output power over 1 W is easily expected by using DC-YDF. Thus, DC-YDF amplifier is suitable for high-power ultra-short pulse generation. Recently, high power THz generation ($> 6.5\,\mu\mathrm{W}$) from GaP using high-power pulse ($> 10\,\mathrm{W}$) was reported.

In this paper, we generate THz pulse pumped by high-power ultra-short pump pulse, amplified by our double-clad Yb-doped fiber amplifier system. From our amplifier, average output power of 700 mW with a pulse width of 230 fs at high repetition ration of 100 MHz is obtained. Using this pulse, we generate and characterize the THz pulse from GaP and DAST crystal. Moreover, we discuss optimum conditions of our amplifier system for high-power broadband THz generation.

Session 3P8a
SC4: Advanced Magnetic Materials for Microwave Applications

Voltage Control of Magnetism in Multiferroic Heterostructures and Low-power Devices
Nian-Xiang Sun, ... 1212
Topological Phenomena of Magnons in Ferromagnets
Shuichi Murakami, ... 1213
Microwave Properties of Ferromagnetic Thin Films — Layering and Magnetic Domain Effects
Jeffrey McCord, ... 1214
Amorphous/Silicone Composites and Their Applications in Microwave Attenuation
Zheng-Wen Li, Zhihong Yang, M. J. Chua, ... 1215
Microwave Application of the Magnetic Rare Earth Intermetallics with in-plane Anisotropy
Fashen Li, Tao Wang, Liang Qiao, Jianqian Wei, ... 1216
X-ray Exposure and Thermal Annealing Effects on Nanocrystals of Y and Co Codoped CeO_2 Diluted Magnetic Oxides
Tai-Sing Wu, Shih-Lin Chang, Horng-Tay Jeng, Yunliang Soo, ... 1217

Voltage Control of Magnetism in Multiferroic Heterostructures and Low-power Devices

Nian X. Sun
Electrical and Computer Engineering Department, Northeastern University, Boston, MA, USA

Abstract— Electrical field control of magnetism has been attracting a great amount of recent interest due to its potential technological impacts. The coexistence of electrical polarization and magnetization in multiferroic materials provides great opportunities for realizing effective electric field control, or vice versa, through a strain mediated magnetoelectric interaction effect in layered magnetic/ferroelectric multiferroic heterostructures. Strong magnetoelectric coupling has been the enabling factor for different multiferroic devices, which however has been hard to achieve, particularly at RF/microwave frequencies. In this presentation, I will cover the most recent progress on novel layered microwave multiferroic heterostructures and devices. We will demonstrate strong magnetoelectric coupling in novel microwave multiferroic heterostructures. These multiferroic heterostructures exhibit a giant electrostatically tunable magnetic field of 3500Oe, and a high electrostatically tunable ferromagnetic resonance frequency range between $1.75 \sim 7.57\,\mathrm{GHz}$, a tunable frequency of $5.82\,\mathrm{GHz}$ or $f_{\max}/f_{\min} = 4.3$. At the same time, we will demonstrate E-field modulation ofanisotropic magnetoresistance, giant magnetoresistance and exchange bias at room temperature indifferent multiferroic heterostructures. Through competition between the E-field induced uniaxial anisotropy and unidirectional anisotropy, large E-field induced tunable exchange field and near 180° deterministic magnetization switching will be demonstrated in exchange coupled multiferroic heterostructures. New multiferroic devices will also be covered in the talk, including multiferroic voltage tunable bandpass filters, voltage tunable inductors, tunable bandstop filters, tunable phase shifters and spintronics.

Topological Phenomena of Magnons in Ferromagnets

S. Murakami[1, 2]

[1]Department of Physics, Tokyo Institute of Technology, Ookayama, Meguro-ku, Tokyo 152-8551, Japan
[2]TIES, Tokyo Institute of Technology, Ookayama, Meguro-ku, Tokyo 152-8551, Japan

Abstract— In electron systems, various kinds of Hall effects are attributed to Berry curvature in momentum space. This Berry curvature involves derivative of the Bloch wavefunction with respect to the wavenumber, and it is determined by the band structure. For electronic systems, the anomalous Hall effect and quantum spin Hall effect (topological insulators) requires the spin-orbit coupling, in order to make Berry curvature nonzero. In the present case of magnons in insulating magnets, we also need a "spin-orbit coupling"; it is realized either by Dyaloshinskii-Moriya interaction or the dipolar interaction. We focus on the dipolar interaction, which can be sensitively controlled by the shape of the magnet. We consider a spin wave in a thin-film ferromagnet, where the wavelength is of the order of microns and spin waves are governed by dipolar interactions (magnetostatic spin waves). We can show that the dipolar interaction gives nonzero Berry curvature, if the magnetic field is out-of-plane. Thermal Hall effect of magnons is predicted in this case, and we can evaluate thermal Hall conductivity.

One can control the magnon band structure by introducing artificial periodicity, i.e., by making magnonic crystals. In some magnonic crystals, the band structure of magnons becomes gapped. In my presentation we also show that in some cases magnonic bands becomes topologically nontrivial, i.e., the integral of the Berry curvature over the Brillouin zone becomes nonzero. This integral becomes an integer called Chern integer, which gives a number of chiral edge modes. Therefore such topological crystal is similar to the quantum Hall effect for electrons, and offers a novel stage for controlling magnon dynamics.

Microwave Properties of Ferromagnetic Thin Films — Layering and Magnetic Domain Effects

Jeffrey McCord
Institute for Materials Science, University Kiel, Germany

Abstract— A lot of high frequency applications in the GHz range depend on the use soft ferromagnetic thin film structures. In a first approximation the general rf magnetization response is directly related to the ferromagnetic material's dynamic properties, which are defined by the precessional frequency and the magnetic damping parameter of the material. In real world applications, however, the films are patterned and also experience interfacial effects that, in addition, strongly influence the effective magneto-dynamic properties. Thereby, understanding the significance of the magnetic domain structure for the dynamic properties of patterned thin film structures is crucial for the optimization of devices for high frequency applications. Moreover, layering of the ferromagnetic films with non-magnetic layers opens an additional path for the tailoring of dynamic magnetic properties.

The role of magnetic domains and magnetic domain walls on the dynamic response will be reviewed in detail. Using time-resolved magneto-optical Kerr microscopy up to the GHz range the magnetic behaviour of the dynamic magnetization response is imaged directly. The role of domain width for the dynamic response of rf-inductors and routes of optimization of the device performance by domain optimization in laminated structures will be explained. Ways of controlling the magnetization response by exchange coupling as well as varying the magnetic damping parameter by the addition of antiferromagnetic materials will be demonstrated. Ion irradiation is used to laterally pattern ferromagnetic films in terms of magnetic damping. The influence of out-of-plane magnetic anisotropy and magnetic stripe domains on the dynamic modes will be discussed.

In general, the bow is spanned from fundamental material aspects to device applications. Aspects of material optimization and device performance are put into comparative context.

Amorphous/Silicone Composites and Their Applications in Microwave Attenuation

Z. W. Li, Z. H. Yang, and M. J. Chua
Temasek Laboratories, National University of Singapore
5A, Engineering Drive 1, Singapore 117411, Singapore

Abstract— Ferromagnetic amorphous materials have relatively high saturation magnetization, very low coercivity and low electric resistivity. Therefore, it can be predicted that the amorphous/silicone composites have high initial permeability, high complex permittivity, and low resonance frequency due to eddy current loss. For microwave attenuation application, in order to retain the advantage of high permeability and to overcome the drawbacks of high permittivity and low resonance frequency, the composites with three types of fillers, namely amorphous flaky-filler with various sizes, amorphous flaky plus ferrite nanoparticle fillers with core-shell-like structure and membrane filler with in-plane arrangement, have been developed using ball-mill and infiltration methods. The experiments show that the composites with core-shell-like fillers are able to greatly reduce permittivity and the composites with in-plane-arrangement fillers can significantly raise complex permeability, as compared to general amorphous-filler composites. Therefore, the prepared membrane-filler composites with core-shell-like structure have better attenuation properties with low reflectivity and broad bandwidth at microwave frequency.

Microwave Application of the Magnetic Rare Earth Intermetallics with in-plane Anisotropy

Fashen Li, **Tao Wang**, **Liang Qiao**, **and Jianqian Wei**
Institute of Applied Magnetics
Key Laboratory of Magnetism and magnetic Materials of the Ministry of Education(MOE) in China
Lanzhou University, Lanzhou, Gansu 730000, China

Abstract— With rapid development of computer technology and communication technology, the working frequency of computers and the data transmision rate appaoches to GHz band [1, 2]. This fact requires a higher natural resonance frequency for the magnetic materials which work in the magnetic divices within microwave band. Because of the SNOEK LIMIT of the traditional magnetic materials which have generally lower natural resonance frequency(1 MHz–100 MHz), they can not fulfill the demand for new technology. So that they have been replaced in the microwave band divices by dielectrical materials, which degrades the impedence matching and the miniaturization of the divices.

Among the magnetic rare earth intermetallics, some of them have none-cubic crystalline structure (hexagonal, tetragonal and so on). Owing to the differences of magnetic crystalline anisitropy between rare earth sublattice and 3d-sublattice, there are two kinds of materials according to the spin configuration at a specified temperature: 1) easy axis materials which have easy magnetization direction along C-axis; 2) easy plane materials which have easy magnetization plane in c-plane or cone-plane. Till now, only easy axis material have been widely used as high quality permanenet magnets (third-and fourth-generation permanent magnets). For easy plane materials, although their crystalline structure and fudamental magnetic properties have been investigated systemetically [3], the technical application of them have not been reported. The results obtained by Lanzhou group have shown that since the out-of-plane anisotropic field are much larger than the in- plane anisotropic field inside the material, they have a higher natural resonance frequency and higher permeability around GHz band. It means that the magnetic rare earth intermetallics with easy magnetization plane have much better magnetic performences around microwave band than that of the microwave soft magnetic materials which we used till now. The magnetic powder composite of easy-plane intermetallics could fulfill the demand of the new generation divices with ever growing working frequency around GHz band. The microwave applications of the easy-plane intermetallics will be discussed.

REFERENCES

1. Gardner, D. S., et al., *IEEE Trans. Magn.*, Vol. 45, 4760–4766, 2009.
2. Kim, S. S., et al., *IEEE Trans. Magn.*, Vol. 47, 4314–4317, 2011.
3. Franse, J. J. M. and R. J. Radwanski, *Handbook of Magnetic Materials*, Chapter 5, Vol. 7, 1993.

X-ray Exposure and Thermal Annealing Effects on Nanocrystals of Y and Co Codoped CeO_2 Diluted Magnetic Oxides

T. S. Wu[1], **S. L. Chang**[1,2], **H. T. Jeng**[1], **and Y. L. Soo**[1,2]

[1]Department of Physics, National Tsing Hua University, Hsinchu, Taiwan
[2]National Synchrotron Radiation Research Center, Hsinchu, Taiwan

Abstract— Structural variationssurrounding Y and Co impurity atoms codoped in nanocrystals of CeO_2 due to x-ray exposure and thermal annealing effects have been investigated using different experimental and theoretical methods. After thermal annealing, the location of the magnetic Co dopant atoms in the CeO_2 host were found by extended x-ray absorption fine structure (EXAFS) and x-ray absorption near edge structure (XANES) to migrate from a distorted substitutional siteto a stable interstitial site, predicted by theoretical calculation using the Vienna *ab initio* simulation package (VASP). However, intensive and prolonged exposure to synchrotron x-rays with photon energy near the Co K edge tends to change their XANES spectra back toward the curveshape of the as-made sample. This observation suggestspossible departure of Co atoms from the stable interstitial site back to a distorted location as a result of x-ray exposure atphoton energies relatedto Co core electron excitation. We have demonstrated an intriguingexample of the interaction between electromagnetic waves and magnetic materials at the hard x-ray regime. The interplay of thermal annealing and x-ray exposure can provide unique opportunity for controlling the structures and magnetism in these nanocrystal diluted magnetic oxides (DMOs). In addition, detailed structural information of the samples with different Y concentration was also obtained using synchrotron radiation and Raman scattering techniques. As revealed by the x-ray diffraction (XRD) data, all nanocrystal samples under investigation have similar average particle size. The concentration of O vacancies in the samples was found to increase with Y doping level as indicated by the Raman spectroscopy, EXAFS, and XANES data. Effects of the structural variations on the magnetic properties of these DMOs will also be discussed.

Session 3P8b
New Materials for EM Shielding — Materials and Technology

Microwave and Terahertz Shielding Properties of PET-MWCNT Composites
Viktor Bovtun, Jan Petzelt, Dmitry Nuzhnyy, Martin Kempa, ... 1220

Graphene/PMMA Sandwich Structures: Toward Electromagnetic Applications in Microwave Range
Polina Kuzhir, Konstantin Batrakov, Alesia G. Paddubskaya, Sophia Voronovich, Sergey A. Maksimenko, Tommi Kaplas, Yuri Svirko, ... 1221

Microwave Dielectric, Magnetic and Shielding Properties of Composites of Metal Nanoparticles and Epoxy Resin
Aleksandra Borisova, Viktor Bovtun, Aleksander Machulyansky, Martin Kempa, Maxim Savinov, Yuriy Yakymenko, ... 1222

The Influence of Magnetic Impurities on the Electromagnetic Absorption of the Foam Silicates in the Wide Frequency Range
Karen Oganisian, D. Hreniak, M. Skrajnowska, W. Strek, ... 1223

Low Frequency Magnetic Field Shielding by Metamaterials
Mustafa Boyvat, Christian Valentin Hafner, ... 1224

Impact of Technology on the Shielding Effectiveness of Barrier Materials Damping Frequency Selected Electromagnetic Fields
Jan Ziaja, Grzegorz Szafran, Maciej Jaroszewski, ... 1225

Microwave and Terahertz Shielding Properties of PET-MWCNT Composites

Viktor Bovtun, **Jan Petzelt**, **Dmitry Nuzhnyy**, **and Martin Kempa**
Department of Dielectrics, Institute of Physics ASCR, Na Slovance 2, 182 21 Prague 8, Czech Republic

Abstract— Poly (ethylene terephthalate) — multiwalled carbon nanotubes composites (PET-xMWCNT, $x = 0$–3 vol.% is the fraction of carbon nanotubes) were prepared and their dielectric permittivity, dielectric loss and *ac* conductivity spectra were studied at room temperature in a very broad frequency range from 10^{-4} Hz to 10^{12} Hz [1]. In addition to the *dc* conductivity of percolated MWCNT clusters, the *ac* conductivity of MWCNT in the finite clusters contributes to the conductivity spectra. The *ac* conductivity increases with frequency and culminates in the THz range for all compositions, achieving ~ 4 S/cm at 1 THz.

The percolation threshold revealed at $x_c \sim 0.07$vol.% is the lowest one observed in the melt-processed polymer composites. Both *dc* and *ac* conductivity of composites can be effectively controlled by the change of MWCNT concentration. The low percolation threshold and ability to modify the microwave conductivity make PET-MWCNT composites attractive for electromagnetic shielding.

The free space reflective and absorptive loss spectra of the composites were calculated for frequencies between 1 MHz and 1 THz from the experimental spectra of dielectric permittivity, dielectric loss and ac conductivity considering the absence of magnetic properties in PET-MWCNT composites. The shielding efficiency was estimated in dependence on the MWCNT concentration, material thickness and frequency. A role of reflective and absorptive losses is analyzed. The compositions and frequency range optimal for shielding applications are discussed.

REFERENCES

1. Nuzhnyy, D., M. Savinov, V. Bovtun, M. Kempa, J. Petzelt, B. Mayoral, and T. McNally, "Broad-band conductivity and dielectric spectroscopy of composites of multiwalled carbon nanotubes and poly (ethylene terephthalate) around their low percolation threshold," *Nanotechnology*, Vol. 24, 055707, 1–9, 2013.

Graphene/PMMA Sandwich Structures: Toward Electromagnetic Applications in Microwave Range

Polina Kuzhir[1], **Konstantin Batrakov**[1], **Alesya Paddubskaya**[1], **Sophia Voronovich**[1], **Sergey Maksimenko**[1], **Tommi Kaplas**[2], **and Yuri Svirko**[2]

[1]Research Institute for Nuclear Problems
Belarusian State University, Republic of Belarus
[2]Department of Physics and Mathematics
University of Eastern, Finland

Abstract— K_a-band (26–37 GHz) is very important slot of microwave radiation, being occupied by satellite communications, uplinks and high resolution targeting radars aboard military airplanes. The problem of electromagnetic compatibility in the K_a-band has recently become an important concern because of drastic increase of "microwave pollution". In this communication we propose a new graphene based thin films with enhanced electromagnetic interference shielding efficiency (EMI SE) in the K_a-band.

The fabricated samples consisted of several layers of graphene sandwiched between Poly (methyl methacrylate) (PMMA) films. The first graphene monolayer was synthesized by chemical vapor deposition (CVD) at 1000 C in methane atmosphere on the copper catalyst and then spin coated by the 600 nm thick PMMA layer. The quality of the graphene was monitored by Raman spectroscopy. The Cu catalyst was wet etched in ferric chloride, while PMMA film with deposited graphene was washed in distilled water and then placed on quartz substrate. By repeating this procedure we fabricated sandwich-like coatings of the silica substrate containing two and three graphene layers.

The microwave measurements were performed using scalar network analyzer R2-408R (ELMIKA, Vilnius, Lithuania). The reflective ability of investigated sample (approx. 25% of incident power) is mostly due to substrate, whereas absorption losses are due to the presence of the graphene layers.

We found that being quasi transparent in IR range (transmittance is 98, 96 and 94% for one-, two- and three-layered graphene samples), graphene/PMMA sandwiches are semi-opaque for microwave radiation. We discovered that the fabricated structures provided remarkably high EMI SE caused by absorption losses, which were as high as 16, 34 and 39% for one-, two- and three-layered graphene/PMMA coatings, respectively. Theoretical modeling based on Fresnel's formulae and boundary conditions in the rectangular waveguide demonstrates excellent coincidence with experimental data obtained for thin sandwich structures, consisting of a few monolayers of graphene and PMMA.

In conclusion, the manufactured graphene sandwiches, being highly conductive at room temperature and quasi transparent in visible range, could be interesting technological material for fabrication of EM interference protective coatings with nm-scale thickness for aerospace applications.

ACKNOWLEDGMENT

This work was partially supported by EU FP7 projects FP7-266529 BY-NanoERA and FP7- 247007 CACOMEL.

Microwave Dielectric, Magnetic and Shielding Properties of Composites of Metal Nanoparticles and Epoxy Resin

Aleksandra Borisova[1], **Viktor Bovtun**[2], **Aleksander Machulyansky**[1], **Martin Kempa**[2], **Maxim Savinov**[2], **and Yuriy Yakymenko**[1]

[1]NTUU "Kyiv Polytechnic Institute", Kyiv, Ukraine
[2]Institute of Physics ASCR, Prague, Czech Republic

Abstract— Composites of metal nanoparticles and epoxy resin (epoxy-xMe, Me = Fe, Ni, Cu, Al; x = 0–40 vol.% is the fraction of metal nanoparticles) were prepared and their dielectric permittivity, dielectric loss and ac conductivity spectra were studied at room temperature in a broad frequency range from 10^{-2} Hz to 10^{10} Hz. Dielectric/conductivity dispersion was observed in the whole frequency range. Both *dc* conductivity of percolated Me clusters and *ac* conductivity of finite Me clusters contribute to the conductivity spectra. The *ac* conductivity increases with a frequency increase and dominates in microwave range. Increase of the metal content results in the increase of dielectric permittivity, loss and conductivity in the whole frequency range, both bellow and above the percolation threshold.

For epoxy-xFe and epoxy-xNi composites, complex permeability spectra were measured at frequencies from 1 MHz to 3 GHz. The microwave permeability dispersion and maximum of magnetic loss between 10 MHz and 1 GHz were revealed. Similar to dielectric permittivity and conductivity, magnetic properties of composites can be controlled by a change of the Me concentration.

The free space reflective and absorptive loss spectra of the composites were calculated for frequencies between 1 MHz and 3 GHz from the experimental dielectric, conductivity and magnetic spectra (or accounting absence of magnetic properties in epoxy-xCu and epoxy-xAl composites). Then shielding efficiency was estimated in dependence on the Me concentration, material thickness and frequency. A role of reflective and absorptive losses is analyzed. Shielding efficiency of composites with and without magnetic properties is compared. The optimal compositions and possible shielding applications are discussed.

The Influence of Magnetic Impurities on the Electromagnetic Absorption of the Foam Silicates in the Wide Frequency Range

Karen Oganisian, D. Hreniak, M. Skrajnowska, and W. Strek
Institute of Low Temperature and Structure Research PAS, Okolna 2, Wroclaw 50-422, Poland

Abstract— The fire-proof thermoinsulating silicate-based foam samples were prepared using a modified sol-gel method based on liquid-glass composition [1, 2]. The silicates were doped at the stage of formation of a porous structure with various magnetic impurities to improve their electromagnetic screening properties that allowed to significantly extend of their application [3]. Electric and magnetic impedance measurements have been performed using the Impedance Analyzer HP 4191A RF the in the frequency range 1–1000 MHz by the Westphal Method [4] and by the method of Concentrated Capacity [5]. The samples were doped with Fe_2O_3, $BaO{\cdot}6Fe_2O_3$ and $(MnZn)Fe_2O_4$ with various concentration of doping. It was found, that doping by $(MnZn)Fe_2O_4$ considerably improve the absorption properties in the wide frequency range. Additionally we investigated the frequency dependence of electrical impedance of sol-gel foam silicates doped by 1–10% of $(MnZn)Fe_2O_4$ in the 1–1000 kHz range. As a result the electrical losses have nonlinear dependence with amount of doped magnetic impurities with the minimum at about 7% of $(MnZn)Fe_2O_4$.

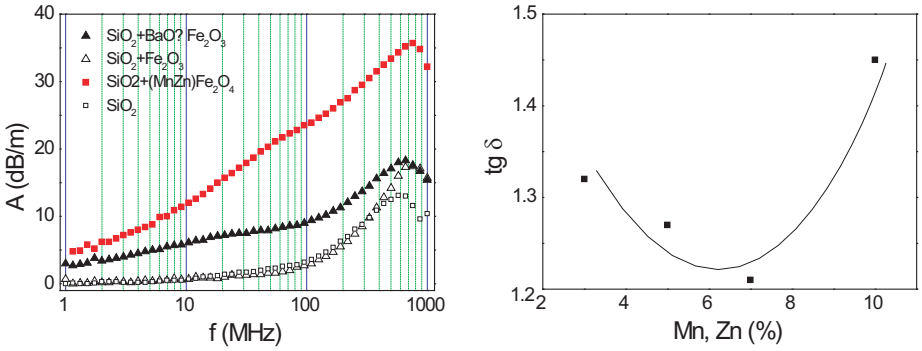

REFERENCES

1. Patent applications: P. 399342(PL), P. 394854(PL), P. 392889(PL), P. 392644(PL), P. 392448(PL), P.388764(PL), PCT/PL2012/050011(WO).
2. Psuja, P., D. Hreniak, M. Pietrzak, and W. Stręk, "Porous thermal insulation silica materials manufactured with the Sol-Gel method," *Materiały Konferencyjne 8th Seminar on Porous Glasses — Special Glasses/Nato Advanced Research Workshop*, 36, Printing House PWr, 2007.
3. Trautnitz, F.-W., "EMC absorbers through the years with respect to the new site VSWR validation procedure in the frequency range from 1 to 18 GHz — A practical approach," *IEEE International Symposium on Electromagnetic Compatibility*, Art No. 4305672, 2007.
4. Technical Report Nr 36, MIT, 1950.
5. Kołodziej, H. and L. Sobczyk, *Acta Phys. Polon. (A)*, Vol. 39, 59, 1971.

Low Frequency Magnetic Field Shielding by Metamaterials

M. Boyvat and Ch. Hafner
Department of Information Technology and Electrical Engineering, ETH Zurich
Gloriastrasse 35, Zurich 8092, Switzerland

Abstract— Metamaterials have been interesting for scientists because they offer unusual electromagnetic properties and the possibility to engineer these properties. They have been explored mostly at high frequencies, i.e., optics and microwave, but the low frequency part of the electromagnetic spectrum had not been considered enough for metamaterials. Recently, it has been shown that metamaterial concept is also promising at very low frequencies and magnetic field shielding by metamaterials has been shown theoretically and experimentally [1, 2].

Metamaterials are structures composed of so-called meta-atoms, which are usually resonating elements. At very low frequencies, wavelength of electromagnetic waves is very large, and this enables using large meta-atoms and reduces the difficulty of fabrication. For very long wavelengths, meta- atoms can be built by lumped circuit elements (i.e., capacitor and inductor) and it is also possible to embed more advanced circuitries into the meta-atoms.

In this talk, first, low frequency metamaterials and design of them for shielding are considered numerically. Due to the possibility to use quasi-static approximation at very low frequencies, the calculations are simplified considerably. This enables calculating total field distribution of a system with a field source and a metamaterial composed of large number of meta-atoms. Moreover, it eases the optimization of metamaterial for shielding.

Due to non-zero resistances on meta-atoms in reality, magnitude and phase deviate from ideal meta-atoms, which results in reduction in the shielding performance of metamaterial. Thus, there is a need to compensate non-zero resistance. Following numerical aspects, the methods to eliminate the undesired effects of non-zero resistance and improve meta-atoms are discussed, which may also provide inspiration for high frequencies.

REFERENCES

1. Boyvat, M. and C. V. Hafner, "Magnetic field shielding by metamaterials," *Progress In Electromagnetics Research*, Vol. 136, 647–664, 2013.
2. Boyvat, M. and C. V. Hafner, "Molding the flow of magnetic field with metamaterials: Magnetic field shielding," *Progress In Electromagnetics Research*, Vol. 126, 303–316, 2012.

Impact of Technology on the Shielding Effectiveness of Barrier Materials Damping Frequency Selected Electromagnetic Fields

Jan Ziaja, **Grzegorz Szafran**, **and Maciej Jaroszewski**
Faculty of Electrical Engineering, Wrocław University of Technology, Poland

Abstract— The present study compared the effects of methods of preparation and the type of material used for shielding effectiveness (SE) selectively chosen frequency electromagnetic field (EMF). Composite materials were obtained by metallization surface of non-woven and polypropylene film. Metallization process was performed by magnetron sputtering and vacuum evaporation (vaccum deposition). Deposited materials are copper (Cu) and Zn-In a composition by weight of 80/20. shielding effectiveness SE of obtained composites was measured according to standard ASTMD 4935-99 (Standard Test Method for Measuring the Electromagnetic Shielding Effectiveness of Planar Materials) in the frequency range 300 MHz–3 GHz. Obtained results of shielding effectiveness are in the range 30–50 dB of attenuation bandwidth of 200 MHz. This width is sufficient to suppress the transmission signal GSM 1800. The results of this study indicate that this type of shielding composite materials can be a significant competitive with currently used conventional materials.

Session 3P9a
SC4: Giant Magneto-impedance and EM Safety

Stable Pico-Tesla Resolution Multi Amorphous Wire GMI Sensor and Its Applications
Tsuyoshi Uchiyama, N. Hamada, Kaneo Mohri, ... 1228

Development and Optimization of High Sensitive Magnetometer Based on Diagonal Magnetoimpedance Effect
Mihail Ipatov, Valentina Zhukova, A. Zhukov, J. Gonzalez, ... 1229

EM-safety: Low Frequency Magnetic Field Exposure in Vehicles with Electrical Powertrains
Alastair R. Ruddle, Lester Low, Andréa Vassilev, ... 1230

Magneto-optical Investigations of Co- and Fe-rich Composite Glass Covered Microwires
Alexander Chizhik, Arkady P. Zhukov, Julian Gonzalez, ... 1231

Ferromagnetic Microwires Enabled Multifunctional Polymer Meta-composites
Faxiang Qin, Hua-Xin Peng, Jie Tang, ... 1232

Optimization of Giant Magnetoimpedance Effect in Thin Composite Microwires
Arkady P. Zhukov, Mihail Ipatov, V. Zhukova, ... 1233

Stable Pico-Tesla Resolution Multi Amorphous Wire GMI Sensor and Its Applications

T. Uchiyama[1], **N. Hamada**[2], **and K.Mohri**[3]

[1]Graduate School of Engineering, Nagoya University, Japan
[2]Aichi Steel Corp., Japan
[3]Nagoya Industrial Science Research Institute (NISRI), Japan

Abstract— Micro sized MI-HIC chips have been in mass production of electronic compasses by Aichi Steel Corp. since 2002 for mobile phones and since 2010 for smart phones. Recently pico-Tesla (10^{-8} Oe) resolution for micro magneto-impedance (MI) sensors is realized [1–3]. Highly sensitive linear micro magnetic-field sensors are constituted utilizing the pulse Magneto-Impedance effect for tension-annealed amorphous wires with wound pick-up coils, combined with the CMOS IC multi-vibrator circuit [2, 3].

In this paper, we present stable pico-Tesla resolution MI sensor. We have already proposed multi amorphous wire head for low noise MI sensor [4]. In this case four amorphous wire cores are included in a pick-up coil. Assuming magnetic noise is a random phenomenon at each amorphous wire in the coil, the total induced noise voltage at the pick-up coil is proportional to $n^{1/2}$, where n is the total number of amorphous wires. On the other hand, the induced voltage depending on external field H_{ex} is proportional to n. Therefore, it is expected that S/N of the sensor system is proportional to $n^{1/2}$. It is confirmed that the noise floor of the multi amorphous wire MI sensor is lower than 1 pT/Hz$^{1/2}$ for the frequency from 20 Hz to 500 Hz.

Figure 1 illustrates progression of the MI sensor projects classified in three groups depending on sensor applications: micro size compatible with integrated circuitry, ultra-high sensitivity with 1 pico-Tesla resolution and portability, and ultra-quick response.

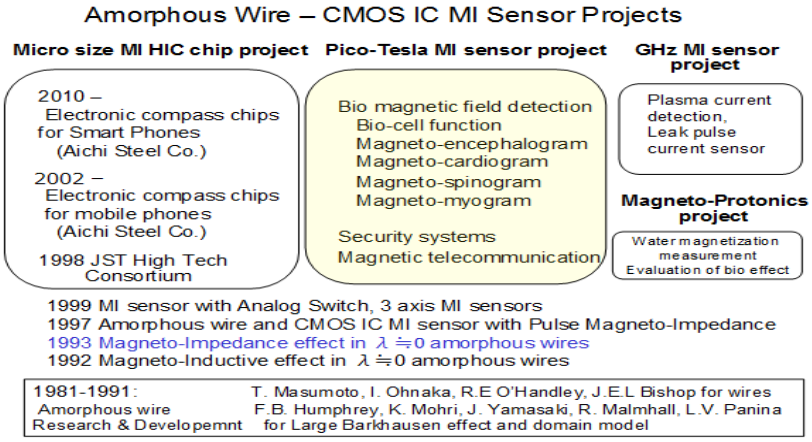

Figure 1: Amorphous wire and CMOS IC MI sensor projects based on three principal advantageous features.

REFERENCES

1. Panina, L. V. and K. Mohri, "Magneto-impedance effect in amorphous wires," *Appl. Phys. Lett.*, Vol. 65, No. 9, 1189–1119, 1994.
2. Mohri, K. and Y. Honkura, "Amorphous wire and CMOS IC based magneto-impedance sensors — Origin, topics, and future," *Sensor Letters*, Vol. 5, No. 1, 267–270, 2007.
3. Uchiyama, T., S. Nakayama, K. Mohri, and K. Bushida, "Biomagnetic field detection using very high sensitive MI sensor for medical application," *Phys. Stat. Solidi. A*, Vol. 206, No. 4, 639–643, 2009.
4. Hamada, N., et. al., *Intermag 2011*, FF-08, 2001.

Development and Optimization of High Sensitive Magnetometer Based on Diagonal Magnetoimpedance Effect

M. Ipatov[1], **V. Zhukova**[1], **A. Zhukov**[1,2], **and J. Gonzalez**[1]

[1]Dpto. de Fís. Mater., UPV/EHU, San Sebastián 20018, Spain
[2]IKERBASQUE, Basque Foundation for Science, Bilbao 48011, Spain

Abstract— The magnetoimpedance (MI) effect has received much attention during the last two decades due to its potential for magnetic sensor applications. Particularly high MI effect was found in amorphous glass coated microwires of nearly zero magnetostriction. In such conductors, the impedance is of tensor form. The longitudinal impedance has appeared generally not to be suitable for magnetic sensors applications as it exhibits a symmetric dependence on the magnetic field. Such dependence does not allow determination the direction of applied magnetic field. Moreover, the MI effect becomes very low approaching zero magnetic field.

Several methods have been proposed for overcoming these drawbacks of diagonal MI such as a shift of MI curve by longitudinal dc bias field or creating the asymmetric MI dependence that consists in combining the induced helical magnetic anisotropy with circumferential bias field produced by the dc current. The later approach was used for obtaining a linear antisymmetric field dependence that can be achieved using a pair of such asymmetrical MI elements [1]. In spite of certain progress in longitudinal MI sensor development, the off-diagonal MI effect that appears due to the cross-magnetization process turn out to exhibit better characteristics and actually is used in commercially available MI sensors. Such an off-diagonal MI sensor allows determination of both the magnitude and the sign of the external magnetic field in the field range below the anisotropy fields whilst in the case that the magnetic field exceeds this range, the sensor can give an erroneous reading.

The present work is based on our previous studies of the longitudinal MI in the wires with induced helical anisotropy and the effect of the bias current on the MI in such microwires [2–4]. In contrast to the previous investigations by the other authors we propose to apply the asymmetry of a single MI element and switching between the MI curves for different values of DC bias current for detection of sign and magnitude of external magnetic field. Also we demonstrate that the longitudinal MI can be used for magnetic field detection in the range higher than the anisotropy field of the wire. In contrast, the off-diagonal MI was found to be negligible at such high fields.

REFERENCES

1. Kitoh, T., K. Mohri, and T. Uchiyama, *IEEE Trans. Magn.*, Vol. 31, 3137–3139, 1995.
2. Ipatov, M., V. Zhukova, A. Zhukov, J. Gonzalez, and A. Zvezdin, *Phys. Rev. B*, Vol. 81, 134421, 2010.
3. Ipatov, M., V. Zhukova, A. Zhukov, and J. Gonzalez, *Appl. Phys. Lett.*, Vol. 97, 252507, 2010.
4. Ipatov, M., V. Zhukova, J. Gonzalez, and A. Zhukov, *J. Magn. Magn. Mat.*, Vol. 324, 4078–4083, 2012.

EM-safety: Low Frequency Magnetic Field Exposure in Vehicles with Electrical Powertrains

A. R. Ruddle[1], **L. Low**[1], **and A. Vassilev**[2]

[1]MIRA Limited, Watling Street, Nuneaton, Warwickshire, CV10 0TU, UK
[2]CEA-Leti, MINATEC Campus, 17 rue des Martyrs, 38054 GRENOBLE Cedex 9, France

Abstract— Vehicle electrification is currently being widely promoted in order to help improve urban air quality, to support efforts to reduce carbon emissions, and to limit reliance on fossil fuels. However, a new feature of hybrid and electric vehicles is that they require significant electrical power (perhaps as high as 200 kW, depending on the vehicle type) to be routed around the vehicle between the on-board power sources (stored and/or generated) and electrical machines that act as traction motors in drive mode or generators under braking conditions. Given the size and space constraints of vehicles, the electrical powertrain components may be located in relatively close proximity to the occupants. Consequently, the occupants of such vehicles will be exposed to low frequency magnetic fields arising from currents flowing in the high voltage power network, traction batteries, and associated devices including inverters and electrical machines. Thus, establishing the electromagnetic safety of the in-vehicle environment will be important to ensure the acceptability of such vehicles to consumers.

Although there are not currently any product standards relating specifically to in-vehicle field exposure, there are general recommendations for field exposure limits from various national and international bodies, such as ICNIRP. Thus, there is a need to develop an understanding of the electromagnetic environment that may result in hybrid/electric vehicles, and to take account of occupant magnetic field exposure in the design and integration of electric vehicle architectures. The FP7 project EM-Safety has therefore undertaken investigations of these issues, and this paper will provide an overview of this work.

Magnetic field measurements have been carried out on a number of representative electric and hybrid vehicles for frequencies up to 2 kHz. A common feature of these measurements is that the highest fields tend to be found where the body is close to high power cables (often near the feet of the driver or front passenger) or traction batteries (e.g., around the lower back for rear passengers in vehicles with batteries located in the rear). Batteries are sometimes also mounted below the occupants in some vehicle architectures, while the electric motor is generally located at the front axle. The power cables may carry current in single-phase or three-phase form, depending on the design of the system. Although the recommended exposure limits for DC magnetic field are very high, single phase high voltage cables also carry current transients containing finite frequency components that could present health risks if the rate of change of magnetic field is sufficiently high.

In measured field spectra the individual frequency components are relatively small compared to the field reference levels. However, ICNIRP requires additive effects to be taken into account for multiple frequencies, and the more frequencies that are present the lower they can be relative to the reference levels. Thus, a simple comparison of spectra against limits is overly optimistic. For non-sinusoidal exposures a time-varying field exposure measure can be derived (based on an inverse Fourier transform) that takes account of the additive effects of multiple frequency exposures but also reflects the phase of the spectral components in order to avoid excessively conservative threat assessments.

Numerical simulations based on a 3D finite element model of a vehicle-like object have been carried out in order to assess the likely impact of vehicle body-shell structures and materials on in-vehicle magnetic fields. More detailed simulations of a small electric vehicle with a steel chassis and dielectric body panels have also been used to derive time-varying field exposure measures from measured cable current transients. Although a lack of detailed current path geometry prevented direct validation of the simulations, the predicted levels for representative configurations encompass the measured fields and are thus considered to be credible. The simulation results indicate that the exposure from battery loop currents can be reduced by a factor of ~ 20 by minimizing the battery loop area, and by a factor of ~ 7 by including a simple steel plate as a battery shield. Other possible field mitigation approaches that have been investigated include twisting of high-voltage power cables in order to obtain enhanced spatial field decay rates.

Magneto-optical Investigations of Co- and Fe-rich Composite Glass Covered Microwires

A. Chizhik[1], **A. Zhukov**[1, 2], **and J. Gonzalez**[1]

[1]Universidad del País Vasco, UPV/EHU, San Sebastián, Spain
[2]IKERBASQUE, Basque Foundation for Science, Bilbao 48011, Spain

Abstract— We have performed wide investigation of composite glass covered magnetic microwires in the frame of task of the miniaturization of active elements of magnetic sensors based on giant magnetoimpedance (GMI) effect. In this work we present the review of the studies of the magnetization reversal and magnetic domain structure in Fe- and Co-rich wires of nano- and micro-metrical scale.

The investigations have been performed using the magneto-optical Kerr effect (MOKE) technique. Application of MOKE magnetometry and MOKE microscopy, as a complementary tools permits to determine the directions of the magnetization in the non-planar surface of studied wires and to study in details the surface magnetization reversal. MOKE experiments have been performed in wide series of Co-and Fe-rich microwires with diameter of metallic nucleus 0.8–100 μm.

For the Fe-rich wires of nano-scale (radius of metallic nucleus of 400 nm, 700 nm, 1000 nm) the MOKE experiments have been performed in the presence of axial tensile stress and torsion stress. It was found that for the microwires of such tiny scale the surface hysteresis loop has a rectangular shape related to the magnetic bistability effect in the form of surface large Barkhausen jump as it was found earlier in the glass covered wires of micrometric scale.

Experiments performed in thick Co-rich microwires (metallic nucleus radius 50 μm, glass coating thickness 20 μm, and a ratio of metallic nucleus diameter to total microwire diameter $\rho = 0.7$) demonstrated four different mechanisms of the magnetization reversal: long distance quick motion of the solitary circular domain walls, the effect of the domain suppression, the drift of wedged domains and the formation and transformation of the vortex domain structure.

Performed investigations permits us now to understand deeper the basic mechanisms of the magnetization reversal in magnetic microwire and to select the optimal magnetic parameters with the purpose to provide the stable operation of magnetic sensors.

Ferromagnetic Microwires Enabled Multifunctional Polymer Meta-composites

F. X. Qin[1,2] H. X. Peng[2], and Jie Tang[1]

[1]1D Nanomaterials Group, National Institute for Materials Science
1-2-1 Sengen, Tsukuba, Ibaraki 305-0047, Japan
[2]Advanced Composite Centre for Innovation and Science, Department of Aerospace Engineering
University of Bristol, University Walk, Bristol, BS8 1TR, UK

Abstract— The last two decades have witnessed intensive studies on the ferromagnetic microwires worldwide. Recent attention has turned to the development of innovative materials and composites derived from these microwires, such as microwire polymer composites. Through incorporating even extremely small concentration of microwires ($\sim 10^{-2}$ vol.%), the resultant composite exhibits a multitude of functionalities which are desirable for a range of technological applications [1]. This talk provides a comprehensive review of the ongoing research on microwire composites from synthesis to structural and property evaluation with a focus on the multi-functionalities presented in these microwire-composites. Starting with an introduction of multifunctional composites and the theories pertinent to the multiple functionalities of microwire composites, a detailed description of fabrication methods of microwire composites is given with a comparison of different processing techniques. Two fundamental effects, namely, giant magnetoimpedance and stress-impedance effects of microwire composites are discussed in relative to the monolithic microwires [2]. Microwave tunable properties are analysed in the presence of magnetic field and stress field [3–6]. We will also show that the ferromagnetic wire composites possess configurable metamaterial characteristics and microwave absorption/shielding capability [7, 8]. With a discussion on the underlying physics of the influence of composite architecture such as material parameters of microwires and microwire periodicity on the performance of resultant composites, useful insights are provided for an effective design of smart composites for specific engineering applications such as structural health monitoring, stress sensing, invisible cloaking, microwave absorption and biomedical applications.

REFERENCES

1. Qin, F. X. and H. X. Peng, *Prog. Mater. Sci.*, Vol. 58, 183, 2013.
2. Qin, F. X., et al., *Composites Part A*, Vol. 41, 1823, 2010.
3. Qin, F. X., et al., *J. Appl. Phys.*, Vol. 107, 09A314, 2010;
4. Qin, F. X., et al., *J. Appl. Phys.*, Vol. 108, 07A310, 2011.
5. Qin, F. X., et al., *Appl. Phys. Lett.*, Vol. 97, 153502, 2010.
6. Qin, F. X., et al., *Appl. Phys. Lett.*, Vol. 101, 152905, 2012.
7. Qin, F. X., et al., *IEEE Trans. Magn.*, Vol. 47, 4481, 2011; *IEEE Trans. Magn.*, DOI. 10.1109/TMAG.2013.2243412.
8. Qin, F. X., et al., *IEEE Trans. Magn.*, DOI. 10.1109/TMAG.2013.2243412.

Optimization of Giant Magnetoimpedance Effect in Thin Composite Microwires

A. Zhukov[1,2], **M. Ipatov**[1], **and V. Zhukova**[1]

[1]Dpto. de Fís. Mater., UPV/EHU, San Sebastián 20018, Spain
[2]IKERBASQUE, Basque Foundation for Science, Bilbao 48011, Spain

Abstract— Giant magneto-impedance (GMI) effect observed in different magnetically soft materials attracted considerable interest in applied magnetism mostly from point of view of applications for sensitive magnetic field microsensors and owing to great sensitivity to low applied magnetic field [1, 2]. The GMI effect is understood as the dependence of the impedance on the external axial magnetic field. The sensitivity of GMI is related with type of magnetic anisotropy and with the value of the magnetic anisotropy constant. Up to now magnetically soft wires exhibiting high circumferential magnetic permeability and excellent soft magnetic properties are considered the best candidates for development of such magnetic microsensors [1]. The outer shell of such wires with vanishing magnetostriction constant presents weak circumferential magnetic anisotropy. On the other hand this magnetic anisotropy can be tailored by the magnetoelastic anisotropy. The magnetoelastic anisotropy depends on the magnetostriction constant (i.e., on the metallic nucleus composition) and on strength of internal and applied stresses. The internal stresses, σ_i, originate during simultaneous rapid quenching of metallic nucleus with diameter d, surrounding by the glass coating and can be controlled by the ρ-ratio ($\rho = d/D$, where D is the total microwire diameter): strength of internal stresses increases decreasing ρ-ratio (i.e., increases with increasing of the glass volume), increasing with decreasing ρ-ratio [3].

We present the results on the optimization of the GMI effect in thin magnetic microwires in extended frequency range. We measured magnetic field, H, dependence of real part, Z_1 of the longitudinal wire impedance Z ($Z = Z_1 + iZ_2$) and GMI ratio, $\Delta Z/Z$, in frequencies range, f, from 1 MHz to 4 GHz in Co-rich microwires with different geometries and different magnetostriction constant. We show, that the frequency dependence of maximum GMI ratio, $\Delta Z/Z_m(f)$, measured in microwires of the same composition and different diameters presents an optimum frequency (at which $\Delta Z/Z_m$ versus f exhibits the maximum) at different frequencies. Thus, for metallic nucleus diameters ranging between 8.5 and 9.0 µm the optimal frequency is about 100 MHz, while for microwires with metallic nucleus diameters between 9 and 11.7 µm the optimal frequency is about 200 MHz. Additionally, heat treatments of microwires affect both magnetoelastic anisotropy and GMI effect.

REFERENCES

1. Jiles, D. C., Vol. 51, 5907, 2003.
2. Zhukova, V., M. Ipatov, and A Zhukov, *Sensors*, Vol. 9, 9216, 2009.
3. Chiriac, H., T.-A. Ovari, and A. Zhukov, *J. Magn. Magn. Mater.*, 254–255, 469, 2003.

Session 3P9b
SC1: Advanced Techniques in Nanoelectromagnetics Applications

The State Space Model for Atomic Interactions
Taner Sengor, ... 1236
New Directions in Plasmonics: SERS and Nanoparticle Superlattice Crystals
George C. Schatz, ... 1237
Mapping Structural and Plasmonic Properties of Gold Nanoparticles
Cecilia Noguez, ... 1238
Simulation of Plasmon Probing with Electrons
Ulrich Hohenester, ... 1239
Designed Surface Waves at an Interface of Plasmonic Nanolayered Metamaterial and Isotropic Dielectric
Slobodan M. Vukovic, Carlos J. Zapata-Rodriguez, J. J. Miret, Zoran Jaksic, ... 1240

The State Space Model for Atomic Interactions

T. Sengor
Yildiz Technical University, Turkey

Abstract— The main goals of this paper is to present a new effective semi-analytical and computational method for manufacturing of the nanoelectromagnetic devices based on system theoretical methods applied on the nanooptical and/or nanoplasmonic structures. The method gives an appropriate looking through the phenomena and techniques in Quantum Electrodynamics within the atomic, molecular, optical, photonic, and nanometer scale focusing on critical issues. The theoretical principles of nanobody-atomic-subatomic structures up to the laser clusters involving the interactions among them are considered. Gaining a global view to scientific development is focused from the approaches given with the state space formalism of simple atomic model, which we call state space model of simple atoms. The model motivates the rapid advances of nanoscience and nanotechnology. These advances offer their need for adequate tools and strategies for fabricating, manipulating, and characterizing the devices at the nanometer scale. Therefore, approaches given in this paper may give an access point to gain a global point of view on nanoscientific developments.

An atomic structure is modeled by a system theoretical approach in this paper. The approach is based on the extended modification of the method given in [1]. The definition of a suitable circuit-like element, which we call atomic system-like element, is given by this approach. We defined atomic circuits, which use atomic system-like element. An atomic circuit is a device designed by atomic system-like materials. The electromagnetic interaction processes give an idea to consider some suitable circuit modelization of sub-atomic processes. This modelization is done by considering an atomic structure as a circuit-like element. We make specific arrangements to do this and derive suitable definitions usable for such circuit-like elements. We call atomic circuit element. We consider the simple case: less electrons and less protons where the constitutive relations are follower:

$$\mathbf{B} = \mathbf{B}(\mathbf{H}, \mathbf{E}) \quad \mathbf{D} = \mathbf{D}(\mathbf{H}, \mathbf{E}) \tag{1}$$

According to analytical restrictions to use the Laplace's transform is convenient: We consider $\mathbf{B}$ is summable over all finite intervals and there is a constant c for which

$$\int_0^\infty |\mathbf{B}| e^{-c|t|} dt < \infty \tag{2a}$$

$$\underline{\mathbf{B}} \triangleq \mathcal{L}\{\mathbf{B}; p\} = \int_0^\infty \mathbf{B} e^{-pt} dt, \quad \mathrm{Re} p > 0 \tag{2b}$$

is exist when $p = \sigma + i\tau$ is such that $\sigma \geq c$. The Laplace transforms of (1) are

$$\underline{\mathbf{B}} = \mathbf{F}_m(\underline{\mathbf{H}}, \underline{\mathbf{E}}) + \mathbf{F}_{m0}(\mathbf{E}_0) \quad \underline{\mathbf{D}} = \mathbf{F}_e(\underline{\mathbf{H}}, \underline{\mathbf{E}}) + \mathbf{F}_{e0}(\mathbf{H}_0) \tag{3}$$

where $\mathbf{E}_0$ and $\mathbf{H}_0$ are initial values (See [1] for analytical details of the essentials of the approach). The using of the above said approaches on sub-atomic processes gives the equations similar to circuit-system equations. We call these equations atomic circuit equations. An atomic circuit element is defined in Laplace transform domain with parameter p by equations derived here. The atomic circuit element is a circuit-like device.

REFERENCES

1. Sengor, T., "A chiralic circuit element and its use in a chiralic circuit," *Complex Computing-Networks, Brain-like and Wave-oriented Electrodynamic Algorithms Series, Springer Proceedings in Physics*, Vol. 104, I. C. Göknar, L. Sevgi, Eds., 2006, ISBN: 3-540-30635-8.

New Directions in Plasmonics: SERS and Nanoparticle Superlattice Crystals

George C. Schatz
Department of Chemistry, Northwestern University, Evanston IL 60208-3113, USA

Abstract— This talk will present theory studies of new substrates for SERS (collaboration with Richard Van Duyne) and applications involving plasmonic superlattice crystals (collaboration with Chad Mirkin). While anisotropic nanoparticles have long been of interest for SERS applications, an important new generation of SERS substrates is based on gold nanoparticles with a small gap ($< 1\,\mathrm{nm}$) as this leads to enhancement factors of $> 10^8$, the structures can be stabilized using silica shells, and they can used for both solution and surface-based measurements. The talk will discuss some of the fundamental theoretical issues involved underlying SERS for these structures, including the importance of dark modes, and of dipole reradiation effects. New studies of nanorod dimer structures, and of immobilized nanorod arrays will be described.

The second part of the talk considers the optical properties of silver and gold nanoparticle superlattice crystals. Motivation for this work has come from recent work in Chad Mirkin's group [1] in which a large variety of superlattice crystal structures have been synthesized using DNA linkers. Optical measurements are only starting to be done, so the present work is aimed using theory to show what optical properties are possible for these structures. The calculations are mostly based on effective medium approximation calculations with Mie theory, FDTD and DDA used for the superlattice crystal. However we have also performed careful studies of the accuracy of the effective medium approximations through comparisons with generalized Mie theory and DDA calculations with explicit particles.

Our calculations for several micron size gold superlattice crystals show that these materials can show both plasmonic resonance behavior and photonic modes, with the former dominating at $< 600\,\mathrm{nm}$ and the latter at $> 700\,\mathrm{nm}$, with a transition region in between. This leads to plasmon enhanced lensing and unusual backscattering properties.

For silver superlattice crystals we find a range of structures and wavelengths for which the real part of the dielectric function is negative, leading to metallic behavior even when the volume fraction is $< 20\%$. And even when the dielectric function is positive, there are unusual resonance shifts for rod-like crystal shapes such that longitudinal resonances can be blue of transverse resonances. Finally, for superlattices made from anisotropic particles, there are parameters which allow both negative permeability in addition to negative permittivity.

REFERENCES

1. Macfarlane, R. J., B. Lee, M. R. Jones, N. Harris, G. C. Schatz, and C. A. Mirkin, "Nanoparticle superlattices engineering with DNA," *Science*, Vol. 334, 204–208, 2011.

Mapping Structural and Plasmonic Properties of Gold Nanoparticles

Cecilia Noguez
Instituto de Física, Universidad Nacional Autónoma de México, Mexico

Abstract— One of the most fascinating aspects of metal nanostructures is the optical response, which is mainly characterized by the surface plasmon resonances. We demonstrate that at the nanoscale, the number, position, width, and intensity of surface plasmons can be tailored by manipulating the size, morphology, composition, and environment of the metal nanostructures. Additionally, metal nanostructures squeeze optical fields into highly confined, nanoscale volumes, which is important for applications such as surface enhanced Raman scattering (SERS) and fluorescence, as biomedical markers and therapy, and for detection and imaging, and for improving plasmon enhanced photovoltaic devices. In this talk, I will discuss our recent contributions of morphology and optical properties of gold nanorods that are obtained using a strategic combination of theoretical and numerical techniques [1, 2]. This combination approach show how the optical properties of gold nanoparticles respond to changes in the size, shape, or temperature, obtained by sampling the optical spectrum over large configuration space, in accordance with the nanoscale phase diagram. Shape-dependent phase diagrams are developed, and the structural and color properties of anisotropic gold nanoparticles are predicted for isotropic and anisotropic gold nanoparticles of different sizes and colloidal concentrations. Calculated maps reveal an intimate relationship between size, morphology, temperature, environment, and optical properties. We conclude that the aspect ratio of nanorods is an important factor influencing the color of the colloidal samples. We also conclude that the nanorod size plays a secondary role, in contrast to common assumption, since the color palette is quite independent of size. Color variations of samples with different refraction indices are also examined in detail, which can modify the relationship between aspect ratio and color transition, although the overall color palette remains the same. As we will show, the theoretical results discussed here are in excellent agreement with experimental observations.

REFERENCES

1. Gonzalez, A. L., C. Noguez, and A. S. Barnard, "Map of the structural and optical properties of gold nanoparticles at thermal equilibrium," *J. Phys. Chem. C*, Vol. 116, No. 26, 14170–14175, 2012.
2. Gonzalez, A. L., C. Noguez, and A. S. Barnard, "Mapping the structural and optical properties of anisotropic gold nanoparticles," *J. Mater. Chem. C*, Vol. 1, No. 18, 3150–3157, 2013.

Simulation of Plasmon Probing with Electrons

Ulrich Hohenester
Institut für Physik, Karl-Franzens-Universität Graz, Universitätsplatz 5, Graz 8010, Austria

Abstract— Surface plasmons, the workhorse of plasmonics, allow to bridge between the micrometer and nanometer length scales of conventional optics and nanodevices. This is achieved by binding or converting light to coherent electron charge oscillations, confined to the surface of metallic nanostructures [1].

In this talk, I will first present the Matlab toolbox MNPBEM which we have developed over the last years and which allows the simulation of particle plasmons in metallic and hybrid nanoparticles [2]. I will then present two case studies where electrons interact with the strong, evanescent plasmon fields, and will compare the experimental results with the simulation results of our toolbox.

First, Electron energy loss spectroscopy (EELS) and microscopy allow probing the evanescent fields of particle plasmons with nanometer resolution. I will discuss the physical processes underlying such EELS mapping. For the prototypical system of a silver nanodisk, results of a recent experimental and theoretical study [3] will be presented that revealed a surprisingly rich plasmonic spectrum, including a breathing mode which does not couple to light and has therefore escaped optical detection.

In the strong evanescent fields of the plasmonic nanoparticle electrons can become liberated and accelerated up to kinetic energies of several tens of eV. Recently, we have used femtosecond laser pulses in combination with time-of-flight spectroscopy to study the details of hot-electron emission from plasmonic nanoparticles, and have identified the physical processes underlying the photoemission process through supplementary simulations [4].

ACKNOWLEDGMENT

Work performed in collaboration with Andreas Trügler, Toni Hörl, Peter Dombi, Franz Schmidt, Harald Ditlbacher, Andreas Hohenau, and Joachim R. Krenn.

REFERENCES

1. Maier, S. A., *Plasmonics: Fundamentals and Applications*, Springer, Berlin, 2007.
2. Hohenester, U. and A. Trügler, *Comp. Phys. Commun.*, Vol. 183, 370, 2012.
3. Schmidt, F., H. Ditlbacher, U. Hohenester, A. Hohenau, F. Hofer, and J. R. Krenn, *Nano Lett.*, Vol. 12, 5780, 2012.
4. Dombi, P., A. Hörl, P. Rácz, I. Márton, A. Trügler, J. R. Krenn, and U. Hohenester, *Nano Lett.*, Vol. 13, 764, 2013.

Designed Surface Waves at an Interface of Plasmonic Nanolayered Metamaterial and Isotropic Dielectric

S. M. Vuković[1,2], C. J. Zapata-Rodríguez[3], J. J. Miret[4], and Z. Jakšić[1]

[1]Center of Microelectronic Technologies and Single Crystals, Institute of Chemistry Technology and Metallurgy, University of Belgrade, Njegoseva 12, Belgrade 11000, Serbia
[2]Texas A & M University at Qatar, P. O. Box 23874, Doha, Qatar
[3]Department of Optics, University of Valencia, Dr. Moliner 50, Burjassot 46100, Spain
[4]Department of Optics, Pharmacology and Anatomy, University of Alicante P. O. Box 99, Alicante, Spain

Abstract— We have investigated surface wave dispersion, diffraction and propagation that take place at an interface between a semi-infinite isotropic dielectric and a semi-infinite nanostructured metal-dielectric planar multilayer cut normally to the layers [1, 2]. In that case, within the framework of the effective-medium approximation (EMA), such a plasmonic multilayer behaves like a uniaxial crystal whose optical axes lies in the interface plane with isotropic dielectric. When the frequency is fixed and metallic losses neglected, bulk electromagnetic wave diffraction can be described by isofrequency surfaces in the k-space. Such surfaces can be closed (sphere, ellipsoid) resembling anisotropic dielectric, or open (hyperboloid with one or two sheets) depending on the metallic filling factor in the binary unit cell of the plasmonic multilayer [3]. Open surfaces show metallic properties in one direction and dielectric in the other (perpendicular). In addition, there are frequencies and the filling factors when only evanescent solutions are possible. Then, plasmonic multilayer resembles anisotropic metal with no propagating bulk waves. However, favourable conditions can appear in that case for propagation of surface modes along and localized near the interface with isotropic dielectric.

Our theoretical analysis shows that various conditions can be designed enabling distinct regimes of surface wave propagation for various cases of isofrequency surfaces. In general, surface waves are hybrid TE-TM polarized, propagate obliquely to the optical axes within the certain range of angles, and are more tightly confined at the interface than the standard surface plasmon polaritons. In our numerical simulations we have studied Ag/Al_2O_3, Ag/TiO_2, as well as Ag/PMMA plasmonic lattices in contact with air. Dissipation due to ohmic losses and nonlocal effects due to a finite layer width, that appear in metallic nanolayers have been studied using finite-element method by means of COMSOL multi-physics software. We would like to emphasise that the "red shift" appears in the propagation constant caused by nonlocal effects. Furthermore, the fields are enhanced on the walls of metallic films, as well as inside the dielectric nanolayers, minimazing dissipation in lossy metamaterial. The imaginary part of the wavevector decreases sharply as compared to EMA estimates, enabling much longer propagation length. Finally, it is worth noting that the properties of surface states rapidly change with the refractive index of isotropic dielectric cladding, suggesting potential applications in chemical and biological sensing and imaging.

REFERENCES

1. Jacob, Z. and E. E. Narimanov, "Optical hyperspace for plasmons: Dyakonov states in metamaterials," *Appl. Phys. Lett.*, Vol. 93, 221109, 2008.
2. Vuković, S. M., I. V. Shadrivov, and Yu. S. Kivshar, "Surface bloch waves in metamaterial- and metal-dielectric superlattices," *Appl. Phys. Lett.*, Vol. 95, 041902, 2009.
3. Krishnamoorty, H. N. S., Z. Jacob, E. E. Narimanov, I. Kretzschmar, and V. M. Menon, "Topological transitions in metamaterials," *Science*, Vol. 336, 205, 2012.

Session 3PK
Poster Session 6

LIPSS Formation on Copper Thin Films Induced by UV Picosecond Laser Pulse
Thi Trang Dai Huynh, Agnès Petit, Nadjib Semmar, ... 1244
High Quality Porous Silicon Multilayer Structures for Infra-red Applications
Zorayda Lazcano Ortiz, Jesus Arriaga, ... 1245
A Metal-dielectric Composited Film Applied to Enhance the Fluorescence Imaging
Taikei Suyama, Xiaowei Ji, Yaoju Zhang, ... 1246
Resonant State Expansion Applied to Two-dimensional Open Optical Systems
Mark B. Doost, Wolfgang Langbein, Egor A. Muljarov, ... 1247
Background Atomic Mercury Detection Using Differential Absorption Lidar System
Liang Mei, Guangyu Zhao, Sune Svanberg, ... 1248
Gas Detection in Wood and Porous Ceramics Using Gas in Scattering Media Absorption Spectroscopy
Liang Mei, Tom Ghenne, Patrik Lund, Jiandong Hu, Sune Svanberg, Gabriel Somesfalean, ... 1249
An Eigenvector Expansion Method for Localized Plasmon Modes: Application to Extinction and Electron Energy Loss Spectra of Isolated and Coupled Metallic Nanoparticles
Stéphane-Olivier Guillaume, F. Javier Garcia de Abajo, Luc Henrard, ... 1250
A New Homogenization Technique for Unfitted Finite Element Electrostatic Analysis
Takeshi Mifune, ... 1251
3D Numerical Modeling of Propagation of Electromagnetic Pulse through Subwavelength Gratings
Ivan A. Goryachev, Vadim D. Levchenko, Andrey V. Zakirov, ... 1253
Generation of Difference-frequency Radiation by Spatially Limited Few-cycle Laser Pulse in Thin Crystal of GaAs
Arsen A. Hakhoumian, Radik M. Martirosyan, Gevorg Davit Hovhannisyan, ... 1254
Numerical Method to Study Three-dimensional Metamaterial Photonic Crystals
Takamichi Terao, ... 1255
Triple Band Planar Monopole Antenna for MIMO Application
Hashimu Uledi Iddi, Muhammad Ramlee Kamarudin, Tharek Bin Abdul Rahman, Amuda Yusuf Abdulrahman, Raimi Dewan, Alyaa Syaza Azini, ... 1256
A Novel Wideband and Dual-polarized Cross-antenna for Satellite Communications
Haiyang Zhang, Yann Mahe, Tchanguiz Razban-Haghighi, ... 1258
Novel Design of Miniaturized Triple Band Square Microstrip Patch Antenna with F Slot for Fixed Service Satellite and Microwave C Band Applications
Faria Jaheen, Abdullah Al Noman Ovi, ... 1259
Highly Compact Broadband LTCC-based Butler Matrix for X-band Applications
Dongsu Kim, Jongkyun Kim, Jong-In Ryu, Jong Min Yook, Youngcheol Park, Jun-Chul Kim, ... 1261
Invariant Embedding Method Modification for Calculation "Woodpile" Photonic Crystal
Valery L. Kuznetsov, Anton S. Rudkovskiy, ... 1263
A Homogeneous Magnetostatic Field Exposure System for Presowing Magnetic Treatment of Seeds
Marco A. Azpurua, Y. Sanchez, Eduardo Javier Paez, ... 1264
Electromagnetic Wave Induced Force and Stress on Metallic Thin Films
Shubo Wang, Jack Ng, Hui Liu, Zhi Hong Hang, Z. Marcet, H. B. Chan, Che Ting Chan, ... 1265
FDTD Based EM Modeling and Analysis for Microwave Imaging of Biological Tissues
Elizabeth Rufus, Zachariah C. Alex, ... 1266
Preliminary Study on Phase-contrast Terahertz Computed Tomography Using Mach-Zehnder Interferometer with Continuous Wave Source
Masayuki Suga, Yoshiaki Sasaki, Takeshi Sasahara, Tetsuya Yuasa, Chiko Otani, ... 1267
Design of Waveguide Structure in Terahertz Quantum Cascade Lasers for Higher Operation Temperature
Norihiko Sekine, Iwao Hosako, ... 1268
Fractal Zone Plates for Terahertz Focusing and Imaging

Walter D. Furlan, V. Ferrando, Arnau Calatayud, Juan A. Monsoriu, ... 1269
A Terahertz Source with High Frequency Accuracy Using a Mach-Zehnder-modulator-based Flat Comb Generator for High Resolution Spectroscopy
Isao Morohashi, Yoshihisa Irimajiri, Takahide Sakamoto, Norihiko Sekine, Tetsuya Kawanishi, Motoaki Yasui, Iwao Hosako, ... 1270
Design of a Substrate Lens for a Terahertz Coplanar Stripline Dipole Antenna
Truong Khang Nguyen, Ikmo Park, ... 1271
Harmonic and Intermodulation Performance of a Radio-frequency Plasma Capacitor
Muhammad Taher Abuelma'atti, ... 1272
Propagation of TE Waves in a Double-layer Nonlinear Cylindrical Waveguide
Evgenii Yu. Smolkin, Dmitry V. Valovik, ... 1273
TE Wave Propagation in a Inhomogeneous Nonlinear Plane Layer
Ekaterina A. Marennikova, Dmitry V. Valovik, ... 1274
Simulation of the Ionospheric Plasma Disturbances Stimulated by the Powerful HF Radio Emission from the SURA Heating Facility
A. S. Belov, Alexander V. Kudrin, L. E. Kurina, ... 1275
Study of the Dispersive Properties of Three-dimensional Magnetized Plasma Photonic Crystals with Diamond Lattices
Hai Feng Zhang, Shaobin Liu, Hai-Ming Li, Bing-Xiang Li, ... 1276
Frequency Multiplier Based on Nonlinear Defective Photonic Crystal
Yi Dai, Shaobin Liu, Xiang-Kun Kong, Hai Feng Zhang, Hui-Chao Zhao, Chen Chen, ... 1277
Collapse of Nonlinear Dust Sound Pulses in Dusty Plasma Waveguides
M. E. Bustos De La Rosa, Volodymyr V. Grimalsky, Svetlana V. Koshevaya, Anatoliy N. Kotsarenko, 1278
Effects of Plasma Formation on Reflection of Laser Light in Ablation of Metals in Air
Olena Benavides, L. De la Cruz May, A. Flores Gil, ... 1279
Reflection of Nanosecond Nd-YAG Laser Pulses in Ablation of Metals in Air and in Vacuum: A Comparative Study
Olena Benavides, L. De la Cruz May, A. Flores Gil, ... 1280
On the Interaction of Electromagnetic Beams and Space-charge Fields in Laser-plasma Systems
A. Bonatto, R. Pakter, C. Bonatto, Felipe Barbedo Rizzato, R. P. Nunes, ... 1281
Effects of Magnetic Field on Low-power Microwave Micro-plasma Excitation
Huan Zhang, Ning Ma, Bin Liao, ... 1282
Analysis of Fractures Detectability by Borehole Radar: A Numerical Study
Sixin Liu, Jiaxin Yu, ... 1283
The Potential of Time-domain Electromagnetic Sounding to Infer the Transpression and Transtension along the Strike-slip Fault in South Andaman — India
Ramanujam Nainar, A. Vignesh, P. Prasad, ... 1284
Volume Scattering Influence on MARSIS and SHARAD Data Inversion
Marco Restano, Giovanni Picardi, Roberto Seu, ... 1285
Electromagnetic Reconstruction of Multi-layered Media Applied to Pavement Profiling
Salvatore Caorsi, Mattia Stasolla, ... 1286
Electromagnetic Susceptibility Analysis of Printed Circuits Board (PCB) and Their Impact to IEC 61000-4-3
Roberto Linares-Miranda, J. H. Caltenco Franca, Raul Peña Rivero, ... 1287
Thin-layer Carbon Coating on Nonwoven Polypropylene Obtained by Low-temperature Glow Discharge Plasma
Janina Pospieszna, Maciej Jaroszewski, Artur Henrykowski, ... 1288
3-phase VSC Modifications for Symmetrical and Asymmetrical Operation
Seyed Mahdi Fazeli, Hew Wooi Ping, Nasrudin Bin Abd Rahim, Boon Teck Ooi, Jeyraj Seelvaraj, .. 1289
Design Optimization of the Exponentially Tapered Microstrip Impedance Matching Sections Using a Cost Effective 3-D-SONNET-based SVRM with the Particle Swarm Intelligence
Mehmet Ali Belen, Salih Demirel, Filiz Gunes, Ahmet Kenan Keskin, ... 1290
Space Gravity Optimization Applied to the Feasible Design Target Space Required for a Wide-band Front-end Amplifier
Nihal Kilinc, Peyman Mahouti, Filiz Gunes, ... 1291
Ultra Wide Band Parabolic Reflector Antenna Design for Forward Looking Ground Penetrating Impulse Radar

Ahmet Serdar Turk, Mustafa Dagcan Senturk, Abdullah Magat, Alper Caliskan, ... 1292
Simulation and Implementation of RF Components
Abdullah Eroglu, ... 1293
Impact of Uncompensated Ionospheric Distortions on MARSIS Data
Marco Restano, Giovanni Picardi, Roberto Seu, ... 1294
Subsurface Geometry Influence on Radar Returns in the Orbiting Ground Penetrating Radar Context
Marco Restano, Giovanni Picardi, Roberto Seu, ... 1295
Consequences of Electromagnetic Stimulation on Hydraulic Conductivity of Soils
Arvin Farid, Sahba Azad, Jim Browning, Elisa Barney-Smith, ... 1296
UWB SAR Landmine-enhanced Imaging Based on Aspect-frequency Characteristics Using Sparse Representation
Fu-Lai Liang, Yuming Wang, Qian Song, Hanhua Zhang, Zhi-Min Zhou, ... 1297
Robust Compressive Imaging Approach to Through-wall Imaging Radar Based on Stepped-frequency and Virtual Aperture
Peng-Yu Wang, Qian Song, Jian Wang, Zhi-Min Zhou, ... 1300
Model for Determination of Territorial Distribution of Surface Radio Refractivity
Mindaugas Zilinskas, Milda Tamosiunaite, Stasys Tamosiunas, Edvinas Brilius, Milda Tamosiuniene, 1302
HEMS with Wireless Power Transmission and Energy Harvesting
Takashi Yoshikawa, ... 1303
A New CPW-fed Circularly Polarized Square Slot Antenna Design with Inverted-L Grounded Strips for Wireless Applications
Erol Karaca, Mesut Kartal, ... 1304
Investigation of Preliminary Breakdown Pulses in Lightning Waveforms
Kamyar Mehranzamir, Behnam Salimi, Zulkurnain Abdul-Malek, ... 1306
A Numerical Hybrid Technique for Radiation and Scattering by Electrically Large Structures with Embedded Substructures
Wasyl Wasylkiwskyj, ... 1308
Antenna Array Spatial Correlation of Wireless Communication Systems with Multipath Fading Channel
Ju-Hong Lee, Jia-Han Lee, ... 1309
Weaker Interhemispheric Correlation of Autism Children: Evidences from Functional near Infrared Spectroscopy
Sailing He, Huilin Zhu, ... 1311

LIPSS Formation on Copper Thin Films Induced by UV Picosecond Laser Pulse

Thi Trang Dai Huynh, **Agnès Petit**, **and Nadjib Semmar**
GREMI-UMR 7344, CNRS/Université d'Orléans, 14, rue d'Issoudun
BP 6744, 45067 Orleans cedex2, France

Abstract— Laser Induced Periodic Surface Structures (LIPSS) have attracted numerous researches because of their applications in micro and nanoscale technology fields such as lithography, high density data storage, micromachining for microelectronics and micro-electromechanical systems (MEMS) LIPSS have been identified with two distinct types: Low Spatial Frequency LIPSS (LSFL) and High Spatial Frequency LIPSS (HSFL) [1, 2]. LSFL have a spatial period close to irradiation laser wavelength. HSFL have a spatial periodic much smaller than laser wavelength. Their orientations can be perpendicular or parallel to the polarization of the incident laser radiation, depending on laser parameters and material properties. These types of LIPSS were frequently identified in the femtosecond regime. In order to understand the mechanism for their morphology transformation in the picosecond regime, detailed studies are required on the relationship among laser parameters. In this paper, the LIPSS formation copper thin film upon irradiation of ps-laser pulsed (Nd : YAG laser: wavelength of 266 nm, duration pulse of 42 ps and repetition frequency of 10 Hz) is studied experimentally. Copper thin films (200 to 1000 nm) are deposited on glass (and silicon) substrate by magnetron sputtering technique. The surface modifications of irradiation laser zone are analyzed by scanning electron microscope (SEM). As expected, two different types of LIPSS are identified with respect to the laser energy, number of laser shots and substrate. Namely, (i) at $N < 1000$ shots, LIPSS are not observable whatever is the laser energy, (ii) at $N \sim 1000$ shots, the appearance of regular spikes and HSFL is starting. (iii) At $N > 1000$ shots, both LIPSS types and regular spikes were formed at the pulse energy $E < 300\,\mu$J. For $E > 300\,\mu$J, the formation of both LSFL ($\Lambda \sim 260$ nm) and HSFL ($\Lambda \sim 150$ nm) have been observed. More generally, the maps of relationship among LIPSS formation, laser energy and number of laser shots on copper thin film with two substrates types were established.

REFERENCES

1. Hohm, S., A. Rosenfeld, J. Kruger, and J. Bonse, "Femtosecond laser-induced periodic surface structures on silica," *Journal of Applied Physics*, Vol. 112, 014901–014909, 2012.
2. Bonse, J., J. Krüger, S. Höhm, and A. Rosenfeld, "Femtosecond laser-induced periodic surface structures," *J. Laser Appl.*, Vol. 24, 042006, 2012.

High Quality Porous Silicon Multilayer Structures for Infra-red Applications

Z. Lazcano and J. Arriaga
Instituto de Física, Benemérita Universidad Autónoma de Puebla
18 Sur y San Claudio, Edif. 110 B, Ciudad Universitaria, Puebla 72570, México

Abstract— Porous silicon (pSi) based structures for optical applications in the visible and near infrared wavelength ranges are constructed with layers with thickness of the order of nanometers, and they are widely studied and successfully fabricated. Examples of these structures include: Bragg reflectors, omnidirectional mirrors, Fabry-Perot microcavities, and rugate filters. However, pSi structures for mid-infrared (MIR) applications require thicker samples, of the order of microns, and they are not easily obtained. This is because pSi layers prepared by electrochemical etching are not perfectly homogeneous throughout their depth [1]. During the etching process of pSi on p-doped substrates the microstructure and porosity of the layers change with depth, and this natural effect becomes significant for layers with thickness of the order of microns. Porous silicon layers with high homogeneity are very important for different applications such as biosensors in the IR range, or ultrasonic devices in the GHz interval of frequencies. In this work we present a systematic method to obtain homogeneous thick pSi layers as well as multilayer structures by introducing etching breaks. During these breaks no current is applied and the electrochemical etching of the Si wafer stops several times during the whole process. The time length of the etch break, the number of repetitions of these breaks, and the total etching time are the parameters that we control to obtain mechanically stable structures with minimum chirp. Since periodic systems present well defined stop-bands in the optical reflectance, we determine the porosity of the constituent layers, by fitting them to the measured spectrum. By comparing the experimental spectrum with the obtained theoretically allow us to evaluate the quality of the samples. The sample thicknesses were measured by profilometry for thin layers (1–10 μm), meanwhile we used an optical microscope for thick layers (more than 20 μm). The theoretical simulations of the reflectivity spectrum in the pSi structures were performed using the transfer matrix method (TMM) [2]. Bruggeman's effective medium approximation was used to estimate the refractive index for layers with different porosities. The reflectance spectrum was measured by Fourier Transform Infrared (FTIR) spectrometry as a function of the wavelength in the MIR range. We successfully grew thick porous silicon single layers with porosities from 43% to 73%, and multilayer periodic structures with large refractive index mismatch for optical application in IR range or acoustic investigation in GHz frequencies.

REFERENCES

1. Foss, S. E., P. Y. Y. Kann, and T. G. Finstad, *J. Appl. Phys.*, Vol. 94, 114909, 2005.
2. Yeh, P., *Optical Waves in Layered Media*, Jhon Wiley and Sons, 1998.

A Metal-dielectric Composited Film Applied to Enhance the Fluorescence Imaging

Taikei Suyama[1], **Xiaowei Ji**[2], **and Yaoju Zhang**[3]

[1]Department of Electrical and Computer Engineering, Akashi National College of Technology Akashi, Japan
[2]Graduate School of Science and Technology, Kumamoto University, Kumamoto, Japan
[3]Department of Physics and Electronic Information, Wenzhou University, Wenzhou, China

Abstract— Fluorescence labeling is the prevailing imaging technique in cell biology research. When they involve statistical investigations on a large number of cells, experimental studies require both low magnification to get a reliable statistical population and high contrast to achieve accurate diagnosis on the nature of the cells' perturbation. Because microscope objectives of low magnification generally yield low collection efficiency, such studies are limited by the fluorescence signal weakness. To overcome this technological bottleneck, E. Le Moal and E. Fort et.al proposed a method based on metal-coated substrates that enhanced the fluorescence process and improved collection efficiency in fluorescence microscope observation and that could be directly used with a common microscope setup. In this paper, we use an Ag-Si_3N_4-Ag multilayer film coated on the substrate and numerically analysis the optical behavior of a fluorophore which was placed above the composited film coated on the substrate. The results shows, using an Ag-Si_3N_4-Ag composited film, the fluorescence imaging can be enhanced markedly.

Resonant State Expansion Applied to Two-dimensional Open Optical Systems

M. B. Doost, **W. Langbein**, **and E. A. Muljarov**
Department of Physics and Astronomy, Cardiff University, Cardiff CF24 3AA, United Kingdom

Abstract— Recently, the resonant state expansion (RSE) a novel perturbation method in electrodynamics has been developed to treat open optical systems [1]. In particular, the RSE is suited to model whispering gallery modes (WGM) in microdisks and microspheres and their perturbations in order to further the development of WGM biosensors. WGM biosensors detect changes to spectra of optical resonators in the presence of perturbations, such as molecules, viruses, etc.. The WGMs in microdisks and microspheres have already been used for the characterization of monolayers [2] and to detect DNA and protein molecules [3].

In this work we demonstrate that the RSE is well suited for modeling open optical resonators with high quality-factors as shown by the convergence and accuracy of the method. The RSE calculates perturbed resonances directly by matrix diagonalization in the basis of known unperturbed resonances which can be known analytically. This is advantageous as compared to, e.g., the finite difference in time domain method which due to slow time decay of WGMs would require large computational domains in space and time and furthermore cannot treat small variations of the structure perturbatively.

The RSE has previously been applied to planar and effectively 1D spherical systems [1, 4]. Here we make an important step forward in the development of the RSE, by extending the method to systems which cannot be reduced to effectively 1D. Specifically, we treat here 3D systems translational invariant in one direction only, which can be reduced to effectively 2D systems [5]. We show, for example, that for a thin wire perturbation of a homogeneous dielectric cylinder the RSE is reproducing the results of an analytic approximation [6] (see Figure 1).

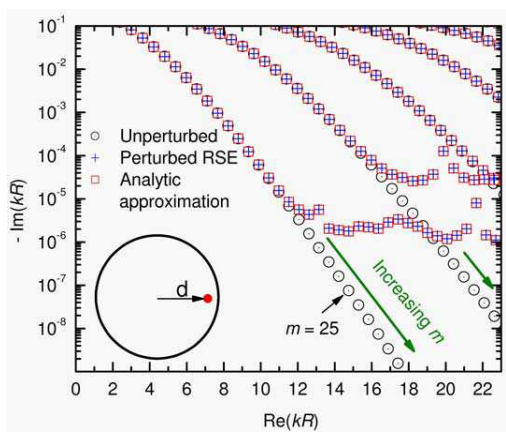

Figure 1: Resonant state wave numbers k of modes which are perturbed by a thin-wire perturbation of a homogeneous dielectric cylinder of refractive index 2 with a thin wire inclusion, calculated via the RSE (crosses) with 2000 basis states and compared with the analytic approximation [6] (empty squares). The unperturbed states are shown as open circles with dots. Inset: Sketch showing the location of the wire as a red dot inside the cylinder.

REFERENCES

1. Muljarov, E. A., W. Langbein, and R. Zimmermann, *Europhys. Lett.*, Vol. 92, 50010, 2010.
2. Noto, N., F. Vollmer, D. Keng, I. Teraoka, and S. Arnold, *Opt. Lett.*, Vol. 30, 510, 2005.
3. Vollmer, F., S. Arnold, D. Braun, I. Teraoka, and A. Libshaber, *Biophys. J.*, Vol. 85, 1974, 2003.
4. Doost, M., W. Langbein, and E. A. Muljarov, *Phys. Rev. A*, Vol. 85, 023835, 2012.
5. Doost, M. B., W. Langbein, and E. A. Muljarov, arXiv:1302.0245v1, 2013.
6. Dettman, C. P., G. V. Morozov, M. Sieber, and H. Waalkens, *Phys. Rev. A*, Vol. 80, 063813, 2009.

Background Atomic Mercury Detection Using Differential Absorption Lidar System

Liang Mei[1,2,3,4], **Guangyu Zhao**[2,3], **and Sune Svanberg**[2,3,4,5]

[1]Center for Optical and Electromagnetic Research, Zhejiang University, Hangzhou 310058, China
[2]Center for Optical and Electromagnetic Research, South China Normal University
Guangzhou 510006, China
[3]Joint Research Center of Photonics, Zhejiang University-South China Normal University
Guangzhou 510006, China
[4]Joint Research Center of Photonics
Zhejiang University-Royal Institute of Technology-Lund University
Hangzhou 310058, China
[5]Physics Department, Atomic Physics Division, Lund University
P. O. Box 118, Lund SE-221 00, Sweden

Abstract— In the present work, we demonstrate a newly developed differential absorption lidar system (DIAL) in Guangzhou, China, which was employed to monitor the background mercury concentration at the campus of South China Normal University (SCNU) located in Guangzhou. The strong absorption line for mercury is due to the transition between the ground $^1S_0$ state and the excited $^3P_1$ state, corresponding to an absorption line around 253.7 nm (vacuum wavelength). An Nd:YAG laser side-pumped dye laser is used as light source of the DIAL system, to generator the fundamental output (507 nm) of the mercury absorption line before a second harmonic frequency generation module. The on- and off-wavelengths of for the mercury measurements are switched shot-to-shot up to 50 Hz by tuning the mirror of the laser cavity using piezoelectric transducer (PZT). The DIAL measurements on atmospheric oxygen lines were also performed for system verification. Strong oxygen absorption lines are situated close to the mercury absorption line. Since the oxygen concentration is well known, expected performance can be predicted thus the performance of the DIAL system could be characterized. The mercury absorption cross section used is obtained from a modeled value based on Einstein spontaneous emission coefficient. A 24-hour continuous monitoring of the atomic mercury background is performed, and a background concentration around 12 ng/m^3 below the altitude of 110 m is obtained on January 11th, 2013 (Temperature 14°C). The system will be integrated in a mobile platform for mercury monitoring in different places of China.

REFERENCES

1. Mei, L., G. Zhao, and S. Svanberg, "Differential absorption lidar system employed for background atomic mercury vertical profiling in South China," in manuscript.

Gas Detection in Wood and Porous Ceramics Using Gas in Scattering Media Absorption Spectroscopy

Liang Mei[1,2,3], **Tom Ghenne**[1], **Patrik Lund**[1,3], **Jiandong Hu**[5], **Sune Svanberg**[1,3,4], **and Gabriel Somesfalean**[1,2,3]

[1]Department of Physics, Lund University, P.O. Box 118, Lund SE-221 00, Sweden
[2]Center for Optical and Electromagnetic Research, Zhejiang University, Hangzhou 310058, China
[3]Joint Research Center of Photonics, Zhejiang University-Royal Institute of Technology-Lund University Hangzhou 310058, China
[4]Center for Optical and Electromagnetic Research, South China Normal University Guangzhou 510006, China
[5]Department of Electrical Engineering, Henan Agricultural University, Zhengzhou 450002, China

Abstract— The presence of gas in porous materials, such as wood and ceramics, can reveal significant structural information which is of fundamental interests in many applications. In this work, we present some of our recent studies on wood and porous ceramics using Gas in Scattering Media Absorption Spectroscopy (GASMAS) [1, 2], see Fig. 1. Measurements on optical properties of various wood samples, including archeological wood, were performed, and gas exchange processes were also carefully studied. The porosity of ceramic samples was investigated, thereby opening up the possibility to use porous ceramics as multipass gas cells.

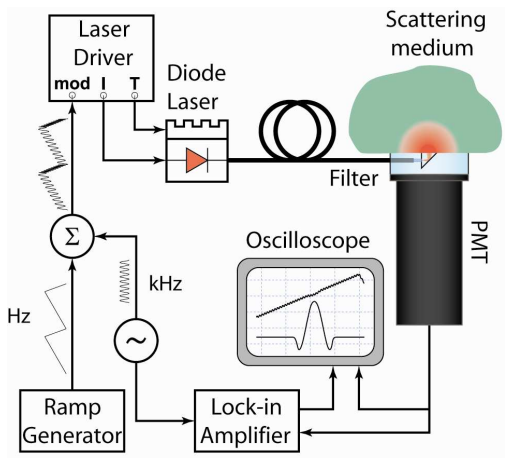

Figure 1: A typical GASMAS setup.

REFERENCES

1. Mei, L., S. Svanberg, and G. Somesfalean, "Combined optical porosimetry and gas absorption spectroscopy in gas-filled porous media using diode-laser-based frequency domain photon migration," *Optics Express*, Vol. 20, 16942, 2012.
2. Mei, L., G. Somesfalean, and S. Svanberg, "Optical characterization of micro-porous ceramics using tunable diode laser," *Proc. SPIE*, 8570, 2013.

An Eigenvector Expansion Method for Localized Plasmon Modes: Application to Extinction and Electron Energy Loss Spectra of Isolated and Coupled Metallic Nanoparticles

Stéphane-Olivier Guillaume[1], **Javier Garcia de Abajo**[2], **and Luc Henrard**[1]

[1]Department of Physics, University of Namur, 61 rue de Bruxelles, Namur, Belgium
[2]IQFR — CSIC, Serrano 119, Madrid 28006, Spain

Abstract— It is well known that the dominant features in the UV/visible spectra of metallic nanoparticles excited electromagnetically are governed by collective oscillations of valence electrons. These resonances are called localized surface plasmon (LSP) and have positions, widths and intensities that depends strongly on the nanoparticle's geometry and environment but also on the nature of the probing excitation. For instance, plane waves excite modes with non-zero dipole moment allowing them to interact with the incident light. For particles with characteristic lengths much smaller than the order of the incident wavelength, only dipolar modes will appear in the spectra. Higher order peaks (quadrupolar, octupolar, etc. ...) appear for larger particles. When one is interested in coupled nanoparticles, the plasmon modes of these systems can be described with an hybridization scheme. With help of this approach, modes can be classified according to the total dipole moment they carry. If it is null, the mode cannot be excited with traditional optical excitation and for this reason we call them 'dark modes' in contrast to 'bright modes' of dipolar nature. A way to overtake this limitation is to use a focused beam of fast electrons as probe instead of plane waves and to measure their energy loss. Indeed, the low spatial extension of the electron's field allows one to locally stimulate the nanoparticles. Their responses will therefore vary with the impact parameter of the electron beam.

In this work, we are interested in the simulation of the extinction and electron energy loss (EEL) spectra of isolated and coupled metallic particles. To achieve this, we have developped a new approach based on the Discrete Dipole Approximation (DDA). Instead of directly solving the full system of dipoles, we calculate the eigenvalues and the associated eigenvectors of the propagator matrix of each particle. This allows us to make an eigenvector expansion of the involved quantities and to truncate it to few hundreds terms compared to the complete basis set containing thousands of vectors. The response of the whole system is then obtained by adding interaction terms which account for multiple scattering between the particles. The advantage of this method is that it reduces significantly the size of the system of equations to be solved (and then the computational effort) when one considers multiparticle systems. The EigenVector Expansion Method (EVEM) has been used to calculate EEL and extinction spectra of isolated and coupled metallic particles of different geometries (such as sphere, triangle, cube, rod, hollow cube. ...) and the results have been confronted to full DDA calculations to validate the approach.

A New Homogenization Technique for Unfitted Finite Element Electrostatic Analysis

T. Mifune
Kyoto University, Japan

Abstract— In the standard finite element method, the domain analyzed is discretized with a fitted mesh, which enforces the mesh lines and is oriented along the material interfaces in the domain. Although the flexibility making this possible is one of the actual benefits of the finite element method, in some practical cases one can take advantage of an *unfitted* mesh [1–3], which can, for example, represent moving interfaces efficiently with no mesh reconstruction.

In this work, we present a new homogenization technique that improves the accuracy of unfitted finite element analysis. The merit of the homogenization is that the technique can be employed with no modification of the basic structure of the finite element algorithm, which differs from other approaches [2, 3].

For simplicity, we consider the following (two-dimensional) electrostatic equations.

$$-\nabla \cdot (\epsilon \nabla V) = 0, \tag{1}$$

where ϵ and V denote the electric permittivity and potential, respectively. The key idea in this work is to determine the electric permittivity tensor in each triangular element so as to guarantee that the finite element solution coincides with the analytical one at least in the simplest situation, where the electric field is uniform in each of two materials around a plain interface. For this purpose, we allow the tensor to be asymmetric.

The test model we used is shown in Figure 1, where the permittivity is set to 10 and 1 in the interior and exterior of a cylinder (denoted by the red line), respectively. Figure 2 compares the maximum error of the electric field obtained from finite element analysis using a simple determination method based on the gravity center of each triangle, the new homogenization technique, and a fitted mesh. The proposed technique achieves an optimal convergence property with respect to the maximum error of the electric field.

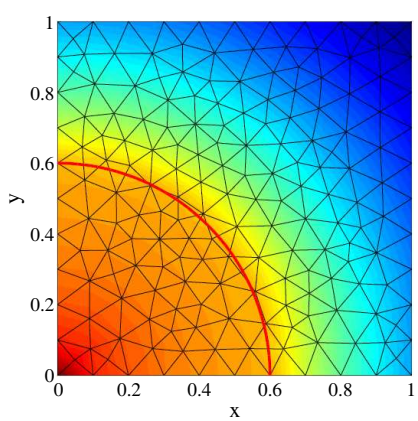

Figure 1: Test model discretized with an unfitted mesh.

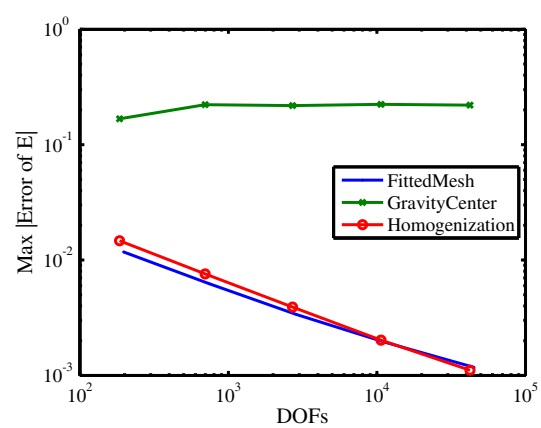

Figure 2: Maximum error of the electric field.

ACKNOWLEDGMENT

This work was supported in part by JSPS KAKENHI Grant No. 23760259.

REFERENCES

1. Watanabe, K., Y. Iijima, K. Kawano, and H. Igarashi, "Voxel based finite element method using homogenization," *IEEE Trans. Magn.*, Vol. 48, No. 2, 543–546, 2012.

2. Hansbo, A. and P. Hansbo, "An unfitted finite element method, based on Nitsche's method, for elliptic interface problems," *Comput. Methods Appl. Mech. Engrg.*, Vol. 191, 5537–5552, 2002.
3. Li, Z., T. Lin, and X. Wu, "New Cartesian grid methods for interface problems using the finite element formulation," *Numer. Math.*, Vol. 96, 61–98, 2003.

3D Numerical Modeling of Propagation of Electromagnetic Pulse through Subwavelength Gratings

I. A. Goryachev, **V. D. Levchenko**, **and A. V. Zakirov**
Keldysh Institute of Applied Mathematics, Moscow, Russia

Abstract— In recent time the fabrication technology of the dielectric thin phase elements are considered. The effective properties of subwavelength grating depend on geometry variation of its structure and the variation of its effective optical index of refraction. The article deals with the computer simulation that is employed for the prediction of a design methodology for synthesizing optical diffractive elements.

Numerical modeling is carried out by the program code CFMaxwell. It exploits LRnLA algorithms by means of large size of computational grid is calculated during the reasonable time. Due to LRnLA algorithms the simulations of such optical elements as diffractive lenses, beam splitters and etc. are possible.

The mathematical model is based on Maxwell's equations in three dimentional spatial region. The equations are solved numerically by FDTD method with PML boundary conditions. Initial electromagnetic pulse is the plane-wave or Gaussian beam with the wavelength lying in optical range. The material features of diffractive grating is close to glass one. The thickness of material is about tens of the wavelength. Geometry shape and size of the cells of the grating is not greater than the wavelength.

The results of numerical modeling are the components of electromagnetic fields in serial time moments. The time evolution of each field component is diagnosed in spatial points to compare the phase shift for various configurations of initial pulse and material features. Also Fourier analysis is employed as addition phase diagnosis. The calculation of pulse energy density as spartial function is possible to determine the effective optical propeties of subwavelength gratings and to research the distorted wavefront.

Generation of Difference-frequency Radiation by Spatially Limited Few-cycle Laser Pulse in Thin Crystal of GaAs

A. A. Hakhoumian[1], **R. M. Martirosyan**[2, 3, 4], **and G. D. Hovhannisyan**[2, 3]

[1]Ashtarak Institute of Radiophysics & Electronics
Alikhanian Bros., 1, IRPhE, Ashtarak 378410, Armenia
[2]Department of Radiophysics, Yerevan State University
A. Manoogian St., Yerevan 375049, Armenia
[3]Department of Microwave Engineering and Communication
Yerevan State University, A. Manoogian St., Yerevan 375049, Armenia
[4]National Academy of Sciences of Armenia
24 Marshal Baghramian Ave., Yerevan 0019, Armenia

Abstract— For theoretical description of difference frequency radiation (DFR) generation due to the interaction of a spatially limited linearly-polarized few-cycle laser pulse with a nonlinear crystal, the diffractive spatial and dispersive temporal spreadings of a broadband laser pulse should be taken into account, which in its turn leads to imposing a limit on the crystal length. At the same time it's evident that decreasing the thickness of nonlinear crystal will allow decreasing the temporal dispersive spreading. At nonlinear interaction of a few-cycle laser pulse with a nonlinear crystal, some pairs of frequency components may be extracted the mixing of which results in DFR generation. For efficient generation of DFR pulses in the process of nonlinear interaction of the spatially limited few-cycle duration pulse, the beam waist variation should be negligible during propagation in nonlinear crystal. In this work we present the results of theoretical study and computational modelling of the DFR generation by interaction of spatially limited few cycle laser pulses with a GaAs thin crystal. We have performed numerical time-integration of the system of nonlinear Maxwell equations by the finite difference method. We considered the laser pulse with central wavelength 1.98 μm, duration 17 fs, beam waist 10 μm, electric field amplitude 100 MV/m and intensity 3.93 GW/cm^2, propagating along the normal to the $\langle 110 \rangle$ plane in 14.7 μm thick GaAs crystal. In the nonlinear part of the medium polarization we take into account the second-order instantaneous nonlinear susceptibility. The action of the beam waist variation on the DFR efficiency generation is studied.

Numerical Method to Study Three-dimensional Metamaterial Photonic Crystals

T. Terao
Faculty of Engineering, Gifu University, 501-1193, Japan

Abstract— We have developed the extended plane-wave expansion method, which is suitable for dispersive metamaterials. Three-dimensional metamaterial photonic crystals (MPC) composed of dispersive left-handed materials and right-handed medium have been investigated.

Introduction: Electromagnetic wave propagation in metamaterials in which permittivity and permeability are simultaneously negative have attracted much attention [1, 2]. Especially, one-dimensional multilayers and two-dimensional photonic crystals consisting of positive- and negative-refractive-index materials have been investigated. It has been demonstrated that such periodic stacking of alternating layers of positive- and negative-index materials leads to a so-called zero-n gap at a characteristic frequency when the average refractive index of the system approaches zero. These phenomena are also observed in one-dimensional aperiodic multilayers and random multilayers with a negative refractive index. In this study, the photonic properties of metamaterial photonic crystals in higher dimension are clarified numerically.

Numerical Method: It is to be noted that both the permittivity and permeability of negative-refractive-index metamaterials are in general frequency dependent. In the past studies of photonic crystals, numerical treatment of such frequency dispersion of materials has been treated by, for example, the finitedifference time-domain (FDTD) method incorporated with the piecewise-linear recursive convolution (PLRC) techniques. In many cases, these numerical techniques can treat only limited cases such as Debye model, Lorentz model, and their variants. Many metamaterials are fabricated using the principle of electromagnetic resonance with fine structures, and their frequency dependence of permittivity and permeability may deviate from such simplified models. From this point of view, a different numerical approach will become requisite for the further study of metamaterials of which the function form of frequency dispersion on permittivity and permeability is not limited.

Conclusion: The author have developed extended plane-wave expansion (E-PWE) method, which is suitable for dispersive metamaterial composites. Using this method, the photonic band structure in three-dimensional metamaterial photonic crystals has been studied numerically.

ACKNOWLEDGMENT

The author also acknowledges the Supercomputer Center, Institute of Solid State Physics at the University of Tokyo, and the Research Center for Computational Science, Okazaki, Aichi, Japan, for the use of their facilities. This work was supported in part by a Grant-in-Aid for Scientific Research from the Ministry of Education, Culture, Sports, Science and Technology, Japan.

REFERENCES

1. Terao, T., "Finite-difference frequency-domain method to study photonic crystals with dispersive metamaterials," *Jpn. J. Appl. Phys.*, Vol. 50, No. 10, 102204-1–102204-5, 2011.
2. Terao, T., "Computing interior eigenvalues of nonsymmetric matrices: Application to three-dimensional metamaterial composites," *Phys. Rev. E*, Vol. 82, No. 2, 026702-1–026702-6, 2010.

Triple Band Planar Monopole Antenna for MIMO Application

Hashimu Uledi Iddi[1,2], **M. R. Kamarudin**[1], **T. A. Rahman**[1], **A. Y. Abdurahman**[1], **R. Dewan**[1], **and A. S. Azini**[1]

[1]Wireless Communication Centre (WCC), Faculty of Electrical Engineering
Universiti Teknologi Malaysia, Malaysia
[2]College of Information and Communication Technologies
University of Dar es Salaam, P. O. Box 35131, Dar es Salaam, Tanzania

Abstract— The high data rate transmission and reduced transmit power demand have increased the interest of many researchers to investigate the use of Multiple Input Multiple output (MIMO) in wireless application. Small size, low profile and simple structure are required some of the antenna array for MIMO application, so that more than one antennas can be placed as close as possible without increasing the mutual coupling between the antenna element [1]. A triple band planar monopole antenna for MIMO application is presented in this paper. The antenna array consists of two triple band monopole antennas with three copper strips, which operate at three frequency bands (2.4, 3.5 and 5.8 GHz). The antenna has been simulated using CST software and the prototype has been fabricated using FR4 substrate.

The antenna has overall dimensions of $20 \times 40 \times 1.6\,\text{mm}^3$ and $40 \times 75 \times 1.6\,\text{mm}^3$ for single triple band monopole antenna and the antenna array respectively, as shown on Figure 1. It has been shown that the antenna array performance is affected by their separation distance. The studies have shown that, when the antenna elements are placed orthogonal to each other, that an optimal distance of 10 mm, which is approximately $\lambda/12$, has been obtained. This yields mutual coupling of -22 dB. As can be seen in Figure 2(a), the proposed antenna's simulated and measured return losses are in close agreement. The proposed antenna array simulated S-parameters are shown in Figure 2(b). The antenna provides the -10 dB bandwidths of 308 MHz (from 2.2275 to 2.5354 GHz), 472 MHz (from 3.337 to 3.809 GHz) and 1.688 GHz (from 5.488 to 7.176 GHz) for 2.4, 3.5 and 5.8 GHz respectively. The results show that the measured and simulated return losses of the optimized antenna have satisfied the requirements for the 2.4/5.8 GHz WLAN and 3.5/5.8 GHz WiMAX applications. The antenna array achieve low mutual coupling of -22 dB at separation distance of 10 mm.

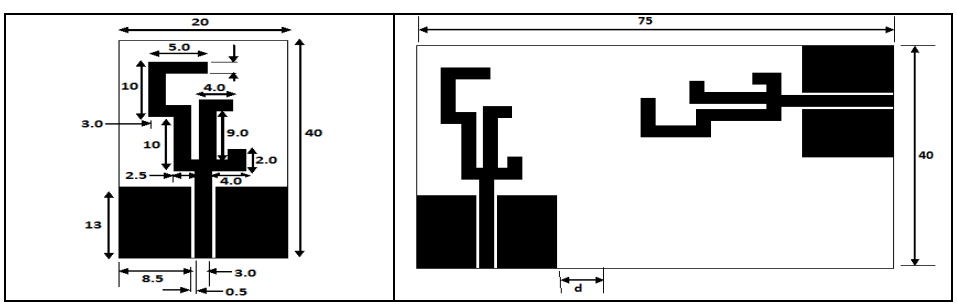

(a) (b)

Figure 1: Geometry of (a) triple band monopole antenna and (b) antenna array of triple band monopole.

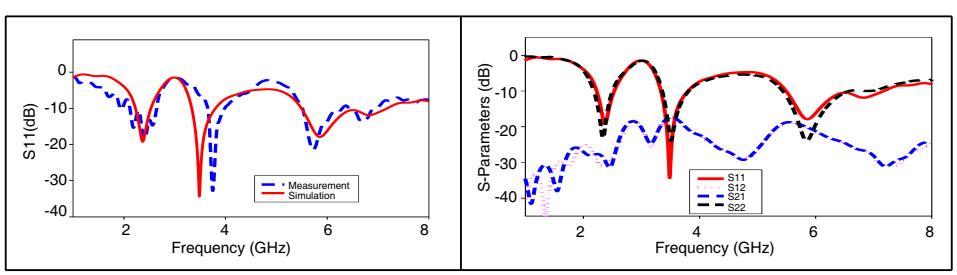

(a) (b)

Figure 2: (a) Measured and simulated return loss of triple band antenna and (b) simulated S-parameters of antenna array.

REFERENCES

1. Karaboikis, M. P., et al., "Integrating compact printed antennas onto small diversity/MIMO terminals," *IEEE Transactions on Antennas and Propagation*, Vol. 56, No. 7, 2067–2078, 2008.

A Novel Wideband and Dual-polarized Cross-antenna for Satellite Communications

Haiyang Zhang, Yann Mahe, and Tchanguiz Razban
IETR UMR 6164, Polytech Nantes, LUNAM Université, Université de Nantes
La Chantrerie, rue C. Pauc, 44306 Nantes cedex 03, France

Abstract— A new broadband and dual-polarization patch antenna was presented. The antenna is composed of two driven patches fed by coaxial cable and five parasitic patches to expand bandwidth. This antenna resonates well in the band 9.0 GHz to 11.2 GHz, while the isolation is better than −16 dB upon the whole band. Using PCB technology, the antenna can be printed on a 1.5 mm thickness TEFLON substrate and the feeding line on the same material with the thickness of 0.8 mm. The structure of the antenna makes it possible to have two orthogonal polarizations of good quality since the cross-polarization is lower than 20 dB compared to the main polarization. The simulation results also indicate that the antenna has a big gain and very high radiation efficiency. It is important to note that the dimensions of this antenna are compatible with networking to increase directivity for satellite communication applications.

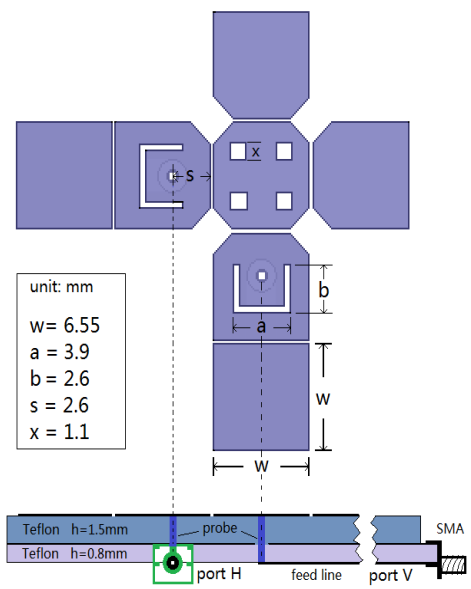

Figure 1: Geometry of the proposed cross antenna with detailed dimensions.

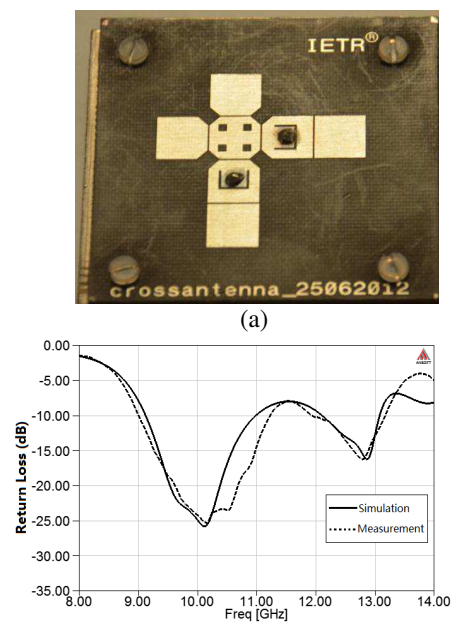

Figure 2: (a) Antenna prototype and (b) S_{11}.

Novel Design of Miniaturized Triple Band Square Microstrip Patch Antenna with F Slot for Fixed Service Satellite and Microwave C Band Applications

Faria Jaheen[1] and Abdullah Al Noman Ovi[2]

[1]American International University, Bangladesh
[2]Bangladesh University of Engineering and Technology, Bangladesh

Abstract— This paper proposes a novel concept of mode modification in miniaturized F slot loaded square microstrip patch antenna for triple band operation. Formerly, mode modification in rectangular microstrip patch antenna was performed using symmetrical rectangular slots closed to radiating edges [1, 2], J slot [3], fractural shaped slot [4], dual T shaped slit [5] and a center rectangular slot and an additional triangular slot [6] etc. Symmetrical slot loading in elliptical patch antenna also lead to the same result [7]. To reduce resonant frequency of TM_{030} mode to act like TM_{010} mode and obtain tri-band operation, an F shaped slot is etched on diminutive square patch (23 mm × 23 mm patch) and the antenna is fed through a coaxial probe. The bandwidth performance of the antenna is quite satisfactory in C band (4 GHz to 8 GHz) range. The simulated results show that the antenna can cover Fixed Service Satellite (FSS) at 3.907 GHz, mobile communication at 4.573 GHz and aeronautic radio navigation at 5.311 GHz. At triple bands (Figure 1) the antenna shows comparable and satisfactory radiation performance with gratifying directivities and gains. The directivities of proposed antenna are about 7.383 dB, 7.685 dB & 7.580 dB as shown in Figures 2, 3 and 4 respectively. A comprehensive analysis of the return loss, Radiation pattern, gain, directivity of the proposed antenna is presented. Parametric study is also included to give an overview for the performance of proposed design. The design and performance of the proposed antenna is carried out using CST Microwave Studio based realistic simulation. In a nutshell, parametric study and realistic numerical simulation of a novel design is included in this paper, considering losses and the presence of the antenna feed, giving an overview of practical realization.

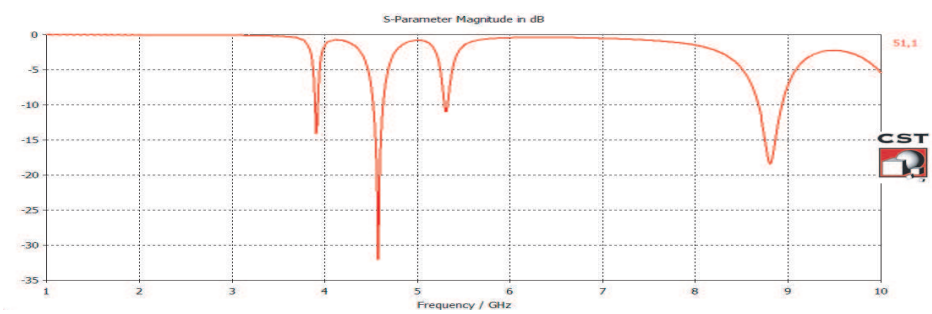

Figure 1: S-parameter performance of the proposed square microstrip patch antenna, TM_{010} mode at 3.907 GHz and $TM_{0\delta 0}$ mode at 4.573 GHz & 5.311 GHz.

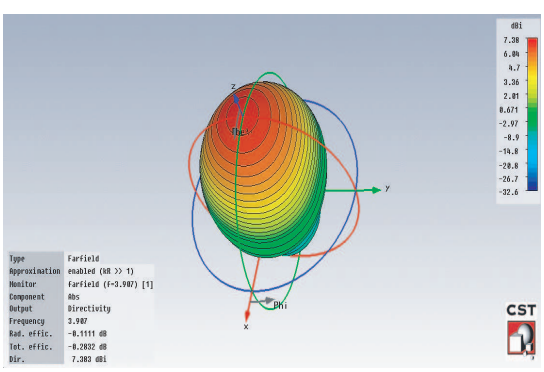

Figure 2: Three dimensional radiation pattern of TM_{010} mode at 3.907 GHz.

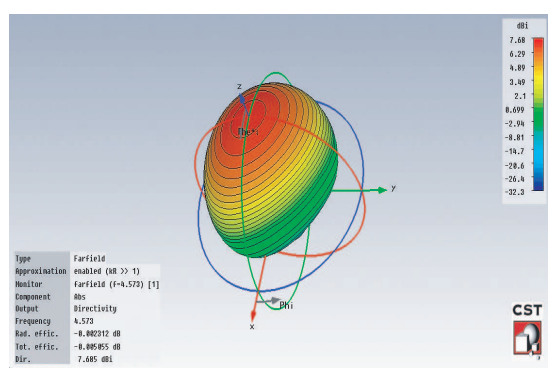

Figure 3: Three dimensional radiation pattern of $TM_{0\delta 0}$ mode at 4.573 GHz.

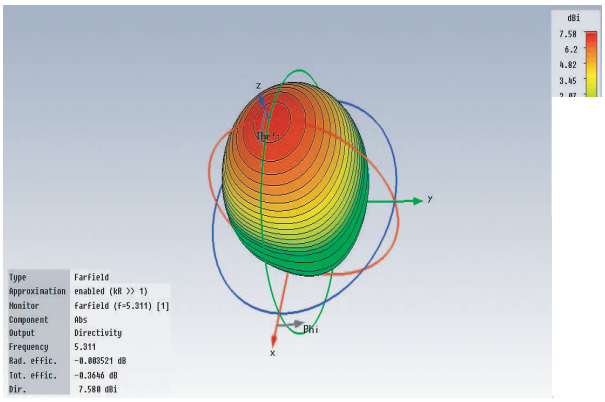

Figure 4: Three dimensional radiation pattern of $TM_{0\delta 0}$ mode at 5.311 GHz.

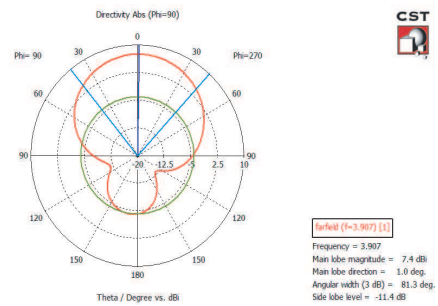

Figure 5: Polar plot of TM_{010} mode at 3.907 GHz.

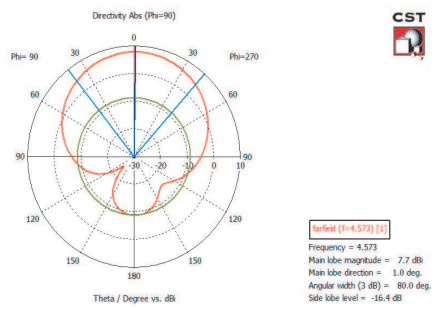

Figure 6: Polar plot of $TM_{0\delta 0}$ mode at 4.573 GHz.

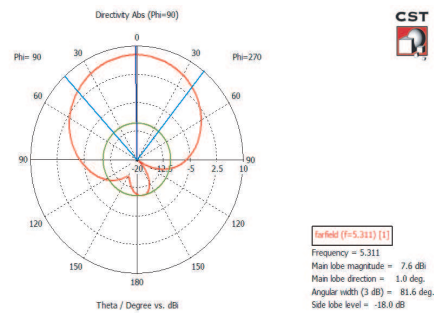

Figure 7: Polar plot of $TM_{0\delta 0}$ mode at 5.31 GHz.

REFERENCES

1. Maci, S., G. Biffi Gentili, P. Piazzesi, and C. Salvador, "Dual-band slot-loaded patch antenna," *IEE Proc. — Microw. Antennas Propag.*, Vol. 142, No. 3, June 1995.
2. Chowdhury, M. R., M. R. A. Zuboraj, A. A. N. Ovi, and M. A. Matin, "Novel design of triple band rectangular patch antenna loaded with metamaterial," *Progress In Electromagnetics Research Letters*, Vol. 21, 99–107, 2011.
3. Noman Ovi, A. A., M. R. Chowdhury, R. A. Zuboraj, and M. A. Matin, "Design of miniaturized dual band microstrip antenna loaded with asymetric J slot," *J. Electr. Eng. Electron. Technol.*, Vol. 2, 1, 2012.
4. Ali, S. A., U. Rafique, U. Ahmad, and M. A. Khan, "Multiband microstrip patch antenna for microwave applications," *IOSR Journal of Electronics and Communication Engineering (IOSR-JECE)*, Vol. 3, No. 5, 43–48, Sep.–Oct. 2012, ISSN: 2278-2834; ISBN: 2278-8735.
5. Mmaidurrahaman, S., Sudiptadas, V. K. Yadaw, A. P. Ramkanu, and A. Karmkar, "New compact tri-band microstrip patch antenna using dual T-shaped slit for wi-max and microwave C band application," *International Journal of Engineering Sciences Research-IJESR*, Vol. 3, No. 05, Sep.–Oct. 2012, ISSN: 2230-8504; e-ISSN-2230-8512.
6. Costantine, J., K. Y. K. Ali EI-Hajj, and M. Rammal, "New multi-band microstrip antenna design for wireless communications," *IEEE Antennas and Propagation Magazine*, Vol. 49, No. 6, Dec. 2007.
7. Noman Ovi, A. A., N. Saha, S. Dey, and N. N. Alam, "Symmetrical slot loaded dual band elliptical microstrip patch antenna," *PIERS Procedings*, 538–541, Moscow, Russia, August 19–23, 2012.

Highly Compact Broadband LTCC-based Butler Matrix for X-band Applications

Dongsu Kim[1], **Jongkyun Kim**[1,2], **Jong-In Ryu**[1], **Jong-Min Yook**[1], **Yeongcheol Park**[2], **and Junchul Kim**[1]

[1]Packaging Research Center, Korea Electronics Technology Institute, South Korea
[2]Electronics Engineering, Hankuk University of Foreign Studies, South Korea

Abstract— This paper presents a highly compact broadband 4×4 Butler matrix using LTCC technology for X-band applications. The Butler matrix is a well-known passive reciprocal beamforming network in a switched beam system [1, 2]. The proposed Butler matrix is composed of four tandem couplers and two Schiffman phase shifters in order to achieve broadband performance. By using LTCC's vertical design and implementation capability, the overall size of the Butler matrix can be less than 20 mm × 10 mm × 1 mm.

Figure 1 shows a schematic diagram of the proposed Butler matrix. Two 8.34-dB coupled lines for 3-dB/90° tandem couplers are realized by broadsidecoupled stripline with diagonally offset between two strip patterns in multi-layered LTCC substrate. The thickness between two layers for 8.34-dB coupling is about 200 µm. Due to the robustness against manufacturing variation by proper design of ground planes and interconnection between them using via holes, this configuration is one of the most promising solutions for LTCC structure. In terms of the phase shifter, which is one of the key elements in this system, the Schiffman differential phase shifter is chosen

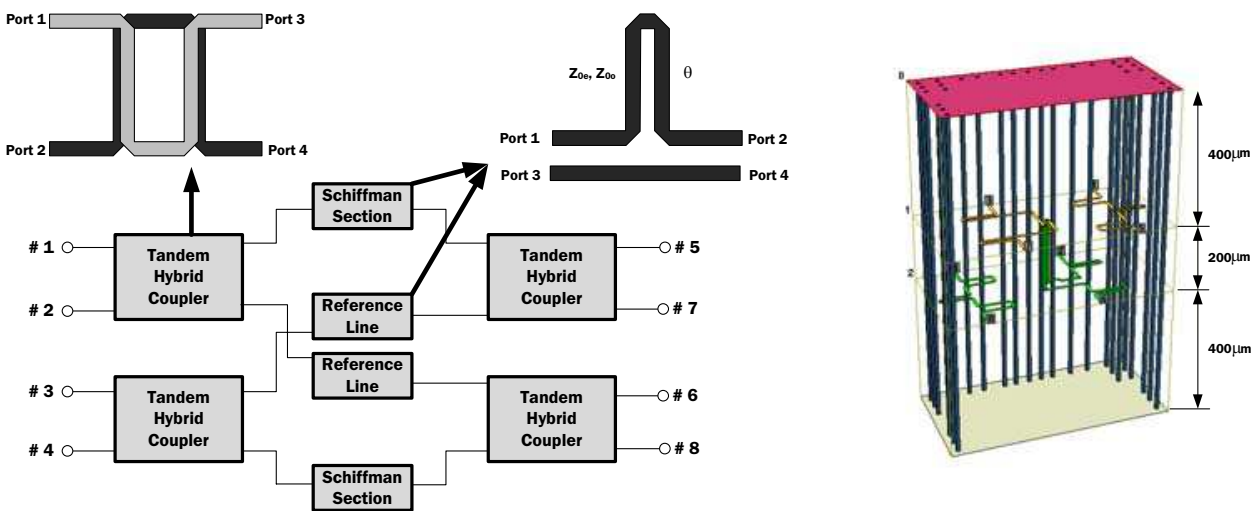

Figure 1: Schematic diagram and 3D view of the proposed Butler matrix.

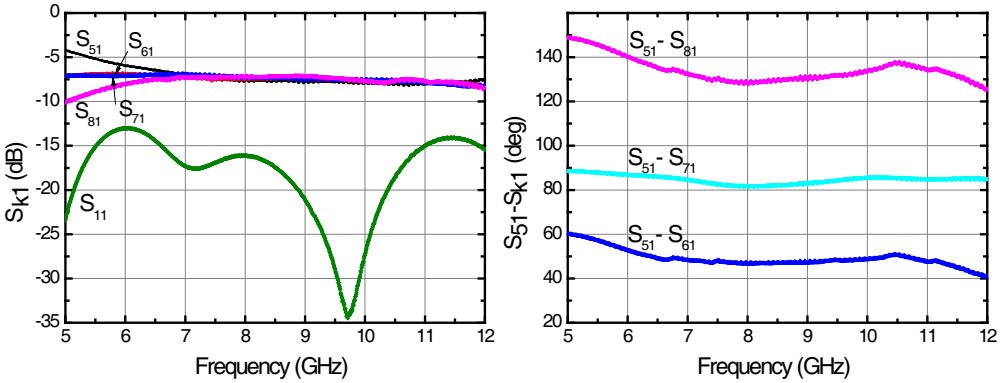

Figure 2: Performance of the proposed Butler matrix.

among several phase shifters' configurations because of its broadband amplitude and phase balance characteristics [3, 4]. The Schiffman phase shifter consists of two transmission lines. One branch is a reference transmission line, and the other is a symmetrical coupled-section line to be dispersive. By properly choosing the even- and odd-mode impedance of the coupled-section line and the length of lines, we can achieve phase difference over broadband.

Figure 2 shows the performance of the proposed Butler matrix based on the measured tandem coupler and the Schiffman phase shifter. It is observed that the average insertion loss and amplitude imbalance of the Butler matrix is about 7.5 dB $\pm$ 0.4 dB from 8 GHz to 10 GHz. The phase imbalance is less than 8° in the frequency band of interest.

REFERENCES

1. Gruszczynski, S. and K. Wincza, "Broadband 4×4 Bulter matrices as a connection of symmetrical multisection coupled-line 3-dB directional couplers and phase correction networks," *IEEE Trans. Micro. Theory Tech.*, Vol. 57, No. 1, 1–9, Jan. 2009.
2. He, J., B.-Z. Wang, Q.-Q. He, Y.-X. Xing, and Z.-L. Yin, "Wideband X-band microstrip Butler matrix," *Progress In Electromagnetics Research*, 131–140, 2007.
3. Quirate, J. L. R., and J. P. Starski, "Novel schiffman phase shifters," *IEEE Trans. Micro. Theory Tech.*, Vol. 41, No. 1, 9–14, Jan. 1993.
4. Guo, Y.-X., Z.-Y. Zhang, and L. C. Ong, "Improved wide-band schiffman phase shifter," *IEEE Trans. Micro. Theory Tech.*, Vol. 54, No. 3, 1196–1200, Mar. 2006.

Invariant Embedding Method Modification for Calculation "Woodpile" Photonic Crystal

V. L. Kuznetsov and A. S. Rudkovskiy
Moscow State Technical University of Civil Aviation, Russia

Abstract— Invariant embedding method should be marked as perspective among the existing methods for the description of PC. Like in transfer matrix methodology [1], it considers scattering medium as a set of elementary layers separated by gaps, but, in contrast to [1], is reduced to embedded equations directly for electromagnetic waves reflection and transmission matrix coefficients [2, 3].

Integration of the embedded equations allows getting these characteristics of the PC for all thicknesses less than specified. However, this advantage, at first glance, of the method leads to necessity of its modification for the analysis of 3D PC Woodpile type. The problem lies in the fact that under certain conditions, evanescent waves can resonate and increase in PC of final thickness. This effect Pendry et al. [4] proposed to use for the possible replacement of metamaterial superlens by 2D PC. The essence of evanescent wave's amplification is explained by unlimited energy supply from the incident wave in the PC. Under such conditions the amplitudes of the diffracted field increases (in time) indefinitely. Note that the problems arising in this way are related to the need to solve self-consistent problem which takes into account the reverse influence of PC at the field source.

We are interested in this issue, because similar resonance effects arise in results of embedded method: for a lossless medium there are thicknesses of PC where some (not all) elements of reflection and transmission matrices corresponding to evanescent modes tend to infinity. And, as in the invariant embedded method implementation one should consequentially increase thicknesses of PC, then at the first resonance calculations stops not allowing to get final results. It is important to note that such singularly resonances arise only in case of evanescent modes which are not interacting with the propagating modes.

In the paper a modification of the invariant embedding method is proposed which allows to "activate" interaction between all possible modes at the initial stage of equations integration. This approach allows to organize the "outflow channel" of energy from the evanescent modes, which were isolated and had resonances under standard method. It should be noted that the simplest way to avoid resonant amplification of evanescent modes is to take into account the energy dissipation in the medium, but it is not acceptable because of the impossibility to check the energy balance. It was shown that the error in this check does not exceed 3×10^{-11} in our calculations.

The paper also presents calculation results for the model under different parameters and shows comparison with the results of physical experiment.

REFERENCES

1. Barnes, C. and J. B. Pendry, "Multiple scattering of waves in random media: A transfer-matrix approach," *Proc. R. Soc. Lond. A*, Vol. 435, No. 1893, 1991.
2. Barabanenkov, Y. N., V. L. Kouznetsov, and M. Y. Barabanenkov, "Transfer relations for electromagnetic wave scattering from periodic dielectric one-dimension interface: TE polarization," *Progress In Electromagnetic Research*, Vol. 24, 39–75, 1999.
3. Barabanenkov, Y. N. and M. Y. Barabanenkov, "Energy invariants to composition rules for scattering and transfer matrices of propagating and evanescent waves in dielectric structures," *PIERS Proceedings*, 10–12, Cambridge, USA, March 26–29, 2006.
4. Luo, C., S. G. Jonson, J. D. Joanopoulos, and J. B. Pendry, "Subwavelength imaging in photonic crystals," *Phys. Rev. B*, Vol. 68, 045115, 2003.

A Homogeneous Magnetostatic Field Exposure System for Presowing Magnetic Treatment of Seeds

M. A. Azpúrua, **Y. Sánchez**, **and E. J. Páez**
Instituto de Ingeniería, Venezuela

Abstract— This paper presents a system for the generation of spatially homogeneous magnetic field, which is intended for the application of magnetic treatments on seeds. The system consists of an array of six coils, which have been sized and located in the space in order to optimize both the spatial homogeneity of the magnitude of magnetic flux density and the average magnitude of it within the volume of interest. The optimization process is implemented using a semi-analytical method that uses the generic equations that model the static magnetic flux density generated by thin wire rectangular coils fed with direct current, within an iterative TABU search algorithm under multiple constraints: the maximum and minimum dimensions of the coils, the maximum number of turns of the windings, the maximum allowable power consumption for each winding and the enameled wire gauge to be used in the windings. The designed system nominal characteristics allow the generation of a magnetic induction up to 10 mT for a current of approximately 14.5 A achieving a spatial homogeneity of 99% in the magnitude of the magnetic flux density over a rectangular volume of 0.5 m × 0.5 m × 1 m (250 lt). The experimental validation was performed following the test protocol that includes measuring the magnetic flux density and power consumption of the coils. The designed device presents a satisfactory performance considering the system constructive tolerances and made possible the implementation of the aforementioned magnetic treatment on large seed samples simultaneously, ensuring control of the exposure dose for further experimental studies on the in influence of static magnetic fields in the process of seed germination, water uptake relations and subsequent developments.

Electromagnetic Wave Induced Force and Stress on Metallic Thin Films

S. B. Wang[1], **Jack Ng**[1], **H. Liu**[2], **Z. H. Hang**[1], **Z. Marcet**[1], **H. B. Chan**[1], **and C. T. Chan**[1]

[1]Department of Physics and William Mong Institute of Nano Science and Technology
The Hong Kong University of Science and Technology, Clear Water Bay, Hong Kong, China
[2]Department of Physics, National Laboratory of Solid State Microstructures
Nanjing University, Nanjing 210093, China

Abstract— It is well known that "optical tweezers" can be used to manipulatesmall particles [1] if light is focused to a small spot. Using light to manipulate objectswithout focusing is more challenging. In particular, it is difficult to induce a strong electromagnetic force in the microwave regime. We have showntheoretically that by utilizing cavity resonance very strong electromagnetic forces can be induced between two parallel metallic plates [2, 3]. We found that the electric field between the plates gives rise to attraction and the magnetic field gives a repulsive force and the total force can be attractive or repulsive depending on whether the electric field can penetrate the metallic plates or not. In the high frequency regime, the field can penetrate the metal and force is attractive and in the microwave regime, the force becomes repulsive. We will show experimental results at the microwave frequency that demonstrate the strong electromagnetic wave induced repulsive force which manifests an enhancement of about two orders of magnitude compared to the normal photon pressure. We will also show numerically that the electromagnetic wave induced stress can deform a metallic thin film and we will compare the deformation calculated numerically with those obtained using an analytic model. The results show that the microwave induced deformation is significantly enhanced at resonance.

REFERENCES

1. Ashkin, A., *Phys. Rev. Lett.*, Vol. 24, 156–159, 1970.
2. Liu, H., J. Ng, S. B. Wang, Z. F. Lin, Z. H. Zhang, C. T. Chan, and S. N. Zhu, *Phys. Rev. Lett.*, Vol. 106, 087401, 2011.
3. Wang, S. B., J. Ng, H. Liu, H. H. Zheng, Z. H. Hang, and C. T. Chan, *Phys. Rev. B*, Vol. 84, 075114, 2011.

FDTD Based EM Modeling and Analysis for Microwave Imaging of Biological Tissues

Elizabeth Rufus[1] **and Zachariah C. Alex**[2]

[1]Department of Engineering, Middle East College, Sultanate of Oman
[2]VIT University, Vellore, India

Abstract— Breast cancer affects many women and early detection is important. The microwave imaging technique can play a vital role in the detection of breast tumor than X-ray mammography and other techniques. The basis of the microwave imaging technique for breast cancer detection and location is the significant contrast in the scattered electromagnetic signals that depends on the dielectric properties of normal and malignant tissues at microwave frequencies. Malignant tissues exhibit higher dielectric properties than normal breast tissues, especially at high frequencies. We have conducted a simulation study to find out the resolution of the microwave imaging using FDTD technique.

In this paper, a Finite Difference Time Domain method is applied to investigate the presence and location of the buried object in a phantom material. The investigation considers a phantom formed by a spherical container filled with material whose permittivity and conductivity are similar to those of normal and abnormal tissues. The study shows that the E field variation in different dielectric mediums can be used for the detection of abnormality.

Preliminary Study on Phase-contrast Terahertz Computed Tomography Using Mach-Zehnder Interferometer with Continuous Wave Source

Masayuki Suga[1], **Yoshiaki Sasaki**[2], **Takeshi Sasahara**[1], **Tetsuya Yuasa**[1], **and Chiko Otani**[2]

[1]Yamagata University, Japan
[2]RIKEN, Japan

Abstract— The terahertz (THz) waves are electromagnetic waves with frequencies ranging from 0.1 to 10 THz, or lying between radio wave and infrared light. The recent development of THz optical devices has accelerated research of THz imaging. A variety of imaging methods have been proposed to take advantage of some excellent characteristics of THz waves. Especially, the high transmissivity of THz waves for some materials enables tomographic imaging analogous to X-ray computed tomography (CT), because projected images can be obtained. However, as many of conventional THz-CTs form images due to attenuation contrast based on attenuation of the incident beam intensity similarly to X-ray CT, remarkable artifacts appear in a reconstructed image at boundaries because of unexpected intensity dissipation from an incident direction, which is caused by refraction, reflection and scattering due to the mismatch of refractive index, leading to impaired quantitative observations. In contrast, the phase-shift is not influenced by the intensity dissipation at the boundaries, so artifact-free reconstruction is expected as long as the transmitted waves can be detected.

In this study, we propose a THz-CT method based on phase contrast for significantly reduced artifacts. The THz-CT is based on the first generation type of CT, which acquires a set of projections by translational and rotational scans using a thin beam. At each data-point, the projection data of phase-shift is estimated by phase modulation technique using Mach-Zehnder interferometer with a continuous wave (CW) source. From the phase-shift projections we reconstruct a spatial distribution of refractive index in a cross section of interest. We constructed a preliminarily system using a continuous wave THz source with a frequency of 0.54 THz to prove the concept, and performed an imaging experiment using a polystyrene foam phantom to investigate imaging properties such as spatial resolution and quantitativeness.

Design of Waveguide Structure in Terahertz Quantum Cascade Lasers for Higher Operation Temperature

Norihiko Sekine and Iwao Hosako
National Institute of Information and Communications Technology, Japan

Abstract— Terahertz quantum-cascade lasers (THz QCLs) have been attracting considerable attention as compact coherent light sources and are expected to be applicable to a variety of applications, such as bio-sensing, security, and environmental monitoring. However, the operation of THz QCLs is still restricted at low temperatures, and to be of practical use, they must operate even at higher temperatures (room temperature and above). To this date, the highest operating temperature of THz QCLs is still less than 200 K [1]. In order to increase the maximum operating temperature ($T_{\max}$), studies have investigated various types of active-region designs, such as bound-to-continuum and LO-phonon-depopulation schemes. However, few studies have investigated waveguide structures in terms of thermal effects. In this work, we have proposed a new waveguide design for improving the performance of the THz QCLs, and we have quantitatively investigated influences on both thermal characteristics and waveguide modes.

In THz QCLs, the width of the waveguide is wider compared to semiconductor lasers used for optical communication systems and is on the order of 100 µm. In such wide waveguides, the active region (AR) temperature (T_{AR}) becomes much higher than the heat-sink temperature (T_{HS}) owing to inefficient thermal dissipation especially at the center of the waveguide. To avoid thermal accumulation around the center of the waveguide, we adopted a metal–metal waveguide with a multi-stripe AR that is buried by materials having higher thermal conductivity. The quantitative study was carried out on a 2D thermo-electrical model using COMSOL [2]. We investigated two waveguide structures: one is a waveguide with a conventional single AR having a width of 100 µm and the other is a waveguide with a 2-stripe AR having a width of 50 µm and a spacing of 5 µm. The height of these waveguides was 10 µm. The results of the numerical simulation showed that the temperature difference ($\Delta T = T_{\mathrm{AR}} - T_{\mathrm{HS}}$) was ~ 60 K for the multi-stripe AR, while ΔT for the single AR was ~ 84 K. Furthermore, it is also numerically confirmed that an electric field distribution of the waveguide with the multi-stripe AR was in a fundamental mode with a high confinement factor ($\Gamma \sim 0.88$). These results indicate that waveguides with multi-stripe AR can enable higher temperature operation in THz QCLs.

ACKNOWLEDGMENT

The authors would like to thank H. Yasuda and Y. Sakasegawa for fruitful discussions. This work is partly supported by JSPS KAKENHI Grant Number 24560434.

REFERENCES

1. Fathololoumi, S., et al., *Opt. Express*, Vol. 20, 3866, 2012.
2. De Naurois, G. M., et al., *Appl. Phys. Lett.*, Vol. 101, 041113, 2012.

Fractal Zone Plates for Terahertz Focusing and Imaging

W. D. Furlan[1], **V. Ferrando**[1,2], **A. Calatayud**[2], **and J. A. Monsoriu**[2]

[1]Departamento de Óptica, Universitat de València, Burjassot 46100, Spain
[2]Centro de Tecnologías Físicas
Universitat Politècnica de València, Valencia 46022, Spain

Abstract— We present novel designs for diffractive lenses with low chromatic aberration to be used in terahertz focusing and imaging. Conventional diffractive lenses (Fresnel zone plates) have been successfully applied in this area due to their low, attenuation, thickness, and weight. However, the strong chromatic aberration of these diffractive lenses limit their application only to systems with narrowband sources. We propose Fractal zone plates (FrZP) as a special type of zone plate where the pattern of the zones is fractal along the square of the radial coordinate. As a result, these lenses produce multiple foci with a fractal structure. The main lobes of the different foci provided by a FrZP coincide in the axial position with those obtained with a conventional Fresnel zone plate, but the subsidiary foci of the FrZP provide an extended depth of focus for each wavelength that partially overlap with the other one, creating an overall extended depth of focus which is less sensitive to the chromatic aberration. We evaluate the different lens designs using Fresnel-Kirchhoff's scalar diffraction theory. We have tested the THz imaging capabilities of FrZPs with broadband sources and compared their performance against a conventional Fresnel zone plate of the same main focal distance. Thus, our proposal overcome the inherent limitations of Fresnel zone plates maintaining the desired large numerical aperture.While our lens designs are tested with THz radiation, the design considerations are applicable also to other regions of the electromagnetic spectrum.

A Terahertz Source with High Frequency Accuracy Using a Mach-Zehnder-modulator-based Flat Comb Generator for High Resolution Spectroscopy

Isao Morohashi, **Yoshihisa Irimajiri**, **Takahide Sakamoto**, **Norihiko Sekine**, **Tetsuya Kawanishi**, **Motoaki Yasui**, **and Iwao Hosako**
National Institute of Information and Communications Technology, Japan

Abstract— Terahertz (THz) waves attract great deal of attention in perspective imaging, gas sensing and so forth. Since photonic technologies are advantageous to versatile signal generation in such a high-frequency region as compared with electronics devices, several techniques based on photomixing have been developed. For this purpose, optical combs are good candidate for seed sources in photomixing. Optical modulator-based comb sources have advantages in the stability and tunabilities. In this paper, we report on a THz source with high frequency accuracy by using a Mach-Zehnder-modulator-based flat comb generator (MZ-FCG).

The MZ-FCG used in the study was driven by an rf signal with the frequency of 10 GHz. The MZ-FCG converted a cw light to a flat comb signal, which has the mode spacing of 10 GHz and the 10 dB-reduction bandwidth of 300 GHz. By using a nonlinear fiber, the bandwidth of the comb signal was broadened to 3 THz. To create optical heterodyne signal, two optical modes are extracted from the comb signal by two narrow-band tunable optical filters. The extracted modes are launched into a uni-traveling carrier photodiodes (UTC-PDs). As a result, generation of THz signals was demonstrated. The nominal bandwidth of the UTC-PD was 1 THz, so that our approach can generate wideband THz signals. Our approach has some merits; (i) the frequency of THz signals can be precisely controlled by the rf signal driving the MZ-FCG, (ii) the stability of the mode spacing of the comb signal is depends on the accuracy of the rf signal.

Design of a Substrate Lens for a Terahertz Coplanar Stripline Dipole Antenna

Truong Khang Nguyen and Ikmo Park
Department of Electrical and Computer Engineering, Ajou University, Suwon, Korea

Abstract— Emitter/receiver antennas are lithographically patterned on a high-resistivity silicon substrate lens to eliminate total internal reflection and to increase the directivity of the radiation pattern through the beam, with a focus on the common implementation of a terahertz time-domain spectroscopy (THz-TDS) system. Despite considerable interest in the characterization of THz-TDS, there have only been a few studies in which the optimization of a substrate lens has been performed [1–4].

In this paper, the influence of a substrate lens on the radiation performance of a coplanar stripline dipole antenna at terahertz frequencies is presented. The antenna gain pattern is investigated by varying the extension length with a fixed hemispherical lens diameter. The result of the antenna gain versus the different ratios of T/R, where T is the extension length and R is the radius of the substrate lens, as a function of frequency shows that a high gain characteristic can be obtained by carefully choosing a particular extension length.

An optimal design was observed in the range of T/R around 0.35. The results indicate that there is a certain range of extension length that results in high gain. In other words, there is a distinct peak in gain at a specific extension length. The observed gain versus frequency curve is useful for predicting the performance of a lens-coupled antenna design. It is important to determine the antenna on a substrate lens that provides the best possible performance, and this is dependent on the specific application that falls within the different frequency bands. For instance, for a unit in imaging antenna arrays, the extension length resulting in peak directivity should be chosen for the best possible packing density in the focal plane. Similarly, for single antenna designs in wireless communication applications, an extension length with a broad beamwidth characteristic resulting in a moderately high gain should be used.

REFERENCES

1. Filipovic, D. F., S. S. Gearhart, and G. M. Rebeiz, "Double-slot antennas on extended hemispherical and elliptical silicon dielectric lenses," *IEEE Trans. Microwave Theory Tech.*, Vol. 41, No. 10, 1738–1749, 1993.
2. Rudd, J. V. and D. M. Mittleman, "Influence of substrate-lens design in terahertz timedomain spectroscopy," *J. Opt. Soc. Am. B*, Vol. 19, No. 2, 319–329, 2002.
3. Woo, I., T. K. Nguyen, H. Han, H. Lim, and I. Park, "Four-leaf clover-shaped antenna for a THz photomixer," *Opt. Exp.*, Vol. 18, No. 18, 18532–18542, 2010.
4. Nguyen, T. K., T. A. Ho, H. Han, and I. Park, "Numerical study of self-complementary antenna characteristics on substrate lenses at terahertz frequency," *J. Infrared Millim. Terahertz Waves*, Vol. 33, No. 11, 1123–1137, 2012.

Harmonic and Intermodulation Performance of a Radio-frequency Plasma Capacitor

Muhammad Taher Abuelma'atti
King Fahd University of Petroleum and Minerals, Box 203, Dhahran 31261, Saudi Arabia

Abstract— In this paper closed-form approximate expressions for the harmonic and intermodulation performance of a radio-frequency plasma capacitor are presented. These expressions are obtained by approximating the nonlinear capacitor-voltage characteristic using a Fourier-series. These expressions are valid over a wide range of the voltage applied across the capacitor and can be used for investigating the large signal performance of the capacitor.

Propagation of TE Waves in a Double-layer Nonlinear Cylindrical Waveguide

Evgenii Yu. Smolkin and Dmitry V. Valovik
Department of Mathematics and Supercomputing, Penza State University, Russia

Abstract— Problem of propagation of TE polarized electromagnetic waves in a double-layer nonlinear dielectric waveguide with circular cross-section is considered. The waveguide is supposed to be lossless and nonmagnetic. The first (inner) layer is filled with constant permittivity medium. The second layer is filled with the permittivity in the form (Kerr law): $\varepsilon = \varepsilon_2(\rho)+\alpha|\mathbf{E}|^2$, where $\varepsilon_2(\rho)$ is a continuous function, which describes the inhomogeneity of the waveguide; α is the Kerr constant; $\mathbf{E}$ is the complex amplitude of an electric field. The outer space is filled with constant permittivity medium.

The physical problem is reduced to a nonlinear eigenvalue problem. The eigenvalues of the problem are propagation constants of the waveguide. The eigenvalue problem for Maxwell's equations is reformulated as an eigenvalue problem for a nonlinear integral equation. The kernel of the integral equation depends on the Green function of a linear eigenvalue problem. Existence of a unique solution of the integral equation is proved with the help of contraction mapping method. Existence of eigenvalues of the waveguide is proved.

Numerical results are presented. One of the main thing that is made is to carry out comparison between two types of waveguides: plane layer and double-layer cylindrical waveguides.

TE Wave Propagation in a Inhomogeneous Nonlinear Plane Layer

Ekaterina A. Marennikova and Dmitry V. Valovik
Department of Mathematics and Supercomputing, Penza State University, Russia

Abstract— Problem of propagation of TE polarized electromagnetic waves in a plane layer nonlinear dielectric waveguide is considered. The waveguide is supposed to be lossless and non-magnetic. The nonlinear layer is located between two half-spaces with constant permittivities. The layer is filled with the permittivity in the form (Kerr law): $\varepsilon = \varepsilon_2(x) + \alpha|\mathbf{E}|^2$, where $\varepsilon_2(x)$ is a continuous function, which describes the inhomogeneity of the waveguide; α is the Kerr constant; $\mathbf{E}$ is the complex amplitude of an electric field.

The physical problem is reduced to a nonlinear eigenvalue problem. The eigenvalues of the problem are propagation constants of the waveguide. The eigenvalue problem for Maxwell's equations is reformulated as an eigenvalue problem for a nonlinear integral equation. The kernel of the integral equation depends on the Green function of a linear eigenvalue problem. Existence of a unique solution of the integral equation is proved with the help of contraction mapping method. Existence of eigenvalues of the waveguide is proved.

We should emphasize that the Green function can not be obtained in an explicit form for any function $\varepsilon_2(x)$. This is the reason why the dispersion equation for propagation constants contains unknown Green function. However, using well-known theory of linear differential operators and their inversions it is possible to prove existence of the roots of the dispersion equation.

Numerical results are presented.

Simulation of the Ionospheric Plasma Disturbances Stimulated by the Powerful HF Radio Emission from the SURA Heating Facility

A. S. Belov, **A. V. Kudrin**, **and L. E. Kurina**
University of Nizhny Novgorod, Russia

Abstract— Modification of the ionosphere has been an important tool for studying the physical processes related to the interaction of high-power radio emissions with a magnetoplasma. The effect of a powerful HF O-mode radio wave on the ionospheric F-region can lead to significant disturbances not only in the pump wave reflection region, but also in the outer ionosphere. An important source of these disturbances is electron heating by the field of plasma waves, which are efficiently excited by the high-power radio wave near its reflection level in the ionosphere. For simulation of the thermal effects stimulated by the powerful HF radio emission from the SURA heating facility, a modified version of the SAMI2 ionospheric model [1] developed at the Naval Research Laboratory (USA) was used. The code has been modified to include the localized Gaussian-shaped heating source in the electron temperature equation [2].

In this work, for the values of the model input parameters which are appropriate to the SURA-DEMETER ionospheric experiments [3], we study the spatial structure of stimulated large-scale disturbances of the electron temperature and plasma density. Typical times of the formation and relaxation of these disturbances have been determined. It is shown that an increase in the ion number density in the artificial ducts formed during these experiments is stipulated by the oxygen ions, whereas the number densities of lighter ions (He^+ and H^+) decrease. The simulation results agree well with the in-situ measurement data obtained by the instruments of the DEMETER satellite, significantly expand them, and provide a better understanding of the processes accompanying ionospheric modification by high-power radio waves.

ACKNOWLEDGMENT

This work was supported by the Russian Foundation for Basic Research (project No. 12–02–00747-a), the Government of the Russian Federation (contract No. 11.G34.31.0048), and the Russian Ministry of Science and Education (contract No. 14.B37.21.0901). The authors thank Dr. J. D. Huba for providing a modified version of the SAMI2 ionospheric model.

REFERENCES

1. Huba, J. D., G. Joyce, and J. A. Fedder, "SAMI2 is another model of the ionosphere (SAMI2): A new low-latitude ionosphere model," *J. Geophys. Res.*, Vol. 105, No. A10, 23035–23053, 2000.
2. Milikh, G. M., A. G. Demekhov, K. Papadopoulos, A. Vartanyan, J. D. Huba, and G. Joyce, "Model for artificial ionospheric duct formation due to HF heating," *Geophys. Res. Lett.*, Vol. 37, No. 7, L07803, 2010.
3. Frolov, V. L., V. O. Rapoport, G. P. Komrakov, A. S. Belov, G. A. Markov, M. Parrot, J. L. Rauch, and E. V. Mishin, "Density ducts formed by heating the Earth's ionosphere with high-power radio waves," *JETP Lett.*, Vol. 88, No. 12, 790–794, 2008.

Study of the Dispersive Properties of Three-dimensional Magnetized Plasma Photonic Crystals with Diamond Lattices

Hai-Feng Zhang[1,2], **Shao-Bin Liu**[1], **Hai-Ming Li**[1], **and Bing-Xiang Li**[1]

[1]College of Electronic and Information Engineering
Nanjing University of Aeronautics and Astronautics, Nanjing 210016, China
[2]Nanjing Artillery Academy, Nanjing 211132, China

Abstract— In this paper, the dispersive properties for two types of three-dimensional (3D) magnetized plasma photonic crystals (MPPCs) composed of homogeneous dielectric and magnetized plasma with diamond lattices (dielectric spheres immersed in magnetized plasma background or vice versa) are theoretically investigated based on a modified plane wave expansion method, as incidence electromagnetic wave vector is perpendicular to the external magnetic field. The influences of plasma collision frequency, filling factor, the external magnetic field and plasma frequency on the dispersive properties of both types of MPPCs are investigated in detail, respectively. From the numerical results, it has been shown that not only the locations but also relative bandwidths of the photonic band gaps (PBGs) for both types of 3D MPPCs can be manipulated by plasma frequency, filling factor and the external magnetic field, respectively. However, the plasma collision frequency has no effect on the PBGs for two types of 3D MPPCs. The locations of flatbands regions can not be tuned by any parameters except for plasma frequency and the external magnetic field.

Frequency Multiplier Based on Nonlinear Defective Photonic Crystal

Yi Dai[1], **Shao-Bin Liu**[1], **Xiang-Kun Kong**[1, 2], **Hai-Feng Zhang**[1], **Hui-Chao Zhao**[1], **and Chen Chen**[1]

[1]College of Electronic and Information Engineering
Nanjing University of Aeronautics and Astronautics, Nanjing 210016, China
[2]Jiangsu Key Laboratory of Meteorological Observation and Information Processing
Nanjing University of Information Science and Technology, Nanjing 210044, China

Abstract— This paper presents a proposal of taking nonlinear material as the structural defects in one-dimensional photonic crystals. The performance of this structure is simulated by using finite-difference time-domain (FDTD) method and transfer matrix method (TMM). The simulation results show that the investigated structure can work as frequency multiplier. In this paper, we introduce nonlinear defective photonic crystals in order to enhance the second harmonic wave and achieve relatively high second harmonic conversion efficiency. By adjusting the parameters of the defective PCs, the position of the defect modes overlap in the position of the fundamental wave ($\lambda_{FW} = 1064\,\mathrm{nm}$) and the harmonic wave ($\lambda_{SH} = 532\,\mathrm{nm}$).

Collapse of Nonlinear Dust Sound Pulses in Dusty Plasma Waveguides

M. E. Bustos De La Rosa[1], **V. Grimalsky**[1], **S. Koshevaya**[1], **and A. Kotsarenko**[2]

[1]CIICAp, Autonomous University of State Morelos (UAEM)
Av. Universidad 1001, Cuernavaca, ZP 62209, Mor., Mexico
[2]Center of Geoscience, UNAM, Campus UNAM, Juriquilla, ZP 76230, Qro., Mexico

Abstract— The dusty plasmas in space, the Earth's ionosphere, in volcano dust clouds, and under laboratory conditions now are under investigations. An important property of dusty plasmas is the support of various waves and oscillations, both linear and nonlinear ones. The dusty plasmas can be bounded and can be the waveguides for plasma waves. In the bounded plasma waves the oscillations of the surface charge take place. Even in the case when the volume nonlinearity is small, the variations of the dust concentration near interfaces can reach essential values. Moreover, because the dust concentration is principally nonnegative, the surface nonlinearity cannot be considered as moderate.

In the report the nonlinear monopulses of dust sound waves in the dusty plasma waveguides bounded by dielectrics are investigated. The waves propagate along OZ-axis, see Fig. 1. The dusty plasma includes the positive ions as the light component and the negative dust as the heavy component. The dusty plasma with different masses of dust particles is considered. The set of hydrodynamic equations for the dust, namely, the continuity equation and the equation for the momentum jointly with the Poisson one are used. The Boltzmann distribution is used for the ions. The electric and hydrodynamic boundary conditions are applied at the interfaces. The initial condition for the electric potential is monopulse-like. The simulations have demonstrated that the monopulses of small amplitudes are the subject to the wave dispersion and the diffraction. But when the moderate nonlinearity manifests, the pulse dynamics changes drastically. Namely, near the interfaces the variations of the dust concentration reach extremely high values, where the collapse of the dust sound waves occurs. The dynamics of the wave collapse depends on the distribution of the masses of the particles within the waveguide. The estimated temporal and spatial scales have demonstrated that it could be possible an appearance of the investigated phenomena of the nonlinear wave collapse in the dust objects under volcano eruptions.

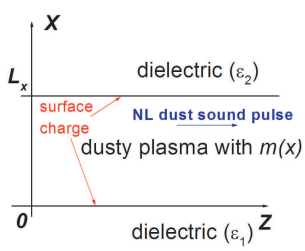

Figure 1: Geometry of the problem.

Effects of Plasma Formation on Reflection of Laser Light in Ablation of Metals in Air

O. Benavides, L. de la Cruz May, and A. Flores Gil
Universidad Autónoma del Carmen, Cd. del Carmen, Campeche, Mexico

Abstract— Processing of materials through laser ablation is widely used in fabrication of devices for photonics, plasmonics, optoelectronics, photovoltaics, microfluidics, and solar energy harvesting. Despite a large number of studies on nanosecond laser ablation, the reflection of high-intensity nanosecond laser pulses is still a poorly studied issue. In this work, we study the total reflectivity of mechanically polished bulk silver and molybdenum samples. In our experiment, a Q-switched Nd : YAG laser that generates 50-ns pulses at a wavelength of 1064 nm is used for ablation of a sample. To measure the total hemispherical reflectivity we use an ellipsoidal light reflector technique. The total hemispherical reflectivity is studied as a function of laser fluence in the range of 0.1–100 J/cm^2. The experiments are performed in air at the atmospheric pressure.

Our study shows that at laser fluences below the plasma formation thresholds the reflectivity of silver and molybdenum samples remains virtually equal to the table room-temperature reflectivity values for mechanically polished surfaces. At the laser fluence of the plasma formation threshold, the total reflectivity begins to undergo a decrease. With increasing laser fluence above the plasma formation threshold, the reflectivity abruptly drops to a value of about 0.17 and 0.11 for silver and molybdenum, respectively, and then remains unchanged with further increasing laser fluence. Our calculations of the surface temperature of the irradiated samples at the plasma formation threshold fluence show that the surface temperature is significantly below the melting point. This indicates an important role of the surface nanostructural defects in the plasma formation on the real sample due to their enhanced heating caused by plasmonic absorption. The observed reflection data are explained using a model of the laser light reflection from a plasma-sample system.

We find that at laser fluences below the plasma formation thresholds the reflectivity of aluminum samples remains virtually equal to the table room-temperature reflectivity value. At the laser fluence of the plasma formation threshold, the total reflectivity begins to undergo a decrease. An interesting feature is that the laser fluence of plasma formation threshold in air is found to be significantly lower than that in vacuum. With increasing laser fluence above the plasma formation threshold, the reflectivity abruptly drops to a value of about 0.14 and 0.24 in the air and vacuum, respectively; and then remains unchanged with further increasing laser fluence. The reflectivity drop in the air is sharper than in vacuum. A considerable difference in the reflection behaviors is due to essentially different properties of laser plasmas induced in ablation under air and vacuum conditions. Mechanisms of the plasma formation in the air and vacuum are discussed based on computing sample surface temperature. The observed reflection data are explained using a model of the laser light reflection from a plasma-sample system.

Reflection of Nanosecond Nd-YAG Laser Pulses in Ablation of Metals in Air and in Vacuum: A Comparative Study

O. Benavides, L. de la Cruz May, and A. Flores Gil
Universidad Autónoma del Carmen, Cd. del Carmen, Campeche, Mexico

Abstract— Nanosecond laser ablation is widely used in many applications such as film deposition, manufacturing of nanomaterials, surface micro/nanopatterning, biomedicine, diamond-like materials and others. Although the nanosecond laser ablation has been extensively studied for many years, a number of its physical processes are not yet well understood. This motivates further research effort.

Among the nanosecond lasers, the Nd:YAG lasers are the most widely used tools in processing of materials. For further advancement in processing of materials with the nanosecond Nd:YAG lasers, a more comprehensive knowledge on ablation is needed. Absorption/reflection of laser light from the irradiated sample is a key physical process in ablation. However, this process is not yet well studied. In this work, we perform a comparative study on the reflection of nanosecond Nd-YAG laser pulses in the ablation of aluminum in the air and in vacuum under the same other experimental conditions.

Our study shows that the reflectivity of mechanically polished aluminum remains virtually equal to the table room-temperature value with increasing laser fluence up to the plasma formation threshold. The values of the plasma formation threshold were found to be significantly different for the ablation in air ($F_{pl} = 1.1\,\mathrm{J/cm^2}$) and in vacuum ($F_{pl} = 3.1\,\mathrm{J/cm^2}$). At the plasma formation threshold, the reflectivity begins to drop both in the air and in vacuum. With increasing laser fluence above the plasma formation threshold, the reflectivity undergoes a sharp drop to a level of about 0.14 and 0.24 in the air and in vacuum, respectively. These reflectivity values remain virtually unchanged with further increasing laser fluence up to the highest studied fluence value of about $200\,\mathrm{J/cm^2}$. Furthermore, the reflectivity drop in the air is sharper than in vacuum. Our study indicates that the surface nano/micro-structural surface defects play the important role in the plasma formation, especially for the ablation in the air, where the plasma formation threshold is found to be by a factor of about 3 smaller than in vacuum.

On the Interaction of Electromagnetic Beams and Space-charge Fields in Laser-plasma Systems

A. Bonatto[1], **R. Pakter** [1], **C. Bonatto**[1], **F. B. Rizzato**[1], **and R. P. Nunes**[2]

[1]Instituto de Física UFRGS, POB 15051, Porto Alegre 91501-970, RS, Brazil
[2]Departamento de Engenharia Elétrica, UFRGS
Ave. Osvaldo Aranha 103, Porto Alegre 90035-190, RS, Brazil

Abstract— In the present analysis we study the weakly nonlinear coupled dynamics involving either pulsed or continuous radiation beams, and space-charge fields in laser-plasmas systems. We direct the analysis to regimes evolving with the co-moving coordinate of the beam frame, but do not make any assumptions on paraxial or underdense conditions. The model thus constructed allows us to perform a wider investigation on equilibrium and nonequilibrium regimes alike.

In the case of continuous beams [1], dependence of equilibrium profiles on control parameters is examined. Beam stability and evolution is then investigated as one adds small mismatches to the ideally matched equilibrium. Details of beam evolution depend on initial conditions. However, independently of the precise form of initial conditions, mismatched beams evolve to incoherent space-time patterns.

In the case of pulsed beams, we first re-examine the conditions needed for soliton formation in planar geometries. Then we add transverse effects and study how far can solitons travel before being destroyed by diffraction and the transverse component of the ponderomotive forces generated by the high-frequency carrier of the radiation field.

In both cases of pulsed and continuous settings, the numerical results can be well understood with help of a simple linear analysis, as we shall discuss.

ACKNOWLEDGMENT

CNPq and FAPERGS, Brasil, AFOSR Grant FA9550-12-1-0438, USA.

REFERENCES

1. Bonatto, A., R. Pakter, F. B. Rizzato, and C. Bonatto, *Laser Part. Beams*, Vol. 30, 583, 2012.

Effects of Magnetic Field on Low-power Microwave Micro-plasma Excitation

Huan Zhang, Ning Ma, and Bin Liao
School of Information Science and Technology
East China Normal University, Shanghai 200241, China

Abstract— Low-power microwave micro-plasma have many applications in the field of small-scale materials processing, micro-chemical-analysis system, sterilization of bio-MEMs, micro-propeller and micro-illuminant, etc. The microwave micro-plasma source is characteristic of small size, portability, operation at room temperature and atmospheric pressure, little contamination and long life. One of investigations is how to utilize less microwave power to ignite microplasma. In this paper, an approach to using ring magnet is presented and the effects of magnetic field on low-power microwave micro-plasma excitation based on microstrip split-ring resonator (MSRR) at 2.45 GHz are studied.

The microstrip split-ring resonator with round-edge gap of 0.1 mm were optimally simulated using HFSS and fabricated with gold on the dielectric substrate of ceramic. A quartz-glass tube with the diameter of 1.5 cm was used to cover the microstrip split-ring resonator in one side and connected with vaccum system in the other side. The microwave signal was supplied by Agilent E8357A and input through a power amplifier to the microstrip split-ring resonator.

The two types of ring magnets with different magnetic field strength were selected. We obtained the preliminary experimental results at gas pressure of 3.7 Torr in air. When no magnet was used, the microstrip split-ring resonator was resonated at 2.476 GHz and the parameter of S_{11} was -13.53 dB. The input microwave power igniting micro-plasma was 4.45 W.

When the ring magnet of 990G was put outside the quartz-glass tube with the S pole outwards, the microstrip split-ring resonator was resonated at 2.475 GHz and the parameter of S_{11} was -12.94dB. The input microwave power igniting micro-plasma was 2.04 W.

When the ring magnet of 2840G was utilized with the S pole outwards, the microstrip split-ring resonator was resonated at 2.481 GHz and the parameter of S_{11} was -18.08 dB. The input microwave power igniting micro-plasma was decreased to 1.36 W.

The preliminary experimental results show that the input microwave power required to ignite micro-plasma was decreased from 2.04 W to 1.36 W with increase of magnetic field strength at gas pressure of 3.7 Torr in air. The experiments at various gas pressure will be done in near future. The study provides the basis on miniaturization of low-power microwave microplasma source.

ACKNOWLEDGMENT

This work is supported by the National Natural Science Foundation of China under Grant No. 61072007.

Analysis of Fractures Detectability by Borehole Radar: A Numerical Study

Sixin Liu and Jiaxin Yu
Jilin University, Changchun, Jilin, China

Abstract— Fracture is an important geologic phenomenon which is crucial for petroleum and geothermal exploration and exists in various scale and geometry in nature. Borehole radar is the only tool which can image single fractures several to tens meters away from borehole in thousand of meters depth. Borehole radar has several advantages due to its working setting. Since the antennas are located in the borehole, borehole radar can measure the electrical characteristics of surrounding rock or soil. Borehole can sense larger region than surface GPR, and it is less affected by surface electromagnetic interface, and nearer to the interested targets detection.

However, the detectability of various fractures is different. We use FDTD to synthesize borehole radar response to fractures with different dips, different distance from borehole, and filling material such water or air. It is found that water-filled vertical fracture is easiest to detect, and horizontal air-filled fracture is nearly undetectable with only the diffraction from the fracture end. It is found that the fracture orientation affect the borehole radar response greatly from our simulation. Vertical fracture is easiest to detect and the horizontal one is difficult to detect due to the reflected wave cannot reach the receiver effectively. Two ends of a fracture cause the diffractions whether the fracture is horizontal or vertical. The distance of the fracture from the borehole is also an important factor affecting the radar signal. Long travel distance attenuates the signals much. The filling material affects the reflection coefficient. The big dielectric difference results to big reflection coefficient and strong reflection signal. That means the water-filled fracture is easy to detect. We think in practical situation, the detected fractures maybe all water-filled ones. This kind of simulation is helpful for the fracture detection and evaluation.

The Potential of Time-domain Electromagnetic Sounding to Infer the Transpression and Transtension along the Strike-slip Fault in South Andaman — India

N. Ramanujam, **A. Vignesh**, **and P. Prasad**
Department of Disaster Management, Pondicherry University
Port Blair, Andaman Islands 744112, India

Abstract— Andaman-Nicobar Islands are the part of an accretionary complex that forms the outer arc ridge of the northern Sunda subduction zone, where Indian plate is subducting northward below the Eurasian plate obliquely below Burma plate. The structure of the Andaman islands comprises an accretionary prism formed by an imbricate stack of east dipping fault slices and folds that young to the west linked to a westward shifting subduction zone. The geology of the an accretionary prism complex reflecting its dynamic environments and involving subduction folding and thrusting. Several observations of contemporaneous shortening and extension have been made for several orogenic systems with shortening at the edge mountain range and extension in the interior. The shortening in the foreland region is oriented perpendicular to the axis of the orogen and the extension of the interior mountain belt is often oriented parallel to the axis of the orogen. It has been reported that deformation in the overriding plate are further modified by the independent motion of the forearc. Oblique subduction in Andaman region has resulted in the form of shearing component of the relative motion between the two separate faults instead of one fault. The trench normal thrust fault in the subduction zone and trench parallel fault isolate forearc in the form of wedge is called as sliver plate. In the sliver plate distinctive structural features such as strike slip fault and landforms which were the outcome of the orientation of the maximum compressional and extensional tectonic stress parallel to the surface. To study the contemporaneous transpression (shortening) and transtension (extension) of the strike slip fault system in the local condition Transient Electromagnetic Sounding has been selected. As TDEM sounding requires much less measuring array than any conventional DC sounding and has more deeper penetration and reveal valuable information in locating concealed structural features. For the present study the survey with coincident loop size $30 * 30$ m; high resolution time series; windows 10 ms (17 windows); base frequency 50 Hz; stacks 100; channel gain 32 were taken for the two profiles oriented in SE-NW direction in Chidiyatappu and one profile N-S direction in Rose valley. Pseudosection obtained from the survey has identified the concealed structures of horst and graben below 20 to 40 m depth at Chidyatappu and Rose Valley are the strike slip faults and inclined steeply. Rollover anticline above listic normal fault has been located at BadaBalu area at the depth 15 to 90 m. From the study it is seen that the regional shear couple tends to rotate basement rocks and overlying sediments. Tectonic shear couple created domains of extension and compression that has resulted in normal fault and folds in the study area.

Volume Scattering Influence on MARSIS and SHARAD Data Inversion

Marco Restano, **Giovanni Picardi**, **and Roberto Seu**
Department of Information, Electrical and Telecommunication Engineering (DIET)
University of Rome "Sapienza", Italy

Abstract— The Mars Advanced Radar for Subsurface and Ionosphere Sounding (MARSIS) and the Shallow Radar (SHARAD) are currently sounding the crust of Mars providing images of the subsurface structure. Both radars emit an HF chirp pulse that can propagate into the crust down to a depth that depends upon crust composition. MARSIS emits a 1 MHz chirp signal of 250 µs duration over 4 channels (1.8–5 MHz) while SHARAD transmits a 10 MHz chirp signal of 80 µs duration over a 20 MHz carrier frequency. SAR processing is focused on SHARAD and unfocused on MARSIS.

An important task to be performed is the data inversion, i.e., the permittivity estimation of the detected subsurface layers. The inversion process proposed for the Martian south pole relies on investigations performed over flat areas selected according to the Mars Orbiter Laser Altimeter (MOLA) data in order to avoid surface clutter presence. Power backscattered by the surface and subsurface interfaces is used to evaluate crust attenuation by means of a dual channel analysis performed after compensating no flat geometries using Physical and Geometric Optics backscattering models. Nonetheless, attenuation is strongly influenced by volume scattering produced during the propagation in the crust with the consequence that data inversion cannot be assumed correct.

A one dimensional Finite-Difference Time-Domain (FDTD) simulator has been implemented evaluating the volume scattering influence on data inversion for scenarios made up of parallel interfaces as proposed by geologists. Power losses and effects on pulse shape, related to the geometric term correction, are discussed providing new criteria to select and correct data to be used in the inversion process.

Electromagnetic Reconstruction of Multi-layered Media Applied to Pavement Profiling

S. Caorsi and M. Stasolla
Dipartimento di Ingegneria Industriale e dell'Informazione, University of Pavia, Pavia, Italy

Abstract— Pavement profiling is commonly defined as the quality assessment of the pavement via nondesctructive evaluation (NDE). According to the most common design specifications, the pavement is composed of 4 uniform layers — surface/wearing course, binder course, base and subgrade [1] — whose structural conditions must be frequently and rapidly controlled in order to optimize maintenance activities and allow efficient rehabilitation plans.

Amongst the currently available NDE tools for sub-surface inspection, the Ground Penetrating Radar (GPR) has been demonstrated to be particularly suitable for the tracking of stratified geometries, so it has been widely employed in pavement profiling [2, 3]. Nevertheless, well established procedures for data analysis are still missing.

Being a radar system, the GPR collects in the time-domain the backscattering from subsurface structures, whose electromagnetic characteristics will be then related to the travel times and amplitudes of the received signals. Therefore, pavement's cross section can be deduced from radar profiles by means of echo detection and amplitude estimation [4], given that only the signals from interfaces are inverted. Multiple reflections, in fact, represent additive noise which generally interferes with the response of primary reflectors hindering the reconstructions process [5].

In this connection, the authors have recently published an inversion technique for the reconstruction of stratified media that works directly in the time domain and that could be easily applied to pavement profiling. Based on a robust time delay estimation (TDE) algorithm that allows to resolve even overlapping echoes, it iteratively reconstructs the permittivity and thickness of each layer composing the multi-layered medium from the top to the bottom [6]. In addition, it is able to detect and filter multiple reflections, whose presence is usually neglected for simplification [7].

This paper will be therefore devoted to test if the proposed method can be effectively employed also for the reconstruction of a typical pavement's vertical profile, obtained through FDTD numerical simulation. Besides the overall accuracy of the vertical profile's reconstruction, the analysis will also focus on the improvements supplied by the filtering of multiple reflections from the GPR data.

REFERENCES

1. Loizos, A. and C. Plati, "Accuracy of ground penetrating radar horn-antenna technique for sensing pavement subsurface," *IEEE Sensors Journal*, Vol. 7, No. 5, May 2007.
2. Saarenketo, T. and T. Scullion, "Road evaluation with ground penetrating radar," *Journal of Applied Geophysics*, Vol. 43, No. 2–4, 119–138, 2000.
3. Gentili, G. and U. Spagnolini, "Electromagnetic inversion in monostatic ground penetrating radar: TEM horn calibration and application," *IEEE Trans. on Geoscience and Remote Sensing*, Vol. 38, No. 4, Jul. 2004.
4. Le Bastard, C., V. Baltazart, Y. Wang, and J. Saillard, "Thin-pavement thickness estimation using GPR with high-resolution and superresolution methods," *IEEE Trans. on Geoscience and Remote Sensing*, Vol. 45, No. 8, 2511–2519, Aug. 2007.
5. Caorsi, S. and M. Stasolla, "Towards the detection of multiple reflections in time-domain EM inverse scattering of multi-layered media," *Progress In Electromagnetics Research B*, Vol. 38, 351–365, 2012.
6. "Electromagnetic infrastructure monitoring: The exploitation of GPR data and neural networks for multi-layered geometries," *Proc. of IGARSS'10*, Honolulu, Hawaii, USA, Jul. 25–30, 2010.
7. Lahouar, S. and I. L. Al-Qadi, "Automatic detection of multiple pavement layers from GPR data," *NDT&E International*, Vol. 41, No. 2, 69–81, 2008.

Electromagnetic Susceptibility Analysis of Printed Circuits Board (PCB) and Their Impact to IEC 61000-4-3

R. Linares y Miranda, **J. H. Caltenco Franca**, **and R. Peña Rivero**
Instituto Politécnico Nacional, SEPI-ESIME-Zacatenco, Laboratorio de Compatibilidad Electromagnética
Av. IPN, S/N, Unidad Profesional Adolfo López Mateos, Edif. Laboratorios Pesados 1
Col. Lindavista, México, DF, C.P. 07836, México

Abstract— One of the problems that cause failures in devices, equipment and systems that work with electric energy are the Electromagnetic Interference (EMI) of their environment. In order to minimize failures, at Electromagnetic Compatibility (EMC) standards are set limits for electromagnetic energy emission and susceptibility to it. One of the standards applied internationally is the IEC61000-4-3, which specifies the limits and measurement procedures, but not analyzes the phenomenon, since they are complex and in each device, equipment or system may be different. As consequence of the requirements of the electronic equipment with standard IEC61000-4-3, studies of susceptibility to electromagnetic fields of radio frequency in Printed Board Circuits (PCB) trace must be developed; taking into account the geometry and configuration in order to apply mitigation techniques induced currents. This paper a method for predicting the induced current by electromagnetic fields external in PCB traces and ground plane of electronic systems is presented. As a first instance the impedance of a conductor plane and fields that illuminate are determined. The results of the prediction are compared to measurements, which are very similar. This contribution may be used as a design tool for electromagnetic compatibility compliance of immunity test in PCB.

Thin-layer Carbon Coating on Nonwoven Polypropylene Obtained by Low-temperature Glow Discharge Plasma

Janina Pospieszna[1], **Maciej Jaroszewski**[1], **and Artur Henrykowski**[2]

[1]Institute of Electrical Engineering Fundamentals, Wroclaw University of Technology
Wybrzeze Wyspianskiego 27, Wroclaw 50-370, Poland
[2]Institute of Physics, Wroclaw University of Technology
Wybrzeze Wyspianskiego 27, Wroclaw 50-370, Poland

Abstract— One of the material solutions in the area of the electromagnetic field shielding are thin conductive coatings. Presently, the plasma deposition process is becoming an increasingly important methods of their production. This study investigated the possibility of obtaining conductive carbon layers on nonwoven polypropyleneby a low temperature plasma glow discharge in an atmosphere of propane-butane. Optimization of process parameters of plasma coatings application, aiming to obtain a conductive layers with good adhesion to the substrate and resistant to abrasion, requires identifying and determining the ratio of the carbon-generated phases-graphite and diamond. In this work, the Raman spectroscopy method was used for this purpose.

3-phase VSC Modifications for Symmetrical and Asymmetrical Operation

Seyed Mahdi Fazeli, **Wooi Ping Hew**, **Nasrudin Bin Abd Rahim**,
Boon Teck Ooi, **and Jeyraj Seelvaraj**
UMPEDAC, Level 4, Wisma R & D UM, University of Malaya, Kuala Lumpur 59990, Malaysia

Abstract— The paper describes minor modifications required of 3-phase voltage-source converters (VSCs) to accommodate the negative and zero-sequences of asymmetrical operation. It also proposes the Individual-Phase Decoupled P-Q Control which has 2 independent control degrees of freedom for each of the 3 phases. They enable asymmetrical operation to be controlled from the a-b-c frame without having to transform to the d-q frame and without having to use symmetrical component concepts. The methods are applied to a D-STATCOM and the concepts are validated by simulations using PSCAD/EMTDC.

Design Optimization of the Exponentially Tapered Microstrip Impedance Matching Sections Using a Cost Effective 3-D-SONNET-based SVRM with the Particle Swarm Intelligence

Mehmet Ali Belen, **Salih Demirel**, **Filiz Güneş**, **and Ahmet Kenan Keskin**
Department of Electronics and Communication Engineering
Yıldız Technical University, Istanbul, Turkey

Abstract— Non uniform transmission lines are extensively used as impedance-matching sections in microwave circuits. Non uniform transmission lines are widely examined in the literature with the pioneering works [1–3]. In this work, exponential tapered microstrip line are realized by the microstrip lines with the exponentially tapered widths and a robust design optimization procedure is put forward to match a complex load to a given another complex impedance within a bandwidth.

In the first stage of the design procedure, a cost effective 3-D SONNET-based Support Vector Regression Machine (SVRM) model of the microstrip line is completed. The 3D EM-based SVRM microstrip model provides the accurate and fast characterization of the equivalent transmission line in terms of the characteristic impedance Z_0 and the dielectric constant ε_{eff} within the continuous domain of the microstrip width W, substrate parameters (ε, h) and in the work the input variable domain is defined by $\{0.1\,\text{mm} \leq w \leq 4.6\,\text{mm},\ 2 \leq \varepsilon_r \leq 10,\ 0.1\,\text{mm} \leq h \leq 2.2\,\text{mm},\ 2\,\text{GHz} \leq f \leq 14\,\text{GHz}\}$ in an efficient manner. In the modeling process, the substantial reduction (up to 64%) is obtained utilizing sparseness of SVRM in the number of expensive fine discretization training data with the negligible loss in the predictive accuracy using the quasi-TEM microstrip synthesis formulas as the coarse model that allow to identify the regions of the design space requiring denser sampling.

The impedance transformation of anexponential tapered microstrip transmission segment in the differential length $\Delta\ell$ with the variable $Z_0(x)$ and $\varepsilon_r(x)$ is formulated in the second stage. The total length of the transmission line ℓ, the governing parameter α of the exponential variation and maximum value of the width are determined as output of the Particle Swarm Optimization (PSO). The objective of the PSO is to minimize the magnitude of the difference between the desired and input impedances over a defined bandwidth.

In the final stage of the work, a worked example is presented which is design of input matching network of a low-noise amplifier using the exponential tapered microstrip line.

REFERENCES

1. Ahmed, M. J., "Impedance transformation equations for exponential, cosine-squared, and parabolic tapered transmission lines," *IEEE Trans. Microwave Theory Tech.*, Vol. 29, 67–68, 1981.
2. Hamade, A. H., A. B. Kouki, and F. M. Ghannouchi, "An efficient approach suitable for the analysis and design of nonuniform transmission lines," *Microwave Opt. Technol. Letter.*, Vol. 3, 146–150, 1995.
3. Wu, D. and C. Ruan, "Analysis of lossless nonuniform transmission lines with power-law characteristic impedance function," *Microwave Opt. Technol. Letter.*, Vol. 17, 195–197, 1998.

Space Gravity Optimization Applied to the Feasible Design Target Space Required for a Wide-band Front-end Amplifier

Nihal Kılınç, Peyman Mahouti, and Filiz Güneş
Department of Electronics and Communication Engineering
Yıldız Technical University, Istanbul, Turkey

Abstract— In this article, the feasible design target space is determined for the input stage-requirements of an ultra-wide band low-noise front end design using a single transistor. The problem is set as an optimization problem where Space Gravity Algorithm have been used as a search and optimization tool within in the problem domain. The primary reason to use this algorithm is ease of its use, broad applicability and global perspective. The movement of the space objects and their effects on each other has been considered as a typical swarm-based approach to optimization, in which the search algorithm is inspired by the speed, acceleration, mass of the space object/asteroids and the physics law that determines the movement and effect of the space objects due to their masses and distances from each other. In this paper, the Space Gravity Optimization (SGO) algorithm is presented as a new meta-heuristic optimization tool to determine design target space for a microwave amplifier subject to the potential performance of the employed transistor where, the real and imaginary parts of the terminations at the input and output of the transistor will be taken as the coordinates of space objects/asteroids. These coordinates of the asteroids will determine Gain G_T, input VSWR V_{in} and Noise figure F response of the selected transistor. Asteroids with the less cost values will have a higher amount of masses than the others. In this algorithm, the speed and acceleration of the asteroid having the maximum amount of the mass will be accepted as zero while other asteroids with lesser masses will be forced to have accelerations and speeds due to the gravity field of the massivest asteroid. This results in change the coordinates and the costs of the asteroids. Thus, the solution space of the problem domain will be searched until the iteration reaches to its maximum value or the cost value of the massivest asteroid is equal or less than the required cost value. In the final part of the work, the proposed SGO approach is implemented to determine The Feasible Design Target Space of a selected microwave low noise transistor and the numerical results will be compared with their analytical counterparts [1]. Furthermore performance of the SGO algorithm is compared with those of the Particle Swarm Optimization [2], Honey Bee Mating optimization algorithms and advantages and disadvantages are concluded.

REFERENCES

1. Güneş, F., M. Güneş, and M. Fidan, "Performance characterisation of a microwave transistor," *IEE Proceedings — Circuits, Devices and Systems*, Vol. 141, No. 5, 337–344, 1994.
2. Güneş, F., U. Özkaya, and S. Demirel, "Particle swarm intelligence applied to determination of the feasible design target for a low-noise amplifier," *Microwave and Optical Technology Letters*, Vol. 51, No. 5, 1214–1218, May 2009.
3. Mahouti, P., F. Güneş, and S. Demirel, "Honey-bees mating algorithm applied to feasible design target space for a wide-band front-end amplifier," *2012 IEEE International Conference on Ultra-Wideband*, 251–255, 2012.

Ultra Wide Band Parabolic Reflector Antenna Design for Forward Looking Ground Penetrating Impulse Radar

Ahmet Serdar Turk, Mustafa Dagcan Senturk, Abdullah Magat, and Alper Caliskan
Electronics and Telecommunication Engineering Department, Yildiz Technical University
Davutpasa Campus, Esenler, Istanbul 34220, Turkey

Abstract— Ultra-wide band (UWB) technologies have been using for radio frequency (RF) wireless networks, high speed communication, RF jammer and high resolution radar systems. They can employ short-time impulse, wideband noise or stepped frequency signal radiation methods with a very broad frequency band operation. The UWB radar operation yields crucial advantages for small object detection, adaptive range resolution, anti-jamming and improved target imaging performances [1].

In recent years, ground-penetrating radar (GPR) has become a leading non-destructive testing and through-wall imaging technology for the detection, identification, and imaging of subsurface structures and buried objects such as pipes, mines, gaps, water channels, tunnels, roads and concealed bodies. The central frequency and bandwidth of the GPR signal are the key factors for the detection performance. The higher frequencies are needed for better resolution, nevertheless the lower frequency bands are preferred to detect something buried too deep due to the dramatically increased wave attenuation in the soil with increasing frequency. Thus, GPR systems that transmit UWB signals are proposed to benefit from both low and high frequencies. For impulse GPR, the impulse durations can vary from a few nanoseconds to hundred picoseconds corresponding to a broad spectrum from 100 MHz to 10 GHz. It can be extended up 20 GHz for stepped-frequency GPR systems, which use microwave tomography methods for high resolution imaging [2].

The convenient design of the UWB antennas is a major issue for the GPR system performance. The GPR antennas must attain high gain, narrow beam, low side lobe and input reflection level characteristics over the wide band to reach the powerful and adequately shaped impulse radiation. Horn antennas, usually TEM horns, are much popular for vehicle-mounted GPR systems due to better gain-bandwidth characteristics than planar antennas [3]. For example, the partially dielectric loaded TEM (PDTEM) horn has been introduced by Turk with 20 : 1 UWB radiation performances from 500 MHz to 10 GHz [4]. However, forward-looking GPR systems should operate at longer ranges (3–10 meters). Therefore, higher directive and narrower beam antenna types, such as dishes are required for small antenna footprint, which yields improved angular resolution for better subsurface imaging.

This paper proposes the use of Vivaldi shaped PDTEM horn as an UWB feeder for the parabolic reflector (PR) to obtain hyper-wide band antenna characteristics from 500 MHz up to 20 GHz. The hybrid PLTLM (partially loaded transmission line antenna method) and ARM (analytical regularization method) approach is used for proper pre-design of PDTEM horn-fed reflector antenna. The designed antenna models were measured between 0.1–20 GHz by network analyzer. The antenna gain, VSWR and radiation pattern performances are presented and compared with 1–18 GHz standard DRHA. It is shown that PDTEM-PR combination attains highly efficient UWB radiation pattern performances and enhanced gain performances up to 10 dB over 40 : 1 bandwidth ratio. Hence, this novel design can be considered quite suitable for multi-band forward-looking GPR operations.

ACKNOWLEDGMENT

This work was supported by grant 110E222 of TUBITAK (The Scientific and Technological Research Council of Turkey) research fund.

REFERENCES

1. Fontana, R. J., "Recent system applications of short-pulse ultra-wide band technology," *IEEE Trans. Microwave Theory Tech.*, Vol. 52, 2087–2104, 2004.
2. Turk, A. S., A. K. Hocaoglu, and A. A. Vertiy, *Subsurface Sensing*, Wiley, New Jersey, 2011.
3. Scheers, B., M. Acheroy, and A. V. Vorst, "Time-domain simulation and characterization of TEM horns using a normalized impulse response," *IEE Proc. Microwave Antennas Propagation*, Vol. 147, 463–468, 2000.
4. Turk, A. S., "Ultra-wideband TEM horn design for ground-penetrating impulse radar systems," *Microwave and Optical Technology Letters*, Vol. 41, 333–336, 2004.

Simulation and Implementation of RF Components

A. Eroglu
Department of Engineering, Indiana University-Purdue University, Fort Wayne, IN 46805, USA

Abstract— The design of RF components involves formulation of the problem, analytical derivation, simulation for verification and implementation and measurement for validation steps. Simulation is an important part of design process because it greatly expedites the design time and helps optimize the device performance. In addition, it significantly reduces the cost associated with design and development of component or device by reducing the test time and eliminating the trial and error, which is a common engineering practice. Simulation of RF components can be performed using planar electromagnetic simulators such as Sonnet or Ansoft Designer or with 3-D electromagnetic simulators such as HFSS or CST. In this paper, several RF components including planar antennas, couplers and filters are simulated and implemented using planar and 3-D electromagnetic simulators. The components are then implemented and measured. The comparison between simulated and measured results has been performed and accuracy of the simulators has been discussed. Overall, it has been shown that simulation of RF components drastically improve the final design by giving ability to optimize component or device performance. One of the devices that has been discussed and presented in this paper is a 5-pole microstrip low pass filter and its simulation and analytical results have been compared and given in Fig. 1.

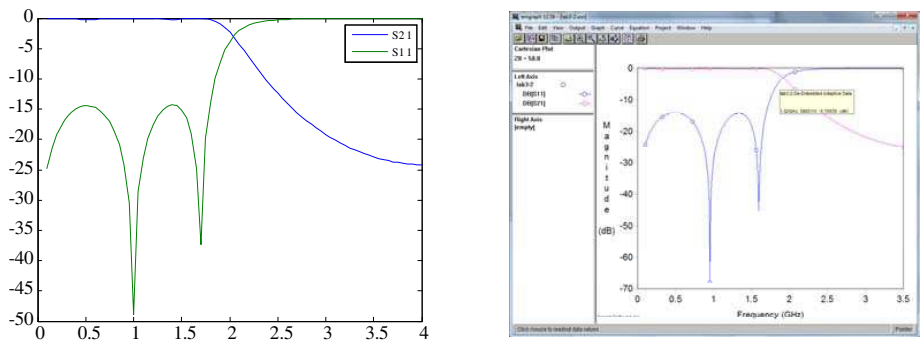

(a) (b)

Figure 1: (a) Analytical results. (b) Simulation results.

Impact of Uncompensated Ionospheric Distortions on MARSIS Data

Marco Restano, Giovanni Picardi, and Roberto Seu
Department of Information, Electrical and Telecommunication Engineering (DIET)
University of Rome, "Sapienza", Italy

Abstract— The Mars Advanced Radar for Subsurface and Ionosphere Sounding (MARSIS) currently operating on Mars needs a fine ionospheric correction in order to deliver products useful for geological investigations. The radar transmits a 1 MHz chirp signal of 250 µs duration over 4 channels (1.8, 3, 4 and 5 MHz) that can propagate into the crust down to a depth that depends upon crust composition. An unfocused SAR processing returns data in three separated Doppler filters.

Currently used ionosphere compensation procedures are based on the Chapman model describing the ionospheric electron density profile. Since recent works, based on the Mars Radio Science Experiment (MaRS), propose different electron density profiles, it is important to quantify the benefit that such profiles would produce on MARSIS data.

Ionosphere influence can be assessed using a new approach based on the finite-difference time-domain (FDTD) method. A simulator based on this formulation has been adopted to simulate the recently discovered electron density profiles evaluating the distortion introduced on MARSIS transmitted chirp signal. A comparison with the Chapman model is reported in terms of signal degradation after range compression.

The recently discovered electron density profiles are then applied on the experimental data proposing a new compensation scheme to be adopted.

So, the proposed work aims to underline the errors introduced by a not perfect knowledge of the ionospheric electron density profile during the compensation procedure. Such effect has a great impact on the data inversion process that aims to estimate the permittivity of the subsurface detected interfaces.

Subsurface Geometry Influence on Radar Returns in the Orbiting Ground Penetrating Radar Context

Marco Restano, Giovanni Picardi, and Roberto Seu
Department of Information, Electrical and Telecommunication Engineering (DIET)
University of Rome "Sapienza", Italy

Abstract— The Mars Advanced Radar for Subsurface and Ionosphere Sounding (MARSIS) and the Shallow Radar (SHARAD) are currently sounding the Martian crust providing products useful for geological investigations. Both radars emit an HF chirp pulse that can propagate into the crust down to a depth that depends upon crust composition. MARSIS emits a 1 MHz chirp signal of 250 µs duration over 4 channels (1.8–5 MHz) while SHARAD transmits a 10 MHz chirp signalof 80 µs duration over a 20 MHz carrier frequency. SAR Processing is focused on SHARAD and unfocused on MARSIS. One of the main task to be accomplished is the data inversion, that aims to estimate the permittivity of the subsurface detected interfaces.

Since very little is known regarding Mars subsurface structure it is important to develop a tool to evaluate the influence that tilted, rough or variously composed subsurface layers would produce on experimental data. So far, only surface backscattering models have been made available but there is no clear study regarding the influence that a rough/tilted surface would have on returns coming from the subsurface.

In order to accomplish such task, a finite-difference time-domain (FDTD) simulator has been developed. MARSIS, SHARAD and the Mars Orbiter Laser Altimeter (MOLA) data have been used to reproduce Martian scenarios in the most accurate way as possible. Crust composition has been modeled according to surface materials discovered by previous missions on Mars as well as on laboratory measurements.

Such analysis will be highly useful to better understand and select data suitable for data inversion.

Consequences of Electromagnetic Stimulation on Hydraulic Conductivity of Soils

A. Farid, S. Azad, J. Browning, and E. Barney-Smith
Boise State University, USA

Abstract— Hydraulic conductivity is a measure of the rate at which water flows through porous media. Because of the dipole properties of water molecules, any electric field can alter the alignment of these dipole molecules and affect the hydraulic conductivity. In this study, the effect of Radio-Frequency (RF) waves on hydraulic conductivity is investigated. This is important both for geophysical measurement of hydraulic conductivity as well as remediation using electromagnetic waves. Bentonite clay and sandy samples are tested in rigid-wall, cylindrical permeameters and stimulated using a CPVC-cased monopole antenna vertically centered in the permeameters. The permeameters are encased within RF cavities constructed of aluminum mesh in order to prevent interference from outside and to confine the RF wave to the medium. Falling-head and constant-head tests are performed to measure the hydraulic conductivity of the clayey and sandy soil samples, respectively. The results show a correlation between the change in the hydraulic conductivity and the characteristics of the RF stimulation. Using frequencies of 80, 94, and 153 MHz, water flow through the clayey sample was sharply decreased for a relatively short period and then stabilized at a lower hydraulic conductivity than that of the unstimulated case. Using various MHz frequencies, water flow through the sandy sample was sharply increased for a relatively short period and then stabilized at a higher hydraulic conductivity than that of the unstimulated case. At 153 MHz, the test was replicated with a gradual decrease of the input RF power from 30 to 10 W. The results revealed that the change in the hydraulic conductivity was larger at the higher input EM power. Measurement of the electric field component of EM waves was collected to map the electric field. In addition, the electric field was simulated using COMSOL Multiphysics for better three-dimensional (3D) visualization and analysis. The possibility of a dielectrophoretic phenomenon governing this effect was then studied for the simulated data. The result of this study was compared with the experimental result of the hydraulic conductivity tests.

UWB SAR Landmine-enhanced Imaging Based on Aspect-frequency Characteristics Using Sparse Representation

Fu-Lai Liang, Yu-Ming Wang, Qian Song, Han-Hua Zhang, and Zhi-Min Zhou
College of Electronic Science and Engineering
National University of Defense Technology, Changsha, Hunan 410073, China

Abstract— Ultra-wideband synthetic aperture radar (UWB SAR) has the characteristics of low-frequency band, large bandwidth and wide accumulated angle. These characteristics guarantee better soil or foliage penetration, high resolution of SAR images, and richer aspect and frequency dependent information of targets, making UWB SAR a promising method for detecting landmines from a safe standoff distance [1–3]. The traditional SAR image mainly shows the intensity of reflectivity from targets. Thus, the weak targets such as the landmine are easy to be masked by the strong clutters with the structures such as trihedral and dihedral. Besides, since little prior knowledge of targets is used in traditional SAR imaging, the targets are treated the same as the clutters. So there exist a lot of clutters in the SAR image. These drawbacks make it a tough problem to detect landmine. Aimed at this problem, the aspect-frequency characteristics of targets contained in UWB SAR data are brought into SAR imaging to enhance targets and suppress clutters.

In traditional SAR imaging, the multi-aspect and multi-frequency signatures are integrated to form a single image, thereby losing some of the explicit aspect and frequency dependence. In contrast, subaperture and subband technique divides the collected returns into several subapertures and subbands, and then form image with the aspect and frequency dependence preserved. Each pixel has a matrix to describe its aspect and frequency dependence.

The finite-difference time domain (FDTD) method for numerical calculation is an effective way to simulate data under various conditions for UWB SAR [4, 5]. We employ the FDTD method to simulate the scattering data of a scene including a landmine (simplified into a cylinder) and a 0.3 m trihedral. The frequency bandwidth is 2 GHz, from 0.5 GHz to 2.5 GHz. The elevation angle is 60°, the aspect angle is from −45° to 45°. The distance between the two targets is 1.414 m. The diameter and height of the cylinder are 0.3 m and 0.1 m, respectively. Fig. 1 shows the pixels corresponding to the landmine and the trihedral. There exist two dominant ridges in aspect-frequency dependence matrix of landmine. But the main characteristics of trihedral are two peaks.

Image sparse representation is used to extract these features contained in aspect-frequency dependence matrix. It can be considered as a process of acquisition the minimums number of α_i, which can be written as

$$\min_{\alpha} \|\alpha\|_0 \quad s.t. \quad f = D\alpha \tag{1}$$

where $\alpha = [\alpha_1, \alpha_2, \cdots, \alpha_I]$. Basis Pursuit (BP) method or Matching Pursuit (MP) method are often adopted in solving Equation (1).

The key is an appropriate dictionary. We choose Gabor atoms to construct the dictionary. Gabor

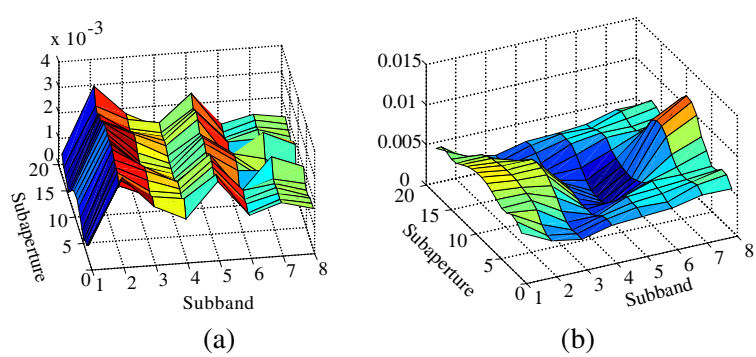

Figure 1: The aspect-frequency characteristics of typical targets. (a) Landmine. (b) Trihedral.

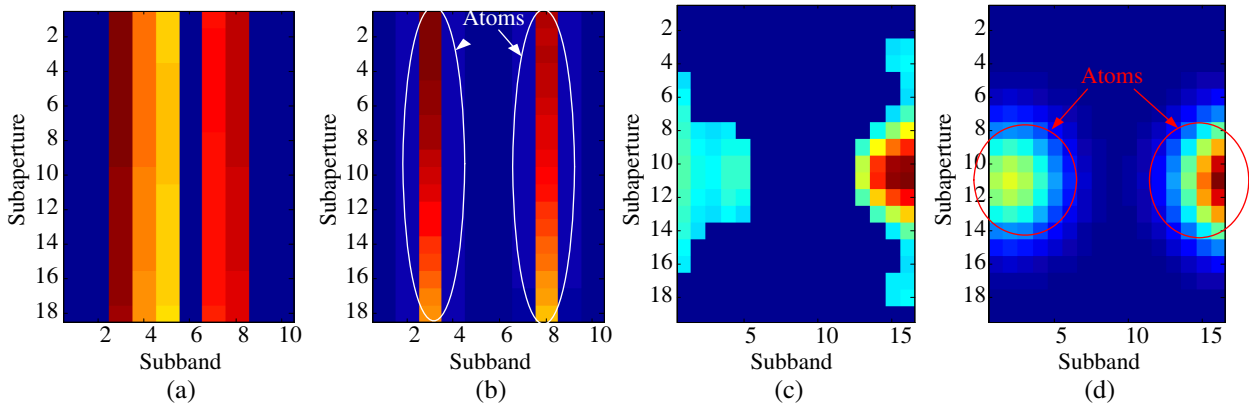

Figure 2: Results of sparse representation. (a) Initial aspect-frequency dependence matrix of landmine. (b) Reconstructed result of (a). (c) Initial aspect-frequency dependence matrix of trihedral. (d) Reconstructed result of (c).

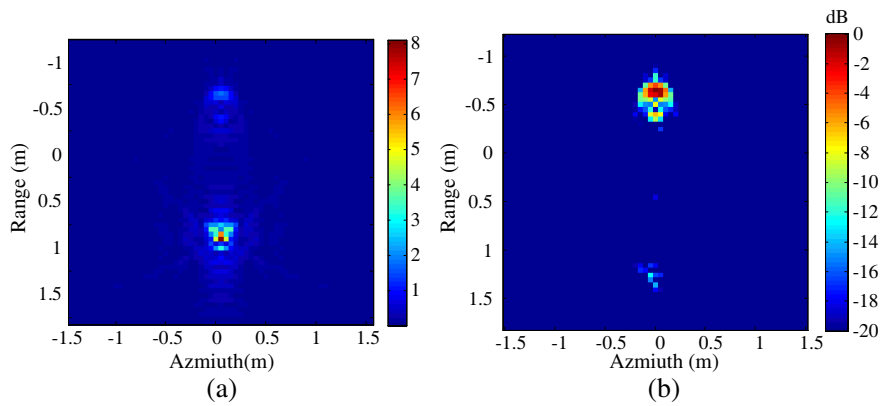

Figure 3: Comparison of results. (a) Traditional SAR image. (b) Landmine-enhanced imaging result.

atoms are defined as follows

$$\begin{aligned} g(x,y,a,b,f,\theta,x_0,y_0) &= \frac{1}{ab}\exp\left[-\pi\left(\frac{x_t^2}{a^2}+\frac{y_t^2}{b^2}\right)\right]\left[\exp(j2\pi f x_t)-\exp\left(-\frac{\pi^2}{2}\right)\right] \\ x_t &= (x-x_0)\cos\theta+(y-y_0)\sin\theta \\ y_t &= -(x-x_0)\sin\theta+(y-y_0)\cos\theta \end{aligned} \tag{2}$$

where a and b are scale factors, x_0 and y_0 are shift factors, f is tuning factor, and θ is rotation angle.

The peaks and ridges are described by atoms with different scale factors and rotation angle. As Fig. 2 shows, the peaks are represented by two atoms whose scale factors are both 6 pixel in subapreture and subband direction. However, the ridges are represented by two atoms whose subapreture scale factors are large but subband scale factors are small. The rotation angles of atoms belonging to landmine are 0, but rotation angles of atoms belonging to trihedral are $\pi/2$.

The extracted atoms show the quantitative analysis of targets, which can be used for enhancement of specific target and classification of targets. In this paper, we concentrate on the method of landmine enhancement. The mean value of subaperture scale factors of the first two atoms is chosen as the weight value of each pixel. Thus, the landmine can be enhanced. As Fig. 3 shows, the landmine in traditional SAR image is much weaker than trihedral. In the enhanced-imaging result, the landmine becomes much stronger than the trihedral. So the proposed method is valid.

REFERENCES

1. Jin, T. and Z. Zhou, "Ultrawideband synthetic aperture radar landmine detection," *IEEE Transactions on Geoscience and Remote Sensing*, Vol. 45, 3561–3573, 2007.
2. Andrieu, J., F. Gallais, V. Mallepeyre, V. Bertrand, B. Beillard, B. Jecko, et al., "Land mine detection with an ultra-wideband SAR system," *Proc. SPIE*, Vol. 4742, 237–247, 2002.

3. Yang, J., X. Huang, T. Jin, J. Thompson, and Z. Zhou, "Synthetic aperture radar imaging using stepped frequency waveform," *IEEE Transactions on Geoscience and Remote Sensing*, Vol. 50, 2026–2036, 2012.
4. Zhang, Y.-Q. and D.-B. Ge, "A unified FDTD approach for electromagnetic analysis of dispersive objects," *Progress In Electromagnetics Research*, Vol. 96, 155–172, 2009.
5. Hu, X.-J. and D.-B. Ge, "Study on conformal FDTD for electromagnetic scattering by targets with thin coating," *Progress In Electromagnetics Research*, Vol. 79, 305–319, 2008.

Robust Compressive Imaging Approach to Through-wall Imaging Radar Based on Stepped-frequency and Virtual Aperture

Pengyu Wang, Qian Song, Jian Wang, and Zhimin Zhou
College of Electronic Science and Engineering
National University of Defense Technology, Changsha, Hunan 410073, China

Abstract— Through-wall imaging (TWI) radar has gained much attention in recent years due to its broad civilian and military applications. Among these applications, target positioning has attracted more and more researchers. That means target electromagnetic scattering characteristic doesnt seem as important as before. Under this condition, the supposition that the targets behind walls can be approximated to point-like reflectors can be considered true. As target number is generally much smaller than the total number of discrete spatial positions, this sparsity just satisfies the premise of applying the new technique known as compressive sensing (CS). Although some challenges need to be overwhelmed before a real CS radar system comes true, the techniques of stepped-frequency (SF) and virtual aperture (VA) have provides the possibility to design a tentative CS-based TWI radar named SFVACS-TWIR. In this paper, we mainly discuss the design and word mode of the SFVACS-TWIR system. And for achieving robust reconstruction, the multi-measurement iterative pixel discrimination (MM-IPD) approach is introduced [1], as well.

Figure 1 shows the system sketch map of SFVACS-TWIR which is consisted of two transmitters and several receivers. For improving the detection efficiency of SFVACS-TWIR, the SF signal generator should work in the mode of ordinal frequency sweep. With the fast switches, the logical controller can achieve the target echo of arbitrary frequency and transmit-receive channel, which just like the measured data achieved by the random measure matrix. Fig. 1(b) shows the work mode of SFVACS-TWIR, where υ represents the frequency scanning number.

Furthermore, the CS is so sensitive in noisy that it is quite difficult for CS to obtain robust reconstruction, especially in low signal-to-noise ratio conditions. Due to the through-wall attenuation, this situation will become even worse in SFVACS-TWIR system. But as mentioned in Ref. [1], the MM-IPD approach can provide a robust solution to this problem. Though the MM-IPD

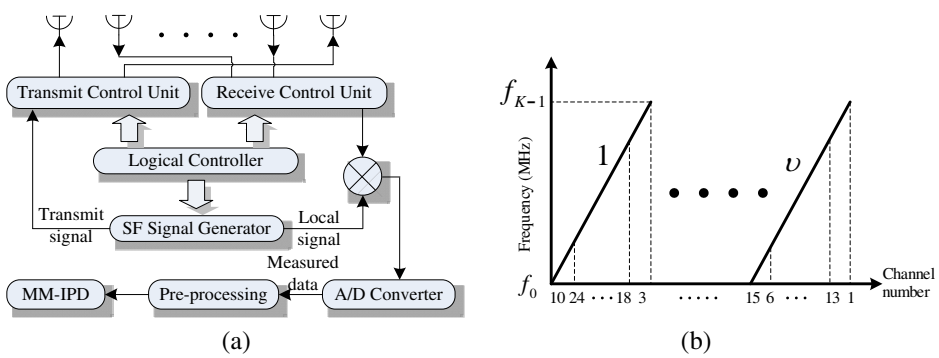

Figure 1: SFVACS-TWIR system, (a) block diagram, (b) work mode.

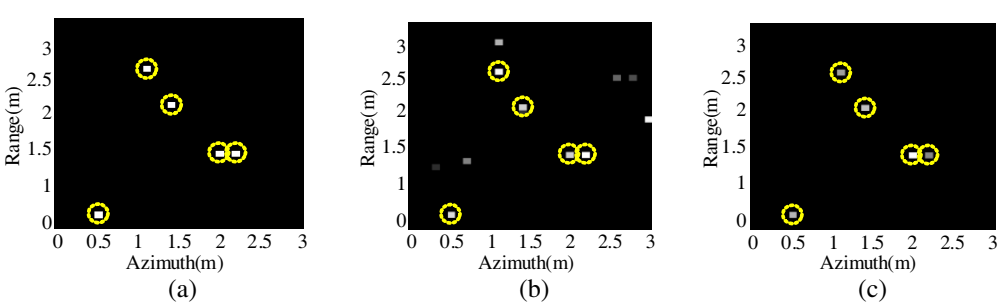

Figure 2: Numerical simulation, (a) target space, (b) result of single CS, (c) result of MM-IPD.

depends on the iterative CS processing and pixel serials clustering, each part of MM-IPD can be replaced by a similar method without affecting the performance. Both the simulated and experimental results have demonstrated the feasibility and effectiveness of the MM-IPD. Fig. 2 shows the simulated results in the noisy environment. Comparing with single CS, the MM-IPD exhibits more robust.

REFERENCES

1. Wang, P., Q. Song, and Z. Zhou, "A physics-based landmine discrimination approach with compressive sensing," *Progress In Electromagnetics Research*, Vol. 135, 37–53, 2013.

Model for Determination of Territorial Distribution of Surface Radio Refractivity

M. Zilinskas[1,2], **M. Tamosiunaite**[3], **S. Tamosiunas**[2,4], **E. Brilius**[2], **and M. Tamosiuniene**[3]

[1]Department of Radio Communication
Communications Regulatory Authority of the Republic of Lithuania, Lithuania
[2]Faculty of Physics, Vilnius University, Lithuania
[3]Semiconductor Physics Institute of Center for Physical Sciences and Technology, Lithuania
[4]Institute of Applied Research, Vilnius University, Lithuania

Abstract— The atmospheric radio refractive index is a ratio of radio wave propagation velocity in free space and its velocity in an atmosphere. The radio refractive index varies in time and location. These changes are negligible. However, they strongly influence the radio wave propagation due to the long length of the track. On purpose to make these changes more noticeable, the term of radio refractivity, N, is used. The N-value is a number in parts per million, which shows how much the refractive index exceeds a unit. This parameter is very important in design of telecommunication systems. It depends on the temperature, pressure, and humidity of air.

The method for determination of N-value has been proposed by International Telecommunication Union (ITU). In the ITU method, the data of air temperature, pressure, and relative humidity are used. In Lithuania the meteorological conditions are very variable and the meteorological parameters are measured only in limited number of localities. Therefore, a specific model for determination of radio refractivity is presented. It is based on the unknown value determination using three known values. Geographically, these reference points make a triangle. Inside the triangle, using the proposed method, the radio refractivity can be calculated when only coordinates of the locality, its altitude, air temperature, and the meteorological parameters, measured in some surrounding reference points, are known.

The calculations were made using average monthly values of meteorological parameters. Therefore, in order to evaluate the possible deviation from the true value of N, several days in different seasons were selected for analysis. The differences in the values, determined using new model, and the model proposed by ITU, were less than one percent in all months, except July. It was concluded that the average monthly relative humidity values should be calculated separately for daytime and nightime hours due to the large daily fluctuations in relative humidity in July.

HEMS with Wireless Power Transmission and Energy Harvesting

Takashi Yoshikawa
Kinki University Technical College, Kasugaoka, Nabari, Mie 518-0459, Japan

Abstract— HEMS (Home Energy Management System) is the most important technology for saving energy. Because conventional HEMS is always mounted into wall of the house so can't satisfy the location free situation, HEMS is not spreading into the public life. Then I propose the novel concept of HEMS which is based on the sensor network technology. Sensor network nodes can be moved everywhere at anytime. This system is characterized as the free from communication wire. But its power source is battery. So we have to change the battery frequently. So as to get rid of the maintenance of changing battery, I introduce the energy harvesting into sensor network nodes. Room illumination and the temperature difference between human body and room atmosphere are regarded as the circumference energy resources. And we can get such energy by using Solar cell and Peltier element. We have to get more than 100 μW power as the average of consumption power of sensor network node by energy harvesting (room illumination and the difference of temperature). Then I've examined the amount of power. Account for room illumination, 100 μW can be obtained under the condition of 200lx. And account for the difference of temperature, 20 μW can be obtained under the temperature. Considering room condition, the room illumination does not always exist for every room, and the difference of temperature always exist. But 20 μW is not enough for the system. Then I've tried to add the extra energy for using magnetic resonance typed wireless power transmission. The target specification for it is transmitting distance is more than 1 m and transmitting loss is more than 0.1% and the diameter of receiving coil must be less than 10 cm for realizing practical HEMS. In this paper we present the calculation result for satisfying the target specification for using different size coils (transmitting coil is very large and receiving coil is very small).

A New CPW-fed Circularly Polarized Square Slot Antenna Design with Inverted-L Grounded Strips for Wireless Applications

Erol Karaca and Mesut Kartal
Istanbul Technical University, Maslak, İstanbul 34469, Turkey

Abstract— In this paper, a new circularly polarized square slot antenna with a coplanar waveguide feed is presented. The proposed antenna composed of 3 Inverted L grounded strips at 3 corners of the square slot. Circular polarization mechanism is related with the L shaped strips, a staircase shaped feed line extension and a thin tuning strip that are proposed in our design. L shaped strips are commonly used in [1–5] in a similar manner to show circular polarization characteristics, but each of these studies use different feed line techniques. The presented compact antenna has $40 \times 40 \times 0.8\,\mathrm{mm}^3$ dimensions. The operation bandwidth for VSWR < 2 is from 3.45 to 8.59 GHz and exhibits a 53.67% (4.73–8.20 GHz) 3 dB axial ratio bandwidth according to the HFSS (ver. 13) simulation results. Compared to the previously reported circularly polarized square slot antenna (CPSSA) structures, the proposed antenna is smaller than [2–10] and same dimensions with [1, 11, 12] references. But our antenna shows wider 3 dB axial ratio bandwidth (about 3.47 GHz) than the reference antennas from [1] to [15]. Furthermore, the antenna supports impedance matching in the whole 3 dB axial ratio bandwidth. To improve VSWR < 2 impedance matching bandwidth, the single strip of the CPW feed line is extended with staircase shaped rectangular extensions and a thin tuning strip. Additionally, the 3 L shaped strips help to enhance impedance matching in the lower frequency intervals. In the meaning of VSWR < 2 radiation bandwidth, the antenna supports a wider bandwidth then [1–4, 6–10, 12–15] references. However, [5, 11] references show wider impedance matching than the proposed antenna. Extended version of this letter, the improvement process of the axial ratio (AR) and S_{11} properties will be discussed in detail. The proposed antenna is appropriate to show circular polarization capability for IEEE 802.11a (5.15–5.35 GHz and an additional band of 5.725–5.825 GHz), and HiperLAN2 (5.47–5.725 GHz) standards. As a result of these properties, the proposed antenna can be deployed in wireless technology supported devices with the advantage of its compact size and wide bandwidth.

REFERENCES

1. Rezaieh, S. A. and M. Kartal, "Broadband CPW-fed circularly polarized square slot antenna with inverted-L strips for wireless applications," *Microwave and Optical Technology Letters,* Vol. 54, No. 6, 1399–1402, Jun. 2012.
2. Felegari, N., J. Nourinia, C. Ghobadi, and J. Pourahmadazar, "Broadband CPW-fed circularly polarized square slot antenna with inverted-L shape grounded strips," *IEEE Antennas and Wireless Propogation Letters,* Vol. 10, 274–277, 2011.
3. Size, J. Y. and C. C. Chang, "Circularly polarized square slot antenna with a pair of inverted-L grounded strips," *IEEE Antennas and Wireless Propogation Letters,* Vol. 7, 149–151, 2008.
4. Size, J. Y., C. I. G. Hsu, Z. W. Chen, and C. C. Chang, "Broadband CPW-fed circularly polarized square slot antenna with lightening-shaped feedline and inverted-L grounded strips," *IEEE Transactions on Antennas and Propogation,* Vol. 58, No. 3, 973–977, Mar. 2010.
5. Pourahmadazar, J., C. Ghobadi, J. Nourinia, N. Felegari, and H. Shirzad, "Broadband CPW-fed circularly polarized square slot antenna with inverted-L strips for UWB applications," *IEEE Antennas and Wireless Propogation Letters,* Vol. 10, 369–372, 2011.
6. Chen, C. and E. K. N. Yung, "Dual-band dual-sense circularly-polarized CPW-fed slot antenna with two spiral slots loaded," *IEEE Transactions on Antennas and Propogation,* Vol. 57, No. 6, 1829–1833, Jun. 2009.
7. Size, J. Y., K. L. Wong, and C. C. Huang, "Coplanar waveguide-fed square slot antenna for broadband circularly polarized radiation," *IEEE Transactions on Antennas and Propogation,* Vol. 51, No. 8, 2141–2144, Aug. 2003.
8. Du, S. and Q. X. Chu, "A CPW-fed broadband circularly-polarized square slot antenna with E-shaped slits in ground plane," *Proceedings of the 39th European Microwave Conference,* Rome, Italy, Oct. 2009.
9. Chou, C. C., K. H. Lin, and H. L. Su, "Broadband circularly polarised crosspatch-loaded square slot antenna," *Electronics Letters,* Vol. 43, No. 9, Apr. 2007.

10. Chen, Y. B., X. F. Liu, Y. C. Jiao, and F. S. Zhang, "CPW-fed broadband circularly polarised square slot antenna," *Electronics Letters,* Vol. 42, No. 19, Sep. 2006.
11. Rezaieh, S. A. and M. Kartal, "A new triple band circularly polarized square slot antenna design with crooked T and F-shape strips for wireless applications," *Progress In Electromagnetics Research,* Vol. 121, 1–18, Oct. 2011.
12. Rezaieh, S. A., M. Abbak, and I. Akduman, "A circularly polarized square slot antenna for wireless applications," *19th Telecommunications Forum TELFOR 2011*, Belgrade, Serbia, Nov. 2011.
13. Size, J. Y., J. C. Wang, and C. C. Chang, "Axial-ratio bandwidth enhancement of asymmetric-CPW-fed circularly-polarised square slot antenna," *Electronics Letters,* Vol. 44, No. 18, Aug. 2008.
14. Zhou, S. W., P. H. Li, Y. Wang, W. H. Feng, and Z. Q. Liu, "A CPW-fed broadband circularly polarized regular-hexagonal slot antenna with L-shape monopole," *IEEE Antennas and Wireless Propogation Letters,* Vol. 10, 1182–1185, 2011.
15. Chen, H. D. and H. T. Chen, "A CPW-fed dual-frequency monopole antenna," *IEEE Transactions on Antennas and Propogation,* Vol. 52, No. 4, 978–982, Apr. 2004.

Investigation of Preliminary Breakdown Pulses in Lightning Waveforms

Kamyar Mehranzamir, Behnam Salimi, and Zulkurnain Abdul-Malek
Institute of High Voltage and High Current (IVAT), Faculty of Electrical Engineering
Universiti Teknologi Malaysia (UTM), Johor Bahru, Malaysia

Abstract— The cloud-to-ground lightning contains one or more sporadic discharges. This process includes a combination of pre-starting sections and return strokes (RSs). The partial discharge trains are investigated by capturing the electric field pulses known as breakdown pulses which precede the return stroke. In a lightning flash, the preliminary breakdown pulses (PBPs) usually happen before the stepped leaders. The characteristics of the lightning breakdown processes are not entirely known yet. The BIL model has been used as the simplest preliminary breakdown pulse analyzer in previous studies. The BIL model is entirely successful in depicting incipient processes of the cloud-to-ground lightning. Although the BIL model is useful as a general depiction, the details of the breakdown process differs from study to study and hence it is not completely standardized. In this paper, the preliminary breakdown pulse (PBP) train is analyzed in cloud-to-ground (CG) lightning waveforms recorded in Malaysia using a broadband antenna.

Introduction: The process within the clouds which contains changes in the electric field configuration is called cloud-to-ground (CG) flashes. These discharges eventuate to streamers, leaders and finally to the return strokes (RSs). There are several descriptions for CG lightning process [1–3]. Clarence and Malan [1] introduced the BIL model, the first and simplest description of the processes for South African lightning. They have reported the characteristic features of preliminary breakdown pulse trains in negative cloud-to-ground flashes. After that several researchers such as Kitagawa and Brook [4], Beasley et al. [5], Brook [6], Cooray and Scuka [7], Cooray and Jayaratne [8], Gomes and Cooray, Mäkelä et al., and Nag and Rakov have done several studies on the PB pulse trains. The pulse trains contain the essential information of the electrical breakdown which leads to the return strokes. Therefore the breakdown characteristics could be extracted from the pulse trains. According to the previous studies, the PBP trains vary in different geographical regions. It means the meteorological conditions may have influence on the breakdown process of the lightning. Consequently, there may be a variety in the initial breakdown processes and characteristics in the clouds at the different regions. For this reason, it is important to analyse and compare the features of the pulse trains in different geographical areas. A few studies have been done on the lightning flashes in equatorial regions [3], however more research are still needed. This research investigates on the characteristics of the lightning waveforms captured in Johor, Malaysia in 2012.

BIL Method: Clarence and Malan defined BIL model, which is the earliest and simplest description of the breakdown processes in a lightning flash. In the BIL model, the flash processes are initiated by below sequential sections [1–3]:

1) An initial breakdown (B): lasting some milliseconds, this radiates intense electromagnetic radiation. This is followed by a quiet intermediate stage with little associated radiation.

2) Intermediate stage (I): lasting up to several hundred milliseconds, ending with the onset of stepped leaders.

3) Stepped leaders (L): lasting a few milliseconds at the most, which again radiates more intensive electromagnetic radiation. The stepped leader stage finally ends with a very intensive return stroke (RS).

According to the previous researches, the BIL model is quite successful in depicting the initial processes in the cloud to ground lightning. Although the BIL model is useful as a general description for the lightning characterization, the manner of the breakdown phenomenon differs in the thunderstorms. Therefore the behavior of the lightning flash varies from study to study, so it is not completely standardized. In the previous studies, it was assumed the breakdown consists of vertical discharges between a negative charge center and a lower positive one. There is some dispute whether the BIL model is able to express correctly the breakdown processes in a lightning flash [3–6].

The BIL model was supported by several researches such as Uman [5], but some researches such as Beasley et al. [5] and Proctor found that the BIL model is not completely fitted to the BIL in

some lightning flashes. Mäkelä et al. done another studies on the preliminary breakdown pulse later and they showed that their observations were fitted to the BIL model.

REFERENCES

1. Clarence, N. D. and D. J. Malan, "Preliminary discharge processes in lightningflashes to ground," *Quarterly Journal of the Royal Meteorological Society*, Vol. 83, 161–172, 1957.
2. Galvan, A. and M. Fernando, "Operative characteristics of a parallel-plate antenna to measure vertical electric fields from lightning fields from lightning flashes," Report UURIE 285-00, Uppsala University, 2000.
3. Baharudin, Z. A., A. Noor Azlinda, M. Fernando, V. Cooray, and J. S. Mäkelä, "Comparative study on preliminary breakdown pulse trains observed in Johor, Malaysia and Florida, USA," *Atmospheric Research*, Vol. 117, 111–121, November 2012.
4. Kitagawa, N. and M. Brook, "A comparison of intracloud and cloud-to ground lightning discharges," *J. Geophys.*, 1189–1201, 1960.
5. Beasley, W., M. A. Uman, and P. L. Rustan, "Electric fields preceding cloud to ground lightning flashes," *J. Geophys*, 4883–4902, 1982.
6. Brook, M., "Breakdown electric fields in winter storms," *Res. Lett. Atmos. Electr.*, 47–52, 1992.
7. Cooray, V. and V. Scuka, "What attracts a lightning to ground," *Proceedings of the 10th International Conference on Atmospheric Electricity*, Osaka, Japan, 1996.
8. Cooray, V. and R. Jayaratne, "What directs a lightning flash towards ground," *Sri Lankan J. Phys.*, Vol. 1, 1–10, 2000.

A Numerical Hybrid Technique for Radiation and Scattering by Electrically Large Structures with Embedded Substructures

Wasyl Wasylkiwskyj
The George Washington University, Washington DC, USA

Abstract— Starting with the boundary integral equation for tangential electromagnetic fields on a closed surface, a matrix formulation for radiation and scattering by electromagnetically penetrable structures is presented that affords a unified framework for numerical modeling of antenna and scattering problems. This is achieved by interpreting the relationship between the interior and exterior boundary value problems in electrical network terms. The result is a novel approach to numerical modeling of (electrically) large structures within which are embedded electrically small sub-structures. An important application is the design of numerically efficient hybrid codes that can optimally combine formulations based on asymptotic high-frequency techniques, such as the GTD or PTD for large exterior supporting structures with FEM or MOM-based approaches for electrically small interior sub-structures. When the FEM is employed in such a hybrid code, the use of an artificial absorbing boundary for the exterior part of the structure becomes unnecessary.

Antenna Array Spatial Correlation of Wireless Communication Systems with Multipath Fading Channel

Ju-Hong Lee[1] and Jia-Han Lee[2]

[1]1Department of Electrical Engineering, Graduate Institute of Communication Engineering
and Graduate Institute of Biomedical Electronics and Bioinformatics, National Taiwan University
No. 1, Sec. 4, Roosevelt Rd., Taipei 10617, Taiwan
[2]Graduate Institute of Communication Engineering, National Taiwan University
No. 1, Sec. 4, Roosevelt Rd., Taipei 10617, Taiwan

Abstract— This paper considers the spatial correlation characteristics of multiple antenna arrays deployed in multiple-input-multiple-output (MIMO) wireless communication systems. In the literature, several reports have considered the impact of both the azimuth of arrival (AOA) and elevation of arrival (EOA) on the characteristics of the spatial correlation function (SCF) for several antenna array configurations like uniform linear array (ULA), uniform circular array (UCA), and uniform concentric ring array (UCRA). First, we present a general closed-form formula for the SCF of a multiple antenna array with a planar array configuration under uniform signal angular energy distribution. Based on this formula, we explore the characteristics of the SCF for several multiple antenna arrays with different array geometries including ULA, UCA, and UCRA. Then, we derive a closed-form formula for the ergodic channel capacity (ECC) of MIMO wireless communication systems with a Rayleigh-Lognormal fading channel (RLFC) model which is appropriate for the urban environments. It is found that a multiple antenna array's SCF affects the ECC of wireless communication systems with a RLFC model. Accordingly, we present a method to find the optimum planar array geometry for a multiple antenna array for maximizing the ECC of the wireless communication systems with a RLFC model. This method develops a novel objective function to incorporate with a chaotic particle swarm optimization (CPSO) algorithm for solving the resulting optimization problem. We present a computer simulation example to confirm the validity of the theoretical work and show the effectiveness of the proposed method.

Example: This example presents the results of using the proposed method for ECC maximization. The parameters used are as follows: the number of antenna array sensors = 6 for both of the transmitter and receiver, the spread of azimuth angle = 20°, the radius of the circular geometry = 5λ on the azimuth plane, where λ denotes the signal wavelength. The signal-to-noise ratio is 10 dB. The number of Monte Caro runs for obtaining the sample average of the expectation ECC is set to 3000. Figure 1 depicts the ECC versus the mean of the azimuth angle of arrival. For comparison, the results of using ULA with length = 5λ (Blue line), UCA with radius = 5λ (Green line), and two types of UCRA (Magenta line for the UCRA Type I and Cyan line for the UCRA Type II) proposed by [1] with radius = 5λ are also included. The red line shows the results of using the proposed method with the multiple antenna array restricted to a circular area of radius = 5λ. We observe from Figure 1 that the proposed method provides the best ECC performance for wireless communication systems with a RLFC model and multiple antenna arrays with a circular geometry.

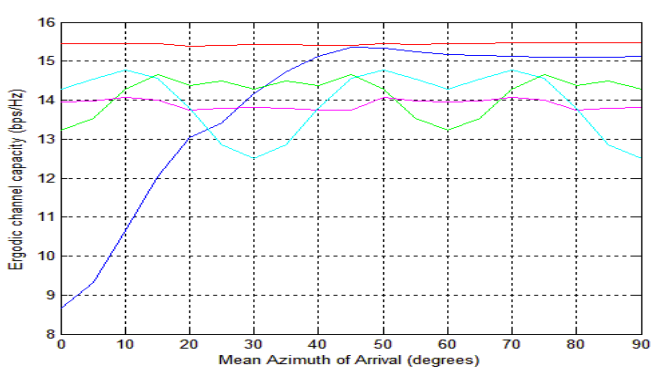

REFERENCES

1. Lee, J.-H. and S.-I. Li, "Spatial correlation characteristics of antenna systems using uniform concentric ring arrays," *Proc. of The 16th International Conference on Digital Signal Processing*, S4C.1, Santorini, Greece, July 2009.

Weaker Interhemispheric Correlation of Autism Children: Evidences from Functional near Infrared Spectroscopy

Sailing He[1,2] **and Huilin Zhu**[1]

[1]Centre for Optical and Electromagnetic Research, ZJU-SCNU Joint Research Center of Photonics
South China Normal University (SCNU), Guangzhou 510006, China
[2]Department of Electromagnetic Engineering, School of Electrical Engineering
Royal Institute of Technology, Stockholm 10044, Sweden

Abstract— Autism has been defined as a neuro-developmental disorder that is characterized by impaired social interactions, communication deficits and a restricted, repetitive pattern of interests and behaviors. fMRI studies have found that autism has abnormalities of neural synchronization, referring as poor functional connectivityat the resting state. In this study, a three wavelength (780 nm, 805 nm, and 830 nm) 44-channel functional near infrared spectroscopy (fNIRS) is applied for the first time to study the difference of connectivity in the left and right inferior frontal cortices (IFC) and superior temporal cortices (STC) between autistic and normally developing children of 7–10 years of age. 27 autistic children and 10 normal ones were recruited in our study for 8 min resting state measurement. In order to estimate the slow drifts and reduce some physiological noise, a band pass filtered between 0.009–0.08 Hz was used and the signal was obtained for each channel. Time cross correlation coefficient was calculated between a channel and its symmetrical channel located on the other hemisphere. Our results showed that the average interhemispheric correlation values of HbO (through its absorption measurement) at STC was significantly lower for the autistic children ($r_{normal} = 0.124 \pm 0.142$) than those for the normal children ($r_{autism} = 0.296 \pm 0.135$). The typical symmetrical pattern found in normal children in a correlation map was lost for the autistic children. These results confirm the feasibility of using an optical method to measure the functional connectivity of a brain and its application to autism diagnosis.

Session 4A1a
2_FocusSession.SC2: Transformation Optics 2

Preventing Reflections from Impedance-mismatched Transformation-optics Devices
Ian R. Hooper, T. G. Philbin, ... 1314
Transforming Optical Forces Using Thin Film Metamaterials
Vincent Ginis, Philippe Tassin, Costas M. Soukoulis, Irina Veretennicoff, ... 1316
Design Lens with Isotropic Transformation Media to Improve Fractional Fourier Transform
Jin Hu, Xiangyang Lu, Ran Tao, ... 1317
Metal-dielectric Metamaterials for Cylindrical Cloaking Devices at Visible Frequencies
Andreas Rottler, ... 1318
Novel Approaches to Quasi-isotropic Transformation Media
Carlos Garcia-Meca, ... 1319

Preventing Reflections from Impedance-mismatched Transformation-optics Devices

I. R. Hooper and T. G. Philbin
Electromagnetic and Acoustic Materials Group, Department of Physics and Astronomy
University of Exeter, Exeter, EX4 4QL, UK

Abstract— Since the seminal works by Leonhardt [1] and Pendry et al. [2] in 2006 a large body of theoretical work has been undertaken developing the tools and framework of Transformation Optics (TO). In reality, however, there have been relatively few designs, and even fewer practical devices resulting from this work. One of the reasons for this is that "pure" TO developed designs require the permittivity and permeability tensors to be equal (in other words the materials prescribed by TO are impedance-matched) which is an enormous challenge from a materials perspective. It is clearthat we must adapt the permittivity and permeability profiles arising from the TO process in order to create functioning devices with available materials.

Appropriate scaling of the permittivity and permeability tensors has been shown to maintain the ray trajectories [3] and, if an appropriate scaling factor is used, the resulting device can be fabricated using all-dielectric materials, but will only work correctly for a single (in-plane) polarisation. Unfortunately, whilst the ray trajectories are maintained, the loss of impedance matching results in strong reflections from the boundaries, potentially limiting the usefulness of any device designed in this way. These reflections can be clearly seen in full wave simulations of a transmuted Eaton lens [4, 5] (an omnidirectional retro-reflector), as shown in Figure 1(a).

We have determined that these unwanted reflections can be eliminated through the addition of a simple boundary condition in the co-ordinate transformation requiring the gradient be continuous. We demonstrate this using the transmuted Eaton lens and show that all reflections from the boundary of the device can be eliminated (Figure 1(b)), but that the out-of-plane polarisation is sacrificed (Figure 1(c)).

Though the method is demonstrated using a relatively simple device, there is no reason why a similar process cannot be used for other TO designed systems, paving the way for transformation optics designed broadband single polarisation devices using non-resonant materials.

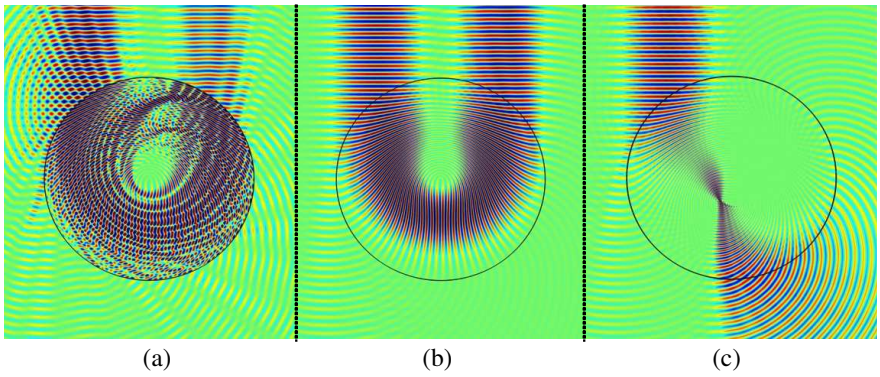

Figure 1: Full wave numerical modeling (COMSOL) of transmuted Eaton lenses. (a) A scaled transmuted Eaton lens consisting of non-magnetic materials (in-plane polarisation), (b) a transmuted Eaton lens consisting of non-magnetic materials using the modified co-ordinate transformation, (c) the same as (b), but for the out-of-plane polarisation.

REFERENCES

1. Leonhardt, U., "Optical conformal mapping," *Science*, Vol. 312, 1777–1780, 2006.
2. Pendry, J. B., D. Schurig, and D. R. Smith, "Controlling electromagnetic fields," *Science*, Vol. 312, 1780–1782, 2006.
3. Danner, A. J., T. Tyc, and U. Leonhardt, "Controlling birefringence in dielectrics," *Nature Photonics*, Vol. 5, 357–359, 2011.

4. Eaton, J. E., "On spherically symmetric lenses," *IRE Trans. Antennas Propag.*, Vol. 4, 66–71, 1952.
5. Tyc, T. and U. Leonhardt, "Transmutation of singularities in optical instruments," *New Journal of Physics*, Vol. 10, 115038 2008.

Transforming Optical Forces Using Thin Film Metamaterials

V. Ginis[1], **P. Tassin**[2], **C. M. Soukoulis**[2], **and I. Veretennicoff**[1]

[1]Applied Physics Research Group (APHY), Vrije Universiteit Brussel
Pleinlaan 2, Brussel 1050, Belgium
[2]Ames Laboratory — U.S. DOE, Department of Physics and Astronomy
Iowa State University, Ames, IA 50011, USA

Abstract— Recently, a lot of interest has been paid to the possibility to dynamically actuate nanoscale devices using optical forces. These forces arise when linear momentum is transferred between electromagnetic fields and matter. In the past decade, optical forces have been used in the field of optomechanics, but they still remain too small for dynamic manipulation in photonic actuation systems. We show how transformation optics can enhance optical forces in such systems by altering the perceived separation distance, resulting in a more than tenfold enhancement of the optical force. This transformation can be implemented using single-negative metamaterial thin films. Additionally, we show how this lensing mechanism is robust to the dissipative loss associated with resonant metamaterials. Therefore, our results provide an alternative way to boost optical gradient forces in nanophotonic actuation systems and may be combined with existing resonator-based enhancement methods to produce optical forces with unprecedented amplitude [1].

REFERENCES

1. Ginis, V., et al., *Phys. Rev. Lett.*, Vol. 110, 057401, 2013.

Design Lens with Isotropic Transformation Media to Improve Fractional Fourier Transform

Jin Hu[1], **Xiangyang Lu**[1, 2], **and Ran Tao**[1]

[1]School of Information and Electronics, Beijing Institute of Technology, Beijing 100081, China
[2]School of Electronic and Information Engineering
Zhongyuan University of Technology, Zhengzhou 450007, China

Abstract— The transformation optics provides a powerful tool for distributing material parameters with prescribed functions. To obtain the desired functions, one needs to construct a particular mapping from a virtual space to a physical space, and usually needs to write down the explicit coordinate-transformation of this mapping to calculate the corresponding material parameters. However, the explicitness of the coordinate-transformation implies that the transformation's global information (such as the boundaries coordinates or shapes of both virtual and physical spaces) should be determined, and sometimes it is difficult to obtain such explicit coordinate-transformation expression directly.

In this talk, we indicate that the deformation view of the transformation optics can help with the material design and parameters calculation. Instead of relying on the explicit coordinate-transformation expression, the deformation view suggests that one can adjust the local principal stretches, which have very clear geometrical meaning, to manipulate the transformed material parameters, therefore the requirement of global information of the space mapping is reduced to local ones. As a result, in some cases it is possible to obtain the desired transformation material parameters without any coordinate-transformation expressions or determine the coordinate-transformation expressions inversely from the local geometrical properties.

As a example, we show that by manipulating the principal stretches during a two-step space mapping, isotropic transformation material can be obtained to extend the input spatial frequency bandwidth of a conventional Fourier lens. Isotropy is important for easy fabrication, low loss, and broadband application. When the designed lens is applied to fractional Fourier transform, the inversely obtained explicit analytical transformation makes it possible to obtain the same results as those of the conventional graded index lens.

Metal-dielectric Metamaterials for Cylindrical Cloaking Devices at Visible Frequencies

Andreas Rottler
Institute of Applied Physics, University of Hamburg, Germany

Abstract— We investigate two metal-dielectric metamaterials that can be utilized as cylindrical cloaking devices in the visible regime. The first metamaterials consists of periodically arranged silver nanoparticles that are embedded in a host medium of PMMA [1]. Contrary to previous work which proposes metal needles of small size that are radially aligned [2], the spherically-shaped inclusions do not need to be specifically orientated in the host medium. This presented metamaterial utilizes the tunability of the plasmonic interactions between the metallic nanoparticles which depend on distance and size. The variation of the particle distances increases or decreases the interaction strength of the particles. This results in a shift of the permittivity at a given frequency of interest, enabling us to obtain the permittivity profile that is needed for cylindrical cloaking.

In a second approach we were able to validate that a metal-rod device, consisting of metal rods that are radially aligned in a dielectric host like PMMA, is also a feasible approach for cylindrical cloaking at visible frequencies [3]. The design is based on stacked radial nanowires, which are straight forwardly realizable with current lithographic methods. We developed a cloaking-shell design model based on the Maxwell-Garnett approximation combined with the Levenberg-Marquardt optimization algorithm to obtain — for a given frequency and materials — design rules for cloaking devices in the visible. Furthermore, we performed full-wave simulations on the cloaking devices designed following the above design model. These full-wave simulations consider the realistic structure of the cloaking devices and their optical parameters including ohmic losses and unambiguously prove their cloaking performance at visible frequencies.

REFERENCES

1. Diedrich, D., A. Rottler, D. Heitmann, and S. Mendach, *New J. Phys.*, Vol. 14, 053042, 2012.
2. Cai, W., U. K. Chettiar, A. V. Kildishev, and V. M. Shalaev, *Nat. Photon.*, Vol. 1, 224, 2006.
3. Rottler, A., B. Krüger, D. Heitmann, D. Pfannkuche, and S. Mendach, *Phys. Rev. B*, Vol. 86, 245120, 2012.

Novel Approaches to Quasi-isotropic Transformation Media

Carlos García-Meca
Nanophotonics Technology Center, Universidad Politécnica de València, Spain

Abstract— Transformation optics enables us to curve optical paths in almost any desired way by suitably engineering the medium through which light propagates. Unfortunately, the material properties required to implement the devices based on this technique are technologically challenging. One of the main difficulties arises from the highly anisotropic character of the optical media based on a transformational design. Although the rapid development of metamaterials provides a way to synthesize materials with exotic properties, the practical realization of many transformation media is still out of reach.

If we restrict ourselves to the two-dimensional case, a possible solution relies on the use of conformal mappings. This type of transformation preserves the isotropy of the original space and facilitates significantly the implementation of transformation media. When a conformal transformation mapping the original region of interest to the desired one does not exist, we can resort to quasi-conformal mappings, which restrict anisotropy to small values. Generally, quasi-conformal mappings are calculated numerically by minimizing some functional or by solving Beltrami or inverse Laplace equations. Apart from being numerical techniques, these methods present several disadvantages. For instance, in standard methods the original domain must be simply connected and have a rectangular shape. In three dimensions the situation worsens, as the only possible conformal mappings are inversions and similarities. Some solutions have been proposed, but they impose strong restrictions such that unidirectional functionality or revolution symmetry.

In this work, we analyze a special class of transformations that enables us to lift some of the above-mentioned limitations in the design of quasi-isotropic devices. We provide several theoretical examples based on the proposed kind of transformations. The examples include illusion optics devices and light squeezers. The functionality of the studied devices is verified via numerical simulations performed with the commercial software COMSOL Multiphysics.

Session 4A1b
3_FocusSession.SC3: Photonics and Optoelectronics in Industry

Photonics and Photonic Materials in Medical Applications
Cees Ronda, ... 1322
Photonics Innovations at Philips Healthcare
J. J. H. B. Schleipen, ... 1323
Progress in Electronic Paper Displays
P. F. Bai, M. L. Jin, L. L. Shui, X. Zhang, Z. C. Yi, R. A. Hayes, Guofu Zhou, ... 1324
Generic InP-based Integration Technology: Present and Prospects
Giovanni Gilardi, Meint K. Smit, ... 1325
Quantum Dots for Display Backlighting
Jonathan Steckel, ... 1326
Wide Band Reflectance Spectrometry and Hyperspectral Imaging for Intraoperative Tissue Recognition
Anna Tchebotareva, R. M. Schols, F. P. Wieringa, L. Alic, N. D. Bouvy, L. P. S. Stassen, E. Van de Steeg, D. Klomp, S. Baumer, A. Statham, P. Dunias, ... 1327

Photonics and Photonic Materials in Medical Applications

Cees Ronda
Philips Group Innovation, Research, High Tech Campus 4, Eindhoven 5656 AE, The Netherlands

Abstract— Photons are increasingly being applied in medical treatments. In this lecture, I will give a review on photonic materials and photonics based procedures for diagnostics and therapies in healthcare applications. To this end, I will discuss the medical use of photons with strongly varying energies. I will also discuss how application needs are translated into research questions.

Photonics Innovations at Philips Healthcare

J. J. H. B. Schleipen
Philips Research, Eindhoven, The Netherlands

Abstract— It is generally well known that our healthcare systems are under continuous stress. An aging population and increasing costs ask for innovative technology solutions that make our healthcare system more affordable and cost effective. Recent advances in molecular diagnostics allow for timely screening of patients in a decentralized setting, resulting in early diagnosis and optimized and personalized treatment. And in the operating room more and more clinical interventions become minimally-invasive, allowing for better and faster patient recovery. Optics and photonics here play a crucial role. In this talk we will focus on two new technologies that have recently been developed by Philips. The Magnotech biosensor technology uses a unique combination of magnetic actuation of magnetic nanoparticles and evanescent field detection, in order to detect troponin, a biomarker for cardiovascular diseases, bringing central lab performance to point of care locations. The second example illustrates the elegant use of fiber Bragg gratings for real-time, 3-dimensional shape reconstruction and precise localization of a catheter inserted into the body, thereby eliminating the need for continuous x-ray fluoroscopy during an interventional procedure.

Progress in Electronic Paper Displays

P. F. Bai, M. L. Jin, L. L. Shui, X. Zhang, Z. C. Yi, R. A. Hayes, and G. F. Zhou
Electronic Paper Display Institute, South China Academy of Advanced Optoelectronics
South China Normal University, Building 5, Higher Education Mega Center, Guangzhou 510006, China

Abstract— Since the successful commercialization of electronic paper displays in Sony e-reader product in 2004, the worldwide e-reader market has become increasingly attractive and is increased by more than 200% per year in the past several years. Electronic paper displays based on electrophoretic principle require ultra-low power and have superior optical contrast in direct sunlight. Recently, the switching speed and brightness are further improved in our group by introducing a new driving scheme without modifying the existing electrophoretic materials/films. Furthermore, color options are generated based on several display principles. In this paper, we will give a short overview on these progresses.

Generic InP-based Integration Technology: Present and Prospects

Giovanni Gilardi and Meint K. Smit
COBRA Research Institute, Technical University Eindhoven
P. O. Box 513, 5600 MB Eindhoven, The Netherlands

Abstract— The generic foundry approach will lead to a revolution in micro and nanophotonics, just as it did in microelectronics thirty years ago. Generic integration leads to a drastic reduction in the entry costs for developing Photonic Integrated Circuits. Integrated circuits using generic integration open up a whole new range of application including datacommunications, fiber-to-the-home, fiber sensors, gas sensing, medical diagnostics, metrology and consumer photonics.

The Concept of Generic Photonic Integration Process: A generic photonic integration process is a process which supports monolithic integration of complex circuits from a small number of basic building blocks (BBs) with high and well defined performances, like such as:

- Waveguides and waveguide-based components (MMI-couplers, AWG demultiplexer, ...),
- Semiconductor Optical Amplifiers (SOAs),
- Phase modulators

These BBs allows for the implementation of complex photonic integrated circuits (PICs). For instance, by integrating SOAs with reflectors, tunable gratings or AWGs, a variety of lasers can be realized. Short SOA-sections can be used as detectors.

The generic integration concept is well known in microelectronics, where very complex circuits are composed of a small set of basic building blocks, like transistors, capacitors and resistors. In photonics it is new.

Multi — Project Wafers Runs: Multi-Project Wafer (MPW) Runs area key concept in the generic foundry model. In an MPW run a number of different designs are combined on a single wafer, so that the costs of the wafer run can be shared by a number of different designs. This becomes possible only if different chips can be fabricated in the same standardized integration process. Through MPW Runs the entry cost for developing Photonic ICs are strongly reduced. In fact a chip designer can use a well-developed high performanceprocess which he does not have to develop himself, and for this designs he can buy some wafer area in an MPW run, which will provide him with a number of his chip without having to pay for the whole run. The designer can use a dedicated design kit, including components libraries which will bring him a guided design based on an automatic design rule check. The MPW Runs will bring PICs within reach for many SMEs and larger companies for which the entry costs of today's technology are too high and sometimes not sustainable.

In the presentation the state of the art in Photonic Integration and the prospects of InP-based Photonic foundry technology will be reviewed.

Quantum Dots for Display Backlighting

Jonathan Steckel
Materials R&D and Manufacturing, QD Vision, Inc., 29 Hartwell Ave., Lexington, MA 02421, USA

Abstract— Quantum dots (QDs) as downconversion materials have several basic properties that have long made them potentially interesting options for the LED lighting and LCD backlight markets, e.g., they are narrowband emitters with a wide range of color tunability. However, limitations such as stability, high temperature operation, and high flux operation have limited QD applicability, as the cost to benefit ratio or value proposition was not previously compelling enough to drive mainstream product adoption. Significant breakthroughs in stability, efficiency and reliability at higher temperatures, as well as large scale investment in manufacturing capacity have eliminated the main barriers to high volume, mainstream product adoptions of QD materials in display devices. In this presentation, we will update the community on the material performance improvements that have broken through these commercialization barriers, and describe how the materials are currently transforming a variety of products and product forms in the marketplace.

Wide Band Reflectance Spectrometry and Hyperspectral Imaging for Intraoperative Tissue Recognition

A. Tchebotareva[1], **R. M. Schols**[1, 2], **F. P. Wieringa**[1], **L. Alic**[1], **N. D. Bouvy**[2], **L. P. S. Stassen**[2], **E. van de Steeg**[1], **D. Klomp**[1], **S. Bäumer**[1], **A. Statham**[1], **and P. Dunias**[1]

[1]Van't Hoff Shared Research Program on Medical Photonics, TNO
Netherlands Organization for Applied Scientific Research, Eindhoven, The Netherlands
[2]Department of Surgery, Maastricht University Medical Center
NUTRIM School for Nutrition, Toxicology and Metabolism
Maastricht University, Maastricht, The Netherlands

Abstract— One of the challenges during surgery is to make a proper distinction between vital tissues, structures and organs, both at the surface of the exposed area and beneath it. Currently, identification of different tissue types relies either on the skills and anatomical knowledge of the surgeon (e.g., nerves, blood vessels, different tissue types), or on the results of off-line histopathological analysis on biopsies for assessment of cancer-free margins. These approaches are observer-dependent, or, as in the case of off-line histopathological analysis, also timeconsuming. A quick, non-invasive, and more observer-independent intraoperative tissue recognition method, applicable both *ex-vivo* and *in-vivo*, would be of great assistance during surgical procedures. Hyper-Spectral Imaging (HSI) has a lot of potential for such applications. It combines high spatial resolution with spectral information at numerous wavelengths that cannot be separated by human eye in the visible, and also beyond the visible spectral range. This technique enables enhanced discrimination between different tissue types based on their specific spectral signatures.

We will describe the approach to HSI which is being developed within van't Hoff Medical Shared Research Program at TNO in collaboration with multiple clinical, academic and industrial partners. We study and analyze wide-band reflectance spectra of different tissues types collected through a fiber-based probe, both *in-vivo* during open surgery procedures and *ex-vivo* on freshly excised tissues. These data are used to identify spectral signatures of different tissue types. Based on this information, we develop data processing techniques to identify and distinguish the target tissues. We also further develop this approach towards a HSI setup for tissue imaging. The first step with such a setup is testing on inorganic phantoms and animal tissues. At a later stage the setup will be employed for *ex-vivo* human tissue analysis, both at the surface and up to several millimeters beneath the surface, with the final goal of *in-vivo* intraoperative tissue recognition and tissue-specific contrast-enhanced imaging.

Session 4A2
SC2: Non-linear Metamaterials and Plasmonics

Shining a (Bright) Light on the Very Small
Romain Quidant, ... 1330
Realization of High-quality Metamaterials Resonators Adding Metallic Structures to Dielectric Slabs
Costas M. Soukoulis, ... 1331
Stopped-Light Lasing in Nanoplasmonic Metasurfaces
Ortwin Hess, ... 1332
Amplification and Lasing with Surface Plasmons
Pierre Berini, ... 1333
Nonlinear Nanoplasmonics: Making Use of Metal Nonlinearities
Pavel Ginzburg, Alexey V. Krasavin, Anatoly V. Zayats, ... 1334
Taking Control of Surface Plasmons
Laurens Kobus Kuipers, ... 1335
Templated Self-assembly of Gold Nanostructures for SERS
Kristjan Leosson, Virginia Merk, ... 1336
Metallic Nanostructures on Ferroelectric Domain Patterns in Nonlinear Laser Crystals
E. Yraola, P. Molina, J. L. Plaza, M. O. Ramirez, Luisa E. Bausa, ... 1337
Nonlinear and Tunable Metamaterials with Superconductors and Graphene
Philippe Tassin, ... 1338
Coulomb-interaction-based Strong Enhancement of Photoluminescence from Semiconductor Quantum Well
Arkadii A. Krokhin, Antony Llopis, Arup Neogi, ... 1339

Shining a (Bright) Light on the Very Small

Romain Quidant[1, 2]

[1]ICFO, The Institute of Photonic Sciences, Castelldefels, Barcelona, Spain
[2]ICREA, Institució Catalana de Recerca I Estudis Avançats, Barcelona, Spain

Abstract— Extensive research in plasmonics over the last decade has demonstrated the ability of noble metal nanostructures to control optical fields on the nanometer scale. Such concentration of light, well beyond the limit of diffraction, potentially opens new opportunities for enhanced interaction with tiny amounts of matter down to the single molecule/atom level. In practice though, fully exploiting the capability of plasmonics requires nanoscale positioning of the molecule/atoms within the hot spot, where the light is concentrated.

In this talk, we first present different experimental strategies to accurately control the interaction of top-down metallic nanostructures with few to single molecules or artificial atoms. We then discuss some applications to different areas including nanochemistry and biosensing.

The first approach we discuss is based on immobilizing a nano-object of interest (either a molecule, a nanoparticle or a qdot) at a predefined location of the plasmonic nanostructure, and more especially in the hot spot where the plasmonic field is concentrated. A first technique consists in combining e-beam lithography with surface chemistry to define a functionalized nanowell in which the nano-object can bind [1]. Along the same line, we report on another technique in which the immobilization within the hot spot is triggered by a photochemical process that creates a chemical bond that acts as a scaffold for the subsequent immobilization of a nano-object of interest [2]. As an illustration of the potential of these techniques, we demonstrate reproducible immobilization of single qdots in the gap of gold dimers. The delivered qdot is used as a nanoprobe of the plasmonic hot spot. By monitoring the change in the X/BX ratio via lifetime measurement, we are able to retrieve the actual local field enhancement within the gap [3].

Beyond permanent immobilization, the second approach we discuss here consists in raster scanning the nano-object of interest above the plasmonic structure. In particular we report on the use of optical tweezers to trap and manipulate an individual diamond nanocrystal hosting a single Nitrogen Vacancy (NV). Remarkably, we find the NV axis is nearly fixed inside the trap and can be controlled in-situ, by adjusting the polarization of the trapping light. By combining this unique spatial and angular control with coherent manipulation of the NV spin and fluorescent lifetime measurements near an integrated photonic and plasmonic systems, we prove optically trapped NV center as a novel route for both 3D vectorial magnetometry and sensing of the local density of optical states [4].

REFERENCES

1. Curto, A. G., et al., *Science*, Vol. 329, 930, 2010.
2. Galloway, C., et al., submitted, 2013.
3. Ureña, E. B., et al., *Adv. Mater.*, Vol. 24, 314, 2012.
4. Geiselmann, M., M. L. Juan, J. Renger, J. M. Say, L. J. Brown, F. J. García de Abajo, F. Koppens, and R. Quidant, *Nature Nanotechnol.*, Vol. 8, 175, 2013.

Realization of High-quality Metamaterials Resonators Adding Metallic Structures to Dielectric Slabs

Costas M. Soukoulis[1, 2]

[1]Ames Laboratory, Department of Physics, Iowa State University, Ames, Iowa 50011, USA
[2]Institute of Electronic Structure and Lasers (IESL), FORTH, Heraklion, Crete 71110, Greece

Abstract— Most metamaterials (MMs) to date consist of small metallic structures that are effectively replacing atoms as the basic unit of interaction with EM waves. Unfortunately, the use of metals results in substantial dissipation due to ohmic heating at optical frequencies. We combine experimental methods with computer simulations to develop a set of novel MMs exhibiting resonances that store energy mainly in a dielectric material. This avoids resonant loss in the metals and we indeed demonstrate electric and magnetic metamaterial resonators with very large quality factors. The resulting structures can be straightforwardly scaled at optical frequencies to create low-loss MMs with a wide range of properties.

Our study shows that bound states in dielectric structures can be used as constituents of resonant metamaterials and allow for much larger quality factors than metallic meta-atoms. Here we have used a bound state on a dielectric slab, but surface states on an array of rods or a 2D/3D photonic crystal could equally be used. The dielectric meta-atoms can also be straightforwardly scaled to terahertz and optical frequencies, where high-performance dielectrics such as fused silica can be taken advantage of and even higher quality factors can be expected. Also, in contrast to Mie resonant dielectric particles, we do not need a particularly large permittivity for the dielectric slab. The main limitation of the metamaterial demonstrated here is that it is highly anisotropic and only works for normal incidence, since the slab can be made thin only in the propagation direction. This is acceptable, though, in many metamaterial applications involving a single normally incident beam, like delay lines, polarization rotation or optical isolation. Here we have demonstrated a slow light metamaterial and a negative-permeability metamaterial, but one could likewise design, e.g., a metamaterial with strong dichroism or optical activity by using a chiral scatterer. In this way, the dielectric meta-atom offers a universal design framework in which we can modify the response of the metamaterial by a well-chosen no resonant secondary scatterer, while at the same time the response is dramatically enhanced by the strong, low-loss resonance of the dielectric meta-atom and the large energy storage in the dielectric material.

Stopped-Light Lasing in Nanoplasmonic Metasurfaces

Ortwin Hess
The Blackett Laboratory, Department of Physics, Imperial College London, SW7 2AZ, UK

Abstract— It has recently been demonstrated that an electronic two-dimensional (2D) material in combination with a photonic 2D metasurface allows to create and exploit structures with extraordinary properties [1]. Indeed, using light-trapping metamaterials [2] and ultra-thin photoactive materials together has shown tremendous potential to make better (i.e., thinner and more efficient) solar cells. This counter-intuitive result is a consequence of singularities in the electronic density of states (van Hove-singularities) that exist in electronic 2D or 1D (but not in 3D) materials. When combined with an optical 2D material realized through photonic metasurfaces, singularities in the optical density of states can (via trapped or stopped-light modes) be engineered that enhance light-matter interactions by at least another order of magnitude (typically a factor 10–100).

Here, it is shown and discussed that the very same fundamental principles that are exploited to fabricate such innovative ultra-thin (surface-like) photovoltaic elements can also be applied to beneficially combine nano-plasmonic meta-materials with quantum gain [4, 5] to realise "stopped light lasing" [6] with unprecedented properties such as ultrafast modulation in an ultra-flat structure.

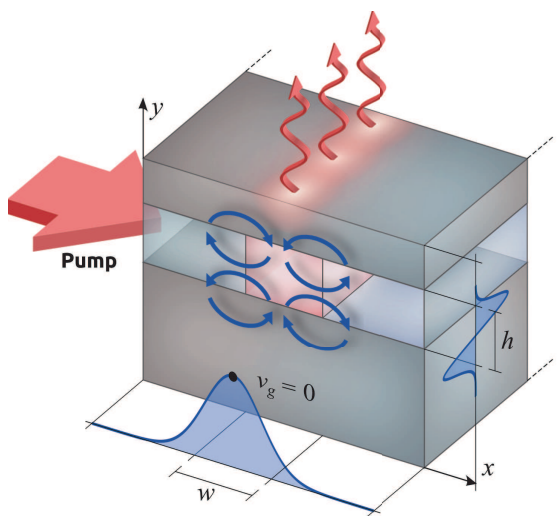

Figure 1: Stopped-light surface lasing in a nanoplasmonic waveguide geometry.

ACKNOWLEDGMENT

Support by the Leverhulme Trust and the EPSRC is acknowledged.

REFERENCES

1. Britnell, L., et al., *Science*, Vol. 340, 1311, 2013.
2. Hamm, M. and O. Hess, *Science*, Vol. 340, 1299, 2013.
3. Pendry, J. B., et al., *Science*, Vol. 337, 549, 2012.
4. Hess, O., et al., *Nature Materials*, Vol. 11, 573, 2012.
5. Hess, O. and K. L. Tsakmakidis, *Science*, Vol. 339, 654, 2013.
6. Pickering, T., J. M. Hamm, A. F. Page, S. Wuestner, and O. Hess, (submitted).

Amplification and Lasing with Surface Plasmons

Pierre Berini[1, 2]

[1]School of Electrical Engineering and Computer Science
University of Ottawa, 161 Louis Pasteur, Ottawa, ON K1N 6N5, Canada
[2]Department of Physics, University of Ottawa
161 Louis Pasteur Ottawa, ON K1N 6N5, Canada

Abstract— This paper discusses the amplification of surface plasmons via propagation through an optically pumped dipolar gain medium (e.g., a dye) incorporated into a cladding adjacent to a metal surface. Physically realisable structures based on the single metal-dielectric interface and on the thin metal slab bounded by dielectrics are described. The gain of the medium is non-uniform close to the metal surface due to position dependence in the dipole lifetime, and to the non-uniform distribution of the pump irradiance. Models of these effects are discussed and merged with the transfer matrix method to compute the modal properties of the propagating surface plasmons. It is found that the non-uniformity of the gain medium limits the mode power gain available from the system. Nonetheless, net amplification of the long-range surface plasmon (LRSPP) in the metal slab has been demonstrated at infrared wavelengths using a reasonable pump power and dipole concentration. The amplifier also produced compelling noise characteristics. The integration of such an amplifier with Bragg gratings is predicted to lead to a single-mode LRSPP laser producing an emission linewidth that is much narrower than that observed in other more confined surface plasmon lasers.

Nonlinear Nanoplasmonics: Making Use of Metal Nonlinearities

P. Ginzburg, A. V. Krasavin, and A. V. Zayats
Department of Physics, King's College London, Strand, London WC2R 2LS, United Kingdom

Abstract— Numerous active plasmonic components based on plasmonic crystals, waveguides components and metamaterials have recently been utilising electric, magnetic, acoustic and optical control signals. All-optical control is especially interesting as it allows achievement of fast response and variety of approaches to be used including nonlinear response dielectric adjacent to the metal as well as metal nonlinearity itself [1]. In this talk, we will overview nonlinear plasmonic effects due to intrinsic, hydrodynamic metal nonlinearity, enhanced by sub-wavelength field confinement and interaction between plasmonic resonances [2–6]. This includes, harmonic generation, solitonic effects and Kerr-nonlinearity-induced switching. In addition to conventional intensity and phase modulations, active control of light polarization presents an important alternative. Nonlinear plasmonic effects present viable route to integrated active plasmonic components with unbeatable size, speed and energy consumption parameters.

REFERENCES

1. Kauranen, M. and A. V. Zayats, "Nonlinear plasmonics," *Nature Photonics*, Vol. 6, 737–748, 2012.
2. Krutyanskiy, V. L., E. A. Gan'shina, P. Evans, I. A. Kolmychek, S. V. Lobanov, T. V. Murzina, R. Pollard, A. A. Stashkevich, G. A. Wurtz, and A. V. Zayats, "Plasmonic enhancement of the nonlinear magneto-optical response of nickel nanorod metamaterials," *Phys. Rev. B*, Vol. 87, 035116, 2013.
3. Wurtz, G. A., R. Pollard, W. Hendren, G. P. Wiederrecht, D. J. Gosztola, V. A. Podolskiy, and A. V. Zayats, "Designed ultrafast optical nonlinearity in a plasmonic nanorod metamaterial enhanced by nonlocality," *Nature Nanotech.*, Vol. 6, 107–111, 2011.
4. Ginzburg, P., A. V. Krasavin, and A. V. Zayats, "Cascaded second-order surface plasmon solitons due to intrinsic metal nonlinearity," *New J. Phys.*, Vol. 15, 013031, 2013.
5. Ginzburg, P., A. Krasavin, Y. Sonnefraud, A. Murphy, R. J. Pollard, S. A. Maier, and A. V. Zayats, "Nonlinearly coupled localized plasmon resonances: Resonant second-harmonic generation," *Phys. Rev. B*, Vol. 86, 085422, 2012.
6. Ginzburg, P., et al., "Manipulating polarization of light with ultrathin epsilon-near-zero metamaterials," to be published.

Taking Control of Surface Plasmons

L. Kobus Kuipers
Stichting FOM, The Netherlands

Abstract— Manipulating light at the nanoscale forms the central theme of nanophotonics. Metal nanostructures can exert a huge control over light at the nanoscale. Subwavelength holes in a metal film can be used to excite and scatter surface plasmons. With a phase-sensitive near-field microscope we, have visualized the field patterns that arise around single holes when a surface plasmons are scattered by those holes. Through a quantitative analysis of the occurring interference patterns, we were able to determine the polarizability of subwavelength holes [1].

Interestingly, the near-field probe used is also a metallic nanostructure. We have used its cylindrical symmetry to induce a light-matter interaction mediated by the magnetic field rather than by the electric field, which usually dominates light-matter interaction at optical frequencies. The circular current induced by the magnetic field impinging on the metallic ring in effect results in a "diamagnetic" light-matter interaction inducing a blue-shift of the resonance frequency of a photonic crystal nanocavity [2]. By modifying the shape of the probe we can even map the magnetic field of light propagating in a photonic structure in addition to its electric field [3].

We also used arrangements of subwavelength holes to launch surface plasmons. Coherent control of the excitation enables the creation of plasmonic "hot spots" at arbitrary positions [4, 5]. Recently, we have succeeded in deterministically scanning the hot spot, thus obtaining a scanning focus of a plasmon microscope [6]. We show that this microscope has a superior resolution.

REFERENCES

1. Rotenberg, N., M. Spasenovic, T. L. Krijger, B. le Feber, F. J. García de Abajo, and L. Kuipers, *Phys. Rev. Lett.*, Vol. 108, 127402, 2012.
2. Burresi, M., et al., *Phys. Rev. Lett.*, Vol. 105, 123901, 2010.
3. Burresi, M., et al., *Science*, Vol. 326, 550–553, 2009.
4. Gjonaj, B., J. Aulbach, P. M. Johnson, A. P. Mosk, L. Kuipers, and A. Lagendijk, *Nature Photon.*, Vol. 5, 360–363, 2011.
5. Gjonaj, B., J. Aulbach, P. M. Johnson, A. P. Mosk, L. Kuipers, and A. Lagendijk, *Nano Lett.*, Vol. 12, 546–550, 2012.
6. Gjonaj, B., J. Aulbach, P. M. Johnson, A. P. Mosk, L. Kuipers, and A. Lagendijk, submitted.

Templated Self-assembly of Gold Nanostructures for SERS

Kristjan Leosson and Virginia Merk
Department of Physics, Science Institute
University of Iceland, Reykjavik IS-107, Iceland

Abstract— Dense (nondiffracting) metal nanostructure arrays with small interparticle distance allow for efficient focusing of light into a high density of hotspots. This results in strong local electric fields and an enhancement of non-linear optical processes at the metal surface. In principle, lithographic methods can be used to fabricate regular nanostructured arrays, but the minimum achievable distance between particles is typically limited. Previous attempts to overcome this limitation require specialized fabrication approaches and/or particular structure designs. In this talk, we present a simple and general method that has been developed to reduce interparticle distance in dense lithographically patterned arrays. Our approach involves repeated deposition and subsequent annealing of ultrathin gold films on top of pre-patterned gold nanoparticles. Surface diffusion of gold results in ripening of the initially patterned particles, thus reducing interparticle distance. The process can be tuned to realize a distinctly bimodal particle size distribution that is beyond the capabilities of any current lithographic method. Such a structure is suitable for focusing incoming radiation to a high density of nanoscale spots, with local field intensity enhancements up to three orders of magnitude compared to the incoming radiation, as confirmed by surface enhanced Raman scattering experiments and finite-difference time-domain calculations.

Metallic Nanostructures on Ferroelectric Domain Patterns in Nonlinear Laser Crystals

E. Yraola, **P. Molina**, **J. L. Plaza**, **M. O Ramírez**, **and L. E. Bausá**
Dept. Física de Materiales and Instituto Nicolás Cabrera
Universidad Autónoma de Madrid, Madrid 28049, Spain

Abstract— Ferroelectrics are key systems for the development of a great number of applications relevant to different fields of science and technology. These materials have been playing an important role in photonics due to their suitable electro-optic and nonlinear properties for light control. They are successfully used as high-speed light modulators, parametric oscillators, or nonlinear frequency converters, covering a wide range of the optical spectrum. Moreover, the extraordinary progress achieved so far in micro-engineering of ferroelectric domains allows frequency conversion processes in a broad spectral range, sometimes only limited by the transparency range of the material. In addition, when conveniently doped with optical active ions they have also demonstrated laser action and intracavity self-frequency conversion processes, which substantially increase their multi-functionality in integrated photonics.

Here, periodic arrays of Ag nanoparticles on Nd^{3+} doped periodically poled $LiNbO_3$ laser crystals are photochemically assembled in chain-like form on the ferroelectric domain walls. The coupling between the optical transitions of Nd^{3+} ions and the localized surface plasmon resonances supported by the metallic nanostructures results in a periodic intensification of the spontaneous emission at the Nd^{3+} laser wavelength of around 80%. The mechanism of enhancement is analyzed taking into account different polarization configurations. Additionally, taking advantage of the nonlinear character of $LiNbO_3$ crystal, the interaction between the metallic nanoparticles and the second harmonic generation is also studied to demonstrate a remarkable intensification of the quadratic nonlinear response, in a factor of 20, which takes place with the periodicity of the metallic arrays.

The results can be extended to the 2D case to exploit the nonlinear properties of different types of alternating ferroelectric domain structures on active materials, which constitutes an alternative approach in the search for sub-micrometer wavelength lasers or gain-enhanced nanoplasmonic metamaterials.

Nonlinear and Tunable Metamaterials with Superconductors and Graphene

Philippe Tassin
Iowa State University, USA

Abstract— The linear properties of metamaterials have received a lot of attention since the conception of metamaterials about a decade ago. Nevertheless, nonlinear constituents may be advantageous to create active and tunable metamaterials and to counteract dissipative loss through gain. First we discuss how dark meta-atoms can be used to enhance nonlinear interaction when they are not homogeneously broadened by radiation loss. This approach is illustrated with a microwave metamaterial based on a hybrid metal-superconductor structure that can switch between two output signals depending on the power of the incident wave. Second, we will describe how graphene can be integrated in metamaterials to obtain tunability. Metals are hard to control, but the resonances of metal-based meta-atoms can be altered through a layer of electrically biased graphene to obtain transmission changes larger than the few percent that can be achieved with a homogeneous graphene flake.

REFERENCES

1. Kurter, C., P. Tassin, A. P. Zhuravel, L. Zhang, T. Koschny, A. V. Ustinov, C. M. Soukoulis, and S. M. Anlage, "Switching nonlinearity in a superconductor-enhanced metamaterial," *Appl. Phys. Lett.*, Vol. 100, 121906, 2012.
2. Zou, Y., P. Tassin, T. Koschny, and C. M. Soukoulis, "Interaction between graphene and metamaterials: Split rings vs. wire pairs," *Opt. Express*, Vol. 20, 12198–12204, 2012.

Coulomb-interaction-based Strong Enhancement of Photoluminescence from Semiconductor Quantum Well

Arkadii Krokhin, **Antony Llopis**, **and Arup Neogi**
University of North Texas, Denton, USA

Abstract— We report a new mechanism of enhancement of light emission from GaN and GaAs quantum wells (QW). This mechanism is due to electrostatic attraction of the carriers to metal nanoparticles (NP) imbedded within a QW. Metal NPs equally attracts electrons and holes through their electrostatic images, causing the carriers to concentrate near metal surface. Increased concentration results in increased probability of e-h recombination and higher quantum efficiency. In our experiments, this manifests as emission enhancement in InGaN (GaAs) quantum wells radiating in the Near-UV (Near-IR) region. Enhanced spectra are shown in Figures 1(a) and (b). Gold (gallium) NPs were incorporated inside the GaN (GaAs) QW with no effect on the quality of the sample structure, Figures 1(c) and (d). The same nitride material system used to demonstrate plasmonic enhancement [1]. It has been shown that gold film do not enhance the emission because of mismatch of surface plasmon energy and the emission energy of the QW. Here we observe the enhancement caused by electrostatic mechanism that *does not require energy matching*. The size of the NP plays a principal role here, determining the increase in concentration. The drift of the carriers towards the NP becomes noticeable if the ratio $\gamma = (e^2/\varepsilon R)/\mathrm{kT}$ of electrostatic energy to thermal energy becomes $\gamma \sim 1$. For the effect to be observable at 300 K, this condition requires that the typical size R of the NP be $R < 50$ nm given that $\varepsilon \sim 10$. This enhancement of emission occurs due to the decrease in the ratio of nonradiative to radiative recombinations near the NPs. Strongly inhomogeneous distribution of emission intensity which is clearly visible in the near-field and micro-PL images a corresponding increase in the IQE, and ~ 20 meV blue shift are signatures of our proposed electrostatic mechanism. The hallmarks of this effect are highly localized light emission, increased IQE and slightly increased decay lifetime (unlike oders of magnitude decrease observed for the plasmonic mechanism), non-dissipative character of enhancement, and saturation at high pump power. Since the mechanism does not require frequency matching, the level of enhancement remains the same for *any* type of metal used.

This new fundamental mechanism provides a new perspective for improving the efficiency of broad-band light emitters and controlling carrier concentration on the nanoscale.

This work is supported by the DOE grant # DE-FG02-06ER46312.

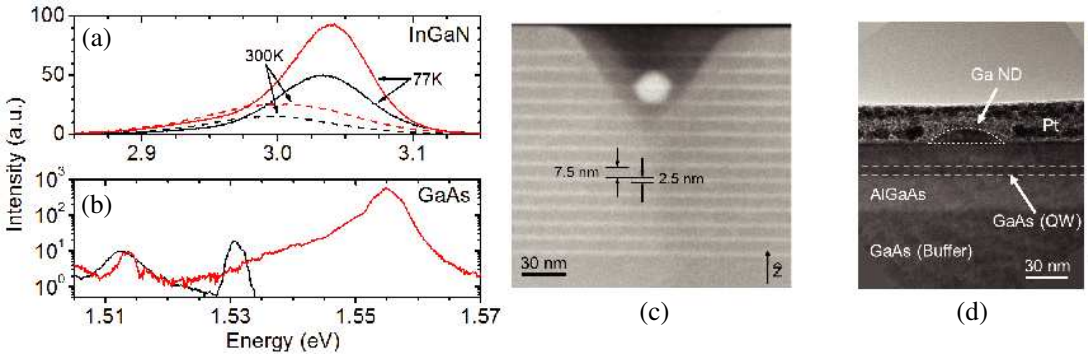

Figure 1: (a) The PL spectra from the reference (black) and gold NP InGaN QWs (red). (b) The same for the GaAs QW with Ga droplets (red) and reference (black) at 11 K. (c) TEM of the InGaN multi-QW showing a gold NP embedded within the naturally occurring pit resulting from threading dislocations. (d) TEM of GaAs QW with a Ga nanodroplet (ND) on the top surface.

REFERENCES

1. Neogi, A., et al., "Enhancement of spontaneous recombination rate in a quantum well by resonant surface plasmon coupling," *Phys. Rev. B*, Vol. 66, 153305, 2002.

Session 4A3
3_FocusSession.SC3: Progress in Optical Sensing and Environmental Monitoring

Laser Spectroscopy in Environmental Sensing
Sune Svanberg, ... 1342

Remote Sensing of Atmospheric Traces and Particulate Matter Using Backscattered Light from Nanosecond and Femtosecond Laser Light
Benjamin Thomas, Gregory David, Christophe Anselmo, Elodie Coillet, Katja Rieth, Alain Miffre, Patrick Rairoux, ... 1343

Photonic Sensing of Reactive Molecules in the Atmosphere: Challenges and Opportunities
Wei Dong Chen, R. Maamary, X. Cui, T. Wu, E. Fertein, C. Coeur, A. Cassez, W. Liu, F. Dong, Y. Wang, W. Zhang, X. Gao, G. Zha, Z. Xu, T. Wang, ... 1344

Quantum Cascade Lasers for Process and Emission Control
Peter Kaspersen, Peter Geiser, ... 1345

NICE-OHMS — A Frequency Modulated Cavity Enhanced Spectroscopic Technique for Sensitive Detection of Gases down to the $10^{-12}\,\mathrm{cm}^{-1}\mathrm{Hz}^{-1/2}$ Range
Ove Axner, Patrick Ehlers, Isak Silander, Junyang Wang, ... 1346

Concentration Extraction of Multiple Gases Based on Shape Analysis of a Single Absorption Line
Patrik Lundin, Liang Mei, Stefan Andersson-Engels, Sune Svanberg, ... 1347

Recent Progress on WindScanners Based on Coherent Doppler Lidars
Mikael Sjöholm, Nikolas Angelou, Farzad Cyrus Foroughi Abari, Per Hansen, Kasper Hjorth Hansen, Guillaume Lea, Jakob Mann, Torben Mikkelsen, Ameya Sathe, Anders Tegtmeier Pedersen, Nikola Vasiljevic, ... 1348

LIDAR Techniques for the Cultural Heritage Sector
Giovanna Cecchi, David Lognoli, Lorenzo Palombi, ... 1349

Field Entomological Applications of kHz Optical Ranging and Sensing
Mikkel Brydegaard, Alem Gebru, ... 1350

Authentication of Jadeite Using Surface Enhanced Raman Spectroscopy
Chi Man Lawrence Wu, Siu Pang Ng, ... 1352

Lorentz Contraction, Apparent or Real
Nils Hugo Abramson, ... 1353

High Speed BOCDA Measurement of Strain Distribution by Longitudinal Sweep Method
Kazuki Washiyama, Masato Kishi, Zuyuan He, Kazuo Hotate, ... 1354

Inverse Obstacle Scattering and Linear Classification
Giovanni Franco Crosta, Yong-Le Pan, Gorden Videen, ... 1356

Laser Spectroscopy in Environmental Sensing

Sune Svanberg[1, 2]

[1]Lund University Laser Centre, Lund University, P. O. Box 118, SE-221 00 Lund, Sweden
[2]Center for Optics and Electromagnetic Research, South China Normal University
University City Campus, Guangzhou 510006, China

Abstract— Laser spectroscopic techniques have brought about a revolution in basic studies of fundamental systems and in numerous applied fields. Environmental monitoring is one of the areas which has much benefitted from new possibilities arising. High sensitivity, selectivity, non-intrusiveness and real-time data availability are all attractive aspects. Many spectroscopic approaches can be taken, including elastic scattering, absorption, fluorescence, Raman and laser-induced break-down spectroscopy. Studies of laboratory samples can be readily performed, but also remote sensing at considerable distances using long-path absorption or laser radar (lidar) techniques. We will illustrate laser-based environmental remote sensing by range-resolved mapping of air pollutants using differential absorption lidar, by fluorescence lidar studies of water, vegetation and the cultural heritage, and by ecological studies focusing on insects and birds. Also, laboratory and short-range applications, mostly based on semiconductor lasers and light emitting diodes, will be presented. Finally, we will discuss the new field of gas in scattering media absorption spectroscopy (GASMAS), which provides many new possibilities for gas monitoring in unconventional environments. Some literature references pertaining to the work presented are listed below.

REFERENCES

1. Andersson, M., R. Grönlund, L. Persson, M. Sjöholm, K. Svanberg, and S. Svanberg, "Laser spectroscopy of gas in scattering media at scales ranging from kilometers to millimeters," *Laser Physics*, Vol. 17, 893, 2007.
2. Svanberg, S., "Laser based diagnostics — From cultural heritage to human health," *Appl. Phys. B*, Vol. 92, 351, 2008.
3. Svanberg, S., "LIDAR," *Springer Handbook of Lasers and Optics*, Invited Book Chapter for F. Träger, Ed., 1031–1052, Springer, Heidelberg 2007.
4. Svensson, T., E. Adolfsson, M. Lewander, C. T. Xu, and S. Svanberg, "Disordered, strongly scattering porous materials as miniature multi-pass gas cells," *Phys. Rev. Lett.*, Vol. 107, 143901, 2011.
5. Svanberg, S., "Fluorescence spectroscopy and imaging of lidar targets," *Laser Remote Sensing*, T. Fujii and T. Fukuchi, Ed., Chapter 7, 433–467, CRC Press, Boca Raton, 2005.
6. Guan, Z. G., M. Brydegaard, P. Lundin, M. Wellenreuther, E. Svensson, and S. Svanberg, "Insect monitoring with fluorescence LIDAR techniques — Field experiments," *Appl. Optics*, Vol. 48, 5668, 2010.
7. Svanberg, S., "Gas in scattering media absorption spectroscopy — From basic studies to biomedical applications," *Lasers and Photonics Reviews*, 2013, Doi 10.1002/Ipor.201200073.

Remote Sensing of Atmospheric Traces and Particulate Matter Using Backscattered Light from Nanosecond and Femtosecond Laser Light

Benjamin Thomas[1], **Gregory David**[1,2], **Christophe Anselmo**[1,2], **Elodie Coillet**[1,2], **Katja Rieth**[1,2], **Alain Miffre**[1,2], **and Patrick Rairoux**[1,2]

[1]Institute of Light and Matter (ILM), Université Lyon1, CNRS, France
[2]LASIM, Université Lyon1, CNRS, France

Abstract— Laser-based optical spectroscopy is becoming a standard for atmosphere observation and survey. Absorption as well as linear and non-linear scattering of laser light by atmospheric compounds are the fundamental processes applied for this purpose. Moreover, atmosphere laser remote sensing capability has found a great interest in local and global environment surveys. In this context, lidar (light detection and ranging) is the well-known and the most used methodology.

The aim of this contribution is to present achievements on the one hand, on laser remote sensing of nanometer-sized range particulate matter content into the atmosphere by using UV and VIS nanosecond laser pulses and, on the other hand, greenhouse gases remote sensing using IR femtosecond laser pulses.

Non-spherical particles, such as volcanic ash or desert dust particles present a wide range of sizes, shapes and chemical composition. These particles exhibit sharp edges as for volcanic ash particles or varying shapes from compact to thin flakes, as for mineral dust particles. After long-range transport in the atmosphere, from a source region to a place where intrusion episodes occur, an aerosol cloud, such as a dust or volcanic ash cloud is composed of both spherical (s) and non-spherical (ns) particles. In this contribution, we specifically address the ns-particles contained in an aerosol cloud (a) with a home-built UV-VIS polarization lidar at Lyon (45.87°N, 4.83°E, France). The achieved sensitivity and accuracy allows distinguishing different aerosols layers having different polarization and backscattering properties. To achieve such observations, three main points have been considered. Firstly, the scattering matrix formalism has been developed for a mixed aerosol cloud (a) = {s, ns}, composed of both s and ns-particles.

The Optical Correlation Spectroscopy methodology (OCS) coupled the lidar technique has been developed to remotely evaluate CH_4 and H_2O greenhouse gas concentrations in the atmosphere. It is based on combining the OCS method with broadband femtosecond laser based lidar. The novelty of this work is that the broadened laser pulses are spectrally shaped in order to be either correlated or not with the specific trace absorption cross-section. The amplitude modulation is obtained thanks to an Acoustic Optical Programmable Dispersive Filter (AOPDF) which avoids the use of a hazardous gas reference cell, as operated in conventional OCS-devices. To evaluate the performance of the OCS-Lidar methodology, statistical and systematical errors have been studied using a theoretical and numerical model based on a Monte Carlo simulation. Moreover the proof of the broadband OCS-Lidar has been recently proven by measuring the water vapor content of the atmosphere.

In summary, we will present at PIERS, application of the basics in laser absorption spectroscopy and on optical scattering that allows to remotely probing the content of traces and particulate matter in the atmosphere.

Photonic Sensing of Reactive Molecules in the Atmosphere: Challenges and Opportunities

W. Chen[1], **R. Maamary**[1], **X. Cui**[1,2], **T. Wu**[1,3], **E. Fertein**[1], **C. Coeur**[1], **A. Cassez**[1], **W. Liu**[2], **F. Dong**[2], **Y. Wang**[2], **W. Zhang**[2], **X. Gao**[2], **G. Zha**[4], **Z. Xu**[4], **and T. Wang**[4]

[1]Laboratory of Physical Chemistry of the Atmosphere
University of the Littoral Opal Coast, Dunkerque, France
[2]Anhui Institute of Optics & Fine Mechanics, Chinese Academy of Sciences, Hefei, China
[3]Key Laboratory of Nondestructive Test, Nanchang Hang Kong University, Nanchang, China
[4]Department of Civil and Structural Engineering
The Hong Kong Polytechnic University, Hong Kong, China

Abstract— Chemically reactive atmospheric species play a crucial role in tropospheric processes that dominate regional air quality and global climate change. Contrary to long-lived species (such as greenhouse gases), real time *in situ* sensing of such short-lived atmospheric molecules represents a real challenge due to their very high reactivity resulting in short lifetimes (of around 1-100 seconds) and ultra-low concentrations that measure in parts per billion by volume (ppbv) to parts per quadrillion by volume (ppqv).

In this talk, we report on our recent progress in the development of photonic instruments for *in situ* trace gas monitoring of nitrous acid (HONO), nitrate radical (NO_3) and nitrogen dioxide (NO_2) in the atmosphere. The experimental arrangements, based on the advanced photonic technologies (such as quantum cascade laser, difference-frequency generation parametric source, light emitting diode) combined with selective and sensitive long optical path length enhanced absorption spectroscopy, as well as their applications to field observation and smog chamber study of environmental and atmospheric interest will be presented.

ACKNOWLEDGMENT

This work is mainly supported by the IRENI program of the Région Nord-Pas de Calais. The financial supports from the French national research agency (ANR) under the NexCILAS (ANR-11-NS09-0002) and the CaPPA (ANR-10-LABX-005) contracts are acknowledged.

REFERENCES

1. Cui, X., C. Lengignon, T. Wu, W. Zhao, G. Wysocki, E. Fertein, C. Coeur, A. Cassez, L. Croisé, W. Chen, Y. Wang, W. Zhang, X. Gao, W. Liu, Y. Zhang, and F. Dong, *J. Quant. Spectrosc. Rad. Transfer*, Vol. 113, 1300–1316, 2012.
2. Wu, T., W. Chen, E. Fertein, F. Cazier, D. Dewaele, and X. Gao, *Appl. Phys. B*, Vol. 106, 501–509, 2012.
3. Chen, W., T. Wu, Q. Zha, Z. Xu, and T. Wang, *SPIE Newsroom*, January 18, 2013, DOI: 10.1117/2.1201301.004689.

Quantum Cascade Lasers for Process and Emission Control

Peter Kaspersen and Peter Geiser
Norsk Elektro Optikk A/S, Solheimveien 62A, Lørenskog 1473, Norway

Abstract— Near infrared tunable diode laser absorption spectroscopy (NIR-TDLAS) has been accepted by industrial users as the best available technology for in-situ emission and process control measurements. However, for some important gases the absorption line strengths and thus the sensitivities are too low (e.g., nitric oxide, NO) or the species does not possess any absorption features in the NIR (e.g., sulfur dioxide, SO_2). The fundamental absorption bands in the mid-infrared spectral region (MIR) are orders of magnitude stronger than the overtone and combination bands in the near infrared. For example, the best absorption line in the 5.2 µm-band of nitric oxide is approx. 1200 times stronger than the best line in the 1.8 µm-band (using telecom diode lasers).

In this paper an example of an important industrial application for a NO measurement and a solution using a quantum cascade laser (QCL) in a TDLAS gas monitor will be presented.

In most combustion processes the emission of nitric oxide into ambient air has to be limited due to environmental protection regulations (e.g., by US EPA or Bundesumweltamtin Germany) and emissions from coal-fired power plants are considered to be one of the major contributors to the poor air quality all over China.

A so called "deNOx process" is used to reduce the NO concentration in industrial gas mixtures. In this process either gaseous ammonia (NH_3) or ammonia-water is used to convert NO and NH_3 into water vapor (H_2O) and nitrogen (N_2). The amount of ammonia depends on the NO content of the process gas. Especially in a dynamic process where the fuel or the fuel composition changes rapidly the variation of the NO concentration can be quite high. To regulate the deNOx process and thus the amount of ammonia added to the process gas the NO content has to be measured in-situ, very accurately, and with a fast time response early in the gas cleaning process. Since the measurement point can be very close to the process the gas temperature can be still very high (up to 400°C). Typical nitric oxide concentrations are in the low ppm range so that the lower detection limit (LDL) of NO instruments used for the regulation should be around 1 ppm· m at 400°C.

State-of-the-art NIR laser spectrometers allow measurements of only around 10 ppm· m at 300°C due to weak absorption line strengths in the NIR and strong water vapor interference at higher gas temperatures. Therefore NIR gas monitors are in general not suitable for this application.As described above in the MIR the line strength is significantly stronger.Software simulations based on HITRAN and HITEMP databases have led to selection of interference-free NO absorption lines in a typical industrial incinerator process gas mixture. Therefore a spectrometer using a mid-infrared laser sourcehas a high potential to meet the LDL required for a deNOx regulation while having no interference from other gases in the process.

In cooperation with a laser manufacturer a quantum cascade laser chip for one of the selected absorption lines in the 5.2-µmm band of NO has been prepared. The QCL was implemented into a spectrometer setup and mounted onto a heated cell (optical path length $L = 0.7$ m; gas-temperature $T_{gas} \leq 400$°C). Tests at 400°C have successfully been performed and showed good agreement with the simulations.

The sensitivity of the spectrometer has been determined to be around $2.5 \cdot 10^{-4}$ [rel. abs.] which leads to a lower detection limit of better than 1 ppm· m at 400°C. The measurement is interference-free from water-vapor concentrations up to 30% at an optical path length of 2 m. Other gases like ammonia (NH_3), methane (CH_4), or nitrous oxide (N_2O) at typical combustion concentration levels do not influence the NO measurement. Results from measurements of NO in relevant industrial processes willbe presented.

The same approach has also led to a spectrometer for sulfur dioxide (SO_2) in the 7.4 µm-band. The sensitivity of the spectrometer has been determined to be around $2 \cdot 10^{-4}$ [rel. abs.] and tests have been performed again with the heated cell. The lower detection limit has been determined to be 1 ppm· m at 300°C. Additionally it has been demonstrated that it is possible to subtract the signal from up to 20% water vapor so that interference-free measurements up to that water vaporlevel are possible.

NICE-OHMS — A Frequency Modulated Cavity Enhanced Spectroscopic Technique for Sensitive Detection of Gases down to the $10^{-12}\,\mathrm{cm}^{-1}\mathrm{Hz}^{-1/2}$ Range

Ove Axner, Patrick Ehlers, Isak Silander, and Junyang Wang
Department of Physics, Umeå University, S-901 87 Umeå, Sweden

Abstract— Noise-Immune Cavity-Enhanced Optical Heterodyne Molecular Spectroscopy (NICE-OHMS) is a laser-based spectroscopic technique originally developed for high precision frequency standard applications at JILA in Boulder, CO, USA, with unique properties. By combining an external cavity for increased interaction length with the sample with frequency modulation for reduced influence of noise, the technique achieves an extraordinary high sensitivity. In addition, by choosing the modulation frequency equal to the free-spectral range of the cavity, the technique obtains immunity to laser frequency noise, which implies that detection can be made as if the cavity would not be there. Finally, both Doppler-broadened and Doppler-free signals can be measured in either absorption or dispersion mode of detection. In its first realization, based on a well stabilized solid state laser, an impressive absorption sensitivity of $10^{-14}\,\mathrm{cm}^{-1}$ was demonstrated for molecular species detection [1]. This is several orders of magnitude better than any other optical detection technique can achieve, which gives NICE-OHMS a large potential for sensitive trace gas analysis.

However, the technique has, for a long time, been considered too complex to be used for practical trace gas analysis. To make the technique more applicable to trace gas detection, our research group has challenged this and is developing the NICE-OHMS technique further, with the main aim of reducing the complexity of the instrumentation while keeping as much as possible of the high sensitivity [2]. The systems developed so far are based narrowband fiber or DFB lasers and have, whenever possible, utilized fiber-coupled components for a more compact realization. Using C_2H_2 as the pilot species, we have scrutinized the dependence of the technique on a variety of parameters for optimum sensitivity, selectivity, and thereby its applicability. Using a cavity with a finesse of 5700, we have demonstrated an absorption sensitivity of $5.6 \times 10^{-12}\,\mathrm{cm}^{-1}\mathrm{Hz}^{-1/2}$, or $\Delta I/I$ of 7.2×10^{-11} over 10 sec, which allows detection of low ppt (parts-per-trillion) concentrations of acetylene in atmospheric samples [3]. The talk will provide a short description of the basic features of the technique and some of the most important results. An NICE-OHMS system based on an OPO for addressing transitions in the MIR range is under development which will allow a large number of species to be detected with unprecedented detection sensitivity, including isotopological assessments, which, in turn, will open up for assessment of species for both environmental issues and medical diagnostics (breath analysis).

REFERENCES

1. Ye, J., L. S. Ma, and J. Hall, "Ultrasensitive detection in atomic and molecular physics: Demonstration in molecular overtone spectroscopy," *J. Opt. Soc. Am. B*, Vol. 15, 6–15, 1998.
2. Foltynowicz, A., F. M. Schmidt, W. Ma, and O. Axner, "NICE-OHMS: Current status and future potential," *Appl. Phys. B*, Vol. 92, 313–326, 2008.
3. Ehlers, P., I. Silander, J. Wang, and O. Axner, "Fiber-laser based NICE-OHMS instrumentation for Doppler broadened detection in the $10^{-12}\,\mathrm{cm}^{-1}\mathrm{Hz}^{-1/2}$ range," *JOSA B*, Vol. 29, 1305–1315, 2012.

Concentration Extraction of Multiple Gases Based on Shape Analysis of a Single Absorption Line

Patrik Lundin[1], **Liang Mei**[1, 2, 3],
Stefan Andersson-Engel[1], **and Sune Svanberg**[1, 4]

[1]Atomic Physics Division, Faculty of Engineering
Lund University, Lund SE-22100, Sweden
[2]Joint Research Centre of Photonics
Zhejiang University-Royal Institute of Technology-Lund University
Hangzhou 310058, China
[3]Center for Optical and Electromagnetic Research
Zhejiang University, Hangzhou 310058, China
[4]Center for Optical and Electromagnetic Research
South China Normal University, Guangzhou 510006, China

Abstract— A commonly used method for gas concentration measurements is TDLAS (Tunable Diode Laser Absorption Spectroscopy). In this technique, the wavelength of a diode laser is tuned across an absorption line of a gas while the transmitted intensity is monitored. The fraction of light absorbed at the peak of the absorption line is, through the Beer-Lambert law, providing information about the gas concentration. A requirement is, however, that the path length is known. We present a related but alternative method for optical measurements of gas concentrations based on line shape analysis instead of on absorption magnitude. The background to the approach is that the broadening and shift of molecular absorption lines are dependent on the concentrations of the other molecules in the buffer gas mixture (apart from on the temperature and pressure). We have used this approach to simultaneously determine the concentrations of multiple gas species in a buffer gas mixture, by performing line shape analysis on single absorption lines of water vapor. Since the width and position of the water vapor line depend on the concentrations of the neighboring molecules in the gas mixture, these can be indirectly measured. The main advantages of the approach are that the concentration of gases lacking absorption lines can be measured, and that the gas concentration can be retrieved even in the case that the path length of light-gas interaction is unknown, e.g., in the application of gas in scattering media absorption spectroscopy.

Recent Progress on WindScanners Based on Coherent Doppler Lidars

Mikael Sjöholm, **Nikolas Angelou**, **Farzad Cyrus Foroughi Abari**, **Per Hansen**, **Kasper Hjorth Hansen**, **Guillaume Lea**, **Jakob Mann**, **Torben Mikkelsen**, **Ameya Sathe**, **Anders Tegtmeier Pedersen**, **and Nikola Vasiljevic**
Department of Wind Energy, Technical University of Denmark
DTU Risø Campus, Frederiksborgvej 399, Roskilde 4000, Denmark

Abstract— Remote optical sensing of wind and turbulence is increasingly finding applications within both research and industry relating to the fields of wind power, aviation, construction and environmental monitoring. In this context, various WindScanners based on coherent Doppler lidars operating at wavelengths around 1.55 micrometer have been developed during the last years at the Department of Wind Energy at the Technical University of Denmark, which now is leading the design and implementation of a distributed European research infrastructure WindScanner facility (www.WindScanner.eu).

The WindScanners are providing novel measurements of the full three-dimensional wind and turbulence fields by measuring the line-of-sight wind speeds along three freely steerable lidar laser beams. Two types of WindScanners have been developed and applied in field experiments. The focused continuous-wave lidars, with steerable dual rotating prism scanners, provide agile beam steering and small sampling volumes at short ranges below a few hundred meters, whereas the pulsed lidars, with steerable dual mirror scanners, provide slower beam steering but measurement ranges of several km.

Here, the technology is presented and results from field campaigns involving comparisons with traditional in-situ instrumentation and examples from applications within aviation, construction, environment and wind power are given. In particular, the measurement of the downwash below a helicopter, the wake of a small building, and the flow that has passed a steep 12-m high escarpment at a small isolated peninsula are presented. In addition, results from a field experiment demonstrating the capabilities of turbine mounted lidars for providing feed-forward control of wind turbines are shown.

The WindScanner development advances the studying of wind and turbulence fields in complex environments remotely without disturbing the flow by meteorological towers, which opens up many new research possibilities. In relation to environmental monitoring, the combination of WindScanners with air pollution concentration mapping differential absorption lidars has the prospects of providing useful measurements of air pollution fluxes in complex industrial environments.

LIDAR Techniques for the Cultural Heritage Sector

Giovanna Cecchi[1,2], **David Lognoli**[1], **and Lorenzo Palombi**[1]

[1]Applied Physics Institute 'Nello Carrara', National Research Council of Italy
Via Madonna del Piano, Sesto Fiorentino 10-50019, Italy
[2]On leave to National Institute of Optics, National Research Council of Italy, Italy

Abstract— Since the nineties, LIDAR sensors have shown good performances in their application to the cultural heritage sector; currently they have reached a good level of maturity in the remote monitoring and diagnostics of monumental sites and works of art.

LIDAR returns exploit both the elastic and inelastic backscattering processes, that are employed for a 3D reconstruction of the object (through the acquisition of point-clouds) and for a physico-chemical characterization of the object (through the laser induced fluorescence spectroscopy). In addition, the possibility of imaging detection enhanced the LIDAR success in their application to the remote sensing of cultural heritage, so that nowadays LIDAR sensors are recognized as a key tool for diagnostics and preservation.

In the sector of cultural heritage, elastic backscattering LIDAR works as a laser-scanner; it is a well established instrument, whose use is expanding rapidly facilitating — for instance — the virtual 3D reconstruction of deteriorated building artifacts and archeological sites. From a technological point of view, fluorescence LIDARs are a more complex instrument; however they are gaining an increasing attention due the large amount of information which can be extracted from the analysis of the fluorescence spectral signal. Actually, a fluorescence LIDAR provides a monitoring of different parameters which turn helpful in the conservation status assessment of monuments and works of art. More in detail, fluorescence LIDARs have been successfully applied in the remote detection and classification of biodeteriogens and protective treatments, in the characterization of stones and other masonry materials. Furthermore, when a fluorescence LIDAR is operated in scanning mode, it is possible to acquire fluorescence hyperspectral images — even over extended areas — from which different thematic maps can be extracted, providing a comprehensive assessment on the status of the whole monument at a spatial definition that cannot be reached by traditional samplings.

Finally, it has to be underlined that the LIDAR technique shows the advantage of being non-destructive and it can be carried out *in situ* without the use of scaffolding that, besides being costly, limits the access to the monument and its fruibility. This peculiar aspect offers the opportunity to acquire repetitive images, opening new perspectives for an accurate monitoring of a monument, repeatable in time, to follow the changes of the monument status.

ACKNOWLEDGMENT

Giovanna Cecchi wishes to thank Valentina Raimondi for her contribution during many years.

Field Entomological Applications of kHz Optical Ranging and Sensing

Mikkel Brydegaard[1, 2, 3] **and Alem Gebru**[1]

[1]Laser Research Institute, Universiteit van Stellenbosch, South Africa
[2]Center for Animal Movement, Lund University, Sweden
[3]Applied Molecular Spectroscopy and Remote Sensing, Lund University, Sweden

Abstract— A major difficulty in field entomology is the quantitative estimation of insect activity and abundance in the atmosphere, where the primarily used tools consist of a variety of traps with unknown biases. In particular behavioral aspects such as landscape dispersal and insect interaction, e.g., in predation, mating or rivalry are difficult to address, not least during night time. Here optical remote sensing and ranging can contribute with a variety of details such as spatial and temporal abundance [1], remote classification of species, genders and age groups [2], flight direction and chasing reaction kinetics [3]. We have recently developed a number of tools in this field, recently in particular focusing on robust, inexpensive and realistic instrumentation [4]. Our latest activities includes the development and testing of a novel 3 W continuous wave LIDAR operating at 810 nm, so far achieving sample frequencies up to 2 kHz. Kilohertz detection is crucial for field entomology [5] in order properly resolve wing beat modulation and its content of high order harmonics. We have also developed daylight scattering tools for remote flight direction assessment using quadrant detectors as well as multiband kHz detection of wing-beat iridescence [6].

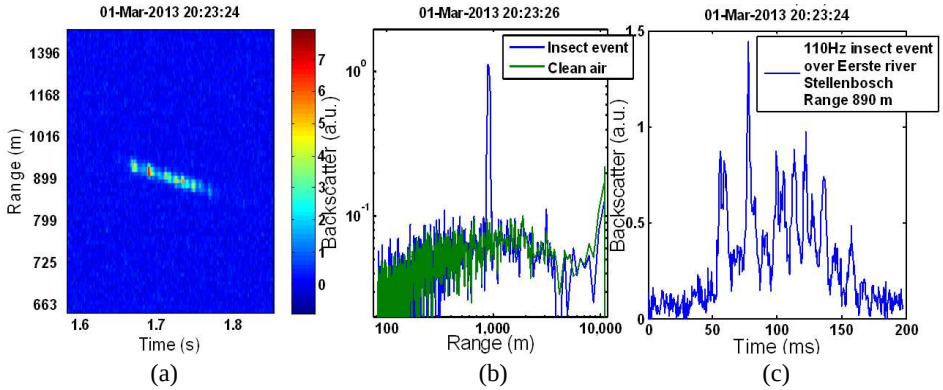

Figure 1: (a) Typical insect event in fast lidar range-time map. The insect was observed roughly 20 m above the adjacent Eerste river. (b) Comparison of an insect echo to the return signal from clear air, the decreased termination echo is seen at 11.4 km range. (c) Ranged time-series of the event showing the wing beat modulation.

REFERENCES

1. Guan, Z., M. Brydegaard, P. Lundin, M. Wellenreuther, A. Runemark, E. Svensson, and S. Svanberg, "Insect monitoring with fluorescence lidar techniques: Field experiments," *Appl. Opt.*, Vol. 49, 1–11, 2010.
2. Sikulu, M., G. F. Killeen, L. E. Hugo, et al., "Near-infrared spectroscopy as a complementary age grading and species identification tool for african malaria vectors," *Parasit. Vectors*, Vol. 3, No. 49, 2010.
3. Runemark, A., M. Wellenreuther, H. Jayaweera, S. Svanberg, and M. Brydegaard, "Rare events in remote dark field spectroscopy: An ecological case study of insects," *IEEE Journal of Selected Topics in Quantum Electronics*, Vol. 18, 1573–1582, 2012.
4. Brydegaard, M. and S. Svanberg, "Multispectral imaging in development," *Europhysics News*, Vol. 42, No. 5, 2011.

5. Carlsten, E. S., G. R. Wicks, K. S. Repasky, J. L. Carlsten, J. J. Bromenshenk, and C. B. Henderson, "Field demonstration of a scanning lidar and detection algorithm for spatially mapping honeybees for biological detection of land mines," *Appl. Opt.*, Vol. 50, 2112–2123, 2011.
6. Brydegaard, M., P. Samuelsson, M. W. Kudenov, and S. Svanberg, "On the exploitation of mid-infrared iridescence of plumage for remote classification of nocturnal migrating birds," *Appl. Spectr.*, May 2013.

Authentication of Jadeite Using Surface Enhanced Raman Spectroscopy

Chi Man Lawrence Wu and Siu Pang Ng
Department of Physics and Materials Science, City University of Hong Kong, Hong Kong SAR, China

Abstract— While the trade of jadeite dominates the gemstone market in China, it is essential to develop effective authentication tools to distinguish counterfeits from genuine stones. Since the price of jadeite generally depends on its visual appearance which diverse greatly, artificial treatments of inferior grade jadeites to improve their attractiveness are popular trick-of-the-trade. One of the typical methods involves the removal of the colorific impurities, followed by impregnation of synthetic dyes and polymers. Although existing Raman spectroscopy is capable of detecting these addictives, high laser power is usually needed if the concentrations are low. Unfortunately, this means that the method involves bulky equipment, making it not very attractive for retailers. Also, the high laser power used may induce surface damage to gemstones to be tested, thus contradicts the initiative to provide a nondestructive analysis. To alleviate these issues, we propose to introduce the surface enhanced Raman scattering (SERS) effect using self-assembly plasmonic nanoparticle for jadeite authentication. Two self-assembly approaches of incorporating the nanoparticles onto the jadeite sample were studied. The results were compared with those with the simple method of applying the nanoparticles, e.g., using pipette. Our experimental results showed that with the appropriate way to apply the nanoparticles, the signal strength with an SERS analysis could be increased by at least an order of magnitude on the added polymer in the gemstone. The results would enable further advancement of the testing methodology in this field, such as the development of portable nondestructive SERS gemstone inspection system in the near future.

Lorentz Contraction, Apparent or Real

Nils H. Abramson
Industrial Metrology, Royal Institute of Technology, Stockholm 10044, Sweden

Abstract— The Michelson Morley interference experiment of 1887 indicated that the velocity of light is independent of the velocities of source and observer. This surprising result was in conflict with earlier calculations. To make theory and experiment in agreement Lorentz stated a contraction of rigid objects parallel to velocity. We discuss if this contraction is real or caused by the interference method of measurement. Our approach is to introduce a sphere of observation based on ultra short light pulses combined to ultra short observations. When the experimenter travels at high velocity this sphere is according to Lorentz contracted into an oblate ellipsoid. According to our proposed theory the sphere is instead elongated into a prolate ellipsoid. The result of this effect is that stationary objects appear contracted. Our results are in full agreement to Einsteins Special Theory of Relativity. To support our statements we introduce a novel method to measure the length of a travelling object that is independent of interferometry.

High Speed BOCDA Measurement of Strain Distribution by Longitudinal Sweep Method

K. Washiyama[1], **M. Kishi**[1], **Z. He**[2], **and K. Hotate**[1]

[1]Department of Electrical Engineering and Information Systems
University of Tokyo, Japan
[2]Shanghai Jiao Tong University, Shanghai, China

Abstract— Research on smart structures and smart materials has been more and more attractive recently. As sensing technology for the smart structures and smart materials, optical fiber sensing is promising for its capability of distributed measurement. In this study, we accomplished a high speed BOCDA (Brillouin optical correlation domain analysis) distributed strain measurement. In BOCDA, pump and probe lightwave propagating in FUT (fiber under test) in opposite directions are modulated in the lasing frequency to realize position-selective excitation of the stimulated Brillouin scattering. By changing the modulation frequency, the distributed measurement is performed.

In the BOCDA system fabricated for this study (Fig. 1), we adopted longitudinal sweep method, in which the mean frequency difference between the pump and probe lightwave and the frequency of the laser FM for sweeping the sensing position are simultaneously changed in order to obtain the distribution of BGS (Brillouin gain spectrum) along the entire FUT in short time. In our preceding study, time constant of lock-in amplifier restricted the measurement speed [1]. In another study, there was difficulty in making appropriate waveform to control the laser current because it adopted time-division pump-probe generation scheme [2].

In this study, we newly proposed the system to overcome these difficulties. In this system, we adopt SSBM (single side band modulator) to control and sweep precisely the pump and probe mean frequency difference. Instead of the lock-in detection, data subtraction of the two cases of pump-on and pump-off is introduced to have the Brillouin gain. Thus, the measurement speed of the BOCDA becomes higher and the operation becomes simpler. Besides, a low pass filter is adopted to realize the position selective measurement in the correlation domain technique. In this system, one distributed measurement with 50 cm spatial resolution along 120 m FUT was done in 50 ms. High speed iterative distributed strain measurement was demonstrated with twelve traces of the distribution measurement per one second, applying 1Hz dynamic strain at a 50 cm fiber portion. Fig. 2 shows the high speed iterative distribution measurement at around the strain applied portion.

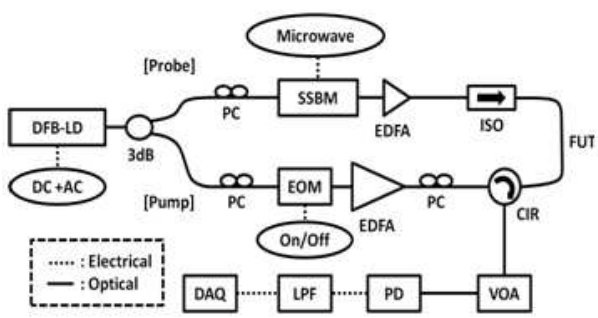

Figure 1: Experimental setup of the high speed BOCDA distributed strain measurement.

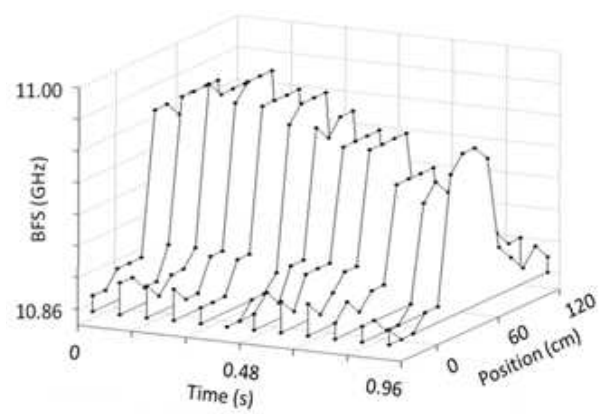

Figure 2: High speed iterative measurement of BFS (Brillouin frequency shift) distribution around the fiber portion where the dynamic strain is applied. Twelve traces of the distribution are measured per one second with 50 cm spatial resolution along 120 m sensing fiber.

REFERENCES

1. Zou, W., Z. Y. He, and K. Hotate, "Realization of high-speed distributed sensing based on Brillouin optical correlation domain analysis," *Conference on Lasers and Electro-Optics, and 2009 Conference on Quantum electronics and Laser Science Conference, CLEO/QELS 2009*, 1–2, 2009.
2. Song, K. Y., M. Kishi, Z. Y. He, and K. Hotate, "High-repetition-rate distributed Brillouin sensor based on optical correlation-domain analysis with differential frequency modulation," *Optics Letters*, Vol. 36, No. 11, 2011.

Inverse Obstacle Scattering and Linear Classification

Giovanni F. Crosta[1], **Yong-Le Pan**[2], **and Gorden Videen**[2]

[1]Inverse Problems & Mathematical Morphology Unit, Department of Earth and Environmental Science
University of Milan-Bicocca, 1, piazza della Scienza, Milan, IT 20126, Italy
[2]U.S. Army Research Laboratory, Adelphi, MD 20783, USA

Abstract—

Experimental: TAOS (two-dimensional angle-resolved optical scattering) is an experimental method to detect single, micrometer-sized airborne material particles, illuminate them by a single pulse of laser ($\lambda = 532\,\text{nm}$, pulse duration $= 30\,\text{ns}$) and record their scattered light intensity patterns over the angular sector $\{75^\circ \leq \theta \leq 135^\circ\} \times \{0^\circ \leq \varphi \leq 360^\circ\}$ at high resolution (one pattern $\doteq 1024^2$ pixels). Particles of reference materials and from outdoor environmental sampling have been analyzed and thousands of scattering patterns (TAOS patterns, hereinafter) have been stored [1]. Examples of reference materials are: 2.8 µm dioctyl phthalate droplets (label: Fq), 1.03 µm dried polystyrene latex spheres (Pq), *Bacillus subtilis* spores (Bq). Examples of environmental materials are: unsorted diesel engine soot (sq) and airborne dust from rooftop sampling (labeled $K0$ to $K5$).

Problem: The Inversion of Scattering Patterns: The problem of determining the size, shape, and complex refractive index of the particle (the scatterer) from its TAOS pattern corresponds to reconstructing an obstacle from a single incident wavevector and the intensity of the scattered wave. No theoretical result is available to date.

Solution: Feature Extraction for Linear Classification: For the past eight years the first author has worked at recasting the inverse problem into statistical terms and replacing obstacle reconstruction by the assignment of a TAOS pattern to a class. An algorithm has been developed, whereby two modules interact: feature extraction [2] and linear classification. In the current implementation (2012 to present) the former module regards the TAOS pattern as an image, applies a windowed Fourier transform followed by non-linear operations and yields a feature vector. The linear classifier applies multivariate statistics to feature vectors. Training and validation are supervised and rely on sequences of training sets made e.g., from Fq, Pq and Bq patterns. Once validated, the classifier is applied to recognize other patterns. The assignment of a TAOS pattern to a class relies on a fusion rule.

Classification Results: One of the goals of classification is the discrimination of bacterial spore patterns (Bq). Figure 2 provides a typical result: a set of 969 $K5$ (outdoor dust) patterns is analysed; 98 patterns (10%) are falsely recognised as Bq (lower halfplane), whereas the remainder is assigned to the other two training classes, Fq (top) and Pq (middle). Further details are provided by the caption.

Each of the 957 $K5$ TAOS patterns is represented by a point on the plane $\{z_1, z_2\}$ of the first two principal components, has a label, and is assigned to a class: Bq (blue), or Pq (green) or Fq (cyan). Counterclockwise, from top left, {pattern, assigned class, label} and, between parentheses, the pattern distinctive feature, which may justify assignment: $\{K5034, Fq, 124\}$ (curls), $\{K5024, Pq, 115\}$ (curls), $\{K5016, Bq, 107\}$ (coarse feature), $\{K5008, Bq, 184\}$ (coarse patch), $\{K5069, Pq, 159\}$ (wide rings), and $\{K5094, Fq, 99\}$ (rings).

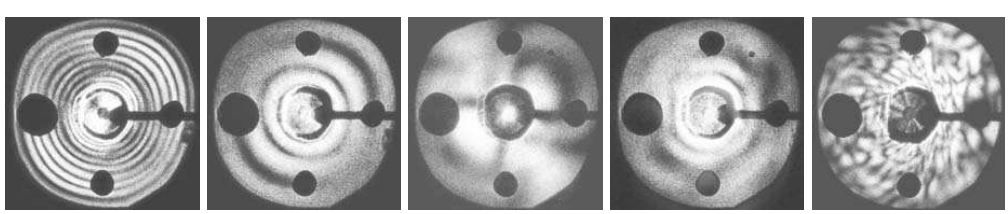

Figure 1: TAOS patterns, left to right, from a dioctyl phthalate droplet (Fq, narrow rings), a dried polystyrene latex sphere (Pq, wide rings), a single *Bacillus subtilis* spore (Bq, bowtie), an aggregate of diesel engine soot particles (sq, no special structure), and outdoor sampling ($K5$, almost random patches). The polarisation of the incident wave is +45 deg. Contrast has been enhanced by the Equalize command of GIMP for display purposes only.

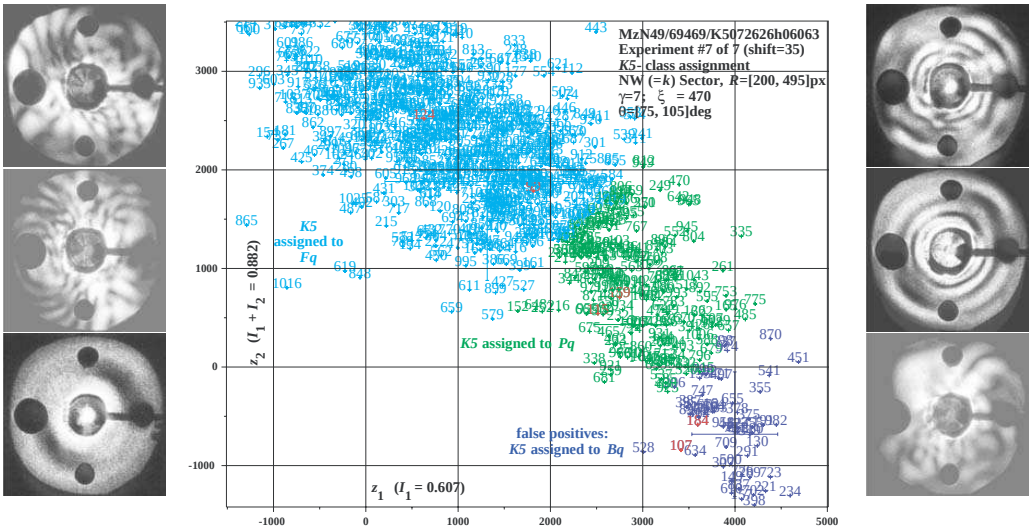

Figure 2: Recognition of 957 TAOS patterns from outdoor sampling ($K5$ set).

ACKNOWLEDGMENT

G. F. C. gratefully acknowledges the financial support of Contract W911NF 11-1-0277 R&D 1449-BC-01 granted to Università Milan-Bicocca by the US Army RDECOM ACQ CTR.

REFERENCES

1. Aptowicz, K. B., R. G. Pinnick, S. H. Hill, Y.-L. Pan, and R. K. Chang, "Optical scattering patterns from single aerosol particles at Adelphi, Maryland, USA: A classification relating to particle morphologies," *J. Geophys. Res.*, Vol. 111, D12212, 2006.
2. Crosta, G. F., "Image analysis and classification by spectrum enhancement: New developments," *Image Processing: Algorithms and Systems VIII — Proceedings of SPIE*, J. T. Astola, K. O. Egiazarian, Ed., Vol. 7532, 75320L-01–75320L-12, SPIE, Bellingham, WA, 2010.

Session 4A4
SC4: Wireless Energy Transmission and Harvesting 1

Adaptive Impedance Matching for 2, 3, 4-coil Wireless Power Systems
Benjamin H. Waters, Vamsi Talla, Brody J. Mahoney, Joshua R. Smith, ... 1360
Magnetic Characterization of Interfering Objects in Resonant Inductive Coupling Wireless Power Transfer
Elisenda Bou Balust, D. Vidal, Raymond J. Sedwick, Eduard Alarcon, ... 1362
Inductive Power Transmission by Toothed Drive Belt
Hans-Jurgen Roscher, K. Wolf, ... 1363
A 1-kW Wireless Power Transfer Link for Welding Rollers
Riccardo Trevisan, Alessandra Costanzo, ... 1364
Frequency Compensation of Wireless Power Transfer for Vehicles
Uooyeol Yoon, Sang Hoon Chung, Dang-Oh Kim, Ja Hyeon Lee, Dong-Ho Cho, ... 1366
Negative-permeability Superlenses for Near-field Magneto-inductive Wireless Power
Yaroslav A. Urzhumov, Guy Lipworth, Joshua Ensworth, Kushal Seetharam, Jae Seung Lee, Paul Schmalenberg, Matthew S. Reynolds, David R. Smith, ... 1367
A Study of Detuning Effects and Losses in Implantable Coils for Biomedical Wireless Power Transfer
Vamsi Talla, Benjamin H. Waters, Joshua R. Smith, ... 1369
Distributed Resonant Coil Systems for Efficient Wireless Power Transfer in Mobile Systems
Matthew J. Chabalko, David S. Ricketts, ... 1370
Q-factor Improvement in Planar RF Inductors by the Use of Ferrite Compensators
Mikhail Makurin, Nikolay Olyunin, Ki Young Kim, Keum-Su Song, Vladimir Mihaylovich Parfenyev, 1371
Obstacle Detection Method Using Array Antenna for Coupled-resonant Wireless Power Transfer
Hiroyuki Yamada, Keishi Miwa, Hiroshi Hirayama, Nobuyoshi Kikuma, Kunio Sakakibara, ... 1372
Superconducting-ferromagnetic Shell for Magnetic Energy Harvesting and Transmission at a Distance
Jordi Prat-Camps, Carles Navau, Alvaro Sanchez, ... 1374

Adaptive Impedance Matching for 2, 3, 4-coil Wireless Power Systems

B. H. Waters[1], **V. Talla**[1], **B. J. Mahoney**[1], **and J. R. Smith**[1, 2]

[1]Department of Electrical Engineering, University of Washington, USA
[2]Department of Computer Science Engineering, University of Washington, USA

Abstract— One of the challenges associated with developing wireless power transfer (WPT) applications that comply with existing regulatory standards for wireless devices is ensuring that nearly all of the energy is transferred across an accepted frequency band. Outside the bandwidths of the accepted frequency bands, the allowable field strength emissions are significantly lower than the permissible field strengths within the regulated bandwidth. Since the most efficient operating frequency can vary for a given set of high quality factor coils, it is difficult to maintain high efficiency across a wide range of distances and misalignments between the coils while operating at a single transmit frequency [1].

Rather than tuning the frequency to maintain high efficiency, adaptive impedance matching networks can be used to enable high efficiency at a single or narrowband transmit frequency. Previous work has demonstrated the benefits of adaptive impedance matching networks for 4-coil WPT systems [2]. Depending on the allowable size of the coils defined by the application and the desirable distance at which maximum efficiency should be achieved, adaptive impedance matching may be more practical for a 2, 3, 4 or n-coil wireless power system.

In this work, adaptive impedance matching networks for 2, 3, 4-coil wireless power systems are compared. Three sets of coils were built using equivalent coils in each case. The 4-coil system consists of a drive loop, transmit coil, receive coil, and receive loop, the 3-coil system consists of a drive loop, transmit coil, and receive coil and the 2-coil system consists of a transmit and receive coil. A vector network analyzer was used to measure S-parameters for a range of distances between the transmit and receive coils in each system. The efficiency of each system is approximated as $|S_{21}|^2$. Figure 1(a) shows the efficiency of each system operating at a single transmit frequency of 13.56 MHz, which corresponds to the resonant frequency of each coil. The efficiency peaks for each system occur at various distances, and the 4-coil system is capable of achieving highest efficiency at the greatest distance. Figure 1(b) shows the efficiency for each system using frequency tracking, which improves the efficiency at short distances because of the frequency splitting effect [3]. Figure 1(c) shows the efficiency using an adaptive impedance matching network (π-match) at both the transmit and receive sides of the system. With adaptive impedance matching, the 2-coil system achieves the greatest improvement in range from the single frequency and frequency tracking cases. The 2-coil system also maintains the highest efficiency at close distances compared to the 2 and 3-coil systems.

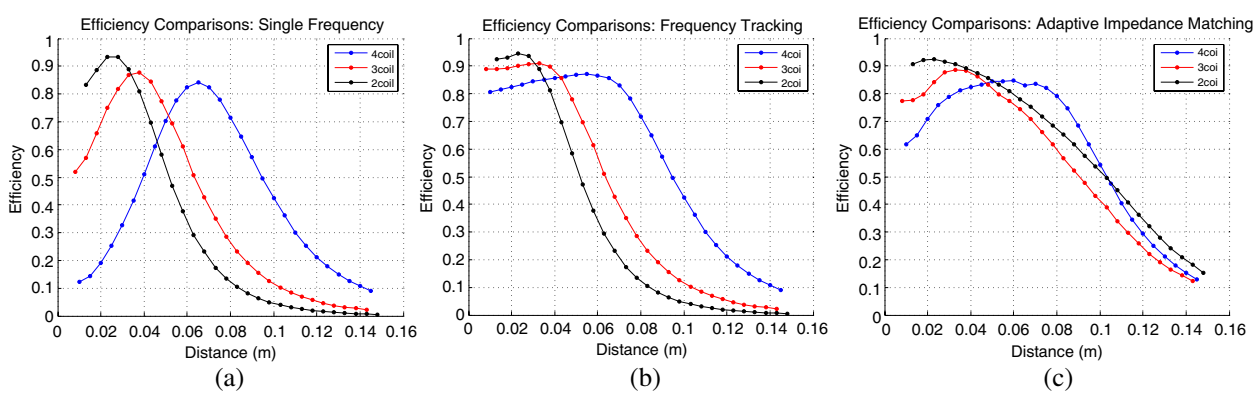

Figure 1: (a) Single frequency operation for 2, 3, 4 coil WPT systems terminated in 50 Ω. (b) Frequency tracking operation for 2, 3, 4 coil WPT systems terminated in 50 Ω. (c) Adaptive impedance matching operation for 2, 3, 4 coil WPT systems terminated in 50 Ω.

REFERENCES

1. Sample, A. P., B. H. Waters, S. T. Wisdom, and J. R. Smith, "Enabling seamless wireless power delivery in dynamic environments," *Proceedings of the IEEE*, Vol. PP, No. 99, 1–16, Jun. 2013.
2. Waters, B. H., A. P. Sample, and J. R. Smith, "Adaptive impedance matching for magnetically coupled resonators," *PIERS Proceedings*, 694–701, Moscow, Russia, Aug. 19–23, 2012.
3. Sample, A. P., D. Meyer, and J. R. Smith, "Analysis, experimental results, and range adaptation of magnetically coupled resonators for wireless power transfer," *IEEE Transactions on Industrial Electronics*, Vol. 58, No. 2, 544–554, Feb. 2011.

Magnetic Characterization of Interfering Objects in Resonant Inductive Coupling Wireless Power Transfer

E. Bou[1], **D. Vidal**[1], **R. Sedwick**[2], **and E. Alarcon**[1]

[1]Technical University of Catalonia UPC BarcelonaTech, Spain
[2]University of Maryland, US

Abstract— Resonant Inductive Coupling (RIC) Wireless Power Transfer is a key technology to provide an efficient and harmless wireless energy channel to consumer electronics, biomedical implants and wireless sensor networks. However, there are two factors that are limiting the applicability of this technology: the effects of distance variation between transmitter and receiver and the effects of interfering objects. While distance variation in WPT has been thoroughly studied, the effects of conductive interfering objects in resonant inductive coupling links are still unclear.

When a conductive element is in the vicinity of a RIC link, both the transmitter and the receiver can experiment a change on their resonant frequencies as well as their impedances. This can greatly affect the efficiency of such WPT link causing it to a) make the transmitter and/or receiver act as a pass-band filter and b) loose part of the transmitter magnetic field through coupling to the interfering object. Depending on the natural resonant frequency of the object and the distances between this object and the transmitter and receiver antennas, this can affect significantly the RIC wireless power transfer link. In this article, we characterize the Magnetic behavior of a resonant inductive coupled link in the presence of a conductive interfering object using a Finite Element Field Solver (FEKO). Several distances between interference and transmitter/receiver are analyzed providing a design space exploration and applicability study of this link.

Inductive Power Transmission by Toothed Drive Belt

H.-J. Roscher and K. Wolf
Fraunhofer Institute for Machine Tools and Forming Technology (IWU)
Chemnitz/Dresden, Germany

Abstract— Toothed drive belts are widely used in both drive and conveyor technologies.

Integrating active elements like sensors and actuators into toothed drive belts opens up more possibilities for the use of toothed drive belts in both assembly automation and handling technology applications.

The traditionally used drag chains can be eliminated by using the toothed drive belt to transmit electricity to and from the units connected by it.

Further advantages are that this concept reduces the moving mass and that it allows for a contactless inductive electricity supply at the point of use.

It is also simple to transmit the electricity from the tooth drive belt to the unit requiring the electricity if the unit in question is firmly fixed to the toothed drive belt.

The concept of conducting electrical current with tooth drive belts necessitates the integration of conductors into the belt. The conductors act as the secondary coil of a transformer.

This transformer is plagued by high secondary leakage inductance because of the geometrical conditions resulting from the long conductors in the belts.

The effect of secondary leakage inductance can be limited by using resonance in the power supply.

The possibility to improve the efficiency of the conductors, by reducing their ohmic resistance, is limited by the extreme high flexibility requirements. The high flexibility requirements can only be satisfied when the diameter of the conductors are very small.

To ensure energy efficient electricity transmission from the supply to the point of use, the voltage drop in relation to the connection voltage must be kept to a minimum.

The solution to ensure good energy efficiency of the system is to use inductive energy transmission from the toothed drive belt to a switchable capacitor which acts as energy store.

The capacitor must be rechargeable with the smallest possible current while only increasing the mass of the moving components marginally. Double layer capacitors are particularly well suited for this purpose, because of their high energy density. They also enable, with ease, the storage of regenerated energy typically produced when motorised units act as brakes.

In order to minimise the current flowing in the conductors, the operation of the equipment must be managed in such a way that there is enough time to recharge the capacitors.

A 1-kW Wireless Power Transfer Link for Welding Rollers

R. Trevisan[1] and A. Costanzo[2]

[1]DEI, University of Bologna, IMA Industries Srl, Italy
[2]DEI, University of Bologna, Italy

Abstract— Rotatable welders are commonly employed in automatic machineries to process materials that slide on a guide. Rotatable welders are often constituted by welding rollers heated up to the setpoint temperature by welding resistors drowned in the rollers. Electrical power is traditionally transferred to the resistors by means of sliding contacts, or slip rings. Because of the mechanical nature of the electrical joint, slip rings suffer from early degradation, fretting, and significant increase in the contact resistance over time. A challenging alternative solution is the realization of contactless energy transfer (CET) system based on rotatable electrical joints to replace slip rings. This solution is expected to lead to better performances, low maintenance requirements, higher reliability, and shorter downtimes. In this work, we describe the implementation of a full wireless power transfer link designed to substitute slip rings in supplying 1.2 kW to welding-roller resistors in a contactless fashion.

An eligible system for contactless energy transfer (CET) in rotatable applications must simultaneously satisfy various requirements, both mechanical, such as preserving axial symmetry, and electrical, such as guaranteeing high power transfer efficiency and power handling capabilities. Among the possible CET near-field approaches, such as capacitive or inductive, the latter is chosen due to the higher efficiency and power capability. Furthermore, inductive links are highly compatible with requirements of many industrial applications, such as robots, manipulators, sensors, and actuators.

As for the rotatable welders, axial symmetry can be obtained by adopting pot-core geometry in the magnetic circuit design (i.e., the transformer). In order to allow rotation of the welding roller with respect to the static part of the machine, the half cores that compose the pot-core transformer must be physically decoupled. This can be obtained by ensuring a small air gap between the halves (the chosen gap for our implementation is 0.6 mm). A rendering of the final system is visible in Figure 1. We will show that by adopting a proper reluctance model of the pot-core transformer it is possible to accurately predict the effect of the gap on the magnetic coupling link performance, as well as the equivalent-inductance values that constitute the electrical model of the transformer.

First, a proper choice of the size of the inductive device need be selected, compatible with the voltage levels to be rectified and switched at CET operating frequency. Second, the winding materials should be properly selected to ensure minimal losses in the operating band, which lies around tens of kHz. At these frequencies the resistance of the windings apparently increases because of skin and proximity effects. To solve this problem we adopted litz wires that are specifically designed to address such issue. Tens or hundreds of individually insulated thin copper strands (diameter of 0.2 mm or less) are generally bound together to form a litz wire. The switching converter may also represent a potential source of power loss, especially during the commutation of the switches. We will describe the design of resonant or quasi-resonant switches, such as zerovoltage and clamped-voltage solutions, to reduce turn-on and turn-off losses of the switching network. A quasi-resonant (or pseudo-resonant) inverter has been obtained by properly designing capacitances in parallel to MOSFET devices and by exploiting the equivalent input inductance of the transformer.

Finally we will discuss some representative simulated and measured results of the developed wireless power link for two configurations that differ on the number of turns of the windings and on the compensation of the transformer's inductances. The first configuration, named 'setup 18/17' (which refers to the turns ratio), fully exploits the transformer's input inductance to achieve the pseudo-resonance of the inverter and limits the losses in the copper by adopting litz wires composed by a high number of thin strands. The second configuration, named 'setup 27/24', reduces the number of litz strands to fit more turns in the winding area of the core; the inductance is partially compensated by adding a series capacitance on the primary side. The partial compensation of the inductance leads to a much more sinusoidal input current, compared to the first setup. To demonstrate the accuracy of adopted model, Figures 2 and 3 show the overlaps of simulated and measured input and output power waveforms of setup 18/17 and setup 27/24, respectively.

One the main goals in industrial applications is the decreasing in the electro-magnetic interferences generated by devices. For this reason, setup 27/24 is chosen — although the copper losses increase — because the analytical model, the FEM analysis, and the experimental measures on the realised prototype agree on the minimal efficiency reduction (in setup 18/14 efficiency is 97.7%, whereas in setup 27/24 efficiency is 95.6%). This makes setup 27/24 more favourable in EMI-aware applications in which circuit complexity, efficiency, and temperature increase due to increased copper losses are not an issue.

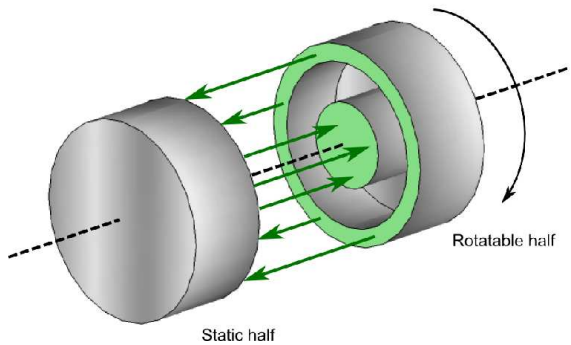

Figure 1: 3D image of two pot half cores and magnetic flux lines.

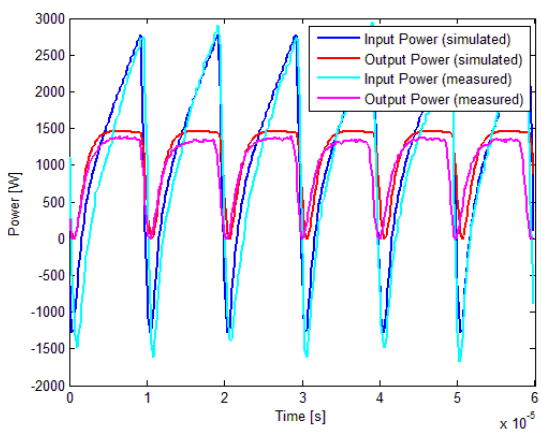

Figure 2: Simulated and measured input and output power waveforms of 'setup 18/17'.

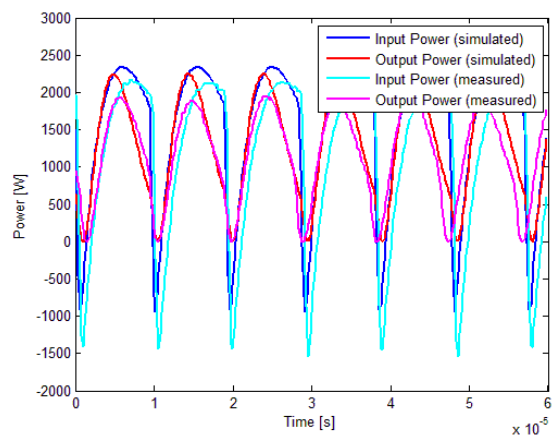

Figure 3: Simulated and measured input and output power waveforms of 'setup 27/24'.

Frequency Compensation of Wireless Power Transfer for Vehicles

Uooyeol Yoon, Sang Hoon Chung, Dang-Oh Kim, Ja Hyeon Lee, and Dong-Ho Cho
Wireless Power Transfer Research Center, KAIST, Daejeon 305-701, Korea

Abstract— For wireless power transfer invehicles with magnetic resonance, the tuning of frequency in resonance is very important for maximal power transfer. Even once the frequency in resonance is set, as the wireless power transfer goeson, there is deviation between the current operating frequency and the frequency in resonance. This deviation comes from heat, electrical change and so on.

In order to compensate this deviation, in this publication, authors propose the way to tune the operating frequency in considering the current output power. In the pilot system authors consider, there are multiple pick-up devices which gather the electro-magnetic field wirelessly from power supply line. Considering the output power from multiple pick-up devices, authors derive and propose the way to adjust the value of the capacitance in each pickup device. Output power from the multiple pick-up devices can be checked from the output power from the DC regulator in the pick-up device. By adjusting the capacitance in the pickup device, the frequency of resonance can be adjusted for achieving the maximal power transfer. This frequency tuning is performed periodically or at the moment when it is detected that there is unbalancing of output power from each pickup device.

Authors verify and analyze the algorithm above by simulation. Simulation is set up in considering the multiple pick-up devices mentioned above. From the simulation, authors verify that in the algorithm authors propose, the frequency in resonance can be tuned effectively within the acceptable range. Authors also apply the proposed the scheme to KAIST OLEV (On-Line Electric Vehicle) system. From the simulation and experiment, authors verify the effectiveness of the proposed scheme.

Negative-permeability Superlenses for Near-field Magneto-inductive Wireless Power

Yaroslav A. Urzhumov[1,2], **Guy Lipworth**[1,2], **Joshua Ensworth**[2], **Kushal Seetharam**[2], **Jae Seung Lee**[3], **Paul Schmalenberg**[3], **Matt Reynolds**[2], **and David R. Smith**[1,2]

[1]Center for Metamaterials and Integrated Plasmonics, Pratt School of Engineering
Duke University, 130 Hudson Hall, Box 90271 Durham, North Carolina 27708, USA
[2]Department of Electrical and Computer Engineering, Duke University
130 Hudson Hall, Box 90271 Durham, North Carolina 27708, USA
[3]Toyota Research Institute of North America, Ann Arbor, Michigan 48105, USA

Abstract— We report theoretical development, fabrication and experimental testing of a near-field wireless power transfer (WPT) device operating at an ISM frequency (13.56 MHz) inside the High-Frequency (HF) band, driven by quasi-magnetostatic field sources and enhanced by a near-field negative-permeability superlens, which is constructed from magnetic metamaterials (MMMs) with three-dimensional response and structure.

Design Methodology: MMMs are designed using a novel implementation of a field-averaging homogenization, based on the calculations of inductance of the unit cells. Unlike the standard S-parameter retrieval, this method allows one to retrieve the normal component of magnetic permeability (and dielectric permittivity, if necessary) for finite-thickness single- or multi-layer slabs of MMM unit cells. The tangential component is also retrievable in this method and has been compared against the standard S-parameter retrieval. Using these homogenization methods, we design a metamaterial with strong (resonantly-enhanced) magnetic response for all three polarizations of the magnetic field. MMM unit cells are 1.66 cm in size and form a cubic lattice. Single, double and triple layer stacks have been designed to demonstrate our ability to engineer multiple, densely packed layers of resonators without a significant broadening of splitting of the resonances.

Fabrication: To fabricate negative-permeability MMMs, we employ standard PCB fabrication methods executed by a commercial PCB vendor. We used 0.01"-thick, low-loss Rogers 4350 clad with 1oz (34.8 µm-thick) copper. To fabricate an array of resonators responding to magnetic field with all possible polarizations, flat sheets were cut into strips, and a double array of orthogonal strips was formed by inserting the strips in a comblike fashion. To complete fabrication, a contiguous flat panel was inserted into the pre-arranged slots on strips.

The transmitter (Tx) and receiver (Rx) of ac power, both resonant magnetic-dipole antennas, were fabricated from copper wire with circular cross-section (4 mm diameter), bent into a circular spiral shape and attached to a low-loss polymer glass substrate for mechanical stability. The outer/inner diameter of the spiral is 34/15 cm, with spiral pitch 1.58 cm and a total of 7.75 turns. Tx and Rx coils were fine-tuned to resonate at 13.558 MHz with Q-factor of about 127.

Metamaterial Characterization: To ensure accurate design of the MMM superlens, we performed in-house characterization of the various components of the MMMs, as well as the full structure. Resonance properties of single unit cells and 3×3 boards were measured using a vector network analyser set to a 10 Hz IF bandwidth with 1600 data points and a 200 kHz span. Single cells resonated at (12.865 ± 0.0006) MHz. The Q-factor of resonances was in the range 74.3–78.0, with an average of $Q = 76$ and standard deviation 1.1.

Testing: The full WPT system was tested in the frequency range from 12–17 MHz (in the HF band), with particular focus on the 13.56 MHz ISM band. VNA is used to measure the S_{11} and S_{21} parameters of the network consisting of a non-resonant coupling coil, resonant spiral Tx coil, MMM slab, resonant Rx coil and another non-resonant coupling coil. The S-parameters are then de-embedded to reveal the transmission coefficient of the Tx-MMM-Rx sub-circuit.

Conclusions: Measurements of PCB-based metamaterial unit cells confirm that we were able to manufacture a magnetic-dipole high-Q resonant composite structure with resonator dimensions of only $\lambda/1333$ at 13.56 MHz. The measured power transfer efficiency through the metamaterial-enhanced system show slower deterioration of efficiency vs transfer distance than in the same measurement without the metamaterial. At Tx-Rx distances greater than 1 m, MMM increases power efficiency of the system, progressively with distance.

REFERENCES

1. Urzhumov, Y. A. and D. R. Smith, *Phys. Rev. B*, Vol. 83, 31, 2011.
2. Huang, D., Y. Urzhumov, D. R. Smith, K.-H. Teo, and J. Zhang, *J. Appl. Phys.*, Vol. 111, 064902, 2012.

A Study of Detuning Effects and Losses in Implantable Coils for Biomedical Wireless Power Transfer

V. Talla[1], B. H. Waters[1], and J. R. Smith[1, 2]

[1]Department of Electrical Engineering, University of Washington, USA
[2]Department of Computer Science Engineering, University of Washington, USA

Abstract— Wireless power transfer (WPT) using magnetically coupled resonators (MCRs) is a promising technology for powering implanted biomedical devices [1, 2]. In typical applications, the receive coil(s) is implanted inside the body and is encapsulated by biological fluids and tissues. Since biological fluids and tissues have high electric constant and loss tangent, the efficiency of WPT degrades as a result of capacitive detuning and conductive losses respectively [3].

In tradition analysis of WPT, the coils are modeled as a series LR circuit where R accounts for the loses in the coil, and the capacitive and conductive losses of the surroundings are neglected. However, when the coil is surrounded by biological material, this model is no longer accurate. This can be seen from Figure 1(c) which shows the imaginary component of the input reflection coefficient for a receive coil (shown in Figure 1(a))) in phantom (saline solution) vs. in air. It can be seen that there is a drastic shift in the resonant frequency and the quality factor (this accounts for losses) of the coil. This change is not accounted for in the previous models.

In this work we propose a new model as shown in Figure 1(b) where C_{par} models the capacitive detuning effect, R_{L_par} models the conductive losses in the surrounding tissues and R_{L_par} accounts for the cumulative losses in the coil inductance. We use this new equivalent model to investigate the performance of WPT for a neural implant application wherein the receive coil is implanted in beneath the skull. We present numerical simulation results, extracted parameters from vector network analyzer and experimental results to verify the accuracy of the proposed model.

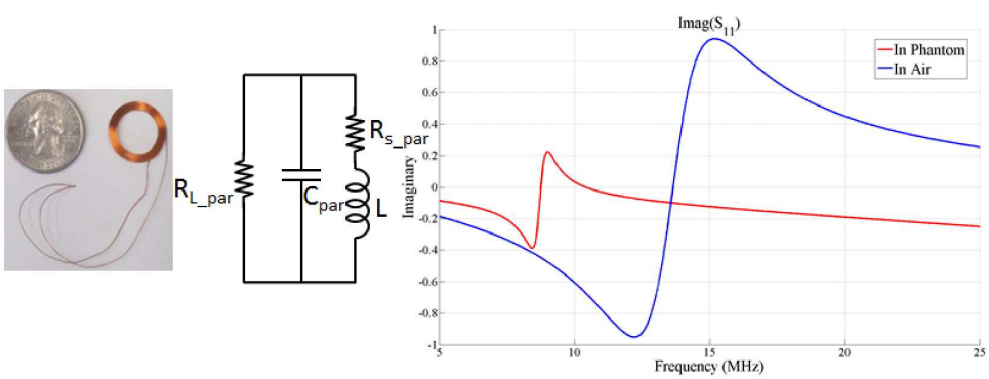

(a) (b) (c)

Figure 1: (a) The receive coil used for implantation. (b) Equivalent circuit model for implanted coils. (c) Plots showing difference in Input impedance of coils in air vs. in phantom (saline).

REFERENCES

1. Waters, B. H., A. P. Sample, P. Bonde, and J. R. Smith, "Powering a ventricular assist device (VAD) with the free-range resonant electrical energy delivery (FREE-D) system," *Proceedings of the IEEE*, Vol. 100, No. 1, 138–149, Jan. 2012.
2. Sample, A. P., D. Meyer, and J. R. Smith, "Analysis, experimental results, and range adaptation of magnetically coupled resonators for wireless power transfer," *IEEE Transactions on Industrial Electronics*, Vol. 58, No. 2, 544–554, Feb. 2011.
3. Gabriely, S., R. W. Lau, and C. Gabriel, "The dielectric properties of biological tissues: II. Measurements in the frequency range 10 Hz to 20 GHz," *Physics in Medicine and Biology*, Vol. 41, No. 11, 222512269, 1996.

Distributed Resonant Coil Systems for Efficient Wireless Power Transfer in Mobile Systems

M. J. Chabalko[1, 2] and D. S. Ricketts[1, 2]

[1]Carnegie Mellon University, Pittsburgh, USA
[2]North Carolina State University, Raleigh, North Carolina

Abstract— The efficacy of wireless power transfer at near and mid-range has been well established in recent years, in particular through the use of resonance for improved impedance matching at longer distances [1, 2]. Most systems examined, however, have been fixed or nearly fixed systems where the WPT problem is well defined over all time. In this paper, we present an analysis of WPT for mid- and far range applications where the source and load move over multiple coil diameters over time. Such systems create a significant challenge as the optimal impedance matching condition changes dramatically with the physical translation of the source/receiver [3]. Moreover, the movement of the receiver from the source by several coil diameters requires additional consideration to achieve high efficiencies. For example, the receiver may be moved far enough away that it no longer significantly overlaps the sources magnetic field, and the coupling becomes effectively zero, reducing WPT efficiency [4]. We will present experimental results from a system of coils where the load is laterally displaced by several coil diameters. We compare and contrast the standard two-coil resonant WPT system with several alternatives: a driven four two-coil repeater system, a driven two two-coil repeater system, and a passive two tow-coil repeater system. We show that high continuous WPT efficiency ($> 75\%$) can be achieved over large translation distances using these systems by using several compensation methods. We also compare and contrast the trade-offs and advantages of each approach.

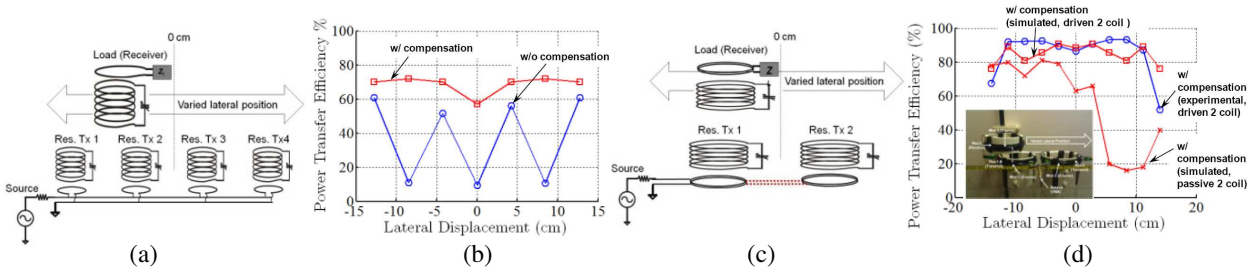

Figure 1: (a) Diagram of the driven four two-coil system. (b) Power transfer efficiency versus lateral displacement of the load with and without compensation. (c) Diagram of both the driven two two-coil system, as well as the passive two two-coil system. The connection indicated by the red dotted lines indicates the configuration for the driven two two-coil system, and the passive two two-coil system is represented by the same diagram, but *without* completing the connection of the dotted red lines. (d) Power transfer efficiency versus lateral displacement of the load (receiver) coil. All results (both simulated and experimental) show the efficiency possible *with* compensation. However note that the passive two-two coil system performs more poorly over the largest separations between source and receiver. The inset shows a photograph of the experimental setup used to measure the efficiency vs. lateral displacement.

REFERENCES

1. Kurs, A., A. Karalis, R. Moffatt, J. D. Joannopoulos, P. Fisher, and M. Soljačić, "Wireless power transfer via strongly coupled magnetic resonances," *Science*, Vol. 317, No. 5834, 83–86, 2007.
2. Ricketts, D. S., M. J. Chabalko, and A. Hillenius, "Experimental demonstration of the equivalence of inductive and strongly coupled magnetic resonance wireless power transfer," *Appl. Phys. Lett.*, Vol. 102, No. 5, 053904–053904, 2013.
3. Ricketts, D. and M. Chabalko, "On the efficient wireless power transfer in resonant multi-receiver systems," *Proceedings of IEEE International Symposium on Circuits and Systems (ISCAS)*, Beijing, China, 2013.
4. Sample, A. P., D. A. Meyer, and J. R. Smith, "Analysis, experimental results, and range adaptation of magnetically coupled resonators for wireless power transfer," *IEEE Trans. Ind. Electron.*, Vol. 58, No. 2, 544–554, 2011.

Q-factor Improvement in Planar RF Inductors by the Use of Ferrite Compensators

Mikhail Makurin[1], **Nikolay Olyunin**[1], **Ki Young Kim**[2], **Keum-Su Song**[2], **and Vladimir Parfenyev**[3]

[1]Samsung R & D Institute Russia, Russia
[2]Future IT Research Center, Samsung Advanced Institute of Technology, Yongin 446-712, Korea
[3]Moscow Institute of Physics and Technology, Russia

Abstract— A method for increasing the Q-factor of planar RF inductors via redistribution of the current density by the use of ferrite material is proposed. According to numerical simulations, the Q-factor increases twice mainly due to the decrease of the ohmic resistance.

The ohmic resistance R of a planar RF inductor is defined mostly by skin and proximity effects (if ferrite material is not used). These effects lead to the concentration of the electric current mainly at the edges of the metal surface, therefore reducing the effective cross-section of the conductor and increasing the ohmic resistance. For reducing the ohmic losses in planar inductors we propose a method based on the use of ferrite material, which is easy to implement.

The method is based on the idea for improvement of the current distribution in a strip-shaped conductor which was proposed in [1]. The essence of the idea is the use of ferrite material near the edge of the strip. Without ferrite, edge current peaks are due to high value of magnetic field component normal to the coil plane near the edge. In presence of ferrite its magnetization provides additional magnetic field. Therefore similar magnetic field near the edge is produced by lower current density near inductor edge. Thus presence of high permeability ferrite changes current density distribution and reduces the ohmic resistance.

The aforementioned idea may be used as well in the case of planar spiral-shaped inductors. The presence of ferrite material near the inner and outer edges of the inductor and further optimization of the width of the turns allows significantly reduce the ohmic resistance of the inductor. This was confirmed in simulation and in experiment.

REFERENCES

1. Kutkut, N. H., D. W. Novotny, D. M. Divan, and E. Yeow, "Analysis of winding losses in high frequency foil wound inductors," *Conference Record of the 1995 IEEE Industry Applications Conference 30th IAS Annual Meeting*, 859–867, October 1985.

Obstacle Detection Method Using Array Antenna for Coupled-resonant Wireless Power Transfer

H. Yamada, K. Miwa, H. Hirayama, N. Kikuma, and K. Sakakibara
Department of Computer Science and Engineering, Nagoya Institute of Technology, Japan

Abstract—

Introduction: Coupled resonant wireless power transfer (WPT) is expected to release power cables from electrical appliances [1]. Since the WPT system handles power of kW order, it is necessary to detect intruded obstacles between transmitting and receiving coils. In this report, we propose a method of detecting intrusion of obstacles by using array antennas for WPT. We verified the feasibility of the proposed method by numerical simulation.

Consideration model is shown in Fig. 1. Element antennas consist of square-shaped two-turn loop coils. The coil is made of copper wire with 1 mm radius thick. TX and RX array antennas consist of four element antennas. At the terminal of the transmitting coils (port1 $\sim$ 4), voltage sources (1 V, 50 Ω) and tuning capacitor of 38.8 pF are connected in series. At the terminals of the receiving coils (port5 $\sim$ 8), 50 Ω load and tuning capacitor are connected in series. The capacitance of the tuning capacitors is determined to resonate at 13.56 MHz for each element antenna. A drink can made of aluminum is modeled for an obstacle with 12.22 cm high and 3.3 cm radius. Standard deviation (SD) of S-parameters between facing antennas (S_{15}, S_{26}, S_{37}, S_{48}) is employed as an index of detection.

First, we analyzed distance characteristics of SD by using method of moments. Position of the obstacle is on the center of the TX1, as shown in Fig. 1. The distance h between the transmitting coils and receiving coils is varied from 6 cm to 20 cm. Fig. 2 shows SD with and without obstacle. It is shown that obstacle detection is possible by setting threshold at -79 dB, which is maximum level of SD without obstacle.

Second, we analyzed effect of position of the obstacle on the SD, shown in Fig. 3. Position of the obstacle is swept within the square region (-30 cm $\leqq (x, y) \leqq 30$ cm). The distance between the transmitting coils and receiving coils is set to 14 cm. It is shown that detection of existence of an obstacleis possibleover the entire regionby settingthreshold at -79 dB exceptthe center.

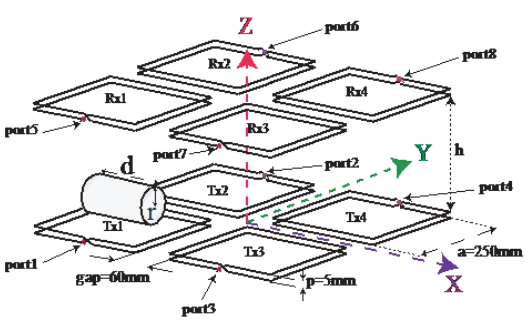

Figure 1: Consideration model.

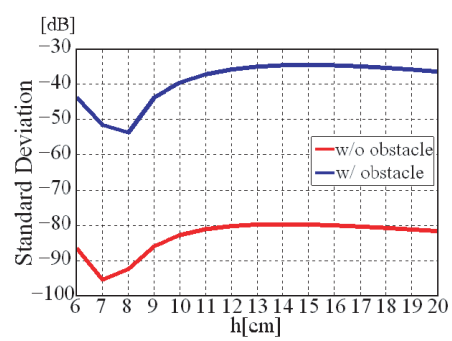

Figure 2: Distance characteristics of standard deviation.

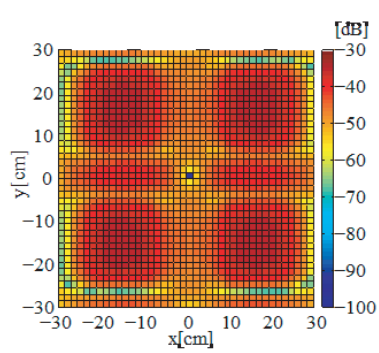

Figure 3: Effect of position of obstacle.

In conclusion, we proposed a detection method of intrusion of obstacle for coupled-resonant wireless power transfer by using standard deviation of S-parameters.

REFERENCES

1. Kurs, A., et al., "Efficient wireless non-radiative mid-range energy transfer," *Annals of Physics*, Vol. 323, 34–48, Apr. 2007.

Superconducting-ferromagnetic Shell for Magnetic Energy Harvesting and Transmission at a Distance

Jordi Prat-Camps, **Carles Navau**, **and Alvaro Sanchez**
Departament de Física, Universitat Autònoma de Barcelona
08193 Bellaterra, Barcelona, Catalonia, Spain

Abstract— We introduce a magnetic shell that allows to concentrate and distribute static magnetic fields with high efficiency and exibility, based on transformation optics technique [1]. The device consists of shell made of a material with a homogeneous and anisotropic magnetic permeability value. Analytical expressions for the field in all regions of space can be obtained when a external field is applied and also when a field source is placed in the interior hole. In the former case it is shown that the shell concentrates the field (and the magnetic energy) in the hole, while in the later field is expelled towards the exterior. The combination of these features allows to demonstrate that magnetic concentrating shells could be used to transfer the magnetic energy from a source to a given distant point or to increase the coupling between magnetic field sources separated by empty space, which could have relevance to wireless power transmission.

This ideal magnetic concentrating shell requires materials with extreme anisotropic permeability components and actual materials with such properties do not exist. Nevertheless a very good approximation consisting of an alternation of homogenoeus superconducting (SC) and ferromagnetic (FM) wedges (or even rectangular prisms) demonstrates an effective behavior very similar to the ideal one. The concentrating capabilities of the discretized version of the shell are studied as a function of the number of pieces and the applied field [2].

Finally, although the SC and the FM parts building an approximate concentrator are feasible (even commercially available), in some situations the use of SC can be unpractical as they require low temperatures. For this reason alternative proposals are being explored, seeking less exact but more practical configurations.

REFERENCES

1. Navau, C., J. Prat-Camps, and A. Sanchez, "Magnetic energy harvesting and concentration at a distance by transformation optics," *Phys. Rev. Lett.*, Vol. 109, 263903, 2012.
2. Prat-Camps, J., A. Sanchez, and C. Navau, "Superconductor-ferromagnetic metamaterials for magnetic cloaking and concentration," To be published in *Supercond. Sci. Tech.*, 2013.

Session 4A5
SC5: High Resolution Imaging with Penetrating Radar Scanners for Detection of Small or Low Contrast Objects

Ultrawideband Radar Future Directions and Benefits
James D. Taylor, ... 1376
Advances in Imaging of Archaeological Structures Using GPR
Salvatore Piro, D. Goodman, ... 1377
High Resolution Imaging with a Holographic Radar Mounted on a Robotic Scanner
Lorenzo Capineri, I. Arezzini, M. Calzolai, Colin G. Windsor, Masaharu Inagaki, Tim Bechtel, Sergey I. Ivashov, ... 1378
Analytical Approach for RASCAN Radar Images of Dinosaur Footprints through Basic Experiments
Masaharu Inagaki, Timothy D. Bechtel, Lorenzo Capineri, Sergey I. Ivashov, Colin G. Windsor, .. 1379
Bringing up the Bodies: High Resolution and Target Definition Using GPR
Erica Utsi, ... 1380
A GPR Study of Parabolic Dune Stratification, White Sands New Mexico
Mark Domaracki, Douglas J. Jerolmack, Tim Bechtel, ... 1381
Concrete Imaging without Information of Incident Field
Toshiyuki Tanaka, Toshifumi Moriyama, Takashi Takenaka, ... 1382
A Novel Method for Developing Receiver Operating Characteristic Curves for Target Discrimination by Penetrating Radar
Timothy D. Bechtel, Lorenzo Capineri, Colin G. Windsor, Masaharu Inagaki, Sergey I. Ivashov, .. 1383
A Real Scale Validator for a High Resolution 3D Imaging GPR Using Geometrical Surface Reconstruction
Mario Duran, Pedro Ramaciotti, Ricardo Hein, ... 1384
An Experimental Study of Through-the-Wall Radar for Lifesign Detection
Betul Yilmaz, Sevket Demirci, Enes Yigit, Caner Ozdemir, ... 1385
QPSK Mapped OFDM Signal Processing on Radar Applications
Arsen A. Hakhoumian, Kh. Tovmasyan, Tigran Zakaryan, ... 1387

Ultrawideband Radar Future Directions and Benefits

James D. Taylor
148 Breezy Bay Drive, Ponte Vedra, FL 32081, USA

Abstract— Practical applications and benefits can determine future ultrawideband (UWB) radar development objectives. Application driven research could produce UWB radar techniques to detect and identify small, low contrast objects from their shape, composition and other characteristics. Tangible benefits could include applications for medical imaging which can give small clinics the capabilities of large hospital.

UWB radar nonsinusoidal signals change waveform and spectrum on transmission, target interaction and reception. Predicting and modeling the waveform changes and return signal spectra could provide the basis for increased detection sensitivity and promote medical, nondestructive testing and other practical applications. Barrett describes this concept in *Resonance and Aspect Matched Adaptive Radar (RAMAR)*.

Previous experimental work shows the possibilities for exploiting side and forward scattered signals as a way to detect objects which have small backscatter due to geometry (size and shape) and a low medium index of refraction contrast. Potential applications include ways to detect small biological tumors, plastic mines, defects in structures or parts in medicine, manufacturing control and materials penetrating imaging. A combination of radar and tomographic approaches could increase the possibilities a small target detection and identification.

These objectives can help UWB medical radar technology provide imaging services only found in hospitals with CT scanners, MRI and X-rays. This can provide a way to image and detect objects in living tissue and identify them as benign or dangerous. A combination of radar and tomographic techniques could provide these possibilities. Continued progress in understanding the theory of UWB back, side and forward scattering could produce a UWB radar based scanner for diagnosis in small clinics and remote areas. It could help emergency medical technicians to detect serious internal injuries quickly.

REFERENCES

1. Taylor, J. D., *Ultrawideband Radar Applications and Design*, CRC Press, Boca Raton, FL, USA, 2012.
2. Barrett, T., *Resonance and Aspect Matched Adaptive Radar (RAMAR)*, World Scientific Publishing, 2012.

Advances in Imaging of Archaeological Structures Using GPR

S. Piro[1] and D. Goodman[2]

[1]ITABC, CNR, P. O. Box 10, Monterotondo Sc., Roma 00015, Italy
[2]Geophysical Archaeometry Laboratory, LA, CA, USA

Abstract— For most archaeological prospections with GPR, detection is the most important aspect of the surveys. If enough density of profiles is recorded across a site, structural information can also be obtained regarding the buried features. Shallow and narrow features may require a very fine line density to get detected. If the profile spacing is large, shallow areas can have no microwaves penetrating the region. At greater penetration depths however, the unsampled region decreases. If small targets are buried close to the ground surface, detection of these features may require a finer line spacing then objects which are buried slightly deeper and within the penetration depth of the antenna.

The smallest detectable size of archaeological materials is in general dependent on the frequency of the transmitting antenna. Smaller antennas can resolve smaller objects better than larger lower frequency antennas. Large antenna can detect very small objects, although the significance of the reflections from those small objects may not be realized by the naked eye on a single radargram profile. These reflections may be so minute that the changes may not be easily visualized. For instance, imaging a buried archaeological debris field, perhaps containing higher concentrations of small fragments of ancient habitation, e.g., flint chips or other materials, may show some scattered energies on the radargrams which may only be one or two digital values different then in areas where no debris are located. Unless a fortunate color transform is used, it is unlikely that these small reflections will ever be noticed within the radargram — vertical slice — dataset.

An alternative method for presenting GPR data from archaeological sites is needed to show these minute changes. Rather than showing the changes in reflected energies along the vertical — radargram — slices of the ground, it is more useful to map horizontal changes of reflected energy across a site. In this case small, but consistent reflections above the background noise can be visualized by using time slice analysis.

There are a variety of imaging and analyses that must be implemented to solve the multitude of subsurface conditions in the archaeological field survey. Among a few of the necessary imaging techniques and analysis to be briefly introduced in this presentation: Time slices, Isosurface rendering and Overlay Analysis.

GPR Case Histories at several important archaeological sites are presented and discussed. The results show some very successful studies with radar to remotely sense and define subsurface archaeology — and all without excavation!

High Resolution Imaging with a Holographic Radar Mounted on a Robotic Scanner

L. Capineri[1], I. Arezzini[1], M. Calzolai[1], C. Windsor[2], M. Inagaki[3], T. Bechtel[4], and S. Ivashov[5]

[1]Department of Information Engineering, University of Florence, Florence 50139, Italy
[2]116 New Road, East Hagbourne, OX11 9LD, UK
[3]Walnut Ltd., 1-19-13, Saiwaicho, Tachikawa, Tokyo 190-0002, Japan
[4]Department of Earth and Environment, Franklin & Marshall College, Lancaster, PA, USA
[5]Remote Sensing Laboratory, Bauman Moscow State Technical University, Moscow, Russia

Abstract— The holographic radar of Rascan 4/4000 type has been demonstrated as a useful instrument for producing images of high spatial resolution from sub-surface dielectric constant discontinuities [1]. The comparison of the incident monocromatic field and the reflected field from a buried shallow object is the basic principle of the holography that in this case is implemented at 4 GHz microwave frequencies. The measured phase variations between incident and received field at different locations on the surface create a sinusoidal modulated baseband signal that can be used to produce gray scale images. From the electromagnetic viewpoint these images are not complete holograms because only the phase variation of the received field is measured while the amplitude information is neglected. However the images have a spatial resolution that is about a $\lambda/4$, where λ is the wavelength in the investigated material at the emitted holographic frequency f_i [2]. Generally the holographic radar transmits and receives signals at discrete frequencies in order to avoid null responses for phase values that null the sinusoidal function. The standard methods to scan a surface is the manual scan that is also used for high frequency subsurface GPR: this method is rather time consuming task as the experiments need a spatially referenced grid alomg which the antenna head is moved along manually. Generally this line grid is implemented on a thin dielectric mat (Plexiglas, rubber or paper). The latter accessory are certainly useful but their use is limited to areas of investigation of rather small size (typically less than 1 square meter) and require a skilled and concentrated operator to avoid uncertainty in the manual movement of the antenna head. Larger surfaces of several square meters are difficult to scan manually with accuracy and require a long time to set-up the reference system. A different approach to this limitation is the development of a robotic scanner where the holographic radar head is moved automatically with high spatial accuracy (better than 1 mm) guaranteed by the optical enconder of the mechanical movements. An area is covered by the composition of a lateral fast (50 cm/s) movement and the advancement slow (2–5 mm/s) motion by two wheels connected to DC motors. This approach is particularly suitable for the compact and light weigh (400 gr) holographic radar 4 GHz head that as to be moved mechanically. In this way the robot scanner can spatially oversample the reflected field and produce averaged low noise images of subsurface objects with the operator that can remotely control the area to be investigated. Examples of this approach will be given for the detection of low dielectric contrast objects like plastic landmines, for rapid scan of infrastructures floors after a natural disaster or for searching dinosaur's tracks in rocks for archeological or paleontological site. Moreover for these applications a light-weight robotic scanner (less than 6 kg) is suitable to avoid loading the surface with the weight of a human operator.

REFERENCES

1. Ivashov, S. I., V. V. Razevig, I. A. Vasiliev, A. V. Zhuravlev, T. D. Bechtel, and L. Capineri, "Holographic subsurface radar of RASCAN type: Development and applications," *IEEE Journal of Selected Topics in Earth Observations and Remote Sensing*, Vol. 4, No. 4, 763–778, December 2011.
2. Ivashov, S. I., L. Capineri, and T. D. Bechtel, "Holographic subsurface radar technology and applications," *UWB Radar: Applications and Design*, 421–444, James J. Taylor, Ed., CRC Press, Taylor & Francis Group, 2012, ISBN 978-1-4200-8986-8.

Analytical Approach for RASCAN Radar Images of Dinosaur Footprints through Basic Experiments

M. Inagaki[1], **T. Bechtel**[2], **L. Capineri**[3], **S. Ivashov**[4], **and C. Windsor**[5]

[1]Walnut Ltd., 1-19-13, Saiwaicho, Tachikawa, Tokyo 190-0002, Japan
[2]Department of Earth and Environment, Franklin & Marshal College, Lancaster, PA, USA
[3]Department of Information Engineering, University of Florence, Florence 50139, Italy
[4]Remote Sensing Laboratory, Bauman Moscow State Technical University, Moscow, Russia
[5]116, New Road, East Hagbourne, OX11 9LD, UK

Abstract— Over very long geological time bones of creatures change to fossils. A dinosaur footprint, which is not the creature itself, but a mold of the creature, is also found as a "trace" fossil. Although no obvious indication appears on the ground surface, a part of the footprint may suddenly be unveiled by even a small blow of a hammer. But the forthcoming work to disclose the whole part takes very long tedious time. The existence of a footprint fossil indicates that some discontinuity occurred at the footprint plane during sedimentation. Soil properties like density might be different in upper and lower part of the footprint plane. Some impurities (such as a clay film) or a very thin air gap might exist at the plane.

Rascan holographic radar reveals the plan shape of buried objects. Its remarkable feature is that concealment of targets by the surface reflection is not a limit as it is for pulse radar. That allows recording of clear shape images of shallow buried objects.

At first, the ability to image very small differences in permittivity was verified. A few lumps of hardened loam soil were buried in powdered loam soil bed. The lumps were made by leaving fully water saturated loam soil for four years, then drying. The powdered loam soil was made by smashing the dried clumps. Rascan holographic radar was scanned over the test bed, and very weak but recognizable reflections showed the existence of the clumps in the radar image. Thus, despite the identical mineralogy, moisture content, and grain size distribution, the textural difference alone may create a difference in permittivity.

In another experiment, holographic radar was scanned over base materials in which a thin layer of impurity material was put. Rubber plates and vinyl chloride plates were used as base materials. Paper and air gaps were used as the inserted thin layer. The scan test showed that the thin layer was significantly identical until minimum 1 mm thin layer for the high contrast combination, rubber plates and air gap. This shows that a thin film of impurity material may develop recognizable reflection.

Finally blind tests were performed for mock and real samples of dinosaur footprints. Artificial footprints were carved on hardened loam soil bed and dried. The test bed was covered with powdered dry loam soil. Holographic radar scan acquired very weak but recognizable reflection from the footprint. But the shape was not so obvious. Replacing the loam soil by sand (perhaps increasing the permittivity contrast), the shape of toes became recognizable. A real dinosaur footprint was used to prepare a cast and mold in carbonate material with a microscopic air gap between cast them. The radar image has no recognizable pattern. However, when the air gap was replaced by very thin clay layer, the shape of the toes became recognizable.

These experiments show that to recognize a dinosaur footprint by radar, only a very subtle or very thin (but stronger) permittivity contrast at the fossil layer is required. Rascan holographic radar has the advantage of making clearer shallow images than impulse pulse radar, because of little influence from surface reflection.

Bringing up the Bodies: High Resolution and Target Definition Using GPR

Erica Utsi
Utsi Electronics Ltd., UK

Abstract— Ground Penetrating Radar (GPR) is an extremely useful non-destructive testing (NDT) and detection technique applied in many different spheres of activity from the common ones of utility detection, concrete investigation, road monitoring and archaeology to the more rarely used ability for forensic and security investigations. Target detection and imaging are inter-related both in terms of the frequency of antenna used and the survey parameters applied. Even for strong reflectors, the density of data collected can make a significant difference to identification, particularly where this is based on pattern recognition.

The definition capability of a 4 GHz antenna used primarily in structural investigations is described. Taking as an example, the two graves discovered beneath the floor of the Cosmati Pavement in front of the High Altar of Westminster Abbey, this paper examines the evidence for extant skeletal remains in GPR data generated using a 4 GHz antenna. These results are then compared with results from a more traditional lower frequency antenna (400 MHz) used for the detection of graves within the Abbey (including the two beneath the mosaic pavement), in forensic searches for missing persons believed to have been buried in open ground and in the archaeological investigation of an area known to contain mediaeval graves. Although faunal remains have been found in such searches, the recognition of weak reflectors such as human remains more often relies upon the recognition of associated material rather than the signals returned by the bodies themselves. The reasons for this are briefly discussed.

The potential effect of increasing data density is discussed with particular reference to the data (4 GHz and 400 MHz) from Westminster Abbey and suggestions made as to how the effect of more intensive survey might assist in the identification of buried human remains, whether in a legitimate grave or not.

A GPR Study of Parabolic Dune Stratification, White Sands New Mexico

M. Domaracki[1], **D. Jerolmack**[1], **and T. Bechtel**[2]

[1]Department of Earth and Environmental Science, University of Pennsylvania, Philadelphia, PA, USA
[2]Department of Earth and Environment, Franklin & Marshall College, Lancaster, PA, USA

Abstract— In an effort to decipher poorly understood depositional and erosional processes that control parabolic dune migration in White Sands National Monument (New Mexico, USA), GPR transects parallel and perpendicular to dune migration direction were recorded using a GSSI SIR3000 impulse radar system with a 400 MHz transducer in survey wheel mode. Transects were recorded for a typical dune, as well as a miniature parabolic dune. Post processing included background removal, topographic correction and raypath correction, as well as a time varying gain adjustment to highlight subtle features. GPR calibration was completed for gypsum sand above the water table by burying a marker to a depth of 30 cm and identifying the marker at depth during initial scanning. Post processing reveals a water table reflection that mimics dune topography with amplitude variations corresponding to salinity changes. Above the water table, subtle dipping reflectors indicate forset bedding and previous dune surfaces that have been buried during dune migration. Since the dune is composed of mineralogically and texturally homogeneous (or nearly so) grains, the presence of permittivity contrasts above the water table is somewhat unexpected, and their source(s) have not been determined definitively. Possible reasons for permittivity contrasts that highlight the internal dune structure may include salt ridges formed at the capillary fringe, microbial/organic mats, and grain flow deposition (creating subtle textural variations). Undulating subsurface features reflect the deeper vadoseaeolian system close to the water table. Determining an in-situ signature of depositional features using GPR ground-truthed with limited test pitting may reveal, with minimal disturbance, more about historical processes and migration of dunes in this unique erosional/depositional environment and ecosystem.

Concrete Imaging without Information of Incident Field

Toshiyuki Tanaka, **Toshifumi Moriyama**, **and Takashi Takenaka**
Graduate School of Engineering, Nagasaki University, Nagasaki 852-8521, Japan

Abstract— Maintenance and management of concrete structures are important to prevent serious accidents. Among a variety of diagnostic approaches ground penetrating radar (GPR) is a non-destructive diagnosis technique for inspection without affecting the current state or any damage to the existing structures. GPR emits an electromagnetic pulse which is radiated into a concrete structure and part of the wave is reflected by reinforcing-bars and defects such as voids in the structure. GPR processes the reflected data to detect or locate them. The use of a tomographic technique for GPR is expected to give more information of the concrete structure than radar-based techniques, e.g., a size of a reinforcing-bar and, the shape and dielectric parameter of defects. Inverse scattering analyses which are the basis of microwave tomography usually assume the knowledge of incident fields. The field radiating from a transmitting antenna of GPR just above a concrete surface is different from the field of GPR located far from the concrete structure since the antenna characteristics are changed due to interaction between the antenna and the structure, so that it is difficult to know accurately the incident field penetrating into the concrete structure.

In this paper, imaging of a concrete structure without information of incident field is discussed. An inverse scattering approach based on the field equivalence principle [1] is extended to apply for reconstruction of spatial profiles of electric parameters (relative permittivity and conductivity) in the concrete structure. If a measurement surface is closed, a problem equivalent to the original scattering problem for the interior region enclosed by the measurement surface can be set up. In the case of concrete evaluation, however, it is impossible to measure the fields on a whole closed surface. Usually transmitting and receiving antennas are limited to one side of a concrete structure. Since a pulsed incident wave does not reach the place far enough from the wave source in a finite observation time, it is not necessary for the measurement surface to be a closed surface. Equivalent surface currents in the equivalent problem are determined by the tangential component of the electric and the magnetic fields on the measurement surface. These equivalent surface currents generate the same electromagnetic field in the region below the measurement surface as does the original incident pulse and yield a null field in the region above the measurement surface. Note that the equivalence holds only when the original source in the region above the measurement surface is removed while the original scatterers remain below the surface. If the original scatterers are replaced by different objects, then there appear non-zero electromagnetic fields in the region above the measurement surface. This allow us to formulate the inverse scattering problem as a minimization problem with a cost function consisting of a magnitude of electromagnetic fields in the region above the measurement surface. Numerical simulations of a reinforcing-bar or a cavity investigation in the concrete structure from only total field data measured on the observation surface are performed in order to show the effectiveness of the proposed inversion method.

REFERENCES

1. Takenaka, T. and T. Moriyama, "Inverse scattering approach based on the field equivalence principle: Inversion without a priori information on incident fields," *Optics Letters*, Vol. 37, 3432–3434, August 2012.

A Novel Method for Developing Receiver Operating Characteristic Curves for Target Discrimination by Penetrating Radar

T. Bechtel[1], **L. Capineri**[2], **C. Windsor**[3], **M. Inagaki**[4], **and S. Ivashov**[5]

[1]Department of Earth and Environment, Franklin & Marshall College, Lancaster, PA, USA
[2]Department of Information Engineering, University of Florence, Florence 50139, Italy
[3]116, New Road, East Hagbourne, OX11 9LD, UK
[4]Walnut Ltd., 1-19-13, Saiwaicho, Tachikawa, Tokyo 190-0002, Japan
[5]Remote Sensing Laboratory, Bauman Moscow State Technical University, Moscow, Russia

Abstract— In some applications, e.g., de-mining or UXO clearance, discrimination of difficult targets is equal in importance to simple detection. That is, classification of unseen subsurface targets into bins such as "mine" versus "clutter" is critical, as is statistical evaluation of the accuracy of such classification using receiver operating characteristic (ROC) curves. For radar systems with automated target recognition that involves some threshold parameter, this is easily accomplished by plotting the detection rate versus the false alarm rate across a range of threshold values. However, for simple imaging systems where interpretation is done visually by the operator, there is no distinct threshold parameter. Instead, the operator makes a "judgment call" based on some level of training and experience. We propose that for visual interpretation of radargrams, differences in judgment between different operators can provide a proxy for a variable threshold parameter. To test this, we recorded numerous images of a 1.5 meter square test bed containing plastic antipersonnel mine casings (filled with granulated sugar having dielectric constant very close to plastique explosive), and clutter items (including crushed cans, nails, rocks, bits of wire, etc.). Each image contained between zero and three mines, and three to seven clutter items. University students with no prior training in mine or UXO recognition where given 15 minutes of instruction on radar imaging and interpretation, and shown a single "teaching scan" portraying just the buried mines. They were then shown the unseen radargrams and asked to identify the mines hidden amongst the clutter. Each student completed this on their own with no consultation, and no possibility to ask questions. The detection and false alarm rate for each test subject across all of the images yielded a single point on an ROC curve. The full test was completed for one group of students, and the ROC curve developed. In addition, the false alarm rate for each clutter item was determined individually. Based on this, it appeared that the rock clutter item was the most frequent false alarm. For a second round of testing with a new group of students, new images were added to the testing set to raise the percentage of rocks as clutter items from 18 to 42 percent. As expected, this slightly changed the shape of the ROC curve, with the area under the curve (a single-parameter measure of the effectiveness of the receiver) being reduced by 21 percent. Additional testing with varying percentages of rocks as clutter items, as well as differing soil surface roughnesses and moisture contents are underway to further quantify not only the effectiveness of this type of scanning, but also this method for receiver assessment. We propose that this method would be useful for validating the performance of simple detection and discrimination systems of any kind that are designed to be used by minimally-trained lay people such as de-miners recruited from within mined communities.

A Real Scale Validator for a High Resolution 3D Imaging GPR Using Geometrical Surface Reconstruction

M. Duran[1], **P. Ramaciotti**[1], **and R. Hein**[2]

[1]Departamento de Ingeniería de Minería, Escuela de Ingeniería
Pontificia Universidad Católica de Chile, Santiago, Chile
[2]Ingenieros Matemáticos Consultores Asociados S.A., INGMAT, Santiago, Chile

Abstract— This article describes the implementation and the results obtained by a validator of a High Resolution 3D imaging ground penetrating radar (GPR) technology using geometrical reconstruction of the surface that separates the image domain from the radar device. This approach uses synthetic aperture radar techniques to scan a large area of underground terrain and lidar measurements to reconstruct the geometrical features of the surface. The surface's geometrical information is then used to resolve buried reflector targets by phase coherence over the synthetic radar data. Different case studies using a real scale validator are presented and discussed, in particular in relation to the system capability for resolving reflecting targets placed next to larger reflectors and performance in other geometrically complex environments.

An Experimental Study of Through-the-Wall Radar for Lifesign Detection

Betul Yilmaz[1], **Sevket Demirci**[1], **Enes Yigit**[2], **and Caner Ozdemir**[1]

[1]Department of Electrical-Electronics Engineering, Mersin University, Mersin, Turkey
[2]Vocational School of Technical Sciences, Mersin University, Mersin, Turkey

Abstract— Through-the-Wall Radar (TWR) is an emerging technology which is very useful for detecting and identifying unknown objects behind the walls. It can be used indifferent applications ranging from survivor detection in rescue or hostage operations to people localization in anti-terrorist operations [1]. Recently, microwave Doppler radars were developed for remote sensing of heartbeat and breathing [2]. Both heartbeat and breathing motions cause changes in frequency, phase, amplitude and arrival time of returned signal from a living human-body. These responses; however, may attenuate drastically due to the thickness and the electrical properties of the wall material. Therefore; getting a successful radar detection of heartbeat or breathing is usually considered to be a challenging task. In this study, we have exploited a stepped frequency continuous wave radar system that has a very large fractional bandwidth (50%). In the experiments, we have utilized a monostatic configuration in front of the concrete wall that has a thickness of 30 cm. A 26 year old man stood still just behind the wall. As a sensor, a C-band pyramidal horn antenna was used while the frequency of the vector network analyzer has varied from of to GHz for 201 linearly stepped points. In the first experiment, the response from a normally breathing man has collected over a period of 20 seconds while the man was standing still. It is well known that the movement of a persons' chest causes varying radar returns with different back-scattering amplitudes. To be able to plot this change in the environment, differential range profile was gathered by subtracting the previous one from the next one. This change detection operation produced the radar images in Fig. 1. This time-varying differential range-profiles of the breathing man are then consecutively displayed to have a two-dimensional (2D) image as plotted in Fig. 1(a). The changes around the 30 cm range distance can be easily detected for all time instants in the image. In Fig. 1(b), the response at 30 cm range is drawn with respect to -the observed time interval. A total of 7 inhaling (for the 16 seconds period) were detected using the figure that is consistent with nominal breathing values of a healthy human. In the second experiment, heartbeat detection has been studied. For this purpose, the person stood still just behind the wall holding his breath for a period of 16 seconds. The experimental set-up and the parameters were kept the same. The resulting radar images are given in Fig. 2. Since the person was not breathing and his chest was not moving, the only change in the scene was his beating heart. The resultant time-varying range-profiles that have weaker reflection when compared to breathing experiment are shown in Fig. 2(a) as a 2D radar image. Again, changes around 30 cm range distance are distinguishable in the image around −50 dB amplitude level. Plotting the response at 30 cm range distance with respect to the observed time interval produces Fig. 2(b). In this figure, the peaks corresponds the heartbeats ofthe person. We have counted a total of 17 peaks that corresponds to 64 pulses/min. This result is again consistent with nominal values of 60 to 80 beats/min for a healthy man.

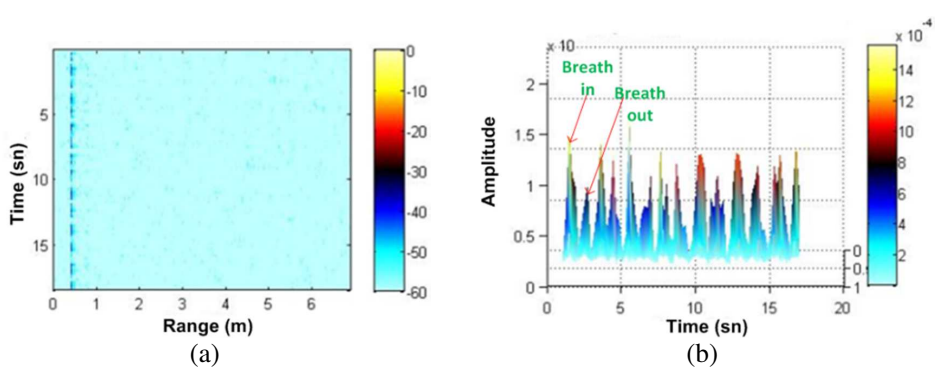

Figure 1: Radar images for breathing person: (a) 2D image constructed by consecutively displaying the differential range-profiles, (b) slice of the resulted image that corresponds to the 30 cm range.

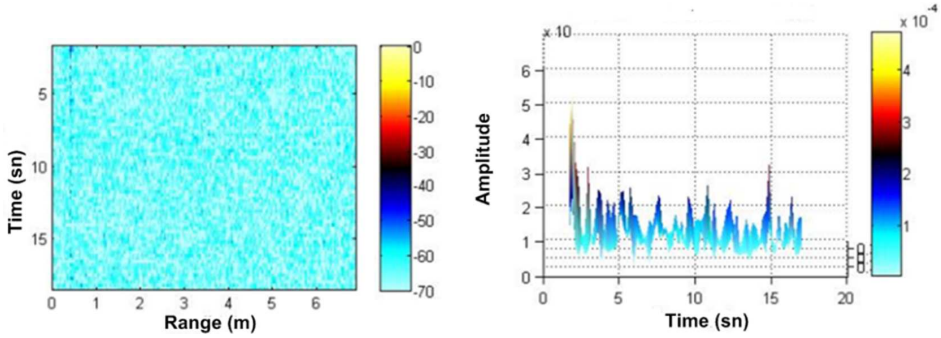

(a) (b)

Figure 2: Radar images for heartbeat: (a) 2D image constructed by consecutively displaying the differential range-profiles, (b) slice of the resulted image that corresponds to the 30 cm range.

REFERENCES

1. Ferris, D. D. and N. C. Currie, "A survey of current technologies for through-the-wall surveillance (TWS)," *Proc. SPIE*, Vol. 3577, 62–72, 1998.
2. Chuang, H. R., Y. Chen, and K. M. Chen, "Automatic clutter canceller for microwave life detection systems," *IEEE Trans. on Instrument. and Measurement*, Vol. 40, 747–750, 1991.

QPSK Mapped OFDM Signal Processing on Radar Applications

A. Hakhoumian, **Kh. Tovmasyan**, **and T. Zakaryan**
Institute of Radiophysics and Electronics, Armenian National Academy of Sciences
Alikhanian st. 1, Ashtarak 0203, Armenia

Abstract— OFDM (Orthogonal Frequency Division Multiplexing) signals have been widely used in communication systems. Recently they have also intensively studied for radar applications. Two major features of OFDM signals which make it suitable in radar applications, are simultaneous long duration and wide spectrum of the same signal. The first one, signal long duration helps to determine Doppler shift very accurately. On the other hand, wide spectrum of the signal gives an opportunity to find a time shift of the received echo signal. Knowing these two values we can decide the velocity of the target and its distance from the radar station respectively.

Several techniques have been proposed to process OFDM signals in radar systems. One of them is based on conventional correlation processing of the received and the transmitted signals which requires huge computation resources. An alternative proposed algorthm operates directly on modulated symbols and overcomes the typical drawbacks of correlation based baseband signal processing.

In present work the Doppler shift and time delay influence on the OFDM QPSK mapped signal constellations have been studied. It is shown that the constellation graph for the reflected signal with the Doppler shift and time delay has been rotated and scaled. Also the results show that the Doppler shift both rotates and scales the graph, meanwhile the time delay just rotates it. Therefore the velocity and distance of the target from the radar station can be defined separately using frequency and time delay bank filters. The results of simulations verifies this approach. The multi-periodical LFM-OFDM signals have been studied to solve multi-target problem as well.

Session 4A6a
SC3&2: Physics and Modeling of Laser-induced Periodic Surface Structures

Surface Reorganization from Laser-induced Instability as Origin of LIPSS
Olga Varlamova, Jürgen Reif, Sergej Varlamov, Michael Bestehorn, ... 1390

Adaptive Generation of Laser Induced Periodic Structures with MEMS Axicons
Alexander Treffer, Susanta Kumar Das, Hamza Messaoudi, Jens Brunne, Ulrike Wallrabe, Ruediger Grunwald, ... 1391

Direct Patterning of a Nanograting with Femtosecond Laser Pulses
Kenzo Miyazaki, Godai Miyaji, ... 1392

"Golden" Principles of Ultimate Surface Nanostructuring by Ultrashort Laser Pulses: The Role of Transient Material Optics and Photo-excitation Conditions
Sergey I. Kudryashov, Andrey A. Ionin, Sergey V. Makarov, Pavel N. Saltuganov, Leonid V. Seleznev, 1393

Role of Multiple Shots of Low-fluence Pulses in Femtosecond-laser-induced Periodic Surface Nanostruture Formation
Godai Miyaji, Kenzo Miyazaki, ... 1394

Basic Stages of Laser-induced Periodical Structures Evolution: From Near-wavelength to Sub-wavelength Gratings
Sergey V. Makarov, Andrey A. Ionin, Sergey I. Kudryashov, Leonid V. Seleznev, Dmitry V. Sinitsyn, 1395

Surface Reorganization from Laser-induced Instability as Origin of LIPSS

Olga Varlamova[1], **Jürgen Reif**[1], **Sergej Varlamov**[2], **and Michael Bestehorn**[2]

[1]LS Experimentalphysik II, Brandenburg University of Technology (BTU) Cottbus
Erich-Weinert-Str. 1, Cottbus 03046, Germany
[2]LS Theoretische Physik II, Brandenburg University of Technology (BTU) Cottbus
Erich-Weinert-Str. 1, Cottbus 03046, Germany

Abstract— Irradiation of dielectrics with femtosecond laser pulses (100 fs, 800 nm) is accompanied by appreciable emission of photoelectrons. Upon action of considerable number of pulses, an electrostatically unstable corrugated thin layer is created on the surface target. Taking into account the laser photon energy ($h\nu = 2.5\,\mathrm{eV}$) and the band gap of the dielectric target ($E_g \sim 10\,\mathrm{eV}$), a thickness of the charged layer is estimated to be about of 100 nm. This electrostatically unstable layer, which is similar to thin liquid film, can relax through explosive emission of particles (Coulomb explosion) that is counterbalanced by thermal surface diffusion. As a result, a periodic surface modulations appear in the laser affected area.

The time evolution of such thin layer instability is considered in nonlinear dynamics and is described by an equation of the Kardar-Parisi-Zhang type, where an interplay between surface erosion and thermal self-diffusion leads to the creation of periodic surface patterns. The influence of polarization and incidence angle of the laser beam are included in the modeling. Numerically calculated patterns are in an excellent agreement with experimental results.

Adaptive Generation of Laser Induced Periodic Structures with MEMS Axicons

Alexander Treffer[1], **Susanta Kumar Das**[1], **Hamza Messaoudi**[1], **Jens Brunne**[2], **Ulrike Wallrabe**[2], **and Ruediger Grunwald**[1]

[1]Max-Born-Institute for Nonlinear Optics and Short-Pulse Spectroscopy, Berlin, Germany
[2]Laboratory for Microactuators Freiburg, Department of Microsystem Engineering
IMTEK, University of Freiburg, Germany

Abstract— The generation of laser-induced periodic surface structures (LIPSS) with ultrashort laser pulses promises to be a simple-to-implement, fast and cost-effective method for structuring solid state materials on the nanoscale. Nanostructured surfaces are of growing importance for applications in biosensing, photovoltaics, electronics and many other fields. Because of its high complexity, however, the relevant physical mechanisms of structure formation depending on energy and number of pulses are the subject of ongoing investigations. For the creation of reproducible structures, the choice of the laser parameters including wavelength, polarization, pulse duration, pulse number or pulse fluence is essential. A well balanced steering of these parameters enables to precisely control the shape, size and orientation of the structures.

Recently we proposed to use adaptive components like spatial light modulators to exploit the specific advantages of flexibly shaping nondiffracting beams for a multichannel LIPSS with spatially structured illumination. Here we present the results of first femtosecond laser LIPSS experiments with a linear micro-electro-mechanical system (MEMS) axicon as an adaptive optical beam shaper.

In our experiments, 120 fs laser pulses were spatially shaped by a linear axicon which consists of a pair of plane aluminum coated silicon mirror segments on top of a soft polydimethylsiloxane (PDMS) layer on a piezo disk. The tilting angle between these two mirrors is changed by controlling the voltage applied to the piezo disk. The interference of the two crossing partial waves leads to the formation of one or multiple light sheets depending on the tilting angle. The working principle is comparable to the classical setup for the formation of holographic gratings but the applied angles are much smaller. With an intermediate lens, the light sheets were focused onto a Si substrate. The dependence of the LIPSS formation on the angle and axial distance was studied systematically. For an axial distance of $z = 11.5$ cm from the MEMS, the required voltage for the formation of a high quality nondiffracting propagation zone was about 1.30 V. The corresponding periods of the LIPSS were found to be in the range of 500 nm. A specific advantage of the MEMS results from the fact that the center of gravity of the focal zone can be shifted via tuning the voltage. This feature together with the large depth of focus of the generated light sheets enables to generate nanostructures on curved surfaces as well as on substrates at different positions or with different height levels. Currently, the application of the LIPSS structures to surface enhanced Raman spectroscopy (SERS), photocatalysis and to the exploration of laser-induced ion physics at high field excitation is under further investigation.

Direct Patterning of a Nanograting with Femtosecond Laser Pulses

Kenzo Miyazaki and Godai Miyaji
Institute of Advanced Energy, Kyoto University, Japan

Abstract— In a recent decade, much attention has been paid on periodic surface nanostructure formation observed with femtosecond (fs) laser pulses, as the sub-wavelength surface structure suggests a new phenomenon at nanoscale dimensions that may provide a promising approach to laser nano-processing of materials. Despite intensive studies on a variety of materials, however, direct patterning of well-designed nanostructures still remains challenging, due likely to the insufficient understanding of the detailed interaction process and the lack of method for manipulating intense fs-laser fields at the nanoscale. In this study we show that a homogeneous nanograting can be fabricated on solid surface in air through the controlled excitation of surface plasmon polaritons (SPPs) in fs laser ablation.

The experiment was made for gallium nitride (GaN) crystal with linearly polarized 800 nm, 100-fs laser pulses from a Ti : sapphire laser system. A simple two-step ablation process was designed for fabricating a nanograting on GaN, based on our model of nanostructuring process [1, 2]. In the first step, as shown in Figure 1(a), an interference pattern was produced on the target surface with a single-pulse ablation, and the scanning probe microscope (SPM) image of the pattern is shown in Figure 1(b). In the second step, the fringe period was reduced by irradiating with superimposed multiple shots of low-fluence fs laser pulses from a single beam (beam 1). Figure 1(c) show the SPM image of a nanograting in the second step. We found that the nanograting period d is equal to $d \sim g/5$ for $L = 940$ nm and discretely changes as $d \sim g/q$ with the integer q, depending on the laser fluence. Cross sectional images of nanogratings were observed with a scanning transmission electron microscope. The image has shown that the bottom of nanograting grooves was deeply ablated at a uniform period on the smooth horizontal level.

The results represent exactly the nature when a single spatial standing SPP wave mode is formed in the downsizing process. A model calculation has supported this mechanism, where the calculated half SPP wavelength is in good agreement with the observed nanograting period.

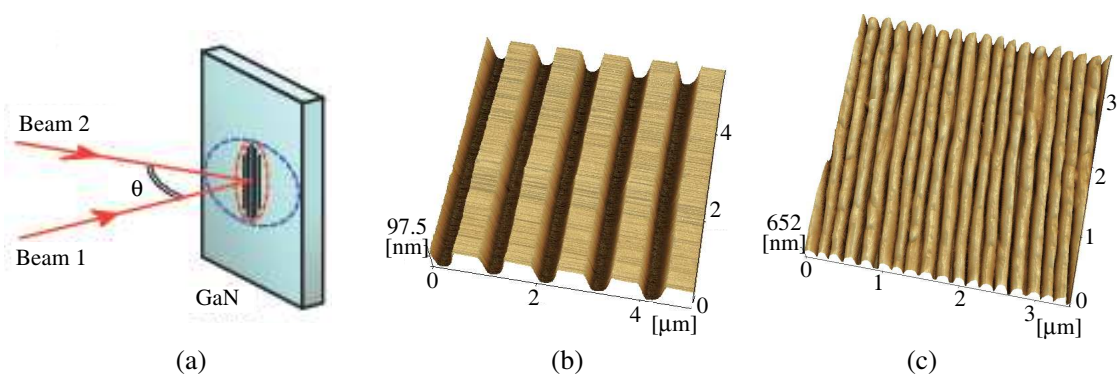

Figure 1: (a) Schematic of optical configuration for the two-step ablation process, (b) SPM image of the interference pattern with the period $L \sim 940$ nm in the first step, and (c) SPM image of the nanograting formed on GaN in the second step. The observed area: (b) $5 \times 5\,\mu\text{m}^2$ and (c) $3.5 \times 3.5\,\mu\text{m}^2$.

REFERENCES

1. Miyaji, G. and K. Miyazaki, *Opt. Express*, Vol. 16, 16265, 2008.
2. Miyaji, G. and K. Miyazaki, *Opt. Express*, Vol. 20, 14848, 2012.

"Golden" Principles of Ultimate Surface Nanostructuring by Ultrashort Laser Pulses: The Role of Transient Material Optics and Photo-excitation Conditions

Sergey I. Kudryashov, Andrey A. Ionin, Sergey V. Makarov, Pavel N. Saltuganov, and Leonid V. Seleznev
P. N. Lebedev Physical Institute, Russian Academy of Sciences, Moscow 119991, Russia

Abstract— Transient optics of diverse photoexcited materials under nanostructuring by ultrashort laser pulses was studied by optical pump/probe reflection technique to enlighten details of surface plasmon-polariton excitation and of their transient "frequency-wavenumber" dispersion relationships. Basing on the experimental studies and their theoretical analysis, optimal photoexcitation conditions were chosen to achieve ultimate (sub-100-nanometer) nanoripple periods and to enhance surface laser-surface plasmon-polariton interactions. Advanced photoexcitation tools were applied to keep dynamically this favorable nanostructuring regime during each nanostructuring ultrashort laser pulse and along their multi-shot series. Appearance of sub-wavelength surface ripples was explained basing on the profound plasmonic description.

Role of Multiple Shots of Low-fluence Pulses in Femtosecond-laser-induced Periodic Surface Nanostruture Formation

Godai Miyaji and Kenzo Miyazaki
Institute of Advanced Energy, Kyoto University, Japan

Abstract— Self-organized periodic nanostructures observed in femtosecond (fs) laser ablation of solid surfaces suggest a potential route to laser nano-processing of materials beyond the diffraction limit. The nanostructuring process appears to strongly depend on the experimental conditions such as target material, its surface roughness, laser parameters, and environment of the target [1], and the exact interaction mechanism of nanostructuring is still under discussion. We notice that superimposed multiple shots of fs laser pulses at low fluence are the common condition for nanostruturing of a variety of material surfaces. Our previous studies have shown that the low-fluence pulses are crucial to initiate the nanoscale ablation with laser-induced near-fields around high curvatures on the target surface [2], and strongly suggest that the excitation of surface plasmon polaritons (SPPs) is responsible for the periodic nano-ablation on the target surface with small roughness or corrugation [3].

For further understanding the role of multiple shots of low-fluence fs laser pulses innanostructuring, we made pump-probe measurements of the reflectivity η of crystalline Si surface in water,using 800-nm, 100-fs laser pulses.Withsuperimposed shots of fs pulses weobserved the fine and course structures with the period of $\sim 150\,\mathrm{nm}$ and $\sim 400\,\mathrm{nm}$. Under the condition of the fine nanostruture formation at the fluence $F = 120\,\mathrm{mJ/cm^2}$, first we measured η for a single pump pulse as a function of the time delay Δt between the pump and probe pulses. The single pump pulse induced neither ablation nor morphological change of the target surface. However, the pump pulse was observed to bring about the rapid decrease in η at $\Delta t \sim 0.5\,\mathrm{ps}$, representing the generation of a high-density of free electrons at the surface, and then η slowly recovered due primarily to the energy transfer from free electrons to the lattice. At the different time delay, η was measured as a function of superimposed shot number N of pump pulses. The results have shown that the multiple shots of fs pulses accumulate the bonding structure change into the amorphous Si, resulting in the decrease in the ablation threshold or the onset of ablation. Once the surface was corrugated, the low fluence fs pulses produced the fine periodic nanostructure. On the other hand, the fine periodic nanostructure was never formed at higher fluence than $F \sim 140\,\mathrm{mJ/cm^2}$.The measurements of η at the high fluence have shown that the surface temperature exceeds the melting point of Si when ablation takes place. This makes it difficult to form the fine nanostructure.

In conclusion, the superimposed multiple shots of low-fluence fs laser pulses are crucial for the accumulation of bonding structure change to decrease the ablation threshold and resulting non-thermal ablation at the surface temperature less than the melting point.

REFERENCES

1. Miyazaki, K., "Nanostructuring of thin film surfaces in femtosecond laser ablation," *Nanophotonics and Nanofabrication*, M. Ohtsu, ed., Chap. 10, 193–214, Wiley-VCH, Weinheim, 2009.
2. Miyaji, G. and K. Miyazaki, *Appl. Phys. Lett.*, Vol. 91, 123102, 2007; *ibid.*, Vol. 89, 191902, 2006.
3. Miyaji, G. and K. Miyazaki, *Opt. Express*, Vol. 16, 16265, 2008; *ibid.*, Vol. 20, 14848, 2012.

Basic Stages of Laser-induced Periodical Structures Evolution: From Near-wavelength to Sub-wavelength Gratings

Sergey V. Makarov, Andrey A. Ionin, Sergey I. Kudryashov, Leonid V. Seleznev, and D. V. Sinitsyn
P. N. Lebedev Physical Institute, Russian Academy of Sciences, Moscow 119991, Russia

Abstract— Three main scenarios of laser-induced periodical surface structures evolution under multipulse femtosecond laser irradiation were studied experimentally and theoretically. They were divided according to laser fluence, which can be higher, near or lower than the structures formation threshold. The main question was what the mechanisms of sub-wavelength periodical structures formation are in these three different regimes of femtosecond laser action? To give an answer, we measured all parameters of the surface structures (geometrical and optical) on different materials, and carried out both analytical and numerical calculations of scattered light distribution on such structures. Obtained results gives good agreement between the experiments and the theory, and deep understanding of the structures formation mechanisms.

Session 4A6b
SC4: Millimeter-Wave and THz Components, Antennas and Arrays

Novel All-dielectric Horn Antennas Based on the Woodpile EBG Structure
Inigo Ederra, Irina Khromova, Ramon Gonzalo, Jorge Teniente, Bastiaan P. de Hon, Karu P. Esselle, 1398

Efficient Horn Antenna Designs for Next Generation Terahertz and Millimeter-wave (Far-infrared) Space Telescopes
Neil Trappe, J. A. Murphy, C. O'Sullivan, M. L. Gradziel, S. Doherty, D. McCarthy, C. Bracken, A. Polegre, ... 1400

Microwave Diode on the Base of Symmetrically and Asymmetrically Doped Semiconductor Heterojunction
Algirdas Sužiedėlis, Steponas Asmontas, Algis Jurgis Kundrotas, Jonas Gradauskas, Andžej Lučun, Aurimas Čerškus, Viktorija Nargelienė, Tomas Anbinderis, Pavel Anbinderis, ... 1401

A Waveguide-to-microstrip Line Transition in Multi-layered Structure for 77 GHz Band Automotive Radar Applications
Ching-Han Tsai, Shyh-Jong Chung, ... 1402

Two-dimensional Angle-of-arrival Analysis by One Enhanced Six-port Structure
Alexander Koelpin, Stefan Lindner, Sebastian Mann, Francesco Barbon, Sarah Linz, Robert Weigel, 1403

Novel All-dielectric Horn Antennas Based on the Woodpile EBG Structure

I. Ederra[1], I. Khromova[1], R. Gonzalo[1], J. Teniente[1], B. P. de Hon[2], and K. Esselle[3]

[1]Universidad Pública de Navarra, Campus Arrosadia, Pamplona, Navarra, E31006, Spain
[2]Department of Electrical Engineering, Eindhoven University of Technology
5600 MB Eindhoven, The Netherlands
[3]Maquarie University, NSW 2109, Australia

Abstract— The scientific and technological interest towards electromagnetic band gap (EBG) structures has been growing rapidly since their discovery. In recent years EBGs have been widely exploited for the purpose of improving the radiation characteristics of different types of antennas. In particular, EBG resonator cavities and defects [1–3] have been used to create antennas with large directivities and high efficiencies. Following the analogy with classical metallic horn antennas, introducing a horn-shaped hollow defect can make the EBG-based system work as a horn antenna. These EBG based antennas could substitute metallic horns in certain applications, which is especially valuable for millimeter and THz devices.

This paper reviews novel concepts for woodpile based horn antennas. Traditionally sectoral horns H-horns embedded in one layer of rods in a woodpile structure have been created. The principal drawback of these woodpile based horn antennas is the absence of mirror symmetry in the stacking direction of a woodpile structure, which results in non-symmetrical radiation patterns. The proposed configurations will overcome these limitations.

First, the concept of evanescent feeding for EBG horn antennas is discussed. It is shown that such horn antennas, realized as hollow defects in a three-dimensional (3D) periodic structure can be coupled to an EBG waveguide via evanescent fields existing in the embedding medium. This concept allows one to design compact arrays of EBG antennas, where horns can share feeds. An example in the F band of this concept and of the radiation patterns which can be obtained are shown in Figures 1(a) and 1(b).

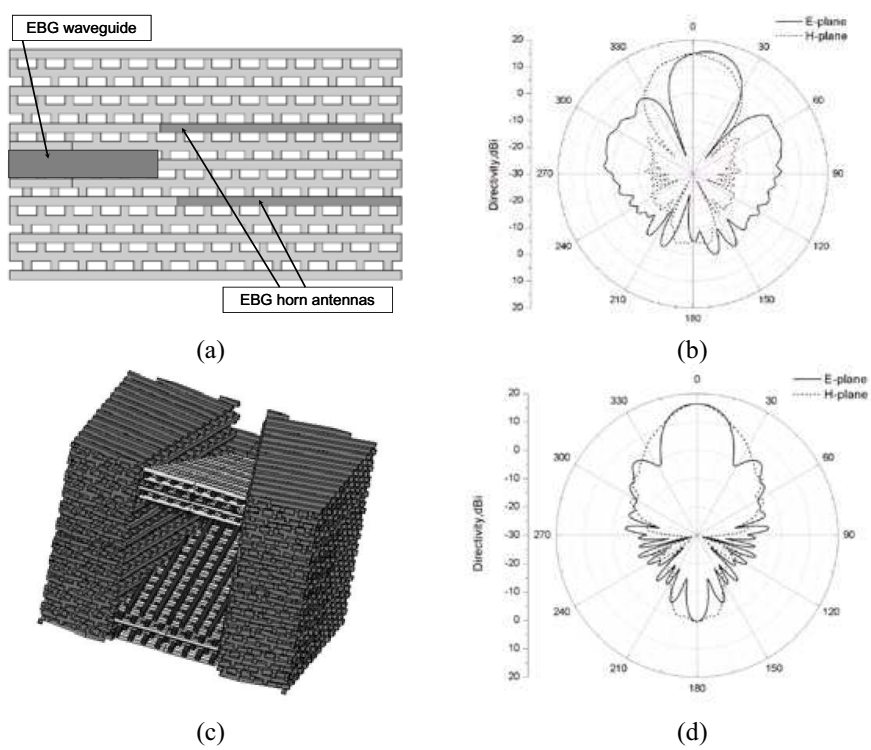

Figure 1: (a) and (b) Evanescently fed woodpile antenna and radiation pattern. (c) and (d) EH-horn antenna and radiation pattern.

In addition to this, this paper presents the design of a novel symmetric EH-horn antenna based on the woodpile structure. The main concept of the design lies in turning the EBG structure at the antenna flare angle and thus forming the EBG "walls" of the horn, as shown in Figure 1(c). This allows obtaining symmetric radiation patterns, as that in Figure 1(d).

REFERENCES

1. Meade, R. D., et al., "Photonic bound states in periodic dielectric materials," *Phys. Rev. B*, Vol. 44, No. 24, 13772–12774, 1991.
2. Noda, S., A. Chutinan, and M. Imada, "Trapping and emission of photons by a single defect in a photonic bandgap structure," *Nature*, Vol. 407, No. 6804, 608–610, 2000.
3. Khromova, I., et al., "Resonance frequency behavior of 3D EBG cavities," *J. Appl. Phys.*, Vol. 106, 014901–01498, 2009.

Efficient Horn Antenna Designs for Next Generation Terahertz and Millimeter-wave (Far-infrared) Space Telescopes

N. Trappe[1], J. A. Murphy[1], C. O'Sullivan[1], M. Gradziel[1], S. Doherty[1], D. McCarthy[1], C. Bracken[1], and A. Polegre[2]

[1]National University, Maynooth, Ireland
[2]ESA ESTEC, Noordwijk, Holland

Abstract— Astronomical observations in the far-infrared are critical for investigation of the early universe and the formation and evolution of planets, stars and galaxies. In the case of space telescope receivers a strong heritage exists for corrugated horn antenna feeds to couple the far-infrared signals to the detectors mounted in a waveguide or cavity structure. For the demands of the future space missions it is clear that the development of new technology solutions for the optimization and simplification of horn antenna structures will be required for large arrays. Horn antennas need to offer excellent control of beam and polarization properties for CMB polarisation experiments satisfying stringent requirements on low sidelobe levels, symmetry and low cross polarization in large arrays.

In this paper, we present a computationally efficient approach for modelling and optimising horn characteristics. We investigate smooth-walled profiled horns that have a performance equivalent to that of the corrugated horns traditionally used for CMB measurements. We discuss the horn optimisation process and the algorithms available to maximise performance of a merit parameter such as low cross polarisation or high Gaussicity.

Microwave Diode on the Base of Symmetrically and Asymmetrically Doped Semiconductor Heterojunction

A. Sužiedėlis[1], **S. Ašmontas**[1], **A. J. Kundrotas**[1], **J. Gradauskas**[1], **A. Lučun**[1], **A. Čerškus**[1], **V. Nargelienė**[1], **T. Anbinderis**[2], **and P. Anbinderis**[2]

[1]Center for Physical Sciences and Technology, Savanoriu Ave. 231, LT-02300 Vilnius, Lithuania
[2]Elmika Ltd, Naugarduko St. 41, LT-03227 Vilnius, Lithuania

Abstract— Microwave Schottky-diode detectors are known to be the most sensitive devices in a wide spectrum range of electromagnetic radiation. However, their poor stability and reliability necessitate search for new alternatives to the Schottky diodes. One of such an alternative is microwave diode on the base of semiconductor heterojunction. Bulk nature of the active region with heterojunction situated far away from the surface promises better stability and reliability of the microwave diode. Planar design of the heterojunction diode makes it possible to apply in both the microwave and infrared ranges, including THz region of the electromagnetic radiation [1].

The n-type GaAs/$Al_xGa_{1-x}As$ semiconductor heterojunction was created in MBE grown structure. Both sides of the heterojunction had the same donor density values $10^{16}\,cm^{-3}$. $Al_xGa_{1-x}As$ compound semiconductor with different AlAs mole fraction x was used for fabrication of different heterojunction diodes. As concerns the voltage sensitivity of the heterojunction microwave diode, optimal composition of the $Al_xGa_{1-x}As$ compound was established to be with $x = (0.2 \div 0.25)$ [2]. However, the best possible design of the heterojunction microwave diode still needs consideration since symmetric doping of the GaAs and AlGaAs sites of the heterojunction results in higher electrical resistance of the junction thus leading to lower voltage sensitivity and lower operational speed of the diode.

New design of the n-GaAs/n-$Al_xGa_{1-x}As$ microwave diode is proposed in this report. Different doping levels at both sides of the heterojunction are taken into consideration. Promising results of the heterojunction diode parameters are obtained after simplified analysis of energetic band structure of the n-GaAs/n-$Al_{0.2}Ga_{0.8}As$ heterojunction.

REFERENCES

1. Gradauskas, J., A. Suziedelis, S. Asmontas, et al., "Sensitive planar semiconductor detector from microwave to infrared applications," *IEEE Sensors Journal*, Vol. 10, No. 3, 662–667, 2010.
2. Sužiedėlis, A., S. Ašmontas, A. J. Kundrotas, J. Gradauskas, A. Čerškus, V. Nargelienė, and T. Anbinderis, "Planar heterojunction diode for millimeter waves detection," *PIERS Proceedings*, 927–930, Moscow, Russia, August 19–23, 2012.

A Waveguide-to-microstrip Line Transition in Multi-layered Structure for 77 GHz Band Automotive Radar Applications

C. H. Tsai and S. J. Chung
Institute of Communications Engineering, National Chao-Tung University, Hsinchu 30010, Taiwan

Abstract— In this paper, a novel waveguide-to-microstrip line transition in the multi-layered substrate which is operated for 77 GHz forward-looking automotive collision warning radar band, is presented. The operating frequency of 77 GHz long range automotive radar is from 76 GHz to 77 GHz, the long range automobile radar antenna required high gain and narrow radiation beamwidth in order to detect target in long distance (> 100 m). Thus, low loss and wide bandwidth of the transition between waveguide and microstrip line is required. In this application, the antenna substrate is a triple-layered structure (3 metal layer, 2 dielectric layer) which is shown in Fig. 1, the thickness of layer M1/2/3 is 5/2.7/20 mil, respectively. The 20 mil layer is antenna layer, the 5 mil layer is circuit layer, the $L1$ is metal layer of microstrip line and RF circuit, $L2$ and $L3$ is ground and antenna layer, respectively. The triple-layered design can separate the radiating elements and RF circuits to the front and back side which creates more room to place more radiation elements and RF circuit. The proposed transition is fed by a standard WR10 rectangular waveguide, the power is coupled from the waveguide into the patch which is located at the center of wavegude and transmit to antenna. Compare to the conventional W-band waveguide-to-microstrip line transition [1–3], the feeding direction of the proposed transition is inverse to those conventional design, the freedom of design is limited cause by this fed direction. Moreover, the stacked-layer structures via size and spacing is restrict by the fabrication rule, via size and spacing is different in each dielectric layer, thus, the complexity of the design increase. Finally, the proposed waveguide-to-microstrip line transition is well design and verified by measurement, this design possess several advances such as small size, low cost, and could easy introduced in the automobile radar application.

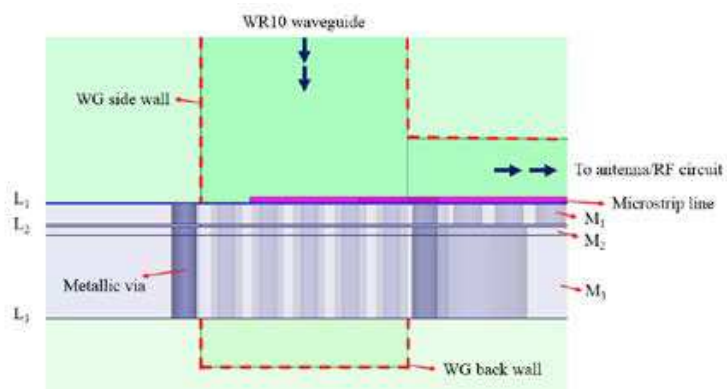

Figure 1: Schemtic of the proposed waveguide-to-microstrip line transition.

REFERENCES

1. Iizuka, H., K. Sakakibara, and N. Kikuma, "Millimeter-wave transition from waveguide to two microstrip lines using rectangular patch element," *IEEE Trans. Microw. Theory Tech.*, Vol. 55, 899–905, 2007.
2. Murase, K., K. Sakakibara, N. Kikuma, and H. Hirayama, "Design of via-less planer microstrip-to-waveguide transition with choke structure," *IEEE iWAT.*, 63–66, 2008.
3. Sakakibara, K., M. Hirono, N. Kikuma, and H. Hirayama, "Broadband and planar microstrip-to-waveguide transitions in millimeter-wave band," *International Conference on ICMMT*, Vol. 3, 1278–1281, 2008.

Two-dimensional Angle-of-arrival Analysis by One Enhanced Six-port Structure

A. Koelpin, S. Lindner, S. Mann, F. Barbon, S. Linz, and R. Weigel
Institute for Electronics Engineering, University of Erlangen-Nuremberg, Germany

Abstract— In this publication the Enhanced Six-Port receiver concept for two-dimensional angel-of-arrival (AoA) measurements will be presented for the first time showing ultra-high accuracy combined with reduced size and low cost implementation. Three antennas detect the impinging wave and feed it to the passive Enhanced Six-Port structure where the three signals are superimposed with four different relative phases. These linear combinations feature the input signals' relative phase shifts in their power due to different free path delays for the received waves at the three antennas. Therefore, the four output signals are converted to DC voltages by simply constructed diode detectors and are digitized. The relative phases can be calculated from the four digitized voltages by digital signal processing. In a last step the relative phases have to be transformed to spherical coordinates resulting in a two-dimensional AoA.

Introduction: Modern manufacturing technologies require precise measurement tools operation in harsh environments. E.g., distance or angle analysis for tools, robot arms, or work pieces have to be determined contact-free with high accuracy in the micrometer or millidegree range for many applications in automated fabrication.

The Enhanced Six-port Receiver: The Enhanced Six-Port receiver has been introduced for simultaneous data reception and one-dimensional AoA by [1] and is based on an extension of a common Six-Port architecture. A classic Six-Port receiver is a passive structure formed by, e.g., microwave couplers superimposing in the microwave domain the two input signals of the system with four different relative phases, e.g., multiples of $\pi/2$. This leads to interference, resulting in four in general different microwave signals coding the relative phase shifts of the signals in their power. Consequently, the four output signals are transfered to equivalent DC voltages by diode detectors.

With this common Six-Port concept one-dimensional AoA analysis featuring high accuracy in the millidegree range has been shown [2]. For this purpose, two antennas are connected to the input ports of the Six-Port. With respect to this antenna plane the AoA of an impinging microwave signal, e.g., backscattered by a corner re ector mounted on top of a robot arm, can be measured by analyzing the relative phase shift of the two antenna signals resulting form the delay in free space transmission due to the AoA. Using two of these Six-Port systems simultaneously will enable two-dimensional AoA detection after transforming the results for both sub-systems. For this concept hardware is doubled compared to one-dimensional AoA.

The approach presented in this paper will show a concept for combining both Six-Port subsystems in one structure, named the Enhanced Six-Port. According to [1] this structure can be regarded as two Six-Port systems with two different input port pairs out of three existing ports having the respective third input port as interfering source featuring a well defined signal, i.e., a phase shifted copy of the received signal of both other input ports. It will be shown that this interferer can be eliminated easily by digital signal processing resulting in two relative phase differences between a first and a second subset of two antennas, respectively. The Enhanced Six-Port concept for 2D AoA analysis will be discussed in theory and demonstrated in detail for the final paper.

REFERENCES

1. Koelpin, A., G. Vinci, B. Laemmle, and R. Weigel, "The enhanced six-port receiver: A new concept for simultaneous data reception and direction of arrival detection," *IEEE MTT-S International Microwave Symposium Digest*, 1–4, Baltimore, USA, June 2011.
2. Vinci, G., A. Koelpin, F. Barbon, and R. Weigel, "A high accuracy direction-of-arrival and misalignment angle detector," *Proc. German Microwave Conference GeMiC 2011*, 1–3, Darmstadt, Germany, March 2011.

Session 4A7
Integrated Optical Passive and Active Components for Communication and Sensing Applications

III-V Semiconductor Quantum Structure Based Electroabsorption Modulators for Communication Applications
Qin Wang, Bertrand Noharet, Stephane Junique, Susanne Almqvist, Andy Zhang, Duncan Platt, Michael Salter, Jan Y. Andersson, ... 1406

Current Distribution in InGaAs/GaAs Transistor Vertical-cavity Surface Emitting Lasers
Yu Xiang, Xingang Yu, Jesper Berggren, Thomas Zabel, Mattias Hammar, Muhammad Nadeem Akram, ... 1407

1.3-μm InGaAs/GaAs VCSELs with Buried Tunnel Junction Current Injection
Xingang Yu, Yu Xiang, Thomas Zabel, Jesper Berggren, Mattias Hammar, ... 1408

Optical Properties of InSb and InGaSb Quantum Dots Grown on InAs
Oscar Gustafsson, Amir Karim, Carl Reuterskiöld Hedlund, Susan Savage, Susanne Almqvist, Qin Wang, Jonas Weissenrieder, Thomas Zabel, Jesper Berggren, Mattias Hammar, ... 1409

Challenges and Solutions for Fabricating Monolithically Integrated EAM-DFB for Radio-over-fiber System
Andy Z. Zhang, Qin Wang, Richard Schatz, Olle Kjebon, Pierre-Yves Fonjallaz, Susanne Almqvist, Marek Chacinski, Stefan Karlsson, Jesper Berggren, Mattias Hammar, ... 1410

Picoliter Volume Glucose Concentration Microsensing Using Micro-abrupt-tapered Fiber Mach-Zehnder Interferometers with Immobilized Glucose Oxidase
Kuen-Yi He, Ming-Yu Lin, Yen-Pei Lu, Tsung-Hsun Yang, Nan-Kuang Chen, Yi-Ning Chen, ... 1411

Stretched-abrupt-tapered Fiber Mach-Zehnder Interferometer for Active Microsensing Applications
Kuen-Yi He, Tsung-Hsun Yang, Hsiang-Ting Peng, Zhao-Ying Chen, Nan-Kuang Chen, ... 1413

Dispersion Properties of Subwavelength Grating SOI Waveguides
Jiri Ctyroky, P. Kwiecien, Ivan Richter, ... 1415

High Finesse Micro Fabry-Perot Resonator Using Thin Tellurite Glass Film over a Tapered Fiber
Yu-Hsin Hsieh, Nan-Kuang Chen, Junjie Zhang, ... 1416

III-V Semiconductor Quantum Structure Based Electroabsorption Modulators for Communication Applications

Qin Wang, **Bertrand Noharet**, **Stephane Junique**, **Susanne Almqvist**, **Andy Zhang**, **Duncan Platt**, **Michael Salter**, **Jan Y. Andersson**
Department of Nanoelectronics, Acreo Swedish_ICT AB, Electrum 236, S-16440 Kista, Sweden

Abstract— Historically one research group at Acreo has exclusively focused on research and development (R&D) of diverse discrete electroabsorption modulators (EAM) and their 1D and 2D arrays based on III-V semiconductor quantum structures for custom orientated device/system prototypings. All aspects of EAM technology from active quantum structure design to device and related module manufacturing have been covered, which has ensured an extensive knowledge platform for us to address various unique communication applications.

This talk will review current the state-of the-art R&D of EAMs, their new challenges/demands/trends and corresponding technology solutions. In particular, EAM activities at Acreo will be presented by a few examples of both surface normal (SN) and travelling wave (TW) type EAMs for individual communication applications. Compared to these two types EAMs, SN EAMs offer significant advantages in terms of polarisation insensitivity, large active apertures, large format (enabling arrays) and low insertion losses. A drawback of the SN modulators is the short interaction length between the incident light and the active medium, thus limiting the contrast ratio. These two types of EAMs provide flexibility to select the suitable one according to different communication scenarios.

One of these examples is GaAs-based quantum well large aperture SN EAMs, which are used for high speed free-space communications in defense, space or bio applications. Using a hybrid integration technique 1D or 2D EAM arrays can be flip-chip mounted on their corresponding 1D/2D driven CMOS or specific designed fanout circuits, which helps this technology for fulfilling high density, multiple channel communication requirements. For example, a 2×128 linear array was used in light wave architectures for the processing of broadband electronic signals.

InP based coupled quantum well structures were utilized as active material in our EAMs for C-band and Ku-band communication cases. Our ongoing EU project working on 1D EAM array in an antenna system can provide broadband connectivity within aircraft cabins will be presented.

A novel monolithic integration approach enabled to use our TW-EAMs for fabricating an analog optical transmitter and an analog optical transceiver to address integrated photonic mm-wave functions for broadband connectivity. The transmitter and transceiver were fabricated by monolithic integration of TW-EAM with a DFB laser or a semiconductor optical amplifier (SOA), respectively.

Current Distribution in InGaAs/GaAs Transistor Vertical-cavity Surface Emitting Lasers

Yu Xiang[1], **Xingang Yu**[1], **Jesper Berggren**[1], **Thomas Zabel**[1], **Mattias Hammar**[1], **and Muhammad Nadeem Akram**[2]

[1]School of Information and Communication Technology, KTH Royal Institute of Technology
Electrum 229, S-164 40 Kista, Sweden
[2]Institute of Micro Nano Systems Technology, University College VestFold, N-3103 Tønsberg, Norway

Abstract— Recently, Feng et al. have introduced so-called transistor-lasers as one possible pathway to satisfy the vast increasing demand for increasing modulation speeds in optical communication networks. This is due to the unique three-terminal operation allowing a fast carrier extraction from the optical active region. However, besides proposed high modulation bandwidths, transistor-lasers are expected to offer additional advantages most prominently the simultaneous electrical and optical output as well as the possibility of inherent feedback operation [1]. One way to further improve this concept is the monolithic combination of transistor lasers and vertical-cavity surface-emitting laser (T-VCSEL). Here, we report on a detailed electro-optical investigation of a 980 nm InGaAs/GaAs heterojunction T-VCSEL based on epitaxial regrowth and intra-cavity carrier injection [2]. The optical active region employs three InGaAs/GaAs quantum wells (QWs) embedded in the transistor base region. The vertical cavity is formed by an undoped bottom semiconductor AlGaAs/GaAs distributed Bragg reflector (DBR) and a dielectric amorphous Si/SiO_2 top DBR. This design facilitates a continuous output power of several mW with a sub-mA threshold base current at room temperature. Interestingly, the high lasing efficiency is maintained even far beyond transistor saturation and does not exhibit the often observed negative differential current gain at lasing threshold. Steady-state numerical simulations show that this is caused by local potential variations strongly influencing the current distribution inside the device. This yields a device locally operating in the active mode while globally being in the saturation regime. Finally, we present preliminary results of the small-signal modulation response for different device configurations.

REFERENCES

1. Holonyak, N. and M. Feng, "The transistor laser," *IEEE Spectrum*, Vol. 43, No. 2, 50, 2006.
2. Yu, X., Y. Xiang, J. Berggren, M. Hammar, N. Akram, W. Shi, and L. Chrostowski, *Electronics Letters*, Vol. 49, No. 3, 208–210, 2013.

1.3-µm InGaAs/GaAs VCSELs with Buried Tunnel Junction Current Injection

X. Yu, Y. Xiang, T. Zabel, J. Berggren, and M. Hammar
School of Information and Communication Technology
KTH Royal Institute of Technology, Isafjordsgatan 22-24, Kista 16440, Sweden

Abstract— Offering a dispersion free transmission the optical communication band centered at 1.3 µm is of greatest significance in optical communication. Due to the requirements on cost and power-efficiency, vertical-cavity surface-emitting lasers (VCSELs) are the preferred light sources for these applications. However, while standard GaAs-based quantum wells (QWs) falls short for this wavelength range, the InP-based materials system is not well-suited for VCSEL applications. In consequence, 1.3-µm VCSELs tend to either be based on complex and difficult-to-fabricate InP-based designs, or exotic alloys lattice-matched to GaAs but with extended emission wavelength. As an alternative we have been exploring standard-type GaAs VCSELs based on highly strained InGaAs QWs and negative gain-cavity tuning to reach the 1.3-µm band [1]. These VCSELs have been based on oxidation confinement or pn-blocking layer regrowth.

Here we present a VCSEL design where the current confinement is due to a InGaAs/GaAs buried tunnel junction; see Fig. 1. Compared to our previous device generations, this design has the advantage of reduced electrical parasitics and optical loss. In addition it has a simplified fabrication as compared to the pn-blocking layer design. These devices are capable of an optical multimode output power in excess of 8 mW at 5°C and 3.5 mW at 80°C, respectively, as well as singlemode emission with an output power of 1.2 mW up to 80°C. In addition, small-signal modulation measurements indicate a 3 dB-bandwidth beyond 9 GHz.

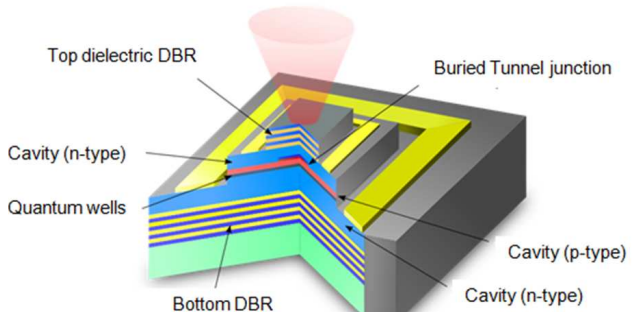

Figure 1: Sketch of InGaAs/GaAs BTJ-VCSEL.

REFERENCES

1. Marcks von Wurtemberg, R., et al., "Performance optimization of epitaxially regrown 1.3-mm vertical-cavity surface-emitting lasers," *IET Optoelectron.*, Vol. 3, No. 2, 112–121, 2009.

Optical Properties of InSb and InGaSb Quantum Dots Grown on InAs

O. Gustafsson[1], **A. Karim**[2], **C. Reuterskiöld Hedlund**[1], **S. Savage**[2], **S. Almqvist**[2], **Q. Wang**[2], **J. Weissenrieder**[1], **T. Zabel**[1], **J. Berggren**[1], **and M. Hammar**[1]

[1]School of Information and Communication Technology
KTH Royal Institute of Technology, Isafjordsgatan 22-24, Kista 16440, Sweden
[2]Acreo AB, Electrum 236, Kista 16440, Sweden

Abstract— Indium-antimonide (InSb) deposited on indium-arsenide (InAs) substrates has been shown to form quantum dots (QD) in a self-assembled manner [1]. These QDs offer a type III band alignment which allows the absorption of light from a confined state in the valence band to a continuum. In combination with the low transition energies of the order of 250 meV this makes InSb quantum dots a very suitable material system for long-wavelength imaging photo detectors in the range of 8–14 µm.

In this contribution, we present a study of the optical properties of InSb based self-assembled QDs deposited by means of metal-organic vapor phase epitaxy. Using photoluminescence spectroscopy we investigate the influence of various growth properties like growth temperature or the amount of deposited material [2].

Furthermore, we will report on the incorporation of gallium (Ga) into such quantum dots which allows for a further red shift of the luminescence energy due to an increased island size stemming from a reduction of the lattice mismatch between InGaSb and InAs compared to InSb and InAs.

We then address the realization of InAs pin diode photo detectors with embedded InSb and InGaSb quantum dots. We show an experimental analysis of the photo response. Here we find that the observed absorption cut-off matches the transition energies determined by photoluminescence spectroscopy. The quantum efficiency of such diodes is up to 1% at 230 K.

REFERENCES

1. Norman, A., et al., *Inst. Phys. Conf.*, Vol. 157, 353–356, 1997.
2. Gustafsson, O., et al., *Optics Express*, Vol. 20, 19, 2012.

Challenges and Solutions for Fabricating Monolithically Integrated EAM-DFB for Radio-over-fiber System

Andy Z. Zhang[1], **Qin Wang**[1], **Richard Schatz**[2], **Olle Kjebon**[2], **Pierre-Yves Fonjallaz**[1], **Susanne Almqvist**[1], **Marek Chacinski**[2], **Stefan Karlsson**[2], **Jesper Berggren**[2], **and Mattias Hammar**[2]

[1]Department of Nanoelectronics, Acreo Swedish_ICT AB
Electrum 236, Kista SE-16440, Sweden
[2]Royal Institute of Technology (KTH), Kista SE-16440, Sweden

Abstract— Monolithic integration is beneficial for small system size and reduction of power consumption. At the same time it can be technologically challenging. In this work, we report on the process technology to fabricate monolithically integrated optical transmitter for distributing RF-signals up to 100 GHz on an optical subcarrier.

The device consists of a Distributed FeedBack (DFB) Laser and a monolithically integrated dual section Traveling Wave Electro-Absorption Modulator (TW-EAM). Both the DFB and the TW-EAM are based on InGaAsP multiple quantum well (MQW) structures, and integrated by butt-joint approach. The DFB grating was defined by e-beam lithography and then transferred into the material using selective wet etch. The grating has a 240 nm period with a duty cycle of 50 percent and 20 nm depth to provide a measured coupling efficiency of $23\,\mathrm{cm}^{-1}$. An etched 1.6 µm narrow waveguide ridge confines the optical mode with low loss. A BCB layer is used below the microwave transmission lines to obtain low capacitance and low loss of the microwave signal. A systematic study of the BCB process was done and good adhesion to the metal of the 5 µm thick BCB was achieved with a 2-step BCB planarization process.

The fabricated lasers had 18 mA threshold, 12 mW output power through the TW-EAM with SMSR > 40 dB. Measurements show good electrical isolation and good optical quality of the butt-joint interface between the DFB laser and the EAM. The modulation efficiency of the modulator was 2.5 mW/V and at 10 mW output power from the laser, the modulator exhibited 12 mA photocurrent at 5 V reverse bias. The devices were used for optical transmission of a 2 Gbps signal on a 60 GHz electrical RF-carrier. The high speed performance can be further improved by a lower resistance of the sputtered microwave load of the TW-EAM.

Picoliter Volume Glucose Concentration Microsensing Using Micro-abrupt-tapered Fiber Mach-Zehnder Interferometers with Immobilized Glucose Oxidase

Kuen-Yi He[1], Ming-Yu Lin[3], Yen-Pei Lu[3], Tsung-Hsun Yang[1], Nan-Kuang Chen[1, 2], and Yi-Ning Chen[1, 2]

[1]Department of Electro-Optical Engineering
National United University, Miaoli 360, Taiwan, R.O.C.
[2]Optoelectronics Research Center
National United University, Miaoli 360, Taiwan, R.O.C.
[3]Instrument Technology Research Center
NARL, Hsinchu 300, Taiwan, R.O.C.

Abstract— We report all-fiber micro Mach–Zehnder interferometers (M-MZIs) with immobilized glucose oxidase (GOD) [1, 2] by introducing two closely-spaced micro-abrupt-tapers in a cladding-reduced highly germanium doped single-mode fiber (Ge-doped SMF) for glucose concentration measurement. In this device, the length L_1 (L_2) and waist diameter d_1 (d_2) of the left (right) abrupt taper is about 252.3 (208.6) µm and 29.7 (41.7) µm, respectively. The total device length of the M-MZI comprising two abrupt tapers and the phase shifter is 889.7 µm, shown in Fig. 1. The working principle of the M-MZI is based on the two beam interference. To make M-MZIs for the microsensing applications, it is very important to excite the very high order cladding mode so as to maximize the OPLD between the reference beam and the sensing beam in a short device length. The high numerical aperture (NA) Ge-doped SMF is a good option to help maximize the optical path length difference (OPLD) because the remaining active dopants at the abrupt taper are still effective to well-confine the core mode in contrast to the conditions in Ge-doped fiber [3, 4]. The single-mode fiber has the NA, core and cladding diameters of 0.28, 3.75, and 80 µm respectively. The GOD is immobilized on M-MZI to increase biospecificity and sensitivity for glucose concentration microsensing. In fabrication, the two micro-abrupt-tapers are introduced on a thinned Ge-doped SMF by a focused CO_2 laser beam, and are coated with GOD at micro-abrupt-tapers. The output power of the CO2 laser is 2.5 Watt. A tiny drop of buffer and glucose solution at a picoliter liquid volume was applied to be trapped at the micro abrupt tapers by capillary. Fig. 2(a) shows the spectral responses of M-MZI with and without immobilized glucose oxidase. It is shown that a slight wavelength shift and an extra 10 dB optical losses could be introduced. In Fig. 2(b), the 300 mg/dL concentration variation for the picoliter volume glucose may give rise to a wavelength shift of 0.2 nm at around 1570 wavelength band. The preliminary results reflect that this M-MZI is promising for picoliter glucose measurement.

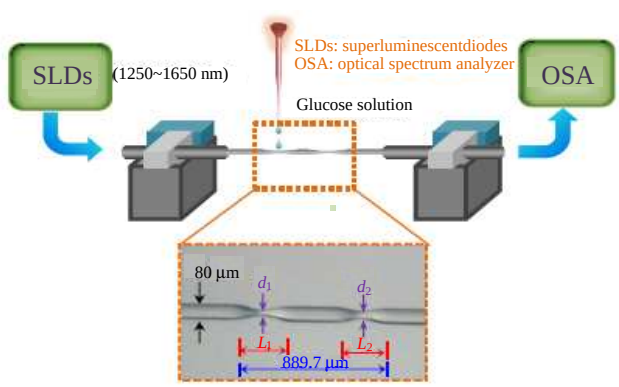

Figure 1: Schematic diagram of the Mach-Zehnder-interferometer and experimental set-up.

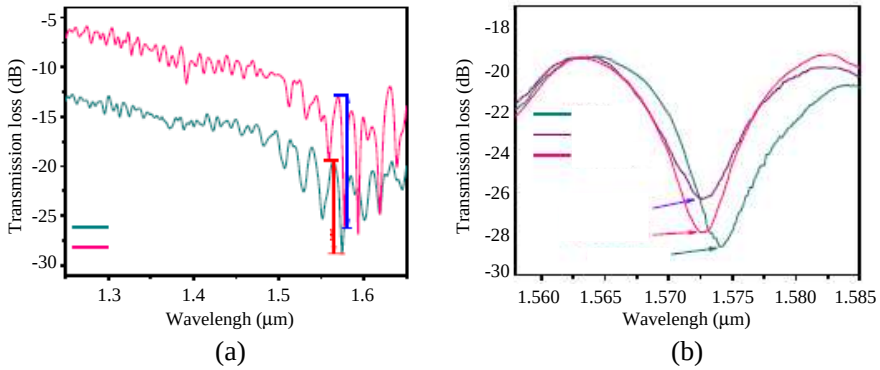

Figure 2: (a) Spectral responses of M-MZI with immobilized glucose oxidase. (b) Spectral responses of the M-MZI when a drop of buffer and glucose solution.

REFERENCES

1. Lin, T. Q., Y. L. Lu, and C. C. Hsu, "Fabrication of glucose fiber sensor based on immobilized GOD technique for rapid measurement," *Opt. Express*, Vol. 18, 27560–27566, 2010.
2. Jiang, D., E. Liu, X. Chen, and J. Huang, "Design and properties study of fiber optics glucose biosensor," *Chin. Opt. Lett.*, Vol. 1, 108–110, 2003.
3. Chen, N. K. and Z. Z. Feng, "Effect of gain-dependent phase shift for tunable abrupt-tapered Mach-Zehnder interferometers," *Opt. Lett.*, Vol. 35, 2109–2111, 2010.
4. Chen, N. K., T. H. Yang, Z. Z. Feng, Y. N. Chen, and C. Lin, "Cellular-dimension picoliter-volume index microsensing using micro-abrupt-tapered fiber Mach-Zehnder interferometers," *IEEE Photon. Technol. Lett.*, Vol. 24, 842–844, 2012.

Stretched-abrupt-tapered Fiber Mach-Zehnder Interferometer for Active Microsensing Applications

Kuen-Yi He[1], **Tsung-Hsun Yang**[1], **Hsiang-Ting Peng**[1], **Zhao-Ying Chen**[1], **and Nan-Kuang Chen**[1, 2]

[1]Department of Electro-Optical Engineering
National United University, Miaoli 360, Taiwan, R.O.C.
[2]Optoelectronics Research Center
National United University, Miaoli 360, Taiwan, R.O.C.

Abstract— We demonstrate micro stretched-abrupt-tapered fiber Mach-Zehnder interferometer (SAT-MZI). In this device, one of the two abrupt tapers is intentionally stretched and thinned down to a diameter of 3.2 µm while the other one remains its diameter to be 51.75 µm. The total device length is 8.77 mm. It is known that the quickly varying evanescent-field surrounding tapered fiber will come along with optical attractive force to propel microparticles or to trap atoms [5]. In this work, the device structure is base on abrupt tapered fiber Mach-Zehnder interferometer (AT-MZI) in which a 1.2-cm-long Er/Yb codoped phosphosilicate fiber (EYDF) is used. This fiber has a numerical aperture of 0.22 and which is advantageous to quickly increase the optical path length difference (OPLD) between core mode and cladding modes. In fabrication, a micro hydrogen flame was used to heat and stretch the fiber to introduce two abrupt tarpers (ATs) on the EYDF. The two ATs have a diameter of over a range of 40–55, one of

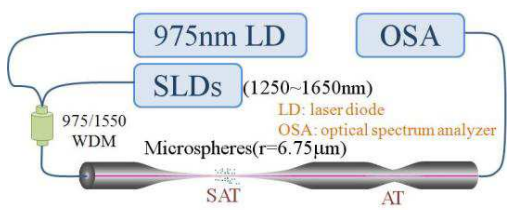

Figure 1: Schematic diagram of the Mach-Zehnder-interferometer and experimental set-up.

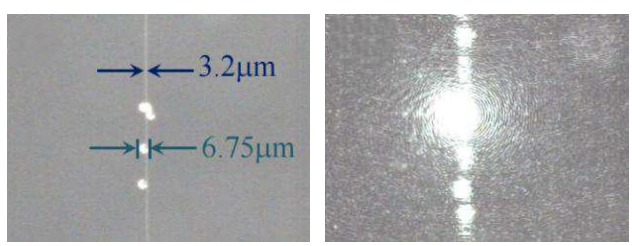

(a) (b)

Figure 2: Microphotographs under a 1000X CCD microscope of (a) SAT-MZI with microspheres (r = 6.75 µm) at SAT, and (b) SAT-MZI with clustering polymeric microspheres at SAT when a laser at 975 nm wavelength is on.

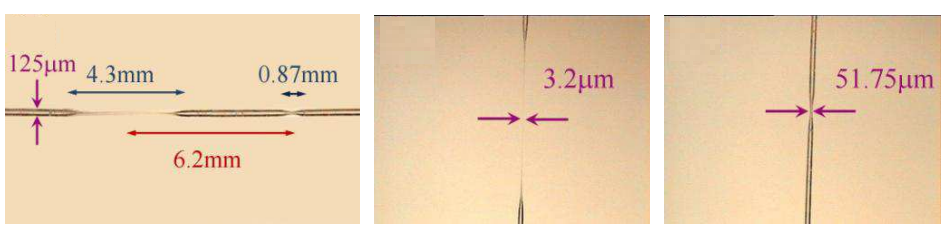

(a) (b) (c)

Figure 3: (a) The total device length of the SAT-MZI is 8.77 mm with an SAT and an AT on an EYDF (Fibercore: DF1500Y.). (b), (c) The SAT and AT have a diameter of 3.2 µm and 51.75 µm, respectively.

the ATs is intentionally stretched at the second stage until the strong optical attractive force can be available at a diameter of around 3 μm. The SAT-MZI was then immersed in the water containing microspheres with an average radius of 6.75 μm. The 975 nm laser was coupled into the SAT-MZI with an input power of 21.7 mW to actively attract the microspheres, as shown in Fig. 2.

REFERENCES

1. Tian, Z., S.-H. Yam, and H. P. Loock, "Refractive index sensor based on an abrupt taper Michelson interferometer in a single-mode fiber," *Opt. Lett.*, Vol. 33, 1105–1107, 2008.
2. Tian, Z. and S.-H. Yam, "In-line abrupt taper optical fiber Mach-Zehnder interferometric strain sensor," *IEEE Photon. Technol. Lett.*, Vol. 21, 161–162, 2009.
3. Lu, P., L. Men, K. Sooley, and Q. Chen, "Tapered fiber Mach-Zehnder interferometer for simultaneous measurement of refractive index and temperature," *Appl. Phys. Lett.*, Vol. 94, 131110-1–131110-3, 2009.
4. Chen, N. K. and Z. Z. Feng, "Effect of gain-dependent phase shift for tunable abrupt-tapered Mach-Zehnder interferometers," *Opt. Lett.*, Vol. 35, 2109–2111, 2010.
5. Brambilla, G., G. Senthil Murugan, J. S. Wilkinson, and D. J. Richardson, "Optical manipulation of microspheres along a subwavelength optical wire," *Opt. Lett.*, Vol. 32, 3041–3043, 2007.
6. Xu, R., H. Xin, Q. Li, X. Yang, H. Chen, and B. Li, "Photothermal formation and targeted positioning of bubbles by a fiber taper," *Appl. Phys. Lett.*, Vol. 101, 054103-1–054103-4, 2012.

Dispersion Properties of Subwavelength Grating SOI Waveguides

Jiří Čtyroký[1], **Pavel Kwiecien**[2], **and Ivan Richter**[2]

[1]Institute of Photonics and Electronics AS CR, v.v.i., Chaberská 57, 182 51 Prague 8, Czech Republic
[2]Department of Physical Electronics, Faculty of Nuclear Sciences and Physical Engineering
Czech Technical University in Prague, Břehová 7, 11519 Prague 1, Czech Republic

Abstract— Segmented subwavelength grating waveguides (SWGW) can be very effectively used to create waveguides with very different properties based on a standard silicon-on-insulator (SOI) fabrication technology using one-lithographic step only [1–4]. In the first approximation of an effective medium theory (EMT), the SWGW can be interpreted as a waveguide with refractive index reduced by interlacing high-index Si segments with a low-index silica (or a suitable polymer) [5–7]. However, for more demanding applications, e.g., in devices utilizing nonlinear optical effects, the mode field confinement and the dispersion properties of such waveguides have to be known with much greater accuracy. In fact, these waveguides are not longitudinally invariant but they represent periodic structures — 1D photonic crystals — supporting propagation of guided Bloch modes [2]. In view of a simple and uniform vertical structure of SOI waveguides, one may think that the complexity of the 3D problem can be reduced to a more easily tractable and computable 2D problem by using the effective-index method. However, our modeling calculations [8] have shown that this approximation can be used to get a rough estimation of the general trends only, but no reliable quantitative prediction can be obtained. In this contribution, we thus present detailed results of a full-vector 3D modeling of SWGW using our proprietary Fourier modal methods recently developed [9, 10]. As the main result, we present dependencies of both phase and group effective indices of Bloch modes in the wide wavelength range (1.2–1.7 μm) on the geometrical parameters of the SWGW. To avoid the uncertainty in optical properties of polymers like SU8, only structures created by a SWG Si nanowire embedded into a SiO_2 environment are analyzed. Three typical values of Si thickness used in SOI technology are considered, namely 200 nm, 220 nm, and 260 nm. Our results are important for the design of SOI waveguide devices in a number of applications as mode transformers and couplers, nonlinear optical devices, sensors, etc..

ACKNOWLEDGMENT

This work was financially supported by the Czech Science Foundation under project P205/10/0046.

REFERENCES

1. Bock, P., et al., *Optics Express*, Vol. 18, 20251, 2010.
2. Bock, P., et al., *Optics Express*, Vol. 18, 16146, 2010.
3. Cheben, P., et al., *Optics Express*, Vol. 14, 4695, 2006.
4. Cheben, P., et al., *Optics Letters*, Vol. 35, 2526, 2010.
5. Lord Rayleigh, J. W. S., *Phil. Mag.*, Vol. 34, 481, 1892.
6. Rytov, S. M., *Sov. Phys. JETP*, Vol. 2, 466, 1956.
7. Lalanne, P. and J.-P. Hugonin, *Journal Optical Society of America A*, Vol. 15, 1843, 1998.
8. Kwiecien, P., I. Richter, and J. Čtyroký, *Proceedings of SPIE*, Vol. 8306, 83060Y-1, 2011.
9. Čtyroký, J., P. Kwiecien, and I. Richter, *18th ECIO 2012*, Sitges, Spain, paper 108, 2012.
10. Čtyroký, J., *Journal of Lightwave Technology*, Vol. 30, 3699, 2012.

High Finesse Micro Fabry-Perot Resonator Using Thin Tellurite Glass Film over a Tapered Fiber

Yu-Hsin Hsieh[1], **Nan-Kuang Chen**[1, 2], **and Junjie Zhang**[3]

[1]Department of Electro-Optical Engineering, National United University, Miaoli 360, Taiwan, R.O.C.
[2]Optoelectronics Research Center, National United University, Miaoli 360, Taiwan, R.O.C.
[3]Shanghai Institute of Optics and Fine Mechanics, Chinese Academy of Sciences, Shanghai 201800, China

Abstract— In this work, we demonstrate the reflection-type micro Fabry-Perot (FP) resonators using high-index thin tellurite glass film attach against the cleaved up-tapered fiber end. Compare with silica, the tellurite glass has a refractive index of higher than 2 so that a high finesse micro FP cavity can be easily achieved when a high index difference at the interface between silica/air and tellurite is formed [1, 2]. To make the high finesse FP resonator, a section of up-tapered single mode fiber was prepared by compressing the fiber axially when the fiber was heated by a hydrogen flame. Based on the up-tapered fiber, the numerical aperture can be decreased due to a larger effective core diameter to make more propagating lights bouncing back and forth in the micro cavity. Accordingly, it is highly promising to achieve a high finesse FP resonator with the significant improvement of decrease the optical insertion losses. Subsequently, the tellurite glass can be melted by a butane flame with a working temperature of around 600°C to cover the cleaved up-taper end. Due to the high cohesion of tellurite glass and the surface tension of the melted tellurite glass, the glass molecules will easily form a symmetric small sphere at the fiber end and the fractional amount of the tellurite glass occupied the end face of cleaved up-taper can be shaped into a microcavity. The best extinction ratio achieved can be high above 21 dB with a thickness less than 10 µm. This high extinction ration micro Fabry-Perot resonator is simple and cost-effective for making sensors.

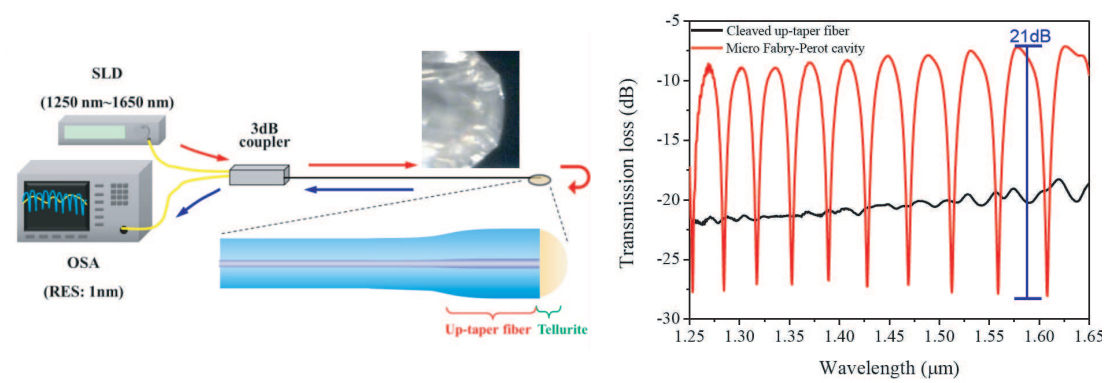

(a) (b)

Figure 1: (a) Experimental set-up of the micro Fabry-Perot resonator. (b) Spectral responses of micro Fabry-Perot resonator.

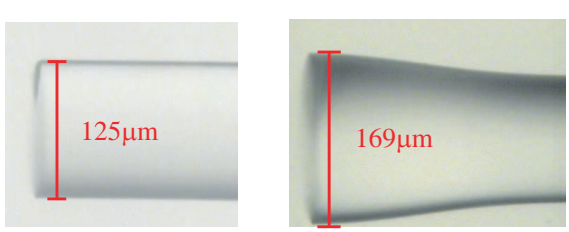

(a) (b)

Figure 2: Side views of (a) standard silica fiber with a diameter of 125 µm and (b) up-taper fiber with a diameter of 169 µm.

REFERENCES

1. Tian, Z., S. S.-H. Yam, and H. P. Loock, "Refractive index sensor based on an abrupt taper Michelson interferometer in a single-mode fiber," *Opt. Lett.*, Vol. 33, 1105, 2008.
2. Greiner, C. M., D. Lazikov, and T. W. Mossberg, "Low-loss silica-on-silicon two-dimensional Fabry-Perot cavity based on holographic Bragg reflectors," *Opt. Lett.*, Vol. 30, 38, 2005.

Session 4A8a
Remote Sensing of the Earth, Ocean, and Atmosphere

Application of MoM to the Calculation of Polarimetric Variables for Ensembles of Rough Hydrometeors
Djordje Mirkovic, Dusan Zrnic, Alexander Ryzhkov, ... 1420

Power Spectra of a Radio Wave Diffracted by Random Electron Density Irregularities
George Vakhtang Jandieri, Akira Ishimaru, ... 1421

Aperture Averaging of Focused Multi-Gaussian Beams
Canan Kamacioglu, Yahya Kemal Baykal, Erdem Yazgan, ... 1422

Real Beam vs. Synthetic Aperture Radar for Slope Monitoring
Massimiliano Pieraccini, ... 1423

Propagation inside a Space Made Up of a Homogeneous Medium Overlying a Duct Having a Linear-square Refractive Index Profile
Christophe Bourlier, Nicolas Pinel, ... 1425

A Dynamical System Perspective of Multi-temporal Remote Sensing: Analysis of MODIS Spectral Index Time Series from Forest Wildfires
Biagio Di Mauro, Giovanni Franco Crosta, Francesco Fava, Lorenzo Busetto, Roberto Colombo, ... 1426

Application of MoM to the Calculation of Polarimetric Variables for Ensembles of Rough Hydrometeors

Djordje Mirković[1, 3, 4], Dušan Zrnić[2], and Alexander Ryzhkov[1]

[1]National Severe Storm Laboratory, University of Oklahoma CIMMS, Norman, OK, USA
[2]National Severe Storm Laboratory, NOAA, Norman, OK, USA
[3]School of Electrical and Computer Engineering, University of Oklahoma, Norman, OK, USA
[4]School of Electrical Engineering, University of Belgrade, Serbia

Abstract— Hydrometeor scattering, until now, has been investigated using simple spheroidal models as representation for the most of the observed precipitation. These simple models provided satisfying result for the uni-polarized network of WSR 88D. The new generation of dual-polarized radars has provided new capabilities in observation of weather phenomena. Thus, it has stimulated development of algorithms capable of quantitatively discriminating between different precipitation types, on the basis of the measured quantities of: differential reflectivity Z_{DR}, differential phase δ and cross-correlation coefficient ρ_{HV}. Furthermore, these capabilities have set a new task to the modeling of the atmospheric scattering volumes to replicate data observed by radars.

Application of spheroidal based modeling has proven to have difficulties quantitatively replicating observed low values of cross-correlation coefficient of wet snow in the melting layer and hail storms, especially in cases when rough hail was observed on ground. These difficulties led to the necessity of developing new modeling approach that would be able to replicate observed data.

Aforementioned difficulties of spheroidal models, disabled usage of widely accepted T-Matrix and similar methods, as they solely rely on the spheroidal geometry, despite of the fact they can introduce different hydrometeor axis ratios and dielectric properties. In order to overcome observed deficiency, new ensemble models need to include rough, spiky hail, as previous studies conducted discovered that the low ρ_{HV} values are related to the protuberances in the hail surface or to the spike-alike protrusions.

Proposed approach, to the aforementioned issue, relays on using the Method of Moments (MoM) software for modeling complex geometries of hydrometeors, which would form larger ensembles. Ensemble formation and ρ_{HV} calculations are performed from the scattering computations stored in scattering matrixes of rough hail, which are produced by Method of Moments (MoM) software WIPL-D that has demonstrated capability of modeling scattering of complex objects. Specific scattering values, dependable of solid angle, are chosen from the overall data set representing pre-defined distribution of hail type size and dielectric parameters.

To the best of our knowledge, this is the first application of WIPL-D, and one of the first attempts to use MoM for hydrometeor scattering. We suggest specific topologies, orientations, sizes, distribution and EM properties for the sampled scatterers. Specifically we suggest models of giant hail resembling observations to replicate drop observed by weather radars.

Power Spectra of a Radio Wave Diffracted by Random Electron Density Irregularities

G. V. Jandieri[1] and A. Ishimaru[2]

[1]Georgian Technical University, Georgia
[2]University of Washington, USA

Abstract— Statistical characteristics of multiply scattered electromagnetic waves in turbulent magnetized and non-magnetized plasma with both electron density and external magnetic field fluctuations are investigated analytically and numerically using experimental data of the F-region of the ionosphere. Analytical expressions for phase fluctuations of scattered radiation in the direction perpendicular to the principle plane is derived using the smooth perturbation method taking into account diffraction effects. Correlation and wave structure functions of the phase fluctuations are obtained for arbitrary correlation functions of fluctuating plasma parameters and external magnetic field. Numerical calculations are carried out for 3 MHz and 40 MHz original electromagnetic wave.

For anisotropic Gaussian correlation function of electron density fluctuations wave structure function oscillates at small distances tending to saturation with increasing distance between observation points. Angleof-arrivals (AOA) are calculated for different angle of inclination of prolate irregularities. Numerical calculations show that at fixed frequency of an incident wave increasing angle of inclination AOA in the principle plane decreases. Investigation has shown that strongly pronounced dip appears in the SPS of scattered ordinary electromagnetic wave along prolate irregularities at oblique illumination of magnetized plasma by mono-directed incident radiation. Double-humped shape has symmetrical form become deeper increasing distance travelling by ordinary wave in magnetized ionospheric plasma. Phase portraits of external magnetic field fluctuations have been constructed and substantially depend on non-dimensional spatial parameters characterizing given problem.

For power-law spectrum of electron density fluctuations SPS having symmetrical form broadens and a gap increases upsizing anisotropy factor of prolate irregularities and a distance travelling by electromagnetic wave in non-magnetized plasma. Formation of a gap in the SPS and evaluation of its doublehumped shape for power-law spectrum at different angle of inclination of prolate irregularities with respect to the external magnetic field is considered for the first time.

The obtained results will have applications at observations of electromagnetic waves propagation in the ionosphere and remote sensing.

Aperture Averaging of Focused Multi-Gaussian Beams

Canan Kamacıoğlu[1], **Yahya Baykal**[2], **and Erdem Yazgan**[3]

[1]Department of Mechatronics Engineering, Çankaya University, Ankara, Turkey
[2]Department of Electronic and Communication Engineering, Çankaya University, Ankara, Turkey
[3]Electrical and Electronics Engineering, Hacettepe University, Ankara, Turkey

Abstract— We investigate the behaviour of the power fluctuations of the focused annular and flat-topped beams when a realistic receiver possessing a finite sized aperture is employed in turbulent atmospheric optics links. Employing our previously derived formulation for the power scintillation index, the variations of the power scintillations and the receiver aperture averaging factor of the focused annular and flat-topped beams are scrutinized. Receiver aperture averaging factor is deduced from the ratio of power scintillation index detected by a finite sized aperture to that obtained by a point aperture. Influence of the receiver aperture radius, the propagation length, the structure constant, the inner and the outer beam sizes for an annular type incidence, flatness parameter for a flat-topped incidence and the focusing parameter for the multi-Gaussian beam in general, on the power scintillation and the receiver aperture averaging factor are studied. It is found that for the focused multi-Gaussian beams, the effect of the receiver aperture averaging factor increases as the aperture radius increases for larger link lengths. Additionally, for the annular incidences in turbulence, the effect of the receiver aperture averaging factor is stronger for larger inner beam source sizes. At a fixed receiver aperture radius, receiver aperture averaging becomes more effective when the structure constant becomes larger. When focused multi-Gaussian beams are compared to their collimated counterparts, it is seen that the receiver aperture averaging is more beneficial for the focused annular and focused flat-topped beams. At large link lengths, increase in the receiver aperture radius decreases the power scintillations.

Real Beam vs. Synthetic Aperture Radar for Slope Monitoring

Massimiliano Pieraccini
Department of Information Engineering, University of Florence, Via Santa Marta, 3 Firenze 50139, Italy

Abstract— In the last years ground-based interferometric radar has become a popular technology for displacement monitoring of landslides and slopes in open pit mines. Several research groups and companies have worked on it, and currently two quite different technologies are emerging: real beam radar and synthetic aperture radar.

The first embryonic idea of SAR (Synthetic Aperture Radar) is probably due the mathematician Carl A. Wiley [1] that in 1951 described a "Doppler Unbeamed Search Radar". It was not a SAR as known today, nevertheless it provided the basis of a radar with improved angular resolution using the Doppler shift of a travelling antenna. Other developments were done in 1950s, but they were covered by military secret. The civil history of SAR begins in 1960, when the idea was first acknowledged publicly [2]. Today SAR is the standard for satellite radars, as they require the best possible angular resolution for focussing on the earth surface operating from an orbit [3]. Since 1990s with the launch of ERS-1 (1991), JERS-1 (1992), RADARSAT-1 and ERS-2 (1995) [4], satellite-based SAR has been able to exploit the phase information of images for detecting ground displacements. These developments had an early follow-up in analogue ground-based radar systems in the late '90s. In 2003 Tarchi et al. [5] proposed for the first time to exploit Ground Based SAR Inteferometry for slope monitoring. Since those early days of ground based SAR, the technique has been developed and tested in the field for about a decade [6, 7] until its consolidation as a commercial equipment [8]. At the same time, more traditional radars with physical aperture antennas have been proposed and used with the same purpose [9]. Currently the two different technologies (Real Beam and Synthetic Aperture) are both popular as instruments for displacement monitoring of natural and engineered slopes. Just for reference, IBIS [8] of IDS company and LisaLab [10] of Ellegi are radars for slope monitoring based on synthetic aperture, SSR of GroundProbe [9], MSR of Reutech and GPRI of Gamma Remote Sensing [11] are radar systems based on physical aperture antennas.

The aim of this paper is to discuss the fundamental differences of the two techniques, with emphasis on the principles rather than on particular implementations and commercial products, on the basis of a decade of experience in the specific field of the author.

REFERENCES

1. Love, A. W., "In memory of Carl A. Wiley," *IEEE Antennas and Propagation Society Newsletter*, 17–18, Jun. 1985.
2. Cutrona, L. J., W. E. Vivian, E. N. Leith, and G. O Hall, "A high-resolution radar combat-intelligence system," *IRE Transactions on Military Electronics*, 127–131, Apr. 1961.
3. Curlander, J. C. and R. N. McDonough, "Synthetic aperture radar: Systems and signal processing," *Wiley Series in Remote Sensing and Image Processing*, 1991.
4. Borgeaud, M., J. Noll, and A. Bellini, "Multi-temporal comparisons of ERS-1 and JERS-1 SAR data for land applications," *Geoscience and Remote Sensing Symposium, 1994; IGARSS'94*, Vol. 3, 1603–1605, 1994.
5. Tarchi, D., N. Casagli, R. Fanti, D. Leva, G. Luzi, A. Pasuto, M. Pieraccini, and S. Silvano, "Landslide monitoring by using ground-based SAR interferometry: An example of application to the Tessina landslide in Italy," *Engineering Geology*, Vol. 68, 15–30, 2003.
6. Pieraccini, M., L. Noferini, D. Mecatti, C. Atzeni, G. Teza, A. Galgaro, and N. Zaltron, "Integration of radar interferometry and laser scanning for remote monitoring of an urban site built on a sliding slope," *IEEE Transactions on Geoscience and Remote Sensing*, Vol. 44, No. 9, 2335–2342, Sep. 2006.
7. Mecatti, D., G. Macaluso, A. Barucci, L. Noferini, M. Pieraccini, and C. Atzeni, "Monitoring open-pit quarries by interferometric radar for safety purposes," *2010 European Radar Conference (EuRAD)*, 37–40, Sep. 30, 2010–Oct. 1, 2010.
8. Severin, E., L. Eberhardt, S. Leoni, and S. Fortin, "Use of ground-based synthetic aperture radar to investigate complex 3-D pit slope kinematics," *Proceedings, Slope Stability 2011: International Symposium on Rock Slope Stability in Open Pit Mining and Civil Engineering*, Vancouver, Canada, Sep. 18–21, 2011.

9. Noon, D., *Slope Stability Radar for Monitoring Mine Walls, Mining Risk Management Conference*, Sidney, 1–12, 2003.
10. Antonello, G., J. Fortuny, D. Tarchi, N. Casagli, C. Del Ventisette, L. Guerri, G. Luzi, F. Mugnai, and D. Leva, "Microwave interferometric sensors as a tool for space and time analysis of active volcano deformations: The Stromboli case," *Second Workshop on Use of Remote Sensing Techniques for Monitoring Volcanoes and Seismogenic Areas, 2008. USEReST 2008*, 1–6, Nov. 11–14, 2008.
11. Werner, C., A. Wiesmann, T. Strozzi, A. Kos, R. Caduff, and U. Wegmiuler, "The GPRI multi-mode differential interferometric radar for ground-based observations," *9th European Conference on Synthetic Aperture Radar, EUSAR*, 304–307, Apr. 23–26, 2012.

Propagation inside a Space Made Up of a Homogeneous Medium Overlying a Duct Having a Linear-square Refractive Index Profile

C. Bourlier and N. Pinel
Laboratory IETR, LUNAM University, Nantes, France

Abstract— For a two-dimensional problem, this paper presents the evaluation of the spatial Green function of environments made up of a homogenous medium overlying a duct having a linear-square refractive index profile. This function must be determined to deal with the more general problem of scattering from a rough sea surface in the presence of a duct. Assuming a slowly-varying refractive index, by using the method of steepest descents, closed-form expressions of the spatial Green function in different regions (illuminated and shadowed) are derived. In addition, they are compared with that obtained from the parabolic wave equation.

Introduction and Results: In the past decades, researchers in the areas of applied electromagnetics and underwater acoustics developed rigorous and asymptotic models for mathematically describing the combined effects of atmospheric conditions (ducting conditions) and surface roughness on the propagation and scattering. To solve this issue, two main methods are available in the literature: the well-known parabolic wave equation (PWE) method [1] and the boundary integral equation (BIE) method [2]. The great advantage of the PWE method is that it can deal with most real-life inhomogeneous environments. Its main drawback is the underlying paraxial approximation leading to an approximation of the propagator (that is, the Green function). By contrast, the advantage of the BIE method is that it is a rigorous method, but its main drawback is that the Green function (propagator) is known only for a small class of refractive index profiles [3].

In this paper, in order to apply the latter method, a closed-form expression of the spatial Green function is derived for environments made up of a homogeneous medium overlying a duct having a linear-square refractive index profile. The four cases, transmitter or/and receiver inside or/and outside the duct, are considered. Then, the exact Green function is expressed in terms of Airy functions. But in the spatial domain, its inverse Fourier transform is not numerically tractable, since the involved integrals are difficult to evaluate even numerically, due to the rapidly oscillatory nature of the integrands. Consequently, an approximate solution obtained from the works of [4, 5], which is valid in the frequency range of interest (i.e., the microwave range), is obtained asymptotically by using the method of SD (Steepest Descents) combined with the WKB approximation (Wentzel-Kramers-Brillouin) [3]. In addition, including this function in the BIE method, preliminary results of the scattering from a rough sea surface are also presented.

ACKNOWLEDGMENT

This project is funded by French Ministry of Defense via DGA under the contract RAPID named "PRORASEM".

REFERENCES

1. Levy, M., "Parabolic equation methods for electromagnetic wave propagation," Electromagnetic Waves Series 45, The institution of Electrical Engineers, London, 2000.
2. Awadallah, R.-S. and G. S. Brown, "Low-grazing angle scattering from rough surfaces in a duct formed by a linear-square refractive index profile," *IEEE Trans. Ant. Prop.*, Vol. 48, No. 5, 1461–1474, 2000.
3. Brekhovskikh, L. M., *Waves in Layered Media*, 2nd Edition, Academic Press, New York, 1980.
4. Fock, V. A., *Electromagnetic Diffraction and Propagation Problems*, Pergamon Press, Paris, 1965.
5. Kukushkin, A., *Radio Wave Propagation in the Marine Boundary Layer*, Wiley-VCH, British Library, 2004.

A Dynamical System Perspective of Multi-temporal Remote Sensing: Analysis of MODIS Spectral Index Time Series from Forest Wildfires

Biagio Di Mauro[1], **Giovanni Franco Crosta**[2], **Francesco Fava**[1], **Lorenzo Busetto**[1,3], **and Roberto Colombo**[1]

[1]Remote Sensing of Environmental Dynamics Laboratory
Department of Earth and Environmental Sciences, University of Milano-Bicocca, Milan, Italy
[2]Inverse Problems and Mathematical Morphology Unit
Department of Earth and Environmental Sciences, University of Milano-Bicocca, Milan, Italy
[3]European Commission, Joint Research Centre
Institute for Environment and Sustainability, Via E. Fermi 2749, Ispra, VA, Italy

Abstract— Land surface satellite time series can be interpreted as the output of a dynamical system which generates a process of interest. In this research, the qualitative theory of dynamical systems is applied to understand seasonal time series, which correspond, respectively, to spectral indexes and to the reflectance of single wavelengths from Alpine areas affected by wildfire.

A collection of 293 images acquired from MODerate resolution Imaging Spectroradiometer (MODIS) sensor aboard the NASA-Terra satellite platform was analysed in order to study the dynamics of mountain vegetation (broadleaf, needleleaf and prairies) before and after wildfires in the Alps. Satellite images of the Normalized Difference Vegetation Index (NDVI), the Enhanced Vegetation Index (EVI) and the Normalized Burnt Ratio (NBR) with spatial resolution of 250 m and time resolution of 16 days in the years 2000–2012 were used. Wildfire affected areas (> 40 ha) in Lombardy between 2000 and 2010 were selected. For each burned area, an undisturbed adjacent control site was located on the basis of a digital elevation model (DEM), historical aerial orthophotographs and land-use/land-cover maps.

A set of multi-dimensional arrays (multi-temporal imagery) was created for each spectral index (NDVI and EVI), single band (red, blue, near infra-red, short wave infra-red, all in units of radiance) and for each of the MODIS acquisition meta data (Quality Assurance, Usefulness Index, Shadow, Pixel Reliability, Sun Zenith angle, View Zenith angle and Day Of Year). The time series of these variables thus become available for each pixel of the area. Data pre-processing consisted in the smoothing of MODIS time series for noise removal; in this procedure a SAVITZKY-GOLAY recursive filter was applied, where the weighting scheme is based on the quality parameters of MODIS acquisitions.

Due to the periodic energy input to ecosystems, the vegetation growth cycle in Alpine environments exhibits marked seasonal oscillations. The optical properties vegetation and the related spectral indices are affected accordingly. The process is therefore modelled by a stable periodic orbit of a dynamical system. Wildfire is a perturbation, which alters the system parameters, hence its phase portrait. The effect of the perturbation was visualised by creating a set of yearly scatter plots of different spectral indexes and single wavelengths, extracted from burned and reference areas. Each plot is a sequence of points on the plane, which are the vertices of a generally self-intersecting polygonal chain; these were characterized by a set of morphological descriptors (area, perimeter, centroid coordinates, moments and tensor of inertia). Principal Components Analysis of these descriptors was applied and some representative wildfires could be qualitatively analyzed in the plane of the first two components.

Session 4A8b
SC5: Advances in EM Imaging and Detection of Concealed Objects or People through Walls

Overview of EM Imaging and Detection of Concealed Objects: EM Modeling, Efficient Signal Processing and Experimental Results
Patrick Millot, Brahim Boudamouz, Nadia Maaref, Xavier Ferrieres, Laurent Casadebaig, Christian Pichot, ... 1428

FDTD Based EM Modeling and Analysis for Detection of Tumors
Elizabeth Rufus, Zachariah C. Alex, ... 1429

An Approach for on Body Concealed Weapon Detection Using Continuous Wavelet Transform
Ali Saied Atiah, Nicholas John Bowring, ... 1430

Improving Non-coherent Multistatic UWB Impulse Radar System for through-the-wall Applications
Vincent Mérelle, Omar Benahmed Daho, Alain Gaugue, Jamal Khamlichi, Michel Ménard, ... 1431

UWB MIMO EM Radar Imaging for the Detection of Human Beings inside Buildings
Brahim Boudamouz, Patrick Millot, Xavier Ferrieres, Christian Pichot, ... 1433

Overview of EM Imaging and Detection of Concealed Objects: EM Modeling, Efficient Signal Processing and Experimental Results

Patrick Millot[1], **Brahim Boudamouz**[1], **Nadia Maaref**[1], **Xavier Ferrières**[1], **Laurent Casadebaig**[1], **and Christian Pichot**[2]

[1]DEMR (Electromagnetism and Radar Department)
ONERA, The French Aerospace Lab, France
[2]LEAT laboratory, CNRS-University of Nice Sophia-Antipolis, France

Abstract— In many areas of remote sensing like military surveillance applications, homeland security, non destructive testing or medical imaging, one needs to "see" the invisible. Using EM waves and the principle of radar, it is possible to detect objects, defects or even people through opaque matter. Radar or EM imaging can deliver a map of contrast of dielectric permittivity inside or through materials. EM wave can penetrate matter as long as the EM attenuation is low enough. There is a trade-off to be found between wave penetration and space resolution that depends on the wave-length and the frequency bandwidth (UWB). Of course, the performances of EM imaging depend also on signal processing. In this paper, numerous examples of EM imaging and detection will be given:

- Humanitarian mine detection (0.5–8 GHz)
- Non destructive control of lossy material (1–10 GHz)
- Breast cancer diagnostic (0.5–3 GHz)
- Detection of human beings through walls (1–5 GHz)
- Through cloth detection of weapons and explosives (8–12 GHz)

EM modeling (2D and 3D), mainly FDTD based in the context of UWB is presented and has taken large advantage of parallel computing. For processing, we have considered spotlight synthetic aperture radar imaging (with UWB and near-field corrections) with or without a simplified Green's kernel, Time Reversal processing, High Resolution Imaging (MUSIC), Inverse Problem Imaging, and MIMO multi-static imaging. Different computing efficiencies and robustness's to noise and to propagation medium are discussed. Last, various experimental set-ups (including antennas) are presented as well as experimental results.

FDTD Based EM Modeling and Analysis for Detection of Tumors

Elizabeth Rufus[1] and Zachariah C. Alex[2]

[1]Department of Engineering, Middle East College, Sultanate of Oman
[2]VIT University, Vellore, India

Abstract— Breast cancer affects many women and early detection is important. The microwave imaging technique can play a vital role in the detection of breast tumor than X-ray mammography and other techniques. The basis of the microwave imaging technique for breast cancer detection and location is the significant contrast in the scattered electromagnetic signals that depends on the dielectric properties of normal and malignant tissues at microwave frequencies. Malignant tissues exhibit higher dielectric properties than normal breast tissues, especially at high frequencies.

In this paper a Finite Difference Time Domain (FDTD) algorithm is developed to analyze the wave propagation into the dielectric medium to obtain an insight into the capabilities of the microwave imaging for detection and location of tumors. The algorithm solves for the six field components in a 3-D rectilinear space made up of Yee cells. The main program is written in C++ and acts as a driver housing all the subroutines for the problem space, structure geometry, Electric and Magnetic field algorithms, incident wave generation and the absorbing boundary conditions.

Finite Difference Time Domain investigation in this work considers a phantom formed by a spherical container filled with material whose permittivity and conductivities are similar to those of normal and abnormal tissues. The study shows that the Electric field variation in different dielectric mediums can be used for the detection of abnormality. Snap shots of the Electric field distribution inside the computational domain is viewed by writing a MATLAB code. The results show the presence of a tumor as small as that having radius 2 mm.

An Approach for on Body Concealed Weapon Detection Using Continuous Wavelet Transform

A. Atiah[1] and N. J. Bowring[2]

[1]Alzaetona University, Libya
[2]Manchester Metropolitan University, UK

Abstract— The demand to remotely and automatically detect concealed weapons at the entrance of public places such as airport and government buildings has been a major security challenge. In the application of detecting the response of concealed on body weapons, powerful signal processing algorithms that accurately extract the target signature is needed [1, 2]. New approach for concealed weapon detection based on a CWT applied to the scattering response of a target being detected has been successfully tested. A series of experiments were conducted to test the CWT performance on the new approach of this detection system which involved on and off body objects such as, knives, handheld guns. Experimental results illustrated the success of the approach of using the CWT in analyzing the LTR signature. Spectral response for every target could be seen as a distribution in which the energy level and life-time depended on the target material and geometry. Onbody target detection results show that use of the CWT technique is capable of detecting the existence or absence of target objects concealed onbody and is also capable to discriminate between different objects. The signature of both an on body knife and on body handgun was verified the feasibilities of using TFDs to study transient scattering from on body concealed targets. The spectral density provides very powerful information concerning target complexity and geometry. As a result of that it can be confirmed that the CWT response is directly identifies the response of the unknown concealed target and could be a very powerful tool in the detection of any on body concealed object.

REFERENCES

1. Harmer, S., D. Andrews, N. Rezgui, and N. Bowring, "Detection of handguns by their complex natural resonant frequencies," *IET Microwaves, Antennas & Propagation*, Vol. 4, 1182–1190, 2010.
2. Atiah, A. and N. Bowring, "Design of flat gain UWB tapered slot antenna for onbody concealed weapons detections," *PIERS Online*, Vol. 7, No. 5, 491–495, 2011.

Improving Non-coherent Multistatic UWB Impulse Radar System for through-the-wall Applications

V. Mérelle, **O. Benahmed Daho**, **A. Gaugue**,
J. Khamlichi, **and M. Ménard**
Laboratory of Informatics Image and Interaction (L3i)
La Rochelle University, France

Abstract— Through-the-wall (TTW) radar is a strategic research topic because of its outstanding applications in major fields such as antiterrorism and urban security. This paper presents an experimental TTW radar in multilateral configuration based on pulsed Ultra Wide Band technology. The major drawbacks of such systems are technical aspects: high bandwidth, fast acquisition speed and precise time synchronisation. Moreover pulse signals are highly sensitive to environment noise and need some preprocessing to be exploitable. In return, the wall effects, mainly constituted by the first received impulse, can be easily removed. The imaging reconstruction algorithms are straightforward with trilateration based algorithms, without needs of some time-consuming FFT to get the distances as in the case of FMCW radar.

The radar demonstrator developed is composed with a pulson P210 pulse generator of the Time Domain Corp with an omnidirectional antenna. The emitted signal is a Gaussian pulse modulated by a sinusoid at a 4.6 GHz frequency, and 3.2 GHz of bandwidth. The receiver part is composed with four directional antennas uniformly distributed in line around the transmitter's antenna.

The acquisition of the received signals is done by a 6 GHz bandwidth oscilloscope (Agilent 54855A DSO). The system quality is based on the property of the emitted signal and the precision of the acquisition time. Thus, the emitter is wired directly to the transmitter antenna and the trig signal of the oscilloscope is generated by an extra antenna placed closed to the transmitter antenna. In that way, we obtain a clean signal with a good amplitude, and which can meet the full performance of the oscilloscope trigger circuit which exhibits 1 ps RMS of jitter.

This performance allows to make some equivalent time sampling [1] by delaying acquisitions of a step of few picoseconds and sorting them to obtain datasets with a new time step equal to the delay value, typically 10 ps. To minimize the noise, an average of the signals is systematically applied.

The imaging technique used in this radar system is a non-coherent method based on the TOA. This time is obtained by computation of the signal envelope. Usually this envelope is provided by Hilbert transform. In our case, we used the higher order statistics method [2] which has the twin advantages of removing some noise in the signal and vanishing phase-uncoupled harmonics to get the envelope.

Then, the image is built with a modified cross-correlated back projection algorithm [3]. The back projection technique superimposed all the received signals on a screen to bring out the scatter points. This result is correlated with two reference antennas in order to reduce the inherent artefacts. The modification consists in a moving average on the correlation with a subset size equal to the impulse time.

The article presents a new methodology of acquiring the data with a commercial oscilloscope and new preprocessing operations. It was tested with a scene composed with two targets behind a wallboard of 7 cm thickness [4]. The images were formed with a modified cross-correlated back projection algorithm to gain in fidelity. It points out good results compared to others TTW systems.

REFERENCES

1. Yang, Y. and A. E. Fathy, "Development and implementation of a real-time see-through-wall radar system based on FPGA," *IEEE Transactions on Geoscience and Remote Sensing*, Vol. 47, 1270–1280, 2009.
2. Tungnait, J. K., "Time delay estimation with unknown spatially correlated Gaussian noise," *IEEE Transactions on Signal Processing*, Vol. 41, 549–558, Feb. 1993.
3. Zetik, R., J. Sachs, and R. Thomas, "Modified cross-correlation back projection for UWB imaging: Numerical exemples," *2005 IEEE International Conference on Ultra-Wideband, ICU 2005*, Sep. 2005.

4. Zhao, X., A. Gaugue, C. Lièbe, J. Khamlichi, and M. Ménard, "Through the wall detection and localization of a moving target with a bistatic UWB radar system," *Enropean Radar Conference (EuRAD)*, 204–207, 2010.

UWB MIMO EM Radar Imaging for the Detection of Human Beings inside Buildings

Brahim Boudamouz[1], **Patrick Millot**[1], **Xavier Ferrieres**[1], **and Christian Pichot**[2]

[1]The French Aerospace Lab, Electromagnetism and Radar Department, DEMR, ONERA, France
[2]LEAT Laboratory, CNRS, University of Nice Sophia Antipolis, France

Abstract— The ability of electromagnetic (EM) waves to penetrate buildings or opaque materials and sense targets at stand-off makes radar systems attractive for indoor detection. Here we address EM detection in urban context with the emerging radar technique named multiple-input multiple-output (MIMO) radar. MIMO radar concept consists in using several transmitting antennas and several receiving antennas. To be precise, we focus on human beings EM detection inside buildings. It is well known that detection systems through buildings are of great use in law enforcement operations.

Nevertheless, EM wave propagation through the walls (TTW), especially heterogeneous walls like concrete bricks or cinder blocks, induces EM signals deformations. They encounter strong attenuation with respect to frequency and incidence and also wave-front distortions. To overcome these EM wave propagation limitations and improve detection performances, TTW radar systems use Ultra Wide Band to obtain frequency diversity to mitigate TTW propagation effects. More, apart an increase in image resolution, the MIMO concept brings some antenna diversity for TTW detection and gives new perspectives to improve indoor detection.

These improvements due to MIMO have been first observed with with a Finite Difference Finite Domain (FDTD) full wave simulator. FDTD computations allow addressing both through wall propagation effects and indoor multi-path effects. The simulator allows modelling different kind of wall: homogeneous wall (concrete) or heterogeneous wall (cinder blocks). Other elements can also been added to simulation scenarii like human beings or furniture.

In TTW radar, detection and localization is realized with the help of an EM imaging processing. Thus, simplified signal model have been proposed to take into account TTW propagation effects. Then radar imaging algorithm applied to the MIMO configuration have been derived. Results of radar imaging for different scenario are presented.

At the same time, an experimental FMCW MIMO radar have been developed. The UWB system is 2 GHz bandwidth, has 4 transmitting antenna and 8 receiving antennas and use Time-Multiplexing to address antennas. The system allows detection and localization through wall. Some EM imaging results on cinder blocks walls with experimental data are presented.

Session 4AK
Poster Session 7

Single-particle Plasmonic Switching Realized by Coating Polyaniline on Colloidal Gold Nanorods
Nina Jiang, Lei Shao, Jianfang Wang, ... 1438

Dependence of Slow Light Characteristics of Photonic Crystal Waveguides on the Properties of Holes Surrounding the Line Defect
Fulya Bagci, Baris Akaoglu, ... 1439

Magnetron Sputtered Optical Nanogradient Coatings
Nikolay F. Abramov, Oleg D. Volpian, Yuri A. Obod, Sergey V. Schkatula, ... 1440

Examples of UV Measurements under 400 kV Powerlines in Finland
Rauno Paakkonen, Leena Korpinen, Fabriziomaria Gobba, ... 1441

Multi-core Liquid Photonic Crystal Fiber Based Localized Surface Plasmon Resonance Temperature Sensor
Ying Lu, Congjing Hao, ... 1442

Stochastic Electromagnetic Plane-wave Pulse with Non-uniform Correlation Distribution
Chaoliang Ding, Liuzhan Pan, ... 1443

Polarization Changes of Stochastic Electromagnetic Bessel-Gauss Pulsed Beams through a Dispersive Aperture Lens
Haixia Wang, Chaoliang Ding, Zhiguo Zhao, Liuzhan Pan, ... 1444

Nonlinear Dissipative Dynamics and Optical Properties of Quantum Dots for Nanomedicine
Vladimir D. Krevchik, Vladimir I. Volchikhin, Igor I. Artemov, Mikhail B. Semenov, Roman V. Zaitsev, Alexey V. Razumov, Ascar K. Aringazin, Kenji Yamamoto, ... 1445

Effects of Extremely High Frequency EMI on Growth and Some Parameters of Wheat Seedlings Nuclei
Liya A. Minasbekyan, M. R. Darbinyan, ... 1446

Increasing of Fermentative and Antiinflamatory Activity of the Pleurotus Ostreatus (Jacq.:Fr.) Kumm. Culture by Modification of Growth Conditions by MM-waves
Inessa A. Avagyan, Siranush G. Nanagulyan, Liya A. Minasbekyan, ... 1447

3-D Reconstruction of the Breast Surface for Microwave Breast Cancer Imaging Applications
Ahmet Hakan Tunçay, P. Tunçay, Ibrahim Akduman, ... 1448

A Flexible RF Exposure Setup for Long-term Electrophysiological Investigations on Biological Samples in Vitro
Stefan Oster Oster, Andreas Daus, Michael Goldhammer, Ulrich Bochtler, Christiane Thielemann, 1449

Influence of Near Earth Electromagnetic Resonances on Human Cerebrovascular System in Time of Heliogeophysical Disturbances
Elena A. Sazanova, A. V. Sazanov, Nadezda P. Sergeenko, V. G. Ionova, Yu. Ya. Varakin, ... 1450

MRI Imaging of the Physiology of Fungal Pathogens in Cultivated Plants
Eliska Hutová, Karel Bartušek, Radim Korinek, Radovan Pokorny, ... 1451

Comparison and Display of the Water Contained in Early Somatic Embryos
Eliska Hutová, Radim Korinek, Karel Bartušek, Ladislav Havel, ... 1452

Methods for the Sensing of Ionosphere Changes
Michael Hanzelka, Pavel Fiala, Martin Friedl, ... 1453

Thermal Conductivity and Heat Capacity Measurement of Biological Tissues
Jan Hrozek, Dusan Nespor, Karel Bartušek, ... 1454

Multi-resolution Analysis Technique for Lung Cancer Detection in Computed Tomograpic Images
Muhammad Usman, Muhammad Shoaib, Mohamad Rahal, ... 1455

Development of Biological Tissue-equivalent Agar-based Solid Phantom in HF Band
Mizuki Inoue, Ryotaro Suga, Kazuyuki Saito, Masaharu Takahashi, Koichi Ito, ... 1456

Novel Magnetic Lens for Static Magnetic Field Enhancement
Fei Sun, Sailing He, ... 1457

Impact of Electromagnetic Field Generated nearby High Voltage Alternating Current Transmission Lines on Prooxidant-antioxidant Balance in Selected Internal Organs of Rats

Pawel Sowa, Karolina Sieron-Stoltny, Grzegorz Jan Cieslar, Aleksander Sieron, ... 1458
System Information Therapy as a Tool in Personalized Medicine
Alberto Foletti, Settimio Grimaldi, ... 1459
System Information Therapy in the Management of Pain: A Pilot Study
Paolo Baron, Giuseppe Bucci, Alfio Rinaudo, Roberto Rocco, Eugenio Sclauzero, Alberto Foletti, .. 1460
The Thermal Analysis of Some Light Sources
A. Yasin Citkaya, S. Selim Seker, Osman Cerezci, ... 1461
EM System to Guide Visually Impaired Running Athlete
Valerio Petrini, Valentina Di Mattia, Marco Pieralisi, Lorenzo Scalise, Valter Mariani Primiani, Alfredo De Leo, Paola Russo, Graziano Cerri, ... 1462
Characteristics of an Optical Bowtie Nanoantenna
Ahmed Abbas, Mostafa El-Said, Samir F. Mahmoud, ... 1464
Characteristic of Novel Elliptical-spiral Photonic Crystal Fibre with Arbitrary Gold Wires Embedded in Cladding Air Holes
Ahmed Mahmoud Heikal, Salah Sabry Ahmed Obayya, ... 1465
Near Field Optics of Plasmonic Nanostructures Presenting High Aspect Ratio
Yacoub Ould Agha, G. Colas des Francs, ... 1467
Localized Plasmons and Interface Reflections: Fano Interference and Complete Light Annihilation
Mikael Svedendahl, P. Johansson, Mikael Kall, ... 1468
Redshift by Design for Plasmonic Enhancement of Ultrathin Infrared Detectors
Marko Obradov, Zoran Jaksic, Milija Sarajlić, Danijela Randjelović, ... 1469
Gain Assisted Surface Plasmon Polariton Propagation in a Schottky Junction Based Cylindrical Structure
Thamani Manjula Wijesinghe, Malin Premaratne, ... 1470
Novel, Compact and Multiband Antenna for Mobile and Wireless Communication
Kamel Salah Sultan, Haythem Hussein Abdullah, Esmat Abdel-Fattah Abdallah, Essam Abdel Haleem Hashish, ... 1472
Gold Plating Carbon Nano Tube Antenna Integrated with Voltage Control Oscillator
Kuan-Ting Lin, Jian-Yu Hsieh, Yu-Jen Chen, Shuo-Hung Chang, Ying-Jay Yang, Shey-Shi Lu, .. 1473
Dual-band Antenna for In-building Repeater Systems
Ho-Jun Lee, Min-Ki Woo, Nae-In Lee, Gene Yoo, ... 1474
Development of Textile Antennas for Smart Clothing Applications
Kuo-Sheng Chin, Chi-Sheng Wu, Chih Chun Chang, ... 1475
MIMO Reference Antennas for OTA Applications
Shuai Zhang, Kun Zhao, Zhinong Ying, Sailing He, ... 1476
Theoretical Analysis of AC Resistance of Coil Made by Copper Clad Aluminum Wires
Chihiro Kamidaki, Ning Guan, ... 1477
A Hybrid Optimization of Wireless Power Transfer with Intermediate Coils
Tie Jun Cui, Shuo Liu, Linhui Chen, ... 1478
A Rectenna for Wireless Power Transmission
Jwo-Shiun Sun, Si-Jyun Hung, Yi-Ching Huang, Tsung-Lin Li, Guan-Pu Pan, ... 1479
Compact Design of a Flexible and Wearable Tri-band Rectenna
Diego Masotti, Alessandra Costanzo, Massimo Del Prete, Martino Aldrigo, Riccardo Trevisan, ... 1480
Wireless Power Transmission by Enlarging the Near Field
Konstantin Meyl, ... 1482
Numerical Study on the Radiative Transmission Efficiency of Dipolar Sources
Charles Luke Moorey, William Holderbaum, Ben A. Potter, ... 1483
An Energy Management Circuit Based on Up-conversion to Power Wireless Sensor Nodes
Shiqiang Pan, Ping Li, Yumei Wen, Ziqiang Zhang, Dan Lu, Dengfeng Sun, ... 1484
Self-contained Self-powered Wireless Sensing Node for AC Power Supply Cords Monitoring
Dan Lu, Yumei Wen, Ping Li, Shiqiang Pan, Ziqiang Zhang, ... 1486
Symmetric Ridge-type Semiconductor Laser with Selectively Formed Double-sided Antiguiding Cladding Layers
Daiya Katsuragawa, Takahiro Numai, ... 1487
Design of Narrow Core Structure for High Power Pickup Device in Railroad Application
Sang Hoon Chung, Bo Yune Song, Dang-Oh Kim, Uooyeol Yoon, Jaegue Shin, Yangsu Kim, Chung Hee Lee, Guho Jung, ... 1488

A 200 GHz on-chip Active Antenna
Bing Zhang, Li Wei, Mingquan Bao, Yinggang Li, Herbert Zirath, ... 1489
A Compact Energy Pattern Reconfigurable Antenna
Junrui Zhang, Shao-Qiu Xiao, ... 1490
Scanning Range Expanding of Time Domain Array with Energy Pattern Reconfigurable Antenna Elements
Junrui Zhang, Shao-Qiu Xiao, ... 1492
Design of Ultra Wideband Balanced Antipodal Vivaldi Antenna for Hyperthermia Treatment
Khaled A. Alsulaiman, Mohammed Al alShaykh, Sulaiman Alsulaiman, Ibrahim M. Elshafiey, ... 1494
Label-free Acoustic and Optical Biosensors Playing on Evanescent Waves
Yihui Wu, Guigen Liu, Peng Hao, Junfeng Wu, Yongbo Deng, Yongshun Liu, Ming Xuan, ... 1495
The Estimation of a Gold Nanoparticles Distribution Using the Evanescent Electric Field in Gold Nanoparticles Filled Surface Plasmon Resonance Biosensing
Chardchai Korjittavanit, Rardchawadee Silapunt, Boonsong Sutapun, ... 1496
Numerical Analysis of Passively Q-switched Er and Yb Doped Fiber Laser
Dan Savastru, Roxana Savastru, Sorin Miclos, Ion Lancranjan, ... 1497
Vector Magnetic Field Detecting with a Single Nitrogen Vacancy Center in Diamond
Xiangdong Chen, Changling Zou, Fangwen Sun, ... 1498
Low-pass Filter Design from EBG Waveguides Periodically Loaded with Metal Ridges
Stephan Marini, Pablo Soto, Angela Coves, Benito Gimeno Martinez, Vicente E. Boria, ... 1499
Monte-Carlo MPSTD Analysis on Scattering of Cylinders Buried in a Layered Half Space with Random Rough Interface
Yueyang Dai, Wei Liu, Xiao-Bang Xu, ... 1500
Design of Multiband Reflection Filters with Dielectric Frequency Selective Surfaces
Angela Coves Soler, Benito Gimeno Martinez, Miguel Vicente Andres, ... 1501
Method of Pseudodifferential Equations for Problems of Electromagnetic Wave Diffraction by Closed Screens
A. Ilyinsky, Yury G. Smirnov, ... 1502
Nonlinear Optical Limiting in Suspensions of Carbon Nanotubes
Andrey Yu. Vlasov, Anastasia Venediktova, Ivan M. Kislyakov, Dmitry A. Videnichev, Elena D. Obraztsova, Ekaterina P. Sokolova, ... 1503
A 12-cavity Relativistic Magnetron with Optimized Design of Diffraction Output
Meiqin Liu, C. Liu, Edl Schamiloglu, ... 1504
Rabi Splitting in Acoustics
Xu Ni, Li-Yang Zheng, Ze-Guo Chen, Ming-Hui Lu, Yan-Feng Chen, ... 1505
Near Zero Index in Phononic Crystal Induced by Flat Branch
Li-Yang Zheng, Xu Ni, Ze-Guo Chen, Ming-Hui Lu, Yan-Feng Chen, ... 1506
Fabrication and Characteristic of Nanometal(Shell)-silica(Core) Composite Particles by Ultrasonic Electrodeposition
Jun Qi, Yue Feng Tang, Yi Zhang, Yan-Feng Chen, ... 1507
Enhanced Rotation of the Polarization of a Light Beam Transmitted through a Silver Film with an Array of Perforated S-shaped Holes
Shan Wu, Xuejin Zhang, Yongyuan Zhu, ... 1509

Single-particle Plasmonic Switching Realized by Coating Polyaniline on Colloidal Gold Nanorods

Nina Jiang, **Lei Shao**, **and Jianfang Wang**
Department of Physics, The Chinese University of Hong Kong, Shatin, Hong Kong SAR, China

Abstract— Plasmonics, an emerging branch in photonics, has the potential in developing various nanoscale photonic devices for integrated photonic circuits. A number of plasmon-based optical devices, such as filters, waveguides, resonators, and lenses, have been demonstrated. Metal nanostructures, owing to their extraordinary localized surface plasmon resonance (LSPR) properties, have been widely used in fabricating such plasmon-based devices. Optical switches are essential components in integrated photonic circuits. Developing robust optical switches will be crucial for integrated photonic circuits and many other optical applications.

Polyaniline (PANI) has been considered as the most promising conductive polymer owing to its low cost, convenient synthesis, good environmental stability, and processability. Its conductivity depends on two variables, i.e., the oxidation and protonation degrees. Through the control of either variable, PANI can transform completely from an insulator to a conductor.

PANI has been combined with Au nanostructures in previous studies for fabricating active plasmonic devices. The PANI synthesis and device fabrication in those studies are very time-consuming and complicated. Au nanostructures have been fabricated by electron beam lithography. PANI has been synthesized through electrochemical polymerization. This polymerization method can neither ensure the uniform coating of PANI on Au nanostructures, nor give similar conductivities to those obtained by chemical oxidative polymerization.

Herein, we describe the coating of PANI on colloidal Au nanorods at varying thicknesses and the realization of plasmonic switching on single PANI-coated Au nanorods. The coating of PANI was through surfactant-assisted chemical oxidative polymerization. The resultant core/shell nanostructures were embedded on a microfluidic chip. By injecting acidic and basic solutions alternately, the longitudinal plasmon peak of single Au nanorods was reversibly switched at two wavelengths, with the plasmon shifts reaching up to 100 nm. The unprecedented plasmon shifts, easily observable by eyes, between the two switching states was understood to arise from the proton-doped and undoped states of PANI. Moreover, we also simulated the plasmonic switching behaviors of the PANI-coated Au nanorods. The simulated spectra were in reasonable agreement with the experimental ones. Our plasmonic switches will be useful for many optofluidic applications. They can further be adapted for the fabrication of smart windows with controllable transmissions and colors.

Dependence of Slow Light Characteristics of Photonic Crystal Waveguides on the Properties of Holes Surrounding the Line Defect

Fulya Bagci and Baris Akaoglu
Department of Engineering Physics, Faculty of Engineering, Ankara University
Besevler, Ankara 06100, Turkey

Abstract— Slow light, naturally occurring near the band edges of the photonic crystal waveguides (PCW), is restricted to a narrow bandwidth region and shows great group velocity dispersion (GVD) which causes the degradation of optical signals. A variety of design approaches have been proposed to eliminate these drawbacks. Among these methods, changing the radius and position of the rows of holes adjacent to the line-defect have been the most applied procedures for generating slow light. On the other hand, ring-shaped holes are attractive in PCWs due to their enhanced sensing property. In this study, slow light properties of various PCWs embedded in silica is studied by plane wave expansion method and finite-difference time-domain calculations. By changing the position of the rows and the type of holes in these rows adjacent to the line-defect separately and in combination, the mechanism of controlling slow light properties has been investigated. We point that shifting of the first and second rows adjacent to the line-defect have different impacts on group index-frequency curves and are rather associated with different sections of the guided mode which offers a strategy to design flatter bands. The anticrossing point shifts to smaller wave-numbers as outer radius of ring-shaped holes increases, which removes the slow light region more from the Brillouin-zone edge. Almost constant normalized delay-bandwidth products of about 0.28 have been found for a variety of group indices and photonic crystal waveguide configurations. In the slow light bandwidth, the maximum GVD parameters are determined for various amounts of shifts.

Magnetron Sputtered Optical Nanogradient Coatings

Nikolay F. Abramov[1], **Oleg D. Volpian**[1], **Yuri A. Obod**[2], **and Sergey V. Schkatula**[2]

[1]JSC "M. F. Stelmakh R&D Institute Polyus", Russian Federation
[2]Scientific-Manufacturing Enterprise "Fotron-Auto Ltd.", Russian Federation

Abstract— Energetic, spatial and spectrum characteristics of optical system parts greatly depend on deposited optical coatings properties. For example, in order to provide operating characteristics for modern laser systems, optical coatings must meet the following complex requirements: simultaneous multiple-wavelengths functioning, hard-driving modulation of optical characteristics, low optical losses, high resistance to high-power radiation and strong thermal and humid influences. The increasing requirements for operating characteristics of optical and laser systems have shown the need of novel optical coatings development, which will meet these requirements. Among these are nanogradient coatings, where the refractive index greatly changes along the layer thickness in a thin dielectric layers structure (for the thickness less than 100 nm) [1]. Gradient coatings, made of metamaterials and described in some sources are perspective for these applications [2].

Production of nanogradient coatings is a difficult technological problem. According to our research the best technique for high-quality optical dielectric thin-films production is the pulse magnetron sputtering technique in reactive gas medium [3]. The automated equipment for precision nanogradient optical coatings production using the dual-magnetron sputtering deposition technique has been created in JSC "M. F. Stelmakh R&D Institute "Polyus" and "SME "Fotron-Auto" Ltd. The technology of production of $1D_z$ gradient sub wave-thickness coatings has been developed using this equipment.

Moreover, novel analytical-numerical method for nanogradient optical coatings engineering for required spectral characteristics was developed. It is based on the combination of two algorithms: the analytical one for coating engineering, and the heuristic one for coating structure optimization. New engineering software of computer-based modeling was developed on the base of this novel method. Furthermore, developed control equipment and software let execute in situ reengineering of their structure when producing complex coatings. As a result, the reproducible nanogradient optical structures with divers profile and modulation of refractive index were produced.

Test results for the nanogradient coatings, which were produced using the developed equipment and software, have shown the conformity to radiation, climatic and mechanical requirements for onboard optical and laser systems. These optical and laser coatings have been successfully implemented and operated in avionic and space devices since some years.

REFERENCES

1. Kuzmichev, A. I., A. B. Shvartsburg, O. D. Volpian, Y. A. Obod, and P. P. Yakovlev, "Polarized light in nanogradient metamaterials," *Optical Complex Systems: OCS11*, Marseille, France, September 5–8, 2011.
2. Volpian, O. D. and A. I. Kuzmichev, "Negative waves refraction. Introduction in physics and technology of electromagnetic metamaterials," *Kiev*, Avers, 2012.
3. Volpian, O. D., A. I. Kuzmichev, Y. A. Obod, and P. P. Yakovlev, "Optical nanogradient metacoatings production using the reactive magnetron sputtering," *Mat. Of 15th Intern. Conf.*, "High technologies in the industry of Russia — Materials and devices of functional electronics and microphotonics," *22th Intern. Symp.*, "Thin-films in electronics," 447–450, Moscow, 2009.

Examples of UV Measurements under 400 kV Powerlines in Finland

Rauno Pääkkonen[1], **Leena Korpinen**[2], **and Fabriziomaria Gobba**[3]

[1]Finnish Institute of Occupational Health, Tampere, Finland
[2]Department of Electronics and Communications Engineering
Tampere University of Technology, Tampere, Finland
[3]Department of Public Health Sciences, University of Modena and Reggio Emilia, Italy

Abstract— Ultraviolet radiation exposure in Finland is relatively low compared to other European countries, for example, in Italy. However, the Nordic skin type is often lighter, and thus the risk of adverse effects can also exist in Finland. Approximately 30% of Finnish persons have skin type I-II, and most of Finns have skin type III. Therefore, at least 30% of Finns have a relatively high risk of sunburn if they are exposed to the sun in summer in Finland.

The Finnish limit value at work for weighted ultraviolet radiation (UV-BC) is $30\,\mathrm{J/m^2}$ for 8 h exposure (based on European directive (2006/25/EU)), which is not applicable to sunshine. We measured UV-BC weighted radiation with a meter Solar PMA2100 equipped with a safety probe PMA2120 (calibrated 2010 at the factory), and we received a dose of $0.65\,\mathrm{J/m^2}$ over one hour and $1.23\,\mathrm{J/m^2}$ when the measurement period was over 3 hours and 51 minutes. If we calculate from this a daily dose, we receive a value of less than $3\,\mathrm{J/m^2}$, which is about 10% of our exposure limit value.

Secondly, we measured instantaneous values of irradiances to be 2–150 $\mathrm{mW/m^2}$, which exceeds, for example, the ACGIH (American Conference of Industrial Hygienists) recommended value of $1\,\mathrm{mW/m^2}$ over 8 hours. This also means that in Finland, the erythema dose can be exceeded in a light skinned person if protection measures, such as entering a shaded are or applying sun lotions are not employed. In Finland, the recommended midsummer exposure recommendation is less than one hour for type II skin.

Multi-core Liquid Photonic Crystal Fiber Based Localized Surface Plasmon Resonance Temperature Sensor

Ying Lu and Congjing Hao
College of Precision Instrument and Opto-electronics Engineering, Tianjin University, China

Abstract— We demonstrate a kind of multi-core photonic crystal fiber (PCF) -based localized surface plasmon resonance temperature sensor in this paper. The gold nanowires with the mixed liquid (the ratio of chloroform and ethanol is 7:3) with large thermo-optic coefficient are embedded in the PCF to guarantee the total internal reflection sensing mechanism. With the scattering boundary condition, a full-vector finite element method is used to calculate the fiber model and investigate the temperature sensing properties. The numerical results indicate that a blue-shift in the localized surface plasmon resonance related peak with the temperature increases, as well as the narrowing of the plasmon resonance shift. This can be explained by that the temperature variations will influence on the coupling efficiencies between the plasmonic mode and the core-guided mode. And the simulation results for the loss spectra show that the rensonance wavelength of the PCF-based temperature sensors with $-20°$C, $-10°$C, $0°$C, $10°$C, $20°$C, and $30°$C temperature is in the range of 550–580 nm. Moreover, the confinement loss curves demonstrate a declining trend with the temperature increases. It is namely that the higher temperature confines the fiber core and surface plasmon mode resonance, which makes the energy of light field in the core has lower loss. In our work, with the simulation results, a temperature sensitivity of 1100 pm/°C is achieved, which is higher than many formerly reported structures. And if 10 pm can be accurately detected, the corresponding sensor resolution is 9.09×10^{-3}°C. Moreover, the proposed PCF-based temperature sensor design indicates that it shows higher sensitivity for low temperature detection than that for high temperature detection range. So the proposed structure may be more useful for cryogenic temperature. And we expect that the PCF-based LSPR temperayure sensor can provide an effective platform and will be very convenient for many sensing fields.

Stochastic Electromagnetic Plane-wave Pulse with Non-uniform Correlation Distribution

Chaoliang Ding and Liuzhan Pan
Department of Physics, Luoyang Normal University, Luoyang 471022, China

Abstract— Recently, more and more attention is being paid to a stochastic beam with non-uniform correlation distribution. Up to now, only few papers were devoted to the propagation properties of non-stationary stochastic light with non-uniform correlation distribution. In this paper, the stochastic electromagnetic plane-wave (SEPW) pulse with non-uniform correlation distribution is introduced. The realizability condition for such pulse is derived. It is found that the evolution properties of the intensity and the degree of polarization of a SEPW pulse with non-uniform correlation distribution in dispersive media are much different from those of a SEPW pulse with uniform correlation distribution.

Polarization Changes of Stochastic Electromagnetic Bessel-Gauss Pulsed Beams through a Dispersive Aperture Lens

Haixia Wang, **Chaoliang Ding**, **Zhiguo Zhao**, **and Liuzhan Pan**
Department of Physics, Luoyang Normal University, Luoyang 471022, China

Abstract— The analytical expression for the cross-spectral density function of spatially and spectrally partially coherent electromagnetic Bessel-Gauss pulsed beams through a dispersive aperture lens is derived and used to study the changes in the degree of polarization at the focal plane. The effect of pulse duration, temporal coherence length and dispersion of different orders on the degree of polarization of electromagnetic Bessel-Gauss pulsed beams is illustrated through numerical calculations.

Nonlinear Dissipative Dynamics and Optical Properties of Quantum Dots for Nanomedicine

V. D. Krevchik[1], **V. I. Volchikhin**[1], **I. I. Artemov**[1], **M. B. Semenov**[1], **R. V. Zaitsev**[1], **A. V. Razumov**[1], **A. K. Aringazin**[2], **and K. Yamamoto**[3]

[1]Penza State University, Russia
[2]Eurasian National University, Kazakhstan
[3]International Medical Center, Japan

Abstract— The aim of this work is theoretical and experimental study of the effect of doping for semiconductor quantum dots on their photoluminescence (PL), which has important applications both for nanomedicine and nanoelectronics devices to create the controlled properties. An experimental study of the surface treatment effect for quantum dots (QDs) of CdSe on their photoluminescence (PL) has been fulfilled. It is shown that the highest intensity of photoluminescence yield QD with surface treated by the donor electron impurity. The role of the QD doping by impurities has been theoretically studied. It is shown that the PL intensity in this case can be increased considerably. The development of the 1d-dissipative tunneling theory for structures with quantum dots in the system of combined AFM/STM in an external electric field at a finite temperature has been proposed. The probability of the 1d-dissipative tunneling in a double-well model oscillator potential in the external electric field with accuracy of the pre-exponential factor has been calculated. Theoretical investigation of features for the field dependence of the tunnel probability is allowed to offer the controlled growth method of colloidal gold QD, based on the transformation of the oscillator double-well potential in the external electric field. The applicability of nanoscale dots (QD) from colloidal gold for nanomedicine has been discussed. For example, QD from colloidal gold are used as carriers of drugs, as well as for the diagnosis and treatment of cancer. Optical response for QD from colloidal gold (surface enhanced Raman spectroscopy) is 200 times brighter than for semiconductor quantum dots. Optical and transport properties of the doped semiconductor QDs with bio-conjugated shells can be used as fluorescent labels for imaging of biological objects and in nanomedicine for the diagnosis and treatment of a number of serious diseases, including cancer.

Effects of Extremely High Frequency EMI on Growth and Some Parameters of Wheat Seedlings Nuclei

L. A. Minasbekyan and M. R. Darbinyan
Department of Biophysics, Yerevan State University, 1 Alek Manukyan St, Yerevan 0025, Armenia

Abstract— Low intensively EHF EMI capable to cause the replay of the biological system, appearing on all level of the organizations of the alive organism. Initial unit of the biological influence of EMI is the lipid layers of membrane, which stimulate peroxidation of lipids.

The phospholipids (PL) content of nuclear soluble fraction and membrane of wheat seedlings have been investigated. Under treatment of soak seeds by EM mm-waves of different frequency, to the 3-D day of germination occur redistribution in PL composition of seedlings nuclear subfraction. EM mm-waves influence not only on the PL content of nuclear envelope, but act and on the chromatin conformation, DNA melting parameters and DNA methylation, and by this path controlling of permeability of nuclear membrane and its surface charge.

We have study as well as electrokinetic property of intact nuclei from wheat seeds-control and treated by different EMI (extremely high frequency) in the range 45–53 GHz, *in vitro* and *in vivo*. Have been investigated biochemical content (DNA, RNA and protein) of nuclear envelope too. Nuclear envelope and its charge play significant role in the transport of macromolecules between nucleus and cytoplasm through nuclear pore complexes. The significant effect was observed at exposition of 40 min treated *in vitro* intact nuclei led to the increasing of EKP, that evidence that EMI change surface charge on the nuclei. The biological effective frequencies are narrow range 49–53 GHz with the expressed resonant frequencies close to 50.3 GHz and 51.8 GHz are revealed. On the basis of our study we suggested that EMI of this diapason increase of preservation system of living organisms. Biological replay directs to the surviving of organisms and an adaptive reaction of organism against to the stress of physical factors of environment.

Increasing of Fermentative and Antiinflamatory Activity of the Pleurotus Ostreatus (Jacq.:Fr.) Kumm. Culture by Modification of Growth Conditions by MM-waves

I. A. Avagyan[1], S. G. Nanagulyan[1], and L. A. Minasbekyan[2]

[1]Department of Botany and Mycology, Yerevan State University
1 Alek Manukyan St, Yerevan 0025, Armenia
[2]Department of Biophysics, Yerevan State University
1 Alek Manukyan St, Yerevan 0025, Armenia

Abstract— Epidemiological studies have indicated that almost all cases of cancer are associated with environmental factors including foods. Mushrooms have recently become attractive as health beneficent foods. Mushrooms have been used traditionally to treat many types of cancers. In mushroom's content there are such valuable compounds as the isoflavones genestein, β-glucans, glioxal-oxidase et al.. Plants contain isoflavones in primarily in glucoside forms and need in β-glucosidase which converts glucoside isoflavones in more potent aglicone forms. The unique feature of mushrooms in their content of β-glucosidase enzyme and various type of active peroxidases.

We have examined the most popular edible wood-decaying mushroom — *Pleurotus ostreatus* (Jacq.:Fr.) Kumm., which is wide-spreading in the forests, under influence of such an abiotic factor as the extremely high frequency waves in the interval of 45–53 GHz during 20 and 40 min on the 7-th day of mycelial culture's growth. The some conditions of such treatment led to significant rising of the peroxidase activity in mycelia culture homogenate. After the treatment of culture at the 3-th and 4-th days we examined the influence these waves on physiological parameters of the growth, changes in the protein content and fermentative activity. Such treatments and conditions will allow us to produce mushrooms with high content of active enzymes and high protein content without genetically transformation, which provides us with high valuable pharmaceutical raw materials.

We study antiinflammatory property obtained extracts from mushroom cultures with increased fermentative activity. Antiinflammatory activity of mushroom's extract investigate on the model of ear acute inflammation stimulated by xylol on white underbred rat-male. Antiinflammatory activity estimated by mass difference after 90 min of administration of the fresh extract from mushroom's culture, treated by various frequency of mm-waves. As evidence our investigations intraperitoneal introduction of led to the decreasing of induced by xylol ear swelling compare with control up to 85%.

Obtained data evidence about high antiinflammatory activity of extracts from culture of wood-decaying mushroom's, due to increased fermentative systems, having antioxidant activity and be able to inhibited ferments, participated in synthesis and metabolism of prostaglandins.

3-D Reconstruction of the Breast Surface for Microwave Breast Cancer Imaging Applications

A. H. Tunçay[1], **P. Tunçay**[2], **and İ. Akduman**[1]

[1]Electronics & Communications Department, Istanbul Technical University, Istanbul, Turkey
[2]Department of Satellite Communication and Remote Sensing
Istanbul Technical University, Istanbul, Turkey

Abstract— Microwave imaging of the human breast emerged as a promising multidisciplinary area for early breast cancer detection concerning bioelectromagnetics and signal processing. In the last decade, nearly hundreds of studies published on the subject. Theoretical studies benefit from the realistic breast phantoms during the development of different imaging approaches and methodologies. These breast phantoms can be numerical for computer simulations as well as chemical realistic phantoms for practical experiments. In both cases, shape of the phantoms is needed to be known in order to make accurate computations. On the other hand, in clinical applications, breast shape varies from patient to patient. Therefore its shape must be modeled accurately in each imaging session.

In this study, we design and implement a 3-D reconstruction methodology for the breast surface in order to be used in clinical microwave breast imaging applications. Presented method uses 2-D images of the breast acquired at different angles and then reconstructs a 3-D volume. For this purpose, we integrate an optical camera working on visible spectrum into our microwave measurement system. The camera rotates around the breast acquiring enough number of images at certain angles. Then, several morphological operations are applied to those acquired images to obtain the necessary edge information [1]. Breast surface is then reconstructed using parallel beam [2] and cone-beam [3] reconstruction algorithms.

We implemented our method on both the simulation data of a 3-D numerical realistic breast phantom and our microwave breast imaging instrument. Parallel and cone-beam reconstructions of the breast surface are compared with each other in terms of microwave breast imaging requirements. The root mean square error (RMSE) is used to quantify the reconstructed 3-D image quality by numerical tests with the realistic breast phantom. Both the application and the simulation results show that, the breast surface can be accurately modeled with the proposed method using both parallel and cone-beam reconstruction techniques.

REFERENCES

1. Gonzalez, R. C. and R. E. Woods, *Digital Image Processing*, 2nd Edition, Prentice-Hall, Upper Saddle River, NJ, 2002.
2. George, A. K. and Y. Bresler, "Shear-based fast hierarchical backprojection for parallel-beam tomography," *IEEE Transactions on Medical Imaging*, Vol. 26, No. 3, 317–334, Mar. 2007.
3. Wang, G., T.-H. Lin, P. Cheng, and D. M. Shinozaki, "A general cone-beam reconstruction algorithm," *IEEE Transactions on Medical Imaging*, Vol. 12, No. 3, 486–496, Sep. 1993.

A Flexible RF Exposure Setup for Long-term Electrophysiological Investigations on Biological Samples in Vitro

Stefan Oster[1], **Andreas W. Daus**[1], **Michael Goldhammer**[2], **Ulrich Bochtler**[2], **and Christiane Thielemann**[1]

[1]Biomems Lab, University of Applied Sciences Aschaffenburg, Germany
[2]Laboratory for EMC, University of Applied Sciences Aschaffenburg, Germany

Abstract— Since long the health of the human brain is an issue in biological radiation research and the question whether weak radio frequency electromagnetic fields, for instance according to GSM-standard for mobile communication, could affect neuronal activity is a serious concern. Although there is only little evidence of major health risk arising from the exposure of the human body to EMF at mobile phone frequencies, a few of the published results are inconsistent and lead to contentious interpretations. Throughout all results, there is a lack of reproducibility and so it is not surprising that concerns about possible health risks, frequently arise amongst public.

In-vitro studies are widely used to investigate possible interactions between biological tissue and radio frequency electromagnetic fields (RF-EMF) in a controlled environment. Cell culture models grown on petri dishes or Micro Electrode Array (MEA)-Chips are considered suitable to imitate in-vivo like conditions. In a former publication, we showed that reaggregates of cardiac myocytes on MEA-Chips can be employed to study electrophysiological behaviour following RF-EMF exposure [1]. A flexible, hands-on TEM-cell based setup, a so-called stripline, for electromagnetic exposure of the biological samples was used. This setup is not based on standing waves and hence suitable for a large range of sample bins, frequencies and field strength, respectively SAR levels.

To study developing and mature neuronal networks in long-term experiments, the stripline has been integrated into a CO_2 incubator to keep ambient conditions like temperature and gas concentration stable. Investigations have been done in order to address problems like field homogeneity and accurate dosimetry. Conditions in the stripline were simulated at 900 MHz by finite element calculation and the setup was optimized in terms of SAR homogeneity and temperature stability.

For electrophysiology recordings were conducted with metal microelectrode arrays. As well known, electrical conductors can have an influence on electric field lines, which is obviously a disadvantage of wire electrodes. Simulations of the MEA metal structure have been performed in the exposition setup and show that chip position and electrodes' aspect ratio are important parameters. For the given microelectrode geometry, we found that induced field modifications are minor and can be neglected. As a consequence we state that the MEA chip is an excellent device to investigate potential electrophysiological effects caused by RF-EMF. Moreover temperature measurements were performed to avoid thermal effects. During exposure, temperature stability was below 0.1 K and it can be assumed that these alterations do not affect neuronal activity.

REFERENCES

1. Daus, A. W., M. Goldhammer, P. G. Layer, and C. Thielemann, "Electromagnetic exposure of scaffold-free three-dimensional cell culture systems," *Bioelectromagnetics*, Vol. 32, 351–359, 2011.

Influence of Near Earth Electromagnetic Resonances on Human Cerebrovascular System in Time of Heliogeophysical Disturbances

E. A. Sazanova[1], **A. V. Sazanov**[2], **N. P. Sergeenko**[2], **V. G. Ionova**[3], **and Yu. Ya. Varakin**[3]

[1]Clinical Hospital of Russian Academy of Sciences, Moscow, Russia
[2]Pushkov Institute of Terrestrial Magnetism, Ionosphere and Radio Wave Propagation (IZMIRAN), RAS Moscow, Russia
[3]Scientific Center of Neurology RAMS, Moscow, Russia

Abstract— Problems of adaptation of the person are actual in the conditions of heliogeophysical disturbances at its life-support, both on the Earth, and in space. Changes of fluidity of blood, levels of catecholamins of blood on different phases of heliogeomagnetic disturbances are analyzed.

The physical processes influencing on cerebrovascular shifts at people during indignations are discussed. Physical characteristics of environment (bioeffective frequencies of ionospheric resonators) are compared with own frequencies human body. It is supposed, that the human body is the difficult nonlinear self-oscillatory system exposed to resonant influence. It is supposed, that in a storm initial stage the stochastic resonance can be one of physical mechanisms of influence of external weak periodic signals against noise. External electromagnetic fluctuations can synchronize or desynchronize rhythms of electromagnetic fluctuations of cells of a brain and blood. Ionosphere disturbances lead to fluctuations of frequencies and the periods of the ionosphere Alfen's resonator which, in turn, can influence on rhythms of components of an organism, first of all on a brain and rheological properties of blood, as in experiences in vitro, and in vivo.

Also possibility of direct influence of geomagnetic variations during storms on a brain and the system of blood connected witht influence of an electromagnetic field on dynamics of process of aggregation — disaggregation of erythrocytes and DF (an adenosinediphosphatase acid) — induced platelet aggregation. (ADF-AT) in a blood stream is discussed.

The found out effects are statistically authentic and specify presence of direct influences of physical processes during indignations on blood cells.

The received results allow to assume, that, one of leading mechanisms of influence of indignations on cerebrovascular system of the person are their effects on rheological properties of blood. Ionosphere and geomagnetic disturbances can be the indicator of influences of physical processes during heliogeophysical disturbances on health of people.

MRI Imaging of the Physiology of Fungal Pathogens in Cultivated Plants

E. Hutová[1], K. Bartušek[2], R. Kořínek[2], and R. Pokorný[3]

[1]Department of Theoretical and Experimental Electrical Engineering
Brno University of Technology, Technicka 12, Brno 612 00, Czech Republic
[2]Institute of Scientific Instruments, Academy of Sciences of the Czech Republic
Kralovopolska 147, Brno 612 64, Czech Republic
[3]Department of Crop Science, Breeding and Plant Medicine (FA)
Mendel University in Brno, Zemedelska 1, Brno 613 00, Czech Republic

Abstract— The imaging of the physiology of fungal pathogens is currently feasible by means of the microscopic technique or the photographic approach. However, these methods do not provide dependable results, mainly because their description of the physiology of pathogens is either too detailed or lacks the necessary aspects. The authors of this paper have analyzed the possibility of visualizing the physiology of pathogen mycelia via the MRI method. This approach provides an overall image of the pathogens and enables the mapping of the plant infestation stage. MRI imaging also appears to be a suitable tool to support further research of the pathogens and their influence on the attacked plants or other biological material.

Comparison and Display of the Water Contained in Early Somatic Embryos

E. Hutova[1], **R. Korinek**[2], **K. Bartusek**[2], **and L. Havel**[3]

[1]Department of Theoretical and Experimental Electrical Engineering
Brno University of Technology, Technicka 12, Brno 612 00, Czech Republic
[2]Institute of Scientific Instruments, Academy of Sciences of the Czech Republic
Kralovopolska 147, Brno 612 64, Czech Republic
[3]Department of Crop Science, Breeding and Plant Medicine (FA)
Mendel University in Brno, Zemedelska 1, Brno 61300, Czech Republic

Abstract— This paper compares two methods that allow determining the total volume of water that occurs in early somatic embryos (ESEs). The first measurement was the measurement of proton density (PD) of early somatic embryos. This measurement was performed using MRI views (ISI ASCR Brno). The second technique was the weighing of dry sample of ESEs (Mendel University, Brno). These two methods were compared and the correlation coefficient of the two techniques was 0.816. Another important issue of the experiment was comparing the images of ESEs which were to show the biological processes in ESEs used relaxation times T_1 and T_2 to show the transition between the plant and the culture substrate.

Methods for the Sensing of Ionosphere Changes

M. Hanzelka, **P. Fiala**, **and M. Friedl**
Department of Theoretical and Experimental Electrical Engineering
Brno University of Technology, Technická 3082/12, Brno 616 00, Czech Republic

Abstract— The impact of the environment upon living organisms constitutes a crucial problem examined by today's science. In this context, research institutes worldwide analyze diverse positive and negative factors affecting the biological system of the human body; one such factor consists in the influence of the surrounding electromagnetic field. This paper presents the results of investigation focused on ionosphere parameter changes and their effect on the basic function of the nervous system. It is a well-known fact that the frequency of the so-called alpha waves of brain activity [1] ranges within 6–8 Hz. Changes in the electromagnetic and chemical composition of the Earth's surface may cause variation of signals in the above-defined frequency region of 6–8 Hz. Detailed examination of the overall impact inflicted by environmental factors upon the human organism is performed within a large number of medicinal disciplines. The research presented within this paper is concentrated on the sensing and detection of changes in the region of very low frequencies of the electromagnetic field; the authors apply both theoretical and experimental procedures to define the effects influencing brain activity.

ACKNOWLEDGMENT

The research described in the paper was financially supported by a grant of the Czech Ministry of Industry and Trade, No. FR-TI1/001, Czech Science Foundation GACR 13-09086S, a project of the BUT Grant Agency, No. FEKT-S-11-5/1012 and project from Education for Competitiveness Operative Programme CZ.1.07.2.3.00.20.0175 and CZ.1.07/2.3.00/30.0005.

REFERENCES

1. Ferris, J., "The brain generates an electric field that influences its own activity," *Scientific American Mind*, Vol. 21, 10, 2010, Published online: October 28, 2010, doi:10.1038/scientificamericanmind1110-10a.

Thermal Conductivity and Heat Capacity Measurement of Biological Tissues

J. Hrozek[1], **D. Nespor**[1], **and K. Bartusek**[2]

[1]Deptartment of Theoretical and Experimental Electrical Engineering, Brno University of Technology
Kolejni 2906/4, Brno 612 00, Czech Republic
[2]Institute of Scientific Instruments, Academy of Sciences of the Czech Republic
Kralovopolska 147, Brno 612 64, Czech Republic

Abstract— This paper deals with a measurement of temperature dependencies of thermal properties only by one measure system. Specific heat and thermal conductivity are two general thermal properties subscribed here. Thermal properties of each matter are dependent on their own temperature and are various in whole temperature range. Temperature dependencies of many commercial materials are well known. But temperature dependencies of biological tissues are very bad to find. However knowledge of these parameters is very important for the thermal processes computer simulation. The methodology described here is based on deficiencies of current measuring devices and methods. The thermal conductivity of biological tissues is measured with special needle (very thin and quite long) called the needle probe. This method has some good known deficiencies which are described in this paper. Specific heat is measured with Differential Scanning Calorimetry (DSC). The DSC is conventional method without serious deficiencies. Big disadvantage of current thermal properties measurement is in necessary using of both methods, i.e., two devices must be used. Simultaneous measurement of thermal conductivity and specific heat is the main advantage of our methodology. Results of temperature dependencies measurement will be used in computer simulation for hypothermia cancer destroying.

Multi-resolution Analysis Technique for Lung Cancer Detection in Computed Tomograpic Images

Muhammad Usman[1], **Muhammad Shoaib**[2], **and Mohamad Rahal**[1]

[1]Department of Electrical Engineering, University of Hail, P. O. Box 2440, Hail, Saudi Arabia
[2]Department of Mathematics, University of Hail, P. O. Box 2440, Hail, Saudi Arabia

Abstract— Lungs cancer ranked fourth in the number of deaths related with cancer in Saudi Arabia. In most cases Lung cancer does not show any symptoms in the initial stages. It is often suspected initially from chest x-ray or Computed Tomography (CT) scans done to evaluate a cough or chest pain. Several researchers have recommended Computer Aided Diagnosis (CAD) systems which facilitate early detection of lung cancer nodules at more curable stages. The First stage of those CAD systems requires the segmentation of the Lung parenchyma from the CT or x-ray Scan images. Improper segmentation of the Lung parenchyma will highly affect the accuracy of the Lung nodule detection or lung diseases classification algorithms. This research proposed a multi-resolution based Lung parenchyma segmentation method to segment the lung lobes at accuracy levels acceptable for clinical applications. The methodology incorporates statistical models together with multi-resolution analysis techniques in order to enhance the accuracy of the overall system. In this research, the image quality and accuracy of detecting the cancer affected area are the key factors. The assessment of image quality and improvements are depending on the enhancement stage where different techniques have been used. Mainly Gabor filter and Fourier Transforms have been used for image enhancement and Pixel Percentage and Mask Labelling techniques have been used for detecting the area of interest.

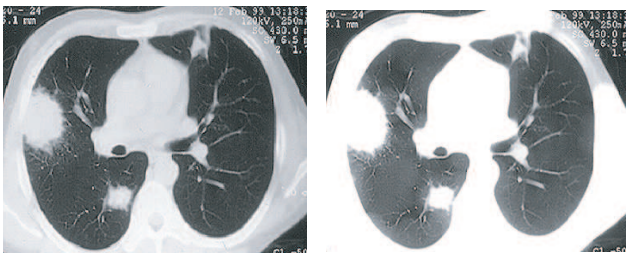

(a) (b)

Figure 1: (a) Original CT scan image. (b) Enhanced image.

Development of Biological Tissue-equivalent Agar-based Solid Phantom in HF Band

Mizuki Inoue, **Ryotaro Suga**, **Kazuyuki Saito**,
Masaharu Takahashi, **and Koichi Ito**
Chiba University, Japan

Abstract— In recent years, radiofrequency devices, which are usually placed in the vicinity of the human body, are widely used. In addition, these devices are used around human body in various situations, for example, telecommunications, broadcast, home electrical appliance (e.g., microwave oven, induction heating (IH) and medical applications (e.g., hyperthermia, magnetic resonance imaging (MRI) system). Therefore, the evaluation of the interaction between electromagnetic waves and the human body, which is radiated by the devices, is indispensable. The interaction is generally estimated from numerical simulations and experimental evaluations. In these evaluations, biological tissue-equivalent phantoms, which are adjusted to have the same dielectric constants of human tissues, are usually used. Until now, various investigations have been made on phantoms. However, most of these previous studies have focused on phantom for VHF (Very High Frequency) band and above. Until now, various investigations have been mainly made on the interaction between the mainly cellular phones and the human body at ultra high frequency (UHF) band. For the future, it is necessary to evaluate the interaction between the EM waves and human body in other situations (e.g., frequency, devices, etc.). Therefore, it is necessary to develop phantoms for HF band. In this study, some agar-based phantoms with a mixture of aluminum powder and sodium chloride (NaCl) for HF band are proposed. In addition, electric constants in HF band of phantoms are measured by using impedance analyzer. As a result of a example, it is clear that the biological tissue-equivalent phantom can realize the electrical properties of high water content tissues at 13.56 MHz.

Novel Magnetic Lens for Static Magnetic Field Enhancement

Fei Sun[1,2] **and Sailing He**[1,2]

[1]Centre for Optical and Electromagnetic Research
Zhejiang Provincial Key Laboratory for Sensing Technologies
JORCEP, East Building #5, Zijingang Campus, Zhejiang University, Hangzhou 310058, China
[2]Department of Electromagnetic Engineering, School of Electrical Engineering
Royal Institute of Technology (KTH), S-100 44 Stockholm, Sweden

Abstract— We design a passive lens for static magnetic field enhancement by using transformation optics. In our previous study, our attention is focused on two dimensional (2D) structures. In this paper, we extend our design to three dimensional (3D) structures and good static magnetic field enhancement performance has also been verified by using 3D finite element method (FEM). This novel magnetic lens can greatly enhance the static magnetic field without additional power consumption from a weak background magnetic field, which may have potential applications in Magnetic resonance imaging (MRI) and other compact high-field-magnet systems.

The designed lens is a ring with inner radius R_1 and outer radius R_2 in x-y plane and length h in z axis (see Fig. 1(a)). The performance of the 3D lens is shown in the Fig. 1(b). When the weak background static magnetic field 1 T incidents from z direction onto the lens, we can obtain an enhanced magnetic field about 25 T in the center part of the lens. The more interesting is that the enhanced magnetic field is almost uniform.

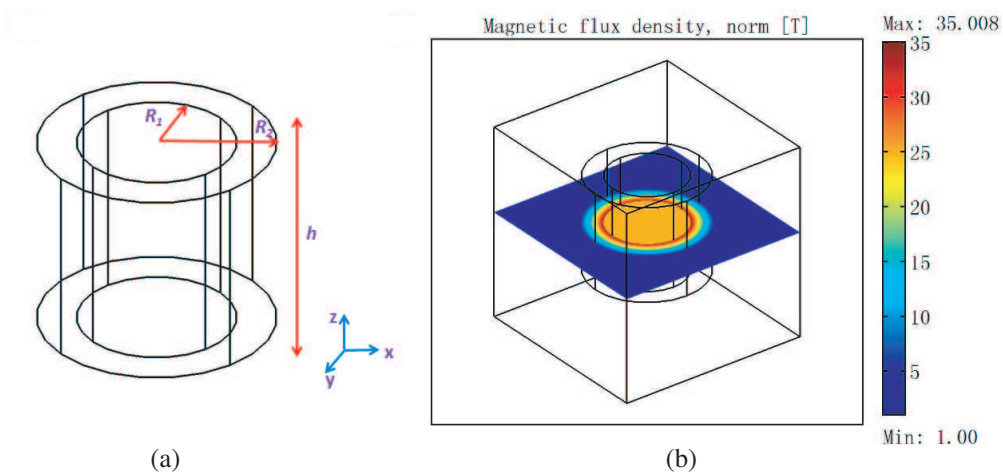

(a) (b)

Figure 1: (a) The geometric structure of the lens. (b) 3D FEM simulation result. The parameters of the magnetic lens is $R_1 = 0.2\,\mathrm{m}$, $R_2 = 0.3\,\mathrm{m}$, $R_3 = 1\,\mathrm{m}$ and $h = 0.5\,\mathrm{m}$. The background magnetic flux incidents from z direction with amplitude 1 T onto the lens. We plot the magnetic flux distribution on a cross section of the lens which passes through the center of the lens.

Impact of Electromagnetic Field Generated nearby High Voltage Alternating Current Transmission Lines on Prooxidant-antioxidant Balance in Selected Internal Organs of Rats

P. Sowa[1], **K. Sieron-Stoltny**[2], **G. Cieslar**[3], **and A. Sieron**[3]

[1]Institute of Power System and Control, Silesian University of Technology, Poland
[2]Department of Physical Medicine, Medical University of Silesia, Katowice, Poland
[3]Department and Clinic of Internal Diseases, Angiology and Physical Medicine
Medical University of Silesia, Poland

Abstract— Nowadays human population is permanently exposed to electromagnetic fields with industrial frequency generated by high voltage alternating current transmission lines. In this study the impact of whole-body exposure to 50 Hz electromagnetic field generated nearby those lines on prooxidant/antioxidant balance in selected internal organs of male rats was estimated, by means of analysis of the contents of markers of membrane lipid peroxidation and oxidative stress: malone dialdehyde (MDA) and total oxidant capacity (TOC), respectively, as well as the activity of antioxidant enzymes: superoxide dismutase (SOD), catalase (CAT), glutathione peroxidase (GPx), glutathione reductase (GR) and glutathione S-transferase (GST), in homogenates of kidney, heart and lung tissue. The experiment was performed on 20 male Wistar rats, in mean age of 10 weeks, divided into 2 equal groups (consisting of 10 animals), subjected to long-term exposure to electromagnetic field or to sham-exposure, respectively. Rats from examined group were exposed to electromagnetic field with physical parameters generated by typical high voltage electric current transmission lines ($f = 50\,\mathrm{Hz}$, $E = 10\,\mathrm{kV/m}$), 22 hours a day (with a break between 8^{00} and 10^{00}) for 28 succeeding days. Rats from control group were exposed for 28 succeeding days to sham-exposure, during which they stayed in identical as examined animals environmental conditions, excluding the influence of electromagnetic field. During the exposure rats were stayed in plastic cages placed between two round electrodes of experimental system supplied with an alternating current. After the end of a cycle of 28 daily exposures to electromagnetic field or sham-exposures (control rats), animals were starved by 24 hours, then anaesthetized and next the abdominal cavity was opened and samples of kidney, heart and lung were taken. In the homogenates prepared from the obtained samples the contents of TOC and MDA, as well as the activity of SOD, CAT, GPx, GR and GST were measured. The biochemical analyses were performed by means of routine spectrophotometric and kinetic methods. As a result of repeated exposures, in electromagnetic field-exposed group of rats in kidney tissue homogenates a significant increase in the contents of TOC and in the activity of SOD and GPx, as well as a significant decrease in the activity of GR and GST was observed, in heart tissue homogenates a significant decrease in the contents of TOC and in the activity of GST, as well as a significant increase in the activity of GPx was found, while in lung homogenates a significant increase in the contents of MDA and in the activity of CAT was confirmed, as compared to control sham-exposed rats. On the basis of the obtained results it was found, that 4-week lasting exposure of rats to electromagnetic field with physical parameters generated by high voltage alternating current transmission lines causes a slight intensification of oxidant processes in the tissue of examined internal organs with accompanying compensatory, multidirectional changes of antioxidant enzymes activity, enabling the maintenance of prooxidant/antioxidant balance only in heart tissue.

System Information Therapy as a Tool in Personalized Medicine

Alberto Foletti[1, 2] **and Settimio Grimaldi**[2]

[1]Department of Innovative Technologies
University of Applied Sciences of Southern Switzerland-SUPSI, Manno, Switzerland
[2]Institute of Translational Pharmacology, C.N.R., Rome, Italy

Abstract— By bridging physics and biology living organisms can nowadays be viewed as dynamic processes sustained by a ceaseless flows of matter, energy and information within specific space-time quanta defined as morphogenetic fields. Life is a far from equilibrium process described as dissipative structure. A more dynamic approach replaced the old static concept of omeostasis and the process aimed to keep stability through dynamic changes has been recently defined as allostasis. Allostatic load is the expression of the effort due to the total amount of stress the whole system has to cope to maintain allostasis. Allostasis lead to strengthen of health potential toward salutogenesis while allostatic load lead to a decrease of health potential toward pathogenesis. Allostasis and allostaic load are in a dynamic relationship as an expression of the flow of information due to adaptive dynamics. And here we are: health and disease can be better understood as an expression of the allostasis/allostatic load dynamics. Information flows in biological system can be studied either by a chemical and molecular description either by an electromagnetic signals emission and processing approach. It has been established, in the last decays, that electromagnetic signals are endogenously generated at different level in many cell components and supposedly play an active role in synchronizing either inner cell function at microscopic level either systemic adaptive response of organs, apparatus and whole organism. In this framework all the adaptive response both at microscopic and at macroscopic level, either local or holistic, could be identified by their specific electromagnetic signals emission. Each specific adaptive reaction, being unique for any person at any time, will have his own specific and personal electromagnetic signature. System Information Therapy is a developing clinical methodology employing medical devices (such as Med Select 729) working by a combination of endogenous and external electromagnetic signals with the aim of restoring the self regulation and self regeneration capability of the human being. This process has been clarified at the microscopic level with evidence of repatterning of cell menbrain components or at epigenetic level with evidence of selective mRNA expression induction. At macroscopic level the self regulation effect has been, for instance, demonstrated in postural repatterning with evidence of disappearance of fluctuating asymmetry, a clinical correlate to allostatic load, or in pain management. System Information Therapy is a new effective and efficient tool in personalized medicine allowing to cure each person by her own specific dysfunctional or pathological electromagnetic signals at local or systemic level. Moreover System Information Therapy is also a suitable tool in preventive medicine allowing to manage allostatic load in order to keep allostasis and coping efficiently with everyday stress of life.

REFERENCES

1. Brizhik, L. S., E. Del Giudice, F. A. Popp, W. Maric-Oeler, and K. P. Schlebusch, "On the dynamics of self-organization in living organisms," *Electromagn. Biol. Med.*, Vol. 28, No. 1, 28–40, 2009.
2. McEwen, B. S. and J. C. Wingfield, "The concept of allostasis in biology and biomedicine," *Horm. Behav.*, Vol. 43, No. 1, 2–15, 2003.
3. Liboff, A. R., "Toward an electromagnetic paradigm for biology and medicine," *J. Altern Complement Med.*, Vol. 10, No. 1, 41–47, 2004.
4. Liboff, A. R., "Local and holistic electromagnetic therapies," *Electromagn Biol. Med.*, Vol. 26, No. 4, 315–325, 2007.
5. Foletti, A. and S. Grimaldi, "Systems information therapy and the central role of the brain in allostasis," *J. Phys: Conf. Ser.*, Vol. 329, 012027, 2011.

System Information Therapy in the Management of Pain: A Pilot Study

Paolo Baron[1], **Giuseppe Bucci**[1], **Alfio Rinaudo**[1], **Roberto Rocco**[1], **Eugenio Sclauzero**[1], **and Alberto Foletti**[2, 3]

[1]General Practictioners, Regione Friuli Venezia Giulia, Italy
[2]Institute of Translational Pharmacology, National Research Council — CNR
Via Fosso del Cavaliere, 100, Rome 00133, Italy
[3]Deartment of Innovative Technologies
University of Applied Sciences of Southern Switzerland — SUPSI
Galleria 2, Manno 6928, Switzerland

Abstract— Dealing with pain is an important daily part of current medical practice. Biophysical methods by use of medical devices (such as Med Select 729 in this trial) allows to perform very personalized treatment using endogenous signals of the patient leading to the definition of a System Information Therapy (SIT) approach. An open labeled clinical trial was designed to assess the effectiveness of a biophysical treatment compared to a common anti inflammation drug (ibuprofen) and compared to placebo. Methods: patients has been divided in three groups: **Group 1** System Information Therapy patients receiving two steps of treatment by the Med Select 729 medical device: 1st step delivered with a program called regulation therapy with recording of endogenous input signals at the painful region and delivery of therapeutic output signals at systemic level by mean of an electromagnetic mattress on which the patient lied — 2nd step delivered with the program called pain therapy: recording endogenous input signals at the painful region and delivery of therapeutic output signals at the pain site, moreover a copy of therapeutic signals has been recorded on a commercial available aqueous system (Nomabit Base). **Group 2** Pharmacological therapy: receiving ibuprofen 600 mg twice a day for 10 days. **Group 3** Placebo group: receiving only Nomabit Base solution as placebo. A total of 66 patients was enrolled: 26 in System Information Therapy group (17 f, 9 m), 23 in the pharmacological group (11 f, 9 m); 17 in the placebo group (12 f, 5 m). Evaluation of follow up was performed by a visual analogue scale at the beginning, after one week, after one month, and after three months. After one week biophysical therapy shows similar effect than ibuprofen and after one month the statistical significance was $\chi^2 = 12.153$ with $p < 0.02$. In conclusion the biophysical therapy protocol demonstrated the same effectiveness than usual pharmacological therapy with ibuprofen at first week reaching statistical significance after one month of administration and maintaining the effect at tree month. System information therapy seems, therefore, to be an effective and safe method in the management of pain in current medical practice representing a possible resource especially for patients with chronic disease and multiple comorbidities in order to reduce drug overload.

REFERENCES

1. Foletti, A. and S. Grimaldi, "Systems information therapy and the central role of the brain in allostasis," *J. Phys.: Conf. Ser.*, Vol. 329, 012027, 2011.
2. Baron, P., G. Bucci, A. Rinaudo, R. Rocco, E. Sclauzero, and A. Foletti, "Biophysical therapy in the management of pain in current medical practice," *Proceedings of the 2nd International Symposium, "Biophysical Aspects of Complexity in Health and Disease",* 37–38, Lugano, Switzerland, May 18–19, 2012.

The Thermal Analysis of Some Light Sources

A. Yasin Citkaya[1], **S. Selim Seker**[1], **and Osman Cerezci**[2]

[1]Department of Electrical-Electronic Engineering, Bogazici University, Bebek, Istanbul 34342, Turkey
[2]Department of Electrical-Electronic Engineering, Sakarya University, Esentepe, Sakarya 54187, Turkey

Abstract— Incandescent, fluorescent, compact fluorescent lamps (CFL), High Intensity Discharge (HID) sources including mercury vapor, metal halide, High Pressure Sodium (HPS), Low Pressure Sodium (LPS) are the common light source types. Many indoor lamps, emit at UVA, UVB and sometimes even UVC wavelengths. The goal of this study, which is to inspect the photo-thermal effects due to interaction with commonly used light sources with biological tissue, is planned to be reached via first simulating the interaction with a human skin model, then using the findings of the model, compare them with the experimental results obtained with a tissue subject to various kinds of light sources.

Thermoregulation of skin is another vital process that skin is thermally responsible for through heat generation, absorption, transmission, conduction, radiation, and vaporization. An exact representation of light propagation in skin requires a model that characterizes the spatial distribution and the size distribution of tissue structures, their absorbing qualities.

The numerical procedure developed for the solution of the bio-heat equation analyzes the dynamics of spatial- temporal temperature distribution $T(x, y, x, t)$ in biological tissues. An optothermal model of the skin obtained from different sources has been implemented in computer software program, such that the tissue, with a volume of $5\,\mathrm{mm} \times 5\,\mathrm{mm} \times 4\,\mathrm{mm}$, is considered to be composed of six layers from the optical point of view where some limitations are inevitable due to the multilayered structure. Thermal behavior of skin tissue that is exposed to light source is analyzed through the numerical method which utilizes Finite Element Method (FEM) by solving the diffusion and Bioheat equations under the effect of dominating boundary conditions. Having completed the modeling steps in the Finite Element Solver software by creating geometries, putting up the parameters and defining the boundary and sub domain settings, the simulations were done. The post processed results clearly show that temperature distribution inside the tissue is generally non-monotonic function of depth, due to varying optothermal parameters of tissue layers, like absorption coefficient, heat conductivity and so on. As the exposure duration increases, maximum temperature induced on tissue increases. When it comes to effects of two different InfraRed light sources, one clear and other with a red filter are used. We found that two light sources have different thermal effects on tissue even though the lamp output powers are set to be equal. It is also seen that as exposure duration gets longer, difference in maximum temperature induced in tissue models increases and gets more significant for the two different types of light sources. Hence, the obtained results are in line with the expected results in such a way that red filtered lamp should and actually do cause less temperature increase in tissue. Analyzing possible range of the induced thermal effects on biological tissues due to exposure with different light sources requires an extensive effort with numerical methods, since parameters of both tissue and the light sources chosen show quite variations. In this work, experimental analysis offers more realistic data with comparative advantages to numerical study. Additionally, the effect of distance between light sources and tissue is verified via a comparative study made with the same light source. The experimental setup, consists of a light source directed to in vitro biological tissue (namely chicken meat covered with skin), and the thermal interaction between them is monitored via a thermal camera. Distance between tissue and light source, d_1, is set to 30 cm and thermal camera is held at a distance d_2 of 50 cm for the best visual results, because of the limitation from the focus distance of camera which is 40 cm. As we observed from our the temperature curves behave in the same way for both experimental and numerically obtained results. It can be inferred that there is about 2% difference between the results, which is generally in acceptable limits. Having obtained experimental results that are in good agreement with numerical analysis, distance variation was illustrated. For this purpose, one experiment is carried out at 50 cm distance between tissue and lamp (InfraRed light with red filter). It should not be so surprising that as exposure distance rises, maximum induced temperature gets low. Hence, it becomes easy to conclude that less photo thermal damage occurs at large exposure distances. In this regard, safety limits can be defined to minimize the hazardous effects of light.

From our results, the experimental results can be used to compare the thermal effects of different light sources. Those with high power outputs, such as IR, Halogen and UV, some of which are designed for usage especially in heating applications, display higher temperature increases during the exposure period.

EM System to Guide Visually Impaired Running Athlete

Valerio Petrini[1], **Valentina Di Mattia**[1], **Marco Pieralisi**[1], **Lorenzo Scalise**[2], **Valter Mariani Primiani**[1], **Alfredo De Leo**[1], **Paola Russo**[1], **and Graziano Cerri**[1]

[1]Department of Information Engineering, Università Politecnica delle Marche
via Brecce Bianche, Ancona 60131, Italy
[2]Department of Industrial Engineering and Mathematical Science
Università Politecnica delle Marche, via Brecce Bianche, Ancona 60131, Italy

Abstract— In this abstract is presented an electromagnetic (EM) warning system aiming to guide a blind or visually impaired (VI) athlete during running. The system has been designed in order to be able to create a virtual hallway by means of two transmitting antennas located on a bike or vehicle running before the athlete. Whenever the VI runner is getting closer to one of the two EM borderlines of the track, a receiving wearable system, located on the user's chest, warns him through two vibrating transducers positioned on the user's left and right arm. The final scope is to improve VI athlete autonomy, designing a system capable to allow him to freely perform (without the need for a running guide on his/her side) and to maintain always the right position along the pathway.

Introduction: Worldwide, about 285 million people are visually impaired: 39 million are blind and 246 million suffer of low vision conditions [1]. Mobility tasks, in particular in outdoor environments, are the main issues for these subjects who can be strongly limited in their social and professional life. Nevertheless, many people with disabilities participate in high performance, competitive and/or recreational sports. Although a wide range of Electronic Travel Aids (ETAs) to assist mobility has been designed so far [2, 3], no electronic devices have been conceived yet to improve their autonomy during sports and in particular for running athletes. Most of the time, VI athletes run linked to a guide runner by means of a non-stretchable tether tied around their wrists or held between their fingers thus limiting the sport act [4]. For these reasons, the EM system proposed in this work has been thought to support and guide athletes while training or running.

System Description: As an overview, the system draws an invisible track that should be followed by the runner, by means of the generation of two EM walls, as illustrated in Fig. 1. To make sure that the athlete always remains inside the virtual hallway, it is necessary to generate a warning whenever he is getting close to the borderlines so as to encourage the runner to move toward the central position.

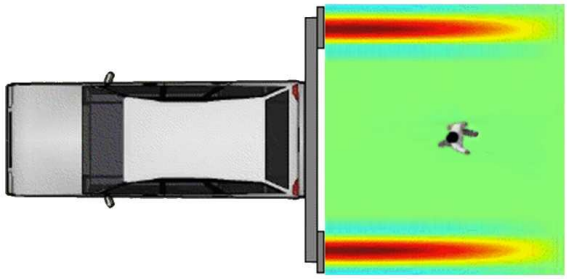

Figure 1: Virtual hallway.

To this aim the whole system has been divided into transmitting and receiving subsystems. The transmitting subsystem includes: Two radiating elements, to be placed on a car running in front of the user, that generate the two EM walls, and two amplitude modulators at two different frequencies to discriminate between left and right boundary. On the other side, the receiving system is composed of a receiving antenna, an AM demodulator, two bandpass filters, a Micro Controller Unit (MCU) for thresholds settings and further signal processing, and two vibration transducers to communicate a warning signal to the blind athlete.

Antennas Design and Characterization: To date, our work has been focused on the design and realization of the transmitting and receiving antennas, working at about 10.4 GHz. Since to generate an EM wall the radiation pattern should be narrow on the horizontal plane and wide

on the vertical one (fan-shaped), a slot antenna has been chosen as radiating element. Before realization, its design and characterization have been performed using commercial software [5]. With regards to the receiving element, it has been designed in order to have a lightweight and wearable device with a radiation characteristic similar to (but less restrictive than) those of the transmitting antennas. A microstrip array antenna of four elements has been modelled and realized on a PCB.

The combination of the transmitting and receiving radiation patterns leads to different levels of the received signal. As the position of the runner with regard to the transmitting antennas changes, the level of the received signal changes accordingly and it can be used to drive the warning signal.

Further Developing: Currently we are developing the electronic board which demodulates and filters the LF signals, and consequently generates appropriate outputs to vibration transducers.

REFERENCES

1. National Federation of the Blind, May 8, 2009, [Online], Available at: http://www.nfb.org/.
2. Roentgen, U. R., G. J. Gelderblom, M. Soede, and L. P. De Witte, "Inventory of electronic mobility aids for visually impaired persons — A literature review," *Journal of Visual Impairment & Blindness*, Vol. 102, 702–724, 2008.
3. Scalise, L., V. Mariani Primiani, D. Shahu, A. De Leo, P. Russo, V. Di Mattia, and G. Cerri, "Electromagnetic aids for visually impaired users," ICEmB II Convegno Nazionale, "Interazioni fra campi elettromagnetici e biosistemi," Bologna, 2012.
4. "Paralympics 2012: the guide runners," September 2012, [Online], Available at: http://www.telegraph.co.uk/sport/olympics/paralympic-sport/paralympics-gb/9529080/Paralympics-2012-the-guide-runners.html.
5. CST, Computer Simulation Technology, 3D Electromagnetic Simulation Software, [Online], at: http://www.cst.com.

Characteristics of an Optical Bowtie Nanoantenna

Ahmed Abbas, **Mostafa El-Said**, **and Samir F. Mahmoud**
Electronic and Communication Engineering Department, Cairo University, Egypt

Abstract— Optical nanoantennas have recently found several applications in areas such as near field probing in optical microscopy, as optical tweezers, and in biomedical applications. The optical nanoantenna is composed of a resonant length of rare metal, such as silver or gold, placed on glass or any dielectric layer. By illuminating the antenna with a light wave, optical plasmon is formed at the metal-dielectric interface. Unlike ordinary metallic wire antennas, where the electric current wave has the same phase velocity as the radiated field, the current wave on the optical nanoantenna is much slower than the radiated optical wave. This leads to considerably compact antenna, which is much shorter than half the free space wavelength [1].

In this paper, we study the performance of Bow-Tie antenna on glass (see Figure below) and obtain a simple transmission line model for the nanoantenna that accounts for the gap length and end effects. It is shown that the peak value of E_z across the gap coincides with resonance of the impedance Z_{TM} defined as:

$$Z_{TM} = \frac{E_z}{H_x} \quad \text{at} \quad z = x = 0 \tag{1}$$

So at the resonant frequency when Z_{TM} is purely real, the field E_z shows a peak value in the gap. At this frequency the effective length of the bow tie is equal to half the plasmon wavelength (after taking the gap and end effects into account). Using our transmission line model we predict the dependence of the resonant frequency on the gap length 'g' and compare it with simulation results. We also obtain results for the input impedance Z_{in} defined as the ratio of voltage across the gap to the total displacement current crossing the gap [2]. It is found that the resonance of Z_{in} occurs at a higher frequency compared with that corresponding to peak E_z at the gap.

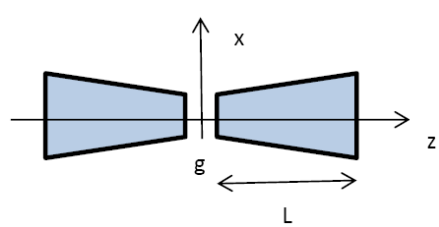

REFERENCES

1. Biagioni, P., et Al., "Nanoantennas for visible and infrared radiation," *Rep. Prog. Phys.*, Vol. 75, 024402, Feb. 2012.
2. Alu, A. and N. Engheta, "Input impedance, nanocircuit loading and radiation tuning of optical nanoantennas," *Physical Review Letters*, Vol. 101, 043901, Jul. 2008.

Characteristic of Novel Elliptical-spiral Photonic Crystal Fibre with Arbitrary Gold Wires Embedded in Cladding Air Holes

A. M. Heikal and S. S. A. Obayya
Centre for Photonics and Smart Materials, Zewail City of Science and Technology
Sheikh Zayed District, 6th of October City, Giza, Egypt

Abstract— In this paper, a novel design of elliptical-spiral photonic crystal fibre (ES-PCF) with arbitrary metal wires embedded in cladding air holes is proposed and analyzed using full vectorial finite difference frequency domain method for linear oblique and curved interface (FVFD-LOCI). First, the coupling characteristic between the core guided mode and surface plasmon polaritons (SPPs) excited on the surface of gold wire is presented. Then, a highly polarization-dependent transmission characteristic in (ES-PCF) is obtained by embedding multiple gold wires closely arranged in cladding air hole. Moreover, the effect of changing the cladding refractive index on the polarization characteristic of ES-PCF has been studied.

Recently, PCF with other air hole arrangements such as equiangular spiral PCF (ES-PCF) has attracted the interest of many researchers due to their useful properties. ES-PCF with small effective mode area, high nonlinearity and ultraflattened dispersion has been reported by Hossain et al. [1]. In addition, ES-PCF was designed for nonlinear applications in visible region [2]. Therefore, it is expected that unique and useful properties may be obtained by tailoring the ES-PCF design for fiber-optic communication system. Optical characteristic of silica-air PCFs can be controlled by filling the cladding air holes with different materials such as liquid crystal [3], semiconductor [4], or metal [5]. In metal-filled photonic crystal fibres (MF-PCFs), coupling occurs between surface plasmon polaritons (SPPs) formed on the metal wires and the core guided mode when the phases of them match [6]. The coupling between the core mode and SPPs occurs at specific frequencies, so MF-PCFs have highly wavelength-dependent transmissions. Figure 1 shows cross section of the suggested ES-PCF. The proposed design relies on using ES-PCF with eight arms with seven holes in each arm. The background of the suggested design is silica. A gold wire is embedded into the cladding air hole. Sellmeier equation for the dispersion of silica [7], and Drude-Lorentz model for metal [8] are used. The second hole in each arm is at a normal distance $D = 2\,\mu\text{m}$ to the line between the centers of two neighboring holes in the first ring as shown in Figure 1. Similarly, the third hole in each arm is at a normal distance D to the line between the centers of two neighboring holes in the second ring. The elliptic core has ellipticity $a/b = 1.45$. All the cladding holes have the same radius $r_h = 1\,\mu\text{m}$.

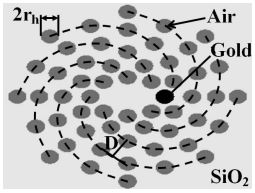

Figure 1: Cross section of the suggested ES-PCF.

REFERENCES

1. Hossain, M. N., M. S. Alam, D. M. N. Hasan, and K. M. Mohsin, "A highly nonlinear spiral photonic crystal fiber for tailoring two zero dispersion wavelengths in the visible region," *Photon. Lett.*, Vol. 2, 143–145, Poland, 2010.
2. Hossain, N., M. S. Alam, D. M. N. Hasan, and K. M. Mohsin, "Design of a spiral silica photonic crystal fiber for nonlinear applications in visible region," *Opt. Eng.*, Vol. 50, No. 7, 070503, Jul. 2011.
3. Noordegraaf, D., L. Scolari, J. Lægsgaard, T. Tanggaard Alkeskjold, G. Tartarini, E. Borelli, P. Bassi, J. Li, and S.-T. Wu, "Avoided-crossing-based liquid-crystal photonic-bandgap notch filter," *Opt. Lett.*, Vol. 33, No. 9, 986–988, 2008.
4. Tyagi, H. K., M. A. Schmidt, L. N. Prill Sempere, and P. St. J. Russell, "Optical properties of photonic crystal fiber with integral micron-sized Ge wire," *Opt. Express*, Vol. 16, No. 22, 17227–17236, 2008.

5. Schmidt, M., L. Prill Sempere, H. Tyagi, C. Poulton, and P. Russell, "Waveguiding and plasmon resonances in two-dimensional photonic lattices of gold and silver nanowires," *Phys. Rev. B*, Vol. 77, No. 3, 033417, 2008.
6. Schmidt, M. A. and P. St. J. Russell, "Long-range spiralling surface plasmon modes on metallic nanowires," *Opt. Express*, Vol. 16, No. 18, 13617–13623, 2008.
7. Agrawal, G. P., *Nonlinear Fiber Optics*, Academic Press, San Diego, CA, 1989.
8. Vial, A., A.-S. Grimault, D. Macías, D. Barchiesi, and M. de la Chapelle, "Improved analytical fit of gold dispersion: Application to the modeling of extinction spectra with a finite-difference time-domain method," *Phys. Rev. B*, Vol. 71, No. 8, 085416, 2005.

Near Field Optics of Plasmonic Nanostructures Presenting High Aspect Ratio

Y. Ould Agha and G. Colas Des Francs
Laboratoire Interdisciplinaire Carnot de Bourgogne (ICB), UMR 5209
CNRS-Université de Bourgogne, 9, Avenue Alain Savary, BP 47870, Dijon 21078, France

Abstract— Plasmonic nanostructures concentrates light on subwavelength scales, opening the way to promising applications such as nano-optical antennas, surface enhanced spectroscopies or quantum plasmonics [1–3]. In the last decade, strong efforts have been done in modeling and simulation of these structures, in order to predict and determine the best configuration for specific applications. Particularly, the electric field quickly decays away from the metal surface so that dedicated methods have to be developed to correctly describe near-field optics properties of plasmonic systems. Additionally, high aspect ratio shapes are often needed to control their resonance position. Fast field decay and high aspect ratio shapes leads to strong numerical difficulties for methods based on the object discretization, notably in term of memory cost and computational time.

In this communication we use the dyadic Green technique based on the integral method developed by G. Gao and C. Torres Verdin [4]. Specifically, the object is meshed with cells of various aspect ratios. Then, we calculate the electric near-field of elongated silver nanorod consisting of cylindrical rod capped with hemispherical ends. For silver, we use the bulk dielectric function tabulated by Johnson and Christy [5]. We successfully determine an optimum cell shape. We demonstrate that when the elementary cells present an aspect ratio similar to the one of the full object, we achieve excellent convergence with limited memory requested and low computational time. To assess the reliability of our method, we compare the numerical results to those obtained from a commercial software (COMSOL Multiphysics) based on the finite element method. Finally, we compute the local density of modes (LDOS) of the considered structures.

REFERENCES

1. Muskens, O. L., V. Giannini, J. A. Snchez-Gil, and J. Gmez Rivas, "Optical scattering resonances of single and coupled dimer plasmonic nanoantennas," *Optics Express*, Vol. 15, No. 26, 17736–17746, 2007.
2. Stockman, M. I., "Nanoplasmonics: Past, present, and glimpse into future," *Optics Express*, Vol. 19, No. 22, 22029–22106, 2011.
3. Baik, J. M., S. J. Lee, and M. Moskovits, "Polarized surface-enhanced raman spectroscopy from molecules adsorbed in nano-gaps produced by electromigration in silver nanowires," *Nano Letters*, Vol. 9, No. 2, 672–676, 2009.
4. Gao, G., C. Torres-Verdin, and T. M. Habashy, "Analytical techniques to evaluate the integrals of 3D and 2D spatial dyadic Green's functions," *Progress In Electromagnetics Research*, Vol. 52, 47–80, 2005.
5. Johnson, P. B. and R. W. Christy, "Optical constants of the noble metals," *Phys. Rev B*, Vol. 6, 4370–4379, 1972.

Localized Plasmons and Interface Reflections: Fano Interference and Complete Light Annihilation

M. Svedendahl[1], **P. Johansson**[1,2], **and M. Käll**[1]

[1]Chalmers University of Technology, Göteborg, Sweden
[2]Örebro University, Örebro, Sweden

Abstract— We show that reflections from short range ordered gold nanodisks immobilized on a glass substrate show highly asymmetric line-shapes and a spectral red-shift of the LSP resonance of about 0.2 eV, as the incidence angle, θ_i, was varied from normal to grazing incidence. These properties may be understood as a Fano resonance between the spectrally narrow LSP resonance and the broad bare interface reflection. Above the critical angle, θ_c, the destructive interference between these two components can be tuned into a critical coupling mode, where all light is absorbed by the nanoparticles.

Introduction: The interaction of light and subwavelength structures, supporting so-called localized surface plasmons (LSPs), show great promise in the development of, for example, solar harvesting technology and bio/chemical sensors. As a first approximation, the LSPs in metal nanoparticles can be described as a damped harmonic oscillator yielding a Lorentzian polarizability. Many plasmonic resonances are, however, better described by an asymmetric line-shape, conveniently described by the Fano function.

Results: Gold nanodisk arrays were fabricated on glass microscope slides by Hole Mask Colloidal Lithography (HCL). Figure 1 show experimentally acquired s-polarized reflection spectra from a gold nanoparticle array at various incidence angles [1]. Above θ_c the arrays can be designed to fulfill a critical coupling condition, where all incident light is absorbed [2]. We experimentally illustrate the absorption by measuring the temperature of the substrate with a heat camera as a function of θ_i, showing maximum absorption around the critical coupling angle.

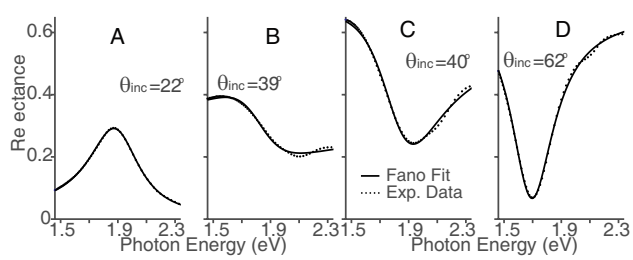

Figure 1: Specular reflection spectra for varying angles of incidence. Dotted lines correspond to experimental data, and solid lines are fits to the Fano formula.

Conclusion: The asymmetry factor can be controlled by altering the incidence angle and/or the surface density of nanoparticles. These results may, for instance, be used in material specific refractometric biosensing and more efficient excitation of the nanoparticle LSPs, useful in near-field intensity based applications, such as SERS or optical trapping methodologies.

REFERENCES

1. Svedendahl, M. and M. Käll, "Fano interference between localized plasmons and interface reflections," *ACS Nano*, Vol. 6, No. 8, 7533–7539, 2012.
2. Svedendahl, M., P. Johansson, and M. Käll, "Complete light annihilation in an ultrathin layer of gold nanoparticles," 2013, submitted.

Redshift by Design for Plasmonic Enhancement of Ultrathin Infrared Detectors

Marko Obradov, **Zoran Jakšić**, **Milija Sarajlić**, **and Danijela Randjelović**
Centre of Microelectronic Technologies and Single Crystals
Institute of Chemistry, Technology and Metallyrgy
University of Belgrade, Njegoševa 12, Belgrade 11000, Serbia

Abstract— In order to maximize sensitivity and specific detectivity of photodetectors, one has to ensure optimal light concentration within the active area. This is especially important in situations where the optical thickness (absorption coefficient-thickness product) of the device is relatively small. Such situations are met in thin film photovoltaics for solar energy harvesting and in narrow-bandgap semiconductor infrared detectors, whose optical thickness may be much smaller than the operating wavelength. One possible approach to light management in such devices is the use of plasmonics [1].

We considered light trapping based on surface plasmon resonance (SPR) in infrared detectors for night vision purposes. Since typical plasmonic metals like gold or silver have their resonance in the ultraviolet or visible part of the spectrum, we had to investigate possibilities for alternative approaches to redshifting plasmonic characteristics into infrared. To this purpose we considered both ordered and disordered thin-film structures to be deposited over the active region of the detector. Such structures couple incident light into guided modes within semiconductor, thus simultaneously serving as an antireflective structure and redistributor of light within the detector. We investigated redshifting by the replacement of metal with transparent conductive oxides (TCO) like indium tin oxide and zinc oxide, which also have a Drude-type relative dielectric permittivity, but with lower absorptive losses and with a resonance frequency shifted towards infrared [2]. The amount of the wavelength shift is dependent on the level of doping of TCO and on the details of the fabrication procedure. The two main geometries we investigated included thin dielectric host with TCO nanoparticle fillers [3] and spoof (designer) plasmon structures [4].

We performed numerical optimization of the influence of different factors of plasmonic light trapping structures, including their geometry and electromagnetic properties. We investigated parallel use of different redshifting strategies. As far as the detectors were concerned, we investigated epitaxial mercury cadmium telluride devices with a typical active layer thickness of 4–8 micrometer. Our results show that detector performance in atmospheric windows (3–5) and (8–14) micrometers can be significantly enhanced through plasmonics. Both sensitivity and specific detectivity can be improved without impairing other detector characteristics. Since the overall level of intrinsic noise in a night vision detector (especially generation-recombination noise due to Auger processes) is dependent on the volume of the active region [5], our results point out to a conclusion that even thinner active areas than those we considered could be readily used, thus suppressing intrinsic noise and even further boosting specific detectivity.

REFERENCES

1. Atwater, H. A. and A. Polman, "Plasmonics for improved photovoltaic devices," *Nature Mater.*, Vol. 9, No. 3, 205–213, 2010.
2. Boltasseva, A. and H. A. Atwater, "Low-loss plasmonic metamaterials," *Science,* Vol. 331, No. 6015, 290–291, January 21, 2011.
3. Jakšić, Z., M. Milinović, and D. Randjelović, "Nanotechnological enhancement of infrared detectors by plasmon resonance in transparent conductive oxide nanoparticles," *Journal of Mechanical Engineering,* Vol. 58, No. 6, 367–375, 2012.
4. Pendry, J. B., L. Martín-Moreno, and F. J. Garcia-Vidal, "Mimicking surface plasmons with structured surfaces," *Science,* Vol. 305, No. 5685, 847–848, 2004.
5. Rogalski, A., *Infrared Detectors*, CRC Press, Bocca Raton, 2010.

Gain Assisted Surface Plasmon Polariton Propagation in a Schottky Junction Based Cylindrical Structure

T. M. Wijesinghe and M. Premaratne
Advanced Computing and Simulation Laboratory (AχL)
Department of Electrical and Computer Systems Engineering
Monash University, Clayton, VIC 3800, Australia

Abstract— Surface plasmon polartions (SPPs) are hybrid transverse magnetic optical waves that are bounded and propagate along metal based interfaces and oscillate collectively with free electrons in the metal. SPPs have proven to be effective in nanoscale as its ability to confine and manipulate photonic energy through subwavelength structures, overcoming constraints imposed by the fundamental diffraction limit. The fundamental SPP properties have been opened up intensive research avenues in areas such as photonics and integrated optics, biomedical imaging and sensing, spectroscopy, nanolithography and metamaterials [1, 2].

SPP waveguides considered to be a major topic in photoelectronics which lead to efficient integration of photonics elements with electronic circuitries. Recent studies analysed SPP waveguides from metal stripes to nanowires and nanoparticle chains, demonstrating more improved SPP manipulations. However, the ohmic losses in metallic elements cause SPP propagation distance limit to few tenths of micrometers. The ability of energy gain by interacting SPP with an active media has been studied in recent research literature for cases such as planar metal stripe waveguides, nanoparticles and nanowires incorporating gain media contain dye molecules, polymers and semiconductor heterostructures [3, 4].

In this research we focus on partial compensation of SPP power loss in the metal by supplying gain to the SPP mode propagate in the waveguide using the semiconductor active medium in order to improve the mode propagation length. We consider a cylindrical structure similar to a nanowire which is formed by a metal core and a semiconductor shell (shown in the figure below). The cylindrical structure has more ability to confine SPP mode than a planer structure. Interface between a metal and semiconductor is known as a Schottky junction. A Schottky junction with a high barrier height could form an inversion layer in its space charge region under the forward biased condition [5]. This leads to a population inversion in the junction, resulting a stimulation emission process. Accordingly the radial Schottky junction with an ohmic coating in the surface can be used to obtain an improved SPP propagation length under forward biased conditions.

In this work, we derive analytical expressions for the carrier behavior in the radial Schottky junction and demonstrate the effct of externally applied voltage, donor concentration and core radius on inversion region and hence on material gain in the active region. Further, we define the modal gain coefficient for TM_{00} SPP mode propagates along the cylindrical structure which is formed using Au core and n-$In_{0.53}Ga_{0.47}As$ shell. Then we analyse the power loss coefficient for the mode and estimate the net modal gain experienced by SPPs. Accordingly, we show the improvement in mode propagation length when the radial Schottky junction is forward biased. This arrangement is more simple and efficient as the gain is supplied by minority carrier injection method. This analysis gives vital information for design and utilization of radial Schottky junction as active waveguides for routing SPPs in integrated circuitry.

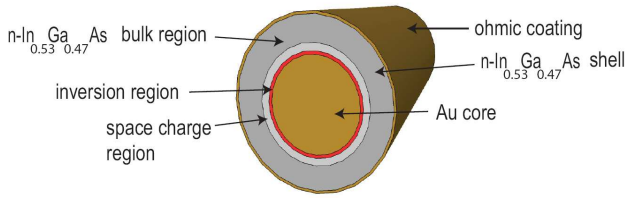

REFERENCES

1. Barnes, W. L., A. Dereux, and T. W. Ebbesen, "Surface plasmon subwavelength optics," *Nat. Photonics*, Vol. 424, 824–830, 2003.
2. Ozbay, E., "Plasmonics: Merging photonics and electronics at nanoscale dimensions," *Science*, Vol. 311, 189–193, 2006.

3. Maier, S. A., "Gain-assisted propagation of electromagnetic energy in subwavelength surface plasmon polariton gap waveguides," *Opt. Commun.*, Vol. 258, 295–299, 2006.
4. Gather, M. C., K. Meerholz, N. Danz, and K. Leosson, "Net optical gain in a plasmonic waveguide embedded in a fluorescent polymer," *Nat. Photonics*, Vol. 4, 457–462, 2010.
5. Fedyanin, D. Y. and A. V. Arsenin, "Surface plasmon polariton amplification in metal-semiconductor structures," *Opt. Express*, Vol. 19, 12524–12531, 2011.

Novel, Compact and Multiband Antenna for Mobile and Wireless Communication

Kamel S. Sultan[1], **Haythem H. Abdullah**[1], **Esmat A. Abdallah**[1], **and Essam A. Hashish**[2]

[1]Electronics Research Institute, Dokki, Giza, Egypt
[2]Faculty of Engineering, Cairo University, Giza, Egypt

Abstract— In this paper, an open slot antenna fed by a U shaped monople is introduced. The slot antenna radiates in the range from 1.6 to 3.44 GHz and from 3.8 to 5.7 GHz. The slot is formed by an open ring of quarter wavelength at 900 MHz. Thus, the ring acts as a monopole at 900 MHz in addition to a wideband slot radiator in the high frequency range. In order to serve the LTE700 MHz band, another ringe monopole is added to the antenna. The proposed antenna has a -10 dB bandwidth which extends from 674 to 750 MHz, from 872 to 976 MHz, from 1.6 to 3.44 GHz, and from 3.8 to 5.7 GHz. The antenna size is $23 \times 31 \times 1.5\,\mathrm{mm}^3$. A prototype of the antenna was fabricated using FR4 substrate ($\varepsilon_{\mathbf{r}} = 4.5$) with 1.5 mm thickness and loss tangent of 0.025. This paper proposes a new mobile handset antenna structure with low SAR values with compact size that cover most of the mobile operating bands and other wireless applications. The covered bands are the GSM900, DCS1800, PCS1900, UMTS2100, and most of the LTE bands including the LTE700 band. Furthermore, it covers the ISM, WIMAX and the WLAN bands. The SAR calculations are done using the CST2012 commercial package and the voxel head modal. The SAR values are calculated at different operating bands, different distances, and different orientations. The effect of the human body on the performance of the antenna is tested by calculating the radiation pattern in the presence of the body. The simulation results are compared to the experimental measurements and a good agreement is observed.

Gold Plating Carbon Nano Tube Antenna Integrated with Voltage Control Oscillator

Kuan-Ting Lin[1], **Jian-Yu Hsieh**[1], **Yu-Jen Chen**[2], **Shuo-Hung Chang**[2], **Ying-Jay Yang**[1], **and Shey-Shi Lu**[1],

[1]Graduate Institute of Electronics Engineering, National Taiwan University, Taiwan, R.O.C.
[2]Department of Mechanical Engineering, National Taiwan University, Taiwan, R.O.C.

Abstract— With the dramatic development of wireless communication technology in recent years, high-speed wireless applications have become popular, including cloud services, video streaming, and data communications. In order to meet the high data rate requirements, millimeter-wave applications which have wide bandwidth for data communication are the trend to serve the needs. The antenna is the first component in the transceiver and combining the antenna and chip concurrently in millimeter-wave integrated circuits is difficult.

In this paper, gold plating of the bundled carbon nano tube (CNT) antenna which is integrated with a voltage control oscillator (VCO) is proposed. The integration of the antenna and VCO is performed by silver paste. This integration not only saves a V-band signal generator but also demonstrates an on-chip antenna implementation. Owing to gold plating, the antenna and radiation efficiency can be improved. The length and width of the bundled carbon nano tube are equal to 520 um and 54 um, respectively. The design of the V-band complementary VCO is fabricated in 90nm CMOS technology with transistors, varactors, and inductors.

Measurements show a 51 GHz VCO operating from 1 V with phase noise of −88 dBc/Hz at 1 MHz offset and power consumption of 3 mW, which delivers −15 dBm of differential output power. The figure of merit is −177.4 dBc/Hz for the implemented VCO. In order to obtain the antenna properties of the bundled CNT, the measuring equipment includes a V-band horn antenna and spectrum analyzer are used. The measurement results of the antenna indicate that the radiation power is −49.9 dBm for 50.7 GHz. The radiation power is about 10 dB larger than the radiation power of the VCO without the CNT antenna. The experimental results show that the CNT is suitable to be an antenna and may be considered as a useful component in future millimeter-wave applications.

Dual-band Antenna for In-building Repeater Systems

Ho-Jun Lee[1], **Min-Ki Woo**[2], **Nae-In Lee**[2], **and Gene Yoo**[2]

[1]Convergence Communication Components Research Center
Korea Electronics Technology Institute, South Korea
[2]Innonet Co., Ltd., South Korea

Abstract— In this paper, we proposed a novel design of dual-band antenna for in-building repeater systems. The proposed antenna configuration is shown in Figure 1. Antennas in this paper are simulated by using CST Microwave Studio. A prototype of this antenna was fabricated on FR4 substrate with thickness $h = 0.6$ mm and dielectric constant $\varepsilon_r = 4.4$. The measurements of electrical characteristics such as radiation patterns, VSWR, and return loss of the implemented antenna were conducted in an anechoic chamber equipped with a PNA network analyzer and far field measurement system. Figure 2 shows return loss (S_{11}) characteristics. The measured impedance bandwidth of the antenna is from 1.7 to 2.2 GHz for VSWR < 2. Figure 3 shows a photograph of the fabricated antenna. We manufactured the antenna based on the results of optimized simulation results and measured characteristics of the suggested antenna in the anechoic chamber. Details of the proposed antenna designs are described, and typical experimental results are presented and discussed.

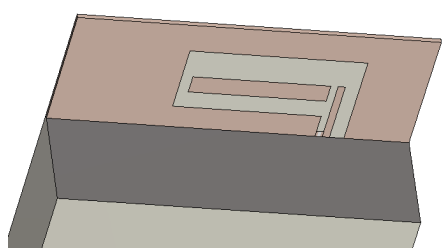

Figure 1: Proposed antenna.

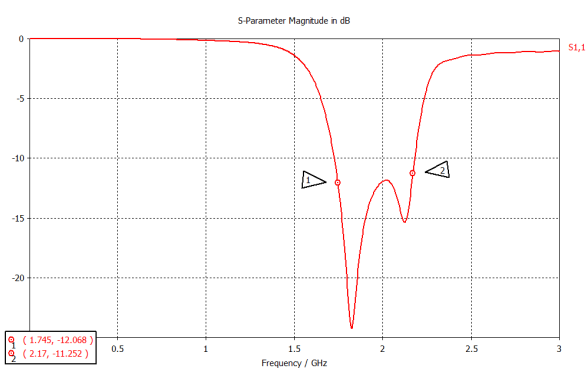

Figure 2: Return loss.

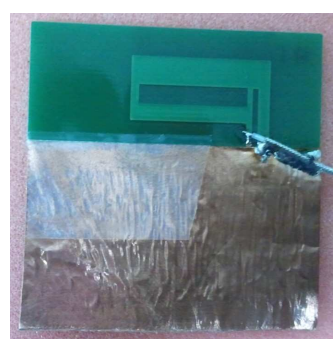

Figure 3: Photograph of the fabricated antenna.

REFERENCES

1. Stutzman, W. L. and G. A. Thiele, *Antenna Theory and Design*, 2nd Edition, Hohn Wiley & Sons, New York, 1998.
2. Balanis, C. A., *Antenna Theory Analysis and Design*, 2nd Edition, Wiley & Sons, 1997.

Development of Textile Antennas for Smart Clothing Applications

Kuo-Sheng Chin, **Chi-Sheng Wu**, **and Chih-Chun Chang**
Department of Electronic Engineering, Chang Gung University, Tao-Yuan 333, Taiwan, R.O.C.

Abstract— This paper presents three different structures of microstrip antennas constructed on textiles for smart clothing applications. Conductive material, a copper plated polyester fabric, was used as the antenna radiators and ground planes. Substrate used in the design is insulating neoprene fabric with a thickness of 4 mm and the permittivity of 1.4. The value of permittivity was determined experimentally based on the resonance method. Conductive material was attached to the substrate using acrylic adhesive. These three antennas are low-profile, lightweight, flexible, and washable, which is most suitable for wearable applications.

Recently, a study on body-centric wireless communications has become an attractive area of research because of its increasing applications in personal communication systems. Smart clothing is a typical wearable personal communication system, which can be used for eldercare, emergency medical, firefighting, military, and athlete monitoring. Textile antennas show great promise due to their ease of integration with other textile materials. This paper presents the design of three textile antennas: (a) rectangular microstrip patch antenna, (2) annular slot antenna, and (3) microstrip PIFA antenna, in the 2.45 GHz WLAN band for smart clothing applications. Fig.1 shows photos and the measured radiation patterns of the textile patch antennas with a maximum gain of 5.96 dBi and a bandwidth of 14.2%. The gain and bandwidth of the annual slot antenna are 4.4 dBi and 12%, respectively, while a little lower than the patch antenna. The PIFA antenna has the widest bandwidth of 19.5% but the smallest gain of 2 dBi. The radiation patterns show that the patch antenna has a lower back radiation than the PIFA and the slot antenna, which is beneficial to reduce the radiation towards human body for achieving low SAR. The performance deterioration of the proposed antennas is also analyzed under bent conditions to check compatibility with wearable applications. Detailed results and parametric comparison between the designed antenna structures are presented in this paper.

(a) (b) (c)

Figure 1: Fabricated textile patch antenna: (a) Photo of the patch antenna. (b) Photo of the smart clothing with a patch antenna. (c) Measured radiation patterns.

ACKNOWLEDGMENT

This work was partially supported by the National Science Council, Taiwan, R.O.C., (NSC 101-2221-E-182-052), the High Speed Intelligent Communication (HSIC) Research Center, and the Healthy Aging Research Center (HARC), Chang Gung University.

MIMO Reference Antennas for OTA Applications

Shuai Zhang[1,2], **Kun Zhao**[1,3], **Zhinong Ying**[3], **and Sailing He**[1,2]

[1]School of Electrical Engineering, KTH-Royal Institute of Technology, Stockholm SE-100 44, Sweden
[2]Centre for Optical and Electromagnetic Research, Zhejiang University, Hangzhou 310058, China
[3]Research and Technology, Corporate Technology Office
Sony Mobile Communications AB, Lund SE-221 88, Sweden

Abstract— In this paper, MIMO reference antennas with different correlation coefficients are proposed for Over-The-Air (OTA) applications. The correlation can be simply controlled through a slot etched on a dual-feed PIFA with the similar total efficiency. Three kinds of situations are investigated with the proposed method: high correlation (HC), mid correlation (MC), and low correlation (LC). In order to verify the introduced idea, the measurements of correlations and efficiencies are carried out in a reverberation chamber. The simulation and measurement agree well with each other.

Theoretical Analysis of AC Resistance of Coil Made by Copper Clad Aluminum Wires

C. Kamidaki and N. Guan
Power and Telecommunication Cable System R&D Department, Fujikura Ltd., Japan

Abstract— In wireless power transfer systems using inductive coupling through magnetic fields, power transfer efficiency is significantly influenced by the quality factor $Q = \omega L/R_{ac}$ of its coil, where ω, L and R_{ac} are the angular frequency, inductance and AC resistance, respectively. In order to obtain a higher Q, higher frequency and lower R_{ac} are desirable, but R_{ac} increases quickly with frequency due to the skin effect as well as proximity effect which comes from the eddy currents induced by current flowing in neighbor wires.

We have proposed the replacement of copper (Cu) wires by copper clad aluminum (CCA) wires, which are aluminum (Al) wires coated with thin Cu layer via metallic bond. The CCA coils are not only cost-effective, light-weight and solderable as Cu, but also show lower R_{ac} than Cu under certain circumstance, as shown in Fig. 1.

In the paper, both the skin and proximity effects for a circular metallic wire with multiple layers are theoretically analyzed and the AC resistance is formulated by

$$R_{ac} = R_s + \alpha^2 D_p \tag{1}$$

where R_s and D_p are the AC resistance related to the skin effect and the loss caused by the proximity effect, respectively, and α is a shape factor for coils. R_s and D_p are theoretically given and α is related to the intensity of magnetic field affecting by neighboring wires. Assuming a coil is wound with T turns, α is given by

$$\alpha = \sqrt{\frac{\sum_{k=1}^{T} 2\pi R_k H_k^2}{\sum_{k=1}^{T} 2\pi R_k i_k^2}} \tag{2}$$

where i_k, H_k and R_k are the intensity of current, the intensity of magnetic field and the radius of the k-th wire, respectively. α is determined from the coil geometry. By this formulation, the AC resistance of CCA coils are numerically analyzed with good agreement with measurement, as shown in Fig. 1.

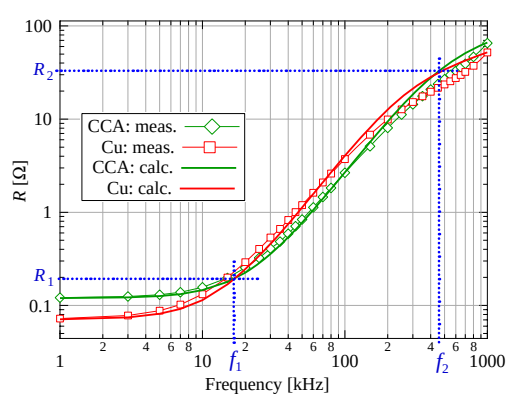

Figure 1: Measured and calculated result of AC resistance of CCA and Cu coils.

In practical applications, frequencies f_1 and f_2 between which CCA wires are superior to Cu ones are very important parameters. They and corresponding resistances R_1 and R_2 are also quantitatively analyzed in this paper.

A Hybrid Optimization of Wireless Power Transfer with Intermediate Coils

Tiejun Cui, **Shuo Liu**, **and Linhui Chen**
School of Information Science and Engineering, Southeast University, China

Abstract— Transmitting power without wires has been one of the most exciting researches in recent years, which may finally eliminate cables from mobile devices such as cell phones and cameras. It is a significant improvement on the transfer distance when the non-radiated magnetic resonant coupling technique was suggested by the MIT group in 2007. However, the transferred energy is still restricted to about one coil diameter. Recently, the wireless power transfer (WPT) with one or more intermediate coils, which is called a relay system, have been investigated and showed great improvement to the extending of the effective transfer distance.

In this paper, we propose a hybrid scheme to optimize the wireless power transfer (WPT) with intermediate coils. First, the total transfer efficiency is expressed by the product of several sub-efficiencies. By simulations with the function of total efficiency, we have given the optimized load impedance for the most common intermediate WPT, where only the coupling coefficient k between adjacent coils is considered.

Second, as shown in our previous work "An Optimizable Circuit Structure for High-Efficiency Wireless Power Transfer", the overall transfer efficiency can be calculated by the Q-factors and coupling coefficient of coils. Therefore, how to design the shape of coils and their relative position are also critical to the design of a WPT system. We have presented a complete scheme to optimize the transfer efficiency of a relay WPT system directly from the 3D model, which gives us a more intuitive and convenient way of design than the previous circuit-level analysis. First, the full-wave simulation software, CST Microwave Studio, is used to exact the S-parameter of the relay WPT system. Then, the S-parameter is sent to Agilent Design System (ADS) for further processing of the transfer efficiency and the corresponding matching network. Hence CST and ADS together provide us a comprehensive method to simulate from the physical structure of coils to the final transfer efficiency of an arbitrary WPT system.

Experiments of the WPT systems with one intermediate coil and two intermediate coils are conducted to validate the analysis of the intermediate WPT system. Each coil has a diameter of 10 cm and is winded with copper wires with 2.5-mm diameter around the Plexiglas armatures by five turns. A Vector Network Analyzer is used to help tuning the system into the resonant status. Then we use a frequency generator and an oscilloscope to measure the input and output voltage of the system for the calculation of the total efficiency. Experiments have shown that the relay system with two intermediate coils achieve much higher efficiency than that of the non-intermediate WPT system, which agrees well with simulation results.

A Rectenna for Wireless Power Transmission

Jwo-Shiun Sun, Si-Jyun Hung, Yi-Ching Huang, Tsung-Lin Li, and Guan-Pu Pan
Institute of Computer and Communication Engineering
National Taipei University of Technology, Taipei, Taiwan

Abstract— A designed circularly polarized (CP) antenna for wireless power transmission (WPT) shows its 3 dB axial ratio bandwidth of 180 MHz, from 2390 to 2570 MHz with 3.2 dBi gain. A balun and Schottky barrier diodes are chosen for the rectifying circuit. The designed rectenna with the CP antenna and one half-wave voltage-doubler rectifying circuit exhibits a maximum output voltage of 8.2 V and conversion efficiency about 80% is attainable.

Compact Design of a Flexible and Wearable Tri-band Rectenna

Diego Masotti[1], **Alessandra Costanzo**[2], **Massimo Del Prete**[2], **Martino Aldrigo**[1], **and Riccardo Trevisan**[3]

[1]D.E.I., University of Bologna, Viale Risorgimento 2, Bologna 40136, Italy
[2]D.E.I., University of Bologna, Via Venezia 52, Cesena 47521, Italy
[3]D.E.I., University of Bologna/IMA Industries, Bologna, Italy

Abstract— Nowadays several applications can be supported by small amounts of power (ranging from a few μW to a few hundreds of μW), such as ultra-low power microcontrollers and sensors requiring power consumption few times per day. In this paper we demonstrate that highly efficient multi-band wearable rectennas (rectifying antennas) can provide this energy by exploiting ubiquitously available RF sources, operating at different bands, with unknown directions of incidence and polarizations. The original solution adopted for the present design is described in Figure 1: in order to meet compactness requirements, high radiation and conversion performances, we resort to a multi-layer structure, with a single radiating/rectifying section: these choices allow the use of different kinds of flexible materials suitably selected for technical clothing solutions and to minimize both unwanted electromagnetic couplings and rectifying diode losses.

The substrate supporting the antenna consists of a 4 mm-thick pile, whose relative permittivity has been measured by means of resonant methods, and results to be 1.23. The Global EMC shielding fabric is chosen as the antenna conductive material for its low surface resistivity (0.02 Ω/sq), and its minimal fraying with respect to other fabrics. A thermo-adhesive is used at each pile-conductive fabric interface. The lower feeding circuitry (matching network, phase shifter, power divider and rectifier) is realized on a 0.1 mm-thick flexible Kapton ($\varepsilon_r = 3.4$, $\tan\delta = 0.002$), whose area is limited to the minimum needed, in order to guarantee a more comfortable wearable solution. The rest of the antenna ground plane is provided by attaching the Kapton to the Global EMC fabric. Large ground planes can thus be easily obtained by increasing the pile and the conductive fabric areas: superior antenna performances and prevention from back-radiation into human tissues are guaranteed.

A unique slotted annular-ring patch antenna provides the multi-band behaviour of the scavenging system, by exploiting different resonant modes. In order to harvest from two cell phone standards and from WiFi three mode frequencies are tuned by modifying the positions and dimensions of the slots etched in the patch metallization (Figure 1). The Kapton feeding network consists of a broadband 90° phase shifter/divider: by means of two apertures obtained from the Kapton ground plane the contemporaneous excitation of two in-quadrature orthogonal modes is achieved,

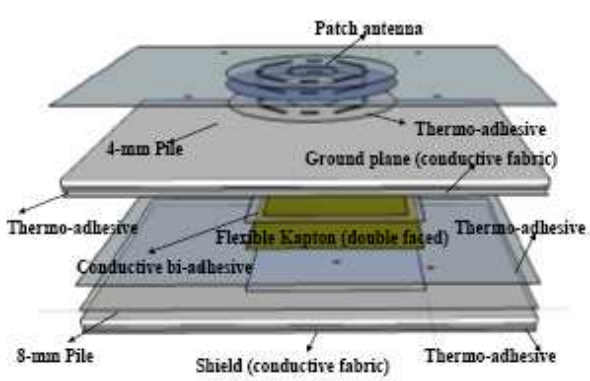

Figure 1: Stack-up of the proposed solution.

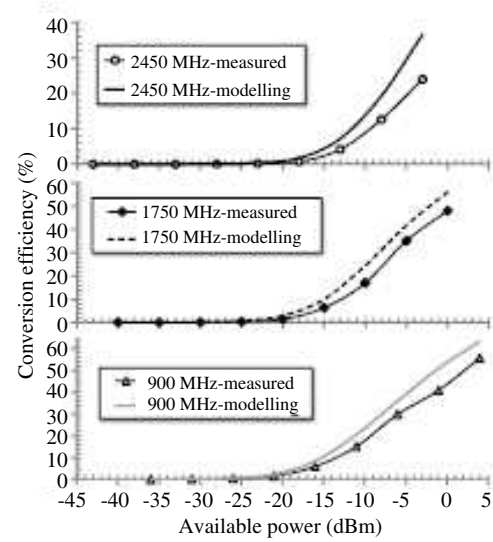

Figure 2: Conversion efficiencies at the three operating frequencies.

for circular polarization purposes. The adopted approach allows to represent layout-wise the entire passive sub-circuit (antenna, matching network, and feeding network) by the broadband scattering matrix derived by EM simulation and to optimize the rectenna as a whole by means of a multi-tone HB nonlinear technique: the network function to be maximized is the conversion efficiency, defined as the ratio between the DC output power delivered to the optimum load and the actual RF power available at the rectifier input. By means of this rigorous approach several crucial phenomena, such as power mismatch between antenna and receiver front end, and the simultaneous presence of different RF sources are automatically included in all the evaluations. The effectiveness of the procedure is demonstrated by the results shown in Figure 2: good agreement between simulated and measured conversion efficiencies is obtained for all the operating frequencies, even in the indoor office scenario here considered. In this case, a realistic description of the channel within the multi-platform CAD tool is mandatory, too.

Wireless Power Transmission by Enlarging the Near Field

Konstantin Meyl
Faculty of Computer and Electrical Engineering, Furtwangen University, Germany

Abstract— Continuing the contribution about "wireless power transmission by scalar waves", presented in Moscow 2012, this paper goes deeper, explaining the different types and properties of waves described by the wave equation. Starting with the wave description of Maxwell an extended version of the Laplace equation is derived, expanding the standard derivations of the near field, showing how to influence the zone, where the longitudinal wave parts occur. We come to the conclusion that the near field zone is enlarging, if the longitudinal parts of a wave or the antenna voltage are accelerated. This relationship is essential for the wireless transmission of energy. In addition this exciting new result could be tested experimentally. The simple experiment will be demonstrated at PIERS 2013 in Stockholm. Only by changing the antenna design, it will be shown how both, the speed of propagation and the near field are enlarging proportional to each other. In all practical applications as discussed in PIERS Proceedings 2012, the extended near field is the key of success.

Numerical Study on the Radiative Transmission Efficiency of Dipolar Sources

C. L. Moorey, W. Holderbaum, and B. A. Potter
University of Reading, UK

Abstract— Accurate calculation of the transfer efficiency between a source and a receiver in radiative wireless power transmission relies heavily on the accurate computation of the electromagnetic fields existing in the free space surrounding the source. For source structures that exhibit complex geometry, no closed-form solution is usually possible. In these cases, emphasis is placed upon numerical methods to obtain electromagnetic field solutions. Dipoles, however, are simple enough objects to derive closed-from solutions for [1]. For radiative wireless power transfer, dipoles can be used to model the power flow due to an electrically small source [2], or more importantly, to create a linear superposition of such dipoles that produces a radiation pattern which maximises the transfer efficiency (e.g., a "high-gain" dipole array) [3]. To this end, accurate computation of their electromagnetic fields is vital. Furthermore, it is undesirable to have to limit a field solution to a given region, such as the near- or far-field, as for high frequency sources this severely limits the spatial freedom of the solution. Computation of the radiation transmission efficiency of the dipoles using the full-field expressions (no near- or far-field approximations) for the electromagnetic fields demonstrates a singularity at a distance $r = \lambda/\sqrt{2\pi}$ from the dipole [4]. Numerical solutions for the dipoles are obtained using Remcom XFDTD 7 software to investigate the existence and nature of this singularity. Comparisons between the numerical and analytical solutions are made. Specific focus is given to the variation of the radiative transmission efficiency with respect to frequency and spatial location.

REFERENCES

1. Hammond, P., *Applied Electromagnetism*, Pergamon Press, 1971.
2. Fan, H. and F. Schlagenhaufer, "Far-field approximation of electrically moderate-sized structures by infinitesimal electric and magnetic dipoles," *IEEE Electromagnetic Compatibility*, Vol. 52, No. 1, 82–88, 2010.
3. Lerideau, G., J.-M. Floc'h, A. K. El Sayed Ahmad, A.-C. Tarot, R. Loison, S. Thizon, and S. Pied, "High gain printed dipole array with reflectors and directors," *2011 11th Mediterranean Microwave Symposium (MMS)*, No. 1, 61–63, Sep. 2011.
4. Moorey, C. L., W. Holderbaum, and B. A. Potter, "Radiative transmission from dipolar sources," to be published in *Proceedings of IEEE WPTC 2013 Perugia Conference*, 2013.

An Energy Management Circuit Based on Up-conversion to Power Wireless Sensor Nodes

S. Q. Pan, P. Li, Y. M. Wen, Z. Q. Zhang, D. Lu, and D. F. Sun
Research Center of Sensors and Instruments, Department of Optoelectronic Engineering
Chongqing University, Chongqing 400044, China

Abstract— Since wireless sensor nodes (WSNs) own many characterizations, such as low power consumption and miniaturization, they can exhibit an evidential advantage to detect the current and temperature of the electric wires which are generally installed in the unapproachable and dangerous environments relative to other traditional detecting approaches To improve the operation lifespan of WSNs, the power supplies must be considered. The conventional solution to power WSNs with batteries is troublesome due to their infinite lifetime and bulk mass. Harvesting energy from ambient environment as the power supplies of WSNs is gradually becoming an excellent alternative to the batteries. Since the electromagnetic energy extensively distributes around the current-carrying electric wire, it can be conveniently transduced into the electric energy to be as the energy sources of WSNs by an electromagnetic transducer. To store and govern the weak energy from the electromagnetic transducer, an energy management circuit exhibits an extremely important role. However, traditional energy management circuits don not accomplish fine impedance matching and cannot accumulate energy from transducer to drive WSNs under weak current across the electric wire circumstances due to their weak energy harvesting capability. Hence, to ensure the regular operation of WSNs, more energy must be extracted from the electric wire and stored into the energy reservoir by a high power energy management circuit.

This paper presents an energy management circuit based on up-conversion to power WSNs, as shown in Fig. 1. The electromagnetic energy around the electric wire can be transduced into electric energy by the transducer which is a specially designed electromagnetic coil. The proposed energy management circuit based on up-conversion can convert the electric signal with 50 Hz induced from the electric wire into a narrow bandwidth signal focused on a higher frequency. Since the generated high-frequency electric signal exhibits a more powerful charging capability for the storage capacitor, the energy management circuit can achieve good impedance matching and the output load of management circuit can be improved. Thus, more weak energy from the transducer can be accumulated in the storage capacitor and the charging time of storage capacitor can also be improved. Experimental results demonstrate that the storage capacitor of 0.1 F can be charged to 3.3 V at a charging time of 30 minutes by the proposed management circuit under 1 A current across the electric wire, as shown in Fig. 2. The energy accumulated in the storage capacitor can be released to drive a wireless sensor node, of which the power consumption is 13 mW in acquiring data mode (199 ms) and 70 mW (1 ms) in transmitting data mode at a communication distance of 10 m respectively. Since the proposed energy management circuit can efficiently scavenge weak energy from the transducer, the approach based on up-conversion to harvesting energy can also be applied in other weak input situations.

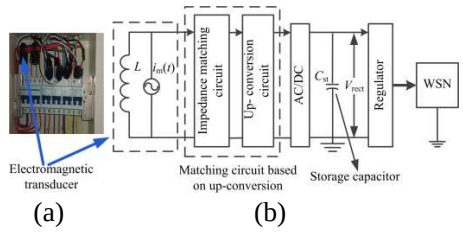

Figure 1: (a) 220 V distribution box. (b) Schematic diagram of energy management circuit.

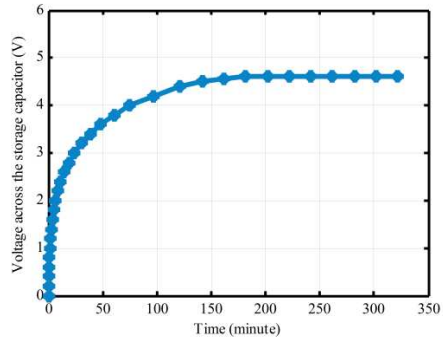

Figure 2: Charging process of storage capacitor (0.1 F) under 1 A current across the electric wire.

ACKNOWLEDGMENT

This work is financially supported by the National Natural Science Foundation of China (Grant Nos. 50830202 and 61071042) and the National High Technology Research and Development Program of China (863 Program) (No. 2012AA040602).

Self-contained Self-powered Wireless Sensing Node for AC Power Supply Cords Monitoring

D. Lu, Y. Wen, P. Li, S. Pan, and Z. Zhang
Research Center of Sensors and Instruments, Department of Optoelectronic Engineering
Chongqing University, Chongqing 400044, China

Abstract— Energy harvesting is thought to be a promising solution for sustainably powering wireless sensors. As a matter of fact, in general ambience, it is quite difficult to sustainably scavenge adequate and sufficient energy from fixed ambient sources for power supply. However there are guaranteed electric/magnetic fields along power cords carrying AC currents. Thus, it is ready to develop self-powered sensor systems in actual applications connected with power lines. Harvesting the energy aroused from AC current carrying power lines has been applied for powering monitoring systems of power transmission lines and substations, in which cases, the line voltage reaches kV-level [1]. There are also self-powered sensors used for the power supply cords, which voltage is typically 110 V $\sim$ 380 V [2]. In the case of wireless sensing of power cord condition, a battery usually has to be contained in the wireless node [3]. Here, for wireless monitoring low-voltage AC power supply cords of electric appliances, a self-contained self-powered sensing node is proposed.

The self-contained and self-powered sensing node for power line monitoring consists of an energy harvester, a current sensor, a temperature sensor and a wireless communication module. The node is designed to be self-contained for monitoring AC power supply cords of electric appliances exclusive of using battery or externally physical connection of power supply. The underlying component of the node is a magnetic core, which embraces the monitored cord in operation. For easy installation, the core is designed as a disengaging split-core. There are two sets of coils wound around the core, one is sensing the current and another is scavenging the magnetic energy originated from the carried-on AC current. The output of the energy harvesting coil is connected with the power management circuit to produce adequate DC supply for the wireless sensing node. The outputs of the current and temperature sensors are connected to the communication module for wireless transmission.

Tests have been conducted on the performance of the self-contained and self-powered sensing node. The energy scavenged from the AC power supply cord can drive the wireless sensing node, whose power consumption is 6.4 μW during the sleep interval and 54 mW during the transmission cycle. The wireless sensing node operates while the carried-on current is from less than 1 A to 100 A with a wireless distance of 10 meters. Because of the compact size and self-contained device architecture, the sensing node can be easily installed to encircle a power cord without interruption of the power supply from the monitored cord, and the sensing data is wirelessly transmitted at a data loss rate less than 5‰. The wireless sensor network is constructed in a star topology distributively with the proposed self-contained self-powered sensing nodes.

REFERENCES

1. Du, L., C. Wang, X. Li, L. Yang, Y. Mi, and C. Sun, "A novel power supply of online monitoring systems for power transmission lines," *IEEE Transactions on Industrial Electronics*, Vol. 57, No. 8, 2889–2895, 2010.
2. Xu, Q., M. Seidel, I. Paprotny, R. M. White, and P. K. Wright, "Centralized electric current monitoring system using PEM AC current sensors," *IEEE Sensors Journal*, Vol. 13, No. 3, 1055–1064, 2013.
3. Zhang, Y., J. Lu, H. Hiroshima, T. Itoh, and R. Maeda, "Simulation and design of micro inductor for electromagnetic energy scavenging at low AC frequency in wireless sensor network," *Power MEMS 2009*, 253–256, Freiburg, Germany, Nov. 28–29, 2009.

Symmetric Ridge-type Semiconductor Laser with Selectively Formed Double-sided Antiguiding Cladding Layers

Daiya Katsuragawa and Takahiro Numai
Ritsumeikan University, Japan

Abstract— High power 980-nm semiconductor lasers are indispensable for pumping sources of erbium doped optical fiber amplifiers. Generally, 980-nm semiconductor lasers have ridge structures so as not to expose their active regions to air during their fabrication, because the active regions are easily oxidized and degraded in air. In the ridge structures, higher-order transverse modes as well as the fundamental transverse mode are confined. As a result, with an increase in injected current, higher-order transverse modes lase; kinks appear in their current versus light-output (I-L) curves. These kinks are attributed to changes in the local gain profile and refractive index owing to spatial hole burning, the free-carrier plasma effect, and heating. To obtain high fiber-coupled optical power, semiconductor lasers with high kink levels operating in the fundamental transverse mode are required. To date, to increase kink levels, coupling of the optical field to the lossy metal layers outside the ridge, highly resistive regions in both sides of ridge stripe, and incorporation of a graded V-shape layer have been demonstrated. To increase kink level and decrease the threshold current further, a ridge structure with optical antiguiding layers have been proposed, but the fabrication process is fairly complicated.

In this paper, in order to make the fabrication process more simple and increase kink level, a symmetric ridge-type semiconductor laser with selectively formed double-sided antiguiding cladding layers is proposed and simulated. In the proposed ridge structure, kink-free laser operation is obtained up to the injected current of 2 A by suppressing spatial hole burning and lowering optical gains for higher-order transverse modes with the step of the antiguiding cladding layer.

ACKNOWLEDGMENT

This research was partially supported by the Japan Society for Science, Grant-in-Aid for Scientific Research (C) 24560429, 2013.

Design of Narrow Core Structure for High Power Pickup Device in Railroad Application

Sang Hoon Chung, **Bo Yune Song**, **Dang-Oh Kim**, **Uooyeol Yoon**, **Jaegue Shin**, **Yangsu Kim**, **Chung Hee Lee**, **and Guho Jung**
Wireless Power Transfer Technology Research Center, KAIST, Daejeon 305-701, Korea

Abstract— In this paper, design of narrow core structure for high power pickup device in railroad application is described. The proposed core structure for pickup device in this paper is designed to show 60 kW output power at 70 mm air gap (90 mm core to core distance) when applied to a pickup device. This new structure has its advantages in its reduced width while showing a same level of energy harvesting performance compared to the ones designed in previous studies.

While numerous researches on wireless power transfer pickup device for bus and railroad application has been carried out by KAIST over the past few years and has successfully developed this pickup device, it still has room for improvements through further studies. We sought this possibility in changing structure of core. Compared to previous designs in bus applications, the newly designed structure in this paper has its width reduced up to 30% and hence its volume being reduced by 30%. Since railroad application requires much larger power output (9.8 MW for the largest train in Korea), it is imperative that pickup device becomes smaller in size. Smaller pickup core structure requires primary core to be narrower as well and this brings out a large reduction in cost. Above all, the fact that it gets cheaper will be able to provide short path to commercialization of railroad non-contact power transfer system. This will allow various railroad systems to be cheaper and less space-occupying since the conventional catenary and pantograph are no longer needed. In this study, we designed a narrower (compared to previous designs) pickup core structure that is capable of having 60 kW output power at 60 kHz resonance frequency. Then we carried out FE analysis to verify the feasibility of narrow core structure for 60 kW pickup devices in railroad application.

A 200 GHz on-chip Active Antenna

Bing Zhang[1], **Li Wei**[1], **Mingquan Bao**[2], **Yinggang Li**[2], **and Herbert Zirath**[1]

[1]Microwave Electronics Laboratory, Department of Microtechnology and Nanoscience (MC2)
Chalmers University of Technology, Gothenburg SE-41296, Sweden
[2]Microwave and High Speed Electronics Research Center
Ericsson Research, Ericsson AB, Mölndal SE-43184, Sweden

Abstract— For the available broad bandwidth and variant atmospheric attenuation, the millimeter-wave (mmWave) spectrum is preferable for either short- or long-range high date rate wireless communication. For example, the 60-GHz band with large atmospheric attenuation is regulated for short-range usage of nearly 9 GHz unlicensed bandwidth. One of the atmospheric windows 200–250 GHz is preferred for radio backhauling over miles of range for its low atmospheric attenuation. In late 1990s, Y. P. Zhang initiated the idea that for the small wavelength, the integration of antenna with other devices on a single chip or in a package became possible. After then, the mainstream of antenna designed for mmWave applications could be categorized as antenna-in-package (AiP) and antenna-on-chip (AoC). However, because of the large dielectric loss of the substrate in AoC applications, antennas usually do not feature desirable gain. To overcome this problem, the co-design of antennas with amplifiers is widely preferred to compensate the substrate loss. But the required lossy on-chip power combiner for multi-transistor amplification is another limitation on the improvement of on-chip antenna's gain. In this work, we present a 200 GHz on-chip active antenna, which is co-designed with driving amplifiers and reflection amplifiers, on the 5 µm thick benzocyclobutene (BCB) dielectric layer ($\varepsilon_r = 2.7$, $\tan\delta = 0.006$ and 5 µm thickness) of a 250 nm indium phosphide (InP) double heterojunction bipolar transistor (HDBT) process. The antenna is composed of four conductor arms. Each of the arms is equally folded, which has 3 µm thickness and one guided wavelength at 200 GHz ($\lambda_g = 600$ µm) in length. By exciting the arm at one end through a driving amplifier, the output power of the driving amplifier is radiated by the antenna and combined simultaneously in space. The properly designed reflection amplifier at the other end of the arm helps to reflect, re-radiate and re-combine continuously without oscillation, thus forms a power cycle with the driving amplifier. By doing this, the large on-chip dielectric loss is compensated by the co-designed amplifiers, the widely adopted lossy on-chip power combiner becomes unnecessary, and the power utilization is improved. Moreover, the proposed antenna features either linear or circular polarization by different feeding phases.

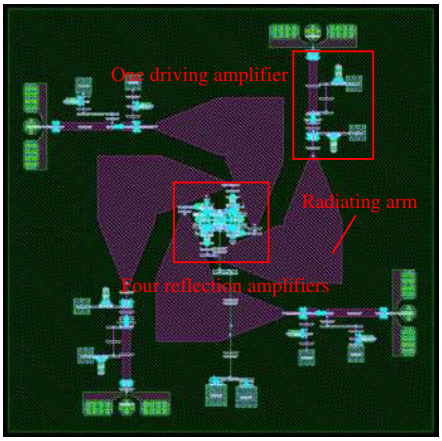

A Compact Energy Pattern Reconfigurable Antenna

Junrui Zhang and Shaoqiu Xiao
Institute of Applied Physics, University of Electronic Science and Technology of China, China

Abstract— Energy patterns and waveform fidelity factors are usually adopted to depict the time domain performance of a pulse radiating antenna [1–3]. An energy pattern reconfigurable pulse radiating antenna operating in $2 \sim 6$ GHz was presented in [4], the structure presented was $70 \times 60 \times 1.6\,\text{mm}^3$. This paper aims to realize energy pattern reconfiguration in a more compact area.

The proposed antenna (shown in Figure 1) is mounted on a $24 \times 18 \times 1.6\,\text{mm}^3$ FR4 substrate ($\varepsilon_r = 4.4$, $\tan\delta = 0.0254$). Ideal model of PIN diode switches (i.e., 4 Ohm series resistor for ON mode and 0.025 pf series capacitor for OFF mode) is adopted to simulate the reconfiguration characteristics of the proposed antenna. The simulation results are given by CST 2012 MICROWAVE STUDIO and post-processing of a MATLAB program. According to different configurations of the two "switches", the antenna operates in two STATEs (Table 1) whose energy patterns in the xoy plane are mirror of each other (Figure 2). Due to symmetrical property of the structure, the S_{11} of both STATEs are the same (Figure 3). The proposed antenna can radiate a $2 \sim 6$ GHz Gaussian pulse with high fidelity (Table 2).

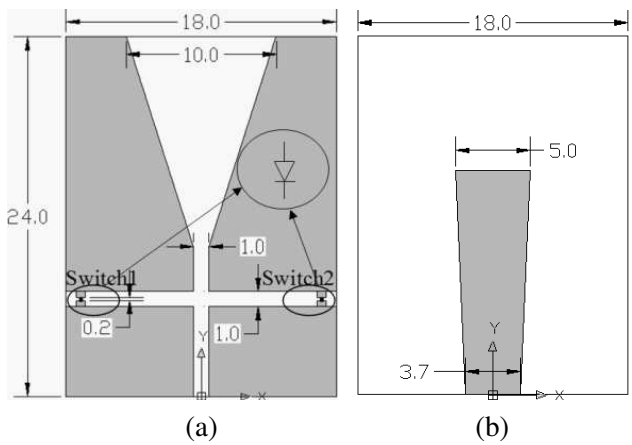

Figure 1: Proposed structure (units: mm). (a) Top side, (b) bottom side.

Table 1: Operating STATEs of proposed antenna.

	Switch1	Switch2
STATE1	ON	OFF
STATE2	OFF	ON

Table 2: Fidelity factors of proposed antenna.

STATE1	68°	22°	114°
	0.983	0.981	0.966
STATE2	−68°	−22°	−114°
	0.983	0.981	0.966

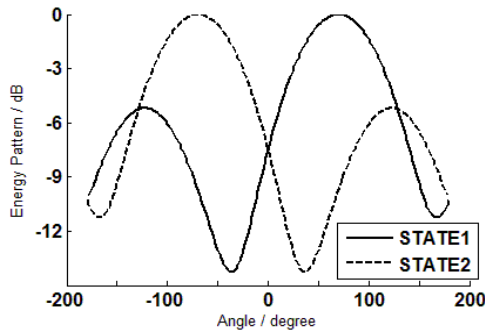

Figure 2: Normalized energy pattern, 3 dB lobe: $-114^\circ \sim 22^\circ$ STATE2, $-22^\circ \sim 114^\circ$ STATE1.

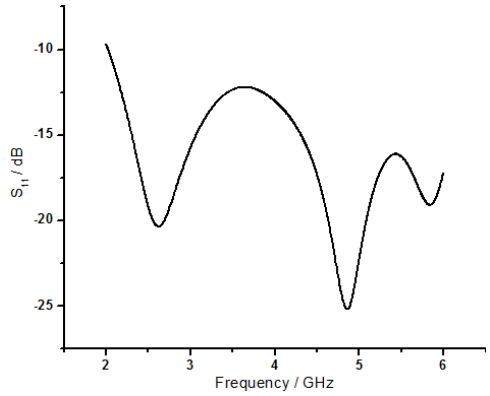

Figure 3: Reflection coefficient S_{11}.

REFERENCES

1. McLean, J. S., H. Foltz, and R. Sutton, "Pattern descriptors for UWB antennas," *IEEE Transactions on Antennas and Propagation*, Vol. 53, No. 1, 553–559, Jan. 2005.
2. Zhang, G. M., J. S. Hong, B. Z. Wang, et al., "Design and time-domain analysis for a novel pattern reconfigurable antenna," *IEEE Antennas and Wireless Propagation Letters*, Vol. 10, 365–368, 2011.
3. Lamensdorf, D. and L. Susman, "Baseband-pulse-antenna techniques," *IEEE Antennas and Propagation Magazine*, No. 36, No. 1, 20–30, Feb. 1994.
4. Zhang, J. R., S. Xiao, et al., "Time domain characteristics of a novel pattern reconfigurable pulse radiating antenna," *IEEE Antennas and Wireless Propagation Letters*, Vol. 11, 1202–1205, Oct. 2012.

Scanning Range Expanding of Time Domain Array with Energy Pattern Reconfigurable Antenna Elements

Junrui Zhang and Shaoqiu Xiao
Institute of Applied Physics, University of Electronic Science and Technology of China, China

Abstract— Energy pattern scanning is useful in real-time tracking and grating lobe elimination ([1], scanning range $\pm 20°$). Reconfigurable antenna was used as elements in [2] to expand the scanning range of a narrow band array. This paper exploits the ability of wide-angle scanning with energy pattern reconfigurable elements.

4 antenna elements (element structure shown in Figure 1) lay abreast in the x-axis direction (Figure 2), with an element distance of 40 mm. The element exhibits energy pattern reconfiguration characteristics (Figure 3) and can radiate a $2 \sim 6$ GHz Gaussian pulse in two different directions at different time. According to the main lobe direction, the operating states of an element are defined as L-mode and R-mode. When all the elements operate in one of the two modes simultaneously, the array is able to scan in a wide range in the same quadrant as the functioning mode radiates. For example, when all the elements operate in L-mode, with proper delay configurations between adjacent elements [1], the main beam of the array scans from $-4°$ to beyond $-40°$ (Figure 4 & Table 1). Time delay in Table 1 refers to the feed delay of element n minus that of element $n+1$. Symmetrically, with R-mode elements, the array scans through $4° \sim 40°$. The results are given by CST 2012 MICROWAVE STUDIO simulation and a MATLAB program post-processing. According to Figure 4, when scanning around $0°$, the peak value of the array pattern drops very sharply, which is due to the element pattern property around $0°$. Thus, a "bridging" state that makes up the gap around $0°$ (i.e., a STATE where the element energy pattern pointing to $0°$) is necessary, or a higher level of overlapping [3] between the L and R modes' energy pattern is needed.

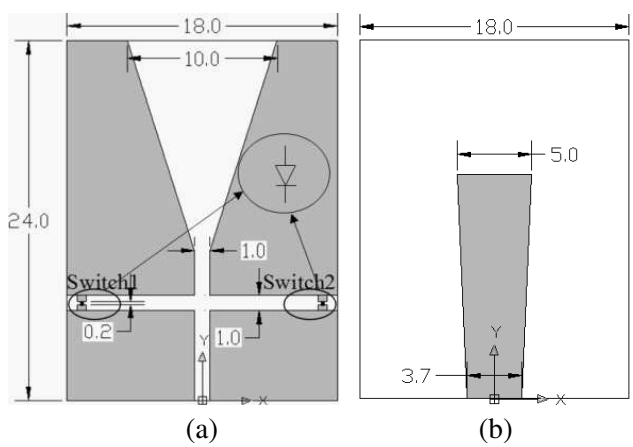

Figure 1: Proposed structure (units: mm). (a) Top side, (b) bottom side.

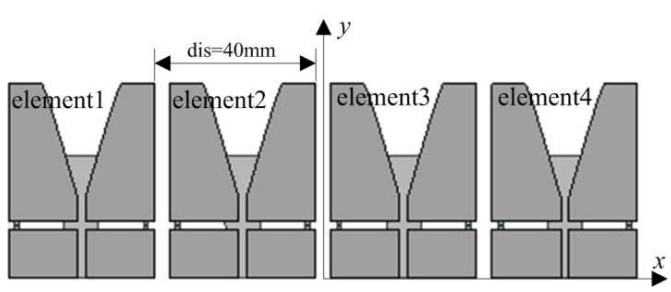

Figure 2: Array structure.

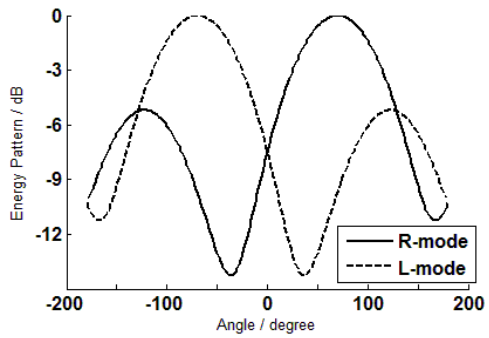

Figure 3: Normalized element energy pattern, 3 dB lobe: $-114^\circ \sim 22^\circ$ L-mode.

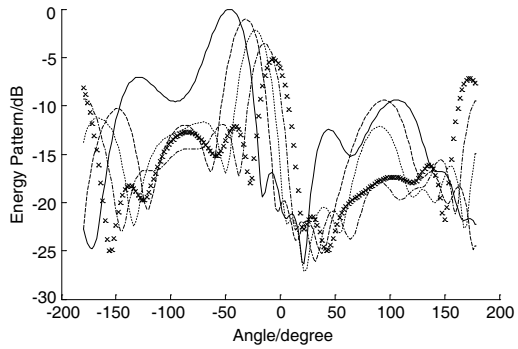

Figure 4: Beam scanning of normalized array energy pattern.

Table 1: Energy pattern scanning property.

Beam direction	Beam range	Side lobe	Back lobe	Time delay
-4°	$-15^\circ \sim 7^\circ$	-7 dB	-2 dB	0 ns
-12°	$-23^\circ \sim -1^\circ$	-8.5 dB	-5.7 dB	0.02 ns
-20°	$-33^\circ \sim -9^\circ$	-9.5 dB	-9 dB	0.04 ns
-30°	$-43^\circ \sim -17^\circ$	-8.6 dB	-8.4 dB	0.06 ns
-44°	$-61^\circ \sim -31^\circ$	-9.3 dB	-7 dB	0.09 ns

REFERENCES

1. Liao, C. H., P. Hsu, and D. C. Chang, "Energy patterns of UWB antenna arrays with scan capability," *IEEE Transactions on Antennas and Propagation*, Vol. 59, No. 4, 1140–1147, Apr. 2011.
2. Bai, Y. Y., S. Q. Xiao, M. C. Tang, et al., "Wide-angle scanning phased array with pattern reconfigurable elements," *IEEE Transactions on Antennas and Propagation*, Vol. 59, No. 11, 4071–4076, 2011.
3. Zhang, J. R., S. Q. Xiao, X. Geng, et al., "Time domain characteristics of a novel pattern reconfigurable pulse radiating antenna," *IEEE Antennas and Wireless Propagation Letters*, Vol. 11, 1202–1205, Oct. 2012.

Design of Ultra Wideband Balanced Antipodal Vivaldi Antenna for Hyperthermia Treatment

Khaled A. Alsulaiman, **Mohammed Al alShaykh**,
Sulaiman Alsulaiman, **and Ibrahim Elshafiey**
Department of Electrical Engineering, King Saud University, Riyadh, Saudi Arabia

Abstract— Hyperthermia is an emerging modality for the treatment of cancer. The principle of hyperthermia involves the increase of tumor temperature, leading to the destruction of cancer cells causing tumors to shrink, and eventually to disappear. Hyperthermiatreatment has been shown to enhance the effectiveness of other treatment modalities such as chemotherapy and radiotherapy. Various techniques are used for inserting energy into to the tumor including. Microwave energy based applicators are attractive solutions for hyperthermia treatment since they allow external application of energy and also focusing the energy into a specified local area. Conventional hyperthermia treatment systems depend on single antenna operating at a single or narrow band frequency. Such systems have no energy localization and offer no flexibility in treatment. To enhance the localization process, the used antenna has to be of wide and low operating frequency band. It has to be geometrically small to allow operation into an array system. In this paper, we introduce a hyperthermia applicator for tumor treatment in the head and neck region. Various configurations were investigated. SEMCAD X software was used in performing numerical simulations. The system is based on an array of UWB, electrically small antenna. The designed antenna is a balanced antipodal Vivaldi antenna structure proposed in [1]. The modified antenna design has dimensions of $80 \times 44 \times 9.2$ mm including the SMA attachments antenna as shown in Fig. 1. The antenna is simulated with water background, and the simulation results shows a reflection coefficient less than -10 dB at a frequency range from 50 MHz to 3.75 GHz, as presented in Fig. 2. The paper contains an overview of hyperthermia, theoretical aspects of Vivaldi antennas, simulation of phantom model exposed to radiation from four antenna arrayto observe the impact on SAR. Investigation of the use of nanoparticles to control the electrical conductivity and permittivity of the tumoris presented.

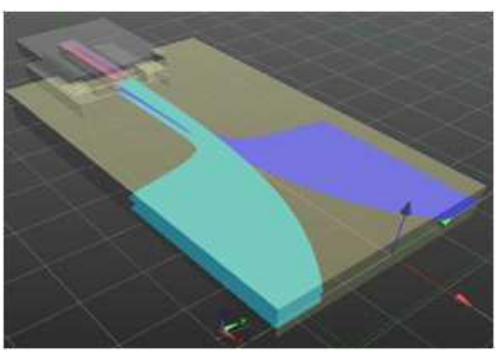

Figure 1: BAVA SEMCAD X model.

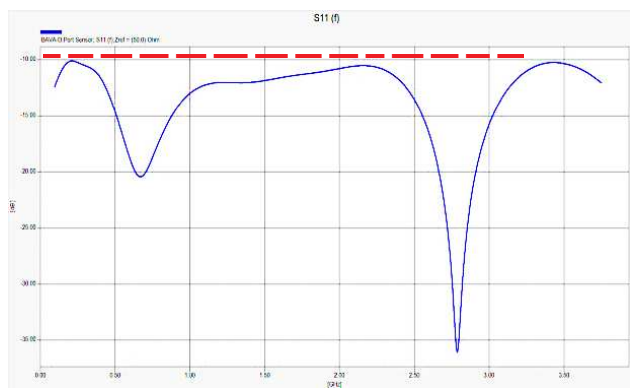

Figure 2: S_{11} parameter.

REFERENCES

1. Bourqui, J., "Balanced antipodal vivaldi antenna with dielectric director for near-field microwave imaging," *IEEE Transactions on Antennas and Propagation*, Vol. 58, No. 7, July 2010.

Label-free Acoustic and Optical Biosensors Playing on Evanescent Waves

Yihui Wu, **Guigen Liu, Peng Hao, Junfeng Wu**, **Yongbo Deng, Yongshun Liu, and Ming Xuan**
State Key Laboratory of Applied Optics, Changchun Institute of Optics, Fine Mechanics and Physics
Chinese Academy of Sciences, Changchun 130033, China

Abstract— Development of sensitive, reliable, high-throughput, label-free detection techniques is an issue with increasing emphasis because the labelling strategies that most of the microarray applications have employed, such as fluorescent, chemiluminescent and radioactive labelling, have synthetic challenges, multiple label issues and may exhibit interference with the binding sites. Label-free detection techniques monitor biomolecular interactions and simplify the bioassays by eliminating the need for secondary reactants.

Especially, biosensors based on evanescent waves often have high sensitivities by recording the changes caused by the molecule interaction near the sensor surface within the evanescent field, and moreover they provide quantitative information for the binding kinetics. For example, the fiber-optic biosensors developed by our group reached a detection limit of 10 pg/mL. Owing to recirculation of photons which allows multiple sampling of the refractive index perturbation introduced by target molecules, microcavities serve as another powerful tool to achieve even lower detection limits. There have been lots of efforts on fabricating microcavities in an array format. Acoustic ones can be made by MEMS process with extremely small size and integrated on silicon substrate to realize array and high-throughout detections. However, the sensitivities and Q factors of all the acoustic biosensors still need to be improved. For example, the Q factor obtained by the point defect mode of a phononic crystal in vacuum reached 49800 in our group, but it's difficult to get such a high Q when the phononic crystal is placed in water. Actually, acoustic and optical sensors are sensitive to different parameters, thus it is expected to verify the feasibility of several measurements at different scales. It is possible to achieve multi-parameter detections of the changes of optical refractive index, density, and viscosity within a liquid and even the temperature compensation can be accomplished simultaneously.

In this article, we will describe the similarity of sound waves and electromagnetic waves, review these two types of label-free techniques, such as photonic, phononic and acousto-optical biosensors. The theoretical and technical outlines behind the sensing principles, such as the evanescent waves scattering, interference, resonance and tunnel effects, will be analysed. The physical mechanisms to modulate waves by micro/nano structures, which localize the waves, amplify the signal/noise ratio and increase Q factor for high sensitivity and high resolution, will also be discussed. Moreover, the promising acousto-optic biosensing mechanism with multi-parameter decoupling will be discussed, and their potential applications, prospects, merits and challenges are also provided.

The Estimation of a Gold Nanoparticles Distribution Using the Evanescent Electric Field in Gold Nanoparticles Filled Surface Plasmon Resonance Biosensing

Chardchai Korjittavanit[1], **Rardchawadee Silapunt**[1], **and Boonsong Sutapun**[2]

[1]Department of Electronic and Telecommunication
King Mongkut's University of Technology Thonburi, Bangkok 10140, Thailand
[2]School of Telecommunication Engineering
Suranaree University of Technology, Nakhon Ratchasima, Thailand

Abstract— The estimation of a gold nanoparticles (AuNPs) distribution using the evanescent electric field in AuNPs filled surface plasmon resonance (SPR) biosensing is proposed here. In this study, AuNPs distribution models are divided into uniform and non-uniform distributions in 1- and 2-row vertical arrays. The number of AuNPs arrays is defined to imitate the techniques of biomolecules binding detection by single AuNPs and AuNP pairs. Maxwell's equations are then employed to determine average evanescent electric fields in the 2-dimensional (2D) sensing structure containing thin gold and saline layers, in a direction normal to the gold/saline interface. The location and distribution of the AuNPs can be estimated by analyzing the evanescent field or equivalent power density profiles. For the uniform AuNPs distribution of both types of arrays, the profiles show very prominent electromagnetic (EM) interactions between AuNPs and gold surface and between AuNP pairs. Figures 1 and 2 illustrate the evanescent power density profiles, $|E_0|^2$, as a function of the distance z, normal to the interface. The arrays are placed 50 nm above the gold surface. For the 2-row uniform AuNPs array, the gaps between AuNP pairs are varied at 10, 30, and 60 nm, respectively. The degree of the EM interaction can be enhanced by reducing the gaps between the AuNPs array and gold surface and between AuNP pairs, such as the 10 nm gap profile shown in Figure 2. The profiles of non-uniform AuNPs distribution for both types of arrays are easily identified by comparing with those of the uniform AuNPs distribution. For the 2-row array with each row having different NP distributions, the EM interaction in one is actually stronger than the other after accounting for the natural decay. The shifts in shape or magnitude of these evanescent field profiles are easily observed compared to those determined by the Fresnel model with the application of modified Maxwell-Garnett (MG) equations. This approach can then be utilized effectively to estimate AuNPs distributions in AuNPs-filled SPR sensing.

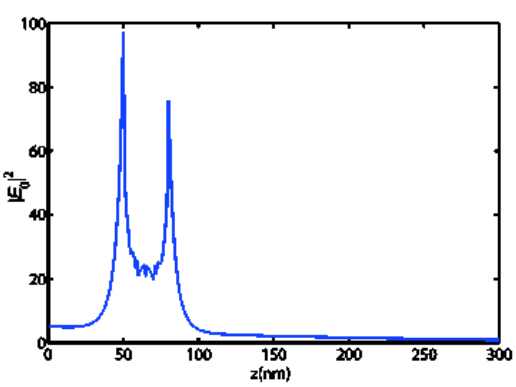

Figure 1: The evanescent power density profile of the 1-row uniform AuNPs array.

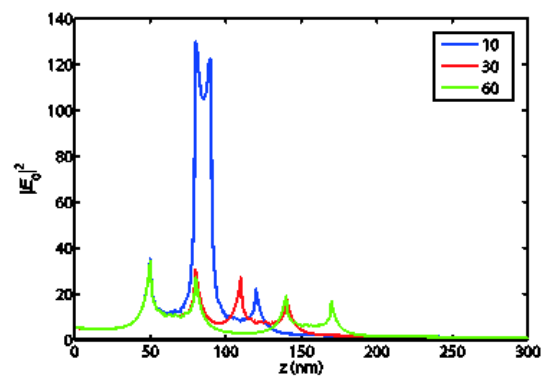

Figure 2: The evanescent power density profile of the 2-row uniform AuNPs array at 10, 30, and 60 nm gaps between AuNP pairs.

Numerical Analysis of Passively Q-switched Er and Yb Doped Fiber Laser

Dan Savastru, **Roxana Savastru**, **Sorin Miclos**, **and Ion Lancranjan**
National Institute of R&D for Optoelectronics — INOE 2000
409 Atomistilor St., Magurele, Ilfov RO-077125, Romania

Abstract— The main purpose of the paper consists in presenting simulation results obtained in analysis of linear and ring structures of single or double clad fiber laser using Er^{3+}, Yb^{3+}, Er^{3+}/Yb^{3+} or $Er^{3+}/Yb^{3+}/Cr^{3+}$ as active lasing centers and operated in passive Q-switching regime. Several types of passive Q-switch cells manufactured of materials such as $Co^{2+}:MgAl_2O_4$ bulk crystals or nano-crystals embedded in phosphate glass, $Co^{2+}:ZnSe$, $Co^{2+}:ZnS$, UO^{2+} embedded in phosphate glass and $LiF:F_2^-$ (lithium fluoride with F_2^- color centers) are considered. The use of an un-pumped Er^{3+} doped fiber optic as a passive Q-switch cell is also investigated. Both the doped fiber optic active medium and passive Q-switch cell spectroscopic characteristics are analyzed concerning the lasing function. The saturation dynamics of the investigated passive Q-switch cells is separately analyzed using a FTDT method. The simulation results are obtained by solving the coupled rate equations describing the laser dynamics and considering as accurate as possible differential equation coefficients describing the investigated laser systems. The linear and ring fiber laser structures simulations are performed considering the influence of various factors including ASE on power and temporal output characteristics of eye-safe erbium laser. Also the thermal effects appearing in the passive Q-switch cells during laser operation are investigated. The paper is pointing to present simulation results which are part of a design procedure for construction of linear or ring fiber laser emitters, including the "Eye Safe" ones operated at approximately 1550 nm for various industrial, laboratory or military applications. These fiber lasers are intended to be used as optical sensors in various domains.

Vector Magnetic Field Detecting with a Single Nitrogen Vacancy Center in Diamond

Xiangdong Chen, **Changling Zou**, **and Fangwen Sun**
Key Lab of Quantum Information, University of Science and Technology of China
Hefei 230026, China

Abstract— As the magnetic field plays an important role in various areas, many methods are developed to detect the magnetic field. Recently the magnetometry based on nitrogen vacancy (NV) centers were proposed. The general idea of this method is that the electron spin energy levels change with the external magnetic field due to the electron Zeeman effect. Because of small size and long spin coherence time, the NV center magnetometry can be used to detect small magnetic field with high spatial resolution.

However, the electron Zeeman shift mainly depends on the magnetic field along the NV symmetry axis, the traditional NV magnetometry is not suitable for vector magnetic field sensing. In this work, we developed a new method to detect vector magnetic field by a single NV, with the assistance of a ^{15}N nuclear spin. A single ^{15}NV center was used for this detection. Since the distance between nuclear spin and the electron spin of NV is less than 1 nm, high spatial resolution can be maintained. The magnetic field in parallel with the axis of NV is obtained by detecting the electron Zeeman shift, while the perpendicular to the axis is measured through the nuclear spin Larmor precession. The magnetical sensitivity of the nuclear spin precession is improved by the hyperfine interaction between nuclear spin and electron spin. The electron Zeeman effect and the nuclear precession can be detected through the fluorescence from the defect. Therefore, the magnitude and polar angle of the vector magnetic field are obtained. By additional calibrated magnetic fields, all the vector information can be deduced. Also our method is temperature insensitive, it can be operated conveniently at room temperature.

REFERENCES

1. Balasubramanian, G., I. Y. Chan, R. Kolesov, M. AlHmoud, J. Tisler, C. Shin, C. Kim, A. R. Wojcik, P. Hemmer, A. Krueger, T. Hanke, A. Leitenstorfer, R. Bratschitsch, F. Jelezko, and J. Wrachtrup, "Nanoscale imaging magnetometry with diamond spins under ambient conditions," *Nature*, Vol. 455, 648–651, 2008.
2. Maertz, B. J., A. P. Wijnheijmer, G. D. Fuchs, M. E. Nowakowski, and D. D. Awchalom, "Vector magnetic field microscopy using nitrogen vacancy centers in diamond," *Appl. Phys. Lett.*, Vol. 96, 092504, 2010.

Low-pass Filter Design from EBG Waveguides Periodically Loaded with Metal Ridges

S. Marini[1], **P. Soto**[2], **A. Coves**[3], **B. Gimeno**[4], **and V. E. Boria**[2]

[1]Departamento de Física, Ingenieria de Sistemas y Teoría de la Señal
Instituto de Física Aplicada a las Ciencias y Tecnologías, Universidad de Alicante, Spain
[2]Departamento de Comunicaciones, Instituto de Telecomunicaciones y Aplicaciones Multimedia
Universidad Politécnica de Valencia, Spain
[3]Departamento de Ingeniería de Comunicaciones, Universidad Miguel Hernández de Elche, Spain
[4]Departamento de Física Aplicada, Instituto de Ciencia de los Materiales
Universidad de Valencia, Spain

Abstract— Periodic structures are currently receiving a renewed interest due to their potential use in the microwave and millimeter-wave frequency bands. For filtering applications, such structures are reported to offer reduced physical size and improved stopband performance [1]. The E-plane waveguide technology, periodically loaded with metal ridges, offers a convenient way for realizing Electromagnetic Bandgap (EBG) passive waveguide structures [2].

The dispersion diagram of the infinite periodic structure is useful for the practical design of waveguide filters. Analyzing the pass- and stop-bands (gaps) in the dispersion diagram of a unit cell, it is possible to generate a finite structure with a very similar electrical response. Low-pass filters from passive structures based on EBG waveguides periodically loaded with metal ridges are analyzed and designed in this work. For this purpose, a very efficient Integral Equation (IE) technique is followed to model the planar steps involving arbitrary waveguides, and the well-known Boundary Integral — Resonant Mode Expansion (BI-RME) method is also used to obtain the modal chart of the ridged waveguides [3, 4].

Once the dispersion diagram of the infinite periodic structure has been computed, it is necessary to match the Bloch impedance with the impedance of the TE_{10} rectangular mode in the access ports to obtain a real low-pass filter (i.e., implemented with a finite number of cells). In order to achieve an adequate level of scattering parameters, a stepped ridged waveguide transformer [5] has been designed and added to the finite periodic structure. An improved five-order and a new eight-order low-pass filter have been obtained after an optimization step, thus demonstrating the practical application of an EBG ridged waveguide structure.

ACKNOWLEDGMENT

This work was supported by the Ministerio de Economía y Competitividad (MINECO), Spanish Government, under the coordinated R & D project TEC2010-21520-C04, and by the University of Alicante under the project GRE10-22.

REFERENCES

1. Goussetis, G. and D. Budimir, "Novel periodically loaded E-plane filters," *IEEE Microwave and Wireless Comp. Letters*, Vol. 13, No. 6, 193–195, 2003.
2. Goussetis, G., A. Feresidis, and P. Kosmas, "Efficient analysis, design, and filter applications of EBG waveguide with periodic resonant loads," *IEEE Transactions on Microwave Theory and Tech.*, Vol. 54, No. 11, 3885–3892, 2006.
3. Cogollos, S., S. Marini, V. E. Boria, P. Soto, A. Vidal, H. Esteban, J. V. Morro, and B. Gimeno, "Efficient modal analysis of arbitrarily shaped waveguides composed of linear, circular, and elliptical arcs using the BI-RME method," *IEEE Transactions on Microwave Theory and Tech.*, Vol. 51, No. 12, 2378–2390, 2003.
4. Marini, S., A. Coves, V. E. Boria, and B. Gimeno, "Efficient modal analysis of periodic structure loaded with arbitrarily shaped waveguides," *IEEE Transactions on Microwave Theory and Tech.*, Vol. 58, No. 3, 529–536, 2010.
5. Hoefer, W. J. R. and M. N. Burton, "Closed-forms expressions for the parameters of finned and ridged waveguides," *IEEE Transactions on Microwave Theory and Tech.*, Vol. 30, No. 12, 2190–2194, 1982.

Monte-Carlo MPSTD Analysis on Scattering of Cylinders Buried in a Layered Half Space with Random Rough Interface

Yueyang Dai, **Wei Liu**, **and Xiao-Bang Xu**
Holcombe Department of Electrical and Computer Engineering
Clemson University, Clemson, SC 29634-0915, USA

Abstract— Analysis of electromagnetic scattering of buried objects is of practical interest in subsurface investigations. In reality, the earth is of layered structure with random rough interface. The layered structure and the roughness of the random rough interface need to be considered in the analysis, because they both contribute to the scattering signature and hence affect the detection of buried objects.

In this paper, we present a Monte-Carlo multidomain psuedospectral time-domain (MPSTD) numerical technique developed for the analysis of electromagnetic scattering of an object buried in a layered lower half space with random rough interface. The random rough interface may be of finite length or of extensive periodic structure. The MPSTD method [1] is employed and further developed to solve Maxwell's equations in the layered structure in time domain. And the Monte-Carlo method is used to obtain a statistic average of the solution involving a random rough interface. In the development, special attention is paid to the treatment of the random rough interface, and the wave propagation in the layered structure is investigated. Using the numerical technique developed, sample numerical results are obtained, presented, and analyzed. In particular, the impact of the roughness of the random rough interface and the electromagnetic properties of the layered half space on the scattering signature are investigated. Also, the correctness of the numerical results is validated.

REFERENCES

1. Liu, Q. and G. Zhao, "Advances in PSTD techniques," *Computational Electromagnetics, The Finite-Difference Time-Domain Method*, A. Taflove and S. C. Hagness, Ed., 3rd Edition, Chapter 17, Artech House, 2005.

Design of Multiband Reflection Filters with Dielectric Frequency Selective Surfaces

A. Coves[1], **B. Gimeno**[2], **and M. V. Andrés**[2]

[1]Departamento de Ingeniería de Comunicaciones, Universidad Miguel Hernández de Elche
Elche, Alicante 03202, Spain
[2]Departamento de Física Aplicada y Electromagnetismo, Instituto de Ciencia de los Materiales
Universidad de Valencia, Burjassot, Valencia 46100, Spain

Abstract— The frequency selectivity behavior of multilayered periodic structures, both dielectric and metallic, has led to a growing interest in the study and application of this type of structures at microwave frequencies and in the visible range. Thus, multilayered structures formed by the cascade connection of periodic metallic surfaces printed on dielectric homogeneous layers have found a wide field of application in antennas and satellite communication systems as reflection and transmission filters [1]. On the other side, a recent interest has arisen in the application of thin dielectric structures that combine the use of homogeneous and periodic layers [2–4] which have a periodic variation along some layers. At millimeter frequencies, these structures have the advantage of having low absorption losses compared to metal surfaces. These structures have been given multiple applications including transmission and reflection filters, antenna reflectors, couplers, multiplexers, holograms, optical sensors, Bragg gratings, etc..

This work focuses on the study and design of reflection filters, using multilayered periodic dielectric structures with periodicity in one dimension, under plane wave excitation. To this end, the formulation developed in [4, 5] based on a vectorial modal method is used. These structures have already been previously designed as reflection filters under plane wave excitation [3], using a single periodic dielectric grating with a rectangular modulation of the dielectric permittivity. The frequency response of the periodic grating is determined by the resonance effect of guided modes in the grating, giving rise to strong reflections (total reflection) at certain frequencies, with practically no reflection in the frequency bands adjacent to the resonant frequency. The position of the resonance frequency of the grating is determined by the phase matching condition in the periodic layer [2, 4].

This paper demonstrates that it is possible to design multiband reflection filters using structures containing various periodic gratings with different period, where the resonant frequencies are determined by the resonances of the individual periodic gratings. It has been found that the frequency shift between the total reflection peaks of the filter can be adjusted by changing the periods of the different periodic gratings.

ACKNOWLEDGMENT

This work was supported by the Ministerio de Ciencia e Innovación, Spanish Government, under the coordinated project TEC2010-21520-C04-02.

REFERENCES

1. Mittra, R., C. H. Chan, and T. Cwik, "Techniques for analyzing frequency selective surfaces — A review," *Proceedings of the IEEE*, Vol. 76, No. 12, 1593–1615, Dec. 1988.
2. Bertoni, H. L., L. H. S. Cheo, and T. Tamir, "Frequency-selective reflection and transmission by a periodic dielectric layer," *IEEE Transactions on Antennas Propagat.*, Vol. 37, No. 1, 78–83, Jan. 2006.
3. Tibuleac, S., R. Magnusson, T. A. Maldonado, P. P. Young, and T. R. Holzheimer, "Dielectric frequency-selective structures incorporating waveguide gratings," *IEEE Transactions on Microwave Theory and Tech.*, Vol. 48, No. 4, 553–561, Apr. 2000.
4. Coves, A., B. Gimeno, J. Gil, M. V. Andrés, A. A. San Blas, and V. Boria, "Full-wave analysis of dielectric frequency-selective surfaces using a vectorial modal method," *IEEE Transactions on Antennas Propagat.*, Vol. 52, 2091–2099, Aug. 2004.
5. Coves, A., B. Gimeno, A. A. San Blas, A. Vidal, V. E. Boria, and M. V. Andrés, "Three-dimensional scattering of dielectric gratings under plane-wave excitation," *IEEE Antennas Wirel. Propagat. Lett.*, Vol. 2, 215–218, 2003.

Method of Pseudodifferential Equations for Problems of Electromagnetic Wave Diffraction by Closed Screens

A. Ilyinsky and Yury G. Smirnov
Penza State University, Russia

Abstract— The paper is devoted to investigation of vector electromagnetic diffraction problems on system of closed screens. We consider the vector problem of diffraction of an electromagnetic field by a system of bounded, perfectly conducting screens of arbitrary shape. The problem is reduced to a vector integrodifferential equation on the screens. The purpose of this work is to extend the method of pseudodifferential equations to electromagnetic wave diffraction problems on system of closed surfaces. The integrodifferential equation is considered as a pseudodifferential equation. The problems of diffraction is analyzed in the case of closed surfaces by considering PDOs on manifolds that act in special Sobolev spaces of the cross sections of vector bundles. The Sobolev vector spaces will be chosen in order to satisfy physical requirements of the diffraction problem.

We will call this approach the method of pseudodifferential equations [1]. The main idea of the approach is in the transition to the analysis of a PDO. We analyze differential operators and PDOs using the calculus of the symbols of PDOs.

Fredholm property of the operator with the zero index for the equation is proved. We perform a diagonal splitting of the PDO on subspaces, which is a key point in the analysis of its properties. By considering the restriction of PDOs on subspaces, we reveal the structure of the complete symbol of the operator and prove the Fredholm property of the operator with the zero index. Knowledge of the structure of a PDO is very important when one has to perform a correct choice of an appropriate numerical method for solving a pseudodifferential equation and basis and probe functions in the Galerkin method.

REFERENCES

1. Ilyinsky, A. S. and Yu. G. Smirnov, *Electromagnetic Wave Diffraction by Conducting Screens*, VSP, Utrecht, The Netherlands, 1998.

Nonlinear Optical Limiting in Suspensions of Carbon Nanotubes

Andrey Yu. Vlasov[1,2], **Anastasia Venediktova**[1,2], **Ivan M. Kislyakov**[2,3], **Dmitry A. Videnichev**[2,3], **Elena D. Obraztsova**[4], **and Ekaterina P. Sokolova**[1]

[1]Department of Chemistry, St. Petersburg State University
26, Universitetsky Pr., St. Petersburg 198504, Russia
[2]S. I. Vavilov State Optical Institute, 12, Birzhevaya line, St. Petersburg 199034, Russia
[3]St. Petersburg National Research University ITMO
49, Kronverksky pr., St. Petersburg 197101, Russia
[4]A. M. Prokhorov Institute of General Physics, Russian Academy of Sciences
38, Vavilov Str., Moscow 119991, Russia

Abstract— Systems able to perform nonlinear optical limiting (OPL) of high intensity laser irradiation have been drawing attention of researchers during the last decade because of the extensive use of lasers: low-power lasers are employed in DVD-recording, laser-pointers, medicine; while high-power lasers are ubiquitous in industry, scientific research and military applications. Suspensions of single-walled carbon nanotubes (SWCNT) are among the most perspective OPL-materials. The driving mechanism of the OPL in SWCNT suspensions is light-induced scattering: nanotubes convert laser irradiation energy into heat and convey it to the nanotube microenvironment and solvent, the successive laser pulses being scattered on the formed bubbles of the boiling solvent. The OPL-parameters of SWCNT suspensions are controlled by a number of properties of the suspension components, viz., nanomaterial *per se*, stabilizing micro-evironment, dispersing medium. However relative significance of energy conversion isn't yet clear: it can either, in first instance, scatter on the surface plasmon and then upon its retardation — on the phonons of the carbon lattice, or alternatively can get transferred straight onto phonons.

We give a go to monitoring the dependences of OPL-behavior upon the properties of system components, to juxtaposing channels of laser energy conversion and to comparing mechanisms of interaction between the SWCNT and the amphiphile stabilizer (aggregation vs. adsorption). We report the dependency of the OPL-behavior upon concentration and degree of SWCNTs de-bundling, phase and aggregative properties of the amphiphile stabilizer alongside the reciprocal of the bleaching resistibility against the solvent properties. We also give account of suspensions stability at sub-zero temperatures in mixed solvents "water+antifreeze" (glycerol, polyethilenglycol-400, alcohols). Issues of energy conversion were tackled by a study of the OPL response on variations of plasmon peak position through altering surfactants used as stabilizing microenvironment and by variations in numbers of defects on nanoparticles.

ACKNOWLEDGMENT

The authors were supported by RFBR (grants # 13-03-01111 and #11-03-01106-a) and Ministry of Science of Russia (2013-1.3-14-513-0018 and GOSK #14.513.12.0003).

A 12-cavity Relativistic Magnetron with Optimized Design of Diffraction Output

M. Liu[1], C. Liu[1], and E. Schamiloglu[2]

[1]Key Laboratory of Physical Electronics and Devices of the Ministry of Education
Xi'an Jiaotong University, Xi'an 710049, China
[2]Department of Electrical and Computer Engineering
University of New Mexico, Albuquerque, NM 8713-0001, USA

Abstract— The possibility of mode switching from one pulse to the next in a 6-cavity gigawatt and 12-cavity gigawatt magnetron with diffraction output (MDO) using a single frequency RF signal was demonstrated using particle-in-cell (PIC) simulations in our earlier work [1–3]. For the 12-cavity gigawatt magnetron, a splitting of the radiation frequency for each eigenmode owing to its different longitudinal distribution was also demonstrated. In this paper, we optimize the 12-cavity gigawatt magnetron to improve the electronic efficiency and output power, and calculate the eigenmodes for the optimized 12-cavity gigawatt magnetron. When the relativistic magnetron is operated using an applied 400 kV voltage pulse, electrons emitted from the cathode with high energy strike the anode block and secondary electron and backscattering electron emission occurs. The emitted secondary current will lower the output power of the 12-cavity relativistic magnetron and will complicate the spectrum when the applied magnetic field approaches the boundary of neighboring modes. This is especially the case for a short applied voltage pulse. This phenomenon changes the boundary between neighboring modes as well as the boundary between splitting neighboring longitudinal modes with the same transverse field structure. Also, this makes choosing stable modes complicated when considering a boundary for mode switching.

The result of this paper will provide reference for 12-cavity gigawatt magnetron mode switching experiments when selecting the boundary between neighboring modes.

REFERENCES

1. Fuks, M. I. and N. F. Kovalev, "Relativistic magnetron with diffraction output," *Program and Abstracts of XI Int. Conf. on High-power Electromagnetics*, 18, 1998.
2. Liu, M., C. Michel, S. Prasad, M. Fuks, E. Schamiloglu, and C. L. Liu, *Appl. Phys. Lett.*, Vol. 97, 251501–3, 2010.
3. Fuks, M. and E. Schamiloglu, *IEEE Trans. Plasma Sci.*, Vol. 38, 1302–1312, 2010.

Rabi Splitting in Acoustics

Xu Ni, **Li-Yang Zheng**, **Ze-Guo Chen**, **Ming-Hui Lu**, **and Yan-Feng Chen**
National Laboratory of Solid State Microstructures and Department of Materials Science and Engineering
Nanjing University, Nanjing 210093, China

Abstract— In recent years, Rabi splitting has received much attention in this relative field on the interaction between light and matter. Two conditions might be satisfied for the observation of Rabi splitting, one is the existence of a resonance cavity and an atom (two-level system), and the other is the possibility for the coupling (between cavity mode and transition of two levels) to happen. To observe Rabi splitting in the microwave regime, the atom could be replaced by an artificial one, using metamaterials with negative permittivity or negative permeability or both. However, all these research are based on the electromagnetic waves, the possibility for Rabi splitting to happen in other classical waves remains uncertain. Acoustic wave is an important form of waves, having broad applications in our daily life. The research on acoustic metamaterials and sonic crystals are in fast development, with the observation of many novel physical effects, such as extraordinary acoustic transmission, negative modulus realized by using Helmholtz resonance cavities. Some quantum effects have classical counterparts in acoustics such as tunneling, Bloch oscillations. However, as far as we know, Rabi splitting in acoustics is not reported. In this paper, we use a finitely long subwavelength slit as the Fabry-Perot (FP) resonance cavity and a resonance cavity as the artificial atom. Rabi splitting in acoustics is achieved by the coupling of FP fundamental resonance mode with the resonance mode of the artificial atom. This effect is verified by experiment, simulation and calculation. This research will broaden physical insight on Rabi splitting, and show the common sense between quantum and classical problems. In addition, our work will improve the research of extraordinary sound transmission and acoustic metamaterials, and then it will bring large potential applications in acoustics.

Near Zero Index in Phononic Crystal Induced by Flat Branch

Li-Yang Zheng, **Xu Ni**, **Ze-Guo Chen**, **Ming-Hui Lu**, **and Yan-Feng Chen**
National Laboratory of Solid State Microstructures & Department of Materials Science and Engineering
Nanjing University, Nanjing 210093, China

Abstract— Recently, zero-refractive-index (ZRI) materials have drawn worldwide attention. Since waves do not experience any spatial phase change in a zero-refractive-index material, such peculiar materials have many interesting wave-manipulating properties, such as tunneling of electromagnetic energy through subwavelength channels and bends, tailoring of the radiation phase pattern of electromagnetic sources and super-reflection or cloaking under specific boundary conditions. Although tunneling effect with epsilon-near-zero (ENZ) materials filled in a narrow channel has been experimentally realized, the impedance mismatch at the interface is still very huge. However, a perfect match material known as zero-refractive-index material is proposed. By accidental degeneracy induced Dirac cones at the center of the Brillouin zone, materials with both permittivity and permeability are zero at the same time are demonstrated. But the Dirac cones do not always contribute to zero-refractive-index and their relationship seems a little subtle. Here, we show that by designing and fabricating proper phononic crystals, a peculiar dispersion with a flat branch can be achieved at the center of the Brillouin zone at $f = 0.537c/a$. This flat band supports the transverse mode in nature and can be excited because the phononic crystal consisted of discrete steel rods is not perfectly homogeneous. We further illustrate that this flat band contributes to an effective near-zero material under the description of the effective medium theory. Finally, numerical and experimental demonstrations have been implemented to confirm our speculation. This work provides a simple way to design and fabricate effective near zero index materials. Since zero materials possess many fascinating characters to manipulate waves, our work will facilitate many applications of near-zero materials.

Fabrication and Characteristic of Nanometal(Shell)-silica(Core) Composite Particles by Ultrasonic Electrodeposition

Jun Qi, **Yue Feng Tang**, **Yi Zhang**, **and Yan Feng Chen**
National Laboratory of Solid State Microstructures, Department of Materials Science and Engineering
Nanjing University, Nanjing 210093, China

Abstract— In recent years, the deposition of nanoscaled metal on various substrates has attracted considerable attentions. These composite particles have greatly potential applications in various fields such as surface enhanced Raman scattering, modulation of optical properties, photonics, biological detection, electronics, ultrahighdensity magnetic storage and catalysis, etc. [1–7]. Among metals, iron has been paid much attention because it has the highest magnetic moment among the 3d transition ferromagnetic metals. Moreover, because iron metal has high activity, we can use it as template to deoxidize other metals. To achieve excellent properties, it is important to explore appropriate synthesis techniques for the iron-coating silica nanocomposites.

In general, this kind of core-shell structure was fabricated by depositing nanoscaled metal particles on various substrates with various methods. For example, pretreatment of electroless deposition, seeding plating, polyol process, surface functionalization and layer by layer process [8–11]. However it is relatively complex because these metal coating processes usually involved multistep processes and it is difficult to obtain dense and uniform nanoscaled metal layer with high purity. In addition, simplicity and controllability of the process are necessary for industrial applications. Therefore, further exploring and evaluating the deposition methods are necessary for the preparation of the interesting materials. The electrochemical processes had been employed by synthesizing the insoluble metal powders [12–17] and metal-dielectric nanocomposites [18]. The advantages of electrochemical processes include clean preparation (no need to separate from the reducing agent), easy isolation and the possibility of size-selectivity. In this communication, a facile and one-step ultrasonic electrodeposition method is applied to deposit iron nanoparticles onto the surface of dielectric silica spheres. The effects of experimental conditions such as the current density (I), the concentration of electrolyte (C) on the size and the dispersive uniformity are investigated.

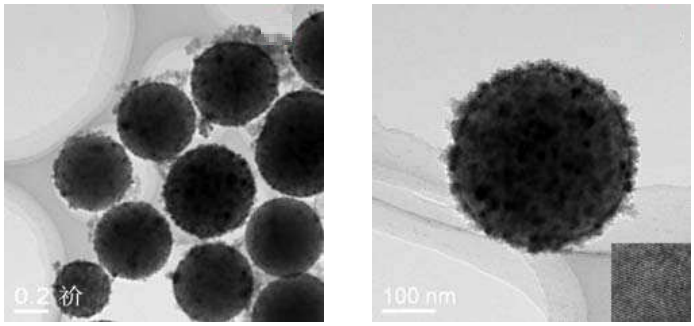

(a) (b)

Figure 1: TEM micrographs of (a) as-synthesized sample of iron coated on amorphous silica; (b) magnification image of micrograph (a).

REFERENCES

1. Nie, S. and S. R. Emory, *Science*, Vol. 275, 1102–1106, 1997.
2. Averitt, R. D., S. Westcott, and N. J. J. Halas, *Opt. Soc. Am.*, Vol. 16, 1824–1832, 1999.
3. Lu, Y., Y. Yin, Z. Y. Li, and Y. Xia, *Nano. Lett.*, Vol. 2, 785–788, 2002.
4. Loo, C., A. Lowery, N. Halas, J. West, and R. Drezek, *Nano. Lett.*, Vol. 5, 709–711, 2005.
5. Peto, G., G. L. Molnar, Z. Paszti, O. Geszti, A. Beck, and L. Guczi, *Mater. Sci. Eng. C*, Vol. 19, 95–99, 2002.
6. Stoeva, S. I., F. W. Huo, J. S. Lee, and C. A. Mirkin, *J. Am. Chem. Soc.*, Vol. 127, 15362–15363, 2005.

7. Phadtare, S., A. Kumar, V. P. Vinod, C. Dash, D. V. Palaskar, M. Rao, P. G. Shukla, S. Sivaram, and M. Sastry, *Chem. Mater.*, Vol. 15, 1944–1949, 2003.
8. Kobayashi, Y., V. Salgueirino-Maceira, and L. M. Liz-Marzan, *Chem. Mater.*, Vol. 13, 1630–1633, 2001.
9. Zhu, M. W., G. D. Qian, Z. L. Hong, Z. Y. Wang, X. P. Fan, and M. Q. Wang, *J. Phys. Chem. Solid.*, Vol. 66, 748–752, 2005.
10. Graf, C. and A. van Blaaderen, *Langmuir*, Vol. 18, 524–534, 2002.
11. Cassagneau, T. and F. Caruso, *Adv. Mater.*, Vol. 14, 732–736, 2002.
12. Natter, H., T. Krajewski, and R. Hempelmann, *Ber. Bunsenges. Phys. Chem.*, Vol. 100, 55–64, 1996.
13. Natter, H. and R. Hempelmann, *J. Phys. Chem.*, Vol. 100, 19525–19532, 1996.
14. Zoval, J. V., R. M. Stiger, P. R. Biernacki, and R. M. Penner, *J. Phys. Chem.*, Vol. 100, 837–844, 1996.
15. Whitney, T. M., J. S. Jiang, P. C. Searson, and C. L. Chien, *Science*, Vol. 261, 1316–1319, 1993.
16. Xu, L., W. L. Zhou, C. Frommen, R. H. Baughan, A. A. Zakhidov, L. M. Malkinski, J. Q. Wang, and J. B. Wiley, *Chem. Commun.*, 997–998, 2000.
17. Bartlett, P. N., P. R. Birkin, and M. A. Ghanem, *Chem. Commun.*, 1671–1672, 2000.
18. Tang, S. C., Y. F. Tang, F. Gao, Z. G. Liu, and X. K. Meng, *Nanotechnology*, Vol. 18, 295607, 2007.

Enhanced Rotation of the Polarization of a Light Beam Transmitted through a Silver Film with an Array of Perforated S-shaped Holes

Shan Wu, Xuejin Zhang, and Yongyuan Zhu
National Laboratory of Solid State Microstructures, Nanjing University, Nanjing 210093, China

Abstract— In this letter, we realized an enhanced optical rotation of the zero-order transmitted light through a silver film with an array of perforated S-shaped holes. Different to the previous studies, this effect results from the contribution of both the localized surface plasmons (LSPs) and surface plasmon polaritons (SPPs). The rotation angle can be modulated with the thickness due to the phase-retardation of the SPPs when tunneling to the emitted surface. With a sample thickness 245 nm, a near-complete cross-polarization conversion (90° optical rotation) can be achieved, representing a major advance in performance compared to the previously reported planar chiral structures.

Session 4P1
2_FocusSession.SC2: Microwave Metamaterials and Applications 2

RCS Reduction Based on Random Scattering via Artificial Metamaterials
Qiang Cheng, Jie Chen, Di Sha Dong, Jie Zhao, Tie Jun Cui, ... 1512
Narrow-band Wave Block by Chiral Metamaterials
Nantakan Wongkasem, Amornthep Sonsilphong, ... 1513
Extraordinary Transmission Induced by Thin Metamaterial Layers with Longitudinal Electric Resonances
S. C. Li, J. Luo, Yun Lai, Bo Hou, ... 1514
Experimental Demonstration of High-performance Grin Lens Antenna with Controllable Aperture Field
Mei-Qing Qi, W. X. Tang, Di Bao, Hui-Feng Ma, Tie Jun Cui, ... 1515
Some Characteristics of Gyrator Using Magnetoelectric Effect
Makoto Tsutsumi, ... 1516
Hybrid Resonance of SRR Metamaterials: A Circuit Model
Rui-Xin Wu, Min Liu, Yin Poo, ... 1517
Ray Tracing in an Arbitrary Cloak in Two Dimensions
Haroonhaider Sidhwa, R. P. R. C. Aiyar, S. V. Kulkarni, ... 1518
Broadband Flattened Luneburg Lens with Ultra-wide Angle Based on a Liquid Medium
Lingling Wu, Ming Yin, Xiaoyong Tian, Dichen Li, ... 1519
A 3D Electromagnetic Wave Concentrator Realized with Gradient Index Woodpile Structure in Metamaterial Regime
Ming Yin, Lingling Wu, Xiaoyong Tian, Dichen Li, ... 1520
Electromagnetic Behavior of SRR Loaded Microstrip Transmission Lines: Investigation for Different SRR Types and Array Topologies
Gokay Disken, Fazil Pala, Esra Demir, H. Demet Korucu, Evren Ekmekci, ... 1521
The High Directivity Antenna Based on Metamaterials
Wanzhao Cui, Tiancun Hu, ... 1522
Microwave Focusing by a Wire Medium
Joaquim J. Barroso, Antonio Tomaz, Ugur C. Hasar, Alberto Jose de Faro Orlando, ... 1523

RCS Reduction Based on Random Scattering via Artificial Metamaterials

Qiang Cheng, **Jie Chen**, **Di Sha Dong**, **Jie Zhao**, **and Tie Jun Cui**
State Key Laboratory of Millimetre Waves
Southeast University, Nanjing, Jiangsu 210096, China

Abstract— In the past few years, more and more technologies have been proposed for RCS reduction of military targets, such as the Radar absorbent materials, purpose shaping and active cancellation. Here we will introduce the random scattering technology based on metamaterials, which can dramatically decrease the directive energy reflection from the targets. We have constructed a random meta-surface with a number of metallic patches on a grounded substrate. Due to the difference of the patch dimensions, various phase shifts will be produced when they are illuminated by the incident waves. We have shown that when the phase shifts of the metallic patches tend to be randomly distributed, the reflected energy from the metallic targets will be dispersed in various directions, resulting in the reduced RCS as desired.

The main limitation for previous designs is the narrow frequency bandwidth. Usually we have to use multilayer structures for broadband applications. However, in this work, only one single layer has been used for simplicity. In the meanwhile, a broadband radiating element has been employed to meet the related bandwidth requirement, which is actually a windmill-shaped patch. This patch consists of an inner ring and an outer ring with several branches attached. We can control the phase of the reflected field ranging from 0° to 360° stochastically by tuning the dimensions of the rings and the branches.

Full wave simulations have shown that the backward RCS of the metallic plate can be reduced at least 10 dB in the whole X band when it is covered by the proposed random surface. The results show that this method can be applied potentially in the radar stealth technology in the future.

Narrow-band Wave Block by Chiral Metamaterials

Nantakan Wongkasem and Amornthep Sonsilphong
Metasolver Laboratory, Department of Electrical Engineering
Faculty of Engineering, Khon Kaen University, Khon Kaen 40002, Thailand

Abstract— EM wave block design using double-layer chiral metamaterials in microwave regimes is proposed. One of the well-known chiral structures, C8, proven to have low loss narrow bandwidth, is employed in this design. The first layer is used to block one of the CP waves, while the other CP wave is filtered out by the same chiral structure with opposite handedness. Different distances between the two chiral layers are observed for the stopband location. These proposed designs are additional promising candidates in EM wave block applications.

Extraordinary Transmission Induced by Thin Metamaterial Layers with Longitudinal Electric Resonances

S. C. Li, **J. Luo**, **Y. Lai**, **and B. Hou**
Wave Functional Materials Lab, School of Physical Science and Technology
Soochow University, Suzhou, China

Abstract— The discovery of the extraordinary optical transmission (EOT) through hole arrays or slits in an otherwise opaque metallic film [1, 2] has aroused tremendous research interest in the past decade. The existence of EOT usually relies on the surface plasmons or spoof surface plasmons on the metal surface which are both critically related to the periodicity of the hole array or slits.

In this work [3], we theoretically and experimentally investigated the case of adding thin metamaterial layers with longitudinal electric resonances to the metallic film. We find such layers of longitudinal resonance are capable of inducing extraordinary transmissions that are nonexistent before. They are not related to the periodicity of the hole arrays or slits. We note that longitudinal magnetic resonances which produce zero index have been previously used to create total transmission or reflection depending on the thickness of the metal film [4]. But here the transmission peaks are also irrespective of the thickness of the metal film. In fact, they are only related to the longitudinal resonance frequencies. As a result, this new mechanism provides a perfect tool to achieve extraordinary transmission at desired frequencies and through metallic films with non-periodic or even random patterns. By using microwave experiments, we have confirmed this unique extraordinary transmission behavior induced by metamaterials with longitudinal resonance.

REFERENCES

1. Ebbesen, T. W., H. J. Lezec, H. F. Ghaemi, T. Thio, and P. A. Wolff, *Nature*, Vol. 391, 667, 1998.
2. García de Abajo, F. J., *Rev. Mod. Phys.*, Vol. 79, 1267, 2007.
3. Li, S. C., et al., to be published.
4. Ma, H. F., J. H. Shi, B. G. Cai, and T. J. Cui, *New J. Phys.*, Vol. 14, 123010, 2012.

Experimental Demonstration of High-performance Grin Lens Antenna with Controllable Aperture Field

M. Q. Qi, **W. X. Tang**, **D. Bao**, **H. F. Ma**, **and T. J. Cui**
State Key Laboratory of Millimeter Waves, Southeast University, Nanjing 210096, China

Abstract— The radiation pattern is one of the most important properties for antennas that have been widely used in modern science and technology. Different applications have different specific requirements to the radiation patterns (directivity, gain, bandwidth, etc.). Traditionally, phased arrays have been used to control the radiation patterns by adjusting the field amplitudes and phases on the array units. Unfortunately, they are usually narrow-band and expensive due to the complicated feeding network. Hence it is significant to seek alternatives to control the radiation patterns over wide frequency bands. One promising way is to employ the metamaterials, which is well known for its ability to control electromagnetic (EM) waves with high flexibility. To the author's knowledge, metamaterials have been mostly used to engineer only the phase distribution of EM waves on the antenna aperture (e.g., to transform spherical waves into plane waves), and therefore, are not able to easily optimise the far-field performance and consequently to tailor the radiation patterns. In this work, we have developed and experimentally demonstrated a new method to design high-performance gradient refractive-index (GRIN) lens antenna with optimised radiation patterns using metamaterials. On the one hand, the distribution of refractive index in a GRIN lens can determine the phase of aperture field of the lens. By carefully designing the refractive index distribution in the lens, a uniform phase is formed on the flat aperture and a high-gain antenna in the direction normal to the flat lens is therefore achieved. On the other hand, the distribution of refractive index in the former designed GRIN lens can be further optimised to modify the amplitude distribution on the lens aperture, which has been proved to have a significant impact on the radiation pattern in the far field. For example, an aperture field distribution with Taylor circle array amplitude and uniform phase results in extremely low side-lobes as well as high directivity. For experimental demonstration, a prototype metamaterial lens has been designed, fabricated and measured. Drilled-hole dielectrics are chosen as unit cells and the refractive index covers all the required values ranging from 1.1 to 1.627. It has been tested that in the near field the amplitude distribution on the lens aperture agrees very well with the Taylor circular array distribution, and the phase front distributes quite uniformly on the lens aperture except on the two edges. And in the far field, high gain and low side-lobes have been verified by both simulated and measured results over a broad frequency band from 12 GHz to 18 GHz.

Some Characteristics of Gyrator Using Magnetoelectric Effect

Makoto Tsutsumi
Okaminami Machi 14-5, Hirakata, Osaka 573-0033, Japan

Abstract— Magnetoelectric effect offers magnetization by the electric field, $(\mathrm{ME})_{\mathrm{E}}$ effect and electric polarization by the magnetic field, $(\mathrm{ME})_{\mathrm{H}}$ effect. In recent years material studies on ME effect have been very active in new ME element like z type hexagonal ferrite $Sr_3CO_2Fe_{24}O_{41}$ [1, 2], piezoelectric PZT — magnetostriction material and also metamaterials. Gyrator has been proposed by Tellegen in more than half century ago but with brief ME transmission line model.

In this paper, exact characteristics of ME gyrator were treated theoretically [3] and with related electromagnetic field problems.

ME gyrator circuit is shown in Fig. 1, it consists of mutual coupling circuit between capacitance created by a ME disk and coil around disk. Equivalent circuit of ME gyrator was derived under assumption of diagonal tensor of ME susceptibility α. Scattering parameters on lumped element gyrator was estimated numerically. Broadband microwave gyrator characteristics were found for developed ME materials. While ME gyrator geometry was analyzed electromagnetically through Maxwell's equation, and a mixed state of TE and TM resonance modes in a ME disk was estimated with electric field patterns of E_r and E_θ as shown in Fig. 2.

Next distributed ME gyrator was proposed with parallel plate transmission line model where nondiagonal ME susceptibility was loaded. Nonreciprocal characteristic of line was found in the dispersion relation, and condition to form distributed gyrator was defined as $2\omega\alpha_{xx}L = \pi$, where ω is a angular frequency, L is a length of transmission line. Finally sensitive phase characteristic of distributed gyrator was discussed.

To realize practical microwave gyrator, ME effect materials having $\alpha = 0.1/c$ (c = light velocity) should be required with high frequency response.

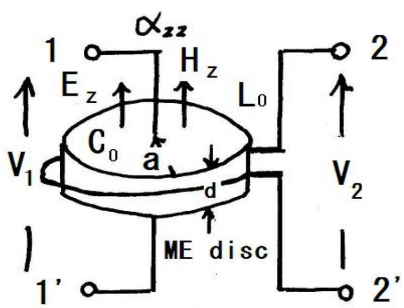

Figure 1: Geometry of the ME gyrator.

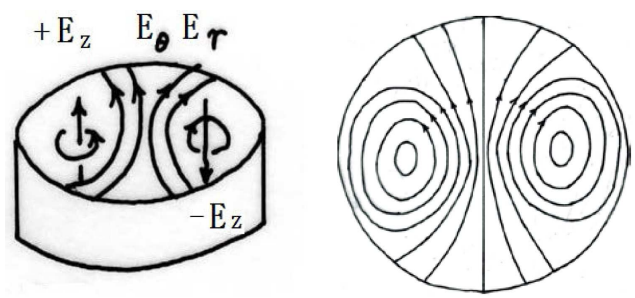

Figure 2: (a) Fields in the ME disk. (b) Electric field pattern.

REFERENCES

1. Kitagawa, Y., Y. Hiraoka, T. Honda, T. Ishikura, H. Nakamura, and T. Kimura, "Low field magnetoelectric effect at room temperature," *Nature Materials Letters*, Vol. 9, 797–802, Oct. 2010.
2. Ebnabbasi, K., C. Vittoria, and A. Widom, "Converse magnetoelectric experiments on a room temperature spirally ordered hexaferrite," *Physical Review*, Vol. B86, 024430, 2012.
3. Tsutsumi, M., T. Tomiya, and K. Aoyagi, "On the circuit analysis containing magnetoelectric effect," *IEEE Trans. Circuit Theory*, Vol. 17, No. 3 339–344, Aug. 1970.

Hybrid Resonance of SRR Metamaterials: A Circuit Model

Rui-Xin Wu, **Min Liu**, **and Yin Poo**
School of Electronic Sciences and Engineering, Nanjing University, Nanjing 210093, China

Abstract— Metamaterials, whose electromagnetic responses can be tailored by engineering, provide a new way to control the electromagnetic (EM) wave propagation. Many abnormal phenomena, such as negative refraction, superlensing and cloaking have been predicted and demonstrated by using the metamaterials. The building elements of the metamaterials, the artificial "atoms", can be designed to yield desired electric and magnetic moments. As these "atoms" have subwavelength scale, the metamaterials are usually modeled by effective medium; their EM responses are the average responses of the "atoms". However, the theory cannot explain some other phenomena, especially those caused by interelement coupling, the interaction between the elements within the unit cell, which may be significant in some circumstances. Recent studies show that the interelement coupling lead to some novel phenomena that do not exist in conventional metamaterials. Hybrid resonance and optical activity are of the examples. It is considered that the hybrid resonance is due to the very strong interactions between the interelements. The hybridization model, which was originally used to describe the plasmon response of complex nanostructures, was applied to the metamaterials to understand the coupling effects of the "atoms". For example, by means of Lagrangian formalism this model has explained the split of resonance frequencies in the paired split ring resonators (SRRs) and its variation with respect to the relative position of the rings. However, the interelement coupling effects have not yet been well appreciated.

In this work, we theoretically study the interelement coupling effects on paired SRRs metamaterial. We have developed an intuitive circuit model for hybrid resonance and derived its eigenfrequencies. This model can identify and evaluate the electric and magnetic coupling, and the breakdown of the hybridization. With this model, the electric and magnetic couplings with respect to the space between the rings are evaluated, and the hybrid resonance states are analyzed. The results reveal that the mutual inductance and the mutual capacitance between the rings can greatly change the resonance states, and the hybrid resonance does not necessary need a very strong coupling. The results of our model are demonstrated by simulations. It is expected that this model could be further extended to model the couplings of other kinds of metamaterials, which offers a simple way to explore the new phenomena and applications of metamaterials with coupled interelements.

ACKNOWLEDGMENT

This work is supported by the NSFC (61271080, 61071007, and 61001017) and RFDP (20110091110030, 20100091120045). RXW thanks partial support from STP of Jiangsu Province (BK2012722).

Ray Tracing in an Arbitrary Cloak in Two Dimensions

H. H. Sidhwa[1], **R. P. Aiyar**[2], **and S. V. Kulkarni**[1]

[1]Department of Electrical Engineering, Indian Institute of Technology, Bombay, India
[2]CRNTS, Indian Institute of Technology, Bombay, India

Abstract— Electromagnetic wave behaviour in an anisotropic medium with two dimensional arbitrary geometry is studied. The aim is to trace the path of a ray in such a complex medium for the purpose of achieving cloaking (invisibility). The region to be cloaked is represented as an arbitrary closed curve in a two dimensional space (XY plane). The dimension along the Z direction is assumed to be infinity. For the purpose of cloaking the region inside the domain is to be mapped to an annular region similar to the approach given by Li and Li [1]. A coordinate transformation is carried out for the formulation of an annular region at the centre of the structure whose topology is a scaled geometry of outer boundary of the structure. We use the approach for the initial formulation of the problem given in [1]. Expressions for permittivity and permeability in the anisotropic medium in the transformed medium are calculated. For verification of the method, we assume that the arbitrary geometry is elliptical in nature. The Hamiltonian is formulated using the approach given in [2] by including terms dependent on cylindrical polar coordinate, θ. Since computations of the determinant of permittivity tensor are cumbersome, we do not evaluate it. We solve the resulting Hamiltonian equation taking into account the variation of r with respect to θ. The Hamiltonian is calculated in terms of cylindrical polar coordinates but the ray tracing is carried out in Cartesian coordinates. Therefore, at every step there is a need for transformation from Cartesian to polar coordinates. The elliptical surface is defined by a function $r = R_0(\theta)$ for the outer boundary. The inner boundary is scaled by a factor $\tau < 1$ and defined as $r = \tau R_0(\theta)$. The annular region between these two surfaces is the region to be cloaked. A plot of path of a plane wave incident on such a medium is generated to indicate that cloaking has been achieved. Further if we put the ellipticity of the ellipse as 0 (a circular cylinder), we get the same expression as given by Shurig et al. [2].

REFERENCES

1. Li, C. and F. Li, "Two-dimensional electromagnetic cloaks with arbitrary geometries," *Optics Express*, Vol. 16, 13414–13420, August 2008.
2. Shurig, D., J. Pendry, and D. Smith, "Calculation of material properties and ray tracing in transformation media," *Optics Express*, Vol. 14, 9794–9804, October 2006.

Broadband Flattened Luneburg Lens with Ultra-wide Angle Based on a Liquid Medium

Lingling Wu, Ming Yin, Xiaoyong Tian, and Dichen Li
State Key Laboratory of Manufacturing Systems Engineering
Institute of Advanced Manufacturing Technique, Xi'an Jiaotong University, China

Abstract— A flattened Luneburg lens with an ultra-wide viewing angle has been realized based on a liquid medium approach in our present work. The field-of-view angle of the achieved Luneburg lens is up to 180° over the microwave regime. The transformed lens is realized in two-dimensional and three-dimensional case respectively by using a low-loss liquid medium and a large variation of refractive index from 1 to 4.18 is achieved. The non-resonant property of the liquid ensures a broadband and low-loss performance of the lens from 12.4 GHz to 18 GHz. The high directivity and relatively low loss of the proposed lens were demonstrated by simulation and experimental results. As all the materials needed in the process are cheap and easily accessible, this approach proves to be a feasible way to promote the practical applications of the flattened Luneburg lens.

A 3D Electromagnetic Wave Concentrator Realized with Gradient Index Woodpile Structure in Metamaterial Regime

Ming Yin, Lingling Wu, Xiaoyong Tian, and Dichen Li
State Key Laboratory of Manufacturing Systems Engineering
Institute of Advanced Manufacturing Technique, Xi'an Jiaotong University, China

Abstract— Artificial effective "optical black hole", which is inspired by cosmic phenomena, has been proposed as an optical analogue of celestial mechanics and was later realized in two-dimensional (2D) cases. Such devices which function as EM wave absorbers may have applications in energy harvesting and radiation detector. Here we present the first realized three-dimensional (3D) practical implementation of the so called "optical black hole" in microwave frequencies, which is a broadband and omnidirectional electromagnetic (EM) concentrator. In a broad bandwidth, incident radiation from all directions is bended towards inside and absorbed effectively by the core. The 3D "EM black hole" is realized with non-resonant gradient index (GRIN) 3D photonic crystals (PCs) structure in metamaterial regime. Stereo lithography (SL) and a compound liquid medium approach were utilized to fabricated the device. Simulations and experimental results validated the omnidirectional EM wave capture and absorbing ability of the device in a broad bandwidth. The proposed device is highly integrated and behaves like a 3D EM wave concentrator, which may find applications in energy harvesting and radiation detector for 3D situation. Furthermore, by changing the photosensitive material used in SL process, and the composition in the compound liquid medium, more flexible effective index range can be realized. Also, the proposed structure is all dielectric and non-resonant, which can be extended to optical regime. The approach reported here can be further applied to realizing other 3D designs and practical devices with 3D GRIN profile.

Electromagnetic Behavior of SRR Loaded Microstrip Transmission Lines: Investigation for Different SRR Types and Array Topologies

G. Disken, F. Pala, E. Demir, H. D. Korucu, and E. Ekmekci
Department of Electronics and Communication Engineering
Suleyman Demirel University, Isparta, Turkey

Abstract— The conventional SRR (Split Ring Resonator) structure is a well-known metamaterial structure that shows negative values of effective permeability over a specific frequency band around its resonance frequency. Recently, the uses of SRR type resonator structures have become very popular especially on filter, antenna, imaging, cloaking and sensor applications. Single SRR structure is modeled by an equivalent LC resonant circuit. However, the array behaviors of these special resonator structures are very important, as well since they are widely used in array forms. Especially, for the microstrip filter, antenna and sensor applications, providing the best possible coupling between the resonator structure and the microstrip feed line are very important to obtain maximum device performances.

In this study we concentrate on microstrip transmission lines loaded by SRR structures in various types, numbers and topologies. The SRR types that are used in this study are shown in Figure 1. We investigate the loading effects of single, double and quadruple SRR structures having different gap directions, different inter-element spacings, different separation distances to the microstrip feeding line and different ring widths. These structures are characterized numerically with the use of CST Microwave studio. Basically, magnitudes of S_{11} (i.e., $|S_{11}|$) and S_{21} (i.e., $|S_{21}|$) are observed and compared by that of unloaded (empty) microstrip transmission line. For an unloaded and matched microstrip transmission line, $|S_{21}|$ is expected to be around 0 dB and $|S_{11}|$ is expected to be below -40 dB. For the SRR loaded cases, we expect $|S_{21}|$ to be lower than -10 dB, and $|S_{11}|$ to be higher than -3 dB, as the figure of merit.

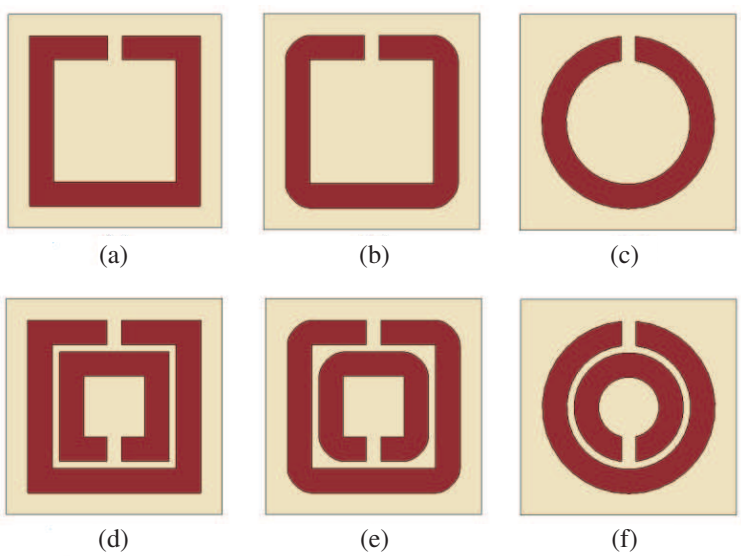

Figure 1: The SRR geometries that are used in this study. (a) Square-shaped single ring SRR, (b) square-shaped single ring SRR smoothened at the corners, (c) circular-shaped single ring, (d) square-shaped double ring SRR, (e) square-shaped double ring SRR smoothened at the corners, (f) circular-shaped double ring.

The High Directivity Antenna Based on Metamaterials

Wanzhao Cui and Tiancun Hu
Science and Technology on Space Microwave Laboratory
Xi'an Institute of Space Radio Technology
Xi'an 710100, Shannxi Province, China

Abstract— Metamaterials, artificially fabricated by densely arranged sub-wavelength inclusions, have been attracting tremendous interests during the last years due to supernatural electromagnetic characteristics not found in normal, naturally occurring media. They offer the possibility to create independent tailored electric and magnetic responses to incident radiation in nearly any frequency band. Owing to this tailored property, effective materials with permittivity or permeability less than that of vacuum or with negative values have been successfully achieved in every technologically relevant spectral range from radio to optical, which could be used to design and build novel devices, such as super lenses which can overcome the diffraction limit, enhanced tunneling effect devices, or invisibility cloaks. Recently, metamaterials with "near-zero" permittivity or permeability have also attracted a lot of interest. With the near-zero refractive index of the metamaterial, the rays emitted by the source inside the metamaterial will be refracted at the air-metamaterial interface into a small angular range centered along the normal of the surface. Therefore, an enhancement of the directivity compared with the original radiation can be expected based on which an antenna with high directivity can be realized.

In this paper, we make an anisotropic slab made of metallic symmetrical rings with dispersive permeability near to zero and show by theoretical analysis, simulation and experiments that when several such slabs with the near-zero refractive index are arranged properly, a multi-beam antenna with high directivity can be achieved in a limited frequency band. The experimentally measured results agree well with theoretical one. This new design provides an alternative way to design the multi-beam antenna.

Microwave Focusing by a Wire Medium

Joaquim J. Barroso[1], **Antônio Tomaz**[2], **Ugur C. Hasar**[3], **and Alberto J. Faro Orlando**[2]

[1]Instituto Nacional de Pesquisas Espaciais (INPE), São José dos Campos, SP, Brazil
[2]Instituto Tecnológico de Aeronáutica (ITA), São José dos Campos, SP, Brazil
[3]University of Gaziantep, Gaziantep 27310, Turkey

Abstract— As a versatile electroheat method, microwave heating offers advantages over conventional heating because energy is directly transferred into the absorbing material without thermal conductivity delay and without passing through an interface. In this regard, the present paper demonstrates the ability of a wire medium to focus microwave radiation in the 8–14 GHz frequency range. Despite the considerable operating wavelength, microwave focusing is achieved in a small volume to produce localized energy dissipation processes and high-temperature gradients. The wire medium is implemented with 0.5-mm-diameter metallic wires symmetrically arranged on a square lattice (spacing constant of 10.0 mm) to build a rectangular parallelepiped 17-wire long and 15-wire wide; then a square of 5×5 wires is removed from the downstream edge to form a reentrant slab symmetric along is length, as displayed in Fig. 1(a). Using the CST MWS software, full-wave electromagnetic simulation is carried out on the rectangular bounding box, with boundary conditions the top and bottom faces as perfectly conducting metallic planes, and the transverse walls as magnetic surfaces. The upstream red colored end face [Fig. 1(a)] is used as an input port from which a normally incident plane wave is launched into the medium with the electric field polarized along the wires. The simulated return loss (S_{11} scattering parameter) is shown in Fig. 1(b), where over the first pass band are identified 16 sharp dips, which are related with the 16 resonant eigenmodes supported by the periodic medium thus constructed with 17 layers. Above the pass band there extends a Bragg stopband starting from 15 GHz, the frequency at which its half wavelength is just the periodic distance $p = 10.0$ mm. In the second pass band, above the band gap ($\lambda/2 < p$), the wire medium behaves as a photonic crystal, where diffraction and scattering phenomena dominate, and as such the periodic structure cannot be characterized by an effective refractive index. On the other hand, in the first passband ($\lambda/2 > p$), the propagating fields see the structure as a homogeneous and refractive medium. In fact, at 9.77 GHz we see in Fig. 1(c) that the parallel wavefronts of the input wave plane converge to a focal line after passing through the reentrant region in the wire medium. Other frequencies corresponding to the resonance dips in Fig. 1(b) would give similar electric-field patterns. But the resonance frequency can be tuned by removing or adding extra wire layers. For instance, by removing the first layer of 15 wires the third dip at 8.49 GHz in Fig. 1(b) shifts down to 8.45 GHz. In the corresponding electric-field pattern shown in Fig. 1(d), we see that the incoming plane wave becomes

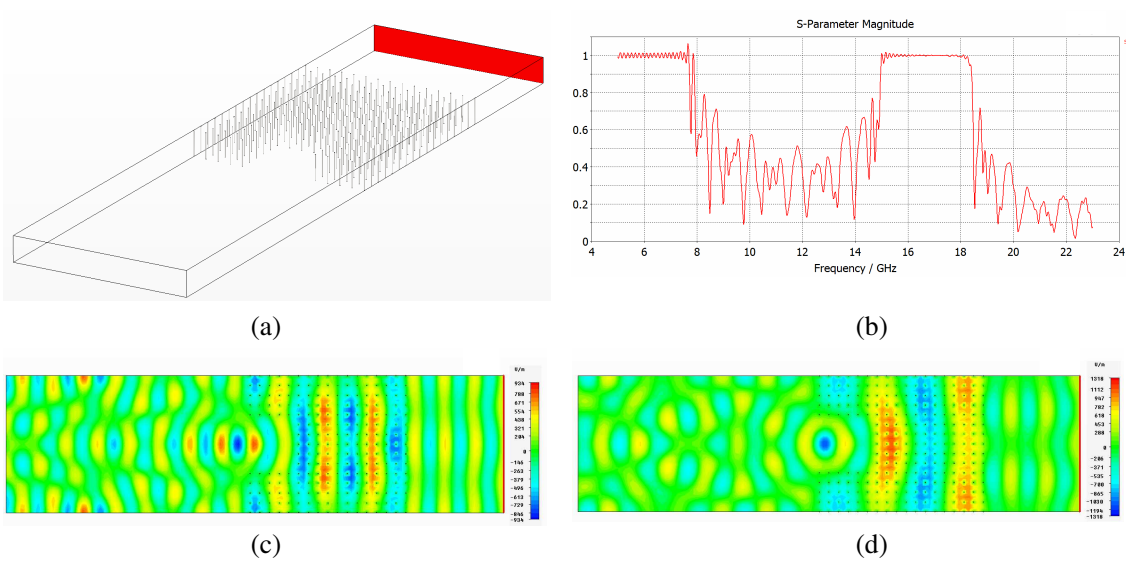

Figure 1: (a) Three-dimensional view of the wire medium, (b) magnitude of S_{11}, (c) top view of the E-field pattern at 9.77 GHz, (d) E-field pattern at 8.45 GHz with the first wire layer (next to the input port) removed.

strongly concentrated on a circular spot, thus demonstrating the focusing action of the designed wire medium. In this paper, in addition to the physics underpinning the refraction mechanism, other examples are discussed in connection with the refractive index retrieved from scattering parameters.

Session 4P2
SC2: New and Novel Concepts on Metamaterials/Plasmonics

Controlling Light at Subwavelength Scales: The Nonlocal and Quantum Tunnelling Effects
Yu Luo, Antonio I. Fernandez-Dominguez, Stefan A. Maier, John B. Pendry, ... 1526
Plasmonic Phase Retardation in Anisotropic Nanodots: Modeling and Increased Sensor Figure of Merit
Wen-Yu Chen, Chun-Hung Lin, Wei-Ting Chen, ... 1527
Giant Photobleaching Suppression Using the Strong Purcell Effect of Plasmonic Nanostructures
Yongmin Liu, Hu Cang, Xiang Zhang, ... 1528
Chirality in the Interaction between Plasmons, Light, and Vortex Electron Beams
Ana Asenjo-Garcia, F. Javier Garcia de Abajo, ... 1529
Multipole Nanodisk Plasmons Excited by Cylindrical Vector Beams
Kyosuke Sakai, Takeaki Yamamoto, Kensuke Nomura, Yoshito Tanaka, Keiji Sasaki, ... 1530
Effective Model for Plasmonic Coupling: A Rigorous Derivation
Meng Qiu, Bin Xi, Shiyi Xiao, Hao Xu, Lei Zhou, ... 1531
Invisibility through Radial Anisotropy
Henrik Kettunen, Henrik Wallen, Ari Henrik Sihvola, ... 1532
Calculating the van der Waals Interaction Using Transformation Optics
Rongkuo Zhao, Yu Luo, Antonio I. Fernandez-Dominguez, John B. Pendry, ... 1533
Metamaterials Simulators for Topological Excitations in Condensed Matters
Wei Tan, Yong Sun, Shun-Qing Shen, Hong Chen, ... 1534
Novel Realizations for Optical Magnetism and Magnetic Metamaterials Down to Ultraviolet Wavelengths
Jianwei Tang, Sailing He, ... 1535
Designer Magnetoplasmonics in Anisotropic Nanoferromagnets
Kristof Lodewijks, Irina Zubritskaya, Randy Dumas, Johan Akerman, Alexandre Dmitriev, ... 1536
Refraction and Reflection of Surface Plasmon Polaritons with Parasitic Scattering Suppression
Evgeni A. Bezus, L. L. Doskolovich, ... 1538
Super-absorbing Plasmonic Metamaterials: From Visible to Mid-infrared
Michaël Lobet, Olivier Deparis, Luc Henrard, ... 1539
Direct Observation of Plasmon Enhanced Four Wave Mixing (FWM)
Po-Wen Tang, Wen-Hsiang Yu, Chao-Yi Tai, ... 1541

Controlling Light at Subwavelength Scales: The Nonlocal and Quantum Tunnelling Effects

Yu Luo, **Antonio I. Fernández-Domínguez**, **Stefan A. Maier**, **and J. B. Pendry**
Department of Physics, Imperial College London, London, UK

Abstract— Metallic nanoparticles that support localized surface plasmon resonances can harvest light into a deep-subwavelength volume, thereby achieving very large field enhancement. Many emerging nanophotonic technologies rely on the careful control of this field enhancement, including cancer therapy, improved photovoltaic devices, and optical antennas for enhanced light-matter interactions. However, at deep subwavelength scales, classical continum electrodynamics fails to describe the optical responses of nanoparticles owing to nonlocal screening and the spill-out of electrons. Electron correlations that are driven by these effects require a new model of nonlocal transport, which is crucial in nanoscale optoelectronics. In this contribution, I will present a systematic strategy, based on transformation optics, to study the plasmonic interaction at subnanometer scales. Our approach incorporates radiative, nonlocal, and quantum tunnelling effects, and thus can be applied to design realistically sized plasmonic systems. As an example, I will use this method to elucidate the optimum shape of a nanoparticle that maximizes its absorption and field enhancement capabilities.

Plasmonic Phase Retardation in Anisotropic Nanodots: Modeling and Increased Sensor Figure of Merit

Wen-Yu Chen[1], **Chun-Hung Lin**[1, 2], **and Wei-Ting Chen**[2]

[1]Department of Photonics, National Cheng Kung University, Tainan 701, Taiwan
[2]Advanced Optoelectronic Technology Center, National Cheng Kung University, Tainan 701, Taiwan

Abstract— Localized surface plasmon resonances (LSPR) [1] always attract great interests for their applications of sensing. LSPR based sensors often suffer from broad full width at half maximum (FWHM) and therefore decline their performance. Previous efforts contributed on the FWHM narrowing by using the approaches such as the substrate excited mode from a silver nanocube [2], the interference between LSPR and Rayleigh anomaly [3], and the detuned resonances of perpendicular polarizations by an oblique incidence [4]. In this study, we demonstrated the phenomenon of plasmonic phase retardation in anisotropic nanodots. The investigated configuration and the corresponding transmission and phase spectra are illustrated in Figure 1. LSPRs induce phase transitions for transmission waves polarized along the symmetric axes, and these phase transitions are spectrally detuned by the anisotropy of the nanodots. Therefore, the phase difference at the LSPR wavelength exhibits an extremely narrow FWHM. The phase signal can be measured by transmission ellipsometry, and thus boosts the figure of merit (FOM) for refractive index sensing. To improve our understanding, we used temporal coupled-mode theory (TCMT) [5] to model the LSPR. The agreement between the TCMT equations and the spectra reveals the origin of the phase transition in the LSPR. Then, we numerically adjusted the aspect ratio of the nanodots and thus controlled the FWHM of the ellipsometric parameter. The FOM is improved over 20-fold compared to the FOM for intensity detection in the simulations. We also experimentally examined the arrangement, and the results highly agree with the corresponding simulations. This working principle can be further applied to various plasmonic nanoparticles to obtain highly improved FOM.

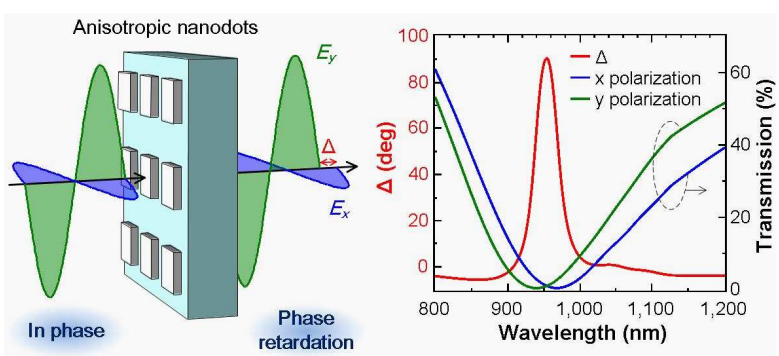

Figure 1: Plasmonic phase retardation in anisotropic nanodots.

REFERENCES

1. Mayer, K. M. and J. H. Hafner, "Localized surface plasmon resonance sensors," *Chemical Reviews*, Vol. 111, 3828–3857, 2011.
2. Sherry, L. J., S. H. Chang, G. C. Schatz, R. P. van Duyne, B. J. Wiley, and Y. N. Xia, "Localized surface plasmon resonance spectroscopy of single silver nanocubes," *Nano Letters*, Vol. 5, 2034–2038, 2005.
3. Offermans, P., M. C. Schaafsma, S. R. K. Rodriguez, Y. Zhang, M. Crego-Calama, S. H. Brongersma, and J. Gómez Rivas, "Universal scaling of the figure of merit of plasmonic sensors," *ACS Nano*, Vol. 5, 5151–5157, 2011.
4. Lodewijks, K., W. van Roy, G. Borghs, L. Lagae, and P. van Dorpe, "Boosting the figure-of-merit of LSPR-based refractive index sensing by phase-sensitive measurements," *Nano Letters*, Vol. 12, 1655–1659, 2012.
5. Fan, S. H., W. Suh, and J. D. Joannopoulos, "Temporal coupled-mode theory for the Fano resonance in optical resonators," *Journal of the Optical Society of America A*, Vol. 20, 569–572, 2003.

Giant Photobleaching Suppression Using the Strong Purcell Effect of Plasmonic Nanostructures

Yongmin Liu[1,2], **Hu Cang**[3], **and Xiang Zhang**[4,5]

[1]Department of Mechanical and Industrial Engineering, Northeastern University, USA
[2]Department of Electrical and Computer Engineering, Northeastern University, USA
[3]Waitt Advanced Biophotonics Center, Salk Institute for Biological Studies, USA
[4]NSF Nanoscale Science and Engineering Center (NSEC), University of California, Berkeley, USA
[5]Materials Sciences Division, Lawrence Berkeley National Laboratory, USA

Abstract— Photobleaching, an irreversible light-induced chemical reaction, changes the structure of a fluorescent molecule and permanently destroys the molecule's fluorescence capability [1]. It imposes a fundamental limit of the total number of photons that one can harvest from the molecule. Considerable effort has been devoted to suppress the photobleaching, which culminates primarily in chemical-based strategies: making the local environment more chemically inert to fluorophores, or modifying the structure and energy landscape of the fluorophores to be more resistant to photobleaching.

Here, we demonstrate that the strong Purcell effect [2] of a plasmonic nanostructure could effectively steer a fluorophore away from photobleaching and prolong a fluorophore's lifespan, offering a "physical" approach to manipulate the photochemical reactions of bleaching. The underlying mechanism lies in the fact that the two channels — the relaxation and the bleaching — compete with each other during fluorescence process. As a result, we can reduce the probability of the molecule entering the bleaching channel by enhancing the relaxation process with plasmonic structures. Experimentally, up to 1,000 folds more photons have been harvested from a single fluorescent molecule located in a plasmonic cavity, in good agreement with theoretical predictions. Such a giant suppression of photobleaching is well beyond conventional chemical schemes. Our findings will not only accelerate single-molecule fluorescence applications, but also open up a new avenue to electromagnetic control of chemical reactions.

REFERENCES

1. Moerner, W. E. and D. P. Fromm, "Methods of single-molecule fluorescence spectroscopy and microscopy," *Review of Scientific Instruments*, Vol. 74, 3597, 2003.
2. E. M. Purcell, "Spontaneous emission probabilities at radio frequencies," *Phys. Rev.*, Vol. 69, 681, 1946.

Chirality in the Interaction between Plasmons, Light, and Vortex Electron Beams

A. Asenjo-Garcia[1] **and F. J. García de Abajo**[2]

[1]IQFR, CSIC, Serrano 119, Madrid 28006, Spain
[2]ICFO, Spain

Abstract— We have studied the interaction of plasmonic chiral matter with both circularly polarized light and vortex electron beams. For light, we compare the calculations based upon multiple scattering theory with recent observations of circular dichroism (CD) in nanoparticles assembled using DNA origami. We analyze the effect of varying distance between the particles and particle sizes as well as the influence of the material in the CD signals showing that it is possible to optimize the position of the particles to enhance the CD signal or to reverse its sign just with minor displacements. For electrons, we predict strong dichroism in the electron energy-loss spectroscopy (EELS) signal by using electron vortex beams. These vortex beams carry orbital angular momentum that can be exchanged in the interaction with chiral plasmons: when an electron looses energy by interacting with a chiral sample and it passes through a fork mask, different beams are diffracted (each with different orbital angular momentum), and the energy lost by the components with opposite units of angular momentum will be different. Incidentally, this method benefits from high spatial resolution of electron microscopes and might be really useful for magnetic dichroism imaging.

Multipole Nanodisk Plasmons Excited by Cylindrical Vector Beams

Kyosuke Sakai, Takeaki Yamamoto, Kensuke Nomura, Yoshito Tanaka, and Keiji Sasaki
Research Institute for Electronic Science, Hokkaido University, N-20 W-10, Kita-ku, Sapporo, Japan

Abstract— Multipole (high-order) plasmon modes typically show lower radiative losses and higher quality (Q) factors compared to dipole plasmon modes [1]. Thus, applications such as plasmon lasing, plasmon enhanced luminescence, and biosensing can substantially benefit from multipole plasmons. However, coupling of the incident plane wave to multipole plasmons is very weak, although possible through phase retardation or symmetry breaking [2, 3]. Here, we present a novel method that enables strong excitation of multipole plasmons of a planar nanodisk. We theoretically demonstrate that an efficient coupling of the incident light to multipole plasmons is possible, if we use cylindrical vector beams [4, 5].

Figure 1(a) shows the calculation model, where the incident light propagates downward from the top surface to the gold nanodisk. Figure 1(b) shows the near-field intensity spectrum of the dipole plasmon excited by linearly polarized Gaussian beam. The inset shows the near-field intensity and electric-field distributions around the nanodisk at the peak wavelength. Figure 1(c) shows the results for the quadrupole plasmon excited by cylindrical vector beam. Sharper resonant peak at shorter wavelength and quadrupole intensity profile (inset) evidence that the strong excitation of multipole plasmon is possible using cylindrical vector beam. The current method can be extended to even higher-order modes, e.g., hexapole, and should make multiple plasmons better suited for above mentioned applications.

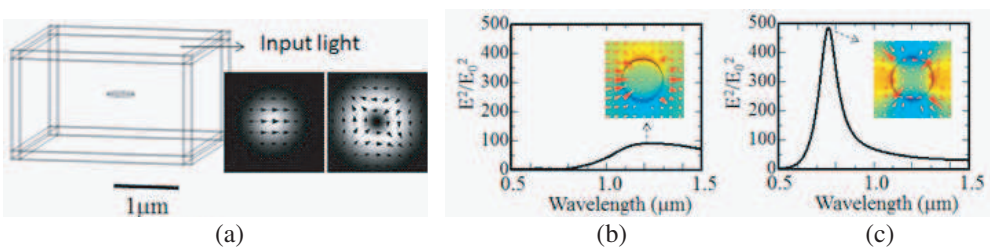

Figure 1: (a) Calculation model. Dimension of nanodisk is diameter = 400 nm, thickness = 30 nm. (b) Near-field spectrum of dipole plasmon excited by linearly polarized Gaussian beam. (c) Near-field spectrum of quadrupole plasmon excited by cylindrical vector beam. The inset shows near-field profile around the nanodisk (arrow: electric field vector). The spectrum intensity ($|E|^2$) was normalized by the field intensity ($|E_0|^2$) that was obtained for the same model but without the gold nanodisk.

REFERENCES

1. Verellen, N., P. V. Dorpe, D. Vercruysse, G. A. E. Vandenbosch, and V. V. Moshchalkov, "Dark and bright localized surface plasmons in nanocrosses," *Opt. Exp.*, Vol. 19, 11034–11051, 2011.
2. Hao, F., E. M. Larsson, T. A. Ali, D. S. Sutherland, and P. Nordlander, "Shedding light on dark plasmons in gold nanorings," *Chem. Phys. Lett.*, Vol. 458, 262–266, 2008.
3. Wang, H., Y. Wu, B. Lassiter, C. L. Nehl, J. H. Hafner, P. Nordlander, and N. J. Halas, "Symmetry breaking in indivisual plasmonic nanoparticles," *Proc. Natl. Acad. Sci.*, Vol. 103, 10856–10860, 2006.
4. Iwahashi, S., Y. Kurosaka, K. Sakai, K. Kitamura, N. Takayama, and S. Noda, "Higher-order vector beams produced by photonic-crystal lasers," *Opt. Exp.*, Vol. 19, 11963–11968, 2011.
5. Kitamura, K., K. Sakai, N. Takayama, M. Nishimoto, and S. Noda, "Focusing properties of vector vortex beams emitted by photonic-crystal lasers," *Opt. Lett.*, Vol. 37, 2421–2423, 2012.

Effective Model for Plasmonic Coupling: A Rigorous Derivation

Meng Qiu, Bin Xi, Shiyi Xiao, Hao Xu, and Lei Zhou
Physics Department, Fudan University, Shanghai 200433, China

Abstract— Plasmonic properties of noble-metal nanoparticles (NPs) have drawn much attention recently. When multiple number of NPs aggregate to form a cluster, couplings between neighboring NPs generate fascinating physical phenomena, which can be utilized to realize certain practical applications. However, theoretical understandings on such problems are relatively behind the fast experimental developments. Most theoretical efforts are based full wave simulations, which are not only computational complicated but also physically less transparent. Here, based on the generalized tight-binding theory for dispersive photonic systems [1], we found the explicit form of the mutual coupling constant $t_{1,2}$ between two NPs

$$t_{12} = t_{pp} + t_{pp}^{rad} + t_{pm} + t_{mm} \quad (t_{pp} \gg t_{pp}^{rad} > t_{pm} > t_{mm}) \tag{1}$$

with t_{pp} and t_{mm} being the standard dipolar interactions between electric and magnetic dipoles in different NPs, and t_{pp}^{rad} is the electric dipolar interaction contributed from radiation effect, and t_{pm} describes the interaction between electric and magnetic dipoles [2]. For the double gold nano-ellipsoids system depicted in the inset to Fig. 1(a), our theory predicts

$$\Delta f = 2t_{pp} \approx f_0 \left(1 - 3\cos^2\theta\right) |\vec{p}|^2 / \left(4\pi\varepsilon_0 d^3\right). \tag{2}$$

As shown in Figs. 1(a)–(b), the numerically simulated frequency splitting (open circles) does follow the above dipolar interaction model (solid line) very well. The magnetic dipolar interaction term t_{mm} can be singled out only when the electric dipole moment of the NP vanishes. We use the broadside-coupled split ring resonator (BC-SRR) structure, whose lowest resonance is a purely magnetic mode [6]. In this case, our theory predicts that

$$\Delta f = 2t_{mm} \approx f_0\mu_0 \left(1 - 3\cos^2\theta\right) |\vec{m}|^2 / \left(4\pi\varepsilon_0 d^3\right) \tag{3}$$

Simulations (Figs. 1(c) and (d)) verified Eq. (3). We will introduce the details of the theoretical derivation and more applications of our effective model in the conference.

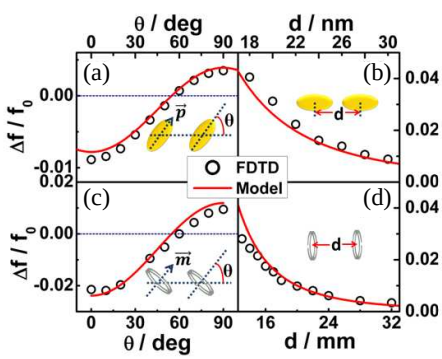

Figure 1: Resonance frequency splitting between (a), (b) two gold NPs and (c), (d) two BC-SRR structures against the distance between two NPs and the angle between dipole and center-center line, obtained by simulations (symbols) and model calculations.

REFERENCES

1. Xi, B., H. Xu, S. Xiao, and L. Zhou, *Phys. Rev. B*, Vol. 83, No. 16, 165115, 2011.
2. Xi, B., M. Qiu, S. Xiao, H. Xu, and L. Zhou, Unpublished.

Invisibility through Radial Anisotropy

H. Kettunen[1], **H. Wallén**[2], **and A. Sihvola**[2]

[1]Department of Mathematics and Statistics, University of Helsinki, Finland
[2]Department of Radio Science and Engineering
Aalto University School of Electrical Engineering, Finland

Abstract— Invisibility cloaking is inarguably one of the most intriguing topics in metamaterials research. The probably best-known suggested cloak constructions are based on transformation optics [1, 2]. The realization of such cloaks is, however, very difficult considering the complexity of the required material parameters. Another idea is based on scattering cancellation, where the cloaked object is covered by a metamaterial coating that cancels out the dipole moment of the object [3]. This cloak works well in the long-wavelength limit. The design of the cloak, however, depends on the size and the material of the cloaked object.

In this presentation, we propose a simple approximative non-magnetic cloaking realization based on radial anisotropy. A *radially anisotropic* (RA) geometry has well-defined radial and tangential directions and its permittivity components in these directions, $\varepsilon_{\mathrm{rad}}$ and $\varepsilon_{\mathrm{tan}}$, respectively, differ from each other. Such geometries include *polarly radially anisotropic* (PRA) cylinders and *spherically radially anisotropic* (SRA) spheres. In practice, radially anisotropic geometry could be constructed, for instance, using radially oriented needle-shaped inclusions [4] or by stacking several thin concentric layers on top of each other [5]. The RA cloak can be considered a generalization of the idea presented in [3] and a simplification of the constructions considered in [6, 7]. The operating principle of our cloak, however, resembles more the cloaks designed by transformation optics, except that the RA cloak only works perfectly in the quasi-static limit.

We consider the electrostatic responses of the aforementioned RA geometries. We show that with certain choices of $\varepsilon_{\mathrm{rad}}$ and $\varepsilon_{\mathrm{tan}}$ the RA structures become invisible. Simultaneously increasing $\varepsilon_{\mathrm{tan}}$ and decreasing $\varepsilon_{\mathrm{rad}}$ make the potential levels inside the RA object bend such that a nearly constant potential, and a zero field, is created around the center of the object. This zero field region can serve as a cloak, where an inserted object is not polarized at all and cannot thus be observed from the outside. The cloak design is therefore independent of the permittivity, shape or number of the inclusions to be hidden. By simulations, we show how the cloak can be used in cloaking a dielectric object of arbitrary shape. We also study the performance of the cloak in a dynamic case where it is excited by a propagating electromagnetic wave.

REFERENCES

1. Leonhardt, U., "Optical conformal mapping," *Science*, Vol. 312, No. 5781, 1777–1780, 2006.
2. Pendry, J. B., D. Schurig, and D. R. Smith, "Controlling electromagnetic fields," *Science*, Vol. 312, No. 5781, 1780–1782, 2006.
3. Alù, A. and N. Engheta, "Achieving transparency with plasmonic and metamaterial coatings," *Phys. Rev. E*, Vol. 72, No. 1, 016623-1–9, 2005.
4. Cai, W., U. K. Chettiar, A. V. Kildishev, and V. M. Shalaev, "Optical cloaking with metamaterials," *Nat. Photonics*, Vol. 1, No. 4, 224–227, 2007.
5. Tricarico, S., F. Bilotti, and L. Vegni, "Scattering cancellation by metamaterial cylindrical multilayers," *J. Eur. Opt. Soc. — Rapid*, Vol. 4, 09021-1–10, 2009.
6. Gao, L., T. H. Fung, K. W. Wu, and C. W. Qiu, "Electromagnetic transparency by coated spheres with radial anisotropy," *Phys. Rev. E*, Vol. 78, No. 4, 046609-1–11, 2008.
7. Ni, Y., L. Gao, and C.-W. Qiu, "Achieving invisibility of homogeneous cylindrically anisotropic cylinders," *Plasmonics*, Vol. 5, No. 3, 251–258, 2010.

Calculating the van der Waals Interaction Using Transformation Optics

Rongkuo Zhao, **Yu Luo**, **A. I. Fernández-Domínguez**, **and J. B. Pendry**
The Blackett Laboratory, Department of Physics
Imperial College London, London SW7 2AZ, United Kingdom

Abstract— van der Waals (vdW) forces between nanostructures, which arise from the electromagnetic interaction between instantaneous quantum fluctuation-induced charges, play an important role in surface adhesion and friction, colloidal stability and crystallization, and nanoparticle self-assembly. Exact calculation of the van der Waals interaction between closely spaced plasmonic nanoparticles with a "singular" separation is challenging both numerically and analytically due to the strong concentration of the electromagnetic fields at the nearly touching nanometric gap between them. The technique of transformation optics, capable of mapping a small volume into any desired length scale, enables us to shed physical insight into the intricate behavior of electromagnetic fields in extremely small gaps. Through transforming two closely spaced spheres with a "singular" gap into an annulus one that possesses higher symmetry and less "singular" (see Fig. 1), we have not only obtained fast convergence of exact calculations, but also obtained very accurate analytical approximations which can be used directly by a broad range of people from all disciplines without requiring special knowledge. Our generic method can also be applied to the study of radiative heat transfer and non contact van der Waals frictions.

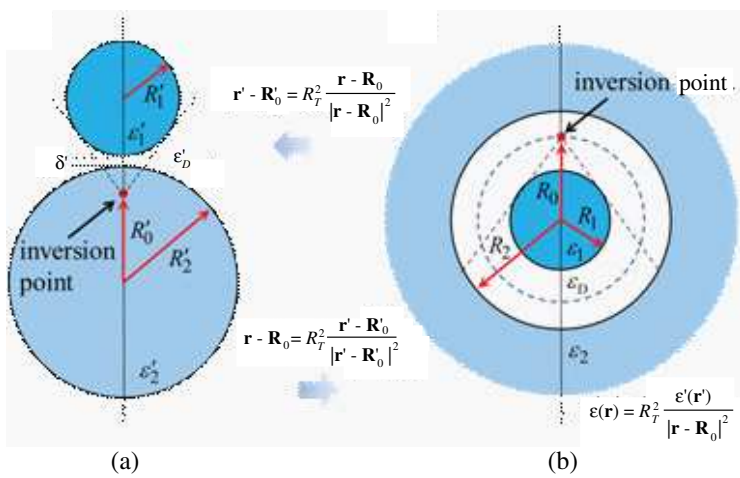

Figure 1: Applying an inversion transformation about the point $\mathbf{R}'_0$, two separated spheres (a) are mapped into an annulus (b), and vice versa. The annulus geometry comprises an inner solid sphere and an outer hollow one. The geometric inversion is accompanied by a transformation of the system permittivities. The small gap inside the cone indicated by the two dashed lines in (a) is enlarged in the annulus and is located further from the inversion point in (b). The opening angle of the cone in (a) is unchanged under the conformal transformation.

ACKNOWLEDGMENT

For our support we thank the following: AIFD and JBP the Gordon and Betty Moore Foundation, JBP the AFOSR, RZ the Royal Commission for the Exhibition of 1851, YL and JBP the Leverhulme Trust.

Metamaterials Simulators for Topological Excitations in Condensed Matters

Wei Tan[1], **Yong Sun**[1], **Shun-Qing Shen**[2], **and Hong Chen**[1]

[1]Key Laboratory of Advanced Micro-structured Materials, MOE, Department of Physics
Tongji University, Shanghai 200092, China
[2]Department of Physics, The University of Hong Kong, Pokfulam Road, Hong Kong, China

Abstract— Metamaterials with left-handed chirality and condensed matter systems with topological order have attracted recently extensive interests in the fields of optics and physics. In this talk, we will describe our recent studies trying to connect these two seemly unrelated concepts. We propose to establish the relation between the chirality in metamaterials and the topological order in condensed matter systems, by transforming explicitly Maxwell's equations to the Dirac equation in one dimension (1D). In terms of electric and magnetic parameters such as electric and magnetic fields E_z and H_y, permittivity (permeability) of the media ε_0 and ε_r (μ_0 and μ_r), the transformed Maxwell's equations can be written as

$$[-i\sigma_x\partial_x + m(x)\sigma_z + V(x)]\,\varphi = E\varphi$$

where the spinor is defined as $\varphi = \begin{pmatrix} \sqrt{\varepsilon_0}E_z \\ \sqrt{\mu_0}H_y \end{pmatrix}$, the effective mass $m(x) = \frac{\omega}{2c}(\varepsilon_r - \mu_r)$, the potential $V(x)$ and energy $EV(x) - E = \frac{\omega}{2c}(\varepsilon_r + \mu_r)$, c is the speed of light in vacuum, and $\sigma_{x,y,z}$ are the three Pauli matrices.

It is noted that the effective mass in the transformed Dirac equation is given by the permittivity and permeability, which can be tailored by artificial structures in metamaterials. The signs of permittivity and permeability determine the chirality of electromagnetic wave in optical media: the electric field, magnetic field and the wave vector obey the right-handed or left-handed triad. On the other hand, it is known that the sign change of the effective mass is closely related to the topological order of a condensed matter system. Therefore, the above transformation establishes the possible relation between chirality feature in metamaterials and topological order in condensed matters. We believe that this relation will open a new route to mimic topological phases and excitations of Dirac equation in designed metamaterials in one way. In the other way, we may understand and even explore some exotic phenomena in metamaterials from a point of view of the Dirac equation.

Microwave experiments based on transmission-line metamaterials are carried out to simulate topological excitations described by the Dirac equation in 1D condensed matter systems, such as the band structure inversion from a positive to negative mass, topological excitation or soliton in 1D polymer, end states in 1D lattice topological phase of the Su-Schrieffer-Heeger model.

Novel Realizations for Optical Magnetism and Magnetic Metamaterials Down to Ultraviolet Wavelengths

Jianwei Tang[1] **and Sailing He**[1, 2]

[1]Centre for Optical and Electromagnetic Research
JORCEP [Sino-Sweden Joint Research Center of Photonics]
Zhejiang Provincial Key Laboratory for Sensing Technologies
Zhejiang University, Zijingang Campus, East Building No. 5, Hangzhou 310058, China
[2]Department of Electromagnetic Engineering, Royal Institute of Technology, Stockholm 100 44, Sweden

Abstract— We first proposed a hybrid metal-dielectric ring resonator mainly composed of a high index dielectric material TiO_2 with some gaps filled with metal (e.g., Ag). The hybrid metal-dielectric ring resonator is able to overcome both the saturation problem of split-ring resonators and the homogenization problem of all-dielectric magnetic resonators, and therefore can form homogenizable magnetic metamaterials at short wavelengths down to the ultraviolet wavelength range. An analytical LC model was developed to describe the magnetic resonances of ring resonators, including the proposed hybrid ring resonator, the split-ring resonator and the all-dielectric ring resonator. In the framework of the LC model, we compared the hybrid ring resonator with the split-ring resonator to interpret how hybrid ring resonator can overcome the saturation problem to exhibit strong magnetic resonance down to ultraviolet wavelengths, and we compared the hybrid ring resonator with the all-dielectric ring resonator to interpret how hybrid ring resonator can overcome the homogenization problem to form homogenizable magnetic metamaterials. We also demonstrated optical magnetism down to UV wavelengths from an anti-symmetric plasmonic mode in a single silver nanostrip. Strong anti-symmetric plasmonic modes are usually supported by coupled metal strips, but not by a single metal strip. We used only a single metal strip to support a strong anti-symmetric plasmonic mode by sandwiching it with TiO_2 layers. The underlying physics of the anti-symmetric plasmonic mode was explained using a "truncated insulator/metal/insulator waveguide" model. Our design and analysis may lead to deeper understanding of plasmonic coupling and is promising for inspiring novel plasmonic designs. Homogenizable magnetic metamaterials down to UV wavelengths can be formed by periodically arrayed TiO_2-sanwiched silver nanostrips. We experimentally fabricated arrays of TiO_2-sanwiched silver nanostrips to realize magnetic metamaterials in the blue, violet and part of ultraviolet light range.

Designer Magnetoplasmonics in Anisotropic Nanoferromagnets

Kristof Lodewijks[1], **Irina Zubritskaya**[1], **Randy Dumas**[2], **Johan Åkerman**[2], **and Alexandre Dmitriev**[1]

[1]Applied Physics, Chalmers University of Technology, Fysikgränd 3, Göteborg 412 96, Sweden
[2]Physics Deparment, Gothenburg University, Fysikgränd 3, Göteborg 412 96, Sweden

Abstract— The interaction between magnetic materials and plasmon resonances has been extensively studied in the field of magnetoplasmonics. It was recently shown that ferromagnetic nickel nanoparticles support localized surface plasmon resonances that can be exploited to modify the magneto-optical behavior at will [1]. As such, the Kerr rotation angle that is measured in spectroscopic Magneto-Optical Kerr Effect (MOKE) experiments can change both in sign and magnitude depending on the excitation wavelength and its relative position with respect to the localized surface plasmon resonance (LSPR) frequency. This tunability originates from the large phase change between both spectral sides of the LSPR and the intrinsic phase shift that the magnetization of the ferromagnetic material induces. Here we show that symmetry breaking adds one more degree of freedom by modifying both the magnetic and optical behavior of the nanoparticles. We studied the magnetization behavior of round and elliptical nickel nanoparticles in longitudinal spectral MOKE, measuring along the different symmetry axes of the system, as illustrated in Figure 1.

From the MOKE loops, it can be seen directly that the short and long axis of the nanoparticles behave as a hard- (red) and easy (blue) axis for the magnetization, which severely alters the magnetization behavior compared to simple round disks (black). When we compare the coercivity

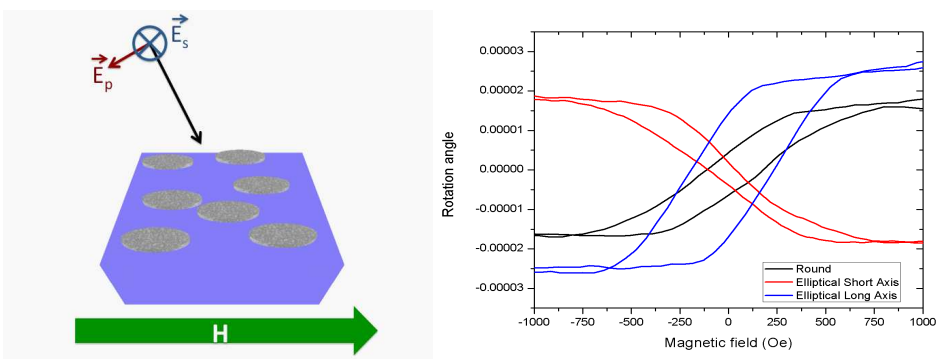

Figure 1: Schematic overview of the measurement configuration in L-MOKE (left) and magnetization loops measured with 800 nm wavelength along the different symmetry axis of round (170 nm) and elliptical (170/240 nm) particles in P-polarization.

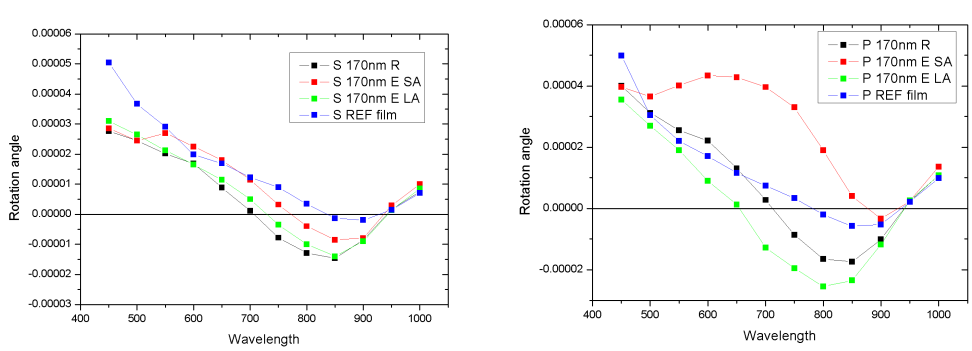

Figure 2: Spectroscopic dependence of the rotation angle in L-MOKE for P- and S-polarization and different sample orientation.

between the different particles we observe an increase (decrease) along the long (short) axis with respect to the values for round nanoparticles. Moreover, the particles also support 2 pronounced localized plasmon resonances along the 2 symmetry axes of the system, which adds one more degree of freedom that can be exploited to tailor the magnetoplasmonic response of the system.

For the different samples in S-polarization, the behavior looks very similar to what was observed before in round nanoparticles [1]. For P-polarization however, we observe that the Kerr rotation angle moves in the opposite direction (compared to a reference film) when the LSPR is excited along the short axis, which differs significantly from what we observed before in round nanoparticles or what is observed when the LSPR is excited along the long axis. As such, it turns out that breaking the symmetry of ferromagnetic nanoparticles offers us another degree of freedom to tune the Kerr rotation at will.

REFERENCES

1. Bonanni, V., et al., *Nano Lett.*, Vol. 11, 5333, 2011.

Refraction and Reflection of Surface Plasmon Polaritons with Parasitic Scattering Suppression

E. A. Bezus[1,2] **and L. L. Doskolovich**[1,2]

[1]Image Processing Systems Institute of the Russian Academy of Sciences, Samara 443001, Russia
[2]Technical Cybernetics Department, Samara State Aerospace University, Samara 443001, Russia

Abstract— Electromagnetic waves supported by the interfaces between metal and dielectric media (surface plasmon polaritons, SPP) have attracted a lot of interest during recent decades due to their potential applications in optical sensors, lithography and photovoltaics. Optical information processing at the nanoscale has been a key direction, where the use of SPP is especially promising [1]. While various types of dielectric plasmonic elements have been proposed, the efficiency of the most of them is dramatically affected by the parasitic scattering. Scattering losses typical for SPP diffraction on a dielectric block located directly on the propagation surface amount 30–50%. In our previous work [2], we have proposed a simple and efficient way for SPP scattering suppression using a two-layer dielectric structure made of isotropic materials. However, in [2], only normal incidence of the SPP has been considered.

In the present work, we extend the proposed approach for SPP scattering suppression to oblique SPP incidence. The results of numerical simulations based on the rigorous coupled-wave analysis technique demonstrate that the scattering losses can be decreased by an order-of-magnitude almost for all combinations of angle of incidence and structure length. Is is also shown that with the used scattering suppression approach, the SPP reflection and transmission coefficients can be well approximated by analytical expressions corresponding to the Fresnel formulas for an equivalent TE-polarized plane wave model. Applications of the proposed approach for the design of low-scattering plasmonic lenses and Bragg reflectors are discussed.

ACKNOWLEDGMENT

This work was financially supported by RFBR grants Nos. 12-07-00495, 13-07-00464, 12-07-33018, and 12-07-31116 and RF Presidential grant No. NSh-4128.2012.9.

REFERENCES

1. Gramotnev, D. K. and S. I. Bozhevolnyi, "Plasmonics beyond the diffraction limit," *Nature Photonics*, Vol. 4, 83–91, 2010.
2. Bezus, E. A., L. L. Doskolovich, and N. L. Kazanskiy, "Scattering suppression in plasmonic optics using a simple two-layer dielectric structure," *Appl. Phys. Lett.*, Vol. 98, 221108 (3pp), 2011.

Super-absorbing Plasmonic Metamaterials: From Visible to Mid-infrared

M. Lobet, O. Deparis, and L. Henrard
Laboratoire de Physique du Solide, Université de Namur
61 rue de Bruxelles, Namur B-5000, Belgium

Abstract— In recent years, the need for thin films structures that absorb electromagnetic radiation over a broadband spectrum has been shown to be paramount in solar harvesting for photovoltaic cells, thermal emitters or infrared detectors systems operating in 1–3 µm and in 3–5 µm atmospheric windows used for both civilian and military applications. Recently, Cui & al. [1] presented saw-toothed anisotropic metamaterials acting as thin film broadband absorbers in the infrared regime using alternating gold and dielectric layers. The full absorption normalized width at half the maximum was $\Delta\omega/\omega = 86\%$ over the 3 µm to 5.5 µm wavelength range.

In the present work, we design a metamaterial absorber (MMA) showing averaged absorptivity of $\overline{A} = 91.01\%$, over a much broader spectrum, between 200 nm and 6.5 µm. This MMA is made of a periodical array of truncated pyramids with a squared base disposed in air. The truncated pyramids deposited on a semi-infinite gold substrate consist of 20 layers a stratified medium with alternating Au (thickness $t_{\mathrm{Au}} = 15$ nm) and Ge (thickness $t_{\mathrm{Ge}} = 35$ nm) slices whose lateral side linearly reduces from $L = 600$ nm at the basis to $L = 150$ nm at the top of the pyramid. A stack of twenty layers is used in the present MMA resulting to a 1 µm high thin structure. The periodicity is set to 800 nm and, though Ge has a band gap at 0.67 eV, we consider it to be non dispersive ($\varepsilon_{\mathrm{Ge}} = 4$) while Au permittivity is described using tabulated data. Numerical results (Figure 1(a)) were obtained using a rigorous coupled-wave analysis (RCWA) method, which is perfectly suited for periodic systems. Since the gold substrate is semi-infinite, no transmission ($T = 0$) occurs, and the absorption (A) is directly deduced from reflectivity (R) calculations using $A = 1 - R$. We distinguish three parts in the absorption spectrum: a first part ranging from 200 nm to 2.6 µm (*UV*, *visible*, *NIR*, *MIR*) with an averaged absorption of $\overline{A_I} = 94.47\%$, a second part encompassing wavelengths between 2.6 µm and 4 µm (*MIR*) showing a weaker absorption of $\overline{A_{II}} = 85.38\%$ and, finally, a third part from 4 µm to 6.5 µm (*MIR*) with an absorption of $\overline{A_{III}} = 90.20\%$. The absorption mechanism is attributed to the excitation of localized surface plasmon (LSP) at the interface between metal and dielectric layers. Each layer of the pyramid contributes to several narrow absorption peaks and, since LSP are shape and size dependent, the associations of different sizes of the layers sum up constructively, boosting absorption in a broadband manner.

Modelling of the absorption of individual layers was conducted using a Discrete Dipole Approximation DDSCAT code and enabled to identify several modes optically active in individual systems. We identified several peaks in absorption spectra of square parallelepipeds of thickness

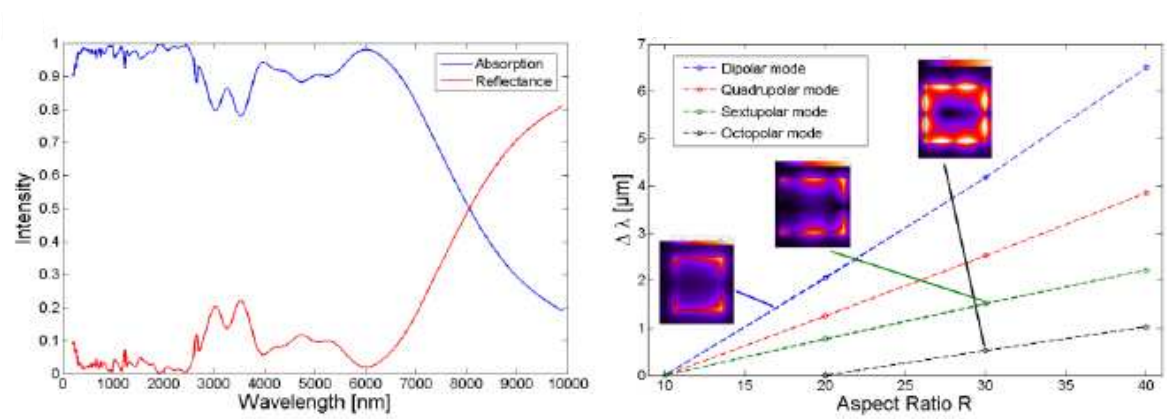

(a) (b)

Figure 1: (a) Absorption and reflection spectra of the proposed MMA obtained by RCWA method, (b) wavelength shift of plasmonic modes according to aspect ratio R of the slides of the MMA obtained by DDSCAT code. Insets: field maps of three modes.

$t_{\mathrm{Au}} = 15\,\mathrm{nm}$ and length $L = 15\,\mathrm{nm}$, $300\,\mathrm{nm}$, $450\,\mathrm{nm}$ and $600\,\mathrm{nm}$ embedded in a Ge dielectric medium. Those peaks correspond to dipolar, quadrupolar, sextupolar and octopolar modes, according to field map distributions. In Figure 1(b), we show the mode resonance wavelength shift $\Delta\lambda$ with respect to the resonance of the smallest system ($L = 150\,\mathrm{nm}$) as a function of the aspect ratio $R = L/t$. This proves that, when L increases, longer wavelengths are absorbed, which explains the broadband spectrum. A comparison with dispersion relations of laterally infinite Au film embedded in Ge host will be presented, in order to support the hypothesis of the size dependence of the LSP excitations. Additional simulations of square towers of alternating dielectric and metallic layers will be presented, in order to take into analyses the coupling effect between adjacent metallic layers. The ultra-broadband characteristics of the MMA, extending from visible to mid-IR ranges, give huge versatility for the design of various devices.

REFERENCES

1. Cui, Y., K. H. Fung, J. Xu, H. Ma, Y. Jin, S. He, and N. X. Fang, "Ultra broadband light absorption by a sawtooth anisotropic metamaterial slab," *Nano Lett.*, Vol. 12, 1443, 2012.

Direct Observation of Plasmon Enhanced Four Wave Mixing (FWM)

Po-Wen Tang, Wen-Hsiang Yu, and Chao-Yi Tai
Department of Optics and Photonics
National Central University, No. 300, Jhongda Rd., Jhongli 32001, Taiwan

Abstract— We demonstrate plasmon enhanced optical nonlinearities by multiplex four wave mixing (FWM) in gold thin films. The experimental setup is shown in Fig. 1(a). Light from a mode-locked Ti-sapphire laser operated at repetition rate of 80 MHz, pulse duration of 100 fs, and average power of 1 W passes through a beam splitter to split pulse into two parts. One acts as the pump, and the other one was used for pumping the photonic crystal fiber (PCF), generating a white light continuum (WLC) with pulse duration of ∼1 ps The WLC is filtered by a long pass filter ($\lambda_{LP} = 830$ nm) and is subsequently joined collinearly with the pump beam with the time delay scanned from -2.5 ps to $+2.5$ ps. The combined beam is then focused onto the gold film via a 100×, $NA = 1.25$ microscope objective, and the multiplexed FWM signal was collected using the same lens in the epi-direction. As shown in Fig. 1(b), the maximum intensity of the FWM lies around $\lambda = 610$ nm which is coincident to the plasmon resonance of Au. Beside, the bandwidth of the multiplexed FWM is equal to that of the pump as shown in Fig. 1(c). Since the spectrum of the WLC is very flat from $\lambda = 990$ nm to $\lambda = 1040$ nm, as shown in Fig. 1(c), the significant FWM generation at $\lambda = 610$ nm is attributed to the plasmon enhanced effect.

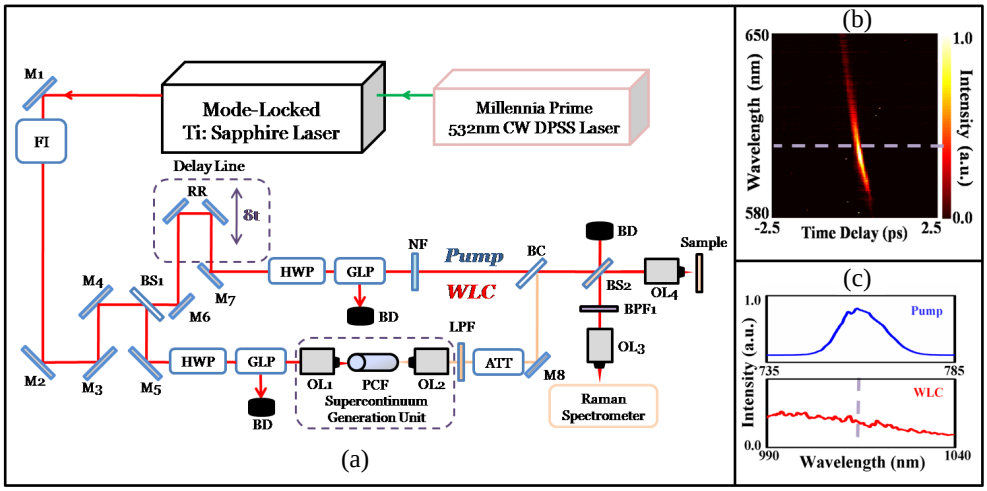

FI: Faraday Isolator, M: Mirror, BS: Beam Splitter, RR: Retro-Reflector, HWP: Half Wave Plate, GLP: Glan Laser Polarizer, BD: Beam Dump, NF: Notch Filter, LPF: Longpass Filter, BC: Beam Combiner, OL: Objective Lens, ATT: Attenuator, BPF: Bandpass Filter

Figure 1: (a) Experimental setup for FWM. (b) Intensity of FWM as functions of the time delay and wavelength. (c) Spectra of the pump and the WLC beams.

Session 4P3
SC2: Plasmonic Nanomaterials and Nanostrcutures for Photovoltaics and Optoelectronics in Energy 2

Comprehensive Study of Plasmonic Effects in Organic Solar Cells
Wei E. I. Sha, Wallace C. H. Choy, Weng Cho Chew, ... 1544
Plasmonic Harvesting of Solar Energy for Chemical Reactions
Jianfang Wang, ... 1545
Plasmonic Enhancement of Organic Optoelectronic Devices with Metallic Nanostructures
Jianxin Tang, ... 1546
Black Macroporous Silicon Film for Thin-silicon Photovoltaics
Xianyu Ao, Sailing He, ... 1547
Plasmonic Solar Cells beyond the Shockley-Queisser Limit
Krzysztof Kempa, F. Ye, M. J. Burns, M. J. Naughton, ... 1548
The Use of Metal Nanoparticles in Photovoltaic Junctions
Philipp Reineck, Udo Bach, ... 1549
Planar Heterojunction Small-molecule Organic Solar Cell with Plasmonic Anode Structure
Shun-Po Yang, Tien-Lung Chiu, Meng-Lin Tsai, Jr-Hau He, Jiun-Haw Lee, Chi-Feng Lin, ... 1550
Achieving 8% Efficiency Inverted Organic Solar Cells by Using Room-temperature Solution-process Ag Nanoparticles Doped Hole Transport Layer
Xinchen Li, Wallace C. H. Choy, Fengxian Xie, Shaoqing Zhang, Jianhui Hou, ... 1551
Encapsulated Au Nanorods Serving as Plasmonic Materials in Dye-sensitized Solar Cells
Shuai Chang, Tao Chen, ... 1552
Graphene Nanoantenna with Tunable Optical Properties
Xingang Ren, Wei E. I. Sha, Wallace C. H. Choy, ... 1553

Comprehensive Study of Plasmonic Effects in Organic Solar Cells

Wei E. I. Sha[1], **Wallace C. H. Choy**[1], **and Weng Cho Chew**[2]

[1]Department of Electrical and Electronic Engineering
The University of Hong Kong, Pokfulam Road, Hong Kong, China
[2]Department of Electrical and Computer Engineering
University of Illinois, Urbana-Champaign, Illinois, USA

Abstract— Environmentally friendly organic solar cell (OSC), which has a bright outlook to meet the urgent demand in clean energy, draws much attention in recent years due to their merits of large-area production, low-cost processing and mechanical flexibility. Proposing and optimizing new device architectures plays a key role in designing high-performance OSCs. Having unique features of tunable resonance and unprecedented near-field concentration, plasmon is an enabling technique for light manipulation and management. Introducing metallic nanostructures to OSCs can enhance the optical absorption of OSCs and shows a great potential to break the 10% efficiency barrier. We compressively studied plasmonic effects in OSCs based on a rigorous solution of Maxwell's equations and principle of wave physics. The optical response of OSCs incorporating metallic nanogratings, nanospheres, nanoprisms and their hybrids with different material composition and spatial position are investigated systematically. We employed finite-difference, integral equation and mode matching methods to simulate complicated 2D and 3D plasmonic OSC device structures and extracted important physical quantities, such as enhancement factor, total absorptivity, near-field distribution, scattering/absorption cross section, power flux, etc.. Based on our first-principle calculations, the versatile resonant mechanism involving Fabry-perot mode, quasi-guided mode, low and high-order plasmonic modes and mode hybridization are explored and manipulated for achieving broadband and angle insensitive optical absorption. Particularly, some misleading concepts or arguments are clarified by our rigorous models.

Moreover, we find that nonuniform distributions of optical near-fields induced by plasmonic nanostructures will significantly affect the carrier transport in OSCs. This is confirmed by our multiphysics model where Maxwell's equations and semiconductor equations (Poisson, drift-diffusion and continuity equations) are solved simultaneously with a unified finite-difference method. Besides their optical effects, the electrical effects induced by plasmonic resonances will open up a new way to design emerging plasmonic organic photovoltaics.

Plasmonic Harvesting of Solar Energy for Chemical Reactions

Jianfang Wang
Department of Physics, The Chinese University of Hong Kong, Shatin, Hong Kong SAR, China

Abstract— The efficient use of solar energy has received wide interests due to the increasing energy and environmental concerns. Besides the tremendous efforts made on improving the efficiencies of photovoltaic devices, the exploration of new harvesting means will also be essential. A potential means in chemistry is sunlight-driven catalytic reactions. Herein I report on the direct harvesting of light from the visible to near-infrared region for chemical reactions by use of plasmonic Au/Pd nanostructures, which serve simultaneously as an energy converter and a catalyst for Suzuki coupling reactions. The plasmonic excitation enables and accelerates the targeted catalytic reaction through pure-metal plasmonic photocatalysis and plasmonic photothermal heating. The intimate integration of the plasmonic energy converter and the catalyst facilitates the efficient light energy conversion and utilization. The effect of pure-metal plasmonic photocatalysis becomes more important when the incident light is at the plasmon resonance wavelength or the resonant incident light power is increased.

Plasmonic Enhancement of Organic Optoelectronic Devices with Metallic Nanostructures

Jianxin Tang
Institute of Functional Nano & Soft Materials (FUNSOM)
Soochow University, Suzhou 215123, China

Abstract— Organic optoelectronic devices, including organic light-emitting devices (OLEDs) and organic photovoltaic cells (OPVs) have been attracting considerable interest as next-generation lighting source and renewable energy applications. Significant progress on the device performance of OLEDs and OPVs with nearly 100% internal quantum efficiency has been made in recent years via the incorporation of new materials, morphology control, interface engineering, and device fabrication processes. However, further improvement in external quantum efficiency is still required for practical applications as a cost competitive and sustainable technology. Surface plasmonic effect induced by metallic nanostructures has been proposed to enhance light out-coupling in OLEDs and to enhance the photon absorption in OPVs, respectively. Here, we will introduce our recent advances in the plasmonic enhanced OLEDs and OPVs by using metallic nanostructures. An observable enhancement in electroluminescence is achieved by incorporating the synthesized Au nanoparticles (NPs) in the hole injection layer of OLEDs due to the Au NPs-generated plasmonic near-field enhancement. The increased light absorption and exciton generation rate in OPVs is demonstrated by blending the solution processable Au and Ag NPs into the anodic buffer layer, which can be ascribed to the near-field enhancement arising from the excitation of the localized surface plasmon resonance of NPs.

REFERENCES

1. Xiao, Y., J. P. Yang, P. P. Cheng, J. J. Zhu, Z. Q. Xu, Y. H. Deng, S. T. Lee, Y. Q. Li, and J. X. Tang, *Appl. Phys. Lett.*, Vol. 100, 013308, 2012.
2. Yang, J. P., Y. Xiao, Y. H. Deng, S. Duhm, N. Ueno, S. T. Lee, Y. Q. Li, and J. X. Tang, *Adv. Funct. Mater.*, Vol. 22, 600, 2012.
3. Cheng, P. P., G. F. Ma, J. Li, Y. Xiao, Z. Q. Xu, G. Q. Fan, Y. Q. Li, S. T. Lee, and J. X. Tang, *J. Mater. Chem.*, Vol. 22, 22781, 2012.
4. Fan, G. Q., Q. Q. Zhuo, J. J. Zhu, Z. Q. Xu, P. P. Cheng, Y. Q. Li, X. H. Sun, S. T. Lee, and J. X. Tang, *J. Mater. Chem.*, Vol. 22, 15614, 2012.

Black Macroporous Silicon Film for Thin-silicon Photovoltaics

Xianyu Ao[1] **and Sailing He**[1, 2]

[1]Centre for Optical and Electromagnetic Research, SCNU-ZJU Joint Research Center of Photonics
South China Academy of Advanced Optoelectronics, South China Normal University
Guangzhou 510006, China
[2]Department of Electromagnetic Engineering, School of Electrical Engineering
Royal Institute of Technology, SE-100 44 Stockholm, Sweden

Abstract— We present a viable scheme for antireflection and light-trapping in thin crystalline silicon (c-Si) solar cells. Such a scheme is demanding in order to improve the energy conversion efficiency and also reduce silicon material consumption [1, 2]. The salient feature of our scheme is that, the c-Si film itself and the antireflection/light-trapping structures are produced at the same time by means of low-cost wet etching ("one-step strategy"), rather than rely on a pre-prepared c-Si film, in contrast to previous publications. The film, called "modulated macroporous silicon film", with nano/micro-hybrid multiscale texture, has very high absorptance and short-circuit current density (close to the Yablonovitch limit [2]), and much better performance and smaller surface area, than a pure nano-hole silicon film studied previously [1]. Small surface area is important in order to ensure that a nano- or micro-structure would really improve the efficiency of a solar cell, as the enhancement in optical absorption should overwhelm the increase in surface recombination loss. We also compared our result with a very recent result [2], i.e., a solid film with optimized nanocone gratings on both surfaces, and showed that our porous film has better light trapping capability in the near infrared region and thus overall higher short-circuit current density.

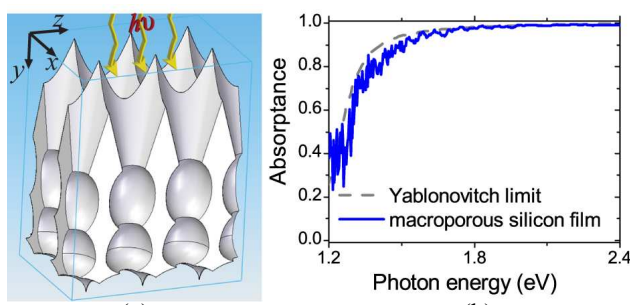

(a) (b)

Figure 1: (a) Schematic drawing of the modulated macroporous silicon film, consisting of truncated cones and ellipsoids of air in a silicon film. The pores were arranged in a square pattern with a lattice constant of 2 µm. The pore shape is chosen to mimic a structure we fabricated. (b) Calculated absorption of the macroporous silicon film and the Yablonovitch limit with the equivalent silicon thickness.

REFERENCES

1. Han, S. E. and G. Chen, "Optical absorption enhancement in silicon nanohole arrays for solar photovoltaics," *Nano Letters*, Vol. 10, 1012–1015, 2010.
2. Wang, K. X., Z. Yu, V. Liu, Y. Cui, and S. Fan, "Absorption enhancement in ultrathin crystalline silicon solar cells with antireflection and light-trapping nanocone gratings," *Nano Letters*, Vol. 12, 1616–1619, 2012.

Plasmonic Solar Cells beyond the Shockley-Queisser Limit

K. Kempa, F. Ye, M. J. Burns, and M. J. Naughton
Boston College, USA

Abstract— We show that by combining two metamaterial effects, resonant light trapping and plasmonic protection of hot electron energy, solar cells with efficiencies well beyond the Shockley-Queisser limit can be produced. The first effect employs distributed subwavelength metallic nanopatterns embedded in the volume or on the surface of an ultrathin absorber. The metamaterial and plasmonic actions of the nanopatterns dramatically increase absorbance of light in ultrathin absorbers, over a broad frequency band. Preliminary results (simulations plus experiments) on near-field scattering-enhanced optical absorption using embedded metallic nanopatterns suggest the ability to increase the efficiency of ultrathin PV cells using CdTe by $\sim 80\%$, and CIGS, *a*-Si and *a*-SiGe cells by $\sim 60\%$. The second effect employs another similar metamaterial/plasmonic micropattern on the surface of an ultrathin solar cell, acting as a plasmonic reservoir, where plasmonic resonance can be tuned to match that of characteristic hot electron energies. Resonant energy transfer from those hot electrons into plasmons of the array can then occur, on time scales faster than irreversible phonon emission. Since plasmon-phonon and plasmon-photon scattering processes can be relatively slow in such structures, this could provide a "plasmonic protection" mechanism for the excess free energy of the excited hot electrons. Our simulations show that the protected energy could maintains available about 5 times longer in the collective, plasmonic electronic form, before dissipating into heat. This may be sufficient to collect significant numbers of hot carriers in ultrathin solar cells since, as we've recently shown, such cells already collect a small fraction of hot electrons even without plasmonic protection. By combining the two above schemes, solar cells with efficiencies well beyond the Shockley-Queisser limit could be developed.

The Use of Metal Nanoparticles in Photovoltaic Junctions

Philipp Reineck[1] **and Udo Bach**[1, 2, 3]

[1]Department of Materials Engineering, Faculty of Engineering
Monash University, Clayton, Victoria 3800, Australia
[2]Commonwealth Scientific and Industrial Research Organization
Materials Science and Engineering, Clayton South, Victoria 3169, Australia
[3]The Melbourne Centre for Nanofabrication
151 Wellington Road, Clayton, Victoria 3168, Australia

Abstract— We observed that gold and silver nanoparticles located at the interface between TiO_2 and an organic charge transport material generate sustainable photocurrents upon excitation of the particles' localized surface plasmon resonance. The photocurrent response closely follows the plasmonic absorption characteristics of the nanoparticles. We introduce a simple method for the electrostatic self-assembly of metal nanoparticles allowing for the controlled creation of dense nanoparticle monolayers with well-defined interparticle separations. Absorbed photon-to-electron conversion efficiencies of up to 15% were observed with these metal nanoparticle sensitized flat heterojunctions. Three mechanisms for surface plasmon resonance based charge carrier separation are proposed and discussed. In the second part of this talk we will describe a detailed study of energy transfer phenomena between metal nanoparticles and organic chromophores in a colloidal model system. This energy transfer potentially enables the use of metal nanoparticles as 'light harvesting antennas' in photovoltaic devices. We study the distance and wavelength dependence of fluorescence quenching via steady state and time-resolved fluorescence spectroscopy. The results are compared to predictions derived from electrodynamic theory.

Planar Heterojunction Small-molecule Organic Solar Cell with Plasmonic Anode Structure

Shun-Po Yang[1], **Tien-Lung Chiu**[1], **Meng-Lin Tsai**[2], **Jr-Hau He**[2], **Jiun-Haw Lee**[2], **and Chi-Feng Lin**[3]

[1]Department of Photonics Engineering, Yuan Ze University, Chung-Li, Taiwan
[2]Graduate Institute of Photonics and Optoelectronics
Department of Electrical Engineering, National Taiwan University, Taipei, Taiwan
[3]Department of Electro-Optical Engineering
National United University, Miaoli 36003, Taiwan

Abstract— In this paper, we demonstrate an organic solar cell (OSC) based on planar heterojunction small molecule organic materials with plasmonic anode structure exhibiting improved short circuit current (Jsc) and power conversion efficiency. Compared with mixed or bulk-heterojunction OSC, planar heterojunction device exhibits fewer donor-acceptor interfaces which has the potential for boosting up open circuit voltage (Voc). Besides, carrier recombination and trapping are suppressed in planar heterojunction structure which is beneficial to obtain high fill factor (FF). However, on the other hand, thin donor and acceptor layers are required to efficiently dissociate the excitons which limits the light absorption in a heterojunction OSC. To improve light absorption in such a thin film structure, we fabricated 2-D Ag grating structure on the top of the indium-tin-oxide (ITO) anode. ITO/Ag mixed anode was treated with UV ozone for 30 sec to: (1) clean the anode surface, (2) improve the workfunction of ITO, and (3) form AgOx for better hole-extraction capability. Then, PEDOT : PSS was spun on the anode surface to improve the hole conduction and partially relief the corrugation structure. Donor and acceptor materials were chloroaluminium phthalocyanine (ClAlPc) and C60, respectively, with the thicknesses of 20 and 40 nm. 7-nm bathocuproine (BCP) and 100-nm Ag were then deposited sequentially as the exciton blocking layer and cathode. A significant enhancement was observed in Jsc of our plasmonic OSC compared to conventional ITO-based device, while Voc and FF were nearly the same. From external quantum efficiency spectrum, the improvement was at 400–500 nm, which was designed for the plasmonic resonant absorption.

Achieving 8% Efficiency Inverted Organic Solar Cells by Using Room-temperature Solution-process Ag Nanoparticles Doped Hole Transport Layer

Xinchen Li[1], **Wallace C. H. Choy**[1], **Fengxian Xie**[1], **Shaoqing Zhang**[2], **and Jianhui Hou**[2]

[1]Department of Electrical and Electronic Engineering
The University of Hong Kong, Pokfulam Road, Hong Kong, China
[2]Institute of Chemistry, Chinese Academy of Sciences, Beijing 100190, China

Abstract— While metal oxide interfacial layers are typically formed by high-temperature and sputtering deposited processes, we report a new approach with the features of room-temperature, water-free and solution-based process for forming molybdenum oxide (MoO_x) hole transporting interfacial layer of inverted organic solar cells (OSCs) by proposing vacuum treatment at room temperature and selecting appropriate solvent. Remarkably, our results and analysis of the ultraviolet photoelectron spectroscopy (UPS) measurement and high-resolution X-ray photoelectron spectroscopy (XPS) measurement indicate that the vacuum treatment can introduce oxygen vacancies in the molybdenum oxide interfacial layer and modify its work function for functioning as an efficient hole transporting layer. The performances of inverted OSCs using this room-temperature solution-process MoO_x as hole transporting layer have comparable performance with the commonly used thermal evaporated molybdenum oxide film in OSCs. To further improve the performances of inverted OSCs and the hole transporting layer, silver nanoparticle-molybdenum oxide (Ag NP-MoO_x) composite film is demonstrated by the introduction of Ag nanoparticles in the solution. Evidences and explanations of wideband enhancement of incident photon to converted electron (IPCE), hole dominated devices and transient photo-generated voltage (TPV) measurement, confirm that OSCs performance enhancement is mainly due to the improvement of the electrical properties of Ag NP-MoO_x composite film. Moreover, inverted OSCs with high power conversion efficiency (PCE) of 7.94% are achieved with this composite hole transporting interfacial layer. Through the demonstration of highly efficient inverted OSCs with different polymer materials, the water-free, room-temperature and solution-processed MoO_x can contribute to the evolution of high performance OSCs such as inverted and tandem OSCs and other optoelectronic devices.

Encapsulated Au Nanorods Serving as Plasmonic Materials in Dye-sensitized Solar Cells

Shuai Chang and Tao Chen
Department of Physics, The Chinese University of Hong Kong, Shatin, Hong Kong SAR, China

Abstract— Dye-sensitized solar cells (DSSCs) have attracted increasing interest primarily due to its easy fabrication and reasonably high solar-to-electric power conversion efficiency. Extending the response of dye sensitizers to a broader range of the solar spectrum is a key step in further improving the device efficiency. However, so far there is no dye possessing high extinction coefficient in the range from full visible to near-infrared.

Noble metal nanocrystals have demonstrated strong ability in light engineering. Surface plasmon resonance (SPR) of metal nanocrystals can effectively trap light to increase sunlight utility in solar cells. The use of plasmonic effect for light trapping can be an efficient way to make full use of the dyes and explore the new possibilities of achievable efficiency. Here, we present a method for implementing plasmon effect of Au nanorods (NRs) into DSSCs.

By proper incorporation of Ag_2S-encapsulated AuNRs into a TiO_2 based photoanode, photocurrent generation at longer wavelengths (600–720 nm) can be enhanced by 37.6% [1]. Our results clearly indicate that AuNRs can effectively improve the low energy sunlight harvesting in DSSCs. Since most of the conventional dyes or quantum dots show rapidly decreased absorption coefficients at longer wavelengths, we can envisage that the use of plasmon induced light trapping would find wide applications in enhancing solar spectrum response of the solar cells.

REFERENCES

1. Chang S, Q. Li, X. Xiao, K. Y. Wong, and T. Chen, "Enhancement of low energy sunlight harvesting in dye-sensitized solar cells using plasmonic gold nanorods," *Energy & Environ. Sci.*, 9444–9448, 2012.

Graphene Nanoantenna with Tunable Optical Properties

Xingang Ren, **Wei E. I. Sha**, **and Wallace C. H. Choy**
Department of Electrical and Electronic Engineering, The University of Hong Kong
Pokfulam Road, Hong Kong, China

Abstract— Nanoantennas play a fundamental role in the nanotechnology due to their capabilities to confine and enhance the light through converting the localized fields to propagating electromagnetic fields, and vice versa. The characteristics of nanoantennas can be modified by carefully designing the geometric size and shape as well as choosing different materials of nanoantennas. However, the features cannot be dynamically tuned once the nanoantenna is fabricated. In the literatures, the pristine graphene has been used as a transparent electrode due to the properties of high optical transmittance and electrical conductivity. Meanwhile, due to the forbidden interband transitions by the Pauli blocking, the chemically or electrostatically doped graphene can support strong plasmonic effects particularly at the far-infrared or terahertz regime. These capabilities of dynamically modifying chemical potentials enable to fabricate controllable devices by introducing the graphene sheet.

Here we propose to utilize tunable properties of the doped graphene sheet to achieve a controllable nanoantenna. The conceptual architecture comprises a gold (Au) dipole antenna composed of two Au arms separated by a feed gap, a graphene sheet, and an aluminum oxide (Al_2O_3) as the insulator inserted between the dipole antenna and graphene. The thickness of the insulator is chosen as 12 nm so that electrical (quantum) tunneling effect from the graphene to metal can be ignored. The dispersion relation of the graphene sheet on the insulator with tunable chemical potential is investigated to demonstrate the possibility of the mode couplings between the graphene sheet and the metallic nanoantenna, which is further confirmed by the rigorous numerical simulation. Interestingly, our results show that the in-phase and out-of-phase couplings between metallic plasmonics and graphene plasmonics not only split the single resonance frequency of the convectional metallic dipole antenna but also modify the near-field and far-field responses of the metal-graphene nanoantenna. Furthermore, the bandwidth of full width at half maximum (FWHM) modified by the graphene sheet is enhanced by 17.1%. In addition, the far-field radiation intensity is drastically reduced by 50% due to the optical absorption induced through the graphene plasmonics. The most important property of the metal-graphene hybrid nanoantenna lies at its tunable or switch on/off feature. We show that the low resonant peak of the two split frequencies can be dynamically tunable through increasing the chemical potential. Especially, the hybrid nanoantenna can be restored to the conventional metallic dipole antenna by simply employing an intrinsic graphene or electrostatically tuning the chemical potential of graphene. This work is of a great help to design high-performance electrically-tunable nanoantennas applicable both in nano-optics and nano-electronics fields.

Session 4P4
SC2: Plasmonics beyond the Common Local-response Approximation

Ab Initio Plasmonics: Beyond Classical Local Electromagnetic Theory
Peter Nordlander, ... 1556
Quantum Plasmonics from First Principles
Kristian Sommer Thygesen, ... 1557
Hybrid Quantum/Classical Calculations by Real-time Classical Electrodynamics and Time-dependent Density Functional Theory
Arto Sakko, T. Rossi, R. M. Nieminen, ... 1558
Performance of Non-local Optics When Applied to Plasmonic Nanostructures
Lorenzo Stella, Pu Zhang, Francisco J. Garcia-Vidal, Angel Rubio, Pablo Garcia-Gonzalez, ... 1559
Robust Subnanometric Plasmon Ruler by Rescaling of the Non-local Optical Response
T. V. Teperik, Peter Nordlander, A. G. Borisov, Javier Aizpurua, ... 1560
Spatial Dispersion in Plasmonics and Metamaterials
Pavel Ginzburg, Viktor A. Podolskiy, Anatoly V. Zayats, ... 1561
Nanoplasmonics: Hydrodynamic Approach to Nonlocal Response
Martijn Wubs, N. Asger Mortensen, ... 1562
Inclusion of Nonlocal Effects in the Hydrodynamic Description of Metal Surfaces with Smooth Density Profiles
Christin David, F. Javier Garcia de Abajo, ... 1563
The Impact of Plasmonic Nonlocality on Field Enhancement
Cristian Ciraci, David R. Smith, ... 1564
Nonlocal Effects in Three-dimensional Nanoplasmonic Devices
Antonio I. Fernandez-Dominguez, ... 1565
Nonlocal Response in Waveguides
Soren Raza, Thomas Christensen, Martijn Wubs, Sergey I. Bozhevolnyi, N. Asger Mortensen, ... 1566
Nonlocal Effects in a Hybrid Plasmonic Waveguide for Nanoscale Confinement
Qiangsheng Huang, Fanglin Bao, Sailing He, ... 1567
Nonlocal Response in Plasmonic Waveguiding
Giuseppe Toscano, ... 1568
Perfect Imaging and ENZ Phenomena for Metallic Slabs in the Scope of Nonlocal Effects
Christin David, Niels Asger Mortensen, J. Christensen, ... 1569

Ab Initio Plasmonics: Beyond Classical Local Electromagnetic Theory

Peter Nordlander
Laboratory for Nanophotonics, Department of Physics and Astronomy
Rice University, Houston TX77251, USA

Abstract— An *ab initio*quantum mechanical approach for the description of plasmonic and excitonic nanoparticles and their interactions with light has been developed [1, 2]. Quantum effects can have a pronounced influence on the electric field enhancements near the nanoparticle surfaces and on the optical properties of nanoparticles. For closely spaced metallic nanoparticles, electron tunneling can result in a charge transfer plasmon where oscillatory electric tunneling current flows between the particles nanoparticles and give rise to new spectral features and a significantly reduced electric field enhancement [3, 4]. Nonlocal effects introduced by the spill out of the plasmon induced surface charges can significantly reduce the field enhancements near a nanoparticle surface [5]. Quantum mechanical effects can introduce a strong nonlinear optical response of a nanoparticle dimer [6] and enhance the coupling to molecules in the junction [7–9]. For the coupled plasmonic-excitonic system where hybrid plexciton states are formed, quantum effects can induce highly nonlinear optical response [10, 11].

REFERENCES

1. Prodan, E. and P. Nordlander, *Nano Lett.*, Vol. 3, 543, 2003.
2. Prodan, E. and P. Nordlander, *Nano Lett.*, Vol. 3, 1411, 2003.
3. Zuloaga, J., et al., *Nano Lett.*, Vol. 9, 887, 2009.
4. Esteban, R., et al., *Nat. Comm.*, Vol. 3, 825, 2012.
5. Zuloaga, J., et al., *ACS Nano*, Vol. 4, 5269, 2010.
6. Marinica, D. C., et al., *Nano Lett.*, Vol. 12, 1333, 2012.
7. Song, P., et al., *J. Chem. Phys.*, Vol. 134, 074701, 2011.
8. Song, P., et al., *Phys. Rev. B*, Vol. 86, 121410, 2012.
9. Thongrattanasiri, S., et al., *Laser Phot. & Rev.*, 2013, 10.1002/lpor.201200101.
10. Manjavacas, A., et al., *Nano Lett.*, Vol. 11, 2318, 2011.
11. Manjavacas, A., et al., *ACS Nano*, Vol. 6, 1724, 2012.

Quantum Plasmonics from First Principles

Kristian S. Thygesen
Center for Atomic-scale Materials Design (CAMD) and Center for Nanostructured Graphene (CNG)
Department of Physics, Technical University of Denmark
Fysikvej 1, 2800 Kgs. Lyngby, Denmark

Abstract— When the size of a plasmonic structure reaches the nano-scale, quantum effects begin to play a dominant role and the widely used classical models of electronic response break down. To explore the role of these effects on the energy, life time, and spatial shape of the plasmons and to identify the range of validity of the classical models, we have applied linear response time-dependent density functional theory (TDDFT) to obtain the plasmon eigenmodes of different types of metallic nanostructures including metallic thin films, freestanding nanowires and coupled nanowire dimers. The quantum plasmon modes are computed as the eigenstates of the non-local and frequency dependent dielectric matrix corresponding to zero eigenvalues [1]. This method provides a real-space visualization of the plasmon modes, and includes quantum mechanical effects such as electron spill-out, quantum confinement, surface scattering, coupling to single-particle transitions, and non-local response. In general we find that for simple metals, quantum confinement and the effect of spill out leads to a red shift of the plasmon energies for smaller structures. This is contradictory to observations for silver nanoparticles where a blue shift was observed, and indicates the importance of interband transitions for plasmons in noble metals. For two structures in close proximity, electron tunneling is found found to influence the energy and shape of the hybridized plasmon modes for distances below $\sim 1.5\,\mathrm{nm}$, and leads to the formation of a new charge transfer plasmon around 2Å separation. If time allows, I will present TDDFT calculations for the conventional and acoustic surface plasmons on the noble metal surfaces Au(111), Ag(111), and Cu(111). These calculations clearly demonstrate the important role of screening arising from interband transitions between the occupied d-band and the free electron s-band.

REFERENCES

1. Andersen, K., K. W. Jacobsen, and K. S. Thygesen, "Spatially resolved quantum plasmon modes in metallic nano-films from first principles," *Phys. Rev. B*, Vol. 86, 245129, 2012.
2. Yan, J., K. W. Jacobsen, and K. S. Thygesen, "Conventional and acoustic surface plasmons on noble metal surfaces: A time-dependent density functional theory study," *Phys. Rev. B*, Vol. 86, 241404(R), 2012.

Hybrid Quantum/Classical Calculations by Real-time Classical Electrodynamics and Time-dependent Density Functional Theory

A. Sakko, **T. Rossi**, **and R. M. Nieminen**
COMP Centre of Excellence, Department of Applied Physics, Aalto University, Finland

Abstract— Failure of classical electrodynamics in describing the optical properties of sub-nm scale structures has led to an increasing interest in extending quantum mechanical simulations for nano-photonic applications. For instance, recent works have demonstrated the need for electronic structure calculations in simulating nanoscale plasmonics [1]. Another example is the electrodynamical coupling between sharp metal structures and nearby molecules (as realized in, e.g., surface-enhanced Raman scattering), whose accurate simulation requires quantum mechanical treatment of at least the molecule. Unfortunately, the combination of different length scales often hinders such simulations: the molecular part requires sophisticated electronic structure calculations, but the present day computational power is not sufficient for treating the whole complex quantum mechanically. Therefore development and evaluation of novel multiscale methods for combining quantum and classical simulations is required.

In this work we present hybrid quantum/classical simulations for the optical properties of realistic nano-plasmonic materials. The method is based on simulating the real-time evolution of the charge density that contains both classical and quantum mechanical contributions. The classical charge density is propagated using a recently introduced method, which neglects the propagating transverse solutions of the Maxwell equations [2, 3]. The quantum mechanical charge density is treated by the time-dependent density functional theory. We present calculations for quantum mechanically treated molecules that are adsorbed on classically treated metal nanoparticles. We compare our results with previous calculations and experimental data. We discuss the theoretical background of the scheme and describe its implementation in an electronic structure calculation code. We also discuss the limitations and possible applications of the method.

REFERENCES

1. Morton, S. M., D. W. Silverstein, and L. Jensen, "Theoretical studies of plasmonics using electronic structure methods," *Chem. Rev.*, Vol. 111, No. 6, 3962–94, 2011.
2. Coomar, A., C. Arntsen, K. Lopata, S. Pistinner, and D. Neuhauser, "Near-field: A finite-difference time-dependent method for simulation of electrodynamics on small scales," *J. Chem. Phys.*, Vol. 135, No. 8, 084121, 2011.
3. Gao, Y. and D. Neuhauser, "Dynamical quantum-electrodynamics embedding: Combining time-dependent density functional theory and the near-field method," *J. Chem. Phys.*, Vol. 137, No. 7, 074113, 2012.

Performance of Non-local Optics When Applied to Plasmonic Nanostructures

Lorenzo Stella[1, 2], **Pu Zhang**[3], **F. J. García Vidal**[3], **Angel Rubio**[1], **and Pablo García-González**[3]

[1]Nano-Bio Spectroscopy Group, Universidad del País Vasco, San Sebastian, Spain
[2]Department of Physics, King's College London, United Kingdom
[3]Departamento de Física Teórica de la Materia Condensada
Universidad Autónoma de Madrid, Spain

Abstract— The resonant interaction of light with metallic nanostructures is dominated by the appearance of surface plasmons. As a result, the induced electromagnetic near-field can be concentrated and enhanced in regions that are much smaller than the wave length of the incident field. This is the basis of a number of present and prosprective applications in the emerging field of nanoplasmonics. Therefore, there is a clear need for accurate theoretical tools able to predict optical properties of complex nanoplasmonic devices.

The main characteristics of a plasmon (frequency and lifetime) depend very sensitively on a delicate interplay between the geometrical details and the optical properties of a given nanostructure. Thus, time-dependent density functional theory (TDDFT) emerges as the method of choice to perform a full quantum description of collective excitations in metals. However, the range of application of TDDFT is limited by the size of the system under study. Then, simplified tools such a non-local optics based on the hydrodynamic approximation emerge as a promising alternative able to provide results with enough predictive accuracy at a much lower computational cost.

With the aim of confirming this idea, we obtain the non-local optical absorption spectra and the induced near-field in a model nanoplasmonic device (two metallic nanowires) in which there are spatial gaps between the components at nanometric and sub-nanometric scales. After a comparison against TDDFT calculations, we conclude that hydrodynamic non-local optics provides absorption spectra exhibiting qualitative agreement but not quantitative accuracy. This lack of accuracy, which is manifest even in the limit where induced electric currents are not established between the constituents of the device, is mainly due to the poor description of induced electron densities.

Robust Subnanometric Plasmon Ruler by Rescaling of the Non-local Optical Response

T. V. Teperik[1], **P. Nordlander**[2], **A. G. Borisov**[3], **and J. Aizpurua**[4]

[1]Institut d'Electronique Fondamentale
UMR 8622 CNRS — Université Paris-Sud, Bâtiment 220, Orsay Cedex 91405, France
[2]Laboratory for Nanophotonics, Department of Physics and Astronomy, M.S. 61
Rice University, Houston, Texas 77251-1892, USA
[3]Institut des Sciences Moléculaires d'Orsay
UMR 8214 CNRS — Université Paris-Sud, Bâtiment 351, Orsay Cedex 91405, France
[4]Material Physics Center CSIC-UPV/EHU and Donostia International Physics Center, DIPC
Paseo Manuel de Lardizabal 5 20018, Donostia-San Sebastían, Spain

Abstract— We present the optical response of two large interacting metallic wires within local and nonlocal approaches. A full quantum mechanical calculation within a time-dependent density functional theory (TDDFT) gives exact account of nonlocal and tunneling effects as the wires approach down to subnanometric separation distances. A comparison with a nonlocal response based on a hydrodynamical model shows the limitations of the latter. Most importantly, we find that the full nonlocal quantum mechanical results are equivalent to those from classical approaches when the separation between the surfaces is rescaled to the distance between the centroids of the induced charges at the interfaces. This establishes a plasmon ruler for subnanometric distances universally valid once this rescaling is adopted within each model. Such a ruler not only impacts the basis of many applications of plasmonics, but also establishes a robust rule of thumb for subnanometric metrology.

Spatial Dispersion in Plasmonics and Metamaterials

Pavel Ginzburg[1], **Viktor A. Podolskiy**[2], **and Anatoly V. Zayats**[1]

[1]Department of Physics, King's College London, UK
[2]Department of Physics and Applied Physics, University of Massachusetts Lowell, USA

Abstract— Nonlocal optical response of materials, important at the nanometric scale, influences numerous fundamental phenomena, such as electromagnetic field confinement and spectral characteristics of plasmonic nanoparticles and their composites (metamaterials).

Recently, various nanostructured media have been used to control light-matter interaction and to achieve and design advanced nanophotonic functionalities, such as functionalized surfaces and films, metamaterials [1] and transformation-optics designs [2]. In many cases, nanostructured media are inherently spatially dispersive, due to either nonlocal response of material components [3] or from collective response of strongly coupled objects [4, 5]. The material contribution could be in turn approximately subdivided in classical nonlocality due to collective electronic effects and quantum one due to finite size of the electron wavefunction [6].

In this paper we will give a review on recent investigations on optical nonlocalities in nanophotonic structures. While the significant attention has been paid to the 'hydrodynamic model' [7], as it provide sufficient modelling tool for some experimental demonstrations of nonlocality signatures, we will present comprehensive classification of nonlocal phenomena, in order to make an attempt to unify the nonlocalities within the universal yet phenomenological model.

ACKNOWLEDGMENT

This work has been supported in part by ERC, EPSRC (UK) and US Army Research Office (grant #W911-NF-12-1-0533). PG acknowledges the Royal Society for the Newton International Fellowship.

REFERENCES

1. Cai, W. and V. M. Shalaev, *Optical Metamaterials: Fundamentals and Applications*, Springer, 2010.
2. Pendry, J. B., D. Schurig, and D. R. Smith, "Controlling electromagnetic fields," *Science*, Vol. 312, 1780, 2006.
3. Agranovich, V. M. and V. L. Ginzburg, *Spatial Dispersion in Crystal Optics*, Springer-Verlag, 1984.
4. Belov, P. A., R. Marques, S. I. Maslovski, I. S. Nefedov, M. Silverinha, C. R. Simovski, and S. A. Tretyakov, "Strong spatial dispersion in wire media in the very large wavelength limit," *Phys. Rev. B*, Vol. 67, 113103, 2003.
5. Pollard, R. J., A. Murphy, W. R. Hendren, P. R. Evans, R. Atkinson, G. A. Wurtz, A. V. Zayats, and V. A. Podolskiy, "Optical nonlocalities and additional waves in epsilon-near-zero metamaterials," *Phys. Rev. Lett.*, Vol. 102, 127405, 2009.
6. Ginzburg, P. and A. V. Zayats, "Localized surface plasmon resonances in spatially dispersive nano-objects," submited to *ACS Nano*.
7. Raza, S., G. Toscano, A. Jauho, M. Wubs, and N. A. Mortensen, "Unusual resonances in nanoplasmonic structures due to nonlocal response," *Phys. Rev. B*, Vol. 84, 121412(R), 2011.

Nanoplasmonics: Hydrodynamic Approach to Nonlocal Response

Martijn Wubs and N. Asger Mortensen
Departments of Photonics Engineering, Technical University of Denmark, Denmark

Abstract— Nanoplasmonic structures may exhibit nonlocal response when shrinking their critical dimensions to a regime where quantum phenomena are commonly expected to become important. This talk will address a semi-classical hydrodynamic description as a first natural attempt that goes beyond the common description based on the local-response approximation, i.e., Ohm's law. Including the hydrodynamic response of the Fermi gas adds an intrinsic length scale to the electrodynamics, thus smearing the possible development of singular response inherent to a local-response approximation. In contrast to insight from the local-response approximation, transverse-light excitation may also exhibit oscillations above the plasma frequency with a longitudinal nature, i.e., bulk-like plasmons. Starting from a generalized nonlocal wave equation, consequences for plasmonic structures supporting enhanced light-matter interactions will be discussed.

Inclusion of Nonlocal Effects in the Hydrodynamic Description of Metal Surfaces with Smooth Density Profiles

C. David and F. J. García de Abajo
Instituto de Química-Física Rocasolano, Consejo Superior de Investigaciones Científcas, Spain

Abstract— We demonstrate that a hydrodynamic description of the electron gas can reasonably well describe the nonlocal effects that arise from collective electron quantum interactions in plasmonic metal surfaces and narrow gaps between metals including the spill out of valence electrons.

We extend the hydrodynamic model to describe metal surfaces with a smoothly changing conduction electron density and an abrupt jellium edge. By choosing densities and a dielectric background corresponding to simple metals and transition metals, we are capable of reproducing experimentally determined plasmon redshifts in simple metals and plasmon blueshifts in noble metals. Systems involving small gaps display a regime of tunnelling electrons, which is partially captured in the classical picture by overlapping electron densities.

We apply our method to planar structures and cylinders, which allows us to describe charge-transfer plasmons (CTPs) and other nonlocal effects.

The Impact of Plasmonic Nonlocality on Field Enhancement

C. Ciracì and D. R. Smith
Center for Metamaterials and Integrated Plasmonics
Department of Electrical and Computer Engineering
Duke University, Durham NC 27708, USA

Abstract— Plasmonic nanoparticles can convert optical radiation into deeply sub-wavelength-localized fields. As light is squeezed into sub-wavelength regions, the field spatial variation is no longer defined by the wavelength of the radiation, but rather by the ability of plasmonic structures to harvest and concentrate the electromagnetic radiation. In such systems, the impact of quantum nature of the electrons of the metal becomes important, placing strict bounds on the ultimate field enhancement [1]. We investigate the properties of plasmon resonant nanoparticles separated by a dielectric nanometric spacer from a metallic film. When a nanoparticle is brought in close proximity to a metallic film, it couples to its electromagnetic image, exhibiting a strong optical spectral shift that increases with decreasing distance to the film. The film-coupled nanoparticle system provides a precise and robust platform for producing surfaces with controlled reflectance properties [2]. Alternatively this spectral shift can be related to the dielectric function of the metal, and thus it can be used as a signature, providing information on the material properties. As the gap between film and nanoparticle is closed, the local field enhancement rises dramatically, accompanied by an increasing red-shift in the plasmon resonance. Structures that are singular in some sense, such as spheres touching at a point, have been predicted to produce unbounded field enhancements, based on a simple Drude-Lorentz model of the metal [3]. The singular behavior, of course, indicates the failure of the conventional model for the response of the conduction electrons of a metal, which ignores effects due to the quantum nature of the electrons. In this context, we show that the hydrodynamic model of electron response in metals is a valuable tool that can generate accurate predictions and can be easily incorporated into computational techniques [4]. The hydrodynamic model includes a quantum pressure term, which introduces spatial derivatives into the equation of motion for the electrons; the electronic response acquires a nonlocal character that becomes increasingly important as light is increasingly confined to sub-nanometer regions. To confirm the applicability of this model, we correlate the spectral shifts in numerically simulated film-coupled plasmonic nanoparticles with the nonlocality of the conduction electron response. Though the hydrodynamic model is likely an incomplete description of the electron response [1], it nevertheless provides a quantitative prediction for the spectral shifts as a function of gap distance that is in remarkable agreement with experiments [5, 6]. For devices that depend on the field enhancement of plasmonic systems, the nonlocal response of the metal will likely represent the ultimate limitation to the device performance.

REFERENCES

1. Zuloaga, J., E. Prodan, and P. Nordlander, "Quantum description of the plasmon resonances of a nanoparticle dimer," *Nano Letters*, Vol. 9, 887–891, 2009.
2. Moreau, A., C. Ciracì, J. J. Mock, R. T. Hill, Q. Wang, B. Wiley, A. Chilkoti, and D. R. Smith, "Controlled-reflectance surfaces with film-coupled colloidal nanoantennas," *Nature*, Vol. 492, 86–89, 2012.
3. Fernández-Domínguez, A. I., S. A. Maier, and J. B. Pendry, "Collection and concentration of light by touching spheres: A transformation optics approach," *Physical Review Letters*, Vol. 105, No. 26, 266807, 2010.
4. Toscano, G., S. Raza, A.-P. Jauho, N. A. Mortensen, and M. Wubs, "Modified field enhancement and extinction by plasmonic nanowire dimers due to nonlocal response," *Optics Express*, Vol. 20, No. 4, 4176–4188, 2012.
5. Ciracì, C., R. Hill, J. J. Mock, Y. Urzhumov, A. I. Fernández-Domínguez, S. A. Maier, J. B. Pendry, A. Chilkoti, and D. R. Smith, "Probing the ultimate limits of plasmonic enhancement," *Science*, Vol. 337, 1072–1074, 2012.
6. Savage, K. J., M. M. Hawkeye, R. Esteban, A. G. Borisov, J. Aizpurua, and J. J. Baumberg, "Revealing the quantum regime in tunnelling plasmonics," *Nature*, Vol. 491, 574–577, 2012.

Nonlocal Effects in Three-dimensional Nanoplasmonic Devices

A. I. Fernández-Domínguez
The Blackett Laboratory, Department of Physics
Imperial College London, London SW7 2AZ, United Kingdom

Abstract— The miniaturization trend in the experimental production of plasmonic devices is rapidly approaching the limit where the local solutions of macroscopic Maxwell's equations do not describe accurately their electromagnetic properties [1]. Due to their simpler numerical treatment, most theoretical investigations so far have focused on the analysis of failure of the local picture in two-dimensional nanostructures. In this talk, we will explore the occurrence of nonlocal effects due to electron confinement in threedimensional geometries, such as plasmonic tips, nanocrescents, or gapped nanoparticles [2, 3].

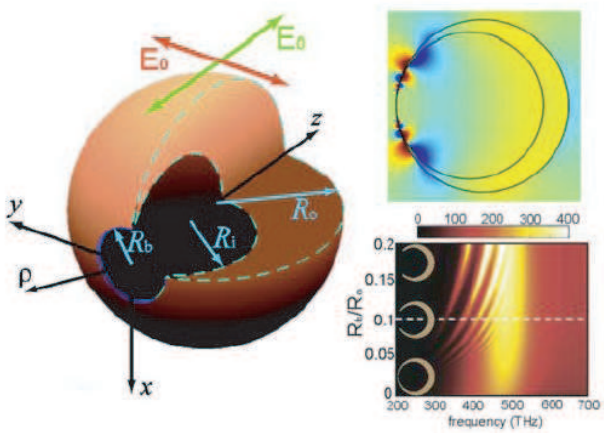

Figure 1: The left panel shows a gold three-dimensional crescent-shaped nanoparticle. The upper right panel shows the electric field component parallel to the crescent symmetry axis for a perfect ($R_b = 0$) geometry. The lower right panel renders the nanocrescent absorption spectrum as a function of the blunt radius, R_b. In this nanostructure, the phenomenology associated to blunt effects is similar to the one linked to the emergence of spatial nonlocality [3].

REFERENCES

1. Ciraci, C., et al., *Science*, Vol. 337, 1072, 2012.
2. Wiener, A., et al., *Nano Lett.*, Vol. 12, 3308, 2012.
3. Fernández-Domínguez, A. I., et al., *Nano Lett.*, Vol. 12, 5946, 2012.

Nonlocal Response in Waveguides

Søren Raza[1], **Thomas Christensen**[2], **Martijn Wubs**[2],
Sergey I. Bozhevolnyi[3], **and N. Asger Mortensen**[2]

[1]Center for Electron Nanoscopy, Department of Photonics Engineering
Technical University of Denmark (DTU), Kongens Lyngby DK-2800, Denmark
[2]Center for Nanostructured Graphene, Department of Photonics Engineering
Technical University of Denmark (DTU), Kongens Lyngby DK-2800, Denmark
[3]Institute of Sensors, Signal and Electrotechnics University of Southern Denmark
Odense DK-5230, Denmark

Abstract— Guiding of light at metal-dielectric interfaces has attracted a lot of attention in recent years due to the subwavelength light confinement achievable by excitation of propagating surface plasmon polariton (SPP) modes. In this context, the metal-insulator (MI) waveguide along with the symmetric metal-insulator-metal (MIM) and insulator-metal-insulator (IMI) waveguides (see Fig. 1) are the most fundamental of such waveguide structures, which provide the basic understanding of more complex plasmonic waveguides. While the MIM and IMI waveguides have been extensively studied theoretically, the by far most used method of calculating the SPP modes of these waveguides has been to apply the local-response approximation (LRA) of the response of the free electrons in the metals.

In this study, we go beyond the LRA and determine the dispersion relations of the SPP modes of the MI, IMI and MIM waveguides taking into account nonlocal response, retardation effects and interband transitions in the metals. The nonlocal response is described by a linearized semiclassical hydrodynamic model, which includes the quantum kinetics of the free-electron gas described by Thomas-Fermi theory.

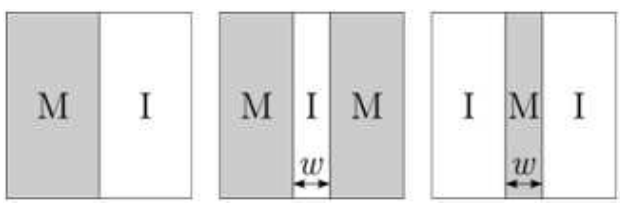

Figure 1: ketch of the metal-insulator, metal-insulator-metal and insulator-metal-insulator waveguides.

Nonlocal Effects in a Hybrid Plasmonic Waveguide for Nanoscale Confinement

Qiangsheng Huang[1], **Fanglin Bao**[1], **and Sailing He**[1, 2]

[1]Centre for Optical and Electromagnetic Research
JORCEP [Sino-Sweden Joint Research Center of Photonics]
Zhejiang Provincial Key Laboratory for Sensing Technologies, Zhejiang University
East Building No. 5, Zijingang Campus, Zhejiang University, Hangzhou 310058, China
[2]Department of Electromagnetic Engineering, Royal Institute of Technology, Stockholm 100 44, Sweden

Abstract— The effect of nonlocal optical response is studied for a novel silicon hybrid plasmonic waveguide. Finite element method is used to implement the hydrodynamic model and the propagation mode is analyzed for a hybrid plasmonic waveguide of arbitrary cross section. We demonstrate the validity of our method by comparing our simulating results with some analytical results for a metal cylindrical waveguide and a metal slab waveguide in a wide wavelength range. The novel silicon hybrid plasmonic waveguide is composed of an inverted metal nano-rib, which enables nanoscale light confinement. Our theoretical investigation has shown that the mode area could be of $10^{-6}\lambda^2$ size in a wide wavelength range from 1.3 µm to 2 µm, and the propagation distance still remains several microns. The figure of merit (FoM) is also improved in the same time, compared to the pervious hybrid plasmonic waveguide. We also investigate how nonlocal effects alter the confinement of the hybrid plasmonic waveguide. However, we don't consider the quantum effect at the metal surface. This is because the effect of electron tunneling between the metal and the dielectric is weaker than that between the metal nanoparticles. For this hybrid plasmonic waveguide, we find that the nonlocal effects can give less loss and better confinement. In particular, we explore the influence of the radius of the rib's tip on the loss and the confinement. We show that the nonlocal effects change the sensitivity of the electromagnetic field to the radius of the tip. We have shown that when the radius of the rib's tip is approaching zero, the mode area gets saturated in the nonlocal model, instead of monotonous decrease in the Drude model.

Nonlocal Response in Plasmonic Waveguiding

G. Toscano
Department of Photonics Engineering, Technical University of Denmark
DK-2800 Kgs. Lyngby, Denmark

Abstract— The study of the free-electron optical response of metallic nanostructures is usually based on the classical Drude model. The ongoing miniaturization of plasmonic devices to size comparable to the Fermi wavelength of the gas, calls for a description that includes quantum effects. One of the models that have been proposed is the *hydrodynamic model*, that describes the free-electrons as a compressible Fermi-gas subject to the electromagnetic force. The pressure waves in the gas give rise to the nonlocal optical response. The most important feature of this model is the finite thickness of the volumetric charges, that extend on a region of the dimension of the Fermi wavelength. These charges allow the electromagnetic field to smear out over a finite volume, and to obtain a finite field even for infinitely sharp features [1–4].

Here I will survey a novel wave equation for linearized plasmonic response, that is derived by combining the coupled real-space differential hydrodynamic equations for the electric field and the current density equation. Nonlocal response is fully accounted for, and the formulation is very well suited for numerical implementation of waveguide problems, allowing us to study dispersion relations for waveguides with subnanometer cross-sections exhibiting extreme light confinement [5]. The numerical solutions of the wave equation were calculated by means of the standard commercial software Comsol Multiphysics, and three structures were analyzed: cylindrical waveguide, V-groove and Λ-wedge. The results of these simulations showed that V-groove and Λ-wedge waveguides have a fundamental lower limit in their mode confinement, not captured by a local-response approximation. This limitation translates into an upper limit for the corresponding Purcell factors, and consequently it has important implications for quantum plasmonics.

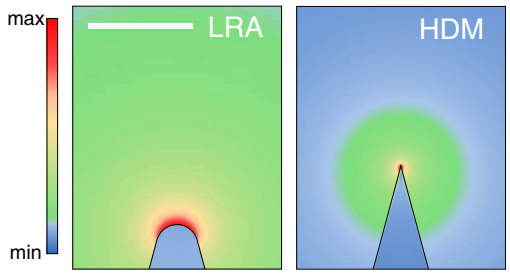

Figure 1: Field-intensities (white scale bars are 5 nm long) at $\lambda = 600$ nm for a Λ-wedge structure with aperture angle $\theta = 30°$. LRA indicates the Local Response Approximation, while HDM stands for hydrodynamic model. The LRA intensities are with rounding $r = 1$ nm, while $r = 0$ is used for the HDM map.

REFERENCES

1. Raza, S., G. Toscano, A.-P. Jauho, M. Wubs, and N. A. Mortensen, "Unusual resonances in nanoplasmonic structures due to nonlocal response," *Phys. Rev. B*, Vol. 84, 121412(R), 2011.
2. Toscano, G., S. Raza, A.-P. Jauho, N. A. Mortensen, and M. Wubs, "Modified field enhancement and extinction by plasmonic nanowire dimers due to nonlocal response," *Optics Express*, Vol. 20, No. 4, 4176–4188, 2012.
3. Toscano, G., S. Raza, S. Xiao, M. Wubs, A.-P. Jauho, S. I. Bozhevolnyi, and N. A. Mortensen, "Surface-enhanced Raman spectroscopy (SERS): Nonlocal limitations," *Optics Letters*, Vol. 37, No. 13, 2538–2540, 2012.
4. Mortensen, N. A., G. Toscano, S. Raza, N. Stenger, W. Yan, A.-P. Jauho, S. Xiao, and M. Wubs, "Nanoplasmonics beyond Ohm's law," *AIP Conf. Proc.*, Vol. 1475, 28, 2012.
5. Toscano, G., S. Raza, W. Yan, C. Jeppesen, S. Xiao, M. Wubs, A.-P. Jauho, S. I. Bozhevolnyi, and N. A. Mortensen, "Nonlocal response in plasmonic waveguiding with extreme light confinement," arXiv:1212.4925, Submitted to *Physical Review Letters*.

Perfect Imaging and ENZ Phenomena for Metallic Slabs in the Scope of Nonlocal Effects

C. David[1, 2], **N. A. Mortensen**[2], **and J. Christensen**[2, 3]

[1]Instituto de Química-Física Rocasolano
Consejo Superior de Investigaciones Científcas, Spain
[2]DTU Fotonik, Department of Photonics Engineering
Technical University of Denmark, Denmark
[3]Institute of Sensors, Signals and Electrotechnics (SENSE)
University of Southern Denmark, Denmark

Abstract— We study the implications of nonlocal properties of metal slabs and MIM waveguide structures on perfect lensing, ENZ and other relevant optical phenomena. Although nonlocal effects arise from the quantum nature of the free conduction band electrons, classical theories such as the Mermin dielectric function in the framework of the specular reflection model and the hydrodynamical model can well describe the observed effects. Based on the semiclassical hydrodynamic approach, we derive analytical expressions for the nonlocal analogue of Fresnel's coefficients, indicate differences in the expected performance of metal devices at specific resonances and study the figure of merit of waveguides. This yields a parallel wave vector dependent frequency mismatch and reduced band width under perfect imaging conditions. Additional nonradiative decay channels and coupling to longitudinal modes not present in the local approximation, explain most of the observed effects.

Session 4P5a
SC4: Wireless Energy Transmission and Harvesting 2

Analysis, Design and Experimental Verification of Modified Folded Loop Antennas for RF Harvesting and RFID Applications on Metal Objects
Hubregt J. Visser, ... 1572

Wireless Energy Harvester with a Switching Passive Charge Pump Rectifier
Andre Luis Rodrigues Mansano, Wouter A. Serdijn, ... 1573

Theoretical and Numerical Investigation of a Mid-infrared Energy-harvesting System
Martino Aldrigo, Alessandra Costanzo, Diego Masotti, Riccardo Trevisan, ... 1574

Novel Rectenna Using Modified Ground Plane for RF Energy Harvesting
Jung-Ick Moon, In-Kui Cho, Seong-Min Kim, Soon-Ik Jeon, Jae-Ick Choi, ... 1576

A High-efficiency Matching Technique for Low Power Levels in RF Harvesting
Iker Anchustegi-Echearte-Atienzar, David Jiménez-López, Manel Gasulla, Francesco Giuppi, Apostolos Georgiadis, ... 1577

Co-design of a 90 nm CMOS Rectifier and Small Loop Antenna for Large Range RF Energy Harvesters
Mark Stoopman, S. Keyrouz, H. J. Visser, Kathleen Philips, Wouter A. Serdijn, ... 1578

Analysis, Design and Experimental Verification of Modified Folded Loop Antennas for RF Harvesting and RFID Applications on Metal Objects

Hubregt J. Visser
Holst Centre/IMEC, Eindhoven, The Netherlands

Abstract— To reduce energy consumption in buildings, wireless sensors are needed to measure temperature, lighting conditions and presence of persons. Lighting and heating may then be adjusted based on these readings. This Smart Building Integration concept [1] relies on the widespread use of sensors. Powering of these sensors may be accomplished through RF [2]. For this remote powering, the antenna needs to have a specific complex input impedance, the value depending on the rectifier circuit used and the RF power level incident upon the antenna [2].

To be able to realize this desired input impedance, the antenna needs to have sufficient geometrical features for impedance tuning. Such an antenna has recently been introduced in [3]. The antenna consists of an asymmetrical, printed, folded dipole antenna on a dielectric substrate with (asymmetrically placed) short circuits in both arms, see Figure 1. The antenna design has been verified for free-space applications. In [3], first full-wave simulation results of this antenna, placed on a EBG ground plane were shown for the antenna placed on a (metallic) object, see Figure 2. In this paper, we describe a two-phase approach to the design of an EBG-backed, modified folded dipole antenna having a desired complex input impedance and the experimental verification of the design. The antenna is designed for free space using the approximate analytic model developed in [3, 4]. The EBG ground plane is designed separately, using an approximate analytic model that is based on an equivalent circuit model of a gridded square-loop FSS [5]. The antenna characteristics are verified through full-wave simulations and input impedance measurements on a realized prototype. The EBG ground plane characteristics are verified also through full-wave simulations and through a microstrip transmission line measurement of a realized prototype. Finally, the antenna is placed on top of the EBG ground plane. This structure is full-wave characterized and the input impedance of the antenna is measured as a function of frequency. A fine-tuning scheme for a final design will be discussed.

Figure 1: Antenna prototype.

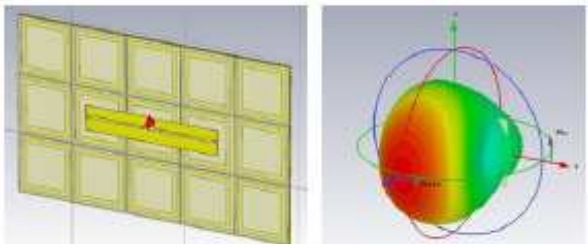

Figure 2: Antenna above EBG ground plane and simulated radiation pattern.

REFERENCES

1. Snoonian, D., "Smart buildings," *IEEE Spectrum*, Vol. 40, No. 8, 18–23, August 2003.
2. Visser, H. J., "Indoor wireless RF energy transfer for powering wireless sensors," *Radioengineering*, Vol. 21, No. 4, 963–973, December 2012.
3. Visser, H. J., "Printed folded dipole antenna design for rectenna and RFID applications," *Proceedings EuCAP*, 4 pages, 2013.
4. Visser, H. J., *Approximate Antenna Analysis for CAD*, John Wiley & Sons, Chichester, UK, 2009.
5. Yilmaz, A. and M. Kuzuoglu, "Design of the square loop frequency selective surfaces with particle swarm optimization via the equivalent circuit model," *Radioengineering*, Vol. 18, No. 2, 95–102, 2009.

Wireless Energy Harvester with a Switching Passive Charge Pump Rectifier

Andre L. R. Mansano and Wouter Serdijn
Biomedical Electronics Group, Delft University of Technology, The Netherlands

Abstract— The conception of a wireless energy harvester with a switching passive charge pump rectifier and a passive voltage-boosting network (VBN) is presented. The VBN makes use of a inductive antenna to boost input voltage at the charge pump rectifier (CPR) terminals. To improve the power conversion efficiency (PCE), the VBN also provides control signals for switching action of the CPR which comprises MOS transistors as voltage-controlled switches in order to reduce conduction losses. Analytical models for the CPR are presented and compared to simulation results at low ISM band (13.56 MHz). Simulation results, in a 90 nm standard CMOS technology, shows a DC voltage of 1.35 V and a PCE of 11.9% for a 5-stage high ISM band (915 MHz) CPR with a 1 Mohm load at −18.2 dBm available input power (PS, AV) . To show technology scalability of the design, the CPR is also validated using a 0.18 µm high-voltage (HV) CMOS technology. Moreover, scalability to operate over multiple sub-GHz ISM frequency bands has been proved.

Theoretical and Numerical Investigation of a Mid-infrared Energy-harvesting System

Martino Aldrigo[1], **Alessandra Costanzo**[1], **Diego Masotti**[1], **and Riccardo Trevisan**[2]

[1]D.E.I., University of Bologna, Viale Risorgimento 2, Bologna 40136, Italy
[2]D.E.I., University of Bologna/IMA Industries, Bologna, Italy

Abstract— In this contribution we discuss the theoretical and numerical aspects of a novel energy-harvester in the Infra-Red (IR) region, exploiting a misaligned-arms 8-element bow-tie antenna array as the radiating system, and a numerically-optimized Metal-Oxide-Metal (MOM) tunnel diode as the THz-power rectifying device [1]. In order to overcome the intrinsic limitations of solar panels (area occupation, raw-material cost, sensitivity to visible light and Ultra-Violet (UV) radiation only upon direct illumination), we propose a new way to deploy IR energy, which covers the frequencies up to about 400 THz and represents more than 40% of the total energy radiated by the sun. After choosing the operating frequency to be 100 THz ($\lambda \approx 3\,\mu$m), starting point of the CAD design (via CST Microwave Studio®) has been the modeling of the materials used for the substrate (SiO_2) and the metallization (gold): the first has negligible losses around 100 THz, whereas the latter exhibits (like all other metals) a strongly lossy dispersive behavior at such IR frequencies. The novel idea of misaligned printed monopoles stems from the traditional antenna-coupled-to-MOM-diode configuration and allows to design a compact bow-tie antenna array with a balanced corporate feed (i.e., with symmetric traces on opposite faces of the substrate) and only one diode: this way, the array factor can be constructively exploited to focus all the sun radiation received by the system into the nonlinear device. Each monopole is printed on a 100-nm thick SiO_2 layer and is made of a 35-nm thick gold deposition, whose overall dimensions are: width (W) of 987 nm and length (L) of 840 nm. The final optimized CAD project consists in a 4 rows-by-2 columns matrix with a $0.8 * \lambda$-spacing along the x-(horizontal) and y-(vertical) direction. Figure 1(a) shows the proposed solution, whereas in Figure 1(b) the simulated radiation surface (linear scale) of the E-field at 100 THz is plotted. Finally, the whole system made of the aforementioned bow-tie array and a customized futuristic MOM diode model with a strongly asymmetric and nonlinear behavior has been characterized by means of a nonlinear simulator [2], in order to predict the theoretical rectifying performance in presence of realistic solar-power levels incident onto the system itself (see Figure 2). In spite of the adopted MOM model, poor rectification properties have to be taken into account for solar energy-harvesting applications. A possible countermeasure could be represented by a multi-array macro-system, which would be still easy-to-be-embedded thanks to its nanometer-scale overall size. Moreover, the same system could be much more profitably exploited by using a dedicated IR high-power source.

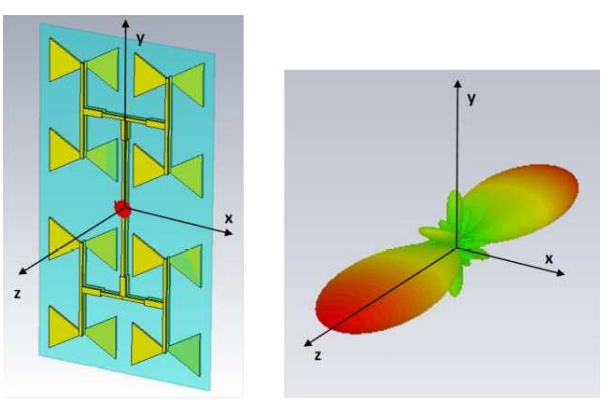

(a) (b)

Figure 1: (a) 4-by-2 misaligned bow-tie antenna array; (b) simulated radiation surface (linear scale) of the E-field at 100 THz.

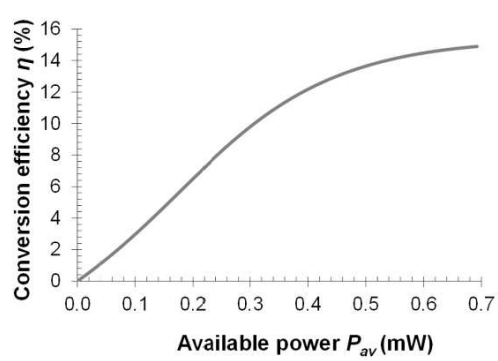

Figure 2: Conversion efficiency $\eta(\%)$ of the proposed bow-tie array as a function of the available power P_{av}. The maximum predicted value for η is about 15%.

REFERENCES

1. Sanchez, A., C. F. Davis, K. C. Liu, and A. Javan, "The MOM tunneling diode: Theoretical estimate of its performance at microwave and infrared frequencies," *J. Appl. Phys.*, Vol. 49, No. 10, 5270–5277, Oct. 1978.
2. Costanzo, A., A. Romani, D. Masotti, N. Arbizzani, and V. Rizzoli, "RF/baseband co-design of switching receivers for multiband microwave energy harvesting," *Elsevier Journal on Sensors and Actuators A: Physical*, Vol. 179, No. 1, 158–168, Mar. 2012.

Novel Rectenna Using Modified Ground Plane for RF Energy Harvesting

Jung-Ick Moon, In-Kui Cho, Seong-Min Kim, Soon-Ik Jeon, and Jae Ick Choi
Radio Technology Research Department
Electronics and Telecommunications Research Institute (ETRI), Korea

Abstract— In this paper, a novel antenna using modified ground plane for RF energy harvesting was proposed. This antenna is composed of the main radiator and the modified ground plane. The main radiator designed as a dipole type covers WCDMA-band in Korea and the ground plane is used to harvest the RF energy from the main radiators, which don't disturb the main radiator's electrical performance. The ground plane has a rectangular structure with vertical metallic walls in order to suppress and harvest the back-lobe of the antenna. The amount of the harvested energy from this rectenna is approximately 1% of the originally radiated power. The simulated gain of the proposed antenna is almost same with that of the printed dipole without the metallic walls. And the back-lobe of the proposed rectenna was reduced to 7.0 dB.

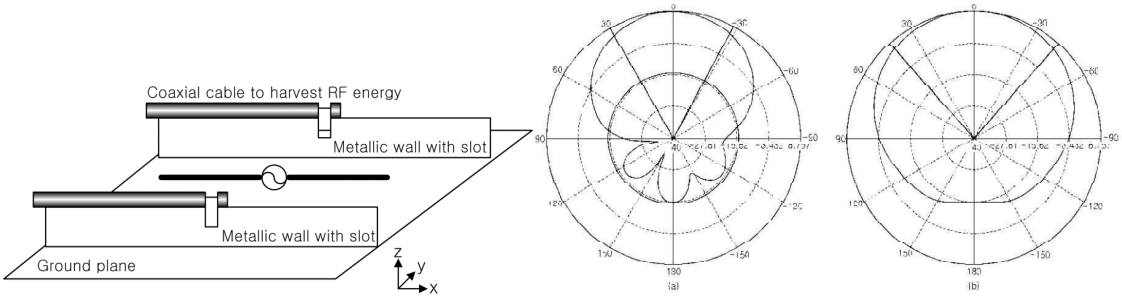

Figure 1: The proposed rectenna structure and its radiation patterns on E & H-plane.

ACKNOWLEDGMENT

This research was funded by the MSIP(Ministry of Science, ICT & Future Planning), Korea in the ICT R & D Program 2013.

REFERENCES

1. Heo, S., "Efficient maximum power tracking of energy harvesting using a µcontroller for power savings," *ETRI Journal*, Vol. 33, No. 6, Dec. 2011.
2. Siu, L. and K.-M. Luk, "Unidirectional antenna with loaded dielectric substrate," *IEEE Antenna and Wireless Propagation Letters*, Vol. 7, 2008.

A High-efficiency Matching Technique for Low Power Levels in RF Harvesting

I. Anchustegui-Echearte[1], **D. Jiménez-López**[1], **M. Gasulla**[1], **F. Giuppi**[2], **and A. Georgiadis**[2]

[1]Department of Electronic Engineering, Universitat Politècnica de Catalunya, Catalonia, Spain
[2]Centre Tecnològic de Telecomunicacions de Catalunya, Catalonia, Spain

Abstract— Powering low-power devices (e.g., autonomous sensors) from electromagnetic waves has been proposed in the literature [1–5]. Radiofrequency (RF) energy can be harvested either from the surrounding environment or from dedicated sources. A conventional RF harvester is mainly composed by an antenna, a matching network and a rectifier. Reported RF-to-DC power efficiencies are higher for increasing power levels at the RF input. In [3], efficiencies around 70% and 40% are achieved for RF power levels of 10 dBm and −10 dBm, respectively. The circuits and diodes used for each power range are different in order to optimize the performance.

This work focuses on the matching network stage in order to achieve high efficiencies at low input power levels, in particular at −10 dBm. At this power level, the corresponding voltage amplitude at the antenna is low and comparable to the voltage drop of the diodes used in the rectifier. So, in order to increase the rectifier efficiency, a boost of the antenna voltage is required before driving the rectifier. Here, an L-network is proposed with a resonant frequency of 868 MHz (ISM band). As the voltage is boosted by the matching network there is no need to further boost it by using the rectifier and thus a single-diode half-wave rectifier was used.

First, a theoretical analysis was performed that takes into account the parasitic capacitance of the diode. A zero-bias Schottky diode (HSMS2850) was selected. Then, simulations with ADS (Harmonic Balance) were carried out taking into account the circuit layout. The antenna was simulated by an RF generator with an output impedance of 50 Ω. The selected components for the L-network were a 0.5 pF capacitor and a 27 nH inductor. Finally, a PCB implementation was performed achieving an RF-to-DC efficiency of 45% at 868 MHz and at −10 dBm with an optimum load of 2.5 kΩ. The input power was generated by an RF generator. Efficiencies of 34.5% and 22.5% were achieved at −15 dBm and −20 dBm, respectively.

ACKNOWLEDGMENT

The work of I. Anchustegi-Echearte, D. Jiménez-López and M. Gasulla was supported by the Spanish Ministry of Economy and Competitivity under Project TEC2011-27397. The work of A. Georgiadis and F. Giuppi was supported by the Spanish Ministry of Economy and Competitivity under Project TEC2012-39143 and by EU Marie Curie project FP7-PEOPLE-2009-IAPP 251557.

REFERENCES

1. Soltani, H. N. and F. Yuan, "A high-gain power-matching technique for efficient radio-frequency power harvest of passive wireless microsystems," *IEEE Trans. Circuits Syst. I, Reg. Papers*, Vol. 57, No. 10, 2685–2695, 2010.
2. Nintanavongsam, P., U. Muncuk, D. R. Lewis, and K. R. Chowdhury, "Design optimization and implementation for RF energy harvesting circuits," *IEEE J. Emerg. Sel. Topic Circuits Syst.*, Vol. 2, No. 1, 24–33, 2012.
3. Marian, V., B. Allard, C. Vollaire, and J. Verdier, "Strategy for microwave energy harvesting from ambient field or a feeding source," *IEEE Trans. Power Electron.*, Vol. 27, No. 11, 4481–4491, 2012.
4. Costanzo, A., F. Donzelli, D. Masotti, and V. Rizzoli, "Rigorous design of RF multi-resonator power harvesters," *Proc. 4th European Conference on Antennas and Propagation (EuCAP)*, 1–4, Apr. 12–16, 2010.
5. Andia Vera, G., A. Georgiadis, A. Collado, and S. Via, "Design of a 2.45 GHz rectenna for electromagnetic (EM) energy scavenging," *Proc. 2010 IEEE Radio and Wireless Symposium (RWS)*, 61–64, Jan. 10–14, 2010.

Co-design of a 90 nm CMOS Rectifier and Small Loop Antenna for Large Range RF Energy Harvesters

Mark Stoopman[1], **S. Keyrouz**[2], **H. J. Visser**[2], **Kathleen Philips**[2], **and Wouter A. Serdijn**[1]

[1]Electronics Research Laboratory, Delft University of Technology, The Netherlands
[2]Imec-NL, Holst centre, Eindhoven, The Netherlands

Abstract— The main design challenge for current state-of-the-art RF energy harvesters is to improve the sensitivity (wireless range), efficiency and robustness simultaneously. Generating a sufficiently large voltage to activate the rectifier with a few μW of power is the first concern as MOS transistors inherently are voltage-controlled devices. To address these issues, a design methodology is described for the co-design and integration of a CMOS rectifier and small loop antenna for highly sensitive RF energy harvesters. It is shown that the choice of antenna-rectifier interface impedance plays a crucial role in this optimization. Following this methodology, a 5 stage cross-connected bridge rectifier is designed that is brought at resonance with a high-Q loop antenna by means of a 7-bit binary weighted capacitor bank. A feedback controlled voltage boosting and tuning network compensates any impedance variation in the interface that may occur in a realistic environment, making the RF energy harvester very robust while fully benefiting from the passive voltage boost obtained from the high-Q network. Subsequently, a small loop antenna is designed which meets the specific requirements obtained from the rectifier impedance.

The rectifier and capacitor bank have been implemented in standard 90 nm CMOS technology, includes ESD protection and are integrated on the antenna. Measurements in an anechoic chamber at 868 MHz show a −27 dBm sensitivity for 1 V output across a capacitive load and 27 meter range for a 1.78 W RF source in an office corridor. The maximum power conversion efficiency equals 40% at −17 dBm.

Session 4P5b
Antenna and Array

Phase Characterization of X-band Minkowski Reflectarray Antennas Using 3-D CST Microwave Studio-based Neural Network Model Included Dielectric Properties
Selahattin Nesil, Filiz Gunes, Salih Demirel, ... 1580

Antenna Array Synthesis, Using Method of Compressed Cosines
Peter Stoyanov Apostolov, ... 1581

High-gain ***S***-band Slotted Waveguide Antenna Arrays with Elliptical Slots and Low Sidelobe Levels
Mohammed Al-Husseini, Ali El-Hajj, Karim Y. Kabalan, ... 1582

Large Impedance Ground Plane Antennas for mm-accuracy of GNSS Positioning in Real Time
Dmitry V. Tatarnikov, Andrey Astakhov, ... 1584

The Proposal of a Printed Dipole Array Antenna with Partial Drive through Transmission Line Coupling
Hiroyuki Hosono, Kuniaki Shibata, Kenji Saegusa, Tadashi Takano, ... 1585

Omni-directional Leaky-wave Coaxial Antenna
Ahmed Mohamed Attiya, ... 1586

Comparison of Radiation Patterns of Transmission Antennas for Marathon Race Considering Frequency Migration of Field Pick-up Units
Naoto Kogo, Tetsuomi Ikeda, ... 1587

Robust Beamforming Using Weighted Directional Constraints and Wavelet Blocking Matrix
Said Esmail El-Khamy, Mohamed R. M. Rizk, Roshdy K. Korayem, ... 1589

Phase Characterization of X-band Minkowski Reflectarray Antennas Using 3-D CST Microwave Studio-based Neural Network Model Included Dielectric Properties

Selahattin Nesil[1], **Filiz Güneş**[2], **and Salih Demirel**[2]

[1]Department of Electrical and Electronics Engineering, Fatih University, Istanbul, Turkey
[2]Department of Electronics and Communication Engineering
Yıldız Technical University, Istanbul, Turkey

Abstract— Modern wireless communication system requires low profile, light weight, high gain, and simple structure antennas to assure reliability, mobility, and high efficiency characteristics. Microstrip reflectarray (RA) antenna satisfies all of these requirements. This antenna provides all of the advantages of printed circuit technology. In addition, they do not require any complicated feeding network. The flat-plate microstrip reflectarray offers advantage of profile size reduction as compared to its counterpart parabolic reflector. The limitations of microstrip RA antennas are narrow frequency band and disability to operate at high power levels of waveguide, coaxial line or even strip line. Therefore, the challenge in microstrip RA antenna design is to increase the bandwidth and gain that necessitates the design optimization of the unit element together with the substrate [1]. The phasing method using variable size patches is a preferable choice in many designs due to its simplicity. To meet the larger phasing range on a single layer substrate, the novel, complicated patch configurations are needed to be worked in which the structure to be optimized presents a lot of degrees of freedom and all concur to the performances of the whole antenna. Since a 3-D EM simulator is very inefficient to be used within an optimization procedure, the accurate and rapid models are desperately needed in the design optimization of the reflectarrays. In recent years, Multilayer Perceptron (MLP) type of Artificial Neural Network (ANN) has been used in the modeling of microstrip reflectarray (RA) s [2]. Our research group has worked with the Minkowski shape [3, 4] which is from the 1st iteration of fractals and the Minkowski radiator is shown to have an optimum phasing characteristic with the fairly large linear region and easy fabrication [6]. In this work, adding dielectric property ε_r of the substrate to the modeling, a complete MLP NN model is built to be used in both the design and performance analysis of the Minkowski RAs for the X-band applications. Thus, the designer will be able to obtain the optimum Minkowski geometry not only on a defined substrate, at the same time, on the most suitable substrate with the optimum dielectric property ε_r and thickness h. The work can briefly be summarized as building a complete, rapid and accurate model for the reactive impedance behavior of a Minkowski unit radiator. For this purpose, the MLP NN with the Levenberg-Marquardt algorithm is used and the training and validation data sets are obtained from the 3-D CST simulation of a unit Minkowski reflective element placed at the end of a standard X-band waveguide, by varying the geometrical parameters of the patch for each substrate (ε_r, h) at each operation frequency f within the defined input domain. Thus the reflection phase of an independent Minkowski radiator is established as a highly nonlinear function within the continuous domain of the element geometry and substrate parameters (ε_r, h) in a defined bandwidth centered the resonant frequency of the microstrip patch. The reflection phase characterization of the MLP ANN model will be presented as the numerous graphics depicting the variations of the geometry parameters and substrate parameters (ε_r, h) as compared with analysis of the 3-D EM simulator CST and interpreted in terms of design parameters.

REFERENCES

1. Huang, J., and J. A. Encinar, *Reflectarray Antennas*, Wiley-IEEE Press, 2007, ISBN: 978-0470-08491-4.
2. Caputo, D., et al., "Neural network characterization of microstrip patches for reflectarray optimization," *Proceedings of the European Conference on Antennas and Propagation, EuCAP*, 2520–2522, March 23–27, 2009.
3. Nesil, S., F. Güneş, and G. Kaya, "Analysis and design of X-band reflectarray antenna using 3-D EM-based artificial neural network model," *IEEE International Conference on Ultra-Wideband (ICUWB)*, 532, 536, Sept. 17–20, 2012.
4. Zubir, F., M. K. A. Rahim, O. Ayop, A. Wahid, and H. A. Majid, "Design and analysis of microstrip reflectarray antenna with minkowski shape radiating element," *Progress In Electromagnetics Research B*, Vol. 24, 317–331, 2010.

Antenna Array Synthesis, Using Method of Compressed Cosines

Peter Apostolov
High school "College of Telecommunications and Post", Student City
Street "Academician Stefan Mladenov", No. 1, Sofia, Bulgaria

Abstract— In the paper, an application of the method of compressed cosines is shown for synthesis of a three-element linear equidistant antenna array (LEAA). The synthesis is performed by an approximation of a Kronecker Delta function. Two cases of approximations by optimal third-degree polynomials are considered. As a result, directivity diagrams with a high selectivity are obtained. Functional diagrams are proposed for realization of a three-element LEAA and a five-element, two-dimensional LEAA.

High-gain S-band Slotted Waveguide Antenna Arrays with Elliptical Slots and Low Sidelobe Levels

M. Al-Husseini[1], **A. El-Hajj**[2], **and K. Y. Kabalan**[2]

[1]Lebanese Center for Studies and Research, Beirut 2030 8303, Lebanon
[2]American University of Beirut, Beirut 1107 2020, Lebanon

Abstract— This paper presents an S-band slotted waveguide antenna array with elliptical slots made to one broadwall. The antenna is designed for operation at 3 GHz, and for 20 dB of sidelobe level ratio (SLR). At a later stage, two rectangular sheets are added as reflectors, in a symmetrical setting, to increase the gain.

Elliptical slots are known to be more suitable for high power applications. Ten elliptical slots are cut into one broadwall of a WR-284 waveguide ($a = 2.84$ in, $b = 1.37$ in), which is shorted at one end and fed at the other. The slots are spaced at half the guide wavelength, center to center ($\lambda_g = 138.5$ mm). The width of each slot, which is 2 times the minor radius of the ellipse, is fixed at 5 mm. This value is obtained from $0.0625 \times a/0.9$, which is taken in proportionality to the width of a rectangular slot in an X-band waveguide. Because of the elliptical shape, the length of the slots (double the major radius) is going to be larger than half the free space wavelength, so simulations were done, using ANSYS HFSS, to optimize the slot length, assuming all slots are at the same spacing from the broadwall centerline, in an alternating order. For operation at 3 GHz with good reflection coefficient, the uniform spacing is 7.7 mm. The optimized slot length is found to be 54.25 mm. The resulting slotted waveguide antenna, with uniform slot-centerline spacing, has a peak gain of 16.9 dB, and as expected, the SLR is about 13 dB.

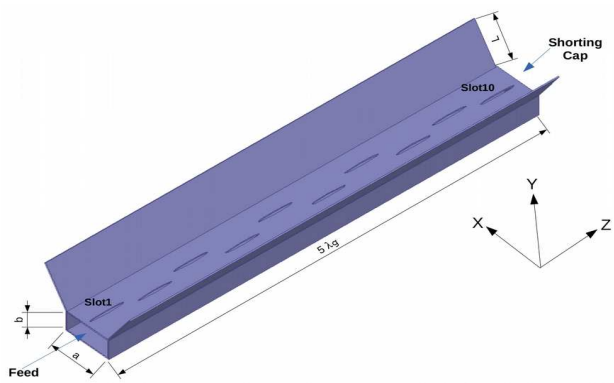

Figure 1: Slotted waveguide with 10 elliptical slots and reflectors added.

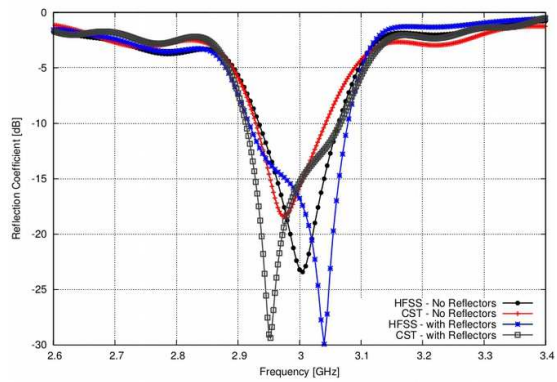

Figure 2: Reflection coefficient without and with the reflectors.

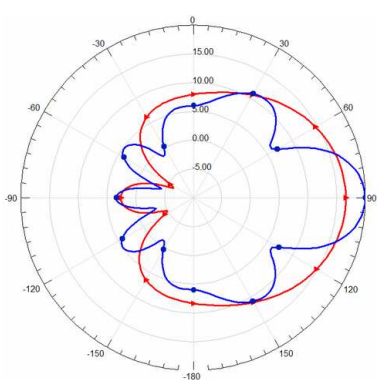

Figure 3: Patterns in the azimuth plane (Red: no reflectors, Blue: with reflectors).

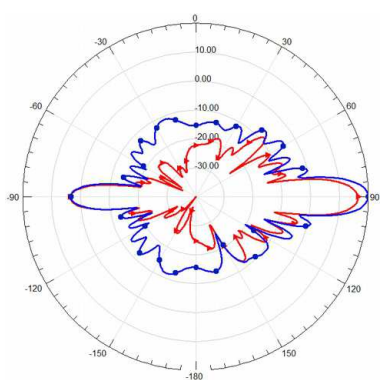

Figure 4: Patterns in the YZ plane (Red: no reflectors, Blue: with reflectors).

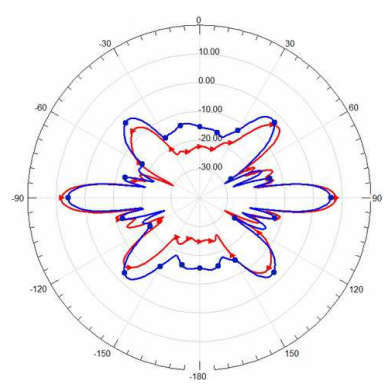

Figure 5: Patterns in the XZ plane (Red: no reflectors, Blue: with reflectors).

Since better SLRs are desirable, the displacements of the slots from the centerline are changed, to non-uniform, using a heuristic method. For an example SLR of 20 dB, the displacements are: 3.74 mm for Slots 1 and 10, 5.42 mm for Slots 2 and 9, 7.11 mm for Slots 3 and 8, 8.4 mm for Slots 4 and 7, and 9.11 mm for Slots 5 and 6. The alternating position about the centerline should be respected. The length of all slots is kept at 54.25 mm, as in the uniform case. The resonating length of these elliptical slots is not so sensitive to the distance from the centerline. For these values, the antenna still resonates at 3 GHz, the SLR is 20 dB, and the peak gain is 16.8 dB.

Two metal sheets are then attached symmetrically, as shown in Fig. 1, at an angle of 60° with respect to the XZ plane. These 2 sheets act as reflectors, leading to a gain increase of about 3 dB. The value of L is 3 in. With all dimensions kept the same, the antenna retains its resonance at 3 GHz, and the SLR remains around 20 dB. The back lobe level stays about the same, so the main-to-back lobe level ratio also increases by about 3 dB. The S_{11} and pattern results of the two cases, with and without the reflectors, are shown in Figs. 2–5. All results generated in HFSS were verified in CST Microwave Studio, where a match is observed.

Large Impedance Ground Plane Antennas for mm-accuracy of GNSS Positioning in Real Time

D. V. Tatarnikov and A. V. Astakhov
Topcon Positioning Systems, Russia

Abstract— Global Navigation Satellite Systems (GNSS: GPS of the USA, GLONASS of Russia, Galileo of the EC and Compass of China) are recognized as powerful tools for planetary research and have led to a vast variety of practical applications. With the invention of Real Time Kinematic (RTK) algorithm, real-time accuracy of positioning has improved dramatically and currently is about 1–2 cm; unavoidable multipath reflections from the Earth surface that is undelaying the receiver GNSS antenna remain the largest error source. It is widely recognized that to suppress said reflections the antenna is to have a cut-off type pattern in the elevation plane. This calls for the antenna size to be sufficiently large in wavelength scale. Classical ground plane antennas potentially capable of providing with a high signal-to-noise ratio along with multipath suppression would of advantage for many applications. Results of development and implementation of such an antenna are presented in the paper. It has been found out that the ground plane of impedance type could be structured in such a way that both the required antenna gain for directions in top semi-sphere and cut-off pattern behavior while crossing the local horizon would be achieved. Said is valid regardless of the type of impedance surface the ground plane is made of. For practical implementation a high capacitive impedance pins surface has been employed. This is to obtain a broadband functionality to cover the entire GNSS frequency band. Antenna samples with the ground plane of 3 meters in diameter have been built. Multipath error is shown to fall below phase noise of the receiver. By filtering out said noise areal-time positioning accuracy of $1.2, \ldots, 2$ mm in vertical has been obtained. Potential applications to geo-spatial networks and robotic machine control are discussed.

The Proposal of a Printed Dipole Array Antenna with Partial Drive through Transmission Line Coupling

Hiroyuki Hosono, **Kuniaki Shibata**, **Kenji Saegusa**, **and Tadashi Takano**
College of Science and Technology, Nihon University, Japan

Abstract— A phased array antenna (PAA) is esteemed to be an appropriate solution for a spacetenna aboard a solar power satellite (SPS), because of (1) flexibility to cope with any size of an antenna, (2) flat mechanical structure, and (3) capability to scan the beam. On the other hand, a PAA should include a feeding network from a microwave generator to each radiating element. The feeding network increases the weight and cost more than a parabolic reflector antenna with a single radiating element. For these reasons to replace the driven elements with parasitic elements or parasites, the concept of partial drive was proposed. In the former partial drive technique, which contributes to the cost reduction of array antenna (AA), a part of the whole radiating elements are driven, and the rest are excited by spatial coupling. This technique can realize the performance approximately equivalent to that of a fully driven AA (FDAA). But the configuration is limited in design freedom due to spatial coupling. In that case, it is necessary to optimally determine the height and the spacing of elements. Thus we have proposed a method to connect the driven and parasitic elements by using a transmission line in order to get sufficient coupling even in a printed antenna, and named it "a partially driven array antenna (PDAA) with transmission line coupling".

In this paper, we have examined the influence of the feeding method and the transmission path configuration on the antenna characteristics. We showed the influence on the antenna characteristics by changing the feeding method and the transmission path shape about PDAA. S_{11} can be decreased by optimizing the position of the feeding point and the transmission path. Especially, it is important to adjust the connection point to decrease S_{11}.

Omni-directional Leaky-wave Coaxial Antenna

Ahmed M. Attiya
Microwave Engineering Department, Electronics Research Institute, Egypt

Abstract— There is an increasing interest in directive omni-directional antennas with a conical radiation pattern in different applications like satellite communication, wireless systems and mobile base stations. Zhao et al. [1] introduced simplified modal analysis and design procedure for planar leaky wave antenna based on transverse equivalent network of a planar waveguide composed of a grounded dielectric substrate and covered with a partially reflecting artificial impedance surface. The aim of the present paper is to extend the analysis of [1] to the case of a coaxial leaky wave antenna with a partially reflecting outer surface to obtain an efficient and simplified procedure for the analysis and design of this antenna structure.

In this paper, we present detailed analysis of a coaxial leaky wave antenna composed of inner perfect electric conductor and outer impedance surface separated by a dielectric layer as show in Fig. 1. This analysis is used to introduce design steps for this coaxial leaky wave antenna. These design steps are used to obtain the physical parameters of this coaxial structure like the outer radius and the surface impedance of the outer surface for specific values of inner radius and dielectric material to obtain certain scanning angle at a certain operating frequency. The artificial impedance surface is implemented by periodic slits in a conducting sheet. Primary estimates for the dimensions of these slits which satisfy the required impedance surface are obtained by simple analytical form. All these parameters are combined together and compared with the results of a full wave numerical simulation by using HFSS.

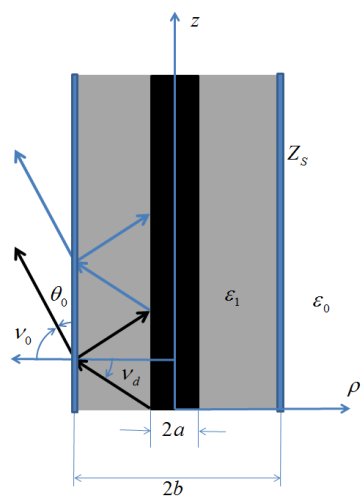

Figure 1: Geometry of a coaxial structure with inner conductor and partially reflecting outer surface.

REFERENCES

1. Zhao, T., D. R. Jackson, J. T. Williams, and A. A. Oliner, "General formulas for 2-D leaky-wave antennas," *IEEE Trans. Antennas Propag.*, Vol. 53, No. 11, 3525–3533, Nov. 1993.

Comparison of Radiation Patterns of Transmission Antennas for Marathon Race Considering Frequency Migration of Field Pick-up Units

Naoto Kogo and Tetsuomi Ikeda
Science & Technology Research Laboratories, NHK, Japan

Abstract— Outside broadcasting (OB) is the term used to describe the production of television or radio programs away from a purpose-built studio and is typically used to broadcast live events such as sports, festivals, and breaking news. During live OB of road races, such as marathons and ekiden (Japanese term for long-distance relay running races), video images are captured using cameras on moving OB vans, and the signals of the video images are transmitted to the receiving stations. The multiple receiving points are set on the top of buildings, telegraph poles, and mountains along the marathon course and the signals are transmitted by a field pick-up unit (FPU), which is an OFDM transmission system in the 700-MHz band (770–806 MHz) [1]. However, the Ministry of Internal Affairs and Communications (MIC), Japan is considering reallocating the frequencies used by FPUs for mobile relays from this 700-MHz band to the 1.2-GHz (1.24–1.3 GHz) and 2.3-GHz (2.33–2.37 GHz) bands as part of a frequency-reallocation action plan.

To achieve high reliability of the wireless links between an OB van and receiving stations, even after this frequency migration, the location of receiving points, the selection of receiving antennas, and the performance of transmission antennas are important [2, 3]. There are many types of equipment installed on the roof of an OB van; therefore, it is assumed that the radiation pattern of the transmission antenna is affected by this equipment and the shape of the OB van. However, few studies have been conducted concerning the effect of OB vans on the radiation patterns by taking into account the frequency migration.

We designed transmission antennas and an OB van and calculated the radiation patterns in the 700-MHz, 1.2-GHz, and 2.3-GHz bands. Given that the scale of the radiation pattern analysis in the 1.2-GHz and 2.3-GHz bands is large, which makes analysis difficult to conduct on a standard workstation, we decided to use the TSUBAME2.0 [4] supercomputer managed by the Tokyo Institute of Technology. We found that the antenna height is a significant parameter for characteristics of the radiation patterns on OB vans.

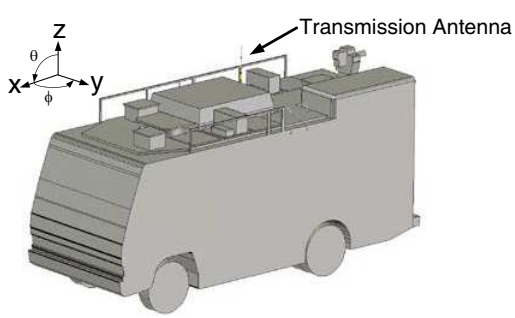

Figure 1: Calculation model of OB van.

Figure 2: Photograph of OB van.

ACKNOWLEDGMENT

The numerical calculations were carried out on the TSUBAME2.0 supercomputer at the Tokyo Institute of Technology supported by the MEXT Open Advanced Research Facilities Initiative.

REFERENCES

1. Moriyama, S., K. Tsuchida, M. Sasaki, and S. Yamazaki, "Digital outside-broadcasting-link using OFDM modulation scheme," *IEEE Trans. on Broadcasting*, Vol. 42, No. 3, 266–271, Sep. 1996.

2. Hirono, J. and N. Kawashima, "Live transmission system for the "Tokyo Marathon" using 800 MHz COFDM links from moving vehicle," *Proc. of 53rd NAB Broadcast Engineering Conference*, 577–584, Apr. 1999.
3. Kogo, N., M. Yatagai, F. Murakami, and T. Ikeda, "Performance improvement of transmission antenna installed on outside broadcasting van for live broadcast of road race," *Proc. of ISAP2012*, 4B1-2, 1325–1328, Nov. 2012.
4. Matsuoka, S., "TSUBAME 2.0 begins — The long road from TSUBAME 1.0 to 2.0 (part one)," *TSUBAME e-Science Journal*, Vol. 2, 2–10, Oct. 2010.

Robust Beamforming Using Weighted Directional Constraints and Wavelet Blocking Matrix

Said E. El-Khamy, **Mohamed R. M. Rizk**, **and Roshdy K. Korayem**
Department of Electrical Engineering, Faculty of Engineering
Alexandria University, Alexandria, Egypt

Abstract— The Constrained Least Mean Square (CLMS) is one of the used techniques to adapt the beam-pattern of the sensor array. It minimizes the output power and in the same time satisfies some constraints (e.g., directional constraints). CLMS is distinguished over Least Mean Square (LMS) by it does not need a reference signal. It depends on satisfying constraints instead of minimizing the error signal. Error in constraints' detection is one of the large problems which the CLMS suffers from.

In the case of directional constraints, CLMS algorithms (e.g., sidelobe canceller) fail to capture the Signal Of Interest (SOI) if there is an error in the Direction Of Arrival (DOA) estimation. Moreover it will consider the SOI as an interferer and create null in the desired. The large gain will be toward the wrong (detected) direction. Several techniques may be used to overcome this problem. We are interested in two of them. First, constrain the pattern derivative(s) to be equal to zero at the DOA to create constant gain around the detection angle. The second is dividing the interval of uncertainty into smaller intervals. The desired beamformer is the sum of the ideal beamformers of the mid-points of the intervals weighted by some weights. Constant weight and the probability density function of the random variable θ namely Bayesian weights, θ is the DOA, are two examples of the weights may be used.

The Sidelobe Canceller (SLC) is one of the used techniques to implement LCMV beamformer. It depends on processing the input signal using two branches. The first branch (the quiescent filter) bypasses the constraints while the other branch blocks them using blocking matrix. The SLC is adapted using weights located after the blocking matrix. The design problem of the SLC is designing the quiescent filter and the blocking matrix. In the case of conventional design the sidelobe canceller suffers from the problem of performance degrading due to the DOA detection error like conventional LCMV. To overcome this degrading, the problem of detection error has to be taken into account when designing the quiescent filter and the blocking matrix.

Wavelet based blocking matrix employs the wavelet property of vanishing moments to block wider interval. This needs to bypass the same interval in the quiescent filter. Normally, derivative constraints are used in the quiescent filter. The pass interval through the derivative constraints depends on the derivative order, it is difficult to be accurately calculated and designed. It has been noticed in our analysis that the pass band is small and does not employ the whole blocked interval.

In the paper which we introduce an abstract, in aim to control the quiescent filter band we replaced the derivative constraints in the quiescent filter by dividing the interval of uncertainty and used weighted directional constraints. Constant weight and Bayesian weight schemes have been studied. The constant weight scenario succeeds to keep constant gain around the detected DOA for longer interval than the derivative constraints. The Bayesian weight scenario succeeds to track the user with high directivity although there is an error in the direction of arrival estimation.

Session 4P6a
Electromagnetic Modeling, Inversion and Applications

Design of Elliptic-Function Microstrip Filters with Defected Ground Structures
Agâh Oktay Ertay, Serkan Simsek, ... 1592
Shape Reconstruction of a Dielectric Coated PEC through Generalized Impedance Boundary Conditions
Birol Aslanyurek, Tolga Ulas Gurbuz, Hulya Sahinturk, ... 1593
Electromagnetic Stimulation of Transport in Water for Geoenvironmental Applications
Arvin Farid, Mahsa Azad, Jim Browning, Elisa Barney-Smith, ... 1594
Inversion of Planetary Rough Surface Permittivity and Thickness from Radar Sounder Observations
Hongxia Ye, ... 1595
Wave Propagation Characteristics of Layered Uniaxially Anisotropic Media
Y. H. Lee, Abdullah Eroglu, Jay Kyoon Lee, ... 1596

Design of Elliptic-Function Microstrip Filters with Defected Ground Structures

A. O. Ertay and S. Şimşek
Electrical and Electronics Eng. Faculty, Istanbul Technical University, Istanbul, Turkey

Abstract— Determination of design objectives of microwave filters is one of the most important points in filter design as regards practical requirements. Microwave filter designers follow specific design procedures to meet design objectives [1].

Filters may have frequency characteristics like bandpass, low pass, and high pass and bandstop responses. Practically, any filter has no ideal characteristics like infinite attenuation at stopband, zero insertion loss at passband [2] and steep transition region from passband to stopband. In addition, some of designer's goals may be compacting of the design structure, smooth curve of group delay, wider bandwidth or stopband. Therefore, it is desired to approach these ideal cases for proposed filter characteristics.

Recently, considerable attention attracted for defected ground structures due to their implementations used for microstrip component designs. Slots etched on the ground plane, which permit interaction between microstrip and defected ground plane, are employed for microwave filter design [3]. Many applications such as power dividers, microstrip antennas and microwave filters are based on defected ground structures.

In this study, it is proposed to improve the frequency characteristics of elliptic function microstrip filters with defected ground structures using a design procedure which includes three steps for the filter design. Firstly, a conventional filter design is presented using elliptic filter prototype. Following the first step, normalized element values of elliptic low pass filter prototype are calculated and desired filter transformation is carried out. Secondly, microstrip filter transformation of obtained elliptic low pass filter is attained. Lastly, ground plane is etched using different shapes like donut, square, V-shape, U-shape, interdigital and fractal versions of different geometries with appropriate modifications. In this case, an improvement of microstrip filter design is achieved using DGSs. MATLAB and full wave electromagnetic simulators are used to model the proposed filters. Scattering parameters of microstrip elliptic filter are extracted and plotted in commercial EM design environments. Modifications of ground plane with different geometries are applied to the microstrip elliptic filter via EM software tools and simulation results are consistent with our design objectives.

REFERENCES

1. Şimşek, S., E. Topuz, and E. Niver, "A novel design method for electromagnetic bandgap based waveguide filters with periodic dielectric loading," *AEU Int. J. Electron. Commun.*, Vol. 66, No. 3, 228–234, 2012.
2. Pozar, D. M., *Microwave Engineering*, 4th Edition, John Wiley, 2012.
3. Hong, J.-S., *Microstrip Filters for RF/Microwave Applications*, 2nd Edition, John Wiley, 2011.

Shape Reconstruction of a Dielectric Coated PEC through Generalized Impedance Boundary Conditions

Birol Aslanyürek[1], **Tolga Ulaş Gürbüz**[2], **and Hülya Şahintürk**[1]

[1]Mathematical Engineering Department, Yildiz Technical University, Davutpasa, Istanbul 34210, Turkey
[2]Electrical-Electronics Engineering Faculty, Istanbul Technical University, Maslak, Istanbul 34469, Turkey

Abstract— Generalized Impedance Boundary Conditions (GIBCs) enable simplification of the mathematical and numerical complexities in the solution of electromagnetic scattering problems since GIBCs defined on the surface of a scatterer include the information about the geometrical and material properties of the object. Thus, GIBCs are widely used to model imperfectly conducting obstacles, scatterers with corrugated or rough surfaces, dielectric resonators, conductive thin sheets, etc. Apart from these, in [1, 2], GIBCs are defined on the outer boundary of a thin dielectric coating with constant thickness. On the other hand, for dielectric coatings with variable thickness, GIBC expressions up to third order with respect to the thickness are derived in [3].

In this study, we deal with the inverse scattering problem of reconstructing the shape of a Perfectly Electric Conductor (PEC) with a thin dielectric coating having variable thickness through the GIBC expressions in [3]. This can be achieved by determining the thickness function in the expressions of the GIBCs. However, it is first required to calculate the total field and its normal and higher order tangential derivatives on the outer boundary of the coating. These required fields appearing in the GIBCs are obtained by the analytical continuation of the measured data to the coating surface through the single layer potential representation. Then, the GIBC expression for each order is transformed into a system of integro-differential equations which is finally reduced to a system of nonlinear algebraic equations by expanding the thickness function in a series of exponentials. The resulting systems of equations are solved for the coefficients of the exponential series iteratively via the Newton-Raphson method. The proposed approach is tested with several examples in order to see its efficiency and accuracy as well as applicability. It is shown that it yields accurate results for the coatings whose thickness is less than one-tenth of wavelength of the incident field.

REFERENCES

1. Haddar, H. and P. Joly, "Stability of thin layer approximation of electromagnetic waves scattering by linear and nonlinear coatings," *J. Comput. Appl. Math.*, Vol. 143, No. 2, 201–236, 2002.
2. Bendali, A. and K. Lemrabet, "Asymptotic analysis of the scattering of a time-harmonic electromagnetic wave by a perfectly conducting metal coated with a thin dielectric shell," *Asymptot. Anal.*, Vol. 57, Nos. 3–4, 199–227, 2008.
3. Aslanyürek, B., H. Haddar, and H. Şahintürk, "Generalized impedance boundary conditions for thin dielectric coatings with variable thickness," *Wave Motion*, Vol. 48, No. 7, 681–700, 2011.

Electromagnetic Stimulation of Transport in Water for Geoenvironmental Applications

A. Farid, M. Azad, J. Browning, and E. Barney-Smith
Boise State University, USA

Abstract— Air sparging is a popular soil remediation technique, which enables the removal of contaminants through diffusing air into saturated zones of soil. The removal process is, however, slow. The goal of this work is to study the effect of electromagnetic (EM) waves — with minimal heat generation — on transport mechanisms such as diffusion, in order to improve airflow or contaminant transport and expedite the cleanup process using air sparging or similar technologies. This effect is studied through an experimental setup that examines the diffusion of a nonreactive dye in water. The setup was tested at a range of frequencies, 50–200 MHz. Measurement of the electric field component of EM waves was taken to map the electric field. In addition, the electric field was simulated using COMSOL Multiphysics for better 3D visualization and analysis. A dielectrophoretic study was then performed using the simulated electric field data. The result of this study is in agreement with the experimental result of the dye flow. Recording the temperature change of the medium at different individual frequencies shows the same trend of the temperature change (less than 1°C throughout the duration of the stimulation) for all tests. However, only at the specific frequency of 65 MHz, the dye flow was different from all other frequencies. The dye was also contained at 76 MHz. Therefore, this observation suggests that thermal effects are not controlling the movement of the dye through convective flow in the water. Since the flow of the dye is in the direction of the dielectrophoretic forces, it is believed that the governing mechanism for the dye transport is mainly dielectrophoresis.

Inversion of Planetary Rough Surface Permittivity and Thickness from Radar Sounder Observations

Hongxia Ye
Key Lab of Wave Scattering & Remote Sensing Information, Fudan University, China

Abstract— In planetary remote sensing, e.g., explorations of Moon and Mars layering media, high frequency radar sounder has been implemented to investigation of the surface/subsurface features. This communication presents an approach to retrieve the physical properties of the surface/subsurface media. Based on our numerical simulations of rough surface scattering, radar range echo images, the dielectric permittivity and layer thickness of the planetary surface is inverted from the radar sounder echoes.

Firstly, according to the derivations of rough surface scattering with zero slope approximation and the KA approach, it is found that the received echo at nadir direction preserves the functional dependence of the surface reflectivity $P_r = \vartheta(kh, kl, \theta_i, A) \cdot R^2$. It leads to the inversion of the real part of ε_{r1} derived from the ratios of the received echo powers and the medium reflectivity. Then the surface layer depth d can be retrieved from the measured range images, $d = R_{sub}/\sqrt{\varepsilon_{r1}}$. Chosen two locations with DEM data, the imaginary part of ε_{r1} can be further determined from power attenuation, and the permittivity ε_{r2} of the subsurface medium can be similarly obtained. Employing the numerical calculation of the cratered rough surface based on the tangent plane approximation, the dataset of Mars DEM (digital elevation mapping) is applied to validate the derivations.

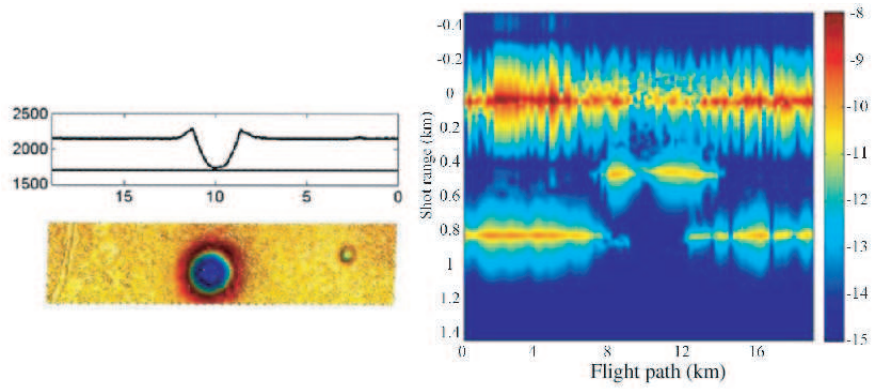

Figure 1: The range echo image.

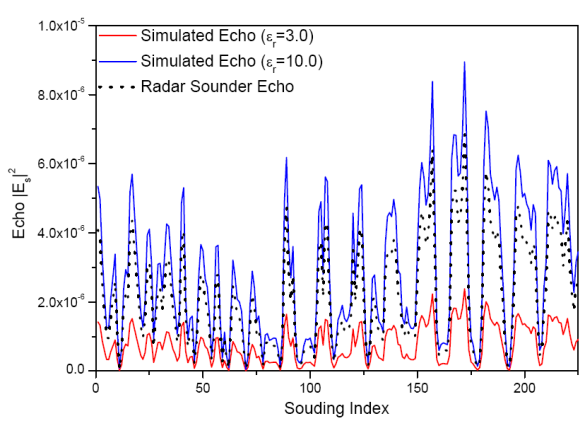

Figure 2: Echo curve along the flight path.

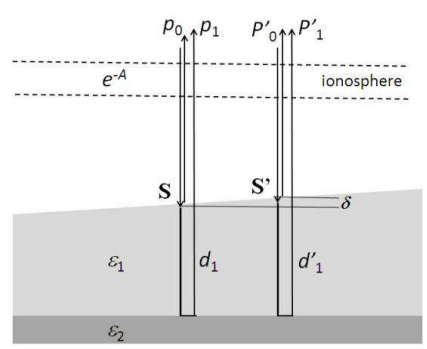

Figure 3: Inversion model for layer surface.

ACKNOWLEDGMENT

This work was supported by the National Natural Science Foundation of China No. 61001007.

Wave Propagation Characteristics of Layered Uniaxially Anisotropic Media

Y. H. Lee[1], **A. Eroglu**[2], **and J. K. Lee**[3]

[1]Telecommunication R&D Center, Samsung Electronics, Seoul, Korea
[2]Department of Engineering, Indiana University — Purdue University, Fort Wayne, IN 46805, USA
[3]Department of Electrical Engineering and Computer Science
Syracuse University, Syracuse, NY 13244-1240, USA

Abstract— Material properties carry great importance in microwave device applications due to several constraints including efficiency, loss characteristics, and agility. Use of anisotropic materials in device design brings several of these benefits due to its inherent electrical properties of the medium [1]. Hence, the understanding of the wave propagation characteristics is important in better performance of microwave devices.

The wave propagation for two layered and three layered uniaxially anisotropic media have been analyzed in [2, 3]. In [2], Fresnel coefficients were obtained with an arbitrarily oriented optic axis when the optic axis is tilted only in one direction for two-layered uniaxially anisotropic media. In [3], closed form relations for Fresnel coefficients were given with an arbitrarily oriented optic axis when the optic axis is tilted in two directions for three-layered unaxially anisotropic media. A generalized form of Snell's law for anisotropic media is given in [4] where refraction angles are obtained numerically when optic axis is normal to the boundary. Furthermore, the wave reflection and transmission at the anisotropic-isotropic interface with an optic axis tilted in one direction were studied in [5].

In this paper, wave propagation characteristics of layered uniaxially anisotropic media are investigated in detail when an arbitrary optic axis is tilted in one direction. Brewster and critical angles for the two-layered anisotropic media are obtained and numerical results depending on the material properties, polarization of the wave, and incident angles for positively and negatively uniaxial media are presented. The physical interpretation of the results including their impact on device performance is discussed. The results of this paper can be used in microwave device design for the identification of the substrate that will be implemented when anisotropic material properties are needed to improve the device performance.

REFERENCES

1. Eroglu, A., *Wave Propagation and Radiation in Anisotropic and Gyrotropic Media*, 1st Edition, Springer, 2010.
2. Lee, J. K. and J. A. Kong, "Dyadic Green's functions for layered anisotropic medium," *Electromagnetics*, Vol. 3, 111, 1983.
3. Eroglu, A., Y. H. Lee, and J. K. Lee, "Wave propagation and fresnel coefficients for three layered uniaxially anisotropic media with arbitrarily oriented optic axes," *Progress In Electromagnetics Research B*, Vol. 47, 63–86, 2013.
4. Slawinski, M. A., R. A. Slawinski, and R. J. Brown, "A generalized form of Snell's law in anisotropic media," *Geophysics*, Vol. 65, 632–637, Mar.–Apr. 2000.
5. Lee, Y. H. and J. K. Lee, "Electromagnetic wave reflection and transmission at an anisotropicisotropic interface," *IEEE Antennas and Propagation/URSI Symposium*, Chicago, IL, Jul. 18–25, 1992.

Session 4P6b
SC4: MIMO Antennas

Modeling of Ultra Wideband Antenna Arrays
Yvan Duroc, ... 1598
A Method of Dual-frequency Decoupling for Two-element MIMO Antenna
Hiroshi Sato, Yoshio Koyanagi, Koichi Ogawa, Masaharu Takahashi, ... 1599
Body-effect-adaptive Compact Wideband LTE MIMO Antenna Array with Quad Elements for Mobile Terminals
Shuai Zhang, Kun Zhao, Zhinong Ying, Sailing He, ... 1600
Multiple-feed Coupling Measurements for Luneburg Lens Antenna
Debora Franco-Vazquez, María Vera-Isasa, M. Edita De Lorenzo Rodriguez, ... 1601
Planar MIMO Antenna System for Laptop Applications
Amira El-Tokhy Ali, Deena A. Salem, ... 1602
The Study of Loss Effect on the LTE MIMO Antenna in Mobile Handset
Kun Zhao, Shuai Zhang, Zhinong Ying, Erik Bengtsson, Sailing He, ... 1603

Modeling of Ultra Wideband Antenna Arrays

Yvan Duroc
Grenoble Alpes University, LCIS, F-26900, Valence, France

Abstract— This paper presents system approaches for modeling the antenna arrays and the mutual coupling. The modeling based on the characterization of linear time invariant systems can be exploited in the case of UWB antenna arrays for different issues: the expression of the beampattern of an array of N-antennas, the determination of a time-frequency model of TX antenna arrays, and the characterization of the mutual coupling between two elements.

A Method of Dual-frequency Decoupling for Two-element MIMO Antenna

Hiroshi Sato[1, 2], **Yoshio Koyanagi**[2], **Koichi Ogawa**[3], **and Masaharu Takahashi**[1]

[1]Chiba University, Japan
[2]Panasonic Mobile Communications Co., Ltd., Japan
[3]Toyama University, Japan

Abstract— MIMO (Multiple-Input Multiple-Output) technologies using multiple antennas are situated in the stage of practical use, stepping forward to implementing in many wireless terminals, such as portable telephones and local area network devices, for the purpose of an increase in transmission rate and communication quality. There is a limited space available for installing a number of antenna elements in these wireless terminals, and consequently mutual coupling has a great impact on radiation efficiency and antenna correlation, resulting in reduction of transmission rate, due to a small distance between antenna elements. If closely spaced MIMO antennas are placed without mutual coupling, the volume occupied by antenna elements and transmission losses resulting from RF lines can be reduced, so that one can get a freedom of designing a wireless terminal in terms of a good appearance and compactness of the terminal. In previous studies, a large number of publications regarding decoupling techniques have been presented, but most of them were considered only on a single frequency.

This paper presents a method of dual-frequency antenna decoupling between closely spaced 2-element monopole. The method utilizes a newly developed decoupling circuit between two elements, realizing a reduction of mutual coupling in the two frequency bands simultaneously. A simple design procedure for the dual-frequency decoupling circuit has been demonstrated. It is confirmed that MIMO antennas using the proposed decoupling technique provide higher radiation efficiency and lower antenna correlation than those without decoupling. From this unique feature, it is anticipated that large throughput can be achieved by using MIMO antennas accommodating the proposed decoupling technique.

Body-effect-adaptive Compact Wideband LTE MIMO Antenna Array with Quad Elements for Mobile Terminals

Shuai Zhang[1,2], **Kun Zhao**[1,3], **Zhinong Ying**[3], **and Sailing He**[1,2]

[1]School of Electrical Engineering, KTH-Royal Institute of Technology, Stockholm SE-100 44, Sweden
[2]Centre for Optical and Electromagnetic Research, Zhejiang University, Hangzhou 310058, China
[3]Research and Technology, Corporate Technology Office
Sony Mobile Communications AB, Lund SE-221 88, Sweden

Abstract— A body-effect-adaptive compact wideband LTE MIMO antenna array with quad elements for mobile terminals is proposed in this paper. It can cover the bands of 750–960 and 1700–2700 MHz with a low envelope correlation coefficient. Through different combinations two of the four elements can be utilized as dual element LTE MIMO antenna array to reduce three kinds of body effects (head and hand; single hand; dual hands) with the other two ports open. Some common rules about the body effects are introduced. The conclusions about the optimal chassis locations of LTE MIMO antenna elements to improve MIMO performance are also presented.

Multiple-feed Coupling Measurements for Luneburg Lens Antenna

D. Franco-Vazquez, M. Vera-Isasa, and E. de Lorenzo Rodríguez
Universidade de Vigo, Spain

Abstract— Luneburg lenses have being studied extensively and recently have been proposed as an effective solution for high-gain commercial antenna for WiMax, 4G or LTE [1], as well as direction of arrival (DOA) estimation [2]. Since every point on the surface of an ideal Luneburg lens is the focal point for parallel radiation on the opposite side, this antenna is a valuable choice for multi-beam applications. However, the spherical symmetry and its behavior change dramatically when the lens is fed by an antenna array, leading to blockage or coupling between feeds depending on the angle of arrival of the signal. Despite this drawback, few studies of mutual coupling between feeds illuminating a Luneburg lens can be found in literature [3].

This paper presents measurements of mutual coupling and gives the critical spacing between feeders for a Luneburg lens. The antenna under test consists of a 365 mm diameter Luneburg lens illuminated by WR90 waveguides. The transmitter is placed 9 m away from the Luneburg lens to accomplish the far field condition. Transmitter and receivers are connected to a four-port Rhode & Schwartz ZVA-67 network analyzer. Measurements are obtained for several settings, varying the number of waveguide elements (one to four) and the spacing between them. In a first step, measurements involve only two WG, one in a fixed position whereas the other is moved around the lens. In a second step, the coupling between four elements placed simultaneously around the lens is measured. The S_{21} parameter given by the analyzer is recorded at every feeds arrangement within a frequency range from 8 GHz to 12 GHz for further processing. Mutual coupling measurements and conclusions about feed spacing related to the antenna performance will be presented in this communication.

REFERENCES

1. Matytsine, L., P. Lagoiski, M. Matytsine, and S. Matitsine, "Large size, lightweight, Luneburg Lenses for multi-beam antenna applications," *2012 6th European Conference on Antennas and Propagation (EUCAP)*, 2266–2270, Mar. 26–30, 2012.
2. Liang, M., X. Yu, S.-G. Rafael, W.-R. Ng, M. E. Gehm, and X. Hao, "Direction of arrival estimation using Luneburg lens," *2012 IEEE MTT-S International Microwave Symposium Digest (MTT)*, 1–3, Jun. 17–22, 2012.
3. Nikolic, N. and J. S. Kot, "Analysis of mutual coupling in a multi-beam Luneburg lens antenna using a hybrid method," *2007 IEEE Antennas and Propagation Society International Symposium*, 4999–5002, Jun. 9–15, 2007.

Planar MIMO Antenna System for Laptop Applications

Amira El-Tokhy Ali[1] and Deena A. Salem[2]

[1]Electrical and Communication Department, Modern Science and Arts University (MSA)
6th October City, Egypt
[2]Microstrip Department, Electronic Research Institute (ERI), Dokki, Cairo, Egypt

Abstract— Multi-Input Multi-Output (MIMO) antenna systems have attracted considerable interest as an effective way of improving reliability and increasing the channel capacity. MIMO antennas are suitable for wireless communication systems that require high speed and high quality transmission involving large amount of data transfer such as Wireless LAN systems, to achieve speeds that exceeds 100 Mbits/sec [2]. A significant parameter is the mutual coupling since it may marginally change the performance of the system especially at the receiver end [1].

In [3] an ISM MIMO E-shaped antenna system was presented using four back-to-back elements for laptop applications. The antennas were placed on the upper rim of the laptop screen, with separation of 0.66λ. The main concern of the research in Ref. [3] was to study the effects of electromagnetic interaction between human body and a laptop integrated MIMO antenna array from the performance viewpoint and EM dosimetry.

In this research four printed Yagi-Uda antennas were used to construct a WLAN MIMO system for laptop applications. The four elements are placed coplanar in the back corners of the laptop screen. The four elements are orthogonal to each other so that the combined radiation patterns form an omni-directional one. In the simulations the screen was modeled as a PEC sheet of different dimensions, to study the radiation pattern and mutual coupling between the antennas for different laptop sizes. The prototype element of the used antenna dimensions are $60 \times 24 \times 1.5$ mm. The operational bandwidth of the single element extended from 5.09–5.36 GHz to include WLAN applications, with gain 8.45 dB.

Simulations were carried out for different separations between the elements namely $\lambda/4$, λ, 2λ, 3λ and 4λ. The results showed very low mutual coupling that didn't exceed -20 dB for the smallest separation. The gain of the MIMO system deteriorated slightly from that of the single element to become 6.8 dB with minor variations for different separations. This may be attributed to the nature of the element used and the orientation of the elements in the MIMO system relative to each other.

REFERENCES

1. Mallahzadeh, A. R., S. Es'haghi, and A. Alipour, "Design of an E-shaped MIMO antenna using IWO algorithm for wireless application at 5.8 GHz," *Progress In Electromagnetics Research*, Vol. 90, 187–203, 2009.
2. Kurosaki, S., Y. Asai, T. Sugiyama, and M. Umehira, "SDM-COFDM scheme using feed-forward inter-channel interference canceller for broadband mobile communications," *IEEE 55th Vehicular Technology Conference, VTC*, Vol. 3, 1079–1083, May 2002.
3. Guterman, J., A. Moreira, C. Peixeiro, and Y. Rahmat-Samii, "Antenna-user interaction in MIMO-enabled laptops," *Radioengineering*, Vol. 18, No. 4, 418–424, Dec. 2009.

The Study of Loss Effect on the LTE MIMO Antenna in Mobile Handset

Kun Zhao[1,2], **Shuai Zhang**[1,2,3], **Zhinong Ying**[2], **Erik Bengtsson**[2], **and Sailing He**[1,3]

[1]Department of Electromagnetic Engineering, School of Electrical Engineering
KTH-Royal Institute of Technology, Stockholm SE-100 44, Sweden
[2]Research and Technology, Corporate Technology Office
Sony Mobile Communications AB, Lund SE-221 88, Sweden
[3]Centre for Optical and Electromagnetic Research, Zhejiang University, Hangzhou 310058, China

Abstract— Due to the bandwidth extension in the LTE communication, carrier aggregation technology is deployed in mobile handset antennas [1]. The carrier aggregation on mobile antennas can be realized by using MEMS switches, to make antennas be tunable among different frequency bands correspond to the different states of MEMS switches. However, MEMS switches will introduce the insertion loss, and can change the radiation property of antennas: Especially for MIMO antennas, not only the efficiency but also the correlation of MIMO antennas will be influenced. In this paper, we proposed a dual elements MIMO antenna for LTE mobile handset with two MEMS switches. The antenna's performances (S-parameter, efficiency and envelope correlation) with different insertion loss value from MEMS switches are presented and analyzed as well. Furthermore, as some inductors are also used in our antenna designs, this will also increase insertion loss and thus, the influence of inductors' insertion loss is also discussed in this paper. The structure of our MIMO antenna is shown in Figure 1 (a). Both elements are located on the same end of the ground plane and with C-fed structure. There are two resonates in the lower band of LTE, one is between 850 MHz to 950 MHz, and the other one can be tuned from 700 MHz to 850 MHz correspond to different states of the MEMS switch (grounding, opening or 10 nH inductor).

The insertion loss of MEMS can reduce the efficiency of our proposed antenna, which has been known well. However, for MIMO antennas, the insertion loss will also reduce the envelope correlation. In Figure 1(b), the envelop correlation with different value of insertion loss ($r = 0$, 0.25, 0.5, 1, 3, 5) when MEMS switches are in open state are shown. This is mainly due to the variation of Q factor of the antenna [2]. In the full paper, we will present more results of our study and provide detail analysis.

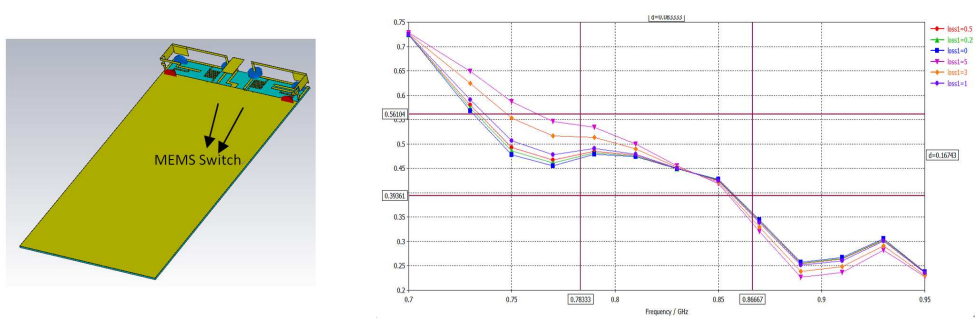

(a) (b)

Figure 1: (a) The structure of our antenna, (b) the variation of envelope correlation efficiency with different value of insertion loss when MEMS switches are in open state.

REFERENCES

1. Ghosh, A., R. Ratasuk, B. Mondal, N. Mangalvedhe, and T. Thomas, "LTE-advanced: Next-generation wireless broadband technology [Invited Paper]," *IEEE Wireless Communications*, Vol. 17, No. 3, 10, 22, Jun. 2010.
2. Zhang, S., A. Glasunov, Z. Ying, and S. He, "Reduction of the envelope correlation coefficient with improved total efficiency for mobile LTE MIMO antenna arrays: Mutual scattering mode," *IEEE Trans. Antennas and Propag.*, No. 99, Feb. 2013.

Session 4P7
Microwave and Millimeter Wave Circuits and Devices, CAD

Asymetrical Interdigital Dual-band Bandpass Filter Using Grounded inside Arms with via Holes
Ram Krishna Maharjan, Nam-Young Kim, ... 1606

Low Profile Planar Composite Inductor Design for High Power Applications
Abdullah Eroglu, ... 1607

A Design of Multi-harmonics Load Network for Class-S Power Amplifier
Girdhari Chaudhary, Phirun Kim, Yongchae Jeong, Chan-Sei Yoo, ... 1608

Systematic Study of the Effective Permittivity in a Periodically Drilled Substrate Integrated Waveguide
Rodrigo Isidro, Angela Coves Soler, Miguel Ángel Sanchez-Soriano, German Torregrosa-Penalva, Enrique Bronchalo, Maurizio Bozzi, ... 1609

Design of a Single-board Two-port Analyzer for Microwave Dielectrometry
Roberto Olmi, Filippo Micheletti, ... 1611

A 2.45 GHz High Figure-of-Merit Reflection Type Phase Shifter
François Burdin, Zyad Iskandar, Florence Podevin, Philippe Ferrari, ... 1612

A Compact Hybrid EBG Microstrip Bandstop Filter for Digital Clock Suppression in a Power Supply System
Raul Peña Rivero, A. Mendoza-Tellez, Roberto Linares-Miranda, J. A. Tirado-Mendez, ... 1613

Switchable Band-stop to All Pass Filter Using Stepped Impedance Resonator
Amine Adoum Bakhit, Peng Wen Wong, ... 1614

Study of Dynamic-periodic Transmission Lines
Jose Roberto Reyes Ayona, Peter Halevi, ... 1615

A Length-reduced Microstrip Line with Inductive and Capacitive Perturbations
Jongsik Lim, Kyunghoon Kwon, Kolet Mok, Yongchae Jeong, Sang-Min Han, Dal Ahn, ... 1616

Effect of the Ionizing Radiation on the Harmonic and Intermodulation Performance of the CMOS Inverting Amplifier
Muhammad Taher Abuelma'atti, ... 1617

Design Optimization of Microstrip Matching Circuits Using a Honey Bee Mating Algorithm Subject to the Transistor's Potential Performance
Peyman Mahouti, Salih Demirel, Filiz Gunes, ... 1618

Asymetrical Interdigital Dual-band Bandpass Filter Using Grounded inside Arms with via Holes

Ram Krishna Maharjan and Nam-Young Kim
RFIC Center, Kwangwoon University, 447-1 Wolgye-dong, Nowon-ku, Seoul 139-701, Korea

Abstract— A planar novel asymmetrical interdigital dual-band bandpass filter (BPF) based on the bended-inside arms' using via ground holes is presented for C-band applications. By optimizing the orientation of internal and external interdigital-arms with via holes, as well as consequently analyzing the transmission and reflection coefficients in scattering parameters, a useful dual-band filter response is realized. A simple planar interdigital topology is proposed with low cost dielectric material like Teflon having a low dielectric constant. Each of inside arms in the structure is short-circuited using via ground holes at one end and both of outside arms are open-circuited at the opposite sides. The interdigital arms also called resonator elements are seemed those open-circuited arms being arranged in a parallel array with the positions of the short-circuited ends. Two pass-bands are produced by a pair of grounded via holes into the bended ends of the inside arms of the asymmetrical interdigital structure. The designed interdigital resonator-based dual-band filter is fed by asymmetric feeder lines, and four transmission zeros are obtained at the both sides of bands in order to improve the band selectivity and spurious suppression. The grounded arms enhance to flow electric and magnetic field significantly. Hence the orientation of the both arms helps to build up strong electromagnetic (EM) coupling effectively through the open gaps and via holes themselves with maintaining adequate transmission and reflection coefficients for dual-band frequencies. The first and second band resonant frequencies were measured at 3.5 GHz and 5.6 GHz, respectively. The measured return losses (S_{11}) of the fabricated filter are of -18.6 dB and -19.2 dB; and insertion losses (S_{21}) are of -0.48 dB and -1.02 dB, at the first and the second resonant frequencies of the dual-band bandpass filter, respectively. The spurious suppression was measured to be less than -32 dB at out-band frequencies in all of four transmission zeros. To validate the methods applied in the design, the proposed filter is fabricated and measured. It is compared and demonstrated by the predicted simulation and measurement results that the proposed dual-band filter has both good performance and selectivity. The designed filter can be useful to the C-band application in satellite communication systems.

Low Profile Planar Composite Inductor Design for High Power Applications

A. Eroglu
Department of Engineering, Indiana University-Purdue University, Fort Wayne, IN 46805, USA

Abstract— Practical high power planar composite planar inductor design method for Industrial, Scientific and Medical (ISM) applications up to 30 MHz is given. Ceramic substrate and soft magnetic material are used to form high performance RF inductor. Different configurations of composite structure have been tested using planar electromagnetic simulators. The characteristics of the composite structure such as power loss and field distribution have been obtained. The final design is built and tested. Measured results and simulated results have been compared and found to be very close. The measured improvement and percentage change in the inductance value is shown in Fig. 1.

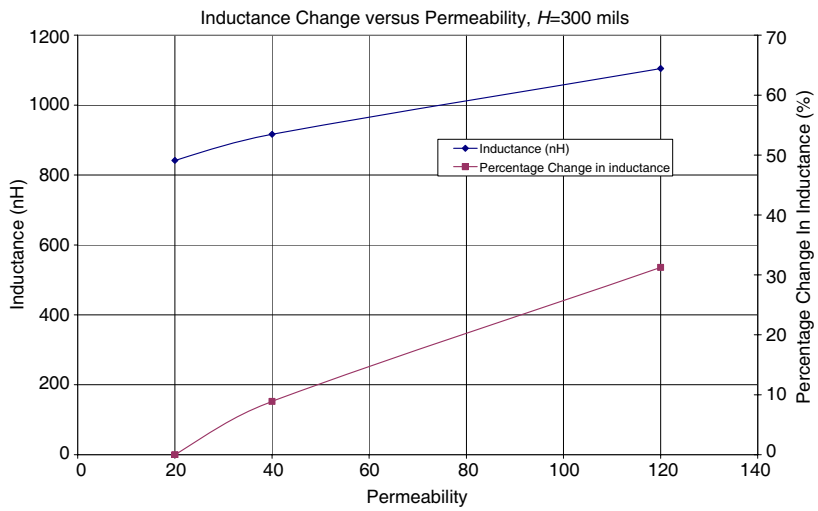

Figure 1: Change in inductance value versus magnetic material permeability.

A Design of Multi-harmonics Load Network for Class-S Power Amplifier

Girdhari Chaudhary[1], **Phirun Kim**[1], **Yongchae Jeong**[1], **and Chan-sei Yoo**[2]

[1]Chonbuk National University, Republic of Korea
[2]Korea Electronics Technology Institute (KETI), Republic of Korea

Abstract— Abstract Today's wireless communications systems require higher transmit and receive data rates in order to fulfill the demands of customers including features such as email, internet browsing, and video downloads with faster rates. This results in greater power consumption in power amplifiers. Therefore, minimizing the power consumption of wireless devices is a critical challenge for both system and circuit design. For this purpose, highly efficient switching-mode power amplifiers (PAs) such class-S are attractive solution because their high efficiency can potentially extend the battery life, lower cost of heat-sinking and increase the device reliability. In highly efficient switching mode PAs, the product of current and voltage should ideally zero at all frequencies except the fundamental frequency. Therefore, the load network for the voltage mode class-S PA is proposed in this paper. The load network for the voltage mode class-S PA requires infinite impedances at harmonic frequencies except the fundamental as shown in Fig. 1. For designing load network, the first shunt stub transmission line should be $\lambda/4$ at highest harmonic frequency which will be transferred to open by transmission line of electrical length $\theta_1 = \lambda/4$ at this harmonic frequency. Similarly, second shunt stub of $\lambda/4$ long at second highest harmonic frequency is added after line of electrical length θ_2. This line will help to make total electrical length of the series transmission line $\theta_1 + \theta_2 = \lambda/4$ at this frequency and will transfer impedance at open (Fig. 1). This process is repeated until lowest harmonic frequency. To verify design concept, the load network for $n = 3$ (2nd and 3rd harmonic suppression) at the fundamental frequency (f_0) of 0.955 GHz is designed and fabricated as shown in Fig. 2. From simulation and measurement results, it was found that load impedance at harmonic frequencies ($3f_0$ and $2f_0$) is almost infinite and is matched to $2\,\Omega$ at f_0 respectively, as shown in Figs. 3 and 4. Similarly, the attenuation characteristics are greater than 30 dB at harmonic frequencies as shown in Fig. 5. The proposed design method is applicable for multi-harmonics and will help in efficiency enhancement of the voltage-mode class-S PA.

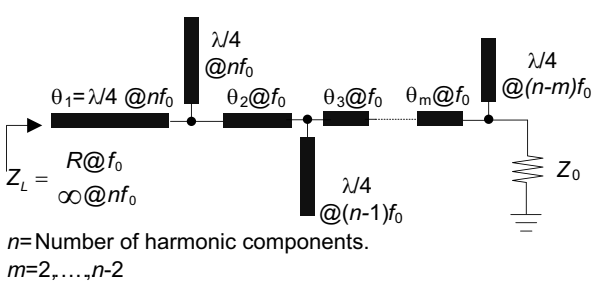

Figure 1.

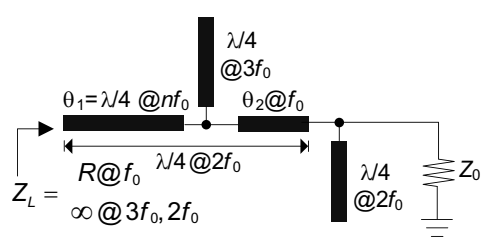

Figure 2.

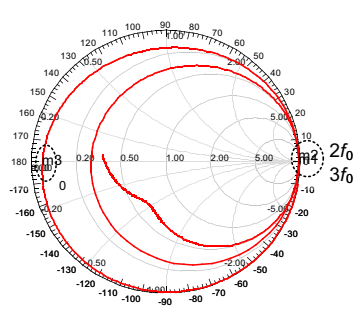

Figure 3.

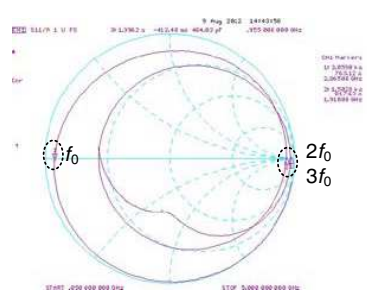

Figure 4.

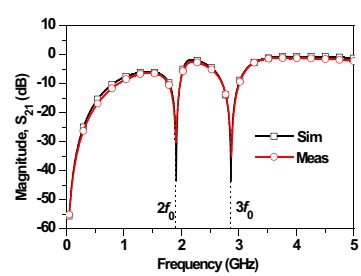

Figure 5.

Systematic Study of the Effective Permittivity in a Periodically Drilled Substrate Integrated Waveguide

R. Isidro[1], **A. Coves**[1], **M. A. Sánchez-Soriano**[2], **G. Torregrosa**[1], **E. Bronchalo**[1], **and M. Bozzi**[3]

[1]Departamento de Ingeniería de Comunicaciones
Universidad Miguel Hernández de Elche, Elche, Alicante 03202, Spain
[2]Lab-STICC, Université Bretagne Occidentale, Brest, France
[3]Department of Electrical, Computer and Biomedical Engineering
University of Pavia, Pavia, Italy

Abstract— In recent years, many papers have been published on a new type of transmission line called SIW (Substrate Integrated Waveguide) [1, 2]. This low-cost realization of the traditional rectangular waveguide takes the advantages of planar lines for easy integration with other circuits, and low radiation losses of waveguides. Furthermore, this new technology has been used for making a large number of microwave devices such as filters, antennas, multiplexers, etc. [3–5]. On the other hand, the use of different dielectric materials along a rectangular guide [6] can be applied to the design of filtering structures [6].

This paper presents the results of a systematic study of the effective permittivity in a SIW waveguide in which arrays of air holes are added along the waveguide in order to synthesize a lower effective permittivity. The study is performed by using the commercial software tool HFSS [7]. For each geometry analyzed, only one period along the propagation direction is simulated, and by applying periodic conditions at each edge of the periodic cell, the obtained cutoff frequency of the waveguide provides its effective permittivity. Different holes patterns are analyzed, and for each one, the effect of the variation of the hole diameters is also studied. Such study demonstrates that the effective permittivity in the drilled waveguide can not be rigorously approximated through a surface weighted average, mainly due to the drilling of the metal surfaces. The radiation effect by the air holes in the drilled SIW has also been studied, concluding that radiation losses are not important if some design considerations are followed.

The results of this study will be used in a new topology of bandpass filters in SIW technology based on coupled cavities of different permittivity, which is achieved by the introduction of air holes in the lower relative permittivity sections. In the case of drilled waveguides, a decrease of the dielectric losses, which are more relevant at high frequencies, is expected due to the removal of material.

ACKNOWLEDGMENT

This work was supported by the Ministerio de Ciencia e Innovación, Spanish Government, under the coordinated project TEC2010-21520-C04-02.

REFERENCES

1. Deslandes, D. and K. Wu, "Design consideration and performance analysis of substrate integrated waveguide components," *32nd European Microwave Conference Proceedings*, Vol. 2, 881–884, Sep. 2002.
2. Cassivi, Y., L. Perregrini, P. Arcioni, M. Bressan, K. Wu, and G. Conciauro, "Dispersion characteristics of substrate integrated rectangular waveguide," *IEEE Microw. Wirel. Compon. Lett.*, Vol. 12, No. 9, 333–335, Sep. 2002.
3. Yan, L., W. Hong, G. Hua, J. Chen, K. Wu, and T. J. Cui, "Simulation and experiment on SIW slot array antennas," *IEEE Microw. Wirel. Comp. Lett.*, Vol. 14, No. 9, 446–448, Sep. 2004.
4. Chen, X. P., K. Wu, and Z. L. Li, "Dual-band and triple-band substrate integrated waveguide filters with Chebyshev and quasielliptic responses," *IEEE IEEE Trans. Microw. Theory Tech.*, Vol. 55, No. 12, 2569–2578, Sep. 2007.
5. Bozzi, M., A. Georgiadis, and K. Wu, "Review of substrate integrated waveguide (SIW) circuits and antennas," *IET Microw. Antennas Propagat.*, Vol. 5, No. 8, 909–920, Jun. 2011.
6. Gómez, A., A. Lakhtakia, A. Vegas, and M. A. Solano, "Band-gaps electromagnéticos unidimensionales en guía de onda rectangular," *Actas del XVIII Simposium Nacional de la Unión Científica Internacional de Radio*, La Coruña (España), Sep. 2008.

7. *HFSS: 3D Full-wave Electromagnetic Field Simulation*, Available: http://www.ansoft.com/products/hf/hfss, 2007.

Design of a Single-board Two-port Analyzer for Microwave Dielectrometry

R. Olmi and F. Micheletti
Institute for Applied Physics — National Research Council, IFAC-CNR
Via Madonna del Piano, 10, Sesto Fiorentino (Firenze) 50019, Italy

Abstract— Several diagnostics applications based on the measurement of the dielectric properties or on the detection of dielectric contrast between materials require using an impedance analyzer as the heart of the diagnostic system.

Applications of that kind of instruments exist in very different fields, from the diagnostics/monitoring of cultural heritage, to the on-field analysis of snow or soils, to industrial applications in the agri-food sector and more. In particular, the system here described is part of a diagnostics equipment used for the detection and measurement of sub-surface moisture content and salts in artistic wall paintings.

Such applications can greatly benefit from the availability of low-cost measurement systems fulfilling a number of basic requirements, including low-weight and reduced size and low-consumption battery operation. Often also an easy to use solution is required where final equipment should be used by non-specialized people.

In this work design solutions are proposed for realizing a single-board microwave system suitable for two-port transmission measurement. The system has been purposely designed to operate with a two-port resonant sensor for dielectric spectrometry, measuring the scalar transmission coefficient between the two ports, but it can be easily transformed in a one-port device for measuring the vector reflection coefficient, that is a general purpose low-cost vector network analyzer.

A system-level approach is adopted, based on the choice of a commercially available single-chip device for differential gain measurement and phase detection.

RF power and frequency requirements are shown presenting a block schematic of the different sections that are separately discussed and a power budget analysis of the whole system is developed.

Specific attention is posed on typical design issues that can invalidate system working or, at least, limit its performance.

A 2.45 GHz High Figure-of-Merit Reflection Type Phase Shifter

F. Burdin[1], **Z. Iskandar**[2], **F. Podevin**[1], **and P. Ferrari**[1]

[1]IMEP-LAHC, University of Grenoble, UMR CNRS 5130, Grenoble, France
[2]LAIR/DACLE, CEA/Léti, 17 rue des Martyrs, 38054 Grenoble cedex 9, France

Abstract— Phase shifters are key components for the fabrication of phased arrays, which are nowadays attractive devices in order to address modern telecommunications schemes where mobile networking and autonomy in terms of energy are mandatory. Phase shifters can be realized by three main approaches, (i) periodically loading a transmission line with tunable elements (i.e., varactors, MEMS, ...) [1], (ii) switching transmission lines having different electrical lengths [2], and (iii) loading a 3-dB coupler by two identical reflective loads, e.g. the Reflection Type Phase Shifter (RTPS) topology [3]. Among these three solutions, the RTPS offers a good compromise between matching, surface area and Figure-of-Merit (FoM), defined as the ratio of the maximum phase shift over the maximum insertion loss in dB. The objective of this paper is to show the design and characterization of a 2.45 GHz RTPS optimized for a high FoM and low magnitude imbalance. The RTPS topology studied herein is given in Figure 1.

The 3-dB hybrid coupler was loaded by a transmission line (Z_1, θ_1) in cascade with a varactor modeled by a variable capacitance C in series with a resistance R. Z_T and Z_{IN} represent the impedance seen at the coupler output, in direction of the coupler for Z_T and of the varactor for Z_{IN}. The equations corresponding to this topology were carried out and the RTPS was optimized by varying all the design elements (Z_T, Z_1, θ_1, $C_{\max}$ and $C_{\min}$).

The optimized RTPS was realized in a PCB technology for a 2.45-GHz working frequency. Rogers RO4003c substrate was used (dielectric constant $\varepsilon_r = 3.38$, thickness 813 µm), with MACOM varactors MA46H071, giving a variable capacitance between $C_{\min} = 0.45$ pF and $C_{\max} = 2.72$ pF. $Z_1 = 100\,\Omega$, $\theta_1 = 35°$ and $Z_T = 20\,\Omega$. The measured relative phase shift obtained by varying the varactor capacitance from $C_{\min}$ to $C_{\max}$ is given in Figure 2. The maximum phase shift reaches 243° for a DC bias varying from 0 ($C_{\max}$) to 20 V ($C_{\min}$) . The insertion loss varies from 0.43 dB to 0.89 dB, leading to a FoM equal to 273°/dB, much higher than the current state-of-the-art.

The detailed design methodology will be given in the final paper, along with a careful comparison with the state-of-the-art.

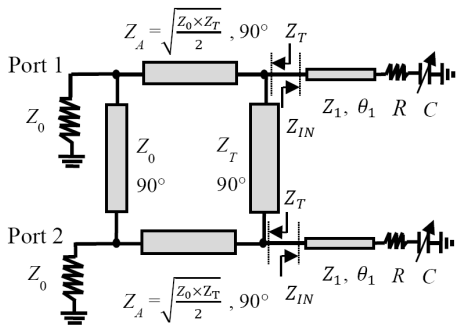

Figure 1: RTPS topology.

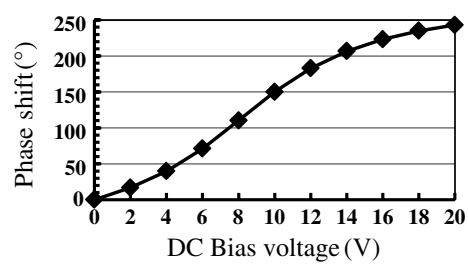

Figure 2: Measurement results.

REFERENCES

1. Bourtoutian, R., A. Jrad, and P. Ferrari, "A tapered distributed analog tuneable phase shifter with low insertion and return loss," *IEE Electronics Lett.*, Vol. 41, No. 15, 852–854, July 2005.
2. Gong, S., H. Shen, and N. S. Barker, "A 60-GHz 2-bit switched-line phase shifter using SP4T RF-MEMS switches," *IEEE Transactions on Microwave Theory and Techniques*, Vol. 59, No. 4, 894–900, April 2011.
3. Hardin, R. N., E. J. Downey, and J. Munushian, "Electronically-variable phase shifters utilizing variable capacitance diodes," *Proc. IRE*, Vol. 48, 944–945, May 1960.

A Compact Hybrid EBG Microstrip Bandstop Filter for Digital Clock Suppression in a Power Supply System

R. Peña-Rivero, **A. Mendoza-Tellez**, **R. Linares y Miranda**, **and J. A. Tirado-Mendez**
Laboratorio de Compatibilidad Electromagnetica Escuela Superior de Ingeniería Mecanica y Electrica
Instituto Politécnico Nacional, UPALM. Av. IPN s/n Col. Lindavista, México DF 07738, Mexico

Abstract— In this paper, a compact novel wide band microstrip bandstop filter for digital clock suppression in power supply systems is presented. Filter combines the effects of electromagnetic bandagap structure (EBG) with surface mount technology (SMT) capacitor. Parameters are optimized via numerical simulations to achieve a stopband of 12 GHz for a reject of the first nine harmonics of a 1.35 GHz digital clock frequency. A FR4 substrate of relative permittivity 4.7 is used, where mushrooms like EBG structure of rectangular patches connected to ground by vias are built. Four SMT capacitor of 1 pF to the EBG structure are added. With this is possible to obtain a rejection band at −3 dB form 1 GHz to 13.1 GHz within a small circuit area of 225 mm^2.

Switchable Band-stop to All Pass Filter Using Stepped Impedance Resonator

A. A. Bakhit and W. P. Wong
Universiti Teknologi PETRONAS, Bandar Seri Iskandar, 31750 Tronoh, Perak, Malaysia

Abstract— The exponential growth of modern wireless communications market creates an unprecedented demand for compact-size, low-cost, high-performance and a reconfigurable filter. Due to this recent development, much attention has been devoted to compact microwave reconfigurable filters. The first condition that must be met by a reconfigurable filter is that it must be capable of inducing microwave transmitters and receivers to be adaptable to multi-band operations using a single filter, which is highly desirable in the current wireless communication technology. Among the many techniques found in recent literature, reconfigurable filters for cognitive system prove to be a popular technique. Up till now, different structures of micro-strip reconfigurable filters have been proposed. These structures are innovative, however, a switchable band-stop to all pass filters suitable for the integration into a switchable, narrow band system has not been demonstrated as of yet. This paper is concerned with the design and the implementation of a novel switchable band-stop to all pass filters with new capabilities not found in previous designs. This filter is realized by using a stepped impedance resonator, with the PIN diodes incorporated into the topology as switching elements. It provides two modes of operation under two conditions; in the first condition, the filter will produce a band-stop response when the PIN diodes are switched '*ON*', and in the second condition, the filter will produce an all pass response when the PIN diodes are switched '*OFF*'. Theoretical analysis of the approach is presented in this paper, and the feasibility of the approach has been experimentally verified with a micro-strip circuit prototype. Figure 1(a) shows the photography of the microstrip circuit prototype. The measured result shows that the insertion loss S (1, 2) in band-stop mode of operation is around 38 dB, and the return loss S (1, 1) is around 27 dB. For the all-pass mode of operation, the insertion loss is totally at at 0 dB, and the return loss is around 17 dB, which makes it suitable for wireless communication.

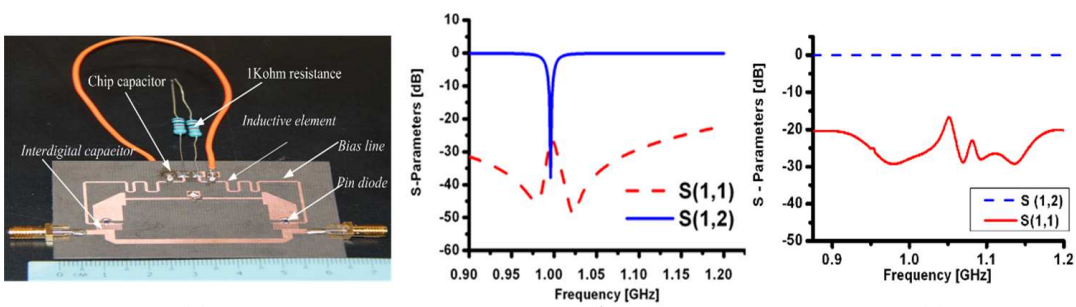

(a) (b) (c)

Figure 1: (a) Photography of switchable band-stop to all pass filter, (b) band-stop mode of operation, (c) all pass mode of operation.

Study of Dynamic-periodic Transmission Lines

J. Roberto Reyes-Ayona and P. Halevi
Instituto Nacional de Astrofisica Óptica y Electrónica
Luis Enrique Erro # 1, Sta. María Tonantzintla, Puebla 72840, Mexico

Abstract— When an incident wave of frequency ω excites a dielectric medium whose dielectric constant $\varepsilon r(t)$ varies periodically in time at a frequency $\Omega/(2\pi)$, the transmitted and reflected waves exhibits the harmonics (ω-$n\Omega$ with $n = 0, \pm 1, \pm 2 \ldots$) and the band structure is periodic in the modulation frequency Ω rather than in the wavevector k [1]. The transmission and reflection can be resonant if the exciting frequency ω equals $n\Omega/2$, with n an odd integer, and for slab thicknesses that meet a specific condition [2]. In the long-wavelength limit this medium can be realized in the microwave region by means of a transmission line (TL) that consists of a linear periodic array of cells of length a, composed of series inductors L and time changing shunt capacitors (varactors) $C(t)$ ($C(t) = \bar{C}[1 + M \sin \Omega t]$ where $\bar{C}$ is the static capacitance value and M is the modulation strength ≤ 1). For the long-wave limit ($ka \ll 1$), a dynamic TL can be characterized by the following effective permittivity and permeability [3]:

$$\varepsilon_o \varepsilon_r(t) = \bar{C}(t)/a, \quad \mu_0 \mu_r = L/a, \tag{1}$$

Here we present a more realistic study of the TL which considers the effect of finite TL copper conductance (the inductors are made of copper lines) modeled as a series resistance R, dielectric losses modeled as a shunt conductance G, and the modulation source modeled as a voltaje source V_Ω and resistance R_Ω (Figure 1).

Dispersion curves present frequency periodicity and could present wavevector bandgaps (instead of frequency bandgaps). Figure 2(a) shows four bands for a dynamic medium and a dynamic TL with $L = 2\,\text{nH}$, $\bar{C} = 2\,\text{pF}$, $G = 0.001$, $\Omega/2\pi = 1.5\,\text{GHz}$. Figure 2(b) shows four bands for the same values excepting $\Omega/2\pi = 2\,\text{GHz}$. For certain values of M (R or Ω_N), the imaginary part of the wavevector k become zero at $\omega = \Omega/2$, if and only if, the real part of k has a bandgap. $\Omega_N = \Omega/\omega_0$, where ω_0 is the static resonant frequency.

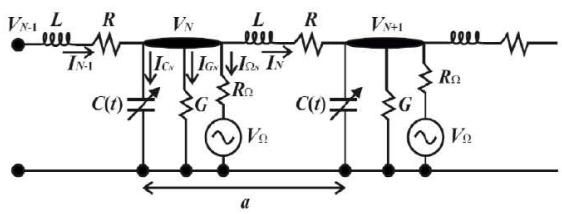

Figure 1: Unit cell of TL.

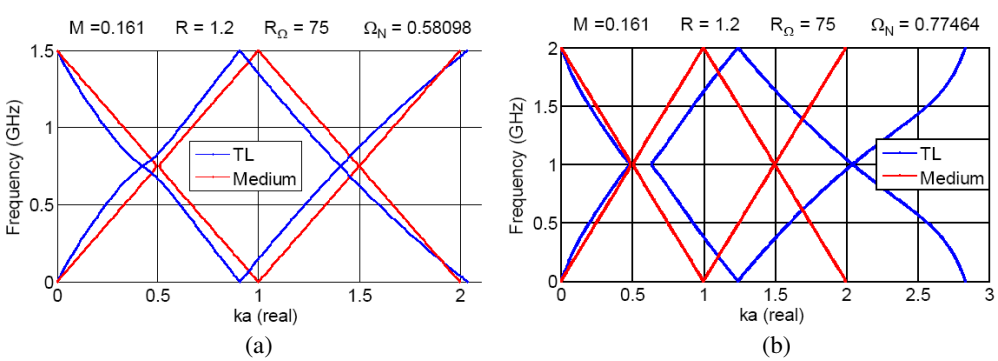

Figure 2: Dispersion curves for (a) $\Omega_N = 0.58098$, and (b) $\Omega_N = 0.77464$.

REFERENCES

1. Zurita-Sánchez, J. R., P. Halevi, and J. C. Cervantes-González, *Phys. Rev. A*, Vol. 79, 053821, 2009.
2. Zurita-Sánchez, J. R. and P. Halevi, *Phys. Rev. A*, Vol. 81, 053834, 2010.
3. Halevi, P., U. Algredo-Badillo, and J. R. Zurita-Sánchez, *Proc. SPIE*, Vol. 8095, 80950I, 2011

A Length-reduced Microstrip Line with Inductive and Capacitive Perturbations

Jongsik Lim[1], **Kyunghoon Kwon**[1], **Kolet Mok**[2], **Yongchae Jeong**[2], **Sang-Min Han**[1], **and Dal Ahn**[1]

[1]Soonchunhyang University, Republic of Korea
[2]Chonbuk National University, Republic of Korea

Abstract— It is well known that the characteristic line impedance (Z_c) of ideal transmission lines strongly depends on the ratio of equivalent inductance (L) to capacitance (C) per unit length, and is expressed as $Z_c = (L/C)^{1/2}$. Fig. 1 shows the normal structure of microstrip line. The properties of microstrip transmission lines change when a periodic perturbation structure is added to dielectric substrates. Representatively, if DGS (defected ground structure) or PBG (photonic bandgap) patterns (Fig. 2), which are equivalently inductive-adding structures, combine with a normal microstrip line, the Z_c and electrical length increase. So the line width increases and physical length becomes shorter if compared to normal microstrip lines for a specified line impedance and electrical length. Similarly when a capacitive-adding perturbation such as SIAD (substrate integrated artificial dielectric) structure (Fig. 3) is combined with a microstrip line, the Z_c becomes lower and electrical length increases. So the line width is getting narrower and physical length becomes shorter for the specified line impedance and electrical length. Even though the physical length can be reduced effectively by adding a perturbation structure, however sometimes the resultant line width may be too narrow to be realized or abnormally wide to be treated as a transmission element In order to solve this problem, the microstrip line structure with both DGS(inductive)- and SIAD(capacitive)-adding perturbations is proposed in this work (Fig. 4) Because the inductive- and capacitive-adding perturbation structures lead to the increased and decreased line width, respectively, the final line width with both perturbations is close to that of the normal microstrip line for a specified Z_c (Table 1). It is noted that the physical length of the microstrip line with both perturbations for a fixed electrical length is shorter than the other three lines; normal one, DGS-loaded one, and the microstrip line with SIAD structure So the proposed microstrip line with both perturbations can be widely applied in reducing the size of high frequency circuits.

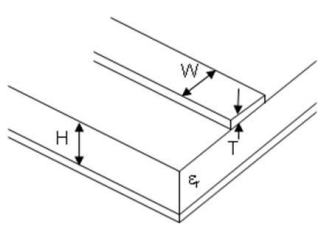

Figure 1.

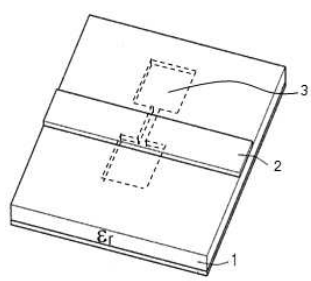

Figure 2.

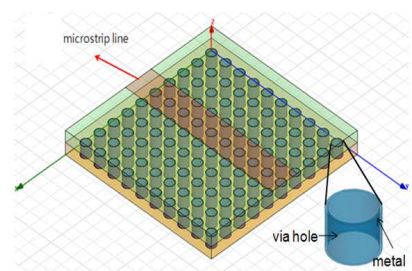

Figure 3.

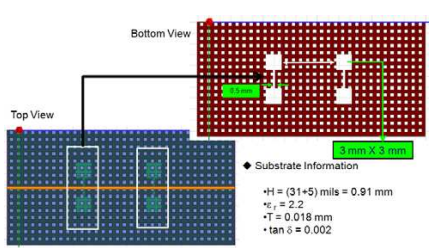

Figure 4.

	Normal Line	With DGS	With SIAD	With DGS+SIAD
Width (W)	2.87	3.87	1.28	1.68
$\lambda/4$@1 GHz	53.71	44.31	41.92	33.77
Remarks	$H = (31+5)$ mils $= 36$ mils, $\varepsilon_r = 2.2$, $T = 0.018$ mm, $Z_c = 50\,\Omega$, Unit = mm			

Table 1.

Effect of the Ionizing Radiation on the Harmonic and Intermodulation Performance of the CMOS Inverting Amplifier

Muhammad Taher Abuelma'atti
King Fahd University of Petroleum and Minerals, Box 203, Dhahran 31261, Saudi Arabia

Abstract— This paper presents a simple mathematical model for the transfer characteristic of the CMOS inverting amplifier. The model, basically a Fourier series, can accommodate the influence of the irradiation and can yield closed-form expressions for the amplitudes of the harmonic and intermodulation components of the output voltage resulting from a two-tone input voltage. The results show that the harmonic and intermodulation performance of the CMOS inverter is strongly dependent on the irradiation condition and the amplitudes of the input tones.

Design Optimization of Microstrip Matching Circuits Using a Honey Bee Mating Algorithm Subject to the Transistor's Potential Performance

Peyman Mahouti, Salih Demirel, and Filiz Güneş
Department of Electronics and Communication Engineering, Yıldız Technical University Istanbul, Turkey

Abstract— In this work, the same Honey Bee Mating Optimization as in [1] this time is applied to design of the input and output microstrip matching circuits to provide the source Z_S and load Z_L terminations ensuring the selected performance quadrate to the transistor, respectively for the desired performance triplets (V_{in}, $F(f)$, G_T) [1, 2]. In this implementation, the populations of the Queen Candidates and Drones are defined in terms of the widths $\vec{W}$ and lengths $\vec{\ell}$ of the input and output microstrip matching circuits to determine the fitness values or estrogen values of the bees. Among the female bees probabilistically mating with the drones, the one with the fittest gens or estrogen level will be chosen as the Queen bee, in the other words, the best solution for optimization problem. On the other hand, the multi-objective design optimization procedure of the amplifier is reduced into the single objective design procedures of the input/output matching circuits using Darlington realizations of the quadrate Z_S, Z_L terminations. It can be concluded that in this work, all the constituents of the HBMO design optimization are defined rigorously and at the output, all the microstrip lengths and widths of the input and output matching circuits are obtained to be printed on a selected dielectric substrate. Finally as a work example the design of a typically ultra-wide band low noise amplifier with NE3512S02 is presented on a substrate of Rogers 4350 ($\varepsilon_r = 3.48$, $h = 1.524\,\text{mm}$, $\tan\delta = 0.003$, $t = 0.001\,\text{mm}$) within 2–5 GHz satisfying ($V_{in} = 1.5$, $F = F_{\min}(f)$, $G_T = 10\,\text{dB}$) triplet using the T type of microstrip matching circuit and verified using the circuit simulator AWR.

REFERENCES

1. Mahouti, P., F. Güneş, and S. Demirel, "Honey-bees mating algorithm applied to feasible design target space for a wide-band front-end amplifier," *IEEE International Conference on Ultra-Wideband*, 251–255, 2012.
2. Güneş, F., M. Güneş, and M. M. Fidan, "Performance characterisation of a microwave transistor," *IEE Proceedings-Circuits, Devices and Systems*, Vol. 141, No. 5, 337–344, 1994.
3. Afshar, A., O. B. Haddad, M. A. Marino, and B. J. Adams, "Honey-bee mating optimization (HBMO) algorithm for optimal reservoir operation," *Journal of the Franklin Institute*, Vol. 344, 452–462, 2007.

Session 4P8a
Medical Electromagnetics, Biological Effects

Electromagnetic Information Delivery as a New Perspsctive in Medicine
Alberto Foletti, Settimio Grimaldi, Mario Ledda, Antonella Lisi, ... 1620

A Novel Conformal Antenna for Ingestible Capsule Endoscopy in the MedRadio Band
Konstantinos A. Psathas, Asimina Kiourti, Konstantina S. Nikita, ... 1622

Impact of Electromagnetic Field Generated by Mobile Phone on Prooxidant-antioxidant Balance in Selected Internal Organs of Rats
Pawel Sowa, Karolina Sieron-Stoltny, Grzegorz Jan Cieslar, Aleksander Sieron, ... 1624

Electric and Magnetic Fields Due to the Operation of Roof Mounted Photovoltaic Systems
Anastasia S. Safigianni, Aristotle M. Tsimtsios, ... 1625

Experimental Study about the Thermal Effects of EM Sources on Human Skin Tissue
A. Yasin Citkaya, S. Selim Seker, Osman Cerezci, ... 1626

Optimized Nanocage for Cancer Photothermal Therapy and Comparison with Other Nanoparticles
Sameh Kessentini, Dominique Barchiesi, ... 1627

Electromagnetic Information Delivery as a New Perspsctive in Medicine

Alberto Foletti[1,2], **Settimio Grimaldi**[2], **Mario Ledda**[2], **and Antonella Lisi**[2]

[1]Department of Innovative Technologies
University of Applied Sciences of Southern Switzerland-SUPSI, Galleria, Manno 2,6928, Switzerland
[2]Institute of Translational Pharmacology, National Research Council-CNR
Via Fosso del Cavaliere, 100, Rome 00133, Italy

Abstract— Since the time of Hyppocrates it is very well known that is possible to transfer biochemical information for the treatment of human diseases by using molecules as active principle.

This strategy has been the most efficient one until the time of Becker [1–8] and Fröhlich [9, 10] when we become aware that it was also possible transfer effective information to biological target by the use of electromagnetic field in the ELF range.

Later on Benveniste suggested that for every chemical molecule there is only and only one electromagnetic image a kind of electromagnetic signature.

Benveniste and coworkers [11] demonstrated that picking up the physical signals of a chemical compound and transferring it to an aqueous system by mean of an electronic device this procedure was mimicking the same effect of the chemical source molecule.

The transfer of the physical activity is probably mediated and can be amplified by water biophysical re-patterning [12–14].

Electromagnetic Information Transfer of Specic Molecular Signals according to previous report [15–17] and ours [18, 19] was performed in order to understand the possible role of water in mediating the electro-magnetic information transfer of biological active molecules such as retinoic acid (RA).

The electromagnetic information signals from the retinoic acid solution (RA-EMIT) was captured and transferred to the target by a commercially available oscillator (Vegaselect 719).

The retinoic acid signals was transferred to a cell culture medium (RPMI).

Neuroblastoma Cell Line (LAN-5) was seeded and grown up for four days in presence of Retinoic Acid signal and/or chemical molecule.

The experimental findings demonstrated that the RA signal shows the tendency to behave as a differentiating agent such as the original retinoic acid molecule.

REFERENCES

1. Becker, R. O. and D. G. Murray, "A method for poducing cellular dedifferentiation by means of very small electrical currents," *Transactions of the New York Academy of Sciences*, Vol. 29, No. 5, 606–615, 1967.
2. Friedman, H., R. O. Becker, and C. H. Bachman, "Effect of magnetic field on reaction time performance," *Nature*, Vol. 213, No. 5079, 949–950, 1967.
3. Becker, R. O., "The electrical control of growth processes," *Med. Times*, Vol. 96, No. 6, 657–669, 1967.
4. Becker, R. O., "The basic biological data transmission and control system influenced by electrical forces," *Annals of the New York Academy of Sciences*, Vol. 238, 236–241, 1974.
5. Baker, B., J. Spadaro, A. Marino, and R. O. Becker, "Electrical stimulation of articular cartilage regeneration," *Annals of the New York Academy of Sciences*, Vol. 238, 491–499, 1974.
6. Marino, A. A. and R. O. Becker, "Biological effect of extremely low frequency electric and magnetic field: A review," *Physiol. Chem. Phys.*, Vol. 9, No. 2, 131–147, 1977.
7. Becker, R. O., "Electromagnetism and the revolution in medicine," *Acupunct Electrother Res.*, Vol. 12, No. 1, 75–79, 1987.
8. Becker, R. O., "Induced dedifferentiation: a possible alternative to embryonic stem cell transplant," *Neuro Rehabilitation*, Vol. 17, No. 1, 23–31, 2002.
9. Fröhlich, H., "Coherent electric vibrations in biological systems and the cancer problem," *IEEE Transactions on Microwave Theory and Techniques*, Vol. 26, 613–617, 1978.

10. Fröhlich, H., "The extraordinary dielectric properties of biological molecules and the action of enzymes," *Proc. Nat. Acad. Sci.*, Vol. 72, 4211–4215, USA, 1975.
11. Thomas, Y., M. Schiff, L. Belkadi, P. Jurgens, L. Kahhak, and J. Benveniste, "Activation of human neutrophils by electronically transmitted phorbol-myristate acetate," *Medical Hypotheses*, Vol. 54, 3–39, 2000.
12. Smith, C. W., "Quanta and coherence effects in water and living systems," *J. Altern. Complement. Med.*, Vol. 10, No. 1, 69–78, 2004.
13. Del Giudice, E., G. Preparata, and M. Fleischman, "QED coherence and electrolyte solutions," *Journal of Electroanalytical Chemistry*, Vol. 482, 110–116, 2000.
14. Del Giudice, E., M. Fleischmann, G. Preaparata, and G. Talpo, "On the 'unreasonable' effects of ELF magnetic field upon a system of ions," *Biolectromagnetics*, Vol. 23, No. 7, 522–530, 2002.
15. Endler, P. C., M. Citro, W. Pongratz, C. W. Smith, C. Vinattieri, and F. Senekowitsch, "Transfer of molecular information using a bioresonance instrument (BICOM) in amphibian trial," *Acta Medica Empirica*, Vol. 44, No. 3, 1–16, 1995.
16. Kreisl, P., "Test on the transduction of acetic acid information via an electronic amplifier," *Acta Medica Empirica*, Vol. 47, No. 3, 17–24, 1998.
17. Heredia-Rojas, J. A., A. C. Torres-Flores, A. O. Rodriguez-De la Fuente, B. D. Mata-Cardenas, L. E. Rodriguez-Flores, M. P. Barron-Gonzales, A. C. Torres-Pantoja, and G. M. Alcocer-Gonzales, "Entamoeba histolytica and trichomonas vaginalis: Trophozoite growth inhibition by metronidazole electro-transferred water," *Exp. Parasitol.*, Vol. 127, No. 1, 80–83, 2011.
18. Foletti, A. and S. Grimaldi, "Differentiation of human LAN-5 neuroblastoma cells by electronically transmitted retinoic acid (RA)," *PIERS Online*, Vol. 6, No. 6, 518–522, 2010.
19. Foletti, A., S. Grimaldi, M. Ledda, and A. Lisi, "Electromagnetic information transfer of specific molecular signals mediated through aqueous systems: Experimental findings on two human cellular models," *PIERS Proceedings*, 1590–1592, Marrakesh, Morocco, Mar. 20–23, 2011.

A Novel Conformal Antenna for Ingestible Capsule Endoscopy in the MedRadio Band

Konstantinos A. Psathas, **Asimina Kiourti**, **and Konstantina S. Nikita**
Biomedical Simulations and Imaging Laboratory (BIOSIM)
School of Electrical and Computer Engineering
National Technical University of Athens
9 Iroon Polytechniou Str., Athens 15780, Greece

Abstract— Traditional wired endoscopy methods do not allow the entire examination of the small intestine (length of 6.5–7.5 m) and offer limited diagnostic capabilities [1]. Nowadays, the development of ingestible microcapsules with imaging capabilities and embedded sensors and antennas enables non-invasive wireless capsule endoscopy (WCE), and has the potential to revolutionize wireless medical telemetry. Such endoscopy capsules are designed to send images of the gastrointestinal (GI) tract in real-time and at high data rates, thus requiring transmitting antennas with wide-bandwidth capabilities. Omni-directivity is also a pre-requisite for ingestible antennas in order to transmit signals independent of their position and orientation which are, in principle, unknown. Given the miniature dimensions of the capsule and the limited space left from the integration of sensors, electronics and batteries [1, 2], size becomes yet another significant concern for ingestible antennas. Miniaturization becomes even more intriguing in the widely-used low-frequency band of Medical Device Radiocommunication Services (MedRadio, 401–406 MHz) [3].

In this work, a miniature conformal antenna is proposed for ingestible capsule endoscopy in the MedRadio band. The antenna exhibits a microstrip structure and is designed on a flexible substrate material which allows its conformance to the shape of the capsule (Rogers RT/duroid 5880, $\varepsilon_r = 2.2$). A flexible superstrate covers the structure to preserve its biocompatibility and robustness. Thickness of the substrate and superstrate layers is limited to 0.127 mm, each. The conformal radiating patch is of square shape, with meanders being inserted to increase the length of the current flow and decrease its size to 18 mm × 18 mm. Design of the proposed antenna while wrapped around a cylindrical capsule (radius of 5 mm, height of 18 mm) is shown in Fig. 1(a). Finite Element (FE) numerical simulations are performed assuming the capsule to be immersed inside muscle tissue. The exhibited reflection coefficient ($|S_{11}|$) frequency response and 3D far-field gain radiation pattern are shown in Figs. 1(b) and 1(c), respectively. The antenna resonates at 403 MHz with a wide 10 dB-bandwidth of 31 MHz, and exhibits nearly omni-directional radiation with maximum far-field gain of −30 dB. Assuming a power of 1 mW incident to the antenna, the 1 g- and 10 g-averaged Specific Absorption Rate (SAR) values in the surrounding muscle tissue do not exceed 4.78 W/kg and 25.58 W/kg, respectively.

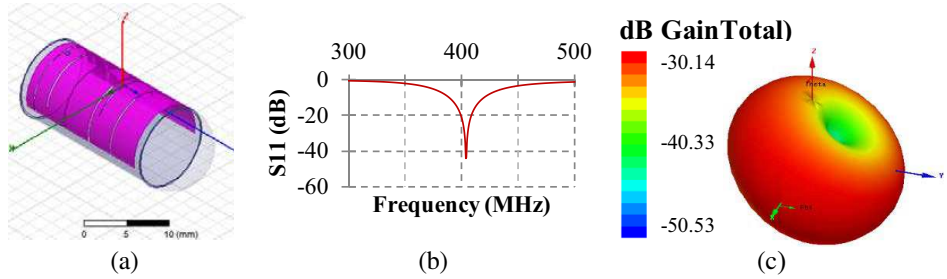

Figure 1: Proposed ingestible antenna: (a) geometry, (b) reflection coefficient frequency response, and (c) 3D far-field gain radiation pattern.

REFERENCES

1. Ciuti, G., A. Menciassi, and P. Dario, "Capsule endoscopy: From current achievements to open challenges," *IEEE Reviews in Biomedical Engineering*, Vol. 4, 59–72, 2011.
2. Izdebski, P. M., H. Rajagopalan, and Y. Rahmat-Samii, "Conformal ingestible capsule antenna: A novel chandelier meandered design," *IEEE Transactions on Antennas and Propagation*, Vol. 57, No. 4, 900–909, April 2009.

3. Kiourti, A. and K. S. Nikita, "A review of implantable patch antennas for biomedical telemetry: Challenges and solutions," *IEEE Transactions on Antennas and Propagation*, Vol. 54, No. 3, 210–228, June 2012.

Impact of Electromagnetic Field Generated by Mobile Phone on Prooxidant-antioxidant Balance in Selected Internal Organs of Rats

P. Sowa[1], **K. Sieron-Stoltny**[2], **G. Cieslar**[3], **and A. Sieron**[3]

[1]Institute of Power System and Control, Silesian University of Technology, Poland
[2]Department of Physical Medicine, Chair of Physiotherapy
Medical University of Silesia in Katowice, Poland
[4]Department and Clinic of Internal Diseases, Angiology and Physical Medicine
Silesian Medical University, Poland

Abstract— In recent years human population is commonly exposed to electromagnetic fields with frequency of 900–1800 MHz generated by mobile phones. In this study the impact of whole-body exposure to electromagnetic field with a frequency of 900 MHz generated by mobile phone on prooxidant/antioxidant balance in selected internal organs of male rats was estimated, by means of analysis of the contents of markers of membrane lipid peroxidation and oxidative stress: malone dialdehyde (MDA) and total oxidant capacity (TOC), respectively, as well as the activity of antioxidant enzymes: superoxide dismutase (SOD), catalase (CAT), glutathione peroxidase (GPx), glutathione reductase (GR) and glutathione S-transferase (GST), in homogenates of kidney, heart and lung. The experiment was performed on 20 male Wistar rats, in mean age of 10 weeks, divided into 2 equal groups (consisting of 10 animals), subjected to long-term exposure to electromagnetic field or to sham-exposure, respectively. Rats from examined group were exposed for 28 succeeding days to electromagnetic field with frequency of 900 MHz generated by mobile phone Nokia 5110, that was turned on every 1/2 hour by 8 hours daily and emitted signal for 15 s. The mean value of power density of the electromagnetic field registered during initializing of connection was 85.3 $\mu W/m^2$, and during lasting connection was 17.0 $\mu W/m^2$. Rats from control group were exposed for 28 succeeding days to sham-exposure, during which they stayed in identical as examined animals environmental conditions, excluding the influence of electromagnetic field. During the exposure the mobile phone was placed under a cage with animals. After the end of a cycle of 28 daily exposures to electromagnetic field or sham-exposures (control rats), animals were starved by 24 hours, then anaesthetized and next the abdominal cavity was opened and samples of kidney, heart and lung were taken. In the homogenates prepared from the obtained samples the contents of TOC and MDA, as well as the activity of SOD, CAT, GPx, GR and GST were measured. The biochemical analyses were performed by means of routine spectrophotometric and kinetic methods. As a result of repeated exposures, in electromagnetic field-exposed group of rats, in kidney tissue homogenates a significant increase in the contents of TOC, as well as a significant decrease in the activity of GR and GST was observed, in heart tissue homogenates a significant decrease in the contents of MDA and in the activity of SOD, CAT, GR and GST was found, while in lung tissue homogenates a significant increase in the contents of TOC and in the activity of GR, as well as a significant decrease in the activity of SOD and CAT was confirmed, as compared to control sham-exposed rats. On the basis of the obtained results it was found, that 4-week lasting exposure of rats to electromagnetic field with physical parameters generated by mobile phone working in a frequency range of 900 MHz, causes a slight intensification of oxidant processes in the tissue of examined internal organs with accompanying compensatory, multidirectional changes of antioxidant enzymes activity, enabling the maintenance of prooxidant/antioxidant balance only in heart tissue.

Electric and Magnetic Fields Due to the Operation of Roof Mounted Photovoltaic Systems

A. S. Safigianni and A. M. Tsimtsios
Electrical and Computer Engineering Department
Democritus University of Thrace, Xanthi, Greece

Abstract— Exposure to man-made electromagnetic fields has been steadily increasing during the previous century. The benefits of using electricity in everyday life and health care are unquestioned but during the last years the scientific community as well as the general public have become increasingly concerned about potential health hazards of exposure to electric and magnetic fields (EMFs) at extremely low frequencies (ELF).

These fields have been suspected of causing or contributing to adverse health effects. Although some health effects have been statistically related to ELF EMFs exposure, these effects are poorly understood and may exist only as statistical or scientific errors. The final conclusion of the relevant work done by several expert working groups all over the world is that more research is required in order to give an accurate answer to the question "do ELF EMFs present a human health hazard?".

Nowadays, national standards as well as generally accepted guidelines define reference levels for safe public and occupational exposure to ELF EMFs.

Various researchers have treated extensively the EMFs generated by transmission lines, power stations and substations of various voltage levels, domestic appliances etc.

In Greece, during the last years a huge number of independent producer applications have been submitted and approved, concerning ground and roof mounted photovoltaic systems connected to the distribution network. The Greek Government subsidises the production of these 'green' kWhs in order to meet the environmental constraints established by the Kyoto Protocol and other government initiatives primarily concerning fuel saving.

This paper investigates the electric and magnetic fields due to the operation of roof mounted photovoltaic units. The close proximity of these units to houses and work places causes anxiety among people over possible health hazards from the resultant electric and magnetic fields. For this reason, first, basic topological, constructional and operational data of these systems are provided. Electric and magnetic field measurements in roof mounted photovoltaic systems having different nominal power and inverter types (single or three phase) have been performed. The main measurement results are presented in relevant tables and diagrams. These results are evaluated according to the reference levels for safe public exposure given by international guidelines. Conclusions, concerning safe public exposure to electric and magnetic fields caused by the operation of roof mounted photovoltaic systems, are finally derived.

Experimental Study about the Thermal Effects of EM Sources on Human Skin Tissue

A. Yasin Citkaya[1], **S. Selim Seker**[1], **and Osman Cerezci**[2]

[1]Department of Electrical-Electronics Engineering, Bogazici University
Bebek, Istanbul 34342, Turkey
[2]Department of Electrical-Electronics Engineering, Sakarya University
Esentepe, Sakarya 54187, Turkey

Abstract— The assessment of exposure level to commonly used light sources needs specific attention in today's technology of lighting. The main reason behind this concern is that unless exposure levels are known, the biological results and necessary safety limits cannot be determined with accuracy.

Interaction of light with tissue is widely investigated in different perspectives: physics of propagation of light through media and its biological effects to the absorbing media; some of which have found great applications in life for photo-thermal curing techniques. Neverthough, certain exposures remain potentially hazardous and require specific attention in terms of safety standards. The ultimate goal of inspecting the photo-thermal effects due to interaction with commonly used light sources with biological tissue is planned to be reached via experimental studies made with human subject whose arm is exposed to various kinds of light and heat sources.

Skin is the largest organ as an integrated structure in human body and serves as the first line of defense from the environmental insults. This crucial role of skin makes it the subject for our experimental study to inspect its thermal response under artificial light and heat sources. This study will also provide valuable basis for further numerical studies about thermal interaction of skin, which are currently rather complicated due to complex optical properties of skin.

CFL, LED and Halogen lamps, held at 30 cm distance from human arm, and Infrared heaters with different power specifications at 100 cm distance are chosen in order to illustrate the effects of spectral variations and also the durational impact on temperature increases. Basically, as it can be expected from daily life, even the power specifications of light sources are smaller relatively than heat sources, these light sources also cause temperature increase on skin tissue. In the experiments, it has been observed that some light sources caused temperature increase in the surrounding air, which has also affected the thermal induction in skin tissue in a similar way as in everyday life occupational exposure. Distance variation will illustrate obvious and expected results on thermal effects of exposure that less photo thermal damage occurs at large exposure distances. With higher power specifications of an Infrared heater, induced temperature increase rate is much higher. Additionally from the final skin temperatures obtained from Infrared heater experiments, one can easily expect that under such tissue temperature values near and above 45°C, irreversible chemical reactions might take place, in the end of which serious health hazards may arise for live tissues. All these experimental results are line with theoretical expectations, they as well can be compared with results of further numerical studies.

The ever-rising diffusion of artificial light and heat sources in many application areas brings the question of possible health effects. In this respect, temporal distributions related to exposures from different kinds of light and heat sources are investigated with in-vivo experiments are made on human arm tissue. From a detailed analysis of the outputs, it can be stated that at certain times the maximum temperature increase induced on the tissue can reach very high and dangerous levels. There is no doubt that high exposure can be tolerated by human body for very short durations if under controlled conditions.

Considering the lack of scientific studies on heating effects of light sources on human skin and the lack of definition of safety limits for light and heat exposure, thermal analysis carried out in this work will undeniably be useful to get a step forward in the ultimate goal of providing safety exposure limits.

Optimized Nanocage for Cancer Photothermal Therapy and Comparison with Other Nanoparticles

Sameh Kessentini and Dominique Barchiesi
Project Group for Automatic Mesh Generation and Advanced Methods
Gamma3 Project (UTT-INRIA), University of Technology of Troyes, France

Abstract— The purpose of this study is to get more efficient gold nanocages for photothermal therapy (PTT) of cancer. Therefore a numerical maximization of the absorption efficiency (generating heat) is achieved. Two therapeutic cases (using visible and infrared laser) are considered. The optimization leads to an improved absorption of the nanocages compared with previous studies. The optimized nanocages are also compared with other gold nanoparticles (nanorods, hollow nanospheres and nanoshells) and are shown to be more absorbent when infrared light is used.

The predominating benefits of PTT with gold nanoparticles conjugated to antibodies are both safety and efficiency as PTT limits the possible damage of healthy cells unlike other treatments [1]. Huang et al. [2] found that the laser energy threshold for cell death of the malignant cells using gold nanorods with aspect ratio of 3.9 ($10\,\mathrm{W/cm^2}$) is about half that needed to cause cell death of the nonmalignant cells (that start to be injured at $15\,\mathrm{W/cm^2}$ and are obviously injured at $20\,\mathrm{W/cm^2}$). Au et al. [3] showed that the damage for cancer cells (percentage of cellular damage) treated with the immuno gold nanocages increases linearly as power densities (from $1.6\,\mathrm{W/cm^2}$ to $6.4\,\mathrm{W/cm^2}$). These results suggest that nanoparticles can be used as a selective and efficient photothermal agent for cancer therapy using a low-energy laser.

The laser energy threshold for death of the malignant cells could be reduced provided that more absorbent nanoparticles are used and thus the treatment would be more selective (less damage to healthy cells). The absorption efficiency of gold nanoparticles depends on their shape, size and treatment conditions (e.g., laser illumination). Therefore, maximizing the absorption of nanoparticles can be achieved by tailoring their shape and size for a given therapy. In a previous study [4] we optimized nanorods, nanoshells and hollow nanospheres for targeted photothermal therapy cases. The optimization was found to yield improved results compared to results reported in previous studies and the above optimized nanoparticles are compared to each other. In this study, we complete the comparison by considering the gold nanocage [3, 5, 6]. The optimized nanocages are shown to be the most absorbent when a near infra red illumination is used. Moreover, the results show an improved efficiency compared with previous studies (the absorption efficiency is at least twice). Therefore, with such nanocages, the laser power used in therapeutics could be reduced for more control (avoiding any injury of surrounding cells).

REFERENCES

1. Liu, C., C. C. Mi, and B. Q. Li, "Energy absorption of gold nanoshells in hyperthermia therapy," *IEEE Trans. in Nanobioscience*, Vol. 7, 206–214, 2008.
2. Huang, X., I. H. El-Sayed, W. Qian, and M. A. El-Sayed, "Cancer cell imaging and photothermal therapy in the near-infrared region by using gold nanorods," *J. Am. Chem. Soc.*, Vol. 128, 2115–2120, 2006.
3. Au, L., D. Zheng, F. Zhou, Z.-Y. Li, X. Li, and Y. Xia, "A quantitative study on the photothermal effect of immuno gold nanocages targeted to breast cancer cells," *ACS Nano*, Vol. 2, 1645–1652, 2008.
4. Kessentini, S. and D. Barchiesi, "Quantitative comparison of optimized nanorods, nanoshells and hollow nanospheres for photothermal therapy," *Biomed. Opt. Express*, Vol. 3, 590–604, 2012.
5. Von Maltzahn, G., J.-H. Park, A. Agrawal, N. K. Bandaru, S. K. Das, M. J. Sailor, and S. N. Bhatia, "Computationally guided photothermal tumor therapy using long-circulating gold nanorod antennas," *Cancer Res.*, Vol. 69, 3892–3900, 2009.
6. Khlebtsov, B. N., V. A. Khanadeev, I. L. Maksimova, G. S. Terentyuk, and N. G. Khlebtsov, "Silver nanocubes and gold nanocages: fabrication and optical and photothermal properties," *Nanotechnologies in Russia*, Vol. 5 454–468, 2010.

Session 4P8b
SC3: Nonlinear Optics: Structured Materials, Functional Devices and Applications 2

Dynamic Frequency Conversion in an Ultrahigh-Q Fiber Grating Cavity
Zhangwei Yu, Irina V. Kabakova, Patrik Rugeland, Pierre-Yves Fonjallaz, Oleksandr Tarasenko, C. Martijn de Sterke, Walter Margulis, ... 1630

Third Harmonic Generation by Optimized Hyperfine Aperiodic Optical Superlattice
Cheng-Wei Hsu, Jui-Yu Lai, Shangda Yang, ... 1631

Enhanced Visible-harmonic Generations in an Azo-polymer Resonant Waveguide Grating
Jian-Hung Lin, Georg W. Rieger, Hung-Chih Kan, Ching-Ting Lee, Jeff F. Young, Chia Chen Hsu, 1632

Fiber-based Ultrafast Frequency Conversion Sources for Multiphoton Microscopy
Yen-Yin Lin, Shi-Wei Chu, Yuan Yao Lin, ... 1633

Tunable Plasmonic Behaviour of Micro-structured Composite Materials
Roberto Caputo, Luciano De Sio, Marco Castriota, Cesare P. Umeton, ... 1634

Gap Solitons in Coupled Bragg Gratings with Cubic-quintic Nonlinearity
Md. Jahedul Islam, Javid Atai, ... 1635

Dispersion Engineering of Suspended Silicon Photonic Waveguides for Broadband Mid-infrared Wavelength Conversion
Xibin Li, Ping Zhou, Shiming Gao, Sailing He, ... 1636

Dual Wavelength Switching by a Bare Fiber Butt Joint in an Erbium-doped Fiber Ring Laser
Fang-Wen Sheu, Yu-Han Kao, ... 1637

Dynamic Frequency Conversion in an Ultrahigh-Q Fiber Grating Cavity

Zhangwei Yu[1,2], **I. V. Kabakova**[3], **P. Rugeland**[1,2],
P.-Y. Fonjallaz[2], **O. Tarasenko**[2], **C. M. de Sterke**[3], **and W. Margulis**[1,2]

[1]Department of Applied Physics, Royal Institute of Technology (KTH)
Roslagstullbacken 21, Stockholm 10691, Sweden
[2]Department of Fiber Optics, Acreo Swedish ICT AB
Electrum 236, Kista 16440, Sweden
[3]CUDOS and IPOS, School of Physics, University of Sydney
New South Wales 2006, Australia

Abstract— In this Paper, switching and dynamic frequency conversion in an ultrahigh-Q fiber grating cavity with high-voltage electrical pulses is studied experimentally and numerically. The ultrahigh-Q cavity is formed by a phase-shifted grating inscribed in a twin-hole silica fiber. A pair of 28.8-µm-diameter holes is filled with 8-cm-long BiSn alloy creating resistive electrodes inside the fiber, one of which is connected to SMA contacts. Following high current in an electrode, resistive heating induces thermal expansion of the electrode and mechanical stress is applied to the silica walls of the metal-filled holes. This stress induces through the photo-elastic effect an acoustic wave, which changes the refractive index of the fiber core within a few nanoseconds. The cavity dynamics is studied using a heterodyne technique in which the frequency-shifted light, leaking from the grating cavity at a rate determined by its Q factor, is beating with the reflected probe light at the incident frequency. The oscillating beat signal can be easily measured by an oscilloscope. The beat period is inversely proportional to the frequency shift. Due to a slight birefringence of the used fiber, two resonance peaks exist at different wavelengths corresponding to the fiber's two orthogonal polarization modes. Very different dynamics are observed for the two linear polarizations. Simulations accurately describe observations. The beating seen for the x-polarization (parallel to the two holes) is relatively simple. The refractive index of the core oscillates due to the bouncing acoustic wave but does not allow refilling of the cavity by the probe laser light, for the electrical power used here. For the y-polarization (perpendicular to the two holes), however, the oscillations make the grating pass through the original wavelength a number of times, during which the fiber grating cavity is refilled. This results in a succession of beating events, a behavior that could be explored or eliminated, by mechanically matching the fiber and the surrounding environment.

Third Harmonic Generation by Optimized Hyperfine Aperiodic Optical Superlattice

Cheng-Wei Hsu[1], **Jui-Yu Lai**[1,2], **and Shang-Da Yang**[1]

[1]Institute of Photonics Technologies, National Tsing Hua University, Hsinchu 30013, Taiwan
[2]HC Photonics Corp., R&D Division, 4F, No. 2, Technology Rd. V
Hsinchu Science Park, Hsinchu 30078, Taiwan

Abstract— Arbitrary spectral grids of second-harmonic generation (SHG) efficiency have been realized by hyperfine aperiodic optical superlattice (HAOS) optimized by iterative domino algorithm with unprecedented overall conversion efficiency. In this report, HAOS scheme is extended to third harmonic generation (THG) by designing two artificial wave numbers K_{SHG}, K_{SFG} that can phase-match SHG and sum-frequency generation (SFG) processes in a monolithic structure, respectively. We compared the performances of HAOS and conventional cascade structure composed of two periodic quasi-phase matching (QPM) gratings of the same length but different periods Λ_{SHG}, Λ_{SFG} numerically and experimentally. Simulation shows that HAOS outperforms the cascade structure in two aspects. (1) The THG efficiency of HAOS is 1.65 times higher than that of the cascade structure when the third-order QPM is used for SFG ($\Lambda_{\mathrm{SFG}} = 6\pi/K_{\mathrm{SFG}}$). (2) THG of any pump wavelength λ can be achieved by HAOS, while cascade structure could only permit discrete λ's due to finite resolution of mask patterning. For example, the achievable λ's (around 1595 nm) are spaced by $\sim$ 2 nm for cascade periodically poled congruent lithium niobate with 50-nm mask patterning resolution. We made a 5-cm-long QPM sample with HAOS and cascade channels to prove the concept. The HAOS channel gave a conversion efficiency of 1.0×10^{-6} at a CW pump of 500-mW average power and 1547.35-nm wavelength. In contrast, the THG signal produced by the cascade channel was below the sensitivity ($\sim$ 1 nW) of our measurement system. This is mainly attributed to the larger misalignment between the SHG, SFG efficiency spectra of the cascade channel arising from the deviation of actual wave numbers K_{SHG}, K_{SFG} from the designed values. We also proposed a three-section structure consisting of HAOS sandwiched between two first-order QPM gratings to exceed the maximum THG efficiency $\eta_{\max}$ achieved by cascade structure with two first-order QPM gratings. An analytical procedure shows that an optimal three-section structure can achieve $1.21\eta_{\max}$, which is the highest THG efficiency to the best of our knowledge.

Enhanced Visible-harmonic Generations in an Azo-polymer Resonant Waveguide Grating

Jian Hung Lin[1], **Georg W. Rieger**[2], **Hung-Chih Kan**[1], **Ching-Ting Lee**[3], **Jeff F. Young**[2], **and Chia Chen Hsu**[1]

[1]Department of Physics, National Chung Cheng University, Ming Hsiung, Chia Yi 621, Taiwan
[2]Department of Physics and Astronomy, University of British Columbia, Vancouver, V6T 1Z1, Canada
[3]Institute of Microelectronics, Department of Electrical Engineering
National Cheng Kung University, Tainan, Taiwan

Abstract— In this work, we demonstrate the enhancement of second- and third-harmonic generation (SHG and THG) in anazo-polymer resonant waveguide grating (RWG) structure. Comparing with a sample without RWG, the SHG and THG output can be enhanced by 1000 times thanks to the guided-mode resonance (GMR) effect in the WGS. The RWG structure is composed of a nonlinear azo copolymer layer, 1D sinusoidal waveguide grating (TiO_2) and a cladding layer (SU-8) on the backside of an indium-tin-oxide (ITO) glass substrate. The RWGstructure was fabricated using the two-beam interference and electron-beam deposition techniques. Toproduce SHG the corona electric field poling technique was employed to align azocopolymer to form non-centro symmetric distribution. To measure THG and SHG generated from the azo copolymer RWG, atunable wavelengthoptical parametric oscillator (OPO) laser beam with 10 ns pulse width, 10 Hz repetition rate and an average power of 5 mW was used as afundamental beam. The collimated fundamental beam was normally transmitted through the WGS sampleand the THG and SHG output weredetected by a spectrometer. The strong THG and SHG outputs appear at particular fundamental wavelengths where GMR occur. From a simulation, we found at GMR wavelength, strong localized electric field is generated at the interface betweenazo copolymer and TiO_2 layers. The strong SHG and THG resonance are associated with the GMR related local field enhancement effect.

Fiber-based Ultrafast Frequency Conversion Sources for Multiphoton Microscopy

Yen-Yin Lin[1], **Shi-Wei Chu**[2], **and Yuan-Yao Lin**[1]

[1]Department of Electrical Engineering, Institute of Photonics Technologies
National Tsinghua University, Hsinchu, Taiwan
[2]Department of physics, National Taiwan University, Taipei, Taiwan

Abstract— Ultrafast lasers play an important in a verity of applications. The goal of this study is to provide more versatile, compact, and efficient ultrafast light sources for arbitrary spectral regions from the visible to mid-IR. Since mode-locked fiber lasers are more compact, lighter, and more efficient, they are ideal pump laser sources to achieve our goal. We have demonstrated high efficiency optical parametric amplifiers (OPA) and optical parametric generation (OPG). In this talk, we present our fundamental finding in these OPA and OPG.

Ultrafast lasers wrote an important chapter in the history of science, because they can provide higher electric fields to materials without damage and thermal problems. Therefore, whole spectral ultrafast light sources are desirable for a verity of applications, such as pump-probe spectroscopy, multiphoton microscopy/spectroscopy, and high harmonic generation. In this study, we investigated the basic properties of ultrafast optical parametric amplifiers (OPA). The advantage of this OPA is that the seeding was a generated from the same laser of OPA pump, so the timing jitter can be ignored. Fig. 1 shows the dependencies of measured conversion efficiency versus pump power for (a) doubly (signal+idler) seeded OPA.

In these experiments, we find that the doubly-seeding configuration will restrict phase matching condition in the MgO:PPLN crystal; therefore, initial phase relations between pump, signal, and idler waves were critical in the doubly-seeding configuration. Finally, the laser system will combine to a microscope for multiphoton microscopy.

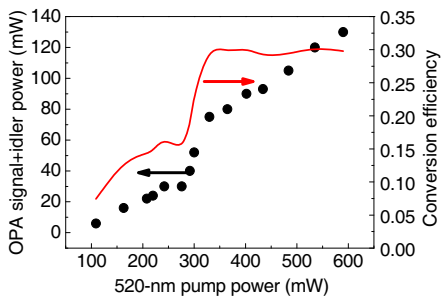

Figure 1: The dependency of OPA output power (black dots) and conversion efficiency (red line).

Tunable Plasmonic Behaviour of Micro-structured Composite Materials

R. Caputo, L. De Sio, M. Castriota, and C. Umeton
LICRYL (Liquid Crystals Laboratory, IPCF-CNR)
Center of Excellence CEMIF.CAL, Department of Physics
University of Calabria, Arcavacata di Rende (CS) 87036, Italy

Abstract— Fabrication of samples showing plasmonic properties is fundamental for the realization of devices exhibiting peculiar electromagnetic properties. A hot-topic is the fabrication of devices whose plasmonic functionalities are also tunable. In this paper we report our approach for obtaining such systems by adopting a micro-structured composite material including metallic sub-entities.

Wide interest is actually devoted to the realization of materials showing Plasmonic properties. These materials are of great interest for many applications such as integrated optics [1], plasmonic circuits [2], biosensing [3] and quantum information processing [4]. Their unique properties derive from the collective oscillation of the free conduction electrons induced by the interaction of metallic nanoparticles with an external electromagnetic field, the so-called Localized Surface Plasmon Resonance (LSPR). The plasmonic response of a system containing metal nanoparticles (NPs) is usually evidenced by a very intense color, absent in the bulk material, as well as in individual atoms. Surrounding the plasmonic entities with a medium whose dielectric constant is also tunable can enable control of the spectral position of the plasmonic resonance [5]. Here we report on our attempts to realize such tunable plasmonic systems by combining "hard" and "soft" matter, e.g., liquid crystals (LCs) and gold nanoparticles [6]. Results show that both blue- and red-shift can be achieved depending whether the tunability is obtained through the application of an external electric field or by changing the sample temperature.

ACKNOWLEDGMENT

The research leading to reported results has received funding from the European Union's Seven Framework Programme (FP7/2007-2013) under grant agreement No. 228455.

REFERENCES

1. Shalaev, V. M. and S. Kawata, *Nanophotonics with Surface Plasmons (Adv. In Nano-optics and Nano-photonics)*, Elsevier, 2007.
2. Ebbesen, T. W., C. Genet, and S. I. Bozhevolnyi, *Phys. Today*, Vol. 61, 44, 2008.
3. Anker, J. N., W. P. Hall, O. Lyandres, N. C. Shah, J. Zhao, and R. P. Van Duyne, *Nat. Mater.*, Vol. 7, 442, 2008.
4. Childress, L., J. M. Taylor, A. S. Sorensen, and M. D. Lukin, *Phys. Rev. A*, Vol. 72, 052330, 2005.
5. Mie, G., *Ann. Phys.*, Vol. 25, 377, 1908.
6. De Sio, L., R. Caputo, U. Cataldi, and C. Umeton, *J. Mat. Chem.*, Vol. 21, No. 47, 18967, 2011.

Gap Solitons in Coupled Bragg Gratings with Cubic-quintic Nonlinearity

Md. Jahedul Islam and Javid Atai
School of Electrical and Information Engineering, The University of Sydney, NSW 2006, Australia

Abstract— It is well known that the effective dispersion induced by a fiber Bragg grating (FBG) is up to six orders of magnitude greater than the chromatic dispersion of the medium [1]. At sufficiently high intensities, nonlinearity and the grating-induced dispersion can be balanced giving rise to gap solitons (GSs). GSs have been studied extensively in various nonlinear media over the past two decades [1–5]. In particular, in Ref. [6] the existence and stability of GSs in two linearly coupled Bragg gratings in cubic nonlinearity have been reported.

In this paper, we investigate the existence and stability of GSs in a model of two linearly coupled FBGs in a cubic-quintic nonlinear medium. Starting from Maxwell's equations, one can derive the following set of normalized equations:

$$iu_{1t} + iu_{1x} + \left(\frac{1}{2}|u_1|^2 + |v_1|^2\right) u_1 - \eta \left(\frac{1}{4}|u_1|^4 + \frac{3}{2}|u_1|^2|v_1|^2 + \frac{3}{4}|v_1|^4\right) u_1 + v_1 + \lambda u_2 = 0 \quad (1)$$

$$iv_{1t} - iv_{1x} + \left(\frac{1}{2}|v_1|^2 + |u_1|^2\right) v_1 - \eta \left(\frac{1}{4}|v_1|^4 + \frac{3}{2}|v_1|^2|u_1|^2 + \frac{3}{4}|u_1|^4\right) v_1 + u_1 + \lambda v_2 = 0 \quad (2)$$

$$iu_{2t} + iu_{2x} + \left(\frac{1}{2}|u_2|^2 + |v_2|^2\right) u_2 - \eta \left(\frac{1}{4}|u_2|^4 + \frac{3}{2}|u_2|^2|v_2|^2 + \frac{3}{4}|v_2|^4\right) u_2 + v_2 + \lambda u_1 = 0 \quad (3)$$

$$iv_{2t} - iv_{2x} + \left(\frac{1}{2}|v_2|^2 + |u_2|^2\right) v_2 - \eta \left(\frac{1}{4}|v_2|^4 + \frac{3}{2}|v_2|^2|u_2|^2 + \frac{3}{4}|u_2|^4\right) v_2 + u_2 + \lambda v_1 = 0 \quad (4)$$

where $u_{1,2}$ and $v_{1,2}$ are the amplitudes of the forward- and backward-propagating waves in the cores 1 and 2, respectively. $\eta > 0$ is a real parameter and accounts for the strength of the quintic nonlinearity. λ is the coefficient of the linear coupling between the cores.

Using analytical and numerical techniques, we have found that Eqs. (1)–(4) admit both symmetric ($u_1 = u_2, v_1 = v_2$) and asymmetric soliton ($u_1 \neq u_2, v_1 \neq v_2$) solutions. It is also found that within each of these categories there exist two disjoint families of solutions that are separated by the curve $1 - \omega - \lambda = 27/(160\eta)$. The soliton families differ in their amplitudes, phase structures and parities. By means of systematic numerical stability analysis, we have identified stability regions for various values of λ in the (η, ω) plane.

REFERENCES

1. De Sterke, C. M. and J. E. Sipe, *Prog. Opt.*, Vol. 33, 203, 1994.
2. Eggleton, B. J., R. E. Slusher, C. M. de Sterke, P. A. Krug, and J. E. Sipe, *Phys. Rev. Lett.*, Vol. 76, 1627, 1996.
3. Atai, J. and B. A. Malomed, *Phys. Lett. A*, Vol. 284, 247, 2001.
4. Mok, J. T., C. M. de Sterke, I. C. M. Littler, and B. J. Eggleton, *Nature Phys.*, Vol. 2, 775, 2006.
5. Neill, D. R., J. Atai, and B. A. Malomed, *J. Opt. A: Pure and Appl. Opt.*, Vol. 10, 085105, 2008.
6. Mak, W. C. K., P. L. Chu, and B. A. Malomed, *J. Opt. Soc. Am. B*, Vol. 15, 1685, 1998.

Dispersion Engineering of Suspended Silicon Photonic Waveguides for Broadband Mid-infrared Wavelength Conversion

Xibin Li, **Ping Zhou**, **Shiming Gao**, **and Sailing He**
Centre for Optical and Electromagnetic Research
State Key Laboratory of Modern Optical Instrumentation
Zhejiang University, Hangzhou 310058, China

Abstract— Integrated photonic technique based on silicon-on-insulator (SOI) waveguides has attracted much attention in the past decade due to the high refractive index contrast which leads to a tight confinement of light and the compatibility to the CMOS fabrication technology. Silicon-based integrated function devices using linear and nonlinear optical effects have played an important role in optical communication systems. In particular, nonlinear silicon waveguides have been demonstrated to realize many all-optical signal processing functions, such as wavelength converters, logic gates, and parametric amplifiers. Moreover, silicon has been found that it also have excellent optical performances in mid-infrared band. In addition, the nonlinear absorptions in silicon, which greatly obstructs the nonlinear applications in telecommunication band, are effectively reduced in the short-wavelength infrared (1.7–2.2 μm) and mid-wavelength infrared (2.2–5 μmm) bands. It provides the possibility to develop mid-infrared nonlinear silicon devices. However, a new coming problem is that the silica cladding used in the SOI platform shows a large propagation in mid-infrared region and suspended silicon photonic waveguides have shown their competition by replacing the silica cladding with air. In this paper, we investigate wavelength conversion based on four-wave mixing in a suspended silicon photonic waveguide. The relationship of the dispersion curve and the waveguide dimensions is analyzed and the dispersion is tried to engineer by optimizing the cross section of the waveguide. As a result, the phase mismatch is effectively reduced and a broad conversion bandwidth in the mid-infrared band is obtained. Simulation results show that a 3 dB conversion bandwidth of 700 nm can be achieved, using a 7-mm-long suspended silicon photonic waveguide.

Dual Wavelength Switching by a Bare Fiber Butt Joint in an Erbium-doped Fiber Ring Laser

Fang-Wen Sheu and Yu-Han Kao
Department of Electrophysics, National Chiayi University, Chiayi 60004, Taiwan

Abstract— The wavelength tunable erbium-doped fiber ring laser with a tapered fiber tip has been reported [1, 2]. Here, we try to alternatively make use of a bare fiber butt joint to realize the wavelength switching in a similar ring-cavity structure. The dual wavelength switching can be achieved by this proposed technique. The experimental setup is shown in Figure 1. The two bare fiber ends of two optical fibers form a butt joint. The transmitting-end optical fiber is connected to the output port of an erbium-doped fiber amplifier (EDFA, SDO EFAS1P112PP02). The receiving-end optical fiber is further connected to two successive fiber couplers in order to measure the optical power and optical spectrum of the fiber laser output light with the power meter (ADVANTEST TQ8215) and the optical spectrum analyzer (OSA, ADVANTEST Q8384). An additional optical fiber is used to guide the laser light emanating from the first fiber coupler to the input port of the EDFA, forming a ring-type resonant cavity. The drive current of the EDFA is set at 190 mA. The relative positions of the bare fiber ends are initially tuned to achieve maximum laser output power. The output wavelength of this erbium-doped fiber ring laser with a bare fiber butt joint can be switched from 1558 nm to 1531 nm approximately by transversely or longitudinally displacing the butt-joint bare fiber ends. We attribute the possible mechanism to the dynamic variation in the nonlinear gain characteristics (population inversion) of erbium-doped fiber. This dual wavelength switchable erbium-doped fiber ring laser with a simple setup might find useful application if a fast spatial tuning device can be incorporated into the system.

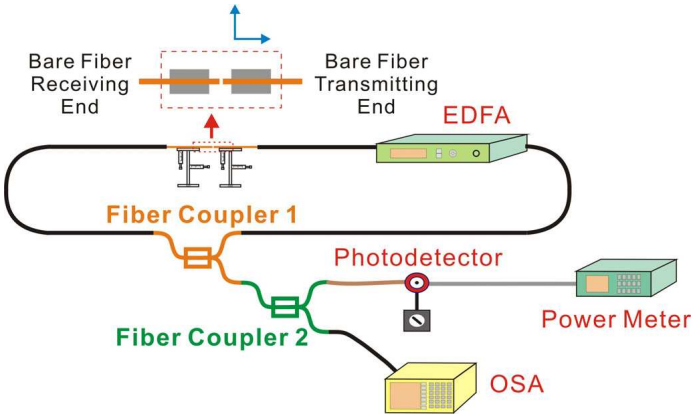

Figure 1: The experimental setup.

REFERENCES

1. Li, Y. and X. Bao, *Appl. Phys. Lett.*, Vol. 93, 261107, 2008.
2. Wang, X., Y. Li, and X. Bao, *Appl. Opt.*, Vol. 48, 6827, 2009.

Author Index

Abari Farzad Cyrus Foroughi, 1348
Abass Aimi, 1156
Abbak Mehmet, 108
Abbas Ahmed, 1464
Abdallah E., 576
Abdallah Esmat Abdel-Fattah, 571, 850, 874, 979, 1472
Abdelwahab Khaled A., 979
Abdul-Malek Zulkurnain, 1306
Abdulkareem Seevan F., 855
Abdullah Haythem Hussein, 850, 1472
Abdulrahman Amuda Yusuf, 1256
Abenius E., 322
Aboufoul Tamer, 521
Abovyan M. S., 144
Abramov Nikolay F., 130, 1440
Abramson Nils Hugo, 1353
Abuelma'atti Muhammad Taher, 1057, 1272, 1617
Acharyya Aritra, 426
Adami Kristian Z., 296
Adato Ronen, 326, 336, 921
Addamo Giuseppe, 293
Afacan Erkan, 1182
Agba Basile L., 1199
Agha Yacoub Ould, 1467
Agneessens Sam, 992
Aguila Víctor Velázquez, 731
Ahmad A. Izwan, 399
Ahmad Mohd Riduan, 880, 1201
Ahmadsimab M., 1103
Ahn B., 46
Ahn Chang-Soo, 618
Ahn Dal, 1616
Aiazzi Bruno, 499
Aiyar R. P. R. C., 1518
Aizpurua Javier, 218, 219, 1096, 1560
Akahane Kouichi, 931
Akaoglu Baris, 1439
Akbarzadeh Alireza, 463
Akduman Ibrahim, 108, 109, 111, 1448
Akerman Johan, 1536
Akgun Ozlem, 119
Akhtar Mohammad Jaleel, 210, 623
Akiyama Tomohide, 112
Akleman Funda, 391, 815
Akram Adeel, 552
Akram Muhammad Nadeem, 1407
Aksimsek Sinan, 629, 771
Al alShaykh Mohammed, 1494
Al-Husseini Mohammed, 168, 442, 849, 1582
Al-Jarro A., 99
Alabidi Ebrahim Sailan, 164
Alarcon Eduard, 1362
Albayrak Yalçin, 487
Albert F., 934
Aldrigo Martino, 1480, 1574
Alekseev Stanislav I., 994
Alex Zachariah C., 1266, 1429
Alexandrov Yuriy, 697
Alexeeva T. A., 448
Ali Amira El-Tokhy, 638, 1602
Ali Jawad K., 617, 855
Ali Mohamed Mamdouh Mahmoud, 80, 560
Alic L., 1327
Alici Kamil B., 24
Alkumru Ali, 807
Almqvist Susanne, 1406, 1409, 1410
Aloi Daniel N., 863
Alomainy Akram, 521, 989
Alonso Julian, 956
Alonso Miguel A., 352, 733
Alqaisy Mushtaq A., 617
Alsulaiman Khaled A., 1494
Alsulaiman Sulaiman, 1494
Altimiras Carles, 675
Altug Hatice, 326, 336, 921
Alzina F., 471
Amaya Iván, 878
Ameya Michitaka, 742
Amin Yasar, 552, 556
Anand Srinivasan, 474
Anbinderis Pavel, 1401
Anbinderis Tomas, 1401
Anchustegi-Echearte-Atienzar Iker, 1577
Anderson Christopher R., 379
Anderson P. N., 724
Andersson Anders, 775
Andersson Jan Y., 1406
Andersson L. Mauritz, 730
Andersson S., 983
Andersson-Engels Stefan, 696, 1347
Andonegui Imanol, 666
Andrei Mihail-Iulian, 373
Andres Miguel Vicente, 1501
Andronov Ivan Viktorovitch, 762
Angelou Nikolas, 1348
Angermann Lutz, 120, 367, 581
Anh Duc Vu, 98
Anselmo Christophe, 1343
Antezza Mauro, 708
Antkowiak Bozena, 447
Ao Xianyu, 1547
Apostolov Peter Stoyanov, 1581
Aragon Ana M., 875
Arai Hiroyuki, 744
Arakawa Yasuhiko, 657, 926
Araujo J. P., 843
Arbabian Amin, 290
Arce Cristina Lerma, 1014
Ardenne Arnold Van, 985
Ardila Gustavo, 271
Areed Nihal F. F., 1043
Arezzini I., 1378
Argyropoulou Eftychia, 774
Aringazin Ascar K., 444, 1445
Aris Skander, 894
Ariza-Flores A. David, 885
Arju Nihal, 24, 326
Arkhipov A. I., 1064
Arnold Cord L., 722
Arranz-Andres Javier, 875
Arrebola Manuel, 299
Arriaga Jesus, 1162, 1171, 1245
Artar Alp, 336
Artemov Igor I., 368, 444, 1445
Artemov V. G., 151
Arwin H., 418
Aryanfar I., 31
Asenjo-Garcia Ana, 436, 1102, 1529
Ashizawa Yoshito, 1010, 1012
Aslanyurek Birol, 109, 1593
Asmontas Steponas, 1401
Assous Franck, 380
Astakhov Andrey, 1584
Atai Javid, 1635
Ates S., 633
Atia Khaled Sami R., 826
Atiah Ali Saied, 1430
Atkins Phillip R., 59, 1115
Attiya Ahmed Mohamed, 1586
Au Minh, 1199
Auffeves Alexia, 681
Auslender Mark, 261
Avagyan Inessa A., 1447
Avalos Monica V., 1086
Avci Sinem, 111
Awelemdy Anwuna Kingsley, 390
Axner Ove, 1346
Aydogan Ahmet, 815
Aydogmus Tugrul, 487

Ayona Edgar Reyes, 1162
Ayona Jose Roberto Reyes, 620, 1615
Azad Mahsa, 1594
Azad Sahba, 1296
Azini Alyaa Syaza, 1256
Azpurua Marco A., 1264

Babuty Arthur, 247
Bach Udo, 1549
Backstrom Mats, 1194
Badics Zsolt, 1000
Bagci Fulya, 1439
Bagci Hakan, 376–378
Baghai-Wadji Alireza R., 126, 407
Baghchehsaraei Zargham, 284
Bai Benfeng, 232
Bai P. F., 1324
Bakhit Amine Adoum, 1614
Bakir B. Ben, 66
Balust Elisenda Bou, 1362
Balzano Quirino, 736
Bandres Miguel A., 352
Banerjee Joyoti Prasad, 426
Banerjee Suranjana, 426
Bang Jeong-Ju, 895
Bansal Rajeev, 481
Bao Di, 1515
Bao Fanglin, 1567
Bao Mingquan, 1489
Bao Y., 709
Barak Serkan, 807
Barba Mariano, 299
Barbastathis George, 457
Barbon Francesco, 1403
Barchiesi Dominique, 1627
Barnes Jack A., 1021
Barney-Smith Elisa, 1296, 1594
Barnthaler A., 329
Baron Paolo, 1460
Barroso Joaquim J., 909, 1523
Bartušek Karel, 642, 797, 801, 1451, 1452, 1454
Barut Basak Isik, 198
Basov Dmitri N., 14
Bastrakov Sergey, 1001
Batchelor J. C., 517
Batrakov Konstantin, 1221
Baudot C., 70
Baumberg Jeremy J., 94, 218, 219, 535, 1104
Baumer S., 1327
Bausa Luisa E., 1337
Baykal Yahya Kemal, 1422
Bazin Alexandre, 659
Bechtel Tim, 1378, 1381
Bechtel Timothy D., 1379, 1383
Beetz Johannes, 658
Beggs Daryl M., 661
Behunek I., 798, 799, 1052
Behunin Ryan, 717
Bekkali Abdelmoula, 748
Belen Mehmet Ali, 1290
Belhadj Chokri Ahmed, 821
Belkin Mikhail E., 152
Bellomo B., 708
Belov A. S., 1275
Ben-Abdallah Philippe, 244
Benavides Olena, 1279, 1280
Benavides-Cruz Manuel, 888
Benech Philippe, 271
Benes Vladimir, 1052
Bengtsson Erik, 1603
Bennett Anthony J., 932
Bennett John, 361
Berec Vesna I., 684
Berezin M., 339
Berg Markus, 166
Berggren Jesper, 1407–1410
Berggren Martin, 89
Berglind Eilert, 732
Berini Pierre, 1333
Berrier Audrey, 536
Berry Simon James, 906
Bertet Patrice, 675
Bertini Federica, 116
Berzin A. A., 150
Besieris Ioannis M., 346, 348
Bestehorn Michael, 1390
Bezus Evgeni A., 1538
Bharadwaj Richa, 989
Bharathi P. A., 606
Bhaskaran Madhu, 236
Bhat Harish, 372
Bhat Harish S., 387
Bhattacharjea Rajib, 379
Bhattacharya Avik, 606
Bhatti Farooq Ahmad, 884
Bian Bo-Rui, 260, 416, 615
Biancalana Fabio, 345
Bichurin Mirza Imamovich, 140, 423, 1083
Bieler Mark, 1207
Bienstman Peter, 65, 1014
Bierwirth Micha, 941
Bilgin Egemen, 628
Binhammer T., 722
Biris Claudiu G., 99
Birowosuto Muhammad Danang, 656, 930
Biswas Anjan, 810
Bitar Mohamad-Ali, 442
Bjork G., 732
Bjork Gunnar G. E., 730
Bjorninen Toni, 550, 739, 990
Blanco Alvaro, 467
Blanco J. M., 1061
Blanco Oscar Gutiérrez, 1079
Bleuse J., 933
Bliokh Yury P., 15
Blumenstock Thomas, 1060
Bochtler Ulrich, 1449
Bock Martin, 353
Bodera Pawel, 447
Boeuf F., 70
Bogacheva Elena, 736
Boggild Peter, 289
Bogy David D., 252
Boilot J.-B., 98
Bojorges Nidia Escamilla, 731
Bolognesi Colombo R., 276
Bonatto A., 1281
Bonatto C., 1281
Bonoto J. C., 397
Booth Tim, 289
Borderies Pierre, 825
Bordo Vladimir G., 508, 1133
Borghs Gustaaf, 324
Boria Vicente E., 1499
Borisov A. G., 219, 1560
Borisov Andrei G., 218
Borisov Andrey G., 1096
Borisova Aleksandra, 1222
Bormann Dierk, 814
Borries O., 320
Boubakri Akram, 845
Boudamouz Brahim, 1428, 1433
Boudet A., 595
Bourayou A., 894
Bourlier Christophe, 1425
Bouville D., 70
Bouvy N. D., 1327
Bovtun Viktor, 1220, 1222
Bowring Nicholas John, 1430
Boyarkin S. V., 170
Boyarskii D. A., 448
Boyvat Mustafa, 1224
Bozhevolnyi Sergey I., 240, 751, 1566
Bozzi Maurizio, 282, 553, 1609
Bracken C., 1400
Braggio C., 706
Brauer Chris, 1021
Bravo Cristina L., 485
Brevik Iver, 710
Bril Andrey, 1060
Brilius Edvinas, 1302
Brocklesby W. S., 724
Broekmans Onno D., 1123
Brogioni Marco, 498

Bronchalo Enrique, 564, 1609
Brown Anthony Keith, 292, 296
Brown Lisa V., 914
Browning Jim, 1296, 1594
Bruckner Stephan, 194
Brunne Jens, 1391
Bruscaglioni Piero, 887
Bryan Rebecca, 319
Brydegaard Mikkel, 1350
Bryllert Tomas, 283
Bucci Giuseppe, 1460
Budaev Bair V., 252
Buhmann Stefan Yoshi, 713
Buisson Olivier, 681
Bukhari S. S., 1181
Bukhtiyarov I. V., 877
Buljan Hrvoje, 17
Bunea Alina Cristina, 1071, 1072
Burdin François, 1612
Burgdorfer J., 329
Burns M. J., 1548
Buron Jonas Due, 289
Busetto Lorenzo, 1426
Butcher T. J., 724
Butera Salvatore, 707
Bykov Alexandr S., 132
Bykov Dmitry Alexandrovich, 331
Byun Woo-Jin, 544

Caduff Rafael, 497
Cai K., 783
Cai Long, 1129
Cai Zhiping, 963
Calatayud Arnau, 1269
Calegari F., 45
Caliskan Alper, 1292
Caloz Christophe, 35
Caltenco-Franca Jose Hector, 1086
Calvo Isidro, 666
Calzolai M., 1378
Campagne-Ibarcq P., 672
Campenhout Joris Van, 69
Canalias C., 532
Cang Hu, 1528
Cao Qing, 822
Caorsi Salvatore, 1286
Capasso Federico, 230, 231
Capineri Lorenzo, 1378, 1379, 1383
Capovilla C. E., 397, 1081
Capozzoli Amedeo, 1003
Caputo Roberto, 1634
Cardinali Alessandro, 127
Carrasco Eduardo, 235, 299, 1189
Cartwright Natalie A., 808
Carugno G., 706
Carvalho Camille, 583
Casadebaig Laurent, 1428
Cassan Eric, 70
Cassez A., 1344
Castriota Marco, 1634
Caymax Matty, 69
Cayoren Mehmet, 108, 111
Cecchi Giovanna, 1349
Ceccuzzi Silvio, 546
Centi Sonia, 689
Cerezci Osman, 1461, 1626
Cerrada Maria L., 875
Cerri Graziano, 1462
Cerskus Aurimas, 1401
Cerullo Giulio, 43
Cervera Sergio, 592
Cervinkova Katerina, 143
Cetin A., 209
Cetiner Bedri A., 1087
Chabalko Matthew J., 1370
Chacinski Marek, 1410
Chae Keun Hwa, 609
Chahat Nacer, 994
Chakrabarty Chandan Kumar, 617
Chakraborty Ajay, 897
Chan Che Ting, 1108, 1265
Chan H. B., 1265
Chan Ho Bun, 709
Chan K. H. A., 932
Chang Chih Chun, 1475
Chang Darrick, 216
Chang Jun-Yan, 614
Chang Kao-Der, 1172
Chang Liann-Be, 614
Chang Liann-Bie, 945, 1015
Chang Shih-Lin, 92, 1217
Chang Shuai, 1552
Chang Shuo-Hung, 1473
Chang The-Nan, 437
Chang Wei-Ling, 562
Chang Wen-Hao, 225
Chang Wenmo, 496
Chang Wonkeun, 725
Chang Yao-Tang, 396
Chapuis Pierre-Olivier, 247
Charbonnier B., 66
Chattoraj Neela, 640, 852
Chaudhary Girdhari, 619, 1608
Che W., 1036
Cheah Kok Wai, 233
Chefanov S. G., 627
Chefranov A. G., 627
Chekurov Nikolai, 284
Chembo Yanne Kouomou, 506
Chen Chen, 1277
Chen Fu-Chiarng, 1009
Chen Gang, 704
Chen Goong, 116
Chen Guan-Hua, 1116
Chen Hong, 1534
Chen Hongsheng, 905
Chen Hsin-Yi, 92
Chen Huai-Yi, 610
Chen Huanlei, 1036
Chen Hung-Ying, 225
Chen Jiajie, 1154
Chen Jianping, 68
Chen Jie, 1512
Chen L., 667
Chen Lih-Juann, 225
Chen Linhui, 1478
Chen Nan-Kuang, 856, 858, 860, 1154, 1411, 1413, 1416
Chen Qiang, 552, 556
Chen Shumei, 233
Chen Tao, 1157, 1552
Chen Tuo, 26
Chen Wei Dong, 1344
Chen Wei Ting, 239
Chen Wei-Sheng, 1063
Chen Wei-Ting, 1527
Chen Weijian, 1021
Chen Wen-Yu, 1527
Chen X., 1019
Chen Xiangdong, 876, 1498
Chen Xianzhong, 232
Chen Xiaodong, 976, 1206
Chen Xuewen, 1141
Chen Yan-Feng, 1505–1507
Chen Yi-Ning, 1411
Chen Yongpin, 1115
Chen Yu-Jen, 1473
Chen Yu-Qing, 415
Chen Ze-Guo, 1505, 1506
Chen Zhanli, 841
Chen Zhao-Ying, 858, 1413
Chen Zhijun, 986
Cheng Chung-Wei, 1159
Cheng Gia-Ling, 858
Cheng Ming-Hsiung, 419
Cheng Pan-Pan, 1047
Cheng Qiang, 1512
Chesnel Lucas, 583
Chevrier Joel, 248, 251
Chew Weng Cho, 59, 480, 1114–1116, 1544
Chia Shih-Hsuan, 43
Chiang Yen-Chung, 191, 565
Chien W. C., 676
Chin Albert, 1204

Chin Kuo-Sheng, 1475
Chisaka Tadashi, 743
Chiu Hsien-Chin, 192
Chiu Tien-Lung, 1550
Chizhik Alexander, 1231
Chizhik Dmitry, 572
Cho Chi-Hyun, 1080
Cho Dong-Ho, 1366
Cho In-Kui, 1576
Cho Seunghyun, 862
Cho Sung-Jin, 868
Cho Yong Heui, 544
Choi Duck-Kyun, 1076
Choi Hyoung Jin, 593
Choi Hyung-Do, 201
Choi In-O., 780
Choi Jae-Ick, 1576
Choi Se-Hwan, 870, 871, 1048
Choi Suna, 199
Choi Won-Kyu, 438
Chong H. M. H., 1019
Chou Min-Li, 192
Choubeni Fethi, 845
Chouhan Sanjay, 897
Chousseaud Anne, 303
Choy Wallace C. H., 195, 1046, 1115, 1118, 1154, 1155, 1544, 1551, 1553
Christensen J., 1569
Christensen Thomas, 1566
Christiansen Mads B., 507
Chu Anthony, 697
Chu Fang-Dar, 1063
Chu Pei-Tze, 92
Chu Shi-Wei, 1633
Chu W.-C., 45
Chua M. J., 1215
Chui Siu-Tat, 1164
Chung Boon Kuan, 85, 411
Chung Pei-Kang, 509
Chung Sang Hoon, 1366, 1488
Chung Shyh-Jong, 301, 1402
Churyukanova M., 1061
Cieslar Grzegorz Jan, 1458, 1624
Cifra Michal, 142, 143
Cinar Gokhan, 771, 775
Cinar Ozge Yanaz, 629, 771
Ciraci Cristian, 1564
Cirmi Giovanni, 43
Cismasu Marius, 969
Citkaya A. Yasin, 1461, 1626
Ciuprina Gabriela, 373
Claes Tom, 1014
Claudon Julien, 933
Clavier T., 295
Close Sigrid, 175
Cluzel Benoit, 76
Coeur C., 1344
Coillet Elodie, 1343
Colombo Roberto, 1426
Colomer Jean-François, 96
Comin Fabio, 248
Conley Ray, 609
Constantinou Constantinos, 995
Cooray Vernon, 880, 1201
Correa Rodrigo, 878
Cortona Pietro, 937
Costa J. W. C. A., 843
Costanza Gabriele, 125
Costanzo Alessandra, 1364, 1480, 1574
Courvoisier Francois, 350
Coves Angela, 1499
Craeye Christophe, 295, 297
Crandles David A., 272
Crepaz A., 498
Crisp Michael J., 748
Crosta Giovanni Franco, 116, 812, 1356, 1426
Crozat P., 70
Crozier Kenneth B., 923
Cruz E. Motta, 303
Cruz Sara Cruz y, 731
Csete Mária, 510
Ctyroky Jiri, 630, 1415
Cui Tie Jun, 241, 764, 766, 767, 902, 1113, 1478, 1512, 1515
Cui Wanzhao, 621, 622, 1522
Cui X., 1344
Cuinas Inigo, 392, 485, 592
Curcio Claudio, 1003

D'Agosta Roberto, 937
Da Cunha Migliano Antonio Carlos, 632
Dabidian Nima, 225, 326
Dahlback Robin, 283
Daho Omar Benahmed, 1431
Dai Chunyang, 203
Dai Daoxin, 752
Dai Yi, 1277
Dai Yitang, 962
Dai Yueyang, 1500
Dalarsson Mariana, 773
Dall Jorgen, 356
Dalvit Diego A. R., 60, 717
Daly S., 701
Dambre Joni, 65
Damgaci Yasin, 1087
Dang Mau-Chien, 557
Danner Aaron J., 463
Darbinyan M. R., 1446
Darson D., 672
Dartora C. A., 393, 639
Darwish A., 141
Darwish Ali M., 421
Das Susanta Kumar, 1391
Daskalaki Paraskevi N., 1190
Daskalaki V., 1186
Daus Andreas, 1449
David Christin, 1563, 1569
David Gregory, 1343
De Abajo F. Javier Garcia, 436, 1102, 1250, 1529, 1563
De Adana Francisco Saez, 1079
De Araujo Humberto Xavier, 397, 1081
De Faro Orlando Alberto Jose, 632, 909, 1523
De Fornel Frederique, 76
De Hon Bastiaan P., 1398
De la Cruz May L., 1279, 1280
De La Cruz W., 272
De La Rosa M. E. Bustos, 1278
De la Torre José Ignacio I niguez, 1058
De Leo Alfredo, 1462
De Lera Acedo Eloy, 295, 297
De Lorenzo Rodriguez M. Edita, 485, 1601
De Luca Jayme Vicente, 1027
De Sio Luciano, 1634
De Sterke C. Martijn, 1630
De Wilde Yannick, 247
De Zuani Stefano, 536
Debaes Christof, 999
Decca Ricardo S., 55, 711
Declercq Frederick, 992
Dedkova Jarmila, 644, 1039
Dekoster Johan, 69
Delga A., 933
Dellinger Jean, 76
Delsing Per, 254, 674, 678
Demir Esra, 1521
Demirci Sevket, 781, 784, 786, 1385
Demircioglu Erdem, 211
Demirel Salih, 1290, 1580, 1618
Deng Yongbo, 1495
Denisov Anton D., 587
Deparis Olivier, 96, 1539
Derevyanchuk Ekaterina D., 365
Descardeci Jose-Ricardo, 639
Descharmes Nicolas, 470
Deutscher Nicholas M., 1060
Devoret Michel H., 671, 672
Dewan Raimi, 1256
Dharanipathy Ulagalandha Perumal, 470

Dhia Anne-Sophie Bonnet-Ben, 583
Dholakia Kishan, 342, 692
Diao Zhaolu, 470
Dias L. P., 1081
Diaz-Guerrero Dan Sidney, 885, 1055, 1056
Diebold Alain C., 25
Diepkilé Adama, 1067
Dierck Arnaut, 992
Ding Chaoliang, 625, 1443, 1444
Ding Jianfeng, 75
Ding K., 755
Ding Kung-Hau, 490
Diniz Igor, 681
Disken Gokay, 1521
Diziain Severine, 477
Djafari-Rouhani Bahram, 471
Dlugach Janna M., 179
Dmitriev Alexandre, 1536
Dohe Susanne, 1060
Doherty S., 1400
Dohnal Premysl, 839, 840
Dolatsha Nemat, 290
Domaracki Mark, 1381
Domonkos Mária, 414
Donaire Manuel, 715
Dong Chun-Hua, 338
Dong Di Sha, 1512
Dong F., 1344
Dong Jianji, 954
Dong Zhenchao, 1106
Donnan Robert S., 1205
Doost Mark B., 1247
Dorlas Tony C., 680
Dorpe Pol Van, 324
Doskolovich L. L., 331, 1538
Douchin Nicolas, 173, 595
Drakinskiy Vladimir, 283
Dressel Martin, 536
Driscoll Tom, 1109
Du Chunguang, 226
Duan G.-H., 66
Dubrouil A., 45
Dudkin Fedir, 831
Dudley John M., 350
Dumas Randy, 1536
Dumur Etienne, 681
Dunias P., 1327
Dunsby Chris, 697
Dupre Matthieu, 1184
Duran Mario, 1384
Durgin Gregory David, 379
Durgut Kadir, 807
Duroc Yvan, 1598
Dutta Rahul, 347
Dvorak Pavel, 801
Dwivedi Surabhi, 445, 446, 1088

Ederra Inigo, 1398
Edquist Anders, 87, 88
Effendi Mohammad Ridwan, 616
Efimenko E. S., 375
Efimenko Evgeny S., 1001
Eggeling Christian, 1126
Eggleton Benjamin J., 31
Ehlers Patrick, 1346
Eibert Thomas F., 777, 1036
Eich Manfred, 71
Eisenstein G., 927
Eizawa Toru, 118
Ekebrand T., 983
Ekins-Daukes Ned J., 1158
Ekmekci Evren, 1521
El Ahdab Zeina, 391
El Helw Amr, 429
El Misilmani Hilal, 168
El Naschie Mohamed S., 128, 864
El-Dahab Mohamed Aboul, 979
El-Gendy Mohamed S., 850
El-Hadidy Mohamed, 141, 421, 571, 576
El-Hajj Ali, 168, 849, 1582
El-Henawy Hadia M., 874
El-Jallal S., 471
El-Khamy Said Esmail, 429, 1589
El-Sabban Salwa, 612
El-Said Mostafa, 1464
El-Sallabi Hassan, 394, 575
El-Shaarawy Heba B., 874
Elgaid Khaled, 285
Elhennawy H., 571, 576
Elkady A., 141
Elshafiey Ibrahim M., 1494
Emrich Anders, 983
Enciso-Aguilar Mauro Alberto, 888
Endo Takashi, 931
Enfield Joey, 701
Ensworth Joshua, 1367
Erdogan Melike, 108
Eroglu Abdullah, 1293, 1596, 1607
Erokhin Nikolay Sergeevich, 584
Erramilli Shyamsunder, 336
Ertay Agâh Oktay, 184, 1592
Esa Mona Riza Mohd, 880, 1201
Escobar Eric R., 1188
Eshrah Islam A., 421
Esquivel-Sirvent Raul, 61
Esselle Karu P., 1398
Essen Hanno, 1024, 1025
Esteban Carolina Redondo, 1058
Esteban R., 219
Esteban Ruben, 218
Esteve Daniel, 675
Ettabaa Karim Saheb, 449, 896
Ezerskaya Anna A., 433
Ezzahri Y., 246

Fabbri F., 98
Faccio Daniele, 345
Fahmy Hossam A. H., 421
Fan Bixuan, 678
Fan Jinglong, 265
Fan Jingtao, 721
Fan S., 31
Fan Yifeng, 273, 908, 1192
Fang Shaobo, 43
Fanti Alessandro, 1037
Farah Imed Riadh, 896
Farah Petros, 535
Farhat Eman O., 296
Farid Arvin, 1296, 1594
Farinello Paolo, 43
Farooqui Muhammad Zunnoorain, 293
Farrer I., 932
Farsari Maria, 694
Fattahpoor Sartoon, 658
Fava Francesco, 1426
Favaro Alberto, 122
Fawky A., 571, 576
Fawzy Ahmed Mohamed, 612
Fazeli Seyed Mahdi, 1289
Fedeli J.-M., 66, 70
Fedotov Mikhail V., 587
Feist Johannes, 220
Felbacq Didier, 708, 1111
Fellman Vineta, 696
Feng C., 45
Feng Yijun, 265, 454, 910
Fennel Thomas, 46
Fenollosa Roberto, 100
Feofanov Alexey, 681
Fernandez-Dominguez Antonio I., 222, 1526, 1533, 1565
Ferrando V., 1269
Ferrari Philippe, 1612
Ferreiro Teresa I., 48
Ferrieres Xavier, 1428, 1433
Fertein E., 1344
Fhager Andreas, 772
Fiala J., 417

Fiala Pavel, 794, 797–799, 839, 840, 1052, 1453
Fichte Lars Ole, 1195
Fiers Martin, 65
Filho Horacio Tertuliano, 393, 639
Filonenko Konstantin, 1133
Fink M., 1184
Fink Mathias, 269
Fiolhais Miguel C. N., 1024, 1025
Fiore Andrea, 658, 936
Fischer Joachim, 1127
Fletcher Alexander, 175
Floc'h Jean-Marie, 523
Flores A. G., 1089
Flores Ana García, 1058
Flurin E., 671, 672
Foletti Alberto, 1459, 1460, 1620
Foltz Heinrich D., 515, 971
Fonjallaz Pierre-Yves, 1410, 1630
Forchel A., 934
Ford Kenneth Lee, 268
Forg B., 46
Forsberg Erik, 903
Forster M., 46
Fortaki Tarek, 894
Fozdar David Y., 24
Franca J. H. Caltenco, 1287
Franco-Vazquez Debora, 1601
Francs G. Colas des, 1467
Frandsen Lars Hagedorn, 64
Frassetto F., 45
Freilikher Valentin D., 15
French Paul M. W., 697
Frey J. G., 724
Freymann Georg Von, 655
Frezza Fabrizio, 204, 542
Friberg Ari T., 347
Friden Jonas, 778
Friedl Martin, 799, 1052, 1453
Froehly L., 350
Frongillo Marcello, 763
Fu Hongyan, 963
Fueser Heiko, 1207
Fukasawa Toru, 745
Fuks Mikhail I., 879
Fukumoto Y., 123
Fukusako Takeshi, 518
Fumeaux Christophe, 236
Funcia Víctor Javier Raposo, 1058
Furfaro L., 350
Furlan Walter D., 1269
Furst Josef U., 505, 867
Futter Peter, 82, 318
Gabbouj Moncef, 362
Gaceb Youcef, 207
Gacoin T., 98
Gaeta Alexander L., 528, 723
Gaggero Alessandro, 658
Gaggero-Sager Luis Manuel, 885, 1055, 1056
Gagnon Dany Sebastien Ly, 999
Gagnon F., 1199
Galaz-Larios M., 888
Galeazzi G., 706
Galili Michael, 64, 959
Gallinet Benjamin, 333
Gallo Katia, 475
Gambassi Andrea, 712
Gampala Gopinath, 82
Gao Jinlan, 554
Gao Shiming, 1636
Gao X., 1344
Garcia Fernando Tomas Pachon, 370
Garcia Martin Lopez, 667
Garcia Pierre-Antoine, 303
Garcia-Adeva Angel J., 666
Garcia-Garcia Joan, 956
Garcia-Gonzalez Pablo, 1559
Garcia-Meca Carlos, 1319
Garcia-Ripoll Juan Jose, 673
Garcia-Vidal Francisco J., 1559
Garcinuno José Antonio Encinar, 299
Gardiner Tom, 48
Garzelli Andrea, 499
Gasulla Manel, 1577
Gaugue Alain, 1431
Gay-Fernandez Jose Antonio, 592
Gebru Alem, 1350
Geburt Sebastian, 223
Gehler Stefan, 329
Geiser Peter, 1345
Geiss Reinhard, 477
Genc Kerim, 319
Gennarelli Gianluca, 763
Genov Dentcho A., 455
Georgiadis Apostolos, 1577
Georgiev Georgi Nikolov, 805
Georgieva-Grosse Mariana Nikolova, 805
Gerard Jean-Michel, 933
Gerhard Christoph, 156, 193, 194
German Vitaly A., 157
Gharsallah Ali, 854
Ghenne Tom, 1249
Ghosh Ankit Kumar, 165, 182
Ghulinyan Mher, 503
Giannini Vincenzo, 1158
Gibson Lachlan J., 693
Gil A. Flores, 1279, 1280
Gilardi Giovanni, 1325
Ginis Vincent, 1316
Ginzburg Pavel, 1334, 1561
Giraldi Maria T. R., 843
Giuppi Francesco, 1577
Giust R., 350
Glazunov Andres Alayon, 574
Glineur F., 295
Gluchowski P., 600
Gobba Fabriziomaria, 1441
Gobin Vincent, 825
Gogineni Prasad, 356
Goita Kalifa, 359, 1067
Gokten Mesut, 211
Golden Kenneth Morgan, 358
Goldhammer Michael, 1449
Golovastikov N. V., 331
Gomez-Rivas Jaime, 220, 1095
Gomis-Bresco J., 471
Gompf Bruno, 536
Gona Stanislav, 264
Gonoskov Arkady, 1001
Gonzalez J., 1229
Gonzalez Jorge, 878
Gonzalez Julian, 1231
Gonzalez-Legarreta L., 1061
Gonzalez-Ovejero David, 295, 297
Gonzalo Ramon, 1398
Goodman D., 1377
Goonan Christopher, 121, 624
Goryachev Ivan A., 1002, 1253
Goulielmakis Eleftherios, 42
Goussetis George, 242
Grachev Vladimir I., 157
Gradauskas Jonas, 1401
Gradziel M. L., 1400
Graf C., 46
Granet Gérard, 539, 543
Granqvist C. G., 418
Gratus Jonathan, 842
Graves William S., 52
Gready D., 927
Grebennikov Dymitro, 272
Green Alan, 110, 626
Greenhalgh Stewart, 110, 626
Greenleaf Allan, 453, 458, 459
Greffet Jean-Jacques, 247, 248
Gregersen Niels, 933
Grigorenko Alexander N., 1140
Grimaldi Settimio, 1459, 1620
Grimalsky Volodymyr V., 1278
Griol A., 471
Grivet-Talocia Stefano, 949
Grosse P., 66

Grunwald Ruediger, 353, 1391
Gschneidtner Tina, 729
Gu Chengling, 721
Gu Xiang, 604, 1059
Guan Ning, 1477
Gubin Tikhon A., 444
Gubsky D. S., 488
Guegan Mikael, 312
Guerreiro A., 843
Guesquiere A., 680
Guichard Wiebke, 681
Guillaume Stéphane-Olivier, 1250
Guizal Brahim, 1111
Gumen Lyudmila, 1162, 1171
Gunes Filiz, 185, 1290, 1291, 1580, 1618
Guo Changjian, 196, 313
Guo Chu-Cai, 504
Guo Guang-Yu, 239
Guo Guangcan, 338
Guo J., 722
Guo Weiming, 69
Guo Yingjie Jay, 242
Guraliuc Anda Raluca, 993, 994
Gurbuz Tolga Ulas, 109, 1593
Guren O., 111
Gustafsson Mats, 514, 776, 969, 975, 977
Gustafsson Oscar, 1409
Guttowski Stephan, 941
Gwo Shangjr, 225
Gyimothy Szabolcs, 1000

Ha Deock-Ho, 891
Hadji Emmanuel, 76
Hafner Christian Valentin, 1224
Hakhoumian Arsen A., 1254, 1387
Hakkarainen Anssi, 493
Hakonen Pertti J., 435, 676
Halas Naomi J., 18, 217, 914
Halevi Peter, 1615
Hall Peter S., 995
Hallikainen Martti Tapani, 493
Hallynck Elewout, 1014
Hamada Lira, 738
Hamada N., 1228
Hamazaki Junichi, 1209
Hamdi Med Ali, 449, 896
Hameed Mohamed Farhat O., 1043
Hamié Ali, 312
Hammar Mattias, 1407–1410
Hammoodi Ali I., 855
Hamze Mohamad, 312
Han Kyu-Won, 395
Han Sang-Min, 1616
Hanaffi Farhan, 1119
Hang Zhi Hong, 1166, 1265
Hanninen Jari J., 482
Hanning Johanna, 283
Hansen Kasper Hjorth, 1348
Hansen Per, 1348
Hanzelka Michael, 1453
Hao Congjing, 1442
Hao Peng, 1495
Hao Y., 300
Hao Yang, 273, 908, 995, 1192
Hao Yufeng, 24
Harada Yoshinori, 112
Harrabi Amal, 854
Harris J., 297
Harris Justin T., 100
Hartmann J. M., 70
Hasar Ugur C., 1523
Hasar Ugur Cem, 909
Hasek Jiri, 143
Hashish Essam Abdel Haleem, 1472
Hassan Emadeldeen, 89
Hassel J., 435
Hauer Martin, 505, 867
Hava Shlomo, 261
Havel Ladislav, 1452
Havelka Daniel, 142
Haw Goh Jia, 85
Hawkeye Matthew M., 218, 219
Hay Stuart G., 305
Hayashi Shinichiro, 287
Hayes R. A., 1324
He Dong Feng, 439
He Ji-Huan, 864
He Jr-Hau, 1550
He Kuen-Yi, 1411, 1413
He Qiong, 238, 239, 907
He Sailing, 26, 33, 138, 313, 314, 597, 599, 601, 613, 691, 828, 903, 1053, 1311, 1457, 1476, 1535, 1547, 1567, 1600, 1603, 1636
He Songbai, 427
He Wenping, 415
He Xin-Yi, 783
He Yingran, 138, 599
He Yu, 603
He Zuyuan, 1354
Hedlund Carl Reuterskiöld, 1409
Heikal Ahmed Mahmoud, 1465
Hein Ricardo, 1384
Helhel Selcuk, 487, 1084
Hell Stefan W., 688, 1123, 1124
Heller Iddo, 1123
Hellmann D., 250
Helszajn Joe, 187
Henaux C., 1038
Henkel Carsten, 255
Henrard Luc, 1250, 1539
Henrykowski Artur, 1288
Heo Yoon-Seok, 871
Herben Matti H. A. J., 280
Hermannsson Petur G., 507
Hernandez-Gomez Pablo, 1089
Hernando B., 1061
Hess Ortwin, 1332
Heuck Mikkel, 660
Heyl C. M., 722
Hibbins Alastair P., 906
Hirayama Hiroshi, 1372
Hirose Haruka, 1006
Hirose Masanobu, 742
Hirose Miyuki, 577
Hisham Nurbaizatul Badrul, 398
Hjorvarsson Bjorgvin, 1100
Ho Aaron Ho-Pui, 1154
Ho Ho-Pui, 195
Ho Ying-Lung Daniel, 667
Hoang Thang Ba, 658, 936
Hock Goh Chin, 617
Hodjat-Kashani F., 180
Hoefling Sven, 658
Hofheinz Max, 675
Hofinghoff Jan-Florian, 90
Hofling S., 934, 936
Hofrichter Jens, 754
Hohenester Ulrich, 1239
Hoi Io-Chun, 678
Holderbaum William, 1483
Holtby Daniel Graham, 268
Holzer Philipp, 725
Hommelhoff Peter, 46
Hong J.-S., 274
Hong Jun, 646
Hong Sheng-Rong, 420
Hong Xuezhi, 314, 1053
Hooper Ian R., 1314
Hopfmann C., 934
Horak Peter, 724
Horner Marc, 319
Horsley S., 906
Horsley Simon A. R., 57
Horst Folkert, 754
Hosako Iwao, 1209, 1268, 1270
Hosono Hiroyuki, 1585
Hoste Jan-Willem, 1014
Hotate Kazuo, 1354
Hou Bo, 1514
Hou Jianhui, 1551
Houdre Romuald, 470

Hovhannisyan Gevorg Davit, 1254
Howells Ian, 737
Hoye Johan S., 710
Hraimel Bouchaib, 961, 1150
Hreniak D., 1223
Hrozek Jan, 1454
Hsieh Hong-Wen, 509
Hsieh Jian-Yu, 1473
Hsieh Li-Zen, 614
Hsieh Ya-Ping, 95
Hsieh Yu-Hsin, 1416
Hsu Cheng-Wei, 1631
Hsu Chia Chen, 478, 636, 1632
Hsu Chiu-Hsiang, 565
Hsu Chuan-Lun, 271
Hsu Der-Yi, 856
Hsu Ken-Yuh, 635
Hsu Pu-Jian, 431
Hsueh Yung-Ta, 181
Hu Hao, 64
Hu Jiandong, 1249
Hu Jin, 1317
Hu Jun, 440
Hu Leiting, 699
Hu Ming-Lie, 721
Hu Tiancun, 621, 622, 1522
Hu Zhebin, 427
Huang C. S., 1015
Huang Ci, 910
Huang Fan-Hsiu, 192
Huang Guo-Wei, 562
Huang Hsi-Ting, 610
Huang Jian Hao, 636
Huang Jun Z., 1115, 1116
Huang Lingchen, 196, 313
Huang Lingling, 232
Huang Qiangsheng, 205, 440, 1567
Huang Rong, 1075
Huang Tung-Wuu, 945
Huang Yi-Ching, 1479
Huang Yong-Zhen, 504
Huang Yu Chung, 636
Huangfu Jiangtao, 37
Huard Benjamin, 671, 672
Huber Rupert, 49
Hugo Bender, 69
Huh Chang-Su, 895
Humphreys David, 741
Hung Si-Jyun, 1479
Hussein Mohamed, 1043
Hutová Eliska, 642, 643, 797, 1451, 1452
Huyart Bernard, 389
Huynh Thi Trang Dai, 1244
Hwang Soon-Mi, 424, 1085
Hwang Sun-Mook, 895
Hylton Nicholas P., 1158

Ibarra-Escamilla Baldemar, 310
Ibbotson Lindsey Anne, 94
Ibrahim Ibrahim I., 612
Iddi Hashimu Uledi, 164, 1256
Idrobo Juan Carlos, 25
Ikeda Tetsuomi, 1587
Ilyinsky A., 1502
Imeci S. Taha, 211
Inagaki Keizo, 931
Inagaki Masaharu, 1378, 1379, 1383
Ince Turker, 362
Iniguez J., 1089
Inoue Mizuki, 1456
Intravaia Francesco, 717
Ioan Daniel, 373
Ioannidis Andreas, 580
Ioannidis Andreas D., 125, 774, 775
Ionin Andrey A., 1393, 1395
Ionova V. G., 1450
Iovine Renato, 695
Ipatov Mihail, 1061, 1229, 1233
Irimajiri Yoshihisa, 1270
Ishii Nozomu, 738
Ishimaru Akira, 1421
Isidro Rodrigo, 1609
Iskandar Zyad, 1612
Islam Md. Jahedul, 1635
Ismail Muhammad Yusof, 206
Itami Go, 112
Ito Koichi, 1456
Iupikov Oleg, 984
Ivanov V., 927
Ivashina Marianna V., 984
Ivashov Sergey I., 1378, 1379, 1383
Iwamoto S., 657
Iwashita Takeshi, 830
Izak Tibor, 414

Jablan Marinko, 17
Jackson Aaron D., 327
Jacob Zubin, 1138
Jacquot M., 350
Jaheen Faria, 1259
Jakobus Ulrich, 318
Jakovels Dainis, 698
Jaksic Zoran, 846, 1240, 1469
Jandieri George Vakhtang, 1421
Jandieri Vakhtang, 541, 547
Jang Kyoung Won, 862
Janipour M., 180
Janner Davide, 952
Janstch Axel, 556
Jaroszewski Maciej, 1225, 1288
Jen Alex K. Y., 71
Jeng Horng-Tay, 1217
Jeng Jer-Ming, 1015
Jeng Ming-Jer, 614
Jensen Asger Sellerup, 64
Jeon Dayeong, 862
Jeon Se-Yeoun, 430
Jeon Seeon, 197
Jeon Soon-Ik, 1576
Jeong Seung-Hwan, 438
Jeong Yongchae, 619, 1608, 1616
Jepsen Peter Uhd, 289, 959
Jerolmack Douglas J., 1381
Jessen Bjarke Sorensen, 289
Ji Hua, 64
Ji Ruiqiang, 75
Ji Wei, 534
Ji Xiaowei, 1246
Ji Yuefeng, 962
Jiang L. J., 1115
Jiang Lijun, 178, 480, 947, 1114, 1116
Jiang Nina, 1438
Jiang Tian, 265, 454, 910
Jimenez-Barco Antonio, 370
Jimenez-Lopez David, 1577
Jin Guofan, 232
Jin M. L., 1324
Joannopoulos John D., 37
Johanesson H., 679
Johannsen U., 280
Johansson Goran, 253, 677, 678, 1098
Johansson P., 1017, 1098, 1468
Johansson Peter, 729
Johnson S. G., 709
Johnson Steven G., 58
Joly Nicolas Y., 725
Jonsson B. Lars G., 302, 977
Jonsson J., 983
Jorge Pedro A. S., 843
Jorgensen Erik, 320
Joseph Wout, 992
Joshi Mohit Kumar, 165, 182
Joulain Karl, 246, 247
Jourdan Guillaume, 248
Joyez Philippe, 675
Jr. Patrick Ciarlet,, 583
Juan Ta-Ko, 239
Juan Yu-Shan, 955
Junesand Carl, 73, 757
Jung Guho, 1488
Jung Jae-Young, 395
Jung Tae-Sung, 873
Junginger Friederike, 49

Junior Eduil Nascimento, 393, 639
Junique Stephane, 1406

Ka Min-Ho, 197, 430
Kabakova Irina V., 1630
Kabalan Karim Y., 168, 442, 849, 1582
Kadlec Radim, 798, 839, 840
Kadri Abdullah, 748
Kahya Gizem, 487
Kaina Nadege, 269
Kaiser Thomas, 571, 576
Kaklyugin Alexander S., 137
Kall Mikael, 729, 1017, 1098, 1468
Kaloshkin S., 1061
Kamacioglu Canan, 1422
Kamarudin Muhammad Ramlee, 164, 1256
Kamenetskii Eugene O., 330, 339, 683
Kamidaki Chihiro, 1477
Kaminer Ido, 352
Kamp Martin, 658, 934
Kampan Adchara, 746
Kampfrath Tobias, 661
Kan Hung-Chih, 478, 636, 1632
Kanatas Athanasios G., 1186, 1190
Kang Ho-Je, 895
Kang Kyongok, 792
Kang Ming, 233
Kang No-Weon, 1080
Kang Xueyan, 604, 1059
Kang Zhiwen, 1154
Kanno Atsushi, 931
Kanth Rajeev Kumar, 552, 556
Kao Cheng-Lung, 1009
Kao Hsuan-Ling, 192, 1204
Kao Ti Yi, 478
Kao Yu-Han, 1637
Kapaklis Vassilios, 1100
Kaplas Tommi, 1221
Karaca Erol, 1304
Karchevskiy Evgeny M., 401
Karim Amir, 1409
Karlsson Stefan, 1410
Kartal Mesut, 1304
Kartner Franz X., 43
Kasilingam Dayalan Prajith, 121, 624
Kaspersen Peter, 1345
Kataja Juhani, 890
Kataria Himanshu, 73, 757
Kato T., 1012
Katsuragawa Daiya, 1487
Kawanishi Tetsuya, 931, 1270
Kawano M., 824
Kawase Kodo, 287
Kazim M. Imran, 280
Ke Po-Yu, 192
Kelly Richard, 492
Keltikangas Kirsti, 486
Kempa Krzysztof, 1548
Kempa Martin, 1220, 1222
Keskin Ahmet Kenan, 1290
Kessentini Sameh, 1627
Kettunen Henrik, 1532
Keyrouz S., 1578
Khader Shaaban EL-Shahat Mohamed, 893
Khaled Elsayed Esam M., 80, 560, 851
Khaleghi Hamidreza, 308
Khaliel Maher Mohamed Ahmed, 571, 576
Khalil Diaa, 612
Khamlichi Jamal, 1431
Khanikaev Alexander, 326
Khanikaev Alexander B., 24
Kharitonov Andrey L., 866
Khatun Afroza, 573
Khedr Mona El-Shahat Mohamed, 893
Kholmanov Iskandar, 24
Kholodnyak Dmitry V., 274
Khoo Iam-Choon, 531
Khorshid A., 141
Khorshid Ahmed Eissa Fathy, 421
Khromova Irina, 1398
Kikuma Nobuyoshi, 1372
Kildal Per-Simon, 983
Kilic Emre, 777
Kilinc Nihal, 1291
Kim Byung Chan, 201
Kim Chul-Hee, 1085
Kim D., 46
Kim Dang-Oh, 1366, 1488
Kim Dongsu, 1261
Kim Eunkyoung, 1160
Kim Heung-Euy, 871
Kim J. S., 929
Kim Jin-Sup, 870, 871
Kim Jisun, 225
Kim Jong-Kyu, 870
Kim Jongkyun, 1261
Kim Jun-Chul, 1261
Kim Ki Young, 1371
Kim Nam, 602
Kim Nam-Young, 561, 868, 898, 899, 1606
Kim Phirun, 619, 1608
Kim Sang-Kuk, 870
Kim Sangkil, 553
Kim Seok, 197, 430
Kim Seong-Min, 1576
Kim Sin, 862
Kim Sungil, 946
Kim Tae-Young, 873
Kim Yangsu, 1488
Kim Young Sik, 618, 872
Kim Young-Ho, 1076
Kim Zee Hwan, 1093
Kiourti Asimina, 1622
Kiranyaz Serkan, 362
Kirkagac Yagmur, 441
Kirsch Nicholas J., 1188
Kirsch Stefan, 1032
Kiselev Aleksei P., 344
Kiselev Dmitry A., 132
Kishi Masato, 1354
Kishimoto Seiya, 1010
Kislyakov Ivan M., 1503
Kiss Imre, 1000
Kitajyo Takafumi, 114
Kitano Masao, 816
Kittel Achim, 250
Kivshar Yuri S., 328
Kjebon Olle, 1410
Klemm Maciej, 817
Kley Ernst-Bernhard, 477
Kling Matthias F., 46
Klomp D., 1327
Knoblauch Tobias, 536
Ko D. H., 1015
Kobayashi Kazuya, 118, 804
Kobayashi T., 577
Koci R., 1052
Kockum Anton F., 678
Kodera Toshiro, 35
Koelpin Alexander, 1403
Koenderink A. Femius, 916
Kogo Naoto, 1587
Kolitsidas Christos I., 302
Komiyama Akira, 811
Kondo Toshiaki, 922
Konev Leonid S., 818
Kong Xiang-Kun, 260, 615, 1277
Konig Karsten, 697
Kontu Anna, 494
Kopcal İnan, 487
Korayem Roshdy K., 1589
Korepanov Valeriy, 831
Korgel Brian A., 100
Korinek Radim, 1451, 1452
Korjittavanit Chardchai, 1496
Korkmaz Veysel, 209
Korpinen Leena, 886, 889, 1441
Korucu H. Demet, 1521
Koshevaya Svetlana V., 1278
Koski Karoliina, 990

Kosta Y. P., 1088
Kosta Yogesh P., 445, 446
Kostitcyna E., 1061
Kotsarenko Anatoliy N., 1278
Kou Pengfei, 613
Kovac Michal, 1052
Koyanagi Yoshio, 1599
Krasavin Alexey V., 759, 1334
Krauss Thomas F., 661
Krausz Ferenc, 46
Kravchenko I. I., 709
Krepelka Pavel, 642, 645, 796
Krevchik Vladimir D., 368, 444, 1445
Kristensen Anders, 507
Kristensen Philip T., 660
Kristensson Gerhard, 776
Kriz Tomas, 644, 794, 795, 1039
Krokhin Arkadii A., 1162, 1171, 1339
Kromka Alexander, 414
Kropatsch W. G., 801
Kroutilová Eva, 839, 840
Kruger M., 46
Krzyzowska Malgorzata, 447
Ksenich S. V., 132
Kubasek Radek, 794
Kudrin Alexander V., 809, 1275
Kudryashov Sergey I., 1393, 1395
Kuei Ping-Yu, 945
Kuhl U., 329
Kuipers Laurens, 661
Kuipers Laurens Kobus, 1335
Kulish Petr, 679
Kulkarni S. V., 1518
Kumar Harish, 556
Kumar K. S., 676
Kumar Sunil, 697
Kundrotas Algis Jurgis, 1401
Kung Andy, 533
Kung Bruno, 681
Kung Wen-Ting, 239
Kunter Fulya Callialp, 441
Kurata Hiroyuki, 608
Kurina L. E., 1275
Kurizki Gershon, 62
Kurokawa Satoru, 742
Kurylev Yaroslav, 453, 458, 459
Kushnin Roman, 104
Kusiek Adam, 161–163, 189, 190, 1033, 1050
Kuster Niels, 736
Kuzhir Polina, 1221
Kuzin E. A., 310
Kuzmenko Alexey B., 34
Kuzmiak Vladimir, 630
Kuzmichev Anatoly I., 133
Kuzmina Ilona, 698
Kuznetsov Valery L., 170, 1263
Kwak Sang Il, 201
Kwiecien P., 417, 630, 1415
Kwon Do-Hoon, 544
Kwon Kyunghoon, 1616
Kypraios Ioannis, 74

L'Huillier A., 722
Lagae Liesbet, 324
Lagendijk Ad, 664
Lagovsky Boris A., 374
Lahlil K., 98
Lahteenmaki Pasi, 435
Lai C. S., 1015
Lai Jui-Yu, 1631
Lai Yun, 461, 1169, 1514
Lakadamyali Melike, 1125
Lancranjan Ion, 101, 1497
Landesa Luis, 1112
Landy Nathan, 1109
Lang Klaus-Dieter, 941
Langbein Wolfgang, 1247
Langley Richard, 1187
Langley Richard J., 268
Lansaker Pia C., 418
Lanteri Stephane, 817
Lassailly Y., 98
Lassas Matti, 453, 458, 459
Laurell Fredrik, 532
Lavery Martin P. J., 728
Lavrentieva Ksenia Valerievna, 1083
Le Nguyen-Ngan, 557
Lea Guillaume, 1348
Leahy Martin J., 701
Lech Rafal, 161–163
Ledda Mario, 1620
Leduc Carole, 994
Lee Bongsoo, 862
Lee Cherl-Hee, 596
Lee Chien-Chih, 1063
Lee Ching-Ting, 1632
Lee Chow, 1015
Lee Chung Hee, 1488
Lee Dong-Joon, 1080
Lee E. H., 929
Lee El Hang, 613
Lee Ho-Jun, 1049, 1474
Lee Hyunwook, 873
Lee Ik-Jae, 609
Lee Ja Hyeon, 1366
Lee Jae Seung, 1367
Lee Jae-Young, 1048
Lee Jaegook, 873
Lee Jay Kyoon, 1596
Lee Jia-Han, 1309
Lee Jin-Fa, 176, 177
Lee Jiun-Haw, 1550
Lee Jong-Chul, 873
Lee Jonghun, 596
Lee Ju-Hong, 1179, 1309
Lee Juseop, 618, 872
Lee Kan-Hua, 1158
Lee Kangho, 618, 872
Lee Kwan-Hun, 424, 1085
Lee Kyu-Bok, 1048
Lee Nae-In, 1049, 1474
Lee Seung Woo, 602
Lee Tae Yun, 197, 430
Lee Tae-Hak, 618, 872
Lee Y. H., 1596
Lee Yi-Kun, 860
Lee Young Chul, 425, 1078
Lee Yun-Jui, 301
Lefevre Y., 1038
Lehmuskero Anni, 729
Lei Ting, 1016
Leite Ivo T., 843
Leitenstorfer Alfred, 49
Lem Stefan, 519
Lemmetyinen Juha, 494, 496
Lenz Martin O., 697
Leon A., 187
Leone Marco, 943
Leonhardt Ulf, 459
Leoni Roberto, 658
Leosson Kristjan, 1336
Lermer Matthias, 658, 934, 936
Lerosey Geoffroy, 269, 1184
Lesnak Michal, 545
Leung Michael, 507
Leus Vladimir A., 404
Levchenko Vadim D., 388, 1002, 1253
Lewander Märta, 696
Li Bin-Xiang, 416
Li Bing-Xiang, 1276
Li Bo, 258
Li Bo-Hong, 225
Li Borui, 138
Li Chun-Fang, 734
Li Chunyong, 345
Li D. B., 755
Li Dichen, 1519, 1520
Li Dong, 788, 789
Li Elaine, 326
Li Er Ping, 940, 948
Li Fashen, 1216
Li Guixin, 232, 233
Li Hai-Ming, 1276
Li J., 950
Li Jensen, 233, 460

Li Jian, 676
Li Jianqiang, 962
Li Jiansheng, 603
Li Jie, 525
Li Jie-Ai, 1047
Li L. H., 936
Li Liang, 646, 841
Li Lizhi, 525
Li M.-K., 59
Li Ping, 1484, 1486
Li Qiang, 753
Li Renkai, 39
Li S. C., 1514
Li Sha, 986
Li Shangyuan, 1147
Li Tsung-Lin, 1479
Li Wen-Yuan, 440
Li Wenxing, 522
Li Xiao, 995
Li Xiaofeng, 1158
Li Xibin, 1636
Li Xin, 238, 907
Li Xinchen, 1551
Li Xuanhua, 195
Li Y., 898, 899
Li Yanqing, 1047
Li Yinggang, 1489
Li Yingsong, 522
Li Yongdong, 879
Li Yue-Heng, 478
Li Zheng-Wen, 1215
Li Zhouyuan, 1087
Liang Anhui, 699
Liang Bingyang, 304
Liang Fu-Lai, 1297
Liang Xingdong, 203
Liao Bin, 1282
Liao Chun Yen, 239
Libisch Florian, 329
Lienau Christoph, 50, 1136
Lihachev A., 698
Lihacova Ilze, 698
Liljeberg Pasi, 552, 556
Liljestrand C., 532
Lim Christina, 1148
Lim Dong-Joon, 870
Lim Jongsik, 619, 1616
Lim Soo Yong, 390
Limonov Mikhail F., 328
Lin C.-D., 45
Lin Chi-Feng, 1550
Lin Ching-Chi, 945
Lin Chun-Hung, 1527
Lin Jian-Hung, 478, 636, 1632
Lin June Hua, 635
Lin Jyun-Ming, 437
Lin Kuan-Hao, 856
Lin Kuan-Ting, 1473
Lin Ming-Yu, 1411
Lin Peng, 1046
Lin Ray-Ming, 614
Lin Shiuan Huei, 635
Lin Y. T., 1015
Lin Yen-Yin, 1633
Lin Yi-Hong, 1159
Lin Yih-Chuan, 431
Lin Yu-Fan, 1051
Lin Yuan Yao, 1633
Lin Zhifang, 1164
Linares-Miranda Roberto, 1086, 1287, 1613
Lindberg Sven, 696
Lindell Ismo Veikko, 122
Lindner Stefan, 1403
Linfield E. H., 936
Ling Jonathan, 572
Link Stephan, 1094
Linz Sarah, 1403
Lioumpas A. S., 988
Lipson Michal, 38, 249
Lipworth Guy, 1367
Liseno Angelo, 1003
Lisi Antonella, 1620
Liu C., 1504
Liu Feng-Zhou, 856
Liu Fu, 460
Liu Guigen, 1495
Liu Hui, 455, 1108, 1265
Liu Jin, 633
Liu Kexin, 33
Liu Luyi, 1187
Liu Meiqin, 1504
Liu Min, 1517
Liu Qi, 205
Liu Qing, 304
Liu Qing Huo, 1117
Liu Shaobin, 260, 415, 416, 615, 1276, 1277
Liu Shiyang, 1164
Liu Shuo, 1478
Liu Sixin, 1283
Liu Taijun, 961, 1150
Liu Tao, 962
Liu W., 1344
Liu Wei, 1500
Liu Wen-Chung, 1051
Liu Xiaoming, 1206
Liu Yongmin, 1528
Liu Yongshun, 1495
Liu Z. C., 755
Llopis Antony, 1339
Lo Wen-Chen, 1179
Lo Y. H., 178
Lobet Michaël, 1539
Lodahl Peter, 633, 935, 1132
Lodewijks Kristof, 324, 1536
Lognoli David, 1349
Loh Tian Hong, 741
Lombardi A., 706
Loncar Marko, 215, 469
Loock Hans-Peter, 1021
Lopez Alicia Casanueva, 187
Lopez Cefe, 466
Lorek E., 722
Lorke M., 633
Lou Fei, 758
Lourdudoss Sebastian, 73, 757
Low Lester, 1230
Lu Dan, 1484, 1486
Lu Haifei, 195, 1154
Lu Hua, 962
Lu Liangjun, 68
Lu Ming-Hui, 1505, 1506
Lu Ming-Yen, 225
Lu Shey-Shi, 1473
Lu T., 709
Lu Xiangyang, 1317
Lu Xiaotang, 100
Lu Yang, 1053
Lu Yen-Pei, 1411
Lu Yi-Long, 160
Lu Ying, 1442
Lu Yu-Jung, 225
Lu Zejiang, 1206
Luan Pi-Gang, 1172
Lubeck Eric, 1129
Lucamarini M., 932
Lucun Andžej, 1401
Ludiyati Hepi, 1074
Lui Hoi-Shun, 772
Lumia Mauro, 293
Lund Patrik, 1249
Lundin Patrik, 696, 1347
Luo J., 461, 1514
Luo Jingdong, 71
Luo Ma, 1117
Luo Yu, 917, 1526, 1533
Luo Yuan, 457
Luo Ziqian, 828
Lush David C., 1028
Lutif Ellen Yoshie Sudo, 632
Lv Meng, 605

Ma Ben, 416
Ma Guancong, 1173
Ma Hui-Feng, 1515
Ma Huifeng, 902
Ma Ning, 1282
Ma Yungui, 462
Ma Zu-Hui, 1114
Maalej Nabil M., 821
Maamary R., 1344
Maaref Nadia, 1428
Macatangay Ronald, 1060

Machulyansky Aleksander, 1222
Mackowski D. W., 179
Madalinski G., 1019
Madhavi Devabhaktuni, 637
Maeda Hiroshi, 547
Maema Hiroyuki, 518
Maes Bjorn, 1156
Magat Abdullah, 1292
Maharjan Ram Krishna, 561, 1606
Mahdy Azza, 429
Mahe Yann, 854, 1258
Maher Simon, 404
Mahmoud Korany Ragab, 568
Mahmoud Mohamed Mamdouh, 851
Mahmoud Samir F., 1464
Mahoney Brody J., 1360
Mahouti Peyman, 1291, 1618
Mahrlein Sebastian, 49
Mai Nicholas, 116
Maier Stefan A., 221, 223, 1092, 1158, 1526
Mak K. F., 725
Makarov Sergey V., 1393, 1395
Maksimenko Sergey A., 1221
Makurin Mikhail, 1371
Malek Fareq, 398–400
Malek Mohd Fariz Abd, 398, 400
Malek Mohd Fariz bin Haji Abd, 399
Maliatsos K., 1186
Malinkovich Mikhail D., 132, 136
Malko Aleksandra, 283
Malkov Yu. A., 375
Mallet Francois, 671, 672
Malomed Boris A., 538
Maltseva Olga A., 865
Mamay I. V., 488
Mametsa Henri-Jose, 173
Manara Giuliano, 991
Manente Marco, 127
Manin Generosa F., 485
Manjavacas Alejandro, 436
Mann Jakob, 1348
Mann Sebastian, 1403
Mansano Andre Luis Rodrigues, 1573
Manson J., 272
Mansson Daniel, 1197
Mantzke Andreas, 943
Manzoni Cristian, 43
Marcet Z., 709, 1265
Marennikova Ekaterina A., 1274
Margulis Walter, 1630
Marin Pilar, 875
Marini Stephan, 1499
Marinica Dana-Codruta, 1096
Marpaung David, 953
Marris-Morini Delphine, 70
Martens Daan, 1014
Martinelli L., 98
Martinez Alejandro, 471
Martinez Benito Gimeno, 1499, 1501
Martinez Cynthia, 956
Martinez-Iranzo Ursula, 956
Martirosyan Radik M., 1254
Marynowski Wojciech, 161–163, 189, 190, 1033, 1050
Mascher P., 272
Mashanovich Goran Z., 1019
Masiello David J., 918
Masotti Diego, 1480, 1574
Masuda Hideki, 922
Mathis A., 350
Matovic Jovan, 846
Matsuda T., 824
Matsumoto Mitsuji, 1151
Matt R., 351
Matteini Paolo, 689
Mattia Valentina Di, 1462
Mattioli Francesco, 658
Matzler Christian, 491, 494, 497
Maurer Hansruedi, 110, 626
Mauritsson J., 722
Mauro Biagio Di, 1426
Mayer Bernhard, 49
Mazets Igor E., 62
Mazhar Waqas, 884
Mazur J., 190, 1033
Mazur Jerzy, 189
Mazur Mateusz, 1050
Mazzarella Giuseppe, 1037
McCarthy D., 1400
McCauley Alexander P., 709
McCord Jeffrey, 1214
McCormack Matthew Jack, 842
McIntosh Alex, 1205
McLean James S., 515, 971
Medeiros Allan, 389
Medhat A., 141
Meerovich Victor, 1090
Mehranzamir Kamyar, 1306
Mei Jun, 1173
Mei Liang, 1248, 1249, 1347
Meincke P., 320
Melander Emil, 1100
Melazzi Davide, 127
Meles Giovanni, 110, 626
Menard Michel, 1431
Mendoza Z. Gress, 731
Mendoza-Tellez A., 1613
Menezo Sylvie, 66
Meng Chao, 39
Meng Chinchun, 562
Meng Zhi Qi, 106
Menshova Sverlana B., 368
Menyuk Curtis R., 506
Merckling Clement, 69
Merelle Vincent, 1431
Merilampi Sari, 550
Merk Virginia, 1336
Meseguer Francisco, 100
Messai Abderraouf, 894
Messaoudi Hamza, 1391
Messina R., 708
Metaferia Wondwosen, 73, 757
Meyerov Iosif, 1001
Meyl Konstantin, 800, 1482
Meza Juan C., 387
Michailidis Emmanouel T., 1190
Michel Alain, 87, 88
Micheletti Filippo, 183, 1611
Michishita Naobumi, 743
Miclos Sorin, 101, 1497
Midolo Leonardo, 658, 936
Miffre Alain, 1343
Mifune Takeshi, 1251
Mikkelsen Torben, 1348
Mikulka Jan, 799
Miljkovic Vladimir D., 1017
Miller David A. B., 999
Miller Philip, 741
Miller R. J. Dwayne, 51
Millot Patrick, 1428, 1433
Min Bumki, 22
Min Rui, 75
Minamide Hiroaki, 287
Minasbekyan Liya A., 144, 1446, 1447
Ming Feng, 646
Miranda M., 722
Miret J. J., 1240
Mirkovic Djordje, 1420
Mirrahimi M., 672
Mishchenko Michael I., 179
Mishra Vivekanand, 445, 446, 1088
Miskovic Zoran L., 25
Misran Norbahiah, 206
Misrikhanov M. Sh., 371
Mitchell Arnan, 236
Mitchell-Thomas R. C., 300
Mitin Vladimir, 19
Mitra Monojit, 426
Mitsuya K., 30

Mittra Raj, 483, 522, 904, 966
Miwa Keishi, 1372
Miyaji Godai, 1392, 1394
Miyashita Hiroaki, 745
Miyazaki Kenzo, 1392, 1394
Mizumoto Tetsuya, 30
Mkrtchian V. E., 255
Mohamed Ahmed Magdy, 568
Mohamed Hesham Abd Elhady, 874
Mohan Akhilesh, 165, 182
Mohri Kaneo, 1228
Mojon Artemio, 485
Mok Kolet, 1616
Molina P., 1337
Molinet Frederic, 762, 765
Monari Jader, 293
Mondes V., 46
Monnier Paul, 659
Monroy Idelfonso Tafur, 1145
Monsoriu Juan A., 1269
Moodie S., 272
Moon Joo-Hyun, 862
Moon Jung-Ick, 1576
Moorey Charles Luke, 1483
Mopidevi Hema Swaroop, 1087
Mora Nicolas, 1196
Moradi Bahareh, 956
Moradi Elham, 990
Moraru Luminita, 810
Morel Pascal, 308
Morfin P., 672
Morino Isamu, 1060
Moriyama Toshifumi, 107, 360, 1382
Mork J., 933
Mork Jesper, 660
Moro Riccardo, 553
Morohashi Isao, 1270
Morosov Alexander I., 150
Morrison Keith, 361
Mortensen N. Asger, 1135, 1163, 1562, 1566
Mortensen Niels Asger, 1101, 1168, 1569
Moshchalkov Victor V., 1104
Mosk Allard P., 664
Mouchet Sébastien, 96
Mousavi Hossein, 326
Mousavi S. Hossein, 24
Mozhaeva N. S., 865
Muecke Oliver D., 43
Mueller G., 245
Muhlenbernd Holger, 232
Muinonen K., 179
Mukai Sonoyo, 1065, 1066
Muljarov Egor A., 1247
Mulvad Hans Christian Hansen, 64
Muneeb M., 1019
Munir Achmad, 616, 1073, 1074
Munoz Claudio, 1079
Munro Ian, 697
Munsch M., 933
Murakami Shuichi, 1213
Murata Hiroshi, 277
Murphy J. A., 1400
Murzanev A. A., 375
Murzin S. G., 371

Nagaoka Tomoaki, 998
Nagarkoti Deepak Singh, 273, 1192
Nagasaka Takashi, 804
Nagy B., 571, 576
Nainar Ramanujam, 1284
Nakagawa Katsuji, 1010, 1012
Nakamura Shigehisa, 1068–1070
Nakanishi Toshihiro, 816
Nakano Hisamatsu, 820, 1008, 1011
Nakashima Hiroshi, 830
Nakata Josuke, 1045
Nakata Makiko, 1065, 1066
Nakata Yosuke, 816
Nanagulyan Siranush G., 1447
Nargeliene Viktorija, 1401
Nasser Y., 442
Nasser Youssef, 849
Nassiopoulou Androula G., 271
Nastasovic Aleksandra, 846
Naud Cecile, 681
Naughton M. J., 1548
Nauroze S. A., 262
Nauwelaers Bart K. J. C., 278
Navarro Miguel Ángel, 1079
Navarro-Urrios D., 471
Navau Carles, 1374
Nawata Kouji, 287
Ndip Ivan, 941
Nechayev Yuriy I., 995
Neculoiu Dan, 1071, 1072
Nedeljkovic M., 1019
Neil Mark A. A., 697
Nelson Florence J., 25
Neogi Arup, 1339
Nepa Paolo, 991
Nerudova Michaela, 143
Nesil Selahattin, 1580
Nespor Dusan, 643, 794, 1454
Neto Adriao Duarte Doria, 389
Ng Jack, 1265
Ng Siu Pang, 1352
Nguyen Dat-Son, 557
Nguyen Truong Khang, 1271
Ni J., 274
Ni Xu, 1505, 1506
Nielsen Ulrik Dam, 356
Nieminen R. M., 598, 1558
Nieminen Timo A., 693
Nikita Konstantina S., 988, 1622
Niklasson Gunnar A., 418
Nikoskinen Keijo, 486, 573
Nilsson Borje, 580, 771, 775
Nilsson Hans-Erik, 554
Nilsson Johan, 720
Nilsson Jonas, 932
Ning Cun Zheng, 755
Nirmalathas Ampalavanapillai, 1148
Nishimori Kentaro, 747
Nishio Kazuyuki, 922
Nisoli M., 45
Noda Susumu, 650
Noguez Cecilia, 1238
Noharet Bertrand, 1406
Nomura Kensuke, 1530
Nordebo Sven, 580, 771, 775
Nordlander Peter, 214, 219, 334, 914, 1556, 1560
Norgren Martin Karl, 105, 770, 773
Nori Franco, 15
Notholt Justus, 1060
Notomi Masaya, 656, 930
Ntouni Georgia D., 988
Numai Takahiro, 1487
Nunes R. P., 1281
Nuzhnyy Dmitry, 1220

O'Sullivan C., 1400
Oakes Ben, 1200
Obayya Salah Sabry Ahmed, 826, 1043, 1465
Obelleiro Fernando, 1112
Oberhammer Joachim, 284
Obod Yuri A., 130, 133, 135, 1440
Obradov Marko, 1469
Obraztsova Elena D., 1503
Ocket Ilja, 278
Offrein Bert Jan, 754
Oganisian Karen, 600, 1223
Ogawa Koichi, 1599
Ogier Robin, 729
Ogrisek Matthias, 223
Oh Sang-Hyun, 1020, 1122
Ohashi Eriko, 744
Ohnuki Shinichiro, 1010, 1012
Ohtera Yasuo, 1006

Oikawa Takuto, 1008
Oksanen Jani, 97
Okun Oleksandr, 886, 889
Okuno Yoichi, 824, 828
Olivadese S. B., 949
Olivier Richard, 69
Olmi Roberto, 183, 1611
Olmos J. J. Vegas, 1145
Olsson David, 883
Olsson Magnus, 321
Olyunin Nikolay, 1371
Ooi Boon Teck, 1289
Opran Constantin, 101
Orta Renato, 293
Ortiz Zorayda Lazcano, 1245
Orul Tuna, 1182
Orzechowski K., 600
Orłowski Sławomir, 1034
Osgood, Jr. Richard M., 28
Oshchepkov Sergey, 1060
Osley Edward J., 1134
Osman Lotfi, 854
Ostanina Ksenia, 644
Oster Stefan Oster, 1449
Ostman Erik, 1100
Ota Yasutomo, 657
Otani Chiko, 1267
Otero David Navas, 1058
Otobo Theoma M. Sanchez, 393, 639
Otsuji Taiichi, 19
Otten F. W. M. Van, 936
Ottens Richard S., 245
Oubaid Rania, 1038
Oudich M., 471
Oulton Rupert F., 223
Ouyang Min, 227
Overmeyer Ludger, 90
Ovi Abdullah Al Noman, 1259
Oxenlowe Leif Katsuo, 64
Oxenlwe Leif K., 959
Oyeka D. O., 517
Ozaki Ryosuke, 823
Ozaki Shingo, 820
Ozdemir Caner, 781, 784, 786, 1385
Ozen Sukru, 487, 1084
Ozkaya Ufuk, 185

Paakkonen Rauno, 1441
Paddubskaya Alesia G., 1221
Padgett Miles J., 728
Paez Eduardo Javier, 1264
Pagliano F., 936
Pajewski Lara, 546
Pajot A., 173
Pakizeh Tavakol, 180, 1103
Pakter R., 1281
Pala Fazil, 1521
Paladugu Mohan, 69
Palomaki Tauno, 678
Palombi Lorenzo, 1349
Paloscia S., 499
Paloscia Simonetta, 498
Paltsev Yu. P., 877
Paluch Malgorzata, 447
Pampaloni Paolo, 498
Pan Guan-Pu, 1479
Pan Jin, 480
Pan Liuzhan, 625, 1443, 1444
Pan Shilong, 960
Pan Shiqiang, 1484, 1486
Pan Yong-Le, 1356
Panagamuwa Chinthana J., 737, 1178
Panda Debendra Kumar, 897
Paniagua-Sanchez Jesus Manuel, 370
Panoiu Nicolae C., 99, 1134
Pant Ravi, 31
Pantaleev Miroslav, 982, 983
Pantelides Sokrates T., 25
Pantouvaki Marianna, 69
Papaioannou Evangelos Th., 1100
Papke Jessica, 497
Paraoanu Gheorghe Sorin, 435, 676
Parfenyev Vladimir Mihaylovich, 1371
Parini Clive, 521
Parini Clive G., 976, 989
Park Byung Gi, 862
Park Chan-Won, 395, 438
Park Ikmo, 869, 1271
Park Jeong-Il, 1080
Park Joung-Geun, 873
Park Sang-Hong, 780
Park Se-Hoon, 1076
Park Seungkeun, 199
Park Woo-Chul, 895
Park Youngcheol, 1261
Parker Edward A., 517
Parkhomenko Yuriy N., 136
Parkomenko Yuriy N., 132
Parlavecchio Olivier, 675
Pashkin Alexej, 49
Pasiskevicius Valdas, 532
Passante Roberto, 707
Patalay Rakesh, 697
Pavarin Daniele, 127
Pavo Jozsef, 1000
Pavone Francesco S., 700
Pedersen Anders Tegtmeier, 1348
Pelleg Joshua, 1090
Pellegrini Alice, 995
Peltz C., 46
Penades J. Soler, 1019
Pendry John B., 452, 714, 917, 1526, 1533
Peng Hsiang-Ting, 856, 858, 1413
Peng Hua-Xin, 1232
Peng Jie, 1116
Peng Liang, 1101, 1168
Peng Shao-Wei, 955
Peng Zhen, 176, 177
Pennec Y., 471
Pennycook Stephen J., 25
Penttila Antti, 179
Penty Richard V., 748
Perepelkina A. Yu., 1002
Peretti J., 98
Perini Federico, 293
Peropadre B., 673
Perov Sergey Yu., 736, 877
Perruisseau-Carrier Julien, 235, 1189
Persson Kristin, 776
Persson Mikael, 772
Pertsch Thomas, 477
Peterman Erwin J. G., 1123
Petersen Dirch Hjort, 289
Petit Agnès, 1244
Petri Christof, 1060
Petrini Valerio, 1462
Petrov Alexander Yu., 71
Petrov Roman Valer'evich, 140, 423, 1083
Petrov Vladimir M., 1083
Pettinato Simone, 499
Petzelt Jan, 1220
Peverini Oscar Antonio, 293
Peyrade David, 76
Phaiboon Supachai, 746
Pham Tien-Thong, 557
Phan Gia-Tam, 557
Philbin T. G., 1314
Philbin Thomas G., 56
Philips Kathleen, 1578
Picard Emmanuel, 76
Picardi Giovanni, 1285, 1294, 1295
Pichot Christian, 1428, 1433
Pieraccini Massimiliano, 1423
Pieralisi Marco, 1462
Piksarv Peeter, 351
Pinel Nicolas, 1425
Ping Hew Wooi, 1289
Pini Roberto, 689
Pirkkalainen J.-M., 676
Piro Salvatore, 1377
Pistora Jaromir, 545

Pitot P., 595
Pizzocchero Filippo, 289
Platt Duncan, 1406
Plaza J. L., 1337
Plenge J., 46
Pleshchinskii Nikolai B., 412, 413, 585
Poddubny Alexander N., 328
Podevin Florence, 1612
Podgorny Yu, 149
Podlipenko Yury, 113
Podolskiy Viktor A., 1561
Poirier Jean-Rene, 825, 1038
Pokhodzey L. V., 877
Pokorny Radovan, 1451
Polegre A., 1400
Poletto L., 45
Ponti Cristina, 546
Poo Yin, 39, 1517
Poon Andrew Wing On, 1016
Poon Joyce K. S., 502
Popov Maksym A., 32, 911
Porras Miguel A., 349
Porta Antonio La, 754
Portier Fabien, 675
Pospieszna Janina, 1288
Potapov Alexander A., 157
Potter Ben A., 1483
Pottiez Olivier, 310
Poulton Christopher G., 31
Praludi Teguh, 616
Prasad Harishankar, 623
Prasad P., 1284
Prasad Prafulla Chandra, 852
Prat-Camps Jordi, 1374
Preece Daryl, 693
Premaratne Malin, 1470
Prete Massimo Del, 1480
Primiani Valter Mariani, 1462
Prochazka Marek, 414
Prochnow O., 722
Prokopenko Alexander S., 587
Proksch M., 494
Pronin A. V., 151
Prorok Stefan, 71
Proska Jan, 414
Prozheev I. V., 433
Pruneri V., 952
Psaltis Demetri, 530
Psathas Konstantinos A., 1622
Pu Minhao, 64
Pu Ye, 530
Pucci Annemarie, 915
Puerto D., 471
Pulliainen J., 494
Pun Edwin Yue-Bun, 233
Purtseladze David, 24
Pyatakova Zoya A., 1064, 1170
Qaraqe Khalid A., 394, 575
Qi Jun, 1507
Qi Mei-Qing, 1515
Qian S., 274
Qiao Liang, 1216
Qin Faxiang, 1232
Qin Qiming, 159
Qin Xuefei, 1042
Qiu Cheng-Wei, 232, 457, 463
Qiu Meng, 1531
Qiu Min, 753
Qiu Xianggang, 225
Qu Che, 238
Qu De-Xin, 1075
Quetschke V., 245
Quevedo-Teruel Oscar, 300
Qui Junyi, 1205
Quidant Romain, 1330
Quinlan James A., 863
Qurratulain, 640

Rachidi Farhad, 1196
Radovanovic Filip, 846
Raev M. D., 448
Rahal Mohamad, 158, 1455
Rahim Hasliza A., 398–400
Rahim Nasrudin Bin Abd, 1289
Rahman Tharek Bin Abdul, 164, 1256
Rahmat-Samii Yahya, 990
Raichik I., 380
Raineri Fabrice, 659
Rairoux Patrick, 1343
Raj Rama, 659
Rajab Khalid Z., 273, 908, 1192
Raju C. K., 1026
Ramaciotti Pedro, 1384
Ramirez Ivan Dario Arellano, 1062
Ramirez M. O., 1337
Rampone Thierry, 308
Ran Lixin, 37
Randjelović Danijela, 1469
Rao C. Subba, 86
Rao Neeraj, 973
Raposo V., 1089
Rarity John G., 667
Rashid Amir Khurrum, 262, 266
Rasigade G., 70
Ratto Fulvio, 689
Raucy C., 297
Rautiainen K., 494
Raza Soren, 1566
Razavi-Ghods Nima, 295, 297
Razban-Haghighi Tchanguiz, 303, 854, 1258
Razumov Alexey V., 444, 1445
Rebane O., 348
Rebholz Marc, 49
Reddy B. Rama Sanjeeva, 648
Reddy C. J., 82, 84, 318
Reduzzi M., 45
Reed G. T., 1019
Reichl Herbert, 941
Reid Derryck T., 48
Reid M. T. Homer, 58, 709
Reif Jürgen, 1390
Reineck Philipp, 1549
Reinhard Bjoern M., 919
Reinhard Bjorn M., 335
Reithmaier Johann Peter, 927
Reitze D. H., 245
Reitzenstein Stephan, 934
Ren Xingang, 1553
Renaut Claude, 76
Renner Michael, 655
Repina I. A., 448
Restano Marco, 1285, 1294, 1295
Rettinger Markus, 1060
Rey Isabella H., 661
Reynolds Matthew S., 1367
Rez Jiří, 795
Rhee Seung-Yeup, 602
Ribeiro L. R., 1081
Riccio Giovanni, 763
Richards Simon, 319
Richter Frank, 507
Richter Ivan, 417, 630, 1415
Ricketts David S., 1370
Rida Ibrahim, 158
Rieger Georg W., 1632
Rieth Katja, 1343
Rigelsford Jonathan M., 520, 1187
Rikken G. L. J. A., 715
Rinaudo Alfio, 1460
Ritchie D. A., 932
Rivero Raul Pe na, 1287, 1613
Rizk Mohamed R. M., 1589
Rizzato Felipe Barbedo, 1281
Rmili Hatem, 523
Rocco Roberto, 1460
Roch N., 671, 672
Roche Patrice, 675
Rodíguez Méndez, 888
Roder Robert, 223
Rodriguez Alejandro W., 58, 709, 716
Rodriguez Isabelle, 100
Rodriguez Jose Luis, 1112

Rodriguez Marcelino Zazo, 1058
Rodriguez S. R. K., 220
Roelkens Gunther, 1019
Roger Thomas W., 345
Rogier Hendrik, 992
Rolin E. Cherubini, 393, 639
Ronda Cees, 1322
Ronning Carsten, 223
Roscher Hans-Jurgen, 1363
Rossi Francesca, 689
Rossi T., 1558
Rossi Tuomas, 598
Rostovskiy Ivan, 886
Rotenberg Nir, 661
Rotter Stefan, 329
Rottler Andreas, 1318
Roubal Zdeněk, 645, 795
Rouissi Ines, 523
Rousseau Emmanuel, 248
Roy Langis, 281
Roy Samudra, 345
Roy Wim Van, 324
Rubins Uldis, 698
Rubinstein Marcos, 1196
Rubinsztein-Dunlop Halina, 693
Rubio Angel, 1559
Rubtsova Nina B., 371, 736, 877
Rudawski P., 722
Ruddle Alastair R., 1230
Rudkovskiy Anton S., 1263
Rufo-Perez Maria Montana, 370
Rufus Elizabeth, 1266, 1429
Rugeland Patrik, 1630
Ruhl E., 46
Ruoff Rodney S., 24
Ruoso Giuseppe, 706
Rusakov A. S., 274
Russell P. St. J., 725
Russo Paola, 1462
Rybin Mikhail V., 328
Ryken Jef, 324
Ryu Heung-Gyoon, 848
Ryu Jong-In, 1076, 1261
Ryzhii Elena, 594
Ryzhii Maxim, 19, 594
Ryzhii Victor, 19
Ryzhkov Alexander, 1420

Saad Ayman Ayd Ramadan, 80, 560, 851
Saari Peter, 348, 351
Saastamoinen Kimmo, 347
Saberi Nastaran, 492
Sadi Toufik, 97
Saegusa Kenji, 1585
Safigianni Anastasia S., 1625
Sagnes Isabelle, 659
Sahin Dondu, 658
Sahinturk Hulya, 1593
Saint-Nom Roxana, 1079
Saito Kazuyuki, 1456
Saito Shingo, 1209
Sakai Kyosuke, 1530
Sakai Osamu, 112
Sakakibara Kunio, 1372
Sakamoto Takahide, 1270
Sakko Arto, 598, 1558
Sakoda Kazuaki, 93, 472
Salazar Edwin Andres Quintero, 1062
Saleh Mohammed F., 345
Salem Deena A., 638, 1602
Salim Ali J., 855
Salimi Behnam, 1306
Salonen Erkki T., 166
Salter C. L., 932
Salter Michael, 1406
Saltuganov Pavel N., 1393
Salvatore Stefano, 535
Salvo Elia Di, 542
Samanta Kamal K., 279
Sambles J. Roy, 906
Sammut Charles V., 296
Samokhin Alexander B., 123, 374
Sanchez Alvaro, 1374
Sanchez Angel Mediavilla, 187
Sanchez Manuel Garcia, 392
Sanchez Y., 1264
Sanchez-Romaguera V., 517
Sanchez-Soriano Miguel Ángel, 564, 1609
Sanders Alan, 218
Sanders Charlotte E., 225
Sano Itaru, 1065, 1066
Sansone Giuseppe, 45
Santi E., 499
Santi Emanuele, 498
Santos W. J., 1081
Sarafis Panagiotis, 271
Sarajlić Milija, 1469
Sarma N. V. S. N., 648
Sasahara Takeshi, 1267
Sasaki Keiji, 325, 1530
Sasaki Yoshiaki, 1267
Sathe Ameya, 1348
Sathyamoorthy Sankar R., 678
Sato Hiroshi, 1599
Sato Motoyuki, 114
Satou Akira, 19
Sauleau Ronan, 993, 994
Saunders John E., 1021
Savage Kevin J., 218, 219
Savage Susan, 1409
Savastru Dan, 101, 1497
Savastru Roxana, 101, 1497
Savinov Maxim, 1222
Sayed Sadeed Bin, 378
Sayed Samir, 568
Sazanov A. V., 1450
Sazanova Elena A., 1450
Sazli Murat H., 211
Scalise Lorenzo, 1462
Schamiloglu Edl, 879, 1504
Schatz George C., 1237
Schatz Richard, 1410
Scheel Stefan, 54, 705
Scheid Claire, 817
Schettini Giuseppe, 546
Schkatula Sergey V., 1440
Schleipen J. J. H. B., 1323
Schmalenberg Paul, 1367
Schmidt Christian, 49
Schneebeli Marin, 491
Schneebeli Martin, 494
Schneider Bendix, 65
Schneider C., 934
Schneider Matthias, 1060
Schols R. M., 1327
Schotz J., 46
Schrauwen Benjamin, 65
Schrempel Frank, 477
Schubert Olaf, 49
Schuhmann Rolf, 1032
Schwank Mike, 494
Schwefel Harald G. L., 505, 867
Sciaini German, 51
Sclauzero Eugenio, 1460
Seager Robert D., 1178
Sedlmeir Florian, 505, 867
Sedwick Raymond J., 1362
Seelvaraj Jeyraj, 1289
Seetharam Kushal, 1367
Segars Paul, 319
Segev Mordechai, 352
Seiffert L., 46
Seker S. Selim, 1461, 1626
Sekine Norihiko, 1209, 1268, 1270
Seleznev Leonid V., 1393, 1395
Semba Kazuki, 830
Semenjako Janis, 104
Semenov A. N., 124, 386
Semenov Mikhail B., 368, 444, 1445
Semmar Nadjib, 1244
Seng Kah Phooi, 390
Sengor Taner, 586, 1236
Sengul Orhan, 211
Senturk Mustafa Dagcan, 1292

Seppänen Jaakko, 493
Serdijn Wouter A., 1573, 1578
Sergeenko Nadezda P., 866, 1450
Serpedin Erchin, 394, 575
Seu Roberto, 1285, 1294, 1295
Sha Wei E. I., 178, 195, 947, 1115, 1544, 1553
Shaarawi Amr M., 346
Shafiei Farbod, 326
Shah Charan Manish, 236
Shah Umer, 284
Shahine Mohamad Y. Abou, 849
Shahmoon Ephraim, 62
Shao Lei, 1438
Shao Yang, 176
Sharaiha Ammar, 308, 312
Sharkov E. A., 448
Shavit Reuven, 330, 339
Shcherbachev Kirill D., 136
Shegai Timur, 1017, 1098
Sheikh Muntasir, 523
Shen Dongya, 961, 1150
Shen Shun-Qing, 1534
Shen Xiaopeng, 241
Shen Zhongxiang, 258
Sheng C., 455
Sheng P., 1169
Sheng Ping, 1173
Sheng Xin-Qing, 480
Sheppard Colin J. R., 343, 354
Shestopalov Yury V., 113, 124, 365, 366, 401, 582
Shete Manisha, 210
Sheu Fang-Wen, 1637
Shevchenko Sergey, 886, 889
Shevchenko V. V., 386
Shi J. C., 498
Shi Lei, 100
Shi Xiaojin, 604, 1059
Shibata Kuniaki, 1585
Shibayama Jun, 820, 1008
Shields A. J., 932
Shigenaga Yukinori, 1011
Shih Chien-Fu, 945
Shih Chih-Kang, 225
Shih Tien-Tsorng, 181, 419, 420
Shin Jaegue, 1488
Shin Sang Hun, 862
Shipman Stephen P., 327
Shiwa Mitsuharu, 439
Shkatula Sergey V., 135
Shoaib Imran, 976
Shoaib Muhammad, 1455
Shoaib Nosherwan, 976
Shoaib Sultan, 976
Shoji Yuya, 30
Shpolyanskiy Yuri A., 818
Shu Fang-Jie, 338
Shui L. L., 1324
Shumeiko Vitaly, 685
Shur Michael S., 19
Shuvaeva E., 1061
Shvartsburg Alexander Borisovich, 131, 584
Shvets Gennady, 24, 225, 326
Sibille Alain, 569
Sicard Etienne, 950
Sichkovskyi V., 927
Siden Johan, 554
Sidhwa Haroonhaider, 1518
Sidiropoulos Themistoklis P. H., 223
Sieron Aleksander, 1458, 1624
Sieron-Stoltny Karolina, 1458, 1624
Siew Wah Hoon, 1119
Sigov Alexander S., 148–150
Sihvola Ari Henrik, 1167, 1532
Silander Isak, 1346
Silapunt Rardchawadee, 1496
Sillanpaa Mika A., 676
Silva Anderson Oliveira, 843
Silva F. R. L., 1081
Silveira Francisco Eugenio Mendonca Da, 793
Silveri Matti P., 676
Simone M., 1037
Simsek Serkan, 1592
Sinder Misha, 1090
Singer F., 246
Singh G., 606
Sinitsyn Dmitry V., 1395
Sipos Áron, 510
Siria Alessandro, 248
Sitters Gerrit, 1123
Sjoberg Daniel, 484
Sjoholm Mikael, 1348
Skiba-Szymanska J., 932
Skrajnowska M., 1223
Sliman Sana, 1196
Smirnov Aleksander P., 124, 386
Smirnov Yury G., 365, 443, 1502
Smit Meint K., 1325
Smith Cameron L. C., 507
Smith David R., 1109, 1367, 1564
Smith Joshua R., 1360, 1369
Smith Ray T., 404
Smolders A. Bart, 280
Smolkin Evgenii Yu., 1273
Smolyanskaya O. A., 433
So Peter T. C., 354
Sobis Peter J., 283
Soganci Ibrahim Murat, 754
Sokolov Alexey V., 368
Sokolova Ekaterina P., 1503
Sokolovsky Vladimir, 1090
Soler Angela Coves, 564, 1501, 1609
Solis D. M., 1112
Solis Diego M., 176
Soljacic Marin, 17, 37
Solovey Aleksey, 171
Soloviev Alexander Nikolaevich, 140, 1083
Solovjev Ivan N., 140, 1083
Somesfalean Gabriel, 696, 1249
Somjit Nutapong, 284
Son Haewon, 438
Song Bo Yune, 1488
Song Jin Dong, 929
Song Keum-Su, 1371
Song Qian, 1297, 1300
Song Yi, 753
Song Zhengyong, 907
Sonnefraud Yannick, 221, 332, 1092
Sonsilphong Amornthep, 1513
Soo Yunliang, 1217
Sosa-Pedroza Jorge R., 888
Soto Pablo, 1499
Sotomayor-Torres C. M., 471
Soukoulis Costas M., 21, 1316, 1331
Souleiman Bassel, 896
Sounas Dimitrios L., 35
Sowa Pawel, 1458, 1624
Spigulis Janis, 698
Sprafke Alexander, 653
Srinivasan Gopalan, 32, 911
Sriram Sharath, 236
Stace Thomas M., 678
Stake Jan, 283
Stamp Gordon W. H., 697
Stankiewicz Wanda, 447
Stasolla Mattia, 1286
Stassen L. P. S., 1327
Statham A., 1327
Steckel Jonathan, 1326
Steel M. J., 31
Stefanski Tomasz P., 172, 1034, 1035
Steiner Ullrich, 535
Stella Lorenzo, 1559
Stepanov A. N., 375
Sterner Mikael, 284
Stevenson R. M., 932
Stierle J., 46
Stobbe S., 633

Stock E., 934
Stockmann Hans-Jurgen, 329
Stoja Endri, 204, 542
Stolcova Lucie, 414
Stolin Alexander, 679
Stoopman Mark, 1578
Strand Bo, 322
Strek W., 600, 1223
Strepitov E. A., 433
Strozzi Tazio, 497
Stumpf Theresa M., 356
Su Tao, 647
Suβmann Frederik, 46
Subhash Hrebesh Molly, 701
Sudarchikova V., 1061
Sudhakar Alapati, 86, 637
Suer Can, 184
Suga Masayuki, 1267
Suga Ryotaro, 1456
Suhrke Michael, 1198
Suk Ji Won, 24
Suksmono Andriyan Bayu, 1074
Sultan Kamel Salah, 1472
Sumikura Hisashi, 656, 930
Sun Dengfeng, 1484
Sun Fang-Wen, 338
Sun Fangwen, 876, 1498
Sun Fei, 1457
Sun Jwo-Shiun, 1479
Sun Nian-Xiang, 1212
Sun Shulin, 238, 239, 1165
Sun Wei, 603
Sun Xiaomeng, 68
Sun Yanting, 73, 757
Sun Yaoming, 286
Sun Yong, 1534
Sung Nark-Eon, 609
Surendar Manickam, 606
Surmin Igor, 1001
Sushko Oleksandr, 1205
Sussman Ralf, 1060
Sutapun Boonsong, 1496
Sutton Robert, 515, 971
Suyama Taikei, 828, 1246
Suziedelis Algirdas, 1401
Svanberg Emilie Krite, 696
Svanberg Katarina, 696
Svanberg Sune, 696, 1248, 1249, 1342, 1347
Svedendahl Mikael, 1468
Svirko Yuri, 1221
Swaminathan Madhavan, 948
Sydanheimo Lauri, 550, 739, 990
Syu Jin-Siang, 562
Szabo Z., 799
Szafran Grzegorz, 1225
Szekeres Gábor, 510
Szenes András, 510

Ta Son Xuat, 869
Tababe K., 926
Taboada Jose Manuel, 176, 1112
Tagirdzhanov Azat M., 344
Tahir Farooq Ahmad, 266, 884
Tai Chao-Yi, 1541
Takahashi Eiji J., 44
Takahashi Kazunori, 114
Takahashi Masaharu, 1456, 1599
Takahashi Yasuhito, 830
Takano Tadashi, 1585
Takano Y., 1012
Takeda Hiroyuki, 93, 663
Takenaka Takashi, 107, 1382
Takezawa Ryosuke, 738
Takiguchi M., 930
Talaat A., 1061
Talbot Clifford B., 697
Talla Vamsi, 1360, 1369
Tamosiunaite Milda, 1302
Tamosiunas Stasys, 1302
Tamosiuniene Milda, 1302
Tan Peng Seng, 356
Tan Qiaofeng, 232
Tan Shurun, 496
Tan Wei, 1534
Tanaka Toshiyuki, 107, 1382
Tanaka Yoshito, 1530
Tandaechanurat Aniwat, 657
Tang Aik-Yean, 283
Tang Jianwei, 597, 1535
Tang Jianxin, 1047, 1546
Tang Jie, 1232
Tang Po-Wen, 1541
Tang W. X., 1515
Tang Yue, 160
Tang Yue Feng, 1507
Tang Yueying, 604, 1059
Tanghe Emmeric, 992
Tani F., 725
Tani Koji, 830
Taniguchi Jun, 607
Tanner David B., 245
Tao Ran, 1317
Tarar M. A., 266, 884
Tarasenko Oleksandr, 1630
Tarparelli Richard, 695
Taryana Yana, 1073
Tascone Riccardo, 293
Tassin Philippe, 23, 337, 1316, 1338
Tatar Kaya, 24
Tatarenko Alexander Sergeevich, 423
Tatarnikov Dmitry V., 1584
Tatematsu Akiyoshi, 1196
Tatini Francesca, 689
Taverne Mike P. C., 667
Taylor James D., 1376
Tchebotareva Anna, 1327
Tedeschi Nicola, 542
Tedjni Smail, 557
Teixeira J. M., 843
Tenhunen Hannu, 552, 556
Teniente Jorge, 1398
Tennant Alan, 268
Tentzeris Manos M., 553
Teperik T. V., 1560
Terao Takamichi, 1255
Thi Tam Hoang, 1151
Thielemann Christiane, 1449
Thienpont Hugo, 999
Thomas Benjamin, 1343
Thompson Dane, 319
Thourhout Dries Van, 69
Thuneberg Erkki V., 676
Thygesen Kristian Sommer, 1557
Thylen Lars, 750, 758
Tian Bin, 69
Tian Jie, 753
Tian Xiaoyong, 1519, 1520
Tibaldi Alberto, 293
Tienda Carolina, 299
Tiggelen Bart A. Van, 715
Tikhonov Vasiliy V., 448
Tilmann Wittig, 81
Timofeev A., 435
Timoshkin Igor, 1119
Tirado-Mendez J. A., 1613
Tirado-Mendez Jose Alfredo, 1086
Tokarskij A. Yu., 371
Tomasek Pavel, 264, 366
Tomaz Antonio, 909, 1523
Tomomatsu Yasunori, 931
Tonin Mario, 470
Topa Antonio L., 402
Topfer Fritzi, 284
Tornberg Lars, 678
Tornero Jose Luis Gomez, 242
Torre Patrick Van, 992
Torregrosa-Penalva German, 564, 1609
Toscano Giuseppe, 1568
Toso Giovanni, 1003
Tosun Pinar Deniz, 1084
Tounsi Mohamed Lamine, 207
Tovmasyan Kh., 1387
Toyoshima Hidenori, 738

Trad Imen Ben, 523
Trappe Neil, 1400
Travers John C., 725
Treffer Alexander, 1391
Trevisan Riccardo, 1364, 1480, 1574
Trofimov Vyacheslav A., 587
Trushin S., 46
Tsai Ching-Han, 1402
Tsai Din Ping, 239
Tsai Meng-Lin, 1550
Tsai Pei-Chang, 478
Tsang Leung, 490, 496
Tsiang Raymond Chien-Chao, 95, 1159
Tsimtsios Aristotle M., 1625
Tsutsumi Makoto, 1516
Tulkki J., 97
Tumakov D. N., 585
Tunçay Ahmet Hakan, 1448
Tunçay P., 1448
Tuncer E., 418
Tunnermann Andreas, 477
Tuorila Jani, 676
Tuovinen Tommi, 166
Turgaliev V. M., 274
Turhan-Sayan Gonul, 198
Turk Ahmet Serdar, 1292
Turki B. M., 517
Turner R. Brough, 1188
Turunen Jari, 347
Tyc Tomas, 463

Uchino Osamu, 1060
Uchiyama Tsuyoshi, 1228
Uchizono Yosuke, 820
Uhlmann Gunther, 453, 458, 459
Ukkonen Leena, 550, 739, 990
Ulku Huseyin Arda, 376–378
Ullah Shan, 262, 266, 884
Umeton Cesare P., 1634
Umezawa Toshimasa, 931
Underhill Michael James, 403, 405
Unno Noriyuki, 607
Urade Yoshiro, 816
Urban Robert, 643
Urzhumov Yaroslav, 1109
Urzhumov Yaroslav A., 1367
Usman Muhammad, 158, 1455
Utsi Erica, 1380
Uysal Ismail Enes, 377

Vaaja Matti, 493
Vaerenbergh Thomas Van, 65
Vaisman G., 330
Vakula Damera, 648
Valdmann A., 351
Valenzuela Reinaldo A., 572
Valev Ventsislav K., 218, 535, 1104
Valle F. Della, 706
Vallozzi Luigi, 992
Valovik Dmitry V., 364, 1273, 1274
Valtna-Lukner Heli, 351
Valyukh I., 418
Valyukh Sergiy, 234
Van de Steeg E., 1327
Vandoorne Kristof, 65
Vannahme Christoph, 507
Varakin Yu. Ya., 1450
Varlamov Sergej, 1390
Varlamova Olga, 1390
Vasiljevic Nikola, 1348
Vassilev Andréa, 1230
Vaz Garnet J., 372, 387
Vegni Lucio, 695
Velazco Voltaire, 1060
Vena Arnaud, 990
Venakides Stephanos, 327
Vendik Irina B., 274
Venediktova Anastasia, 1503
Venkataraman G., 606
Venugopal Vinay, 627
Vepsalainen Antti, 676
Vera-Isasa María, 1601
Verbiest Thierry, 1104
Veretennicoff Irina, 1316
Vermeeren Guenter, 992
Verschuuren M. A., 220
Veselago Victor G., 134
Vesely Alessandro Alberto, 1040
Vesely Sara Liyuba, 1040
Vesterdal N., 320
Viöl Wolfgang, 156, 193, 194
Vidal D., 1362
Vidal F. J. Garcia, 220
Vidal Francisco, 389
Videen G., 179
Videen Gorden, 1356
Videnichev Dmitry A., 1503
Vigneron Jean-Pol, 96
Vignesh A., 1284
Vignolini Silvia, 535
Vilamot R., 1038
Vincent Julien, 825
Vion Denis, 675
Viquerat J., 817
Virkki Johanna, 550
Virone Giuseppe, 293
Virot L., 66, 70
Vishnevskiy A., 149
Vishwakarma Dinesh Kumar, 973
Visser H. J., 1578
Visser Hubregt J., 519, 1572
Vivien Laurent, 70
Vlasov Andrey Yu., 1503
Vlcek Jaroslav, 545
Vogt A., 600
Volchikhin Vladimir I., 444, 1445
Volkov Alexander A., 151
Volpian Oleg D., 130, 133, 135, 1440
Volz Sebastian, 248, 937
Vorobyev Oleg B., 409, 967
Voronovich Sophia, 1221
Vorotilov Konstantin, 149
Vos Willem L., 651, 664
Voutilainen Jukka, 739
Vrba Jan, 142, 143, 145
Vrba, Jr. Jan, 881, 1174
Vrbova Barbora, 145
Vukovic Slobodan M., 1240

Wadbro Eddie, 89
Wahl Pierre, 999
Wakabayashi Yuu, 1011
Wallen Henrik, 1167, 1532
Waller Erik, 655
Wallrabe Ulrike, 1391
Wallraff Andreas, 670
Wan Jian, 841
Wang C., 898, 899
Wang Chao, 957
Wang Chia-Ling, 562
Wang Chih-Ming, 239
Wang Ching-Yue, 721
Wang Chun-Yuan, 225
Wang Haixia, 1444
Wang Hsiang-Chen, 95, 1159
Wang Jian, 1300
Wang Jianfang, 1438, 1545
Wang Jiawei, 1016
Wang Jing, 753
Wang Jingyu, 37
Wang Junyang, 1346
Wang Nan, 159
Wang Peng-Yu, 1300
Wang Qin, 1406, 1409, 1410
Wang Shubo, 1265
Wang T., 1344
Wang Tao, 1216
Wang Xin, 848
Wang Xuchen, 440
Wang Y., 455, 1344
Wang Yi-Hao, 1159
Wang Yi-Sheng, 95
Wang Yuming, 1297

Wang Zhechao, 69
Wang Zheng, 37
Wang Zhiyu, 37
Wang Zixin, 647
Wangle Dawei, 196
Warburton Paul A., 1134
Ward M. B., 932
Warren Sean, 697
Washiyama Kazuki, 1354
Wasylkiwskyj Wasyl, 1308
Watanabe Koki, 540
Watanabe Soichi, 738, 998
Waters Benjamin H., 1360, 1369
Wegener Martin, 1127
Wehrspohn Ralf B., 653
Wei Fan, 1147
Wei Jianqian, 1216
Wei Li, 1489
Weigel Robert, 1403
Weissenrieder Jonas, 1409
Weissl Thomas, 681
Wen Geyi, 942
Wen Weijia, 1173
Wen Yumei, 1484, 1486
Weng Zi-Hua, 836–838
Werquin Sam, 1014
Whittow William, 522, 737, 1181
Widenberg Björn, 776
Widengren Jerker, 1128
Wieringa F. P., 1327
Wiesmann A., 494
Wiesmann Andreas, 497
Wijesinghe Thamani Manjula, 1470
Wiktor Michal, 1035
Willatzen Morten, 1133
Willets Katherine A. (Kallie), 1097
Wilson C. M., 678
Windsor Colin G., 1378, 1379, 1383
Withayachumnankul Withawat, 236
Witting-Larsen E., 722
Woldering Léon A., 651
Wolf K., 1363
Wong Peng Wen, 1614
Wongkasem Nantakan, 1513
Woo Min-Ki, 1049, 1474
Worbes L., 250
Wosinski Lech, 473, 758
Wright Selwyn Edgar, 381, 408
Wu Chao-Ming, 1051
Wu Chi Man Lawrence, 1352
Wu Chi-Sheng, 1475
Wu Chien-Pai, 191
Wu Chihhui, 225, 326
Wu Jianfei, 950
Wu Junfeng, 1495
Wu Lingling, 1519, 1520
Wu Linxiao, 910
Wu Ping-Han, 1159
Wu Rui-Xin, 39, 1517
Wu Shan, 1509
Wu T., 1344
Wu Tai-Sing, 1217
Wu Xianyue, 995
Wu Y., 1169
Wu Yaw-Dong, 181, 419, 420
Wu Yihui, 1495
Wu Yirong, 203
Wu Yumao, 1115
Wubs Martijn, 1163, 1562, 1566
Wuite Gijs J. L., 1123
Wunch Debra, 1060
Wustmann Waltraut, 685

Xi Bin, 1531
Xia T., 936
Xiang Yu, 1407, 1408
Xiao Jin-Long, 504
Xiao Sanshui, 20
Xiao Shao-Qiu, 1490, 1492
Xiao Shiyi, 238, 239, 907, 1531
Xie Fengxian, 1046, 1551
Xie Jingya, 68
Xin Zi-Hua, 734
Xing Shuai, 603
Xiong Shiyun, 937
Xiong X., 498
Xiong Xiaoyan Y. Z., 178, 947
Xu Chris, 47
Xu Dan-Xia, 1021
Xu Hao, 1531
Xu Hongxing, 920
Xu Kun, 962, 1144
Xu Lei, 512
Xu Qing, 603
Xu Su, 905
Xu Xiao-Bang, 1500
Xu Xiaolan, 490, 496
Xu Xun, 828
Xu Ying-Ying, 440
Xu Z., 1344
Xu Zuowei, 963
Xuan Ming, 1495

Yadav Ajit, 1178
Yagoub Mustapha C. E., 207
Yakymenko Yuriy, 1222
Yam Chi-Yung, 1116
Yam Scott S.-H., 1021
Yamada Hirohito, 1006
Yamada Hiroyuki, 1372
Yamada Kai, 607
Yamada Takashi, 830
Yamada Yoshihide, 743
Yamamoto Keiko, 608
Yamamoto Kenji, 444, 1445
Yamamoto Manabu, 607, 608
Yamamoto Naokatsu, 931
Yamamoto Takeaki, 1530
Yamanoi Toshio, 931
Yamasaki Tsuneki, 823
Yamauchi Junji, 820, 1008, 1011
Yan Min, 753
Yan Wei, 1163
Yan Xingjing, 304
Yan Yihua, 986
Yanagi Takashi, 745
Yanagishita Takashi, 922
Yang Bin, 1205
Yang Changhe, 841
Yang Cheng, 1206
Yang De-Cao, 948
Yang Huan, 260, 615
Yang J., 983
Yang Jhe-Ming, 95
Yang Jheng-Hong, 509
Yang Jian, 298, 984
Yang Kaike, 937
Yang Kuang Yu, 239
Yang Lin, 75
Yang Liu, 613
Yang Min, 1173
Yang Shangda, 1631
Yang Shun-Po, 1550
Yang Tsung-Hsun, 856, 1411, 1413
Yang Xinwu, 962
Yang Yan, 39
Yang Yehua, 647
Yang Ying-Jay, 1473
Yang Yizhuo, 1148
Yang Yue-De, 504
Yang Zhihong, 1215
Yang Zhiyu, 1173
Yanik Ahmet Ali, 326
Yano Akira, 1045
Yao Yuan, 1206
Yapar Ali, 628
Yashiro Keníchiro, 174
Yashwanth A. V., 86
Yasui Motoaki, 1270
Yasumoto Kiyotoshi, 541, 547
Yasumoto Masayoshi, 1066
Yatsyk Vasyl V., 120, 367, 581
Yazgan Erdem, 1422
Ye F., 1548
Ye Hongxia, 1595

Ye Jundong, 1075
Yeates S. G., 517
Yeganegi Elahe, 664
Yen Shun-Tung, 509
Yew Elijah Y. S., 354
Yi Z. C., 1324
Yigit Enes, 781, 784, 786, 1385
Yilmaz Betul, 781, 784, 786, 1385
Yin Feifei, 962
Yin Jie, 962
Yin L. J., 755
Yin Ming, 1519, 1520
Ying Zhinong, 966, 978, 1476, 1600, 1603
Ymbern Oriol, 956
Yokoo A., 930
Yokota Tatsuya, 1060
Yoo Chan-Sei, 1608
Yoo Gene, 1049, 1474
Yoo Wook Jae, 862
Yook Jong Min, 1076, 1261
Yoon Ki-Cheol, 873
Yoon Uooyeol, 1366, 1488
Yoon Young Joong, 201
Yoshida Shuhei, 607, 608
Yoshida Yuki, 1146
Yoshida Yukio, 1060
Yoshikawa Takashi, 1303
You Baiqiang, 304, 525
You Fei, 427
You Jianwei, 1113
Young Jeff F., 529, 1632
Young Philippe, 319
Yraola E., 1337
Yu Fa-Xin, 905
Yu Jiaxin, 1283
Yu Jiwoong, 197, 430
Yu Junsheng, 1206
Yu Nanfang, 231
Yu Wen-Hsiang, 1541
Yu Xianbin, 959
Yu Xingang, 1407, 1408
Yu Y., 660
Yu Yufeng, 205
Yu Zhangwei, 963, 1630
Yu Zhengzhong, 454
Yuasa Tetsuya, 1267
Yueh Simon H., 490, 496
Yvind K., 660
Yvind Kresten, 64

Zabel Thomas, 1407–1409
Zaboronkova T. M., 809
Zaihasra W. N., 206
Zaitsev Roman V., 444, 1445
Zaitseva Anna S., 809
Zakaryan Tigran, 1387
Zakirov Andrey V., 388, 1253
Zanello D., 706
Zapata-Rodriguez Carlos J., 1240
Zavislyak Igor V., 32, 911
Zayats Anatoly V., 759, 1334, 1561
Zazo M., 1089
Zemlyakov Viacheslav V., 488, 566
Zeng Jianhua, 538
Zengin G., 1098
Zentgraf Thomas, 232
Zha G., 1344
Zhadobov Maxim, 993, 994
Zhai Wenshuai, 604, 1059
Zhan Qiu Qiang, 691
Zhan Yaohui, 1158
Zhang Andy, 1406
Zhang Andy Z., 1410
Zhang Baile, 457, 905
Zhang Bin, 37
Zhang Bing, 1489
Zhang Bohai, 427
Zhang Di, 1046
Zhang Hai Feng, 415, 416, 615, 1276, 1277
Zhang Haixi, 1154
Zhang Haiyang, 1258
Zhang Han, 313
Zhang Hanhua, 1297
Zhang Hanyi, 1147
Zhang Huan, 1282
Zhang John Xiupu, 961, 1150
Zhang Jun, 764, 766
Zhang Junjie, 1416
Zhang Junrui, 1490, 1492
Zhang Limeng, 721
Zhang Meng, 265
Zhang Pu, 1559
Zhang Runren, 905
Zhang Shaoqing, 1551
Zhang Shuai, 1476, 1600, 1603
Zhang Shuang, 232
Zhang W., 1344
Zhang Wei, 83
Zhang Weichun, 753
Zhang Wen Ling, 593
Zhang Wen Xun, 480
Zhang X., 1324
Zhang Xiang, 1528
Zhang Xizhou, 599
Zhang Xuejin, 1509
Zhang Yaoju, 1246
Zhang Yi, 1507
Zhang Yongwei, 292, 296
Zhang Yuan, 601, 903
Zhang Yunhua, 604, 788, 789, 1059
Zhang Z. Q., 1169
Zhang Zhaowei, 48
Zhang Ziqiang, 1484, 1486
Zhao Guangyu, 1248
Zhao Huan, 283
Zhao Hui-Chao, 260, 615, 1277
Zhao Jie, 1512
Zhao Junming, 454, 910
Zhao K., 914
Zhao Kun, 1476, 1600, 1603
Zhao Rongkuo, 714, 1533
Zhao Wen-Sheng, 440
Zhao Yang, 525
Zhao Zhiguo, 1444
Zheng Li-Rong, 552, 556
Zheng Li-Yang, 1505, 1506
Zheng X., 667
Zheng Xiaoping, 1147
Zherebtsov S., 46
Zhong Xing Jian, 1075
Zhou Bin, 861
Zhou Bingkun, 1147
Zhou Guofu, 1324
Zhou Jianhua, 304, 525
Zhou Lei, 238, 239, 907, 1047, 1165, 1531
Zhou Liangjiang, 203
Zhou Linjie, 68
Zhou M., 320
Zhou Ping, 1636
Zhou Weidong, 1042
Zhou Wu, 25
Zhou Xiao, 767
Zhou Zhi-Min, 1297, 1300
Zhu Bo, 454, 910
Zhu Haike, 68
Zhu Huilin, 1311
Zhu Ningli, 83
Zhu Ran, 1150
Zhu S. N., 455
Zhu Shi-Ning, 1108
Zhu Yongyuan, 1509
Zhukov A., 1229
Zhukov Arkady P., 1061, 1231, 1233
Zhukov Roman N., 132
Zhukova V., 1233
Zhukova Valentina, 1061, 1229
Ziaja Jan, 1225
Ziebell M., 70
Zieniutycz Wlodzimierz, 1050
Zilinskas Mindaugas, 1302
Zilk Matthias, 477
Zirath Herbert, 1489
Zohar Moshe, 261
Zou Chang-Ling, 338

Zou Changling, 876, 1498
Zou J., 709
Zou Longfang, 236
Zou Zhi, 68
Zrnic Dusan, 1420
Zubko E., 179
Zubritskaya Irina, 1536
Zueco D., 673
Zukauskas A., 532
Zwol P. J. Van, 251